ENCYCLOPEDIA of SNOW, ICE AND GLACIERS

Edited by
Vijay P. Singh, Pratap Singh and
Umesh K. Haritashya

Springer

ENCYCLOPEDIA of EARTH SCIENCES SERIES

ENCYCLOPEDIA *of* SNOW, ICE AND GLACIERS

Encyclopedia of Earth Sciences Series

ENCYCLOPEDIA OF SNOW, ICE AND GLACIERS

Volume Editors

Vijay P. Singh holds the Caroline and W. N. Lehrer Distinguished Chair in Water Engineering, and is also Professor of Biological and Agricultural Engineering, and Civil and Environmental Engineering at Texas A & M University. He has authored 16 text and reference books, edited 49 books, authored 72 book chapters, and published more than 550 refereed journal articles, 320 conference proceedings papers and 70 technical reports. He is Editor-in-Chief of the Water Science and Technology Book Series of Springer, the ASCE Journal of Hydrologic Engineering, and Water Science and Engineering. He has received more than 60 national and international awards and numerous honors, including the ASCE's Arid Lands Hydraulic Engineering Award; Distinguished Research Master Award from Louisiana State University; ASCE's Ven Te Chow Award; AIH's Ray K. Linsley Award; Hon. Ph.D. from University of Basilicata, Italy; and Hon. Diplomate from American Academy of Water Resources Engineers. He is a fellow of ASCE, AWRA, IE, IAH, ISAE, and IWRS. He is a member/fellow of 10 international science and engineering academies. His research interests include surface and groundwater hydrology, hydraulic engineering, irrigation engineering, and mathematical and stochastic modeling.

Pratap Singh has over 30 years experience in snow and glacier hydrology with an emphasis on modeling of snow and glacier melt runoff. He developed a snow melt model (SNOWMOD), which has been applied for streamflow simulation for snow- and glacier-fed rivers. He has published over 100 technical papers in international/national journals and co-authored with Professor V.P. Singh a book on *Snow and Glacier Hydrology*, published by *Kluwer Academic Publishers*, The Netherlands. He is Associate Editor for the Hydrological Sciences Journal, Wallingford, UK.

Umesh K. Haritashya is a faculty member in the Department of Geology at the University of Dayton, where he teaches courses in glacial geology, geomorphology and remote sensing. He has extensive experience of working on many mountain regions around the world. His research interests include debris cover glacier characterization, glacier dynamics, contribution of glaciers to sea level rise, impact of climate change on mountain glaciers, and glacier hydrology. He is also associated with NASA's GLIMS project and is an editorial board member of the Journal of Hydrologic Engineering, the Open Hydrology Journal, and Himalayan Geology.

Editorial Board

Aims of the Series

The *Encyclopedia of Earth Sciences Series* provides comprehensive and authoritative coverage of all the main areas in the Earth Sciences. Each volume comprises a focused and carefully chosen collection of contributions from leading names in the subject, with copious illustrations and reference lists.

These books represent one of the world's leading resources for the Earth Sciences community. Previous volumes are being updated and new works published so that the volumes will continue to be essential reading for all professional earth scientists, geologists, geophysicists, climatologists, and oceanographers as well as for teachers and students. See the dustjacket of this volume for a current list of titles in the *Encyclopedia of Earth Sciences Series*. Go to http://www.springerlink.com/reference-works/ to visit the "Earth Sciences Series" online.

About the Series Editor

Professor Charles W. Finkl has edited and/or contributed to more than eight volumes in the Encyclopedia of Earth Sciences Series. For the past 25 years he has been the Executive Director of the Coastal Education & Research Foundation and Editor-in-Chief of the international *Journal of Coastal Research*. In addition to these duties, he is Research Professor at Florida Atlantic University in Boca Raton, Florida, USA. He is a graduate of the University of Western Australia (Perth) and previously worked for a wholly owned Australian subsidiary of the International Nickel Company of Canada (INCO). During his career, he acquired field experience in Australia; the Caribbean; South America; SW Pacific islands; southern Africa; Western Europe; and the Pacific Northwest, Midwest, and Southeast USA.

Founding Series Editor

Professor Rhodes W. Fairbridge (deceased) has edited more than 24 Encyclopedias in the Earth Sciences Series. During his career he has worked as a petroleum geologist in the Middle East, been a WW II intelligence officer in the SW Pacific and led expeditions to the Sahara, Arctic Canada, Arctic Scandinavia, Brazil and New Guinea. He was Emeritus Professor of Geology at Columbia University and was affiliated with the Goddard Institute for Space Studies.

ENCYCLOPEDIA OF EARTH SCIENCES SERIES

ENCYCLOPEDIA *of* SNOW, ICE AND GLACIERS

edited by

VIJAY P. SINGH
Texas A&M University
College Station, Texas
USA

PRATAP SINGH
New Delhi
India

UMESH K. HARITASHYA
University of Dayton
Dayton, Ohio
USA

Springer

Library of Congress Control Number: 2011922317

ISBN: 978-90-481-2641-5
This publication is available also as:
Electronic publication under ISBN 978-90-481-2642-2 and
Print and electronic bundle under ISBN 978-90-481-2643-9

Published by Springer
P.O. Box 17, 3300 AA Dordrecht, The Netherlands

Printed on acid-free paper

Cover illustration: photo 81332975 from Photos.com. © 2011 Photos.com

Dedicated to Snow, Ice and Glacier Scientists around the World

Contents

Contributors

James S. Aber
Emporia State University
Emporia, KS 66801-5087
USA
jaber@emporia.edu

Vladimir Aizen
College of Science, Mines Building
University of Idaho
Moscow, ID 83844-3025
USA
aizen@uidaho.edu

Ian Allison
Australian Antarctic Division and Antarctic Climate and Ecosystems CRC
Private Bag 80
Hobart, Tasmania 7001
Australia
ian.allison@utas.edu.au

John T. Andrews
Institute of Arctic and Alpine Research
and Department of Geological Sciences
University of Colorado
Boulder, CO 80309
USA
andrewsj@colorado.edu

Manoj K. Arora
Department of Civil Engineering
Indian Institute of Technology Roorkee
Roorkee 247667
India
manojfce@iitr.ernet.in

Monohar Arora
National Institute of Hydrology (NIH)
Roorkee 247667, UA
India
arora@nih.ernet.in

Cliff Atkins
School of Geography, Environment and Earth Sciences
Victoria University of Wellington
P.O. Box 600
Wellington 6140
New Zealand
Cliff.Atkins@vuw.ac.nz

David B. Bahr
Department of Physics and Computational Science
Regis University
3333 Regis Blvd
Denver, CO 80221-1099
USA
dbahr@regis.edu

Ian Baker
Thayer School of Engineering
Dartmouth College
Hanover, NH 03755
USA
Ian.Baker@Dartmouth.edu

Jostein Bakke
Department of Geography/Bjerknes Centre for Climate Research
University of Bergen
Fosswinckelsgate 6
5020 Bergen
Norway
Jostein.Bakke@geog.uib.no

Lars Bengtsson
Department of Water Resources Engineering
Lund University
P.O. Box 118
22100 Lund
Sweden
Lars.Bengtsson@tvrl.lth.se

Martin Beniston
Interdisciplinary Institute for Environmental Dynamics
University of Geneva
7 route de Drize
1227 Carouge, Geneva
Switzerland
martin.beniston@unige.ch

Matthew R. Bennett
The School of Applied Sciences
Bournemouth University Talbot Campos
Fern Barrow
Dorset BH12 5BB
UK
MBennett@bournemouth.ac.uk

Andrzej Ber
Polish Geological Institute – Polish Research Institute
Warszawa
Poland
andrzej.ber@pgi.gov.pl

Etienne Berthier
LEGOS/CNRS/UPS
14 av. Ed. Belin
31400 Toulouse
France
etienne.berthier@legos.obs-mip.fr

Nancy A. N. Bertler
Joint Antarctic Research Institute
Victoria University of Wellington and GNS Science
P.O. Box 600
Wellington 6140
New Zealand
Nancy.Bertler@vuw.ac.nz

Achim A. Beylich
Quaternary Geology and Climate Group
Geological Survey of Norway (NGU)
Leiv Eirikssons vei 39
7491 Trondheim
Norway
and
Department of Geography
Norwegian University of Science and Technology (NTNU)
Dragvoll
7491 Trondheim
Norway
achim.beylich@NGU.NO

Mahendra R. Bhutiyani
Hazard Assessment and Forecasting Division
Snow and Avalanche Study Establishment
Plot No. 1, Sector 37 A, Him Parisar
Chandigarh 160036
India
mahendra_bhutiyani@yahoo.co.in

Richard Bintanja
Royal Netherlands Meteorological Institute (KNMI)
Wilhelminalaan 10
3732 De Bilt
The Netherlands
R.Bintanja@knmi.nl

Farjana S. Birajdar
Centre of Studies in Resources Engineering
Indian Institute of Technology Bombay
Powai, Mumbai 400076, Maharashtra
India

Michael P. Bishop
Department of Geography and Geology
University of Nebraska-Omaha
6001 Dodge Street
Omaha, NE 68182
USA
mpbishop@mail.unomaha.edu

Tobias Bolch
Department of Geography
University of Zürich-Irchel
Winterthurerstr. 190
8057 Zürich
Switzerland
tobias.bolch@geo.uzh.ch

Sarah Boon
Department of Geography
University of Lethbridge
4401 University Dr
Lethbridge, AB T1K 3M4
Canada
sarah.boon@uleth.ca

David A. Braaten
Center for Remote Sensing of Ice Sheets
Department of Geography
University of Kansas
Lawrence, KS 66045
USA
braaten@ku.edu

Roger J. Braithwaite
Geography Programme, School of Environment and Development
University of Manchester
Oxford Road
Manchester M13 9PL
UK
r.braithwaite@manchester.ac.uk

Claudio Bravo
Centro de Estudios Científicos, CECS
Arturo Prat 514
Valdivia
Chile
cbravo@cecs.cl

Gary J. Brierley
School of Environment
The University of Auckland
10 Symonds Street
Private Bag 92019, Auckland 1142
New Zealand
g.brierley@auckland.ac.nz

Jason P. Briner
Department of Geological Sciences
University at Buffalo
Buffalo, NY 14260
USA
jbriner@buffalo.edu

Margo M. Burgess
Geological Survey of Canada
Natural Resources Canada
601 Booth Street
Ottawa, ON K1A 0E8
Canada
Margo.Burgess@nrcan-rncan.gc.ca

Paolo Burlando
Institute of Environmental Engineering
ETH Zurich
8093 Zurich
Switzerland
paolo.burlando@ifu.baug.ethz.ch

Katie Burles
Department of Geography
University of Lethbridge
4401 University Dr
Lethbridge, AB T1K 3M4
Canada

Andrew B. G. Bush
Department of Earth and Atmospheric Science
University of Alberta
1-26 Earth Sciences Building
Edmonton, AB T6G 2E3
Canada
andrew.bush@ualberta.ca

David R. Butler
Mountain GeoDynamics Research Group
Department of Geography
Texas State University-San Marcos
San Marcos, TX 78666-4616
USA
db25@txstate.edu

Fay Campbell
Department of Geographical and Earth Sciences
University of Glasgow
Glasgow G12 8QQ
UK

Norm R. Catto
Department of Geography
Memorial University of Newfoundland
St. John's, NL A1B 3X9
Canada
ncatto@mun.ca

Fiona Cawkwell
Department of Geography
University College Cork
Cork
Ireland
f.cawkwell@ucc.ie

Anny Cazenave
Laboratoire d'Etudes en Géophysique et Océanographie Spatiales (LEGOS)
LEGOS-CNES, Observatoire Midi-Pyrénées
18 Av. E. Belin
31400 Toulouse
France
Anny.Cazenave@legos.obs-mip.fr
anny.cazenave@gmail.com

Stanley A. Changnon
University of Illinois
Urbana, IL 61853
USA
schangno@illinois.edu

Arun Chaturvedi
Antartic Division
Geological Survey of India
NH 5P
Faridabad 121001
India
arun.daak@gmail.com

Anju Chaudhary
Water Resources System Division
National Institute of Hydrology
Roorkee 247667
India
anju@nih.ernet.in

Jie Cheng
College of Global Change and Earth System Science
Beijing Normal University
19 Xinjiekouwai Street
Beijing 100875
China
brucechan2003@126.com

Jessica Ellen Cherry
International Arctic Research Center and Institute of Northern Engineering
University of Alaska Fairbanks
930 Koyukuk Dr.
Fairbanks, AK 99775-7335
USA
jcherry@iarc.uaf.edu

Poul Christoffersen
Scott Polar Research Institute
University of Cambridge
Lensfield Road
Cambridge CB2 1ER
UK
pc350@cam.ac.uk

John J. Clague
Department of Earth Sciences
Centre for Natural Hazard Research
Simon Fraser University
8888 University Drive
Burnaby, BC V5A 1S6
Canada
jclague@sfu.ca

J. Graham Cogley
Department of Geography
Trent University
Peterborough ON, K9J 7B8
Canada
gcogley@trentu.ca

Jeffrey D. Colby
Department of Geography and Planning
Appalachian State University
Boone, NC 28608
USA
colbyj@appstate.edu

Simon J. Cook
Centre for Glaciology
Institute of Geography and Earth Sciences
Aberystwyth University
H5, Llandinam
Ceredigion, Wales SY23 3DB
UK
smc@aber.ac.uk
basalice@gmail.com

Luke Copland
Department of Geography
University of Ottawa
Ottawa, ON K1N 6N5
Canada
luke.copland@uottawa.ca

Michel Crucifix
Georges Lemaitre Centre for Earth and Climate Research
Université catholique de Louvain
2 chemin du Cyclotron
1348 Louvain-la-Neuve
Belgium
michel.crucifix@uclouvain.be

Ronald P. Daanen
Geophysical Institute
University of Alaska Fairbanks
903 Koyukuk Dr.
Fairbanks, AK 99775-7320
USA
rdaanen@alaska.edu

Prem Datt
Research and Design Center (RDC)
Snow and Avalanche Study Establishment
Plot No-1, Sector 37-A
Himparishar 160036, Chandigarh
India
datt_prem@rediffmail.com

Carmen de Jong
The Mountain Institute
University of Savoy
73376 Pôle Montagne, Le Bourget du Lac
France
carmen.dejong@institut-montagne.org

Reynald Delaloye
Department of Geosciences
Geography University of Fribourg
Ch. du Musee 4
1700 Fribourg
Switzerland
reynald.delaloye@unifr.ch

Philip Deline
EDYTEM Lab
Université de Savoie, CNRS
73376 Le Bourget du Lac
France
pdeli@univ-savoie.fr

Michael N. Demuth
Glaciology Section, Geological Survey of Canada
Earth Sciences Sector Program on Climate Change
Geoscience
Natural Resources Canada
601 Booth Street
Ottawa, ON K1A 0E8
Canada
Mike.Demuth@NRCan-RNCan.GC.CA

Stephen J. Déry
Environmental Science and Engineering Program
University of Northern British Columbia
3333 University Way
Prince George, BC V2N 4Z9
Canada
sdery@unbc.ca

Guglielmina Diolaiuti
Department of Earth Sciences "A. Desio"
University of Milano
Via Mangiagalli 34
20133 Milano
Italy
guglielmina.diolaiuti@unimi.it

D. P. Dobhal
Wadia Institute of Himalayan Geology
33, General Mahadev Singh Road
Dehradun 248001, Uttarakhand
India
dpdobhal@rediffmail.com

Florent Domine
Laboratoire de Glaciologie et Géophysique de l'Environnement
CNRS
BP 96, 54 rue Molière
38402 Saint Martin d'Hères
France
florent@lgge.obs.ujf-grenoble.fr

Divya Dudeja
Department of Geology
DBS (P.G.) College
Dehradun 248001, Uttarakhand
India
divyadudeja@yahoo.co.in

Michael Durand
Byrd Polar Research Center
Ohio State University
108 Scott Hall, 1090 Carmack Road
Columbus, OH 43210
USA
durand.8@osu.edu

Jürgen Ehlers
Geologisches Landesamt
Billstrasse 84
20539 Hamburg
Germany
juergen.ehlers@bsu.hamburg.de

Heidi Escher-Vetter
Commission for Glaciology
Bavarian Academy of Sciences and Humanities
Alfons-Goppel-Strasse 11
80539 Munich
Germany
Heidi.Escher@kfg.badw.de

Richard Essery
School of GeoSciences
University of Edinburgh
Edinburgh EH9 3JW
UK
richard.essery@ed.ac.uk

Steven Fassnacht
Snow Hydrology, Watershed Science Program
Colorado State University
Natural Resources Building Room 335
Fort Collins, CO 80523
USA
srf@warnercnr.colostate.edu

Jiang Fengqing
Xinjiang Institute of Ecology and Geography, CAS
Chinese Academy of Sciences
40-3 South Beijing Road
Urumqi, Xinjiang 830011
China
jiangfengqing@gmail.com
jiangfq@ms.xjb.ac.cn

Xavier Fettweis
Institute for Marine and Atmospheric Research
Utrecht University
Princetonplein 5
3584 CC Utrecht
Netherlands
and
Department of Geography
University of Liège
Allée du 6 Août, 2
4000 Liège
Belgium
xavier.fettweis@ulg.ac.be

Charles Fierz
WSL Institute for Snow and Avalanche Research SLF
7260 Davos Dorf
Switzerland
fierz@slf.ch

Sean J. Fitzsimons
Department of Geography
University of Otago
P.O. Box 56
Dunedin 9054
New Zealand
sjf@geography.otago.ac.nz

Andrew G. Fountain
Department of Geology
Portland State University
P.O. Box 751
Portland, OR 97207-0751
USA
andrew@pdx.edu

Hugh M. French
University of Ottawa (retired)
10945 Marti Lane
North Saanich, British Columbia V8L 5S5
Canada
hmfrench@shaw.ca

Ping Fu
Department of Earth and Atmospheric Sciences
Purdue University
550 Stadium Mall Dr
West Lafayette, IN 47907
USA
pfu@purdue.edu

Yoshinori Furukawa
Research Group for Phase Transition Dynamics of Ice
Institute of Low Temperature Science
Hokkaido University
N19 W8
Sapporo 060-0819
Japan
frkw@lowtem.hokudai.ac.jp

Olivier Gagliardini
Laboratoire de Glaciologie et Géophysique de
l'Environnement du CNRS/UJF
54, rue Molière BP 96
38402 Grenoble
France
gagliardini@lgge.obs.ujf-grenoble.fr

Isabelle Gärtner-Roer
Glaciology, Geomorphodynamics and Geochronology
Department of Geography
University of Zürich
Winterthurerstrasse 190
8057 Zürich
Switzerland
isabelle.roer@geo.uzh.ch

John R. Giardino
Department of Geology and Geophysics
Texas A&M University
College Station, TX 77843-3115
USA
rickg@tamu.edu

Philip Gibbard
Quaternary Palaeoenvironments Group, Cambridge
Quaternary
Department of Geography
University of Cambridge
Downing Street
Cambridge CB2 3EN
UK
plg1@cam.ac.uk

Alan R. Gillespie
Department of Earth and Space Sciences
Quaternary Research Center
University of Washington
Seattle, WA 98195-1310
USA
arg3@u.washington.edu

Neil F. Glasser
Centre for Glaciology, Institute of Geography & Earth
Sciences
Aberystwyth University
Aberystwyth, Ceredigion, Wales SY23 3DB
UK
nfg@aber.ac.uk

Manmohan Kumar Goel
Water Resources System
National Institute of Hydrology
Roorkee 247667, Uttarakhand
India
goel_m_k@yahoo.com
mkg@nih.ernet.in

Gavin Gong
Department of Earth and Environmental Engineering
Henry Krumb School of Mines
Columbia University
500 West. 120th Street, MC4711
New York, NY 10027
USA
gg2138@columbia.edu

Alastair G. C. Graham
Ice Sheets Programme, British Antarctic Survey
High Cross, Madingley Road
Cambridge CB3 0ET
UK
alah@bas.ac.uk

Amanda M. Grannas
Department of Chemistry
Villanova University
800 Lancaster Ave
Villanova, PA 19085
USA
amanda.grannas@villanova.edu

Thomas C. Grenfell
Department of Atmospheric Sciences
University of Washington
Seattle, WA 98195-1640
USA
tcg@atmos.washington.edu

G. Hilmar Gudmundsson
British Antarctic Survey
High Cross Madingley Road
Cambridge CB3 0ET
UK
ghg@bas.ac.uk

Ravi P. Gupta
Department of Earth Sciences
Indian Institute of Technology Roorkee
Roorkee 247667, UA
India
rpgupta.iitr@gmail.com
rpgesfes@iitr.ernet.in

Wilfried Haeberli
Glaciology, Geomorphodynamics & Geochronology
Geography Department
University of Zurich
Winterthurerstrasse 190
8057 Zurich
Switzerland
wilfried.haeberli@geo.uzh.ch

Brenda L. Hall
Department of Earth Sciences and
Climate Change Institute
Bryand Global Sciences Center
University of Maine
Orono, ME 04469
USA
BrendaH@maine.edu

Dorothy K. Hall
Crysopheric Sciences Branch
Code 614.1, NASA/Goddard Space Flight Center
Greenbelt, MD 20771
USA
dorothy.k.hall@nasa.gov

Michael J. Hambrey
Centre for Glaciology
Institute of Geography & Earth Sciences
Aberystwyth University
Aberystwyth, Ceredigion, Wales SY23 3DB
UK
mjh@aber.ac.uk

Jonathan Harbor
Department of Earth and Atmospheric Sciences
Purdue University
550 Stadium Mall Dr
West Lafayette, IN 47907
USA
jharbor@purdue.edu

Douglas R. Hardy
Climate System Research Center and
Department of Geosciences
University of Massachusetts
Morrill Science Center
611 North Pleasant Street
Amherst, MA 01003-9297
USA
dhardy@geo.umass.edu
doug.hardy@valley.net

Spencer P. Hardy
Hanover High School
41 Lebanon St
Hanover, NH 03755
USA

Chelamallu Hariprasad
Centre for Studies in Resource Engineering
Indian Institute of Technology, Bombay
Powai, Mumbai 400076, Maharashtra
India
chariprasad@iitb.ac.in

Umesh K. Haritashya
Department of Geology
University of Dayton
300 College Park
Dayton, OH 45469-2364
USA
ukharit@yahoo.com
Umesh.Haritashya@notes.udayton.edu

Stephan Harrison
School of Geography, Archaeology and Earth Resources
University of Exeter
Cornwall Campus
Penryn, Cornwall TR10 9EZ
UK
stephan.harrison@exeter.ac.uk

Kenneth Hewitt
Cold Regions Research Centre
Wilfrid Laurier University
75 University Avenue West
Waterloo, ON N2L 3C5
Canada
khewitt@wlu.ca

Christopher A. Hiemstra
Cold Regions Research and Engineering Laboratory (CRREL)
U.S. Army Corps of Engineers, ERDC
P.O. Box 35170
Fort Wainwright, AK 99703-0170
USA
Christopher.A.Hiemstra@usace.army.mil

Richard Hodgkins
Department of Geography
Loughborough University
Leicestershire LE11 3TU
UK
r.hodgkins@lboro.ac.uk

Bryn Hubbard
Centre for Glaciology
Institute of Geography and Earth Sciences
Aberystwyth University
Llandinam Building
Aberystwyth, Ceredigion, Wales SY23 3DB
UK
byh@aber.ac.uk

Philip D. Hughes
Geography, School of Environment and Development
The University of Manchester
Arthur Lewis Building
Manchester M13 9PL
UK
philip.hughes@manchester.ac.uk

Terry Hughes
Department of Earth Science
University of Maine
Orono, ME 04469-5790
USA
and
Climate Change Institute
University of Maine
Orono, ME 04469-5790
USA
terry.hughes@maine.edu

Lasafam Iturrizaga
Department of Geography/High Mountain Geomorphology
Institute of Geography
University of Göttingen
Goldschmidtstr. 5
37077 Göttingen
Germany
liturri@gwdg.de

C. K. Jain
National Institute of Hydrology
Centre for Flood Management Studies
G. S. Road, Sapta Sahid Path, Mathura Nagar
Dispur, Guwahati 781006, Assam
India
ckj_1959@yahoo.co.in

Manoj K. Jain
Department of Hydrology
Indian Institute of Technology
Roorkee 247667, Uttarakhand
India
jain.mkj@gmail.com

Sanjay K. Jain
National Institute of Hydrology
Roorkee, 247667 Uttarakhand
India
Sjain@nih.ernet.in

Adrian Jenkins
British Antarctic Survey
Natural Environment Research Council
High Cross, Madingley Road
Cambridge CB3 0ET
UK
ajen@bas.ac.uk
a.jenkins@bas.ac.uk

Hester Jiskoot
Department of Geography
University of Lethbridge
4401 University Drive W
Lethbridge, AB T1K 3M4
Canada
hester.jiskoot@uleth.ca

Jerome B. Johnson
Institute of Northern Engineering
University of Alaska Fairbanks
P.O. Box 755910
Fairbanks, AK 99775-5910
USA
jerome.b.johnson@alaska.edu

Tobias Jonas
Snow Hydrology Research Group
WSL Institute for Snow and Avalanche Research SLF
7260 Davos
Switzerland
jonas@slf.ch

M. Torre Jorgenson
Alaska Ecoscience
Fairbanks, AK 99709
USA
tjorgenson@abrinc.com

Andreas Kääb
Department of Geosciences
University of Oslo
Sem Sælands vei 1, 1047
Blindern, 0316 Oslo
Norway
kaeaeb@geo.uio.no

M. Z. Kanevskiy
Department of Civil and Environmental Engineering
University of Alaska Fairbanks
245 Duckering Building, P.O. Box 755900
Fairbanks, AK 99775-59000
USA
mkanevskiy@alaska.edu

Shichang Kang
Key Laboratory of Tibetan Environmental Changes and Land Surface Processes
Institute of Tibetan Plateau Research
Chinese Academy of Sciences
No.18, Shuangqing Rd., P.O. Box 2871
Haidian District, Beijing 100085
China
and
State Key Laboratory of Cryospheric Sciences
Chinese Academy of Sciences
Lanzhou 730000
China
Shichang.Kang@itpcas.ac.cn

Martin Kappas
Cartography, GIS and Remote Sensing Section
Institute of Geography
Georg-August University Göttingen
Goldschmidtstr. 5
37077 Göttingen
Germany
mkappas@gwdg.de

Rijan B. Kayastha
Himalayan Cryosphere, Climate and Disaster Research Center (HiCCDRC)
Kathmandu University
Dhulikhel, Kavre
P.O. Box 6250, Kathmandu
Nepal
rijan@ku.edu.np

Matt A. King
School of Civil Engineering and Geosciences
Newcastle University
Cassie Building
Newcastle upon Tyne NE1 7RU
UK
m.a.king@ncl.ac.uk

Martin P. Kirkbride
Geography, School of the Environment
University of Dundee
Perth Road
Dundee DD1 4HN, Scotland
UK
m.p.kirkbride@dundee.ac.uk

Peter G. Knight
School of Physical and Geographical Sciences
Keele University
William Smith Building
Staffordshire ST5 5BG
UK
p.g.knight@esci.keele.ac.uk

Johannes Koch
Department of Earth Sciences
Simon Fraser University
Burnaby, BC V5A 1S6
Canada
jkoch@sfu.ca

Lynn Koehler
University of Victoria Tree-Ring Laboratory
Department of Geography
University of Victoria
Victoria, British Columbia V8W 3R4
Canada
lynn.koehler@gmail.com

Markus Konz
Institute of Environmental Engineering
Hydrology and Water Resources Management
ETH Zürich
Wolfgang-Pauli-Str. 15
8093 Zurich
Switzerland
markus.konz@ifu.baug.ethz.ch

Nadine Konz
Institute of Environmental Geosciences
University of Basel
4003 Basel
Switzerland
nadine.konz@unibas.ch

Akhouri Pramod Krishna
Department of Remote Sensing
Birla Institute of Technology (BIT)
Deemed University
P.O. Mesra
Ranchi 835215, Jharkhand
India
apkrishna@ewca.eastwestcenter.org
apkrishna@bitmesra.ac.in

Matthias Kuhle
Department of Geography and High Mountain Geomorphology
Geographical Institute
University of Göttingen
Goldschmidtstr. 5
37077 Göttingen
Germany
mkuhle@gwdg.de

Amit Kumar
Department of Geology
Centre of Advanced Study in Geology
Punjab University
Sector-14
Chandigarh 160014, Punjab
India
amithydrocoin@gmail.com
amitwalia@wihg.res.in

Bhishm Kumar
Hydrological Investigations Division
National Institute of Hydrology
Roorkee 247667, Uttarakhand
India
bk@nih.ernet.in
bhishm_nih@yahoo.co.in

Rajesh Kumar
School of Engineering and Technology
Sharda University
32–34, Knowledge Park-III
Greater Noida 201306, NCR
India
and
Remote Sensing Division
Birla Institute of Technology, Extension Centre Jaipur
27, Malviya Industrial Area
Jaipur 302017, Rajasthan
India
rajeshbhu@yahoo.com

Vijay Kumar
National Institute of Hydrology
Roorkee 247667, Uttarakhand
India
vijay@nih.ernet.in
vk_nih@yahoo.com

Christophe Lambiel
Institute of Geography
University of Lausanne
Bâtiment Anthropole
1015 Lausanne
Switzerland
christophe.lambiel@unil.ch

Wendy Lawson
Department of Geography
University of Canterbury
Private Bag 4800
Christchurch 8140
New Zealand
wendy.lawson@canterbury.ac.nz

Daniel J. Leathers
Department of Geography
University of Delaware
Newark, DE 19716-2541
USA
leathers@udel.edu

Jean-Michel Lemieux
Département de géologie et de génie géologique
Université Laval
1065 avenue de la Médecine
Québec, QC G1V 0A6
Canada
jmlemieux@ggl.ulaval.ca

Eric M. Leonard
Department of Geology
Colorado College
14E Cache la Poudre
Colorado Springs, CO 80903
USA
eleonard@coloradocollege.edu

Matti Leppäranta
Department of Physics
University of Helsinki
P.O. Box 64, (Gustaf Hällströmin katu 2a)
00014 Helsinki
Finland
matti.lepparanta@helsinki.fi

Delphis F. Levia
Department of Geography
University of Delaware
Newark, DE 19716-2541
USA
dlevia@udel.edu

Shunlin Liang
Department of Geography
University of Maryland
2181 LeFrak Hall
College Park, MD 20742
USA
sliang@umd.edu

Kenneth G. Libbrecht
Department of Physics
Caltech
264-33 Caltech
Pasadena, CA 91125
USA
kgl@caltech.edu

Ron Lindsay
Polar Science Center
Applied Physics Laboratory
University of Washington
1013 NE 40th Street
Seattle, WA 98105-6698
USA
lindsay@apl.washington.edu

Glen E. Liston
Cooperative Institute for Research in the Atmosphere
Colorado State University
1375 Campus Delivery
Fort Collins, CO 80523-1375
USA
liston@cira.colostate.edu

Jingshi Liu
Institute of Tibetan Plateau Research
Chinese Academy of Sciences
18 Shuangqing Rd.
Haidian District, Beijing 100085
China
jsliu@itpcas.ac.cn

Yongqin Liu
Laboratory of Tibetan Environment Changes and Land Surface Processes (TEL)
Institute of Tibetan Plateau Research
Chinese Academy of Sciences
No. 18 Shuangqing Rd, P.O. Box 2871
Haidian District, Beijing 100085
China
yqliu@itpcas.ac.cn

Christopher Lloyd
Department of Geography
University of Sheffield
Sheffield S10 2TN
UK
ggp08ctl@sheffield.ac.uk

Rachel W. Lomonaco
Thayer School of Engineering
Dartmouth College
Hanover, NH 03755
USA

Reginald D. Lorrain
Département des Sciences de la Terre et de l'Environnement
Université Libre de Bruxelles
Bruxelles
Belgium
rlorrain@ulb.ac.be

Mira Losic
Department of Geography
University of Calgary
Earth Sciences 356, 2500 University Dr NW
Calgary, AB T2N 1N4
Canada
mlosic@ucalgary.ca

Sven Lukas
Department of Geography
Queen Mary University of London
Mile End Road
London E1 4NS
UK
S.Lukas@qmul.ac.uk

Juha P. Lunkka
Institute of Geosciences
University of Oulu
P.O. Box 3000
90014 Oulu
Finland
juha.pekka.lunkka@oulu.fi

Kelly MacGregor
Geology Department
Macalester College
1600 Grand Avenue
Saint Paul, MN 55105
USA
macgregor@macalester.edu

William C. Mahaney
Quaternary Surveys
26 Thornhill Ave
Thornhill, ON L4J 1J4
Canada
arkose@rogers.com
bmahaney@yorku.ca

Shawn J. Marshall
Department of Geography
University of Calgary
Earth Sciences 356, 2500 University Dr NW
Calgary, AB T2N 1N4
Canada
shawn.marshall@ucalgary.ca

Richard A. Marston
Department of Geography
Kansas State University
118 Seaton Hall
Manhattan, KS 66506-2904
USA
Rmarston@ksu.edu
Rmarston@k-state.edu

Christoph Marty
WSL Institute for Snow and Avalanche Research SLF
Flüelastr. 11
7260 Davos
Switzerland
marty@slf.ch

Robert D. McCulloch
School of Biological and Environmental Science
University of Stirling
Stirling FK9 4LA, Scotland
UK
robert.mcculloch@stir.ac.uk

Brian Menounos
Geography Program and Natural Resources and
Environmental Studies Institute
University of Northern British Columbia
3333 University Way
Prince George, BC V2N 4Z9
Canada

Justin R. Minder
Department of Atmospheric Science
University of Washington
Box 351640
Seattle, WA 98195-1640
USA
juminder@atmos.washington.edu

Debasmita Misra
Department of Mining and Geological Engineering
College of Engineering and Mines
University of Alaska Fairbanks
P.O. Box 755800
Fairbanks, AK 99775-5800
USA
debu.misra@alaska.edu

Vanya I. Miteva
Department of Biochemistry and Molecular Biology
The Pennsylvania State University
211 South Frear
University Park, PA 16802
USA
vim1@psu.edu

Thomas Mölg
Center for Climate & Cryosphere
University of Innsbruck
6020 Innsbruck
Austria

Peter Molnar
Institute of Environmental Engineering
ETH Zurich
8093 Zurich
Switzerland
molnar@ifu.baug.ethz.ch

Bruce F. Molnia
U.S. Geological Survey
562 National Center, 12201 Sunrise Valley Drive, 12201
Reston, VA 20192
USA
bmolnia@usgs.gov

Brian Morse
Department of Civil and Water Engineering
Laval University
1065, ave de la Médecine
Quebec, QC G1V 0A6
Canada

Nozomu Naito
Department of Global Environment Studies
Hiroshima Institute of Technology
Miyake 2-1-1, Saeki-ku
Hiroshima 731-5193
Japan
naito@cc.it-hiroshima.ac.jp

Jacob Napieralski
Department of Natural Sciences
University of Michigan-Dearborn
Dearborn, MI 48128
USA
jnapiera@umd.umich.edu

Atle Nesje
Department of Earth Science\Bjerknes Centre for Climate Research
University of Bergen
Allégaten 41
5007 Bergen
Norway
atle.nesje@geo.uib.no

Thomas A. Neumann
NASA Goddard Space Flight Center
Greenbelt, MD 20771
USA
thomas.neumann@nasa.gov

Peter W. Nienow
School of Geosciences
University of Edinburgh
Drummond Street
Edinburgh EH8 9XP
UK
pnienow@geo.ed.ac.uk

David C. Nobes
Department of Geological Sciences
University of Canterbury
Private Bag 4800
Christchurch 8140
New Zealand
david.nobes@canterbury.ac.nz

Rachel W. Obbard
Thayer School of Engineering
Dartmouth College
Hanover, NH 03755
USA
Rachel.w.obbard@dartmouth.edu

Øyvind Paasche
Bjerknes Centre for Climate Research
University of Bergen
Allégaten 55
5007 Bergen
Norway
and
Department of Research Management
University of Bergen
Professor Keysers gt. 8
5020 Bergen
Norway
oyvind.paasche@uni.no

Thomas H. Painter
Jet Propulsion Laboratory/Caltech
4800 Oak Grove Drive
Pasadena, CA 91109
USA
Thomas.Painter@jpl.nasa.gov

Pratima Pandey
Centre of Studies in Resources Engineering
Indian Institute of Technology Bombay
Powai, Mumbai 400076, Maharashtra
India
pratimapandey@iitb.ac.in

Himali Panthri
Department of Geology
D.B.S (P.G) College
Dehradun 248001, Uttarakhand
India
himali.geo@gmail.co

Frank Paul
Department of Geography
University of Zurich
Winterthurerstrasse 190
8057 Zurich
Switzerland
frank.paul@geo.uzh.ch

Francesca Pellicciotti
Institute of Environmental Engineering
ETH Zurich
8093 Zurich
Switzerland
francesca.pellicciotti@ifu.baug.ethz.ch

Mauri S. Pelto
Department of Environmental Science
Nichols College
Dudley, MA 01571
USA
mauri.pelto@nichols.edu

Christine Pielmeier
WSL Institute for Snow and Avalanche Research SLF
Warning and Prevention
Flüelastrasse 11
7260 Davos Dorf
Switzerland
pielmeier@slf.ch

Jan A. Piotrowski
Department of Earth Sciences
University of Aarhus
Høegh-Guldbergs Gade 2
8000 Aarhus C
Denmark
and
Department of Geography
University of Sheffield
Sheffield S10 2TN
UK
jan.piotrowski@geo.au.dk

Philip R. Porter
Division of Geography and Environmental Sciences
School of Life Sciences
University of Hertfordshire
Hatfield, Hertfordshire AL10 9AB
UK
p.r.porter@herts.ac.uk

George Postma
Faculty of Geosciences
EUROTANK Laboratories
P.O. Box 80.021
3508 TA Utrecht
The Netherlands
gpostma@geo.uu.nl

P. Pradeep Kumar
Department of Atmospheric and Space Sciences
Pune University
Pune 411007, Maharashtra
India
ppk@physics.unipune.ac.in

Daniel J. Pringle
Arctic Region Supercomputing Center and Geophysical Institute
University of Alaska
Fairbanks, AK 99775
USA
danielpringle75@gmail.com

John C. Priscu
Department of Land Resources and Environmental Sciences
Montana State University
Bozeman, MT 59717
USA
jpriscu@montana.edu

Duncan J. Quincey
Institute of Geography and Earth Sciences
Penglais Campus
Aberystwyth University
Aberystwyth, Wales SY23 3DB
UK

Camilo Rada
Centro de Estudios Científicos, CECS
Arturo Prat 514
Valdivia
Chile

Y. S. Rao
Centre of Studies in Resources Engineering
Indian Institute of Technology
Powai, Mumbai 400076
India
ysrao@iitb.ac.in

Donald Rapp
Independent Contractor
1445 Indiana Avenue
South Pasadena, CA 91030
USA
drdrapp@earthlink.net

Rasik Ravindra
National Centre for Antarctic and Ocean Research
Headland Sada, Vasco-Da-Gama
Goa 403804
India
rasik@ncaor.org

Netra R. Regmi
Department of Geology and Geophysics
Texas A&M University
College Station, TX 77843-3115
USA
netraregmi@neo.tamu.edu

Helen E. Reid
School of Environment
The University of Auckland
10 Symonds Street
Private Bag 92019, Auckland 1142
New Zealand
h.reid@auckland.ac.nz

Alan W. Rempel
Department of Geological Sciences
University of Oregon
Eugene, OR 97403-1272
USA
rempel@uoregon.edu

Jeffrey Ridley
Met Office, Hadley Centre
FitzRoy Road
Exeter EX1 3PB
UK

George A. Riggs
SSAI
10210 Greenbelt Road, Suite 600
Lanham, MD 20706
USA
george.a.riggs@nasa.gov

Eric Rignot
Department of Earth System Science
University of California Irvine
Irvine, CA 92697
USA
and
Jet Propulsion Laboratory
4800 Oak Grove Drive
Pasadena, CA 91214
USA
erignot@uci.edu

Vinvent Rinterknecht
School of Geography and Geosciences
University of St Andrews
North Street
St Andrews KY16 9AL, Scotland
UK
vr10@st-andrews.ac.uk

Daniel Riseborough
Geological Survey of Canada
601 Booth Street
Ottawa, ON K1A 0E4
Canada
drisebor@nrcan.gc.ca

Andrés Rivera
Centro de Estudios Científicos, CECS
Arturo Prat 514
Valdivia
Chile
and
Universidad de Chile
Marcoleta 250
Santiago
Chile
and
Centro de Ingeniería de la Innovación, CIN
Arturo Prat 514
Valdivia
Chile
arivera@cecs.cl

Gerard H. Roe
Department of Atmospheric Science
University of Washington
Box 351640
Seattle, WA 98195-1640
USA
and
Department of Earth and Space Sciences
University of Washington
2206 N41 St
Seattle, WA 98103
USA
gerard@ess.washington.edu

Neil Ross
School of Geosciences
University of Edinburgh
Geography Building
Drummond Street
Edinburgh EH8 9XP
UK
neil.ross@ed.ac.uk

Anders Schomacker
Institute of Earth Sciences
University of Iceland
Askja, Sturlugata 7
101 Reykjavík
Iceland
and
Department of Geology
Norwegian University of Science and Technology
7491 Trondheim
Norway
anders@hi.is

Bob E. Schutz
Center for Space Research
University of Texas at Austin
Austin, TX 78759
USA
schutz@csr.utexas.edu

Annette Semádeni-Davies
Department of Water Resources Engineering
Lund University
22100 Lund
Sweden
annette.davies@tvrl.lth.se

Hung Tao Shen
Department of Civil and Environmental Engineering
Clarkson University
P.O. Box 5710
Potsdam, NY 13699-5710
USA
htshen@clarkson.edu

Arun B. Shrestha
International Centre for Integrated Mountain Development (ICIMOD)
Khumaltar, Lalitpur, GP.O. Box 3226
Kathmandu
Nepal
abshrestha@icimod.org

John F. Shroder
Department of Geography and Geology
University of Nebraska at Omaha
6001 Dodge Street
Omaha, NE 68182
USA
jshroder@mail.unomaha.edu

Aparna Shukla
Uttarakhand Space Application Centre
Dehradun
India
aparna.shukla22@gmail.com

Yuri Shur
Department of Civil and Environmental Engineering
University of Alaska Fairbanks
245 Duckering Building, P.O. Box 755900
Fairbanks, AK 99775-59000
USA
yshur@alaska.edu

Martin J. Siegert
School of GeoSciences
University of Edinburgh
Grant Institute
West Mains Road
Edinburgh EH9 3JW
UK
m.j.siegert@ed.ac.uk

Oddur Sigurðsson
Veðurstofu Íslands
Icelandic Meteorological Office
Bústaðavegi 9
150 Reykjavík
Iceland
oddur@vedur.is

A. K. Singh
DIAT (Deemed University)
Girinagar
Pune 411025, Maharashtra
India
draksingh@hotmail.com
aksingh@diat.ac.in

Gulab Singh
Centre of Studies in Resources Engineering
Indian Institute of Technology Bombay
Powai
Mumbai 400076, Maharashtra
India
gskaliar@iitb.ac.in

Pratap Singh
Integrated Natural Resources Management (INRM)
Consultants Pvt. Ltd
An Incubatee Company of IIT Delhi
New Delhi
India
and
Hydro Tasmanier Consulting
Nehru Place
New Delhi 110019
India
pratap_singh_1@yahoo.com
pratapsingh.iitd@gmail.com

Vijay P. Singh
Department of Biological and Agricultural Engineering
Texas A&M University
Scoates Hall
2117 TAMU
College Station, TX 77843-2117
USA
vsingh@tamu.edu

Subhajit Sinha
DBS College
Dehradun, Uttarakhand
India
sinha_subho@rediffmail.com

Claudio Smiraglia
Department of Earth Sciences "A. Desio"
University of Milano
Via Mangiagalli 34
20133 Milano
Italy
claudio.smiraglia@unimi.it

Andy M. Smith
British Antarctic Survey, High Cross
Madingley Road
Cambridge CB3 0ET
UK
amsm@bas.ac.uk

Dan J. Smith
University of Victoria Tree-Ring Laboratory
Department of Geography
University of Victoria
Victoria, British Columbia V8W 3R4
Canada

Sharon L. Smith
Geological Survey of Canada
Natural Resources Canada
601 Booth Street
Ottawa, ON K1A 0E8
Canada
Sharon.Smith@nrcan-rncan.gc.ca

Rudolph R. Stea
Stea Surficial Geology Services
851 Herring Cove Road
Halifax, Nova Scotia B3R 1Z1
Canada
ralphstea@eastlink.ca

Chris R. Stokes
Department of Geography
Durham University
Science Site, South Road
Durham DH1 3LE
UK
c.r.stokes@durham.ac.uk

Tim Stott
Physical Geography and Outdoor Education
Liverpool John Moores University
I. M. Marsh Campus, Barkhill Road
Liverpool L17 6BD
UK
t.a.stott@ljmu.ac.uk

Edward A. Sudicky
Department of Earth and Environmental Sciences
University of Waterloo
Waterloo, ON N2L 3G1
Canada
sudicky@sciborg.uwaterloo.ca

Kazuyoshi Suzuki
Research Institute for Global Change
Japan Agency for Marine-Earth Science and Technology
3173-25 Showa-machi
Yokohama 236-0001
Japan
skazu@jamstec.go.jp

Ryohei Suzuki
Graduate School of Environmental Studies
Nagoya University
c/o Hydrospheric Atmospheric Research Center
Furo-cho Chikusa-ku
Nagoya 464-8601
Japan
cryosuzuki@nagoya-u.jp

Darrel A. Swift
Department of Geography
University of Sheffield
Sheffield S10 2TN
UK
D.A.Swift@sheffield.ac.uk

Nozomu Takeuchi
Department of Earth Sciences
Graduate School of Science
Chiba University
1-33 Yayoicho, Inage-ku, Chiba-city
Chiba 263-8522
Japan
ntakeuch@faculty.chiba-u.jp

Renoj J. Thayyen
Western Himalayan Regional Centre
National Institute of Hydrology
Jammu (J&K) 180003
India
renojthayyen@gmail.com

Malte Thoma
Bavarian Academy and Sciences, Commission for Glaciology
Alfons-Goppel-Str. 11
80539 Munich
Germany
and

Alfred Wegener Institute for Polar and Marine Research
Bussestrasse 24
27570 Bremerhaven
Germany
Malte.Thoma@awi.de

David N. Thomas
School of Ocean Sciences, College of Natural Sciences
Bangor University
Menai Bridge, Anglesey LL59 5AB
UK
d.thomas@bangor.ac.uk

Anita M. Thompson
Department of Biological Systems Engineering
University of Wisconsin-Madison
230 Ag. Eng. Building, 460 Henry Mall
Madison, WI 53706
USA
amthompson2@wisc.edu

Thierry Toutin
Canada Centre for Remote Sensing
Natural Resources Canada
Ottawa, ON K1A 0Y7
Canada
thierry.toutin@ccrs.nrcan.gc.ca

Martyn Tranter
Bristol Glaciology Centre
School of Geographical Sciences
University of Bristol
University Road
Bristol BS8 1SS
UK
m.tranter@bristol.ac.uk

Donna F. Tucker
Department of Geography
University of Kansas
1475 Jayhawk Blvd., Room 213
Lawrence, KS 66045-7613
USA
dtucker@ku.edu

Hugh Tuffen
Lancaster Environment Centre
Lancaster University
Lancaster LA1 4YQ
UK
h.tuffen@lancaster.ac.uk

Fiona Tweed
Department of Geography
Staffordshire University
College Road
Stoke-on-Trent, Staffordshire ST4 2DE
UK
f.s.tweed@staffs.ac.uk

Michiel Van den Broeke
Institute for Marine and Atmospheric Research
Utrecht University
Princetonplein 5
3584 CC Utrecht
Netherlands
m.r.vandenbroeke@uu.nl

C. J. van der Veen
Department of Geography and
Center for Remote Sensing of Ice Sheets
University of Kansas
203 Lindley Hall
1475 Jayhawk Blvd
Lawrence, KS 66045-7613
USA
cjvdv@ku.edu

Veerle Vanacker
TECLIM, Earth and Life Institute
University of Louvain
Place L. Pasteur, 3
1348 Louvain-la-Neuve, BW
Belgium
veerle.vanacker@uclouvain.be

Dominic Vella
Department of Applied Mathematics and Theoretical Physics
Institute of Theoretical Geophysics
University of Cambridge
Wilberforce Road
Cambridge CB3 0WA
UK
d.vella@damtp.cam.ac.uk

G. Venkataraman
Centre of Studies of Resources Engineering
Indian Institute of Technology Bombay
Mumbai 400076
India
gv@iitb.ac.in

Ashok Kumar Verma
Department of Geography and Environmental Studies
Cold Regions Research Center
Wilfrid Laurier University
75 University Ave. West
Waterloo, ON N2L 3C5
Canada
ashokpph@gmail.com
verm3620@wlu.ca

Andreas Vieli
Department of Geography
Durham University
Durham DH1 3LE
UK
Andreas.Vieli@durham.ac.uk

Timo Vihma
Finnish Meteorological Institute
Erik Palménin aukio 1, P.O. Box 503
00101 Helsinki
Finland
timo.vihma@fmi.fi

John D. Vitek
Department of Geology and Geophysics
Texas A&M University
College Station, TX 77843-3115
USA
jvitek@neo.tamu.edu

Mathias Vuille
Department of Atmospheric and Environmental Sciences
University at Albany
State University of New York
1400 Washington Avenue
Albany, NY 12222
USA
mathias@atmos.albany.edu

John Wahr
Department of Physics and CIRES
University of Colorado
Boulder, CO 80309-0390
USA
wahr@lemond.colorado.edu

Stephen J. Walsh
Department of Geography
University of North Carolina
Chapel Hill, NC 27599-3220
USA
swalsh@email.unc.edu

Charles R. Warren
School of Geography and Geosciences
University of St. Andrews
Irvine Building
St. Andrews, Fife KY16 9AL, Scotland
UK
charles.warren@st-andrews.ac.uk

Daniel J. Weiss
Department of Geography
University of North Carolina
Chapel Hill, NC 27599-3220
USA

John Wettlaufer
Yale University
New Haven, CT 06520-8109
USA
john.wettlaufer@yale.edu

Roger Wheate
Geography Program and Natural Resources and
Environmental Studies Institute
University of Northern British Columbia
3333 University Way
Prince George, BC V2N 4Z9
Canada
wheate@unbc.ca

Ian C. Willis
Department of Geography
Scott Polar Research Institute
University of Cambridge
Lensfield Road
Cambridge CB2 1ER
UK
iw102@cam.ac.uk

John Woodward
Division of Geography
School of Applied Sciences
Northumbria University
Ellison Place
Newcastle upon Tyne NE1 8ST
UK
john.woodward@unn.ac.uk

Cunde Xiao
State Key Laboratory of Cryospheric Sciences
Cold and Arid Regions Environmental and Engineering
Research Institute, Chinese Academy of Sciences
Lanzhou, Gansu 730000
China
cdxiao@ns.lzb.ac.cn
cdxiao@cams.cma.gov.cn

Zhang Yanwei
Xinjiang Institute of Ecology and Geography
Chinese Academy of Sciences
40-3 South Beijing Road
Urumqi, Xinjiang 830011
China

Tandong Yao
Laboratory of Tibetan Environment Changes and Land Surface Processes (TEL)
Institute of Tibetan Plateau Research
Chinese Academy of Sciences
No. 18 Shuangqing Rd, P.O. Box 2871
Haidian District, Beijing 100085
China
tdyao@itpcas.ac.cn

Jacob C. Yde
Center for Geomicrobiology
University of Aarhus
Ny Munkegade building 1540
8000 Århus C
Denmark
and
Bjerknes Centre for Climate Research
University of Bergen
Allégaten 55
5007 Bergen
Norway
yde@phys.au.dk

Wusheng Yu
Laboratory of Tibetan Environment Changes and Land Surface Processes (TEL)
Institute of Tibetan Plateau Research
Chinese Academy of Sciences
No. 18 Shuangqing Rd, P.O. Box 2871
Haidian District, Beijing 100085
China

Tingjun Zhang
National Snow and Ice Data Center
Cooperative Institute for Research in Environmental Sciences
University of Colorado at Boulder
Boulder, CO 80309-0449
USA
tzhang@nsidc.org

Huabiao Zhao
Laboratory of Tibetan Environment Changes and Land Surface Processes (TEL)
Institute of Tibetan Plateau Research
Chinese Academy of Sciences
No. 18 Shuangqing Rd, P.O. Box 2871
Haidian District, Beijing 100085
China

H. J. Zwally
NASA Goddard Space Flight Center
Greenbelt, MD 20771
USA
zwally@icesat2.gsfc.nasa.gov

Preface

Snow, ice and glaciers (SIG) are the components constituting what is called cryosphere. They exist at all latitudes and contain the majority of the earth's fresh water. Due to their dominant prevalence, they influence weather, climate, ecosystems, vegetation, and life and human activities in a variety of ways. Indeed they shape human civilization. Owing to looming climate change and global warming, temperature changes now seem inevitable and are changing the landscape of snow, ice and glaciers, or even the existence thereof. In fact, the changes occurring in SIG can be construed as major indicators of climate change. The nature of cryosphere is highly interdisciplinary and calls for an updated interdisciplinary account of its dynamics. Recent decades have witnessed increasing attention to SIG and scientific communities have started working collectively to develop the basic foundation upon which the broad understanding of cryosphere rests. However, there is still a long way to go.

Discussions on climate change and global warming now seem to be occupying the center stage in public debates, professional forums, news media, and political dialog. As a result, the general public has become much more aware of what is happening to our climate. Since both climate change and climate variability have been found to be closely linked with the cryosphere, it is important for scientists and professionals in the field of earth, environmental, oceanic and atmospheric sciences to develop a better understanding of this sphere from conceptual, theoretical, technical and applied viewpoints. This is especially important for snow, ice and glacier covered areas, since they are rarely stable and are continuously changing in their thickness, areal extent, and flow speeds. Recent advances in field-based studies and quantitative and numerical modeling have provided answers to several key questions but have also highlighted the urgent need for cryospheric studies in many areas, for example, contribution of snow, ice and glacier melt to the sea level rise; importance of snow and glacier to water resources; and so on.

The objective of this Encyclopedia is to present the current state of scientific understanding of various aspects of earth's cryosphere – snow, glaciers, ice caps, ice sheets, ice shelves, sea ice, river and lake ice, and permafrost – and their related interdisciplinary connections under one umbrella. Therefore, every effort has been made to provide a comprehensive coverage of cryosphere by including a broad array of topics, such as the atmospheric processes responsible for snow formation; snowfall observations; snow cover and snow surveys; transformation of snow to ice and changes in their properties; classification of ice and glaciers and their worldwide distribution; glaciation and ice ages; glacier dynamics; glacier surface and subsurface characteristics; geomorphic processes and landscape formation; hydrology and sedimentary systems; hydrochemical and isotopic properties; permafrost modeling; hazards caused by cryospheric changes; trends of glacier retreat on a global scale along with the impact of climate change; and many more quantitative estimates of various glacier parameters, such as degree-day, mass balance, extent and volume, and downwasting. Also included are articles on GPS application, and satellite image application in glaciology; GPR analysis; and sea level rise.

For purposes of the Encyclopedia 463 articles were selected. Literature on snow, ice and glaciers has grown too large to be fully treated in a single volume; therefore, the selection of articles included some subjectivity but was reviewed by many experts who have long been at the forefront of research in the field of cryosphere. We truly understand that given the scope of this subject it is almost impossible to include each and every topic in this type of reference book, but we have tried our best to avoid any glaring omissions or miss something which could significantly hamper the quality of the Encyclopedia. Therefore, we have made the contents of the Encyclopedia exhaustive, but we understand that we might have missed certain topics. We are also aware of some partial omissions. As it frequently happens, willing contributors

cannot unfortunately be always found for all the suggested topics. It may be noted that if the reader does not see an entry for the particular topic that interests him or her, then he or she should look in the index because that topic may have been covered under a different heading and perhaps in more than one article. In making the list exhaustive, it is possible that there might be a little bit of repetition here and there, but we do not want readers to read two articles to understand one.

The material presented in the articles consists of established information on a particular topic and represents easily accessible digested knowledge. The level of material is such that a graduate student can benefit from the presentation which is not necessarily from his or her area of expertise. An effort has been made such that each article stands on its own, without an assumption that a reader will be seeing any other portion of the Encyclopedia. Although entries are presented in alphabetical order, they have been organized under major compilation headings which should become particularly obvious when the reader uses the cross-references with each entry. This is not an exhaustive list but hopefully it gives a structure to the Encyclopedia's contents. Of equal value are the many references given with the entries.

This *Encyclopedia of Snow, Ice and Glaciers* is supposed to provide clear explanations of current topics, and is not structured as a student textbook, but it is rather for quick access to particular terms and concepts in self-contained entries. We hope that this volume will also tempt the casual reader to browse through and become curious about the different facets and foci of cryosphere.

The contributors represent varying backgrounds and many of them represent WHO'S WHO in the cryosphere. It is hoped that the Encyclopedia will serve as a reference to scholars and students. The Encyclopedia will also be a valuable resource for geologists, geographers, climatologists, hydrologists, and water resources engineers; as well as to those who are engaged in the practice of agricultural and civil engineering, earth sciences, environmental sciences and engineering, ecosystems management, and other relevant fields.

The encyclopedia is comprised of articles under three categories: A, B, and C. Tables 1, 2 and 3 provide a list of major headings of articles included in the encyclopedia for a quick reference (see List of Articles, pages 1233–1237). 64 articles in category A represent major divisions and review topics. These also serve to coordinate the widely scattered entries of categories B and C. 182 Category B articles constitute building block items, inspired by textbook subheads, but also the cookbook items. 217 articles in category C are mini-entries dealing with materials, fancy terms, or outdated concepts. All these categorical entries on different topics are compiled in an alphabetical order, with their length being related to their relative importance.

March 2011

Vijay P. Singh
Pratap Singh
Umesh K. Haritashya
(Editors-in-Chief)

Acknowledgments

This Encyclopedia is a result of the collective contributions of the authors who were gracious, generous and willing to write different articles. These authors, representing five continents, have synthesized the body of knowledge in their particular area, and therefore the quality of the Encyclopedia is a reflection of the quality of their efforts. We are grateful to these authors. Any drawbacks are editors', not authors'. The preparation of this Encyclopedia was greatly aided by the assistance we received from our International Advisory Board members:

Richard Armstrong, NSIDC, Boulder, Colorado, USA;
Michael P. Bishop, University of Nebraska-Omaha, USA;
Helgi Björnsson, Institute of Earth Sciences, Iceland;
Wilfried Haeberli, WGMS, University of Zurich, Iceland;
Johannes Oerlemans, University of Utrecht, Netherlands;
John F. Shroder, University of Nebraska-Omaha, USA;
Martyn Tranter, University of Bristol, UK;

We wish to express our deep gratitude to them for their invaluable support and encouragement.

All category A articles and major category B articles were peer reviewed. Reviewers of these articles are gratefully acknowledged for their constructive reviews. Their efforts have greatly enhanced the quality of contributions contained in the Encyclopedia. Special thanks goes to Tom Allen, Andrew Bush, Etienne Berthier, Poul Christoffersen, Graham Cogley, Luke Copland, Moritz Dick, Thomas Grenfell, William Harrison, Robert Hellstrom, Kenneth Jezek, Richard Lindzen, Frederick Nelson, Mauri Pelto, Donald Rapp, and Cornelis Vanderveen.

We would also like to acknowledge the constant support and help we received from Petra van Steenbergen, Senior Publishing Editor, Earth Sciences and Geography, Dr. Sylvia Blago, Associate Editor MRW and Simone Giesler, Editorial Assistant, Springer.

Our families (V.P. Singh: wife Anita, son Vinay, daughter-in-law Sonali, and daughter Arti; P. Singh: wife Anju, sons Arpit and Aman; and U.K. Haritashya: wife Namrata and daughter Vanshika) allowed us to work during holidays, weekends and in night away from them. They provided support and help whenever we needed. Without their patience and love, this volume might not have been completed, and we are much grateful to them.

Guide to the Reader

For the beginners, it is good to start with a general article, then track the list of cross-references provided at the end of the article to locate similar or relevant articles. For example, if one wants to learn about hydrological aspects of snow and glaciers, then one should go to Glacier Hydrology and Snow Hydrology, then Melt Runoff Modeling, then Impacts of Snow and Glaciers on Runoff, then Hydrochemical Characteristics of Snow, Ice and Glaciers, then Hydropower: Hydroelectric Power Generation from Alpine Glacier Melt, or several other specific Snow or Glacier Hydrology related articles. The list of cross-references provided at the end of the article is not exhaustive, otherwise it would lead to a long listing, rather it is a guide for the reader to find other relevant articles, which are further cross-referenced.

Experts or other readers with background in cryosphere may directly search for specific topics. For example, Ice Age Cycles: Data, Models, and Uncertainties, or Basal Sediment Evacuation by Subglacial Drainage Systems. If one does not find the topic one is looking for, it is possible that it may have been covered under a different heading. Therefore, one should go to the index that would lead to the articles that may cover the topic of interest. If a reader is looking for more explanation than what is already described under any particular topic, then most articles provide important and landmark bibliographic references that relate to both general and research articles. Some articles provide older references which allow readers to find the historical aspect of the topic.

A

ABLATION DEPRESSION

Lasafam Iturrizaga
Geography/High Mountain Geomorphology,
Geographical Institute, University of Göttingen,
Göttingen, Germany

Synonyms

Ablation valley; Ablation valley complexes; Lateroglacial valley; Randkluft; Valley-side depression

Definition

The ablation depression ("ablation valley") is an element of the lateroglacial landform system. The term refers to a depression in-between the glacier and the adjacent valley flank or the sediment mantling the valley flank. It is mainly formed by solar insolation processes. Its width ranges generally from several meters to some tens of meters. The ablation depression might act as important sediment trap.

Geographical distribution

Ablation depressions may occur along the lateral margins of any glaciers worldwide as long as they are flanked by slopes of bedrock or sediments (Figure 1). Ablation effects by the emission of long-wave radiation occur in all geographical latitudes, but at different extents. The optimal distribution area of ablation valleys is located along glaciers in subtropical latitudes, such as in the Andes (Jordan, 1991) or in High Asia (Kuhle, 1991). They are best developed in the extensively glaciated Karakoram Mountains (Visser, 1938; Röthlisberger, 1986) and attain their highest altitudinal distribution worldwide in this mountain region (Iturrizaga, 2003, 2007) (Figure 2). Low rates of humidity promote a high transparency of the air leading to insolation rates that may almost reach values of the solar constant. Ablation valleys occur from altitudes around the snow line at about 4,800–5,200 m down to 2,900 m (Iturrizaga, 2007; cf. Visser, 1938). However, they are also reported from glaciers in high latitudes, such as along Norwegian glaciers, where they are developed in smaller size (Gresswell, 1958).

Their distribution is influenced by aspect (Visser, 1938). Therefore, they are supposed to show an asymmetric allocation along the glaciers and occur preferentially in South-aspect at W-E running glaciers. However, topographical-controlled factors, such as debris supply by the tributary valleys into the lateroglacial environments, might predominate the aspect-controlled distribution of the ablation depressions.

Formation process

Ablation depressions have been firstly documented as glaciological landforms of heat radiation from the Himalayas (Strachey, 1847). Oestreich (1906) introduced the nongenetic term of "Randtälchen" (*small marginal valleys*) for these lateroglacial depressions. Visser (1938) has investigated the lateroglacial landforms in a more systematic approach and recognized that they are characteristic key forms of subtropical high-mountain areas. He introduced the term "ablation valley" (*Ablationstal*), but it has been subsequently widely confused with the landform of a "lateral moraine valley" (Röthlisberger, 1986; Hewitt, 1993). Because this landform is no true valley, that means it possesses no continuous gradient and is in general only some tens to hundreds of meters long, the term "ablation depression" has been introduced.

The formation of an ablation depression is a direct consequence of solar insolation and reflection effects of the bedrock. Due to the heating of the rock and the subsequent emission of long-wave radiation, the glacier ice is melting back at its margins forming a striking void. Temperature values of the bedrock surface can rise to over 30°C along

Vijay P. Singh, Pratap Singh & Umesh K. Haritashya (eds.), *Encyclopedia of Snow, Ice and Glaciers*, DOI 10.1007/978-90-481-2642-2,

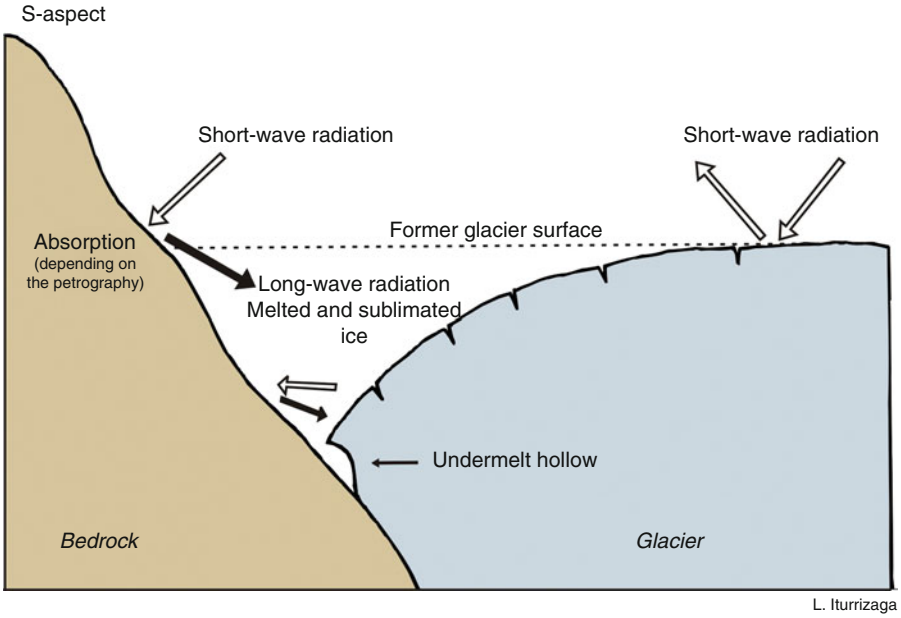

Ablation Depression, Figure 1 Cross section through an ablation depression.

Ablation Depression, Figure 2 Ablation depression in combination with lateroglacial sedimentation complexes at 3900 m at the Yazghil glacier in the Karakoram Mountains. (Photo: L. Iturrizaga 18.07.2001.)

the glacier margins, even at altitudes of 5,000 m depending on the color and mineralogical composition of the geological parent material (Visser, 1938; Iturrizaga, 2007). Ablation processes include the melting and runoff or evaporation and sublimation of the glacier ice, which results in wasting of the ice and mass loss. Sublimation processes play a major role in the dry air in the formation of the ablation depressions.

In principle, ablation depressions can occur at clean ice, debris-covered glaciers, advancing glaciers, and also along avalanche cones at the base of south-exposed valley flanks in the form of ablation crevasses. They can be mixed up with valley-side depressions as a result of general ice shrinkage and the backwasting of the glacier at its marginal sides.

The formation of ablation depressions may be enforced by lateroglacial rivers, which widen the gap between glacier and valley flank. Once an ablation depression has been built up, dumping processes of supraglacial moraine material at the glacier margins may cover the clean ice surfaces and protecting the glacier ice to a certain extent from further melting processes. The ablation depressions can

act subsequently, as well as sediment traps forming lateral moraine valleys.

Summary

To conclude, ablation depressions are rather short-lived lateroglacial landforms. They might be easily mistaken as indicators of glacier shrinkage. After the formation of an ablation valley, the steep glacier marginal cliffs may be covered by a lateral moraine and transformed into a more stable and long-lasting lateral moraine valley.

Bibliography

Gresswell, R. K., 1958. Glacier and Glaciations. Hulton Educational publications LTD, 128 pp.
Hewitt, K., 1993. Altitudinal oranization of Karakoram geomorphic processes and depositional environments. In Shroder, J. F., Jr. (ed.), *Himalaya to the Sea. Geology, Geomorphology and the Quaternary*. London: Routledge, pp. 159–183.
Iturrizaga, L., 2003. The distribution and genesis of lateroglacial valleys in the Karakoram Mountains (Pakistan). In *Zeitschrift für Geomorphologie* N.F., Suppl.–Bd. **130**, 51–74.
Iturrizaga, L., 2007. Die Eisrandtäler im Karakorum: Verbreitung, Genese und Morphodynamik des lateroglazialen Sedimentformenschatzes. In *Geography International.* Aachen: Shaker Verlag, Vol. 2, 389 pp.
Jordan, E., 1991. *Die Gletscher der Bolivianischen Anden. Erdwissenschaftliche Forschung*. Stuttgart: Franz Steiner Verlag, 365 pp.
Kick, W., 1956. Der Chogo-Lungma-Gletscher im Karakorum. *Zeitschrift für Gletscherkunde und Glazialgeologie*, **3**, 335–347.
Kuhle, M., 1991. Glazialgeomorphologie. *Wissenschaftliche Buchgesellschaft Darmstadt*, 213 pp.
Oestreich, K., 1906. Die Täler des nordwestlichen Himalaya. In Ergänzungsheft Nr. 155 zu Petermanns Geographische Mitteilungen, 106 pp. Gotha, Justus Perthes.
Röthlisberger, F., 1986. 10 000 Jahre Gletschergeschichte der Erde. Verlag Sauerländer.
Strachey, R., 1847. A Description of the Glaciers of the Pindur and Kuphinee Rivers in the Kumaon Himalaja. *Journal of the Asiatic Society of Bengal*, **16**, 794–809.
Visser, P. C., 1938. Glaziologie. In Visser, Ph.C., and Visser Hooft, J. (eds.), Wissenschaftliche Ergebnisse der Niederländischen Expeditionen in den Karakorum und die angrenzenden Gebiete in den Jahren 1922, 1925 und 1929/30. Band II, 215 pp.

Cross-references

Lateroglacial
Lateroglacial Landform Systems

ABLATOMETER

Rijan B. Kayastha
Himalayan Cryosphere, Climate and Disaster Research Center (HiCCDRC), Kathmandu University, Dhulikhel, Kavre, Nepal

Definition

An ablatometer is an instrument used for measuring the rate of surface ablation of exposed ice or snow. The sensing element may be a potentiometer linked to a movable metal tube, supported between two poles that are drilled at least 2 m into the surface to minimize subsidence of the supports, as in the Lewkowicz (1985) ablatometer. The sensing tube has a foot constructed of wood for ice and plastic for snow, which rest on the surface, thus following it down as ablation occurs. The ablatometer operates by converting an extension of the slide into a change in the electrical resistance of the potentiometer. The later is wired into a micro-logger for continuous recording of ablation.

The star ablatometer, as explained by Muller and Keeler (1969), consists of a 1 m long six-arm metal star mounted on a stake. Thirty-six points are measured by the lowering of a thin rod through the six sleeved holes in each arm. The rod contacts a variety of surface points, including both peaks and depressions of the microrelief, and penetrates the larger cryoconite holes and some of the spaces between loose crystals. Thus, the star ablatometer provides some information on the changes within the weathering crust in the surface lowering value and therefore yields a more accurate measure of ablation than the straightedge method. The instrument is removed between measurements, thus obviating the interference that additional stakes would cause.

Bibliography

Lewkowicz, A. G., 1985. Use of an ablatometer to measure short-term ablation of exposed ground ice. *Canadian Journal of Earth Sciences*, **22**, 1767–1773.
Muller, F., and Keeler, C. M., 1969. Errors in short-term ablation measurements on melting ice surfaces. *Journal of Glaciology*, **8**(52), 91–105.

ACIDITY OF GLACIER ICE

Cunde Xiao
State Key Laboratory of Cryospheric Sciences, Cold and Arid Regions Environmental and Engineering Research Institute, Chinese Academy of Sciences, Lanzhou, Gansu, China

Synonyms

Acidity of snow; Alkalinity of glacier ice

Definition

The acidity of glacier ice is the degree of acidity (content of $[H^+]$) of glacier ice, reflecting the dissolved anionic contents among the grain boundaries of glacier ice.

Acidity of glacier ice

The acidity of glacial ice is determined by the anionic contents of aerosols captured by snow and ice. When no extra

ions are in input, then ionic balance in current polar snow/ice can be represented as:

$$\Delta C = [Na^+] + [NH_4^+] + [K^+] + [H^+] + [Ca^{2+}] + [Mg^{2+}] - [F^-] - [Cl^-] - [NO_3^-] - [SO_4^{2-}] - [CH_3SO_3^-] - [HCOO^-] - [CH_3COO^-]$$

Usually there are very low concentrations of Ca^{2+}, Mg^{2+}, and Cl^- in the polar ice sheets. Therefore the acidity is mainly determined by Cl^-, NO_3^-, and SO_4^-. Therefore, the above equation can be reduced as:

$$[H^+] = [Cl^-] + [NO_3^-] + [SO_4^{2-}].$$

While in extra-polar regions, HCO_3^- and CO_3^{2-} are important anions due to larger areas of bare rock/soil surface. It can be represented as:

$$[H^+] = [Cl^-] + [NO_3^-] + [SO_4^{2-}] + [HCO_3^-] + [CO_3^{2-}]$$

Acidity of glacial ice is always reflected by electrical properties of solid ice. Ice conductance is often measured using electrical conductivity method (ECM) or dielectric profiling (DEP), which rapidly detects impurity ions incorporated into the ice lattice and at grain boundaries. High ECM or DEP reflects high acidity. When detecting ECM and DEP along ice cores, high signals reveal past volcanic events that characterized by high SO_4^{2-} concentrations in ice layers.

In mountainous glaciers in the mid-latitudes, it is found that electric conductivity (EC) of glacial melt water is a useful proxy for the total concentrations of dissolved ions. Therefore, alkalinity (OH^-) of glacial ice has positive relationship with major cations such as Ca^{2+}, Mg^{2+}, Na^+, and K^+, which derives mainly from dust aerosols. Therefore, higher dust loading of glacier ice corresponds to lower acidity.

Summary or conclusions

Acidity of glacier ice is a useful proxy for the past climatic and environmental changes. Volcanic events recorded in ice cores were detected using this proxy. Anthropogenic pollution can also be reflected by high degree of acidity in the ice. Loadings of alkaline dust can reduce the acidity of glacier ice.

ACTIVE ICE WEDGE

Pratima Pandey
Centre of Studies in Resources Engineering, Indian Institute of Technology, Bombay, Mumbai, Maharashtra, India

Definition

An *ice wedge* is defined as a crack in the frozen ground. It may have an opening at the ground surface of the order of few meters which reduces with depth. Ice-wedge is abundantly found along the Arctic coast and in many permafrost areas of the world. The formation and growing of ice wedges have been backed by the thermal contraction theory. In general, the melting of snow and its refreezing in thermal contraction cracks are accepted as the main reason for recent ice wedge formation. Due to thermal contraction, cracks open in winter and filled in with water in summer and form ice veins. The wedges which are still evolving and growing because of repeated but not necessarily annual winter cracking are defined as active ice wedges. Permafrost is the region where most ice wedges remain active. Ice wedge cracking is sensitive to climatic factors, particularly the winter snowfall. The long-term monitoring of ice wedge cracks can play an important role in climatic change–related studies.

ADFREEZE

Pratima Pandey
Centre of Studies in Resources Engineering,
Indian Institute of Technology, Bombay, Mumbai,
Maharashtra, India

Definition

Adfreezing is the process by which two objects are bonded together by ice formed between them and that anchors piles or buried foundations in permafrost, so that they can be unaffected by frost heave occurring in the active layer. Adfreeze (adfreeze strength) is the shear or tensile strength that has to be overcome to separate two objects that are bonded together by ice. The shear stress required to separate an object from the frozen ground is frequently referred to as the "tangential adfreeze strength."

AERIAL PHOTOGRAMMETRY FOR GLACIAL MONITORING

Martin Kappas
GIS and Remote Sensing Section, Institute of Geography, Georg-August University Göttingen, Göttingen, Germany

Definition

Before starting with the main text, some photogrammetry terms and some standard technical terms of photogrammetry are introduced. As defined after the fifth edition of the Manual of Photogrammetry: "Photogrammetry is the art, science and technology of obtaining reliable information about physical images and patterns of electromagnetic radiant energy and other phenomena." In short it is the "science of measuring in photos." It belongs to the broader field of remote sensing. The principle of *stereoscopic viewing* is used to derive three-dimensional information in photogrammetry.

Photo: The original photo on film
Image: The photo in digital representation – scanned or directly digitally captured by a digital camera
Stereo model: Two neighboring images within a flight strip that have an area with stereoscopic overlap
Strip: All overlapping images within a flight line
Block: All images of all strips
Base: Distance between the projection centers of two neighboring photos
Oriented image: A digital image that has both the interior and exterior orientations known
Rectified image: A digital image, in which the pixels have been corrected to a vertical projection and errors resulting from the non-verticality of the camera have been removed
Orthophoto: A digital image in which the pixels have been corrected to an orthogonal projection, removing errors due to tilt and terrain displacement
Monitoring: To observe or measure an object from time to time

Introduction

Glaciers are three-dimensional objects, which change their shape in length, width, and height. The monitoring of these changes is one major field of airborne-based or satellite-based (e.g., ASTER) photogrammetry. To measure three-dimensional coordinates, a method is needed to get the third dimension. In photogrammetry, the so-called stereoscopic viewing is used to get three-dimensional information: If two or more photos from the same object (glacier) are taken from different positions, the three-dimensional coordinates (x, y, z) of any point that is represented in both or more photos can be easily calculated. In general, for any object point represented in at least two photos, three-dimensional object (terrain- or surface-) coordinates can be calculated. If the height in point P (on the glacier surface) is changing, the corresponding points P′ and P″ are linearly moved along their epipolar lines. Figure 1 illustrates the geometry in an oriented stereo model. Each point on the glacier surface (object point) is detectable in at least two photos. If all geometric parameters of the situation during photo shooting are known, the three-dimensional coordinates (x, y, z) of the point P on the glacier surface can be calculated by setting up the equations for the rays (P′ → P) and (P″ → P).

Measurement in photos means also to measure points on the object without a physical contact to the object. Therefore, photogrammetry is useful for glaciers or for situations in which the object cannot easily be reached (often the case for glaciers).

A brief history of photogrammetry

From a historical view, photos are the first "remotely sensed" data of the earth surface. Therefore, photos about glaciers offer an important historical data archive about the glaciers state and development over time, which can be used for monitoring purposes. The history of

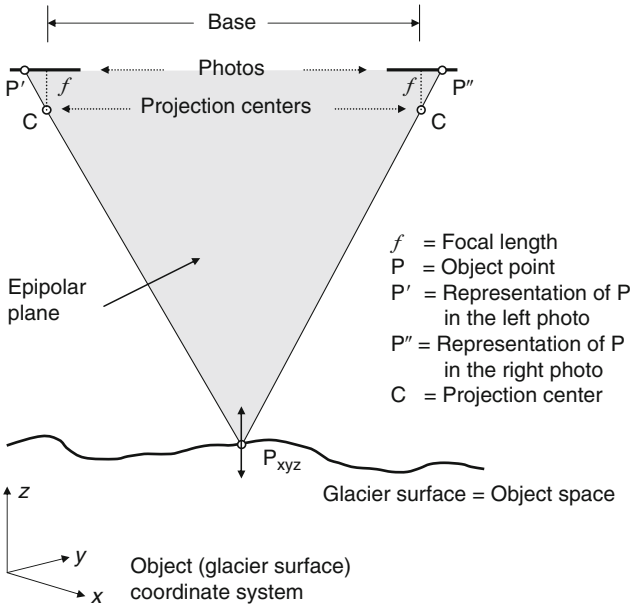

Aerial Photogrammetry for Glacial Monitoring,
Figure 1 Geometry in an oriented stereo model (modified after Linder, 2006).

photogrammetry and in particular the history of photogrammetry for glacier monitoring is covered here in terms of time periods corresponding to the emergence of specific photogrammetric technologies. In brief, three different era's can be highlighted: During the first era, the *Analogue Era*, photogrammetry developed into an advanced and coherent technology with the evolution of aviation and the development of optical-mechanical devices that replicated perspective image geometries and offered the first opportunity for precise spatial measurements from stereo imagery. It can be said that aerial photography made its first serious debut in 1912, and since then it has been subject to constant development in both technology and application. The second period, the *Analytical Era*, started with the advent of electronic computing clearing the way for photogrammetric exploitation of imagery by replacing analogue instruments with mathematical modeling. With the advent of computers, the main idea was to no more reconstruct the orientation analogue but algorithmic – via algorithms and their coefficients. This work was still done with real (analogue) photos and needed a high precision mechanical and optical piece of equipment, the so-called analytical plotter. According to that, this time period was called "Analytical Photogrammetry". The last era is the *Digital Era*, which developed with the accelerated progress of the age of electronics. At present, appliances are provided to acquire, store, and exploit images in digital form. At the beginning of the twenty-first century, imagery is captured and exploited in all digital environments, offering vast opportunities for rapid, accurate, and economical measurements of glaciers. Today, our conventional (large format 23 cm²) air cameras have been

subject to considerable change – mainly a reflection of new modern technology. Forward-motion image compensation (FMC) is today an accepted standard in all well-known air cameras, such as the Wild (RC 30) or Zeiss (RMK TOP and LMK 2000) cameras with additional image stability reinforced by stabilized mounts. Further GPS navigation (INS) is integrated with computer terminals such as flight planning, navigation, camera operation, and even post-flight analysis that can be retraced by survey flight management systems.

Geometric principles for monitoring glaciers by photogrammetry

The distance between camera position and object (in our case flight height above glacier for vertical air-photos or distance to the glacier terminus for oblique-air-photos) affects the quality of the air-photos. The smaller the distance between camera position and object and the wider the lens angle, the greater are the displacements considering the central perspective. Vice versa: The greater the distance between camera position and object and the smaller the lens angle (tele-view), the smaller are the displacements. Figure 2 summarizes the effect of different camera positions and lens angles in relation to displacements inside the photos. If we would like to transform a single air-photo about a glacier to a given map projection, it would be best to take the photo from as high as possible to reduce the displacements (comparable to satellite images). On the contrary, the displacements (radial-symmetric) are a prerequisite to measure pairs of images stereoscopically. Because an aerial photo is based upon central projection, it is subject to distortion and displacement. Distortion is any shift in the position of an image on a photo that alters the perspective characteristics of the image. Displacement is any shift in the position of an image that does not alter the perspective characteristics. Topographic displacement, or terrain displacement, is a serious concern, because it alters scale inside the image. Areas of higher elevation of the glacier lie closer to the camera and appear bigger than areas lying in lower elevation. Objects on the glacier are also displaced on the photo by the camera on the aircraft, which is not perfectly horizontal at the moment of the exposure. This phenomenon is known as tilt. Tilt is a basic characteristic of all aerial photos and it is used to classify photos as either vertical or oblique.

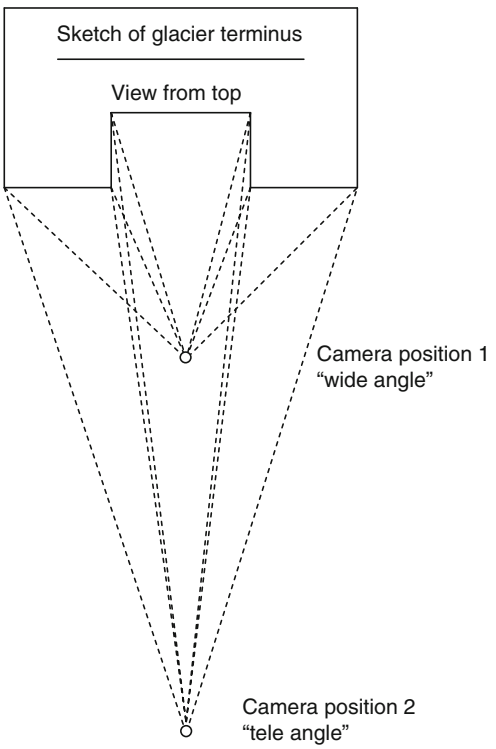

Aerial Photogrammetry for Glacial Monitoring, Figure 2 Different camera positions and lens angles.

The first step in using aerial photos about glaciers will be the reconstruction of the orientation of each photo (image). This means that first the exact position of all photos, which are to be used inside the object (glacier-terrain) coordinate system, should be defined. In general, three image orientation steps can be distinguished: interior, exterior, and absolute orientation. The interior orientation consists of the camera's focal length, photo's principal point x location, and photo's principal point y location. The exterior orientation is made up of three positions (or translations) X, Y, Z and three tilts (or rotations): φ (phi) = nose of the airplane up or down; ω (omega) = wing of the airplane up or down; κ (kappa) = swing, crab, or yaw. At large, there are nine orientation elements of an aerial photo. There are six elements associated with the camera position in space, which include the three positions of the camera relative toward the ground (X, Y, Z) and three rotations of the camera (φ, ω, κ). The values of φ and ω will normally be near zero. In the case of being exactly zero, the photo is called *nadir photo*. In practice, all air photos show deviations from zero due to wind drift and small motions of the aircraft.

If the coordinates of the projection centre, the three rotation angles (against the x-, y-, z-axis, e.g., Figure 3), and the focal length of the camera are known, the position of the photo in the 3D-space is defined. To get three-dimensional coordinates of objects on a glacier, at least two images from our target are needed, whereas the pictures must be taken from different positions. This is the principle of stereoscopy, which is based on the relative camera positions. The accuracy of height measurements derived from stereo models is a function of the distance of observation (in case of vertical aerial photos = flying height; in case of oblique aerial photos = distance to object) and the distance between points of observation (air base). The air base corresponds to the distance of two camera positions (see Figure 4). Let D be the distance between the glacier and the cameras and DC the distance between both camera positions (base), then

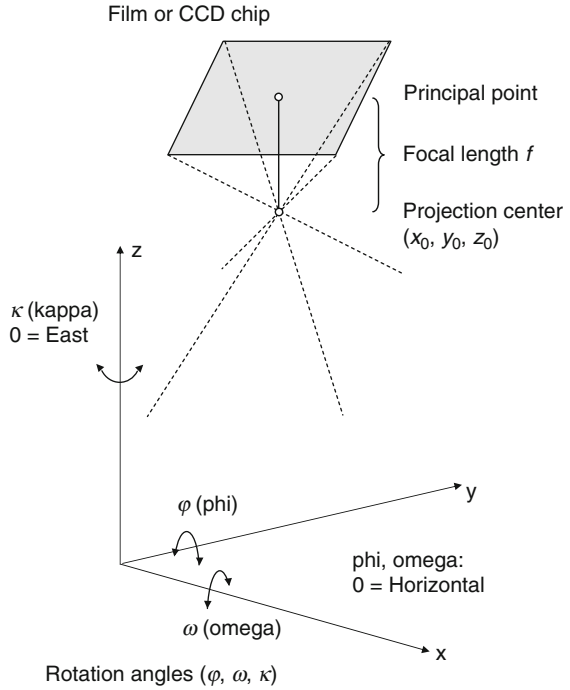

Aerial Photogrammetry for Glacial Monitoring, Figure 3 Focal length, projection center, and rotation angles (modified after Linder, 2006).

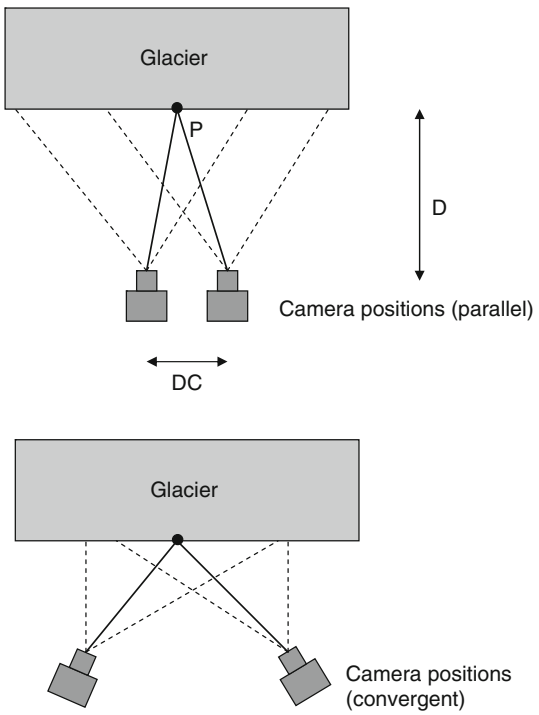

Aerial Photogrammetry for Glacial Monitoring, Figure 4 Camera positions for parallel (*above*) and convergent (*below*) situations (modified after Linder, 2006).

the angle between both projection rays (continuous lines) depends on the ratio D/DC. This ratio is called height/base-ratio. Generally spoken, the larger the value of the height/base-ratio, the more accurate the measurement. The accuracy of the calculated coordinates P (x, y, z) can be improved by increasing the base (the distance between two camera positions). If the overlap area (stereo model) gets to small, convergent camera positions can be used. The disadvantage of the convergent case is that additional perspective distortions are produced. Normally, the parallel case is suitable for stereo viewing and automatic surface reconstruction. The convergent or oblique case can often lead to a higher precision particularly in z direction. Another geometric consideration is that the height/base-ratio is equal to the focal length/aerial base-ratio. For precise height measurements, the photos are preferably taken with a short focal length camera in order to get a large base/height-ratio.

Summary of the geometry of a single photo

- A map has one scale – a photo has many.
- A map is based upon orthographic projection – a photo upon central projection.
- Displacement of images on the photo is caused by tilt and ground terrain (also height of objects).
- Camera coordinate axes are expressed in lower-case letters (x, y, z), where x is parallel with the flight direction and y is perpendicular.
- A photo has three centers:
  - Principal point, where principal axis intersects the film plane. The principal point is defined by the intersection of lines coming from the diagonally opposing corners (mostly fiducial marks).
  - Nadir, is the point vertically beneath the camera.
  - Isocenter is the point, which falls on a line halfway between the principal point and the Nadir (for small angles).
- There are nine elements for a complete orientation.
- Focal length and flying height affect scale and ground coverage.
- Scale = focal length/flying height.

A typical workflow for using photogrammetry for glacier monitoring is summarized in Figure 5. Starting with the capturing of the photo or images, the orientation parameters of all images that will be used in the analysis will be calculated. After completion of the different orientation steps, object coordinates inside the model can be measured and various products like surface models or orthophotos can be derived.

Analogue and digital cameras for glacier monitoring

The evolution of photogrammetry is closely connected with the development of aviation and photography. For more than over 100 years, photos have been taken on glass plates or film material (negative or positive). In general, specific photogrammetry cameras (also called metric

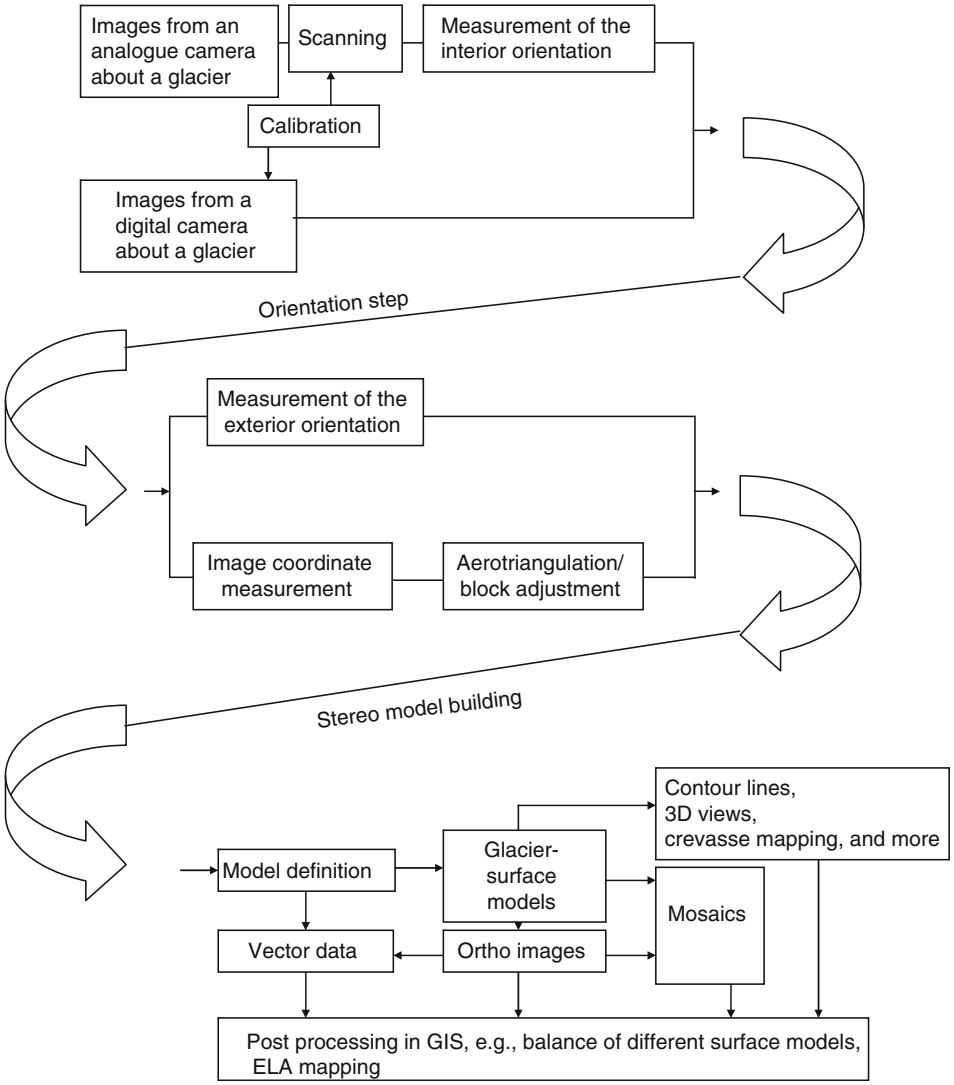

Aerial Photogrammetry for Glacial Monitoring, Figure 5 Typical workflow for monitoring glaciers with photogrammetry (modified after Linder, 2006).

cameras) work in the same way as amateur cameras do. The differences arise from the high-quality demands. Besides high precision mechanics and optics, aerial cameras also use a large film format. Amateur cameras normally use the size of 24 by 36 mm. Aerial cameras use a size of 230 by 230 mm (9 by 9 in.). This is essential for a good ground resolution inside the photos. As a result of the large format, the focal lengths ("wide angle," "normal angle," "tele angle") differ from those normally known. The frequently used wide angle aerial camera has a typical focal length of about 153 mm. The normal angle has a focal length of about 305 mm. Furthermore, the lens system of aerial cameras is constructed as a unit within the camera. There is no "zoom" or lens change possible in order to provide high stability and good lens correction. Today, digital aerial cameras dominate the photogrammetry market. For the close-range domain, the transition from film to digital cameras can be characterized in the way that existing film cameras are still used, but if a camera is replaced, the new one will be a digital camera system. Small and medium format cameras like those from Rollei (D7 metric, D30 metric, or the AIC) are well suitable for the aerial domain. There are two main construction strategies: One strategy is to maintain the central perspective principle which is well-known from existing film cameras. This strategy offers the advantage that existing software for data processing can be used. For this strategy, an area sensor is required (frame camera). The problem for this solution is that a high-resolution area sensor providing the same information as 230 by 230 mm photos captured on film would be very expensive. One solution for this problem is for instance to use four

overlapping smaller sensors and to match these four images together (like Digital Mapping Camera, DMC from Intergraph). Another strategy is to use a line sensor across the flight direction. This technique is comparable to sensors on satellites or from hyper-spectral scanners (e.g., Leica's ADS 40).

Urgent suggestions for using a digital camera for glacier monitoring:

- *Manually parameter setting*: In general, it should be possible to choose and set the parameters as focal length, exposure time, focus, and *f*-number manually.
- *Focus* or *distance setting*: It should be possible to deactivate the auto focus system.
- Evaluating the *Focal length range*: The optical range is decisive and not the digital (interpolated) range.
- *Number of pixels* or *resolution*: The physical or real resolution, and not the interpolated resolution, is important. Resolution increases with the number of pixels.
- *Exposure time* and *f-number*: The maximum f-number or lens opening should not be less than 1:2.8. The exposure time should have a range of at least 1–1/1,000 s.
- *Image storage*: In general, images are stored in a format like JPEG or TIFF. The image compression rate should be selectable or the image compression itself should be able to be switched off.

Essential concepts and applications in glacier monitoring

Today, photogrammetry is the leading concept in monitoring glaciers. Digital photogrammetry offers a high amount of automation in the generation of glacier surface models. At the same time, light detection and ranging (LIDAR) and interferometric synthetic aperture radar (IFSAR) systems are increasingly used to collect and produce high quality elevation data about glaciers.

LIDAR systems primarily produce elevation data but can also produce intensity images. A LIDAR system is an active sensor that employs a high performance inertial measuring system combined with GPS to measure the sensors' attitude and position. During the aircraft flight, position, attitude, and range to the ground and glacier surface are measured. Typical LIDAR systems scan the surface with laser pulses. Regarding the wavelengths used, they often cannot penetrate clouds or heavy moisture compared to passive optical photogrammetry, but unlike optical photogrammetry, LIDAR systems work well at night. LIDAR systems also record the returned intensity for each laser pulse. The main result is an intensity image at the same density as the elevation points. The intensity images can be used to check the quality of the elevation data. The high accuracy of the LIDAR products (5–30 cm) gives them many advantages over other methodologies such as photogrammetry. The quality of the LIDAR elevation products for a glacier depends on many factors such as:

- Position and attitude measurement quality
- System calibration quality
- Point density
- Flying height and speed
- Amount and density of objects

LIDAR outputs include grid formats and/or irregular formats. They often produce 10,000–80,000 data points per second and this produces very large datasets of dense elevation data. Typical elevation models range from 0.5 m horizontal spacing to 5 m horizontal spacing on the ground. Vertical accuracies typically vary from 5 to 30 cm range.

Interferometric synthetic aperture radar (IFSAR) is another concept to derive information about the glacier surface. IFSAR systems produce raw elevation data and intensity images that can be processed into elevation and orthophoto products. Comparable to LIDAR system, IFSAR systems use active sensors which measure the aircraft's position and attitude while also measuring the range and received intensity of the radar pulse from the ground. IFSAR systems use two antennae and measure the phase difference of the received signals. Typical IFSAR products are elevation data in form of grids or TIN's and image products such as orthophotos and mosaics. IFSAR systems produce high quality elevation and image data at faster data rates than LIDAR systems. Typical IFSAR systems use short wave lengths such as X or C bands, which gain high resolution data. A typical format of IFSAR data is grid based and owns a resolution between 2 and 10 m. IFSAR elevation products typically have accuracies of 0.5–2 m. Accuracies depend on many factors such as:

- System calibration
- Position and attitude measuring system quality
- The base length between the two IFSAR antennae
- Flying height and speed

A well-known example of IFSAR data products is the elevation coverage from the shuttle radar topography mission (SRTM). The SRTM-mission collected elevation data of nearly 80% of the earth's landmass at a resolution of approximately 30 m. Much of these data is today available in grid formats with an accuracy of 20 m horizontally and 16 m vertically. In many cases, these data are too coarse for glacier monitoring.

A future trend in monitoring glaciers will be the combination of data derived from stereo photogrammetry, LIDAR, and IFSAR. The elevation data produced from LIDAR and IFSAR systems can be edited or checked using photogrammetric means.

A further concept to monitor glaciers is to derive orthophotos to map and monitor the glaciers' elongation. Orthophotos are comparable to topographic maps and use the same projection as topographic maps. Today, most orthophotographs are produced by digital image processing methods utilizing aerial photographs as input, which have been converted into a digital form using a photogrammetric film scanner. Mostly, the differential rectification technique is applied through a suitably

designed software package on the basis of existing DEM (digital elevation model), which may be generated using any one the methods listed below:

- Through the automatic correlation of stereopairs of photographs in digital photogrammetric workstations (DPW);
- Directly from airborne laser scanning or interferrometric SAR (InSAR) data;
- Interpolation of digitized contours from an existing map.

Current investigations also use oblique photogrammetry to gather information about glaciers. The rationale behind this is based on frequently bad weather conditions over glaciers that prevent the monitoring of the glaciers by means of vertical photogrammetry or satellite images. Contrary to the standard aerial survey methods, oblique aerial photography from relatively low altitudes can often be accomplished when weather conditions preclude traditional vertical aerial stereo-photography (Figure 6) (Gleitsmann and Kappas, 2005).

Hence, close range digital multiple-image-photogrammetry (convergent or multi-image-photogrammetry with 100% image overlap) method can be used for aerial surveys even when weather would anticipate standard survey flights. The combination of a German survey camera and Dutch photogrammetric software facilitates the measurement of changes in the ice volume of glacier ablation zones and other geomorphic features of mountain areas. A small single engine airplane with far less operational costs than the normal aerial survey airplane is ideally suited for this. A current project of the University of Göttingen analyzes ice volume changes on several glaciers in south-central Alaska. Recently, most glaciers of the region showed a significant retreat and loss of substance, which is being documented in this project with the help of oblique photogrammetry. A modern digital multiple-image-photogrammetry system is used to process the imagery. Similar to stereo-vertical imagery, automated surface measurements are possible. However, photogrammetric analysis of a surface is limited in the same way as traditional stereo-photo analysis is limited by a lack of identifiable features on the target. Naturally, fresh unbroken snow surfaces in the accumulation areas of glaciers cannot be measured by photogrammetry.

Weather conditions are a limiting factor for aerial survey flights over glaciers, and waiting for favorable weather can cost too much time and money in some circumstances, especially in survey areas that are often

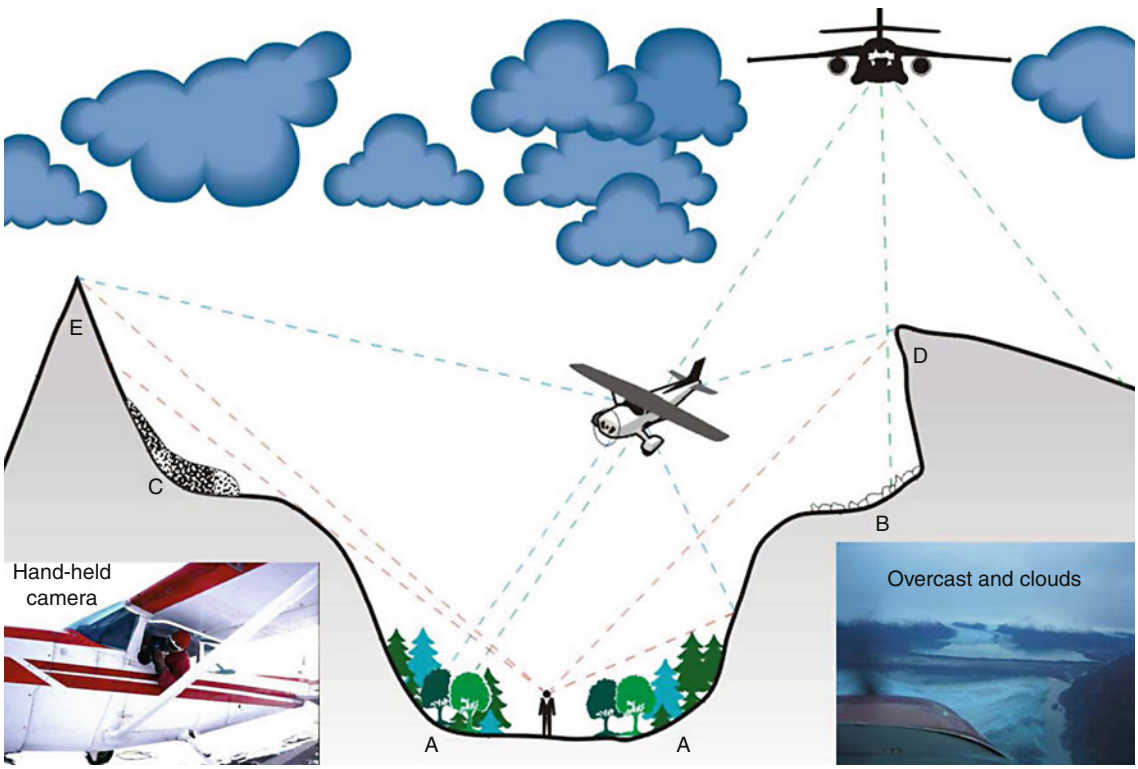

Aerial Photogrammetry for Glacial Monitoring, Figure 6 Considerable advantages exist with oblique aerial photography, instead of stereo-vertical imagery in high mountain environments with adverse weather conditions. *Image*: Schematic of a high mountain valley, with a cirque glacier (C) and a rare overhang (D) with debris talus (B) on a shoulder of a U-shaped glacially formed valley. In Alaska's oceanic influenced areas, the cloud base would be typically under the elevation of the mountain peaks (E); in a Himalayan scenario the clouds would be present within the valley in monsoon-influenced times of the year.

cloudy. In most cases, the optical sensors of satellites have the very same problem, since any cloud cover, even if very high based, does affect them. In the case of this study of the Göttingen University over south central Alaska's glaciers, located in the coastal mountain ranges under an oceanic climate regime, an innovative aerial survey method that can deal with adverse conditions regarding weather and terrain was applied. Conditions in this climate regime often prevent vertical stereo-image survey flights, flown from a high altitude above the ridges and peaks of the terrain, because of cloud cover and turbulence. Modern camera mounts have improved the situation with wind and turbulence somewhat, but not to an extent that makes a difference in this operational scenario. The glaciers and ablation areas studied here are separate targets with limited surface areas, so they can be surveyed with not too many multiple image clusters. Additionally, it is comparatively cheap regarding the equipment requirements and extraordinarily cheap regarding the "platform," a small single engine airplane. Thus, a real world alternative system was developed and tested for survey flights with limited financial resources that focus on smaller target areas under cloud cover (Gleitsmann and Trabant, 2005).

Due to the nature of this study with oblique photogrammetry, a comparison to other methods in use in this field of remote sensing and glacier and snow surface measurements appears appropriate. In the last years, this field of work has seen the introduction of several new survey techniques, and this method should be put in context with them, especially from the financial and practical point of view. The use of the SAR and InSAR satellite data in this field of work, with the high mountain environment, seems to be related to many inherent problems. Radar penetration into a snow surface is difficult to quantify, because it depends on moisture content, and results in the imaging of a measured surface below the real snow surface. With both these methods, large areas can be densely sampled with very high relative accuracy at relatively low cost, after high initial costs of the equipment (Bäumker et al., 2004). Changes in snow-moisture content, melting, fresh snowfall, and snow creep can all lead to loss of interferometric coherence, while steep terrain produces radar shadow, image distortion, and layover resulting in lost data. This is also limiting the availability of useful ground control points. Therefore, the control of the survey often consists entirely on DGPS/INS (Figure 7). The initial

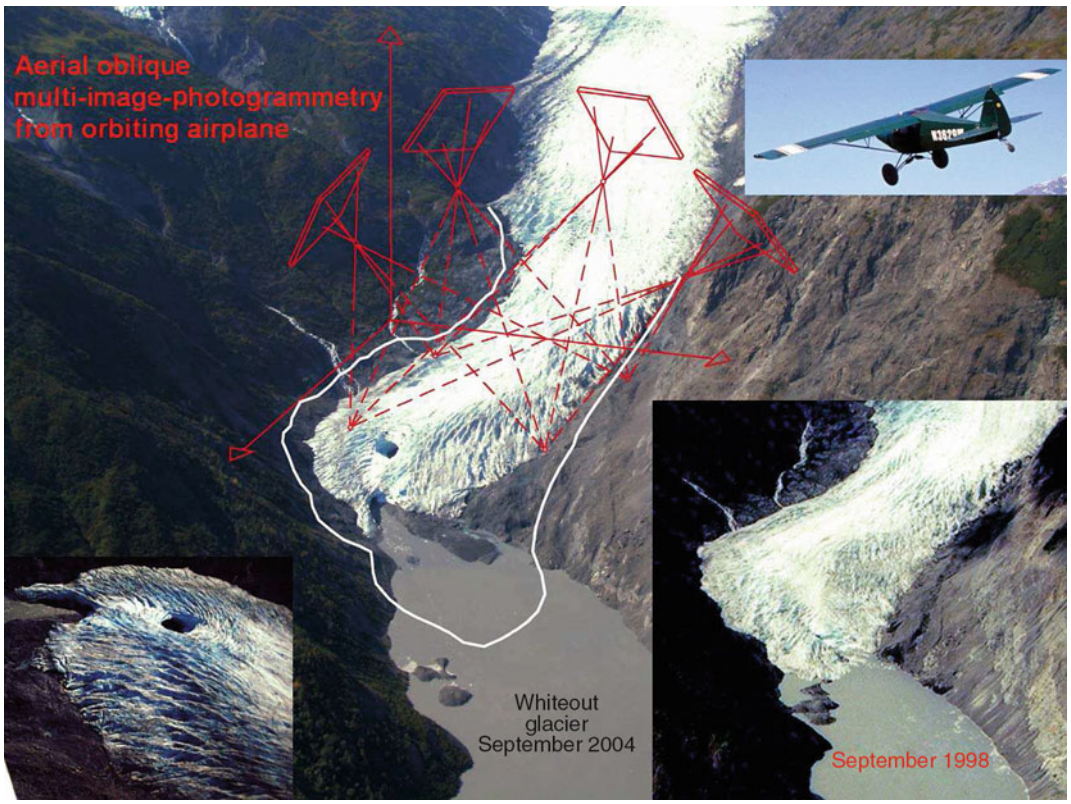

Aerial Photogrammetry for Glacial Monitoring, Figure 7 Aerial Picture of Whiteout Glacier, Alaska; taken on August 24, 2004. *White line* shows extent of Glacier terminus, as documented in September 1998. Graphics in *red* illustrate the concept of multiple-image-photogrammetry, with four image planes of the oblique aerial photography, and a coordinate system based on four ground control points. The points are DGPS measured and are located on bedrock surfaces, not on the glacier surface. Small single engine airplanes are ideal to reach the necessary camera-positions, like in this example, depicted as four red focal-planes. Note the completely different habitus and glacier snout of the receding terminus compared to 1998.

expense of about 50,000 USD for the complete multiple-image-photogrammetry system compares with much higher initial costs for a LIDAR system (Kääb and Volmer, 2000). The expense and the low availability of airborne laser scanning LIDAR (laser-induced direction and range) systems, combined with operational technical (platform) problems to employ them, often prevents a widespread use. Also, the systems seem to be extremely intolerant toward the usual aircraft landing forces, since they have to be reset and serviced after most landings, which is expensive and time consuming. With the LIDAR systems, the content of moisture in the air seems to be a very limiting factor, since even moisture content below the visible level, or any haze, will prevent gathering of LIDAR data. Also, with laser technology, wet ice, which is a widespread phenomenon on coastal glaciers, tends to create a heavy backscatter and rough signal. But, specific limitations apply to any photogrammetric topographic mapping of snow-covered glaciers within steep mountain terrain (Houghton et al., 2001).

Example of glacier-monitoring in South Central Alaska using oblique-convergent aerial photogrammetry as the survey method

Study area

Funded by the German Science Foundation (DFG), the Project of the Remote Sensing Department of the Institute of Geography of the University of Goettingen, Germany, has studied the surface changes of several glaciers in south central Alaska, mainly in the Knik glacier area, 90 km east-north-east of Anchorage. The glaciers under investigation are the USGS benchmark Wolverine Glacier (Figure 8) (Mayo et al., 2004), the Knik (Trabant and Mayo, 1979), Lake George, and Colony Glacier. All of them are located in the Chugiak Mountains of south central Alaska, the last three in the Knik area northeast of Anchorage, while the Wolverine Glacier is located in the eastern Kenai peninsula, which has an even more oceanic climate with extremely high winter precipitation. The Knik glacier got infamous in the past due to its

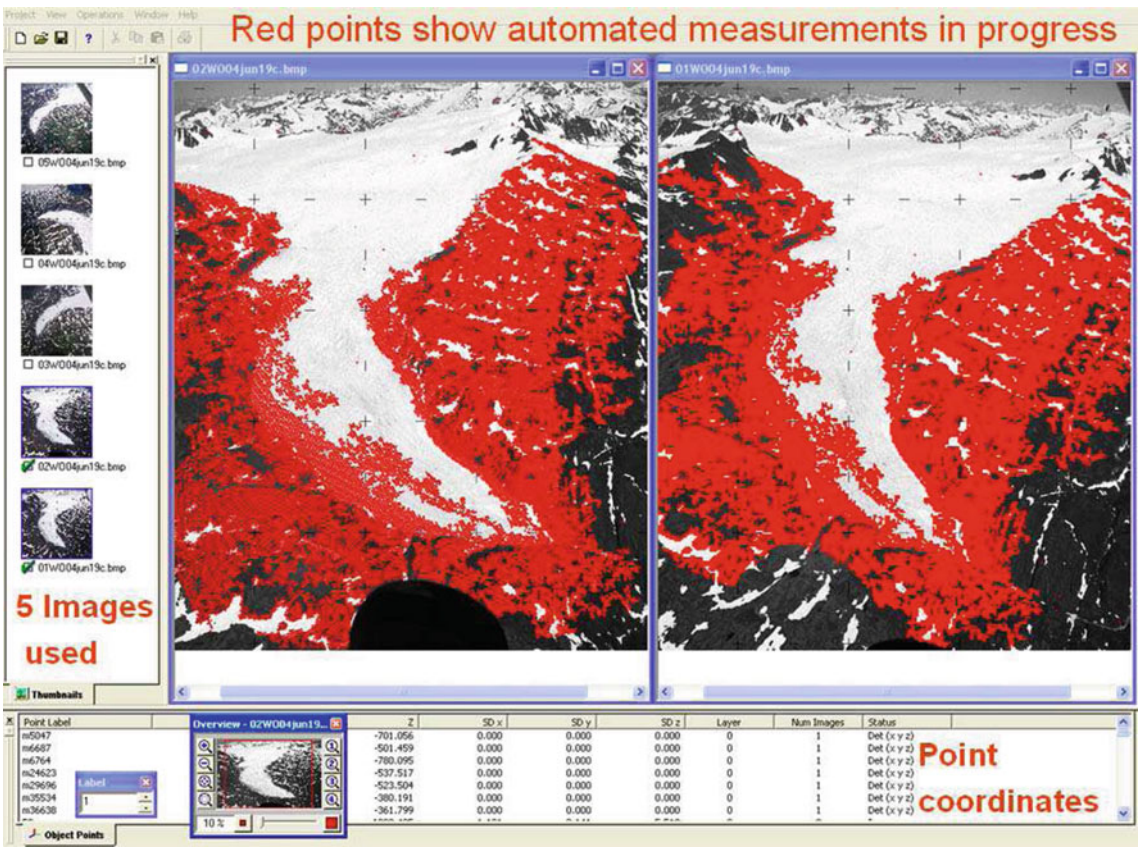

Aerial Photogrammetry for Glacial Monitoring, Figure 8 Images of Wolverine Glacier in June 2004, shown in "Polarphox" software while automated matching process is underway; if completed, all surfaces of the target with identifiable features would be depicted with red measurement points. The fresh snow patches on the areas around the glacier are not covered, since they are only white and featureless.

responsibility for creating one of the largest ice dammed lakes in Alaska (Hulsing, 1981) and regularly triggering dangerous GLOF's (glacier lake outburst floods), which destroyed the railroad and road connections to Anchorage, Alaska's largest city.

Methods

The project investigates the areas under the snow line of several Alaskan glaciers. Aerial survey pictures of the studied glaciers are taken twice a year, in the spring, after the snowmelt, and in the autumn, before the first snowfall. At the same time, fieldwork on the ground is done to create GCPs (ground-control-points) in order to be able to set positions, level, altitude, and scale to the digital models using the photogrammetric measurements. The GCPs are either recognizable features on rock outcrops or painted markers on rock surfaces or aluminum foil coated rocks set together on tundra surfaces. They are identifiable in the imagery, and are surveyed with DGPS, tachymeter and triangulation, and laser distance measurement equipment. The GCPs used at the Wolverine Glacier are the most accurately surveyed points in the project, and are ideal to evaluate the accuracy of the aerial oblique multiple-image-photogrammetry system that is employed here (see Figure 9). In general terms, the aerial multiple-image-photogrammetry survey of a target object works as follows:

Ideally, starting out from a high position vertically above the object (if weather/cloud base permits), the light aircraft that is used as the camera platform performs a gradual downward spiral, orbiting the object. All the time, pictures are taken of the object with a hand-held medium format specialized survey camera out of the open window of the aircraft. A large number of pictures, from any direction, including vertical, if desired, is thus created. This allows for the certain possibility to select the best geometric configuration of images for the multiple-image swathe of the target. The lattice model of photogrammetric measurements gets to be especially accurate due to the higher number of images used for every measurement (Wester-Ebbinghaus, 1990). Depending on the shape of the target, images from all sides are not even always necessary, if the target structure is simple enough, only four pictures from two sides of it may be enough for accurate measurements, provided every piece of surface can be seen in at least three pictures and the angles of the pictures aiming at the target are about 30° apart from each other. Therefore, this method is less affected by weather and low cloud base. If any vertical pictures cannot be taken due to weather, the multiple-image-photogrammetry still works. The camera is a 6 × 6 cm medium format with a réseau plate that creates a grid on commonly available film. The software "réseau-transforms" the digitally scanned photograph ensuring that the digital image is restored to the exact proportions it had when the photographic exposure was made. This digital rectifying produces a more precise rendering of features on the image than the traditional vacuum-plate flattening of film in large format survey cameras. Obviously, the réseau grid cannot be removed from the image. During the processing, common natural points (tie points), which can be identified with high accuracy on the target surface, are used for tying the multi-image composition together. With the points marked, the multiple-image-orientation is the next step. Then, the camera positions are known relative to each other. With the knowledge of the position of at least three points on the target surface, the systems-orientation is done; this produces the scale and the level, as well as the geographical coordinates to every measurement. Then the camera positions can also be identified with very good approximate positions. Following these work steps, every optically identifiable point visible in three pictures of the

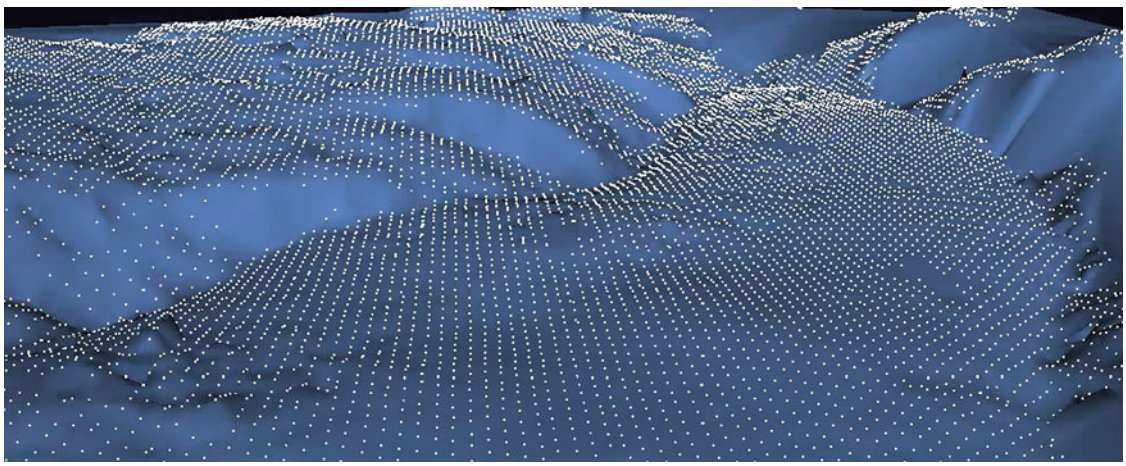

Aerial Photogrammetry for Glacial Monitoring, Figure 9 Uncorrected DEM of the Wolverine Glacier surface, with point measurements shown. The réseau-crosses reappear on the glacier surface, because they have to be masked out on the images for the automated grayscale-differences matching process. Apart from that, the depiction of the surface itself is very realistic.

multiple image composition can be measured with three-dimensional accuracy. The software used in this study is able to automatically generate surfaces from a minimum of three oblique images and can measure the position of points equivalently to a stereo-photogrammetry system (see Figure 8).

The comparison of the resulting surface models of different dates in order to quantify the volume and surface changes of the studied glacier termini is the main method of this study based on oblique photogrammetry. Successful automated surface measurements with the multiple-image-photogrammetry software "Polarphox" were so far conducted for five different surveys (multitemporal) of the Wolverine Glacier and one of the Colony glacier (Figure 10). In general, the measurements worked satisfactory, covering the whole ablation area of the targeted glaciers. The results were found to depend distinctively on the quality of the scans being used, and on the selection of the right patch size for the matching process, depending on the natural size and scale depiction of the surface features to be measured on the glacier surface. Naturally, areas with insufficient surface features, like fresh snowdrifts on the glacier terminus, cannot be measured. But the findings show that the measurements extend to the outermost perimeter of recognizable features, which is very satisfactory (see Figure 9). Cloud shadows going over the glacier in high winds still pose a problem, similar dark shadows of mountains on the ice. Most of those problems can be countered by the use of enough pictures to get the ideal perspectives and by selecting the right time of the day. Very few glaciers are so smooth on their surface below the firn line that points are difficult to measure. The higher the rate of debris coverage is, the easier the measurements are, because the debris provides identifiable features. This makes the Wolverine Glacier the most difficult target, since it has no medial or upper moraine or debris coverage whatsoever, and its surfaces of the terminus are characterized by the runoff of surface water due to its steepness. This creates line features in contrast to the easier to measure point features, which are more prominent on the other glaciers.

Today, photogrammetry can work and automatically measure points despite unknown camera positions and convergent oblique aerial photos, without straight flightlines, using near 100% image overlap, and ideal convergence angles. This technological change makes the use of small (or medium) format survey cameras for mapping of limited sized areas, a competitive option that was impossible until recently. The inherent problem of photogrammetry cannot be countered, of course; if there are no surface features because of fresh, white snow, no measurements are possible. Especially with glaciers as the target of the study, this factor is very significant. Due to this, it seems a combination approach of LIDAR data for the dry and snowy areas above firn line, combined with photogrammetry at the wet terminus of the glacier, would yield the ideal results. In the area around the equilibrium line (ELA) of the glacier where both systems start to encounter their difficulties, the combination of the data would allow for both cross-evaluation of the methods and more dense measurements.

The recent results clearly show the possibility of an aerial application of digital multiple-image-photogrammetry with automated surface measurements, which are based on matching algorithm and grayscale-differences in a search patch. With the use of a medium format camera for aerial surveys, the highest available scan quality with low image noise is necessary. Consumer product type scanners have proven unsatisfactory. The general reasoning for use of oblique imagery for detailed evaluations in high mountain terrain appears as a valid method, especially with the possible use despite adverse weather. The remaining question is,

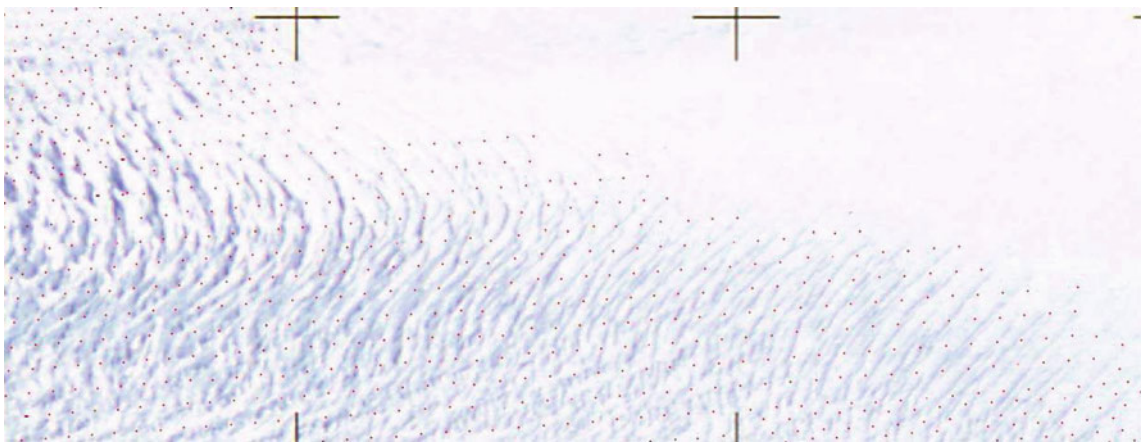

Aerial Photogrammetry for Glacial Monitoring, Figure 10 A fraction of the surface of Wolverine Glacier in the "Polarphox" photogrammetry software, after automated surface point measurements. The extent of the red measurement points shows the satisfactory use of available surface features and the inherent problem with fresh snow cover.

if the automated surface measurements can produce an accurate surface model over the full extent of the whole target area under these special conditions. For many earth science studies in remote or unsurveyed areas, this approach should open up new possibilities of making use of otherwise unattractive aerial surveys. The low cost and enhanced adverse weather ability should be significant enough to get access to data that would be not attainable otherwise. Adding positioning data from a differential global positioning receiver and mounting an inertial navigation system to the survey camera may eliminate the need for establishing ground control points in the target area in the near Future.

Summary

The last decades have shown a significant retreat of glaciers and seasonal sea ice boundaries, along with changes to permafrost and vegetation zones. Still, there are some glaciers that are advancing (Echelmeyer et al., 2003). The complexity of those observed changes may very well be related to those phenomena known as "global climate change." Many scientific studies have focused on this in recent years, employing a large variety of methods (Mayo et al., 2004). Since climatic change produces changes of the glaciers and also geomorphologic changes and effects, especially in high mountain terrain and in the arctic and sub-arctic latitudes, these areas get more into focus. Many previously uninhabited high mountain areas all over the world are under use now. In these areas, the changes are often observed as an increasing occurrence of natural hazards. Thus, there is a great motivation to study the geomorphology of those areas, and due to the idiosyncrasies of nature in these areas, a need for innovative survey techniques exists. Today, analogue and digital photogrammetry are powerful and adopted techniques to monitor glaciers. In the future, the combination of aerial photogrammetry with new techniques as LIDAR and SAR will be a powerful tool to monitor glaciers. But for historical studies of glaciers, the traditional photos are the only source of knowledge.

Bibliography

Albota, M. C., 1976. Short Chronological History of Photogrammetry. Proceedings of XIII Congress of the International Society for Photogrammetry, Commission VI, Helsinki, 20 pp.

Bäumker, M., Brechtken, R., Heimes, F.-J., and Richter, T., 1998. Hochgenaue Stabilisierung einer Sensorplattform mit den Daten eines (D)GPS-gestützten Inertialsystems. In Zeitschrift für Photogrammetrie und Fernerkundung ZPF, Heft 1/98, 15–22 pp.

Echelmeyer, K., Harrison, W., Lingle, C., Truffer, M., Arendt, A., Valentine, V., and Zirnheld, S., 2003. The Contribution of Alaskas Glaciers to Global Sea Sea Level Rise. In SEARCH open science meeting, oct 27,2003, Seattle WA, USA.

Gleitsmann, L., and Kappas, M., 2005. Glacier monitoring survey flights below clouds in Alaska: Oblique aerial photography utilizing digital multiple-image photogrammetry methods to cope with adverse weather. In EARSeL e-proceedings LIS-SIG (Land Ice and Snow) Workshop, Berne, February 21–23, 2005.

Gleitsmann, L., and Trabant, D., 2005. Digital multi-image photogrammetry combined with oblique aerial photography enables glacier monitoring survey flights below clouds in Alaska, a new tool for climate change studies and natural hazard assessment? In Erasmi, S., Cyffka, B., and Kappas, M. (Hrsg.): Remote Sensing for Environmental Studies: Applications in Geography. Göttinger Geographische Abhandlungen, Bd. 113, S.151–S.159.

Houghton, J. T., Ding, Y., Griggs, D. J., Noguer, M., van der Linden, P. J., and Xiaosu, D. (eds.), IPCC, 2001. Climate Change 2001. The Scientific Basis; Contribution of Working Group I to the Third Assessment Report of the Intergovernmental Panel on Climate Change (IPCC). Cambridge, England: Cambridge University Press.

Hulsing, H., 1981. *The Breakout of Alaska's Lake George*. Denver, Colorado, U.S.A: USGS. 15 pp.

Kääb, A., and Volmer, M., 2000. Surface geometry, thickness changes and flow fields on creeping mountain permafrost: automatic extraction by digital image analysis. *Permafrost and Periglacial Processes*, **11**, 315–326.

Kappas, M., 2009. *Klimatologie. Klimaforschung im 21. Jahrhndert – Herausfordrung für Natur-und Sozialwissenschaften*. Heidelberg: Spektrum Akademischer Verlag.

Kostka, R., 1993. The Problems of high mountain Cartography. Lecture in memory of Erwin Schneider. *Journal of the Nepal Research Centre*, Vol. IX. Kathmandu. pp. 1–15.

Linder, W., 2006. *Digital Photogrammetry*. New York: Springer.

Mayo, L. R., and Trabant, D. C., 1982. Geodetic Trisection, Altitude, and Ice-Radar Surveying Techniques used at Knik Glacier, Alaska, and Summary of 1979, 1980, and 1981 Data. USGS Open-File Report 82-685, Fairbanks, Alaska, U.S.A., 26 pp.

Mayo, L. R., Trabant, D. C., and March, R. S., 2004. A 30-Year Record of Surface Mass Balance (1966–1995) and Motion and Surface Altitude (1975–1995) at Wolverine Glacier, Alaska; USGS Open-File Report 2004-1069, Fairbanks, Alaska, U.S.A., 105 pp.

Pritchard, H., Murray, T., Strozzi, T., Luckman, A., and Barr, S., SAR Interferometry Derived Topographic Data for Studies of Changing Glacial Flux at: http://www.rspsoc.org/calendar/calendarArchive/calendar0102/mt010117.htm#Westaway

Trabant, D. C., and Mayo, L. R., 1979. Knik Glacier, Alaska – May 1979 Monument and Glacier Survey, USGS Open-File Report 80-48, Fairbanks, Alaska, 20 pp.

Warner, W. S., Graham, R. W., and Read, R.E., 1996. *Small Format Aerial Photography*. Caithness, Scottland: Whittles, G.B. 348 pp.

Wester-Ebbinghaus, W., 1990. High precision industrial Photogrammetry. Photogrammetric Record, 8. London, pp. 37–68.

Wester-Ebbinghaus, W., 1989. Das Réseau im photogrammetrischen Bildraum. *Zeitschrift für Photogrammetrie und Fernerkundung*, **57**(3), 64–71.

Würländer, R., and Eder, K., 1998. Leistungsfähigkeit aktueller photogrammetrischer Auswertemethoden zum Aufbau eines digitalen Gletscherkatasters. *Zeitschrift für Gletscherkunde und Glazialgeologie*, **34**(2), 167–185.

Cross-references

Digital Elevation Model Generation Over Glacierized Region
Glacial Geomorphology and Landforms Evolution
GPS in Glaciology, Applications
Ground Penetrating Radar Measurements Over Glaciers
LIDAR in Glaciology
Optical Remote Sensing of Alpine Glaciers
Radar Application in Snow, Ice, and Glaciers
Synthetic Aperture Radar (SAR) Interferometry for Glacier Movement Studies

ALASKAN GLACIERS

Bruce F. Molnia
U.S. Geological Survey, Reston, VA, USA

Definition

All glaciers located in the Alaska, USA, in North America.

Background

In spite of Alaska's remoteness, its glaciers have been studied for more than 150 years. More than 1,000 journal articles, books, and U.S. Geological Survey publications present details about individual glaciers or glacierized regions. Today, most Alaskan glaciers at lower elevations are retreating. However, about a dozen large valley glaciers, including Hubbard, Harvard, Meares, Taku, and Lituya Glaciers (all tidewater or former tidewater glaciers), are currently thickening and advancing. At higher elevations glaciers are thickening or exhibit no change.

Introduction

Glaciers cover about 75,000 km^2 of Alaska (Post and Meier, 1980), about 5% of the State. As shown in Figure 1, the glaciers are situated on 11 mountain ranges (Alaska Range, Aleutian Range, Brooks Range, Chugach Mountains, Coast Mountains, Kenai Mountains, Kigluaik Mountains, St. Elias Mountains, Talkeetna Mountains, Wood River Mountains, and the Wrangell Mountains), one large island (Kodiak), an island chain (the Aleutian Islands), and one archipelago (the Alexander Archipelago).

Alaskan glaciers range in elevation from above 6,000 m to below sea level. Alaska's glaciers extend geographically from the far southeast at latitude 55°19′N., longitude 130°05′W., about 100 km east of Ketchikan; to the far

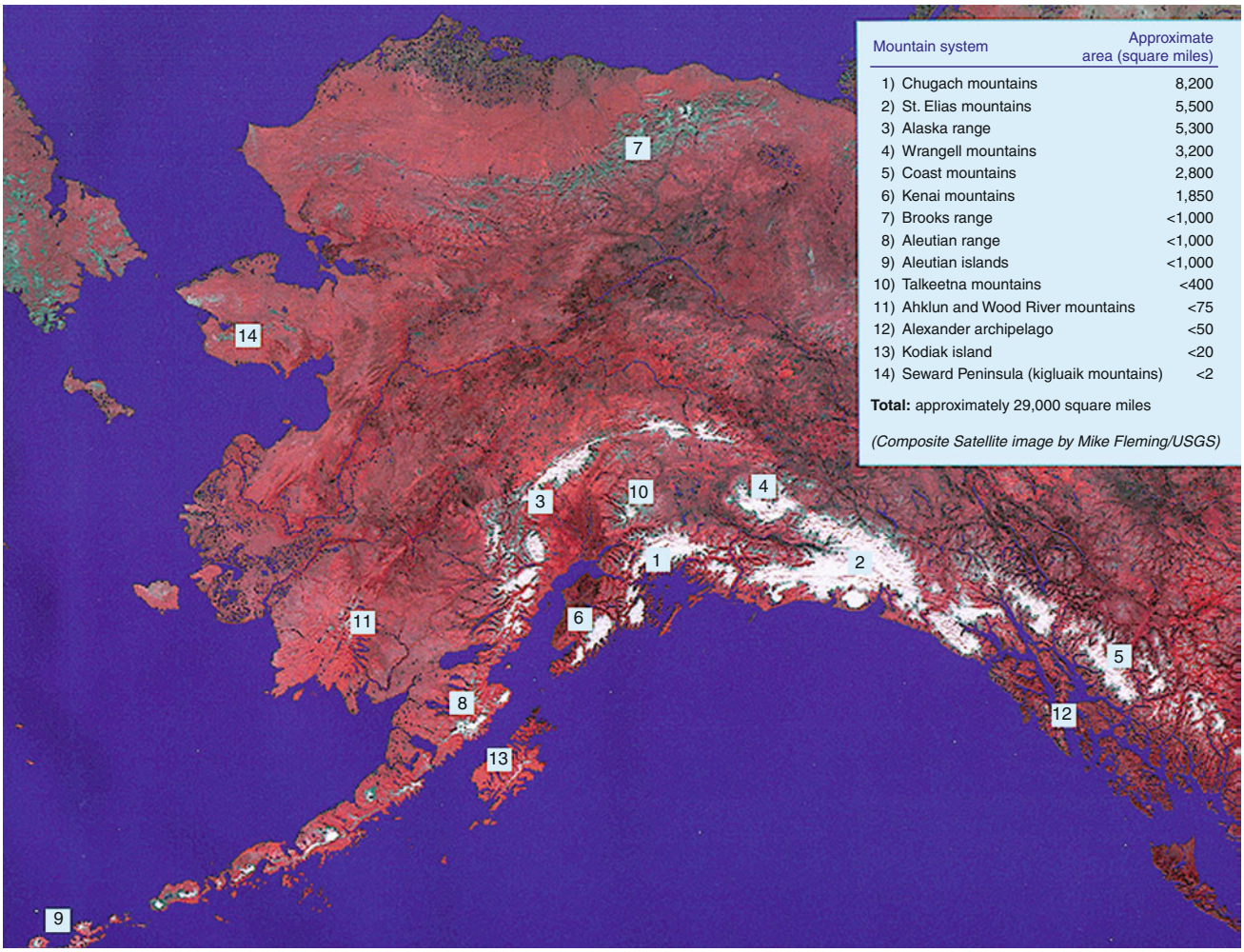

Alaskan Glaciers, Figure 1 Location map, showing the location of Alaska's 14 glacier hosting regions.

southwest at Kiska Island at latitude 52°05′N., longitude 177°35′E., in the Aleutian Islands; and as far north as latitude 69°20′N., longitude 143°45′W., in the Brooks Range. Nearly all mountain glaciers in Alaska are temperate. As the glaciers of Alaska melt, their meltwaters flow into the Gulf of Alaska and into the Bering, Chukchi, and Beaufort Seas, contributing to global (eustatic) sea-level rise.

During the Little Ice Age, Alaska's glaciers expanded significantly. Since then, the total area and volume of glaciers in Alaska has decreased. In some areas this retreat began during the eighteenth century (Lawrence, 1950). In others, it only started during the twentieth century (Molnia, 2007, 2008).

Of the 153 1:250,000-scale topographic maps that cover the State of Alaska, 63 sheets depict the presence of glaciers. Although the number of extant glaciers has never been systematically counted and is thus unknown, the total probably is greater than 100,000. Only about 600 glaciers (about 1%) have been officially named by the U.S. Board on Geographic Names (Molnia, 2008). There are about 50 active tidewater glaciers in Alaska (Viens, 1995). Within the glacierized mountain ranges of southeastern Alaska and western Canada, 205 glaciers (75% in Alaska) have a history of surging (Post, 1969).

Hundreds of retreating Alaskan glaciers have ice-marginal lakes. Many also form ice-dammed lakes. Post and Mayo (1971) documented that more than 53 present and 7 former large ice-dammed lakes produced jökulhlaups. Ice-capped volcanoes on mainland Alaska and in the Aleutian Islands have a potential for jökulhlaups caused by subglacier volcanic and geothermal activity.

Because of the size of the area covered by glaciers and the lack of large-scale maps of the Alaskan glacierized areas, satellite imagery and other satellite remote-sensing data are the only practical means of monitoring regional changes in the area and volume of Alaska's glaciers in response to short- and long-term changes in the maritime and continental climates of the State.

Distribution and recent behavior of Alaska's glaciers

A review of satellite imagery and historical literature for each of the 14 glacierized areas of Alaska was conducted to determine both the individual and the regional status of Alaskan glaciers and to characterize changes in thickness and terminus position of representative glaciers in each mountain range or island group (Molnia, 2008). In many areas, observations used for determining change date from the late eighteenth or early nineteenth centuries.

For each region, a detailed assessment of Landsat Multispectral Imagery (Figure 2) collected between 1972 and 1982 was made. This decade was selected as the baseline from which to assess recent glacier response to changing climate. The analysis determined that every mountain range and island group investigated can be characterized by significant glacier retreat, thinning, and (or) stagnation,

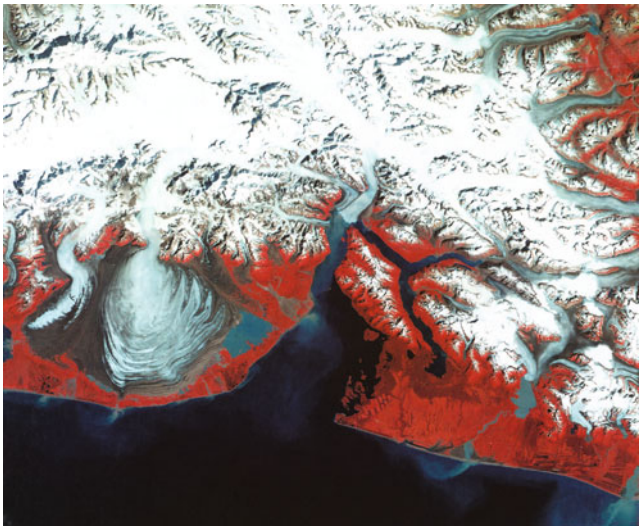

Alaskan Glaciers, Figure 2 A Landsat 2 Multispectral Scanner false-color composite image of the Malaspina Glacier (piedmont outlet glacier), tidewater Hubbard Glacier, and other glaciers in the St. Elias Mountains, Alaska. (Landsat 2 MSS image 21675-19482; 24 August 1979; Path 67, Row 18 from the EROS Data Center, Sioux Falls, SD). Hubbard Glacier has been thickening and advancing since the later part of the nineteenth century, while the Malaspina Glacier has been thinning and retreating for more than a century. The numerous folded moraines visible on the Malaspina's surface are evidence of its complex surge behavior.

especially those glaciers that end at lower elevations. At some locations, glaciers completely disappeared during the twentieth century. In other areas, retreat that started as early as the early eighteenth century has continued into the twenty-first century. Ironically, in several areas, retreat is resulting in an increase in the total number of glaciers; even though individual glaciers are separating, the volume and area of ice continue to decrease.

Temperature records at all Alaskan meteorological recording stations document a twentieth and early twenty-first century warming trend. Therefore, characterizing the response of Alaska's glaciers to changing climate helps to quantify potential sea-level rise from past, present, and future melting of glacier ice (Shulski and Wendler, 2007).

During the Little Ice Age, the total glacier-covered area and the number of mountain ranges and islands having glacier cover were significantly larger than they were during the "baseline" period. Since the end of the Little Ice Age, there has been a decrease in the glacier area and the thickness of most of the Earth's glacierized areas in the middle and low latitudes, along with advances of individual glaciers in some areas including about a dozen in Alaska. However, the timing, magnitude, and complexity of this post-Little Ice Age glacier change have been different in each of Alaska's 14 glacierized areas. Although thinning of lower elevation glaciers and retreat of glacier

termini are ubiquitous throughout Alaska, the current status of Alaska's glaciers varies significantly from area to area and with elevation.

Although most Alaskan glaciers at lower elevations are retreating, not all are doing so. At elevations below about 1,500 m, about a dozen glaciers, including Hubbard, Harvard, Meares, Taku, and Lituya Glaciers (all tidewater or former tidewater glaciers), are currently thickening and advancing. Many glaciers at higher elevations are thickening or exhibit no change. Several volcanoes, including Redoubt Volcano, had twentieth century eruptions that melted summit glaciers, but these events were followed by the formation of new glaciers in their craters.

The following region-by-region summary details the observed changes in glaciers described by Molnia (2008).

Coast Mountains – The glacierized area of the Coast Mountains is approximately 10,500 km^2. From south to north, the largest glaciers in the southern Coast Mountains are: Chickamin Glacier, with an length of 26 km and an area of about 140 km^2 (26 km, 140 km^2); Le Conte Glacier, the southernmost tidewater in Alaska (36 km, 472 km^2); Baird Glacier (50 km, 784 km^2); Dawes Glacier (37 km, 653 km^2); Sawyer Glacier (37 km, 399 km^2); and South Sawyer Glacier (50 km, 683 km^2). With the exception of Chickamin Glacier, all are outlet glaciers of the Stikine Icefield. To the north, the advancing Taku Glacier (60 km, 831 km^2) is the largest outlet glacier of the 1,955 km^2 Juneau Icefield. Taku's recent behavior was summarized by Motyka et al. (2001). In the 1970s, Taku, Hole-in-the-Wall, and Mead Glaciers were advancing. All other valley and outlet glaciers in the Coast Mountains were thinning and retreating. At the end of the twentieth century and early in the twenty-first century, Taku Glacier's advance continued, while Hole-in-the-Wall Glacier was stable. All other valley and outlet glaciers in the Coast Mountains continued to thin and retreat.

The longest field mass balance measurement in Alaska is from the Juneau Icefield. There studies of Taku and Lemon Creek Glaciers (Miller and Pelto, 1999) have documented significant annual variability and long-term volume loss.

Alexander Archipelago – On mid-twentieth century USGS 1:250,000-scale topographic maps, several hundred small unnamed mountain glaciers were mapped in the mountainous areas of six of the islands in the Alexander Archipelago: Revillagigedo, Prince of Wales, Kupreanof, Baranof, Chichagof, and Admiralty Islands. In the 1970s, the Alexander Archipelago had a glacierized area of less than 150 km^2. The largest of these was an unnamed glacier on Baranof Island that extended for about 5 km on a ridge between 1,100-m-high Mount Furuhelm and an unnamed 1,624-m peak. Since then, due to their small size, low elevation, and southerly latitude, all have thinned and retreated, and some have melted completely and no longer exist.

St. Elias Mountains – The glacierized area of the Alaskan St. Elias Mountains is approximately 11,800 km^2. Included are parts of the three largest temperate glaciers in North America. Two, Bering and Malaspina Glaciers, are piedmont outlet glaciers, each with areas greater than 5,000 km^2; and the third, Hubbard Glacier, is a tidewater glacier (114 km, 3,900 km^2). More than 50 glaciers in the St. Elias Mountains have lengths greater than 8 km. East of Glacier Bay, the largest glacier is Davidson Glacier (20 km, 115 km^2), located in the Chilkat Range. In the Glacier Bay area, about a dozen glaciers have lengths exceeding 15 km, the longest and largest is Grand Pacific Glacier (60 km, 650 km^2), which originates in Alaska, flows through British Columbia, and terminates in Alaska. Brady and Carroll Glaciers also have areas that exceed 500 km^2. Glacier Bay has a length of more than 100 km. About 250 years ago, Glacier Bay did not exist. Its basin was filled by a single large ice mass that reached into Icy Strait. Larsen et al. (2005, 2007) calculated that the ice volume that was lost during post-Little Ice Age retreat was about 3,700 km^3, about 3,450 km^3 was lost above sea level and 250 km^3 below sea level. Figure 3 presents three images that document the rapid retreat of Muir Glacier, the dominant glacier in the East Arm of Glacier Bay between 1941 and 2004. Most of the twentieth century ice loss from Glacier Bay occurred in East Arm.

During the 1970s, Johns Hopkins, Grand Pacific, Margerie, Brady, North Crillon, Lituya, Hubbard, and Turner Glaciers were advancing. La Perouse and South Crillon Glacier were stable, although the positions of their termini fluctuated from year to year. All other valley and outlet glaciers in the St. Elias Mountains were thinning and retreating. At the beginning of the twenty-first century, North Crillon, Lituya, Hubbard, and Turner Glaciers were advancing. Johns Hopkins, La Perouse, and South Crillon Glacier were stable, although the positions of their termini also fluctuated from year to year. All other observed valley and outlet glaciers in the St. Elias Mountains were thinning and retreating.

Chugach Mountains – The glacierized area of the Chugach Mountains is approximately 21,600 km^2. Included are most of Bering Glacier, which surged at least five times during the twentieth century (Molnia and Post, 1995), and more than 20 valley and tidewater glaciers with areas greater than 100 km^2. These include Martin River Glacier, (48 km, 290 km^2), Miles Glacier (52 km, 225 km^2); Bremner Glacier, which has three distinct outlets: Middle Fork Lobe, North Fork Lobe, and Tana Lobe (44 km, 150 km^2); Tana Glacier (68 km, 100 km^2); the western Jefferies Glacier (55 km, 300 km^2), a complex glacier with many outlet glaciers that is contiguous with the Tana Glacier; Sheridan Glacier (24 km, 101 km^2); Scott Glacier (24 km, 160 km^2); Woodworth Glacier (23 km, 185 km^2); Schwan Glacier (23 km, 131 km^2); Allen Glacier (31 km, 230 km^2); Childs Glacier (19 km, 100 km^2); Valdez Glacier (34 km, 158 km^2); Shoup Glacier (30 km, 146 km^2); Columbia Glacier (59.5 km, 1,121 km^2); Meares Glacier (25 km, 142 km^2); Yale Glacier (32 km, 194 km^2); Harvard Glacier (39 km, 524 km^2); Matanuska Glacier (46 km, 324 km^2); Nelchina

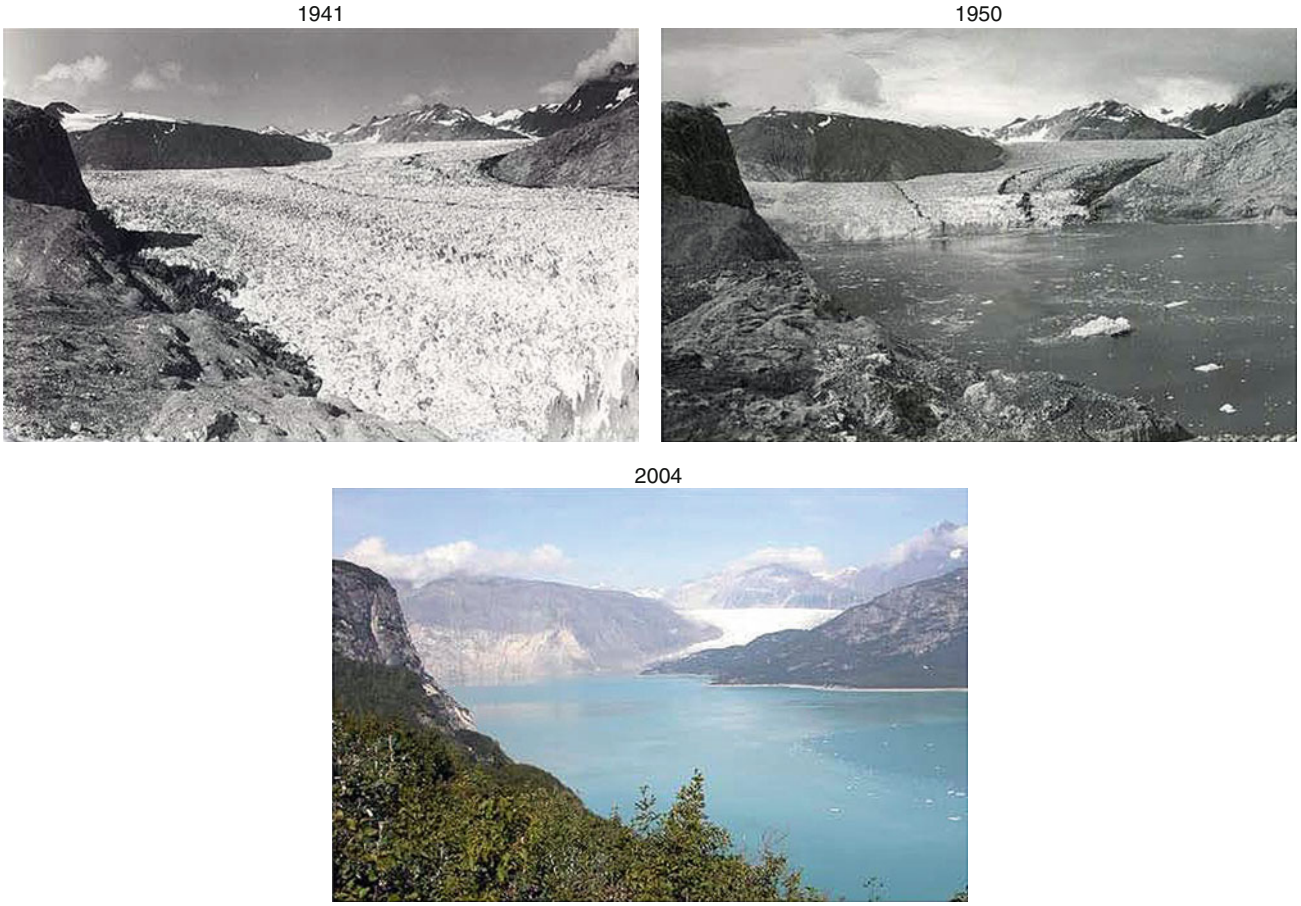

Alaskan Glaciers, Figure 3 Three northeast-looking photographs taken in Muir Inlet, Glacier Bay National Park and Preserve, Alaska, document changes that have occurred to Muir Glacier during the 63 years between August 13, 1941 and August 31, 2004. The 1941 photograph shows the lower reaches of Muir Glacier, then a large, tidewater calving valley glacier and its tributary Riggs Glacier. The ice thickness in the center of the photographs is more than 0.7 km. For nearly two centuries prior to 1941, Muir Glacier had been retreating. Maximum retreat exceeded 50 km. In places, more than a 1.0 km thickness of ice had been lost. Note the absence of any identifiable vegetation and the numerous bare bedrock faces present on both sides of the glacier (W. O. Field, # 41–64, courtesy of the National Snow and Ice Data). The August 4, 1950 photograph documents the significant changes that have occurred during the 9 years between it and the 1941 photograph. Muir Glacier has retreated more than 3 km, exposing more of Muir Inlet, and thinned 100 m or more. However, it still is connected with tributary Riggs Glacier. White Thunder Ridge continues to be devoid of vegetation. (W. O. Field, # F50-R29, courtesy of the Glacier Bay National Park and Preserve Archive). The August 31, 2004 photograph documents the significant changes that have occurred during the 63 years between the first and third photographs and during the 54 years between the second and third photographs. Muir Glacier has retreated out of the field of view and is now located more than 7 km to the northwest. Riggs Glacier has retreated as much as 0.6 km and thinned by more than 250 m. Note the dense vegetation, dominated by *Alnus,* that has developed on the till cover of White Thunder Ridge. Also note the correlation between Muir Glacier's 1941 thickness and the trimline on the left side of the 2004 photograph. (USGS Photograph by Bruce F. Molnia.)

Glacier (39 km, 328 km^2); Tazlina Glacier (47 km, 398 km^2); Knik Glacier (49 km, 380 km^2); and Colony Glacier (29 km, 237 km^2). With the exception of the advancing Harvard and Meares Glaciers, all of these glaciers are currently retreating and thinning. Since the early 1980s, Columbia Glacier has been catastrophically retreating (Krimmel, 2001; Pfeffer et al., 2000; Pfeffer, 2007).

Kenai Mountains – The glacierized area of the Kenai Mountains is approximately 4,600 km^2. The region contains several hundred glaciers. Seven have lengths of about 20 km, and 2 exceed 30 km. Most of the glaciers in the Kenai Mountains originate from two large ice fields, the Sargent and the Harding Icefields, and two smaller unnamed ice fields, one north of the Sargent Icefield between Kings Bay and Portage and the other southwest of the Harding Icefield. With the exception of Aialik and McCarty Glaciers, both of which advanced more than 500 m during the second half of the twentieth century, all of the valley and tidewater glaciers in the Kenai

Mountains continued to stagnate, thin, and (or) retreat. Wolverine Glacier, a USGS Benchmark Glacier, has a mass balance record that exceeds 30 years (Josberger et al., 2007).

Kodiak Island – During the 1970s, the glacierized area of Kodiak Island was less than 15 km^2, significantly reduced from the island's Little Ice Age glacier extent. Here, all glaciers are small and poorly studied. Their small size, low elevation, and location on an island that has undergone a temperature increase and is surrounded by temperate ocean water suggest that these glaciers are continuing to thin and retreat.

Aleutian Range –The glacierized area of the Aleutian Range is approximately 1,250 km^2. The range contains more than 30 glaciers having lengths of 8 km or more. The largest, Blockade Glacier, is 44 km long and has an area of about 250 km^2. Large, non-surge-type valley glaciers in the Aleutian Range are generally stagnant, thinning, and (or) retreating. Several glaciers surged during the 1970s, but no termini advances were reported. At the end of the twentieth century and into the early twenty-first century, all of the valley and outlet glaciers in the Aleutian Range continued to thin, stagnate, and retreat. Several small glaciers in the Glacier Fork drainage were reported to be advancing during the 1990s. When Tuxedni Glacier was observed in 2000, it showed some evidence of a recent terminus advance. However, trimlines and abandoned moraines document a long-term history of retreat and thinning. The 1912 eruption of Mount Katmai melted and beheaded a number of summit and flank glaciers (Griggs, 1922). Following the eruption, two small glaciers formed on the talus beneath the crater rim. They continue to exist. Similarly, following the 1989–1990 eruption of Mount Redoubt, snow and glacier ice accumulating in the crater have replaced snow and ice melted during the eruption.

Aleutian Islands – During the 1970s, the glacierized area of the Aleutian Islands was approximately 960 km^2, with glaciers present on at least ten islands in the eastern and central part of the Aleutian Islands. From east to west, islands where glaciers have been reported are Unimak, Akutan, Unalaska, Umnak, Herbert, Atka, Great Sitkin, Tanaga, Gareloi, and Kiska Islands. All of the mapped glaciers of the Aleutian Islands descend from the summits of active or dormant volcanoes, extending into either calderas or down their flanks. All head at elevations greater than 1,200 m. Very little information exists about the status of Aleutian Islands glaciers, either historically or today.

Wrangell Mountains – The glacierized area of the Wrangell Mountains is approximately 8,300 km^2. Many of its glaciers are surge-type. About 50 outlet glaciers have lengths of 8 km or more. The largest, Nabesna Glacier, is 87 km long, and has an area of 819 km^2. It is the largest inland glacier in North America. With the exception of Athna Glacier and South and Center Mackeith Glaciers (Sturm et al., 1991) which were advancing, apparently in response to heat-flow-related non-climatic forcing, all of the valley and outlet glaciers in the Wrangell Mountains appear to be retreating, thinning, or stagnant.

Talkeetna Mountains – During the 1970s, the glacierized area of the Talkeetna Mountains was approximately 800 km^2. Several hundred glaciers were present including seven with lengths of more than 8 km. The longest, an unnamed glacier located above the headwaters of the northwest-flowing Sheep River, had a length of 17.7 km, and an area of 77 km^2. Chickaloon Glacier (14.5 km, 33 km^2) and Talkeetna Glacier (11.6 km, 25 km^2) are the largest named glaciers. Collins (1975) analyzed the comparative sizes and numbers of glaciers shown on topographic maps made from 1948 to 1952 aerial photography with later photography. The result was clear evidence that all of the glaciers of the Talkeetna Mountains were thinning, retreating, and (or) stagnant. Every glacier observed from the air in 2000 and 2007 by the author showed continuing evidence of thinning and retreat, and that many smaller glaciers had completely disappeared.

Alaska Range – The glacierized area of the Alaska Range is approximately 13,900 km^2. The Alaska Range consists of a number of adjacent and discrete mountain ranges that extend in an arc more than 750 km long. The Alaska Range supports thousands of glaciers which range in size from tiny unnamed cirque glaciers with areas of less than 1 km^2 to very large valley glaciers with lengths up to 76 km and areas of greater than 500 km^2. From east to west, the largest include: Johnson Glacier (33 km, 183 km^2); an unnamed glacier (24 km, 108 km^2), which forms the headwaters of the West Fork of Robertson River; Gerstle Glacier (24 km, 80 km^2), which forms the headwaters of the Gerstle River; Gakona Glacier (32 km, 112 km^2); Canwell Glacier (24 km, 89 km^2); Trident Glacier (28 km, 222 km^2); Gillam Glacier (25 km, 144 km^2); Yanert Glacier (35 km, 183 km^2), which advanced about 5 km in a 1942 surge, stagnated for more than 57 years, and surged again in 2000 and 2001; West Fork Glacier (41 km, 311 km^2); Susitna Glacier (36 km, 323 km^2), which surged about 5 km in 1952 or 1953; Black Rapids Glacier (40 km, 341 km^2); Muldrow Glacier (61 km, 516 km^2); Yentna Glacier (51 km, 487 km^2); Kahiltna Glacier (76 km, 580 km^2); Tokositna Glacier (44 km, 240 km^2); Ruth Glacier (63 km, 449 km^2); Eldridge Glacier (48 km, 485 km^2); Peters Glacier (27 km, 123 km^2), which surged in 1986; Straightaway Glacier (22 km, 71 km^2); Foraker Glacier (25 km, 74 km^2); Herron Glacier (25 km, 79 km^2); and Chedotlothna Glacier (27 km, 97 km^2). Non-surge-type valley glaciers in the Alaska Range are stagnant, thinning, and (or) retreating.

Gulkana Glacier, a USGS Benchmark Glacier, has a mass balance record that exceeds 30 years (Josberger et al., 2007). West Gulkana Glacier, a 4-km-long valley glacier was mapped in 1957 (AGS, 1960) and again in 1987 (Thompson and Smith, 1988). A comparison of the maps shows that the glacier retreated about 520 m and thinned and narrowed in the 30 years between surveys.

Wood River Mountains – A GIS analysis of USGS 1:63,360-scale topographic maps of the Wood River Mountains by Manley (1999) determined that 106 glaciers exist in the Wood River Mountains. The analysis quantified 32 different parameters of these 106 glaciers and determined that the total glacier-covered area was approximately 60 km^2 and that individual glaciers ranged in area from 0.05 to 6.4 km^2 (median area 0.26 km^2). They ranged in average elevation from 581 to 1,176 m (median elevation 937 m), in length from 0.25 to 4.38 km (median length 0.61 km), in width from 0.17 to 2.97 km (median width 0.72 km), and in perimeter from 1.0 to 23.8 km (median perimeter 2.6 km). The ELAs ranged from 545 to 1,155 m (average 929 m) and displayed high local variability. The largest glacier, Chikuminuk Glacier, was mapped in 1957 and 1958 during the IGY (AGS, 1960). Since then, its terminus region has thinned and retreated. However, at elevations above 1,000 m, it has thickened by an average of about 10 m.

Kigluaik Mountains – As recently 1986, three very small valley glaciers, Grand Union, Thrush, and Phalarope Glaciers, which have a collective glacierized area of less than 3 km^2, existed in the Kigluaik Mountains (Kaufman and Calkin, 1988). Their field investigations confirmed that other glaciers that existed during the early twentieth century had completely disappeared. They also documented that the remaining three Kigluaik Mountain glaciers were continuing to decrease in area and length. Given the rate at which these three glaciers were retreating and thinning, it is possible that one or more of them may have subsequently disappeared.

Brooks Range – The Brooks Range is the northernmost mountain group in Alaska, containing about a dozen named generally east–west-trending contiguous mountain ranges. Here, polythermal glaciers cover an area of 723 km^2 (C. Suzanne Brown, oral communication, 1992). The largest glaciers are located in the Romanzof Mountains. There, at least 188 glaciers with a combined area of 260 km^2 existed during the 1970s (Denton, 1975). Four had lengths of 5 km or more, including 8.3-km-long Okpilak Glacier and 7.6-km-long McCall Glacier. Details of mass loss at McCall Glacier have been presented by Nolan et al. (2005). All Brooks Range glaciers are retreating.

The general thinning and retreat of lower elevation temperate glaciers is one of the most visible manifestations of the post-Little Ice Age response of Alaska's glaciers to changing regional climate. As the regional summaries of the status of Alaska's glaciers clearly show, most Alaskan mountain glaciers at lower elevations are stagnant and (or) retreating and thinning in response to a post-Little Ice Age regional warming. In fact, more than 98% are currently thinning, retreating, or stagnant. As has also been shown, local and regional variability has given every glacier in Alaska its own complex and unique history of change. For example, many glaciers in southeastern Alaska – such as most of the glaciers of the Glacier Bay and the Lynn Canal areas – began to retreat as early as the mid-eighteenth century. Today while most of Alaska's glaciers continue to retreat, others, like the tidewater Harvard and Hubbard Glaciers, have been advancing for more than a century.

Airborne and spaceborne measurements of changes in Alaskan glaciers

Numerous airborne and spaceborne geophysical missions have provided insight into elevation and volume change of many glacier-covered regions and individual glaciers. For instance, Arendt et al. (2002) synthesized the result of more than a decade of geodetic airborne laser profiling of 67 glaciers in Alaska and adjacent Canada, representing about 20% of the glacierized area of Alaska and adjacent Canada. They concluded that the total annual volume change of Alaska glaciers, expressed as water equivalent, to be -52 ± 15 km^3/year for the period from the 1950s to the early 1990s and -96 ± 35 km^3/year for the period from the middle 1990s to the late 1990s. These volumes are equivalent to a rise in sea level of 0.14 ± 0.04 mm a-1 during the early period and 0.27 ± 0.10 mm a-1 during the more recent period.

More recently, Arendt et al. (2006, 2009), Berthier et al. (2010), and VanLooy et al. (2006) used spaceborne sensors to make measurement of glacier elevation changes in Alaska that confirm and expand the earlier airborne studies. Numerous studies, such as Arendt et al. (2008), Chen et al. (2006), Luthcke et al. (2008), and Tamisiea et al. (2005), have used the Gravity Recovery and Climate Experiment (GRACE) satellite mission to document mass changes in Alaskan glaciers. For example, Chen and his colleagues determined that monthly gravity data, spanning April 2002–November 2005, showed a prominent glacial melting trend in the mountain regions around the Gulf of Alaska equal to 101 ± 22 km^3/year.

Summary

This entry presents a summary of the distribution, size, behavior, and characteristics of the glaciers of Alaska. It has documented that today, most of Alaska's approximately 2,000 valley glaciers are retreating, thinning, and/or stagnating. Additionally, many lower elevation mountain and cirque glaciers have disappeared in post-Little Ice Age time. In spite of the regional trend of significant ice loss, about a dozen large valley glaciers are currently thickening and advancing. All of these are near the Pacific Ocean and generally possess significant higher elevation accumulation areas. At higher elevations, generally above 2,000 m, glaciers are thickening or exhibit no change.

Several volcanoes, including Redoubt Volcano, had twentieth century eruptions that melted summit glaciers. Post-eruption conditions resulted in the formation of new glaciers in their craters. Recently, space-based investigations have confirmed the role of melting Alaskan glaciers in global sea-level rise and documented the acceleration of the rate of melting and retreat at many locations.

Bibliography

American Geographical Society (AGS), 1960. *Nine Glacier Maps, Northwestern North America*. New York: American Geographical Society Special Publication No. 34, p. 37, 9 pls.

Arendt, A. A., Echelmeyer, K. A., Harrison, W. D., Lingle, C. S., and Valentine, V. B., 2002. Rapid wastage of Alaska glaciers and their contribution to rising sea level. *Science*, **297**(5580), 382–386.

Arendt, A. A., et al., 2006. Updated estimates of glacier volume changes in the western Chugach Mountains, Alaska, and a comparison of regional extrapolation methods. *Journal of Geophyscial Research*, **111**(F3), F03019.

Arendt, A., Luthcke, S., Larsen, C., Abdalati, W., Krabill, W., and Beedle, M., 2008. Validation of high-resolution GRACE mascon estimates of glacier mass changes in the St. Elias Mountains, Alaska, USA using Aircraft Laser Altimetry. *Journal of Glaciology*, **54**(188), 778–787.

Arendt, A. A., Walsh, J., and Harrison, W., 2009. Changes of glaciers and climate in northwestern North America during the late 20th century. *Journal of Climate*, **22**(15), 4117–4134.

Berthier, E., Schiefer, E., Clarke, G. K. C., Menounos, B., and Remy, F., 2010. Contribution of Alaskan glaciers to sea level rise derived from satellite imagery. *Nature Geoscience*, **3**(2), 92–95.

Chen, J. L., Tapley, B. D., and Wilson, C. R., 2006. Alaskan mountain glacial melting observed by satellite gravimetry. *Earth and Planetary Science Letters*, **248**(1–2), 368–378.

Collins, S. G., 1975. Glaciers of the Talkeetna Mountains, Alaska. In Field, W. O. (ed.), *Mountain Glaciers of the Northern Hemisphere*. Hanover: US Army Corps of Engineers, Cold Regions Research and Engineering Laboratory, Vol. 2, pp. 543–548.

Denton, G. H., 1975. Glaciers of the Brooks Range. In Field, W. O. (ed.), *Mountain Glaciers of the Northern Hemisphere*. Hanover: US Army Corps of Engineers, Cold Regions Research and Engineering Laboratory, Vol. 2, pp. 651–662.

Griggs, R. F., 1922. *The Valley of the Ten Thousand Smokes*. Washington, DC: The National Geographic Society, p. 341.

Josberger, E. G., Bidlake, W. R., March, R. S., and Kennedy, B. W., 2007. Glacier mass-balance fluctuations in the Pacific Northwest and Alaska, USA. *Annals of Glaciology*, **46**, 291–296.

Kaufman, D. S., and Calkin, P. E., 1988. Morphometric analysis of Pleistocene moraines in the Kigluaik Mountains, northwestern Alaska, U.S.A. *Arctic and Alpine Research*, **20**(3), 273–284.

Krimmel, R. M., 2001. *Photogrammetric Data Set, 1957–2000, and Bathymetric Measurements for Columbia Glacier, Alaska*. Tacoma: US Geological Survey. Water-Resources Investigation Report 01–4089, p. 40. 1 CD-ROM.

Larsen, C. F., Motyka, R. J., Freymueller, J. T., Echelmeyer, K. A., and Ivins, E. R., 2005. Rapid viscoelastic uplift in southeast Alaska caused by post-Little Ice Age glacial retreat. *Earth and Planetary Science Letters*, **237**, 548–560.

Larsen, C. F., Motyka, R. J., Arendt, A. A., Echelmeyer, K. A., and Geissler, P. E., 2007. Glacier changes in southeast Alaska and northwest British Columbia and its contribution to sea level rise. *Journal of Geophysical Research*, **112**, 11. doi:10.1029/2006JF000586.

Lawrence, D. B., 1950. Glacier fluctuations for six centuries in southeastern Alaska and its relation to solar activity. *Geographical Review*, **40**(2), 191–223.

Luthcke, S. B., Arendt, A. A., Rowlands, D. D., McCarthy, J. J., and Larsen, C. F., 2008. Recent glacier mass changes in the Gulf of Alaska region from GRACE mascon solutions. *Journal of Glaciology*, **54**(188), 767–777.

Manley, W. F., 1999. GIS assessment of glaciers, equilibrium line altitudes and climate sensitivity – an example from southwestern Alaska. *Geological Society of America Annual Meeting, Programs and Abstracts*, **31**(7), 366.

Miller, M. M., and Pelto, M. S., 1999. Mass balance measurements on the Lemon Creek Glacier, Juneau Icefield, Alaska 1953–1998. *Geografiska Annaler Series a-Physical Geography*, **81A**(4), 671–681.

Molnia, B. F., 2007. Late nineteenth to early twenty-first century behavior of Alaskan glaciers as indicators of changing regional climate. *Global Planet Change*, **56**(1–2), 23–56.

Molnia, B. F., 2008. Glaciers of Alaska. In Williams, R. S., Jr., and Ferrigno, J. G. (eds.), *Satellite Image Atlas of Glaciers of the World*. Washington: US GPO. U.S. Geological Survey Professional Paper 1386-K, p. 525.

Molnia, B. F., and Post, A., 1995. Holocene history of Bering Glacier, Alaska: a prelude to the 1993–1994 surge. *Physical Geography*, **16**(2), 87–117.

Motyka, R. J., Echelmeyer, K., and Elsberg, D., 2001. Taku Glacier on the move again: active deformation of proglacial sediments. *EOS. Transactions of the American Geophysical Union*, **82**(47, Fall Meeting Supplement, Abstract IP52A–0745), F556.

Nolan, M., Arendt, A., Rabus, B., and Hinzman, L., 2005. Volume change of McCall Glacier, Arctic Alaska, USA, 1956–2003. *Annals of Glaciology*, **42**, 409–416.

Pfeffer, W. T., 2007. A simple mechanism for irreversible tidewater glacier retreat. *Journal of Geophysical Research*, **112**, 03S25, doi:10.1029/2006JF000590.

Pfeffer, W. T., Cohn, J., Meier, M. F., and Krimmel, R. M., 2000. Alaskan glacier beats a dramatic retreat. *EOS. Transactions of the American Geophysical Union*, **81**(48), 577, 584.

Post, A., 1969. Distribution of surging glaciers in western North America. *Journal of Glaciology*, **8**(53), 229–240.

Post, A., and Meier, M. F., 1980. A preliminary inventory of Alaskan glaciers. In *World Glacier Inventory Workshop: Proceedings*, Reideralp, September 17–22, 1978. Dorking, Surrey, UK: International Association of Hydrological Sciences (IAHS) Publication No. 126, pp. 45–47.

Post, A., and Mayo, L. R., 1971. *Glacier-Dammed Lakes and Outburst Floods in Alaska*. Washington: US Geological Survey. Hydrologic Investigations Atlas HA–455, p. 10, 3 pls.

Shulski, M., and Wendler, G., 2007. *The Climate of Alaska*. Fairbanks: University of Alaska Press, p. 207.

Sturm, M., Hall, D. K., Benson, C. S., and Field, W. O., 1991. Nonclimatic control of glacier-terminus fluctuations in the Wrangell and Chugach Mountains, Alaska, U.S.A. *Journal of Glaciology*, **37**(127), 348–356.

Tamisiea, M. E., Leuliette, E. W., Davis, J. L., and Mitrovica, J. X., 2005. Constraining hydrological and cryospheric mass flux in south eastern Alaska using space-based gravity measurements. *Geophysical Research Letters*, **32**(20), L20501.

Thompson, L. S., and Smith, S. E., 1988. Constructing a 5-meter contour map and determining volumetric change from digital data, West Gulkana Glacier, Alaska. In Marcus, M. G., and Reynolds, W. J. (eds.), *Glacier and Climate Studies, West Gulkana Glacier and Environs, Alaska*. Tempe: Arizona State University, Department of Geography. Arizona State University, Department of Geography Publications Series No. 4; United States Military Academy, Department of Geography and Computer Science Research Paper No. 1, Vol. 1, p. 142, and map.

VanLooy, J., Forster, R., and Ford, A., 2006. Accelerating thinning of Kenai Peninsula glaciers, Alaska. *Geophysical Research Letters*, **33**(21), L21307.

Viens, R. J., 1995. *Dynamics and Mass Balance of Temperate Tidewater Calving Glaciers of Southern Alaska.* M.S. dissertation, Seattle, University of Washington, p 149.

ALBEDO

Thomas C. Grenfell
Department of Atmospheric Sciences, University of Washington, Seattle, WA, USA

Definition

Albedo: The fraction of incident solar radiative energy flux, or irradiance, reflected and scattered upward from a surface integrated over the solar spectrum from 300 to approximately 3,000 nm.
Spectral Albedo. The ratio of upwelling to incident irradiance versus the wavelegth of the radiation.

Introduction

Heat exchange over snow and ice is strongly affected by the interaction of solar radiation with the surface. A quantitative understanding of this interaction is critical in treating a wide variety of problems involving both the state and evolution of the surface, the subsurface layers, and the overlying atmosphere. The concept of surface albedo has been introduced as an essential tool for specifying the *surface energy balance*. The albedos of surfaces across the Arctic and Antarctic as well as snow-covered and glaciated areas at lower latitudes have been an ongoing topic of observations and modeling for many years. Pioneering work has been carried out by Dunkle and Bevans (1956), and Langleben (1971). Albedo values have been obtained with progressively increasing accuracy and with a variety of modern instruments. Developments in radiative transfer theory make it possible to examine the physical principles involved in great detail. Many of the principles given here apply to terrestrial surfaces in general, but the present discussion will be limited to surfaces consisting of various forms of snow and ice. For these media, the albedo is typically dominated by volume scattering and absorption of light that penetrates below the surface, while surface scattering or reflection is usually a secondary effect.

In winter, with a thick snow cover on the surface, the albedo is spatially quite uniform, for example, over the large continental ice sheets and some areas of the Arctic. In general, however, the albedo of a given region can be quite complex due to spatial inhomogeneities in the surface such as undulations, crevasses, or windswept zones giving rise to areas where the snow is shallow. Vegetation both in and extending above the snow generally lowers the albedo. These considerations are particularly important in the spring and summer during the melt season that occurs near sea level at almost all latitudes as well as over a significant fraction of the Greenland ice sheet and around the margins of Antarctica. As the snow becomes thinner and finally melts away, patches of the underlying surface are exposed or meltwater accumulates on or percolates below the surface. Underlying ice surfaces such as sea ice and glacier ice continue to melt throughout the summer producing further spatiotemporal variations. In these cases, changes in albedo can affect both vertical and lateral melting rates, which in turn can modify the local and regional albedo producing a decrease that accelerates the melting. In recent climate modeling studies, these effects are referred to as "snow-albedo or ice-albedo feedback" and they act to accelerate the changes in the properties of the surface, in the albedo, and in the total energy balance of the area in question. An understanding of how the albedo varies in response to changes in the state of the surface is a central component in understanding the climate of ice-covered regions and the climate in general.

Definition of surface albedo

To understand the physical principles determining the albedo, we consider the radiative energy flux or irradiance, integrated over the upward (F_{up}) or downward (F_o) hemisphere, which is commonly expressed in units of watts per square meter. The albedo, denoted by α, is expressed simply as the ratio

$$\alpha = F_{up}/F_o. \tag{1}$$

The downwelling irradiance at the surface, F_o, consists of total direct plus scattered solar radiation over the wavelength range from about 350 to 3,000 nm. This is often referred to as "shortwave radiation" in contrast to thermal infrared radiation emitted by terrestrial surfaces and by the atmosphere. F_{up} is the total shortwave irradiance redirected upward as a result of scattering and reflection by the near-surface layers. On clear days, F_o consists primarily of direct solar radiation with a secondary diffuse component due to Rayleigh and aerosol scattering by the atmosphere. On days with uniform overcast skies, F_o is diffuse and nearly isotropic. The incident radiation is attenuated in its passage through the atmosphere more strongly in the infrared than at visible and UV wavelengths due primarily to water vapor absorption. Representative examples of F_o for the Arctic are shown in Figure 1. F_o has a strong dependence on wavelength, λ, consisting of a blackbody spectrum with a maximum near 500 nm and superposed spectral absorption bands. Because the absorption properties of ice and snow also have a strong wavelength dependence, it is important to define the concept of spectral irradiance $F(\lambda)$ and the corresponding spectral albedo, α_λ, where

$$\alpha_\lambda = F_{up}(\lambda)/F_o(\lambda). \tag{2}$$

The total albedo is given by:

$$\begin{aligned}\alpha &= \int_{SW} \alpha_\lambda \cdot F_o(\lambda)\, d\lambda \Big/ \int_{SW} F_o(\lambda)\, d\lambda \\ &= \int_{SW} \alpha_\lambda \cdot F_o(\lambda)\, d\lambda \Big/ F_o,\end{aligned} \tag{3}$$

where SW denotes the shortwave radiation band.

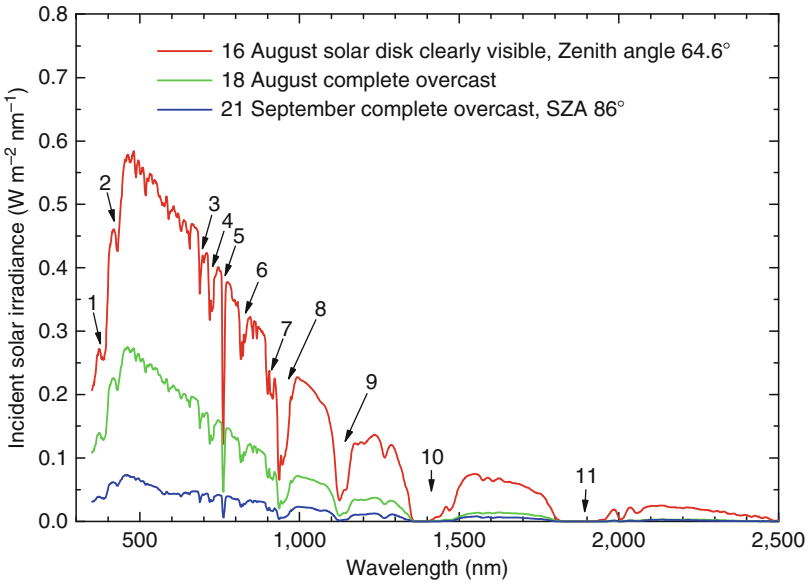

Albedo, Figure 1 Incident solar radiation spectra over Arctic sea ice with the solar disk clearly visible on 16 August 2005 and for overcast skies on 18 August and 21 September 2005 (Grenfell and Perovich, 2008). The following atomic and molecular absorption features are present: **1**. Ca II H/K, 393–396 nm; **2**. Fe/Ca, 431 nm; **3**. O_2 B, 686–688 nm; **4**. H_2O, 718–729 nm; **5**. O_2, 759–765 nm; **6.** H_2O, 820 nm; **7.** H_2O, 910 nm; **8.** H_2O, 933–946 nm, **9.** H_2O, 1,118–1,144 nm, **10.** H_2O, 1,350–1,480 nm; **11.** H_2O, 1,810–1,950 nm.

It is important to realize that the albedo is an *apparent* optical property. This means that it depends on the angular distribution and spectral composition of the ambient radiation field as well as on the *inherent* optical properties, which depend only on the structural and optical properties of the medium. This is evident from Equation 3 but also depends on the transfer of radiation within the medium. Spectral albedo depends in general on the solar elevation and cloud cover and thus is also an apparent optical property, but it is insensitive to many natural variations in the ambient radiation field related to the spectral distribution of the radiation. Because α_λ depends strongly on wavelength for all snow and ice surfaces as does $F_o(\lambda)$ in general, an understanding the physical principles governing the albedo require detailed understanding of the spectral albedo. In order to categorize α_λ for comparison purposes, it is most convenient to specify its values under conditions of diffuse illumination encountered beneath a uniform cloud cover, avoiding complications due to daily and seasonal variations in $F_o(\lambda)$. Conveniently, heavy cloud cover is common over large areas of melting snow and ice. The techniques discussed in Radiative Transfer Modeling can then be used to calculate corresponding values of α_λ appropriate for the full range of solar elevations and a wide variety of cloud conditions. Note that the α_λ under diffuse illumination for snow and ice is equal to the value for clear skies for a solar zenith angle of approximately 50° (Wiscombe and Warren, 1980). Because clouds absorb preferentially in the solar infrared leaving more radiation in the visible where α_λ is greater, it can be seen from Equation 3 that cloudy conditions modify the value of α, producing an increase in α for solar zenith angles near 50° for example.

Underlying principles

To model the albedo of a snow or ice medium in terms of its physical properties, it is necessary to take into account the layer structure, grain and bubble size distributions, and impurity contents as appropriate. In the following it is assumed unless stated otherwise that the total snow or ice layer in question is locally plane parallel and "optically thick," i.e., sufficiently thick that the albedo would not increase if the thickness were increased. In this case, the albedo is not influenced by the properties of the underlying medium. In practical terms this applies to a snow layer of at least 5–10 cm in thickness while other more transparent surface types such as bare sea ice or lake ice would need to be at least ten times thicker. Also required are the inherent optical properties of ice and water as functions of wavelength, including the refractive indices and absorption coefficients, together with the scattering coefficients for ice grains, bubbles, and other inhomogeneities. The scattering coefficients depend, in general, on the size distribution function, $n(r)$, and shapes of the particles as well as on the optical constants of ice and of any foreign inclusions. In modeling albedo, when we refer to "grain size" we mean effective grain radius derived from the actual size distribution, $n(r)$, by an expression such as the equation

$$r_{eff} = \int r^3 \cdot n(r) \cdot dr \Big/ \int r^2 \cdot n(r) \cdot dr \qquad (4)$$

introduced by Hansen and Travis (1974).

The most recent compilation of values for absorption coefficient and refractive index for ice (Warren and Brandt, 2008) is shown in Figure 2a and b. Corresponding values for pure water (Segelstein, 1981) are also needed for wet or melting snow and ice. To model the volume scattering, the size distribution and shapes of the scattering particles are needed. Although falling snow grains are usually hexagonal, the shape of the grains in the upper layers of the snow on the surface quickly become rounded even under polar conditions (Figure 3) and can often be well approximated as spheres or more generally by the method of equivalent spheres (Grenfell and Warren, 1999) for which Mie scattering theory provides a rigorous solution. For other cases such as snow in the atmosphere or very new snow, the grains can be hexagonal or irregular with very complex shapes such as multibranched dendrites, and ridged, ruffled, or rimed surfaces. Considerable progress has been made in recent years in modeling the scattering functions of many of these types of nonspherical particles, but specifying the actual shapes and size distributions of such particles in a given situation is very complex and is a topic of current research.

The modeling study by Wiscombe and Warren (1980) clarified the dependence of albedo on the structure of snow. For a thick snowpack, the albedo is sensitive primarily to the size of the snow grains in the sense that as the snow grain radius increases the albedo decreases. The decrease is greater in the infrared because the absorption coefficient of ice is greater at longer wavelengths. This can be understood in physical terms by noting that

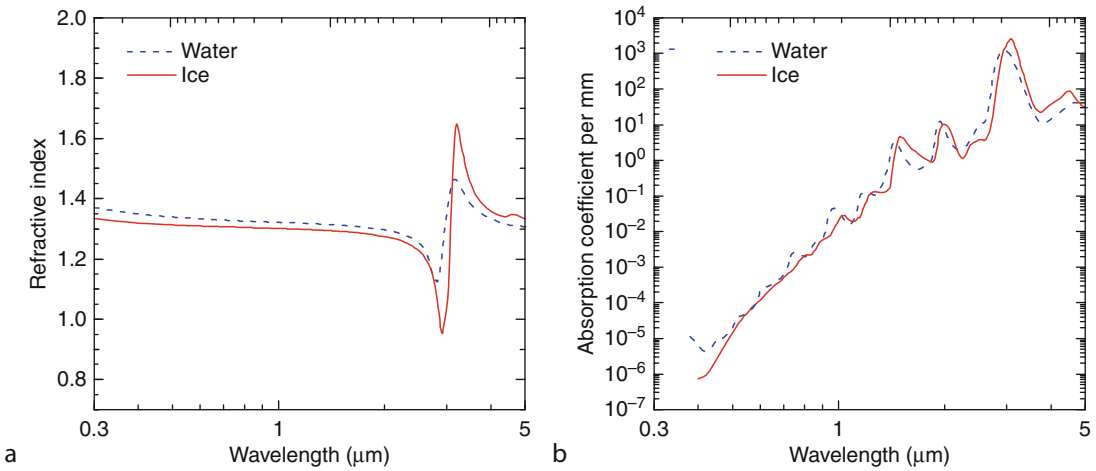

Albedo, Figure 2 Index of refraction (**a**) and absorption coefficient (**b**) for ice and water from 0.2 to 5 μm. Ice data from Warren and Brandt (2008). Water data from Segelstein (1981) and Pope and Fry (1997). Values in the ultraviolet between 0.3 and 0.4 μm are very low for both ice and water and are presently uncertain.

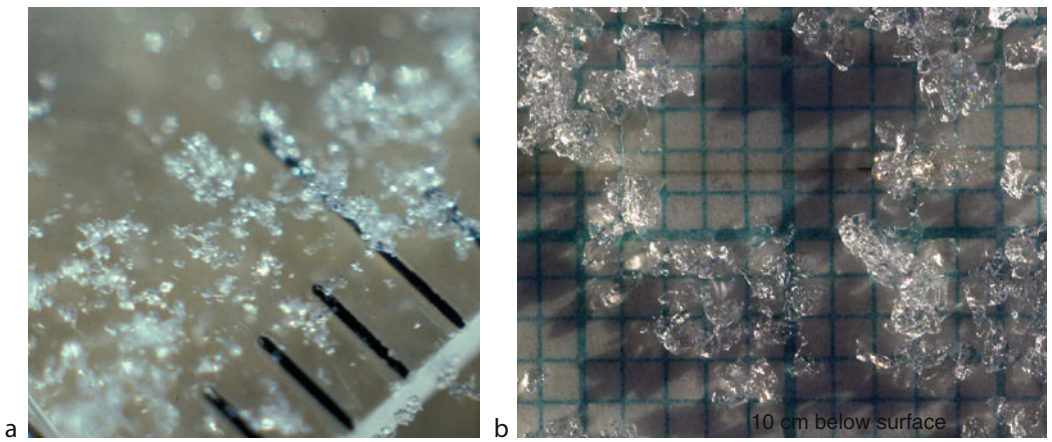

Albedo, Figure 3 Rounded and eroded snow grains from (**a**) the surface layer near South Pole Station; and (**b**) from 10 cm below the surface near Dome C Station. The spacing between the black lines in (**a**) and between the thinner blue lines in (**b**) is 1 mm.

snow grains scatter radiation predominantly in forward directions so that downward propagating rays must be scattered by many grains before they reemerge at the surface. Further since the grains are very large compared with the wavelength of the light, about the same number of scattering events is needed to redirect an incident ray back out of the snow regardless of grain size. Then from Figure 4 cases A and B we see why a homogenous snowpack with larger grains will have a lower albedo than one with smaller grains. The total absorption path length for a ray emerging from the snow is the distance traveled through ice grains and the path length through ice is greater for larger grains. If the grains are compacted to increase the density (case C), the number of scattering events for a ray to emerge will remain about the same so the absorption path length will be the same as for case A. Hence the albedo will remain the same even though the penetration depth varies. From case D, it is can be seen that emergent rays that have entered the snow closer to the vertical have experienced a larger number of scattering events and hence greater absorption, thus the albedo under clear skies will decrease as the solar elevation increases for constant snow-pack structure. The grain size dependence of α_λ is illustrated by the model results shown in Figure 5.

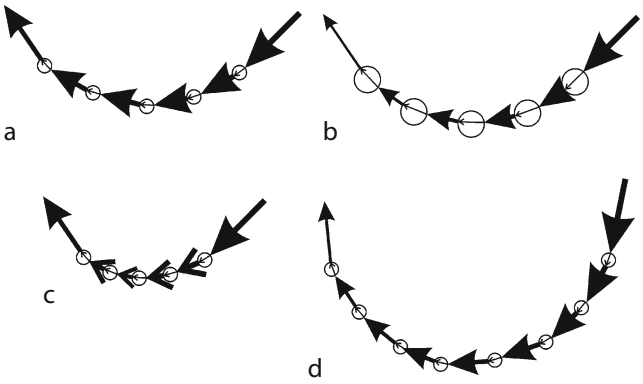

Albedo, Figure 4 Schematic diagram showing the influence of grain size, density, and solar elevation on albedo. Width of arrows external to the grains indicates the relative intensity. Case (**a**). Small grains, low absorption, high albedo; Case (**b**). Larger grains, greater absorption path length through ice, lower albedo than Case (**a**); Case (**c**). Small grains, greater snow density, absorption path length and albedo equal to case (**a**). Case (**d**). Small grains, higher sun angle, more scattering events, greater absorption path length and lower albedo than case (**a**).

Radiative transfer theory has been shown to model accurately the spectral and total albedo of thick snow on the Antarctic Plateau (Grenfell et al., 1994). This is an ideal test location where the snow is extremely pure and snow conditions are very stable. For snow in other areas, extra absorption usually arises from inclusions of foreign material such as soot, dust, and biological organisms. For other ice types including sea-ice and glacier ice, brine inclusions and vapor bubbles play a central role, and foreign materials are also usually present. Modeling of albedo in these cases requires an investigation of the size and shapes and optical properties of all inclusions.

Since bubbles and other air inclusions are also strongly forward scattering, analogous considerations apply for lake ice (Mullen and Warren, 1988), continental ice sheets, and glacier ice. A greater number density of bubbles gives

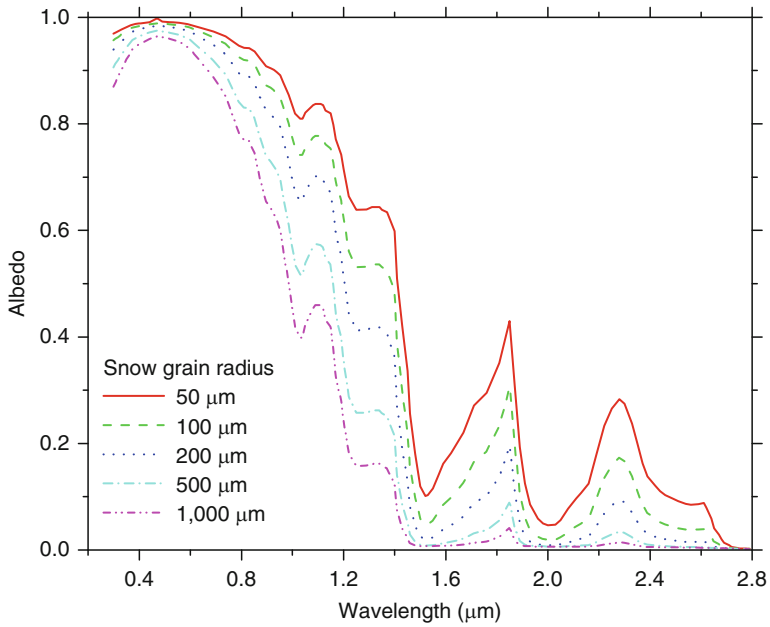

Albedo, Figure 5 Radiative transfer model results of spectral albedo of pure snow for different effective snow grain radii for a solar zenith angle of 60° from Wiscombe and Warren (1980), transcribed.

more volume scattering and thus a higher albedo while larger bubbles for a given number density imply lower albedo (Grenfell, 1983). The bulk structure in these cases typically includes additional complexity such as cracks, variable surface topography, and thickness variations due to deformation events. The determination of $n(r)$ is in general complex and can be quite sensitive to the number very small bubbles, which are at or near practical limits of resolution and can exhibit considerable spatial variability.

Other factors that can be significant in determining the albedo, depending on the ice type in questions, are the presence of subsurface ice layers, surface roughness (e.g., sastrugi), and inhomogeneities such as cracks on varying scales from microscale to crevasses. In addition, these quantities typically show spatial variations particularly over meter and larger scales as well as temporal variations especially associated with melting and refreezing events in the spring and fall. For these cases, modeling is much more complex and considerable work remains to obtain a quantitative understanding the intricacies involved.

Instruments and techniques

To understand how to measure albedo, it is useful to consider the following expansion of Equation 2:

$$\alpha_\lambda = \int_{\text{upper hemisph.}} I_{up}(\lambda,\mu,\varphi)\,\mu\,d\mu\,d\varphi \Big/ \int_{\text{lower hemisph.}} I_{dn}(\lambda,\mu,\varphi)\,\mu\,d\mu\,d\varphi, \tag{5}$$

where μ is the cosine of the angle of incidence (zenith or nadir as appropriate), φ is the azimuth angle, the subscript "up" or "dn" denotes upwelling or downwelling radiation, which is integrated over the appropriate hemisphere. From Equation 4 it follows that an ideal receptor for measuring $F_{\text{up}}(\lambda)$, $F_{\text{o}}(\lambda)$, and spectral albedo should have a hemispherical field of view with a sensitivity that is proportional to μ and independent of φ under uniform illumination by a beam of constant intensity. Such an instrument is said to have an ideal "cosine" response and its output is directly proportional to the irradiance incident upon it regardless of the angular distribution of the radiation field incident upon it. An instrument to measure wavelength integrated values should also have a sensitivity that is independent of wavelength over the shortwave spectral region.

A major development in studying α has been the development of a remarkable class of instruments called pyranometers that closely satisfy the above requirements for radiation incidence angles from 0° to between 70° and 75°. These instruments make use of a thermocouple array or thermopile covered with a nearly ideal black coating that is exposed directly to and heated by the radiation. Pyranometers measure the temperature difference between the thermopile and a reference mass inside the instrument that is shielded from the radiation and kept at ambient air temperature. The thermopile is protected by a pair of hemispherical quartz domes that limit the detected radiation to the shortwave region and provide shielding from the wind while introducing no angular bias in sensitivity. These instruments have a linear response over a large range in light intensity. They are lightweight, compact, easy to deploy, and require no external power source. Units consisting of a matched pair of sensors looking up and downward simultaneously are now available from Kipp and Zonen (www.kippzonen.com). A wide variety of low-power solid-state recorders are also available to record the output, making it feasible to carry out long-term unattended observations. The main challenge is that the outer domes often collect condensation, rime, or frost, which must be removed to obtain accurate results.

Pyranometers are not suitable for high resolution α_λ measurements because their sensitivity is too low. Modern photo-optical sensors, such as photodiode arrays and more recently CCD arrays, have overcome the sensitivity problem, and spectrophotometric instruments that provide measurements over the full shortwave spectrum are now available. One of the major concerns with these instruments is to produce a sensor with a true cosine response at all wavelengths or to correct the measurements for departures from the ideal response.

The first spectrophotometers for field use in the Polar Regions were restricted to the 400–1,100 nm wavelength range. Grenfell and Maykut (1977) reported observations of spectral albedo for sea ice and snow, but extrapolation to longer wavelengths was necessary to determine total albedo, limiting the accuracy of the results. A prototype instrument produced the first set of accurate spectral albedo observations over the full wavelength range for clean snow and ice in the Antarctic (Grenfell et al., 1994). The turret receptors in use had significant deviations from an ideal cosine response, particularly in the infrared, and significant wavelength-dependent corrections had to be applied. Commercial instruments are now available with improved sampling speed, accuracy, sensitivity and spectral resolution, and broad-band cosine receptors whose response is much closer to the ideal cosine dependence.

Calibrations

Observations can be made directly with matched upward and downward-looking instruments or by orienting a single instrument alternately upward and downward and recording the ratio of the signals. In the latter case, it is important to have an external reference instrument with similar response characteristics to monitor changes in the incident radiation field, particularly when clouds are present.

Albedo measurements have also been made with a receptor with a limited field of view looking downward alternately at the surface and then at a diffusely scattering reference plate such as Spectralon® that scatters the incident radiation toward the receptor. In this case, corrections

for the departure of the reference plate from a perfect diffuse scatterer can be applied because its directional reflectance properties are well characterized (Bruegge et al., 2001; Voss and Zhang, 2006). It is necessary to compensate properly for the angular distribution of the upwelling radiance from the surface outside the field of view of the detector.

For either mode of measurement, it is necessary to determine a shadowing correction to account for the obstruction of the ambient radiation fields by the presence of the instrument and other obstructions. Corrections for both α and α_λ range from about 0.005 to 0.04 for typical configurations (Grenfell et al., 1994), but shadowing corrections can be significantly larger if the instruments are mounted on a ship or aircraft or near taller buildings and must be determined on a case-by-case basis (Allison et al., 1993).

Albedo observations have been reported using only a photodiode detector system with a response over the spectral range from about 350 to 1,100 nm. These must be corrected for the effects of solar radiation at longer wavelengths since about half the incident irradiance lies at wavelengths between 700 and 3,000 nm. Approximation by reference to existing tabulations or radiative transfer modeling can be used; however, significant uncertainties remain in the incident infrared portion of the spectrum due to fluctuations in atmospheric water vapor and in the structure of the near surface layers of the snow or ice.

Considerable effort has been devoted to inferring spectral and total surface albedos using satellite observations. These require at least two important additional corrections. First it is necessary to account for attenuation and scattering by the atmosphere, whose properties can vary on time scales as short as a few seconds. Many satellite studies make use of surface-based albedo data as standards to infer optical properties of the atmosphere. Second, satellites view a given surface element with a very narrow field of view and from only a single direction or at most a few different directions; however, to extrapolate the observations over the upward hemisphere requires a knowledge of the hemispherical reflectance distribution function (HRDF). This is closely related to the bidirectional reflectance distribution function (BRDF) that describes the directional dependence of radiation scattered upward from a collimated incident beam. The HRDF describes the distribution of upwelling radiation from actual illumination conditions under clear skies taking into account the diffuse sky component as well as that of the direct solar beam. Values have been reported for broadband use for a selection of reference surfaces including cold snow covers (Taylor and Stowe, 1984; Kato and Loeb, 2005). Spectral values for Antarctic snow have been presented by Hudson et al. (2006) and for glacier ice by Greuell and de Ruyter de Wildt (1999). Accurate HRDF observations are very difficult to carry out under general field conditions due to the need to take a large series of observations rapidly while compensating for changes in ambient lighting. Spatial and temporal variations of surface properties introduce further uncertainties. Automated steering mechanisms for the receptor have been developed that have produced significant improvements providing the capability to measure values of HRDF rapidly (e.g., Painter and Dozier, 2004). Theoretical interpretation of these results is considerably more involved than for α_λ, which is much less sensitive to much of the fine-scale angular dependence of the upwelling radiation field.

Observations of snow and ice surfaces

Observational results from a variety of surfaces from different stages in the seasonal cycle are presented in this section. Almost all the surfaces discussed below undergo an annual cycle consisting of a cold period where the upper layers consist of snow deposited in the current year followed by a melt season where much or all of the snow melts away exposing an ice or ground surface underneath. The surface albedos vary over the annual cycle. Only on the high altitude ice sheets of Antarctica and Greenland are there large areas where summer melting does not occur and the optical properties of the surface layers are much more stable throughout the year (Liljequist, 1956). The magnitude of actual seasonal and interannual variations in reflectance patterns have recently been reported by Jin et al. (2008). These regions are of particular interest as stable reference surfaces for remote sensing measurements.

Snow

Spectral albedos for a thick clean snow cover have been reported from observations on the Antarctic plateau (Figure 6). Volume scattering is very strong and nearly constant across the entire shortwave band. Consequently,

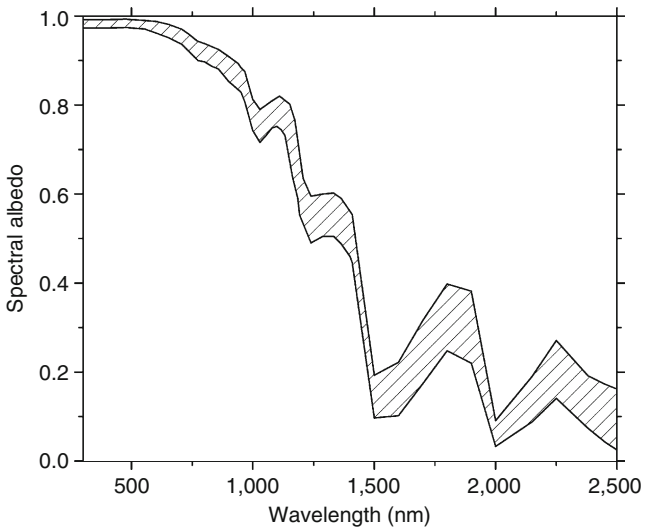

Albedo, Figure 6 Envelope of the observed spectral albedos of snow on the Antarctic Plateau from South Pole, Vostok, and Dome C stations. Data from austral summers of 1985–1986, 1990–1991, and 2004 (Grenfell et al., 1994; Hudson et al., 2006). Mean $\alpha = 0.85$.

α_λ at visible wavelengths where ice is very weakly absorbing closely approaches unity. At longer wavelengths, ice absorption increases by many orders of magnitude (Figure 2b), and α_λ decreases to very low values in the infrared. The corresponding total albedos for diffuse illumination are 0.85 ($\pm$0.02). The results of observations made under uniform cloud cover at different locations and in different years are essentially the same indicating the stability of the albedo of snow on the Antarctic plateau. The observations have been successfully matched by radiative transfer models (Grenfell et al., 1994). Similar studies in other polar regions (Aoki et al., 2000; Grenfell and Perovich, 2004) have also shown good agreement between observation and theory but impurities in the snow influence the results resulting in lower values, particularly at visible wavelengths as discussed below.

Spectral bidirectional reflectance observations of snow on the Antarctic Plateau have been analyzed and parameterized by Hudson et al. (2006) for the full range of local solar zenith angles over the full solar spectrum. The values are characterized in general by a strong enhancement in the direction of the sun with nearly isotropic values at other angles. A representative example is shown in Figure 7. A very similar pattern has been reported for a temperate snowpack (Painter and Dozier, 2004).

Sea ice

Albedos for sea ice have been reported at various locations and times of year since the early 1960s. A summary is given by Grenfell and Maykut (1977). An annual cycle of α for thick multiyear sea ice has been reported from the Surface Heat and Energy Budget of the Arctic (SHEBA) experiment in 1997/1998 as shown in Figure 8.

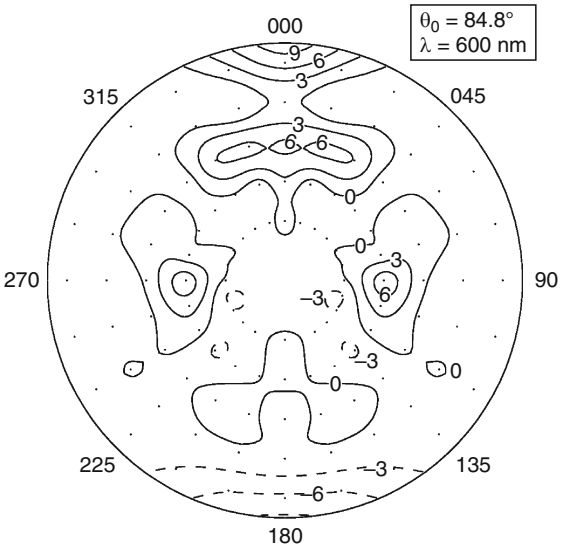

Albedo, Figure 7 Polar contour plot of anisotropic reflectance factor of snow at Dome C Station, Antarctica, for a solar zenith angle of 84.8° and a wavelength of 600 nm (Hudson et al., 2006).

During the cold season from October to late-May, the sea ice was covered with a layer of snow about 30 cm in thickness and the albedo was quite stable. The fluctuations were mainly due to changes in illumination conditions and variations in grain size. Significant changes occurred as soon as the snow began to melt in the Spring, and they continued throughout the melt season and into the fall until the snow cover and cold Winter conditions resumed.

The spectral albedo of thick winter sea ice is quite similar to the pure snow albedos shown in Figure 6. The spectral albedo of growing thin and young ice ranges from a low almost wavelength-independent value near 0.067 increasing with ice thickness and accumulation of surface frost and snow. The development of the albedo of young ice types can be influenced by episodic events such as air temperature variations and snowfall. Representative sequences have been presented for specific situations (Grenfell et al., 1998; Brandt et al., 2005).

The summer ice cover consists of drained white ice and melt ponds. Selected values of α_λ are shown in Figure 9. The spectral albedo of white ice is nearly constant across the visible part of the spectrum decreasing in the infrared. In this case, α_λ is quite stable throughout the summer because of the presence of a drained layer above freeboard level whose thickness and structure are maintained by hydrostatic adjustment as water from the melting surface drains off the floes. Melt ponds occur in local depressions where the melt water can collect. The albedo of melt ponds is primarily determined by the amount of volume scattering in the ice beneath the water while the dependence on water depth in the ponds is relatively weak (Makshtas and Podgorny, 1996). Both light and dark melt ponds occur for cases where the volume scattering is greater or smaller respectively. For dark melt ponds the maximum

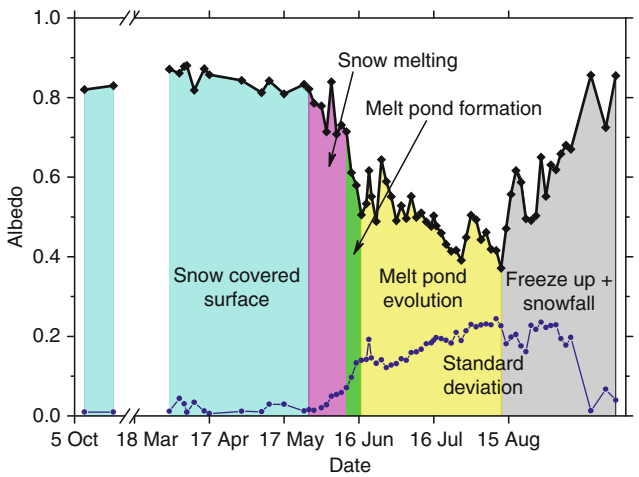

Albedo, Figure 8 Time series of wavelength-integrated albedo of sea ice in October 1997 and from 1 April 1998 through 27 September 1998. Values were averaged over a 200-m-long albedo line. The standard deviation of albedo measured along the albedo line for each is plotted as *solid blue circles*. From Perovich et al., 2002 with modifications.

values of α_λ, near 500 nm, are smaller than those shown in Figure 9, but they taper off to the same values in the near-infrared where the water is opaque. Because of the decrease in α_λ from 500 to 750 nm the ponds look blue or greenish blue. The regional albedo of melting sea ice floes is determined primarily by the albedos and areal coverage of the melt ponds, both of which are quite variable.

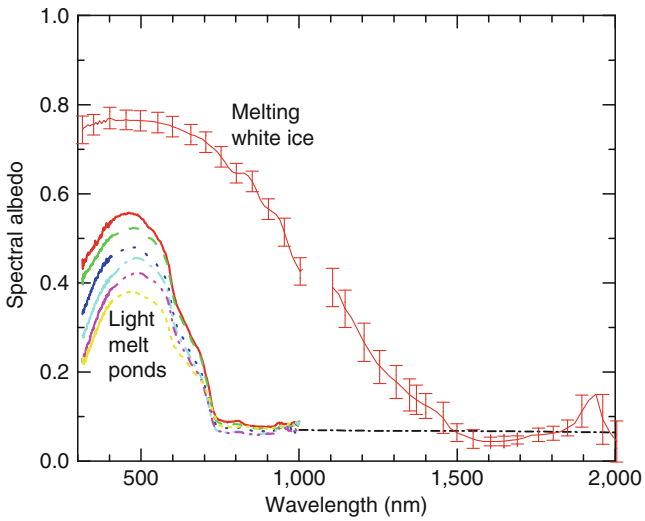

Albedo, Figure 9 Spectral albedos of bare drained sea ice (white ice) during the melt season from 7 July through 14 August 1998 ($\alpha = 0.65$) and light melt ponds over approximately the same interval (Perovich et al., 2002). *Dashed line* is an extrapolation of melt pond albedo based on Fresnel reflection coefficients using the active index values for ice.

Aircraft surveys of the fractional area of pond coverage during SHEBA recorded values as high as 25%. The melt pond coverage is thus very important for the regional shortwave energy balance.

An additional surface type associated with sea ice is open water in leads and polynyas formed by separation of ice floes, exposing the ocean beneath. The spectral albedos are nearly independent of wavelength and are dominated by specular reflection from the upper surface. Plankton and algae in the water can produce some volume scattering resulting in a slight increase across the visible part of the spectrum. Values of $\alpha = 0.066 \pm 0.007$ have been measured for diffuse illumination (Pegau and Paulson, 2001; Brandt et al., 2005). Because of their low albedo, the areal coverage of leads and polynyas are also very important in the seasonal energy balance.

Glaciers

The albedo of glaciers in temperate zones undergoes a strong seasonal cycle where the winter values of uniform surfaces closely resemble those of cold snow, and summer values range from melting coarse grained snow (~0.65) to lower values for exposed melting firn and bare ice. The volume scattering that dominates the albedo is due to snow grains near the surface and vapor inclusions formed as the snow is compressed into impermeable ice at depth, trapping the air between the grains. To illustrate the annual cycle of glacier albedo, a 1-year record of albedo and snowfall events from the ablation zone of the Morteratschgletscher (Oerlemans and Knapp, 1998) is shown in Figure 10. The main variations shown were shown to be due to snowfall events and changes in the thickness of the annual snow cover. An example of α_λ from late

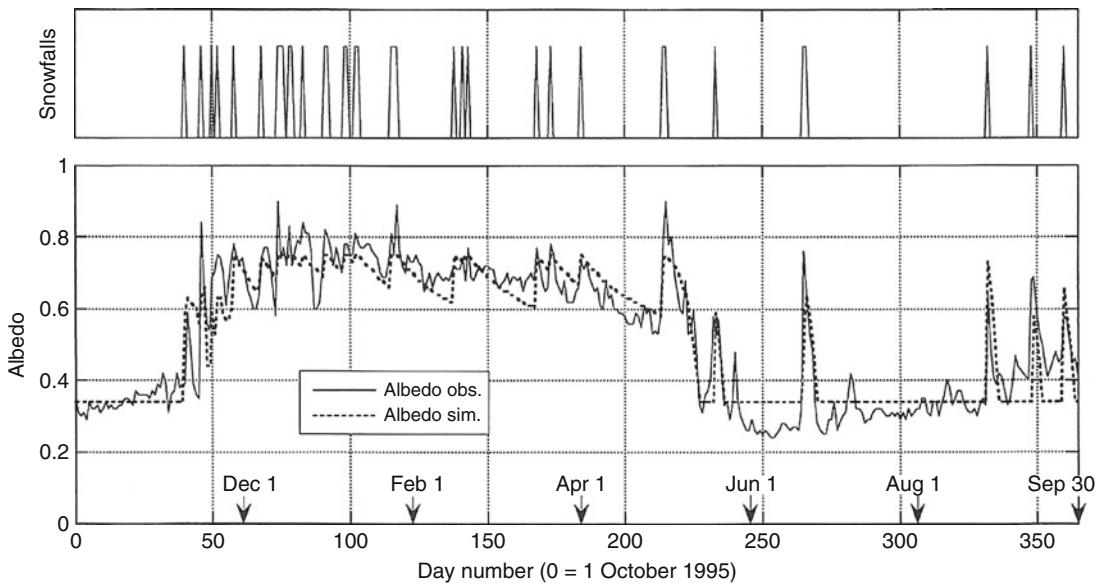

Albedo, Figure 10 A record of albedo (*lower panel*) and snowfall events (*upper panel*) from the ablation zone of the Morteratschgletscher from 1 October 1995 through 30 September 1996 (Oerlemans and Knapp, 1998).

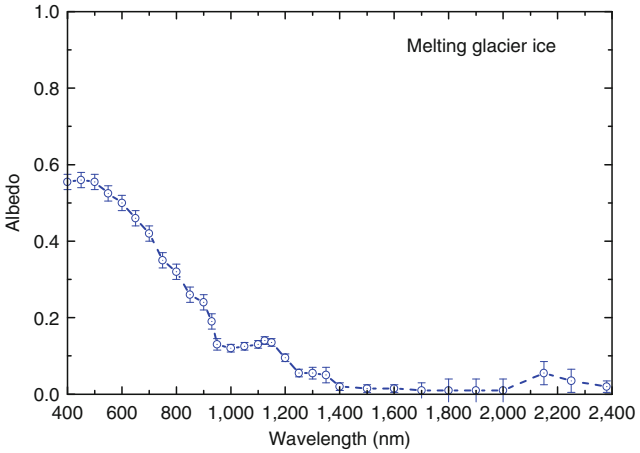

Albedo, Figure 11 Bare melting glacier ice in the ablation zone of Athabasca Glacier 16 September 1981. $\alpha = 0.34$ (GP 84). Variable amounts of dust and debris from neighboring mountains can result in large local and regional variations in glacier albedo.

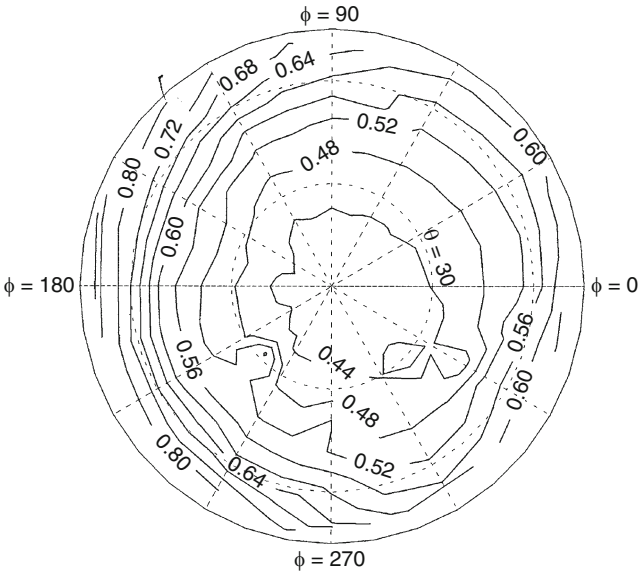

Albedo, Figure 12 Directional reflectance observations of glacier ice in the ablation zone of the Morteratschgletscher for solar zenith angle 74° and wavelength 540 nm (Greuell and de Ruyter de Wildt, 1999).

summer for the ablation zone of the Athabasca glacier is shown in Figure 11 for which the total albedo was 0.34. Since glacier ice almost always accumulates windblown dust from the surrounding mountains, both the surface snow and the underlying ice are not usually clean. The albedo is quite variable and thus difficult to model on both small and regional spatial scales, due not only to varying amounts of dust but to dynamically introduced features such as crevasses, stress cracks, medial moraines, etc. As described below, the apparent albedo can be strongly influenced by the tilt of the surface, a significant consideration for ice in mountainous terrain.

Directional reflectance observations for glacier ice (Figure 12) have been carried out, for example, by Greuell and de Ruyter de Wildt (1999) together with concurrent albedo observations to derive parameterizations relating the HDRF to the albedo for a given viewing geometry in the Landsat TM 2 and 4 bands. The reflectance patterns show a less distinct forward peak than that of Antarctic snow and a greater degree of anisotropy particularly at near nadir viewing angles.

Lake ice

Representative values of spectral albedos from three different stages during the annual cycle are shown in Figure 13. In winter, lake ice can have a thick snow cover with a resulting albedo similar to that of snow in Figure 6; however, if the snow has been removed exposing the bare ice, the spectral albedo is much lower (green circles in Figure 13). For this case, α_λ at visible wavelengths was relatively low but remained at about 0.1 throughout the solar infrared due to the strong specular reflection due to the large solar zenith angle at the time of the experiment ($\sim$70°). During the spring melt season, the ice near the

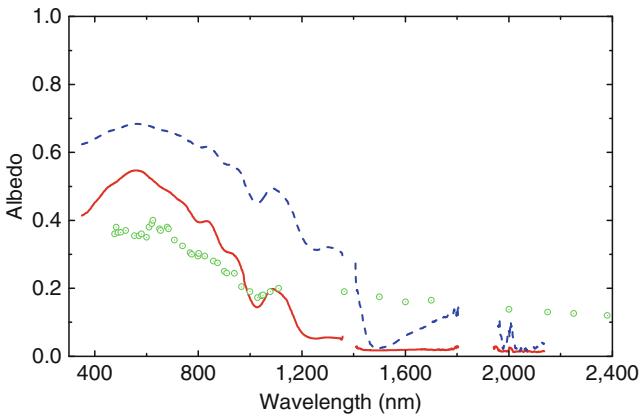

Albedo, Figure 13 Albedos for snow-free lake ice. Melting ice, Imikpuk Lake, Barrow AK, 13/18 June 2001, overcast, $\alpha = 0.39$ (*solid red curve*), and 20–22 June 2001, overcast, $\alpha = 0.54$ (*dashed blue curve*), (Grenfell and Perovich, 1984, 2004) edited. Cold bare lake ice, Moses Lake WA 17 January 1984 clear sky, solar zenith angles from 68° to 75° (*green circles*) (Mullen and Warren, 1988, transcribed).

lake surface melted preferentially at the contact planes of the ice crystals, establishing an array of anisotropic ice grains (horizontal dimensions $\sim$1 cm, vertical dimensions $\sim$10 cm) above the local water table that gave rise to increased volume scattering and a decrease in specular reflection component. As a result, α_λ at visible wavelengths was higher than for the winter case while in the infrared it decreased to values near 0.01 (red solid curve). As melting progressed the surface granular layer

thickened, the ice grains fell apart decreasing the grain size, and the albedo resembled that of melting sea ice (blue dashed curve). When the ice has melted completely, the albedo depends on the depth and clarity of the water, and for deep lakes values it is similar to those of leads and polynyas discussed above. If the lake is shallow and the water clear, α_λ depends on the optical properties of the material at the bottom of the lake.

Underlying surfaces

Spectral albedos for snow and ice-free surface types are important for interpreting the albedo of areas with thin or patchy snow cover. Values of α_λ measured in the Arctic coastal zone near Barrow AK in late May and early June are shown in Figure 14. Tundra albedo increased across the visible and into the near infrared resulting in a brown surface. The albedos of mud (brownish) and gravel (gray) were also low across the shortwave band with less pronounced increases across the visible. This is opposite to the behavior of α_λ for snow and ice surfaces so these types of surfaces can be distinguished from snow or ice.

Remote sensing and regional values

Predictions of regional albedo values using the above results in combination with satellite imagery have been carried out in order to identify various features or areas detectable from space and provide important spatial and temporal information on regional albedo and surface type distribution for sea ice and polar land areas. Studies of Antarctic sea ice combining surface-based albedo observations with a determination of the distribution of surface types based on visible estimates from ship traverses in conjunction with total ice fraction provided by the satellite imagery have been reported by Allison et al. (1993) and Brandt et al. (2005). The satellite data do not provide direct albedo values per se and rely at present on the accuracy of the surface-based measurements and parameterizations. Satellite studies provide an immense amount of useful information about the earth's surface, but there are considerable uncertainties still involved in inferring albedos from the imagery. The recently deployed polar orbiting MISR instrument offers the potential to observe the same scene from nine different viewing angles and determine much of the HRDF directly. MISR data were used, for example, to explain how clouds over snow alter the BRDF (Hudson and Warren, 2007).

The spectral dependence of upwelling scattered radiation has been used to infer effective snow grain size by Nolin and Dozier (2000). In conjunction with radiative transfer calculations, this information can be used to reconstruct the albedo over a broad range of illumination conditions avoiding many of the difficulties mentioned above, but the technique relies on the assumption that the snowpack is optically thick and spatially homogeneous over distances of many tens of meters to kilometers depending on the resolution of the satellite in question.

Additional uncertainties

An important potential source of error in albedo measurement under clear skies is the tilt of the surface away from horizontal. Particularly in mountainous regions, surface slope can introduce errors because of the large slope angles. Even small slopes can cause significant error due to the large solar zenith angles. A case study at South Pole station (Grenfell et al., 1994) for a surface slope of 2°

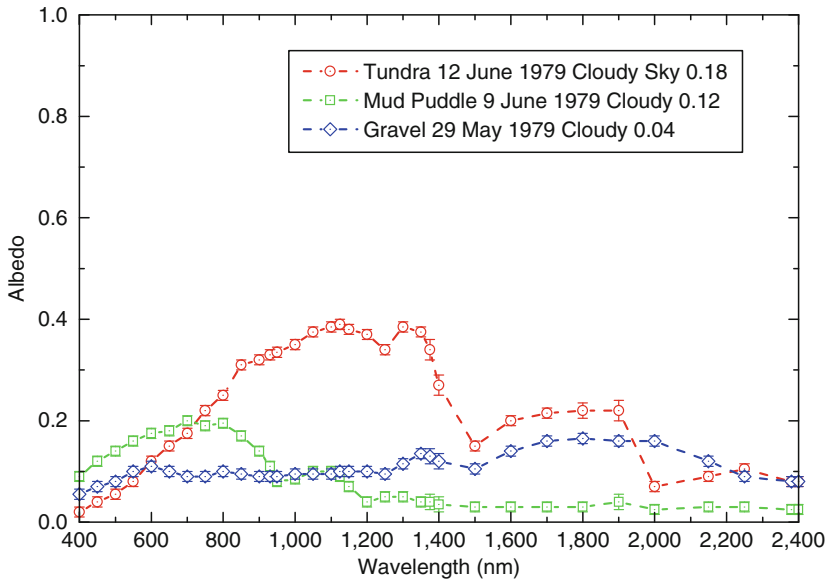

Albedo, Figure 14 Representative albedos for snow-free and ice-free Arctic surfaces early in the melt season 1979: Bare Tundra albedo, Mud, Gravel (Grenfell and Perovich, 1984).

showed deviations above and below the true albedo of up to 10% depending on the solar azimuth. The effect was well matched using a small slope model; however, Dozier and Frew (1990) have presented the following general formulation for any surface slope where the sun remains above the local horizon:

$$\alpha_\lambda(apparent) = \alpha_\lambda(true)\cdot \frac{\cos(\theta_{sun})\cos(\theta_{surf}) + \sin(\theta_{sun})\sin(\theta_{surf})\cdot\cos(\phi_{sun})}{\cos(\theta_{sun})}, \quad (6)$$

where φ_{sun} is the solar azimuth angle defined as 0° in the downhill direction, and the θ values indicate solar zenith angle (sun) or surface tilt angle (surf). Taking into account the surface tilt is of particular important for glacier ice, where slopes can be large (Klok et al., 2003). Aligning the instrument with its optical axis perpendicular to the local surface rather than vertical is preferred to remove the bias; however, if distant terrain is in the field of view of the upward looking sensor, a shadowing correction should also be taken into account (Grenfell et al., 1994; Grenfell and Perovich, 2008).

A thin snow or ice cover with finite optical thickness over a darker underlying surface such as soil, rock, or ocean water would give a lower combined albedo with the greatest reduction at visible wavelengths. In cases where the snow is optically thin, less than 10 cm or so, the snow cover is frequently patchy exposing the surface below producing a spectral albedo that is flattened out in the visible and mimics the response of a dirty continuous snow cover.

The grain size in a snowpack typically increases with depth due to metamorphism. This can also have a significant effect on the albedo and on the interpretation of its spectral distribution. Because absorption by ice increases into the infrared, there is a corresponding decrease in penetration depth of the radiation. Thus in the infrared near 2,000 nm, for example, α_λ will be influenced by the grains right at the surface while at visible wavelengths the radiation will interact with grains well below the surface whose radius can be much larger. As a result, a multilayer model is needed in general to explain α_λ across the solar spectrum.

Impurities

The presence of soot, dust, sediment, or biological material can modify the albedo of both snow and ice. Soot in particular has been identified as being important for global energy balance (Hansen and Nazarenko, 2004). Warren and Wiscombe (1980) presented demonstrating the effect of varying levels of soot in a thick uniform snowpack. For a particular soot loading, the main effect is that the visible albedo decreases most strongly compared with clean snow while the infrared albedo is less affected. This is because ice absorbs weakly in the visible but very strongly

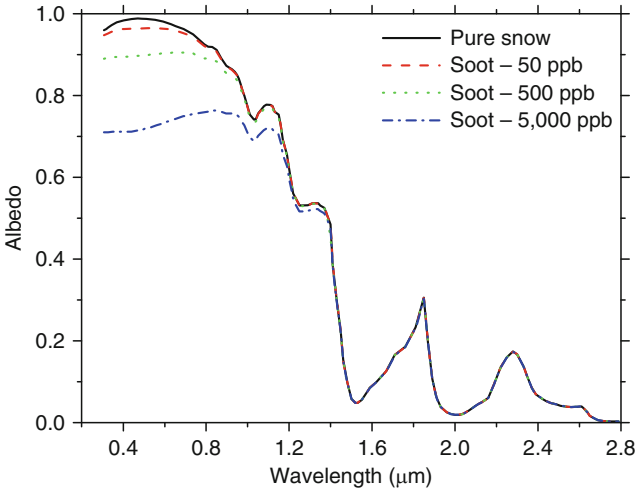

Albedo, Figure 15 Model results for varying amounts of soot in snow. Snow grain radius 100 μm, snow density 100 kg/m^3, solar zenith angle 60°. (Warren and Wiscombe, 1980). Median background soot levels in the Arctic are presently less than 50 ppb.

in the infrared so that the addition of small amounts of another absorber can have a significant effect in the visible but little effect at longer wavelengths. The effect of soot on α_λ is shown in Figure 15 for soot concentrations up to 5,000 ppb. At three locations on the Antarctic Plateau, background soot levels in the snow have been measured in the range 0.1–1 ppb (Warren and Clarke, 1990; Grenfell et al., 1994). This is sufficiently low that the resulting albedo reduction is not detectable and is not important for climate. In the Arctic, median background soot concentrations in the snow have been reported in the range 1–50 ppb (Clarke and Noone, 1985) for which the resulting decreases in α can be as large as about 0.04 depending on snow grain size (Warren and Wiscombe, 1985). A recent study (Hegg et al., 2009) has shown that most of the soot in the perennial snow cover of the Arctic comes from biomass burning and current median background levels range from 1 to ~30 ppb. Because of the relatively small variations in albedo associated with these levels, soot concentrations are presently below the levels of uncertainty in satellite studies and need to be determined from surface-based observations.

Summary

The physical principles involved in the determination of the albedo of snow and ice covered surfaces as well as the uncertainties in the observational techniques are well understood. Modern instrumentation has significantly improved the accuracy and ease of obtaining surface-based observations, and a wide range of satellite borne sensors now provide the potential to extend monitoring over the full extent of both polar regions. Table 1 presents representative values and uncertainty for the albedos of selected surface types.

Albedo, Table 1 Representative median values of albedo for selected surface types under conditions of diffuse illumination. The uncertainties represent natural variability due to differences in bubble or crystal size distribution or variations in foreign impurities such as dust and soot

Surface	Albedo	Uncertainty
Snow-covered ice on Antarctic Plateau	0.85	0.02
Cold snow-covered arctic sea ice	0.83	0.03
Melting snow-covered arctic sea ice	0.75	0.05
Melting bare multiyear sea ice	0.65	0.02
Cold snow-covered glacier ice	0.8	0.05
Melting glacier ice	0.35	0.1
Melting bare lake ice	0.45	0.1
Melt ponds on arctic sea ice	0.26 to 0.1	0.15
Cold bare lake ice	0.2	0.1
Calm deep water (open water in sea ice and deep lakes)	0.067	0.005
Arctic tundra	0.18	0.04
Dry arctic beach gravel	0.04	0.01

Agreement has been achieved between radiative transfer models and field observations of clean flat snow covers, but natural snowpacks are generally more complex. The approximations of homogeneous flat surfaces or pure snow do not apply in many situations where the surface is rough, tilted, or inhomogeneous complicating our understanding of the albedos of natural surfaces in general. Impurities in snow and ice have been identified in selected areas as being large enough to be important to affect the earth's climate, but large-scale spatial and temporal distributions of these impurities are not yet well quantified. The study of the albedo of snow and ice-covered surfaces thus remains an active area of scientific study.

Bibliography

Allison, I., Brandt, R. E., and Warren, S. G., 1993. East Antarctic sea ice: Albedo, thickness distribution, and snow cover. *Journal of Geophysical Research*, **98**, 12417–12429.

Andreassen, L. M., Van Den Broeke, M. R., Giesen, R. H., and Oerlemans, J., 2008. A five-year record of surface energy and mass balance from the ablation zone of Storbreen, Norway. *Journal of Glaciology*, **54**(185), 245–258.

Aoki, Te., Aoki, Ta., Fukabori, M., Hachikubo, A., Tachibana, Y., and Nishio, F., 2000. Effects of snow physical parameters on spectral albedo and bidirectional reflectance of snow surface. *Journal of Geophysical Research*, **105**, 10219–10236.

Brandt, R. E., Warren, S. G., and O'Rawe Hinton, P., 1988. Effect of surface roughness on bidirectional reflectance of Antarctic snow. *Journal of Geophysical Research*, **103**, 25789–25807.

Brandt, R. E., Warren, S. G., Worby, A. P., and Grenfell, T. C., 2005. Surface albedo of the Antarctic sea-ice zone. *Journal of Climate*, **18**, 3606–3622.

Bruegge, C., Chrien, N., and Haner, D., 2001. A Spectralon BRF data base for MISR calibration applications. *Remote Sensing of Environment*, **76**, 354–366.

Clarke, A. D., and Noone, K. J., 1985. Soot in the arctic snowpack: a cause for perturbations in radiative transfer. *Atmospheric Environment*, **19**, 2045–2053.

Dozier, J., and Frew, J., 1990. Rapid calculation of terrain parameters for radiation modeling from digital elevation data. *IEEE TGRS*, **28**(5), 963–969.

Dunkle, R. V., and Bevans, J. T., 1956. An approximate analysis of the solar reflectance and transmittance of a snow cover. *Journal of Meteorology*, **13**, 212–216.

Grenfell, T. C., 1983. A theoretical model of the optical properties of sea ice in the visible and near infrared. *Journal of Geophysical Research*, **88**, 9723–9735.

Grenfell, T. C., 1991. A radiative transfer model for sea ice with vertical structure variations. *Journal of Geophysical Research*, **96**(C9), 16,991–17,001.

Grenfell, T. C., and Maykut, G. A., 1977. The optical properties of ice and snow in the Arctic Basin. *Journal of Glaciology*, **18**, 445–463.

Grenfell, T. C., Perovich, D. K., and Ogren, J. A., 1981. Spectral albedos of an alpine snow pack. *Cold Regions Science and Technology*, **4**, 121–127.

Grenfell, T. C., and Perovich, D. K., 1984. Spectral albedos of sea ice and incident solar irradiance in the southern Beaufort Sea. *Journal of Geophysical Research*, **89**, 3573–3580.

Grenfell, T. C., Warren, S. G., and Mullen, P. C., 1994. Reflection of solar radiation by the Antarctic snow surface at ultraviolet, visible, and near-infrared wavelengths. *Journal of Geophysical Research*, **99**, 18669–18684.

Grenfell, T. C., Barber, D. G., Fung, A. K., Gow, A. J., Jezek, K. C., Knapp, E. J., Nghiem, S. V., Onstott, R. G., Perovich, D. K., Roesler, C. S., Swift, C. T., and Tanis, F., 1998. Evolution of electromagnetic signatures of sea ice from initial formation to the establishment of thick first-year ice. *IEEE TGRS*, **36**(5), 1642–1654.

Grenfell, T. C., and Warren, S. G., 1999. Representation of a nonspherical ice particle by a collection of independent spheres for scattering and absorption of radiation. *Journal of Geophysical Research*, **104**(D24), 31,697–31,709.

Grenfell, T. C., and Perovich, D. K., 2004. Seasonal and spatial evolution of albedo in a snow-ice-land-ocean environment. *Journal of Geophysical Research*, **109**, C01001, doi:10.1029/2003JC001866.

Grenfell, T. C., and Perovich, D. K., 2008. Incident spectral irradiance in the Arctic Basin during the summer and fall. *Journal of Geophysical Research*, **113**, D12117, doi:10.1029/2007JD009418.

Greuell, W., and de Ruyter de Wildt, M., 1999. Anisotropic reflection by melting glacier ice: measurements and parametrizations in Landsat TM Bands 2 and 4. *Remote Sensing of Environment*, **70**, 265–277.

Hansen, J. E., and Travis, L. D., 1974. Light scattering in planetary atmospheres. *Space Science Reviews*, **16**, 527–610.

Hansen, J., and Nazarenko, L., 2004. Soot climate forcing via snow and ice albedos. *Proceedings of the National Academy of Sciences USA*, **101**, 423–428.

Hegg, D. A., Warren, S. G., Grenfell, T. C., Doherty, S. J., Larson, T. V., and Clarke, A. D., 2009. Source attribution of back carbon in arctic snow. *Environmental Science & Technology*, **43**(11), 4016–4021.

Hudson, S. R., Warren, S. G., Brandt, R. E., Grenfell, T. C., and Six, D., 2006. Spectral bidirectional reflectance of Antarctic snow: measurements and parameterization. *Journal of Geophysical Research*, **111**, D18106, doi:10.1029/2006JD007290.

Hudson, S. R., and Warren, S. G., 2007. An explanation for the effect of clouds over snow on the top-of-atmosphere bidirectional reflectance. *Journal of Geophysical Research*, **112**, D19202, doi:10.1029/2007JD008541.

Jin, Zh., Charlock, T. P., Yang, P., Xie, Y., and Miller, W., 2008. Snow optical properties for different particle shapes with application to snow grain size retrieval and MODIS/CERES radiance

comparison over Antarctica. *Remote Sensing of Environment*, **112**, 3563–3581.
Kato, S., and Loeb, N. G., 2005. Top-of-atmosphere shortwave broadband observed radiance and estimated irradiance over polar regions from Clouds and the Earth's Radiant Energy System (CERES) instruments on Terra. *Journal of Geophysical Research*, **110**, D07202, doi:10.1029/2004JD005308.
Klok, E. J., Gruell, W., and Oerlemans, J., 2003. Temporal and spatial variation of the surface albedo of Morteratschgletscher, Switzerland, as derived from 12 Landsat images. *Journal of Glaciology*, **49**(167), 491–502.
Langleben, M. P., 1971. Albedo of melting sea ice in the southern Beaufort Sea. *Journal of Glaciology*, **10**, 101–104.
Liljequist, G. H., 1956. Energy exchange of an Antarctic snow field: shortwave radiation (Maudheim 71°01′ S, 10°65′ W), Norwegian-British-Swedish Antarctic Expedition, 1949–1952. *Scientific Results*, **2**(1A).
Makshtas, A. P., and Podgorny, I. A., 1996. Calculation of melt pond albedos on arctic sea ice. *Polar Research*, **15**(1), 43–52.
Mullen, P. C., and Warren, S. G., 1988. Theory of the optical properties of lake ice. *J. Geophys. Res.*, **93**(D7), 8403–8414.
Nolin, A. W., and Dozier, J., 2000. A hyperspectral method for remotely sensing the grain size of snow. *Remote Sensing of Environment*, **74**(2), 207–216.
Oerlemans, J., and Knapp, W. H., 1998. A one-year record of global radiation and albedo from the ablation zone of the Morteratschgletscher, Switzerland. *Journal of Glaciology*, **44**, 231–238.
Painter, T. H., and Dozier, J., 2004. Measurements of the hemispherical-directional reflectance of snow at fine spectral and angular resolution. *Journal of Geophysical Research*, **109**, D18115, doi:10.1029/2003JD004458.
Pegau, W. S., and Paulson, C. A., 2001. The albedo of arctic leads in summer. *Annals of Glaciology*, **33**, 221–224.
Perovich, D. K., Grenfell, T. C., Light, B., and Hobbs, P. V., 2002. The seasonal evolution of arctic sea-ice albedo. *Journal of Geophysical Research*, **107**, C10, doi:10.1029/2000JC000438.
Pirazzini, R., 2004. Surface albedo measurements over Antarctic sites in summer. *Journal of Geophysical Research*, **109**, D200118, doi:10.1029/2004JD004617.
Pope, R. M., and Fry, E. S., 1997. Absorption specturm (380–700 nm) of pure water. II. Integrating cavity measurements. *Applied Optics*, **36**(33), 8710–8723.
Segelstein, D., 1981. *The Complex Refractive Index of Water.* M.S. Thesis, University of Missouri, Kansas City.
Taylor, V. R., and Stowe, L. L., 1984. Reflectance characteristics of uniform earth and cloud surfaces derived from Nimbus-7 ERB. *Journal of Geophysical Research*, **89**, 4987–4996.
Voss, K. J., and Zhang, H., 2006. Bidirectional reflectance of dry and submerged Labsphere Spectralon plaque. *Applied Optics*, **45**(30), 7924–7927.
Warren, S. G., 1982. Optical properties of snow. *Reviews of Geophysics and Space Physics*, **20**, 67–89.
Warren, S. G., and Wiscombe, W. J., 1980. A model for the spectral albedo of snow, 2, Snow containing atmospheric aerosols. *Journal of Atmospheric Sciences*, **37**, 2734–2745.
Warren, S. G., and Clarke, A. D., 1990. Soot in the atmosphere and snow surface of Antarctica. *Journal of Geophysical Research*, **95**, 1811–1816.
Warren, S. G., and Wiscombe, W. J., 1985. Dirty snow after nuclear war. *Nature*, **313**, 467–470.
Warren, S. G., Brandt, R. E., and Grenfell, T. C., 2006. Visible and near-ultraviolet absorption spectrum of ice from transmission of solar radiation into snow. *Applied Optics*, **45**, 5320–5334.
Warren, S. G., and Brandt, R. E., 2008. Absorption spectrum of ice from the ultraviolet to the microwave: a revised compilation. *Journal of Geophysical Research*, **113**, D14220, doi:10.1029/2007JD009744.
Wiscombe, W. J., and Warren, S. G., 1980. A model for the spectral albedo of snow, 1, pure snow. *Journal of Atmospheric Science*, **37**, 2712–2733.

Cross-references

Antarctica
Arctic Hydroclimatology
Atmosphere-Snow/Ice Interactions
Digital Image Information Extraction Techniques for Snow Cover Mapping from Remote Sensing Data
Greenland Ice Sheet
Physical Properties of Snow
Radiative Transfer Modeling
Sea Ice
Surface Energy Balance

ALPS

Martin Beniston
Interdisciplinary Institute for Environmental Dynamics, University of Geneva, Carouge, Geneva, Switzerland

Definition and introduction: the Alps and alpine climates

Although mountains differ considerably from one region to another, one common feature is the complexity of their topography, which results in some of the sharpest gradients found in continental areas. Related characteristics include rapid and systematic changes in climatic parameters, in particular temperature and precipitation, over very short distances (Beniston, 2003); greatly enhanced direct runoff and erosion; systematic variation of other climatic (e.g., radiation) and environmental factors (e.g., differences in soil types). Mountains in many parts of the world are susceptible to the impacts of a rapidly changing climate, and provide interesting locations for the early detection and study of the signals of climatic change and its impacts on hydrological, ecological, and societal systems. All these features have a bearing on the location, behavior, and evolution of alpine cryospheric systems.

The Alps cover just over 200,000 km^2 and consist of an arc that stretches in a north–south direction from the Mediterranean in France to Switzerland, then curves eastward through Switzerland to finally reach as far as eastern Austria. Alpine climates are governed by four major factors, in increasing order of importance: latitude, continentality, topography, and altitude (Barry, 2008). Altitude is certainly the most distinguishing and fundamental characteristic of mountain climates, because atmospheric density, pressure, and temperature decrease with height in the troposphere. Mountains often serve as elevated heat sources, whereby diurnal temperatures are higher than at similar altitudes in the free atmosphere. Topographic features play a key role in determining local climates, in particular due to the slope, aspect, and exposure of the surface to climatic elements. These factors tend to govern the

redistribution of solar energy as it is intercepted at the surface, as well as precipitation that is highly sensitive to local site characteristics. Precipitation is generally observed to increase with height in the Alps and even modest topographic elements can exert an often disproportionate influence on precipitation amount. These climatic and topographic factors control, to a large extent, the extent and behavior of alpine glaciers that, currently, occupy about 2,900 km^2, and permafrost that is estimated to occupy up to 3–5% of the surface area of the mountain chain (Harris et al., 2001). At the synoptic scale, the Alps are subject to the competing influences of Mediterranean, Atlantic, Continental, and Polar weather regimes.

The importance of the alpine cryosphere for natural and socioeconomic systems

Snow is an essential component of numerous aspects of the alpine environment, and any changes in the amount, duration, and timing of the snowpack can have long-lasting environmental and economic consequences (e.g., Stewart et al., 2004). Snow determines the timing of peak river discharge during the melting of the snowpack in the spring and, in many instances, maintains river flows even during warm and dry summer periods. The timing of snowmelt is also a major determinant for initiating the vegetation cycle of many alpine plant species, and hence its quantification is necessary when assessing the response of vegetation to year-to-year climate variability or long-term climatic change (e.g., Keller and Körner, 2003). Körner (1999) has shown that for many parts of the Alps, the length of the snow season and minimum temperatures are the most important factors for high alpine vegetation because they determine the growth and survival rates of numerous species at high altitudes. Furthermore, in many parts of the French, Italian, Swiss, and Austrian Alps, snow is intimately linked to tourism based on winter sports, on which numerous mountain resorts depend for a substantial part of their income (OECD, 2006).

Changes in the alpine snowpack

A quantification of the amount of snow in the mountains and the changes that occur with shifts in climate is crucial for assessing the amount of water that will ultimately runoff and be routed into the numerous river systems originating in the Alps in the spring and early summer. The Alps in general and Switzerland in particular, have in the past been referred to as "the water tower of Europe" (Mountain Agenda, 1998). Any substantial changes in the mountain snow pack inevitably has a significant impact on the flow of many major river basins, not only because of changes in the amount and timing of runoff, but also because of the potential for enhanced flooding, erosion, and associated natural hazards.

The two principal determinants of snow are temperature and precipitation; as climate changes, subsequently modifying temperature distributions and precipitation patterns, so does snow amount and duration. In mountain regions, an average rise of 1 °C is accompanied by a general rise of about 150 m in the altitude of the snowline (Beniston, 2004). Regional studies of climatic change in Switzerland (e.g., Schär et al., 2004) suggest that alpine temperatures could rise by 3-5 °C by 2100 (for the IPCC SRES A-2 Scenario; Nakicenovic et al., 2000), with possibly increased precipitation in winter but a substantial decrease in summer (e.g., Frei et al., 1998). For the Swiss Alps, a warming of this amplitude would push the snowline upward by at least 500–800 m in winter.

The length of the snow season has tended to decrease at many locations since the early 1970s (Beniston, 2004), although the behavior of the snow cover exhibits high interannual variability. In a climate where winters may experience a rise in average temperatures by 3-5 °C compared to today, and a possible increase in precipitation by 5-20% (e.g., Beniston et al., 2003), there could be more abundant snowfall in the higher reaches of the mountains, but much reduced snow at lower levels where precipitation is more likely to fall in the form of rain. The "crossover" level where snow becomes more abundant under milder conditions is located at around 2,000 m above sea level. The volume of snow, which is a key variable for assessing peak flow from snowmelt in river systems originating in the Alps, may decrease by 50–100% (i.e., an inverse relationship with altitude, roughly 10% reduction per degree of warming at 2,000 m above sea level and 20% reduction per °C at 1,000 m height). The projected increase in precipitation will not be sufficient to compensate for the rise in mean winter temperatures.

Behavior of alpine glaciers

The volume of ice in a mountain glacier, and correspondingly its surface area, thickness, and length, is determined by the balance between inputs (accumulation of snow and ice) and outputs (melting and calving). As climate changes, this balance may be altered, thereby modifying the equilibrium line altitude of the glacier (the altitude at which accumulation and ablation are in approximate balance) and resulting in a change in thickness and the advance or retreat of the glacier (e.g., Zemp et al., 2007). Most of the alpine glaciers with the exception of those at very high altitudes (above 3,500 m above sea level) have surface and internal temperatures very close to the freezing point, so that any small rise in temperatures beyond the 0 °C threshold results in a very sensitive response of the glaciers.

Since 1850, the glaciers of the European Alps have lost about 30–40% of their surface area and about half of their volume (Haeberli and Beniston, 1998), a feature that has been observed in many other mountain glaciers of the world, both in the midlatitudes and in the tropics; this serves to emphasize the global nature of atmospheric temperature increase (Paul et al., 2007). Empirical and

energy-balance models indicate that 30–50% of existing mountain glacier mass could disappear by 2100 according to the rate of warming project by global climate models (Haeberli and Beniston, 1998). The smaller the glacier, the faster it will respond to changes in climate. For most mountain glaciers in the temperate parts of the world, there exists a close linear relationship between the equilibrium line altitude of the glacier and the precipitation and temperature controls on glacier mass. In order to maintain the equilibrium line altitude of a glacier, it is estimated that roughly 300 mm of additional precipitation per degree of warming would be necessary. Projections from regional climate models (e.g., the PRUDENCE Project; Christensen et al., 2002) suggest that warming will be accompanied by an average reduction of annual precipitation, with strong reductions in summer that any local increases in winter will not compensate for. This will result in rapidly waning glaciers until they perhaps find a new equilibrium at much higher elevations, with substantially reduced volume and surface area; some may disappear entirely as the equilibrium line altitude may ultimately end up well above the glacier catchment area (IPCC, 2007).

Shrinking glaciers will lead to changes in the hydrological response of certain regions compared to today; as glaciers melt rapidly, they will provide enhanced runoff, but as the ice mass diminishes, the runoff will wane.

Mountain permafrost

The interpretation of recent changes in the alpine permafrost is much more complex than that of glaciers or the snow pack. This is because the exact extent and depth of permanently frozen soils is not fully known, in part because it can also exist intermittently at altitudes well below those where permafrost would usually be expected to occur. Some limited direct measurements of permafrost have taken place in the Alps through the monitoring of the temperature profile at depth in boreholes. There seems to be a general increase in the temperature at depth over time (e.g., Haeberli, 1990), implying that the signal of climate warming is penetrating deeper into the surface. Modeling studies for a warmer climate suggest that this trend will continue and accelerate into the future (Salzmann et al., 2007), although all of the complexities of heat transfer within the ice-packed soils are not fully understood.

Permafrost degradation has in the past already shown the potential for increasing instability of mountain slopes as a result of the reduced cohesion of mountain soils. With the melting of the present permafrost zones at high elevations, material released by the melting subsurface ice will be available to fuel more frequent and probably more severe rock and mud slides and debris flows. These events in turn will cause problems for high-mountain infrastructure such as buildings and cable-car suspension pylons.

Summary and conclusions

Because the Alps are a key source region for many of Europe's rivers, the impacts of climatic change on hydrology are likely to have significant repercussions not only in the mountains themselves but also in populated lowland regions that depend on rivers like the Rhine, the Rhone, the Po and, indirectly, the Danube for domestic, agricultural, energy, and industrial purposes. Water resources for populated lowland regions are influenced by the alpine climates and cryosphere; meltwater from snow feeds into the hydrological basins and acts as a control on the timing of water runoff in the spring and summer months, supplemented by seasonal thawing of glaciers. Significant shifts in cryosphere regimes in a warming climate will inevitably disrupt the quantity and seasonal distribution of water and its consequent use for a wide range of economic activities.

Bibliography

Barry, R. G., 2008. *Mountain Weather and Climate*, 3rd ed, Cambridge University Press, 506pp.

Beniston, M., 2003. Climatic change in mountain regions: a review of possible impacts. *Climatic Change*, **59**, 5–31.

Beniston, M., 2004. *Climatic Change and Impacts; A Review Focusing on Switzerland*. Dordrecht: Kluwer Academic (now Springer), p. 296.

Beniston, M., Keller, F., and Goyette, S., 2003. Snow pack in the Swiss Alps under changing climatic conditions: an empirical approach for climate impacts studies. *Theoretical and Applied Climatology*, **74**, 19–31.

Christensen, J. H., Carter, T. R., and Giorgi, F., 2002. PRUDENCE employs new methods to assess European climate change. *EOS. Transactions of the American Geophysical Union*, **83**, 147.

Frei, C., Schär, C., Lüthi, D., and Davies, H. C., 1998. Heavy precipitation processes in a warmer climate. *Geophysical Research Letters*, **25**, 1431–1434.

Haeberli, W., 1990. Glacier and permafrost signals of 20th century warming. *Annals of Glaciology*, **14**, 99–101.

Haeberli, W., and Beniston, M., 1998. Climate change and its impacts on glaciers and permafrost in the Alps. *Ambio*, **27**, 258–265.

Harris, C., Haeberli, W., Vonder Mühll, D., and King, L., 2001. Permafrost monitoring in the high mountains of Europe: the PACE project in its global context. *Permafrost and Periglacial Processes*, **12**, 3–11.

IPCC, 2007. *Contribution of Working Group I to the Fourth Assessment Report of the Intergovernmental Panel on Climate Change*. Solomon, S., Qin, D., Manning, M., Chen, Z., Marquis, M., Averyt, K. B., Tignor M., and Miller H. L., (eds.), Cambridge University Press, 996pp.

Keller, F., and Körner, C., 2003. The role of photoperiodism in alpine plant development. *Arctic, Antarctic and Alpine Research*, **35**, 361–368.

Körner, C., 1999. *Alpine Plant Life*. Heidelberg: Springer, p. 338.

Mountain Agenda. 1998. Mountains of the World. Water Towers for the 21st Century, prepared for the United Nations Commission on Sustainable Development. Institute of Geography, University of Berne (Centre for Development and Environment and Group for Hydrology) and Swiss Agency for Development and Cooperation. Bern: Paul Haupt, 32pp.

Nakicenovic, N., et al., 2000. *IPCC Special Report on Emission Scenarios*. Cambridge/New York: Cambridge University Press, p. 599.
OECD, 2006. *The Impacts of Climatic Change on the European Alps*. Paris: OECD, p. 129.
Paul, F., Kääb, A., and Haeberli, W., 2007. Recent glacier changes in the Alps observed by satellite: consequences for future monitoring strategies. *Global and Planetary Change*, **56**, 111–122.
Salzmann, N., Frei, C., Vidale, P.-L., and Hoelzle, M., 2007. The application of Regional Climate Model output for the simulation of high-mountain permafrost scenarios. *Global and Planetary Change*, **56**, 188–202.
Schär, C., Vidale, P. L., Lüthi, D., Frei, C., Häberli, C., Liniger, M., and Appenzeller, C., 2004. The role of increasing temperature variability in European summer heat waves. *Nature*, **427**, 332–336.
Stewart, I., Cayan, D. R., and Dettinger, M. D., 2004. Changes in snowmelt runoff timing in western North America under a "Business as Usual" climate change scenario. *Climatic Change*, **62**, 217–232.
Zemp, M., Hoelzle, M., and Haeberli, W., 2007. Distributed modelling of the regional climatic equilibrium line altitude of glaciers in the European Alps. *Global and Planetary Change*, **56**, 83–100.

Cross-references

Cirque Glaciers
Climate Change and Glaciers
Dynamics of Glaciers
Inventory of Glaciers
Quaternary Glaciation

ALTAI-SAYAN GLACIERS

Vladimir Aizen
College of Science, University of Idaho, Moscow, ID, USA

Synonyms

Alpine glaciers; Altai-Sayan; Glaciers of central Asia; Glaciers of mid-latitudes; Glaciers of south Siberia, Russia, Mongolia, China, and Kazakhstan; Glaciers in Ob' and Yenisei river basins

Definition

Altai-Sayan glaciers are the alpine glaciers of the mid-latitudes that are existing in the Altai-Sayan high mountains in south Siberia and north-western Mongolia continental climate.

The Altai-Sayan mountain system stretching between 45°–54°N and 84°–103°E. Glaciers of Altai-Sayan mountains are located in the most northern periphery of the central Asian mountain system and the southern periphery of the Asian Arctic basin (Figures 1 and 2). The highest part of the Altai-Sayan mountains (Katun, South Chuya, and North Chuya ridges) hold 70% of

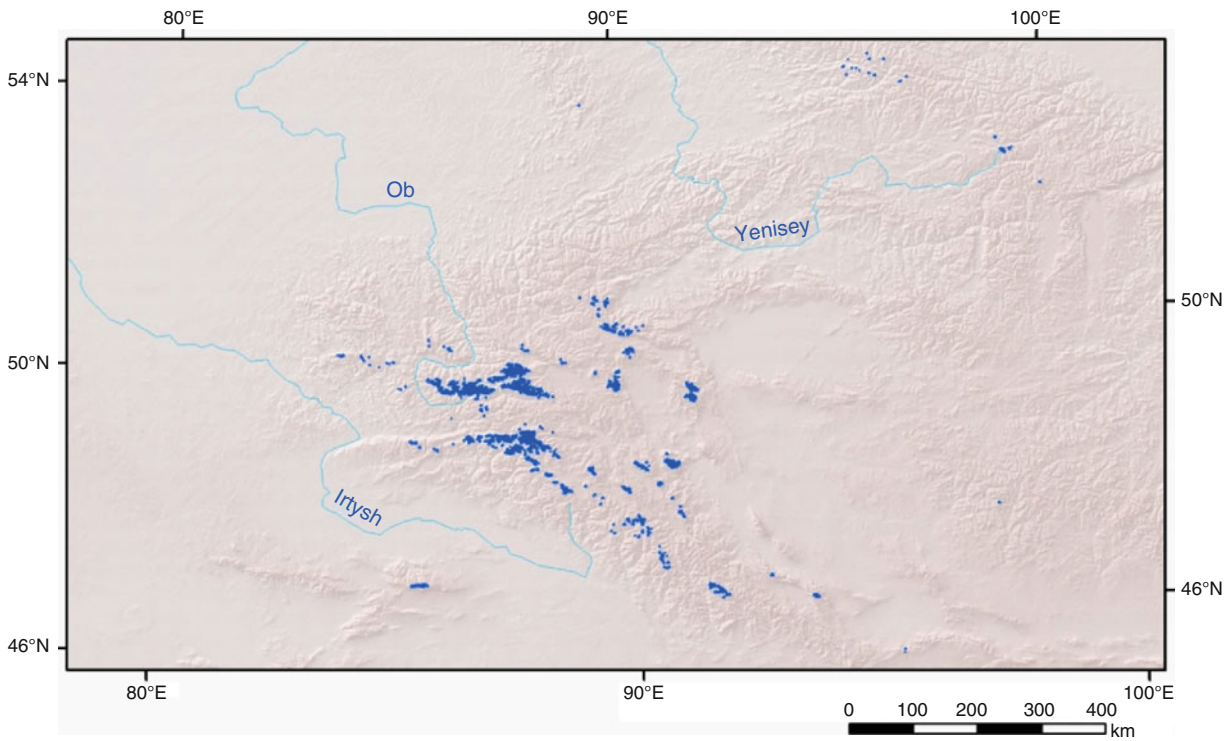

Altai-Sayan Glaciers, Figure 1 Glaciers of the Altai-Sayan Mountains. The Aktru Glacier basin highlighted by *red* square.

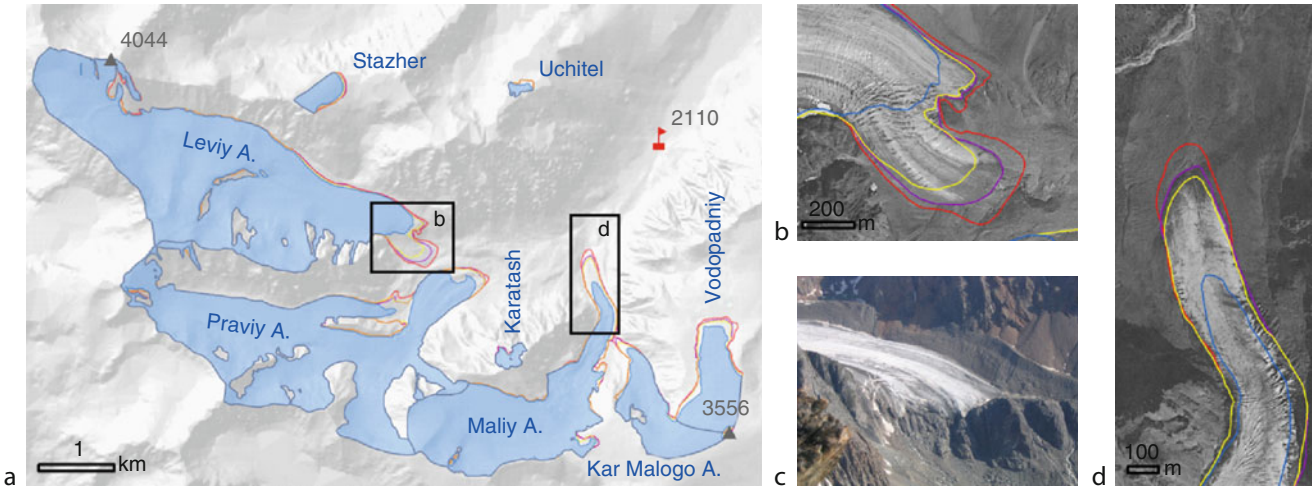

Altai-Sayan Glaciers, Figure 2 (**a**) The Aktru glacier basin in Altai and multitemporal glacier boundaries: 2006 in *blue*, 1975 in *yellow*, 1966 in *violet*, 1952 in *red*. The *red* marker shows location of the Aktru meteorological station. (**b**) The Leviy Aktru glacier terminus position overlaid on the 1966 Corona image. (**c**) A 2006 ground photograph of the Leviy Aktru glacier terminus. (**d**) The Maliy Aktru glacier terminus position overlaid on the 1966 Corona image.

all south Siberian glaciers. The latest investigation in Altai-Sayan mountains based on remote sensing data numbers 2,340 glaciers with total area of 1,562 km^2 (Surazakov et al., 2010). Altai-Sayan glaciers feed the major Siberian Rivers (Ob and Yenisei) in Arctic Basin and the north-western, inner, Mongolia Plateau endorheic basin. Altai-Sayan glaciers distributed between 2,100 and 4,500 m a.s.l. An average glacier equilibrium line elevation (ELA) 2,800 m a.s.l. Average thickness of the Altai-Sayan glaciers is 57 m reaching 328 m in Central Altai (Katun basin glaciers). The total ice volume of Altai-Sayan glacier is 42,565 km^3 estimated by calculation based on passive radar measurements (Nikitin et al., 2010). Taldurinskiy Glacier is the largest Atai-Sayan glacier, which is 7.5 km length and 28.2 km^2 in area (Chagan-Uzun River basin). Between 1950 and 2000, Altai-Sayan glaciers lost 14% area and 10% ice volume on average. The accelerated glacier recession in Altai-Sayan Mountains is mainly the result of increased summer air temperatures by 1.03°C in the last 50 years, which intensify glacier's melt.

Bibliography

Nikitin, S. A., Surazakov, A. B., and Aizen, V. B., 2010. Altai-Sayan glacier-water resources from passive-radar ice thickness measurements and simulation. *Journal of Hydrology* (submitted).

Surazakov, A. B., Nikitin, S. A., and Aizen, V. B., 2010. Changes of area of Altai-Sayan glaciers from 1953 to 2009. *Journal "The Cryosphere"* (submitted).

ANABATIC WINDS: IN RELATION WITH SNOW/GLACIER BASIN

Umesh K. Haritashya[1], Vijay P. Singh[2], Pratap Singh[3]
[1]Department of Geology, University of Dayton, Dayton, OH, USA
[2]Department of Biological and Agricultural Engineering, Texas A&M University, College Station, TX, USA
[3]Tahal Consulting Engineers Ltd, New Delhi, India

Definition

A local wind which blows up a slope heated by sunshine.

Anabatic winds: in relation with snow/glacier basin

An anabatic wind flows upslope of a mountain from lower valleys during daytime (Figure 1). It occurs due to radiational warming of the lower slopes by convection, which allows the warm and less dense air to rise and cold denser air to sink. This type of wind is most common in summer season when slopes are snow free and drier, which allow vertical sun rays to heat the ground faster. In winter, lower slopes are mostly snow covered and do not allow sun radiation to be absorbed and generate convective heating due to high albedo. There appears to have a significant relation between the type of a wind and how it affects snow melting, but theories in this respect have yet to be completely developed. Also, melting is mostly radiation driven, and therefore researchers have mostly focused on developing

Anabatic Winds: In Relation with Snow/Glacier Basin, Figure 1 Anabatic winds flowing upslope during daytime. Chhota Shigri Glacier in the Western Himalaya can be seen on the background. Photo by Umesh Haritashya June 20, 2006.

relations between melting and other meteorological parameters, including wind velocity. In general, anabatic winds are considered to be responsible for producing lower melt rates than the katabatic (downslope) winds (Hannah and McGregor, 1997), and they are also less stronger than katabatic winds. For details see the article entitled *Atmosphere-Snow/Ice Interactions*, and *Katabatic Wind: In Relation with Snow and Glaciers*.

Bibliography

Hannah, D. M., and McGregor, G. R., 1997. Evaluating the impact of climate on snow- and ice-melt dynamics in the Taillon basin, French Pyrenees. *Journal of Glaciology*, **43**(145), 563–568.

Cross-references

Atmosphere-Snow/Ice Interactions
Katabatic Wind: In Relation with Snow and Glaciers

ANCHOR ICE

D. P. Dobhal
Wadia Institute of Himalayan Geology,
Dehradun, Uttarakhand, India

Definition

Anchor ice is formed on ground stones and other objects at the bottom of running water and thus remains attached or anchored to the ground. Ice crystals are formed and may coalesce or adhere to submerged objects like stones, marine organisms, rocks, man-made structures, etc. Anchor ice is most commonly observed in fast-flowing rivers during periods of extreme cold, in the shallow sub or inter-tidal during or after storms when the air temperature is below the freezing point of the water, and in the sub tidal in the Antarctic along ice shelves or near floating glacier tongues. The flow of the rivers having anchor ice is disturbed because it works as a barrier to the flowing water.

ANDEAN GLACIERS

Mathias Vuille
Department of Atmospheric and Environmental Sciences,
University at Albany, State University of New York,
Albany, NY, USA

Definition

Andean glaciers: All glaciers located in the Andes of South America.

Introduction

In all Andean countries of South America, the highest peaks are covered by glaciers. These can be subdivided into tropical glaciers, located in Venezuela, Colombia, Ecuador, Peru, Bolivia and northernmost Chile, and extratropical glaciers, located in central and southern Chile and Argentina. The latter also include the northern and southern Patagonian ice fields (*Patagonia*, qv). While most Andean glaciers outside of Patagonia are

fairly small and contain a limited amount of ice, they are nonetheless very unique and important. The tropical Andes, for example, are home to more than 99% of all tropical glaciers (Kaser, 1999) and they provide very important environmental services, such as freshwater during the dry season to downstream populations. Andean glaciers are also unique with regard to their mass and energy balance and their sensitivity to climate change (*Climate Variability and High Altitude Temperature and Precipitation*, qv), which is very different from glaciers at mid- and high latitudes.

Tropical Andean glaciers

Glacier evolution over the past centuries and current extent

The northernmost tropical glaciers are located in Venezuela, but the country has lost more than 95% of its glacier-covered area since the mid-nineteenth century and the few remaining glaciers total less than 2 km^2 (Vuille et al., 2008a). In Colombia, six different mountain ranges still have some glacier coverage, but glaciers are rapidly retreating there as well. In Ecuador, glaciers are mostly located on volcanoes along the country's two mountain chains, the Cordillera Occidental and the Cordillera Oriental. These glaciers reached a maximum extent during the Little Ice Age (LIA) and have retreated since, interrupted by short periods of advance. Peru contains the largest fraction of all tropical glaciers (~70%) and is home to the world's most extensively glacier-covered tropical mountain range, the Cordillera Blanca. As in all other Andean countries, glaciers reached their maximum extent during the Little Ice Age and have retreated since. In the Cordillera Blanca, for example, the ice coverage decreased from ~850 to 900 km^2 during the LIA to 620 km^2 in 1990. The ice coverage at the end of the twentieth century was slightly less than 600 km^2. Glaciers in Bolivia can be found in two main mountain ranges, the Cordillera Occidental along the western border with Chile and the Cordilleras Apolobamba, Real, Tres Cruces, and Nevado Santa Vera Cruz in the east. The maximum glacier extent in Bolivia was reached during the second half of the seventeenth century (Rabatel et al., 2006). Afterwards glaciers started to retreat, with recession accelerating after 1940 and especially since the 1980s. In many locations of the Cordillera Real glaciers have lost between 60% and 80% of their LIA size and much of the surface and volume loss occurred over the past 30 years (Rabatel et al., 2006). In some instances such as on Chacaltaya, glaciers have disappeared altogether within the past 10 years (Francou et al., 2003). Chile also has a few glaciers along the border with Bolivia that can be considered tropical in the broadest sense (Vuille et al., 2008a). Figure 1 summarizes the retreat of glacier tongues and the reduction of surface area of ten glaciers in the Andes of Peru and Bolivia (from Vuille et al., 2008a).

Tropical Andean glacier mass and energy balance

In tropical locations, temperature stays more or less the same throughout the year but the *Hydrologic Cycle and Snow* (qv) shows a pronounced separation into wet and

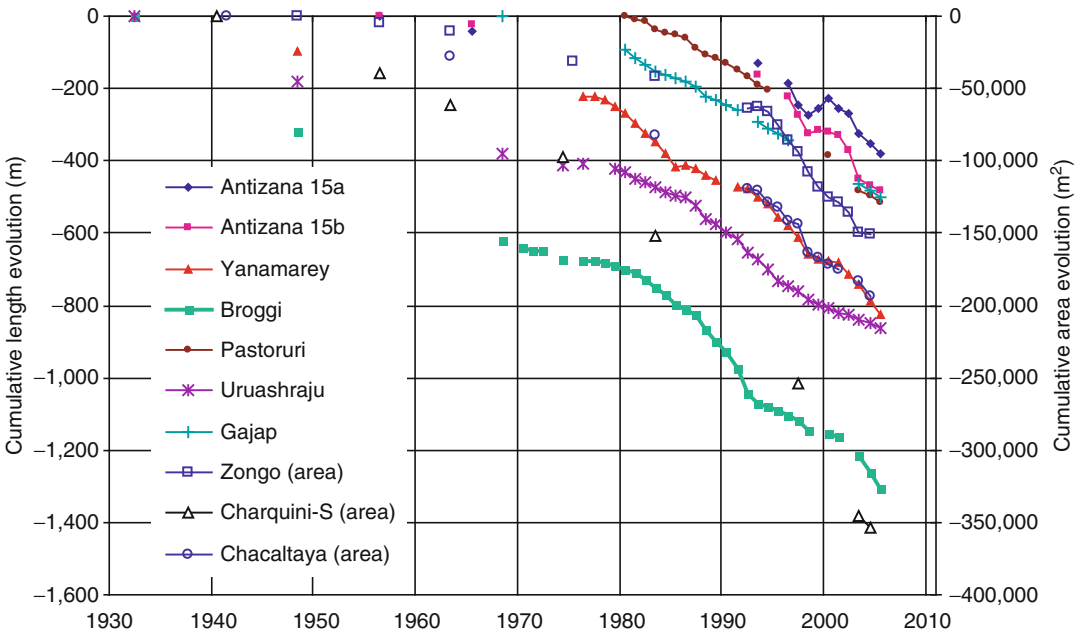

Andean Glaciers, Figure 1 Change in length and surface area of ten tropical Andean glaciers from Ecuador (Antizana 15a and 15b), Peru (Yanamarey, Broggi, Pastoruri, Uruashraju, Gajap), and Bolivia (Zongo, Charquini, Chacaltaya) between 1930 and 2005. (Reproduced from Vuille et al., 2008a. With permission from Elsevier.)

dry seasons. Therefore, the mass and *Surface Energy Balance* (qv) of tropical glaciers is fundamentally different from mid- and high-latitude glaciers (Kaser, 2001). While at mid- and high latitudes winter represents the accumulation and summer the ablation season, ablation and accumulation occur at the same time on tropical glaciers. Also, because temperature does not change much throughout the year, ablation occurs predominantly in the ablation zone below the Equilibrium Line Altitude (ELA), and accumulation is restricted to regions above the snow-rain line that remains at a more or less constant altitude throughout the year (Vuille et al., 2008a). Actual mass and energy balance studies on Andean glaciers are fairly limited because they have to be restricted to glaciers that are easily accessible and safe to work. The longest continuous mass balance measurements with stake networks are located on Zongo and Chacaltaya glaciers in Bolivia (Francou et al., 2003). These studies reveal that the largest mass loss and gain occurs during the wet seasons, while mass balance is almost always near equilibrium during the dry and cold months. On interannual timescales, the El Niño-Southern Oscillation phenomenon (ENSO) appears to play a prominent role, dictating mass balance variability, with El Niño years featuring a strongly negative mass balance and La Niña events producing a nearly balanced or even slightly positive mass balance on glaciers in Bolivia (Wagnon et al., 2001; Francou et al., 2003), Peru (Vuille et al., 2008b), and Ecuador (Francou et al., 2004). These results can be explained by the dominant influence of ENSO on climate in the tropical Andes with La Niña years tending to be cold and wet, while warm and dry conditions usually prevail during El Niño years. Energy balance studies on several tropical Andean glaciers indicate a strong sensitivity to changes in atmospheric humidity, which governs sublimation, but also to the timing, amount and phase of *Precipitation* (qv), as this determines the glacier reflectance or albedo, and hence the amount of absorbed shortwave radiation. Net radiation receipts at the glacier surface are further affected by cloudiness, which controls the incoming long-wave radiation. Hence, the sensitive heat flux does not appear to play an equally important role as on mid- and high-latitude glaciers (Wagnon et al., 2001).

Tropical Andean glaciers, climate change, and water resources

The observed glacier retreat in the tropical Andes may soon lead to water shortages in many parts of the tropical Andes, especially in Bolivia and Peru (Vuille et al., 2008a). Studies show that temperature has increased significantly throughout the region (Vuille et al., 2003) and projections of future climate change indicate a significant rise in freezing levels (*Global Warming and its Effect on Snow/Ice/Glaciers*, qv) and hence the Equilibrium Line Altitude over the course of the twenty-first century (Bradley et al., 2006; Urrutia and Vuille, 2009).

This situation is of grave concern as Andean glacier *Discharge/Streamflow* (qv) provides water for human consumption, agriculture, hydropower production, etc., and is also crucial to maintain the integrity of threatened Andean ecosystems. On the Pacific side of Peru, most of the water resources originate from snow and ice in the Andes. Many large cities in the Andes are located above 2,500 m and thus depend almost entirely on high altitude water stocks to complement rainfall during the dry season. In addition, as glaciers retreat and lose mass, they add to a temporary increase in runoff (*Runoff Observations*, qv) to which downstream users quickly adapt, even though this increase is temporary and not sustainable once the glaciers become too small to sustain dry season runoff. Indeed it is estimated that in rivers draining the western side of the Cordillera Blanca 10–20% of the water is from nonrenewed glacier melt and that during the dry season this value jumps up to ∼40% (Mark and Seltzer, 2003). Simulations with a tropical glacier-climate model suggest that glaciers will continue to retreat in the twenty-first century and in some cases (depending on location and climate change scenario considered) completely disappear (Juen et al., 2007). As a result dry season runoff will be significantly reduced, while wet season runoff may actually be higher due to the larger glacier-free areas and the enhanced direct runoff (Juen et al., 2007; Vuille et al., 2008a). Hence, while the overall discharge may not change very much, water availability during the dry season, when it is the most needed, will be significantly reduced.

Extratropical Andean glaciers

South of ∼18°S glaciers are absent along the Andean cordillera due to the extreme aridity, with the snow line reaching above 6,000 m, before they reappear as small ice caps in the central Andes of Chile and Argentina south of the "South American Arid Diagonal" at ∼29°S. Due to the enhanced winter *Precipitation* (qv) and high topography (including the highest elevation in the Southern Hemisphere, Aconcagua at 6,954 m), glaciers to the south of 31°S rapidly increase in size and form true valley glaciers. The total area covered by glaciers south of the arid diagonal but north of 35°S was estimated to be about 2,200 km^2 in 1998 (Lliboutry, 1998). Between ∼35°S and the northernmost limit of the Patagonian ice fields (*Patagonia,* qv) at ∼46°S more than 35 isolated volcanoes, many of them active, have elevations high enough to support glacier ice (Lliboutry, 1998). Glaciers in this region are famous for their penitents, east-west oriented formations of ice in the shape of blades, tilting toward the sun, and created by intense solar radiation and differential ice sublimation rates.

Snow and ice from this part of the Andes helps sustains some of the richest agriculture and large population centers on both sides of the Andes. Despite their importance for regional water supply, little is known about glacier

mass balance in this region. Consistent with the meridional gradient in precipitation both accumulation and ablation values increase southward, with the net balance in the accumulation zone reaching values as low as 30 cm water equivalent (w. eq.) at Cerro Tapado (29°S) to a record value of 1,540 cm w. eq. at glacier Tyndall in Patagonia (Casassa et al., 2006). Mass balance also shows a clear east-west gradient, in particular south of 33°S, due the prevailing westerly circulation, which leads to higher accumulation on the western, windward side of the Andes. On interannual timescales, mass balance is closely related to ENSO events, with dry La Niña years and wet El Niño years (Casassa et al., 2006).

Glacier monitoring on the Chilean side of the central Andes between 32°S and 41°S has revealed a significant tongue retreat, area shrinkage and ice thinning (*Thinning of Glaciers*, qv) over the past decades, with the trend accelerating over the most recent period (Rivera et al., 2006). A glacier inventory (*Inventory of Glaciers*, qv) of nearly 1,600 glaciers with a total ice area of ca. 1,300 km^2 shows a total volume loss due to thinning (*Thinning of Glaciers*, qv) and retreat of 46 $\pm$ 17 km^3 of water equivalent between 1945 and 1996 (Rivera et al., 2006), most likely attributable to a combination of atmospheric warming (*Global Warming and its Effect on Snow/Ice/Glaciers*, qv) and a significant reduction in *Precipitation* (qv) (Bown and Rivera, 2007).

Summary

Glaciers exist in all Andean countries and can be subdivided into tropical glaciers, located in Venezuela, Colombia, Ecuador, Peru, Bolivia, and northernmost Chile and extratropical glaciers, located in central and southern Chile and Argentina. They are mostly fairly small in size and contain a limited amount of ice, but provide important environmental services, such as freshwater during the dry season to downstream populations. Glaciers in the tropical Andes are also unique in terms of their mass and energy balance (*Surface Energy Balance*, qv), which is fundamentally different from mid- and high-latitude glaciers, as accumulation and ablation seasons are not separated into distinct seasons, but occur at the same time. Andean glaciers have been in retreat over the past few decades and many are projected to completely disappear in the twenty-first century.

Bibliography

Bown, F., and Rivera, A., 2007. Climate changes and glacier responses during recent decades in the Chilean Lake District. *Global and Planetary Change*, **59**, 79–86.

Bradley, R. S., Vuille, M., Diaz, H. F., and Vergara, W., 2006. Threats to water supplies in the tropical Andes. *Science*, **312**, 1755–1756.

Casassa, G., Rivera, A., and Schwikowski, M., 2006. Glacier mass balance data for southern South America (30°S–56°S). In Knight, P. G. (ed.), *Glacier Science and Environmental Change*. Oxford: Blackwell, pp. 239–241.

Francou, B., Vuille, M., Wagnon, P., Mendoza, J., and Sicart, J. E., 2003. Tropical climate change recorded by a glacier in the central Andes during the last decades of the 20th century: Chacaltaya, Bolivia, 16°S. *Journal of Geophysical Research*, **108**(D5), 4154.

Francou, B., Vuille, M., Favier, V., and Cáceres, B., 2004. New evidence for an ENSO impact on low latitude glaciers: Antizana 15, Andes of Ecuador, 0°28'S. *Journal of Geophysical Research*, **109**, D18106.

Juen, I., Kaser, G., and Georges, C., 2007. Modeling observed and future runoff from a glacierized tropical catchment (Cordillera Blanca, Perú). *Global and Planetary Change*, **59**(1–4), 37–48.

Kaser, G., 1999. A review of the modern fluctuations of tropical glaciers. *Global and Planetary Change*, **22**, 93–103.

Kaser, G., 2001. Glacier–climate interaction at low latitudes. *Journal of Glaciology*, **47**(157), 195–204.

Kaser, G., Ames, A., and Zamora, M., 1990. Glacier fluctuations and climate in the Cordillera Blanca, Peru. *Annals of Glaciology*, **14**, 136–140.

Lliboutry, L., 1998. Glaciers of Chile and Argentina. In Williams, R. S., and Ferrigno, J. G. (eds.), *Satellite Image Atlas of the Glaciers of the World – South America*. Washington: USGS Professional Paper 1386-I, pp. 109–206.

Mark, B. G., and Seltzer, G. O., 2003. Tropical glacier meltwater contribution to stream discharge: a case study in the Cordillera Blanca, Peru. *Journal of Glaciology*, **49**(165), 271–281.

Rabatel, A., Machaca, A., Francou, B., and Jomelli, V., 2006. Glacier recession on Cerro Charquini (16°S), Bolivia since the maximum of the Little Ice Age (17th century). *Journal of Glaciology*, **52**(176), 110–118.

Rivera, A., Acuña, C., and Casassa, G., 2006. Glacier variations in central Chile (32°S–41°S). In Knight, P. G. (ed.), *Glacier Science and Environmental Change*. Oxford: Blackwell, pp. 246–247.

Urrutia, R., and Vuille, M., 2009. Climate change projections for the tropical Andes using a regional climate model: temperature and precipitation simulations for the end of the 21st century. *Journal of Geophysical Research*, **114**, D02108.

Vuille, M., Bradley, R. S., Werner, M., and Keimig, F., 2003. 20th century climate change in the tropical Andes: observations and model results. *Climatic Change*, **59**(1–2), 75–99.

Vuille, M., Francou, B., Wagnon, P., Juen, I., Kaser, G., Mark, B. G., and Bradley, R. S., 2008a. Climate change and tropical Andean glaciers: past, present and future. *Earth Science Reviews*, **89**, 79–96.

Vuille, M., Kaser, G., and Juen, I., 2008b. Glacier mass balance variability in the Cordillera Blanca, Peru and its relationship with climate and the large-scale circulation. *Global and Planetary Change*, **62**(1–2), 14–28.

Wagnon, P., Ribstein, P., Francou, B., and Sicart, J. E., 2001. Anomalous heat and mass budget of Glaciar Zongo, Bolivia, during the 1997–98 El Niño year. *Journal of Glaciology*, **47**, 21–28.

Cross-references

Climate Variability and High Altitude Temperature and Precipitation
Global Warming and its Effect on Snow/Ice/Glaciers
Inventory of Glaciers
Patagonia
Precipitation
Surface Energy Balance
Thinning of Glaciers

ANISOTROPIC ICE FLOW

Olivier Gagliardini
Laboratoire de Glaciologie et Géophysique de l'Environnement, CNRS/UJF, Grenoble, France

Definition

Anisotropy. A material is anisotropic if it has a response that differs according to the direction of the loading.
Ice anisotropy. In this article, we focus on the viscous part of the ice deformation. Elastic response of ice is also anisotropic but much less pronounced than its viscous part.

Introduction

The size of an ice crystal varies from few millimeters to few tens of centimeters, whereas the typical size of a glacier or an ice sheet is few kilometers to thousands of kilometers. The strong viscous anisotropy of the ice crystal and the way the crystals are orientated influence the flow of glaciers and ice sheets. This article explains how these very different scales are related and coupled, leading to special features that can only be explained by an anisotropic behavior.

Anisotropy of the ice crystal

Terrestrial ice presents a hexagonal symmetry that induces a strong viscous anisotropic behavior. The principal mechanism responsible for the crystal deformation is the displacement of screw dislocations within the basal planes, perpendicular to the symmetry axis, also called optical-axis or *c*-axis. The ice crystal behaves like a deck of cards: non-basal deformation under a given prescribed strain rate requires stresses 50–60 times larger than for an easy glide-oriented crystal. Owing to this strong anisotropy, a crystal within a polycrystal tends to deform mainly by basal glide and its deformation differs from that of the polycrystal. Satisfaction of the continuity conditions involves a reorientation of the crystal by lattice rotation. This process is responsible for the development of strain-induced fabrics.

Deformation mechanisms

Although strain rates and deviatoric stresses are very low, it is now commonly accepted that deformation processes along polar ice cores are dominated by the viscoplastic mechanism of dislocation, which glide mainly along the basal plane. Diffusional creep, commonly associated with such conditions in many materials, yields a viscosity much higher than that deduced from field data (Lliboutry and Duval, 1985). Deformation by basal glide of dislocations is associated with efficient processes of accommodation such as normal grain growth and dynamic recrystallization.

Strain-induced fabrics and polycrystal anisotropy

An ice polycrystal is composed by hundreds to thousands of crystals, and its viscous behavior depends on its fabric, which describes how all the crystals are oriented. Near an ice-sheet surface, all the grain orientations are, more or less, randomly distributed and the polycrystal response is close to isotropy. At the other extreme, when all the crystals have the same orientation, as observed for height deeps at some places in Antarctica or Greenland, such textured polycrystals are about ten times easier to shear perpendicular to the main orientation than the corresponding isotropic sample. In between these two extremes, the polycrystal anisotropy is entirely determined by its fabric.

On an other hand, the actual fabric can give indications on the strain history undergone by the polycrystal, as far as other recrystallization processes is concerned – grain rotation are not active.

One-maximum fabric or single maximum fabric is characteristic of a uniaxial compression in the direction of the main orientation, whereas a girdle type fabric indicates a uniaxial tension perpendicular to the plane containing the crystal orientations.

Effects of recrystallization processes on fabric

There are three main dynamic recrystallization regimes for polar ice:

1. Normal grain growth that has no direct effect on fabric, except modifying the size of the grains.
2. Rotation or continuous recrystallization (also called polygonization) which, for a vertical compression, is expected to counteract the normal growth of grain and slow down the fabric development.
3. Migration or discontinuous recrystallization that produces grains orientated favorably to the state of stress and has the effect to produce four-maxima fabrics inducing a more or less isotropic behavior.

How anisotropy influences ice flow

The most known effect of anisotropy in ice sheets is the enhancement of the flow induced by the development of one-maximum fabrics vertically oriented. This anisotropy effect induces surface velocities five to ten times larger than the ones expected with an isotropic rheology.

The coupling between the fabric evolution and the anisotropy can conduct heterogeneous deformation of adjacent layers. If two adjacent layers have different initial viscosity, which could be explained by a difference in grain size or in impurities content, then we have a positive feedback: strengthened fabric is easier to shear that again leads to a more strengthened fabric (Paterson, 1991). Such positive feedback can explain a sharp strengthening of fabric in relation to a climatic transition as observed in some ice cores (Paterson, 1991; Durand et al., 2006).

Due to the non-colinearity between deviatoric stress and strain-rate tensors and the presence of rheological inhomogeneities, anisotropy can induce the folding of layers (Thorsteinsson and Waddington, 2002).

Summary

The ice single crystal is one of the most anisotropic natural materials. At the scale of the polycrystal, the viscous behavior is also anisotropic, and it depends on the fabric that evolves from place to place and with depth. Fabric acts, therefore, in controlling the ice flow, but also as a marker of the cumulated deformation. For a single maximum fabric, like those observed below a dome, the flow can be enhanced by a factor up to 10 in comparison to the isotropic case. Moreover, the coupling between fabric evolution and anisotropic behavior can result in the development of heterogeneous flow and layer folding.

For more details, the reader can refer to the two review papers from Placidi et al. (2006) and Gagliardini et al. (2009).

Bibliography

Durand, G., Gillet-Chaulet, F., Svensson, A., Gagliardini, O., Kipfstuhl, S., Meyssonnier, J., Parrenin, F., Duval, P., and Dahl-Jensen, D., 2007. Change of the ice rheology with climatic transitions – implication on ice flow modelling and dating of the EPICA Dome C core. *Climate of the Past*, **3**, 155–167.

Gagliardini O., Gillet-Chaulet, F., and Montagnat, M., 2009. A review of anisotropic polar ice models: from crystal to ice-sheet flow models. In "*Physics of Ice Core Records II*." Supplement Issue of Low Temperature Science, 68, December 2009.

Lliboutry, L., and Duval, P., 1985. Various isotropic and anisotropic ices found in glacier and polar ice caps and their corresponding rheologies. *Annales Geophysicae*, **3**(2), 207–224.

Paterson, W. S. B., 1991. Why ice-age is sometimes soft. *Cold Regions Science and Technology*, **20**, 75–98.

Placidi, L., Hutter, K., and Faria, S., 2006. A critical review of the mechanics of polycrystalline polar ice. *GAMM-Mitt*, **29**(1), 77–114.

Thorsteinsson, T., and Waddington, D., 2002. Folding in strongly anisotropic layers near ice-sheet centers. *Annals of Glaciology*, **35**, 480–486.

Cross-references

Plastic Flow
Recrystallization of Ice

ANTARCTICA

Rasik Ravindra[1], Arun Chaturvedi[2]
[1]National Centre for Antarctic and Ocean Research, Headland Sada, Vasco-Da-Gama, Goa, India
[2]Antartic Division, Geological Survey of India, Faridabad, India

Definition

Antarctica is the southernmost continent on the globe, the fifth largest of the seven continents on the earth. The name originated from "Anti-Arctic," which was used to denote an imaginary landmass, postulated on the opposite pole of the globe with respect to the Arctic (Bernadette Hince, 2000). Much later, in the 1820s, it was first sighted from ship (U.S. Congress, 1989).

Introduction

Today, Antarctica is defined as the entire area of land–ice–water south of the Antarctic Circle (i.e., South of 66° 33 min), where there is at least 1 day of 24-h sun during the polar summer. However, for purposes of the Antarctic Treaty System (ATS), "all areas south of 60° South Latitude" are included in this demarcation (Bastmeijer, 2003).

The Antarctic continent has an area of ~14 million km^2. It is surrounded on all sides by the Southern Ocean. In every winter, the seawater surrounding the continent freezes from ~600 to ~1,000 km from the coast. During peak winter, the area of the surrounding sea ice touches nearly 150% of the size of the continent. As this sea ice remains attached to the main landmass, it nearly doubles the area of the continent. With the arrival of summer season, this sea ice breaks up into floating packs and the area of the continent is reduced back to its original. Since this process of expansion and contraction is repeated every year, Antarctica has also been called "the pulsating continent" (Sharma, 1986).

The floating packs of sea ice during the summer season make navigation difficult in Antarctic waters. This barrier of sea ice sheltered Antarctica from the wooden ships of the past which could not advance much into it. That is the main reason why Antarctica remained undiscovered until the 1800s. Even in the age of modern icebreaker ships, the exploration of Antarctica is still difficult and expensive and Antarctic continues to be the least known part of the globe.

For the past few millions of years, snowfall has accumulated in the interior of the continent, where, due to the extreme cold, there is no melting. The successive deposition of these snow layers has given birth to a thick ice sheet over the continent. On an average, this ice sheet is ~2,500 m thick, while at places its maximum thickness touches ~4,700 m (Kotlyakov, 1966).

In the inner reaches of the continent, the ice makes a high plateau. This has resulted in giving a "flat-bottomed-inverted-bowl-shape" to the continent; where the margins of the landmass are either at or ~50–100 m above the mean sea level (MSL), while the interior of the continent is ~3,000–3,300 m above the MSL. This gives Antarctica the highest average elevation among continents (Stonehouse, 2002).

The total ice volume of Antarctica is ~29 million km^3, which is 90% of all the ice on the globe. It is equivalent of about 65% of all the freshwater on earth. If it melts completely, it could raise the worldwide sea levels by ~60–70 m. Even the annual snow deposition on Antarctica has the capacity to change the global sea levels

by ~5–6 mm if it were to all melt into the ocean (Herzfeld, 2004).

The flow pattern of this huge ice mass is basically domal, starting from the center of the ice sheet on the polar plateau toward the peripheral coasts.

Antarctica is usually divided into East Antarctica and West Antarctica, loosely separated by the Transantarctic Mountain chain. The entire basement is hidden below a thick ice sheet but geophysical soundings have revealed that the East Antarctic Ice Sheet generally rests on bedrock (the Antarctic Shield) above the MSL, while the West Antarctic Ice Sheet rests on bedrock where topographic highs are separated by deep basins below the MSL. If the ice sheet were to melt, western Antarctica would no longer be a single landmass but would become a large group of islands (Michael, 1998; Garrett and Michael, 2002).

The location of the continent at the southern pole of the globe and the presence of a huge ice sheet make Antarctica the coldest place on earth. The usual temperatures in the coastal areas range from +5°C (during summer) to −35°C (during winter). On the Antarctic plateau, the general summer temperatures are about −25°C, while the winter temperatures are around −70°C. The lowest natural temperature ever recorded on earth was recorded at a Russian polar plateau station, "Vostok," in 1983, which was −89.2°C (Greg, 2005).

The large temperature gradient between the interior of the continent and the surrounding sea gives rise to giant low pressure circulatory systems. These systems touch a diameter ranging from 500 to 2,500 km. The rotation of the earth affects the direction of movement of these systems, which always rotate in a clockwise direction around Antarctica. The systems follow each other in rapid succession, making Antarctica the windiest continent, with wind speeds exceeding 300 km/h. Powder-snowdrifts because of these powerful winds, making blizzards common in Antarctica (Riffenburgh, 2007).

Another common meteorological phenomenon is the flow of heavy cold air from the polar plateau toward to the coast, particularly following sunset in the spring and fall. This type of wind is called a "gravity wind" or "katabatic wind," which often reaches speeds of ~60 km/h (McGonigal and Woodworth, 2005).

These peculiarities combine to make Antarctica the highest, coldest, windiest, least vegetated, most isolated, and least explored continent of our globe. It is also the only place on earth which has no native population (Riffenburgh, 2007).

Antarctic ice sheet

The Antarctic Ice Sheet is the largest accumulation of ice on this planet. The ice sheet is flat and wide; but due to the basement/bed topography, it acquires a dome shape. The ice in the sheet flows at a low velocity, generally toward the ice margins.

About 98% of Antarctica is covered by ice and only ~2% of its landmass is exposed on the surface. The outcrops of land protrude through the ice cover like islands inside a sea. When these rocky projections are small and are surrounded by ice, they are called "nunataks" (Figure 5).

Topographic and dating evidence reveal that the area of the Antarctic ice sheet was significantly larger during the Last Glacial Maxima (LGM), that is, about 18,000 years before present (BP); but it has retreated to its present geographic extent since the Last Interglacial Transition, that is, about 8,000 years BP (Riffenburgh, 2007).

The interior of Antarctica has a snowfall of about 5–6 cm of rainfall-equivalent, while the peripheral areas receive about 15–20 cm of rainfall-equivalent snow. When fresh snow falls over the ice sheet, its surface density is ~0.3 gm/cm^3. Old snow metamorphoses and recrystallizes during burial into a denser material termed "firn," with a density of ~0.4 gm/cm^3. The air spaces within the firn are still connected to each other. With further densification of snow, when the air spaces are separated into air bubbles, the firn is said to be converted into "ice," which has a density of ~0.8–0.9 gm/cm^3. With deeper burial, these icy layers are further compacted and ultimately reach a density of ~0.9–0.92 gm/cm^3. This old dense ice may be exposed in zones of ablation, where the top cover is removed, to reveal areas of "blue ice" (Riffenburgh, 2007; McGonigal, 2009).

In the areas of accumulation of snow, various Aeolian snow-forms are carved out by strong winds. The smallest of these are snow-ripples, very similar to the ripples in the sands of the deserts. On a larger scale, a series of undulations (~1–2 m high) is quite common on the polar plateau, these are called "sastrugis." The largest of these structures are dunelike formations made by the winds, these are called "snow barchans" (Kotlyakov, 1966; Riffenburgh, 2007).

The mass balance, an account of the sums of additions and removals of ice mass, of the ice sheet in Antarctica depends on many variables, such as the annual accumulation of snow, drifting of deposited snow, surface evaporation, melting, calving of icebergs, etc. The mass balance in western Antarctica is generally negative, while some parts of eastern Antarctica show a positive mass balance. However, as a whole, there is a general overall tilt toward negative mass balance (Riffenburgh, 2007).

The Antarctic Ice Sheet influences many natural processes of the globe, and there are two important modes of influence on the global climate. The first is through the interactions between the ocean and the continental ice (along with sea ice), while the second is due to the exchanges between the atmosphere and the continental ice along with sea ice (and Ray, 1998; Riffenburgh, 2007).

It is inferred from geological evidence that Antarctica had become an isolated continent ~23 million years BP and tectonically it gradually drifted to its southern location. This location started cooling the continent. About 12 million years BP, ice started covering the entire continent and reflected most of the solar radiation back into the atmosphere. This process accelerated the cooling and

the ice cap thickened. For the past 1 million years, the ice cap has acquired its present thickness (Riffenburgh, 2007; McGonigal, 2009).

Antarctic glaciers

A glacier is a body of ice that moves in a direction dictated by gravity. As the ice sheet moves over the mountains and valleys, it gets divided into a number of glaciers and ice streams, which have variable rates of flow, starting from a meter per annum to a few kilometers per annum (Tulacyyk, 2006; Riffenburgh, 2007). The largest Antarctic glacier is Lambert Glacier in the Prince Charles Mountains of East Antarctica, which is ~400 km long and ~40 km wide; it moves at ~230 m/h near its entry to the mountains (Riffenburgh, 2007) (Figure 4).

The fastest moving Antarctic glacier is Shirase Glacier in eastern Dronning Maud Land, which moves ~2.3 km/year at the grounding line, while accelerating to ~3.11–3.5 km/year at the terminus of the floating ice tongue (Nakamura et al., 2007).

Two distinct types of glacier ice are distinguished in Antarctica: the first is "temperate ice" which is at a pressure melting point at the bottom of the ice sheet and the second is "cold ice" in the layers above it. During movement, the inland ice sheet moves basically by stratified flow of its internal layers, in which the upper layers move faster. In the mountain glaciers, in addition to this stratified flow, another possibility is of moving by glacier sliding over the rocky bedrock.

An "ice stream" is part of an inland ice sheet in which the ice moves much more rapidly than the surrounding ice. Most ice streams drain rapidly into the Antarctic Ocean. The terminal part of an ice stream becomes afloat into the ocean and forms a floating tongue or ice shelf. The largest ice stream–ice shelf system is the Lambert Glacier/Amery Ice Shelf system, located in East Antarctica.

Glaciers and ice streams carry rock debris and deposit the debris either along the way or at the terminus; these deposits are called "moraines." The debris formed below the glacier are termed "ground moraine," debris along the sides of the glacier are called "lateral moraines," debris moving along the central line of the glacier at the surface are "medial moraines," and debris deposited at the end of the glacier are named "terminal moraines" (Clifford and King, 1975). When a glacier recedes, it leaves imprints behind in the form of debris, which can provide evidence of the extent of past glaciation. These moraines can also be dated by Thermoluminscence Dating (TL) method, which provides quantified data about the glacial history of that area (Philip and Leonard, 2004).

Antarctic ice shelf

An "ice shelf" or a "glacier tongue" is glacier ice, which while moving seaward floats on seawater but still remains connected to the mainland (Figure 2). An ice shelf becomes progressively thinner toward the sea. Ultimately, it breaks under the effects of tidal swells and glacial push to give rise to icebergs.

While floating, ice shelves keep growing in thickness both from snow deposition on the surface, as well as from bottom freezing of seawater. During the polar summer, the ice shelves waste mostly by calving into icebergs. A smaller amount is also lost by surface melting, streaming, evaporation, and ablation (William and Christiansen, 2004).

The grounding line of a glacier is defined as the line of transition of grounded ice (ice moving over rocks) to floating ice (ice over sea waters) of a glacier that extends from land to ocean. Often the glaciers have a "grounding zone," rather than a clear-cut grounding line. The ice shelves are very thick at the grounding line, at times exceeding 1,000 m, but when they reach the seacoast, the thickness is reduced to ~100–150 m. Depending on the original thickness and the local conditions, the thickness of the ice shelf projecting above the sea level ranges between ~2 and 50 m (Herzfeld, 2004).

There are two huge ice shelves in Antarctica, namely the Ross Ice Shelf and Filchner Ice Shelf. The Ross Ice Shelf in the Ross Sea exceeds ~550,000 km^2 in area, while the Filchner Ice Shelf in Weddell Sea is ~420,000 km^2.

An "ice rise" is an ice-covered island. It is dome shaped but the bedrock may or may not rise above the sea level. It represents a localized grounding of the ice shelf.

An "ice-doline" or "ice-crater" is a large oval-shaped depression in an ice shelf, where ice has caved in. Depressions or undulations on the surface of normally flat ice shelves are due to uneven flow of ice. These depressions are more common within the last 30–50 km from the coast and their amplitude ranges from 5 to 10 m in height and 1–5 km in length. Near the grounding of ice shelves over the seabed or over submerged islands, the grounded ice generates a damming resistance, resulting in pressure waves within the spreading ice. The result is the formation of depressions on the landward side of the grounded area. When the surface ice melts during the polar summer, some of the near-coast depressions become filled with freshwater that is potable (Herzfeld, 2004).

Any differential movement of outlet glaciers or ice streams over the glacier bed, for example, where the bed topography is uneven, generates cracks within the ice. These cracks are termed "crevasses." Some of the deep crevasses can extend right down to the basement, that is, to a depth of ~2,000 m or more in the Antarctic ice. Also, when the ice shelves rise and fall under the effects of swells and tides, crevasses are generated. Crevasses on the ice shelf can also form near ice rises or obstructions. Most of the Antarctic crevasses get camouflaged by snowfall and snowdrift and can be detected only by aerial reconnaissance of the glacier area.

Ice shelves continually break into the sea, so forming icebergs. The ice shelf may act as a barrier to glacier flow, and ice shelf disintegration may result in glacier surging, which in turn may lead to elevated discharge of land-based

ice into the sea. Discharge of land-based ice above MSL is a net contribution to rising sea levels (Riffenburgh, 2007).

Antarctic icebergs

An iceberg is a large floating piece of ice that has broken off from the ice shelf (Figure 9). The breaking process generating an iceberg from the ice shelf is termed "calving." Freshly calved icebergs are often tabular and flat. Some of the larger iceberg such as the one calved out from Filchner Ice Shelf in 1986 had an area of about 210×92 km.

Basal melting and selective side erosion by sea wave action makes an iceberg unstable, causing it to tilt or even rotate in the water. This gives birth to oddly shaped icebergs, which can be domal, pinnacled, pyramidal or blocky, etc. Sometimes tunnel through icebergs is also observed.

The floating upper side of the ice, projecting over the waters, is termed the "hummock"; while the downward projection of the ice, which is hidden below the seawater, is termed the "bummock." These bummocks are dangerous for ships navigating in Antarctic waters.

Icebergs may disintegrate into smaller pieces, around the size of small houses, called "bergy bits," which typically have a height of less than 5 m and an area of about 300 m^2.

Further breaking up leads to the formation of "growlers." Growlers typically have a height of less than 1 m above the water and an area of $\sim$20 m^2. Being so small, the growlers are difficult to detect on the radars; yet these can still have a mass of more than 100 tons. Growlers pose the gravest risks for ships navigating in Antarctic Ocean, even for the modern well-equipped ships (Riffenburgh, 2007).

Lastly, the growlers may disintegrate into "brash ice," which is made up of wrecked fragments of other ice, with each fragment less than 2 m in size.

Sometimes, the broken fragments of ice get frozen together again due to a sudden drop in air temperature, giving the appearance of small rafts which are welded together; this is termed "ice breccia."

Icebergs are used as proxies for global warming. With increasing temperatures, more ice shelves are likely to disintegrate, leading to birth of a larger number of icebergs (Walton and Doake, 1987).

Antarctic sea ice

Seawater, being highly saline, does not freeze at 0°C, but at a temperature of $\sim$1.9°C. The first freezing of seawater produces tiny crystals of ice in suspension, termed "frazil ice" (Figure 1).

Later, these tiny ice crystals coagulate to form an oily or soupy surface on the seawater, which is called "grease ice."

With further freezing, small spongy white lumps of ice are formed, which are a few centimeter across; these aggregations of ice crystals are termed "shuga."

Antarctica, Figure 1 Frazil ice.

Antarctica, Figure 2 Ice shelf in Central Dronning Maud Land.

These floating fragments of ice coalesce together to form bigger pieces of "pancake ice" or "ice cakes" (Figure 7). Pancakes generally range from 30 cm to 3 m in size. The rims of the pancakes are raised by the constant collisions with one another.

With further freezing, the pancakes join together to form "floes." These may become interlocked by thrust-fingers alternately over and under each other, and are then termed "finger rafted ice."

When the thickness of finger rafted ice is less than 10 cm, it acquires a thin elastic crust of ice, which bends easily with waves and swells; this is termed "nilas."

Nilas, which are less than 5 cm thick, are usually rather dark in color and are thus called "dark nilas"; while those that are more than 5 cm thick, gradually acquire a lighter color and are termed "light nilas."

Nilas form only in saline waters, as the salt content gives it the typical elasticity. When freshwater or water of low salinity freezes, the growing ice crystals exclude solute and are almost free of salt; the result is a similar feature but lacking in elasticity, these rigid ice forms are termed "ice rinds."

With further freezing, the nilas become thicker and lose their elasticity; the resultant sea ice is thicker than 10–15 cm and it is termed "gray ice." Under the effect of waves and swells, it rafts and breaks. Further cooling increases the thickness of gray ice and when it goes up to ~70 cm, it is called "white ice."

"Ice cakes" are an intermediate stage in the freezing of pancake ice into floes, where the size of each cake is typically less than 20 m. By contrast, small floes are 20–100 m in size and big floes may range from 500 to 2,000 m.

A collection of floes constitutes a "pack." When the floes are not in contact with each other or are loosely lumped together with many leads and polynyas, the concentration of ice on the surface of the sea is generally less than 60%. This type of sea ice is termed "open pack ice." When the floes are very densely packed, with a concentration of 70–80%, it is termed "close pack ice." When no water is visible between the floes, then the pack ice has a concentration of 100% and is termed "compact pack ice" (Riffenburgh, 2007).

An area of pack ice less than 10 km across is called an "ice patch," while if it is more than 10 km in extent it is termed an "ice field."

When two different types of pack ice are seen together, the line of transition between the two pack areas is termed a "concentration boundary."

When individual floes of pack ice are pushed by winds or currents and ride over each other, these are termed "pressure ridges" or "ridged ice" (Figure 6).

If hummocks of ridged ice coalesce together and project to a height of more than 5 m above the water, and if these are floating separately from any other sea ice, then it is termed a "floeberg." This is fundamentally different from a typical iceberg because it is composed of saline ice, whereas an iceberg is made up of freshwater ice.

Coelescence of floes results in the formation of large "pack sheets." These float freely in Antarctic waters for tens of kilometers. Ultimately, they may bond together to form an unbroken continuity, termed "fast ice." The term originated because the fast ice is a sea ice which is "still holding fast to the coast," remaining attached to a rocky coast, an ice wall, an ice shelf, or even to a grounded iceberg. Fast ice typically extends for hundreds of kilometers from the coast.

Fast ice reaches its maximum extent in September and October every year. The average extent of fast ice is generally about 600 km from the coast. The greatest expanse of fast ice is seen in the Weddell Sea, where in peak winters it extends to ~2,500 km from the coast of Antarctica. The maximum total area of sea ice has been observed around Antarctica is ~20 million km^2, greater than the area of the continent itself is ~14 million km^2 (Gordon et al., 2000).

Open ocean water reflects about 5% of the solar radiation back into the atmosphere, while pack ice has a much higher albedo and reflects back about 85% of the incoming solar radiation. Thus, pack ice has a major impact on the energy balance of the Antarctic region.

The thickness of fast ice is generally 1–2 m. Fast ice of only one winter's growth is termed "young ice" and its thickness is typically 30 cm to 2 m. When the sea ice survives for at least two seasons, it becomes thicker, usually up to ~3 m, and is termed "multiyear ice."

Overall, wherever pack ice is present in a reasonable quantity, it hampers swell thus calms the sea surface. Static water freezes more readily compared to moving water, and therefore this surface calming promotes more rapid freezing. Thus, the very presence of pack ice acts like a nucleus around which more sea ice grows.

The boundary separating fast ice from pack ice or open water is termed the "fast ice edge." If the fast ice edge is full of chaotic pieces, it is termed a "flaw." If the flaw becomes wide and can be navigated by ship, it is termed a "flaw-lead" or simply a "lead."

An open water anomaly within the sea ice is termed a "Polynya" (Figure 10). Depending on its location, it is termed "shore polynya," "flaw polynya" or "recurring polynya," etc.

When the fast ice disintegrates and moves away from the coast, sometimes a narrow fringe of ice remains as a stable leftover on the coast, unmoved by the waves and tides; this is called the "ice foot." If this ice strip covering a coastal strip of low-lying area is backed by mountains, then the ice foot is termed "ice piedmont." These ice piedmonts rise gradually from the sea side and merge into ice walls or ice shelves. A very narrow ice piedmont, which is less than 1 km wide, is called an "ice fringe."

The contact of fast ice and the ice shelf is usually marked by a long coastal crack because of the cyclic action of the tides; this is termed a "tidal crack."

In the final stages of decomposition, all sea ice becomes honeycombed, marked with many holes. It is then termed "rotten ice."

Antarctic ice cores and climate change

In the interior of Antarctica, snowfall occurs every year and accumulates, due to the intense cold that precludes melting. This process has been going on for the past few million years. The pointers or proxies to the past climate, which are trapped within the ice, are atmospheric gases, traces of volcanic eruptions, particles of dust, pollen, and cosmic dust. In addition to these, the ratio of the oxygen isotopes within the ice gives information about the prevailing temperatures. Thus, ice cores can provide the atmospheric composition of that particular period, along with the air temperature at the time of snowfall, the season of the snowfall (summer or winter), and the amount of

Antarctica, Figure 3 Ice core retrieved in Antarctica.

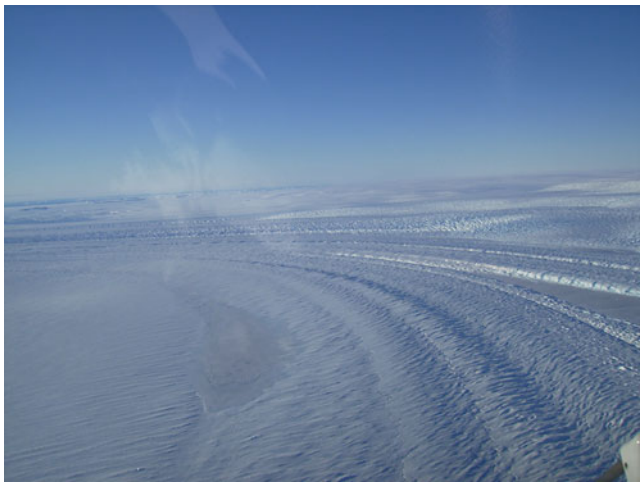

Antarctica, Figure 4 Lambert glacier Amery coast.

Antarctica, Figure 5 Nunatak in Schirmacher area of East Antarctica.

precipitation (Cuff and Goudie, 2008; Petit et al., 1999) (Figure 3).

The Antarctic ice sheet on an average is ~2,000 m thick. In the basins of Wilkes Land, an ice thickness can be greater than 4 km, with a maximum of almost 4,700 m. The Antarctic ice sheet is an unparalleled repository climatic information of the past ~0.8 million years, which is the oldest age obtained from deep ice cores to

Antarctica, Figure 6 Hummocky ice.

Antarctica, Figure 7 Pancake ice.

date (Figure 8). The ice has preserved records for studying global climatic change, environmental pollution levels, mega volcanic eruptions, paleo-temperatures, and the composition of atmospheric gases through ages past (Cuff and Goudie, 2008; Petit et al., 1999).

At a burial depth of about 300 m, the specific gravity of ice touches 0.82 and then the interconnecting air passages within the ice are broken into individual confines, so creating individual air bubbles. When the snow is buried to a depth of more than a kilometer, the pressure of burial is so great that these air bubbles are squeezed into waxy gas clathrates that convert back into air bubbles when the pressure on the ice is released, for example, during the retrieval of ice cores from depth. These air bubbles provide very rare and unique samples of the past atmosphere (Hitoshi and Langway, 1982; Petit et al., 1999).

Oxygen has three stable isotopes – ^{16}O, ^{17}O, and ^{18}O; where the number of neutrons in the atomic nucleus varies from 8 to 10, respectively. The first isotope, ^{16}O,

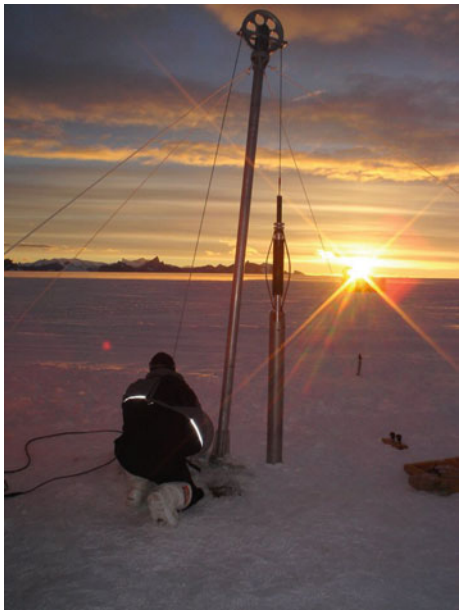

Antarctica, Figure 8 Ice core drilled in Antarctica.

Antarctica, Figure 9 Tabular iceberg.

is the dominant one, accounting for less than 99% of the oxygen in natural waters. The heaviest isotope, ^{18}O, is quite rare, accounting for less than 0.2% of the oxygen in natural waters. At the time of snowfall, lower temperatures increase the proportion of ^{18}O in the snow. The ratio of $^{18}O/^{16}O$ obtained from the ice, when compared to that of the oceanic water (called Standard Mean Ocean water or SMOW), can be used to estimate the temperature at the time of snowfall. This ratio, termed $\delta^{18}O$, has become a standard tool in paleoclimatic studies of ice cores. By finding the temperature at the time of snowfall, individual snow layers can be labeled for summer and winter seasons and thus yearly cycles can be counted. Annual layers within the ice core samples can be counted back and dated just like annual tree rings (Petit et al., 1999).

The amount of carbon dioxide gas (CO_2) in the atmosphere is a crucial component that affects the climate. Ice cores from Antarctica are the only available direct source of information about the exact content of CO_2 in different periods during the past hundreds of thousands of years (Cuff and Goudie, 2008; Petit et al., 1999).

Attempts have been made to date the CO_2 gas present within the air bubbles by means of AMS ^{14}C dating methods. As far as precision is concerned, the results have been encouraging. The date of actual formation of the ice differs from the CO_2 gas age inside the bubbles by a few hundred years, due to the time lag that always occurs before air bubbles are sealed and cut off completely from the outside gases during burial. Thus, radiocarbon dating methods are not much used for ice core dating and isotopic analysis is mainly limited to oxygen and hydrogen isotopes (Petit et al., 1999; Morgan and van Ommen, 1997).

The individual seasonal layers within the Antarctic ice cores can occasionally be detected by visually observing the internal stratification. In places, the annual summer layers are slightly highlighted by the presence of dust particles. However, with greater depth of burial, the visual record becomes almost indistinguishable. Then the best tool for detection of seasonal layers is to analyze the cores at very short regular intervals for $\delta^{18}O$ values (Grootes et al., 2002). When the accumulation rates are high and when there is no melting and refreezing of layers, this method is very successful. But with increasing depths, the seasonal layers become more and more compact and it becomes difficult to use even this tool. At very great depths, especially near the bedrock, ice gets deformed by plastic flow, which almost eliminates seasonal snow layering (Petit et al., 1999; Budd and Radok, 1971).

Sometimes marker horizons can be detected within ice cores, which are recorded at many other places for comparisons. Major volcanic eruptions in the history of the earth, which affected global climate, have their signatures in Antarctic ice also. If these eruptions were of an explosive nature with a lot of ash content, the signatures are quite emphatic. In places, the ash particles are so characteristic of one particular eruption that these can be compared well with other global sites, leading to a very precise marker horizon (De Angelis et al., 1985; Laluraj et al., 2009).

Apart from ash and volcanic dust particles, volcanic gases also leave their imprints within the ice. Sulfur dioxide and hydrogen sulfide in particular are dissolved in cloud water and are scavenged from the atmosphere by snowfall dilute traces of sulfuric acid. This results in a more acidic snowfall, leading to acidity of glacier ice. After drilling, these acidic layers within the ice cores can be detected by abrupt changes in electrical conductivity of the cores and also by precise analyses of the chemical composition of snow and ice (De Angelis et al., 1985; Laluraj et al., 2009).

Antarctica, Figure 10 Ship birthed along ice shelf in a Polynya.

Recent nuclear explosions also leave global signatures and their fallouts can be detected in Antarctic ice cores, providing another type of recent markers (Wolff, 1990).

Climatic warming is amplified in the polar regions. The northern Antarctic Peninsula has warmed by ~2.5°C in the last 50 years, while the Southern Hemisphere appears to have warmed by ~1.5°C during the same period. As a consequence, many ice shelves in the peninsula, which were stable for the last 1,800 years, have suffered dramatic disintegration (British Antarctic Survey, 2001).

A few very deep ice cores has been extracted from the Antarctic ice sheet, including the Vostok, EPICA, Dome-C, and Byrd cores. These provide ice cores from depths of 3,000 m or more. The paleoclimatic record from these ice cores goes to a maximum of ~450,000 to ~800,000 years BP (Petit et al., 1999).

The analysis of air extracted from air bubbles in the EPICA-Dome C ice core shows that present-day levels of green house gases are higher than at any point during the past 650,000 years. The CO_2 is higher by 30%, while methane is higher by 170%. In the year 1780, the CO_2 levels were ~278 ppm, while now they are ~380 ppm, and still rising by $\sim 2 \times 10^{-6}$ atm every year. The methane content in ice cores is more variable but still correlates well with the advancing industrial age on earth. About 40% of CO_2 is absorbed by the oceans but 60% remains in the atmosphere. With the present trend, atmospheric CO_2 concentrations are likely to double by 2050. The CO_2 invasion may be leading to a transition in the oceanic carbon cycle, with unforeseen consequences (NPP, 2007).

The mass balance of the Antarctic ice sheet and glaciers should remain constant to avoid any rise in the sea levels. Surface warming and basal sliding may give rise to to a powerful feedback: more surface melting causes faster sliding and increased calving, which in turn leads to lowered surface, less resistance to sliding, and hence more melting (NPP, 2007).

A warmer atmosphere enhances snowfall in the interiors of large ice sheets, but increases ablation at the marginal zones. Satellite data have suggested that Greenland and Antarctic ice sheets are thickening in their interiors, while rapidly thinning at the peripheral areas (NPP, 2007).

Outlook

Antarctic ice is one of the most important climatic indicators today. Its icy layers have preserved an unbroken continuity of the climatic record for the past ~1 million years. Recent climate change (during the past ~200 years) is very distinctly observed in the ice. The air bubbles trapped within the ice also provide actual samples of the composition of the atmosphere, changing year by year. A clear and quantifiable relationship between the greenhouse gases (carbon dioxide, methane, and nitrous oxide) and the global temperature gradients is established by these annual records. This provides a unique opportunity to study the gradual changes taking place in our recent climate and thus helps in the design of models for forecasting the climate of the coming decades (Petit et al., 1999; Riffenburgh, 2007; Philippe, 1990).

Even the mass balance of the present ice sheet and sea ice is good indicators of the climatic changes that are taking place today. The scientific observations show that the peripheral parts of the Antarctic continental ice are shrinking very rapidly. The coastal ice edge of the glaciers is melting and retreating, the ice shelves are disintegrating

and floating away into the ocean, and the inland glaciers are surging and accelerating toward to the sea. All this suggests that the peripheral mass balance is negative and the ice sheet in the coastal areas is melting away (Riffenburgh, 2007).

However, in the interior of the continent, there are some scientific observations that show that the thickness of the ice sheet is increasing. Added to this is also the observation that the sea ice cover is also increasing. Satellite data has established that in 2007 the sea ice cover was the most extensive in the past 3 decades (Susan, 2007).

Even these two contradictory aspects fit well with current climatic models of global warming. The warming of the oceans provides more moisture to the huge circulatory systems around Antarctica, leading to more snowfall everywhere. While the higher snowfall in the coastal areas melts away due to rising temperatures, the interior of the continent never melts and preserves this extra precipitation.

The climatic models predict that with further rise in global temperatures, the sea ice in Antarctica would start "thinning" as is happening today in the Arctic. The coastal ice shelves would break away, leading to accelerated surge of the inland ice streams toward the sea. The slight rise in the thickness of the interior ice sheet would not be able to balance this huge mass-loss and Antarctic melting would substantially contribute to rising MSLs (Riffenburgh, 2007).

Since sea-level rise and changing climatic trends are crucial factors for the survival of human civilization, Antarctica remains a key scientific observatory for studying these changes. Observations on snow, ice, glaciers, ice shelves, and sea ice of Antarctica, coupled with analysis of shallow depth ice cores, are major tools for elucidation of contemporary climatic change. The scientific research stations spread around the Antarctic continent provide precious inputs for the prediction of climatic change on the planet and help to form part of an early warning system for rising global temperatures.

Bibliography

Bastmeijer, K., 2003. *The Antarctic Environmental Protocol and its Domestic Legal Implementation*. Netherland: Kluwer Law International, Martinus Nijhoff, p. 517.

British Antarctic Survey, 2001–2002 and 2007–2008, Annual Report.

Budd, W. F., and Radok, U., 1971. Glaciers and other large ice masses. *Reports on Progress in Physics*, **34**(1), 25–36.

Clifford, E., and King, Cuchlaine A. M., 1975. *Glacial Geomorphology.* University of California: Wiley, p. 573.

Cuff, D. J., and Goudie, A., 2008. *The Oxford Companion to Global Change*. Oxford: Oxford University Press, p. 684.

De Angelis, M., Fehrenbach, L., Jehanno, C., and Maurette, M., 1985. Micrometer-sized volcanic glasses in polar ice and snows. *Nature*, **317**, 52–54.

Garrett, N., and Michael, W., 2002. *Cold Environments: Processes and Outcomes*. Cheltenham: Nelson Thornes, p. 96.

Gordon, C., Cooper, C., Senior, C. A., Banks, H., Gregory, J. M., Johns, T. C., Mitchell, J. F. B., and Wood, R. A., 2000. The simulation of SST, sea ice extents and ocean heat transports in a version of the Hadley Centre coupled model without flux adjustments. *Climate Dynamics*, **16**(2–3), 147–168.

Greg, R., 2005. *Antarctica: The Frozen Continent.* Black Rabbit Books, RIC publication, Green Wood Western Australia, p. 32.

Grootes, P. M., Steig, E. J., Stuiver, M., Waddington, E. D., Morse, D. L., and Nadeau, M. J., 2002. The Taylor Dome Antarctic $\delta^{18}O$ record and globally synchronous changes in climate. *Quaternary Research*, **56**, 289–298.

Herzfeld, U. C., 2004. *Atlas of Antarctica: Topographic Maps from Geostatistical Analysis of Satellite Radar Altimeter Data*. Berlin: Springer, p. 364.

Hince, B., 2000. *The Antarctic Dictionary: A Complete Guide to Antartic English*. Collingwood: CSIRO Publishing, p. 394.

Kotlyakov, V. M., 1966. *The Snow Cover of the Antarctic and Its Role in the Present Day Glaciation of the Continent.* Israel Program for Scientific Translations, University of California, pp. 256.

Laluraj, C. M., Krishnan, K. P., Thamban, M., Rahul, M., Chaturvedi, A., Naik, S. S., Dsouza, W., and Ravindra, R., 2009. Origin and characterisation of microparticles in an ice core from the Central Dronning Maud Land. East Antarctica. *Environmental Monitoring and Assessment*, **149**(1–4), 377–383.

McGonigal, D., 2009. *Antarctica: Secrets of the Southern Continent*. University of California: Frances Lincoln, p. 400.

McGonigal, D., and Woodworth, L., 2005. *Antarctica: The Blue Continent*. University of California: Frances Lincoln, p. 224.

Michael, O., 1998. Global warming and the stability of the West Antarctic Ice Sheet. *Nature*, **393**, 325–332.

Morgan, V., and van Ommen, T. D., 1997. Seasonality in late-Holocene climate from ice-core records. *Holocene*, **7**(3), 351–354.

Nakamura, K., Doi, K., and Shibuya, K., 2007. Estimation for seasonal changes of Shirase Glacier flow by using JERS-1/SAR image correlation. *Polar Science*, **1**, 73–83.

Netherlands Polar Programme, 2007–2010.

Petit, J. R., Jouzel, J., Raynaud, D., Barkov, N. I., Barnola, J. M., Basile, I., Bender, M., Chappellaz, J., Davisk, M., Delaygue, G., Delmotte, M., Kotlyakov, V. M., Legrand, M., Lipenkov, V. Y., Lorius, C., Pepin, L., Ritz, C., Saltzmank, E., and Stievenard, M., 1999. Climate and atmospheric history of the past 420,000 years from the Vostok ice core, Antarctica. *Nature*, **399**, 429–436.

Philip, J. E., and Leonard, G., 2004. *Quaternary Glaciations: Extent and Chronology.* Amsterdam: Elsevier, p. 310.

Philippe, H., 1990. A 3-D model for the Antarctic ice sheet: a sensitivity study on the glacial-interglacial contrast. *Climate Dynamics*, **5**(2), 79–92.

Ray, G. P., and Warren, B. W., 1998. Slow oceanic teleconnections linking the Antarctic Circumpolar Wave with the tropical El Niño-Southern Oscillation. *Journal of Geophysical Research*, **103**(C11), 24,573–24,583.

Riffenburgh, B., 2007. *Encyclopedia of the Antarctic*. Routledge: CRC Press, p. 1272.

Sharma, R. C., 1986. *Growing Focus on Antarctica.* University of California: Rajesh Publications, p. 286.

Shoji, H., and Langway, C. C. Jr., 1982. Air hydrate inclusions in fresh ice core. *Nature*, **298**, 548–550.

Stonehouse, B., 2002. *Encyclopedia of Antarctica and the Southern Oceans*. Chichester: Wiley. 391.

Susan, S., 2007. *Climate Change 2007: The Physical Science Basis: Contribution of Working Group I to the Fourth Assessment Report of the Intergovernmental Panel on Climate Change*. Cambridge: Cambridge University Press, p. 996.

Tulacyyk, S., 2006. Fast Glacier flow and ice streaming. In Knight, P. G., and Knight, P., (eds.), Glacier Science and Environmental Change. Wiley-Blackwell, Garsington Road Oxford OX4 2DQ, UK, p. 527.

U.S. Congress, Office of Technology Assessment, 1989. *Polar Prospects: A Minerals Treaty for Antarctica*. Washington: US. Government Printing Office, p. 218.
Walton, D. W. H., and Doake, C. S. M., 1987. *Antarctic Science*. CUP Archive. pp. 280.
William, K. H., and Christiansen, E. H., 2004. *Earth's Dynamic Systems*. Pearson Education: Prentice Hall, p. 759.
Wolff, E. W., 1990. Signals of atmospheric pollution in polar snow and ice. *Antarctic Science*, **2**, 189–205.

ANTI-ICING

Rijan B. Kayastha
Himalayan Cryosphere, Climate and Disaster Research Center (HiCCDRC), Kathmandu University, Dhulikhel, Kavre, Nepal

Definition

Anti-icing is the practice of applying chemicals to roadways to prevent forming of frost or ice from forming. It prevents bonding of frozen precipitation to road surface. Anti-icing chemicals are applied in liquid form (brine) to road surfaces. Liquid sodium chloride (NaCl) is the most effective choice for anti-icing above −10°C. The other anti-icing products are calcium chloride, magnesium chloride, potassium acetate, and calcium magnesium acetate. Each chemical has its own advantages and disadvantages. The major benefits of anti-icing are reduction in road accident, de-icing material, labor, and de-icer residue, winter cleanup work and costs, and accumulation of sand in drainage systems and beneath guardrails. Anti-icing practice is used mostly on roads to prevent forming of frost or ice. Initial applications can be made either as a pretreatment in advance of a storm event or as an early storm period treatment.

ANTI-SYNGENETIC ICE WEDGE

Pratima Pandey
Centre of Studies in Resources Engineering, Indian Institute of Technology, Bombay, Mumbai, Maharashtra, India

Definition

An ice wedge that grows progressively downward into a receding slope and in a direction perpendicular to the surface is called anti-syngenetic ice wedge.

Ice wedges or cracks in ground ice are generally classified into two main types: epigenetic and syngenetic. Epigenetic wedges grow wider rather than deeper whereas syngenetic wedges grow both wider and deeper more or less simultaneously. Field studies show that there is a third type, an anti-syngenetic wedge, which grows downward on receding slopes in a direction normal to the slope.

APPALACHIAN GLACIER COMPLEX IN MARITIME CANADA

Rudolph R. Stea
Stea Surficial Geology Services, Halifax, Nova Scotia, Canada

Definition

The Appalachian Glacier Complex is defined as a series of local ice centers and divides that developed in Maritime Canada during the Wisconsinan glaciation, effectively barring Laurentide ice from the region.

Introduction

At the turn of the last century when the first geological maps were being completed in the Maritime Provinces of Canada (Figure 1), a controversy emerged about the nature of glaciation in the area that still resonates today. Was the ice local, originating in Appalachian upland areas or was it part of the Laurentide Ice Sheet (LIS) with its center in Québec.

These two opposing models of glaciation for the Maritime Provinces have come to be known as the "minimum" and "maximum" models. The maximum model invokes the LIS covering the entire region during the last glacial maximum (LGM) (~20 kyr BP) (Flint, 1971; Mayewski et al., 1981; Dyke et al., 2002). The minimum model evolved from the recognition of autonomous local glaciers in Maritime Canada (Chalmers, 1895), into a concept of small glaciers restricted to lowland terrestrial areas, and terminating just offshore of the land areas during the LGM (Grant, 1977; Dyke and Prest, 1987; Grant, 1989; 1994). The minimum model was found to be invalid when the land-locked ice margins defined in that model were radiocarbon dated at 13 ka ^{14}C years BP (Stea and Wightman, 1987), and the maximum extent of LGM glaciers was defined at the edge of the continental shelf (Mosher et al., 1989).

Recent studies have emphasized the role of ice streams in the Bay of Fundy and Laurentian Channel in the ablation of the LIS and in the formation of local ice divides (e.g., Mayewski et al., 1981; Belknap et al., 1989; Grant, 1989; Shaw, 2003). The model that eventually emerged to counter both extreme models is one of large, local ice divides situated over maritime Canada collectively termed the Appalachian Glacier Complex (AGC) that developed during the last glaciation (Wisconsinan), effectively barring the LIS from most of the region (Prest and Grant, 1969; Stea et al., 1998; Stea, 2004; Shaw et al., 2006).

Evidence that precludes the Laurentide Ice Sheet from the region

1. Ice flow patterns in Nova Scotia, Prince Edward Island, and eastern New Brunswick (NB) are dominated by a variety of local ice flow trends rather than

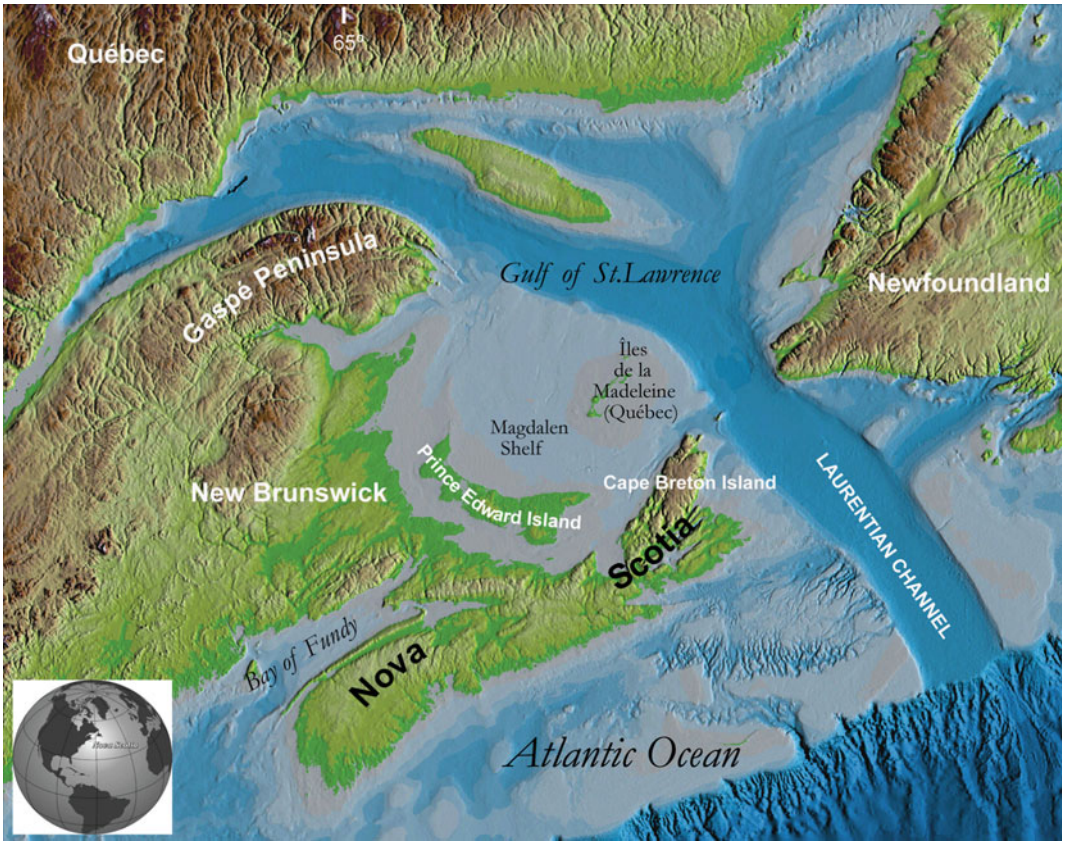

Appalachian Glacier Complex in Maritime Canada, Figure 1 Location map and topography of the study area.

a pervasive regional southward trend that would likely be the result of flow from the LIS centered in northern Quebec (Figures 1 and 2). A crucial area is northeastern NB and the Gaspé Peninsula where mapped flow patterns are dominated by Appalachian glaciers to the south rather than ice flow from the Laurentide in north (Pronk et al., 1989; Parkhill and Doiron, 2003) and erratics on the Chic-Choc range of the Gaspé Peninsula are exclusively Appalachian in origin (Olejczyk and Gray, 2007).

2. The coasts of eastern New Brunswick, northern Nova Scotia, and Cape Breton have been extensively surveyed by both bedrock and Quaternary geologists and Canadian Shield erratics have not been reported. Laurentide erratics from the Precambrian rocks of the Laurentian Highlands of Quebec, to the north of the St. Lawrence River, are known only from the area of the Saint John River valley in the northwestern part of New Brunswick (Figure 1; Rampton et al., 1984). If Laurentide ice centered in Quebec had crossed the region during the LGM abundant erratics would be expected as they are found in many areas of central Canada 300–500 km south of the shield margin (Prest et al., 2001). A petrologic and geochemical study of erratics from a type section along the Atlantic coast near Halifax, for example, confirmed the Appalachian origin of all crystalline erratics found there (Stea and Pe-Piper, 1999). Prest and Nielsen (1987) did report an anorthosite boulder in western PEI and suggested a Canadian Shield source, but the preponderance of Devonian-age Appalachian granite erratics associated with it and the known occurrences of anorthosite in the highlands of southern New Brunswick (Barr et al., 2001) suggest the possibility that the erratic assemblage is solely Appalachian in origin. More detailed petrologic or dating work needs to be done to define the sources of crystalline erratics in these regions.
3. One of the main lines of evidence supporting the minimum model and against the ingress of the LIS was the minimal loading of the lithosphere as defined by the degree of marine submergence (Grant, 1977). The 0 isobase (line of no submergence) occurs well within the Gulf of St. Lawrence and was taken as a proxy for the LGM ice margin. Stea et al. (2001), however, argued that the lack of submergence features was not a result of an ice margin but the delayed melting of local glaciers. Nonetheless, areas such as the head of the Bay of Fundy deglaciated at around the same time as regions covered by the LIS in the Gulf show considerably less submergence.

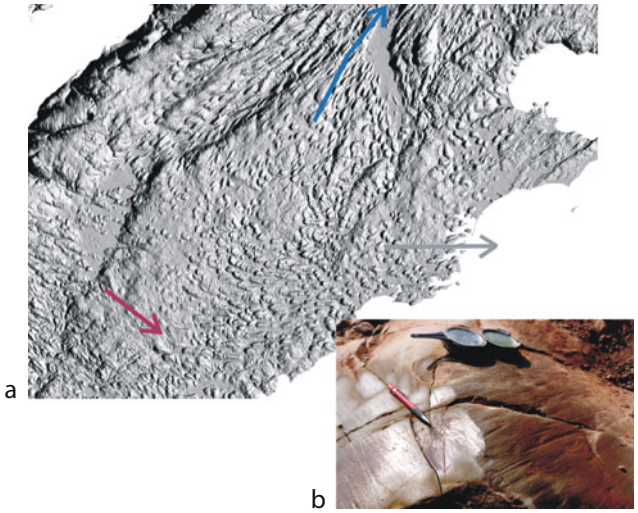

Appalachian Glacier Complex in Maritime Canada, Figure 2 (**a**) A drumlin field in southeast Cape Breton showing the juxtaposition of several temporally-separate ice flow phases as shown by varying orientations of drumlins, palimpsest drumlins and superimposed fluting on drumlins. Caledonia Phase eastward flow (grey) represented by eastward-trending drumlins in the southern part. Scotian Phase ice stream flow (blue) shown by converging, attenuated drumlins trending northeastward and late Chignecto Phase flow (purple) indicated by southeastward trending forms. The angular discordance and superposition of these drumlin trends within the same area precludes synchroneity of formation. (**b**) Crossing glacial striae, southeast Cape Breton Island. Early Caledonia Phase eastward striae (90°), preserved on the lee slope of an outcrop, with a younger southeastward ice flow imprinted on the top surface of the outcrop (Chignecto Phase-150°).

Similar lines of evidence were used to propose that Newfoundland was not covered by LIS during the LGM in spite of being much closer the to the Laurentide ice center (e.g., Grant, 1977). The Gaspé highlands (>1,000 m) formed a topographic barrier that probably blocked the LIS from the western part of the region and the 500 m deep Laurentian Channel funneled LIS ice streams away from the highland rimmed maritime provinces. These topographic entities defined the configuration of the LIS and AGC in Atlantic Canada.

Summary: Evolution of the Appalachian Glacier Complex during the last glaciation (Marine Isotope Stages 4-2; 75-12 ka BP)

The ice centers and divides of the AGC shifted in time and place over the LGM producing a palimpsest of glacial landforms (Stea, 1994). These landforms include cross-striated bedrock outcrops and drumlin fields showing multiple long-axis trends, superimposed fluting, and lobate forms (Figure 2). Based on till provenance, offshore glacial sediments were correlated to their terrestrial counterparts, establishing crucial links between ice flow patterns on land and radiocarbon-dated ice margins offshore (King, 1996; Stea et al., 1998). From these empirical data five major flow phases were defined along with their offshore margins (Figure 3). During the Caledonia Phase in the early part of the last glaciation (Marine Isotope Stage MIS 4-75-60 ka BP), both eastward and southeastward-flows are recorded from glaciers in the Appalachian Highland of eastern Maine and central New Brunswick.The age and extent of the early eastward flow, stemming from Appalachian upland sources, is uncertain and may also represent a pre-Wisconsinan flow. These flows likely crossed Nova Scotia and extended to the continental shelf edge. The Caledonia Phase ended with a global period of ice retreat during MIS 3 (60-25 ka BP). During MIS 3 the Laurentian Channel cleared of ice but adjacent land areas remained covered by glaciers (Dredge and Thorleifson, 1987). During the subsequent cooling in the Late Wisconsinan (MIS 2-25-12 ka BP) remnant glacier ice on the Magdalen Shelf (Figure 1) re-formed into an ice divide (Escuminac Ice Divide-EID) and southward flow from this divide has been termed the Escuminac Phase (Figure 3). Ice flow from the EID was generally southward over the region and extended out to the edge of the continental shelf. In previous publications, the Escuminac Phase was attributed to multiple ice centres, one in central New Brunswick (Gaspereau Ice Center-Seaman, 2004) and one over the Magdalen Shelf (Escuminac Ice Center – Rampton et al., 1984; Stea et al., 1998).

Just after 20 ka BP, at the start of a period of global warming the EID was reorganized as ice streams developed in marine channels bordering the Magdalen Shelf and in the Bay of Fundy. The progressive thinning of ice in the Magdalen Shelf and in the Bay of Fundy produced an ice divide (Scotian Ice Divide-SID) over mainland Nova Scotia and a general reversal of ice flow termed the Scotian Phase. Ice flow in northern mainland Nova Scotia rotated from northeastward to north-northwestward as the calving margin in the Laurentian Channel migrated landward. The margin of SID is marked offshore by the Scotian Shelf End Moraine Complex dated between 20 and 16 ka BP (Figure 3; King, 1996).

Responding to rapid global warming after 16.0 ka BP the SID reorganized into an east-west trending feature as the Bay of Fundy ice stream picked up momentum. Ice flow rotated from northwestward during the Scotian Phase to westward to southwestward into the Bay of Fundy from an ice divide over Prince Edward Island and northern mainland Nova Scotia (Northern Nova Scotia Ice Divide). This westward and southwestward ice flow pattern was termed the Chignecto Phase (Rampton et al., 1984; Seaman, 2004; Stea, 2004).

Between 16 and 12 ka BP local centers advanced and retreated, responding to mass balance changes during a time of fluctuating northern hemisphere climate. Chignecto Phase glaciers eventually dissipated and their margins retreated landward. Isolated marine and terrestrial remnants of the Chignecto Phase glaciers re-advanced significantly during the Collins Pond Phase (Younger Dryas) just after 12.9 ka BP (Stea and Mott, 2005).

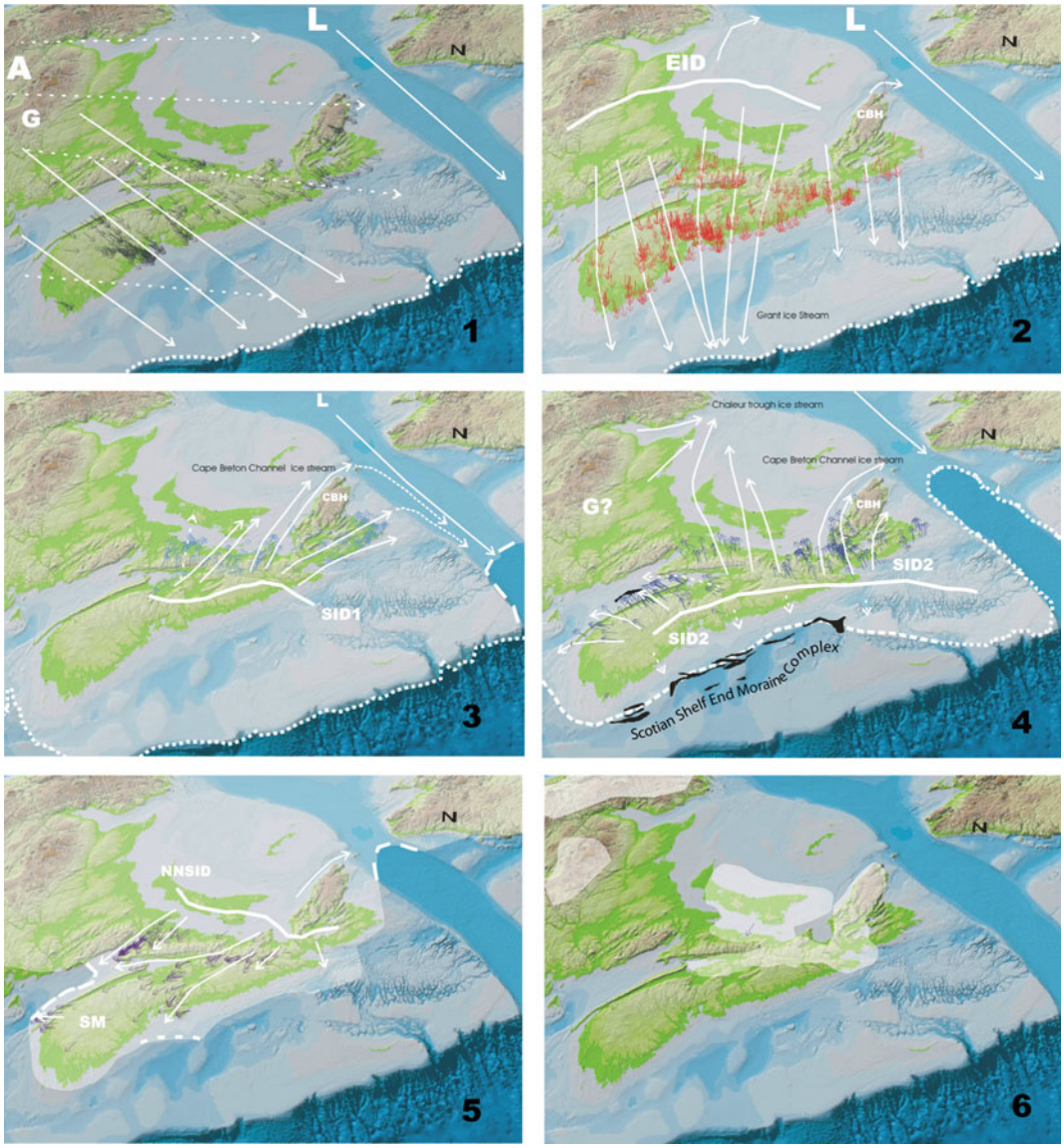

Appalachian Glacier Complex in Maritime Canada, Figure 3 Ice flow "phases", glacier flow lines and ice divides defined by landforms (drumlins, fluting, striae) indicative of glacier flow. Striation data plotted on the figures from Stea et al., (1992) and Grant (1994). An ice flow "phase" is defined as discrete, regionally mappable trends of striations and streamlined landforms of the same relative age (cf. Rampton et al., 1984). 1-Caledonia Phase (earlier eastward flow from Maine (A)) (Northumberland Glacier- Chalmers, 18). southeastward flow from the Gaspereau Ice Center (Rampton et al., 1984). 2. Escuminac Phase (dotted line) early eastward flow may represent pre-Wisconsinan flow phase southward flow from Escuminac Ice Divide (EID), Grant Ice Stream funneled into a marine channel offshore. 3. Scotian Phase ice flow initial NE flow phase and the development of the Scotian Ice Divide (SID 1), calving bay migration in the Laurentian Channel. 4. Main Scotian Phase with a linear ice divide straddling the peninsula of Nova Scotia and ice flow northwest and southeast from the divide (SID 2). Outlined in black offshore Nova Scotia is the Scotian End moraine Complex (King, 1996). 5. Chignecto Phase southwestward ice flow from an ice divide in northern mainland Nova Scotia (NNISD). 6. Collins Pond Phase ice flow from a local glacier advance during the Younger Dryas Chronozone.

Bibliography

Barr, S. M., White, C. E., Venugopal, D. V., Hamilton, M. A., and Stirling, J. A. R., 2001. Petrology and age of the lower Coverdale high-Ti, P, and V gabbro-anorthosite complex and associated granite, Moncton area. In Abstracts Volume; Annual Review of Activities, New Brunswick, Minerals and Energy Division, Report: 2001-1, pp. 3–6.

Belknap, D. F., Shipp, R. C., Kelley, J. T., and Schnitker, D., 1989. Depositional sequence modelling of late Quaternary geologic history, west central Maine. In Tucker, R. D., and Marvinney, R. G. (eds.), *Studies in Maine Geology.* Augusta, Maine: Geological Survey of Maine. Quaternary Geology, Vol. 5, pp. 29–46.

Chalmers, R., 1895. Report on the surface geology of eastern New Brunswick, north-western Nova Scotia and a Portion of Prince

Edward Island. Geological Survey of Canada, Annual Report, 1894, 1(7), pt. m.
Dredge, L. A., and Thorleifson, L. H., 1987. The middle Wisconsinan history of the Laurentide ice sheet. *Géographie physique et Quaternaire*, **41**(2), 215–236.
Dyke, A. S., and Prest, V. K., 1987. Late Wisconsinan and Holocene history of the Laurentide ice sheet. In Fulton, R. J., and Andrews, J. T. (eds.), *The Laurentide Ice Sheet*. *Géographie physique et Quaternaire*, **41**, 237–264.
Dyke, A. S., Andrews, J. T., Clark, P. U., England, J. H., Miller, G. H., Shaw, J., and Veillette, J. J., 2002. The Laurentide and Innuitian ice sheets during the Last Glacial Maximum. *Quaternary Science Reviews*, **21**(1–3), 9–31.
Flint, R. F., 1971. *Glacial and Quaternary Geology.* New York: Wiley, 892 p.
Grant, D. R., 1977. Glacial style and ice limits, the Quaternary stratigraphic record and changes of land and ocean level in the Atlantic Provinces, Canada. *Géographie physique et Quaternaire*, **31** (3–4), 247–260.
Grant, D. R., 1989. Quaternary Geology of the Atlantic Appalachian region of Canada. In Fulton, R. J. (ed.), *Chapter 5 Quaternary Geology of Canada and Adjacent Greenland*, Geological Survey of Canada, Geology of Canada, pp. 393–440.
Grant, D. R., 1994. *Quaternary Geology, Cape Breton Island*. Geological Survey of Canada, Bulletin 482, 159 p.
King, L. H., 1996. Late Wisconsinan ice retreat from the Scotian Shelf. *Geological Society of America Bulletin*, **108**, 1056–1067.
Mayewski, A., Denton, G. H., and Hughes, T. J., 1981. Late Wisconsin Ice Sheets in North America; Chapter 2. In Denton, G. H., and Hughes, T. J. (eds.), *The Last Great Ice Sheets*. New York: Wiley, pp. 67–178.
Mosher, D. C., Piper, D. J. W., Vilks, G. V., Aksu, A. E., and Fader, G. B., 1989. Evidence for Wisconsinan glaciations in the Verrill Canyon area, Scotian Slope. *Quaternary Research*, **31**, 27–40.
Olejczyk, P., and Gray, J. T., 2007. The relative influence of Laurentide and local ice sheets during the last glacial maximum in the eastern Chic-Chocs Range, northern Gaspé Peninsula, Quebec. *Canadian Journal of Earth Sciences*, **44**(11), 1603–1625.
Parkhill, M. A., and Doiron, A., 2003. Quaternary geology of the Bathurst Mining Camp and implications for base metal exploration using drift prospecting. In Goodfellow, W. D., McCutcheon, S. R., and Peter, J. M., (eds.), *Massive Suphide Deposits of the Bathurst Mining Camp, New Brunswick and Northern Maine,* Economic Geology Monograph 11, pp. 631–660.
Prest, V. K., and Grant, D. R., 1969. Retreat of the last ice sheet from the Maritime Provinces – Gulf of St. Lawrence region. *Geological Survey of Canada Paper 6933*, 15 p.
Prest, V. K., Donaldson, J. A., and Mooers, H. D., 2001. The omar story: The role of omars in assessing glacial history of west-central North America. *Géographie physique et Quaternaire*, **54**, 257–270.
Prest, V. K., and Nielsen, E., 1987. The Laurentide ice sheet and long distance transport. In Kujansuu, R., and Saarnisto, M. (eds.), *INQUA Till Symposium, Finland 1985*. Geological Survey of Finland Special Paper, Vol. 3, pp. 91–102.
Pronk, A. G., Bobrowsky, T., and Parkhill, M. A., 1989. An interpretation of the late Quaternary glacial flow indicators in the Baie des Chaleurs region, northern New Brunswick. *Géographie physique et Quaternaire*, **43**(2), 179–190.
Rampton, N., Gauthier, R. C., Thibault, J., and Seaman, A. A., 1984. *Quaternary Geology of New Brunswick*. Geological Survey of Canada, Memoir, 416, 77 pp.
Seaman, A., 2004. Late Pleistocene history of New Brunswick, Canada. In Ehlers, J., and Gibbard, P. L. (eds.), *Quaternary Glaciations Extent and Chronology, Part II North America*. Amsterdam: Elsevier, pp. 151–167.
Shaw, J., 2003. Submarine moraines in Newfoundland coastal waters: Implications for the deglaciation of Newfoundland and adjacent areas. *Quaternary International*, **99–100**, 115–134.
Shaw, J., Piper, D. J. W., Fader, G. B. J., King, E. L., Todd, B. J., Bell, T., Batterson, M. J., and Liverman, D. G. E., 2006. A conceptual model of the deglaciation of Atlantic Canada. *Quaternary Science Reviews*, **25**, 2059–2081.
Stea, R. R., 1994. Relict and palimpsest glacial landforms in Nova Scotia, Canada. In Warren, W. P., and Groot, D. G. (eds.), *Formation and Deformation of Glacial Deposits*. Rotterdam: Balkema, pp. 141–158.
Stea, R. R., 2004. The Appalachian Glacier Complex in Maritime Canada. In Ehlers, J., and Gibbard, P. L. (eds.), *Quaternary Glaciations Extent and Chronology, Part II North America*. Amsterdam: Elsevier, pp. 213–232.
Stea, R. R., and Mott, R. J., 2005. Younger Dryas glacial advance in the southern Gulf of St. Lawrence, Canada: analogue for ice inception? *Boreas*, **34**(3), 345–362.
Stea, R. R., and Pe-Piper, G., 1999. Using whole-rock geochemistry to locate the source of igneous erratics from drumlins on the Atlantic coast of Nova Scotia. *Boreas*, **28**, 308–325.
Stea, R. R., and Wightman, D. M., 1987. Age of the Five Islands Formation, Nova Scotia and the deglaciation of the Bay of Fundy. *Quaternary Research*, **27**, 211–219.
Stea, R. R., Conley, H., and Brown, Y., (compilers) 1992. Surficial geology of the Province of Nova Scotia. *Nova Scotia Department of Natura1 Resources*, Map 92-1, Scale 1: 500,000.
Stea, R. R., Piper, D. J. W., Fader, G. B. J., and Boyd, R., 1998. Wisconsinan glacial and sea-level history of Maritime Canada, a correlation of land and sea events. *Geological Society of America Bulletin*, **110**(7), 821–845.
Stea, R. R., Fader, G. B. J., Scott, D. B., and Wu, P., 2001. Glaciation and relative sea-level change in Maritime Canada. In Weddle, T. K., and Retelle, M. J. (eds.), *Deglacial History and Relative Sea-Level Changes, Northern New England and Adjacent Canada,* Geological Society of America, Special Paper 351, pp. 35–49.

Cross-references

Laurentide Ice Sheet
Sediment Entrainment, Transport, and Deposition

ARCTIC HYDROCLIMATOLOGY

Jessica Ellen Cherry
International Arctic Research Center and Institute of Northern Engineering, University of Alaska Fairbanks, Fairbanks, AK, USA

Synonyms

Arctic hydrometeorology; Arctic water cycle; Cold region climatology; Northern hydrology

Definition

Arctic hydroclimatology is the study of water in the climate system of the far north. It can be differentiated from Arctic hydrometeorology in that it is generally concerned with longer than synoptic timescales. Physical climatologists typically focus on trying to quantify the fluxes and stocks of freshwater in the Arctic. The domain of

interest includes the Arctic hydrologic catchment, which extends as far south as 45°N, but also includes transport of freshwater in the ocean and atmosphere in and out of the Northern Regions.

Fluxes of liquid, vapor, and frozen water between the land and the atmosphere include precipitation, evapotranspiration, and sublimation. Water stored on land includes that in snow cover, glaciers, lakes, rivers, in vegetation, and in ice-rich permafrost. Fluxes of water in the coastal areas include river runoff, air–sea interactions, and atmospheric transport and may be strongly influenced by distributions of sea ice in the shoulder seasons. Freshwater in the ocean is mixed, evaporated, stored, and transported as liquid as well as sea ice. Clouds also play an important role in the climate of the Arctic, not only as a means for moisture transport, but also as a driver of both radiative warming and cooling, depending on the cloud type and location.

System components

The balance between precipitation and evapotranspiration is the fundamental driver of freshwater storage in the Arctic. Annual and seasonal patterns of precipitation vary widely from south to north and between coastal and continental climates. In general, there is more precipitation in the south than in the north, because relatively warm moist air is being transported to these regions from the midlatitudes. By the time these air masses reach the high Arctic, much of that heat and moisture has been lost *en route*. Coastal regions in the Arctic tend to get more precipitation than inland locations, whereas those in the midlatitudes tend to have more moderate seasonal differences in temperature and precipitation patterns. Values can range from 1,600 mm per year in coastal Norway to 150 mm per year in Northern Greenland (AARI, 1985). In most locations throughout the Arctic, more precipitation falls in the warm season than in the cold season, although the ground may be covered with snow for much of the year.

The precise amount and distribution of precipitation and evapotranspiration in the Arctic are both poorly known. Continuous, long-term observations (50 years or more) of precipitation exist at only a few locations. While hundreds of additional stations were added throughout the Arctic during the latter part of the twentieth century, many of these were closed or converted to automated observations toward the end of the century. Stations where enough measurements are made to credibly calculate evapotranspiration are limited to a handful across the whole Arctic. Precipitation, in addition to being sparsely observed in the Arctic, is extremely difficult to measure. Large biases occur in the measurement of solid precipitation, because precipitation gauges are subject to wind-induced undercatch. The gauge itself creates a disturbance in the flow of the atmosphere that causes particles, particularly snowflakes, to fall preferentially away from the gauge. Intercomparison studies of gauge performance (Yang et al., 2005) have estimated wind-induced undercatch to be up to 150% or more of recorded precipitation in Arctic conditions. Because solid precipitation can occur at any time of year in the Arctic, this measurement bias is particularly detrimental to accurate estimates of total precipitation. Other types of measurement biases include mechanical failures (especially problematic for automated gauges), evaporation and wetting losses (when liquid sticks to the inside of the gauge and is not measured). Gauges also fail to measure trace precipitation, which may account for a large portion of total precipitation in the Arctic (Yang et al., 1998).

River discharge, where it is measured, is considered to be one of the more robust hydroclimatological system observations. However, geophysical features such as permafrost cause considerable braiding of rivers in the far north, making discharge in all but the mouths of the larger rivers difficult to estimate. Ice flow during breakup can make it difficult to capture the peak discharge if sensors get damaged. Finally, large numbers of the Arctic rivers remain entirely ungauged. Remote sensing and other techniques are being explored to remedy this problem and the other challenges of hydrologic measurements, but have limitations for estimating historical fluxes. McClelland et al. (2006) report the average combined discharge of rivers into the Arctic Ocean as approximately 2,500 km^3/year over the period 1964–2000 and they also suggest that discharge has increased over 10% during this era. The cause of this increase is the source of considerable debate and may include increases in precipitation, thawing of ground ice, increased contributions from groundwater, and glacial melt.

Shallow lakes are a prominent feature of the Arctic, in part because continuous permafrost can act as an impermeable boundary for liquid water. For example, the Arctic Coastal Plain, which has a total area of 55,964 km^2, has 9,545 km^2 (~17%) of its surface covered by lakes (Arp and Jones, 2009). Bathymetry data and therefore direct estimates of volume have been measured in only a handful of these lakes, although Jefferies et al. (1996) and others have developed techniques to estimate volume from remote sensing. The balance of water in these lakes is generally driven by the difference between precipitation and evapotranspiration in the drainage, however, warming soil or other landscape disturbances may cause degradation of permafrost and lake drainage. The prominence of surface waters in the Arctic poses an interesting juxtaposition: as a measure of annual precipitation, the Arctic is very dry. However, long winters and impermeable permafrost causes what water there is to be mainly trapped at the surface. The result is a large amount of recycling of water between the land and atmosphere during the summer months.

A discussion of the role of glaciers in the Arctic hydroclimatology will be left for other entries in this encyclopedia. Suffice it to say that glacier mass balance is closely tied to precipitation and temperature trends and that glacial melt constitutes a significant portion (10% or

more) of river discharge in regions such as Southeast Alaska and Scandinavia.

Freshwater in the ocean, including sea ice, has important interactions with climate over longer timescales than it does on land or in the atmosphere. River discharge and maritime precipitation are both significant sources of freshwater in the ocean. Formation of sea ice rejects most of the brine back into the water, creating a layer of dense water. The balance of ice formation and freshwater inputs contribute, along with temperature differences, to buoyancy-driven circulation in the ocean. In turn, this influences the fluxes of heat and moisture between the atmosphere and ocean that modulate not only arctic climate, but also the whole Earth. Measurements of changes in ocean freshwater are also difficult to obtain. Remote sensing can be used to estimate precipitable water in the atmosphere, but is limited to the satellite era and the fluxes of water between the atmosphere and ocean are not directly measured. In the ocean, manual salinity measurements and automated sensors on moorings can be used to monitor freshwater content, but are very expensive to obtain and are limited to a single point (on a mooring) or a temporary transect in a research vessel, typically in late summer during the sea ice cover minimum.

Natural variability and anticipated hydroclimate changes in a warmer world

All components of the Arctic hydroclimate cycle have a strong component of interannual variability. Large-scale climate dynamics such as those associated with the El Niño-Southern Oscillation, the Pacific Decadal Oscillation, and the Arctic Oscillation also tend to drive variability in the arctic water cycle on the timescale of several years to decades. In addition to this, frequent variability is thought to be long-term variability associated with a large-scale planetary warming. However, the scale of natural variability in most components of the hydroclimate system is several orders of magnitude larger than the scale associated with climate change.

Although the change may be small and for the reasons discussed above difficult to measure, precipitation and evapotranspiration are both expected to increase in the warmer climate projected by the Intergovernmental Panel on Climate Change (IPCC, 2007). A warmer atmosphere will drive additional evaporation, which will lead to enhanced precipitation.

It is debatable whether this climate change signal is evident in historical precipitation, for example. However, there is relative consensus that the increase in Arctic river discharge over the twentieth century is associated with climate change and intensification of the hydroclimate cycle, as well as with natural variability (Déry et al., 2005; McClelland et al., 2006). Melting of ground ice is thought to be a much smaller component of this increase in discharge than is increased precipitation (McClelland et al., 2004).

Vegetation changes in the Arctic have also been observed, particularly an expansion of shrubs that utilize more water than existing biomes. The consequences of vegetation change for other climate feedbacks are considerable. A few examples include interception of snow by shrubs leading to changes in ground thermodynamics; they have a different color than existing vegetation that alters the energy absorption and spring snow melt, and they transpire at a different rate than other plants.

Warming and degradation of permafrost will alter the hydroclimate of the Arctic considerably. As the land surface warms, the seasonally thawed portion of the soil deepens, and the soil can store more water. This could lead to less surface water storage by draining lakes. There is already evidence of this in Siberia, in regions of discontinuous permafrost (Smith et al., 2005). If precipitation were to remain constant, this could lead to less recycling of moisture between the land and atmosphere. How an increase in precipitation would balance with an increase in the subsurface storage of water is unknown.

Summary

Arctic hydroclimatology includes many components of the physical climate system that interact regionally as well as feedback on the global climate system. The remoteness and harsh environment make quantification of the arctic hydroclimate system components difficult. Measurement biases and high natural variability make long-term change detection challenging, but experts anticipate this to become more evident with time and the development of better measurement techniques.

Bibliography

AARI, 1985. Atlas arktiki (Atlas of the Arctic). Treshnikov, A. F. (ed.), Arctic and Antarctic Research Institute, State Committee of the USSR for Hydrometeorology and environmental monitoring, Directorate-General for Geodesy and Cartography of the USSR Council of Ministers, Moscow, 204p. (in Russian, English summaries) (AAR Figure 2.6).

Arp, C. D., and Jones, B. M., 2009. Geography of Alaska lake districts: identification, description, and analysis of lake-rich regions of a diverse and dynamic state: U.S. Geological Survey Scientific Investigations Report 2008–5215, 40p.

Déry, S. J., Sheffield, J., and Wood, E. F., 2005. Connectivity between Eurasian snow cover extent and Canadian snow water equivalent and river discharge. Journal of Geophysical Research, **110**, D23, D23106, doi:10.1029/2005JD006173.

IPCC, 2007. Summary for policymakers. In Parry, M. L., Canziani, O. F., Palutikof, J. P., van der Linden, P. J., and Hanson, C. E., (eds.), *Climate Change 2007: Impacts, Adaptation and Vulnerability.* Contribution of Working Group II to the Fourth Assessment Report of the Intergovernmental Panel on Climate Change. Cambridge: Cambridge University Press, pp. 7–22.

Jefferies, M., Morris, K., and Liston, G., 1996. A method to determine lake depth and water availability on the north slope of Alaska with spaceborne imaging radar and numerical ice growth modeling. *Arctic*, **49**(4), 367–374.

McClelland, J. W., Holmes, R. M., Peterson, B. J., and Stieglitz, M., 2004. Increasing river discharge in the Eurasian Arctic: Consideration of dams, permafrost thaw, and fires as

potential agents of change. *Journal of Geophysical Research*, **109**, D18102, doi:1010292004JD004583.
McClelland, J. W., Déry, S. J., Peterson, B. J., Holmes, R. M., and Wood, E. F., 2006. A Pan-Arctic evaluation of changes in river discharge during the latter half of the 20th century. *Geophysical Research Letters*, **33**, L06715, doi:10.1029/2006GL025753.
Smith, L. C., Sheng, Y., Macdonald, G. M., and Hinzman, L. D., 2005. Disappearing Arctic lakes. *Science*, **308**, 1429.
Yang, D., Goodison, B. E., Ishida, S., and Benson, C. S., 1998. Adjustment of daily precipitation data at 10 Climate stations in Alaska: Application of World Meteorological Organization Intercomparison Results. *Water Resources Research*, **34**, 241–256.
Yang, D., Kane, D., Zhang, Z., Legates, D., and Goodison, B., 2005. Biaas corrections of long-term (1973–2004) daily precipitation data over the northern regions. *Geophysical Research Letters*, **32**, L19501, doi:1010292005GL024057.

Cross-references

Frozen Soil Hydrology
Permafrost

ARTIFICIAL GROUND FREEZING

Rijan B. Kayastha
Himalayan Cryosphere, Climate and Disaster Research Center (HiCCDRC), Kathmandu University, Dhulikhel, Kavre, Nepal

Definition

Artificial ground freezing (AGF) is a technique of freezing of pore water in saturated and partially-saturated soil which changes the thermal and mechanical properties such as stiffness, strength, and creep behavior of soil. This change in properties increases the load-carrying capacity of the frozen soil which is exploited in various construction works. Originally, the AGF was first developed by F.H. Poetsch in 1883. Poetsch's process involves the circulation of a refrigerated coolant through a series of subsurface pipes to extract heat, thus converting the soil water to ice, creating a strong, watertight material. Most ground freezing systems are quite similar in principle, with subtle differences in the engineering aspects of the individual sites. The single most important component of a ground freezing system is the subsurface refreezing system, consisting of a series of refrigeration pipes installed with various drilling techniques. The quantity, spacing, depth, and size of the refrigeration pipes are unique to each site, and determined on the basis of the thermal and hydraulic properties of soils, construction schedule, and cost effectiveness.

The cooling medium varies depending on the required application. Where very rapid freezing is required, liquid nitrogen is used with temperatures well below −150°C. For most applications however, a secondary coolant such as calcium chloride (brine) or ethylene glycol is used. This secondary coolant is chilled using large portable refrigeration plants which employ ammonia as a primary refrigerant. These refrigeration plants are typically mounted on conventional over-the-road trailers and are electrically powered using commercially available electricity.

Once the system has been drilled and installed, it operates continuously as a closed system requiring constant monitoring with occasional plant adjustment and coolant flow modifications. After the initial freezing has been completed and the frozen barrier is in place, the required refrigeration capacity is significantly reduced to maintain the frozen barrier.

Use: AGF is employed in tunneling, during open excavations, and for retaining structures.

ARTIFICIAL PRODUCTION OF SNOW

Carmen de Jong
The Mountain Institute, University of Savoy, Le Bourget-du-Lac, France

Synonyms

Artificial snow; Man-made snow; Programmed snow; Snow production; Technical snow

Definition

Artificial snow is produced by rapidly freezing water into ice crystals under high pressure.

Introduction

The artificial production of snow serves two objectives: on the one hand, artificial snow is necessary for laboratory experiments to simulate snow and avalanche processes, on the other hand, it is produced commercially as a surrogate for natural snow to cover ski runs where natural snowfall is missing or uncertain. It is also produced in indoor centers for skiing as well as outdoors in cities for events. It can be produced in virtually all climate zones, even in hot, arid countries like Israel. Dubai hosts the world's largest indoor ski center. Artificial snow is now produced on nearly all ski runs globally that are affected by large variations in snowfall, that have insufficient natural snowfall or that are effected by climate change. This includes the Alps, Pyrenees, Rockies, Andes, Carpathians, nearly all skiable Mediterranean mountains (e.g., Mount Hermon) and newer developments such as in the Yabuli mountains (China), etc. Some ski runs are covered by 100% artificial snow (layered with natural snow), in particular in the United States. However, many ski runs especially in the Alps and semiarid regions rely entirely on artificial snow for part of their season.

Short history of artificial snow

Artificial snow was first produced and patented from snow canons to cover ski runs by Art Hunt, Dave Richey, and Wayne Pierce in 1950 in the United States. In Europe,

artificial snow production was introduced only in the 1970s. Since then, artificial snow has been used commercially. Artificial snow production has increased exponentially and is now produced at a large scale and altitudinal range worldwide. In the European Alps, it covers up to 70% of the ski runs (for example in Italy) up to an altitude of 3,200 m. The most dynamic increase in artificial snow infrastructure has occurred since the mid-1980s, parallel with strong climate change marked by more erratic snowfall events and the increase in global warming. Nowadays, artificial snow is produced for all world cup winter sport events to ensure homogenous ski runs.

In the Alps, nearly 250 km^2 of ski runs are prepared using artificial snow, costing nearly 3 billion Euros per year for construction and maintenance and consuming approximately 600 GWh per year. At present 1 m^3 of artificial snow costs between 2.50 and 5.00 Euros.

Production of artificial snow

There are two principal methods used for producing artificial snow, based on internal and external mixing of air and water. For the first method, water is cooled to just above the freezing point and then pumped under high pressure together with compressed air into a mixing chamber inside the snow gun or snow canon (Figure 1). It is then ejected through one principal nozzle as a mixture of air and water to the outside. For the second method, compressed air and compressed water are channelled separately inside the snow gun or snow cannon to the outside and mixed during the ejection. The compressed water exits several primary and secondary nozzles and is mixed outside with the compressed air that exits via two principal valves perpendicular to the water nozzles.

The most important processes occur within the first 50 cm outside the snow canon. As the water and air mixture exit the nozzle, it expands and cools off rapidly. This zone is dominated by atomization of water into fine droplets (on average between 200 and 300 µm in size), accompanied by the onset of nucleation and seeding. Nucleation is part of a first-order phase change, in this case it is the process by which the water droplets freeze into ice particles (on average 50 nm in size). Seeding is the process by which water vapor condenses around a seeding nucleus, in this case an ice crystal, causing ice crystal growth (on average between 5 and 100 µm in size). However, water vapor and the potential for seeding, is limited to °C temperatures. Within the range of 50–100 cm, nucleation dominates followed by seeding. In the zone between 100 and 200 cm, seeding dominates and evaporation begins. At 200–500 cm, evaporation of water attached to the ice crystals dominates, supporting further cooling of the ice-crystals, freezing the remainder, and causing the ice crystals to grow in size. Dispersal occurs across a range of 1–80 m and includes evaporation and convection. Depending on the type of snow canon/gun, snow can be distributed over 20–80 m. Snow canons are mobile and placed on the ground, so that artificial snow can be pumped from 1 to 2 m height at a distinct angle into the air. Snow guns are fixed installations, usually at 10 m height pumping artificial snow at an angle towards the ground. The third method, used mainly in indoor centers, is to freeze water by compressing air together with water and liquid nitrogen. Nowadays the production of artificial snow is computer controlled. Large purpose-built reservoirs supply water to a central "snow factory" which then pumps both water and air at high pressure through a network of underground

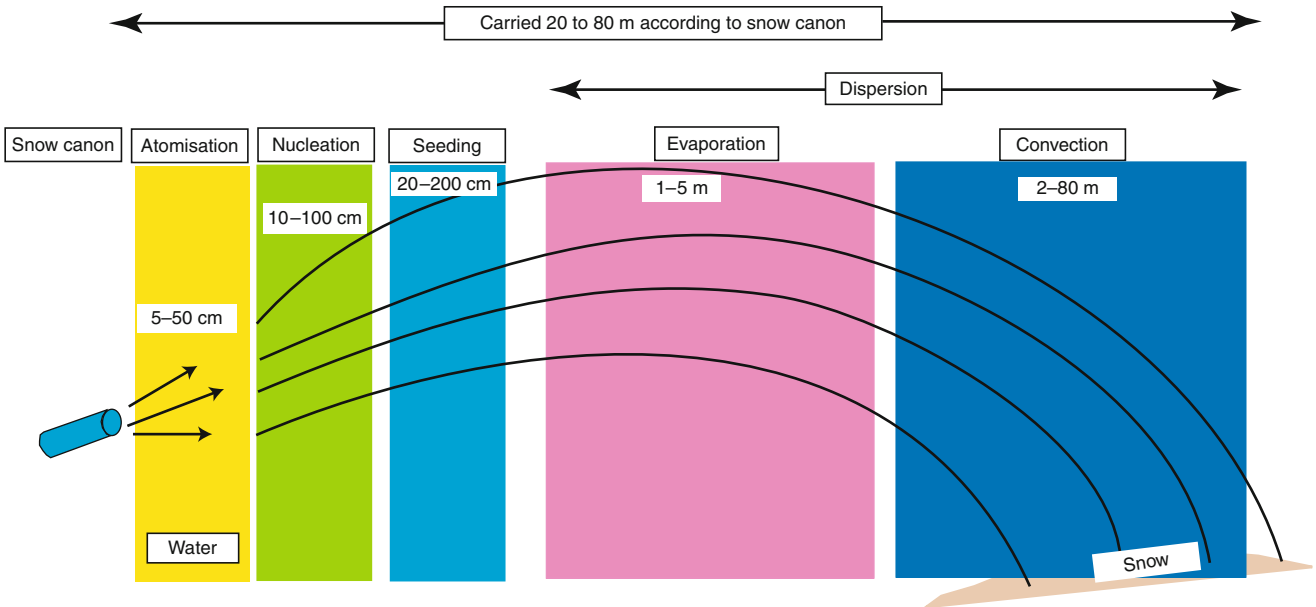

Artificial Production of Snow, Figure 1 Production of artificial snow.

pipes to a series of snow-guns/canons. The snow guns/canons automatically switch the snow-making process on and off according to the prevailing local meteorological conditions.

Optimal conditions for snow production include low relative humidity, low wind speeds, and temperatures below −3°C. At high wind speeds, artificial snow is dispersed into the atmosphere rather than deposited on the ground and can be carried away for long distances. Temperatures above −3°C are suboptimal for snow production since the water droplets do not freeze rapidly enough and will fall to the ground as cold rain (Figure 2). Another problem is that if the water droplets freeze but the ground is still too warm, the ice crystals melt when reaching it. Unless enough snow is produced to cool the ground to low temperatures to keep the snow, this technique is not very energy efficient. In Zermatt, Switzerland and Pitztal glacier, Austria however, a snow production machine has been installed that can produce artificial snow even at air temperatures of +20°C (IDE snowmakers). This technique could be used to upgrade downhill runs with sufficiently low surface temperature even under unfavorable warm weather conditions. In order to produce artificial snow at temperatures above −3°C, some countries authorize the addition of condensation nuclei, such as ash, silver iodide, kaolin, soaps and detergents, fungi, or lichens. The most widely-used additive is "Snomax," a freeze-dried protein powder derived from the Pseudomonas syringae bacterium that helps initialising ice crystallization. Snomax is authorized in Switzerland and the United States.

Modern snow guns can produce up to 96 m^3/h of snow transmitting a water flow rate of up to 638 L/min.

Characteristics of artificial snow

The grain size distribution of artificial snow lies between 0.05 and 2 mm. Compared to natural snow, with a grain size of 0.2 to several mm, artificial snow crystals are much smaller and also have a different grain size and shape. Whereas natural snow is dendritic in shape, artificial snow is spherical, consisting of small, rounded particles. Since artificial snow is produced very rapidly, the ice crystals may still contain a pocket of air, a bulge or may even be broken (Figure 3) (Fauve and Ryner, 2004). Artificial snow resembles the final stage of natural snow after several weeks of metamorphosis through sublimation and melting and refreezing.

Due to its small grain size and high degree of compaction, artificial snow has a much higher density (300–500 kg/m^3) than uncompacted, fresh natural snow, on the whole it is four times denser (Rixen et al., 2003; Jones and Devarennes, 1995). Its conductivity is more than ten times higher than natural snow, typically above 85 μS/cm. This is due to its high density and high ion concentration. Depending on the geology of the water source area, mineral concentration can be considerably higher, for example, magnesium and calcium can be 40 times and 10 times higher respectively. Due to its high density, artificial snow can be 60 times harder than natural snow. Snow hardness measurements of 36 N for artificial snow compared to 0.6 N for uncompacted natural snow (Keller et al., 2004).

The thermal properties of artificial snow also differ from natural snow. During the winter season (e.g., from December to April), measurements show that the temperatures remain homogenous, fluctuating around the 0°C

Artificial Production of Snow, Figure 2 Artificial snow production at temperatures above −3°C (Photo: Kees Woolthorn).

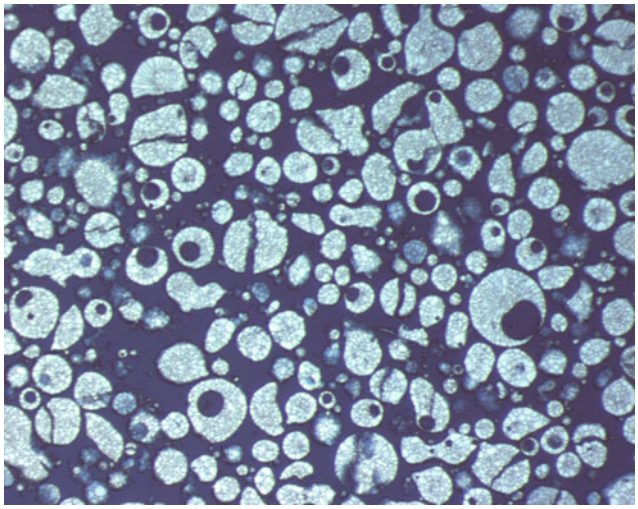

Artificial Production of Snow, Figure 3 Crystal shape of artificial snow, showing broken crystals (Photo: Mathieu Fauve).

(Rixen et al., 2003). In contrast, compacted natural snow stays well below 0°C at −3°C to −5°C under the same atmospheric conditions. The isothermal conditions render artificial snow more prone to melting and refreezing during the daytime.

Chemical/mineral properties

The salinity of meltwaters from artificial snow is extremely high compared to natural snow (Jones and Devarennes, 1995) (see above, conductivity). On average, the mineral and ion concentration in artificial snow meltwater is four times higher than in the surrounding streams causing a local input of ions (Rixen et al., 2003). This is because water used for snowmaking is abstracted from groundwater and river water that has a higher mineral concentration than precipitation. It is also possibly due to enrichment effects of stagnating snow as water vapor sublimates and evaporates into the atmosphere.

Climate change and artificial snow

Since the mid-1980s, climate change has clearly visible effects on the frequency of snowfall events, snowpack thickness, and snow duration. Most mountains, together with the whole northern hemisphere, show a clear decrease in total amount of snow and the length of the winter season. In the Col du Porte, (Massif Chartreuse, altitude 1,505 m) France, snow height has decreased by more than half a meter over the last 50 years and the snow season has decreased by several weeks (Meteo France). In other higher latitude sites there has been more than 4 m decrease in snow depth (Barth, 2007). Since skiing is based primarily on snow as a natural resource, the inconsistency of snowfall and snow duration associated with climate change has caused more and more ski resorts to resort to the artificial production of snow. As the regional snowline is climbing higher, the replacement of natural snow by artificial snow guarantees continuous skiing on the ski runs.

The exponential increase in snow production infrastructure goes parallel with the current trend of global warming temperatures. More and more ski resorts worldwide are being equipped with snow-making infrastructure to ensure snow during the whole season and over all runs.

However, global warming itself is limiting snow production, with some ski resorts already unable to produce snow at temperatures above the threshold during warm winters (Steiger and Mayer, 2008). Local conditions such as aspect (orientation) of ski slope, altitude, patterns of inversion, and exposure to foehn winds play a major role. With the expected increase in temperatures between 1.5°C and 6°C by the end of the century, the altitudinal limit of snow making could rise by between 250 and 1,000 m. As the periods with subzero temperatures will be shorter, the preseason preparation of artificial snow will also become more uncertain.

Another major limiting factor is the availability of water. Large quantities of water are necessary for snow production, approximately 3,300 m^3/year per hectare, (up to 0.2 m^3/s and snow cannon). Under the current trend of climate change, water is distributed more unequally over time and its availability at high altitudes is limited due to the limited catchment size and groundwater reservoirs.

Environmental effects of artificial snow

Meteorological

Artificial snow is commonly produced in large amounts during a whole week in the autumn, that is, October in preparation of the winter ski season. The amount of artificial snow produced is usually the equivalent of natural snowfall during the whole winter season. It is stored in large mounts for later redistribution over the ski runs shortly before the ski runs are opened. The snow is not produced during natural snowfall. During its production, tiny particles from evaporating snow crystals are emitted into the atmosphere. The local ultrafine particle concentration during artificial snow production can reach numbers comparable to polluted atmospheres ~20,000/cm^3 in contrast to approximately 5–800/cm^3 under normal clean conditions (Junkermann, personal communication). First results show that 90% of the artificial snow produced particles are smaller than 50 nm in size. These particles are too small to act as cloud nucleation nuclei (CCN), since cloud nucleation nuclei have to exceed 50 nm in size to allow condensation of water for the formation of rain or snow. On a regional scale, the remaining 10% still can double the number of climate relevant CCN.

Hydrological

Artificial snow perturbates the water cycle at two stages: firstly when water is abstracted from sources, streams, groundwater and interbasin transfer and stored in

preparation for snow production resulting in a local, temporary deficit in water. This deficit is caused not only by the direct abstraction of discharge from the streams and groundwater but also by a loss in evaporation at three stages: in the water storage reservoirs, during its production, and during its redistribution and storage over the ski runs. It is estimated that about 30% of water is lost by evaporation and is not re-issued into the basin (Wemplel et al., 2007). Since artificial snow requires large amounts of water, water has to be stored in appropriate reservoirs. These can reach volumes of up to 400,000 m^3 comparable to a medium-sized dam. As water availability is becoming more and more limited, the construction of artificial snow water reservoirs is becoming more and more widespread. Unfortunately, theses have major impacts on the landscape and hydrology (Figure 4). Often reservoirs are built in depressions that are either wet zones and therefore environmentally sensitive areas or even biodiversity hotspots.

Secondly, when water is re-issued into the environment through snowmelt from the local catchments or is imported from other catchments, a local surplus of water can result. A shift in the seasonality of discharge and an increase in flood discharge have been modelled (de Jong and Barth, 2007). Meltwater from artificial snow runs produces on average two times more runoff than natural snow because of the increased thickness of artificial snow on ski runs and its higher density (Rixen et al., 2004).

Water quality and health

Several studies have been carried out on the effects of the additive "Snomax," derived from the Pseudomonas syringae bacteriumn. Although the bacterium is sterilized before use and no traces of it are found after use, the mixture is favorable to the proliferation of other potentially pathogenic bacteria (Dinger, 2006). Poor water quality used for snow production, derived from reused water can also have effects on human health (AFSSET, 2008).

Ecological

Changes in snow density of artificial snow can cause significant changes in soil and vegetation processes (Rixen et al., 2008; Wipf et al., 2005). The dense, thin snow cover of artificial snow leads to changes in soil insulation and relatively higher soil temperatures, which consequently increases net N mineralization. A denser snow cover furthermore results in a delay in plant phenology of up to 5 weeks after melt-out.

Soil and ecology are affected by the nature and duration of artificial snow cover. Since it is highly compacted and further compressed by piste preparation and machine grading, artificial snow remains on the ski runs on average 3–4 weeks longer than natural snow (Keller et al., 2004; Teich et al., 2007). This delays vegetation development and reduces the length of vegetation period (Wipf et al., 2005). In addition, the compaction of snow and soil causes both to become impermeable, preventing water infiltration and causing increased surface runoff. This often triggers erosion. Local water logging and permanent change in plant community can occur where slope profiles are short (Pröbstl et al., 2006).

Noise pollution by snowmaking machines can perturbate wildlife. For example, lower bird species diversity was detected in the coniferous forests along ski runs

Artificial Production of Snow, Figure 4 Water storage reservoir being built for artificial snow production (Photo: Benjamin Damelet).

with artificial snow production in the western Italian Alps due to negative edge effects caused by noise (Laiolo and Rolando, 2005).

Summary

Although artificial snow is produced on skis runs for over 50 years, scientific literature on artificial snow still remains very limited. Technical details of snowmaking are available in detail, showing that conditions for snowmaking are limited to certain meteorological conditions, such as temperatures below –3°C. The scientific basis of an artificial snow climatology is in the process of development. It shows that snowmaking may be limited through climate change in the future. The environmental impacts of artificial snow are very diverse and require interdisciplinary analysis.

Bibliography

AFSSET (2008) La neige de culture: Évaluation des risques sanitaires lies à l'utilisation d'adjuvants pour la fabrication de la neige de culture (Artificial snow: evaluation of sanitary risks associated with the use of additives for the fabrication of artificial snow), Report by the Afsset. (*French Agency for health, environmental and work security*), p. 104.

Barth, T. "Etude de l'impact du transfert d'eau du basin versant d'Arc 2000 au basin versant des Arcs 1600–1800, dans le cadre de l'enneigement culture." (Study of the impact of water transfer of the basin of Arc 2000 to Arcs 1600-1800 in the frame of artificial snow production) *Master Thesis* Science and Technology. Applied Mountains Sciences, University of Savoy, p. 286, September 2007.

de Jong, C., 2007. "Artificial snow drains mountain resources" *EnvironmentalResearchWeb*, Talking Point Article. http://environmentalresearchweb.org/cws/article/opinion/30703, August 2007.

de Jong, C., and Barth, T., 2007. Challenges in Hydrology of Mountain Ski Resorts und Changing Climate and Human Pressures. ESA, 2nd Space for Hydrology workshop, *Water Storage and Runoff: Modeling, In-Situ data and Remote Sensing*, Geneva (Switzerland).

Dinger, F., 2006, Snomax, neige de culture et environnement, *Revue générale du froid*, pp. 30–37.

Fauve, M., and Ryner, H. U., 2004. Physical description of snowmaking process using the jet technique and properties of produced snow, *Snow Engineering,* V. Bartlet, Adams, Christen, Sack and Sato (Eds), Taylor and Francis, pp. 215–218.

Hudson, S., 2000. Snow business. A study of the International Ski Industry. Cassell

IDE snowmakers Israel. http://www.ide-snowmaker.com/FCKeditor/_sec/php/english/news/ide1.htm.

Jones, H. G., and Devarennes, G., The chemistry of artificial snow and its influence on the germination of mountain flora, Biogeochemistry of Seasonally Snow-Covered Catchments. In *Proceedings of a Boulder Symposium, July 1995*. IAHS Publication no. 228, pp. 355–360.

Junkermann, W. http://imk-ifu.fzk.de/21_746.php.

Keller, T., Pielmeier, C., Rixen, Ch, Gadient, F., Gustafsson, D., and Stähli, M., 2004. Impact of artificial snow and ski-slope grooming on snowpack properties and soil thermal regime in a sub-alpine ski area. *Annals of Glaciology*, **38**, 314–318.

Laiolo, P., and Rolando, A., 2005. Forest bird diversity and ski-runs: a case of negative edge effect. *Animal Conservation*, **8**(1), 9–16, doi:10.1017/S1367943004001611.

Meteo France. http://france.meteofrance.com/.

Pröbstl, U., and Pröbstl, U., 2006. Kunstschnee und Umwelt (Artificial Snow and the Environment). Entwicklungen und Auswirkungen der technischen Beschneiung (Developments and Impacts of technical snowmaking). Haupt, Bern.

Rixen, Ch., and Stoeckli, V., 2000. La neige artificielle et ses effets sur l'environnement. (Artificial snow and its effects on the environment). Annual Report, No. 11, *WSL,* Switzerland.

Rixen, C., Stoeckli, V., and Ammann, W., 2003. Does artificial snow production affect soil and vegetation of ski pistes? A review. *Perspectives in Plant Ecology, Evolution and Systematics*, **5**(4), 219–230.

Rixen, C., Haeberli, W., and Stockli, V., 2004. Ground temperatures under ski pistes with artificial and natural snow. *Arctic, Antarctic, and Alpine Research*, **36**(4), 419–427.

Rixen, C., Freppaz, M., Stoeckli, V., Huovinen, C., Huovinen, K., and Wipf, S., 2008. Altered snow density and chemistry change soil nitrogen mineralization and plant growth. *Arctic, Antarctic, and Alpine Research*, **40**(3), doi: 10.1657/1523-0430(07-044)[RIXEN]2.0.CO; **2**, 568–575.

Steiger, R., and Mayer, M., 2008. Snowmaking and climate change. Future options for snow production in tyrolean ski resorts. *Mountain Research and Development*, **28**(3/4), 292–298, doi:10.1659/mrd.0978.

Teich, M., Lardelli, C., Bebi, P., Gallati, D., Kytzia, S., Pohl, M., Pütz, M., and Rixen, Ch, 2007. *"Klimawandel und Wintertourismus: Ökonomische und ökologische Auswirkungen von technischer Beschneiung. Report*. Schnee und Landschaft WSL, Birmensdorf: Eidg. Forschungsanstalt für Wald, p. 169.

Wemplel, B., Shanley, J., Denner, J., Ross, D., and Mills, K., 2007. Hydrology and water quality in two mountain basins of the northeastern US: assessing baseline conditions and effects of ski area development. *Hydrological Processes*, **21**, 1639–1650, doi:10.1002/hyp. 6700.

Wipf, S., Rixen, Ch, Fischer, M., Schmid, B., and Stoeckli, V., 2005. Effects of ski piste preparation on alpine vegetation. *Journal of Applied Ecology*, **42**, 306–316.

Cross-references

Alps
Canadian Rockies and Coast Mountains of Canada
Climate Variability and High Altitude Temperature and Precipitation
Hydrologic Cycle and Snow
Melting Processes
Seasonal Snow Cover
Snow Crystal Structure
Snow Density
Snow Grains
Sublimation from Snow and Ice

ATMOSPHERE-SNOW/ICE INTERACTIONS

Timo Vihma
Finnish Meteorological Institute, Helsinki, Finland

Definition

Interactions between the atmosphere and snow/ice are due to exchange of heat, mass, and momentum at the air-snow/ice interface. Through the exchange, interactive dynamic and thermodynamic processes take place at a wide range of spatial and temporal scales in the atmosphere and snow/ice.

Introduction

The atmosphere-snow/ice heat exchange includes solar shortwave and thermal longwave radiation, as well as turbulent fluxes of sensible and latent heat, the latter related to sublimation/condensation. The heat exchange processes modify the heat content of snow/ice and the atmospheric boundary layer (ABL), defined as the air layer, typically 0.1–1 km high, where the direct effects of the earth surface are felt at time scales of hours. The changes in the heat content result in metamorphosis, melt, freeze, or transport of liquid water or water vapor in snow/ice and in buoyant or stabilizing dynamic forces in the ABL. Cooling of sloping snow/ice surfaces commonly results in generation of katabatic winds and sometimes katabatic jumps. Mass exchange includes precipitation, sublimation/condensation, surface erosion due to drifting or blowing snow, and deposition of aerosols. Mass exchange results in thickening or thinning of the snow cover, changes in the surface properties, and changes in the atmospheric water content. Changes in the snow/ice surface properties further affect the surface heat balance and exchange of momentum, while changes in the atmospheric water content affect the radiative transfer, convection, condensation, and precipitation. The exchange of momentum is due to wind stress over the snow/ice surfaces. The wind stress depends on the aerodynamic characteristics of the snow/ice surface and the thermal stratification. Depending on the resistance of surface particles (or larger bodies, such as sea ice floes) against motion, the wind stress may solely result in the dissipation of momentum or also in sea ice or snow drift.

A schematic presentation of the atmosphere–snow/ice interaction processes is shown in Figure 1. The surface fluxes of momentum, heat, and moisture, as well as the surface temperature and albedo (see *Albedo*) interact with both the material properties of the snow/ice surface and the structure of and processes in the ABL. Some of these interactions are discussed here in more detail. For deposition of atmospheric impurities, not addressed here, see *Chemical and Microbe Records in Snow and Ice*, and *Chemical Processes in Snow and Ice*.

Thermal interaction between the atmosphere and snow/ice

Snow and ice surfaces have properties that generate particular boundary conditions for the radiative and turbulent heat exchange. First of all, the surface conditions are affected by both thermodynamic and dynamic processes. The latter, including sea ice and snow drift, may generate rapid changes in the boundary conditions for radiative and turbulent fluxes. Second, snow has a low heat conductivity (see *Snow*). Hence, the snow surface temperature rapidly adapts to changes in the atmospheric forcing. While remaining low compared to other surface types in the earth, the snow heat conductivity may, however, rapidly vary due to the changes in snow wetness. Also, the snow thickness and density (see *Snow Density*) vary a lot in time and space. Hence, the conductive heat flux and the response of the surface temperature to atmospheric forcing changes in time and space. Further, while the turbulent fluxes of sensible and latent heat usually depend interactively on the surface-air differences in temperature and moisture, this is not the case over melting snow. The temperature of melting snow does not exceed 0°C, which eliminates the effect of the turbulent fluxes on the surface temperature.

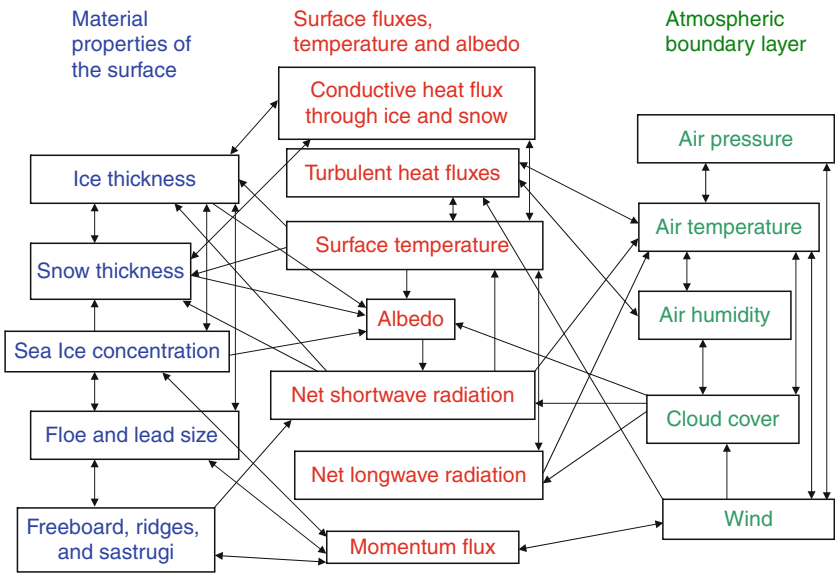

Atmosphere-Snow/Ice Interactions, Figure 1 Schematic diagram of atmosphere–snow/ice interactions.

Surface energy balance

The surface energy balance over snow and ice can be presented as:

$$H + \mathrm{LE} + (1-\alpha_S)(1-\beta)\,\mathrm{SWR}\downarrow + (1-\alpha_L)\mathrm{LWR}\downarrow + \mathrm{LWR}\uparrow + C + P = 0 \quad (1)$$

where SWR↓ is the downward solar shortwave radiation, α is the surface albedo, β is the fraction of the shortwave radiation penetrating below the surface, LWR↓ is the downward longwave radiation, LWR↑ is the upward longwave radiation, C is the conductive heat flux from below the surface, and P is the heat flux due to precipitation. All fluxes are here defined positive to the snow/ice surface. Accordingly, $(1-\alpha_L)\,\mathrm{LWR}\downarrow$ is always positive, the net shortwave radiation $(1-\alpha_S)(1-\beta)\,\mathrm{SWR}\downarrow$ is always positive or zero, and LWR↑ is always negative, while the sign of H, LE, C, and P varies from case to case. Four terms in Equation 1 (H, LE, LWR↑, and C) directly depend on the surface temperature. Hence, Equation 1 provides an equation for surface temperature, assuming the snow/ice surface as an infinitely thin layer with no heat capacity.

In the absence of solar radiation in winter, the major terms in Equation 1 are usually the net longwave radiation, $(1-\alpha_L)\mathrm{LWR}\downarrow + \mathrm{LWR}\uparrow$, and H (Persson et al., 2002). The net longwave radiation is in winter usually negative, of the order of a few tens of W m^{-2}, and balanced by H and C. Due to the larger heat conductivity of ice than snow, C is larger for ice, in particular for thin sea ice (see *Heat and Mass Transfer in Sea Ice*). For a snow surface, C may be significant during conditions of rapid surface cooling: a large temperature gradient in the upper snow layers compensates for the low heat conductivity. The direct effect of precipitation is usually negligible in Equation 1, but precipitation affects the snow/ice mass balance and surface albedo (Pirazzini, 2004), and thus indirectly also the heat balance. In the case of sea ice, precipitation affects the mass balance via snow ice formation due to ocean flooding and superimposed ice formation due to refreezing of melt water.

In summer, the solar radiation usually dominates in Equation 1, in particular over ice surfaces with α_S lower than that for snow. Under a thick cloud cover, the net longwave radiation is close to zero or even positive. Compared to solar radiation, the turbulent fluxes are usually minor, in particular over sea ice, where thermal differences between the atmosphere, ocean, ice, and snow are minor in summer (Vihma et al., 2009). Under cloudy skies with a strong wind, the magnitudes of turbulent fluxes may, however, exceed the net shortwave and net longwave radiation.

Radiative fluxes

From the point of view of solar radiation, the particular properties of snow and ice are: (a) snow and ice crystals are subject to metamorphosis, (b) the surface albedo is high and highly variable (see *Albedo*), (c) solar radiation penetrates inside the snow and ice cover, and (d) the snow extinction coefficient is highly variable. All these properties interact mutually.

The instantaneous incoming flux of solar shortwave radiation over snow and ice is controlled by the solar zenith angle, cloud fraction, cloud properties (liquid water and ice content and droplet/crystal size distribution), air humidity, and amount of aerosols. The cumulative daily flux additionally depends on the length of the day, reaching its maximum in clear sky conditions during summer solstice in the South Pole and North Pole. In the latter, however, clear-sky conditions are rare in summer. Under cloudy skies, the transfer of solar radiation is a very complex process due to, among others, multiple reflections between the cloud base and snow/ice surface (Pirazzini and Räisänen, 2008). A recently discovered effect on the absorption of solar radiation in the Arctic is the soot concentration in snow.

The LWR↑ depends on the fourth power of the surface temperature (T_S) and on the surface emissivity (ε), which for snow and ice surfaces is typically 0.97–0.98:

$$\mathrm{LWR}\uparrow = \varepsilon\,\sigma\,T_S^4 \quad (2)$$

where σ is the Stefan–Boltzmann constant (5.67×10^{-8} W m^{-2} K^{-4}). The LWR↓ depends on the vertical profiles of the air temperature and emissivity, and is accordingly affected by the amount of water vapor, cloud fraction, and cloud properties. Under clear skies at an air temperature of 0°C, LWR↓ varies by 25 W m^{-2} depending on the amount of water vapor in the atmosphere (Prata, 1996). In the case of cloud formation, LWR↓ is even much more strongly affected (Curry et al., 1996). From the point of view of longwave radiation, snow is approximately a gray body, i.e., the emissivity is close to absorptivity. Hence, α_L is typically 0.02–0.03, but strongly increases for melting snow.

In polar regions, the cloud radiative forcing at the sea surface is positive for most of the year, i.e., clouds increase the downward longwave radiation more than they reduce the downward shortwave radiation. In the Arctic Ocean the period of negative cloud radiative forcing may be as short as 2 weeks in the melting season (Intrieri et al., 2002).

Turbulent surface fluxes

The turbulent air–snow/ice exchange of heat consists of the fluxes of sensible and latent heat. Within a few millimeters of the air–snow/ice interface the exchange is, in fact, due to molecular diffusion. The turbulent fluxes above this viscous sub-layer control, however, the efficiency of the air–snow/ice exchange. The direction and magnitude of the sensible heat flux is controlled by the potential temperature difference between snow/ice surface and air. The latent heat flux is related to sublimation: the flux of latent heat is the water vapor flux (in kg m^{-2} s^{-1}) multiplied by the sum of the latent heats of evaporation

and melting. The direction and magnitude of the latent heat flux is controlled by the air-surface difference in specific humidity. The specific humidity of snow/ice surface is the saturation specific humidity corresponding to the snow/ice surface temperature. Both in the case of sensible and latent heat, the magnitude of the flux is also affected by the wind speed, aerodynamic roughness of the surface, and the atmospheric stratification, which control the efficiency of turbulent mixing above the snow/ice surface.

Hence, in numerical models for snow thermodynamics, weather prediction, and climate simulations, the fluxes of sensible heat (H) and latent heat (LE) are parameterized using the so-called bulk-aerodynamic formulae:

$$H = \rho\, c_p C_{HEZ}(\theta_Z - \theta_S)V_Z \tag{3}$$

$$\mathrm{LE} = \rho\, \lambda\, C_{HEZ}(q_Z - q_S)V_Z \tag{4}$$

where θ is the potential temperature, q is the specific humidity, ρ is the air density, c_p is the specific heat of air, C_{HEZ} is the turbulent exchange coefficient for heat and moisture, and V is the wind speed. Subscript "s" refers to the surface and "z" to a height in the air. In addition to height z, the exchange coefficient C_{HEZ} depends on the roughness lengths for momentum (z_0) and heat/moisture (z_T), and on the thermal stratification usually expressed by the Monin–Obukhov theory (Monin and Obukhov, 1954). For a snow cover without vegetation penetrating through it, z_T depends on the roughness Reynolds number (Andreas, 1987), while for a snow-covered forest $z_T \approx 0.1 \times z_0$. The z_0 of snow and ice is discussed in the section on dynamic interactions.

In conditions of stable stratification, i.e., $\theta_Z > \theta_S$, H is directed from air to snow. With increasing stability under a constant wind speed (increasing $\theta_Z - \theta_S$), the downward H first increases. When the stratification becomes very stable, as often over snow and ice during calm, clear-sky nights, the reduced turbulent mixing starts to dominate over the effects of increasing $\theta_Z - \theta_S$, and H starts to decrease. This acts as a positive feedback mechanism for the increase of $\theta_Z - \theta_S$. Hence, the air and snow surface become thermally decoupled, and $\theta_{2m} - \theta_S$ may reach 10 K. The low heat conductivity of snow favors decoupling, as C does not contribute much to prevent θ_S from decreasing. In such conditions the parameterization of H and, hence, the modeling of the evolution of surface and air temperatures are sensitive to the exact presentation of the stability dependence of C_{HE}, which represents a major challenge for both numerical weather prediction and climate models.

The direction and magnitude of H and LE strongly depend on the air-mass origin. In cases of warm-air advection over snow/ice, H is downward (as sometimes also LE), and a shallow, stably stratified ABL develops (Tisler et al., 2008). The largest sensible heat fluxes are observed in such cases: the warm-air advection is often associated with moderate or strong winds, which prevents the decoupling. On the contrary, if the air mass originates from large ice sheets, it is usually close to thermal equilibrium with the underlying surface, and the turbulent fluxes are smaller.

In temperatures of $-10°C$ and lower, the latent heat flux is a minor component in Equation 1. The saturation specific humidity is so low that even with the air humidity approaching zero, the difference $q_z - q_s$ and thus also LE keep small in magnitude. In melting conditions under dry air, for example under Föhn winds, LE may become a large component in Equation 1 (Granskog et al., 2006).

The heat exchange processes are particularly complex over sea ice, which is typically broken by cracks, leads, and polynyas. In winter, these areas of open water release large amounts of heat to the atmosphere; the sum of H and LE may be several hundred W m^{-2} below zero, while over sea ice (usually covered by snow), H is typically positive and LE close to zero (Persson et al., 2002). Accordingly, extreme variations in the surface fluxes take place even at spatial scales of meters.

The turbulent surface fluxes can be measured by the so-called eddy-correlation technique, which is based on the measurement of high-frequency fluctuations in the vertical wind component, air temperature, and specific humidity. A sampling rate of approximately 20 Hz is needed to resolve the contribution of small turbulent eddies to the vertical transport of heat and moisture. In the case of sensible heat flux, the measurements are usually made by applying a sonic anemometer: the travel times of three orthogonal ultrasonic signals are measured, and the wind components and air temperature are solved from them. For latent heat flux, fast-response hygrometers are used.

Boreal forest

From the point of view of atmosphere-snow heat exchange, boreal forest represents a particular environment because (a) snow is present both on the ground and trees, (b) the aerodynamic roughness of forest is much higher than that of snow/ice surfaces without penetrating vegetation, and (c) radiative transfer through the forest is a complex process (see *Snow Cover and Snowmelt in Forest Regions*). The exchange of sensible and latent heat takes place both between the air and the snow on the ground and between the air and the trees, which may be partly snow-covered. The air within the forest canopy is sheltered: both wind speeds and the solar radiation flux are reduced from their values above the canopy. Hence, the canopy air acts as a buffer for heat exchange between snow and the atmosphere above the forest canopy.

The surface albedo (α_S) of bare ground and snow-free trees is much lower than that of the snow surface and snow-covered trees. In spring, trees become snow-free earlier than the forest ground. Hence, the amount of shortwave radiation reflected from the forest-snow-ground system strongly depends on the solar zenith angle and the forest density. During large zenith angles in dense forest, most of the solar radiation is absorbed in the snow-free trees, while for small zenith angles and sparse forest,

a larger part of the solar radiation reaches the snow-covered ground and is reflected back to the atmosphere. The energy balance of a boreal forest is a challenge for climate and numerical weather prediction models. See Bartlett et al. (2006) for recent model developments.

Effects of snow/ice surfaces on atmospheric thermodynamics

The basic mechanisms for snow/ice surfaces to affect atmospheric thermodynamics are related to the effective cooling of the surface and, in warming conditions, to the upper limit of 0° for the surface temperature. If we compare the state of the ABL over snow/ice surfaces and neighboring bare ground or open sea, we practically always observe lower surface temperatures over the snow/ice surface (sea ice in summer is an exception). Over continents, the colder surface is most commonly due to the high shortwave albedo and longwave emissivity, but the low heat conductivity of the snow pack may also play a role. Over sea ice, this insulating effect dominates in winter.

Due to the cold surface, H often becomes positive and the ABL becomes stably stratified. This reduces turbulent mixing, prevents convective circulations, and reduces near-surface wind speeds (Stull, 1988). Under very stable stratification, the air temperature increases upwards, i.e., there is a temperature inversion. The generation of a temperature inversion is not necessarily only via surface cooling; also the heat advection in or above the ABL and direct radiative cooling of the air are often important. The mechanisms may also involve positive feedbacks: surface cooling decreases convection and favors subsidence in the atmosphere, which reduce cloud formation. This further enhances longwave cooling of the surface and the air itself, yielding to stronger inversions.

Hence, it is not surprising that strong temperature inversions are common over snow/ice cover. King and Turner (1997) reported a case measured in the winter of 1967 at the Plateau Station, Antarctica (79.2°S, 40.5°E, 3,624 m above sea level) calling it "...probably the most strongly stably stratified boundary layer observed anywhere on Earth." The air temperature increased by 21 K from the snow surface to the height of 32 m in the air. Also, the mean temperature profiles in the Antarctic and Arctic include strong temperature inversions. Over the Arctic Ocean in winter, the inversion is usually surface-based, extending to the height of 1.2 km with a temperature increase of 10–12 K (Serreze et al., 1992). In summer the inversions are weaker, typically 5 K, and their base is elevated some 200–400 m from the surface. In the Antarctic sea ice zone, the sea ice is mostly seasonal and thinner (0.6–1 m) than in the Arctic. Further, the sea ice concentration is lower and sea ice is located in lower latitudes on average. Hence, the winter-time temperature inversions are assumed to be weaker than in the Arctic, but there are not much data to prove this. Temperature inversions also favor condensation of fog and low clouds, in particular in cases of warm-air advection over snow/ice surface.

In polar regions in summer, although the Sun does not set or only sets for a few hours, the variations in the solar zenith angle may generate diurnal cycles in the surface heat balance components over snow and ice, although strongly reduced from those over land surfaces. In the Antarctic sea ice zone, Vihma et al. (2009) observed diurnal cycles in 15 surface or near-surface variables. A simplified picture of the causal chain is that the driving force, the incoming shortwave radiation, most directly affects the diurnal cycles in the reflected solar radiation and snow surface temperature. These further affect the outgoing longwave radiation, surface albedo, and the turbulent fluxes of sensible and latent heat. The diurnal cycles in the air temperature as well as the specific and relative humidity follow in this causal chain, where the variables most indirectly affected are the incoming longwave radiation and wind speed. The base height of low clouds is affected by the air temperature and moisture, as well as the incoming and reflected shortwave radiation.

The snow and ice surface temperature cannot exceed 0°C. In the melting season, the snow/ice surface and the ABL are closely coupled via the sensible heat flux and longwave radiation. Hence, if the air temperature tends to rise significantly above zero, the heat is used to melt snow or ice. If the air temperature tends to drop much below zero, meltwater in the snow or, in the case of sea ice, leads to freezing, and the latent heat of freezing is released, preventing a significant decrease of the near-surface air temperature. The effectiveness of these processes is demonstrated in Figure 2, which shows the year-round time series of 2-m air temperature (T_{2m}) in the drifting ice station SHEBA (Persson et al., 2002). In the melting season (days 515–600 in Figure 2), the variability in T_{2m} is much smaller than in winter. The maximum T_{2m} in the melting season is 2.1°C and the minimum was −4.5°C, while in winter T_{2m} varies even by 20° at the time scale of days.

The latent heat of melting plays a role also in the climate change in the Arctic. Vihma et al. (2008) compared the air temperature observations at the drifting ice station Tara in the Arctic Ocean in spring-summer 2007 against Russian drifting station data in 1937–1938 and 1950–1991. Although the Tara data showed 7.0°C higher mean T_{2m} for April, the mean T_{2m} for July was the same as at the Russian station (−0.2°C).

Dynamic interaction between atmosphere and snow/ice

Orographic effects of ice/snow slopes on the atmospheric dynamics

In conditions of a temperature inversion, the densest air is located closest to the snow/ice surface. Hence, over a sloping surface, the gravity force generates a downward flow. Such flows are called katabatic winds, the name originating from the Greek word katabatikos – going

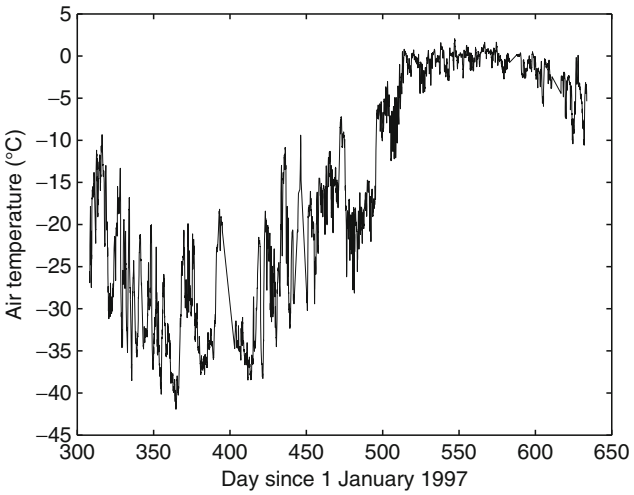

Atmosphere-Snow/Ice Interactions, Figure 2 Time series of 2-m air temperature at the drifting ice station SHEBA in the Beaufort Sea in 1997–1998.

downhill. According to a strict definition, only winds with gravity as the dominating force are katabatic. Due to the large scale of the sloping glaciers in the Antarctic and Greenland, Coriolis force becomes important, and therefore downslope flows are not pure katabatic winds, although usually called such.

Katabatic winds typically occur in the lowermost tens or a few hundreds of meters of the atmosphere, and the maximum speed often occurs a few meters or a few tens of meters above the surface. Katabatic winds may occur in a large range of spatial and temporal scales. Local katabatic winds are developed at night time on mountain slopes in mid and low latitudes. In the case of large mountain glaciers, katabatic winds may prevail through the day even in mid-latitudes. In the Antarctic and Greenland, katabatic winds are remarkably unidirectional, persistent, and strong (King and Turner, 1997). Due to their shallowness and sensitivity to small-scale variations in the topography, katabatic winds represent a challenge for numerical weather prediction and climate models.

Already Prandtl (1952) and Ball (1960) developed simple analytic models for katabatic winds, based on the equations for advection and turbulent diffusion of momentum and sensible heat in a gravity-driven flow. Despite the simplicity of these models, they performed well in reproducing the large-scale features of the wind field over Antarctica. In coastal regions with steeper and more complex topography, the analytic models are, however, not applicable, and high-resolution numerical models are needed. Experiments applying numerical models have also resulted in new points of view on the factors controlling the wind field over the Antarctic ice sheet. On the basis of model sensitivity tests excluding the radiative cooling of the snow surface, Parish and Cassano (2003) suggested that the role of katabatic winds in the Antarctic boundary layer may be overemphasized and that the adjustment process between the ambient pressure field and the orography of the continental ice surface may be the primary cause of the Antarctic wind field.

Katabatic winds may also be accompanied by a katabatic jump (King and Turner, 1997). In the upper parts of the slope the katabatic flow takes place in a shallow layer with blowing snow, and the Froude number (Fr) of the flow exceeds unity. The flow is affected by surface friction, leading to the convergence of momentum. In the narrow region of the katabatic jump, turbulence and vertical velocities are strong, lifting snow as a high wall. A lot of turbulent kinetic energy is dissipated, and downstream of the katabatic jump the downslope flow is much weaker ($Fr < 1$) but takes place in a thicker layer. The katabatic jump is basically similar to the common hydraulic jumps in rivers, but the physics is more complicated, as the flow includes both air and snow.

Frictional effects of snow/ice surfaces on the atmosphere

In the ABL, the momentum balance is achieved between the Coriolis force (term in the left side of Equations 5a and 5b), the pressure gradient force (first term in the right side), and the frictional force (second term in the right side):

$$-f\,v = -\frac{1}{\rho}\frac{\partial p}{\partial x} + \frac{\partial}{\partial z}\left(\frac{\tau_X}{\rho}\right) \tag{5a}$$

$$f\,u = -\frac{1}{\rho}\frac{\partial p}{\partial y} + \frac{\partial}{\partial z}\left(\frac{\tau_Y}{\rho}\right) \tag{5b}$$

where f is the Coriolis parameter, p is the atmospheric pressure, and τ is the momentum flux, with components in the orthogonal horizontal directions x and y. τ depends on the wind speed and the drag coefficient C_{DZ}, and can be parameterized at the atmosphere-snow/ice interface as

$$\tau = \rho\, C_{\mathrm{DZ}}\, V_{\mathrm{Z}}^2 \tag{6}$$

where subscript "z" indicates the reference height for C_{DZ} and V_{Z}. C_{DZ} further depends on the aerodynamic roughness length z_0 and the thermal stratification:

$$C_{\mathrm{DZ}} = \left(\frac{k}{\ln(z/z_0) - \psi_{\mathrm{M}}}\right)^2 \tag{7}$$

where k is the von Karman constant (0.4) and Ψ_{M} is an empirical function describing the effects of thermal stratification on the vertical mixing of momentum. Ψ_{M} depends on the stability parameter z/L, where L is the Obukhov length (Obukhov, 1971).

To quantify the frictional effects of snow and ice surfaces on atmospheric dynamics, we need information on z_0. Laboratory experiments can be made to develop relationships between z_0 and the geometric properties of the surface, but field measurements are usually needed to

reliably determine z_0 over snow and ice. The aerodynamic roughness of snow-covered surfaces typically ranges from 10^{-5} to 10^{-4} m (King et al., 2008), but during summer in glacier ablation zones z_0 may reach 0.1 m (Smeets et al., 1998). Over boreal forest, the presence of snow cover does not significantly change z_0, which is year-round about one tenth of the canopy height (Stull, 1988).

If generated, sastrugi may affect z_0 of snow-covered surfaces. As sastrugi are streamlined by the wind, z_0 does not necessarily increase with increasing geometric dimensions of sastrugi, analogously to ocean waves (large waves in balance with the actual wind have a very small z_0). More important is the alignment of wind with respect to the orientation of sastrugi. Lowest z_0s are observed when wind has blown long from a constant direction, while z_0 is largest after changes in the wind direction. On the basis of measurements over Antarctic sea ice, Andreas and Claffey (1995) found that when the wind continued from a constant direction and streamlined the surface, C_{DN10m} could decrease by as much as 30% in 12 h. If the wind direction then shifted by as little as 20°, C_{DN10m} immediately increased significantly.

The presence of drifting or blowing snow also affects the properties of turbulence in the ABL. This is partly due to the exchange of heat and moisture between the snow flakes and air and partly due to the exchange of momentum.

Effects of wind on snow

Sastrugi affect the wind field, while the formation of sastrugi depends on the capability of the wind to lift snow in the air. Drifting snow is defined as snow lifted by wind up to a height of 2 m. Drifting snow is rolling and bouncing turbulently above the surface. Blowing snow is defined as snow lifted to a height of 2 m or more above the surface, and existing in such quantities that horizontal visibility is reduced to less than 11 km. During blowing snow events, it is in practice usually not possible for a ground-based observer to distinguish between the snow lifted by the wind and eventual snow fall. The presence of blowing snow is one of the requirements for a storm to be called as a blizzard. The preconditions for drifting or blowing snow are that the wind speed is strong enough, typically at least 6–8 m s^{-1}, and the snow density is small. Wet snow will not be lifted even by a strong wind. Andreas and Claffey (1995) observed that when the wind speed exceeded 8 m s^{-1} the surface was continually changing due to drifting or blowing snow: sastrugi were building and eroding. Due to formation of sastrugi, snow-covered surfaces are not isotropic, but have a preferred direction dictated by the wind history.

An important problem related to the living conditions in harsh climates is the difficulty in keeping roads open during snow storms. Visibility reduced by blowing snow also poses problems for aviation. By depositing snow on roofs and around entrances, drifting/blowing snow also generates problems for buildings. Hence, operational forecasts of drifting and blowing snow are needed. Drifting or blowing snow is also important with respect to the release of avalanches. Deposits of snow drifts in the starting zones of snow avalanches contribute substantially to the release of avalanches as well as their sizes. Hence, sophisticated avalanche forecasting systems include components to estimate the amounts of drifting/blowing snow. Coupled with atmospheric models, dynamic snow models have been developed to simulate drifting and blowing snow. The most sophisticated ones include predictive equations for concentration, mass mixing ratio, shape parameter, fall velocities, and radar reflectivity for blowing snow, as well as visibility in blowing snow.

When snow particles are in the air, the exchange of heat and moisture is strongly enhanced as each particle is continuously ventilated on its entire surface. Hence, in addition to operational applications, information on the sublimation from drifting/blowing snow and the transport of snow by wind are needed in climatological studies. For example, Gordon et al. (2006) showed that the inclusion of blowing snow sublimation improves the results for snow depth predictions in Canada. Dery and Yau (2002) suggested that the combined processes of surface and blowing snow sublimation remove significant amounts of annual precipitation over Antarctica and the Arctic Ocean. Large amounts of snow may be transported by wind, but the effects of this transport on the snow mass balance are usually only locally important. Averaged over large areas, the divergence of mass transport through wind redistribution is generally two orders of magnitude less than surface and blowing snow sublimation (Dery and Yau, 2002). Coastal regions and sea ice margins make, however, an exception: snow transported to the open sea represents a sink for the snow mass balance.

Another effect of wind on the snow cover is wind packing, which results in an increase in snow density (see *Snow Density*).

Effects of wind on sea ice

Sea ice consists of undeformed ice cover as well as rafted and ridged ice flows of variable thickness, in places separated by cracks, leads, and polynyas. Compared to most snow-free continental surfaces, the surface of ice-covered seas is in any case relatively homogeneous with respect to roughness, but in winter very heterogeneous with respect to temperature (Vihma and Haapala, 2009). The surface type may change rapidly due to ice motion, and more slowly due to ice and snow thermodynamics. Over the marginal ice zone, the ABL is often under modification, adjusting to its changing boundary conditions. Hence, wind forcing on sea ice drift is an interactive process.

Already Nansen (1902) observed that in the Arctic Ocean the mean drift speed of ice is 2% of the wind speed and the drift direction deviates 30° to the right from the wind. Somewhat larger drift-to-wind speed ratios have been observed in the Antarctic sea ice zone, where the average ice concentration is smaller, which reduces the

internal ice resistance. Through its effects on the ice drift, the wind forcing also generates divergence, shear, and vorticity in the ice motion field.

As indicated in Equations 6 and 7, the air–ice momentum flux τ depends on the wind speed, surface roughness, and stratification. The large-scale roughness length z_0 of a broken sea ice cover depends on the skin friction of level ice and the form drag generated by pressure ridges, flow edges, and sastrugi. Hence, relevant parameters for z_0 of sea ice are the ice concentration (area fraction covered by ice flows), freeboard (depends on the ice and snow thickness according to the Archimedes law), flow size distribution, as well as ridge height and density (number of ridges per unit area). Taking into account the effect of sastrugi is more challenging because the effect depends on the history of wind direction with respect to the ice flow. Over sea ice, the stratification in the ABL is typically stable, which reduces τ. Localized convection may, however, occur over leads and polynyas, which enhance the turbulent mixing and τ. In winter, the effect of stratification may dominate the variability of C_{DZ} (Uotila (2001). Lüpkes and Birnbaum (2005) and Stössel et al. (2008) have improved parameterizations of z_0 and τ in the atmosphere, sea ice, and ocean models. In practice, problematic aspects in modeling the momentum flux over sea ice are that the sea ice conditions change rapidly, and we often lack accurate information on the essential parameters.

Atmospheric moisture transport and its effects on precipitation in the Arctic and Antarctic

The mass budgets of the Antarctic and Greenland ice sheets are controlled by precipitation, iceberg calving, melt water discharge, basal melt of underwater parts of the ice sheets, sublimation, evaporation, condensation, and net export of blowing snow. Precipitation is the only significant source term in the mass budget. As evaporation and sublimation are close to zero over most parts of the ice sheets, there are no significant sources of water vapor to the atmosphere. Hence, precipitation is dependent on the atmospheric moisture transport from the surrounding oceans. Further, via the cloud radiative forcing the moisture transport strongly affects the heat budget of ice sheets.

The atmospheric moisture transport to the Arctic and Antarctic has been studied on the basis of rawinsonde soundings, surface-based observations on precipitation and evaporation, and satellite data, and atmospheric reanalyses. Atmospheric model results have been applied to analyze the modeled precipitation minus evaporation and to calculate the meridional moisture flux and its convergence. The effects of cyclones on the moisture transport have been addressed and the origins of weather systems that have precipitated over the Antarctic have been identified by trajectory analyses.

The poleward moisture transport can be divided into the contributions of mean meridional circulation (MMC), stationary eddies (SE), and transient eddies (TE), i.e., moving cyclones. The total moisture transport is dominated by transient eddies both in the Arctic (Sorteberg and Walsh, 2008) and Antarctic (Tietäväinen and Vihma, 2008). In the Antarctic coastal areas, the mean meridional circulation contributes to the northward transport, but this effect is compensated for by the southward transport by stationary eddies. The convergence of the meridional water vapor transport, yielding precipitation, is at its largest at the Antarctic coastal and sea ice zones. Interannual variations in the water vapor transport are related to a large-scale circulation pattern called the Southern Annual Model.

In the Arctic, the largest northward moisture transport takes place in the Atlantic and North Pacific sectors, while weaker southward transport prevails over the Canadian archipelago. The meridional moisture transport and net precipitation are in winter and spring related to the Arctic Oscillation (AO) index. The interannual variability in moisture transport is mainly driven by the cyclone activity over the Greenland Sea and East Siberian Sea (Sorteberg and Walsh, 2008). In the polar regions, most of the moisture transport takes place in the lowermost 2 km of the atmosphere.

Conclusions

The interactions between the atmosphere and snow/ice take place at a wide range of spatial and temporal scales. Differences exist between sea ice, terrestrial snow, and glaciers in the way they interact with the atmosphere. These are related to the differences in the thickness and heat capacity, which affect the time scale of interactions, and the mobility of the surface, which affects the nature of interactions. The physics of direct interactions is, however, basically similar for sea ice, terrestrial snow, and glaciers. The direct interactions at the air-snow/ice interface are microscale processes: absorption, reflection, and emission of radiation, dissipation of momentum, and molecular diffusion of heat and moisture. The turbulent exchange of momentum, heat, and moisture is characterized by spatial scales from 10^{-2} to 10^{2} m, i.e., the processes take place in the ABL. The ABL wind, air temperature, air humidity, clouds, and fog are typically affected by the surface exchange processes at time scales of hours. The properties of the ABL affect the synoptic-scale weather and further the large-scale circulation and transport of heat and moisture.

In addition to their general effects on the evolution of weather, atmosphere–snow/ice interactions include particular processes that require attention in operational forecasting. These are avalanches, drifting snow, freezing of roads, snow storms with blowing snow, advection fog over snow and ice, strong katabatic winds, and sea ice growth, drift, and ridging. To improve operational services for the general public, navigation, aviation, road traffic, and skiers, research on atmosphere–snow/ice interactions has been carried out for decades. With the recent growing signals of climate change and its polar amplification, research on atmosphere–snow/ice interactions has

extended and oriented more towards climate-scale processes. Still, large uncertainties remain in the quantitative knowledge on several key climate processes, calling for more research efforts. These processes include (a) the natural and anthropogenic factors controlling the snow/ice surface albedo, (b) the interaction of albedo, radiative transfer, and cloud physics, (c) turbulence in the very stable ABL, (d) radiation-turbulence interactions, (e) interaction of katabatic and synoptic-scale winds, (f) factors controlling the meridional transport of heat and moisture to polar regions, and (g) the effects of the decadal-scale reduction of snow and ice cover on the atmospheric heat and moisture budget and circulation.

Bibliography

Andreas, E. L., 1987. A theory for the scalar roughness and the scalar transfer coefficients over snow and sea ice. *Boundary-Layer Meteorology*, **38**, 159–184.

Andreas, E. L., and Claffey, K. J., 1995. Air-ice drag coefficients in the western Weddell Sea: 1. Values deduced from profile measurements. *Journal of Geophysical Research*, **100**, 4821–4831.

Ball, F. K., 1960. Winds on the ice slopes of Antarctica. In *Antarctic Meteorology*. London: Pergamon, pp. 9–16.

Bartlett, P. A., MacKay, M. D., and Verseghy, D. L., 2006. Modified snow algorithms in the Canadian Land Surface Scheme: Model runs and sensitivity analysis at three boreal forest stands. *Atmosphere-Ocean*, **44**, 207–222.

Curry, J. A., Rossow, W. B., Randall, D., and Schramm, J. L., 1996. Overview of Arctic cloud and radiation characteristics. *Journal of Climate*, **9**, 1731–1764.

Dery, S. J., and Yau, M. K., 2002. Large-scale mass balance effects of blowing snow and surface sublimation. *Journal of Geophysical Research*, **107**, 4679.

Gordon, M., Simon, K., and Taylor, P. A., 2006. On snow depth predictions with the Canadian land surface scheme Including a parametrization of blowing snow sublimation. *Atmosphere-Ocean*, **44**, 239–255.

Granskog, M., Vihma, T., Pirazzini, R., and Cheng, B., 2006. Superimposed ice formation and surface fluxes on sea ice during the spring melt-freeze period in the Baltic Sea. *Journal of Glaciology*, **52**, 119–127.

Intrieri, J., Fairall, C. W., Shupe, M. D., Persson, P. O. G., Andreas, E. L., Guest, P. S., and Moritz, R. E., 2002. An annual cycle of Arctic surface cloud forcing at SHEBA. *Journal of Geophysical Research*, **107**, 8039, doi:10-1029/2000JC000439.

King, J. C., and Turner, J., 1997. *Antarctic Meteorology and Climatology*. Cambridge: Cambridge University Press.

King, J. C., Pomeroy, J. W., Gray, D. M., Fierz, C., Fohn, P. M. B., Harding, R. J., Jordan, R. E., Martin, E., and Plüss, C., 2008. Snow-atmosphere energy and mass balance. In Armstrong, R. L., and Brun, E. (eds.), *Snow and Climate. Physical Processes, Surface Energy Exchange and Modeling*. Cambridge: Cambridge University Press, pp. 70–124.

Lüpkes, C., and Birnbaum, G., 2005. Surface drag in the Arctic marginal sea-ice zone: a comparison of different parameterization concepts. *Boundary-Layer Meteorology*, **117**, 179–211.

Monin, A. S., and Obukhov, A. M., 1954. Dimensionless characteristics of turbulence in the surface layer (in Russian). *Trudy Geofiz. Inst. Akademia Nauk SSSR*, **24**, 163–187.

Nansen, F., 1902. *The Norwegian North Polar Expedition, 1893–1896. Scientific Results. Volume III*. London: Christiania.

Obukhov, A. M., 1971. Turbulence in an atmosphere with a non-uniform temperature. *Boundary-Layer Meteorology*, **2**, 7–29.

Parish, T. R., and Cassano, J. J., 2003. The role of katabatic winds on the Antarctic surface wind regime. *Monthly Weather Review*, **131**, 317–333.

Persson, P. O. G., Fairall, C. W., Andreas, E. L., Guest, P. S., and Perovich, D. K., 2002. Measurements near the atmospheric surface flux group tower at SHEBA: Near-surface conditions and surface energy budget. *Journal of Geophysical Research*, **107**, 8045, doi:10.1029/2000JC000705.

Pirazzini, R., 2004. Surface albedo measurements in Antarctic sites in summer. *Journal of Geophysical Research*, **109**, D20118, doi:10.1029/2004JD004617.

Pirazzini, R., and Räisänen, P., 2008. A method to account for surface albedo heterogeneity in single column radiative transfer calculations under overcast conditions. *Journal of Geophysical Research*, **113**, D20108, doi:10.1029/2008JD009815.

Prandtl, L., 1952. *Essentials of Fluid Dynamics: With Applications to Hydraulics, Aeronautics, Meteorology and Other Subjects. (English translation)*. London: Blackie & Son.

Prata, A. J., 1996. A new long-wave formula for estimating downward clear-sky radiation at the surface. *Quarterly Journal of the Royal Meteorological Society*, **122**, 1127–1151.

Serreze, M. C., Kahl, J. D., and Schnell, R. C., 1992. Low-level temperature inversions in the Eurasian Arctic and comparisons with Soviet drifting station data. *Journal of Climate*, **5**, 599–613.

Smeets, C. J. P. P., Duynkerke, P. G., and Vugts, H. F., 1998. Observed wind profiles and turbulence fluxes over an ice surface with changing surface roughness. *Boundary-Layer Meteorology*, **92**, 101–123.

Sorteberg, A., and Walsh, J. E., 2008. Seasonal cyclone variability at 70°N and its impact on moisture transport into the Arctic. *Tellus, Series A*, **60A**, 570–586.

Stössel, A., Cheon, W.-G., and Vihma, T., 2008. Interactive momentum flux forcing over sea ice in a global ocean GCM. *Journal of Geophysical Research*, **113**, C05010, doi:10.1029/2007JC004173.

Stull, R. B., 1988. *An Introduction to Boundary-Layer Meteorology*. Dordrecht: Kluwer.

Tietavainen, H., and Vihma, T., 2008. Atmospheric moisture budget over Antarctica and the Southern Ocean based on the ERA-40 reanalysis. *International Journal of Climatology*, **28**, 1977–1995, doi:10.1002/joc.1684.

Tisler, P., Vihma, T., Müller, G., and Brümmer, B., 2008. Modelling of warm-air advection over Arctic sea ice. *Tellus, Series A*, **60A**, 775–788.

Uotila, J., 2001. Observed and modelled sea ice drift response to wind forcing in the northern Baltic Sea. *Tellus, Series A*, **53A**, 112–128.

Vihma, T., and Haapala, J., 2009. Geophysics of sea ice in the Baltic sea – a review. *Progress in Oceanography*, **80**, 129–148, doi:10.1016/j.pocean.2009.02.002.

Vihma, T., Launiainen, J., and Uotila, J., 1996. Weddell Sea ice drift: kinematics and wind forcing. *Journal of Geophysical Research*, **101**, 18279–18296.

Vihma, T., Jaagus, J., Jakobson, E., and Palo, T., 2008. Meteorological conditions in the Arctic Ocean in spring and summer 2007 as recorded on the drifting ice station Tara. *Geophysical Research Letters*, **35**, L18706, doi:10.1029/2008GL034681.

Vihma, T., Johansson, M. M., and Launiainen, J., 2009. Radiative and turbulent surface heat fluxes over sea ice in the western Weddell Sea in early summer. *Journal of Geophysical Research*, **114**, C04019, doi:10.1029/2008JC004995.

Cross-references

Albedo
Antarctica
Arctic Hydroclimatology

Climate Change and Glaciers
Global Outlook of Snowcover, Sea Ice, and Glaciers
Heat and Mass Transfer in Sea Ice
Radiative Transfer Modeling
Sea Ice
Snow Cover and Snowmelt in Forest Region
Thinning of Arctic Sea Ice

ATMOSPHERIC CIRCULATION AND GLACIOCHEMICAL RECORDS

Shichang Kang
Key Laboratory of Tibetan Environmental Changes and Land Surface Processes, Institute of Tibetan Plateau Research, Chinese Academy of Sciences, Beijing, China
State Key Laboratory of Cryospheric Sciences, Chinese Academy of Sciences, Lanzhou, China

Synonyms

Glaciochemical records; Ice core records

Definition

Atmospheric circulation. Patterns of horizontal and vertical air movements above earth surface, mainly including movement strength and direction.
Glaciochemical records. Chemical species data recorded in glacier snow/ice.

Since chemical species were analyzed from ice cores retrieved from glaciers or ice sheet and were used to investigate climate and environmental changes in 1960s, the environmental significances of glaciochemical records has been acknowledged by the researchers. Glaciochemistry is mainly influenced by atmospheric chemistry which has been stored in the glacier by dry and wet deposition. Atmospheric chemical species are affected by their sources and transport strength (namely atmospheric circulation change). Therefore, the glaciochemical records have been used not only in reconstructing the paleoenvironmental changes, but also for understanding the changes in atmospheric circulation.

In Arctic, glaciochemical records have been used to investigate changes in atmospheric circulation patterns over the Greenland Ice Sheet (Mayewski et al., 1994, 1997; Appenzeller et al., 1998) and Mt. Logan (Kang et al., 2005) since 1990s. For example, major ion series developed from a sub-annual scale sampling of the GISP2 ice core from central Greenland were calibrated with instrumental series of sea level pressure (SLP) to provide proxy records of major marine (Icelandic Low) and terrestrial (Siberian High) atmospheric circulation over the past 1,400 years (Meeker and Mayewski, 2002). Using sodium concentrations from a Mt. Logan ice core, a 292-year history of the Aleutian Low was constructed which revealed a dramatic intensification of atmospheric circulation over the North Pacific region since the twentieth century.

On a hemispheric scale, more detailed relationships between glaciochemical records and atmospheric circulation in spring were provided. For an instance, an enhanced spring Arctic High weakens dust aerosol transport from central Asia to subarctic regions (e.g., southern Greenland and Yukon Territory), but strengthens transport of dust to the Himalaya (e.g., Mt. Everest). An intensification of the Siberian High may strengthen transport of dust aerosols to Greenland, and an enhancement of the Tibetan High strengthens transport to Himalaya and Yukon regions in spring. A stronger spring Azores High favors dust transport to both the Himalayas and south Greenland. On a regional scale, a deepened spring Icelandic Low and Aleutian Low increases transport of dust aerosols to Greenland and the Yukon Territory, respectively (Kang et al., 2002, 2003).

In Antarctic, glaciochemical records from the western and eastern Antarctic Sheet are closely correlated with atmospheric circulations over the southern hemisphere which was used to reconstruct changes in SLP and wind strength (Reusch et al., 1999; Kreutz et al., 2000; Souney et al., 2002; Xiao et al., 2004; Yan et al., 2005). For example, crustal ion concentrations from three West Antarctica ice cores (Siple Dome, ITASE00-1, and ITASE01-5) are closely correlated with circumpolar zonal wind and westerly wind, as well as Antarctic Oscillation (Yan et al., 2005). A 250-year multivariate glaciochemical record from Princess Elizabeth Land was used to reconstruct SLP over the southern Indian Ocean, which has a strong coherency summer transpolar index, and its decadal-scale variability suggests shifting of the polar vortex (Xiao et al., 2004).

Summary

Relationships developed between glaciochemical records from bipolar and Asia and atmospheric circulation (such as SLP, wind strength) demonstrate that ice core records provide a proxy for the reconstruction of atmospheric circulation. Furthermore, understanding the changes in atmospheric circulation is one of great contributions for global change research.

Bibliography

Appenzeller, C., Schwander, J., Sommer, S., and Stocker, T. F., 1998. The North Atlantic Oscillation and its imprint on precipitation and ice accumulation in Greenland. *Geophysical Research Letters*, **25**, 1939.
Kang, S., Mayewski, P. A., Qin, D., Yan, Y., Hou, S., Zhang, D., Ren, J., and Kreutz, K., 2002. Glaciochemical records from a Mt. Everest ice core: relationship to atmospheric circulation over Asia. *Atmospheric Environment*, **36**, 3351.
Kang, S., Mayewski, P. A., Yan, Y., Qin, D., Yao, T., and Ren, J., 2003. Dust records from three ice cores: relationships to spring atmospheric circulation over the Northern Hemisphere. *Atmospheric Environment*, **37**, 4823.
Kang, S., Yan, Y., and Mayewski, P. A., 2005. A 290-year record of atmospheric circulation over the North Pacific from a Mt. Logan ice core, Yukon Territory. *Acta Oceanologica Sinica*, **24**, 81.

Kreutz, K. J., Mayewski, P. A., Pittalwala, I. I., Meeker, L. D., Twickler, M. S., and Whitlow, S., 2000. Sea level pressure variability in the Amundsen Sea region inferred from a west Antarctic glaciochemical record. *Journal of Geophysical Research*, **105**, 4047.

Mayewski, P. A., Meeker, L. D., Whitlow, S., Twickler, M. S., Morrison, M. C., Bloomfield, P., Bond, G. C., Alley, R. B., Gow, A. G., Grootes, P. M., Meese, D. A., Ram, M., Taylor, K. C., and Wumkes, W., 1994. Changes in atmospheric circulation and ocean ice cover over the North Atlantic during the last 41,000 years. *Science*, **263**, 1747.

Mayewski, P. A., Meeker, L. D., Twickler, M. S., Whitlow, S., Yang, Q., Lyons, W. B., and Prentice, M., 1997. Major features and forcing of high latitude northern hemisphere atmospheric circulation using a 110,000-year-long glaciochemical series. *Journal of Geophysical Research*, **102**, 26345.

Meeker, L. D., and Mayewski, P. A., 2002. A 1400 year long record of atmospheric circulation over the North Atlantic and Asia. *The Holocene*, **12**, 257.

Meeker, L. D., Mayewski, P. A., and Bloomfield, P., 1995. A new approach to glaciochemical time series analysis. In Delmas, R. J. (ed.), *Proceedings of NATO Advanced Research Workshop on Biochemical Cycles, NATO ASI Ser. I*. New York: Springer, Vol. 30, p. 383.

Reusch, D. B., Mayewski, P. A., Whitlow, S., Pittalwala, I. I., and Twickler, M. S., 1999. Spatial variability of climate and past atmospheric circulation patterns from central West Antarctic glaciochemistry. *Journal of Geophysical Research*, **104**, 5985.

Souney, J. M., Mayewski, P. A., Goodwin, I. D., Meeker, L. D., Morgan, V., Curran, M. A. J., Van Ommen, T. D., and Palmer, A. S., 2002. A 700-year record of atmospheric circulation developed from the Law Dome ice core. *Journal of Geophysical Research*, **107**, 4608, doi:10.1029/2002JD002104.

Xiao, C., Mayewski, P. A., Qin, D., Li, Z., Zhang, M., and Yan, Y., 2004. Sea level pressure variability over the southern Indian Ocean inferred from a glaciochemical record in Princess Elizabeth Land, east Antarctica. *Journal of Geophysical Research*, **109**, D16101, doi:10.1029/2003JD004065.

Yan, Y., Mayewski, P. A., Kang, S., and Meyerson, E. A., 2005. An ice core proxy for Antarctic circumpolar zonal wind intensity. *Annals of Glaciology*, **41**, 121.

Cross-references

Antarctica
Geochemistry of Snow and Ice
Himalaya

AUTOMATED GLACIER MAPPING

Frank Paul
Department of Geography, University of Zurich, Zurich, Switzerland

Synonyms

Glacier mapping; Glacier outline digitizing; Multispectral classification

Definition

Automated glacier mapping generates digital glacier outlines in a vector format from automated classification of remote sensing data.

Historical background

Glaciers and icecaps were in the focus of satellite observations at the time when the first data from the Landsat mission (1972) became available. While the large regions covered by satellite data were always considered as a benefit for glacier related applications, mapping of glacier extent was introduced quite late. Early applications focused on discriminating snow from ice and mapping of snowlines (Østrem, 1975; Rott, 1976) or analysis of glacier movement and flow characteristics (Krimmel and Meier, 1975). It has to be noted that in the early days of data analysis (1970s), most work was performed on contrast enhanced photographic prints rather than with digital data (e.g., Dowdeswell and Cooper, 1986). The full potential of directly analyzing the digital data from computer compatible tapes (CCTs) was delayed until appropriate computers became available in the late 1980s. The use of Landsat digital data in the context of glacier mapping was forwarded by Rundquist et al. (1980). Howarth and Ommanney (1986) discussed the possibility to use Landsat data for creating glacier inventories, and Della Ventura et al. (1987) compared mapped glacier extents with inventory data. Compared to the 4-band MultiSpectral Scanner (MSS) sensor at about 80 m spatial resolution that was used for these early studies, an important step forward was achieved in 1984 with the availability of higher resolution (30 m) data in six spectral bands from the Thematic Mapper (TM) sensor. With its capability to discriminate snow from clouds and the increasing computer performance, largely automated glacier mapping at a global scale became feasible.

The first methods for automated snow cover mapping from TM were proposed (Dozier, 1984; Dozier and Marks, 1987) and a number of spectral investigations of glaciers with TM data were conducted (e.g., Hall et al., 1987, 1988, 1989, 1990; Orheim and Lucchitta, 1987; Rott and Markl, 1989; Williams et al., 1991). Techniques for the largely automated mapping of glacier extent was first presented in the 1990s (e.g., Bayr et al., 1994; Aniya et al., 1996; Binaghi et al., 1997; Jacobs et al., 1997) followed by a comparison of different glacier mapping techniques by Sidjak and Wheate (1999). In that year, the satellites Landsat 7 (sensor ETM+) and Terra (sensor ASTER) were launched and glaciers were one of the main targets from the beginning (Raup et al., 2000; Bindschadler et al., 2001). The related initiative Global Land Ice Measurements from Space (GLIMS) was started (Kieffer et al., 2000) and glacier mapping from simple and robust semi-automated techniques (Paul, 2002a) combined with GIS-based glacier data assessment were established (Paul et al., 2002).

In parallel to these applications, the global terrestrial network for glaciers (GTN-G) was established (Haeberli et al., 2000) within the framework of global climate related observing programs (GCOS/GTOS). Within GTN-G, repeated glacier inventories from satellite data were constituted at the Tier 5 level (e.g., Haeberli, 2006).

The sensitive reaction of glaciers to small climatic fluctuations designated them as key climatic indicators (IPCC, 2007) and it become clear that the point information as stored in the former world glacier inventory (WGI) from the 1970s (WGMS, 1989) is difficult to use for change assessment. To overcome this drawback, the GLIMS glacier database was designed to store glacier outlines in a digital vector format (Raup et al., 2007). Indeed, the most efficient way to fill this database is by applying largely automated glacier mapping techniques to large amounts of satellite scenes.

The recent opening of the entire USGS Landsat archive for the public (USGS, 2008) and the availability of accurate and robust mapping methods for clean to slightly dirty glacier ice (Albert, 2002; Paul and Kääb, 2005) will largely facilitate the generation of a more or less complete global digital baseline data set of glacier outlines. Apart from the global aspect of glacier mapping and inventory creation (e.g., for improved calculation of their contribution to sea-level rise), also regional (e.g., hydropower, discharge), and local aspects (tourism, natural hazards), have created much attention for the requirement of establishing a global baseline glacier inventory (GCOS, 2006; Raper and Braithwaite, 2006; Schiermeier, 2010). Only such a 2D vector dataset of glacier outlines will allow to perform the required change assessment for sufficiently large and representative samples.

Below, the applied semi-automated glacier mapping methods are described and challenges to be considered are discussed. The focus is on multispectral (optical) rather than microwave sensors and especially on Landsat TM/ETM + type sensors, which are most frequently used for glacier mapping. In principal, the methods work with all sensors that have similar spectral bands. A disadvantage of optical sensors is their dependence on cloud conditions, i.e., glaciers can only be mapped when they are not covered by (optically thick) clouds. Another important point to consider is snow conditions. Seasonal snow can mask the true glacier perimeter, which implies that glacier mapping becomes difficult or impossible. In order to reduce the workload for processing, the available satellite images should be carefully analyzed for cloud and snow conditions before they are processed.

Spectral properties and available sensors

The surface of a glacier is composed of snow, firn (i.e., 1 year old snow), ice, water, and debris (e.g., rock, pebbles, dust, soot) with a highly variable fraction of each component from glacier to glacier and in the case of ice, snow, and water also in the course of a year. With a focus on temperate glaciers as they appear at the end of the ablation season and neglecting debris cover and liquid water, the physical properties of the glacier surface are determined by snow with variable grain size (i.e., glacier ice can be seen as metamorphosed snow with large grain size). This implies that methods which automatically map snow cover (e.g., Dozier, 1989) do also work for glacier mapping. In the following, the focus is on the optical properties of snow; an overview for other parts of the electromagnetic spectrum (e.g., microwaves) is given by Rees (2005). The spectral characteristics of the debris cover on a glacier strongly depend on the lithology of the source material and vary from place to place. Debris on glaciers can in general not be automatically distinguished from other debris (e.g., in the glacier forefield) using spectral or other techniques (e.g., Bishop et al., 2001; Paul et al., 2004a) but should be included as a part of the glacier (Raup and Khalsa, 2007). Hence, glacier outlines have to be inspected and corrected manually during post-processing. This is in most cases accurately possible as human recognition is able to trace the glacier perimeter based on very subtle reflectance variations, but for such glaciers the extent mapping from spectral classification is better called semi-automated.

The spectral properties of snow have been investigated in the field (e.g., Grenfell et al., 1981; Qunzhu et al., 1985) and modeled numerically (e.g., Dozier, 1989; Warren, 1982). Both approaches reveal a high spectral reflectance of snow in the visible part of the spectrum (with a large dependence on contamination and a very small one on grain size), a decreasing reflectance in the near infrared (with decreasing dependence on contamination and an increasing one on grain size), and very low reflectance in the middle or shortwave infrared (with little dependence on contamination and a strong one on grain size). Spectral reflectance obtained from satellite data have frequently been used to distinguish between ice and snow zones (facies) that are partly different from those identified in the field (e.g., Bronge and Bronge, 1999; Hall et al., 1987; Williams et al., 1991; Williams and Hall, 1998; Winther, 1993). For example, a superimposed ice zone (belonging to the accumulation area) cannot be detected due to the spectral similarity with the ice in the ablation zone.

The distinct spectral reflectance characteristics of ice and snow with the low reflectance in the shortwave infrared (SWIR) could thus be used for a thematic classification. As the related spectral range is located in a region of high atmospheric transparency (see Figure 1), a sensor covering the SWIR is found on several satellites (e.g., Landsat TM/ETM+, Terra ASTER/MODIS, SPOT HRV, IRS 1 C/D LISS III). A brief overview of major sensor characteristics is compiled in Table 1. Automated classification of clean glacier ice is based on the reflectance differences of a SWIR sensor with a sensor in the visible to near infrared (VNIR). As spatial resolution is closely related to swath width (following the rule: the higher, the smaller), the optimum sensor for glacier mapping combines high spatial resolution with a large area covered. In this regard, the Landsat TM/ETM + sensors are close to an optimum as the smallest reasonable glacier size might be close to 0.01 km^2 which is about 11 TM pixels. Under optimum mapping conditions this number of glacier pixels is well recognizable with TM. For higher spatial resolution panchromatic sensors, it is an asset for glacier mapping when the spectral range of the sensor does not extend

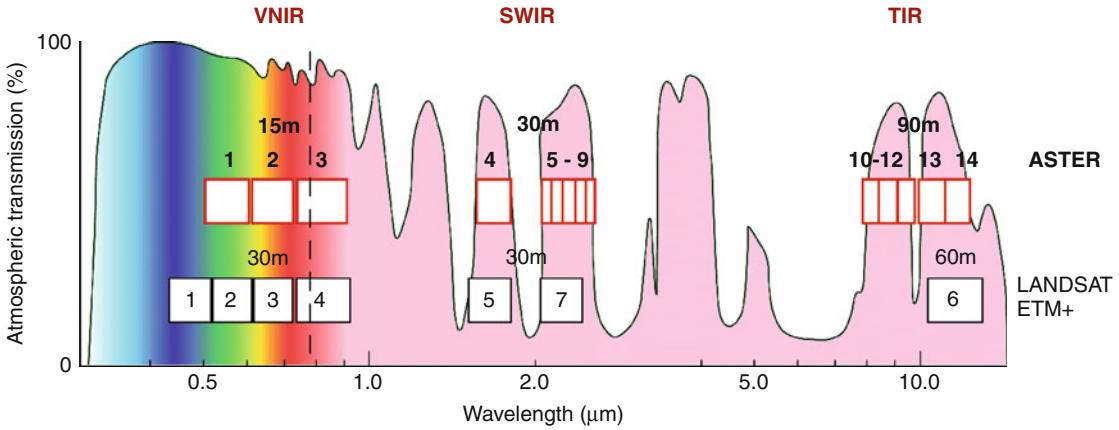

Automated Glacier Mapping, Figure 1 Atmospheric transmission and location of ASTER and ETM + spectral bands (Figure courtesy of A. Kääb).

Automated Glacier Mapping, Table 1 Spectral bandwidths of reflective bands from the different sensors (in μm). Data from http://geo.arc.nasa.gov/sge/health/sensor/cfsensor.html

	Landsat TM	Landsat ETM+	Terra ASTER	SPOT 2/3 HRV	IRS-1 C LISS III
1 (Blue)	0.45–0.52	0.45–0.52	–	–	–
2 (Green)	0.52–0.60	0.53–0.61	0.52–0.60	0.50–0.59	0.52–0.59
3 (Red)	0.63–0.69	0.63–0.69	0.63–0.69	0.61–0.68	0.62–0.68
4 (NIR)	0.76–0.90	0.75–0.90	0.76–0.86	0.78–0.89	0.77–0.86
5 (SWIR)	1.55–1.75	1.55–1.75	1.60–1.70	1.58–1.75	1.55–1.70
7 (SWIR)	2.08–2.35	2.09–2.35	2.15–2.43[1]	–	
Pan	–	0.52–0.90	–	0.51–0.73	0.50–0.75

[1]Summary of five individual bands

too much in the near infrared, as this strongly degrades the contrast between bare glacier ice and surrounding rock.

Applied methods for glacier mapping

In general, the processing of satellite images can be divided into three phases: pre-, main, and post-processing. Some of the required steps for pre-processing have been discussed above (scene selection based on quicklooks). Additional steps include data download and format conversion, preparation of RGB composites for later editing and maybe orthorectification. The latter corrects the elevation dependent location shifts of each pixel and requires a digital elevation model (DEM) and a set of ground control points. The main processing is then the application of the selected mapping method and creation of glacier outlines using raster to vector conversion. In the post-processing phase, glacier outlines are visually controlled using the contrast enhanced RGB composites and corrected where required. These corrections include in general wrongly mapped water surfaces (with or without ice on it), debris-covered glacier tongues, attached seasonal snowfields, and sometimes regions in cast shadow. For multitemporal applications it is recommended to digitize a separate glacier basin layer that also separates possible seasonal snowfields from the main glacier and provides ice-ice divides in the accumulation area (Paul, 2002b; Paul et al., 2002; Paul and Kääb, 2005). This will guarantee that change assessment always refers to the same entities. A set of rules that should be considered when contiguous ice masses are separated into individual entities is given by Raup and Khalsa (2007).

Automated methods that have been used for mapping of clean glacier ice include maximum likelihood classification (mlc), ISODATA clustering (iso), principal component analysis (pca), normalized difference snow index (NDSI), and band ratios (Paul, 2001). In principal, all these methods work on raw digital numbers (DN), which implies that atmospheric or terrain correction is not required. Empirical tests have shown that results are even worse after such corrections, because the required DEM introduces noise and blurs the spectral signal as a result of coregistration errors (Paul et al., 2002). The result of the mlc, iso, and pca methods (along with some others) does depend on the scene content and requires a considerable pre-processing workload for each image. Moreover, the obtained results are less accurate than from the other two methods (e.g., Albert, 2002), which implies that they are used only seldom. From the point of frequent monitoring or application to hundreds of scenes, more simple methods are preferable. Also for this reason the

NDSI [(TM2 − TM5)/(TM2 + TM5)] and simple band ratios (TM3 or 4/TM5) are more popular (cf. Racoviteanu et al., 2008). A direct comparison of both methods has shown that they are of a similar accuracy but the NDSI has a somewhat higher pre-processing workload (Paul and Kääb, 2005). The following discussion is thus restricted to the ratio method.

The most flexible and accurate version of the ratio method is based on TM/ETM + bands 1, 3 and 5 (ASTER 1, 2 and 4) and uses two thresholds (t_1, t_2) that have to be interactively selected by on-screen comparison. In pseudo-code the algorithm for each pixel of the scene is (Figure 2):

IF (TM3/TM5 > t_1) and (TM1 > t_2) then
pixel = glacier else pixel = other

While the first threshold (t_1) separates glaciers from other terrain, t_2 allows to correct misclassification in regions of cast shadow without glaciers. The general rule is to select the correct thresholds in shadow regions with the aim of minimizing the workload for post-processing. This decision is scene dependent as it depends on the distribution of (small) glaciers in steep alpine terrain versus large glaciers or ice fields. When ice in deep shadows is correctly mapped, often rock in shadow (without ice) that is lit by bright snow surfaces through scattering is also mapped. When this misclassification can be corrected faster than for the glaciers in deep shadow, the t_2 threshold should be selected to map the (small) glaciers correctly. A threshold value of 2.0 (+/−0.5) for t_1 and 50 (+/−20) for t_2 provide in most cases a good glacier map as a starting point. The pixel value for "glacier" should be set to zero (black) and for "other" to 255 (white) in order to facilitate visual comparison.

Depending on the scene conditions (seasonal snow patches, noise in shadow regions), the application of a 3 by 3 median filter to the black and white glacier map can improve the classification further by removing isolated (snow) pixels and closing gaps due to a medial moraine (e.g., Svoboda and Paul, 2009). However, the filter also closes gaps at mountain ridges and reduces the size of small glaciers to a certain extent (the smaller the glacier the stronger the reduction in relative terms). A careful test and analysis of its influence is thus recommended.

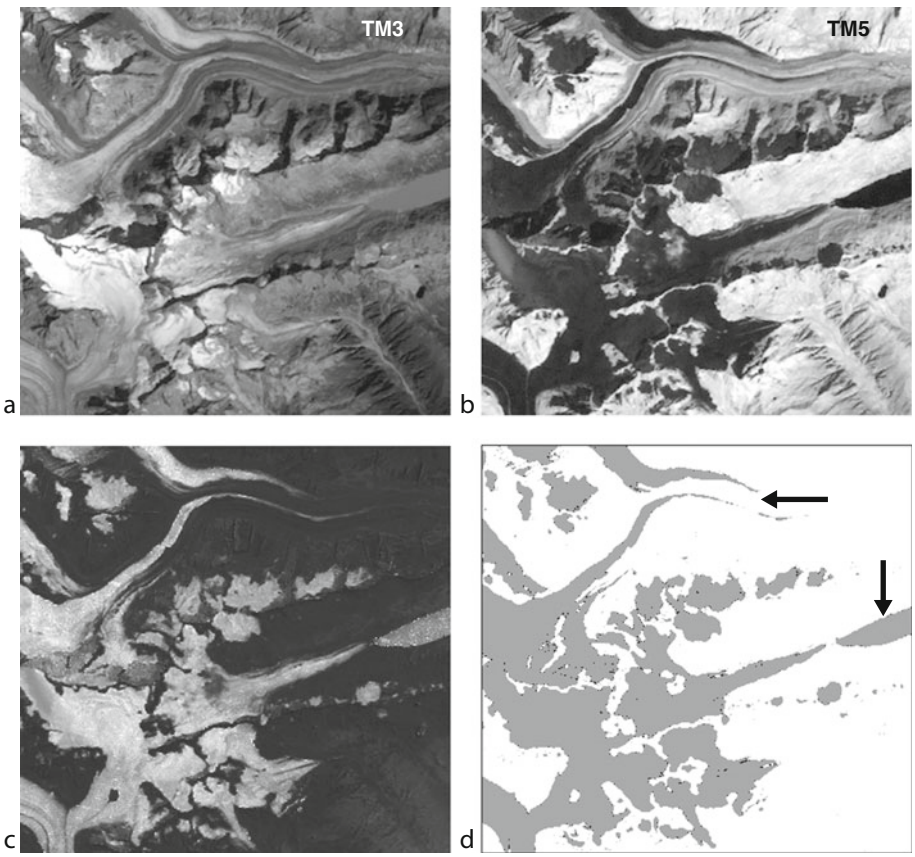

Automated Glacier Mapping, Figure 2 Automated glacier mapping for a test site in the Swiss Alps. (**a**) Landsat TM band 3, (**b**) Landsat TM band 5, (**c**) TM3/TM5 ratio image, and (**d**) resulting glacier map (*dark grey*) after thresholding. Black pixels are added by the median filter, and light grey pixels are deleted. The *arrows* denote: missing debris cover (*top*) and a wrongly classified turbid lake (*middle*).

The ratio method does correctly map glaciers under optically thin clouds (Paul and Andreassen, 2009), scattered debris or a polluted surface (dust, soot), and deep shadows where it sometimes even surpasses human recognition. Compared to other methods the simple band ratio provides most accurate results and is very fast to apply (Albert, 2002). It is also quite robust as a change of the threshold value by 0.1 has little influence on the mapped glacier extent (Paul and Hendriks, 2010). In absolute terms the accuracy of the glacier mapping is difficult to determine as a comparable ground truth (e.g., same date, same spectral bands and higher resolution) is often not available (cf. Paul and Andreassen, 2009). Comparisons with manually delineated glacier outlines from higher resolution data sets indicate that the error is in general smaller than 3% of the total area but increases toward smaller glaciers (Paul and Kääb, 2005; Paul et al., 2003). Compared to the manual digitization of outlines for clean glaciers, the automated method is more consistent and not generalized, which is a great advantage for creating reproducible results. Though manual delineation must be applied for editing of classification errors during post-processing, also here large errors can occur in particular for debris-covered glaciers (Hall et al., 2003).

Post-processing

As mentioned above, there are some cases that require manual editing during post-processing. An overview on some frequent issues (e.g., debris cover, ice divides, snow conditions) is given in Racoviteanu et al. (2009). The maybe still largest bottleneck for generating accurate glacier outlines is debris-covered glacier ice. While it is in autumn images (end of the ablation season) in mid-latitudes still possible to identify debris-covered glacier ice from subtle illumination differences, this can be impossible toward lower latitudes with high solar elevations (e.g., western Himalaya). In part, additional data like slope information derived from a DEM (Paul et al., 2004a) or more sophisticated classification algorithms based on geomorphometric analysis (Bishop et al., 2001) and/or decision-tree classifiers (Bolch et al., 2007; Shukla et al., 2010) do provide very suitable first estimates of potentially debris-covered glacier regions. However, manual corrections and editing by a specialized analyst remains to be done to obtain the required accuracy. The problem of properly identifying debris cover on glaciers is also illustrated in Figure 3 a and b for a region in Alaska and Pakistan, respectively. In the latter case with high solar elevation, it is nearly impossible to recognize the glacier at all. Even at a much higher spatial resolution (1 m) it is very difficult to determine the outline and terminus of the glacier. So this issue is still an open area for scientific advancement.

Assuming that cloud-free images are available, another challenge for accurate glacier mapping is related to seasonal snow. At a first place, the number of suitable images are greatly reduced when only scenes are considered that have (nearly) no snow outside of glaciers. Once a scene with good mapping conditions is identified, regional characteristics of the topography can result in persistent seasonal snowfields that might partly hide glaciers in the accumulation region and lead to the related uncertainties of the true glacier extent. In other regions such snowfields might be perennial (i.e., exist more than a year) and do not change their extent for decades. Often it is not possible to decide whether ice is underneath such perennial snow fields or not (Paul and Andreassen, 2009) and it has been recommended to either exclude or mark them for an inventory (Paul et al., 2009c). The problem of identifying debris cover on glaciers is also illustrated in Figure 3a and b for a region in Alaska and Pakistan, respectively. In the latter case it is nearly impossible to recognize the glacier at all. The problem of distinguishing seasonal from perennial snow or ice is illustrated in Figure 3c. Many of the elongated snow ridges have probably ice underneath but this could not be decided based on this image alone.

In Arctic regions, lakes could still be covered by ice at the end of the ablation period or sea ice is found on ocean water. Both features will be classified as glaciers with any method and manual correction is required. While sea ice or ice bergs can be easily identified and removed from the classification, a TM band 4, 3, 2 composite supports the identification of ice covered lakes (it is also helpful for editing lakes that are not covered by ice). However, when frozen lakes look very similar to flat ice caps, even human recognition might fail to distinguish them (Figure 3d).

A special case is related to optically thick clouds (e.g., cumulus), which might cover a glacier partly or completely and lead to errors in the derived surface area. At first, all clouds have to be identified. This could be done on a band 5, 4, 3 false color composite (FCC) where only clouds are white (exceptions exist for low and thin clouds). In the case of a small cloud that is completely surrounded by glacier ice it can be assumed that ice is also underneath and the cloud outline can be deleted. A cloud that partly hides the glacier perimeter in the ablation area could be corrected for short sections by considering glacier flow and surrounding rock walls. When both options do not apply, multitemporal analysis and image mosaicing can be considered to correct the outline, or the glacier has, finally, to be excluded from the analysis.

A further special case is volcanic ash on the glacier surface. It could be found on several ice caps in Iceland (e.g., Vatnajøkul) and other glaciers close to volcanoes in Alaska or South America. While optically thick, the ash layers could be very thin in reality and might have the same surface temperature than the underlying ice. In this case, the thermal band (TM6) can be used instead of TM5 for the ratio method. The lower spatial resolution of the sensor is in general not a problem on large ice caps, but the DNs of TM6 should be resampled bilinearly to the resolution of the other sensors before.

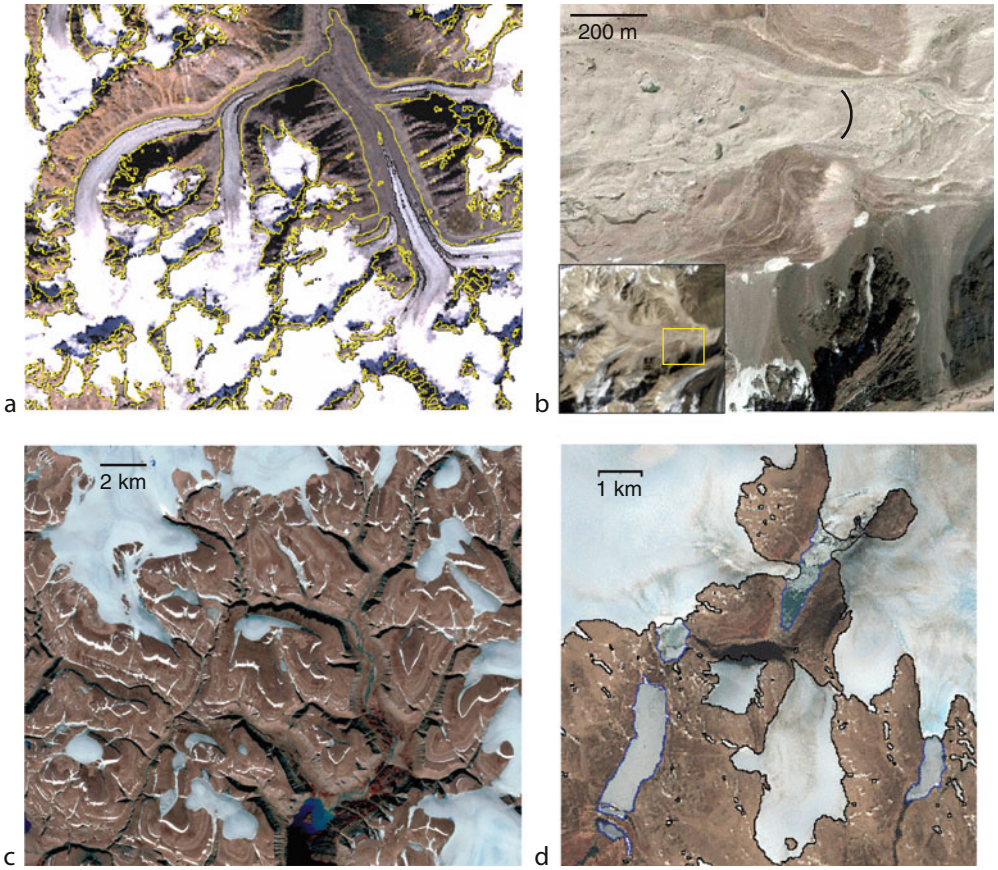

Automated Glacier Mapping, Figure 3 Examples of four challenging regions that require careful manual editing. (**a**) Debris-covered glaciers (Alaska Range, USA). The *black lines* indicate the extent from the automated mapping, the *yellow lines* show the extent after manual correction. (**b**) A small and highly debris-covered glacier in Pakistan as seen with Landsat TM (inset). The *yellow square* denotes the region of the large image that is taken from Google maps. Even at this high resolution (about 1 m) it is nearly impossible to determine the glacier terminus (probably located at the *black line*). (**c**) Seasonal or perennial snow fields (*white*) with probable ice (*grey*) underneath (Devon Icecap, Canada). (**d**) Frozen lakes (*blue outlines*) that are hardly distinguishable from flat icecaps (Baffin Island, Canada).

Applications

Once glacier outlines have been determined, a large number of further applications are possible. Combined with a DTM, the creation of glacier inventory data (e.g., Paul et al., 2002; Paul and Kääb, 2005; Paul and Andreassen, 2009) is likely a next step. Change detection using mutlitemporal analysis will also be in the focus of applications in the coming years (e.g., Paul et al., 2004b). Combined with other satellite based products, a larger number of additional glaciological investigations can be performed (cf. Bamber, 2006; Racoviteanu et al., 2008; Paul et al., 2009b). This includes mapping of snow extent and subsequent determination of mass balance terms (e.g., Rabatel et al., 2005), determination of flow velocities from multitemporal analysis (e.g., Kääb, 2005; Berthier et al., 2004), calculation of glacier specific thickness change from DEM comparison (e.g., Paul and Haeberli, 2008), or distributed mass balance modelling over larger regions (Paul et al., 2009a).

Conclusions

Overall, the largely automated glacier mapping from thresholded ratio images is simple, fast, and accurate. It is not fully automatic as pre-, main and post-processing requires human intervention and expertise (e.g., threshold selection and final editing). However, it allows to map all areas covered by ice and snow independent of their size and is reproducible. Debris cover on glaciers and some special cases (clouds, frozen lakes, volcanic ash) require particular attention during post-processing but can be handled in most cases by an experienced analyst. The opening of the USGS Landsat archive and the free availability of the SRTM DEM and ASTER GDEM have set the stage

for a completely new dimension of glacier inventory creation (outlines and topographic parameters) from satellite data at a global scale.

Bibliography

Albert, T., 2002. Evaluations of remote sensing techniques for ice-area classifications applied to the tropical Quelccaya ice cap, Peru. *Polar Geography*, **26**, 210–226.

Aniya, M., Sato, H., Naruse, R., Skvarca, P., and Casassa, G., 1996. The use of satellite and airborne imagery to inventory outlet glaciers of the southern Patagonia Icefield, South America. *Photogrammetric Engineering and Remote Sensing*, **62**, 1361–1369.

Bamber, J., 2006. Remote sensing in glaciology. In Knight, P. (ed.), *Glacier Science and Environmental Change*. Oxford: Blackwell, pp. 370–382.

Bayr, K. J., Hall, D. K., and Kovalick, W. M., 1994. Observations on glaciers in the eastern Austrian Alps using satellite data. *International Journal of Remote Sensing*, **15**, 1733–1742.

Berthier, E., Arnaud, Y., Baratoux, D., Vincent, C., and Rémy, F., 2004. Recent rapid thinning of the "Mer de Glace" glacier derived from satellite optical images. *Geophysical Research Letters*, **31**, L17401.

Binaghi, E., Madella, P., Montesano, M. P., and Rampini, A., 1997. Fuzzy contextual classification of multisource remote sensing images. *IEEE Transactions on Geoscience and Remote Sensing*, **35**, 326–339.

Bindschadler, R., Dowdeswell, J., Hall, D. K., and Winther, J.-G., 2001. Glaciological applications with Landsat-7 imagery: early assessments. *Remote Sensing of Environment*, **78**, 163–179.

Bishop, M. P., Bonk, R., Kamp, U., and Shroder, J. F., Jr., 2001. Terrain analysis and data modeling for alpine glacier mapping. *Polar Geography*, **25**, 182–201.

Bolch, T., Buchroithner, M. F., Kunert, A., and Kamp, U., 2007. Automated delineation of debris-covered glaciers based on ASTER data. In Gomarasca, M. A. (ed.), *GeoInformation in Europe: Proceedings of the 27th Symposium of the European Association of Remote Sensing Laboratories (EARSeL), Bolzano/Bozen, Italy, 4–7 June 2007*. Netherlands: Millpress, pp. 403–410.

Bronge, L. B., and Bronge, C., 1999. Ice and snow-type classification in the Vestfold hills, East Antarctica, using Landsat-TM data and ground radiometer measurements. *International Journal of Remote Sensing*, **20**, 225–240.

Della Ventura, A., Rampini, A., and Serandrei Barbero, R., 1987. Development of a satellite remote sensing technique for the study of alpine glaciers. *International Journal of Remote Sensing*, **8**, 203–215.

Dowdeswell, J. A., and Cooper, A. P. R., 1986. Digital mapping in polar regions from Landsat photographic products: a case study. *Annals of Glaciology*, **8**, 47–50.

Dozier, J., 1984. Snow reflectance from Landsat 4 Thematic Mapper. *IEEE Transactions on Geoscience and Remote Sensing*, **GE-22**, 323–328.

Dozier, J., 1989. Spectral signature of alpine snow cover from Landsat 5 T. *Remote Sensing of Environment*, **28**, 9–22.

Dozier, J., and Marks, D., 1987. Snow mapping and classification from Landsat Thematic Mapper data. *Annals of Glaciology*, **9**, 97–103.

Grenfell, T. C., Perovich, D. K., and Ogren, J. A., 1981. Spectral albedos of an alpine snow pack. *Cold Regions Science and Technology*, **4**, 121–127.

Haeberli, W., 2006. Integrated perception of glacier changes: a challenge of historical dimensions. In Knight, P. G. (ed.), *Glacier Science and Environmental Change*. Oxford: Blackwell, pp. 423–430.

Haeberli, W., Barry, R., and Cihlar, J., 2000. Glacier monitoring within the Global Climate Observing System. *Annals of Glaciology*, **31**, 241–246.

Hall, D. K., Ormsby, J. P., Bindschadler, R. A., and Siddalingaiah, H., 1987. Characterization of snow and ice zones on glaciers using Landsat Thematic Mapper data. *Annals of Glaciology*, **9**, 104–108.

Hall, D. K., Chang, A. T. C., and Siddalingaiah, H., 1988. Reflectances of glaciers as calculated using Landsat 5 Thematic Mapper data. *Remote Sensing of Environment*, **25**, 311–321.

Hall, D. K., Chang, A. T. C., Foster, J. L., Benson, C. S., and Kovalick, W. M., 1989. Comparison of in situ and Landsat derived reflectances of Alaskan glaciers. *Remote Sensing of Environment*, **28**, 493–504.

Hall, D. K., Bindschadler, R. A., Foster, J. L., Chang, A. T. C., and Siddalingaiah, H., 1990. Comparison of in situ and satellite derived reflectances of Forbindels glacier, Greenland. *International Journal of Remote Sensing*, **11**, 493–504.

Hall, D. K., Bayr, K. J., Schöner, W., Bindschadler, R. A., and Chien, J. Y. L., 2003. Consideration of the errors inherent in mapping historical glacier positions in Austria from the ground and space (1893–2001). *Remote Sensing of Environment*, **86**, 566–577.

Howarth, P., and Ommanney, C. S., 1986. The use of Landsat digital data for glacier inventories. *Annals of Glaciology*, **8**, 90–92.

IPCC, 2007. *Fourth Assessment Report*. Cambridge and New York: Intergovernmental Panel on Climate Change.

Jacobs, J. D., Simms, E. L., and Simms, A., 1997. Recession of the southern part of Barnes ice cap, Baffin island, Canada, between 1961 and 1993, determined from digital mapping of Landsat TM. *Journal of Glaciology*, **43**(143), 98–102.

Kääb, A., 2005. Combination of SRTM3 and repeat ASTER data for deriving alpine glacier flow velocities in the Bhutan Himalaya. *Remote Sensing of Environment*, **94**, 463–474.

Kieffer, et al., 2000. New eyes in the sky measure glaciers and ice sheets. *EOS, Transactions, American Geophysical Union*, **81**(24), 270.

Krimmel, R. M., and Meier, M. F., 1975. Glacier applications of ERTS-1 images. *Journal of Glaciology*, **15**(73), 391–402.

Orheim, O., and Lucchitta, B. K., 1987. Snow and ice studies by Thematic Mapper and Multispectral Scanner Landsat images. *Annals of Glaciology*, **9**, 109–118.

Østrem, G., 1975. ERTS – 1 data in glaciology – an effort to monitor glacier mass balance from satellite imagery. *Journal of Glaciology*, **15**(73), 403–415.

Paul, F., 2001. Evaluation of different methods for glacier mapping using Landsat TM. *EARSeL eProceedings*, **1**, 239–245.

Paul, F., 2002a. Changes in glacier area in Tyrol, Austria, between 1969 and 1992 derived from Landsat 5 TM and Austrian glacier inventory data. *International Journal of Remote Sensing*, **23**, 787–799.

Paul, F., 2002b. Combined technologies allow rapid analysis of glacier changes. *EOS, Transactions, American Geophysical Union*, **83**(23), 253, 260, 261.

Paul, F., and Andreassen, L. M., 2009. Creating a glacier inventory for the Svartisen region (Norway) from Landsat ETM + satellite data: challenges and results. *Journal of Glaciology*, **55**(192), 607–618.

Paul, F., and Haeberli, W., 2008. Spatial variability of glacier elevation changes in the Swiss Alps obtained from two digital elevation models. *Geophysical Research Letters*, **35**, L21502.

Paul, F., and Hendriks, J., 2010. Optical remote sensing of glaciers. In Pellikka, P., and Rees, W. G. (eds.), *Remote Sensing of Glaciers – Techniques for Topographic, Spatial and Thematic Mapping of Glaciers*. Leiden: CRC Press, Taylor and Francis, pp. 137–152.

Paul, F., and Kääb, A., 2005. Perspectives on the production of a glacier inventory from multispectral satellite data in the Canadian Arctic: Cumberland peninsula, Baffin island. *Annals of Glaciology*, **42**, 59–66.
Paul, F., Kääb, A., Maisch, M., Kellenberger, T. W., and Haeberli, W., 2002. The new remote sensing derived Swiss glacier inventory: I Methods. *Annals of Glaciology*, **34**, 355–361.
Paul, F., Huggel, C., Kääb, A., and Kellenberger, T. W., 2003. Comparison of TM-derived glacier areas with higher resolution data sets. *EARSeL eProceedings*, **2**, 15–21.
Paul, F., Huggel, C., and Kääb, A., 2004a. Combining satellite multispectral image data and a digital elevation model for mapping of debris-covered glaciers. *Remote Sensing of Environment*, **89**, 510–518.
Paul, F., Kääb, A., Maisch, M., Kellenberger, T. W., and Haeberli, W., 2004b. Rapid disintegration of Alpine glaciers observed with satellite data. *Geophysical Research Letters*, **31**, L21402.
Paul, F., Escher-Vetter, H., and Machguth, H., 2009a. Comparison of mass balances for Vernagtferner obtained from direct measurements and distributed modeling. *Annals of Glaciology*, **50**, 169–177.
Paul, F., Kääb, A., Rott, H., Shepherd, A., Strozzi, T., and Volden, E., 2009b. GlobGlacier: mapping the world's glaciers and ice caps from space. *EARSeL eProceedings*, **8**, 11–25.
Paul, F., Barry, R., Cogley, G., Frey, H., Haeberli, W., Ohmura, A., Ommanney, S., Raup, B., Rivera, A., and Zemp, M., 2009c. Recommendations for the compilation of glacier inventory data from digital sources. *Annals of Glaciology*, **50**(53), 119–126.
Qunzhu, Z., Meisheng, C., Xuezhi, F., Fengxian, L., Xianzhang, C., and Wenkun, S., 1985. A study of spectral reflection characteristics for snow, ice and water in the north of China. *International Association of Hydrological Sciences*, **145**, 451–462.
Rabatel, A., Dedieu, J. P., and Vincent, C., 2005. The use of remote sensing data to determine equilibrium line altitude and mass balance time series validation on three French glaciers for the 1994–2002 period. *Journal of Glaciology*, **l51**(175), 539–546.
Racoviteanu, A. E., Williams, M. W., and Barry, R. G., 2008. Optical remote sensing of glacier characteristics: a review with focus on the Himalaya. *Sensors*, **8**, 3355–3383.
Racoviteanu, A. E., Paul, F., Raup, B., Khalsa, S. J. S., and Armstrong, R., 2009. Challenges in glacier mapping from space: recommendations from the Global Land Ice Measurements from Space (GLIMS) initiative. *Annals of Glaciology*, **50**(53), 53–69.
Raper, S. C. B., and Braithwaite, R. J., 2006. Low sea level rise projections from mountain glaciers and icecaps under global warming. *Nature*, **439**, 311–313.
Raup, B. H., and Khalsa, J. S., 2007. GLIMS analysis tutorial (Online). Available from World Wide Web: http://www.glims.org/MapsAndDocs/assets/GLIMS_Analysis_Tutorial_a4.pdf
Raup, B. H., Kieffer, H. H., Hare, T. M., and Kargel, J. S., 2000. Generation of data acquisition requests for the ASTER satellite instrument for monitoring a globally distributed target: glaciers. *IEEE Transactions on Geoscience and Remote Sensing*, **38**, 1105–1112.
Raup, B. H., Kääb, A., Kargel, J. S., Bishop, M. P., Hamilton, G., Lee, E., Paul, F., Rau, F., Soltesz, D., Khalsa, S. J. S., Beedle, M., and Helm, C., 2007. Remote sensing and GIS technology in the Global Land Ice Measurements from Space (GLIMS) project. *Computers and Geosciences*, **33**, 104–125.
Rees, W. G., 2005. *Remote Sensing of Snow and Ice*. Boca Raton, London, New York: Taylor & Francis, p. 312.
Rott, H., 1976. Analyse der Schneeflächen auf Gletschern der Tiroler Zentralalpen aus Landsat Bildern. *Zeitschrift für Gletscherkunde und Glazialgeologie*, **12**, 1–28.
Rott, H., and Markl, G., 1989. Improved snow and glacier monitoring by Landsat Thematic Mapper. In *Proceedings of a Workshop on Landsat Thematic Mapper Applications*. ESA, SP-1102, pp. 3–12.
Rundquist, D. C., Collins, S. C., Barnes, R. B., Bussom, D. E., Samson, S. A., and Peake, J. S., 1980. The use of Landsat digital information for assessing glacier inventory parameters. *International Association of Hydrological Sciences*, **126**, 321–331.
Schiermeier, Q., 2010. Glacier estimate is on thin ice. *Nature*, **463**, 276–277.
Shukla, A., Arora, M. K., and Gupta, R. P., 2010. Synergistic approach for mapping debris-covered glaciers using optical thermal remote sensing data with inputs from geomorphometric parameters. *Remote Sensing of Environment*, doi:10.1016/j.rse.2010.01.015.
Sidjak, R. W., and Wheate, R. D., 1999. Glacier mapping of the Illecillewaet icefield, British Columbia, Canada, using, Landsat TM and digital elevation data. *International Journal of Remote Sensing*, **20**, 273–284.
Svoboda, F., and Paul, F., 2009. A new glacier inventory on southern Baffin island, Canada, from ASTER data: I. Applied methods, challenges and solutions. *Annals of Glaciology*, **50**(53), 11–21.
USGS, 2008. Opening the Landsat Archive. USGS Factsheet 2008–3091. URL: http://pubs.usgs.gov/fs/2008/3091/pdf/fs2008-3091.pdf
Warren, S. G., 1982. Optical properties of snow. *Reviews of Geophysics and Space Physics*, **20**, 67–89.
WGMS, 1989. World glacier inventory – status 1988. In Haeberli, W., Bösch, H., Scherler, K., Østrem, G., and Wallén, C. C. (eds.), *World Glacier Monitoring Service*. Zurich: IAHS (ICSI)/UNEP/UNESCO, p. 458.
Williams, R. S., Jr., and Hall, D. K., 1998. Use of remote-sensing techniques. In Haeberli, W., Hoelzle, M., and Suter, S. (eds.), *Into the Second Century of Worldwide Glacier Monitoring: Prospects and Strategies*. Paris: UNESCO, pp. 97–111.
Williams, R. S., Jr., Hall, D. K., and Benson, C. S., 1991. Analysis of glacier facies using satellite techniques. *Journal of Glaciology*, **37**(125), 120–127.
Winther, J. G., 1993. Landsat TM derived and in situ summer reflectance of glaciers in Svalbard. *Polar Reserach*, **12**, 37–55.

Cross-references

Alps
Arctic Hydroclimatology
Climate Change and Glaciers
Debris
Digital Elevation Model Generation Over Glacierized Region
Digital Image Information Extraction Techniques for Snow Cover Mapping from Remote Sensing Data
Glacier Field Studies: Important Things to Notice
Inventory of Glaciers
Normalized-Difference Snow Index (NDSI)
Optical Remote Sensing of Alpine Glaciers
Physical Properties of Snow
Summer Accumulation Type Glaciers
Temperate Glaciers
Winter Accumulation Glacier

B

BASAL SEDIMENT EVACUATION BY SUBGLACIAL DRAINAGE SYSTEMS

Darrel A. Swift
Department of Geography, University of Sheffield, Sheffield, UK

Definition

Basal sediment: The debris layer that exists at the ice–bedrock interface of a glacier or ice sheet and that is produced by glacial erosion of the underlying bedrock.
Basal sediment evacuation: The removal of basal sediment from the ice–bed interface by glacial and/or glaciofluvial sediment transport; most frequently used to describe the flushing of basal sediment from the ice–bedrock interface by subglacial water.
Subglacial drainage system: The network of drainage pathways at the ice–bed interface that convey water to the glacier margin or terminus.

Introduction

Contemporary observations and theoretical analyses demonstrate that, for *Temperate Glaciers* (qv), the entrainment and transport of basal sediment by fluvial processes dominates all other glacial sediment transport (*Sediment Entrainment, Transport, and Deposition*, qv) processes (see Hallet et al., 1996; Alley et al., 1997). Basal sediment evacuation by the *Subglacial Drainage System* (qv) therefore dominates in glacial *Sediment Budgets* (qv) (Alley et al., 1997), and the high *Suspended Sediment Load* (qv) of most glacier-fed rivers presents a major difficulty for the management and use of meltwater (Østrem, 1975; Bezinge et al., 1989; Bogen, 1989).

Sediment entrainment by subglacial water is difficult to observe directly. However, the relatively rapid transit of water through the subglacial drainage system means that the suspended load of glacier-fed streams should reflect closely the processes of sediment entrainment at the glacier bed. Analysis of the sediment load of glacier-fed streams has therefore been applied widely as a means of elucidating the processes of basal sediment evacuation (e.g., Gurnell et al., 1992; Clifford et al., 1995; Hodgkins, 1996; Willis et al., 1996; Hodson and Ferguson, 1999; Swift et al., 2005a).

Controls on basal sediment entrainment and evacuation

Investigation of basal sediment evacuation has been confined largely to the analysis of suspended sediment time series from glacier-fed rivers in temperate alpine environments (see, e.g., reviews by Gurnell [1987a, 1995] and Gomez [1987]). These studies have highlighted considerable temporal variation in basal sediment evacuation at a wide range of scales (e.g., Bogen, 1988, 1996; Collins, 1990; Clifford et al., 1995) (*Suspended Sediment Dynamics*, qv) that has been linked to a complex array of subglacial processes. Nevertheless, hydrologically-driven seasonal evolution of the subglacial drainage system (*Glacier Hydrology*, qv) has been shown to exert a key control on rates and patterns of basal sediment evacuation because it greatly influences how and where subglacial water accesses, entrains, and transports basal sediment (e.g., Gurnell et al., 1992; Swift et al., 2005a).

Essential concepts

The processes of subglacial erosion and subsequent comminution of erosion products at the ice–bedrock interface (*Glacial Erosion*, qv) generate significant quantities of debris characterized by an extremely wide size distribution. The extent to which such debris accumulates at the ice–bedrock interface in the form of a basal sediment layer (*Till*, qv) will depend largely on the efficacy of sediment evacuation by glacial and fluvial processes. Fluvial

Vijay P. Singh, Pratap Singh & Umesh K. Haritashya (eds.), *Encyclopedia of Snow, Ice and Glaciers*, DOI 10.1007/978-90-481-2642-2,

sediment transport is widely appreciated to dominate basal sediment evacuation (e.g., Alley et al., 1997), but the efficiency of basal sediment evacuation by fluvial processes is dependent on subglacial water having sufficient competence and capacity to entrain and transport available sediment, as well as being able to access basal sediment sources and/or stores.

Fluvial sediment entrainment and transport processes in the subglacial environment are largely similar to those that operate in subaerial streams (e.g., Alley et al., 1997). Notably, the efficiency of sediment transport or evacuation reflects, on the one hand, the competence and capacity of flow, and on the other, the size and accessibility/availability of sediment. Flow strength is therefore critical because it determines both flow competence (the largest particle a given flow is able to carry) and flow capacity (the total quantity of sediment of a given size that the flow can carry). Although flow strength is best defined in terms of flow energy or boundary shear stress, many sediment transport studies use flow velocity or discharge (*Discharge/Streamflow*, qv), which in general provide convenient and acceptable approximations.

Both discharge and suspended sediment transport can easily be measured in glacier-fed streams (*Suspended Sediment Concentration*, qv). As a result, the predictably strong relationship between these two factors has been demonstrated by a very large number of studies. However, many such studies have also reported changes in basal sediment transport that have occurred irrespective of discharge, and these range from short-term flushes of sediment lasting minutes or hours, to longer-term changes over a single melt season or a series of melt seasons. Such changes have been attributed to both the subglacial processes that determine basal sediment availability and the ease with which available sediment sources and/or stores can be accessed by elements of the subglacial drainage system.

Importance of subglacial drainage system morphology

Two morphologically distinct types of subglacial drainage exist beneath most temperate glaciers and, in the case of polythermal glaciers, beneath warm-based ice. The most widespread system, both spatially and temporally, will be some form of *distributed system*. Such systems convey small volumes of water derived largely from *basal melting* via a physically tortuous flowpath that may include flow within linked cavities, thin water films, and/or porous sediments. Changes in discharge within this system are accommodated largely by changes in the number or size of individual flowpaths and not by changes in flow velocity. Hence, despite being spatially extensive, such systems entrain and transport only the very finest fractions of available sediment (e.g., Humphrey and Raymond, 1994; Willis et al., 1996; Alley et al., 1997).

The efficiency of basal sediment evacuation increases significantly if a *channelized drainage system* is present. Channel systems typically form in summer in response to the very large quantities of surface melt that are conveyed to the glacier bed via *Moulins* (qv) and *Crevasses* (qv). Although physically and temporally discrete, channels convey large discharges at very high velocities, and are also sufficiently large to transport all but the very largest fractions of basal sediment. The resulting competence and capacity of the channel system is such that the annual glacial sediment budget may be dictated almost entirely by the annual spatial and temporal extent of channelized drainage (e.g., Alley et al., 1997; Swift et al., 2005a). Furthermore, a number of mechanisms related to the inception and growth of the channel network are considered to influence temporal patterns of basal sediment evacuation.

One important reason why the channelized system is so efficient at transporting sediment is because the increase in flow velocity that occurs as a function of discharge is extremely nonlinear when flow is confined within a subglacial channel. Alley et al. (1997) demonstrated theoretically that the transport capacity of unconfined channels typically varies as Q^2 because changes in discharge can be accommodated equally by changes in flow depth, width, and velocity. However, for subglacial channels, which can only be enlarged by melting of the channel walls, rapid changes in discharge will be accommodated almost exclusively by changes in flow velocity, such that transport capacity will vary up to $Q^{4.5}$. Swift et al. (2005a) demonstrated that such relationships were a major factor behind seasonal changes in the efficiency of basal sediment evacuation at Haut Glacier d'Arolla, Switzerland, where sediment transport during periods of distributed drainage was shown to vary as $Q^{\sim 2.3}$, and during periods of channelized drainage was shown to vary as $Q^{\sim 3.2}$.

Observations at surging glaciers (*Glacier Surging*, qv), such as Variegated Glacier, Alaska, also demonstrate the importance of drainage system morphology for basal sediment evacuation (e.g., Humphrey et al., 1986; Kamb and Engelhardt, 1987; Humphrey and Raymond, 1994). Surging occurs when the channelized drainage system fails to develop as expected, promoting high basal water pressures and hence rapid basal sliding that further discourages channel formation. These studies show that basal sediment evacuation remains low during each surge, despite distributed drainage having wide access to the glacier bed, and despite high rates of basal sliding that should enhance rates of both basal sediment disturbance and subglacial erosion. In contrast, flushing of basal sediment occurs as the surge ceases and channelized drainage is reestablished.

Importance of basal sediment availability

Changes in sediment availability (and also accessibility) are believed to be significant because the sediment loads of glacier-fed streams are often only weakly correlated with discharge at annual scales. For example, Bogen (1989, 1996) linked poor correlation between annual sediment load and discharge from various Norwegian glaciers to changes in subglacial erosion rate, but also changes in the

location of arterial subglacial channels across successive melt seasons. Similarly, Gurnell (1995) linked annual sediment load from Tsidjiore Nouve, Switzerland to the rate of glacier advance, citing changes in sediment availability as a result of the rate of disturbance of subglacial drainage.

Studies of sediment transport in glacier-fed streams at shorter timescales have identified changes in sediment availability during specific periods of the melt season. For example, enhanced availability of basal sediment has commonly been observed in spring and has been explained in terms of: (1) a build-up of basal sediment over winter as a result of the absence of surface melt reaching the glacier bed (e.g., Liestøl, 1967; Hooke et al., 1985; Collins, 1989, 1990); (2) unprecedented access of water to the glacier bed as surface melt swells the distributed system (see previous references); (3) enhanced disturbance of existing subglacial drainage pathways and/or sediments as a result of enhanced rates of *Glacier Sliding* (qv) (e.g., Collins, 1989; Hooke et al., 1985); and (4) drainage system reorganization associated with the rapid incision and growth of a channelized drainage network (e.g., Collins, 1989, 1990; Anderson et al., 1999).

Another common observation is an overall decline in sediment availability during the melt season. This has been attributed both to the reduced ability of water to access basal sediment as flow becomes increasingly confined to discrete channels (e.g., Collins, 1989, 1990; Gurnell, 1987b; Gurnell et al., 1992) and to the exhaustion of sediments that are accessible to such channels (e.g., Østrem, 1975; Hooke et al., 1985). Nevertheless, a number of studies have demonstrated increasingly efficient evacuation of basal sediment during the melt season (e.g., Clifford et al., 1995; Vatne et al., 1995). Swift et al. (2005a) demonstrated that this may be a result of the increasing peakedness of surface melt production during the melt season, as this should promote: (1) an associated increase in the sediment transport capacity of subglacial channel flow (Clifford et al., 1995; Swift et al., 2005b); and (2) an increasingly strong diurnally reversing subglacial hydraulic gradient that should encourage basal sediment to flow or deform toward channels (Vatne et al., 1995; Swift et al., 2005b).

Short-term controls on basal sediment evacuation

On hourly to weekly timescales, temporal patterns of sediment transport are controlled largely by discharge, particularly the diurnal changes in discharge that reflect the temporal pattern of surface melt production (e.g., Gurnell, 1987b; Clifford et al., 1995; Willis et al., 1996). However, diurnal patterns of sediment transport are complicated both by *Hysteresis* (qv), where sediment concentrations at equivalent discharges on the discharge hydrograph are observed to be higher on the rising limb than on the falling limb, and by flushes of sediment on a variety of temporal scales that may or may not be related to changes in discharge.

Hysteresis is commonly evident both during individual diurnal discharge cycles (e.g., Leistøl, 1967; Østrem, 1975; Collins, 1979; Bogen, 1980; Hammer and Smith, 1983; Gurnell, 1982, 1987b; Willis et al., 1996) and over multiple discharge cycles or events, notably where the magnitude of a discharge peak fails to equal or exceed that of a previous peak (e.g., Leistøl, 1967; Østrem et al., 1967; Church, 1972; Collins, 1979; Gurnell, 1982, 1987b; Richards, 1984; Schneider and Bronge, 1996). Leistøl (1967) suggested that such hysteresis occurred because changes in discharge in a subglacial channel are accommodated at least partly by changes in flow width, such that flow on the rising limb accesses successively larger areas of the glacier bed, whereas flow on the falling limb is confined to areas that have been stripped of basal sediment. Transport hysteresis might also reflect velocity hysteresis, which describes the characteristically higher flow velocities that occur on the rising limb (e.g., Richards, 1984).

Flushes of sediment lasting hours or days have been linked to rapid changes in flow routing. For example, flushes commonly occur during spring as surface melt promotes the reorganization of distributed drainage pathways into discrete channels (Collins, 1989, 1990) and as incipient channels release stored water and sediment from within a swollen distributed system (Warburton and Fenn, 1994; Anderson et al., 1999). Flushes have also been linked to short-term injections of water into the distributed system resulting from intense rainfall (e.g., Raymond et al., 1995; Denner et al., 1999), the drainage of ice-marginal or intra-glacial water stores (e.g., Collins, 1979; Beecroft, 1983), or temporary blockages in subglacial channels (e.g., Collins, 1990). The injection of water into the distributed system may further facilitate flushing by enhancing ice-bed separation and basal sliding (e.g., Anderson et al., 1999; Hooke et al., 1985; Raymond et al., 1995; Swift et al., 2005a).

Shorter pulses of sediment, often lasting only seconds or minutes, can also contribute significantly to the total annual sediment load (Gurnell and Warburton, 1990). These have been linked largely to instabilities in elements of the subglacial drainage system, including: (1) the establishment of new drainage pathways or the migration of existing ones (e.g., Collins, 1979, 1989, 1990; Gurnell, 1982, 1995; Gurnell and Warburton, 1990; Gurnell et al., 1992; Willis et al., 1996; Hodson et al., 1997; Vatne et al., 1995; Hodson and Ferguson, 1999); (2) disturbance of basal sediment or subglacial flowpaths by sudden changes in the rate of basal sliding (e.g., Willis et al., 1996; Swift et al., 2005a); (3) blockage of channels by channel-roof failure (e.g., Lawler et al., 1992); and (4) the deformation and/or collapse of basal sediment toward or into adjacent channels (Collins, 1979; Vatne et al., 1995; Clifford et al., 1995; Bogen, 1996).

Feedbacks and significance for glacial erosion rates and sediment yields

Efficient evacuation of basal sediment is likely to be very important in glacial systems (*Glacial Ecosystems*, qv) because erosion of subglacial bedrock will be limited

where debris at the ice–bedrock interface accumulates to form a basal sediment layer (Alley et al., 1997). Efficient flushing of debris is likely to maintain glacial erosion by enhancing ice–bedrock interaction that is also likely to enhance the comminution of larger debris (*Crush*, qv) that is produced at the ice–bedrock interface by subglacial quarrying (Swift et al., 2002). The efficiency of basal sediment evacuation by subglacial drainage is therefore likely to be a dominant control on glacial *Erosion Rate* (qv) and *Sediment Yield* (qv).

The high sediment competence and transport capacity of subglacial channels indicates that the extent to which a spatially extensive channelized drainage network evolves during the melt season is also likely to be extremely important in dictating erosion rates and annual sediment yields (Swift et al., 2002; Swift et al., 2005b). Glaciers that evolve limited channelized systems and have predominantly distributed drainage are likely to have thicker and more extensive basal sediment layers that discourage ice–bedrock interaction and promote the entrainment and transport of sediment by glacial processes. The efficiency of basal sediment evacuation by subglacial drainage is therefore likely also to influence rates and styles of proglacial sediment deposition (Swift et al., 2002).

Areas of controversy and future research potential

Present understanding of basal sediment evacuation by subglacial drainage is limited largely to temperate ice masses. Few studies have been conducted at *polar* or *polythermal glaciers* (e.g., Hodgkins, 1996; Hodson and Ferguson, 1999), especially those glaciers that emanate from larger ice masses such as the Greenland ice sheet, even though the potential for surface melt to reach the ice–bed interface of such glaciers has now been demonstrated widely. As a result, the processes of basal sediment evacuation in such environments, including those that are associated with the seasonal evolution of subglacial drainage system morphology, may play an important but as yet poorly understood role in a wide array of subglacial processes at ice sheet scales.

The significance of fluvial sediment evacuation in glacial geomorphic systems is also poorly understood, most notably in terms of the importance of basal sediment evacuation in controlling rates of glacial erosion and resulting patterns of landscape evolution (*Glacial Geomorphology and Landforms Evolution*, qv) . Widely variable sediment yields (e.g., Hallet et al., 1996) indicate that glacier-to-glacier variation in the efficiency of basal sediment evacuation may be a critical control on rates of glacial erosion. Sediment transport by subglacial drainage may also play a critical role in the evolution of glacier-bed overdeepenings (*Glacial Overdeepening*, qv) (Alley et al., 2003) and their geomorphic impacts (*Glaciohydraulic Supercooling*, qv) (e.g., Swift et al., 2002; Cook et al., 2006). However, understanding is limited by an absence of sufficiently long-term records of sediment transport in glacier-fed streams, particularly with respect to bed-load (e.g., Alley et al., 2003).

Summary

Basal sediment evacuation by subglacial meltwater plays a key role in glacial systems. Notably, the efficiency of basal sediment evacuation is likely to determine the extent to which the products of glacial erosion are retained at the ice–bed interface (Alley et al., 1997), which is likely to dictate not only rates and patterns of subglacial erosion and glacial sediment yield, but also the proportion of debris in glacial versus fluvial sediment transport pathways, and as a result will greatly influence rates and styles of sediment deposition in ice-marginal environments (*Moraine*, qv) (see Swift et al., 2002). Nevertheless, the importance of basal sediment evacuation by subglacial water for glacial geomorphic processes has largely until recently been neglected by the glaciohydrological and glaciogeomorphological literature.

Bibliography

Alley, R. B., Cuffey, K. M., Evenson, E. B., Strasser, J. C., Lawson, D. E., and Larson, G. J., 1997. How glaciers entrain and transport basal sediment: physical constraints. *Quaternary Science Reviews*, **19**, 1017–1038.

Alley, R. B., Lawson, D. E., Larson, G. J., Evenson, E. B., and Baker, G. S., 2003. Stabilizing feedbacks in glacier-bed erosion. *Nature*, **424**, 758–760.

Anderson, S. A., Fernald, K. M. H., Anderson, R. S., and Humphrey, N. F., 1999. Physical and chemical characteristation of a spring flood event, Bench Glacier, Alaska, USA: evidence for water storage. *Journal of Glaciology*, **45**, 177–189.

Beecroft, I., 1983. Sediment transport during an outburst from Glacier de Tsidjiore Nouve, Switzerland, 16–19 June, 1981. *Journal of Glaciology*, **29**, 185–190.

Bezinge, A., Clark, M. J., Gurnell, A. M., and Warburton, J., 1989. The management of sediment transported by glacial meltwater streams and its significance for the estimation of sediment yield. *Annals of Glaciology*, **13**, 1–5.

Bogen, J., 1980. The hysteresis effect of sediment transport systems. *Norsk Geografisk Tidsskrift*, **34**, 45–54.

Bogen, J., 1988. A monitoring programme of sediment transport in Norwegian rivers. In Bordas, M. P., and Walling, D. E. (eds.), *Sediment Budgets*, IAHS Publication No. 174, pp. 149–159.

Bogen, J., 1989. Glacial sediment production and development of hydro-electric power in glacierized areas. *Annals of Glaciology*, **13**, 6–11.

Bogen, J., 1996. Erosion rates and sediment yields of glaciers. *Annals of Glaciology*, **22**, 48–52.

Bridge, C. W., and Rannie, W., 1967. Glacio-hydrology, discharge and sediment transport in the decade glacier area, Baffin Island, N.W.T. *Geografiska Annaler*, **49A**, 268–282.

Church, M., 1972. Baffin Island Sandurs: A study of Arctic fluvial processes. *Geological Survey of Canada Bulletin*, **216**, 208.

Clifford, N. J., Richards, K. S., Brown, R. A., and Lane, S. N., 1995. Scales of variation of suspended sediment concentration and turbidity in a glacial meltwater stream. *Geografiska Annaler*, **77A**, 45–65.

Collins, D. N., 1979. Sediment concentration in meltwaters as an indicator of erosion processes beneath an alpine glacier. *Journal of Glaciology*, **23**, 247–257.

Collins, D. N., 1989. Seasonal development of subglacial drainage and suspended sediment delivery to meltwaters beneath an Alpine glacier. *Annals of Glaciology*, **13**, 45–50.
Collins, D. N., 1990. Seasonal and annual variations of suspended sediment transport in meltwaters draining from an Alpine glacier. In Lang, H., and Musy, A. (eds.), *Hydrology in Mountainous Regions 1: Hydrological Measurements; the Water Cycle*, IAHS Publication No. 193, pp. 439–446.
Cook, S. J., Waller, R. I., and Knight, P. G., 2006. Glaciohydraulic supercooling: the process and its significance. *Progress in Physical Geography*, **30**, 577–588.
Denner, J. C., Lawson, D. E., Larson, G. J., Evenson, E. B., Alley, A. B., Strasser, J. C., and Kopczynski, S., 1999. Seasonal variability in hydrologic-system response to intense rain events, Matanuska Glacier, Alaska, USA. *Annals of Glaciology*, **28**, 267–271.
Gomez, B., 1987. Bedload. In Gurnell, A. M., and Clark, M. J. (eds.), *Glacio-fluvial Sediment Transfer: An Alpine Perspective*. Chichester: Wiley, pp. 355–376.
Gurnell, A. M., 1982. The dynamics of suspended sediment concentration in a proglacial stream system. In Glen, J. W. (ed.), *Hydrological Aspects of Alpine and High-Mountain Areas*. New York: Wiley, pp. 59–85.
Gurnell, A. M., 1987a. Fluvial sediment yield from Alpine, glacierized catchments. In Gurnell, A. M., and Clark, M. J. (eds.), *Glacio-fluvial Sediment Transfer: An Alpine Perspective*. Chichester: Wiley, pp. 415–420.
Gurnell, A. M., 1987b. Suspended sediment. In Gurnell, A. M., and Clark, M. J. (eds.), *Glacio-fluvial Sediment Transfer: An Alpine Perspective*. Chichester: Wiley, pp. 305–354.
Gurnell, A. M., 1995. Sediment yield from Alpine glacier basins. In Foster, I. D. L., Gurnell, A. M., and Webb, B. W. (eds.), *Sediment and Water Quality in River Catchments*. Chichester: Wiley, pp. 407–435.
Gurnell, A. M., and Warburton, J., 1990. The significance of suspended sediment pulses for estimating suspended sediment load and identifying suspended sediment sources in Alpine glacier basins. In Lang, H., and Musy, A. (eds.), *Hydrology in Mountainous Regions. 1: Hydrological Measurements; the Water Cycle*, IAHS Publication No. 193, pp. 463–470.
Gurnell, A. M., Clark, M. J., and Hill, C. T., 1992. Analysis and interpretaion of patterns within and between hydroclimatological time series in an Alpine glacier basin. *Earth Surface Processes and Landforms*, **17**, 821–839.
Hallet, B., Hunter, L., and Bogen, J., 1996. Rates of erosion and sediment evacuation by glaciers: a review of field data and their implications. *Global and Planetary Change*, **12**, 213–235.
Hammer, K. M., and Smith, N. D., 1983. Sediment production and transport in a proglacial stream, Hilda Glacier, Alberta, Canada. *Boreas*, **12**, 91–106.
Hodgkins, R., 1996. Seasonal trends in suspended sediment transport from and Arctic glacier, and implications for drainage system structure. *Annals of Glaciology*, **22**, 147–151.
Hodson, A. J., and Ferguson, R. I., 1999. Fluvial suspended sediment transport from cold and warm-based glaciers in Svalbard. *Earth Surface Processes and Landforms*, **24**, 957–974.
Hodson, A. J., Tranter, M., Dowdeswell, J. A., Gurnell, A. M., and Hagen, J. O., 1997. Glacier thermal regime and suspended sediment yield: a comparison of two high-Arctic glaciers. *Annals of Glaciology*, **24**, 32–37.
Hooke, R. L., Wold, B., and Hagen, J. O., 1985. Subglacial hydrology and sediment transport at Bondhusbreen, southwest Norway. *Geological Society of America Bulletin*, **96**, 388–397.
Humphrey, N. F., and Raymond, C. F., 1994. Hydrology, Erosion and Sediment Production in a Surging Glacier – Variegated Glacier, Alaska, 1982–83. *Journal of Glaciology*, **40**, 539–552.
Humphrey, N., Raymond, C., and Harrison, W., 1986. Discharges of turbid water during min-surges of Variagated Glacier, Alaska, USA. *Journal of Glaciology*, **32**, 195–207.
Kamb, B., and Engelhardt, H., 1987. Waves of accelerated motion in a glacier approaching surge: the mini-surges of Variagated Glacier, Alaska, USA. *Journal of Glaciology*, **33**, 27–46.
Lawler, D. M., Dolan, M., Tomasson, H., and Zophoniasson, S., 1992. Temporal variability of suspended sediment flux from a subarctic glacial river, southern Iceland. In Bogen, J., Walling, D. E., and Day, T. (eds.), *Erosion and Sediment Transport Monitoring Programmes in River Basins*, IAHS Publication No. 210, pp. 233–243.
Liestøl, O., 1967. Storbreen glacier in Jotunheimen, Norway. *Norsk Polarinstitutt Skrifter*, **141**, 1–63.
Østrem, G., Bridge, C. W., and Rannie, W. F., 1967. Glacio-hydrology, discharge and sediment transport in the decade glacier area, Baffin Island, N.W.T. *Geografiska Annaler*, **49A**, 268–282.
Østrem, G., 1975. Sediment transport in glacial meltwater streams. In Jopling, A. V., and McDonald, B. C. (eds.), *Glaciofluvial and Glaciolacustrine Sedimentation*. Tusla: Society of Economic Paleontologists and Mineralogists. Special Publication No. 23, pp. 101–122.
Raymond, C. F., Benedict, R. J., Harrison, W. D., Echelmeyer, K. A., and Sturn, M., 1995. Hydrological discharges and motion of Fels and Black Rapids Glaciers, Alaska, USA: implications for the structure of their drainage systems. *Journal of Glaciology*, **41**, 290–304.
Richards, K., 1984. Some process observations on suspended sediment dynamics in Storbregrova, Jotunheim. *Earth Surface Processes and Landforms*, **9**, 101–112.
Schneider, T., and Bronge, C., 1996. Suspended sediment transport in the Storglaciären drainage basin. *Geografiska Annaler*, **78A**, 155–161.
Swift, D. A., Nienow, P. W., Spedding, N., and Hoey, T. B., 2002. Geomorphic implications of subglacial drainage system configuration: rates of basal sediment evacuation controlled by seasonal drainage system evolution. *Sedimentary Geology*, **149**, 5–19.
Swift, D. A., Nienow, P. W., and Hoey, T. B., 2005a. Basal sediment evacuation by subglacial meltwater: suspended sediment transport from Haut Glacier d'Arolla, Switzerland. *Earth Surface Processes and Landforms*, **30**, 867–883.
Swift, D. A., Nienow, P. W., Hoey, T. B., and Mair, D. W. F., 2005b. Seasonal evolution of runoff from Haut Glacier d'Arolla, Switzerland and implications for glacial geomorphic processes. *Journal of Hydrology*, **309**, 133–148.
Vatne, G., Etzelmuller, B., Sollid, J. L., and Ødegård, R. S., 1995. Hydrology of a polythermal glacier, Erikbreen, northern Spitsbergen. *Nordic Hydrology*, **26**, 169–190.
Warburton, J., and Fenn, C. R., 1994. Unusual flood events from an Alpine glacier: observations and deductions on generating mechanisms. *Journal of Glaciology*, **40**, 176–186.
Willis, I. C., Richards, K. S., and Sharp, M. J., 1996. Links between proglacial stream suspended sediment dynamics, glacier hydrology and glacier motion At Midtdalsbreen, Norway. *Hydrological Processes*, **10**, 629–648.

Cross-references

Discharge/Streamflow
Erosion Rate
Glacial Drainage Characteristics
Glacial Erosion
Glacier Hydrology
Glaciohydraulic Supercooling

Sediment Budgets
Sediment Entrainment, Transport, and Deposition
Sediment Yield
Subglacial Drainage System
Subglacial Processes
Suspended Sediment Concentration
Suspended Sediment Dynamics
Suspended Sediment Load

BASE FLOW/GROUNDWATER FLOW

Debasmita Misra[1], Ronald P. Daanen[2], Anita M. Thompson[3]
[1]Geological Engineering, College of Engineering and Mines, University of Alaska Fairbanks, Fairbanks, AK, USA
[2]Geophysical Institute, University of Alaska, Fairbanks, AK, USA
[3]Department of Biological Systems Engineering, University of Wisconsin-Madison, Madison, WI, USA

Synonyms

Drought flow; Groundwater recession flow; Low flow; Seepage flow; Infiltration; Deep percolation; Soil moisture redistribution

Definition

Base Flow: Between storms and runoff events, stream flow is maintained by groundwater discharge known as base flow, as long as the water table remains above the stream bottom (Delleur, 1999).
Groundwater: Groundwater is the liquid water flowing through aquifers. However, technically it includes soil moisture, permafrost, immobile water in very low permeability bedrock, and deep geothermal and oil formation water. It is the water (or ice) that resides beneath the ground surface in soil pore spaces and in the fractures of lithologic formations.
Aquifer: Aquifers are units of rock or an unconsolidated soil formation that can store and transmit a usable quantity of water.
Groundwater Flow: Groundwater flow occurs in soil and rock formations due to difference in hydraulic head or hydraulic potential within the unit or aquifer. The flow or discharge of groundwater is governed by Darcy's law, which is the product of the hydraulic conductivity or permeability of the rock or soil, the hydraulic gradient of the fluid, and the cross-sectional area of the aquifer.

Introduction

Groundwater is a component of the hydrologic cycle. Precipitation that falls on the land surface infiltrates into the ground until the rate of infiltration becomes less than the rate at which precipitation occurs. The excess precipitation at that point runs off the land surface into ditches, lakes, or streams and is called overland runoff. The amount of precipitation that infiltrates into the ground forms the groundwater. After entering the ground, the groundwater flows as lateral seepage due to capillary action of the soil pore spaces or percolates deeper into the subsurface to reach the groundwater table (top of groundwater saturation) and thus recharging the aquifer. Aquifers are bounded by streams. Groundwater discharges into streams when the water table rises above the streambed. This process is often referred to as the base flow. The amount of base flow a stream receives is closely linked to the permeability of rock or soil in the watershed. Readers are referred to Fitts (2002), Fetter (2001), Freeze and Cherry (1979), or McWhorter and Sunada (1977) for detailed description and hydraulics of groundwater flow and base flow.

Precipitation can occur in form of rain or snow. While the infiltration of rainfall has been studied extensively, the study of infiltration due to snowmelt and its impact on groundwater flow has been limited so far. Similarly, the study of base flow in seasonally freezing streams has also been limited. In northern latitudes, the dynamics of active layer (seasonally freezing soil) that stores significant quantity of infiltrated water as ice in winter or releases those as liquid water in spring has also been hardly studied. Williams (1970) studied groundwater flow in permafrost underlain lands in Alaska. He reports,

> Although groundwater in permafrost regions in Alaska occurs according to the same geologic and hydrologic principles prevailing in temperate regions, subfreezing temperatures result in profound modification of groundwater flow systems. Frozen ground is an impermeable layer, which restricts recharge, discharge, and movement of groundwater; acts as a confining layer; and limits the volume of consolidated deposits and bedrock in which liquid water may be stored.

Boulton et al. (1995) report,

> Ice sheets melting basally inject water into subglacial permeable beds under a maximum head equivalent to the total ice pressure." They conclude from their study on large aquifers in Sweden, the Netherlands, and Germany "that these large aquifers had a sufficient transmissivity to drain all subglacial meltwater; that groundwater heads, potential gradients and fluxes during glacial periods were very much larger than during interglacials; that proglacial permafrost played an important role in sustaining fluid overpressures in the ice sheet terminal zone; that during glacial periods major pressure pulses were driven through aquifer systems; and that groundwater systems were completely reorganized." Singh and Singh (2001) report, "The base flow (in glacial fed basins) is controlled by storage characteristics of the glacier and is determined by the delayed response of the basin.

Groundwater flow and base flow in permafrost regions

The study of groundwater flow and base flow systems in environments that are dominated by permafrost is quite sparse. Kane and Slaughter (1973) state that the understanding of groundwater flow in permafrost environments

have been grossly hindered due to the lack of subsurface data on permafrost. Kane and Slaughter state,

> Groundwater flow systems may be simply considered as comprising three components: recharge area, transmission zone, and discharge area... In permafrost settings, all three components (recharge, transmission, and discharge zones) can be affected by presence of local or regional areas of frozen ground. Permafrost in the recharge area can act as a barrier to downward water movement, thus restricting aquifer recharge. The presence of permafrost can affect groundwater movement in the transmission zone. For *suprapermafrost* groundwater, the permafrost forms an impermeable base; for *subpermafrost* groundwater, the permafrost acts as an overlying confining bed and thus creates a confined aquifer. Wells that penetrate permafrost to the subpermafrost groundwater are commonly artesian. The presence of permafrost in discharge zones can similarly influence the groundwater movement and yield.

Delleur (1999) states,

> ... permafrost under the right temperature may contain a mixture of unfrozen water and ice, or it may contain only ice. The unfrozen water exists as thin films adsorbed on surfaces of mineral particles and the thicknesses of the films are functions of temperature... Hydraulic conductivity in permafrost layers is a function of the temperature of the permafrost system, the thermal gradient and the available cross-sectional area of interconnected films of unfrozen water. Movement of groundwater is retarded in movement through permafrost, but permafrost acts more like a semi-confining bed of very low hydraulic conductivity and not like a completely confining bed of zero hydraulic conductivity. If the permafrost layers are fractured significantly, the higher overall hydraulic conductivity can be expected to be much higher than in unfractured permafrost.

An effect of base flow in the permafrost regions results in the formation of wetlands. Ford and Bedford (1987) provide a thorough review of the hydrology of Alaskan wetlands. They state,

> Little is known about the hydrologic behavior of arctic and subarctic wetlands (Roulet and Woo, 1986), including those that occur in Alaska... In the arctic and subarctic climates found in Alaska, water is present in solid phase for much of the year, and the influence of such typical high-latitude phenomena as glaciers, permafrost, and naleds (massive winter icings that occur in river valleys) on the volume, areal distribution, rate, and timing of water release become critical in understanding the hydrology of these high-latitude wetlands... Wetlands in continuous permafrost regions often have a perched water table in the active layer. The active layer is confined at the bottom by solid ice rich permafrost. The active layer thaws every year giving it a moving bottom boundary. This results in base flow change over the season and the runoff responds of a watershed on rain events therefore changes as the thaw season progresses. Climate change may affect the annual active layer development and change the rain fall responds and base flow of arctic streams (Reinhart and Jones, pers. com.). Ford and Bedford (1987) also state, "In discontinues permafrost zones little is known about how Alaskan wetlands affect groundwater recharge or about the areal extent and geographic distribution of wetlands maintained by groundwater discharge. However, some inferences can be drawn from the literature on individual arctic and sub-arctic drainage basins that are known to contain wetlands... Information on groundwater-flow systems in permafrost regions is sparse, although the pace of investigation is accelerating as development pressures encroach on high-latitude systems (e.g., Tolstikhin, 1978). Several characteristics distinguish groundwater hydrology in permafrost regions from that in other areas. First, rates of groundwater movement are generally lower than in equivalent temperate regions because of the increased viscosity of water at low temperatures (1.2–1.8 times higher) (Brandon, 1966; Church, 1974). Second, "ground-water" in these regions includes subpermafrost, intra-permafrost, and suprapermafrost (active layer) groundwater. In regions of deep, continuous permafrost, little or no hydraulic connection exists between the subpermafrost and suprapermafrost zones. Permafrost can act as an upper confining bed on the subpermafrost aquifer, which is typically artesian (Williams and Waller, 1966; Cederstrom, 1963; Kane and Slaughter, 1973; Linell, 1973)... In regions of discontinuous permafrost, there may be hydraulic connections between supra- and subpermafrost groundwater through unfrozen zones (taliks) that occur under lakes, rivers, and valley bottoms, and on south-facing slopes. Some taliks that are saline are also known as cryopegs (e.g., Cederstrom, 1961), and talik temperatures are therefore often below 0°C. If a thawed zone links the shallow and deep aquifers, artesian pressure can result in discharge to both wetlands and ponds (as base flow). In the larger northern river systems, groundwater discharge can be an important source of winter flow (Church, 1974). In many areas, however, seasonal frost can reach the permafrost table, restricting groundwater flow, increasing the hydrostatic pressure, and forcing water through cracks in the ice cover. As the continuous winter base flow rises to the surface and freezes in the frigid winter air, thick stream and river icings are created that can range in size from a few square yards to thousands of hectares (Dean, 1984)... these icings (also referred to as aufeis, or naleds) serve to redistribute total water discharge from small, continuous outputs during the cold season to a single, short-duration, catastrophic output at the beginning of the warm season (Sokolov, 1978). In spring, aufeis melt can comprise a significant portion of the total annual water volume of a river (Sokolov, 1978).

Snowmelt and groundwater flow or base flow

Bengtsson (1982) reports,

> There are often discussions about whether the snowmelt runoff takes place as overland flow at the base of the snowpack on the frozen ground, or whether the meltwater first infiltrates the frozen soil and thereafter contributes to an increase of the groundwater discharge. The problem has recently been discussed by Rodhe (1981), who from isotope studies found that most of the streamflow from a forested area in mid Sweden originated from groundwater. Similar studies have been made by Dincer et al. (1970) and Martinec (1975). Also in these investigations it was found that the main contribution to the peak streamflow was from groundwater (as base flow). Many hydrologists support the view that since the melt rate is rather low most of the melted snow infiltrates; others claim that since the ground below a snowpack is frozen, most of the meltwater flows along the ground. Of course, depending on the conditions both theories may be correct. The characteristics of overland flow and groundwater flow are, however, quite different... During a long cold winter runoff also takes place from a large groundwater basin. The

response of such basins to infiltrating meltwater is slow. The runoff from small groundwater basins ceases almost completely during a long winter. The interaction between infiltrating meltwater and streamflow depends on the characteristics of the groundwater basin and also on the conditions in the soil moisture zone (as the ground freezes). . . Observations over 6 years in the Luleâ region, cf. Bengtsson (1981), have shown that all the first meltwater infiltrates, and that the infiltration capacity of the frozen soil is very limited in the final phase of a long melt period. If it is assumed that the relatively large infiltration at the beginning of a melt period corresponds to a high recharge to the groundwater, and that the recharge is reduced in the later phase of the snowmelt, a steady state groundwater discharge is obtained also for aquifers of moderate hydraulic conductivity. . . From field measurements, Stephenson and Freeze (1974) found in their study that the mechanism of streamflow generation was subsurface delivery of meltwater over limited distances through shallow, highly permeable, low-porosity formations. From interpretation of the measurements by a mathematical model of transient saturated-unsaturated subsurface flow they also concluded that the peak streamflow came from early snowmelt near the stream. In their final discussion they showed that for soil conditions of very high and very low hydraulic conductivities, snowmelt is delivered promptly to stream channels as subsurface and overland flow respectively. The minimum response will occur in basins just permeable enough to sustain subsurface throughflow.

Glacial melt and groundwater flow or base flow

Most of the studies on interaction of glacial melt with groundwater systems has been based on reconstruction of geologic events from the past (e.g., Boulton et al., 1993 and references therein). Singh and Singh (2001) note that,

> An examination of streamflow from glacierized basin illustrates a considerable flow in the form of base flow during summer period. This base flow is controlled by storage characteristics of the glacier and is determined by the delayed response of the basin. Continuous drainage of water from various parts/locations governs the volume of base flow. It indicates that only a portion of the melt water produced each day reaches the snout on the same day. The remaining melt water is stored within the glacier, which gets delayed and adds to later day melt contribution (Martinec, 1970). In fact, the diurnal cycle of runoff also consists of a part of this continuing base flow. Investigations based on the tracer experiments, isotope studies and analysis of the runoff distribution suggest that the major contribution to base flow results from continuous runoff from the accumulation area (firn area), continuous drainage from the glacier lakes, water filled cavities and groundwater flow (Lang et al., 1979; Elliston, 1973; Collins, 1982; Stenborg, 1970; Tangborn et al., 1975). The base flow dominated with melt water from the accumulated area has higher time of concentration as compared with melt water generated in the ablation area.

Summary

Groundwater flow and base flow are impacted by snow, ice, permafrost, and glacial melt. Groundwater in permafrost regions occurs according to the same geologic and hydrologic principles prevailing in temperate regions; however, subfreezing temperatures result in profound modification of groundwater flow systems. Isotope studies have revealed that most of the streamflow from snowmelt runoff and main contribution to the peak streamflow originated from groundwater. An examination of streamflow from glacierized basin illustrates a considerable flow in the form of base flow during summer period. This base flow is controlled by storage characteristics of the glacier and is determined by the delayed response of the basin.

Bibliography

Bengtsson, L., 1981. Infiltration in frozen soils (English summary). *TULEA*, **1981**, 21.

Bengtsson, L., 1982. Groundwater and meltwater in the snowmelt induced runoff. *Hydrological Sciences Journal – des Sciences Hydrologiques*, **27**(2), 147–158.

Boulton, G. S., Slot, T., Blessing, K., Glasbergen, P., Leijnse, T., and van Gijssel, K., 1993. Deep circulation of groundwater in overpressured subglacial aquifers and its geological consequences. *Quaternary Science Reviews*, **12**(9), 739–745.

Boulton, G. S., Caban, P. E., and Van Gijssel, K., 1995. Groundwater flow beneath ice sheets: Part I – Large scale patterns. *Quaternary Science Reviews*, **14**(6), 545–562.

Brandon, L. V., 1966. Evidences of ground water flow in permafrost regions. In *Permafrost: Proceedings of an International Conference, Lafayette, Indiana, Nov. 11–15, 1963*. National Research Council Publication 1287. Washington, DC: National Academy of Sciences–National Research Council, pp. 176–177.

Cederstrom, D. J., 1961. Origin of a salt-water lens in permafrost at Kotzebue, Alaska. *Geological Society of America Bulletin*, **71**, 1427–1432.

Cederstrom, D. J., 1963. *Groundwater resources of the Fairbanks area, Alaska*. US Geological Survey Water Supply Paper, 1590. 84 pp.

Church, M., 1974. Hydrology and permafrost with references to northern North America. In *Permafrost Hydrology: Proceedings of a Workshop Seminar (1974)*. Ottawa: Canadian National Committee for the International Hydrological Decade, pp. 7–20.

Collins, D. N., 1982. Temporal variations of meltwater runoff from an Alpine glacier. In *Proceedings of the Symposium on Hydrological Research Basins*. Bern, Sonderheft, Landeshydrologie, Vol. 3, pp. 781–789.

Dean, K. G., 1984. Stream-icing zones in Alaska. Report of Investigations 84-16. Fairbanks, AK: Alaska Department of Natural Resources, Division of Geological and Geophysical Survey, 15 pp.

Delleur, J. W., 1999. *The handbook of groundwater engineering*. Boca Raton, FL: CRC Press.

Dincer, T., Payne, B. R., Florkowski, T., Martinec, J., and Tongiorgi, E., 1970. Snowmelt runoff from measurements of tritium and oxygen-18. *Water Resources Research*, **6**(1), 110–124.

Elliston, G. R., 1973. Water movement through the Gornergletscher. In *Proceedings of the Symposium on the Hydrology of Glaciers*. Cambridge Symposium. IASH Publ. No. 95, pp. 79–84.

Fetter, C. W., 2001. Applied Hydrogeology, Prentice Hall, USA, 598 pp.

Fitts, C. R., 2002. *Groundwater science*. San Diego: Academic.

Ford, J., and Bedford, B. L., 1987. The hydrology of Alaskan wetlands, USA: a review. *Arctic and Alpine Research*, **19**(3), 209–229.

Freeze, R. A., and Cherry, J. A., 1979. *Groundwater*. Englewood Cliffs, NJ: Prentice Hall.

Kane, D. L., and Slaughter, C. W., 1973. Recharge of a central Alaskan lake by subpermafrost groundwater. In *Permafrost – North American Contribution to Second International Conference on Permafrost, Yakutsk, Siberia, July 13–18, 1973*. Washington, DC: National Academy of Sciences, pp. 458–462.

Lang, H., Leibundgut, C., and Festel, E., 1979. Results from the tracer experiments on water flow through Altschgletscher. *Zeitschrift für Gletscherkunde und Glazialgeologie*, **15**, 209–218.
Linell, K. A., 1973. Risk of uncontrolled flow from wells through permafrost. In *Permafrost – North American Contribution to Second International Conference on Permafrost, Yakutsk, Siberia, July 13–18, 1973*. Washington, DC: National Academy of Sciences, pp. 462–468.
Martinec, J., 1970. Recession coefficient in glacier runoff studies. *Bulletin of the IASH*, **15**(1), 87–90.
Martinec, J., 1975. Subsurface flow from snowmelt traced by tritium. *Water Resources Research*, **11**(3), 496–498.
McWhorter, D., and Sunada, D. K., 1977. *Ground-water hydrology and hydraulics*. LLC, Highlands Ranch, CO: Water Resources.
Rodhe, A., 1981. Spring flood – meltwater or groundwater? *Nordic Hydrology*, **12**(1), 21–30.
Roulet, N. T., and Woo, M.-K., 1986. Hydrology of a wetland in the continuous permafrost region. *Journal of Hydrology*, **89**, 73–91.
Singh, P., and Singh, V. P., 2001. *Snow and glacier hydrology*. Dordrecht, The Netherlands: Kluwer Academic.
Sokolov, B. L., 1978. Regime of naleds. In Sanger, F. J. (ed.), (with assistance of P. J. Hyde), *Permafrost-USSR Contribution to Second International Conference on Permafrost, Yakutsk, Siberia, July 13–18, 1973*. Washington, DC: National Academy of Sciences, pp. 408–411.
Stenborg, T., 1970. Delay of runoff from a glacier basin. *Geografiska Annaler*, **52A**(1), 1–30.
Stephenson, G. R., and Freeze, R. A., 1974. Mathematical simulation of subsurface flow contributions to snowmelt runoff, Reynolds Creek watershed, Idaho. *Water Resources Research*, **10**(2), 284–294.
Tangborn, W. V., Krimmel, R. M., and Meier, M. F., 1975. A comparison of glacier mass balance by glaciological, hydrological and mapping methods, South Cascade Glacier, Washington. In *Proceedings of the Snow and Ice Symposium*. Moscow Symposium, IASH Publ. No. 104, pp. 185–196.
Tolstikhin, N. I., 1978. Groundwater of the permafrost region of the USSR. In Sanger, F. J. (ed.) (with assistance of P. J. Hyde), *Permafrost-USSR Contribution to Second International Conference on Permafrost, Yakutsk, Siberia, July 13–18, 1973*. Washington, DC: National Academy of Sciences, pp. 724–733.
Williams, J. R., 1970. *Groundwater in the permafrost regions of Alaska*. Professional paper 696, U.S. Geological Survey, Washington DC.
Williams, J .R., and Waller, R. M., 1966. Groundwater occurrence in permafrost regions of Alaska. In *Permafrost: Proceedings of an International Conference, Lafayette, I ndiana, Nov. 11–15, 1963*. National Research Council Publication 1287. Washington, DC: National Academy of Sciences- National Research Council, pp. 159–164.

Cross-references

Permafrost
Talik

BED (BOTTOM) TOPOGRAPHY

Vijay Kumar
National Institute of Hydrology, Roorkee, India

Bed topography represents the shape and features of the riverbed. The shape of a riverbed is largely determined by the relief of the terrain through which river crosses. Riverbed topography varies due to local controls imposed by boulder, log, and gravel bar obstructions. Increased flow, as during a flood or high rainfall season, can make permanent changes to the riverbed by displacing rocks and boulders or by deposition of alluvium. In a meandering river, the riverbed topography is modified by the development of point bars at the inner side of each bend because of the localized deposition and erosion processes.

The riverbed topography affects the flow characteristics of a river. The frictional effects related to the riverbed topography make the flow of water in a river cross-section nonuniform. The river water may exhibit strong turbulence caused in part by certain features of the river topography. Riverbed topography is considered as a primary factor in creating rapids. Variation in riverbed topography influences the potential energy distribution at the boundary between the river and subsurface and could be a significant control on surface–subsurface interactions in the mountain rivers. Streambed topography influences groundwater–surface water interactions at a scale as small as channel bed slope units by creating localized pathways for stream flow in the subsurface that return to the surface a short distance downstream (Harvey and Bencala, 1993).

Measurement of riverbed topography plays a key role in validating sedimentary processes in experimental hydraulics. The repetitive measurement of riverbed topography is one of the common approaches used to estimate gravel load in rivers. The riverbed topography can be obtained by the measurement of set range lines by conventional land surveying equipment and techniques. New techniques of digital photogrammetry and image analysis (Westaway et al., 2003) and airborne LIDAR (Hilldale and Raff, 2008) can be used to generate riverbed topography.

Bibliography

Harvey, J. W., and Bencala, K. E., 1993. The effect of streambed topography on surface-subsurface water exchange in mountain catchments. *Water Resource Research*, **29**, 89–98.
Hilldale, R. C., and Raff, D., 2008. Assessing the ability of airborne LiDAR to map river bathymetry. *Earth Surface Processes and Landforms*, **33**(5), 773–783.
Westaway, R. M., Lane, S. N., and Hicks, D. M., 2003. Remote survey of large-scale braided, gravel-bed rivers using digital photogrammetry and image analysis. *International Journal of Remote Sensing*, **24**(4), 795–815.

BED FORMS (FLUVIAL)

Vijay Kumar
National Institute of Hydrology, Roorkee, India

Bed form can be defined as the feature developed on the bed of an alluvial channel due to the flow of water.

Bed forms are structures that are molded on beds where deposition takes place due to flowing water. Natural channels rarely have flat beds. When water carries loose grains across a horizontal bed of unconsolidated sediment, regular geometric patterns develop on the surface of the bed. Any particle that is larger than approximately 0.7-mm diameter will form visible topographic features on the riverbed or streambed. Shear stresses above the critical for transport will mold cohesion-less beds into discernible forms whose geometry depends on flow characteristics which in turn are influenced by those forms, resulting in complex feedback relationship (Knighton, 1998). Various concealed bed forms most commonly associated with sand bed are ripples, dunes, plane bed, and antidunes. Pebble clusters, transverse ribs, riffle-pool sequence, and step-pool systems are some of the bed forms developed in gravel bed streams. Sequences of steps and pools are generally formed in steep rocky channels.

The size and shape of bed forms depend on the flow strength and grain size. Very fine sand and silt are very easy to transport and erode. They form nice ripples, but do not form dunes when transported by water. Coarse sand and larger sediment are too hard to transport and erode to get ripples. For a given bed material size in the sand range, the sequence of ripples, dunes, plane beds, and antidunes is correlated with increasing flow intensity. At very low discharges, the bed of a sand stream may be dominated by ripples. As flow increases, sand dunes begin to appear on the bed. If discharge continues to increase, a point is reached when the flow velocity mobilizes the sand on the streambed and the entire bed converts again to a planar form. If discharge increases further still, antidunes may form.

Bibliography

Knighton, D., 1998. *Fluvial Forms & Processes: A New Perspective*. London: Arnold, p. 383.

BED ROUGHNESS

Vijay Kumar
National Institute of Hydrology, Roorkee, India

Bed roughness develops due to stream surface relief at the base of a flowing fluid and it exerts frictional effect on the flow in the stream. Bed roughness is considered to be smooth or rough depending on whether sediment particles project through the viscous sublayer at the base of the flow. Roughness generally increases with increasing particle size.

There are two components of bed roughness: (a) grain roughness which relates to the effects of the individual grains making up the channel bed and (b) form roughness which refers to features of bed forms such as ripples and dunes, created when certain alluvial substrates are moulded by the flow. Grain roughness refers to the shear forces created by sediment particles at the flow boundary. Grain roughness is mainly a function of relative roughness which is defined as the ratio of depth of flow and bed material size. Grain roughness can be the dominant component of the bed roughness where stream beds consist of gravel or cobbles.

The shape and size of in-stream sediment deposits, or bed forms contribute to the bed roughness. In sand-bed streams, form roughness is often considered more important than grain roughness (Knighton, 1998). Bed forms like ripples and dunes increase the roughness of the stream bottom, which tends to slow velocity and increase the depth of flow. Sediment cover of different sizes increases bed roughness.

Bed roughness plays an important role in streams. It helps to determine the depth or stage of flow in a stream reach. As flow velocity slows in a stream reach due to roughness, the depth of flow has to increase to maintain the volume of flow that enters the upstream end of the reach (a concept known as flow continuity).

Bibliography

Knighton, D., 1998. *Fluvial Forms & Processes: A New Perspective*. London: Arnold. 383 pp.

BED STRENGTH

Vijay Kumar
National Institute of Hydrology, Roorkee, India

Bed strength (shear) represents the internal strength of the bed. It is determined by the amount of internal frictional resistance within the bed material. Bed strength depends on the sediment composition and the state of consolidation of bed. Shear strength increases when sediment grains are tightly packed together. Silt and clay particles, if present in a bed material, tend to stick together as a result of cohesive (attractive) electrochemical forces between the particles and so help in erosion resistance. Under normal flow conditions, there is a balance between the erosive power of the flow and the strength of the bed material. The changes in the channel form during major flood events, when the erosive power of the flow is greatly increased, depend on how much resistance is provided by the bed and banks. Bed erosion takes place when the bottom shear stress exceeds the strength, i.e., resistance forces, of the bed. The shear strength of the cohesive sediment bed is generally a linear function of the bed bulk density. Flowing water exerts shear stress on the bed material in the direction of flow. Shear stress is the frictional force per unit of bed area exerted on the bed by the flowing water. The faster the water velocity, the greater is the shear stress.

BENCHMARK GLACIER

Tobias Bolch
Department of Geography, University of Zürich-Irchel, Zürich, Switzerland

Synonyms

Reference glacier

Definition

A benchmark glacier is a glacier on which detailed direct measurements of seasonal glacier mass changes, meteorological environment, and streamflow variations are collected for an indefinite period, and which should be representative for a particular region.

Benchmark glacier, reference glacier and glacier monitoring

The term "benchmark glacier" was established as part of the monitoring strategy of the United States Geological Survey (USGS) (Fountain et al., 1997). The similar term "reference glacier" is in the monitoring strategy of the Global Terrestrial Network for Glaciers (GTN-G, http://www.fao.org/gtos/gt-netGLA.html) a glacier with a long-term, continuous, and continuing programme of mass balance observations. The benchmark and reference glacier concepts are similar; however, the reference glacier does not claim to be representative for other glaciers in a mountain range. The majority of benchmark glaciers were established during the 1960s as part of the International Hydrological Decade. The main objective here was to measure "typical" mass and energy processes on glaciers and to provide data on the resulting effect on streamflow in each mountain range in different climatic regions around the world (Fountain et al., 1997; UNESCO/IAHS, 1970). Hence, the selected benchmark glaciers are intended to be representative for a selected region or mountain range. Detailed direct measurements of seasonal glacier mass changes, glacier geometry, meteorological environment, and streamflow variations are to be collected at each benchmark glacier. Glacier mass balance shows a direct response to the climate variables and is hence a valuable component of climate monitoring. Front variation measurements are important complements to the mass balance measurements as they are less laborious, have a better global coverage (data available for about 1,700 glaciers worldwide, WGMS, 2008) and they extend much further back in time. The main drawback is that the length variations show an indirect climate signal, only.

Earliest glacier monitoring was initiated in 1894 for about 50 glaciers in the European Alps with the establishment of the International Glacier Commission (Haeberli, 1998). The longest record of continuous long-term measurements of glacier mass balance with ablation stakes on the glacier started at Storglaciären, Sweden in 1945. The benchmark glaciers have attracted new interest in the past decade because they are used to further understanding of the contribution of alpine glaciers to river run-off and global sea-level rise. The majority of the monitored glaciers have strong negative mass balances series. The global average shows moderate ice loss since the 1960s followed by accelerating mass loss since the middle or end of the 1980s up to recent years (WGMS, 2008).

Distribution of benchmark glaciers and their representativeness for major mountain ranges

The distribution of benchmark glaciers with mass balance measurements are biased towards the northern hemisphere and Europe (Figure 1). Only about 10% are situated in the southern hemisphere. The longest mass balance series are found in the European Alps and Scandinavia. Other long-term measurements are located in North America and the high mountains of Asia. There is only one long-term measurement in the tropics (1979–1996, Lewis Glacier, Mt. Kenya). The large ice masses situated around the two ice sheets in Greenland and Antarctica, South America, and Northern Eurasia with few and short-term measurements are strongly underrepresented (Zemp et al., 2009). Altogether, there are mass balance measurements available from 228 glaciers, but only about 30 glaciers have continuous measurements since 1976 (Table 1). Mass balance measurements for 97 glaciers on the globe exist for the hydrological year 2006 (Zemp et al., 2009). Some measurements were begun in recent years in previously underrepresented regions such as the Andes, the Southern Alps in New Zealand, the Indian Himalaya, on the Tibetan Plateau, and the Antarctica in order to expand the worldwide coverage. However, other measurements were discontinued in the 1990s, especially in the high mountains of Asia (Caucasus, Tien Shan, Altay) (WGMS, 2008).

The intention in this chosen distribution of benchmark glaciers was to obtain representative data for mountain ranges in different climatic regimes. However, the choice of glaciers was often motivated by logistic considerations (e.g., accessibility). Hence, even when mass balance measurements do exist, their representativeness is often unclear. Fountain et al. (2009) found in a study on northwest USA that its benchmark glacier (South Cascade Glacier) is much larger, has a lower slope and its mass loss is greater than most other glaciers in the region. The glacier AX010 in the Nepal Himalayas with little longer term mass balance measurements (Fujita et al., 2001) is comparatively small (0.42 km² in 1999), low in altitude, and has no debris cover. Hence, it cannot be seen as representative for the Himalaya, as larger debris-covered glaciers are common in these mountains. In addition, its elevation is relatively low.

Discussion

The existing data from the benchmark glaciers are an important source of information on glacier changes over

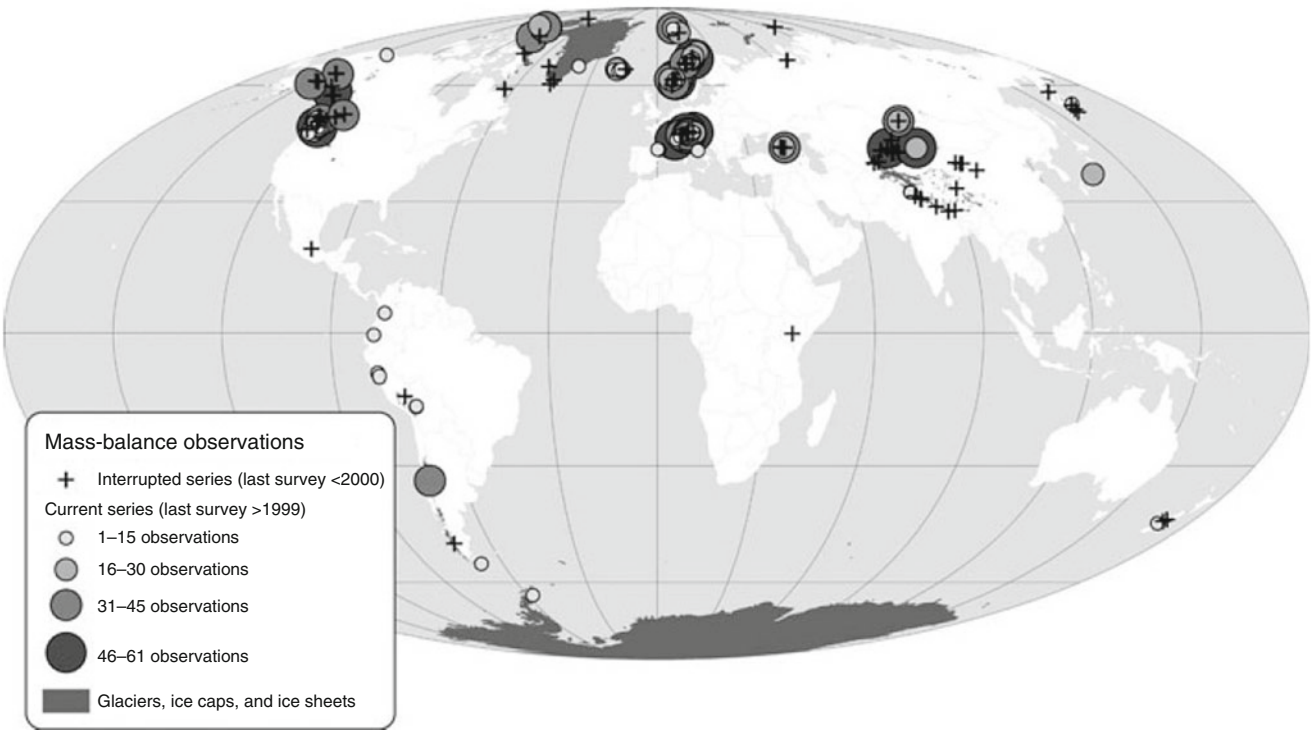

Benchmark Glacier, Figure 1 Distribution of glaciers with mass balance observations (Source: Zemp et al., 2009, reprinted from the Annals of Glaciology with permission of the International Glaciological Society).

the corresponding period. However, further analysis is recommended in order to assess the representativeness of these glaciers for the corresponding mountain ranges and climatic zones (Fountain et al., 2009; Haeberli et al., 2007). Less intensive field studies on the mass balance of glaciers in the surrounding region ("Secondary Glacier Network," Fountain et al., 1997), front variation measurements, analysis of the Little Ice Age moraines, and remote-sensing-based analysis provide important supplemental data in order to assess the complexity for each glacierized region. A suitable method for assessing the representativeness of benchmark glaciers, besides measuring of length changes of surrounding glaciers, is the differencing of digital elevation models (DEM) (Paul and Haeberli, 2008). The glacier mass change is derived from a change in elevation over time (dh/dt). This so-called geodetic method requires exact elevation information for at least two periods in time (Bhamber and Rivera, 2007). Elevation data can be obtained by different methods such as altimetry (e.g., airborne LiDAR, ICESat GLAS); photogrammetry (stereo airborne or spaceborne imagery, such as from ASTER, SPOT); and interferometric synthetic aperture radar (InSAR, from repeat pass or single pass observations such as from ERS, Terra-SAR-X or the SRTM-Mission). Aerial imagery and data from reconnaissance satellite imagery such as Corona are suitable sources for extending the data back in time (Bolch et al., 2008). Topographic maps should be used with caution due to variing accuracy of the glacier outlines (Bhambri and Bolch, 2009). High accuracy can be obtained by airborne laser scanning (LiDAR). Geodetic derived mass balances and especially the latter method is an important source for calibrating the field measurements on mass balance as it can cover the entire glacier. The main advantage of remote sensing is that data can be obtained from glaciers or glacier sections which are difficult or not possible to access. Hence, new benchmark glaciers for remote-sensing-based monitoring could be selected. Remote sensing methods offer great opportunities for the future but cannot substitute for detailed field measurements on benchmark glaciers, as not all relevant data such as runoff can be obtained. In addition, all remote sensing methods need ground truth for verification and calibration.

Most of the relevant glacier data are collected by individual researchers and institutions with little funding, and compiled for public availability through WGMS. Not all data, however, is available through WGMS or other generally accessible databases such as the National Snow and Ice Data Center in Boulder/Colorado (www.nsicd.org). In order to improve the knowledge about the worldwide glacier changes and their consequences (e.g., sea-level rise), an approach combining detailed field investigations on benchmark glaciers with remote sensing

Benchmark Glacier, Table 1 Characteristics of the most important benchmark glaciers with ongoing, continuous mass balance measurements (Source: Zemp et al., 2009; Cox and March, 2004; Demuth and Pietroniro, 1999)

Name	Country/region	Mountain range	Area (km²)	Begin measurements
Gulkana glacier	USA/Alaska	Alaska Range	17.1 (1999)	1966
Wolverine glacier	USA/Alaska	Kenai Mountains	172 (1995)	1966
Peyto glacier	Canada	Rocky Mountains	~12 (1990s)	1966
Place glacier	Canada	Coast Mountains	3.2 (2005)	1965
South cascade glacier	USA	Cascades	1.9 (2003)	1953
Echaurren Norte	Chile	Andes	0.4 (2000)	1976
Austre Brøggerbreen	Norway	Spitsbergen	6.1 (1995)	1967
Midtre Lovénbreen	Norway	Spitsbergen	5.5 (1999)	1968
Ålfotbreen	Norway	Scandes	4.5 (2005)	1963
Engabreen	Norway	Scandes	3.6 (2005)	1970
Gråsubreen	Norway	Scandes	2.3 (2005)	1962
Hardangerjøkulen	Norway	Scandes	17.1 (2005)	1963
Hellstugubreen	Norway	Scandes	3.0 (2005)	1962
Nigardsbreen	Norway	Scandes	47.8 (2005)	1962
Storbreen	Norway	Scandes	5.4 (2005)	1949
Storglaciären	Sweden	Scandes	3.2 (2005)	1946
Sait Sorlin	France	Alps	3.0 (2000)	1957
Serennes	France	Alps	0.5 (2000)	1949
Gries	Switzerland	Alps	6.2 (2001)	1962
Silvretta	Switzerland	Alps	3.0 (2003)	1960
Hintereisferner	Austria	Alps	7.5 (2005)	1953
Kesselwandferner	Austria	Alps	3.9 (2005)	1953
Sonnblickkees	Austria	Alps	1.4 (2005)	1959
Vernagtferner	Austria	Alps	8.4 (2005)	1965
Caresr	Italy	Alps	2.8 (2005)	1967
Djankuat	Russia	Caucasus	2.7 (2005)	1968
Leviy Aktru	Russia	Altai	6.0 (2000)	1977
Maliy Aktru	Russia	Altai	2.7 (2000)	1962
Vodopadniy (No. 125)	Russia	Altai	0.75 (2000)	1977
Ts. Tuyuksuyskiy	Kazakhstan	Tien Shan	2.5 (2005)	1957
Urumqihe S. No. 1	China	Tien Shan	1.7 (2000)	1959

analysis and distributed mass balance modelling is recommended (Haeberli et al., 2007). New benchmark glaciers with intensive field studies in so far underrepresented regions should be established. These glaciers should be carefully selected based on statistical considerations concerning climate and glacier characteristics (size, dynamics, debris cover, accumulation area ratio, etc.) in order to match the goal to be representative. However, they need to be also accessible in order to be able to perform continuous measurements.

Conclusions

Benchmark glaciers have long-term continuous measurements and should be representative for a certain region. The existing detailed measurements on the selected glaciers are of high importance but they have to be checked for their representativeness. If required, the data has to be adjusted so as to be seen as representative. It is recommended to publish all available records, to extend the monitoring network to previously underrepresented regions with no or few measurements, and to monitor glaciers based on remote sensing in order to reach the major objectives of the benchmark glacier concept: to obtain a worldwide overview of glacier variability based on detailed measurements on selected representative glaciers.

Bibliography

Bamber, J. L., and Rivera, A., 2007. A review of remote sensing methods for glacier mass balance determination. *Global and Planetary Change*, **59**(1–4), 138–148.

Bhambri, R., and Bolch, T., 2009. Glacier mapping: a review with special reference to the Indian Himalayas. *Progress in Physical Geography*, **33**(5), 672–704.

Bolch, T., Buchroithner, M. F., Pieczonka, T., and Kunert, A., 2008. Planimetric and volumetric Glacier changes in Khumbu Himalaya since 1962 using Corona, Landsat TM and ASTER data. *Journal of Glaciology*, **54**(187), 592–600.

Cox, L. H., and March, R. S., 2004. Comparison of geodetic and glaciological mass-balance techniques, Gulkana Glacier, Alaska, USA. *Journal of Glaciology*, **50**(170), 363–370.

Demuth, M., and Pietroniro, A., 1999. Inferring glacier mass balance using radarsat: results from Peyto glacier, Canada. *Geografiska Annaler A*, **81**(4), 521–540.

Fountain, A. G., Krimmel, R. M., and Trabant, D. C., 1997. A strategy for monitoring glaciers. *U.S. Geological Survey Circular*, **1132**, 19.

Fountain, A. G., Hoffman, M. J., Granshaw, F. D., and Riedel, J., 2009. The "benchmark glacier" concept - does it work? Lessons from the North Cascade Range, USA. *Annals of Glaciology*, **50**, 163–168.
Fujita, K., Kadota, T., Rana, B., Shresta, R. B., and Ageta, Y., 2001. Shrinkage of Glacier AX010 in shorong region, Nepal Himalayas in the 1990s. *Bulletin of Glaciological Research*, **18**, 51–54.
Haeberli, W., 1998. Historical evolution and operational aspects of worldwide glacier monitoring. Into the second century of worldwide glacier monitoring: prospects and strategies. Haeberli, W., Hoelzle, M., Suter, S., UNESCO Studies and Reports in Hydrology. Vol. 56, pp. 35–51.
Haeberli, W., Hoelzle, M., Paul, F., and Zemp, M., 2007. Integrated monitoring of mountain glaciers as key indicators of global climate change: the European Alps. *Annals of Glaciology*, **46**, 150–160.
Paul, F., and Haeberli, W., 2008. Spatial variability of glacier elevation changes in the Swiss Alps obtained from two digital elevation models. *Geophysical Research Letters*, **35**, L21502, doi:10.1029/2008GL034718.
UNESCO/IAHS, 1970. Perennial ice and snow masses – a guide for compilation and assemblage of data for the world glacier inventory. Technical Papers in Hydrology, No. 1.
WGMS, 2008. Global Glacier Changes: facts and figures. In Zemp, M., Roer, I., Kääb, A., Hoelzle, M., Paul, F., and Haeberli, W. (eds.), UNEP, World Glacier Monitoring Service, Zurich, Switzerland, 88 pp.
Zemp, M., Hoelzle, M., and Haeberli, W., 2009. Six decades of glacier mass balance observations - a review of the worldwide monitoring network. *Annals of Glaciology*, **50**, 101–111.

Cross-references

Glacier Mass Balance

BIOGEOCHEMISTRY OF SEA ICE

David N. Thomas
School of Ocean Sciences, College of Natural Sciences, Bangor University, Menai Bridge, Anglesey, UK

Synonyms

Land-fast ice; Pack ice

Definition

Salinity: The sum of all dissolved salts in grams per kilogram of seawater
Primary production: Photosynthetic carbon fixation per unit area, per unit of time.
Autotrophy: The ability to utilize inorganic carbon (usually CO_2) as the sole source of carbon for organic synthesis, based on energy from light (photoautotrophic) or from oxidation of inorganic compounds (chemoautotrophic).
Heterotrophy: The ability of an organism to obtain carbon for organic synthesis by metabolizing organic materials.
Psychrophilic: Describing an organism that lives and grows optimally at relatively low temperatures, usually below 15°C, and cannot grow above 20°C. Psychrophiles consist mainly of bacteria, algae, fungi, and protozoans; extreme psychrophiles can grow at subzero temperatures.

Introduction

Every autumn and winter, a fundamental transition occurs in the surface waters of the Arctic and Southern Oceans, and nonpolar seas such as the Baltic, Caspian, and Okhotsk. The surface waters of millions of square kilometers freeze to form an ice layer that varies from a few centimeters through to several meters thick, and which effectively separates the ocean from the atmosphere above. Ice made from seawater is a porous, semisolid matrix permeated by a labyrinth of brine channels and pores, and within these a diverse microbial assemblage, including viruses, archaea, bacteria, flagellates, and unicellular algae can thrive (Figure 1). The microbial assemblages are in turn a rich food source for grazing proto- and zooplankton, especially in winter when food in the water column is scarce (Brierley and Thomas, 2002).

The study of biogeochemical processes in sea ice originated from the long-established ecological studies of organisms living in or at the peripheries of ice floes in the Southern and Arctic Oceans. In the past 30 years, our knowledge of the diversity of organisms associated with the oceanic cryosphere and the ecological interactions of sea ice assemblages has received considerable research effort and these works are extensively reviewed (contributions in Thomas and Dieckmann, 2010). In an effort to more clearly emphasize the biological drivers for current sea ice research, Arrigo and Thomas (2004) concluded that the term ecobiogeochemistry would be a better reflection of current of the way must sea ice research is conducted. It will become clear during this short review that there is a case for describing the current multidisciplinary study of sea ice under the rather impractical term

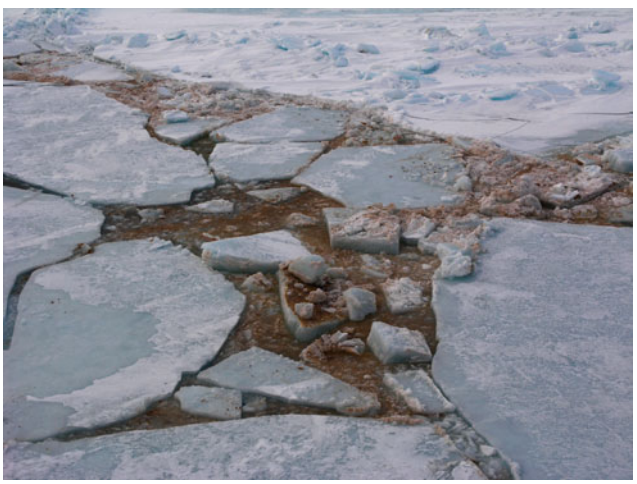

Biogeochemistry of Sea Ice, Figure 1 Antarctic ice floes demolished by an ice-breaking research ship. Within the debris, the dark brown color of extensive sea ice assemblages is revealed.

of physico-ecobiogeochemistry: The unique temperature and salinity and space limitations within the frozen sea ice matrix mean that any study of biology, chemistry, or geochemistry that does not consider the pertinent abiotic drivers is considerably compromised.

Freezing of seawater

It is important to keep in mind that sea ice is ephemeral, and for most systems on Earth the life span of most ice formed in autumn or winter is less than 6 months. There are regions where multiyear sea ice is well documented, and in the past thick multiyear ice floes (over 5 years old) where a characteristic of the Arctic system that was often cited as one of the main characteristics that differentiated Arctic and Southern Ocean systems. However, with the recent well-recorded changes in Arctic sea ice extent and thickness (Serreze et al., 2007), it is predicted that within the next 2 decades, 90% of the sea ice on Earth will not be older than 1 year, and the majority of this will be probably only last less than 6 months.

When seawater freezes (at −1.86°C) ice crystals form and float to the surface of the water column where they collect. On further freezing, the crystals coalesce to form a rigid structure of ice, the form of which is greatly influenced by the nature of the turbulence of the waters in which the crystals are formed. As ice crystals grow, the dissolved constituents of the water are expelled, and this results in the formation of a system of channels and pores permeating the ice matrix. These are filled with concentrated brines derived from the ice crystal mass. Since temperature determines the mass of ice, therefore it also determines the volume of brine and the concentration of dissolved constituents, or salinity of that brine (Figure 2). At −6°C, the brine salinity is 100, at −10°C it is 145, and at −21°C it is 216. The brines are not static and gravity results in a high proportion of the brine draining out of thickening ice sheets and in time the ice becomes desalted. The bulk properties of ice integrate the ice mass and brine, so that although a piece of ice at −10°C may contain brines with a salinity of 145, the bulk salinity of ice when melted is less than 10. In the absence of any other processes (i.e., biological), the relationship between dissolved constituents (gases and ions) should lie on a conservative dilution line, and it is the correlation of measurements made on bulk ice samples with calculated dilution lines that are the fundamental of sea ice biogeochemical studies: Below the dilution line implies the biology has consumed the constituent, above that the biological activity has produced the constituent.

Ultimately, the distribution of biology in sea ice is limited by the space available, for example, a millimeter sizes crustacean cannot live in a micrometer-sized pore or channel. For this reason, the most concentrated biological accumulations in sea ice are found at the peripheries of ice floes (Figure 3), because they are in contact with the surrounding water or close to the freezing point of seawater. This means that the pore/channel space is large and the exchange of seawater means that replenishment or exchange of gases and nutrients is possible. However, typically just 5–10 cm into the ice away from the peripheral edges temperatures are of such that brine volumes are low and exchange processes are severely restricted (Figure 4).

Sea ice biological and chemical interactions

The biology that lives within the sea ice matrix exhibits a wide range of metabolic, physiological, and, in some cases, life-history strategies that enable them to withstand the temperature, salinity, and light gradients that exist across any ice floe (Thomas and Dieckmann, 2002). However, it should not be forgotten that any organism that is found in the ice is recruited from the open water plankton. It is true that many of the protists are psychrophilic and some have only been described in ice and so must

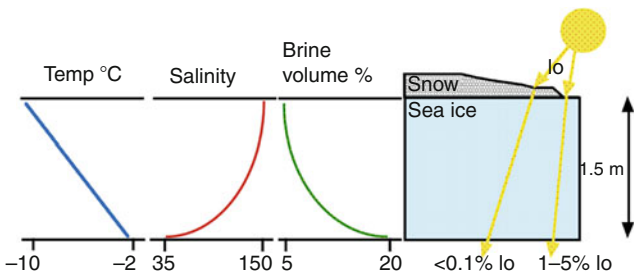

Biogeochemistry of Sea Ice, Figure 2 The physical nature of an ice floe is dominated by gradients in temperature, which in turn determine the salinity of brines and brine volume (porosity) of the ice. Likewise, the ice determines the light availability for photosynthesis. The incident irradiation (I_o) is very much reduced by the bottom of an ice floe where much of the biology is. This is significantly more reduced if snow covers the ice floe.

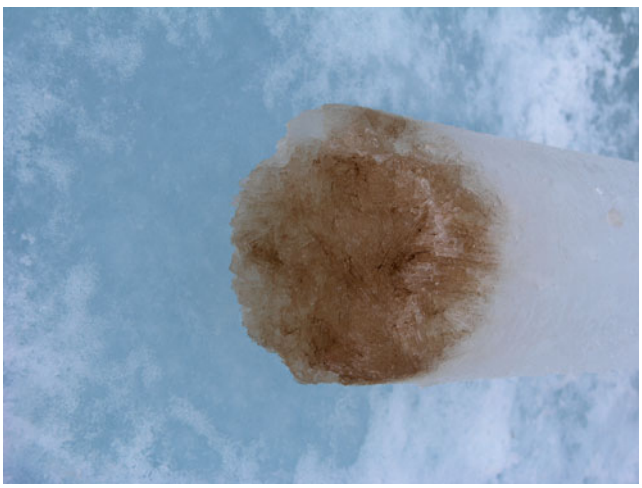

Biogeochemistry of Sea Ice, Figure 3 This tilted ice floe illustrates that the peripheries of the ice floe are where the biology concentrates.

Biogeochemistry of Sea Ice, Figure 4 The bottom of an ice core (9 cm in diameter) illustrating that most of the biology is restricted to the bottom 10 cm in the ice floe from which this core was taken.

be present in the plankton as dormant stages or cysts (e.g., ciliates and bacteria); however, there are many examples of organisms that are equally flourished in the plankton and ice.

When thinking about biogeochemical processes in aquatic systems, the balance between autotrophic and heterotrophic production and organic matter cycling and inorganic nutrient regeneration is mainly mediated through a complex microbial network. In the open ocean, the efficiency and impact of this network is strongly influenced by the distribution: for example, in reality there can be relatively large distances between microalgal autotrophs releasing organic matter into the water column and the bacteria that use such matter for growth. Resupply of nutrients or removal of gases are diffusion-driven, and as such are strongly influenced by turbulence on various scales from the micro through to the overturning of water masses. Organisms living within sea ice are of course very much more concentrated than in the water column, and therefore there is the potential that the biogeochemical processes are considerably more efficient, quicker, and enhanced. In contrast to this concept, naturally the light, salinity and temperature constraints in sea ice greatly influence the metabolism/physiologies of organisms, and the kinetics of biogeochemical processes, and in many cases these are slower than would be measured in open-water conditions. Therefore, in overall biogeochemical processes terms the consequences of dense accumulations of enhanced biological interactions may be a compensation for the suboptimal biochemical reaction rates.

It seems prudent to consider sea ice accumulations of biology and the biogeochemical characteristics that they have as being more akin to marine surface sediments in shallow waters and/or biofilms, rather than simply being a concentrated open-water network (Krembs and Deming, 2008). A consequence of life in the ice is that some metabolic processes cause significant biochemical changes in organisms that can markedly alter the geochemical "signatures" of the organisms when they sink to the ocean floor and are incorporated into marine sediments. An obvious result of this is that biochemical markers of previous sea ice extent over geological time are available to researchers (e.g., Belt et al., 2008).

Sea ice bacteria from Arctic ice have been shown to be active at temperatures down to −20°C, and motile down to −10°C (Deming, 2002; Deming and Eicken, 2007). It is thought that cryoprotectants such as antifreeze may be produced to inhibit ice crystal formation. The antifreeze proteins produced by bacteria are possibly part of the large pool of extracellular polymeric substances (EPS) located on the cell surface. In particular, the CFB group of bacteria is known for its abundant slime EPS production under decreasing temperatures. Such EPS have been found in other cold adapted bacteria and by unicellular algae isolated from sea ice. As a consequence, EPS concentrations in sea ice can be very high (Krembs and Deming, 2008).

There are ice-active substances (IASs) or ice-binding proteins (IBPs) produced by sea ice diatoms and bacteria. These (mainly glycoprotein's) have been shown to bind preferentially to ice crystals, causing pitting in the ice crystal surfaces. This pitting may in turn alter the optical properties of sea ice and may also help to maintain fine pore space structure. However, it might be that some interaction of the IASs/IBPs on the surface of cells increases the ability of cells to stick to ice surfaces, or is involved

in protecting cells from freeze-thaw damage (reviewed by Mock and Thomas, 2005, 2008).

Besides avoiding freezing, the transport of essential nutrients and gases through the cell membranes has to be guarantied under low temperatures and high salt concentrations. Hence, change increase in membrane fluidity is one of the most important acclimations during temperature reduction and is therefore well-documented particularly for bacteria. It is clear that a decrease in temperature leads to one or some combinations of the following changes: An increase in fatty acid unsaturation, a decrease in average chain length, an increase in methyl branching, and an increase in the ratio of anteiso-branching relative to iso-branching. Furthermore, polyunsaturated fatty acids (PUFA) are not normally detected in temperate bacteria but ω3 and ω6 fatty acids such as 20:5($n-3$) are often found in significant amounts in lipids of sea ice bacteria (reviewed by Mock and Thomas, 2005, 2008).

Besides temperature, salinity is probably the factor that has the greatest influence on the organisms living within the brine channel system, especially in cold ice where the brine salinities are typically three or four times seawater concentrations. The ability for diatoms to acclimate to hyperosmotic brine solutions is based on their ability to synthesize intracellular compatible solutes including amino acids such as proline and other cryoprotectants such as dimethylsulfoniopropionate (DMSP). Antarctic researchers have shown that very high concentrations of DMSP can be produced by ice algae assemblages reaching concentrations of over 1,500 nM, considerably more than seawater values that are typically below 50 nM (Trevena and Jones, 2006). DMSP is broken down to dimethylsulphide (DMS) and in remote ocean regions, DMS accounts for most of the non-sea salt sulfate in the atmosphere, and the oxidation of DMS in the atmosphere to aerosol particles and cloud condensation nuclei is part of a complex system of localized and global climate control. The greatest release of DMS from sea ice regions is associated with melting ice and the corresponding reduction in ambient salinity, when cells containing hypersaline-induced high concentrations of DMSP are released into the seawater. Periods of ice melt are also times when elevated grazing activity in ice edge waters will increase the release of DMS into surface waters and therefore into the atmosphere (Stefels et al., 2007). Of particular interest is the breakdown of DMSP to DMS and subsequently into methanesulphonic acid (MSA) which can be used as a proxy in glacial ice cores for past sea ice extent estimations (Curran et al., 2003; Dixon et al., 2005).

The still limited data on dissolved gases in sea ice brines indicate that when there is high primary production, and accumulation of large algal standing stocks in sea ice, the brines are characterized by substantial reductions in total inorganic carbon, pH values up to 11, and O_2 supersaturation (Papadimitriou et al. 2007). As stated previously, at high diatom standing stocks in the ice in general species diversity decreases. Gleitz and Thomas (1993) showed that as first-year sea ice grew and high algal standing stocks established the assemblages were dominated by only a very few small diatom species, and they suggested that pore and channel size was the major determining factor. However, Gleitz et al. (1998) subsequently concluded that it was the physiological capacity of these species to maintain high growth rates in the spring and summer, in connection with their life-history cycles, that may be the key to the prominence of so few diatom species in the ice for example. The ability to sustain photosynthesis at high O_2 and low CO_2 in a strongly alkaline environment will be a critical prerequisite for survival of algae within the ice. For example, the ability of algae actively to assimilate HCO_3^- at very low CO_2 (aq) concentrations is considered to be a decisive factor for the success of small diatom species common in sea ice algal assemblages (Gleitz et al., 1998).

Not all biogeochemical processes in sea ice are mediated by biology, and at low temperatures and high salinities, physicochemical processes are known to occur: Mineral precipitation from sea ice brine has been well characterized and the most thermodynamically consistent sequence of minerals precipitating from seawater derived brines during freezing is known as the Gitterman pathway and consists of calcite ($CaCO_3$) at −2.2°C, mirabilite ($Na_2SO_4.10H_2O$) at −6.3°C, gypsum ($CaSO_4.2H_2O$) at −22.9°C, hydrohalite ($NaCl.2H_2O$) at −22.9°C, sylvite (KCl) at −33.0°C, and $MgCl_2.12H_2O$ at −36.2°C. Documented observations of mineral precipitation in sea ice are still scarce in natural settings, but there is recent field evidence for ikaite formation in Antarctic late-winter sea ice (Dieckmann et al., 2008).

Summary

The frozen oceans and seas have held a wide-reaching fascination ever since the first explorers ventured into these realms. In the last 30 years or so, researchers have discovered that the ice is far from being a barren wasteland devoid of life. In contrast, sea ice supports a rich diversity and prolific life that is a vital part of the ecosystems over which the ice covers. The biogeochemical processes within sea ice have profound implications for the biogeochemistry of underlying waters and the ocean–atmosphere interactions. Our understanding of these processes is still hampered by the logistical difficulties in operating in such environments although this is being addressed in recent years as technology is developed that permits long-term programs of research to be established (see contributions in Thomas and Dieckmann, 2010).

Bibliography

Arrigo, K., and Thomas, D. N., 2004. The importance of sea ice for the Southern Ocean ecosystem. *Antarctic Science*, **16**, 471–486.

Belt, S. T., Massé, G., Vare, L. L., Rowland, S. J., Poulin, M., Sicre, M.-A., Sampei, M., and Fortier, L., 2008. Distinctive ^{13}C

isotopic signature distinguishes a novel sea ice biomarker in Arctic sediments and sediment traps. *Marine Chemistry*, **112**, 158–167.
Brierley, A. S., and Thomas, D. N., 2002. On the ecology of Southern Ocean pack ice. *Advances in Marine Biology*, **43**, 171–278.
Curran, M. A. J., van Ommen, T. D., Morgan, V. I., Phillips, K. L., and Palmer, A. S., 2003. Ice core evidence for Antarctic sea ice decline since the 1950s. *Science*, **302**, 1203–1206.
Deming, J. W., 2002. Psycrophiles and polar regions. *Current Opinion in Microbiology*, **5**, 301–309.
Deming, J. W., and Eicken, H., 2007. Life in ice. In Sullivan, W. T., and Baross, J. A. (eds.), *Planets and Life: The Emerging Science of Astrobiology*. Cambridge: Cambridge University Press, pp. 292–312.
Dieckmann, G. S., Nehrke, G., Papadimitriou, S., Gottlicher, J., Steininger, R., Kennedy, H., Wolf-Gladrow, D., and Thomas, D. N., 2008. Calcium carbonate as ikaite crystals in Antarctic sea ice. *Geophysical Research Letters*, **35**, L08501, doi:10.1029/2008GL033540.
Dixon, D., Mayewski, P. A., Kaspari, S., Kreutz, K., Hamilton, G., Maasch, K., Sneed, S. B., and Handley, M. J., 2005. A 200 year sulfate record from 16 Antarctic ice cores and associations with Southern Ocean sea-ice extent. *Annals of Glaciology*, **41**, 155–166.
Gleitz, M., and Thomas, D. N., 1993. Variation in phytoplankton standing stock, chemical composition and physiology during sea ice formation in the southeastern Weddell Sea, Antarctica. *Journal of Experimental Marine Biology and Ecology*, **173**, 211–230.
Gleitz, M., Bartsch, A., Dieckmann, G. S., and Eicken, H., 1998. Composition and succession of sea ice diatom assemblages in the Weddell Sea, Antarctica. In Lizotte, M. P., and Arrigo, K. R. (eds.), *Antarctic Sea Ice Biological Processes, Interactions and Variability*, American Geophysical Union, Washington D.C. Antarctic Research Series, Vol. 73, pp. 107–120.
Krembs, C., and Deming, J. W., 2008. The role of exopolymers in microbial adaptation to sea ice. In Margesin, R., Schinner, F., Marx, J.-C., and Gerday, C. (eds.), *Psychrophiles: From Biodiversity to Biotechnology*. Berlin: Springer, pp. 247–264.
Mock, T., and Thomas, D. N., 2005. Recent advances in sea ice microbiology. *Environmental Microbiology*, **7**, 605–619.
Mock, T., and Thomas, D. N., 2008. Microalgae in Polar regions: Linking functional genomics and physiology with environmental conditions. In Margesin, R., Schinner, F., Marx, J.-C., and Gerday, C. (eds.), *Psychrophiles: From Biodiversity to Biotechnology*. Berlin: Springer, pp. 285–312.
Papadimitriou, S., Thomas, D. N., Kennedy, H., Hass, C., Kuosa, H., Krell, A., and Dieckmann, G. S., 2007. Biochemical composition of natural sea ice brines from the Weddell Sea during early austral summer. *Limnology and Oceanography*, **52**, 1809–1823.
Serreze, M. C., Holland, M. M., and Stroeve, J., 2007. Perspectives on the Arctic's shrinking sea-ice cover. *Science*, **315**, 1533–1536.
Stefels, J., Steinke, M., Turner, S., Malin, G., and Belviso, S., 2007. Environmental constraints on the production and removal of the chemically active gas dimethylsuphide (DMS) and implcations for ecosystem modelling. *Biogeochemistry*, **83**, 245–275.
Thomas, D. N., and Dieckmann, G. S., 2002. Antarctic sea ice - A habitat for extremophiles. *Science*, **295**, 641–644.
Thomas, D. N., and Dieckmann, G. S. (eds.), 2010. *Sea Ice*, 2nd edn. Oxford: Wiley-Blackwell.
Trevena, A. J., and Jones, G. B., 2006. Dimethylsulphide and dimethylsulphoniopropionate in Antarctic sea ice and their release during sea ice melting. *Marine Chemistry*, **98**, 210–222.

Cross-references

Atmosphere-Snow/Ice Interactions
Palaeoclimate and Past Glaciations
Sea Ice

BLUE ICE

Richard Bintanja
Royal Netherlands Meteorological Institute (KNMI),
De Bilt, The Netherlands

Definition

Localized bare-ice regions on the Antarctic polar plateau.

Blue ice areas, which until now have only been found on the Antarctic ice sheet, are formed when wind conditions can erode the snow. These are often more localized regions, usually only a few square kilometers in area, where the topography has induced a surface wind field that favors continuous erosion of snow, leaving bare (blue) ice. Usually, but not exclusively, these blue ice areas are found in the wake of mountains protruding through the ice surface. Over the course of time, strong, turbulent surface winds erode the entire snow deck. Once the ice layers are surfaced, snow is unable to stick to the smooth ice, preventing the blue ice area from being covered by snow again. Blue ice areas are characterized by subzero temperatures, so that melting is insignificant, which differentiates them from regular glacial ablations zones.

The persistence of blue ice areas is reinforced by strong sublimation rates. Since blue ice is darker than the adjacent snow fields, and hence the surface albedo lower, heating through solar radiation is more vigorous, creating a relatively mild local climate in which the ice surface loses mass through sublimation. While only a tiny fraction of Antarctica is covered by blue ice, their bluish appearance makes them fairly easily recognizable from space. If climate-induced changes in local temperature and wind somehow affect the spatial extent of blue ice areas, these regions may be used as an indicator of climate variations taking place over the southern continent.

Blue ice areas feature a number of scientific and practical applications. First, since the ice originates from compacted snow accumulated long ago in adjacent snow regions, it may be very old with the potential of yielding paleoclimatic information from the air bubbles inside the ice. Second, blue ice areas are essentially the ablation zone of a much wider catchment area, where under favorable conditions meteorites that fall into this catchment area can accumulate by converging ice flows. The vast majority of meteorite specimens found on Earth were collected on Antarctic blue ice areas on the polar plateau. Finally, because of their smoothness, blue ice areas are commonly used as landing strips for aviation; the regular occurrence of wind-induced surface ripples provides the grip required.

Bibliography

Bintanja, R., 1999. On the glaciological, meteorological and climatological significance of Antarctic blue ice areas. *Reviews of Geophysics*, **37**(3), 337–359.
Bintanja, R., Reijmer, C. H., and Hulscher, S. J. M. H., 2001. Detailed observations of the rippled surface of Antarctic blue ice areas. *Journal of Glaciology*, **47**, 387–396.

BOTTOM MELTING OR UNDERMELT (ICE SHELF)

Ashok Kumar Verma
Cold Regions Research Center, Department of Geography & Environmental Studies,
Wilfrid Laurier University, Waterloo, ON, Canada

The basal melting of a snowpack or a glacier is termed as bottom melting. This term often related with glacier ablation, or under-melt for sea ice (Menzies, 1995). Various convective phenomena are responsible for the bottom melting which mainly depends upon the bulk temperature and velocity of the water and for the sea ice, would be salinity. The addition of sensible heat can cause the internal melting of the ice cover which could be added to the ice through conduction or radiative process. The overall effect of heat flux is to raise the bulk temperature of the ice to the point where preferential melting begins. The presence of snow at the upper surface may affect the process and magnitude of the bottom melting as it diverges the heat transfer to the underlying ice layers (Lock, 1990).

The process of melting initiates at the vicinity of impurities and the grain boundaries. The effect of impurities following the melting can be seen as rotten ice which is a reflection of granular structure of the ice. These effects can be seen in the sea ice with the formation of different colors and forms of sea ice (Weeks and Ackley, 1986) (Armstrong et al., 1973). Intergranular melting weakens the ice cover in combination of several other mechanical actions arising due to the wind and water behavior. The combined effect of the thermal expansion and undercurrents are capable of opening fissures in the cover. Wind magnifies the effects of opening fissures to the fragmentation of the ice covers. Warming of surface layer of water induce the convective instabilities which accelerate the bottom melting processes.

Bibliography

Armstrong, T., Roberts, B., and Swithinbank, C., 1973. *Illustrated Glossary of Snow and Ice*. Cambridge: Scott Polar Research Institute.
Lock, G. S. H., 1990. *The Growth and Decay of Ice*. Cambridge: Cambridge University Press, pp. 365–367.
Menzies, J., 1995. *Modern Glacial Environments: Processes, dynamics and sediments*. Oxford: Butterworth-Heinemann, Vol. 1.
Weeks, W.F. and Ackley, S.F., 1986. *The Growth, Structure and Properties of Sea Ice.* US Army Cold regions Research and Engineering Laboratory Monograph 82-1.

BRASH ICE

Chelamallu Hariprasad
Centre for Studies in Resource Engineering,
Indian Institute of Technology, Bombay, Powai,
Mumbai, Maharashtra, India

Accumulation of floating ice made up of fragments less than about 2 m across is called brash ice. Brash ice often forms between the ice floes. Brash ice consists of frazil

Brash Ice, Figure 1 Description: Brash ice forming at sundown in calm glacier bay, Patagonia, Chile (http://www.dreamstime.com/abstract-brash-ice-image1851031, Dated on April 27, 2009).

Brash Ice, Figure 2 Description: Brash ice, icebergs on an ocean as smooth and shiny as a mirror, Neko Harbor, Andvord Bay, Antarctica (http://www.dreamstime.com/brash-ice-icebergs-on-an-ocea-image2131394, Dated April 27, 2009).

ice that grows during freeze-up as well as rudiments of fracturing and colliding floes. Brash ice also originates from sea ice that is breaking up or commonly as debris from calving ice bergs or ice bergs that break up as part of their ongoing erosion. Whenever one large piece of ice falls off another, brash is generated and can cover quite large amounts of sea. Brash ice is considered ideal for studies of the properties of completely fresh sea ice, particularly because brash ice is a slushy mixture of ice and water that characterizes the first phase of ice formation in turbulent water, forms more rapidly than ice that freezes solid (Figures 1 and 2).

C

CALVING GLACIERS

Charles R. Warren
School of Geography and Geosciences, University of St. Andrews, St. Andrews, Scotland, UK

Calving glaciers terminate in water and lose mass by calving, the process whereby masses of ice break off to form icebergs. Since they may consist of temperate or polar ice, may be grounded or floating, and may flow into the sea or into lakes, many types exist. They are widely distributed, but while lake-calving glaciers may exist in any glacierized mountain range, tidewater glaciers (Tidewater Glaciers) are currently confined to latitudes higher than 45°. Typically, calving glaciers are fast flowing and characterized by extensional (stretching) flow near their termini, resulting in profuse crevassing (Crevasses). They usually terminate at near-vertical ice cliffs, which are typically a few tens of meters in height but are sometimes as much as 80 m high. Calving activity above the waterline comprises a continuum from small fragments of ice to pillars the full height of the cliff. Below the waterline much ice may be lost through melting, but, in deep water, buoyancy causes infrequent but high magnitude calving events. In some settings, thermal erosion (melting) at the waterline can cause calving by undercutting the cliff. The calving process permits much larger volumes of ice to be lost over a given time than melting; this is seen spectacularly at the margins of ice shelves (Ice Shelf) from which tabular icebergs (Iceberg) with surface areas of many tens of square kilometers can be released. For example, over 35 days in 2002, an area of 3,250 km^2 of the Larsen Ice Shelf in Antarctica calved catastrophically, releasing 720 km^3 of ice into the ocean.

Glaciers calve faster in deeper water. This correlation between calving rate ($\underline{u}_c$ in meters per annum) and water depth (h_w) is linear, and can be simply expressed as $\underline{u}_c = c\underline{h}_w$. The value of the coefficient c varies greatly in different settings, being highest for temperate glaciers and lowest for polar glaciers. Also, for any given water depth, calving is an order of magnitude faster in fjords (Fjords) than in lakes, largely as a result of the effect of the different water densities on the buoyancy forces acting on the ice. Much of our understanding of the dynamics of calving glaciers stems from intensive studies of a small number of Alaskan glaciers (Alaskan Glaciers), particularly Columbia Glacier and LeConte Glacier (Meier, 1997; O'Neel et al., 2001). This work established the empirical u_c/h_w relationship, but left the physical processes behind it unclear. Modeling has subsequently shown that this relationship, and the contrasting calving rates in tidewater and freshwater, can be understood with reference to intricate feedbacks between calving and glacier dynamics (Dynamics of Glaciers) (Van der Veen, 2002; Benn et al., 2007). In essence, calving rates are controlled primarily by variations in longitudinal strain rates and ice velocities (especially sliding speeds), which determine the density and depth of crevassing.

Calving glaciers are significant for three main reasons:

1. *Glacier dynamics.* Calving glaciers comprise the most dynamic elements of many of the world's ice masses, and calving is the major means of ice loss from the two continental ice sheets of Antarctica and Greenland (Antarctica and Greenland Ice Sheet) (Rignot and Kanagaratnam, 2006). An understanding of calving processes is therefore critical for predicting cryospheric response to future climate change and consequent sea-level rise; our present limited understanding of the links between climate and ice dynamics hinders such predictions (Nick et al., 2009). During the waning stages of Quaternary glacial periods

Vijay P. Singh, Pratap Singh & Umesh K. Haritashya (eds.), *Encyclopedia of Snow, Ice and Glaciers*, DOI 10.1007/978-90-481-2642-2,

(Quaternary Glaciation), calving was the dominant process of mass loss around the midlatitude ice sheets, and calving processes strongly affected their patterns of growth and decay. Armadas of icebergs discharged during ice sheet collapses are believed to have caused global climate change by altering oceanic circulation. Calving has also accounted for the rapid collapse of ice shelves around the Antarctic Peninsula in recent decades, most notably the Larsen ice shelves.

2. *Non-climatic behavior*. Calving glacier fluctuations are highly sensitive to topographic controls, with advances and retreats often being punctuated by stillstands at topographic pinning points – locations of relative narrowing and shallowing. Some tidewater glaciers fluctuate cyclically, in ways unrelated to climate, over distances of tens of kilometers and over timescales of centuries to millennia. Therefore, neither the contemporary behavior of calving glaciers nor the geomorphological records from past fluctuations can be interpreted straightforwardly as indicators of climatic change (Warren, 1992; Vieli et al., 2001).
3. *Socioeconomic impacts*. Calving glaciers can provide resources for society, but they also represent significant hazards. Resources include tourism and the medium-term possibility of harnessing Antarctic tabular icebergs as a source of freshwater, while hazards include icebergs and glacier lake outburst floods (Glacier Lake Outburst Floods). With continued global warming (Global Warming and Its Effect on Snow/Ice/Glaciers), calving may lead to rapid and sustained loss of ice from the marine ice sheet (Marine Ice Sheet) of West Antarctica, in turn causing global sea-level rise of 3–4 m (Sea-Level).

Bibliography

Benn, D. I., Warren, C. R., and Mottram, R. H., 2007. Calving processes and the dynamics of calving glaciers. *Earth Science Reviews*, **82**, 143–179.

Meier, M. F., 1997. The iceberg discharge process: observations and inferences drawn from the study of Columbia Glacier. In van der Veen, C. J. (eds.), *Calving Glaciers: Report of a Workshop, Febuary. 28–March 2, 1997*. Byrd Polar Research Centre Report No. 15. Columbus, Ohio: The Ohio State University, pp. 109–114.

Nick, F. M., Vieli, A., Howat, I. M., and Joughin, I., 2009. Large-scale changes in Greenland outlet glacier dynamics triggered at the terminus. *Nature Geoscience*, **2**, 110–114.

O'Neel, S., Echelmeyer, K. A., and Motyka, R. J., 2001. Short-term flow dynamics of a retreating tidewater glacier: LeConte Glacier, Alaska, U.S.A. *Journal of Glaciology*, **47**, 567–578.

Rignot, E., and Kanagaratnam, P., 2006. Changes in the velocity structure of the Greenland Ice Sheet. *Science*, **311**, 986–990.

Van der Veen, C. J., 2002. Calving glaciers. *Progress in Physical Geography*, **26**, 96–122.

Vieli, A., Funk, M., and Blatter, H., 2001. Flow dynamics of tidewater glaciers: a numerical modelling approach. *Journal of Glaciology*, **47**, 595–606.

Warren, C. R., 1992. Iceberg calving and the glacioclimatic record. *Progress in Physical Geography*, **16**, 253–282.

Cross-references

Alaskan Glaciers
Antarctica
Dynamics of Glaciers
Fjords
Glacier Lake Outburst Floods
Global Warming and its Effect on Snow/Ice/Glaciers
Greenland Ice Sheet
Ice Shelf
Marine Ice Sheet
Quaternary Glaciation
Sea-Level
Tidewater Glaciers

CANADIAN ROCKIES AND COAST MOUNTAINS OF CANADA

John J. Clague[1], Brian Menounos[2], Roger Wheate[2]
[1]Department of Earth Sciences, Simon Fraser University, Burnaby, BC, Canada
[2]Geography Program and Natural Resources and Environmental Studies Institute, University of Northern British Columbia, Prince George, BC, Canada

Definition

Alpine glaciers cover about 26,000 km^2 of British Columbia and westernmost Alberta. The glacier source areas are cirques and plateaus above about 1,500-m elevation in several mountain ranges that trend northwest through the two provinces. Some glaciers in the Coast and St. Elias Mountains extend down to elevations below 500 m asl and one (Grand Pacific Glacier) calves into the sea. This article summarizes the distribution of glaciers in British Columbia (B.C.) and Alberta, discusses the mass balance and climatology of the glaciers, and describes historical changes in ice cover.

Introduction

The total area of glaciers in British Columbia (B.C.) and Alberta is about 26,000 km^2, which is about one quarter of the area of alpine ice cover in North America, but only 0.2% of the total on Earth. The number of glaciers, although difficult to establish, is approximately 15,000, of which about 1,000 are in Alberta. Nearly 70% of the total glacierized area in B.C. and Alberta is in the Coast Mountains, a series of northwest-trending ranges bordering the Pacific coast and extending about 1,000 km from the B.C.–Washington border on the south to the B.C.–Yukon border on the north (Figure 1). The highest peaks in the Coast Mountains are in the southern part of the mountain system, culminating in Mount Waddington (4,016 m asl). The southern part of the St. Elias Mountains extends into northern B.C. along its border with Alaska, and peaks in that area exceed 4,000 m asl, the highest being Mount Fairweather (4,663 m asl).

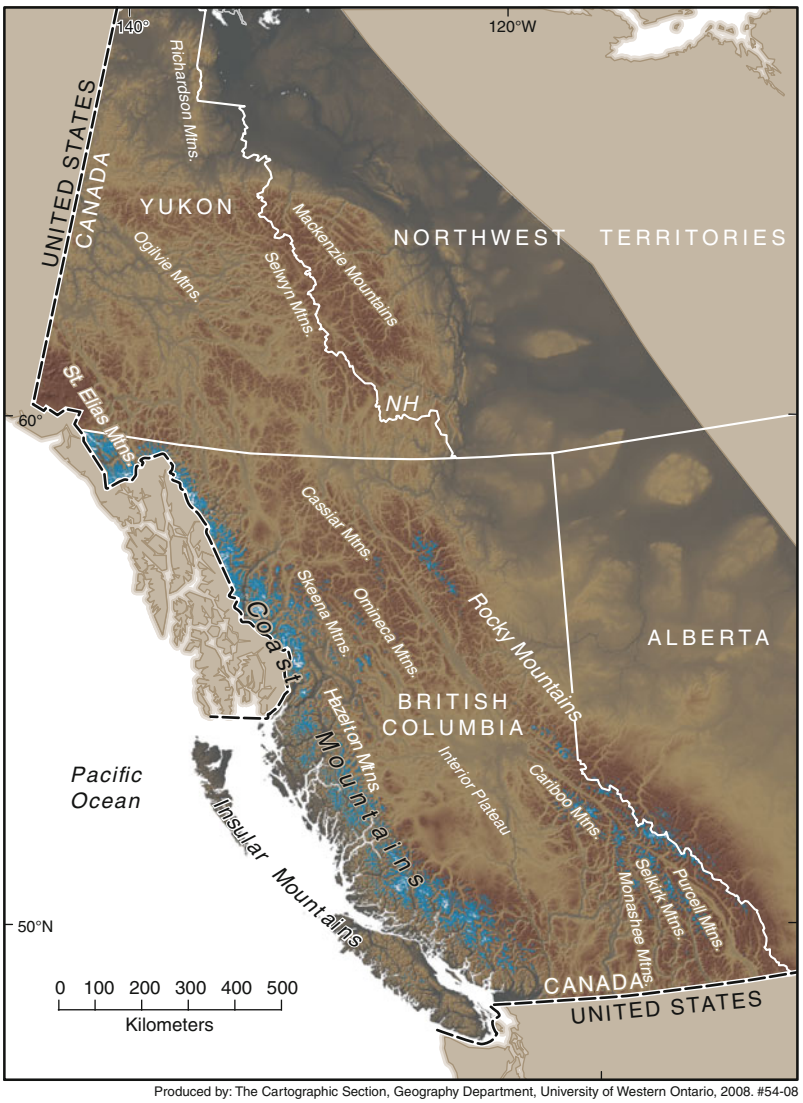

Canadian Rockies and Coast Mountains of Canada, Figure 1 Relief map of western Canada, showing major mountain systems and ranges. Blue shading shows present-day ice cover.

Ice cover is greater in the northern and southern Coast Mountains than in the central part of the system, where lower elevations limit the size and number of glaciers. Overall elevations are greater in the southern Coast Mountains than in the northern Coast Mountains. More extensive ice cover in the northern Coast Mountains results from the decrease in the glaciation limit from south to north due to lower mean temperatures and locally greater precipitation (Østrem, 1966). As a consequence, 36% of the total glacierized area in B.C. and Alberta is in the northern Coast Mountains, 26% in the southern Coast Mountains, and 7% in the central part. The B.C. portion of the St. Elias Mountains has about 12% of the total ice cover.

The glaciation limit generally rises to the east across B.C. due to the more continental environment and generally lower amounts of precipitation in the interior ranges than along the coast (Østrem, 1966). The total glacierized area in the B.C. interior ranges and Alberta Rocky Mountains thus is much less than in the Coast Mountains – glaciers in the Rocky Mountains represent 8.7% of the total area of ice cover; those in the southern B.C. interior, 7.5%; and those in the mountains of the northern interior, 2.3%. Approximately 60 small glaciers on Vancouver Island have a combined area of only 20 km^2.

Most glaciers are remote and not easily accessible except by helicopter, but some are close to roads or established hiking trails. Notable among these are Athabasca and Saskatchewan glaciers in the Alberta Rocky Mountains; Illecillewaet Glacier in the Selkirk Mountains of eastern B.C.; Hudson Bay Glacier near Smithers, B.C.; Helm, Sphinx, and Sentinel glaciers in the southern Coast

Mountains, and Salmon Glacier in the northern Coast Mountains. Athabasca Glacier, located along the Icefields Parkway in Jasper National Park, is the most visited glacier in North America (Figure 2). It flows from the Columbia Icefield, which has an area of nearly 325 km^2 and feeds six major glaciers. Athabasca Glacier is presently about 6 km long, has an area of about 6 km^2, and a maximum thickness of about 300 m.

Mapping British Columbia and Alberta glaciers

Western Canadian glaciers were mapped at scales of 1:50,000 and 1:250,000 as part of the National Topographic Survey (NTS) completed during the second half of the twentieth century. No single date can be associated with the areal extent of the glaciers depicted on NTS maps. Glaciers in B.C. were mapped at 1:20,000-scale during the initial Terrain Resources Inventory Management (TRIM) program between 1981 and 1989. The total glacier cover, estimated from aerial photographs acquired for TRIM mapping, is about 28,500 km^2 (Schiefer et al., 2007). Glacier cover in the Alberta Rocky Mountains for the same period was approximately 1,050 km^2. Some small glaciers have subsequently disappeared, and others have disintegrated into multiple smaller ice masses.

Links between climate and glaciers

A prominent feature of British Columbia's climate is the regular occurrence of mid-latitude cyclones during winter. These systems originate in the North Pacific Ocean, track eastward across the coast, and deliver large amounts of snow to the mountains of B.C. A high-pressure center commonly forms off western North America during summer and steers storm systems along more northerly tracks. Summer is thus typically warm and dry in southern B.C. and Alberta (Moore et al., 2009). The interior ranges of B.C. and the Canadian Rockies experience frequent convective storms during summer, and snow can fall during these storms at high elevations.

The strongest links between regional climate and glacier mass balance in B.C. are during winter when the atmosphere is most active. Wintertime circulation is strongly influenced by the Pacific North American Pattern (PNA), a recurring pattern of high-and low-pressure centers (Wallace and Gutzler, 1981) that can either direct or divert winter storms across southern and middle latitudes of B.C. A persistent ridge of high pressure over B.C. during the strong phase of the PNA favors reduced snowfall. In contrast, cool, wet conditions characterize the weak phase of the PNA, especially in maritime locations of southern B.C. and the U.S. Pacific Northwest (Moore, 1996; Moore and McKendry, 1996).

PNA-like atmospheric patterns are linked to large sea-surface temperature anomalies in the equatorial Pacific or in the North Pacific. These temperature anomalies are associated with the El Niño-Southern Oscillation (ENSO) and the Pacific Decadal Oscillation (PDO). ENSO events typically last 1–2 years and recur every 2–7 years, whereas PDO events tend to last for periods of one to several decades (Mantua et al., 1997). Both El Niño conditions and the warm phase of the PDO favor higher-than-average sea surface temperatures along the west coast of North America and lower-than-average sea-surface temperatures in the central North Pacific. In contrast, cool sea surface temperatures are common during La Niña events and the cold phase of the PDO.

Canadian Rockies and Coast Mountains of Canada, Figure 2 Athabasca Glacier, the most visited glacier in North America. The glacier has retreated more than 1.5 km since the middle 1800s.

Glacier mass balance and frontal variations

Mountain glaciers respond to climate over a range of temporal scales. At annual timescales, for example, glaciers may gain mass if winter accumulation outpaces melting during summer. A persistent imbalance between accumulation and ablation will eventually cause glaciers to adjust their thickness, length, or area to reach a new equilibrium with climate. Adjustments in length and area can take decades or centuries, whereas changes in thickness occur over timescales of years.

Detailed glacier mass balance studies in western Canada began at the start of the International Hydrologic Decade in 1965. Early researchers chose glaciers along a west–east transect through southern B.C. and westernmost Alberta to examine links between climate and mass balance from maritime (Sentinel and Helm glaciers) to continental (Peyto and Ram River glaciers) environments (Østrem, 1966). Berendon Glacier in the northern Coast Mountains was added after 1965 to establish a north–south transect. Only Place and Peyto glaciers, however, have mass balance records longer than 30 years.

Yarnal (1984) showed that mass balance changes at Sentinel and Peyto glaciers are partly controlled by recurring synoptic features during the accumulation and ablation seasons, determined from charts of the geopotential surface (500 hPa). Both glaciers gain mass during periods of cyclonic activity in winter and under synoptic conditions that favor cloudy conditions. Similar synoptic mass balance relations were shown by Walters and Meier (1989), who analyzed a longer and more complete data set for other North Pacific glaciers (South Cascade, Sentinel, Place, Peyto, Wolverine, and Gulkana glaciers). They suggested that wintertime mass balance variability can be largely explained by changes in atmospheric circulation similar to those controlled by the PNA.

The mass balance of western Canadian glaciers is strongly affected by winter precipitation (Hodge et al., 1998; Bitz and Battisti, 1999). In addition to the direct influence of precipitation on accumulation, winter precipitation can also influence summer ablation (Moore et al., 2009): years with heavy snowfall can delay exposure of ice in the ablation season, thus maintaining a high surface albedo and reducing melt during summer (Young, 1981; Moore and Demuth, 2001). Weather and synoptic conditions during summer influence the balance of glaciers in the interior ranges and Rocky Mountains (Letréguilly, 1988; Bitz and Battisti, 1999).

The average winter balance at Peyto Glacier averaged 1.51 m water equivalent (we) per year from 1965 to 1976, but decreased to 1.01 m we per year over the period 1977–1999 interval, following a Pacific climate shift in 1976 (Watson and Luckman 2004; Moore et al., 2009). Place Glacier and glaciers in the U.S. Pacific Northwest experienced similar declines in winter mass balance following 1976, in concert with a shift in climate involving the warm phase of the PDO and more frequent El Niño conditions (McCabe and Fountain, 1995; Moore and Demuth, 2001).

Historical glacier changes and links to climate

Glaciers in B.C. and Alberta remained near their Little Ice Age positions until the early twentieth century, when climate abruptly warmed in western North America (Jones et al., 1999; Menounos, 2006; Koch et al., 2009). Athabasca Glacier in the Rocky Mountains retreated only about 200 m between 1844 and 1906, but receded over 1 km during the next 75 years and lost nearly half its volume (Luckman et al., 1999). Likewise, Helm Glacier in the southern Coast Mountains and Illecillewaet Glacier in Columbia Mountains retreated about 200 m in the late 1800s, followed by about 1 km of retreat between 1900 and 1988 (Osborn and Luckman, 1988; Koch et al., 2009).

Fluctuations of glaciers in B.C. and Alberta also mirror changes in climate on decadal timescales. Most glaciers rapidly retreated during the period 1920–1950. Glacier recession slowed after 1950, and in some cases glaciers advanced during the 1960s and 1970s. After about 1980, glaciers resumed their retreat, a trend that has continued to the present (Koch et al., 2009; Moore et al., 2009). Periods of glacier recession coincide with positive phases of the PDO, when the climate of B.C. was relatively warm and dry. The minor advances of the 1960s and 1970s occurred during a negative, cool phase of the PDO. Rates of glacier retreat in the southern Coast Mountains were highest (30 m a^{-1}) between about 1920 and 1950 (Menounos et al., 2005; Koch et al., 2009). Illecillewaet Glacier in eastern B.C. retreated 20–40 m a^{-1} between 1900 and 1960, but only about 6 m a^{-1} between 1960 and 1980 (Osborn and Luckman, 1988).

Analysis of 2005 Landsat satellite imagery shows that the total glacierized area in B.C. and Alberta decreased 10.8% (±2.9%) and 25.4 (±3.4%), respectively, over the preceding 20-year period (Bolch et al., 2010). The average annual retreat rate of 0.55% a^{-1} is comparable to late twentieth century rates reported for other mountain regions, including the European Alps and the Himalayas.

Areal changes in ice cover during the past 3 decades

The Coast and St. Elias Mountains have the greatest glacierized area and show the greatest total ice loss – about 2,400 km^2 between 1985 and 2000. Regions with less ice cover, however, have the highest relative areal ice losses – 24% in the northern interior ranges and 25.4% in the Alberta Rocky Mountains, compared with 7.7% and 10.3% in the northern and southern Coast Mountains, respectively. These losses are only part of the total reduction in ice cover since the Little Ice Age. For example, in Garibaldi Provincial Park, ice cover was 16% less in 2005 than in 1987, but was 49% less in 2005 than in the eighteenth century (Koch et al., 2009). Many valley glaciers have retreated more than 1 km since

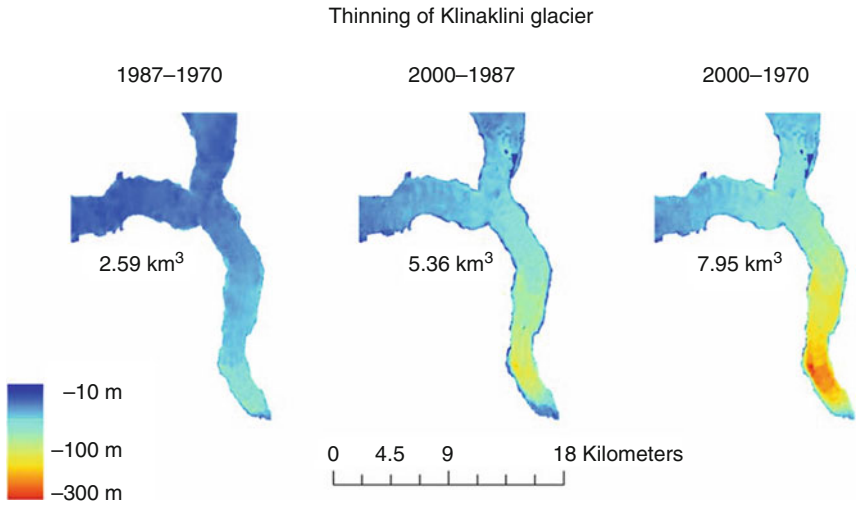

Canadian Rockies and Coast Mountains of Canada, Figure 3 Elevation change of Klinklini Glacier between 1970 and 2000. Colors denote elevation loss in the ablation zone of the glacier over three periods. Changes in the glacier surface were obtained by differencing digital elevation models produced from the National Topographic Database maps (1970), Terrain Resource Inventory Maps (1987), and Shuttle Radar Topographic Mission imagery (2000).

1900, based on visible trim lines. Small glaciers have experienced the highest percentage areal losses and, in some cases, have disappeared. Conversely, many small cirque glaciers in sheltered topographic locations experienced relatively little reduction in area (DeBeer and Sharp, 2007, 2009).

Volume losses

Geodetic methods and area-volume scaling provide volume loss estimates for glaciers in B.C. and Alberta (Schiefer et al., 2007; Bolch et al., 2010). In the case of small glaciers, terminus retreat explains much of the volume loss; for large glaciers, downwasting in the ablation zone dominates mass loss. The total estimated ice loss in B.C. between 1985 and 2000, based on the TRIM and the Shuttle Radar Topographic Mission (SRTM) digital elevation models, is 22.5 ($\pm$5.5) km^3 a^{-1}, which corresponds to an average thinning rate of 0.78 $\pm$ 0.19 m a^{-1}. Thinning rates are highest where ice cover is greatest (i.e., the Coast and St. Elias Mountains) and lowest in the B.C. interior and the northern Rocky Mountains (Figure 3).

Summary

There are about 15,000 glaciers, covering a total area of 26,000 km^2, in British Columbia and western Alberta. About 36% of the ice cover is in the northern Coast Mountains, 26% is in the southern Coast Mountains, and 12% is in the B.C. portion of the St. Elias Mountains; the remainder is in the central part of the Coast Mountains.

The mass balance of western Canadian glaciers is strongly affected by winter precipitation, although weather and synoptic conditions during summer influence the summer balance of glaciers in the interior ranges and Rocky Mountains. Wintertime circulation in British Columbia is controlled by the Pacific North American Pattern (PNA). A persistent ridge of high pressure over B.C. during the strong phase of the PNA favors reduced snowfall. In contrast, cool, wet conditions typify the weak phase of the PNA, especially in maritime locations of southern B.C. PNA-like atmospheric patterns are linked to large sea-surface temperature anomalies in the equatorial Pacific or in the North Pacific, which in turn are associated with the El Niño-Southern Oscillation (ENSO) and the Pacific Decadal Oscillation (PDO).

Most glaciers in British Columbia and Alberta retreated between 1920 and 1950. Glacier recession slowed after 1950, and in some cases glaciers advanced during the 1960s and 1970s. After about 1980, glaciers continued their retreat, a trend that has continued to the present. Periods of glacier recession coincide with positive phases of the PDO. The minor advances of the 1960s and 1970s occurred during a negative, cool phase of the PDO.

Glacier cover in the Coast and St. Elias Mountains decreased by about 2,400 km^2 between 1985 and 2000. The average annual loss in ice volume over this period is 22.5 ($\pm$5.5) km^3 a^{-1}, which corresponds to an average thinning rate of 0.78 $\pm$ 0.19 m a^{-1}.

Bibliography

Bitz, C. M., and Battisti, D. S., 1999. Interannual to decadal variability in climate and the glacier mass balance in Washington, western Canada, and Alaska. *Journal of Climate*, **12**, 3181–3196.

Bolch, T., Menounos, B., and Wheate, R., 2010. Landsat-based inventory of glaciers in western Canada, 1985 to 2005. *Remote Sensing of the Environment*, **114**, 127–137.

DeBeer, C. M., and Sharp, M. J., 2007. Recent changes in glacier area and volume within the southern Canadian Cordillera. *Annals of Glaciology*, **46**, 215–221.

DeBeer, C. M., and Sharp, M. J., 2009. Topographic influences on recent changes of very small glaciers in the Monashee Mountains, British Columbia, Canada. *Journal of Glaciology*, **55**, 1–10.
Hodge, S. M., Trabant, D. M., Krimmel, R. M., Heinrichs, T. A., March, R. S., and Josberger, E. G., 1998. Climate variations and changes in mass of three glaciers in western North America. *Journal of Climate*, **11**, 2161–2179.
Jones, P. D., New, M., Parker, D. E., Martin, S., and Rigor, I. G., 1999. Surface air temperature and its changes over the past 150 years. *Review of Geophysics*, **37**, 173–199.
Koch, J., Menounos, B., and Clague, J. J., 2009. Glacier change in Garibaldi Provincial Park, southern Coast Mountains, British Columbia, since the Little Ice Age. *Global and Planetary Change*, **66**, 161–178.
Letréguilly, A., 1988. Relation between mass balance of western Canadian mountain glaciers and meteorological data. *Journal of Glaciology*, **34**, 11–18.
Luckman, B. H., Kavanagh, T. A., Craig, I., and St. George, R. S., 1999. Earliest photograph of Athabasca and Dome glaciers, Alberta. *Géographie physique et Quaternaire*, **53**, 401–504.
Mantua, N. J., Hare, S. R., Zhang, Y., Wallace, J. M., and Francis, R. C., 1997. A Pacific interdecadal climate oscillation with impacts on salmon production. *Bulletin of the American Meteorological Society*, **78**, 1069–1079.
McCabe, G. J., and Fountain, A. G., 1995. Relations between atmospheric circulation and mass balance of South Cascade Glacier, Washington, USA. *Arctic and Alpine Research*, **27**, 226–233.
Menounos, B., 2006. Anomalous early 20th century sedimentation in proglacial Green Lake, British Columbia, Canada. *Canadian Journal of Earth Sciences*, **43**, 671–678.
Menounos, B., Clague, J., Gilbert, R., and Slaymaker, O., 2005. Environmental reconstruction from a varve network in the southern Coast Mountains, British Columbia, Canada. *Holocene*, **15**, 1163–1171.
Moore, R. D., 1996. Snowpack and runoff responses to climatic variability, southern Coast Mountains, British Columbia. *Northwest Science*, **70**, 321–333.
Moore, R. D., and Demuth, M. N., 2001. Mass balance and streamflow variability at Place Glacier, Canada, in relation to recent climate fluctuations. *Hydrological Processes*, **15**, 3473–3486.
Moore, R. D., and McKendry, I. G., 1996. Spring snowpack anomaly patterns and winter climatic variability, British Columbia, Canada. *Water Resources Research*, **32**, 623–632.
Moore, R. D., Fleming, S., Menounos, B., Wheate, R., Fountain, A., Holm, C., and Jakob, M., 2009. Glacier change in western North America: influences on hydrology and geomorphic hazards and water quality. *Hydrologic Processes*, **23**, 42–61.
Osborn, G. D., and Luckman, B. H., 1988. Holocene glacier fluctuations in the Canadian Cordillera (Alberta and British Columbia). *Quaternary Science Reviews*, **7**, 115–128.
Østrem, G., 1966. The height of the glaciations limit in the southern British Columbia and Alberta. *Geografiska Annaler*, **48A**, 126–138.
Schiefer, E., Menounos, B., and Wheate, R., 2007. Recent volume loss of British Columbian glaciers, Canada. *Geophysical Research Letters*, **34**, L16503, doi:10.1029/2007GL030780.
Wallace, J., and Gutzler, D., 1981. Teleconnections in the geopotential height field during the Northern Hemisphere winter. *Monthly Weather Review*, **109**, 784–812.
Walters, R. A., and Meier, M. F., 1989. Variability of glacier mass balances in western North America. In Peterson, D. H. (ed.), *Aspects of Climate Variability in the Pacific and Western Americas*. Geophysical Monographs, Vol. 55, pp. 365–374.
Watson, E., and Luckman, B. H., 2004. Tree-based mass-balance estimates for the past 300 years at Peyto Glacier, Alberta, Canada. *Quaternary Research*, **62**, 9–18.
Yarnal, B., 1984. Relationships between synoptic-scale atmospheric circulation and glacier mass balance in south-western Canada during the International hydrological Decade, 1965–1974. *Journal of Glaciology*, **30**, 188–198.
Young, G. J., 1981. The mass balance of Peyto Glacier, Alberta, Canada, 1965 to 1978. *Arctic and Alpine Research*, **13**, 307–318.

Cross-references

Alaskan Glaciers
Cascade Mountains, USA
Climate Change and Glaciers
Rocky Mountains

CASCADE MOUNTAINS, USA

Rijan B. Kayastha
Himalayan Cryosphere, Climate and Disaster Research Center (HiCCDRC), Kathmandu University, Dhulikhel, Kavre, Kathmandu, Nepal

Synonyms

Canadian cascade; Cascade range; Cascadia; North cascade

Definition

The Cascade Mountains, USA, is a major mountain range of western North America. It extends for about 1120 km in the north–south direction from northern California through Oregon and Washington State, and for a short distance into British Columbia, Canada. The Cascades derive their name from the cascades (waterfalls) of the Columbia River. The Cascade Mountains include both nonvolcanic mountains, including the rugged spires of the North Cascades and the notable volcanoes known as the High Cascades. Major peaks in Cascade Mountains in California are Lassen Peak and Mount Shasta; in Oregon are Mount Hood and Mount Jefferson and in Washington State are Mount Adams, Mount Baker, Mount St Helens, and Mount Rainier.

The Cascade Mountains are part of the Pacific Ring of Fire, the ring of volcanoes and associated mountains around the Pacific Ocean. The most active volcanoes in the USA, excluding Alaska and Hawaii, are found in the Cascade Range, e.g., Mount Rainier (4,392 m), Mount Shasta (4,317 m), and Mount Adams (3,751 m). Mount Rainier is the highest Peak in the Cascade Mountain USA. Mount St Helens in Washington (2,549 m), which had been dormant since 1857, erupted violently in 1980 and 1982. Minor eruptions of Mount St. Helens have also occurred, most recently in 2006.

The core of the Cascade Mountains is formed by old crystalline rocks but above their crest line are many volcanic cones, whose lava flows have covered much of the lower slopes. Because of the Cascade Mountain's proximity to the Pacific Ocean, these mountains receive good

precipitation, especially on the western slopes, with annual accumulations of up to 3,800 mm in some areas. It is not uncommon for some places in the Cascades to have over 5,500 mm of snow accumulation, such as at Lake Helen (near Lassen Peak), one of the snowiest places in the world. Most of the High Cascades are therefore white with snow and ice year round. However, the annual rainfall drops to 200 mm on the eastern foothills due to a rain shadow effect.

CASCADE SYSTEM

Rijan B. Kayastha
Himalayan Cryosphere, Climate and Disaster Research Center (HiCCDRC), Kathmandu University, Dhulikhel, Kavre, Kathmandu, Nepal

Definition

Cascade system is defined as a system in which the flow of energy and/or matter from one element passes to next element in the series. The concept of cascade system is used in the distributed hydrological modeling for simulating runoff from a basin. In this concept, a basin is divided into number of sub-basins say, Tank 1, Tank 2, Tank 3, . . ., Tank n, from upstream to downstream as shown in Figure 1. The inflow on the starting tank, Tank 1, in the upstream end of the basin will be rainfall and after evapotranspiration, infiltration, and other initial losses, the remaining water (outflow of Tank 1) will be inflow to the lower tank, Tank 2. Similarly, outflow of the Tank 2 will be will become the inflow to Tank 3 in the series and so on. This process will continue to the lowermost tank of the basin which will give the actual runoff from the basin.

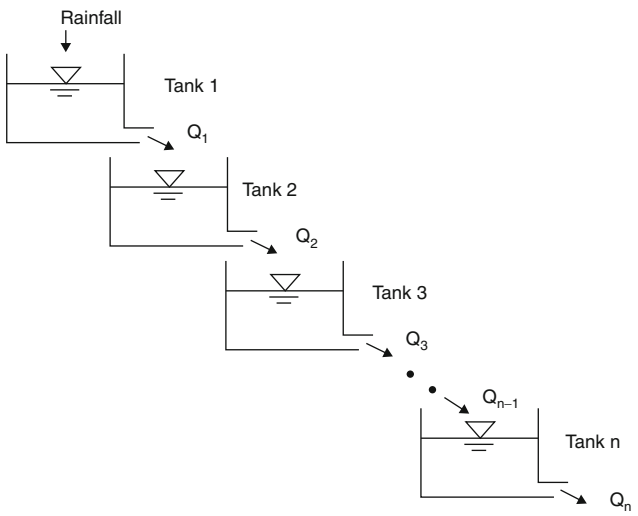

Cascade System, Figure 1 Cascade system in runoff modeling.

CATASTROPHIC FLOODING

Fiona Tweed
Department of Geography, Staffordshire University, Stoke-on-Trent, Staffordshire, UK

Synonyms

High magnitude floods; Superfloods

Definition

The term "catastrophic flooding" is generally used to describe the occurrence of exceptional or rare high magnitude floods.

The term catastrophic flooding has its origins in the diluvial theory of the biblical flood and derives from the thinking that catastrophic events shaped the Earth's surface. Floods can be attributed catastrophic status on the basis of their impacts on channel morphology and/or sedimentology or the amount of sediment that they transport. Catastrophic floods create substantial monetary and human losses in the areas in which they occur. Whether a flood is catastrophic or not can depend on the timescale over which the impacts of the flood are considered; for example, an event may appear catastrophic over a short timescale but over a longer timescale may be one of a number of similar events and therefore be relatively "non-catastrophic" (Wolman and Miller, 1960; Wolman and Gerson, 1978; Maizels and Russell, 1990a, b; Russell, 2004). Preservation of erosional landforms and sedimentary evidence of floods over geological timescales is likely to reflect truly catastrophic events and the conditions appropriate for their impacts to be preserved (Russell, 2004). If considered over shorter timescales a flood could be defined as catastrophic if it results in irreversible changes in fluvial systems.

The largest known catastrophic floods are associated with deglaciation as well as high-intensity rainfall. In glaciated environments, catastrophic processes associated with high-energy flows (such as *Ice-Dammed Lakes*, *jökulhlaups/glacier lake outburst floods (GLOFs), etc.*, see entries *Hydrology of Jökulhlaups*; *Glacier Lake Outburst Floods*.) can cause substantial landscape change. The main causes of catastrophic flooding in glaciated terrain comprise rainfall, melting of ice, and natural or man-made dam failure, which generate sudden and large inputs of water to flood routeways (e.g., Mayer and Nash, 1987; Evans and Clague, 1994; Tweed and Russell, 1999; Clague and Evans, 2000; Martini et al., 2002). The Channeled Scablands of Washington, USA, are believed to have been shaped by catastrophic flooding from the drainage of proglacial lakes during the late *Pleistocene Epoch* (Baker, 1981).

Bibliography

Baker, V. R., 1981. *Catastrophic flooding: The Origin of the Channeled Scabland*. Stroudsburg: Dowden, Hutchinson & Ross.

Baker, V. R., 1996. Megafloods and glaciation. In Martini, I. P. (ed.), *Late Glacial and Postglacial Environmental Changes*. New York: Oxford University Press, pp. 98–108.
Clague, J. J., and Evans, S. G., 2000. A review of catastrophic drainage of moraine-dammed lakes in British Columbia. *Quaternary Science Reviews*, **19**, 1763–1783.
Evans, S. G., and Clague, J. J., 1994. Recent climate change and catastrophic geomorphic processes in mountain environments. *Geomorphology*, **10**, 107–128.
Maizels, J. K., and Russell, A. J., 1990a. Catastrophic drainage and the quaternary record. I. Criteria for defining 'catastrophic' drainage. *Quaternary Newsletter*, **61**, 12–18.
Maizels, J. K., and Russell, A. J., 1990b. Catastrophic drainage and the quaternary record II. Environmental significance of 'catastrophic' floods: possible applications in the UK and development of a database. *Quaternary Newsletter*, **61**, 18–23.
Martini, P.I., Baker, V.R., and Garzón, G. (eds.), 2002. *Flood and Megaflood Processes and deposits: Recent and Ancient Examples*, International Association of Sedimentologists, Special Publication, 32.
Mayer, L., and Nash, D., 1987. *Catastrophic Flooding*. Binghamton Symposium in Geomorphology, 18. London: Allen & Unwin.
Russell, A. J., 2004. Sedimentary processes – catastrophic floods. In Selley, R. C., Cocks, L. R. M., and Plimer, I. R. (eds.), *Encyclopedia of Geology*. Oxford: Elsevier B.V, pp. 628–641.
Tweed, F. S., and Russell, A. J., 1999. Controls on the formation and sudden drainage of glacier-impounded lakes: implications for jökulhlaup characteristics. *Progress in Physical Geography*, **23**, 79–110.
Wolman, M. G., and Gerson, R., 1978. Relative scales of time and effectiveness of climate in watershed geomorphology. *Earth Surface Processes and Landforms*, **3**, 189–203.
Wolman, M. G., and Miller, J. P., 1960. Magnitude and frequency of forces in geomorphic processes. *Journal of Geology*, **68**, 54–74.

Cross-references

Glacier Lake Outburst Floods
Hydrology of Jökulhlaups
Ice-Dammed Lakes
Pleistocene Epoch

CATASTROPHIC ROCK SLOPE FAILURES AND MOUNTAIN GLACIERS

Kenneth Hewitt[1], John J. Clague[2], Philip Deline[3]
[1]Cold Regions Research Centre, Wilfrid Laurier University, Waterloo, ON, Canada
[2]Centre for Natural Hazard Research, Department of Earth Sciences, Simon Fraser University, Burnaby, BC, Canada
[3]EDYTEM Lab, Université de Savoie, CNRS, Le Bourget-du-Lac, France

Definition

"Catastrophic rock slope failure" is the sudden failure and downslope movement of a large mass of intact rock. The failed rock mass rapidly disintegrates and may flow a long distance at speeds up to 100 m s^{-1} before coming to rest, in some instances kilometers beyond the source. The mobility of the streaming debris is enhanced as it travels over snow and ice. Catastrophic rock slope failures and other types of landslides are common in mountains around the world, but are particularly numerous in high glacierized ranges where glaciers have eroded steep slopes and where recent glacier retreat has left unstable slopes unsupported. Thaw of alpine permafrost in a warming climate has also been implicated in many landslides in glacierized mountains. We describe the interplay between catastrophic rock slope failures and glaciers in the Karakoram Himalaya and western North America, two areas with some of the highest relief and largest alpine glaciers on Earth, and thirdly in the European Alps, with one of the most detail records.

Introduction

Rock slope failures in glacierized mountains may generate rock avalanches that affect mountain glaciers (Figure 1). The runout and emplacement geometry of rock avalanches are affected when they travel over ice (Evans and Clague, 1988; Deline, 2009), and substantial modifications of glacier activity, mass balance, and sedimentation can follow (Huggel, 2008; Hewitt, 2009). If the landslides descend over glaciers into ice-free valleys, they can develop even greater mobility and can, if they reach inhabited areas, result in singular catastrophes (Pflaker and Ericksen, 1978; Hauser, 2002;

Catastrophic Rock Slope Failures and Mountain Glaciers, Figure 1 Rock avalanche onto the accumulation zone of a glacier in the Southern Alps of New Zealand.

Huggel et al., 2008). Rock avalanches occurring in ice-free areas below glaciers can affect ice-margin and proglacial sedimentation, even terminal fluctuations. When landslides dam valleys at or near glacier termini, lakes may cause the ice to float (Hewitt, 2001; Deline, 2005b).

Rock avalanches occur in almost all mountain ranges (Table 1), but most reported examples are in presently or formerly glacierized mountain valleys. Many detachment zones are on slopes over-steepened by glacial erosion. Glacial retreat and debuttressing may be important factors in destabilizing such slopes (Evans and Clague, 1993;

Catastrophic Rock Slope Failures and Mountain Glaciers, Table 1 Examples of large (>10^6 m^3) rock avalanches descending onto glaciers

Mountain system	Examples	No.	Reference
North American Cordillera			
Alaska	1945–1963	11	Post, 1967
	1964 earthquake	>50	McSaveney, 1978
	1964–1965	4	Reid, 1969
British Columbia	Pandemonium Creek 1959		Evans and Clague, 1988
	Devastation Glacier 1975		
	North Creek 1986		
	Mount Meager 1986		
Washington, USA	Mount Rainier:		Crandell 1971
	Prehistoric	"frequent"	Fahnestock, 1978
	Emmons Glacier 1963	"several"	
Greenland	Holsteinsborg sixteenth to seventeenth centuries		Kelly, 1980
South American Cordillera			
Peru, Cordillera Blanca	Nevados Hascaran		Pflaker and Ericksen, 1978
	Prehistoric, 1962, 1970	>3	
Chile, Andes	Rio Colorado,		Hauser, 2002
	Three prehistoric		
	Estero Paraguirre 1987		
Argentina, Andes	Aconcagua	2	R. Hermanns, pers. comm.
Antarctica, S.Georgia,	Lyell Glacier 1975	1	Gordon et al., 1978
New Zealand, S. Alps	Mt. Cook 1873, 1991	McSaveney, 2002	
	Mt. Fletcher 1991		
	Mt. Thomson 1996		
	Mueller Glacier 1960		
	Mt. Isobel 1950s		
European Alps	Triolet Glacier, Italy < 1000, 1717	2	Porter and Orombelli, 1980
			Deline and Kirkbride, 2009
	Brenva Glacier, Italy,	>10	Valbusa, 1921
	c. 2500 BP, c. 500, 1300, 1767, 1920, 1997		Deline, 2001, 2005a, 2005b
	Rossbodergletscher,		
	Switzerland, 1901		
	Miage Glacier, Italy, 1921,	>10	Deline, 2009
	1945, 1988		
	Aletsch Glacier,	>3	Alean, 1984
	Switzerland, 1937		
	Thurwieser, Italy, 2004		Sosio et al., 2008
Caucasus	Urukh River/Glacier ca. 1959		A Strom, personal communication
	Kolka-Karmadon 2002		Haeberli et al., 2004
			Huggel et al., 2005
Pamir	Rgo Glacier 2003?		Schneider, 2004
Karakoram Himalaya	Prehistoric	21	This article
	Historic	8	
	Bualtar Glacier 1986		
	Chillinji Glacier 1991		
	Aling Glacier 1990?		
	North Te-Rong 2002		
Nepal Himalaya	Kali Gandaki, prehistoric	"many"	Fort, 2000
	Ghasa Gompa, Dhampu		
	Annapurna		Weidinger, 2004
	Langthang, "Tsergo Ri"		Heuberger et al., 1984

Ballantyne and Benn, 1996; Bovis and Stewart, 1998; Dadson and Church, 2005).

Investigations are revealing a much higher incidence of rock avalanches in glacierized mountains than formerly realized and impacts there have been underestimated (McSaveney, 2002; Deline, 2009). As such, they must be considered an important factor in denudation, sedimentation, and landscape evolution in these mountains.

Our topic involves new and challenging notions for the relations between mass movements and mountain glaciers. Hitherto, studies of the phenomenon have focused mainly on modern events, commonly treated as singular cases (Voight, 1978). These studies have elucidated the processes involved, but the broader implications of regional concentrations of events received little attention until recently.

Rockslide-rock avalanches

Catastrophic rock slope failures are referred to as *rockslide-rock avalanches* (Mudge, 1965), *rock avalanches* (Eisbacher and Clague, 1984), and *sturzstroms* (Heim, 1932; Hsü, 1975, 1978; Hutchinson, 1988). They are characterized by sudden failures of large (10^6–10^{10} m^3) intact masses of rock, followed by rapid runout and emplacement of relatively thin sheets of crushed and pulverized debris. Maximum runout distances are commonly five to ten times total fall height. The debris generally travels at velocities exceeding 100 km h^{-1}, in some instances more than 250 km h^{-1}. When the speed falls below a threshold, the debris comes to an abrupt halt through frictional "freezing" (Hewitt et al., 2008).

The majority of known rock avalanches are in glacierized mountains, but those actually falling on glaciers must be greatly underestimated, mainly because they are unlikely to be recognizable after a few decades. Burial of landslide debris by snow in glacier accumulation zones, or its dispersal by ice movement and ablation as described below, greatly reduce the chances that their legacy will be recognized (McSaveney, 2002). Because most occur in rugged, often uninhabited terrain that is difficult of access, many modern events must have been missed, at least prior to satellite imaging. Most catastrophic rock slope failures are triggered in earthquakes or severe weather, further reducing the chances of direct observation. And dozens of surviving rock-avalanche deposits have been misidentified as moraines or till (Heim, 1932; Porter and Orombelli, 1980; Hewitt, 1999; Blikra et al., 2006; Deline and Kirkbride, 2009). Misidentification is an understandable mistake in rugged environments with many different sources of coarse, poorly stratified, or massive debris.

Landslide–glacier interactions

The impact of a landslide on a glacier depends partly on the size and character of the rock slope failure, partly on its location relative to the glacier, and partly on the behavior of the rock avalanche from inception to cessation of flow. The size of the rock avalanche relative to that of the glacier, the steepness and relief of the rock-avalanche path, the orientation of path relative to that of the glacier, and the steepness of the glacier bed and surface are important factors.

Several distinct contexts and some sub-types can be recognized. First are rock avalanches that occur entirely on ice and do not reach beyond the margins of the glacier. Important sub-categories are events largely restricted to the glacier's accumulation area (Figure 1) and those affecting mainly the ablation zone (Figure 2). Second are rock avalanches that originate in glacierized basins and travel onto ice-free valley floors (Figure 3). A rare variant of this group is rock avalanches that significantly erode the glaciers onto which they fall, producing highly mobile, mixed flows of debris, and ice that travel far beyond the glacier terminus. An example is the disastrous 2002 Kolka-Karmadon event in the Russian Caucasus (Haeberli et al., 2004; Huggel et al., 2005). An avalanche of rock and ice fell onto Kolka Glacier, eroding almost all its ice. A massive flow of rock and ice continued 20 km down valley, where it came to rest at the entrance to a gorge. There, it transformed into a mudflow that traveled for another 15 km. The rock-ice avalanche killed about 140 people and caused massive destruction. Third are rock avalanches that originate on slopes of ice-free valleys and travel over the termini of active glaciers. In addition, rock avalanches that originate and are wholly emplaced in ice-free valleys may affect up-valley glacier behavior (Figure 4). This article deals mainly with the first group of events, where landslide material is emplaced on active ice, but in terms of natural hazards the second and third types are more dangerous (Figure 5).

An important contextual variant, not dealt with here, is glacierized volcanoes. The cataclysmic eruption of Mt. St. Helens in 1980 triggered a huge rock avalanche and lahars, and indicated something of the scale and diversity of mass movements that occur on glacier-clad volcanoes during eruptions (Waitt et al., 1983).

Significant processes and developments

Glacier effects on rock-avalanche movement

From a study of 17 examples, Evans and Clague (1988) concluded that travel over glaciers tends to increase rock-avalanche mobility. Snow and ice surfaces over which the debris travels are typically flat or gently sloping, allowing unobstructed flow, and frictional resistance is much lower than in situations where the landslide travels over rock or sediment surfaces. During landslides in 1986 at Bualtar Glacier in the Karakoram Himalaya, rapid melting of ice by the frictionally heated debris helped to remove surface irregularities (Hewitt, 1988). These conditions also mean the debris sheets on glaciers are characteristically thin; average thicknesses are generally 1–3 m, and large areas of bare or nearly bare ice may occur within the sheet (Figure 6).

Channeling by lateral moraines or in glacial troughs increases the runout distances of rock avalanches by

Catastrophic Rock Slope Failures and Mountain Glaciers, Figure 2 Rock-avalanche deposit on Black Rapids Glacier, Alaska. The deposit has a volume of about 10×10^6 m^3 and averages about 2 m in thickness. The rock avalanche was triggered by a magnitude-7.9 earthquake in November 2002. (Photo: J. J. Clague, 2007.)

limiting or preventing lateral spreading (Evans et al., 1989). For instance, downwasting of the Brenva Glacier since 1988 had converted its moraines into ramparts that channeled the 1997 rock avalanche. In contrast, most deposition in the 1920 rock avalanche occurred outside the moraines because the advance of the glacier that started in 1913 had raised its surface above the moraine crests (Deline, 2009).

Observations of what happens in accumulation zones of glaciers during rock avalanches are few because the landslide material is soon buried under new snow. Many high-elevation landslides occurred during the 1964 and 2005 earthquakes in Alaska; observations after these events suggest that soft snow, ploughed up and melted by the landslide, may affect its movement (Post, 1967; McSaveney, 1978; Harp et al., 2003; Jibson et al., 2006). Debris typically moves away from the main body of the rock avalanche in linear tongues, sometimes anchored by large blocks of rock (Figure 7). Some rock avalanches, such as at Brenva Glacier in 1997, erode through the firn of the accumulation zone and incorporate large amounts of ice. At Kolka-Karmadon in 2002, a large part of the glacier was removed (Huggel, 2008).

Effects of rock avalanches on glacier movement and supraglacial debris

A landslide onto the accumulation zone of a glacier may have some, as yet undetermined, effect on glacier flow. Clearer and more significant consequences for glacier behavior and the fate of the landslide debris are in the ablation zone where the debris is continuously exposed. Deline (2009, 1073) has identified two types of supraglacial units derived from rock avalanches in his work on Miage Glacier, the main debris-covered glacier on the Mont Blanc massif. One type is flow-parallel stripes derived from rock avalanches and rock falls in the accumulation zone that have subsequently been transported englacially. A straight stripe is associated with a short englacial transport path, and a curved stripe results from longer englacial transport. However, it is unlikely debris transported from the accumulation zone will, when it reemerges, be ablated out as a more or less continuous and pure sheet of rock-avalanche debris. Rather, it will undergo irregular and gradual emergence at the surface over a long period with a degree of modification that is greater than with earlier emergence. The second type comprises irregular sheets of rock-avalanche and rock-fall deposits emplaced on bare ice in the ablation zone and subsequently transported entirely supraglacially.

Whatever the origin of the debris, it is progressively modified as it is transported down the glacier. The original form of the debris sheet is distorted by glacier flow that occurs at typical rates of tens to hundreds of meters per year. Surface features common to rock-avalanche deposits in other environments, including ridges transverse and parallel to rock-avalanche flow may be preserved for decades, but become less distinct with time. Even thin layers of rock debris insulate the underlying ice surface, leading to rapid and significant elevation of the debris sheet above the surrounding bare ice. Debris-draped ice plateaus may develop at rates of several meters per year and reach heights of many tens of meters as they move down valley toward the glacier terminus (Figure 8). Observations in the Karakoram, described below, indicate a limit as to how high the protected ice will become,

Catastrophic Rock Slope Failures and Mountain Glaciers, Figure 3 Rock-avalanche debris (*foreground*) blocks the Hunza and Hispar valleys, Central Karakoram. The rock avalanche originated on the rock walls of Ultar Peak (7,388 m asl) and traveled down the glacier in the background. (Photo: K. Hewitt, 2005.)

probably as a result of compensating flow displacement at depth (Hewitt, 2009). Eventually, debris adjusts to surface irregularities by sliding into depressions or moulins.

The fabric and thickness of the debris change as a result of these processes. In glaciers with tributaries, crevasse fields, icefalls, and changes of direction, there is ample opportunity for redistribution and modification of the debris. With time, it becomes difficult to distinguish rock-avalanche debris from other supraglacial materials. The impacts on glacial transport and ablation are likely to be significant, but techniques hardly exist to even identify the phenomenon, let alone the scale of the impacts.

When a rock avalanche blankets part or all of the ablation zone with debris, it initiates a series of disturbances that affect mass balance and ice dynamics. A source of positive mass balance – a large area of insulated glacier ice – becomes a moving "accumulation" anomaly localized in the ablation zone. Ice thickening and accelerated movement may lead to overriding of ice-free margins and advance of the glacier terminus. A consequence is that the normal relations between accumulation and ablation zones are compromised, and the glacier may respond in a different manner from other glaciers in the region. Fluctuations of Brenva Glacier, Italy, over the past century have been associated with repeated burial and reduced ablation under rock-avalanche debris (Valbusa, 1921; d'Agata et al., 2005; Deline, 2005a). The 1920 rock avalanche augmented the debris cover in the ablation zone, causing the glacier to advance 490 m between 1920 and 1941; in contrast, neighboring glaciers retreated from the mid-1920s onward. Bualtar and Aling glaciers in the Karakoram continued advancing for almost 15 years after being blanked by rock-avalanche debris, while surrounding glaciers retreated (Hewitt, 2009). These two also are examples of glaciers that have surged following rock avalanches (Gardner and Hewitt, 1989). Unlike typical surges, however, the advances may continue long after the surge.

Landslide debris alters sedimentation at the glacier margin. Ice-margin and proglacial fluvial sedimentation may, over the course of a disturbance episode, exceed normal rates by one or two orders of magnitude. Most of the rock-avalanche material is dispersed to the glacier margin and forefield within a few decades or centuries. In contrast, rock avalanches emplaced on ice-free ground may resist removal for millennia, even tens of millennia (Voight, 1978; Hewitt, 2002). A consequence is that many lateral and end moraines may include a substantial legacy of reworked and transported rock-avalanche debris. They may even be, as Deline (2009, 1082) suggests ". . . long-term archives of rock-avalanche activity." In some cases, moraines may consist entirely of rock-avalanche debris, in which case they carry no climatic implications. The distal flank of one of Brenva Glacier's lateral moraines has a pronounced concave slope that differs from the typical rectilinear distal slope of a dump moraine; it is attributed to successive deposits of Holocene rock avalanches. Finally, certain morainic complexes extend farther down valley than neighboring ones and lack ordered concentric moraines. They record glacier advances driven, not by climate, but by rock avalanches. Examples have been described in the Barpu-Bualtar basin, Pakistan (Hewitt, 2009) and at Triolet Glacier, Italy (Deline, 2009; Deline and Kirkbride, 2009).

Glaciers affected by rock avalanches also have significant contributions from smaller, but far more frequent rock fall. Patches or tongues of rock-fall debris are common on these glaciers. The two need to be considered together when assessing the role of rock-wall processes on long-term denudation in glacierized terrain (Deline, 2009).

The large amounts of fine debris emplaced during rock avalanches are readily flushed away by on-ice processes, making it progressively more difficult to distinguish the residual coarse fraction from rock-fall material. Nevertheless, it is now evident that in many glaciated mountains, moraines may include a substantial legacy of reworked

Catastrophic Rock Slope Failures and Mountain Glaciers, Figure 4 The Bhurt rock avalanche in the Western Karakoram crossed the Karambar valley from a source behind the camera. Rock-avalanche debris blocks the valley of the tributary Bhurt Glacier (*upper background*); almost all sediment from the glacier is trapped behind the debris barrier. (Photo: K. Hewitt, 1998.)

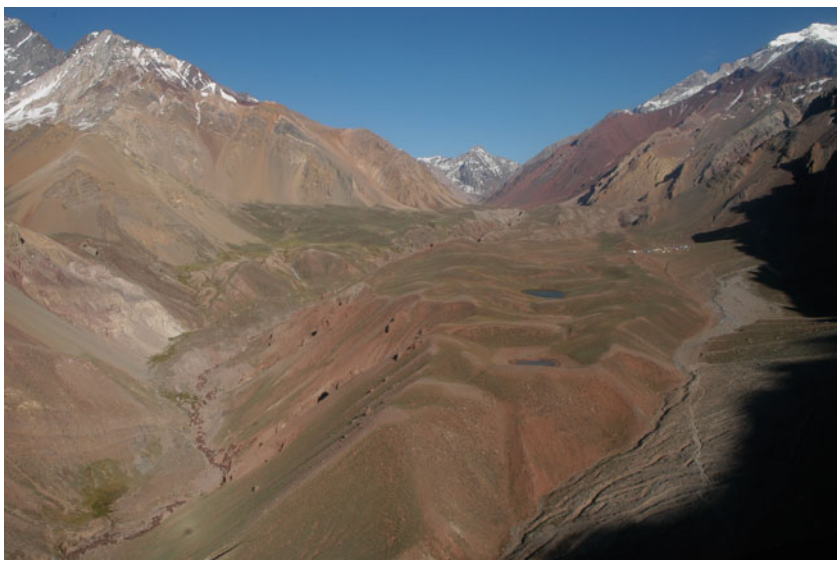

Catastrophic Rock Slope Failures and Mountain Glaciers, Figure 5 Up to 200 m of debris filling the valley in the foreground originated as a rock avalanche from Mount Aconcagua (6,962 m asl; *top right background*). The landslide traveled over Horcones Glacier and incorporated large quantities of ice, snow, and additional debris to become an extremely large (>3 km ^{3}) and very mobile mass flow. The landslide traveled another 15 km down the valley below the photograph to dam the main valley where the Trans-Andean Highway is located today. (Photo: K. Hewitt, 2006.)

and transported rock-avalanche debris produced by the same events that left intact, unmodified deposits at the glacier margins (Hewitt, 2002).

Effects of recent glacier retreat on slope stability

Thinning and retreat of alpine glaciers appear to be responsible for some catastrophic rock slope failures in glacierized mountains (Evans and Clague 1994, 1999; Holm et al., 2004). Many marginally stable slopes that were buttressed by glacier ice during the Little Ice Age failed after they became deglaciated in the twentieth century. An ancillary factor that may have contributed to such failures is steepening of rock slopes by cirque and valley glaciers during the Little Ice Age.

Catastrophic Rock Slope Failures and Mountain Glaciers, Figure 6 The boulder surface of the 1986 rock avalanche on Bualtar Glacier, Karakoram Himalaya. (Photo: K. Hewitt, 1987.)

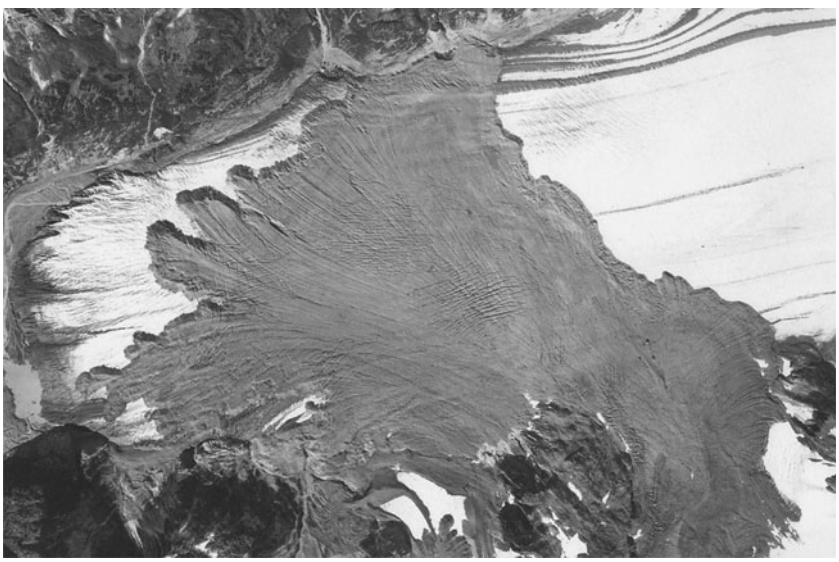

Catastrophic Rock Slope Failures and Mountain Glaciers, Figure 7 Aerial photograph of the deposit of the 1964 Sherman Glacier rock avalanche, taken in August 1967. Note the digitate margin of the debris sheet; lobes of debris ploughed through snow ahead of the main body of debris.

These effects are most pronounced in mountain ranges with the greatest ice cover (Himalaya, St. Elias Mountains, and Coast Mountains) because it is there that ice losses in the twentieth century have been largest. An extreme example is Glacier Bay, Alaska, which until the end of the eighteenth century was completely occupied by glacier ice. Since then, the bay has become deglaciated, with the loss of over 1,000 km^2 of ice. The ice loss is so great that the land is rising due to isostatic rebound (Larson et al., 2005).

Other mechanisms besides debuttressing can cause or trigger landslides. Temperatures in high glacierized mountains are normally below freezing. They may rise rapidly, however, during warm spells, melting snow and ice. The water generated by this melting can infiltrate fractures in marginally stable rock masses (Davies et al., 2001). When

Catastrophic Rock Slope Failures and Mountain Glaciers, Figure 8 Thin sheet of rock-avalanche debris overlying an ice platform in the ablation zone of Black Rapids Glacier. The debris sheet, which is 2 m thick, insulates the underlying ice. In the 7 years since the rock avalanche, the bare glacier surface adjacent to the debris sheet has downwasted nearly 20 m, leaving the elevated platform of debris-covered ice. (Photo: J.J. Clague.)

temperatures fall below freezing, water within the fractures may freeze or the fractures may be sealed by freezing at the surface. In either case, pore water pressures rise, producing extensional forces on an already weak rock mass. A related process is thawing of permafrost beneath high-elevation rock slopes (Gruber et al., 2004; Fischer et al., 2006; Gruber and Haeberli, 2007; Noetzli and Gruber, 2009). The lowest elevation of alpine permafrost has risen in most or all mountains in the twentieth century due to global warming (Zhang et al., 2006). Thawing has lowered the strength of rock with fractures or other structural discontinuities, because water in the fractures melts.

Illustrative of these processes is the unusually large number of rock falls that happened in the European Alps during the exceptionally warm summer of 2003. The rock falls posed a significant hazard to climbers and attracted the attention of scientists and the public. Larger landslides have also occurred more recently, for example in 2004 at Thurwieser Peak in the central Italian Alps and in 2007 at Monte Rosa in the northwestern Italian Alps, both areas visited by large numbers of tourists.

Examples from western North America

The Canadian and Alaskan parts of the North American Cordillera have supported glaciers for at least 10 million years, and during the Pleistocene much of this region repeatedly was enveloped by the Cordilleran ice sheet (Clague, 1989). This recurrent and repeated glaciation has left a strong imprint on the physiography of the region: local relief is great, steep slopes are common, and classic glacial landforms, including U-shaped valleys, fiords, cirques, and arêtes, abound. Glaciers remain common within the Cordillera, covering approximately 125,000 km^2 of region.

Pandemonium Creek

In 1959, a rock spur became detached from the glacially debuttressed headwall of a cirque near Pandemonium Creek in the southern Coast Mountains of British Columbia (Evans et al., 1989). Approximately 5×10^6 m^3 of blocky, gneissic quartz diorite debris traveled across a small glacier and then 9 km along a highly irregular path, descending a vertical distance of 2 km to the valley of South Atnarko River (Figure 9). The high mobility of the rock avalanche is manifested by super-elevation in valley bends, two runups, and two right-angle changes in flow direction. This mobility is due, in part, to peculiarities in the path of the landslide (lateral moraines, for example, funneled and accelerated the debris) and, in part, to travel over a glacier below the detachment zone. Although most of the debris came to rest on the upper part of a fan at the mouth of Pandemonium Creek, one lobe traversed the fan and entered Knot Lakes, where it generated displacement waves that destroyed trees along the shore. Runup and superelevation data indicate that the debris was moving between 81 and 100 m s^{-1} as it entered the runup zone at Pandemonium Creek and 21–38 m s^{-1} in Pandemonium valley to the east. The Pandemonium Creek landslide is similar in many respects to much larger, highly mobile rock avalanches involving glacier ice in other parts of the world, for example, Huascaran, Peru (Pflaker and Ericksen, 1978). It is illustrative of the extreme mobility of relatively small rock avalanches that interact with glaciers.

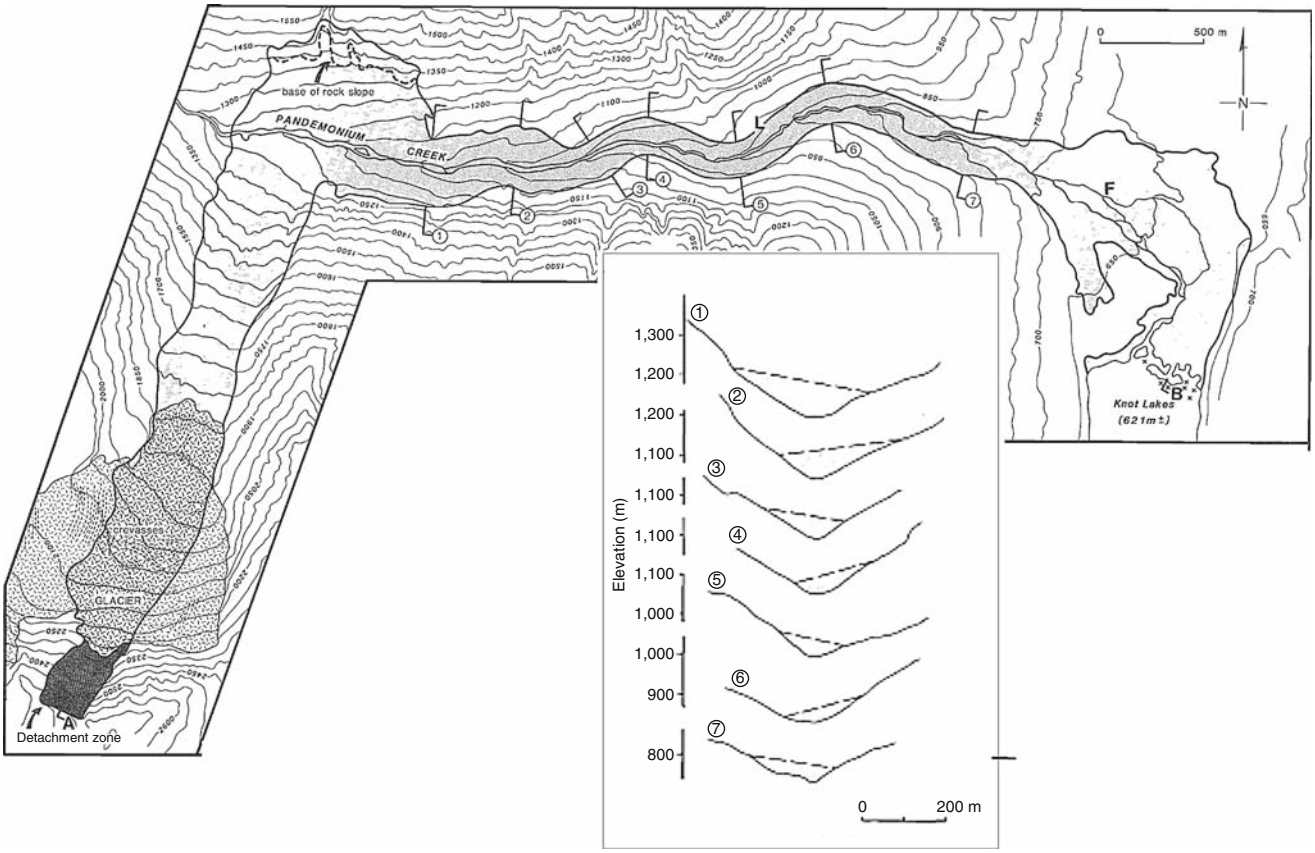

Catastrophic Rock Slope Failures and Mountain Glaciers, Figure 9 Topography, longitudinal profile, and cross-sections of the 1959 Pandemonium Creek rock avalanche, British Columbia. (Adapted from Evans et al., 1989, Figures 4 and 10.)

Mount Munday

Sometime between May 25 and July 10, 1997, a large rock avalanche occurred on the south flank of Mount Munday (3,367 m asl) in the British Columbia Coast Mountains (Evans and Clague, 1998). The site is 6.5 km southeast of Mount Waddington (4,019 m asl), the highest peak in the Coast Mountains. About 3.2×10^6 m^3 of debris flowed across and down the Ice Valley Glacier, forming a spectacular tongue-shaped deposit covering 220 ha of the glacier surface (Figure 7). The landslide involved highly resistant gneissic rocks that form a number of high peaks in the area. Failure was controlled by the foliation and by a steeply dipping planar fault surface that has a more southerly strike and cuts across the foliation at a lower dip angle.

The detached rock mass first traveled in a southwest direction across Ice Valley Glacier. It ran up the opposing slope to a height of about 100 m above the glacier surface and was deflected about 90° downglacier in a northwest direction, in a manner similar to a bobsled. Below the bobsled bend, the debris traveled up to 2.6 km over the snow-covered glacier surface on a slope of only 6°. Ridges of snow were pushed up at the margins of the debris. At the distal limit of the debris, a lobe approximately half the width of the main debris sheet moved a distance of 900 m on a slope of 5°.

The geometry of the rock-avalanche path below the bobsled bed indicates a coefficient of kinetic friction of approximately 0.11 (6°) for the interface between the debris and snow. Clearly defined, overlapping flow lines were evident in the debris following the rock avalanche. In places along the travel path, debris was thin or absent, exposing the glacier surface beneath.

Glaciers in the Mount Waddington area have thinned and retreated due to atmospheric warming, and glacier ice loss is likely a factor in the Mount Munday event. The immediate trigger of the failure may be related to the exceptional precipitation in southwest British Columbia during the first half of 1997 and a pronounced period of warm weather in the days before the failure.

Examples from the European Alps

A recent inventory of rock avalanches and rock falls in the Alps includes 301 events, of which about half are dated and most are historic (Schoeneich et al., 2008). Few of the landslides are known from glacierized environments, partly because the deposits in these environments typically are not preserved. However, since 1997 five rock

avalanches have descended in part or totally on glaciers in the western Alps – Brenva Glacier (1997), Punta Thurwieser (2004), the west face of Les Drus (2005), and the east face of Monte Rosa (2006, 2007). Research on the Italian side of the Mont Blanc massif suggests that many others occurred during the Holocene (Haeberli et al., 2002; Ravanel and Deline, 2008; Deline, 2009).

Brenva Glacier

Small rock falls occur regularly on the steep slopes bordering Brenva Glacier. In addition, two large rock avalanches have occurred during the twentieth century (Figures 10 and 11), and several others in the late Holocene. In January 1997, part of Eperon de la Brenva collapsed, mobilizing 2×10^6 m^3 of rock debris and $>4.5 \times 10^6$ m^3 of ice and snow. The avalanche of rock, ice, and snow traveled 5,750 m horizontally and 2,325 m vertically before coming to rest. On reaching the lower part of the glacier, it spread in two directions: one lobe overflowed the south lateral moraine, whereas the main lobe was channeled by the lateral moraines and reached the glacier terminus.

In November 1920, four separate rock masses detached from the east face of the Grand Pilier d'Angle. The total volume of failed rock is in the range $2.4–3.6 \times 10^6$ m^3; an additional $7.6–9.9 \times 10^6$ m^3 of ice was mobilized in the four events. Maximal horizontal and vertical displacements were 5,150 m and 2,660 m, respectively (Figure 11).

Based on observations of these historic events, the strong asymmetry of the south lateral moraine of Brenva Glacier probably is the result of numerous rock avalanches onto the glacier during the Holocene. Thus far, however, only four Holocene rock avalanches prior to the twentieth century have been identified – AD 1767 (Deline, 2005a), early fourteenth century, after AD 426–615, and 2750–2350 calendar years BP (Deline, 2005b).

Examples from the Karakoram Himalaya

More than 320 rock avalanches have been identified in the Karakoram Himalaya, and at least 29 of them spread in part or whole over glaciers. Most events in the inventory are prehistoric, but 11 rock avalanches descended onto glaciers between 1986 and 2009, and one is reported from the nineteenth century (Table 2). For reasons noted earlier, these numbers are underestimates. If recent reports are at all representative, as many as 4,000 rock avalanches may have traveled over glaciers in the Karakoram, Nanga Parbat, and Hindu Raj ranges in the Holocene. The glaciers have a total area of some 18,000 km^2. By comparison, surveys of postglacial rock avalanches at lower elevations and in ice-free areas suggest much lower incidences – 1,000–1,500 Holocene events over an area of some 80,000 km^2. Yet, even these rates are among the highest global concentrations yet known. These lower areas may also have experienced more frequent rock

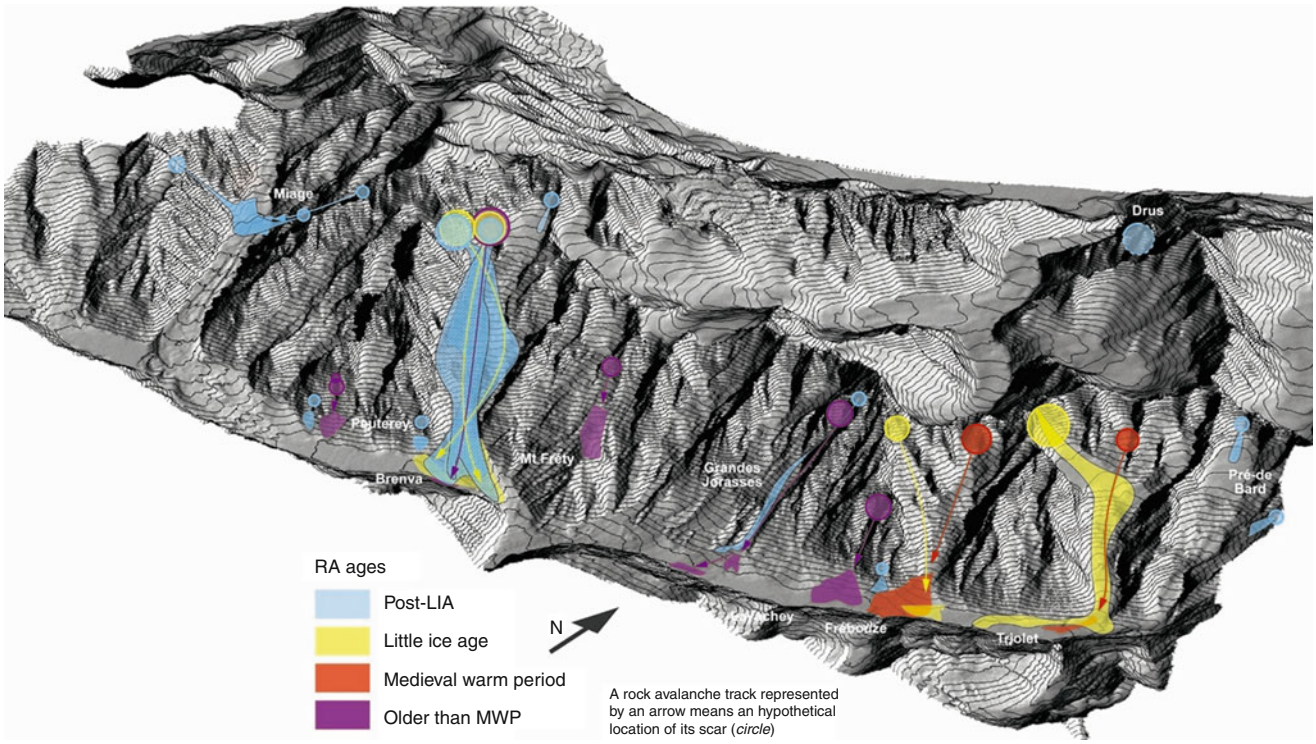

Catastrophic Rock Slope Failures and Mountain Glaciers, Figure 10 Late Holocene rock avalanches on the Italian side of the Mont Blanc massif. Most of the rock avalanches traveled onto glaciers.

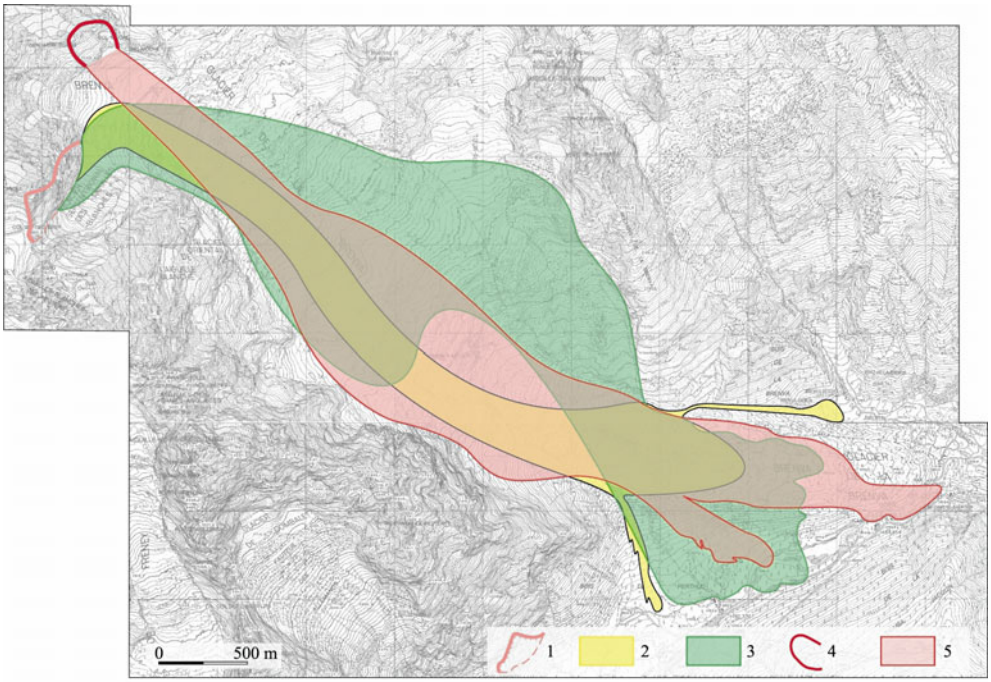

Catastrophic Rock Slope Failures and Mountain Glaciers, Figure 11 Brenva rock avalanches in 1920 and 1997. 1 – 1920 scar. 2 – 14 November 1920 track. 3 – 19 November 1920 track. 4 – 1997 scar. 5 – 18 January 1997 track.

Catastrophic Rock Slope Failures and Mountain Glaciers, Table 2 Selected rock avalanches that have descended onto glaciers in the Karakoram Himalaya and their dimensions

Rock avalanche	River	Glacier	Volume (10^6 m^3)	Area (km^2)	Comment
Ghorsit	Hushe/Shyok	Charakusa	300	2.5+	Prehistoric, partly covered terminus
Lokpar	Hushe/Shyok	Aling	20	3.0	1992; surge of Lokpar and Aling terminus
Masherbrum	Hushe/Shyok	Masherbrum	2	1.5	Late 1980s
Unnamed	Shyok	Unnamed	600+	>30	Prehistoric; from small glacier basins
Tsok	Dumordo	Unnamed	150	8	Descent over small tributary below Panmah Glacier
Naltar Lakes	Naltar	Kuto	300	14	Dams outflow of glacier
Baltit-Sumayar	Hunza	Ultar	400	8	Dammed ice-free Hunza and Hispar valleys
Yashbandan-Barut	Hunza	Pasu and Ghulkin	>250	21	Covered termini of two glaciers
Bligim Platt I	Hunza	Batura	5	3	Covered outer moraines
Bilgim Platt II	Hunza	Batura	3	2	Covered outer moraines
Shikarjerab	Hunza	Unnamed	12	>8	Prehistoric
Qalandar Uwin	Karambar	Chhateboi	>600	>15	Prehistoric
North Te-Rong	Nubra	North Te-Rong	?	5	2002
Buldar Basin	Nanga Parbat	Kappen	11	2.3	2003
Astor basin	Nanga Parbat	Chhichi	1.5	0.5	2005?

avalanches in late-glacial time, as glaciers that covered almost the entire region thinned and retreated. If so, the evidence for this activity has been largely removed from the landscape.

Bualtar and Aling glaciers, central Karakoram

In August 1986, three rock avalanches descended from the same rock wall onto the ablation zone of Bualtar Glacier. By 2005, the landslide debris had been transported about 9 km down valley, about one-third of the distance in glacier surges (see below). During this 20-year period, the landslide debris was fully reworked. The average debris thickness was reduced from about 7 to 8 m in 1986 to about 2 m in 2005, and the debris became less readily distinguishable from supraglacial debris generated by snow avalanches and rock fall, which are widely present on

Catastrophic Rock Slope Failures and Mountain Glaciers, Figure 12 A rock avalanche descended onto the Lokpar tributary glacier (*upper left*) in 1992. The following year the glacier surged into the main Aling Glacier which rapidly advanced 2.5 km. (Photo: K. Hewitt, 1999.)

Karakoram glaciers. Nevertheless, throughout this time, the debris sheet remained much thicker than debris anywhere else on Bualtar Glacier before 1986, and thicker than most debris covers on glaciers examined elsewhere in the region. As a result, it reduced ablation to a much greater extent, and a large area of thickened ice persisted beneath the rock avalanche material. The debris cover had a positive impact on mass balance, equivalent to a 20% increase in annual accumulation (Hewitt, 2009). The area of thickened ice moved along with debris through the ablation zone, and within 10 years it was equivalent to the mass transferred in the surges.

The 1986 Bualtar rock avalanches represent a fivefold increase in supraglacial debris on the glacier. Rock-avalanche debris carried to the margins of the glacier within 30 years of the failures will equal almost 500 years of normal supraglacial transport by the glacier. Similarly, the events represent a doubling of average rate of denudation during this period.

A few months after the rock avalanches, in January 1987, Bualtar Glacier surged at and below the debris sheet (Gardner and Hewitt, 1989). Over the summer, a wave of fast-moving ice traveled down the valley from the vicinity of the rock avalanches. Measured ice velocities were between 7 and 11 m day^{-1}, an order of magnitude higher than pre-surge rates (<0.8 m day^{-1}). A second surge of similar scale occurred in 1989. During the two surges, ice overtopped lateral moraines that had been ice-free for at least a few decades. Ice and meltwater undercut the glacier margins and triggered landslides and debris flows. Meltwater that had ponded at the sides of the glacier escaped in a series of small outburst floods.

The surges initially did not affect the terminus, but over the next 5 years the glacier advanced some 2.5 km and it continued to advance more slowly for another 10 years. It reached to within a kilometer of the Hispar River, farther than at any time since the 1920s (Mason, 1930).

A rock avalanche appears to have been responsible for another glacier surge in the Karakoram. The rock avalanche descended onto Lokpar Glacier, a tributary of Aling Glacier (Figure 12). Shortly thereafter, Lopkar Glacier surged, in turn causing Aling Glacier to advance some 3 km. In other recent cases, glaciers affected by rock avalanches did not surge, but their rates of flow increased and they thickened down valley (Hewitt, 2009).

Concluding remarks

Rock avalanche–glacier interactions involve mutual disturbance of two different Earth surface process systems. The behavior and deposits of one process system cannot be understood without reference to the other. Glacier behavior, landforms, and sedimentary deposits are affected by landslides throughout an extended period of debris transport, disturbed mass balance, and sedimentation. Each period has a distinctive character and sequence, and spatial relations are organized and lagged accordingly.

Bibliography

Alean, J., 1984. Ice avalanches and a landslide on Grosser Aletschgletscher. *Zeitschrift für Gletscherkunde und Glazialgeologie*, **20**, 9–25.

Ballantyne, C. K., and Benn, D. I., 1996. Paraglacial slope adjustment during recent deglaciation and its implication for slope

evolution in formerly glaciated environments. In Anderson, M. G., and Brooks, S. M. (eds.), *Advances in Hillslope Processes*. British Geomorphological Research Group Symposia Series, Vol. 12, 1173–1195.

Blikra, L. H., Longva, O., Braathen, A., Anda, E., Dehl, J. F., and Stalsberg, K., 2006. Rock slope failures in Norwegian fjord areas: Examples, spatial distribution and temporal patterns. In Evans, S. G., Scarascia Mugnozza, G., Strom, A. L., and Hermanns, R. L. (eds.), *Landslides from Massive Rock Slope Failure*. *Proceedings of NATO Advanced Research Workshop*, Celano, Italy. Springer, Dordrecht, pp. 475–496.

Bovis, M. J., and Stewart, T. W., 1998. Long-term deformation of a glacially undercut rock slope, southwest British Columbia. In Moore, D., and Hungr, O. (eds.), *Proceedings of the Eight International Congress*. International Association for Engineering Geology and the Environment. Rotterdam: A. A. Balkema, pp. 1267–1276.

Clague, J. J., 1989. Quaternary geology of the Canadian Cordillera. Chapter 1, In Fulton, R. J. (ed.), *Quaternary Geology of Canada and Greenland*. Geological Survey of Canada Geology of Canada, Vol. 1, pp. 15–96.

Clague, J. J., 1997. Evidence for large earthquakes at the Cascadia subduction zone. *Reviews of Geophysics*, **35**, 439–460.

Crandell, D. R., 1971. Postglacial lahars from Mount Rainier Volcano, Washington. *U. S. Geological Survey Professional Paper*, 677.

D'Agata, C., Smiraglia, C., Zanutta, A., and Mancini, F., 2005. Recent variations of a debris-covered glacier (Brenva glacier) in the Italian Alps monitored by comparison of maps and digital orthophotos. *Journal of Glaciology*, **51**, 183–185.

Dadson, S. J., and Church, M., 2005. Postglacial topographic evolution of glaciated valleys; a stochastic landscape evolution model. *Earth Surface Processes and Landforms*, **30**, 1387–1403.

Davies, M. C. R., Hamza, O., and Harris, C., 2001. The effect of rise in mean annual temperature on the stability of rock slopes containing ice-filled discontinuities. *Permafrost and Periglacial Processes*, **12**, 137–144.

Deline, P., 2001. Recent Brenva rock avalanches (Valley of Aosta): New chapter in an old story? *Supplementi di Geografia Fisica e Dinamica Quaternaria*, **5**, 55–63.

Deline, P., 2005a. Change in surface debris cover on Mont Blanc massif glaciers after the 'Little Ice Age' termination. *Holocene*, **15**, 302–309.

Deline, P., 2005b. Large rock avalanches on glaciers since 2500 BP on the Italian flank of the Mont Blanc massif. *European Geosciences Union, General Assembly, Vienna, Austria, Abstracts*, EGU05-A-03434.

Deline, P., 2009. Interactions between rock avalanches and glaciers in the Mont Blanc massif during the late Holocene. *Quaternary Science Reviews*, doi:10.1016/j. quascirev. 2008.09.025.

Deline, P., and Kirkbride, M. P., 2009. Rock avalanches on a glacier and morainic complex in Haut Val Ferret (Mont Blanc massif, Italy). *Geomorphology*, **103**, 80–92.

Eisbacher, G. H., and Clague, J. J., 1984. Destructive Mass Movements in High Mountains. *Geological Survey of Canada Paper*, 84–16.

Evans, S. G., and Clague, J. J., 1988. Catastrophic rock avalanches in glacial environments. In Bonnard, C. (ed.), *Landslides: Proceedings of Fifth International Symposium on Landslides*. Rotterdam: Balkema, pp. 1153–1158.

Evans, S. G., and Clague, J. J., 1993. Glacier-related hazards and climate change. In Bras, R. (ed.), *The World at Risk: Natural Hazards and Climate Change*. American Institute of Physics Conference Proceedings, Vol. 277, pp. 48–59.

Evans, S. G., and Clague, J. J., 1994. Recent climatic change and catastrophic geomorphic processes in mountain environments. *Geomorphology*, **10**, 107–128.

Evans, S. G., and Clague, J. J., 1998. Rock avalanche from Mount Munday, Waddington Range, British Columbia, Canada. *Landslide News*, **11**, 23–25.

Evans, S. G., and Clague, J. J., 1999. Rock avalanches on glaciers in the Coast and St. Elias Mountains, British Columbia. In *Proceedings of the 13th Annual Vancouver Geotechnical Conference*. Richmond: BiTech, BC, pp. 115–123.

Evans, S. G., Clague, J. J., Woodsworth, G. J., and Hungr, O., 1989. The Pandemonium Creek rock avalanche, British Columbia. *Canadian Geotechnical Journal*, **26**, 427–446.

Fahnestock, R. K., 1978. Little Tahoma Peak rockfalls and avalanches, Mount Rainier, Washington, U.S.A. In Voight, B. (ed.), *Rockslides and Avalanches 1: Natural Phenomena*. New York: Elsevier, pp. 181–196.

Fischer, L., Kääb, A., Huggel, C., and Noetzli, J., 2006. Geology, glacier retreat and permafrost degradation as controlling factor of slope instabilities in a high-mountain rock wall: The Monte Rosa east face. *Natural Hazards and Earth System Sciences*, **6**, 761–772.

Fort, M., 2000. Glaciers and mass wasting processes: Their influence on the shaping of Kali Gandaki valley, Nepal. *Quaternary International*, **65**(66), 101–119.

Gardner, J. S., and Hewitt, K., 1989. Surge of the Bualtar Glacier, Karakoram Ranges, Pakistan: A possible landslide trigger. *Journal of Glaciology*, **32**, 27–29.

Gordon, J. E., Birnie, R., and Timmis, R., 1978. A major rockfall and debris slide on the Lyell Glacier, South Georgia. *Arctic and Alpine Research*, **10**, 49–60.

Gruber, S., and Haeberli, W., 2007. Permafrost in steep bedrock slopes and its temperature-related destabilization following climate change. *Journal of Geophysical Research*, **112**, F02S18, doi:10.1029/2006JF000547.

Gruber, S., Hoelzle, M., and Haeberli, W., 2004. Permafrost thaw and destabilization of alpine rock walls in the hot summer of 2003. *Geophysical Research Letters*, **31**, 4pp.

Haeberli, W., Käab, A., Paul, F., Chiarle, M., Mortara, G., Mazza, A., Deline, P., and Richardson, S., 2002. A surge-type movement at Ghiacciaio del Belvedere and a developing slope instability in the east face of Monte Rosa, Macugnaga, Italian Alps. *Norsk Geografisk Tidsskrift*, **56**, 104–111.

Haeberli, W., Huggel, C., Kääb, A., Zgraggen-Oswald, S., Pollkvoj, A., Galushkin, I., Zotikov, I., and Osokin, N., 2004. The Kolka-Karmadon rock/ice slide of 20 September 2002; an extraordinary event of historical dimensions in North Ossetia, Russian Caucasus. *Journal of Glaciology*, **50**, 533–546.

Harp, E. L., Jibson, R. W., Kayen, R. E., Keefer, D. K., Sherrod, B. L., Carver, G. A., Collins, B. D., Moss, R. E. S., and Sitar, N., 2003. Landslides and liquefaction triggered by the M 7.9 Denali Fault earthquake of 3 November 2002. *GSA Today*, **13**(8), 4–10.

Hauser, A., 2002. Rock avalanche and resulting debris flow in Estero Parraguire and Rio Colorado, Region Metropolitana, Chile. In Evans, S. G., and Degraff, J. V. (eds.), *Catastrophic Landslides: Effects, Occurrence, and Mechanisms*. Geological Society of America Reviews in Engineering Geology, Vol. 15, pp. 135–148.

Heim, A., 1932. *Bergsturz und Menschenleben*. Zürich: Fretz and Wasmuth.

Heuberger, H., Masch, L., Preuss, E., and Strecker, A., 1984. Quaternary landslides and rock fusion in Central Nepal and the Tyrolean Alps. *Mountain Research and Development*, **4**, 345–362.

Hewitt, K., 1988. Catastrophic landslide deposits in the Karakoram Himalaya. *Science*, **242**, 64–67.

Hewitt, K., 1999. Quaternary moraines vs catastrophic rock avalanches in the Karakoram Himalaya, Northern Pakistan. *Quaternary Research*, **51**, 220–237.

Hewitt, K., 2001. Catastrophic rock slides and the geomorphology of the Hunza and Gilgit Basins, Karakoram Himalaya. *Erdkunde*, **55**, 72–93.
Hewitt, K., 2002. Styles of rock avalanche depositional complex in very rugged terrain, Karakoram Himalaya, Pakistan. In Evans, S. G., and Degraff, J. V. (eds.), *Catastrophic Landslides: Effects, Occurrence, and Mechanisms*. Geological Society of America Reviews in Engineering Geology, Vol. 15, pp. 345–378.
Hewitt, K., 2009. Rock avalanches that travel onto glaciers: Disturbance regime landscapes, Karakoram Himalaya, Inner Asia. *Geomorphology*, **103**, 66–79.
Hewitt, K., Clague, J. J., and Orwin, J., 2008. Legacies of catastrophic rock slope failures in mountain landscapes. *Earth Science Reviews*, **87**, 1–38.
Holm, K., Bovis, M., and Jakob, M., 2004. The landslide response of alpine basins to post- Little Ice Age glacial thinning and retreat in southwestern British Columbia. *Geomorphology*, **57**, 201–216.
Hsü, K. J., 1975. Catastrophic debris streams (sturzströms) generated by rock falls. *Geological Society of America Bulletin*, **86**, 129–140.
Hsü, K. J., 1978. Albert Heim: Observations of landslides and relevance to modern interpretations. In Voight, B. (ed.), *Rockslides and Avalanches 1, Natural Phenomena*. New York: Elsevier, pp. 70–93.
Huggel, C., 2008. Recent extreme slope failures in glacial environments: Effects of thermal perturbation. *Quaternary Science Reviews*, doi:10.1016/j.quascirev.2008.06.007.
Huggel, C., Zgraggen-Oswald, S., Haeberli, W., Kääb, A., Polkvoj, A., Galushkin, I., and Evans, S. G., 2005. The 2002 rock/ice avalanche at Kolka/Karmadon, Russian Caucasus; Assessment of extraordinary avalanche formation and mobility, and application of QuickBird satellite imagery. *Natural Hazards and Earth System Sciences*, **5**, 173–187.
Huggel, C., Caplan-Auerbach, J., and Wessels, R., 2008. Recent extreme avalanches triggered by climate change? *EOS (Transactions, American Geophysical Union)*, **89**(47), 469–470.
Hutchinson, J. N., 1988. General report: morphological and geotechnical parameters of landslides in relation to geology and hydrology. In Bonnard, C. (ed.), *Landslides: Proceedings of Fifth International Symposium on Landslides*. Rotterdam: Balkema, pp. 3–35.
Jibson, R. W., Harp, E. L., Schulz, W., and Keefer, D. K., 2006. Large rock avalanches triggered by the M 7.9 Denali Fault, Alaska, earthquake of 3 November 2002. *Engineering Geology*, **83**, 144–160.
Kelly, M., 1980. A prehistoric catastrophic rock avalanche at Holsteinsborg, West Greenland. *Geological Survey of Denmark Bulletin*, **28**, 73–79.
Larson, C. F., Motyka, R. J., Freymueller, J. T., Echelmeyer, K. A., and Ivins, E. R., 2005. Rapid viscoelastic uplift in Southeast Alaska caused by post-Little Ice Age glacial retreat. *Earth and Planetary Science Letters*, **237**, 548–560.
Mason, K., 1930. The Glaciers of the Karakoram and Neighbourhood. *Records of the Geological Survey of India*, LXIII/2, Government of India, Central Publications Branch, Calcutta.
McSaveney, M. J., 1978. Sherman Glacier rock avalanche, Alaska, USA. In Voight, B. (ed.), *Rockslides and Avalanches, 1 Natural Phenomena*. New York: Elsevier, pp. 197–258.
McSaveney, M. J., 2002. Recent rockfalls and rock avalanches in Mount Cook National Park, New Zealand. In Evans, S. G., and Degraff, J. V. (eds.), *Catastrophic Landslides: Effects, Occurrence, and Mechanisms*. Geological Society of America Reviews in Engineering Geology, Vol. 15, pp. 35–70.
Mudge, M. R., 1965. Rock avalanche and rockslide avalanche deposits at Sawtooth Range, Montana. *Geological Society of America Bulletin*, **76**, 1003–1014.
Noetzli, J., and Gruber, S., 2009. Transient thermal effects in Alpine permafrost. *The Cryosphere*, **3**, 85–99.
Pflaker, G., and Ericksen, G. E., 1978. Nevados Huascaran avalanche, Peru. In Voight, B. (ed.), *Rockslides and Avalanches, 1 Natural Phenomena*. New York: Elsevier, pp. 277–314.
Porter, S. C., and Orombelli, G., 1980. Catastrophic rockfall of September 12, 1717 on the Italian flank of the Mont Blanc massif. *Zeitschrift fur Geomorphologie, N.F.*, **24**, 200–218.
Post, A. S., 1967. Effects of the March 1964 Alaska Earthquake on Glaciers. *U.S. Geological Survey Professional Paper*, 544-D.
Ravanel, L., and Deline, P., 2008. La face ouest des Drus (massif du Mont-Blanc): Évolution de l'instabilité d'une paroi rocheuse dans la haute montagne alpine depuis la fin du petit âge glaciaire. *Géomorphologie*, **4**, 261–272.
Reid, J. R., 1969. Effects of a debris slide on 'Sioux Glacier', south-central Alaska. *Journal of Glaciology*, **8**, 353–367.
Schneider, J. F., 2004. Risk assessment of remote geohazards in Central and Southern Pamir/Tajikistan, Gbao, Tajikistan. In Abdrakhmatov, K., Evans, S. G., Hermanns, R., Scarascia-Mugnozza, G., and Strom, A. L. (eds.), *Security of Natural and Artificial Rockslide Dams: Extended Abstracts Volume*. Bishkek, Kyrgyzstan: NATO Advanced Research Workshop, pp. 164–169.
Schoeneich, P., Hantz, D., Deline, P., and Amelot, F., 2008. A new database of Alpine rock falls and rock avalanches. In *Proceedings, Interpraevent 2008 – Dornbirn*, Vol. 2, pp. 243–250.
Sosio, R., Crosta, G. B., and Hungr, O., 2008. Complete dynamic modeling calibration for the Thurwieser rock avalanche (Italian Central Alps). *Engineering Geology*, **100**, 11–26.
Valbusa, U., 1921. La prima frana-valanga del Monte Bianco sul ghiacciaio della Brenva (14 novembre 1920). *Societa Geografica Italiana Bolletino*, Series VI, Vol. 8, pp. 118–125.
Voight, B. (ed.), 1978. *Rockslides and Avalanches, 1 Natural Phenomena*. New York: Elsevier.
Waitt, R. B., Jr., Pierson, T. C., MacLeod, N. S., Janda, R. J., Voigt, B., and Holcomb, R. T., 1983. Eruption-triggered avalanche, flood, and lahar at Mount St. Helens – Effects of winter snowpack. *Science*, **221**, 1394–1397.
Weidinger, J. T., 2004. Case histories of Pleistocene to Recent rockslide dams in the Himalayas (India, Nepal) and Qin Ling Mountains (China). In Abdrakhmatov, K., Evans, S. G., Hermanns, R., Scarascia-Mugnozza, G., and Strom, A. L. (eds.), *Security of Natural and Artificial Rockslide Dams: Extended Abstracts Volume*. Bishkek, Kyrgyzstan: NATO Advanced Research Workshop, pp. 189–201.
Zhang, Y., Chen, W., and Riseborough, D. W., 2006. Temporal and spatial changes of permafrost in Canada since the end of the Little Ice Age. *Journal of Geophysical Research*, **111**(D22), 14pp.

Cross-references

Alaskan Glaciers
Alps
Canadian Rockies and Coast Mountains of Canada
Debris-Covered Glaciers
Glacier Surging
Glaciers of the Karakoram Himalaya
Himalaya
Hindu Kush
Ice-Marginal Deposition
Natural Hazards Associated with Glaciers and Permafrost
Optical Remote Sensing of Alpine Glaciers
Rocky Mountains
Sediment Entrainment, Transport, and Deposition

CATCHMENT GLACIER

D. P. Dobhal
Wadia Institute of Himalayan Geology,
Dehradun, Uttarakhand, India

Definition

The catchment glacier represents the superficial area of a glacier from where the glaciers receive and release the snow/ice material in different form and maintain the equilibrium of a glacier. The catchment of a glacier may be formed by single or more ice body, slowly moving on the downward slope and from a huge glacier reservoir system. All processes by which snow or ice are added or removed from or to a glacier are considered on its catchment basis.

CAUCASUS MOUNTAINS

Chris R. Stokes
Department of Geography, Durham University,
Durham, UK

The Caucasus Mountains are aligned west-northwest to east-southeast between 40–44°N and 40–49°E and span the borders of Russia, Georgia, Armenia, and Azerbaijan. They consist of two separate mountain systems: the Greater Caucasus extends for ~1,300 km between the Black Sea and the Caspian Sea, while the Lesser Caucasus runs parallel but approximately 100 km to the south. The Greater Caucasus contains several peaks above 5,000 m, the highest of which is Elbrus at 5,642 m (18,506 ft). The mountains originate from collision between the Arabian plate to the south and the Eurasian plate to the north and the region is tectonically active, with numerous small earthquakes.

In addition to altitudinal variations in climate, the Caucasus Mountains are characterized by strong longitudinal gradients that produce a maritime climate in the west and a more continental climate in the east. Trends in *Precipitation* (qv), for example, reveal that westernmost areas typically receive around three to four times as much as eastern areas (Horvath and Field, 1975). The southern slopes are also characterized by higher temperatures and precipitation, which can be up to 3,000–4,000 mm a^{-1} in the southwest (Volodicheva, 2002). Much of this precipitation falls as *Snow* (qv), especially on windward slopes of the western Greater Caucasus, which are subjected to moist air masses sourced from the Black Sea. The high snowfall and steep slopes (>25°) result in one of the highest levels of *avalanche* activity in the whole of Russia (Seliverstov et al., 2008).

Glaciers (*Glacier*, qv) cover large parts of the Caucasus, particularly on north-facing slopes of the central Caucasus, with estimates ranging from 1,400 (Bazhev, 1989) to 1,805 km^2 (Horvath and Field, 1975). There are over 2,000 glaciers, mainly classed as small, *mountain*, or *Cirque Glaciers* (qv); but the highest summits can be covered by larger *ice fields* drained by several glaciers, for example, Elbrus, which is covered by a 123-km^2 ice field (Volodicheva, 2002).

The most recent glacier advances are associated with the "Little Ice Age" and maximum positions have been dated to AD 1680, 1750, and 1850 (Volodicheva, 2002). Glaciers have subsequently retreated from these positions (probably by as much as 30%) and widespread *Terminus* (qv) retreat has been documented between 1972 and 2000 (Bedford and Barry, 1995; Stokes et al., 2006). Analysis of the mass balance (*Glacier Mass Balance*, qv) of Djankuat Glacier, one of ten *Benchmark Glacier* selected by the *World Glacier Monitoring Service* (*WGMS* (*World Glacier Monitoring Service*), qv) because of its continued measurement since 1967, indicate that this retreat is being driven by increased summer temperatures, with no compensating increase in winter precipitation (Shahgedanova et al., 2005). Furthermore, glacier retreat appears to be associated with expansion of supraglacial debris (*Supra-Glacial Debris Entrainments*, qv) cover and ice-contact/*Proglacial Lakes* (qv) (Stokes et al., 2007), which may increase the likelihood of glacier-related hazards and debris flows. Unfortunately, such hazards are relatively common in this region and have led to major loss of life. On September 20, 2002, for example, a catastrophic ice-debris flow, including almost complete mobilization of the Kolka Glacier, traveled 19 km down the Genaldon Valley, North Ossetia, and killed over 100 people (Evans et al., 2009).

Bibliography

Bazhev, A. B., 1989. Modern glaciation: snow-ice resources. In Badenkov, Y. P. (ed.), *Guidebook for the Pre-Conference Excursion "Transformation of Mountain Environments: Regional Development and Sustainability; Consequences for Global Change"*. Moscow: USSR Academy of Sciences, Institute of Geography.

Bedford, D. P., and Barry, R. G., 1995. Glacier trends in the Caucasus, 1960s–1980s. *Physical Geography*, **15**(5), 414–424.

Evans, S. G., Tutubalina, O. V., Drobyshev, V. N., Chernomorets, S. S., McDougall, S., Petrakov, D. A., and Hungr, O., 2009. Catastrophic detachment and high-velocity long-runout flow of Kolka Glacier, Caucasus Mountains, Russia in 2002. *Geomorphology*, **105**, 314–321.

Horvath, E., and Field, W. O., 1975. The Caucasus. In Field, W. O. (ed.), *Mountain Glaciers of the Northern Hemisphere*. Hanover: Cold Regions Research and Engineering Laboratory.

Seliverstov, Y., Glazovskaya, T., Shnyparkov, A., Vilchek, Y., Sergeeva, K., and Martynov, A., 2008. Assessment and mapping of snow avalanche risk in Russia. *Annals of Glaciology*, **49**, 205–209.

Shahgedanova, M., Stokes, C. R., Gurney, S. D., and Popovnin, V., 2005. Interactions between mass balance, atmospheric circulation, and recent climate change on the Djankuat Glacier, Caucasus Mountains, Russia. *Journal of Geophysical Research*, **110**, D04108, doi:10.1029/2004JD005213, 2005.

Stokes, C. R., Gurney, S. D., Shahgedanova, M., and Popovnin, V., 2006. Late-20th-century changes in glacier extent in the

Caucasus Mountains, Russia/Georgia. *Journal of Glaciology*, **52**(176), 99–109.
Stokes, C. R., Popovnin, V., Aleynikov, A., Gurney, S. D., and Shahgedanova, M., 2007. Recent glacier retreat in the Caucasus Mountains, Russia, and associated increase in supraglacial debris cover and supra-/proglacial lake development. *Annals of Glaciology*, **46**, 196–203.
Volodicheva, N., 2002. The Caucasus. In Shahgedanova, M. (ed.), *The Physical Geography of Northern Eurasia*. Oxford: Oxford University Press, pp. 350–376.

CHARACTERISTICS OF SNOW AND GLACIER FED RIVERS IN MOUNTAINOUS REGIONS WITH SPECIAL REFERENCE TO HIMALAYAN BASINS

Akhouri Pramod Krishna
Department of Remote Sensing, Birla Institute of Technology (BIT), Deemed University, Ranchi, Jharkhand, India

Definition

Snow and glacier fed rivers of the Himalaya usually originate from the high mountains with their morphogenetic regions in perennial high snow fields and glaciers.

Introduction

Interactions between the processes that control the snow and glacier-melt contribution to runoff vary considerably between different climatic regions. In mid- and high-latitude mountain ranges, for example, seasonal snow cover exerts a strong influence on runoff variability, whereas glaciers are the dominant source of water during the dry season at low latitudes (Hock and Rees, 2006). In mountainous regions, snow- and glacier-fed rivers usually have their origins in the high snow fields. Upper morphogenetic regions of such rivers have their sources in perennial high snow fields and glaciers (Krishna, 2005). Meltwater contributions from snow cover, glaciers, and permafrost (permanently frozen ground) play an important role for generating the innumerable streams that feed the perennial river systems of the high mountain regions, e.g., Himalayan region. Himalayan glacier-fed rivers supply water to one third of the world's population. Since such rivers and their tributaries are fed perennially by snow cover and glacier ice, the extent of snow-covered areas has great bearing on their discharge and runoff (Krishna, 1996). Glaciers act as buffers and regulate the runoff water supply from high mountains to the plains during both dry and wet spells, which are inherent phenomena in a tropical environment. Estimated total volume of water stored globally in ice is 700 times greater than the volume of the annual river runoff (Hall and Martinec, 1985). Their hydrological implications are significant due to snow-fed origins in addition to their glacial meltwater regime and fluctuating rainfall they receive through different altitudinal zones. Snow- and glacier-fed rivers may not only be good indicators of climate change, but also may be suitable testing grounds for examining ecological concepts (Brittain and Milner, 2002).

Central Asia with an estimated total ice cover of 114,800 km^2 has as its dominant mountain range the Himalaya (WGMS, 2009). With 15% of its area covered by glaciers, the Himalaya constitutes the largest glacier system in the world outside Antarctica and Greenland (cf. Racoviteanu et al., 2008). Whereas in comparison, there are over 100,000 glaciers in Alaska, although overall ice cover is only 5% of this state (Anonymous, 2002). Himalayan glaciers form the largest body of ice outside the polar caps (Jain, 2008). Himalayan ranges are home to some of the longest glaciers in the world such as Siachen, Bara Shigri, Gangotri, Zemu, Milam, and Kedarnath. Ice mass covering the Himalayan-Hindu Kush mountain range is the third largest in the world, after the polar icecaps. Snow and glacier together are the source of largest rivers of Asia. These glacial masses store precipitation in the form of snow and ice, regulating water distribution and providing continuous flows during the dry months (World Bank, 2009). Runoff from rain-fed rivers may change in the future such that a reduction in snowmelt water may put the dry-season flow of these rivers relatively under more stress than the present situation (IPCC, 2000). River flow from glacier areas in the Himalaya is influenced both by intra-annual variations in precipitation and energy availability, and by longer-term changes in storage of water as glacier ice. High specific discharge from ice melt often dominates flow for considerable distances downstream, particularly where other sources of runoff are limited, providing a major water resource (Rees and Collins, 2005). Snow-fed basins are more sensitive in terms of reduction in water availability due to a compound effect of increase in evaporation and decrease in melt. For a complex type of basin, the decrease in melt from seasonal snow may be counterbalanced by increase in melt from glaciers (Singh and Bengtsson, 2005).

Himalayan glaciers feed many significant rivers of Asia ensuring a year-round water supply to hundreds of millions of people in the Indian subcontinent and China (Taylor, 2005). These glaciers, which release an estimated 8.6 million cubic meters of water annually, have nourished seven great rivers of Asia – Ganga, Indus, Brahmaputra, Salween, Mekong, Yangtze, and Huang Ho. Ancient civilizations sprang up and thrived along the shores of these rivers (Gopal Raj, 2007). Swiss and French Alps, Rocky Mountains, Colorado and across the US, Europe, and Antarctica have provided clear indications of rise in temperature during the twentieth century. Former Soviet Union except in eastern Siberia, the Baltic Republics, some locations in Caucasus, and low elevations in Central Asia show a rising trend. The rise in temperature has been felt almost in every region. An increase or decrease in the river discharge is one of the strongest evidences for climate change (Joshi, 2009). As glacier water flows dwindle, the energy potential of hydroelectric power

may decrease, causing problems for industry, while reduced irrigation means lower crop production. Heavy snowfall is very beneficial as with the onset of summers, snow starts melting. Thus, snow-fed rivers become replete with water as more of water is discharged. In case this diminishing trend of glaciers and hydrological disruptions continue, regime of snow-fed rivers in the region may be adversely affected. For suitable planning of micro and mini hydroloelectric power stations, there is a need to take up snow and glacier-melt run-off studies of snow- and glacier-fed river catchments (Kulkarni et al., 1999; Singh and Jain, 2002).

As per a recent WWF report on "Overview of Glaciers, Glacier Retreat and Subsequent Impacts in Nepal, India and China," rate of retreat of Himalayan glaciers are accelerating. The report suggested that three of Nepal's snow-fed rivers had declining trends in discharge. In case of China, the report stated that Qinhai Plateau's wetlands had declining lake water levels, lake shrinkage, absence of water flow in rivers and streams, and the degradation of swamp wetlands. In India, several glaciers are receding, which eventually result in water shortages for hundreds of millions of people who rely on glacier-dependent rivers in China, India, and Nepal.

Physical characteristics

According to Braddock (1998), glaciers contribute to flows throughout the year, but most melt occurs during the warmer spring and summer seasons. Glacier-fed rivers reach their peak discharge during hot summer weather. As the seasonal snow resource is depleted, the glacier surface is exposed to melt. The amount of melt generated is largely dependent on the prevailing synoptic situation of the period. Glaciers have three main influences: they contribute to river flows, delay the peak seasonal flow, and reduce the year-to-year variability of flow. Systematic and sustained studies of hydrometeorological processes of snow and glacial regime are necessary for evaluating changes in the hydrology of mountain rivers due to glacier recession and climate change (Thayyen et al., 2007).

Discharge regimes

The alpine and high mountainous areas of the world play an important and distinctive role in the hydrological processes of the planet and in the regional hydrology of all continents (Verbunt et al., 2003). One of the most important tasks related to snow and glacier hydrology in mountainous regions is river-flow forecasting. Snow is more convenient than rain for river-flow forecasting as water is retained in a basin for weeks or months before being released (Hall and Martinec, 1985). Such delays allow the forecasters more time for evaluating the hydrometeorological situation and getting more collateral inputs acquired through remote sensing data, etc. Remote sensing data may help in avoiding discharge forecasting failures particularly in the years which deviate from the usual run-off patterns, especially during snowmelt seasons. Better forecast possibilities in case of snow- and glacier-fed rivers lead to benefits in terms of various utility projects downstream, namely, power generation, irrigation, flood control and drinking water supply, etc. Impact of glaciers and snow cover on river hydrology are often not considered in water resources management policies at lower reaches of the glacier-fed rivers due to lack of information on hydrological processes of snow/glacier regime (Thayyen et al., 2007). Estimation of the snow and glacier contribution in the annual runoff of various Himalayan rivers is necessary for the development and efficient management of water resources, which include flood forecasting, reservoir operation, design of hydraulic structures, etc. (Kumar et al., 2007).

Snow cover built up in the higher altitudinal regions during the winter months melts in the spring and on a seasonal basis contributes the largest volume of water to river flow and to groundwater recharge in particular areas (Bandyopadhyay et al., 1997). Snowmelt runoff from mountains is the primary input to river discharge and is the major source of water for the populations of adjacent lowlands (Price and Barry, 1997). Seventy percent of the world's freshwater is frozen in glaciers, which buffer ecosystems against climate variability by releasing water during dry seasons or years. In tropical areas, glaciers melt year-round, contributing continuously to streamflow and often providing the only source of water for humans and wildlife during dry parts of the year (WWF, 2009). According to Braddock (1998), many rivers of the South Island are sourced from the glacierized catchments of the Southern Alps. Those that drain into hydro storage lakes rely on the regular flows from these catchments, ensuring close to full lake levels for the coming winter peak electricity demand. During summer, glaciers act to supplement flows with water when it is otherwise scarce. In winter, a large proportion of precipitation falls as snow, contributing to storage rather than directly to runoff, thereby reducing flows. In effect, glaciers influence the amount and timing of river flows throughout the year. At an annual scale, the water balance can be used to estimate the meltwater quantity to river flows.

For a better management of water resources, the information on water stored in a basin in the form of snow is of immense use (Singh et al., 2000; Singh et al., 1997). On a short term, fast-melting glaciers provide a bounty for some rivers, as more ice turns to water. But when the glaciers shrink too much, summer stream flows are expected to drop off (Cornwall, 2006). Glaciers are very sensitive to climate change. Their size, life span, and history of growth and retreat all depend strongly on climate conditions (Thapa, 2004). Availability of water from snow-fed rivers may increase in the short term but decrease in the long term. Runoff from rain-fed rivers may change in the future, although a reduction in snowmelt water would result in a decrease in dry-season flow of these rivers. Larger populations and increasing demands in the agricultural, industrial, and hydropower

sectors will put additional stress on water resources. Global Warming is melting glaciers in every region of the world, putting millions of people at risk from floods, droughts, and lack of drinking water. Pressure will be most acute on drier river basins and those subject to low seasonal flows. Hydrological changes in island and coastal drainage basins are expected to be small, apart from those associated with sea-level rise. Heavy snowfall proves fortuitous for the rivers, especially snow-fed ones which would have abundant water during summers when the snow melts, and boosts hydropower generation. Glaciers exert a direct influence on the hydrologic cycle by slowing the passage of water through the cycle. Like lakes and groundwater reservoirs, glaciers are excellent natural storehouses, releasing water when it is needed most (Anonymous, 2008). "Himalayan catchment" is one of the three distinct glacio-hydrologic regimes of the Himalaya. Other two are the winter snow dominated Alpine catchment and cold-arid region of the Ladakh (Thayyen and Gergan, 2009). At the foot of the Himalayas, vast plains receive much of their fresh water from thousands of glaciers high up in the mountains (Harris, 2007).

Geomorphology

Glacial landforms commonly found around high snow fields and glaciers constitute a variety of erosional features, namely, moraines, eskers, drumlins, braided streams, etc. Braided glacial rivers exhibit a highly predictable annual flow pulse caused by the freeze–thaw cycle onto which summer dale discharge fluctuations and unpredictable spates induced by rainfall are superimposed (Rothlisberger and Lang, 1987). Glaciers and subsurface aquifers are the main water sources that interact over time and space to produce a dynamic riverscape made of contrasting glacial water fed channels and groundwater-fed channels (Brown et al., 2003). The mountainous topography causes great spatial variations of all processes of snow cover formation and ablation. The main controlling factors are precipitation, air temperature, albedo, and the heating balance equation and all with more or less strong dependence on altitude (Verbunt et al., 2003).

Rivers of fluvio-glacial origin release large amounts of meltwater in summer months. Glaciers exert tremendous forces on the rocks over which they slowly flow. This action grinds the rocks to a fine silt known as glacial or rock flour. This means that one could begin with relatively dilute glacial water at the toe of an ice mass, then flow downstream with the associated suspended flour, dissolving the major constituents within, and quickly end up with water relatively high in dissolved salts (Ahearn, 2002). Thus, glaciers contribute a huge quantity of sediment and dissolved salts to the glacier-fed rivers every year. Meltwater transports glacially eroded material to the outwash plain, an alluvial plain at the edge of retreating glaciers. Discharge often occurs in surges with wide channels and vast quantities of water. These rivers usually flow in high-energy environment rendering them capable of eroding and transporting. Glaciers feeding the rivers in the high mountains show glacio-fluvial erosional and depositional features such as zones of ablation and accumulation along with glacial moraine features (Krishna, 1999). Fowler and Archer (2005) have illustrated that summer runoff on the high-altitude glacier-fed catchments shows significant positive correlation with summer temperatures. Winter precipitation is strongly correlated with summer runoff on the snow-fed catchments. However, temperature and runoff are negatively correlated on middle altitude (snow-fed) catchments. In middle altitude snow-fed catchments, Singh and Bengtsson (2005) have found that increased temperature results in increased evaporative loss and (since snow cover volume is limiting) reduced runoff.

Sediment transport and load

Magnitude of sediment transported by rivers has become a serious concern for the water resources planning (Jain et al., 2003). An attempt has also been made to quantify the suspended sediment load carried by the stream draining the Satopanth and Bhagirath Kharak Glaciers in Ganges basin in the Indian Himalayas (Chauhan and Hasnain, 1993). The suspended sediment concentration exhibits diurnal variation, an increase in discharge leading to a rise in the suspended load. Relationship between suspended sediment load and discharge allows an assessment of sediment transport and yield. In fluvial processes associated with snow- and glacier-fed rivers, sediment transport relates to rivers/streams, periglacial flows, flash floods, and glacial lake outburst floods (GLOF). Such rivers carry sediments ranging in size from sand, gravel extending even upto cobbles and boulders. Morphogenetic regions of snow- and glacier-fed rivers generally have erosional and depositional glacial-periglacial features present in the area. Fluvio-glacial characteristics of the snow- and glacier-fed rivers over their entire catchments are important to understand. As per IPCC Special Report (2001), Himalayas play a crucial role in the provision of water to continental monsoon Asia. Increased temperature and increased seasonal variability in precipitation may lead to accelerated recession of glaciers and increasing danger from glacial lake outburst floods. A reduction in flow of snow-fed rivers, accompanied by increases in peak flows and sediment yields, would have major impacts on hydropower generation, urban water supply, and agriculture.

Chemical characteristics

Chemical characteristics of meltwaters discharged from glaciers can be distinguished in terms of chemical activity from other aqueous systems (Chauhan and Hasnain, 1993). They further state that the data available on the geochemistry of meltwaters show that apparent rate of denudation in glaciarized basins is highly significant. Based

on studies on a significant Himalayan glacier, Hasnain et al. (1989) reported that meltwaters from the glacial surface had low solute content. Whereas after passing through the glacier, waters were found to be chemically enriched. Variations of solute concentration in meltwaters at the snout were related to their discharge.

Anderson et al. (1997) found that sediment yields were high from glaciers, which suggested that water flux, rather than physical erosion, exerted the primary control on chemical erosion by glaciers. They further stated that although glaciers did not influence total chemical denudation rates at a given runoff, they might yield compositionally distinctive chemical fluxes to the oceans. As such, geology of the area is a primary control on stream chemistry. Some of the findings state that clear water tributaries of snow-fed rivers are characterized by low temperatures, high dissolved oxygen concentrations, low total dissolved solids, and water rich in calcium and bicarbonate. Dilution of dissolved salts takes place due to factors like (i) high specific run-offs and (ii) seasonal variations. Conversely, glacially fed tributaries have a slightly higher dissolved load and in order of magnitude, greater turbidity and suspended sediment loads (Maurer and Scott, 1992).

Biological characteristics

Hydrological flow-paths and the connectivity of chemical weathering environments with sources of oxygen are key controls on the redox potential of the environments that microbes colonize (Tranter et al., 2005). The subglacial environment, comprising sediment and water beneath glaciers and debris-rich ice accreted to the glacier sole, was historically considered to be devoid of life, and subglacial geochemical activity was explained exclusively in terms of abiotic processes. However, this view has been superseded with the discovery of microbial communities in the refrozen lake water above an Antarctic subglacial lake and at the beds of alpine and high Arctic glaciers (Bhatia et al., 2006).

Understanding riverscape dynamics is of particular importance because the relative proportion, life span, and spatial arrangement of these contrasting water bodies control biodiversity and bioproduction within the braided band (Malard et al., 2006). Based on studies on glaciers in Switzerland by Sharp et al. (1999), it is suggested that bacterial populations found in subglacial meltwaters and basal ice are comparable to those in the active layer of permafrost and orders of magnitude larger than those found in ice cores from large ice sheets. Populations increase with sediment concentration, and 5–24% of the bacteria are dividing or have just divided, suggesting that the populations are active. These findings (1) support inferences from recent studies of basal ice and meltwater chemistry that microbially mediated redox reactions may be important at glacier beds, (2) challenge the view that chemical weathering in glacial environments arises from purely inorganic reactions, and (3) raise the possibilities that redox reactions are a major source of protons consumed in subglacial weathering and that these reactions may be the dominant proton source beneath ice sheets where meltwaters are isolated from an atmospheric source of CO_2.

Glacier and Nival systems: variations downstream

Glacier-fed (more properly, glacionival) rivers play a central hydrologic role in many regions, including much of North America, Europe, and the Indian subcontinent; they are typically spatially interspersed with nival rivers, and a growing body of evidence suggests that the two types of fluvial system can respond quite differently to climatic variability (Fleming, 2004). Nival ecosystems comprise of moraines, eternal snow, and glaciers. Nival systems, especially glaciers, play the important role in formation of a river drain and climatic conditions of a region.

Dery et al. (2009) found that runoff from pluvial, nival, and glacial catchments differ in the timing and the quantity of flow. They have further stated that the flows in rain-dominated rivers in western Canada peak during fall and winter and are low during summer. In contrast, high flows in nival and glacial rivers occur in spring and summer with low flows during winter. Nival rivers show a more pronounced and narrower peak in river discharge driven by snowmelt, whereas glacial rivers have an extended period of high flows with an attenuated recession following snow and glacial melt. Accordingly, cumulative annual discharge rises more steadily in rain-dominated rivers than in nival or glacial rivers.

Growing interest in the differential responses of glacial and nival rivers to climatic forcing, and in ecological distinctions between the two streamflow regimes, suggests the need for a better comparative understanding of how the annual hydrologic cycle differs with presence or absence of catchment glacial cover (Fleming, 2005). A nival-glacial system is an environmental system characterized by the dominant role of snow cover and ice, where moisture and energy exchanges may have central importance and in all processes that affect the evolution of the system and its interaction with the environment (Il'yina, 1991). Annual peak flow generally occurs in a certain month in pluvial rivers, whereas this happens between some other periods for nival and glacial rivers.

Summary

Snow- and glacier-fed rivers particularly emanating from high mountains are of significance to understand their characteristics. This is owing to the fact that such rivers receive significant discharge from the snow and glacier covered morphogenetic regions giving them a perennial character. Thus they carry runoff, from such regions which are considered rich frozen deposit of water, downstream fulfilling various needs of the regions through which they travel. Glacier and nival regimes together leads to distinct nature of seasonal hydrological discharge as a result of meltwater from the catchment. Understanding of detailed characteristics of rivers of such origins may facilitate forecasting of seasonal run-off pattern, appropriate discharge

forecasts for hydroelectric power generation, irrigation, drinking water supplies, and many allied types of requirements and prevention against floods, flash floods, and other forms of channel disturbances downstream. In addition, global climate-change investigations are also being facilitated a lot through various hydrological and glaciofluvial indicators in the morphogenetic regions. Present day approach to detail snow- and glacier-fed rivers tend to consider their physical, chemical, and biological characteristics as well. Inherent natural processes with respect to high mountain catchment areas of snow- and glacier-fed rivers are necessarily referred to in terms of fluvio-glacial and hydrological characteristics. This may lead to better understanding of conceptual and practical aspects of the genesis as well as utility and services being provided by snow- and glacier-fed rivers.

Bibliography

Ahearn, D., 2002. The biogeochemistry of glacial and spring-fed streams in the Copper river watershed, South Alaska. http://watershed.ucdavis.edu/copper_river/background/data/Alaska%20Paper.pdf (accessed March 2009).

Anderson, S. P., Drever, J. I., and Humphrey, N. F., 1997. Chemical weathering in glacial environments. *Geology*, **25**(5), 399–402.

Anonymous, 2002. Icefields and Glacieras. http://www.fs.fed.us/r10/tongass/forest_facts/forest_facts.shtml (accessed March 2009).

Anonymous, 2008. Glaciers – nature's frozen rivers. http://www.ec.gc.ca/envhome.html (accessed April 2009).

Bandyopadhyay, J., Rodda, J. C., Kettelmann, R., Kundzewicz, Z. W., and Kraemer, D., 1997. Highland waters – a resource of global significance. In Messerli, B., and Ives, J. D. (eds.), *Mountains of the World – A Global Priority*. New York: Parthenon, pp. 131–155.

Bayr, J. J., Hall, D. K., and Kovalick, W. M., 1994. Observations on glaciers in the eastern Austrian Alps using satellite data. *International Journal of Remote Sensing*, **15**(9), 1733–1742.

Bhatia, M., Sharp, M., and Foght, J., 2006. Distinct bacterial communities exist beneath a high Arctic polythermal glacier. *Applied and Environmental Microbiology*, **72**(9), 5838–5845.

Braddock, D. H., 1998. The influence of glaciers on runoff, Southern Alps, New Zealand, *GeoVoice*, issue 1 (article based on MSc thesis of 1998). http://geovoice.otago.ac.nz/issue001/mvandergoes.html (accessed April 2009).

Brittain, J. E., and Milner, A. M., 2002. Ecology of glacier-fed rivers: current status and concepts. *Freshwater Biology*, **46**(12), 1571–1578.

Brown, L. E., Hannah, D. M., and Milner, A. M., 2003. Alpine stream habitat classification: an alternative approach incorporating the role of dynamic water source contributions. *Arctic, Antarctic, and Alpine Research*, **35**, 313–322. *cf.* Malard, F., Uehlinger, U., Zah, R., and Tockner, K., 2006. Flood pulse and riverscape dynamics in a braided glacial river. *Ecology*, **87**(3), 704–716.

Chauhan, D. S., and Hasnain, S. I., 1993. Chemical characteristics, solute and suspended sediment loads in the meltwaters draining satopanth and bhagirath kharak glaciers, Ganga Basin, India. In *Snow and Glacier Hydrology* (*Proceedings of the Kathraandu Symposium*, Kathmandu, November 16–21, 1992), IAHS Publ. no. 218.

Cornwall, W., 2006. State's shrinking glaciers: going ... going ... gone? *Seattle Times*, November 2, 2006. http://seattletimes.nwsource.com/html/home (accessed April 2009).

Déry, S. J., Stahl, K., Moore, R. D., Whitfield, P. H., Menounos, B., and Burford, J. E., 2009. Detection of runoff timing changes in pluvial, nival, and glacial rivers of western Canada. *Water Resources Research*, **45**, W04426, doi:10.1029/2008WR006975.

Fleming, S. W., 2004. *Comparative statistical hydroclimatology of glacial and nival rivers in southwest Yukon and northwest British Columbia*. PhD thesis, Vancouver, University of British Columbia.

Fleming, S. W., 2005. Comparative analysis of glacial and nival streamflow regimes with implications for lotic habitat quantity and fish species richness. *River Research and Applications*, **21**, 363–379, doi:10.1002/rra.810.

Fowler, H. J., and Archer, D. R., 2005. Hydro-climatological variability in the Upper Indus Basin and implications for water resources. In *Regional Hydrological Impacts of Climatic Change – Impact Assessment and Decision Making* (*Proceedings of Symposium S6 Held During the Seventh IAHS Scientific Assembly*, Foz do Iguaçu, April 2005). IAHS Publ. 295.

Gopal Raj, N., 2007. The great Himalayan meltdown. *The Hindu* (online edition; April 10, 2007). http://epaper.thehindu.com/ (accessed March 2009).

Hall, D. K., and Martinec, J., 1985. *Remote Sensing of Ice and Snow*. London: Chapman & Hall, p. 189.

Harris, J., 2007. Linking glacial melt to food. *Planet Earth*, **Summer** (2007 Issue), 28–29.

Hasnain, S.I., Subramanian, V., and Dhanpal, K., 1989. Chemical characteristics and suspended sediment load of meltwaters from a Himalayan glacier in India, *Journal of Hydrology*, **106** (1–2), 99–108.

Hock, R., and Rees, G., 2006. Contribution from glaciers and snow cover to runoff from mountains in different climates. *Hydrological Processes*, **20**, 2089–2090.

Il'yina, E. A., 1991. Characteristics of nival-glacial systems at high latitudes in a marine climate. In *Glaciers-Ocean-Atmosphere Interactions* (*Proceedings of the International Symposium*, St. Petersburg, September 1990). IAHS Publ. no. 208.

IPCC, 2000. *The regional impacts of climate change – an assessment of vulnerability: summary for policymakers*. Intergovernmental Panel on Climate Change Special Report on Emissions Scenarios, UNEP/WMO. http:/www.grida.no/climate/ipcc/regional (accessed March 2009).

IPCC, 2001. *IPCC Special Reports on Climate Change* – complete online versions, UNEP/GRID-Arendal Publications, p. 45.

Jain, S. K., 2008. Impact of retreat of Gangotri glacier on the flow of Ganga River. *Current Science*, **95**(8), 1012–1014.

Jain, S. K., Singh, P., Saraf, A. K., and Seth, S. M., 2003. Estimation of sediment yield for a rain, snow and glacier fed river in the western Himalayan region. *Water Resources Management*, **17**(5), 377–393.

Joshi, V. K., 2009. Himalayan rivers reflect climate shift. http://www.boloji.com/environment/index.htm (accessed April 2009).

Krishna, A. P., 1996. Satellite remote sensing applications for snow cover characterization in the morphogenetic regions of upper Tista River basin, Sikkim Himalaya. *International Journal of Remote Sensing*, **17**(4), 651–656.

Krishna, A. P., 1999. Snow cover and glacier assessments in parts of the Sikkim Himalaya by remote sensing and GIS. In *Proceedings of NSSW'99 National Snow Science Workshop, Snow and Avalanche Study Establishment (SASE)*, Manali, DRDO, Govt. of India; pp. 33–40.

Krishna, A. P., 2005. Snow and glacier cover assessment in the high mountains of Sikkim Himalaya. *Hydrological Processes*, **19**, 2375–2383. Publ. online in Wiley Interscience, doi:10.1002/hyp.5890.

Kulkarni, A. V., Basak, P., Randhawa, S. S., and Sood, R. K., 1999. Estimation of winter snow contribution into snow-melt run-off model. In *Proceedings of NSSW'99 National Snow Science*

Workshop, Snow and Avalanche Study Establishment (SASE), Manali. DRDO, Govt. of India, pp. 153–156.
Kumar, V., Singh, P., and Singh, V., 2007. Snow and glacier melt contribution in the Beas River at Pandoh Dam, Himachal Pradesh, India. *Hydrological Sciences–Journal–des Sciences Hydrologiques*, **52**(2), 376–388. Publ. IAHS.
Lundquist, J. D., Dettinger, M. D., and Cayan, D. R., 2005. Snow-fed streamflow timing at different basin scales: case study of the Tuolumne River above Hetch Hetchy, Yosemite, California. *Water Resources Research*, **41**, W07005, doi:10.1029/2004WR003933.
Maurer, M. A., and Scott, R., 1992. Copper river highway environmental impact studies: water quality of surface waters. Public data file 92-23, State of Alaska, Department of Natural Resources (cf. Ahearn, Dylan 2002, *The biogeochemistry of glacial and spring-fed streams in the Copper river watershed, South Alaska*, GEL 198). http://watershed.ucdavis.edu/copper_river/background/data/Alaska%20Paper.pdf.
Price, M. F., and Barry, R. G., 1997. Climate change. In Messerli, B., and Ives, J. D. (eds.), *Mountains of the World – A Global Priority*. New York: Parthenon, pp. 409–445.
Racoviteanu, A. E., Williams, M. W., and Barry, R. G., 2008. Optical remote sensing of glacier characteristics: a review with focus on the Himalaya. *Sensors*, **8**, 3355–3383, doi:10.3390/s8053355.
Rees, W. G., 2006. *Remote Sensing of Snow and Ice*. Taylor & Francis – CRC Press, Singapore.
Rees, H. G., and Collins, D. N., 2005. Regional differences in response of flow in glacier-fed Himalayan rivers to climatic warming. *Hydrological Processes*, **20**(10), 2157–2169.
Rothlisberger, H., and Lang, H., 1987. Glacial hydrology. In Gurnell, A. M., and Clark, M. J. (eds.), *Glacio-Fluvial Sediment Transfer*. Chichester: Wiley, pp. 207–284. *cf.* Malard, F., Uehlinger, U., Zah, R., and Tockner, K., 2006. Flood pulse and riverscape dynamics in a braided glacial river. *Ecology*, **87**(3), 704–716.
Sharp, M., Parkes, J., Cragg, B., Fairchild, I. J., Lamb, H., and Tranter, M., 1999. Widespread bacterial populations at glacier beds and their relationship to rock weathering and carbon cycling. *Geology*, **27**, 107–110.
Singh, P., and Bengtsson, L., 2005. Impact of warmer climate on melt and evaporation for the rainfed, snowfed and glacierfed basins in the Himalayan region. *Journal of Hydrology*, **300**, 140–154.
Singh, P., and Jain, S. K., 2002. Snow and glacier melt in the Satluj river at Bhakra Dam in the western Himalayan region. *Hydrological Science Journal*, **47**, 93–106.
Singh, P., Jain, S. K., and Kumar, N., 1997. Estimation of snow and glacier contribution to the Chenab river, western Himalaya. *Mountain Research and Development*, **17**, 49–55.
Singh, P., Huebl, H., and Weinmeister, H. W., 2000. Use of the recession characteristics of snowmelt hydrographs in the assessment of snow water storage in a basin. *Hydrological Processes*, **14**(1), 91–101.
Taylor, J. M., 2005. Himalayan glacier alarms, *Environment and Climate News*, Publ. The Heartland Institute, Chicago.
Thapa, A. B., 2004. Himalayan glaciers and Nepal. *Nepalnews.com*, **23**(37), April 2–8, 2004 (Chaitra 20, 2060).
Thayyen, R. J., and Gergan, J. T., 2009. Role of glaciers in watershed hydrology: "Himalayan catchment" perspective. *The Cryosphere Discussion*, **3**, 443–476.
Thayyen, R. J., Gergan, J. T., and Dobhal, D. P., 2007. Role of glaciers and snow cover on headwater river hydrology in monsoon regime – Micro-scale study of Din Gad catchment, Garhwal Himalaya, India. *Current Science*, **92**(3), 376–382.
Tranter, M., Skidmore, M., and Wadham, J., 2005. Hydrological controls on microbial communities in subglacial environments. *Hydrological Processes*, **19**, 995–998.
Verbunt, M., Gurtz, J., Jasper, K., Lang, H., Warmerdam, P., and Zappa, M., 2003. The hydrological role of snow and glaciers in alpine river basins and their distributed modeling. *Journal of Hydrology*, **282**, 36–55.
WGMS, 2009. *Global glacier changes: facts and figures*, GRID-UNEP, World Glacier Monitoring Service, University of Zurich.
World Bank, 2009. Climate change; water: South Asia's lifeline at risk, South Asia Region. The World Bank Group. http://www.worldbank.org/sar (accessed March 2009).
WWF, 2009. Climate change and global glacier decline. http://www.panda.org/climate/glaciers (accessed March 2009).

Cross-references

Aerial Photogrammetry for Glacial Monitoring
Direct Surface Runoff
Glacial Drainage Characteristics
Glacier Hydrology
Global Outlook of Snowcover, Sea Ice, and Glaciers
Himalaya
Hydropower: Hydroelectric Power Generation from Alpine Glacier Melt
Impacts of Snow and Glaciers on Runoff
Snow Hydrology
Streamflow Trends in Mountainous Regions

CHEMICAL COMPOSITION OF SNOW, ICE, AND GLACIERS

Amanda M. Grannas
Department of Chemistry, Villanova University, Villanova, PA, USA

Incorporation of chemicals in snow/ice

Snow is formed by the condensation of water vapor onto an ice forming nucleus (IFN) or by riming, a process whereby supercooled liquid droplets freeze onto growing ice crystals. IFN and cloud condensation nuclei can thus introduce impurities to snow. Supercooled liquid droplets can also scavenge gas phase and aerosol species from the atmosphere, which will eventually be incorporated into the snow. Rimed snow generally has higher impurity concentrations than snow formed solely by vapor condensation. Snow crystals can scavenge aerosol and gas phase species from the atmosphere during precipitation. Gases can also be taken up or emitted from freshly fallen snow. Further discussion of snow physical properties can be found in the section *Physical Properties of Snow*.

Postdepositional metamorphism is an important factor in both the physical characteristics and chemical composition of snow. Sublimation/condensation can alter individual snow grain characteristics and cause changes to snowpack such as porosity, specific snow surface area, hardness, density, etc. (*Physical Properties of Snow*, qv). These physical processes have the ability to release/trap dissolved species. As snowpack begins to melt, wet metamorphism can have significant impacts on the chemical composition of the snow. More highly water soluble species, such as acids and ions, have a higher affinity for the liquid

phase and can be readily removed during the first stages of snowmelt. There is evidence, however, for the preferential elution of some ions (e.g., SO_4^{2-}, Ca^{2+}, Mg^{2+}, K^+, Na^+) before others (NO_3^-, NH_4^+, Cl^-, F^-). Nonpolar organic molecules can also be found in meltwater, but are less easily removed by percolation. Although particulate material can be incorporated into percolating water, such entrainment rarely occurs in the early stages of melt and particulates may remain in the snow until the final stages of melting. An extensive discussion of snow physics, particularly as related to chemistry occurring in snow, can be found in the recent review of Dominé et al. (2008).

Both glaciers and ice cores represent important archives of environmental information. Where summer melting is absent, accumulation of snow (subsequently transformed into ice) allows for the preservation of chemical, isotopic, and insoluble composition signatures from the atmosphere in oftentimes well-defined stratigraphic sequences. High snow accumulation sites result in thicker layers that can allow for determination of variability of inputs on seasonal timescales, while low accumulation sites can provide longer sequences, but with arguably less-resolved information.

Inorganic species

Snow and ice contain a number of inorganic species. The dominant contributors depend in part on the proximity to continental and oceanic inputs. Dominant ions include H^+, Na^+, Ca^{2+}, Mg^{2+}, NH_4^+, Cl^-, NO_3^-, SO_4^{2-}, and carboxylic acids. Greenland ice contains significantly more NH_4^+ and carboxylic acids as compared to Antarctica, likely due to the larger input from continental biosphere sources. The reviews of Delmas (1992) and Legrand and Mayewski (1997) discuss the chemical composition of polar ice cores, including inorganic species, dust, and gases, and the environmental information that can be obtained by careful analysis of ice core inputs. Snowfall composition in the high Arctic has shown that the major ions present are Ca^{2+}, Na^+, H^+, NH_4^+, SO_4^{2-}, Cl^-, and NO_3^-. Organic acids are also present, although in smaller quantities (about 2% of the ionic balance). Seasonal differences are evident in many species, influenced both by anthropogenic sources as well as localized snowpack chemistry.

Metals can also be found in snow and ice. Evidence of atmospheric metal emission increases from anthropogenic activities, as compared to preindustrial levels, is apparent in Greenland ice cores. Increase in Zn, Cu, Cd, and Pb (in some cases several orders of magnitude) is observed when comparing post-1950 ice to preindustrial levels. Heavy metal records in Antarctic ice cores are also available for select sites. Heavy metal and metalloid records from an East Antarctic ice core date back 672,000 years, one of the longest records available to date. Deciphering ice core records of heavy metals can be challenging, however, due to the low concentrations present in polar ice, and the potential for contamination during the drilling process. Careful decontamination procedures allow for reliable records to be obtained. Mercury is also found in polar snow and ice, as well as glacial ice, and is deserving of special attention due to its toxicity and propensity to bioaccumulate (in organomercury forms). Steffen et al. (2008) discuss the existing polar atmospheric and snow/ice measurements of mercury and review its cycling in the environment, particularly as related to active snow chemistry that can alter the oxidation state and chemistry of this particular metal.

Organic species

Snow is an efficient scavenger of organic chemicals from the atmosphere, more efficient than rain in some cases. Snow can remove both particle-bound and gas phase organics from the atmosphere. A general measure of the organic carbon content of snow/ice can be determined by total organic carbon (TOC) measurements. These have been reported for snow and ice in a variety of sites, including the high Arctic, Greenland, Antarctica, and midlatitude sites with widely ranging values (from <10 to $>3{,}000$ μg C L^{-1}). Organics can exist in both the dissolved and particulate phases, so it is important to distinguish dissolved and particulate fractions. Recent measurements have focused on the water soluble component of organic carbon (WSOC) in air and surface snow at Summit, Greenland. Large firn air concentrations of gas phase WSOC suggested that the snowpack was a source for this material, consisting mainly of formic and acetic acids. Despite recent work aimed at better understanding the relative contributions of dissolved and particulate organic carbon to the total organic carbon pool, the fraction of organic carbon that is distributed between the aqueous and particulate phases is still not well understood.

Organic carbon present in snow and ice can be of both natural and anthropogenic origin, and can be from primary or secondary sources. Only recently has the complex nature of organic matter in snow and ice been fully appreciated. Previous work has quantified small molecules like hydrocarbons, formaldehyde, and methanesulfonic acid in snow, firn, and ice. Other species present in snow and ice include black carbon, carboxylic acids, and anthropogenic materials such as PAHs, pesticides, and industrial chemicals. Higher molecular weight materials are also present in snow and ice. Biogenic materials such as lignin, humic, and fulvic acids and larger polycarboxylic acids have been identified in snow and ice from a variety of locations, including Antarctica. A recent review (Grannas et al., 2007) discusses much of the available literature describing organic matter incorporation into snowpack and the nature of organic materials found in polar snow.

Biological inputs are important in snow and ice as well. Bacteria can act as effective ice nucleation sites, thus becoming incorporated into ice and snow crystals during formation. Recent investigations indicate that snow, glaciers, and ice sheets are biologically active, containing algae, bacteria, viruses, and other organisms. In some

cases, the microorganisms present have the ability to degrade organic compounds found in snow/ice (e.g., propionate, acetate, and formate) and could play a role in both snow chemistry and the carbon cycle as a whole. Additionally, microbial sequestration of nutrients from the atmosphere can play a major role in annual fluxes of, for example, nitrogen from glacier surfaces. It could be the case that snow, ice, and glacial environments should be considered as a separate ecosystem in their own right.

Release of chemicals from snow, ice, and glaciers

Melting snow, ice, and glaciers can lead to release of chemicals in short and concentrated pulses delivering nutrients and contaminants to terrestrial and aquatic environments, possibly affecting ecosystem health. Although much is known about the fate of inorganic species during snowmelt, release of organic contaminants from melting snow is less well studied. Several factors will affect the behavior of organic materials during melt including solubility, vapor pressure, Henry's law equilibria, association with the dissolved phase or particles, etc.

Snow/ice may also release species to the gas phase from chemical processes occurring in the condensed phase. Examples of such releases include nitrogen oxides, formaldehyde, acetaldehyde and acetone, small carboxylic acids, molecular halogens, organohalogens, etc. These processes are seemingly ubiquitous, having been observed in the Arctic, Antarctic, and midlatitudes. The sources of these emissions are discussed in further depth in Chemical Processes in Snow and Ice.

Summary

The chemical composition of snow, ice, and glaciers is an important area of continuing research. It is important to better understand the potential effects of chemical transfer upon snowmelt, as the release of nutrients and contaminants to surrounding terrestrial and aquatic areas could play an important role in ecosystem health. Additionally, the presence of various inorganic and organic species (both soluble and insoluble) as well as trapped gases in glacial and polar ice cores can serve as an important record of past atmospheric and climatic histories. Advanced analytical techniques are continually being developed to better characterize the oftentimes low concentrations of a variety of species at higher resolution than previously available. As these techniques develop, better glaciochemical records will become available, allowing for a better understanding of past climate and potentially help us better understand the potential impacts of future climate change scenarios.

Bibliography

Delmas, R. J., 1992. Environmental information from ice cores. *Reviews of Geophysics*, **30**(1), 1–21.

Dominé, F., Albert, M., Huthwelker, T., Jacobi, H.-W., Kokhanovsky, A. A., Lehning, M., Picard, G., and Simpson, W. R., 2008. Snow physics as related to snow photochemistry. *Atmospheric Chemistry and Physics*, **8**, 171–208.

Grannas, A. M., Jones, A. E., Dibb, J., Ammann, M., Anastasio, C., Beine, H., Bergin, M., Bottenheim, J., Boxe, C. S., Carver, G., Crawford, J. H., Domine, F., Frey, M. M., Guzman, M. I., Heard, D., Helmig, D., Hoffmann, M. R., Honrath, R. E., Huey, L. G., Jacobi, H.-W., Klan, P., McConnell, J., Sander, R., Savarino, J., Shepson, P. B., Simpson, W. R., Sodeau, J., von Glasgow, R., Weller, R., Wolff, E., and Zhu, T., 2007. An overview of snow photochemistry: evidence, mechanisms and impacts. *Atmospheric Chemistry and Physics*, **7**, 4329–4373.

Legrand, M., and Mayewski, P., 1997. Glaciochemistry of polar ice cores: a review. *Reviews of Geophysics*, **35**, 219–243.

Steffen, A., Douglas, T., Amyot, M., Ariya, P., Aspmo, K., Berg, T., Bottenheim, J., Brooks, S., Cobbett, F., Dastoor, A., Dommergue, A., Ebinghaus, R., Ferrari, C., Gardfeldt, K., Goodsite, M. E., Lean, D., Poulain, A. J., Scherz, C., Skov, H., Sommar, J., and Temme, C., 2008. A synthesis of atmospheric mercury depletion event chemistry in the atmosphere and snow. *Atmospheric Chemistry and Physics*, **8**, 1445–1482.

Cross-references

Chemical Processes in Snow and Ice
Snow
Snow Crystal Structure
Snow Metamorphism
Transformations of Snow at the Earth's Surface and its Climatic and Environmental Consequences

CHEMICAL AND MICROBE RECORDS IN SNOW AND ICE

Liu Yongqin
Laboratory of Tibetan Environment Changes and Land Surface Proceses (TEL), Institute of Tibetan Plateau Research, Chinese Academy of Sciences, Haidian District, Beijing, China

Definition

Microbe records in snow and ice. Microbe is an organism that is microscopic. Microbes include bacteria, algae, fungi, archaea, and protists. Microbe records in snow and ice mostly focus on the bacteria and algae.

Chemical records in snow and ice. Chemical ions and anions, such as Ca^{2+}, Mg^{2+}, K^{+}, Na^{+}, NH_4^{+}, SO_4^{2-}, NO_3^{-}, Cl^{-}, in the snow and ice are frequently analyzed. They are found closely connected with climatic and environment change.

Introduction

Snow falling on polar and high altitude regions carries lots of biotic and abiotic material. Ice is formed from accumulated snow as a result of compression and immured these materials. Chemical records in snow and ice from polar ice sheets or mountain glacier provide information about natural and anthropogenic atmospheric content, atmospheric circulation, and aerosol and contaminant transport and deposition. Chemical analyses of ice cores have been

made to reconstruct high-resolution paleoclimate and environmental change (Mayewski et al., 1997; Thompson et al., 1997, 2000; Kang et al., 2002; Yao et al., 2004).

Despite the wealth of information about chemical records in snow and ice, little information exists on the microorganisms. Snow is a significant climatic and ecological system that covers ca. 35% of the Earth's surface permanently or for varying times during the year (Miteva, 2007). Snow ecological systems are dynamic nutrient and microbial reservoirs (Jones, 1999). Microbes play important roles in snow ecology (Hoham and Duval, 2001). Snow algae serve as primary producers that sustain heterotrophic communities on the glaciers (Yoshimura et al., 1997; Hoham and Duval, 2001; Painter et al., 2001; Takeuchi, 2001; Stibal et al., 2006). Diverse bacteria habiting in snow were recovered by culture and unculture method. Early in 1933, snow samples were collected in the south polar region in the course of the Byrd Antarctic Expedition II. *Bacillus mesentericus*, *B. subtilis*, *B. tumescens*, *Achromobacter delicatulum*, *A. liquidum*, *Micrococcus freudenreichii*, *Flavobacteriu devorans*, and unidentified *Bacillus* were obtained using cultivation methods (Darling and Siple, 1941). Employing molecular methods, Carpenter et al. (2000) obtained rRNA gene sequences related to *Thermus-Deinococcus*-like organisms, and report the low rates of bacterial DNA and protein synthesis in South Pole snow. In Arctic, Amato et al. (2007) report the bacterial concentrations are about 2×10^4 cells mL^{-1} in snow cover at Spitsbergen, Svalbard. They recovered that strains have the capacity to degrade organic compounds at moderate temperature, which suggests that bacteria were actively involved in the chemistry of the Arctic snow cover (Amato et al., 2007). In the low and mid latitudes, bacterial abundance in the snow at Mount Sonnblick, Austria, and in the Tyrolean Alps ranges from 10^3 to 10^5 cells mL^{-1}(Alfreider et al., 1996; Sattler et al., 2001). The snow bacterial biomass at the Tateyama Mountain, Japan, varied seasonally due to rapid bacterial growth during summer (Segawa et al., 2005).

The Tibetan Plateau (TP) contains the largest concentration of the world's snow and ice outside of Antarctica and Greenland. Abundant bacteria existed in snow at the world highest plateau. Bacterial diversity and cell abundance in the snow of the four glaciers (Guoqu, Zadang, East Rongbuk, and Palong No.4) located in different climatic zones of the TP were investigated through culture-independent molecular analysis of 16S rRNA gene clone library and flow cytometry approaches. Cell abundance ranged from 676 to 7.2×10^5 cells mL^{-1}. Most of them were similar to those in the Antarctica, and less than those in the Arctic and other high mountains. Snow bacteria at the northern glaciers were higher than that at the southern ones. Cell abundance were related with Ca^{2+} concentration (index of the input dust) but did not show obvious correlation with the concentration of total organic carbon and total nitrogen. The snow bacteria spatial variation was agreed with the snow chemistry in the TP. The ion concentrations in snow from the northern of the plateau are higher than that from the southern of the plateau. The spatial patterns of snow chemistry demonstrated that continental dust originates mainly from the deserts to the north, while monsoon sources of moisture exert greater influence on snow chemistry on the southern of the plateau (Xiao et al., 2002). The result suggested that snow bacteria could be a good index of climate and environment as other chemical parameters in the snow.

Unexpected high diverse bacteria dwelled in snow over the TP. Bacterial 16S rRNA gene sequences affiliated to 13 phyla and 82 genera. Fifteen common genera (genera *Acinetobacter, Acidovorax*, *Arthrobacter, Bacillus*, *Bradyrhizobium*, *Brevibacterium, Curvibacter*, *Hymenobacter, Kocuria, Ochrobactrum*, *Polaromonas*, *Pseudomonas, Ralstonia* , *Rhodoferax*, *Sphingomonas*) distributed widely in glaciers located at different regions of the plateau, implying that the same selective mechanism occurs at the plateau. The bacterial diversity in the snow at different glaciers was related to the surrounding environments. The Guoqu Glacier, to the north near the desert zone and with the lowest temperature, preserved more bacteria closely related to a cold environment and soil than the other glaciers. However, in the Palong No. 4 Glacier located in the south warm region around vegetation, most bacteria were phylogenetically related to plant-associated bacteria (Liu et al., 2009a).

Bacteria in snow over the TP were seasonal various. Under the influence of various atmospheric circulation and temperature, bacteria in snow varied seasonally with different manners at different regions. High bacterial abundances occurred during monsoon season at the East Rongbuk Glacier located in the southern of the TP, but exhibited during no-monsoon season at the Guoqu Glacier in the central of the TP. Bacterial diversity seasonal variation at the Guoqu Glacier was more distinct than that at the East Rongbuk (Liu et al., 2006, 2009b).

Glacier ice immures microbial life in extreme environment for hundreds of thousands of years. Microbe in ice core firstly drew biologists' attentions. Bacteria were recovered from the Vostok ice core in the Antarctic (Priscu et al., 1999; Christner et al., 2001), GISP2 ice core in the Arctic (Sheridan et al., 2003; Miteva et al., 2004; Miteva and Brenchley, 2005), Guliya ice core in TP (Christner et al., 2003), and ice cores in the Andes and New Zealand (Christner et al., 2000). The diversity, evolution, survival mechanism of microorganism, and in situ microbial activity were revealed (Christner et al., 2000; Priscu and Christner, 2003; Miteva, 2007).

During recent years, microbe in ice core attracted glaciologist's attention because glacier ice is a unique ecosystem preserving microbial life and past climate changes chronologically. In the TP, bacteria and chemical features in the ice cores were analyzed together to explore the relationship between microorganisms and climatic and environmental changes. In the 102-m-deep ice core from Malan glacier, microbial concentrations were negatively correlated to temperature in four different temperature

phases and positively correlated with mineral particle concentrations (Yao et al., 2006).

Vertical profile of bacterial DNA structures at different depths in the Puruogangri ice core (83.45 m) were investigated by the denaturing gradient gel electrophoresis (DGGE) DNA fingerprinting technique. DGGE profiles indicated that the bacterial species diversity in glacial ice is high, and indigenous species represented by common bands in all samples may grow on the glacial surface. Bacterial diversity was comparable to that of soil habitats and had a positive correlation with Ca^{2+} concentration. This suggested that the soil ecosystem was the main source of bacteria in this glacier. The low similarity indices (0–43%) were found between the ice-core samples, which corresponded to the episodic deposition under defined climatic conditions and low activity of microorganisms in glacial ice. The profile of bacterial species composition in glacial ice is a bioindicator of climatic changes (Zhang et al., 2006).

Annual bacterial abundances in ice deposited over the past 70 years and trapped within a core retrieved from Mt. Geladaindong were recovered. The bacterial abundance was lowest in 1938 and highest in 1997. Analyses of correlations between bacterial abundance and $\delta^{18}O$ and Ca^{2+} concentrations indicate that bacterial abundance correlates positively with both temperature and amount of dust transported onto the glacier. These correlations imply that both higher temperatures and more frequent dust deposition influence bacterial abundance in the Geladaindong ice core (Yao et al., 2008).

Summary

Chemical and microbe records in snow and ice contain plenty of information about climate, environment, and anthropogenic active. They were both good indicators of paleoclimatic and paleoenvironmental change. However, microbes in ice core need further work in the future.

Bibliography

Alfreider, A., Pernthaler, J., Amann, R., Sattler, B., Glockner, F., Wille, A., and Psenner, R., 1996. Community analysis of the bacterial assemblages in the winter cover and pelagic layers of a high mountain lake by In Situ Hybridization. *Applied and Environmental Microbiology*, **62**, 2138–2144.

Amato, P., Hennebelle, R., Magand, O., Sancelme, M., Delort, A. M., Barbante, C., Boutron, C., and Ferrari, C., 2007. Bacterial characterization of the snow cover at Spitzberg, Svalbard. *FEMS Microbiology Ecology*, **59**, 255–264.

Christner, B. C., Mosley-Thompson, E., Thompson, L. G., Zagorodnov, V., Sandman, K., and Reeve, J. N., 2000. Recovery and identification of viable bacteria immured in glacial ice. *Icarus*, **144**, 479–485.

Christner, B. C., Mosley-Thompson, E., Thompson, L. G., and Reeve, J. N., 2001. Isolation of bacteria and 16S rDNAs from Lake Vostok accretion ice. *Environmental Microbiology*, **3**, 570–577.

Christner, B. C., Mosley-Thompson, E., Thompson, L. G., and Reeve, J. N., 2003. Bacterial recovery from ancient glacial ice. *Environmental Microbiology*, **5**, 433–436.

Darling, C. A., and Siple, P. A., 1941. Bacteria of Antarctica. *Journal of Bacteriology*, **42**, 83–98.

Hoham, R. W., and Duval, B., 2001. Microbial ecology of snow and freshwater ice with emphasis on snow algae. In Jones, H. G., Pomeroy, J. W., Walker, D. A., and Hoham, R. W. (eds.), *Snow Ecology: An Interdisciplinary Examination of Snow-Covered Ecosystems*. Cambridge: Cambridge University Press, pp. 168–228.

Jones, H. G., 1999. The ecology of snow-covered systems: a brief overview of nutrient cycling and life in the cold. *Hydrological Processes*, **13**, 2135–2147.

Kang, S., Mayewski, P. A., Qin, D., Yan, Y., Hou, S., Zhang, D., Ren, J., and Kruetz, K., 2002. Glaciochemical records from a Mt. Everest ice core: relationship to atmospheric circulation over Asia. *Atmospheric Environment*, **36**, 3351–3361.

Liu, Y. Q., Yao, T. D., Kang, S. C., Jiao, N. Z., Zeng, Y. H., Shi, Y., Luo, T. W., Jing, Z. F., and Huang, S. J., 2006. Seasonal variation of snow microbial community structure in the East Rongbuk glacier, Mt. Everest. *Chinese Science Bulletin*, **51**, 1476–1486.

Liu, Y. Q., Yao, T. D., Jiao, N. Z., Kang, S. C., Xu, B. Q., Zeng, Y. H., Huang, S. J., and Liu, X. B., 2009a. Bacterial diversity in the snow over Tibetan plateau glaciers. *Extremophiles*, **13**(1), 89–99.

Liu, Y. Q., Yao, T. D., Jiao, N. Z., Kang, S. C., Zeng, Y. H., and Liu, X. B., 2009b. Snow bacteria in two glaciers at the Tibetan Plateau and their relationship with climate and environment. *Frontiers of Earth Science in China*, **3**, 80–90.

Mayewski, P. A., Meeker, L. D., Twickler, M. S., Whitlow, S., Yang, Q. Z., Lyons, W. B., and Prentice, M., 1997. Major features and forcing of high-latitude northern hemisphere atmospheric circulation using a 110,000-year-long glaciochemical series. *Journal Of Geophysical Research, Oceans*, **102**, 26345–26366.

Miteva, V., 2007. Bacteria in snow and glacier ice. In Margesin, R., Schinner, F., and Marx, J.-C. (eds.), *Psychrophiles: from Biodiversity to Biotechnology*. Berlin: Springer, pp. 31–50.

Miteva, V. I., and Brenchley, J. E., 2005. Detection and isolation of ultrasmall microorganisms from a 120,000-year-old Greenland glacier ice core. *Applied and Environmental Microbiology*, **71**, 7806–7818.

Miteva, V. I., Sheridan, P. P., and Brenchley, J. E., 2004. Phylogenetic and physiological diversity of microorganisms isolated from a deep Greenland glacier ice core. *Applied and Environmental Microbiology*, **70**, 202–213.

Painter, T. H., Duval, B., Thomas, W. H., Mendez, M., Heintzelman, S., and Dozier, J., 2001. Detection and Quantification of Snow Algae with an Airborne Imaging Spectrometer. *Applied and Environmental Microbiology*, **67**, 5267–5272.

Priscu, J. C., and Christner, B. C., 2003. *Earth's icy biosphere*. Washington, DC: AMS Press.

Priscu, J. C., Adams, E. E., Lyons, W. B., et al., 1999. Geomicrobiology of subglacial ice above Lake Vostok, Antarctica. *Science*, **286**, 2141–2144.

Sattler, B., Puxbaum, H., and Psenner, R., 2001. Bacterial growth in supercooled cloud droplets. *Geophysical Research Letters*, **28**, 239–242.

Segawa, T., Miyamoto, K., Ushida, K., Agata, K., Okada, N., and Kohshima, S., 2005. Seasonal change in bacterial flora and biomass in mountain snow from the Tateyama Mountains, Japan, analyzed by 16S rRNA gene sequencing and Real-Time PCR. *Applied and Environmental Microbiology*, **71**, 123–130.

Sheridan, P. P., Miteva, V. I., and Brenchley, J. E., 2003. Phylogenetic analysis of anaerobic psychrophilic enrichment cultures obtained from a Greenland glacier ice core. *Applied and Environmental Microbiology*, **69**, 2153–2160.

Stibal, M., Sabacka, M., and Kastovska, K., 2006. Microbial communities on glacier surfaces in Svalbard: impact of

physical and chemical properties on abundance and structure of cyanobacteria and algae. *Microbial Ecology*, **52**, 644–654.
Takeuchi, N., 2001. The altitudinal distribution of snow algae on an Alaska glacier (Gulkana Glacier in the Alaska Range). *Hydrological Processes*, **15**, 3447–3459.
Thompson, L. G., Yao, T., Davis, M. E., Henderson, K. A., Mosley Thompson, E., Lin, P. N., Beer, J., Synal, H. A., ColeDai, J., and Bolzan, J. F., 1997. Tropical climate instability: the last glacial cycle from a Qinghai-Tibetan ice core. *Science*, **276**, 1821–1825.
Thompson, L. G., Yao, T., Mosley-Thompson, E., Davis, M. E., Henderson, K. A., and Lin, P. N., 2000. A high-resolution millennial record of the South Asian Monsoon from Himalayan ice cores. *Science*, **289**, 1916–1919.
Xiao, C., Kang, S. C., Qin, D., Yao, T. D., and Ren, J. W., 2002. Transport of atmospheric impurities over the Qinghai-Xizang (Tibetan) Plateau as shown by snow chemistry. *Journal of Asian Earth Sciences*, **20**, 231–239.
Yao, T. D., Wu, G. J., Pu, J. C., Jiao, K. Q., and Huang, C. L., 2004. Relationship between calcium and atmospheric dust recorded in Guliya ice core. *Chinese Science Bulletin*, **49**, 706–710.
Yao, T. D., Xiang, S. R., Zhang, X. J., Wang, N. L., and Wang, Y. Q., 2006. Microorganisms in the Malan ice core and their relation to climatic and environmental changes. *Global Biogeochemical Cycles* **20**, GB1004, doi:1010.1029/2004GB002424.
Yao, T. D., Liu, Y. Q., Kang, S. C., Jiao, N. Z., Zeng, Y. H., Liu, X. B. and Zhang, Y. J., 2008. Bacteria variabilities in a Tibetan ice core and their relations with climate change. *Global Biogeochemical Cycles* **22**, doi:10.1029/2007GB003095.
Yoshimura, Y., Kohshima, S., and Ohtani, S., 1997. A community of snow algae on Himalayan glacier: change of algal biomass and community structure with altitude. *Arctic and Alpine Research*, **29**, 126–137.
Zhang, X., Yao, T., An, L. Z., and Tian, L. D., 2006. A study on the vertical profile of bacterial DNA structure in the Puruogangri (Tibetan Plateau) ice core using denaturing gradient gel electrophoresis. *Annals of Glaciology*, **43**, 160–166.

Cross-references

Antarctica
Atmosphere-Snow/Ice Interactions
Chemical Processes in Snow and Ice
Glacier
Ice
Snow
Tibetan Plateau

CHEMICAL PROCESSES IN SNOW AND ICE

Amanda M. Grannas
Department of Chemistry, Villanova University, Villanova, PA, USA

Introduction

Recent studies have identified important chemical processes occurring in snow and ice in polar, alpine, and midlatitude regions that can influence the chemical composition of snow/ice and the surrounding environment. Many processes are photochemically driven and can significantly impact the composition of the atmosphere overlying these chemically active snowpacks. Observations include both ozone and mercury depletion in the lower atmosphere, driven by interactions between the atmosphere and photochemically active snow/ice. These processes may also impact the overall oxidizing capacity of the tropospheric boundary layer.

Photochemical processes in snow and ice

In the mid-1980s scientists made the shocking discovery of complete ozone removal from the marine boundary layer in the Arctic. Concentrations of ozone in the lowest portion of the atmosphere were occasionally significantly depleted from typical background levels of 40 ppb (parts per billion). It was found that the ozone depletion was inversely correlated with particle-phase bromine concentrations and subsequent studies have better elucidated the role of halogens in the ozone depletion chemistry. It is now apparent that chemistry occurring in the sunlit snowpack plays a key role in the cycling of photochemically active halogens (Br_2 and BrCl) by oxidation of seasalt (a review of halogen chemistry as related to ozone depletion events can be found in Simpson et al., 2007). Associated with the observed ozone depletion events are simultaneous atmospheric mercury depletion events (Steffen et al., 2008).

Many chemical processes are now known to occur in sunlit snow and ice. The chemistry occurring within this frozen medium can produce species such as NO_x, HONO, H_2O_2, HCHO, CH_3CHO and acetone, alkenes, molecular halogens, organic acids, and CO and can cause destruction of ozone within the snowpack interstitial air. The various locations of the measurement sites indicate that snow photochemistry may indeed be a ubiquitous process, as snowpack production of chemicals has been observed in both Arctic and Antarctic sites, as well as midlatitude areas. An extensive review of snow photochemistry can be found in Grannas et al. (2007).

The production of such varied species can have an important impact on the overlying atmosphere, as well as the surrounding ecosystem. Oxidation of sea-salt halogens in sunlit snow/ice is presumed to be the primary mechanism of halogen activation that leads to tropospheric ozone depletion events witnessed every spring in the Arctic (Simpson et al., 2007). Additionally, the observed snowpack source of H_2O_2, HCHO, and HONO can significantly impact the oxidant budget of the overlying atmosphere. Mercury cycling (an important toxic chemical that, depending on its form and oxidation state, can bioaccumulate) is also perturbed by snowpack photochemistry, as described in detail in the review of Steffen et al. (2008). This can have important ramifications for ecosystem health.

The impact of the physical nature of snow and ice on chemistry

Chemical processes occurring in snow and ice are impacted by the physical nature of the frozen medium.

It has been shown that a liquid-like (quasi-liquid or disordered) layer exists on the surface of pure ice and that this quasi-liquid layer is also found on the surface of ambient snow crystals and ice at environmentally relevant temperatures. Many processes can take place when freezing a solution that could impact the location and chemistry of dissolved species, including the formation of grain boundaries (the surface between two monocrystalline ice grains), veins (the linear intersections of grain boundaries), and nodes (the junction of veins). As liquid water freezes, solutes can be excluded from the ice phase into the quasi-liquid layer, grain boundaries, veins, or nodes, increasing their apparent aqueous concentration, known as the freeze concentration effect. Fast, nonequilibrium freezing can also cause solutes to become trapped in micropockets of highly concentrated solution. These processes lead to a chemically enriched liquid-like layer at the surface, grain boundaries, and interstitial pores of snow and ice that can impact the nature and rates of chemistry occurring in snow and ice.

As water freezes, anions and cations can become distributed unevenly between ice and solution, leading to a "freezing potential." H_3O^+ or OH^- then migrates to neutralize the potential, leading to highly variable pH in the liquid layer. This too can have an effect on chemical processes occurring in snow and ice. For example, Takenaka et al. (1996) found that the rate of reaction of nitrous acid with dissolved oxygen in laboratory experiments was accelerated 10^5 times upon freezing, due in large part to the freezing potential effect. Field measurements of nitrogen oxide production also support the idea that the pH of the snow will play a role in the release of chemicals from sunlit snowpack. It has been shown that HONO production ceased in alkaline snow. This is supported by the fact that HONO formation is highly dependent on pH of the quasi-liquid layer, with no HONO production at pH $\geq$ 5 (HONO pKa is 2.8 in solution).

It is thus apparent that the nature of the snow and ice, as well as its history (e.g., postdepositional metamorphism) can potentially impact the chemical processing of species (Physical Properties of Snow). This is discussed in further detail in the reviews of Grannas et al. (2007) and Dominé et al. (2008).

Summary

The ability of snow and ice to act as a chemically reactive medium is only a recently discovered phenomenon. The production of photochemically and oxidatively active species can have a number of impacts on the overlying atmosphere, including the initiation of ozone and mercury depletion events and alteration of the oxidizing capacity of the boundary layer. Both field and laboratory measurements have advanced the field significantly, yet our understanding of the fundamental behavior of solutes in snow and ice, partitioning of chemicals between air/snow/ice, and a molecular level understanding of many reaction mechanisms remain limited.

Bibliography

Dominé, F., Albert, M., Huthwelker, T., Jacobi, H.-W., Kokhanovsky, A. A., Lehning, M., Picard, G., and Simpson, W. R., 2008. Snow physics as related to snow photochemistry. *Atmospheric Chemistry and Physics*, **8**, 171–208.

Grannas, A. M., Jones, A. E., Dibb, J., Ammann, M., Anastasio, C., Beine, H., Bergin, M., Bottenheim, J., Boxe, C. S., Carver, G., Crawford, J. H., Domine, F., Frey, M. M., Guzman, M. I., Heard, D., Helmig, D., Hoffmann, M. R., Honrath, R. E., Huey, L. G., Jacobi, H.-W., Klan, P., McConnell, J., Sander, R., Savarino, J., Shepson, P. B., Simpson, W. R., Sodeau, J., von Glasgow, R., Weller, R., Wolff, E., and Zhu, T., 2007. An overview of snow photochemistry: evidence, mechanisms and impacts. *Atmospheric Chemistry and Physics*, **7**, 4329–4373.

Simpson, W. R., von Glasow, R., Riedel, K., Anderson, P., Ariya, P., Bottenheim, J., Burrows, J., Carpenter, L. J., Friess, U., Goodsite, M. E., Heard, D., Hutterli, J., Jacobi, H.-W., Kaleschke, L., Neff, B., Plane, J., Platt, U., Richter, A., Roscoe, H., Sander, R., Shepson, P., Sodeau, J., Steffen, A., Wagner, T., and Wolff, E., 2007. Halogens and their role in polar boundary-layer ozone depletion. *Atmospheric Chemistry and Physics*, **7**, 4375–4418.

Steffen, A., Douglas, T., Amyot, M., Ariya, P., Aspmo, K., Berg, T., Bottenheim, J., Brooks, S., Cobbett, F., Dastoor, A., Dommergue, A., Ebinghaus, R., Ferrari, C., Gardfeldt, K., Goodsite, M. E., Lean, D., Poulain, A. J., Scherz, C., Skov, H., Sommar, J., and Temme, C., 2008. A synthesis of atmospheric mercury depletion event chemistry in the atmosphere and snow. *Atmospheric Chemistry and Physics*, **8**, 1445–1482.

Takenaka, N., Ueda, A., Daimon, T., Bandow, H., Dohmaru, T., and Maeda, Y., 1996. Acceleration mechanism of chemical reaction by freezing: The reaction of nitrous acid with dissolved oxygen. *The Journal of Physical Chemistry*, **100**, 13874–13884.

Cross-references

Chemical Composition of Snow, Ice, and Glaciers
Physical Properties of Snow
Snow
Snow Crystal Structure
Snow Metamorphism
Transformations of Snow at the Earth's Surface and its Climatic and Environmental Consequences

CIRCULATION AND MIXING IN ICE-COVERED LAKES

Lars Bengtsson
Department of Water Resources Engineering, Lund University, Lund, Sweden

Definition

Circulation is the water movement and mixing is the dispersion of particles. The circulation, as well as the dispersion in ice-free lakes is mainly caused by the wind. When a lake is ice covered, the wind does not act on the water surface, and the water movements are much determined by thermal processes and by the vertical movement of the ice cover.

Introduction

Knowledge about circulation processes in lakes is essential when planning for the use of a lake for water supply or receiving waters. The conditions controlling the dynamics of ice-covered lakes are different from those of an ice-free lake. The ice cover prevents heat losses to the atmosphere and direct generation of wind mixing. As in ice-free lakes, a river running through a lake induces currents. In an ice-free lake, the dynamics are dominated by the directly induced wind mixing. There are also oscillations caused by set-up of the water surface by the wind. Such oscillations occur also in ice-covered lakes. The wind causes the ice cover to oscillate, thereby causing back and forth movements of water mass. However, much of the mixing is caused by thermal processes. The thermal conditions and the heat fluxes are responsible for convection and mixing of different character. Heat accumulated in the sediments during summer is released to the water in ice-covered lakes. The heat flux is largest at shallow water, where the water is cold and lighter than the deep water. When the water gains heat from the sediment, it becomes warmer and denser and the water slides downwards generating a large convection cell. In the spring, when the snow is free from ice and the solar radiation can penetrate into the lake water and heat the water close to the ice, density instabilities arise, local convection takes place, and a top mixing layer develops. While the currents in ice-free lakes are typically 2% of the wind speed, that is 20 cm/s when the wind is 10 m/s, the currents in an ice-covered lake are very much lower. The oscillation movements may be 1 cm/s back and forth. The currents caused by thermal processes are of the order mm/s or even less. Still, these movements result in vertical mixing and changed temperature conditions in the course of the winter.

River through-flow

A river that runs through a lake generates currents, but after initial mixing near the inlet, the river water can be traced only if the river is large. In ice-covered lakes, it has been observed thinner ice on the right-hand side indicating upwelling of warm bottom water with secondary currents induced as an effect of the earth's rotation, but most studies show that the current is rather uniformly directed in the upper part of a cross section. When the river flow is large and the lake elongated like a fjord lake, a cold top layer, where the flow takes place, develops over a pronounced thermocline separating the cold layer from a warmer bottom layer. The dispersion (dispersion coefficient D) in this top layer can be determined as for a river (D = coef R U*), only that the friction velocity (U*) is related to the friction against the ice. The hydraulic radius (R) is the distance between the underside of the ice and the thermocline.

Oscillating currents induced by ice movement

When a wind acts on the ice of a lake, the ice cover is tilted and oscillates. The water particles underneath are forced to move back and forth over very short distances, in the order of meters. The maximum velocities in lakes 1–10 km^2 seem to be 1–3 cm/s. The net movement is close to nil, although a slow horizontal circulation pattern can be induced. Although the net movement is close to nil, mixing occurs and particles are dispersed. Dye experiments in Swedish lakes, where the oscillation period is about 20 min, have shown that the horizontal dispersion coefficient is in the range 10–200 cm^2/s. It can be stated that some kind of oscillatory currents are always present in ice-covered lakes and they significantly contribute to the horizontal mixing.

Currents induced by heat released from the sediments

Water that gains heat from the sediment near the shores moves slowly along the bottom towards the deeper parts of the lake, generating large convective circulation cells as shown in Figure 1. As compensation for the downward movement along the bottom, there is an upward movement in the central part. The convective velocities can be crudely estimated from mathematical model experiments and from crude dye measurements. The velocities involved seem to be well below 1 mm/s. Instead of considering the physics of convective motion, it is instead possible to determine a vertical mixing coefficient from the change over time of the vertical temperature profile. The thermal vertical diffusivity is well below 0.1 cm^2/s. Detailed measurements in the Karelian Lake Vendyurskoe reveal that the diffusion coefficients increase from the ice downwards, being molecular at the top 20 cm and increasing linearly to six times the molecular ($7*10^{-3}$ cm^2/s) value at 2 m below the ice. The bottom water is mixed due to the convection induced by the heat flow from the sediments. However, once the water has reached the temperature of maximum density, 4°C, the water does not take part in the mixing process; the convection takes place above this 4°C water. The bottom water in subbasins of a lake may be isolated from the water in the main basin and remain stagnant for many months.

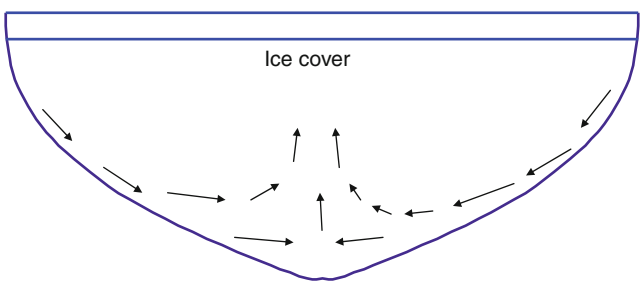

Circulation and Mixing in Ice-Covered Lakes, Figure 1 The principle of large-scale convective circulation generated by heat flux from sediment to water.

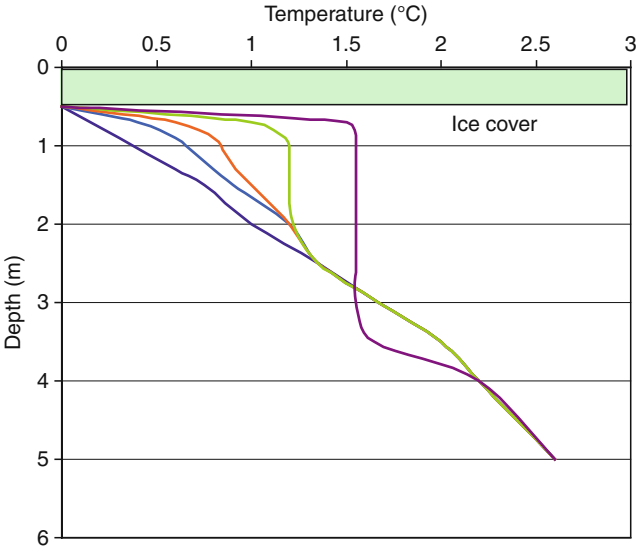

Circulation and Mixing in Ice-Covered Lakes,
Figure 2 Convective mixing during 5 consecutive days (the first day being the lower line with linearly increasing temperature with depth, the last day being the top line with constant temperature between 0.5 m and 3.5 m) in Lake Vendyurskoe due to penetration of solar radiation through the ice. Ice thickness 0.5 m.

Convective solar radiation induced mixing

When the solar radiation is able to penetrate through the ice, the water below the ice gains heat and becomes denser than the water further down. Convective mixing is initiated as the warm water sinks. A mixed layer may develop down to considerable depths, but it is depended on the extinction coefficient of the lake water and to how far the shortwave radiation reaches. The mixed layer deepens rather fast, maybe 0.5 m/day. An example of deepening of the mixed layer is shown in Figure 2. The convective vertical velocity involved in the mixing process is about 1 mm/s.

Summary

Although a lake is ice covered, there are mixing and slow currents below the ice. Currents are generated by rivers through flow, by oscillation of the ice cover, and by heat released from the sediments. There is intense convection below the ice in late spring, when the ice is free from snow and some solar radiation can penetrate the ice. The net currents are of the order mm/s, but still important for the vertical mixing and the development of the temperature profile.

Bibliography

Bengtsson, L., 1986. Dispersion in ice-covered lakes. *Nordic Hydrology*, **17**(4), 151–170.
Bengtsson, L., 1996. Mixing in ice covered lakes. *Hydrobiologia*, **322**, 91–97.
Bengtsson, L., Malm, J., Terzhevik, A., Petrov, M., Boyarinov, P., Glinsky, A., and Palshin, N., 1996. Field investigation of winter thermo- and hydrodynamics in a small Karelian lake. *Limnology and Oceanography*, **41**, 1502–1513.
Colman, J. A., and Armstrong, D. E., 1983. Horizontal Diffusivity in a Small, Ice-Covered Lake. *Limnology and Oceanography*, **28**, 1020–1026.
Jonas, T., Terzhevik, A. Y., Mironov, D. V., and Wuest, A., 2003. Radiatively driven convection in an ice-covered lake investigated by using temperature microstructure technique. *Journal of Geophysical Research*, **108**, 3183.
Kenney, B. B., 1996. Physical limnological processes under ice. *Hydrobiologia*, **322**, 85–90.
Malm, J., 1998. Bottom buoyancy layer in an ice-covered lake. *Water Resources Research*, **34**(11), 2981–2993.
Malm, J., 1999. Some properties of currents and mixing in a shallow ice-covered lake. *Water Resources Research*, **35**(1), 221–232.
Malm, J., Terzhevik, A., Bengtsson, L., Boyarinov, P., Glinsky, A., Palshin, N., and Petrov, M., 1997a. Temperature and salt content regimes in three shallow ice-covered lakes: 1 Temperature, salt content, and density structure. *Nordic Hydrology*, **28**, 99–128.
Malm, J., Terzhevik, A., Bengtsson, L., Boyarinov, P., Glinsky, A., Palshin, N., and Petrov, M., 1997b. Temperature and salt content regimes in three shallow ice-covered lakes: 2 Heat and mass fluxes. *Nordic Hydrology*, **28**, 129–152.
Malm, J., Terzhevik, A., Bengtsson, L., Boyarinov, P., Glinsky, A., Palshin, N., and Petrov, M., 1998. A field study on currents in a shallow ice-covered lake. *Limnology and Oceanography*, **43**, 295–322.
Matthews, P. C., and Heaney, I., 1987. Solar heating and its influence on mixing in ice-covered lakes. *Freshwater Biology*, **18**, 135–149.
Petrov, M. P., Terzhevik, A. Y., Zdorovennov, R. E., and Zdorovennova, G. E., 2006. The thermal structure of a shallow lake in early winter. *Water Research*, **33**, 135–143.
Stefanovic, D. L., and Stefan, H. G., 2002. Two-dimensional temperature and dissolved oxygen dynamics in the littoral region of an ice-covered lake. *Cold Regions Science and Technology*, **34**, 159–178.

Cross-references

Ice Covered Lakes
Thermal Regime of Ice-Covered Lakes

CIRQUE GLACIERS

Øyvind Paasche
Department of Research Management, University of Bergen, Bergen, Norway

Synonyms

Mountain glacier

Definition

Cirque glacier. Small glacier found in half-open, semicircular shaped niches, or hollows located on mountainsides or in upper part of valleys. The French term *cirque* originates from the Latin word *circus* meaning *circle*.

Introduction

Cirque glaciers are among the most frequent types of glacier found on Earth, and typically observed in any Alpine landscape where climate condition allows glacier formation. *Cirque glacier* is a true hybrid concept referring both to the landform it creates through erosion and evacuation of rocks and sediments (Glacial Erosion: Glaciological Variables Controlling Glacial Erosion; Glacial Geomorphology and Landforms Evolution), and to the ice body occupying it in the first place. In certain areas of the world such as the Himalayas and the Andes, cirque glaciers represent vital water reservoirs that are critical for agriculture and human living conditions. Because of their small size and volume they are extremely sensitive to changing climate conditions, which is emphasized by the fact that cirque glaciers worldwide are receding at an unprecedented rate (e.g., Oerlemans, 2005; Haeberlie et al., 2007), suggesting that they are among the most vulnerable parts of the now ever-diminishing Cryosphere (Cryosphere).

Morphology and size

The shape of any cirque glacier is to a large extent determined by the surrounding topography, which not only constrains the morphology, but also directs the flow and movement of the ice mass (cf. Lewis, 1960). Because cirques (i.e., the landform) come in such a wide variety of forms, the glaciers hosting these hollows also exist in many shapes. Evans (2007) offers a rigid classification of different types of cirques, divided into five grades (ranging from premature to mature). He also demonstrates that the length and the width of cirques in Wales and the English Lake District are positively correlated to the overall size of the cirque, which suggests that the glaciers tend to increase in size and volume with cirque enlargement. As the cirque evolves, the more sheltered the glacier occupying it will be by steepening sidewalls and headwall, which outline its basin. Through this slow process, certain positive feedbacks will be amplified such as added accumulation through wind-drifted snow, snow avalanching, and net shading. An example of a cirque glacier is shown in Figure 1.

Another aspect that influences the morphology of a cirque glacier is its thermal regime, which to some extent also controls its erosional capacity. Glaciers are by convention defined as being either temperate, polythermal, or polar (the old classification would be temperate, subpolar, and polar (Ahlmann, 1935). The thermal regime of an ice body is usually different in the accumulation area (usually the upper part, but not exclusively) and the ablation area (Glaciology, Glacier Mass Balance). In polythermal glaciers, which usually are warm based in the upper part and cold based in the lower part, the erosional efficiency would be highest in the upper part (e.g., Richardson and

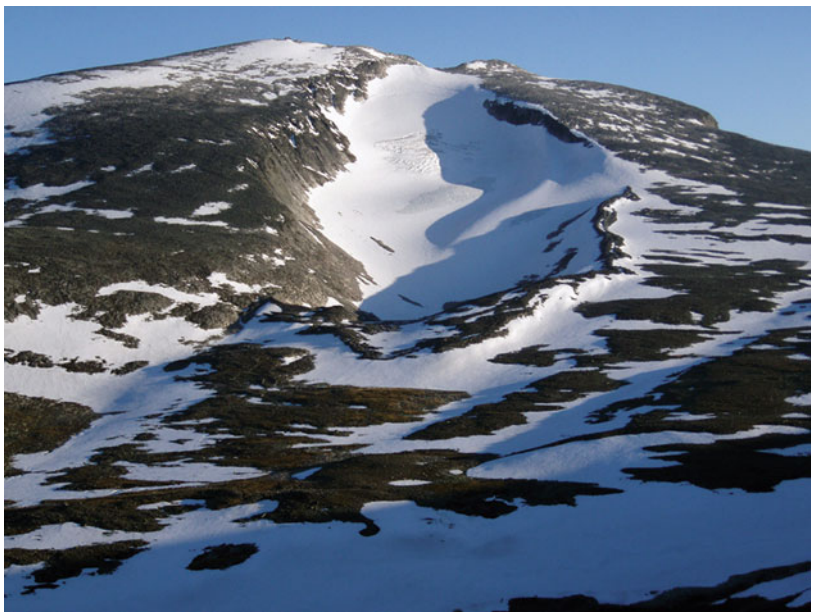

Cirque Glaciers, Figure 1 A small cirque glacier in the mountain massif called Snøhetta (2,286 m) located in central Norway. The glacier, which appears to be of a polythermal character, has been steadily retreating for the last 10 years. The ice-cored moraine damming up a small proglacial lake has yet to be breached, but erosion along proximal sides of the moraines indicates that this is bound to happen in near future. The age of the moraine is uncertain, but it shows that the cirque glacier has been considerably larger than at present. The author took the picture in 2007.

Holmlund, 1996). The frequently observed low-relief base of cirques agrees well with such an erosional system. Since cirque glaciers are found within all three classes of thermal regimes, so their shapes also vary significantly, which simply adds to the complexity of the glacier morphology (Polythermal Glaciers).

It should be kept in mind when relating glacier physics to cirque geometry that the development of a mature cirque arguably takes several 100,000 years (e.g., Benn and Evans, 1998). This implies that reoccurring cirque glaciers of different thermal regimes have eroded the same cirque over the period in question, including non-glacial processes.

In a slightly outdated, but comprehensive glacier inventory from 1973, covering Northern Norway and Sweden, most of the 1,491 registered glaciers are categorized as cirque glaciers (Østrem et al., 1973). They are often smaller than 0.5 km^2 and certainly smaller than 3 km^2. A more up-to-date survey carried out for southwestern Greenland shows similar numbers (Weidicke et al., 1992). Out of 1,473 mapped mountain glaciers, the majority is labeled as cirque glaciers. They are on average 1 km^2, with a mass volume of around 0.1 km^3 and a corresponding thickness of 20–50 m (see also Østrem et al., 1988).

Inception and decay of cirque glaciers

A cirque glacier may develop from a perennial snowfield, ice apron, or glacieret that is already established in concave, often steep, mountainsides. Leeward sides and shaded areas are favored places for cirque glacier inception.

Separating perennial snowfields from cirque glaciers are, however, not straightforward, although in theory it is simple, that is, when the ice mass starts to deform it is per se a glacier. Benn and Ballantyne (1994) suggest, for instance, that the threshold boundary separating a snowfield from becoming a glacier is related to the length measured from the headwall to the terminus of the snowfield, which is set to be 30–70 m. Whenever exceeding this threshold limit, the overlying pressure will be big enough to trigger the existing ice mass to start flowing. The average temperature of the snowfield is critical to this approach because colder temperatures will slow the annual process of transforming snow to ice, and it will also increase the pressure required to instigate and sustain deformation (cf. Paterson, 1994). Once a glacier is established, it will quickly start to erode the substratum (Formation and Deformation of Basal Ice).

A cirque glacier that expands beyond the outer limit of the rock basin can develop, often by coalescing with other advancing cirque glaciers, into a valley glacier – a process that can be reversed.

How fast can cirque glaciers develop? In theory, this will depend solely on climate conditions promoting growth, that is, temperature, precipitation, and prevailing wind direction. Few empirical studies currently exist that addresses this question, perhaps because most glaciers currently are receding. One option for obtaining estimates on cirque glacier development is by reconstructing the behavior of paleoglaciers.

A thoroughly studied cirque glacier system, once located on a small island in Western Norway, might shed light on this issue. At this site (called Kråkenes) a small, but temperate glacier (0.14 km^2) formed due to the transient cooling of the North Atlantic realm referred to as the Younger Dryas, which existed from 12,900 to 11,700 calendar years BP (cf. Rasmussen et al., 2006). The reconstruction of this glacier is based on exceptionally well-dated downstream lake sediments that efficiently track its inception and subsequent decay. According to a novel study carried out by Jostein Bakke and coworkers the glacier formed within 90 years and disappeared in 55 years (Bakke et al., 2009).

Modern observations of receding cirque glaciers indicate that the recession rate can be even faster than what the paleodata predicts for the Lateglacial–Holocene transition. At South Georgia (54°S, 34°W), Hodges Glacier was still present in 1982 with a size of 0.19 km^2, even producing a terminal moraine at the time (Gordon and Timmis, 1992). By 2008, it had completely disappeared (author's observation, unpublished). The initial size of the glacier, as it starts to retreat will obviously impact the time it takes to melt it completely. A massive loss of cirque glaciers is nevertheless to be expected for the coming century, as global temperatures keep getting warmer. However, as valley glaciers diminish and tributary glaciers become separated from their main glacier trunk, a significant number of glaciers will be reclassified as cirque glaciers.

A molder of landscapes

Glaciers erode through physical processes such as abrasion, abrading, and plucking, and chemically through meltwater interaction (Subglacial Weathering; Mechanical Weathering; Hydrochemical Characteristics of Snow, Ice, and Glaciers). The erosional capacity of cirque glaciers is obvious from the many empty cirques, Alpine horns, and arêtes, but they are also responsible for shaping mountain ranges with peaks rising above the regional equilibrium line altitude (ELA) (Equilibrium-Line Altitude (ELA)). The influence and significance of mountain glaciers, and particularly cirque glacier, as chief landscape molders led Mitchell and Montgomery (2006) to launch the concept of "glacial buzzsaw," arguing that the formation of glaciers on mountain ranges that gradually elevates, due to tectonic movements, will constantly lower the range as long as it keeps rising. Their case study area was the Cascade Range in central Washington, USA. In a long-term perspective with climates significantly warmer than present day, this theory might be less valid, but for average Quaternary (<3 million years) conditions (cf. Porter, 1989) there is

abundant empirical work to support it (Oskin and Burbank, 2005; Mitchell and Montgomery, 2006 and references therein; Foster et al., 2008).

Climatic indicator

Of all glaciers used as indicators of climate change, cirque glaciers are probably the optimal ones to use. Due to their small size and volume, their response time to positive or negative changes in mass balance is rapidly manifested, often within a couple of years. This implies that a sustained negative mass balance, lasting no less than a decade, will rapidly lead to a reduction in size and vice versa. In the European Alps, cirque glaciers (including other types of mountain glaciers) have since 1850 lost more than 50% of their volume, and the rate of melting keeps increasing toward present with an ongoing loss of 2–3% a^{-1} (Haeberlie et al., 2007).

If moraines have been deposited, that later can be mapped, the accumulation area ratio (AAR) can be invoked in order to estimate the corresponding ELA (Andrews, 1975; Osmaston, 2005). Given that the moraines can be properly dated, either directly or indirectly, they can be used as proxies for past climate change.

Because downstream lakes are extremely efficient in trapping suspended sediments (Suspended Sediment Dynamics), they currently represent the only possibility to produce continuous glacier reconstructions. The fact that most cirque glaciers have such defined catchments is an advantage for reconstructions utilizing lake sediments precisely because it reduces the risk of unwanted "sediment pollution" by extraglacial sediment sources (cf. Paasche et al., 2007). Another advantage with using cirque glaciers for the purpose of reconstructing past climate conditions is that they very rarely surges, which otherwise would seriously hamper the quality of the reconstruction.

Summary

Cirque glaciers are small and extremely responsive to changing climate conditions. Currently, such glaciers are in a global state of demise. Because of their swift response to changing climate conditions, they are preferred for continuous reconstructions of past glacier activity. Cirque glaciers erode the hollows they occupy, which tends to be enlarged through time. In a long perspective, they are probably among the most important molders of mountain ranges such as the Alps, the Himalayas, and the Andes.

Bibliography

Ahlmann, H. W., 1935. Contribution to the physics of glaciers. *Geographical Journal*, **86**, 97–107.

Andrews, J. T., 1975. *Glacial systems: an approach to glaciers and their environments*. Duxbury Press, 191 pp.

Bakke, J., Lie, Ø., Heegaard, E., Dokken, T., Haug, G. H., Birks, H. H., Dulski, P., and Nilsen, T., 2009. Rapid oceanic and atmospheric changes during the Younger Dryas cold period. *Nature Geoscience*, **2**, 202–205.

Ballantyne, C. K., and Benn, D. I., 1994. Glaciological constraints on protalus rampart development. *Permafrost and Periglacial Processes*, **5**, 145–153.

Benn, D. I., and Evans, D. J. A., 1998. *Glaciers and Glaciation*. London: Edward Arnold, p. 734.

Evans, I. S., 2007. Glacial landforms, erosional features: major scale forms. In Elias, S. A. (ed.), *Encyclopedia of Quaternary Science*. Amsterdam: Elsevier, pp. 838–852.

Foster, D., Brocklehurst, S. H., and Gawthorpe, R. L. (2008). Small valley glaciers and the effectiveness of the glacial buzzsaw in the northern Basin and Range, USA. *Geomorphology*, **102**, 624–639.

Gordon, J. E., and Timmis, R. J., 1992. Glacier fluctuations on South Georgia during the 1970s and early 1980s. *Antarctic Science*, **4**, 215–226.

Haeberli, W., Hoelzle, M., Paul, F., and Zemp, M., 2007. Integrated monitoring of mountain glaciers as key indicators of global climate change: the European Alps. *Annals of Glaciology*, **46**, 150–160.

Lewis, W. V. (ed.), 1960. Norwegian Cirque Glaciers, R.G.S. Research Series. London: Royal Geographical Society, Vol. 4, 104 p.

Mitchell, S. G., and Montgomery, D. R., 2006. Influence of a glacial buzzsaw on the height and morphology of the Cascade Range in central Washington State, USA. *Quaternary Research*, **65**, 96–107.

Oerlemans, J., 2005. Extracting a climate signal from 169 glacier records. *Science*, **308**, 675–677.

Oskin, M., and Burbank, D. W., 2005. Alpine landscape evolution dominated by cirque retreat. *Geology*, **33**, 933–936.

Osmaston, H., 2005. Estimates of glacier equilibrium line altitudes by the Area x Altitude, the Area x Altitude Balance Ratio and the Area x Altitude Balance Index methods and their validation. *Quaternary International*, **138**, 22–31.

Østrem, G., Haakensen, M., and Melander, O., 1973. *Atlas over breer i Nord-Skandinavia*. Hydrologisk avdeling, Norges Vassdrags-og Energiverk, Meddelelse, Vol. 22, 315 pp.

Østrem, G., Selvig, K. D., and Tandberg, K., 1988. *Atlas over Breer i Sør-Norge*. Norges Vassdrags-og Energiverk: Oslo.

Paasche, O., Dahl, S. O., Bakke, J., Løvlie, R., and Nesje, A., 2007. Cirque glacier activity in arctic Norway during the last deglaciation. *Quaternary Research*, **68**, 387–399.

Paterson, W. S. B., 1994. *The Physics of Glaciers*. Oxford: Butterworth-Heinemann, 481 pp.

Porter, S. C., 1989. Some geological implications of average quaternary glacial conditions. *Quaternary Research*, **32**, 245–261.

Richardson, C., and Holmlund, P., 1996. Glacial cirque formation in northern Scandinavia. *Annals of Glaciology*, **22**, 102–106.

Rasmussen, S. O., et al., 2006. A new Greenland ice core chronology for the last glacial termination. *Journal of Geophysical Research-Atmospheres*, **111**.

Weidick, A., Bøggild, C. E., Knudsen, N. T., 1992. Glacier inventory and atlas of west Greenland. Rap-port Grønlands Geologiske Undersøgelse, p. 158.

Cross-references

Equilibrium-Line Altitude (ELA)
Formation and Deformation of Basal Ice
Glacial Erosion
Glacial Geomorphology and Landforms Evolution
Glacier Mass Balance
Glaciology
Hydrochemical Characteristics of Snow, Ice, and Glaciers
Ice
Mechanical Weathering
Polythermal Glaciers
Subglacial Weathering

CLIMATE CHANGE AND GLACIERS

Arun B. Shrestha
International Centre for Integrated Mountain Development (ICIMOD), Kathmandu, Nepal

Definition

Ablation area: The area of a glacier where more glacier mass is lost than gained.
Accumulation area: Area of a glacier where more mass is gained than lost.
Climate: Climate in a narrow sense is usually defined as the "average weather," or more rigorously, as the statistical description in terms of the mean and variability of relevant quantities over a period of time ranging from months to thousands or millions of years. The classical period is 30 years, as defined by the World Meteorological Organization (WMO). These quantities are most often surface variables such as temperature, precipitation, and wind. Climate in a wider sense is the state, including a statistical description, of the climate system.
Climate change: IPCC definition – Climate change refers to a statistically significant variation in either the mean state of the climate or in its variability, persisting for an extended period (typically decades or longer). Climate change may be due to natural internal processes or external forcings, or to persistent anthropogenic changes in the composition of the atmosphere or in land use.
UNFCC Definition: A change of climate which is attributed directly or indirectly to human activity that alters the composition of the global atmosphere and which is in addition to natural climate variability observed over comparable time periods.
Glacial retreat (advance): When the position of a mountain glacier's terminus is farther upvalley (downvalley) than before. Glacial retreat occurs when a glacier ablates more (less) ice at its terminus than it transports into that region.
Glacier: A mass of ice that originates on land, usually having an area larger than one tenth of a square kilometer; many believe that a glacier must show some type of movement; others believe that a glacier can show evidence of past or present movement.
Mass balance: Difference between accumulation and ablation of a glacier in a given time interval.

Glaciers and climate

Glaciers can form anywhere in the world where snow deposited during the cold/humid season does not entirely melt during the warm/dry times. The seasonal snow, as it accumulates, gradually becomes denser and transforms into perennial firn (rounded, well-bonded snow that is older than 1 year) and finally, after the voids connecting the grains are closed off, into ice. The ice from such accumulation area flows under the influence of its own weight and the surface topography down to the lower altitudes, where it melts. The lower areas where temperatures are high and where melting occurs are termed as ablation areas. Accumulation and ablation areas are separated by equilibrium line, where the balance between gain and loss of ice mass is exactly zero.

The glacier-climate change response system is a complex chain of processes. Changes in atmospheric conditions (such as solar radiation, air temperature, precipitation, wind and cloudiness) influence the mass and energy balance at the glacier surface (Kuhn, 1981; Oerlemans, 2001). Air temperature plays a predominant role, as it is related to the radiation balance and turbulent heat exchanges, and also determines whether precipitation falls as snow or rain. Over time periods of years and decades, changes in energy and mass balance cause changes in volume and thickness, which in turn affect the flow of ice through internal deformation and basal sliding.

This dynamic relation eventually leads to changes in the size of the glacier more visually manifested by the retreat and advance of the glacier terminus. In simple terms, the glacial mass balance is directly linked with annual atmospheric conditions – with no delay – whereas the advance or retreat of glacier tongues is an indirect, delayed, and filtered signal of climate change.

The climate of the specific location determines the nature of the glaciers. In humid-maritime climates the equilibrium line is at a relatively low altitude because for ablation to take place, warm temperatures and long melting seasons are necessary. The climatic regions are dominated by temperate glaciers with relatively rapid flow. The ice caps and valley glaciers of Patagonia and Iceland, the western Cordillera of North America, and the mountains of New Zealand and Norway are examples of this type of glaciers. In dry continental areas, on the other hand, such as northern Alaska, Arctic Canada, subarctic Russia, parts of Andes near Atacama Desert and many Central mountain chains, the equilibrium line is at relatively high elevation with cold temperatures and short melting seasons. These glaciers have low mass turnover.

Glaciations and climate change of the last 2.5 million years

Evidences from Europe, North America, and other parts of the world show clear sequences of expansion and contraction of glaciers and sheets in the last 2.5 million years. The fluctuations in the ice masses were better understood in proper time frame after studying deep-sea sediments. The large-scale fluctuations in the glaciers and ice sheets were clearly related to similar large-scale changes in the climate of the earth, mainly due to changes in the earth's orbital parameters with very regular cyclic behavior. Variations in Earth's eccentricity, axial tilt, and precession comprise the three dominant cycles, collectively known as Milankovitch Cycles for Milutin Milankovitch, the Serbian Astronomer who calculated the variations in the orbital forcings in 1914 while detained as a political prisoner.

Eccentricity is, simply, the measure of how elliptic is the Earth's orbit around the Sun (Figure 1). This constantly fluctuating, orbital shape ranges between more and less elliptical (0–5% ellipticity) on a cycle of about 100,000 years. These oscillations, from more elliptic to less elliptic, are of prime importance to glaciations in that it alters the distance from the Earth to the Sun, thus changing the distance the Sun's short wave radiation must travel to reach Earth, subsequently reducing or increasing the amount of radiation received at the Earth's surface in different seasons.

Axial tilt, the second of the three Milankovitch Cycles, is the inclination of the Earth's axis in relation to its plane of orbit around the Sun. Oscillations in the degree of Earth's axial tilt occur on a periodicity of 41,000 years from 21.5° to 24.5° (Figure 2). Today the Earth's axial tilt is about 23.5°, which largely accounts for our seasons. Because of the periodic variations of this angle the severity of the Earth's seasons changes. With less axial tilt the Sun's solar radiation is more evenly distributed between winter and summer. However, less tilt also increases the difference in radiation receipts between the equatorial and Polar Regions. One hypothesis for Earth's reaction to a smaller degree of axial tilt is that it would promote the growth of ice sheets. This response would be due to a warmer winter, in which warmer air would be able to hold more moisture, and subsequently produce a greater amount of snowfall. In addition, summer temperatures would be cooler, resulting in less melting of the winter's accumulation. At present, axial tilt is in the middle of its range.

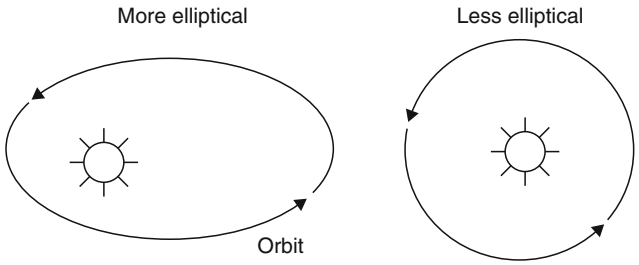

Climate Change and Glaciers, Figure 1 Eccentricity of the Earth's orbit.

The third and final of the Milankovitch Cycles is Earth's precession. Precession is the Earth's slow wobble as it spins on axis. This wobbling of the Earth on its axis can be likened to a top running down, and beginning to wobble back and forth on its axis. The precession of Earth wobbles from pointing at Polaris (North Star) to pointing at the star Vega (Figure 3). When this shift to the axis pointing at Vega occurs, Vega would then be considered the North Star. This top-like wobble, or precession, has a periodicity of 23,000 years. Due to this wobble a climatically significant alteration must take place. When the axis is tilted toward Vega the positions of the Northern Hemisphere winter and summer solstices will coincide with the aphelion and perihelion, respectively. This means that the Northern Hemisphere will experience winter when the Earth is furthest from the Sun and summer when the Earth is closest to the Sun. This coincidence will result in greater seasonal contrasts. At present, the Earth is at perihelion very close to the winter solstice.

These variables are only important because the Earth has an asymmetric distribution of landmasses, with virtually all (except Antarctica) located in the Northern Hemisphere. Even when all of the orbital parameters favor glaciations, the increase in winter snowfall and decrease in summer melt would barely be enough to trigger glaciations, not to grow large ice sheets. Ice sheet growth requires the support of positive feedback loops, the most obvious of which is that snow and ice have a much lower albedo than ground and vegetation, thus ice masses tend to reflect more radiation back into space, thus cooling the climate and allowing glaciers to expand. The positive feedback also involves thickening of ice sheets which reduces the temperature at the surface.

Glaciations and climate change of past 21,000 years

The large extension of glaciers occurred about 21,000 years ago, in period known as last glacial maximum (LGM), when glaciers covered up to 30% of the land. Glacier fluctuations can be reconstructed back to that time using a variety of scientific techniques and this knowledge has become central to understanding the causes and possible future of contemporary glacier change. Historical reconstruction of glaciers in the Alps, Scandinavia, Alaska, the Canadian Rockies, Patagonia, the Tropics of

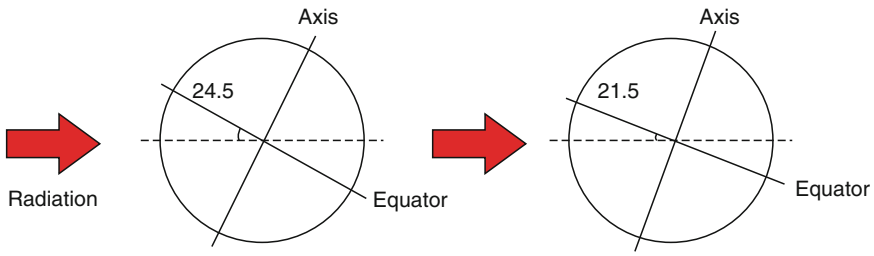

Climate Change and Glaciers, Figure 2 Changes in Earth's axial tilt.

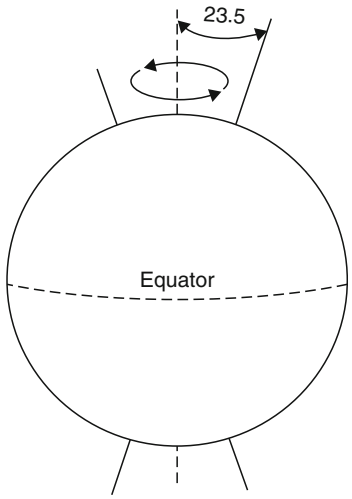

Climate Change and Glaciers, Figure 3 Precession of the Earth's axis.

South America, Tibet, the Arctic, and Antarctica shows that the fluctuations in the state of the glaciers are largely consistent with the reconstruction of climatic and environmental changes provided by other indicators, such as ice-cores, tree-line shifts, pollen records, and lake sediments (Solomina et al., 2008). General warming during the transition from the Late Glacial period (between the Last Glacial Maximum and about 10,000 years ago) to the early Holocene (about 10,000 to 6,000 years ago) led to a drastic general glacier shrinkage with intermittent periods of expansion. About 11,000 to 10,000 years ago, this pronounced warming reduced the glaciers in most mountain areas to sizes comparable with conditions at the end of the twentieth century. In northern Europe and western North America, which were still influenced by the remnants of the great ice sheets, this process was delayed until about 6,000 to 4,000 years ago. Several early-Holocene re-advances, especially those in the North Atlantic and North Pacific as well as possibly in the Alps, cluster around an event about 8,000 years ago, and were likely triggered by changes in the ocean thermohaline circulation and subsequent cooling resulting from the outbursts of Lake Agassiz (Solomina et al., 2008). On a timescale of hundreds of years there were periods of synchronous glacier advance around the world – peaking in the late Holocene in the Northern Hemisphere, and in the early Holocene in the Southern Hemisphere (Koch and Clague, 2006). The difference in the amount of sunlight that reaches the Earth's surface in the two hemispheres (Solanki et al., 2004) accounts for these differences in long-term glacier evolution (Koch and Clague, 2006).

About 5,000 years ago, there was a period of increasing warming around Earth as recorded through pollen and other indicators. Glaciers in the tropics were rather small or even absent during this period, gradually re-advancing from about 4,000 years ago, probably as a result of increasing humidity (Abbott et al., 2003). During medieval times there was a general warming, at least as recorded in Europe. Starting about 1300 A.D. the climate began to deteriorate drastically. Circumstantial evidence suggests that the cooling was caused by decrease in the Sun's heat output. Vikings who had settled on Greenland vanished by the fifteenth century and the year 1645 A.D. was the coldest year modern Europeans have ever experienced. Thereafter the climate gradually warmed until the middle of the nineteenth century. The period from 1300 A.D. to 1820 A.D. has been called the "Little Ice Age." The moraines (accumulations of unsorted, unstratified mixtures of clay, silt, sand, gravel, and boulders deposited by the glaciers) that were formed during the so-called Little Ice Age (from the early fourteenth to the mid-nineteenth centuries) can be found in many regions of the world, although the timing is asynchronous.

There has been a general retreat of glaciers worldwide since their Holocene maximum extent, toward the end of the Little Ice Age, between the seventeenth and the second half of the nineteenth century, with intermittent periods of glacier re-advance in certain regions.

From the paleoclimatic evidences, it is clear that climate change and glacier fluctuations are closely connected phenomena.

Glacier response to climate change

There are two main ways that a body of snow or ice can lose mass: through melting (conversion of solid into liquid) or sublimation (conversion of solid into vapor). Both transformations require energy. It takes 8.5 times as much energy to convert a kilogram of ice into water vapor by sublimation as it does to convert the same kilogram into liquid water by melting. Therefore, if conditions allow the glacier surface to warm to 0°C, the amount of ablation that can be sustained by a given energy input increases dramatically. Sublimated water vapor is always carried away by the air, but the fate of meltwater has a strong effect on ablation by melting. Runoff from steep ice-cliffs, or through subglacial flow driven by water percolating through pores or fractures, will convert a high fraction of melting into ablation. If meltwater percolates into the glacier and re-freezes, the effect on ablation is more limited and indirect.

Lower altitude portions of a glacier can be warmed directly by year-round exposure to above-freezing air, but at higher altitudes absorption of sunlight ultimately supplies all the energy, which sustains ablation. However, the other terms in the energy balance directly or indirectly affect the amount of absorbed solar radiation which is available for ablation. These terms are sensitive to air temperature, atmospheric humidity, cloudiness, and wind. The daytime glacier surface temperature typically has to be greater than the air temperature in order to close the energy budget; in consequence, melting can occur even when the air temperature remains below freezing. Because melting is so much more

energetically efficient than sublimation, the main way that moderate changes in atmospheric conditions – including air temperature – affect ablation is through changing the number of hours during which melting occurs, and the amount of energy available for melting. In particular, through infrared and turbulent heating effects, an increase in air temperature forces the glacier surface to warm, and makes it easier for melting to occur.

In addition to adding mass to a glacier, precipitation has an indirect effect on glacier mass balance by changing the amount of sunlight the glacier absorbs. This occurs because fresh snow is much more reflective than old snow or bare ice. The reflectivity effect can be almost ten times more important than the effect of mass directly added by precipitation. Because a thin layer of snow is just as reflective as a thick layer, the reflectivity effect depends more on the seasonal distribution of snowfall than the annual average amount.

A healthy glacier has an accumulation zone at high elevations and an ablation zone at lower elevations; ice flow from the accumulation zone continually feeds glacier tongues that penetrate into the ablation zone. The altitude separating the accumulation zone from the ablation zone is known as the equilibrium line altitude. Glaciers shrink when climate change causes the equilibrium line to rise, but they stop at a new equilibrium size with smaller accumulation zone. However, if the equilibrium line rises to the summit of the mountain, the accumulation zone disappears altogether and the glacier is doomed. This has happened on Chacaltaya and, according to limited recent observations (Mölg and Hardy, 2004), also on the summit glaciers of Kilimanjaro. Glacier AX010 in Shorong Himal, Nepal has its equilibrium line above the highest point on the glacier (Fujita et al., 2001).

Seasonal glacier-balance data, including winter balance, b_w, and summer balance, b_s, provide estimates of precipitation and summer temperature distributions in high-mountain and high-latitude areas where observational climatic data are both rare and biased. Very few long-term climatic stations exist above 3,000 m in altitude, and those that do grossly underestimate the actual precipitation as compared to observed glacier winter balances. Winter balance and precipitation also obey rather different spatial statistics. Unlike temperature, precipitation is not spatially homogeneous parameter, especially in mountainous environment. Winter balance, on the other hand, shows a higher autocorrelation at these distances, and drops to only about 0.5 at 2,000 km. This suggests that accumulation values are well correlated spatially, and are less influenced by local variations.

Another important measure of glacier–climate interactions is the vertical gradient in mass balance, d_b/d_z (Shumskiy, 1947; Meier and Post, 1962; Kuhn, 1980, 1984; Dyurgerov and Dwyer, 2001). While a good network of glaciers with long record of mass balance studies is lacking, Dyurgerov and Meier (2004) collected available data and found that d_b/d_z is getting steeper in recent years with warmer climate conditions (Figure 4). This is a result of glaciers losing mass at low altitudes due to higher temperatures. On the other hand, it is also due to glaciers gaining mass at high altitudes because of increasing snow accumulation that indicates intensification of precipitation in the higher altitude, although this might have some regional exceptions.

Apart from the change in the mass balance gradient, Dyurgerov and Meier (2004) also noted the increase in the equilibrium line altitude (ELA) and the decrease in ratio of glacier area above the ELA to the total glacier area

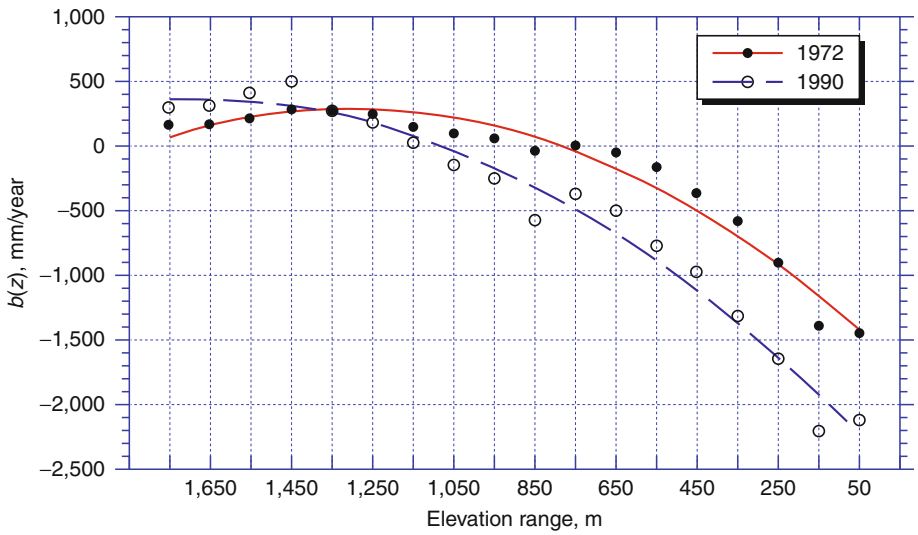

Climate Change and Glaciers, Figure 4 Change in mass balance gradient between cold and warm years; mass balance data have been averaged for 21 Northern Hemisphere glaciers and adjusted to the same elevation (Source: Dyurgerov and Meier, 2005).

(the accumulation-area ratio, AAR). One interesting indication of recent shifts in glacier mass balances is seen in the averaged AAR data plotted as standard departures (Figure 5); this shows an accelerated decrease in the AAR around the year 1977 and again in the early 1990s, in common with other evidence of increased glacier wastage. Except for debris covered glaciers, measurements of AAR can be made from satellite images, so this is an especially useful metric, particularly for glacial hydrological modeling.

The current increases in winter balances at high elevations have been especially rapid in the last decade, and have not been paralleled by appreciable increases in precipitation as measured at (lower altitude) climate stations. This also suggests a significant increase in the intensity of the hydrologic cycle at high elevations. The increase in b_w is even more remarkable considering the simultaneous decrease in glacier accumulation areas. An appropriate measure of this change in both major components of glacier mass balance is the glacier mass turnover, the average of the absolute values of b_w plus b_s (Meier, 1984). Another important measure is the sensitivity of mass balance to air temperature, db/dT. These observations show that both demonstrate changes in the recent warm decades of the twentieth century; these have not been predicted by, or used in, glacier-climate models. The spatialtemporal changes in glacier mass balances appear to be forced by changes in air temperature, which has increased globally. The study shows that an acceleration in volume wastage started in some regions as early as the 1970s (e.g., in Central Asia) and was completed by the end of the twentieth century in other regions (e.g., Arctic).

Glaciers: indicators of climate change

Glaciers have been considered to be excellent indicator of climate change (Oerlemans and Reichert, 2000; GTOS, 2008). Fluctuations of a glacier, which are not influenced by thick debris covers, calving or surge instabilities, are a reaction to climatic forcing. Thereby, the glacier length change (i.e., the advance or retreat) is the indirect, delayed, filtered but also enhanced signal to a change in climate, whereas the glacier mass balance (i.e., the change in thickness/volume) is the direct and undelayed response to the annual atmospheric conditions (Hoelzle and Haeberli, 1995). The mass balance variability of glaciers is well correlated with air temperature over distances of several hundred kilometers (Lliboutry, 1974; Schöner et al., 2000; Greene, 2005). However, the glacier mass balance change provides an integrative climatic signal, and the quantitative attribution of the forcing to individual meteorological parameters is not straight forward. The energy and mass balance at the glacier surface is influenced by changes in atmospheric conditions (e.g., solar radiation, air temperature, precipitation, wind, cloudiness). Air temperature thereby plays a predominant role as it is related to the radiation balance, turbulent heat exchange, and solid/liquid precipitation ratio (Kuhn, 1981; Ohmura, 2001). The climatic sensitivity of a glacier not only depends on regional climate variability but also on local topographic effects and the distribution of the glacier area with elevation, which can result in two adjacent glaciers featuring different specific mass balance responses (Kuhn et al., 1985). As a consequence, the glacier sensitivity to a climatic change is much related to the climate regime in which the ice is located. The mass balance of temperate glaciers

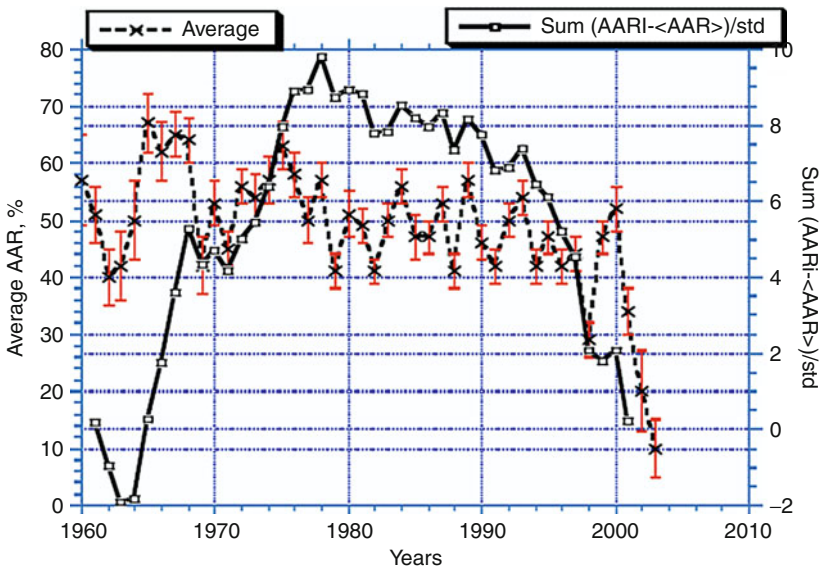

Climate Change and Glaciers, Figure 5 Annual variability and the change with time of the accumulation-area ratio <AAR> in terms of standardized cumulative departure. The data are averaged for all time series longer than 5 years; bars are standard errors. The time of <AAR> shifts to a decrease at the end of 1970s and again the early 1990s; data after 2001 are incomplete (Source: Dyurgerov and Meier, 2005).

in the mid-latitudes is mainly dependent on winter precipitation, summer temperature, and summer snow falls (temporally reducing the melt due to the increased albedo). In contrast, the glaciers in the low-latitudes, where ablation occurs throughout the year and multiple accumulation seasons exist, are strongly influenced by variations in atmospheric moisture content which affects incoming solar radiation, precipitation and albedo, atmospheric longwave emission, and sublimation (Wagnon et al., 2001; Kaser and Osmaston, 2002). In the Himalaya, influenced by the monsoon, most of the accumulation and ablation occurs during the summer (Ageta and Fujita, 1996; Fujita and Ageta, 2000). Cold glaciers in high altitude and the polar regions can receive accumulation in any season (Chinn 1985). As described in the text, strongly diverse mass balance characteristics also exist between glaciers under dry continental conditions and in maritime regions. As a consequence, analytical or numerical modeling is needed to quantify the above mentioned topographic effects as well as to attribute the glacier mass changes to individual meteorological or climate parameters (e.g., Kuhn, 1981; Oerlemans, 2001). Modeling is further needed in combination with measured and reconstructed glacier front variations, to compare the present mass changes with the (pre-) industrial variability (e.g., Haeberli and Holzhauser, 2003).

Recently, attempts have been made to relate the glacial dynamics with climate change. Differences in the climate sensitivity and response time of glaciers are taken into account. Oerlemans (2005) made an attempt to reconstruct past climate based on glacier length fluctuations data of 169 glaciers distributed around the world. The records are not spread equally over the globe. There is a strong bias toward the European Alps, where a wealth of documents exists and glacier monitoring was introduced relatively early. Fluctuations of some glaciers in Iceland and Scandinavia before 1800 have also been documented well (Sigurdsson, 1998; Østrem et al., 1976; Bogen et al., 1989).

The response of a glacier to climate change depends on its geometry and on the climatic setting. To unravel the climate signal contained in the glacier length records, Oerlemans (2005) discriminated glaciers with respect to the climate sensitivity c and to the response time t (the time a glacier needs to approach a new equilibrium state). Similar to other climate proxies, glacier length fluctuations are the product of variations in more than one meteorological parameter. Glacier mass balance depends mainly on air temperature, solar radiation, and precipitation. Extensive meteorological experiments on glaciers have shown that the primary source for melt energy is solar radiation but that fluctuations in the mass balance through the years are mainly due to temperature and precipitation (Greuell and Smeets, 2001).

Mass-balance modeling for a large number of glaciers has shown that a 25% increase in annual precipitation is typically needed to compensate for the mass loss due to a uniform 1 K warming (Oerlemans, 2001). These results, combined with evidence that precipitation anomalies normally have smaller spatial and temporal scales than those of temperature anomalies (Follard and Karl, 2001), indicate that glacier fluctuations over decades to centuries on a continental scale are primarily driven by temperature. Here, the climate sensitivity c is therefore defined as the decrease in equilibrium glacier length per degree temperature increase. The simplest approach that deals with lag effects is the response equation (Oerlemans, 2005):

$$\frac{\mathrm{d}L'(t)}{\mathrm{d}t} = -\frac{1}{\tau[cT'(t) + L'(t)]}$$

Here, t is time, L' is the glacier length with respect to a reference state, T' is a temperature perturbation (annual mean) with respect to a reference state, c is climate sensitivity, and τ is response time. The inverse model is now obtained by solving for T':

$$T'(t) = -\frac{1}{c\left[L'(t) + \tau\frac{\mathrm{d}L'(t)}{\mathrm{d}t}\right]}$$

For any glacier length record, the corresponding temperature history can be obtained with above equation once the climate sensitivity and response time are known.

The temperature reconstruction obtained using this method is shown in Figure 6. The interpretation of the temperature curves before 1800 should be done with caution, because the number of records is small. From 1860 onward, most regions show a temperature increase. In the first half of the twentieth century the temperature rise is notably similar for all regions: about 0.5 K in 40 years. After 1945, the global mean temperature drops slightly until 1970, when it starts to rise again. For North America, the reconstruction shows a marked cooling after 1940. The global mean temperature shown in Figure 6 is a weighted mean for the period from 1834 to 1990.

The derived global temperature record is in broad agreement with other reconstructions and for the last part also with the instrumental record (Figure 7). However, the glacier reconstruction shows somewhat larger amplitude on the century timescale. Because glaciers need time to react and the number of records drops sharply after 1995, the warming seen in the instrumental record over the past 15 years is not yet reflected in the reconstruction. Temperature curves appear to be very similar for glaciers with low and high median elevation. Low and high glaciers are classified as glaciers with median elevation below and above 2,850 m, respectively. For this threshold, the number of glaciers in both classes is approximately equal. Although the evidence is not conclusive because only a limited altitudinal range is considered, the glacier record does not show any sign of a height dependence of the global warming signal.

Summary

Glacier are widely distributed over the globe and form where over longer time periods snow deposited during cold/humid season does not entirely melt during warm/dry seasons. The glacier-climate change response system

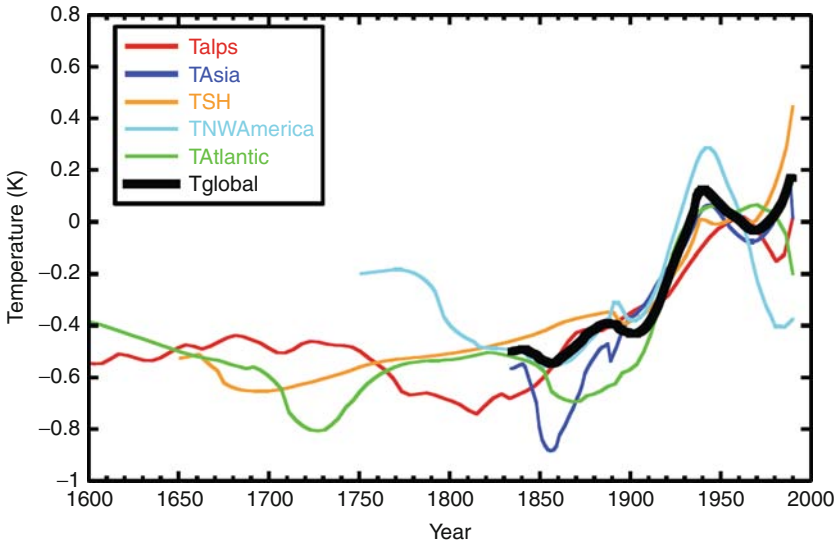

Climate Change and Glaciers, Figure 6 Temperature reconstruction for various regions. The black curve shows an estimated global mean value, obtained by giving weights of 0.5 to the Southern Hemisphere (SH), 0.1 to Northwest America, 0.15 to the Atlantic sector, 0.1 to the Alps, and 0.15 to Asia (Source: Oerlemans, 2005).

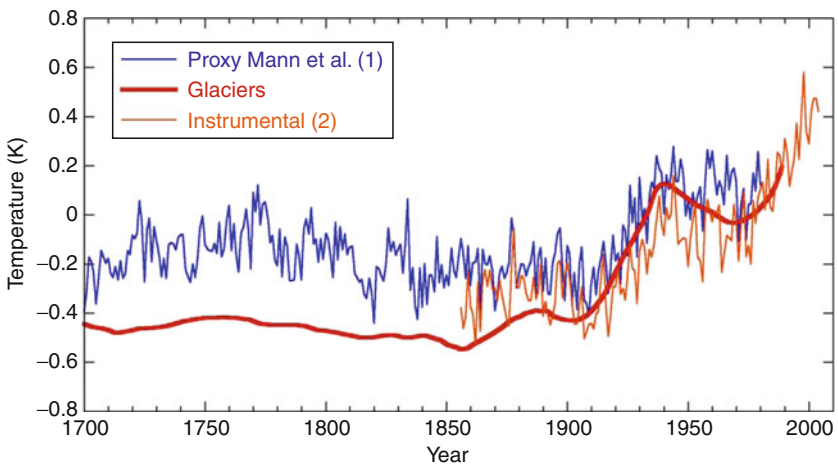

Climate Change and Glaciers, Figure 7 A comparison of global mean temperature series (Source: Oerlemans (2005) Supporting Materials).

is a complex chain of processes. The dynamic relationship between climate and glacier leads to changes in the size of the glacier, which is visually evident by advance and retreat of glacial front. The terminus fluctuation closely represents the changes in the mass balance of glaciers. A healthy glacier has accumulation zone at high elevation and ablation zone at lower elevations. The equilibrium line separates the two zones. Glaciers shrink when climate change causes the equilibrium line to rise and stop at a new equilibrium size.

The relationships between glacier fluctuation and climate change existed throughout the history of the Earth. The correlation exists in varying timescales: from several years to several hundred thousand years. At time scales of tens of thousands to hundreds of thousands of years, glacial variations were caused by climate change, which in turn was due to solar variations and variations in orbital and axial parameters of the Earth.

The excellent relationship between glacier and climate provides the opportunity of using glacier fluctuations as indicators of climate change. Seasonal glacier-balance data, including winter balance and summer balance provides estimates of precipitation and summer temperature distributions in high-mountain and high-latitude areas where

observational climatic data are both rare and biased. Glacier mass balance provides an integrative climatic signal, which is very much dependent on the geometry of the glaciers.

Bibliography

Abbott, M. B., Wolfe, B. B., Wolfe, A. P., Seltzer, G. O., Aravena, R., Mark, B. G., Polissar, P. J., Rodbell, D. T., Rowe, H. D., and Vuille, M., 2003. Holocene paleohydrology and glacial history of the central Andes using multiproxy lake sediments studies. *Palaeogeography, Palaeoclimatology, Palaeoecology*, **194**, 123–138.

Ageta, Y., and Fujita, K., 1996. Characteristics of mass balance of summer-accumulation type glaciers in the Himalayas and Tibetan Plateau. *Zeitschrift fur Gletscherkunde unde Glaczialgeologie*, **32**, 61–65.

Bogen, J., Wold, B., and Østrem, G., 1989. In Oerlemans, J. (ed.), *Glacier Fluctuations and Climatic Change*. Dordrecht: Kluwer, pp. 305–323.

Chinn, T. J., 1979. How wet is the wettest of the wet West Coast. New Zealand. *Alpine Journal*, **32**, 85–88.

Chinn, T. J. H., 1985. Structure and equilibrium of the Dry Valleys glaciers. N. Z. *Antarc. Rec*., 6, Special Supplement, 73-88.

Dyurgerov, M., and Dwyer, J. D., 2001. The steepening of glacier mass balance gradients with northern hemisphere warming. *Zeitschrift für Gletscherkunde und Glazialgeologie*, **36**, 107–118.

Dyurgerov, M., and Meier, M. F., 2004. Glaciers and the study of climate and sea-level change. In Bamber, J. L., and Payne, A. J. (eds.), *Mass Balance of the Cryosphere: Observations and Modelling of Contemporary and Future Changes*. Cambridge: Cambridge University Press, pp. 579–622.

Dyurgerov, M. D., and Meier, M. F., 2005. *Glaciers and Changing Earth System: A 2004 Snapsot*. Boulder: Institute of Arctic and Alpine Research, University of Colorado, p. 117.

Folland, C. K., and Karl, T. R., 2001. In Houghton, J. T., et al. (eds.), *Climate Change 2001: The Scientific Basis*. Cambridge: Cambridge University Press, pp. 101–181.

Fujita, K., and Ageta, Y., 2000. Effect of summer accumulation on glacier mass balance on the Tibetan Plateau revealed by mass balance model. *Journal of Glaciology*, **46**, 244–252.

Fujita, K., Kadota, T., Rana, B., Kayastha, R. B., and Ageta, Y., 2001. Shrinkage of Glacier AX010 in shorong region, Nepal Himalayas in the 1990s. *Bulletin of Glaciological Research*, **18**, 51–54.

Greene, A. M., 2005. A time constant for hemispheric glacier mass balance. *Journal of Glaciology*, **51**(174), 353–362.

Greuell, W., and Smeets, C. J. J. P., 2001. *Journal of Geophysical Research*, **106**, 31717.

GTOS, 2006. Global Terrestrial Observing System Biennial Report 2004–2005. GTOS-40.

GTOS, 2008. Terrestrial Essential Climate Variables for Climate Change Assessment, Mitigation and Adaptation. GTOS-52. http://www.fao.org/gtos/doc/pub52.pdf.

Haeberli, W., and Holzhauser, H., 2003. Alpine glacier mass changes during the past two millennia. *PAGES News*, **11**(1), 13–15.

Hoelzle, M., and Haeberli, W., 1995. Simulating the effects of mean annual air temperature changes on permafrost distribution and glacier size. An example from the Upper Engadin, Swiss Alps. *Annals of Glaciology*, **21**, 400–405.

Kaser, G., and Osmaston, H., 2002. *Tropical Glaciers*. Cambridge: Cambridge University Press. UNESCO International Hydrological Series, p. 207.

Koch, J., and Clague, J. J., 2006. Are insolation and sunspot activity the primary drivers of Holocene glacier fluctuations? *PAGES News*, **14**(3), 20–21.

Kuhn, M. (1980). Climate and glaciers. IAHS Publication No. 131: 3–20.

Kuhn, M., 1981. Climate and glaciers. *IAHS*, **131**, 3–20.

Kuhn, M., 1984. Mass budget imbalances as criterion for a climatic classification of glaciers. *Geografiska Annaler*, **66A**(3), 229–238.

Kuhn, M., Markl, G., Kaser, G., Nickus, U., and Obleitner, F., 1985. Fluctuations of climate and mass balance. Different responses of two adjacent glaciers. *Zeitschrift für Gletscherkunde und Glazialgeologie*, **2**, 409–416.

Kuhn, M., Dreiseitl, E., Hofinger, S., Markl, G., Span, N., and Kaser, G., 1999. Measurements and models of the mass balance of Hintereisferner. *Geografiska Annaler*, **81 A**(4), 659–670.

Lliboutry, L., 1974. Multivariate statistical analysis of glacier annual balance. *Journal of Glaciology*, **13**, 371–392.

Meier, M. F., 1984. Contribution of small glaciers to global sea level. *Science*, **226**, 1418–1421.

Meier, M. F., Post, A. S., 1962. Recent variations in mass net budgets of glaciers in western North America. International Association of Scientific Hydrology Publication **58** (Symposium at Obergurgl 1962 - Variations of Glaciers), 63–77.

Mölg, T., and Hardy, D. R., 2004. Ablation and associated energy balance of a horizontal glacier surface on Kilimanjaro. *Journal of Geophysical Research*, **109**, D16104, doi:10.1029/2003JD004338.

North America. Commission des Nieges et des Glaces (Commission of Snow and Ice), Colloque D'Obergurgl, September 10–18, 1962, *Symposium of Obergurgl. International Association of Scientific Hydrology*, 58: 63–77.

Oerlemans, J., 2001. *Glaciers and climate change*. Lisse: Balkema.

Oerlemans, J., 2005. Extracting a climate signal from 169 glacier records. *Science*, **308**, 675–677.

Oerlemans, J., and Reichert, B. K., 2000. Relating glacier mass balance to meteorological data by using a seasonal sensitivity characteristic. *Journal of Glaciology*, **46**, 1–4.

Ohmura, A., 2001. Physical basis for the temperature-based melt-index method. *Journal of Applied Meteorology*, **40**, 753–761.

Østrem, G., Liestøl, O., and Wold, B., 1976. *Norsk Geografisk Tidsskrift*, **30**, 187.

Schöner, W., Auer, I., and Böhm, R., 2000. Climate variability and glacier reaction in the Austrian eastern Alps. *Annals of Glaciology*, **31**(1), 31–38.

Shumskiy, P. A., 1947. *Energiya oledeneniya i zhisn' lednikov (Energy of glaciation and life of glaciers)*. Moscow: Geographgiz, p. 60. Russian.

Sigurdsson, O., 1998. Glacier variations in Iceland 1930–1995. From the database of the Iceland Glaciological Society. *Jökull*, **45**, 3.

Solanki, S. K., Usoskin, I. G., Kromer, B., Schüssler, M., and Beer, J., 2004. Unusual activity of the sun during recent decades compared to the previous 11, 000 years. *Nature*, **431**, 1084–1087.

Solomina, O., Haeberli, W., Kull, C., and Wiles, G., 2008. Historical and Holocene glacier-climate variations: General concepts and overview. *Global and Planetary Change*, **60**(1–2), 1–9.

Wagnon, P., Ribstein, P., Francou, B., and Sicart, J. E., 2001. Anomalous heat and mass budget of Glaciar Zongo, Bolivia during the 1997/98 El Niño year. *Journal of Glaciology*, **47**(156), 21–28.

Cross-references

Debris
Equilibrium-Line Altitude (ELA)
Firn
Glacier Mass Balance
Himalaya
Ice
Last Glacial Maximum Glaciation (LGM/LGP) in High Asia (Tibet and Surrounding Mountains)
Little Ice Age
Precipitation
Temperate Glaciers

CLIMATE VARIABILITY AND HIGH ALTITUDE TEMPERATURE AND PRECIPITATION

Mathias Vuille
Department of Atmospheric and Environmental Sciences, University at Albany, State University of New York, Albany, NY, USA

Definition

High altitude temperature and precipitation variability: It is the inherent characteristic of precipitation and temperature to change over time. Variability is measured as the temperature or precipitation deviations (anomalies) over a given period of time from a climate statistic (long-term mean) averaged over a reference period.

Introduction

Mountains give rise to very distinct climates at their highest peaks where glaciers exist, and this mountain climate varies in ways that is quite different from nearby low elevations. Mountain-induced dynamic and thermodynamic processes modify synoptic weather systems and create regional-scale atmospheric circulation regimes that generate distinct wind systems, cloudiness, Precipitation patterns, etc., and lead to a very unique mountain climate (e.g., Barry, 2008). However, climate variability at high altitude (including temperature and precipitation variability) is not nearly as well understood as similar variations at lower elevations. The remoteness and difficulty in accessing many high elevation sites, combined with the complications of operating automated weather stations (AWS) at high elevations, make long-term measurements very challenging. Furthermore, the complex topography of high elevation sites often leads to very site-specific measurements that are not always representative of a larger regional mountain environment.

Climate observations at high elevation

While some high elevation observatories, in particular in the Alps, have maintained climate records for over 100 years, most mountain regions of the world are difficult to access and essentially devoid of any high-altitude observations. New advances in instrumentation, satellite telemetry, and power supply through solar panels have made high elevation measurements more feasible in these regions over the past decade. For example, new and unique measurements have become available from remote glacier sites in the tropical Andean Glaciers, the Himalayas, and Mt. Kilimanjaro, thanks to the installation of such AWS – locations, where previously no climatic information existed (e.g., Hardy et al., 1998, 2003; Georges and Kaser, 2002; Moore and Semple, 2004; Mölg et al., 2009). Figure 1 shows an example from an AWS installed and operated by the University of Massachusetts, Amherst on the summit of Quelccaya ice cap in Peru (14°S) at 5,670 m above sea level. Still, to be truly useful for climate research it is imperative that these

Climate Variability and High Altitude Temperature and Precipitation, Figure 1 Automated weather station (AWS) on the summit of Quelccaya ice cap, located at 14°S in the eastern Peruvian Andes (Cordillera Vilcanota) at 5,670 m above sea level. Photo courtesy of Douglas R. Hardy.

AWS remain operational for several years and ideally decades to allow detection of trends and variability on interannual to decadal timescales (e.g., Bradley et al., 2004).

Characteristics of temperature and precipitation at high elevations

In the free atmosphere temperature decreases with height at a rate of about 6°C km^{-1} (Environmental Lapse Rate), although this rate varies by region, season, time of day, and by the type of air mass. Similarly the diurnal temperature range also decreases with elevation in the free atmosphere; an effect that can also be observed on mountain slopes and summits where mixing of slope air with the free atmosphere occurs (Barry, 2008). The comparison between near-surface observations at high elevations and measurements in the surrounding free atmosphere at the same elevation, however, is not straightforward (e.g., Pepin and Seidel, 2005) as temperature in the free

atmosphere is generally colder than its near-surface counterpart due to both latent and sensible heating of the atmosphere above elevated surfaces. Therefore, temperature lapse rates on a mountain slope may bear a close resemblance to the free atmospheric lapse rate or may be almost independent (Barry, 2008).

Precipitation distribution and amount are also strongly affected by mountain barriers; but in many mountain regions the exact mechanisms and impacts on Precipitation are still poorly understood due to paucity of data and problems related to accurate measurements of snowfall totals, in particular at exposed, windy, high-elevation sites (e.g., Falvey and Garreaud, 2007). In general, high elevations sites are affected by mountain-induced Orographic Uplift or convective instability that lead to regionally enhanced Precipitation. In typical convective patterns, common on tropical mountains, Precipitation is usually highest near the cloud base (generally at or below 1,500 m) and decreases significantly at higher elevations. The zone of maximum Precipitation tends to occur at higher elevations in drier climates. In mid-latitudes where Precipitation is derived primarily from advective situations, at least during the winter season, forced large-scale ascent over a barrier can lead to enhanced Precipitation even at 3,000 m or above on the windward side, due to both higher intensity and longer duration of Precipitation events (Barry, 2008). On the leeward side, however, the remaining moisture that spills over the mountain crest is usually insufficient to induce significant condensation and Precipitation amounts tend to be much lower than on the windward side.

Climate variability and change at high elevation

In many mountain ranges of the world both Precipitation and temperature vary on interannual timescales in response to changes in the large-scale circulation, forced by major modes of ocean–atmosphere interactions. In the Alps, for example, winter precipitation is sensitive to the phase of the North Atlantic Oscillation, with decreased snowfall and higher temperatures during its positive phase (e.g., Beniston, 1997, 2006). Similarly Precipitation in parts of the Rocky Mountains, the Cascades, and the Alaskan coastal range (Alaskan Glaciers) are influenced by the Pacific Decadal Oscillation, while snowfall amounts in the mountains of East Africa and the Himalayas are sensitive to the phase of the Indian Ocean dipole and the El Niño–Southern Oscillation (ENSO) phenomenon (e.g., Vuille et al., 2005; Chan et al., 2008). Temperature and snowfall variations in the tropical Andean Glaciers are also primarily a reflection of ENSO variability (Vuille et al., 2000; Garreaud et al., 2003), while the southern Andean Glaciers are more strongly influenced by the state of the Antarctic Oscillation (Gillett et al., 2006).

Superimposed on these natural climate variations, caused by ocean–atmosphere interactions, are long-term trends in temperature and Precipitation that have become discernible at many high-elevation sites over the past decades. There is clear evidence from many mountain ranges that the temperature increase over the past 100 years has been significantly amplified at high elevations when compared with low elevations or the global average temperature (e.g., Beniston et al., 1997; Diaz and Bradley, 1997), and that the warming is more closely related to an increase in daily minimum temperature than a change in the daily maximum (Diaz and Bradley, 1997; Beniston, 2006; Giambelluca et al., 2008).

The differential temperature trends with altitude are particularly apparent in the Alps and on the Tibetan Plateau. In the Alps many locations have seen an increase in minimum temperature of 2°C or more during the twentieth century (Beniston, 2006). Liu and Chen (2000) reported a significant warming on the Tibetan Plateau since the 1950s (0.16°C per decade), and especially during winter (0.32°C per decade). They observed an amplified warming at higher elevations, which was later attributed primarily to a strong elevation dependence of trends in minimum temperature (Liu et al., 2009). However, this dependence does not seem to hold for temperature extremes (You et al., 2008). In the mountains of the western United States (Rocky Mountains) the strongest warming (0.5–0.6°C between 1950 and 2000) seems to have occurred below 2,000 m (Diaz, 2005), although strong summertime warming at high elevations has lead to a significant reduction of alpine tundra (Diaz and Eischeid, 2007). In East Africa the lack of an adequate observational network has so far precluded a definite assessment of temperature changes at high altitudes. While some suggest that temperature has also increased significantly at highest elevations of the East African Mountains (e.g., Taylor et al., 2006), this has been questioned by others (e.g., Mölg et al., 2006). In the tropical Andean Glaciers the observed warming is stronger at higher elevation only on the eastern slope, while on the western side the strongest warming is recorded close to sea level (Vuille and Bradley, 2000; Vuille et al., 2003). This differential response may be related to changes in cloud cover and the lack of a seasonal snow cover at high elevations, which precludes an amplified warming due to a snow-albedo feedback (e.g., Pepin and Lundquist, 2008). Nonetheless, temperatures at high elevations in the tropical Andean Glaciers have increased by about 0.68°C over the past 70 years (Vuille et al., 2008), consistent with the observed increase in the freezing level height (altitude at which air temperature is close to 0°C) of about 1.43 m $year^{-1}$ between 1948 and 2000 (Diaz et al., 2003). Much of the warming in the high elevation tropics and hence the increase in freezing levels can be traced back to warmer tropical sea surface temperatures SST (Diaz and Graham, 1996; Diaz et al., 2003; Vuille et al., 2003). In the southern Andean Glaciers of central Chile the freezing level has also increased by 122 m during winter and 200 m during summer between 1975 and 2001 (Carrasco et al., 2005), leading to a rise in the glacier equilibrium line altitude (Snow Line) (Carrasco et al., 2008).

Projections of future climate change under different Greenhouse Gas emission scenarios suggest that in many locations higher elevations will continue to experience the strongest warming (Global Warming and its Effect on Snow/Ice/Glaciers). Fyfe and Flato (1999) report that the strongest twenty-first century warming in the Rocky Mountains will occur at the highest elevations. Similarly model projections in the tropical Andean Glaciers suggest that both surface and free-tropospheric temperature changes will be largest at higher elevations where glaciers are located (Bradley et al., 2006; Vuille et al., 2008; Urrutia and Vuille, 2009). Simulations with regional climate models in the Alps also project a significant warming of 4–6°C by the end of the twenty-first century, when compared to the 1961–1990 average. In general winters will be warmer and more humid in the Alps, while summers will also be warmer, but drier than today (see Beniston, 2006 and references therein). For the Tibetan Plateau Liu et al. (2009) project increases between 2.9°C (below 500 m) and 3.9°C (above 5,000 m) by the end of the twenty-first century.

While there is strong evidence for warming in most mountain regions, the picture for changes in Precipitation is much more mixed. In the northwestern Alps winter precipitation has increased significantly during the twentieth century (up to 30% in the last 100 years) but decreased by the same amount in the southeast (Schmidli et al., 2005; Schär and Frei, 2005). Vuille et al. (2003) found a positive Precipitation trend in the tropical Andean Glaciers north of about 10°S and a negative trend further south, but in general the trends were weak and statistically not significant. Bhutiyani et al. (2009) reported a significant decline in summer monsoon Precipitation over the northwestern Himalayas during the past 140 years, but found no change in the amount of winter Precipitation. In general changes in timing or amount of Precipitation are much more ambiguous and difficult to detect and there is no clear evidence of significant changes in Precipitation patterns in most mountain regions. Nonetheless Precipitation characteristics at high elevation will change significantly over the next 100 years as the increase in temperature will lead to more Precipitation falling in the form of rain. For roughly every °C rise in temperature the snow/rain transition will rise by about 150 m (e.g., Beniston, 2003).

Summary

Temperature and Precipitation variability are still poorly understood at many high elevation sites due to the lack of an adequate long-term monitoring network, but studies on mountain-induced dynamic and thermodynamic processes have advanced our understanding of climate variability at high altitude. In many mountain ranges of the world large-scale ocean-atmosphere interactions are the main driver for observed variability in both Precipitation and temperature. Over the past 100 years long-term warming trends (Global Warming and its Effect on Snow/Ice/Glaciers) have been superimposed on this natural variability and become increasingly evident at most high altitude sites. In many mountain regions of the world high altitudes appear to experience a stronger warming than the surrounding lowlands. Projections of future climate change in the twenty-first century suggest continued warming and rising freezing levels, combined with altered Precipitation patterns in many high altitude locals.

Bibliography

Barry, R. G., 2008. *Mountain Weather and Climate, 3rd edn*. Cambridge: Cambridge University Press, 506pp.

Beniston, M., 1997. Variations of snow depth and duration in the Swiss Alps over the last 50 years: Links to changes in large-scale forcings. *Climatic Change*, **36**, 281–300.

Beniston, M., 2003. Climatic change in mountain regions: a review of possible impacts. *Climatic Change*, **59**, 5–31.

Beniston, M., 2006. Mountain weather and climate: a general overview and a focus on climatic change in the Alps. *Hydrobiologia*, **562**, 3–16.

Beniston, M., Diaz, H. F., and Bradley, R. S., 1997. Climatic Change at high elevation sites: an overview. *Climatic Change*, **36**, 233–251.

Bhutiyani, M. R., Kale, V. S., and Pawar, N. J., 2009. Climate change and the precipitation variations in the northwestern Himalaya: 1866–2006. *International Journal of Climatology,* **30**(4), 535–548.

Bradley, R. S., Keimig, F. T., and Diaz, H. F., 2004. Projected temperature change along the American cordillera and the planned GCOS network. *Geophysical Research Letters*, **31**, L16210.

Bradley, R. S., Vuille, M., Diaz, H. F., and Vergara, W., 2006. Threats to water supplies in the tropical Andes. *Science*, **312**, 1755–1756.

Carrasco, J. F., Cassasa, G., and Quintana, J., 2005. Changes of the 0°C isotherm and the equilibrium line altitude in central Chile during the last quarter of the 20th century. *Hydrological Sciences Journal*, **50**(6), 933–948.

Carrasco, J. F., Osorio, R., and Casassa, G., 2008. Secular trend of the equilibrium-line altitude on the western side of the southern Andes derived from radiosonde and surface observations. *Journal of Glaciology*, **54**, 538–550.

Chan, R. Y., Vuille, M., Hardy, D. R., and Bradley, R. S., 2008. Intraseasonal precipitation variability on Kilimanjaro and the East African region and its relationship to the large-scale circulation. *Theoretical and Applied Climatology*, **93**, 149–165.

Diaz, H. F., 2005. Monitoring climate variability and change in the western United States. In Huber, U. M., Bugmann, H. K. M., and Reasoner, M. A. (eds.), *Advances in Global Change Research - Global Change and Mountain regions*. Dordrecht: Springer, pp. 267–274.

Diaz, H. F., and Bradley, R. S., 1997. Temperature variations during the last century at high elevation sites. *Climatic Change*, **36**, 253–279.

Diaz, H. F., and Eischeid, J. K., 2007. Disappearing "alpine tundra" Koppen climatic type in the western United States. *Geophysical Research Letters*, **34**(18), L18707.

Diaz, H. F., and Graham, N. E., 1996. Recent changes in tropical freezing heights and the role of sea surface temperature. *Nature*, **383**, 152–155.

Diaz, H. F., Eischeid, J. K., Duncan, C., and Bradley, R. S., 2003. Variability of freezing levels, melting season indicators and snow cover for selected high elevation and continental regions in the last 50 years. *Climatic Change*, **59**, 33–52.

Falvey, M., and Garreaud, R. D., 2007. Wintertime precipitation episodes in central Chile: Associated meteorological conditions and orographic influences. *Journal of Hydrometeorology*, **8**, 171–193.
Fyfe, J. C., and Flato, G. M., 1999. Enhanced climate change and its detection over the Rocky Mountains. *Journal of Climate*, **12**, 230–243.
Garreaud, R., Vuille, M., and Clement, A. C., 2003. The climate of the Altiplano: Observed current conditions and mechanisms of past changes. *Palaeogeography, Palaeoclimatology, Palaeoecology*, **194**, 5–22.
Georges, C., and Kaser, G., 2002. Ventilated and unventilated air temperature measurements for glacier-climate studies on a tropical high mountain site. *Journal of Geophysical Research*, **107**(D24), 4775.
Giambelluca, T. W., Diaz, H. F., and Luke, M. S. A., 2008. Secular temperature changes in Hawai'i. *Geophysical Research Letters*, **35**, L12702.
Gillett, N. P., Kell, T. D., and Jones, P. D., 2006. Regional climate impacts of the Southern Annular Mode. *Geophysical Research Letters*, **33**, L23704.
Hardy, D. R., Vuille, M., Braun, C., Keimig, F., and Bradley, R. S., 1998. Annual and daily meteorological cycles at high altitude on a tropical mountain. *Bulletin of the American Meteorological Society*, **79**(9), 1899–1913.
Hardy, D. R., Vuille, M., and Bradley, R. S., 2003. Variability of snow accumulation and isotopic composition on Nevado Sajama, Bolivia. *Journal of Geophysical Research*, **108**(D22), 4693.
Liu, X., and Chen, B., 2000. Climatic warming in the Tibetan plateau during recent decades. *International Journal of Climatology*, **20**, 1729–1742.
Liu, X., Cheng, Z., Yan, L., and Yin, Z.-Y., 2009. Elevation dependency of recent and future minimum surface air temperature trends in the Tibetan Plateau and its surroundings. *Global and Planetary Change*, **68**(3), 164–174.
Mölg, T., Rott, H., Kaser, G., Fischer, A., and Cullen, N. J., 2006. Comment on "Recent glacial recession in the Rwenzori mountains of East Africa due to rising air temperature" by Richard, GT. Taylor, Lucinda Mileham, Callist Tindimugaya, Abushen Majugu, Andrew Muwanga, and Bob Nakileza. *Geophysical Research Letters,* **33**, L20404.
Mölg, T., Cullen, N. J., Hardy, D. R., Winkler, M., and Kaser, G., 2009. Quantifying climate change in the tropical midtroposphere over East Africa from glacier shrinkage on Kilimanjaro. *Journal of Climate*, **55**, 292–302.
Moore, G. W. K., and Semple, J. L., 2004. High Himalayan meteorology: Weather at the South Col of Mount Everest. *Geophysical Research Letters*, **31**, L18109.
Pepin, N. C., and Lundquist, J. D., 2008. Temperature trends at high elevations: Patterns across the globe. *Geophysical Research Letters*, **35**, L14701.
Pepin, N. C., and Seidel, D. J., 2005. A global comparison of surface and free-air temperatures at high elevations. *Journal of Geophysical Research*, **110**, D03104.
Schär, C., and Frei, C., 2005. Orographic precipitation and climate change. In Huber, U. M., Bugmann, H. K. M., and Reasoner, M. A. (eds.), *Advances in Global Change Research – Global Change and Mountain regions*. Dordrecht: Springer, pp. 255–266.
Schmidli, J., Schmutz, C., Frei, C., Wanner, H., and Schär, C., 2005. Mesoscale precipitation in the Alps during the 20th century. *International Journal of Climatology*, **22**, 1049–1074.
Taylor, R. G., Mileham, L., Tindimugaya, C., Majugu, A., Muwanga, A., and Nakileza, B., 2006. Recent glacial recession in the Rwenzori Mountains of East Africa due to rising air temperature. *Geophysical Research Letters*, **33**, L10402.
Urrutia, R., and Vuille, M., 2009. Climate change projections for the tropical Andes using a regional climate model: Temperature and precipitation simulations for the end of the 21st century. *Journal of Geophysical Research*, **114**, D02108.
Vuille, M., and Bradley, R. S., 2000. Mean annual temperature trends and their vertical structure in the tropical Andes. *Geophysical Research Letters*, **27**, 3885–3888.
Vuille, M., Bradley, R. S., and Keimig, F., 2000. Interannual climate variability in the central Andes and its relation to tropical Pacific and Atlantic forcing. *Journal of Geophysical Research*, **105**, 12447–12460.
Vuille, M., Bradley, R. S., Werner, M., and Keimig, F., 2003. 20th century climate change in the tropical Andes: observations and model results. *Climatic Change*, **59**(1–2), 75–99.
Vuille, M., Werner, M., Bradley, R. S., Chan, R. S., Keimig, F., 2005. Stable isotopes in East African precipitation record Indian Ocean Zonal mode. *Geophysical Research Letters*, **32**(21), L21705, doi:10.1029/2005GL023876.
Vuille, M., Francou, B., Wagnon, P., Juen, I., Kaser, G., Mark, B. G., and Bradley, R. S., 2008. Climate change and tropical Andean glaciers: past, present and future. *Earth Science Reviews*, **89**, 79–96.
You, Q., Kang, S., Pepin, N., and Yan, Y., 2008. Relationship between trends in temperature extremes and elevation in the eastern and central Tibetan Plateau, 1961–2005. *Geophysical Research Letters*, **35**, L04704.

Cross-references

Alaskan Glaciers
Alps
Andean Glaciers
Global Warming and its Effect on Snow/Ice/Glaciers
Kilimanjaro
Precipitation
Rocky Mountains
Snow Line
Temperature Lapse Rates in Glacierized Basins
Tibetan Plateau

CLOUDBURST

Vijay Kumar
National Institute of Hydrology,
Roorkee, India

Cloudbursts have no strict meteorological definition. The term usually signifies a sudden, heavy fall of rain over a small area in a short period of time. Cloudburst represents cumulonimbus convection in conditions of marked moist thermodynamic instability and deep, rapid dynamic lifting by steep orography. The phenomenon occurs due to sudden upward drift of moisture-laden clouds as a tall vertical column termed "Cumulonimbus clouds." The ascending moisture-laden clouds become heavier and at certain point they produce violent rainstorm within a short interval. Orographic lifting of moist unstable air releases convective available potential energy necessary for a cloudburst (Das et al., 2006).

A cloudburst is a devastating weather phenomenon representing sudden burst of highly concentrated rain associated with thunderstorm over a small geographical area, generally not exceeding 20–30 km^2. Cloudbursts are generally accompanied by lightening, thunder, and strong gusts of winds. Rain from a cloudburst is usually of the shower type with a fall rate equal to or greater than 100 mm/h. During a cloudburst, more than 20 mm of rain may fall in a few minutes. The hard rain characteristic of a cloudburst is caused by a phenomenon known as langmuir precipitation in which drops of rain fuse together to create large drops as they fall, falling ever more quickly as they grow.

Cloudbursts in India occur when monsoon clouds associated with low-pressure area travel northward from the Bay of Bengal across the Ganges plains onto the Himalayas and "burst" in heavy downpours (Das et al., 2006). Cloudbursts are common to all hilly areas but the states of Himachal Pradesh and Uttaranchal are most affected due to topographical conditions. Most of the damages to properties, communication system, and human casualties are as a result of flash floods. Prediction of cloudbursts is challenging and requires high-resolution numerical models and meso-scale observations, high-performance computers, and Doppler weather radar (Das et al., 2006).

Bibliography

Das, S., Ashrit, R., and Moncrieff, M. W., 2006. Simulation of a Himalayan cloudburst event. *Journal of Earth System Science*, **115**(3), 299–313.

COHESION

P. Pradeep Kumar
Department of Atmospheric and Space Sciences, Pune University, Pune, Maharashtra, India

Definition

Cohesion means cling together or sticking together. The force holding the molecules of the same substance is cohesion. The cohesion of molecules gives the phenomena of surface tension, which is responsible for the spherical shape of the cloud or rain drops as they fall through the air. Cohesion is important for fluid flow. Cohesion is important for snow avalanches.

Bibliography

Chang, M., 2003. *Forest Hydrology: An Introduction to Water and Forests*. Boca Raton, FL: CRC Press, p. 373. ISBN 0849313635, 9780849313639.
McClung, D., and Schaerer, P., 2006. *The Avalanche Handbook*, 3rd edn. Seattle, WA: The Mountaineers Books, p. 342. ISBN 0898868092, 9780898868098.

COLD-BASED GLACIERS

Reginald D. Lorrain[1], Sean J. Fitzsimons[2]
[1]Département des Sciences de la Terre et de l'Environnement, Université Libre de Bruxelles, Bruxelles, Belgium
[2]Department of Geography, University of Otago, Dunedin, New Zealand

Definition and synonyms

Cold-based glaciers are glaciers with their basal part entirely below the pressure melting point and therefore sometimes called "dry-based glaciers" (through lack of liquid water). Floating ice bodies are not considered in this entry.

Antonyms are respectively warm-based glaciers and wet-based glaciers.

This terminology emphasizes the importance of basal conditions of glaciers. In a happy turn of phrase, Knight (1999, p. 78) justifies this point of view telling that the basal part is the "business end" of glaciers because, among other factors, the rheology of the basal ice layer which accommodates the bulk of movement in many glaciers is critical to glacier dynamics and the basal ice acts as an agent of glacier impact on the landscape. In fact, as we will see below, nearly always, it is possible to equate cold-based glaciers with cold glaciers (and warm-based glaciers with warm – or temperate – glaciers). But this dichotomy is too simple an approach because very often, different parts of the same glacier can fall into one or the other category. That is the reason why these transitional forms are referred to as polythermal glaciers. The twofold classification also leads to another oversimplification implying that there is no liquid water at all at the base of cold-based glaciers so that they are firmly frozen to their bed. As a result, they are thought to be ineffective agents of erosion and, after retreat, leaving nearly no evidence of their former existence in the landscape. Very large surfaces are thought to have been protected from glacial erosion because of the cold-based Pleistocene ice caps and ice sheets (Kleman and Hatterstrand, 1999; Sugden and John, 1976). This has been suggested by many observations of relatively fragile landforms as tors which are widespread in formerly glaciated regions. In fact, even if such observations are undeniable, the conclusion of the general absence of basal motion and, hence, of erosion by cold-based glaciers is questionable.

Basal thermal regime

Vertical temperature profiles in glaciers show that below an upper layer of 10–15 m thick affected by seasonal variations and eventually refreezing of percolating meltwater, there is a general increase in temperature with depth. This situation results from internal and basal heating. But, where the bed is below the melting point, the basal temperature is mainly governed by the geothermal heat flux and only secondarily by friction heat. This means that, if the ice mass

is stagnant, the steady state temperature distribution is determined as soon as the temperature gradient and the near surface temperature (below the depth of 10–15 m) are known. Because any heat flux is proportional to the temperature gradient, this heat flux determines the temperature gradient that must develop throughout the ice mass (Hooke, 1977). For a typical geothermal flux of 50 mW m^{-2} (Paterson, 1994), the gradient is 0.021 K m^{-1} since the thermal conductivity of ice is 2.39 W m^{-1} K^{-1} (at −20°C). For a 100 m ice thickness, this means that, if the near surface temperature is −20°C, the basal temperature will be −17.9°C.

Now, if the ice mass is moving, the effects of vertical and horizontal velocities have to be taken into account. Hooke (1977) has calculated temperature profiles for realistic combinations of ice thickness and vertical velocity, reproduced in Figure 1. It is clearly visible that the basal temperature increases markedly with increasing vertical velocity in the ablation zone while it is the contrary in the accumulation zone.

Considering the effect of horizontal velocity, Hooke (1977) indicates that temperature gradients in the horizontal direction are generally so small that very little warming or cooling of the ice occurs. But, because the velocity decreases with depth, there is shear deformation in the horizontal direction which produces heat. The rate of deformation increases with temperature so that in cold glaciers, the shear is particularly concentrated close to the bed. The frictional heat released is added to the geothermal heat with the result that the temperature gradient at the bed is that much higher. With the typical basal shear stresses of about 0.5 bars given by Hooke, it appears that for producing an amount of heat comparable to the geothermal heat, the horizontal velocity must be several tens of meters per year. However such velocities are far to be reached everywhere. Moreover, horizontal velocities increase from the highest places of the accumulation areas to the equilibrium lines and than decrease from these to the margins.

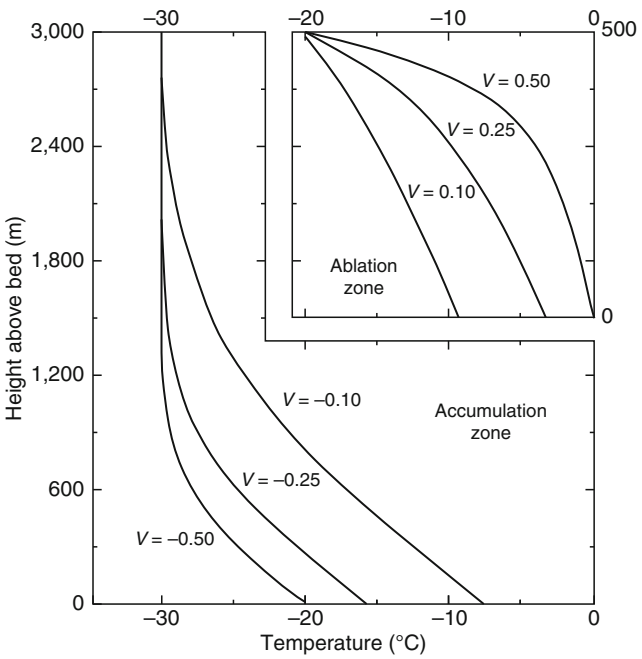

Cold-Based Glaciers, Figure 1 Illustrative temperature profiles [v = vertical velocity at glacier surface (in m a^{-1}) and is positive upwards]. In the ablation zone (*upper right*), v is upward. In the accumulation zone (*lower left*), v is downward; horizontal conduction and advection and internal heat generation is ignored in all cases. Vertical velocity is assumed to decrease linearly with depth. After Figure 3 in Hooke (1977).

From the considerations developed above, one can easily understand that at the places where they are cold-based, glaciers are at subfreezing temperature from top to bottom except in certain cases for a surface layer of about 10–15 m thick where the temperature can reach the melting point seasonally. It is also obvious that they can only exist in regions where the mean annual temperature is markedly negative, that is, in high latitude and high altitude areas.

Now, as the temperature gradient above the glacier sole determines the amount of heat that can enter the glacier per unit time, there are three possible situations (Weertman, 1961):

1. More heat (from the geothermal flux and from frictional heating) is provided than can be conducted upwards through the glacier; then, the excess heat is consumed by melting ice at the base.
2. The heat amount provided is equal to that which can be conducted upwards through the glacier; there is thus a balance between melting and freezing.
3. The heat amount provided is smaller than the amount which can be removed through the glacier (even if latent heat is released locally by freezing of meltwater flowing in from an adjacent zone). In this case which is the only one relevant to our subject, the glacier is frozen to its bed and impedes (or reduces) sliding considerably so that the forward movement of the glacier is mainly due to internal flow.

From this threefold alternative, it appears clearly that different thermal zones can coexist at the base of glaciers (e.g., Robinson, 1984) and ice sheets, so explaining why they can be polythermal. The areal distribution of these zones is likely to change in the course of time as a result of climatic changes. Moreover, these changes can result in thickening or thinning of the glacier and in consequent changes in the velocity field. However, some glaciers are exclusively cold-based. A cold base is favored by smaller ice thickness, low surface temperature, low basal velocity, and low geothermal heat flux.

Glacier margin morphology

As remarkably analyzed by Chinn (1991), cold-based glaciers display a variety of margin forms which have in common a three-part structural sequence of: (1) white glacier ice, terminating at (2) an inner moraine, which is surrounded by (3) an outer apron structure (Figure 2).

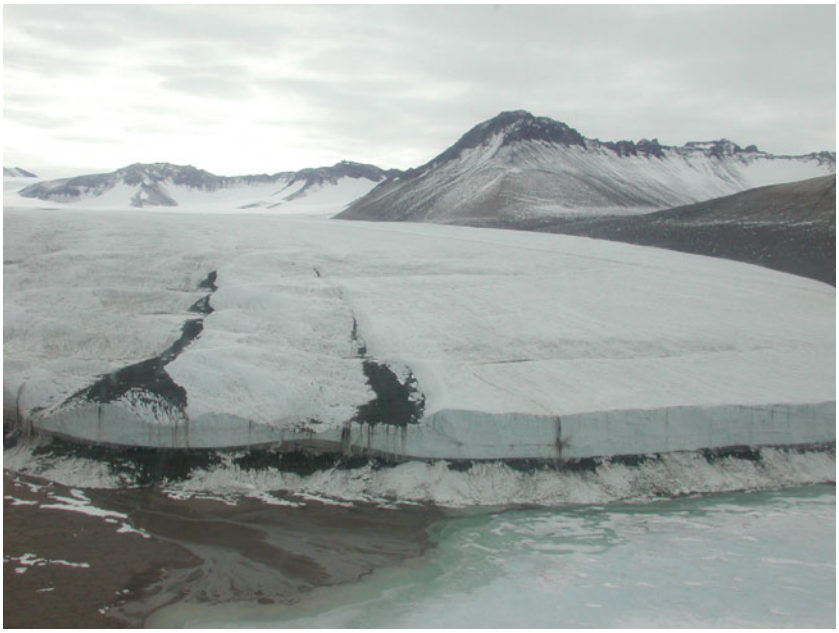

Cold-Based Glaciers, Figure 2 Victoria Upper Glacier (Victoria Valley, Antarctica). This typical cold-based glacier is showing its terminal cliff, about 40 m high towering above the apron mainly formed by successive cliff collapses. Debris coming out at the upper part of the apron is progressively forming a shear moraine.

The forms and behavior of these margins result from the effects of internal zones of different viscosity and the fact that basal ice is frozen to the bed. Where the ice thins to nearly 20 m as it approaches to the glacier margin, the upper "semi rigid zone" (Chinn, 1991, p. 29) becomes grounded and basal debris is upwarded against this obstructing ice to appear at the surface as a shear moraine. A wedge of drifted snow and ice usually forms in the inflection between the glacier and the ground to form an kind of scree called "apron" (Chinn, 1991) around the glacier margin.

Sliding at subfreezing temperatures

As indicated above, ice masses with basal temperature below the pressure melting point are traditionally assumed to display neither sliding nor bed deformation even if Shreve (1984), theorizing on glacier sliding at subfreezing temperatures had already predicted nonzero sliding speeds.

It is highly significant in this respect that in the authoritative "The Physics of Glaciers," by Paterson (1994), there is only one page on sliding at sub-freezing temperatures out of 26 on glacier sliding. However, as pointed out by Waller (2001), there is growing field evidence that directly contradicts the generally accepted view. As far as contemporary glacial environments are concerned, this evidence has been first derived from field work conducted by, e.g., Echelmeyer and Wang (1987), Fitzsimons (1996), and Cuffey et al. (1999).

The first cited authors described observations they made in a tunnel at the base of the predominantly cold-based Urumqi Glacier n°1 in North-Western China. They found that 60–85% of the overall glacier motion occurred within the lowermost 1–2% of the glacier thickness, mainly through deformation of the subglacial sediments. The latter were displaying a 100-fold reduction in creep strength relative to clean ice at the same temperature (here $< -1.75°C$). A small but significant amount of basal sliding was measured at the ice–drift interface (0.5 mm day^{-1}) and basal sliding at an ice–rock interface was also detected. Among different conclusions, the authors suggested that cold-based glaciers are able to mobilize and entrain permafrozen, subglacial material *en masse*, due to transmission of basal shear stress across the ice–bed interface. Following Waller (2001), the greatest merit of Echelmeyer and Wang's work is that it demonstrates that the basal processes beneath a cold-based ice-mass may contribute in an extremely important way to its total surface motion, even though they are only accommodating flow rates of the order of up to a few meters per year. However, it should be noted that the basal temperature in this case is not very negative, which allows to suspect that liquid water could still be present, for instance in the case of high solute concentrations frequently found in water within sediments.

Fitzsimons (1996) has shown that several cold-based glaciers in the Dry Valleys of McMurdo (Antarctica) have prominent end moraines which contradict the previously accepted idea that these glaciers are geomorphologically inactive. They are thrust-block moraines consisting of blocks of lacustrine sediments often interbedded with ice. All previous explanations of the formation of thrust-block moraines depend on the presence of subglacial

meltwater and thus appear inappropriate for the cold-based glaciers in question, having basal temperature as low as −17°C. The author has proposed a model based on the presence of ice-marginal lakes. Transient wet-based conditions can occur as ice flows onto the unfrozen sediments of the lake bottom, creating conditions favorable for the entrainment of sediments and for ice accretion by water freezing. This model has been proved to be valid by an ice-composition study of the basal part of Suess Glacier (Taylor Valley) where stable isotope and gas composition have allowed discriminating between meteoric glacier ice and basal refrozen water from the adjacent lake (Lorrain et al., 1999).

Concerning the work of Cuffey et al. (1999), it showed that sliding is occurring at very cold (−17°C) ice–rock interface beneath Meserve Glacier situated in another of the Dry Valleys of McMurdo (Wright Valley, Antarctica). This observation is interpreted as manifestations of thin water films at ice–rock interfaces. These interfacial films can exist due to a reduction of the chemical potential of water very close to the surface of a foreign solid which depresses the melting point. It is to be noted that recent work by Samyn et al. (2005) have given some weight to this hypothesis thanks to gas composition analyses performed in the basal ice of another cold-based glacier of the dry Valleys. Their results point to the occurrence of water phase changes involving minute liquid water bodies present despite the ice temperature of −17°C. Coming back to the work of Cuffey et al. (1999), an interesting point is that cavities were observed in the lee of boulders on the bed and that the cavity roofs are striated. Displacement transducers were inserted 1and 30 mm above the bed just upstream of a prominent cavity. These markers moved downglacier at a rate more than an order of magnitude faster than due to shear strain and therefore measuring sliding (Cuffey et al., 1999). The markers showed a sliding rate of about 8 mm a^{-1}. Theoretical treatment based on Gilpin's (1979) interfacial film theory allowed the authors to explain the relatively rapid sliding of this cold glacier by the presence of very high solute content of unfrozen water within interfacial films at the ice–rock interface. In a later paper, Cuffey et al. (2000) reported on their investigations in the same tunnel and confirmed their previous interpretation, using compositional analyses (gas and stable isotopes) of the different types of ice observed at the base. They showed that active entrainment occurs at the bed. They were also able to calculate that, as the Dry Valleys have been cold and dry for at least 10^7 years, entrainment may have formed the U-shaped trough containing the glacier, assuming that the modern debris flux they measured is representative of long-term rates. Their general conclusion was: "The common assumption that cold-based glaciers are protective rather than erosional is not true in the absolute sense although it's accurate relative to temperate glaciers." (Cuffey et al., 2000, p. 354).

The Dry Valleys are particularly interesting in that context because they concentrate on a small territory a number of cold-based glaciers which are relatively accessible and, therefore have attracted many investigations. Examination of their basal zone has demonstrated a wide variety of types of basal ice (Fitzsimons, 2006). More specifically, it has shown that, in the case of glaciers that rest on unconsolidated sediments, the thickness, composition, and structure of basal ice are distinctly different from those confined to the valley sides, such as Meserve Glacier. Tunnels excavated into several of the former glaciers (Suess, Wright Lower, and Taylor glaciers) have provided an opportunity to closely examine the composition, structure, and behavior of basal ice (with temperature always lower than −16°C) and glacier beds. The configuration and composition of this basal ice show that, in several cases, no simple clear boundary does separate basal ice from a frozen substratum. In Suess Glacier for instance, the compound velocity profile (Figure 3) together with measurements of sliding demonstrate that the glacier bed is not a simple ice-substrate contact that can be adequately described by a power law like Glen's Law. Following Fitzsimons (2006), the measured velocity structure is the product of variability in the rheological behavior of ice with distinct physical and chemical composition. In other words, the zero-based velocity of cold-based glaciers is simplistic and in reality, the situation is likely to be much complicated. There is abundant evidence to suggest that deformation of the glacier substrate has resulted in both *en masse* entrainment of the glacier substrate and mixing of material from the glacier substrate with basal ice. Ultimately, the point of zero velocity in any glacier is governed by the thermal and mechanical processes which vary in space and time. Accordingly, where a glacier rests on an unconsolidated substrate, the base is likely to be a zone rather than a boundary. In the case of the cold-based Antarctic glaciers cited above, this zone has developed as a result of folding, faulting and shearing that has produced a complex mosaic of ice-rich sediment and debris-rich ice within which many structural characteristic of the

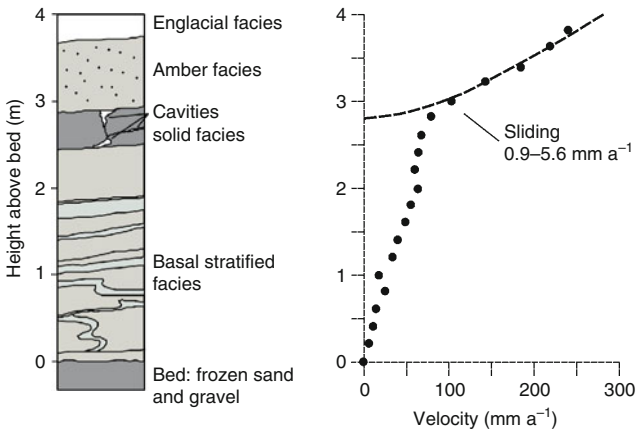

Cold-Based Glaciers, Figure 3 Ice composition, structure, and deformation at the base of Suess Glacier (Taylor Valley, Antarctica).

substrate are preserved after the material has been entrained (Fitzsimons, 2006).

Perspectives and conclusion

In a recent paper, Alley et al. (2008) have attracted attention on the fact that surface meltwaters that seasonally form lakes on top of the Greenland Ice sheet can drain catastrophically into the ice sheet, delivering heat rapidly to the bed. In a warming world, intensification of this phenomenon would deliver sufficient heat to thaw areas where the bed is currently frozen. Accelerations comprised between twofold and more than an order of magnitude could occur especially where extensive regions with soft sediments were to thaw. As such events would clearly influence future sea level change, we plead for an increasing research effort devoted to studying basal characteristics of the soft-bedded cold-based glaciers.

Bibliography

Alley, B., Fahnestock, M., and Joughin, I., 2008. Understanding glacier flow in changing times. *Science*, **322**, 1061–1062.

Chinn, T. J. H., 1991. Polar glacier margin and debris features. *Memorie Della Societa Geologica Italiana*, **46**, 25–44.

Cuffey, K. M., Conway, H., Hallet, B., Gades, A. M., and Raymond, C. F., 1999. Interfacial water in polar glaciers and glacier sliding at –17°C. *Geophysical Research Letters*, **26**(6), 751–754.

Cuffey, K. M., Conway, H., Gades, A. M., Hallet, B., Lorrain, R., Severinghaus, J. P., Steig, E. J., Vaughn, B., and White, J. W. C., 2000. Entrainment at cold glacier beds. *Geology*, **28**, 351–354.

Echelmeyer, K., and Wang, Z., 1987. Direct observation of basal sliding and deformation of basal drift at subfreezing tremperature. *Journal of Glaciology*, **45**, 361–369.

Fitzsimons, S. J., 1996. Formation of thrust-block moraines at the margin of dry-based glaciers, South Victoria Land, Antarctica. *Annals of Glaciology*, **22**, 68–74.

Fitzsimons, S., 2006. Mechanical behaviour and structure of the debris-rich basal ice layer. In Knight, P. G. (ed.), *Glacial Science and Environmental Change*. Oxford: Blackwell, pp. 329–335.

Gilpin, R. R., 1979. A model of the liquid-like layer between ice and a substrate with application to wire regelation and particle migration. *Journal of Colloid and Interfacial Science*, **68**, 235–251.

Hooke, R. Le B., 1977. Basal temperatures in polar ice sheets: a qualitative review. *Quaternary Research*, **7**, 1–13.

Kleman, J., and Hatterstrand, C., 1999. Frozen-bed Fenoscandian and Laurentide ice shheets during the last Glacial Maximum. *Nature*, **402**, 63–66.

Knight, P. G., 1999. *Glaciers*. Cheltenham: Stanley Thornes.

Lorrain, R., Fitzsimons, S. J., Vandergoes, M. J., and Stiévenard, M., 1999. Ice composition evidence for the formation of basal ice from lake water beneath a cold-based Antarctic glacier. *Annals of Glaciology*, **28**, 277–281.

Paterson, W. S. B., 1994. *The Physics of Glaciers*, 3rd edn. Oxford: Burtterworth Heinemann.

Robinson, P. H., 1984. Ice dynamics and thermal regime of Taylor Glacier, South Victoria Land, Antarctica. *Journal of Glaciology*, **105**, 153–160.

Samyn, D., Fitzsimons, S., and Lorrain, R., 2005. Strain induced phase changes within cold basal ice from Taylor Glacier, Antarctica indicated by textural and gas analyses. *Journal of Glaciology*, **51**, 611–619.

Shreve, R. L., 1984. Glacier sliding at subfreezing temperatures. *Journal of Glaciology*, **30**, 341–347.

Sugden, D. E., and John, B. S., 1976. *Glaciers and Landscape*. London: Edward Arnold.

Waller, R. L., 2001. The influence of basal processes on the dynamic behaviour of cold-based glaciers. *Quaternary International*, **86**, 117–128.

Weertman, J., 1961. Mechanism for the formation of inner moraines found near the edge of cold ice caps and ice sheets. *Journal of Glaciology*, **3**, 965–978.

Cross-references

Frictional Melting
Glacial Erosion
Glacier Motion/Ice Velocity
Glacier Sliding
Landscapes of Glacial Erosion
Polythermal Glaciers
Refreezing of Meltwater
Solutes in Glacier Ice
Subglacial Processes

CONDENSATION NUCLEI

P. Pradeep Kumar
Department of Atmospheric and Space Sciences, Pune University, Pune, Maharashtra, India

Definition

Condensation nuclei are very small atmospheric particles in the range of 1 nm–0.1 μm on which water can condense at very high supersaturations. Atmospheric aerosols upon which water vapor can condense at lower supersaturations are called as Cloud Condensation Nuclei (CCN). Only a small fraction of aerosols serve as CCN (about 1% in continental air and about 10–20% in maritime air). Most of the CCN would be a mixture of soluble and insoluble components.

Bibliography

Wallace, J. M., and Hobbs, P. V., 1977. *Atmospheric Science: An Introductory Survey*. New York, NY: Academic, p. 467.

CONFLUENCE OF RIVERS

Anju Chaudhary
Water Resources System Division, National Institute of Hydrology, Roorkee, India

Definition

Confluence of rivers is defined as a meeting point of two or more rivers. In other words it usually refers to the point where a tributary joins a major river, called the mainstream. In general, downstream of the confluence, the river having the combined flow of rivers/streams is known as the main stream, but in some cases a new name is also given to the river after the meeting of two streams/rivers. Two examples of confluence of rivers are given below (Figures 1 and 2).

Confluence of Rivers, Figure 1 Confluence of Spiti river with Satluj river in the Himachal Pradesh (India).

Confluence of Rivers, Figure 2 Confluence of Alaknanda river with Bhagirathi river at Deoprayag in the Uttrakhand (India). This river is known as Ganga after confluence of Alaknanda and Bhagirathi rivers.

CONGELATION ICE

Pratima Pandey
Centre of Studies in Resources Engineering, Indian Institute of Technology Bombay, Mumbai, Maharashtra, India

Definition

Congelation ice forms as water freezes on the bottom of the ice cover, and the latent heat of crystallization is conducted upward through the ice and snow to the atmosphere. Formation of sea ice on the bottom of an established sea ice cover in the form of platelets, which coalesces to form solid ice, is also represented by congelation ice. Its growth rate is proportional to the rate at which energy is transferred from the bottom surface of the ice layer to the air above. Congelation ice is often referred to as *black ice* because it has a high optical depth that permits significant light transmission to the underlying water. It forms as a stable ice sheet with a smooth bottom surface.

CRACK

Pratima Pandey
Centre of Studies in Resources Engineering, Indian Institute of Technology, Bombay, Mumbai, Maharashtra, India

Definition

A crack is defined as a narrow rift/fracture in the ice. As ice expands, it causes stresses through its depth and across its breadth which results in crack of ice. Cracks are found in glaciers and floating ice in the sea. Wider cracks can be termed as "crevasses" in the glaciers.

CREEP

Christophe Lambiel[1], Reynald Delaloye[2], Isabelle Gärtner-Roer[3]
[1]Institute of Geography, University of Lausanne, Lausanne, Switzerland
[2]Department of Geosciences, Geography, University of Fribourg, Fribourg, Switzerland
[3]Glaciology, Geomorphodynamics and Geochronology, Department of Geography, University of Zürich, Zürich, Switzerland

Definition

Creep is the slow deformation of rock, debris, soil, or ice.

Introduction

Regarding geomorphological processes, creep or flow, respectively, is one form of mass movement and may occur in bedrock (e.g., sagging, Sackung), debris (e.g., rock glacier), as well as soil (e.g., solifluction) (Dikau et al., 1996). In general, creep is driven by gravity and shows slow, plastic deformation with rates of mm, cm, and dm per year. Creep can be continuous or periodical (seasonal). In addition, creep is also defined for glacier movement. Regarding cryospheric processes, creep characteristics are detailed for ice (glacier) and ice–debris mixtures (rock glacier).

Creep of ice

Creep is the motion that results from ice crystal deformation and movement between individual ice crystals (Benn and Evans, 1998). Glacier ice deforms internally because it is subject to stress. The average shear stress within a glacier can be approximated as:

$$\tau = \rho_i g h \sin a$$

where ρ_i is the density of ice, g is the gravitational acceleration, h is the ice thickness, and a is the surface slope of ice. This equation indicates that the shear stress at the base of the glacier depends on the glacier thickness and on the slope. An increase in glacier thickness will increase the shear stress and thus increase the rate of movement. It also indicates that the deformation is maximal in the basal layers because shear stress is the highest.

The typical creep curve for glaciers, when polycrystalline ice is subject to a constant stress, displays an initial elastic deformation, followed by a primary creep in which the strain rate decreases continuously (Paterson, 1981). Then, a period of constant strain, which is called secondary or steady state creep, occurs. After this, the strain rate increases (tertiary creep). Most glaciers are thought to be in a permanent state of secondary creep.

Numerous laboratory studies have shown how the ice responds to stress. The law most often used is the Glen's flow law (Glen, 1955):

$$\varepsilon = A\tau^n$$

where ε represents the strain rate, A and n are constants, and τ is the shear stress. A correlates strongly with temperature. Thus, it signifies that the rate of deformation depends on shear stress and temperature. This explains the slower movement of cold ice, which is less plastic at lower temperatures. The flow law exponent n also varies, but is usually close to 3.

In reality, strain rates often differ from values predicted from laboratory experiments, especially because of orientation of crystals in the ice and of the presence of impurities in the form of dissolved ions, gas bubbles (which soften the ice) and rock particles, whose role on ice deformation is of great importance (Hubbard and Sharp, 1989; Benn and Evans, 1998).

Creep of ice-supersaturated permafrost

Rock glaciers are landforms resulting of the deformation of ice-supersaturated sediment (e.g., Barsch, 1996). By

definition, debris content in rock glaciers is important. In many cases, ice is present only in the pores between the particles, which reduces the cohesive strength.

Like glaciers, rock glaciers are thought to be in a permanent secondary creep (steady state creep) (Haeberli, 1985). It is generally assumed that the deformation rate of frozen sediment is strongly dependant on its external (slope gradient) and internal characteristics (ice content, particle size, etc.) and on its temperature. The presence of unfrozen water also influences the creep rate at temperatures close to the melting point (Barnes et al., 1971). Arenson (2002) showed in laboratory experiments that, for low stress conditions, creep is more influenced by the temperature than by the ice content and that creep rate may vary by an order of magnitude, even for small temperature changes, close to the melting point. Arenson and Springman (2005) confirmed that warm, ice-rich permafrost exhibits higher creep rate. However, if modelling the entire creep process is possible for ice, it is much more challenging for rock glaciers, since their internal structure is extremely heterogeneous (Haeberli et al., 2006).

A shear horizon was identified in some rock glaciers at various depths (e.g., Arenson et al., 2002). It was shown that a large part of total deformation occurs in this relatively thin layer. Thus, the surface movement of ice-supersaturated material is the addition of sliding in a shear horizon and internal deformation. Deformation at the base can be also possible (Roer et al., 2008).

Data on the internal deformation of rock glaciers is sparse, because of the high cost of boreholes. Thus, most of the information come from surface measurements, either by remote sensing (e.g., Kääb, 2005) or by terrestrial measurements (e.g., Lambiel and Delaloye, 2004). The strong dependency of rock glacier creep on permafrost temperature is illustrated by the velocity differences between arctic and alpine rock glaciers. Whereas cold arctic rock glaciers have velocities of some cm a^{-1} (Kääb et al., 2002), velocities of alpine rock glaciers are generally higher, typically between 20 cm and 1 m a^{-1} (e.g., Kääb et al., 2007; Lambiel et al., 2008).

Interannual variations of velocities of warm rock glaciers – which could be not frozen at their base – can be large, due to their dependency on external climatic factors, such as characteristics of the snow cover or summer temperatures (Delaloye et al., 2008), or seasonal snowmelt water refilling the rock glacier system (Ikeda et al., 2008). As observed since the beginning of the 1990s in the Alps, the increase of the ground surface temperatures leads to an increase in rock glacier creep (Kääb et al., 2007). Possibly in connection with this, recent observations of rock glaciers with velocities up to 4 m a^{-1} and in a destabilization phase have been reported (Roer et al., 2008).

Conclusion

Creep is a widely held process in cryosphere. With basal sliding, it is the major process of glacier advance and motion of perennially frozen sediments. As indicated by the Glen's flow law, temperature of the material is a critical parameter for creep. The effect of the ongoing warming on the deformation rates of ice-associated landforms is best expressed by the increasing velocities of rock glaciers.

Bibliography

Arenson, L. U., 2002. *Unstable alpine permafrost: a potentially important natural hazard–variations of geotechnical behaviour with time and temperature*. Doctoral thesis No. 14801, ETH Zurich.

Arenson, L. U., and Springman, S. M., 2005. Mathematical description for the behaviour of ice-rich frozen soils at temperatures close to zero centigrade. *Canadian Geotechnical Journal*, **42**, 431–442.

Arenson, L. U., Hoelzle, M., and Springman, S. M., 2002. Borehole deformation measurements and internal structure of some rock glaciers in Switzerland. *Permafrost and Periglacial Processes*, **13**, 117–135.

Barnes, P., Tabor, D., and Walker, J. C. F., 1971. Friction and creep of polycristalline ice. *Proceedings of the Royal Society of London, Series A*, **324**, 155–155.

Barsch, D., 1996. *Rockglaciers: Indicators for the Present and Former Geoecology in High Mountain Environments*. Berlin: Springer.

Benn, D. I., and Evans, D. J. A., 1998. *Glaciers and Glaciation*. London: Arnold.

Delaloye, R., Perruchoud, E., Avian, M., Kaufmann, V., Bodin, X., Hausmann, H., Ikeda, A., Kääb, A., Kellerer-Pirklbauer, A., Krainer, K., Lambiel, C., Mihajlovic, D., Staub, B., Roer, I., and Thibert, E., 2008. The short-term response of rock glaciers creep to recent warm periods in the European Alps (2002–2007). In *Proceedings of the Ninth International Conference on Permafrost*. Fairbanks, Alaska, Vol. 1, pp. 343–348

Dikau, R., Brunsden, D., Schrott, L., and Ibsen, M.-L., 1996. *Landslide Recognition – Identification, Movement and Causes*. Chichester: Wiley.

Glen, B. J., 1955. The creep of polycristalline ice. In *Proceedings of the Royal Society of London, Series A*. Mathematical and Physical Science, Vol. 228, pp. 519–538.

Haeberli, W., 1985. Creep of mountain permafrost: internal structure and flow of alpine rock glaciers. *Mitteilungen der Versuchsanstalt für Wasserbau, Hydrologie und Glaziologie*, **77**.

Haeberli, W., Hallet, B., Arenson, L., Elconin, R., Humlum, O., Kääb, A., Kaufmann, V., Ladanyi, B., Matsuoka, N., Springman, S., and Vonder Mühll, D., 2006. Permafrost creep and rock glacier dynamics. *Permafrost and Periglacial Processes*, **17**, 189–214.

Hubbard, B., and Sharp, M. J., 1989. Basal ice formation and deformation: a review. *Progress in Physical Geography*, **13**, 529–558.

Ikeda, A., Matsuoka, N., and Kääb, A., 2008. Fast deformation of perennially frozen debris in a warm rock-glacier in the Swiss Alps: an effect of liquid water. *Journal of Geophysical Research*, **113**, F01021.

Kääb, A., 2005. *Remote Sensing of Mountain glaciers and permafrost creep*. Schriftenreihe Physische Geographie, Glaziologie und Geomorpholdynamik, Universität Zürich, 48.

Kääb, A., Isaksen, K., Eiken, T., and Farbrot, H., 2002. Geometry and dynamics of two lobe-shaped rock glaciers in the permafrost of Svalbard. *Norwegian Journal of Geography*, **56**, 152–160.

Kääb, A., Frauenfelder, R., and Roer, I., 2007. On the response of rockglacier creep to surface temperature increase. *Global and Planetary Change*, **56**, 172–187.

Lambiel, C., and Delaloye, R., 2004. Contribution of real-time kinematic GPS in the study of creeping mountain

permafrost: Examples from the Western Swiss Alps. *Permafrost and Periglacial Processes*, **15**, 229–241.
Lambiel, C., Delaloye, R., Strozzi, T., Lugon, R., and Raetzo, H., 2008. ERS InSAR for assessing rock glacier activity. In *Proceedings of the Ninth International Conference on Permafrost.* Fairbanks, Alaska, Vol. 1, pp. 1019–1024.
Paterson, W. S. B., 1981. *The Physics of Glaciers*, 2nd edn. Oxford: Pergamon.
Roer, I., Haeberli, W., Avian, M., Kaufmann, V., Delaloye, R., Lambiel, C., and Kääb, A., 2008. Observations and considerations on destabilizing active rockglaciers in the European Alps. In *Proceedings of the Ninth International Conference on Permafrost*. Fairbanks, Alaska, Vol. 2, pp. 1505–1510.

Cross-references

Formation and Deformation of Basal Ice
Glacier
Glacier Motion/Ice Velocity
Global Warming and Its Effect on Snow/Ice/Glaciers
Gravity Flow (Mass Flow)
Ice
Mountain Geomorphology
Natural Hazards Associated with Glaciers and Permafrost
Periglacial
Permafrost
Permafrost and Climate Interactions
Plastic Deformation
Rock Glaciers

CREVASSES

C. J. van der Veen
Department of Geography and Center for Remote Sensing of Ice Sheets, University of Kansas, Lawrence, KS, USA

Definition and introduction

Crevasses are intimidating fractures or cracks in the ice, a few tens to thousands of meters long and up to several meters wide and tens of meters deep, cutting through the surfaces of most glaciers. A crevasse may be covered or bridged by snow, thus masking its presence. Most explorers and glaciologists tend to consider these features as an impediment to safely traversing the glacier surface, especially those crevasses that have been bridged over and are all but invisible. On the other hand, it has been recognized that patterns of fracturing may provide information on how glaciers deform and move. Recent years have seen a modest resurgence of scientific studies on crevasse formation and propagation, motivated in part by efforts to better understand processes involved in iceberg calving and break up of ice shelves and floating ice tongues. Further, meltwater-driven crevasse propagation has been suggested as a mechanism by which surface meltwater can drain rapidly to the base of an ice sheet.

Opening criteria

As early as the mid-1800s, it was recognized that crevasses form as a result of tensional stresses. The earliest mathematical model was presented in 1843 at the Cambridge Philosophical Society by William Hopkins who argued that a fracture will form when the maximum tension is greater than the cohesive strength of the ice. While some studies relate first occurrence of crevasses to a critical strain rate, more complete compilations support the existence of a critical stress for crevasse formation. Strain rates are converted to stresses using the flow law for glacier ice, accounting for varying ice temperatures. A tensile stress between 90 and 320 kPa, altered by differences in crevasse spacing, is required for crevasses to occur. In a field of closely-spaced crevasses, a larger tensile stress is required for crevasse opening compared to a single crevasse due to the "blunting" effect that neighboring crevasses have on an individual one. Within the thin slabs of ice separating adjacent crevasses, no tensile stress can exist and there are no large stress concentrations near the crevasse tip that would otherwise promote downward propagation. This coupling between tensile stress and crevasse spacing may explain why in some places a few large crevasses exist while elsewhere crevasses occur in fields of smaller ones.

Penetration depth

For an air-filled crevasse at the glacier surface, the net longitudinal stress is the sum of the tensile stretching stress, which tends to open a crevasse, and the weight-induced lithostatic stress that causes the crevasse to close. In first approximation, the depth to which a crevasse will penetrate can be estimated from the depth at which the lithostatic stress balances the tensile stress such that the net longitudinal stress is zero. For a tensile stress of 150 kPa, this gives a depth of ca. 30 m. For individual crevasses, the penetration depth is greater because stress concentrations at the crevasse tip partly counter the lithostatic stress, thereby allowing the crevasse to extend deeper into the ice. Such stress concentrations become smaller in fields of crevasses and all but vanish if crevasses are closely spaced.

An expedient model to describe downward crevasse propagation that accounts for stress concentrations at crevasse tips is one based on linear elastic fracture mechanics (LEFM). This approach is based on the assumption that materials contain small cracks and flaws that may develop into large fractures through stress concentration near the crack tip. If the concentrated stresses are large enough to overcome the cohesion of the material, further crack growth is possible and under certain conditions, this process can become self-sustaining with crack growth leading to larger stress concentrations, allowing further growth, etc. Formally, this is described through the stress intensity factor, which is a measure for the concentrated stresses at the tip and that can be estimated from the geometry of the fracture (most notably its depth) and the net longitudinal stress acting on the fracture. Crack growth occurs where the stress intensity factor is larger than a critical value, called the fracture toughness, and will continue to the

depth at which the stress intensity factor equals the fracture toughness.

The LEFM approach to describing crevasse propagation on glaciers may be challenged for several reasons. First, ice is not a linear elastic material and viscous flow and deformation may affect the stress concentration at the crevasse tip. For surface crevasses that form in the upper firn layers, it is not clear how important this effect is. Second, initiation and growth of mature crevasses requires the presence of starter cracks of at least a few centimeters for tensile stresses typical of glaciers. Little is known about the origins and dimensions of these starter cracks. They may develop from millimeter-scale microfractures in the crystal structure through subcritical crack propagation as has been observed in rocks and other materials. Subcritical growth can occur when the stress intensity factor is less than the fracture toughness and proceeds at slow speeds until the stress intensity factor exceeds the fracture toughness and further growth is described by LEFM. There are no field or laboratory data on ice that can be used to test this model. Alternatively, centimeter-scale defects in firn may result from burial of sastrugi and sun crusts, or from folding of internal layers with different densities.

If the crevasse is water-filled, the water pressure compensates part or all of the lithostatic stress in the ice, thereby allowing the crevasse to penetrate deeper. Because the density of water is greater than that of ice, if the water level remains close to the glacier surface, water pressure increases more rapidly with depth than does the lithostatic stress associated with the weight of the ice, allowing the crevasse to penetrate the full ice thickness. The observation that most ice-shelf break-up events in the Antarctic Peninsula have occurred during longer melt season during which melt ponds formed on the surface, led to the suggestion that crevasse propagation driven by meltwater ponding is the main mechanism by which ice shelves weaken and rapidly disintegrate into a myriad of icebergs. Similarly, calving rates on tidewater glaciers and Greenland outlet glaciers increase in the spring with the onset of surface melting, lending support to the hypothesis that full-thickness fracturing of water-filled crevasses is an important control on iceberg calving.

Orientation

The assumption that crevasses form perpendicular to the direction of the principal tensile force was first applied by Hopkins (1862) to explain the orientation of crevasses as frequently observed on valley glaciers in the European Alps. If A represents the normal force in the direction of flow (generally along the axis of the glacier), B the normal force in the direction perpendicular to ice flow, and F the tangential or shearing force, the direction of the principal tensile stress, P, is given by

$$\tan 2\alpha = \frac{2F}{A-B}$$

where α represents the angle between the direction of P and the ice flow. Consider the principal surface strain rates and crevasse orientation measured on Blue Glacier in the Olympic Mountains, shown in Figure 1. Towards the margins, the ice velocity decreases and the dominant force is the tangential force, F, representing lateral drag originating at the valley walls. Setting $A = B = 0$ in the above equation gives an angle of 45° with the axis of the glacier as the direction of principal tension. Thus, near the glacier margin, crevasses will strike at an angle of 45° as in region I in Figure 1. Near the centerline of the glacier, drag from the margins is small ($F = 0$) and the force responsible for crevasse opening is the normal tension, A, acting in the flow direction so that crevasses open perpendicular to this axis (region II in Figure 1). Where the valley walls diverge, longitudinal or splaying crevasses may form. As the ice spreads laterally, the speed decreases and A becomes compressive (negative) while the other normal force, B, is tensile (positive). Where the tensile force in the cross-flow direction becomes sufficiently large, fracturing in the direction of glacier flow can occur. The diverging flow causes these crevasses to splay radially, resulting in the pattern in region III.

While in many cases crevasse patterns predicted by the Hopkins model agree with observations, there are exceptions, in particular where crevasses meet glacier margins. On many glaciers, including Blue Glacier shown in Figure 1, crevasses are oriented perpendicular to the margins. Further, a number of observations indicate strike-slip or shear displacement of crevasse walls, suggesting that mixed-mode fracturing may better describe crevasse growth. Thus, for modeling crevasse propagation along the glacier surface, it may be more appropriate to consider a combination of fracturing modes. Traditionally, crevasses are associated with Mode I fracturing ("opening mode") with displacements of the fracture surfaces in the direction of the tensile stress. Allowing also for Mode II fracturing ("sliding mode"), in which the fracture surfaces slide parallel to the plane of fracturing, shows that the predicted crevasse orientation can deviate from the direction perpendicular to the principal tensile stress. While this model can explain at least in a qualitative sense some of the observations, a rigorous test based on measurements and theory is still lacking.

Crevasses often persist over periods of several years and can be used to estimate surface velocity if individual and distinct crevasses can be identified on successive images. As crevasses are advected by ice flow, their orientation may change, especially where the velocity field is characterized by strong shear. However, several studies that compare calculated rotation with observed crevasse orientation along glaciers do not show good agreement. For example, on Whillans Ice Stream, west Antarctica, progressive rotation is not evident on a map of crevasse trains despite the presence of strong velocity shear. This may indicate that crevasses are more transient features with old and inactive ones disappearing once they are no

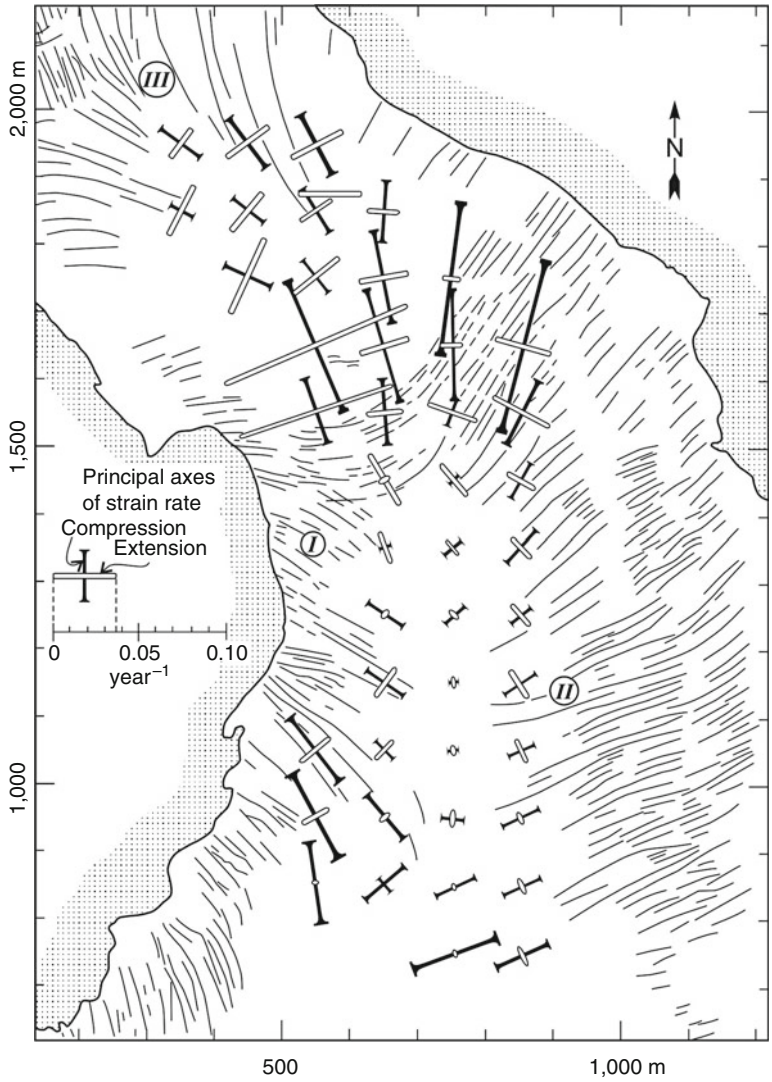

Crevasses, Figure 1 Principal surface strain rates and crevasse orientation on Blue Glacier, Olympic Mountains, Washington, USA. Ice flow is towards the top of the figure. From Meier et al. (1974).

longer oriented perpendicular to the principal tensile stress. The process whereby new crevasses are constantly formed while older ones are closed may explain why crevasses in fields often intersect at shallow angles. If crevasses formed as a result of surface tension, one would expect a crevasse, once formed, to relieve this tension, thus disfavoring formation of new crevasses. It has been suggested that crevasses reflect processes acting at some depth below the surface. In low-density firn, the tensile stress may increase with depth below the surface as density increases and the firn becomes stronger and able to support larger stresses. This raises the possibility that crevasse initiation occurs at some depth below the surface, rather than at the surface as commonly assumed. Ground-penetrating radar measurements on Rutford Ice Stream, west Antarctica, show subsurface crevasses occurring at depths ranging from 3 to 20 m in areas where surface crevasses are absent. Application of LEFM models shows that subsurface crevasse initiation is (theoretically) possible.

Bottom crevasses

Bottom crevasses extend from the base upward into the ice and can exist on floating ice shelves and on grounded glaciers where abundant basal water at sufficiently high pressure is available for the crevasse to remain water-filled. The water pressure, together with a tensile longitudinal stress, must be large enough to overcome the weight-induced lithostatic stress, which reaches its maximum at the glacier base. In practice, this means that the ice must be at or very near to flotation. Observational evidence supports this conclusion. Bottom crevasses have been observed using radar sounding on ice shelves, floating ice tongues, and in the vicinity of grounding lines.

Extensive radar sounding over Greenland and Antarctica, indicates that bottom crevasses are very rare in the more interior regions.

Summary

Crevasses remain among the least studied and understood features on glaciers and are usually not included in models of glacier flow. From an ice-dynamics perspective, there may not be any compelling reason for incorporating crevasses in glacier models. However, better understanding of crevasse initiation and propagation is needed for modeling transfer of surface meltwater to the glacier base, and for developing more realistic models for iceberg calving. This requires more systematic observations of crevasse properties (depth and spacing) and concurrent measurements of surface strain rates.

Bibliography

Hopkins, W., 1862. On the theory of the motion of glaciers. *Philosophical Transactions of the Royal Society of London*, **152**, 677–745.

Meier, M. F., Kamb, W. B., Allen, C. R., and Sharp, R. P., 1974. Flow of blue glacier, Olympic Mountains, Washington, USA. *Journal of Glaciology*, **13**, 187–212.

Van der Veen, C. J., 1999. Crevasses on glaciers. *Polar Geography*, **23**, 213–245.

Cross-references

Alaskan Glaciers
Antarctica
Calving Glaciers
Crack
Englacial Conduit
Englacial Processes
Glacial Drainage Characteristics
Glacier Hydrology
Ice Shelf
Meltwater Conduit
Moulins
Structural Glaciology
Tidewater Glaciers

CRITICAL TEMPERATURE

Pratima Pandey
Centre of Studies in Resources Engineering, Indian Institute of Technology, Bombay, Maharashtra, India

Definition

The *critical temperature* of a substance is the temperature at and above which vapor of the substance cannot be liquefied, regardless of the pressure applied on the substance. Gases become more difficult to liquefy as the temperature increases because the kinetic energies of the particles that make up the gas also increase. Every substance has a critical temperature. For example, for water critical temperature is 374°C.

CRUSH

Pratima Pandey
Centre of Studies in Resources Engineering, Indian Institute of Technology, Bombay, Mumbai, Maharashtra, India

Definition

Crushing is the process which results from pressure exerted by the debris and ice carried by the glacier during erosion. A glacier can erode rock by a mixture of abrasion, crushing and fracturing, and plucking. Crushing causes mineral boundaries to disintegrate into separate minerals. Glaciers crush, grind, and move large rocks and scour bedrock to form the floor and wall of mountain valleys.

CRUST

Pratima Pandey
Centre of Studies in Resources Engineering, Indian Institute of Technology Bombay, Mumbai, Maharashtra, India

Definition

An upper hard layer of snow or a film of ice or compacted snow lying upon a softer layer where liquid water has refrozen into grain fabric is known as crust. It represents a crisp, firm, outer surface upon snow. Freezing rain, direct sunlight, wind, or the melting and refreezing of snow helps in forming the snow crust.

CRYOCONITE

Nozomu Takeuchi
Department of Earth Sciences, Graduate School of Science, Chiba University, Inage-ku, Chiba-city, Chiba, Japan

Definition

Cryoconite: Dark-colored sediment deposited on snow or ice surfaces of glaciers.
Cryoconite hole: A water-filled cylindrical hole on glacial ice surface, in which cryoconite is deposited.
Cryoconite granule: A spherical aggregate of mineral particles, organic matter, and microbes in cryoconite.

Introduction

Cryoconite was first noted by an Arctic explorer, A. E. Nordenskjöld, on his trip over the Greenland ice sheet (Nordenskjöld, 1875). He observed numerous water-filled cylindrical pits sunk into ice. The bottom of these pits was covered with fine dust. He named the dust cryoconite after the Greek *kruos* (ice) and *konis* (dust), and called the pits

cryoconite holes. As the cryoconite absorbs solar radiation and promotes melting of the ice beneath it, the cylindrical holes are formed. Constituents of cryoconite have been studied mineralogically and biologically. Cryoconite contains mineral particles supplied from surrounding ground by wind and, on some glaciers, micrometeorite collected by glacial flow. It also contains abundant microbes and organic matter. The microbes are cold-tolerant species living on the glacial surface. Cryoconite holes seem to play a role of favorable habitats on glaciers for such organisms. Recently, cryoconite and cryoconite holes have been studied biogeochemically to understand their ecological roles on biological communities on glaciers. Dynamics of cryoconite holes have also been investigated in terms of the heat balance of glacier surface. The formation process of cryoconite holes is strongly associated with physical conditions on glacier surface and also can affect total ablation of glaciers (Figure 1).

Components of cryoconite

Terrestrial mineral particles are major components of cryoconite. They usually include quartz, feldspar, mica, calcite, and clay minerals. Fine mineral particles (0.1–10 μm in diameter) are supplied from surrounding grounds by wind. They are also carried from a far away desert in arid regions. Coarser mineral particles (>10 μm in diameter) are derived from rock wall, nunataks, and moraines of glaciers.

Other major components of cryoconite are microbes and organic matter. A large amount of photosynthetic microbes, such as snow algae and cyanobacteria, are commonly observed in cryoconite. They photosynthetically produce organic matter in the holes and sustain other heterotrophic microbes, such as rotifers, tardigrada, fungi, and bacteria. These organisms are specialized taxa that have adapted to cold environments.

Dark-colored organic matter, which is often contained in cryoconite, is humic substances (Takeuchi et al., 2001). Humic substances are thought to be highly polymerized compounds of residues that remain after bacterial decomposition of organic matter. The dark-colored humic substances effectively absorb solar radiation and result in the formation of cryoconite holes.

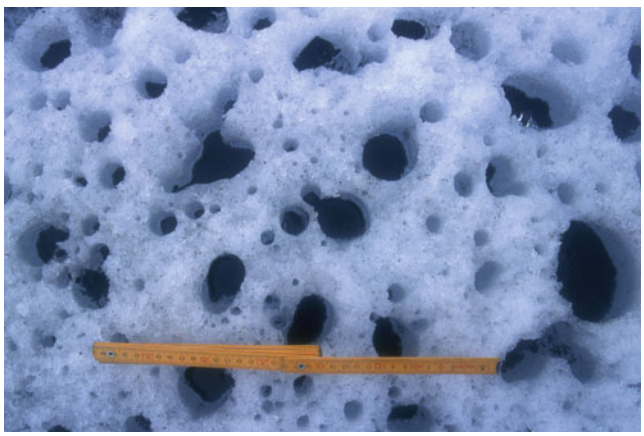

Cryoconite, Figure 1 Cryoconite holes on a Himalayan glacier.

These constituents, such as mineral particles, microbes, and other organic matter, usually conglomerate into small spherical granules, called cryoconite granules (Takeuchi et al., 2001). The granules are dark colored and 0.5–2.0 μm in diameter. The surface of the granule is usually covered with filamentous cyanobacteria. The spherical shape of the granules is maintained by the entanglement of filamentous cyanobacteria and adhesive substances around the mineral or organic particles.

Micrometeorites have been reported in cryoconite on the Greenland ice sheet (e.g., Maurette et al., 1987). The meteorites that fall on the ice sheet can be concentrated in cryoconite holes by ice flow and ablation. The cryoconite in Greenland is well known as the richest and best-preserved mines of cosmic dust grains found on the Earth. Their size is usually less than 1 mm in diameter. Micrometeorites can be identified by morphology and element analyses. They usually have evidence of surface heating such as glassy coatings or thin rims of Fe-rich material. And, they contain terrestrially less abundant elements such as Ir, Ni, Co and Cr.

The ecological aspects of cryoconite holes

Cryoconite holes play important roles in glacial ecosystems. As mentioned above, holes are inhabited by various kinds of organisms. For example, on Himalayan glaciers, there are rotifers, tardigrada, copepods, and larvae of midges sustained by snow algae and cyanobacteria. On North American glaciers, ice worms and collembolas are commonly observed in cryoconite holes. Organisms found in cryoconite holes on worldwide glaciers have been listed in Mueller et al. (2001). Although there are still a few measurements on photosynthetic rate of snow algae and cyanobacteria in cryoconite holes, the rate is comparable to other aquatic ecosystems in polar regions (Hodson et al., 2008). Wharton et al. (1985) suggested that cryoconite holes are individual ecosystems with distinct boundaries, energy flow, and nutrient cycling. The holes trap nutrient-rich particles, prevent nutrient washout by meltwater, and provide a semi-stagnant aquatic habitat for various algae and animals. Furthermore, cryoconite holes have recently gained attention because they may furnish refugia of organisms during glacial periods (Warton et al., 1985). They may play in the survival of microorganisms during ice ages and the colonizing of newly exposed areas after a glacier retreats. Also, cryoconite holes are possible analogues for similar structures on icy planets, such as Mars and Europa, or on the Earth during its hypothesized global glaciations (Snowball Earth) 600–800 million years ago (Fountain et al., 2008).

Dynamics of cryoconite holes

Formation and evolution of cryoconite holes are associated with physical conditions of glaciers. The size of cryoconite holes usually ranges from 1 to 50 cm in

diameter and from 3 to 50 cm in depth, and varies among places, times, and geographical locations of glaciers. Generally, holes are deeper on polar glaciers (20–50 cm), compared with those on middle- and low-latitude mountain glaciers (3–20 cm). On the other hand, the diameter of holes is not related to latitude, but probably to the age of holes.

The depth of the holes is determined by the balance of melting rate between the hole bottom and the surrounding ice surface (McIntyre, 1984). Depths should reach an equilibrium when the hole-deepening rate matches the ablation rate of the glacier surface. The heat sources of glacier surface are solar and long-wave radiations, and sensible and latent heats from air. On the other hand, those of the hole bottom are the circulation of warm water within the holes, solar radiation transmitted obliquely through the ice, diffuse and direct radiation entering the hole from the top, and heat generated metabolically by the microbes in cryoconite. The equilibrium depth of holes is determined by relative importance of these different energy sources. Average hole depth on a glacier temporally changes due to weather conditions. It also changes decadally or in longer timescales with climate (e.g., Gajda, 1958; Fountain et al., 2008; Takeuchi et al., 2000).

The horizontal growth of cryoconite holes occurs through coalescence of holes located close to each other or by trapping of more material into the holes. Since shrinkage in size or division of holes are rarely observed, the diameter of cryoconite holes generally reflect age of the holes.

The life span of cryoconite holes ranges from weeks to months on mountain glaciers, to more than years on polar glaciers. The holes on glaciers where melt rates are high are easy to collapse due to daily variation of the hole depth or to meltwater flows on the glacier surface. The cryoconite may be washed into streams and may accumulate in new deposits that often result in the formation of new holes. In contrast, on less melt rate glaciers in polar regions, a life span of 100–200 years was suggested to be possible. Analyses of the water chemistry of cryoconite holes on Antarctic glaciers showed life spans of 10 years or more (Fountain et al., 2008). On the Antarctic glaciers, ice-riddled cryoconite holes have been observed. The cryoconite in such holes is isolated from the atmosphere for 10 years or more.

Effect of cryoconite on glacier melting

In Antarctica, although cryoconite holes cover only a small portion of the entire glacial surface, they create a significant amount of meltwater runoff at near-surface hydrologic system. The contribution of meltwater produced by cryoconite to the total runoff on a glacier in the Mcmurdo Dry Valleys has been estimated approximately 15% (Fountain et al., 2008).

On some glaciers, the cryoconite lies not only in cryoconite holes, but also on whole glacier surfaces in the ablation area. It substantially reduces albedo and thus accelerates melting of the glacier surface (e.g., Takeuchi et al., 2008; Kohshima et al., 1993). The effect was first suggested on Greenland ice sheet (Gaja, 1958). A surface coating of cryoconite was observed close to the ice margins as well as farther back from it, and had a significant effect on melting of the ice. Kohshima et al. (1993) observed that the albedo of the intact surfaces bearing the cryoconite was substantially lower than that of the surface from which the cryoconite was artificially removed (5% versus 37%) on a Himalayan glacier. The melting rates of the intact surfaces were reported to be three times larger than that of the surfaces without the cryoconite. Thus, cryoconite on the glacier surface has a major influence on the glacial mass balance on such glaciers. On Asian glaciers, the effect is particularly significant compared to those in other regions (Takeuchi et al., 2008). Comparison of the amount of cryoconite on the glacier surface shows that the Asian glaciers, including the Himalayan, Tibetan, and Tienshan mountains, were more than 200 g m^{-2} in dry weight of cryoconite, whereas glaciers in the Arctic, Alaska, and Patagonia were less than 100 g m^{-2}. The large amounts of cryoconite on Asian glaciers are probably due to a large supply of windblown desert sand and a high biological production. In particular, the organic fraction in cryoconite is optically effective on the surface albedos as organic particles in cryoconite are usually dark colored and large in volume. Therefore, biological productivity on the glacier surface plays a significant role in glacial ablation.

Summary

Cryoconite is dark-colored sediment on glacier surface, and usually deposited at the bottom of water-filled cylindrical pits, called cryoconite holes. Cryoconite and cryoconite holes can be commonly observed from polar ice sheets to low-latitude mountain glaciers in the world. Cryoconite consists of mineral particles supplied from surrounding ground by wind, biogenic organic matter produced by microbes living on the glacial surface, and also micrometeorites in some glaciers. These constituents are usually conglomerated into small granules, called cryoconite granules. Abundant microbes in cryoconite indicate that glaciers are biologically active environments. Thus, it is important to study cryoconite to understand the ecology of organisms in such cold environments. Furthermore, dynamics of cryoconite holes are strongly related with physical conditions on glacier surface and can affect total ablation of glaciers. Thus, physical process of cryoconite holes is important to evaluate mass balance of glaciers. The information on cryoconite and holes, however, is still limited on particular glaciers, further studies, therefore, are necessary to understand them both biologically and physically on worldwide glaciers.

Bibliography

Fountain, A. G., Nylen, T. H., Tranter, M., and Bagshaw, E., 2008. Temporal variations in physical and chemical features of cryoconite holes on Canada Glacier, McMurdo Dry Valleys, Antarctica. *Journal of Geophysical Research*, **113**, G01S92, doi:10.129/2007JG000430.

Gajda, R. T., 1958. Cryoconite phenomena on the Greenland ice cap in the Thule area. *Canadian Geographer*, **3**(12), 35–44.
Hodson, A., Anesio, A. M., Tranter, M., Fountain, A., Osborn, M., Priscu, J., Laybourn-Parry, J., and Satteler, B., 2008. Glacial ecosystems. *Ecological Monographs*, **78**(1), 42–67.
Kohshima, S., Seko, K., and Yoshimuram, Y., 1993. Biotic acceleration of glacier melting in Yala Glacier, Langtang region, Nepal Himalaya. In *Snow and Glacier Hydrology. Proceeding of the Kathumandu Symposium,* November 1992*, IAHS*, **218**, pp. 309–316.
Maurette, M., Jehanno, C., Robin, E., and Hammer, C., 1987. Characteristics and mass distribution of extraterrestrial dust from the Greenland ice cap. *Nature*, **328**, 699–702.
McIntyre, N. F., 1984. Cryoconite hole thermodynamics. *Canadian Journal of Earth Sciences*, **21**, 152–156.
Muller, D. R., Vincent, W. F., Pollard, W. H., and Fritsen, C. H., 2001. Glacial cryoconite ecosystems: a biopolar comparison of algal communities and habitats. *Nova Hedwigia*, **123**, 173–197.
Nordenskjöld, N. E., 1875. Cryoconite found 1870, July 19th–25th, on the inland ice, east of Auleitsivik Fjord, Disco Bay, Greenland. Geological Magazine, Decade 2, **2**, 157–162.
Takeuchi, N., and Li, Z., 2008. Characteristics of surface dust on Ürümqi Glacier No. 1 in the Tien Shan Mountains, China. *Arctic, Antarctic, and Alpine Research*, **40**(4), 744–750.
Takeuchi, N., Kohshima, S., Yoshimura, Y., Seko, K., and Fujita, K., 2000. Characteristics of cryoconite holes on a Himalayan glacier, Yala Glacier Central Nepal. *Bulletin of Glaciological Research*, **17**, 51–59.
Takeuchi, N., Kohshima, S., and Seko, K., 2001. Structure, formation, darkening process of albedo reducing material (cryoconite) on a Himalayan glacier: a granular algal mat growing on the glacier. *Arctic Antarctic and Alpine Research*, **33**, 115–122.
Wharton, R. A., McKay, C. P., Simmons, G. M., and Parker, B. C., 1985. Cryoconite holes on glaciers. *Bioscience*, **35**, 449–503.

Cross-references

Glacial Ecosystems

CRYODESSICATION

P. Pradeep Kumar
Department of Atmospheric and Space Sciences, Pune University, Pune, India

Definition

Freeze drying (cryodessication) combines the virtues of dehydration and chilling for preserving. Freeze drying works by freezing the material and then reducing the surrounding pressure and adding enough heat to sublime the ice.

The mars analogue carbonate deposits in subglacial volcanic complex on Svalbard (Norway) is believed to have been formed through a process of cryodessication and/or thermal evaporation.

Bibliography

http://www.kgbanswers.com/what-13-cryodessication/823335
http://en.wikipedia.org/wiki/Freeze-drying
Rummel, J., Hoehler, T., and Eigenbrode, J., 2008. Astrobiology, 8(2), 347–355, doi:10.1089/ast.2008.1238.

CRYOFRONT

P. Pradeep Kumar
Department of Atmospheric and Space Sciences, Pune University, Pune, India

Definition

The cryofront is defined as the "zero degree isotherm in a soil profile" and it may be referred as the "leading edge of the cold." In other words it represents the boundary between cryotic and noncryotic ground as indicated by the position of the 0°C isotherm in the ground.

Bibliography

National Snow and Ice Data Centre (NSIDC), http://nsidc.org/cgi-bin/words/letter.pl?C

CRYOGENESIS

P. Pradeep Kumar
Department of Atmospheric and Space Sciences,
Pune University, Pune, India

Definition

Cryogenesis is the combination of thermophysical, physicochemical, and physicomechanical processes occurring in freezing and thawing earth materials.

Soil cryogenesis is defined as a process dictating many important properties and regimes of cold and permafrost-affected soils. Soil cryogenesis is influenced by climatic parameters, the earth–atmosphere interactions, the properties of soils, and the conditions of the permafrost.

Bibliography

http://nsidc.org/cgi-bin/words/letter.pl?C
Khudyakov, O. I., 2002. Permafrost, soil cryogenesis, and soil formation. *Eurasian soil science*, **35**(10), 1085–1091.

CRYOGENIC AQUICLUDE

P. Pradeep Kumar
Department of Atmospheric and Space Sciences,
Pune University, Pune, India

Definition

Aquiclude can be defined as layer of rock that has almost no porosity and does not allow the flow of water. Cryogenic aquiclude can be considered as layer of ground which, because of its frozen state, has a low enough permeability to act as a confining bed for an aquifer.

In cryogenic mountainous stony organic soils, the peat usually covers 25 or 30 cm or more and the permafrost

table lies at 100 cm as aquiclude. The cryogenic acquiclude slows down the migration of organic matter through iron elements through soil profile.

Bibliography

http://nsidc.org/cgi-bin/words/letter.pl?C
Kimble, J.M., 2004. *Cryosols: Permafrost-Affected Soils*. Springer, p. 726, ISBN 3540207511, 9783540207511.

CRYOGENIC FABRIC

P. Pradeep Kumar
Department of Atmospheric and Space Sciences,
Pune University, Pune, India

The distinct soil micromorphology is produced due to the effects of freezing and thawing processes and is termed as cryogenic fabric. Layers, lenses, and streaks of segregation ice are typical elements of the cryogenic fabric of ice-saturated frozen soil of loamy and clay texture. The formation of cryogenic fabric can be influenced by the mineralogical composition in the soil.

Bibliography

Jackson, J. A., Mehl, J. P., Neuendorf, K. K. E., 2005. *Glossary of geology*, American Geological Institute, Contributor Neuendorf, K. K. E., Springer Science & Business, p. 779, ISBN 0922152764, 9780922152766.
Kimble, J. M., 2004. *Cryosols: Permafrost-Affected Soils*. Springer, p. 726, ISBN 3540207511, 9783540207511.

CRYOLITHOLOGY

P. Pradeep Kumar
Department of Atmospheric and Space Sciences,
Pune University, Pune, India

Definition

Cryolithology is the study of the genesis, structure, and lithology of frozen earth materials. The study of development, nature, and structure of underground ice, especially ice in permafrost regions. Cryolithology is relevant to understanding the history of perennially frozen regions.

Bibliography

http://nsidc.org/cgi-bin/words/letter.pl?C
Jackson, J. A., Mehl, J. P., Neuendorf, K. K. E., 2005. *Glossary of Geology*, American Geological Institute, Contributor Neuendorf, K. K. E., Springer Science & Business, p. 779, ISBN 0922152764, 9780922152766.

CRYOPEG

P. Pradeep Kumar
Department of Atmospheric and Space Sciences,
Pune University, Pune, India

Cryopeg is a layer of unfrozen ground that is perennially cryotic (forming part of the permafrost) in which freezing is prevented by freezing-point depression due to the dissolved-solids content of the pore water. Cryopegs remain liquid at the in situ temperature of −9°C to −11°C and make up the only habitat on the Earth that is characterized by permanent subzero temperatures, high salinity, and the absence of external influence during geological time. Cryopegs are mineralized headwater lenses below the Arctic massive ground ice bodies.

Bibliography

Gilichinsky, D., et al., 2005. Biodiversity of cryopegs in permafrost. *FEMS Microbiology Ecology*, **53**, 117–128.
http://the2050project.com.
Ozerskaya, S. M., Ivanushkina, N. E., Kochkina, G. A., Fattakhova, R. N., and Gilichinsky, D. A., 2004. Mycelial fungi in cryopegs. *International Journal of Astrobiology*, **3**(4), 327–331.

CRYOSOL

P. Pradeep Kumar
Department of Atmospheric and Space Sciences, Pune University, Pune, Maharashtra, India

Definition

Soil formed either in mineral or organic materials having permafrost either within 1 m below the surface or if the soil is strongly cryoturbated, the 2 m below surface and having a mean annual ground temperature below 0°C. Cryosol are also referred to the pumpable mixtures of brine and ice (ice slurries) used for coolants in cold storage equipments.

Bibliography

Christian, D., and Falk, M., 2003. Cold transport and cold storage with cryosol. *Euroheat & Power*, **32**(10), 34–39.
Jackson, J. A., Mehl, J. P., and Neuendorf, K. K. E., 2005. *Glossary of Geology*. Berlin: Springer Science & Business, p. 779. ISBN 0922152764, 9780922152766. (American Geological Institute, Contributor Klaus K. E. Neuendorf.)
National Snow and Ice Data Center (NSIDC), http://nsidc.org/cgi-bin/words/letter.pl?C

CRYOSTATIC PRESSURE

Pratima Pandey
Centre of Studies in Resources Engineering,
Indian Institute of Technology Bombay, Mumbai, India

Definition

Cryostatic pressure is the pressure exerted on the rock/soil by existing ice body such as glaciers, ice sheets, etc. It is represented by the product of the weight and the thickness of ice. Such pressure is responsible for cracks in rocks resulting in higher rate of erosion from the underneath rocks and soil.

CRYOSTRUCTURE

Pratima Pandey
Centre of Studies in Resources Engineering,
Indian Institute of Technology Bombay, Mumbai, India

Definition

Cryostructure is the structural characteristics of frozen earth materials. The time dependent mechanical properties of ice-rich frozen soils such as creep and long-term strength are studied in relation to their cryostructure. Through cryostructure, the permafrost geology is related to the time dependent mechanical properties of frozen soils.

CRYOTURBATION

P. Pradeep Kumar
Department of Atmospheric and Space Sciences,
Pune University, Pune, India

Cryoturbation (mixing of soil layers due to repeated freeze-thaw processes) is a major soil-forming process in Arctic regions or periglacial regions. It represents the churning up of rocks and soil. Cryoturbation may contribute to long-term storage of carbon in soils of northern latitudes. Cryoturbation, therefore, may lead to additional long-term storage of carbon in the system by (1) retarding decomposition processes of buried organic material and (2) enabling the soil to restart carbon accumulation in topsoil layers.

Bibliography

Kaiser, C., Meyer, H., Biasi, C., Rusalimova, O., Barsukov, P., Richter, A., 2007. Conservation of soil organic matter through cryoturbation in arctic soils in Siberia. *Journal of Geophysical Research*, **112**(G2), Cite ID G02017.

Van Vliet-Lanoë, B., 2006. The significance of cryoturbation phenomena in environmental reconstruction. *Journal of Quaternary Science*, **3**(1), 85–96.

D

DATING GLACIAL LANDFORMS

Jason P. Briner
Department of Geological Sciences, University at Buffalo, Buffalo, NY, USA

Definition

Dating glacial landforms. Applying geochronological tools (e.g., relative- and absolute-dating methods, etc.) to glacial landforms (e.g., moraines) to yield the timing of past glaciation (Moraine and Glacial Geomorphology and Landforms Evolution).

Introduction

Ever since scientists first recognized that glaciers and ice sheets were once larger in the past, they have desired to know the precise timing of past glaciation. Today, there is a more urgent need to tightly constrain patterns of past glaciation through time and space as projections of future global change rely upon knowledge from the past. Crude approaches have given way to complex techniques with increasing precision and decreasing uncertainty. Certainly, however, we are only a short way down a long path that carries us closer to a complete understanding and ability to date glacial landforms.

The techniques employed to date glacial landforms have been cleverly devised. For example, determining the growth rate of lichens and then measuring lichen diameters on moraine boulders to elucidate their exposure age (hence the timing of moraine deposition), using the patterns of tree-ring thickness to "cross-date" exhumed stumps that were eroded by a former glacier advance, and measuring the accumulation of isotopes in rocky surfaces that result from the bombardment of cosmic radiation to calculate the time elapsed since glaciers retreated. Our current understanding of when former glaciations occurred is better than ever, but is far from complete. Even with the dating techniques currently available, we could vastly improve our current understanding with more resources and time.

Here, I focus on dating glacial landforms, such as moraines and outwash terraces (depositional landforms), and glacially-eroded bedrock features and U-shaped troughs (erosional landforms). Thus, not included are the wide variety of techniques used to date stratigraphic sequences of glacial sediments. In some cases, the boundaries of dating glacial landforms and dating glacial sediments are blurred. For example, moraines comprise glacial sediments, and dating sediments associated with a landform can constrain landform age. However, focus on dating landforms inherently results in omitting certain landforms from this entry whose age in absolute time can only be constrained by dating glacial stratigraphy, such as subglacial depositional landforms (e.g., eskers) or depositional/erosional landforms (e.g., drumlins). Of course, dating both landforms and glacial sediments, combined with additional information, such as records of global ice volume from $\delta^{18}O$ measurements from benthic marine organisms, has led to the present understanding of the timing of Earth's glaciations.

The focus on dating glacial landforms inherently results in discussion of recent (middle and late Quaternary) landforms. In some cases, landforms survive from pre-late Pleistocene glaciations, which can be a result of slow rates of landform degradation and the survival from erosion from successive glaciations. However, in most cases where old landforms remain intact on the landscape (e.g., pre-late Pleistocene), the ability to date them is hampered by the limits of the method or by the increasing uncertainty of dating techniques back in time. Finally, this entry focuses on the dating tools that are widely used today. Although some commonly used relative- and

Vijay P. Singh, Pratap Singh & Umesh K. Haritashya (eds.), *Encyclopedia of Snow, Ice and Glaciers*, DOI 10.1007/978-90-481-2642-2,

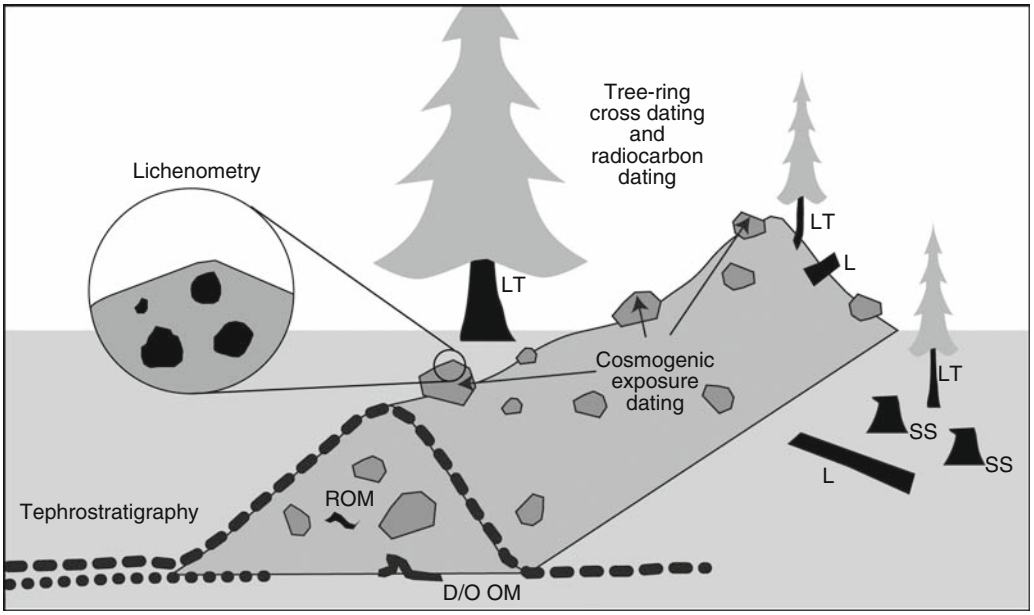

Dating Glacial Landforms, Figure 1 Common methods used to date moraines. Targets for radiocarbon and tree-ring cross dating are labeled: *LT* living tree, *L* log, *SS* sheared stump, *ROM* reworked organic material, *D/O OM* deformed/overridden organic material. *Dashed* and *dotted lines* represent tephra layers.

calibrated-dating techniques are discussed, more emphasis is placed on the absolute-dating techniques that are most commonly applied to glacial landforms (Figure 1).

Relative-dating techniques

The initial and most fundamental approach to dating glacial landforms is ordering landscape features in a relative sense. In terms of moraines, those closer to the ice source are younger because in almost all cases subsequent glaciations obliterate prior surface features beneath their footprint. When dealing with moraines deposited by alpine glaciers (i.e., moraines in mountain valleys), assigning relative ages to moraines is fairly straightforward. Much like assigning relative ages to rock layers (stratigraphy), there is a relative age assignment to surface features (morphostratigraphy). In some cases, moraines can be cross-cutting, where younger moraines are deposited on top of, and truncate, older moraines. A classic example is Bloody Canyon, eastern Sierra Nevada, USA (see Phillips et al., 1990), but there are a surprising number of other examples.

In rare cases, for example where polar ice sheets are cold-based, the obliterative nature of glacier flow is replaced by non-erosive characteristics. In these settings, it is possible to preserve glacial landforms that were formed during previous glacial cycles, and the relative ordering of landforms is more complicated. On the other hand, this rarely happens in alpine landscapes. In other cases, subglacial bedforms (e.g., drumlins, megaflutes, etc.) in areas that were occupied by Pleistocene ice sheets reveal shifting flow directions. The preservation of these stacked sequences of bedform orientations reveals that, at least in some locations, bedforms can be preserved from not just the most recent flow direction.

Slightly more sophisticated approaches to the relative dating of glacial landforms rely on the physical and chemical weathering that takes place on and within glacial deposits. The application of soil chronosequences to moraine and outwash surfaces has been used to assess the relative age of these features, and in some cases to correlate glacial landforms from valley to valley in a given mountain range. In particular, soil thickness, B-horizon thickness, B-horizon development, and weathering-rind thickness measured in clasts in soil profiles have been used as indicators of relative age (Porter, 1975; Burke and Birkeland, 1979; Colman and Pierce, 1986; Birkeland et al., 1991). The weathering of surface rocks has also been employed as a relative-age indicator, specifically, characteristics such as the abundance and depth of pitting, grussification, and hardness have been used to make relative subdivisions of moraines (e.g., Birkeland et al., 1979). The degree of degradation of depositional landforms (landform morphology) has also been used as a relative-dating parameter. Because moraines are originally deposited with relatively steep slopes that degrade with time, the steepness of moraine slopes, or degree of surface roughness within hummocky moraine belts that we see on the landscape today is partly of function of moraine age. Slope angle, crest width, and the degree of gullying are parameters that have been measured and linked with relative age (e.g., Kaufman and Calkin, 1988).

Despite the factors that complicate the accuracy of relative-dating techniques, they nonetheless remain useful. Relative-dating techniques are useful for correlating moraines from valley to valley, provide the only chronology in many cases where materials for absolute dating are absent, and act as an aid even when absolute dating is available. Furthermore, it is generally less time-consuming and less expensive to employ relative-dating techniques versus absolute-dating methods, and thus characteristics of many more moraines can be included in a dataset. Finally, because of the high cost of many absolute-dating techniques, using relative-dating methods to correlate a low number of landforms with absolute-age control to many more landforms of the same properties across a region is a powerful approach.

Lichenometry

Lichenometry is a surface-exposure dating method that uses lichen-growth rates to infer the age of young (few thousand years old or younger) glacial landforms, typically bouldery deposits such as moraines. The technique combines measurements of the size of lichens growing on rocky glacial deposits with independently derived lichen growth rates to derive lichen age, and thus moraine age. Lichen types that grow radially and regularly are used, most commonly the crustose lichen genus *Rhizocarpon*, where *R. geographicum* is specifically targeted in most cases, but field identification to the species level is difficult (Figure 2). The method has been widely applied since its development in the mid-twentieth century (Beschel, 1950).

Several approaches have been employed to measure lichens, and a distinct advantage of lichenometry over other techniques is its simplicity (Bradwell, 2009). One approach is to measure the diameter of dozens to hundreds of semi-circular lichens on boulders scattered about on a moraine surface. The largest diameter measured, or the average of the five largest diameters measured, can be used with the growth curve to obtain a surface age. Additional approaches include determining the size frequency of all lichens in a representative area, or measuring the total lichen cover on a substrate. Ongoing research includes more advanced statistical approaches to extract the most meaningful age from field measurements (cf. Bradwell, 2009) and placing more emphasis on the controls on the pattern of lichen growth (Loso and Doak, 2006).

Used in the right circumstances, lichenometry can be a successful numerical-dating method. This success relies on several factors. First, because lichen-growth rates are a function of a variety of conditions (e.g., regional climate, substrate, microenvironment, species competition), the growth rate needs to be well constrained in the area of application (Figure 2). Independently dated surfaces upon which lichens grow that are commonly used for calibration include tombstones, mining waste, and archaeological sites. Furthermore, because growth rate is not linear, but rather has an initial period of fast growth, followed by a slower, linear growth rate, multiple calibration points are required to quantify the growth rate through time (Figure 2). With a well-constrained growth rate that spans the same time period of study and that was measured on similar substrates, the lichenometry method can be reasonably accurate. Because of increasing uncertainty back in time, changing climatic conditions through time, and the intersection of individual lichens as surfaces become heavily colonized, the lichenometry method becomes less reliable beyond a few thousand years. The highest accuracy with lichenometry is its application to glacial landforms deposited within the last millennium.

There are many uncertainties with lichenometry. Many involve how applicable the growth curve is to any single area of study. As with any surface-exposure dating technique, lichenometry best dates the timing of landform stabilization, as in the case of moraines (Putkonen et al., 2008). Furthermore, there is an unknown amount of time it takes for lichens to colonize a surface, but this is thought

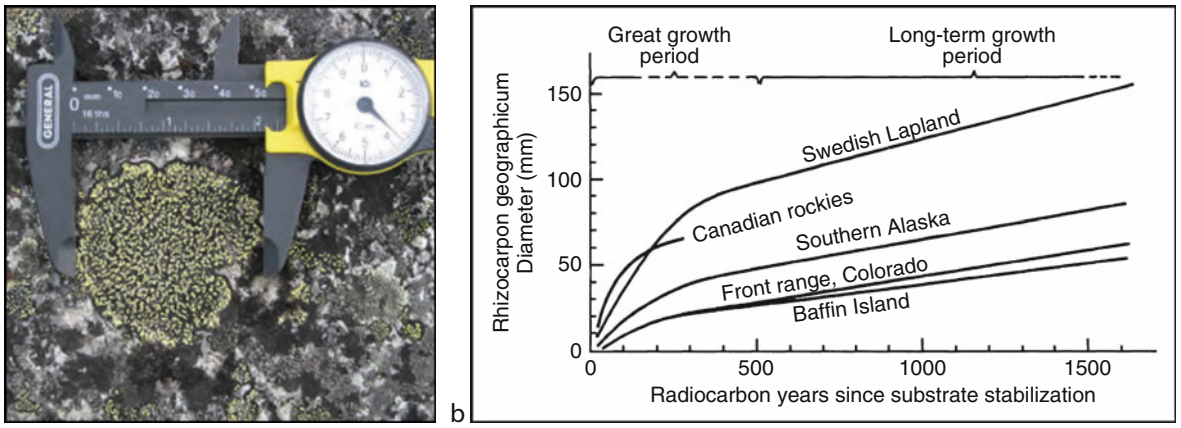

Dating Glacial Landforms, Figure 2 (**a**) Photograph of *R. geographicum* thallus measured on a moraine boulder (from Young et al., 2009). (**b**) Selected *R. geographicum* growth curves (from Calkin and Ellis, 1980).

to be years to decades, not centuries. Finally, it should be mentioned that even where well-constrained lichen growth curves are absent, lichenometry can still serve as a valuable relative-dating technique. For example, determining the largest lichen diameters on individual moraines among a sequence can be useful where correlating moraines between valleys across a mountain range. Additionally, the full range of lichen diameters present on a large group of moraines might indicate whether all the moraines are of similar age, or whether moraine ages span millennia (Solomina and Calkin, 2003; Barclay et al., 2009a).

Association with volcanic deposits

In regions where glaciers exist in proximity to volcanoes, glacial landforms can be dated by their association with volcanic flows that are radiometrically dated. In addition, where glaciation takes place near volcanic arcs or other areas with explosive volcanism, the age of glacial landforms can be constrained by tephrostratigraphy. These techniques are useful throughout the Quaternary, spanning the time period represented by the record of glacial landforms.

One example of dating glacial landforms by their association with dated volcanic flows took place near the summit of Mauna Kea, Hawaii (Figure 3). Mauna Kea periodically supported an ice cap during the Pleistocene, from which outlet glaciers flowed radially part way down the volcano flanks. Potassium–argon dating of lava flows that overlie and underlie drift units associated with two of the most recent moraines deposited on Mauna Kea provided bracketing ages on moraine age (Porter, 2005). A second example regards dating moraines in Patagonia

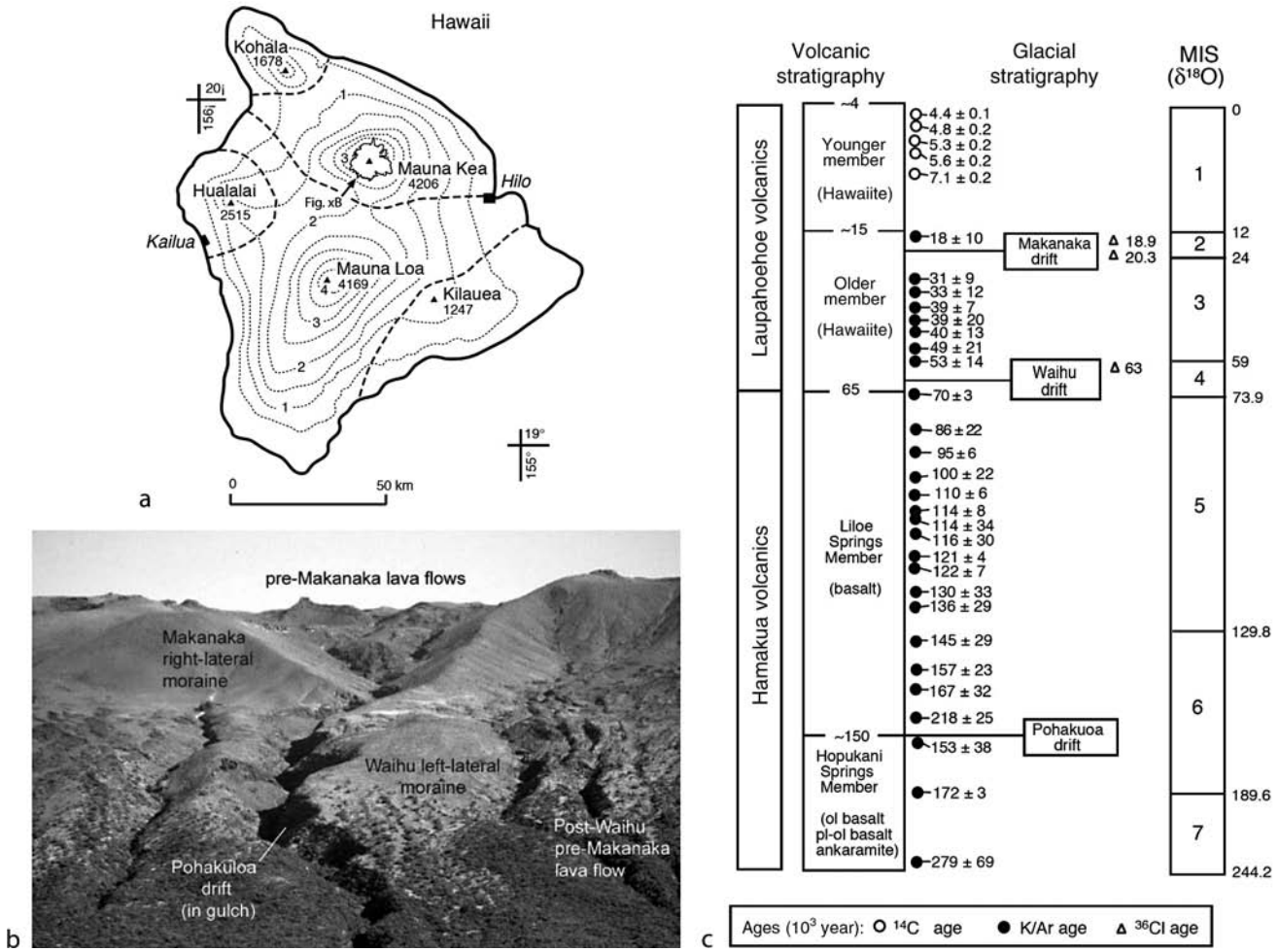

Dating Glacial Landforms, Figure 3 Example of dating volcanic deposits to constrain moraine age from Hawaii modified from Porter (2005). (**a**) Hawaii showing location of Mauna Kea. (**b**) Oblique photograph showing late Pleistocene moraines deposited on flank of Mauna Kea. (**c**) Summary diagram showing K/Ar ages on lava flows interbedded with glacial drift units; in particular the K/Ar ages constrain the deposition of the Waihu and Makanaka moraines. Note how K/Ar ages compare to ^{36}Cl exposure ages from boulders on the moraine surface.

bounded by basalt lava flows. Argon–argon and potassium–argon dating was used to constrain the age of several moraines deposited during the middle and late Pleistocene (Singer et al., 2004). In some locations (e.g., Iceland), volcano-glacier landforms occur, such as table mountains (or tuyas), which are volcanoes that erupt subglacially and eventually emerge through the ice, ending in a subaerial eruption phase. These features can be dated radiometrically using volcanic materials (Kaufman et al., 2001), or by cosmogenic-exposure dating (see below) on the subaerial surface lava flows (Licciardi et al., 2007).

Volcanic ash, or tephra deposits, that lie beneath or overlie moraines can be used to constrain moraine age. Tephrostratigraphy is the field of matching unknown tephras at a study site with a database based on prior work of tephras of known ages and chemistries. By analyzing tephra chemistry at a study site and comparing it to a database, tephras and their ages can be identified. Because tephras are airfall deposits, they form stratigraphic layers on the Earth's surface. Thus, they can underlie or overlie glacial landforms like moraines, and provide maximum and minimum ages, respectively (Figure 1). In some cases, tephra can be reworked into glacial depositional landforms, which can also provide a maximum age of moraine deposition. In this way, moraines can be dated by their association with tephras. Some examples are dating moraines in Alaska (e.g., Begét, 1994), and in the Cascade Range, western U.S. (e.g., Porter, 1976; Heine, 1998).

Radiocarbon dating

Radiocarbon dating is probably the single most important dating method in Quaternary science. With a usable age range between ~300 and ~40,000 years in most applications, and sample types that include most organic-material, radiocarbon dating is widely used to date sediments and landforms. Typical analytical uncertainties are ~2–5%, although uncertainty typically becomes larger when ages are calibrated into calendar years. In terms of dating glacial landforms, radiocarbon dating has been most useful for dating moraines, although ultimately the dating of the moraine itself arises by dating the sediments that comprise the moraine, or sediments associated with moraines (Figure 1). Studies have applied radiocarbon dating to sediments below, within, and above moraines to provide maximum (below and within) and minimum (above) age constraints.

Dating moraines with radiocarbon works best in environments where glaciers flow across forested landscapes. Radiocarbon dating of wood is used to constrain moraine age in several ways. When a glacier advances into a forest, its proglacial sediments sometimes partly bury tree trunks. By the time the glacier snout reaches these partly buried trees, it shears them off part way up the tree trunk. Following moraine deposition and glacier retreat, the in-situ sheared tree trunks become exhumed and available for sampling. Radiocarbon dating of their outer rings provides a maximum age on moraine formation. In other cases, sheared trees become incorporated in moraine sediments, become deposited on the landscape as erratic logs, or are deposited in till blanketing the landscape, and eventually exposed or washed out. In these cases, radiocarbon dating outer rings of glacially transported logs also provides maximum ages on moraine formation. There are many good examples of using radiocarbon dating to date Holocene moraine formation from southern Alaska (e.g., Barclay et al., 2009a), western Canada (Menounos et al., 2009), and in the Alps (Joerin et al., 2006). In rare cases, glacier snouts tilt trees as they deposit moraines; in this case, radiocarbon dating the damaged tree can provide a close-limiting age on moraine formation. Where logs are involved, radiocarbon dating is commonly used in conjunction with tree-ring cross dating, which is a more precise method to constrain moraine age (see below) (Figure 4).

There are many cases, of course, where entire logs are not preserved, but rather pieces of wood or cones and other organic material are reworked and incorporated into moraine sediments. In places where glaciers advance through marine embayments and fjords, they can rework fossiliferous marine sediments into their moraines. In Greenland, for example, radiocarbon dating of reworked fossil material, including marine bivalves, whale bones, and even a walrus tusk provided maximum constraints on the age of late Holocene moraine formation (Weidick et al., 2004). In some cases, glaciers overrun lakes or bogs and deform peat; in these cases radiocarbon dating of the uppermost layers of disturbed peat provide close maximum age constraints on moraine formation (Mercer and Palacios, 1977; Buffen et al., 2009).

In most cases, finding organic materials below or within moraines is rare. More widely used are organic deposits that accumulate behind or on top of moraines. Obtaining so-called basal radiocarbon ages from lakes and bogs is a powerful approach to providing minimum constraints on moraine age in both alpine and continental ice sheet settings (e.g., Thackray et al., 2004; Lowell et al., 2005).

Radiocarbon dating of glacial landforms includes features in addition to moraines. Organic deposits on top of, beneath, and incorporated into outwash deposits allow radiocarbon dating to constrain the age of outwash terraces (e.g., Porter et al., 1983; Hamilton, 1986). Radiocarbon dating has also been used extensively to date raised glaciomarine landforms, such as ice-contact deltas, that are deposited during ice retreat in isostatically recovering (emerging) landscapes (Dyke, 1999). In these cases, radiocarbon ages of in-situ bivalves from the delta sediments provide a direct age on ice-contact delta formation.

Tree-ring cross dating

Tree-ring cross dating is a precise means to date logs, and where logs are associated with moraines (see above), tree-ring cross dating can provide more precise age control than radiocarbon dating alone (Wiles et al., 1996).

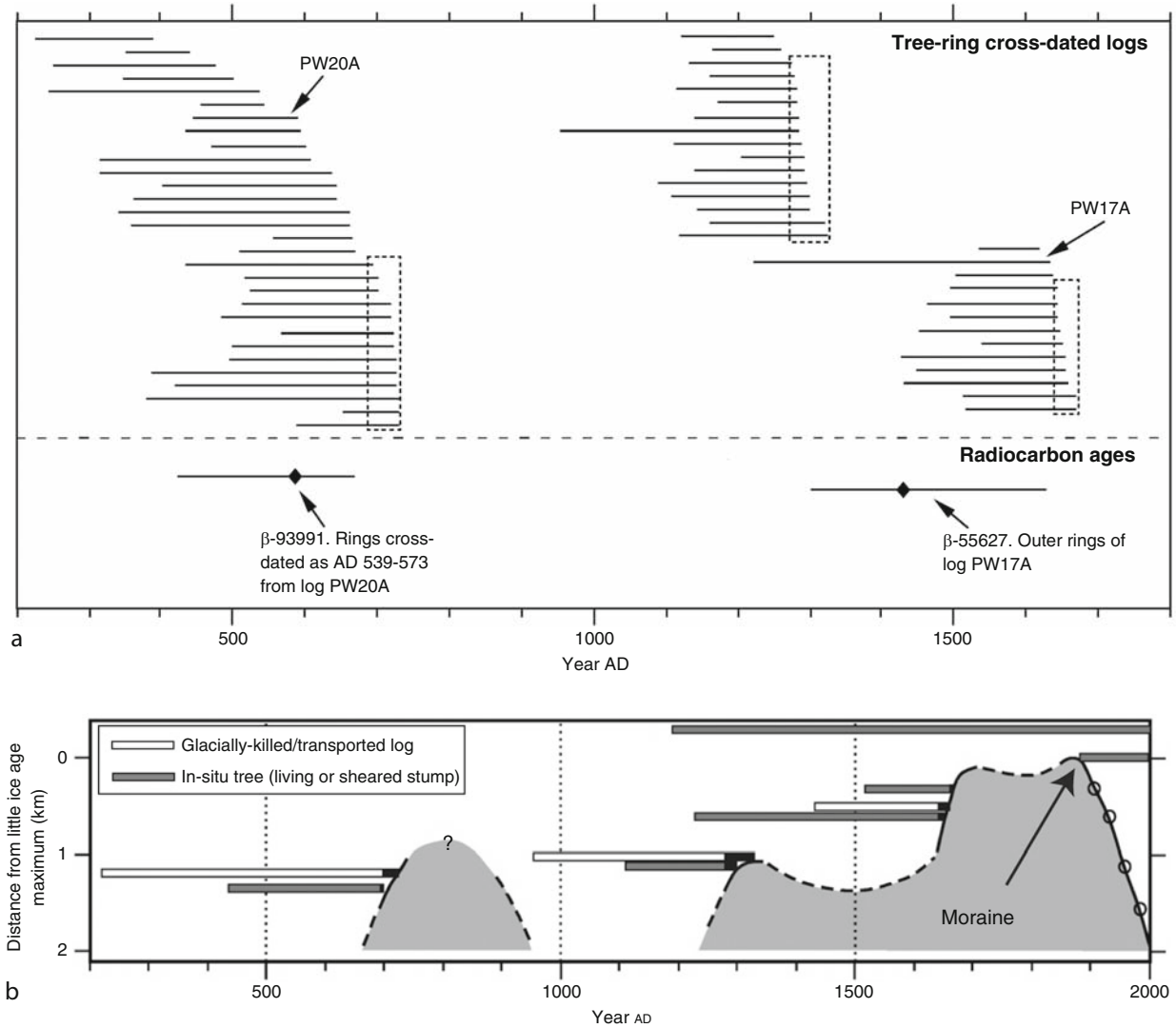

Dating Glacial Landforms, Figure 4 Example of using radiocarbon and tree-ring cross dating. (**a**) *Horizontal black lines* in upper portion of figure represent the lifespan of each cross-dated log found in front of a retreating glacier in south Alaska; *dashed line boxes* represent timing of glacier advance when the majority of the trees were killed, indicating glacier advance. The lower portion shows the 2-σ age range (*black bar*) and median (*diamond*) of radiocarbon ages of the outer rings of select logs. Modified from Barclay et al. (2009a). (**b**). Time-distance diagram of the Tebenkof Glacier, south Alaska, constrained by tree-ring cross dating of glacially transported trees and in-situ sheared stumps that were killed upon glacier advance and living trees growing on and outboard of the Little Ice Age moraine. Modified from Barclay et al. (2009b).

The principles rely on wiggle-matching patterns of tree-ring widths between a "master" tree-ring width series and tree rings in a specimen of which the age is unknown. In this manner, logs can be placed in absolute time, and their age of death in some cases can be constrained to a single year. Thus, over time periods spanned by a master ring-width series, using tree-ring cross dating to determine the age of trees can be much more precise than radiocarbon dating.

Because of regional variations in climate and other factors that influence tree growth, tree-ring master series are constructed and applied within specific regions. Because living tree-ring width time series only go back a few centuries in time, subfossil trees are used to extend the time series farther back in time. Once master chronologies exist, placing glacially transported logs and sheared stumps into an absolute age provides tight age control on moraine formation. For example, when glacially-transported logs in glacier forefields are dated by cross dating, they reveal when a stand of trees were glacially overrun, and hence provide a maximum age for moraine formation (Barclay et al., 2009b). Similarly, in-situ stumps that have been sheared from advancing glaciers also provide maximum ages of moraine formation, and also

pinpoint the exact location of glacial overriding (Barclay et al., 2009b; Menounos et al., 2009) (Figure 4). Tree-ring counting from living trees that grow on moraines can provide a close minimum age of moraine formation, but the method can be complicated somewhat by the ecesis time (the time it takes for a tree to germinate on fresh glacial deposits). In some cases, glaciers that advance into forests can damage or tilt trees in the processes of moraine deposition. In these cases, cross-dated damaged trees can provide a precise time of moraine formation (Wiles et al., 1996; Barclay et al., 2003).

Cosmogenic-exposure dating

Cosmogenic-exposure dating (also referred to as surface-exposure dating and terrestrial cosmogenic-nuclide dating) has emerged over the last two decades as the premier chronological tool to date glacial landforms such as moraines, erratic boulders, and glacially eroded bedrock. As with the other dating methods above, the details of the method are not discussed herein, but rather focus is placed on its application to dating glacial landforms. See Gosse and Phillips (2001) for a thorough treatment of background and fundamental principles.

Briefly, a family of isotopes is produced in Earth's rocky surface (mostly in the upper few meters) as a result of cosmic-ray bombardment. Many of the resulting "cosmogenic" isotopes are radioactive (e.g., ^{14}C, ^{10}Be, ^{26}Al, ^{36}Cl), whereas others are stable (e.g., ^{3}He, ^{21}Ne). Some of the isotopes are produced solely from cosmic ray bombardment (e.g., ^{10}Be), whereas others can be formed by additional means (e.g., ^{36}Cl). The different isotopes have differing target, or parent, minerals. For example, applications of ^{10}Be mainly use quartz-bearing rocks, whereas applications of ^{3}He commonly rely on olivine phenocrysts in igneous rocks. And, some methods use a "whole-rock" approach because there are several parent elements that produce the cosmogenic isotope (e.g., ^{36}Cl). Furthermore, the radioactive cosmogenic isotopes (radionuclides) are used for different applications depending on their varying half lives.

Because organic matter and glacial deposits are rarely associated, radiocarbon dating cannot be applied in many areas. On the other hand, cosmogenic-exposure dating can be used in more widespread locations because the target materials are rocky deposits typical of glacial landscapes. Moraines, more specifically boulders on moraine surfaces (Figure 1), have been the primary target of cosmogenic-exposure dating, although there have been many other applications. Ultimately, because the target samples (e.g., boulders and bedrock) for cosmogenic-exposure dating are different, and perhaps more common, from organic material required for radiocarbon dating, and are more common than materials targeted for other dating techniques mentioned above, cosmogenic-exposure dating has revolutionized the ability to date glacial landforms. Furthermore, although radiocarbon dating is usable only to about 40,000 years ago, the analytical limit of cosmogenic-exposure dating extends back hundreds of thousands to millions of years.

Early studies that applied cosmogenic-exposure dating to moraines and glacial boulders took place primarily in the western U.S. and Antarctica (e.g., Phillips et al., 1990; Brook et al., 1993). Since then, there have been dozens of studies that have generated moraine chronologies from around the globe. These studies range from moraines deposited by mountain glaciers in tropical latitudes (e.g., Smith et al., 2005a), middle latitudes (e.g., Phillips et al., 1997), and high latitudes (e.g., Briner et al., 2005a). Moraines deposited by ice sheets have also been targeted (e.g., Balco et al., 2002). Until recently, most research has focused on late Pleistocene deposits (~120,000–11,700 years ago), and most specifically, on deposits created during the peak of the last glaciation (~25,000 to ~11,700 years ago). This time period has the advantage of being geologically young enough such that moraines are not too intensely weathered and degraded, yet old enough that concentrations of cosmogenic nuclides are high enough to be analytically measurable. In some locations with apparently slow rates of erosion and moraine degradation, exposure dating works reasonably well farther back in time (Smith et al., 2005b; Licciardi and Pierce, 2008; Porter and Swanson, 2008), but in general, moraine chronologies become increasingly scattered beyond 50,000–100,000 years ago. Recently, as analytical techniques and chemical procedures in preparation laboratories have improved, dating moraines deposited during the Holocene (last 11,700 years), and even during the last millennium, has become more common (Schaefer et al., 2009; Licciardi et al., 2009).

Producing reliable moraine chronologies with low uncertainty relies on several important criteria (Figure 5). To ensure that boulders receive constant exposure to cosmic-ray bombardment since their deposition, the upper, skyward-facing surfaces of large boulders (usually >1 m high, but even larger boulders typically are more stable on moraines) are sampled. Because there are a number of geologic and analytical uncertainties that can affect any given boulder age, researchers typically average cosmogenic-exposure ages from five to ten boulders per moraine crest. Although analytical uncertainties can be significant (particularly for young surfaces), geologic uncertainties, and uncertainties in isotope production rates and spatial scaling rules are typically more significant. Because this entry emphasizes the application, the discussion herein is limited to the most important geologic uncertainties.

Because moraines are depositional features, gravity efficiently decreases moraine slope angles and thus moraines degrade through time (Bursik, 1991). The tilting and rolling of surface boulders, and the exhumation of subsurface boulders to the surface, yield cosmogenic exposure ages that are younger than the true timing of moraine deposition (Figure 6). Thus, moraine degradation severely hampers tightly-clustered moraine chronologies, and skews average ages toward a younger age. In addition

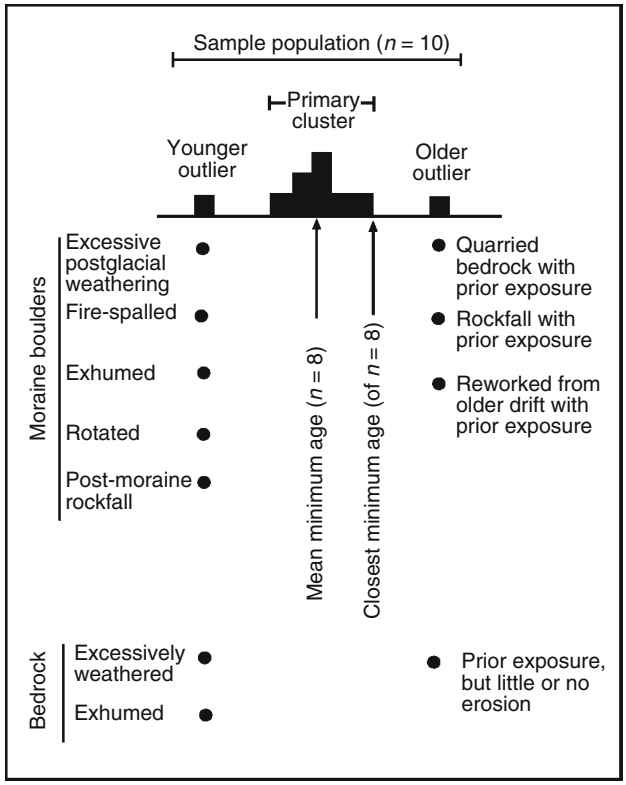

Dating Glacial Landforms, Figure 5 Complicating factors that potentially influence the distribution of cosmogenic exposure ages of moraine boulders (*top*) and glacially-eroded bedrock (*bottom*). In addition, the diagram provides guidelines for interpreting a population of cosmogenic exposure ages of moraine boulders, such as identifying outliers and interpreting an age cluster as the mean minimum age versus closest minimum age. From Porter and Swanson (2008).

to moraine degradation, rock-surface erosion acts upon boulder surfaces and is a process that decreases the cosmogenic-isotope inventory, and thus decreases cosmogenic-exposure age. Despite rock-surface erosion being most important for poorly indurated lithologies and/or for pre-latest Pleistocene moraines, it is commonly difficult to determine how much rock-surface erosion has taken place, and thus remains a potential complication (Figure 6). Sampling boulder surfaces that retain glacial striations or polish avoids this issue, but these features are rarely preserved. Multiple cosmogenic isotopes with different depth-production profiles have also been used to solve for surface erosion (Phillips et al., 1997). Finally, partial burial of moraine boulders by loess or seasonal snowfall also yields cosmogenic exposure ages that are younger than the timing of moraine deposition. Correcting for snow and loess cover is challenging because it is difficult to reconstruct the magnitude of shielding for the duration of a sample's surface history. Most researchers collect samples from tall boulders on high parts of the landscape to increase the likelihood that boulder surfaces are windswept. In some cases, collecting samples during the snow season to evaluate modern snow cover is helpful. In any case, these three complications (moraine degradation, boulder-surface erosion, snow/loess shielding) lead to ages younger than the true timing of moraine formation, which further complicates determining their relative importance. In all cases, careful field sampling can significantly reduce these complications.

Another type of geologic uncertainty arises from isotopic inheritance (Figure 6). Isotopic inheritance refers to cases where moraine boulders are deposited on a moraine surface already containing some inventory of cosmogenic isotopes. These isotopes are "inherited" from a period of prior exposure, a situation that results from inefficient glacial erosion, rockfall onto a glacial surface, or reworking of older materials. In cases where eroded and transported blocks are deposited with their previously exposed surface facing skyward, a chance exists that inherited isotopes combine with isotopes that accumulate during the targeted period of exposure. Thus, these boulders yield cosmogenic exposure ages that pre-date the actual time of moraine deposition. In many cases, inheritance is a much less likely complication than moraine degradation. However, certain contexts exist in which the likelihood of inheritance occurring significantly increases. Primarily, inheritance occurs where glaciers are cold-based or polythermal, and thus do not deeply erode landscapes. There are several examples at high latitude study areas of the prevalence of inheritance and the complication that it imposes in producing moraine chronologies (e.g., Briner et al., 2005b). Indeed, in many settings the presence/absence of isotope inheritance has been used to elucidate patterns of glacial erosion (Sugden et al., 2005; Briner et al., 2006). Another likely context in which inheritance can be common is in short glaciers (e.g., cirque glaciers) where the proportion of head- and valley-wall-sourced boulders is relatively high compared to subglacially sourced boulders. Finally, in some cases, very near the terminus of glaciers and ice sheets, erosion becomes less efficient, and reworked boulders have a better chance of appearing in younger deposits (e.g., Balco et al., 2002).

Assessing the various geologic means by which scatter in a population of cosmogenic-exposure ages arises is critical to ultimately assigning moraine age (Figure 5). To date, there have been several investigations regarding the relative importance of these major complicating factors (Hallet and Putkonen, 1994; Putkonen and Swanson, 2003). In most cases, these studies document the stronger and more typical influence of moraine degradation on a suite of cosmogenic-exposure ages. For this reason, many researchers interpret cosmogenic-exposure ages as providing the timing of moraine abandonment and hence the onset of deglaciation following a glacier advance. That is, boulders that are sampled at the moraine surface were the last deposited on the moraine crest just prior to retreat of the ice margin. In addition, due to the prevalence of moraine degradation, many researchers interpret cosmogenic exposure ages as minimum ages for the onset

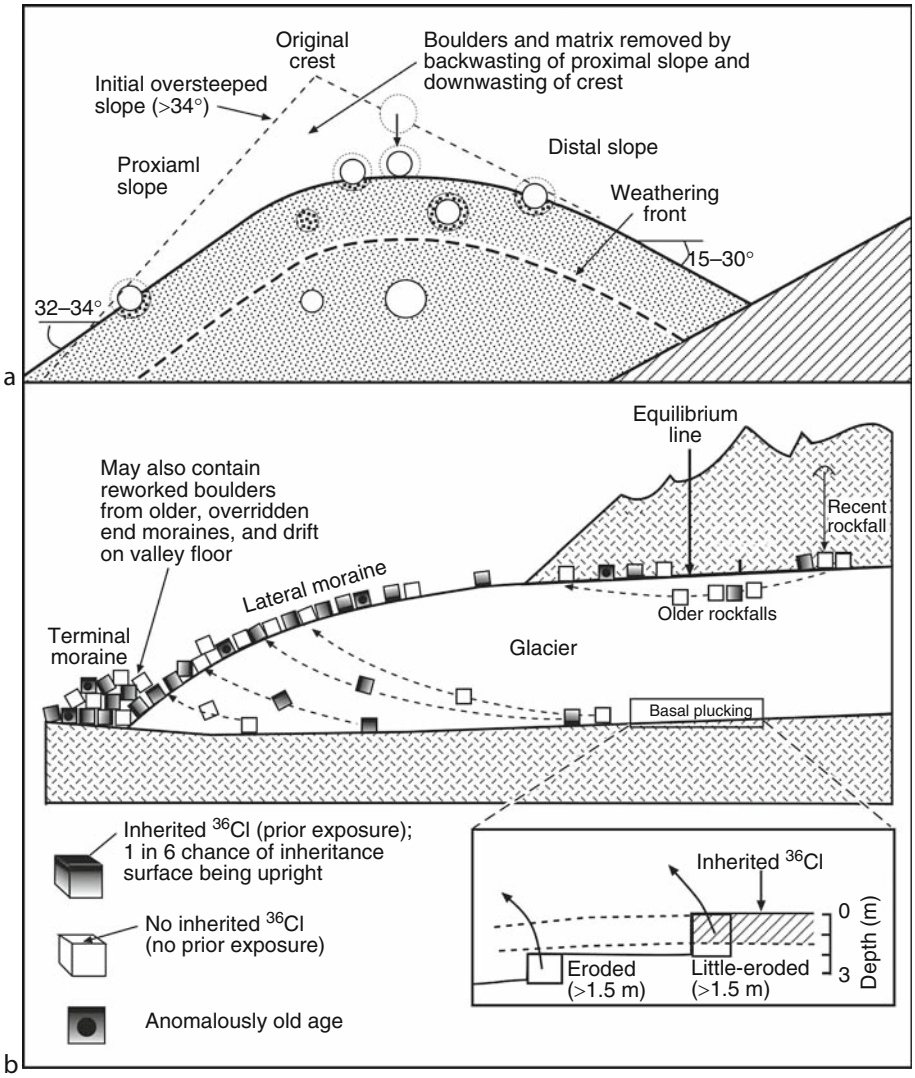

Dating Glacial Landforms, Figure 6 (**a**) Diagram illustrating complication of applying cosmogenic exposure dating to degrading moraines, in particular, the issue of boulders exhumed to the moraine surface as the crest lowers through time. The additional complication of boulder erosion is also illustrated; "zoned" boulders indicate weathering rinds and grussification. (**b**) Sketch showing different processes that lead to inherited cosmogenic isotopes (e.g., ^{36}Cl) in moraine boulders. Modified from Porter and Swanson (2008).

of deglaciation. In some rare cases where moraine crests are stacked together, the outermost moraine crest may not date the onset of deglaciation (Gosse et al., 1995). A misconception that still arises in the literature is that cosmogenic-exposure ages yield the timing of glacier advances, or the timing of glacier maxima. This can result in incorrectly assigning leads/lags between one study area compared with glacier and climate-change records from elsewhere. Thus, it is critical to have a firm understanding of complications in producing cosmogenic-exposure dating chronologies, and to acknowledge what part of the glacial cycle the ages constrain.

In addition to moraines, cosmogenic-exposure dating has been applied to other glacial landforms with great success. Common glacial landforms targeted with cosmogenic-exposure dating are outwash and marine terraces (e.g., Anderson et al., 1996). Because fine-grained sediments (as opposed to large boulders on moraine surfaces) can become mixed after their deposition by soil and bioturbation processes, merely dating a collection of surface pebbles potentially would yield an age younger than the true timing of sediment deposition. An additional complication is that a small proportion of inherited isotopes can be present in sediments. Both of these complications can be elucidated by collecting samples of sediment along a depth profile, measuring cosmogenic isotope concentrations in each, and matching the resulting profile of concentration versus depth to the expected theoretical

profile. In this manner, inheritance can be detected (if, with depth, concentrations decrease to a value above zero, which represents the inherited component). Furthermore, the depth profile can be extrapolated to the surface to estimate the surface exposure age. Although useful, this approach does require multiple measurements for a single surface age.

Dating glacial erosional landforms

Glacial-erosional landforms, such as the variety of bedrock landforms common in glaciated landscapes (e.g., roche moutonnées, whalebacks, etc.), are commonly polygenetic features (depending on their size). In many cases, these bedrock features have been reshaped during the most recent period of glaciation. Cosmogenic-exposure dating has been employed with success to assign ages to glacially eroded bedrock surfaces. Dating the landform, in most cases, is accomplished to place timing on the most recent period of ice recession. Many studies have successfully placed constraints on ice sheet thinning (e.g., Stone et al., 2003) and recession (e.g., Briner et al., 2009) using transects of samples from glacially eroded bedrock landforms.

In some ways, cosmogenic-exposure dating can also constrain the actual age of erosional landforms. For example, where cosmogenic-isotope inheritance exists, the magnitude of glacial reshaping of the landform during the last glacial cycle can be determined to be minimal. In fjord landscapes, the spatial distribution of isotope inheritance can constrain how much these large-scale glacial landforms evolved during the most recent glaciation (e.g., Sugden et al., 2005; Briner et al., 2006). In some cases, researchers have used two isotopes with different half lives (e.g., ^{10}Be and ^{26}Al) to assess glacial erosion not only for the most recent period of glaciation, but the general magnitude of erosion and landscape modification during prior glaciations (e.g., Bierman et al., 1999). An additional tool applied to determine the timing of formation of large-scale glacial erosional features, such as fjords, is thermochronology. In particular, low temperature thermochronology techniques (e.g., (U-Th)/He and ^{4}He/^{3}He; Reiners and Brandon, 2006) have recently placed constraints on the evolution of glacial landscapes and the timing of major fjord incision (Shuster et al., 2005).

Summary

Reliably, dating glacial landforms are fundamental to the field of paleoclimatology. All dating methods have uncertainties and room for improvement. Just as multiple proxies are needed to reconstruct past climate change, or multiple climate models should be used to predict future climate change, more than one geochronological tool should be employed wherever possible to date glacial landforms. Newer and more powerful techniques (e.g., cosmogenic-exposure dating) need to be used in concert with relative-dating techniques, beginning with a foundation of geomorphic mapping and morphostratigraphic relationships. The geochronologic toolbox employed to date glacial landforms is expanding, and it is exciting to think about what additional techniques will be available in the future. At the same time, however, the tools already in hand are sufficient to read landscapes upon which there are widespread traces of former glacier change.

Bibliography

Anderson, R. S., Repka, J. L., and Dick, G. S., 1996. Explicit treatment of inheritance in dating depositional surfaces using in situ ^{10}Be and ^{26}Al. *Geology*, **24**, 47–51.

Balco, G., Stone, J. O. H., Porter, S. C., and Caffee, M. W., 2002. Cosmogenic-nuclide ages for New England coastal moraines, Martha's Vineyard and Cape Cod, Massachusetts, USA. *Quaternary Science Reviews*, **21**, 2127–2135.

Barclay, D. J., Wiles, G. C., and Calkin, P. E., 2003. An 850 year record of climate and fluctuations of the iceberg calving Nellie Juan Glacier, south central Alaska, USA. *Annals of Glaciology*, **36**, 51–56.

Barclay, D. J., Wiles, G., and Calkin, P. E., 2009a. Holocene glacier fluctuations in Alaska. *Quaternary Science Reviews*, **28**, 2034–2048.

Barclay, D. J., Wiles, G. C., and Calkin, P. E., 2009b. Tree-ring crossdates for a First Millennium AD advance of Tebenkof Glacier, southern Alaska. *Quaternary Research*, **71**, 22–26.

Begét, J. E., 1994. Tephrochronology, lichenometry and radiocarbon dating at Gulkana Glacier, central Alaska Range, USA. *Holocene*, **4**, 307–313.

Beschel, R. E., 1950. Flechten als Altersmassstab rezenter Moränen. *Zeitschrift für Gletscherkunde und Glazialgeologie*, **1**, 152–161.

Bierman, P. R., Marsella, K. A., Patterson, C., Davis, P. T., and Caffee, M., 1999. Mid-Pleistocene cosmogenic minimum-age limits for pre-Wisconsin glacial surfaces in southwestern Minnesota and southern Baffin Island: a multiple nuclide approach. *Geomorphology*, **27**, 25–39.

Birkeland, P. W., Colman, S. M., Burke, R. M., Shroba, R. R., and Meierding, T. C., 1979. Nomenclature of alpine glacial deposits, or, what's in a name? *Geology*, **7**, 532–536.

Birkeland, P. W., Berry, M. E., and Swanson, D. K., 1991. Use of soil catena field data for estimating relative ages of moraines. *Geology*, **19**, 281–283.

Bradwell, T., 2009. Lichenometric dating: a commentary, in the light of some recent statistical studies. *Geografiska Annalar*, **91**A, 61–69.

Briner, J. P., Kaufman, D. S., Manley, W. F., Finkel, R. C., and Caffee, M. W., 2005a. Cosmogenic exposure dating of late Pleistocene moraine stabilization in Alaska. *Geological Society of America Bulletin*, **117**, 1108–1120.

Briner, J. P., Miller, G. H., Davis, P. T., and Finkel, R. C., 2005b. Cosmogenic exposure dating in arctic glacial landscapes: implications for the glacial history of northeastern Baffin Island, Arctic Canada. *Canadian Journal of Earth Sciences*, **42**, 67–84.

Briner, J. P., Miller, G. H., Davis, P. T., and Finkel, R. C., 2006. Cosmogenic radionuclides from fiord landscapes support differential erosion by overriding ice sheets. *Geological Society of America Bulletin*, **118**, 406–420.

Briner, J. P., Bini, A. C., and Anderson, R. S., 2009. Rapid early Holocene retreat of a Laurentide outlet glacier through an Arctic fjord. *Nature Geoscience*, **2**, 496–499.

Brook, E. J., Kurz, M. D., Achert, R. P. J., Denton, G. H., Brown, E. T., Raisbeck, G. M., and Yiou, F., 1993. Chronology of Taylor Glacier advances in Arena Valley, Antarctica, using in situ cosmogenic ^{3}He and ^{10}Be. *Quaternary Research*, **39**, 11–23.

Buffen, A. M., Thompson, L. G., Mosely-Thompson, E., and Huh, K. I., 2009. Recently exposed vegetation reveals Holocene changes in the extent of the Quelccaya Ice Cap, Peru. *Quaternary Research*, **72**, 157–163.

Burke, R. M., and Birkeland, P. W., 1979. Reevaluation of multiparameter relative dating techniques and their application to the glacial sequence along the eastern escarpment of the Sierra Nevada, California. *Quaternary Research*, **11**, 21–51.

Bursik, M. I., 1991. Relative dating of moraines based on landform degradation, Lee Vining Canyon, California. *Quaternary Research*, **35**, 451–455.

Calkin, P. E., and Ellis, J. M., 1980. A Lichenometric Dating Curve and Its Application to Holocene Glacier Studies in the Central Brooks Range, Alaska. *Arctic and Alpine Research*, **12**, 245–264.

Colman, S. M., and Pierce, K. L., 1986. Glacial sequences near McCall, Idaho – weathering rinds, soil development, morphology, and other relative-age criteria. *Quaternary Research*, **25**, 25–42.

Dyke, A. S., 1999. Last glacial maximum and deglaciation of Devon Island, Arctic Canada: Support for an Innuitian Ice Sheet. *Quaternary Science Reviews*, **18**, 393–420.

Gosse, J. C., and Phillips, F. M., 2001. Terrestrial in situ cosmogenic nuclides: theory and application. *Quaternary Science Reviews*, **20**, 1475–1560.

Gosse, J. C., Klein, J., Evenson, E. B., Lawn, B., and Middleton, R., 1995. Be-10 dating of the duration and retreat of the last Pinedale glacial sequence. *Science*, **268**, 1329–1333.

Hallet, B., and Putkonen, J., 1994. Surface dating of dynamic landforms – young boulders on aging moraines. *Science*, **265**, 937–940.

Hamilton, T. D., 1986. Late Cenozoic glaciation of the central Brooks Range. In Hamilton, T. D., Reed, K. M., and Thorson, R. M. (eds.), *Glaciation in Alaska – The geologic record*. Anchorage: Alaska Geological Society, pp. 9–50.

Heine, J. T., 1998. Extent, timing, and climatic implications of glacier advances, Mount Rainier, Washington, U.S.A., at the Pleistocene/Holocene transition. *Quaternary Science Reviews*, **17**, 1139–1148.

Joerin, U. E., Stocker, T. F., and Schlüchter, C., 2006. Multicentury glacier fluctuations in the Swiss Alps during the Holocene. *Holocene*, **16**, 697–704.

Kaufman, D. S., and Calkin, P. E., 1988. Morphometric analysis of Pleistocene glacial deposits in the Kigluaik Mountains, Northwestern Alaska, U.S.A. *Arctic and Alpine Research*, **20**, 273–284.

Kaufman, D. S., Manley, W. F., Forman, S. L., and Layer, P., 2001. Pre-late-Wisconsin glacial history, coastal Ahklun Mountains, southwestern Alaska – New amino acid, thermoluminescence, and $^{40}Ar/^{39}Ar$ results. *Quaternary Science Reviews*, **20**, 337–352.

Licciardi, J. M., and Pierce, K. L., 2008. Cosmogenic exposure-age chronologies of Pinedale and Bull Lake glaciations in greater Yellowstone and the Teton Range, USA. *Quaternary Science Reviews*, **27**, 814–831.

Licciardi, J. M., Kurz, M. D., and Curtice, J. M., 2007. Glacial and volcanic history of Icelandic table mountains from cosmogenic ^{3}He exposure ages. *Quaternary Science Reviews*, **26**, 1529–1546.

Licciardi, J. M., Schaefer, J. M., Taggart, J. R., and Lund, D. C., 2009. Peruvian Andes indicate northern climate linkages. *Science*, **325**, 1677–1679.

Loso, M. G., and Doak, D. F., 2006. The biology behind lichenometric dating curves. *Population Ecology*, **147**, 223–229.

Lowell, T. V., Fisher, T. G., Comer, G. C., Hajdas, I., Waterson, N., Glover, K., Loope, H. M., Schaefer, J. M., Rinterknecht, V., Broecker, W., Denton, G., and Teller, J. T., 2005. Testing the Lake Agassiz meltwater trigger for the Younger Dryas. *EOS Transactions*, **86**, 365–373.

Menounos, B., Osborn, G., Clague, J. J., and Luckman, B. H., 2009. Latest Pleistocene and Holocene glacier fluctuations in western Canada. *Quaternary Science Reviews*, **28**, 2049–2074.

Mercer, J. H., and Palacios, O. M., 1977. Radiocarbon dating of the last glaciation in Peru. *Geology*, **5**, 600–604.

Phillips, F. M., Zreda, M. G., Smith, S. S., Elmore, D., Kubik, P. W., and Sharma, P., 1990. Cosmogenic chlorine-36 chronology for glacial deposits at Bloody Canyon, eastern Sierra Nevada. *Science*, **248**, 1529–1532.

Phillips, F. M., Zreda, M. G., Gosse, J. C., Klein, J., Evenson, E. B., Hall, R. D., Chadwick, O. A., and Sharma, P., 1997. Cosmogenic ^{36}Cl and ^{10}Be ages of Quaternary glacial and fluvial deposits of the Wind River Range, Wyoming. *Geological Society of America Bulletin*, **109**, 1453–1463.

Porter, S. C., 1975. Weathering rinds as relative-age criterion: Application to subdivision of glacial deposits in the Cascade Range. *Geology*, **3**, 101–104.

Porter, S. C., 1976. Pleistocene glaciation in the southern part of the North Cascades Range, Washington. *Geological Society of America Bulletin*, **87**, 61–75.

Porter, S. C., 2005. Pleistocene snowlines and glaciation of the Hawaiian Islands. *Quaternary International*, **138–139**, 118–128.

Porter, S. C., and Swanson, T. W., 2008. ^{36}Cl dating of the classic Pleistocene glacial record in the northeastern Cascade Range, Washington. *American Journal of Science*, **308**, 130–166.

Porter, S. C., Pierce, K. L., and Hamilton, T. D., 1983. Late Wisconsin mountain glaciation in the western United States, In Porter, S. C. (ed.), Late Quaternary Environments of the United States, Vol. 1, The Late Pleistocene: Minneapolis, University of Minnesota Press, pp. 71–111.

Putkonen, J., and Swanson, T., 2003. Accuracy of cosmogenic ages for moraines:. *Quaternary Research*, **59**, 255–261.

Putkonen, J., Connolly, J., and Orloff, T., 2008. Landscape evolution degrades the geologic signature of past glaciations. *Geomorphology*, **97**, 208–217.

Reiners, P. W., and Brandon, M. T., 2006. Using thermochronology to understand orogenic erosion. *Annual Review of Earth and Planetary Sciences*, **34**, 419–466.

Rodbell, D. T., 1993. The timing of last deglaciation in Cordillera Oriental, northern Peru, based on glacial geology and lake sedimentology. *Geological Society of America Bulletin*, **105**, 923–934.

Schaefer, J. M., Denton, G. H., Kaplan, M., Putnam, A., Finkel, R. C., Barrell, D. J., Andersen, B. G., Schwartz, R., Mackintosh, A., Chinn, R., and Schlüchter, C., 2009. High-frequency Holocene glacier fluctuations in New Zealand differ from the northern signature. *Science*, **324**, 622–625.

Shuster, D. L., Ehlers, T. A., Rusmore, M. E., and Farley, K. A., 2005. Rapid Glacial Erosion at 1.8 Ma Revealed by $^{4}He/^{3}He$ Thermochronometry. *Science*, **310**, 1668–1670.

Singer, B. S., Ackert, R. P., and Guillou, H., 2004. $^{40}Ar/^{39}Ar$ and K-Ar chronology of Pleistocene glaciations in Patagonia. *Geological Society of America Bulletin*, **116**, 434–450.

Smith, J. A., Seltzer, G. O., Farber, D. L., Rodbell, D. T., and Finkel, R. C., 2005a. Early local Last Glacial Maximum in the Tropical Andes. *Science*, **308**, 678–681.

Smith, J. A., Finkel, R. C., Farber, D. L., Rodbell, D. T., and Seltzer, G. O., 2005b. Moraine preservation and boulder erosion in the tropical Andes: interpreting old surface exposure ages in glaciated valleys. *Journal of Quaternary Science*, **20**, 735–758.

Solomina, O., and Calkin, P. E., 2003. Lichenometry as applied to moraines in Alaska, USA, and Kamchatka, Russia. *Arctic, Antarctic and Alpine Research*, **35**, 129–143.

Stone, J. O., Balco, G. A., Sugden, D. E., Caffee, M. W., Sass, L. C., Cowdery, S. G., and Siddoway, C., 2003. Holocene deglaciation of Marie Byrd Land, West Antarctica. *Science*, **299**, 99–102.

Sugden, D. E., Balco, G., Cowdery, S. G., Stone, J. O., and Sass, L. C., 2005. Selective glacial erosion and weathering zones in the coastal mountains of Marie Byrd Land, Antarctica. *Geomorphology*, **67**, 317–334.
Thackray, G. D., Lundeed, K. A., and Borgert, J. A., 2004. Latest Pleistocene alpine glacier advances in the Sawtooth Mountains, Idaho, USA: Reflections of midlatitude moisture transport at the close of the last glaciation. *Geology*, **32**, 225–228.
Weidick, A., Kelly, M., and Bennike, O., 2004. Late Quaternary development of the southern sector of the Greenland Ice Sheet, with particular reference to the Qassimiut lobe:. *Boreas*, **33**, 284–299.
Wiles, G. C., Calkin, P. E., and Jacoby, G. C., 1996. Tree-ring analysis and Quaternary geology: Principles and recent applications. *Geomorphology*, **16**, 259–272.
Young, N. E., Briner, J. P., and Kaufman, D. S., 2009. Late Pleistocene and Holocene glaciation of the Fish Lake valley, northeastern Alaska Range, Alaska. *Journal of Quaternary Science*, **24**, 677–689.

DEAD ICE

D. P. Dobhal
Wadia Institute of Himalayan Geology, Dehradun, Uttarakhand, India

Definition

The dead ice is defined as the ice which does not move, that is, it becomes stagnant. Generally, dead ice is formed due to detachment of/from the active glacier and topographic conditions do not allow for its movement, and it is covered with thick piles of moraine/debris, which act as insulator and protect from quick melting. It is also known as stagnant ice.

DEBRIS

Tobias Bolch
Department of Geography, University of Zürich, Zürich, Switzerland

Synonyms

Boulder; Detritus; Scree material

Definition

Unconsolidated sediment, larger than 1 mm, of angular or rounded angular fragments of boulders (clasts), predominantly originating from physical weathering.

Introduction

Debris occurs in a wide range of environments, but most significantly in those where physical weathering rates dominate, such as periglacial environments. Hence debris is common in glacierized areas, affecting glaciers and ice in the ground, as well as their appearance and characteristics, in a great variety of ways. Debris e.g. significantly influences the glacier melt and the glacier movement. Debris can be found on the surface of glacier ice (supraglacial), within glacier ice (englacial), as well as below (subglacial) and beside glacier ice. Coarse debris in periglacial scree slopes plays an important role in the development of so-called rock glaciers (Barsch, 1996, Haeberli et al., 2006). The focus here is on debris related to glacial environments.

Debris sources

The principal sources of debris are mass movements such as rockfalls, rock avalanches, debris flows, debris-laden ice, and snow avalanches from surrounding mountain slopes (Hambrey et al., 2008; Kirkbride, 1993). These sudden and sometimes vast events of debris relocation are common phenomena in alpine regions. The amount of debris that reaches a given glacier depends on the characteristics and extent of the catchment area, especially its weathering and erosion rates (Haeberli, 1986). These again are influenced by the lithology of the source material. Scree slopes (debris deposits) situated in a periglacial environment favor the development of firn patches and rock glaciers due to the different thermal regime of blocky material (Haeberli et al., 2006). An additional source of debris is recycled material from lateral moraines. These moraines become unstable as the glacier lowers and permafrost thaws, enabling moraine material to fall onto the glaciers (Nakawo et al., 1986). Debris eroded from the glacier bed may also become entrained into the ice. The extent of subglacial entrainment depends mainly on thermal regime and substrate erodibility.

Distribution of debris

The spatial distribution of debris in and on the glacier is the result of three main processes (supraglacial, englacial, and subglacial; Hambrey et al., 2008, Nakawo et al., 1986), and depends primarily on the location of the entrainment zone and the transport of the sediment away from it. Debris supplied in the accumulation zone is buried by snow and becomes entrained into the ice, while debris supplied in the ablation zone usually remains on the surface due to emergent glacier flow. Debris supplied from below generally remains in the ice. However, some basal or even subglacial debris can also reach the glacier surface along shear horizons and become supraglacial debris (Hambrey et al., 2008). On the other hand, debris can become entrained in crevasses and then into the ice by falling from the surface (Gulley and Benn, 2007). The distribution of debris is usually inhomogeneous. Debris from point sources usually accumulates in planar shapes (debris septa) or as discrete bodies of variable geometry. Supraglacial debris can cover whole or substantial parts of the glacier tongue (debris-covered glacier), given low surface slope values (Paul et al., 2004). Supraglacial debris cover can also form at the margin of glaciers

(side moraines), or over the glacier surface in longitudinal strips (medial moraines). The latter can develop only where debris is supplied almost continuously. This is typically the case when two or more glaciers join and the side moraines converge into medial moraines (Anderson, 2000). Debris from supraglacial sources is generally dominated by angular clasts (Benn and Owen, 2002). Fluvially rounded gravel or sand can be found on debris-covered glaciers, indicating the existence of debris redistribution due to meltwater (Hambrey et al., 2008). Englacial debris is found mainly in lenticular bands, but discordances and folded forms exist as well due to the action of compressive flow (Gulley and Benn, 2007). Boulders commonly retain their size, although they might become slightly rounded during the englacial transport due to clast collisions. The shapes are altered efficiently in the englacial fluvial environment. They rapidly become rounded and break down into platy clasts.

Glaciological effects of debris

Debris influences the glacier system in fundamental ways. Most important are the effects on ablation and mass balance, glacier rheology and glacier dynamics. Depending on its thickness, thermal conductivity, and thermal gradient, debris can cause ablation to increase or decrease. In general, thin (~15–80 mm) and dispersed debris cover enhances ice melt, while the insulating effect increases as the debris cover becomes thicker (Nakawo and Young, 1981; Tangborn and Rana, 2000). However, significant melt rates do occur on a glacier with a thick debris cover if it has steep ice slopes and glacier ponds (Sakai et al., 2000). Large individual boulders reduce ablation and glacier (or "boulder") tables develop, while cryocronites are a sign of enhanced melt due to small debris. Englacial debris influences the rheology (deformational behavior) of the ice. The existence of undeformable material in the glacier reduces the creep rate of ice (Nickling and Bennet, 1984). Debris has an indirect effect on ice crystal growth. A thick supraglacial layer on the ablation zone of the glacier alters glacier dynamics and its sensitivity to climate. Reduced ablation causes glacier tongues to be more stable and to react with greater delay to climate fluctuations than clean ice glaciers. In addition, some debris-covered glacier tongues contain stagnant ice parts at their fronts (Bolch et al., 2008a; Quincey and Glasser, 2009). Debris cover can also hamper the identification of the actual terminus, and the reaction of the glacier to climate influences can be recognized mainly by the downwasting that occurs (Bolch et al., 2008b). Conversely, large rockfalls onto glaciers can trigger glacier advances (Porter and Orombelli, 1981).

Conclusions

Debris is widespread in glacier environments and affects glaciers in a variety of ways. Although knowledge about the influence of debris on glaciers has increased significantly in the last decades, especially through remote sensing, modeling, and field investigations, much still remains to be discovered in this regard.

Bibliography

Anderson, R. S., 2000. A model of ablation-dominated medial moraines and the generation of debris-mantled glacier snouts. *Journal of Glaciology*, **46**(154), 459–469.

Barsch, D., 1996. *Rock Glaciers. Indicators for the Present and Former Geoecology in High Mountain Environments*. Berlin: Springer.

Benn, D. I., and Owen, L. A., 2002. Himalayan glacial sedimentary environments: a framework for reconstructing and dating the former extent of glaciers in high mountains. *Quaternary International*, **97–98**, 3.

Bolch, T., Buchroithner, M. F., Bajracharya, S. R., Peters, J., and Baessler, M., 2008a. Identification of glacier motion and potentially dangerous glacier lakes at Mt. Everest area/Nepal using spaceborne imagery. *Natural Hazards and Earth System Sciences*, **8**(6), 1329–1340.

Bolch, T., Buchroithner, M. F., Pieczonka, T., and Kunert, A., 2008b. Planimetric and volumetric Glacier changes in Khumbu Himalaya since 1962 using Corona, Landsat TM and ASTER data. *Journal of Glaciology*, **54**(187), 592–600.

Gulley, J., and Benn, D. I., 2007. Structural control of englacial drainage systems in Himalayan debris-covered glaciers. *Journal of Glaciology*, **53**(182), 399–412.

Haeberli, W., 1986. Factors influencing the distribution of rocky and sedimentary glacier beds. *Mitteilung. VAW/ETHZ*, **90**, 48–49.

Haeberli, W., Hallet, B., Arenson, L., Elconin, R., Humlum, O., Kääb, A., Kaufmann, V., Ladanyi, B., Matsuoka, N., Springman, S., and Vonder Mühll, D., 2006. Permafrost creep and rock glacier dynamics. *Permafrost and Periglacial Processes*, **17**(3), 189–214.

Hambrey, M. J., Quincey, D. J., Glasser, N. F., Reynolds, J. M., Richardson, S. J., and Clemmens, S., 2008. Sedimentological, geomorphological and dynamic context of debris-mantled glaciers, Mount Everest (Sagarmatha) region. *Nepal Quaternary Science Reviews*, **27**, 2341–2360.

Kirkbride, M. P., 1993. The temporal significance of transitions from melting to calving termini at glaciers in the central Southern Alps of New Zealand. *Holocene*, **3**, 232–240.

Nakawo, M., and Young, G., 1981. Field experiments to determine the effect of a debris layer on ablation of glacier ice. *Annals of Glaciology*, **2**, 85–91.

Nakawo, M., Iwata, S., Watanabe, O., and Yoshida, M., 1986. Processes which distribute supraglacial debris on the Khumbu Glacier, Nepal Himalaya. *Annals of Glaciology*, **8**, 129–131.

Nickling, W. G., and Bennett, L., 1984. The shear strength characteristics of frozen coarse granular debris. *Journal of Glaciology*, **30**, 348–357.

Paul, F., Huggel, C., and Kääb, A., 2004. Combining satellite multispectral image data and a digital elevation model for mapping of debris-covered glaciers. *Remote Sensing of Environment*, **89**(4), 510–518.

Porter, S. C., and Orombelli, G., 1981. Alpine rockfall hazards. *American Scientist*, **69**(1), 67–75.

Quincey, D. J., and Glasser, N. F., 2009. Morphological and ice-dynamical changes on the Tasman Glacier, New Zealand, 1990–2007. *Global and Planetary Change*, **68**(3), 185.

Sakai, A., N. Takeuchi, K. Fujita, and Nakawo, M., 2000. Role of supraglacial ponds in the ablation process of a debris-covered

glacier in the Nepal Himalayas. IAHS 264 (=Debris-Covered Glaciers), pp. 119–130.
Tangborn, W., and Rana, B., 2000. Mass balance and runoff of the partially debris-covered Langtang Glacier, Nepal IAHS Publication 264 (=Debris-Covered Glaciers), pp. 99–108.

Cross-references

Cryoconite
Debris Thermal Properties and Impact on Ice Ablation
Debris-Covered Glaciers
Dynamics of Glaciers
Englacial Processes
Glacier Motion/Ice Velocity
Mechanical Weathering
Moraine
Rock Glaciers
Subglacial Processes

DEBRIS THERMAL PROPERTIES AND IMPACT ON ICE ABLATION

Ryohei Suzuki
Hydrospheric Atmospheric Research Center, Graduate School of Environmental Studies, Nagoya University, Nagoya, Japan

Definition

Debris thermal properties. The thermal conductivity of the debris, which varies with mineralogy, porosity, and moisture content. In this chapter, the thickness of the debris layer is also discussed as a factor of thermal properties.

Introduction

Debris layers often cover the surface of ablation zones in *valley glaciers* surrounded by steep, bare rock walls (Debris-Mantled Glacier Snouts). Because supraglacial debris affects the transfer of heat between the atmosphere and ice surface, the ice *melt rates* under these layers depend on the thermal properties (e.g., debris thickness, thermal conductivity, and heat capacity) of the debris as well as the *meteorological conditions* on the glacier. This means that the methodologies for observing and estimating *mass balances* of debris-free glaciers cannot be applied to debris-covered glaciers without taking into account the influence of debris on ice melt.

The spatial distribution of debris thermal properties is heterogeneous even in an ablation area. Furthermore, each glacier has its own characteristics of thermal properties and their spatial distribution. Such characteristics are determined by the different supply mechanisms of the debris, which depend on the type of rock and the topographic and climatic conditions (Debris).

Due to the factors described above, there exists a necessity to clarify the state of debris thermal properties on glaciers in order to understand the physical processes involved and evaluate the glacier melt under debris layers. This chapter illustrates the relationship between debris thermal properties and impact on ice ablation along with the development of studies in this field.

Debris thickness and ice melt rate under debris layers

The relationship between debris thickness and ice melt rate under debris layers has been studied since the late 1950s. Early experimental research focused on debris layers with a thickness of several centimeters. The results of these studies were often expressed in graph form, with the horizontal axis indicating debris thickness and the vertical axis indicating ice melt rate under the debris layer (e.g., Mattson et al., 1993).

The absorbed amount of solar radiation on a glacier surface increases where the debris layer has a thickness of several centimeters because such a debris layer causes a decrease in *albedo*. Although the range may not be uniform, the ice melt rate is sometimes several times faster than that of a bare ice surface. On the other hand, a thicker debris layer leads to an increase in heat release from the surface. This means that a thick debris layer acts as a heat insulator that reduces the transfer of heat to the ice surface. At the critical thickness of debris, the ice melt rate under the layer equals that on the bare ice surface. Where the debris layer is thick in comparison with the critical thickness, the ice melt rate is smaller than that of bare ice. In other words, the ice melt rate is suppressed by the debris layer.

Although the above studies showed some common characteristics, the ice melt rate differed quantitatively from case to case. For instance, some experiment results showed the maximum values were twice that of bare ice, whereas other studies showed only a 20% increase. It is also important to note that the value of critical thickness differed from study to study, and some values were more than twice others. Additionally, some studies showed ice melt rates that were two or three times slower than others where the ice melt rate was suppressed by debris layer thickness (e.g., Mattson et al., 1993).

The causes of the above differences can be understood as follows: the ice melt rate is accelerated only if the albedo of the debris surface is lower than that of the glacier ice. This means that the ice melt rates of each study depend on the albedo of the debris used in each experiment. Because the values of albedo on bare ice are not uniform, we cannot regard the ice melt rate on bare ice as a basis for evaluating the influence of debris by comparing the ice melt rates under the debris layers. Additionally, because the impact of differences in albedo depends on the intensity of solar radiation, meteorological conditions must also be considered as controlling factors in ice melt rates.

The studies mentioned above discussed ice melt rates as a function of debris thickness only, but the use of thermal properties to evaluate ice melt rate should not be neglected if a thick debris layer covers the ice. The fact that the thermal conductivity of debris layers is different from

case to case is one possible reason why differing ice melt rates were found.

As mentioned above, applying the physical parameters concerning energy balance calculations at one point on a glacier to other areas causes considerable discrepancies in ice melt rate estimation. Furthermore, most debris-covered glaciers are located in remote high mountain areas and the topographic conditions of their ablation areas are so arduous that in-situ observations are hardly feasible. These factors show the limitations of using a methodology based on the debris thickness function to evaluate the ice melt rates of a whole ablation area on a single glacier or multiple glaciers.

Thermal resistance as an index of debris thermal properties

Taking into account the above issues, Nakawo and Young (1981, 1982) proposed a physical parameterization of thermal resistance that is defined as a value of thickness divided by thermal conductivity of a debris layer to estimate ice melt rates. This methodology is based on Fourier's law of heat conduction; the heat used for ice melt under a debris layer can be estimated using the relations among the heat provided from the surface, temperature profile, and heat conductivity of the debris layer. The *energy balance* method, for which the input parameters are the surface temperature of the debris layer and the meteorological conditions, specifies the heat amount conducted from the surface to the bottom of the debris layer. This method assumes that all the heat derived from the energy balance calculation is transferred to the debris layer. The temperature at the bottom of the debris layer can be assumed to be the ice melt point during glacier melt season for *temperature glaciers*. Therefore, we only have to measure the surface temperature to obtain the temperature difference between the top and bottom of the debris layer. If a linear temperature profile in a debris layer is assumed, the temperature gradient can be calculated by the temperature difference divided by the thickness of the debris layer. Here, we cannot solve the equation because it contains two parameters that are usually unknown: the thickness and heat conductivity of the debris layer. However, by replacing these two parameters with the value for the thermal resistance and treating them as a single parameter, thermal resistance can be solved for the equation of Fourier's law.

Thermal resistance increases with an increase in debris thickness and a decrease in heat conductivity; the ice melt rate under the debris layer decreases with an increase in thermal resistance. Because variations of debris thickness and heat conductivity over a period of several years should be negligible on average, thermal resistance is often assumed to be a constant value. This means that the ice melt rate under a debris layer can be derived if the thermal resistance is known and meteorological data for an adequate and appropriate period of time can be obtained. By combining two equations regarding energy balance and heat conduction, we can solve the equation numerically for the heat used for ice melt without having to remeasure the surface temperature.

As mentioned above, one of the advantages of using thermal resistance is that two unknown parameters can be combined into a single parameter. Although investigating the states of these parameters on a debris-covered glacier also has been essayed (e.g., Conway and Rasmussen, 2000), no study has found a method that is sufficiently versatile to be applied extensively on glaciers due to the difficulties in making the requisite observations. Similarly, there is currently no known feasible method for collecting surface temperatures over a period of time on debris-covered glaciers. These reasons indicate that the method for estimating ice melt rate under debris layers by using thermal resistance which is derived from combining surface temperature data at a point in time and data about meteorological conditions over a period of time is another advantage for overcoming the difficulties in observations.

Nakawo and Young (1981, 1982) showed that the ice melt rates that were estimated from the above method are compatible with measured ice melt rates using sample debris layers of which thermal resistances were previously known. Rana et al. (1997) and Nicholson and Benn (2006) also support the validity of this methodology when using daily meteorological data for the input.

Satellite utilization

Since the methodology using thermal resistance was proposed, it has been applied to optical satellite remote sensing data (Satellite Applications on Snow, Ice, Glacier Studies), for example, obtained from LANDSAT TM and ASTER, which observe the reflected solar radiation between visible to near infrared wavelengths and the emission of infrared light on ground surfaces (e.g., Rana et al., 1997; Nakawo et al., 1999; Suzuki et al., 2007). These multi-spectral sensors provide spatial distributions of surface temperature and albedo of ground surfaces as digital images in the range of about 60–180 km square. The idea of applying satellite data was originally proposed by Nakawo et al. (1993). After that, Rana et al. (1997) compared the estimated runoff from the Langtang glacier in the Himalayas to the measured runoff to show the validity of estimation. Combining the other data, for example, the ice flow vectors derived from SPOT-HRV, has been shown to discuss the variations in the Khumbu glacier of in the Himalayas (Nakawo et al., 1993).

The advantage of utilizing satellite data is not only that spatial distributions of physical parameters can be collected, but also that the complex debris-covered areas can be averaged into the pixel sizes of each satellite sensor. There are ponds and ice cliffs on the ablation areas of debris-covered glaciers and their absorbed heat is roughly ten times larger than that under a debris layer (Sakai et al., 2000). Because such areas can be averaged spatially by using satellite data, thermal resistance calculated from these data represent averaged thermal properties on target

areas (Nakawo et al., 1993). On the other hand, the limitations on taking optical satellite data (mainly due to cloud cover) make the study of thermal properties of debris more difficult.

Summary

The study of the relationship between debris thermal properties and ice ablation has developed from experimental research into debris thickness and ice melt rates to observational research using satellite remote sensing. With the escalated concern over global warming of recent years, the importance of clearly understanding the facts about glacier mass balances in debris-covered glaciers is also increasing. One example of an important issue on which attention has been focused is the impact of variations in glacier mass balances on local water environments, such as the *Glacier Lake Outburst Floods (GLOFs)* that are often caused by *moraine-dammed lakes*. Since ice ablation has direct impact on development of glacier lakes, the studies to specify the thermal properties of debris and ice melt rates under the debris layer play important roles in such field, too.

Bibliography

Conway, H., and Rasmussen, L. A., 2000. Summer temperature profiles within supraglacial debris on Khumbu Glacier, Nepal. In Nakawo, M., Raymond, C. F., and Fountain, A. (eds.), *Debris-Covered Glaciers.* IAHS Publication No. 264, pp. 89–97.

Mattson, L. E., Gardner, J. S., and Young, G. J., 1993. Ablation on debris covered glaciers: an example from the Rakhiot Glacier, Punjab, Himalaya. In Young, G. J. (ed.), *Snow and Glacier Hydrology.* IAHS Publication No. 218, pp. 289–296.

Nakawo, M., and Young, G. J., 1981. Field experiments to determine the effect of a debris layer on ablation of glacier ice. *Annals of Glaciology*, **2**, 85–91.

Nakawo, M., and Young, G. J., 1982. Estimate of glacier ablation under a debris layer from surface temperature and meteorological variables. *Journal of Glaciology*, **28**, 29–34.

Nakawo, M., Moroboshi, T., and Uehara, S., 1993. Satellite data utilization for estimating ablation of debris covered glaciers. In Young, G. J. (ed.), *Snow and Glacier Hydrology.* IAHS Publication No. 218, pp. 75–83.

Nakawo, M., Yabuki, H., and Sakai, A., 1999. Characteristics of Khumbu Glacier, Nepal Himalaya: recent change in the debris-covered area. *Annals of Glaciology*, **28**, 330–334.

Nicholson, L., and Benn, D. I., 2006. Calculating ice melt beneath a debris layer using meteorological data. *Journal of Glaciology*, **52**, 463–470.

Rana, B., Nakawo, M., Fukushima, Y., and Ageta, Y., 1997. Application of a conceptual precipitation-runoff model (HYCYMODEL) in a debris-covered glacierized basin in the Langtang Valley, Nepal Himalaya. *Annals of Glaciology*, **25**, 226–231.

Sakai, A., Takeuchi, N., Fujita, K., and Nakawo, M., 2000. Role of supraglacial ponds in the ablation process of a debris-covered glacier in the Nepal Himalayas. In Nakawo, M., Raymond, C. F., and Fountain, A. (eds.), *Debris-Covered Glaciers.* IAHS Publication No. 264, pp. 119–130.

Suzuki, R., Fujita, K., and Ageta, Y., 2007. Spatial distribution of thermal properties on debris-covered glaciers in the Himalayas derived from ASTER data. *Bulletin of Glaciological Research*, **24**, 13–22.

Cross-references

Albedo
Debris
Debris-Covered Glaciers
Glacier Lake Outburst Floods
Glacier Mass Balance
Ice-Dammed Lakes
Optical Remote Sensing of Alpine Glaciers
Specific Melt Rate
Surface Energy Balance
Temperate Glaciers
Topographic Normalization of Multispectral Satellite Imagery

DEBRIS-COVERED GLACIERS

Martin P. Kirkbride
Geography, School of the Environment, University of Dundee, Dundee, Scotland, UK

Synonyms

Debris-mantled glaciers; Glaciers noirs

Definition

A glacier where part of the ablation zone has a continuous cover of supraglacial debris across its full width. Some authors apply a more rigorous definition of debris cover over at least 50% of the ablation zone.

Debris covered-glaciers probably exist in all the major mountain regions of the world, and are the dominant valley glacier type in high-relief orogenic belts, where high denudation rates of mountain faces supply copious quantities of rock debris by rockfall, rock avalanching, and mixed snow/ice/rock avalanching. They are especially well-developed in the Himalaya (Racoviteanu et al., 2008a), Karakoram (Owen and Derbyshire, 1993; Shroder et al., 2000), Caucasus (Stokes et al., 2007), Alaska, New Zealand (Kirkbride, 1993) and parts of the Andes (Racoviteanu et al., 2008b). Small covered glaciers are also widespread in some regions of cirque glaciation such as northern Iceland and the Sierra Nevada, California (Clark et al., 1994). Supraglacial debris covers form where debris supply is high and ice flow is slow relative to bare-ice ablation, so that a glacier is unable to evacuate rock debris efficiently. Debris covers therefore develop mostly on the lower parts of ablation zones.

Though varied in extent and form, supraglacial debris covers tend to thicken downstream to between 0.5 and 2.0 m maximum thickness, and to comprise sandy boulder-gravels (Hambrey et al., 2008). A distinct vertical sorting often exists in which a surficial openwork clast layer overlies more matrix-rich gravels of lower void ratio. Eluviation of fines through the layer may coat the ice surface with sandy silt. While angular rockfall material dominates, debris covers may also contain comminuted basal debris, fluvially rounded clasts and sand, and aeolian and anthropogenic material. The composition of any debris

cover depends on the local availability of debris from different sources and on the large-scale structure and thermal regime of the glacier.

Debris covers are functional components of glacier systems because of their influence on sub-debris ice melt and mass balance. Debris cover extent varies inversely with mass balance as glaciological conditions alternate between transport-dominant (higher velocities, lower ablation) and ablation-dominant (lower velocities, high ablation) conditions (Kirkbride, 2000). The insulating effect of supraglacial debris was quantified in a classic study by Østrem (1959). Dispersed debris and thin covers enhance melting above "clean" (uncovered) ice rates because low-albedo rock surfaces absorb much of the incoming short-wave radiation. However, under a continuous clast-thick cover, heat transfer to the debris-ice interface is reduced due to the low thermal conductivity of the void-rich debris layer (typically 0.8–1.5 W m^{-2}). Melt rate declines asymptotically with increasing debris thickness: a 10 cm layer may reduce ablation by 60% and a 50 cm layer by 90%. Many experimental studies using fine debris (sand, volcanic ash, coal dust) show these relationships well (e.g., Nakawo and Rana, 1999; Adhikary et al., 2000), but the threshold debris loads associated with optimum enhancement of ablation and with the onset of reduced ablation are not well established for coarse debris on real glaciers. Energy balance modeling of the thermal behavior of debris covers is complex, as models have to integrate energy transfers across the atmosphere–debris and debris–ice interfaces, as well as time-dependent variations in heat storage and transfer within the debris layer itself (Bozhinskiy et al., 1986; Mattson and Gardner, 1989; Nicholson and Benn, 2006; Brock et al., 2010). The complexity derives from the fact that all three are to varying degrees related by feedback mechanisms and lags in heat flow.

At the glacier scale, the insulation of ice beneath debris covers means that a greater ablation area is required to maintain equilibrium mass balance (Benn et al., 2003). Accumulation-area ratios (AARs) of Himalayan debris-covered glaciers are typically 0.25–0.50 instead of the 0.60 typical of uncovered valley glaciers. Ablation zones tend to be long, narrow, and gentle and ice velocities at the terminus are very low. Climatic fluctuations of the glacier tend to be expressed as thinning and thickening of the ablation zone rather than as advance and retreat of the terminus, and the maximum amplitude of change is located near the upstream margin of the continuous cover. The common maxim that debris-covered glaciers are "unresponsive" to climate variation refers only to the subdued fluctuations of glacier termini: glacier volume adjusts sensitively to climate but volume losses are redistributed by the insulating debris cover.

Geomorphologically, such glaciers are inefficient at evacuating their debris loads into the proglacial system, and may build lateral moraines tens to hundreds of meters high. Different forms of terminus may develop from the sluggish flow of debris-covered ice. These may include moraine-dammed raised-bed glaciers such as Hatunraju, Peru (Lliboutry, 1977), outwash-head termini such as Tasman Glacier, New Zealand (Kirkbride, 1993), and rock-glacier-type lobes such as Sachen Glacier, Pakistan (Shroder et al., 2000). Where bounding moraines are breached by overspilling ice lobes, multi-lobed termini will develop, for example, Miage Glacier, Italy (Deline and Orombelli, 2005). Which form develops depends on the discharge and stability of the outwash stream, the slope of the proglacial area, and the debris load of the glacier itself, but their interrelationships are not well understood. Over millennial timescales and multiple mass-balance cycles, geomorphic and chronological evidence suggests that some heavily debris-covered and moraine-bounded glaciers have progressively expanded while nearby uncovered glaciers have retreated. This suggests a long-term net accumulation of supraglacial debris on lengthening glacier tongues, in which glaciological feedbacks promote further supraglacial debris accumulation, reduced mean specific net balance, and therefore a long-term dynamic in which the ablation zone must expand to maintain equilibrium mass balance of ice (Kirkbride, 2000). At shorter timescales, recent climatic amelioration in alpine ranges is associated with increasing supraglacial debris loads due to higher rates of rockfall supply, such as at Miage Glacier (Figure 1), where a continuous debris cover has developed since the maximum of the Little Ice Age (Deline, 2005).

Much of the research interest in these glaciers is because their retreat dynamics endanger downstream populations (Quincey et al., 2005). Recent retreats of debris-covered valley glaciers have resulted in the formation of calving ice cliffs in moraine-dammed lakes. Catastrophic floods may result from calving waves overtopping the moraine dams, and/or sudden lake drainage due to dam failure. Fatal incidents of glacial lake outburst floods (GLOFs) have occurred in recent decades,

Debris-Covered Glaciers, Figure 1 Debris-covered Miage Glacier (Mont Blanc massif, Italy). Photograph by Ben Brock.

leading to early-warning systems and engineering operations being introduced at some glaciers to manage the risk.

Conclusions

Debris-covered glaciers have recently become the focus for much research, notably using remote-sensing techniques (Quincey et al., 2005; Racoviteanu, 2008a, b) to monitor changing debris-cover areas, and geohazard monitoring in relation to lake outburst floods. Much remains to be discovered about the topographical, geological, and glaciological controls on debris cover evolution, and on how such covers modify the responses of such glaciers to climate change.

Bibliography

Adhikary, S., Nakawo, M., Seko, K., and Shakya, B., 2000. Dust influence on the melting process of glacier ice: experimental results from Lirung Glacier, Nepal Himalayas. In Nakawo, M., Raymond, C. F., and Fountain, A. (eds.), *Debris-Covered Glaciers*. IAHS, Vol. 264, pp. 43–52.

Benn, D., Kirkbride, M. P., Owen, L. A., and Brazier, V., 2003. Glaciated valley landsystems. In Evans, D. J. A. (ed.), *Glacial Landsystems*. London: Edward Arnold, pp. 372–406.

Bozhinskiy, A. N., Krass, M. S., and Popovnin, V. V., 1986. Role of debris cover in the thermal physics of glaciers. *Journal of Glaciology*, **32**, 255–266.

Brock, B., Mihalcea, C., Kirkbride, M., Diolaiuti, C., Cutler, M., and Smiraglia, C., 2010. Meteorology and surface energy fluxes in the 2005–2007 ablation seasons at Miage debris-covered glacier, Mont Blanc Massif, Italian Alps. *Journal of Geophysical Research (Atmospheres)*, **115**, D09106, DOI:10.1029/2009JD013224.

Clark, D. H., Clark, M. M., and Gillespie, A. R., 1994. Debris-covered glaciers in the Sierra Nevada, California, and their implications for snowline reconstruction. *Quaternary Research*, **41**, 139–153.

Deline, P., 2005. Change in surface debris cover on Mont Blanc Massif glaciers after the "Little Ice Age" termination. *Holocene*, **15**, 302–309.

Deline, P., and Orombelli, G., 2005. Glacier fluctuations in the western Alps during the Neoglacial, as indicated by the Miage morainic amphitheatre (Mont Blanc massif, Italy). *Boreas*, **34**, 456–467.

Hambrey, M. J., Quincey, D. J., Glasser, N. F., Reynolds, J. M., Richardson, S. J., and Clemmens, S., 2008. Sedimentological, geomorphological and dynamic context of debris-mantled glaciers, Mount Everest (Sagarmatha) region, Nepa. *Quaternary Science Reviews*, **27**, 2341–2360.

Kirkbride, M. P., 1993. The temporal significance of transitions from melting to calving termini at glaciers in the central Southern Alps, New Zealand. *Holocene*, **3**, 232–240.

Kirkbride, M. P., 2000. Ice-marginal geomorphology and Holocene expansion of debris-covered Tasman Glacier, New Zealand. In Nakawo, M., Raymond, C. F., and Fountain, A. (eds.), *Debris-Covered Glaciers*. IAHS, Vol. 264, pp. 211–217.

Lliboutry, L. A., 1977. Glaciological problems set by the control of dangerous lakes in the Cordillera Blanca. Peru. II. Movement of a covered glacier embedded within a rock glacier. *Journal of Glaciology*, **18**, 255–273.

Mattson, L. E., and Gardner, J. S., 1989. Energy exchange and ablation rates on the debris-covered Rakhiot Glacier, Pakistan. *Zeitschrift für Gletscherkunde und Glazialgeologie*, **25**, 17–32.

Nakawo, M., and Rana, B., 1999. Estimate of ablation rate of glacier ice under and debris layer. *Geografiska Annaler*, **81A**, 695–701.

Nicholson, L., and Benn, D. I., 2006. Calculating ice melt beneath a debris layer using meteorological data. *Journal of Glaciology*, **52**, 463–470.

Østrem, G., 1959. Ice melting under a thin layer of moraine and the existence of ice cores in moraine ridges. *Geografiska Annaler*, **41A**, 228–230.

Owen, L. A., and Derbyshire, E., 1989. The Karakoram glacial depositional system. *Zeitschrift für Geomorphologie Supplement Bund.*, **76**, 33–73.

Owen, L. A., and Derbyshire, E., 1993. Quaternary and Holocene intermontane basin sedimentation in the Karakoram Mountains. In Shroder, J. F. (ed.), *Himalaya to the Sea*. London: Routledge, pp. 108–131.

Quincey, D. J., Lucas, R. M., Richardson, S. D., Glasser, N. F., Hambrey, M. J., and Reynolds, J. M., 2005. Optical remote sensing techniques in high-mountain environments: applications to glacial hazards. *Progress in Physical Geography*, **29**, 475–505.

Racoviteanu, A. E., Williams, M., and Barry, R., 2008a. Optical remote sensing of glacial characteristics: a review with focus on the Himalayas. *Sensors*, **8**, 3355–3383.

Racoviteanu, A., Arnaud, Y., Williams, M., and Ordoñez, J., 2008b. Decadal changes in glacier parameters in the Cordillera Blanca, Peru derived from remote sensing. *Journal of Glaciology*, **54**, 499–510.

Shroder, J. F., Bishop, M. P., Copland, L., and Sloan, V. F., 2000. Debris-covered glaciers and rock glaciers in the Nanga Parbat Himalaya, Pakistan. *Geografiska Annaler*, **82A**, 17–31.

Stokes, C. R., Popovnin, V., Aleynikov, A., Gurney, S. D., and Shahgedanova, M., 2007. Recent glacier retreat in the Caucasus Mountains, Russia, and associated increase in supraglacial debris cover and supra-/proglacial lake development. *Annals of Glaciology*, **46**, 195–203.

Cross-references

Alps
Caucasus Mountains
Debris
Debris Thermal Properties and Impact on Ice Ablation
Glacier
Glaciers of the Karakoram Himalaya
Global Warming and its Effect on Snow/Ice/Glaciers
Himalaya
Ice-Dammed Lakes
Ice-Marginal Processes
Iceland Glaciers
Little Ice Age
Moraine
Retreat/Advance of Glaciers
Rock Glaciers
Supra-Glacial Debris Entrainments

DEGLACIATION

Vinvent Rinterknecht
School of Geography and Geosciences, University of St Andrews, St Andrews, Scotland, UK

Definition

Deglaciation refers to the uncovering of land and water that was previously covered by ice. The process corresponds to the retreat of the glacier terminus or the ice sheet

margin toward its source area (cirque, ice sheet center). This occurs when the ice mass transfer from the accumulation zone to the ablation zone (see *Glacier Mass Balance* for details) is not sufficient to replace the ice lost by melting or calving. As glaciers and ice sheets are highly sensitive to climate variations, their mass balance budget will primarily reflect prevailing climate conditions: cooling (ice advance), warming (ice decay), and stable (ice stagnation). In the case of the deglaciation, more ice will melt in the ablation area than could be replaced by precipitation (mostly as snow) in the accumulation area, resulting in a net glacier/ice sheet margin retreat.

Mechanisms of deglaciation

Warming temperature

The main mechanism involved in deglaciation is the melting of ice due to air temperature warming. While the accumulation usually happens during winter time, the ablation season or melting season usually occurs during the summer months. The direct consequence of warmer summer temperatures is an increase in the rate of glacial meltwater. The increased melting rate results in a negative mass balance and ultimately in the retreat of the glacier to higher altitudes.

Glaciologists use the equilibrium line altitude (ELA) to define the boundary between the accumulation zone and the ablation zone. The elevation of this line defines where a glacier is in balance, i.e., where the volume of ice accumulated equals the volume ablated. As the mass balance becomes increasingly negative (more ablation than accumulation), the ELA will shift progressively to higher elevations, corresponding to glacier recession. Ultimately, if the ELA is higher than the highest topography for a sustained period of time, glaciers will retreat continuously until deglaciation is complete.

For glaciers and ice sheets terminating in water, the water temperature also plays a role in deglaciation. Recently, Holland et al. (2008) demonstrated that increased ocean water temperature had a direct effect on the retreat rate of the Jakobshavn Isbræ because of rapid basal thinning of the floating ice tongue.

Decreasing precipitation

The process of ice flow from the accumulation zone to the ablation zone dictates the ice mass transfer (Paterson, 1994). This means that a decrease in precipitation will affect negatively the mass balance by decreasing the accumulation, resulting in net retreat. Such a scenario could occur when the climate becomes drier or when the source of precipitation does not reach the interior of an ice sheet, literally starving the ice sheet.

Successive negative mass balance for years due to reduction or absence of precipitation could lead to the surface of the glacier becoming entirely prone to ablation (ELA above the elevation of the glacier surface). In turn, this could result in catastrophic downwasting by areal stagnation.

Calving

A particular case of a deglaciation mechanism can be observed for glaciers and ice sheets terminating in lakes or oceans (tidewater glaciers). Calving allows much faster ablation as compared to melting, by removing large blocks of ice from the ice margin (Figure 1). Glaciers terminating in water are subject to increased calving when water levels are increasing. This can happen in lakes when the water level is raised by damming (by ice, landslide, or lava flow), forcing the glacier to a new grounding line. For example, in Argentina, the Moreno glacier periodically dams an arm of Lake Argentino, increasing the lake water level upstream from the ice dam. Once the water level builds up sufficient pressure, the ice margin bursts and retreats to its original grounding line near the lake shore.

In the case of tidewater glaciers or ice shelves, water level fluctuation in conjunction with increasing air temperature could lead to catastrophic events, such as the ongoing breakup of the Wilkins shelf in Antarctica.

Long-term monitoring of calving glaciers shows that lake-terminating glaciers calve much slower than ocean-terminating glaciers, which are subject to the constant action of waves and tides (van der Veen, 2002).

Consequences of deglaciation

New landscape

Deglaciation produces new landforms and sediments that provide an endless source of information to understand glacial processes (Benn and Evans, 2010). Modern glacial retreat produces landforms such as sandar (singular: sandur), push moraines, kettle holes, or leaves on the newly-exposed landscape typical features such as eskers, roches moutonnées, and perched erratic boulders. These glacial features provide the foundations for our understanding of glacial processes, as the bases of active glaciers and ice sheets are mostly inaccessible and, thus, very rarely studied.

Sea level rise

During deglaciation, more water is lost by glaciers and ice sheets via melting and calving than is stored via precipitation. The net addition of water from land-based glaciers and ice sheets to the ocean results in an increase of sea level. This has been recorded for the last deglaciation. At the time of the last glacial maximum ~21,000 years ago, when glaciers and ice sheets reached their maximum volumes, the relative sea level was lowered by ~120 m compared to today's sea level. Most of the sea level rise occurred in the following 14,000 years. In today's context of global warming, ice sheets and glaciers are monitored by remote sensing and ground surveys. These studies tell us that the melting of ice is contributing to the global sea level rise, although detailed figures are still elusive (Meier et al., 2007; Pfeffer et al., 2008; Siddall et al., 2009).

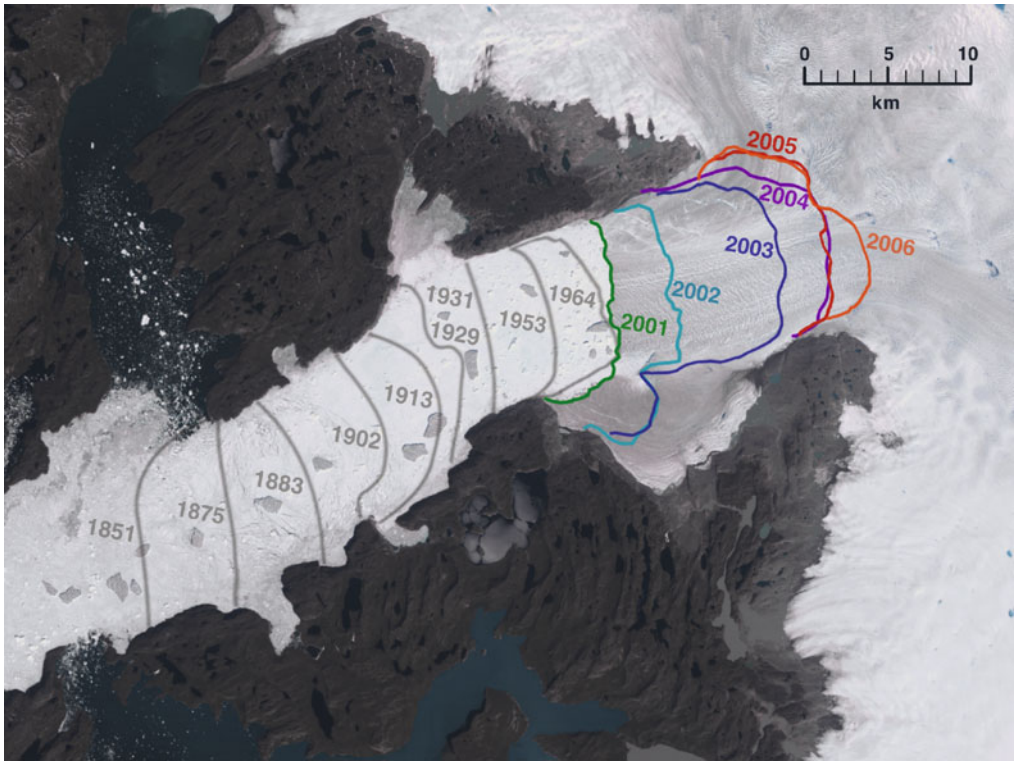

Deglaciation, Figure 1 The Jakobshavn glacier, Western Greenland, shows the changes in the glacier's calving front between 1851 and 2006 (note the scale in kilometers). Historic calving front locations, 1851 through 1964, were compiled by Anker Weidick and Ole Bennike, and are shown here in gray. Recent calving front locations, 2001 through 2006, derived from satellite imagery are shown in colors (source: NASA/Goddard Space Flight Center Scientific Visualization Studio, accessed 07/08/09).

Glacial isostatic adjustment

Landmasses respond to the unloading of ice by rising with respect to the relative sea level. The process can be illustrated primarily as a postglacial rebound of the landmass, but is in fact accompanied by a range of adjustments, such as downward land movements, changes in the Earth's gravity field, changes in the Earth's rotational motion, and can possibly trigger earthquakes. An example of glacial isostatic adjustment can be found in the United Kingdom where the Scottish coast is slowly rising in response to the unload of the last Scottish ice cap (11,000 years ago), and where the southern English coast is virtually sinking due to faster sea level rise compared to land uplift rates.

Deglaciation information

The deglaciation process is rarely uniform, and the ice margin could display a retreat punctuated by a succession of stillstands, leaving behind a characteristic landscape, such as moraine sequences. Geomorphology and dating techniques such as surface exposure dating using cosmogenic nuclides (^{10}Be, ^{26}Al, ^{36}Cl) provide information that helps us to understand deglaciation in the past (Rinterknecht et al., 2009; Briner et al., 2009). From these studies, it is possible to estimate the rate of glacial retreat and infer possible patterns and mechanisms of deglaciation. Rinterknecht et al. (2006) used a multi-proxy approach using cosmogenic ^{10}Be dates and ^{14}C ages to provide a new and comprehensive chronology that constrains the timing of fluctuations of the southern margin of the Scandinavian Ice Sheet in central and Eastern Europe (Figure 2). These results allowed the assessment of the contribution of the ice sheet to the large and often abrupt sea level and climate changes since the last glacial maximum 21,000 years ago. The results also provide the first direct evidence that the ice sheet contributed to the abrupt rise in sea level 19,000 years ago, but not to the similar abrupt sea level event 14,600 years ago. Not surprisingly, the authors found that the ice sheet responded to the abrupt climate changes originating in the North Atlantic Ocean. However, what is surprising is that they were able to demonstrate that those responses varied as a function of the mean climate state; warming during a cold climate caused ice sheet advance, whereas warming during a warm climate caused ice sheet retreat. These responses are exactly of the kind that are expected for the Antarctic (cold climate) and Greenland (warm climate) ice sheets as the Earth's surface temperature warms in the coming century, and thus provides a striking validation of such behavior.

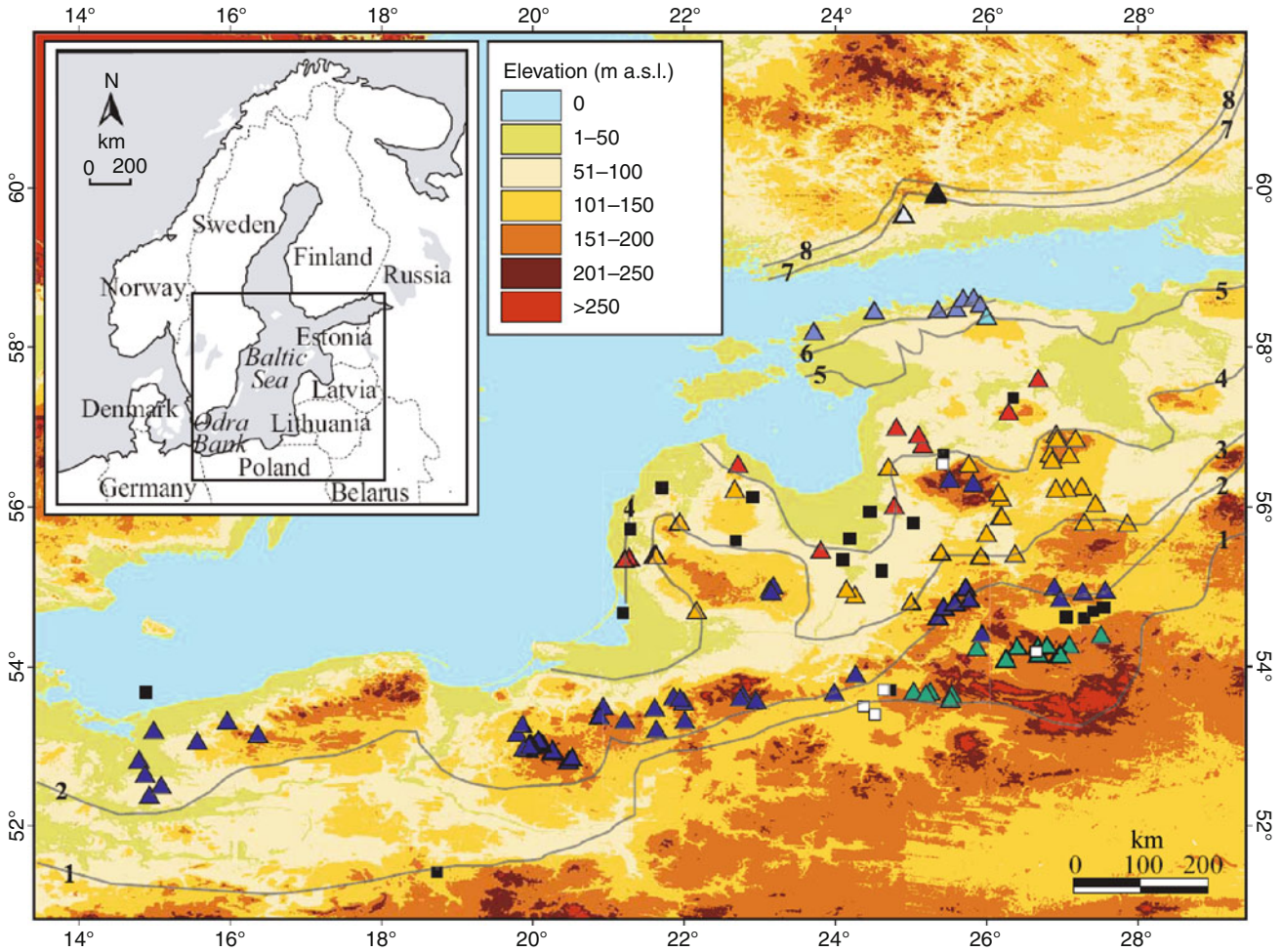

Deglaciation, Figure 2 Digital elevation model of Northern Europe (Adapted from http://lpdaac.usgs.gov, accessed 24-06-2005), with main palaeo ice-marginal positions outlined in gray: 1, LGM Moraine; 2, Pomeranian Moraine; 3, Middle Lithuanian Moraine; 4, North Lithuanian Moraine; 5, Pandivere Moraine; 6, Palivere Moraine; 7, Salpausselkä I Moraine; 8, Salpausselkä II Moraine. ^{10}Be sites: LGM Moraine (*green-blue triangles*), Pomeranian Moraine (*dark blue triangles*), Middle Lithuanian Moraine (*orange triangles*), North Lithuanian Moraine (*red triangles*), Pandivere Moraine (*light blue triangle*), Palivere Moraine (*purple triangles*), Salpausselkä I Moraine (*gray triangle* represents nine samples), Salpausselkä I Moraine (*black triangle* represents four samples). ^{14}C sites: *white squares* and *black squares* represent various studies. (Figure from Rinterknecht et al., 2006.)

Link with the atmosphere and ocean

Ice masses have a direct influence on the air masses that are in direct contact. As deglaciation occurs and glaciers disappear, specific winds like katabatic winds will no longer be generated. As such, deglaciation has a direct influence on the local state of the atmosphere. At the hemispheric scale, the maximum extents of ice sheets in the past are known to have influenced the position of the jet stream, pushing it southward compared to its present position, and thus creating a different overall atmospheric circulation. With the decay of the northern hemisphere ice sheets at the end of the last glaciation, the jet stream migrated northward to its present position, resulting in the global atmospheric circulation with which we are familiar. If tomorrow the last two remaining ice sheets were to disappear, a new pattern of atmospheric circulation would emerge.

Melting ice masses also influence the ocean circulation. Currently, the shallow Gulf Stream brings warmth from the southern latitudes to Western Europe. This oceanic current then sinks in the North Atlantic, where deep water is formed, and flows southward as part of the great oceanic conveyor (Broecker, 1991). Deep sea core sediment data document that the thermohaline circulation (driven by sea temperature and salinity differences) has undergone major shifts in the past. Major inputs of freshwater by: (1) quick release of meltwater stored in proglacial lakes, or (2) rapid surging of ice sheets, are among the current theories to explain the Younger Dryas cold interval (11,000 years ago), and possibly the 8.2 kyr cold event

(8,200 years ago). By adding freshwater to the North Atlantic, the supply of warmth from the southern latitudes would have been decreased or suppressed during these cold events. While these events involved far more extensive decaying of ice sheets than currently observable in both poles, these kinds of cooling episodes are not expected to happen in the future.

Bibliography

Benn, D. I., and Evans, D. J. A., 2010. *Glaciers and Glaciation*. 2nd edn. London: Hodder Education.

Briner, J. P., Bini, A. C., and Anderson, R. S., 2009. Rapid early Holocene retreat of a Laurentide outlet glacier through an Arctic fjord. *Nature Geoscience*, **2**, 496–499.

Broecker, W. S., 1991. The great ocean conveyor. *Oceanography*, **4**, 79–89.

Carlson, A. E., Legrande, A. N., Oppo, D. W., Came, R. E., Schmidt, G. A., Anslow, F. S., Licciardi, J. M., and Obbink, E. A., 2008. Rapid early Holocene deglaciation of the Laurentide ice sheet. *Nature Geoscience*, **1**, 620–624.

Holland, D. M., Thomas, R. H., de Young, B., Ribergaard, M. H., and Lyberth, B., 2008. Acceleration of Jakobshavn Isbræ triggered by warm subsurface ocean waters. *Nature Geoscience*, **1**, 659–664.

Meier, M. F., Dyurgerov, M. B., Rick, U. K., O'Neel, S., Pfeffer, W. T., Anderson, R. S., Anderson, S. P., and Glazovsky, A. F., 2007. Glaciers Dominate Eustatic Sea-Level Rise in the 21st Century. *Science*, **317**, 1064–1067.

Paterson, W. S. B., 1994. *The Physics of Glaciers*. Oxford: Pergamon.

Pfeffer, W. T., Harper, J. T., and O'Neel, S., 2008. Kinematic constraints on glacier contributions to 21st-century sea-level rise. *Science*, **321**, 1340–1343.

Rinterknecht, V. R., Clark, P. U. M., Raisbeck, G. M., Yiou, F., Bitinas, A., Brook, E. J., Marks, L., Zelcs, V., Lunkka, J.-P., Pavlovskaya, I. E., Piotrowski, J. A., and Raukas, A., 2006. The last deglaciation of southeastern sector of the Scandinavian ice sheet. *Science*, **311**, 1449–1452.

Rinterknecht, V. R., Gorokhovich, Y., Schaefer, J., and Caffee, M., 2009. Preliminary ^{10}Be chronology for the last deglaciation of the western margin of the Greenland Ice Sheet. *Journal of Quaternary Science*, **24**, 270–278.

Siddall, M., Stocker, T. F., and Clark, P. U., 2009. Constraints on future sea-level rise from past sea-level change. *Nature Geoscience*, **2**, 571–575.

van der Veen, C. J., 2002. Calving glaciers. *Progress in Physical Geography*, **26**, 96–122.

DEGREE-DAYS

Roger J. Braithwaite
Geography Programme, School of Environment and Development, University of Manchester, Manchester, UK

Synonyms

Degree-day factor; Degree-day methods; Degree-day total or positive degree-day sum

Definition

Degree-day methods. The melting of snow and ice is assumed to be related to air temperature as long as air temperature is above a critical threshold, usually close to the melting point of ice. In particular, the amount of snow or ice melted at a certain place, during a certain period, is assumed proportional to the sum of positive temperatures (on the Celsius scale) at the same place and in the same period. The amount of melt is linked to this *positive degree-day sum* by the *degree-day factor*. In the present entry, *air temperature* refers to conventional measurements made c. 2 m above the snow or ice surface, or extrapolated from a similar station in the same region.

The melting of snow and ice and air temperature

By the end of the nineteenth century, the general importance of air temperature for the melting of snow and ice was widely recognized (Hann, 1903) although few data were then available. Finsterwalder and Schunk (p. 82, 1887) assume "in the absence of direct observations" that ice ablation on a glacier depends on the length of the snow-free period and on the average temperature above the freezing point during that period. The product of these two factors is clearly related to our degree-day sum. Finsterwalder and Schunk (1887) made no connection but temperature sums above some critical threshold were already widely used in discussion of temperature control of vegetation (Hann, 1903).

The full history of degree-day methods in hydrology remains to be written but the relation between snowmelt runoff and degree-day sums was already well known to Wilson (1941) who tried to explain it in thermodynamic terms. Early workers appear to have compared snowmelt runoff from a whole basin with the degree-day sum at a particular site so the numerical value of any factor linking the two variables has no general significance and is not usually published. The degree-day approach is still widely used for estimating runoff from melting snow although, significantly, De Walle and Rango (2008) do not include values of the degree-day factor in their detailed table of Snow Runoff Model (SRM) applications and results for 112 case studies. The TS-variable developed by Hoinkes and Steinacker (1975) is also based on the degree-day concept and gives a reasonably high correlation with annual mass balance series but, again, the numerical value of the factor linking the TS-variable to the annual balance is not given.

Zingg (1951), de Quervain (1979), and Kuusisto (1984) estimate degree-day factors for seasonal snow by comparing data from snow stakes with air temperature data at the same site, and their degree-day factors can therefore be compared, see Hock (2003).

The key role of air temperature in variations of glacier mass balance may seem obvious to us today but Hoinkes (1955) explicitly downplayed the role of air temperature in controlling glacier melt. Slater (1927) may have been the first worker to measure ablation and air

temperature at the same location. Leaving aside the crudity of his instruments, his result is equivalent to a degree-day factor for melting ice of 9.1 mm d^{-1} K^{-1}. From various glaciers in the former Soviet Union, Krenke and Khodakov (1966) suggest degree-day factors of 4.5 and 7 mm d^{-1} K^{-1} for snow and ice respectively. Orheim (1970) also calculated degree-day factors for melting ice over 2 years on a Norwegian glacier and found values of 6.1 and 6.5 mm d^{-1} K^{-1}, which are not included in Hock (2003).

The measurement of daily melt on glaciers by Müller and Keeler (1969) in parallel with meteorological measurements was a significant development and allowed Braithwaite (1981) to model daily ablation in terms of air temperature and energy balance. He obtained an average degree-day factor of 6.3 ± 1.1 mm d^{-1} K^{-1} for the four series studied, equivalent to a total of 123 days of record. Daily measurements of ice melt were made over a number of summer seasons (1979–1986) at two sites on the Greenland ice-sheet margin at Nordbogletscher (415 days) and Qamanârssûp sermia (512 days) (Braithwaite, 1995).

Variations in degree-day factors

There are substantial variations between degree-day factors at various sites on glaciers. For example, see extensive tables and discussion in Braithwaite (1995), Braithwaite and Zhang (2000), Hock (2003, 2005), and especially some previously unpublished values from the high mountains of China in Zhang et al. (2006). These results are mainly based on melt data from stakes on glaciers but Braithwaite (2008) has also used a simple model to assess degree-day factor at the equilibrium line altitude (ELA) of 66 glaciers.

Degree-day factors are generally lower for snow and higher for ice (Table 1). Monthly estimates of degree-day factors for melting ice at Nordbogletscher and Qamanârssûp sermia (Braithwaite, 1995) describe time variations in degree-day factor. Similarly, time variations are illustrated by a 28-year series of snow melt data from Weissfluhjoch, Switzerland (de Quervain, 1979). Degree-day factors listed by Hock (2003) for both ice (32 sites) and snow (18 sites) illustrate variations between different locations and periods. Results from Braithwaite (2008) reflect different locations (66 glaciers) but also different methods based on either winter balance or "winter balance plus summer precipitation" from Ohmura et al. (1992).

From Table 1, it is clear that degree-day factors for ice and snow are not precise single values, even at the same place. Variations in degree-day factor in Table 1 are denoted by standard deviations but field data (Krenke and Khodakov, 1966) and analysis of the energy balance (Braithwaite, 1995) both suggest that very high degree-day factors for ice should only occur at low temperatures and not at random. The generally lower degree-day factor for melting snow compared with ice is mainly due to higher albedo which reduces the energy available for melting (Braithwaite, 1995), while time variations at the same locations presumably reflect differing weather conditions as expressed by variations in the surface energy balance.

Insofar as we can expect the different terms in the energy balance to vary geographically and temporally (Braithwaite, 1995; Guðmundsson et al., 2009), we may expect some systematic variations in degree-day factor and there is some evidence for this. Zhang et al. (2006) claims a clear geographic variation in degree-day factor for ice from low values (2–3 mm d^{-1} K^{-1}) in the relatively continental Tien Shan in Northwest China to high values (15 mm d^{-1} K^{-1}) in the relatively maritime mountains of South China. Fausto et al. (2009) have suggested different degree-day factors for ice over colder and warmer parts of the Greenland ice sheet, i.e., 15 and 7 mm d^{-1} K^{-1}, respectively. Huss and Bauder (2009) claim to detect multiyear variations in glacier-averaged degree-day factor for Swiss glaciers (roughly equal to the degree-day factor for snow?) which they explain in terms of secular variations in global radiation.

Estimation of degree-day sums

The calculation of degree-day totals from raw temperature data is a trivial one of summing all the positive temperatures in a time series, and a computer can do this easily. However, it would be very laborious to find and store long series of daily, or better sub-daily, temperature data if all

Degree-Days, Table 1 Mean and standard deviation of degree-day factors for melting ice or snow (from Braithwaite, 2008)

		Degree-day factor mm d^{-1} K^{-1}		
Location	Type	Mean	St. devn.	Sample
Nordbogletscher Braithwaite (1995)	Glacier ice	6.9	±1.1	Nearly daily data for 14 months
Qamanârssûp sermia Braithwaite (1995)	Glacier ice	7.8	±1.0	Nearly daily data for 21 months
Hock (2003)	Glacier ice	8.9	±3.7	32 sites
Weissfluhjoch, Switzerland De Quervain (1979)	Seasonal snow on land	4.2	±1.0	28 melt seasons
Hock (2003)	Snow on glaciers	5.1	±2.2	18 sites
Braithwaite (2008) using data from Ohmura et al. (1992)				
(1) Winter balance	Snow at ELA	3.5	±1.4	66 glaciers
(2) Winter balance plus summer precipitation	Snow at ELA	4.6	±1.4	66 glaciers
(1) and (2) Combined	Snow at ELA	4.1	±1.5	2 × 66 glaciers

we want to do is to calculate monthly or annual sums. Braithwaite (1985) therefore suggested that monthly degree-day totals can be calculated from monthly mean temperature by assuming that temperature is normally distributed within the month with standard deviations of about ±2 to ±4 K. The advantage of this approach is that monthly mean temperatures are now more widely available in digital form for individual climate stations, or for cells in a gridded climatology like that of New et al. (1999).

Reeh (1991) extended the approach of Braithwaite (1985) by noting that monthly mean temperatures can be approximated by a sine curve around the annual mean temperature if the annual temperature range is prescribed. Temperatures at any particular time are then assumed to be normally distributed around the sine curve. Carlov and Greve (2005) revisit the calculations of Braithwaite (1985) and Reeh (1991) and propose a much more efficient algorithm suitable for the many repeated calculations needed for long-term simulations of the Greenland ice sheet.

Degree-day models

A degree-day model is one where snow and ice melt are calculated according to the degree-day method, for example, as opposed to the energy-balance model, although extra procedures are needed to account for snow accumulation and refreezing of melt water. According to Hock (2003), degree-day models are widely used for four reasons: (1) wide availability of air temperature data, (2) relatively easy interpolation and forecasting possibilities for air temperature, (3) generally good model performance despite their simplicity, and (4) computational simplicity.

The reported success of the degree-day approach to ice and snow melt at two sites in Greenland (Braithwaite and Olesen, 1989) inspired Reeh (1991) to further develop the model and test it with the limited amount of data from other sites in Greenland. Huybrechts et al. (1991) then used the degree-day model to calculate mass balance forcing for their model of ice dynamics for the whole Greenland ice sheet, assuming degree-day factors of 3 and 8 mm d^{-1} K^{-1} for snow and ice, respectively. Many of the current models of Greenland mass balance follow Huybrechts et al. (1991).

Laumann and Reeh (1993), Jóhannesson et al. (1995), Jóhannesson (1997), Marshall and Clarke (1999), Braithwaite and Zhang (2000), Braithwaite et al. (2002), De Woul and Hock (2005), Raper and Braithwaite (2006), Anderson et al. (2006), Braithwaite and Raper (2007), Liu et al. (2009), Shea et al. (2009), Hughes and Braithwaite (2008), and Rasmussen and Wenger (2009) use different variants of the degree-day model to calculate mass-balances of glaciers outside Greenland. The relevant degree-day factors are either found by tuning models onto field data or are prescribed. In general, modelled accumulation depends upon the degree-day factor for snow, and mass–balance sensitivity depends upon the degree-day factor for ice (Braithwaite and Raper, 2007). Balance gradients near the ELA depend on both degree-day factors with higher gradient in the upper ablation area and lower gradient in the lower accumulation area (Braithwaite and Raper, 2007). This predicted nonlinearity of the balance gradient is in reasonable agreement with observations (Furbish and Andrews, 1984; Rea, 2009).

Many workers use a simpler approach than the degree-day model whereby glacier melt is assumed to be a function of summer mean temperature. With appropriate choice of averaging period, e.g., June–August, May–September, or May–October, the summer mean temperature mainly represents the effects of temperatures above freezing point. For example, Krenke and Khodakov (1966) assume a power-law relation between melt and summer mean temperature and their equation was used in constructing the *World Atlas of Snow and Ice Resources* (Kotlyakov et al., 1997). Other workers follow Ahlmann (1924) in using an exponential relation to link melt to summer mean temperature (Nesje and Dahl, 2000). As the degree-day model predicts a family of curves linking melt to summer mean temperature (Reeh, 1991: Braithwaite, 2008) these different approaches are not in serious conflict as long as it is accepted that there can be no single curve linking melt to summer mean temperature.

Summary and outlook

There is generally a relation between the melting of snow and ice and air temperature which can be modelled using degree-day methods. No doubt the relative merits of degree-day and energy-balance methods will continue to be discussed but more climate data from glaciers in different climatic regions should be collected using modern data loggers that can be left unattended for long periods. At the same time, running degree-day and energy models in parallel may also be a fruitful line for future work in trying to understand the possible variations in degree-day factor. In particular, the role of sublimation in the energy balance of very high mountains in the Andes and High Asia deserves further study as does the effect of debris cover.

Bibliography

Ahlmann, H. W., 1924. Le niveau de glaciation comme function de l'accumulation d'humidité sous forme solide. *Geografiska Annaler*, **6**, 223–272.

Anderson, B., Lawson, W., Owens, I., and Goodsell, B., 2006. Past and future mass balance of 'Ka Roimata o Hine Hukatere' Franz Josef Glacier, New Zealand. *Journal of Glaciology*, **52**(179), 597–607.

Braithwaite, R. J., 1981. On glacier energy balance, ablation, and air temperature. *Journal of Glaciology*, **27**(97), 381–391.

Braithwaite, R. J., 1985. Calculation of degree-days for glacier-climate research. *Zeitschrift für Gletscherkunde und Glazialgeologie*, **20**, 1–8.

Braithwaite, R. J., 1995. Positive degree-day factors for ablation on the Greenland ice sheet studied by energy-balance modelling. *Journal of Glaciology*, **41**(137), 153–160.

Braithwaite, R. J., 2008. Temperature and precipitation climate at the equilibrium-line altitude of glaciers expressed by the degree-day factor for melting snow. *Journal of Glaciology*, **54**(186), 437–444.

Braithwaite, R. J., and Olesen, O. B., 1989. Calculations of glacier ablation from air temperature, West Greenland. In Oerlemans, J. (ed.), *Glacier Fluctuations and Climatic Change*. Dordrecht: Kluwer Academic Publishers, pp. 219–233.

Braithwaite, R. J., and Zhang, Y., 2000. Sensitivity of mass balance of five Swiss glaciers to temperature changes assessed by tuning a degree-day model. *Journal of Glaciology*, **46**(152), 7–14.

Braithwaite, R. J., and Raper, S. C. B., 2007. Glaciological conditions in seven contrasting regions estimated with the degree-day model. *Annals of Glaciology*, **46**, 297–302.

Braithwaite, R. J., Zhang, Y., and Raper, S. C. B., 2002. Temperature sensitivity of the mass balance of mountain glaciers and ice caps as a climatological characteristic. *Zeitschrift für Gletscherkunde und Glazialgeologie*, **38**(1), 35–61.

Carlov, R., and Greve, R., 2005. A semi-analytical solution or the positive degree-day model with stochastic temperature variations. *Journal of Glaciology*, **51**(172), 173–175.

de Quervain, M., 1979. Schneedeckenablation und Gradtag im Versuchsfeld Weisfluhjoch. *Mitteilung VAW/ETH Zürich*, **41**, 215–232.

De Walle, D. R., and Rango, A., 2008. *Principles of Snow Hydrology*. Cambridge: Cambridge University Press.

De Woul, M., and Hock, R., 2005. Static mass-balance sensitivity of Arctic glaciers and ice-caps using a degree-day approach. *Annals of Glaciology*, **42**, 217–224.

Fausto, R. S., Ahlstrøm, A. P., van As, D., Bøggild, C. E., and Johnsen, S. J., 2009. A new present-day temperature parameterization for Greenland. *Journal of Glaciology*, **55**(189), 95–105.

Finsterwalder, S., and Schunk, H., 1887. Der Suldenferner. *Zeitschrift des Deutschen und Österreischischen Alpenvereins*, **18**, 72–89.

Furbish, D. J., and Andrews, J. T., 1984. The use of hypsometry to indicate long-term stability and response to valley glaciers to changes in mass-transfer. *Journal of Glaciology*, **30**(105), 199–211.

Guðmundsson, S. H., Björnsson, F. P., and Haraldsson, H. H., 2009. Energy balance and degree-day models of summer ablation on the Langjökull ice cap, SW Iceland. *Jökull*, **59**, 1–18.

Hann, J., 1903. *Handbook of Climatology: Part 1*. The MacMillan Company: General Climatology. New York.

Hock, R., 2003. Temperature index melt modelling in mountain areas. *Journal of Hydrology*, **282**(1–4), 104–115.

Hock, R., 2005. Glacier melt: a review of processes and their modelling. *Progress in Physical Geography*, **29**(3), 362–391.

Hoinkes, H., 1955. Measurements of ablation and heat balance on alpine glaciers. *Journal of Glaciology*, **2**(17), 497–501.

Hoinkes, H., and Steinacker H., 1975. Hydrometeorological implications of the mass balance of Hintereisferner, 1952–53 to 1968–69. In *Proceedings of the Snow and Ice Symposium, Moscow 1971*. IAHS Publication 104, pp. 144–149.

Hughes, P. D., and Braithwaite, R. J., 2008. Application of a degree-day model to reconstruct Pleistocene glacial climates. *Quaternary Research*, **69**(1), 110–116.

Huss, M., and Bauder, A., 2009. 20th-Century climate change inferred from four long-term point observations of seasonal mass balance. *Annals of Glaciology*, **50**, 207–214.

Huybrechts, P., Letréguilly, A., and Reeh, N., 1991. The Greenland ice sheet and greenhouse warming. *Palaeogeography, Palaeoclimatology, Palaeoecology* (*Global and Planetary Change Section*), **89**, 399–412.

Jóhannesson, T., 1997. The response of two Icelandic glaciers to climatic warming computed with a degree-day glacier mass–balance model coupled to a dynamic glacier model. *Journal of Glaciology*, **43**(144), 321–327.

Jóhannesson, T., Sigurdsson, O., Laumann, T., and Kennett, M., 1995. Degree-day glacier mass balance modelling with applications to glaciers in Iceland, Norway and Greenland. *Journal of Glaciology*, **41**(138), 345–358.

Kotlyakov, V. M., Golubev, G. N., Dreyer, N. N., and Kravtsova, V. I., 1997. *World Atlas of Snow and Ice Resources*. Moscow: Russian Academy of Sciences, Institute of Geography, Vol. 2.

Krenke, A. N., and Khodakov, V. G., 1966. O svyazi poverkhnostnogo tayaniya lednikov s temperaturoy vozdukha [The relationship between surface ice melting and air temperature]. *Mater. Glyatsiol. Issled.*, **12**, 153–164 [In Russian with English summary].

Kuusisto, E. 1984. *Snow accumulation and snowmelt in Finland*. National Board on Waters, Finland. Publication of the Water Research Institute 55.

Laumann, T., and Reeh, N., 1993. Sensitivity to climate change of the mass balance of glaciers in southern Norway. *Journal of Glaciology*, **39**(133), 656–665.

Liu, S., Zhang, Y., Zhang, Y., and Ding, Y., 2009. Estimation of glacier runoff and future trends in the Yangtze River, source region, China. *Journal of Glaciology*, **55**(190), 353–362.

Marshall, S. J., and Clarke, C. K. C., 1999. Ice sheet inception: subgrid hypsometric parameterization of mass balance in an ice sheet model. *Climate Dynamics*, **15**, 533–550.

Müller, F., and Keeler, C. M., 1969. Errors in short-term ablation measurements on melting ice surfaces. *Journal of Glaciology*, **8**(52), 91–105.

Nesje, A., and Dahl, S. O., 2000. *Glaciers and Environmental Change*. London: Arnold.

New, M., Hulme, M., and Jones, P., 1999. Representing twentieth century space-time climate variability. I. Development of a 1961–1990 mean monthly terrestrial climatology. *Journal of Climate*, **12**(3), 829–856.

Ohmura, A., Kasser, P., and Funk, M., 1992. Climate at the equilibrium line of glaciers. *Journal of Glaciology*, **38**(130), 397–411.

Orheim, O., 1970. Glaciological investigations of Stor Supphellebre, west-Norway. Norsk Polarinstitut. Skrifter 151.

Raper, S. C. B., and Braithwaite, R. J., 2006. Low sea level rise projections from mountain glaciers and icecaps under global warming. *Nature*, **439**(7074), 311–313.

Rasmussen, L. A., and Wenger, J. M., 2009. Upper-air model of summer balance on Mount Rainier, USA. *Journal of Glaciology*, **55**(192), 619–624.

Rea, B. R., 2009. Defining modern day Area-Altitude Balance Ratios (AABRs) and their use in glacier-climate reconstructions. *Quaternary Science Reviews*, **28**(3–4), 237–248.

Reeh, N., 1991. Parameterization of melt rate and surface temperature on the Greenland ice sheet. *Polarforschung*, **59**(3), 113–128.

Shea, J. M., Moore, R. D., and Stahl, K., 2009. Derivation of melt factors from glacier mass-balance records in western Canada. *Journal of Glaciology*, **55**(189), 123–130.

Slater, G., 1927. Studies on the Rhone Glacier, 1927: the relationship between the average air temperature and the rate of melting of the surface of the glacier. *Quarterly Journal Royal Meteorological Society*, **55**, 385–393.

Wilson, W. T., 1941. An outline of the thermodynamics of snowmelt. *Transactions of the American Geophysical Union*, **41**, 182–195.

Zhang, Y., Liu, S., Xie, C., and Ding, Y., 2006. Observed degree-day factors and their spatial variation on glaciers in western China. *Annals of Glaciology*, **43**, 301–306.

Zingg, T., 1951. Beziehung zwischen Temperatur and Schmelzwasser und ihre Bedeutung für Niederschlags- und Abflussfragen. IAHS Publication 32, pp. 266–269.

DEPLETION OF SNOW COVER

Sanjay K. Jain
National Institute of Hydrology, Roorkee, Uttarakhand, India

A snow cover is formed by deposition of snow on the ground surface and has different characteristics as compared with fresh snow. The term areal extent of snow cover may be defined as the extent of ground area covered by snow irrespective of its depth and water equivalent, while a snow pack refers to the total volume of snow on the catchment. In warm conditions, the snow may melt away just after its fall or stay for a short period. Snow cover that stays only for a few days and then depletes away due to climate conditions is known as temporary snow cover. The snow cover accumulated during accumulation period called as seasonal snow cover area, melts away during the next summer season. Depletion curves of snow-covered areas continuously indicate the gradual areal diminishment of the seasonal snow cover during the snowmelt season. The snow cover depletion curves normally relate the areal extent of the snow cover to elapsed time. Or in simple words, snow-cover variations during the snowmelt season are displayed as depletion curves. Snow-covered area of a zone or basin is usually obtained from a depletion curve. A variety of sources of snow-cover area may be used to compile the depletion curves including ground observation, aircraft photography, and satellite imagery. If data are available, it is recommended that satellite imagery be used since it is the easiest to analyze and also quite accurate, depending on the basin size.

Satellite products have the potential for obtaining snow-cover area data in near-real time. Snow-cover area is an important natural element that is mapped successfully by satellite remote sensing owing to its high albedo. Since the first mapping of the snow cover from satellites, the spectral and spatial resolution of the available sensors has been much improved. The high spatial resolution satellites (Earth Resources observation satellites) such as Land sat, SPOT, Indian Remote Sensing Satellite (IRS) and Japan's Earth Resources Satellite (JERS), and the medium resolution satellites such as NOAA and MODIS are widely used for mapping snow cover. The Landsat Multispectral Scanning System (MSS) and IRS Linear Imaging Self Scanner-1 (LISS-I) have a spatial resolution of about 79 and 72 m, respectively, and are suitable for snow mapping in basins larger than 10 km^2. Improved spatial resolution has been available from Landsat Thematic Mapper TM (30 m), IRS LISS-II (36 m), JERS Optical Sensor System (OPS) (20 m) and High Resolution Visible instrument (HRV) from the French SPOT satellite (20 m in multi spectral mode and 10 m in panchromatic mode), and IRS Resourcesat/Cartosat ISS IV (5.6 m). However, the repetition cycles of Landsat 1, 2, 3, (18 days) Landsat 4, 5 (16 days), SPOT 1, 2, 3 (26 days), IRS 1A, 1B (22 days), IRS-P2 (24 days), and JERS-1 (44 days) have serious limitations for frequent periodical snow-cover mapping in connection with snowmelt runoff forecast, because all the acquired images cannot be used owing to extensive cloud cover or their acquisition after new snowfall. In the case of the above satellites, the period between two usable satellite images is often more than one month. This may not be sufficient during periods of maximum change of snow cover for an adequate determination of the snow-cover depletion. The sampling period may be improved for snow-cover depletion studies by taking multisensor data from various high spatial resolution satellites into consideration.

Now there are many sensors providing images with great spectral, spatial, and temporal resolution, which can be used, based on the need of the study. With the availability of a large number of satellite data, it is now left up to the choice and requirement of the user community to use particular data. A long interval between the measurements increases the uncertainty and risk of errors in drawing these curves. For a precise derivation of the depletion curves, weekly satellite images are necessary, therefore satellite with larger revisit time such as NOAA and MODIS are better than satellite with low frequency.

The depletion curves are prepared periodically monitoring for snow-covered area and for snowmelt runoff simulations. The snow-cover depletion curves for different bands in Satluj basin located in Western Himalayan regions are shown in Figure 1. These depletion curves are, as explained, influenced by different factors and are not predictable. Due to the temperature lapse rate, maximum accumulation of snow is not synchronous at different altitudes, while the snowmelt season starts in the lower parts, the accumulation of snow continues at the higher altitudes. A fast decrease of the snow-covered area can mean a shallow snow pack or high melt rates. On the other hand, a slow decrease is the result of either a high snow accumulation or of low melt rates. The snow cover must be monitored again in each new year because the depletion curves always take a different course depending on the initial snow reserves, meteorological conditions, and intermittent precipitation during the snowmelt season.

In order to simulate the runoff in a new climate, it is necessary to determine a new set of snow-cover depletion curves that would result from higher temperatures and changes in precipitation. For a more confidential interpretation of the climatic differences between the basins, "modified depletion curves" have to be introduced. The new depletion curve (for use in the climate change study) can thus be plotted by using the modified curve. There will be a shift of the conventional depletion curve for a new warmed climate, because in a warmer climate a greater part of the winter precipitation will be rain instead of snow. This will cause the snow accumulation at the start of the snowmelt season to decrease so that the decline of the snow-covered area will be accelerated.

In many situations, however, the climate change will result in an increase in winter precipitation, which will probably offset the decline of the amount of solid

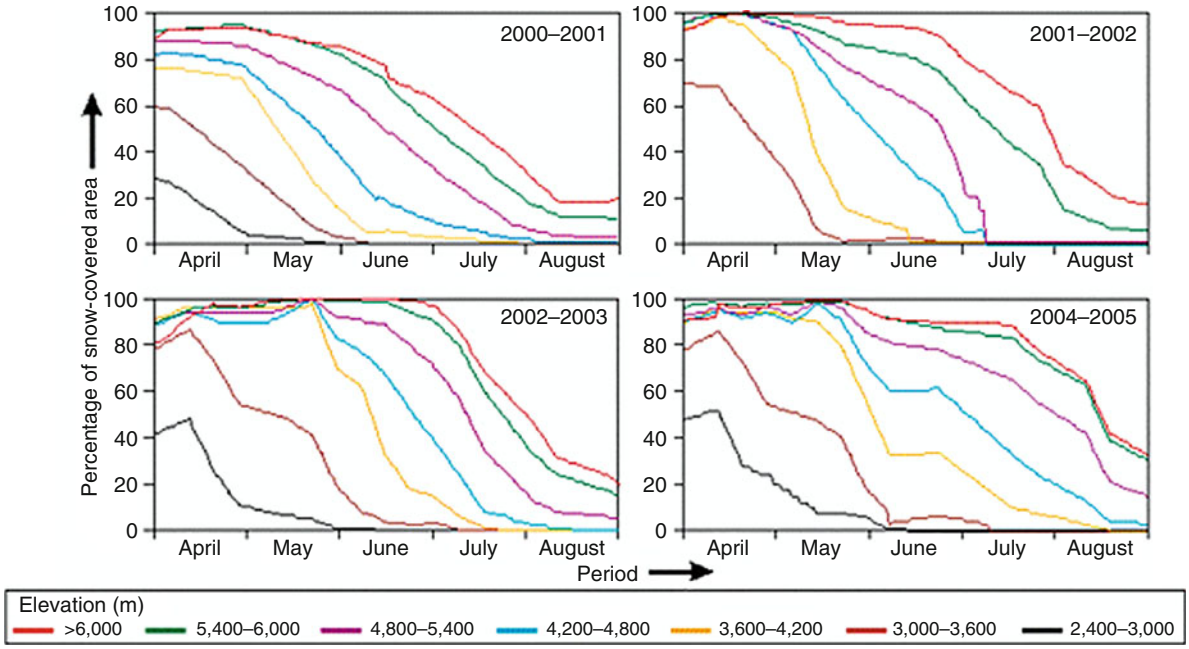

Depletion of Snow Cover, Figure 1 Snow cover depletion curves for different bands in Satluj basin.

precipitation. The shape of a depletion curve in a given basin is determined by the initial accumulation of snow and by the changing melt rates, which depend mainly on the air temperature. Conventional depletion curves, which relate the percentage of a basin or zone covered by snow to the elapsed time during the snowmelt season, do not enable these effects to be identified. Therefore, modified curves have been introduced (Martinec, 2000) in which the time scale is replaced by accumulated degree days. Since the effect of temperature fluctuations in the different weeks or months is eliminated, the decline of these curves is steep in a year with a shallow snow cover and slows in a year with a deep snow cover. Rango and Martinec (1994) outlined a procedure for generating snow depletion curves for changed climatic scenarios and applied the procedure to a number of basins. For warmer temperature scenarios, a modified depletion curve for a zone is obtained by relating snow-cover area to the cumulative snowmelt corresponding to the temperature scenarios.

DEPOSITION FROM DEBRIS-RICH ICE

Gulab Singh, Farjana S. Birajdar
Centre of Studies in Resources Engineering, Indian Institute of Technology Bombay, Powai, Mumbai, India

Definition and origin

Deposition within the glacier system can occur in numerous ways. Rock fall can deposit boulders or sediment on top of the glacier, which then are transported and redeposited in a different glacial environment. Deposition can also occur in a proglacial environment through the process of glaciofluvial actions, or even marine environments. Glacial deposits are composed of different amounts and shapes of till (Trenhaile, 2007). Till is a general term used to describe all the unsorted rock debris deposited by glaciers. Till is composed of rock fragments ranging from clay to boulder size. Till is generally identified by being unsorted (all the rock is jumbled together) and unlayered. The glacier will often carry large boulders, sometimes as large as cars or small homes, as they advance. When the glacier retreats, these large boulders are left behind, often dropped among much smaller glacial till. These large boulders are called erratics (Dreimanis, 1988).

The main glacial deposits are as follows.

Moraines

Moraines (ablation, lateral, medial, and terminal moraine): The term "moraine" covers a wide range of depositional features associated with glaciers and normally consists of unstratified material. Moraines may be categorized on the basis of their position (lateral, medial, or end moraines), their state of activity (active – in contact with ice, or inactive – not in contact with ice), and their method of formation(ablation or ground moraine) (Embleton and King, 1975). Ablation moraine is a conspicuous layer of active moraine on the surface of glacier.

Esker

An esker is a long-winding ridge of stratified sand and gravel, examples of which occur in glaciated and formerly

glaciated regions of Europe and North America. Eskers are frequently several miles long and, because of their peculiar uniform shape, are somewhat like railroad embankments.

Most eskers are believed to form in ice-walled tunnels by streams which flowed within (englacial) and under (subglacial) glaciers. After the retaining ice walls melt away, stream deposits remain as long-winding ridges.

The concentration of rock debris in the ice and the rate at which sediment is delivered to the tunnel by melting and from upstream transport determines the amount of sediment in an esker. The sediment generally consists of coarse-grained, water-laid sand and gravel, although gravelly loam may be found where the rock debris is rich in clay. This sediment is stratified and sorted, and usually consists of pebble/cobble-sized material with occasional boulders. Bedding may be irregular but is almost always present, and cross-bedding is common (Easterbrook, 1999).

Bibliography

Dreimanis, A., 1988. Tills: Their genetic terminology and classification. In Goldthwaite, R. P, Matsch, C. L (eds.), *Genetic Classification of Glacigenic Deposits*. Rotterdam: A.A. Balkema, pp. 17–83.

Easterbrook, D. J., 1999. *Surface Processes and Landforms*. New Jersey: Prentice Hall, p. 352. ISBN ISBN 0 13 860958 6.

Embleton, C., and King, C. A. M., 1975. *Periglacial Geomorphology (Their Glacial and Periglacial Geomorphology*, 2nd edn. London: Edward Arnold, Vol.2, ISBN-13: 9780713157932; 0713157933.

Trenhaile, Alan, 2007. *Geomorphology: A Canadian Perspective*. Don Mills: Oxford University Press, pp. 188–191. ISBN 0-19-542474-3.

DIGITAL ELEVATION MODEL GENERATION OVER GLACIERIZED REGION

Thierry Toutin
Canada Centre for Remote Sensing, Natural Resources Canada, Ottawa, ON, Canada

Introduction

Digital elevation models (DEM) represent one of the most important data source for investigating the geophysical science of glaciated regions, not only the Earth's Polar Regions, but also the inland ice caps and the high-mountain ice fields. To name a few applications: (1) Multi-date multisource DEMs enable derivation of 3D glaciers parameters, such as elevation and volume changes, surface displacements, surface mass balance (since Krabill et al., 1995 to Bamber and Rivera, 2007). (2) Regions of basin can be determined with highly accurate DEM (Hardy et al., 2000). (3) Hazards assessments due to rapid changes of high mountains environment can be performed with continuous monitoring based on regular remote sensing observations (Kääb et al., 2005). Stereo-photogrammetry applied to air photos acquired at different dates can be used to simultaneously computed DEM and velocity fields (Kääb et al., 2005). Because most of these applications are addressed in this Encyclopedia, this entry only gives an in-look for the generation of DEMs using Earth observation (EO) data from multi-platform and multi-sensor.

Some data and methods for DEM generation could have some limits (orbit inclination, elevation accuracy and grid spacing, strong terrain slopes) in their usefulness for some applications in glaciated regions. The synergy of terrestrial, airborne, spaceborne data from various sensors in the visible and microwave spectrum using different methods and algorithms (clinometry, stereoscopy, interferometry, and altimetry) could thus overwhelm these limitations.

Relevant sensor technologies

The relevant sensors are easier to distinguish as a function of the energy wavelength: the optical sensors in the visible and infrared (VIR) spectrum and the radar in the microwave spectrum. The following gives the basic description for each sensor useful for the comprehension of DEM generation over glaciated regions.

Optical sensors

The main optical sensors used for elevation extraction and/or DEM generation are: (1) the digital scanners and (2) the laser altimeter or the Light detection and ranging (Lidar).

Digital scanners (ASTER, SPOT)

The two main satellites with stereo capability (Toutin, 2001) of specific interest for DEM generation over large glaciated regions are:

1. The Advanced Spaceborne Thermal Emission and Reflection Radiometer (ASTER), a Japanese instrument launched on December 19, 1999, on the Terra platform as part of National Aeronautics and Space Administration's (NASA) Earth Observing System (EOS).
2. The SPOT-1 to -5 series (*Satellite Pour l'Observation de la Terre*) with the high-resolution, optical imaging sensors, as part of Earth observation strategy of the Centre National d'Etudes Spatiales (CNES), the French Space Agency.

As a matter of fact, ASTER is the prime instrument that is used to produce an inventory of glaciers around the world as part of the Global Land Ice Measurements from Space (GLIMS) project due to the high resolution (15 m) of the visible and near infrared (VNIR) subsystem and its along-track stereo capability. ASTER has been developed and launched in order to provide a new source of topographic data for the land surface of the Earth (Welch et al., 1998). In summary, the most important specifications of the ASTER stereo subsystem that govern the DEM generation capabilities include: along-track

same-date stereo geometry; one nadir-viewing and one 27.7° aft-viewing telescope; base-to-height (B/H) of 0.6; ground resolution of 15 m; 9 s required to acquire a 60 × 60 km scene; 64 s required to acquire a stereo pair; bandpass of 0.76–0.86 μm (near infrared) in channel 3N (nadir) and 3B (aft). In October 2009, the distribution of an ASTER global DEM (GDEM) for all the land regions between ±83° latitude (http://www.ersdac.or.jp/GDEM/E/2.html) generated using all available stereo-pairs started: the size of each tile is 1° by 1° with 30-m posting interval and an estimated elevation accuracy (standard deviation) of 10 m.

Since February 22, 1986, the SPOT series include five satellites with two fully-operational: SPOT 4, launched on March 24, 1998, and SPOT 5, launched on May 3, 2002. They maintain the main features of its predecessors but with enhanced resolutions, and SPOT 5 has also new along-track stereo sensors, High Resolution in Stereoscopy (HRS), with 10-m resolution to measure relief elevation (Figure 1).

The most important specifications of the SPOT series that govern the DEM generation capabilities include:

- For SPOT 1-4 HRV, 10 m panchromatic images and across-track stereo capability with variable B/H up to 1.1; 60 × 60 km scene; bandpass of 0.50–0.73 μm but 0.61–0.68 μm for SPOT 4
- For SPOT 5 HRG, 2.5–5-m panchromatic images and across-track stereo capability with variable B/H up to 1.1; 60 × 60 km scene; bandpass of 0.48–0.71 μm
- For SPOT 5 HRS, 10 by 5-m panchromatic images and along-track same-date stereo capability; B/H of 0.8; 120 × up to 600 km long scene; bandpass of 0.48–0.70 μm

Laser altimeter (Lidar, laser scanning, ICESat)

The laser altimeter, or Lidar or airborne laser swath mapping (ALSM), is an optical remote sensing technology (micropulse lidar system and short wavelengths) that measures properties of scattered light to find range and/or other information of a distant target. The range to an object is determined by measuring the time delay between transmission of a pulse and detection of the reflected signal. In addition to the 3D surface mapping capability of the Lidar, a laser scanning sensor can also record the intensity of the backscattered pulse energy returned from the surface. The intensity return is a function of the pulse range, the pulse footprint, the angle of incidence, and the spectral characteristics of the optical sensor in combination with the surface and object imaged on the ground.

There are several major components to a lidar system: (1) the *Laser* (generally 1,047, 1,064, 1,550 nm, beam divergences of 0.3–0.5 mrad); (2) the *Scanner and optics* (displacement of the platform provides the along-track distribution of pulses while the scanner redistributes pulses in the across-track direction ±40° being the more common); (3) the *Receiver and receiver electronics*; and (4) the *Position and navigation systems* (GPS receiver, IMU or star-tracker system). Better target resolution is achieved with shorter pulses, and the pulse footprint is a function of beam divergence, range, and angle of incidence.

January 13, 2003, a spaceborne laser altimeter (ICESat) was launched with the objectives of monitoring ice-surface elevation in a short-term period over Artic and Antarctic ice sheets (http://icesat.gsfc.nasa.gov/). One lidar of the Geoscience Laser Altimeter System (GLAS) transmits short pulses (4 ns) at 1,064-nm wavelength for deriving topography using also a GPS receiver and a star-tracker attitude determination system. The specific near-circular near-polar orbit of ICESat results in across-track spacing at the equator of about 84 km, reduced to around 54 km at latitude of 50°, and provides coverage to ±86° latitude (full Greenland and Artic ices masses and much of Antarctic) with orbital crossovers to estimate elevation changes in Antarctica (Zwally et al., 2002).

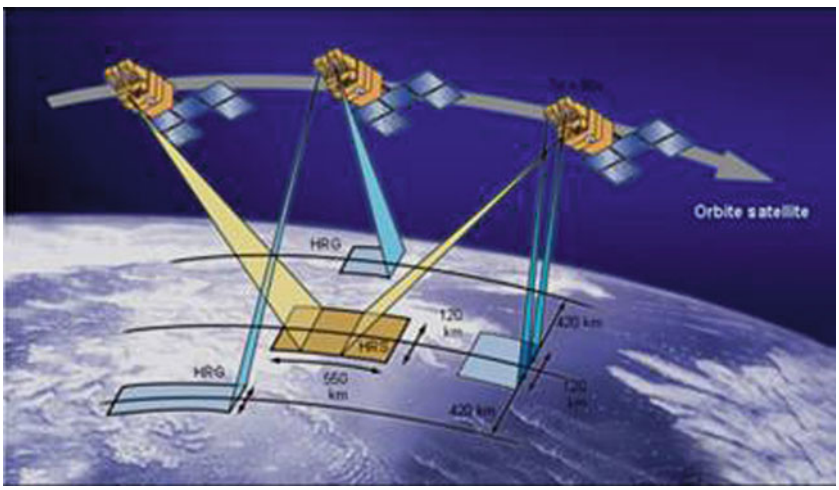

Digital Elevation Model Generation Over Glacierized Region, Figure 1 Stereo geometry of SPOT-5 and its sensors HRG and HRS.

The footprint is 76 m in diameter with 175-m along-track spacing. The planimetric location of footprints is better than 6 m, and the satellite-surface distance has accuracy better than 10 cm under clear-sky conditions, diminishing to about 1 m at the Pole. However, the computed elevation accuracy varies from 30 cm over low slopes ice-sheet regions to 80 cm when slopes are 1–2°, while elevation changes can be estimated within 60 cm. The forward scattering in thin clouds and the errors in laser pointing are, however, the main limiting factors (Thomas et al., 2004). Because the return pulse width increases with surface roughness and/or slopes, its characteristics are used for determining these parameters (Brenner et al., 1983), but some imprecision can occur because the surface height represents a mean value over the footprint. Due to technical issues, the different GLAS lasers operated since February 20, 2003, in burst of 4–5 week long-periods three times a year during 16 operational campaigns (http://glo.gsfc.nasa.gov/).

GLAS data can be obtained from the National Snow and Ice Data Center (NSIDC) DAAC, which archived 15 Level-1 and Level-2 data products via FTP Pull or FTP Push (http://nsidc.org/data/icesat/index.html). Data also include the laser footprint gelocation and reflectance, as well as geodetic, instrument, and atmospheric corrections for range measurements. One Level-2 altimetry product is of special interests for surface elevations over ice sheets is GLA12 (GLAS/ICESat L2 Antarctic and Greenland Ice Sheet Altimetry Data). The GLA12 data from the first seven operational periods (from February 2003 through June 2005) were used to provide new surface elevation grids of the ice sheets and coastal regions, with greater latitudinal extent and fewer slope-related effects than radar altimetry. The DEMs of Antarctica and Greenland are reported on polar stereographic 500-m and 1-km grids, respectively, as centimeters above the datum relative to WGS84 ellipsoid and EGM96 geoid.

Microwave sensors

Only the active form of microwave sensing providing their own source of microwave radiation (approximately 1 cm to 1 m in wavelength) to illuminate the target can be used for elevation extraction or DEM generation on glaciated regions. Longer wavelength microwave radiation can penetrate through cloud cover, haze, dust, and all but the heaviest rainfall as the longer wavelengths are not susceptible to atmospheric scattering which affects shorter optical wavelengths. This property allows detection of microwave energy under almost all weather and environmental conditions so that data can be collected at any time. They are generally divided into two distinct categories: (1) *imaging*, the *Ra*dio *d*etection and *r*anging (radar) and the synthetic aperture radar (SAR) and (2) *non-imaging*, the radar and SAR altimeter.

Imaging: Radar and SAR

The sensor transmits a microwave (radio) signal toward the target and detects the backscattered portion of the signal. The strength of the backscattered signal is measured to discriminate between different targets and the time delay between the transmitted and reflected signals determines the distance (or *range*) to the target. Such radar systems will require long antenna to achieve fine resolution radar imagery, which is unacceptable for spaceborne radar. The solution is to combine information from the moving antenna to synthesize a long antenna: such radar systems are called synthetic aperture radar (SAR). Radar backscatter is sensitive to physical and structural properties of the target (dielectric properties, surface roughness, shape, etc) as a function of the wavelength, polarization, and incidence angle. More information on SAR and their applications can be obtained in the *Manual of Remote Sensing*, 3rd edition (1998) and the particular radar-target interactions with snow/firn medium in this Encyclopedia.

Since the 1980s, several research and commercial airborne radar systems around the world have been developed and are operational. Since the first ESA's ERS-1 (1991) to Radararsat-2 (2007), numerous spaceborne SAR data are available in different configurations. The most important characteristics for DEM generation can be summarized as follows:

- Single or multiple spatial resolutions between 1 m and 30 m
- Single or multiple radar frequencies: most popular wavelengths are X (2.4–3.75 cm), C (3.75–7.5 cm), and L (15–30 cm) bands
- Single/multiple polarization or full polarimetric modes
- Single or multiple incidence angles between 20° and 60°
- Swath coverage between 20 and 100 km (and 500 km for ScanSAR)
- Revisit time of few days (3–35)

Non-imaging: Altimeter (radar, SAR, CryoSat)

The primary method to provide the spatial coverage and density with sufficient elevation accuracy for mass balance and sea level assessments of large low-slope ice sheets is the radar altimeter (RA). Because they are nadir-viewing instruments, using the ranging capability, they provide a topographic profile of the Earth below the satellite track (Figure 2). Surface elevation is the difference between the satellite's position on orbit with respect to an arbitrary reference surface (the Earth's center or a rough approximation of the Earth's surface: the reference ellipsoid) and the satellite-to-surface range. In a first step, the time delay between the pulse emission and the returned echo from the surface is converted into an accurate measure of the satellite height with the knowledge of the propagation velocity. In a second step, the surface elevation is thus computed from the satellite ephemeris using several locating systems (Laser tracking, GPS system, DORIS instrument from Doppler location, Precise Range and Range-rate Equipment, PRARE, using range determination). This is a straightforward concept, but more difficult to understand in all details because the RAs emits pulses not in narrow beam, such as a laser but

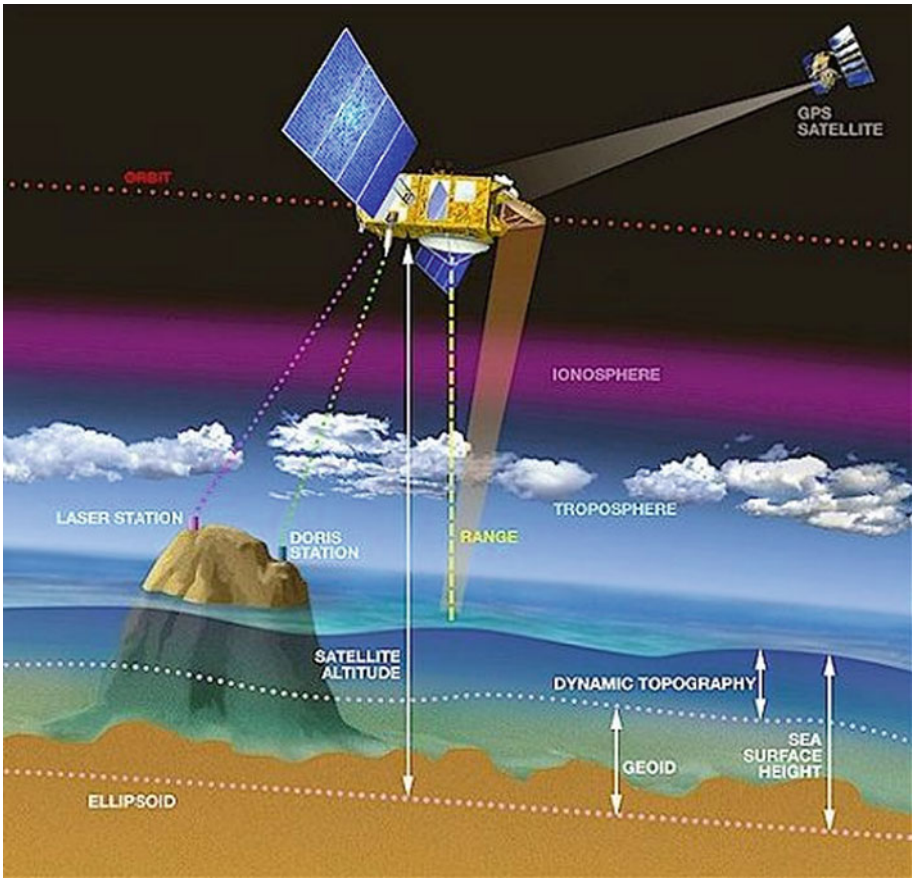

Digital Elevation Model Generation Over Glacierized Region, Figure 2 The principle of altimetry. (Credits and reproduced with the permission of CNES and D. Ducros) (http://www.altimetry.info).

in a wider beam (more than 1°), which becomes wider the further it travels. Further details and discussions can be found in Rémy et al. (2001) and Rosmorduc et al. (2009).

The theoretical use of an active ranging system for mapping elevation of ice sheets was first proposed by Robin (1966). Its theoretical concept was thus scientifically demonstrated on inland ice sheets with Seasat (SEAfaring SATellite) in June 1978 and Geosat (GEOdetic SATellite) from April 1985 to January 1990 because of 72° latitudinal limit providing coverage of the southern half of Greenland and about one fifth of Antarctica. The ERS (European Remote Sensing) series starting 1991 resolved the problem of high-latitude coverage with 81.5° latitudinal limit, generating a continuous record from 1991 covering almost the whole Greenland and four fifths of Antarctica. Finally, Envisat (Environmental Satellite) carries ten complementary instruments, including dual-frequency RA-2 altimeter. Dual-frequency RA is useful (1) for ionospheric corrections over the oceans with the determination of atmospheric electron content, which affects the radar signal path delay, and (2) for measuring the amount of rain in the atmosphere (Rosmorduc et al., 2009), and (3) to be less sensitive to temporal snowpack artifacts.

A second generation of RA has been proposed that could resolve most of the problems encountered with the traditional pulse-limited footprint RAs, such as latitudinal limit, coverage, footprint size, surface gradient larger than the antenna beamwidth, poor accuracy in steep slopes (more than about 1°) and marginal outer regions, melting zones, etc. (Wingham, 1995). This novel-design RA is an altimeter/interferometer (Drinkwater et al., 2004): the SAR Interferometric Radar Altimeter (SIRAL) to be launched on ESA's CryoSat II in 2010, which can be operated in three modes (Rosmorduc et al., 2009):

1. A conventional low-resolution, nadir-pointing altimeter mode measuring the satellite-Earth's surface distance.
2. A conventional SAR mode: because SIRAL will send at 50-μs interval a burst of pulses, processed in one operation, it thus generates 250-m wide across-track strip using Doppler shifts in the forward- and aft-looking parts of the beam.

3. An interferometric SAR (InSar) mode, which uses a second receive antenna to measure the arrival angle. The radar echo is thus received by the two antennas with 1-m across-track interferometric baseline and will be processed with interferometric algorithms using the phase difference.

The last RA generation is the Glacier and Land Ice Surface Topography Interferometer (GLISTIN) using Ka-band radar wavelength, which was developed to support International Polar Year studies. During their first airborne mission on May 1, 2009, scientists from JPL and Dryden Flight Research Center, Calif. USA, applied for the first time, millimeter-wave interferometry with two receiving antennas, separated by about 0.25 m. They evaluated the ability to map ice surface topography of Greenland. About 250,000 km^2 were mapped during 110 h of data collection. The elevation should be accurate to within 0.1 m of elevation with a ground footprint equivalent to spaceborne lidar. Scientists expect GLISTIN to penetrate the snow and ice by just centimeters, rather than by meters, as current microwave radars do.

Various methods: description and results

Clinometry (shape from shading)

Using the principle that an image of a smooth object known to have a uniform surface will exhibit gradations of brightness, or shading, the shape can be determined to map the height of this surface. Because there are two degrees of freedom to surface orientation, the reflectivity does not uniquely determine the local normal but a set of possible normal directions. These directions describe a cone, whose axis is the illumination direction, and the half-angle the incidence angle. Consequently, local operation on the brightness alone cannot be used to determine the shape of the surface and its orientations. Additional constraint must therefore be added: generally the surface is assumed to be continuous and smooth, so that the surface orientations of neighboring surface elements are not independent. If the reflectivity function (a general Lambertian model) and the position of the illumination source are known, the shape can thus be obtained from the shading. In summary, the accuracy of this technique with remote sensing data is limited by intrinsic radiometric and geometric ambiguities (Toutin, 2001; Toutin and Gray, 2000):

1. The reflectivity is not only dependent on the local incidence angle, but also on the albedo related to land cover, rugosity, humidity, etc., as a function of the sensor (radiometric ambiguity).
2. The determined incidence angle yields to a set of potential orientations whose normal directions describe a cone (conic ambiguity). Some reference elevation information is thus needed to derive the absolute elevation, and the accuracy is limited by the height error propagation.

Consequently, clinometry remains a marginal technique, except on homogeneous low-slope terrain surfaces, such as ice sheets/caps: the radiometric/geometric ambiguities (albedo vs. reflectance; incidence angle with Lambertian surfaces) can these be resolved more easily.

Application with VIR (Landsat, SPOT, AVHRR, and MODIS)

Lodwick and Paine (1985) used two Landsat-1 and 2 MSS images (July and October) over an ice cap on Baffin Island, Canada, to obtain high and low sun angles and maximum difference in sun azimuth. Because they demonstrated that the reflectance conditions of an ice cap are non-Lambertian for a large range of incidence angles, they applied a simple linear model between typical maximum slopes in the "sun facing and away facing" directions and the reflectance values at the 1% level of the gray value histogram. Finally, a weighted third-order surface adjustment is carried out with nine control points to transform the 50-m posting slopes in the sun-azimuth direction into elevations. The results for the basic shape of the ice cap surface compared well with the base map. Some variations could be partly explained by the surges (melting and refreezing) of the ice-cap surface. No quantitative accuracy was performed due to the lack of accurate topographic information. Other experiments were thus developed either using Landsat or SPOT images (Dowdeswell and McIntyre, 1987; Bingham and Rees, 1999; Cooper, 1994). Different assumptions were made: (1) slopes are less than 2°; (2) surfaces have uniform reflecting properties; (3) the maximum slopes is smaller than the incidence angle; and (4) the sensor is not saturated. While quantitative accuracy evaluations were limited, it seems that the first solution (±2 m rms with Fourier domain, Cooper, 1994) achieved better results than the second one (±15–20 m rms with cosine of illumination angle, Bingham and Rees, 1999) for solving the Lambertian scattering properties.

On the other spatial range, Scambos and Fahnestock (1998) also applied the method with two low-resolution (1.1 km) cloud-free Advanced Very High-Resolution Radiometer (AVHRR) data and a coarse radar-altimetry-derived DEM (5-km grid spacing) previously generated over the northeast Greenland ice stream. The extracted slopes are transformed into elevation data adding topographic details to the coarse DEM with spatial scales of around 3–20 km. This was then confirmed by the comparison with airborne laser elevation profiles. Scambos and Haran (2002) applied the method with 44 AVHRR images using the full Greenland DEM (Bamber et al., 2001). The same experiments were performed in Antarctica with MODIS data taking profit of an improved spatial (250 m) and radiometric (12 bits) resolutions and input coarse DEMs derived from satellite laser and radar altimetry (Haran et al., 2008). However, the first conclusion of the first experiment that an ice cap is a non-Lambertian surface for a large range of incidence angles was never taken into

account in these experiments, which applied Lambertian reflectivity with large field-of-view images (Landsat, MODIS, and AVHRR).

Stereoscopy

To obtain good geometry for better DEM generation, the intersection angle (or B/H) should be large in order to increase the stereo exaggeration factor, or equivalently the observed parallax, which is used to determine the terrain elevation: B/H of 0.6 (ASTER) to 1.1 (SPOT) are a typical value to meet the requirements of topographic mapping (Toutin, 2001). Whatever the data sources, the different processing steps to produce DEMs using stereo images can be roughly described (Figure 3):

1. Data acquisition and pre-processing: the rawest available stereo images and their metadata and stereo GCPs
2. 3D geometric model computation: least-squares bundle adjustment using the stereo GCPs
3. DEM generation: image matching and editing in the quasi-epipolar geometry and cartographic reprojection with regular grid spacing

The image matching applied on the quasi-epipolar images can be based on single primitive approach (gray level, feature-based, etc.) or hybrid approach by combining multi-primitive geometrically constrained least-square matching, both using pyramid multi-scale algorithm. DEM editing includes blunder removal, mismatched filling by interpolation or with seed points, filtering and smoothing, as well as correction of land cover heights. The final step is to resample the epipolar DEM into the user map projection with regular grid spacing.

Analog (Finsterwalder, 1954), analytical (Reinhardt and Rentsch, 1986) and digital (Baltsavias et al., 2001) photogrammetry has demonstrated the relevance and benefit of air photos for topographic mapping of glaciers. The photo archives to compare multi-date photogrammetric DEMs of glaciated regions can also be exploited (Hopkinson, 1997; Bindschadler and Vornberger, 1998). Besides all these advantages (archives, stable geometry, resolution, level of details, customer control), airborne photogrammetry is mainly used for small-to-medium size mountains glaciers. However, the difficulty to collect GCPs and the image matching in snow fields are two key issues, which can lead to large DEM errors exceeding any measured changes in glacier volume. These DEMs are mainly limited to altitudes below the equilibrium line where crevasses and other features provide enough contrast (Howat et al., 2008).

For large remote regions with difficult ground accessibility satellite data are recommended. To obtain stereoscopy with images from VIR satellite scanners, two solutions are possible:

1. The along-track same-date stereoscopy from the same orbit (ASTER, SPOT5 HRS)
2. The across-track multi-date stereoscopy from two different orbits (SPOT HRV/HRG)

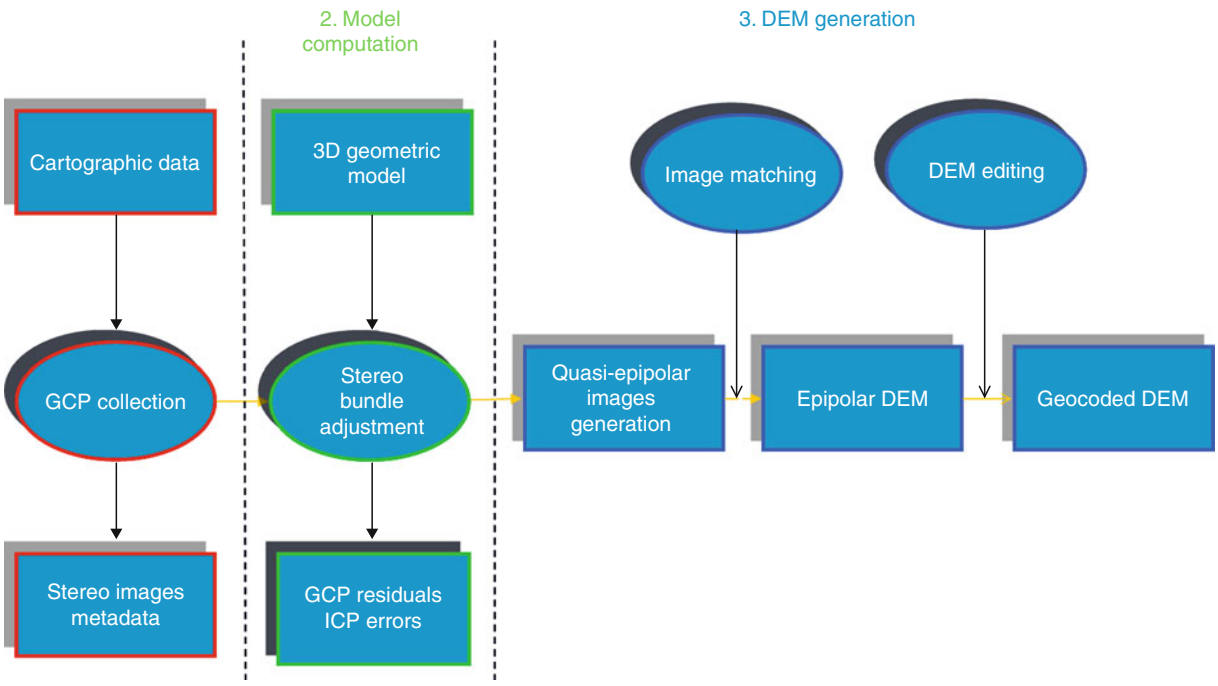

Digital Elevation Model Generation Over Glacierized Region, Figure 3 Processing flow for DEM generation by stereoscopy.

The almost-simultaneous along-track stereo-data acquisition gives a strong advantage in terms of radiometric variations versus the multi-date stereo-data acquisition with across-track stereo (Toutin, 2001): mainly in the image matching success due to less temporal radiometric difference. In addition, glacier flow (up to a few meters per day) during this few-day interval can bias the topographic measurement (Berthier and Toutin, 2008).

The advantages of using satellite data are:

- Images cover large regions: 60 by 60 km for SPOT HRV/HRG and ASTER, but 120 by 600 km for SPOT-5 HRS.
- Strips formed with consecutives images from the same-date orbital path and block of several strips can be simultaneously processed over large regions.
- Less processing is required with one satellite image than with a block of aerial photos.
- Less GCPs with a relaxed accuracy related to sensor resolution (10 m for ASTER and 2–5 m for SPOT) are required.

Some disadvantages specific to ice regions are related to the lower resolution of satellite sensors (Berthier and Toutin, 2008): sufficient variation of albedo over few pixels for a better image matching; frequent cloud cover over mountainous and polar regions; surface features greater than the sensor resolution; and elevation changes greater than the stereo capability. Numerous researches generating DEM over mountain glaciers have been reported within GLIMS projects (Kääb et al., 2005), and the fourth International Polar Year (IPY) projects (Berthier and Toutin, 2008; Korona et al., 2009) over the glaciers of the Antarctic and Greenland ice sheets (Howat et al., 2008). Elevation errors equivalent to the resolution, e.g., 15 m for ASTER and 5–10 m for SPOT (Kääb et al., 2005; Berthier et al., 2004) were generally reported when comparing with limited or not-always-accurate ground truth (old photogrammetric DEM, SRTM, bedrocks profiles, ICESat data, independent check points, etc.). An almost linear correlation between accuracy and terrain-slopes was also found (Berthier et al., 2004; Korona et al., 2009).

US Geological Surveys and the Earth Remote Sensing Data Acquisition Centre in Japan have agreed to produce high-quality global DEM (GDEM) from the ASTER data acquired within 83° latitudinal limit. It thus covers all the land on Earth and the majority of glaciated regions. These data are freely available to all users whatever the area size and location. Because the ASTER GDEM (30 m grid spacing; 7-m accuracy 1σ) is developed based on a grid of 1° × 1° in latitude and longitude, no scene selection or mosaicking is required (http://www.ersdac.or.jp/GDEM/E/1.html).

Interferometry

Radar interferometry, using the coherent property of modern SAR, is a better alternative to the conventional stereoscopic method. Imaging interferometric SAR (InSAR) combines complex images recorded either by two antennas at different locations (across-track) or with the same antenna at two different times (repeat-pass). Both systems can be applied with air- and spaceborne SAR. Analysis of the differential phase between the SAR images can lead to information on terrain elevation or, with observations with the same antenna at different times, to terrain displacements. The InSAR processing for DEM generation is summarized (Figure 4), but more information can be found in (Rosen et al., 2000).

There are numerous public/private airborne InSAR systems around the world (Canada, USA, Denmark, France, Germany, China, etc.) using generally across-track and along-track interferometry from multiple SAR wavelength bands and polarizations. Depending of the wavelengths and the volumetric content of water in the snow, the SAR penetration can largely vary from the full depth of glaciers (P-band) to few centimeters (X-band over wet snow). Consequently, airborne SAR interferometry can provide either elevation of the bed rock or the top of glaciers (Figure 5). For most of the experiments, few-meter accuracy (1–3 m, 1σ) is achieved in horizontal and vertical directions, but can be dependent of the altitude and local incidence angle (Muskett et al., 2003) and of the SAR backscatter and penetration depth (Magnússon et al., 2005). It is also recommended to apply a multi-look process for reducing SAR noise (phase and speckle) and post-process the DEM for filtering/smoothing and removing noisy regions.

To date, only one across-track single-pass interferometric satellite mission, SRTM, derived DEMs, but only between 56° South and 60° North. It was thus used in mountain glaciers and ice caps (Kääb et al., 2005). The general vertical accuracy is around 16 m (better in some regions) with bias (10 m) at high altitudes, maybe due to SAR problems in mountains (Berthier et al., 2006). The fusion of SRTM DEM with air-photo DEMs could thus be a valid combination for mountain glaciers.

A recent interferometric satellite launched in 2010, TanDEM-X (TerraSAR-X add-on for Digital Elevation Measurement), is the name of TerraSAR-X's twin satellite, a German Earth observation satellite using X-band SAR. It is a second, almost identical spacecraft to TerraSAR-X launched in 2007. TanDEM-X is also the name of the satellite mission flying the two satellites in a closely controlled formation with typical distances between 250 and 500 m. The primary mission objective is to use almost-simultaneous across-track interferometry for the generation of a consistent global DEM with an unprecedented accuracy according to better than Digital Terrain Elevation Data (DTED) Level 2 specifications. The new DEM resolution will roughly correspond to DTED Level 3 (post spacing of better than 12 m) and a height accuracy of better than 2 m. However, the accuracy will degrade to tens of meters in mountainous regions. On July 2010, researchers at the German Aerospace Center facility in Oberpfaffenhofen published the first 3D images from the TanDEM-X satellite mission

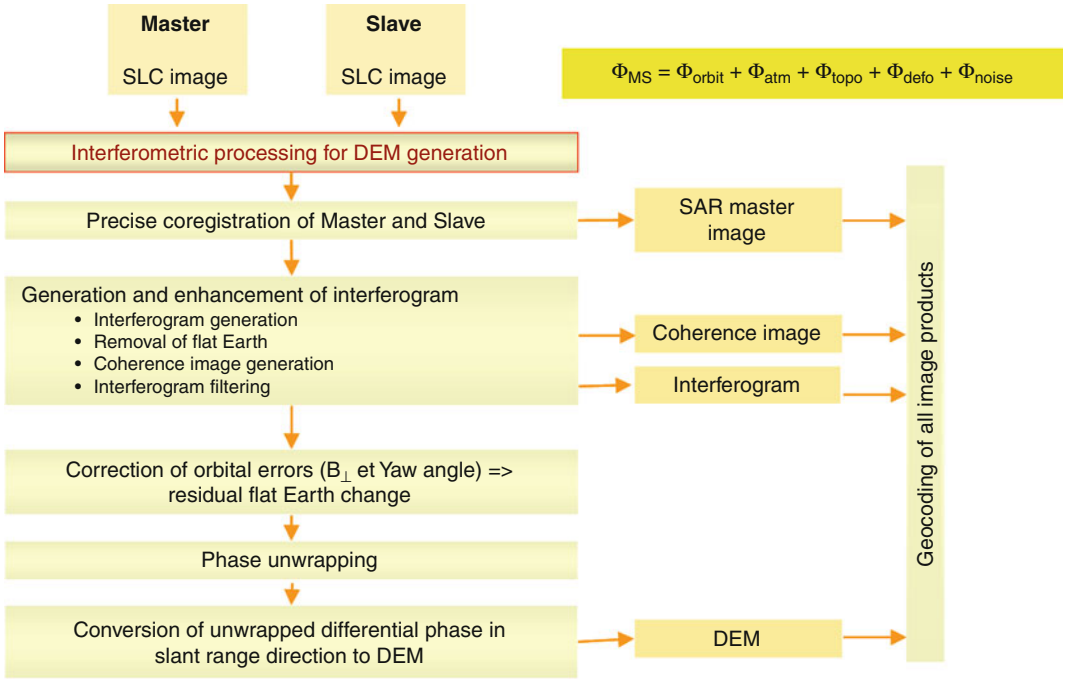

Digital Elevation Model Generation Over Glacierized Region, Figure 4 Interferometric SAR processing for DEM generation.

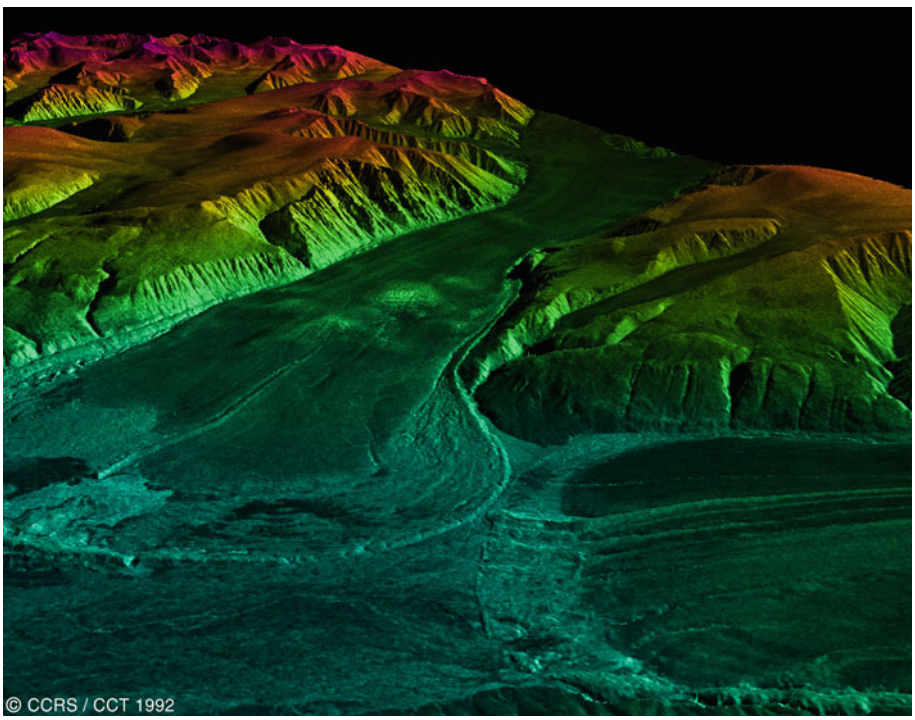

Digital Elevation Model Generation Over Glacierized Region, Figure 5 This north-looking perspective of a section of the Bylot Island, Canada, using CCRS Convair580 InSAR DEM shows peaks and plateau ice caps of the Byam Martin Mountains. An unnamed glacier flows southward, and its terminal lobe almost meets the terminus of a westward flowing glacier, on their common outwash plain. Many geological features are clearly visible: crevasses (**a**), super glacial streams (**b**), lateral and terminal moraines. The raised medial moraines, and ablation moraines (**c**), and a dammed lake (**d**) are evidence of glacial retreat (Gray et al., 1995). http://www.ccrs.nrcan.gc.ca/radar/airborne/cxsar/sbinter_e.php.

(http://www.spacedaily.com/reports/TanDEM_X_Delivers_First_3D_Images_999.html). A group of icy Russian islands of the Severnaya Zemlya group in the Arctic Ocean was selected for the first test: the October Revolution island showed in 3D an ice cap with a diameter of 30–40 km and 700 m high, which is located on a landscape of snow and ice and where the drainage channels run from the ice cap. In 2014, this homogenous DEM will be available for the Earth's entire land surface, i.e., 150 Mio square kilometers. Without doubt, it will be of interest for all glaciological applications.

On the other hand, repeat-pass interferometry can be applied with ERS-1/-2, Radarsat-1/2 and TerraSAR-X at higher latitudinal coverage (80°) for covering ice sheets, but with limitations due to temporal decorrelation of the signal (mainly over moving glaciers) and the separation of topographic and displacement phases. However, the ERS tandem mission (1 day) gives a better temporal resolution than repeat-pass ERS-1 (3 days) and Radarsat (24 days). To name few examples: ERS-1 SAR data from one or more tracks were used over various outlet glaciers in Greenland to generate wide-area homogeneous DEM with 3–5 m accuracy (Joughin et al., 1996).

Altimetry

Lidar

The airborne lidar processing includes: (1) the determination of the absolute position of the laser scan system during the flight by analysis of the time-synchronized GPS and INS data, (2) the computation of the relative coordinates, (3) the system calibration with external data, (4) the calculation of the coordinates in a ground reference system, and (5) the post-processing of the DEM (Arnold et al., 2006). The uncertainties in the laser range (around 7 cm) and the GPS position (around 10 cm) are the main factors in the final elevation accuracy (Kennett and Eiken, 1997). In addition, the effect of calibration drift over time can generate 7-cm elevation drift for 1-h flight (Davenport et al., 2004). An airborne Lidar sensor with a good calibration can achieve 10–20 cm accuracy in the three axes (Davenport et al., 2004), but dependent of terrain slopes (Hodgson and Bresnahan, 2004). In addition to laser scanning, the Lidar DEM can be used to ortho-rectify the intensity image of the laser pulse return from the ground surface and to generate other 3D added-value products. The first experiments for 3D glaciological applications were performed with laser profiling (a single measurement line below the aircraft) in Iceland/ Greenland (Garvin and Williams, 1993) and Alaska (Echelmeyer et al., 1996) and then with laser scanning over Greenland (Krabill et al., 1995; Bindschadler et al., 1999), alpine glaciers (Kennett and Eiken, 1997), and small inland glaciers (Baltsavias et al., 2001; Arnold et al., 2006). They also have been used for calibration/validation over Greenland (Bindschadler et al., 1999; Bamber et al., 2001).

While the primary goal of ICESat is to measure elevation and its change of the vast polar ice sheets, it also collects data over large temperate glaciers (Patagonia, Alaska). Even if these glaciers display rougher surfaces and steeper zones, individual footprint rather than averaging over large regions or relying on crossovers can be used to estimate glacier elevation. A partial DEM over Antarctica (north of 86°S, 500-m spacing) was produced using only ICESat data (DiMarzio et al., 2008) or combined with slope-weighted data of scanning radar altimeter (SRA) for expanding Antarctica's DEM (Bamber et al., 2005). However, most of the experiments used ICESat data for calibration/validation of DEMs over Antarctica (Bamber and Gomez-Dans, 2005), ice sheets and caps (Korona et al., 2009) or glaciers (Berthier and Toutin, 2008).

SAR

To calculate precise ice surface elevations, the altimeter range measurements need to be referenced to a common datum and corrected for tracker misalignment of the waveform due to the undulating and nonuniform nature of ice surface. The corrected altimeter range measurement is then subtracted from a precision orbit to calculate a corrected surface height. The slope correction post-processing corrects for the largest errors (10–150 m). Then, the waveform retracking post-processing is required over ice sheets because the leading edge of the ice-sheet return waveform deviates from the onboard altimeter tracking gate, causing an error (±15 m) in the telemetry-range measurement. Finally, the atmospheric delay post-processing includes correction for dry and wet tropospheric refractions (1.5–2.5 m) and ionospheric refraction (0.02–0.10 m).

Before the 1990s, the topography of ice sheets was only known with few measurements and errors of hundreds of meters. Afterward, SRAs, in particular from ERS, have been one of the major sources for the generation of DEMs (5-km grid spacing) over Greenland (Bindschadler et al., 1989; Bamber et al., 2001) and Antarctica (Bamber et al., 2005). Elevation measurements can be adjusted at orbit crossover, mainly at the high latitudes. Over the latitudinal limit of the satellite (around 81.5°S), terrestrial measurements have been used to complete the Antarctic DEM (Bamber and Rivera, 2007) or to provide a better spatial sampling in low relief (Liu et al., 1999). More recently, the combination of slope-weighted ERS-SRA data with a good spatial coverage but a poor vertical accuracy, and the Lidar ICESat data with a poor spatial coverage but a good vertical accuracy maximized the grid spacing and the vertical accuracy of the final Antarctic DEM (http://nsidc.org/data/nsidc-0422.html). The spatial grid spacing of this ERS1-2 + ICESat DEM was then improved over West Antarctica using MODIS imagery with shapelets and krigging methods (Haran et al., 2008). The data and method cumulation was also applied to Greenland and Antarctica DEMs generated from ERS-SRA data with airborne laser, AVHRR or MODIS data using clinometry (Scambos and Haran, 2002).

Summary

Most geoscientific applications using georeferenced cartographic data need a good knowledge and visualization of the topography of the Earth's surface: three-dimensional (3D) information, such as digital elevation models (DEM), has to be generated or is to be added for a better interpretation of the two-dimensional (2D) data.

Since the early emergence of earth observation satellites, researchers have investigated different methods of extracting 3D information using satellite data. Apart from a few early stereo-images acquired with handheld cameras during the Gemini and Apollo missions, the first experiments to extract 3D data using stereo viewing from space began with the Earth Terrain Camera (ETC) flown onboard SkyLab in 1973–1974.

Since these early experiments, various analog or digital sensors in the visible or in the microwave spectrum have been flown to provide researchers and geoscientists with spatial data for extracting and interpreting 3D information of the earth's surface. Although the shape-from-shading technique can be applied to optical sensor images in ice sheets and caps with low slopes, stereo-viewing using airborne cameras or digital scanner images was, and still is the most common method used by the mapping, photogrammetry, and remote sensing communities. However, airborne and spaceborne altimeters, such as lidar become more and more popular.

On the part of the spectrum, radar data gives also the opportunity to extract 3D information using image-processing techniques appropriate to the nature of the data. With SAR data, three main methods have been developed: radargrammetry, interferometry, and altimetry. Radargrammetry is roughly similar to photogrammetry with stereo images acquisition from different viewpoints. Interferometry uses mainly the SAR signal data instead of the image, and altimetry becomes important sources of data in the 1990s with the scanning radar altimeter to generate small-scale DEMs.

The chapter reviews the different methods and sensors used to extract absolute or relative elevation and assess their performance applied to glaciated regions using the results from various research and university organizations. It also discusses the respective advantages, difficulties, and constraints of the sensors, the methods, and the technologies to take into account the strength of each when integrating them (input, algorithms, and outputs).

Concluding remarks

Elevation modelling from satellite data has been a vibrant R&D topic for the last 30 years since the launch of the first civilian remote sensing satellite. Different data (space photographs, VIR scanner, SAR, altimeter) in different formats (analog, digital) can be processed by different methods (clinometry, stereoscopy, interferometry, altimetry) taking advantage of the different sensor and image characteristics (geometric, radiometric, phase) using different types of technology (analog, analytical, digital) and processing (interactive, automatic).

Most of the techniques have been proposed and tested in the early years. Shape from shading provides cues all over the studied surface, but can be applied successfully only on homogeneous surfaces, and the method thus remains well adapted to glaciated regions, despite some of its disadvantages.

On the other hand, stereoscopy is generally the preferred method by the mapping, photogrammetry and remote sensing communities, most likely due to the heritage of the well-developed stereo photogrammetry. With the launch of Radarsat-1 in 1995, there is renewed interest in radargrammetry because researchers could take advantages of the R&D in image matching realized for SPOT at the end of the 1980s, and in the new computer technologies. Therefore, the DEM generation has become more automated, but not completely with occasional unmatched expectations, mainly in difficult terrain conditions, such as the glaciated regions, especially in mountain glaciers.

When ERS-1 was launched, scientists became enthusiastic over interferometric techniques using previously developed parametric modelling. Most research efforts have then focused in the first years on image processing (coherence image, phase unwrapping) and afterward on the newly identified physical artifacts (atmospheric conditions, sensor calibration, etc.). All these issues are of importance when generating DEMs in northern glaciated regions.

Finally, altimetry first remained more at the level of scientific interest in the physical parametric modelling and in data or image processing development in the academic and governmental institutions. They are now largely used over ice sheets or caps and alpine and small inland glaciers. They also are well used for calibration/validation of DEMs produced with other methods.

Since any sensor, system, or method has its own advantages and disadvantages, solutions already exploit the complementarity between the different sensors, methods, and processing. It has already been optimized in stereoscopy combining VIR and SAR data where the radiometric content of the VIR image is combined with the SAR's high sensitivity to the terrain relief and its "all-weather" capability. The complementarity of methods has already been applied with SAR combining altimetry and clinometry or to generate an approximate DEM to help the phase unwrapping in interferometry. In the same way, Lidar and SRA were combined to take advantages of their good vertical accuracy and good spatial coverage, respectively.

It seems obvious that the R&D for glaciated regions will then focus on the use of the new high-resolution satellites (VIR and SAR) and the development of their associated technologies. Already large data sets acquired from these types of new satellites (Ikonos, WorldView, KOMPSAT, etc.) have demonstrated their real potential for DEM generation and could potentially be used as primary DEM source or complementary sources for

improving the existing DEMs in glaciated regions, such as it has been shown with the first DEM over ice-cap islands generated from the high-resolution interferometric TanDEM-X mission in July 2010.

Bibliography

Arnold, N. S., Rees, W. G., Devereux, B. J., and Amable, G. S., 2006. Evaluating the potential of high-resolution airborne LiDAR data in glaciology. *International Journal of Remote Sensing*, **27**(6), 1233–1251.

Baltsavias, E. P., Favey, E., Bauder, A., Bosch, H., and Pateraki, M., 2001. Digital surface modelling by airborne laser scanning and digital photogrammetry for glacier modelling. *The Photogrammetric Record*, **17**(98), 83–94.

Bamber, J., and Gomez-Dans, J. L., 2005. The accuracy of digital elevation models of the Antarctic continent. *Earth and Planetary Science Letters*, **237**, 516–523.

Bamber, J. L., and Rivera, A., 2007. A review of remote sensing methods for glacier mass balance determination. *Global and Planetary Change*, **59**, 138–148.

Bamber, J. L., Ekholm, S., and Krabill, W. B., 2001. A new high-resolution digital elevation model of Greenland fully validated with airborne laser altimeter data. *Journal of Geophysical Research*, **10**(B4), 6733–6745.

Bamber, J. L., Gomez-Dans, J. L., and Griggs, J. A., 2005. A new 1 km digital elevation model of the Antarctic derived from combined satellite radar and laser data – part 1: data and methods. *The Cryosphere*, **3**, 101–111.

Berthier, E., and Toutin, Th., 2008. SPOT-5 HRS digital elevation models and their applications to the monitoring of glacier changes: a case study in North-West Canada and Alaska. *Remote Sensing of Environment*, **112**(5), 2443–2454.

Berthier, E., Arnaud, Y., Baratoux, D., Vincent, C., and Remy, F., 2004. Recent rapid thinning of the "Mer de Glace" glacier derived from satellite optical images. *Geophysical Research Letters*, **31**(17), L17401-1–L17401-7.

Berthier, E., Arnaud, Y., Vincent, C., and Remy, F., 2006. Biases of SRTM in high-mountain regions: implication for the monitoring of glacier volume changes. *Geophysical Research Letters*, **33**(8), L08502-1–L08502-5.

Bindschadler, R. A., and Vornberger, P. L., 1998. Changes in West Antarctic ice sheet since 1963 from Declassified Satellite Photography. *Science*, **279**, 689–692.

Bindschadler, R. A., Zwally, H. J., Major, J. A., and Brenner, A. C., 1989. *Surface Topography of the Greenland Ice Sheet from Satellite Radar Altimetry.* NASA SP-503, 65 p.

Bindschadler, R., Fahnestock, M., and Sigmund, A., 1999. Comparison of Greenland Ice Sheet Topography measured by TOPSAR and Airborne Laser Altimetry. *IEEE Transactions on Geoscience and Remote Sensing*, **37**(5), 2530–2535.

Bingham, A. W., and Rees, W., 1999. Construction of a high-resolution DEM of an Artic ice cap using shape-from-shading. *International Journal of Remote Sensing*, **20**(15–16), 3231–3242.

Brenner, A. C., Bindschadler, R. A., Thomas, R. H., and Zwally, H. J., 1983. Slope induced errors in radar altimetry over continental ice sheets. *Journal of Geophysical Research*, **88**(C3), 1617–1623.

Cooper, A. P. R., 1994. A simple shape-from-shading algorithm applied to images of ice-covered terrain. *IEEE Transactions on Geoscience and Remote Sensing*, **32**(6), 1196–1198.

Davenport, I. J., Holden, N., and Gurney, R. J., 2004. Characterizing errors in airborne laser altimetry data to extract soil roughness. *IEEE Transactions on Geoscience and Remote Sensing*, **42**(10), 2130–2141.

DiMarzio, J., Breener, A. C., Schutz, R., Schuman, C. A., and Zwally, H. J., 2008. GLAS/ICESat 500 m laser altimetry digital elevation model of Antarctica. National Snow and Ice Data Center. Digital Media. http://nsidc.org/data/nsidc-0304.html

Dowdeswell, J. A., and McIntyre, N. F., 1987. The surface topography of large ice masses from Landsat imagery. *Annals of Glaciology*, **33**, 16–23.

Drinkwater, M. R., Francis, R., Ratier, G., and Wingham, D. J., 2004. The European Space Agency's Earth Explorer Mission CryoSat: measuring variability in the cryosphere. *Annals of Glaciology*, **39**, 313–320.

Echelmeyer, K. A., Harrison, W. D., Larsen, C. F., Sapiano, J., Mitchell, J. E., Demallie, J., Rabus, B., Adalgeirsdottir, G., and Sombardier, L., 1996. Airborne surface profiling of glaciers: a case study in Alaska. *Journal of Glaciology*, **42**, 538–547.

Finsterwalder, R., 1954. Photogrammetry and glacier research with special reference to glacier retreat in the Alps. *Journal of Glaciology*, **2**, 306–315.

Garvin, J. B., and Williams, R. S., 1993. Geodetic airborne laser altimetry of Breiðamerkurjökull and Skeiðarárjökull, Iceland and Jakobshavns Isbræ, West Greenland. *Annals of Glaciology*, **17**, 379–385.

Gray, A. L., Mattar, K. E., and van der Kooij, M. W. A., 1995. Cross-track and along-track Airborne Interferometric SAR at CCRS. In *Proceedings of the 17th Canadian Symposium on Remote Sensing*, June 13–15, Saskatoon, pp. 232–237.

Haran, T. M., Scambos, T. A., Fahnestock, M. A., and Csatho, B. M., 2008. New enhancements of an ERS1-2 + ICESat digital elevation model of West Antarctica using MODIS imagery, shapelets and krigging. *Eos Transactions*, *AGU*, **89**, Fall meeting 2008, Abstract #C31A-0461.

Hardy, R. J., Bamber, J. L., and Orford, S., 2000. The delineation of major drainage basins on the Greenland ice sheet using a combined numerical modelling and GIS approach. *Hydrological Processes*, **14**(11–12), 1931–1941.

Hodgson, M. E., and Bresnahan, P., 2004. Accuracy of airborne lidar-derived elevation: empirical assessment and error budget. *Photogrammetric Engineering and Remote Sensing*, **70**(3), 331–340.

Hopkinson, C., 1997. The net volumetric loss of glacier cover within the Bow Valley above Banff, Alberta. In *Proceedings of the Joint Eastern Snow Conference/Western Snow Conference*, Banff, pp. 270–278.

Horn, B., 1975. *Obtaining Shape from Shading Information. The Psychology of Computer Vision (Chapter 4)*. New York: McGraw-Hill, pp. 115–155.

Howat, I. M., Joughin, I., Fahnestock, M., Smith, B. E., and Scambos, T. A., 2008. Synchronous retreat and acceleration of southeast Greenland outlet glaciers 2000-06: ice dynamics and coupling to climate. *Journal of Glaciology*, **54**(187), 646–660.

Joughin, I., Winebrenner, D., Fahnestock, M., Kwok, R., and Krabill, W., 1996. Measurement of ice-sheet topography using satellite-radar interferometry. *Journal of Glaciology*, **42**(140), 10–22.

Kääb, A., Huggel, C., Fischer, L., Guex, S., Paul, F., Roer, I., Salzmann, N., Schlaefli, S., and Schmutz, K., 2005. Remote sensing of glacier- and permafrost-related hazards in high mountains: a review. *Natural Hazards and Earth System Sciences*, **5**, 527–554.

Kennett, M., and Eiken, T., 1997. Airborne measurement of glacier surface elevation by scanning laser altimeter. *Annals of Glaciology*, **24**, 86–91.

Korona, J., Berthier, E., Bernard, M., Rémy, F., and Thouvenot, E., 2009. SPIRIT. SPOT 5 stereoscopic survey of Polar Ice: reference images and topographies during the fourth International Polar Year (2007–2009). *ISPRS Journal of Photogrammetry and Remote Sensing*, **64**(2), 204–212.

Krabill, W., Thomas, R., Jezek, K., Kuivinen, K., and Manizade, S., 1995. Greenland ice sheet thickness changes measured by laser altimetry. *Geophysical Research Letters*, **22**(17), 2341–2344.
Liu, H. X., Jezek, K. C., Li, B. Y., 1999. Development of an Antarctic digital elevation model by integrating cartographic and remotely sensed data: a geographic information system based approach. *J Geophys Res-Solid Earth*, **104**, 23199–23213.
Lodwick, G. H., and Paine, S. H., 1985. A digital elevation model of the Barnes Ice-Cap Derived from Landsat-MSS Data. *Photogrammetric Engineering and Remote Sensing*, **51**(12), 1937–1944.
Magnússon, E., Björnsson, H., Pálsson, F., and Dall, J., 2005. The 20th century retreat of ice caps in Iceland derived fromairborne SAR: W-Vatnajökull and N-Mýrdalsjökull. *Earth and Planetary Science Letters*, **237**, L05504.
Muskett, M. M., Lingle, C. S., and Rabus, B. T., 2003. Multidecadal elevation changes on Bagley Ice Valley and Malaspina Glacier, Alaska. *Geophysical Research Letters*, **30**(16), 1857-1–1857-4.
Reinhardt, W., Rentsch, H., 1986. Determination of changes in volume and elevation of glaciers using digital elevation models for the Vernagtferner, Ötztal Alps, Austria. *Ann Glaciol*, **8**, 151–155.
Rémy, F., Legrésy, B., and Testut, L., 2001. Ice sheets and satellite altimetry. *Surveys in Geophysics*, **22**(1), 1–29.
Rippin, D., Willis, I., Arnold, N., Hodson, A., Moore, J., Kohler, J., and BjöRnsson, H., 2003. Changes in geometry and subglacial drainage of Midre Lovénbreen, Svalbard, determined from digital elevation models. *Earth Surface Processes and Landforms*, **28**(3), 273–298.
Robin, G., and de, Q., 1966. Mapping the Antarctic ice sheet by satellite altimetry. *Canadian Journal of Earth Sciences*, **3**(6), 893–901.
Rosen, P. A., Hensley, S., Joughin, I. R., Li, F. K., Madsen, S. N., Rodríguez, E., and Goldstein, R. M., 2000. Synthetic aperture radar interferometry. *Proceedings of the IEEE*, **88**(35), 333–382.
Rosmorduc, V., Benveniste, J., Lauret, O., Maheu, C., Milagro, M., and Picot, N., 2009. *Radar altimetry tutorial*. In Benveniste, J., and Picot, N. (eds.), http://www.altimetry.info
Scambos, T. A., and Fahnestock, M. A., 1998. Improving digital elevation models over ice-sheets using AVHRR-based photoclinometry. *Journal of Glaciology*, **44**(146), 97–103.
Scambos, T. A., and Haran, T. M., 2002. An image-enhanced DEM of the Greenland ice sheet. *Annals of Glaciology*, **34**, 291–298.
Thomas, R. H., Rignot, E., Casassa, G., Kanagaratnam, P., Acuña, C., Akins, T., Brecher, B., Frederik, E., Goginini, P., and Krabill, W., 2004. Accelerated sea-level rise from West-Antartica. *Science*, **306**(5694), 255–258.
Toutin, Th., 2001. Elevation modelling from satellite visible and infrared (VIR) data: a review. *International Journal of Remote Sensing*, **22**(6), 1097–1125.
Toutin, Th., and Gray, A. L., 2000. State-of-the-art of extraction of elevation data using satellite SAR data. *ISPRS Journal of Photogrammetry and Remote Sensing*, **55**(1), 13–33.
Welch, R., Jordan, R. T., Lang, H., and Murakani, H., 1998. ASTER as a source for topographic data in the late 1990s. *IEEE Transactions on Geoscience and Remote Sensing*, **36**(4), 1282–1289.
Wingham, D., 1995. The limiting resolution of ice-sheet elevations derived from pulse-limited satellite altimetry. *Journal of Glaciology*, **41**(138), 414–422.
Zwally, H. J., Schutz, B., Abdalati, W., Spinhirne, J. D., Bentley, C., Brenner, A., Bufton, J., Dezio, J., Hancock, D., and Harding, D., 2002. ICESat's laser measurements of polar ice, atmosphere, ocean and land. *Journal of Geodynamics*, **34**(3–4), 405–445.

Cross-references

Automated Glacier Mapping
Glacier Mass Balance
Glacier Motion/Ice Velocity
GRACE in Glaciology
Greenland Ice Sheet
Ground Penetrating Radar Measurements Over Glaciers
Ice Sheet Mass Balance
ICESat Data in Glaciological Studies
LIDAR in Glaciology
Optical Remote Sensing of Alpine Glaciers
Synthetic Aperture Radar (SAR) Interferometry for Glacier Movement Studies

DIGITAL IMAGE INFORMATION EXTRACTION TECHNIQUES FOR SNOW COVER MAPPING FROM REMOTE SENSING DATA

Manoj K. Arora[1], Aparna Shukla[2], Ravi P. Gupta[3]
[1]Department of Civil Engineering, Indian Institute of Technology Roorkee, Roorkee, India
[2]Uttarakhand Space Application Centre, Dehradun, India
[3]Department of Earth Sciences, Indian Institute of Technology Roorkee, Roorkee, India

Definition

Digital image information extraction. A set of image-processing techniques applied to the satellite images in digital form for the enhancement and extraction of the required information.
Snow-cover mapping from remote sensing data. Mapping of the snow-covered areas in the satellite image by application of the specialized digital image information extraction techniques.

Introduction

Snow is one of the most sensitive and vital natural resources. Over the years, gradual technological progress in mapping of snow-covered areas using remote sensing data has been influenced by several interrelated factors. These include advancements in the satellite sensor and image-processing technologies, and increasing demand for accurate and frequent monitoring of snow-covered areas due to mounting pressures from rapid industrialization, urbanization, and changing climate. Thus, regular and precise mapping of snow-covered regions is important at various scales due to several reasons such as:

1. On global and continental scales, snow due to its highly reflective nature and large surface coverage (snow can cover up to 40% of the Earth's land surface during the Northern Hemisphere winter) has great impact on climate variations, surface radiation balance, and energy exchange (Wang and Li, 2003).
2. On a regional scale, snow cover estimates constitute the primary input parameter for hydrological modeling

(Rango and Martinec, 1981; Shiyin et al., 2003; Fukushima et al., 1991).
3. On a local scale, accurate estimates of snow cover areas form key inputs to the mass balance studies, volumetric estimates, meltwater runoff modeling and snow hazard prediction modeling (Haeberli et al., 1998 and 2001; Berthier et al., 2007; Oerlemans et al., 2007; Quincey et al., 2005; Khromova et al., 2006; IPCC, 2007; Kulkarni et al., 2007).

Remote sensing data acquired in relevant parts of the electromagnetic spectrum have been widely employed for mapping of snow-covered area throughout the world (Konig et al., 2001; Hall et al., 2005; Bamber, 2006). Present status of snow-cover mapping can broadly be described based on:

1. The scale of mapping (small, medium, or large) both at pixel and sub-pixel levels
2. The region of electromagnetic spectrum utilized, namely, ultraviolet, visible, infrared, or microwave (active or passive)
3. The type of sensor used (Landsat TM and ETM+, SPOT VGT, NOAA AVHRR, IRS LISS-III, IV, Terra MODIS and ASTER, etc.)
4. The image information extraction techniques employed on remote sensing data

The aim of this chapter is to review the status of snow-cover mapping based on image information techniques. First, the conventional techniques of snow-cover mapping have been reviewed and their limitations highlighted, which are followed by a discussion on the importance of remote sensing in mapping of snow cover. A number of digital image information techniques employed for mapping of snow-covered areas, till date, have been conversed.

Conventional approaches of snow-cover mapping

Traditionally, snow cover has been mapped using ground (Potts, 1944; Miller, 1953) and aerial photographic surveys. Ground surveys may not be as complete as aerial surveys because of the field of vision and other obstructions, such as hills. Aerial photographic surveys provide more comprehensive information of the snow cover as compared to the ground surveys. It, however, also has some limitations such as time required to process a large number of photographs covering a big basin, high costs of operation of the aircraft, and difficulty in interpretation of snow cover in the forested areas (Singh and Singh, 2001). Further, reliability of the snow cover estimates from extrapolation of the snow cover information from meteorological stations depends heavily on the density of the weather stations, which is often quite insufficient. The temperature lapse-rate method for snow cover area approximation ignores the snow cover area lying outside the glacier and assumes snow, glacial ice, and debris-covered glacial ice as one homogeneous body.

Remote sensing for snow-cover mapping

In view of the vastness, inaccessible nature and harsh climatic conditions of the snow-covered areas, remote sensing is perhaps the most effective tool for comprehensive and repetitive study of these areas in a cost-effective manner. The remote sensing data can be obtained at a range of spectral, spatial, and temporal resolutions, which make them suitable for snow-cover mapping and monitoring. In fact, the high albedo of snow presents a high contrast with most other land cover types (except clouds) and for this reason maps of snow-covered area were one of the first products of satellite remote sensing (Tarble, 1963).

Understanding of spectral characteristics of snow forms an important prerequisite in its mapping from the satellite remote sensing data. Significant studies on the reflective properties of snow have been done by Wiscombe and Warren (1980), Warren and Wiscombe (1980), Warren (1982), and Zeng et al. (1984). Discussion of factors influencing snow reflectance have been given by Foster et al. (1987), Winther and Hall (1999), and Winther et al. (1999). As shown in Figure 1, snow reflectance is very high in the visible and much lower in the infrared region of the electromagnetic spectrum. Reflectance of snow is influenced by various factors such as grain size, contamination, solar zenith angle, cloud cover, metamorphism and age factor, and liquid water content.

In visible wavelengths (400–700 nm), snow reflectance is quite sensitive to minor amounts of contamination like carbon soot, volcanic ash, continental dust, etc. In the near- and middle-infrared region (700–3,000 nm), snow reflectance is sensitive to the grain size. The metamorphism of the snow cover, in general, results in a decrease of reflectance. Liquid water content in the snowpack has the effect of increasing the effective grain size and thus lowering the snow albedo (Konig et al., 2001).

Reflectance of snow is anisotropic and dependent on incidence and view angle. This dependence is described by the bidirectional reflectance distribution function (BRDF) (Knap and Reijmer, 1998). However, most satellite-derived albedo studies have generally not taken into account the anisotropic reflectance behavior of snow. The effect of anisotropic reflection increases as snow metamorphoses, for example, with increasing grain size and surface melt-freeze processes that sometimes produce a highly specular surface ("firnspiegel") (Konig et al., 2001).

Recently, there have been several commendable attempts to employ satellite remote sensing for mapping and monitoring of some major characteristics (such as area, depth, volume, and albedo) of snow as these constitute vital input parameters for hydrological, climatological, and hazard prediction models. Though, remote sensing greatly facilitates the mapping and monitoring of snow cover. However, mapping snow cover from remotely sensed data may also be fraught with a number of snags, which may be data and technology dependent. The main problem with data from visible and near-infrared sensors is their weather dependency (e.g., influence of the

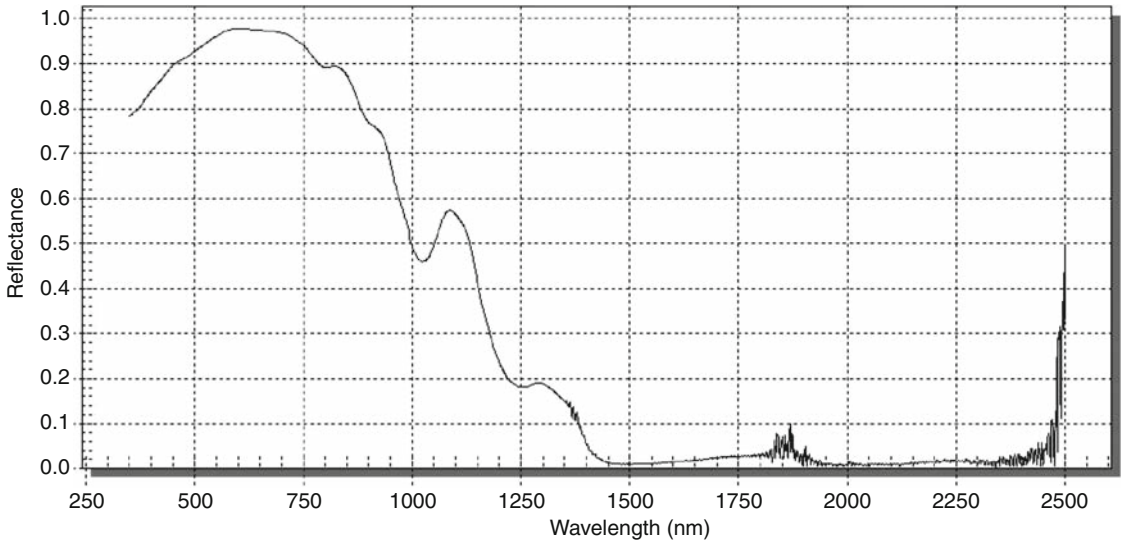

Digital Image Information Extraction Techniques for Snow Cover Mapping from Remote Sensing Data, Figure 1 Ground-based spectral reflectance curve of snow.

atmosphere on these data, especially the existence of cloud cover). A number of approaches have been suggested to get over the problem of cloud cover. Utilization of active and passive microwave data may overcome this problem. However, passive microwave data underestimates snow cover, perhaps due to their inability to map snow cover under forest and to distinguish wet snow from surrounding terrain. Basin-wide or large-scale snow and ice mapping has also been attempted using active microwave data obtained through Synthetic Aperture Radar (SAR) sensors since these sensors can discriminate between snow and bare ground at a spatial resolution that is compatible with topographic variation in mountainous basins. However, SAR data suffers from several limitations such as difficulties in interpretation of the recorded backscatter (Konig et al., 2001), complex image-processing requirements, and problems in distinguishing between wet snow and other smooth surfaces (Shi and Dozier, 1997). Data from different regions of the electromagnetic spectrum have also been used in combination for snow-cover mapping (Tait et al., 1999; Solberg et al., 2005; Liang et al., 2008).

Mountain shadows are also impediment to the determination of the snow line or the extent of snow-covered areas of a basin, especially in steep mountain terrains. A way out may be to combine the visible data with terrain features to minimize the effect of shadow. Alternatively, a number of ratio images and spectral indices may also be devised to map the snow cover extent (Dozier, 1989; Hall et al., 1995b).

Another problem faced in mapping of snow cover is the forest cover. A major part of the snow falling over forested areas reaches the ground after filtering through the forest canopy. Depending on the forest density, a part of fresh snowfall may stay atop the forest canopy. A dense forest cover may obscure underlying snow. Therefore, much attention is being paid to effectively determine snow-covered areas in forested regions (Klein et al., 1998; Vikhamar and Solberg, 2002, 2003; Shimamura et al., 2006). These include, using some vegetation indices such as the Normalized Difference Vegetation Index (NDVI) (Klein et al., 1998), formulating special indices for mapping snow cover under forests by using the near-infrared band (Shimamura et al., 2006) and by utilizing spectral signatures of snow cover under forests separately (Vikhamar and Solberg, 2002, 2003).

It is thus clear that mapping snow cover from remote sensing data is an intricate task and requires effective digital image information extraction techniques to extract these from a variety of aircraft- and satellite-based data acquired at varied spectral, spatial, and temporal resolutions. The use of ancillary data in this process may also not be undermined.

Digital image information extraction techniques for snow-cover mapping

A number of image information extraction techniques have been developed in view of the increasing demands for improved areal estimates of snow cover for varied applications. These techniques, as discussed in the next section, may be categorized as:

1. Manual delineation
2. Change detection–based method
3. Spectral ratios
4. Spectral indices
5. Per pixel image classification
6. Sub-pixel image classification

In order to demonstrate the implementation of these techniques and their comparison, results from a case study in mapping snow cover in a test glacier located in the Chenab basin, Western Himalaya, India, have also been presented.

Manual delineation

Manual delineation involves on-screen digitization of the satellite images based on the visual interpretation of snow-covered areas using a set of interpretation elements namely tone, texture, shape, size, association, pattern, and shadow applied individually or in combination. It has been widely used for mapping of glacial ice and snow extents, and in particular, for the estimation of retreat and deglaciation in various parts of the world (Hall et al., 1995a; Williams et al., 1997; Williams and Hall, 1993; Khromova et al., 2006; Kulkarni et al., 2007). Though being effective, the manual delineation is a very tedious and time-consuming task and may not be appropriate for mapping at operational level. Moreover, since the technique involves high degree of subjectiveness, therefore results from different sources may seldom match due to varying degrees of accuracy and bias involved.

Change detection–based method

In the change detection–based method, a snow-free satellite image is used as a reference image and is digitally compared, pixel by pixel, to record snow and non-snow-covered pixels. The brightness of the images may have to be adjusted to account for the daily and seasonal solar illumination angle differences. This method was developed initially by the U.S National Weather Station (NWS) for operational snow-cover mapping with AVHRR and Geostationary Environmental Satellite (GOES) sensors (Allen and Mosher, 1985; Holroyd et al., 1989). The method was found suitable for identification of snow in coniferous forested areas (Baumgartner and Rango, 1991). A variant of this change detection method was developed by Lillesand et al. (1982), which accounted for the inherent variations within cover types, for between-date variations within similar cover types, and for differing site characteristics (Baumgartner and Rango, 1991).

Spectral ratios

Formation of spectral ratios involves pixel-by-pixel division of the two bands of an image, which are selected in such a way that these maximize the spectral contrast between snow cover and other classes. The ratio image is then segmented using appropriate threshold values for mapping the snow cover. Band ratioing has been found to be a useful method for enhancing snow cover features in the multispectral images (e.g., Hall et al., 1987, 1988; Jacobs et al., 1997; Paul et al., 2004; Boresjö Bronge and Bronge, 1999; Williams et al., 1991). It has also been used to reduce the variable effects of solar illumination and topography besides enhancing the spectral information in the images (Justice et al., 1981; Gupta, 2003). The bands used to create ratios for mapping of snow-covered areas rely on its fundamental spectral characteristics, that is, high reflectance in visible region and strong absorption in the infrared region of the electromagnetic spectrum. Some typical spectral ratios for snow-cover mapping as cited in the literature have been compiled in Table 1.

Hall et al. (1987) used the ratio of TM4 (NIR) and TM5 (SWIR) bands to characterize snow and ice zones on glaciers using their spectral properties. Ratio values of raw Digital Numbers (DNs) (i.e., spectral response of pixels) were thresholded to generate a glacier mask by Hall et al. (1988). Rott and Markl (1989) found that spectral ratio TM3/TM5 revealed better results in shadowed areas than those obtained from TM4/TM5, whereas the latter showed better performance in mapping glacier areas facing the sun.

Jacobs et al. (1997) used atmospherically corrected spectral reflectance images obtained from TM4/TM5 and TM3/TM5, respectively, to obtain glacier mask after thresholding. Williams et al. (1991) found the TM4/TM5 ratio to be useful for discriminating glacier facies for temperate glaciers. Boresjö Bronge and Bronge (1999) found that the TM3/TM4 ratio resulted in the most accurate discrimination between blue ice and other snow types. Further, this ratio was also insensitive to the influence of thin clouds and cloud shadows. Paul (2000), while comparing various methods for glacier mapping using Landsat TM data, found that segmentation of a ratio image (TM4/TM5) with raw DNs yielded accurate glacial mapping.

Digital Image Information Extraction Techniques for Snow Cover Mapping from Remote Sensing Data, Table 1 Basic formulations of spectral ratios for snow-cover mapping

S.No.	Popular name	Formulation	Used by
1	$TM4/TM5$	$\frac{\text{NearInfrared(NIR)}}{\text{ShortwaveInfrared(SWIR)}}$	Hall et al. (1987, 1988); Rott and Markl (1989); Jacobs et al. (1997); Williams et al. (1991); Bronge and Bronge (1999); Paul (2000, 2003); Paul et al., (2002, 2004).
2	$TM3/TM5$	$\frac{\text{Red}}{\text{ShortwaveInfrared(SWIR)}}$	Rott and Markl (1989); Jacobs et al. (1997); Bronge and Bronge (1999).
3	$TM3/TM4$	$\frac{\text{Red}}{\text{NearInfrared(NIR)}}$	Bronge and Bronge (1999).

For demonstrating the snow mapping capabilities of spectral ratios, the most widely used NIR/SWIR ratio was selected in the study conducted in Chenab basin (Figure 2) and was applied to an IRS P6 AWiFS (Advanced Wide Field Sensor) image of the test glacier. The histogram of NIR/SWIR ratio image (Figure 2c) was studied for the determination of an appropriate threshold value. Snow-ice binary glacier terrain maps were generated using arbitrary thresholds of 1.5 and 2.0 (commonly used threshold; Paul, 2003) (Figure 2d and 2e, respectively). It can be seen that the ratio is unable to segregate the snow and ice class and fail to map the mixed ice and debris (MID) and supraglacial debris (SGD) classes (encircled areas in Figure 2a, 2d and 2e) toward the glacier snout. Thus, although spectral ratioing constitutes a fast and robust method for mapping snow- and ice-covered areas, the subjectivity involved in the derivation of appropriate thresholds and its inability to precisely differentiate between snow and ice zones limit its use.

Spectral indices

Besides the ratios, several empirical spectral indices have also been devised (Dozier, 1989; Hall et al., 1995b; Xiao et al., 2001; Shimamura et al., 2006; Keshri et al., 2009) for segregation and mapping of the snow and ice classes. Some of these spectral indices, their utility, and cited reference have been compiled in Table 2. Spectral indices characterize the basic spectral differences in the classes to be separated as well as assist in diminishing the radiometric effects of differential solar illumination and topography.

Normalized Difference Snow Index (NDSI), as defined in Table 2, was formulated by Dozier (1989) and Hall et al. (1995b). The basis of index is the high reflectance of snow in the visible region and a very low reflectance in the SWIR region, thereby providing high values of NDSI for snow-covered areas (Hall et al., 1995b; Nolin and Liang, 2000).

The main advantages of using NDSI are:

1. Discrimination between snow and clouds
2. Removal of mountain shadows to some extent

Winther and Hall (1999) used NDSI for snow cover area estimation to provide input for hydrological models for snow runoff modeling. Wang and Li (2003) compared NDSI with other methods and found it to be a valid and rational method for extracting snow cover areas. Kulkarni et al. (2006) employed an NDSI-based algorithm for producing snow cover products (5- and 10-day products) using data from IRS-P6 AWiFS sensor in Himalayan region.

MODIS snow-cover mapping algorithm referred as SNOWMAP is also based on the NDSI with few additional thresholds. SNOWMAP is a computationally frugal algorithm and thus is simple to implement at global scale (Hall et al., 1995b; Riggs et al., 1994; Riggs et al., 1996; Hall et al., 1998; Klein et al., 1998).

On similar lines, Xiao et al. (2001) proposed the Normalized Difference Snow and Ice Index (NDSII-1) (Table 2) for mapping snow and ice cover utilizing VEGETATION (VGT) sensor of SPOT 4. For Landsat TM data, they found that NDSII-1 yielded almost similar results as compared to NDSI. Later, NDSII-1 has also been used by them for spatial and temporal analysis of snow and ice cover over Asia and pan-Arctic zone using multi-temporal VGT sensor data.

Gupta et al. (2005) utilized NDSI along with a DEM for mapping dry and wet snow using IRS LISS-III data. The results (the area covered by dry snow) of this method were validated and compared with the area of non-melting zone from the temperature lapse method. The two were found to be in close correspondence (i.e., differences were $<15\%$).

Shimamura et al. (2006) intercompared NDSI with another index S3 (initially proposed by Saito and Yamazaki (1999) for GLI sensor of ADEOS) using Landsat ETM + data and found that S3 index was advantageous for mapping snow cover under dense forests. They argued that similar to other studies while the S3 index (calculated using red, NIR, and SWIR bands) was able to map snow cover under forested areas without any reference data (e.g., NDVI image), the NDSI could not.

Keshri et al. (2009) have recently proposed two indices (Normalized Difference Glacier Index (NDGI) and Normalized Difference Snow and Ice Index (NDSII-2)) for detailed mapping of supraglacial terrain. The indices facilitate three-step discrimination. First, the snow and ice are separated from rest of the terrain using NDSI, then snow and ice from ice-mixed-debris class using NDGI, and finally snow from ice using NDSII-2.

For the case study in Chenab basin, an NDSI image was created using Green and SWIR bands of the IRS P6 – AWiFS image of the test glacier. Thereafter, its frequency distribution (Figure 3c) was analyzed and two binary glacier terrain maps (Figure 3d and 3e) were generated at 0.4 (commonly used thresholds, Dozier, 1989; Hall et al., 1995b) and 0.5 thresholds. It can be seen that on increasing the threshold value from 0.4 to 0.5 for reducing the misclassification of glacial lake water, the ice area near the snout also diminishes (Figures 3d and e). Thus, creation of empirical spectral indices, such as NDSI, may assist in quick segregation of snow and ice classes from the rest of the classes under various terrain conditions (e.g., shadow, highly rugged topography, and forest cover). However, selection of an appropriate threshold value is a crucial task, as even a slight variation in threshold values may lead to over- or underestimation of snow cover. Moreover, the thresholds may vary with different satellite sensors as well as seasons (Dozier, 1989, Hall et al., 1995b).

Digital image classification

Digital image classification is perhaps the major image-processing task for extracting useful information from remote sensing data. The aim is to produce thematic maps where each pixel in the image is assigned a class (e.g., snow) on the basis of its spectral response to produce a classification. The per-pixel (PP) classification is

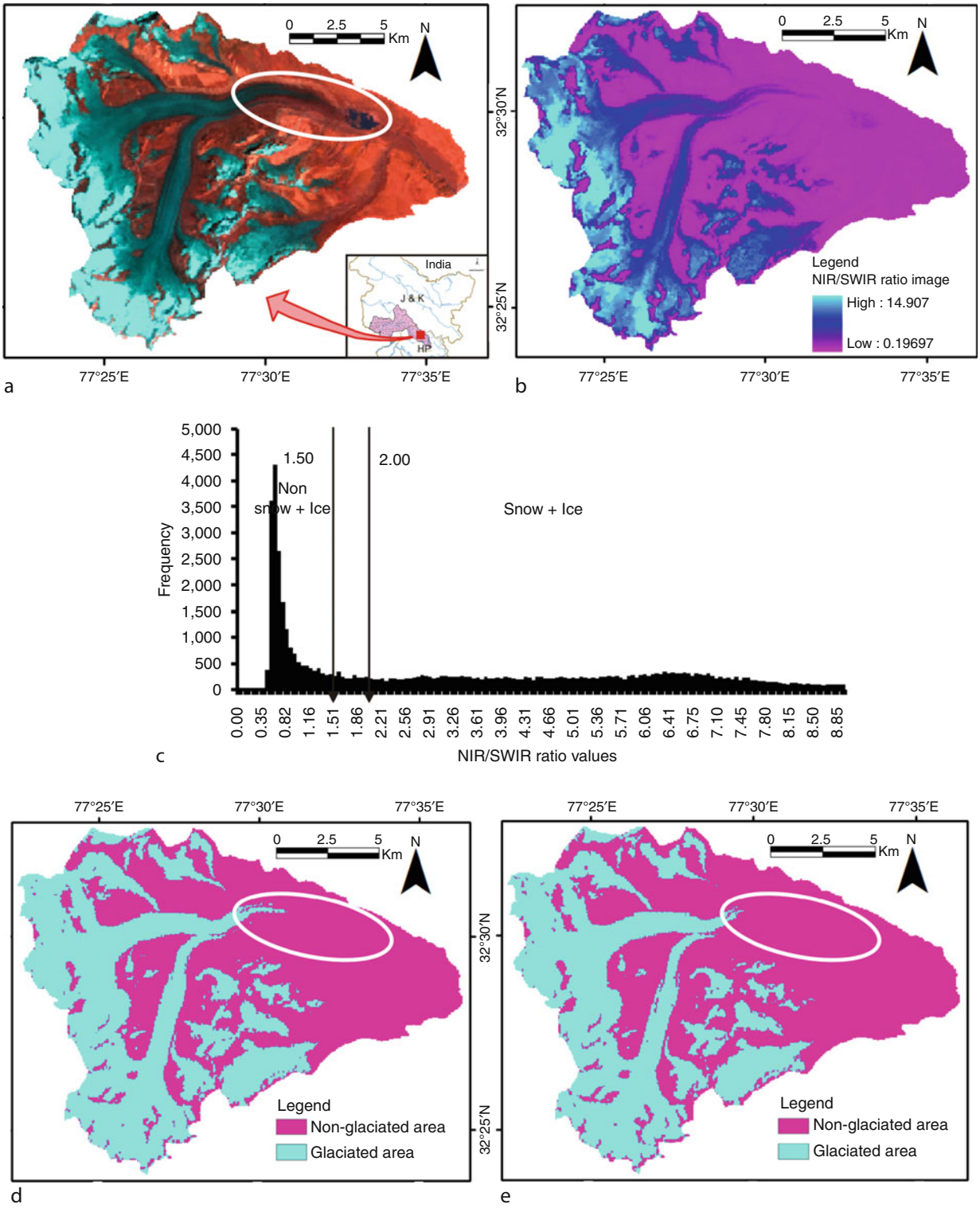

Digital Image Information Extraction Techniques for Snow Cover Mapping from Remote Sensing Data, Figure 2 Snow-cover mapping using NIR/SWIR ratio. **(a)** An FCC (R = B5, G = B4, B = B3) of AWiFS image of a test glacier, **(b)** NIR/SWIR ratio image, **(c)** histogram of NIR/SWIR image, and **(d)** and **(e)** binary glacier terrain maps derived from NIR/SWIR ratio image at 1.5 and 2.0 threshold values.

Digital Image Information Extraction Techniques for Snow Cover Mapping from Remote Sensing Data, Table 2 Formulations and utility of various spectral indices

Name of the index	Cited reference	Formulation	Utility
Normalized Difference Snow Index (NDSI)	Dozier (1989), Hall et al. (1995b)	$\text{NDSI} = \frac{\text{Green} - \text{SWIR}}{\text{Green} + \text{SWIR}}$	For mapping and differentiation of snow-ice covered areas from non-snow and ice areas.
Normalized Difference Snow and Ice Index (NDSII-1)	Xiao et al. (2001)	$\text{NDSII} = \frac{\text{Red} - \text{SWIR}}{\text{Red} + \text{SWIR}}$	For mapping and differentiation of the snow-ice covered areas from non-snow and ice areas.
S3 Index	Shimamura et al. (2006)	$\text{S3} = \frac{\text{NIR}(\text{red} - \text{SWIR})}{(\text{NIR} + \text{red})(\text{NIR} + \text{SWIR})}$	For mapping snow and ice cover under forest covered areas.
Normalized Difference Glacier Index (NDGI)	Keshri et al. (2009)	$\text{NDGI} = \frac{\text{Green} - \text{Red}}{\text{Green} + \text{Red}}$	For mapping and differentiating between snow-ice and mixed ice and debris class.
Normalized Difference Snow and Ice Index (NDSII-2)		$\text{NDSII} = \frac{\text{Green} - \text{NIR}}{\text{Green} + \text{NIR}}$	For mapping and differentiating between snow and ice class.

suitable when the image pixels are pure (i.e., one pixel area is covered by a single class). However, as the spatial resolution becomes coarser, the proportion of mixed pixels (i.e., pixels containing more than one class) increases, which leads to erroneous per-pixel classification. Therefore, sub-pixel classification has been suggested. The output from a sub-pixel (SP) classification is set of fraction images (equal to the number of classes being mapped) each depicting spatial extent of a class. Both supervised and unsupervised approaches can be used to produce per-pixel and sub-pixel classifications.

Supervised classification is one of the most widely used one in various remote sensing studies, and involves four stages, as depicted in Figure 4. The salient characteristics of some of the supervised and unsupervised classifiers are given in Table 3. The following section focuses on the review of per-pixel image classifiers for mapping snow cover.

Snow-cover mapping using per-pixel image classification

Della Ventura et al. (1983) developed a technique for automatic glacier-cover mapping (i.e., mapping of ice, snow, and other classes) using Landsat MSS data. Later, Della Ventura et al. (1987) applied a decision tree classifier and achieved more accurate results than the previous attempt. A supervised maximum-likelihood classification was applied to Landsat MSS and TM scenes by Gratton et al. (1990) to map seven classes. However, in that study, misclassification between clouds, shadows, and water, particularly in debris-covered glaciers, was observed due to which the maps had to be corrected manually. An inventory of the entire Southern Patagonian Icefield (SPI) based on TM data of year 1986 was prepared by Aniya et al. (1996) using cluster analysis (ISODATA) of TM bands 1, 4, and 5 to produce three classes (snow, ice, and rock). A parallelepiped classification was performed. In case of misclassification between ice in shade and supraglacial till, manual correction was applied (Paul, 2003).

The fuzzy set theory was used by Binaghi et al. (1997) for glacier classification. Although, a high classification accuracy was achieved, the method being technically intensive, was quite complex and moreover, debris cover on glaciers could not be mapped (Paul, 2003).

Ehrler and Seidel (1995) developed an algorithm for mapping snow and ice areas using Landsat TM and MSS and SPOT XS data via supervised classification for snow runoff modeling (SRM). The images were segmented into four illumination classes depending on the local incidence angle. Each illumination class was separately classified into bare ice, snow, transition zone, and snow free (aper). Wang and Li (2003) also performed supervised classification of images from Landsat TM, Terra MODIS, and NOAA-AVHRR to map three classes (old snow, fresh snow, and firn) using minimum distance classifier and intercompared with other snow and ice mapping techniques.

Additional information from sources other than spectral data (such as transformed spectral bands, DEM, and its derivatives) have also been utilized in the supervised classification process by some researchers either to simply augment the snow cover classifications (Boresjö Bronge and Bronge, 1999; Sidjak and Wheate, 1999).

Boresjö Bronge and Bronge (1999) applied supervised MLC to the principal components (PCs) of Landsat TM image for mapping blue ice of different characteristics as well as snow with various degrees of metamorphism. Although, the major snow and ice classes could be discerned, snow misclassifications were observed for image pixels covered with clouds and shadows. Sidjak and Wheate (1999) applied the supervised MLC using different input bands (PCs, TM4/TM5 ratio, NDSI, TM543 composite image) for mapping the glacier extent and discriminating glacier zones. The approach was able to

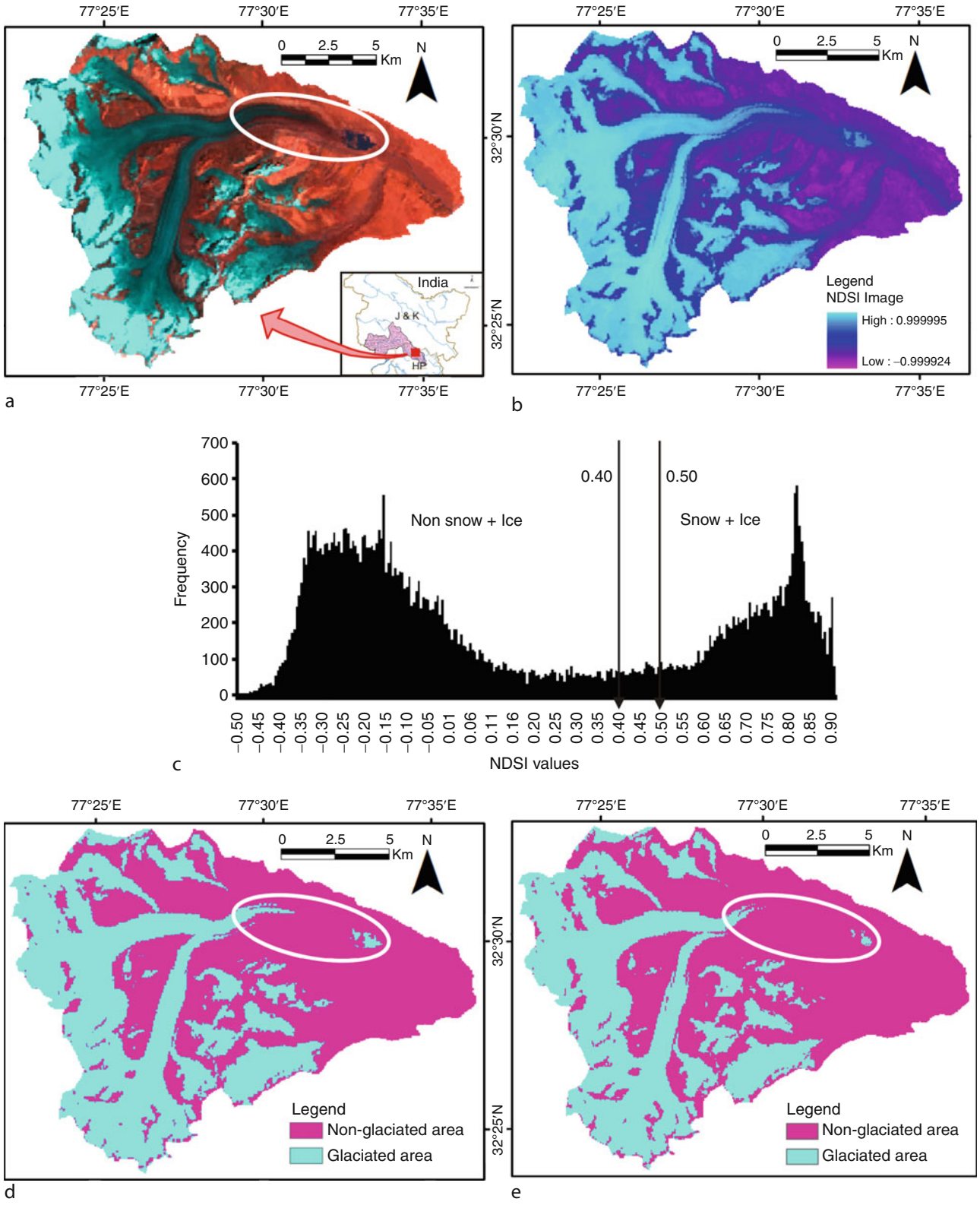

Digital Image Information Extraction Techniques for Snow Cover Mapping from Remote Sensing Data, Figure 3 Snow-cover mapping using NDSI. **(a)** FCC (R = B5, G = B4, B = B3) of AWiFS image, **(b)** NDSI image, **(c)** histogram of NDSI image, and **(d)** and **(e)** binary glacier terrain maps derived from NDSI ratio image at 0.4 and 0.5 thresholds.

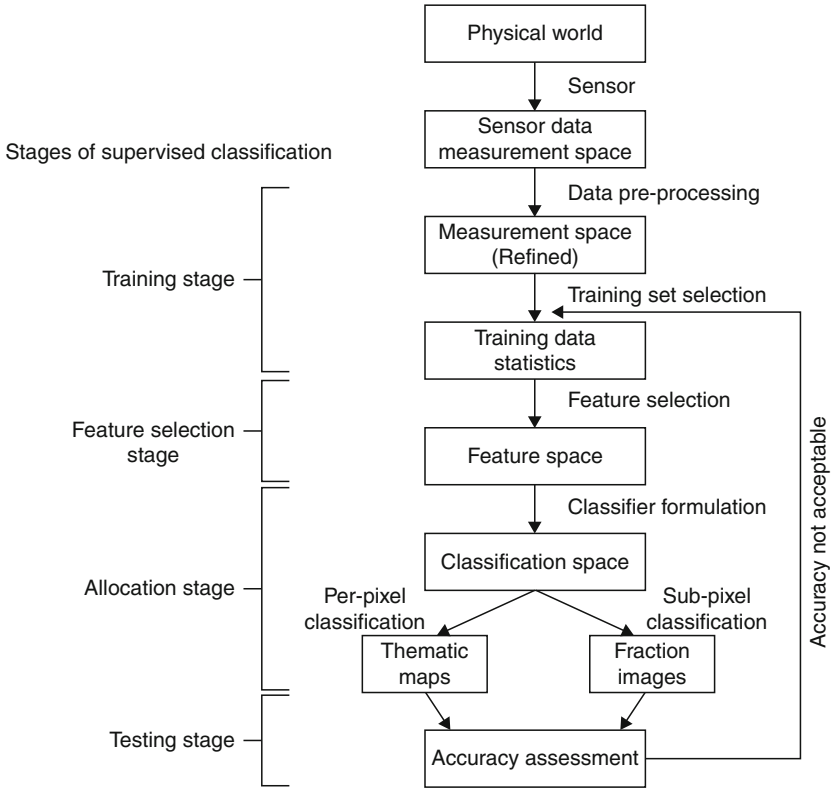

Digital Image Information Extraction Techniques for Snow Cover Mapping from Remote Sensing Data, Figure 4 Typical flowchart of a supervised classification process (Modified after Gupta, 2003).

accommodate problems of sensor saturation and shadowed areas, and thus refining the discrimination of debris-mantled ice and ice marginal water bodies.

In order to assess the influence of ancillary data together with spectral data and their transformations in the classification process, snow-cover mapping in Chenab basin was carried out using AWiFS image via MLC. Use of three different datasets, namely, only reflectance data, reflectance data + NDSI, and reflectance data + thermal data (ASTER TIR data), was made in the classification to produce three glacier terrain maps of the area (Figure 5). Comparing these maps those produced from other snow-cover mapping methods, it can be clearly observed that MLC is able to differentiate snow from all the major glacier terrain classes in the study area and therefore, seems superior to other existing techniques.

Figure 5 shows that classification of only reflectance data leads to precise estimation of snow cover. A comparative evaluation of the three snow-cover maps reveals that while integration of data from sources (i.e., NDSI and thermal data) with reflectance data reduces the misclassification of shadow class (Figures 5b and c) and facilitates the segregation of periglacial and supraglacial debris classes (Figures 5b and d), it does not have much influence on the accuracy of snow-cover mapping.

Thus, these studies clearly demonstrate the potential of per-pixel image classification techniques for snow-cover mapping. However, in per-pixel classification, a pixel is assigned a single class, which may lead to misclassification and misrepresentation of mixed pixels especially in case of coarse spatial resolution data of sensors such as NOAA-AVHRR, Terra-MODIS, IRS-P6-AWiFS, etc. For example, MODIS snow-cover mapping algorithm SNOWMAP classifies a pixel as snow covered if it has at least 60% snow, resulting in over-estimation of snow covered area. Thus, a number of sub-pixel classification techniques for snow-cover mapping have been proposed.

Sub-pixel image classification

The output of a sub-pixel image classification is a set of fraction images equal to the number of classes being mapped. A fraction image is a grayscale image representing pixels values as the proportion of the class to which it belongs. Some sub-pixel classification techniques include MLC in soft form, spectral mixture modeling (SMM) (Settle and Drake, 1993), Fuzzy set–based methods (Bezdek et al., 1984), Evidential Reasoning (ER) (Peddle, 1993), Artificial Neural Networks (ANN) (Foody, 1995), Support Vector Machines (SVMs) (Brown et al., 1999) and Decision-tree classification (Min et al., 2005) etc.

Digital Image Information Extraction Techniques for Snow Cover Mapping from Remote Sensing Data, Table 3 Formulations and descriptions of some supervised and unsupervised image classification algorithms

Classifier	Basic formulations	Description	Supervised	Unsupervised	PP	SP
Parallelepiped Classifier	$\overline{x}_{ck} - S_{ck} \leq DN_{ijk} < \overline{x}_{ck} + S_{ck}$	It defines thresholds for each class (c) using their mean ($\overline{x}_{ck}$) and standard deviation (S_{ck}) in each band (k) and uses these to determine whether a pixel falls in that class.	✓	✗	✓	✗
Minimum Distance to Mean Classifier	Euclidean distance = $d(x,\overline{x_c}) = \left[\sum_{c=1}^{M}(x_c - \overline{x_c})^2\right]^{1/2}$ and $x \in \omega_c$ if $d(x,\overline{x_c})^2 < d\left(x,\overline{x_p}\right)^2$ for all $p \neq c$ where x is a pixel, $\overline{x_c}$ is the mean of the cth class, and ω_c is a set of spectral classes M (total number of spectral classes).	The distances between the pixel to be classified and each class center are compared. The pixel is assigned to the class whose center is the closest to the pixel.	✓	✗	✓	✗
Maximum Likelihood Classifier (MLC)	$p(x/c) = \frac{1}{(2\pi)^{n/2}\lvert\Sigma_c\rvert^{1/2}} e^{\left(-1/2\left[(\mathbf{x}-\overline{x}_c)^T\Sigma_c^{-1}((\mathbf{x}-\overline{x}_c))\right]\right)}$ where $p(x/c)$ is the probability density function of a pixel x as a member of class c, n is the number of bands, $\mathbf{x}$ is the vector denoting spectral response of pixels, $\overline{x}_c$ is the vector of class mean and $\sum_c$ is the variance covariance matrix.	It allocates each pixel to the class with which it has the highest probability of membership and requires the data to follow a normal distribution.	✓	✗	✓	✓

Artificial Neural Network Classifier (ANN)	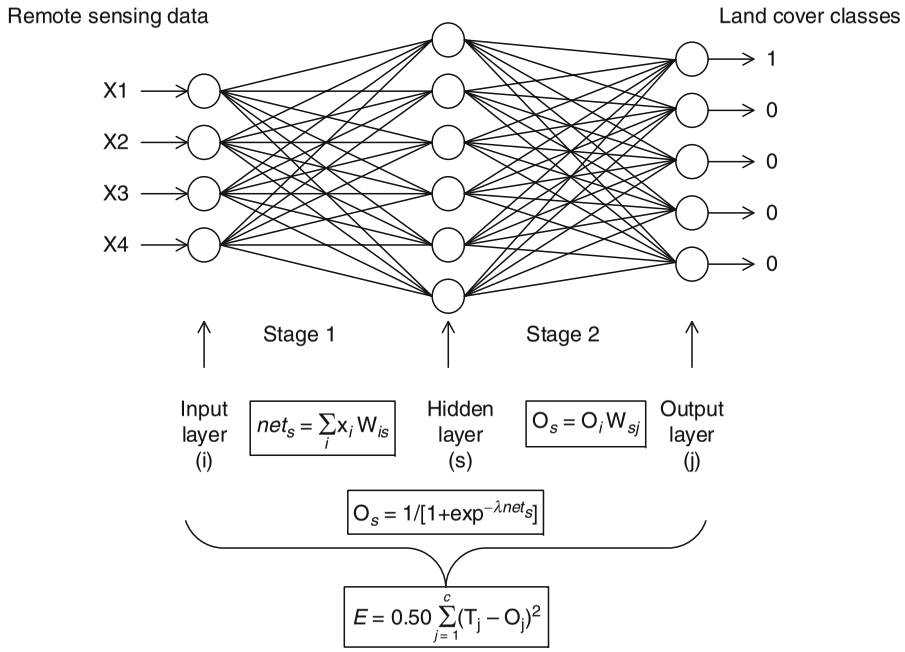	ANN consists of several nodes arranged in three basic layers (input, hidden, and output). The neural network uses the training data to adjust the weights connecting the units until it is able to correctly identify class membership. This is achieved with the aid of an iterative learning process.	✓	✗	✓	✓
	x_i = Input pixel vector; W_{is} = weights between input and hidden l ayer node connections; net_s = net input for hidden layer nodes; O_s = is the output of the sth hidden node. O_j = is the output of the jth unit of the output layer; W_{sj} = weights between hidden and output layer node connections; E = Error function determined from training data and network output. This is to be minimized					
Fuzzy c-Means Clustering Classifier (FCM)	$J_m(U,V) = \sum_{i=1}^{N}\sum_{j=1}^{c} (\mu_{ij})^m \left\|\mathbf{x}_i - v_j\right\|_A^2$ subject to constraints, $\sum_{j=1}^{c} \mu_{ij} = 1$ for all i; $\sum_{i=1}^{N} \mu_{ij} > 0$ for all j; $0 \le \mu_{ij} \le 1$ for all i, j where $\mathbf{x}_i$ is the vector denoting spectral response of a pixel i, V is the collection of vector of cluster centers, v_j, μ_{ij} are class membership values of a pixel (members of fuzzy c-partition matrix), c and N are number of clusters and pixels respectively, m is a weighting exponent ($1 < m < \infty$), $\left\|X_i - v_j\right\|_A^2$ is the squared distance between $\mathbf{x}_i$ and v_j.	FCM measures the fuzzy membership value of data for each cluster based on the distance between the cluster center and the data in the feature space of remotely sensed imagery.	✓	✓	✗	✓

Digital Image Information Extraction Techniques for Snow Cover Mapping from Remote Sensing Data, Table 3 (Continued)

Classifier	Basic formulations	Description	Supervised	Unsupervised	PP	SP
Spectral Mixture Modelling (LMM)	$x_k = \sum_{c=1}^{n} f_c M_{kc} + e_k$ where, M_{kc} is the endmember spectra representing the mean class spectral responses of cth class in kth band, f_c are the fraction of cth class in a pixel, and the term e_k is the error term for kth band, which expresses the difference between the observed spectral response and the model derived spectral response of the pixel, respectively.	It assumes that the spectral response of an individual pixel is a linear sum of the mean spectral responses of its components (i.e. land cover classes) weighted by their relative proportions on the ground and thus calculates the proportion of each class	✓	✗	✗	✓
Evidential Reasoning (ER)	Mass function For one band, the mass function of a class c, for a DN value x is given as, $m_c(x) = \frac{\text{no. of pixels with value } x \text{ intraining sample of class } c}{\text{Total number of pixels intraining sample of class } c}$ Orthogonal summation If m_1 and m_2 are two mass functions defined on inputs from two sources, the combined mass function m_{12} is given by the equations, $m_{12}(A) = \frac{\sum_{B \cap C = A} m_1(B) m_2(C)}{1-k}$ where $A \neq \Phi$ where K is a normalization factor for ignoring conflicting evidence and is mathematically expressed as, $K = \sum_{B \cap C = \Phi} m_1(B) m_2(C)$	The mathematical theory of evidence actually refers to the Dempster–Shafer theory. The theory provides a general heuristic basis for combining information from independent sources, and can be applied to any problem where a choice is to be made from a set of well-known alternatives, based on information from various sources.	✓	✗	✓	✓

Decision Tree Classifier (DT)	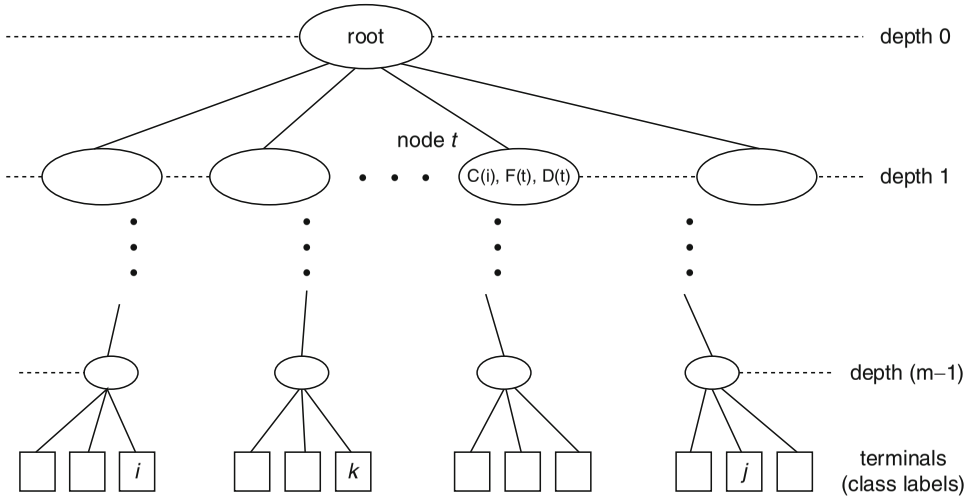 *C*(*t*)- subset of classes accessible from node *t* *F*(*t*)- feature subset used at node *t* *D*(*t*)- decision rule used at node *t*	Decision tree is a nonparametric classifier and involves a recursive partitioning of the feature space, based on a set of rules that are learned by an analysis of the training set. A tree structure is developed where at each branching a specific decision rule is implemented, which may involve one or more combinations of the attribute inputs.	✓	✗	✓
K-Means Clustering	Given a set of observations $(\mathbf{x}_1,\mathbf{x}_2,\ldots,\mathbf{x}_n)$, where each observation is a d-dimensional real vector, then k-means clustering aims to partition this set into k *(M)* partitions ($k < n$) so as to minimize the within-cluster sum of squares : $\underset{\omega}{\operatorname{argmin}} \sum_{c=1}^{k} \sum_{x_c \in \omega_c} \|x_c - \overline{x_c}\|^2$	It is an iterative clustering algorithm. First an arbitrary initial cluster mean vector is assigned. The second step classifies each pixel to the closest cluster mean. In the third step the new cluster mean vectors are calculated based on all the pixels in one cluster. The second and third steps are repeated until the “change” between the iteration is small.	✗	✓	✓

Digital Image Information Extraction Techniques for Snow Cover Mapping from Remote Sensing Data, Table 3 (Continued)

Classifier	Basic formulations	Description	Supervised	Unsupervised	PP	SP
ISODATA	Same as *k*-means with additional merging and splitting of clusters.	The ISODATA algorithm has some further refinements by splitting and merging of clusters. Clusters are merged if either the number of members (pixel) in a cluster is less than a certain threshold or if the centers of two clusters are closer than a certain threshold. Clusters are split into two different clusters if the cluster standard deviation exceeds a predefined value and the number of members (pixels) is twice the threshold for the minimum number of members.	✗	✓	✓	

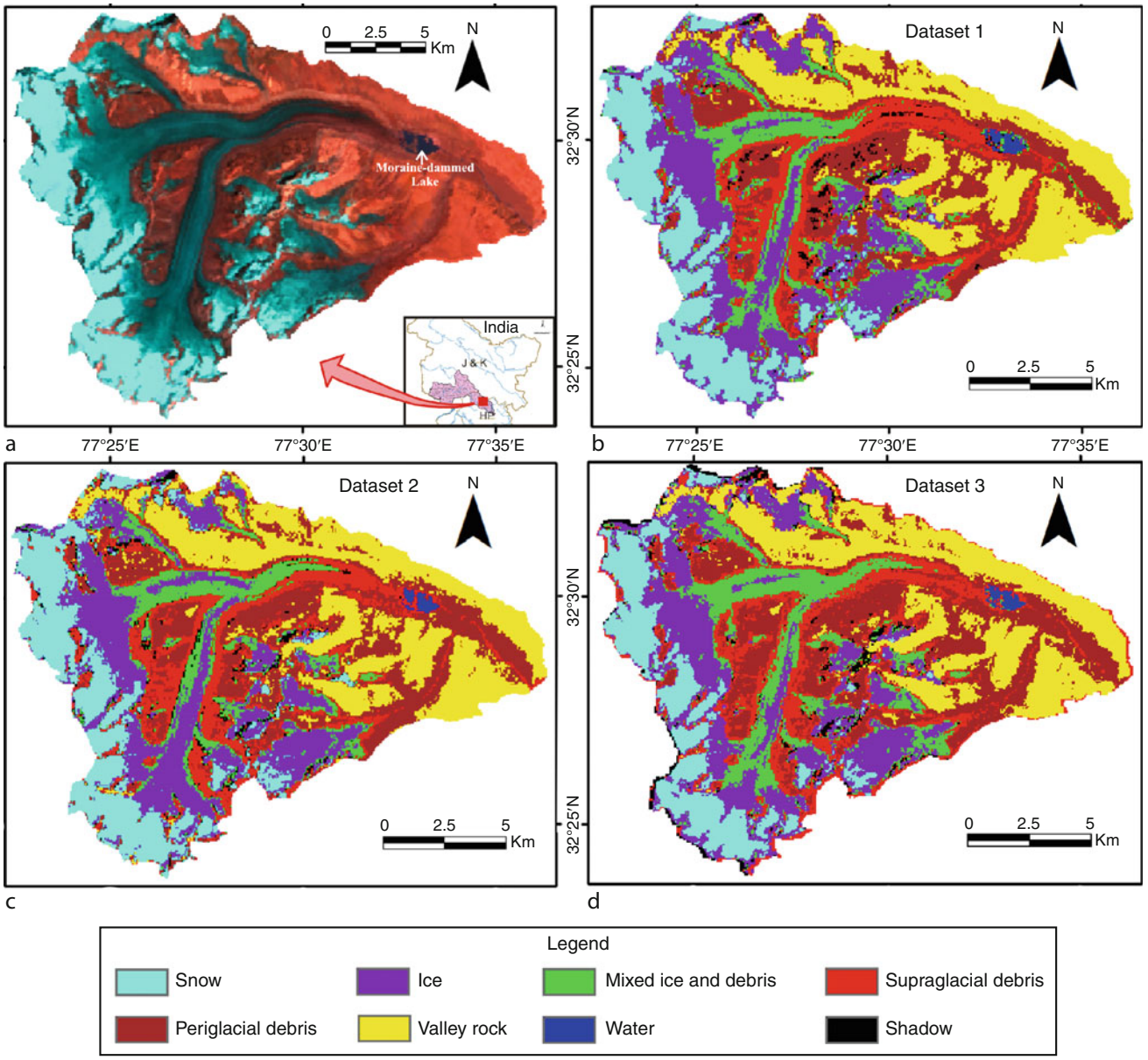

Digital Image Information Extraction Techniques for Snow Cover Mapping from Remote Sensing Data, Figure 5 Snow-cover mapping using per-pixel image classification: **(a)** An FCC (R = B5, G = B4, B = B3) of AWiFS image of a test glacier, **(b)** Glacier terrain map derived from reflectance data, **(c)** Glacier terrain map derived from reflectance data + NDSI, and **(d)** Glacier terrain map derived from reflectance data + thermal data.

Among these, very few have been applied for snow cover estimation. The prevalent approaches of fractional snow-cover mapping include the techniques using empirical relationships (Andersen, 1982; Kaufman et al., 2002; Salomonson and Appel, 2004, 2006), SMM and its variations (Nolin et al., 1993; Painter et al., 2003; Vikhamar and Solberg, 2002, 2003; Sirguey et al., 2008 and 2009), and fuzzy set–based approaches (Rampini et al., 2002). Among all these, SMM has been used most widely in glaciological studies.

Empirical relationships–based snow-cover mapping

In these techniques, an empirical relationship between snow cover and some other property such as reflectance or NDSI, etc., is established, which is used to back calculate the percentage of snow cover in a pixel. Keeping in view the requirements of an operational sub-pixel snow-cover mapping algorithm, techniques based on empirical relationships have been developed (Andersen, 1982; Kaufman et al., 2002; Salomonson and Appel, 2004, 2006). Andersen (1982) developed a fractional snow-cover

mapping algorithm based on an empirical "reflectance to snow-cover" relationship. The model was calibrated by providing two points on the reflectance function: highest reflectance for 0% snow cover, and lower reflectance for 100% snow cover. This algorithm is used by the Norwegian Water Resources and Energy Directorate (NVE) to produce snow-cover maps from NOAA-AVHRR sensor.

Kaufman et al. (2002) devised an empirical technique for the estimation of fractional snow cover, based on principles of remote sensing of aerosol over the land. Both aerosol and sub-pixel snow are dark at 2.1 μm and much brighter at 0.66 μm. A relationship between directional reflectance of the non-snow areas (vegetation and soil) at these wavelengths was used to predict the reflectance at 0.66 μm. The results were validated with the snow fractions obtained from SMM (Rosenthal and Dozier, 1996) as the ground truth. The results showed a difference of only 1–2% between the snow fractions derived from the two techniques.

Salomonson and Appel (2004) conducted a study with the aim to evaluate the utility of NDSI in estimating the fractional snow cover within a 500-m MODIS pixel. For this, the data from Landsat ETM + scenes covering a wide variety of snow cover conditions was acquired as ground truth. All the Landsat scenes were classified as snow or non-snow using the current SNOWMAP algorithm of MODIS. An ordinary least squares regression approach was then applied to derive linear relationships between the snow fraction (FRA) and NDSI corresponding to the 500-m grid cells. Results from this technique proved to be superior, with lowest RMS error in the range of 0.10–0.12 and highest correlation in the range of 0.95–0.97.

Spectral Mixture Modeling

The SMM is widely used for producing class proportions within mixed pixels (Settle and Drake, 1993). SMM models the pixel spectrum with a least squares fit as a linear combination of the spectral responses of classes present within the pixel. The surface spectral responses of classes (also called as endmembers) are thus determined from other sources and the fractional cover of each class is obtained (Konig et al., 2001).

Nolin et al. (1993) were probably the first to apply SMM for mapping fractional snow cover in the mountainous regions of Sierra Nevada, California using AVIRIS data. Two multiband subset images containing 16 and 18 bands in the visible and NIR wavelengths, out of the available 224 bands were used. The SMM was run for each image to calculate the fraction images for each endmember. Deviations between the model and the data were calculated as residuals and RMS error images as well as an overall RMS error were also computed for each image. Overall RMS errors for the two subsets were found to be 3.4 Wm^{-2} μm^{-1} sr^{-1} and 3.0 Wm^{-2} μm^{-1} sr^{-1}, respectively, which are quite low. Therefore, they were able to successfully map deep snow, thin snow, shaded snow, and snow mixed with vegetation.

For operational snow-cover mapping, Rosenthal and Dozier (1996) estimated fractional snow cover using SMM for only a few representative regions and found that the technique was able to accurately identify surfaces without topographic correction (Konig et al., 2001). Recently, Sirguey et al. (2009) have presented a method for production of snow-cover maps with improved spatial resolution of 250 m, using MODIS data, at sub-pixel level. Image fusion techniques (wavelet fusion and "ARSIS" concept, Sirguey et al., 2008) were used to merge the relatively high resolution MODIS band 1 and band 2 (250 m) with MODIS bands 3–7 (500 m) data. A constrained SMM was applied on radiometrically corrected MODIS images. The eight endmembers, namely, ice, debris, rocks, medium granular snow, coarse granular snow, transformed snow, rain-forest + bush, and pasture were identified using ground measurements and photointerpretation. The accuracy of the resultant snow cover fractions was assessed against the reference snow-cover maps derived from fine-resolution ASTER data. The overall RMSE and mean absolute error (MAE) showed an improvement of 25%, while R^2 increased by 5.6% when the MODIS images with improved spatial resolution were used.

Some variations of SMM have also been reported especially in regions of rugged topography through the use of multiple snow endmembers (Painter et al., 2003). A method for sub-pixel mapping of snow cover in forests was developed by Vikhamar and Solberg (2002). The method was based on SMM of snow, trees, and snow-free ground. The focus had been on development of a physically based reflectance model that uses a forest-cover map as prior information. Later they tried to derive a simplified reflectance model suitable for operational snow-cover mapping in forests (Vikhamar and Solberg, 2003).

Although an effective technique, SMM has its own limitations such as that arisen from its basic assumption that the spectral response of a pixel is a linear weighted sum of its constituent classes. Nonlinearities are generated by the adjacency effect of bright pixels (i.e., pixels with high reflectance) next to dark pixels (pixels with low reflectance) adding some unaccounted-for path radiance and by the anisotropic distribution of reflected radiation from snow (particularly in the near-infrared wavelengths), as well as by the presence of adsorbed impurities in snow that can be adequately modeled as an intimate mixture (Nolin et al., 1993). In order to overcome the limitations of SMM, other sub-pixel classification techniques, which account for nonlinearity in spectral mixing have been proposed.

Fuzzy Set–Based Approaches

Fuzzy c-means clustering (FCM) is a popular fuzzy clustering method, which may be employed to partition pixels of remote sensing image into different class membership values or fractions. FCM measures the fuzzy membership value of data for each cluster based on the distance between the cluster center and the data in the feature space

of remotely sensed imagery and may be used in both supervised and unsupervised modes (Table 2). Rampini et al. (2002) used a supervised FCM classifier to extract eight land cover classes (snow, ice, rocks, wood, grass, lakes, clouds, and shadow) from Landsat TM and ETM + images to estimate the changes in the glacier cover from 1986 to 1999. The overall accuracy in all the classes was found to be above 90%.

In order to demonstrate the sub-pixel classification techniques, snow cover was estimated using MLC in soft form, FCM, and Evidential Reasoning (ER) from the AWiFS image in the Chenab basin (Figure 6). The SMM was ruled out due to the constraint that the number of classes to be mapped (eight in present case) should be one less than the number of spectral bands (four in present case of AWiFS data). Visual inspection of the snow cover fraction images from the three classifiers reveals that FCM has been relatively more successful in classifying snow cover as compared to MLC and ER. MLC and ER seem to underestimate and misclassify snow cover.

Summary

Mapping of snow- and ice-covered area has always been one of the major global scientific studies such as the mass balance studies, volumetric estimations of cryospheric components, meltwater runoff modeling, snow hazard prediction modeling, climatological modeling, etc. Conventional snow-cover mapping techniques include ground and aerial surveys, extrapolation of point data from weather stations, from topographic maps, and by application of temperature lapse rate method. The advances in satellite remote sensing have virtually revolutionized the global scenario of cryospheric studies in general, and

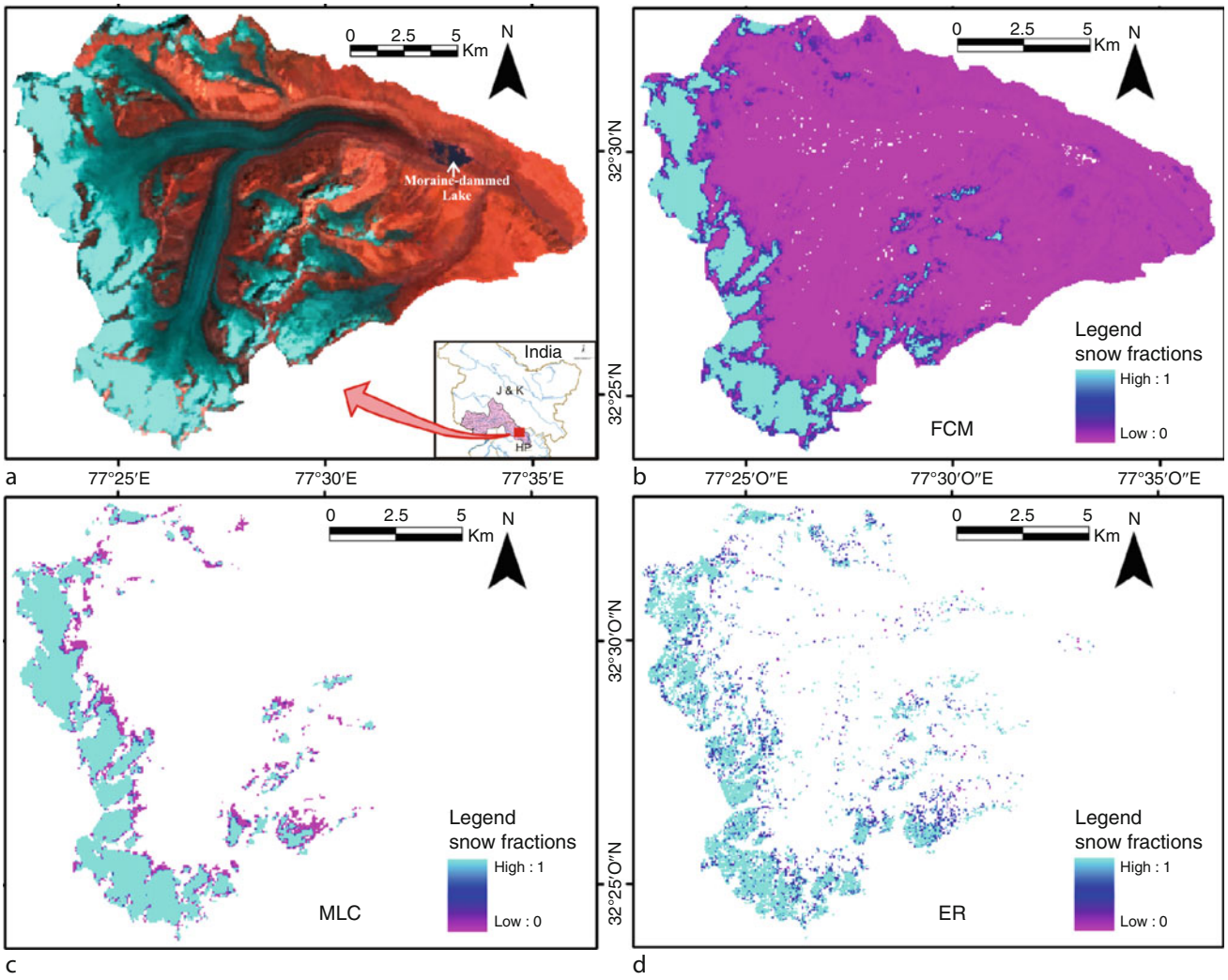

Digital Image Information Extraction Techniques for Snow Cover Mapping from Remote Sensing Data, Figure 6 **(a)** An FCC (R = B5, G = B4, B = B3) of AWiFS image of a test glacier; Pseudo-color snow cover fraction images from **(b)** FCM, **(c)** MLC, and **(d)** ER algorithms.

mapping of snow-covered areas in particular. Parallel to the advancements in the satellite sensor technology and availability of much refined data, the techniques of digital information extraction have also been enhanced. From simple change detection and manual delineation techniques to image ratios, spectral indices, and digital image classification–based mapping of snow-covered areas, there has been an exponential growth in snow-cover mapping at per-pixel and sub-pixel scales. Each technique, discussed in this chapter, has its merits and demerits. For example, while image ratioing and empirical spectral indices are appropriate for operational level tasks, the technically sound methods of digital image classification are more appropriate than others for detailed basin scale studies. Moreover, the results from digital image classification can also be augmented for further improvement by incorporation of data from sources. Moreover, work has also been carried out to exploit potential of the coarse spatial resolution data for snow-cover mapping using sub-pixel techniques, largely based on spectral mixture modeling. The utility of other techniques for snow-cover mapping at operational level needs to be explored. Besides, incorporation of ancillary data at sub-pixel level to enhance the classification accuracy and moving from sub-pixel classification to sub-pixel mapping or "super resolution mapping" of snow-covered areas constitute some areas for future research.

Conclusively, it may be stated that rapidly advancing tool of remote sensing has yet not reached its zenith and would continue to evolve and grow and in order to keep pace with it and imbibe its advantages in the field of snow-cover mapping.

Bibliography

Allen, N. W., and Mosher, F. R., 1985. Interactive snow cover mapping with geostationary satellite data over the western United States. In *Summaries, 19th International Symposium on Remote Sensing of Environment*, Ann Arbor, Michigan, p. 153.

Andersen, T., 1982. Operational snow mapping by satellites. In *Hydrological aspects of Alpine and high mountain areas. Proceedings of the Exeter Symposium*, July 1982. Wallingford: IAHS Publ. 138, pp. 149–154.

Aniya, M., Sato, H., Naruse, R., Skvarca, P., and Casassa, G., 1996. The use of satellite and airborne imagery to inventory outlet glacier of Southern Patagonian Icefield, South America. *Photogrammetric Engineering and Remote Sensing*, **62**, 1361–1369.

Bamber, J., 2006. Remote sensing in glaciology. In Knight, P. G. (ed.), *Glacier Science and Environmental Change*. Malden, MA: Wiley, 527 p.

Baumgartner, M. F., and Rango, A., 1991. Snow cover mapping using microcomputer image processing systems. *Nordic Hydrology*, **22**, 193–210.

Berthier, E., Arnaud, Y., Kumar, R., Ahmad, S., Wagnon, P., and Chevallier, P., 2007. Remote sensing estimates of glacier mass balances in the Himachal Pradesh (Western Himalaya, India). *Remote Sensing of Environment*, **108**(3), 327–338.

Bezdek, J. C., Ehrlich, R., and Full, W., 1984. FCM: The fuzzy c-means clustering algorithm. *Computers and Geosciences*, **10**, 191–203.

Binaghi, E., Madella, P., Montesano, M. P., and Rampini, A., 1997. Fuzzy contextual classification of multisource remote sensing images. *IEEE Transactions on Geoscience and Remote Sensing. GE-35*, **2**, 326–339.

Bronge, L. B., and Bronge, C., 1999. Ice and snow type classification in Vestfold Hills, East Antarctica, using LANDSAT TM data and ground radiometer measurements. *International Journal of Remote Sensing*, **20**(2), 225–240.

Brown, M., Gunn, S. R., and Lewis, H. G., 1999. Support vector machines for optimal classification and spectral unmixing. *Ecological Modelling*, **120**, 167–179.

Della Ventura, A., Rampini, A., Rabagliati, R., and Serandrei-Barbero, R., 1983. Glacier monitoring by satellite. *Il Nuovo Cimento, C-1*, **6**, 211–221.

Della Ventura, A., Rampini, A., and Serandrei-Barbero, R., 1987. Development of a satellite remote sensing technique for the study of alpine glaciers. *International Journal of Remote Sensing*, **8**, 203–215.

Dozier, J., 1989. Spectral signature of alpine snow-cover from the Landsat Thematic Mapper. *Remote Sensing of Environment*, **28**, 9–22.

Ehrler, C., and Seidel, K., 1995. Mutual effects of the climate change and the alpine snow cover and their influence on the runoff regime evaluated with the aid of satellite remote sensing. In Stein, T. I. (ed.), *IGARSS'95; Quantitative Remote Sensing for Science and Applications*. Italy: Florence, Vol. 3, pp. 1973–1975.

Foody, G. M., 1995. Land cover classification by an artificial neural network with ancillary information. *International Journal of Remote Sensing*, **16**, 527–542.

Foster, J. L., Hall, D. K., and Chang, 7., 1987. Remote sensing of snow. *Eos, Transaction of the American Geophysical Union*, **68**(32), 682–684.

Fukushima, Y., Watanabe, O., and Higuchi, K., 1991. Estimation of streamflow change by global warming in a glacier-covered high mountain area of the Nepal Himalaya. In Proceedings of Bergmann, H., Lang, H. P., Frey, W., Issler, D., and Salm, B. (eds.), *International symposium snow, hydrology and forests in high alpine areas Vienna*, August 11 –24, 1991. International association of hydrological sciences. IAHS/AISH Publication, 205, pp. 181–188.

Gratton, D. J., Howarth, P. J., and Marceau, D. J., 1990. Combining DEM parameters with Landsat MSS and TM imagery in a GIS for mountain glacier characterization. *IEEE Transactions on Geoscience and Remote Sensing*, **28**, 766–769.

Gupta, R. P., 2003. *Remote Sensing Geology*, 2nd edn. Berlin: Springer Publication, p. 655.

Gupta, R. P., Haritashya, U. K., and Singh, P., 2005. Mapping dry/wet snow cover in the Indian Himalayas using IRS multispectral imagery. *Remote Sensing of Environment*, **97**(4), 458–469.

Haeberli, W., Hoelzle, M., and Suter, S., 1998. Into the second century of worldwide glacier monitoring: prospects and strategies. *A contribution to the International Hydrological Programme (IHP) and the Global Environment Monitoring System* (*GEMS*), *UNESCO Studies and Reports in Hydrology*, 56, 228 p.

Haeberli, W., Kääb, A., Vonder Mühll, D., and Teysseire, P., 2001. Prevention of outburst floods from periglacial lakes at Grubengletscher, Valais, Swiss Alps. *Journal of Glaciology*, **47**(156), 111–122.

Hall, D. K., Ormsby, J. P., Bindschadler, R. A., and Siddalingaiah, H., 1987. Characterization of snow and ice zones on glaciers using Landsat Thematic Mapper data. *Annals of Glaciology*, **9**, 104–108.

Hall, D. K., Chang, A. T. C., and Siddalingaiah, H., 1988. Reflectances of Glaciers as calculated from the Landsat 5 Thematic Mapper data. *Remote Sensing of Environment*, **25**, 311–321.

Hall, D. K., Riggs, G. A., and Salomonson, V. V., 1995a. Development of methods for mapping global snow-cover using moderate

resolution spectroradiometer data. *Remote Sensing of Environment*, **54**, 127–140.
Hall, D. K., Benson, C. S., and Field, W. O., 1995b. Changes of glaciers in Glacier Bay, Alaska, using ground and satellite measurements. *Physical Geography*, **16**(1), 27–41.
Hall, D. K., Foster, J. K., Verbyla, D. L., Klein, A. G., and Benson, C. S., 1998. Assessment of snow-cover mapping accuracy in a variety of vegetation-cover densities in Central Alaska. *Remote Sensing of Environment*, **66**(2), 129–137.
Hall, D. K., Kelly, R. EJ., Foster, J. L., and Chang, A. T. C., 2005. Estimation of snow extent and snow properties. In Anderson, M. G., (eds.), *Encyclopedia of Hydrological Sciences.* New York: Wiley, pp. 811–828.
Holroyd, E. W., Verdin, J. P., and Carroll, T. R., 1989. Mapping snow cover with satellite imagery: comparison of results from three sensor systems. In *Proceedings of the 57th Annual Western Snow Conference*, Ft. Collins, Colorado, pp. 59–68.
IPCC, 2007. Climate Change 2007: The physical science basis. In Solomon, S., Qin, D., Manning, M., Chen, Z., Marquis, M., Averyt, K. B., Tignor, M., and Miller, H. L. (eds.), *Contribution of Working Group I to the Fourth Assessment Report of the Intergovernmental Panel on Climate Change*. Cambridge: Cambridge University Press, 996 pp.
Jacobs, J. D., Simms, E. L., and Simms, A., 1997. Recession of the southern part of Barnes Ice Cap, Baffin Island, Canada, between 1961 and 1993, determined from digital mapping of Landsat TM. *Journal of Glaciology*, **43**(143), 98–102.
Justice, C. O., Wharton, S. W., and Holben, B. N., 1981. Application of digital terrain data to quantify and reduce the topographic effect on Landsat data. *International Journal of Remote Sensing*, **2**(3), 213–230.
Kaufman, Y. J., Kleidman, G. R., Hall, D. K., Martins, J. V., and Barton, J. S., 2002. Remote Sensing of sub-pixel snow-cover using 0.66 and 2.1 m channels. *Geophysical Research Letters*, **29**(16), 28–1–28–4.
Keshri, A., Shukla, A., and Gupta, R. P., 2009. ASTER ratio indices for supraglacial terrain mapping. *International Journal of Remote Sensing*, **30**(2), 519–524.
Khromova, T. E., Osipova, G. B., Tsvetkov, D. G., Dyurgerov, M. B., and Barry, R. G., 2006. Changes in glacier extent in the eastern Pamir, Central Asia, determined from historical data and ASTER imagery. *Remote Sensing of Environment*, **102** (1–2), 24–32.
Klein, A. G., Hall, D. K., and Riggs, G. A., 1998. Improving snow-cover mapping in forests through the use of caopy reflectance model. *Hydrological Processes*, **12**, 1723–1744.
Knap, W. H., and Reijmer, C. H., 1998. Anisotropy of the reflected radiation field over melting glacier ice: measurements in Landsat TM bands 2 and 4. *Remote Sensing of Environment*, **65**, 93–104.
Konig, M., Winther, J. G., and Isaksson, E., 2001. Measuring snow and glacier ice properties from satellite. *Reviews of Geophysics*, **39**(1), 1–27.
Kulkarni, A. V., Singh, S. K., Mathur, P., and Mishra, V. D., 2006. Algorithm to monitor snow cover using AWiFS data of RESOURCESAT-1 for the Himalayan region. *International Journal of Remote Sensing*, **27**(12), 2449–2457.
Kulkarni, A. V., Bahuguna, I. M., Rathore, B. P., Singh, S. K., Randhawa, S. S., Sood, R. K., and Dhar, S., 2007. Glacier retreat in Himalayas using Indian Remote Sensing satellite data. *Current Science*, **92**(1), 69–74.
Liang, T., Zhang, T., Xie, H., Wu, C., Feng, Q., Huang, Q., and Chen, Q., 2008. Toward improved daily snow cover mapping with advanced combination of MODIS and AMSR-E measurements. *Remote Sensing of Environment*, **112**(10), 3750–3761.
Lillesand, T. M., Meisner, D. E., LaMois-Downs, A., and Denell, R. L., 1982. Use of GOES and TirosINOAA satellite data for snow cover mapping. *Photogrammetric Engineering and Remote Sensing*, **48**(2), 251–259.
Miller, D. H., 1953. Snow cover depletion and runoff. *Snow Hydrology.* Portland: U. S Army Corps of Engineers.
Min, X., Watanachaturaporn, P., Varshney, P. K., and Arora, M. K., 2005. Decision tree regression for soft classification of remote sensing data. *Remote Sensing of Environment*, **97**(3), 322–336.
Nolin, A., and Liang, S., 2000. Progress in bidirectional reflectance modelling and application for surface particulate media: snow and soils. *Remote Sensing Reviews*, **14**, 307–342.
Nolin, A. W., Dozier, J., and Mertes, L. A. K., 1993. Mapping alpine snow using spectral mixture modeling technique. *Annals of Glaciology*, **17**, 121–124.
Oerlemans, J., Dyurgerov, M., and Van de Wal, R. S. W., 2007. Reconstructing the glacier contribution to sea-level rise back to 1850. *The Cryosphere Discuss*, www.the-cryospherediscuss.net/1/77/2007/, **1**: 77–97.
Painter, T. H., Dozier, J., Roberts, D. A., Davis, R. F., and Green, R. O., 2003. Retrieval of sub-pixel snow covered area and grain size from imaging spectrometer data. *Remote Sensing of Environment*, **85**, 64–77.
Paul, F., 2000. Evaluation of different methods for glacier mapping using Landsat TM. *EARSEL eProceedings*, **1**, 239–244.
Paul, F., 2003. *The new Swiss glacier inventory 2000: application of remote sensing and GIS*. PhD thesis. Zürich, Department of Geography, University of Zürich, 198 pp.
Paul, F., Kääb, A., Maisch, M., Kellenberger, T., and Haeberli, W., 2002. The newremote-sensing-derived Swiss glacier inventory: I Methods. *Annals of Glaciology*, **34**, 355–361.
Paul, F., Kääb, A., Maisch, M., Kellenberger, T., and Haeberli, W., 2004. Rapid disintegration of Alpine glaciers observed with satellite data. *Geophysical Research Letters B*, **31**(21), L21402, doi:10.1029/2004GL020816.
Peddle, D. R., 1993. An empirical comparison of evidential reasoning, linear discriminate analysis and maximum likelihood algorithm for Alpline land cover classification. *Canadian Journal of Remote Sensing*, **19**, 31–42.
Potts, H. L., 1944. A photographic survey method of forecasting runoff. *Transactions – American Geophysical Union*, **25**(1), 153–194.
Quincey, D. C., Lucas, R. M., Richardson, S. D., Glasser, N. F., Hambrey, M. J., and Reynolds, J. M., 2005. Optical remote sensing techniques in high-mountain environments: application to glacial hazards. *Progress in Physical Geography*, **29**(4), 475–505.
Racoviteanu, A. E., Williams, M. W., and Barry, R. G., 2008. Optical remote sensing of glacier characteristics: a review with focus on the Himalaya. *Sensors*, **8**, 3355–3383.
Rampini, A., Brivio, P. A., Rota Nodari, F., and Binaghi, E., 2002. Mapping Alpine glaciers changes from space. *IEEE Transactions on Geoscience and Remote Sensing Symposium*, 2199–2201.
Rango, A., and Martinec, J., 1981. Accuracy of snowmelt runoff simulation. *Nordic Hydrology*, **12**, 265–274.
Riggs, G. A., Hall, D. K., and Salomonson, V. V., 1994. A snow index for the Landsat thematic mapper and moderate resolution imaging spectroradiometer. In *Proceedings of the International Geoscience and Remote Sensing Symposium, IGARSS '94*, August 8–12, 1994, Pasadena, CA, pp. 1942–1944.
Riggs, G. A., Hall, D. K., and Salomonson, V. V., 1996. Recent progress in development of the moderate resolution imaging spectroradismeter snow cover algorithm and product. In *Proceedings of the International Geoscience and Remote Sensing Symposium, IGARSS '96*, Lincoln, NE, pp. 139–141.
Rosenthal, W., and Dozier, J., 1996. Automated mapping of montane snow-cover at sub-pixel resolution from the Landsat Thematic Mapper. *Water Resources Research*, **100**, 115–130.

Rott, H., and Markl, G., 1989. Improved snow and glacier monitoring by the Landsat Thematic Mapper. In *Proceedings of a workshop on the Landsat Thematic Mapper applications,* ESA SP-1102, pp. 3–12.
Saito, A., and Yamazaki, T., 1999. Characteristics of spectral reflectance for vegetation ground surfaces with snowcover: Vegetation indices and snow indices. *Journal of Japan Society of Hydrology and Water Resources*. **12**, 28–38.
Salomonson, V. V., and Appel, I., 2004. Estimating fractional snowcover from MODIS using the normalised difference snow index. *Remote Sensing of Environment*, **89**, 351–360.
Salomonson, V. V., and Appel, I., 2006. Development of the Aqua MODIS NDSI fractional snow cover algorithm and validation results. *IEEE Transactions on Geoscience and Remote Sensing*, **44**(7), 1747–1756.
Settle, J. J., and Drake, N. A., 1993. Linear mixing and the estimation of ground cover proportions. *International Journal of Remote Sensing*, **14**, 1159–1177.
Shi, J., and Dozier, J., 1997. Mapping seasonal snow with SIR-C/X-SAR in mountainous areas. *Remote Sensing of Environment*, **59**(2), 294–307.
Shimamura, Y., Izumi, T., and Matsumaya, H., 2006. Evaluation of a useful method to identify snow-covered areas under vegetation – comparisons among a newly proposed snow index, normalized difference snow index and visible reflectance. *International Journal of Remote Sensing*, **27**(21), 4867–4884.
Shiyin, L., Wenxin, S., Yongping, S., and Gang, L., 2003. Glacier changes since the Little Ice Age maximum in the western Qilian Shan, northwest China, and consequences of glacier runoff for water supply. *Journal of Glaciology*, **49**, 117–124.
Sidjak, R. W., and Wheate, R. D., 1999. Glacier mapping of the Illecillewaet icefield, British Columbia, Canada, using Landsat TM and digital elevation data. *International Journal of Remote Sensing*, **20**(2), 273–284.
Singh, P., and Singh, V. P., 2001. *Snow and Glacier Hydrology.* The Netherlands: Kluwer Academic Publishers, pp. 742.
Sirguey, P., Mathieu, R., Arnaud, Y., Khan, M. M., and Chanussot, J., 2008. Improving MODIS spatial resolution for snow mapping using wavelet fusion and ARSIS concept. *IEEE Geoscience and Remote Sensing Letters*, **5**(1), 78–82.
Sirguey, P., Mathieu, R., and Arnaud, Y., 2009. Subpixel monitoring of the seasonal snow cover with MODIS at 250 m spatial resolution in the Southern Alps of New Zealand: methodology and accuracy assessment. *Remote Sensing of Environment*, **113**, 160–181.
Solberg, R., Malnes, E., Amlien, J., Koren, H., Eikvil1, L., and Storvold, R., 2005. Multi-sensor/multi-temporal approaches for snow cover area monitoring. In *Proceedings of EARSeL LIS-SIG Workshop,* Berne, February, 2005.
Tait, A. B., Hall, D. K., Foster, J. L., and Armstrong, R. L., 1999. Utilizing multiple datasets for snow-cover mapping. *Remote Sensing of Environment*, **72**, 111–126.
Tarble, R. D., 1963. Areal distribution of snow as determined from satellite photographs. *IAHS Publication*, **65**, 372–375.
Vikhamar, D., and Solberg, R., 2002. Subpixel mapping of snow cover in forests by optical remote sensing. *Remote Sensing of Environment*, **84**, 69–82.
Vikhamar, D., and Solberg, R., 2003. Snow-cover mapping in forests by constrained linear spectral unmixing of MODIS data. *Remote Sensing of Environment*, **88**, 309–323.
Wang, J., and Li, W., 2003. Comparison of methods of snow cover mapping by analyzing the solar spectrum of satellite remote sensing data in China. *International Journal of Remote Sensing*, **24**(21), 4129–4136.
Warren, S. G., 1982. Optical properties of snow. *Reviews of Geophysics*, **20**(1), 67–89.
Warren, S. G., and Wiscombe, W. J., 1980. A model for the spectral albedo of snow, II, Snow containing atmospheric aerosols. *Journal of Atmospheric Sciences*, **37**, 2734–2745.
Williams, R. S., Jr., and Hall, D. K., 1993. Glaciers. In Gurey, R. J., Foster, J. L., and Parkinson, C. L. (eds.), *Atlas of Satellite Observations Related to Global Change*. Cambridge: Cambridge University Press, 401–421.
Williams, R. S., Hall, D. K., and Benson, C. S., 1991. Analysis of glacier facies using satellite techniques. *Journal of Glaciology*, **37**, 120–128.
Williams, R. S. Jr., Hall, D. K., Sigurdsson, O., and Chein, J. Y. L., 1997. Comparison of satellite-derived with ground- based measurements of the fluctuations of the margins of Vatnajokull, Iceland, 1973–1992. *Annals of Glaciology*, **24**, 72–80.
Winther, J. G., and Hall, D. K., 1999. Satellite derived- snow coverage related to hydropower production in Norway: present and future. *International Journal of Remote Sensing*, **20**(15–16), 2991–3008.
Winther, J. G., Gerland, S., Orback, J. B., Ivanov, B., Blanco, A., and Boike, J., 1999. Spectral reflectance of melting snow in a high Arctic watershed on Svalbard: some implications for optical satellite remote sensing studies. *Hydrological Processes*, **13**(12–13), 2033–2049.
Wiscombe, W. J., and Warren, S. G., 1980. A model for the spectral albedo of snow, I, Pure snow. *Journal of Atmospheric Sciences*, **37**, 2712–2733.
Xiao, X., Shen, Z., and Qin, X., 2001. Assessing the potential of VEGETATION sensor data for mapping snow and ice cover: a normalized difference snow and ice index. *International Journal of Remote Sensing*, **22**(13), 2479–2487.
Zeng, Q., Cao, M., Feng, X., Liang, F., Chen, X., and Sheng, W., 1984. A study of spectral reflection characteristics for snow, ice and water in the north of China. In *Hydrological Applications of Remote Sensing and Remote Data Transmission: Proceedings of the Hamburg Symposium.* Wallingford, UK: IAHS Publ. 145, pp. 451–462.

DIRECT SURFACE RUNOFF

Lars Bengtsson
Department of Water Resources Engineering, Lund University, Lund, Sweden

Definition

Direct surface runoff is the rain or meltwater that runs off during the rain or melt event as overland flow or in the vegetation cover above a frozen soil.

The meltwater and the rain falling onto snow or on frozen ground reach a stream along different pathways. It may be as groundwater after vertical infiltration in macropores or through the soil matrix. It may be as saturated overland flow or as Hortonian overland flow on concrete frozen soil; or as flow in cracks just below the ground surface. The water reaching a stream during or just after snowmelt or after a storm event may be old subsurface water forced forward by new water, or it may be event water, that is, meltwater or event rain water. The quality of the stream water depends on the pathways and on the interactions with the soil during the particles route to the stream.

The ground under a snow cover is usually frozen. In very cold climate with thin snow cover, the frost depth is deep. When the ground is snow covered early with much snow, the snow isolates the soil and the frost depth is minor. When the ground freezes at high moisture content, the frozen soil becomes almost impermeable; while if the soil moisture is low, melt water can infiltrate into frozen soil especially into cracks and macropores. In a forest and at meadows with bushes, there is much litter and moss vegetation, many small stones, and macropores. The infiltration capacity is high. The soil seldom has high moisture content. Even when the soil is frozen, all the meltwater can infiltrate and percolate to the groundwater through the macropore system. Snowmelt occurs over extended time so the groundwater level is increasing throughout the snowmelt. At the bottom of the slopes, the groundwater reaches the surface. Saturated overland flow occurs.

In agricultural soils, there is no litter on top of the ground, macropore systems are less developed, and soils usually have clay content, all resulting in much more concrete-like frost than at forested sites. The first meltwater may infiltrate into cracks in the top ploughed soil layer, but once these are filled a saturated layer builds up and runoff occurs just below the ground surface, or if the melt proceeds over long time at the base of the snow pack. At a subdrained agricultural field, much of the water first moves horizontally in the crack-system and then vertically through drainage zones of coarse sand and gravel into the subdrains. If the soil had very high soil moisture content when the soil froze, the infiltration capacity may be almost completely reduced. Always where the ground is hard and the soil is packed, there is almost no infiltration into frozen soil, even if the soil was rather dry when the soil froze. The meltwater runs off as Hotonian flow at the base of the snow cover. The very first part of the horizontal runoff process in the snow may be considered as Darcian flow. When the melt proceeds, flow channels develop at the bottom of the snow pack. Then to match theory and observations, hydraulic conductivity 0.1–1.0 m/s may have to be used. Preferential flow takes place and the flow is faster than true Darcian flow.

Snowmelt is a slow process. Melt intensity is low compared to rainfall intensity. The velocity at which the meltwater moves in the snow is also low. Overland flow

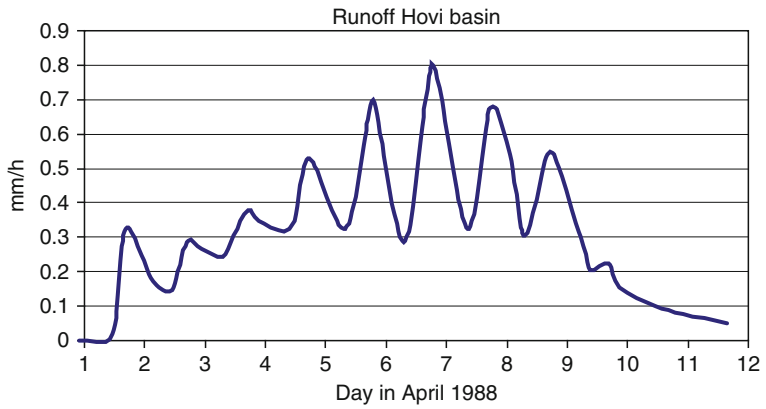

Direct Surface Runoff, Figure 1 Runoff from the Hovi agricultural basin in Finland.

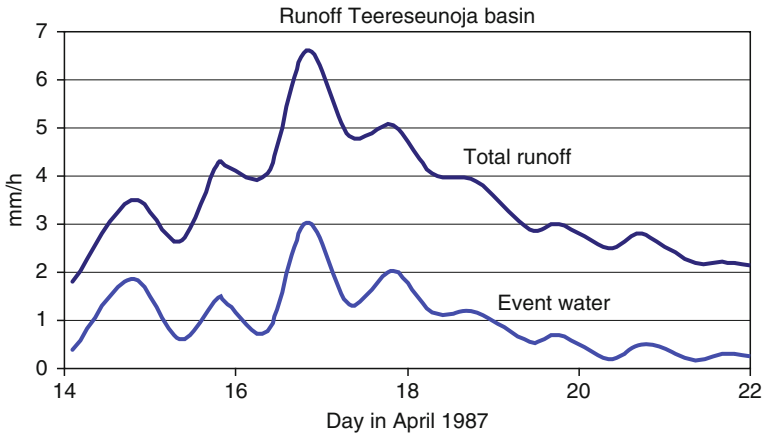

Direct Surface Runoff, Figure 2 Total runoff and runoff of Event water from the Teereseunoja forested basin in Finland.

proceeds through the night at the base of the snow pack even when melt occurs only during daytime. An example from the Hovi agricultural basin in Finland is shown as Figure 1. The distance from the top of the basin to the outlet is 400 m. The slope is about 0.01. The runoff is during the three days of most intense melt 0.7 mm/h at the end of the day and 0.3 mm/h after the night. Most of the water is snowmelt event water as determined from isotope analysis.

The diurnal runoff fluctuations are less in small forested basins compared to an agricultural one, as seen in Figure 2 from the Teereseunoja basin in Finland, mainly due to large fractions of pre-event water. In the very runoff peak of almost 0.7 mm/h, the fraction of event water is 40% but of the total runoff during melt less than 20% is event water. The ground slope towards the stream is about 10%. About one fourth of the basin is peat moor with trees. The event water contribution varies over the day in the range 0.2 mm/h in the afternoon to 0.07 mm/h in the morning and can, to a large extent, be attributed to the direct surface runoff on the moor. The diurnal runoff fluctuations are entirely attributed the event water.

Bibliography

Bengtsson, L., 1982a. Ground- and meltwater in the snowmelt induced runoff. *IAHS-Hydrological Sciences Journal*, **27**(2), 147–158.

Bengtsson, L., 1982b. Percolation of meltwater through a snowpack. *Cold Regions Science and Technology*, **6**, 73–81.

Bengtsson, L., and Singh, V. P., 2000. Model sophistication in relation to scales in snowmelt runoff modeling. *Nordic Hydrology*, **31**, 267–286.

Bengtsson, L., Saxena, R. K., and Dressie, Z., 1987. Soilwater movements estimated from isotope tracers. *IAHS Hydrological Sciences Journal*, **32**(4), 497–520.

Bengtsson, L., Seuna, P., Lepistö, A., and Saxena, R. K., 1992. Particle movement of meltwater in a subdrained agricultural basin. *Journal of Hydrology*, **135**, 383–398.

Beven, K., 1982. On subsurface stormflow: predictions with simple kinematic theory for saturated ann unsaturated flows. *Water Resources Research*, **18**, 1627–1633.

Boggild, C. E., 2000. Preferential flow and melt water retention in cold snow packs in West-Greenland. *Nordic Hydrology*, **31**, 287–300.

Carey, S. K., and Woo, M.-K., 1998. Snowmelt hydrology of two subarctic slopes, southern Yukon. *Canada, Nordic Hydrology*, **29**, 331–346.

Colbeck, S. C., 1978. The physical aspects of water through snow. *Advances in Hydroscience*, **11**, 165–206.

Dunne, T., Price, A. G., and Colbeck, S. C., 1976. The generation of runoff from subarctic snowpacks. *Water Resources Research*, **12**, 677–685.

Kane, D. L., 1980. Snowmelt infiltration into seasonally frozen soil. *Water Resources Research*, **16**, 153–161.

Singh, V. P., Bengtsson, L., and Westerström, G., 1997a. Kinematic wave modelling of vertical movement of snowmelt water through a snowpack. *Hydrological Processes*, **11**, 149–167.

Singh, V. P., Bengtsson, L., and Westerström, G., 1997b. Kinematic wave modelling of saturated basal flow in a snowpack. *Hydrological Processes*, **11**, 177–187.

Young, K. L., 2008. Role of snow in the hydrology of a high arctic riparian wetland. *Hydrology Research*, **39**, 277–286.

Cross-references

Frozen Soil Hydrology
Hydrographs
Isotopic Characteristics of Ice, Snow, and Glaciers
Percolation Zone
Runoff Generation
Snow Cover and Snowmelt in Forest Regions
Specific Melt Rate

DISCHARGE/STREAMFLOW

Debasmita Misra[1], Ronald P. Daanen[2], Anita M. Thompson[3]
[1]Geological Engineering, College of Engineering and Mines, University of Alaska Fairbanks, Fairbanks, AK, USA
[2]Geophysical Institute, University of Alaska Fairbanks, Fairbanks, AK, USA
[3]Department of Biological Systems Engineering, University of Wisconsin-Madison, Madison, WI, USA

Synonyms

Glacier-melt; Meltwater; River flow; Snowmelt

Definition

Discharge. Discharge is the rate of water output resulting from melting of snow, ice, or glaciers.
Streamflow. Streamflow is the resulting rate of water flow in a stream or river draining a basin that contains snow, ice, or glacier.

Introduction

Generation of streamflow from snowmelt discharges includes processes that produce meltwater within the snowpack, those that store and delay the liquid water within the snowpack and those that channel the meltwater through watersheds to streams or rivers. Glacier-melt discharge is more complex than snowmelt discharge due to additional processes that are involved in melting of glaciers (Singh and Singh, 2001; Hock, 2005). In addition to seasonal snowpack melt, internal movement of glacier ice and the sliding of a glacier body are responsible for significant amount of melt discharge from the glaciers. Depending on elevation there are different stages within glaciers of liquid water movement from storage in firn to channel flow in the lower regions of the glacier.

Snowmelt discharge and streamflow

The depth of snow cover, the snow water equivalent, and the aerial extent of snow cover influence the amount of snowmelt runoff that will occur during the melt season. The snow water equivalent is the depth of water obtained by melting the snow cover and an estimate can be computed using the depth of snow and the density of the snowpack. The rate of snowmelt is determined by

snowpack and atmospheric conditions. The melt rate of snow is lower in the beginning of the melt season and increases in summer. Maximum snowmelt rates as high as 70 mm/day have been observed in New Zealand (Singh and Singh, 2001).

According to DeWalle and Rango (2008),

> Outflow of liquid water from a snowpack represents water from melt and rainfall and internal changes in liquid-water holding capacity due to metamorphosis. During non-rain periods, nearly all outflows are due to melting. Daily melt rates up to 2 cm d^{-1} occur frequently and maximum daily rates of 7–8 cm d^{-1} have been noted (Kuchment, 1997; Cooley and Palmer, 1997). Hourly melt rates can reach 0.1 to 0.3 cm h^{-1}. Meltwater generated at the surface of the snowpack can refreeze deeper within unripe snowpacks or be temporally stored as liquid water within the snowpack by ice layers. Thus the timing of outflow at the snowpack base can be altered considerably by storage and transmission within the snowpack.

Snow meltwater can experience significant lag in migration through the snowpack. Such conditions can occur when the liquid refreezes in subfreezing snowpacks due to significant cold content or is subjected to satisfying the liquid water holding capacity of the snowpack. Transmission of liquid water through the porous matrix of the snowpack experiences significant resistance and hence is delayed in discharging (Daanen and Nieber, 2009).

Once the discharge from snowpacks reaches the surface of the landscape, it can be rapidly transported to streamflow due to soil frost, permafrost, or saturated ground depending upon the hydraulic flow paths that are active (DeWalle and Rango, 2008). Snow that falls directly into channels or streams could discharge and flow rapidly and contributes to the initial stages of streamflow response to precipitation. Meltwater that is delivered to the soil surface in excess of the soil infiltration rate that eventually reaches a stream or river can be significant in quantity depending upon the permeability of the frozen soil or if the soil is underlain with permafrost (Semadeni-Davies, 1998; Gibson et al., 1993; Bengtsson et al., 1992; Bengtsson and Westerstrom, 1992; Kane and Stein, 1983).

DeWalle and Rango (2008) note,

> "Rapid delivery of meltwater is a particular problem in arctic basins with permanently frozen ground or permafrost (Woo, 1986). Prèvost et al. (1990) found that the low infiltration capacity of frozen soil caused overland flow and contributed to high peak streamflows during spring snowmelt at Lac Laflamme in Quebec, Canada. In an Arctic watershed, McNamara et al. (1997) found from isotope studies that runoff in spring was primarily (90%) due to event meltwater from the snowpack, but runoff in summer was typically sustained (70%) by older water released from storage by thawing of the shallow soil layer or active layer above the permafrost. A soil infiltration index was needed to account for frozen soil effects in models for accurate peak-streamflow prediction. Prediction of the depth of soil frost and the infiltration capacity of the frozen ground can be quite important to successful modeling of streamflow from snowmelt."

Streamflow hydrographs from snowmelt are strongly coupled to the energy supply for melt. The streamflow hydrograph, or time distribution of streamflow during snowmelt, depends on the physical characteristics of the drainage basin and the characteristics of the snowmelt. For example, the snowmelt discharge hydrograph for the Sierra Nevada is characterized by a *spring pulse* or the first surge in snowmelt-driven river discharge in spring, *maximum snowmelt discharge*, and *base flow* or low river discharge supported by groundwater in fall (Peterson et al., 2005). The timing of the spring pulse is primarily influenced by air temperature, but solar radiation plays a major role in mountainous terrain. The maximum daily snowmelt discharge is primarily influenced by the initial snow water equivalent. The timing of the spring pulse is mid-April, maximum daily snowmelt discharge is late May/early June, and base flow is late fall (Peterson et al., 2005).

Glacier-melt discharge and streamflow

In recent years, approximately 3,000 km^3 of water is released from the glaciers per year (Knight, 1999 and references therein). Most of the water transferred back to the hydrological system is due to ablation. Knight (1999) noted that water released from glaciers is transferred to surface streams, groundwater, directly into the ocean, or by evaporation and sublimation to the atmosphere. The discharge from a glacierized basin is characterized by a diurnal rhythm superimposed on the baseflow (Singh and Singh, 2001). This rhythm distinguishes glacier fed streams. There is also considerable baseflow in glacier fed streams during the summer. The majority of discharge from glaciers occurs during the summer months of June–August. For example, the glaciers of Alaska discharge meltwater equivalent of 2.5×10^6 m^3 of water for each km^2 of glacier during the months of July and August (Knight, 1999 and references therein).

Glaciers melt both on the surface and at the base. The surface melting occurs due to solar radiation and turbulence in the atmosphere. The basal melting occurs due to energy supplied from the bedrock underlying the glacier. Singh and Singh (2001) note, "Surface melting is seasonal and reaches a peak value usually in late summer, whereas basal melting fluctuates less markedly and generally exists throughout the entire year". They further comment that additional melting in glaciers occur due to internal movement of the glacier and the glacier sliding process when the glacier base is at pressure melting point.

Knight (1999) noted,

> Meltwater (discharge in glaciers) can be produced supraglacially, englacially, and subglacially. Supraglacial melting of snow and ice is driven by insolation, turbulent heat transfer, precipitation, and other heat sources. Englacial melting occurs due to strain heating during flow, or heat transfer into the body of the glacier. This heat transfer can occur due to percolating meltwater and by conduction from the surface or from the bed. Melting can occur at the base as a result of a variety of processes including geothermal heating, frictional heating, variations in melting point due to pressure

fluctuations during flow across the bed, heat transfer by water flowing at the bed, flow of ice between zones of different basal thermal regimes, and volcanic activity.

Timing of meltwater release from glaciers is often complicated due to different regimes of water movement with glaciers. Snowmeltwater is stored in porous snow and firn as it slowly moves toward the multiyear ice as Darcian flow. In the multiyear ice the pore structure does not support Darcian flow and most of the liquid water is stored and moves through cracks in the solid ice body. These cracks are often not connected and can therefore pond water for longer periods and even refreeze. These ponds are released when cracks and crevasses grow, which can lead to a liquid pulse release from the glacier. At the lowest stage of glacier hydrology is the channel flow where major flow paths near the bottom of the glacier funnel the water away from the glacier (Hock, 2005). These large channels tend to collect rocks and debris from the mountains and can become smaller or larger over time. These rock collection channels are also known as eskers when the glacier recedes.

Global warming has a profound effect on glacier fed stream flow, because glaciers need a long time to adjust to changing climate conditions. During a warming period glacier melt will be faster and can cause more river runoff and can offer a greater potential for hydropower generation. This trend is however not sustainable and will diminish when the glacier is reduced to a new equilibrium state. The new state is however very hard to predict and some glacier runoff may already be declining (Hock, 2005). When a new equilibrium is reached, more runoff will be generated from snowmelt during spring and rain events during the summer and much less from the melting glacier.

Summary

Discharge as a result of melt from snow and glaciers depends on a combination of snowpack and glacier physical characteristics and atmospheric conditions. Glacial melt is more complex than snowmelt due to internal movement of glacier ice and sliding of the glacier body. Snow meltwater can contribute quickly to streamflow via overland flow when the ground is frozen or saturated. Meltwater stored within the soil profile can contribute to streamflow over longer time scales. Snow melt contributions to streamflow are greatest during spring months while glacier fed streams have significant baseflow during summer months when the majority of glacial discharge occurs. Glacial melt occurs at both the surface and the base of the glacier with the timing of meltwater release complicated due to different regimes of water movement within glaciers.

Bibliography

Bengtsson, L., and Westerstrom, W., 1992. Urban snowmelt and runoff in northern Sweden. *Hydrological Sciences*, **37**, 263–275.

Bengtsson, L., Seuna, P., Lepisto, A., and Saxena, R. K., 1992. Particle movement of melt water in a subdrained agricultural basin. *Journal of Hydrology*, **135**, 383–398.

Cooley, K. R., and Palmer, P., 1997. Characteristics of snowmelt from NRCS SNOTEL (SNOwTELemetry) sites. *Proceedings of the 65th Annual Western Snow Conference*, Banff, Alberta, Canada, pp. 1–11.

Daanen, R. P., and Nieber, J. L., 2009. Model for Coupled Liquid Water Flow and Heat Transport with Phase Change in a Snowpack. *Journal of Cold Regions Engineering ASCE*, **23**(2), 43–68.

DeWalle, D. R., and Rango, A., 2008. *Principles of Snow Hydrology*. Cambridge: Cambridge University Press.

Gibson, J. J., Edwards, T. W. D., and Prowse, T. D., 1993. Runoff generation in a high boreal wetland in northern Canada. *Nordic Hydrology*, **24**, 213–224.

Hock, R., 2005. Glacier melt: a review of processes and their modelling. *Progress in Physical Geography*, **29**, 362–391.

Kane, D. L., and Stein, J., 1983. Water movement into seasonally frozen soils. *Water Resources Research*, **19**(6), 1547–1557.

Knight, P. G., 1999. *Glaciers*. Routledge: Taylor and Francis. 261 pp.

Kuchment, L. S., 1997. Estimating the risk of rainfall and snowmelt disastrous floods using physically-based models of river runoff generation. In *Destructive Water: Water Caused Natural Disasters, Their Abatement and Control, Conference Proceedings*, IAHS Publication No. 239, Anaheim, CA, pp. 95–100.

McNamara, J. P., Kane, D. L., and Hinzman, L. D., 1997. Hydrograph separation in an Arctic watershed using mixing model and graphical techniques. *Water Resources Research*, **33**, 1707–1719.

Peterson, D., Smith, R., Stewart, I., Knowles, N., Soulard, C., and Hager, S., 2005. Snowmelt Discharge Characteristics Sierra Nevada, California. *U.S. Geological Survey Report SIR-2005-5056*. U.S. Geological Survey, U.S. Department of the Interior.

Prèvost, M., Barry, R., Stein, J., and Plamondon, A. P., 1990. Snowmelt runoff modeling in a balsam fir forest with a variable source area simulator (VSAS2). *Water Resources Research*, **26**(5), 1067–1077.

Semadeni-Davies, A., 1998. Modelling snowmelt induced waste water inflows. *Nordic Hydrology*, **29**(4/5), 285–302.

Singh, P., and Singh, V. P., 2001. *Snow and Glacier Hydrology*. Dordrecht, The Netherlands: Kluwer.

Woo, M.-K., 1986. Permafrost hydrology in North America. *Atmosphere Ocean*, **24**(3), 201–234.

Cross-references

Melt Runoff Modeling
Riverflow
Runoff Observations

DISTRIBUTARY CHANNELS

Anju Chaudhary
Water Resources System Division, National Institute of Hydrology, Roorkee, India

Definition

Distributary channel is a stream that carries water away from the main river channel and distributes it to other area. Distributary channel has bifurcating channels that persists relatively independent of the parent stream. However, they may rejoin the parent channel or each other. Distributary channels are a common feature of river deltas.

Distributaries are usually formed as a stream nears the lake or the ocean, but they can occur inland as well. In some cases, a minor distributary can take so much water from the main channel that it can become the main route. The opposite of a distributary is a tributary.

DIURNAL CYCLE OF RUNOFF

Darrel A. Swift
Department of Geography, University of Sheffield, Sheffield, UK

Definition

Runoff. The flow of surface water, derived from snow melt, glacier melt, precipitation, or other sources, from a defined drainage area, such as a glacierized basin.
Diurnal cycle. The daily rise and fall of discharge/streamflow that is characteristic of runoff derived from snow and ice melt, most notably in glacierized basins.

Introduction

The important contribution of snow and ice melt to runoff from mountainous or glacierized basins causes *Discharge/Streamflow* (qv) to exhibit a distinctive diurnal cycle. The rate of melting of snow and ice is determined predominantly by the intensity of solar radiation (qv *Melting Processes*), such that runoff from these sources rises and falls daily, with diurnal maxima (i.e., daily peak flow) occurring shortly after the diurnal peak in melt. The form of the diurnal cycle varies as a result of both seasonal and spatial variations in the sources of melt, the efficiency with which solar energy is converted into melt, and the efficiency with which the resulting runoff is routed to the glacier or basin terminus (qv *Specific Melt Rate*; *Snow Hydrology*; *Glacier Hydrology*).

Diurnal cycle characteristics and their significance

Discharge Observations (qv *Discharge/Streamflow*) in mountainous or glacierized basins commonly demonstrate marked diurnal changes in discharge/streamflow superimposed on a *Base Flow/Groundwater Flow* (qv) that changes more slowly (Paterson, 1994). Diurnal changes are most obvious during fine summer weather when they are dominated by changes in the volume of runoff from snow and ice melt that has followed hydraulically efficient flow pathways (e.g., via open channels); this results in a strong diurnal runoff cycle where diurnal maxima occur only a few hours after the peak in melt. Base flow comprises snow and ice melt plus water from other sources, including groundwater, that has at least in part followed less hydraulically efficient flow pathways (e.g., via seepage through the snowpack itself, qv *Snow Hydrology*); as a result, such runoff takes a great many hours or days to reach open channels. The volume of the base flow component is typically estimated from diurnal minima (i.e., daily minimum flow). Key features of the diurnal cycle – notably, the diurnal minima and maxima, separated by periods of rising and falling (or recessional) discharge – are evident from *Hydrographs* (qv).

Discharge records from glacierized basins at the peak of the melt season demonstrate very pronounced diurnal runoff cycles (e.g., Elliston, 1973) because a number of factors maximize both the efficiency with which solar energy is converted into melt and the efficiency of flow pathways that connect runoff sources to the glacier terminus. Firstly, because the *Albedo* (qv) of glacier ice is very low in comparison to that of fresh snow, the exposure of large areas of glacier ice – as a result of the melting of accumulated winter snowfall – produces large volumes of ice melt with a highly-peaked diurnal cycle (e.g., Gordon et al., 1998). Secondly, because glacier ice is effectively impermeable at intermediate scales, runoff from ice melt is routed rapidly across the glacier surface, typically in open channels. Thirdly, highly-peaked glacier surface runoff has been shown to result in the evolution of hydraulically-efficient subglacial channel networks (e.g., Nienow et al., 1998), such that runoff from ice melt that accesses the glacier bed via moulins is also routed rapidly to the glacier terminus. Diurnal variation in discharge/streamflow may cease temporarily if summer snowfalls re-cover the glacier surface, and the cessation of surface runoff over winter allows hydraulically efficient subglacial channel networks to close.

Runoff cycle evolution in glacierized basins

The diurnal cycle of runoff from glacierized basins evolves during the melt season, from low and steady base flow with no superimposed diurnal cycle, to high base flow with highly peaked superimposed diurnal cycles whose diurnal maxima may be two or more times greater than the diurnal minima (e.g., Elliston, 1973). Base flow is initially low and stable because runoff is derived largely from Bottom Melting or Undermelt (Ice Shelf) (qv *Bottom Melting or Undermelt (Ice Shelf)*), groundwater, and the slow release of water from temporary englacial and/or subglacial storage (qv *Meltwater Storage*). As the melt season begins, base flow increases as a result of snow and ice melt following hydraulically inefficient supraglacial and subglacial flow pathways, while the diurnal cycle increases in amplitude simultaneously largely as a result of an increasing proportion of runoff being derived from ice melt, and to a lesser extent snow melt, that is able to follow hydraulically efficient flow pathways. Base flow volume is also influenced by the length and form of the recession curve from the previous diurnal peak (qv *Recession of Discharge*), which itself reflects the efficiency with which runoff from various sources is routed through the glacier (e.g., Gurnell, 1993).

The ease with which *Discharge/Streamflow* (qv) can be obtained has resulted in the characteristics of the diurnal cycle and their relationship with meteorological variables – for example, the lag times between diurnal

maxima in runoff cycles and air temperature or incident radiation, and the relative magnitudes of the diurnal and base flow components – being used widely to characterize the hydrological evolution of glacierized basins (e.g., Gurnell et al., 1992; Fountain, 1992; Hodson et al., 1998). Most recently, the controls on diurnal runoff cycle evolution have been explored using statistical analyses of hydrograph form (e.g., Hannah et al., 1999, 2000; Swift et al., 2005a). For example, Swift et al. (2005a) statistically classified diurnally-peaked hydrographs from Haut Glacier d'Arolla, Switzerland into three types that demonstrated systematic evolution of the diurnal cycle that is characteristic of many temperate glacierized basins (e.g., Elliston, 1973; Lang, 1973; Gurnell et al., 1992; Fountain, 1992; Raymond et al., 1995); however, the timing and extent of runoff cycle evolution varied significantly between melt seasons as a result of the influence of the glacier-surface snowpack on the sources of melt and the routing of the resulting runoff (cf. Willis et al., 2002).

A notable feature of diurnal cycle evolution is the appearance of progressively earlier diurnal maxima, and therefore an increasingly rapid rise to peak discharge from the diurnal minima, which Elliston (1973) suggested reflects the more efficient routing of runoff as a result of the enlargement of subglacial channels. However, Fountain (1992) has argued that channel size should have a negligible effect, since the delay between peak melt and peak runoff should be a function of the time required for a pressure wave to propagate over the same distance. Swift et al. (2005a) therefore suggested that the timing of diurnal maxima may be affected by changes in glacier-surface characteristics that effect the efficiency of melt production and the routing of the resulting runoff – for example, changes in albedo as melting concentrates englacial debris on the ice surface, and the development of more efficient (i.e., less tortuous and better-connected) supraglacial, englacial, and subglacial drainage networks – as the melt season progresses (cf. Seaberg et al., 1988; Hock and Hooke, 1993; Fountain, 1996).

The glaciological factors that control the evolution of the size of the diurnal cycle relative to base flow are also poorly understood. Observations at many glaciers indicate that the amplitude of the diurnal cycle at the peak of the melt season may be only 50% of the volume of base flow (e.g., Elliston, 1973; Lang, 1973; Raymond et al., 1995), perhaps because a large proportion of runoff from ice melt that accesses the glacier bed does so in areas of hydraulically inefficient subglacial drainage. This theory is given support by observations at Haut Glacier d'Arolla that are consistent with the corollary; in other words, moulins at Haut Glacier d'Arolla that allow surface runoff to reach the glacier bed are located largely above preferential subglacial drainage axes (Sharp et al., 1993), and diurnal maxima at the peak of the melt season are typically in excess of two times base flow volume (Swift et al., 2005a). Nevertheless, it might be possible for channel flow to elevate base flow if diurnal maxima are sufficient to force channel flow into adjacent areas of hydraulically inefficient subglacial drainage (cf. Hubbard et al., 1995) and/or delay flow within the inefficient system from entering arterial channels (Swift et al., 2005a).

Significance of the runoff cycle for glaciology

The form of runoff cycles in glacierized basins is highly significant because the large amplitude of runoff cycles produced by ice melt have been shown to drive the evolution of hydraulically efficient subglacial drainage systems (e.g., Gordon et al., 1998; Nienow et al., 1998) and to dictate water pressure variations within such systems (cf. Hubbard et al., 1995) that influence glacier motion (cf. Willis, 1995; Nienow et al., 2005) (qv *Dynamics of Glaciers*; *Glacier Sliding*). Such diurnal water pressure variations will increase in amplitude with the increasing peakedness of the runoff cycle, and, should increasingly peaked runoff cycles result in open flow conditions in subglacial channels for longer periods of the diurnal cycle (cf. Sharp et al., 1993), adjustments in the cross-sectional area of channels should further increase water pressures at peak flows (Swift et al., 2005a). Swift et al. (2005b) have shown that the peakedness of the diurnal cycle also appears to control the efficiency of basal sediment evacuation by subglacial drainage, presumably because high water pressure variation promotes extreme discharge gradients within subglacial channels and a strong diurnally-reversing hydraulic gradient between channels and adjacent areas of hydraulically inefficient drainage (cf. Hubbard et al., 1995) (qv *Subglacial Drainage System*).

Summary

Diurnal cycles in runoff are common in mountainous and glacierized basins, but are especially pronounced in glacierized basins during fine summer weather at the peak of the melt season, when large areas of exposed glacier ice generate large volumes of ice melt that is efficiently routed to the glacier terminus by hydraulically efficient subglacial channel networks. The form of runoff cycles is also influenced by the sources of melt and the efficiency with which melt is produced, such that the removal of accumulated winter snowfall from the glacier surface during the summer is a critical control on the timing and extent of runoff cycle evolution, as well as being a significant source of base flow as a result of flow through the snowpack being highly inefficient. The amplitude of the diurnal cycle is critical in many important glacial processes, including the evolution of hydraulically efficient subglacial channels, and rates of basal sliding and sediment evacuation. Nevertheless, as a result of the compexities of runoff sources, the processes that generate melt, and the routing of the resulting runoff, the controls on the form and evolution of key components of the diurnal cycle remain poorly understood.

Bibliography

Elliston, G. R., 1973. Water movement through the Gornergletscher. *Symposium on the Hydrology of Glaciers*. IASH Publication No. 95, pp. 79–84.

Fountain, A. G., 1992. Subglacial water flow inferred from stream measurement of South Cascade Glacier, Washington, USA. *Journal of Glaciology*, **138**, 113–119.

Fountain, A. G., 1996. Effect of snow and firn hydrology on the physical and chemical characteristics of glacial runoff. *Hydrological Processes*, **10**, 509–521.

Gordon, S., Sharp, M., Hubbard, B., Smart, C., Ketterling, B., and Willis, I., 1998. Seasonal reorganisation of subglacial drainage inferred from measurements in boreholes. *Hydrological Processes*, **12**, 105–133.

Gurnell, A. M., 1993. How many reservoirs? An analysis of flow recessions from a glacier basin. *Journal of Glaciology*, **39**, 409–414.

Gurnell, A. M., Clark, M. J., and Hill, C. T., 1992. Analysis and interpretaion of patterns within and between hydroclimatological time series in an Alpine glacier basin. *Earth Surface Processes and Landforms*, **17**, 821–839.

Hannah, D. M., Gurnell, A. M., and McGregor, G. R., 1999. A methodology for investigation of the seasonal evolution in proglacial hydrograph form. *Hydrological Processes*, **13**, 2603–2621.

Hannah, D. M., Smith, B. P. G., Gurnell, A. M., and McGregor, G. R., 2000. An approach to hydrograph classification. *Hydrological Processes*, **14**, 317–338.

Hock, R., and Hooke, R. L., 1993. Evolution of the internal drainage system in the lower part of the ablation area of Storglaciären, Sweden. *Geological Society of America Bulletin*, **105**, 537–546.

Hodson, A. J., Gurnell, A. M., Washington, R., Tranter, M., Clark, M. J., and Hagen, J. O., 1998. Meteorological and runoff time-series characteristics in a small, high-Arctic glaciated basin, Svalbard. *Hydrological Processes*, **12**, 509–526.

Hubbard, B. P., Sharp, M. J., Willis, I. C., Nielsen, M. K., and Smart, C. C., 1995. Borehole water level variations and the structure of the subglacial hydrological system of Haut Glacier d'Arolla, Valais, Switzerland. *Journal of Glaciology*, **41**, 572–583.

Lang, H., 1973. Variations in the relation between glacier discharge and meteorological elements. IASH Publication No. 95, pp. 85–94.

Nienow, P., Sharp, M., and Willis, I., 1998. Seasonal changes in the morphology of the subglacial drainage system, Haut Glacier d'Arolla, Switzerland. *Earth Surface Processes and Landforms*, **23**, 825–843.

Nienow, P. W., Hubbard, A. L., Hubbard, B. P., Chandler, D., Mair, D. W. F., Sharp, M. J., and Willis, I. C., 2005. Hydrological controls on diurnal ice flow variability in valley glaciers. *Journal of Geophysical Research*, **110**, F04002, doi:10.1029/2003JF000112.

Paterson, W. S. B., 1994. *The Physics of Glaciers*. Oxford: Pergamon.

Raymond, C. F., Benedict, R. J., Harrison, W. D., Echelmeyer, K. A., and Sturn, M., 1995. Hydrological discharges and motion of Fels and Black Rapids Glaciers, Alaska, USA: implications for the structure of their drainage systems. *Journal of Glaciology*, **41**, 290–304.

Seaberg, S. Z., Seaberg, J. Z., Hooke, R. L., and Wieberg, D. W., 1988. Character of the englacial and subglacial drainage system in the lower part of the ablation area of Storglaciären, Sweden, as revealed by dye-trace studies. *Journal of Glaciology*, **34**, 217–227.

Sharp, M., Richards, K., Willis, I., Arnold, N., Nienow, P., Lawson, W., and Tison, J.-L., 1993. Geometry, bed topography and drainage system structure of the Haut Glacier d'Arolla, Switzerland. *Earth Surface Processes and Landforms*, **18**, 557–571.

Swift, D. A., Nienow, P. W., Hoey, T. B., and Mair, D. W. F., 2005a. Seasonal evolution of runoff from Haut Glacier d'Arolla, Switzerland and implications for glacial geomorphic processes. *Journal of Hydrology*, **309**, 133–148.

Swift, D. A., Nienow, P. W., and Hoey, T. B., 2005b. Basal sediment evacuation by subglacial meltwater: suspended sediment transport from Haut Glacier d'Arolla, Switzerland. *Earth Surface Processes and Landforms*, **30**, 867–883.

Willis, I. C., 1995. Intra-annual variations in glacier motion: a review. *Progress in Physical Geography*, **19**, 61–106.

Willis, I. C., Arnold, N. S., and Brock, B., 2002. Effect of snowpack removal on energy balance, melt and runoff in a small supraglacial basin. *Hydrological Processes*, **16**, 2721–2749.

Cross-references

Albedo
Basal Sediment Evacuation by Subglacial Drainage Systems
Base Flow/Groundwater Flow
Bottom Melting or Undermelt (Ice Shelf)
Catchment Glacier
Direct Surface Runoff
Dynamics of Glaciers
Glacial Drainage Characteristics
Glacier Hydrology
Hydrographs
Impacts of Snow and Glaciers on Runoff
Meltwater Storage
Precipitation
Runoff Generation
Runoff Observations
Snow Hydrology
Specific Melt Rate
Streamflow Trends in Mountainous Regions
Subglacial Drainage System

DIVERGING ICE FLOW

Gulab Singh, Farjana S. Birajdar
Centre of Studies in Resources Engineering, Indian Institute of Technology Bombay, Powai, Mumbai, India

Definition

Diverging ice flow represents the slow-moving ice flow. The divergence of glacial flow is directly linked to ice velocity and sediment transport to the glacial terminus. Slow-flowing areas of ice sheets (or glaciers) are often associated with divergent flow line gradient, little basal erosion, and low sediment supply to continental slope. Diverging flow occurs where flow lines diverge and lateral stresses are tensional results in decrease in forward velocity. Diverging flow occurs at locations where there is a transverse gradient in the slope of the ice (e.g., zone of ablation in a valley glacier). Under such conditions, streaming ice becomes unconfined. On the other hand, converging flow where flow lines converge and lateral stresses are compressive results in an increase in velocity. This type of flow is observed in the accumulation zone of an alpine glacier or where unconfined flow becomes

confined or channeled into a valley. The significance of *divergent ice flow* direction can be probably linked to the mode of deglaciation.

Bibliography

Dowdeswell, J. A., and Cofaigh, C., 2002. *Glacier-influenced sedimentation on high-latitude continental margins*. London: Geological Society.

DRIFT GLACIER/ICE/SNOW

Gulab Singh, Farjana S. Birajdar
Centre of Studies in Resources Engineering, Indian Institute of Technology Bombay, Powai, Mumbai, India

Definition

Drift Glacier is movement of glacier which results in transportation of rock material by glacial ice. Glacial drift occurs as scattered rock fragments, as till, and as outwash. The erosive action of glaciers generates considerable amount of sediment. Drift could be deposited by ice, by a combination of melt water and ice, or reorganized completely by melt water. Mainly, the material transported by glaciers is gravel, sand, or clay.

The drift ice is defined as the movement of ice fields or floes in water bodies caused by wind or currents, whereas drift snow is a deposit of snow created by wind into a mound during snowstorms.

Bibliography

Allen, T. R., 1998. Topographic context of glaciers and perennial snowfield, Glacial national park, Montana. *Geomorphology*, **21**, 207–216.

DRY AND WET SNOW LINE/ZONE

Ravi P. Gupta
Department of Earth Sciences, Indian Institute of Technology Roorkee, Roorkee, UA, India

Definition

Dry and wet snow line/zone essentially separates that part of the snow cover in the mountain basin where snowmelt arises (wet) from that where no snowmelt arises (dry).

Dry and wet snow line/zone

1. Dry and wet snow line/zone essentially separates that part of the snow cover where snowmelt arises (wet) from that where no snowmelt arises (dry). Snow at the time of precipitation from clouds has a dry granular-flaky form with soft and open structure and possesses low relative density. With the onset of melting season as the environmental temperature rises and crosses the melting point (0°C), the snow starts to melt, and almost invariably at this time undergoes repeated cycles of partial melting (day) and refreezing (night). This leads to development of bigger recrystallized ice crystals with increased density and this forms the typical melting seasonal snow.
2. Sun is the main source of heat energy leading to the melting of snow, and the intensity of solar radiation reaching the individual snow-covered topographic slope/facet is the most important factor in the snow-melting process. Therefore, the dry and wet snow line/zone is influenced by a complex interplay of various factors, such as sun direction and angle vis-à-vis local topographic slope and aspect, time of the day, latitude–longitude, besides various atmospheric–meteorological factors. Thus, the dry and wet snow line/zone could vary in altitude/location within a basin.
3. Further, the dry and wet snow line/zone is a transient feature that changes position with time within a basin. It exhibits a systematic gradual movement toward higher elevation with time as the snowmelt season advances. The boundary between dry and wet snow is gradational and fuzzy; therefore, in field the term zone is more appropriate, whereas on small-scale maps, it may appear as a line.
4. Snowpack constitutes an important source of fresh water in many parts of the world. Melting seasonal snow, most of which is névé, is relatively less recognized and described in literature, but is of great importance as snowmelt is concerned. Out of the entire snow-cover area in a basin on a particular date, snowmelt is generated only from the snow-cover area that lies below the dry and wet snow line/zone, as the snow-cover area above it remains essentially dry and does not produce any melt. Snowmelt runoff models (SRMs) are developed to predict snowmelt runoff in the ensuing summer melting season on a daily basis, and it is very important to map dry/wet snow line/zone for estimating snowmelt runoff.
5. Field investigations for mapping of dry and wet snow line/zone are very difficult to carry out and may be tedious, arduous, and too time consuming. On the other hand, the position of the line/zone rapidly changes with time. Therefore, satellite remote sensing systems are most optimally suited to collect synoptic data for mapping of dry and wet snow line/zone. The melting seasonal snow consists of small snow-ice crystals, possibly with moisture film during the daytime. This leads to a reduced near-infrared reflectance as compared to the dry snow (Dozier and Painter, 2004; Hall et al., 1992) (Figure 1). Thus, on satellite sensor images, the wet snow is characterized by marked reduced reflectance in the near-infrared part of the spectrum in comparison to the dry snow, which exhibits very high reflectance, facilitating their mutual discrimination.
6. Although, wet snow and glacial ice appear similar on remote sensing satellite images, the two can be differentiated from each other on the basis of shape, site,

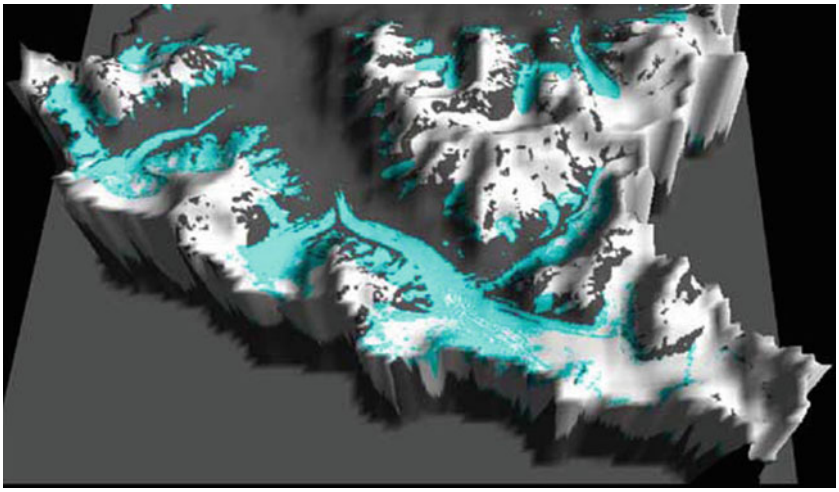

Dry and Wet Snow Line/Zone, Figure 1 Boundary and relative distribution of dry snow (*white*) and wet snow (*cyan-blue*) in the Gangotri basin (the origin of the Ganges river), Himalaya. Dry snow occurs at higher altitudes and is fringed by the melting seasonal wet snow on relatively lower altitudes. Perspective view generated by draping IRS-satellite image over the digital elevation model (Gupta et al., 2005).

and repetivity in occurrence on different temporal images. The ice body occurs only in glacial valley, is lingulate, has a sharp boundary and a permanent position, i.e., is repeatedly shown at the same place in various images, whereas the wet snow occurs as a fringe adjoining the dry snow all over on hill slopes and valleys, and this fringe changes position with time in the melting season, i.e., appears at different heights/places on images of different dates (Gupta et al., 2005).

7. Anomalous local deviations in dry and wet snow line/zone, e.g., late occurrence in the accumulation season and advance presence in the melting season, may indicate local higher geothermal gradients, e.g., due to hot springs.

Summary

In summary, it may be stated that dry and wet snow line/zone is basin morphology dependent, fuzzy, and transient. Its delineation is extremely important for various purposes such as water resources modeling and management. As field investigations are tedious, arduous, and too time consuming, satellite remote sensing techniques are most optimally suited for such resources applications.

Bibliography

Dozier, J., and Painter, T. H., 2004. Multispectral and hyperspectral remote sensing of alpine snow properties. *Annual Review of Earth and Planetary Sciences*, **32**, 465–494.

Gupta, R. P., Haritashya, U. K., and Singh, P., 2005. Mapping dry/wet snow cover in the Indian Himalayas using IRS multispectral imagery. *Remote Sensing of Environment*, **97**, 458–469.

Hall, D. K., Foster, J. L., and Chang, A. T. C., 1992. Reflectance of snow as measured in situ and from space in sub-arctic areas in Canada and Alaska. *IEEE Transactions on Geoscience and Remote Sensing*, **30**(3), 634–637.

Cross-references

Dry Snow

DRY SNOW

Ravi P. Gupta
Department of Earth Sciences, Indian Institute of Technology Roorkee, Roorkee, UA, India

Definition

When snowfall occurs in a condition such that the temperature of the troposphere (the lowermost layer of the earth's atmosphere which contains most of the atmospheric water vapor) and the temperature of the earth's surface, both, are below freezing point, then in that condition the snow falling on the earth's surface is crystalline, granular, flaky material with dendritic or highly branched crystals possessing very low relative density. This is essentially dry snow. Such conditions of snowfall generally occur during winter months at high altitudes and high latitudes. The dry snow comprises of solid crystals with no melt or moisture film on crystal surfaces and has a minimal amount of water content. Snow is considered wet or dry based on the water content, that is, "snow to liquid equivalent," a ratio used to indicate the amount of liquid water produced as snow melts. Wet snow has this ratio as usually 10:1 (means 10 cm of snow produces 1 cm of melt water), whereas for dry snow the ratio could 30:1, implying presence of more air pockets in the (dry) snow medium. Dry snow has a very high reflectance, reflecting more than 90% of the incident solar radiation. Further, it is not "sticky" or cohesive, and can be hardly

used for making snowballs or snowmen. Being non-cohesive, it is also susceptible to avalanches. The dry snow zone is the region where no melt occurs and is great for skiing.

DYE TRACER INVESTIGATIONS OF GLACIER HYDROLOGY

Peter Nienow
School of Geosciences, University of Edinburgh, Edinburgh, UK

Definition

Dye tracing. Dye tracing involves the input of a fluorescent dye into a hydrological system and subsequent detection of the dye after it has flowed through the system under investigation. Analysis of the dye breakthrough curve enables inferences to be made concerning the structure and flow conditions of the hydrological system that has been traced.

Introduction

Salt and dye tracers have been used for over a century to investigate glacial drainage systems. These tracers provide direct information on water flow characteristics between an input site, usually a freely-draining, ice-surface moulin or crevasse (Figure 1), and a detection site located on the proglacial stream close to the glacier snout. If detection of an internal drainage connection is the sole aim of a tracer test, the hydraulic properties of the tracer are unimportant. However, if the tracer is to be used for estimation of flow velocity or other quantitative parameters, it is essential that the hydraulic behavior of the tracer is equal or very similar to that of the water itself (Hotzl, 1990). Most modern applications of dye tracing are concerned with the quantitative analysis of dye breakthrough curves and therefore require advanced fluorometric equipment. Fluorescent dyes such as rhodamine and fluorescein are the most commonly used tracers, since they can be detected by a fluorometer at concentrations below 1 ppb upon emergence in the proglacial stream. Water samples are collected either manually or by pump or gravity-driven continuous flow (Fountain, 1993; Sharp et al., 1993). With the latter technique, dye concentration is usually recorded at regular intervals using automated data loggers. Dye concentration breakthrough curves can be analyzed to yield a number of parameters that can be related to the character of the glacier hydrological system that has been traced.

Hydrological flow parameters derived from tracer tests

Subglacial and englacial drainage systems are largely inaccessible. Glaciologists have therefore developed a range of remote techniques for determining the character of these systems including dye tracing in addition to investigations of bulk meltwater discharge and chemistry, proglacial bedrock characteristics, and borehole studies (Hubbard and Nienow, 1997). Dye tracing has been used to investigate glacier hydrology across a variety of glacial environments including temperate glaciers in the Alps (e.g., Behrens et al., 1975) and polythermal glaciers in the High Arctic (Bingham et al., 2005) and Greenland. Extensive tracer campaigns conducted over the course of a melt-season can be used to infer both temporal and spatial variations in subglacial drainage system characteristics (Hock and Hooke, 1993; Nienow et al., 1998). The parameters that can be derived from a suite of dye tracer tests to infer the structure and flow characteristics of glacier hydrological systems are outlined below:

Dye Tracer Investigations of Glacier Hydrology, Figure 1 Rhodamine dye flowing into a moulin during a tracer experiment on a glacier near the margin of the Greenland ice sheet.

- Internal drainage connections

  The simplest application of any fluid tracer is to provide positive evidence of the existence of a hydrological connection between a point of injection and a point of detection. Tracing of water for this purpose is clearly only of value when the routing of the water is unobservable. For these reasons, tracers have been used for many years to determine hydrological

connections in karst, groundwater, and subglacial drainage systems (Ford and Williams, 1989).

The earliest attempts to study glacial drainage connections using dye tracers involved the injection of dye into moulins and relied on the visual detection of dye emerging from portals at the glacier snout (Forel, 1898; Vallot and Vallot, 1900). This method of detection has been used more recently when advanced fluorometric equipment has been unavailable or when more than one dye has been used (e.g., Theakstone and Knudsen, 1981; Burkimsher, 1983). This simple technique allows a basic reconstruction of subglacial drainage pathways. If multiple streams are discharging water from a glacier and each is sampled for dye after an injection, it is possible if multiple injection sites are used, to determine whether the glacier is underlain by a number of discrete drainage catchment basins (Stenborg, 1969; Willis et al., 1990; Fountain, 1993; Sharp et al., 1993).

- Dye flow velocity

  A minimum estimate of the mean flow velocity of water during a tracer test can be obtained from the time elapsed between dye injection and peak concentration at the detection site and the straight-line distance between these two sites. The flow velocity through the englacial and subglacial drainage system is dependent on the character of the flow pathways via which the water has travelled. Return velocities from tracer tests made into moulins and boreholes have varied between 0.0031 m s^{-1} for a winter trace at Findelengletscher, Switzerland (Moeri and Leibundgut, 1986) and 1.8 m s^{-1} at Austre Okstindbreen, Norway (Theakstone and Knudsen, 1981).

  Rapid transit velocities of greater than 0.2 m s^{-1} are interpreted in terms of flow through hydraulically efficient channelized drainage systems (e.g., Stenborg, 1969; Behrens et al., 1975; Burkimsher, 1983). In contrast, lower through-flow velocities have usually been interpreted in terms of flow through an inefficient "distributed" hydrological system such as a linked-cavity configuration, a thin basal water film, or a permeable basal sediment layer (Theakstone and Knudsen, 1981; Iken and Bindschadler, 1986; Kamb, 1987; Willis et al., 1990). In some studies, velocities of less than 0.1 m s^{-1} have also been interpreted as flow through highly sinuous hydraulically inefficient anabranching channels (Seaberg et al., 1988: Hock and Hooke, 1993; Fountain, 1993).

- Velocity–discharge relationships

  If water discharge is monitored, then the mean cross-sectional area of a drainage system can be calculated by dividing that discharge by the mean flow velocity derived from a tracer test. With this cross-sectional area information, it is possible to use turbulent flow theory to calculate the expected flow velocity through a variety of alternative drainage configurations (Seaberg et al., 1988; Kohler, 1995). By comparing the predicted velocities with those determined from dye tracer experiments, inferences can be made about the likely character of the drainage pathways followed. Furthermore, by analyzing the relationship between velocity and discharge, inferences can be made about both the hydraulic geometry and the flow conditions in a drainage system (Leopold and Maddock, 1953; Seaberg et al., 1988; Willis et al., 1990; Hock and Hooke, 1993; Fountain, 1993; Nienow et al., 1996a; Schuler et al., 2003).

- Percentage dye recovery

  The percentage of dye recovered during a tracer test can be determined by multiplying the integral of the dye breakthrough curve by the proglacial stream discharge. Recoveries of less than 50% typically indicate storage of the tracer within the glacier's hydrological system (Theakstone and Knudsen, 1981). These returns are more likely in a hydrologically complex drainage system, since efficient channels route water rapidly, as a concentrated slug of dye, with little potential for storage. However, a number of non-hydrological variables may result in erroneous estimates of dye recovery and caution must be exercised when using this parameter for interpreting glacial drainage systems (Nienow, 1993). For example, loss of dye may result from sorption onto sediment surfaces (Bencala et al., 1983) while certain suspended sediments fluoresce at the same wavelength as the tracer causing a spurious increase in fluorometer reading resulting in apparent overestimation of the volume of dye recovered (Smart and Laidlaw, 1977).

- Dye dispersion

  The shape of a dye return curve is determined by dispersive processes that spread dye out during its passage through a flow system (Taylor, 1954; Fischer, 1968). This dispersion results from two main mechanisms: (i) advection in the fluid flow (mechanical dispersion) and (ii) molecular diffusion. Since these processes are controlled by flow hydraulics, which are themselves controlled by the structure of the flow path, the shape of a dye return curve may be interpreted in terms of the structure of the flow pathways followed by that water. An increasingly dispersed dye cloud can result from two main characteristics of flow: (i) an increase in the variation of flow velocities within the drainage routeway and (ii) an increase in the volume of storage locations or immobile zones along the course of the drainage routeway. In all glacial flow systems, both characteristics cause dispersion of a dye cloud although in general, dispersion resulting from variations in flow velocity dominates, particularly in channelized systems, while dispersion resulting from storage retardation becomes increasingly significant in hydraulically inefficient flow systems.

While the shape of a dye return curve can provide a wealth of information on the structure of the drainage system which has generated the curve, visual interpretations of return curve shapes are highly subjective. An objective

method of describing the properties of return curves requires physically meaningful and empirically reproducible results. The most commonly used parameter derived from the shape of breakthrough curves is *dispersivity* (d), in m, which represents the rate of spreading of a tracer cloud (described by the *dispersion coefficient, D,* in $m^2\ s^{-1}$) relative to the rate of advection of the dye or salt during transit through a flow system (u), in $m\ s^{-1}$ (Fischer, 1968; Seaberg et al., 1988; Hock and Hooke, 1993):

$$d = D/u \tag{1}$$

The most commonly adopted form of D in glaciology is that derived by Brugman (1986) as:

$$D = \frac{\left(x^2(t_m - t_i)^2\right)}{(4t_m t_i \ln(2(t_m/t_i)^{0.5}))} \tag{2}$$

In general, more dispersed tracer returns ($d > \sim 10$ m) reflect inefficient drainage pathways (e.g., Seaberg et al., 1988; Nienow et al., 1998), while highly-peaked, less dispersed ($d < 10$ m) curves are interpreted in terms of flow through efficient channels (e.g., Burkimsher, 1983). Irregularities on the rising or falling limbs of breakthrough curves (including the occurrence of multiple tracer peaks) are interpreted in terms of flow divergence in the drainage pathways (Collins, 1982).

The interpretation of dye return curve shapes is the most complex area of dye tracer analysis and the one most susceptible to conflicting interpretations between different workers. However, to ensure that the parameters derived from the return curves are accurate and comparable between tests, a minimum sampling interval should be used which is no greater than *tm*/16 where *tm* is the time to peak dye concentration (Nienow et al., 1996b).

Tracer investigations in the snowpack and firn

While dye tracing techniques have been most commonly used in glacial environments for investigating the routing and flow characteristics of englacial and subglacial drainage systems, the same methods can be applied for investigating the hydrology of the snowpack (Gerdel, 1954; Schneebeli, 1995, Kattelmann and Dozier, 1999) and firn. Observations of the movement of dye-stained water through an alpine snowpack reveal qualitatively the complexity of flow patterns and the influence of ice layers and preferential flow zones in controlling percolation through the snowpack, and fluorometric techniques can be used to yield flow rates for percolation through the snowpack of between 0.13 and 0.49 $m\ h^{-1}$ (Campbell et al., 2006). The changing form of dye-return curves can also be used to determine changes in percolation rates over the course of a melt season and thus in the efficiency with which the snowpack transmits meltwater (Campbell et al., 2006).

A more recent application of tracers has been to determine, through visual observation of shallow ice cores, the depths to which summer meltwaters percolate before refreezing in the percolation zone of the firn on a High Arctic ice cap. Rhodamine dye was spread over the surface of the snowpack in spring, and cores were retrieved in Autumn down to depths of ~3m to visually determine the depths to which the surface meltwaters had percolated prior to refreezing (Bell et al., 2008).

Summary

Dye tracing provides a simple, inexpensive, and valuable technique for investigating glacial drainage systems which is today usually reliant on the use of a fluorometer which can detect dye in concentrations as low as 0.05 ppb. This equipment provides the potential for obtaining extremely detailed information on both the routing of water through and flow conditions within a glacial drainage system. The raw data which can be obtained from tracer tests enable the investigator to determine (i) the portals at which dye emerges from the system; (ii) the water flow velocities through the system; (iii) the shape of the dye return curves emerging from the system; and in conjunction with discharge; (iv) the proportion of dye recovered after an injection into the system; and (v) the hydraulic geometry and the flow conditions in the drainage system.

From these data, a considerable amount of information can therefore be gained about the drainage conditions through and under a glacier. Furthermore, since dye can be injected at any point where water enters the englacial drainage system, extensive spatial coverage can be provided by tracer tests on any given glacier. Tests can also be carried out over the course of a melt-season to provide evidence for the temporal evolution of subglacial drainage systems (Hock and Hooke, 1993; Nienow et al., 1998; Bingham et al., 2005). Despite this excellent spatial and temporal resolution, however, dye breakthrough curves can only be interpreted in terms of the net influence of the flow pathways separating the injection and detection sites. The technique therefore provides only limited evidence for spatial variability in the flow pathways followed by dye clouds.

Bibliography

Behrens, H., Bergmann, H., Moser, H., Ambach, W., and Jochum, O., 1975. On the water channels of the internal drainage system of Hintereisferner, Otztal Alps, Austria. *Journal of Glaciology*, **14**, 375–382.

Bell, C., Mair, D., Burgess, D., Sharp, M., Demuth, M., Cawkwell, F., Bingham, R., and Wadham, J., 2008. Spatial and temporal variability in the snowpack of a High Arctic ice cap: implications for mass-change measurements. *Annals of Glaciology*, **48**, 159–170.

Bencala, K. E., Jackman, A. P., Kennedy, V. C., Avanzino, R. J., and Zellweger, G. W., 1983. Kinetic analysis of strontium and potassium sorption onto sands and gravels in a natural channel. *Water Resources Research*, **19**(3), 725–731.

Bingham, R., Nienow, P., Sharp, M., and Boon, S., 2005. Subglacial drainage processes at a High Arctic polythermal valley glacier. *Journal of Glaciology*, **51**, 15–24.

Brugman, M. M., 1986, unpublished. *Water Flow at the Base of a Surging Glacier*. PhD thesis (Part 2), California Institute of Technology, Pasadena.

Burkimsher, M., 1983. Investigations of glacier hydrological systems using dye-tracer techniques: observations at Pasterzengletscher, Austria. *Journal of Glaciology*, **29**, 403–416.
Campbell, F., Nienow, P., and Purves, R., 2006. Role of the supraglacial snowpack in mediating meltwater delivery to the glacier system as inferred from dye tracer investigations. *Hydrological Processes*, **20**, 969–985.
Collins, D. N., 1982. Flow-routing of meltwater in an alpine glacier as indicated by dye tracer tests. *Beiträge zur Geologie der Schweiz – Hydrologie*, **28**(II), 523–534.
Fischer, H. B., 1968. Methods for predicting dispersion coefficients in natural streams, with applications to lower reaches of the Green and Duwamish Rivers, Washington. U.S. Geological Survey, Professional Paper, 582-A.
Ford, D., and Williams, P., 1989. *Karst Geomorphology and Hydrology*. London: Unwin Hyman.
Forel, F.-A., 1898. Circulation des eaux dans le Glacier du Rhone. *Bulletin de la Societe de Speleologie (Spelunca)*, **4**, 156–158.
Fountain, A. G., 1993. Geometry and flow conditions of subglacial water at South Cascade Glacier, Washington State, USA; analysis of tracer injections. *Journal of Glaciology*, **39**, 143–156.
Gerdel, R. W., 1954. The transmission of water through snow. *Transactions, American Geophysical Union*, **35**(3), 475–485.
Hock, R., and Hooke, R. Le B., 1993. Evolution of the internal drainage system in the lower part of the ablation area of Storglaciären, Sweden. *Geological Society of America Bulletin*, **105**, 537–546.
Hooke, R. Le B., 1989. Englacial and subglacial hydrology: a qualitative review. *Arctic and Alpine Research*, **21**, 221–233.
Hotzl, H., 1990. Advantages and limitations in the use of artificial tracers in the study of complex aquifers. *Memoires of the 22nd Congress of the International Association of Hydrogeologists*, Lausanne, **22**, 183–193.
Hubbard, B., and Nienow, P., 1997. Alpine subglacial hydrology: research status and implications for glacial geology. *Quaternary Science Reviews*, **16**(9), 939–956.
Iken, A., and Bindschadler, R. A., 1986. Combined measurements of subglacial water pressure and surface velocity of Findelengletscher, Switzerland: conclusions about drainage system and sliding mechanism. *Journal of Glaciology*, **32**, 101–119.
Kamb, B., 1987. Glacier surge mechanism based on linked cavity configuration of the basal water conduit system. *Journal of Geophysical Research*, **92**(B9), 9083–9100.
Kattelmann, R., and Dozier, J., 1999. Observations of snowpack ripening in the Sierra Nevada, California, U.S.A. *Journal of Glaciology*, **45**, 409–416.
Kohler, J., 1995. Determining the extent of pressurized flow beneath Storglaciären, Sweden, using results of tracer experiments and measurements of input and output discharge. *Journal of Glaciology*, **41**, 217–231.
Leopold, L. B., and Maddock, T., 1953. The hydraulic geometry of stream channels and some physiographic implications. *United States Geological Survey Professional Paper*, **252**, 1–57.
Moeri, T., and Leibundgut, C., 1986. Winter dye tracer experiments on the Findelengletscher (Canton Wallis, Switzerland). *Zeitschrift Gletscherkunde und Glazialgeologie*, **22**, 33–41.
Nienow, P. W., 1993, unpublished. *Dye Tracer Investigations of Glacier Hydrological Systems.* PhD thesis, University of Cambridge.
Nienow, P., Sharp, M., and Willis, I., 1996a. Velocity-discharge relationships derived from dye-tracer experiments in glacial meltwaters: implications for subglacial flow conditions. *Hydrological Processes*, **10**, 1411–1426.
Nienow, P., Sharp, M., and Willis, I., 1996b. Sampling-rate effects on the properties of dye breakthrough curves from glaciers. *Journal of Glaciology*, **42**, 184–189.
Nienow, P., Sharp, M., and Willis, I., 1998. Dye tracer investigations at the Haut Glacier d'Arolla, Switzerland: the late-summer configuration of the of the subglacial drainage system. *Earth Surface Processes and Landforms*, **23**, 825–843.
Schneebeli, M., 1995. Development and stability of preferential flow paths in a layered snowpack. In Tonnessen K. A., Williams M. W., and Tranter, M., (eds.), *Biogeochemistry of Seasonally Snow-Covered Catchments*, IAHS Publication No. 228. Wallingford: IAHS Press, pp. 89–95.
Schuler, T., Fischer, U. H., and Gudmundsson, G. H., 2003. Diurnal variability of subglacial drainage conditions as revealed by tracer experiments. *Journal of Geophysical Research*, **109**, F02008, doi:10.1029/2003JF000082.
Seaberg, S. Z., Seaberg, J. Z., Hooke, R. Le B., and Wiberg, D. W., 1988. Character of the englacial and subglacial drainage system in the lower part of the ablation area of Storglaciären, Sweden, as revealed by dye-tracer studies. *Journal of Glaciology*, **34**, 217–227.
Sharp, M. J., Richards, K., Willis, I., Arnold, N., Nienow, P., Lawson, W., and Tison, J.-L., 1993. Geometry, bed topography and drainage system structure of the Haut Glacier d'Arolla, Switzerland. *Earth Surface Processes and Landforms*, **18**, 557–572.
Smart, P. L., and Laidlaw, I. M. S., 1977. An evaluation of some fluorescent dyes for water tracing. *Water Resources Research*, **13**(1), 15–33.
Stenborg, T., 1969. Studies of the internal drainage of glaciers. *Geografiska Annaler*, **51A**, 13–41.
Taylor, G. I., 1954. Dispersion of matter in turbulent flow through a pipe. *Proceedings of the Royal Society of London*, **223**(A), 446–468.
Theakstone, W. H., and Knudsen, N. T., 1981. Dye tracer tests of water movement at the glacier Austre Okstindbreen, Norway. *Norsk Geografisk Tidsskrift*, **35**(1), 21–28.
Vallot, G., and Vallot, J., 1900. Experience sur la vitesse de la circulation de l'eau dans les torrents et sous les glaciers. *Annales de l'Observatoire Meteorologigue, Physique et Glaciare, Mont Blanc, Tom.*, **4**, 19–34.
Willis, I. C., Sharp, M. J., and Richards, K. S., 1990. Configuration of the drainage system of Midtdalsbreen, Norway, as indicated by dye-tracing experiments. *Journal of Glaciology*, **36**, 89–101.

Cross-references

Catchment Glacier
Discharge/Streamflow
Englacial Conduit
Glacier Hydrology
Meltwater Storage
Moulins
Percolation Zone
Snow Hydrology
Subglacial Drainage System

DYNAMICS OF GLACIERS

Hester Jiskoot
Department of Geography, University of Lethbridge, Lethbridge, AB, Canada

Synonyms

Glacier adjustment to climate; Glacier length changes; Glacier motion; Glacier movement; Ice velocity

Definition

Dynamics of glaciers are the resulting ice flow processes caused by the interplay of the physical mechanism causing a glacier to move (gravity) and forces resisting this movement (e.g., friction). Alternatively it can be defined as a glacier's response to climate change or to other external or internal forcings.

Internal deformation (or *creep*) is the movement of an ice mass through the deformation of glacier ice itself.

Basal motion is the movement of ice relative to the substrate, either through basal sliding or through bed deformation of a soft sedimentary substrate (till), or both.

Basal sliding is the movement of ice along the bed, as a result of *enhanced creep*, *regelation* (melting of basal ice under higher pressure on the upstream side of bed obstacles, and refreezing of this ice in the lower pressure regime on the lee side of these obstacles), or complete *decoupling* from the bed.

Soft bed deformation is the movement of the subglacial sediments (substrate) causing some of the forward motion of a glacier or ice sheet.

Normal stress is the force per unit area that is applied perpendicular to a plane. In the case of glacier dynamics, the normal stress is usually considered the stress acting on the ice through vertical loading.

Shear stress is the force per unit area that is applied parallel or tangential to a plane. In the case of glacier dynamics it is most often the force that is applied to glacier ice due to the ice surface slope.

Yield stress is the stress at which a material begins to deform plastically. At stresses equal or higher than the yield stress the deformation is instantaneous and irreversible, and the resulting stress is limited to the yield stress. The yield stress is dependent on the *yield strength* of a material: yield strength of glacier ice is generally much higher than that of till (100 ± 50 kPa and 2–90 kPa, respectively: Paterson, 1994; Murray, 1997).

Longitudinal stress is the force per unit area that is pushing or pulling on an ice mass in the along-flow direction.

The *constitutive relationship* relates applied stress to deformation rate (also called stress–strain relationship). This relationship is dependent on the rheology of the specific material. The *rheology of ice* is the way glacier ice responds (deforms/strains) to applied stress.

Anisotropy is the property of ice that causes the deformation rate to differ, depending on the direction of applied stress. Anisotropy mainly results from the stress loading history, which can orient individual ice crystals. Anisotropy results in so-called ice *fabric* (preferential orientation of the ice crystals).

Ice overburden pressure (or normal pressure) is the force exerted by the ice on the substrate due to its weight (expressed as ρgH: ice density × gravitational acceleration × ice thickness).

Hydrostatic pressure is the magnitude at which the basal water pressure exactly counteracts the ice overburden pressure. If the basal water pressure exceeds the hydrostatic pressure, the ice can be lifted off its bed (effectively floating the glacier).

Introduction

Glaciers are like large rivers of ice that slowly make their way downslope under the pull of gravity. They move because the surplus ice mass from years of accumulation in the upper parts of the glacier (the accumulation area) needs to be compensated by outflow of ice to the lower parts of the glacier (ablation area), where ice loss through melting and calving needs to be replenished by the inflow of ice. If this redistribution of ice mass would not take place a glacier would become steeper infinitely. Theoretically, glaciers discharge ice from the accumulation area to the ablation area through movement in order to maintain a steady-state glacier profile: this is the balance flux. The corresponding velocity, the balance velocity, is controlled by mass balance conditions and glacier geometry (Clarke, 1987a). However, because glacier motion is a delayed effect of the amount of accumulation received, with individual glacier response time depending on glacier type and size, mass balance fluctuations result in asynchronous, filtered and time-lagged decadal to century-long velocity fluctuations and corresponding advance and retreat rates (e.g., Jóhannesson et al., 1989). Although ice masses often flow with speeds corresponding to their balance velocities, in some glaciers the balance flux is much lower or higher than the measured fluxes. If this occurs over a prolonged time, glacier depletion (mass wasting) or pulsating behavior with sudden switches between slow and fast flow can occur. Pulsating glaciers include unstable tidewater glaciers, ice streams, and surge-type (Clarke, 1987a).

The velocity and motion in glaciers and ice sheets is determined by the geometry of the ice (ice thickness, surface slope) and by its physical properties (temperature, impurities, density), by the valley shape or lack of valley walls in the case of ice sheets, by the conditions at the glacier bed (frozen versus thawed bed, hard bedrock versus soft deformable substrate, type of subglacial drainage system), by the amount of ice that is floating in adjacent water (lake, sea or ocean) as a floating tongue or an ice shelf, and by the average accumulation and ablation rates (the surface mass balance, or net amount of snow received and melted over several years). Dependent on all of these factors, average ice flow velocities for valley glaciers are generally less than a few hundreds of meters per year (m a^{-1}) and for outlet glaciers up to several kilometers per year (Paterson, 1994). Most glaciers have seasonal velocity fluctuations, with the faster flow occurring in the early melt season when the available large quantities of meltwater cannot be discharged efficiently yet because the subglacial drainage systems have not been fully developed. An enigma that has been part of research into glacier dynamics for a long time is the behavior of pulsating glaciers, and in particular that of surging glaciers and ice streams (Meier and Post, 1969; Harrison and Post,

2003). Glacier surging is a quasi-periodic oscillation between long periods (tens to hundreds of years) of slow flow or quiescence, and shorter periods of typically 10–1,000 times faster flow or surge. During a surge, the flow velocity increases abruptly, and fast flow is maintained over some time and over a wide area. The switch from slow to fast flow is an internally triggered ice flow instability, reflecting sudden changes within the glacier system. These changes can sometimes be associated with external factors (e.g., weather, climate, and earthquakes), but only if the glacier system is already close to a critical threshold.

Because glaciers move, they scrape and pluck the landscape causing bedrock erosion. This material is then transported by the glaciers and deposited hundreds of meters to over a thousand kilometers downglacier, leaving layers of glacial sediment (till), which are sometimes molded or pushed up into pronounced landforms (e.g., moraines, flutes, etc.). Moving ice is therefore a geomorphological agent altering the landscape. Additionally, glaciofluvial, glaciolacustrine and iceberg calving action can alter the landscape as well. Further, thick ice masses (from hundreds of meters to several kilometers in thickness for present and past ice sheets) isostatically depress the asthenosphere and overlying lithosphere up to about one-third of the ice thickness, which is followed by isostatic rebound of the crust after the ice thins or completely melts away. This effect is lagging behind the growth and shrinkage of ice sheets, and regions under the former Pleistocene ice sheets still experience differential uplift, affecting relative sea level in those regions.

Historical perspective

The first scientist to measure the movement of a glacier was Franz Josef Hugi, who built a rock hut on the medial moraine of Unteraargletcher in the Swiss Alps. Hugi visually observed his hut to have moved several hundreds of meters between 1827 and 1836 (Clarke, 1987b). In 1938, Louis Agassiz started a field campaign drilling holes in the ice of Unteraargletcher, and in 1842 James D. Forbes, who had joined Agassiz in the field in 1941 but with whom he had fallen out after he had published his results independently, had started his measurements using a theodolite on Mer de Glace, France. Both Agassiz and Forbes, as well as eighteenth- and nineteenth-century physicists, mathematicians, chemists, and geologists, including Horace de Saussure, John Tyndall, Lord Kelvin, William Hopkins, and Harry Reid, speculated about the mechanisms of movement, and several theories were developed (Clarke, 1987b). Although most of these theories were untenable, important observations included that (a) ice behaves both in a brittle and viscous way, (b) ice is layered, (c) ice velocity at the surface of a glacier may be submergent or emergent rather than parallel to the ice surface, (d) ice moves both through plastic deformation and sliding along the base, (e) the force driving glacier movement is opposed by a resisting shearing force, and (f) ice deformation is temperature dependent (e.g., Mathews, 1870).

Although several early twentieth century scientists worked on the properties of ice, it was not until the mathematical work by Nye (1951, 1957) and experimental work by Glen (1952, 1955) that a generalized flow law was developed for the creep, or internal deformation, of glacier ice. This law, known as "Glen's Flow Law" is to this day being used by glaciologists, although it has been adjusted for cases outside the temperature and stress regimes that it was originally tested for, as well as to account for a range of glacier ice properties (impurities, water, and anisotropy) (see Marshall, 2005). Also in that period, Shumskii (summarized in Shumskii, 1964) extensively studied the geochemistry and geophysics of glacier ice, Weertman (1957) and Lliboutry (1958) recognized the two main processes of basal sliding (regelation and enhanced creep) and developed a "sliding law," and Ahlmann (1948) executed field studies to link climate change to glacier fluctuations. Not until a decade later, the important roles of water pressure and cavitation in the process of sliding were identified (Lliboutry, 1968), which led to mathematical theories on how switches in the subglacial drainage system control sliding speed and related flow instabilities (Iken, 1981; Bindschadler, 1983; Kamb, 1987). A *paradigm shift* (Boulton, 1986) in thinking about ice flow elucidated the importance of motion within subglacial soft deformable substrate (till) in the overall motion of glaciers and ice sheets (Blankenship et al., 1986; Alley et al., 1986), and led to the development of a first (viscous) till rheology (Boulton and Hindmarsh, 1987). While laboratory experiments and field observations have now led to the development of a plastic till rheology, the viscous rheology is still occasionally used because of its simplicity. We now also have a much better understanding of the mechanical and hydraulic properties of till (Clarke, 1987c), of till discontinuity and heterogeneity causing sticky spots (Alley, 1993), of the effects of frozen till on ice flow (Murray et al., 2000), and some have observed that till deformation is not as widespread and pervasive as originally proposed (e.g., Piotrowski et al., 2001 and 2004).

On a larger scale, the flow and response of glaciers, and in particular ice sheets, have been explored using mathematical and numerical (computer) models, starting with the work of Nye (1965) through works of Budd (e.g., Budd and Jenssen, 1971) using numerical techniques, and Oerlemans (1980) and Pollard (1982) on glacial cycles, and continuously involving more complex processes, including fast flow in ice streams, flow of marine ice sheets and ice shelves, the role of shear margins, calving, subglacial lakes, and the role of thermomechanical coupling and longitudinal stresses in ice flow (overviews in Hutter, 1983; Hindmarsh, 1997; Hughes, 1998; Van der Veen, 1999; Hindmarsh, 2004; Marshall, 2005; Pattyn et al., 2008). Lastly, the developments and increased use

of remote sensing and geophysical techniques in glaciology over the last half century have led and continue to lead to a more detailed understanding of glacier dynamics (see e.g., Clarke, 1987b; Bingham et al., 2010).

Basic principles: force balance and constitutive relationship

Glaciers flow due to the force of gravity pulling them down because of their weight. The rates of ice flow are dependent on the stresses that act on a glacier, on the way in which ice can deform (creep) and whether or not, and how, a glacier can slide over its bed. Glacier flow can be described with a force-balance equation (as accelerations are negligible), where the gravitational driving stress is balanced by a resistive stress (or stresses). The gravitational driving stress is determined by the gravitational acceleration, the average density of glacier ice, and the ice thickness and surface slope of a glacier. Thickening of the accumulation area and thinning in the ablation area result in a steeper surface slope, increasing the gravitational driving stress. Glacier flow is therefore intricately related to a glacier's surface mass balance. On most (grounded) glaciers, resistive stresses act mainly at the base of the glacier in the form of *basal drag*, but can also include *lateral drag* from the valley walls or shear margins (in the case of ice streams in an ice sheet), and *dynamical resistance* to flow through pulling and pushing due to longitudinal stress gradients within the ice.

In the most simple case, the gravitational driving stress of a glacier is compensated by the basal shear stress (basal drag). This basal shear stress, τ (in Pa), is related to glacier thickness, the steepness of the surface slope, and the shape of the glacier valley, which for a rectangular section in a glacier equals:

$$\tau = f\rho g H \sin\alpha, \tag{1}$$

where ρ is the density of ice (830–917 kg m^{-3}: the maximum in this range is usually taken as a standard and represents bubble-free glacier ice at depth), g the gravitational acceleration (9.8 m s^{-2}), H the ice thickness (m), α the ice thickness gradient (dH/dx) which equals the ice surface slope on a horizontal bed, and f a dimensionless shape factor related to the glacier profile and valley shape (Paterson, 1994). Typical values for basal shear stress are ~10 kPa for ice streams and ~100 kPa for valley glaciers (Paterson, 1994). The shape factor (f) is a dimensionless term included to represent friction along the bed as a fraction of the net basal drag, which is one of the driving stresses. In valley glaciers, however, part of the driving stresses is resistance by lateral drag or friction along the valley walls. Therefore, f can be expressed as the ratio between the "hydraulic radius" (defined as the cross-sectional area of the glacier divided by the "wetted perimeter" or the length of the glacier/ground interface), and the centerline ice thickness (Nye, 1965). Theoretically f can be between 0 and 1, but the usual range is between 0.7 and 0.9 for valley glaciers. A shape factor of $f = 1$ is for an infinitely wide glacier (an ice sheet), while a very low ratio (e.g., $f = 0.6$) is for a glacier in a deep narrow valley. Shape factors can be easily calculated from the ratio (W) between the half-width of a glacier and its ice thickness at the centerline, and a range of values are given in Paterson (1994).

There are some extrapolations to this simple case of the force balance, to account for cases where the gravitational driving stress is not balanced by the basal shear stress alone. For scales where basal shear stress is calculated from ice thickness and surface slopes averaged over distances equal or larger than the ice thickness (the so-called shallow ice approximation or SIA: see e.g., Paterson, 1994), Equation 1 is a good approximation. However, for shorter distances, longitudinal stresses that act within the glacier system need to be included. If these longitudinal stresses are unbalanced (i.e., they are "pushing" or "pulling"), then the basal shear stress can be significantly larger or smaller than in Equation 1.

The three major components of ice flow

In response to the driving stress, glaciers can move due to three independent ice flow processes: (1) internal deformation (creep), (2) basal sliding, and (3) soft bed deformation. These components contribute, sometimes in ensemble, to the overall movement of a glacier. While all glaciers move due to creep flow, only glaciers that are not frozen to their beds (temperate and polythermal glaciers) demonstrate sliding as a major component, and only glaciers that are underlain by soft deformable substrate (till) experience bed deformation. Where sliding and/or bed deformation are activated, these factors often contribute well over 50% of the total velocity measured at the glacier surface, and are orders of magnitude greater than internal deformation velocities (e.g., Boulton and Hindmarsh, 1987). The net ice flow measured at the glacier surface (U) can be described as the sum of deformation velocity (creep velocity), sliding velocity, and bed deformation velocity (Figure 1: $U = U_c + U_s + U_d$), where the last two terms are sometimes combined as basal motion (U_b). Where glaciers move predominantly through internal deformation, the velocity decreases as a fourth-order polynomial with depth, from a maximum velocity at the glacier surface to almost zero at the base (Figure 1: U_c). For glaciers dominated by internal deformation, the transverse velocity profile (velocity distribution across the glacier) has a parabolic shape (with maximum velocities in the center of the valley and tapering off toward the valley walls; Figure 2), whereas for glaciers dominated by basal motion, a more uniform (flat) transverse velocity profile results. The extreme case of the latter is called "plug flow" (Sharp, 1988), and has well-defined shear margins on either side at the transitions between stationary rock/ice and moving ice (Figure 2). Plug flow is common in tidewater glacier tongues and glaciers that are surging. The descriptions of the different flow mechanisms that follow will help explain these differences in velocity profiles.

Internal deformation

Glacier ice is polycrystalline and behaves as a nonlinear visco-plastic material in the stress regime commonly found in glaciers. If large stresses are applied rapidly glacier ice can break, which results in crevasses (this is clearly visible in many glaciers and ice sheets, as well as in icebergs that are breaking off, and in rifts that form in ice shelves). However, if glacier ice is subject to stresses that are applied slowly and over a long time, as is the case inside a glacier, then the ice becomes permanently deformed in a plastic rather than a brittle way. The range of stresses experienced in normal glacier flow is 50–200 kPa (Paterson, 1994). The ice deformation rate (or shear strain rate) under a constant shear stress is initially high but then tapers off to a constant value, also called the secondary strain rate. The exact value of the constant shear strain rate is dependent on the amount of stress applied, on the ice temperature, on the stress history, and on impurities within the ice.

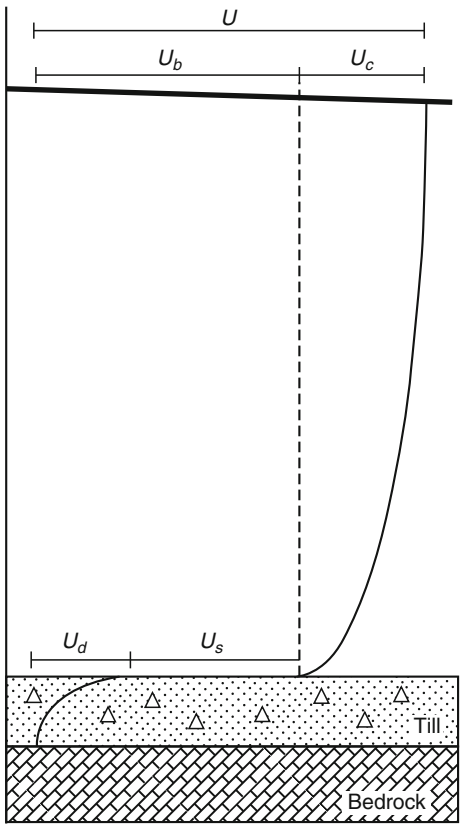

Dynamics of Glaciers, Figure 1 Cross section of vertical velocity distribution and surface velocity (U) in a glacier with the three components of ice motion: internal deformation (U_c), basal sliding (U_s), and bed deformation (U_d). U_s and U_d combined can also be denoted as basal motion (U_b).

Stress–strain relationship: Glen's Flow Law

Through laboratory experiments where the deformation rate was measured in a block of ice subject to a range of stresses and a range of temperatures, Glen (1955) derived the constitutive relationship of glacier ice (the relation between secondary shear strain rate, $\dot{\varepsilon}$, and applied stress, τ). This empirical flow law for ice, known as *Glen's Flow Law,* in steady-state ice creep, is expressed as:

$$\dot{\varepsilon} = A\tau^n, \tag{2}$$

where A is the ice "*softness parameter*" depending on ice temperature and activation energy according to the Arrhenius relation (Glen, 1955). Rigsby (1958) showed that parameter A is not affected by hydrostatic pressure, provided that the temperature is taken relative to the freezing point (hydrostatic pressure depresses the freezing point). A ranges from 10^{-14} to 10^{-17} s^{-1} kPa^{-3} and decreases log-linearly with temperature for temperatures well below the freezing point, but at a higher rate close to the freezing point (Paterson, 1994). The exponent n is a constant that depends on applied stress and is in the range $1.5 < n < 4.2$ with a mean of $\sim$3 for temperate valley glaciers (Paterson, 1994). Thus, for temperate valley glaciers the deformation rate is proportional to the vertical shear stress cubed, which is a function of depth. However, from laboratory experiments, borehole deformation measurements, and ice sheet models it was derived that for the low stress (<40 kPa) environments in central regions of polar ice sheets the exponent n is closer to 1 or 2 (e.g., Pettit and Waddington, 2003). The temperature dependence of A and n reflects the fact that ice is stiffer at lower

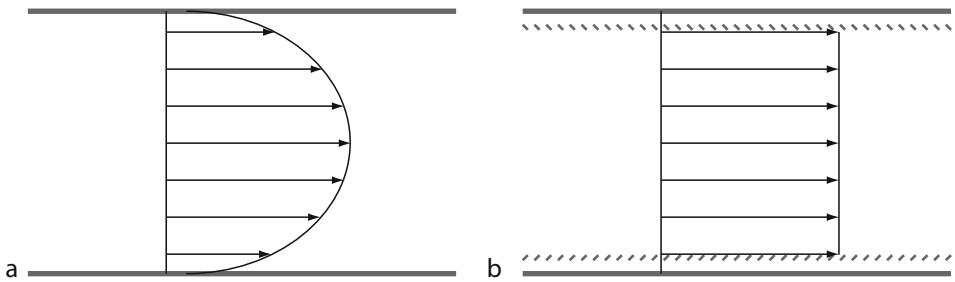

Dynamics of Glaciers, Figure 2 Diagrams of two end-members of transverse velocity profiles in glaciers (**a**) Approximate parabolic flow, and (**b**) plug flow. Hatched lines represent shear margins.

temperatures: cooling ice from −10°C to −25°C reduces the internal deformation by a factor of 5 (Paterson, 1994). Instead of parameter A, some use B or β, where $B = A^{-n}$. Because it is now well known that complex microscale processes influence ice deformation, recent advances have been made to improve on Glen's Flow Law and to include anisotropy, grain size evolution, recrystallization, grain-boundary migration, and the deformation rate of glacier ice outside the commonly tested stress and temperature ranges. See Pettit and Waddington (2003) and Schulson and Duval (2009) for overviews of these efforts.

Deformation velocity (creep)

By adding up (integrating) the shear strain throughout the thickness of a glacier, a deformation velocity profile can be produced. The sum of all these layers of ice deforming is expressed as the velocity at the glacier surface. The vertically averaged horizontal deformation (creep) flow velocity (U_c) can be described as:

$$U_c = c_I H \tau^n, \tag{3}$$

where the constant c_I depends on the values for A and n from Glen's Flow Law (Equation 2), H is ice thickness, and τ is basal shear stress (Equation 1) (Kamb and Echelmeyer, 1987). The geometrical controls in this relationship are clear: steeper and thicker glaciers have a larger internal deformation rate than thin ones with shallow slopes. It can also be seen that the relation between applied stress and glacier flow is nonlinear, and approximately proportional to the fourth power of ice thickness (H^4) and the third power of ice surface slope (α^3). Therefore, if the surface mass balance of a glacier changes that glacier's ice thickness or surface slope, or both, very large changes in ice flow solely due to the mechanism of internal deformation can result.

Basal sliding

When glaciers are not frozen to the substrate (bedrock or sediments) additional movement may occur through glaciers sliding over their beds.

Sliding without cavitation

Two processes, first recognized by Weertman (1957), are fundamental to the mechanism of glacier sliding without cavitation or ice-substrate separation: enhanced creep and regelation. Enhanced creep is the result of bedrock protuberances causing a local increase in stress on the upstream side of these bumps, which can increase the amount of creep around such obstacles. The process of regelation results from local increases in pressure on the upstream sides of bedrock bumps that lower the melting point and cause some ice to melt, which then moves to the leeside of the bump where the pressure is lower and where refreezing occurs. While enhanced creep is most efficient for large bedrock obstacles, regelation is most efficient with small obstacles. Bed roughness is therefore an important factor controlling this process.

Sliding with cavitation

Enhanced creep and regelation can occur without bed separation. However, high water pressures can cause cavities (voids) to form on the leeside of obstacles. This cavitation can cause sliding with bed separation if the water pressures in these cavities are high enough to lift the glacier partly off its bed, which drastically reduces basal friction. The importance of cavitation in controlling sliding velocity was emphasized by Lliboutry (1968). He postulated that glacier sliding would be a multivalued function of the basal shear stress and effective pressure. A multivalued sliding law has two "modes" of sliding for the same basal shear stress. According to present understanding, the "slow mode" is for subglacial drainage through conduits (Röthlisberger channels), and the "fast mode" for drainage through linked cavities. Given the water pressure–water flux relation of conduit systems is inverse and that of linked-cavity systems is direct, the effective pressures are generally low in conduit systems, but can be close to overburden pressure in linked-cavity systems, lifting the glacier off its bed causing bed separation (Kamb, 1987). Switches in these two subglacial drainage systems can therefore cause sudden changes in sliding velocity that are directly related to the amount of bed coupling (Lliboutry, 1968; Bindschadler, 1983; Kamb, 1987). These types of switches have been observed as a result of seasonal changes in water input to the glacier (Iken, 1981) as well as in the sudden changes in flow velocity related to glacier surging (Kamb et al., 1985; Kamb, 1987).

Sliding velocity

Basal boundary conditions for the sliding velocity (U_s) are the basal shear stress (τ) and the effective pressure (N_e), which is the difference between ice overburden pressure ($p_i = \rho g H$) and water pressure (p_w). Water pressure is dependent on the pressure–flux relations in the subglacial drainage system. Efficient fast draining Röthlisberger channel systems generally have low water pressure while discharging large volumes of water, while slow distributed subglacial drainage systems (e.g., linked-cavity systems) have high water pressure and low water flux. The lower the effective pressure the higher the sliding velocity. At water pressures exceeding the ice overburden pressure the glacier can start to "float," which means that complete ice-bed decoupling occurs. A general form for the sliding velocity flow law is:

$$U_s = \frac{k \tau^m}{N_e} \tag{4}$$

where k and m are constants (k is a function of bed roughness, and $m > n$) and N_e is the effective normal pressure (Bindschadler, 1983). However, the commonly used sliding relationships neither take into account realistic hard bed morphologies (bumps of different sizes and shapes) nor sliding over soft beds (e.g., Tulaczyk, 1999). Recent attempts have been made to improve the mathematical description of sliding over irregular beds, where both

drowning of bed features and cavitation play a role in the sliding velocity (e.g., Schoof, 2005). This work has also confirmed the theoretical upper limit to sliding velocity, the "Iken's bound" (after Iken, 1981), for general bed geometries. Further complications to the general sliding laws, such as Equation 4, are that they ignore the effects of frictional forces between rock particles frozen in the basal ice and the underlying bedrock (Hallet, 1981; Iverson et al., 2003), and the effects of chemical reactions in bedrock or in impurities within the basal ice due to melting and refreezing (Hallet, 1976). Additionally, the sliding speed itself controls the amount of basal sliding, as faster flow produces more frictional heat.

Soft bed deformation

Subglacial till is a non-sorted to poorly sorted mixture of unconsolidated sediments, ranging in size from boulders to clay. Thicknesses of till in the order of 1–20 m have been inferred under ice streams, outlets from ice caps, and glaciers. Because the finer sediments (clay to sand) lack cohesion and are almost frictionless, they can readily deform under applied shear stress if a large fraction of their pore space is filled with water under high pressure. Ice underlain by matrix-supported till is therefore likely to have soft bed deformation as a proportion of its basal motion. Where a glacier is underlain by such a soft deformable substrate, then, if the basal shear stress exceeds the yield strength of the till, some or all of the shear stress can be accommodated by bed deformation. The yield strength of till is highly dependent on the grain size distribution, the fractional water content and the water pressure within the till, and its deformation history. Low yield strength (as low as 2–10 kPa) has been reported for tills underlying present and past ice streams and outlets from ice caps (especially in Iceland), and the fast flow velocities of these ice masses at relatively low basal shear stresses (<50 kPa) have by some been attributed to the soft bed deformation mechanism in these subglacial tills (Alley et al., 1986; Blankenship et al., 1986). Although rapid bed deformation generally occurs under warm bedded glaciers, bed deformation can also play a role under polythermal glaciers, where the till can be partly or temporarily thawed (Murray, 1997).

Ice flow through bed deformation

Ice flow over a soft bed is often a combination of basal sliding and bed deformation, where the latter can be (a) pervasive and deep-seated (an entire till layer is involved), (b) through plowing at the ice-sediment or the sediment-bedrock interface, or (c) along internal stratigraphic boundaries (Fischer and Clarke, 1994; Murray, 1997; Kjær et al., 2006; Fleisher et al., 2006). The type and amount of bed deformation is dependent on till thickness, till composition, and water pressure. Because these factors can vary temporally as well as spatially, till is a complex and highly heterogeneous material and it is quite difficult to construct a constitutive relationship or general flow law for soft bed deformation. Most soft bed deformation flow laws assume an average deformability of till of a certain composition, which can be based on field measurements of till properties combined with ice flow velocities (e.g., Boulton and Hindmarsh, 1987), on empirical laboratory experiments with till samples (e.g., Iverson et al., 1998), or on mathematical treatments of till physics with specific designated properties (e.g., Fowler, 2003).

Although subglacial till is not a viscous material, a quasi-viscous constitutive relationship was proposed by Boulton and Hindmarsh (1987) ("the B–H rheology") on the basis of sparse field observations. This B–H rheology was later modified by Fowler and Walder (1993). The modified viscous B–H rheology is still occasionally used because of its simplicity, but laboratory experiments and field studies have proven that till behaves almost like a perfectly plastic material, but one where the deformation rate is dependent on the amount of stress (Iverson et al., 1998; Tulaczyk et al., 2000). This is sometimes expressed as an exponential quasi-viscous flow law of the form

$$\dot{\varepsilon} = A_2 \mathrm{e}^{\frac{\tau}{b\tau_0}}, \tag{5}$$

where A_2 is a constant related to a reference strain rate, b a constant that is dependent on pre-consolidation stresses and texture of the till, and τ_0 the stress taken at a reference shear strain rate (larger than the Mohr–Coulomb yield strength) (Hooke, 2005). This relationship implies that small increases in shear stress should result in large increases in till deformation, which is often related to unstable runaway flow of glaciers over soft deformable beds which in extreme cases could result in surges.

Piotrowski et al. (2001, 2004) recently argued that till deformation is not as widespread and pervasive as originally thought, and that so-called "sticky spots" appear to be the norm rather than the exception, at least under ice sheets. Sticky spots are patches where till is frozen or of increased stiffness or absent (e.g., bedrock protrudes), and influence the proportion of forward motion contributed to soft bed deformation (Alley, 1993; Murray et al., 2000; Kjær et al., 2006). These sticky spots are sometimes considered ephemeral in nature (i.e., that they can be created and destroyed in response to variations in subglacial water pressure, temperature, or through redistribution of till). An additional factor in the heterogeneity of soft bed deformation is the fact that cavitation over soft deformable sediments plays an important role both in the overall soft bed deformation velocity and in basal sliding over soft beds (e.g., Schoof, 2007).

Dynamic adjustments to variations in driving forces

Deviations from balance velocity result from changes in the driving forces and the resistive forces. Small perturbations in the driving forces such as in accumulation rate, basal conditions, subglacial hydrology (especially fluctuations in volume, pressure and distribution of meltwater), nonuniformities in the deformation rate and calving events

can initiate stress irregularities which may lead to short-term perturbations in flow speed (e.g., Hutter, 1983). Short-term perturbations in surface mass balance, for example, excess accumulation over some winter seasons, can be transmitted downglacier more rapidly in the form of "kinematic waves," which are topographic waves (bulges) that travel through the ice at rates much higher than the overall ice flow velocity. Kinematic wave theory was first applied to glaciology by Nye (1963), and further developed and used by many. At longer timescales, changes in driving forces can be caused by variations in surface mass balance related to a change in climate. This mechanism is called "climate forcing." As the adjustment to climate forcing is not instantaneous, but occurs according to a specific response time, glaciers are constantly adjusting to the large-scale variability in mass balance conditions and are in disequilibrium with their present mass balance. It is therefore complicated to deduce changes in surface mass balance (or indeed a climate signal) from changes in length of glaciers of different shapes and sizes worldwide (e.g., Oerlemans, 2005).

Ice flow adjustment to calving events and breakup of ice shelves can be quite instantaneous and significant, but can also have long-term effects. Floating ice, with virtually no basal shear stress, has a surface gradient approaching zero. This implies that stresses in ice shelves are generally low (<40 kPa, Paterson, 1994). The driving stress is partly compensated by the back pressure exerted by the frictional drag on the ice shelf edges (most ice shelves are confined in an embayment) and by basal drag on islands in the embayment (ice rises) (Menzies, 1995). Rapid changes in these systems have resulted in sudden collapse of ice shelves. Collapse of ice shelves in the Antarctic peninsula region due to regional warming of surface and ocean temperatures has lead to rapid adjustments upstream by increasing ice flow of the land-based glaciers that were once buttressed by those ice shelves, and has in some cases resulted in rapid retreat of these glaciers (Rignot, 2006). Through positive feedback, this retreat can then lead to sea-level rise, which may destabilize large parts of the (marine) West Antarctic ice sheet, which will lead to further retreat of the ice sheet. Reversely, positive feedback effects involving resistive stresses can also slow down glaciers: Catania et al. (2006) found from geophysical field measurements with ice-penetrating radar that the sudden stagnation of Kamb ice stream (Ice Stream C) was due to changes in basal conditions where reduced basal lubrication in the subglacial tills related to negative changes in water input and subsequent refreezing of the ice stream to its bed.

Because changes in mass balance influence ice thickness and glacier slope, glaciers respond dynamically to these changes. Dynamic adjustment to changes in mass balance due to climate forcing is important to understand because it can determine how sensitive a glacier is to climate change, and how fast it adjusts to such a change (response time).

Response time

Response time is the observed delay in the dynamic response of glaciers and ice sheets to longer-term changes in climate and is usually measured as length and/or volume adjustment to a new perturbed state. Response time is usually expressed as the sum of reaction time, or delay between the change in mass balance and initiation of a change, and adjustment time, the subsequent time it takes to adjust to the change in mass balance. Response times generally range from a few decades to a century for alpine glaciers and from centuries to millennia for ice sheets. In general, glacier with a steeper mass balance gradient (e.g., temperate maritime glaciers) have higher balance velocities (or turnover rates) than glaciers in continental regions where the precipitations rates are much lower (if their ablation rates are not extreme), and glaciers with higher turnover rates tend to respond faster to a given climate forcing. Further, glaciers with contrasting hypsometries (e.g., top-heavy, equidimensional, bottom-heavy) appear to have intrinsically different response times (Furbish and Andrews, 1984), and it is also clear that thermal regime can directly affect glacier response (e.g., Hutter, 1993). Therefore, glaciers with different geometry show different net balance histories for the same climate forcing. These observations led to research in individual response time of glaciers of different sizes and types, using principles of the kinematic wave theory (Nye, 1965), and the requirement of mass continuity and the height mass balance feedback (Jóhannesson et al., 1989; Oerlemans, 1989; Haeberli and Hoelzle, 1995). This research is done both by analytical and numerical modeling and by using direct observations of glacier length and/or volume changes in a variety of regions around the world. Response time determined from modeling is usually a dynamic adjustment to a step-change in climate, whereas climate forcing in nature causes glaciers to respond to a complex history of climate variability. Therefore, glacier response time determined from both methods might elucidate slightly different combinations of controls on response time.

Instrumental mathematical research by Jóhannesson et al. (1989) showed that volume response time can be expressed in terms of the ratio between the characteristic glacier thickness and the balance rate at the glacier terminus, in which case the response time is independent of terminus dynamics, which is contrary to that originally suggested using the kinematic wave theory (Nye, 1965). Subsequent research into volume and length response times has included the influence of bed slope, balance gradient, glacier size, and average surface elevation (e.g., Bahr et al., 1998; Harrison et al., 2001; Oerlemans, 2008). Generally, large glaciers, with gentle slopes and small balance gradients have longer response times than small glaciers with steep gradients and large balance gradients, thus response time is inversely proportional to both bed slope and balance gradient (Oerlemans, 2008). Therefore, arctic glaciers have a longer response time than

mid-latitude glaciers, and maritime glaciers a shorter response time than continental glaciers of the same size. Further, when large spatial and temporal scales are considered (>50 years) temperature is a much more important driving force than precipitation, and response time can be scaled according to glacier length, slope, and average annual precipitation (Oerlemans, 2005).

Response time research based on observed glacier terminus and area behavior has revealed many of the controls mentioned above. On the basis of three typical response patterns of glaciers in the North Cascades since the Little Ice Age, Pelto and Hedlund (2001) concluded that glacier slope, terminus velocity, average thickness, and accumulation rate determine response time and climate sensitivity. In their dataset, the reaction time, or delay between the change in mass balance and initiation of a change, was 4–16 years, while the response time or full adjustment to that change was 20–100 years, where glaciers with steeper slopes were on the lower end of this range, and glaciers with shallower slopes on the upper end. Hoelzle et al. (2003) showed that specific combinations of glacier size and slope (proxies for basal shear stress) in the Swiss Alps determined response to climatic forcing, with small steep glaciers showing high frequency variability with low amplitude, and large shallow glaciers showing low frequency response with high amplitude. This concurred with the terminus behavior of glaciers worldwide, where glaciers larger than 8 km with shallow slopes show greater retreat than smaller glaciers (Hoelzle et al., 2003). Using data from the World Glacier Inventory and assuming that glacier area is always symmetrically distributed around the ELA (here ELA = median elevation) Raper and Braithwaite (2009) suggest that the volume response time depends directly upon the mean glacier thickness, and indirectly on glacier altitude range and vertical mass balance gradient. They therefore relate response time to glacier hypsometry, as was already suggested by Furbish and Andrews (1984). Raper and Braithwaite (2009) further show that the type of relation between volume response and glacier area is not straightforward, but rather dependent on geographical region: in the Arctic the relation is positive (response time increases with glacier area), in wet maritime regions it appear to be inverse, and in maritime subarctic regions they found that glacier area (size) is not related to response time.

A separate type of glacier response is that of glacier survival (Schwitter and Raymond, 1993; Pelto, 2010), which is the viability of a glacier to cease to exist under a certain climatic condition. Glacier survival response is dependent the ratio between glacier thinning in the accumulation zone and thinning at the terminus, where when this ratio is approximately 0.2–0.4 the glacier is thinning much more rapidly at the terminus than in the accumulation area and the glacier is retreating to a new stable position. However, if the ratio approaching 1 then the glacier is thinning at an equal rate everywhere and the glacier is unlikely to survive under unchanged climate conditions (Pelto, 2010).

Modeling ice dynamics

Many modern numerical glacier and ice sheet models include full thermomechanical coupling to calculate ice flow and response to mass balance. Although most models include the ice dynamic processes and mechanisms as outlined above, many are still based on the shallow ice approximation (SIA) and do not include longitudinal or transverse stress gradients or other complex mechanisms. Longitudinal and transverse stress gradients are particularly important for transition zones (e.g., between ice sheet and ice shelf flow or at the onset regions of ice streams). A relatively easy way to solve this has been to include an enhancement factor representing these longitudinal stresses (Marshall, 2005). However, models that include higher-order stress gradients (including longitudinal stresses), called higher-order models, are becoming more common. Some of these models apply the Full Stokes solution to resolve the stress field, following pioneering work by Blatter (1995). An additional improvement of application of the Full Stokes models to model the behavior of glaciers and ice sheets over time is that in the SIA models the response of glaciers to a climate forcing is almost immediate, whereas in Full Stokes models it is delayed, which is more realistic (Oerlemans, 2008). Efforts are also underway to couple models of subglacial hydrology directly with ice sheet models (see Marshall, 2005), and to understand and model the stability and ice flow over large Antarctic subglacial lakes, where lake drainage is a common feature (e.g., Wingham et al., 2006). Further, calving and the flow in ice shelves can now be incorporated in ice dynamics models of tidewater glaciers and ice sheets. Most of these models resolve the strain rate at the calving front that determines the fracture propagation of crevasses, while some include a calving criterion, such as the height of the calving cliff above the water or crevasse depth (e.g., Benn et al., 2007).

Summary

Glaciers move as a result of the gravitational driving force, and the processes of movement include internal deformation (usually expressed as secondary plastic creep), basal sliding, and soft bed deformation. Although these three processes can act in ensemble, the activation of the basal motion components is dependent on specific conditions such as temperature at the base of a glacier, bed morphology, subglacial water volume and pressure distribution (related to surface melt and configuration of the subglacial drainage system), as well as the presence, properties, and distribution of till. Therefore, with the same driving stress, glaciers can flow with vastly different speeds, ranging from a few meters per year to kilometers per year. It is obvious that subglacial water pressure, the volume and the distribution of water under a glacier or ice sheet, and in its underlying till, are of crucial importance in glacier dynamics, as these can reduce basal friction, and are directly linked to glacier sliding and bed deformation.

All in all, glaciers are complex systems and glacier dynamics are dependent on the properties of all materials involved (glacier ice, water, till, and bedrock), as well as on the configuration of the subsystems within, under, or in front of a glacier. Many of these factors exhibit temporal and/or spatial variability, such as ice temperature, hydrology, bed configuration, and till properties and distribution. Most relationships in glacier dynamics are nonlinear and therefore small changes in certain properties can have large "runaway" effects on the glacier movement. The dynamic adjustment of glacier geometry, as well as of other subsystems, to this movement can further rapidly change other properties, and can cause positive or negative feedback effects in the dynamic response of glaciers. It is therefore not surprising that individual glaciologists often specialize in specific aspects of the glacier system. A combination of field and remote sensing observations and measurements of glacier (sub)systems, empirical laboratory experiments (ice and till properties), and conceptual, mathematical analytical, and numerical models of glaciers and ice sheets is needed for the advancement of understanding of glacier dynamics. This understanding will then provide us with the tools to model and predict recent and future changes in these glacier systems, as well as to understand past ice sheet behaviour.

For a more detailed treatment of many aspects of the dynamics of glaciers, I refer to the following books, ranging from early expositions on ice flow to very advanced treatment of the physics of glaciers, and mathematical and numerical modeling of glaciers and ice sheets (Shumskii, 1964; Hutter, 1983; Drewry, 1986; Sharp, 1988; Paterson, 1994; Menzies, 1995; Hughes, 1998; Van der Veen, 1999; Hooke, 2005; Schulson and Duval, 2009).

Bibliography

Ahlmann, H. W:son., 1948. *Glaciological research on the North Atlandtic Coast*. RGS Series, 1, 83 pp.

Alley, R. B., 1989. Water-pressure coupling of sliding and bed deformation: I Water system. *Journal of Glaciology*, **35**(119), 108–118.

Alley, R. B., 1993. In search of ice-stream sticky spots. *Journal of Glaciology*, **39**(133), 447–454.

Alley, R. B., Blankenship, D. D., Bentley, C. R., and Rooney, S. T., 1986. Deformation of till beneath ice stream B, West Antarctica. *Nature*, **322**(6074), 57–59.

Bahr, D. B., Pfeffer, W. T., Sassolas, C., and Meier, M. F., 1998. Response time of glacier as a function of size and mass balance: (1) Theory. *Journal of Geophysical Research*, **103**, 9777–9782.

Benn, D. I., Warren, C. R., and Mottram, R. H., 2007. Calving processes and the dynamics of calving glaciers. *Earth Science Reviews*, **82**, 143–179.

Bindschadler, R., 1983. The importance of pressurized subglacial water in separation and sliding at the glacier bed. *Journal of Glaciology*, **29**(101), 3–19.

Bingham, R. G., King, E. C., Smith, A. M., and Pritchard, H. D., 2010. Glacial geomorphology: towards a convergence of glaciology and geomorphology. *Progress in Physical Geography*, **34**(3), 327–355.

Blankenship, D. D., Bentley, C. R., Rooney, S. T., and Alley, R. B., 1986. Seismic measurements reveal a saturated, porous layer beneath an active Antarctic ice stream. *Nature*, **322**(6074), 54–57.

Blatter, H., 1995. Velocity and stress fields in grounded glaciers: a simple algorithm for including deviatoric stress gradients. *Journal of Glaciology*, **41**, 333–344.

Boulton, G. S., 1986. A paradigm shift in glaciology? *Nature*, **322**, 18.

Boulton, G. S., and Hindmarsh, R. C. A., 1987. Sediment deformation beneath glaciers: rheology and geological consequences. *Journal of Geophysical Research*, **92**(B(9)), 9059–9082.

Budd, W. F., 1970. The longitudinal stress and strain-rate gradients in ice masses. *Journal of Glaciology*, **9**(55), 19–27.

Budd, W. F., and Jenssen, D., 1971. Numerical modeling of glacier systems. *IAHS-AISH*, **104**, 257–291.

Catania, G., Scambos, T., Conway, H., Raymond, C., 2006. The sequential shutdown of Kamb Ice Stream, West Antarctica. *Geophysical Research Letters*, 22 (L14502): doi:10.1029/2006GL026430.

Clarke, G. K. C., 1987a. Fast glacier flow: ice streams, surging, and tidewater glaciers. *Journal of Geophysical Research*, **92**(B9), 8835–8841.

Clarke, G. K. C., 1987b. A short history of scientific investigations on glaciers. *Journal of Glaciology*, Special Issue: 4–24.

Clarke, G. K. C., 1987c. Subglacial till: a physical framework for its properties and processes. *Journal of Geophysical Research*, **92**, 9023–9036.

Drewry, D. J., 1986. *Glacial Geologic Processes*. London: Edward Arnold, 276 pp.

Fischer, U. H., and Clarke, G. K. C., 1994. Ploughing of subglacial sediment. *Journal of Glaciology*, **40**, 97–106.

Fleisher, P. J., Lachniet, M. S., Muller, E. H., and Bailey, P. K., 2006. Subglacial deformation of trees within overridden foreland strata, Bering Glacier, Alaska. *Geomorphology*, **75**, 201–211.

Fowler, A. C., 2003. On the rheology of till. *Annals of Glaciology*, **37**, 55–59.

Fowler, A. C., and Walder, J. S., 1993. Creep closure of channels in deforming subglacial till. *Proceedings of the Royal Society of London. Series A*, **441**, 17–31.

Furbish, D. J., and Andrews, J. T., 1984. The use of hypsometry to indicate long-term stability and response of valley glaciers to changes in mass transfer. *Journal of Glaciology*, **30**(105), 199–211.

Glen, J. W., 1952. Experiments on the deformation of ice. *Journal of Glaciology*, **2**(12), 111–114.

Glen, J. W., 1955. The creep of polycrystalline ice. *Proceeding of the Royal Society of London. Series A*, **228**, 519–538.

Haeberli, W., and Hoelzle, M., 1995. Application of inventory data for estimating characteristics of and regional climate-change effects on mountain glaciers: a pilot study with the European Alps. *Annals of Glaciology*, **21**, 206–212.

Hallet, B., 1976. The effect of subglacial chemical processes on glacier sliding. *Journal of Glaciology*, **17**(76), 209–221.

Hallet, B., 1981. Glacial abrasion and sliding: their dependence on the debris concentration in basal ice. *Annals of Glaciology*, **2**, 23–28.

Harrison, W. D., and Post, A. S., 2003. How much do we really know about glacier surging? *Annals of Glaciology*, **36**, 1–6.

Harrison, W. D., Elsberg, D. H., Echelmeyer, K. A., and Krimmel, R. M., 2001. On the characterization of glacier response by a single time-scale. *Journal of Glaciology*, **47**(159), 659–664.

Hindmarsh, R. C. A., 1997. Deforming beds: viscous and plastic scales of deformation of subglacial sediment. *Quaternary Science Reviews*, **16**, 1039–1056.

Hindmarsh, R. C. A., 2004. A numerical comparison of approximations to the Stokes equations used in ice-sheet and glacier modeling. *Journal of Geophysical Research,* **109**(F): doi:10.1029/2003JF000065.

Hoelzle, M., Haeberli, W., Dischl, M., and Peschke, W., 2003. Secular glacier mass balances derived from cumulative glacier length changes. *Global and Planetary Change*, **36**(4), 295–306.
Hooke, R. L., 2005. *Principles of Glacier Mechanics*, 2nd edn. Cambridge: Cambridge University Press, 448 pp.
Hughes, T. J., 1998. *Ice Sheets*. New York: Oxford University Press, 343 pp.
Hutter, K., 1983. *Theoretical Glaciology*. Dordrecht: Reidel, 510 pp.
Hutter, K., 1993. Thermo-mechanically coupled ice-sheet response – cold, polythermal, temperate. *Journal of Glaciology*, **39**(131), 65–86.
Iken, A., 1981. The effect of subglacial water pressure on the sliding velocity of a glacier in an idealized numerical model. *Journal of Glaciology*, **27**(97), 407–422.
Iverson, N. R., Hooyer, T. S., and Baker, R. W., 1998. Ring shear studies of till deformation; Coulomb plastic behaviour and distributed strain in glacier beds. *Journal of Glaciology*, **44**(148), 634–641.
Iverson, N. R., Cohen, D., Hooyer, T. S., Fischer, U. H., Jackson, M., Moore, P. L., Lappegard, G., and Kohler, J., 2003. Effects of basal debris on glacier flow. *Science*, **301**(5629), 81–84.
Jóhannesson, T., Raymond, C. F., and Waddington, E. D., 1989. Time-scale for adjustment of glaciers to changes in mass balance. *Journal of Glaciology*, **35**, 355–369.
Kamb, B., 1987. Glacier surge mechanisms based on linked cavity configuration of the basal water conduit system. *Journal of Geophysical Research*, **92**(B9), 9083–9100.
Kamb, B., 1991. Rheological nonlinearity and flow instability in the deforming bed mechanism of ice stream motion. *Journal of Geophysical Research*, **96**(B10), 16585–16595.
Kamb, B., and Echelmeyer, K. A., 1987. Stress-gradient coupling in glacier flow: I Longitudinal averaging of the influence of ice thickness and surface slope. *Journal of Glaciology*, **32**(111), 267–284.
Kamb, B., et al., 1985. Glacier surge mechanism: 1982–1983 Surge of Variegated Glacier, Alaska. *Science,* **227**(4686), 469–479.
Kjær, K. H., et al., 2006. Subglacial decoupling at the sediment/bedrock interface: a new mechanism for rapid flowing ice. *Quaternary Science Reviews*, **25**, 2704–2712.
Lliboutry, L., 1958. Contribution à la théorie du frottement du glacier sur son lit. *Comptes rendus Hebdomadaires des Séances de l'Académie des Sciences*. Paris, **247**(3), 318–320.
Lliboutry, L., 1968. General theory of subglacial cavitation and sliding of temperate glaciers. *Journal of Glaciology*, **7**(49), 21–58.
Marshall, S. J., 2005. Recent advances in understanding ice sheet dynamics. *Earth and Planetary Science Letters*, **240**(2), 191–204.
Mathews, W., 1870. Mechanical properties of ice, and their relation to glacier motion. *Nature*, **1**, 534–535.
Meier, M. F., and Post, A., 1969. What are glacier surges? *Canadian Journal of Earth Sciences*, **6**, 807–817.
Menzies, J. (ed.), 1995. *Modern glacial environments: processes, dynamics and sediments. Glacial Environments:* Vol. 1. Oxford: Butterworth-Heinemann, 621 pp.
Murray, T., 1997. Assessing the paradigm shift: deformable glacier beds. *Quaternary Science Reviews*, **16**(9), 995–1016.
Murray, T., Stuart, G. W., Miller, P. J., Woodward, J., Smith, A. M., Porter, P. R., and Jiskoot, H., 2000. Glacier surge propagation by thermal evolution at the bed. *Journal of Geophysical Research*, **135**(B6), 13491–13507.
Nye, J. F., 1951. The flow of glaciers and ice-sheets as a problem in plasticity. *Proceedings of the Royal Society of London. Series A*, **207**, 554–572.
Nye, J. F., 1957. The distribution of stress and velocity in glaciers and ice-sheets. *Proceedings of the Royal Society of London. Series A*, **239**, 113–133.
Nye, J. F., 1963. The response of a glacier to changes in the rate of nourishment and wastage. *Proceedings of the Royal Society of London. Series A*, **275**, 87–112.
Nye, J. F., 1965. The flow of a glacier in a channel of rectangular, elliptic or parabolic cross-section. *Journal of Glaciology*, **5**(41), 661–690.
Oerlemans, J., 1980. Model experiments on the 100,000-yr glacial cycle. *Nature*, **287**, 430–432.
Oerlemans, J., 1989. On the response of valley glaciers to climatic change. In Oerlemans, J. (ed.), *Glacier Fluctuations and Climate Change*. Dordrecht: Kluwer Academic, pp. 353–371.
Oerlemans, J., 2001. *Glaciers and Climate Change*. Rotterdam: A.A. Balkema, 148 pp.
Oerlemans, J., 2005. Extracting a climate signal from 169 glacier records. *Science*, **308**(5722), 675–677.
Oerlemans, J., 2008. *Minimal Glacier Models*. Utrecht Publishing and Archiving Services: Igitur, 90 pp.
Paterson, W. S. B., 1994. *The Physics of Glaciers*, 3rd edn. Oxford: Pergamon, 480 pp.
Pattyn, F., et al., 2008. Benchmark experiments for higher-order and full-Stokes ice sheet models (ISMIP–HOM). *The Cryosphere*, **2**, 95–108.
Pelto, M. S., 2010. Forecasting temperate alpine glacier survival from accumulation zone observations. *The Cryosphere*, **4**, 67–75.
Pelto, M. S., and Hedlund, C., 2001. Teminus behaviour and response time of North Cascade glaciers, Washington, USA. *Journal of Glaciology*, **47**(158), 497–506.
Pettit, E. C., and Waddington, E. D., 2003. Ice flow at low deviatoric stress. *Journal of Glaciology*, **49**(166), 359–369.
Piotrowski, J. A., Mickelson, D. M., Tulaczyk, S., Krzyszkowski, D., and Junge, F., 2001. Were subglacial deforming beds beneath past ice sheets really widespread? *Quaternary International*, **86**(1), 139–150.
Piotrowski, J. A., Larsen, N. K., and Junge, F. W., 2004. Reflections on soft subglacial beds as a mosaic of deforming and stable spots. *Quaternary Science Reviews*, **23**(9–10), 993–1000.
Pollard, D., 1982. A simple ice sheet model yields realistic 100 kyr glacial cycles. *Nature*, **296**, 334–338.
Raper, S. C. B., and Braithwaite, R. J., 2009. Glacier volume response time and its links to climate and topography based on a conceptual model of glacier hypsometry. *The Cryosphere*, **3**, 183–194.
Rignot, E., 2006. Changes in ice dynamics and mass balance of the Antarctic ice sheet. *Philosophical Transactions of the Royal Society of London Series A*, **364**, 1637–1655.
Rigsby, G. P., 1958. Effect of hydrostatic pressure on the velocity of shear deformation of single ice crystals. *Journal of Glaciology*, **3**(24), 261–272.
Schoof, C., 2005. The effect of cavitation on glacier sliding. *Proceedings Royal Society of London*, **A461**, 609–627.
Schoof, C., 2007. Cavitation on deformable glacier beds. *SIAM Journal on Applied Mathematics*, **67**(6), 1633–1653.
Schulson, E. M., and Duval, P., 2009. *Creep and Fracture of Ice*. Cambridge: Cambridge University Press, 401 pp.
Schwitter, M. P., and Raymond, C. F., 1993. Changes in the longitudinal profiles of glaciers during advance and retreat. *Journal of Glaciology*, **39**(133), 582–590.
Sharp, R. P., 1988. *Living Ice: Understanding Glaciers and Glaciation*. Cambridge: Cambridge University Press, 248 pp.
Shumskii, P. A., 1964. *Principles of structural glaciology.* (Translated from the Russian by D. Kraus), New York: Dover, 497 pp.
Truffer, M., Harrison, W. D., and Echelmeyer, K. A., 2000. Glacier motion dominated by processes deep in underlying till. *Journal of Glaciology*, **46**(153), 213–221.
Tulaczyk, S., 1999. Ice sliding over weak, fine-grained tills: dependence of ice-till interactions on till granulometry. In Mickelson, D. M., Attig, J. (eds.), GSA Special Paper 337, Glacial Processes: Past and Modern, pp. 159–177.

Tulaczyk, S. M., Kamb, B., and Engelhardt, H. F., 2000. Basal mechanics of Ice Stream B, West Antarctica. I. Till mechanics. *Journal of Geophysical Research*, **105**(B1), 463–481.
Van der Veen, C. J., 1999. *Fundamentals of Glacier Dynamics*. Rotterdam: Balkema, 406 pp.
Weertman, J., 1957. On the sliding of glaciers. *Journal of Glaciology*, **3**(21), 33–38.
Wingham, D. J., Siegert, M. J., Shepherd, A., and Muir, A. S., 2006. Rapid discharge connects Antarctic subglacial lakes. *Nature*, **440**(7087), 1033–1036.

Cross-references

Glacier Hydrology
Glacier Mass Balance
Glacier Motion/Ice Velocity
Glacier Sliding
Glacier Surging
Hypsometry
Retreat/Advance of Glaciers
Structural Glaciology
Subglacial Drainage System

E

ELONGATION RATIO

Vijay Kumar
National Institute of Hydrology, Roorkee, India

Definition

Elongation ratio is one of the main areal properties of basin. Areal properties express the overall plan form and dimensions of the basin. The elongation ratio (R_e) is defined by Schumm (1956) as the ratio of the diameter of a circle with the same area as that of the basin to the maximum basin length:

$$R_e = \frac{D_c}{L_b}$$

where

D_c, diameter of the circle with the same area as that of the basin
L_b, maximum basin length

The value of R_e approaches 1.0 as the shape of a drainage basin approaches to a circle. The ratio varies from 0.6 to 1.0 over a wide variety of climatic and geologic regimes. Typical values are close to 1.0 for regions of very low relief and are between 0.6 and 0.8 for regions of strong relief and steep ground slope.

The elongation ratio has important hydrological consequences because, in contrast to more circular catchments, precipitation delivered during a storm in highly elongated basins has to travel a wide range of distances to reach the basin outlet. The resulting delay in the arrival of a proportion of the storm flow consequently leads to a flattening of the storm hydrograph. Statistical analyses of the glacio-morphometric parameters of glaciers of Indian Himalayas by Ahmad et al. (2004) indicated that the higher relief area gradient and higher elongation ratio are the favorable morphometric condition for surviving the glaciations for a glacier. Elongated body is more influenced by surrounding reflected diffuse energy and vice versa.

Bibliography

Ahmad, S., Hasnain, S. I., and Selvan, M. T., 2004. Morpho-metric characteristics of glaciers in the Indian Himalayas. *Asian Journal of Water Environment and Pollution*, **1**(1, 2), 109–118.
Schumm, S. A., 1956. Evolution of drainage systems and slopes in badlands at Perth Amboy, New Jersey. *Geological Society of American Bulletin*, **67**, 597–646.

ENGLACIAL CONDUIT

D. P. Dobhal
Wadia Institute of Himalayan Geology, Dehradun, Uttarakhand, India

Definition

Englacial conduits are the primary water transporting system from the surface of glacier to the base of a glacier. Supraglacial melt water either flows over the ice surface or descends vertically into the ice via holes called Moulin, where the water connects in the form of pipes or conduits of the englacial system. Moulin can go all the way to the bottom of the glacier. Englacial melt water is often connecting to sub-glacier flow system at the base of the glacier. Geometry and hydraulics of englacial conduits depends on the structure of the glacier.

Vijay P. Singh, Pratap Singh & Umesh K. Haritashya (eds.), *Encyclopedia of Snow, Ice and Glaciers*, DOI 10.1007/978-90-481-2642-2,

ENGLACIAL PROCESSES

Andrew G. Fountain
Department of Geology, Portland State University, Portland, OR, USA

Definition

Englacial processes refer to the body of the glacier, or that region between the surface and the bed. In practice it refers to the ice, as opposed to firn, part of the englacial region away from the surfaces. Although no formal distance away from the surface is adopted, the term generally implies that portion of the ice body which is not directly affected by the atmosphere. In this view, the englacial region starts below average crevasse depth from the atmosphere-ice interface. At the bed, no implicit or explicit distance away from this interface exists.

Characteristics

The englacial region is generally considered to be entirely composed of ice, although rock debris, water-filled voids (in temperate glaciers), and air-filled voids may be present. Other impurities that may be scavenged by precipitation descending through the atmosphere, or that may be blown onto the snow surface in the accumulation zone become incorporated in the englacial region (Cuffey and Paterson, 2010). Ice sheets, and to some degree polar glaciers, are generally free of large englacial inclusions, as revealed by ice radar. Instead, reflecting horizons in ice sheets are common and can be followed for hundreds of kilometers (Figure 1; Siegert and Hodgkins, 2000; Welch and Jacobel, 2003). These horizons are thought to result from changes in snow (ice) chemistry due to volcanic or other dust events that cover the snow surface for long distances (Fujita et al., 1999). In contrast, temperate glaciers exhibit many reflectors and are thought to be water-filled inclusions of unknown origin (Figure 2; Murray et al., 2000). Indeed, the number density of these reflectors were such that early versions of ice radar technology could not penetrate significant distances into the ice and it wasn't until the application of long wavelength radar that the bottom of the glacier could be detected.

For the remainder of this discussion, we focus on the englacial characteristics of temperate glaciers. Investigations of the englacial region have relied strongly on theoretical considerations, and on three empirical approaches. First, ground penetrating radar, often called "ice radar," has been employed with great success in the polar ice sheets to explore the stratigraphic horizons (Figure 1). Application to temperate glaciers has been less successful due to the large number of radar-scatters in the ice, as previously discussed. The hope has been to unambiguously map the location and extent of englacial conduits and other hydraulic features with only a few successful efforts to date. Better success has been achieved in estimating the water fraction within the ice; however, this has not been independently tested. The second approach is to inject tracers using the travel time and dispersion to infer the geometry of the flow system. However, the tracer is typically routed through subglacial pathways before exiting the glacier clouding interpretations of englacial hydraulics. Finally, the most direct approach is to drill a borehole into a glacier and examine the englacial region directly using submersible video cameras. In addition, hydraulic tests can be conducted to measure the permeability of the region. Ground penetrating radar antennas have also been lowered in boreholes to better detect deep englacial structures.

In temperate glaciers the englacial region contains significant volumes of water. At the microscopic scale water is present along the grain boundaries where three or more ice crystals meet (Raymond and Harrison, 1975). Given that the ice is near its melting temperature in such glaciers,

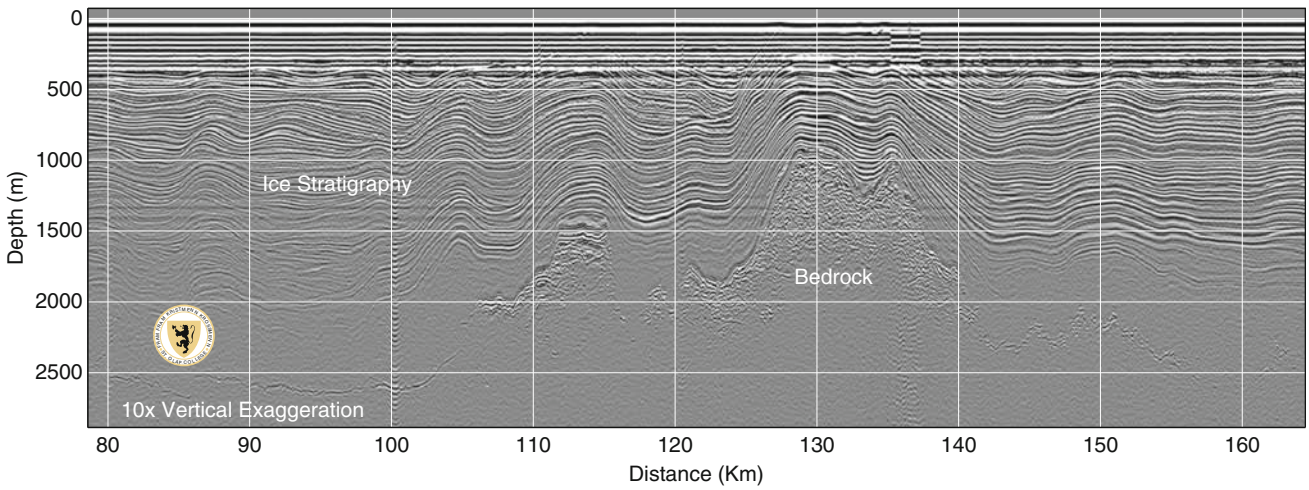

Englacial Processes, Figure 1 Radar reflections within the Antarctic ice sheet. The x-axis is kilometers. Note the parallel horizons that extend from tens to hundreds of kilometers. Taken from Welch and Jacobel (2005).

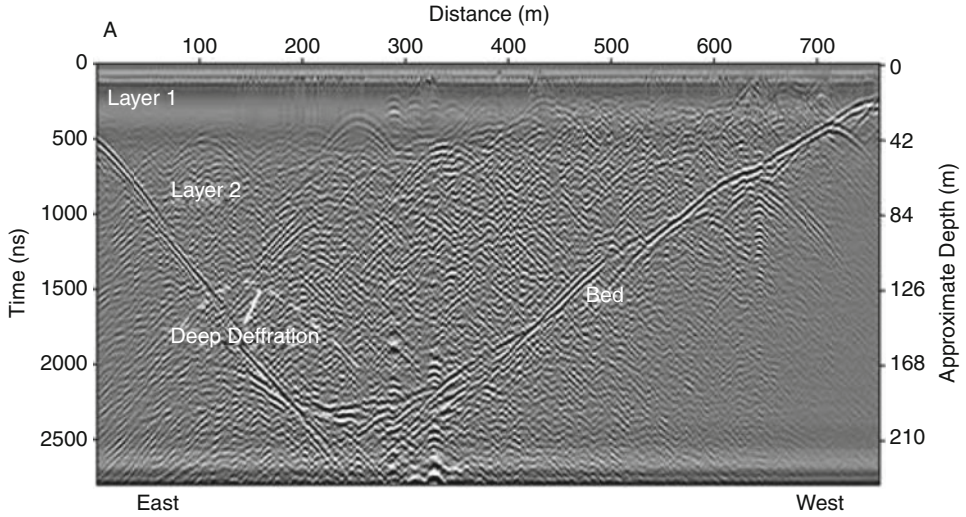

Englacial Processes, Figure 2 25 MHz GPR data with a 2-4-15-30 MHz bandpass filter applied layer 1 has few reflectors, whereas layer 2 exhibits apparently random reflectors. Taken from Bradford and Humphrey (2005).

thermodynamics considerations predict the presence of water at the boundaries. It was once thought that a network of passageways through the grain boundaries routed water from the glacier surface to bottom; however, the presence of air bubbles and the surface tension of water precludes significant water flux rates (<1 m s^{-1}) (Lliboutry, 1976). Nearly all rain and surface meltwater enters the body of the glacier through crevasses and moulins (e.g., Stenborg, 1973). Crevasses are the most important avenue for water because they are more numerous than moulins and are found over the entire glacier, whereas moulins are generally restricted to the ablation zone. Water-filled crevasses are not common, indicating that they efficiently route water into the body of the glacier. This conclusion is supported by Stenborg's (1973) work showing that moulins develop from crevasses. Neither the nature of hydraulic links between crevasses and the body of the glacier nor the formation of such links is well understood.

Conventional wisdom envisions englacial water flow in semi-circular ice-walled conduits (Fountain and Walder, 1998). The mechanics of steady flow in englacial conduits have been described theoretically. These conduits exist if the tendency for closure, from the inward creep of ice, is balanced by the melt enlargement resulting from the energy dissipated by flowing water. Englacial conduits should form an upward branching arborescent network, with the mean flow direction oriented steeply down-glacier, as determined by the gradient of the total potential (gravity and ice pressure) driving the flow. Observations of englacial conduits, with typically shallow slopes, near a glacier terminus and lower ablation zone are relatively common (Figure 3). In a particularly nice study of conduit geometry Gulley and Benn (2007) showed that conduits that developed from debris-filled crevasses exhibit a wide variety of cross-sectional geometries and formed a sinuous flow path. Empirical results based on the dispersion and travel time of numerous tracer injections in crevasses support the arborescent-network hypothesis. Most of the information bearing on the distribution and geometry of englacial passageways or on englacial water pressures and flow rates comes from boreholes drilled to the glacier bottom using a jet of hot water. About half of all such boreholes drain before the glacier bed is reached, indicating that they intersect englacial. Measurements of water level, water quality, and flow direction in boreholes and measurements of tracers injected into boreholes strongly suggest the presence of englacial passageways. However, the hydraulic inferences are contaminated by the hydraulic connections between the englacial passageway and a subglacial connection at the bottom of the borehole. Therefore, distinguish variations in flow/pressures in the subglacial connection versus that in englacial connections cannot be separated with certainty.

A number of direct measurements of englacial passages exist including englacial voids with typical vertical extents of ~0.1 m, and small (~mm in radius), arborescent, passages, but whether these voids or passages were part of an active hydraulic system was unclear. (Void is used here to mean a water-filled pocket in the ice, which may or may not be part of the englacial hydraulic system. Isolated voids are known to exist.) Englacial conduits have been observed where they connect to subglacial tunnels. Video cameras lowered into boreholes revealed multiple englacial voids through nearly the entire ice thickness. Voids that intersected opposite sides of the borehole wall were interpreted as englacial conduits; typically, one or two such features were encountered in each borehole, with diameters typically ~0.1 m (e.g., Harper and Humphrey, 1995). Pohjola (1994) determined that water was flowing in a few englacial conduits and estimated a flow speed in one of 0.01–0.1 m/s, the same range estimated by Hooke et al. (1988) using dye tracers. Fountain et al. (2005a) intersected two adjacent semi-circular

Englacial Processes, Figure 3 An exceptionally well-developed englacial conduit with incised floor in Ngozumpa Glacier. Taken from Gulley and Benn (2007).

englacial conduits at a depth of about 42 m. The diameters were 0.03 m and 0.1 m and within the conduit water flow speeds were about 0.1 m s^{-1}. Most conduits seen by borehole video seemed to be nearly horizontal.

In the search for englacial conduits Fountain et al. (2005b) found water-filled hydraulically connected fractures conveying englacial water to be ubiquitous in the ablation zone of an alpine glacier. Conduits were not encountered until the search included a small region around moulins. The fracture aperture openings averaged about 4 cm and were found from near surface to 96% of the local ice depth. Water flow speeds in the fractures were 1–2 cm s^{-1}. The fractures were near vertical in orientation and associated with clear ice. From this they inferred that the fractures are probably partly refrozen crevasses. That these features were also found near the bottom of the glacier points to a possible subglacial origin for deep fractures. Surface fractures/crevasses can be propagated deep into a glacier through hydrofracturing (Boon and Sharp, 2003; van der Veen, 2007) if it is water filled. The common occurrence of englacial fractures and the lack of conduits contest the traditional hypothesis that englacial conduits route surface water through the englacial region of temperate glaciers. Englacial conduits may be limited to regions down-glacier of moulins and fractures may convey most of the water up-glacier of moulins (Figure 4).

The multiple radar reflections and ubiquity of fracture observations suggests that the englacial region of a glacier may be quite heterogeneous and rather than a solid mass of ice and a few conduits it is highly fractured with water-filled fractures. The implications for glacier hydrology are clear; however, how such a composition affects glacier motion is less obvious.

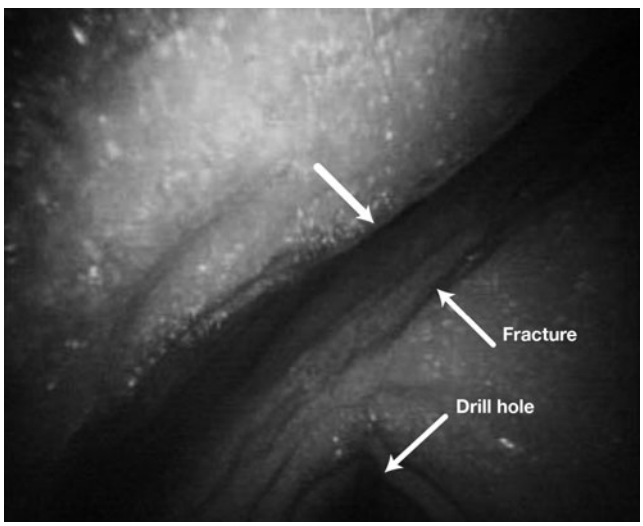

Englacial Processes, Figure 4 Englacial fracture in Storglaciaren, Sweden. The view is looking vertically downward, note the drill hole at the bottom. Width of the fracture at the *arrows* is approximately 4 cm. Taken from Fountain et al. (2005b).

Understanding how water is routed through the englacial region is of key importance for understanding the motion of temperate glaciers and glacier hydrology. Water routing to the bottom of a glacier is an important control on the basal hydrology and therefore basal drag and glacier motion. Basal water pressure partially offsets ice pressure on the bed reducing sliding friction. In addition, the presence of basal water bodies transfers the bulk shear stress to areas

of ice-substrate contact. The influence of englacial routing on subglacial hydraulics can be argued as follows. Where large fluxes of surface water are focused to a few crevasses, we presume efficient flow pathways, moulins and englacial/subglacial conduits, develop to route the water. In regions where input is much smaller and more disperse among numerous crevasses, other pathways can accommodate the water flux and a different configuration of subglacial hydraulic features can develop.

Temperate glaciers can store and catastrophically release water impounded in ice-dammed lakes or stored internally, presumably in englacial or subglacial regions. Although the evolution of ice-dammed flooding behavior has been well-outlined theoretically and largely explains the observations, the processes of storage and release are essentially unknown. Outburst floods are an important hazard in many alpine regions, particularly in the Himalaya Hindu-Kush region. Also, temperate glaciers play an important role in alpine hydrology, particularly during the hot-dry summer months when rainfall is a minimum. Understanding glacier controls on stream flow variations is a relevant concern for dams and other human infrastructure in such regions. In some alpine regions of Norway and Switzerland, water is drained from beneath some glaciers to drive hydroelectric facilities.

Bibliography

Boon, S., and Sharp, M., 2003. The role of hydrologically-driven ice fracture in drainage system evolution on an Arctic glacier. *Geophysical Research Letters*, **30**, 1916, doi:10.1029/2003GL018034.

Bradford, J., and Harper, J., 2005. Wave field migration as a tool for estimating spatially continuous radar velocity and water content in glaciers. *Geophysical Research Letters*, 32, doi:10.1029/2004GL021770.

Cuffey, K., and Paterson, W., 2010. The physics of glaciers, 4th edn. Academic Press, ISBN: 978-0-12-369461-4, 704 pp.

Fountain, A., and Walder, J., 1998. Water flow through temperate glaciers. *Reviews of Geophysics*, **36**, 299–328.

Fountain, A., Schlichting, B., Jansson, P., and Jacobel, R., 2005a. Observations of englacial flow passages: a fracture dominated system. *Annals of Glaciology*, **40**, 25–30.

Fountain, A., Schlicting, R., Jacobel, R., and Jansson, P., 2005b. Fractures as main pathways of water flow in temperate glaciers. *Nature*, **433**, 618–621.

Fujita, S., Maeno, H., Uratsuka, S., Funukawa, T., Mae, S., Fiujii, Y., and Watanabe, O., 1999. Nature of radio echo layering in the Antarctic ice sheet detected by a two-frequency experiment. *Journal of Geophysical Research*, **104**, 13013–13024.

Gulley, J., and Benn, D., 2007. Structural control of englacial drainage systems in Himalayan debris-covered glaciers. *Journal of Glaciology*, **53**, 399–412.

Harper, J., and Humphrey, N., 1995. Borehole video analysis of a temperate glacier's englacial and subglacial structure: implications for glacier flow models. *Geology*, **23**, 901–904.

Lliboutry, L., 1976. Temperate ice permeability, stability of water veins and percolation of internal meltwater. *Journal of Glaciology*, **42**, 201–211.

Murray, T., Stuart, G. W., Fry, M., Gamble, N., and Crabtree, M., 2000. Englacial water distribution in a temperate glacier from surface and borehole radar velocity analysis. *Journal of Glaciology*, **46**, 389–398.

Pohjola, V., 1994. TV-video observations of englacial voids in Storglaciaren, Sweden. *Journal of Glaciology*, **40**, 231–240.

Raymond, C., and Harrison, W., 1975. Some observations on the behavior of the liquid and gas phases in temperate glacier ice. *Journal of Glaciology*, **71**, 213–234.

Siegert, M., and Hodgkins, R., 2000. A stratigraphic link across 1100 km of the Antarctic ice sheet between the Vostok ice-core site and Titan Dome (near south pole). *Geophysical Research Letters*, **27**, 2133–2136.

Stenborg, T., 1973. Some viewpoints on the internal drainage of glaciers, in hydrology of glaciers. *IAHS Publications*, **95**, 117–129.

van der Veen, C., 2007. Fracture propagation as means of rapidly transferring surface meltwater to the base of glaciers. *Geophysical Research Letters*, 34, doi:10.1029/2006GL028385.

Welch, B., and Jacobel, R., 2003. Analysis of deep-penetrating radar surveys of west Antarctica, US-ITASE 2001. *Geophysical Research Letters*, **30**, 1444, doi:10:1029/2003GL017210.

Welch, B., and Jacobel, R., 2005. Bedrock topography and wind erosion sites in east Antarctica: observations from the 2002 US-ITASE traverse. *Annals of Glaciology*, **41**, 92–96.

Cross-references

Crevasses
Firn
Glacier Lake Outburst Floods
Glacier Hydrology
Ground Penetrating Radar Measurements Over Glaciers
Moulins
Subglacial Processes
Temperate Glaciers

ENVIRONMENTAL ISOTOPES

Bhishm Kumar
Hydrological Investigation Division, National Institute of Hydrology, Roorkee, Uttarakhand, India

Definition

Environmental isotopes may be defined as those isotopes, both stable and radioactive, which occur in the environment in varying concentration over which the investigator has no control (Payne, 1983).

These can be stable or unstable isotopes. Some examples of stable isotopes include ^{2}H, ^{3}He, ^{6}Li, ^{11}B,^{13}C, ^{15}N, ^{18}O, ^{34}S, etc., and some unstable or radioactive isotopes are ^{3}H, ^{14}C, ^{36}Cl, ^{137}Cs ^{210}Pb, etc. These are principal elements of hydrological, geological, and biological systems. The stable isotopes of these elements serve as tracers of water, carbon, nutrient, and solute cycling. Radioactive environmental isotopes are also important in hydrogeology. The environmental radioisotopes, whether naturally occurring due to cosmic ray interaction with various gaseous molecules or anthropogenically produced and become the part of hydrological cycle, are safe in normal conditions and do not pose any threat to human health. Environmental radionuclide such as ^{14}C and ^{3}H decay with time so that they can be used to estimate the age or circulation of groundwater.

Uses

Since glaciers are known to preserve the precipitation of the past in an unbroken sequence, it might seem that they are especially well suited for the study of the isotopic composition of precipitation and its variation with time. Dansgaard (1964) first proposed that the ^{18}O and D contents in glacier ice might reflect climatic conditions of the past. The other applications include study of accumulation rates, run-off ratio, dating of the ice-core, ice-flow pattern, drifting sea ice, and paleoclimates (Clark and Fritz, 1997).

Bibliography

Clark, I., and Fritz, P., 1997. *Environmental Isotopes in Hydrogeology*. Boca Raton, FL/New York: Lewis.

Dansgaard, W., 1964. Stable isotopes in precipitation. *Tellus*, **16**, 436–438.

Payne, B. R., 1983. *Guidebook on Nuclear Techniques in Hydrology*. Technical Report Series No. 91. Vienna: International Atomic Energy Agency.

EPIGENETIC ICE

Chelamallu Hariprasad
Centre for Studies in Resource Engineering, IITB, Mumbai, Maharashtra, India

Definition

The ground ice refers to all types of ice formed in freezing and frozen ground. Broadly ground ice can be categorized as epigenetic and syngenetic. Epigenetic ground ice forms in situ as permafrost aggrades while syngenetic ground ice forms in combination with deposition. Thus Epigenetic is a type of ground ice, formed in situ under conditions of permafrost in the subsoil. In general, frozen ground or permafrost represents the area which existed below 0°C for over few years (at least 2 years).

EPIGLACIAL MORPHOLOGY

Claudio Smiraglia, Guglielmina Diolaiuti
Department of Earth Sciences "A. Desio", University of Milano, Milano, Italy

Synonyms

Epiglacial environment; Epiglacial landscape; Epiglacial system; Supraglacial morphology

Definition

Epiglacial or supraglacial. Processes acting or features being evident at the glacier surface.

Epiglacial morphology. Complex of features deriving from processes active at the glacier surface, such as differential ablation or meltwater flow.

Introduction

Epiglacial morphology due to the large amplitude of topographical features plays a crucial role in determining the distinctive landscape of glacial system; in addition it creates the actual epiglacial environment which is well known to trekkers, alpine climbers, and mountain travellers (Benn and Evans, 1998). Crevasses and ice falls, supraglacial lakes and water ponds, medial moraines and debris-covered glacier snouts are among the best-known features belonging to the glacial landscape.

By analyzing the main epiglacial morphology features it is possible to deepen the knowledge on ice flow and strain rate and on debris transfer through the glacial system.

A large number of processes, which are different in complexity and mutual relations, are driving the epiglacial morphology giving a large amplitude of forms. For sorting the epiglacial forms and describing their development and evolution, a basic and qualitative classification can be applied: (1) forms related to glacier motion and flow, (2) forms related to epiglacial meltwater, and (3) forms related to differential ablation.

The above classification, although useful for describing the main features of epiglacial morphology, is not fully exhaustive, since the largest part of epiglacial forms is polygenic and actually results from the interactions among different processes which create a unique complex morpho-dynamic system where glacier flow, epiglacial drainage, and differential ablation are connected by several positive and negative feedback mechanisms.

The driving factors shaping the glacier surface and determining the different types of epiglacial forms are well expressed on temperate glaciers. In the following sections we will focus on this glacier type. It is also important to consider the brief time span covered by epiglacial form evolution: they generate, develop, and end in a short time frame, thus being considered ephemeras forms which, in particular on the lower sectors of glacier ablation tongues, may fast change their shape or disappear after a few days.

Epiglacial forms related to glacier motion

Crevasses are glacier fractures which can be listed among structural forms. Glacier fractures occur when ice cannot creep fast enough to allow a glacier to adjust its shape under stress. Crevasses are fractures formed where ice is pulled apart by tensile stresses; these fractures are fairly superficial features because at depth creep rates are higher and ice will flow faster than it can split (Figure 1). On *temperate* glaciers, characterized by "soft" ice, they rarely extend deeper than 30–40 m, whereas on polar and *cold* glaciers they may be much deeper. Crevasses are surely the most prominent and well-known features related to glacier flow, since they represent the most serious hazards

Epiglacial Morphology, Figure 1 Crevasses in the Mont Blanc area (Alps, at the boundary between France and Italy).

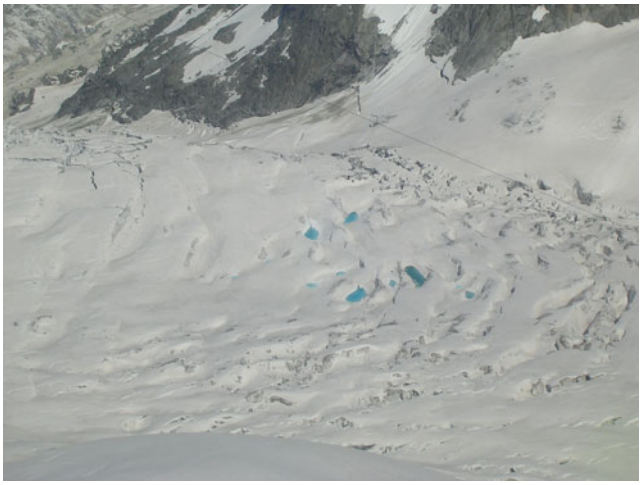

Epiglacial Morphology, Figure 2 Crevasses with some epiglacial ponds (Glacier du Geant, French Alps).

faced by mountaineers; they are present at the surface of several glacier types ranging from small cirque glaciers to ice sheets.

Generally, crevasses are grouped into a well-defined set as it occurs on valley glaciers (Nye, 1952) and from their analysis several types of information on glacier ice stresses can be derived.

Chevron crevasses are among the more common cleft patterns; they are linear breaks with an oblique orientation from the boundaries to the inner glacier sector aligned approximately at 45° to the valley walls; they originate from friction between mountain walls and glacier ice which makes ice velocity increase in the central glacier sector.

In the case of valley glaciers under extending flow conditions, which make glaciers accelerate, *transverse crevasses* occur; the main strain results to be parallel to ice flow and breaks open perpendicularly to the central flow line, slightly bending down valley (Figure 2).

When ice flow becomes compressive, that is the case of lower glacier sectors, *splaying crevasses* take place; they are curved and quite parallel to the ice flow direction in the inner glacier area, instead close to the margins they become bending at a smaller than 45° angle.

Bergschrund is a special crevasse type, a deep transverse one that occurs at the head of a glacier and can be also several hundreds of meters long.

Crevasses, after their genesis, flow down within the glacier reaching areas with different stress conditions which may cause their closure; in this latter case they leave linear scars named *crevasse traces,* layers of blue ice made by regelation of melting water inside the crevasse (before it closes off), or levels of white bubble ice made by snow filling the crevasse before its closure (Hambrey, 1994).

When glaciers flow on very steep slopes they increase their velocity (the acceleration can reach values up to ten times speedier than the normal ones), break in a chaotic totally broken surface, and give rise to *ice falls* with ice

Epiglacial Morphology, Figure 3 Seracs on a tributary of Forni Glacier, the widest Italian valley glacier (Alps).

towers named *séracs* (Figure 3). Generally these towering and unstable blocks of ice convince climbers to find an alternative route. In the areas where ice falls occur, large explosive sounds are not infrequent to be heard as house-size chunks of ice break off and collapse. The Khumbu Icefall on Mount Everest is a classic zone of unstable ice that climbers are forced to traverse.

At the base of ice falls, where ice flow becomes compressive, the most striking glacier structures, *ogives,* occur. These forms are curving bands or waves convex downflow each usually several meters wide, alternating bands of dark and light ice; they (sometimes called *Forbes bands*) are formed annually and each dark-light pair represents 1 year of glacier movement. They reflect the alternate season passage of dirty ice (in summer) and snow-covered ice (in winter) along the ice fall (Nye, 1958). *Layered structures*

are also present at the glacier surface, in any case the driving processes are different in the accumulation area with respect to the ablation one.

When a layered structure (*sedimentary stratification*) develops in the accumulation basin, it reflects yearly accumulation with layers generally parallel to the glacier surface. Layering consists of two kinds of alternating single stratum: thicker strata of coarse-grained white or light blue bubble ice (compacted winter snow and converted to ice by pressure) and thinner strata of dark blue dirty ice (layers saturated with water, that concentrates wind-blown dust, and afterward refrozen). In the ablation area, instead, the ice is characterized by *foliations,* a new layered structure with layers closer and less continuous derived by deformation of sedimentary stratification. The foliation orientation depends on the arrangement of primary stratification and on the sequence of deformations occurred during glacier flow.

Meltwater flow and related epiglacial forms

Meltwater derived from surface ablation is important, together with that derived from basal melting, not only because it influences glacier behavior and geomorphological processes (e.g., flow rate and basal sliding depend on the presence and distribution of liquid water), but also because it may form very peculiar epiglacial features. During the early summer, the winter snow packs may become saturated with water that accumulates in the snow and in the low-relief areas may form zone of *snow swamps* or *slush swamps*.

When on the glacier surface a slope is found, melt water drains away thus originating rills and giving rise to an actual glacier drainage system; the latter develops in the ablation areas like a surface stream network due to the low primary permeability of glacier ice.

The development of epiglacial meltwater streams (named *bédières*) depends on many ice factors (temperature, ablation rate, strain rate) and on features as crevasse occurrence and distribution, or foliation presence and pattern.

The drainage network characterizing epiglacial meltwater streams shows similarities with the ones occurring outside glacier areas (i.e., on glacial sediments or on rock surfaces); nevertheless some differences are present: on glacier surface the drainage density is stronger and higher order streams are absent due to ice flow and ablation that inhibit the development of an integrated drainage network; moreover on glacier surface the drainage pattern shows several subparallel channels which reflect the structural control (mainly crevasse distribution and foliations); the channel density is diminishing in the upper sectors (which is strongly different from the situation found on drainage networks outside glaciers) due to decreasing meltwater production at higher elevations; the channel patterns are fast changing since ablation processes are continuously shaping and modifying the glacier surface. In addition, new crevasses can develop, thus interrupting and intercepting the drainage network (Sugden and John, 1976).

The epiglacial streams are characterized by different depths, from a few centimeters in the case of small rills to several meters in the case of huge canyons which can represent giant obstacles to be traversed by climbers and mountaineers. Glacier streams show smooth sides which offer small resistance to water flow. The epiglacial drainage systems can easily develop on slow moving or stagnant glaciers not strongly crevassed and with small or absent surface moraines. Under these conditions, streams may form a dendritic pattern or a meandering with great regularity of wavelength and amplitude and with the concave slope of their bends characterized by steep gradient walls (Figure 4).

Crevasses are also found to be factors driving the development of peculiar epiglacial forms which are able to reach the inner and deeper glacier sectors. In fact, crevasse traces and/or developing crevasses produce planes of weakness which allow melt water to create vertical holes in the ice called *glacier mills* or *moulins,* analogous to pothole in the limestone of the karst countries. They have a diameter from less than a meter to more than 10 m and may penetrate deep into the glacier for many tens of meters; they in fact form the most important way for the glacier surface meltwater to reach the bed or the internal drainage network. Investigations and descents of moulins by means of speleological techniques have been performed since the end of nineteenth century (J. Vallot in 1898 explored the moulins of the Mer de Glace on Mont Blanc Massif), nevertheless only at the end of the twentieth century investigations became systematic and a new branch of glaciology saw the birth (i.e., glacio-speleology).

From field investigations it results in the higher sector of moulins to be generally vertical and regular, the deeper zone, instead, results to be inclined downvalley and quite always water filled. The water level of glacier moulins shows intense and fast changes and when more water enters the system with respect to the one drained by the englacial and subglacial network (as it occurs during periods of fast melting or after strong rainstorms) the

Epiglacial Morphology, Figure 4 Epiglacial meltwater streams (*bédière)* on the tongue of Dosdè Glacier (Italian Alps).

higher water level is found. The persistence of active moulins is driven by forms related to glacial flow; in the case a crevasse develops at higher elevations than a moulin, it can capture the drainage thus giving the rise, on the same supraglacial stream, of a new moulin at higher elevations (Holmlund, 1988).

Surface meltwater is not only flowing at the glacier surface or in glacier moulins, it may also be temporarily stored up in *epiglacial lakes* or *water ponds* (Figures 2–8). These forms are newly witnessing the complexity and the synergic action played by glacier processes which create epiglacial morphology. Generally epiglacial lakes develop on glacier lower areas like closed-off remnants of crevasses or inactive partially filled moulins. They form during the ablation period and in subpolar regions or wherever ice is below the pressure melting point, and can persist all the melt season due to the impossibility of melt waters to penetrate into the inner ice layers. On temperate glaciers the epiglacial lakes are more ephemeral (a proper example could be the *Effimerous Lake,* which developed in 2001 on Belvedere Glacier, Monte Rosa, Italy), they normally form early in the ablation season but rapidly drain when the drainage network becomes more active or the accelerating glacier flow forms new crevasses (Benn and others, 2001).

A peculiar type of epiglacial lake is spread where glaciers are covered by large amounts of debris (i.e., on debris-covered glaciers) and their development is caused by differential melting or ablation. In this case lakes and water ponds act as increasing glacier absorption of incoming energy (water albedo is lower than ice one, moreover water heat capacity is high and convective fluxes occur) and thus rising glacier ablation. In several cases they are found to enlarge their size, to become coalescent, and they may give rise to GLOF phenomena.

Differential ablation processes

The most impressive and diffuse features of epiglacial morphology derive from differential ablation processes. Differential ablation is defined as the ratio between the melt rate of bare or debris-free ice and the melt rate occurring at debris-covered ice at the same elevation. Supraglacial debris cover plays a key role in determining rates and magnitudes of buried ice ablation (Østrem, 1959; Nakawo and Young, 1982). The debris influence on ice ablation is due to its different albedo, generally lower than the one of bare ice, thus increasing the absorption of incoming solar radiation and ice ablation. Differently, supraglacial debris, whenever thicker than the *critical* value (Mattson et al., 1993), reduces the magnitude and rates of glacier ice ablation; the melt reduction in the case of thick debris layer is due to the prevailing insulating effect played by rock debris. On the glacier surface, especially in the lower part, during the ablation season, an amount of debris ranging in grain size from fine material as silt or sand to rubble or huge blocks of rock is visible. This supraglacial debris derives from different sources: (1) mass movements from adjacent mountain slopes, (2) wind-blown dust, (3) volcanic eruptions, (4) salt and microorganisms from sea-spray, (5) meteorites, and (6) pollutants from human sources (Hambrey, 1994; Kirkbride, 1995; Benn and Evans, 1998). The weight played by the different source types depends on the geographic setting: on areas where volcanic activity is important (e.g., Island) volcanic ash and tephra play the major role; on ice sheet surfaces (e.g., Antarctica) far from rock exposures the main debris sources are volcanoes and meteorites; on mountain glaciers nested by rock walls and with the occurrence of *nunataks* and rock exposures the main debris sources are slope processes (e.g., rock-falls and rock-slides, snow and ice avalanches, creep, debris and mud flows).

There are also several mechanisms of debris transport: supraglacial cover can receive material from subglacial glacier sector; in this case debris transport occurs in the basal shear zone of glaciers (*active transport*, Boulton, 1978). Then debris comes upwards the glacier surface in the ablation zone; debris may also be transported in supraglacial and englacial positions (*passive transpor*t, Boulton, 1978), in the latter case debris reaches the glacier surface when ablation of the nesting ice occurs.

Summarizing, the effect of a debris cover on the ablation rate of the underlying ice depends on the thermal conductivity of the debris, the ice density, the latent heat of ice melting, the surface debris temperature, and most of all, if the other factors are constant, the debris layer thickness.

Differential ablation features

The complex pattern and distribution of epiglacial debris, which may alternate areas with coverage thicker than the critical value or large boulders and areas with debris layer thinner than this threshold, give rise to different epiglacial features. In the case of thin and fine debris cover, ablation tends to form depressions, such as small and a few centimeters deep holes that riddle ice giving it a honeycombed appearance (at the bottom of the holes is well visible the small pebble or the dust that promotes melting). In some situations, where the surface melting waters are able to collect and accumulate a thin deposit of small particles, many water filled holes, on the average 10–20 cm long and large and a few centimeters deep, with the bottom covered by a few millimeters thick black fine debris layer are developed in large numbers (*cryconites*). When the fine debris collected in a hollow by surface stream becomes thicker than the critical value, differential ablation tends to remove more ice from surrounding areas than below the debris layer, producing an upstanding dirt mound; it is called *dirt cone*, formed by a relatively thin veneer of debris, almost sand, covering a cone of ice (Figure 5). Where on the glacier surface, isolated large boulders, even many decimeters thick, are diffused, the rock protects the ice from melting and as a result it tends to be perched on the top of a pedestal of ice that in some large Asian glaciers can more than a man be tall (*glacier table*) (Figure 6).

Epiglacial Morphology, Figure 5 A dirt cone on the surface of Forni Glacier.

Epiglacial Morphology, Figure 7 The ablation tongue of Forni Glacier: a bigger medial moraine (ISI type) is visible together with some thinner moraines (AD type). Ice seracs, transverse and chevron crevasses, rock outcrops are appreciable as well.

Epiglacial Morphology, Figure 6 Glacier table with glaciologists on the Morteratsch Glacier (Switzerland).

The narrow stripes, sometimes sinuous, of the *medial moraines* are among the most striking and spectacular features of valley glaciers due to differential ablation. They are formed by a long dark ridge of coarse debris, a few centimeters thick, that hides the underlying ice and overhangs even for some meters the ice free glacier surface. They may derive from a glacier confluence and be the morphological expression of the merging of two epiglacial lateral moraines; in that case a glacier composed by the confluence of two basins will have one single medial moraine, whereas the basins are three the medial moraines are two. This kind of moraine is called *ice stream interaction* (ISI). When the debris forming the moraine derives from emerging through melt-out of englacial material, the moraine is defined *ablation-dominant* (AD). In the case the debris derives from a rock fall event, the moraine is defined *avalanche-type* (AT) (Eyles and Rogerson, 1978) (Figure 7).

Penitentes are the most fascinating epiglacial features due to differential ablation; they are pinnacles of snow or ice which grow over all glaciated and snow-covered areas in the Dry Andes above 4,000 m (Lliboutry, 1954). They range in size from a few centimeters to over 5 m (Naruse and Leiva, 1997). They take the form of tall thin blades of hardened snow or ice closely spaced with the blades oriented toward the general direction of the sun. Penitentes were first described by Darwin (1839) during his travel from Santiago de Chile to Mendoza (Argentina). Darwin described *penitente*s as features formed by the strong winds of the Andes; this explanation had persisted until the recent times when deeper investigations on these epiglacial features were performed. Lliboutry noted that the key climatic condition for the differential ablation that leads to the formation of *penitentes* is that the dew point is always below freezing. Thus, snow will sublimate, which requires higher energy input than melting. Once the process of differential ablation starts, the surface geometry of the evolving *penitente* produces a positive feedback mechanism, and radiation is trapped by multiple reflections between the walls. The hollows become almost a black body for radiation, while decreased wind leads to air saturation, increasing the dew point temperature and the onset of melting. In this way peaks, where mass loss is only due to sublimation, will remain, as well as the steep walls, which intercept only a minimum of solar radiation. In the troughs ablation is enhanced, leading to a downward growth of *penitentes* (Betterton, 2001; Corripio and Purves, 2005).

Epiglacial Morphology, Figure 8 The debris-covered tongue of Baltoro Glacier (Karakoram). An epiglacial lake is visible as well.

Debris-covered glacier snout features

In some glaciarized areas, where a high relief mountain environment dominates, many glaciers have a continuous debris mantle covering most of their ablation tongue with maximum thickness usually present in the lower part of the glacier. Some typical examples can be seen in Karakoram, Himalaya, Alps of New Zealand, where a large volume of debris is delivered on the glacier surface by rock-falls and other mass wasting processes (Figure 8). The great spatial variability in debris thickness and grain size favors the differential ablation processes that produce a strong gravitational and meltwater reworking of the former debris-covered surface. The flanks of dirt cones and of medial moraines become gradually more steep, the abundance of debris and water produces debris flows and sliding, all processes that redistribute sediments on the glacier surface, change the pattern of differential ablation and create in the deglaciation phases very characteristic and distinctive features. The final phase of the gravitational reworking is the development of a low-relief topography on the very thick debris mantle that reduces strongly ice ablation rates. On actual debris-covered glaciers the larger ice losses are mainly concentrated at the debris-free areas such as the walls of open crevasses and other holes on the glacier surface and steep marginal areas. Ablation proceeds by the preferential melting and retreat of such slopes in a process known as *backwasting* (Eyles, 1979). This process enlarges holes and produces a chain of a circular depression filled with water, favors the collapse of the roofs of englacial and subglacial water conduits (Kirkbride, 1993); the process results in a sequence of landscapes similar to the evolution of karst features on limestone terrains and thus defined as *glacier karst* (Clayton, 1964).

Summary

Epiglacial morphology includes all the forms and features characterizing the glacier surface. Among the most important factors driving epiglacial forms are: glacier flow and dynamics (generating crevasses and foliations), melt water drainage (originating *bédières* and *moulins*), and differential ablation (creating giant forms, medial moraines, or small morphologies – glacier tables).

On the ablation tongue of temperate and subpolar glaciers, where supraglacial debris creates continuous mantles, the most impressive epiglacial forms can be found: supraglacial lakes and water ponds fast changing their shape and giving rise to coalescence features, ice collapse, backwasting. The landscape morphology in such areas resembles the one belonging to the karstic system and is frequently reported as *glacier karst.*

Bibliography

Benn, D. I., and Evans, D. J. A., 1998. *Glaciers and Glaciation*. London: Arnold.

Benn, D. I., Wiseman, S., and Hands, K., 2001. Growth and drainage of supraglacial lakes on the debris-mantled Ngozumpa Glacier, Khumbu Himal. *Journal of Glaciology*, **47**, 626.

Betterton, M. D., 2001. Theory of structure formation in snowfields motivated by penitentes, suncups, and dirt cones. *Physical Review E*, **63**(056129), 12.

Boulton, G. S., 1978. Boulder shapes and grain-size distribution of debris as indicators of transport paths through a glacier and till genesis. *Sedimentology*, **25**, 773.

Clayton, L., 1964. Karst topography on stagnant glaciers. *Journal of Glaciology*, **5**, 107.

Corripio, J. G., and Purves, R. S., 2005. Surface energy balance of high altitude glaciers in the central andes: the effect of snow penitentes. In de Jong, C., Collins, D., and Ranzi, R. (eds.), *Climate and Hydrology in Mountain Areas*. London: Wiley.

Darwin, C., 1839. *Journal of Researches into the Geology and Natural History of the Various Countries Visited by H. M. S. Beagle, Under the Command of Captain Fitz Roy, R. N., 1832 to 1836*. London: H. Colburn.
Eyles, N., 1979. Facies of supraglacial sedimentation on Icelandic and alpine temperate glaciers. *Canadian Journal of Earth Sciences*, **16**, 1341.
Eyles, N., and Rogerson, R. J., 1978. A framework for the investigation of medial moraine formation: Austedalsbreen, Norway, and Berendon Glacier, British Columbia, Canada. *Journal of Glaciology*, **20**, 99.
Hambrey, M. J., 1994. *Glacial Environments*. London: UCL Press.
Holmlund, P., 1988. Internal geometry and evolution of moulins, Storglaciärien, Sweden. *Journal of Glaciology*, **34**, 242.
Kirkbride, M. P., 1993. The temporal significance of transitions from melting to calving termini at glaciers in the central Southern Alps of New Zealand. *Holocene*, **3**, 232.
Kirkbride, M. P., 1995. Processes of transportation. In Menzies, J. (ed.), *Glacial Environments, Vol. I: Modern Glacial Environments: Processes, Dynamics and Sediments*. Oxford: Butterworth-Heinemann, pp. 261–292.
Lliboutry, L., 1954. The origin of penitentes. *Journal of Glaciology*, **2**, 331.
Mattson, L. E., Gardner, J. S., and Young, G. J., 1993. Ablation on debris covered glaciers: an example from the Rakhiot Glacier, Punjab, Himalaya. In Young, G. J. (ed.), *Snow and Glacier Hydrology*. Wallingford, Oxon: International Association of Hydrological Sciences Press, pp. 289–296 (IAHS Publication 218).
Nakawo, M., and Young, G. J., 1982. Estimate of glacier ablation under debris layer from surface temperature and meteorological variables. *Journal of Glaciology*, **28**, 29.
Naruse, R., and Leiva, J. C., 1997. Preliminary study on the shape of snow penitents at Piloto Glacier, the Central Andes. *Bulletin of Glacier Research*, **15**, 99.
Nye, J. F., 1952. A method of calculating the thickness of ice sheets. *Nature*, **169**, 529.
Nye, J. F., 1958. Surges in glaciers. *Nature*, **181**, 1450.
Østrem, G., 1959. Ice melting under a thin layer of moraine and the existence of ice in moraine ridges. *Geografiska Annaler*, **41**, 228.
Sugden, D. E., and John, B. S., 1976. *Glaciers and Landscape*. London: Arnold.

Cross-references

Crevasses
Debris-Covered Glaciers
Debris Thermal Properties and Impact on Ice Ablation
Melting Processes

EQUILIBRIUM-LINE ALTITUDE (ELA)

Jostein Bakke[1], Atle Nesje[2]
[1]Department of Geography/Bjerknes Centre for Climate Research, University of Bergen, Bergen, Norway
[2]Department of Earth Science/Bjerknes Centre for Climate Research, University of Bergen, Bergen, Norway

Synonyms

Snow line

Definition

The equilibrium-line altitude (ELA) marks the area or zone on a glacier separating the accumulation zone from the ablation zone and represents where annual accumulation and ablation are equal.

Introduction

The equilibrium-line altitude (ELA) on glaciers is the average elevation of the zone where accumulation equals ablation over a 1-year period. The ELA can rarely be observed as a line at the same elevation across the entire width of the glacier due to local topographic and climatic variations in accumulation and ablation (Figure 1). Thus, the ELA is the average altitude of the equilibrium line. The ELA is very closely related to the local climate, particularly winter precipitation and summer air temperature. Variations in the ELA can therefore commonly be attributed to changes of these two variables. This can best be illustrated by its relationship to the net balance. The term net mass balance is the net gain or loss of ice and snow. The mass balance is highly dependent on the climate conditions. If the annual mass balance of the glacier as a whole is negative, the ELA rises, and when the balance is positive, the ELA falls. The steady-state ELA is defined as the ELA when the annual net balance is zero, as the glacier mass and the geometry are in balance with climate. The concept is very useful because it provides a measure of the climatic means related to certain glacier positions and geometries. The climatic ELA is the average ELA over a 30-year period (corresponding to a climate "normal" [30-year mean] period). Variations in ELA and net mass balance have been measured for many glaciers worldwide (e.g., Storglaciären in Sweden (since 1946) and Storbreen in Norway (1947). For details, see www.geo.unizh.ch/wgms). These time series underpin how fluctuations in the ELA provide an important indicator of glacier response to climate change and allow reconstructions of former climates and the prediction of future glacier behavior. Although the ELA is determined by local weather conditions, it is a good indicator of regional climate because glacier mass-balance fluctuations are commonly strongly correlated over distances of c. 500 km (Letreguilly and Reynaud, 1989).

Climate influencing the ELA

The accumulation on a glacier includes all materials that add mass to the glacier, such as snow, refrozen slush, hail, rain, and avalanched snow and ice. The ablation includes direct ice melt, iceberg calving, wind erosion/deflation, and sublimation. On most glaciers, accumulation is dominant in the winter months, whereas ablation mainly occurs during the summer. Where an ice sheet or glacier terminates in water, however, iceberg calving may occur throughout the year. Commonly, accumulation exceeds ablation on the upper part of a glacier, whereas ablation is larger than the accumulation in the lower parts. For a "regular" glacier fed by snowfall in its accumulation area and that loses mass by melting of "clean" ice in its ablation area, altitudinal mass-balance gradients are approximately linear, with ablation gradients tending to be steeper than

Equilibrium-Line Altitude (ELA), Figure 1 The southern part of the Folgefonna glacier in western Norway. The ELA can be seen as a meandering line between snow and blue ice (Photo: Jan Rabben).

accumulation gradients (Schytt, 1967; Furbish and Andrews, 1984). The links between climate and glacier mass changes have also been investigated by using mathematical models to find the climatic combinations required to "grow" or "melt" glaciers of a known size in a specified time frame. The most detailed models calculate accumulation and ablation totals by considering changes in all contributions to accumulation input and energy balance within defined time window (e.g., Gruell and Oerlemans, 1986; Kuhn, 1989; Braithwaite and Olesen, 1990). Depending on their complexity, these models incorporate a number of meteorological input parameters and simulate the temporal evolution of mass-balance terms (accumulation and ablation) in the course of a year or over several years (Oerlemans, 2001). The atmospheric forcing is usually provided by weather station data near to or on the glacier surface, which are interpolated to the required horizontal resolution of the mass-balance model. In addition, glacier characteristics (i.e., extent and a digital elevation model [DEM]) are needed as input to the model. More simple models integrate the climatic controls into two or more easily calculated parameters such as annual effective precipitation, mean temperature during the ablation season, or ablation–altitude relationships (e.g., Budd and Smith, 1981; Laumann and Reeh, 1993; Reeh, 1991). Such models can easily be used to calculate ELA also on reconstructed glaciers based on e.g., dated terminal moraines.

Wind influencing the ELA

Climate processes influencing the ELA on glaciers involve ablation (mainly controlled by summer temperature, T) and direct snowfall (precipitation, P), giving the TP-ELA. In addition, wind (W) transport of dry snow is an important factor for the glacier mass balance, in particular during the accumulation season. On plateau glaciers, snow deflation and drifting dominate on the windward side, whereas snow accumulates on the leeward side. By calculating the mean ELA in all glacier quadrants on a plateau glacier, the influence of wind on plateau glaciers may be negligible. The resulting ELA is therefore defined as the TP-ELA (temperature/precipitation ELA). The TP-ELA reflects the combined influence of the accumulation-season precipitation and ablation-season temperature (Dahl and Nesje, 1992). On wind-exposed mountain plateaux, the snow may deflate and accumulate in lower cirques and valleys, either by direct accumulation on the cirque/valley glaciers, or by avalanching from the mountain slopes. The accumulation on the cirque/valley glaciers may therefore be significantly higher than the local precipitation indicates (Figure 2) (Dahl and Nesje, 1992). The mean ELA on a plateau glacier therefore defines the TP-ELA, whereas the ELA on a cirque glacier, commonly influenced by wind-transported snow, gives the TPW-ELA. Therefore, the TPW-ELA is commonly lower than the TP-ELA. Leeward accumulation of windblown snow, including avalanching from the cirque walls, is an important factor influencing the mass balance of cirque glaciers. Due to the potential upslope transport of dry snow by wind, the additional accumulation of snow in a cirque is commonly difficult to estimate. One possible approach to this problem is to calculate the ratio between the catchment area above the TPW-ELA (D) and the reconstructed glacier accumulation area (A) as a rough measure of the potential for additional of snow by wind transport and avalanching in cirques (Dahl et al., 1997). Another approach to calculate this ratio is to define the prevailing wind direction and calculate the area in quadrants upslope and upwind of the glacier surfaces, including plateaux, all

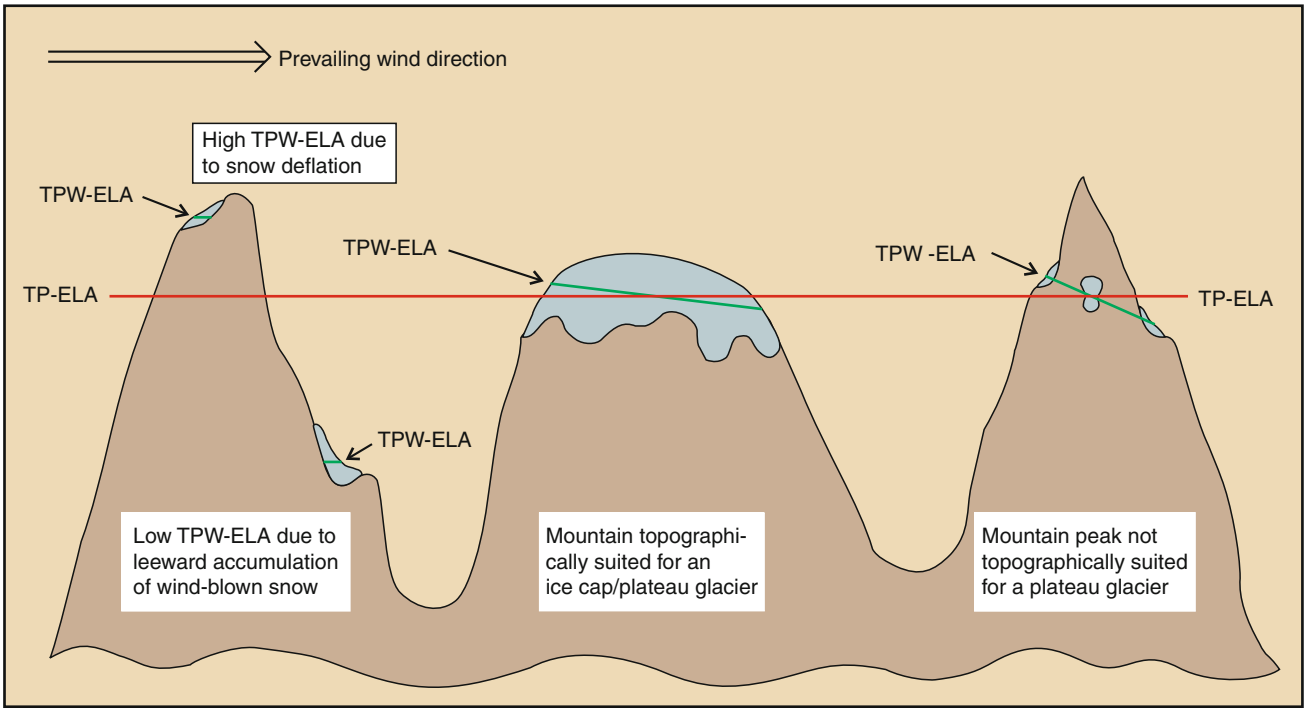

Equilibrium-Line Altitude (ELA), Figure 2 The effect of windblown snow can on some glaciers contribute with a large amount of snow. Therefore, the term temperature-precipitation-wind (TPW) ELA can be useful when describing the altitudinal distribution of glaciers in an alpine terrain (Dahl and Nesje, 1992).

glacier-facing slopes and all other plateau-edge slopes with gradients $<5^{o}$ irrespective of orientation (Benn and Ballantyne, 2005). Further, to take into account snow avalanching, all slopes $>25^{o}$ overlooking the glaciers are calculated. As the two categories frequently overlap, the results must be combined into a single snow-contributing area factor (Ballantyne, 2006). This factor can then be subtracted when calculating the regional ELA in an area. When studying the ELA distribution along a western transect in Scotland during Loch Lomond stadial, the above approach was applied by Ballantyne (2006).

Relationships between precipitation/temperature and the ELA

There is a very close connection between the ELA and local climate, in particular winter accumulation (snowfall), summer temperature, and wind strength causing transport of dry snow during the accumulation season. The ELA is therefore sensitive to perturbations of these variables; high winter snowfall combined with low summer temperatures the following summer gives a low ELA, whereas low winter accumulation followed by a warm summer yields a high ELA. Fluctuations in the ELA over time are therefore an important indicator of climate change and commonly allow reconstructions of past climates. Thus, palaeoclimatic reconstructions based on former glacier extent commonly make use of reconstructed ELAs. Data on past variations of ELAs therefore provides an important source of proxy palaeoclimatic data in glaciated regions around the world.

Relationships between temperature and precipitation at ELAs on glaciers have been established by statistical/analytical approaches (e.g., Liestøl in Dahl et al., 1997; Nesje and Dahl, 2000; Ohmura et al., 1992; Shi et al., 1992; Sissons, 1979). The positive correlation between these two variables for a wide range of glaciers reflects the fact that higher values of mass turnover at the ELA require higher ablation (higher summer temperatures) to balance the annual specific mass budget. The approaches of Ohmura et al. (1992) and Nesje and Dahl (2000), however, deviate significantly for temperature and precipitation $>4°C$ and $>3{,}500$ mm, respectively. Some of the discrepancy may be explained by the fact that Ohmura et al. (1992) used winter accumulation plus summer precipitation at the ELAs, whereas Nesje and Dahl (2000) used only winter (1 Oct–30 Apr) precipitation.

The temperature-precipitation relationship also explains the regional rise in glacier ELAs with increasing distance from moisture sources. In areas of lower precipitation, the temperature required to melt the annual accumulation at the ELA does not need to be as high as in areas of high precipitation. Consequently, ELAs tend to be at higher elevations in areas with low ablation-season temperatures than in areas with higher ablation-season temperatures. If palaeo ELAs have been reconstructed and if palaeotemperatures

are reconstructed from independent proxies (pollen, faunal remains, etc.) nearby, former winter or total precipitation at the ELA can be calculated from temperature-precipitation relationships (e.g., Dahl and Nesje, 1996). Regional variations of glacier ELAs can be used to infer former precipitation gradients that may allow prevailing moisture sources and circulation patterns to be reconstructed (Lehmkuhl, 1998; Lehmkuhl et al., 1998; Miller et al., 1975). In addition, reconstructed ELAs of former glaciers have been used to correlate moraines in mountain regions (e.g., Maisch, 1982). The term ELA has, however, been applied to several altitudinal indices calculated for past glaciers. The relationship between some of these indices and climate has, however, not been firmly established. Palaeoclimatic reconstructions based on these indices may therefore be inaccurate (Benn and Lehmkuhl, 2000). In some high mountain regions, however, the relationship between climate and glacier ELAs may be complicated due to avalanches and debris cover on the glacier surface. It is also complicated by different types of accumulation cycles where the most important types are: (a) winter accumulation type, with a well-defined winter accumulation season and summer ablation season; (b) summer accumulation type, with maxima in accumulation and ablation occurring simultaneously during the summer months: and (c) year-round ablation type, with one or two accumulation maxima coinciding with wet seasons.

Based on the "Liestøl-equation," three equations derived from a close exponential glacier-climate relationship at the ELA of Norwegian glaciers were implemented in a geographical information system (Lie et al., 2003). The equations enable calculation of (1) the minimum altitude of areas climatically suited for present glacier formation, (2) quantification of the glacial build-up sensitivity (GBS) in an area, and (3) calculation of the theoretical climatic temperature-precipitation ELA (TP-ELA) (based on temperature and precipitation data from meteorological stations in southern Norway) in presently non-glaciated areas by combining GBS with terrain altitude. The approach is primarily intended for reconstruction of palaeo ELAs in areas with no present glaciers.

Identifying ELA on modern glaciers

The ELA for any given year can be identified by observing the distribution of snow and ice on the glacier surface at the time of year when glacier mass is at a minimum (in the end of the accumulation season). Commonly, the ELA coincides with the transient snow line. This information can be obtained by field survey or from any photographic source (e.g., aerophoto, satellite images). On temperate glaciers, the ELA can give immediate information of the state of the glacier in relation to the last mass-balance year, and also the longer term state of the glacier. Paterson (1994) lists the following situations that give signs of the relationship between the glacier and climate over the last year(s):

1. A low snow line possessing a sharp boundary with bare ice indicates a positive net balance (the glacier is growing).
2. A similar boundary but at a high altitude indicates that a period of accumulation has interrupted long period of negative balance.
3. A snow line separated from bare ice by an area with old firn indicates a more negative balance than the preceding few years.

Approaches of calculating palaeo ELAs

When calculating the ELAs when a glacier was larger than at present, or when the glacier was melted completely, several approaches for calculating/estimating the ELAs of former glaciers from geomorphological evidence have been developed (see review by Benn and Lehmkuhl, 2000; Gross et al., 1976; Meierding, 1982; Torsnes et al., 1993). Former variations in ELA are a valuable palaeoclimatic proxy as it is also possible to isolate the winter component of the proxy (see above). The concepts of the different methods vary significantly, as do their reliability and ease of use. Some approaches are based on detailed evaluation of mass balance and glacier hypsometry (distribution of glacier area over its altitudinal range). Others are based on the large-scale morphology of the glacier catchment, the altitude of marginal moraines, and the cirque floor. A literature survey indicates that ELA depressions from modern values during the last glacial maximum, Younger Dryas and the "Little Ice Age" were typically in the range of 1,000 $\pm$ 300 m, 500 $\pm$ 200 m, and 100 $\pm$ 50 m, respectively. It is likely that many of the methods discussed below will be redundant by simple mass-balance models for calculation also of former ELAs.

The maximum elevation of lateral moraines (MELM)

Due to the nature of glacier flow toward the center above the ELA and toward the margin of the glacier below the ELA, lateral moraines are theoretically only deposited in the ablation zone below the ELA. As a result, the maximum elevation of lateral moraines should ideally reflect the corresponding ELA. This method is considered best suitable for long valley glaciers with large, continuous lateral moraines. There are, however, several problems with this approach. First, englacial material may not reach the glacier surface immediately below the equilibrium line. Thus, lateral moraines may not form at, but below the actual ELA. Second, it is difficult to assess whether or not a lateral moraine is preserved entirely in the upper part due to degradation on steep slopes. Consequently, ELA estimates derived from eroded/degraded lateral moraines may be too low. Third, the valley sides may be too steep for deposition of lateral moraines, giving estimates of the former ELA that are too low. Finally, if initial glacier retreat is slow, additional moraine material could be deposited in the prolongation of the former steady-state

lateral moraine. The MELM approach is, despite the problems, considered the most reliable method where former glaciers were covered by debris and the mass-balance gradient is poorly or not known.

The median elevation of a glacier (MEG)

This approach places the ELA half altitudinal difference between the glacier front and the top of the glacier. Empirical evidence from modern glaciers, however, suggests that the MEG overestimates the ELA. In addition, this method fails to take into account variations in valley morphology, which strongly affects the area-elevation distribution of a glacier. However, it works reasonably well for small glaciers with an even area/altitude distribution. The main problem is commonly to define the headward limit of a former glacier.

The toe-to-headwall altitude ratio (THAR)

This method assumes that the ELA lies at a fixed proportion of the vertical distance between the highest and lowest part of a former glacier. A ratio between the maximum and minimum altitude of a glacier (toe-to-headwall altitude ratio [THAR]) has been used as a quick estimate to calculate the ELA. Ratios of 0.35–0.4 were used by Meierding (1982) for glaciers in Colorado. Values of 0.4–0.5 were used by Porter et al. (1983) for "clean"-ice glaciers. The THAR approach is considered a rough way of estimating former ELAs because it does not take into account glacier hypsometry and mass balance. In addition, a major problem is to define the headward limit of a former glacier. The THAR approach allows rapid estimates of former ELAs in remote areas with poor or inaccurate maps.

Toe-to-summit altitude method (TSAM)

A way to overcome the problem of defining the upper limit of a former glacier is to use the maximum altitude of the glacier catchment. Louis (1955) suggested that the ELA may be calculated from the arithmetic mean of the altitude of the highest mountain and the terminal moraine. For the European Alps, Gross et al. (1976) demonstrated that this approach yields ELAs that are about 100 m too high. For modern glaciers in the northernmost mountain range of the Mongolian Altai, the inferred values are in agreement with snowlines on glaciers observed in the field and on aerial photographs (Lehmkuhl, 1998). The TSAM method gives, despite its crudeness, rapid estimates of former ELAs in remote areas. ELA estimates based on the TSAM method should be determined for each region separately because they may be due to significant variation due to variations in glacier type.

The accumulation area ratio to the total glacier area (AAR)

The ratio of the accumulation area to the total area (AAR) is based on the assumption that the steady-state AAR of former glaciers is typically 0.55–0.65 (Porter, 1975). An AAR of 0.6 ± 0.05 is generally considered to characterize steady-state conditions of valley/cirque glaciers. Ice caps and piedmont glaciers may, however, differ significantly from this ratio. Gross et al. (1976) inferred a mean AAR value of 0.67 for glaciers in the European Alps. The AAR of a glacier varies mainly as a function of its mass balance; ratios below 0.5 indicating negative mass balance; 0.5–0.8 corresponding to steady-state conditions, and values above 0.8 reflecting positive mass-balance regimes. For modern mid- and high-latitude glaciers, steady-state AARs typically lie in the range 0.5–0.8. The AAR approach requires contour maps of former glacier surfaces, and this method can therefore only be used where detailed topographic data/maps are available. Information about mass-balance gradients is not required for the AAR method. The largest source of inaccuracy related to the AAR method of determining the ELA on former glaciers is the reconstruction of the surface contours, especially if the glacier margins intersect valley-side topographic contours at small angles or coincide with them for some distance. A theoretical evaluation of the AAR approach, using changing slope angles and valley morphology on idealized glaciers, shows that glaciers advancing into flat areas underestimate the ELA depression, whereas glaciers moving into areas of increasing slope angle overestimate the climatic ELA difference. Consequently, topographical and morphological effects on calculated ELA depressions on glaciers must be carefully evaluated.

The balance ratio (BR) method

The balance ratio (BR) method is a refinement of the AAR approach. As demonstrated above, one shortcoming of the AAR method, and also the MEG approach, is that they do not fully account for variations in the hypsometry. To overcome this problem, a balance ratio (BR) method was developed by Furbish and Andrews (1984). This approach takes account of both glacier hypsometry and the shape of the mass-balance curve and is based on the fact that, for glaciers in equilibrium, the total annual accumulation above the ELA must balance the total annual ablation below the ELA. This can be expressed as the areas above and below the ELA multiplied by the average accumulation and ablation, respectively. The BR approach assumes that the accumulation and ablation gradients are approximately linear, that the ratio between the two is known, and that the hypsometry of the glacier is known. The BR method can thus only be used where detailed topographic maps are available and the surface contours of former glaciers can be reconstructed in detail (Benn and Gemmel, 1997). Because accumulation and ablation gradients are controlled by different climatic variables, the accumulation and ablation gradients generally have different values, with the ablation gradient somewhat steeper than the accumulation gradient. In a study of 22 glaciers in Alaska, Furbish and Andrews (1984) found that balance ratios clustered around 1.8, meaning that the ablation gradient is 1.8 times greater than the accumulation gradient.

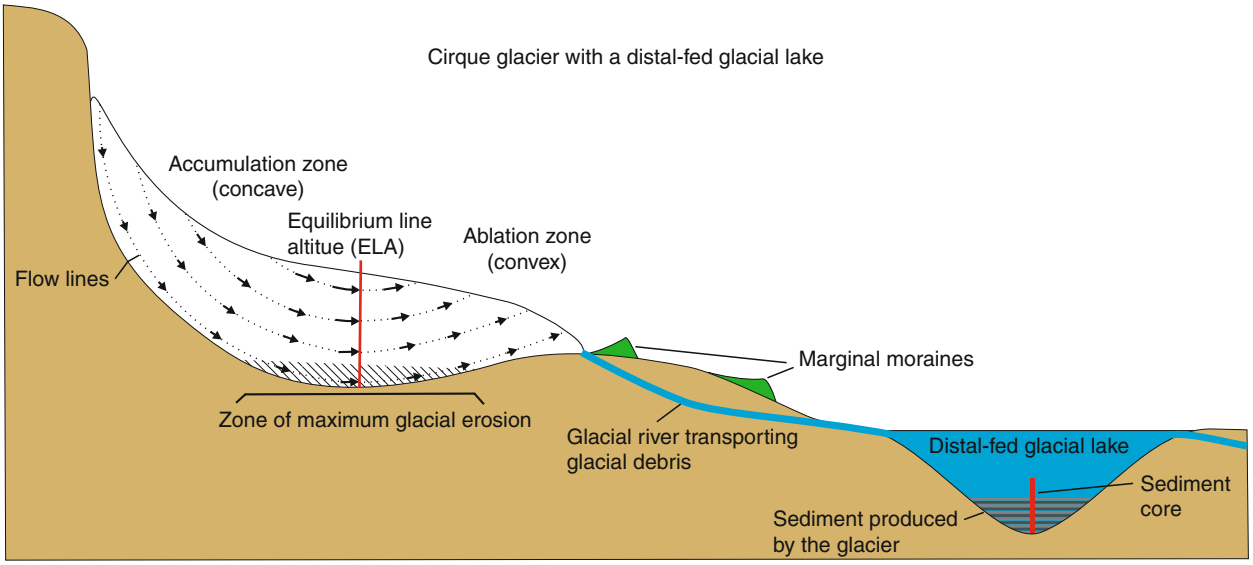

Equilibrium-Line Altitude (ELA), Figure 3 Erosion beneath the glacier produces "rock-flour," which is deposited in downstream proglacial lakes. Quantification of these sediments and later correlation between periods with known glacier size form the fundamentals for doing continuous reconstructions of the ELA in the past.

Benn and Gemmel (1997) published a spreadsheet program that rapidly calculates glacier ELAs using the balance ratio method that allows hypsometric variations to be accounted for in ELA reconstructions. Later another spreadsheet was made available for calculation of the Area-Altitude Balance Ratio (AABR) (Osmaston, 2005). These spreadsheets are becoming increasingly used in palaeoglacier reconstruction for estimating ELA and subsequently deriving quantitative estimates of palaeoclimate. However, there are still only a few studies that have established, from contemporary environments, AABR/BR ratios. Rea (2009) provides an empirically derived dataset characterizing AABR ratios, which may be used for ELA estimation in palaeoglacier reconstructions and for palaeoclimate quantification based on data from World Glacier Monitoring Service, US Geological Survey, and Norwegian Water Directorate.

Cirque floor altitudes

Cirque floor levels or altitudes have been used as indicators of the elevation of former glacier snowlines for Pleistocene glaciers. The elevation of the cirque floor/basin does not, however, have a close relationship with the ELA of the glacier that formed it (see Benn and Lehmkuhl, 2000). Cirques develop cumulatively over many glacial cycles and they can therefore not be attributed to any particular glacial event. They may, however, give some insight into regional trends in glaciation levels and average climatic conditions over longer time scales.

Proglacial sites

Several approaches have been applied to record past variations in ELAs based on lacustrine and terrestrial proglacial sites (Figure 3). These approaches are based on quantification of ELA fluctuations based on analyses of sediments deposited in distal glacier-fed lakes. Several groups worldwide have worked with this approach; here we give some examples from Scandinavian glaciers. Dahl et al. (2003) presented a conceptual model of glacier-meltwater-induced sedimentation in which a variety of proxies are related to the occurrence and size variations (as a response to variations in the ELA) of a glacier in a catchment. In order to quantify glacier reconstructions, it is necessary to validate that the sediments is of glacial origin (not from any mass movement or sub aquatic process) (Bakke et al., 2005b). This can be done by different sediment analyses such as grain-size variations, dry bulk density (DBD), magnetic properties, and X-ray (and XRF). When sediment DBD and glacier size based on the analyses have been established, the altitudinal position of the moraine can be used to calibrate the ELA curve by a correlation between ELA and DBD (Figure 4). The moraines need to be independently "dated" by the use of lichenometry and/or historical sources/or by exposure dating. Periods with anomalies in the sediment parameters are removed from the ELA reconstruction (open squares in Figure 4). The approach has been tested against a net-balance model in a lake downstream from the Folgefonna glacier in Norway. Tvede (1979) established some equations for modeling of the glacier mass balance (Bw/Bs and Bn) of Folgefonna based on temperature and precipitation from the Bergen-Florida meteorological station (station. no. 5054/56). The equation was later reformulated (Elvehøy, 1998) and established also for the northern part of Folgefonna:

$$B_n = 444 + 2.16^{*}P - 54^{*}T_3 \quad (1)$$

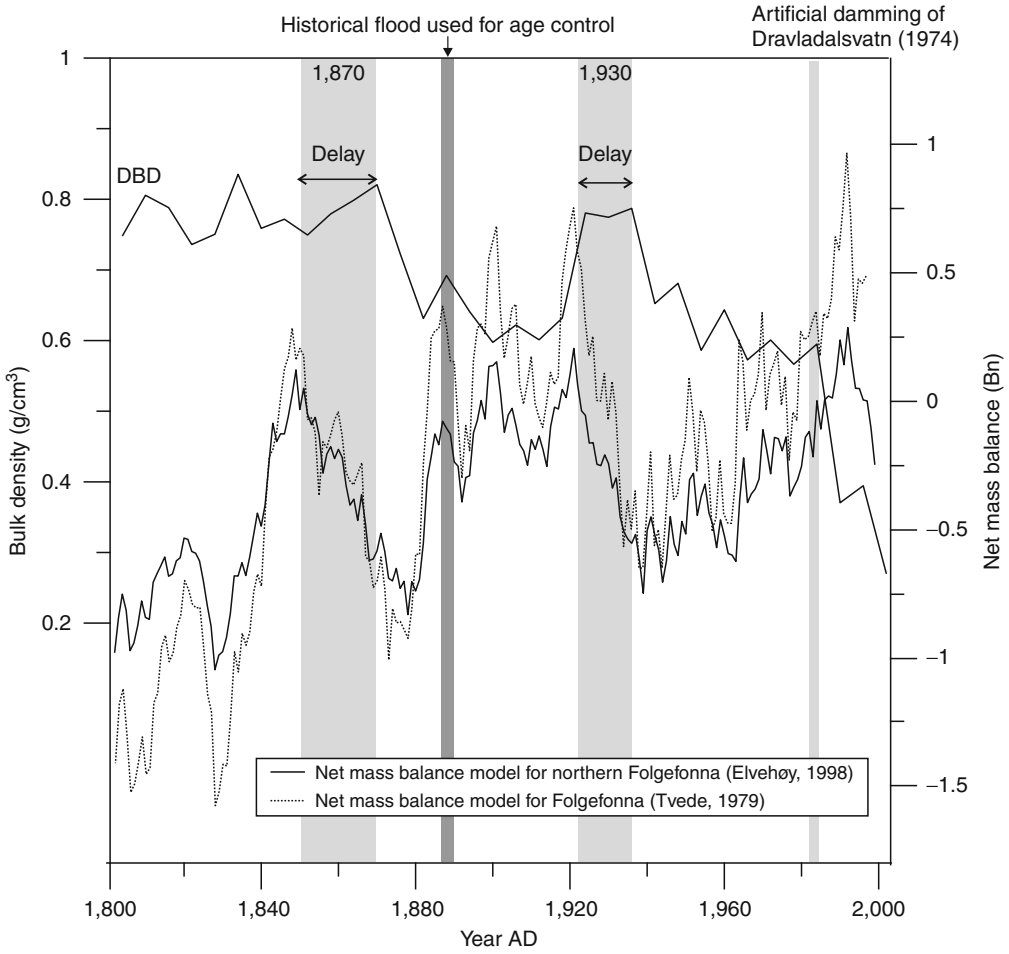

Equilibrium-Line Altitude (ELA), Figure 4 Dry bulk density (DBD) compared to two different glacier net mass-balance models for the Folgefonna and the northern Folgefonna glaciers. The dotted line shows a model developed by Tvede (1979) for the southern part of the Folgefonna glacier, whereas the black line was produced for northern Folgefonna in this study. Both models are compared with a glacier net mass-balance model and net-balance measurements from AD 1963 to 1997 (Elvehøy, 1998) at Folgefonna. The reconstruction is based on temperature and precipitation records from Bergen and Ullensvang (Birkeland, 1932). Thick gray-shaded areas indicate periods with moraine formation in front of the glacier (Bakke et al., 2005b).

where P is winter precipitation in Bergen (01.10–31.05) and T_3 is average summer temperature (01.06–31.08). The equation gives high predictability compared to the net mass balance from 1963 to 1997 ($r^2 = 0.84$). In the reconstruction, temperature and precipitation records from Bergen back to AD 1841 (data from Meteorological Institute) were put into the equation, whereas a temperature record from Ullensvang was used from AD 1800 to 1840 (Birkeland, 1932). As there is a lack of precipitation records for this time span, a linear regression model between the January, February, and March temperatures ($r = 0.6$) to reconstruct the winter precipitation was used. Both models reproduce the AD 1870 (late LIA) glacier advance and the AD 1930 glacier advances, which correspond to two independently dated terminal moraines. The low B_n values from AD 1800 to 1840 reflect the retreat of the glacier after the AD 1750 glacier event, and may explain the high DBD values during the time span (Figure 5). Based on the assumption that the age depth model is correct, another interesting feature is that there apparently exist lags in the bulk-density record with 10 years from a change in net balance to increased bulk-density values. This is suggested to reflect the frontal time lag time of the glacier to mass-balance perturbations.

ELA reconstructions – learning from the past

The use of proglacial lake sediments to reconstruct continuously ELA variations makes it possible to do high-resolution palaeoclimatic analyses. The quantification of sediment variability and better dating techniques make it possible to infer detailed information about the climatic factors affecting the ELA (accumulation and ablation).

In Scandinavia, this approach has been applied in many glaciated areas (Nesje and Dahl, 1991; Nesje et al., 1995;

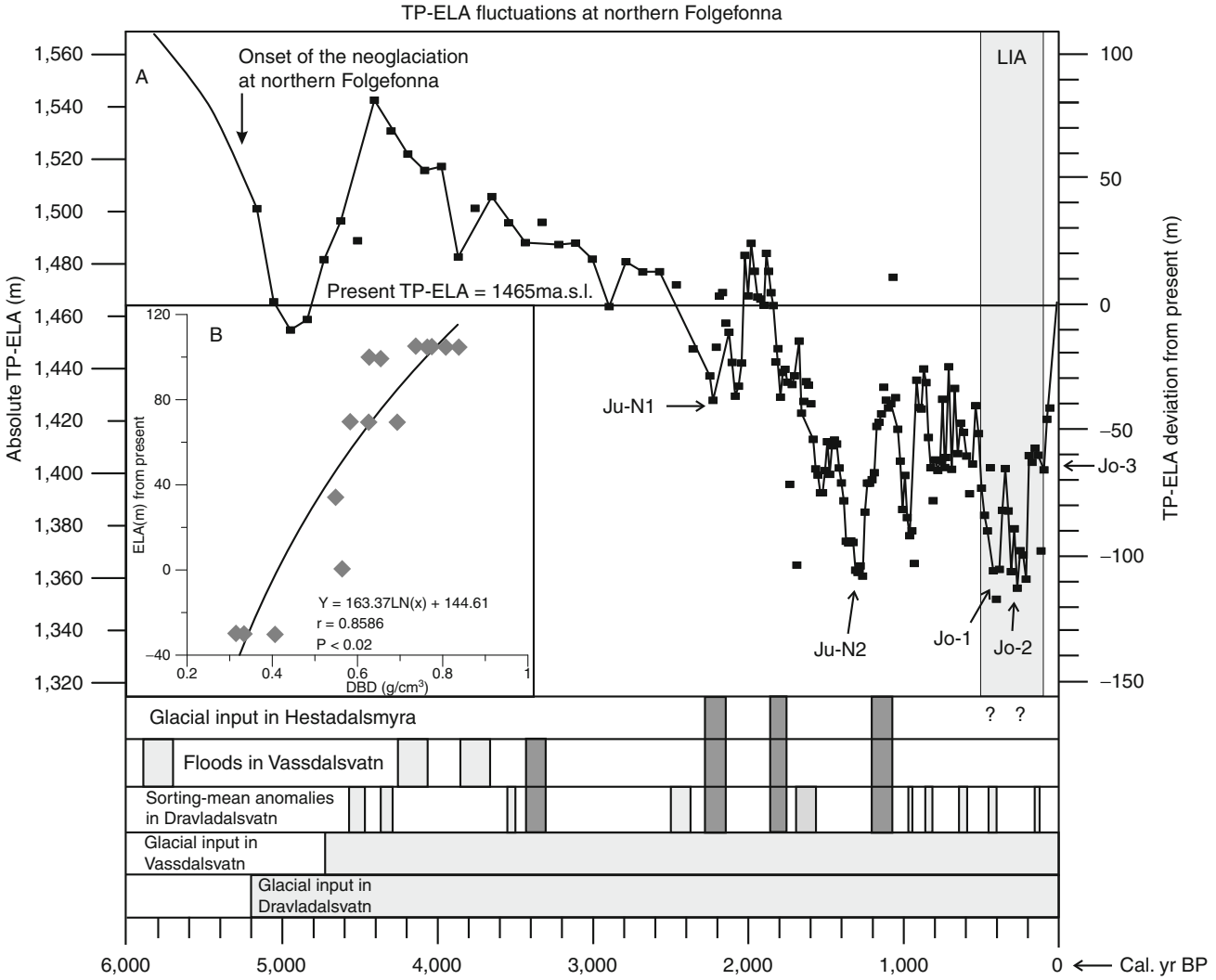

Equilibrium-Line Altitude (ELA), Figure 5 (**a**) TP-ELA curve for northern Folgefonna based on a record of bulk-density record. The lower part of the figure is a summary of sources for validating the ELA record; the peat bog in Hestadalsmyra, floods in Lake Vassdalsvatn, sorting anomalies in Dravladalsvatn, glacial input in Vassdalsvatn, and record of glacial input to Dravladalsvatn. (**b**) Regression between periods with known ELA (calibrated against the moraine chronology) and bulk-density values. The regression model is used to transfer the bulk-density record to a continuous TP-ELA curve (Bakke et al., 2005b).

Dahl and Nesje, 1996; Nesje et al., 2000; Nesje et al., 2001; Seierstad et al., 2002; Bakke et al., 2005a; Bakke et al., 2005b). The overall evolution of maritime glaciers along the western coast of Norway shows a gradual decrease in ELA from 5,200 cal. yr BP until after the termination of the "Little Ice Age." This pattern fits well with the general insolation curve for 65°N that may indicate a close linkage between glacier growth and solar orbital forcing at high latitudes during the late Holocene. Wetter conditions combined with lower summer insolation made the climate favuorable for glacier growth in Scandinavia, especially at maritime sites along the North Atlantic coast of Norway (e.g., Nesje et al., 2001). The linkage to solar insolation also makes it clear that the retreat of maritime glaciers along the entire western Scandinavia over the last century is unprecedented in the entire Neoglacial period spanning the last 5,200 years. Hence, this observation puts the reported glacier retreat in the twentieth century (Oerlemans, 2005) into a long-time western North Atlantic perspective as an anomaly. However, some of the most maritime glaciers in Southern Norway with short response time to climate have shown expansion during the latest decade of the last millennium with a retreat toward the present. This is proven to be a response to larger winter precipitation due to positive winter NAO during some years in the early 1990s (Nesje et al., 2005).

Summary

The equilibrium-line altitude (ELA) marks the area or zone on a glacier where accumulation is balanced by ablation

over a 1-year period. The ELA is sensitive to several meteorological factors, such as variations in winter precipitation, summer temperature, and wind transport of dry snow. When the annual net mass balance is negative, the ELA rises, and when the annual net mass balance is positive, the ELA falls. Fluctuations in the ELA provide an important indicator of glacier response to climate change that allows reconstructions of palaeoclimate (accumulation-season precipitation, ablation-season temperature, and prevailing snow-bearing wind directions). Palaeoclimatic reconstructions based on former glacier extent commonly include estimates of equilibrium-line altitudes (ELAs) and depression of ELAs from present values. Several methods have been developed to estimate steady-state ELAs of former glaciers as a tool to reconstruct palaeoclimates in glaciated regions. A survey of literature related to ELA depressions during the last glacial maximum, Younger Dryas, and the "Little Ice Age" shows lowerings from modern values in the order of 1,000 ± 300 m, 500 ± 200 m, and 100 ± 50 m, respectively. High-resolution reconstructions of ELA give valuable palaeoclimatic information from the terrestrial realm allowing comparison with other high-resolution archives, e.g., ice core and marine sediment records.

Bibliography

Bakke, J., Dahl, S. O., Paasche, O., Lovlie, R., and Nesje, A., 2005a. Glacier fluctuations, equilibrium-line altitudes and palaeoclimate in Lyngen, northern Norway, during the Lateglacial and Holocene. *Holocene*, **15**(4), 518–540.

Bakke, J., Lie, Ø., Nesje, A., Dahl, S. O., and Paasche, Ø., 2005b. Utilizing physical sediment variability in glacier-fed lakes for continous glacier reconstructions during the Holocene, northern Folgefonna, western Norway. *Holocene*, **15**(2), 161–176.

Ballantyne, C., 2006. The Loch Lomond Readvance on north Arran, Scotland: glacier reconstruction and palaoclomatic implications. *Journal of Quaternary Science*, **22**(4), 343–359.

Benn, D. I., and Ballantyne, C., 2005. Palaeoclimatic reconstruction from Loch Lomond Readvance glacier in the West Drumochter Hills. *Scotland Journal of Quaternary Science*, **20**(6), 577–592.

Benn, D. I., and Gemmel, A. M. D., 1997. Calculating equilibrium-line altitudes of former glaciers by the balance ratio method: a new computer spreadsheet. *Glacial Geology and Geomorphology*, http://ggg.qub.ac.uk/ggg/.

Benn, D. I., and Lehmkuhl, F., 2000. Mass balance and equilibrium-line altitudes of glaciers in high-mountain environments. *Quaternary International*, **65/66**, 15–29.

Birkeland, B. J., 1932. Altere meteorologische beobachtungen in Ullensvang, luftdruck und temperatur seit 100 Jahren Geofysiske publikasjoner IX (6), Det norske videnskaps-akademi i Oslo.

Braithwaite, R. J., and Olesen, O. B., 1990. A simple energy balance model to calculate ice ablation at the margin of the Greenland ice sheet. *Journal of Glaciology*, **36**, 222–228.

Budd, W. F., and Smith, I. N., 1981. The growth and retreat of ice sheets in response to orbital radiation changes. In Allison, I., (ed.), *Sea Level, Ice and Climatic Change*, Oxfordshire: IAHS Publication 131, pp. 369–409.

Dahl, S. O., and Nesje, A., 1992. Paleoclimatic implications based on equilibrium-line altitude depressions of reconstructed younger dryas and holocene cirque glaciers in inner Nordfjord, Western Norway. *Palaeogeography, Palaeoclimatology, Palaeoecology*, **94**(1–4), 87–97.

Dahl, S. O., and Nesje, A., 1996. A new approach to calculating Holocene winter precipitation by combining glacier equilibrium-line altitudes and pine-tree limits: a case study from Hardangerjokulen, central southern Norway. *Holocene*, **6**(4), 381–398.

Dahl, S. O., Nesje, A., and Øvstedal, J., 1997. Cirque glaciers as morphological evidence for a thin Younger Dryas ice sheet in east-central southern Norway. *Boreas*, **26**(3), 161–180.

Dahl, S. O., Bakke, J., Lie, Ø., and Nesje, A., 2003. Reconstruction of former glacier equilibrium-line altitudes based on proglacial sites: an evaluation of approaches and selection of sites. *Quaternary Science Reviews*, **22**, 275–287.

Elvehøy, H., 1998. Samanlikning av massebalanse på Hardangerjøkulen og Folgefonna. In Elvehøy, H. (ed.), *Oppdragsrapport*. Norway: Norges vassdrag-og energiverk, pp. 1–27.

Furbish, D. J., and Andrews, J. T., 1984. The use of hypsometry to indicate long-term stability and response to valley glaciers to changes in long-term stability and response of valley glaciers to changes in mass transfer. *Journal of Glaciology*, **30**, 199–211.

Gross, G., Kerschner, H., and Patzelt, G., 1976. Metodische Untersuchungen über die Schneegrenze in alpinen Gletschergebieten. *Zeitschrift für Gletscherkunde und Glazialgeologie*, **12**, 223–251.

Gruell, W., and Oerlemans, J., 1986. Sensitivity studies with a mass-balance model including temperature profile calculations inside the glacier. *Zeitschrift für Gletscherkunde und Glazialgeologie*, **22**, 101–124.

Kuhn, M., 1989. The response of the equilibrium line altitude to climate fluctuations: theory and observations. In Oerlemans, J. (ed.), *Glacier Fluctuations and Climate Change*. Dordrecht: Kluwer, pp. 407–417.

Laumann, T., and Reeh, N., 1993. Sensitivity to climate change of the mass balance of glaciers in southern Norway. *Journal of Glaciology*, **39**, 656–665.

Lehmkuhl, F., 1998. Quaterary glaciations in central and western Mongolia. *Quaternary Proceedings*, **6**, 153–167.

Lehmkuhl, F., Owen, L. A., and Derbyshire, E., 1998. Late Quaternary glaciel history of Northeast Tibet. *Quaternary Proceedings*, **6**, 121–142.

Leonard, E. M., 1985. Glaciological and climatic controls on lake sedimentation, Canadian Rocky Mountains. *Zeitscrift für Gletcherkunde und Glazialgeologie* **21**, 35–42.

Letreguilly, A., and Reynaud, L., 1989. Spatial patterns of mass balance fluctuations of North American glaciers. *Journal of Glaciology*, **35**, 163–168.

Lie, Ø., Dahl, S. O., and Nesje, A., 2003. Theoretical equilibrium-line altitudes and glacier buildup sensitivity in southern Norway based on meteorological data in a geographical information system. *Holocene*, **13**, 373–380.

Liestøl, O., 1967. *Storbreen glacier in Jotunheimen*. Norway: Norsk Polarinstitutt Skrifter 141.

Louis, H., 1955. Schneegrenze und Schneegrenzbestimmung. *Geographisches Taschenbuch* 1954/55, pp. 414–418.

Maisch, M., 1982. Zur Gletscher- und Klimageschichte des alpinen Spätglazials. *Geographica Helvetica*, **37**, 93–904.

Meierding, T. C., 1982. Late Pleistocene glacial equilibrium-line in the Colorado front range, A comparison of methods. *Quaternary Research*, **18**, 289–310.

Miller, G. H., Bradley, R. S., and Andrews, J. T., 1975. The glaciation level and lowest equilibrium line altitude in the high Canadian Arctic: maps and climatic interpretation. *Arctic and Alpine Research*, **7**, 155–168.

Nesje, A., and Dahl, S. O., 1991. Holocene glacier variations of Blaisen, Hardangerjokulen, Central Southern Norway. *Quaternary Research*, **35**(1), 25–40.

Nesje, A., and Dahl, S. O., 2000. *Glaciers and Environmental Change*. London: Arnold.
Nesje, A., Dahl, S. O., and Lovlie, R., 1995. Late Holocene glaciers and avalanche activity in the Alfotbreen area, Western Norway – Evidence from a Lacustrine Sedimentary Record. *Norsk Geologisk Tidsskrift*, **75**(2–3), 120–126.
Nesje, A., Dahl, S. O., Andersson, C., and Matthews, J. A., 2000. The lacustrine sedimentary sequence in Sygneskardvatnet, western Norway: a continuous, high-resolution record of the Jostedalsbreen ice cap during the Holocene. *Quaternary Science Reviews*, **19**(11), 1047–1065.
Nesje, A., Matthews, J. A., Dahl, S. O., Berrisford, M. S., and Andersson, C., 2001. Holocene glacier fluctuations of Flatebreen and winter-precipitation changes in the Jostedalsbreen region, western Norway, based on glaciolacustrine sediment records. *Holocene*, **11**(3), 267–280.
Nesje, A., Jansen, E., Birks, H. J. B., Bjune, A., Bakke, J., Dahl, C. A., Dahl, S. O., Kiltgaard-Kristensen, D., Lauritzen, S. E., Lie, Ø., Risebrobakken, B., and Svendsen, J. I., 2005. Holocene climate variability in the northern North Atlantic region: a review of terrestrial and marine evidence. In Drange, H., Dokken, T., Furevik, T., Rüdiger, G., and Bergen, W., (eds.), *The Nordic Seas: An Integrated Perspective*, Geophysical Monograph Series, American Geophysical Union, Washington, 158, pp. 289–322.
Oerlemans, J., 2001. Glaciers and climate change: a meteorologist's view. Rotterdam: A.A. Balkema.
Oerlemans, J., 2005. Extracting a climate signal from 169 glacier records. *Science*, **308**(5722), 675–677.
Ohmura, A., Kasser, P., and Funk, M., 1992. Climate at the equilibrium line of glaciers. *Journal of Glaciology*, **38**, 397–411.
Osmaston, H., 2005. Estimates of glacier equilibrium line altitudes by the area x altitude, the area x altitude balance ratio and the area x altitude balance index methods and their validation. *Quaternary International*, **138**, 22–31.
Paterson, W. S. B., 1994. *The physics of glaciers*. Oxford: Pergamon.
Porter, S. C., 1975. Equilibrium line altitudes of late quaternary glaciers in the Southern Alps, New Zealand. *Quaterary Research*, **5**, 27–47.
Porter, S. C., Pierce, K. L., and Hamilton, T. D., 1983. Late Pleistocene glaciation in the western United States. In Porter, S. C., (ed.), *Late Quaternary Environments in the United States*. Minneapolis: University of Minnesota Press, pp. 71–111.
Rea, B. R., 2009. Defining modern day area-altitude balance ratios (AABRs) and their use in glacier-climate reconstructions. *Quaternary Science Reviews*, **28**(3–4), 237–248.
Reeh, N., 1991. Parameterization of melt rate and surface temperature on the Greenland ice sheet. *Polarforschung*, **59**, 113–128.
Schytt, V., 1967. A study of "ablation gradient". *Geografiska Annaler*, **49A**, 327–332.
Seierstad, J., Nesje, A., Dahl, S. O., and Simonsen, J. R., 2002. Holocene glacier fluctuations of Grovabreen and Holocene snow-avalanche activity reconstructed from lake sediments in Groningstolsvatnet, Western Norway. *Holocene*, **12**(2), 211–222.
Shi, Y., Zheng, B., and Li, S., 1992. Last glaciation and maximum glaciation in the Qinghai-Xizang (Tibet) Plateau: a controversy to M. Kuhle's ice sheet hypothesis. *Zeitschrift für Geomorphologie*, B.F. (Suppl) 84, 19–35.
Sissons, J. B., 1979. The loch lomond stadial in the British Isles. *Nature*, **280**, 199–203.
Torsnes, I., Rye, N., and Nesje, A., 1993. Modern and little ice age equilibrium-line altitudes on outlet valley glaciers from Jostedalsbreen, Western Norway: an evaluation of different approaches to their calculation. *Arctic and Alpine Research*, **25**, 106–116.
Tvede, A. M., 1979. Likninger til beregning av nettobalansen fra værdata. In Wold, B., and Repp, K. (eds.), *Glasiologiske undersøkelser i Norge 1978*, Norway: Norges Vassdrags og elektrisitetsvesen, p. 71.

Cross-references

Alps
Calving Glaciers
Cirque Glaciers
Climate Change and Glaciers
Debris-Covered Glaciers
Dynamics of Glaciers
Proglacial Lakes
Retreat/Advance of Glaciers
Temperature Lapse Rates in Glacierized Basins

EROSION OF HARD ROCK BED

D. P. Dobhal
Wadia Institute of Himalayan Geology, Dehradun, Uttarakhand, India

Definition

As the river passes over the hard rock bed, it scours rock. The continuous scouring of the rock produces a vertical drop in the river channel. It behaves like the waterfall. The energy of the falling water will continue to erode the bed of the river so that eventually a plunge pool will develop at the base of the waterfall. The plunge pool develops initially because the force of the falling water creates a slightly deeper pool in the bed of the river. As the rivers' bed load falls into the pool it swirls and scours the base of the pool causing it to deepen.

EROSION RATE

Subhajit Sinha
DBS College, Dehradun, Uttarakhand, India

Definition

Sedimentation is the process by which material is deposited from the water column to the bed. Conversely, erosion occurs when material is removed. A long-term (say more than 30 years) average annual erosion rate is the average amount of erosion that occurs from a watershed or study area. The sedimentation/erosion rate in waterways is naturally variable because of the variability in natural processes influencing it such as water-current/flow patterns, climate (rainfall, seasonality), geology, slope (or topography), etc. Human activity (e.g., dredging, impoundments, hydrodynamic alterations, land clearing, etc.) may also result in changes to sedimentation/erosion rates. Increased sedimentation/erosion rates can result in important changes to the form and function of waterways. For example, they may cause changed shoreline and mudflats

area, channel infilling, habitat/benthic community smothering or removal, community composition changes, increased turbidity levels, and the burial or re-suspension of nutrients, trace elements, toxicants, and organic matter. In general erosion rate from the active glaciers is very high.

ESTIMATION OF GLACIER VOLUME AND VOLUME CHANGE BY SCALING METHODS

David B. Bahr
Department of Physics and Computational Science, Regis University, Denver, CO, USA

Definition

Scaling relationship. A power-law exponential equation that relates two quantities such as volume and area.

Estimating volume

Glacier volume V can be estimated from the glacier surface area A using the scaling relationship

$$V = kA^{\gamma} \quad (1)$$

where γ and k are derived from either data or theory (Figure 1). Typical values are $\gamma = 1.36$ and $k = 0.033$ km$^{3-2\gamma}$ for valley glaciers (Macheret et al., 1988; Chen and Ohmura, 1990; Bahr et al., 1997; Bahr, 1997). In many cases, measurements of the glacier volume would be preferable, but this has been done for relatively few glaciers (less than 200), and generally cannot be accomplished without considerable time or expense. The most common measurement technique uses ground-penetrating radar (see entry "*Ground Penetrating Radar Measurements Over Glaciers*"), but with crevasses and inaccessible terrain, hundreds of thousands of glaciers cannot be practically measured using this approach.

In contrast, a scaled estimate like Equation 1 uses a power law to relate an easily measured quantity like surface area to a difficult to measure property like volume. Other power-law scaling relationships involving glacier length, thickness, width, and various quantities have been derived from both theory and data. For example, surface velocity scales with thickness and therefore volume (Bahr, 1997). Many of these power laws can be used to estimate volume (Radic et al., 2008), but glacier area is one of the easiest quantities to measure, and abundant area data have made Equation 1 the most common volume-scaling relationship.

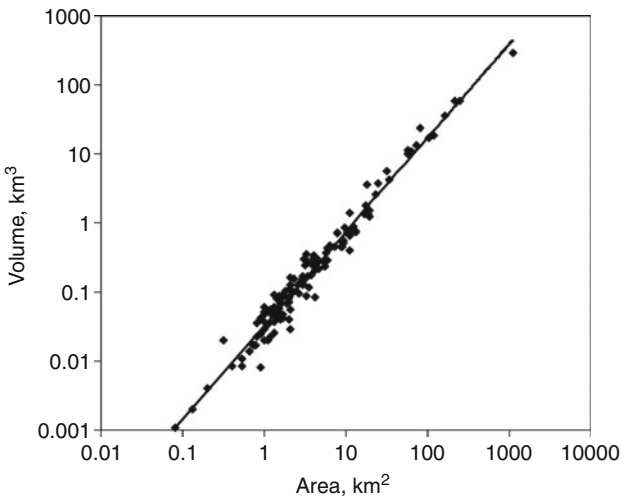

Estimation of Glacier Volume and Volume Change by Scaling Methods, Figure 1 On a log-log plot, glacier area and volume scale linearly. For this set of 144 temperate valley glaciers from around the world, $V = 0.033\ A^{1.36}$ with a squared correlation coefficient of $R^2 = 0.97$. Data are available on request.

Deriving volume–area scaling

The principle of volume–area scaling can be illustrated with a box (Figure 2). Given the surface area A of a square box, we can calculate the length, width, and depth as the square root of the area, $A^{1/2}$. The volume V of the box becomes the cube of the length or $V = A^{3/2}$. Therefore, for a box, the volume–area scaling exponent is 3/2. Similarly, the volume of a glacier is related to its area by a somewhat smaller exponent that reflects a glacier's more elongated shape caused by flowing ice. In this case, the volume–area scaling exponent can be derived directly from the equations of glacier flow.

Glacier flow is described by mass and momentum conservation along with a constitutive relationship that relates deviatoric stresses to strain rates, most commonly Glen's flow law or a similar modification (see entry "*Dynamics of Glaciers*"). Mass conservation (or mass balance) leads to the continuity equation (see entry "*Glacier Mass Balance*"). Momentum conservation leads to the force balance equations (see entry "*Dynamics of Glaciers*"). To derive scaling

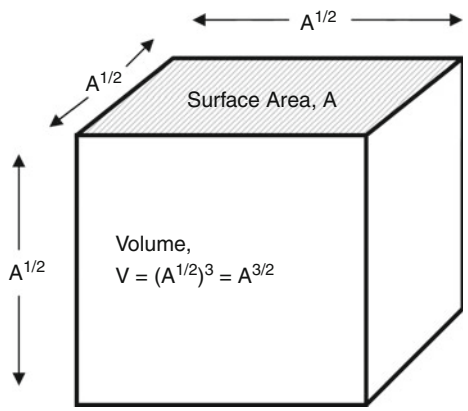

Estimation of Glacier Volume and Volume Change by Scaling Methods, Figure 2 The volume of a box can be derived from its surface area, similar to a glacier.

relationships, each physical quantity in these equations can be rescaled by multiplying by a constant factor. This leads to the stretching symmetries of the differential equations (Bahr and Rundle, 1995).

For example, horizontal velocity v can be stretched or rescaled as $v_{\text{stretched}} = \lambda^a v$, where λ^a is a constant. Similarly, thickness h can be rescaled as $h_{\text{stretched}} = \lambda^b h$ where λ^b is another constant. Length x can be rescaled as $x_{\text{stretched}} = \lambda^c x$. Mass balance rate $\dot{b}$ can be rescaled as $\dot{b}_{\text{stretched}} = \lambda^d \dot{b}$, and so on with stretching constants applied to each variable. Substituting these stretched quantities into the original equations and factoring out λ gives a set of relationships between the exponents a, b, c, d. In other words, if the length of the glacier is stretched by a certain amount, then the thickness (and other quantities) will have to be stretched by another specified amount to maintain consistency within the equations.

These stretching relationships give nondimensional numbers for glaciers that are analogous to Reynolds, Froude, and other quantities from the linear-viscous Navier–Stokes equations. For example, the nondimensional number arising from the continuity equation is

$$\frac{\dot{b}\,x}{vh} = C \tag{2}$$

for some constant C. Equivalently by rewriting, $\dot{b}\,x \propto vh$, and we see that this nondimensional number relates two well-known quantities that describe the response time of glaciers (Jóhannesson et al., 1989).

By combining Equation 2 with other nondimensional numbers from force balance and the constitutive relationship, we can relate volume to surface area as in Equation 1 (Bahr et al., 1997; Bahr, 1997). The scaling exponent γ becomes a function of the flow law exponent n and the slope. For $n = 3$ and shallow slopes like ice caps, $\gamma = 1.25$. For $n = 3$ and steeper slopes, $\gamma = 1.375$. These values are in notable agreement with available data which suggest values of ~1.22 for ice caps (Meier and Bahr, 1996) and ~1.36 for glaciers (Bahr et al., 1997).

The scaling constant k is derived as a combination of the nondimensional numbers like C in Equation 2 (using the same combination of nondimensional numbers that produce the volume–area scaling relationship). Just like rivers which can have different Reynolds numbers depending on the amount of turbulence, every glacier can have a unique set of nondimensional numbers associated with its dynamics. However, unlike rivers, most glaciers have relatively similar flow regimes. So while rivers can have both high and low Reynolds numbers (indicating turbulent flow versus laminar flow), most glaciers will have similar nondimensional numbers and therefore similar scaling constants. Data suggests that the volume–area scaling constant has a well-defined normal distribution with a mean value of 0.034 $\text{km}^{3-2\gamma}$ and a standard deviation of 0.013 when volume and area are measured in kilometers (Bahr, 1997). A value of 0.12 $\text{m}^{3-2\gamma}$ has also been derived by assuming a total worldwide volume of ice and tuning the scaling relationship accordingly (Van de Wal and Wild, 2001).

Limitations of volume scaling

When applied to a single glacier, volume–area scaling should be treated as a reasonable but low-order approximation. Any single glacier is expected to fall along the power-law curve but may deviate slightly as illustrated in Figure 1. As discussed above for nondimensional numbers, the volume has a distribution of possible values with the mean falling on the volume–area curve. For linear regressions on a log-log plot, the standard deviations for large glaciers are more pronounced than deviations for small glaciers.

Volume–area scaling works most accurately when applied to large sets of glaciers. Errors that overestimate one glacier will be offset by errors that underestimate another glacier. For example, the total volume summed from many glaciers will be more accurate than the volume estimate of any single glacier (Bahr et al., 2009). The number of glaciers necessary for a sufficiently large set is a statistical question and depends in part on the quality of the data as well as sampling biases such as preferentially choosing larger glaciers over smaller glaciers. However, as seen in Figure 1, an order of magnitude of 100 glaciers appears sufficient and in many applications far fewer glaciers may be reasonable.

Although published examples exist, volume–area scaling cannot be applied to parts or subsections of a glacier. The stretching relationships and nondimensional numbers are derived from the equations for the entire glacier. As an example, consider a box again with the scaling relationship $V = A^{3/2}$ (Figure 1). If the square surface A of the box is subdivided by a grid into nine equally sized smaller squares (Figure 3), then each smaller part has a length that is one-third of the original and has an area that is one-ninth of the original. Using the scaling relationship, the volume

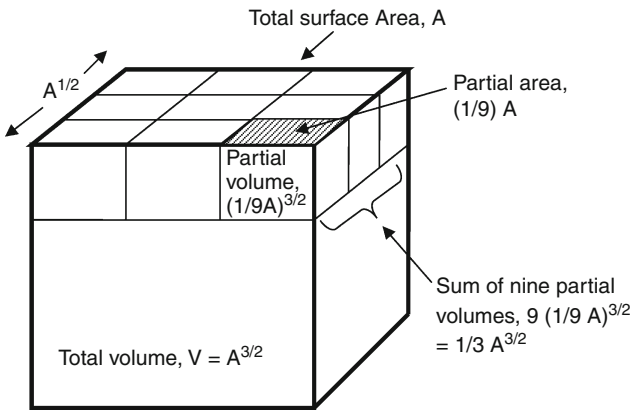

Estimation of Glacier Volume and Volume Change by Scaling Methods, Figure 3 Volume–area scaling cannot be applied to subsections of a glacier. As illustrated with a box, subdividing the surface into nine parts and then applying scaling will give a fraction of the correct total volume.

of each smaller part will be 1/27 the original. If we add up all nine subsections, the total volume will be only one-third of the correct volume. Although the scaling exponent is different for glaciers, using subsections of a glacier would result in similar underestimates of the volume. Only linear scaling relationships with an exponent of 1.0 can be subdivided in this manner.

Estimating volume changes

The derivation of stretching symmetries does not assume steady-state conditions, and volume–area scaling can be used to analyze changing volume with time. A number of numerical simulations have tested the accuracy and demonstrated the application of scaling to changes in volume in both steady-state and non-steady-state conditions (Pfeffer et al., 1998; Church et al., 2001; Van de Wal and Wild, 2001; Radic et al., 2008). In a straightforward approach, a derivative of Equation 1 gives

$$\partial V = k\gamma A^{\gamma-1}\partial A \tag{3}$$

In other words, a change in the volume can be estimated from the original area as well as the subsequent change in the area. However, Equation 3 is only exact for the infinitesimal changes for which the derivative is calculated. As the change in area grows large, Equation 3 will become a poor estimate, and an integration of small changes will be necessary.

Alternatively, finite changes in area can be used. From Equation 1,

$$V + \Delta V = k(A + \Delta A)^{\gamma} \tag{4}$$

where ΔV is a finite change in volume caused by a finite change in area ΔA. Dividing by the volume gives

$$(1 + p_v) = (1 + p_A)^{\gamma} \tag{5}$$

where $p_v = \Delta V/V$ and $p_A = \Delta A/A$ are the fractional changes in volume and area (Bahr et al., 2009). Equation 5 will work well for glaciers affected by climate change, most of which have experienced large fractional changes in area. Conveniently, the scaling constant k is not necessary when estimating fractional changes in volume from Equation 5. This eliminates a potential source of measurement error.

The change in area necessary for a glacier to reach equilibrium with the current climate (where the glacier is neither gaining nor losing mass) can be estimated from its accumulation-area ratio, *AAR*. Using the relationship between *AAR* and glacier surface areas,

$$p_A = AAR/AAR_0 \tag{6}$$

where AAR_0 is the glacier's accumulation-area ratio when in equilibrium (Bahr et al., 2009). Data show that the worldwide average AAR_0 is 0.57 ± 0.01. Consequently, a volume change to AAR scaling relationship is derived by combining Equations 5 and 6, and the fractional change in volume p_v is easily estimated from the glacier's current accumulation-area ratio. The total change in glacier volume is just $p_v V$. By summing $p_v V$ over all glaciers, estimates of glacier meltwater contributions to sea-level rise are possible.

Summary

While difficult to measure directly, glacier volume can be more easily approximated by measuring surface area and applying a power-law scaling relationship. The volume–area scaling relationship has been predicted and well established from field data, theory, and numerical modeling. As a glacier changes size, the consequent changes in glacier volume also can be estimated and predicted by derivations from the same volume–area relationship. Summing such changes over all the world's glaciers gives a convenient measure of global changes in sea level.

Bibliography

Bahr, D. B., 1997. Global distributions of glacier properties: a stochastic scaling paradigm. *Water Resources Research*, **33**, 1669–1679.

Bahr, D. B., and Rundle, J. B., 1995. Theory of lattice Boltzmann simulations of glacier flow. *Journal of Glaciology*, **41**, 634–640.

Bahr, D. B., Meier, M. F., and Peckham, S., 1997. The physical basis of glacier volume-area scaling. *Journal of Geophysical Research*, **102**(B9), 20355–20362.

Bahr, D. B., Dyurgerov, M., and Meier, M. F., 2009. Sea-level rise from glaciers and ice caps: a lower bound. *Geophysical Research Letters*, **36**, L03501, doi:10.1029/2008GL036309.

Chen, J., and Ohmura, A., 1990. Estimation of alpine glacier water resources and their change since the 1870s. *International Association of Hydrological Sciences Publications*, **193**, 127–135.

Church, J. A., et al., 2001. Changes in sea level. In Houghton, J. T., et al. (eds.), *Climate change 2001: the scientific basis. Contribution of Working Group I to the Third Assessment Report of the Intergovernmental Panel on Climate Change*. Cambridge: Cambridge University Press, pp. 639–693.

Jóhannesson, T., Raymond, C., and Waddington, E., 1989. Time-scale for adjustment of glaciers to changes in mass balance. *Journal of Glaciology*, **35**, 355–369.

Macheret, Y. Y., Cherkasov, P. A., and Bobrova, L. I., 1988. Tolschina I ob'em lednikov Djungarskogo Alatau po danniy arororadiozondirovaniya. *Materialy Glyatsiologicheskikh Issledovaniy, Khronika Obsuzhdeniya*, **62**, 59–71.

Meier, M. F., and Bahr, D. B., 1996. Counting glaciers: use of scaling methods to estimate the number and size distribution of the glaciers of the world. *CRREL Special Reports*, **96–27**, 89–94.

Pfeffer, W. T., Bahr, D. B., and Sassolas, C., 1998. Response time of glaciers as a function of size and mass balance: II. Numerical experiments. *Journal of Geophysical Research*, **103**(B5), 9783–9789.

Radic, V., Hock, R., and Oerlemans, J., 2008. Analysis of scaling methods in deriving future volume evolutions of valley glaciers. *Journal of Glaciology*, **54**, 601–612.

Van de Wal, R. S. W., and Wild, M., 2001. Modelling the response of glaciers to climate change by applying volume-area scaling in combination with a high resolution GCM. *Climate Dynamics*, **18**, 359–366.

Cross-references

Dynamics of Glaciers
Glacier Mass Balance
Ground Penetrating Radar Measurements Over Glaciers
Sea-Level

ESTUARY ICE COVER

Brian Morse
Departement of Civil and Water Engineering, Laval University, Quebec, QC, Canada

What is an estuary?

An estuary is a semi-enclosed coastal body of water (Figure 1). The downstream limit is where seawater is measurably diluted by fresh river water. Its upper boundary extends as far as tidal effects are felt. Often, the interpretation of the estuary's limits will depend on the phenomena of interest. For example, some may use a narrow interpretation such as the brackish zone near the mouth of a river. Others may use biological markers that could well extend up into the zone where the water is always fresh but where the tidal signal is still important for flora in shallow zones. If regional processes are of interest, then the definition can cover areas as large as the Arctic Ocean (Macdonald, 2000) since most of the saltwater within it is indeed diluted by the many rivers entering it. Therefore, the working definition of an estuary depends, to a certain extent, on the phenomenon of interest. The important element of an estuary is that there is a mix (to a greater or lesser extent) of sea- and land-based processes.

Estuary classification

Estuaries may be classified according to their geographical location (e.g., Arctic; Sub-Arctic; Continental; etc.); their overall aspect (Archipelago; Delta; Bay; Sound; Fjord; Lake; Gulf; etc.); their size; their shape (e.g., narrow; open; funnel); their depth; their direction of flow (northerly, etc.); their source of freshwater: glacier (fjord) or river (ria); their geological origin (sea level rise; sediment deposition; etc.); their tidal amplitude (macrotidal; mesotidal, or microtidal); the fresh/saltwater mix profile (salt wedge, partially mixed, well mixed, or frozen); the longitudinal salinity gradient (positive or negative); as polluted or pristine; as healthy, recovering or sick; as productive or dead; as urban or natural; and, of course, as ice-covered or not.

River and sea dynamics

All these characterizations are useful and necessary to help describe and understand particular phenomena of interest. Another viewpoint that can help understand estuaries is to view them as battle zones of competing forces and processes. From the watershed, the river enters an estuary and must fully succeed in transporting into it, its load of water, sediment, suspended particulates, dissolved gases, nutrients, fish, mammals, plants, and pollutants. At the downstream end, the sea enters the estuary and must accept the river's load but not, however, without imposing its own characteristics. The sea's saltwater is heavier than freshwater, its temperature is normally very different than the river's, its point of fusion is suppressed (typically $-1.9°C$ for fully saline water); and as the brackish water travels upstream, it does so with the erosive force of its waves, currents and most importantly, its tides. Seawater comes with its own chemistry, fish, plants, mammals, nutrients, and purity or pollutants. The river and the sea battle for physical, chemical, and biological dominance; the river wins mostly in the upstream reaches while the sea wins mostly in downstream flats. In the middle is a unique habitat where

Estuary Ice Cover, Figure 1 Ice on the tidal flats of the St. Lawrence Fluvial Estuary at Quebec City, Canada. February 12, 2010 (W. Boone with permission).

the plants, fish, and birds present there can adapt to rapidly changing salinity, water levels, waves, and currents.

The two bodies of water (fresh and saline) are normally totally out of sync with each other and therefore the fight between river and sea is somewhat cyclical. The timing and intensity of the river's transport is dictated by processes dependent on the river's characteristics and on its watershed size, relief, shape, aspect, content, anthropogenic activity, climate, season and weather. Seawater is governed by longer term weather patterns, changes in ocean currents and salt content; the wave intensity is due to large weather systems, storm surges, and tides that are dictated by the earth's rotation and the relative position of heavenly bodies (i.e., moon and sun) having nothing to do with land-based dynamics.

Atmospheric dynamics

The third actor on the battle field could be described as the atmosphere whose characteristics include humidity; precipitation (rain, snow); wind (speed and direction); airborne particles (inert, organic, living spores, and pollutants); incoming radiation (short and long wave); insects, and birds. The estuary has no choice but to adapt itself to these inputs.

Anthropogenic influence

The fourth influence is comprised of human interactions with the estuaries and includes shore protection; channel dredging; harbor construction; river training; wetland infilling; thermal additions (e.g., thermal plumes from power plants); fishing and overfishing; exotic species invasions; oxygen depletion (by pollution and excess nutrients); and oil, nuclear, and toxic spills, ice management, and ice-breaking activities.

The spatial nature of the estuary and ice

The spatial extent is sculpted by the relative strengths of river's discharge, the atmosphere's wind, the anthropogenic activities, and the sea's tide. On the flip side, the estuary's spatial character will highly influence the nature of the interactions, providing a relative advantage to one over the other and will therefore dictate how the four actors interact. The estuary physical space is defined by its geographical location; size; width; length; shape; orientation; bathymetry; the presence or absence of islands; the extent of its shelf; sediment size; vegetative cover, and the presence of ice in all its many forms.

The ice cover as a barrier between water and atmosphere

The presence of an ice cover dramatically changes the nature of the battlefield and may go so far as to absolutely change the character of an estuary (if only seasonally). An ice cover normally reduces mixing (leading to stabilization and stratification of the water column) because it provides a barrier between the wind and water diminishing the strength of the sea waves, longshore currents, and Ekman flows. The cover arrests light penetration affecting plant growth and fish dynamics. It limits heat and mass transfer (modifying evaporation rates and protecting tidal flat animals from freezing). It cuts off airborne particles drastically reducing sediment transport, limiting reoxygenation and other gaseous exchanges. The cover is a physical barrier forcing sea mammals to come up through ice holes to breathe and preventing ships from navigating. It offers a platform providing support for bears to fish upon; to support people and animals to traverse; to enable caribou to find salt and to enable wolves to attack animals upon.

The ice cover as a barrier between fresh- and saltwater

The ice cover can also be a pathway or a barrier between fresh- and saltwater that can damp tidal amplitudes (e.g., the presence of sea ice formed over the greater Canadian Archipelago reduces James Bay tidal amplitudes from 1.5 m in summer to 1.0 m in winter at the inlet to La Grande River). The ice sheet can provide conditions allowing large freshwater penetration under the ice into the sea in Russian Arctic estuaries and those of Eastern Hudson's Bay. At the edge of the cover, a ridge can be built up into a deep (>20 m) ridge. Virtually all of the Mackenzie's winter flow (0.3 m tide) is stored locally behind this barrier in a unique vertically and longitudinally stratified system known as a "winter" estuary (Macdonald, 2000). It is then released in sync with the spring freshet providing a dramatic freshwater pulse to the Beaufort Sea. In the case of the mesotidal Churchill Estuary (3.3–4.2 m tide), the ridge's role only delays the outpouring of the freshwater into the Western Hudson's Bay by a few days but ice is still the dominant feature of the estuary that highly influences physical and biological processes: "Until late May, the rubble zone partially impounded river discharge, influencing the surface salinity, stratification, flushing time, and distribution and abundance of nutrients in the estuary. The river discharge, in turn, advanced and enhanced sea ice ablation in the estuary by delivering sensible heat. Weak stratification, the supply of riverine nitrogen and silicate, and a relatively long flushing time (6 days) in the period preceding melt may have briefly favored phytoplankton production in the estuary when conditions were still poor in the surrounding coastal environment. However, in late May, the peak flow and breakdown of the ice-rubble zone around the estuary brought abrupt changes, including increased stratification and turbidity, reduced marine and freshwater nutrient supply, a shorter flushing time, and the release of the freshwater pool into the interior ocean. These conditions suppressed phytoplankton productivity while enhancing the inventory of particulate organic matter delivered by the river. The physical and biological changes observed in this study highlight the variability and instability of small frozen estuaries during winter/spring transition, which implies sensitivity to climate change" (Kuzyk et al., 2008).

Ice impact on the physical boundaries

An ice cover and the presence of grounded ice on tidal flats reduce the spatial boundaries of an estuary. In macrotidal estuaries (e.g., Bay of Fundy, Canada (16 m tide)), estuary ice can reach very significant thickness on the tidal flats. In a matter of days, the 5-m-thick stranded ice accumulated on the Petitcodiac Estuary's tidal flats forms "ice walls" that change the channel's trapezoidal shape (with side walls 1 V to 3.5 H) into a rectangular shape (Desplanque and Bray, 1986). As such, the tidal prism and associated flow rates are substantially reduced. In the 5.9-km long mesotidal Portneuf Estuary, Canada, no tidal walls were noted but nevertheless, the midwinter fast ice cover (0.5 m thick), through the combined effects of change in bathymetry and increased wetted perimeter, attenuates the neap tidal range (1.9 m) and spring tidal range (4.0 m) by 17% and 37%, respectively, near the upstream end of the estuary. The arrival of low water is also delayed by about 1.5 h. At the mouth, the cover attenuates the peak ebb tide flow (200 m^3/s) and flood tide flow (500 m^3/s) by approximately 18% and 13% (the river's winter discharge is 20 m^3/s). In general, the ice cover attenuates peak velocities by 12% to 20%, although at certain times and locations, its presence could increase velocities. The ice cover also retards and diminishes the salt wedge intrusion (Morse et al., 2006).

Ice as a barrier between water forces and sediment transport

Bottom fast ice can protect permafrost and can help shape the estuary's beach profile. Ice on tidal flats can be present as a smooth cover or multilayered pieces of drift ice that are frozen together. This ice can rest on the beach, float, or be frozen into the bottom. It provides a barrier between currents, waves, and the shore and can thereby protect the shore from coastal erosion. However, through freezing contact, it can also pick up significant amounts of sediment and organic material and can be an important agent of tidal flat formation. Some ice pieces grow into huge blocks laden with sediment and weigh several tons. They can be lifted on a flood tide and moved. Since they can potentially be both neutrally and negatively buoyant, they represent a significant risk to boats, fishing nets, and marine infrastructure (such as tidal power installations).

Ice as storage

The fast ice preserves water (primarily fresh) until breakup. Depending on the severity of the climate and the tidal range, a substantial amount of water is stored as ice. This implies that the freshwater output from the estuary is significantly reduced in winter. As freshwater goes into storage, brine is released leading to salinization and the creation of a locally "negative" estuary (Macdonald, 2000). The eventual melting of the ice is normally in sync with the spring freshet and thus the freshwater yield (volume of water divided by spatial area) from the estuary to the sea can be significantly increased. This has many implications for primary productivity, for ocean currents and for atmospheric–ocean interactions.

The ice ridge–ice flaw system

Another feature of some ice-covered estuaries is the existence of an open flaw lead (polynya) separating the ice ridge and the mobile sea ice pack. In some cases, the flaw exists in absence of the ridge. The lead can generate a great amount of ice and therefore a great amount of brine resulting in significant vertical mixing. The interplay between the lead, the rubble ridge and the ice cover is fascinating and is documented by Macdonald et al., (1999).

Global coverage of estuaries subjected to ice processes

Many estuaries of the world form an ice cover. The frequency and duration depend primarily on the local climate (particularly the number of degree-days) and the water temperature of the local sea. In some cases, a cover forms each winter (Canada, USA, Alaska, Northern Europe and Russia where it lasts for 9 months), whereas in lower latitudes ice on estuaries is present infrequently (e.g., Columbia Estuary, OR, USA; Chesapeake Bay, VA, USA or the Garonne Estuary at Bordeaux, France). In the following paragraphs, some chosen estuaries from different geographic locations will be discussed.

Continental macrotidal estuaries

Ice cover formation in estuaries depends primarily on the tidal amplitude, the estuary's spatial layout and the wind speed and direction. After presenting an estuarine ice terminology, Desplanque and Bray (1986) provide a detailed discussion of ice formation in a macrotidal estuary in eastern Canada: In the upstream zone of the estuary, a classic river-type of ice cover forms. In the second zone (delineated at the upstream end by high water at spring tide and at the downstream end by high water at neap tide), a series of layers of drift ice stacking up on the tidal flats forms ice walls. The third zone is delineated at the downstream end by the low water associated with spring tides. It is characterized by vast intertidal mud flats whereon drift ice may become temporarily stranded and frozen to the sediment. The fourth zone is always covered with water having a salinity of 10–25‰. This vast zone produces most of the ice (slush, pan, cake) that is transported up the estuary as drift ice. Zone 5 is too deep to cool to the freezing point and therefore produces no ice.

Nelson and Whitney (1996) describe the macrotidal Cook Inlet, Alaska. It "is unique in that it has a very high suspended sediment load, high tides (10 m), a moderate snow fall and an air freezing index of 1,400°C days per year. These conditions combine to cause low visibility, extreme tidal currents (8 kts) and unique modes of ice generation within the inlet. The major mode of formation of floating ice is identified as slush ice formation. The slush then coalesces in the turbulent waters to form various ice features. Ice features with depths greater than 2 m that formed in less

than 7 days are described. Ice buildup on shore based structures results in significant downward and upward vertical forces as well as potential horizontal forces."

Continental mesotidal estuaries

One of the most striking descriptions of an ice cover formation is given by Meese et al., 1987 for an inner estuary having a 3 m tide near Newington, NH known as Great Bay. The authors note that freshwater inflow is very modest (only about 2% of tidal flow) and that the salinity is typically 23‰. "The first stage of the freezing process was characterized by growth of frazil crystals that began forming on the surface of the water on 17 December 1983, giving it a greasy appearance. These crystals, up to 2 cm in diameter, coalesced to form the initial ice sheet. Two days later, wave action caused this sheet to break up into circular-shaped masses (pancakes) that developed raised rims due to collisions with other masses. Frazil continued to grow between the pancakes until, on 22 December, a continuous sheet of ice had formed. By 28 December the ice had thickened to 12 cm and the sheet extended to the edge of the cove. Beneath the frazil ice a structural transition was observed that was characterized by a change in the crystalline texture of the ice that led ultimately to the formation of relatively large columnar-shaped crystals exhibiting brine lamella ice plate substructure, the trademark of typical congelation sea ice. Locally, snow ice was found, formed by the flooding of a snow-covered ice surface by seawater. This results in the formation of slush which subsequently freezes to form the top layer of the ice sheet. The crystals in this layer are generally fine-grained and have a random orientation. Mixing of snow with rain or melt water followed by freezing produces a similar result." The authors go on to note that the snow-ice layer can contain a high degree of salinity when the sheet is flooded by estuarine water or may have a very low salinity when the sheet is flooded by rain. The frazil ice layer had a low salinity. The columnar ice layer's salinity depended on its age. The older it was the more time it had to reject brine and the fresher it was.

Morse et al. (2006) describe the ice cover in midwinter in a mesotidal estuary and its subsequent breakup. In this case, the cover was similar to a river's with the exception of a very large number of longitudinal fissures outlining the principal channel (thalweg); the precarious nature of the ice; the thinning of the ice cover from the banks toward the deeper portions; and a number of local ice effects (e.g., slush balls) related to a tidally dynamic environment. Breakup is also described and is shown to occur as a specific sequence over a few spring tide semidiurnal cycles. On the first ebb tide, ice from the main channel is removed over a certain distance (~1–2 km). On the next ebb tide, ice from the adjacent tidal flats is removed as is the next upstream section of ice cover in the channel portion. After the third ebb tide, thick ice pieces got stranded along the main channel bottom at low tide creating a series of weirs that the water cascaded over. On the following ebb tide, virtually all the ice was gone.

The Saint Lawrence estuary

Ice formation and breakup on the St. Lawrence is also of great interest because of its length and socio-economic-environmental importance. Ice on the Estuary is surveyed about three times a week and is available online from Environment Canada. The St. Lawrence is a huge system and therefore ice processes vary greatly. Upstream of Montreal are vast expanses of water commonly referred to as lakes where, until they are frozen over, large quantities of floating sheets are generated. These are broken up through the rapids near Montreal wherein frazil ice and anchor ice can also be added to the mix. From Montreal to Sorel, although the River is affected by the tides, the diurnal amplitude signal is absent and therefore, this reach acts just like any river wherein shore ice forms near the banks and the drift ice increases in thickness and concentration as it moves down the River. The Sorel to Trois-Rivières reach is so vast that it is referred to locally as a lake. It has a very small (10–20 cm tide) and is very shallow (3 m) except through the middle of it where a 12 m navigation channel is maintained. As such, the shallow portions quickly form a cover (held in place by artificial islands and booms) and the drift ice continues down the navigation channel. Because of the very small river slope, this reach is particularly susceptible to forming jams under adverse wind conditions. The Trois-Rivières (30 cm tide) to Québec (6 m tide) reach has high concentrations of drift ice moving down the river, frazil ice is formed in the water column causing blockages of local water intakes and blocks of ice are stranded on the tidal flats. Near Québec, ice on the flats can build into walls and ice elements on tidal flats have strong interaction with sediment processes. Downstream of Québec, there is primarily drift ice consisting of very large floes. Late in the winter season, during cold years and under unfavorable wind conditions, ice thickness and concentrations can reach significant levels and ships must be escorted by ice breakers (Smith et al., 2006).

Canadian arctic estuaries

The ice features of the Churchill (Hudson's Bay) mesotidal Arctic estuary are beautifully described by Kuzyk et al., 2008 (some elements are presented above). Prior to the major flow diversion to the Nelson River in the mid-1970s, the inner Churchill estuary ice was primarily composed of freshwater having an increased salt content as one travels downstream. Pratte (1975) gives an insight into the ice formation at the Port of Churchill, noting that "operations are forced to stop for ice formed upstream in the rapids, which comes down at ebb tide, jamming against the ships at the dock . . . breaking mooring lines."

Ice features of the microtidal Mackenzie estuary are fully described by Macdonald in a large number of papers (e.g., Macdonald et al., 1999). One particular ice-growth hypothesis for the Mackenzie is the formation of frazil ice in the overlying freshwater layer because of the colder

saltwater layer below. An associated article incorporating local ecological knowledge is presented by Carmack and Macdonald (2008). It is also compared to the neighboring Husky lake estuary of a very different nature (Macdonald, 2000). In all cases, the main winter features of the McKenzie are a smooth thin ice cover in the river portion of the estuary bounded by a significant ice ridge outside the mouth, a flaw lead on the other side and mobile pack ice further out. The nature of Beaufort nearshore ice and some explanations for the ice ridge are provided by Timco (2008) and the role of tidal jacking in the Canadian Arctic is discussed by Stander et al. (1988) for inlets north of Baffin Island.

Some biological processes are described by Emmerton et al., 2008. During river passage through the Mackenzie estuary, particulate matter, dissolved organic carbon and inorganic nutrients showed sedimentation, dilution and biological uptake patterns common to other arctic and non-arctic estuaries. Alternatively, inorganic content of particles increased offshore and dissolved organic N and P increased substantially over the shelf, reaching concentrations among the highest reported for the Arctic Ocean. These observations are consistent with the presence of a remnant ice-constrained ("stamukhi") lake from the freshet period and a slow flushing river plume constrained by sea-ice in close proximity to shore.

Making the link with biological processes, "snow and sea ice cover melt and/or break-up controls the timing of the phytoplankton bloom but primary producers (ice algae and phytoplankton) on the outer shelf are essentially nutrient limited. The total annual primary production (22.7 to 27.7 g-C m^{-2}) is thus controlled by nutrient "preconditioning" in the previous fall and winter and by the depth of wind mixing that is controlled in part by the supply of freshwater at the end of spring (ice melt or runoff)" (Lavoie et al., 2009).

According to Barnes (1999), ice causes the most important disturbance to polar benthic communities. "This occurs in four main forms: the ice-foot, ice scour, anchor ice and fast ice, each of which influences benthos in a very different temporal and spatial manner. The four described forms of ice disturbance are all seasonal, but combined, influence communities throughout the year. The magnitude of ice mediated disturbance is often catastrophic and as a result both dominates benthic community structure and makes recolonization and development rates critical."

The role of water on the ice cover in reducing the albedo and promoting spring melt due to surface melting prior to breakup and the imposition of the massive freshet water. The importance of overlying spring water on the nearby Simpson Lagoon, Alaska, is discussed by Matthews and Stringer (1984).

Russian arctic estuaries

Because of their large freshwater discharge rates, Russian rivers dominate the Arctic Ocean. An overview or these estuaries is given by Dolgopolova and Mikhailova (2008). They note that a "distinguishing feature of freeze-up of Siberian rivers is the beginning of ice formation at the supercooled anchor ice then lifting up to the water surface." Furthermore, "hanging dams are usually formed at the northern rivers . . . meeting the firm estuary ice cover" that normally reaches 2 m thick. Of particular interest is the role of ice jams upstream in drastically diminishing the flow in the estuary that can lead to stagnation there: "its color becomes reddish that results in suffocation of fish." Also of interest is the formation of an intermediate "cold layer of brackish water, which is kept after ice formation" in nontidal estuaries. In fact, one of the interesting elements of this paper is that the estuaries are presented as a function not only of estuary mouth type but, more importantly, as a function of tidal range that increases from East to West in the Russian Arctic Ocean.

Eicken et al. (2005) present a very important paper on the Lena and Yana "open" estuaries of the Laptev Sea. What makes the paper so interesting is the direct comparison of these estuaries with the Mackenzie. They show that Russian estuaries are "winter" estuaries (having a unique saline stratification due to the presence of ice) but that they do not have the very important ice rubble ridge to confine freshwater. "Freshening of under-ice waters during winter and north-/northeastward spreading of the river plume with under-ice spreading rates of 1.0–2.7 cm s^{-1}" (about ten times faster than the spreading in the Mackenzie). For the years studied, the Laptev brackish water plume extended to a depth of 10 m. Stable-isotope data show that the landfast shelf ice is composed of about 62% of river water, locking up 24% of the total annual Lena and Yana discharge. Inside the mouth (delta), the ice samples contained virtually no salt. In the nearshore, salinity of the cores increased as a function of distance from the mouth and as such there is a gradual 10% (0.2 m) decrease in fast ice cover thickness.

Arkhipov et al. (1997) present the results of a two-dimensional laterally averaged model developed to describe the hydrodynamic and thermohaline processes in the Ob and Tas Rivers estuary. Koziy et al. (1998) developed a one-of-a-kind 3-D model for the assessment of contamination in coastal seas and inland water bodies. It includes a high resolution numerical hydrodynamic submodel, a dynamic-thermodynamic ice submodel, and submodels for suspended sediment and pollution transport. Presented are simulations for the assessment of the consequences of the possible release of radionuclides from scuttled nuclear reactors in the Novaya Zemlya fjords and the East Novaya Zemlya Trough of the Kara Sea.

Northern European estuaries

According to Carstensen (2008), "ice events may naturally occur on the German coasts. Ice at the Baltic Sea coast exists mainly as drifting ice. In coastal regions a continuous ice cover over a wide area forms only in very severe winters also due to the salinity of the water. These ice covers are then

generally broken up when storms cause water level fluctuations and the resulting ice floes are subsequently carried out to the sea or onshore depending on the currents (induced by wind or tides) and/or the wind. Ice events such as ridging (ca. 0.5 m high) or hummocking can force ice to pile up to several meters in height. Such ice events can greatly damage coastal protection structures and in the worse case make them unfit for use." Furthermore, "when spray water or defrosting water freezes on pile constructions or groynes above the water surface level, ice is accumulated, building formations several times the diameter of the structure. Due to these accreted formations, rising water levels may exert buoyant forces on these structures therewith pulling them up and diminishing there stability against collapse and usability." Water quality parameters in northern Germany estuaries are described by Grisard (1994).

Ice floes are widely known to abrade surfaces of structures constructed in seawater areas where ice floes move actively in the Gulf of Bothnia, Sweden.

Although people use to skate most winters on Norwegian fjords, over last 2 decades, there has been virtually no ice. This, of course, is a significant cultural loss and the fjords are changing because they are now open to much stronger winter storms. Much further north, the interplay of icebergs and bergy bits with currents and sediment processes for Kongsfjorden, northwest Spitsbergen are described in detail in Dowdeswell and Forsberg (1992).

Conclusion

Estuary ice has many interesting features (smooth cover, hummocks, ridges, stamukha, blocks, ice feet, hanging dams, ice weirs, ice walls, slush balls, frazil ice, anchor ice, landfast ice, bottomfast ice, cakes, pans, floes, brash, nilas, huge lengths of thick ice in Arctic Estuaries known as "massives," slush ice, spray ice, grease ice, bellycatters, etc.). Many of these are related to the stratification and salinity of the water; tidal fluctuations (particularly over tidal flats); wind and waves; and the associated currents. Spray, drifting ice and neutrally buoyant ice can all damage structures and vessels; bottom fast ice can protect shores but can rip also them apart; ice walls and stranded ice can reduce flow rates and currents and protect organisms from freezing; ice covers can impede commercial navigation, change mammal behavior, block out heat, cold and sun; separating water from wind (significantly reducing the fetch required for erosional processes), ice covers can cause unique and very stable salinity vertical and longitudinal stratification known as "winter estuaries"; ice covers can impede or encourage freshwater plumes in the nearshore; ice pressure ridges can form a barrier separating the estuary from the sea that can retard freshwater's voyage by days, weeks, or months; ice can dominate biological processes, can dictate ocean currents, and can jam up inside the mouth causing significant flooding that can damage infrastructure but can also revitalize ecological communities.

When present, an ice cover has a tendency to provide great stability to the estuary, however, covers can disappear very rapidly thereby dramatically changing the nature of the estuary with all the associated impacts on local biota and far-field ocean currents. Depending on the geographical location, the estuary could be very vulnerable to climate change. In isolated cases, the impact is only local but should a group of estuaries change regime, there could be "a strong impact on the thermohaline circulation and sea-ice regimes over the shelves and in the Arctic Basin" (Eicken et al., 2005).

One can only conclude that estuaries are terribly fascinating because of their spatial diversity and the intricacy of the interplay between cryological, hydrodynamic, atmospheric, oceanographic, astronomical, sedimentary, biological, anthropological, and climatic processes.

Bibliography

Arkhipov, B. V., Solbakov, V. V., and Tsvetsinsky, A. S., 1997. Hydrothermodynamic model of the Ob and Tas Rivers estuary. In *Proceedings of the International Offshore and Polar Engineering Conference*, Vol. 3, pp. 772–777.

Barnes, D. K. A., 1999. The influence of ice on polar nearshore benthos. *Journal of the Marine Biological Association of the UK*, **79**, 401–407.

Carstensen, D., 2008. Ice conditions and ice forces. In *Chinese-German Joint Symposium on Hydraulic and Ocean Engineering*, August 24–30, 2008, Darmstadt, pp. 283–287.

Desplanque, C., and Bray, D. I., 1986. Winter ice regime in the tidal estuaries of the Northeastern portion of the Bay of Fundy, New Brunswick. *Canadian Journal of Civil Engineering*, **13**(2), 130–139.

Dolgopolova, E., and Mikhailova, M., 2008. Classification of arctic river mouths and regularities of currents in icecovered estuaries. In *Proceedings of the 19th IAHR International Symposium on Ice*. Vancouver, British Columbia, Canada.

Dowdeswell, J. A., and Forsberg, C. F., 1992. The size and frequency of icebergs and bergy bits derived from tidewater glaciers in Kongsfjorden, northwest Spitsberben. *Polar Research*, **11**(2), 81–91.

Eicken, H., Dmitrenko, I., Tyshko, K., Darovskikh, A., Dierking, W., Blahak, U., Groves, J., and Kassens, H., 2005. Zonation of the Laptev Sea landfast ice cover and its importance in a frozen estuary. *Global and Planetary Change*, **48**(1–3), 55–83.

Emmerton, C. A., Lesack, L. F. W., and Vincent, W. F., 2008. Nutrient and organic matter patterns across the Mackenzie River, estuary and shelf during the seasonal recession of sea-ice. *Journal of Marine Systems*, **74**(3–4), 741–755.

Grisard, K., 1994. Eight years experience with the Elbe estuary environmental survey net. In *Proceedings OCEANS 94*. (Cat. No.94CH3472-8), p I/38–43 vol. 1.

Koziy, L., Maderich, V., Margvelashvili, N., and Zheleznyak, M., 1998. Three-dimensional model of radionuclide dispersion in estuaries and shelf seas. *Environmental Modelling and Software*, **13**(5–6), 413–420.

Kuzyk, Z. A., Macdonald, R. W., Granskog, M. A., Scharien, R. K., Galley, R. J., Michel, C., Barber, D., and Stern, G., 2008. Sea ice, hydrological, and biological processes in the Churchill River estuary region, Hudson Bay. *Estuarine, Coastal and Shelf Science*, **77**, 369–384. Elsevier.

Lavoie, D., Macdonald, R. W., and Denman, K. L., 2009. Primary productivity and export fluxes on the Canadian shelf of the Beaufort Sea: a modelling study. *Journal of Marine Systems*, **75**(1–2), 17–32.

Macdonald, R. W., 2000. Arctic estuaries and ice: a positive-negative estuarine couple. In Lewis, E. L. (ed.), *The Freshwater*

Budget of the Arctic Ocean. Netherlands: Kluwer, pp. 383–407.

MacDonald, R. W., Carmack, E. C., and Paton, D. W., 1999. Using δ18O composition in landfast ice as a record of arctic estuarine processes. *Marine Chemistry*, **65**(1–2), 3–24.

Matthews, J. B., and Stringer, W. J., 1984. Spring breakup and flushing of an Arctic lagoon estuary. *Journal of Geophysical Research*, **89**(C2), 2073–2079.

Meese, D. A., Gow, A. J., Mayewski, P. A., Ficklin, W., and Loder, T. C., 1987. Chemical, physical and structural properties of estuarine ice in Great Bay, New Hampshire. *Estuarine, Coastal and Shelf Science*, **9**(1), 833–840.

Morse, B., Ringô, B., Messier, D., Thanh-Quach, T., and Stander, E., 2006. Hydrodynamics of a mesotidal estuary in winter. *Journal of Cold Regions Engineering*, **20**(3), 95–115.

Nelson, W. G., and Whitney, J. W., 1996. Description of summer and winter environmental conditions within Cook Inlet, Alaska. In *Proceedings – SPE Annual Western Regional Meeting,* Denver, CO, pp. 381–392.

Pratte, B. D., 1975. Churchill River salt water tidal model. National Research Council of Canada, *Quarterly Bulletin of the Division of Mechanical Engineering*, 27–36.

Smith, G. C., Saucier, F. J., and Straub, D., 2006. Response of the lower St. Lawrence estuary to external forcing in winter. *Journal of Physical Oceanography*, **36**(8), 1485–1501.

Stander, E., Frederking, R. M. W., and Nadreau, J.-P., 1988. The effects of tidal jacking on ice displacement and strain in the nearshore environment. In *9th IAHR International Symposium on Ice*, Sapporo, Japan, August 23–27. Vol. 1, pp. 526–536.

F

FAST ICE

D. P. Dobhal
Wadia Institute of Himalayan Geology, Dehradun, India

Definition

Fast ice is defined as the sea ice that has frozen along coasts ("fastened" to them), along the shoals, or to the sea floor over shallow parts of the continental shelf, and extends out from land into the sea. In the Antarctic area, fast ice may also extend between grounded icebergs. Unlike drift ice, it does not move with currents and wind.

FINGER RAFTING

Dominic Vella[1], John Wettlaufer[2]
[1]Department of Applied Mathematics and Theoretical Physics, Institute of Theoretical Geophysics, University of Cambridge, Cambridge, UK
[2]Yale University, New Haven, CT, USA

Synonyms

Thrust structures

Definition

The formation of interlocking fingers when two "*ice floes*" alternately over- and under-ride one another during "*rafting*."

Generation: Finger rafting is caused by two ice floes being forced together under the influence of atmospheric and oceanic stresses (Weeks and Anderson, 1958). It is understood that finger rafting is initiated by the presence of small overlapping regions. Such a region leads to vertical displacements of the two floes that are exactly out of phase with one another so that further forcing causes them to "cut" the fingers out of each other (Vella and Wettlaufer, 2007).

Occurrence: Finger rafting is generally observed in young, thin sea ice with thickness up to approximately 15 cm. The interaction of thicker ice floes leads to simple "*rafting*" for intermediate thicknesses or pressure ridging for thickness above around 1 m (Vella and Wettlaufer, 2008). Laboratory models using thin ($\approx 100\,\mu$m) floating wax sheets have demonstrated that finger rafting is not unique to ice but is observed in brittle floating sheets (Vella and Wettlaufer, 2007).

Properties: The width, w, of the fingers created by the rafting of equally thick ice elastic sheets is (Vella and Wettlaufer, 2007):

$$w = 3.32\left(\frac{B}{\rho g}\right)^{1/4},$$

where B is the bending stiffness of the sheet (dependent on thickness and elastic modulus), ρ is the density of the liquid, and g is the acceleration due to gravity.

Bibliography

Vella, D., and Wettlaufer, J. S., 2007. Finger rafting: a generic instability of floating elastic sheets. *Physical Review Letters*, **98**, 088303.
Vella, D., and Wettlaufer, J. S., 2008. Explaining the patterns formed by ice floe collisions. *Journal of Geophysical Research*, **113**, C11011.
Weeks, W. F., and Anderson, D. L., 1958. Sea ice thrust structures. *Journal of Glaciology*, **3**, 173–175.

Vijay P. Singh, Pratap Singh & Umesh K. Haritashya (eds.), *Encyclopedia of Snow, Ice and Glaciers*, DOI 10.1007/978-90-481-2642-2,

FIRN

Rachel W. Obbard, Ian Baker, Rachel W. Lomonaco
Thayer School of Engineering, Dartmouth College, Hanover, NH, USA

Definition

Crystal – A solid material whose constituent atoms, molecules, or ions are arranged in an orderly repeating pattern such that regularly spaced atomic planes are found in three dimensions.
Firn – Compacted snow that has survived at least one melt season in a temperate glacier, or, in a Polar Region, compacted snow that underlies fresh snow, if any, and has undergone some metamorphism.
Firn-ice transition – The change from a packed granular material containing interconnected pores to a polycrystalline solid containing individual bubbles.
Grain – A small single piece of a substance. In firn, the term is used to refer to a single connected piece of ice, regardless of its atomic arrangement; hence, it could include one or more actual crystals. In polycrystalline ice, the terms crystal and grain are used interchangeably (Snow Grains).
Pore close-off depth – The depth at which only individual bubbles are found, rather than interconnected pores.
Snowpack – An area of naturally accumulated snow.

Introduction

When fallen snow accumulates and the snowpack persists past the depositional season, it undergoes metamorphism and becomes firn.

In temperate glaciers (Temperate Glaciers), firn is defined as snow that has survived at least one melt season. In Polar Regions, where there is no melt season per se, firn is found under the snowpack, or, in areas of low accumulation, such as the Antarctic Plateau, even at the surface. It differs from fresh snow however, in that it has undergone sintering and metamorphism, described.

At the other end of the firn column, which can be several tens of meters to more than 100 m thick, the depth at which pores are no longer interconnected defines the beginning of glacial ice. The depth of pore close-off, and the firn-ice transition, depends on accumulation rate and temperature.

Glaciologists and climatologists use ice cores to study past climate, which can be understood by analyzing the structure and chemistry of the ice, and in particular the contents of gas inclusions (Chemical and Microbe Records in Snow and Ice). Firn is of interest because atmospheric air penetrates it to several tens of meters of depth, permitting chemical exchange and resulting in differences of up to 7,000 years in the age of meteoric ice and the gas it contains (Bender et al., 2006).

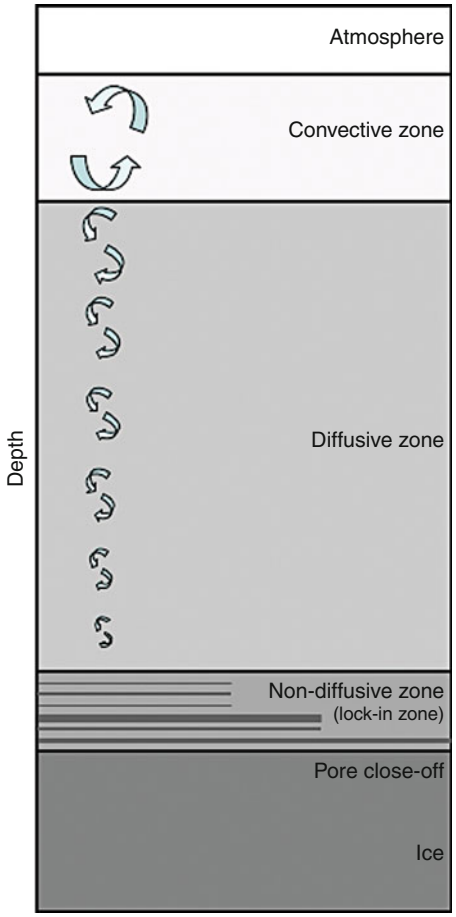

Firn, Figure 1 Schematic of the interstitial air column in firn with labeled mixing zones. Arrows indicate the magnitude of mixing where large convection occurs near the surface and a net downward diffusion occurs in the lower portions of the firn column.

Firn has three zones that can be distinguished by the extent of gas transport taking place there (Figure 1). In the uppermost "convective zone," gas is freely exchanged with the local troposphere through convection. This exchange is the reason that the gas entrained in glacial ice is younger than the ice itself. Below this is the "diffusive zone" in which diffusion within the firn itself takes place, but there is no exchange of gases with the overlying atmosphere. In this zone, the gas becomes increasingly enriched with the nitrogen isotope ^{15}N, and other heavy gas isotopes, due to barometric pressure (Sowers et al., 1992) (Isotopic Characteristics of Ice, Snow, and Glaciers). The thickness of the diffusive zone can vary dramatically, depending on local snow accumulation rates, and the age of trapped gases becomes especially hard to determine in regions such as the Antarctic Plateau where accumulations rates are low and diffusion takes place for many thousands of years (Bender et al., 2006). Below

the diffusive zone is a "non-diffusive zone" in which local cap layers have formed that trap gases and limit diffusion.

Because firn occupies the region between freshly fallen snow and glacial ice, it is a region of great change. The morphology of firn, that is its grain size, porosity, and pore connectivity, plays an important role in convection and diffusion and is key to interpreting the climate record contained in ice cores.

Metamorphism and the development of firn

Snow falls as individual crystals and aggregates of crystals (Snow Grains) and is packed by the force of gravity and the accumulation of more snow. Where the individual crystals contact one another, they sinter, and in time, the geometry of these bonded areas changes. This process, which is called metamorphism, is driven by temperature gradients and results in a reduction in surface free energy. It leads to changes in density, pore shape and size, crystal size, diffusion, chemistry, and impurity distribution. The rate of metamorphism, and grain growth, is related to the local snowfall accumulation rate and surface temperature (Spencer et al., 2006).

Metamorphism can take place as either a wet or dry process. Wet metamorphism takes place where all three phases (solid, liquid, and gas) of water are present, in temperate glaciers (Glacier) for example, whereas dry metamorphism requires only two phases (ice and water vapor), such as is found in Polar Regions.

After deposition (snowfall), there is a period of rapid deformation as the more delicate snowflake structures are destroyed. This "destructive metamorphism" is due to mechanical processes and chemical potential, the preferential sublimation of highly curved surfaces. During this process, angles become more rounded and individual grains approach a more spherical shape (Colbeck, 1983).

The thermal gradient in the snowpack, a function of changing tropospheric temperatures, geothermal heat (Geothermal Heat), and the insulating properties of the snow, affects the structural changes found in the firn. Low mean temperature and small temperature gradients permit particle coarsening and lead to equilibrium structures characterized by relatively small, rounded grains that are well bonded. Large temperature gradients (i.e., >10°C m^{-1}) produce kinetic structures characterized by relatively large faceted structures (Colbeck, 1983). Seasonal variations in climate result in layering, with kinetic structures produced in summer and equilibrium structures produced in winter. This stratigraphy of structure (and density) is preserved during densification (Stratigraphy of Snowpacks) and can be used to identify annual layers (Bender et al., 1997) (Layering of Snow).

Sintering describes a process during which particles are bonded to one another to reduce overall surface free energy. Sintering does not require the presence of liquid water (Domine et al., 2003). Material will migrate and become redistributed in order to minimize surface curvature (and thus length). Under stress (Overburden Pressure), it may also compress vertically and expand laterally, producing an anisotropic microstructure. In its initial stage, adjacent grains bond to produce a neck, or circle of contact. The neck grows until individual particles are no longer distinguishable and pores connected by a network of channels are produced. Finally, the pore spaces become isolated and spherical (Swinkels and Ashby, 1980). There are six primary mechanisms for mass transport and sintering. Surface, lattice, and vapor diffusion, all from surface sources, transport mass between particle surfaces. Grain boundary diffusion from a grain boundary source, lattice diffusion from a dislocation source and lattice diffusion from a grain boundary source densify the matrix (Swinkels and Ashby, 1980). The relative effect of each of the six mechanisms depends on the driving forces present.

There are three main driving forces: temperature gradient, chemical potential gradient, and overburden pressure. Temperature gradients result in the redistribution of mass from warmer surfaces to colder ones, a process that begins with sublimation. When the saturation vapor pressure at a given temperature is greater than the vapor pressure over an ice particle, sublimation from the solid phase to the vapor phase occurs to eliminate the imbalance. Warmer particles have higher saturation vapor pressure and are more likely to sublimate. When the bottom of an ice column is warmer than the surface, there exists a temperature gradient that produces mass transport from the bottom upward. Lower, warmer particles tend to sublimate and the vapor produced condenses on the downward-facing surfaces of higher, colder particles. Atmospheric air that circulates into the snowpack and firn results in vapor pressure imbalances that produce a continual supply of vapor. As the air travels downward, it is warmed and takes up material from the surrounding solid. As it rises, it cools and deposits vapor locally on the bottoms of particles.

Chemical potential gradients lead to grain growth by surface and vapor diffusion that is governed by equilibrium thermodynamics (Colbeck, 1983). Specifically, vapor pressure is lower over concave surfaces and large particles, and higher over convex surfaces and small particles. This leads to local variations in vapor pressure that seek equilibrium. Molecules migrate from regions of higher vapor pressure to regions of lower vapor pressure, or from small particles and sharp edges to large particles and broad junctions between particles (Colbeck, 1983). The overall effect is coarsening of firn texture.

Overburden pressure produces a vertical stress field that increases with depth. This induces strain that leads to densification. Grains merge and displaced material moves along the grain boundary or through the crystal lattice to new bonding sites. Chemical potential gradients also govern this diffusion. Molecules on convex surfaces have higher surface free energy, arising from relatively fewer shared bonds. The amount of overburden pressure

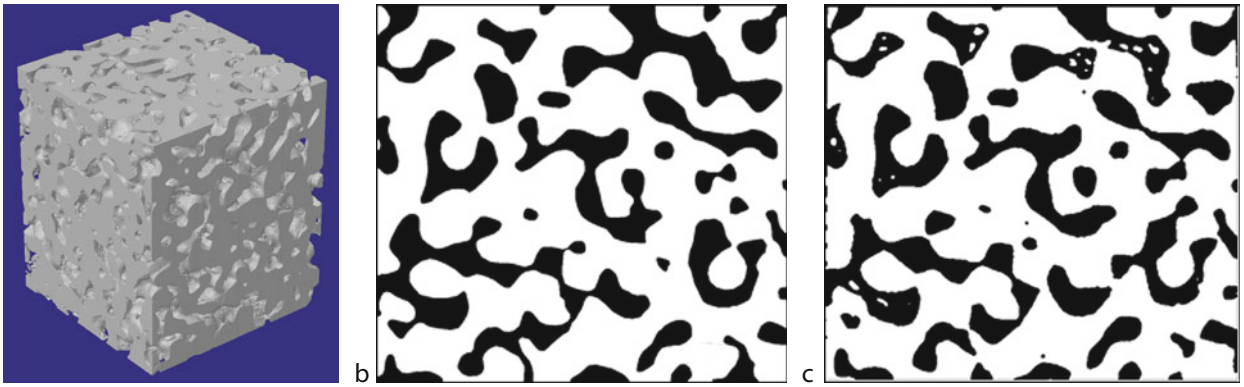

Firn, Figure 2 (**a**) Reconstructed MicroCT image of firn sample (from 27 m, Summit, Greenland) 8 mm^2 on the base, with (**b**) binarized scanning electron microscope image of a horizontal cross section later made from the sample, compared to (**c**) a binarized MicroCT image of the same cross section of the original sample.

is determined by accumulation rate and is most influential at great depths.

Firn morphology and microstructure

The microstructure of polycrystalline ice is described by its texture (crystal size and shape) and fabric. As discussed in the preceding section, firn coarsens with depth, time, and temperature due to mechanisms that tend to minimize free energy.

Traditionally, the structure of firn has been studied using optical microscopy. The sample is permeated with a hydrocarbon such as dimethyl phthalate (melting point 2°C, density 1.19 g cm^{-3}), and then the ice matrix is allowed to sublimate away. This leaves a negative impression of the interconnected pore structure, which can be sectioned and studied using optical microscopy (Albert and Shultz, 2002). This has the disadvantage that very small or isolated pores may not be preserved with the infiltrate. More recently, X-ray micro computed tomography (MicroCT) has been used to nondestructively image pore space in three dimensions, and scanning electron microscopy of sectioned samples used to verify the MicroCT results (Figure 2) and examine grain boundaries in firn in more detail (Figure 3).

Overburden pressure in glacier ice is often sufficient to induce slip within the crystal lattice, and this leads to preferred crystal orientation. The development of preferred orientation has not been observed in firn.

Air movement in firn

Isotopic ratios preserved in interstitial air present in firn and air bubbles are important to determine past atmospheric compositions. Thus, the cycling of air through firn needs to be understood before the atmospheric record preserved in bubbles can be interpreted.

In the convective zone, (as deep as 20 m) rapid air movement takes place. Here, air interacts with the atmosphere by ventilation and natural convection. Ventilation, also known as wind pumping, is the process by which atmospheric pressure changes cause interstitial air movement in firn and snow. Barometric changes, turbulent surface winds, and surface topography produce pressure changes that drive movement (Colbeck, 1989; Albert, 1996, 2002).

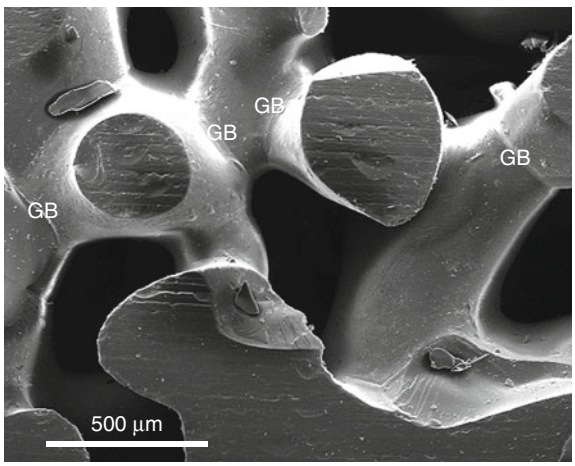

Firn, Figure 3 Scanning electron microscope image of firn (from 10 m, Summit, Greenland). Note the interconnected pores and the grain boundaries (GB) separating the sintered crystals.

In the diffusive zone, air mixes by atomic and molecular diffusion due to thermal and chemical gradients (Bender et al., 1997; Schwander et al., 1997). Gravitational fractionation leads to an enrichment of heavy isotopes with depth because of their superior settling ability based on mass (Craig et al., 1988; Sowers et al., 1992; Schwander et al., 1997).

As depth increases, firn porosity decreases and air mixing becomes more restricted (Schwander et al., 1997; Bender et al., 1997). Seasonal layering can also affect the rate of air movement through firn (Albert, 1996) and may produce impermeable layers in the non-diffusive zone. These prevent air from equilibrating with that in the diffusive zone (Sowers et al., 1992; Schwander et al., 1997). While air may mix locally, within the summer layer for example, impermeable winter layers impede its vertical diffusion (Fain et al., 2008).

Firn measurements

Borehole logging is used to measure firn properties in situ. These include temperature, density, and vertical strain. Unlike snow, which must be sampled at depth by digging a large snow pit and sampling from the sides, firn has enough cohesion (Cohesion) to permit the extraction of intact cores that are used to measure density, porosity and permeability, grain size, and anisotropy.

Because firn is compressible, seasonal layers thin with depth. It is also porous and subject to the migration of chemical species deposited with the snow (Chemical Composition of Snow, Ice, and Glaciers). Both of these aspects can complicate age-depth calculations. Where annual layers cannot be distinguished optically or from the geochemical record, a density profile produced from a borehole log of vertical strain or measurements of mass, length, and diameter of core sections can reveal seasonal layering.

Summary

A transitional state between fallen snow and meteoric ice, firn is a complex material where vast morphological and chemical changes are taking place.

Bibliography

Albert, M., 1996. Modeling heat, mass and species transport in polar firn. *Annals of Glaciology*, **23**, 138–143.

Albert, M. R., 2002. Effects of snow and firn ventilation of sublimation rates. *Annals of Glaciology*, **35**, 52–56.

Albert, M. R., and Shultz, E. F., 2002. Snow and firn properties and air-snow transport processes at Summit, Greenland. *Atmospheric Environment*, **36**(15/16), 2789–2798.

Bender, M., Sowers, T., and Brook, E., 1997. Gases in ice cores. *Proceedings of the National Academy of Science*, **94**, 8343–8349.

Bender, M. L., Floch, G., Chappellaz, J., Suwa, M., Barnola, J.-M., Blunier, T., Dreyfus, G., Jouzel, J., and Parrenin, F., 2006. Gas age-ice age differences and the chronology of the Vostok ice core, 0–100 ka. *Journal of Geophysical Research*, **111**(D21), 115–125.

Colbeck, S. C., 1983. Theory of metamorphism of dry snow. *Journal of Geophysical Research*, **88**, 5475–5482.

Colbeck, S. C., 1989. Air movements in snow due to wind pumping. *Journal of Glaciology*, **35**, 209–213.

Craig, H., Horibe, Y., and Sowers, T., 1988. Gravitation separation of gasses and isotopes in polar ice caps. *Science*, **242**, 1675–1678.

Domine, F., Lauzier, T., Cabanes, A., Legagneux, L., Kuhs, W. F., Techmer, K., and Heinrichs, T., 2003. Snow metamorphism as revealed by scanning electron microscopy. *Microscopy Research and Technique*, **62**, 33–48.

Fain, X., Ferrari, C. P., Dommergue, A., Albert, M., Battle, M., Arnaud, L., Barnola, J. M., Cairns, W., Barbante, C., and Boutron, C., 2008. Mercury in the snow and firn at Summit Station, central Greenland and implications for the study of past atmospheric mercury levels. *Atmospheric Chemistry and Physics*, **8**, 3441–3457.

Hawley, R., Waddington, E. D., Morse, D. L., Dunbar, N. W., and Zielinski, G. A., 2002. Dating firn cores by vertical strain measurements. *Journal of Glaciology*, **48**(162).

Schwander, J., Sowers, T., Barnola, J. M., Blunier, T., Fuchs, A., and Malaize, B., 1997. Age scale of air in the summit ice: implications for glacial-interglacial temperature change. *Journal of Geophysical Research*, **102**, 19483–19493.

Sowers, T., Bender, M., Raynard, D., and Korotkevich, Y. S., 1992. $\delta^{15}N$ of N_2 in air trapped in polar ice: a tracer of gas transport in the firn and a possible constraint on ice age-gas age differences. *Journal of Geophysical Research*, **97**(D14), 15,683–15,697.

Spencer, M. K., Alley, R. B., Fitzpatrick, J. J., 2006. Developing a bubble number-density paleoclimatic indicator for glacier ice. *Journal of Glaciology*, **52**(178), 358–364.

Swinkels, F. B., and Ashby, M. F., 1980. A second report on sintering diagrams. *Metallurgica*, **29**, 259–281.

Cross-references

Antarctica
Chemical and Microbe Records in Snow and Ice
Chemical Composition of Snow, Ice, and Glaciers
Cohesion
Geochemistry of Snow and Ice
Glacier
Ice
Isotopic Characteristics of Ice, Snow, and Glaciers
Layering of Snow
Overburden Pressure
Snow Grains
Stratigraphy of Snowpacks
Temperate Glaciers

FJORDS

Umesh K. Haritashya[1], Vijay P. Singh[2], Pratap Singh[3]
[1]Department of Geology, University of Dayton, Dayton, OH, USA
[2]Department of Biological and Agricultural Engineering, Texas A&M University, College Station, TX, USA
[3]Tahal Consulting Engineers Ltd, New Delhi, India

Synonyms

Fiord

Definition

Fjords are long, narrow, and over-deepened features with steep sides and are carved into bedrock by the glacial activity and flooded by melting water (Figure 1).

Fjords, Figure 1 Fjord as seen in Milford Sound, New Zealand. Photo courtesy Dr. Luke Copland.

Fjords are erosional landforms that represent the movement of a glacier within a confined channel along the valley bottom. The movement of a glacier and formation of fjords is entirely controlled by topography. They are common in the polar regions, but can also be found in subpolar and temperate regions (Table 1). Fjords have existed for millions of years and they range from a few kilometers to several tens of kilometers wide and several kilometers long. Because of their location and relationship with the sea level on one side and tectonically active high mountains on the other side, they are an important feature. They also possess unique characteristics of oceanic processes and ice-ocean interface (Straneo et al., 2010), and therefore, they are appropriately termed as one of the complex and dynamic landsystems that provide information about glacial, fluvial, and oceanographic features.

Most fjords are a Palimpsest feature which makes them an extremely important feature, because they can provide information about the successive glaciations through floor sediments. However, these sediments need to be carefully analyzed, since they may have been buried by younger glacimarine sediments. Fjords act as natural sediment traps and typically have high sediment accumulation rates, providing the potential for high-resolution palaeoclimatic and palaeoenvironmental studies on decadal to centennial timescales and presenting a unique opportunity to study land–ocean interactions. Cowan et al. (2010) used the fjord sediment to identify two prominent glacial erosion surfaces associated with Last Glacial Maximum advance and Little Ice Age advance. Fjords comprise several rock basins, but many of them are deepest at the beginning and become gradually shallower toward the sea. This could be related to the erosive power of glaciers, which becomes lesser and lesser toward the end of the feature.

Sediment deposition in fjords can be related to retreating glaciers by depositional zones moving in the upward direction and hiatuses in retreat by push moraines or morainal banks. Powell and Molnia (1989) has shown various depositional system models associated with retreating glaciers, and he (Powell, 2003) has discussed such models in various types of environment from polar to temperate. Sediment deposition can also be related to advancing glaciers in the form of increasing till thickness from head of a fjord toward the sea limit.

Fjords also provide critical information about marine limits and relate to with the isostaic uplift of deglaciated outer coasts.

Bibliography

Cowan, E. A., et al., 2010. Fjords as temporary sediment traps: history of glacial erosion and deposition in Muir Inlet, Glacier Bay National Park, southeastern Alaska. *GSA Bulletin*, **122**(7-8), 1067–1080, doi:10.1130/B26595.1.

Powell, R. D., 2003. Subaquatic landsystems: fjords. In Evans, D. J. A. (ed.), *Glacial Landsystems*. London: Arnold, pp. 313–347.

Powell, R. D., and Molnia, B. F., 1989. Glacimarine sedimentary processes, facies and morphology of the South-southeast Alaska shelf and fjords. *Marine Geology*, **85**, 359–390.

Straneo, F., et al., 2010. Rapid circulation of warm subtropical waters in a major glacial fjord in East Greenland. *Nature Geoscience*, **3**, 182–186, doi:10.1038/ngeo764.

Cross-references

Sediment Core and Glacial Environment Reconstruction

Fjords, Table 1 Some of the major local controls on modern fjord landsystems (Adopted from Powell, 2003)

						Sediment contribution										
						Glacial		Glacifluvial		Marine			Terrestrial			
Climatic zone	Glacial flow velocity	Internal ice condition	Bed condition	Subglacial water free	Glacier terminus	Sub-	En-/supra	Sub-	En-/supra	icebergs	Sea ice	biogenic	Fluvial	Mass flow	Wind	Modern examples
Temperate	Fast	Temperate	Deforming till, local	Conduit flow	Tidewater cliff	2	2	5	1	2		1	3	3	1	Alaska, British Columbia, Chile
Subpolar	Fast	Slightly cold	Deforming till	Conduit flow	Tidewater cliff	3	1	3	1	1	2	1	3	1	1	Svalbard, Canadian and Russian Arctic
	Moderate	Cold	Mostly frozen, local till	None to minor conduit flow	Short floating tongue or tidewater cliff	2		2		1		2	1		1	Antarctic Peninsula
Polar	Fast	Cold	Deforming till	Local conduit thin film	Floating tongue	3	1	3		3	1	1	2	1	1	Greenland, Ellesmere Island, Baffin Island
	Moderate	Very cold	Deforming till	None	Floating tongue	3	1			1	1	1	1	1	3	Antarctica (Mackay)
	Slow	Very cold	Mostly frozen, some till	None	Floating tongue or tidewater cliff	1	1			1	1	1		1	3	Antarctica (Ferrar and Blue)

FOLIATION

Gulab Singh
Centre of Studies in Resources Engineering, Indian Institute of Technology Bombay, Mumbai, India

Synonyms

Type of layering in glacier

Definition

Foliation is a planner or layered structure that developed in glacier ice during flow.

Origin

The foliation is subjected to stress and strain effects with the glacier sliding down slope and consequently folia (Raina and Srivastva, 2008). Foliation is usually formed by the deformation of preexisting inhomogeneities in the ice. The major inhomogeneities are sedimentary bands, faults, and shear zones and exhibit fold pattern (Paterson, 1994; Raina and Srivastva, 2008).

Type of foliation

Generally two types of foliation, namely, transverse and longitudinal with respect to the direction of ice flow can be observed.

Transverse Foliation: Transverse foliation perpendicular to the linear movement of the ice. These foliation plains of ice often exhibit a highly folded nature.

Longitudinal Foliation: These foliation planes are parallel to the linear movement of the ice.

Bibliography

Paterson, V., 1994. *The Physics of Glaciers*, 3rd edn. UK: Pergamon. ISBN 0080379443, 185 pp.
Raina, V. K., and Srivastva, D., 2008. *Glacier Atlas of India*, 1st edn. *Geological Society of India*, ISBN: 81-85867-80-9.

FORBES BAND

Gulab Singh
Centre of Studies in Resources Engineering, Indian Institute of Technology Bombay, Powai, Mumbai, India

Definition and origin

Alternating convex bands of light and dark ice on a glacier usually found down the glacier from steep narrow icefalls and considered to be the result of different velocity and ablation rates in summer and winter. Forbes band is also known as band ogives. Forbes band are generally formed first at the foot of icefalls. Because forbes band are always formed in icefalls as series of undulation in the surface, the amplitude of these series of undulation decreases toward the terminus (snout) of the glacier. Figure 1 shows an example of the light and dark band in the surface of Panchi Nala Glacier (Bhaga Catchment in Indian Himalaya, Himachal Pradesh). The combined width of one light and one dark band corresponds to the distance the ice moves in a year. It can form on surging glaciers also. It's useful in velocity calculations and identifies basal features. Forbes bands are one of the most enigmatic indicators of glacier flow. Stratification is preserved in these bands.

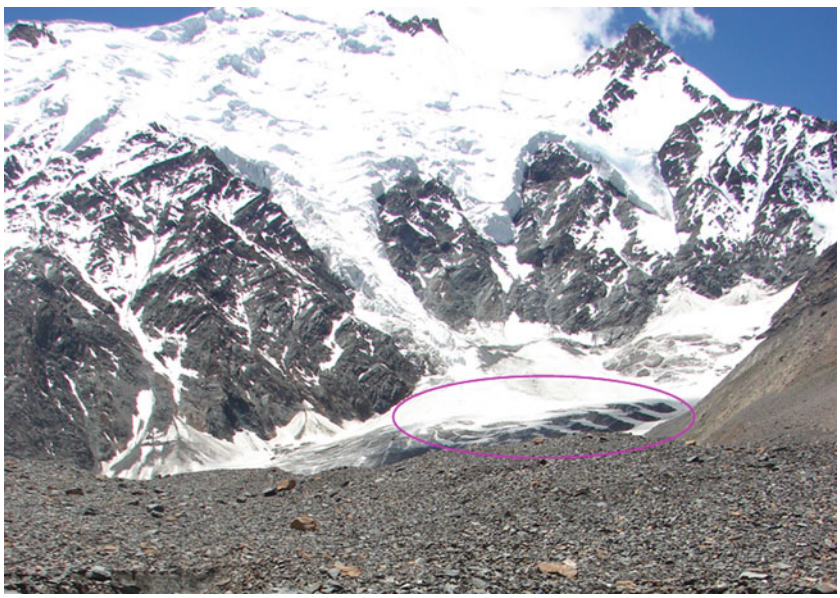

Forbes Band, Figure 1 Panchi Nala Glacier (Photo: CSRE, IIT Bombay Team).

Uses:

1. Forbes bands can be used for stratification.
2. Used to determine velocities or surge intervals.
3. These band can be used to predict crevasse formation by identifying crevasse scars.

Bibliography

Paterson, W. S. B., 1994. *The Physics of Glaciers*, 3rd edn. UK: Pergamon, ISBN: 0080379443, 185 p.

FORMATION AND DEFORMATION OF BASAL ICE

Simon J. Cook
Centre for Glaciology, Institute of Geography and Earth Sciences, Aberystwyth University, Ceredigion, UK

Definition

Basal ice. Ice at the glacier base which has acquired distinctive physical and/or chemical characteristics that differ from those of meteorically derived englacial ice due to its formation and/or metamorphosis by processes operating at or near to the glacier bed.

Introduction

Many glaciers exhibit a layer of basal ice which is conditioned primarily by processes acting at or near to the bed. Where it exists, the basal ice layer can be on the order of a few millimeters to tens of meters in thickness, and is typically more debris rich than the overlying englacial ice (Figure 1), although may not necessarily contain any debris. Basal ice may be absent where basal thermal conditions do not allow the net buildup of ice at the glacier base, or where basal ice is formed but destroyed by subsequent melting (e.g., by glacier sliding or by subglacial water flow), or simply where the requisite conditions to permit the operation of basal ice formation processes are not met. Ice and sediment may accrete to the glacier base through a number of different processes, and may then be altered by processes of melting, refreezing, and deformation. Basal ice thus inherits physical and/or chemical characteristics that are distinct from the overlying englacial ice. Basal ice exerts an important influence on glacier motion, sediment transport and deposition, and geomorphology as a result of these unique characteristics (e.g., Knight, 1997).

Tectonic incorporation of debris into ice

One of the oldest theories for basal debris entrainment is the shearing of subglacial debris into a glacier to create debris bands (e.g., Chamberlin, 1895). This process involves the thrusting of sediment from the bed along shear zones penetrating upward into the ice. Weertman (1961) criticized this model suggesting that it could not account for the varied appearance or the millimeter-scale spacing of debris bands, nor was there sufficient evidence that "scraping" of debris along shear planes from a subglacial position could actually occur. More recent studies suggest, however, that shearing and thrusting can be important for basal ice development, especially where there is intense longitudinal compression at the margin to allow differential movement between ice either side of a thrust plane. The requisite conditions for thrusting may occur in polythermal glaciers where warm-based ice from the interior flows against cold-based ice at the margin, or during glacier surges (e.g., Hambrey et al., 1999). Folding of sediment into the basal zone has also been observed to be important for basal ice development.

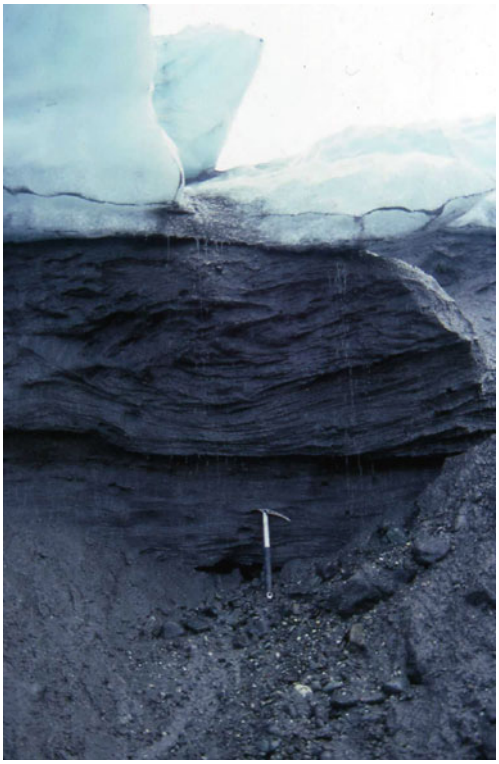

Formation and Deformation of Basal Ice, Figure 1 Debris-rich "stratified" facies basal ice (*dark*) overlain by clean, bubble-rich firnified englacial ice, Matanuska Glacier, Alaska (Photograph by Richard Waller).

Accretion of new ice to the glacier base

Regelation around bedrock obstacles

Weertman (1957) described a process of pressure melting and refreezing around bedrock obstacles important in *Glacier Sliding* (qv). Ice flow against a bedrock obstacle generates high pressure on the stoss side of the obstacle causing the ice to melt. Meltwater flows around the obstacle along the ice–rock interface to the low-pressure area in the lee of the obstacle where it refreezes, with the potential to entrain sediment particles. Latent heat released during ice formation is conducted back through the bedrock obstacle

to promote continued melting on the stoss-side face. This process, often termed "Weertman regelation," can operate around bedrock obstacles smaller than 1 m in amplitude, but the resultant basal ice layer is typically limited to just a few centimeters in thickness because regelation layers may be destroyed by subsequent phases of regelation. Basal ice produced in this manner tends to exhibit alternating millimeter-scale layers of sediment and ice.

Regelation into subglacial sediments

Vertical regelation allows ice to intrude into substrates composed of unconsolidated sediments (e.g., Iverson and Semmens, 1995). In this case, ice melts above individual grains and refreezes below them at speeds proportional to the downward pressure gradient across the particles. Ice can penetrate downward into the substrate until the point where basal melting equals the rate of regelation, producing debris-bearing basal ice up to 1 m in thickness.

The "heat pump" effect

Robin (1976) described basal ice accretion through a "heat pump" effect which results as a consequence of regelation around bedrock obstacles. Upstream of the obstacle water that exists in the vein network between ice crystals is squeezed out of the ice along a pressure gradient toward low-pressure subglacial water films that exist in the overlying ice. Unless there remains some free water in the ice that can release latent heat when the pressure is released, the ice will remain at a colder pressure melting point until the ice mass can warm again by thermal conduction and heating due to internal friction. This process may produce a cold patch several meters in diameter in which subglacial water freezes to the glacier sole. This process may be sufficient to chill a basal layer of up to 2 m by 1°C, and is suggested by Robin to account for the bubble-free nature of the glacier sole where air is expelled with the squeezed water. Additionally, Knight (1997) described how the debris-poor "clotted facies," which contains predominantly silt-sized debris at 3-grain ice crystal intersections, could be formed by the squeezing of water and sediment away from the bedrock in the manner described by Robin (1976).

Basal adfreezing

The term "basal adfreezing" typically refers to the model of basal ice formation proposed by Weertman (1961) associated with cyclic shifts in basal thermal regime. Meltwater may exist beneath a glacier where heat supplied to the glacier sole by geothermal sources and by sliding friction exceeds heat loss by conduction through the ice thickness. As meltwater flows to the glacier margin, the thickness of the overlying ice decreases, thus the temperature gradient between the air and the glacier base steepens allowing meltwater to freeze. Where meltwater flows through subglacial sediments, freezing will also incorporate sediment to form debris-rich basal ice. Basal ice may be partially or completely destroyed in the summer as warmer air intrudes to the glacier base through crevasses and fractures in the thin marginal ice. Debris bands or laminations may develop as a result of freeze-on of new ice beneath any preexisting basal ice.

Glaciohydraulic supercooling

Glaciohydraulic Supercooling (qv) is a process that allows subglacial water to exist in a liquid state at a temperature below the ambient pressure melting point, and subsequently for this *Supercooled Water* (qv) to freeze to the glacier base to produce basal ice (see Cook et al., 2006 for a review). Supercooling of subglacial water occurs where the pressure melting point of water ascending the adverse slope of an overdeepened subglacial basin rises faster than it can be warmed by viscous dissipation. For the water to remain in thermal equilibrium with the overlying temperate ice, some of this water must freeze to release latent heat, resulting in the production of *Frazil* (qv) (porous aggregates of lozenge-shaped crystals) and *Anchor Ice* (qv) (ice platelets anchored to the glacier or substrate). Sediment-laden water percolates through anchor and frazil ice until pore spaces freeze shut, and subsequent debris – ice segregation produces debris-laden "stratified facies" basal ice. Glaciohydraulic supercooling has been suggested to explain anomalously thick basal ice (i.e., greater than 1 m) which is characteristically debris rich (>25% debris by volume) and often layered (hence "stratified").

Freeze-on of porewater

Christoffersen and Tulaczyk (2003) described a process of basal freeze-on beneath ice streams analogous to the process of frost-heave in permafrost environments. In fine-grained subglacial till water is unable to freeze due to interfacial tension effects and insufficient space for crystal growth. In polar ice streams, basal temperatures may be reduced by ice thinning, or by fast downward advection of cold surface ice. Reduced basal temperatures are accompanied by a decrease in water pressure at the ice–water interface producing a hydraulic gradient that drives the supercooled porewater to the freezing front where it freezes to produce basal ice which may comprise solid debris with only interstitial ice, massive ice comprising stacked debris laminae, laminated ice, or clear ice with only dispersed debris aggregates.

Accretion of preexisting ice

Apron entrainment

Ice Apron (qv) entrainment involves the attachment to the glacier sole of ice that already exists in front of the glacier. Shaw (1977) recognized the importance of apron entrainment for debris-rich basal ice formation at arid polar glaciers where basal adfreezing, which is dependent on meltwater generation, cannot operate to produce basal ice. This involves the glacier advancing and overriding pro-glacial accumulations of snow, superimposed ice, and ice-cored debris. Sharp et al. (1994) recognized the process of apron entrainment at the surge-type Variegated

Glacier where they found that "basal diffused" facies was physically indistinguishable from englacial ice, and hence likely formed from fallen ice blocks that had been tectonically incorporated into the basal ice during the surge.

Subglacial ice entrainment

Tison and Lorrain (1987) explained how ice coatings form in subglacial cavities and are entrained into basal ice. Ice coatings form where water enters a subglacial cavity and freezes due to the penetration of cold air into the cavity (e.g., overnight). Debris layers are formed where debris is carried in by water or falls from the cavity ceiling and is covered by freezing of water on top. In some cases, the downward movement of the glacier as it enters the cavity drags the ice coatings along, detaching them from the bedrock and causing them to fold. At the down-glacier margin of the cavity, the folded ice coatings and debris layers are pinched between the sole and the bedrock and become recumbent allowing the repetition of debris layers within the basal ice sequence.

Deformation of basal ice

Although deformation processes do not create new basal ice, they are important in controlling basal ice thickness, the evolution of basal ice character, and can be important for basal sediment entrainment. Glacier ice can be regarded as a metamorphic rock deforming at temperatures very close to, or below the pressure melting point, and this deformation is enhanced close to the glacier bed where basal ice is subject to intense simple shear.

Numerous deformation structures have been identified within basal ice layers. Sharp et al. (1994) identified recumbent folding, thrust faulting, and nappe overriding in the basal ice of Variegated Glacier. Basal ice deformation at this glacier was enhanced by intense longitudinal compression associated with the down-glacier propagation of a surge front. Sharp et al. listed three tectonic processes that occurred during the surge that accounted for the geometry of the basal ice layer: (1) apron overriding which explained the inclusion of flattened blocks of ice that had fallen from the glacier surface and had been overridden and incorporated into the basal ice; (2) intrusion of ductile basal ice into the core of large frontal anticlines which became overturned to produce up-glacier-dipping debris bands that outcropped on the glacier surface after the anticlines had been unroofed by ablation; (3) upward ramping of imbricate thrust faults from the basal décollement through the overturned limbs of growing anticlines.

Deformation in the basal zone promotes the mixing and intercalation of different basal ice facies to produce different sub-facies. Waller et al. (2000) described how deformation could explain the generation of different sub-facies within the debris-rich "stratified facies" basal ice at the Russell Glacier. After initial entrainment, intense shear stress at the glacier base caused frozen sediment within the basal ice to fracture along lines of weakness and to disaggregate under imposed stresses. They observed recumbent folds in the stratified facies basal ice comprising a core of "solid sub-facies" (high sediment content with interstitial ice) surrounded by a folded layer of "discontinuous sub-facies" ice (ice with typically lower debris content interstratified with solid sub-facies). Waller et al. (2000) suggested, therefore, that discontinuous sub-facies ice was tectonically attenuated from the solid sub-facies. This work was an extension of previous work which suggested that after initial debris entrainment by adfreezing or regelation, continued ice movement would tend to attenuate ice-sediment layers and cause sediment to migrate upward through the basal ice profile. Hence a debris band would evolve into a thinner debris band, then into a debris aggregate, and finally into individual particles.

Summary

Basal ice may be formed and deformed by a range of processes, the operation of which varies over time and space dependent upon local environmental conditions. Thus, there is usually complexity in basal ice sequences at point locations, and across entire glacier margins. Study of basal ice characteristics can be used to infer *Subglacial Processes* (qv) and conditions, which in turn play a major role in controlling ice dynamical behavior. The fact that new mechanisms of basal ice formation continue to be identified from analysis of basal ice cores and sections (e.g., Christoffersen and Tulaczyk, 2003) suggests that there is much yet to learn about the controls on ice mass behavior, and how such controls may vary over time and space.

Bibliography

Chamberlin, T. C., 1895. Recent glaciological studies in Greenland. *Bulletin of the Geological Society of America*, **6**, 199–220.

Christoffersen, P., and Tulaczyk, S., 2003. Response of subglacial sediments to basal freeze-on: I. Theory and comparison to observations from beneath the West Antarctic ice sheet. *Journal of Geophysical Research*, **108**(B4), 2222.

Cook, S. J., Waller, R. I., and Knight, P. G., 2006. Glaciohydraulic supercooling: the process and its significance. *Progress in Physical Geography*, **30**, 577–588.

Hambrey, M. J., Bennett, M. R., Dowdeswell, J. A., Glasser, N. F., and Huddart, D., 1999. Debris entrainment and transfer in polythermal valley glaciers. *Journal of Glaciology*, **45**, 69–86.

Iverson, N. R., and Semmens, D. J., 1995. Intrusion of ice into porous media by regelation: a mechanism of sediment entrainment by glaciers. *Journal of Geophysical Research*, **100**(B7), 10219–10230.

Knight, P. G., 1997. The basal ice layer of glaciers and ice sheets. *Quaternary Science Reviews*, **16**, 975–993.

Robin, G., De, Q., 1976. Is the basal ice of a temperate glacier at the pressure melting point? *Journal of Glaciology*, **16**, 183–196.

Sharp, M. J., Jouzel, J., Hubbard, B., and Lawson, W., 1994. The character, structure and origin of the basal ice layer of a surge-type glacier. *Journal of Glaciology*, **40**, 327–340.

Shaw, J., 1977. Tills deposited in arid polar environments. *Canadian Journal of Earth Sciences*, **14**, 1239–1245.

Tison, J.-L., and Lorrain, R. D., 1987. A mechanism of basal ice-layer formation involving major ice-fabric changes. *Journal of Glaciology*, **33**, 47–50.

Waller, R. I., Hart, J. K., and Knight, P. G., 2000. The influence of tectonic deformation on facies variability in stratified debris-rich basal ice. *Quaternary Science Reviews*, **19**, 775–786.

Weertman, J., 1957. On the sliding of glaciers. *Journal of Glaciology*, **3**, 965–978.
Weertman, J., 1961. Mechanism for the formation of inner moraines found near the edge of cold ice caps and ice sheets. *Journal of Glaciology*, **3**, 965–978.

Cross-references

Frazil
Glacier Sliding
Glaciohydraulic Supercooling
Ice Apron
Subglacial Processes
Supercooled Water

FRAZIL

Gulab Singh
Centre of Studies in Resources Engineering, Indian Institute of Technology Bombay, Powai, Mumbai, India

Synonyms

Lolly ice or slushy ice (Disorganized, slushy ice crystals in the water column)

Definition

"Frazil" is the name given to ice crystals in suspension in water and form in very cold water. The first stage of freezing gives an oily or opaque appearance to the surface of the water. The frazil ice is also called "lolly ice" or "slush."

Formation

It sporadically forms in open, turbulent, supercooled water. When the water surface begins to lose heat at a very quick rate, the water becomes supercooled. Turbulence, caused by strong winds or flow from a river, mixes the supercooled water throughout its entire depth. The supercooled water allows the formation of small ice crystals (frazil ice), and the crystals get taken to the bottom of the water body. Frazil ice is the first stage in the formation of sea ice. Through a crystallization process, the crystals quickly increase in number, and because of its supercooled surrounding, the crystals continue to grow. This process of crystallization is known as nucleation.

The accumulation of frazil ice in rivers frequently causes flooding and damage to various water objects, such as trash racks. And since frazil ice is found below the surface of water, it makes it very difficult for humans to detect its formation. Damage could be reduced by promoting designated flood regions with mechanical structures. There are several ways to control frazil ice buildup. They include suppression, mechanical control, thermal control, vibration, prior thought, and damage mitigation.

Bibliography

Daly, S. F., 1991. *Cold Region Technical Digest No. 91-1* "Frazil Ice Blockage of Intake Trash Racks." March 1991, http://en.wikipedia.org/wiki/Frazil_ice

FREEZING BOTTOM (ICE SHELF)

Gulab Singh
Centre of Studies in Resources Engineering, Indian Institute of Technology Bombay, Powai, Mumbai, India

Synonyms

Freezing of water to the bottom of Floating glacier tongues and of ice shelves

Definition

Freezing bottom of floating glacier tongues and of ice shelves is controlled by the temperature of the water in which they float. Water (ocean) supercooling leads to ice shelf bottom freezing (i.e., freezing bottom is a process to freeze of sea water from below Floating glacier tongues and ice shelves).

An *ice shelf* is a thick, floating platform of ice on the sea but attached to the land or to a grounded ice sheet. Ice shelf forms where a glacier or ice sheet flows down to a coastline and onto the ocean surface. The boundary between the floating ice shelf and the grounded (resting on bedrock) ice that feeds it is called the grounding line or grounding zone (Paterson, 1994). Ice shelves are in hydrostatic equilibrium with the water in which they float, so their melting would not contribute directly to a sea level rise (Knight, 1999).

Ice shelves are found much in Antarctica, Greenland, and Canada. They are nourished by flow from the ice sheets and by snow accumulation. The world's largest ice shelves are the Ross Ice Shelf and the Filchner-Ronne Ice Shelf in Antarctica (Paterson, 1994).

Origin

Ice shelves can also occur by the freezing of the water from the ocean below onto the base of the shelf (Paterson, 1994). The freezing of freshwater can be identified to the base of shelf ice, where meltwater become trapped between the base of the ice shelf and more saline deeper water. Cold meltwater produced at the base of shelf ice close to the grounding line. Because of the pressure dependence of the freezing point, the rising limb of the cell can cause ice platelets to form and accrete to the bottom of the shelf. Thermo-haline circulation cell beneath an ice shelf is causing the form of marine ice at the shelf bottom. Melting (near to the grounding zone) produced low salinity and low density water that rises and flows outward along the shelf bottom and with decreasing depth the pressure-dependent freezing point rises, and supercooled water releases ice platelets that accumulate at the ice shelf bottom (Knight, 1999).

Bibliography

Knight, P. G., 1999. *Glaciers*, 1st edn. Cheltenham, UK: Stanly Thomes. ISBN 0-7487-4000-7.
Paterson, W. S. B., 1994. *Physics of Glaciers*, 3rd edn. Tarrytown, NY: Pergamon Press/Elsevier Science. ISBN 0080 37944-3.

FREEZING MELTWATER

Gulab Singh, F. S. Birajdar
Centre of Studies in Resources Engineering, Indian Institute of Technology Bombay, Mumbai, Maharashtra, India

Synonyms

Glacial meltwater

Definition

Melt water is the water released by the melting of snow or ice, including ice sheets and ice shelfs over oceans. Meltwater is often found in the ablation zone of glaciers, where the rate of snow cover is reducing. Meltwater can be produced during volcanic eruptions, in a similar way in which the more dangerous wave/currents are formed. When meltwater pools (rather than flowing) on the ground surface or ice surface, it forms melt ponds. As the weather gets colder, meltwater often re-freezes, known as freezing meltwater. Meltwater can pool or melt under the ice's surface. These pools of water, known as sub-glacial lakes, can form due to geothermal heat and friction.

Bibliography

Greenland ice sheet flows faster during summer melting. *NASA Earth Observatory News*. Retrieved January 16, 2008.

FREEZING AND THAWING INDEX

Jiang Fengqing, Zhang Yanwei
Xinjiang Institute of Ecology and Geography/ Chinese Academy of Sciences, Urumqi, Xinjiang, China

Definition

Freezing and melting index is defined as the cumulative degree-days within a certain time interval (Cheng et al., 2003).

The freezing index is given by the summation of the degree-days for a freezing season with daily mean temperature below zero (Cheng et al., 2003).

Freezing and thawing index

A number of concepts and methods are available for the computation of the freezing and thawing indices. Thorough review of these methods can be found in literatures (e.g., Frauenfeld et al., 2007). Cheng et al. (2003) proposed a method to calculate the freezing and thawing indices of the surface of a railway base based on the annual mean maximum and minimum air temperatures. In general, the freezing and thawing indices can be calculated using daily air temperature observations. However, the monthly air temperature can be used to estimate these indices in some places where almost no data are available for analysis, especially in high-latitude areas and the alpines (Zhang et al., 1997). The freezing and thawing index are defined as the cumulative number of degree days for a given time period. Areas where the thawing index is much lower than the freezing index may be covered by permafrost, while areas with smaller thawing indices and larger freezing indices may have underlying continuous permafrost (Frauenfeld et al., 2007).

The freezing index can be computed as (Frauenfeld et al., 2007; Jiang et al., 2008):

$$\mathrm{FI} = \int_{t_0}^{t_1} |T| \mathrm{d}t, \quad T < 0^\circ\mathrm{C}$$
$$= \sum_{i=1}^{N_F} |Ti| \qquad Ti < 0^\circ\mathrm{C}$$

where the first equation is for theoretical computation and FI is the freezing index with unit in °C. The second one of the aforementioned equations is empirical, which simply defines the freezing index as the cumulation of absolute values of temperature below 0°C in freezing season. In the aforementioned equation, $i = 1, 2, 3, \ldots$; T_i is the daily mean temperature.

Similar to the definition of freezing index, the thawing index is given by the summation of the degree-days with daily mean temperature above 0°C for a thawing season.

Generally, the thawing index can be determined as (Frauenfeld et al., 2007; Jiang et al., 2008):

$$\mathrm{TI} = \int_{t_0}^{t_2} T \mathrm{d}t, \quad Ti > 0^\circ\mathrm{C}$$
$$= \sum_{i=1}^{N_F} Ti \qquad Ti > 0^\circ\mathrm{C}$$

where the first equation is for theoretical computation and FI is the thawing index with unit in °C. The second one of the aforementioned equations is empirical, which simply defines the thawing index as the cumulation of temperature above 0°C in thawing season. In the aforementioned equation, $i = 1, 2, 3, \ldots$; T_i is the daily mean temperature.

Bibliography

Fengqing, J., Ruji, H. U., and Zhen, L. I., 2007. Variation trends of the freezing and thawing index along the Qinghai-Xizang railway for the period 1966–2004. *Acta Geographica Sinica*, **62**(9), 935–945.

Frauenfeld, O. W., Zhang, T., and Mccreight, J. L., 2007. Northern hemisphere freezing/thawing index variations over the twentieth century. *International Journal of Climatology*, **27**, 47–63.

Guodong, C., Hao, J., Keli, W., and Qingbai, W., 2003. Thawing index and freezing index on the embankment surface in permafrost regions. *Journal of Glaciology and Geocryology*, **25**(6), 603–607.

Zhang, T., Osterkamp, T. E., and Stamnes, K., 1997. Effects of climate on the active layer and permafrost on the north slope of Alaska, U.S.A. *Permafrost and Periglacial Processes*, **8**, 45–67.

FREQUENCY ANALYSIS OF SNOW STORMS

Stanley A. Changnon
University of Illinois, Urbana, IL, USA

Definition

Snowstorm data based on events when 15 cm or more occurred in 1 or 2 days were the basis for developing heavy snowfall frequency information for the United States. Data on such snowstorms were available for 204 locations (first-order weather stations) with historical snowfall records for the 1948–2001 period. This was sufficiently long to accurately determine recurrence interval values for return periods of 5 and 10 years.

Introduction

Information essential to designing and planning for heavy snowfall events is data on snowfall amounts expected for various frequencies of occurrence. Structures impacted by snow loads need design information for heavy amounts apt to occur. Planning for snow removal and management of snow-impacted activities requires knowledge of how often and how much snow is apt to occur. Snowfall amounts do not always equate to snow loads, which are dependent on the amount of water in the snow.

Analysis

Analysis of original weather records from weather stations with long-term daily snowfall records revealed that many of the cases when 15 cm or more fell in 2 days were situations when the total snow had fallen in less than 24 h. Nearly 85% of all 2-day events were cases of the total snow falling in 24 h or less. Events of 15 cm or more in 1 or 2 days were defined as snowstorms. The values of snowfall for these snowstorms were the data used in this frequency assessment. The station values were sorted and ranked from high to low to allow fitting to statistical distributions.

Various statistical distributions were tested for applicability in fitting the extreme snowstorm values of each station following established approaches for analyzing extremes of precipitation. A partial duration series was developed for each station using the 54 largest values in the 54-year period of data. Distributions considered included log normal, Frechet, and log-Pearson. Log-log and semi-log fitting procedures were also investigated. The assessment of these various fitting methods for the snowstorm data at the 204 station across the United States showed that the log-log method provided the best fit for recurrence intervals of 2 years or longer. Hence, a log-log analysis was used for the final derivation of the frequency relations.

Examination of the distributions for the 204 stations revealed that stations with lower snowstorm amounts had steeper trend than did those of the stations with heavier snowfalls. The 5- and 10-year recurrence interval values were determined from the linear best fit for each station.

Regional variations

Frequency values determined for selected stations in the eastern half of the United States are listed in Table 1. The record highest values exceed 40 cm at most locations. Comparison of the station values reveals sizable differences between stations and varying locations in the United States. The 5-year values vary from 7 cm at Dallas to 44 cm at Buffalo. Other interesting differences include the 5-year values at Boston and New York, which are similar, but their 10-year values are more different.

The national pattern of snowfall values expected to be equaled or exceeded at a point at least once every 5 years, as based on the 204 stations, shows a general latitudinal distribution from lowest to highest across the central United States. Values are less than 2 cm along the Gulf Coast and range from 25 to 35 cm along the Canadian border. The Great Lakes exert an influence by increasing snowfalls in storms around all the lakes. For example, the 5-year amounts around Lake Michigan show 2 to 5 cm more on the lake's west side and 5 to 10 cm more from storms on the east side. The Appalachian Mountains enhance values from North Carolina north through Virginia, Pennsylvania, and New York. Five-year values in central Maine are 40 cm, and at similar latitudes in North Dakota, the values are 25–28 cm. The mountain and lake effects interact to produce 5-year values of 45 cm or more in upstate New York. In the west, there are notably high values from the central Rockies north into Montana, ranging from 27 to 40 cm. Isolated very high values occur at Flagstaff (57 cm), Mt. Shasta in California (80 cm), in the central Cascades in California (90 cm), and at Stampede Pass in Washington (70 cm).

The national pattern of 10-year values is similar to the 5-year pattern. These include a latitudinal distribution in

Frequency Analysis of Snow Storms, Table 1 Snowfall amounts (cm) for selected stations in the eastern United States

Station	5-year amount	10-year amount	Record highest
Boston, MA	36	52	70
New York, NY	34	43	67
Buffalo, NY	44	52	91
Pittsburgh, PA	26	35	65
Richmond, VA	23	32	44
Asheville, NC	23	29	52
Cleveland, OH	31	34	49
Sault Ste. Marie, MI	34	37	60
Minneapolis, MN	36	44	63
Dallas, TX	7	13	18
Goodland, KS	31	36	55
Bismarck, ND	32	39	49
Indianapolis, IN	23	29	47
Des Moines, IA	26	31	38

the central United States; high values in the western and eastern mountain ranges; and high values around the Great Lakes. The 10-year values in the South are 5–7 cm, approximately double the magnitudes of the 5-year values, and farther north, the 10-year values are 45–55 cm. In the Appalachian Mountains the 10-year values were 12% (north with 40 cm) to 25% (south with 29 cm) higher than the 5-year values. In the western mountains the 10-year values were 33–45 cm, differences that ranged from 10 to 18% higher than the 5-year values. In general, the 10- and 5-year differences were least in the higher snowfall regions of the United States (Table 1).

Summary

The point magnitude of snowfall from storms with 5- and 10-year recurrence intervals is lowest along the Gulf Coast and highest in the mountains of the western United States. The magnitude of the 10-year values is 25–30% greater than the magnitude of the 5-year values. Most locations in the United States have had record snowstorms that produced more than 40 cm.

Bibliography

Changnon, S. A., 2006. Frequency distribution of heavy snowfall from snowstorms in the United States. *Journal of Hydrologic Engineering*, **11**, 427–431.

Changnon, S. A., 2008. Space and time distributions of major winter storms in the United States. *Natural Hazards*, **45**, 1–9.

Changnon, S. A., Changnon, D., Karl, T. R., and Houston, T., 2008. *Snowstorms Across the Nation: An Atlas about Storms and Their Damages*. Asheville, NC: National Climatic Data Center. 96 pp.

Cross-references

Cascade Mountains, USA
Orographic Precipitation
Rocky Mountains

FRESH WATER STORAGE

Pratima Pandey
Centre of Studies in Resources Engineering, Indian Institute of Technology Bombay, Mumbai, Maharashtra, India

Definition

Freshwater is naturally occurring water on the earth. The source of almost all freshwater is precipitation (rain and snow). Snow and glaciers are considered as a huge storehouse of freshwater. The release of fresh water from the glaciers provides valuable natural resources in the form of rivers, lakes, springs, and streams. Freshwater can be defined as water with less than 500 parts per million (ppm) of dissolved salts.

FRICTIONAL MELTING

Pratima Pandey
Centre of Studies in Resources Engineering, Indian Institute of Technology Bombay, Mumbai, Maharashtra, India

Definition

When glacier moves over a terrain, friction occurs at the sides and bottom of the ice mass. This friction caused melting of glacier ice. This type of melting is called frictional melting. Frictional melting is the result of the conversion of mechanical deformation to heat under adiabatic conditions of slip. The pathway to friction melting is controlled by the mechanical properties of a rock's constituent minerals.

FROST

Alan W. Rempel
Department of Geological Sciences, University of Oregon, Eugene, OR, USA

Synonyms

Hoar; Ice deposition (opposite of sublimation); Icing (as in: *aircraft icing* – the term "icing" is also sometimes used to refer to ice formation on a surface from supercooled liquid)

Definition

Frost is the ice deposited from water vapor.

Introduction

Frost formation is caused by the decrease in saturation vapor pressure with reduced temperature, which leads to the removal of water from chilled air by the heterogeneous nucleation of ice on available surfaces. Frost typically occurs at and near the ground surface following radiative heat losses on winter nights in temperate and colder climates. "Frost" also forms the beginning of a number of open compound words (e.g., frost action, frost creep, frost heave, etc.) that refer to phenomena that involve ice that is present near the ground surface, but that are otherwise not at all related to ice deposition from the air. Several of these phenomena are discussed in the following sections.

Frost action

Frost action refers to the weathering, or damage, of near-surface natural materials and anthropogenic structures by the build-up of ice. The degree of damage often correlates with repeated freeze–thaw transitions between liquid water and solid ice. Because liquid water has a higher density than solid ice, when a fixed mass of liquid water is frozen its volume increases. In a closed system that is at fixed volume, freezing can cause large increases in pressure and

these have been suggested as the source of frost action. Though plausible under special circumstances, this cause of frost action may be rare in nature if closed-system freezing is not common. Research that traces its roots to experiments by Taber (1929, 1930), and includes several recent notable developments (e.g., Walder and Hallet, 1985; Hallet et al., 1991; Murton et al., 2006), demonstrates that frost action is more typically associated with increases in ice mass that accompany a migration of liquid water towards colder temperatures where freezing occurs. Because (a) the pathways for this liquid migration are more permeable at temperatures close to the melting point, (b) higher temperature gradients promote more rapid liquid flow, and (c) more water is available for transport towards colder regions when thawing occurs nearby, the correlation of frost damage with freeze–thaw cycles is also predicted by the modern explanation of frost action that is supported by the aforementioned controlled experiments. The physical mechanisms that lead to the observed increases in ice mass are closely related to the phenomena of frost heave, which is discussed below; the density difference between liquid water and ice is incidental to this behavior.

Frost and permafrost

Permafrost is the term given to soil that is at or below the ice melting temperature for 2 or more years. Permafrost is often insulated from atmospheric conditions by an "active layer" of soil that undergoes seasonal temperature excursions above the melting point. Frost is typically more transient than permafrost since it forms by deposition at the ground surface where it is susceptible to changes in atmospheric temperature and vapor content. Vapor transport through permafrost soil can occur under conditions that allow frost to form at depth and remain stable for much longer time spans. Locations where this is important include the Dry Valleys of Antarctica (e.g., Sugden et al., 1995; Ng et al., 2005) and the surface of Mars (e.g., Schorghoffer, 2007).

Frost blister

Frost blisters are seasonal frost mounds (see below).

Frost boils

Frost boils form low elevation mounds in regions that have much less vegetative cover than their surroundings. The reduced thermal insulation causes a component of frost heave to push material outwards from the boil center.

Frost churning

Frost churning refers to the movement of soil that accompanies frost heave and frost action over long time periods.

Frost cracking

Frost cracks form in ice-bound sediments that are subjected to significant and rapid cooling. The patterns of cracking are similar to contraction cracks that form from other causes, common examples of which include mud cracks and columnar basalt. Over long time periods, frost cracking can lead to frost wedging (see below).

Frost creep

The motion of sediments down a slope caused by frost action is known as frost creep. Since frost heave acts parallel to temperature gradients, sediment is lifted normal to the slope of the ground surface during freezing. Upon melting, the sediment settles downwards under gravity. Over many freeze-thaw cycles, frost creep can cause significant down-slope movement (for a review, see Matsuoka [2001]).

Frost heave

Frost heave refers to the upwards displacement of the ground surface that is caused by the formation of ice within frost susceptible sediments. The fact that ice is less dense than liquid water has been suggested as the most obvious explanation for the resulting ground deformation. However, the volume of a fixed mass of ice is only about 10% greater than the same mass of liquid water, and the void fraction (porosity) of soils is typically less than 50%. If the expansion of water upon freezing was responsible, the displacement of the ground surface would be limited to roughly 5% of the depth to the freezing front. In fact, as Taber (1929, 1930) noted in his pioneering work, observed heave often exceeds this by an order of magnitude or more. Taber's experiments conclusively showed that the mass of ice in frost-heaved sediments is greater than the mass of liquid water originally present in the pore space. Additional moisture is transported from warmer regions towards the ground surface, where it freezes in layers known as *ice lenses* that form parallel to isotherms and grow to produce the observed heave.

The presence of ice lenses in frozen sediments has long been recognized; Beskow (1935) gives an extensive survey of the early literature as it relates to the construction of roads and railroads. As heat is extracted from the ground surface, growth of the lowest lens is supplied by liquid water that flows through unfrozen sediments at greater depths and along microscopic liquid films that separate the ice from the sediment grains near the solidification front. This growth continues until a new lens forms lower down in the sediment column and stems the flow.

O'Neill and Miller's (1985) "rigid ice" theory of frost heave has been the basis for many subsequent models that have been successful at predicting observed heaving behavior. We now understand that the pathways for liquid transport in partially frozen soils are in equilibrium at temperatures below the normal melting temperature both because of intermolecular interactions between the ice and sediment across thin liquid films, and because of the energy associated with highly curved ice–liquid interfaces. The equilibrium coexistence of a liquid with its solid below the melting temperature is referred to as premelting (for a recent review, see Dash et al. [2006]).

Premelting is common to the phase behavior of other solids, so it should not be surprising that "frost heave" phenomena have also been observed during solidification experiments with benzene and nitrobenzene (Taber, 1930), helium (Mizusaki and Hiroi, 1995), and argon (Zhu et al., 2000). For each of these other materials the density of the solid is greater than that of its liquid. The intermolecular interactions that cause the solid to be wetted by premelted films are responsible for producing the net force that enables heave to take place and liquid to be drawn towards colder temperatures (Dash, 1989; Rempel et al., 2004; Worster and Wettlaufer, 2006). The conditions of lens initiation and growth can be predicted by continuum treatments that examine the balance of heat, mass, and momentum as freezing progresses.

In their most basic form the models descended from O'Neill and Miller's (1985) treatment only account for relative motion between sediment particles that are separated by a lens.

Recent investigations of freezing in colloidal suspensions have demonstrated that patterns of ice growth, including lensing behavior, also emerge from models that treat the Brownian diffusion of colloid particles and describe the equilibrium melting temperature as a function of their local concentration (Peppin et al., 2006, 2007, 2008). Experiments and theory demonstrate that the concentration and temperature profiles resemble those seen during the solidification of alloys. Growth of a planar ice lens can be disrupted by a morphological instability that produces dendritic growth – with new lenses potentially forming as side-branches to the primary dendrites.

Frost mound

A frost mound is a hill with a core of ice that has formed in the active layer above permafrost. Many frost mounds are seasonal features, but there are also perennial examples, known as pingos. The ice in frost mounds can result from the lens formation that causes frost heave, but elevated artesian water pressures are also sometimes implicated.

Frost susceptibility

The frost susceptibility of a sediment gauges its tendency to host the ice-lens growth that causes frost heave. It is difficult to nucleate ice lenses in coarse-grained sediments such as gravels, and only very restricted liquid pathways are present below the melting temperature when pore sizes are large; such sediments have low frost susceptibility. It is difficult to transport water to supply lens growth in very fine-grained sediments such as clays, so lenses nucleated within these sediments grow slowly; these sediments have an intermediate frost susceptibility. Moderately fine-grained sediments such as silts can both host the nucleation of ice lenses and facilitate relatively rapid liquid transport to supply lens growth; these sediments have high frost susceptibility.

Frost weathering

Synonym for frost action – see above.

Frost wedging

Frost wedges are ice deposits that develop over many seasons in the contraction cracks formed by frost cracking. Ice-infiltrated sediments that have sufficient cohesion to resist inter-particle deformation can fail by cracking as a result of thermal contraction. Wind-blown material and meteoric water subsequently infiltrate cracks to form vertically oriented ice deposits. Over many seasons, cracking in the same location can cause frost wedges to grow many decimeters across.

Summary

Though frost itself forms from vapor deposition, many of the periglacial processes and associated landforms that incorporate frost within their names are more commonly associated with ice formed by freezing of liquid water. Thin films of premelted water that remain unfrozen at the interfaces between ice and sediment particles at subzero temperatures enable significant water redistribution. This behavior leads to frost action, frost creep, frost heave, and the formation of numerous geomorphic features.

Bibliography

Beskow, G., 1935. Soil Freezing and Frost Heaving with Special Application to Roads and Railroads. The Swedish Geological Society, C, no 375, Year Book no. 3 (translated by J. Osterberg). Technological Institute, Northwestern University. Reprinted in: *Historical perspectives in Frost Heave Research* (ed. P. B. Black and M. J. Hardenberg). CRREL Special Report 91–23:37.

Dash, J. G., 1989. Thermomolecular pressure in surface melting: motivation for frost heave. *Science*, **246**, 1591.

Dash, J. G., Rempel, A. W., and Wettlaufer, J. S., 2006. The physics of premelted ice and its geophysical consequences. *Reviews of Modern Physics*, **78**, 695.

Hallet, B., Walder, J. S., and Stubbs, C. W., 1991. Weathering by segregation ice growth in microcracks at sustained sub-zero temperatures: verification from an experimental study using acoustic emissions. *Permafrost and Periglacial Proceedings*, **2**, 283.

Matsuoka, N., 2001. Solifluction rates, processes and landforms: a global review. *Earth Science Reviews*, **55**, 107.

Mizusaki, T., and Hiroi, M., 1995. Frost heave in He. *Psysica B*, **210**, 403–410.

Murton, J. B., Peterson, R., and Ozouf, J.-C., 2006. Bedrock fracture by ice segregation in cold regions. *Science*, **314**, 1127.

Ng, F., Hallet, B., Sletten, R. S., and Stone, J. O., 2005. Fast-growing till over ancient ice in Beacon Valley, Antarctica. *Geology*, **33**, 121.

O'Neill, K., and Miller, R. D., 1985. Exploration of a rigid ice model of frost heave. *Water Resources Research*, **21**, 281.

Peppin, S. S. L., Elliott, J. A. W., and Worster, M. G., 2006. Solidification of colloidal suspensions. *Journal of Fluid Mechanics*, **554**, 147.

Peppin, S. S. L., Worster, M. G., and Wettlaufer, J. S., 2007. Morphological instability in freezing colloidal suspensions. *Proceedings of the Royal Society A*, **463**, 723.

Peppin, S. S. L., Wettlaufer, J. S., and Worster, M. G., 2008. Experimental verification of morphological instability in freezing aqueous colloidal suspensions. *Physical Review Letters*, **100**, 238301.
Rempel, A. W., Wettlaufer, J. S., and Worster, M. G., 2004. Premelting dynamics in a continuum model of frost heave. *Journal of Fluid Mechanics*, **498**, 227.
Schorghofer, N., 2007. Theory of ground ice stability in sublimation environments. *Physical Review E*, **75**, 041201.
Sugden, D. E., Marchant, D. R., Potter, N., Jr., Souchez, R. A., Denton, G. H., Swisher, C. C., III, and Tison, J.-L., 1995. Preservation of Miocene glacier ice in East Antarctica. *Nature*, **376**, 412.
Taber, S., 1929. Frost heaving. *Journal of Geology*, **37**, 428.
Taber, S., 1930. The mechanics of frost heaving. *Journal of Geology*, **38**, 303.
Walder, J., and Hallet, B., 1985. A theoretical model of the fracture of rock during freezing. *Geological Society of America Bulletin*, **96**, 336.
Worster, M. G., and Wettlaufer, J. S., 2006. Premelting dynamics. *Annual Review of Fluid Mechanics*, **38**, 427.
Zhu, D.-M., Vilches, O. E., Dash, J. G., Sing, B., and Wettlaufer, J. S., 2000. Frost heave in argon. *Physical Review Letters,* **85**, 4908–4911.

Cross-references

Artificial Ground Freezing
Cracks
Creep
Cryostatic Pressure
Cryoturbation
Frozen Soil Hydrology
Interstitial Ice
Periglacial
Pingo
Solifluction

FROZEN SOIL HYDROLOGY

Ronald P. Daanen[1], Debasmita Misra[2]
Anita M. Thompson[3]
[1]Geophysical Institute, University of Alaska Fairbanks, Fairbanks, AK, USA
[2]Department of Geological Engineering, College of Engineering and Mines, University of Alaska Fairbanks, Fairbanks, AK, USA
[3]Department of Biological Systems Engineering, University of Wisconsin-Madison, Madison, WI, USA

Synonyms

Hydrology in frozen porous media

Definition

Frozen soil hydrology. The study of water behavior in soil below the freezing point of liquid water.

Permafrost. Ground with a temperature below 0.0°C for at least two consecutive years.

Segregated ice. Discrete layers or lenses of ice in freezing mineral or organic soils, as a result of the migration (and subsequent freezing) of pore water.

Massive ice. A comprehensive term used to describe large masses of ground ice, including ice wedges, pingo ice, buried ice, and large ice lenses.

Pingo. An eskimo term for a perennial frost mound consisting of a core of massive ice with soil and vegetation cover; the size can range from a few meters to tens of meters, in both diameter and height; can be found in continuous and discontinuous permafrost zones.

Talik. A layer or body of unfrozen ground occurring in a permafrost area due to a local anomaly in thermal, hydrological, hydrogeological, or hydrochemical conditions.

Injection ice. Also called intrusion ice, is formed when liquid water under hydraulic pressure forms an ice core and pushes the soil surface up. The ice is a form of massive ice and can be found in a pingo core.

Regelation. Motion of an object through ice by melting and freezing that is caused by pressure differences; this process allows a glacier to slide past small obstacles on its bed.

Ice wedge. A epigenetic ice wedge is a solid ice mass that can be up to 4 m (13 ft) wide near the ground surface, and extends as much as 10 m (33 ft) down. A syngenetic ice wedge is a solid ice mass that can be up to 2 m (7 ft) wide near the ground surface, and extends as much as 30 m (99 ft) down, due to sedimentation on the surface. These features form when the ground temperature decreases during the winter, which leads to contraction of the ground and cracking of the ice wedge; these cracks fill with snowmelt and freeze; the ice wedge expands again in summer, thereby pushing the soil on both sides of the ice wedge upward.

Patterned ground

Sorted patterned ground:

Sorted circles. A patterned ground form that is equidimensional in several directions, with a dominantly circular outline, and a sorted appearance commonly due to a border of stones surrounding a central area of finer material.

Sorted nets. A type of patterned ground with cells that are equidimensional in several directions, neither dominantly circular nor polygonal, with a sorted appearance commonly due to borders of stones surrounding central areas of finer material.

Sorted polygon. A patterned ground form that is equidimensional in several directions, with a dominantly polygonal outline, and a sorted appearance commonly due to a border of stones surrounding a central area of finer material.

Sorted step. A patterned ground feature with a step-like form and a downslope border of stones embanking an area of relatively fine-grained bare ground upslope.

Sorted stripe. A patterned ground with a striped and sorted appearance, due to parallel strips of stones and intervening strips of finer material, oriented down the steepest available slope.

Non-sorted patterned ground:

Non-sorted circles. Sometimes referred to as *frost boils* are approximately 1–3 m in diameter and generally have little vegetation on them due to excessive soil expansion from ice accumulation during winter. Non-sorted circles are, however, typically surrounded by dense vegetation, which acts as an insulator against winter cooling, leading to preferential formation of ice within the circles.

Non-sorted stripes. These features are similar to non-sorted circles, but elongated downslope due to gravity.

Non-sorted polygons. Polygonal shaped features often formed by desiccation cracking of the surface, with vegetation establishment in the cracks. These features are often accentuated on hill slopes where they are also called turf hummocks.

Ice-wedge polygons. A polygon outlined by ice wedges underlying its boundaries.

Introduction

Frozen soil hydrology is a cold climate phenomenon. Approximately 50% of the northern hemisphere experiences frozen soil conditions. Freezing has a profound effect on hydrology in general, but in particular on soils where ice crystals form in soil pores and change the characteristics of the porous medium. These changes can be beneficial and detrimental. Agriculture benefits from freezing and thawing processes, because it increases the porosity of soils, which helps grow crops. Freezing and thawing processes drive cryoturbation, which is an important process for carbon storage in the arctic tundra. Detrimental effects of frozen soils include degradation of infrastructure and foundations, flooding, and hazardous road conditions.

Properties of water in frozen conditions

The properties of water are unique compared to properties of all other matter known to science. Without this unique behavior of water, life would not be possible in cold climates. Phase change from the liquid phase to the solid phase releases a significant amount of heat and the volume of a kilogram of water increases from 1 L to approximately 1.1 L, thus reducing the density of water in the solid form. These two properties (phase change and reduction in density) make ice float on water and prevent lakes in the arctic from freezing to the bottom. The large buffer for heat consumption also prevents permafrost from degrading during the summer months. The negative effects of expansion are bursting water pipes if not protected from cold weather.

Soil water-ice characteristics and frost heave

In soils, the expansion of water upon freezing causes frost heave. There are two components of frost heave, primary and secondary frost heave. Primary frost heave is expansion of liquid water in the soil pores. Secondary frost heave is caused by liquid water movement in the soil while it is freezing and expanding. Many people have recognized this process and have worked on understanding its mechanisms (Henry, 2000).

Liquid water in porous media freezes at the point where the soil temperature drops below the freezing temperature of liquid water. This freezing temperature is not constant, but rather a function of the soil texture, liquid water content, ice pressure, and contaminant concentration under freezing condition. The liquid pressure inside a porous media experiences forces that result in an increase in the pressure as the porous media dries. The same principle works for a freezing soil, that is, as the soil becomes more frozen, the liquid experiences a greater pressure (Dash et al., 2006; Koopmans and Miller, 1966; Spaans and Baker, 1996). An example of the relation between temperature and liquid water content of a freezing soil is illustrated in Figure 1 for a clayey silt loam.

The freezing characteristics curve (Figure 1) can be described with the use of the van Genuchten equation and the Clapeyron equation. The van Genuchten equation was developed for non-freezing soil moisture characteristic relations and proposed by van Genuchten (1980) as

$$S_l = \left(\frac{1}{|\alpha\psi_m|^n + 1}\right)^m \tag{1}$$

where $m = 1 - \left(\frac{1}{n}\right)$.

Where S_l is the pore saturation (%), ψ_m is the matric pressure head (m), and α, n, and m are empirical parameters. For a clayey silt loam soil, values for $\alpha = 0.1$ and

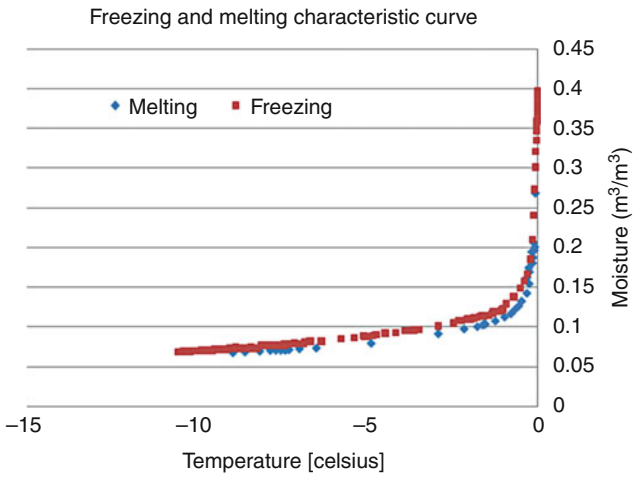

Frozen Soil Hydrology, Figure 1 Soil freezing characteristics measured in Northern Alaska (Data procured by Dr. Ronald P. Daanen using NSF grants of Prof. Vladimir Romanovsky, Permafrost Laboratory, University of Alaska Fairbanks, Grant Numbers ARC 0632400 and ARC 0856864).

$n = 1.6$. These values describe the pores size and structure of a particular soil.

The general Clapeyron equation is used to relate the matric pressure head with the temperature for the freezing characteristic curve, assuming an ice pressure head of zero. This thermodynamic relation is the basis of phase change and can be described as

$$\psi_m = \left(\frac{L_f}{273.15 \times g}\right) T + \psi_i \tag{2}$$

where L_f is the latent heat of fusion (334 kJ/kg), g is the acceleration due to gravity, ψ_m and ψ_i are the matric and ice pressure heads, and the constant 273.15 is the reference freezing point of liquid water at atmospheric pressure.

Examples of these combined equations in sand, loam, and clay are illustrated in Figure 2.

Frost susceptibility of a soil

Frost heave is caused by a supply of liquid water in the soil to feed growing ice lenses that are established in a thermal gradient and capable of displacing the soil in the perpendicular direction to the gradient. The liquid water content below the freezing temperatures of the porous medium and the hydraulic conductivity of frozen soils quantifies the frost susceptibility of a soil. We can describe the liquid water hydraulic conductivity by van Genuchten's (1980) relationship as

$$K = K_S S_e^{0.5} \left(1 - \left(1 - \left(S_e^{(1/m)}\right)\right)^m\right)^2 \tag{3}$$

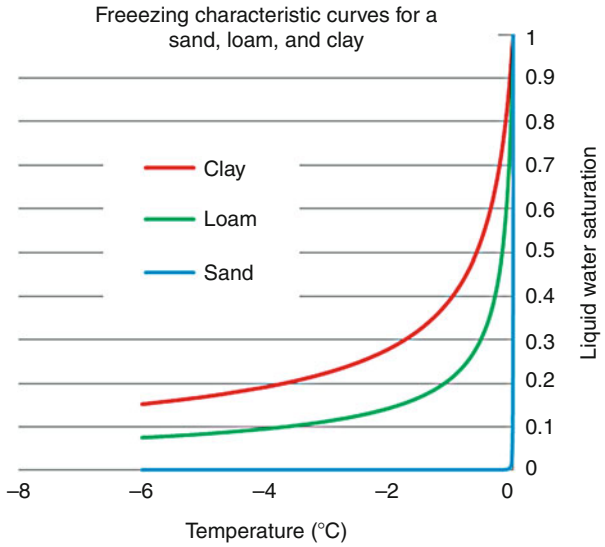

Frozen Soil Hydrology, Figure 2 Examples of freezing characteristic curves for sand, loam, and clay using the combination of van Genuchten equation and Clapeyron equation.

where, the effective saturation (S_e) is related to the soil temperature through the general Clapeyron equation and the freezing characteristic function. The value for K_s (saturated hydraulic conductivity) is dependent on the temperature of the super cooled liquid.

Usually, silty and loamy soil types are susceptible to frost heave. Frost susceptibility can easily be visualized by using Equations 1–3 and varying the soil temperature and temperature gradient to determine heat and water fluxes, while keeping the ice pressure zero. The induced liquid water flow and the induced heat conduction can be expressed as an energy flux. Phase change from liquid to ice is used to express the liquid water flow in an energy flux condition as illustrated in Figure 3.

From Figure 3 it becomes clear that frozen soil processes are highly nonlinear and difficult to solve numerically. Ice pressure was kept constant in the curves of Figure 3, but it has a major influence on the liquid water content, liquid water movement, and heat flux from latent heat during freezing. A value for the ice pressure is hard to obtain but attempts have been made to incorporate it in the mathematical equations governing frost heave (Rempel, 2007). Secondary frost heave described here is the main force behind degradation of foundations, road beds, and plant roots.

Hydraulic conductivity of frozen soil

The understanding and quantification of the hydraulic conductivity of frozen soil has gained interest due to the need of improved prediction methods and control of frost heave (Nixon, 1991), development of an understanding of transport and control of contaminants (especially

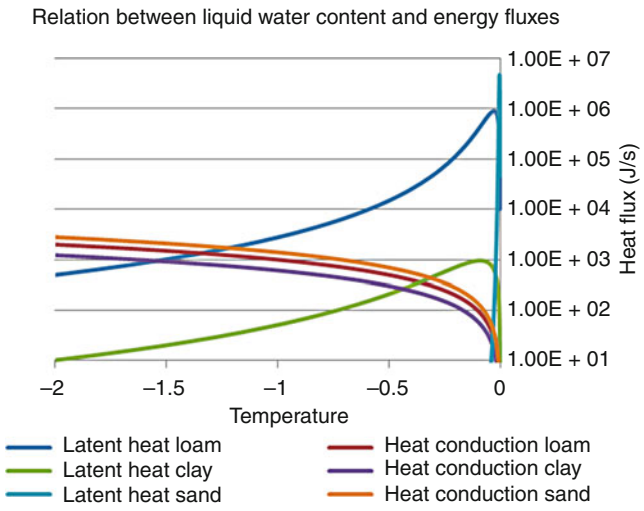

Frozen Soil Hydrology, Figure 3 Frost susceptibility expressed as energy fluxes. The maximum frost heave occurs when heat conduction and latent heat consumption are equal. This point occurs at a different level of heat flow for different soils, loam has the most favorable properties for frost heave with a maximum at a temperature of −1.3°C.

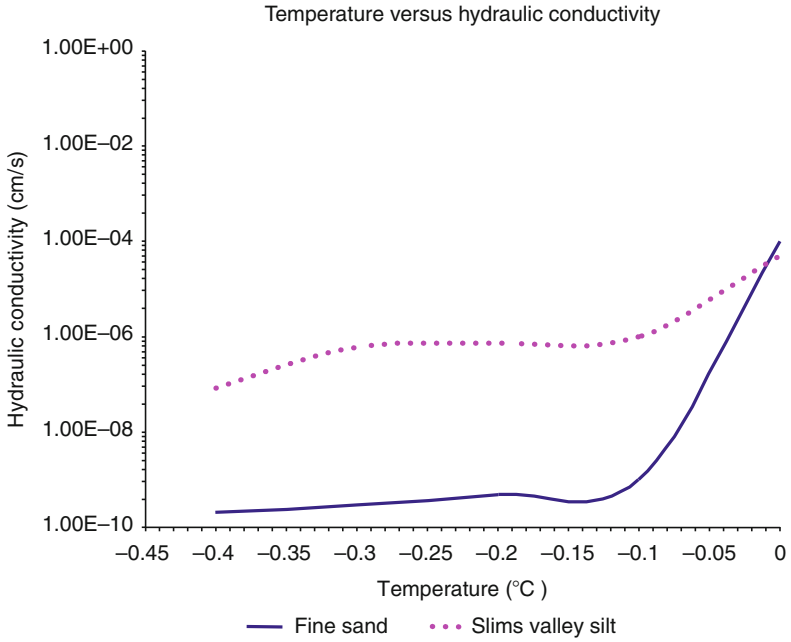

Frozen Soil Hydrology, Figure 4 Variation of hydraulic conductivity with temperature (adapted from Burt and Williams, 1976).

hydrocarbons from surface spillage) in permafrost underlain areas (Biggar et al., 1998), design of containment and remediation of hazardous liquid waste contaminants using frozen soil barriers (Vick, 1994), and remediation of dense nonaqueous phase liquids from soils in cold regions using permeability modification (D'Cunha et al., 2009). The hydraulic conductivity of the soil is directly proportional to the intrinsic permeability, which is usually a constant for any permeable material with a given porosity characteristics (see e.g., Fitts, 2002 or Andersland and Ladanyi, 2004). A change in soil ice content will change the intrinsic permeability of the soil and thus impact the overall hydraulic conductivity of the freezing soil.

The existence of liquid water in freezing or frozen soils allows migration of water under a hydraulic gradient. Experimental investigation by Burt and Williams (1976) indicated that ice formation was faster in high permeability zones (large grained soils) than the low permeability zones (fine grained soils) in a soil. Thus, at below freezing temperatures, large grained soils demonstrated lower hydraulic conductivity than fine grained soils (Figure 4).

D'Cunha et al. (2009) demonstrated through experimental investigation that the rate of change of hydraulic conductivity as a function of decreasing temperature was lower in fine grained soils compared to coarse grained soils (Figure 5). Such understanding has implications in engineering designs in cold regions.

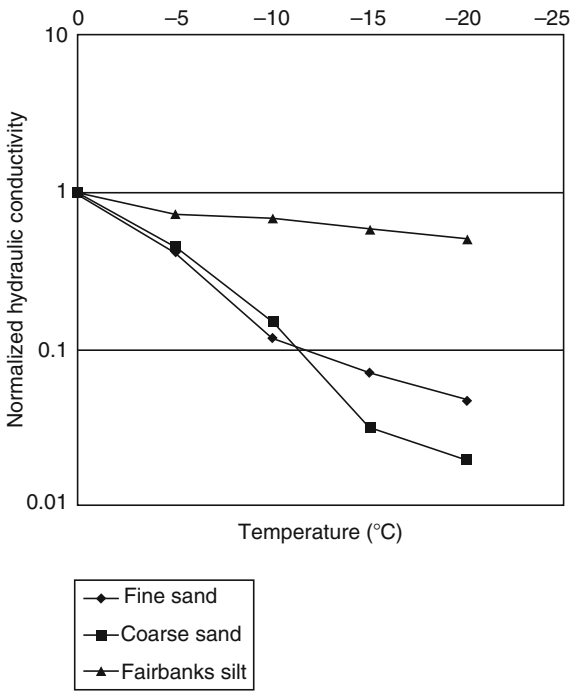

Frozen Soil Hydrology, Figure 5 Rate of change of hydraulic conductivity of three soils as a function of temperature.

Frost features and engineering

Thermokarsts, slides and flows, and aufeis are among the frost processes that are of special concern in engineering (Eranti and Lee, 2000). Thermokarsts are caused by thawing of ice-rich permafrost due to change in the ground thermal regime caused by disturbance in vegetation cover, for example, those that are caused by fire, heavy traffic, or alteration of the ground drainage due to construction. Thermokarsts cause erosion, sinkholes, and beaded

streams that impact structures and landscape. Flows and landslides are also caused due to change in soil thermal regime along slopes underlain with permafrost. Groundwater emerges to the surface due to blocked path (caused by vertical migration of freezing front into soils) in the winter and freezes on the surface causing aufeis conditions. All these features have extensive effect on roads and other structures in cold regions.

Frozen ground usually provides very strong support to short-term loads. However, creep occurs in frozen ground due to long-term loading especially in warm ice-rich frozen ground. Thaw settlement occurs due to such loading over time. The active layer (freezing and thawing regime of the soil) poses the major problems to engineering. Only clean coarse-grained minerals and ice-free bedrocks are not affected by frost action (Eranti and Lee, 2000). According to Eranti and Lee (2000), if the soil contains a few percent of grains that are smaller than 0.02 mm, then the soil is frost susceptible and hence prone to heave. Frost susceptible soils pose significant problems in engineering that includes frost heave, thaw weakening, and thaw settlement.

Impact of freezing soil on landscape

A process related to water migration in frozen soil is the formation of *segregated ice* and *massive ice* in the ground. *Ice wedge polygons* are an example of *massive ice* and responsible for the formation of polygonal patterned ground. *Pingos* are ice mounds formed in drained lake beds. The water from the *talik* underneath the lake slowly freezes and pressurizes to form a large ice core, which lifts the lake bottom up to form the mound. *Injection ice* or intrusion ice is associated with massive ice in pingo formation core, but can also occur along streams at the bottom of hill sides where water in the active layer can pressurize during fall. The top of the active layer along the hill slope freezes in the fall to form shallow confined aquifer, thus pressurizing water beneath the frozen layer. The pressurized water is injected out at the bottom of the hill where ice forms.

Preferential ice formation under rocks and stones caused by thermal conductivity differences drives a sorting process. During freezing of a mixture of soil and rocks, the rocks migrate slowly upward and get pushed out of the ground. Local macro scale thermal differences in the surface then drive a three-dimensional sorting similar to the theory for *non-sorted circles* (Daanen et al., 2008) which form *sorted circles* (Kessler and Werner, 2003), *sorted nets*, and *sorted polygons*.

Another form of sorting also known as *regelation* happens when objects are completely submerged in the ice, for example at the bottom of a glacier where ice moves around rocks and sediments as the glacier slides down the slope (Rempel, 2008). This movement happens under the influence of a temperature or pressure gradient from one to the other side of the object. On the cold end of the object the ice forms, but on the warm end the ice melts. Water migrates through a pre-melt thin film of water from the melting side to the freezing side, and heat flows the opposite way.

On a landscape level, frozen ground affects soil hydrology significantly. Flooding during spring snowmelt is often caused directly by frozen ground. Soil pores are blocked with ice, which reduces infiltration into the soil and increases the amount of water available for runoff. In agricultural regions, the excess water lingers in local depressions where it saturates the root zone and damages the crops in spring due to oxygen deprivation. Frozen ground in these depression-focused groundwater recharge areas thaws preferentially in narrow pockets. After these pockets form, they drain the depression in just a few hours.

Impact of frozen soil on bio- and ecosystems

Biological processes are hindered, but also benefit from frozen soil hydrological processes. For many microorganisms, it is not the temperature that limits their survival or respiration rate, but rather the abundance of liquid water. As we know from the previous sections, liquid water is present at temperatures below freezing, albeit in very thin layers surrounding soil particles. The organisms that survive in these small pores can also be active. An example is soil respiration during winter months in cold regions (Grogan and Jonasson, 2006; Schimel et al., 2006; Zimov et al., 1996). An added effect of the frozen ground is that tension cracks form, which are filled with air. These cracks are conduits for oxygen flow into the ground during the frozen season. Oxygen can reach depths that are usually oxygen depleted due to saturation of the soil profile during the warm season. Besides oxygen, there is also enrichment of nutrients in the thin liquid layers in the frozen soil. This enrichment is caused by solute exclusion from the pore and segregated ice as the water freezes (Konrad and Mccammon, 1990).

Perennial species of plants have to survive the winter months with enough roots to anchor themselves and stay upright so there is a chance to develop new roots in spring. Repeated freeze and thaw cycles create ice lenses within the root zone of plants, which has a negative effect on winter varieties of cereals (Shaw and Blackett, 1966). Besides crops, there is also a negative effect on ecosystems in northern regions. *Permafrost* (frozen ground for at least two consecutive years) limits drainage and controls summer root temperatures, which strongly limits plants from colonizing northern latitudes. In addition, ice lens formation and cryoturbation causes soil movement which has a strong negative effect on the vegetation. A clear example of this phenomenon is ice lens formation, which limits vegetation succession in *non-sorted circles* (Daanen et al., 2007; Daanen et al., 2008).

Summary

Frozen soil hydrology is a cold climate phenomenon. Approximately 50% of the northern hemisphere experiences frozen soil conditions. In soils, the expansion of water upon freezing causes frost heave. Most of this heave is caused by liquid water movement in the soil while it is freezing and expanding. Liquid water in porous media

freezes at the point where the soil temperature drops below the freezing temperature of liquid water. This freezing temperature is not constant, but rather a function of the liquid water and ice pressure. The liquid water content below the melting temperature of a porous medium and the hydraulic conductivity of frozen soils quantifies the frost susceptibility of a soil. Rate of change of hydraulic conductivity in frozen soils are lower in fine grained materials as opposed to coarse grained materials. Frost susceptibility leads to ice lens formation and frost heave, which limits vegetation succession in *non-sorted circles*. Preferential ice formation under rocks and stones caused by thermal conductivity differences drives a sorting process, which leads to sorted patterned ground. Regelation is another sorting process where impurities in ice can move, due to melting and freezing. On a landscape, level frozen ground affects soil hydrology dramatic. Flooding during spring snowmelt is often caused by frozen ground. Soil pores are blocked with ice which reduces infiltration into the soil and increases the amount of water available for runoff. Biological processes are hindered, but also benefit from frozen soil hydrological processes. Liquid water with increase nutrient concentrations in thin films and added oxygen through cracks in the frozen ground can sustain microorganisms during the cold season.

Bibliography

Andersland, O. B., and Ladanyi, B., 2004. *Frozen Ground Engineering*. New York: Wiley.

Biggar, K. W., Haidar, S., Nahir, M., and Jarrett, P. M., 1998. Site investigations of fuel spill migration into permafrost. *Journal of Cold Regions Engineering*, **12**, 84–104.

Burt, T. P., and Williams, P. J., 1976. Hydraulic conductivity in frozen soils. *Earth Surface Process*, **1**, 349–360.

D'Cunha, N. J., Misra, D., and Thompson, A., 2009. An Investigation into the Applications of Natural Freezing and Curdlan Biopolymer for Permeability Modification to Remediate DNAPL Contaminated Aquifers in Alaska. *Cold Regions Science and Technology*, doi:10.1016/j.coldregions.2009.05.005, 59:42–50.

Daanen, R. P., Misra, D., and Epstein, H., 2007. Active-layer hydrology in nonsorted circle ecosystems of the arctic tundra. *Vadose Zone Journal*, **6**, 694–704.

Daanen, R. P., Misra, D., Epstein, H., Walker, D., and Romanovsky, V., 2008. Simulating nonsorted circle development in arctic tundra ecosystems. *Journal of Geophysical Research-Biogeosciences*, **113**, 10.

Dash, J. G., Rempel, A. W., and Wettlaufer, J. S., 2006. The physics of premelted ice and its geophysical consequences. *Reviews of Modern Physics*, **78**, 695–741.

Eranti, E., and Lee, G. C., 2000. *Cold Region Structural Engineering*. USA: McGraw Hill.

Fitts, C. R., 2002. *Groundwater Science*. USA: Academic.

Grogan, P., and Jonasson, S., 2006. Ecosystem CO_2 production during winter in a Swedish subarctic region: the relative importance of climate and vegetation type. *Global Change Biology*, **12**, 1479–1495.

Henry, K. S., 2000. A review of the thermodynamics of frost heave, Report, Cold Regions Research and Engineering Laboratory.

Kessler, M. A., and Werner, B. T., 2003. Self-organization of sorted patterned ground. *Science*, **299**, 380–383.

Konrad, J. M., and Mccammon, A. W., 1990. Solute Partitioning in Freezing Soils. *Canadian Geotechnical Journal*, **27**, 726–736.

Koopmans, R. W. R., and Miller, R. D., 1966. Soil freezing and soil water characteristic curves. *Soil Science Society of America Proceedings*, **30**, 680–685.

Nixon, J. E., 1991. Discrete ice lens theory for frost heave in soils. *Canadian Geotechnical Journal*, **28**, 843–859.

Rempel, A. W., 2007. Formation of ice lenses and frost heave. *Journal of Geophysical Research-Earth Surface*, **112**, F02036.

Rempel, A. W., 2008. A theory for ice-till interactions and sediment entrainment beneath glaciers. *Journal of Geophysical Research-Earth Surface*, **113**, F01013.

Schimel, J. P., Fahnestock, J., Michaelson, G., Mikan, C., Ping, C. L., Romanovsky, V. E., and Welker, J., 2006. Cold-season production of CO_2 in arctic soils: Can laboratory and field estimates be reconciled through a simple modeling approach? *Arctic Antarctic, and Alpine Research*, **38**, 249–256.

Shaw, M. W., and Blackett, G. A., 1966. Unusual frost injury to winter sown wheat and barley. *Plant Pathology*, **15**, 119–120.

Spaans, E. J. A., and Baker, J. M., 1996. The soil freezing characteristic: Its measurement and similarity to the soil moisture characteristic. *Soil Science Society of America Journal*, **60**, 13–19.

van Genuchten, M. Th., 1980. A closed-form equation for predicting the hydraulic conductivity of unsaturated soils. *Soil Science Society of America Journal*, **44**, 892–898.

Vick, J. D., 1994. Description of the Hanford Cryobarrier Demonstration Project. In Notes from Cryobarrier Technology Workshop, Richmond, Wash.

Zimov, S. A., Davidov, S. P., Voropaev, Y. V., Prosiannikov, S. F., Semiletov, I. P., Chapin, M. C., and Chapin, F. S., 1996. Siberian CO_2 efflux in winter as a CO_2 source and cause of seasonality in atmospheric CO_2. *Climatic Change*, **33**, 111–120.

Cross-references

Frost
Glacier Hydrology
Thermokarst

FROZEN TOE (OUTER ZONE OF GLACIER SNOUT)

Pratima Pandey
Centre of Studies in Resources Engineering, Indian Institute of Technology, Bombay, Powai, Mumbai, Maharashtra, India

The frozen toe is a leading edge of a glacier formed due to the glaciotectonism or the thrust which takes place beneath a glacier. It is the frozen outer zone of the snout and has a shape of a boot (shoes) or toe.

G

GELISOLS

Divya Dudeja
Department of Geology, DBS (PG) College, Dehradun, Uttarakhand, India

Gelisol comes from the Latin word "gelare" meaning "to freeze". These are soils of very cold climates that contain permafrost within about 100 cm of the soil surface and/or have gelic materials. Gelic materials are mineral or organic soil materials that have evidence of cryoturbation (frost churning), ice segregation in the active layer, or the upper part of the permafrost. Low soil temperatures cause soil-forming processes such as decomposition of organic materials to proceed very slowly. As a result, most gelisols store large quantities of organic carbon which accumulates in the upper layer and yield black or dark brown color to gelisol layers. Despite the influence of glaciation in most areas where gelisols occur, chemically they are not highly fertile because nutrients, especially calcium and potassium, are very easily leached above the permafrost. The vegetation supported is mostly lichens, mosses, sedges, shrubs, black spruce, and white spruce. Engineering use of gelisols is also limited due to permafrost as large structures are adversely affected by frost heaving and thaw weakening. Gelisols are found chiefly in Siberia, Alaska, and Canada. Smaller areas are found in the Andes (mainly near the intersection between Chile, Bolivia, and Argentina), Tibet, northern Scandinavia, and the ice-free parts of Greenland and Antarctica.

GEOCHEMISTRY OF SNOW AND ICE

Tandong Yao, Yongqin Liu, Huabiao Zhao, Wusheng Yu
Laboratory of Tibetan Environment Changes and Land Surface Processes (TEL), Institute of Tibetan Plateau Research, Chinese Academy of Sciences, Haidian District, Beijing, China

Definition and introduction

The geochemistry of snow and ice is a very broad subject. This chapter includes only the chemistry associated with major ions (Na^+, NH_4^+, K^+, Mg^{2+}, Ca^{2+}, NO_3^-, SO_4^{2-}, and Cl^-) because of limitations of space and the current state of knowledge. As generally known, atmospheric aerosols are scavenged by snow, and dry deposition and/or other forms of wet deposition, such as rain and mist, may add solute to snow cover. The snow on a glacier incorporates impurities and eventually transforms into ice by compaction and recrystallization with time. In this way, airborne constituents can be faithfully recorded by the chemical compositions of glacier ice in suitable locations. Postdepositional effects, such as ablation, sublimation, and snow drifting, may impact on the geochemistry of ice cores. However, ice cores recovered from polar ice sheets and mid- to low-latitude glaciers and ice caps provide numerous proxy records representing past climatic and atmospheric environmental parameters over a wide range of time scales.

Vijay P. Singh, Pratap Singh & Umesh K. Haritashya (eds.), *Encyclopedia of Snow, Ice and Glaciers*, DOI 10.1007/978-90-481-2642-2,

Polar ice sheets

Polar ice sheets contain a wealth of environmental history because of their geographical position and prevailing meteorological conditions. Information retrieved from polar ice sheets has hemispheric or global significance due to their remoteness from local aerosol sources (Delmas, 1992), and holds important historical clues for a better understanding of modern global climatic and environmental changes (Wolff, 1990; Legrand and Mayewski, 1997; Meeker et al., 1997; Wagenbach et al., 1998; Banta et al., 2008; Burkhart et al., 2009).

Studies of impurities in polar snow allow the determination of relationships in chemical concentrations between snow and the atmosphere. These then permit interpretation of ice core records based on changes in sources and transport processes. In the past, researchers generally assumed that snow concentrations change proportionally with the atmospheric concentrations from which they derive (Wolff, 1990). However, some solutes do not always follow this generalization because of the post-depositional effects, such as diffusion from the gas phase to the ice crystalline lattice and redistribution in firn after snow deposition (Mayewski and Legrand, 1990; Staffelbach et al., 1991; De Angelis and Legrand, 1995; Wolff et al., 1998). Therefore, caution must be applied when attempting to use chemical compositions in snow and ice as proxies for past atmospheric concentrations.

Impurities within polar snow have a variety of sources including both natural and anthropogenic emissions (Figure 1). Winds from oceanic and continental surfaces introduce primary aerosols directly into the atmosphere, or as secondary aerosols through chemical reactions with trace gasses (Legrand and Mayewski, 1997). Concentrations of soluble species in snow show significant spatial and seasonal variabilities over the Greenland and Antarctic ice sheets (Kreutz and Mayewski, 1999; Bertler et al., 2005; Burkhart et al., 2009). Therefore all species present in snow and ice must be studied in order to better understand and reconstruct the original associations among the various constituents.

Natural aerosols

Natural aerosols dominate in the polar ice sheets due to the long distances from human habitation. Sea salt (e.g., Na^+, Cl^-) deposition in polar snow is very high in coastal areas but decreases rapidly inland as a function of elevation, distance from the sea, and snow accumulation (Mulvaney and Wolff, 1994; Yang et al., 1996; Goktas et al., 2002; Suzuki et al., 2002; Bertler et al., 2005). Sodium exhibits well-delineated maximum concentrations during winter and glacial periods in both central Greenland and Antarctic ice cores as a consequence of more enhanced advection of marine air masses during winter over ice sheets (Herron, 1982; Legrand and Delmas, 1984), and/or due to the existence of highly saline brines and fragile frost flowers on newly formed sea ice in winter, both very effective sources of sea salt (Rankin et al., 2002; Wolff et al., 2003). Temporal correlations of sea salt concentrations in Antarctica (Kreutz et al., 2000) and Greenland (Meeker and Mayewski, 2002) suggest that oceans contribute a strong influence on the transport to these sites. High sea salt fluxes indicated in the Dome C and Dome Fuji ice cores during the LGM (Last Glacial Maximum) correspond to significantly increased production of winter sea ice on both the Indian and Atlantic sides of Antarctica (Wolff et al., 2003). The significantly increased concentrations of sea salt species in Antarctica (Röthlisberger et al., 2002) and Greenland (Mayewski et al., 1997) during the LGM suggest the influence of both enhanced atmospheric transport and local sea ice extent. Cl^- shows less seasonal variation than does Na^+ in the snowpack owing to additional input or loss of HCl, which could smooth the initial seasonal cycle (Legrand and Delmas, 1988; De Angelis et al., 1997).

Calcium, which derives from marine as well as the terrestrial sources, exhibits little variation in Antarctica, whereas distinct spring maxima appear in Greenland snow (Legrand and Mayewski, 1997). Assuming that Na^+ comes solely from sea salt, the respective contributions of sea salt (ss) and non-sea salt (nss) to the other species can be calculated based on standard seawater ion

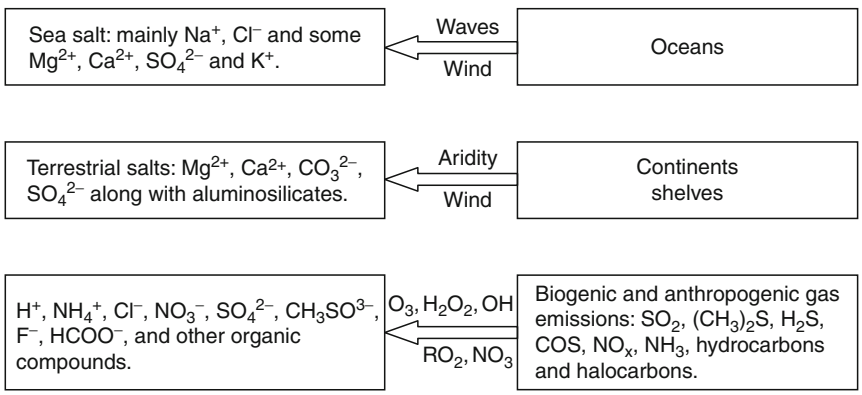

Geochemistry of Snow and Ice, Figure 1 Various soluble impurities likely to be trapped in polar snow layers and their corresponding origins and sources. (Adapted from Legrand and Mayewski (1997) (copyright AGU).)

ratios. In this way, nssCa^{2+} (De Angelis et al., 1997; Wolff et al., 2006, 2007), and nssMg^{2+} (Legrand et al., 1988; De Angelis et al., 1997), can be used as good indicators of the continental input in polar snow and ice from areas of exposed bedrock in Antarctica (Kreutz, 2007), South America (De Angelis et al., 1992; Fischer et al., 2007), and Asia (Whitlow et al., 1992; Meeker and Mayewski, 2002). However, the terrestrial dust usually contributes little to modern polar snow (Legrand and Mayewski, 1997). Similar to the sea salt species, nssCa^{2+} concentrations show dramatic increases in Antarctic and Greenland ice cores from glacial periods (Fuhrer et al., 1993; Mayewski et al., 1996; Petit et al., 1999; Röthlisberger et al., 2002; Werner et al., 2002), which may be caused by changes in climate and vegetation over source areas during those times (Kreutz, 2007).

Natural SO_4^{2-} derives from multiple sources: marine (Legrand, 1995), evaporites (Legrand, 1997), and volcanic eruptions (Hammer, 1977), and is often used to reconstruct marine bioactivity and volcanic events. Volcanic eruptions emit large quantities of SO_2 into the atmosphere. Sulfate aerosols formed from the atmospheric oxidation of SO_2 and gas-to-particle conversions can be transported to, and deposited on, polar ice sheets. These processes often augment the SO_4^{2-} concentrations in polar ice for 1 or 2 years after large volcanic eruptions (Kreutz, 2007). Thus, SO_4^{2-} records in ice cores provide a powerful tool for investigating the impact of individual eruptions on climate and the atmospheric environment (Zielinski et al., 1994; Robock, 2000). Furthermore, the SO_4^{2-} layers of peak concentrations corresponding with well-known volcanic events can be used as marker horizons in ice core dating (Udisti et al., 2000). In addition to SO_4^{2-}, volcanic aerosols can also contribute other species including Cl^- and F^- to the overall solutes (Herron, 1982; De Angelis et al., 1997).

Various natural sources of NO_x (nitrogen oxides, mainly atmospheric precursors of NO_3^-) include soil exhalation, biomass burning, lightning, cosmic rays, stratospheric oxidation of N_2O, and ionospheric dissociation of N_2, and can contribute to the NO_3^- budget in polar precipitation (Legrand and Kirchner, 1990). Although a large amount of snow and ice core NO_3^- data exists, the major sources of NOx influencing the Polar Regions still cannot be identified, because of the reactive NOx cycling between the snow and the surface boundary layer (Mayewski and Legrand, 1990; Wolff et al., 1998; Ginot et al., 2001; Röthlisberger et al., 2002; Wolff et al., 2002). The nonuniform spatial variability of NO_3^- concentrations across polar ice sheets (Burkhart et al., 2004, 2009; Bertler et al., 2005) results from postdepositional alterations by temperature, accumulation, and other factors (Burkhart et al., 2004; Grannas et al., 2007; Wolff et al., 2007). Consequently, one needs to consider spatial variables to properly account for trends and variability in the NO_3^- record from polar ice cores.

NH_4^+ concentrations are usually one order of magnitude lower in Antarctica than in Greenland ice. In view of the geographical locations of the two ice sheets, such a discrepancy supports the idea that continental emissions such as plants, soils, bacterial decomposition, burning of biological materials, and animal activities dominate the atmospheric ammonia content (Legrand and Mayewski, 1997). NH_4^+ concentrations in aerosols and snow from coastal Antarctica vary considerably and most likely relate to the presence of large penguin populations near the site during the austral summer (Legrand et al., 1998). In contrast, high mean NH_4^+ concentrations with strong summer maxima in Greenland snow layers probably relate to NH_3 biospheric emissions from the northern continents (Legrand et al., 1992; Fuhrer and Legrand, 1997). In Greenland, the temporal profile of NH_4^+ concentrations has been used to reconstruct the history of forest fires in the high-latitude Northern Hemisphere (Savarino and Legrand, 1998). On multidecadal to glacial–interglacial timescales, NH_4^+ concentrations in Greenland mainly relate to continental biogenic emissions from soils; and no evidence has been found for a significant marine contribution (Kreutz, 2007). Furthermore, NH_4^+ in central Greenland shows no overall anthropogenic increase, but a doubling of springtime concentrations during the second half of the twentieth century, which may be caused by influence of Eurasian sources and enhanced long-range transport associated with high SO_2 and NO_x emissions (Fuhrer et al., 1996).

Anthropogenic aerosols

Emissions of SO_2 and NO_x from industrial activities and fossil fuel combustion provide significant sources for SO_4^{2-} and NO_3^- found in Greenland (Goto-Azuma and Koerner, 2001). The chemical profiles of ice cores covering the last 200 years provide a wealth of information on the impact of human activities on atmospheric compositions. The nssSO_4^{2-} concentrations in Greenland ice cores reveal an increase at the end of the nineteenth century (Mayewski et al., 1990; Fischer et al., 1998). The south Greenland nssSO_4^{2-} trend resembles that of North American SO_2 emissions (Mayewski et al., 1986, 1990), while the more pronounced nssSO_4^{2-} increase after 1940 in central Greenland might result from a stronger influence of Eurasian sources (Fischer et al., 1998). Greenland ice core samples from after 1980 also show a decreasing trend of nssSO_4^{2-}, which likely reflects the reduction of SO_2 emissions in industrialized countries. Concurrent increases of NO_3^- concentrations since around 1950 in several ice cores in Greenland exclude postdepositional effects, suggesting that the growing NOx emissions in the northern hemisphere originate mainly from fossil fuel burning (Mayewski et al., 1990; Fischer et al., 1998; Goto-Azuma and Koerner, 2001). At the present time, no convincing evidence exists for an anthropogenic impact on SO_4^{2-} and NO_3^- concentrations in Antarctica (Kreutz, 2007). In addition to SO_4^{2-} and NO_3^-, increases in Cl^- could be related to direct anthropogenic HCl emissions from coal burning and waste incineration (Legrand et al., 2002).

Generally, polar ice cores contain one of the better archives for chemical information regarding the composition of the atmosphere in the past. These cores have been widely used to investigate the past changes of global atmospheric circulation, climate in possible source areas, and environmental impacts of human activities. However, the processes that transfer pollutants between the atmosphere and snow under modern conditions provide the best foundation for interpreting ice core records.

Mid- and low-latitude glaciers and ice caps

Analyses of ice from polar ice sheets depict an unprecedented picture of past climatic and environmental changes for the scientific community. However, weather patterns and climate changes in Polar Regions differ from those in mid- and low-latitude regions. Environmental changes cause great concern at mid- and low-latitude regions of our Earth simply because these areas support about 85% of the global population. Thus, understanding potential environmental change in these nonpolar regions takes on prime importance, and can best be accomplished using information retrieved from alpine glaciers. Furthermore, mid- and low-latitude glaciers allow more reliable assessment of anthropogenic contributions that exceed the natural environmental variability because of their proximity to populated areas.

Because of their moderate temperatures, only a few mid- and low-latitude glaciers preserve accurate records of environmental changes over an extended time. For greatest preservation, these sites must have the following characteristics: high elevation, relatively simple ice-flow dynamics, flat- to low-angle bedrock topography, limited redistribution of snow, minimal snowmelt during the summer season, and a large ice thickness for maximum record length (Cecil et al., 2000). Quite a few ice cores have been recovered from mid- and low-latitude regions, such as the Andes (Thompson et al., 1995; Vuille et al., 2008), Rocky Mountains (Naftz et al., 1996, 2002), Alps (Döscher et al., 1996; Schwikowski et al., 1999a), and Central Asia (Yao et al., 1997; Kreutz et al., 2001). Because of the extensive scientific achievements having been made in snow/glacier chemistry from alpine glaciers, this chapter cannot cover all of the research work. Therefore, this section reviews studies of major ions from a small selection of these glaciers in the Alps and the Tibetan Plateau region to illustrate the more extensive work.

Glaciers in the Alps

Surrounded by densely populated and heavily industrialized countries, the Alps exemplify a suitable area for investigating the direct impacts of man-made compounds in the atmosphere (Maggi et al., 2006). Postdepositional processes can significantly remove, redistribute, and alter the chemical information about environmental change that arrives with the snowflakes falling on the surface of mid- and low-latitude glaciers (Schotterer et al., 2004). For example, a drastic disturbance of the concentration record of certain ionic species in a 13-m long firn section of an ice core from Grenzgletscher has been attributed to inflow of surface meltwater along a crevasse system in the glacier (Eichler et al., 2001). Although the seasonal pattern for NH_4^+, F^-, Cl^-, and NO_3^- was more or less well preserved, concentrations of K^+, Na^+, Mg^{2+}, Ca^{2+}, and SO_4^{2-} were significantly reduced (Eichler et al., 2001). Despite various postdepositional effects, ten different sites remain suitable for paleo-chemical investigations in four high-altitude areas in the Alps (Funk, 1994).

Very little postdepositional alteration of chemical solutes occurs at the high-accumulation alpine sites, such as in the Col du Dôme glacier (Mont Blanc Massif). Consequently, the ionic species show a sharply pronounced seasonal pattern, with concentrations low in winter and high in summer (Maupetit et al., 1995; Preunkert et al., 2000; Maggi et al., 2006), which can be used as reference horizons in ice core dating (Eichler et al., 2000; Largiuni et al., 2003). Many studies have demonstrated that the seasonal patterns of major ions in snow and ice from high-altitude glaciers generally correlate with each other, commonly attributed to the behavior of the planetary boundary layer. During winter, stable, low-altitude thermal inversions limit the vertical exchange between the boundary layer and the free troposphere, thus limiting the transport of ground-emitted pollutants to high-elevation locations In summer, convection circulates polluted air vertically, even up to the highest summits in the Alps (Schwikowski et al., 1999b; Largiuni et al., 2003; Maggi et al., 2006). The seasonal pattern of NH_4^+ concentrations in the Alpine glaciers can also be exacerbated by the increased emissions of NH_3 during summer (Maupetit et al., 1995; Kuhn et al., 1998).

Published records include concentrations of various chemical species obtained from the different Alpine ice cores. These records clearly demonstrate the effects of anthropogenic emissions on the chemical compositions of snow. The following discusses only SO_4^{2-}, NO_3^-, and NH_4^+.

The total SO_4^{2-} profile shows a constant level between 1756 and 1870, followed by an increasing trend, reaching maximum values between 1970 and 1985, followed by declining concentrations (Schwikowski et al., 1999b; Preunkert et al., 2001). The Na^+ and Ca^{2+} values provide sea salt and mineral dust tracers, respectively, for calculating the $exSO_4^{2-}$ (SO_4^{2-} concentration after correction for the sea salt and the terrestrial contribution). Because the natural SO_4^{2-} from sea salt and mineral dust had no trend during this period, the increasing trend in total SO_4^{2-} was attributed to anthropogenic SO_2 emissions (Schwikowski et al., 1999b; Schwikowski, 2004) (Figure 2). In order to identify potential source areas of anthropogenic SO_4^{2-} in high Alpine ice cores, the long-term changes of $exSO_4^{2-}$ concentrations in summer and in winter were compared with past SO_2 anthropogenic emission estimates from several combinations of countries in Europe. Preunkert et al. (2001) concludes that countries having an impact on the high-elevation Alpine sites for the Mont Blanc area

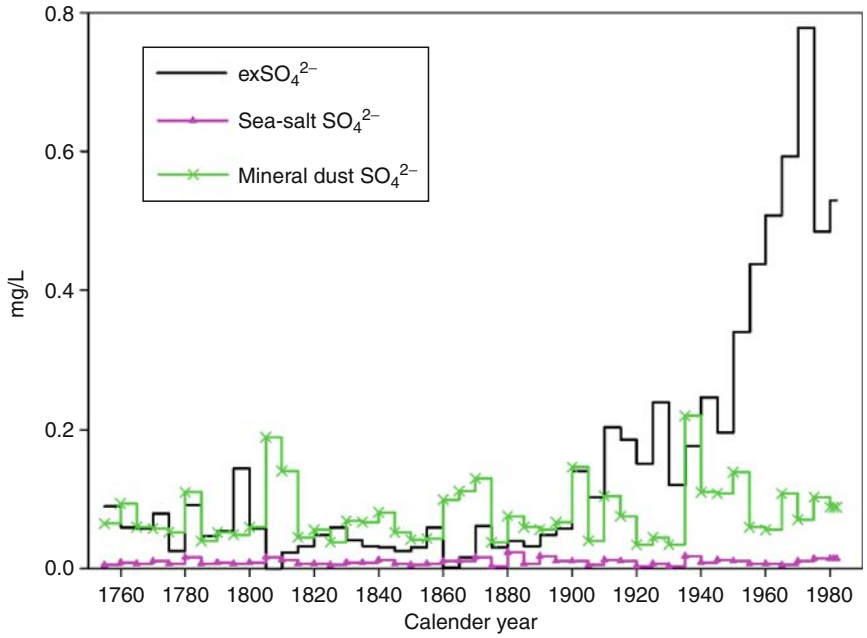

Geochemistry of Snow and Ice, Figure 2 Record of 5-year averages of $exSO_4^{2-}$ (SO_4^{2-} concentration after correction for the sea salt and terrestrial contributions) in Colle Gnifetti (Monte Rosa area) ice core, along with the corresponding records of sea salt and mineral dust derived SO_4^{2-}. (Adapted from Schwikowski et al., 1999b (copyright Munksgaard).)

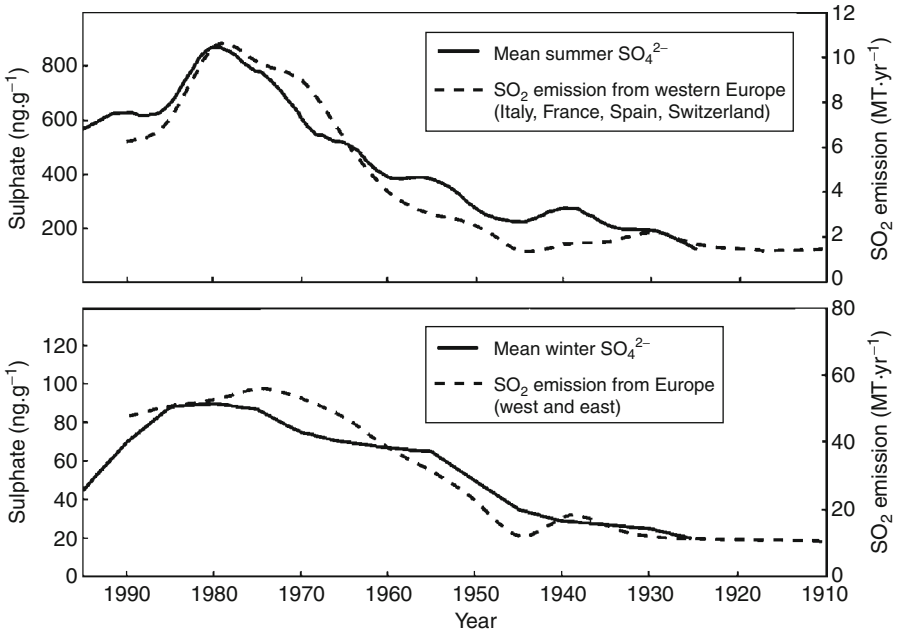

Geochemistry of Snow and Ice, Figure 3 Comparison of Col du Dôme SO_4^{2-} profiles with the European SO_2 emission history. (Adapted from Preunkert et al., 2001 (copyright AGU).)

in summer include regions located within 700–1,000 km of the Alps, with emissions from France, Spain, Italy, and Switzerland having the major influence. In the winter record, $exSO_4^{2-}$ concentrations reflect limited contamination of the free troposphere, with contributions from all of Europe and possibly from the USA (Figure 3).

The nitrate record from an ice core at Colle Gnifetti (in the Monte Rosa area) shows that between the two time

periods of 1850–1880 and 1965–1981, the mean NO_3^- concentration more than doubled (Döscher et al., 1995). Nitrate concentrations remain constant in the ice core record prior to 1930, but after 1930 they increase sharply to 1965 (Döscher et al., 1995). Similar to the SO_4^{2-} example above, Preunkert et al. (2003) also examined the winter and summer trends of NO_3^- record from a Col du Dôme ice core separately. From 1960 to 1980, the summer nitrate changes follow rather closely with the estimates of growing NO emissions from the neighboring European industrialized countries (Italy, France, Switzerland, and Spain) within about 1,000 km (Preunkert et al., 2003). Data from 1980 to 2001 show a minor increase in summer NO_3^- levels, inconsistent with NO emission estimates, which show a decrease after 1993 (Preunkert et al., 2003). The reason for the discrepancy remains unknown. Data indicate that NO_3^- concentrations in rain have not changed much at most monitoring sites in the Alps in the last 15–20 years (Rogora et al., 2006). A weaker increase in winter than in summer seen in the NO_3^- record from 1930 to 1990 in the same ice core may correspond to less contamination of the wide European mid-troposphere (Preunkert et al., 2003).

NH_4^+ forms in the atmosphere via neutralization of NH_3, neutralizing up to 70% of the original acidity in precipitation (Buijsman et al., 1987). As pointed out in previous work on Alpine glaciers (Maupetit et al., 1995; Schwikowski et al., 1999a; Preunkert et al., 2000), NH_4^+ concentrations in high-elevation ice cores show the most pronounced seasonal pattern among all the major ions, with concentrations about one order of magnitude higher in summer than in winter. Within the Alpine regions, high NH_4^+ concentrations generally accompany high concentrations of SO_4^{2-} and NO_3^- (Maggi et al., 2006), because ammonia is always involved in the conversion of SO_2 and NO_x into the aerosol phase (Schwikowski, 2004). A 200-year-long record of NH_4^+ concentrations from the Colle Gnifetti ice core shows an increase in concentrations by a factor of 3 between 1870 and 1980 (Döscher et al., 1996), indicating that NH_3 emissions in Europe substantially increased in the twentieth century.

Sea salt transported together with mineral dust, mainly from the Saharan area, makes up the major source of Cl^- in the Southern Alps. However, an average 16% of the Cl^- deposition in the period 1937–1994 could be related to HCl emissions from anthropogenic sources (Eichler et al., 2000). The sharp increase of nssCl^- in the late 1960s record has been attributed to HCl emissions from waste incineration in some areas of Europe (Eichler et al., 2000; Legrand et al., 2002). Also, Saharan dust plumes can sporadically reach the Alps (De Angelis and Gaudichet, 1991) and disturb the snow chemistry by entraining additional species, such as Ca_2^+, Na^+, Mg^{2+}, and Cl^-, in the Alpine glaciers (Legrand et al., 2002; Maggi et al., 2006).

Cold glaciers from high-altitude regions in the Alps have provided very valuable natural archives for reconstructing variations in the atmospheric components over the last decades and centuries. In addition to the natural variability of the ice core records, several chemical species reveal an unambiguous anthropogenic contribution to mid-troposphere pollution during the second half of the twentieth century (Maggi et al., 2006). On a positive note, Alpine glaciers also reliably demonstrate the progress achieved in environmental protection (Schwikowski, 2004). Many of the pollutants in Alpine ice clearly show decreasing levels since around 1970, resulting directly from various air quality measures.

Glaciers on the Tibetan Plateau and surrounding regions

The Tibetan Plateau and surrounding regions contain over 46,000 glaciers, amounting to a total glacial area of about 59,400 km^2 (Yao et al., 2007) – the highest concentration of glaciers outside of polar regions. Some of these glaciers are suitable for the recovery of ice cores that extend back thousands of years and allow for the development of detailed, high-resolution records of climatic and environmental change in the region. These records provide important insights, considering the critical role of High Asia in regional and global atmospheric circulation, and the importance of the Asian monsoons in providing life-sustaining rains to more than half the world's population (Wake et al., 2001). Research on spatial and temporal changes in snow and ice core records over this broad area contributes greatly to the study of global change.

The influx of dust from the arid and semiarid regions in central Asia primarily controls the spatial distribution of snow chemistry in the region (Wake et al., 1993). These glaciers adjacent to vast arid regions display very high concentrations of dust-related major ions such as Ca^{2+}, Mg^{2+}, K^+, and Na^+. Glaciers more distant from major dust source regions show intermediate levels of major ions, while glaciers on the southern slopes of the Himalaya are relatively free from the influence of desert dust (Wake, 2007). By contrast, fluxes of sea salt species in the glaciers over the Tibetan Plateau show strong spatial gradients, with decreasing concentrations as the distance increases between the glaciers and the Indian Ocean (Wake et al., 1990, 1993; Xiao et al., 2002). Wake et al. (2004) analyzed the gradients of glaciochemical parameters across the crest of the Himalaya based on data from six glaciers in the eastern and central Himalaya: three on the southern slopes and three on the northern slopes. The results show dust-related major ions (Ca^{2+}, Mg^{2+}, and Na^+) to be two to three orders of magnitude greater for northern slope sites compared to the southern slope sites, and appear strongly influenced by dust derived from the arid regions in central Asia (Wake et al., 2004). However, the major and trace elements record from a new Mt. Everest ice core indicates that the dominant winter dusts come from the Arabian Peninsula, Thar Desert, and northern Sahara (Kaspari et al., in press).

The seasonal patterns of major ion concentrations and fluxes exist in the Himalayan glaciers as a result of interactions between the Indian summer monsoon and the

continental air mass (Kang et al., 2000, 2004; Balerna et al., 2003). Kang et al. (2004) summarized the ion concentrations in fresh snow in the vicinity of Mt. Everest from recent research (Figure 4). The seasonal differences in ion concentrations occur both during the monsoon and pre-monsoon seasons. For example, pre-monsoon Ca^{2+} concentrations exceed the monsoon values by an order of magnitude (Kang et al., 2004). While in north central Asia, dust deposition predominantly influences the soluble chemistry of snow and ice, with high ion concentrations coinciding with Asian dust storm events (Wake et al., 1992; Li et al., 1995; Yao et al., 1995; Kreutz et al., 2001). Consequently, the Ca^{2+} record from the Guliya ice cap, which lies adjacent to the dust sources, provides a good proxy for atmospheric dust loading in the region (Yao et al., 2004).

The ionic concentration records from high-resolution ice cores in High Asia can provide valuable contributions for documenting and understanding decadal-to-century-scale variability of the related atmospheric circulations. Through comparisons of the FER (Far East Rongbuk glacier, located on the northern slope of Mt. Everest) Ca^{2+} record with a variety of climate indices, Wake et al. (2001) established a relationship between dust deposition in the Himalaya and the strength of the Asian Low. A strong Asian Low corresponds to a strong Asian monsoon. This relationship indicates an increase in the strength of the Asian monsoon during the second half of the twentieth century. Glaciochemical records from an 80.4-m ice core on the East Rongbuk glacier (also on the northern slope of Mt. Everest) demonstrate that the majority of the crustal ions relate to the winter Mongolian High and the remainder of the crustal species relate to the summer Mongolian Low (Kang et al., 2002a). Kaspari et al. (2007) reconstructed the atmospheric circulation over the eastern Himalaya prior to the instrumental record based on the relationships between the May–October pressure in the Mongolian region and Ca^{2+} and $ssCl^-$ concentrations from another East Rongbuk ice core. This reconstruction shows a decrease in large incursions of marine air masses ($ssCl^-$) since ~1330 AD and an overall increase in incursions of continental air masses (Ca^{2+}) since ~1420 AD, indicating a weakening summer monsoon influence in the Everest region since ~1400 AD.

Given the sparse population and minimal industrial activity on the Tibetan Plateau, the area contributes no significant local pollutants to the atmosphere. However, pollutants resulting from the acceleration of industrialization and explosion of population in south Asia can be transported to the Himalayas by favorable circulation patterns (Shrestha et al., 2000; Hindman and Upadhyay, 2002) and deposit onto the glaciers. A doubling of Cl^- concentrations in the Dasuopu (on the north side of Mt. Xixiabangma) ice core since 1860 AD may reflect increased land use, widespread biomass burning, and increased industrialization in Nepal and India during the twentieth century (Thompson et al., 2000). The close correspondence of the SO_4^{2-} concentration trend in the same ice core to SO_2 emissions over southern Asia indicate that south Asian anthropogenic sources have dominated the SO_4^{2-}deposition on Himalayan glaciers since the 1930s (Duan et al., 2007). The sharp increase of annual NH_4^+ concentrations from the 1940s to the 1980s in an East Rongbuk ice core may correspond to the explosion of population resulting in enhanced agricultural activities (Kang et al., 2002b; Qin et al., 2002; Hou et al., 2003).

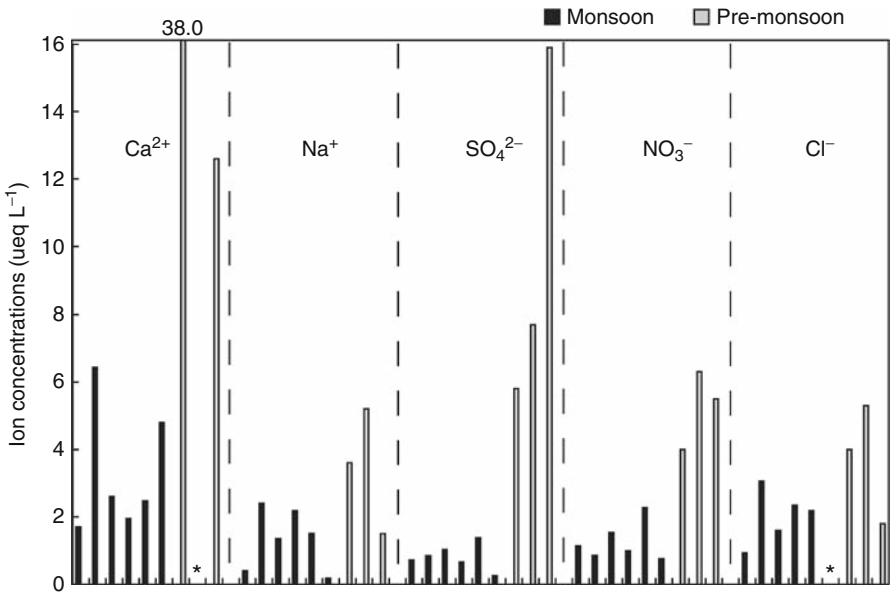

Geochemistry of Snow and Ice, Figure 4 Comparison of ion concentrations between monsoon and pre-monsoon fresh snow samples collected in the vicinity of Mt. Everest, central Himalayas. (From Kang et al., 2004 (copyright Elsevier).)

Although dust-related species dominate the major ion components of snow in central Asia and could mask the anthropogenic signals recorded in the glaciers, information regarding anthropogenic impacts on glaciochemistry can still be recovered. The chemical record from a shallow firn core from the Inilchek glacier (in the Kyrgystan Tien Shan) indicates that a summer increase in atmospheric NH_4^+ may be related to regional agricultural activities (Kreutz et al., 2001). Variations of SO_4^{2-} and NO_3^- records from a Belukha (in the Siberian Altai) ice core reflect SO_2 emissions in Siberia and Kazakhstan from traffic growth and enhanced fertilizer application (Olivier et al., 2003, 2006), respectively. Comparison of SO_4^{2-} and Ca^{2+} concentrations in a Muztagata (in the eastern Pamirs) ice core shows that they shared common trends before mid-1970s because of the masking effect from large terrestrial inputs. But then the SO_4^{2-} concentrations increased more rapidly than Ca^{2+} (Figure 5a), which may indicate that the SO_4^{2-} concentrations in the ice core have been dominated by anthropogenic emissions. Coherent changes between SO_4^{2-} concentration records and SO_2 emission estimates in the CIS (Commonwealth

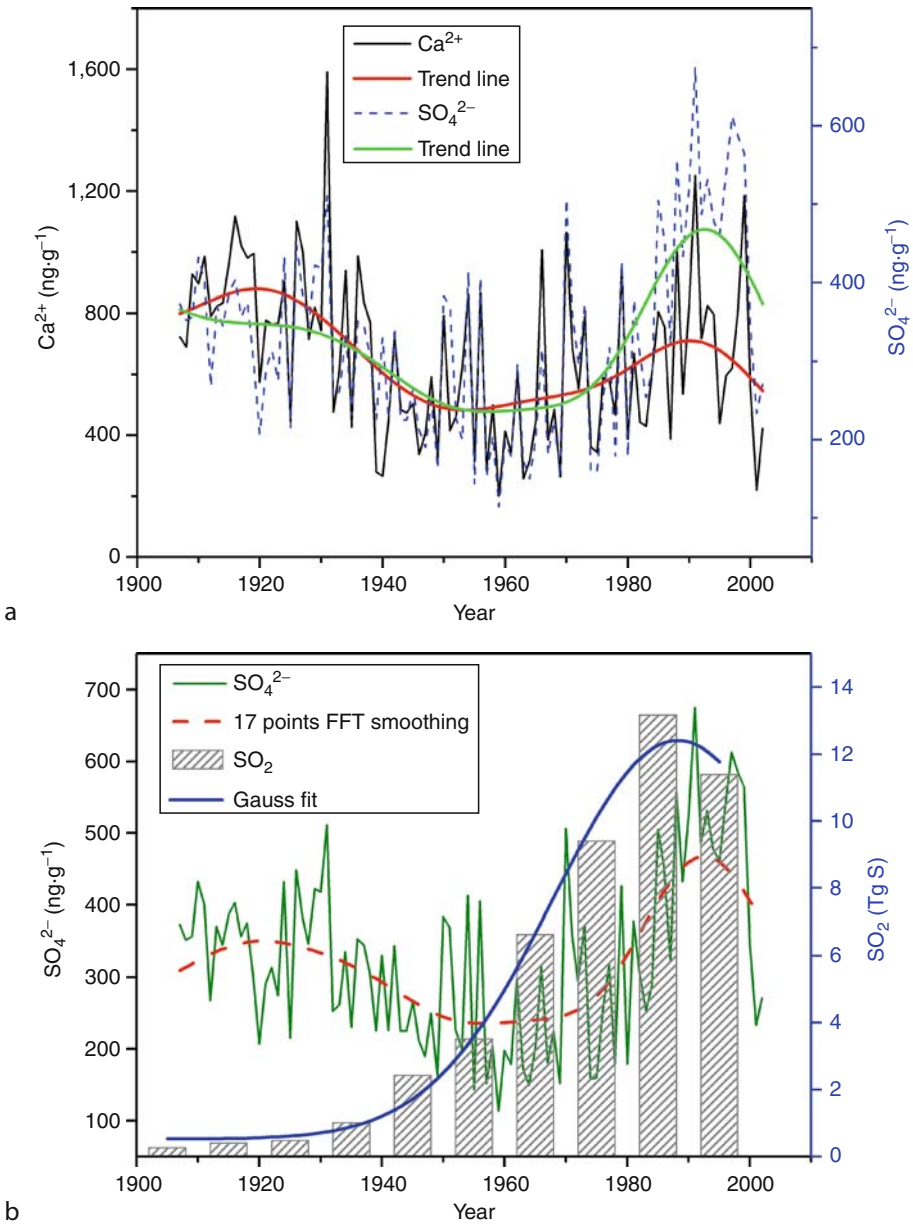

Geochemistry of Snow and Ice, Figure 5 (**a**) The profiles of annual concentrations for SO_4^{2-} and Ca^{2+}, the trend line represents 15-point FFT (Fast Fourier Transform) smoothing; (**b**) Comparison between the SO_4^{2-} concentration record and SO_2 emission estimates in the CIS (Commonwealth of Independent States).

of Independent States) from EDGAR-HYDE 1.3 (Van Aardenne et al., 2001) (Figure 5b) further confirm this conclusion. Of course, quantitatively extracting anthropogenic inputs in central Asian glaciers will require innovative approaches, such as developing detailed records of trace elements, rare earth elements, and sulfur isotopes (Wake et al., 2004).

Multi-parameter glaciochemical records provide the basis for identifying potential sources and transport pathways for major ions and thereby understanding the causes for spatial variability in the major ion records preserved in glaciers. Despite this, there remain considerable gaps in our understanding of the details of climatic and environmental changes in mid- and low-latitude regions. More detailed glacier investigations will be required to resolve these issues.

Bibliography

Balerna, A., Bernieri, E., Pecci, M., Polesello, S., Smiraglia, C., and Valsecchi, S., 2003. Chemical and radio-chemical composition of freshsnow samples from northern slopes of Himalayas (Cho Oyu range, Tibet). *Atmospheric Environment*, **37**(12), 1573–1581.

Banta, J. R., McConnell, J. R., Edwards, R., and Engelbrecht, J. P., 2008. Delineation of carbonate dust, aluminous dust, and sea salt deposition in a Greenland glaciochemical array using positive matrix factorization. *Geochemistry, Geophysics, Geosystems*, **9**, Q07013, doi:10.1029/2007GC001908.

Bertler, N., Mayewski, P. A., Aristarain, A., Barrett, P., Becagli, S., Bernardo, R., Bo, S., Xiao, C., Curran, M., Qin, D., Dixon, D., Ferron, F., Fischer, H., Frey, M., Frezzotti, M., Fundel, F., Genthon, C., Gragnani, R., Hamilton, G., Handley, M., Hong, S., Isaksson, E., Kang, J., Ren, J., Kamiyama, K., Kanamori, S., Karkas, E., Karlof, L., Kaspari, S., Kreutz, K., Kurbatov, A., Meyerson, E., Ming, Y., Zhang, M., Motoyama, H., Mulvaney, R., Oerter, H., Osterberg, E., Proposito, M., Pyne, A., Ruth, U., Simoes, J., Smith, B., Sneed, S., Teinila, K., Traufetter, F., Udisti, R., Virkkula, A., Watanabe, O., Williamson, B., Winther, J. G., Li, Y., Wolff, E., Li, Z., and Zielinski, A., 2005. Snow chemistry across Antarctica. *Annals of Glaciology*, **41**, 167–179.

Buijsman, E., Maas, H. F. M., and Asman, W. A. H., 1987. Anthropogenic NH_3 emissions in Europe. *Atmospheric Environment*, **21**(5), 1009–1022.

Burkhart, J. F., Hutterli, M., Bales, R. C., and McConnell, J. R., 2004. Seasonal accumulation timing and preservation of nitrate in firn at Summit, Greenland. *Journal of Geophysical Research*, **109**, D19302, doi:10.1029/2004JD004658.

Burkhart, J. F., Bales, R. C., McConnell, J. R., Hutterli, M. A., and Frey, M. M., 2009. Geographic variability of nitrate deposition and preservation over the Greenland Ice Sheet. *Journal of Geophysical Research*, **114**, D06301, doi:10.1029/2008JD010600.

Cecil, L. D., Naftz, D. L., and Green, J. R., 2000. Global ice-core research: understanding and applying environmental records of the past. U.S. Geological Survey Fact Sheet FS-003-00.

De Angelis, M., and Gaudichet, A., 1991. Saharan dust deposition over Mont-Blanc (French Alps) during the last 30 years. *Tellus Series B – Chemical and Physical Meteorology*, **43**(1), 61–75.

De Angelis, M., and Legrand, M., 1995. Preliminary investigations of post depositional effects on HCl, HNO_3 and organic acids in polar firn layers. In Delmas, R. (ed.), *Ice Core Studies of Global Biogeochemical Cycles*, NATO ASI Series, Series I. New York: Springer, Vol. 30, pp. 361–381.

De Angelis, M., Barkov, N. I., and Petrov, V. N., 1992. Sources of continental dust over Antarctica during the last glacial cycle. *Journal of Atmospheric Chemistry*, **14**(1–4), 233–244.

De Angelis, M., Steffensen, J. P., Legrand, M., Clausen, H., and Hammer, C., 1997. Primary aerosol (sea salt and soil dust) deposited in Greenland ice during the last climatic cycle: comparison with east Antarctic records. *Journal of Geophysical Research*, **102**(C12), 26681–26698.

Delmas, R. J., 1992. Environmental information from ice cores. *Reviews of Geophysics*, **30**(1), 1–21.

Döscher, A., Gaggeler, H. W., Schotterer, U., and Schwikowski, M., 1995. A 130 years deposition record of sulfate, nitrate and chloride from a high-alpine glacier. *Water, Air, and Soil Pollution*, **85**(2), 603–609.

Döscher, A., Gäggeler, H. W., Schotterer, U., and Schwikowski, M., 1996. A historical record of ammonium concentrations from a glacier in the Alps. *Geophysical Research Letters*, **23**(20), 2741–2744.

Duan, K., Thompson, L. G., Yao, T., Davis, M. E., and Mosley-Thompson, E., 2007. A 1000 year history of atmospheric sulfate concentrations in southern Asia as recorded by a Himalayan ice core. *Geophysical Research Letters*, **34**, L01810, doi:10.1029/2006GL027456.

Eichler, A., Schwikowski, M., and Gaggeler, H. W., 2000a. An Alpine ice-core record of anthropogenic HF and HCl emissions. *Geophysical Research Letters*, **27**(19), 3225–3228.

Eichler, A., Schwikowski, M., Gaggeler, H. W., Furrer, V., Synal, H. A., Beer, J., Saurer, M., and Funk, M., 2000b. Glaciochemical dating of an ice core from upper Grenzgletscher (4200 m a.s.l.). *Journal of Glaciology*, **46**(154), 507–515.

Eichler, A., Schwikowski, M., and Gaggeler, H. W., 2001. Meltwater-induced relocation of chemical species in Alpine firn. *Tellus Series B – Chemical and Physical Meteorology*, **53**(2), 192–203.

Fischer, H., Wagenbach, D., and Kipfstuhl, J., 1998. Sulfate and nitrate firn concentrations on the Greenland ice sheet – 2. Temporal anthropogenic deposition changes. *Journal of Geophysical Research*, **103**(D17), 21935–21942.

Fischer, H., Fundel, F., Ruth, U., Twarloh, B., Wegner, A., Udisti, R., Becagli, S., Castellano, E., Morganti, A., Severi, M., Wolff, E., Littot, G., Rothlisberger, R., Mulvaney, R., Hutterli, M. A., Kaufmann, P., Federer, U., Lambert, F., Bigler, M., Hansson, M., Jonsell, U., de Angelis, M., Boutron, C., Siggaard-Andersen, M. L., Steffensen, J. P., Barbante, C., Gaspari, V., Gabrielli, P., and Wagenbach, D., 2007. Reconstruction of millennial changes in dust emission, transport and regional sea ice coverage using the deep EPICA ice cores from the Atlantic and Indian Ocean sector of Antarctica. *Earth and Planetary Science Letters*, **260**(1–2), 340–354.

Fuhrer, K., and Legrand, M., 1997. Continental biogenic species in the Greenland Ice Core Project ice core: tracing back the biomass history of the North American continent. *Journal of Geophysical Research*, **102**(C12), 26735–26745.

Fuhrer, K., Neftel, A., Anklin, M., and Maggi, V., 1993. Continuous measurements of hydrogen-peroxide, formaldehyde, calcium and ammonium concentrations along the new Grip ice core from Summit, Central Greenland. *Atmospheric Environment. Part A: General Topics*, **27**(12), 1873–1880.

Fuhrer, K., Neftel, A., Anklin, M., Staffelbach, T., and Legrand, M., 1996. High-resolution ammonium ice core record covering a complete glacial-interglacial cycle. *Journal of Geophysical Research*, **101**(D2), 4147–4164.

Funk, M., 1994. Possible Alpine ice-core drilling sites, an overview. In Haeberli, W., and Stauffer, B. (eds.), *Proceedings of the ESF/EPC Workshop on Greenhouse Gases, Isotopes and Trace Elements in Glaciers as Climate Evidence of the Holocene*, VAW Arbeitsheft, Zürich, pp. 40–44.

Ginot, P., Kull, C., Schwikowski, M., Schotterer, U., and Gaggeler, H. W., 2001. Effects of postdepositional processes on snow composition of a subtropical glacier (Cerro Tapado, Chilean Andes). *Journal of Geophysical Research*, **106**(D23), 32375–32386.

Goktas, F., Fischer, H., Oerter, H., Weller, R., Sommer, S., and Miller, H., 2002. A glacio-chemical characterization of the new EPICA deep-drilling site on Amundsenisen, Dronning Maud Land, Antarctica. *Annals of Glaciology*, **35**, 347–354.

Goto-Azuma, K., and Koerner, R. M., 2001. Ice core studies of anthropogenic sulfate and nitrate trends in the Arctic. *Journal of Geophysical Research*, **106**(D5), 4959–4969.

Grannas, A. M., Jones, A. E., Dibb, J., Ammann, M., Anastasio, C., Beine, H. J., Bergin, M., Bottenheim, J., Boxe, C. S., Carver, G., Chen, G., Crawford, J. H., Domine, F., Frey, M. M., Guzman, M. I., Heard, D. E., Helmig, D., Hoffmann, M. R., Honrath, R. E., Huey, L. G., Hutterli, M., Jacobi, H. W., Klan, P., Lefer, B., McConnell, J., Plane, J., Sander, R., Savarino, J., Shepson, P. B., Simpson, W. R., Sodeau, J. R., von Glasow, R., Weller, R., Wolff, E. W., and Zhu, T., 2007. An overview of snow photochemistry: evidence, mechanisms and impacts. *Atmospheric Chemistry and Physics*, **7**(16), 4329–4373.

Hammer, C. U., 1977. Past volcanism revealed by Greenland Ice Sheet impurities. *Nature*, **270**(5637), 482–486.

Herron, M. M., 1982. Impurity sources of F^-, Cl^-, NO_3^- and SO_4^{2-} in Greenland and Antarctic precipitation. *Journal of Geophysical Research*, **87**(20), 3052–3060.

Hindman, E. E., and Upadhyay, B. P., 2002. Air pollution transport in the Himalayas of Nepal and Tibet during the 1995–1996 dry season. *Atmospheric Environment*, **36**(4), 727–739.

Hou, S. G., Qin, D. H., Zhang, D. Q., Kang, S. C., Mayewski, P. A., and Wake, C. P., 2003. A 154a high-resolution ammonium record from the Rongbuk Glacier, north slope of Mt. Qomolangma (Everest), Tibet-Himal region. *Atmospheric Environment*, **37**(5), 721–729.

Kang, S. C., Wake, C. P., Qin, D. H., Mayewski, P. A., and Yao, T. D., 2000. Monsoon and dust signals recorded in Dasuopu glacier, Tibetan Plateau. *Journal of Glaciology*, **46**(153), 222–226.

Kang, S., Mayewski, P. A., Qin, D., Yan, Y., Hou, S., Zhang, D., Ren, J., and Kruetz, K., 2002a. Glaciochemical records from a Mt. Everest ice core: relationship to atmospheric circulation over Asia. *Atmospheric Environment*, **36**(21), 3351–3361.

Kang, S., Mayewski, P. A., Qin, D., Yan, Y., Zhang, D., Hou, S., and Ren, J., 2002b. Twentieth century increase of atmospheric ammonia recorded in Mount Everest ice core. *Journal of Geophysical Research*, **107**(D21), 4595, doi:10.1029/2001JD001413.

Kang, S. C., Mayewski, P. A., Qin, D. H., Sneed, S. A., Ren, J. W., and Zhang, D. Q., 2004. Seasonal differences in snow chemistry from the vicinity of Mt. Everest, central Himalayas. *Atmospheric Environment*, **38**(18), 2819–2829.

Kaspari, S., Mayewski, P., Kang, S., Sneed, S., Hou, S., Hooke, R., Kreutz, K., Introne, D., Handley, M., Maasch, K., Qin, D., and Ren, J., 2007. Reduction in northward incursions of the South Asian monsoon since ~1400 AD inferred from a Mt. Everest ice core. *Geophysical Research Letters*, **34**, L16701, doi:10.1029/2007GL030440.

Kaspari, S., Mayewski, P. A., Handley, M., Kang, S., Hou, S., Sneed, S., Maasch, K., and Qin, D., in press. A high-resolution record of atmospheric dust composition and variability since 1650 AD from a Mt. Everest ice core. Journal of Climate.

Kreutz, K. J., 2007. Ice core records: glaciochemistry. In Elias, S. A. (ed.), *Encyclopedia of Quaternary Science*. Oxford: Elsevier, pp. 1192–1198.

Kreutz, K. J., and Mayewski, P. A., 1999. Spatial variability of Antarctic surface snow glaciochemistry: implications for palaeoatmospheric circulation reconstructions. *Antarctic Science*, **11**(1), 105–118.

Kreutz, K. J., Mayewski, P. A., Pittalwala, I. I., Meeker, L. D., Twickler, M. S., and Whitlow, S. I., 2000. Sea level pressure variability in the Amundsen Sea region inferred from a West Antarctic glaciochemical record. *Journal of Geophysical Research*, **105**(D3), 4047–4059.

Kreutz, K. J., Aizen, V. B., Cecil, L. D., and Wake, C. P., 2001. Oxygen isotopic and soluble ionic composition of a shallow firn core, Inilchek glacier, central Tien Shan. *Journal of Glaciology*, **47**(159), 548–554.

Kuhn, M., Haslhofer, J., Nickus, U., and Schellander, H., 1998. Seasonal development of ion concentration in a high alpine snow pack. *Atmospheric Environment*, **32**(23), 4041–4051.

Largiuni, O., Udisti, R., Becagli, S., Traversi, R., Maggi, V., Bolzacchini, E., Casati, P., Uglietti, C., and Borghi, S., 2003. Formaldehyde record from Lys glacier firn core, Monte Rosa massif (Italy). *Atmospheric Environment*, **37**(27), 3849–3860.

Legrand, M., 1995. Sulphur-derived species in polar ice: a review. In Delmas, R. (ed.), *Ice Core Studies of Global Biogeochemical Cycles*. New York: Springer, pp. 91–120.

Legrand, M., 1997. Ice-core records of atmospheric sulphur. *Philosophical Transactions of the Royal Society of London. Series B: Biological Sciences*, **352**(1350), 241–250.

Legrand, M. R., and Delmas, R. J., 1984. The ionic balance of Antarctic snow: a 10-year detailed record. *Atmospheric Environment*, **18**(9), 1867–1874.

Legrand, M. R., and Delmas, R. J., 1988. Formation of HCl in the Antarctic atmosphere. *Journal of Geophysical Research*, **93**(D6), 7153–7168.

Legrand, M. R., and Kirchner, S., 1990. Origins and variations of nitrate in south Polar precipitation. *Journal of Geophysical Research*, **95**(D4), 3493–3507.

Legrand, M., and Mayewski, P., 1997. Glaciochemistry of polar ice cores: a review. *Reviews of Geophysics*, **35**(3), 219–243.

Legrand, M. R., Lorius, C., Barkov, N. I., and Petrov, V. N., 1988. Vostok (Antarctica) ice core: atmospheric chemistry changes over the last climatic cycle (160, 000 years). *Atmospheric Environment*, **22**(2), 317–331.

Legrand, M., Deangelis, M., Staffelbach, T., Neftel, A., and Stauffer, B., 1992. Large perturbations of ammonium and organic acids content in the Summit-Greenland ice core. Fingerprint from forest fires? *Geophysical Research Letters*, **19**(5), 473–475.

Legrand, M., Ducroz, F., Wagenbach, D., Mulvaney, R., and Hall, J., 1998. Ammonium in coastal Antarctic aerosol and snow: role of polar ocean and penguin emissions. *Journal of Geophysical Research*, **103**(D9), 11043–11056.

Legrand, M., Preunkert, S., Wagenbach, D., and Fischer, H., 2002. Seasonally resolved Alpine and Greenland ice core records of anthropogenic HCl emissions over the 20th century. *Journal of Geophysical Research*, **107**(D12), 4139, doi:10.1029/2001JD001165.

Li, Z., Yao, T., Xie, Z., and Thompson, L. G., 1995. Modern atmospheric environmental records in Guliya Ice Cap of Qinghai-Xizang Plateau. *Chinese Science Bulletin*, **40**(10), 874–875.

Maggi, V., Villa, S., Finizio, A., Delmonte, B., Casati, P., and Marino, F., 2006. Variability of anthropogenic and natural compounds in high altitude – high accumulation alpine glaciers. *Hydrobiologia*, **562**(1), 43–56.

Maupetit, F., Wagenbach, D., Weddeling, P., and Delmas, R. J., 1995. Seasonal fluxes of major ions to a high-altitude cold Alpine glacier. *Atmospheric Environment*, **29**(1), 1–9.

Mayewski, P. A., and Legrand, M., 1990. Recent increase in nitrate concentration of Antarctic snow. *Nature*, **346**(6281), 258–260.

Mayewski, P. A., Lyons, W. B., Spencer, M. J., Twickler, M., Dansgaard, W., Koci, B., Davidson, C. I., and Honrath, R. E., 1986. Sulfate and nitrate concentrations from a South Greenland ice core. *Science*, **232**(4753), 975–977.

Mayewski, P. A., Lyons, W. B., Spencer, M. J., Twickler, M. S., Buck, C. F., and Whitlow, S., 1990. An ice-core record of atmospheric response to anthropogenic sulphate and nitrate. *Nature*, **346**, 554–556.

Mayewski, P. A., Twickler, M. S., Whitlow, S. I., Meeker, L. D., Yang, Q., Thomas, J., Kreutz, K., Grootes, P. M., Morse, D. L., Steig, E. J., Waddington, E. D., Saltzman, E. S., Whung, P. Y., and Taylor, K. C., 1996. Climate change during the last deglaciation in Antarctica. *Science*, **272**(5268), 1636–1638.

Mayewski, P. A., Meeker, L. D., Twickler, M. S., Whitlow, S., Yang, Q. Z., Lyons, W. B., and Prentice, M., 1997. Major features and forcing of high-latitude northern hemisphere atmospheric circulation using a 110,000-year-long glaciochemical series. *Journal of Geophysical Research*, **102**(C12), 26345–26366.

Meeker, L. D., and Mayewski, P. A., 2002. A 1400-year high-resolution record of atmospheric circulation over the North Atlantic and Asia. *Holocene*, **12**(3), 257–266.

Meeker, L. D., Mayewski, P. A., Twickler, M. S., Whitlow, S. I., and Meese, D., 1997. A 110,000-year history of change in continental biogenic emissions and related atmospheric circulation inferred from the Greenland Ice Sheet Project ice core. *Journal of Geophysical Research*, **102**(C12), 26,489–26,504.

Mulvaney, R., and Wolff, E. W., 1994. Spatial variability of the major chemistry of the Antarctic Ice Sheet. *Annals of Glaciology*, **20**, 440–447.

Naftz, D. L., Klusman, R. W., Michel, R. L., Schuster, P. F., Reddy, M. M., Taylor, H. E., Yanosky, T. M., and McConnaughey, E. A., 1996. Little Ice Age evidence from a south-central North American ice core, U.S.A. *Arctic, Antarctic, and Alpine Research*, **28**(1), 35–41.

Naftz, D. L., Susong, D. D., Schuster, P. F., Cecil, L. D., Dettinger, M. D., Michel, R. L., and Kendall, C., 2002. Ice core evidence of rapid air temperature increases since 1960 in alpine areas of the Wind River Range, Wyoming, United States. *Journal of Geophysical Research*, **107**(D13), 4171, doi:10.1029/2001JD000621.

Olivier, S., Schwikowski, M., Brütsch, S., Eyrikh, S., Gäggeler, H. W., Lüthi, M., Papina, T., Saurer, M., Schotterer, U., Tobler, L., and Vogel, E., 2003. Glaciochemical investigation of an ice core from Belukha glacier, Siberian Altai. *Geophysical Research Letters*, **30**(19), 2019, doi:10.1029/2003GL018290.

Olivier, S., Blaser, C., Brütsch, S., Frolova, N., Gäggeler, H. W., Henderson, K. A., Palmer, A. S., Papina, T., and Schwikowski, M., 2006. Temporal variations of mineral dust, biogenic tracers, and anthropogenic species during the past two centuries from Belukha ice core, Siberian Altai. *Journal of Geophysical Research*, **111**, D05309, doi:10.1029/2005JD005830.

Petit, J. R., Jouzel, J., Raynaud, D., Barkov, N. I., Barnola, J. M., Basile, I., Bender, M., Chappellaz, J., Davis, M., Delaygue, G., Delmotte, M., Kotlyakov, V. M., Legrand, M., Lipenkov, V. Y., Lorius, C., Pepin, L., Ritz, C., Saltzman, E., and Stievenard, M., 1999. Climate and atmospheric history of the past 420, 000 years from the Vostok ice core, Antarctica. *Nature*, **399**(6735), 429–436.

Preunkert, S., Wagenbach, D., Legrand, M., and Vincent, C., 2000. Col du Dôme (Mt Blanc Massif, French Alps) suitability for ice-core studies in relation with past atmospheric chemistry over Europe. *Tellus Series B – Chemical and Physical Meteorology*, **52**(3), 993–1012.

Preunkert, S., Legrand, M., and Wagenbach, D., 2001. Sulfate trends in a Col du Dôme (French Alps) ice core: A record of anthropogenic sulfate levels in the European midtroposphere over the twentieth century. *Journal of Geophysical Research*, **106**(D23), 31,991–32,004.

Preunkert, S., Wagenbach, D., and Legrand, M., 2003. A seasonally resolved alpine ice core record of nitrate: Comparison with anthropogenic inventories and estimation of preindustrial emissions of NO in Europe. *Journal of Geophysical Research, [Atmospheres]*, **108**(D21), 4681, doi:10.1029/2003JD003475.

Qin, D., Hou, S., Zhang, D., Ren, J., Kang, S., Mayewski, P. A., and Wake, P. C., 2002. Preliminary results from the chemical records of an 80.4m ice core recovered from East Rongbuk Glacier, Qomolangma (Mount Everest), Himalaya. *Annals of Glaciology*, **35**, 278–284.

Rankin, A. M., Wolff, E. W., and Martin, S., 2002. Frost flowers: Implications for tropospheric chemistry and ice core interpretation. *Journal of Geophysical Research*, **107**(D23), 4683, doi:10.1029/2002JD002492.

Robock, A., 2000. Volcanic eruptions and climate. *Reviews of Geophysics*, **38**(2), 191–219.

Rogora, M., Mosello, R., Arisci, S., Brizzio, M. C., Barbieri, A., Balestrini, R., Waldner, P., Schmitt, M., Stähli, M., Thimonier, A., Kalina, M., Puxbaum, H., Nickus, U., Ulrich, E., and Probst, A., 2006. An overview of atmospheric deposition chemistry over the Alps: Present status and long-term trends. *Hydrobiologia*, **562**(2), 17–40.

Röthlisberger, R., Hutterli, M. A., Wolff, E. W., Mulvaney, R., Fischer, H., Bigler, M., Goto-Azuma, K., Hansson, M. E., Ruth, U., Siggaard-Andersen, M. L., and Steffensen, J. P., 2002a. Nitrate in Greenland and Antarctic ice cores: a detailed description of post-depositional processes. *Annals of Glaciology*, **35**, 209–216.

Röthlisberger, R., Mulvaney, R., Wolff, E. W., Hutterli, M. A., Bigler, M., Sommer, S., and Jouzel, J., 2002b. Dust and sea salt variability in central East Antarctica (Dome C) over the last 45 kyrs and its implications for southern high-latitude climate. *Geophysical Research Letters*, **29**(20), 1963, doi:10.1029/2002GL015186.

Savarino, J., and Legrand, M., 1998. High northern latitude forest fires and vegetation emissions over the last millennium inferred from the chemistry of a central Greenland ice core. *Journal of Geophysical Research*, **103**(D7), 8267–8279.

Schotterer, U., Stichler, W., and Ginot, P., 2004. The influence of post-depositional effects on ice core studies: examples from the Alps, Andes, and Altai. In Cecil, L. D., and Thompson, L. G. (eds.), *Earth Paleoenvironments: Records Preserved in Mid- and Low-Latitude Glaciers*. The Netherlands: Kluwer, pp. 39–59.

Schwikowski, M., 2004. Reconstruction of European air pollution from alpine ice cores. In Cecil, L. D., Green, J. R., and Thompson, L. G. (eds.), *Earth Paleoenvironments: Records Preserved in Mid- and Low-Latitude Glaciers*. The Netherlands: Kluwer, pp. 95–119.

Schwikowski, M., Brutsch, S., Gaggeler, H. W., and Schotterer, U., 1999a. A high-resolution air chemistry record from an Alpine ice core: Fiescherhorn glacier, Swiss Alps. *Journal of Geophysical Research, [Atmospheres]*, **104**(D11), 13709–13719.

Schwikowski, M., Doscher, A., Gaggeler, H. W., and Schotterer, U., 1999b. Anthropogenic versus natural sources of atmospheric sulphate from an Alpine ice core. *Tellus Series B – Chemical and Physical Meteorology*, **51**(5), 938–951.

Shrestha, A. B., Wake, C. P., Dibb, J. E., Mayewski, P. A., Whitlow, S. I., Carmichael, G. R., and Ferm, M., 2000. Seasonal variations in aerosol concentrations and compositions in the Nepal Himalaya. *Atmospheric Environment*, **34**(20), 3349–3363.

Staffelbach, T., Neftel, A., Stauffer, B., and Jacob, D., 1991. A record of the atmospheric methane sink from formaldehyde in polar ice cores. *Nature*, **349**, 603–605.

Suzuki, T., Iizuka, Y., Matsuoka, K., Furukawa, T., Kamiyama, K., and Watanabe, O., 2002. Distribution of sea salt components in snow cover along the traverse route from the coast to Dome Fuji station 1000 km inland at east Dronning Maud Land, Antarctica. *Tellus Series B – Chemical and Physical Meteorology*, **54**(4), 407–411.

Thompson, L. G., Mosleythompson, E., Davis, M. E., Lin, P. N., Henderson, K. A., Coledai, J., Bolzan, J. F., and Liu, K. B., 1995. Late-glacial stage and holocene tropical ice core records from Huascaran, Peru. *Science*, **269**(5220), 46–50.

Thompson, L. G., Yao, T., Mosley-Thompson, E., Davis, M. E., Henderson, K. A., and Lin, P. N., 2000. A high-resolution millennial record of the South Asian Monsoon from Himalayan ice cores. *Science*, **289**(5486), 1916–1919.

Udisti, R., Becagli, S., Castellano, E., Mulvaney, R., Schwander, J., Torcini, S., and Wolff, E., 2000. Holocene electrical and chemical measurements from the EPICA-Dome C ice core. *Annals of Glaciology*, **30**, 20–26.

Van Aardenne, J. A., Dentener, F. J., Olivier, J. G. J., Goldewijk, C. G. M. K., and Lelieveld, J., 2001. A $1^\circ \times 1^\circ$ resolution data set of historical anthropogenic trace gas emissions for the period 1890–1990. *Global Biogeochemical Cycles*, **15**(4), 909–928.

Vuille, M., Francou, B., Wagnon, P., Juen, I., Kaser, G., Mark, B. G., and Bradley, R. S., 2008. Climate change and tropical Andean glaciers: past, present and future. *Earth Science Reviews*, **89** (3–4), 79–96.

Wagenbach, D., Legrand, M., Fischer, H., Pichlmayer, F., and Wolff, E. W., 1998. Atmospheric near-surface nitrate at coastal Antarctic sites. *Journal of Geophysical Research*, **103**(D9), 11,007–11,020.

Wake, C. P., 2007. Ice core records: Chinese, Tibetan Mountains. In Elias, S. A. (ed.), *Encyclopedia of Quaternary Science*. Oxford: Elsevier, pp. 1226–1233.

Wake, C. P., Mayewski, P. A., and Spencer, M. J., 1990. A review of central asian glaciochemical data. *Annals of Glaciology*, **14**, 301–306.

Wake, C. P., Mayewski, P. A., Wang, P., Yang, Q. H., Han, J. K., and Xie, Z. H., 1992. Anthropogenic sulfate and Asian dust signals in snow from Tien-Shan, Northwest China. *Annals of Glaciology*, **16**, 45–52.

Wake, C. P., Mayewski, P. A., Xie, Z. C., Wang, P., and Li, Z. Q., 1993. Regional distribution of monsoon and desert dust signals recorded in Asian glaciers. *Geophysical Research Letters*, **20**(14), 1411–1414.

Wake, C. P., Mayewski, P. A., Qin, D., Yang, Q., Kang, S., Whitlow, S., and Meeker, L. D., 2001. Changes in atmospheric circulation over the south-eastern Tibetan Plateau over the last two centuries from a Himalayan ice core. *Pages News*, **9**(3), 14–16.

Wake, C. P., Mayewski, P. A., and Kang, S., 2004. Climatic interpretation of the gradient in glaciochemical signals across the crest of the Himalaya. In Cecil, L. D., Green, J. R., and Thompson, L. G. (eds.), *Earth paleoenvironments: records preserved in mid- and low-latitude glaciers*. The Netherlands: Kluwer, pp. 81–94.

Werner, M., Tegen, I., Harrison, S. P., Kohfeld, K. E., Prentice, I. C., Balkanski, Y., Rodhe, H., and Roelandt, C., 2002. Seasonal and interannual variability of the mineral dust cycle under present and glacial climate conditions. *Journal of Geophysical Research*, **107**(D24), 4744, doi:10.1029/2002JD002365.

Whitlow, S., Mayewski, P. A., and Dibb, J. E., 1992. A comparison of major chemical-species seasonal concentration and accumulation at the south-Pole and Summit, Greenland. *Atmospheric Environment. Part A: General Topics*, **26**(11), 2045–2054.

Wolff, E. W., 1990. Signals of atmospheric pollution in polar snow and ice. *Antarctic Science*, **2**(3), 189–205.

Wolff, E. W., Hall, J. S., Mulvaney, R., Pasteur, E. C., Wagenbach, D., and Legrand, M., 1998a. Relationship between chemistry of air, fresh snow and firn cores for aerosol species in coastal Antarctica. *Journal of Geophysical Research*, **103**(D9), 11057–11070.

Wolff, E. W., Wagenbach, D., Pasteur, E. C., Mulvaney, R., Legrand, M., and Hall, J. S., 1998b. Relationship between chemistry of air, fresh snow and firn cores for aerosol species in coastal Antarctica. *Journal of Geophysical Research*, **103** (D9), 11,057–11,070.

Wolff, E. W., Jones, A. E., Martin, T. J., and Grenfell, T. C., 2002. Modelling photochemical NO_X production and nitrate loss in the upper snowpack of Antarctica. *Geophysical Research Letters*, **29**(20), 1944, doi:10.1029/2002GL015823.

Wolff, E. W., Rankin, A. M., and Rothlisberger, R., 2003. An ice core indicator of Antarctic sea ice production? *Geophysical Research Letters*, **30**(22), 2158, doi:10.1029/2003GL018454.

Wolff, E. W., Fischer, H., Fundel, F., Ruth, U., Twarloh, B., Littot, G. C., Mulvaney, R., Rothlisberger, R., de Angelis, M., Boutron, C. F., Hansson, M., Jonsell, U., Hutterli, M. A., Lambert, F., Kaufmann, P., Stauffer, B., Stocker, T. F., Steffensen, J. P., Bigler, M., Siggaard-Andersen, M. L., Udisti, R., Becagli, S., Castellano, E., Severi, M., Wagenbach, D., Barbante, C., Gabrielli, P., and Gaspari, V., 2006. Southern Ocean sea-ice extent, productivity and iron flux over the past eight glacial cycles. *Nature*, **440**(7083), 491–496.

Wolff, E. W., Hutterli, M. A., and Jones, A. E., 2007. Past atmospheric composition and chemistry from ice cores - progress and prospects. *Environmental Chemistry*, **4**(4), 211–216.

Xiao, C., Kang, S. C., Qin, D., Yao, T. D., and Ren, J. W., 2002. Transport of atmospheric impurities over the Qinghai-Xizang (Tibetan) Plateau as shown by snow chemistry. *Journal of Asian Earth Sciences*, **20**(3), 231–239.

Yang, Q., Mayewski, P. A., Linder, E., Whitlow, S., and Twickler, M., 1996. Chemical species spatial distribution and relationship to elevation and snow accumulation rate over the Greenland Ice Sheet. *Journal of Geophysical Research*, **101**(D13), 18629–18637.

Yao, T., JIao, K., Tian, L., Li, Z., Li, Y., Liu, J., Huang, C., and Xie, C., 1995. Climatic and environmental records in Guliya Ice Cap. *Science in China. Series B*, **38**(2), 228–237.

Yao, T. D., Shi, Y. F., and Thompson, L. G., 1997. High resolution record of paleoclimate since the little ice age from the Tibetan ice cores. *Quaternary International*, **37**, 19–23.

Yao, T. D., Wu, G. J., Pu, J. C., Jiao, K. Q., and Huang, C. L., 2004. Relationship between calcium and atmospheric dust recorded in Guliya ice core. *Chinese Science Bulletin*, **49**(7), 706–710.

Yao, T., Pu, J., Lu, A., Wang, Y., and Yu, W., 2007. Recent glacial retreat and its impact on hydrological processes on the Tibetan Plateau, China, and sorrounding regions. *Arctic, Antarctic, and Alpine Research*, **39**(4), 642–650.

Zielinski, G. A., Mayewski, P. A., Meeker, L. D., Whitlow, S., Twickler, M. S., Morrison, M., Meese, D. A., Gow, A. J., and Alley, R. B., 1994. Record of volcanism since 7000 B.C. from the GISP2 Greenland ice core and implications for the volcano-climate system. *Science*, **264**(5161), 948–952.

GEOCRYOLOGY

Amit Kumar
Department of Geology, Centre of Advanced Study in Geology, Panjab University, Chandigarh, India

Geocrology is a branch of a more general science which has come into common usage to describe processes and properties of resources having temperatures $<0^\circ$C, and the term frozen is suggested to illustrate the solid phase of water. Geocryology was developed as an integrative discipline with links to geography, geology, engineering,

hydrology, and ecology. The Polish geologist Walery Lozinski used the term "periglacial" to describe the deposits and landforms believed to be the result of frost weathering.

Bibliography

Yershov, E. D., 1998. *General Geocryology*. Cambridge: Cambridge University Press.

GIS IN GLACIOLOGY

Jacob Napieralski
Department of Natural Sciences, University of Michigan-Dearborn, Dearborn, MI, USA

Synonyms

Geographic information science (GISc); Geographic information technologies (GIT); Remote sensing

Definition

Geographic Information Systems (GIS) are designed for interactive queries of data, spatial autocorrelations and pattern analyses, integration, storage and dissemination of data and information, and interactive maps and visualizations. Geographic Information Science (GISc) refers to the study of the theory, development, and application of GIS (Goodchild, 1992).

Introduction

Glaciologists aim to study the nature and distribution of present-day ice or the remnants of paleo-ice sheets and glaciers, with an overall goal of understanding the behavior and patterns of the cryosphere and of glacial landforms. This is best accomplished using technological tools to monitor, measure, manage, and model enormous amounts of spatial data. Consequently, geographic information technologies (GIT), such as global positioning systems (GPS), satellite and aerial imagery (i.e., remote sensing), and GIS, provide an effective tool to process, manage, disseminate, and analyze digital glacial data and assemblages of glacial landforms. In general, glaciologists use GIS to compile and analyze data that represent glacial characteristics and features in time (e.g., chronology of events and radiocarbon dates), space (e.g., position of ice margins and alignment of crevasses), and space-time (e.g., change in ice sheet geometry during stages of growth and decay).

Geographic information systems

Real-world objects, such as glacial features and landforms, are represented in a GIS using two main data models: vector and raster. Raster data, which are comprised of grid cells, are an abstraction of reality and typically associated with remote sensing and elevation datasets. Each grid cell has a spatial location (x, y) and one value (z) that might indicate ice surface elevation, thickness, or velocity. In particular, digital representations of surface topography, referred to as digital elevation models (DEMs) or digital terrain models (DTMs), are used to map surface features and characteristics using techniques such as hillshading, contouring, aspect, slope, and flow accumulation. These techniques have helped identify and locate glacial boundaries, determine the location and elevation of the equilibrium line, and calculate glacier and ice sheet mass balances (Gao and Liu, 2001). DEMs are vital tools in studies of ice surface processes (e.g., modeling flow of supraglacial meltwater), visualizations of glacial geometry and patterns, and the identification and extraction of glacial landforms (e.g., drumlins and moraines). However, it is important to consider the limits of raster datasets in glacier studies, including grid cell size, mixed pixel classification, storage size, and inability to update or modify with relative ease.

Vector data, which represent discrete objects, are frequently associated with glacial boundaries (especially related to change detection of glacial margins), location of linear features (e.g., crevasses and moraines), and orientation data, such as till fabric analyses (a proxy for ice movement). The basic building blocks of vector data are points (a single coordinate feature) which, when combined and connected, can construct lines (multiple points) and polygons (multiple lines). Each feature is spatially referenced (x, y) and dynamically linked to an entry in an attribute table. Vector data are separated into common layers (i.e., thematic layers), such that each layer is a compilation of similar glacial features or landforms. In contrast to raster data, vector data generally require less storage space, are easier to update, register, and reference, and are more compatible with attribute tables and data. However, there are analytical limitations with vector data, especially when exploring continuous data (e.g., ice surface topography).

Data acquisition and distribution

Digital data of glacial features and landforms derive from several sources, including aerial and satellite images, field observation and GPS measurements, and digitization. Most influential to the study of glaciers and glacial terrain has been the acquisition of data using satellite systems, such as Landsat, the Advanced Spaceborne Thermal Emission and Reflection Radiometer (ASTER), and the Ice, Cloud, and land Elevation Satellite (IceSAT). Through various image-processing techniques, such as image restoration, enhancement, and classification, glacier dynamics can be monitored and analyzed over time (i.e., change detection). As a result, background data on ice behavior in isolated and inhospitable regions of the world are captured remotely, including the elevation, thickness and extent of ice, ice velocity, delineation of snow zones, and mapping of glacial features. In addition to spatial extent and ice thickness, analyses of ice surface produce maps of slope angle, profile curvature, aspect,

and flow accumulation, which contribute to glacial mass balance studies and, consequently, studies of the feedbacks between climate forcing and glacier changes. Through the processing of satellite images, supraglacial features, alpine snow, and glacier ice and snow facies have been mapped and analyzed in detail (Bishop et al., 2004). GPS, another common source of glacial data, can assist fieldwork by demarking locations of features and, more commonly, the movement of features over time, such as ice features or crevasses. A series of reflective prisms and an engineer's level, combined with GPS readings, can support the development of a DEM representing land or ice surface or be converted to vector format to study paths and rates of movement. GPS function in all weather conditions, regardless of visibility, which is a valuable attribute when mapping glacial environments. Finally, digitization is the process by which objects from maps or other sources are transferred into a GIS. A static paper map is converted to digital data and is then integrated with other interactive datasets in GIS (e.g., Clark et al., 2004; Napieralski et al., 2007a).

Once digital data are developed and entered into GIS, they can be organized, queried, and distributed with relative ease and efficiency. Spatial and temporal data are interactively queried and revised, a valuable tool for continuous updating and revising to glacial data as data acquisition continues to increase and as the description and classification of glacial landforms and processes evolves. Many organizations share in the compilation of such databases, including ice sheet topographic data, annual extents of sea ice and frozen ground, and global glacier inventories (National Snow and Ice Data Center, NSDIC), glacio-tectonic landforms (International Work Group on Geospatial Analysis of Glaciated Environments, GAGE), and glacial landforms compiled from hundreds of sources from the British Ice Sheet from the Last Glacial Maximum (LGM) (Clark et al., 2004). For example, operating under the auspices of the NSDIC, the Global Land Ice Measurement from Space (GLIMS), an international collaboration to acquire and inventory the world's glaciers, provides GIS and satellite data to visualize and download, including the distribution and visualization of vector glacier data and footprints of satellite images from which data were derived, using a Web-Mapping Service (WMS) (Figure 1). A primary goal of GLIMS, and the aforementioned organizations, is to distribute generic and software-specific formatted data in order to facilitate glacial research and education.

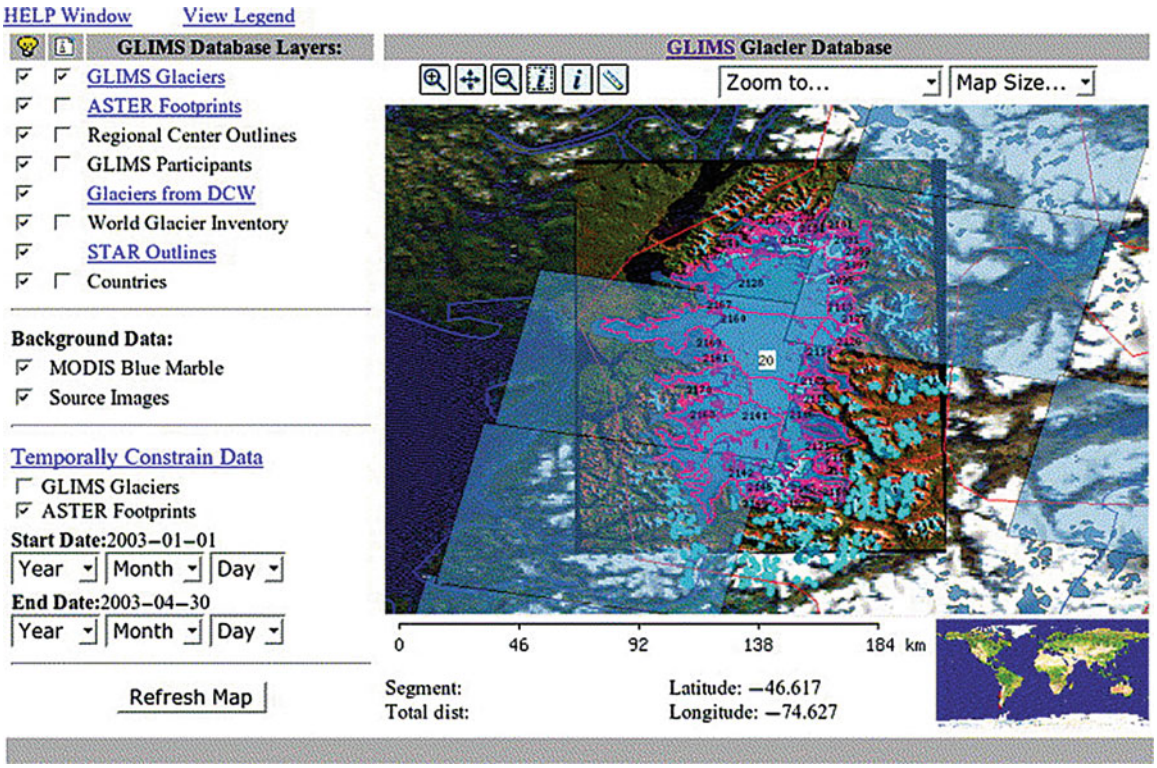

GIS in Glaciology, Figure 1 Example of the GLIMS MapServer interface in a browser. All layers are displayed, and are labeled in the column of check-boxes. Data layers include GLIMS glaciers and program participants, ASTER footprints, and political boundaries. Data received by the GLIMS team are ingested into a spatially enabled database and made available via a web site featuring an interactive map, and a web-based GIS (Web-Mapping Service: WMS) (Raup et al., 2007).

Spatial analyses and modeling

Most GIS contain an abundance of spatial, geostatistical, and modeling functionalities that support the calculation of glacier and landform size, shape, height, orientation, and location. More complex spatial tools, such as density, parallel conformity, distance measuring, and hierarchal clustering (i.e., cluster analyses) have been customized to study patterns in glacial data (Napieralski et al., 2007a). Glacial features and landforms can be digitized (i.e., traced) along the boundary, providing measurements of area or perimeter, or along the spine or long axis, providing length or orientation of a feature or feature group. A GIS can also demark the geographic center (centroid) of a feature. Many of these spatial analyses are used to reevaluate previous studies and to help redefine glacial features based on morphological characteristics. Dunlop and Clark (2006) mapped ribbed moraines (i.e., subglacially formed, transverse ridges) covering over 81,000 km^2 in Canada, Ireland, and Sweden. Their objective was to produce a representative dataset of ribbed moraine morphometry to better assist the ongoing debate regarding moraine formation. In this study, GIS increased analytical efficiency, provided specialized tools to measure landform symmetry and connectability (jigsaw matching), and correlated the distribution of glacial landform structures to elevation.

Morphometric descriptions of glacial landforms also play a critical role in the reconstruction of paleo-ice sheet geometry and behavior, such as suggesting ice flow direction during landform development, locating ice sheet divides and domes, and linking temporal or spatial patterns of erosion–transportation–deposition beneath the ice sheet throughout stages of growth, maximum extent, and decay. To better understand the linkage between ice sheet behavior and the geographic distribution of landform assemblages, two tools developed in ESRI's ArcGIS allowed for an iterative verification of ice sheet model output against sets of glacial landforms (i.e., moraines and lineations). Revised Automated Proximity and Conformity Analysis (R-APCA) and Automated Flow Direction Analysis (AFDA) were specifically developed to quantify the level of correspondence between model output and sets of moraines and flow sets of glacial lineations. R-ACPA systematically quantifies the level of agreement between simulated and observed features using a series of buffers, common GIS tools designed to calculate the distance between features, and overlays (Li et al., 2008). AFDA calculates the offset between the orientation of landforms from each set with the simulated ice flow direction of the ice sheet during different time slices (Figure 2; Li et al., 2007). These two spatial statistical tools compared marginal positions of major end moraines and glacial flow sets against simulations of ice extent for the Scandinavian Ice Sheet during the LGM and Younger Dryas (Napieralski et al., 2007b).

Outlook: future of GIS in glaciology

As GIS continues to evolve, its place in glacial and cryosphere studies will likewise progress, influenced by improved data acquisition techniques (e.g., satellites

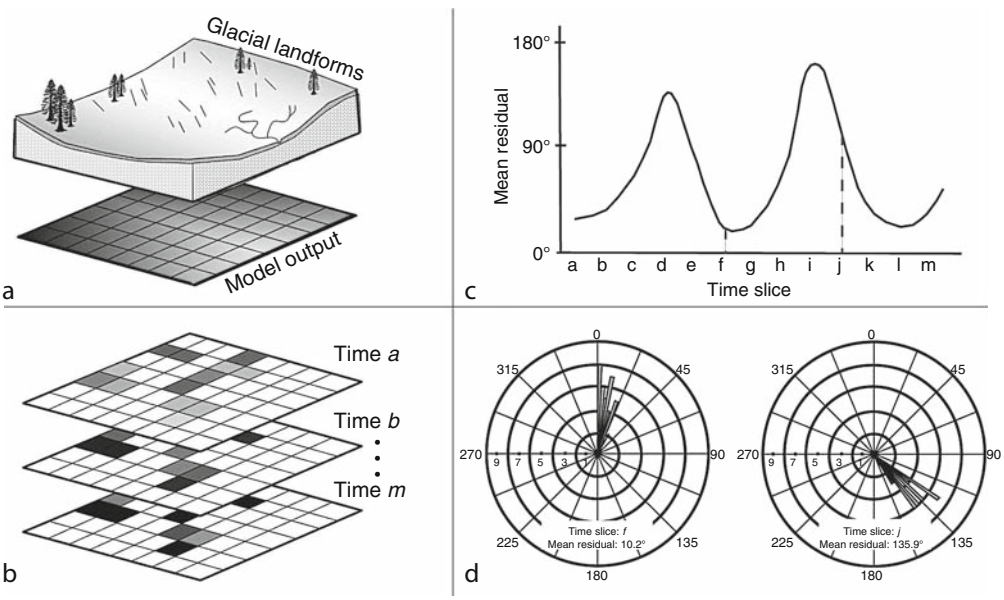

GIS in Glaciology, Figure 2 Steps of AFDA. (**a**) Field-based glacial lineations and model outputs used in analysis. (**b**) Overlay model outputs and field evidence to produce series residual datasets for different time slices. (**c**) Plot resultant mean of residual values against their corresponding time slices to identify temporal patterns of correspondence between predicted directions and field observations. (**d**) Frequency analysis (*rose diagram*) of selected time slices (e.g., f and j) provides detailed information on distribution of residuals across area and can be used to evaluate level of correspondence (Li et al., 2007).

specifically designed for studying polar regions), improved computing technologies, and increased demand for managing and analyzing an ever-growing global collection of spatial data. Only until recently have there been attempts to study glacier evolution and morphology and to link process models to landform assemblages using GIS. Many of the new ideas and tools developed in other disciplines (e.g., hydrology, land use change, remote sensing) can be integrated into glaciology to support complex studies of glacier form and behavior and technological advances, such as web-based GIS (e.g., GLIMS) and mobile GIS, can stimulate data acquisition, dissemination, and collaboration. Overall, future integrations of GIS in glaciology will continue to "make glaciology more dynamic, more analytical, more global, more exploratory, and more predictive in the future" (Gao and Liu, 2001).

Bibliography

Bishop, M. P., Colby, J. D., Luvall, J. C., Quattrochi, D., and Rickman, D., 2004. Remote-sensing science and technology for studying mountain environments. In Bishop, M. P., and Shroder, J. F. (eds.), *Geographic Information Science and Mountain Geomorphology*. New York, NY: Springer-Praxis, pp. 147–187.

Clark, C., Evans, D. A., Khatwa, A., Bradwell, T., Jordan, C. J., Marsh, S. H., Mitchell, W. A., and Bateman, M. D., 2004. Map and GIS database of glacial landforms and features related to the last British Ice Sheet. *Boreas*, **33**, 359–375.

Dunlop, P., and Clark, C. D., 2006. The morphological characteristics of ribbed moraines. *Quaternary Science Reviews*, **25**, 1668–1691.

Gao, J., and Liu, Y., 2001. Applications of remote sensing, GIS and GPS in glaciology: a review. *Progress in Physical Geography*, **25**(4), 520–540.

Goodchild, M. F., 1992. Geographical information science. *International Journal of Geographical Information Systems*, **6**, 31–45.

Li, Y., Napieralski, J., Harbor, J., and Hubbard, A., 2007. Identifying patterns of correspondence between modeled flow directions and field evidence: An automated flow direction analysis. *Computers and Geosciences*, **33**(2), 141–150.

Li, Y., Napieralski, J., and Harbor, J., 2008. A revised automated proximity and conformity analysis method to compare predicted and observed spatial boundaries of geologic phenomena. *Computers and Geosciences*, **34**(12), 1806–1814.

Napieralski, J., Harbor, J., and Li, Y., 2007a. Glacial geomorphology and geographic information systems. *Earth Science Reviews*, **85**(1–2), 1–22.

Napieralski, J., Hubbard, A., Li, Y., Harbor, J., Stroeven, A. P., Kleman, J., and Jansson, K. N., 2007b. Towards a GIS assessment of numerical ice sheet model performance using geomorphological data. *Journal of Glaciology*, **53**(180), 71–83.

Raup, B. H., Racoviteanu, A., Khalsa, S. J. S., Helm, C., Armstrong, R., and Arnaud, Y., 2007. The GLIMS Geospatial Glacier Database: a new tool for studying glacier change. *Global and Planetary Change*, **56**, 101–110.

Cross-references

GPS in Glaciology, Applications
ICESat Data in Glaciological Studies
Optical Remote Sensing of Alpine Glaciers

GLACIAL DRAINAGE CHARACTERISTICS

Richard A. Marston
Department of Geography, Kansas State University, Manhattan, KS, USA

Synonyms

Glacial hydrology; Glacial meltwater; Supraglacial streams

Definition

Supraglacial water. Water that is stored and moves on the surface of the glacier.
Englacial water. Water that is stored and moves within the glacier.
Subglacial water. Water that is stored and moves underneath the glacier.

Glacial drainage characteristics

Water on glaciers moves and is stored on the surface (supraglacial water), inside the glacier (englacial water), and beneath the glacier (subglacial water). Sources of supraglacial and englacial water include melting, precipitation, discharge from water-filled crevasses and moulins, plus small amounts by the heat in supraglacial streams. Basal water can be produced by the geothermal heat flux, which can melt 6 mm/year when the ice is at the pressure melting point (Sugden and John, 1976). Also, basal sliding can produce frictional heat that may melt ice, particularly with pressure melting as the moving ice encounters at topographic obstacle. Most water is produced in the ablation zone of a glacier. Rates of meltwater production are generally highest in martime climates and higher on valley glaciers than on ice sheets because of the longwave radiation from valley sidewalls. One can measure a delay between the maximum daily downsky radiation and the maximum runoff generated on a glacier surface. This lag time varies with meteorological conditions (Marston, 1983). Water that is stored in the subglacial, englacial, and supraglacial environment can be released suddenly, which can generate outburst floods. This hazard, plus the general increase of glacier meltwater production with climate warming are ample reasons to devote attention to the processes and modeling of glacial drainage characteristics. Longwave radiation from valley walls can be an important driver of melting along the margins of alpine glaciers. Glacier meltwater production can be important in late summer months for water users beyond the mountain front after snowmelt and rain have decreased in importance as sources of runoff.

Supraglacial streams form on the glacier surface and are more pronounced when carved in firn than in ice, and when formed in stagnant ice areas. Indeed, supraglacial water leaves the surface via moulins and crevasses, a process that limits development of a surface stream network. In order for supraglacial streams to form, the rate of channel incision must be greater than the rate the glacier

surface is ablating. Some supraglacial streams can incise several meters (Figure 1). Kinetic energy dissipation and frictional heat may be responsible for the small increment of temperature needed to cause this melting (Marston, 1983). When supraglacial streams are not controlled by structures in the ice, they frequently develop a striking meandering pattern (Figure 1). As the streams downcut, they also migrate downglacier, leaving a three-dimensional record of their recent course. The rate and direction of meandering is controlled by meander geometry and stream discharge, as it is for meanders in alluvium.

Englacial water behaves in a manner analogous to groundwater in karst terrain, especially as it moves through spaces connected by structural weakness in the ice. Fountain et al. (2005) found that the majority of englacial water flows through englacial fractures rather than through tunnels. The shape of englacial tunnels will depend on whether hydrostatic pressure exists. Large englacial tunnels grow at the expenses of small ones. A perched water table may exist in glaciers that fluctuates with meteorological conditions and glacier movement. When crevasses are closed at the bottom, meltwater and rainwater can partially or completely fill them. As the glacier moves, crevasses open and release the temporarily stored water into the englacial drainage system. The englacial network of tunnels is best envisioned as a three-dimensional honeycombed network. The tunnels enlarge by melting but can be closed by creep deformation in the glacier. Englacial drainage has been studied by drilling boreholes into the glacier, using ground-penetrating radar and tracers and by lowering cameras into moulins and crevasses.

Glacial Drainage Characteristics, Figure 1 Supraglacial stream meanders, Dinwoody Glacier, Wind River Range, Wyoming. Photo by author.

Subglacial water commonly moves in a dispersed, braided pattern, although subglacial tunnels can form and eventually lead to the formation of fluvial deposits as eskers. Subsurface water can also lubricate the base of the glacier, accelerating ice movement. In Antarctica, large subglacial lakes have been discovered that store water and contribute to basal sliding, which accelerates the velocity of ice streams and outlet glaciers (Bell, 2008).

The runoff from glaciers generally follows a diurnal cycle, increasing during the day as meltwater increases. The timing of peak runoff each day depends on weather and travel time of supraglacial, englacial, and subglacial water to the glacier snout. Glacial meltwater is responsible for creating a variety of erosional and depositional landforms beneath glaciers and ice sheets, in contact with the ice, and in front of the ice (proglacial landforms), discussed elsewhere in this volume.

Summary

Glacial drainage is integrated between the supraglacial, englacial, and subglacial environments. Efforts to develop computer models to describe, explain, and predict glacial drainage have been limited by the availability of careful field measurements. Access to englacial and subglacial environments is especially difficult. Recent developments in field instrumentation are allowing greater access to the three-dimensional glacial drainage systems. Improved modeling will allow more accurate estimates of glacial water discharge for water supply and mitigation of outburst flooding.

Bibliography

Bell, R. E., 2008. The role of subglacial water in ice-sheet balance. *Nature Geoscience*, **1**, 297–304.

Fountain, A. G., Schlichting, R. B., Jansson, P., and Jacobel, R. W., 2005. Observations of englacial water passages: a fracture-dominated system. *Annals of Glaciology*, **40**, 25–30.

Marston, R. A., 1983. Supraglacial stream dynamics on the Juneau Icefield. *Annals of the Association of American Geographers*, **73**, 597–608.

Sugden, D. E., and John, B. S., 1976. *Glaciers and Landscape*. London: Edward Arnold.

Cross-references

Direct Surface Runoff
Discharge/Streamflow
Diurnal Cycle of Runoff
Englacial Processes
Glacier Hydrology
Glacier Lake Outburst Floods
Meltwater Channels
Moulins
Subglacial Drainage System
Subglacial Lakes, Antarctic

GLACIAL ECOSYSTEMS

Nozomu Takeuchi
Department of Earth Sciences, Graduate School of Science, Chiba University, Chiba, Japan

Definition

Glacial ecosystems. A concept to consider glaciers as ecosystems consisting of ice mass and biological community of cold-tolerant organisms.

Introduction

Glaciers have been believed as inhospitable and abiotic environments because of extreme conditions, such as low temperature, high UV radiation, and limited nutrients. However, various organisms have recently been reported to live on glaciers. Photosynthetic microorganisms, such as snow algae and cyanobacteria, grow on the surface of glaciers, and sustain heterotrophic organisms, such as insects, ice worms, rotifers, tardigrada, fungi, and bacteria. These organisms are cold-tolerant special species and adapt their lives to the special conditions of glaciers. Thus, we can consider glaciers as ecosystems consisting of such biological communities and ice mass.

Photosynthetic organisms on glaciers

Photosynthetic organisms, such as snow algae and cyanobacteria, are primary producers in glacial ecosystems. They photosynthetically produce organic matter on snow and ice surfaces of glaciers, and sustain heterotrophic organisms living there. Snow algae and cyanobacteria are commonly observed in most of the glaciers in the world.

Most snow algae found on glaciers are taxonomically green algae (Chlorophyta). More than 100 taxa of green algae have been reported on snow and ice. Visible snow algal blooms are well known as red or green snow. The red snow is caused by red-pigmented cells of the green algae (usually *Chamydomonas nivalis*).

Cyanobacteria are also common photosynthetic organisms on glaciers. They are usually found on ablation ice surface and in cryoconite holes on glaciers. Filamentous cyanobacteria usually form a small granular algal mat with mineral particles and organic matter. The granules are called as cryoconite granules.

Snow algae and cyanobacteria grow in the season when temperature is above freezing point and melt water is available. Although there are still limited measurements on photosynthetic rate of snow algae and cyanobacteria on glaciers, the rate is comparable to other aquatic ecosystems in polar regions (Hodson et al., 2008). For example, the rates of carbon fixation range as 0.63–156.9 μg C L^{-1} h^{-1} on cryoconite on an arctic glacier. The areal rate ranges up to 1,200 mg C m^{-2} h^{-1} on cryoconite, and up to 10 mg C m^{-2} h^{-1} on wet snow surface.

Communities of heterotrophic organisms on glaciers

Cold-tolerant invertebrate and bacterial communities have been reported on most of the glaciers worldwide (Hoham and Duval, 2001). Collembola (springtails or snow flea) are one of common insects on glaciers. Wingless midges and copepods are living on Himalayan glaciers. Stoneflies are found on Patagonian glaciers, and ice worms on North American glaciers. Major microscopic invertebrates on glaciers are tardigrada and rotifers. They are commonly observed on worldwide glaciers. Yeasts also live on snow and ice of glaciers. All these heterotrophic organisms are sustained by algal production and wind-blown organic matter.

Bacteria and virus are also alive on glacier surface (Hodson et al., 2008). The bacteria that grow on the snow and ice are called psychrophilic bacteria. Bacteria can be found in fresh snow, englacial ice, as well as glacier surface. Bacterial concentration ranges from 1 to 4×10^4 cells mL^{-1} on snow or ice surface. Some bacteria are often observed to be attached to cells of snow algae and cyanobacteria. They seem to exchange organic matter and nutrients to live together. This is a concept of "phycoshere" proposed by Jones (1982).

Glaciers as habitats of organisms

The distribution of melt water determines habitable parts for the organisms on glaciers, since liquid water is vital for all organisms (Vincent, 1988; Hodson et al., 2008). The major habitats of organisms with melt water on glaciers are wet snow, bare ice surface, cryoconite holes, streams, and ponds. For example, snow algae grow in the water film of snow grains on glaciers. *Cryoconite* holes, which are cylindrical water-filled holes on glacier ice, are important habitats for many organisms with semi-stagnant liquid water and nutrients on glaciers.

Melt water also exists at the glacier bed and within glacial ice of temperate glaciers, and microbes live in such parts of glaciers. The microbes consist of aerobic and anaerobic bacteria, and virus, and their communities are distinctive from those on the glacier surface. These communities and such environments were proposed as subglacial and englacial ecosystems by Hodson et al. (2008).

Physical conditions as a habitat of organisms on glaciers differ significantly between accumulation and ablation areas. The accumulation area is located at the upper part of glaciers, where the surface condition is usually snow, and air temperature is colder than lower part. Furthermore, frequent snowfalls often cover the glacier surface and prevent photosynthesis of snow algae on the surface. On the other hand, the ablation area is located at the lower part of glaciers and surface condition is bare ice. Since air temperature of the area is higher than in the accumulation area, meltwater is abundant and the growth season of organisms is longer. Therefore, conditions for organisms are generally favorable in the ablation area

compared to the accumulation area. These gradients of conditions on glaciers determine the altitudinal variation of community structures. For example, snow algal biomass on Himalayan glaciers decrease as elevation increases (Yoshimura et al., 1997). Also, species composition changes with elevation. The community in the ablation area mainly consists of ice environment species that prefer to grow on the ice surface. The community in the accumulation area consists of snow environment species that prefer to grow on the snow surface.

Although the velocity of glacial movement is very slow, organisms living on glaciers adapt to the movement. Since the glacier flows downward by gravity, organisms living on the glacier surface have to migrate upward to stay on glaciers. For example, a wingless glacial midge living on a Himalayan glacier walks upward of the glacier in adult stage to recover the distance of movement by glacial flow and meltwater during egg and laval stages (Kohshima, 1985). Microbes may be relocated on a glacier by wind after they are washed out of the glacier by meltwater and dried on the ground. Upstream migration is one of the unique characteristics of glacial ecosystems.

Nutrients, such as nitrogen and phosphorus, are essential for organisms, but usually very limited on glaciers because of a lack of litter and other debris (Hodson et al., 2005). Nutrients are supplied onto the glacier surface by dry and wet depositions. Snow and rain include small amounts of nitrate, ammonium, and phosphate. Marine and terrestrial aerosols are also important sources of these solutes. The nutrient supply may also be episodically enhanced by extreme events. Cryoconite holes play an important role in nutrient cycling in glacial ecosystems. The holes trap nutrient-rich particles, prevent nutrients washout by meltwater, and provide nutrients for various algae and animals in the holes. On mountain glaciers, such as Asian glaciers, a large amount of terrestrial dust is supplied from desert by wind and is deposited on the surface, thus nutrients are relatively abundant. Larger biomass of microbes noted on the Asian glaciers is probably due to the abundant nutrients.

Effect of climate change on glacial ecosystem

Recently, glacial changes, such as alterations in mass balance, snow chemistry, and/or dust concentration have been reported in many parts of the world, and such changes may affect a biological community on the glacial surface (Hodson et al., 2008). In the last few decades, the mass balance of most glaciers worldwide is negative, possibly due to climate warming. More melting of glaciers may enhance the production of photosynthetic microbes, and expand the habitable area on glaciers. The elevation of equilibrium line of such glaciers usually rises upward. The altitudinal distribution of microbial community would also shift upward on the glaciers accompanied by the rising of the equilibrium line. The relative importance of snow and rain in summer may also affect significantly the community of microbes on the glacier surface. The change of windblown solutes and dust due to pollutant, forest fire, and land cover change around glaciers is likely to have a significant impact on biological communities on glaciers. However, evaluation of these effects of climate change on glacial ecosystems is still underway. Ice core studies may reveal how biological communities on a glacier changed in the past. Analyses of snow algae and bacteria in some ice cores have shown that their abundance and community structure have temporally changed with climate (e.g., Yoshimura et al., 2006).

Summary

Glaciers can be considered as ecosystems consisting of ice mass and biological community of cold-tolerant organisms living there. The glacial ecosystems have very unique characteristics, which cannot be seen in other ecosystems. The distribution of melt water determines habitable parts for organisms on glaciers, since liquid water is vital for all organisms. Organisms have to migrate upward to stay on glaciers, since their habitat on the ice moves down by glacial flow. Furthermore, since snow and ice can easily be modified by physical conditions, such as solar radiation, air temperature, and precipitation, glacial ecosystems are highly sensitive to climate change. However, there is still only a few studies on glaciers to regard them as ecosystems, thus further studies are required to understand them.

Bibliography

Hodson, A., Anesio, A. M., Tranter, M., Fountain, A., Osborn, M., Priscu, J., Laybourn-Parry, J., and Satteler, B., 2008. Glacial ecosystems. *Ecological Monographs*, **78**(1), 42–67.

Hodson, A., Mumford, P. N., Kohler, J., and Pynn, P. M., 2005. The high arctic glacial ecosystem: new insights from nutrient budgets. *Biogeochemistry*, **72**, 233–256.

Hoham, R. W., and Duval, B., 2001. Microbial ecology of snow and freshwater ice. In Jones, H. G. et al. (eds.), *Snow Ecology*. Cambridge: Cambridge University Press, pp. 168–228.

Jones, A. K., 1982. Interactions of algae and bacteria. In Bull, A. T., and Slater, J. H. (eds.), *Microbioal Interactions and Communities*. New York: Academic Press, pp. 189–247.

Kohshima, S., 1985. Migration of the Himalayn wingless glacier midge (Diamesa sp.): slope direction assessment by sun compassed straight walk. *Journal of Ethology*, **3**, 93–104.

Vincent, W. F., 1988. *Microbial ecosystems of Antarctica*. Cambridge: Cambridge University Press.

Yoshimura, Y., Kohshima, S., and Ohtani, S., 1997. A community of snow algae on a Himalayan glacier: change of algal biomass and community structure with altitude. *Arctic and Alpine Research*, **29**, 126–137.

Yoshimura, Y., Kohshima, S., Takeuchi, N., Seko, K., and Fujita, K., 2006. Snow algae in a Himalayan ice core: new environmental markers for ice core analyses and their correlation with summer mass balance. *Annals of Glaciology*, **43**, 148–153.

Cross-references

Chemical and Microbe Records in Snow and Ice
Cryoconite
Solutes in Glacier Ice

GLACIAL EROSION

Ping Fu, Jonathan Harbor
Department of Earth and Atmospheric Sciences, Purdue University, West Lafayette, IN, USA

Definition

Glacial erosion includes the loosening of rock, sediment, or soil by glacial processes, and the entrainment and subsequent transportation of this material by ice or meltwater.

Introduction

The wide range of easily recognized landscape features produced by the action of glaciers and ice sheets include many classic landforms produced by glacial erosion, including U-shaped valleys, cirques, arêtes, roches moutoneés, hanging valleys, striations, glacial polish, rock steps, fjords, and glacial grooves. These landforms, which span scales from millimeters to kilometers, result from differential patterns of rock loss. These patterns reflect spatial variations in the glaciological controls on glacial erosion, combined with the history and extent of ice advance and retreat, as well as spatial variations in rock and sediment resistance to erosion.

Some of the earliest published research on glacial erosion identified specific landforms as characteristic of glacial action, and then inferred glaciological variables that must control erosion to produce these specific forms. For example, in the late 1800s W J McGee considered the pattern of erosion necessary to create a glacial U-shaped valley and concluded that glacial erosion rates at different locations are controlled by the weight of the overlying ice and the velocity of the ice movement over the underlying bedrock (reviewed in Harbor, 1989). Subsequent research has considerably increased our understanding of the detailed mechanics of how ice, entrained material, and meltwater all act to loosen and remove rock, sediment, and soil. Combined with the knowledge of glacier and ice sheet history and dynamics, understanding erosion processes is the basis for evaluating how a range of glaciological variables control glacial erosion.

Erosion processes

The primary processes of glacial erosion are plucking, abrasion, and physical and chemical erosion by subglacial water.

Plucking (quarrying)

Plucking, which is also sometimes called quarrying, includes both the fracture of underlying rock and the entrainment by basal ice of rock fragments that result from glacial action or that are due to preexisting fractures in the rock. The results of plucking are seen particularly well on the down-glacier (lee) side of bedrock outcrops where commonly there is angular, fractured bedrock (Figure 1). In some cases, large rock fragments removed from the outcrop occur as a tail of boulders deposited in the down-glacier direction.

Glacial Erosion, Figure 1 Plucking features on the down-glacier side of the bedrock steps.

Fracture of subglacial bedrock

Although plucking can exploit preexisting fractures and joint patterns in rock, active fracture of bedrock under ice is important to maintain erosion once the surface zone of pre-glacial weathered and fractured rock has been removed. Subglacial fracture of bedrock occurs when the pattern of stress induced by the ice and by any clasts embedded in the basal ice causes a tensile stress component in the rock that exceeds the fracture strength of the rock, usually at the tip of a microcrack. The fracture pattern can produce clasts that range in size from very fine rock fragments to large boulders. In addition, as rock is removed by glacial erosion, changes in the in situ rock stress field due to the overall change in load pattern can produce large-scale fracture patterns (Augustinus, 1995).

For a clast embedded in basal ice, a simple model illustrates the stress pattern caused by a normal pressure (Pn) forcing a point on the clast down into the underlying bed (Figure 2a) which induces a shear stress $T_{\max}$ (Equation 1) in the bedrock, as shown in Figure 2b.

$$T_{\max} = -\left(\frac{P_n}{\pi r'}\right)\cos\theta \tag{1}$$

In more realistic conditions of ice flow over an uneven bed, the force applied at the ice-bed contact and the clast-bed contact is tangential to the bed. Thus the surface stress pattern has its maximum down-glacier of the contact point. For ice flowing over a bedrock bump (Figure 3), the maximum stress on bedrock surface occurs on the lee side of the bump, where fractures are most likely to be produced.

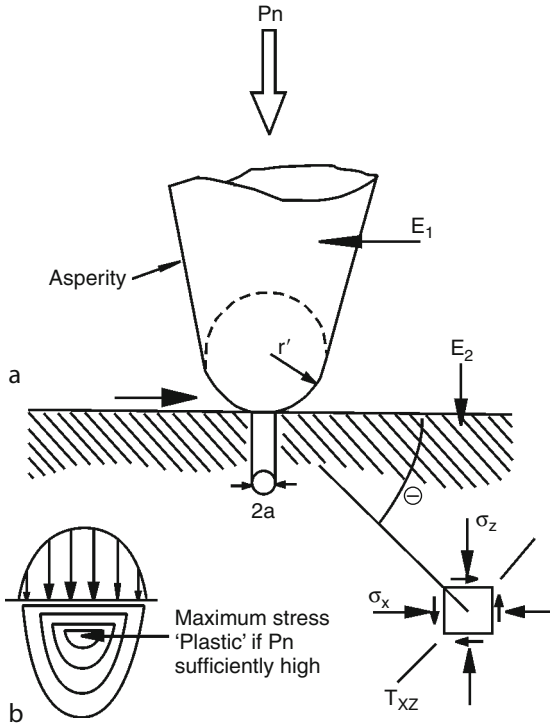

Glacial Erosion, Figure 2 Contact of a spherical asperity with bedrock under a load (Pn). (**a**) The asperity tip has a radius r′. The asperity and bedrock possess Young's moduli of E_1 and E_2, respectively. The pattern of loading through a cross section of the contact area (2a) is shown. Shear (T) and normal (σ) stresses in bedrock resulting from surface loading are also indicated. The load is separated into normal and horizontal components. (**b**) Shows the contours (isolines) of constant maximum shear stress beneath the point (for a normal load only). From Drewry (1986, p. 33).

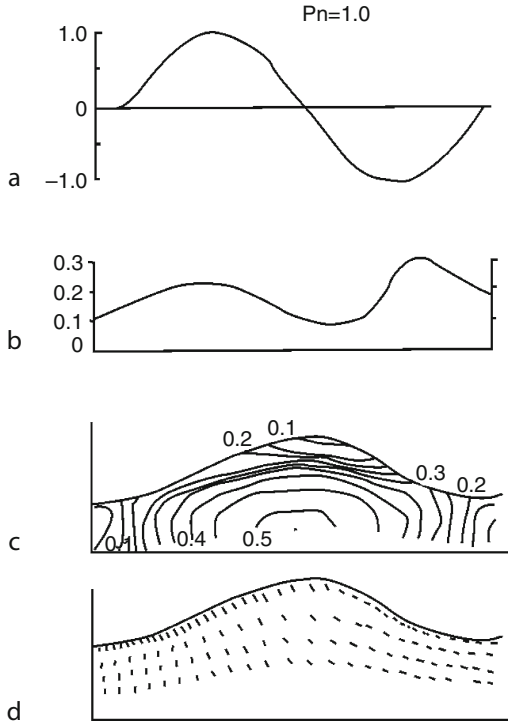

Glacial Erosion, Figure 3 Stress patterns induced in a subglacial bedrock undulation for normal pressure *Pn* = 1.0. Ice flow is from left to right. (**a**) Distribution of normal stress at the interface; (**b**) maximum shear stress at the bedrock surface; (**c**) maximum shear stress contours at depth (MPa); and (**d**) orientation of principle stress axes. From Drewry (1986, p. 41).

Strength and resistance of bedrock. Failure of a rock mass occurs when the shear stress applied is higher than the rock mass' confined or unconfined yield stress (rock strength). The strength of rock is affected by several factors, including the properties of the preexisting discontinuities, degree of weathering, presence and flow of water, presence and properties of material infilling discontinuities, and the loading cycle. In addition to direct glaciologically induced fractures, bedrock areas that are glaciated will have preexisting weaknesses related to the bedrock structure and its history of weathering, which can be exploited by glacial processes (Sugden and John, 1976).

Effective pressure. The force applied to the ice-bed contact or a clast-bed contact is a function of the effective pressure (P_E), which is the difference between the ice overburden pressure (P_i) and the basal water pressure (P_w): $P_E = P_i - P_w$. High effective pressures, and, thus, high fracture rates occur when ice is thick and water pressure at the bed is low. In some cases there are cavities at the glacier bed, resulting from ice flow over bumps at a speed that does not allow deformation of the ice to keep the basal ice in contact with the underlying rock (Hallet, 1996) and (Iverson, 1991). High velocity and low pressure favor the growth of cavities. Cavities reduce the contact area between the ice and the bed, and thus increase the average stress on areas that are in contact. Temporal variations in basal water pressure in cavities also lead to large short-term increases in local stress. In Hallet's model of glacial quarrying (Hallet, 1996), high plucking rates occur at low effective pressure (0.1–1 MPa) and fast sliding velocities, and large stresses are concentrated on bedrock ledges, causing crack propagation (Figure 4).

Fracture growth is enhanced by refreezing of meltwater in cracks resulting from variations in basal pressure and temperature over time at different points on the bed. For example, basal ice melts preferentially on the stoss (up-glacier) side of bedrock bumps because of locally increased pressure, and this meltwater then flows to the lee (down-glacier) side of the bump where pressures are lower and the water refreezes in joints and fractures. Expansion of the water during freezing acts to widen and extend fractures. Cyclic loading of the bed over time increases failure due to fatigue effects (Drewry, 1986), and when a glacier or ice sheet retreats the area that is exposed undergoes an unloading effect (as the weight of

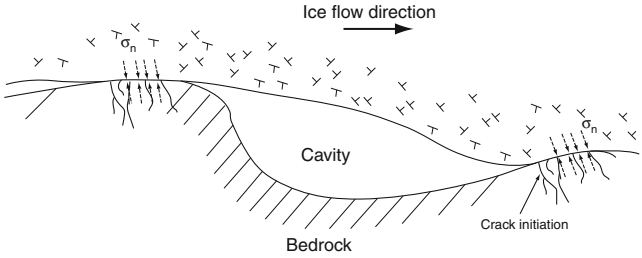

Glacial Erosion, Figure 4 Stresses and location of probable fracture initiation near the corner of a ledge when ice is flowing over bedrock bumps (modified after Hallet, 1996).

the ice is removed) which can result in additional fracture and expansion of joints.

Entrainment of rock fragments by ice

For erosion to occur, material that has been loosened or weakened by fracture must be removed from its original location. The primary mechanism of removal involves incorporation of fragments into basal ice as a function of patterns of melting and freezing.

- Heat-pump effect

  When ice near the pressure-melting point flows over a bedrock bump or step, locally higher pressure occurs on the up-glacier side and produces melting. Meltwater flows around the bump to the lee side region of lower pressure where a cavity may exist. When the lower pressures on the lee side are below the pressure-melting point, the meltwater refreezes forming a frozen ice patch or regelation layer on the down-glacier side of the bump or step. This refreezing of water to the bed incorporates fragments at the bed loosened by fracturing, and these fragments are then removed from the bed as the ice moves further down the glacier. The freezing of meltwater on the lee side releases heat, which is conducted through the bump to the up-glacier side in a positive feedback loop called the heat-pump effect.
- Freeze-on

  In addition to the heat-pump effect, there are larger spatial and temporal changes in basal thermal conditions that produce regions and periods where there is a change from net melting to net freezing of subglacial water, including across boundaries between warm- and cold-based ice patches. Where and when this occurs, clasts and areas of subglacial sediment become frozen in to the basal ice, and are removed from the bed as the ice flows down-glacier. Freeze-on from rising supercooled subglacial water can also significantly affect basal ice growth in some areas and entrain large amounts of basal sediment into the basal ice (Cook et al., 2006).
- Thrust planes

  Large thrust planes in subglacial sediment also form in some cases, in particular at the boundary between areas of warm- and cold-ice regimes, and can incorporate large clasts and blocks of sediment in to basal ice.

Abrasion

Abrasion involves clasts embedded in basal ice scratching and wearing down bedrock over which they pass. It involves small-scale fracture and crushing at the point where a clast touches underlying bedrock, and is most commonly seen where debris-laden ice is forced toward the bed. It is rarely found on the down-glacier side of bedrock humps (where plucking is most common) because the presence of cavities and ice flow away from the bed creates conditions where clasts embedded in basal ice are not forced toward the bedrock. The most common features produced by abrasion are striation marks, which are longitudinal scratches on the order of millimeters across and with lengths from centimeters to meters. Striations are the sum of numerous discrete crushing events at the micro scale, and the removal of the fine rock fragments that are produced. Seen under a microscope, striations consist of numerous crescent-shaped fractures (Benn and Evans, 1998; Iverson, 1995; Liu et al., 2009). Glacial polish is another common feature on glacially eroded rock surfaces, and is generally considered to be the sum of a large number of very small individual striations. However, additional ideas include the removal of large numbers of small protuberances from the bed surface.

Several models have been proposed for the basic mechanics of glacial abrasion; although they have similar basic structure, they differ in conceptions of how the force that is applied to the clast is controlled. In a simple abrasion model (Figure 5a) a clast embedded in basal ice is both forced downward into the underlying bedrock and at the same time moved along the bed by the down-glacier component of ice motion. This results in an indentation in the bed if the clast is harder than the bedrock. As the clast moves across the bed, it leaves a groove behind. The depth of the groove is controlled by the force directed on the clast toward the bed and the relative hardness of the clast and the bedrock, and the bed-parallel velocity controls the length of the striation produced per unit time. As the clast moves across the bed, wear products resulting from erosion, changes in the shape of the asperity, and increased friction between clast and bedrock can inhibit motion of clast causing rotation or lodgment that ends in a particular striation. When a clast rotates (Figure 5b) each time an asperity on the clast contacts the bed, the stresses induced by the contact allow cracks or failures to grow beneath or around the contact point. Discrete contacts between a clast and the bed produce a series of several marks on the bed, called chattermarks. The series continues until the clast is lifted into ice and no longer hits the bed or the clast is totally crushed.

The abrasion rate is affected by

- The force pressing the clast against the bed (defined in various ways in different models), F
- The velocity of the clast relative to the bed, U_p

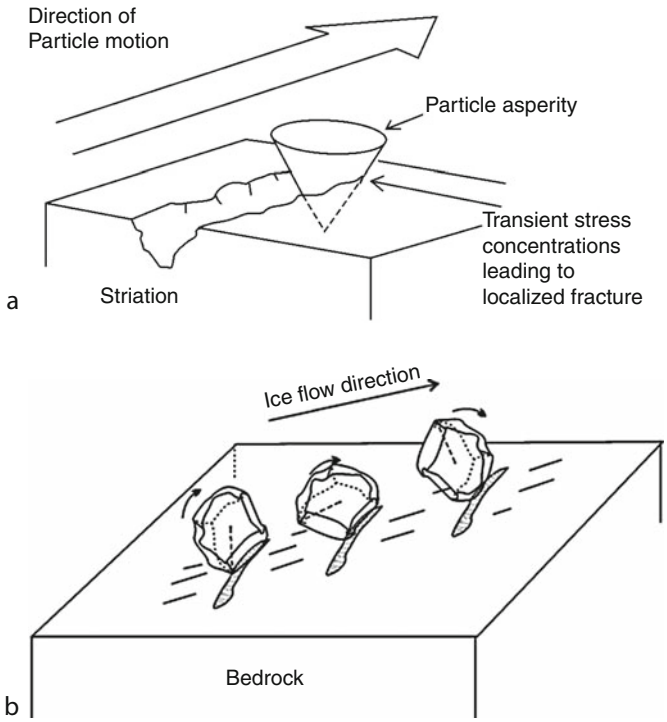

Glacial Erosion, Figure 5 (**a**) Simple model of the striation process. (From Benn and Evans, 1998, modified from Drewry, 1986). (**b**) Set of chattermarks produced by a rolling pattern of movement of a clast across bedrock.

- The concentration of clasts in basal ice, C_o
- The relative hardness of the clast and the bedrock, ΔHd

Three different abrasion models have been developed, reflecting different ways of considering the mechanics of the interaction between sediment in basal ice and the underlying substrate.

Boulton's model

Boulton (1974, 1976) developed a model of glacial abrasion based on an assumption that clasts at the bed of a glacier support the overlying weight of ice: somewhat analogous to sandpaper being rubbed across a surface (Drewry, 1986). For temperate glaciers, basal water pressure in cavities and spaces between clasts also supports some of the weight of the overlying ice; thus, in Boulton's model, the force pressing clasts against the bed (F) is a function of effective pressure, and is given by:

$$F = (\rho_i g h - P_w) A_i \quad (2)$$

where ρ_i is ice density, P_w is water pressure, and A_i is a measure of the contact area between clasts and the bed. In this model, abrasion rates are high under thick ice with low basal water pressure, although under very high effective pressures the velocity of the clast is reduced by friction with the bed and abrasion ceases. Boulton's conception is of a fairly rigid contact interface between the base of a glacier and the underlying bedrock. Although such a situation has been observed in certain field settings (Anderson et al., 1982; Souchez and Lorrain, 1987) and laboratory experiments (Iverson, 1993), in other cases basal ice deforms around basal clasts, suggesting an alternate model for basal conditions and abrasion mechanics is also necessary for some situations.

Hallet's model

In Hallet's conception of conditions at the bed of a glacier, ice behaves as a viscous fluid and deforms around basal clasts (Hallet, 1979, 1981), to create a condition somewhat like a pebble resting on the bottom of a lake (Benn and Evan, 1998). Thus one component of the force between a clast and the underlying bed is the buoyant weight of the clast. However, for clasts at the bed of a temperate glacier, melting of basal ice causes a component of ice flow toward the bed. As ice moving toward the bed deforms around basal clasts, viscous drag results in a bed-directed force on clast. In this case, the force on the clast directed toward the bed is the combination of two components, the buoyant weight (F_b) of clast in ice and viscous drag (F_i) (Equations 3–5), which together exert a tangential force on the contact point. In this model, an increase in clast concentration initially increases the abrasion rate, until the concentration is large enough that it interferes with the flow of ice around clasts toward the bed. This model is considered to be most appropriate for conditions with a relative low basal clast concentration (Schweizer and Iken, 1992).

$$F = F_b + F_i \quad (3)$$

$$F_b = \frac{4}{3}\pi R^3(\rho_r - \rho_i)g\cos\theta \quad (4)$$

$$F_i = \frac{f 4\pi\eta R^3}{R_*{}^2 + R^2} v_n \quad (5)$$

where R_* is the transition radius, which affects regelation and creep and R is the asperity radius, θ is the local down-glacier inclination of the bed, η is the effective viscosity of the ice, $v_n$is the ice velocity normal to the bed, ρ_r, ρ_i are the density of rock and ice, respectively, and f is a parameter describing the bed influence on modifying the viscous drag for a clast in ice (Hallet, 1979).

The primary controlling factors for the Hallet abrasion rate model include:

- Basal melt rate
- Clast concentration
- Clast properties: size and density

According to this model, high abrasion rates will occur with high basal melting rates and clast concentrations that do not impede ice flow toward the bed. The buoyant force is normally insignificant except for very large clasts. For a low roughness bed, Hallet argues that U_p approximately equals U_s (the velocity of ice).

Sandpaper model of Schweizer and Iken, 1992

In a variant of Boulton's conception of bed conditions, Schweizer and Iken (1992) considered a clast-rich sediment layer at the base of the ice that is deformable, in contrast to the rigid contact model of Boulton. In this model, the deformable basal layer is able to adjust to bed undulations. In a similar formulation to Boulton's model, the force pressing the clast to the bed depends primarily on the effective pressure, but this is adjusted by a factor s which is the proportion of the basal layer occupied by water-filled cavities.

$$F = (\rho_i g h - sP_w)A_i \quad (6)$$

Since the force is transmitted to the bed only through the contact points of the asperity and the bed (the real contact area), so larger average normal stress will occur on the contact points when the real contact area is much smaller than the apparent contact area.

On basis of the different conceptions of the abrasion process, abrasion rate tends to (1) for Hallet's model, increase with basal melting and ice velocity and be independent of normal pressure and water pressure, and (2) for Boulton's model and sandpaper model, increase with ice velocity, ice thickness, and lower water pressure. Materials produced by abrasion are removed by subglacial water or entrained in sliding basal ice through the same entrainment mechanisms described in the section on Plucking.

Erosion by glacial meltwater

Glacial meltwater is produced by the melting of surface ice due to heat transfer from contact with air and rain at temperatures above freezing point, and from the energy of incoming solar radiation, or by the melting of basal ice due to pressure, friction, and geothermal heat. Meltwater is important in the evacuation of sediment and rock fragments produced by processes such as abrasion and fracturing. In addition, meltwater flowing in subglacial channels or as films at the ice-rock interface and the sediment carried by meltwater cause erosion of bedrock or sediments by mechanical and chemical processes. Water flowing in subglacial channels responds to the overall pressure gradient in the glacier hydraulic system, which in some cases can result in water flow that is "uphill" relative to the local topography (but down-pressure with respect to the subglacial water system). Thus, channels produced by subglacial water flow can produce erosion in parts of the landscape that would not be likely to be impacted by fluvial action in normal subaerial conditions.

Mechanical erosion

Crushing and abrasion. Crushing and abrasion associated with meltwater are most effective in subglacial streams in which water flows with high velocity and carries a large sediment load. Erosion mechanisms in glacial meltwater streams are the same as in other streams and rivers (see *Glaciofluvial*; *Glacial Erosion*), and crushing and abrasion by clasts being moved by water flow share some of the same mechanics as crushing and abrasion by clasts being moved by ice flow. Clasts being moved by fluvial transport impact the channel bed and produce failures or fractures on the bed and/or the clasts, depending on their relative hardness and preexisting fractures and weaknesses. Flowing water also exerts spatially and temporally variable pressures on the bed directly that in some cases can induce fracture. Factors controlling the effectiveness of crushing and abrasion resulting from glacial meltwater include (Drewry, 1986):

- Water flow velocity
- Angle of attack
  Turbulent flow and winding channels produce large angles of impact, and thus higher erosion rates.
- Clast size, hardness relative to rock hardness, concentration
  High erosion tends to occur with large clast sizes and high clast hardness values relative to the bedrock. Erosion rates increase exponentially with clast concentrations on the order of 1%, which are typical values, and decrease for concentrations over 20%.

Cavitation. When gas bubbles created by turbulences in water flow collapse the resulting pressure wave can damage the surrounding bedrock in a process called cavitation. Gas bubbles form due to low pressures that are produced locally when water flows over an obstacle. These gas bubbles then collapse when water flow takes them into high

pressure regions. This collapse can impart large forces on channel walls and produce failures. The amount of damage caused by cavitation is dictated by the volume and content of the gas, the compressibility of the fluid, and the hardness and preexisting weaknesses of the channel bedrock (Drewry, 1986). Because turbulence favors the growth of bubbles and the collapse of bubbles increases turbulence and rock failure, there is a positive feedback that increases the amount of cavitation that occurs in a meltwater channel.

Chemical erosion

When water freezes, dissolved material in the water is preferentially excluded from the ice that is produced. When this ice melts, it produces water that is relatively pure and reactive, and which has considerable capacity to incorporate and remove material from bedrock and sediments through chemical reactions that, in aggregate, are classified as chemical erosion. Meltwater exiting a glacial system is thus commonly rich in dissolved matter, which primarily reflects exchange between meltwater and the bed and basal sediment. There are three primary mechanisms of chemical erosion:

Dissolution. Chemical dissolution is a process in which water molecules attract ions from minerals that they are in contact with and bond to them, forming ions. Water molecules bond very tightly with positively charged ions, and many common ions in minerals are soluble in water, including calcium (Ca^{2+}), sodium (Na^{+}), potassium (K^{+}), magnesium (Mg^{2+}), and ions of iron (Fe), aluminum (Al), and silica (Si). The removal of these ions is a direct loss of material from the bedrock and sediment, and weakens the remaining structure. Contact with fresh bedrock provides undersaturated meltwater with an abundant supply of ions, but once the most soluble minerals on the bed surface have been dissolved and primarily insoluble minerals, like quartz, remain, dissolution will decrease. However, because the crystal matrix on the rock surface is weakened by the dissolution of soluble ions, the remaining rock is more easily fractured by ice or meltwater, which exposes more fresh rock to dissolution. During periods when the rate of melting is low, the meltwater can become saturated which reduces the rate of dissolution; during seasons of high melt, dissolution is not limited by saturation and maximum rates depend on bedrock mineralogy, and water temperature, acidity, and pressure.

Carbonation. Carbonation is a process in which dissolved carbon dioxide (CO_2) undergoes exchange with Ca from calcite, producing free Ca^{2+} and HCO_3^{-}. As the capacity of the water to hold calcium is pressure- and temperature-dependent, when meltwater flows to lower pressure areas some of the calcium will precipitate. Thus there can be small-scale patterns of solution and precipitation under a glacier in response to local changes in basal water pressure. In terrains with calcite-rich rocks and glacial systems with high discharges of meltwater, chemical erosion can be the most significant component of total erosion.

Cation exchange. Cation exchange takes place on the surfaces of fine sediments, principally clay minerals that contain a high proportion of colloidal-sized material (Drewry, 1986). Clay minerals with negative electrical charges attract dipole water molecules and positive charged ions. The ions absorbed on the surfaces tend to exchange with other cations in meltwater. The large surface areas of fine sediments allow efficient absorption of ions.

In summary, several factors control chemical erosion by meltwater.

- Water flux and degree of undersaturation water
- Large contact surface and time of contact
- Available amount of fresh rock surface
- Concentration of free hydrogen cations
- Dissolved carbon dioxide
- The abundance of fine-grained sediments

Glacial erosion at the landscape scale

The role of basal thermal regime

In addition to considering the details of glacial erosion processes at the scale of millimeters to meters, there are larger-scale patterns of glacial erosion that are also controlled by glaciological variables (Benn and Evans, 1998). One of the primary controls on large-scale patterns of glacial erosion is basal thermal conditions. The glacial erosion processes described above have been widely assumed to be only effective under warm-based ice, because it is under these conditions that basal sliding and meltwater occur, and these are central to the erosion mechanisms described earlier in this entry. Cold-based ice is not at pressure-melting point, and under these conditions there is almost no movement between ice and the underlying bed, and thus there is little or no erosion on the bed. In fact, the traditional view has been that cold-based ice essentially protects and preserves the underlying landforms and landscape. Although this is largely true, detailed studies of erosion beneath cold-based ice have found that basal sliding, abrasion, and bed deformation do exist in these conditions. Echelmeyer and Wang (1987) and Cuffey et al. (1999) demonstrated basal sliding beneath a cold-based glacier, and Cuffey et al. (2000) presented evidence for entrainment of clasts under cold-based ice. Davies et al. (2009) have developed a model for boulder and clast entrainment, and substrate deformation by cold-based glaciers on the basis of the field observations of glacial erosion and deposition. However, although erosion can occur under cold bed conditions, the rate is believed to be very small compared to under temperate ice.

Mountain glaciers can be categorized according to their basal ice temperatures which are controlled primarily by the dominant climate system. For example, glaciers on the southeastern Tibetan Plateau and in the southern

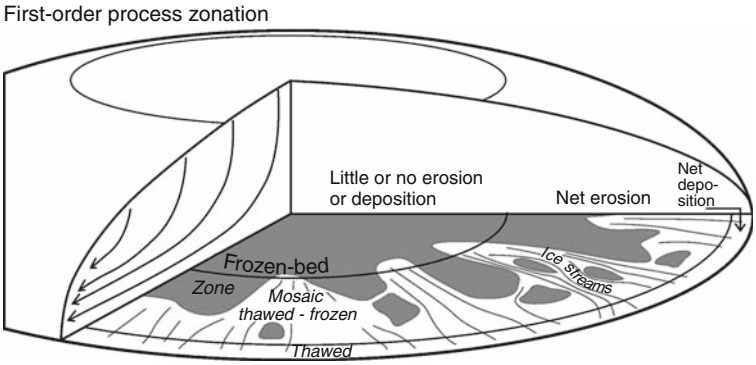

Glacial Erosion, Figure 6 The first-order organization of erosion and deposition zones under a steady-state polythermal mid-latitude ice sheet from Kleman et al. (2008).

Himalaya under monsoon-dominated climates have largely warm-based ice, while glaciers on the central Tibetan plateau under continental westerly dominated climates are typically primarily cold based or polythermal. Consequently, glaciers in the monsoon-dominated areas typically have high rates of glacial erosion and leave behind well-developed glacial landscapes including over-deepened cirques and broad and deep U-shaped valleys, whereas the continental glaciers have low rates of glacial erosion and leave behind landscapes with shallow cirques and poorly developed U-shaped valleys. Such contrasts also occur between areas of differing thermal regimes under past ice sheets. Because of the large scale of ice sheets and variations in underlying topography, different basal ice regimes can exist across the base of an ice sheet. The complex pattern of warm- and cold-ice regime patches and associated landscapes of glacial erosion and protection have been well studied for areas impacted by past ice sheets in Scandinavia (e.g., Kleman and Stroeven, 1997; Kleman et al., 2008; Figure 6). In a region that was covered by multiple past ice sheets occur uplands that have glacial erratics juxtaposed with well-preserved pre-glacial landscape features (such as tors and U-shaped valleys, Figure 7), as well as areas with deep U-shaped valleys and distinctive glacially sculpted bedrock. By comparing this landscape pattern with results from ice-sheet modeling, Napieralski et al. (2007) showed both that large-scale patterns of basal thermal regime under ice sheets likely control such landscape patterns (see also extensive discussion in Sugden and John, 1976), and that such landscape patterns can be used to help refine and calibrate ice sheet models.

The role of ice flow patterns

Ice thermal regime broadly determines whether glacial erosion occurs under a particular region of a glacier or ice sheet, whereas ice flow patterns and velocities exert a control on rates and total amounts of erosion and some of the details of the spatial patterns of glacial erosion. Five distinctive landscapes of glacial erosion have been identified, linked to broad ice-flow pattern types (Sugden and John, 1976; Benn and Evan, 1998; Table 1).

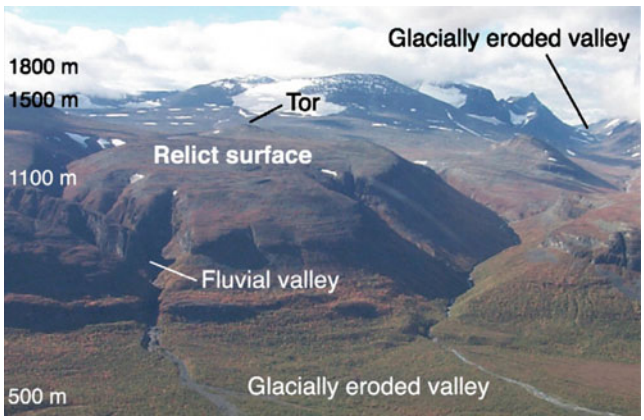

Glacial Erosion, Figure 7 Patchwork of landscape types typical of the northern Swedish mountains. Glacially eroded valleys are juxtaposed with rounded relict surfaces and V-shaped fluvial valleys (from Harbor et al., 2006, after Fabel et al., 2002).

Ice domes and sheet flow

As discussed above, under cold-based ice there is little or no erosion (Figure 7). However, under ice sheets and caps in regions of warm-based ice, relatively uniform flow across large areas produces landscapes with large-scale scouring (Figure 8) in which any major differences in topography relate to patterns of bedrock resistance to erosion. Landscapes of areal scouring include features such as rock knobs, roches moutoneés, and over-deepened rock basins, indicating extensive glacial abrasion and plucking.

Ice stream flow

Large-scale flow patterns under some current and former ice sheets include regions of ice convergence that produce high-velocity streams of warm-based ice, including outlet

Glacial Erosion, Table 1 Classification of landscapes of glacial erosion (after Sugden and John, 1976)

Glacier system	Glacier type	Process	Landscape types
Ice sheets and ice caps	Ice domes Outlet glaciers	Sheet flow Stream flow	1. Little to no erosion 2. Areal scouring 3. Selective linear erosion
Glaciers constrained by topography	Valley glaciers	Stream flow	4. Alpine landscapes 5. Cirque landscapes

Glacial Erosion, Figure 8 Areal scoured formed by ice cap on Haizi Shan Plateau of SE Tibetan Plateau.

Glacial Erosion, Figure 10 Glacial valley formed by paleo outlet glacier on the southeastern Tibetan Plateau.

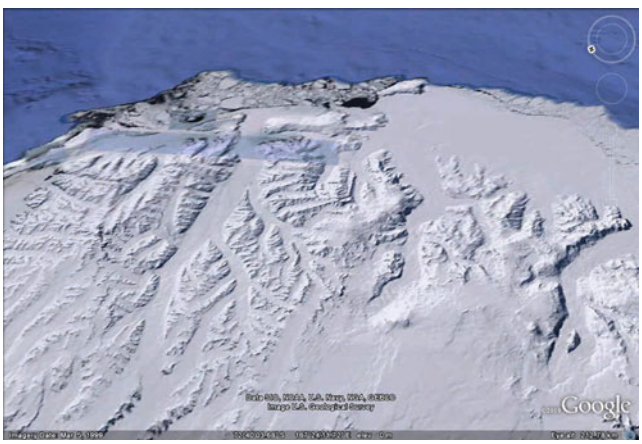

Glacial Erosion, Figure 9 Ice streams on the Antarctic ice sheet (from Google Earth).

Glacial Erosion, Figure 11 Deep glacially eroded fjords with non-eroded uplands, Meta Incognita Peninsula, Baffin Island (from Kleman, 2008).

glaciers as well as regions of high velocity within an ice sheet (Figure 9). Such ice streams produce large-scale glacial troughs, including some classic fjord landscapes (Figures 10 and 11), and typically are areas of maximum erosion by glacial ice (Hambrey, 1994a). As these troughs deepen, the increase in ice thickness and change in thermal gradient can produce a positive feedback with the deeper trough experiencing higher erosion, which in turn increases the depth of the trough. The contrast in erosion rates between the areas of streaming flow and adjacent areas produces a strong contrast in erosion rates that results in landscapes of selective linear erosion.

Summary

Glacial erosion involves a variety of physical and chemical processes that are controlled by glaciological variables on a range of spatial and temporal scales. Abrasion is a commonly recognized process of glacial erosion, and results from clasts embedded in basal ice scratching and wearing bedrock, as a clast at the base of a glacier is forced toward and moved over the bed. Abrasion acts to reduce bed roughness and is involved in features that range from small-scale striations, to larger-scale features that include whalebacks, rock drumlins, and crag and tail. Plucking involves fracture of bedrock due to impact and differential stresses applied by the ice on bedrock, followed by entrainment of the material that is released by fracturing. Plucking typically occurs on the lee sides of obstacles and bedrock steps where tensile stresses fracture large fragments and basal ice entrains the fragments by freeze-on. Glacial plucking tends to maintain roughness of a bed by producing relief in contrast to the abrasional reduction of roughness. Plucking plays an important role in shaping many large-scale landforms; many classic features such as cirques and roches moutoneés are products of a combination of abrasion and plucking (Hambrey, 1994b). Meltwater is important in glacial erosion, both as a mechanism for removing sediment and clasts created by other physical processes, and in removing material by both physical subglacial fluvial processes and chemical erosion. Based on an understanding of how glacial erosion processes work, it is possible to summarize the major glaciological controls on patterns and rates of glacial erosion as:

- Basal thermal dynamics

  Glacial erosion processes are only effective when the basal ice is sliding and there is meltwater, so warm-based ice is of prime importance to glacial erosion. Although there is some evidence that erosion beneath cold-based ice can occur, it is minimal compared to erosion under warm-based ice. Large-scale patterns of erosion are strongly influenced by areas of warm-based ice.
- Basal ice–sliding velocity

  For abrasion, the ice-sliding velocity may play a role in the force that is applied to the bed (Hallet model) and in all models of glacial abrasion it is important in determining the rate at which a clast moves across the bed, and thus striation length per unit time. For plucking, high ice velocity increases the frequency of high stress contacts between the ice or clasts, increasing the rate of fracture of bedrock and producing more rock fragments. The sliding velocity is also an important term in the rate of removal of material produced by plucking or abrasion. Thus glacial erosion is strongly dependent on sliding velocity, and, in erosion equations, the velocity term may be raised to a power greater than 1 to reflect this strong dependence. Large-scale patterns of erosion are strongly influenced by areas of high sliding velocity.
- Availability of meltwater and variability of meltwater pressure

  Meltwater plays an important role in the sliding velocity, but also can enhance fracture as a result of freeze-thaw effects in joints or fractures. In Boulton's abrasion model meltwater pressure is important in reducing effective pressure and in plucking models variability of water pressures over short time periods can produce transient stresses and load effects that enhance rock failure. Meltwater also plays a role in the efficient removal of debris produced by other physical erosion mechanisms, and creates additional erosion through fluvial abrasion, cavitation, and chemical erosion.
- Ice thickness

  Erosion process models that include effective pressure or normal pressure are dependent in part on ice thickness, and Boulton's model of abrasion is particularly sensitive to ice thickness (abrasion increases initially with increasing ice thickness, but then decreases under large ice thicknesses because the large effective pressure causes deposition of basal sediment). Ice thickness also plays a part in controlling sliding velocity, which is important in almost all of the glacial erosion processes.

Bibliography

Anderson, J. B., Kurtz, D. D., and Weaver, F. M., 1982. Sedimentation on the West Antarctic continental margin. In Craddock, C. (ed.), *Antarctic Geoscience*. Madison: University of Wisconsin, pp. 1003–1012.

Augustinus, P., 1995. Glacial valley cross-profile development: the influence of in situ rock stress and rock mass strength, with examples from the Southern Alps, New Zealand. *Geomorphology*, **14**, 87–97.

Benn, G. I., and Evan, D. J. A., 1998. *Glaciers and Glaciation*. Great Britain: Arnold, pp. 118–131. 178–192.

Boulton, G. S., 1974. Processes and patterns of subglacial erosion. In Coates, D. R. (ed.), *Glacial Geomorphology.* Binghamton: State University of New York, pp. 41–87.

Boulton, G. S., 1976. The origin of glacially-fluted surfaces: observations and theory. *Journal of Glaciology*, **17**, 287–309.

Cook, S. J., Waller, R. I., and Knight, P. G., 2006. Glaciohydraulic supercooling: the process and its significance. *Progress in Physical Geography*, **30**, 577–588.

Cuffey, K., Conway, H., Gades, A., Hallet, B., Lorrain, R., Severinghaus, J., Steig, E., Vaughn, B., and White, J., 2000. Entrainment at cold glacier beds. *Geology*, **28**, 351–354.

Cuffey, K. M., Conway, H., Gades, A. M., Hallet, B., and Raymond, C. F., 1999. Interfacial water in polar glaciers and glacier sliding at −17°C. *Geophysical Research Letters*, **26**, 751–754.

Drewry, D. J., 1986. *Glacial Geologic Processes*. London: Edward Arnold, pp. 33–82.

Davies, M. T., Atkins, C. B., Van Der Meer, J. J., Barrett, P. J., and Hicock, S. R., 2009. Evidence for cold-based glacial activity in the Allan Hills, Antarctica. *Quaternary Science Reviews*, **28**, 3124–3137.

Echelmeyer, K., and Wang, Z., 1987. Direct observation of basal sliding and deformation of basal drift at sub-freezing temperatures. *Journal of Glaciology*, **33**, 83–98.

Fabel, D., Stroeven, A., Harbor, J., Kleman, J., Elmore, D., and Fink, D., 2002. Landscape preservation under Fennoscandian ice sheets determined from in situ produced 10Be and 26Al. *Earth and Planetary Science Letters*, **201**, 397–406.
Hallet, B., 1979. A theoretical model of glacial abrasion. *Journal of Glaciology*, **23**, 321–334.
Hallet, B., 1981. Glacial abrasion and sliding: their dependence on the debris concentration in basal cie. *Annals of Glaciology*, **2**, 23–28.
Hallet, B., 1996. Glacial quarrying: a simple theoretical model. *Annals of Glaciology*, **22**, 1–8.
Hambrey, M., 1994a. *Glacial Environments*. England: UCL Press Limited, pp. 241–259.
Hambrey, M., 1994b. *Glacial Environments*. England: UCL Press Limited, pp. 81–109.
Harbor, J., 1989. Early Discoverers XXXVI: W J McGee on glacial erosion laws and the development of glacial valleys. *Journal of Glaciology*, **35**, 419–425.
Harbor, J., Stroeven, A. P., Fabel, D., Clarhäll, A., Kleman, J., Li, Y. K., Elmore, D., and Fink, D., 2006. Cosmogenic nuclide evidence for minimal erosion across two subglacial sliding boundaries of the late glacial Fennoscandian ice sheet. *Geomorphology*, **75**, 90–99.
Iverson, N. R., 1991. Potential effects of subglacial water-pressure fluctuations on quarrying. *Journal of Glaciology*, **37**, 27–36.
Iverson, N. R., 1993. Regelation of ice through debris at glacier beds: implications for sediment transport. *Geology*, **21**, 559–562.
Iverson, N. R., 1995. Processes of erosion. In Menzies, J. (ed.), *Glacial Environments: Processes, Sediments, and Landforms*. Oxford: Butterworth Heinemann, Vol. 1, pp. 241–259.
Kleman, J., 2008. Geomorphology: where glaciers cut deep. *Nature Geoscience*, **1**, 343–344, doi:10.1038/ngeo210. News and Views.
Kleman, J., and Stroeven, A. P., 1997. Preglacial surface remnants and Quaternary glacial regimes in northwestern Sweden. *Geomorphology*, **19**, 35–54.
Kleman, J., Stroeven, A. P., and Lundqvist, J., 2008. Patterns of Quaternary ice sheet erosion and deposition in Fennoscandia and a theoretical framework for explanation. *Geomorphology*, **97**, 73–90.
Liu, G. N., Chen, Y. X., Zhang, Y., and Fu, H. R., 2009. Mineral deformation and subglacial processes on ice-bedrock interface of Hailuogou Glacier. *Chinese Science Bulletin*, **54**(18), 3318–3325.
Napieralski, J., Hubbard, A., Li, Y., Harbor, J., Stroeven, A. P., Kleman, J., Alm, G., and Jansson, K., 2007. Towards a GIS assessment of numerical ice-sheet model performance using geomorphological data. *Journal of Glaciology*, **53**, 71–83.
Schweizer, J., and Iken, A., 1992. The role of bed separation and friction in sliding over an undeformable bed. *Journal of Glaciology*, **38**, 77–92.
Souchez, R. A., and Lorrain, R. D., 1987. The subglacial sediment system. In Gurnell, A. M., and Clark, M. J. (eds.), *Glaciofluvial Sediment Transfer: An Alpine Perspective*. Chichester: Wiley, pp. 147–163.
Sugden, D. E., and John, B. S., 1976. *Glaciers and Landscape: a geomorphological approach*. London: Edward Arnold, pp. 151–191.

Cross-references

Dynamics of Glaciers
Glacial Geomorphology and Landforms Evolution
Glacier Hydrology
Glacier Motion/Ice Velocity
Periglacial

GLACIAL ERRATIC

D. P. Dobhal
Wadia Institute of Himalayan Geology, Dehradun, India

A glacial erratic is a piece of rock that has been eroded and transported by a glacier to a different area and left behind when the glacier/ice melts. Glacial erratic gives information about the direction of ice movement and the distances of the transport of former glacier. Glacial erratic can be of any size from small boulder to large boulder in the size of a house or so.

GLACIAL GEOMORPHOLOGY AND LANDFORMS EVOLUTION

Alan R. Gillespie
Department of Earth and Space Sciences, Quaternary Research Center, University of Washington, Seattle, WA, USA

Synonyms

Evolution: maturation; Geomorphology: physiography; Transformation

Definition

Geomorphology. The study of the surface of the Earth: of surface elements (landforms) and the processes that create and shape them.
Glacial geomorphology. The study of the Earth's surface where it is formed or affected by flowing ice, or by water released by and in the vicinity of flowing ice.
Landscape. The community of landforms and the biological systems they support, generally at the scale of what can be seen and encompassed by an observer on a promontory.
Landscape evolution. The systematic modification over time of the systems of landforms and biota comprising the landscape; here only the systems of landforms are considered.

Introduction

Beginning about 3 Ma, the Earth's climate began a transition from the warm, humid Tertiary Period to the colder, drier Quaternary. This transition is captured in the $^{18}O/^{16}O$ ratio of benthic foraminifera extracted from marine sediment cores (Figure 1). The $^{18}O/^{16}O$ ratio is sensitive to water temperature and, especially, to the global volume of sea level, such that lowered sea levels and lower water temperatures are reflected in greater ratio values. Over the course of the Pleistocene Epoch (2.6 Ma – 11.4 ka) eustatic sea level oscillated in increasingly wide swings, but overall it dropped as more and more ice was captured in the polar ice caps and

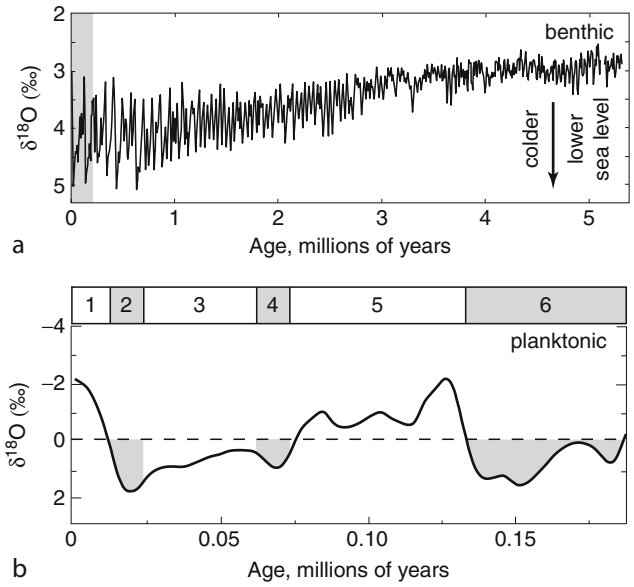

Glacial Geomorphology and Landforms Evolution, Figure 1 Marine oxygen isotope data. (**a**) Sea-level proxy record from 57 globally distributed $^{18}O/^{16}O$ ratios from benthic foraminifera (after Lisiecki and Raymo, 2005). The oxygen ratio is expressed as $\delta^{18}O = 1000\left(\left(\frac{^{18}O}{^{16}O}\right)_s \left(\frac{^{18}O}{^{16}O}\right)_{ref}^{-1} - 1\right)$ where *s* is the sample and *ref* is a reference standard. ^{18}O and ^{16}O are both present in seawater; ^{16}O is preferentially removed during evaporation. During ice ages, water from the oceans is sequestered in ice sheets and the $^{18}O/^{16}O$ ratio in the oceans is increased. This is reflected in the $^{18}O/^{16}O$ ratio in foraminifera; hence $\delta^{18}O$ is a measure of ocean volume. (**b**) Record of the past 0.2 Ma, from $^{18}O/^{16}O$ ratios from planktonic foraminifera. The record shown corresponds to the time covered by the gray bar in a. Marine oxygen isotope stages 1–6, defined by these data, are shown in the horizontal bar above the curve and by shading on the curve itself. The $\delta^{18}O$ of planktonic foraminifera is used as a record of sea surface temperature, which fluctuates along with ocean volume during climatic fluctuations. However, it is problematic because planktonic foraminifera are also sensitive to salinity and other environmental changes. Benthic records are also complex, sensitive to changes in evaporation rates and salinity during deep-water formation.

high-latitude ice sheets. Thus, minima in sea level are associated with glaciations, and maxima are associated with interglacial conditions such as we enjoy now, in the Holocene (11.4 ka – present).

Despite complexities in the interpretation of the $\delta^{18}O$ data shown in Figure 1, these data are commonly used to provide a framework for the discussion of climate during the Quaternary Period, which is divided into odd- and even-numbered marine oxygen isotope stages (MIS) (Figure 1b). During odd-numbered stages, the oceans are high and warm; during even-numbered stages, the ocean levels are low and cool. Although the stages are taken to correspond roughly to glaciations worldwide, the greatest correspondence is to the high-latitude ice sheets. Mountain glaciations show some regional and local variations in the timing of the maximum advances (e.g., Gillespie and Molnar, 1995).

Especially during the latter part of the Quaternary Period, mountain ranges around the world were glaciated repeatedly, along with the expanded high-latitude ice sheets (see entry *Ice Sheet*), during the increasingly cold intervals. This was even true in the tropics, provided the mountains were high enough – for example, >4,000 m in Papua New Guinea (Prentice et al., 2005) and Hawaii (Porter, 2005). During the Quaternary, there have been over 50 oscillations of sea level, and therefore glaciers advanced dozens of times from the mountainous peaks and ridges, down valleys, and sometimes onto the piedmonts. Thus, even if individual glaciers accomplished little, over time they have had the opportunity to modify the landscape of a significant fraction of the land area of the Earth (~20%).

In this entry, the geomorphology of glaciated regions will be reviewed first, with an emphasis on alpine or mountain glaciers. This describes how glaciers modify landscapes and fine and coarse scales. The modification of these landscapes after the glaciers have retreated will then be summarized. More coverage is available in any of several texts, for example, *Glaciers* (Sharp, 1960), *Glacial Geomorphology* (Embleton and King, 1975), *Glaciers and Landscape* (Sugden and Brian, 1976), *Glacial Geology* (Bennett and Glasser, 1996), *Glaciers and Glaciation* (Benn and Evans, 1998), *Surface Processes and Landforms* (Easterbrook, 1998), and *Process Geomorphology* (Ritter et al., 2002).

Glacial geomorphology

Glaciers modify the landscape in characteristic ways, by deposition, by erosion, and even by protection from paraglacial erosion that may affect landscapes in the vicinity of the glaciers themselves (Figure 2). The way in which the landscape is modified depends on the position relative to the glacier, the slope of the land beneath the glacier, and the temperature and thickness of the glacial ice. Thus glacial sculpting of bedrock is most pronounced near range crests, but deposition of till in constructional landforms such as kames (see entry *Kame and Kettle Topography*) and moraines (see entry *Moraine*) is concentrated near the lower part of the glacier where melting of the ice is occurring. Avalanche chutes terminate at the elevation of the glacier's surface; lower down, the glacier shields the mountain wall from the falling snow and rock.

Under very cold conditions, the temperature of the glacier ice may be below 0°C even at its base, and is frozen to the bedrock floor. Such "cold-based" glaciers (see entry *Cold-Based Glaciers*) flow by shear within the ice, and not by basal sliding facilitated by liquid water. Therefore, erosion at the glacier bed is much less than for warm-based glaciers, for which temperatures are at the freezing point, adjusted for the pressure of the overlying ice, for which ice and water can coexist. Erosion on the beds of

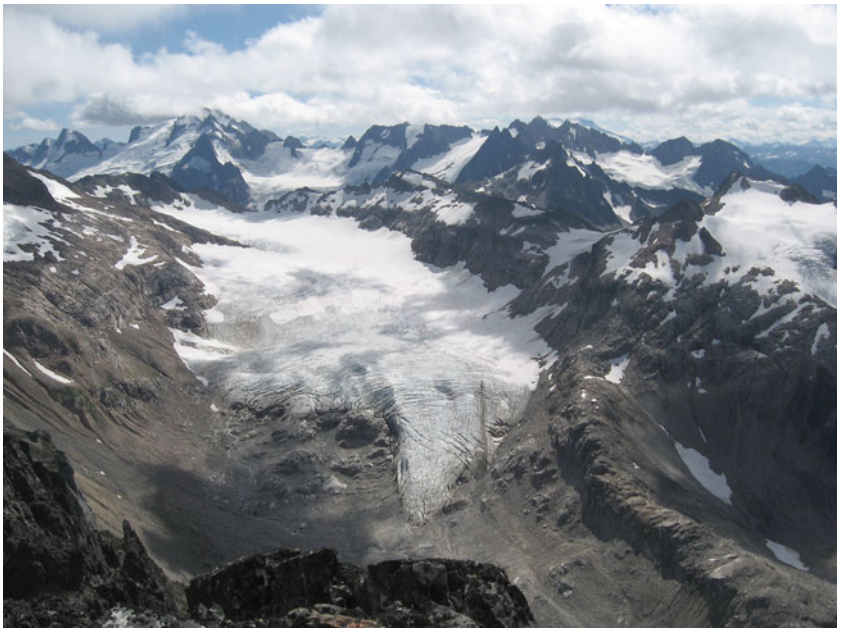

Glacial Geomorphology and Landforms Evolution, Figure 2 Landscape modified by repeated glaciation. South Cascade Glacier from Le Conte Mtn, Cascade Mountains, Washington, USA. The steep cliffs above the lateral margins of the glacier ("trim lines") were produced by glacial erosion and mark the height of the glacier during the last ice age. The crevassed ice (see entry *Crevasses*) at the toe of the glacier is darker than the snow-covered ice at higher elevations. It absorbs more sunlight and ablates more quickly than the reflective snow. View to SE. Photograph: Kurt Parker, 2007.

warm-based glaciers can even take place fluvially, from the flow of subglacial streams.

Hallet et al. (1996) have estimated glacial sediment yields (see entry *Sediment Yield*), including sediment stored in glaciated basins, and find that they vary by orders of magnitude, from 0.01 mm year^{-1} for polar glaciers, to 0.1–1.0 mm year^{-1} for temperate valley glaciers (see entry *Temperate Glaciers*) on diverse bedrock, and to 10–100 mm year^{-1} for large and fast-moving temperate valley glaciers in the tectonically active ranges. Together with solute yields, a small fraction of the suspended load, these sediment rates comprise the erosion rate beneath glaciers (see entry *Glacial Erosion*).

Glacial climate and response

Glaciers advance when more snow falls than can be melted during the summer. For maritime regions, conditions that promote glacial growth are primarily low summer temperatures and high precipitation. Low wind speeds and high humidity also promote accumulation. At high altitudes in arid conditions (<150 mm year^{-1}) where sublimation can be a significant cause of ice mass loss, cloudiness may enhance glacial growth. Summer rain may increase ice melting. The region in which snow accumulates from year to year is called the accumulation zone. As the snow thickens, pressure on the base of the snowfield increases, and the snow is compacted into firn (see entry *Firn*). With further accumulation, the ice exceeds a critical pressure and it begins to creep downhill. The thickness required for this is proportional to the topographic slope:

$$\tau = \rho g\, z \sin(\theta) \tag{1}$$

where τ is the shear stress, ρ is the ice density (0.93 g cm^{-3}), g is gravitational acceleration (9.8 m s^{-2}), z is the depth of the ice in meters, and θ is the topographic slope. Ice begins to slide with a basal shear of about 10^5 Pa (1 bar). Thus, if the bedrock slope is 10°, the glacier will be about 65 m thick. Additional snowfall will lengthen the glacier and may increase the speed of its flow, but will not thicken it. The speed of the flowing ice is determined by the topographic slope, among other factors (see entry *Glacier Motion/Ice Velocity*).

As the ice moves downhill, the atmosphere warms, promoting ablation or melting. At some altitude, the rates of accumulation and ablation balance: this is called the equilibrium line altitude, or ELA (Figure 3) (see entry *Equilibrium-Line Altitude (ELA)*), and is an important measure used in estimating past climatic conditions from the outlines of vanished glaciers. The ELA differs from the snowline in that it represents a long-term average altitude, whereas the snowline fluctuates annually and on shorter timescales. The snow–ice transition shown in Figure 2 corresponds approximately to the snowline.

Below the ELA, ablation dominates, and the glacier loses mass, slows down, and finally stops. As this happens, flow lines rise to the glacier's surface, carrying rock debris to the sides and end of the glacier. They are

left behind as the ice melts, forming moraines of till (Figure 4) – rocky debris with a roughly uniform grain-size distribution and a general lack of fabric.

Most of the erosion by the glacier of its bed occurs because the glacier drags rocky debris over the rock. This is maximized anywhere the flow lines are directed downward, thus especially in the accumulation area.

If the temperature at the base of the glacier is below freezing, such that flow occurs only by deformation within the ice (creep) and not by basal sliding, the glacier will advance much more slowly (by ~2 orders of magnitude: cm day^{-1} instead of m day^{-1}) and may become thicker than if the glacier is warm-based. However, because the freezing temperature is depressed due to the weight of the overlying ice, as the ice continues to thicken ultimately basal melting will occur and the glacier will then advance rapidly and thin (e.g., Meir and Post, 1969). The depth at which the glacier base melts is lessened because of geothermal heat trapped beneath the insulating layer of ice, and therefore the transition from cold- to warm-based glaciers can occur at a range of depths depending on both ambient temperature and heat flow.

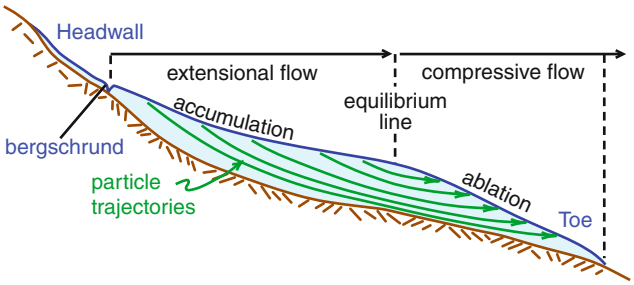

Glacial Geomorphology and Landforms Evolution, Figure 3 Schematic long profile of an alpine glacier. The bergschrund is a crevasse separating the firn and snow mantling the headwall from the moving ice of the glacier. Ice particles in the accumulation area have a downward component to their flow direction as they are buried by new snow. Near the toe of the glacier the flow has an upward component as the ice is ablated from the top of the glacier.

Glacier taxonomy

The unifying characteristic of glaciers is creep or flow under their own weight. Because of the diverse settings in which glaciers are found, and the wide range of climatic conditions under which they exist, a rich descriptive nomenclature has been developed over decades of study. An abbreviated treatment is given here.

Temperature regime... Glaciers are often classified according to their temperature profiles relative to the melting point of ice. Glaciers that are at least seasonally above the melting temperature of ice at the ice/rock interface are called "warm-based." Such glaciers commonly move relatively quickly (e.g., m/day) and erode large amounts of rock. Glaciers that do not exceed the melting point at their bases are called "cold-based" (Figure 5) and are slow moving.

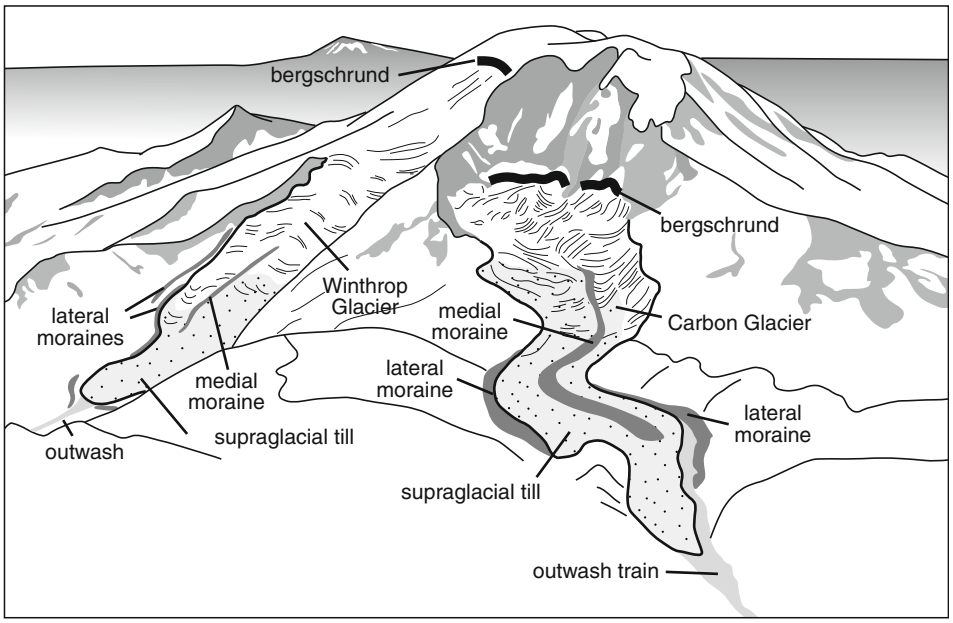

Glacial Geomorphology and Landforms Evolution, Figure 4 Temperate alpine glaciers. Lateral moraines border the glacier below its equilibrium line, where ablation exceeds accumulation and debris entrained in the ice is brought to the surface and left behind as the ice melts. Medial moraines can occur below bedrock obstructions when debris-rich concentrations of ice intersect the ablating surface, or when two glaciers and their lateral moraines merge. Entrained debris may mantle the glacier (supraglacial till) in its ablation zone. Meltwater charged with silt and rocky debris leaves outwash, or reworked till, in valleys below the toe of the glacier. Winthrop (*left*) and Carbon (*right*) glaciers, Mt. Rainier, Washington (USA).

Glacial Geomorphology and Landforms Evolution,
Figure 5 Cold-based Glacier #1 at the head of the Ürümqi River in the Tianshan range of Xinjiang, P. R. China (Echelmeyer, 1987). The glacier today carries very little debris, but the dark-colored Little Ice Age moraines below the glaciers point to earlier times when the glaciers transported more. Photograph: Dr. Ping Kong, Chinese Academy of Sciences, Beijing, China.

The melting temperature of ice depends in part on salinity, which affects sea ice, and pressure, and therefore ice density or porosity. The "pressure melting point" decreases with depth in a glacier at a rate of 0.07 K MPa^{-1}, or about 0.6 K km^{-1}. Glaciers that are below freezing throughout are called "polar," and glaciers that are at the melting point throughout are "temperate." Glaciers that are below the melting point at their base but are at the melting point in their interiors are "subpolar." Many glaciers exhibit considerable spatial complexity, and are "polythermal." For example, since glaciers flow downhill from colder to warmer conditions, some glaciers are cold-based at their tops, and warm-based near their ends. The transport of heat in percolating meltwater plays an important role in controlling the temperature profiles of glaciers.

Their temperature profiles may also change over time. Although these classifications present a simplified picture of glaciers, they form a useful and conventional framework for discussion.

Topographic constraint: Many glaciers occupy canyons or valleys, and may be referred to as "valley glaciers." Ice may also accumulate on an approximately flat upland surface, however. If ice begins to build up on a plateau, it is regarded as a firn cap (firn is intermediate between snow and glacial ice). Eventually, the deepening firn will flow outward under its own weight, driven by the weight and slope of the ice. This body of ice, not confined in a valley, is a kind of glacier called an "ice cap" and has a convex profile (Figure 6a). Larger masses of interconnected glaciers that do not overtop peaks (nunataks) and ridges are known as "ice fields," and coalesced masses of ice that do overtop the terrain are called "ice sheets." These can be very large: during the Pleistocene Epoch ice caps covered much of northern Europe (Fenno-Scandian Ice Sheet) and much of North America (Laurentide and Cordilleran ice sheets).

Coalescence: Distinction is commonly made between isolated and coalesced glaciers even in alpine settings. From the geomorphological viewpoint, this distinction is helpful because the impact of glaciers on the landscape depends in part on whether or not the ridges separating glaciers – commonly sources of rock debris transported to the glacier surface by avalanches and rockfall – are exposed and prone to avalanching, are frozen year round and largely protected by snow or firn cover from mass wasting by firn, as is sometimes the case in cold settings, or are submerged beneath flowing ice and being eroded. Because glacial flow is driven by the slope of the ice surface, and not the bedrock surface, the terrain beneath vanished ice fields and sheets can be complex, with interconnected glacial troughs and modern stream flow sometimes running contrary to the direction of ancient ice flow.

Outlet glaciers and ice streams... As ice caps thicken and coalesce, it is likely that pressure melting and enhanced sliding will occur. This leads to the formation of streams of more rapidly moving ice within the slower-flowing ice field or ice sheet. Some of these emerge from the ice cap as outlet glaciers, usually occupying valleys. In their lower reaches, these may not be easy to distinguish from trunk glaciers – large valley glaciers fed by multiple simple glaciers – but they are treated separately here because of their importance in modifying the landscape underneath the ice sheets themselves, as discussed below.

Glacial modification of the landscape

Fine-scale features

Most people who are casually familiar with glaciated landscapes probably envision temperate alpine glaciers as the responsible geomorphic agent. Glacial modification comprises the construction of relatively minor, short-lived landforms such as moraines, but also coarser-scale, longer-lived erosional features resulting from repeated glacial cycles. Examples of these can be seen in Chamonix (French Alps), Yosemite (Sierra Nevada, California, USA), and many other settings. Downstream from the glacier, glacially eroded and transported rock, gravel, sand, and silt are deposited fluvially as outwash plains that grade to the toe of the glacier. Because available sediment commonly exceeds the capacity of the glacial meltwater to transport it far from the glacier, the glacial streams are meandering and anastomosing, leaving an intermittently flooded plain of gravel bars and channels, intermixed with reworked debris-flow deposits.

The toe of the glacier is often fronted by a terminal moraine, or by a series of recessional moraines if the glacier is in retreat (Figure 7). Moraines (see entry *Moraine*) are one of the most distinctive landforms left by glaciers.

Glacial Geomorphology and Landforms Evolution, Figure 6 An ice cap on Sutai, a 4,226 m peak of the Altai range in western Mongolia. (**a**) Upper ends of the valleys have steepened headwalls and are ice-filled; the lower, V-shaped sections may appear to have been unglaciated, but low moraines at the range front suggest otherwise. (**b**) Lateral moraine left by an outlet glacier from the Sutai ice cap. Notice the linear slopes of the valley walls.

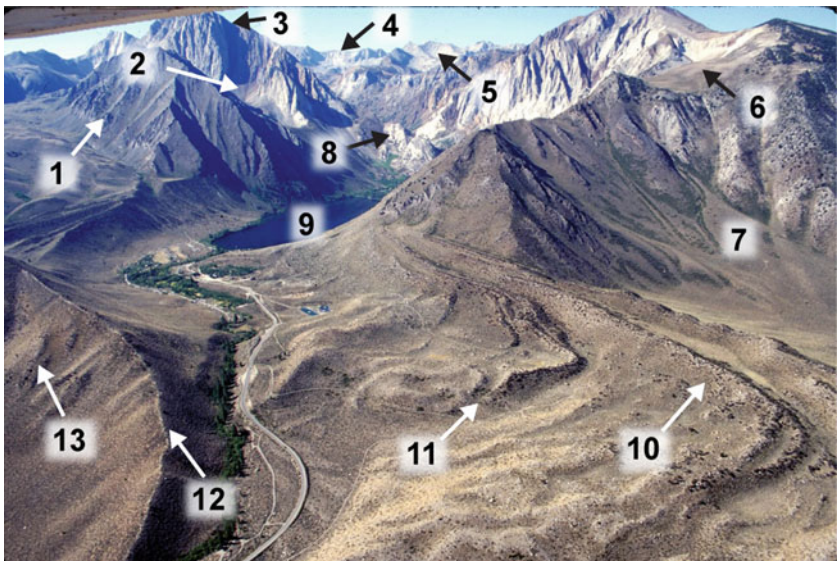

Glacial Geomorphology and Landforms Evolution, Figure 7 Geomorphic features near the toe of an ancient glacier at Convict Creek, California, USA. *1*: Trim line marking upper limit of glacial erosion and height of the ancient glacier. *2*: Hanging valley. *3*: Horn, or sharp peak sculpted on all sides by glacial erosion. *4*: Arête marking a drainage divide – a sharp ridge glacially eroded on both sides. *5*: Cirque. *6*: Felsenmere, a plateau of rocks shattered by freeze/thaw action. *7*: Debris-flow fan. *8*: Cliffs at the site of an icefall. *9*: Lake filling an overdeepened glacial trough. *10*: Recessional end moraine of LGM (MIS 2) age. *11*: Fluvial breach in recessional moraine. Road passes through another breach occupied by the modern stream. *12*: Right-lateral moraine. *13*: Remnants of largely buried older moraine. From a photograph by D. H. Clark.

Because the lateral moraines are deposited only below the ELA (see entry *Equilibrium-Line Altitude (ELA)*), their highest occurrence is one estimate of the ELA of ancient, now-vanished glaciers. Estimating the ELA this way is sometimes referred to as the "maximum elevation of lateral moraine" or MELM technique. Other techniques are also used, based on the ratios of the areas of ice accumulation and ablation, or a known fraction of the elevation difference between the toe of the glacier and the cirque headwall (Meierding, 1982; Selzer, 1994; Benn and Gemmell, 1997).

Moraines are composed of rocky debris ("till") (see entry *Till*) transported within or on top of the glacier and deposited around its perimeter below the ELA. Till is also deposited on the bed of the glacier, especially near its terminus, or mantles the glacier (supraglacial till). During glacier advance, the supraglacial till ultimately becomes part of the end moraine.

Occasionally, supraglacial till is thick enough that the glacier has the appearance of a slow-flowing river of rock: such debris-mantled glaciers are sometimes referred to as rock glaciers. Similar landforms can be created from the

growth of interstitial ice in talus and its subsequent mobilization (Barsch, 1996) (see entry *Rock Glaciers*). A good summary of rock glacier dynamics is found in Haeberli et al. (2006).

Together, primary till left directly by the glacier and till fluvially reworked as outwash are referred to, especially in the classical literature, as "glacial drift." The origins of this term lie in the early history of glacial study, when it was thought that "erratics," or out-of-place boulders littering the glaciated landscape long after the ice is gone, had "drifted" to their resting places during the Noachian Flood. Later, it was recognized that erratics had actually been moved by glaciers (cf. Lyell, 1833).

Large accumulations of drift are common only below the ancient ELA, where the glacial flow lines (Figure 3) are directed upward and where deposition is a dominant geomorphic process. Above the ELA, the ice flows downward and abrades the rocky bed. This leads to an erosional environment anywhere once covered by the flowing ice in the accumulation zone.

In its accumulation zone, the bed of an ancient glacier is rocky and irregular. Roches moutonnées are bedrock knobs that were streamlined by the flowing ice. However, larger resistant bedrock knobs may reverse this asymmetry, with steep upglacier faces and gently sloping lee tails ("crag and tail"). In this case, the crag blocks the flowing ice and reduces its erosive power immediately downglacier.

Cliffs and hollows or basins, now commonly filled with lakes, remain under ancient zones of extending and compressing flow, respectively. The top of the glacier is characteristically marked by a high cliff that once separated the snow and firn high on a mountain from the flowing glacial ice. This cliff is known as the headwall, and forms part of the uppermost basin, or cirque.

Post-glacial modification of glaciated landscapes

During and following glacial retreat, large portions of the once-glaciated landscape are susceptible to modification at a range of scales. This environment is described as "paraglacial" (see entry *Paraglacial Landscape Transformations*). Without the support of the ice and lacking vegetation to retard runoff, for example, moraines are susceptible to rilling and also undercutting by trunk streams meandering in the outwash. This leads to the formation of a catena in which the toeslope of the moraine (in lateral section) is built up at the expense of the upper slopes, which are degraded. Exposed tillstones are also eroded.

Much deglaciated terrain is subject to strong cryoturbation and solifluction, caused by the action of freeze/thaw on soils. Such cryoprocesses can move vast amounts of material downslope, a shallow (~10 cm–1 m) at a time. In this way, the appearance of the glaciated landscape is gradually smoothed.

This smoothing is not restricted to depositional landforms such as moraines, but includes the steep bedrock knobs and cliffs uncovered by the melting of the ice. The fresh bedrock characteristically spalls due to freeze/thaw cycling, and rocky talus and scree slopes build up at the foot of cliffs.

Mass wasting acts at the local scale, but running water redistributes some of the drift downriver far from the glaciated regions, much as outwash itself is transported downstream.

Paraglacial processes

Paraglacial processes (see entry *Paraglacial Landscape Transformations*) are defined by Church and Ryder (1972: 3059) as "nonglacial processes that are directly conditioned by glaciation." The same processes operate in the periglacial environment (see entry *Periglacial*) but their effects are most significant where retreating glaciers have left large supplies of unstable till together, initially, with a large flux of meltwater that can transport it down valley. As might be expected, paraglacial modification of the once-glaciated landscape is greatest immediately after glacial retreat, and diminishes thereafter as slopes and river systems achieve a new equilibrium (Figure 8). Sediment yield for local basins is thus a relaxation phenomenon, but the initial amplitude and the timescale of the relaxation are dependent on local conditions, including lithology

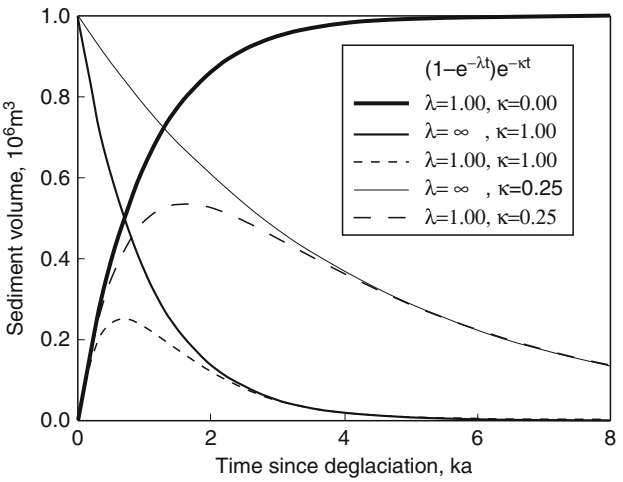

Glacial Geomorphology and Landforms Evolution, Figure 8 Sediment yield from two basins following glacial retreat: a small basin in which unstable till is being reworked, and a larger basin downstream in which sediment is deposited and also eroded and transported downstream. The thick solid curve describes the cumulative amount of the total sediment available upon deglaciation at t = 0 ka (10^6 m^3) that has been removed or stored in the basin over time, for erosion and transport at a constant rate specified by λ = 1.0 ka^{-1} (sediment volume = 10^6 $(1-e^{-\lambda t})$). The two descending solid curves (10^6 $e^{-\kappa t}$) describe sediment loss from the system for two values of κ (1.00 and 0.25 ka^{-1}, for the large and small basins, respectively), where κ is the rate of sediment loss from the sediment store, assuming that no sediment is stored in the basins. The sediment storage over time in the two basins is given by 10^6 $(1-e^{-\lambda t})$ $e^{-\kappa t}$ – after the general steady-state model of paraglacial sediment storage proposed by Ballantyne (2003).

(Ballantyne, 2002a). An excellent summary of paraglacial geomorphology is given by Ballantyne (2002b).

Sediment flux from deglaciated basins: Figure 8 shows the model behavior of two simple steady-state basins following deglaciation, at which time ($t = 0$) it is assumed the 10^6 m^3 of sediment is available for distribution. The amount of sediment remaining after time t is given by 10^6 $e^{-\lambda t}$, where λ is a constant rate of accumulation that is characteristic of the particular basin. The amount of sediment lost to storage or transport downstream is thus 10^6 $(1-e^{-\lambda t})$. The volume of stored sediment is given as 10^6 $(1-e^{-\lambda t})$ $e^{-\kappa t}$, where κ is the rate of loss from the sediment store. Both λ and κ may differ from basin to basin, and application of steady-state models such as this one offers a way to understand how landscapes have responded to glacial inheritance. A detailed treatment is presented by Ballantyne (2003).

The sediment flux from larger basins is also controlled by storage from upriver. Essentially, a wave of sediment moves down the fluvial system as sediment is first transported and then deposited as outwash terraces and fluvial bars and terraces near the glaciers, and then reworked and transported farther downstream. Therefore, the paraglacial sediment erosion and deposition history may be quite varied and complex.

Mass wasting: Paraglacial processes include mass wasting on hillslopes and mixing of the soil or regolith by freeze/thaw – cryoturbation. For example, mountain ridges are commonly scarred by avalanche chutes scoured by falling snow, ice, and rock. The controlling factors are slope, snowfall, and freeze/thaw cycling to loosen the rock. In some areas, such as the Cascade Range of North America, avalanche erosion is active today; in more arid areas such as the Sierra Nevada, avalanching may have been more common in glacial times (Figure 9). In such areas, relict avalanche chutes in cirques and glacier valleys are commonly bottomless, because the rubble ran out on the ancient glacier surface and was carried away. During interglaciations, rocky avalanche debris builds up as talus beneath the chutes. The bottom line of chutes marks in a general way the height of the ancient glacier. Talus from isolated rockfall also builds up beneath cliffs, locally as arcuate or sinuous side-valley ridges known as protalus ramparts (Ballantyne and Benn, 1994). These occur when there is rockfall onto snowbanks at the foot of a slope: the falling rock slides down the snow bank and accumulates at its foot, away from the rock slope.

Mass wasting need not be sudden. Loose rubble and soil is also translated down slopes by soil creep, or solifluction (see entry *Solifluction*). Creep generally occurs in the top few meters of the surface and can be accomplished by expansion and contraction of the soil, for instance by wetting or by freeze/thaw. When soils expand, particles are moved outward perpendicular to the slope, but during contraction (drying or melting) the particle moves downward under the force of gravity, with a resultant in the horizontal direction. Mass wasting can be greatly accelerated by saturated flow in the periglacial environment. Gelifluction (see entry *Gelisols*) is the creep of saturated soil within the active layer above permafrost. Because the viscosity of saturated soil is low, solifluction can occur even on gentle slopes of a degree or less.

Glacial Geomorphology and Landforms Evolution, Figure 9 Avalanche chutes in the Sierra Nevada, California, USA. Most chutes terminate above the cliff that marks the glacial trim line. Absence of talus below them indicates that most chute development preceded deglaciation. One chute (lighter, center) extends through the trim line, and avalanching there appears to have continued during the Holocene. Photograph by D. H. Clark.

Gelifluction and solifluction leave characteristic marks on the landscape. At the fine scale, these marks include headwall scarps and sediment lobes. At the landscape scale, they include hillslope smoothing, tors, and flat-floored box canyons that collect and channel flowing regolith. Figure 10 shows an unglaciated periglacial landscape that has been heavily modified by solifluction and freeze/thaw processes. The top of the mountain is a cryoplanation surface, flanked by two or three large terraces as the slope steepens toward the viewer. Most of the regolith has been stripped from the surface, leaving relatively smooth bedrock. Isolated bedrock knobs, or tors, have been left behind by the general lowering of the surface.

About two-thirds of the way down, the mountain flanks in Figure 10 are stubby valleys with linear slopes, convex only near their tops. Although these valleys host underfit ephemeral streams, they owe their existence and shape to long-term slope-parallel erosion. The regolith is moved down the sides of the valleys to their axes, mainly by solifluction. The sediment temporarily stored on the floors of the stubby valleys is then moved out of the mountain to the broad valley in the foreground by a combination of solifluction and occasional fluvial transport or debris flows. Solifluction is a dominant process of erosion in vast tracts of cold, arid lands where fluvial erosion is suppressed, and is also an important paraglacial process in modifying glaciated terrain.

Modeling sediment flux from hillslopes: Sediment flux from slopes is commonly estimated with diffusion-like models. For low-angle slopes, a linear diffusion equation in which flux q_s is proportional to the topographic gradient ($q_s = KS$) is commonly used, where S is the tangent of the slope angle $\left(S = \frac{dz}{dx}\right)$. This is Fick's Law for diffusion, and the empirical proportionality constant K is the diffusivity. The units of q_s are $m^3\ m^{-1}\ year^{-1}$, or $m^2\ year^{-1}$; values of K vary with lithology, vegetative cover, and other conditions, but for some slopes in unglaciated mountains $K \approx 0.0036 \pm 0.0016\ m^2\ year^{-1}$ (Roering et al., 1999). Hillslopes that erode by linear diffusion should have constant curvature, and should appear parabolic in cross section. However, for soil-mantled slopes curvature approaches zero, and the slopes are linear as in Figure 10. The V-shaped glaciated valley of Figure 6b also has linear slopes, although they are mantled by talus rather than soil.

For steep valley walls such as those in Figures 6b and 10, diffusional sediment flux is more appropriately modeled as a nonlinear function of slope (Roering et al., 1999):

$$q_s = \frac{KS}{1 - \left(\frac{S}{S_c}\right)^2} \tag{2}$$

where S_c is a critical hillslope at which soil flux becomes infinite. Physically, S_c is related to μ, the effective coefficient of friction of the regolith material. Empirically, it has been found that $S_c \approx 1.27 \pm 0.16$. Equation 2 reduces to the linear diffusion model for large values of S_c or for shallow slopes. The diffusion-like models account for creep but not for sediment transport by overland flow.

Sediment fluxes q_s calculated for different diffusivities K and critical slopes S_c are shown in Figure 11. The curve for $K = 0.0036\ m^2\ year^{-1}$ and $S_c = 1.27$ m represents typical values for mountains in the unglaciated Coast Range of Oregon, USA, where much of the analytic work in support of the flux model has been done. The production of sediment from hillslopes becomes increasingly nonlinear with slope for high diffusivities and low critical values (S_c). The hillslopes in the Oregon Coast range are linear, not convex (Roering et al., 1999), like the hillslopes of the glaciated and unglaciated valleys shown in Figures 6b and 10, suggesting that similar models might apply in these cold regions.

The slopes on the stubby valley walls shown in Figure 10 average ~21°, the depths of the valleys are 100–200 m, and the regolith thickness is ~0.5 m. For these slopes, assuming that values of S_c and K found elsewhere apply, the model sediment flux q_s of $\sim 0.002\ m^2\ year^{-1}$

Glacial Geomorphology and Landforms Evolution, Figure 10 Mountain slopes of ~21° at ~2,250 m AMSL extensively modified by prolonged or repeated solifluction in an area of modern discontinuous permafrost in west central Mongolia (48.575° N, 97.225° E) south of Telmen Lake. Vehicles provide scale. Photograph by J. Batbaatar.

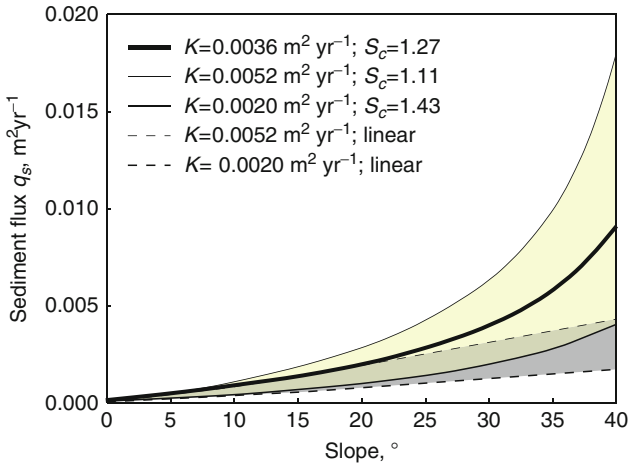

Glacial Geomorphology and Landforms Evolution, Figure 11 Sediment flux from hillslopes as a function of steepness for different soil diffusivities K and critical slopes S_c. bracketing those derived for the Coast Range in Oregon, USA (Table 1: Roering et al., 1999). For high values of S_c sediment production is closely approximated by linear Fickian diffusion.

would be sufficient to erode the entire volume of the valleys since ~200 ka. This is likely an overestimate, suggesting that the regolith has been frozen or inactive much of the time, such that K assumed above was too high or S_c was too low. However, low-diffusivity hillslopes should be convex. It may be that the steady-state sediment flux model may be overly simplified in this setting, as also suggested in general by Whipple (2001).

Nivation: Nivation represents a suite of processes that operate under and below snowfields that develop in the same place year after year. These processes include chemical weathering, creep, and erosion from meltwater flow from beneath the snowfield. Nivation operates in glaciated terrain, but it is not restricted to it.

The main effect of nivation is to create and remove fine sediments. Weathered particles are moved downslope by creep, solifluction, and rill wash. Over time, this leads to the formation of nivation hollows which, when enlarged, can be the beginnings of a cirque. Thorn (1976) reports headward erosion in nivation hollows of 0.0075 m year^{-1}. Maximum erosion requires complete seasonal meltout.

Icing: Icing ("aufeis" or "naled") accumulates during winter along stream and river valleys in arctic and subarctic environments, where it forms by extrusion of water into a freezing environment. It can reach thicknesses of several meters. The source of water may be springs or river water behind ice dams. Aufeis is commonly ephemeral, melting during the summer. As with nivation, aufeis may occur throughout the periglacial environment, but it is a common paraglacial process. For example, it may be found at the toes of glaciers in the winter, where subglacial water emerges into subzero temperatures.

Aufeis may block stream channels and cause their flood plains to widen as spring floodwaters are forced to flow around the ice (Harden et al., 1977). This may also lead to steep bedrock notches at the bottom of V-shaped river canyons. The depth of the notches is roughly the depth of the aufeis, unless the river is actively downcutting. In that case, the depth may be greater, on the order of 10 m.

The bedrock notches commonly show little or no sign of fluvial polishing. It may be that the aufeis serves mainly to hold meltwater between it and the developing notch, leading to enhanced freeze/thaw erosion and plucking of loose rock there.

Landscape-scale features

Above ("Fine-scale features"), some of the prominent effects of glaciers on their beds and immediate vicinities are described. At the coarser scale of landscapes, glaciers also have an impact. Although there is overlap in scale, it is helpful to view suites of the terrain elements, such as roches moutonnées, together with interspersed or adjacent unglaciated landforms such as ridges, as comprising the landscape.

Glaciated landscape is most obviously the work of warm-based glaciers, because they erode more rock quickly and supply larger fluxes of meltwater with which to transport sediments than to polar glaciers. In warm-based glaciers, there is liquid water at the ice/rock interface. Water enables sliding of the ice over the bedrock beneath the glacier, and consequent abrasion of the bedrock. It also enables meltwater erosion there. Although temperate glaciers commonly are warm-based, polythermal glaciers with large parts of cold ice may also have water at the ice/rock interface, and abrade the bedrock.

Glacial valleys and troughs: Perhaps the landscape signature most familiar to many is the straight, wide, parabolic or "U-shaped" valley. Figure 12a shows an example of one glacial trough, Yosemite Valley, viewed from a point just downriver of the late Pleistocene glacier. Near the terminus of the Pleistocene glaciers, as in Figure 12, Yosemite Valley is flat-floored instead of truly parabolic because of in-filling of sediment. The modern Merced River is underfit to the glaciated Yosemite Valley. In Yosemite, the steepening of the walls is enhanced by prominent master joints in the granite, making quarrying by glaciers easier.

Fluvial canyons, in contrast, are taken to have cross sections that are more nearly V-shaped although, as discussed above, the actual shape is determined in large part by hillslope processes that transport sediment from the hillslopes to the river. The contrast of the glacially eroded Yosemite Valley (Figure 12a) with a fluvially eroded canyon, in this case with linearly sloping sides, is shown by an example from the Gobi Desert in Figure 12b, but the same canyon cross section can also be seen in the unglaciated canyon of the Merced River west of the glacial terminus.

How does the glacier work on the landscape to transform a fluvial valley into a parabolic trough? The principal mechanism is the abrasion of the valley walls by the

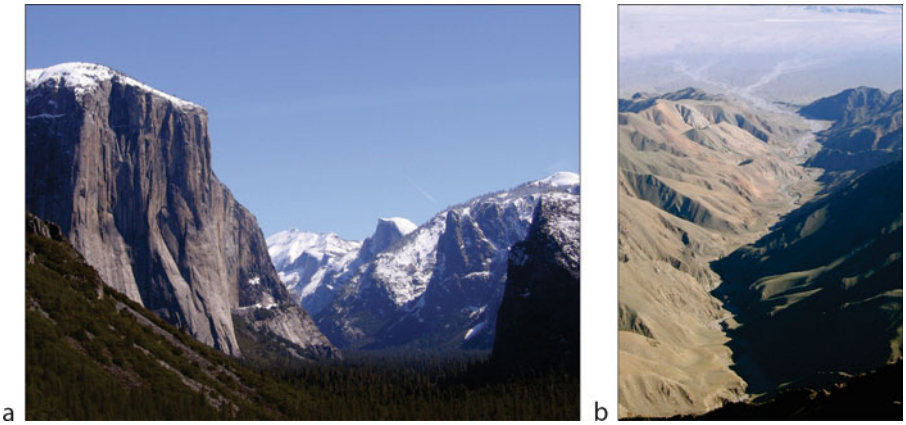

Glacial Geomorphology and Landforms Evolution, Figure 12 Glaciated and unglaciated valleys. (**a**) Yosemite, California, USA, a "classical" U-shaped glacial trough of the Merced River. View is to the east, upriver. Glaciers of the last glacial maximum terminated in the foreground. The steep-sided bedrock walls are due to glacial erosion; the flat valley floor is due to filling of a glacially overdeepened basin that hosted a lake following glacial retreat. (**b**) An unglaciated valley on the northern flank of Ih Bogd, Gobi-Altai. Rapid uplift of the massif along the Gobi-Altai fault on the range front has led to recent incision at the bottom of the V-shaped canyon. The shape of the regolith-covered hillslopes is determined by mass-wasting processes such as debris flows and creep.

glacial ice, especially ice with entrained rocks that are dragged across the rock of the glacier bed. The abrasion is proportional to the ice velocity, which is not everywhere the same, but it also increases with the amount of debris content in the basal ice layer via the influence of friction on sliding (e.g., Schweizer and Iken, 1992). Quantitative models describe two endmember behaviors: one in which rock grains are completely encased by ice and are isolated from each other ("Hallet friction"), and one in which there are so many that they are in contact ("sandpaper friction"). A major difference is that in the former case, glacial sliding may be continuous, whereas in the latter it may be seasonal, stopping in winter when basal water pressure is low. Schweizer and Iken (1992) described the basal sliding velocity μ'_b for "sandpaper friction" by

$$u'_b \approx \left(\frac{\tau'_b}{P'_c - P'_s}\right)^n \; for\, P_{w_s} \le P'_s;$$
$$u'_b \approx \left(\frac{\tau'_b}{P'_c - P_w}\right)^n \; for\, P_{w_s} > P'_s \qquad (3)$$

where τ'_b is the effective basal shear stress, P'_c is the critical pressure at which sliding becomes unstable, P_w is the water pressure, P'_s is the separation pressure necessary to lift the ice from the bed, n is a flow-law parameter (generally 3 or less), and primes ($'$) denote variables depending on friction. As long as $P_w < P'_c$ sliding will be continuous, but when $P_w > P'_c$ sliding will stop. Hallet et al. (1996) estimated that abrasion ranges from 0.01 to 10 mm year^{-1}.

As shown in Figure 13a, when clean ice fills a fluvial valley, the greatest ice velocity – and the greatest erosion – will occur midway up the glaciated sides of the valley. At first, erosion widens the valley more than it deepens it, and moves the locus of erosion farther down the valley walls. Ultimately the walls are steep, and the greatest effect of glacial erosion is then to deepen the valley. However, subglacial erosion proceeds not only from the abrasion by the ice itself, but also by subglacial meltwater flowing in channels under the ice. Meltwater within the glacier, or flowing along its base, can significantly modify the cross section of the glaciated valley, both by erosion of the walls and valley floor and by redistribution of upslope sediment. Strong basal flow can explain glacial erosion far below sea and lake levels (e.g., Zemp et al., 2005), and the sediment from the base of the glacier that occupied the Puget Sound in the northwestern USA was primarily evacuated by subglacial waters (Booth and Hallet, 1993).

Glacial troughs flooded by sea water after glacial retreat, especially in mountainous terrain such as the west coast of Norway or Canada, are known as fjords (see entry *Fjords*). Their overdeepened basins store a significant fraction of the sediment produced by the glaciers (e.g., Cowan et al., 2010), which otherwise would have been transported onto the continental shelves.

The head of the glacier also modifies the landscape characteristically, ultimately producing a wide, steep-headed hollow or cirque, commonly overdeepened. Cirques enlarge laterally as well as deepening. Ultimately, cirques from opposite sides of a mountain meet, leaving only a thin septum (arête) between them. Peaks similarly are eroded into rocky spires or horns, as the three (or more) cirques they shelter enlarge.

Figure 13b depicts the long profile of a glacier in its cirque. Glaciers start when ice accumulates in the head of a fluvial canyon or in a nivation hollow. Modification of the cirque area begins when ice is deep enough to begin flowing. Glacier ice separates from firn at the headwall bergschrund, where blocks are incorporated into the glacier and transported away, steepening the headwall. Downward ice flow in the accumulation area further

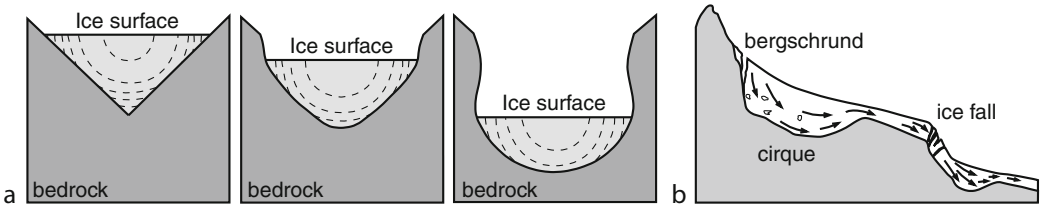

Glacial Geomorphology and Landforms Evolution, Figure 13 Glacial erosion. (**a**) Schematic cross sections of a warm-based alpine glacier evolving over time from an initial V-shaped fluvial valley to a parabolic glacial trough (*left* to *right*). Dashed lines indicate loci of equal ice speed, decreasing from the inner part of the glacier to the contact with the walls. Erosion is proportional to ice speed; therefore, the middle parts of the glaciated valley wall are eroded most quickly at first. As the valley widens, the ice speed over the bottom increases and deepening quickens. After Harbor et al. (1988). (**b**) Schematic long profile of the upper reaches of an alpine glacier. The direction of ice flow is shown by arrows. Glacier ice separates from firn at the headwall bergschrund, where blocks are incorporated into the glacier and transported away, steepening the headwall. Downward ice flow in the accumulation area further erodes and overdeepens the cirque where the ice flow is redirected (*arrows*). Other overdeepened basins (*right*) occur downglacier, typically beneath ice falls or at the confluence of ice streams.

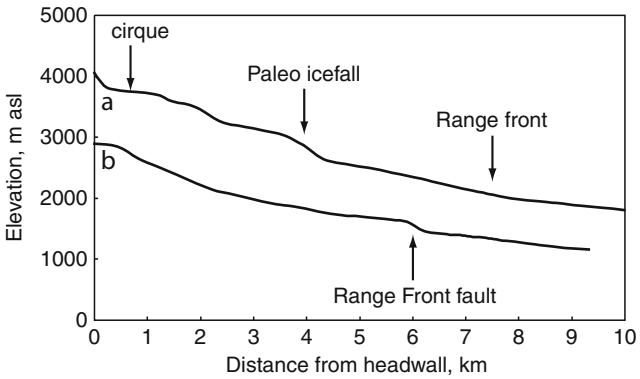

Glacial Geomorphology and Landforms Evolution, Figure 14 Long profiles of (**a**) glacially eroded and (**b**) fluvially eroded valleys (schematic). Lone Pine Creek (**a**) and Olancha Peak (**b**), Sierra Nevada, California (USA). Elevation data: Google Earth.

erodes and overdeepens the cirque where the ice flow is redirected (arrows in Figure 13b). Other overdeepened basins occur downglacier, typically beneath ice falls or at the confluence of ice streams.

Overdeepened basins are a signature for glaciated valleys, although they are not ubiquitous in lightly glaciated regions. Their presence distinguishes glaciated valleys clearly from fluvial valleys. Figure 14 contrasts the long profiles of nearby glaciated and fluvial valleys from the Sierra Nevada (USA). After retreat of the glaciers, the basins are filled by lakes (strings of such lakes are called "paternoster" lakes (see entry *Paternoster Lakes*)). The lakes ultimately trap sediment and become meadows, but until they are filled they ensure that the only sediment transported by the river out of the mountains originates below the lowest step in the glaciated zone.

Ice caps and ice fields: During glaciations, plateaus above the ELA may become covered by ice caps. Valley glaciers themselves may overtop their ridges and coalesce, as is happening today on Mt. Rainier (Figure 4), for example, between the Winthrop Glacier and the Emmons Glacier (unlabelled in the figure) to its left. Figure 15 is a satellite image of a large area of the deglaciated Sayan mountains of Siberia (see entry *Altai-Sayan Glaciers*) that was covered by a large ice field at the end of the Pleistocene, perhaps ~15 ka.

Subglacial rivers and ice streams within the Sayan ice field eroded wide troughs in the bedrock as the ice field thickened and pressure melting caused the basal ice to slide over the bed. These are readily distinguished from the smaller, simple hanging valleys that once contained glaciers tributary to the ice streams. Ultimately, the troughs hosted outlet glaciers that reached beyond the edge of the ice field itself. The traces of such ice streams are locally anastomosing and reflect pressure gradients within the ice cap (i.e., rather than bedrock topography), and therefore appear to run uphill. Some are continuous across modern fluvial divides. In all this they differ dramatically from fluvial networks in unglaciated terrain and from simple drainages once occupied by individual, isolated glaciers. The complex, crossing traces of the abandoned glacial troughs, 2–4 km across, are obvious in the bottom right of Figure 15.

Because erosion of large subglacial troughs may be accomplished by pressurized subglacial fluvial flow (e.g., Piotrowski, 1997; Zemp et al., 2005), it is reasonable to ask what fraction of their erosion was fluvial and what fraction was due to glacial abrasion. In the Sayan mountains, the answer is uncertain, but there seem to be few subglacial channels cut within the trough valleys, and it is clear from moraines along their sides that at least some were occupied by debris-carrying glaciers.

In Figure 15 is a large complex valley trending northeast-southwest. This valley, nearly 8 km across, today hosts an underfit southwest-flowing stream. In its lower elevations (reddish because of increased vegetation cover) are numerous streamlined ridges and knobs, glacially sculpted. The broad valley also hosts smaller canyons with twisting paths, some of which start and end abruptly. These probably were cut by water flowing beneath the glacial ice.

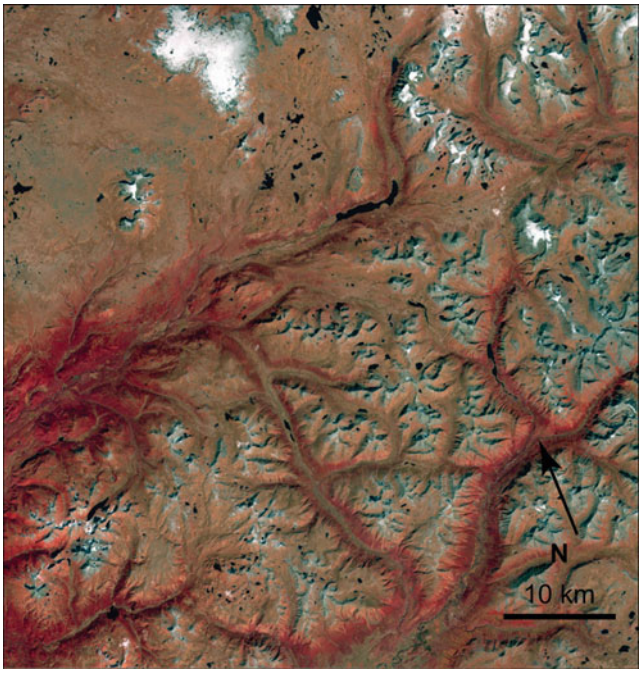

Glacial Geomorphology and Landforms Evolution, Figure 15 NASA ASTER false-color image (vegetation is red) of the Sayan mountains on the Mongolian-Siberian border (52.2°N, 98.5°E), which were mantled by a large Pleistocene ice field. Ice streams within the Sayan ice cap eroded wide troughs in the bedrock that deepened to hoist outlet glaciers reaching beyond the edge of the ice cap itself. The traces of such ice streams may be anastomosing and reflect pressure gradients within the ice cap (i.e., rather than bedrock topography), and therefore appear to run uphill. Image is ~60 km across.

Only the highest terrain protruded from the Sayan ice field, and other ice fields like it, as nunataks. In Figure 15, these ridges appear sharp relative to the smoothed bed of the ancient ice field. Some of these nunataks are snow covered white in (Figure 15) and some are above tree line and appear bluish in the ASTER image, in contrast to the reddish-appearing vegetated slopes. The narrow arêtes and numerous well-developed cirques suggest a terrain heavily modified by glacial erosion.

Cryoplanation surfaces: Nunataks are common in terrain mantled by ice sheets; however, flattened terrain with tors or nunataks can also result from parallel slope erosion due to permafrost action (e.g., Washburn, 1979; Czudek, 1995) and nivation (Reger and Pewe, 1976), which causes mass wasting promoted by the presence of meltwater from permanent snow banks. Such surfaces are called cryoplanation surfaces or terraces. Cryoplanation proceeds in the absence of glacial cover, for example, between glaciations.

The next step in evolution of the glaciated landscape would be the complete erosion of the nunataks, leaving a nearly continuous ice field during glaciations and a smoothed, subdued bedrock topography during interglaciations. Such are terrain can be seen in the northwestern quadrant of Figure 15, in the vicinity of the single isolated nunatak.

A detailed view of an unusual nunatak of schist bedrock that emerged from a different ice field on the southern edge of Siberia is shown in Figure 16. The hanging valleys now filled by lakes are cirques that were occupied by small glaciers after the main ice cap melted. The trunk valley (leading down and to the right in the figure) has a complex long profile (similar to the one in Figure 14a) and bedrock hollows are now occupied by paternoster lakes. The high mountain center is the nunatak. Although its flanks have been sculpted by cirque glaciers, its top is a plateau, possibly a cryoplanation surface but little affected by glacial erosion.

The flanks of the nunatak consist of stepped subhorizontal terraces, themselves a kind of cryplanation terrace (e.g., Figure 9: Lauriol and Godbout, 1988). They are widely – but not ubiquitously – present where there were ice fields in the mountains of northern Central Asia (e.g., Figure 17). The stepped terraces shown in Figure 16 are of interest because they appear to record episodes in the thinning of the ice field (see entry *Thinning of Glaciers*) during deglaciation when freeze/thaw fracture of the exposed bedrock could occur (e.g., Komatsu et al., 2008). In general, however, stepped cryoplanation surfaces can also develop in the periglacial environment.

Loess: Many glaciers produce an abundance of silt-sized finely ground rock during the erosion of their beds, and this silt ("rock flour") is transported to their outwash plains ("sandurs") as long as the glaciers are active. It is this rock flour that colors glacial lakes light blue and green. After deposition with the outwash, this silt is available for aeolian transport and redeposition as loess.

This redeposition is one process by which the influence of glaciers can be felt over great distances. Glacial loess is found on the perimeter of the Laurentide Ice Sheet, in the Mississippi River valley and on the perimeter of the Fenno-Scandian Ice Sheet, for example, in northern Europe. The loess of the Ukranian steppes is as much as ~500 km from the edge of the ice sheet. Glacial loess is also found against smaller ice fields and systems of alpine valley glaciers.

Loess drapes the landscape, changing its form and character. Local drainage networks in loess can be trellised and intricate. Loess deposits hold cliffs especially well, and people have carved houses into them. Loess provides a large surface area of fresh rock, which can weather quickly to provide nutrients for vegetation. However, the organic content is negligible and it therefore takes thousands of years to develop good soils for agriculture. As it erodes, loess can choke river systems, leading to braided channels and rapidly growing deltas, far from the source glaciers.

Not all loess is glacial. The association of loess with warm deserts and drylands has caused some of these deposits to be called "desert loess," and the silt from these

Glacial Geomorphology and Landforms Evolution, Figure 16 Deglaciated terrain near the edge of a former Pleistocene ice cap of the Ulaan Taiga mountains, northern Mongolia (51.43°N, 99.88°E). View is to the south; the central mountain is ~5 km across. Vertical exaggeration: 3×. Image courtesy of Google Earth.

may be created by mechanical weathering of sands caused when the sand grains strike each other and break during wind transport (e.g., Whalley et al., 1982).

Some loess deposits, such as the famous ones of the Loess Plateau in China, are regarded as desert loess because they are downwind from huge sand sheets and dune fields. However, in the source regions of the Taklimakan desert of central Asia, silts are also produced glacially in the high mountains rimming the desert, and the outwash has also provided at least some of the desert sands from which silt is created. Thus, some desert loess may be in part glacial in origin.

Lakes: During and after glacial retreat, one of the main processes of landscape modification is the impounding of water in lakes. The impounding occurs at all scales. As viewed from space, the most obvious of the glacial lakes are the five Great Lakes – Superior, Michigan, Huron, Erie, and Ontario – of North America. These lakes occupy tectonic basins deepened by the Laurentide Ice Sheet. Together, they cover more than 245,000 km^2 and contain a fifth of all the unfrozen fresh water in the world. However, during the retreat of the Laurentide Ice Sheet, much of central Canada was covered by glacial Lake Agassiz. Although largely drained today, at its peak Lake Agassiz covered over 350,000 km^2 and contained half again as much water as the modern Great Lakes.

The effect of glaciocenic lakes was threefold. When they were filled, they acted as sediment traps for glaciogenic silt. Upon their draining, this silt remained behind and – as in the loess belts – formed a rich soil. The lakes also modified the local climate directly, by the "lake effect" in which water was evaporated from the lakes and precipitated downwind. In the case of such large lakes as Lake Agassiz (~600 km diameter), the scale of the lake effect must have been roughly comparable to the scale of cyclonic storms. Lakes also reversed drainages, sending water once bound for one ocean to another. Several examples come from northern Europe, where the Finno-Scandian Ice Sheet impounded north-flowing rivers forming lakes that deepened and finally overflowed down south-flowing rivers such as the Volga until the water flowed south (Arkhipov et al., 1995). Similarly, the Great Lakes once drained down the Mississippi River to the Gulf of Mexico, only switching to the St. Lawrence River and the North Atlantic with the collapse of the Laurentide Ice Sheet. This switching of large volumes of freshwater is thought to have triggered a major climate excursion at the end of the last deglaciation (Rooth, 1982; Broecker et al., 1989).

Not only are large lakes impounded glacially, but numberless smaller ones, too. Often these are in a setting with higher relief, and these lakes are prone to sudden draining. The resulting outburst floods can modify landscape far from the glaciers themselves.

Outburst floods (see entry *Glacier Lake Outburst Floods*): Outburst floods (e.g., O'Connor and Baker, 1992; Komatsu et al., 2008) are among the most dramatic and transformative of the paraglacial processing modifying landscapes. Although they originate near glaciers, they affect not only the near field, but also cause erosion and deposition far from their source.

Outburst floods are of two main kinds: those originating as meltwater stored within glaciers and those from lakes impounded by glaciers. Meltwater can be trapped

in crevasses or thermokarst ponds, and between glaciers and valley walls. Sooner or later, this water escapes subglacially, or as an ice-marginal river. Water can also accumulate in subglacial lakes. It may originate as ice melted by volcanic heat, or simply by pressure melting as the burden of ice above it increases in thickness. Sudden floods erupting from underneath glaciers are called jökulhlaups.

Lakes are also created by glaciers advancing down tributary canyons, damming rivers. The giant Missoula Floods across the state of Washington (USA) are an example (Bretz, 1923). The impounded lake was 2,220 km^3 in volume. It apparently drained catastrophically and refilled more than 40 times between 23 ka and the final retreat of the Cordilleran Ice Sheet in North America (Waitt 1985; Benito and O'Connor, 2003). More than 25 floods had discharges ranging from 10^6 to 10^7 m^3 s^{-1}, and the advancing wall of floodwater where the Columbia passes through the Cascade Mountains was as high as ~200 m. In sum, more than 200 km^3 of rock was eroded in flows exceeding 30 m s^{-1} and deposited downstream as far as the Pacific Ocean. Floods on this scale are transformative events at the landscape scale that widely scour the landscape of soil, widely erode bedrock, and cut new river channels.

Geochronology

Dating is the way we correlate spatially separated landforms and deposits, and the way we link glacial history to global and other records of climate, for example, to the climate and sea-level proxy of Figure 1. There are many techniques that are used to determine the age of deposits in glaciated terrain, such as optically stimulated luminescence and radiocarbon. In geomorphic studies, it is often as important to learn something of the dynamic behavior of landforms as it is to learn their age. The standard approach is to obtain dates in a deposit, from which an age–depth curve can be constructed. The slope of the curve gives depositional rates over time, but the depositional age of the material currently at surface is only a maximum age for the surface itself, since it might be eroding. Furthermore, unless the actual time at which deposition ceased can be established, estimating the rate of erosion is not feasible. Analysis of rock surfaces is likewise difficult and indirect.

Below, one approach that can be used to date the age of eroded surfaces and moraines and other depositional landforms, and also to measure erosion rates directly is briefly reviewed. The approach is based on the concentration of rare nuclides produced by the interaction of cosmic neutrons with atmospheric and earth materials. ^{14}C is one such nuclide, produced in the atmosphere and incorporated in living matter until death, after which concentrations decrease at a constant rate due to radioactive decay. The equation describing the concentration of cosmogenic nuclides such as ^{14}C is

$$N = \frac{N_o}{\lambda} e^{-\lambda t}; \quad \lambda = \frac{\ln(2)}{t_{1/2}} \tag{4}$$

where N is the concentration of the cosmogenic nuclide (e.g., ^{14}C) (atoms g^{-1}), N_o is the concentration at death of the organism, P is the production rate (atoms g^{-1} $year^{-1}$), λ is the decay constant for the radioactive nuclide ($year^{-1}$), t is time elapsed since exposure (year), and $t_{½}$ is the half-life of the nuclide. For ^{14}C, $t_{½} = 5{,}730$ year and $\lambda = 0.000121$ $year^{-1}$. The age can be estimated via inversion of Equation 4 since there is one unknown, t, and one measurement, N.

Other cosmogenic nuclides are produced by exposure of minerals to cosmic rays, for example, ^{10}Be from the silicon in quartz. In this case, the rock absorbs the neutrons such that the production of the cosmogenic nuclides decreases exponentially with depth below the free surface. For eroding surfaces, the growth equation is thus complicated by inclusion of factors describing the shielding and the erosion of the surface since exposure, since erosion will reduce the concentration N of the nuclide available to measure:

$$N = \frac{P}{\left(\rho\varepsilon\Lambda^{-1} + \lambda\right)}\left(1 - e^{-(\rho\varepsilon\Lambda^{-1}+\lambda)t}\right) \tag{5}$$

where ρ is the mineral density (g cm^{-3}), ε is the erosion rate (cm $year^{-1}$), and Λ is an attenuation coefficient (g cm^{-2}) that describes the absorption of neutrons. The exposure age t for a surface sample is calculated from the measured isotope abundance (N) after a correction has been made for radiogenic and geologic background concentrations not shown in (Equation 6) and the decay of the nuclide if it is unstable (Lal, 1988).

For ^{10}Be, $t_{½} = 1.6 \times 10^9$ year ($\lambda = 4.56 \times 10^{-7}$ $year^{-1}$) such that meaningful ages could be found for surfaces hundreds of thousands of years old. However, over most of the Earth erosion is great enough that it precludes simple calculation of age for surfaces older than ~50,000 years. For the geomorphologist, Equation 5 presents an opportunity to measure long-term landscape denudation rates (Bierman, 1994) because, for constant erosion, Equation 5 asymptotically approaches an equilibrium limit between nuclide production, decay, and surface erosion. This can be seen by substituting $t = \infty$ into Equation 6, which then reduces to

$$N = \frac{P}{\left(\rho\varepsilon\Lambda^{-1} + \lambda\right)} \tag{6}$$

from which the erosion rate can be calculated.

The opportunity to measure ε provides the geomorphologist with the opportunity to determine denudation rates for landscape elements for which rates previously had to be inferred less directly. In a study of old landscapes in Namibia, for example, Bierman and Caffee (2001) determined that the surface there was lowering at 3.2 ± 1.5–3.6 ± 1.9 μm $year^{-1}$, consistent in a general way with independent measurements.

Equation 5 is underdetermined, with two unknowns (ε and t) for each measurement (N). By measuring two

nuclides with different decay constants, for instance ^{26}Al and ^{10}Be, from the same sample, it is possible to balance the number of knowns and unknowns, and solve for both ε and t. With the improvements in analytic precision of the past decade, this approach has potential in the analysis of rapidly eroding, youthful terrains, for which it the erosion rate cannot be assumed, and the age is less than several half-lives (e.g., Gillespie and Bierman, 1995).

Concluding comments

Glaciers are powerful forces that have shaped and reshaped a significant fraction of the land surface of Earth during the Quaternary Period, since 2.6 Ma. They occur as high-altitude alpine glaciers even at low latitudes, and as continental-scale ice sheets at high latitudes. Glaciers modify the landscape in characteristic ways by erosion in their upper reaches, and deposition near and below their toes. Glaciers also promote the activity of other powerful forces acting on the landscape, for example, outburst floods.

The overall effect of glaciers on landscapes depends on the amount of time the landscape has been glaciated, and the intensity of competing effects such as tectonism. However, the first stages of alpine glaciation tend to increase terrain relief and straighten and widen glaciated drainages. In the limit, terrain is subdued as the mountain horns and arêtes and other relict terrain features are encroached on by cirques and widening valleys from all sides. Under the limits of former ice fields and sheets, especially at high latitudes, deglaciated terrain is commonly subdued.

Glacial geomorphology is the study of landforms in and around glaciated terrain and the processes of deposition and erosion that create and modify them. The study of these landforms and processes addresses the complex response of the Earth system to climate at the high elevations and latitudes that have experienced glaciation today or in the past.

The motivation for studying glacial geomorphology has changed since it began. Originally, the main goal was to understand in a general way how the landscape came to be the way we found it, and in doing this taxonomic classification was a big early step. Later, analysis shifted in favor of quantitative mathematical models that were based on physically meaningful equations, with values for coefficients empirically determined from field study. Especially for studying vanished ice sheets and glaciers, that could not be inspected directly, the mapping of glacial geomorphologic traces has been of great value for such parameterization and numerical model simulation.

In the context of recent concerns about climate change and the role human activity has had in causing it, glacial geomorphology is important because it is a record of the "natural" climate baseline – the way the Earth's climate system has behaved in the past before the effects of industry, and within what limits. Without this baseline, it is hard to assess the significance of the changes that are occurring today. The predictive forward models discussed in the paragraph above are now called on in a different way, to help with the inference of the past conditions that led to the creation of the evidence. The quantitative models are necessarily simplifications of the "real world" and this model inversion is difficult to the extent that quantitative modeling has not captured the whole picture.

Thus a major challenge lies in inversion of the process models that describe the advance of glaciers in terms of climatic parameters – summer temperatures and cloudiness, and winter precipitation. This inversion is inherently an underdetermined problem: there are too many unknowns and too few meaningful measurements to allow an unambiguous estimation of, for example, paleo precipitation from reconstructed ELAs. Nevertheless, in concert with other investigative approaches – palynology, for example – it is often possible to constrain paleo conditions in a useful way.

The geomorphic record is characterized by spatial detail – today there are 6,000 glaciers in Kyrgyzstan alone – but the record is often incomplete. Early glacial deposits, for example, are often obliterated by later, larger glaciers. In contrast, extracting sediment and ice cores can give a rich and detailed temporal record, but it is expensive and time consuming, and therefore it is hard to capture spatial heterogeneity. The combination of multiple complementary approaches is necessary to tell the whole story.

Bibliography

Arkhipov, S. A., Ehlers, J., Johnson, R. G., and Wright, H. E., Jr., 1995. Glacial drainage towards the Mediterranean during the Middle and Late Pleistocene. *Boreas*, **24**, 196–206.

Ballantyne, C. K., 2002a. A general model of paraglacial response. *The Holocene*, **12**, 371–376.

Ballantyne, C. K., 2002b. Paraglacial geomorphology. *Quaternary Science Reviews*, **21**, 1935–2017.

Ballantyne, C. K., 2003. Paraglacial landform succession and sediment storage in deglaciated mountain valleys: theory and approaches to calibration. *Zeitschrift für Geomorphologie*, **Suppl 132**, 1–18.

Ballantyne, C. K., and Benn, D. I., 1994. Glaciological constraints on protalus rampart development. *Permafrost and Periglacial Processes*, **5**, 145–153.

Barsch, D., 1996. *Rock Glaciers. Indicators for the Present and Former Geoecology in High Mountain Environment*. Heidelberg: Springer.

Benito, G., and O'Connor, J. E., 2003. Number and size of last-glacial Missoula floods in the Columbia River valley between the Pasco Basin, Washington, and Portland, Oregon. *Geological Society of America Bulletin*, **115**, 624–638.

Benn, D. I., and Evans, D. J. A., 1998. *Glaciers and Glaciation*. London: Edward Arnold. 734 pp.

Benn, D. I., and Gemmell, A. M. D., 1997. Calculating equilibrium-line altitudes of former glaciers by the balance ratio method: a new computer spreadsheet. *Glacial Geology and Geomorphology*, http://ggg.qub.ac.uk/ggg/

Bennett, M. R., and Glasser, N. F., 1996. *Glacial Geology: Ice Sheets and Landforms*. Chichester: Wiley. 376 pp.

Bierman, P. R., 1994. Using in situ produced cosmogenic isotope to estimate rates of landscape evolution: a review from the geomorphic perspective. *Journal of Geophysical Research*, **99**(B7), 13-885–13-896.

Bierman, P. R., and Caffee, M., 2001. Slow rates of rock surface erosion and sediment production across the Namib Desert and Escarpment, Southern Africa. *American Journal of Science*, **301**, 326–358.

Booth, D. B., and Hallet, B., 1993. Channel networks carved by subglacial water: observations and reconstruction in the eastern Puget Lowland of Washington. *Geological Society of America Bulletin*, **105**, 671–682.

Bretz, J. H., 1923. The channeled scabland of the Columbia Plateau. *Journal of Geology*, **31**, 617–649.

Broecker, W. S., Kennett, J. P., Flower, B. P., Teller, J. T., Trumbore, S., Bonani, G., and Wolfli, W., 1989. Routing of meltwater from the Laurentide ice sheet during the Younger Dryas cold episode. *Nature*, **341**, 318–321.

Church, M., and Ryder, J. M., 1972. Paraglacial sedimentation: a consideration of fluvial processes conditioned by glaciation. *Bulletin of Geological Society of America*, **83**, 3059–3071.

Cowan, E. A., Seramur, K. C., Powell, R. D., Willems, B. A., Gulick, S. P. S., and Jaeger, J. M., 2010. Fjords as temporary sediment traps: history of glacial erosion and deposition in Muir Inlet, Glacier Bay National Park, southeastern Alaska. *Geological Society of America Bulletin*, **122**, 1067–1080.

Czudek, T., 1995. Cryoplanation terraces – a brief review and some remarks. *Geografiska Annaler*, **77**, 95–105.

Easterbrook, D. J., 1998. *Surface Processes and Landforms*, 2nd edn. New York: Prentice Hall, p. 546.

Echelmeyer, K., 1987. Anomalous heat flow and temperatures associated with subglacial water flow. In *The Physical Basis of Ice Sheet Modelling Proceedings of the Vancouver Symposium*, August 1987. International Association of Hydrological Sciences (IAHS) Publication, Vol. 170, pp. 93–104.

Embleton, C., and King, C. A. M., 1975. *Glacial Geomorphology*. New York: Wiley. 573 pp.

Gillespie, A. R., and Bierman, P. R., 1995. Precision of terrestrial exposure ages and erosion rates from analysis of cosmogenic isotopes produced in situ. *Journal of Geophysical Research*, **100**(B12), 24-637–24-649.

Gillespie, A. R., and Molnar, P., 1995. Asynchronism of maximum advances of mountain and continental glaciations. *Reviews of Geophysics*, **33**, 311–364.

Haeberli, W., Hallet, B., Arenson, L., Elconin, R., Humlum, O., Kääb, A., Kaufmann, V., Ladanyi, B., Matsuoka, N., Springman, S., and Vonder Műhl, D., 2006. Permafrost creep and rock glacier dynamics. *Permafrost and Periglacial Processes*, **17**, 189–214.

Hallet, B., Hunter, L., and Bogen, J., 1996. Rates of erosion and sediment evacuation by glaciers: a review of field data and their implications. *Global and Planetary Change*, **12**, 213–235.

Harbor, J. M., Hallet, B., and Raymond, C. F., 1988. A numerical model of landform development by glacial erosion. *Nature*, **333**, 347–349.

Harden, D., Barnes, P., and Reimnitz, E., 1977. Distribution and character of naleds in northeastern Alaska. *Arctic*, **30**, 28–40.

Komatsu, G., Arzhannikov, S. G., Gillespie, A. R., Burke, R. M., Miyamoto, H., and Baker, V. R., 2008. Cataclysmic floods along the Yenisei River and late Quaternary paleolakes in the Sayan mountains, Siberia. *Geomorphology*, **104**, 143–164.

Lal, D., 1988. In situ-produced cosmogenic isotopes in terrestrial rocks. *Annual Review of Earth and Planetary Science*, **16**, 355–388.

Lauriol, B., and Godbout, L., 1988. Les terrasses de cryoplantation dans le nord du Yukon: distribution, genese et age. *Geographie Physique Et Quaternaire*, **42**, 303–314.

Lisiecki, L. E., and Raymo, M. E., 2005. A Pliocene-Pleistocene stack of 57 globally distributed benthic $\delta^{18}O$ records. *Paleoceanography*, **20**, PA1003, doi:10.1029/2004PA001071.

Lyell, C., 1833. *Principles of Geology*. London: John Murray, Vol. 3. 398 with 83 pp of Appendixes.

Meier, M. F., and Post, A., 1969. What are glacier surges? *Canadian Journal of Earth Science*, **6**, 807–817.

Meierding, T. C., 1982. Late Pleistocene glacial equilibrium-lines in the Colorado Front Range: a comparison of methods. *Quaternary Research*, **18**, 289–310.

O'Connor, J. E., and Baker, V. R., 1992. Magnitudes and implications of peak discharges from glacial Lake Missoula. *Geological Society of America, Bulletin*, **104**, 267–279.

Piotrowski, J. A., 1997. Subglacial hydrology in north-western Germany during the last glaciation: groundwater flow, tunnel valleys and hydrological cycles. *Quaternary Science Reviews*, **16**, 169–185.

Porter, S. C., 2005. Pleistocene snowlines and glaciation of the Hawaiian Islands. *Quaternary International*, **138–139**, 118–128.

Prentice, M. L., Hope, G. S., Maryunani, K., and Peterson, J. A., 2005. An evaluation of snowline data across New Guinea during the last major glaciation, and area-based glacier snowlines in the Mt. Jaya region of Papua, Indonesia, during the Last Glacial Maximum. *Quaternary International*, **138–139**, 93–117.

Reger, R. D., and Péwé, T. L., 1976. Cryoplanation terraces: Indicators of a permafrost environment. *Quaternary Research*, **6**, 99–109.

Ritter, D. F., Kochel, R. C., and Miller, J. R., 2002. *Process Geomorphology*, 4th edn. Boston: McGraw Hill. 576 pp.

Roering, J. J., Kirchner, J. W., and Dietrich, W. E., 1999. Evidence for non-linear, diffusive sediment transport on hillslopes and implications for landscape morphology. *Water Resources Research*, **35**, 853–870.

Rooth, C., 1982. Hydrology and ocean circulation. *Progress in Oceanography*, **11**, 131–149.

Schweizer, J., and Iken, A., 1992. The role of bed separation and friction in sliding over an undeformable bed. *Journal of Glaciology*, **38**, 77–92.

Selzer, G. O., 1994. Climatic interpretation of alpine snowline variations on millenial timescales. *Quaternary Research*, **41**, 154–159.

Sharp, R. P., 1960. *Glaciers*. Eugene: University of Orgeon Press. 78 pp.

Sugden, D. E., and Brian, S. J., 1976. *Glaciers and Landscape: A Geomorphological Approach*. London: Edward Arnold. 376 p.

Thorn, C. E., 1976. Quantitative evaluation of nivation in the Colorado Front Range. *Geological Society of America Bulletin*, **87**, 1169–1178.

Waitt, R. B., Jr., 1985. Case for periodic, colossal jökulhlaups from Pleistocene glacial Lake Missoula. *Geological Society of America Bulletin*, **96**, 1271–1286.

Washburn, A. L., 1979. *Geocryology: A Survey of Periglacial Processes and Environments*. New York: Wiley.

Whalley, W. B., Marshall, J. R., and Smith, B. J., 1982. Origin of desert loess from some experimental observations. *Nature*, **300**, 433–435.

Whipple, K. X., 2001. Fluvial landscape response time: how plausible is steady-state denudation? *American Journal of Science*, **301**, 313–325.

Zemp, M., Kääb, A., Hoelzle, M., and Haeberli, W., 2005. GIS-based modeling of the glacial sediment balance. *Zeitschrift für Geomorphologie*, **Suppl 138**, 113–129.

Cross-references

Crevasses
Equilibrium-Line Altitude (ELA)
Firn
Fjords
Glacial Erosion
Glacier Motion/Ice Velocity
Ice Sheet
Moraine
Paraglacial Landscape Transformations
Paternoster Lakes
Periglacial
Rock Glaciers
Sediment Yield
Temperate Glaciers
Thinning of Glaciers

GLACIAL GROOVES

D. P. Dobhal
Wadia Institute of Himalayan Geology, Dehradun, India

A linear depression, centimeters to meters in length, produced by the removal of rock or sediment by erosive action of a glacier is termed as a glacial groove. Glacial grooves or shallow holes on the bed rock illustrate the movement of the sediment-loaded base of the glacier. Large amounts of coarse gravel and boulders carried along underneath the glacier provide the abrasive power to cut the grooves in the bed rock. This glacial feature is a useful indicator to evaluate the patterns, mass, volume, force/energy of former glacier flow.

GLACIAL OVERDEEPENING

Christopher Lloyd
Department of Geography, University of Sheffield, Sheffield, UK

Definition

Overdeepening. The excavation of the subglacial landscape by the processes of glacial erosion to a level below that which would be expected by other processes. The term is also commonly used to refer to the overdeepened cirques or troughs produced by such processes.

The distinguishing feature of a "true" overdeepening is the adverse slope that forms the lip of the basin or cirque (cirques are further characterized by a steep headwall). Such overdeepenings are characteristic features of almost all formerly glaciated landscapes, where they typically form deep lakes that may become filled with sediment over time. They are commonly found in locations such as cirques and troughs where patterns of ice flow have acted to focus glacial erosion; however, the ability of surface melt to access the glacier bed is also important for maintaining the processes of quarrying and basal sediment evacuation that allow the overdeepening to develop (Hooke, 1991; Alley et al., 2003). Theoretical analysis indicates that moulins and crevasses that form at the upglacier end of the overdeepening will focus water input and hence quarrying toward the head of the overdeepening, resulting in a longitudinal profile that is asymmetrical (Hooke, 1991). Overdeepenings may also be associated with the exploitation by glacial erosion of jointed lithologies.

The idea that valleys could be overdeepened by glacial erosion was first advanced by geographer Henry Gannett in his description of Lake Chelan (Washington State, USA) for the National Geographic magazine (Gannett, 1898). The following year, Albrecht Penck independently reached the same conclusion while studying the Bavarian Alps (see Davis, 1909). Interest in overdeepenings waned until the latter half of the twentieth century, when further descriptive accounts (e.g., Holtedahl, 1967) were followed by largely morphometric investigations (e.g., Aniya and Welch, 1981). Only later did work begin to focus on the importance of "true" overdeepenings in glacial systems (e.g., Rothlisberger and Lang, 1987; Lawson et al., 1998; Alley et al., 2003). Recently, there have been efforts to numerically simulate the evolution of the entire glacial longitudinal profile, including the phenomenon of overdeepenings (e.g., MacGregor et al, 2000; MacGregor et al, 2009). Nevertheless, overdeepenings remain largely a neglected area of academic study.

Bibliography

Alley, R. B., Lawson, D. E., Larson, G. J., Evenson, E. B., and Baker, G. S., 2003. Stabilizing feedbacks in glacier-bed erosion. *Nature*, **424**, 758–760.
Aniya, M., and Welch, R., 1981. Morphometric analyses of Antarctic cirques from photogrammetric measurements. *Geografiska Annaler Series A, Physical Geography*, **63**, 41–53.
Davis, W. M., 1909. The Alps in the Glacial Period. *Geographical Journal*, **34**, 650–659.
Gannett, H., 1898. Lake Chelan. *National Geographic*, **9**, 417–428.
Holtedahl, H., 1967. Notes on the formation of fjords and fjord valleys. *Geografiska Annaler Series A-Physical Geography*, **49**, 188–203.
Hooke, R. L., 1991. Positive feedbacks associated with erosion of glacial cirques and overdeepenings. *Geological Society of America Bulletin*, **103**, 1104–1108.
Lawson, D. E., Strasser, J. C., Evenson, E. B., Alley, R. B., Larson, G. J., and Arcone, S. A., 1998. Glaciohydraulic supercooling: a freeze-on mechanism to create stratified, debris-rich basal ice: 1. Field evidence. *Journal of Glaciology*, **44**, 547–562.
MacGregor, K. R., Anderson, R. S., Anderson, S. P., and Waddington, E. D., 2000. Numerical simulations of glacial-valley longitudinal profile evolution. *Geology*, **28**, 1031–1034.
MacGregor, K. R., Anderson, R. S., and Waddington, E. D., 2009. Numerical modelling of glacial erosion and headwall processes in alpine valleys. *Geomorphology*, **103**, 189–204.
Rothlisberger, H., and Lang, H., 1987. Glacial Hydrology. In Gurnell, A. M., and Clark, M. J. (eds.), *Glacio-Fluvial Sediment Transfer: An Alpine Perspective*. New York: Wiley, pp. 207–284.

GLACIAL STRIATIONS

D. P. Dobhal
Wadia Institute of Himalayan Geology, Dehradun, India

Glacial striations are scratches on the bedrock created by the process of glacial abrasion. Glacial striations usually occur as multiple straight parallel lines, some time scour and polish the bedrock representing the flow direction of the former glacier level. Large amount of area vacated by glaciers due to melting leave behind such features indicating the last glacier maxima that include mass, volume, and energy of glacier flow of the former glaciers.

GLACIAL TROUGH

D. P. Dobhal
Wadia Institute of Himalayan Geology, Dehradun, India

The glacial trough is also called "U" shaped valley, relatively straight, flat-bottomed, deeper, and steep-sided valley formed by glacial erosion (Figure 1). Originally the valley would have in existence as stream/river valley prior to occupation by a glacier. But, after glacier occupies the valley, it modifies it and gives rise to characteristic features that are preserved and can be recognized even after the disappearance of the glacier (deglaciation) and used as a tool for evaluation of past glacier history in terms of existing, paleo-climatic studies. Important features of a glacial trough are as follows:

- A characteristic feature of mountain glaciations: these glacial troughs may be several hundred meters deep and tens of kilometers long.
- Within a glacial trough, several erosional and deposinal features are preserved.
- The main processes involved in the formation of glacial trough are abrasion and plucking.

GLACIAL/INTERGLACIAL CYCLES

Michel Crucifix
Georges Lemaitre Centre for Earth and Climate Research, Université catholique de Louvain, Louvain-la-Neuve, Belgium

Definition

Major waxing–waning cycles of large continental ice sheets in the Northern Hemisphere that characterized the late Pliocene and the Pleistocene Epoch since about 2.7 million years (Myr) ago. By extension, all expressions of environmental changes, including variations in greenhouse gases and ocean circulation that are associated with glacial cycles.

Glacial Trough, Figure 1 Broad view of "U" shaped glaciated valley (Glacial trough), Central Himalaya, India (Photo: Dobhal).

Discovery

The first detailed reports of Alpine Moraine, erratic boulders and "Roches Moutonnees" appear in field reports of the Swiss naturalist H.-B. de Saussure (1779–1796). (For brevity, the most ancient references are not listed in the bibliography list. Well-documented historical accounts are available in Imbrie and Imbrie (1979), Berger (1988), and Bard (2004).) John Playfair (1815) and K. Schimper (1837) (Ice Age) understood that their presence is due to the movement of glaciers, but this is not until Ignace Venetz (1833), Jean de Charpentier (1841) – both inspired by mountain guide J.P. Perraudin – and finally Louis Agassiz (1840) that the *glacial theory* was formulated, according to which ice once extended well outside the Alps. Independently, Esmark (1827) had reached the conclusion that ice once covered the major part of Norway. (cf. also Terraces). Later, Venetz (1861) and, independently, Archibald Geikie (1863) in Scotland concluded that sustained intervals of warm climate intervened between different ice ages. Parallel to these European discoveries, T.C. Chamberlain (1877–1886) and F. Leverett (1897–1935) systematically mapped the moraines of the USA and developed a classification supporting four previous ice ages: Nebraskan (oldest), Kansan, Illinoian, and Wisconsinian (youngest). On the other hand, Penk and Brückner (1909) identified four past Alpine fluvial erosion layers, which they interpreted as the indices of four Alpine glaciations named in alphabetical order according to river valley names: the Günz (oldest), the Mindel, the Riss, and the Würm. This stratigraphical model, used as a reference by W. Köppen and M. Milankovitch to affirm their astronomical theory of glaciations (Explicative Models), was later shown to be partly incorrect (Kukla, 1975).

The first continuous environmental records of the Pleistocene climatic cycles were obtained from sediments sampled in the deep ocean. These sediments are essentially composed of small calcite-shell organisms called foraminifera. Emiliani (1955) proposed a stratigraphic scheme still used today, based on the succession of minima and maxima in the oxygen-18/oxygen-16 isotopic ratio of foraminifera tests sampled from a Caribbean deep-sea core. Isotopic events were numbered from 1 to 16, starting from the most recent. Even numbers represent glacial peaks, the last glacial maximum corresponding to marine isotopic stage 2, and odd numbers point to interglacials. The present interglacial is marine isotopic stage 1. Shackleton (1967) showed that these isotopic fluctuations primarily reflect the effect of the changes in continental ice volume on the isotopic composition of water, although this interpretation was called into question in a later article (Shackleton, 2000) (Isotopic Characteristics of Ice, Snow, and Glaciers and Oxygen Isotopes).

The first reliable estimates of the *timing of glaciations* were permitted by the identification of the Brünhes–Matuyama magnetic reversal in deep-sea cores (–730 kyr, i.e. –730,000 years) and radiocarbon dating of the more recent tests. The latest four glacial–interglacial cycles were found to be roughly 100-kyr long, with glacial buildup taking about five times as long as deglaciation (Broecker and van Donk, 1970). The latter phase was termed "termination" (Broecker and van Donk, 1970; Kukla and Cilek, 1996). Higher-resolution records (Hays et al., 1976) indicated the presence of shorter climatic cycles with periods matching those of the astronomical parameters of precession and obliquity (Berger, 1977). A number of synthetic isotopic records have then been constructed by averaging ("stacking") different marine records. One currently used reference is the LR04 stack combining data from 57 benthic formanifera records dating back to up to 5 Myr (Lisiecki and Raymo, 2005).

Meanwhile, glacial cycles have been indicated in a myriad of paleoenvironmental indicators, just to cite a few: in the succession of paleosols and wind-blown sediments (loess) in China (Liu and Chang, 1964) and Eastern Europe (Kukla, 1975); in indicators of the surface and deep-ocean circulations of the Atlantic (Ruddiman and McIntyre, 1979; Raymo et al., 1989); and in greenhouse gas concentrations, dust, chemical tracers, and isotopic indicators sampled in Antarctica (Petit et al., 1999; Luethi et al., 2008). In particular, the atmospheric concentration in CO_2 oscillated between extremes of 172 parts per million (ppm) at stage 16 and 299 ppm at stage 7 (Luethi et al., 2008) (see *Palaeoclimate and Past Glaciations* for further details about the reconstruction and modeling of glaciers).

Phenomenology

General trends

The current marine isotopic stratigraphy includes 104 *marine oxygen isotopic stages* down to the Gauss magnetic boundary (−2.6 Myr), plus another 112 events numbered according to magnetic polarity, down to the Gilbert magnetic polarity zone, about −5.8 Myr (Shackleton, 1995).

The first major glaciation of the Northern Hemisphere is considered to be marine isotopic stage 100 (−2.5 Myr) (Quaternary Glaciation). This event, early identified as the first major marine oxygen isotopic excursion (Shackleton and Opdyke, 1976), also corresponds to the first major influx of ice-rafted detritus detected in North Atlantic sediments (Shackleton and Hall, 1984; Raymo et al., 1989). Since that period, the marine isotope record indicates an overall increase in amplitude and duration of glacial–interglacial cycles. Near –800 kyr, the glacial–interglacial oscillations shift from a 40-kyr symmetric oscillation to a sawtooth-shaped, 100-kyr cycle (Pisias and Moore, 1981; Ruddiman et al., 1986). This is the mid-Pleistocene transition. The mathematical characterization, timing and the attribution of this transition, remains an open problem (Clark et al., 2006; Lisiecki and Raymo, 2007). Lisiecki and Raymo (2007) suggest –1.4 Myr as the time at which the climate response shifted from a linear regime to a nonlinear one, compatible with the pacemaker theory (Explanations of the 100-kyr periodicity).

The ice-core record (Ice Core) from Dome C, Antarctica (EPICA community members, 2004; Luethi et al., 2008) confirms the significance of another transition near −400 kyr referred to as the mid-Brünhes transition. This event marks the strengthening of the asymmetric character of glacial-interglacial cycles (slow glacial buildup and abrupt termination) and a sudden increase in the greenhouse gases concentrations and Antarctic temperature of interglacial periods.

Sea level

Dated coral terraces and other shoreline geomorphological evidence are used to infer past changes in local sea levels. Their conversion into a global eustatic sea level (a measure of the total amount of ice accumulated on the continents) requires accounting for isostatic and gravitational effects by means of numerical models (Peltier, 1976; Marshall et al., 2002; Yokoyama et al., 2001; Peltier, 2004). The current consensus points to a Last Glacial Maximum eustatic sea level 125–140 m lower than today. This corresponds to about 50×10^6 km^3 of ice, two-thirds of which was located in the North American ice sheet.

Uncertainties in tectonic movements and the erasure of successive glacial terraces make it difficult to find direct sea-level evidence prior to stage 5. Sea-level estimates before that time rely on marine isotopic evidence, possibly complemented by air oxygen isotopic data available in the ice-core record. Fairly sophisticated inverse methods to infer past ice mass from the marine isotopic signal were developed (Bintanja et al., 2005). So far all evidence points to sea-level high stands similar to today ±20 m during the latest four interglacial periods (stages 1, 5, 7, and 9), and low stands of amplitude similar to the last glacial maximum at stages 6, 12, and 16 (Sea-Level).

Power spectrum

Estimating the power spectrum of continental ice-volume variations is a particularly difficult task, given the indirect character of ice-volume evidence (Sea-Level), in-situ perturbations of the sediment and dating uncertainties.

Hays et al. (1976) first observed in ocean records of the late Pleistocene the presence of harmonics matching the orbital periods of 41 (obliquity), 19, and 23 kyr (precession) calculated by Berger (1978). The influence of orbital variations on climate is now indisputable, but the *fraction* of climate change driven by the orbital forcing as well as the identification of the dominant mechanisms are still subjects of debate.

Variance related to the 40-kyr obliquity component clearly dominates the marine oxygen isotope record before the mid-Pleistocene transition (Pisias and Moore, 1981; Lisiecki and Raymo, 2007). After the mid-Pleistocene transition, the 40-kyr variance is still larger than the 20-kyr variance, both in the marine and the Antarctic ice-core records (Mudelsee et al. 2009), but these oscillations are topped by a 100-kyr sawtooth-shaped signal, characteristic of glacial–interglacial cycles.

It was also noted that the fraction of the oxygen isotope record linearly related to orbital variations during the late Pleistocene does not exceed 25% (Kominz and Pisias, 1979) or even 15% (Wunsch, 2003). The power spectrum of the *background noise* corresponds to that of red noise, with a plateau at periods over 100 kyr, and power decreasing almost with the square of the frequency at shorter periods (Kominz and Pisias, 1979; Pelletier, 1997; Huybers and Curry, 2006). Higher-frequency harmonics of periods between 5 and 11 kyr were found in ocean (Pestiaux et al., 1988) and ice-core records (Yiou et al., 1994). They were interpreted as upper harmonics of orbital frequencies excited by nonlinear interactions in the climate system.

Empirical investigation of causal mechanisms

Orbital pacing of terminations

There is statistical evidence that the timing of terminations is controlled by orbital elements. The phase of precession (Raymo, 1997) and obliquity (Huybers and Wunsch, 2004; Huybers, 2007) at the time of major terminations is generally consistent with the Milankovitch hypothesis according to which high summer insolation favors deglaciation (Explicative Models).

Inspection of leads and lags

The analysis of the chronology in the variations of different paleoclimate indicators, such as carbon dioxide, marine oxygen isotopes, and polar temperature proxies requires both a critical analysis of timing assumptions (taking care of avoiding circular reasonings) and state-of-the art time-series analysis methods suited to account for dating uncertainties.

There is firm evidence that the Antarctic deuterium record, which is a proxy for temperature in the Antarctic and over the Southern Oceans, *lead*s the CO_2 variations by about 1 kyr (Mudelsee, 2001). This observation suggests a control of the Southern Hemisphere on atmospheric carbon dioxide concentrations. The relationship between CO_2 and ice volume (or, equivalently, sea level) is more complex. On average over the last 400,000 years, CO_2 tends to lead ice volume (Mudelsee, 2001). The lead is robust over the latest four deglacial terminations (Hargreaves and Abe-Ouchi, 2003) and ranges between 1 and 4 kyr. By contrast, when global ice volume increased from its minimum after termination II, atmospheric CO_2 remained at a high level for about 8 kyr (Mudelsee, 2001).

Since the "Spectral Mapping" (Specmap) project (e.g., Imbrie et al., 1993), a common practice has been to filter paleoclimate time series in the different orbital bands (20, 40, and 100 kyr) and to inspect leads and lags independently in these different bands in order to learn about causal mechanisms. A recent review suggests that CO_2 leads ice-volume variations in the precession (20 kyr) band, while these two quantities are in-phase in the obliquity (40 kyr) band (Ruddiman, 2006). The result yields a conceptual model in which CO_2 responds independently

to precession *and* to ice-volume growth, and ice volume responds to precession, obliquity, and greenhouse gases. Ocean circulation patterns, as reconstructed from $\delta^{13}C$ of foraminifera, have differentiated responses to changes in precession and obliquity (Lisiecki et al., 2008).

Investigations based on filtering methods introduced above suggest a stable phase relationship between orbital eccentricity and climate at the eccentricity period (Imbrie et al., 1984; Raymo, 1997; Shackleton, 2000; Lisiecki et al., 2008). However, this result is difficult to prove rigorously, because the instantaneous phase of eccentricity has no unambiguous meaning in the mathematical sense.

Other time-series analysis

A range of more specialized nonlinear techniques were also applied, such as correlation dimension estimates (Nicolis and Nicolis, 1986; Mudelsee and Statteger, 1994), bicoherence spectra (Hagelberg et al., 1991), or detrended fluctuation analysis (Ashkenazy et al., 2003). Taking advantage of such techniques in the paleoclimate context is not trivial, in part because of the noisy, nonstationary characters of paleoclimate time series and of adverse effects of age uncertainties and sediment mixing.

Continuous or discrete wavelet transforms may constitute an avenue for further investigations, because they are more suited to analyze nonstationary and modulated signals.

Origin of ice ages

History

Joseph Adhémar (1842) formulated the conjecture that the precession of Earth's orbit caused ice ages, because of its effects on the seasonal distribution of incoming solar radiation (insolation). He realized that one season had to be critical given that the changes in winter and summer insolation caused by precession cancel each other (Herschell, 1830). James Croll (1875) further developed the theory and appreciated the importance of the three Earth orbital elements determining insolation: eccentricity, obliquity (angle between the equator and the ecliptic), and the longitude of the perihelion.

Milutin Milankovitch (1920, 1941) is quoted as the first one to have established a self-contained mathematical theory linking orbital elements to insolation and insolation to climate changes. On a suggestion of V. Köppen, he calculated the secular evolution of the summer radiation of the northern latitude (published in Köppen and Wegener, 1925), following the hypothesis that glacial cycles are driven by the effects of changes in summer insolation on snow ablation rate during this season (the conjecture had in fact been earlier expressed by Murphy, 1876, and it contradicted Croll's views). Summer insolation is largest when obliquity is large and/or when summer in the Northern Hemisphere corresponds to the time of perihelion passing. Milankovitch later substantiated the hypothesis by explicitly calculating the effects of radiation changes on the position of the snow line.

By the mid-seventies, the Earth's orbital parameters were known over the last million years to a good accuracy, thanks to the work of several generations of astronomers who based themselves on foundations lain by Laplace and Le Verrier. A decisive step was made by Berger (1978), who expressed in an analytical form the Fourier decomposition of the Earth's orbital parameters relevant for the astronomical theory of paleoclimates. This work constitutes the first demonstration that the spectrum of climatic precession is dominated by periods of 19, 22, and 24 kyr, that of obliquity, by a period 41 kyr, and eccentricity has periods of 400, 125, and 96 kyr. The most accurate solution to date is the La04 (Laskar et al., 2004).

Explanations of the 100-kyr periodicity

The correspondence between the periods found in marine records and astronomical calculations confirmed the existence of an influence of orbital elements on climate. At the same time, the discovery that late Pleistocene glacial cycles are dominated by a 100-kyr cycle constituted a challenge to Milankovitch's theory. Several models were therefore proposed to address this issue.

Quasi-linear forcing by insolation

In this approach, the climate system is effectively *driven* by insolation, but the relationship between insolation and ice growth or melt rate is nonlinear. One much-cited example is the simple dynamical system proposed by Imbrie and Imbrie (1980).

The nonlinearity embedded in this model effectively rectifies the precession signal, which causes a 100-kyr climatic cycle, at the cost of also causing a strong 400-kyr component in the modeled ice-volume time series that is not detected in paleoclimate records.

It was also observed that the fact that both obliquity and precession matter for the timing of glaciation implies that the time between terminations must approximately correspond to an integer number of precession cycles (Raymo, 1997) or both precession and obliquity cycles (Ruddiman, 2006). This idea leads to the concept of the "quantum nature" of glacial cycles, which is used to explain the 80–120 kyr duration of the late Pleistocene ice ages.

The major weakness of these models is that they do not easily explain the massive deglaciation that occurred 400 kyr ago (also called termination IV), a time at which precessional effects were minimal.

Models with instability at high ice volume

These models suppose that climate responds continuously to changes in insolation but there is a background tendency for ice growth. Instability mechanisms are activated when the continental ice volume is too large, causing the rapid collapse of ice sheets characteristic of terminations. This explanation of the 100-kyr cycle has been proposed under different forms including models inferred from

physical principles (Pollard, 1983), more abstract dynamical systems using threshold functions (Paillard, 1998), and more descriptive, empirical conceptual models (Imbrie et al., 1993). One possible instability mechanism is enhanced ice calving under depleted bedrock conditions (Pollard, 1983; Hyde and Peltier, 1987), but other mechanisms were proposed, for example, related to the effects of sea level on deep-water formation and/or carbon-cycle dynamics (Paillard and Parrenin, 2004). Such models claim to successfully explain termination IV.

Self-sustained oscillations (pacemaker)

The 100-kyr cycle may also be explained to some degree as a self-sustained cycle caused by dynamical, nonlinear interactions between the components of the climate system. The existence of runaway feedbacks (implying unstable, multiple equilibria) is now essential. An early attempt is the ice-bedrock model by Oerlemans (1980), but this required an unrealistic isostatic response time. Other models featuring a limit cycle were formulated, notably the ice-sheet–carbon-cycle–ocean models by Saltzman and colleagues (Saltzman et al., 1984; Saltzman and Verbitsky, 1993) and the sea-ice switch model by Gildor and Tziperman (2000). One interesting aspect of such models is that they explain the orbital pacing of terminations through the phenomenon of nonlinear phase locking, well known in dynamical system theory. This is generally referred to as the *pacemaker model*: glacial cycles would occur spontaneously, but the presence of orbital forcing controls the timings of termination and glacial inception (Tziperman et al., 2006).

Nonlinear resonance

The 100-kyr signal appears here as a combination of tones associated with the precession beating (1/109 = 1/23 – 1/19). The idea was proposed by Berger (1977), but formalized as a plausible atmosphere–ice-sheet model by Le Treut and Ghil (1983). For nonlinear resonance to occur, the climate response to orbital forcing must be strongly nonlinear, and this feature is not easily reconciled with the red-noise background of the ocean record. By contrast, it naturally explains the presence of upper harmonics observed in certain paleoclimate records (Power Spectrum).

Several of the above models disagree somewhat with the Milankovitch theory according to which summer insolation controls climate change through its action on the Ice Sheet Mass Balance. For example, Le Treut and Ghil (1983) and Gildor and Tziperman (2000) emphasize the effects of increased snow accumulation on ice sheets with increasing temperatures. Models assuming differentiated effects of precession and obliquity on the ice – carbon-cycle system, have been expressed at the conceptual level (Ruddiman, 2006) (Inspection of Leads and Lags above).

It was remarked that the dominance of the obliquity signal during the early- and mid-Pleistocene is another challenge to the Milankovitch theory (Raymo and Nisancioglu, 2003). One recently proposed explanation views the dominance of the obliquity signal in the ice-volume record as an artifact due to opposite effects of precession on ice-sheet masses lying on Southern and Northern hemispheres (Raymo et al., 2006).

The *mid-Pleistocene transition* is a relatively abrupt event. However, it may have been caused by very gradual changes in environmental conditions, which translated into a rapid variation through a phenomenon of bifurcation. Candidates are tectonically driven changes in carbon dioxide concentration and erosion-induced changes in the sedimentological properties of the bedrock of large ice sheets (Clark et al. 2006).

Physics-resolving models

The models mentioned above are derived from plausible physical hypotheses, but were reduced to small systems of ordinary differential equations. A modeling strategy attempting to resolve the spatiotemporal dynamics of the ice, atmosphere, and oceans is also necessary to deepen the understanding of the mechanisms of ice ages and confirm the relevance of low-order models.

The vertically integrated ice-sheet model by Peltier and Hyde (1984) was an important contribution in that direction. This model gave substantial credit to the hypothesis that large ice sheets may rapidly collapse due to the enhancement of the meridional ice flow under depleted bedrock conditions (Hyde and Peltier, 1987) (Deglaciation).

The model of Gallée et al. (1992) constituted another major step toward model complexity. Vertically integrated ice-sheets dynamics are asynchronously coupled to zonally averaged quasi-geostrophic atmospheric dynamics. The model reproduces the ice-volume record over the last 400 kyr. Experiments based on a three-dimensional ice-sheet model were presented by Tarasov and Peltier (1997, 1999). Progress in computer performance now permits more demanding experiments, either based on three-dimensional general circulation models of the atmosphere (Abe-Ouchi et al., 2007) or on a simplified atmosphere–ocean model synchronously coupled to ice-sheet dynamics (Calov et al., 2005). General circulation models of the atmosphere and ocean, sometimes coupled to global vegetation models, were used to better investigate the response of the complex Earth system to orbital elements (de Noblet et al., 1996; Khodri et al., 2001; Vettoretti and Peltier, 2003) but there is no consensus as whether one mechanism, more than the others, conditions the glacial inception process. A three-dimensional resolution of ice-sheet, ocean, carbon-cycle interactions spanning the Pleistocene still seems beyond reach.

Parallel to these ambitious programs, three-dimensional viscoplastic ice-sheet models were driven by reconstructed climatic scenarios in order to estimate the ice-sheet history over the most recent glacial–interglacial cycles (Huybrechts, 2002; Charbit et al., 2007).

Prediction of the next ice age

Ignoring the anthropogenic perturbation, some numerical models suggest a glacial inception in about 60,000 years from now (e.g., Berger and Loutre, 2002). The anthropogenic perturbation will affect the next glacial inception and possibly delay it by several hundreds of thousand years (Archer and Ganopolski, 2005). By contrast, more conceptual models based on the analysis of the past climate response to orbital forcing lead to the competing paradigm that, lacking an anthropogenic perturbation, glacial inception would have been imminent (Raymo, 1997) or even overdue (Ruddiman, 2007).

The reliability of such climate predictions is restricted by modeling errors, parameter uncertainty, observation errors, and uncertainty on the forcing and climate stochastic perturbations. Statistical methods for assessing the effective horizon of predictability at the glacial–interglacial scales are still in their infancy. A recent exercise drawing on principles of Bayesian statistics suggests that predictability of glacial cycles is poor beyond 60 kyr (Crucifix and Rougier, 2009).

Summary

Glacial–interglacial cycles have paced climate for 2.7 Myr. They are mainly documented from continuous records – marine, ice, and continental archives – but geomorphological and sea-level indicators remain a premium source of knowledge about the timing and amplitude of glaciations. The last glacial–interglacial cycle is one of the largest-amplitude cycles of the Pleistocene. Glacial–interglacial cycles continue to pose challenges at the most fundamental level: there is not yet any universally accepted model of climate response at the timescale of ice ages, even if it is now indisputable that these cycles are somehow controlled by Earth orbital elements. At the same time, these cycles constitute our main source of information about the dynamical and nonlinear interactions between the main components of the climate system at the multimillennium timescale.

Bibliography

Abe-Ouchi, A., Segawa, T., and Saito, F., 2007. Climatic conditions for modelling the Northern Hemisphere ice sheets throughout the ice age cycle. *Climate of the Past*, **3**(3), 423–438.

Archer, D., and Ganopolski, A., 2005. A movable trigger: fossil fuel CO_2 and the onset of the next glacial inception. *Geochemistry Geophysics Geosystem*, **6**(5), Q05003.

Ashkenazy, Y., Baker, D. R., Gildor, H., and Havlin, S., 2003. Nonlinearity and multifractality of climate change in the past 420,000 years. *Geophysical Research Letters*, **30**, Art. 2146.

Bard, E., 2004. Greenhouse effect and ice ages: historical perspective. *Comptes Rendus Geoscience*, **336**, 603–638.

Berger, A., 1977. Support for the astronomical theory of climatic change. *Nature*, **268**, 44–45.

Berger, A. L., 1978. Long-term variations of daily insolation and Quaternary climatic changes. *Journal of Atmospheric Sciences*, **35**, 2362–2367.

Berger, A., 1988. Milankovitch theory and climate. *Reviews of Geophysics*, **26**(4), 624–657.

Berger, A., and Loutre, M. F., 2002. An exceptionally long interglacial ahead? *Science*, **297**, 1287–1288.

Bintanja, R., van de Wal, R. S. W., and Oerlemans, J., 2005. Modelled atmospheric temperatures and global sea levels over the past million years. *Nature*, **437**(7055), 125–128.

Bretagnon, P., 1974. Termes à longues périodes dans le système solaire. *Astronomy and Astrophysics*, **30**, 141–154.

Broecker, W. S., and van Donk, J., 1970. Insolation changes, ice volumes and the O^{18} record in deep-sea cores. *Reviews of Geophysics*, **8**(1), 169–198.

Calov, R., Ganopolski, A., Claussen, M., Petoukhov, V., and Greve, R., 2005. Transient simulation of the last glacial inception. Part I: glacial inception as a bifurcation in the climate system. *Climate Dynamics*, **24**(6), 545–561.

Charbit, S., Ritz, C., Philippon, G., Peyaud, V., and Kageyama, M., 2007. Numerical reconstructions of the Northern Hemisphere ice sheets through the last glacial-interglacial cycle. *Climate of the Past*, **3**(1), 15–37.

Clark, P. U., Archer, D., Pollard, D., Blum, J. D., Rial, J. A., Brovkin, V., Mix, A. C., Pisias, N. G., and Roy, M., 2006. The middle pleistocene transition: characteristics. mechanisms, and implications for long-term changes in atmospheric pCO_2. *Quarterly Science Review*, **25**, 3150–3184.

Crucifix, M., and Rougier, J., 2009. On the use of simple dynamical systems for climate predictions: A bayesian prediction of the next glacial inception. *European Physics Journal – Special Topics*, **174**, 11–31.

de Noblet, N., Prentice, I. C., Joussaume, S., Texier, D., Botta, A., and Haxeltine, A., 1996. Posible role of atmosphere-biosphere interactions in triggering the last glaciation. *Geophysical Research Letters*, **23**, 3191–3194.

Delmas, R. J., Ascencio, J.-M., and Legrand, M., 1980. Polar ice evidence that atmospheric CO_2 20,000yr BP was 50% of present. *Nature*, **284**, 155–157.

Emiliani, C., 1955. Pleistocene temperatures. *Journal of Geology*, **63**, 538–578.

EPICA community members, 2004. Eight glacial cycles from an Antarctic ice core. *Nature*, **429**, 623–628.

Gallée, H., van Ypersele, J. P., Fichefet, T., Marsiat, I., Tricot, C., and Berger, A., 1992. Simulation of the last glacial cycle by a coupled, sectorially averaged climate-ice sheet model. Part II: Response to insolation and CO_2 variation. *Journal of Geophysical Research*, **97**, 15713–15740.

Gildor, H., and Tziperman, E., 2000. Sea ice as the glacial cycles climate switch: role of seasonal and orbital forcing. *Paleoceanography*, **15**, 605–615.

Hagelberg, T., Pisias, N. J., and Elgar, S., 1991. Linear and nonlinear couplings between orbital forcing and the marine record during the late Neogene. *Paleoceanography*, **6**, 729–746.

Hargreaves, J. C., and Abe-Ouchi, A., 2003. Timing of ice-age terminations determined by wavelet methods. *Paleoceanography*, **19**(2), 1035.

Hays, J. D., Imbrie, J., and Shackleton, N. J., 1976. Variations in the Earth's orbit: pacemaker of ice ages. *Science*, **194**, 1121–1132.

Huybers, P., 2007. Glacial variability over the last two millions years: an extended depth-derived age model, continuous obliquity pacing, and the Pleistocene progression. *Quarterly Science Review*, **26**, 37–55.

Huybers, P., and Curry, W., 2006. Links between annual, Milankovitch and continuum temperature variability. *Nature*, **441**, 329–332.

Huybers, P., and Wunsch, C. (2004). A depth-derived Pleistocene age model: Uncertainty estimates, sedimentation variability, and nonlinear climate change. *Paleoceanography*, **19**, PA1028.

Huybrechts, P., 2002. Sea-level changes at the LGM from ice-dynamic reconstructions of the Greenland and Antarctic

ice sheets during the glacial cycles. *Quarterly Science Review*, **21**(1–3), 203–231.
Hyde, W. T., and Peltier, W. R., 1987. Sensitivity experiments with a model of the ice age cycle: The response to milankovitch forcing. *Journal of Atmospheric Sciences*, **44**(10), 1351–1374.
Imbrie, J., and Imbrie, K. P., 1979. *Ice Ages, Solving the Mystery.* New Jersey: Enslow.
Imbrie, J., and Imbrie, J. Z., 1980. Modelling the climatic response to orbital variations. *Science*, **207**, 943–953.
Imbrie, J. J., Hays, J. D., Martinson, D. G., McIntyre, A., Mix, A. C., Morley, J. J., Pisias, N. G., Prell, W. L., and Shackleton, N. J., 1984. The orbital theory of Pleistocene climate: Support from a revised chronology of the marine δO^{18}record. In Berger, A., Imbrie, J., Hays, J., Kukla, J., and Saltzman, B. (eds.), *Milankovitch and Climate, Part I*. Norwell, Mass: D. Reidel, pp. 269–305.
Imbrie, J., Berger, A., Boyle, E. A., Clemens, S. C., Duffy, A., Howard, W. R., Kukla, G., Kutzbach, J., Martinson, D. G., McIntyre, A., Mix, A. C., Molfino, B., Morley, J. J., Peterson, L. C., Pisias, N. G., Prell, W. L., Raymo, M. E., Shackleton, N. J., and Toggweiler, J. R., 1993. On the structure and origin of major glaciation cycles. Part 2: The 100,000-year cycle. *Paleoceanography*, **8**, 699–735.
Khodri, M., Leclainche, Y., Ramstein, G., Braconnot, P., Marti, O., and Cortijo, E., 2001. Simulating the amplification of orbital forcing by ocean feedbacks in the last glaciation. *Nature*, **410**(6828), 570–574.
Kominz, M. A., and Pisias, N. G., 1979. Pleistocene: deterministic or stochastic. *Science*, **204**, 171–173.
Kukla, G., 1975. *Loess stratigraphy of Central Europe. After the Australopithecines.* Den Hague: Mouton, pp. 99–188.
Kukla, G., and Cilek, V., 1996. Plio-pleistocene megacycles: record of climate and tectonics. *Palaeogeography, Palaeoclimatology, Palaeoecology*, **120**(1–2), 171–194.
Laskar, J., Robutel, P., Joutel, F., Boudin, F., Gastineau, M., Correia, A. C. M., and Levrard, B., 2004. A long-term numerical solution for the insolation quantities of the Earth. *Astronomy and Astrophysics*, **428**, 261–285.
Le Treut, H. and Ghil, M. (1983). Orbital forcing, climatic interactions and glaciation cycles. *J. Geophys. Res.*, **88**(C9), 5167–5190.
Lisiecki, L. E., and Raymo, M. E., 2005. A Pliocene-Pleistocene stack of 57 globally distributed benthic $\delta^{18}O$ records. *Paleoceanography*, **20**, PA1003.
Lisiecki, L. E., and Raymo, M. E., 2007. Plio-Pleistocene climate evolution: trends and transitions in glacial cycles dynamics. *Quaternary Science Reviews*, **26**, 56–69.
Lisiecki, L. E., Raymo, M. E., and Curry, W. B., 2008. Atlantic overturning responses to Late Pleistocene climate forcings. *Nature*, **456**(7218), 85–88.
Liu, T., and Chang, T., 1964. The "huangtu" (loess) of china. *Reprinted Sixth INQUA Congress Warsaw 1961*, **4**, 503–524.
Luethi, D., Le Floch, M., Bereiter, B., Blunier, T., Barnola, J.-M., Siegenthaler, U., Raynaud, D., Jouzel, J., Fischer, H., Kawamura, K., and Stocker, T. F., 2008. High-resolution carbon dioxide concentration record 650,000–800,000 years before present. *Nature*, **453**(7193), 379–382.
Marshall, S., James, T., and Clarke, G., 2002. North American ice sheet reconstructions at the Last Glacial Maximum. *Quaternary Science Reviews*, **21**(1–3), 175–192.
Mudelsee, M., 2001. The phase relations among atmospheric CO_2 content, temperature and global ice volume over the past 420 ka. *Quarterly Science Review*, **20**, 583–589.
Mudelsee, M., and Statteger, K., 1994. Plio-/Pleistocene climate modeling based on oxygen isotope time series from deep-sea sediment cores: the Grassberger-Procaccia algorithm and chaotic climate systems. *Mathematical Geology*, **26**, 799–815.
Mudelsee, M., Scholz, D., Röthlisberger, R., Fleitmann, D., Mangini, A., and Wolff, E., 2009. Climate specturm estimation in the presence of timescale errors, *Nonlin*. *Processes in Geophysics*, **16**, 43–56.
Nicolis, C., and Nicolis, G., 1986. Reconstruction of the dynamics of the climatic system from time-series data. *Proceedings of National Academic Science USA*, **83**, 536–540.
Oerlemans, J., 1980. Model experiments on the 100,000-yr glacial cycle. *Nature*, **287**(2), 430–432.
Paillard, D., 1998. The timing of Pleistocene glaciations from a simple multiple-stae climate model. *Nature*, 391.
Paillard, D., and Parrenin, F., 2004. The Antarctic ice sheet and the triggering of deglaciations. *Earth and Planetary Science Letters*, **227**, 263–271.
Pelletier, J. D., 1997. Analysis and modeling of the natural variability of climate. *Journal of Climate*, **10**(6), 1331–1342.
Peltier, W. R., 1976. Glacial isostatic adjustment II – the inverse problem. *Geophysical Journal of the Royal Astronomical Society*, **46**, 669–706.
Peltier, W. R., 2004. Global glacial isostasy and the surface of the ice-age Earth: the ICE-5G (VM2) model and GRACE. *Annual Review of Earth and Planetary Science*, **32**, 111–149.
Peltier, W. R., and Hyde, W., 1984. A model of the ice age cycle. In Berger, A., Imbrie, J., Hays, J., Kukla, G., and Saltzman, B. (eds.), *Milankovitch and Climate, Part II, number 126 in NATO ASI series*. Dordrecht: Reidel, pp. 562–580.
Pestiaux, P., Vandermersch, I., Berger, A., and Duplessy, J. C., 1988. Paleoclimatic variability at frequencies ranging from 1 cycle per 10000 years to 1 cycle per 1000 years – evidence for nonlinear behavior of the climate system. *Climatic Change*, **12**, 9–37.
Petit, J. R., Jouzel, J., Raynaud, D., Barkov, N. I., Barnola, J.-M., Basile, I., Bender, M., Chappellaz, J., Davis, M., Delaygue, G., Delmotte, M., Kotlyakov, V. M., Legrand, M., Lipenkov, V. Y., Lorius, C., Pepin, L., Ritz, C., Saltzman, E., and Stievenard, M., 1999. Climate and atmospheric history of the past 420,000 years from the Vostok ice core, Antarctica. *Nature*, **399**, 429–436.
Pisias, N. G., and Moore, T. C., 1981. The evolution of Pleistocene Climate – a time-series approach. *Earth and Planetary Science Letters*, **52**(2), 450–458.
Pollard, D., 1983. Ice-age simulations with a calving ce-shet model. *Quarterly Research*, **20**, 30–48.
Raymo, M., 1997. The timing of major climate terminations. *Paleoceanography*, **12**(4), 577–585.
Raymo, M. E., and Nisancioglu, K., 2003. The 41 kyr world: Milankovitch's other unsolved mystery. *Paleoceanography*, **18**, 1011.
Raymo, M. E., Ruddiman, W. F., Backman, J., Clement, B. M., and Martinson, D. G., 1989. Late Pliocene variation in Northern Hemisphere ice sheets and North Atlantic deep circulation. *Paleoceanography*, **4**, 413–446.
Raymo, M. E., Lisiecki, L. E., and Nisancioglu, K. H., 2006. Plio-pleistocene ice volume, antarctic climate, and the global delta O-18 record. *Science*, **313**, 492–495.
Ruddiman, W. F., 2006. Orbital changes and climate. *Quarterly Science Review*, **25**, 3092–3112.
Ruddiman, W. F., 2007. The early anthropogenic hypothesis a year later: challenges and responses. *Reviews of Geophysics*, **45**, RG4001.
Ruddiman, W. F., and McIntyre, A., 1979. Warmth of the subpolar North Atlantic Ocean during Northern Hemisphere Ice-Sheet growth. *Science*, **204**, 173–175.
Ruddiman, W. F., Raymo, M., and McIntyre, A., 1986. Matuyama 41,000-year cycles: North Atlantic Ocean and northern

hemisphere ice sheets. *Earth and Planetary Science Letters*, **80**, 117–129.
Saltzman, B., and Verbitsky, M. Y., 1993. Mutiple instabilities and modes of glacial rhytmicity in the Plio-Pleistocene: a general theory of late Cenozoic climatic change. *Climate Dynamics*, **9**, 1–15.
Saltzman, B., Hansen, A. R., and Maasch, K. A., 1984. The late Quaternary glaciations as the response of a 3-component feedback-system to Earth-orbital forcing. *Journal of Atmospheric Sciences*, **41**(23), 3380–3389.
Shackleton, N. J., 1967. Oxygen isotope analyses and Pleistocene temperatures re-assessed. *Nature*, **215**, 15–17.
Shackleton, N. J., 1995. Pliocene stable isotope stratigraphy of site 846. In Pisias, N. G., Mayer, L. A., Janacek, T. R., Palmer-Julson, A., and van Andel, T. H. (eds.), *Proceedings of the Ocean Drilling Program, Scientific Results*, Vol. 138, pp. 337–355.
Shackleton, N. J., 2000. The 100,000-year ice-age cycle identified and found to lag temperature, carbon dioxide and orbital eccentricity. *Science*, **289**, 1897–1902.
Shackleton, N. J., and Hall, M. A., 1984. Oxygen and carbon isotope stratigraphy of deep sea drilling project hole 552A: Plio-Pleistocene glacial history. *Deep Sea Drilling Project Initial Report*, **81**(16), 599–609.
Shackleton, N. J., and Opdyke, N. D., 1976. Oxygen isotope and paleomagnetic stratigraphy of equatorial Pacific core V28-239: Late Pliocene to Latest Pleistocene. In Cline, R. M., and Hays, J. D. (eds.), *Investigation of Late Quaternary Paleoceanography and Paleoclimatology. Vol. 145 of Memoir*. USA: Geological Society of America, pp. 39–55.
Tarasov, L., and Peltier, W. R., 1997. Terminating the 100 kyr ice age cycle. *Journal of Geophysical Research*, **102**, 21665–21693.
Tarasov, L., and Peltier, W. R., 1999. Impact of thermomechanical ice sheet coupling on a model of the 100 kyr ice age cycle. *Journal of Geophysical Research*, **104**, 9517–9545.
Tziperman, E., Raymo, M. E., Huybers, P., and Wunsch, C., 2006. Consequences of pacing the Pleistocene 100 kyr ice ages by nonlinear phase locking to Milankovitch forcing. *Paleoceanography*, **21**, PA4206.
Vettoretti, G., and Peltier, W. R., 2003. Post-Eemian glacial inception. Part II: Elements of a cryospheric moisture pump. *Journal of Climate*, **16**, 912–927.
Wunsch, C., 2003. The spectral description of climate change including the 100 ky energy. *Climate Dynamics*, **20**, 353–363.
Yiou, P., Ghil, M., Jouzel, J., Paillard, D., and Vautard, R., 1994. Nonlinear variability of the climatic system from singular and power spectra of late Quaternary records. *Climate Dynamics*, **9**, 371–389.
Yokoyama, Y., De Deckker, P., Lambeck, K., Johnston, P., and Fifield, L., 2001. Sea-level at the Last Glacial Maximum: evidence from northwestern Australia to constrain ice volumes for oxygen isotope stage 2. *Palaeogeography, Palaeoclimatology, Palaeoecology*, **165**(3–4), 281–297.

Cross-references

Deglaciation
Ice Age
Ice Age Cycles: Data, Models, and Uncertainties
Ice Age Development Theory
Ice Core
Ice Sheet Mass Balance
Isotopic Characteristics of Ice, Snow, and Glaciers
Moraine
Palaeoclimate and Past Glaciations
Quaternary Glaciation
Sea-Level

GLACIATION DURING TIMES OF ENHANCED/REDUCED ATMOSPHERIC CARBON DIOXIDE

Andrew B. G. Bush
Department of Earth and Atmospheric Science, University of Alberta, Edmonton, AB, Canada

Definition

The impact that atmospheric carbon dioxide has on the extent of global glaciation is assessed. Known glacial periods during times of high atmospheric carbon dioxide are contrasted with glaciation during times of low atmospheric carbon dioxide. Mechanisms for the former are discussed.

Introduction and background

Evidence for glaciations has emerged from the geological record as far back in time as the Precambrian era, during the mid-Archaen glaciation approximately 2,900 million years before present (Ma; e.g., Eyles, 2008). In addition, a series of widespread and perhaps global glaciations occurred during the Snowball Earth events of the Neoproterozoic period (e.g., Hoffman et al., 1998; Hoffman and Schrag, 2002). Extensive glaciations occurred during the late Ordovician/early Silurian ~430 Ma (e.g., Le Heron, 2007), at the Carboniferous/Permian transition ~280 Ma (e.g., Bussert and Schrank, 2007) and, more recently, throughout the past 2 million years of the Pleistocene.

Glacial events occurring deep in geologic time, however, are harder to investigate because it is more difficult to reconstruct the environment in which these glaciations occurred. Paleomagnetic reconstructions of continental positions deteriorate in precision through the Paleozoic (~225–570 Ma), as does the proxy evidence for atmospheric composition, although estimates for the amount of atmospheric carbon dioxide through the Phanerozoic have been made (Figure 1a). Nevertheless, from a more theoretical standpoint it appears that there are many factors that can play a role in triggering widespread glaciation. Continental positions play a role, particularly if land exists in high latitudes to support large ice sheets (analogous to modern-day Antarctica and Greenland) or if extensive land with a high albedo exists in the equatorial region where it can reflect a significant amount of incoming solar radiation directly back to space (believed to have been important for the Snowball Earth glaciations; Schrag et al., 2002).

The amount of atmospheric carbon dioxide and other greenhouse gases is an important factor and is, at least for the relatively recent Pleistocene glaciations, highly correlated with the glacial–interglacial temperature cycles (Figure 1b). Solar luminosity, changes in Earth's orbital parameters, changes in ocean circulation due to plate tectonics, volcanism, and (for the more recent glaciations) surface vegetation are all believed to be influential factors.

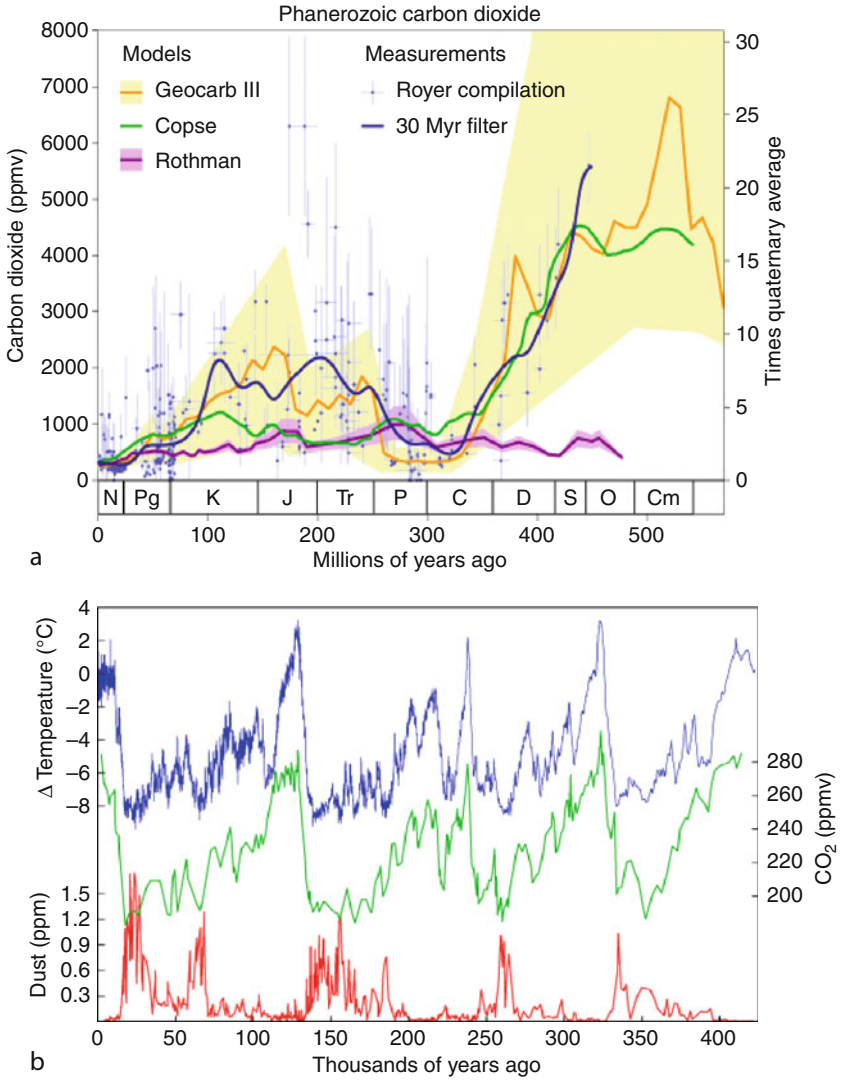

Glaciation During Times of Enhanced/Reduced Atmospheric Carbon Dioxide, Figure 1 (**a**) Estimates of atmospheric carbon dioxide concentration through the Phanerozoic. Image created by Robert A. Rohde/Global Warming Art. Full details are available at http://www.globalwarmingart.com/wiki/File:Phanerozoic_Carbon_Dioxide_png. (**b**) Atmospheric carbon dioxide, temperature, and dust concentration through the late Pleistocene as determined from a Vostok ice core (Petit et al., 1999; data are from http://www.ngdc.noaa.gov/paleo/icecore/antarctica/vostok/vostok_ data.html). Image from the Wikimedia Commons licensed under the Gnu Free Distribution License.

It is likely that more than one factor has contributed to the numerous glacial cycles deduced from the geological record. For example, during the early Pleistocene, glaciations had a ~41,000 year cycle, suggesting that they were regulated by changes in the Earth's angle of obliquity (e.g., Crowley and North, 1992). During the mid-late Pleistocene, however, the glacial cycle switched to a ~100,000-year cycle, suggesting that they were regulated by changes in the Earth's orbital eccentricity. The dynamic mechanism behind this switch to a 100,000-year cycle has proven to be elusive, particularly considering the relative weakness of insolation anomalies associated with the 100,000-year eccentricity changes. It is likely that some internal feedback within the atmosphere–ocean–cryosphere system caused this switch to the longer glaciation cycle. Nevertheless, it appears that the Pleistocene glaciations have been dominantly regulated by changes in the Earth's orbital parameters (the Milankovitch cycles).

The Ordovician/Silurian glaciation is a particularly fascinating one because it is believed to have occurred under times of high atmospheric carbon dioxide, perhaps as high as 10–15 times the preindustrial value (e.g., Berner, 1998; Figure 1a). It is one clear example of glaciation during which multiple factors were at play. Plate tectonic motion formed the supercontinent of Pangaea, which had a large

amount of land over the South Pole (which is now modern-day Africa, from which evidence for glaciation has been discovered in multiple places that are now tropical–subtropical (e.g., Le Heron, 2007; Le Heron et al., 2009)). In addition, solar luminosity was about 3% lower than its modern value (e.g., Endal and Schatten, 1982). The latter two factors, both conducive to glaciation, were sufficient to keep seasonal temperatures below freezing year round near the South Pole despite the enhanced long wave forcing due to the large amount of atmospheric carbon dioxide.

A considerable amount of numerical modeling work has focused on simulating the inception of the most recent glaciation during the Eemian (~116 kyr ago, see Figure 1b; for a review see Mysak, 2008). Milankovich forcing – in particular, high eccentricity, high precession, and low obliquity – reduced summertime insolation in the high northern latitudes during this time. Since glacial inception takes on the order of thousands of years, the numerical models that have been used to investigate the processes involved are referred to as Earth system Models of Intermediate Complexity (EMICs), meaning that the dynamics contained within the models are simplified compared to the fully coupled atmosphere–ocean general circulation models used for climate prediction, yet they retain many of the basic dynamical processes.

Sensitivity experiments using EMICs have determined that many factors in addition to Milankovitch forcing play a role in glacial inception: land surface vegetation and the vegetation-albedo feedback, moisture transport from the oceans to continental high latitudes, the global thermohaline circulation, and atmospheric carbon dioxide are all important factors in generating sufficiently cool conditions over land that perennial snow exists and can be transformed over the course of years into continental ice (Mysak, 2008).

EMICs have also been used to study the future in an attempt to determine whether the postindustrial rise in atmospheric carbon dioxide is sufficient to preclude the next glaciation predicted from Milankovitch theory at the next insolation minimum, 50 kyr from now. Since the uptake of atmospheric carbon by the oceans is a relatively slow process, these models predict that given the anthropogenic increase in atmospheric CO_2, the current interglacial period could last another ~100 kyr (Loutre and Berger, 2000; Archer and Ganapolski, 2005; Cochelin et al., 2006; Mysak, 2008).

Historically, continental ice sheets in general circulation models are static in the sense that they have specified topography and a suitable albedo but they are not allowed to respond to the atmosphere. Ice sheet models, in turn, are typically forced by fields derived from an atmospheric model but do not interact with the atmosphere. The disparity in timescales of large ice sheets operating on the timescale of thousands of years, and the surrounding climate operating on a seasonal timescale, provides some challenges in using a general circulation model to study the dynamic and thermodynamic interactions between continental ice sheets and the climate system. Nevertheless, such models have been recently developed and used to simulate the demise of large ice sheets (Pritchard et al., 2008; Otto-Bleisner et al., 2006; Ridley et al., 2005). Since there is abundant geological evidence for the timing of the demise of the Laurentide ice sheet (e.g., Dyke et al., 2002), one can employ a coupled atmosphere–ice model to determine the factors governing the rate of continental ice retreat. It is found that a critical feedback during deglaciation is a thermodynamic one in which the margins of the ice, during the melt season, have a lower albedo because of the presence of surface melt water (Pritchard et al., 2008). Without this melt water parameterization included, the Laurentide ice sheet does not melt, even under high values of obliquity (such as those found in the early Holocene) and modern carbon dioxide levels (Pritchard et al., 2008).

It is clear, then, that many factors play a role in glacial cycles and that atmospheric carbon dioxide levels are important but are not the only factor. To complicate matters, many of the factors that can regulate glaciations interact with each other creating either positive or negative feedback loops. One advantage of numerical modeling is that each factor can be examined in isolation, keeping the other factors fixed. This article presents general results from a numerical climate model configured for time slices of Earth's history and possible future. It is a fully coupled atmosphere–ocean general circulation model. Since boundary condition data must be known and input into the model (e.g., ice sheet extent and thickness) the representative low CO_2 state is chosen to be the Last Glacial Maximum (LGM), ~21,000 years ago, for which there has been extensive work done on reconstructing the ice sheets and atmospheric composition.

Model details

The global general cirulation model used is a coupled atmosphere–ocean model developed at the Geophysical Fluid Dynamics Laboratory in Princeton, New Jersey, USA. The atmospheric model (Gordon and Stern, 1982) has a spatial resolution of 3.75° of longitude by 2.25° of latitude at the equator. There are 14 levels in the vertical. The ocean model is the Modular Ocean Model v.2 (e.g., Pacanowski, 1995) with a spatial resolution comparable to that of the atmospheric model. The two general circulation models are dynamically and thermodynamically coupled together with an exchange of boundary condition information at 1-day intervals, and each integration simulates 70 years of climate. There is a thermodynamic sea ice formulation included in the model.

The time slices examined are the Last Glacial Maximum (LGM), today (representative of an interglacial period), and a hypothetical doubled atmospheric CO_2 scenario (which may be on the order of 100 years into the future). Ice sheet reconstructions for the LGM simulation are taken from Peltier (1994). The LGM simulation incorporates many of the factors influencing glaciation

discussed previously: Earth's orbital parameters were slightly different (Berger and Loutre, 1991), the continents, though in the same position as today, were more exposed because of the 120-m drop in sea level, surface vegetation was different, and atmospheric CO_2 was 200 ppm. Atmospheric CO_2 in the control simulation of today is 300 ppm, and 600 ppm in the doubled CO_2 experiment.

Since large ice masses are fixed in the model, and there is no parameterization for the snow–firn–ice transition, any potential changes in glaciers and ice masses must be inferred from changes in annual mean snow accumulation. In particular, for alpine glaciers this is all that can be done with a global model since details of mountains are smoothed out given the model's relatively coarse spatial resolution.

Results

Focusing on the pan-Himalaya range from 60 to 105 E, 25 to 45 N, annual mean snow accumulation (Figure 2) indicates large changes between the LGM and today (Figure 2b) and between a doubled CO_2 environment and today (Figure 2c). There is approximately 30% more snow along the Front Range at the LGM, and ~100% more accumulation in the eastern Himalaya. Conversely, there is a ~30% drop in snow accumulation (compared with today) in the center of the front range (~80 E) in a higher CO_2 environment but on the western (72 E) and eastern (90 E) flanks of the range the decreases are 100%. This result would suggest an overall shrinkage of the area in which glaciers could possibly exist, though they could still persist in the center of the range around 80 E where modern snow accumulation is maximum.

Simulated differences between the low CO_2 glacial state and the high CO_2 state (Figure 2d) show that the entire Himalaya is affected with much more snow nearly everywhere when CO_2 is low. This implies that transitions from low to very high CO_2 states are likely to have negatively affected glaciers across the entire Himalaya.

Simulated changes in annual mean snow accumulation are in accord with the annual mean surface temperature changes averaged over the region (Figure 3). The transition from a low CO_2 state to a high CO_2 state brings a warming of approximately 9°C on average. Note that the difference in temperature over this region between today and the LGM (3.8°C, which is close to the global mean value of 4°C) is less than that between a doubled CO_2 state and today (5.3°C) suggesting that potential changes in the area over the next hundred years may be greater in magnitude than between today and the LGM.

In the Arctic, annual mean temperature changes between low and high CO_2 states are also profound, with changes approaching 14°C (averaged over 0–360 E, 60–90 N; Figure 4). This large difference is because at these latitudes the snow/ice albedo feedback plays a stronger role than at lower latitudes, where the surface area of perennial snow and sea ice is relatively small (even

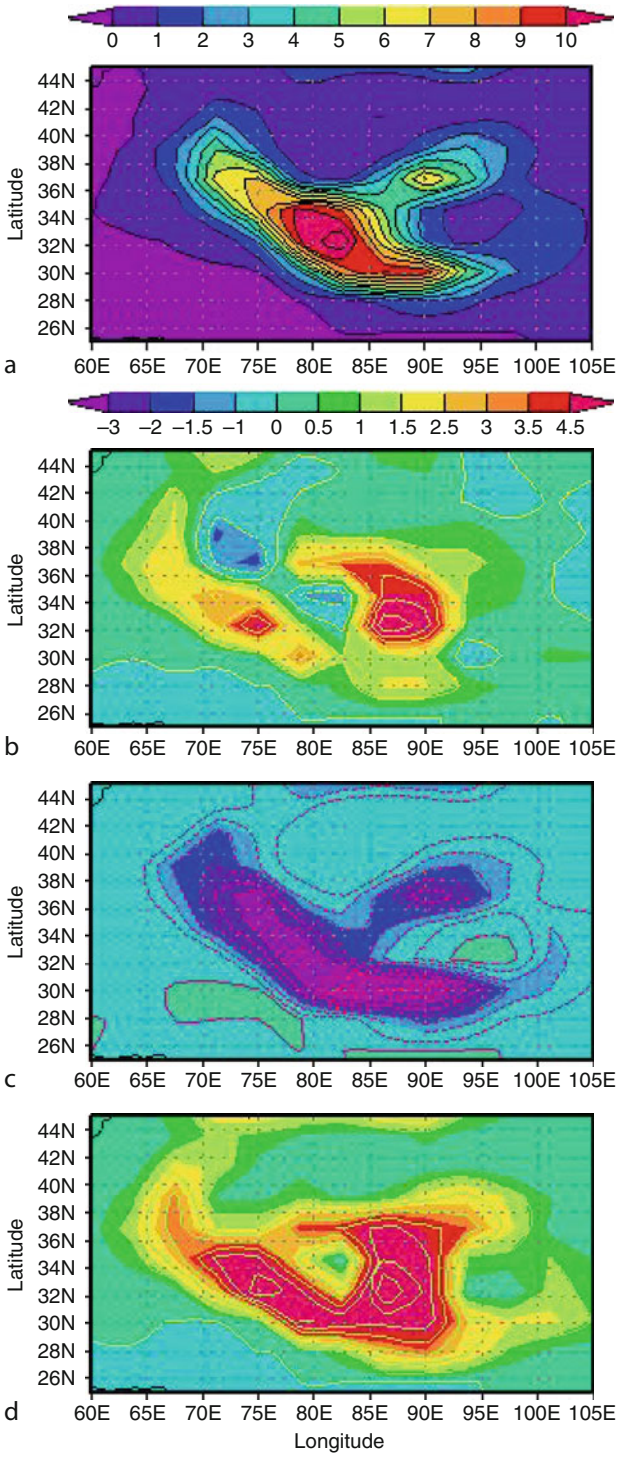

Glaciation During Times of Enhanced/Reduced Atmospheric Carbon Dioxide, Figure 2 (**a**) Annual mean snow accumulation in centimeters of water equivalent in the control simulation. Contour levels are given in the color bar above the panel. (**b**) Last Glacial Maximum (LGM) minus control snow accumulation. (**c**) 2 × CO_2 minus control accumulation. (**d**) LGM minus 2 × CO_2 accumulation. Contour levels for (**b**), (**c**), and (**d**) are given by the color bar above panel (**b**).

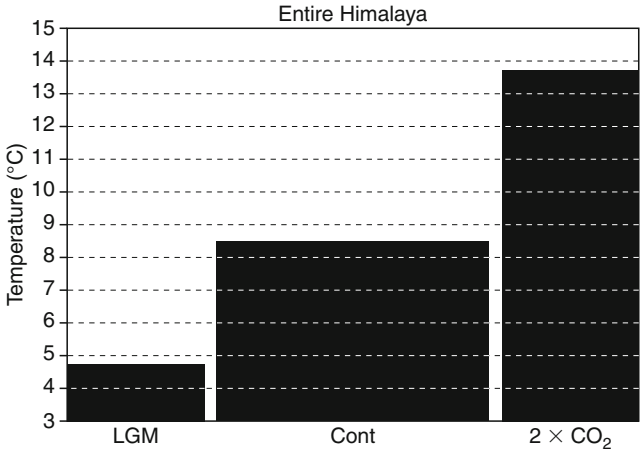

Glaciation During Times of Enhanced/Reduced Atmospheric Carbon Dioxide, Figure 3 Histogram of annual mean surface temperatures in the three simulations, averaged over the entire Himalaya region, 60–105 E, 25–45 N.

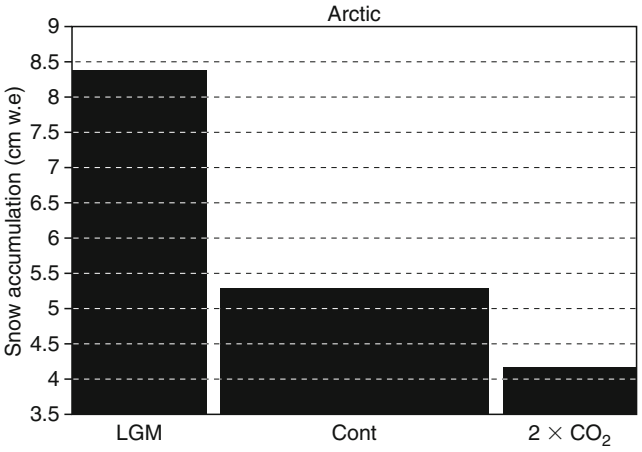

Glaciation During Times of Enhanced/Reduced Atmospheric Carbon Dioxide, Figure 5 Histogram of annual mean snow accumulation in the three simulations, averaged over the entire Arctic region, 0–360 E, 60–90 N.

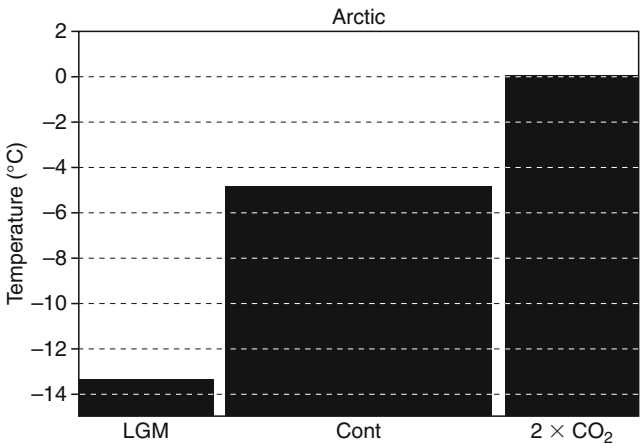

Glaciation During Times of Enhanced/Reduced Atmospheric Carbon Dioxide, Figure 4 Histogram of annual mean surface temperatures in the three simulations, averaged over the entire Arctic region, 0–360 E, 60–90 N.

though insolation is higher). It is interesting to note that in a doubled CO_2 atmosphere, the annual mean temperature of the Arctic is just at the freezing level, implying significantly warmer summer temperature and high rates of ice melt.

Snow accumulation averaged over the Arctic (Figure 5) is in accord with the temperature changes and is not particularly surprising. However, an interesting point may be made with respect to the relatively small change between today and the doubled CO_2 simulation. In a warmer climate, there is increased moisture flux into higher latitudes (e.g., Ross and Elliot, 2001; Wetherald and Manabe, 2003) so if temperatures are sufficiently low that precipitation falls as snow (which, according to Figure 4, would still occur during the wintertime) then the increased moisture implies increased wintertime snowfall. The reason there is still a decrease overall (averaged over 60–90 N) is a combination of increased summertime melt (cf. Figure 4) and the fact that the southern margin of perennial snow migrates further north, thereby decreasing the areal extent of snow covered regions.

Results around Antarctica are fairly uniform through all three simulations, and that is a consequence of the Antarctic ice sheet being fixed in the model (and not that much different at the LGM). This is a weakness of the model where changes in Antarctic climate are likely to influence results for much of the southern hemisphere.

Although there are a number of glaciers in the Andes, the model only captures significant snowfall over southern Patagonia and there is a near 100% drop between the LGM and the doubled CO_2 simulation in that region (not shown).

Discussion and conclusions

Results from a general circulation model are useful in the sense that they give the range of climates under different forcing factors. The two "extreme" climates presented here, that of the LGM and that of a doubled CO_2 atmosphere, bracket the range of possibilities between glacial conditions and a potential future climate state, whereas comparison between the LGM climate and the control brackets the range between glacial and interglacial states (at least through the late Pleistocene).

Between glacial and interglacial states, the variation of atmospheric CO_2 is on the order of 100–150 ppm and in the study regions, this was the primary cause of annual mean temperature changes on the order of 4–5°C over the Himalaya and on the order of 9–10°C over the Arctic

region. The 400-ppm difference in CO_2 between the LGM and the doubled CO_2 simulation produces 9–10°C of temperature change over the Himalaya and 13–14°C of change over the Arctic.

In terms of implications for glaciers, these temperature changes are profound. The temperature dependency of the saturation vapor pressure of the atmosphere is exponential with temperature, implying much more atmospheric water vapor in warmer climates (since evaporation also increases with temperature). This implies more precipitation per event (an event meaning either a synoptic frontal system or, perhaps more importantly for glaciers, orographic uplift). The key issue is whether that precipitation falls as rain or as snow. In a warmer climate, the equilibrium line altitude will shift upward since the shift in precipitation type from rain to snow will shift upward. Theoretically, if the temperature were warm enough then no snow would fall at the highest elevations of the planet. However, the results presented here indicate that a doubling of CO_2 is not sufficient to prevent snow from accumulating at the surface in the Himalaya (cf. Figure 2) it just changes the spatial distribution as well as the net amount. It would be likely, then, that some glaciers could still exist at high elevations in a doubled CO_2 environment, though some that are presently at lower elevations would not be able to exist.

Conversely, in a low CO_2 environment such as that of the LGM, the saturation vapor pressure is lower and precipitation events do not produce as much, but more of what they produce falls as snow in the colder temperatures. As indicated in Figure 2, there is of course spatial variability to the changes in snowfall but on average the increase in snow accumulation at the LGM both over the Himalaya and the Arctic can be attributed primarily to the change in precipitation type. However, there are also changes in wind direction in the LGM simulation that enhances orographic precipitation, particularly in the eastern Himalaya (see Bush, 2002), and there is field evidence to support glacier advances there at the LGM (Richards et al., 2000).

Seasonality also plays a significant role in determining the type of precipitation. In a low CO_2 climate, snowfall events are more likely in the early and late summer months and conversely in a high CO_2 climate rainfall events are more likely in the early and late winter months. On geologic timescales, this fact becomes important on the timescale governing Earth's angle of obliquity (~41,000 years) since high obliquity implies a stronger seasonal cycle. In fact, 6,000 years ago when obliquity was higher than today, the increased seasonality enhanced the summer monsoon winds bringing more moisture to the western Himalaya, which would fall as snow at high elevations, and there is field evidence to support glacier advances at that time (e.g., Phillips et al., 2000; Richards et al., 2000).

The fact that the general circulation model results are in accord with field measurements, at least for the Himalaya (Bush, 2002), implies that the temperature and snow accumulation changes simulated by the model are sufficient to cause glacier advances/retreats. A drawback of the general circulation model is the lack of spatial detail that is necessary to infer changes in specific regions. This deficiency is at present being addressed through the use of regional modeling in which a regional model is driven by data produced by the general circulation model. While this area of research is relatively new, it should give spatial resolutions on the order of kilometers as opposed to the hundreds of kilometers of the general circulation model. Spatial resolution on the order of kilometers would vastly improve the representation of topography in the model (and hence orographic precipitation and topographic radiative shielding of mountain valleys) and should therefore lead to improved results for glacierized regions. However, even this spatial resolution is still relatively coarse compared with the spatial scale of individual alpine glaciers. As of yet there is no direct coupling between regional models and glacier models, so a methodology needs to be developed to take regional atmospheric data and drive some form of glacier model that spans a region large enough to be significant. Such a methodology is currently being developed under the auspices of the Western Canadian Cryospheric Network (http://wcn.unbc.ca).

Bibliography

Archer, D., and Ganapolski, A., 2005. A movable trigger: fossil fuel CO_2 and the onset of the next glaciation. *Geochemistry, Geophysics, Geosystems*, **6**, doi:1029/2004GC000891.

Berger, A., and Loutre, M. F., 1991. Insolation values for the climate of the last 10 million years. *Quaternary Sciences Review*, **10**, 291–317.

Berner, R. A., 1998. The carbon cycle and CO_2 over phanerozoic time: the role of land plants. *Philosophical Transactions of the Royal Society, Series B*, **353**, 75–82.

Bush, A. B. G., 2002. A comparison of simulated monsoon circulations and snow accumulation during the mid-Holocene and at the Last Glacial Maximum. *Global and Planetary Change*, **32**, 331–347.

Bussert, R., and Schrank, E., 2007. Palynological evidence for a latest Carboniferous-Early Permian glaciation in Northern Europe. *Journal of African Earth Sciences*, **49**, 201–210.

Cochelin, A.-S., Mysak, L. A., and Wang, Z., 2006. Simulation of long-term future climate changes with the green McGill paleoclimate model: the next glacial inception. *Climatic Change*, **79**, 381–401.

Crowley, T. J., and North, G. R., 1992. *Paleoclimatology. Oxford Monographs on Geology and Geophysics, No. 18*. New York: Oxford University Press. 339 pp.

Dyke, A. S., Andrews, J. T., Clark, P. U., England, J. H., Miller, G. H., Shaw, J., and Veil-lette, J. J., 2002. The Laurentide and Innuitian ice sheets during the Last Glacial Maximum. *Quaternary Science Reviews*, **21**, 9–31.

Endal, A. S., and Schatten, K. H., 1982. The faint young sun-climate paradox-Continental influences. *Journal of Geophysical Research – Oceans and Atmospheres*, **87**, 7295–7302.

Eyles, N., 2008. Glacio-epochs and the supercontinent cycle after ~3.0 Ga: tectonic boundary conditions for glaciation. *Palaeogeography, Palaeoclimatology, Palaeoecology*, **258**, 89129.

Gordon, C. T., and Stern, W., 1982. A description of the GFDL global spectral model. *Monthly Weather Review*, **110**, 625–644.
Hoffman, P. F., and Schrag, D. P., 2002. The snowball Earth hypothesis: testing the limits of global change. *Terra Nova*, **14**, 129–155.
Hoffman, P. F., Kaufman, A. J., Halverson, G. P., and Schrag, D. P., 1998. A Neoproterozoic snowball earth. *Science*, **281**, 1342–1346.
Le Heron, D. P., 2007. Late Ordovician glacial record of the Anti-Atlas, Morocco. *Sedimentary Geology*, **201**, 93–110.
Le Heron, D. P., Craig, J., and Etienne, J. L., 2009. Ancient glaciations and hydrocarbon accumulations in North Africa and the Middle East. *Earth-Science Reviews*, **93**, 47–76.
Loutre, M. F., and Berger, A., 2000. Future climatic changes: are we entering an exceptionally long interglacial? *Climatic Change*, **46**, 61–90.
Mysak, L. A., 2008. Glacial inceptions: past and future. *Atmosphere-Ocean*, **46**, 317–341.
Otto-Bleisner, B. L., Marshall, S. J., Overpeck, J. T., Miller, G. H., and Hu, A., 2006. Simulating Arctic climate warmth and icefield retreat in the last interglaciation. *Science*, **311**, 1751–1753.
Pacanowski, R. C., 1995. *MOM2 documentation, user's guide, and reference manual*. GRDL Ocean Group Technical Report 3, 232 pp.
Peltier, W. R., 1994. Ice age paleotopography. *Science*, **265**, 195–201.
Petit, J. R., Jouzel, J., Raynaud, D., Barkov, N. I., Barnola, J. M., Basile, I., Bender, M., Chappellaz, J., Davis, J., Delaygue, G., Delmotte, M., Kotlyakov, V. M., Legrand, M., Lipenkov, V., Lorius, C., Ppin, L., Ritz, C., Saltzman, E., and Stievenard, M., 1999. Climate and atmospheric history of the past 420,000 years from the Vostok ice core, Antarctica. *Nature*, **399**, 429–436.
Phillips, W. M., Sloan, V. F., Shroder, J. F. Jr., Sharma, P., Clarke, M. L., and Rendell, H. M., 2000. Asynchronous glaciation at Nanga Parbat, northwestern Himalaya Mountains, Pakistan. *Geology*, **28**, 431–434.
Pritchard, M., Bush, A. B. G., and Marshall, S. J., 2008. Neglecting ice-atmosphere interactions underestimates ice sheet melt in millenial-scale deglaciation simulations. *Geophysical Research Letters*, **35**, LO1503, doi:1029/2007GL031738.
Richards, B. W., Owen, L. A., and Rhodes, E. J., 2000. Timing of Late Quaternary glaciations in the Himalaya of northern Pakistan. *Journal of Quaternary Science*, **15**, 283–297.
Ridley, J. K., Huybrechts, P., Gregory, J. M., and Lowe, A. J., 2005. Elimination of the Greenland ice sheet in a high CO_2 climate. *Journal of Climate*, **18**, 3409–3427.
Ross, J., and Elliot, W., 2001. Radiosonde-based Northern hemisphere tropospheric water vapor trends. *Journal of Climate*, **14**, 1602–1612.
Schrag, D. P., Berner, R. A., Hoffman, P. F., and Halverson, G. P., 2002. On the initiation of a Snowball Earth. *Geochemistry, Geophysics, Geosystems*, **3**, doi:1029/2001GC000219.
Wetherald, R., and Manabe, S., 2003. Simulation of hydrological changes associated with global warming. *Journal of Geophysical Research*, **107**, 1–15, doi:1029/2001JD001195.

Cross-references

Atmosphere-Snow/Ice Interactions
Atmospheric Circulation and Glaciochemical Records
Climate Change and Glaciers
Glacial/Interglacial Cycles
Ice Age
Ice Age Development Theory
Laurentide Ice Sheet
Palaeoclimate and Past Glaciations
Quaternary Glaciation

GLACIATIONS AND GROUNDWATER FLOW SYSTEMS

Jean-Michel Lemieux[1], Edward A. Sudicky[2]
[1]Département de géologie et de génie géologique, Université Laval, Québec, QC, Canada
[2]Department of Earth and Environmental Sciences, University of Waterloo, Waterloo, ON, Canada

Definition and introduction

Pleistocene glaciations had a profound influence on the dynamics of groundwater flow systems. Their impact has not been limited to glaciated regions; they also affected parts of the world that were not glaciated because of the related global perturbations in climatic conditions such as changes in precipitation and eustatic sea levels. As a consequence, groundwater recharge patterns were globally modified and affected groundwater flow dynamics at basinal to continental scales in a wide range of geological environments such as coastal aquifers, intercratonic sedimentary basins and crystalline rocks.

The study of the impact of glaciations on groundwater flow is important for several reasons. First, it can assist in explaining the origins of modern groundwater flow patterns, as well as the geochemistry of waters because it is now recognized that many large-scale groundwater flow systems are not in equilibrium with modern climatic conditions since they are continuing to evolve from past climatic periods (Grasby et al., 2000; Person et al., 2003). Pleistocene waters have geochemical properties that are different than autochthonous waters; their quality is usually good, and in some locations, they are an important source of freshwater (Edmunds, 2001). The sound management of these resources requires a sound scientific understanding of their origin, extent, and the driving forces acting on them. Glacial meltwater is also associated with the generation of biogenic gas resources that are exploited by the petroleum industry in the Michigan and Illinois Basins (McIntosh et al., 2002). Moreover, the lowering of sea level related to the growth of ice sheets have exposed coastal aquifers to freshwater recharge such that, in some locations, the freshwater/sea water interface observed today is not in equilibrium with the current sea level (Akouvi et al., 2008; Person et al., 2003). Pressurized groundwater below ice sheets may also be an important consideration with regard to issues such as the safe long-term disposal of radioactive wastes (Talbot, 1999). Because the suitability of deep geologic repositories must be demonstrated over large timescales, flow patterns under an ice sheet must be understood as they may change drastically.

Supporting evidence

One of the earliest works addressing the direct impact of glaciations on groundwater flow systems was published

by McGinnis (1968) who proposed a groundwater flow reversal close to the margins of the Laurentide Ice Sheet to explain the displacement of brines and formation of Mississippi Valley type (MVT) zinc-lead deposits in Illinois and Wisconsin. This publication did not receive much attention at that time, probably due to the fact that the origin of the MVT deposits were prior explained by another competing mechanism and partly because of the lack of supporting field evidence regarding glacial impacts. However, this publication introduced a new paradigm with regard to the driving forces for groundwater flow. The same concept was later proposed by Boulton et al. (1993), without apparent knowledge of the previous work of McGinnis. Boulton et al. (1993) proposed a theory that pressurized subglacial meltwater from ice sheets would substantially reorganize aquifer flow fields and that groundwater flow would be controlled by the continental-scale topographical form of the ice sheet's surface rather than by the land surface topography, as observed today. His theory was supported by the results from a numerical groundwater flow model that predicted hydraulic gradients sufficient to explain the sediment disruption observed in North-Western Europe. This theory is now widely accepted and has been extensively tested with field observations.

Geochemists also recognized early on that the groundwater chemistry in some regions could not be explained by the recharge of modern precipitation and that paleoclimatic conditions characterized by recharge waters having different geochemical signatures could explain the discrepancies (Clayton et al., 1966). Thus, groundwater chemistries observed today are believed to have recorded the evolution of past climate changes, and early applications of this discovery were tested in non-glaciated regions in order to identify past recharge conditions. For example, Edmunds and Wright (1979) used stable (^{18}O, ^{2}H) and radio-isotope (^{14}C) data measured in groundwaters from the Sirte and Kufra Basins (Libya) to determine the recharge history during the Holocene and the late Pleistocene. Andrews and Lee (1979) also used radio-isotopes (^{222}Rn, ^{4}He, ^{14}C) along with inert gases (Ar, Kr) to infer the temperature and timing of the recharge in England for the late Pleistocene.

In glaciated regions, subglacial recharge is suspected to have penetrated to significant depths in moderately permeable sedimentary aquifers (Siegel and Mandle, 1984) and crystalline environments (Clark et al., 2000). Glacial meltwater is characterized by low ^{18}O, ^{2}H, and total dissolved solids (Clark et al., 2000) and these characteristics are used as the primary indicators to identify the presence of glacial meltwater.

Several other techniques have been proposed for acquiring temporal information from groundwater systems. The techniques and applications are well described in the review by Metcalfe et al. (1998) for dating relative or absolute events such as groundwater recharge or enhanced flow rates. Among these techniques, the most appropriate for Pleistocene events are radioactive isotopes (e.g., ^{13}C, ^{14}C, ^{34}S, ^{222}Rn) to infer the groundwater age and dating groundwater "events" along with noble gas (Ar, Kr, Xe) to estimate groundwater recharge temperatures. The mixing of recharge water with in situ water, however, greatly complicates the interpretation of the geochemical data.

In the recent years, several new lines of evidence have been put forward to demonstrate the strong impact of glaciations on groundwater flow systems in a wide range of geological environments, in both glaciated and non-glaciated regions. This evidence is well summarized by Person et al. (2007) for North America and in a Geological Society of London Special Publication edited by Edmunds and Milne (2001) for Europe.

Important processes

Figure 1 exhibits the hydraulic conditions that may be encountered during a glaciation period. These conditions are much different than observed during the Holocene where the main driving force for groundwater flow is gravity-driven by the topographical forms of the landscape as described by the pioneer works of Hubbert (1940) and Tóth (1962). In the subglacial environment, large hydraulic heads can develop in warm-based regions below the ice sheet where the upward geothermal heat fluxes and subglacial frictional heating are sufficient to raise the temperature above the pressure melting point and thus generate subglacial meltwater. A portion of the pressurized meltwater is driven into the subsurface under ice sheet pressure, which induces a strong downward hydraulic gradient, such that the groundwater recharge rate is significantly modified as compared to values during interglacial periods. The subglacial meltwater that infiltrates into the subsurface will flow from high hydraulic head zones (i.e., under the ice sheet) to lower head zones, which can either be subglacial regions where there is no melting or to distal areas beyond the limits of the ice sheet. Groundwater flow lines therefore mimic in an ancillary way the nature of ice sheet flow lines, and the ice sheet topography has a dominant control on groundwater flow.

The quantity of recharge is dependent on the permeability of the substratum and is much larger for sedimentary basins than for igneous and metamorphic cratons such as the Canadian Shield and the Fennoscandian Shield. When the recharge event is large and sustained long enough, a reversal of the normal flow field can occur (Grasby et al., 2000). At the tip of the ice sheet, large subsurface hydraulic gradients form over short distances, but the permeability is greatly reduced by the presence of the permafrost. These conditions are likely to lead to hydrofracturing in sediments and rocks at the ice sheet margin (Boulton et al., 1993). Laterally beyond the permafrost zone, through local gaps in the discontinuous permafrost, strong upward groundwater flow is likely to occur that will lead to sediment liquefaction, sediment dyke

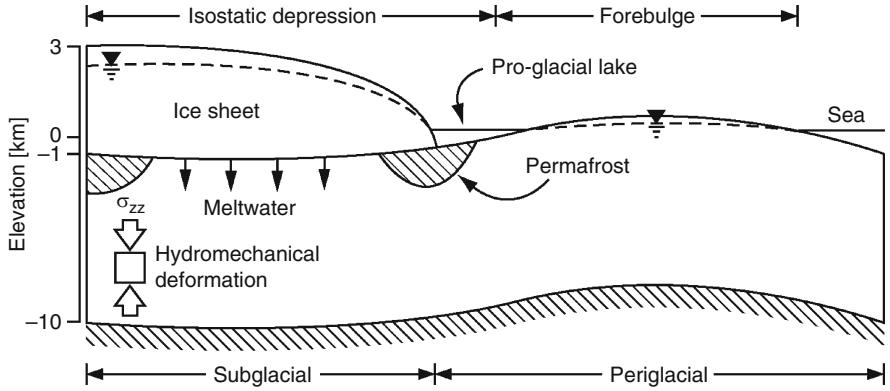

Glaciations and Groundwater Flow Systems, Figure 1 Conceptual model showing relevant processes that may impact groundwater flow systems during a glacial period. The driving forces for groundwater flow are much different than during interglacial periods such as the present time. Important processes include eustatic sea level changes, glacial isostasy (depression and forebulge are identified), permafrost development, hydromechanical deformation due to ice sheet loading, subglacial meltwater recharge, and pro-glacial/periglacial drainage network evolution. Subglacial and periglacial environments are identified and described in the text. The figure is conceptual and not to scale. The depth of 10 km is arbitrary. Modified from Lemieux et al. (2008a, b).

formation, and sediment expulsion structures (Boulton et al., 1993). Recent studies on the dynamic of groundwater recharge suggest that most subglacial recharge occurs during glacial progression while little occurs during glacial regressions, where exfiltration dominates the recharge/discharge dynamics across the land surface (Lemieux et al., 2008a).

In some portions of the subglacial environment, a cold base exists below the ice sheet where no subglacial water is generated and where permafrost occurs. These regions are believed to exist at the ice sheet margins and under the center of ice domes (Boulton et al., 1996; Tarasov and Peltier, 2007) and can reach a depth of 1,000 m in the periglacial environment. The permeability of soils affected by permafrost is greatly reduced (Burt and Williams, 1976) and prevents the movement of groundwater although there is no consensus on the permeability reduction because of the paucity of data. Continuous permafrost prevents surface water from recharging groundwater in the periglacial area and conversely from allowing groundwater to discharge to the surficial regime. Such an interruption in recharge has been documented by Edmunds (2001) for the East European Midlands during the 10–20 ka BP period.

In the periglacial environment, several large proglacial lakes formed during the last deglaciation period (e.g., Lake Agassiz) and their configuration, depth and extent was a result of the interactions between the location of the ice margin, the topography of the newly deglaciated surface, the elevation of the active meltwater outlet along the margins of the ice sheet, and differential isostatic rebound (Teller, 1987). These lakes can affect the ground thermal regime and contribute to the melting of permafrost. They will also strongly interact with the groundwater and have an important role in taliks development. They can also represent a driving force for groundwater recharge or be an outlet for deep pressurized groundwater. In any case, their presence strongly influences subsurface hydraulic gradients over large regions.

Dynamic eustatic sea level variations due to changes in the amount of water stored in ice sheets constantly modifies the sea shore position and coastal water levels during a glaciation cycle, thus exposing the continental shelf to meteoric recharge during glacial maximas. The dynamics of sea level change is such that it regresses more slowly than it transgresses. This has an important repercussion on coastal aquifers where the interface between freshwater and saline waters evolves accordingly. Person et al. (2003) have documented freshwater up to 150 km off the shore of New York, which is not in equilibrium with modern sea level. This could only be explained by meteoric or subglacial Pleistocene recharge.

The weight of an ice sheet causes the Earth's crust to deform such that an isostatic depression develops underneath and a forebulge forms in its distal surroundings. Isostatic depression exceeded 1 km at the last glacial maximum in North America. This modifies large-scale groundwater flow patterns because hydraulic potentials are lowered below the ice sheet and are increased in the forebulge. Another impact of the ice sheet is the additional weight imposed on the geologic medium. Depending on its elastic properties, which are a function of the rock type, compaction can reduce both the porosity and the permeability of the geologic material and hence lead to the development of abnormal pore pressures (Bekele et al., 2003).

Numerical studies have become powerful tools to study the complex interaction among the processes involved during a glaciation period and assess their respective impacts on groundwater flow systems. A comprehensive description of the theoretical

background and applications for basinal to continental scales are given by Person et al. (2007), Lemieux et al. (2008a, b, c), and Bense and Person (2008).

Summary

Pleistocene glaciations had a strong impact on groundwater flow dynamics in a wide variety of geological environments in both the glaciated and non-glaciated parts of the world. Several lines of evidence support this paradigm such as groundwater geochemical imprints, regional disequilibrium in subsurface pore pressures, and sedimentary structures. The study of Pleistocene hydrogeology is complex because of the range of geological and hydraulic processes involved during glacial cycles such as hydromechanical deformation due to glacial loading, glacial isostasy, eustatic sea levels' variations, proglacial drainage evolution, subglacial recharge, and permafrost development. Current groundwater flow in basins affected by Pleistocene glaciations cannot always be interpreted solely on the basis of Holocene conditions and it is likely that several thousands to tens of thousands of years of additional equilibration time will be necessary for systems to reach a new equilibrium state, depending on the system's inertia. On the other hand, the information recorded by the groundwater offers great potential to better understand past climates.

Bibliography

Akouvi, A., Dray, M., Violette, S., de Marsily, G., and Zupp, G. M., 2008. The sedimentary coastal basin of Togo: example of a multilayered aquifer still influenced by a palaeo-seawater intrusion. *Hydrogeology Journal*, **16**(3), 419–436, doi:10.1007/s10040-007-0246-1.

Andrews, J. N., and Lee, D. J., 1979. Inert gases in groundwater from the Bunter sandstone of England as indicators of age and palaeoclimatic trends. *Journal of Hydrology*, **41**(3–4), 233–252.

Bekele, E. B., Rostron, B. J., and Person, M. A., 2003. Fluid pressure implications of erosion unloading, basin hydrodynamics and glaciation in the Alberta Basin. *Journal of Geochemical Exploration*, **78–79**, 143–147.

Bense, V. F., and Person, M. A., 2008. Transient hydrodynamics within inter-cratonic sedimentary basins during glacial cycles. *Journal of Geophysical Research*, **113**, F04005, doi:10.1029/2007JF000969.

Boulton, G. S., Slot, T., Blessing, K., Glasbergen, P., Leijnse, T., and van Gijssel, K., 1993. Deep circulation of groundwater in overpressured subglacial aquifers and its geological consequences. *Quaternary Science Reviews*, **12**, 739–745.

Boulton, G. S., Caban, P. B., van Gissel, K., Leijnse, A., Punkari, M., and van Weert, F. H. A., 1996. The impact of glaciation on the groundwater regime of northwest Europe. *Global and Planetary Change*, **12**(1–4), 397–413.

Burt, T. P., and Williams, P. J., 1976. Hydraulic conductivity in frozen soils. *Earth Surface Processes*, **1**(4), 349–360.

Clark, I. D., Douglas, M., Raven, K., and Bottomley, D., 2000. Recharge and preservation of Laurentide glacial melt water in the Canadian Shield. *Ground Water*, **38**(5), 735–742.

Clayton, R. N., Friedman, L., Graf, D. L., Mayeda, T. K., Meents, W. F., and Shimp, N. F., 1966. The origin of saline formation waters. 1. Isotopic composition. *Journal of Geophysical Research*, **71**(16), 3869–3882.

Edmunds, W. M., and Wright, E. P., 1979. Groundwater recharge and palaeoclimate in the Sirte and Kufra Basins, Libya. *Journal of Hydrology*, **40**(3–4), 215–241.

Edmunds, W. M., 2001. Paleowaters in European coastal aquifers – The goals and main conclusions of the PALAEAUX project. In Edmunds, W. M. and Milne, C. J. (eds.), *Palaeowaters in Coastal Europe: Evolution of Groundwater Since the Late Pleistocene.* London: Geological Society, Special Publication, 189, pp. 1–16.

Edmunds, W. M., and Milne, C. J., 2001. *Palaeowaters in Coastal Europe: Evolution of Groundwater Since the Late Pleistocene.* London: Geological Society, Special Publication, 189.

Grasby, S., Osadetz, K., Betcher, R., and Render, F., 2000. Reversal of the regional-scale flow system of the Williston basin in response to Pleistocene glaciation. *Geology*, **28**(7), 635–638.

Hubbert, M. K., 1940. The theory of groundwater motion. *Journal of Geology*, **48**, 785–944.

Lemieux, J.-M., Sudicky, E. A., Peltier, W. R., and Tarasov, L., 2008a. Dynamics of groundwater recharge and seepage over the Canadian landscape during the Wisconsinian glaciation. *Journal of Geophysical Research*, **113**, F01011, doi:10.1029/2007JF000838.

Lemieux, J.-M., Sudicky, E. A., Peltier, W. R., and Tarasov, L., 2008b. Simulating the impact of glaciations on continental groundwater flow systems: 1. Relevant processes and model formulation. *Journal of Geophysical Research*, **113**, F03017, doi:10.1029/2007JF000928.

Lemieux, J.-M., Sudicky, E. A., Peltier, W. R., and Tarasov, L., 2008c. Simulating the impact of glaciations on continental groundwater flow systems: 2. Model application to the Wisconsinian glaciation over the Canadian landscape. *Journal of Geophysical Research*, **113**, F03018, doi:10.1029/2007JF000929.

McGinnis, L. D., 1968. Glaciation as a Possible Cause of Mineral Deposition. *Economic Geology*, **63**, 390–400.

McIntosh, J. C., Walter, L. M., and Martini, A. M., 2002. Pleistocene recharge to midcontinent basins: Effects on salinity structure and microbial gas generation. *Geochimica et Cosmochimica Acta*, **66**(10), 1681–1700.

Metcalfe, R., Hooker, P. J., Darling, W. G., and Milodowski, A. E., 1998. Dating Quaternary groundwater flow events: a review of available methods and their application. In Parnell, J. (ed.), *Dating and Duration of Fluid Flow and Fluid-Rock Interaction*. Geological Society, London, Special Publication, 144, pp. 233–260.

Person, M., Dugan, B., Swenson, J. B., Urbano, L., Stott, C., Taylor, J., and Willett, M., 2003. Pleistocene hydrogeology of the Atlantic continental shelf, New England. *Geological Society of America Bulletin*, **115**(11), 1324–1343.

Person, M., McIntosh, J., Bense, V., and Remenda, V. H., 2007. Pleistocene hydrology of North America: the role of ice sheets in reorganizing groundwater flow systems. *Reviews of Geophysics*, **45**, RG3007, doi:10.1029/2006RG000206.

Siegel, D. I., and Mandle, R. J., 1984. Isotopic evidence for glacial meltwater recharge to the Cambrian-Ordovician aquifer, north-central United States. *Journal of Quaternary Research*, **22**, 328–335.

Talbot, C. J., 1999. Ice ages and nuclear waste isolation. *Engineering Geology*, **52**(3–4), 177–192.

Tarasov, L., and Peltier, W. R., 2007. Coevolution of continental ice cover and permafrost extent over the last glacial-interglacial cycle in North America. *Journal of Geophysical Research*, **112**, F02S08, doi:10.1029/2006JF000661.

Teller, J. T., 1987. Proglacial lakes and the southern margin of the Laurentide Ice Sheet. In Wright, H. E., and Ruddiman, F. (eds.), *North America and Adjacent Oceans During the Last*

Deglaciation. Boulder, CO: Geological Society of America, pp. 39–67.
Tóth, J., 1962. A theory of ground-water motion in small drainage basins in central Alberta, Canada. *Journal of Geophysical Research*, **67**(11), 4375–4387.

Cross-references

Base Flow/Groundwater Flow
Deglaciation
Frozen Soil Hydrology
Heat and Mass Transfer in Sea Ice
Meltwater Conduit
Subglacial Drainage System
Subglacial Processes
Talik

GLACIER

D. P. Dobhal
Wadia Institute of Himalayan Geology, Dehradun, India

A glacier is a hard, thick and compact ice mass on land that forms through the recrystallization of snow and moves forward under its own weight. Glaciers form over many years of packed snow in areas where more snow accumulates than it melts. A glacier is a dynamic and fragile ice body always moving forward, characterized by three basic components, that is, accumulation, ablation, and terminus zone (Snout) (Figure 1).

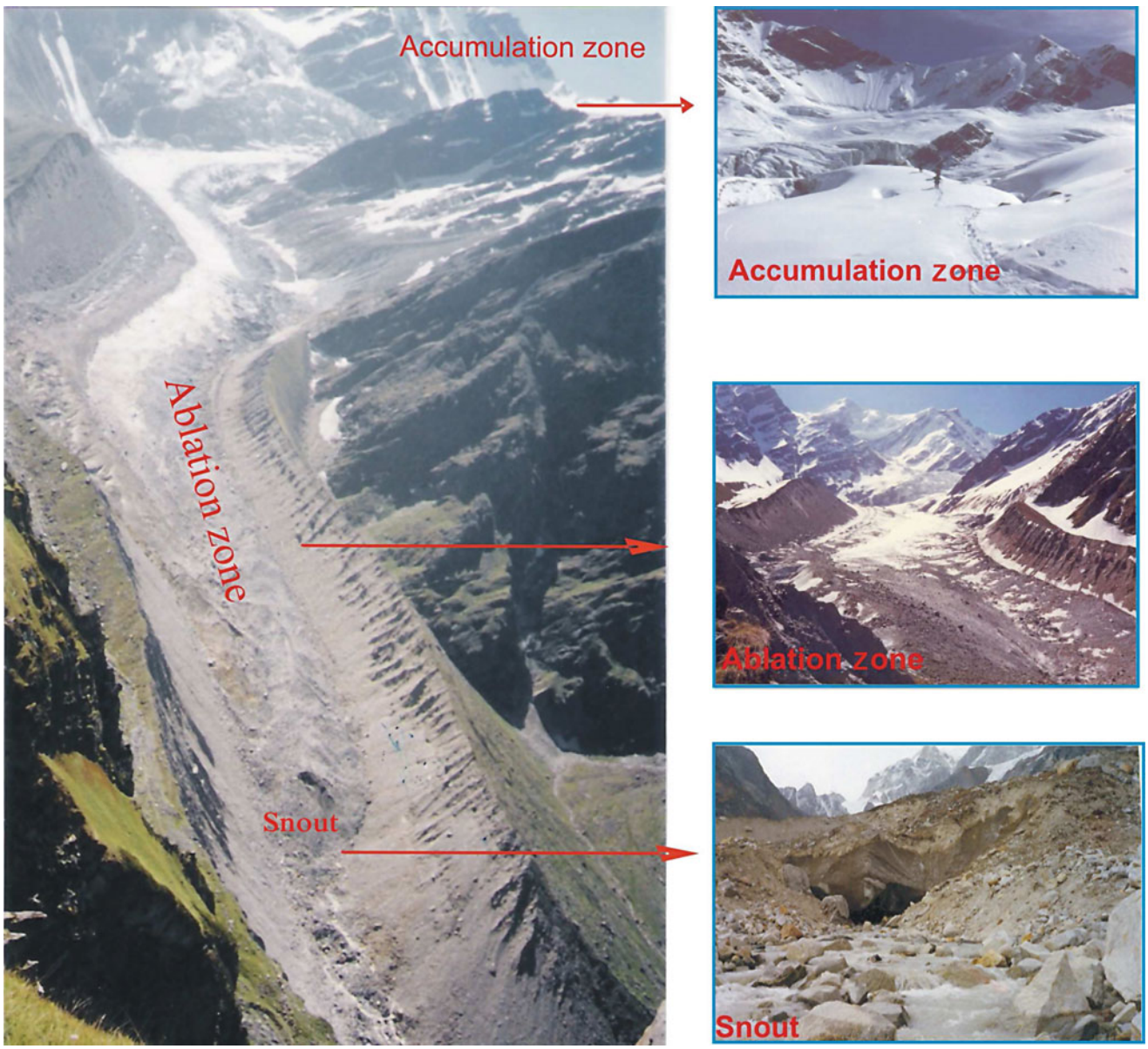

Glacier, Figure 1 Synoptic view of glacier (Dokriani Glacier, Garhwal Himalaya, India) and its components (Photo: Dobhal).

Accumulation Zone: The part of a glacier that is perennially covered with snow, extending between equilibrium line/firn line and brugschund called accumulation zone of the glacier. This occurs through a variety of processes including precipitation, firnification, and wind transportation of snow into a glacier basin from an adjacent area.

Ablation zone: The area extended between the snout and equilibrium line altitudes or firn line is defined as glacier ablation zone. This is the area where ice and snow are lost through a variety of processes including melting and runoff, sublimation, evaporation, calving, and wind transportation of snow out of a glacier basin.

Terminus (snout) zone: The end edge beyond which there is no glacier and from where a stream emerges is called snout/terminus of a glacier. Snout of the glaciers exhibit varying shapes and characters, depending upon the size of glacier, nature of valley, bed rock slope, and of course, mass balance of the glacier.

GLACIER BIRD OF THE ANDES

Douglas R. Hardy[1], Spencer P. Hardy[2]
[1]Climate System Research Center and Department of Geosciences, University of Massachusetts, Morrill Science Center, Amherst, MA, USA
[2]Hanover High School, Hanover, NH, USA

Definition

White-winged Diuca Finch (*Diuca speculifera*) is a bird species that uses glaciers in the High Andes for both roosting and nesting.

Many birds are well adapted to environments seasonally dominated by snow or sea ice, but excepting penguins, birds are not generally associated with glaciers. Even flying over mountain glaciers and ice caps can be hazardous to birds, subjecting them to low oxygen pressure, low temperatures, and harsh environmental conditions such as snowstorms; mortality has been documented from glaciers in Alaska, USA and Yukon Territory, Canada (Krajick, 2002), Greenland (Pfeffer W. T., 2009, personal communication), the Himalaya (Thompson L. G., 2007, personal communication), and on Kilimanjaro (Hardy D. R., 2008, unpublished data).

Conditions on glaciers are usually not well suited for nesting in particular, being cold, actively changing through accumulation and ablation, and at times wet. Until recently the ornithological literature contained only one detailed account of nesting on a glacier, the unusual circumstance where glaciers advancing into Alaska's Prince William Sound overran a Black-legged Kittiwake (*Rissa tridactyla*) colony (Irons, 1988). Previously used nest sites became unavailable and 77 kittiwake nests were constructed on the glacier face; all failed.

One bird species is exceptional, roosting at night within glaciers and perennially nesting on glaciers. This is the White-winged Diuca Finch (*Diuca speculifera* hereafter WWDF), found above 4,500 m elevation in the High Andes of Perú, western Bolivia, and northern Chile (Fjeldså and Krabbe, 1990). Their association with glaciers was first noted at Chacaltaya (5,200 m) near La Paz Bolivia, gathering for the night inside a crevasse (Niethammer, 1953), and Johnson (1967) provides a second-hand report – also from Chacaltaya – of the species nesting in a generalized "ice cave" at 5,300 m. Hardy and Hardy (2008) documented roosting and numerous glacier nests of WWDF in the Cordillera Vilcanota of southern Perú. Nests were found primarily on the near-vertical, retreating glacier margin of the Quelccaya Ice Cap, at elevations up to 5,300 m, over several consecutive years. Observed nests were both in situ on the ice and recently fallen. Supporting evidence, including WWDF eggs and feathers within glacier nests, remains on the ice of WWDF victimized by predation, as well as active WWDF in the area. Glacier nesting by WWDF occurs at Quelccaya Ice Cap despite subfreezing air temperature throughout the year, with extreme night-time radiational cooling whenever cloud cover is low. Furthermore, WWDF is among the highest-elevation nesting bird species of the Western Hemisphere.

Bibliography

Fjeldså, J., and Krabbe, N., 1990. *Birds of the High Andes*. Svendborg: Zoological Museum, University of Copenhagen, and Apollo Books.

Hardy, D. R., and Hardy, S. P., 2008. White-winged Diuca Finch (Diuca speculifera) Nesting on Quelccaya Ice Cap, Perú. *Wilson Journal of Ornithology*, **120**, 613–617, doi:10.1676/06-165.1.

Irons, D. B., 1988. Black-legged Kittiwakes nest on advancing glacier. *Wilson Bulletin*, **100**, 324–325.

Johnson, A. W., 1967. *The birds of Chile and adjacent regions of Argentina, Bolivia and Perú*. Buenos Aires: Platt Establecimientos Gráficos, Vol. 2.

Krajick, K., 2002. Melting glaciers release ancient relics. *Science*, **296**, 454–456.

Niethammer, G., 1953. Zur Vogelwelt Boliviens. *Bonner Zoologische Beiträge*, **4**, 195–303.

GLACIER CAVE

Monohar Arora
National Institute of Hydrology (NIH), Rorkee, UA, India

Caves formed completely in ice are termed as glacier caves and are also very often called ice caves. Glacier caves almost always form from flowing water entering the glacier through cracks or crevasses, which are then enlarged over time, both by erosion and melting. Glacier caves serve as conduits for water through glaciers. Glacier caves are rarely extensive, and may come and go as glaciers recede. Glacier caves are very dynamic and change from year to year. Large glacier cave systems have disappeared as glaciers melt and retreat. The Paradise Glacier Cave system on Mt. Rainier was at one time several

kilometers long, but has melted away as the glacier has receded in recent decades of global warming. Glacier caves are also notoriously unstable, and people have been killed by chunks of falling ice. Glacier caves may be used by glaciologists to study the interior of glaciers. The study of glacier caves themselves is sometimes called glaciospeleology.

GLACIER FIELD STUDIES: IMPORTANT THINGS TO NOTICE

John F. Shroder
Department of Geography and Geology, University of Nebraska at Omaha, Omaha, NE, USA

Definition

Things to notice in field studies include a variety of structures and landforms of both ice and the rock substrate over which the ice rides and interacts.

Four important things

Several points to notice include the quick changeability of ice, whether the ice is present now or was in the past, problems of access onto glaciers, and whether work is to done above or below the equilibrium line.

Lability: In studies of glaciers in the field it is important to pay attention to the high lability of the ice; the fact that it changes more rapidly than any other landform, and what was there last season is likely to be significantly altered in this one. And safety is a paramount concern in such rapidly shifting environments, with deadly crevasses potentially opening up overnight to swallow up the unwary. Field work in these dynamic environments is always interesting and if done well, can be richly rewarding because there is so much to see and to record.

Glacierization versus glaciation: An important first step in glacier field studies is the recognition that two major approaches can be undertaken at the outset: (1) studies of *glacierization* wherein you are working mostly on the surface of any existing ice mass or around its edges, with rare deep probes through the use of drill cores, hotpoint penetration of the ice for installation of cameras, velocity tracking devices and other such internal monitors, and ice penetrating radar, or other remote-sensing techniques to investigate the ice interior; and, (2) studies of *glaciation* where you are observing the results of past glaciations on the rock substrate that was once beneath a thick ice cover. In either case, one is attempting to discover the fundamental ways in which natural processes produce the resulting landforms developed in and of the ice, or in bedrock and in the clastics derived from the bedrock and deposited on it.

Above and below equilibrium line: In working directly upon the ice itself, the position on the ice above or below the equilibrium line where one is located commonly determines what can be observed and some of what one can do, and it very much determines the level of safety and ease of transport from one location to another. Several additional variables that produce significant ice landforms and that control access and trafficability on the ice can also be divided into those above the equilibrium line and those below. Above the equilibrium lines in both alpine and continental ice masses, crevasses are commonly hidden beneath treacherous snow bridges and travel across such regions must be done carefully. In alpine environments above the equilibrium line, the chief dangers at the edges of the glaciers are avalanches of ice and snow down from the great heights on the peaks. At the equilibrium lines, slush avalanches of water-saturated snow on the glacier surface itself commonly transfer significant water and ice masses to lower elevations across the snow lines. Snow pits that are commonly dug to the depth of a few meters above the equilibrium line in mass balance studies reveal the annual increments of snow and firn accumulation that become glacial ice over in 5–10 years' time. Commonly passing through the equilibrium lines from higher to lower altitudes in alpine areas are the unstable ice-block seracs in ice falls, the wave ogives below them, and the lower elevation meltwater streams and lakes. In alpine areas, depending upon the level of lateral ice and snow avalanching that can provide profuse rock rubble to the glacier surface, various thicknesses of debris covers can result. Close to the end of the melt season in any area, the equilibrium lines can be marked where such rubble streams emerge from beneath the snows of the prior season. Above is the zone or accumulation, below, the zone of wastage.

The debris covers on alpine glaciers close to equilibrium lines commonly emerge as lateral moraines that can combine as medial moraines between two or more glaciers merge. These medial moraines at first maintain a certain lithological integrity that exactly samples whatever rock types existed in the surrounding rock walls above that particular ice stream. Further down the ice stream, such medial moraines can merge with others and eventually with the combining of many other tributary glaciers and continued ablation of the ice mass beneath the debris, a more pervasive debris cover results, in which all the sampled rock lithologies become rather chaotically mixed.

Glacier access: Travel over such debris-covered ice is much less dangerous than over the upper firnfields that bridge crevasses, but care must still be exerted where sub- or en-glacial water channels melt out unseen and unstable domes or other openings in the ice beneath thin debris covers thereby producing unsafe situations. In general the thicker the debris cover, and hence the greater its weight, the more stable it is likely to be to support human or pack animal transit. Aside from the shear difficulty of such travel across such potentially unstable rock blocks, however, the occasional shifting of debris covers down the fronts of melt-out ice cliffs also requires vigilance to avoid hazard. With work on surging glaciers, travel through the commonly bewildering and hazardous morass of crevasses may be quite impossible, but some transit can

be done along the common sinuous medial moraines that have also been produced by the surge.

Cold-based ice at high latitudes that is frozen to its bed can present other problems of access in that in many places it rests on the landscape with near vertical walls that are subject to periodic collapse. Once up on such ice, however, data collection can be reasonably straightforward, although care must still be exerted when near surficial meltwater channels, and glacial moulin or meltwater "swallowholes."

Where moving off the ice and onto the lateral margins of alpine or continental glaciers, lateral moraines of tills, and other ice-marginal phenomena are commonly encountered. These include all sorts of full and drained proglacial lakes; Gilbert-type deltas in these existing or former water bodies; kames and kame-terrace sediments that are sorted and stratified by the meltwaters; polygenetic eskers of sub-, en-, and supra-glacial origin, with or without internal ice; various outwash plains pocked with water-filled or dry kettle holes; and other such characteristic glacial landforms and sediments. Walking over these commonly water-saturated sediments can be interesting as they may not support such weight. Commonly in alpine environments with existing glacierization, or below the glacier termini, on the slopes above the existing ice, or in other nearby formerly glaciated valleys, a full suite of landforms and sediments will exit that help in interpretation of what is likely to be concealed beneath the present ice cover.

Summary

Important things to notice in glacier field studies are somewhat in the eye of the beholder but ice, sediment, and landforms can be highly varied and present a host of features to observe and record.

Cross-references

Crevasses
Debris-Covered Glaciers
Equilibrium-Line Altitude (ELA)
Moraine

GLACIER HYDROLOGY

Pratap Singh
Tahal Consulting Engineers Ltd, New Delhi, India

Glacier hydrology

Hydrology of glacierized catchments is being different from nonglacierized basin as usual, because of presence of seasonal snow and ice distribution within the catchments. The study of glaciers forms a part of surface-water hydrology, but because a part of runoff from snow and glaciers behaves like subsurface flow, groundwater hydrology concepts are also invoked. Flow in the stream is made up of the flow due to direct response of the basin to precipitation and the flow from snowmelt/glacier melt and baseflow components. Hydrology of glacierized catchments is an understanding of the Earth's physical processes, which regulate melting processes in hydrological cycle. In order to understand hydrology of glacierized catchments, it is important to understand the physics of snow and glacier melt with other components such as distribution of snow within catchment, energy, and mass balance components.

Any change in hydrological cycle altering implications of climate change, Glaciers are retreating, ice sheets are melting and collapsing, and early snowmelt is augmenting warming rates. Water has the property to move in a hydrological cycle in which it is moved throughout the Earth as it is taken in by plants and animals, condensed and precipitated, infiltrated, as well as by other processes. One of the most significant impacts of climate change is predicted to be shifts in storm intensities, a rise in sea level, and increasingly rapid snow and ice melt.

The runoff generated from the melting of glaciers plays a vital role on the rivers of the highland areas worldwide such as the Alps and the Himalayas and ensures the continuous availability of streamflow for hydropower projects. The snow and glacier melt runoff is considered as highly dependable flow and used for irrigation, drinking water, and generating hydropower particularly during summer, when demand is at peak for power and irrigation. It has been demonstrated that glaciers act as natural frozen reservoirs in the upper part of the basin and provide flows in a regulated manner for the operation of base load and peaking hydropower projects and fresh water supply in lowland areas.

Seasonal and diurnal variations

The presence of snow and glaciers in the upper part of the basins form a unique reservoir of fresh water. For example, in the Himalayan region, glacier meltwater supports rivers such as the Indus, the Ganga, and the Brahmaputra, which are the lifeline of millions of people. The water flowing in these Himalayan rivers is a combined flow from rain, snow, and glaciers. Snow and glacier runoff plays a vital role in making all these rivers perennial, whereas the rainfall contribution during monsoon period is critical for storages in various reservoirs. The summer and spring runoff, comprising mostly of snow melt and glacier melt is a source of water for irrigation, hydroelectric power production, and drinking water supply. Meltwater replenishes stock ponds, infiltrates the soils, and recharges the ground water. The runoff generated from the ground water storage becomes important during the lean season. The water yield of a high Himalayan basin is roughly double that from an equivalent basin area located in the peninsular part of India. This higher water yield is mainly due to the large inputs from the snow and glaciers.

Diurnal variation in streamflow generated from snow and glacier covered part of the basin provides an

understanding of drainage processes of the basin. The daily cycle of solar forcing yields major changes in snow and glacier melt and streamflow over the course of each day, and the difference between the time of highest melt rate and the time of peak discharge provides a measure of average runoff travel times through the river basin.

Discharge variation consists of a cycle of rising and falling flow superimposed on baseflow. A variation in discharge in a glacier-fed river occurs on hourly, daily, and annual cycles based on the prevailing weather systems. The pattern of hydrographs for different years shows very clearly that discharge starts increasing from May onward, reaches its maximum in July and August and after that it starts reducing. Both limbs of hydrograph are almost flat during early and later part of melt season. Rising and falling limbs of the hydrograph become steeper with advancement of the melt season but the rising limb of the hydrograph is always steeper than the recession limb. Such diurnal variations in hydrograph with season can be explained by the changes in physical features of the basin with time.

Runoff delaying and storage characteristics

The runoff from snow and glacier covered basins is mostly temperature controlled and behaves similarly to regulated flow from a water storage. A good estimation of runoff from such basins is very useful for the operation of run-of-the-river hydro projects. Snow and ice storage works as a natural frozen reservoir in the basin, which gradually releases the flow. During the summer period, in the glacier-fed streams only a portion of the meltwater produced each day emerges as runoff from the snout of the glacier on the same day. The remaining meltwater is stored within the glacier. Thus, a considerable contribution to streamflow is received from the meltwater stored in the glacier. Even at diurnal cycle, the runoff also contains a part of this stored meltwater. This shows that the streamflow of a glacier-fed stream is controlled by storage characteristics of the glacier and determined by delayed response of the basin. The size of the glacier, extent of snow cover, depth of snow over the glacier, and drainage network of the glacier are important factors that control the flow rate and volume of the water emerging as runoff. The discharge time response is also a function of the ablation and accumulation area ratio. Runoff dominated by meltwater from the accumulation area has a longer time of concentration as compared to the meltwater generated in the ablation area. The meltwater storage characteristics of two glaciers have been studied using continuous hourly discharge data. Daily (24-h) streamflow records have been subdivided into daytime flow (09:00–20:00 h) and nighttime flow (21:00–08:00 h). Monthly daytime and nighttime discharges for summer months for Gangotri Glacier in Garhwal Himalayas (Haritashya et al., 2006; Singh et al., 2010) are shown in Figure 1. The magnitude of the streamflow during daytime and nighttime indicates that the volume of the nighttime flow is comparable with the daytime flow. Such trends of the daytime and nighttime flows are observed for all the years. As such, very little or no melting takes place on the glacier surface during the night period, but still a high amount of discharge is observed in the stream during the nighttime. It shows that meltwater produced during the daytime is partly stored in the glacier and released later, while such trends in the rain-fed rivers do not exist. This analysis suggests that meltwater storage characteristics of the glacier are much stronger in the early part of the melt season and reduces as the melt season develops. Trends of variations in the ratio of daytime flow to nighttime flow with melt season can be explained on the basis of availability of snow cover on the glacier body and progressive development of the drainage network in the glacier. The greater extent of snow cover in the early part of the melt season along with a poorly developed drainage network amounts to a more delayed response of the meltwater from the basin to the outlet, resulting in reduced difference between daytime and nighttime streamflows. Reduction in the extent of snow cover area and progressive development of

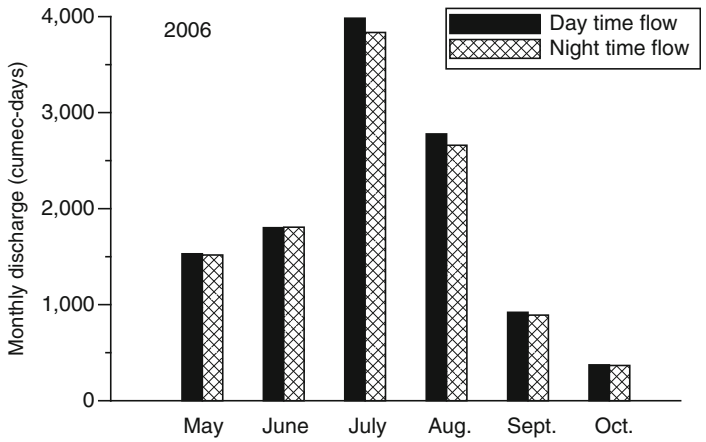

Glacier Hydrology, Figure 1 Monthly distribution of daytime and night time observed discharge near the snout of Gangotri Glacier (Uttarakhand) for summer 2006.

a drainage network with melt season also attribute to a faster response of meltwater in mid or late melt season, which also increases the difference in the daytime and nighttime flows.

Bibliography

Haritashya, U. K., Singh, P., Kumar, N., and Singh, Y., 2006. Hydrological importance of an unusual hazard in a mountainous basin: Flood and landslide. *Hydrological Processes*, **20**, 3147–3154.

Singh, P., Kumar, A., and Kishore, N., 2010. Meltwater storage and delaying characteristics of Gangotri Glacier (Indian Himalayas) during ablation season. *Hydrological Processes* (in press)

GLACIER LAKE OUTBURST FLOODS

Lasafam Iturrizaga
Department of Geography/High Mountain Geomorphology, Institute of Geography, University of Göttingen, Göttingen, Germany

Synonyms

Aluviones; Débâcles; Glacial outwash floods; Gletscherlauf (German); Jökulhlaup (Icelandic); Megafloods and superfloods (Quaternary large-scaled glacier floods)

Definition

Glacier lake outburst floods (GLOFs) refer to sudden and in some cases cyclic release of meltwater from a glacier-dammed or moraine-dammed lake, which can result in a catastrophic flood. Thorarinsson (1939) introduced the term "jökulhlaup" for glacial floods due to the cataclysmic drainage of subglacial lakes in Iceland. It was originally referred to outburst floods triggered by volcanic activity and has been subsequently transferred to a variety of other types of glacial floods. It has become a widely used synonym for describing catastrophic glacial floods in general.

The size of glacial lakes varies considerably and the lakes may hold up to tens of millions of cubic meters of water. Glacier lake outbursts produce flows of water that may be an order of magnitude greater than average rainfall-derived peak flows. Geomorphological impacts and damages of infrastructures can occur up to tens to hundreds of kilometers downstream. Their competence and capacity is high enough to transport large amounts of debris, so that they may occur as hyperconcentrated flow or even debris flow. Catastrophic dam failure may release the reservoir water over a time span of hours to days. Peak flows as high as 30,000 m^3 have been recorded for moraine-dammed lakes, but they are much higher for glacier-dammed lakes. In case the discharge exceeds a flood volume of about $>10^6$ m^3 or peak discharge $>10^6$ m^3/s (Martini et al., 2002; Korup and Tweed 2007) glacier lake outbursts are termed as megafloods. These extremely large paleofloods, which occurred mainly during the end of the Pleistocene, were also termed as superfloods (Rudoy, 2002). Glacier lake outbursts may be caused by different kinds of dam failures depending on the type of natural barrier (Clague and Evans, 1994; Tweed and Russell, 1999). Floods resulting from glacier lake outbursts may pose a severe threat to settlements and their infrastructure. As the spatial interconnection of glacier areas and sedttlement zones has generally increased in the last decades, new concepts and technologies in hazard assessment, evaluation, and mitigation have been developed (Richardson and Reynolds, 2000a, b; Huggel et al., 2004; Kääb et al., 2005a, b; Allen et al., 2009).

Introduction

Glacier lake outbursts have contributed to the largest flood events worldwide and caused large-scaled geomorphological landscape transformations with specific landform assemblages. Glacier lakes generally occur in all glaciated landscapes in different varieties and with specific trigger mechanisms in terms of their catastrophic outbursts. The appearance of glacier lakes and associated floods provide landscapes to study Pleistocene, Holocene, and historical glaciation extent and is therefore an important paleoclimatic key indicator for reconstructing landscape environments and past climate. Moreover, the formation of glacier lakes and subsequent outbursts provide an obvious indicator for glacier dynamics and fluctuations. A striking shift in the distribution pattern of glacier lakes has occurred in the course of the general worldwide glacier recession during the twentieth century. In many glacierized areas, the glacier wastage produced an increase in the number of glacier lakes and lead consequently to an aggravation of the glacier hazard situation of the more and more densely populated glacier forefields and forelands. This is especially true for glaciers that are exploited economically in terms of irrigation and hydropower. Therefore, research on the controlling factors on the development of glacier lakes and glacier lake outbursts in regard to hazard mitigation has increased exponentially in the last decade. Nevertheless, in some regions the glacier recession has caused the disappearance of glacier lakes and produced a decline of glacial flood inundations.

Extensive review papers have been written on different topics of glacier lakes and outbursts (Blachut and Ballanytyne, 1976; Tweed and Russell, 1999; Herget, 2003) providing preferentially case examples from the higher latitudes. This entry gives an overview of the main types of glacier lakes with a special emphasis on lakes in high mountain regions, i.e., on floods occurring in more confined valleys. Glacial lakes are generally impounded either by a glacier or by a moraine or they occur in proglacial depressions caused by glacial overdeepening in the bedrock or sediment. The source area of the lake water may be the meltwater of the damming glacier or the adjacent glaciers. At temperate glaciers, large amounts of meltwater originate as well from basal melting

(Benn and Evans, 1998). The lake size ranges from several square meters up to a million of square kilometers. In principle, three different types of lakes are distinguished: (a) glacier-dammed lakes, (b) moraine-dammed lakes, and (c) internal glacial lakes. Internal glacial lakes (englacial and subglacial) have been discussed elsewhere in this encyclopedia.

Worldwide distribution of glacier lakes prone to lake outbursts

Recent glacier-dammed, moraine-dammed, and internal glacial lakes arise at different scales in the glacierized landscapes of all geographical latitudes. In this regard, regional individual distribution patterns are recognizable (Figure 1). They are a response of the glacier type and therefore of the climatic-controlled nourishment conditions of the glacier, the glacier size, the topographical conditions, and the debris transfer system.

In the Tropics, moraine-dammed lakes occur especially in the Peruvian Andes in the Cordillera Blanca (Huascaran Massif) (8°–10°S) (Ames, 1998). In particular the small, clean-ice glaciers have shrinked rapidly in the last decades due to the fact that they are subject to a all-season ablation regime in the lower glacier parts (Kaser and Osmaston, 2002). In the course of the twentieth century, some of the most devastating glacier lake outbursts have occurred in this region (Carey, 2005; Vilímek et al., 2005). In the inner Tropics, North of 8°S glacier lakes are mostly absent. The topographical preconditions on the steep-sided volcanoes with their small mountaintop glaciations prove to be unfavorable for the formation of moraine and glacier-dammed lakes.

A further distribution area of moraine-dammed lakes is located in subtropical latitude between 28°–34°N in the Himalaya Range, especially in Nepal, Bhutan, and China. The Environmental Programme of the United Nations (UNEP) and the International Centre of Integrated Mountain Development (ICIMOD) have monitored 2,323 glacier lakes in Nepal (Mool et al., 2002a, b). In contrary, in the westward adjacent Karakoram (35–36°N) glacier-dammed lakes are the main type of glacier lakes, mainly generated by advancing tributary glaciers (Hewitt, 1982; Iturrizaga, 2005a, b, c). High-magnitude glacier floods occurred especially at the end of the Little Ice Age until the 1930s. Even nowadays, glacier lake outbursts happen, but to a far lesser extent. In the mid latitudes, such as in the European Alps or the Canadian Rockies with a comparative smaller glacierized area and shorter glaciers, moraine-dammed lakes and numerous new cirque lakes have formed in overdeepened rock and sediment basins (e.g., Trift glacier, Swiss Alps). Another principal distribution area of glacier-dammed lakes is located in the high latitudes (about 60°N) in Alaska (e.g., Abyss Lake) (Post and Mayo, 1971; Stone, 1963; Sturm et al., 1987). The often dendritic trunk glaciers impound the meltwater of their retreating tributary glaciers. Further ice-dammed lakes can be found in Greenland (Russell, 2007) and to a lesser extent in Norway (Howarth, 1968; Knudsen and Theakstone, 1988; Russell, 1994; Breien et al., 2008).

In regard to the hypsometric distribution, glacier-dammed lakes occur from sea level in polar regions up to the high altitudes of the extreme high mountain areas. The largest lakes are located mostly up to 1,500 m below the equilibrium altitude line (ELA), where the meltwater of extensive catchment areas may be impounded by the natural dams. The moraine-dammed lakes arise commonly in the lower part of the ablation area of the glaciers. Some of the highest moraine-dammed lakes appear in the Chinese Himalayas at 5,700 m a.s.l. (Longbasaba and Pida lakes, Xin et al., 2008). The different thermal regimes of

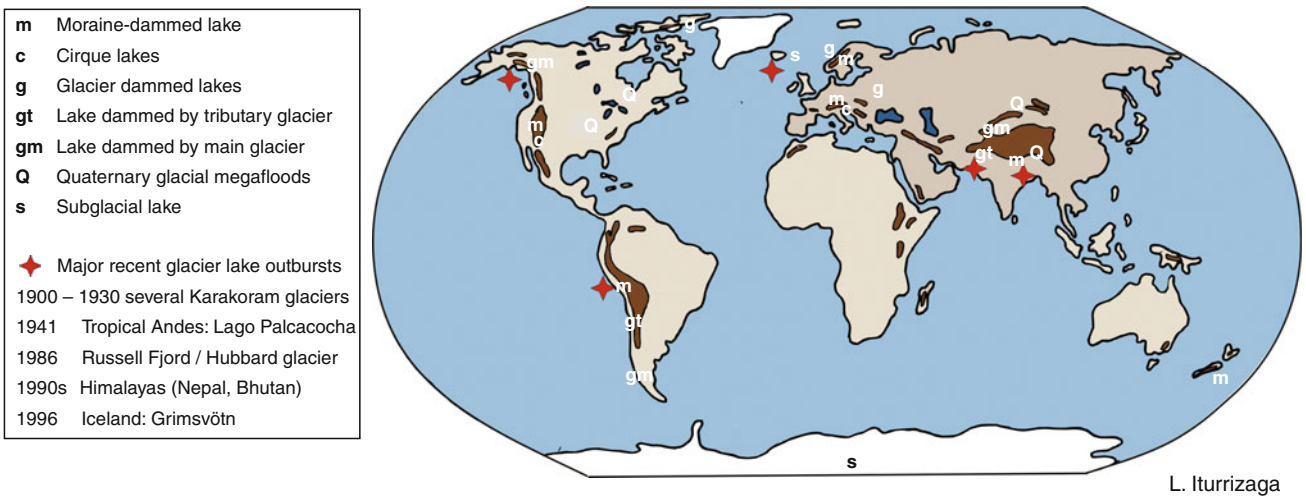

Glacier Lake Outburst Floods, Figure 1 Recent worldwide distribution of glacier lakes and potential glacier lake outbursts areas as well as key localities of Quaternary megafloods. Internal glacier lakes (supraglacial, englacial, subglacial) may exist at all glaciers causing catastrophic floods.

the glaciers (cold and temperate glaciers) have different characteristics for lake formation and corresponding outburst mechanisms.

Quaternary glacier-dammed lakes (megafloods)

Glacier lake outbursts originating from glacier-dammed lakes have contributed to the largest and geomorphologically most significant flood events in the Quaternary (O'Connor and Costa, 2004). During the outbursts of megafloods, gigantic landscape transformations have taken place in only a few hours or days similar to volcanic eruptions, tsunamis, or earthquakes.

After an initial disagreement with the scientific main stream, the reconstruction of the Missoula Flood in North America by Bretz (1923) got widely accepted (Baker et al., 1988). The Missoula Flood area has become a key locality for the landform assemblages of cataclysmic floods. At the end of the Pleistocene before about 16 ka, a southern ice lobe of the Laurentide Ice Sheet impounded during the Wisconsin-Glaciation the Clark Fork River. The maximum lake volume of the Lake Missoula amounted up to 2,184 km^3 with a lake depth of 635 m at the ice dam (Baker and Bunker, 1985). Repetitive lake outbursts showed peak discharges in the order of about 17×10^6 m^3/s (for comparison the Amazonas has a discharge of 370,000 m^3/s, 1953). The Missoula Flood left behind characteristic landforms consisting of (a) erosional forms (Scabland topography, Bretz, 1923) (e.g., cataract complexes, dry falls, spillways, cavitations, P-forms, shorelines) as well as (b) depositional forms (expansion, longitudinal, point and pendant bars, eddy bars, slackwater deposits, and giant or mega ripples).

A Holocene proglacial lake formed at the southern margin of the Laurentide Ice Sheet before about 12 ka, the Lake Agassiz (Clarke et al., 2003), which covered an area of about 1 Mio. km^2 with a water volume of 163,000 km^3 (Teller et al., 2002). The lake drained catastrophically at 8.45 ka into the Hudson Bay. The glacier lake outbursts supposed to be one of the main trigger of the 8.2 ka cooling event. The incoming fresh water from the ice-dammed lake caused a desalinization of the North-Atlantic and lead to the subsequent collapse of the Gulf stream (Clarke et al., 2003). This event accelerated the debate of climate change.

Glacier lakes occurred during the early and middle Weichselian (90–80 ka) and (60–50 ka) at the ice front of the Scandinavian Ice Sheet in Western Russia as well as at the southern margin of the ice sheet, which covered parts of the Barents and Kara Lake (Grosswald, 1980; Mangerud et al., 2004) outreached by far the size of present glacial lakes. It is assumed, that their outbreak had a significant impact on the sea ice formation in the Arctic Ocean and on the regional climate.

A different type locality for the outbreak of glacier-dammed lakes is situated in the Altai Mountains (Southern Siberia) (Baker et al., 1993; Rudoy, 2002; Carling et al., 2002). A glacier dam, 15 km long and several kilometers in width, impounded repetitively the drainage of the Chuja and Kuray Basins and formed a glacial lake (607 km^3) with a maximum depth of 650 m at the ice barrier. The last cataclysmic glacier lake outbursts happened 13 ka during ELA-depressions of 800–1,200 m. The lakes were still in existence about 5 ka. These glacial superfloods had a discharge of about 18×10^6 m^3/s and boulders with a diameter of 11 m have been transported. The outburst landscape is similar to that of the Missoula Flood. Moreover, huge fluvial gravel dunes or megaripples (giant current ripple relief) have been deposited in the Chuja Basin, which are up to 23 m high and 320 m long, and giant diluvial ramparts and terraces-bars (Photos 1 and 2). Interestingly, the landforms have been previously mistaken for glacial deposits. The reconstruction of megafloods in North America and

Glacier Lake Outburst Floods, Photo 1 Megaflood deposits in the Altai mountains (Southern Siberia). Giant ripples in the Chuya Basin.

Glacier Lake Outburst Floods, Photo 2 Megaflood deposits in the Altai mountains (Southern Siberia). Giant gravel terraces at the Katun River (Photos: L. Iturrizaga, August 1995).

Siberia has been the base for interpreting landforms of paleofloods on Mars (Baker, 2001; Fairen and Dohm, 2003).

In the extreme high mountain ranges, such as in High Asia, the number of glacier dams may have been higher than today during the deglaciation of the Last Glacial Maximum (LGM) and during Postglacial times. This is shown by expansive lake sediment sequences throughout the Karakoram valleys (Paffen et al., 1956; Owen, 1996; Cornwell, 1998), such as Lake Guricot in the Astor Valley (Scott, 1992), the Malungutti lake in the Shimshal valley (Iturrizaga, 2005c) and in the lower Chapursan valley (Iturrizaga, 2008). Already in the end of the nineteenth century, glacial lake outburst floods have been discussed as transport agent for the "Punjab erratic boulders" located in the Peshawar Basin at altitudes of only 300–400 m a.s.l. (Cornwell, 1998). As source area of these boulders has been considered a 750 m high ice dam, the Darel-Shatial-moraine in the Indus valley at about 900 m a.s.l. (Bürgisser et al., 1982; Burbank, 1983; Desio and Orombelli, 1983; Shroder et al., 1989; Cornwell, 1998), which would be one of the largest Pleistocene ice barriers in High Asia. In the basin of Chilas, megaripples have been identified (Shroder et al., 1989). However, not only ice-dammed lakes have produced high-magnitude floods in the Indus valley but also landslides, such as the Lichar landslide in 1841, close to the western side of the Nanga Parbat area, 30 km south of Bunji, which reached down to 300 km south of Attock (Shroder, 1993). This fact makes it rather difficult to unravel the source areas of specific flood deposits. In this regard, it has been argued that many of the dams considered as glacier dams, such as the 600 m high Katzarah glacier dam (Dainelli, 1922), were not stable enough to impound a lake of a size of over 170 km. It is doubtful that ice dams provide the conditions for the undisturbed deposition of lake sediments of the size of several hundred meters in thickness (Hewitt, 1998). According to this argument, the existence of rock avalanche barriers is more likely than glacier barriers. The lakes in High Asia have been much smaller in size than those described from Northern America and Northern Eurasia, but due to the high relief energies the outburst floods might have had a tremendous geomorphological impact.

Megafloods have been as well proposed for the outlet glaciers of the Pleistocene (LGM) south Tibetan ice sheet between Cho Oyu and Shisha Pangma (Kuhle, 2002). New field evidence showed further Holocene moraine dams, which may have caused giant (1,011 m^3) lakes with a maximum depth of 680 m in the Tsangpo River gorge in Tibet (Montgomery et al., 2004) with peak discharges higher than the Missoula and Altai floods.

Glacier-dammed lakes

Glacier-dammed lakes may be impounded by the trunk and tributary glacier in different topographical constellations or by small lateroglacial ice lobes. They are also known as ice-dammed lakes in the literature (Blachut and Ballantyne, 1976; Tweed and Russell, 1999). However, glacier barriers of the subtropical high mountain regions are characterized by a high content of debris incorporated in the supraglacial and lateral moraines. This debris material plays a vital role in the mechanics of the glacier lake outbursts and during the subsequent flood events. Therefore, the initial water flood may transform into a hyperconcentrated flow and finally in some cases into a debris flow. For this reason, the superordinated term "glacier-dammed lake" is used, to which the ice-dammed lakes are subordinated. The latter occurs mainly in high latitudes in moderate to low mountain relief with comparatively little glacial sediment transfer. Glacier-dammed lakes are in most cases a reaction of glacier front oscillations and form generally during periods of glacier advance. On a wider time scale, they occur especially during the wastage of an ice-stream network in the transition to individual valley glaciers (Figure 2).

Glacier-dammed lakes are at present time comparatively short-lived and survive often only several months or years. Therefore, lake sediments are rarely deposited. The lake basins fill up rather quickly. Subsequently, a catastrophic drainage may occur. They empty commonly in summer time at the period of highest meltwater discharge.

Types of glacier dams

Tweed and Russell (1999) have summarized the existing classifications of types of glacier-dammed lakes in regard to their topographical settings (Maag, 1969; Blachut and Ballantyne, 1976; Costa and Schuster, 1988) and added the subglacial calderas and englacial or subglacial water bodies as result of volcanic activity.

In principle, the following main categories of glacier dams are differentiated representing the source areas for most of the present glacier lake outbursts.

Tributary glacier dam

A tributary glacier advances into the trunk valley and impounds the river converting it into a lake (Photos 3 and 4). The length of the cross-valley barrier amounts generally not more than 1–2 km with an absolute height of about 250 m. The lowest point of the glacier barrier is located in the contact zone of the glacier tongue and the adjacent valley flank. This is the locality, where the dam may fail in different ways. During a long-lasting glacier terminus position, the glacier may be framed by lateral moraines, which then are an important part of the glacier dam. In case of a glacier advance, the glacier tongue is commonly heavy crevassed. The lateral moraine acts as an additional and rather impermeable barrier.

At present time, tributary glacier barriers are widely distributed in the Karakoram and Hindukush Mountains (Figure 3), which show the greatest glaciation with the longest valley glaciers outside of the polar region. The LGM-ice-stream network (Derbyshire et al., 1984; Kuhle, 2001) has disintegrated into numerous valley glaciers during the deglaciation, which are as long as 72 km (Siachen glacier).

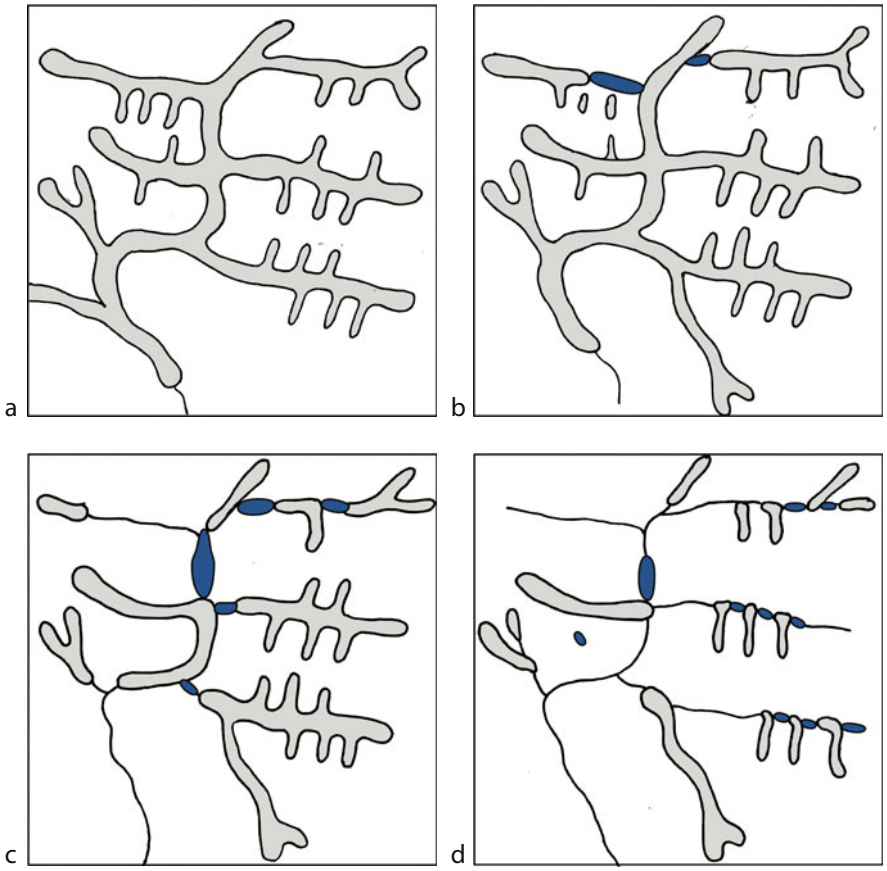

Glacier Lake Outburst Floods, Figure 2 Disintegration of an ice-stream network (**a**) into individual valley glaciers and the transition from main valley glacier-dammed lakes (**b**) to tributary glacier-dammed lakes (**d**). Stage (**c**) shows transitional forms of tributary glacier lakes and proglacial moraine-dammed lakes (double dam formation, cf. Figure 10).

Glacier Lake Outburst Floods, Photo 3 Glacier dams in the Karakoram Mountains. The Khurdopin glacier (47 km long) has been notorious for glacier lake outburst in the twentieth century. The photo shows the 3 km long debris-covered glacier tongue and the Virjerab lake basin. The Virjerab river drains even today subglacially (Photo: L. Iturrizaga, 18.07.2001).

Glacier Lake Outburst Floods, Photo 4 Multiple glacier dams in the Hindukush Mountains. The Chillinji glacier has blocked the Karambar valley about 100 years ago. The glacier tongue is surrounded by up to 250 m high lateral moraines. During dam failure the moraine material is transported with the flood waters causing in some cases hyperconcentrated flows. Most of the Karakoram and Hindukush glaciers are avalanche fed glaciers and highly dynamic (Photo: L. Iturrizaga, 09.2002).

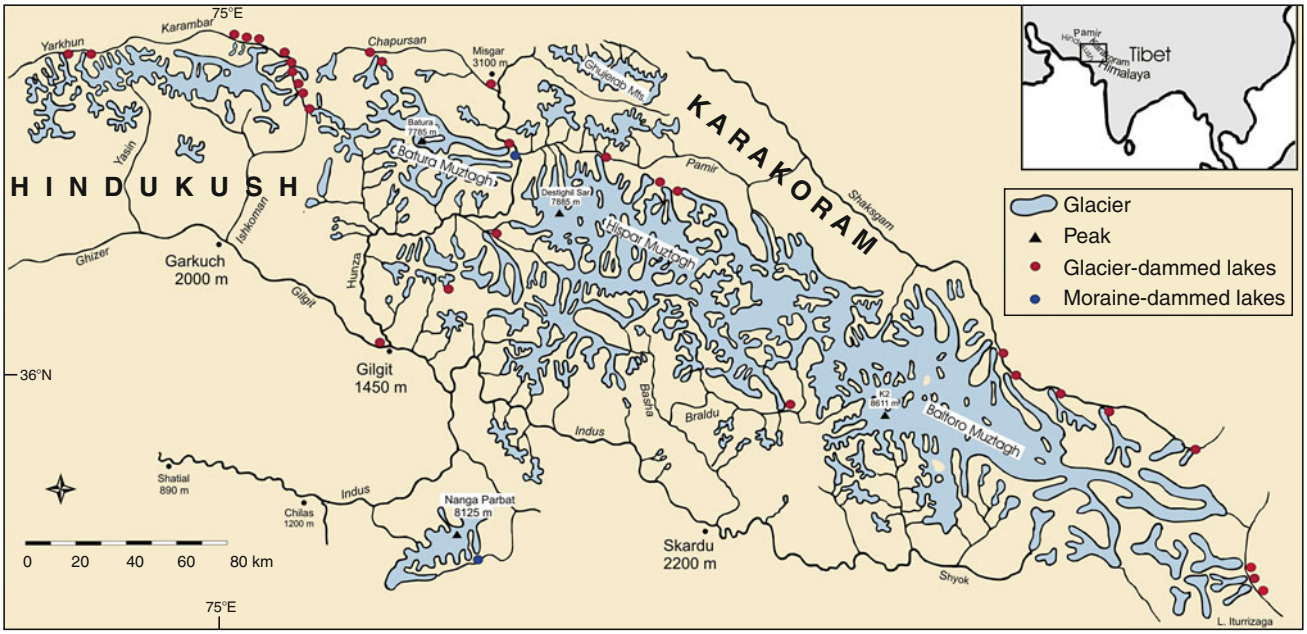

Glacier Lake Outburst Floods, Figure 3 Distribution of glacier-dammed lakes in the Karakoram and E-Hindukush Mountains.

In historical times, about 22 tributary glaciers formed glacier-dammed lakes in the upper Indus catchment area, from which 12 dams were responsible for outburst floods (Hewitt, 1998). Since 1826, 35 glacier lake outbursts have been monitored (Hewitt, 1982), although this number only includes a small selection of past flood events. Two localities were notorious for glacier lake outbursts in the last two centuries: the tributary glaciers of the Shyok valley (East Karakoram) (Mason, 1935; Hewitt, 1982; Feng Qinghua, 1991) as well as side glaciers of the Shimshal valley (North West Karakoram) (Iturrizaga, 1997, 2005c) (Figure 3, Photo 3). The topographic setting is at the current stage of glaciation in the Hindukush–Karakoram region favorable for the formation of this dam type: Tributary glaciers with catchment areas of over 7,000 m in height descend down to low altitudes below 3,000 m into the glacier-free trunk valleys and block temporarily the main river. A remarkable large number of glaciers terminate at confluence positions. Among them occur a lot of white, transversal glaciers in N-aspect. The Karakoram rivers show discharge rates of up to 1,000 m^3/s (Ferguson, 1984). Therefore large-sized lakes, several kilometers in length, may be impounded in a short time period. Lake volumes of up to 3.3×10^9 m^3 are reported from prehistorical glacier dams (Hewitt, 1982). In this region, a seasonal pattern dominates the outburst chronologies. The failures of glacier-dammed lakes mostly occurred between July and August during the time of the highest discharge. Most of the dams fail periodically with irregular possible return intervals of about 1–2 years. The lakes often drain in successive years due to internal changes in the ice barrier itself.

In some valleys, numerous tributary glaciers have formed glacier barriers in the same main valley, so that several glacier lakes may have existed synchronously (Figure 4). In this topographical constellation, an outburst of an upstream-located glacier lake may have triggered the sudden drainage of a lower glacier lake and therefore induced a glacier lake outburst cascade (Iturrizaga, 2005b). Moreover during those flood events, backwater lakes may form further downstream at valley constrictions (Figure 4). In the Karambar valley (Hindukush) at several locations, even about 100 km downward of the glacier dam, backwater lakes developed (Iturrizaga, 2006, Figure 5).

Glacier-dammed lakes are often formed rather spontaneously by surging glacier (Iturrizaga, 2011). In the Aconcagua Mountain Range (Argentinean Andes), the Grande del Nevado Glacier (8 km long), terminating at 3,165 m and flowing down from Cerro de Rio Blanco, has impounded the Rio Plomo and transformed it into a lake, measuring 60×10^6 m^3 in size (Helbig, 1935; Espizúa and Bengochea, 1990). The outbreak in January 1934 produced a flood wave with a run-out-distance of 150 km. In 1984/1985, the Grande del Nevado Glacier has advanced about 2.7 km in less than in 2 months leading to a lake with a surface of over 3 km^2 (Espizua and Bengochea, 1990).

Main valley glacier dam

A main valley glacier barrier blocks the discharge of one or more of its surrounding glaciers in its catchment area.

1. This may be the case when a tributary glacier recedes from a dendritic main glacier (e.g., Tulsequah Glacier

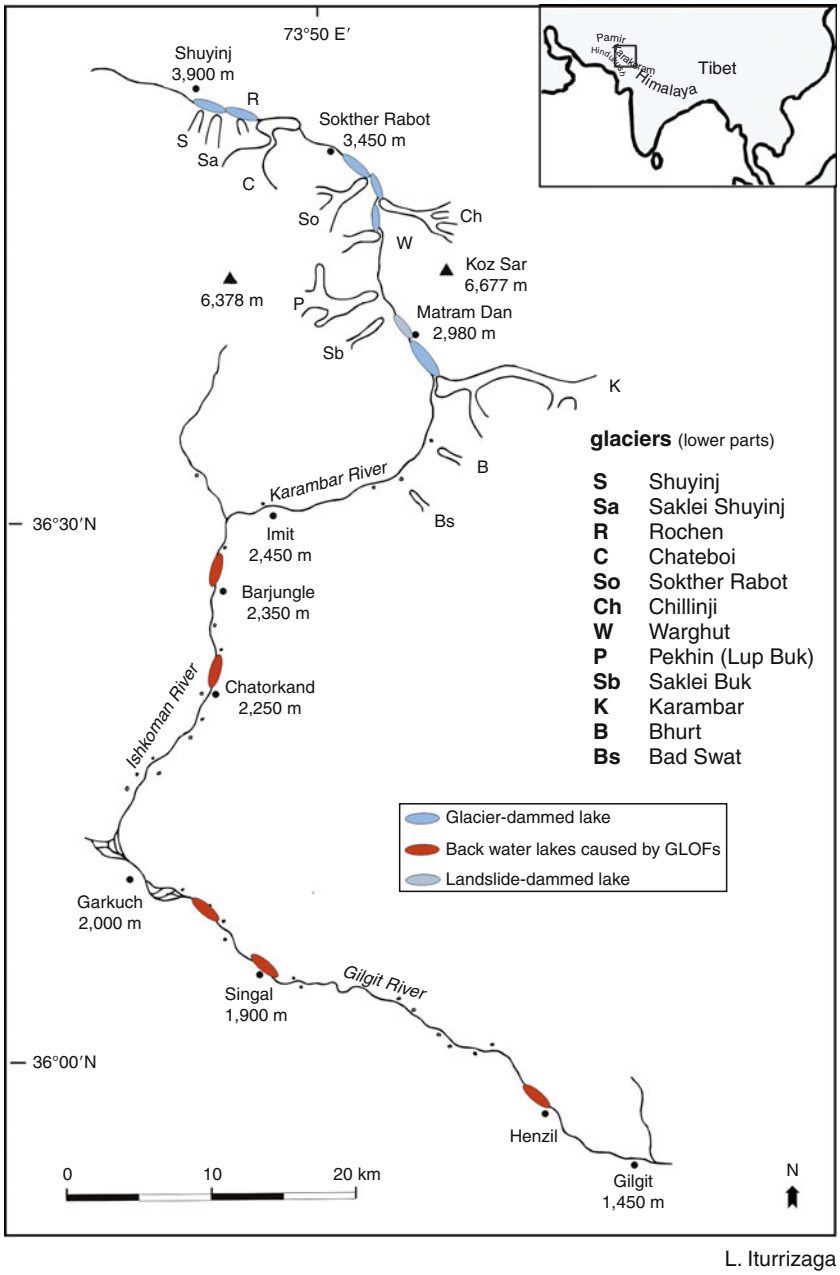

Glacier Lake Outburst Floods, Figure 4 Multiple glacier dams in the Karambar valley in the Hindukush Mountains.

Lake, 195 m in depth, British Columbia, Marcus (1960), Inyltschik glacier, Merzbacher Lake, Tienshan with a depth of 130 m, a length of 4 km, and a width of about 1 km, Mayer et al., 2008). The main distribution area of the glacier dam type is located in Alaska, where over 750 glacier lakes have been monitored (Stone, 1963). The glacier tongues terminate often at sea level and are formed by tidewater glaciers. In case of potential glacier lake outbursts, the run-out-distances are comparatively little. The ice-dammed Lake George (65 km^2), 50 m in depth, impounded by the Knik glacier, east of Anchorage in the Chugach Mountains, showed large annual outbreaks from 1918 to 1967 (Post and Mayo, 1971; O'Connor and Costa, 1993) as a result of downwasting of the ice barrier. Its lake basin is (Inner Lake George) created by an end moraine from the tributary glacier, named Colony glacier. The end moraines are deposited against the lateral margin of the ice barrier of the Knik glacier.

A well-known example from the Alps for the main valley glacier dam is the Lake Märjelen (2,350 m a.s.l.), which was impounded by the longest glacier of

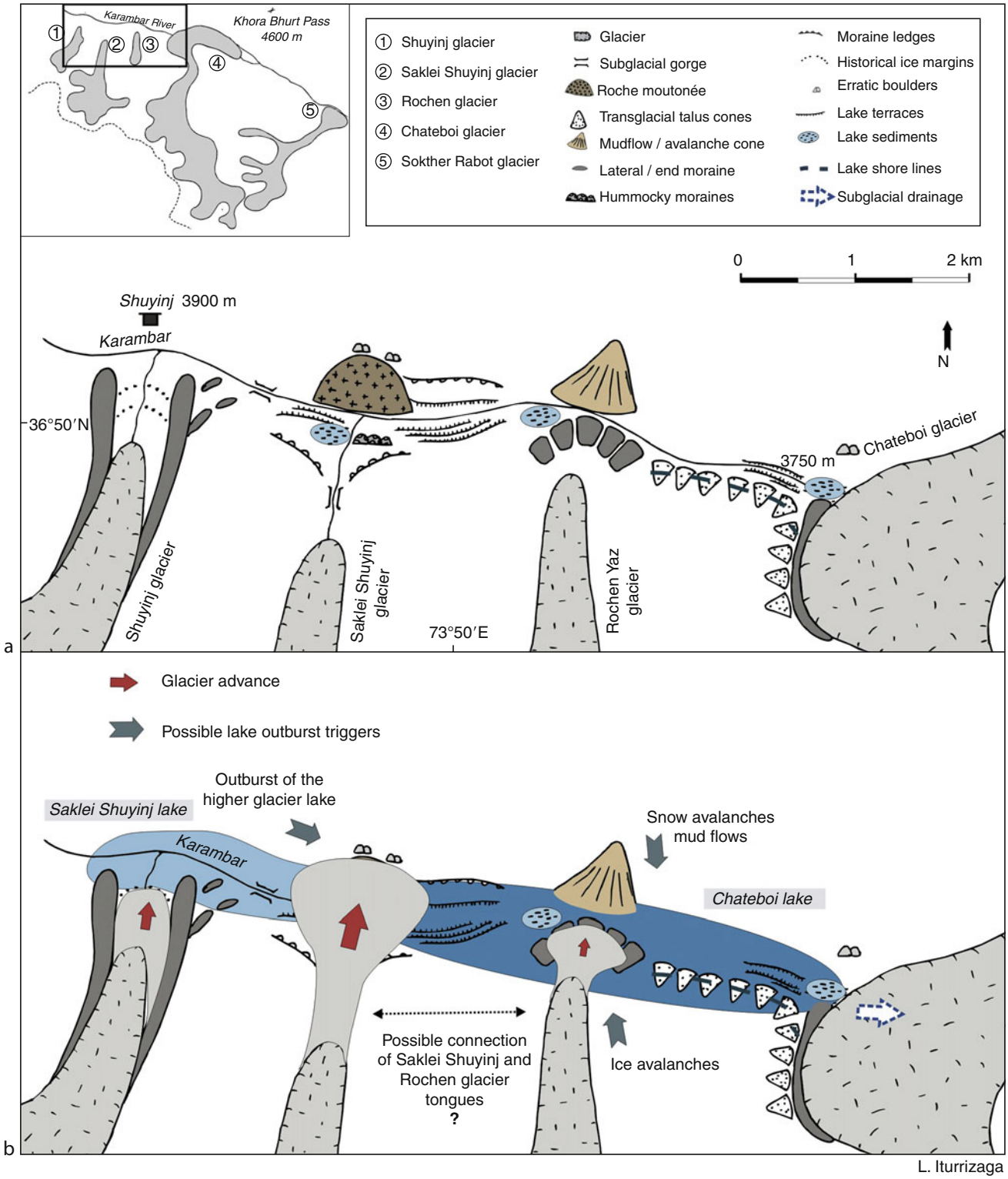

Glacier Lake Outburst Floods, Figure 5 Glacier-dammed lake formation by small tributary glaciers in the upper Karambar valley (Hindukush).

the Alps, the Aletsch glacier, at its margin. It is a transitional form between a lake dammed by the main glacier and a lateroglacial lake. About 25 glacier lake outbursts occurred in-between 1816 and 1896 and devastated the Massa valley downvalley.

2. A main valley glacier barrier may also be formed by the advance of the main glacier, sealing off the discharge of the less or non-glaciated side valleys that show mostly lower catchment areas. This type of glacier barrier is at present rather rare.

Lateroglacial glacier-dammed lakes

At some glaciers, small ice lobes form at the glacier margin in times of irregular ice flow are known as ice-marginal lakes. However, in order to define the lateral location and excluding the proglacial location, the term "lateroglacial" had been introduced (Iturrizaga, 2003, 2007). These ice lobes may in turn block the creeks of the lateroglacial valleys, which flow parallel to the glacier. These lakes mostly drain subglacially through the main glacier. Due to their small volume they do not generally generate high-magnitude floods, but nevertheless they are hazardous.

A special case are lakes that are caused by ice avalanches (Gietro Glacier, European Alps), which may reform as regenerated glaciers at the base of the mountain. In 1595, an outburst flood killed about 140 people in the Val de Bagnes (Tufnell, 1984).

Trigger mechanisms for dam failures of glacier-dammed lakes

Commonly glaciers experience a variety of trigger mechanism, such as fluctuations in ice-dam thickness and length and varying water supply. The initial dam failure often takes places by sub- and englacial gradual widening of the internal glacial conduits due to frictional heat and erosion (Nye, 1976) or by flotation of the ice dam (Thorarinsson, 1939). A variety of trigger mechanisms have been discussed. Most of the assumptions are rather theoretical for the individual glacier lake outburst as direct observations of dam failures are extremely seldom. Trigger mechanisms for dam failures have been mainly described on the base examples of glaciers of higher latitudes. The following listing provides an overview about the main causes of dam failure (Tweed and Russell, 1999):

Simple overspilling

When the lake depth overtops the glacier barrier, supraglacial drainage may take place. Predestined for processes of overspilling of the dam are cold-based glaciers, which are frozen to their glacier bed and characterized by a dry and dense ice, so that they are more impermeable for water (Liestøl, 1956). Moreover, a high debris content of the glacier supposed to be favorable for increasing the density of the glacier and preventing flotation processes (Knight, 1999). Highly crevassed glaciers, which are very common among advancing glaciers, are unfavorable for this outburst mechanism. Overspill processes may be generated by mass movements falling into the glacier lake and causing subsequent displacement waves.

Hydrostatic flotation of the glacier dam

Hydrostatic flotation of the glacier dam is a function of the specific density of glacier ice and water and may be altered by the debris content in the glacier ice. The buoying effect of the ice takes place when the water column of the lake has reached about 90% of the height of the glacier dam (Thorarinsson, 1939). The presence of debris may influence this process, as it increases the density of the ice. Subglacial hollows, which develop under thin glaciers especially at obstacles, may be opened and act as major drainage pathways. After the uplift of the ice barrier, a progressive base water flow occurs at the glacier bed. The emptying of the lake is dependent on the transport capacity of the subglacial channel. The process of flotation was described in detail for the subglacial lake drainage at Grimsvötn in Iceland (Thorarinsson, 1953).

GLEN mechanism

The GLEN mechanism (Glen, 1954) is based upon the assumption that the water pressure of the lake may deform the glacier ice and therefore creates or opens drainage channels at the base of the glacier through the ice, whereby frictional melting processes are involved. At a certain critical height of the water column, the horizontal stress exceeds the vertical stress by the amount of P.

$$P = (pw - pi)\, gh$$

where pw is density of the water, pi is density of the ice, g is gravitational acceleration, and h is height of the water column.

The critical height has been controversially discussed, but generally it is assumed that a height of 150–200 m (Glen, 1954) is necessary for plastic deformation of the glacier ice to operate at the base of the glacier.

Subaerial breach-widening

During the process of subaerial breach-widening, the glacier dam ruptures suddenly or is detached from the adjacent valley flank. Subaerial breach-widening is supposed to be a common outburst trigger in the European Alps (Häberli, 1983) and at glaciers in Alaska (Stone, 1963). It mainly occurs at tributary glaciers that have advanced into main valley. The melting may take place in the contact zone between rock and ice (Walder and Costa, 1996). After the dam break, typically a short, but high-magnitude flood is released from the lake.

The break of the Chong Khumdum glacier in the Karakoram is a case example for a sudden break of the dam (Hewitt, 1982), even though the drainage has been initially started through subglacial drainage conduits.

Subglacial volcanic activity

Subglacial volcanic activity may generate subglacial geothermal heat leading to a thinning of the ice dam or warm

up of the lake water. Moreover, it may accelerate the melting of englacial and subglacial drainage tunnels. A volcanic eruption destabilizes the glacier barrier or even may disrupt it completely (Björnsson, 2003; Magnús, 1997).

Siphoning effect

The mechanism of siphoning at glacier dams is based on changes in water pressure conditions in an existent sub- and englacial drainage system within the glacier barrier (Whalley, 1971) with that the glacier lake is connected. The siphoning process is launched, when the water pressure in the lake exceeds the water pressure of the drainage system. The difference in hydrostatic pressure results in a kind of pull effect caused by the subglacial drainage system. Subsequently, the lake is emptied through the internal conduits in the glacier. At the end of the ablation area, the pressure in the englacial drainage channels is to be lesser than in the lake and the lake may be initiated to drain. It is assumed that the drainage terminates when the pressure conditions are inverted again.

Seismic activity

As in all failures of natural dams, seismic activity in the form of earthquakes and faulting may be involved in the destabilization of the glacier barrier. However, there are few recent examples to underpin this obvious causal relation.

As shown in many natural settings, a combination of the individual trigger mechanisms is highly probable. Moreover, different trigger mechanisms could be responsible for repetitive lake outbursts from same glacier dam.

Moraine-dammed lakes

Moraine-dammed lakes are at their present extent a rather young geomorphological landform. In the textbooks of glacier science of the mid-twentieth century, they have been hardly mentioned as a type of glacial lake. Moraine dam failures resulted in devastating destructions of settlement areas, infrastructure, and loss of human life.

Moraine-dammed lakes are impounded in-between the end moraine complex and the vanishing glacier tongue (Photos 5 and 6). In general, moraine-dammed lakes may be classified in two types that may occur (a) at steep hanging glaciers and (b) at more gently inclined valley glaciers (Figure 6). Smaller lakes are typically associated with shorter and steeper glaciers. Glacier shrinkage commonly takes place by thinning and subsequent ice frontal retreat. In the final stage, the glacier tongue may lose the contact to the lake. The majority of moraine-dammed lakes are retained by moraines of Neoglacial Times and the Little Ice Age. The horizontal extent of the lake is limited along cirque glaciers by the toe of the head wall. At valley glaciers, the maximum reported length for any lake in the Himalayas is about 3.3 km at the Lake Tsho Rolpa (Nepal).

The terminal moraine complex consists of the end moraine, the laterofrontal moraine, and the lateral moraine

Glacier Lake Outburst Floods, Photo 5 Moraine-dammed lakes. Moraine-dammed lake at the Morsarjökull (Iceland) which is dammed by several end moraines. Glaciotectonic processes played a role in forming the depression upstrream of the end moraine complex (Photo: L. Iturrizaga, 09.07.2003).

Glacier Lake Outburst Floods, Photo 6 Moraine-dammed lakes. Moraine-dammed lake basin at the base of the Kanchenjunga South Side (Sikkim Himalaya). The lake has outbursted and left behind the characterical V-shaped incision of the end moraine and a debris flow cone (Photo: L. Iturrizaga, 09.04.2002).

(Figure 7). The end moraine may be the result of a single glacier advance or of several subsequent glacier advances. The inner slopes of the moraines are predominantly extremely oversteepened (up to 80°) and the outer slopes are mostly inclined more gently (20°–35°). The absolute height of the end moraine reaches up to 200 m, whereby the actual dam height of the lake is much smaller. The moraine embracement is often intersected in a narrow and highly instable ridge. The composition of the sediment matrix is diamict. The higher the compaction and the smaller the porosity, the more stable is generally the dam. Glacier lakes in old tongue basins from pre-Neoglacial times are in principle rather stable. Dead ice cores and permafrost lenses may contribute significantly

to the stability of the dam. Water outlets at the outer slopes of the lateral moraines, showing a lesser temperature than the glacier lake, may indicate the presence of ice lenses within the moraine (Lliboutry et al., 1977). Moraine dams may entirely be closed (Tap glacier, Himalaya) or they may also be markedly incised and show a permanent outlet (Müller glacier, New Zealand).

The main distribution areas of hazardous moraine-dammed lakes are the Himalayas and the Andes. In Nepal, over 2,000 glacier lakes exist, of which about 20 have been classified as hazardous. The largest lakes are the Tsho Rolpa, Imja, Lower Barun, and Thulagi lakes, which are situated at an altitude between 4,000 and 5,000 m. The Tsho Rolpa (76×10^6 m^3) with a depth of 130 m and a width of 500 m, is located at an altitude of 4,580 m at the head of the Rolwaling valley and has formed during the last 40 years at the glacier tongue of the Trakarding Glacier (Everest, Nepal) (Figure 8) (Yamada, 1998; Reynolds, 1999). In the Rolwaling valley, the height of the valley floor decreases from 4,500 m to 1,700 m at the confluence with the Bhote Khosi over a vertical distance of only 20 km, providing a rather steep thalweg and high erosional flow velocities of potential floods.

The largest moraine-dammed lakes in the Himalayas are actually dammed by two moraine barriers (Figure 7): the end moraine of the parent glacier and the lateral moraine by a tributary glacier (Tsho Rolpa glacier lake, Imja glacier lake).

In the Cordillera Blanca (Peru) four major lake outbursts occurred between 1938 and 1950, following the glacier ice losses of the 1920s and 1930s (Lliboutry et al., 1977). The most devastating was the 1941 event, in which the Lake Palcacocha drained catastrophically. The event triggered a debris flow (8×10^6 m^3) that destroyed one-third of the town Huaraz. Over 6,000 inhabitants lost their life.

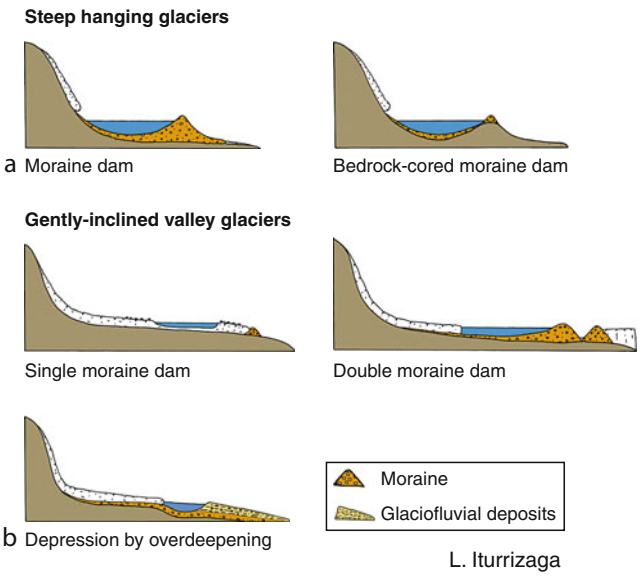

Glacier Lake Outburst Floods, Figure 6 Types of moraine-dammed lakes at short, steep hanging glaciers and gently sloped valley glaciers.

Development of moraine-dammed lakes

The water supply of the moraine-dammed lakes takes place by supraglacial, englacial, and subglacial meltwater, by glacier calving, by tributary rivers, and by precipitation in the form of rain and snow. The amplitude of the lake level may vary several meters during the course of the year

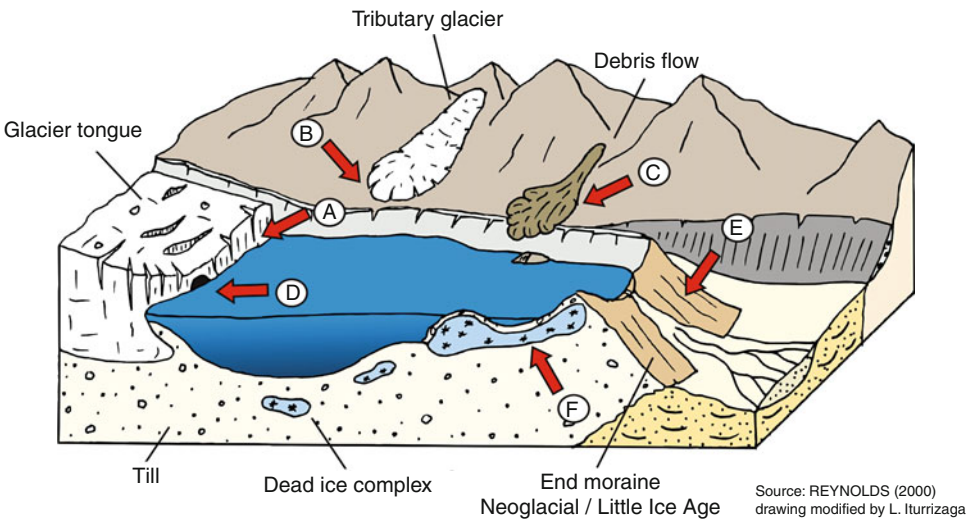

Glacier Lake Outburst Floods, Figure 7 Cross section of a moraine-dammed lake and potential triggers of lake outbursts **A** calving, **B** ice avalanches, **C** debris flows, **D** sudden meltwater drainage (sub-, en-, or supraglacial), **E** failure of the moraine dam, and **F** meltout of dead ice cores.

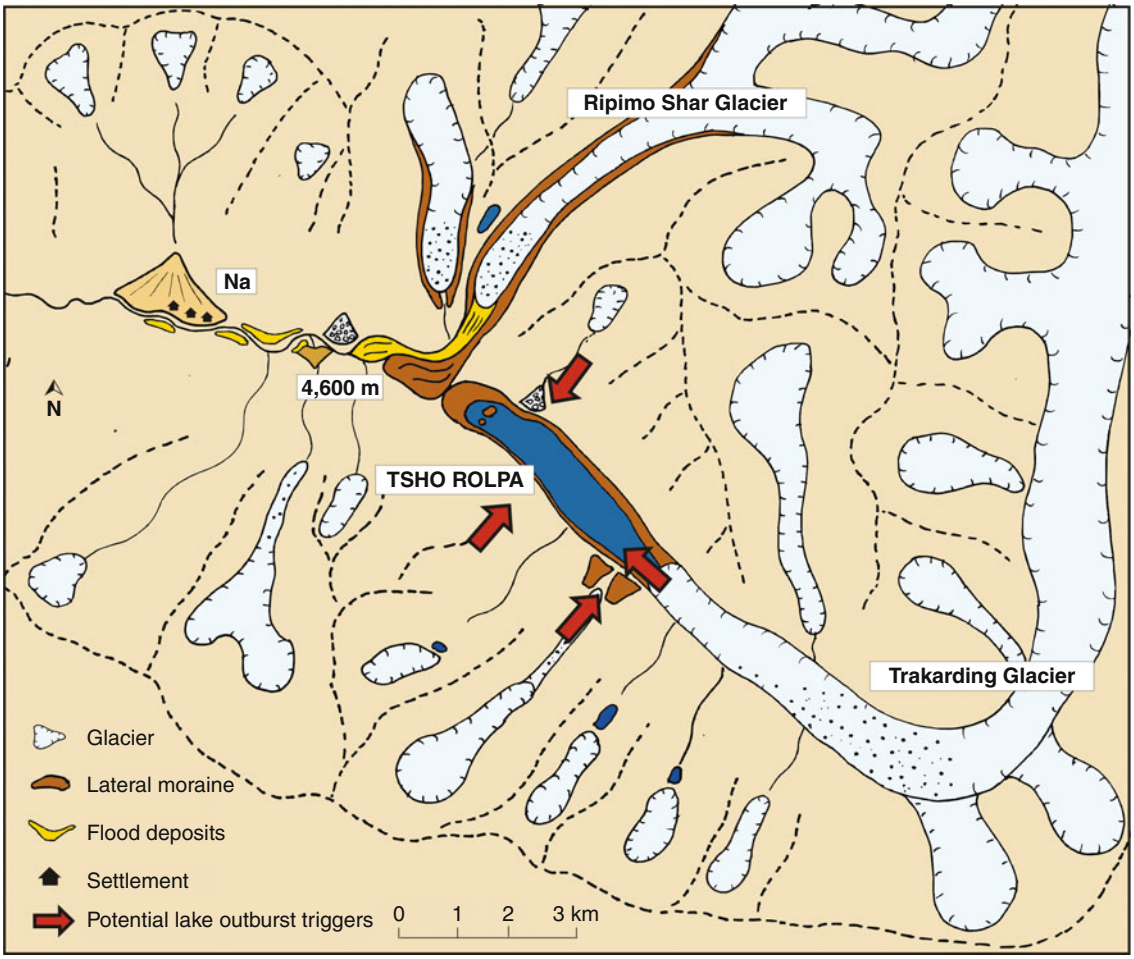

Glacier Lake Outburst Floods, Figure 8 The Tsho Rola Lake with a double dam formation of the former main valley glacier barrier of the Ripmo Shar glacier and the end moraine of the Trakarding glacier.

(3.4 +/– 0.7 m at Lago Paron in the Peruvian Andes, Lliboutry et al., 1977). At valley glaciers, the moraine-dammed lakes possess mostly an oval to elongated form and grow upvalley in longitudinal direction. The lowest point of the lake is situated in the upper third. Debris-covered, warm-based glaciers proved to be very favorable for the development of moraine-dammed lakes. The lake formation is linked with the surface gradient of the glacier (Reynolds, 2000). Larger supraglacial lakes may develop on valley glaciers up to a surface gradient of 2°.

Important for the formation of a large supraglacial lakes is that glacier maintains a stable terminus position over a longer time period. Moreover, the presence of some stagnant ice is favorable. Especially the long valley glaciers are gradually downwasting and thinning and not responding with an immediate glacier front retreat on a negative mass balance.

The initial stages of moraine-dammed lakes at valley glaciers are generally in the form of small supraglacial ponds of a debris-covered glacier. They gradually coalesce to a larger unified lake over time. The formation of supraglacial lakes may begin at undulations or at obstacles at the underground or at crevasse zones (Blachut and Ballantyne, 1976). At first, a vertical expansion of the supraglacial depression occurs at the glacier surface until the shift toward a lateral lake expansion by retreat of the steep ice cliffs. During the enlargement of supraglacial lakes, differential melting und backwasting processes and topographical inversions play a major role, which may result in the development of glacier karst and sink holes (Clayton, 1964). Crucial for the survival of the lakes is that they are not connected to a subglacial or englacial drainage system.

In the following, the lake expands horizontally and also inundates the end moraine. The growing of the supraglacial lake is subject to self-reinforcing processes with increasing vicinity to the end moraine. Due to its higher insolation absorption, the moraine material possesses a higher temperature than the glacier ice (Lliboutry et al., 1977). The direct contact to the lake water favors the

melting of the glacier tongue. The lake formation often starts 1–2 km upvalley of the end moraine, due to the fact that the glacier tongue area is heavily debris-covered. Therefore, the lakes are not that deep and their volume may be overestimated easily.

Progressive enlargement of supraglacial lakes is well researched for glaciers of the Himalayas (Ageta et al., 2000; Benn et al., 2001; Chikita, 2008; Delisle et al., 2003; Fujita et al., 2008; Komori et al., 2003; Reynolds, 2000). In Nepal, glacier lakes increased between 33 and 71 m/a since their formation (Yamada, 1998). The surface area of Tsho Rolpa grew from about 0.23 km^2 in 1959 to 0.62 km^2 by 1972 and 1.3 km^2 by 1990 (Yamada, 1998) (Figure 9). Imja Glacier lake increased from a few small ponds in the 1950s to a single body of water with a surface area greater than 0.5 km^2 in 1984 (Watanabe et al., 1994). In general, the moraine-dammed lakes are not more than 150 m deep. During the lateral expansion of the lake, the lake water may undercut the inner slope of the lake and trigger mass movements into the lake. The Tsho Rolpa is classified as the most dangerous lake in Nepal. The Trakarding glacier recedes by 20 m/a and has increased its size by around eight times in the last decades.

Trigger mechanisms for lake outbursts of moraine-dammed lakes

The failure of moraine dams occurs through a variety of different mechanisms (Reynolds, 2000; Clague and Evans, 2000) (Figure 7).

1. A very common outburst mechanism is the generation of displacement waves generated by ice avalanches or rock fall into the moraine-dammed lake (Dig Sho outburst in Nepal in 1985, Vuichard and Zimmermann, 1987). Subsequently, the flood creates a characteristic V-shaped incision into the moraine (Photo 6) or surges through an existent outlet channel and widens it rapidly. The natural spillway may be enlarged subsequently by retrogressive erosion.
2. Glacier calving may induce displacement waves overtopping the moraine dam. At the glacier tongue, crevasses are located immediately behind the ice cliff and undercutting at the water line may accelerate the calving processes (e.g., Thulagi glacier, Nepal). Calving of glaciers into glacial lakes increases the lake size. Floating glacier tongues are considered to be highly dangerous. They can collapse catastrophically into the lake.
3. Wastage of ice cores increases the volume of the lake and poses a serious risk to dam stability (Richardson and Reynolds, 2000b). Average rates of subsidence due to melting of buried ice in the moraine dam at Imja glacier (Nepal) amounted up to 2.7 m/year (Watanabe et al., 1995).
4. Earthquakes may lead to a dam failure by mass movement and destabilization of the dam (1941 Palcacocha, Huascaran, Peru, Lliboutry et al., 1977).
5. The moraine dam may gradually become instable by seepage, piping, and the enlargement of drainage conduits in the moraine. This natural process is sometimes accelerated accidentally by artificial drainage measurements and leaking of the pipes (e.g., Tsho Rolpa, Grabs and Hanisch, 1993).
6. Catastrophic sub- or englacial drainage of the glacier tongue area into the moraine-dammed lake may lead to a sudden rise of the water level in the proglacial lake (Passu glacier, Karakoram Mountains, in January 2008).

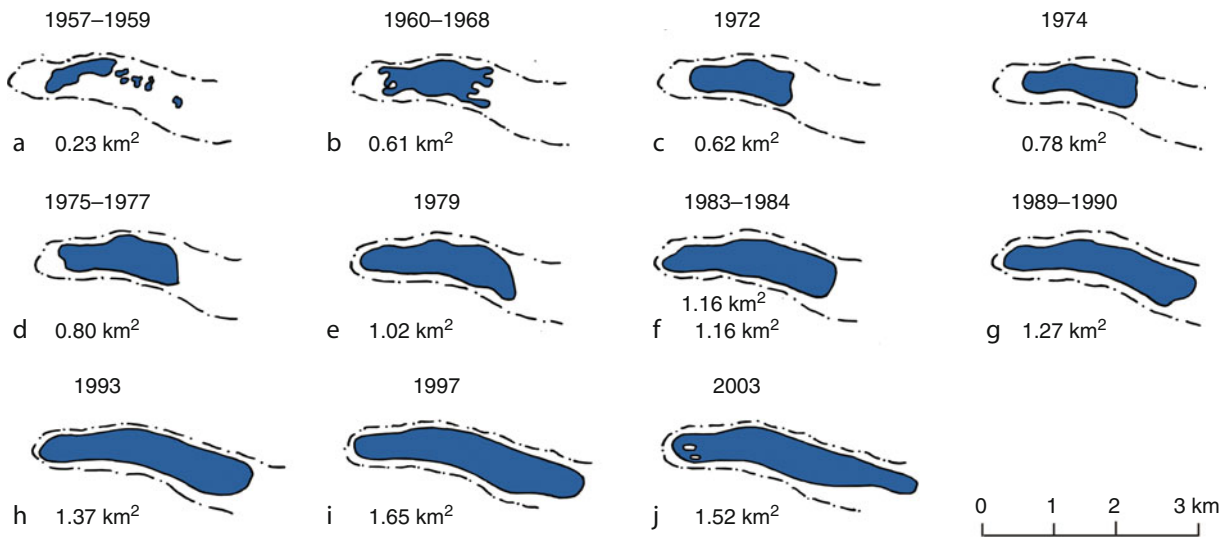

Glacier Lake Outburst Floods, Figure 9 Development of the Tsho Rolpa glacier lake (Reynolds Geo-Sciences Ltd. (2000), Drawing: L. Iturrizaga.

7. Heavy rainfall or snow melt may increase the lake level abruptly and lead to an outburst (Clague and Evans, 2000).

Hazard potential by glacier lake outbursts

Among glacier hazards, glacier lake outburst floods possess the most far-reaching impact zone. The devastating effect itself is significantly dependent from the peak discharge, which is in general much higher than that of floods triggered by rainfall or snowmelt (Clague and Evans, 2000). General hydrology of such floods has been discussed in a separate article entitled *Hydrology of jökulhlaup.*

From the historical record, glacier hazards are comparatively well described from the European Alps, where during the Little Ice Age (1600–1850) especially advancing tributary glaciers have dammed the main valley (e.g., impoundment of the Saaser Vispa by the Allalin glacier). In the Ötztal, the Vernagt glacier and Guslarferner sealed off the Rofental and impounded in 1848 a lake (3×10^6 m^3) with a subsequent outburst flood (Hoinkes, 1969). In total, over 200 glacier lake outbursts have been recorded in the Alps.

The general glacier shrinkage around the world during the twentieth century (Oerlemans, 2001) has lead to a remarkable shift in the glacial landscape systems and therefore in the glacial hazard potential (Evans and Clague, 1994; Häberli et al., 1999; Huggel, 2004; Kääb et al., 2005a, b; Baudo et al., 2007). The glacier retreat has become obvious in the accelerated formation of moraine-dammed lakes in the Himalayas since 1950s (Yamada, 1998; Kattelmann, 2003; Kattelmann and Watanabe, 1997) and the Peruvian Andes (Ames, 1998; Reynolds, 1992; Georges, 2004; Hubbard et al., 2005). With the augmented settlement density in high mountain regions, the hazard potential has increased in some areas. This is especially true for oasis settlements that are dependent on the irrigation of glacial meltwater (Iturrizaga, 1997).

Glacier hazards have reached a wider recognition by the outbreak of the Dig Tsho August 4, 1985. The lake outburst has been triggered by an ice avalanche, falling into the lake and caused a 5 m high flood wave. This type of lake outburst may be one of the major hazards in high mountain areas in the future. A lot of glaciers are in the transition from small-sized valley glaciers, reaching just the foot of the mountain, to hanging glaciers. However, most of the settlements in the Himalayas are located at the slopes or even on mountain ridges, in a rather flood-save location. In contrary, in the Karakoram almost none moraine-dammed lake exist. The main hazards are generated by the outburst of glacier-dammed lakes, which may be several times larger than moraine-dammed lakes. Moreover, their formation and outburst is highly unpredictable. Glacier advances in this region would lead to an increase in glacier-dammed lakes and in turn to a higher hazard potential. A lot of the settlements are situated in flood-prone areas as the slopes are covered with talus accumulations, which are not suitable for housing. Moreover, the oasis settlements are in many cases directly located in the glacier forefields. Settlement loss by glacier lake outbursts amounts up to 300 m in width were reconstructed in the Shimshal valley (Iturrizaga, 1997, Photo 7).

In the Peruvian Andes (Cordillera Blanca), 100 new proglacial lakes have formed during the last century (Ames, 1998). In the 1930s only 30 lakes were monitored, whereas in the 1990s 138 lakes were counted (Ames, 1998; Kaser and Osmaston, 2002). Several glacier lake outbursts, partially triggered by earthquakes and involving subsequent ice avalanches, have seriously affected the settled mountain valley (Welsch and Kinzl, 1970; Patzelt, 1983). Richardson and Reynolds (2000b) have carried out an intensive evaluation with regard to dam stabilities as a base for measurements of technical prevention.

The subsequent technical measurements maybe undertaken to mitigate the risk of the outburst of a moraine-dammed lake (Lliboutry et al., 1977; Grabs and Hanisch, 1993; Richardson and Reynolds, 2000b):

- Selective blasting of instable areas of the parent rock or of the overhanging glacier.
- Installation of mesh wires as protection against rock fall.
- Stabilization of the moraine wall by injection of a cement core.
- Installation of mesh wire at the outer slope of the moraine dam as protection against erosion.
- Artificial heightening of the moraine dam for avoiding the spillover of a displacement wave.
- Lowering of the lake level in order to decrease the pressure on the moraine dam, to reduce the water volume in case of an outburst.
- Drainage of the lake by (a) the stepwise deepening of the natural spillway channel and thus increasing the

Glacier Lake Outburst Floods, Photo 7 The village of Shimshal has lost about 300 m of land by glacier lake outbursts of the Khurdopin glacier (Photo: L. Iturrizaga, 07.07.2001).

drainage rate, effusion of the channel with cement and paving with stones, (b) blasting of parts or the entire moraine dam in its initial stage as prevention measurement (evacuation of the inhabitants), (c) pipes through or below the moraine and stabilization of the pipes with cement, (d) drillings through the bedrock below the moraine dam.

- Method of lowering the lake level by a hydraulic syphon technique with plastic pipes. This method is cost efficient and easily transportable. The system uses the energy, which is produced by the hydraulic gradient between the higher inlet and the lower outlet. The pipes are located at the inlet several meters below the lake level and at the foot of the moraine dam. Leaking of the pipes may be serious problem in destabilizing the dam. In case of a glacier tongue that floats on the lake, the ice may become instable and produce a lake outburst.

Downstream of the moraine dam, the common engineering protection measurements against floods may be installed.

The technical opportunities to prevent an outburst of a glacial-dammed lake are rather limited and in most cases financial funding is as well a key restriction. In general, the hazard potential of glacial-dammed lakes by tributary glaciers has decreased due to the common tendency of glacier retreat.

However, there has been substantial progress in hazard management of moraine-dammed lakes in regard to stabilization techniques and the application of hydraulic siphon techniques. Glacier lake monitoring and potential outburst risks are more and more monitored and evaluated by the analysis of satellite images (Huggel, 2004; Huggel et al., 2004; Quincey et al., 2007; Barry et al., 2008). Statistical remote sensing-based studies have been carried out for estimating the probability of catastrophic drainage from moraine-dammed lakes in southwestern British Columbia (McKillop and Clague, 2007). Flume tanks, which are artificial river channels, have been used to simulate natural river channels and get more insights into glacier lake outbursts sedimentation patterns (Rushmer, 2007). Carrivick (2006) and Herget (2005) have reconstructed computer-based large magnitude floods in two-dimensional (2D) and three-dimensional (3D) flows. These calculations may also be useful for hazard management of artificial dam failures. However, the outbursts of sub- and englacial water pockets, which represent in many mountain areas a serious hazard, are still rather unpredictable (Glacier du Trient). In the European Alps, about 60–70% of the glacier lakes are ice-marginal lakes and 30–40% are water pockets (Häberli, 1983). There are also indications that in the Karakoram Mountains the number of supraglacial lakes is increasing and related with that the danger of englacial lake outbursts (Iturrizaga, 2011). In Nepal, 34 of the existing lakes in the Dudh Khosi catchment area have been increased in size and 24 new lakes have been developed (Bajracharya and Mool, 2009). However, the lake size does not necessarily correspond with a higher risk, as the recent assessment for the Imja Glacier has shown (Watanabe et al., 2009).

Summary

Glacier lakes are indirectly a result of climatic changes expressed by glacier fluctuations. During the earth history glacier lakes have survived only a short time period, but glacier lake outbursts had a profound impact in shaping the landscape. The dominant type of glacial lakes may shift over time from glacier-dammed lakes to moraine-dammed lakes in different glaciation situations in dependence of the topographic setting. In the course of deglaciation, the types of glacier will change and therefore the type of glacial lakes. Glacier-dammed lakes occur mainly in times of glacier advance, but there are also some constellations in which they are the result of glacier retreat. Moraine-dammed lakes are mainly linked to glacier retreat regimes. During the Pleistocene glaciation, ice barriers of several hundred meters in height supposed to have existed. These large ice dams have no pendant at recent times. In general, the number of glaciers increases in the period of deglaciation from an ice-stream network to individual glaciers. Only some glaciers are prone to the formation of moraine-dammed lakes. Their size is in general much smaller than the glacier-dammed lakes. However, glacier lake outbursts from these small lakes can attain extremely high peak discharges by sudden dam failure. As a consequence of topographical and climatic conditions, glacier dynamics and the sediment transfer system glaciers are prone for the formation of moraine-dammed lakes. Therefore, a characteristic distribution pattern of glacier lake types can be recognized in individual mountain areas. In terms of natural hazards, sudden outbursts from small lakes with high peak discharges may have a more severe impact on human settlement than the drainage of large ice-dammed lakes. Not all glacier lake outbursts have to be necessarily released as water floods. They may also occur as debris flow with a high hazard potential.

Bibliography

Ageta, Y., Iwata, S., Yabuki, H., Naito, N., Sakai, A., Narama, C., and Karma, C., 2000. Expansion of glacier lakes in recent decades in the Bhutan Himalayas. In *Proceedings of the Seattle Workshop 2000. Debris-Covered Glaciers*. IAHS, Publication no. 264, pp. 165–175.

Allen, S. K., Schneider, D., and Owens, I. F., 2009. First approaches towards modelling glacial hazards in the Mount Cook region of New Zealand's Southern Alps. *Natural Hazards and Earth System Sciences*, **9**, 481–499.

Ames, A., 1998. A documentation of glacier tongue variations and lake development in the Cordillera Blanca, Peru. *Zeitschrift für Gletscherkunde und Glazialgeologie*, **34**(1), 1–36.

Baker, V., 2001. Water and the martian landscape. *Nature*, **412**, 228–236.

Baker, V. R., Benito, G., and Rudoy, A. N., 1993. Paleohydrology of Late Pleistocene superflooding, Altay Mountains, Siberia. *Science*, **259**, 348–350.

Baker, V. R., and Bunker, R., 1985. Cataclysmic late Pleistocene flooding from glacial lake Missoula: a review. *Quaternary Science Reviews*, **4**, 1–41.

Baker, V. R., Kochel, C. R., and Patton, P. C., 1988. *Flood Geomorphology*. New York: Wiley, p. 503.

Barry, R. G., Williams, M. W., and Racoviteanu, A. E., 2008. Optical remote sensing of glacier characteristics: a review with focus on the Himalaya. *Sensors*, **8**, 3355–3383.

Baudo, R., Tartari, G., and Vuillermoz, E., 2007. *Mountains Witnesses of Global Changes: Research in the Himalaya and Karakoram: Share-Asia Project: Research in the Himalaya and Karakoram: SHAREAsia Project (Developments in Earth Surface Processes)*. Amsterdam: Elsevier, p. 350.

Benn, D. I., and Evans, D. J. A., 1998. *Glaciers and Glaciation*. London: Arnold.

Benn, D. I., Wiseman, S., and Hands, K. A., 2001. Growth and drainage of supraglacial lakes on debrismantled Ngozumpa Glacier, Khumbu Himal, Nepal. *Journal of Glaciology*, **47**(159), 626–638.

Björnsson, H., 2003. Subglacial lakes and jökulhlaups in Iceland. *Global and Planetary Change*, **35**(3–4), 255–271.

Blachut, S. P., and Ballantyne, C. K., 1976. *Ice-Dammed Lakes: A Critical Review of their Nature and Behaviour*. Hamilton, ON: Department of Geography, McMaster University. Discussion Paper 6.

Bajracharya, S. R., and Mool, P., 2009. Glaciers, glacial lakes and glacial lake outburst floods in the Mount Everest region, Nepal. *Annals of Glaciology*, **50**(53), 81–86.

Breien, H., De Blasio, Fabio V., Elverhøi, A., and Høeg, K., 2008. Erosion and morphology of a debris flow caused by a glacial lake outburst flood, Western Norway. *Landslides*, **5**, 271–280.

Bretz, J. H., 1923. The Channeled Scabland of the Columbia plateau. *Journal of Geology*, **31**, 617–649.

Burbank, D. W., 1983. Multiple episodes of catastrophic flooding in the Peshawar Basin during the past 700000 years. *Geological Bulletin University of Peshawar*, **16**, 43–49.

Bürgisser, H. M., Gansser, A., and Pika, J., 1982. Late Glacial lake sediments of the Indus valley area, northwestern Himalayas. *Eclogae Geologicae Helvetiae*, **75**, 51–63.

Carey, M., 2005. Living and dying with glaciers: people's historical vulnerability to avalanches and outburst floods in Peru. *Global and Planetary Change*, **47**, 122–134.

Carling, P. A., Kirkbride, A. D., Parnachov, S., Borodavko, P. S., and Berger, G. W., 2002. Late quaternary catastrophic flooding in the Altai Mountains of south-central Siberia: a synoptic overview and an introduction to flood deposit sedimentology. In Martini, P., Baker, V., and Garon, G. (eds.), *Flood and Megaflood Processes and Deposits*. Oxford: Blackwell, Vol. 32, pp. 17–35.

Carrivick, J. L., 2006. 2D modelling of high-magnitude outburst floods; an example from Kverkfjö ll, Iceland. *Journal of Hydrology*, **321**, 187–199.

Chikita, K. A., 2008. The expansion mechanism of Himalayan supraglacial lakes: observations and modelling. *Himalayan Journal of Sciences*, **2**(4), 118–120.

Clague, J. J., and Evans, S. E., 1994. Formation and failure of natural dams in the Canadian Cordillera. *Bulletin-Geological Survey of Canada*, **464**, 35.

Clague, J. J., and Evans, S. G., 2000. A review of catastrophic drainage of moraine-dammed lakes in British Columbia. *Quaternary Science Reviews*, **19**, 1763–1783.

Clarke, G., Leverington, D., Teller, J., and Dyke, A., 2003. Enhanced: superlakes, megafloods, and abrupt climatic change. *Science*, **301**(5635), 922–931.

Clayton, L., 1964. Karst topography on stagnant glaciers. *Journal of Glaciology*, **5**(37), 107–112.

Cornwell, K., 1998. Quaternary break-out flood sediments in the Peshawar basin of northern Pakistan. *Geomorphology*, **25**, 225–248.

Costa, J. E., 1988. Rheologic, Geomorphic, and Sedimentologic Differentiation of Water Flood, Hyperconcentrated Flows, and Debris Flows. In Baker, V. R., Kochel, R. C., and Patton, P. C. (eds.), *Flood Geomorphology*. New York: Wiley, pp. 113–122.

Costa, J. E., and Schuster, R. L., 1988. The formation and failure of natural dams. *Geological Society of America Bulletin*, **100**, 1054–1068.

Dainelli, G., 1922. Studi sul Glaciale. In Dainelli, G. (ed.), *Relazione Scientifiche della Spedizione Italiana de Filippi, nell'Himalaia, Caracorum e Turchestan Cinese 1913–1914*, Serei II. Resultati geologici e geografici, Vol. 3, volume of plates. Zanichelli, Bologna.

Delisle, G., Reynolds, J. M., Hanisch, J., Pokhrel, A. P., and Pant, S., 2003. Lake Thulagi/Nepal: rapid landscape evolution in reaction to climatic change. *Zeitschrift für Geomorphologie N.F.*, **130**(Suppl), 1–9.

Derbyshire, E., Jijun, L., Perrott, F. A., Suying, X., and Waters, R. S., 1984. Quaternary glacial history of the Hunza Valley, Karakoram Mountains, Pakistan. In Miller, K. J. (ed.), *The International Karakoram Project*. Cambridge: Cambridge University Press, Vol. 2, pp. 456–495.

Desio, A., and Orombelli, G., 1983. The 'Punjab erratics' and the maximum extent of the glaciers in the middle lndus valley (Pakistan) during the Pleistocene. *Atti della Accademia Nazionale dei Lincei*, Series 8, **17**(179), 135–180.

Espizúa, L., and Bengochea, J. D., 1990. Surge of Grande deI Nevado Glacier (Mendoza, Argentina) in 1984: its evolution through satellite images. *Geografiska Annaler*, **72A**(3–4), 255–259.

Evans, S. G., and Clague, J. J., 1994. Recent climatic change and catastrophic geomorphic processes in mountain environments. *Geomorphology*, **10**, 107–128.

Fairen, A. G., and Dohm, J. M., 2003. Episodic flood inundations of the northern plains of Mars. *Icarus*, **165**, 53–67.

Ferguson, R. I., 1984. Sediment load of the Hunza River. In Miller, K. J. (ed.), *The International Karakoram Project*. Cambridge: Cambridge University Press, Vol. 2, pp. 581–598.

Fujita, K., Suzuki, R., Nuimura, T., and Sakai, A., 2008. Performance of ASTER and SRTM DEMs, and their potential for assessing glacial lakes in the Lunana region, Bhutan Himalaya. *Journal of Glaciology*, **54**(185), 220–228.

Glen, J. W., 1954. The stability of ice-dammed lakes and other water-filled holes in glaciers. *Journal of Glaciology*, **2**, 316–318.

Grabs, W. E., Hanisch, J., 1993. Objectives and prevention methods for glacier lake outburst ßoods (GLOFs). In Young, G. J. (ed.), *Snow and Glacier Hydrology.* Wallingford: International Association of Hydrological Sciences Publication 218, pp. 341–352.

Georges, C., 2004. The 20th-century glacier fluctuations in the tropical Cordillera Blanca (Peru). *Arctic, Antarctic and Alpine Research*, **36**(1), 100–107.

Grosswald, M. G., 1980. Late Weichselian ice sheets of Northern Eurasia. *Quaternary Research*, **13**, 1–32.

Gudmunsson, M. T., Sigmundsson, F., and Björnsson, H., 1997. Ice-volcano interaction of the 1996 Gjálp subglacial eruption, Vatnajökull, Iceland. *Nature*, **389**, 954–957.

Häberli, W., 1983. Frequency and characteristics of glacier floods in the Swiss Alps. *Annals of Glaciology*, **4**, 85–90.

Häberli, W., et al., 1999. Eisschwund und Naturkatastrophen im Hochgebirge. Zürich. (Schlussbericht im Rahmen des nationalen Forschungsprogrammes "Klimaänderungen und Naturkatastrophen", NFP 31).

Helbling, R., 1935. The origin of the Rio Plomo ice-dam. *Geographical Journal*, **85**(1), 41–49.

Herget, J., 2003. Eisstausee-Ausbrüche. Ursache für katastrophale Hochwasser. In Geographische Rundschau, 55, Heft Nr. 2, Seite 14–21.

Herget, J., 2005. *Reconstruction of Pleistocene ice-dammed lake outburst floods in Altai-Mountains*. Siberia: Geological Society of America, Special Publication 386, 118 p.

Hewitt, K., 1982. Natural dams and outburst floods of the Karakoram Himalaya. In Glen, J. W. (ed.), *Hydrological Aspects of Alpine and High-Mountain Areas*. International Commission on Snow and Ice (ICSI) Symposium, Exeter, UK, pp. 19–30 July 1982; *Proceedings of International Association of Hydrological Sciences*. IAHS/AISH Publication no. 138, pp. 259–269.

Hewitt, K., 1998. Himalayan Indus streams in the holocene: glacier-, and landslide-"interrupted" fluvial systems. In Stellrecht, I. (ed.), Karakorum –Hindukush–Himalaya: Dynamics of Change. Part I, Culture Area Karakorum. *Scientific Studies*, **4**(1), 3–28.

Hoinkes, H., 1969. Surges of the Vernagtferner in the Ötztal Alps since 1599. *Canadian Journal of Earth Sciences*, **6**, 845–551.

Howarth, P. J., 1968. A supra-glacial extension of an ice-dammed lake, Tunsberg dalsbreen, Norway. *Journal of Glaciology*, **7**, 414–419.

Hubbard, B., Heald, A., Reynolds, J. M., Quincey, D. J., Richardson, S. D., Zapata, M., Santillan, N., and Hambrey, M. J., 2005. Impact of a rock avalanche on a moraine-dammed proglacial lake: Laguna Safuna Alta, Cordillera Blanca, Peru. *Earth Surface Processes and Landforms*, **30**, 1251–1264.

Huggel, C., 2004. Assessment of glacial hazards based on remote sensing and GIS Modeling, University of Zurich. Available from http://www.dissertationen.unizh.ch/2004/huggel/diss.pdf

Huggel, C., Haeberli, W., Kääb, A., Bieri, D., and Richardson, S., 2004. An assessment procedure for glacial hazards in the Swiss Alps. *Canadian Geotechnical Journal*, **41**, 1068–1083.

Iturrizaga, L., 1997. The valley of Shimshal – a geographical portrait of a remote high mountain settlement and its pastures with reference to environmental habitat conditions in the North West Karakorum. In Kuhle, M. (ed.), Tibet and High Asia IV, *GeoJournal*, **42**(2/3), 305–328.

Iturrizaga, L., 2003. The distribution and genesis of lateroglacial valleys in the Karakoram Mountains (Pakistan). *Zeitschrift für Geomorphologie N.F.*, **130**(Suppl), 51–74.

Iturrizaga, L., 2005a. Historical ice-dammed lakes in the Karambar valley, Hindukush (Pakistan). In Kuhle, M. (ed.), Tibet and High Asia (VII): Glaciogeomorphology and Former Glaciation in the Himalaya and Karakorum. *GeoJournal*, **62**(3–4), 1–47.

Iturrizaga, L., 2005b. The historical Saklei Shuyinj and Chateboi glacier dams as trigger for lake outburst cascades in the Karambar valley (Hindukush). *Island Arc*, **14**(4), 389–399.

Iturrizaga, L., 2005c. New observations on glacier lake outbursts in the Shimshal valley. *Journal of Asian Earth Sciences*, **25**, 545–555.

Iturrizaga, L., 2006. Key forms for reconstructing glacier dams, glacier lakes and outburst floods. Historical ice-dammed lakes in the Karambar valley, Hindukush (Pakistan). *Zeitschrift fur Geomorphologie Supplementband*, **142**, 361–388.

Iturrizaga, L., 2007. Die Eisrandtäler im Karakorum: Verbreitung, Genese und Morphodynamik des lateroglazialen Sedimentformenschatzes. In *Geography International*. Aachen: Shaker Verlag, p. 389.

Iturrizaga, L., 2008. Die Talschaft Chapursan – Zur Frage der geomorphologischen Genese von Schutthügellandschaften im Zusammenhang mit historischen Siedlungslandzerstörungen. In Berichte zur Geowissenschaft, Shaker Verlag Aachen, p. 116.

Iturrizaga, L., 2011. Glacial lakes in the Hindukush-Karakoram Mountains and their hazard potential. Geophysical Research Abstracts, Volume 11, EGU2009-8062-1.

Iturrizaga, L., in print. Trends in historical and recent glacier fluctuations in the Karakoram Mountains. In Schrott, L., Otto, J.-C., Stötter, H., Glade, T. (eds.), Zeitschrift für Geomorphologie.

Kääb, A., Huggel, C., Fischer, L., Guex, S., Paul, F., Roer, I., Salzmann, N., Schlaefli, S., Schmutz, K., Schneider, D., Strozzi, T., and Weidmann, Y., 2005a. Remote sensing of glacier- and permafrost related hazards in high mountains: an overview. *Natural Hazards and Earth System Science*, **5**, 527–554.

Kääb, A., Reynolds, J. M., and Haeberli, W., 2005b. Glacier and permafrost hazards in high mountains. In Huber, U. M., Burgmann, H. K. H., and Reasoner, M. A. (eds.), *Global Change and Mountain Regions (A State of Knowledge Overview)*. Dordrecht: Springer, pp. 225–234.

Kaser, G., and Osmaston, H., 2002. *Tropical Glaciers*. Cambridge: Cambridge University Press.

Kattelmann, R., 2003. Glacial lake outburst floods in the Nepal Himalaya: a manageable hazard? *Natural Hazards*, **28** (145–154), 2003.

Kattelmann, R., and Watanabe, T., 1997. Draining Himalayan glacial lakes before they burst. Destructive water: water-caused natural disasters, their abatement and control. In *Proceedings of the Conference*, Anaheim, CA, June 1996. IAHS Publication no. 239, pp. 337–343.

Knudsen, N. T., and Theakstone, W. H., 1988. Drainage of the Austre Okstindbreen icedammed lake, Okstindan, Norway. *Journal of Glaciology*, **34**, 87–94.

Knight, P. G., 1999. *Glaciers*. London: Routledge, 261 pp.

Komori, J., Gurung, D. R., Iwata, S., and Yabuki, H., 2003. Variation and lake expansion of Chubda Glacier, Bhutan Himalayas, during the last 35 years. *Bulletin of Glaciological Research*, **21**, 49–55.

Korup, O., and Tweed, F., 2007. Ice, moraine and landslide dams in mountainous terrain. *Quaternary Science Reviews*, **26**, 3406–3422.

Kuhle, M., 2001. The maximum Ice Age (LGM) glaciation of the Central- and South Karakorum: an investigation of the heights of its glacier levels and ice thicknesses as well as lowest prehistoric ice margin positions in the Hindukush, Himalaya and in East-Tibet on the Minya Konka-massif. In Kuhle, M. (ed.), Tibet and High Asia (VI), Glacio-geomorphology and prehistoric Glaciation in the Karakorum and Himalaya. *GeoJournal*, **54**(2–4), 109–396.

Kuhle, M., 2002. Outlet glaciers of the Pleistocene (LGM) south Tibetian ice sheet between Cho Oyu and Shisha Pangma as potenial sources of former mega-floods. In Martini, P., Baker, V. R., Garzón, G. (eds.), *Flood and Megaflood Processes and Deposits: Recent and Ancient Examples*. Special Publication of the International Association of Sedimentologists (IAS). Oxford: Blackwell Science, Vol. 32, pp. 291–302.

Liestøl, O., 1956. Glacier dammed lakes in Norway. *Norsk Geografisk Tidsskrift*, **15**, 122–149.

Lliboutry, L., Morales, B., Pautre, A., and Schneider, B., 1977. Glaciological problems set by the control of dangerous lakes in the Cordillera Blanca, Peru. I. Historical failures of morainic dams, their causes and prevention. *Journal of Glaciology*, **18**(79), 239–254.

Maag, H., 1969. *Ice Dammed Lakes and Marginal Glacial Drainage on Axel Heiberg Island. Axel Heiberg Island Research Report*. Montreal: McGill University.

Mangerud, J., Jakobsson, M., Alexanderson, H., Astakhov, V., Clarke, G., Henriksen, M., Hjort, C., Krinner, G., Lunkka, J. P., Moller, P., Murray, A., Nikolskaya, O., Saarnisto, M., and John Inge Svendsen, J. I., 2004. Ice-dammed lakes and rerouting of the drainage of northern Eurasia during the Last Glaciation. *Quaternary Science Reviews*, **23**(11–13), 1313–1332. Quaternary Environments of the Eurasian North (QUEEN).

Marcus, M. G., 1960. Periodic drainage of glacier dammed Tulsequah Lake, British Columbia. *Geographical Review*, **50**, 89–106.

Martini, P. I., Baker, V. R., and Garzo´ n, G., 2002. *Flood and Megaflood Processes and Deposits: Recent and Ancient Examples*. Oxford: Blackwell, Vol. 32, Special Publication International Association of Sedimentologists.

Mason, K., 1935. The study of the threatening glaciers. *Geographical Journal*, **85**, 24–41.

Mayer, C., Lambrecht, A., and Hagg, W., 2008. Post-drainage ice dam response at Lake Merzbacher, Inylchek glacier, Kyrgyzstan. *Geografiska Annaler*, Series A, **90A**, 1, 87–96.

McKillop, R. J., and Clague, J. J., 2007. Statistical, remote sensing-based approach for estimating the probability of catastrophic drainage from moraine-dammed lakes. *Global and Planetary Change*, **56**(1–2, Climate Change Impacts on Mountain Glaciers and Permafrost), 153–171.

Montgomery, D. R., Hallet, B., Yuping, L., Finnegan, N., Anders, A., Gillespie, A., and Greenberg, H. M., 2004. Evidence for Holocene megafloods down the Tsangpo River gorge, southeastern Tibet. *Quaternary Research*, **62**, 201–207.

Mool, P. K., Bajracharya, S. R., Joshi, S. P., Sakya, K., and Baidya, A., 2002a. *Inventory of Glaciers, Glacial Lakes and Glacial Lake Outburst Floods Monitoring and early Warning Systems in the Hindu-Kush Himalayan Region, Nepal*. Kathmandu, Nepal: International Center for Integrated Mountain Development, p. 227 S.

Mool, P. K., Wangda, D., Bajracharya, S. R., Kunzang, K., Gurung, D. R., and Joshi, S. P., 2002b. *Inventory of Glaciers, Glacial Lakes and Glacial Lake Outburst Floods Monitoring and Early Warning Systems in the Hindu-Kush Himalayan region, Bhutan*. Kathmandu, Nepal: International Center for Integrated Mountain Development, p. 364 S.

Nye, J. F., 1976. Water flow in glaciers: jökulhlaups, tunnels and veins. *Journal of Glaciology*, **17**, 181–207.

O'Connor, J. E., and Costa, J. E., 1993. Geologic and hydrologic hazards in glacierized basins in North America resulting from 19th and 20th century global warming. *Natural Hazards*, **8**, 121–140. 121.

O'Connor, J. E., and Costa, J. E., 2004. The world's largest floods, past and present: their causes and magnitude. U.S. Geological Survey Circular 1254.

Oerlemans, J., 2001. *Glaciers and Climate Change*. Rotterdam: A. A. Balkema.

Owen, L. A., 1996. Quaternary lacustrine deposits in a high energy semi-arid mountain environment, Karakoram Mountains, northern Pakistan. *Journal of Quaternary Science*, **11**(6), 461–483.

Paffen, K. J., Pillewizer, W., and Schneider, H. J., 1956. Forschungen im Hunza-Karakorum. *Erdkunde*, **10**, 1–33.

Patzelt, G. (ed.), 1983. Die Berg- und Gletscherstürze vom Huascarán, Cordillera Blanca, Peru. Hochgebirgsforschung – High Mountain Research, 6. Arbeitsgemeinschaft für vergleichende Hochgebirgsforschung, München.

Prieto, M. del R., 1986. The glacier dam on the Rio Plomo: a cyclic phenomenon?. Zeitschrift für Gletscherkunde und Glazialgeologie, **22**(H. 1), 73–78 (Innsbruck).

Post, A., and Mayo, L. R., 1971. Glacier-dammed lakes and outburst floods in Alaska: U.S. Geological Survey Hydrologic Investigations Atlas HA-455, 3 sheets, p. 10.

Qinghua, F., 1991. Characteristics of glacier outburst flood in the Yarkant River, Karakorum Mountains. In Kuhle, M., and Daoming, X. (ed.), Tibet and High-Asia, Results of the Sino-German Joint Expeditions (II). *GeoJournal*, **25**(2/3), 255–263.

Quincey, D. J., Richardson, S. D., Luckman, A., Lucas, R. M., Reynolds, J. M., Hambrey, M. J., and Glasser, N. F., 2007. Early recognition of glacial lake hazards in the Himalaya using remote sensing datasets. *Global and Planetary Change*, **56**(1–2), 137–152.

Reynolds, J. M., 1992. "The identification and mitigation of glacier-related hazards: Examples from the Cordillera Blanca, Peru". In McCall, G. J. H., Laming, D. C. J., and Scott, S. (eds.), *Geohazards*. London: Chapman & Hall, pp. 143–157.

Reynolds, J. M., 1999. Glacial HAZARD ASSESSMENT at Tsho Rolpa, Rolwaling, Central Nepal. *Quarterly Journal of Engineering Geology*, **32**, 209–214.

Reynolds, J. M., 2000. On the formation of supraglacial lakes on debris-covered glaciers. In Nakawo, M., Raymond, C. F., Fountain, A. (eds.), *Debris-Covered Glaciers*. Proceedings of a Workshop held at Seattle, Washington, DC, September 2000. Oxford: IAHS Publication, Vol. 264, pp. 153–4161.

Reynolds, J. M., Dolecki, A., and Portocarrero, C., 1998. Construction of a drainage tunnel as part of glacial lake hazard mitigation at Hualcán, Cordillera Blanca, Peru. In Maund, J. G., and Eddleston, M. (eds.), *Geohazards in Engineering Geology.* London: Geological Society, Engineering Geology Special Publications 15, pp. 41–48.

Richardson, S. D., and Reynolds, J. M., 2000a. Degradation of ice-cored moraine dams: implications for hazard development. In Nakawo, M., Raymond, C. F., and Fountain, A. (eds.), *Debris-Covered Glaciers*. Seattle: IAHS Publications, pp. 187–197.

Richardson, S. D., and Reynolds, J. M., 2000b. An overview of glacial hazards in the Himalayas. *Quaternary International*, **65**(66), 31–47.

Rudoy, A. N., 2002. Glacier-dammed lakes and geological work of glacial superfloods in the Late Pleistocene, Southern Siberia, Altai Mountains. *Quaternary International*, **87**(1), 119–140.

Rushmer, E. L., 2007. Physical-scale modelling of jökulhlaups (glacial outburst floods) with contrasting hydrograph shapes. *Earth Surface Processes and Landforms*, **32**, 954–963.

Russell, A. J., 1994. Subglacial jökulhlaup deposition, Jotunheimen, Norway. *Sedimentary Geology*, **91**, 1–14.

Russell, A. J., 2007. Controls on the sedimentology of an icecontact jökulhlaup-dominated delta, Kangerlussuaq, West Greenland. *Sedimentary Geology*, **193**(1–4), 131–148.

Scott, C. H., 1992. *Contemporary sediment transfer in Himalayan glacial systems: Implications for the interpretation of the Quaternary record (Ph.D. thesis)*. Leicester: University of Leicester, 343 pp.

Shroder, J. F., Jr., Khan, M. S., Lawrence, R. D., Madin, I. P., and Higgins, S. M., 1989. Quaternary glacial chronology and neotectonics. In Malinconico, L. L., Lillie, R. J. (eds.), *Tectonics of the Western Himalayas*. Boulder, Colorado: Geological Society of America, Special Paper, 232, pp. 275–294.

Shroder, J. F., Jr., 1993. Himalaya to the Sea: geology, geomorphology and the Quaternary of Pakistan in the regional context. In Shroder, J. F., Jr. (ed.), *Himalaya to the Sea: Geology, Geomorphology and the Quaternary.* New York: Routledge, pp. 1–42.

Stone, K. H., 1963. Alaskan ice-dammed lakes. *Annals of the Association of American Geographers*, **53**, 332–349.

Sturm, M., Beget, J., and Benson, C., 1987. Observations of jökulhlaups from ice-dammed Strandline lake, Alaska: implications for paleohydrology. In Mayer, L., and Nash, D. (eds.), *Catastrophic Flooding*. The Binghampton Symposia in Geomorphology, 18. London: Allen and Unwin, pp. 79–94.

Teller, J. T., Leverington, D. W., and Mann, J. D., 2002. Freshwater outbursts to the oceans from glacial Lake Agassiz and their role in climate change during the last deglaciation. *Quaternary Science Reviews*, **21**(8–9), 879–887.

Thorarinsson, S., 1939. The ice-dammed lakes of Iceland, with particular reference to their values as indicators of glacier oscillations. *Geografiska Annaler*, **21**, 216–242.

Thorarinsson, S., 1953. Some new aspects of the Grímsvötn problem. *Journal of Glaciology*, **2**, 267–274.

Tufnell, L., 1984. *Glacier Hazards*. London: Longman Group, p. 95.
Tweed, F. S., and Russell, A. J., 1999. Controls on the formation and sudden drainage of glacier-impounded lakes: implications for jökulhlaup characteristics. *Progress in Physical Geography*, **23**, 79–110.
Vilímek, V., Zapata Luyo, M., Klimes, J., Patzelt, Z., and Santillan, N., 2005. Influence of glacial retreat on natural hazards of the Palcacocha Lake area, Peru. *Landslides*, **2**, 107–115.
Vuichard, D., and Zimmermann, M., 1987. The 1985 catastrophic drainage of a moraine-dammed lake, Khumbu Himal, Nepal: causes and consequences. *Mountain Research and Development*, **7**, 91–110.
Walder, J. S., and Costa, J. E., 1996. Outburst floods from glacier-dammed lakes: the effect of mode of lake drainage on flood magnitude. *Earth Surface Processes and Landforms*, **21**, 701–723.
Watanabe, T., Ives, J. D., and Hammond, J. E., 1994. Rapid growth of a glacier lake in Khumbu Himal, Nepal: prospects for a catastrophic flood. *Mountain Research and Development*, **14**, 329–340.
Watanabe, T., Kameyama, S., and Sato, T., 1995. Imja Glacier dead-ice melt rates and changes in a supra-glacial lake, 1989–1994, Khumbu Himal, Nepal: danger of lake drainage. *Mountain Research and Development*, **15**, 293–300.
Watanabe, T., Lamsal, D., and Ives, J. D., 2009. Evaluating the growth characteristics of a glacial lake and its degree of danger of outburst flooding: Imja Glacier, Khumbu Himal, Nepal. *Norsk Geografisk Tidsskrift – Norwegian Journal of Geography*, **63**, 255–267.
Welsch, W., and Kinzl, H., 1970. Der Gletschersturz vom Huascarán (Perú) am 31. Mai 1970. die größte Gletscherkatastrophe der Geschichte. *Zeitschrift für Gletscherkunde und Glazialgeologie*, **6**(1–2), 181–192.
Whalley, W. B., 1971. Observations of the drainage of an ice-dammed lake – Strupvatnet, Troms, Norway. *Norsk Geografisk Tidsskrift*, **25**, 165–74.
Xin, W., Shiyin, L., and Wanqin, G., 2008. Assessment and simulation of glacier lake outburst floods for Longbasaba and Pida Lakes, China. *Mountain Research and Development*, **28**(3/4), 310–317.
Yamada, T., 1998. *Glacier Lake and Its Outburst Flood in the Nepal Himalaya*. Tokyo: Data Center for Glacier Research, Japanese Society of Snow and Ice. Monograph No. 1, p. 96.

Cross-references

Alaskan Glaciers
Catastrophic Flooding
Glaciers of the Karakoram Himalaya
Hydrology of Jökulhlaups
Ice-Dammed Lakes
Lateroglacial
Proglacial Lakes

GLACIER MASS BALANCE

Wilfried Haeberli
Glaciology, Geomorphodynamics & Geochronology, Geography Department, University of Zurich, Zurich, Switzerland

Definition

The mass balance of a glacier is the sum of all processes that add mass to a glacier and remove mass from it. Accumulation or addition of mass most commonly takes place in the form of snowfall, often modified by wind and avalanches. Melting of snow and ice is the predominant form of ablation or removal of mass, but calving of tidal glaciers, ice avalanching from steep hanging glaciers or evacuation of windblown snow in dry areas or during cold/dry seasons can locally be of high relative importance. A general overview of the physical processes involved was given by Oerlemans (2001), Kaser et al. (2003) provided a manual for field measurements with related technical nomenclature, Haeberli et al. (1998) compiled an overview of monitoring strategies with their historical background, and described the existing data basis in the international glacier monitoring network. Kaser et al. (2006) and Zemp et al. (2009) summarized the development of glacier mass balance during the past decades (cf. earlier compilations by Dyurgerov and Meier, 1997 and Braithwaite, 2002). Assessments of worldwide glacier mass balance are also regularly contained in the IPCC reports (IPCC, 2007 and earlier issues).

Background and significance

The loss or gain of glacier mass is a direct, undelayed response of a glacier to climatic conditions. It constitutes a key indication of climate change and affects the water cycle and landscape evolution in cold regions on earth (IPCC, 2007; UNEP, 2007). Long-term monitoring of glacier mass balance forms an essential part of internationally coordinated glacier observation (Haeberli, 2004) by the World Glacier Monitoring Service (WGMS) under the umbrella of ICSU (FAGS), IUGG (IACS), UNEP, UNESCO, and WMO within the framework of the Global Terrestrial Network for Glaciers (GTN-G) as part of the Global Terrestrial/Climate Observing System (GTOS/GCOS). Worldwide results from regular measurements are reported through a special biennial "Glacier Mass Balance Bulletin" (WGMS, 2009 and earlier issues) and as part of the more comprehensive series of "Fluctuations of Glaciers" (WGMS, 2008a, b and earlier issues) covering 5-year intervals. Figure 1 illustrates the information from long-term measurements reported in the Glacier Mass Balance Bulletin. Annual and cumulative mass balance are expressed as thickness change in water equivalent (corrected for snow/ice density) averaged over the glacier surface area. The annual values document the interannual variability and the predominant yearly losses, both being of a comparable magnitude. The cumulative values reflect the striking clarity of the negative mass balance as a consequence of increasing temperatures and the overall acceleration of loss rates due to various interactions and feedbacks. Since the turn of the millennium, the mean measured loss rate between 1980 and 1999 roughly doubled and the previous record loss in 1998 was exceeded already three times, in 2006 even by a factor of about two.

Integrative strategies of global climate system observation and related glacier monitoring build on a tiered system of approaches, which help bridging the gap between

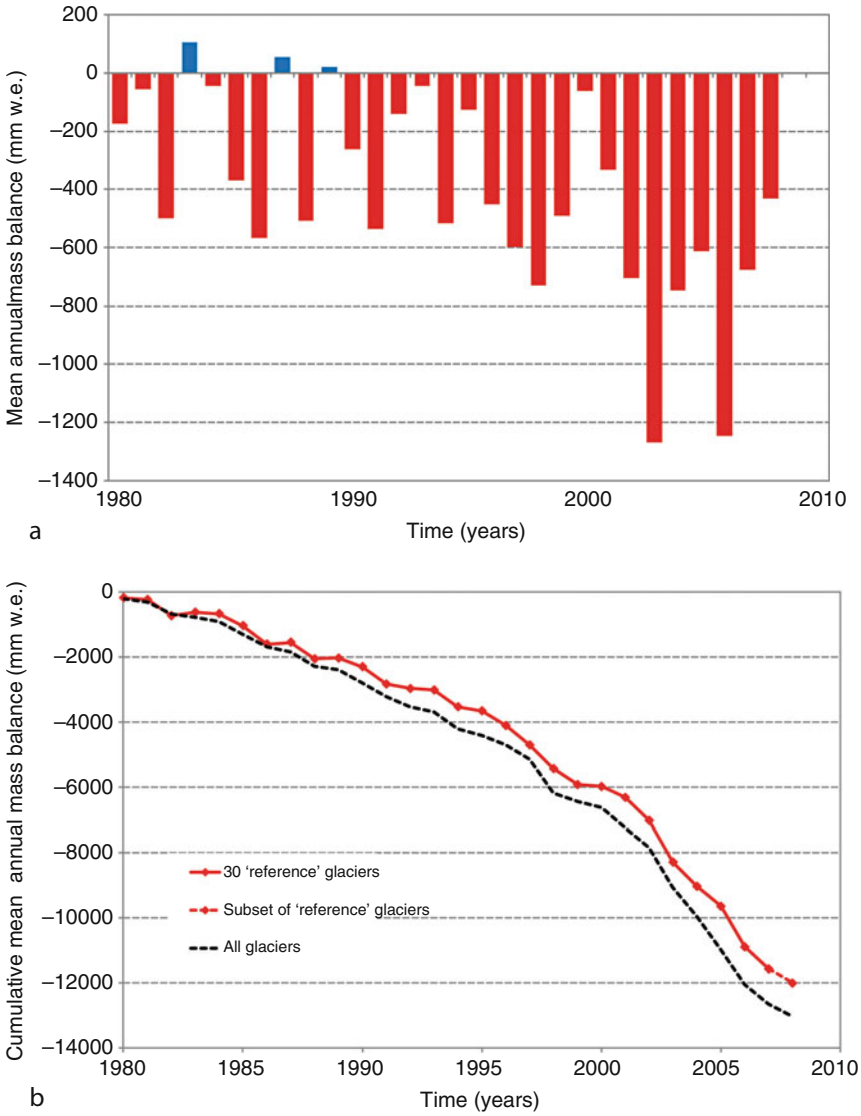

Glacier Mass Balance, Figure 1 Graphs of annual (**a**) and cumulative (**b**) mass balance from about 30 reference glaciers as periodically published in the Glacier Mass Balance Bulletin of the World Glacier Monitoring Service. (From WGMS, 2009.)

detailed local process-oriented observations and global coverage at the pixel resolution of satellite sensors (Haeberli, 2005). The following elements are parts of this tiered approach:

- Extensive and integrative glacier mass balance and flow studies within major climatic zones for improved process understanding and calibration of numerical models;
- Regional observations with cost-saving approaches and monitoring of large glacier ensembles within entire mountain ranges using satellite-based information.

The existing variability of measurement and analysis techniques, as well as application aspects related to long-term studies of glacier mass balance can be structured and explained along such a hierarchical product-oriented perspective.

Integrative, process-oriented mass balance determination

Detailed process understanding and the development and calibration of numerical energy/mass balance and flow models constitute the basis for sensitivity experiments on climate–glacier relations and for extrapolation of mass balance values measured on a few glaciers to regions with less comprehensive measurements or for reconstruction backwards and scenario calculations forward in time. This requires intensive, seasonal, or even more frequent field measurements of mass balance in combination with determinations of glacier flow and hydrometeorological data

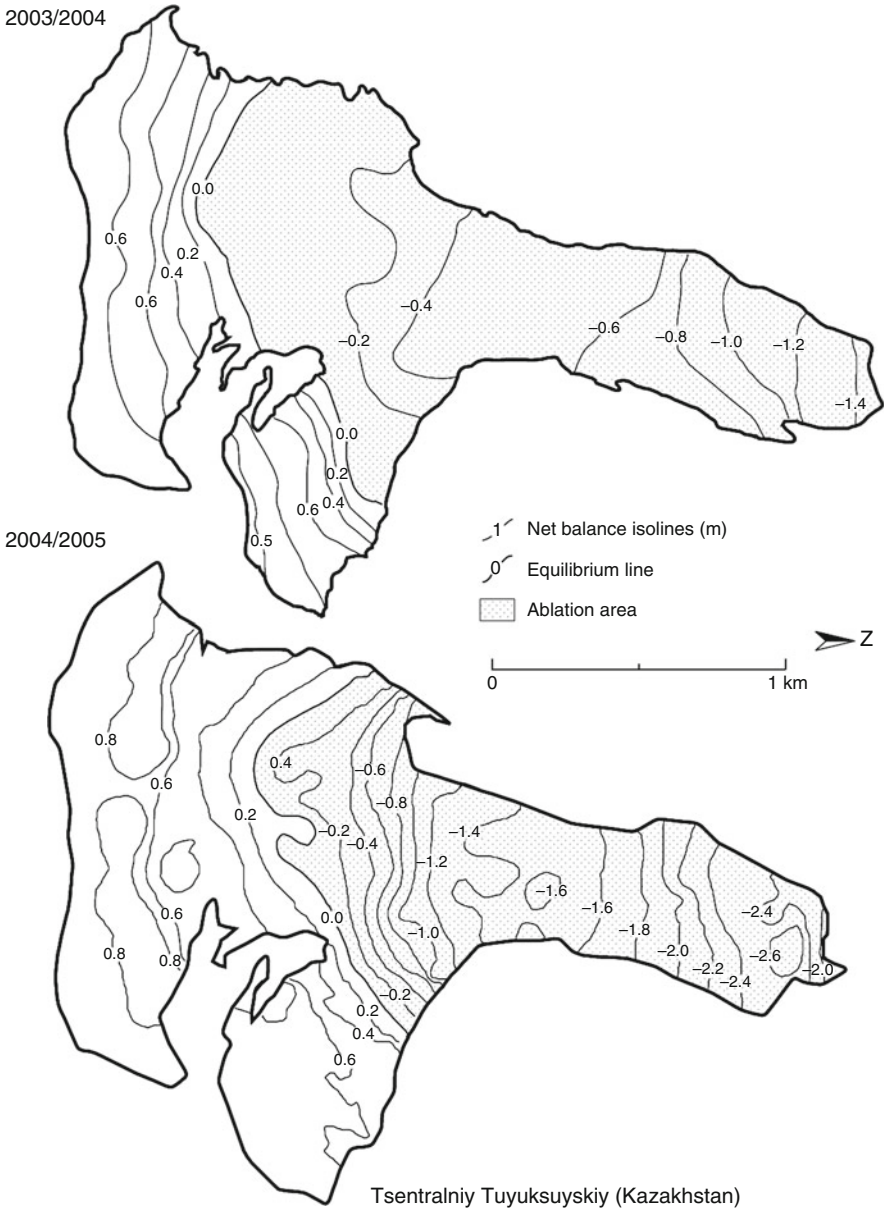

Glacier Mass Balance, Figure 2 Maps of mass balance distribution on Tuyuksu glacier (Kazakhstan/Tien Shan) at the end of the hydrological years 2003/2004 and 2004/2005 from stake/pit-measurements (direct glaciological method). (From WGMS, 2009.)

collection. Networks of ablation stakes and snow pits for accumulation measurements – the so-called direct glaciological method – provide high-resolution quantitative information on spatio-temporal patterns of mass gain and mass loss. Inter- and extrapolation of point measurements to the entire glacier surface area (Figure 2) often uses experience from expert knowledge and earlier, more detailed measurements, patterns of summer snow melt, which remain relatively stable in time, relations between mass balance and altitude, or distributed energy balance modeling using digital terrain information. Such approaches involve uncertainties that must be reduced by repeated mapping of surface area and surface elevation by the so-called geodetic (i.e., terrestrial)-photogrammetric (i.e., air-/spaceborne) method (e.g., Cogley, 2009; Haug et al., 2009; Thibert and Vincent, 2009). Carefully calibrated time series have systematic errors of less than 5 cm water equivalent per year (Thibert et al., 2008). The most commonly used time basis is a fixed-date system with (spring) measurements at the end of the (cold) accumulation period for determining winter balance and (fall) measurements after the (warm) ablation period defining annual balance; summer balance is then calculated by subtracting winter balance from annual balance. Other systems,

however, also exist (stratigraphic system relating to recognizable summer melt surfaces in the firn area) and glaciers in monsoonal climates have specific conditions with accumulation and ablation taking both place in an "active season." The measured and calculated volume change is corrected for density and divided by the surface area to provide a specific mass balance (unit: meters of water equivalent per year). This value represents an easily understood "average rate of thickness change" and is comparable worldwide between large and small glaciers.

Following a number of early observations at individual stakes (e.g., Mercanton, 1916, cf. Huss et al., 2008, 2009), long time series of detailed process-oriented mass balance observations covering entire glaciers and thus enabling worldwide inter-comparability were first initiated in Scandinavia (Storglaciären in Tarfala/Sweden since 1946, Figure 3; Storbreen Jotunheimen/Norway since 1949). These long-term observational time series in Scandinavia were later completed by comparable programs in various parts of the world, providing fundamental insights into basic phenomena and processes of climate/glacier relations (Kuhn, 1981; Oerlemans, 2001). Ablation through melting is the result of the energy balance, involving solar radiation, sensible and latent heat fluxes, while accumulation is primarily related to (solid) precipitation (e.g., Hock, 2005). As air temperature has an influence on all parts of the mass balance via solid–liquid precipitation, longwave radiation, turbulent exchanges, evaporation/condensation and sublimation, it has a predominant influence on glacier mass balance (Braithwaite, 2006; Ohmura, 2001). This predominant influence of air temperature on glacier mass balance together with the efficient mixing of the atmosphere and the well-known relation between air temperature and altitude is the basis for a number of somewhat simplified but nevertheless most important and useful analysis concepts. Such concepts are applied in mass balance modeling, using either full energy balance approaches or statistical relations between measured mass balances and meteorological parameters (for instance, positive degree-days and solid precipitation).

The dependence of glacier mass balance on air temperature causes mass balances to be spatially correlated over large regions (spanning several 100 km: Letréguilly and Reynaud, 1990; Cogley and Adams, 1998). For the same reason, mass balance primarily changes with altitude, from highest ablation at lowest parts to accumulation at higher elevations on the glacier. The equilibrium line where accumulation equals ablation and mass balance is zero separates accumulation from ablation areas on glaciers. As the sum of positive temperature decreases in a non-linear way with altitude, mass balance gradients tend to be smaller at higher altitudes and accumulation areas correspondingly larger than ablation areas for conditions of zero mass balance (continuously updated values can be found in the Glacier Mass Balance Bulletin, cf. Bahr et al., 2009). In humid-maritime regions, large amounts of ablation are required to compensate for heavy snowfall; the equilibrium line remains at altitudes with relatively high air temperature, enabling intense sensible heat flux and strong ice melt during extended ablation seasons. Temperate glaciers at melting temperature, exhibiting high mass turnover and rapid flow dominate these landscapes. The lower parts of such temperate glaciers commonly extend into grassland and forested valleys where summer

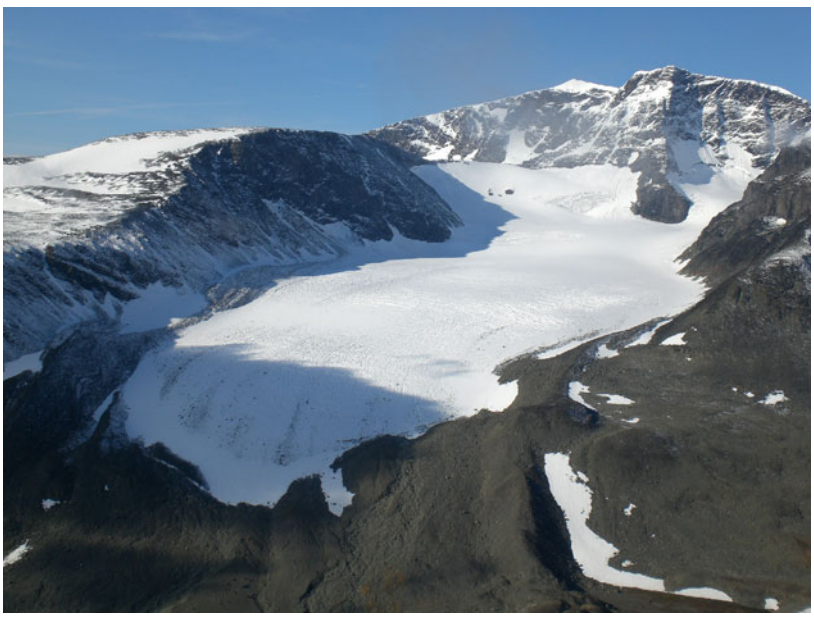

Glacier Mass Balance, Figure 3 Storglaciären near Tarfala in the Kebnekaise region, Swedish Lapland, Photo Th. Koblet. (From WGMS, 2009.)

warmth and winter snow accumulation prevent the development of permafrost (Haeberli and Burn, 2002). Ice caps and valley glaciers of Patagonia and Iceland, the western Cordillera of North America and the coastal mountain chains of New Zealand and Norway are features of this type. In contrast, dry/continental conditions such as they exist in northern Alaska, arctic Canada, subarctic Russia, parts of the Andes near the Atacama desert, or in many central-Asian mountain chains force the equilibrium line to rise to elevations with low air temperatures, short ablation seasons, reduced sensible heat flux, and limited amounts of ice melting (e.g., Braithwaite et al., 2003). In such regions, polythermal or cold glaciers, lying far beyond tree line and often even beyond tundra vegetation, have a low mass turnover, less rapid flow, and are associated with severe periglacial conditions and permafrost (Shumskii, 1964; Haeberli and Burn, 2002). Gradients of mass balance versus altitude can be an order of magnitude higher for temperate glaciers in humid-maritime regions (characteristic annual values are around 1 m of water equivalent per 100 m of elevation difference) than on polythermal/cold glaciers in dry/continental regions (characteristic annual values are about 10 cm per 100 m of elevation difference). In dry/continental regions, the firn of the accumulation zone is cold, causing meltwater produced at the surface to refreeze below surface and not to leave the glacier. For a given increase in temperature, therefore, such glaciers loose considerably less mass than temperate glaciers in maritime regions, where surface melt from the entire glacier surface runs off. As a consequence, there is a strong temperature effect on the sensitivity of glacier mass balance and atmospheric temperature rise. Such differences in mass balance gradients and thermal conditions represent the regional/climatic sensitivity of glacier mass balance (e.g., Kuhn, 1984). As changes in specific mass balance are the product of a shift in equilibrium line altitude (ELA) and the gradient of mass balance with altitude as weighed by the distribution of glacier surface area with altitude (hypsometry), the latter represents the local/individual or topographic part of the glacier mass balance sensitivity. The cumulative mass balances reported for individual glaciers thus not only reflect regional climatic variability but also mark differences in the sensitivity of the observed glaciers. Concerning evolution in time, positive feedbacks relating to surface albedo via changing snow/firn cover or dust deposition (Paul et al., 2005; Oerlemans et al., 2009) and to changing surface elevation can have strong impacts (Raymond et al., 2005) and may even cause self-reinforcing "runaway effects" (down-wasting rather than retreat of glaciers where "vertical" thickness loss is faster than the capacity of a glacier to "horizontally" retreat); increasing debris cover, on the other hand, tends to decouple glaciers from atmospheric influences, and can markedly slow down ice melting and strongly retard tongue retreat (e.g., Smiraglia et al., 2000).

Coupled mass balance and flow models parameterized with data from detailed mass balance observations have been used to simulate glacier reactions to scenarios of climate change (e.g., Oerlemans et al., 1998). Continued atmospheric temperature rise could indeed cause the complete vanishing of glaciers, which constitute the presently existing in-situ mass balance network. In the European Alps, for instance, several glaciers with long observational series of mass balance could disappear within the first half of our century and three of them (Sarennes, Careser, and Sonnblick, cf. Carturan and Seppi, 2007; Le Meur et al., 2007) may even not survive more than a decade or two from now. In order to save the continuity of the mass balance network, mass balance measurements are now being started on still larger- and higher-reaching glaciers. This is, in fact, an urgent task if sufficient overlap in time ought to be assured (Zemp et al., 2009).

Regional observations and monitoring of large glacier ensembles

Long-term integrated mass balance observations are highly demanding. The number of corresponding time series is therefore small (order of magnitude about 10, number changing in time, cf. extensive information in the Glacier Mass Balance Bulletin). A much larger number of glaciers can be observed using reduced stake networks, but still providing annual mass balance values. Repeated glacier inventories and new satellite-based technologies even allow for the calculation of mass changes of large glacier ensembles in entire mountain ranges over time periods of decades (e.g., Larsen et al., 2007, Schiefer et al., 2007). Together with flow considerations and energy balance modeling, calculations are possible of past and potential future regional glacier mass changes. This field of research has been rapidly expanding during the past decade. The following may illustrate characteristic examples.

The annual specific balance as a regional signal can be obtained most economically using geodetic/photogrammetric volume change determinations repeated at time intervals of several years to a few decades in combination with observations on a minimum of three strategically selected index stakes (Haeberli et al., 1998): two stakes should be monitored near the equilibrium line and at some suitable site in the accumulation area where the surface area is most extended and one near the glacier front to determine ablation gradients and to convert cumulative glacier length changes into cumulative mass balance values (Haeberli and Hoelzle, 1995; Hoelzle et al., 2003). Data interpretation can be made by applying a simplified version of the linear balance model (Reynaud et al., 1986), which assumes the mass balance variation at each point of the glacier to be proportional to the mass balance variation of the entire glacier. This concept is an important working tool building on the basic experience that the spatial distribution of mass balance often remains highly similar from year to year: close to the average equilibrium line altitude where surface area and, hence, the influence on the overall mass balance of a glacier is largest (Braithwaite, 2006), the temporal variability in the overall mass balance gradient remains small.

The third stake recommended for a minimum stake network should be installed at the glacier terminus in order to check on the reliability of the linear balance model and to introduce adequate corrections if necessary (cf. Kuhn, 1984; Oerlemans and Hoogendorn, 1989). Many mass balance programs follow this concept or similar simplified approaches. In total, several thousand mass balance values have been reported (until 2008) from 228 glaciers

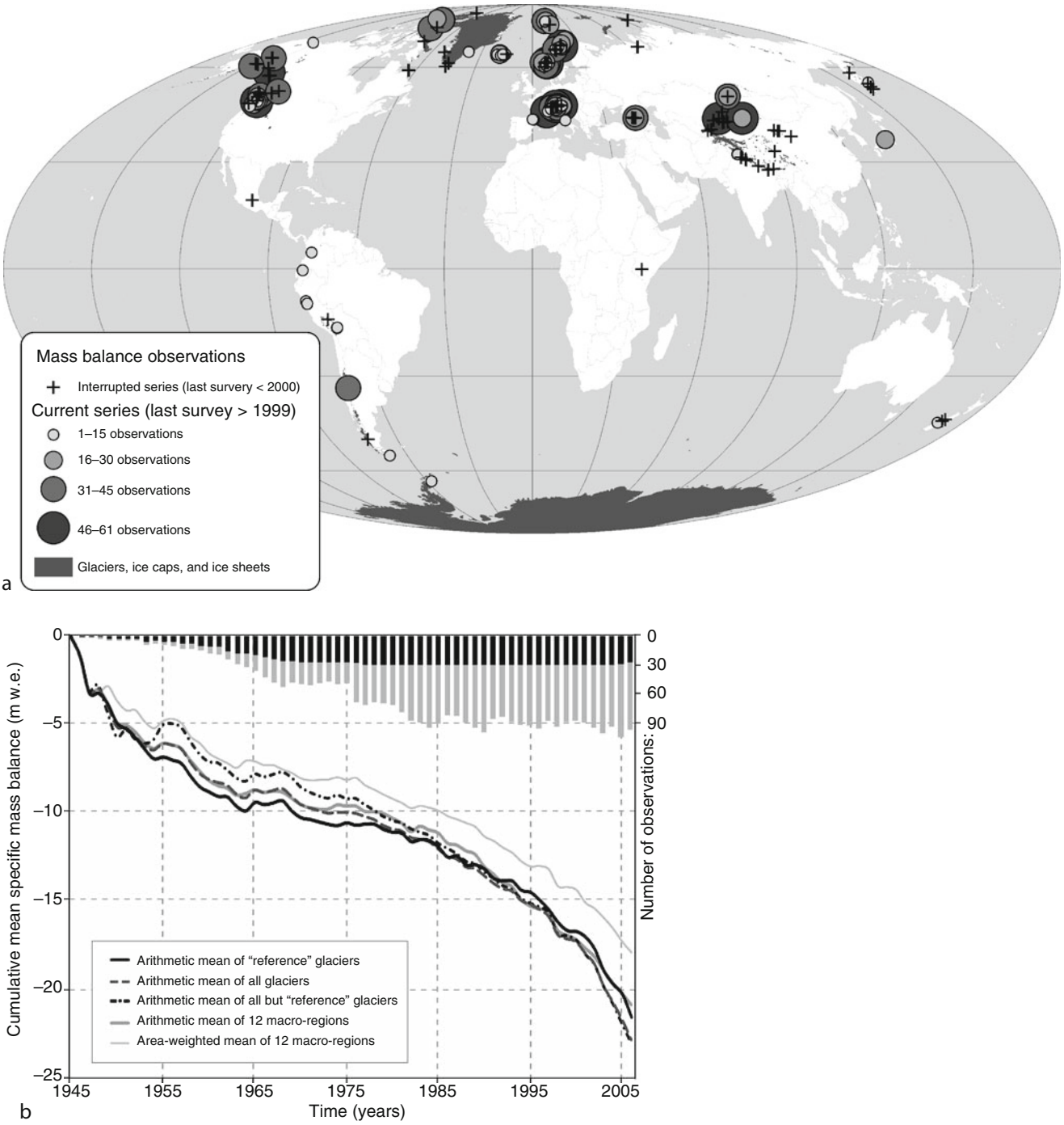

Glacier Mass Balance, Figure 4 Worldwide distribution of long-term mass balance observations (**a**) and evolution of averaged (cumulative) mass balance since 1945. (From Zemp et al., 2009.)

worldwide (Zemp et al., 2009). The sample is strongly biased towards the Northern Hemisphere and Europe and only 30 glaciers have uninterrupted series going back to 1976 (cf. Figure 1). Various statistical techniques have been applied to summarize the data. The results of these approaches differ by less than 0.1 m water equivalent per year, which roughly corresponds to the uncertainty of carefully calibrated time series. Figure 4 shows the averaged development during the past six decades, indicating a strong ice loss as early as the 1940s and 1950s followed by a moderate mass loss until the end of the 1970s and a subsequent acceleration, which continues until now. The compilation also shows an increasing uniformity of the development at a global scale. Reconstruction of past glacier mass balances based on mass conservation and cumulative length change reveal that present loss rates start exceeding characteristic loss rates during the twentieth century (Hoelzle et al., 2003), since the end of the Little Ice Age (Haeberli and Hoelzle, 1995) or even during the past millennia (Haeberli and Holzhauser, 2003). Such reconstructions have a poor time resolution (decades), but are independent of direct mass balance measurements or climatic data. Mass balance reconstructions using numerical mass balance models driven by meteorological data and tuned to data measured in the field confirm this general finding and provide annual values (Huss et al., 2008, Nemec et al., 2009). Annual values reconstructed in this way, however, are not independent of climatic/meteorological data and must be clearly separated from directly measured and independently determined glacier information. The combination of the two approaches, however, increases the confidence in the reported values. They leave no doubt that striking worldwide mass losses of glaciers have taken place during the past century (Ohmura, 2006) and tend to continue at an accelerating rate. In the European Alps, for instance, glaciers have lost about half their total volume (roughly −0.5% per year) between 1850 and around 1975, another 25% (or −1% per year) of the remaining amount between 1975 and 2000, and an additional 10–15% (or −2% to −3% per year) in the first 5 years of this century (Haeberli et al., 2007). Scenario calculations concerning effects of global atmospheric warming (Nesje et al., 2008; Paul et al., 2007; Zemp et al., 2006) clearly confirm earlier regional projections (Haeberli and Hoelzle, 1995) that many mountain ranges could lose major parts of their glacier volumes within the twenty-first century and that the strongest melting in such regions is likely to take place during the coming decades. The rate of mass loss is, in fact, higher than can be explained by radiative forcing and meteorological effects alone. Feedback mechanisms, especially related to albedo lowering (Oerlemans et al., 2009), are therefore likely to play an increasing role.

In recent years, the striking development of glacier mass loss at a global scale and at fast if not accelerating rates was accompanied by rapid developments in observational methodology. Prominent technologies, such as airborne laser altimetry in combination with kinematic GPS (Abdalati et al., 2004); spaceborne digital elevation models (DEMs) from SRTM, ASTER, or SPOT (e.g., Berthier et al., 2004, 2010; Larsen et al., 2007; Rignot et al., 2003; Schiefer et al., 2007; Surazakov and Aizen 2006); and distributed modeling of the climatic accumulation areas or the mass and energy balance for individual glaciers (Arnold et al., 2006) or large glacier ensembles (Machguth et al., 2006a; Zemp et al., 2007), open new dimensions for monitoring and analyzing glacier mass balance and glacier mass changes. The difficulties are still considerable but the perspectives are most promising. Correct determination of complex precipitation and accumulation patterns influenced by wind drift and avalanching remains a fundamental problem for distributed energy and mass balance modeling for large glacier ensembles (Machguth et al., 2006b). The related

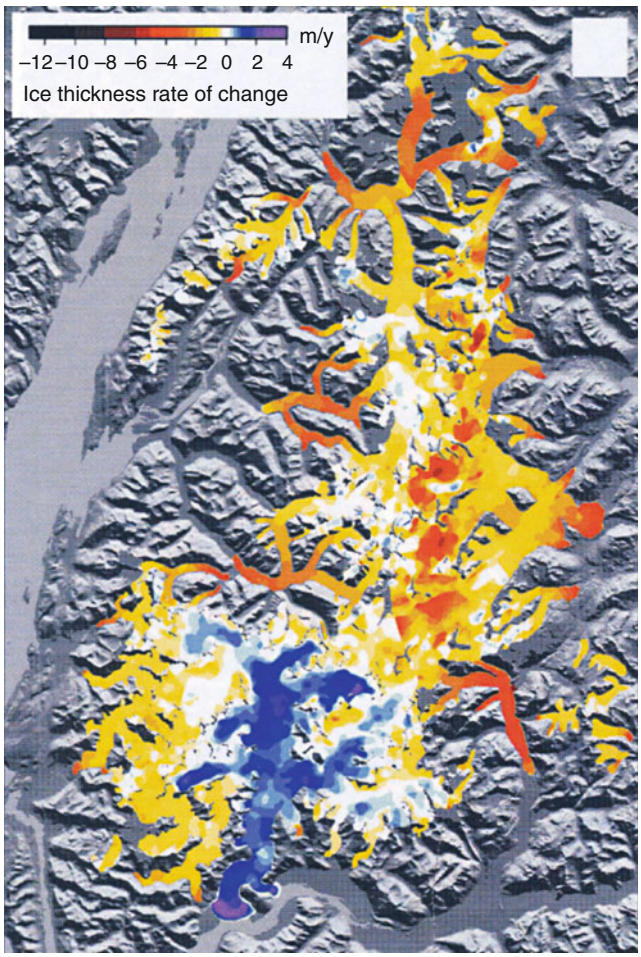

Glacier Mass Balance, Figure 5 Mean annual surface altitude changes of the Juneau Ice Field and its glaciers (southern Alaska) during the past decades (variable time basis) on the basis of DEM-differencing using the Shuttle Radar Topography Mission (SRTM) and older Geological Survey Maps. (From Larsen et al., 2007, reproduced by permission of American Geophysical Union)

uncertainty requires to check the measurements with independent evidence from laser altimetry, which enables very high precision to be reached, or by differencing of DEMs, which is less precise but nevertheless able to document the very large changes during time periods of decades (Kääb, 2008). The example from southern Alaska shown in Figure 5, for instance, shows average thickness losses for a great number of small and large glaciers of several meters per year, in general peaking at the lowermost, flat parts of the glacier tongues. For the first time, such DEM differencing helps establishing, how representative mass balance observations at single glaciers are with respect to all glaciers of a mountain range (Paul and Haeberli, 2008) or even all glaciers on earth. This is especially important with respect to the calculation of glacier contributions to sea-level rise, which mainly involves the largest glaciers on earth with strong dynamic effects – especially calving of tidewater glaciers – on surface mass balance and mass loss (Meier et al., 2007).

Summary

Glacier mass balance as the difference between mass gain through snow accumulation and mass loss through melting and sometimes calving is a rather direct result of fluctuating atmospheric conditions and a key natural indicator of global climate change. International monitoring strategies combine in situ observations at networks of stakes and snow pits (direct glaciological method for process understanding and annual to seasonal time resolution) with repeated mapping (geodetic/photogrammetric method for calibration of field measurements and determination of overall volume/mass change). Modern remote sensing techniques include laser altimetry, radar, gravimetry, and differencing of digital elevation models (DEM) for large glacier ensembles. Long-term in situ mass balance measurements for entire glaciers started after World War II, today involve regular observations at about 100 glaciers worldwide, and reveal a trend of rapidly accelerating mass loss during the past decades.

Bibliography

http://www.wgms.ch/

Abdalati, W., and 9 others. 2004. Elevation changes of ice caps in the Canadian Arctic Archipelago. *Journal of Geophysical Research*, **109**(F4), F04007. (10.1029/2003JF000045.)

Arnold, N. S., Rees, W. G., Hodson, A. J., and Kohler, J., 2006. Topographic controls on the surface energy balance of a high Arctic valley glacier. *Journal of Geophysical Research*, **111**(F2), F02011 (10.1029/2005JF000426).

Bahr, D. B., Dyurgerov, M., and Meier, M. F., 2009. Sea level rise from glaciers and ice caps: a lower bound. *Geophysical Research Letters*, **36**, L03501, (10.1029/2008GL036309)

Berthier, E., Arnaud, Y., Baratoux, D., Vincent, C., and Rémy, F., 2004. Recent rapid thinning of the "Mer de Glace" glacier derived from satellite optical images. *Geophysical Research Letters*, **31**(17), L17401, (10.1029/2004GL020706)

Berthier, E., Schiefer, E., Clarke, G. K. C., Menounos, B., and Rémy, F., 2010. Contribution of Alaskan glaciers to sea-level rise derived from satellite imagery. *Nature Geoscience Letters*, **3**, 92–95.

Braithwaite, R. J., 2002. Glacier mass balance: the first 50 years of international monitoring. *Progress in Physical Geography*, **26**(1), 76–95.

Braithwaite, R., 2006. Measuring and modelling the mass balance of glaciers for global change. In Knight, P. G. (ed.), *Glacier Science and Environmental Change*. Malden, Oxford, Carlton: Blackwell, pp. 418–423.

Braithwaite, R. J., Zhang, Y., and Raper, S. C. B., 2003. Temperature sensitivity of the mass balance of mountain glaciers and ice caps as a climatological characteristic. *Zeitschrift für Gletscherkunde und Glazialgeologie*, **38**, 35–61.

Carturan, L., and Seppi, R., 2007. Recent mass balance results and morphological evolution of Careser Glacier (Central Alps). *Geografia Fisica e Dinamica Quaternaria*, **30**(1), 33–42.

Cogley, J. G., 2009. Geodetic and direct mass balance measurements: Comparison and joint analysis. *Annals of Glaciology*, **50**(50), 96–100.

Cogley, J. G., and Adams, W. P., 1998. Mass balance of glaciers other than the ice sheets. *Journal of Glaciology*, **44**(147), 315–325.

Dyurgerov, M. B., and Meier, M. F., 1997. Mass balance of mountain and subpolar glaciers: a new global assessment for 1961–1990. *Arctic and Alpine Research*, **29**(4), 379–391.

Haeberli, W., 2004. Glaciers and ice caps: historical background and strategies of world-wide monitoring. In Bamber, J. L., and Payne, A. J. (eds.), *Mass Balance of the Cryosphere*. Cambridge University Press: Cambridge, pp. 559–578.

Haeberli, W., 2005. Mountain glaciers in global climate-related observing systems. In Huber, U. M., Bugmann, H. K. H., and Reasoner, M. A. (eds.), *Global Change and Mountain Regions (A State of Knowledge Overview)*. Springer: Dordrecht, pp. 169–175.

Haeberli, W., and Burn, C., 2002. Natural hazards in forests – glacier and permafrost effects as related to climate changes. In Sidle, R. C. (ed.), Environmental Change and Geomorphic Hazards in Forests. IUFRO Research Series, 9, pp. 167–202.

Haeberli, W., and Hoelzle, M., 1995. Application of inventory data for estimating characteristics of and regional climate-change effects on mountain glaciers: a pilot study with the European Alps. *Annals of Glaciology*, **21**, pp. 206–212. Russian translation in: Data of Glaciological Studies, Moscow (Materialy glyatsiologicheskih issledovanii, Moscow, Russia), 82, pp. 116–124.

Haeberli, W., Hoelzle, M., and Suter, S. (eds.) 1998. Into the second century of worldwide glacier monitoring: prospects and strategies. A contribution to the International Hydrological Programme (IHP) and the Global Environment Monitoring System (GEMS). UNESCO – Studies and Reports in Hydrology 56.

Haeberli, W., and Holzhauser, H., 2003. Alpine glacier mass changes during the past two millennia. *Pages News*, **11**(1), 13–15.

Haeberli, W., Hoelzle, M., Paul, F., and Zemp, M., 2007. Integrated monitoring of mountain glaciers as key indicators of global climate change: the European Alps. *Annals of Glaciology*, **46**, 150–160.

Haug, T., Rolstad, C., Elvehøy, H., Jackson, M., and Maalen-Johansen, M., 2009. Geodetic mass balance of the western Svartisen ice cap, Norway, in the periods 1968 1985 and 1985 2002. *Annals of Glaciology*, **50**(50), 119–125.

Hock, R., 2005. Glacier melt: a review of processes and their modelling. *Progress in Physical Geography*, **29**(3), 362–391.

Hoelzle, M., Haeberli, W., Dischl, M., and Peschke, W., 2003. Secular glacier mass balances derived from cumulative glacier length changes. *Global and Planetary Change*, **36**(4), 77–89.

Huss, M., Bauder, A., Funk, M., and Hock, R., 2008. Determination of the seasonal mass balance of four Alpine glaciers since 1865.

Journal of Geophysical Research, **113**, F01015, doi:10.1029/2007JF000803.

Huss, M., Funk, M., and Ohmura, A., 2009. Strong Alpine glacier melt in the 1940s due to enhanced solar radiation. *Geophysical Research Letters*, **36**, L23501, doi: 10.1029/2009GL040789.

IPCC 2007. Climate change 2007: the physical science basis. Contribution of Working Group 1 to the Fourth Assessment Report of the Intergovernmental Panel on Climate Change (eds.: Solomon, S., Qin, D., Manning, M., Chen, Z., Marquis, M. C., Averyt, K., Tignor, M., and Miller, H. L.). Intergovernmental Panel on Climate Change, Cambridge and New York.

Kääb, A., 2008. Glacier volume changes using ASTER satellite stereo and ICES at GLAS laser altimetry. A test study on Edgeøya, Eastern Svalbard. *IEEE Transactions on Geosciences and Remote Sensing*, **46**(10), 2823–2830.

Kaser, G., Fountain, A., and Jansson, P., 2003. A manual for monitoring the mass balance of mountain glaciers with particular attention to low latitude characteristics. A contribution from the International Commission on Snow and Ice (ICSI) to the UNESCO HKH-Friend programme. IHP-VI, *Technical Documents in Hydrology*, No. 59, UNESCO, Paris: 107 pp. + Appendices.

Kaser, G., Cogley, J. G., Dyurgerov, M. B., Meier, M. F. and Ohmura, A. (2006): Mass balance of glaciers and ice caps: Consensus estimates for 1961–2004. *Geophysical Research Letters*, 33(L19501) (doi:10.1029/2006GL027511).

Kuhn, M., 1981. Climate and glaciers. *IAHS*, **131**, 3–20.

Kuhn, M., 1984. Mass budget imbalances as criterion for a climatic classification of glaciers. *Geografiska Annaler*, **66A**(3), 229–238.

Larsen, C. F., Motyka, R. J., Arendt, A. A., Echelmeyer, K. A., and Geissler, P. E., 2007. Glacier changes in southeast Alaska and northwest British Columbia and contribution to sea level rise. *Journal of Geophysical Research*, **112**, F01007. (10.1029/2006JF000586), American Geophysical Union

Le Meur, E., Gerbaux, M., Schäfer, M., and Vincent, C., 2007. Disappearance of an Alpine glacier over the 21st Century simulated from modeling its future surface mass balance. *Earth and Planetary Science Letters*, **261**(3–4), 367–374.

Letréguilly, A., and Reynaud, L., 1990. Space and time distribution of glacier mass balance in the northern hemisphere. *Arctic and Alpine Research*, **22**(1), 43–50.

Machguth, H., Paul, F., Hoelzle, M., and Haeberli, W., 2006a. Distributed glacier mass-balance modelling as an important component of modern multi-level glacier monitoring. *Annals of Glaciology*, **43**, 335–343.

Machguth, H., Eisen, O., Paul, F., and Hoelzle, M., 2006b. Strong spatial variability of snow accumulation observed with helicopter-borne GPR on two adjacent Alpine glaciers. *Geophysical Research Letters*, **33**, L13503, doi:10.1029/2006GL026576.

Meier, M. F., Dyurgerov, M. B., Rick, U. K., O'Neel, S., Pfeffer, W. T., Anderson, R. S., Anderson, S. P., and Glazovsky, A. F., 2007. Glaciers dominate eustatic sea-level rise in the 21st century. *Science*, **317**(5841), 1064–1067.

Mercanton, P. L., 1916. Vermessungen am Rhonegletscher. Neue Denkschriften der Schweizerischen Naturforschenden Gesellschaft 52.

Nemec, J., Huybrechts, Ph, Rybak, O., and Oerlemans, J., 2009. Reconstruction of the annual balance of Vadret da Morteratsch, Switzerland, since 1865. *Annals of Glaciology*, **50**(50), 126–134.

Nesje, A., Bakke, J., Dahl, S. O., Lie, O., and Matthews, J. A., 2008. Norwegian mountain glaciers in the past, present and future. *Global and Planetary Change*, **60**(1–2), 10–27.

Oerlemans, J., 2001. *Glaciers and climate change*. Lisse Abingdon, Exton, Tokyo: A.A. Balkema, p. 148.

Oerlemans, J., Giessen, R. H., and van den Broeke, M. R., 2009. Retraeting alpine glaciers: increased melt rates due to accumulation of dust (Vadret da Morteratsch, Switzerland). *Journal of Glaciology*, **55**(192), 729–736.

Oerlemans, J., and Hoogendorn, N. C., 1989. Mass balance gradients and climatic change. *Journal of Glaciology*, **35**(121), 399–405.

Oerlemans, J., Anderson, B., Hubbard, A., Huybrechts, P., Johannesson, T., Knap, W. H., Schmeits, M., Stroeven, A. P., van de Wal, R. S. W., Wallinga, J., and Zuo, Z., 1998. Modelling the response of glaciers to climate warming. *Climate Dynamics*, **14**(4), 267–274.

Ohmura, A., 2001. Physical basis of the temperature-based melt-index method. *Journal of Applied Meteorology*, **40**(4), 753–761.

Ohmura, A., 2006. Changes in mountain glaciers and ice caps during the 20th century. *Annals of Glaciology*, **43**, 361–368.

Paul, F., and Haeberli, W., 2008. Spatial variability of glacier elevation changes in the Swiss Alps obtained from two digital elevation models. *Geophysical Research Letters*, **35**, L21502, doi:10.1029/2008/GL034718.

Paul, F., Machguth, H., and Kääb, A., 2005. On the impact of glacier albedo under conditions of extreme glacier melt: the summer of 2003 in the Alps. EARSeL Workshop on Remote Sensing of Land Ice and Snow, Berne, 21–23.2. 2005. *EARSeL eProceedings*, **4**(2), 139–149.

Paul, F., Maisch, M., Rothenbühler, C., Hoelzle, M., and Haeberli, W., 2007. Calculation and visualisation of future glacier extent in the Swiss Alps by means of hypsographic modelling. *Global and Planetary Change*, **55**(4), 343–357.

Raymond, Ch, Neumann, T. A., Rignot, E., Echelmeyer, K., Rivera, A., and Casassa, G., 2005. Retreat of Glaciar Tyndall, Patagonia, over the last half-century. *Journal of Glaciology*, **51**(173), 239–247.

Reynaud, L., Vallon, M., and Letréguilly, A., 1986. Mass balance measurements: problems and two new methods of determining variations. *Journal of Glaciology*, **32**(112), 446–454.

Rignot, E., Rivera, A., and Casassa, G., 2003. Contribution of the Patagonia icefields of South America to sea level rise. *Science*, **302**, 434–437.

Schiefer, E., Menounos, B., and Wheate, R., 2007. Recent volume loss of British Columbian glaciers, Canada. *Geophysical Research Letters*, **34**, L16503, doi:10.1029/2007GL030780.

Shumskii, P. A., 1964. *Principles of structural glaciology*. New York: Translated from the Russian by D. Kraus. Dover Publications Inc., p. 497.

Smiraglia, C., Diolaiuti, G., Casati, D., and Kirkbride, M. P., 2000. Recent areal and altimetric variations of Miage Glacier (Monte Bianco massif, Italian Alps). *IAHS*, **264**, 227–233.

Surazakov, A. B., and Aizen, V. B., 2006. Estimating volume change of mountain glaciers using SRTM and map-based topographic data. *IEEE Transactions of Geoscience and Remote Sensing*, **44**(10), 2991–2995.

Thibert, E., and Vincent, C., 2009. Best possible estimation of mass balance combining glaciological and geodetic methods. *Annals of Glaciology*, **50**(50), 112–118.

Thibert, E., Blanc, R., Vincent, C., and Eckert, N., 2008. Glaciological and volumetric mass-balance measurements: error analysis over 51 years for Glacier de Sarennes, French Alps. *Journal of Glaciology*, **54**(186), 522–532.

UNEP, 2007. *Global outlook for ice and snow*. EarthPrint: United Nations Environment Programme, p. 235.

WGMS, (2008a): Global Glacier Changes: Facts and Figures. Zemp, M., Roer, I., Kääb, A., Hoelzle, M., Paul, F., and Haeberli, W. (eds.), UNEP, World Glacier Monitoring Service, Zurich, Switzerland.

WGMS, (2008b): Fluctuations of Glaciers 2000–2005 (Vol. IX, W. Haeberli, M. Zemp, A. Kääb, F. Paul and M. Hoelzle eds). Zurich, Switzerland; ICSU (FAGS), IUGG (IACS), UNEP, UNESCO, WMO.

WGMS, (2009): Glacier Mass Balance Bulletin No. 10 (W. Haeberli, I. Gärtner-Roer, M. Hoelzle, F. Paul and M. Zemp eds.). WGMS, University of Zurich, Switzerland.
Zemp, M., Haeberli, W., Hoelzle, M., and Paul, F., 2006. Alpine glaciers to disappear within decades? *Geophysical Research Letters*, **33**, L13504, doi:10.1029/2006GL026319.
Zemp, M., Hoelzle, M., and Haeberli, W., 2007. Distributed modelling of the regional climatic equilibrium line altitude of glaciers in the European Alps. *Global and Planetary Change*, **56**, 83–100.
Zemp, M., Hoelzle, M., and Haeberli, W., 2009. Six decades of glacier mass balance observations – a review of the worldwide monitoring network. *Annals of Glaciology*, **50**(50), 101–111.

Cross-references

Aerial Photogrammetry for Glacial Monitoring
Albedo
Climate Change and Glaciers
Deglaciation
Degree-Days
Equilibrium-Line Altitude (ELA)
Firn
Glacier
Glacier Mass Balance
Surface Energy Balance
Tidewater Glaciers
WGMS (World Glacier Monitoring Service)

GLACIER MOTION/ICE VELOCITY

Terry Hughes
Department of Earth Science, Climate Change Institute, University of Maine, Orono, ME, USA

Synonyms

Dynamics of glaciers

Definition

Glaciers. Bodies of ice massive enough to thin and spread under their own weight.
Ice sheet. A glacier that covers large parts of a continent or a large island.
Ice shelf. The floating perimeter of parts of an ice sheet grounded in water.
Ice stream. A fast current of ice imbedded in an ice sheet.
Terrestrial ice sheet. Parts of an ice sheet grounded above sea level on land.
Marine ice sheet. Parts of an ice sheet grounded below sea level in water.

Historical background

Glaciers are bodies of ice massive enough to flow under their own weight due to the action of Earth's gravitational field. This definition excludes sea, lake, and river ice, which are moved by wind and water currents, and ice-cemented ground in the permafrost condition, in which ice is trapped in the pores of soil and rock. However, gravity can thin sufficiently thick floating ice and move permafrost down steep slopes. Then these bodies behave like glaciers.

The first recorded scientific studies of glaciers took place in Iceland, the Swiss Alps, and in the mountains of Scandinavia as early as the seventeenth century. Major incentives for these studies were the spectacular appearance of mountain glaciers, the recreational activities these glaciers provided, their essential supply of freshwater to farms and villages, and, later, hydroelectric power provided by this water supply. An early discovery was that these bodies of ice moved downslope, with ice supplied by winter snowfall on the colder upper slopes and lost by summer melting on the warmer lower slopes. It was also noted that these glaciers moved loose material, mostly boulders, gravel, sand, and clay, which could be either carried on the ice surface or entrained in basal ice moving over the bed. Loose material deposited by glaciers is called till.

By the nineteenth century, scientists were pondering the loops of till, now called moraines, that arced around the ends of valleys occupied by glaciers farther upslope. They knew that these glaciers had extended downslope and deposited moraines during a few centuries of unusual cold in Europe that followed a warmer climate in medieval times, which later came to be called the Medieval Climate Optimum. In addition, large boulders called erratics were scattered across the North European Plain and could be traced to source areas in the Scandinavian mountains and elsewhere. These deposits were originally called "drift" on the belief they were transported during the Biblical flood in Genesis. That belief was replaced by the realization that the "flood" had indeed occurred but the water was in its solid state, ice. This is when two new branches of science, glaciology and glacial geology, were born. Glaciologists studied existing glaciers and glacial geologists studied the deposits left by former glaciers. Most of these early scientists were called naturalists, and for them glaciology and glacial geology were the same discipline that studied causes and effects, opposite sides of the same coin.

A Swiss naturalist, Louis Agassiz, did most to popularize the idea that vast sheets of ice spread out from the Alps and the mountains of Scandinavia onto the surrounding lowlands. He came to America and found evidence that a vast sheet of ice had come down from Canada and covered the northeastern USA. The Ice Age Theory was born from such observations by Agassiz and others in the middle and later decades of the nineteenth century. In the early decades of the twentieth century, glacial geology largely separated from glaciology and became incorporated into geomorphology, a branch of geology. These geologists, in mapping glacier deposits in North America, Europe, and western Siberia, soon realized that there had been several massive southward advances of ice, at least four, in these regions. They also found that a smaller advance of ice from the Alps and Scandinavia had occurred at the end of the Medieval Warm Period, but had ended around 1850–1880 when these glacial geologists began mapping

glacier deposits. They called this cold period the Little Ice Age. At the same time, glaciology was being developed as a separate discipline within geology when other scientists who joined explorers to the Arctic and Antarctic regions discovered that Greenland and Antarctica were blanketed by vast sheets of ice, and the highlands of Arctic islands often wore caps of ice. During this period, a whole new scientific vocabulary was developed to describe the great variety of glaciers and the deposits left by them. This encyclopedia presents the new vocabulary, which continues to grow with new discoveries in the twenty-first century.

The primary task of glacial geologists became finding and using ways to date glacial deposits and the landscapes eroded by glaciers, especially by the large continental ice sheets. Dating techniques range from relative ages found by studying organic fossils in stratified deposits linked to glaciers, to absolute ages obtained by counting "varved" layers of sediments deposited seasonally in proglacial lakes, by counting tree rings dating from glacial times, by radiocarbon dating of organic pollen, wood and marine fossils, by other radiometric dating techniques, by seasonal variations of airborne and waterborne trace ions or chemicals usually obtained from cores recovered from glaciers and from sediments on the floors of oceans and lakes, and most recently by dating rocks exposed to damage by "cosmogenic" radiation after glaciers retreated.

The primary task of glaciologists became understanding the mechanisms by which glaciers of all sizes moved over the face of the Earth. This task was undertaken after World War II by physicists, notably in Britain and America, who had been engaged in military applications of ice ("ice ships" that could not be sunk by German torpedoes were the goal of the "Habakkuk Project" in Britain and Canada), and in conducting logistical operations in polar regions (the task of CRREL, the Cold Regions Research and Engineering Laboratory of the U.S. Army in New Hampshire). By 1950, glaciology was being converted from a descriptive branch of geology to an analytical branch of physics. This was the time of the Cold War between East and West, and like the Big Four in that struggle, there was a Big Four in glaciology, John Nye (UK), Louis Lliboutry (France), Petr Shumsky (USSR), and Johannes Weertman (USA). Also notable at that time were John Glen who obtained a "flow law" for glacier ice, Charles Bentley who conducted many of the geophysical measurements (seismic, magnetic, and gravity) along tractor-train traverses across the Antarctic Ice Sheet during and after the International Geophysical Year, Barclay Kamb who determined the other crystal structures of ice that exist at temperatures lower and pressures higher than those found on Earth's surface, Lyle Hansen who developed deep ice drilling and coring technology at CRREL, and Stanley Evans who developed radar-sounding technology. There were many others.

John Nye began by studying flow of glaciers, first in 1951 using plasticity theory in which no flow takes place until a "yield stress" is attained, and then using Glen's flow law. Lliboutry in 1964 produced the first textbook, *Traite de Glaciologie*, that presented a synthesis in which the force balance and the mass balance in glaciers were combined in a systematic way to show how glaciers moved under the force of gravity resisted by "drag" forces at the bed, and how the advance or retreat of glaciers depended on whether accumulation by snowfall at higher elevations was more or less than ablation by melting at lower elevations. Shumsky, largely self-taught and prevented from interacting with the larger glaciological community by Cold War rivalries, created glaciology as a profession in the Soviet Union almost single-handedly. Weertman developed a "sliding law" for glaciers moving over a wet bed and a "flow law" for floating ice spreading under gravity, both in 1957, and was among the first to place the advance and retreat of ice sheets in the larger context of glaciation cycles during the Quaternary Ice Age (the last million years).

These and other glaciologists most active from 1950 to 1970 constitute the Founding Generation of modern glaciology. They trained glaciologists who became a Transitional Generation most active from 1970 to 1990 who trained glaciologists at a time when great advances in technology were being applied to glaciological problems, giving us the present High-Tech Generation from 1990 to 2010. They in turn are training a new generation of glaciologists who will probably become known as the Holistic Generation that incorporates glaciology into climatology with the goal of understanding global climate change, especially rapid change.

A major discovery in the second half of the twentieth century was that ice sheets not only formed on land above sea level, but also formed on land below sea level and produced much the same glacial geology. These "marine" ice sheets had an inherent instability when they ended as floating ice shelves. If the marine bed had become a bowl-shaped depression under the heavy load of ice, the ice-shelf grounding line might retreat irreversibly downslope and rapidly convert the marine ice sheet into a floating ice shelf, which might then disintegrate rapidly, thereby removing the ice sheet from Earth's climate system. This happened to several marine ice sheets shortly after the last glacial maximum and terminated the last glaciation cycle. These ice sheets lost coupling to the bed. Just when ice sheets seemed most stable and permanent, was also when they had depressed their beds farthest below sea level, making them vulnerable to the marine instability. Their rapid collapse into ice shelves that quickly disintegrated into icebergs called attention to the force balance in ice sheets.

The force balance

The force balance describes how glaciers change in shape over time. The fundamental fact of glaciology is that the height of glaciers above the bed is determined by how strongly ice is coupled to the bed. Glaciers thin and spread, a change in shape, when coupling weakens,

thereby changing the balance between gravitational forces causing ice motion and forces that resist motion. Ice-bed coupling weakens first as a frozen bed becomes thawed and then as basal water is able to progressively "float" the overlying ice by drowning bedrock bumps that project up into ice and anchor overlying ice to the bed. In ice sheets, the largest glaciers, ice flow diverges slowly from interior ice domes, gains velocity as it converges on ice streams, and then spreads out as ice lobes grounded on land or as ice tongues floating in water and often imbedded in ice shelves. For sheet flow, gravitational forcing is proportional to the product of ice thickness and ice surface slope, and is resisted primarily by basal drag. For shelf flow, gravitational forcing is proportional to the height of ice floating above water, and is resisted by a tensile stress that resists this gravitational "pulling" for freely floating ice tongues. In ice shelves, additional resistance is provided by shear against the sides of a confining embayment and at basal pinning points where the ice shelf is grounded locally. In stream flow, the gravitational forcing for sheet flow is gradually replaced by the gravitational forcing for shelf flow as a "floating fraction" of ice increases along an ice stream. Gravitational forcing is resisted by a tensile stress that "pulls" upstream ice, a compressive stress that "pushes" downstream ice, side shear against slower moving lateral ice, and basal sliding where ice contacts a thawed bed under ice streams and their terminal ice lobes or confined and pinned ice shelves. Such ice shelves "buttress" ice streams that supply them with ice. Disintegration of a buttressing ice shelf can cause the feeder ice streams to quickly surge, often doubling their velocity, as has been observed for Greenland and Antarctic ice streams in recent years.

Ice velocities shearing against a frozen bed in basal shear, shearing against slower moving ice in side shear, pulling slower ice in tension, or pushing slower ice in compression are linked to gravitational stresses that force ice motion by a "flow law" of ice. The flow law developed by Glen applies to ice shearing over a frozen bed for slow sheet flow. This is analogous to shearing a deck of cards over a tabletop when the bottom card is glued to the table. For floating ice, the flow law applies to ice spreading over the water surface as it thins under the force of gravity. This is analogous to flattening a deck of cards floating in water. Sliding laws apply to ice spreading over a wet bed, but retaining contact with the bed. This is analogous to moving the deck of cards intact over a tabletop when the table is slippery. Weertman developed a sliding law in which only a "film" of water coats bedrock bumps that resist sliding motion, so basal water pressure does not appear in his sliding law. Lliboutry developed a sliding law in which cavities on the lee side of bumps could fill with water and growth of these water-filled cavities could extend ice-bed uncoupling from a local scale to a regional scale. Basal water pressure enters his sliding law. All treatments of glacier sliding on a wet bed spring from these two early efforts. Ongoing efforts center around how to quantify bed roughness and the subglacial hydrology that moves water from sources to sinks on a rough bed. Basal sliding is altered when deformable sediments or till separate basal ice from bedrock. Deformation depends primarily on water content, the size distribution of solid particles, their mineralogy, and on subglacial hydrology that moves basal water from sources to sinks.

Both flow laws and sliding laws of ice begin with a force balance. In deriving a flow law, an external force (such as gravity) is applied to the base of an imaginary triangular pyramid imbedded in ice, and it is balanced by resisting internal forces applied tangent to and normal to the other three triangular faces of the pyramid of ice. Dividing the forces by the areas of faces they contact gives stresses on these faces. These stresses are separated into those that change the size of the pyramid, called confining stresses, and those that change the pyramid shape, called creep stresses (or deviator stresses, because they "deviate" from confining stresses). The flow law is obtained from measuring the rate of ice deformation caused by creep stresses. Simple combinations of creep stresses, such as a compressive stress normal to opposite circular faces of a cylindrical ice specimen or a shear stress parallel to these faces, are applied to the ice specimen and the change in shape of the specimen is measured over time. This change in shape is recorded as strain rates, which are changes in ice velocity measured along the mutually perpendicular axes used to describe the creep stresses as normal stresses or shear stresses. The strain rates are related to the creep stresses in creep experiments in which either temperature is kept constant while stresses change or stresses are kept constant while temperature is changed. Measured strain rates in both cases describe the creep deformation of ice resulting from changing stress and temperature. Creep deformation increases exponentially with linear changes in stress and temperature. This makes creep deformation of ice closer to the purely plastic deformation originally assumed by Nye than to the viscous deformation of fluids in which strain rate varies linearly with creep stress. In sheet flow over a frozen bed, the gravitational deforming stress varies with the product of ice thickness and surface slope, and is resisted by the basal shear stress.

The force balance in sliding laws of ice balances the gravitational driving stress produced by Newton's second law of motion against the resisting force produced by Newton's third law of motion. In Newton's second law, force equals mass times acceleration. Applied to glaciers, it equates ice mass with the product of ice density and ice volume, ice volume being ice height above the bed times unit basal area, and acceleration being the acceleration of gravity resolved along the direction of greatest ice surface slope. In Newton's third law, every force is opposed by an equal and opposite resisting force. Applied to glaciers, the gravitational driving stress causes downslope ice motion that is resisted by a basal drag force equal to the product of the basal shear stress times unit basal area in Newton's third law of motion. When the bed is thawed, a water film between basal ice and the bed cannot transmit the shear stress, so sliding motion of ice must be resisted

by normal stresses acting on faces of bedrock bumps that project up into basal ice. These normal stresses are compressive where ice pushes against bumps and tensile where ice pulls away from bumps. The tensile stress vanishes if water-filled cavities form on the lee side of bumps. When bumps are small, the compressive stress becomes very large because the gravitational driving force acts against a very small area (stress equals force per unit area). This compressive stress crushes ice into water, water occupying a smaller volume for the same mass of ice. The meltwater then flows around the bump and refreezes in the lee of the bump. This process is called regelation (regel means refreeze). The latent heat of freezing is conducted rapidly through small bumps to provide the latent heat of melting for ice being compressed. When bumps are large, regelation shuts down because latent heat is conducted slowly through big bumps. For large bumps, the compressive stress is smaller because the gravitational driving force acts normal to a larger area, so creep in ice moves ice around large bumps. Rates of regelation vary inversely with bump size and rates of creep vary directly with bump size. Basal sliding is controlled by bump sizes for which rates of regelation and creep are the same. These bumps are the "controlling obstacle size" in theories of glacial sliding, since they provide maximum resistance to gravitational forcing.

Ice-bed coupling treated in the force balance is only half the story in understanding the stability and velocity of ice sheets and other glaciers. The other half concerns the mass balance.

The mass balance

The mass balance describes how glaciers change in size over time. These changes, like changes in shape, are partly controlled by the topography of the glaciated landscape. When glaciers occupy valleys, size changes consist mainly in advance and retreat along the valleys. Changes in size of continental ice sheets occur in many directions, with advances in some directions and retreats in others. Glaciers grow in size when accumulation of ice, mostly from snow precipitation over high interior ice elevations, exceeds ablation at low peripheral ice elevations, either by melting when glaciers end on land or by melting and calving of icebergs when glaciers end in water. Glaciers advance when the mass balance is positive and retreat when the mass balance is negative, provided that no major change in ice-bed coupling occurs under the glaciers that may make them thicken because of increased coupling or thin because of decreased coupling. A positive mass balance increases ice volume and a negative mass balance decreases ice volume, apart from changes in the shape of glaciers caused by changes in the force balance.

In mountain glaciers occupying various climatic regimes around the world, advance and retreat of grounded ice margins are very sensitive to changes in the mass balance, and therefore to changes in climate. Typical climatic regimes are cold dry continental climates at high and mid latitudes, cool wet maritime climates at high and midlatitudes, and mixed climates at these latitudes. Continental ice sheets occupy a range of high and midlatitudes and have all these climatic regimes in various sectors. A major effort in documenting climate change since the last glacial maximum (LGM) about 18,000 years ago has been to map and date the looping end moraines deposited by mountain glaciers around the world as these glaciers began their overall retreat, especially during the last 10,000 years called the Holocene when human civilizations arose and attained the advanced industrial societies found today. The rise and fall of many cultures in Africa, Eurasia, and the Americas have been linked to climatic changes documented by changes in dated terminal positions of mountain glaciers around the world caused by changes in their mass balance. An example of this climate research linked to advance and retreat of glaciers has been mapping and dating glacial deposits around the South Pacific rim from Chile in the east to Antarctica in the south to New Zealand in the west by George Denton and colleagues, following earlier correlations in Alaska, Switzerland, and Scandinavia.

Mass balance studies of continental ice sheets are ongoing for both the Greenland and Antarctic ice sheets. These include field studies along ice-sheet margins similar to those conducted for mountain glaciers, monitoring surface changes from Earth-orbiting satellites, and recovering climate records from ice cores. These records consist of measuring ratios of isotopes for oxygen and hydrogen in ice, trace concentrations of ions entrained in the atmosphere by evaporation from oceans, transported by winds, and precipitated with ice crystals over the ice sheets, samples of Earth's atmosphere trapped in air bubbles in ice after surface snow is compressed into ice at depth, and the mineralogy of wind blow dust from volcanoes and deserts around the world. In combination, these measurements give a record of global climate change and guide research seeking the causes of climate change.

The ablation zone of glaciers and ice sheets consists of net melting from surface and basal ice, and calving along vertical ice fronts ending on land and in water. The zone separating the inner accumulation zone from the outer ablation zone is a transition across which summer meltwater soaks into winter snow, transforming dry snow into wet snow. At the base of the wet snow zone is a zone of refrozen meltwater that forms ice superimposed on the ice surface from the previous summer. The snow line occurs when summer melting exposes superimposed ice at the surface. The equilibrium line of the glacier or ice sheet, where the annual mass balance between accumulation and ablation is zero, occurs when summer melting removes superimposed ice. Treating ablation in computer models of ice sheets is complicated by the fact that most ice enters ice streams, fast currents of ice that often cross the ablation zone and end as ice lobes grounded on land or ice tongues floating in water. Ice streams downdraw interior ice, so their surface is lower than flanking ice, which forms ice ridges between closely spaced ice

streams. Shear crevasses separate fast stream flow from the slow sheet flow on either side, so much surface meltwater enters these crevasses and refreezes, instead of draining off the sloping ice surface. If that water is most of the summer meltwater, the "ablation" zone is really still in the accumulation zone of the ice sheet because no true equilibrium line exists. Meltwater filling crevasses to the top will push the cold crevasse walls apart, water being heavier than ice, and will warm the walls by releasing latent heat when meltwater refreezes. This drives the crevasse tips downward and water can drain from the crevasses when the crevasse tips reach the bed and gain access to a subglacial water drainage system. When that happens, the pseudo ablation zone becomes an actual ablation zone because surface meltwater leaves the glacier or ice sheet by way of the basal drainage system. High melting rates can also occur under ice tongues that either float freely or are imbedded in floating ice shelves. In these cases, the floating ice is in an ablation zone even though the surface still has net snow accumulation. The high basal melting rates are caused by warm ocean currents that pass under floating ice. Water-filled bottom crevasses can migrate upward toward the ice surface, and ocean swells that pass under floating ice can cause spectacular calving events along top and bottom crevasses when they meet. Douglas MacAyeal, at the University of Chicago, and his colleagues have studied and modeled these catastrophic ablation mechanisms.

Modeling ice sheets

Modeling past and present ice sheets using high-speed computers began with a steady-state model of the Antarctic Ice Sheet in 1971 by Australian glaciologists, William Budd, Richard Jenssen, and Uwe Radok. They used measurements of temperature, ice accumulation rates, and elevations at the ice surface and measurements of bed topography, mainly along tractor-train traverse routes during the International Geophysical Year in 1958 and thereafter. With this input, their model calculated changing ice temperatures and velocities with depth along ice flowlines in directions of maximum surface slope for specified values of the basal geothermal heat flux. It was the first thermomechanical ice-sheet model. They subsequently applied it to the Greenland Ice Sheet. Their model produced beds that would be nearly wholly thawed or wholly frozen for moderate changes in the unknown basal geothermal heat flux. After Molly Mahaffey showed how ice sheets could be modeled at grid points in the map plane, thermomechanical models proliferated, and became three-dimensional and time dependent. The time dependency showed that basal thermal conditions (basal temperatures for frozen beds and basal melting or freezing rates for thawed beds) depended very strongly on surface conditions, especially accumulation rates, and these basal conditions under present ice sheets were strongly dependent on past surface conditions which were largely unknown. Glacial geology and the climate records extracted from ice cores and cores through ocean and lake sediments showed that past climate conditions, including the elevation of present ice sheets, were highly variable. It was becoming increasingly obvious that these top-down models, using surface conditions as input to extract reliable bed conditions as output, were essentially useless.

Former ice sheets reconstructed from the top down gave unreliable basal thermal conditions, and therefore unreliable ice elevations generated by ice-bed coupling linked to these conditions. Fortunately, glacial geology under former ice sheets could be interpreted to reveal the basal thermal regime, so ice elevations could be reconstructed from the bottom up. Calculating those ice elevations did not require knowing the basal geothermal heat flux or former configurations of the ice sheet through time and were insensitive to surface accumulation rates. Unreliable precipitation rates from models of atmospheric circulation, which depend on knowing the configuration of an ice sheet, did not affect these bottom-up reconstructions. Bottom-up reconstructions of former ice sheets began to restore glaciology and glacial geology to the original cause-and-effect unity they originally had as two sides of the same coin.

An early assumption in modeling ice sheets past and present was that Earth's climate was essentially stable, with the greatest perturbations in climate being the glacial and interglacial maxima of Quaternary glaciation cycles, times when climate changed slowly. This was the guiding assumption of CLIMAP (Climate: Long-range Investigation, Mapping, and Prediction) a project of the International Decade of Ocean Exploration from 1970 to 1980. The last glacial maximum 18,000 years ago and the last interglacial maximum 125,000 years ago were chosen as the primary and secondary goals for reconstructing past climates. Reconstructing ice sheets at these times was needed to provide boundary conditions in models of atmospheric circulation available for CLIMAP. These were the area of ice sheets to determine global albedo, the volume of ice sheets to determine the ocean surface area available for the ocean-to-atmosphere heat exchange, and the elevation of ice sheets to determine the direction and intensity of surface winds and the jet stream. However, records of climate change extracted from ice and sediment cores showed rapid changes within glaciation cycles that had amplitudes comparable to those bracketing glaciation cycles. Perhaps the underlying assumption was wrong. Perhaps Earth's climate is fundamentally unstable, at least within glaciation cycles, and the key to understanding rapid climate change lies in determining what causes the fastest rates of climate change within a glaciation cycle. In this case, ice sheets are not merely passive components of Earth's climate that react slowly to changes in the ocean and atmosphere. Ice sheets may be dynamic components capable of rapid changes independent of the ocean and atmosphere, changes that if big and fast enough could trigger rapid changes in the ocean and atmosphere. This was possible only

from changes in ice-bed coupling at the base of ice sheets. Bottom-up modeling had to constrain top-down modeling.

Holistic ice sheet modeling

In holistic ice sheet modeling, ice sheets must be treated as part of Earth's climatic and tectonic system, and all dynamic components of ice sheets must be modeled and coupled to this system. For example, when ice leaves an ice sheet by calving into icebergs, that ice is entering the oceanic part of the system, and the energy needed to melt that ice must be extracted from ocean water down to the draft of the icebergs. That heat is then unavailable to heat the atmosphere in the ocean-to-atmosphere heat exchange that drives global climate.

Flow in ice sheets consists of slow sheet flow diverging from interior ice domes that mostly converges to become fast stream flow toward ice margins and ends as ice lobes grounded on land and ice tongues floating in water. If ice tongues enter confining embayments, they may merge to become floating ice shelves that are grounded along the sides of the embayment and may be pinned locally to the seafloor at sites that produce ice rumples and ice rises on the ice-shelf surface. Ice rumples are produced when basal ice scrapes across pinning points and ice rises are produced when pinning points penetrate basal ice so basal ice must flow around pinning points. Ice sheets impact most strongly on the ocean and atmosphere when ice shelves either disintegrate catastrophically or release gigantic icebergs. Both events have occurred in parts of the Greenland and Antarctic ice sheets in the last 10 years. These iceberg outbursts can discharge billions of tonnes (metric tons) of ice in periods of weeks to a few years. For each gram of ice, about 10 calories are needed to reach the melting point and another 80 calories are needed for melting. This sensible and latent heat must be extracted from the sensible heat of ocean surface water, where the ocean-to-atmosphere heat exchange takes place. Melting outbursts of icebergs reduces the heat exchange, which then changes climate. These considerations show why glaciologists must study ice sheets as a single dynamic system that may be inherently unstable, with some changes in ice sheets being big and fast enough to trigger changes in Earth's climate. Changes of this magnitude are recorded by the glacial geology of past ice sheets and by climate records in ice and sediment cores.

Holistic ice-sheet modeling that includes transitions from sheet to stream to shelf flow and mechanisms for disintegrating ice shelves and calving gigantic icebergs is necessary to understand how ice sheets may control climate change. Key to this modeling activity is understanding conditions at the base of ice sheets that require bottom-up ice-sheet modeling. Foremost among these basal conditions is the production of basal water and its transport from sources to sinks. Basal water controls ice-bed coupling, and therefore the height of ice above the bed. Models of Earth's tectonic activity combined with modern technology for mapping the distribution and depth of basal water by radar and seismic sounding allow the geothermal heat flux to be mapped for the first time. High rates of geothermal heat output are source areas for basal water. Other source areas are sites of heavy crevassing along ice streams where surface meltwater can enter crevasses, drive the crevasses to the bed by forcing crevasse walls apart, and then flood the bed with surface meltwater. Transport of basal water from sources to sinks occurs beneath ice streams, which discharge up to 90% of the ice and where basal water uncouples ice from the bed and allows fast sliding velocities. Sinks of basal water occur around the perimeter of ice lobes at the ends of terrestrial ice streams and across ungrounding lines of marine ice streams where they become afloat as ice tongues and ice shelves. For marine ice streams, discharge of basal water at the melting point, combined with warm ocean water pumped under ice shelves by tidal cycles, will melt floating ice free from basal pinning points. Confined and pinned ice shelves can buttresses ice streams that supply them. Basal melting and iceberg calving remove pinning points and allow faster ice discharge rates from ice streams and faster ice calving rates from ice shelves. Ice sheets are then downdrawn faster, with no changes in surface conditions other than those caused by lowering the ice surface. Rapid downdraw has the capacity to trigger rapid changes in global climate. Ice shelves can disintegrate catastrophically when external forcing, such as an ocean swell passing under an ice shelf, produces a "tipping point" in the force balance.

When confined and pinned ice shelves disintegrate, they reduce compressive stresses that buttress ice streams supplying the ice shelves. These ice streams may then be able to increase their discharge velocity up to 100-fold, by analogy with surging mountain glaciers. Surges of mountain glaciers last from a few months to a few years, until their ice accumulation regions have become depleted. Ice streams drain much larger areas so their surges can last much longer. Surging mountain glaciers have been studied in some detail, notably by Charles Raymond, Barclay Kamb, and colleagues. During a surge, the glacier thins upslope and advances downslope due to a massive reduction in upslope ice-bed coupling. This occurs independently of the mass balance of surging glaciers, and there is no change in local climate that might trigger surges. These observations can be applied to the ice streams that drain ice sheets. Lobes along the southern margin of the former Laurentide Ice Sheet that blanketed most of North America are surge-like extensions of terrestrial ice streams, and ice-rafted sediments deposited across the North Atlantic have been traced to marine ice streams that may have surged. Some Greenland and Antarctic ice streams appear to be surging, without changes in external conditions.

A key to predicting when and where ice sheets may begin to lower rapidly and discharge vast quantities of icebergs is to monitor changes in ice surface elevations from Earth-orbiting satellites. Surface elevations decrease

fastest at the heads of ice streams. Stream flow is transitional between fully grounded sheet flow and fully floating shelf flow. Ice streams have a concave surface, the only surface that can provide a smooth transition from the high convex surface produced by sheet flow and the low flat surface produced by shelf flow. The gravitational driving stress in sheet flow is proportional to the product of ice height above the bed and the ice surface slope, whereas in shelf flow it is proportional to the height of ice floating above water. In stream flow, gravitational forcing changes downstream from the forcing causing sheet flow to the forcing causing shelf flow. Therefore, a floating fraction of ice increases along marine ice streams from essentially zero at the head of ice streams to essentially unity at their ungrounding lines. Along terrestrial ice streams, the floating fraction increases from zero to nearly unity at their minimum-slope surface inflection line, and then decreases as basal water flows out from beneath terminal ice lobes.

Ice-bed uncoupling in sheet flow is only partial, and occurs when a frozen bed thaws. A melting bed separates a fully frozen bed from a fully thawed bed, with thawed patches growing in number and size as ice flows across a melting bed. The opposite condition exists as ice flows across a freezing bed that separates a fully thawed bed from a fully frozen bed. Melting lowers the ice surface by up to 20% and freezing raises the surface by up to 25%. In both cases, the ice sheet remains intact. Once the bed becomes thawed, further melting of basal ice must drown the bedrock bumps that retard basal sliding and fluidize basal till or sediments, causing them to deform rapidly. Drowning occurs first in ice streams, which generally lie along linear depressions in the subglacial landscape. Although slow sheet flow occurs over some 90% of past and present ice sheets, ice streams discharge up to 90% of the ice. Therefore, ice streams can collapse an ice sheet. As the floating fraction of ice increases over time, ice streams propagate into an ice sheet, pulling out more ice, until the high convex surface of sheet flow collapses to become the low flat surface of shelf flow. The ice surface lowers nearly to sea level if the ice sheet is a marine ice sheet grounded below sea level. Then a calving bay can migrate into ice downdrawn by surging ice streams and carve out what remains of the ice sheet. This terminates a glaciation cycle, as happened when a calving bay migrated up a stagnating post-surge ice steam in Hudson Strait and carved out the heart of the vast Laurentide Ice Sheet centered over Hudson Bay about 8,000 years ago. There is no inherent reason why the same process cannot collapse and disintegrate the ice sheets now covering Antarctica and Greenland, since large parts are grounded below sea level, especially in Antarctica. In this event, global sea level would rise by 70 m, submerging Florida, making Memphis, Tennessee, an ocean port, and converting New England into an island. Whole countries would disappear, from Denmark to Bangladesh, triggering vast migrations of populations that cause worldwide social, political, and economic upheavals.

Summary and outlook

Three facts should guide our understanding of the velocity of glaciers, especially for the large continental ice sheets covering Greenland and Antarctica today. (1) Ice height above the bed is controlled by the strength of ice-bed coupling, reducing ice thickness by some 90% when coupling vanishes. (2) Ice-bed coupling vanishes along ice streams that end as floating ice shelves and drain up to 90% of an ice sheet. (3) Because of (1) and (2), ice sheets can rapidly collapse into ice shelves that can suddenly disintegrate into icebergs, thereby removing ice sheets from Earth's climate system and forcing abrupt climate change and rapidly rising sea levels.

Bibliography

Alley, R. B., and Bindschadler, R. A. (eds.), 2001. *The West Antarctic Ice Sheet: Behavior and Environment. Antarctic Research Series*. Washington, DC: American Geophysical Union.
Andersen, B. G., and Borns, H. W., Jr., 1994. *The Ice Age World*. Oslo: Scandinavian University Press, 208 pp.
Denton, G. H., and Hughes, T. J. (eds.), 1981. *The Last Great Ice Sheets*. New York: Wiley-Interscience. 484 pp.
Hooke, R. LeB., 2005. *Principles of Glacier Mechanics*, 2nd edn. Cambridge: Cambridge University Press, 429 pp.
Hughes, T. J., 1998. *Ice Sheets*. New York: Oxford University Press, 343 pp.
Paterson, W. S. B., 1994. *The Physics of Glaciers*, 3rd edn. Oxford: Butterworth-Heineman. 481 pp.
van der Veen, C. J., 1999. *Fundamentals of Glacier Dynamics*. Rotterdam: A.A. Balkema, 462 pp.

Cross-references

Aerial Photogrammetry for Glacial Monitoring
Antarctica
Calving Glaciers
Climate Change and Glaciers
Creep
Glacial Geomorphology and Landforms Evolution
Glacier Surging
GPS in Glaciology, Applications
Greenland Ice Sheet
Ice Core
Ice Sheet
Marine Ice Sheet
Quaternary Glaciation

GLACIER POTHOLE

Rajesh Kumar
Remote Sensing Division, Birla Institute of Technology, Extension Centre, Jaipur, Rajasthan, India

Glacier pothole is a smooth cavity or hole formed on the rocks by eddy currents of water bearing stones, gravels, and sand. The glacier melt water passing through the crevasses in the glaciers sometimes forms whirlpool at the bottom of the glacier. This water is under very high pressure and carries morainic debris likes large erratic boulder

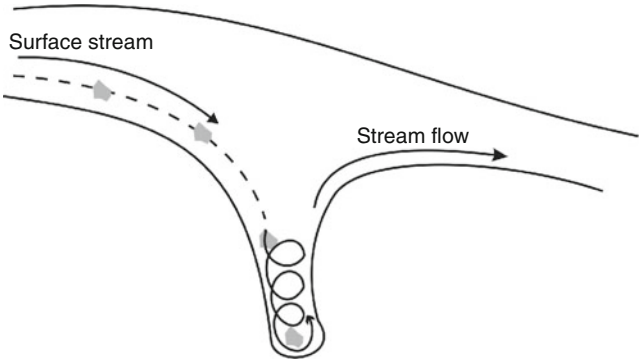

Glacier Pothole, Figure 1 A sketch diagram showing the mechanism of glacier pothole formation under the influence of surface streamflow and rock debris. (Sketch of the concept by Dr. Rajesh Kumar and plot by Randhir Parihar.)

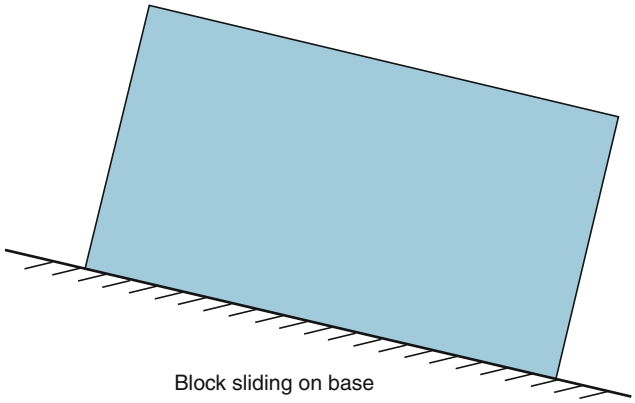

Glacier Sliding, Figure 1 The sketch showing the sliding of the glacier ice under gravity flow on the inclined bed of glacier.

gravels and sand which erodes the underlying bed of the rocks giving rise to the formation of glacier potholes. The erosion is not only caused by the big boulder or gravels but also by the turbid melt water under high pressure and eddy flows. As the potholes are formed through the crevasses/moulin, it also reflects the surging of the glaciers that generate the crevasses.

Potholes are round and almost invariably contain the rounded rock materials that have drilled them (Figure 1). In glacial setting, they may be partially filled by glacial sediments. The initiation of potholes can also be explained as cavitations in very fast flowing deep melt water streams. The resulting cavities subsequently enlarge and deepen by rock materials caught in the turbulent vorticities. It is still not very clear whether erosive mechanism plays an important role in the formation of potholes or not.

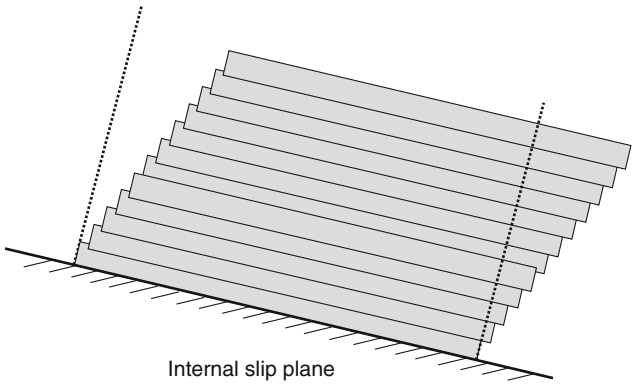

Glacier Sliding, Figure 2 The sketch diagram showing the internal flow of ice mass under the shear stress due to inclined bed and gravitational pull. (Sketch concept by Dr. Rajesh Kumar and plotted by Randhir Parihar (BITEC, Jaipur)).

GLACIER SLIDING

Rajesh Kumar
Remote Sensing Division, Birla Institute of Technology, Extension Centre Jaipur, Jaipur, Rajasthan, India

Sliding of the glacier over bedrock, as shown in Figure 1, occurs only in glacier with ice at the pressure melting point and with enough over pressured water at the base to reduce friction between the ice and substrate. Soft, deformable, water saturated sediments at the base of glaciers enhance basal slippage, hence the faster movement of the glaciers.

The other mechanism for the glacier sliding is internal slippage (Figure 2) along fractures that can occur in any part of the glacier, but is most effective toward the terminus, where thrust faults are developed. In old glacier ice, large crystals are formed strongly elongated down slopes. This is a form of movement and, hence, a contribution to the sliding of glaciers.

The glacier slides at different speeds depending on local environmental conditions Polar glaciers move very slowly like the debris laden margins of the temperate glaciers. The temperate glaciers move usually at a rate of few centimeters per day, however, a few steep glaciers may reach velocities upto 3.0–6.0 m/day.

GLACIER SURGING

Hester Jiskoot
Department of Geography, University of Lethbridge, Lethbridge, Alberta, Canada

Synonyms

Glacier surge dynamics; Glacier surge processes, morphology, and landforms; Surge-type behaviour; Surging

Definition

Glacier surging is a quasiperiodic oscillation between long periods (tens to hundreds of years) of slow flow, called *quiescent phase* or *quiescence*, and shorter periods of typically 10–1000 times faster flow, called *surge phase, active phase*, or *surge*. During a surge, the flow velocity increases abruptly, and fast flow is maintained over some time (1–15 years) and over a wide area. The switch from slow to fast flow is an internally triggered ice flow instability, reflecting sudden changes within the glacier system. These changes can sometimes be associated with external factors (e.g., weather, climate, and earthquakes), but only if the glacier system is already close to a critical threshold. During a surge, a large volume of ice is transported from the *reservoir zone* (upper part) to the *receiving zone* (lower part) of the glacier, which sometimes results in a marked frontal advance. During the surge cycle (from surge through quiescence to the next surge), the morphology and surface characteristics of a glacier undergo dramatic changes that result in morphological features diagnostic for surging: these can be used to identify surge-type glaciers in their quiescent phases, even if a surge proper has not been observed. Only a small percentage of glaciers worldwide exhibit surging behavior, and these surge-type glaciers are clustered in specific glacierized regions. Although surging is more common in valley glaciers, outlets from ice sheets have also been reported to surge.

A *surge-type glacier*, *surge glacier*, *galloping glacier*, or *pulsating glacier* in Russian literature experiences glacier surging or displays morphological evidence that it did so in the past. A surge-type glacier can either be in its surge phase or in its quiescent phase.

A *surging glacier* is in the surge phase of its surge cycle and experiences fast flow and possibly a marked frontal advance. However, this term is sometimes used interchangeably with *surge-type glacier*.

A *normal glacier* or *non-surge-type glacier* does not exhibit surge behavior.

Surge onset/initiation and *surge termination* refer to the start and the end of a surge phase.

A *surge bulge* is a region of thickening that can develop between the reservoir and receiving zones, and which travels downglacier as the *surge front* after surge initiation. Sometimes, a *fore-bulge* develops in the region of compression directly downstream of the surge bulge.

Introduction

Average ice flow velocities for valley glaciers are generally less than a few hundreds of meters per year (m a^{-1}) and for outlet glaciers up to several kilometers a year (Paterson, 1994). Most glaciers have seasonal velocity fluctuations, with the faster flow occurring in the early melt season. Theoretically, glaciers discharge ice from the accumulation area to the ablation area in order to maintain a steady-state glacier profile: this is the balance flux. The corresponding velocity, the balance velocity, is controlled by mass balance conditions and glacier geometry (Clarke, 1987). Studies that model glacier and ice sheet response to climate change often assume that these ice masses flow with speeds corresponding to their balance velocities. Although this is approximately true for most glaciers, in some glaciers the balance flux is much higher than the measured fluxes. If this occurs over a prolonged time, a flow instability can occur through a series of positive feedback mechanisms in the glacier system, which results in pulsating behavior with sudden switches between slow and fast flow. Pulsating glaciers include unstable tidewater glaciers, ice streams, and surge-type glaciers (Clarke, 1987). The latter have internally triggered flow instabilities with a semi-regular cyclic recurrence period (Meier and Post, 1969). The surge cycle involves long periods (tens to hundreds of years) of quiescence, with slow flow velocities much lower than the balance velocity (10–500 m a^{-1}), interspersed with short (1–15 years) active periods, or surges, in which a 10–1000-fold increase in flow results in average velocities of more than 500 m a^{-1}, greatly exceeding the balance velocity (Meier and Post, 1969; Clarke, 1987; Dowdeswell et al., 1991).

Surge behavior has been identified since 1599 for Vernagtferner, Austrian Alps (Hoinkes, 1969), since the eighteenth century in Iceland (Thorarinsson, 1969) and the Caucasus (Glazovskiy, 1996), and for centuries in the oral history of the Tlingit, Alaska (Cruikshank, 2005). The first scientific reports on surging are from observations in Svalbard and Alaska (De Geer, 1910; Tarr and Martin, 1914). Progress in the overall understanding of glacier surging has been summarized in four overview papers (Meier and Post, 1969; Raymond, 1987; Sharp, 1988; Harrison and Post, 2003).

Glacier surging is of great importance in the understanding of ice flow dynamics, as the sudden switches between the slow and fast flow modes reflect dramatic changes in the ice flow processes that are caused by only small changes in the driving stress (Raymond, 1987). It is still elusive what exactly triggers these sudden switches in flow mode, but a number of controlling processes have been identified and substantiated by field evidence. Surging is further considered analogous to modern and past ice stream behavior, where switches between flow modes occur with a cyclicity of hundreds to thousands of years (Boulton and Jones, 1979). Surge-type glaciers are also important as their behavior can obscure the climate signal, and because they can cause a number of natural hazards.

The surge cycle

From detailed field and remote sensing measurements and observations of a small number of well-studied surge-type glaciers, integrated with common patterns from general observations on a large number of surge-type glaciers, a generalized description of glacier surging has been developed that encompasses all surge-type glaciers, although individual surge behavior can vary. This common pattern

is one where the generic surge cycle can be divided into the following three phases:

1. *The buildup phase*, where the glacier profile steepens as a result of a restricted outflow (Meier and Post, 1969). In this phase, the glacier can be divided into an active thickening zone (reservoir zone) and nearly motionless depleted zone (receiving zone), separated by a boundary zone, also called the trigger zone or Dynamic Balance Line (DBL) (Dolgoushin and Osipova, 1975). The reservoir and receiving zones usually do not coincide with a glacier's accumulation and ablation zones, which are separated by the equilibrium line, but instead, the DBL is located where the glacier outflow is restricted (Clarke et al., 1984). A marked ramp of ice, a surge bulge, up to tens of meters in height can form at this boundary (Dolgoushin and Osipova, 1975; Clarke et al., 1984; Murray et al., 1998). In the late stages of this phase, the glacier is on the verge of flow instability and basal shear stress is high. Short periods of speedups, called "mini-surges", can appear, in conjunction with basal water pressure fluctuations and vertical uplift of the glacier surface (Kamb and Engelhardt, 1987). However, it is not clear if these "mini-surges" are directly correlated with the main surge event, as similar sudden switches in flow speed have also been observed in non-surge-type glaciers as a result of seasonal changes in water input to the glacier (e.g., Iken, 1981).
2. *The surge phase*, where the ice is transported from the reservoir to the receiving zone, and ice velocity increases abruptly (Kamb et al., 1985) or gradually (Murray et al., 2003). A surge often initiates in the upper regions and propagates downglacier as a surge front, but sometimes a surge propagates upglacier too (Hodgkins and Dowdeswell, 1994). Above the surge front, ice flow is extensional, resulting in transverse crevassing, while below the surge front ice flow is compressive. A glacier in full surge is often completely crevassed. When the surge front reaches the terminus a marked frontal advance can take place (Meier and Post, 1969). During the surge phase, the glacier becomes less steep due to down-draw in the upper region and thickening of the lower region. The surge termination can either be abrupt, with a sudden slowdown to pre-surge velocities and accompanied by a measurable drop in the ice surface and outburst floods (Kamb et al., 1985), or gradual and extending over months to years (Murray et al., 2003).
3. *The stagnation and depletion phase* is in the first (tens of) years after a surge, where the glacier is virtually stagnant. Crevasses close during this phase, and rapid depletion of the lower regions and a frontal retreat can cause temporary acceleration in the overall ablation rate (Yde and Knudsen, 2007). Part of the lower glacier can detach and be left as dead ice (Weidick, 1988). During this stagnation phase, the glacier surface may look irregular and pitted, partly due to the recent closing of crevasses and related surface drainage patterns (Liestøl et al., 1980; Sturm, 1987; Weidick, 1988). The ice may also become debris-covered, and medial moraines in the ablation zone tend to tower high above the depleted glacier surface (Dolgoushin and Osipova, 1975).

Individual surge characteristics

There is a large variability in the duration of quiescent and surge phases as well as in the velocity development during surges. Although for most individual glaciers the surge cycle (recurrence period of the surges), surge propagation (velocity development), and surge extent and/or maximum advance are similar, large variations occur between and within regions (see Table 1). Even two surge-type glaciers that share accumulation areas do not necessarily surge simultaneously (Paterson, 1994). In fact, the behavior of surge-type glaciers is so diverse and includes such a wide range of surge phenomena, that some argue that it might be necessary to redefine the classical concept of glacier surging and broaden it into a spectrum of flow instabilities. In such a spectrum, glacier surging is part of a continuum that ranges from normal (slow) glacier flow to permanently fast glacier flow.

The highest recorded surge velocity is 125 m d^{-1} for Brúarjökull, Iceland, which also had one of the fastest frontal advances of 10 km in 1 year with maximum advance rates of 1–5 m h^{-1} (Thorarinsson, 1969). The largest recorded advance was ~21 km and observed for Bråsvelbreen, Svalbard (Schytt, 1969) and the fastest daily frontal advance was 105 m d^{-1} for Medveziy glacier, Pamirs (Dolgoushin and Osipova, 1975). In contrast, surge velocities of only 0.1–5 m d^{-1} have been recorded in other regions (Table 1).

Typical surge cycles vary dramatically between regions (Figure 1). The recurrence period of surges in Svalbard is much longer than in other regions (50–500 years instead of 15–50 years), and the surge phase lasts 3–15 years as compared to 1–3 years in other, more temperate, regions (Dowdeswell et al., 1991 and 1995). Furthermore, most Svalbard surge-type glaciers have an overall "sluggish" character, with lower surge velocities, slow initiation, and slow and indistinct termination (Dowdeswell et al., 1991; Murray et al., 2003). A possible exception to this is the 2003–2005 Skobreen-Paulabreen surge, though it is believed to have had a long (>10 years) initiation phase (Benn et al., 2009). For Greenland and the Karakoram, longer surge and quiescent phases have been inferred as well, though not for all glaciers (Weidick, 1988; Jiskoot et al., 2001; Yde and Knudsen, 2007; Hewitt, 2007). Icelandic glaciers have irregular quiescent intervals; 5–30 years for some glaciers, and up to 100–140 for others, while surge advances can be up to 6 years (Björnsson et al., 2003). Mass balance, hence climate, can influence the recurrence interval of surges (Dowdeswell et al., 1995; Harrison et al., 2008) and is suggested to have caused

Glacier Surging, Table 1 Surge characteristics of a selection of surge-type glaciers worldwide, sorted by geographic region: [1]Svalbard, [2]Pamirs, [3]Karakoram, [4]Alaska, [5]Yukon Territory, [6]Greenland, [7]Iceland (After Jiskoot et al., 2001)

Glacier	Length km	Surge advance km	Lowering m	Thickening m	Volume displ. km^3	Calving rate $km^3\ a^{-1}$	Quiescence velocity $m\ d^{-1}$	Surge velocity $m\ d^{-1}$	Surge-front propagation $m\ d^{-1}$	Surge duration y	Quiescence duration y
Bodley[1]	16	2–3.5	−15	+60			0.5	1.4	6.5	7+	
Bakaninbreen[1]	17	0	−15	+40	0.67		0.0005–0.001	0.2–3	2.5–5	5–15	>85
Monacobreen[1]	40	2					0.006–0.008	0.5–5	–	7–11	
Skobreen[1]	8.2	0.2–0.4	−60	+40					7.8	>15	>100
Perseibreen[1]	11.5	0.35						2–2.5			130
Medveziy[2]	13	1.6	−100	+150	0.06		0.001–1.5	68–105	80	0.4–1	10–15
Chiring[3]	15.5	2.5	−150	+130	1–1.5					3	110
Variegated[4]	20	2–5	−50	+100			0.2	14–50	15–80	2	16–26
Bering[4]	200	9.7	−50				1	11–33	90	2–3	20–30
West Fork[4]	40		−60	+123	3.7		0.15	12	23	<1	50
Trapridge[a5]	4	1								10	30
Trapridge[b5]	4	0.45		10	0.00017		<0.02	0.07–0.12	0.08	>20	30
Sortebræ[6]	77	10	−270	+145	22	4.5–5.3	0.1–0.7	5–27	50–330	~2.5	40–50
Storstrømmen[6]	120	10	−80		50	10.8	0.4–0.8	4–5.5		5–6	70
Sermeq peqippoq[6]	10	2.8					0.008–0.01	1–13	190	6–7	>60
Brúarjökull[7]	50	8–10						125		0.4–2	70–100

Note: Trapridge[a] is from the 1940s surge and Trapridge[b] from the 1980s to 2000s slow surge (Frappé and Clarke, 2007).

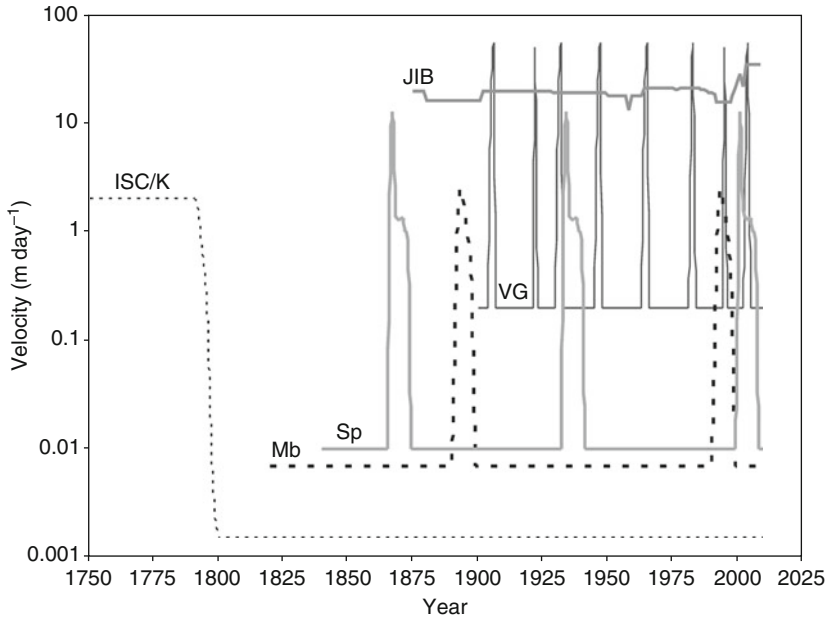

Glacier Surging, Figure 1 Schematic typical velocity fluctuations (logarithmic scale) of ice streams and surge-type glaciers (ISC/K = Ice stream C/Kamb ice stream, Antarctica; JIB = Jakobshavn Isbræ, Greenland; Mb = Monacobreen, Svalbard; Sp = Sermeq peqippoq, East Greenland; VG = Variegated Glacier, Alaska. Timing of pre-1990s surges of Mb and Sp are based on estimated quiescent phases of 100 years (Mb) and 60 years (Sp).

glaciers to change from having surge type to having normal behavior (Jiskoot et al., 2000; Hansen, 2003).

Very short pulses in flow velocity, usually up to a few weeks, that travel downglacier as kinematic waves, are by some coined "mini-surges" (Kamb and Engelhardt, 1987). Dynamically mini-surges show strong similarities to real surges, and some, but not all, may precede a surge (Kamb et al., 1985). Some Greenland glaciers are suggested to have a "periodic" surge on top of a "permanent" surge (Weidick, 1988).

Surges can be differentiated on the basis of the velocity development and concomitant surge characteristics. In a broad sense, surges can either have a two-phase surge cycle, with an abrupt switch between quiescent velocities to surge velocities, sustained fast flow during the surge, with possible fluctuations, and a rapid surge termination (Kamb et al., 1985; Eisen et al., 2005), or a three-phase surge cycle, with a long quiescent phase, an acceleration phase over months to years to peak surge velocity, and a deceleration phase where velocities gradually decline to quiescent phase velocities (Murray et al., 2003; Jiskoot and Juhlin, 2009). These two types of surge cycles and their development have been used to hypothesize that there are at least two different types of surge mechanisms: the Alaskan-type for two-phase surges, and the Svalbard-type for three-phase surges (Murray et al., 2003). Variegated Glacier, a temperate land-based soft-bedded glacier in Alaska, and Monacobreen, a soft-bedded polythermal (subpolar) glacier in Svalbard, can be used as archetypical examples of these types of surge behavior.

Variegated Glacier 1982–1983 surge

Variegated Glacier's surge proper started in the upper glacier with frequent icequakes and increased motion in January 1982, but was preceded by mini-surges for months (Kamb et al., 1985). The location of surge initiation coincided with a bedrock sill. After initiation, a steep (15°) surge front traveled downglacier, creating a leading edge of extremely high longitudinal compression (Raymond, 1987). Rapid velocity increase occurred in early spring, and was followed by rapid deceleration in late June and gradual deceleration until September. Renewed acceleration occurred between October 1982 and May 1983, culminating in peak velocities in June 1983. The surge terminated abruptly at the height of the melt season (mid-July 1983). Surge velocities varied between 10 and 50 m d^{-1}, with maximum velocities of up to 65 m d^{-1} (Kamb et al., 1985). Dye trace experiments, borehole water level measurements, and proglacial hydrological observations revealed that before the surge, the water drained subglacially in an effective low-pressure conduit system, while during the surge high water pressures around overburden occurred consistently, and the basal water flow was retarded and laterally dispersed (Kamb et al., 1985). Peaks in water pressure coincided with oscillatory pulses in glacier movement, and sudden increases in horizontal flow were accompanied by vertical uplifts of the glacier surface, while slowdowns were accompanied by small increases in proglacial discharge. Surge termination was marked by a drop in the ice surface, and coincided within days with a massive outburst flood of

turbid water. After the surge termination, the effective low-pressure drainage system was reestablished, but mini-surges occurred a year after surge termination. Variegated Glacier's 1982–1983 surge occurred in two annual cycles with the peak surge velocities in the second summer. At least two other surges (1964/1965 and 2003/2004) occur in this configuration (Eisen et al., 2005; Harrison et al., 2008). It has undergone eight 1–2-year surges, where the surge intervals of ~15 years appear to be regulated by cumulative mass balance and glacier geometry, at least as long as the preceding surge was "complete" (Harrison et al., 2008). The surge advance is generally ~2 km, and surge velocities 100-fold quiescence velocities.

Variegated Glacier's surge is characterized by a direct link between the subglacial water system and velocity development, and both the winter initiation and summer termination of the surge are rapid events. Surge development and characteristics of a number of other Alaskan glaciers (Harrison and Post, 2003), Medvezyi glacier, Pamirs (Dolgoushin and Osipova, 1975), and Sortebrae, East Greenland (Jiskoot et al., 2001) are similar to that of Variegated Glacier.

Monacobreen 1990s surge

Monacobreen had a months-long acceleration phase (September 1991 to March 1992), and years-long deceleration phase (January 1994 to October 1997 and beyond), punctuated by an increase in flow rate between December 1995 and May 1996 (Murray et al., 2003). Both the surge initiation and termination transitions appear very gradual. The surge started gradually but simultaneously over the entire lower region of the glacier and then propagated upglacier: there was no evidence of a surge front traveling downglacier (Murray et al., 2003). The spatial pattern of both velocity and strain rates were very consistent, and velocity highs and lows remained fixed in location throughout the surge. There was no evidence of elevated subglacial water pressure, or short-lived velocity fluctuations. The increase in velocity during the acceleration phase was about three times faster than its decrease in the deceleration phase. Quiescence velocities are estimated 0.006 to 0.008 m d^{-1}, while maximum measured surge velocities were only 5 m d^{-1}. Surge advance was about 2 km and surge duration 7–11 years (Murray et al., 2003).

Surge development and characteristics of a number of other Svalbard glaciers (Murray et al., 2003), Trapridge Glacier, Yukon Territory (Clarke et al., 1984), as well as Sermeq peqippoq, East Greenland (Jiskoot and Juhlin, 2009) are similar to that of Monacobreen.

Slow surges

Some glaciers have a very slow, incomplete surge-like development, which can only be classified as a "surge" with high-accuracy geodetic measurements. In these glaciers, the surge phase lasts 20 years or more and surge velocities are only five to ten times higher than in quiescence. No marked frontal advance occurs. However, a measurable down-draw of the upper region occurs and a volume is transported from the reservoir to the receiving zone. These "slow" or "partial" surges have only been measured in polythermal glaciers in the Yukon Territory and Svalbard (Frappé and Clarke, 2007; Sund et al., 2009).

Morphological evidence for surging

Many glaciers are situated in remote locations, and even with the modern capabilities of remote sensing a surge may be completely missed or be well under way before it is detected. In addition, a glacier in surge often becomes inaccessible for field research because of rapid movement and crevassing. Fortunately, surge-type glaciers show distinctive geometries and surface characteristics resulting from the changes taking place throughout the surge cycle. This morphological evidence for surge behavior can be detected, both in the surge and quiescent phases, from high-resolution satellite imagery and aerial photographs.

Morphological evidence for surging exists primarily in the form of the appearance of surge-type glaciers (their gradient, overall geometry, surface features, and crevasse patterns) and of surge-related features in the glacier forefield. Whereas some of these morphological features are diagnostic for surging, others could potentially be caused by other dynamic behavior and should only be used in combination with other clear evidence for surging.

Surface gradient and geometry

The surface gradient of a surge-type glacier gradually becomes steeper during quiescence, and rapidly becomes shallower during the surge. Most surge-type glaciers show rapid down-wasting of the frontal area just after a surge, and extensive stagnant tongues during the rest of the quiescent phase (Clapperton, 1975; Meier and Post, 1969). During the surge phase, the glacier gradient is subject to a rapid down-draw of the upper regions and a thickening and potential advance in the lower region. Both end members of the glacier surface gradient are an indication that surge-type glaciers have no steady-state profiles (Paterson, 1994). Trimlines (remnants of snow, ice, and debris left hanging on valley walls), truncated and hanging tributaries, and double cone-shaped snow-avalanche deposits are indications of the dramatic drop in glacier surface during surges (Liestøl, 1969; Dolgoushin and Osipova, 1975; Gardner and Hewitt, 1990).

In some surging glaciers the surge bulge, or surge front, propagates as a wave downglacier and steepens with time. While on Variegated Glacier the ice compression below the surge bulge resulted in the formation of thrust faults, on Trapridge Glacier and Bakaninbreen, pronounced forebulges developed (Clarke et al., 1984; Sharp, 1988; Murray et al., 1998). The latter two are polythermal glaciers, and the surge bulge is at the boundary between a melted and a frozen bed (Clarke et al., 1984; Murray et al., 2000).

If the surge front reaches the glacier margin, the margin steepens and becomes convex (Dolgoushin and Osipova, 1975; Hagen, 1987; Raymond, 1987), and a considerable

advance can occur (Meier and Post, 1969). While convex fronts are typical for land-based surging glaciers, calving glaciers develop near-vertical ice cliffs (Hagen, 1987). Complex lobating of the glacier front and spreading of the glacier tongue have also been associated with surges, as well as thrusting of the surging glacier tongue over others or over dead ice (Kotlyakov, 1980; Sharp et al., 1988; Weidick, 1988).

See Table 1 for down-draw and thickening, surge-front propagation speed, and terminal advance measured for surge-type glaciers worldwide.

Surface features of surge-type glaciers

A range of surface features are indicative of surge-type glaciers. Most of these surface features can be observed any time during the surge cycle, but they are best developed during or just after a surge.

Crevasse patterns in a surging glacier are chaotic and often affect the entire glacier (Meier and Post, 1969). Characteristic crevasse patterns, fractured and pinnacled ice, and their evolvement during the active phase have been observed on numerous surging glaciers, and the orientations of crevasses have been used to investigate tectonic processes typical of surges (Sharp et al., 1988; Hodgkins and Dowdeswell, 1994). Peak crevasse density is often found at the surge front and a mixture of longitudinal and transverse crevassing behind the propagating surge front indicates high compressional stresses as the front arrives and extension as it is passing (Thorarinsson, 1969). In Variegated Glacier, extensional tectonics in the upper part lead to transverse crevassing, superimposed extensional and compressional tectonics at the surge front to intersecting transverse and longitudinal crevasses, while compressional tectonics in the terminus area lead to longitudinal crevassing (Sharp et al., 1988). Large transverse crevasses ("bergschrund") near valley walls are associated with the depression of the glacier surface during surge (Lefauconnier and Hagen, 1991). Active marginal shear is an expression of the block-like "plug flow" indicative of sliding through basal decoupling (Post, 1969; Kotlyakov, 1980; Kamb et al., 1985; Reeh et al., 1994). Transverse crevasses over the width of the glacier can separate the stagnant upper glacier from the surging lower part (Gardner and Hewitt, 1990). From the distribution of crevasse patterns, surge initiation zones have been derived (e.g., Hodgkins and Dowdeswell, 1994; Jiskoot et al., 2001).

Looped and contorted medial moraines are probably the most spectacular surface features of surge-type glaciers, and are considered diagnostic for surging (Meier and Post, 1969). Surge-type medial moraines only develop if supraglacial debris is available and if tributary glaciers are present. Due to the alternating flow regime in surge-type glaciers, a distinct pattern of elongated medial moraine loops is formed (Figure 2). During quiescence, tributaries protrude onto the surface of the stagnant trunk and form bulging moraine loops. During surges, these moraine loops are extended and transported downglacier on the trunk, and are transformed into elongated "tear-shaped" medial moraines (Gripp, 1929; Post, 1972; Figures 1 and 3). Straight medial moraines and loops on the lower tongue can be transformed into tight "accordion" folds during surges (Post, 1972). In late quiescence, medial moraines and moraine loops often stand as prominent ridges above the ice surface of wasted glacier tongues.

Undulations, lakes, and pothole fields can form on surge-type glaciers in quiescence as a result of the highly irregular glacier surface, closing crevasses, and drained supraglacial lakes (Meier and Post, 1969; Liestøl et al., 1980). Potholes or pits are deep circular to elliptic depressions with diameters in the order of 10–100 m (Sturm, 1987). Whereas potholes and lakes generally develop near the equilibrium line on normal glaciers, they are found far down into the ablation area or over the entire surface of surge-type glaciers (Meier and Post, 1969; Weidick, 1988). This gives some surge-type glaciers the appearance

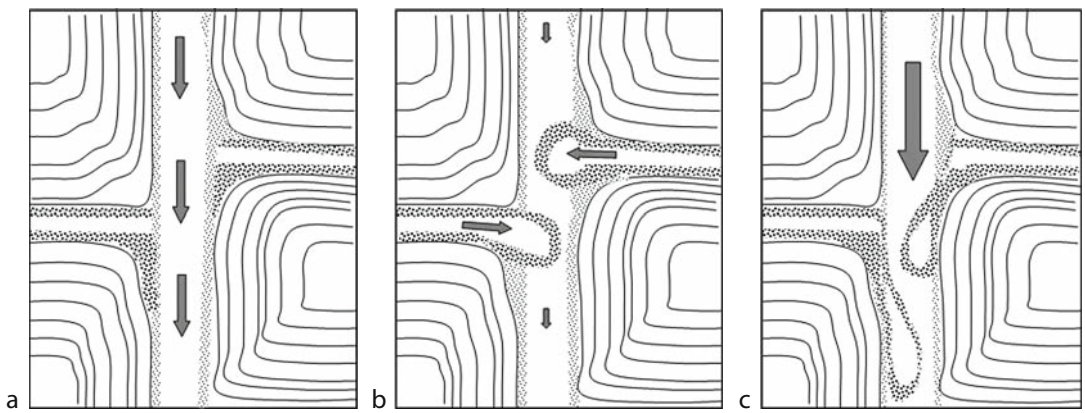

Glacier Surging, Figure 2 Schematic development of surge-related elongated moraine loops. (**a**) normal flow, (**b**) stagnant trunk and active tributaries creating bulging moraine loops, and (**c**) surging trunk forming elongated tear-shaped moraine loops (After Gripp, 1929; Croot, 1988).

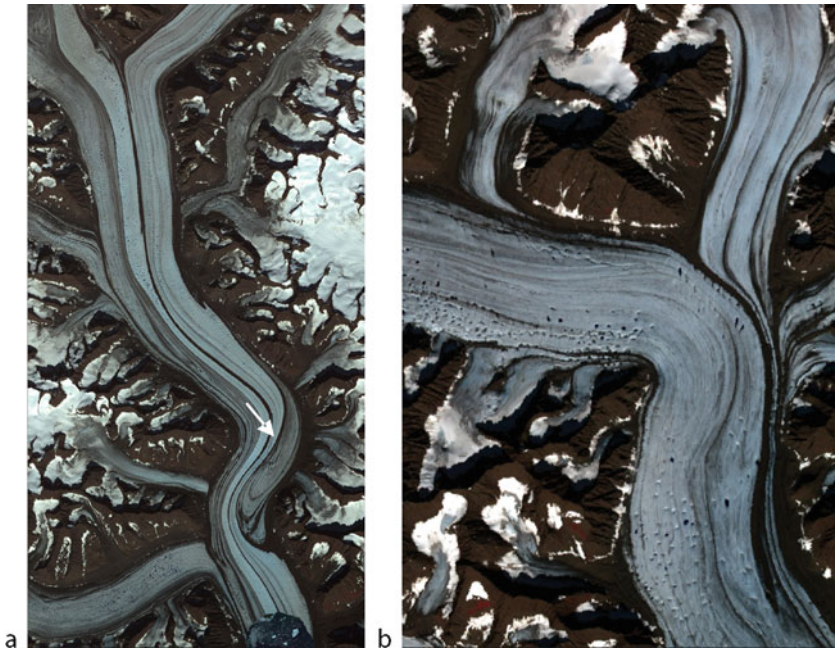

Glacier Surging, Figure 3 East Greenland surge-type glaciers on ASTER images of August 2004. Both glaciers flow downward. (**a**) Sortebræ with elongated tear-shaped moraine loop (arrow) ~10 years after its surge, and (**b**) glacier in quiescence covered in potholes.

of "Swiss cheese" (Weidick, 1997, personal communication, Figure 3). Supraglacial lakes can also develop in early surge, but often drain annually. After such annual drainage on Storstrømmen, NE Greenland, the pressure ridges formed from these lakes by katabatic wind were passively transported downglacier and formed a series of curved ridges, which could be used to estimate surge velocity (Reeh et al., 1994). Ice marginal and ice-dammed lakes can also be associated with surging (Kotlyakov, 1980; Hagen, 1987), especially if these suddenly develop and show extreme turbidity (Jiskoot et al., 2001). Some marginal lakes drain suddenly during surge termination, and can form jökulhlaup features and staircases of strandlines (Kamb et al., 1985; Sharp, 1988).

Proglacial features of surge-type glaciers

Iceberg production, dimensions, and debris content can all be regulated by the process of surging. While in quiescence iceberg production of calving surge-type glaciers can be much lower than that of normal glaciers, in surge, the iceberg production is enhanced due to an increased ice flux and the advance and increased flotation of the calving terminus. Dowdeswell (1989) argues that chaotic crevassing and close spacing of crevasses in surging glaciers enhance the disintegration of ice near the glacier margin, resulting in the production of smaller icebergs. However, Storstrømmen, NE Greenland, produced large tabular icebergs with tidal cracks (Reeh et al., 1994). This difference could be due to a fact that most Svalbard tidewater glaciers are grounded, whereas Storstrømmen is free floating (Reeh et al., 1994). Icebergs calving from glaciers in surge may also contain more debris-rich basal ice than normal glaciers (Dowdeswell, 1989), as the basal ice of surging glaciers is particularly debris rich (Clapperton, 1975).

The proglacial drainage system can undergo rapid changes in discharge and fluvial geometry during a surge. Release of large quantities of turbid water and debris-laden floods are recorded in conjunction with surges, and especially with outburst floods at the surge termination (Kamb et al., 1985; Hagen, 1987; Sharp, 1988). These events cause rapid changes in the proglacial glaciofluvial system and occasionally erosion of alluvial fans (Dolgoushin and Osipova, 1975). There is also evidence of triggering of landslides and mudflows by glacier surges (Kotlyakov, 1980; Gardner and Hewitt, 1990).

Push moraines and proglacial till features are useful in distinguishing between normal and surge-type glaciers in the quiescent phase, as long as they are prominent and not destroyed by subsequent surges. De Geer (1910) and Gripp (1929) already suggested that the extensive push moraines on Spitsbergen were the result of unusually fast glacier flow. These push moraine complexes consist of a series of arclike ridges marking the position of the farthest surge advance, and are evidence of a correlation between glaciotectonics and surging (Croot, 1988). Of note are the "Usherbreen type" moraines, where the surging glacier gradually moved over old terminal ridges to form marked concentric moraine crests (Hagen, 1987). Also in other regions, surge-related push moraine complexes have developed, as well as thrust-block moraines

(Evans and Rea, 2005). However, some push moraine complexes simply indicate the position of the glacier margin during the Last Glacial Maximum or the Little Ice Age (Lefauconnier and Hagen, 1991).

Surging glaciers have characteristic ice marginal sediment sequences, tectonic structure, and architecture (Sharp, 1988; Croot, 1988; Boulton et al., 1996), mostly by thrusting and glaciotectonism of fast advancing ice pushing into a preexisting foreland wedge. This results in a combination of brittle (faulting) and ductile (folding) deformation styles (Benediktsson et al., 2008). In some proglacial areas, dead ice overlain by till evolves into chaotic hummocky topography, on which distinctive rectilinear patterns of till ridges or debris bands can be observed. These are crevasse-fill ridges and reflect the orientation of crevasses in the surging glacier (Sharp, 1988). Smaller-scale features, such as drumlins, flutings, and accordion-eskers, are also related to surging and fast flow. Proglacial signatures of surging can even be found in marine environments (Boulton et al., 1996). On the basis of observations in the forefields of Icelandic surge-type glaciers, Sharp (1988) developed a sedimentation model, and Evans and Rea (2005) a landsystems model for surging glaciers. The sedimentation model links the following glacial sedimentation types to surging behavior: (1) high rates of bedrock erosion, (2) looped and accordion-style moraines, (3) thrusting and overriding of thick sediment sequences in the marginal zone, (4) extensive glaciotectonism, and (5) the formation of crevasse-fill ridges. According to the landsystems model, the geomorphological and sedimentological signature can be arranged in three overlapping zones: (a) an outer (distal) zone of thrust-block and push moraines, (b) a zone of hummocky moraines, and (c) an inner (proximal) zone of flutings, crevasse-squeeze ridges, and concertina eskers with hummocky outwash and remains of overridden zone (a) and (b) signatures.

Classification of surge-type glaciers from morphological evidence

Because of the degree of uncertainty of identifying surge-type glaciers on the basis of morphological evidence, a surge probability index with six classes, rather than a binary surge type and non-surge-type (normal) classification, was developed (Ommanney, 1980). Surge probability is based on the strength of surge evidence, which ranges from an observed surge to complete absence of surge-related morphological evidence. Regional surge classifications with two to six class probability indices have been used for statistical analysis of glacial and environmental controls on surging (e.g., Clarke et al., 1986; Jiskoot et al., 2001).

Hazards related to glacier surging

Surging is associated with a wide range of natural hazards, including outbursts of glacier-dammed lakes (Bruce et al., 1987), deadly rock/ice avalanches (Haeberli et al., 2004), damming and freshening of fjords (Motyka and Truffer, 2007), and overriding of forests (Fleisher et al., 2006). Discharge of large volumes of icebergs from surging glaciers (Table 1) can affect shipping and exploration, and if surging glaciers in the Denali Fault region were to damage the Alaska Pipeline, a major environmental hazard would result.

Why do glaciers surge?

Glazyrin (1978) and Clarke et al. (1984) proposed that downstream resistance to sliding is the cause of surge-type glaciers' unstable flow behavior. Factors that control resistance to sliding and restrict outflow fall into two groups: fixed factors (bedrock topography, valley shape, etc.), and changeable factors that can vary their degree of resistance or spatial location or both (Murray et al., 2003). Possible restrictions in outflow therefore include: (a) factors intrinsic to the glacier (thermal regime, efficiency of hydrological system, etc.), (b) bedrock and substrate properties, (c) valley shape, and (d) interaction with tributary glaciers.

"Sticky spots" are a special type of higher-than-average bed friction. Ideas about "sticky spots" range from bedrock bumps, cavities, thermal lows, and local pressure dips in hard beds to absence of water, increased substrate stiffness or local absence of deformable till (Alley, 1993; Murray et al., 2003; Kjær et al., 2006). Some consider "sticky spots" to be ephemeral in nature, that is, that they can be created and destroyed in response to variations in subglacial water pressure; however, the spatial distribution of velocity lows (sticky spots) and highs (slippery spots) remained fixed throughout the surge of Monacobreen (Murray et al., 2003).

Tributaries that protrude into a quiescent trunk can cause significant longitudinal compression upstream of the confluence, and this process may have the potential to block outflow of the trunk (Gripp, 1929; Glazovskiy, 1996; Jiskoot et al., 2001; Hewitt, 2007). Although statistical tests of the presence of tributaries and surge potential have been inconclusive, entrance angle, slope, depth, relative size, and entrance location may be important factors in determining whether or not a tributary can block a trunk, or vice versa (Kargel et al., 2005).

Flow in surge-type glaciers is governed by longitudinal stresses (pushing and pulling) rather than by basal shear stress alone (Budd, 1975; McMeeking and Johnson, 1986). Local stress gradients can be very sharp at the surge front, and surges tend to initiate at this discontinuity between high and low drag. According to a longitudinal stress model (McMeeking and Johnson, 1986), the rapid up- and downglacier spreading of the low drag region during the surge results in the basal and longitudinal stresses to fall below a critical value, at which the surge terminates. In addition, the attenuation of longitudinal stresses over longer distances might hold a clue to geometrical controls on surging (Jiskoot et al., 2000).

Although they may not be the primary trigger of surges, large rockslides may increase the basal shear

stress to a critical value to enhance sliding, and it has been suggested that they can cause surge-like accelerations (Hewitt, 2009). Since widespread occurrence of rockslides can coincide with the occurrence of large magnitude earthquakes, the long contested "Earth Quake Advance Theory" (Tarr and Martin, 1914) might have some validity after all, though likely only very exceptionally (Post, 1967).

Geographic distribution of surge-type glaciers and controls on surging

Only about 1% of glaciers worldwide are of surge type (Jiskoot et al., 2000), but ongoing research, especially that using advances in remote sensing, adds small numbers of surge-type glaciers to the existing lists on an almost yearly basis. Surging occurs in a wide variety of glacier types and sizes; however, the spatial distribution of surge-type glaciers is nonuniform on both global and regional scales (Post, 1969; Clarke et al., 1986). Most areas are devoid of surge-type glaciers, but clusters of surge-type glaciers exist in Alaska, the Yukon Territory, the Central Andes, Tien Shan, Pamirs, Kamchatka, Karakoram, Iceland, Svalbard, the Canadian and Russian High Arctic, and peripheral to the Greenland Ice Sheet. Within these regions surge-type glaciers are believed to comprise between $<1\%$ and 90% of the total glacier population (Liestøl, 1969; Weidick, 1988).

This geographic clustering suggests that some environmental control(s) exist(s) that make glaciers more likely to exhibit surge-type behavior in certain regions than in others (Post, 1969). Mass balance characteristics in relation to glacier geometry and thermal regime, as well as substrate and topography are likely to be different for surge-type glaciers and can be tested through glacier population analysis. Potential controls cover a range of dependent (glacier system-related) and independent (environmentally related) variables that relate to the distribution of glaciers and affect glacier movement.

According to Raymond (1987), the geometrical evolution of a glacier should be the overriding surge control, with critical geometries for both surge initiation and termination. Budd (1975) suggested that the product of glacier slope and balance flux over width controls surge potential, where this product is constant, irrespective of glacier geometry. Although long glaciers, those in tectonically active mountain ranges, and those with particular hypsometries have a higher likelihood of surging (Post, 1969; Glazyrin, 1978; Clarke et al., 1986; Jiskoot et al., 2000), neither a single characteristic nor combinations thereof can explain the distribution of surge-type glaciers satisfactorily. Combinations of factors that raise the likelihood of surging appear to be regionally specific, and might be an expression of different surge mechanisms (Murray et al., 2003). Since statistical studies use glacier inventory data that include surge-type glaciers in all stages of their surge cycle, the question of critical geometry will likely not be answered with this type of analysis.

Surge mechanisms

The occurrence of surging in a wide range of glaciers and environments suggests that flow instabilities could potentially occur in different components that control glacier flow. Since the 1970s, glaciologists have focused on three broad groups of ideas about the instability mechanisms:

1. Thermal instability
2. Hydrological instability in the subglacial drainage system
3. Instability of a deformable substrate

These surge mechanisms reflect the different types of glaciers that have been observed surging: glaciers overlying different types of beds, valley glaciers versus outlet glaciers, and polar/polythermal and temperate glaciers. Any surge theory should encompass any combination of these three potential instability mechanisms. It was not until the 1980s that any of the proposed surge mechanisms were firmly based on direct measurements of surge/quiescence behavior and on the laws of physics. "Plug flow" (ice flow being relatively uniform across glacier during a surge) and strong shear margins were an indication that basal motion rather than internal deformation or fast creep is the dominant flow process during a surge (Clarke, 1987). This suggests that high basal water pressures might be instrumental in all three mechanisms.

Thermal instability

Robin (1955) argued that surges could be explained by the oscillation of the basal temperature between subfreezing conditions where no sliding is possible, and melting conditions, where sliding is possible. Some surging glaciers have "cold ring" thermal regimes, which is a polythermal structure with an inner core of temperate ice surrounded by a zone of cold ice frozen to bedrock (Schytt, 1969; Clarke et al., 1984). This cold ring may act as a frozen dam during quiescence, which may give in and lead to surging when the zone of temperate ice spreads due to increasing thickness and frictional heat generated in the buildup phase. Alternatively, the polythermal structure has also been suggested to act as a cold-dam preventing the discharge of subglacial water (Murray et al., 2000). As the surge progresses, the progressive thinning of ice will conduct heat from the bed into the cold ice again, through which sliding, and hence the surge, will discontinue.

Hydrological instability

Hydrological instability through lubrication by a subglacial water film (Weertman, 1969) is untenable, because such a water film is not stable under increasing water pressure (Walder, 1982). Instead, cavitation (ice-bed separation through the "hydraulic jack effect") could be controlling sliding velocity, whereby sliding is a multi-valued function of basal shear stress and effective pressure (Lliboutry, 1968; Bindschadler, 1983). Subglacial drainage systems can be distinguished by two types of pressure–flux relations: one

in which water discharge and water pressure are inversely related (the larger the water flux, the lower the pressure: a conduit system of R channels where drainage is fast and localized) and one in which these are directly related (the larger the water flux, the higher the pressure: a linked-cavity system where drainage is slow and dispersed) (Kamb, 1987). Rapid switches between these two drainage systems can occur. A multi-valued sliding law is one where two states of stable sliding velocity exist for the same basal shear stress: "slow sliding" for drainage through conduits and "fast sliding" for drainage through linked cavities. At critical values for the basal shear stress and effective pressure, expressed as an instability parameter or index, sliding could become unstable and switch to the fast sliding mode (Bindschadler, 1983; Kamb, 1987; Fowler, 1987). Thus, rapid switches between fast and slow subglacial drainage systems can result in rapid switches in mode of flow (e.g., at the onset or termination of a surge). This disruption of the hydrological system was originally proposed to explain surges in glaciers overlying hard beds only (Kamb, 1987). However, later observations suggest that most, if not all, surging glaciers are underlain by a soft bed (Harrison and Post, 2003), and that, at critical basal shear stress over soft deformable beds, rapid switches in subglacial drainage systems in till can initiate surges as well (Fowler, 1987; Eisen et al., 2005).

Soft bed deformation

Surges on deformable beds may be triggered in the region of elevated shear stress and water pressure through the destruction of subglacial drainage paths or drainage paths in the subglacial sediment (Boulton and Jones, 1979; Clarke et al., 1984), essentially making this mechanism a hydrologic instability as well. The elevated water pressure results in an increase in till deformability and increasing flow velocities. Because the deformation itself will destroy any possible water drainage ways, the water pressure will remain high and facilitate sustained fast motion. This rapid bed deformation can be pervasive and deep-seated (Truffer et al., 2000), but can also occur through plowing at the ice sediment or the sediment–bedrock interface (Fischer and Clarke, 1994; Kjær et al., 2006), or along internal stratigraphic boundaries (Fleisher et al., 2006). A requirement for this type of instability is the presence of a thick enough layer of fine-grained till and a substantial amount of water stored subglacially at high pressures (Truffer et al., 2000; Fowler et al., 2001). Progressive thinning of the till layer throughout the surge will result in decreased till mobility and eventually leads to surge termination.

Alaskan-type surges: temperate glacier surges regulated by subglacial hydrology and till failure

The velocity development of Alaskan-type surges is bimodal, with sudden switches between the slow and fast flow modes. Alaskan-type surges are generally of short duration (1–3 years) and have short quiescent phases (in the order of decades).

Kamb et al. (1985) postulated from the link between vertical and horizontal velocity, and hydrological characteristics during Variegated Glacier's 1982–1983 surge, that ice flow fluctuations were caused by the process of ice-bedrock separation (basal cavitation). The surge trigger would be a sudden switch in the subglacial drainage system from a conduit-dominated system to a distributed linked-cavity system, which would occur when the main conduit system outgrows itself, destabilizes, and collapses as a result of a sensitive relation between basal shear stress and water-flux-related stability of this fast and efficient drainage system (Kamb, 1987). Surge termination would occur when the conduit system reestablished through frictional heating by large volumes of water. Although this mechanism is, in retrospect, not supported by field observations, the central idea of a sensitive relationship between evolving basal shear stress and subglacial drainage system stability (whether under hard-bedded or soft-bedded glaciers) still holds (e.g., Eisen et al., 2005).

Since bed observations of Alaskan surge-type glaciers suggest that most, if not all, are underlain by a layer of deforming till (Harrison and Post, 2003), the Alaskan-type surging mechanism can clearly not be through ice-bedrock separation. Instead, a soft-bedded surge mechanism was proposed, in which surging in temperate glaciers is associated with the disruption of a soft deformable bed and the drainage system therein (Eisen et al., 2005, building on prior research). This surge mechanism is based on the fact that large amounts of water can be stored englacially, and can gradually move downward into the subglacial till (Lingle and Fatland, 2003), weakening the till's shear strength. At some critical basal shear stress (related to glacier morphology) a surge is promoted by the pervasive failure of the till. This will subsequently destroy the drainage system within the till, redistributing stress and till failure over a larger region, and rapidly leading to a widespread dramatic increase in soft bed deformation. The termination of an Alaskan-type surge is related to a combination of the progressive decrease of the basal shear stress due to the change in glacier morphology during the surge, and a sudden and large increase in the water flux, reestablishing the efficient subglacial drainage system and strengthening the till (Eisen et al., 2005).

Svalbard-type surges: thermally regulated soft bed deformation

Svalbard-type surges have a typical three-phase surge cycle development, a long surge duration (>3 years), and long quiescence (several decades to over a century).

Observations of polythermal regimes and deforming sedimentary beds beneath Svalbard surge-type glaciers (Murray et al., 2000), and the fact that polythermal glaciers overlying sedimentary beds have higher probabilities of surging (Jiskoot et al., 2000), led to the hypothesis of a thermally regulated soft-bedded surge mechanism for

this region. This was verified by measurements on Bakaninbreen in quiescence (Murray et al., 2000) and Monacobreen in surge (Murray et al., 2003), but similar basal conditions also occur beneath Trapridge Glacier, Yukon Territory (Clarke et al., 1984). In East Greenland, a combination of Alaskan and Svalbard-type surges have been observed, and coincide with a transition in thermal regime from temperate to polythermal (Jiskoot et al., 2001; Jiskoot and Juhlin, 2009).

The thermally regulated surging mechanism develops as follows (Fowler et al., 2001; Murray et al., 2003): (1) During quiescence, the glacier is cold-based or polythermal. An increasing area of ice in the reservoir area thickens and reaches the pressure melting point. (2) Once the pressure melting point is reached, basal meltwater is produced. This leads to elevated pore water pressures and weakening of the underlying till, causing till deformation and dilation (weakening through expansion due to opening of pore spaces), which enhances water storage and further weakening. (3) Frictional heat produced by enhanced deformation results in further melting and rising of pore water pressures. (4) The positive feedback between basal motion and meltwater production continues and results in rapid basal motion and full surge development. (5) Through redistribution of ice during the fast flow, ice in the initiation zone will thin until increased heat loss results in refreezing at the glacier bed.

The restricting factors in the weakening of till layers are the thickness of the till layer, and the supply of water (Fowler et al., 2001; Kjær et al., 2006), while the restricting thermal factors are ice thickness and basal movement producing frictional heat. Since these factors change slowly, but progressively, glaciers with a thermally induced soft bed deformation surge mechanism have a typical three-phase surge cycle development.

Timing of surges related to surge mechanism

For Alaskan-type surges (temperate glaciers), surge initiation coincides with low water input into the system when the subglacial drainage system is not yet fully developed and is draining water ineffectively, while surge termination coincides with an abundance of meltwater and the reopening of channels (Kamb et al., 1985; Eisen et al., 2005). This suggests initiation in winter, or at least during absence of abundant surface water, and termination in summer (Raymond, 1987; Harrison and Post, 2003). More specifically, for Variegated Glacier, it has been calculated that surge termination timing is a combined function of total sum of positive degree days (PDD) and record hot days in the late ablation season (Eisen et al., 2005). In contrast, thermally regulated surges are not dependent on the influx of surface meltwater, but on reaching an overall critical thickness, and could therefore start and terminate in any season. However, no systematic comparative studies exist on the seasonality of surge initiation and termination related to surge mechanism.

Summary

Surge-type glaciers have a surge cycle that involves long periods of quiescence, with flow velocities much lower than the balance velocity, interspersed with short surges, in which 10–1000-fold increase of flow results in average velocities greatly exceeding the balance velocity. It is still elusive what exactly triggers these sudden switches in flow mode, but controls that have been identified and for which field evidence exists are thermal regime, configuration of subglacial hydrology, and bed deformation. Basal shear stress, the amount and distribution of subglacially stored water, and type of subglacial drainage system (within or above a soft deformable bed) appear crucial in the process of surging. Two main surge mechanisms have been verified by observations on surging glaciers in different regions: the Alaskan-type mechanism, a hydrological instability in temperate, soft-bedded glaciers, caused by till weakening and a switch in the subglacial drainage system, and the Svalbard-type mechanism, a thermally induced soft bed instability in polythermal (subpolar) surge-type glaciers.

Distinguishing surge-type from normal glaciers by remote sensing can be achieved for glaciers with clear development of the following surface features diagnostic for surging:

- A surge advance
- Elongated "tear-shaped" moraine loops and/or sheared off tributaries
- Trimlines of former ice surface hanging above the present ice surface
- A marked surge bulge
- A completely crevassed glacier (that was not entirely crevassed before)
- A sudden increase in iceberg production
- Potholes covering large parts of the glacier

Only a small percentage of glaciers worldwide are of surge type, and these tend to occur in geographical clusters. No single factor or combination of glacial or environmental factors has been found conclusive determinants of surging. Instead, controls on surging might be regional and related to specific surge mechanisms.

There still remain a number of unresolved questions in the understanding of surge behavior, and many that were posed in Raymond (1987) have not been conclusively answered. Some key questions include: (1) what are the triggers of the flow instabilities leading to surges; (2) which factors control surge initiation, propagation, and termination; (3) what are the critical thresholds between real surges and slow surges, and (4) how are restrictions in outflow related to surging? In the historic line of asking the questions: *What are glacier surges?* (Meier and Post, 1969), *How do glaciers surge?* (Raymond, 1987) and *How much do we really know about glacier surging?* (Harrison and Post, 2003) perhaps future overview papers could address the questions *Why and when do glaciers surge?* and *Why don't all glaciers surge?*

Bibliography

Alley, R. B., 1993. In search of ice-stream sticky spots. *Journal of Glaciology*, **39**(133), 447–454.

Benediktsson, Í. Ö., Möller, P., Ingólfsson, Ó., van der Meer, J. J. M., Kjær, K. H., and Krüger, J., 2008. Instantaneous end moraine and sediment wedge formation during the 1890 glacier surge of Brúarjökull, Iceland. *Quaternary Science Reviews*, **27**, 209–234.

Benn, D. I., Kristensen, L., and Gulley, J. D., 2009. Surge propagation constrained by a persistent subglacial conduit, Bakaninbreen–Paulabreen, Svalbard. *Annals of Glaciology*, **50**(52), 81–86.

Bindschadler, R., 1983. The importance of pressurized subglacial water in separation and sliding at the glacier bed. *Journal of Glaciology*, **29**(101), 3–19.

Björnsson, H., Pálsson, F., and Sigurðsson, O., 2003. Surges of glaciers in Iceland. *Annals of Glaciology*, **36**, 82–90.

Boulton, G. S., and Jones, A. S., 1979. Stability of temperate ice caps and ice sheets resting on beds of deformable sediment. *Journal of Glaciology*, **24**(90), 29–43.

Boulton, G. S., Van der Meer, J. J. M., Hart, J., Beets, D., Rueggs, G. H. J., Van der Wateren, F. M., and Jarvis, J., 1996. Till and moraine emplacement in a deforming bed surge - an example from a marine environment. *Quaternary Science Reviews*, **15**, 961–987.

Bruce, R. H., Cabrera, G. A., Leiva, J. C., and Lenzano, L. E., 1987. The 1985 surge and ice dam of Glaciar Grande del Nevado sel Plomo, Argentina. *Journal of Glaciology*, **33**(113), 131–132.

Budd, W. F., 1975. A first model for periodically self-surging glaciers. *Journal of Glaciology*, **14**(70), 3–21.

Clapperton, C. M., 1975. The debris content of surging glaciers in Svalbard and Iceland. *Journal of Glaciology*, **14**(72), 395–406.

Clarke, G. K. C., 1987. Fast glacier flow: ice streams, surging, and tidewater glaciers. *Journal of Geophysical Research*, **92**(B9), 8835–8841.

Clarke, G. K. C., Collins, S. G., and Thompson, D. E., 1984. Flow, thermal structure, and subglacial conditions of a surge-type glacier. *Canadian Journal of Earth Sciences*, **21**, 232–240.

Clarke, G. K. C., Schmok, J. P., Ommanney, C. S. L., and Collins, S. G., 1986. Characteristics of surge-type glaciers. *Journal of Geophysical Research*, **91**(B7), 7165–7180.

Croot, D. G., 1988. Glaciotectonics and surging glaciers: a correlation based on Vestspitsbergen, Svalbard, Norway. In Croot, D. G. (ed.), *Glaciotectonics: Forms and Processes*. Rotterdam: Balkema, pp. 49–62.

Cruikshank, J., 2005. *Do Glaciers Listen? Local Knowledge, Colonial Encounters, and Social Imagination*. Vancouver: UBC, 312pp.

De Geer, G., 1910. *Guide de l'excursion au Spitzberg*. Stockholm: XIe Congrès Géologique Internationale, 23pp.

Dolgoushin, L. D., and Osipova, G. B., 1975. Glacier surges and the problem of their forcasting. *IAHS-AISH Publications*, **104**, 292–304.

Dowdeswell, J. A., 1989. On the nature of Svalbard icebergs. *Journal of Glaciology*, **35**(120), 224–234.

Dowdeswell, J. A., Hamilton, G. S., and Hagen, J. O., 1991. The duration of the active phase on surge-type glaciers: contrasts between Svalbard and other regions. *Journal of Glaciology*, **37**(127), 338–400.

Dowdeswell, J. A., Hodgkins, R., Nuttall, A.-M., Hagen, J. O., and Hamilton, G. S., 1995. Mass balance changes as a control on the frequency and occurrence of glacier surges in Svalbard, Norwegian High Arctic. *Geophysical Research Letters*, **22**(21), 2909–2912.

Eisen, O., Harrison, W. D., Raymond, C. F., Echelmeyer, K. A., Bender, G. A., and Gordeev, V. V., 2005. Variegated Glacier, Alaska, USA: a century of surges. *Journal of Glaciology*, **51**(174), 399–422.

Evans, D. J. A., and Rea, B. R., 2005. Surging glacier landsystem. In Evans, D. J. A. (ed.), *Glacial Landsystems*, London: Arnold, 532pp.

Fischer, U. H., and Clarke, G. K. C., 1994. Ploughing of subglacial sediment. *Journal of Glaciology*, **40**, 97–106.

Fleisher, P. J., Lachniet, M. S., Muller, E. H., and Bailey, P. K., 2006. Subglacial deformation of trees within overridden foreland strata, Bering Glacier, Alaska. *Geomorphology*, **75**, 201–211.

Fowler, A. C., 1987. A theory of glacier surges. *Journal of Geophysical Research*, **92**(B9), 9111–9120.

Fowler, A. C., Murray, T., and Ng, F. S. L., 2001. Thermal regulation of glacier surging. *Journal of Glaciology*, **47**(159), 527–538.

Frappé, T., and Clarke, G. K. C., 2007. Slow surge of Trapridge Glacier, Yukon Territory, Canada. *Journal of Geophysical Research*, **112**, F03S32, doi:10.1029/2006JF000607.

Gardner, J. S., and Hewitt, K., 1990. A surge of Bualtar Glacier, Karakoram Range, Pakistan: A possible landslide trigger. *Journal of Glaciology*, **36**(123), 159–162.

Glazovskiy, A. F., 1996. The Problem of Surge-Type Glaciers. In Kotlyakov (ed.), *Variations of Snow and Ice in the Past and at Present on a Global and Regional Scale.* IHP-IV Project H-4.1, UNESCO, 78pp.

Glazyrin, G. E., 1978. Identification of surging glaciers by morphometric characteristics. *Materialy Glyatsiologicheskikh Issledovaniy Khronika*, **33**, 136–137.

Gripp, K., 1929. Glaciologische und geologische Ergebnisse der Hamburgischen Spitsbergen-Expedition 1927. *Abhandlungen des Naturwissenschaftlichen Vereins zu Hamburg*, Band XXII 2.-4. Heft: 162–231.

Haeberli, W., et al., 2004. The Kolka-Karmadon rock/ice slide of 20 September 2002: an extraordinary event of historical dimensions in North Ossetia, Russian Caucasus. *Journal of Glaciology*, **50**(171), 533–546.

Hagen, J. O., 1987. Glacier surge at Usherbreen, Svalbard. *Polar Research*, **5**, 239–252.

Hansen, S., 2003. From surge-type to non-surge-type glacier behaviour: midre Lóvenbreen. *Svalbard, Annals of Glaciology*, **36**, 97–102.

Harrison, W. D., and Post, A. S., 2003. How much do we really know about glacier surging? *Annals of Glaciology*, **36**, 1–6.

Harrison, W. D., et al., 2008. Another surge of Variegated Glacier, Alaska, USA, 2003/04. *Journal of Glaciology*, **54**(184), 192–194.

Hewitt, K., 2007. Tributary glacier surges: an exceptional concentration at Panmah Glacier, Karakoram Himalaya. *Journal of Glaciology*, **53**(181), 181–188.

Hewitt, K., 2009. Rock avalanches that travel onto glaciers and related developments, Karakoram Himalaya, Inner Asia. *Geomorphology*, **103**, 66–79.

Hodgkins, R., and Dowdeswell, J. A., 1994. Tectonic processes in Svalbard tide-water glacier surges: evidence from structural geology. *Journal of Glaciology*, **40**(136), 553–560.

Hoinkes, H. C., 1969. Surges of the Vernagtferner in the Ötztal Alps since 1599. *Canadian Journal of Earth Sciences*, **6**, 853–860.

Iken, A., 1981. The effect of subglacial water pressure on the sliding velocity of a glacier in an idealized numerical model. *Journal of Glaciology*, **27**(97), 407–422.

Jiskoot, H., and Juhlin, D. T., 2009. Surge of a small East Greenland glacier, 2001–2007, suggests Svalbard-type surge mechanism. *Journal of Glaciology*, **55**(191), 567–570.

Jiskoot, H., Murray, T., and Boyle, P., 2000. Controls on the distribution of surge-type glaciers in Svalbard. *Journal of Glaciology*, **46**(154), 412–422.

Jiskoot, H., Pedersen, A. K., and Murray, T., 2001. Multi-model photogrammetric analysis of the 1990s surge of Sortebræ, East Greenland. *Journal of Glaciology*, **47**(159), 677–687.

Kamb, B., 1987. Glacier surge mechanisms based on linked cavity configuration of the basal water conduit system. *Journal of Geophysical Research*, **92**(B9), 9083–9100.
Kamb, B., and Engelhardt, H., 1987. Waves of accelerated motion in a glacier approaching surge: the mini-surges of Variegated Glacier, Alaska. *Journal of Glaciology*, **33**(113), 27–46.
Kamb, B., et al., 1985. Glacier Surge Mechanism: 1982–1983 Surge of Variegated Glacier, Alaska. *Science*, **227**(4686), 469–479.
Kargel, J. S., et al., 2005. Multispectral imaging contributions to Global Land Ice Measurements from Space. *Remote Sensing of Environment*, **99**, 187–219.
Kjær, K. H., et al., 2006. Subglacial decoupling at the sediment/bedrock interface: a new mechanism for rapid flowing ice. *Quaternary Science Reviews*, **25**, 2704–2712.
Kotlyakov, V. M., 1980. Problems and results of mountain glaciers in the Soviet Union. *IAHS-AISH Publications*, **126**, 129–137.
Kotlyakov, V. M., Osipova, G. B., and Tsvetkov, D. G., 2008. Monitoring surging glaciers of the Pamirs, central Asia, from space. *Annals of Glaciology*, **48**(1), 125–134.
Lefauconnier, B., and Hagen, J. O., 1991. Surging and calving glaciers in Eastern Svalbard. *Norsk Polarinstitutt Meddelelser*, **116**, 130.
Liestøl, O., 1969. Glacier surges in West Spitsbergen. *Canadian Journal of Earth Sciences*, **6**, 895–897.
Liestøl, O., Repp, K., and Wold, B., 1980. Supra-glacial lakes in Spitsbergen. *Norsk Geografisk Tidsskrift*, **34**, 89–92.
Lingle, C. S., and Fatland, D. R., 2003. Does englacial water storage drive temperate glacier surges? *Annals of Glaciology*, **36**, 14–20.
Lliboutry, L., 1968. General theory of subglacial cavitation and sliding of temperate glaciers. *Journal of Glaciology*, **7**(49), 21–58.
McMeeking, R. M., and Johnson, R. E., 1986. On the mechanism of surging glaciers. *Journal of Glaciology*, **32**(110), 120–132.
Meier, M. F., and Post, A., 1969. What are glacier surges? *Canadian Journal of Earth Sciences*, **6**, 807–817.
Motyka, R. J., and Truffer, M., 2007. Hubbard Glacier, Alaska: 2002 closure and outburst of Russell Fjord and postflood conditions at Gilbert Point. *Journal of Geophysical Research*, **112**, F02004, doi:10.1029/2006JF000475.
Murray, T., Dowdeswell, J. A., Drewry, D. J., and Frearson, I., 1998. Geometric evolution and ice dynamics during a surge of Bakaninbreen, Svalbard. *Journal of Glaciology*, **44**(147), 263–272.
Murray, T., Stuart, G. W., Miller, P. J., Woodward, J., Smith, A. M., Porter, P. R., and Jiskoot, H., 2000. Glacier surge propagation by thermal evolution at the bed. *Journal of Geophysical Research*, **135**(B6), 13491–13507.
Murray, T., Strozzi, T., Luckman, A., Jiskoot, H., and Christakos, P., 2003. Is there a single surge mechanism? Contrasts in dynamics between glacier surges in Svalbard and other regions. *Journal of Geophysical Research*, **108**(B5), 2237, doi:10.1029/2002JB001906.
Ommanney, C. S. L., 1980. The inventory of Canadian glaciers: procedures, techniques, progress and applications. *IAHS-AISH Publications*, **126**, 35–44.
Paterson, W. S. B., 1994. *The physics of glaciers*, 3rd edn. Pergamon: Oxford, 480 pp.
Post, A., 1967. Effects of the March 1964 Alaska Earthquake on Glaciers. *Geological Survey Professional Paper*, 544-D, 41 pp.
Post, A., 1969. Distribution of surging glaciers in western North America. *Journal of Glaciology*, **8**(53), 229–240.
Post, A., 1972. Periodic surge origin of folded medial moraines on Bering piedmont glacier, Alaska. *Journal of Glaciology*, **11**(62), 219–226.
Raymond, C. F., 1987. How do glaciers surge? A review. *Journal of Geophysical Research*, **92**(B9), 9121–9134.
Reeh, N., Bøggild, C. E., and Oerter, C., 1994. Surge of Storstrømmen, a large outlet glacier from the Inland Ice of North-East Greenland. *Rapport. Grønlands Geologiske Undersøgelse*, **162**, 201–209.
Robin, G. de Q., 1955. Ice movement and temperature distribution in glaciers and ice sheets. *Journal of Glaciology,* **2**(18), 523–532.
Schytt, V., 1969. Some comments on glacier surges in Eastern Svalbard. *Canadian Journal of Earth Sciences*, **6**, 867–873.
Sharp, M., 1988. Surging glaciers: geomorphic effects. *Progress in Physical Geography*, **12**(4), 533–559.
Sharp, M., Lawson, W., and Anderson, R.S., 1988. Tectonic processes in a surge-type glacier. *Journal of Structural Geology*, **10**(5), 499–515.
Sturm, M., 1987. Observations on the distribution and characteristics of potholes on surging glaciers. *Journal of Geophysical Research*, **92**(B9), 9015–9022.
Sund, M., Eiken, T., Hagen, J. O., and Kääb, A., 2009. Svalbard surge dynamics derived from geometric changes. *Annals of Glaciology*, **50**(52), 50–60.
Tarr, R. S., and Martin, L., 1914. *Alaskan Glacier Studies of the NGS, Prince William Sound and Lower Copper River Regions*. Washington, DC: National Geographic Society, 498 pp.
Thorarinsson, S., 1969. Glacier surges in Iceland with special reference to the surges of Bruárjökull. *Canadian Journal of Earth Sciences*, **6**, 875–882.
Truffer, M., Harrison, W. D., and Echelmeyer, K. A., 2000. Glacier motion dominated by processes deep in underlying till. *Journal of Glaciology*, **46**(153), 213–221.
Walder, J. S., 1982. Stability of sheet flow of water beneath temperate glaciers and implications for glacier surging. *Journal of Glaciology*, **28**(99), 273–293.
Weertman, J., 1969. Water lubrication mechanism of glacier surges. *Canadian Journal of Earth Sciences*, **6**, 929–942.
Weidick, A., 1988. Surging glaciers in Greenland: a status. *Rapport Grønlands Geologiske Undersøgelse*, **140**, 106–110.
Yde, J. C., and Knudsen, N. T., 2007. 20th-century glacier variations on Disko Island (Qeqertarsuaq), Greenland. *Annals of Glaciology*, **46**, 209–214.

Cross-references

Dynamics of Glaciers
Glacier Lake Outburst Floods
Glacier Motion/Ice Velocity
Glaciostatic Pressure/Stress
Glaciotectonic Structures, Landforms, and Processes
Moraine
Natural Hazards Associated with Glaciers and Permafrost
Retreat/Advance of Glaciers
Structural Glaciology
Subglacial Drainage System

GLACIER SYSTEM

Rajesh Kumar
Remote Sensing Division, Birla Institute of Technology, Extension Centre Jaipur, Jaipur, Rajasthan, India

Each glacier system has its own unique characteristics but with common aspects, such as an accumulation zone and an ablation zone. In order for the glacier to be in equilibrium and have a net zero mass-balance, the mass balance

of water equivalent entering the accumulation zone at higher altitudes in the form of snow must equal to water equivalent leaving the ablation zone. The bigger glaciers also possess the tributary glaciers and have larger glacier system. Hence, glacier's systems are inputs, stores, transfers, and outputs.

Glaciers gain mass as solid precipitation (snow) in the accumulation zone that transform into ice and then flow downhill as gravity flow. Apart from the snow fall, the accumulation zone also gets input from the snow avalanche from the valley side and by the accretion of rime ice by the direct freezing of atmospheric moisture onto the glacier. While coming down, it loses altitude and hence spreads into a higher temperature zone, which is called as ablation zone. The loss of glacier mass is by melting, as a result of warm air temperatures or applied pressure, evaporation, wind erosion, or by calving into icebergs along a floating ice front.

Glacier temperature is an important factor while considering the glacial system. Melt water, erosion, and deposition rates are directly related to the thermal behaviors in the glacier system.

GLACIER TOE

Rajesh Kumar
Remote Sensing Division, Birla Institute of Technology, Extension Centre Jaipur, Jaipur, Rajasthan, India

Glacier toe is the lowest end of a glacier and alternatively called as glacier snout or terminus (Figure 1). The surface streams growing from the snow and ice fields enter into the moulin or crevasse to become the englacial or subglacial flows and emerge out at the glacier toe. Due to this meltwater path, ice caves are formed at glacier toe (Figure 2). There is a general assumption that glacial erosion ends near the toe of a glacier where moraine deposition begins. The glacier toe fluctuations are also representative of the glacier's advance or retreat.

The movement of a glacier's toe back toward the glacier's origin shows the glacier retreat, and forward from the glacier origin reflects the advance of the glacier. If there is no change in the glacier toe position, it is roughly an estimate of glacier in zero balance.

GLACIERS OF THE KARAKORAM HIMALAYA

Kenneth Hewitt
Cold Regions Research Centre, Wilfrid Laurier University, Waterloo, ON, Canada

Definition and introduction

The South West Central Asian mountain system supports several major concentrations of glaciers at high altitude. The largest is in the Greater Karakoram-Hindu Raj, with almost 18,500 km^2 of perennial snow and glacier ice (Table 1). Here are some of the largest valley glaciers outside high latitudes. There are over 5,000 individual glaciers, but the ten largest comprise a third of the cover. Available measurements show maximum ice thicknesses exceeding 1,000 m on glaciers longer than 60 km, and over 500 m in glaciers half as long (Hewitt et al., 1989).

Glacier Toe, Figure 1 A landscape view of glacier toe, Suru glacier, Jammu and Kashmir. (Photograph by Dr. Rajesh Kumar.)

Glacier Toe, Figure 2 The formation of ice cave due to the melt water discharge at the Suru glacier toe. (Photograph by Dr. Rajesh Kumar.)

Glaciers of the Karakoram Himalaya, Table 1 Estimates of the perennial *snow and glacier* areas of the Karakoram and adjacent ranges of the South West Central Asian Mountain System (after von Wissmann, 1959)

Mountain range	K. Hewitt Revised (2007)	von Wissmann
1. Greater Karakoram ("Mustagh")[a]	15,500	(13,655)
2. The Western Karakoram[b]	2,950	(1,480)
Karakoram total	*18,450*[c]	*(15,135)*
3. The Hindu Raj[d]	950	(2,300)
4. Hindu Kush[e]	2,500	(3,900)
Total	21,900	(21,335)
Adjacent areas:		
5. Aghil Mts (Upper Yarkand River)		(1,700)
6. W.Tibet, Depsang, Pangong etc. (upper Indus basin)		(2,200)
7. Himalayan Deosai Mts/Ladakh/ Zanskar etc.		(1,700)
8. Nanga Parbat		(690)
9. Hazara. Indus and Swat Kohistan		(170)
Indus-Yarkand Basins	Total	(27,795)
10. Kun Lun		(14,500)
11. Pamir		(11,980)
Total, SWC Asian Systems		(54,275)

[a]West of the Upper Shyok River to the Hunza valley, north of the main Indus and south of the Shaksgam and Shimshal Rivers.
[b]West of the Hunza River to the Karambar, south of the Chapursan and north of the Gilgit – includes the Batura (740).
[c]*Karakoram draining to Yarkand River* about 1,500 km^2, leaving about 16,000 to Indus.
[d]West of the Karambar, south and east of the Yarkhun River (upper Chitral).
[e]Includes both Pakistan (Chitral) and Afghanistan slopes, but not very large glaciers. The share draining to the Indus is about 2,000 km^2. The remainder flowing to the Amu Darya ("Oxus").

The glaciers may comprise more than 2,000 km^3 stored ice volume and are major stores and sources of surface water in this extreme continental, dry region. However, most glaciers are nourished largely or wholly by snow avalanches from steep rock walls. This makes it difficult to separate permanent snow-covered and snow avalanche source areas from glacier ice and ice streams-proper, or to identify the full extent of the latter. Glacier-ice itself probably comprises less than half the total basin area estimates. Avalanche nourishment is related to another typical

feature, vast areas of debris-covered ice in the lower ablation zones.

The glaciers are part of a range of cryosphere conditions and features. The entire mountain area is covered with seasonal snowfall varying in duration and depth with elevation. Its melting provides about half of stream flows in an average year. Permafrost at intermediate altitudes is more extensive than glaciers and there is widespread patterned ground, hundreds of rock glaciers, erosion, and deposition forms left by snow avalanches. Most, if not all, of the region was glaciated in the Quaternary (Shroder et al., 1993; Kuhle, 2004). Glacier fluctuations in the Holocene also left their mark, especially "Little Ice Age" (LIA) advances (Kick, 1989).

An unusual concentration of surging glaciers is found (Hewitt, 2007a), and a history of ice dams and glacial lake outburst floods (Hewitt, 1998). Scientific work goes back 150 years, but coverage has been patchy in time and space (Visser, 1928; Mason, 1930; Paffen et al., 1956; von Wissmann, 1959; Batura Investigations Group, 1979; Goudie et al., 1984; Hewitt, 2007b).

Glacier climates

Three weather systems affect the region at different times of the year. Two systems bring the snowfall that nourishes the glaciers. A westerly circulation and cyclonic storms dominate the winter, while monsoonal air and storms can bring high altitude snowfall in summer (Mayewski and Jeschke, 1979; Barros et al., 2008). These systems are affected by continental anticyclones over and to the west of the Tibetan Plateau. Meanwhile, anticyclonic conditions bring high levels of solar radiation and nocturnal heat loss critical in summer especially, when clear-versus-cloudy weather is decisive in glacier ablation, direct solar radiations accounting for 80–85% of it. The three very different weather systems vary in relative strength from year to year, and with global climate change.

Equally important are topo-climates; conditions modified by high elevations, relief, and slope orientation. There are strong gradients in precipitation and thermal conditions with elevation (Figure 1). Watersheds of the larger glaciers are in the highest parts of the Karakoram between 6,500 and 8,000 m or more. These glaciers have globally extreme elevation ranges from 3,500 to over 5,000 m. Some termini reach below 2,500 m above sea level (asl); 1,500 m lower than the largest glaciers of Nepal, for example.

Low down, valleys are rain shadowed and semi-arid or arid, with as little as 170 mm annual precipitation. Glacier headwaters just a few kilometers away can receive snowfall up to 2,000 mm water equivalent (w.e.). Average daily temperatures above freezing occur for 7–8 months around 2,500 m asl; between 8 and 4 weeks at 3,800 and 4,800 m respectively, and are rare or absent above 5,000 m. Steep slopes and differences of orientation lead to further variability (Hewitt, 1993).

Mass balance considerations

Glacier mass balance is the relation between accumulation of snow on the upper glacier and ablation on the lower, moderated by the flow of ice in between. Measurements in the central Karakoram show rather more than half of high altitude snow accumulation in winter and somewhat less than half in summer (Wake, 1989). The glaciers are intermediate between the "summer accumulation types" of the Greater Himalaya and "winter accumulation" of

Glaciers of the Karakoram Himalaya, Figure 1 A predominantly avalanche-fed glacier; the upper Choktoi. This tributary of the Panmah Glacier, viewed from 4,500 m asl is hemmed in by rock walls and ice falls up to 7,200 m such that most of the snow descends to the glacier in avalanches. (Photo: Hewitt, June, 2005.)

the Caucasus to the west (Ageta and Fujita, 1996). Precipitation maxima occur in the accumulation zones between 5,000 and 6,000 m asl, much higher than in most of the world's mountains (Barry, 1992, 234).

The interface between the accumulation and ablation zones or equilibrium line altitude (ELA) is usually close to the firn limit, the greatest elevation(s) at which ablation removes all seasonal snowfall and temporarily exposes glacier ice. In the Karakoram, it is usually found at around 5,000 m and in late August, but much higher on south-facing slopes and lower on north-facing ones. The ELA was observed spread out between 4,700 and 5,300 m asl on the Batura Glacier (Batura Investigations Group, 1979).

On avalanche-nourished glaciers, the ELA is lower than the firn limit. Many Karakoram glaciers commence well below 5,000 m asl, linked to the perennial snow zone only by avalanche tracks (Figure 2). Indeed, the larger fraction of glacier ice derives from snow avalanched through 1,000 m elevation or more. However, there are no studies of the contribution of avalanche nourishment to mass balance and little is known of the relative scales and roles of winter, spring, and summer avalanches. They differ in thermal properties, the proportions of powder and wet snow, and debris content.

Ablation zones also involve large gradients with elevation. Some melting occurs for 8–10 months at around 2,500 m asl; for only 4–8 weeks in the most extensive and critical ablation zone areas, and declines to a few days near the ELA. Ablation rates are high under favorable conditions. On the Biafo Glacier, at 4,080 m asl in July, 50–90 mm of ice loss were recorded on clean to dusty ice in clear or slightly cloudy conditions (Hewitt et al., 1989; Hewitt, 2005). Annual ablation here is 5–7 m (w.e). Potential ablation is highest towards glacier termini. Locally, as much as 18.4 m/year was measured near the Batura Glacier terminus (Batura Investigations Group, 1979), but heavy supraglacial moraine suppresses overall melting to just a few centimeters annually. This partly explains the low altitude penetration of many termini (Figure 3). However, dust and thin layers of dirt are more important hydrologically, being decisive in the mid- to upper ablation zones where 70–80% of ablation occurs. Dust particles enhance local absorption of solar radiation and a thin veneer of wet mud can increase ablation rates by over 40% compared to clean ice (Mattson and Gardner, 1989). Dust and dirt on ice surfaces are very sensitive to weather conditions, being quickly washed away on cloudy days, even without rain, and quickly built up again on sunny ones. This also makes them more sensitive to climate change.

To summarize: mass balance in the Karakoram depends critically on events in certain elevations, roughly:

1. 4,500–6,000 m asl for accumulation and glacier nourishment
2. 3,500–4,300 m for ablation, where the most extensive exposed ice areas occur and where dust and dirt enhance ablation
3. below 3500 m, where most ice areas are protected by heavy supraglacial debris

Glacier thermal regimes

Climatic complexity has an indirect effect through ice thermal regimes. Paterson (1994) recognizes four classes,

Glaciers of the Karakoram Himalaya, Figure 2 Rapid buildup of supraglacial moraine in the mid-ablation zone of an avalanche-fed glacier: the Ghondogoro Glacier, Masherbrum range, viewed from 3,800 m asl (Hewitt, July, 2005).

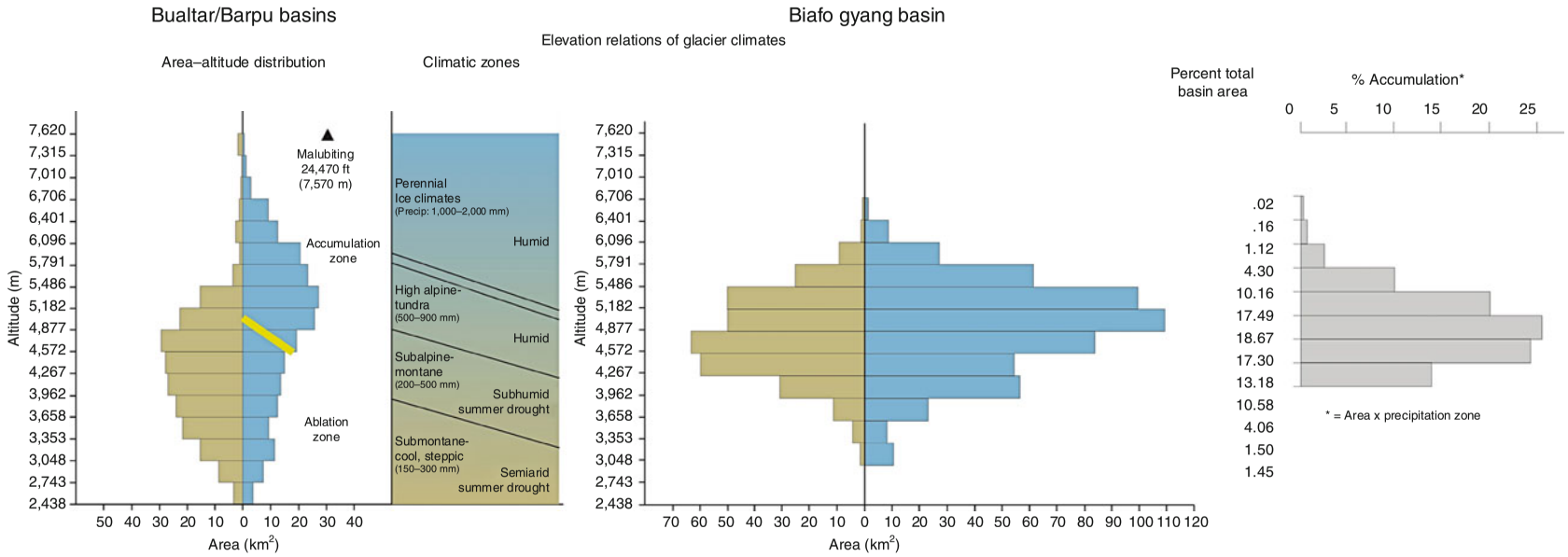

Glaciers of the Karakoram Himalaya, Figure 3 Area-altitude distribution of Karakoram glaciers, and vertical organization of the climatic environment. The Bualtar-Barpu basin in the Rakaposhi Range, Hunza Karakoram, represents the commonest, largely avalanche-fed system. The much larger Biafo Glacier, in the central "Mustagh" Karakoram, is one of the few with a predominance of direct snowfall-fed ice streams from vast high altitude accumulation basins. Most of the measurements and dimensions cited in the text come from investigations in these two basins or nearby areas (after Hewitt, 2005).

commonly identified with different climatic regimes: "polar," "temperate," maritime, and continental. However, all four are present in the Karakoram, usually two in the same glacier, sometimes all four (Batura Investigations Group, 1979; Hewitt, 2005). Ice temperatures affect the deformation rate of ice, which increases with warming of ice below the melting point. Sub-zero ice tends to be frozen to the bed. Unfreezing can dramatically increase movement through sliding at the bed. At present the distribution and full influence of thermal regimes is not known.

Glacier hazards

Among the distinctive and extreme glacial phenomena is a high concentration of glaciers that surge, and a history of glacier dams and outburst floods. In the past 150 years, 32 glacier surges are documented involving 20 glaciers. At least half the surges are of tributary glaciers whose main glacier does not surge, something not yet reported elsewhere (Figure 4). Known surges involve avalanche-fed glaciers. Theories of surging do not invoke a relationship to nourishment, but avalanched snow seems likely to affect the thermal character and debris content of glaciers – which are considered important factors (Sharp, 1988).

Over the past 200 years, 62 glaciers have formed partial or complete cross-valley barriers on Karakoram rivers. More than 60 glacier lake outburst floods (GLOFs) have been reported (Hewitt, 1982). GLOFs from the larger of these ice dams can far exceed weather-generated floods. However, the dangerous moraine-, or dead-ice-ponded lakes associated with rapid retreat in the rest of the Himalaya are locally significant throughout the Karakoram, but the most dangerous ones arise with large tributary glaciers advancing across and damming main river valleys.

Glacier activity and dangers are also affected by catastrophic rock slope failures in glacier basins (Hewitt, 2009b). Some 29 are known to have spread in part or whole over glaciers, and 11 between 1986 and 2009. It is certain the numbers are underestimated due to difficulties of observation, and because active ice rapidly disperses the landslide debris. If recent observations are at all representative, it seems likely that this has been a significant factor in glacier behavior, contributions to denudation, and deposition in the Quaternary.

Concluding remarks: a climatic and/or glacier anomaly?

Various studies suggest glacier fluctuations in the Karakoram are out-of-phase with events elsewhere in the Northern Hemisphere. It is suggested that only minor advances occurred here during the last major Wisconsinian/Wurm glaciation (Shroder et al., 1993), and that LIA advances culminated decades later (Kick,

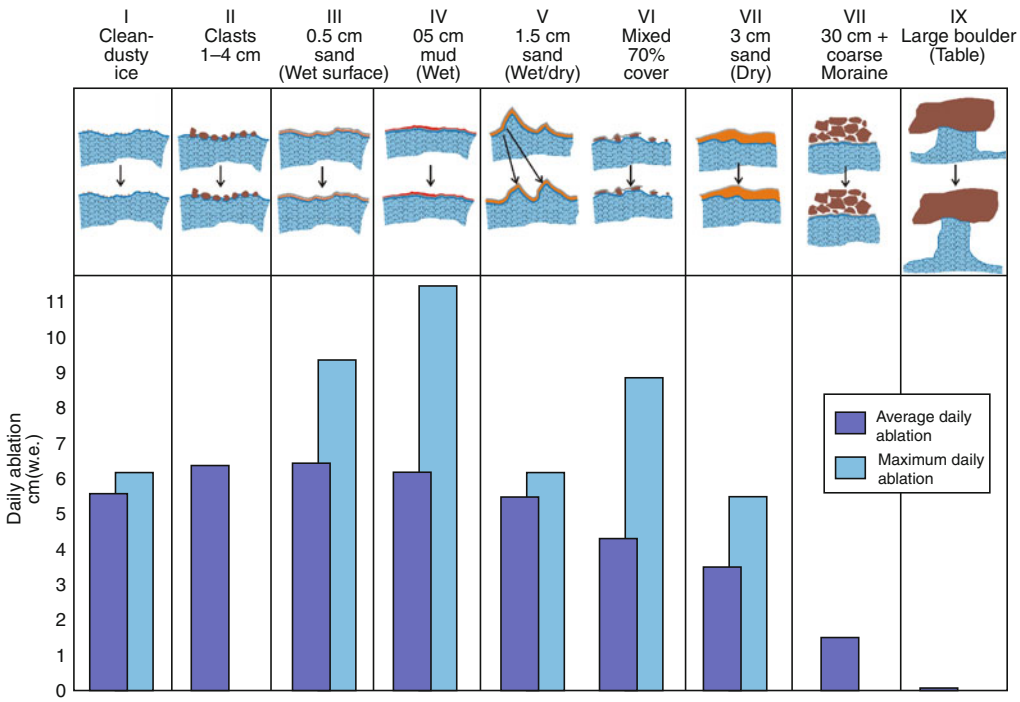

Glaciers of the Karakoram Himalaya, Figure 4 Differential ablation rates due to the thickness and composition of surface dust, dirt, and debris on Biafo Glacier at 4,080 m asl in July 1986. Measurements were made at experimental plots over a 10-day cycle in sunny (maximum rates) and intermittently cloudy weather (after Hewitt, 2005).

Glaciers of the Karakoram Himalaya, Figure 5 Legacies of tributary glacier surges at Panmah Glacier, Mustagh Karakoram. The complex lobes, ridges, and crevasse patterns in the ice stream are the result of four surges (*arrows*) into the main glacier (see Hewitt, 2007a). They occurred in 1994, 2002, and 2005. The ice lobe from a 1970s event 10 km up the glacier to the right had arrived here when the recent ones occurred. The main glacier is 2.5 km wide and some 12 km of its length are shown. (Photo: Hewitt, July, 2005.)

1989). These views do involve contested evidence. Quaternary glacial sequences involve mistaking post-glacial landslide deposits for former ice positions (Hewitt, 1999, 2009a). The LIA anomaly is based on records from glaciers that surge and, therefore, not necessarily in phase with climate fluctuations anyway (Hewitt, 2007a).

Nevertheless, in recent decades reports from the Karakoram suggest little or no disappearance of ice, let alone a catastrophic reduction, unlike the rest of the Himalaya. Some 10% of the ice cover was lost between the early twentieth century and the 1980s. Since the mid-1990s, however, more than 30 glaciers have advanced, and substantial ice storage and reduced melting is indicated in the heavily glacierized Hunza and Braldu basins, and some glaciers on the Yarkand basin, north slope (Archer and Fowler, 2004; Hewitt, 2005; Liu et al., 2006). Glacier change there is, probably due to changes in seasonal snowfall, summer storminess and ablation, and high altitude warming. Yet, through 2009 at least, ice cover is being sustained and may be increasing. A major problem is lack of monitoring of high altitude climate and other controlling conditions in glacier basins to help disentangle the various forcing factors, and how they could affect future ice behavior.

Bibliography

Ageta, Y., and Fujita, K., 1996. Characteristics of mass balance of summer-accumulation type glaciers in the Himalayas and Tibetan Plateau. *Zeitschrift für Gletscherkunde und Glazialgeologie*, **32**, 61–65.

Archer, D. R., and Fowler, H. J., 2004. Spatial and temporal variations in precipitation in the Upper Indus Basin, global teleconnections and hydrological implications. *Hydrology and Earth Systems Science*, **8**, 47–61.

Barros, A. P., Chiao, S., Lang, T. J., Burbank, D., and Putkonen, J. 2008. From weather to climate – Seasonal and Interannual variability of storms and implications for erosion processes in the Himalaya. In Willett, S. D., Hovius, N., Brandon, M. T., and Fisher, D. M. (eds.), *Tectonics, Climate, and Landscape Evolution*. Geological Society of America, Special Paper 398, Boulder, Colorado, pp. 17–38.

Barry, R., 1992. *Mountain Weather and Climate*, 3rd edn. New York: Methuen.

Batura Investigations Group, 1979. The Batura Glacier in the Karakoram Mountains and its variations. *Scientia Sinica*, **22**, 958–974.

Goudie, A. S., Jones, D. K. C., and Brunsden, D., 1984. Recent fluctuations in some glaciers of the western Karakoram Mountains, Pakistan. In Miller, K. J. (ed.), *The International Karakoram Project*. Cambridge: Cambridge University Press. 2, pp. 411–455.

Hewitt, K., 1982. Natural dams and outburst floods of the Karakoram Himalaya. In Glen. J. (ed.), *Hydrological Aspects of Alpine and High Mountain Areas*. International Hydrological Association, (I.A.H.S.) Publ. no.138, pp. 259–269.

Hewitt, K., 1993. Altitudinal organization of Karakoram geomorphic processes and depositional environments. In Shroder, J. F., Jr. (ed.), *Himalaya to the Sea: Geology, Geomorphology and the Quaternary*. New York: Routledge, pp. 159–183.

Hewitt, K., 1998. Glaciers receive a surge of Attention in the Karakoram Himalaya. *EOS, Transactions, American Geophysical Union*, **79**(8), 104–105.

Hewitt, K., 1999. Quaternary moraines vs. catastrophic rock avalanches in the Karakoram Himalaya, Northern Pakistan. *Quaternary Research*, **51**, 220–237.
Hewitt, K., 2005. The Karakoram Anomaly? Glacier expansion and the 'elevation effect', Karakoram Himalaya, Inner Asia, *Mountain Research and Development: Special Issue – Climate Change in Mountains.* **25**, 332–340.
Hewitt, K., 2007a. Tributary glacier surges: an exceptional concentration at Panmah Glacier, Karakoram Himalaya. *Journal of Glaciology*, **53**(181), 181–188.
Hewitt, K., 2007b. Rediscovering colonised landscapes: the first Europeans at the Mustagh Pass, Karakoram Himalaya, Inner Asia. In Gervers, M., Bulag, U., and Long, G. (eds.) *The Exploitation of the Landscape of Central and Inner Asia*, Toronto Studies in Central and Inner Asia, 9. Asian Institute, University of Toronto, pp. 41–67.
Hewitt, K., 2009a. Rock avalanches that travel onto glaciers: disturbance regime landscapes, Karakoram Himalaya, Inner Asia. *Geomorphology*, **103**, 66–79.
Hewitt, K., 2009a. Catastrophic rock slope failures and late Quaternary developments in the Nanga Parbat-Haramosh Massif, Upper Indus basin, Northern Pakistan, *Quaternary Science Reviews*, web version, 1–15. doi:10.1016/j.quascirev.2008.12.019,
Hewitt, K., Wake, C. P., Young, G. J., and David, C., 1989. Hydrological investigations at Biafo Glacier, Karakoram Himalaya, an important source of water for the Indus River. *Annals of Glaciology*, **13**, 103–108.
Kick, W., 1989. The decline of the last Little ice Age in High Asia compared with that in the Alps. In Oerlemans, J. (ed.), *Glacier Fluctuations and Climate Change*. Dordrecht: Kluwer, pp. 129–142.
Kuhle, M., 2004. The Pleistocene Glaciation in the Karakoram-Mountains: reconstruction of past glacier extensions and ice thicknesses. *Journal of Mountain Science*, **1**, 3–17.
Liu, S. Y., Ding, Y. J., Li, J., Shangguan, D. H., and Zhang, Y., 2006. Glaciers in response to recent climate warming in western China'. *Quaternary Sciences*, **26**, 762–771.
Mason, K., 1930. The glaciers of the Karakoram and neighbourhood. *Records: Geological Survey of India*, **63**, 214–227.
Mattson, L. E., and Gardner, J. S., 1989. Energy exchanges and ablation rates on the debris-covered Rakhiot Glacier, Pakistan. *Zeitschrift für Gletscherkunde und Glazialgeologie*, **25**, 17–32.
Mayewski, P. A., and Jeschke, P. A., 1979. Himalayan and transHimalayan glacier fluctuations since AD 1812. *Arctic and Alpine Research*, **11**, 267–287.
Paffen, K. H., Pillewizer, W., and Schneider, H.-J., 1956. Forschungen im Hunza-Karakorum. *Erdkunde*, **10**, 1–33.
Paterson, W. S. B., 1994. *The Physics of Glaciers*, 3rd edn. New York: Pergamon.
Sharp, M. J., 1988. Surging glaciers: behaviour and mechanisms. *Progress in Physical Geography*, **12**, 349–370.
Shroder, J. F., Owen, L., and Derbyshire, E., 1993. Quaternary glaciation of the Karakoram mountains and Nanga Parbat Himalaya. In Shroder, J. F., Jr. (ed.), *Himalaya to the Sea: Geology, Geomorphology and the Quaternary.* New York: Routledge, pp. 132–158.
Visser, Ph C, 1928. Von den Gletschern am Obersten Indus. *Zeitschrift fuer Gletscherkunde*, **16**, 169–229.
von Wissmann, H., 1959. Die heutige Vergletscherung und Schneegrenze in Hochasien mit Hinweisen die Vergletscherung der letzten Eiszeit. *Akademie der Wissenchaften und der Literatur in Mainz*, **14**, 1103–1431.
Wake, C. P., 1989. Glaciochemical investigations as a tool to determine the spatial variation of snow accumulation in the Central Karakoram, Northern Pakistan. *Annals of Glaciology*, **13**, 279–284.

GLACIERET

Rajesh Kumar
Remote Sensing Division, Birla Institute of Technology, Extension Centre Jaipur, Jaipur, Rajasthan, India

Glacierets are very small glaciers or ice masses of indefinite shape in hollows and have little or no movement for at least two consecutive years. Sometimes, it is also termed as a dead glacier. The thickness of the ice is also very less as compared to the normal glaciers. Glacierets are formed either by drifted snow or by snow that has avalanched from above and also under the heavy accumulation in certain years. Glacierets are also formed during the recession stage of the glaciers that has been associated with the climatic conditions and is responsible for the glacier recession after the little ice age. Glacierets commonly occupy cirques that were formed during past glaciations (Figure 1).

GLACIERIZATION

Rajesh Kumar
Remote Sensing Division, Birla Institute of Technology, Extension Centre Jaipur, Jaipur, Rajasthan, India

The word "glacierization" is frequently used as a process of glacier formation and growth, but it also has a meaning of "the covering of large land area by glaciers or ice sheets," that is, the process of glacier growth and development. The growth and decay of glacierization is driven by forces affecting the seasonal cycles of snowfall and snowmelt. The external controlling forces are likely to be variations in the earth's orbit that cause differences in the solar radiation received. Radiational control of snowmelt is also modulated by the seasonal cycles of snow albedo and cloud cover.

GLACIOEUSTASY

Amit Kumar
Department of Geology, Centre of Advanced Study in Geology, Punjab University, Chandigarh, Punjab, India

Glacioeustasy deals with the theory of sea levels rise and fall on the global scale in response to the melting of ice during interglacials and the accumulation of ice during glaciations. The implications of the changing of relative sea level are global in scope. The growth and decay of ice masses, such as glaciers and ice sheets, have direct influence on the changes in sea level. Since the last ice age, sea levels have gradually risen due to decrease in ice mass on the earth.

Glacieret, Figure 1 An example of glacieret observed in the Suru basin in Jammu and Kashmir, India. (Photograph by Dr. Rajesh Kumar on July 23, 2007.)

Read more: eustasy – glacio-eustasy – Sea, Ice, Level, and Global http://science.jrank.org/pages/14742/eustasy.html#ixzz13er6nl00

Bibliography

Miller, K. G., Sugarman, P. J., Browning, J. V., Kominz, M. A., Hernández, J. C., Olsson, R. K., Wright, J. D., Feigenson, M. D., and Van Sickel, W. 2003. Late cretaceous chronology of large, rapid sea-level changes: glacioeustasy during the greenhouse world. *Geology*, **31**(7), 585–588, Geological Society of America.

GLACIOFLUVIAL

Rajesh Kumar
Remote Sensing Division, Birla Institute of Technology, Extension Centre Jaipur, Jaipur, Rajasthan, India

The deposits and landforms or the streams that result by the action of melting glacier are known as glaciofluvial. The fluvial means "produced by the action of a stream," therefore, glaciofluvial simply means "produced by the actions of glaciers."

Glaciofluvial deposits are materials moved by glaciers and subsequently sorted and deposited by streams flowing from the melting ice. The deposits are stratified and may occur in the form of outwash plains, moraines (lateral, medial, and terminal), U-shape valleys, glacial and proglacial lakes, and terraces. Glacial and proglacial lakes are found in a variety of environments and in considerable numbers. Apart from the erosional lake, many lakes are formed as streams and dammed by the ice itself, by glacial deposits, or by a combination of these factors.

GLACIOGENIC DEPOSITS

Rajesh Kumar
Remote Sensing Division, Birla Institute of Technology, Extension Centre Jaipur, Jaipur, Rajasthan, India

The materials having heterogeneous sediments composed of an unconsolidated, heterogeneous mixture of clay, sand, pebbles, cobbles, boulders, and mounds of gravel deposited directly by the retreating glacier ice is called as till. Glacial drift is a general term for the coarsely graded and extremely heterogeneous sediments of glacial origin. Glacial till is that part of glacial drift, which was deposited directly by the glacier.

Till is commonly massive, ideally unsorted and unstratified sediment that may be deposited at the terminal moraine, along the lateral and medial moraines and in the ground moraine of a glacier (Figure 1). It is differentiated on particle size distribution, color, composition, cast shape, roundness, orientation and imbrications, and structure of the deposit. Sometimes, till plains also appear as extensive flat plains of till that form when a sheet of ice becomes detached from the main body of the glacier and melts in place depositing the sediments it carried. Glacial till can form very good soil for the crops to grow. Till may also contain alluvial deposits of gems or other valuable ore minerals.

Glaciogenic Deposits, Figure 1 Glaciogenic deposits, also called as Glacier Till is observed in Suru Basin, Jammu and Kashmir, India. (Photograph by Dr. Rajesh Kumar on July 1, 2008.)

GLACIOHYDRAULIC SUPERCOOLING

Fiona Tweed
Department of Geography, Staffordshire University, Stoke-on-Trent, Staffordshire, UK

Definition

Glaciohydraulic supercooling describes a process that occurs when the pressure melting point of water ascending the adverse slope of a subglacial overdeepening rises faster than the water is heated by viscous dissipation resulting in water remaining liquid below 0°C.

Theory and historical perspective

The theory of glaciohydraulic supercooling was first introduced by Röthlisberger (1972) and further developed by Röthlisberger and Lang (1987), Alley et al. (1998) and Lawson et al. (1998). Beneath thick *ice* at the base of a glacial overdeepening, the melting temperature is depressed by *overburden pressure* and water can continue to be liquid below 0°C (see Figure 1). The pressure gradient forces water to ascend the adverse slope of the overdeepening, and as the *overburden pressure* lessens, the pressure-dependent melting temperature gradually rises. If the adverse bedslope is more than 1.2–1.7 times the gradient of the ice-surface slope (Alley et al., 1998), then the heat generated for the water to remain in thermal equilibrium and the rate of increase in water temperature will be insufficient to match the changing pressure melting point and water will become supercooled (discussed in detail in separate chapter). As supercooled water approaches the *glacier* margin, it can freeze to the *glacier*, resulting in *ice* growth that constricts *meltwater conduits*, forms *frazil ice* and creates *anchor ice* terraces (Lawson et al., 1998; Evenson et al., 1999; Roberts et al., 2002; Tweed et al., 2005).

Glaciohydraulic supercooling has been well-documented at Matanuska Glacier, *Alaska* (Strasser et al., 1996; Lawson et al., 1998; Alley et al., 1999; Evenson et al., 1999), at Bering Glacier *Alaska* (Natel and Fleisher, 1994; Fleisher et al., 1997), and at several glaciers in Iceland (Roberts et al., 2002; Tweed et al., 2005) during normal meltwater flow conditions and during *glacier* floods. Criteria considered indicative of the process comprise water temperatures consistently below freezing despite ambient air temperatures well above freezing; *frazil* crystals and flocs in the discharged water and the growth of *anchor ice* terraces around artesian meltwater vents (Evenson et al., 1999). There is still debate regarding the significance of glaciohydraulic supercooling for the formation of thick basal *ice* sequences beneath temperate glaciers (Lawson et al., 1998; Tweed et al., 2005; Cook et al., 2007) and the role of supercooling in the *dynamics of glaciers* and the development of contemporary and Quaternary landforms and sediments (Lawson et al., 1999; Alley et al., 2003; Larsen et al., 2006; Cook et al., 2006; Knight and Cook, 2008).

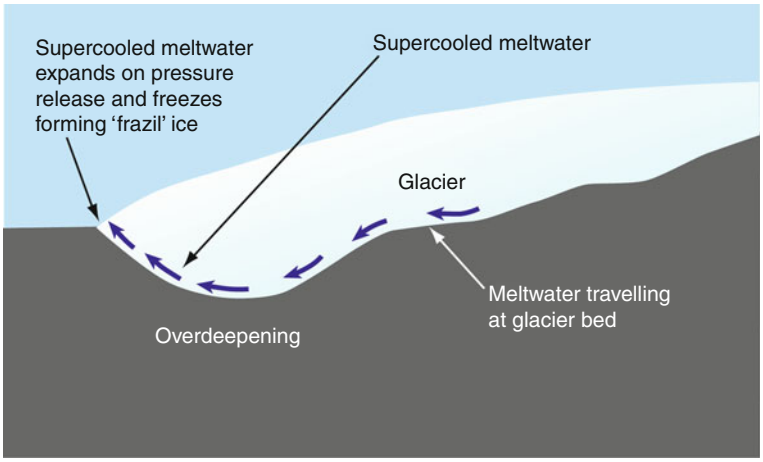

Glaciohydraulic Supercooling, Figure 1 The process of glaciohydraulic supercooling.

Bibliography

Alley, R. B., Lawson, D. E., Evenson, E. B., Strasser, J. C., and Larson, G. J., 1998. Glaciohydraulic supercooling: a freeze-on mechanism to create stratified, debris-rich basal ice: II. Theory. *Journal of Glaciology*, **44**, 563–569.

Alley, R. B., Strasser, J. C., Lawson, D. E., Evenson, E. B., and Larson, G. J., 1999. Glaciological and geological implications of basal-ice accretion in overdeepenings. In Mickelson, D. M., and Attig, J. W. (eds.), *Glacial Processes Past and Present*. Boulder, CO: Geological Society of America. Geological Society of America Special Paper 337, pp. 1–9.

Alley, R. B., Lawson, D. E., Larson, G. J., Evenson, E. B., and Baker, G. S., 2003. Stabilizing feedbacks in glacier-bed erosion. *Nature*, **424**, 758–760.

Cook, S. J., Waller, R. I., and Knight, P. G., 2006. Glaciohydraulic supercooling: the process and its significance. *Progress in Physical Geography*, **30**, 577–588.

Cook, S. J., Knight, P. G., Waller, R. I., Robinson, Z. P., and Adam, W. G., 2007. The geography of basal ice and its relationship to glaciohydraulic supercooling: Svínafellsjökull, southeast Iceland. *Quaternary Science Reviews*, **26**, 2309–2315.

Evenson, E. B., Lawson, D. E., Strasser, J. C., Larson, G. J., Alley, R. B., Ensminger, S. L., and Stevenson, W. E., 1999. Field evidence for the recognition of glaciohydraulic supercooling. In Mickelson, D. M., and Attig, J. W. (eds.), *Glacial Processes Past and Present*. Boulder, CO: Geological Society of America. Geological Society of America Special Paper 337, pp. 23–25.

Fleisher, P. J., Cadwell, D. H., Tormey, B., Lissitschenko, P., and Dell, J., 1997. Post-surge changes and abundant frazil ice, eastern sector, Bering Glacier, Alaska. *Geological Society of America, Abstracts with Programs*, **29**, 216.

Knight, P. G., and Cook, S. J., 2008. Glaciohydraulic supercooling. *Progress in Physical Geography*, **32**, 65–71.

Larsen, G. J., Lawson, D. E., Evenson, E. B., Alley, R. B., Knudsen, O., Lachniet, M. S., and Goetz, S. L., 2006. Glaciohydraulic supercooling in former ice sheets? *Geomorphology*, **75**, 20–32.

Lawson, D. E., Strasser, J. C., Evenson, E. B., Alley, R. B., Larson, G. J., and Arcone, S. A., 1998. Glaciohydraulic supercooling a freeze-on mechanism to create stratified, debris-rich basal ice: I. Field evidence. *Journal of Glaciology*, **44**, 547–562.

Natel, E., and Fleisher, P. J., 1994. Pre-surge meltwater properties in ice-contact lakes, eastern piedmont lobe, Bering Glacier, Alaska. *Geological Society of America, Abstracts with Programs*, **26**, 65.

Roberts, M. J., Tweed, F. S., Russell, A. J., Knudsen, Ó., Lawson, D. E., Larson, G. J., Evenson, E. B., and Björnsson, H., 2002. Glaciohydraulic supercooling in Iceland. *Geology*, **30**, 439–442.

Röthlisberger, H., 1972. Water pressure in intra- and subglacial channels. *Journal of Glaciology*, **11**, 177–203.

Röthlisberger, H., and Lang, H., 1987. Glacial hydrology. In Gurnell, A. M., and Clark, M. J. (eds.), *Glacio-fluvial Sediment Transfer: An Alpine Perspective*. Chichester: Wiley.

Strasser, J. C., Lawson, D. E., Larson, G. J., Evenson, E. B., and Alley, R. B., 1996. Preliminary results of tritium analyses in basal ice, Matanuska Glacier, Alaska, U.S.A.: evidence for subglacial ice accretion. *Annals of Glaciology*, **22**, 126–133.

Tweed, F. S., Roberts, M. J., and Russell, A. J., 2005. Hydrologic monitoring of supercooled meltwater from Icelandic glaciers. *Quaternary Science Reviews*, **24**, 2308–2318.

Cross-references

Dynamics of Glaciers
Frazil
Meltwater Conduit
Overburden Pressure
Supercooled Water

GLACIOISOSTASY

Amit Kumar
Department of Geology, Centre of Advanced Study in Geology, Panjab University, Chandigarh, India

Glacioisostasy is defined as the alteration of the earth crust (lithosphere) through unloading and uploading of ice mass

during major glacial cycles, which attributed to addition and removal of glacial ice. In simplest term glacioisostasy represents the loading or unloading of ice. The worldwide process of glacial isostatic balance results in the process whereby the Earth's shape and gravitational field are made to order in retort to the large-scale changes in surface mass load.

Bibliography

Benn, D. I., and Evans, D. J. A., 1998. *Glaciers and Glaciation*. London: Arnold.

Bennett, M. R., and Glasser, N. F., 1996. *Glacial Geology: Ice Sheets and Landforms*. Chichester: Wiley.

GLACIOLACUSTRINE

Himali Panthri
Department of Geology, D.B.S (P.G) College, Dehradun, Uttarakhand, India

Definition

The term glaciolacustrine is used for the processes and sediments involving a lake that receives meltwater from a glacier.

Lakes are very common in glaciated landscapes. Unique to the glacial lakes is the fact that they receive a major portion of their annual water and sediments from meltwater. Lakes with some portion having direct contact with ice are called *ice contact* lakes, while those located at some distance from ice and fed by outwash streams are known as *noncontact* or *distal* lakes. Glaciolacustrine environments are generally divided into *marginal (proximal)* and *basinal (distal)* ones.

Basinal sub-environments are similar in all glacial fed lakes. Deltas form at the margins of both ice contact and noncontact lakes. Deposition in marginal sub-environment is dominated by mass movement and underflows. Subaqueous fans build where meltwater enters a lake at or near the base of the ice. Ice cliffs or ice ramps (where lake water covers stagnating ice) exist along ice contact lake margins.

In general, deposits formed by sediments carried in bed load of streams are called *glaciolacustrine bed load deposits* (e.g., delta) and those formed by suspended sediments in streams are called *glaciolacustrine suspended deposits*. *Bed load deposits* are the primary deposits during summers when the stream carries greater discharge due to melting while the *suspended deposits* are the major ones during winters due to less melting. Biogenic activities like pelletization, burrowing, may modify glaciolacustrine sediments.

Bibliography

Barnett, D. M., and Holdsworth, G., 1974. Origin, morphology and chronology of sublacustrine moraines, Generator Lake, Baffin island, Northwest Territories, Canada. *Canadian Journal of Earth Science*, **11**, 380–408.

Holdsworth, G., 1973. Ice calving into proglacial Generator Lake, Baffin island N.W.T., Canada. *Journal of Glacialogy*, **12**, 235–250.

GLACIOLOGY

Peter G. Knight
School of Physical and Geographical Sciences, Keele University, Staffordshire, UK

Definition

Glaciology is the scientific study of ice, including glaciers, sea ice, and snow.

The scope of glaciology

Defined broadly, glaciology is the scientific study of ice in all its forms, including glaciers, snow, ice in the atmosphere, ground ice in permafrost regions, sea ice, river ice, the ice that creates problems when it forms on the wings of aircraft, and the ice that keeps drinks cool on a summer afternoon. Attracting the attention of investigators from a wide range of disciplines, including Engineers, Geographers, Geologists, Physicists, Chemists, Meteorologists, Mathematicians, and Climatologists, glaciology is a broad subject. Defined in this way the term glaciology is synonymous with the term cryospheric science: the science of ice in the environment. However, cryospheric science includes distinct subfields that are usually considered independently. For example, permafrost scientists working on frozen ground (geocryologists) do not usually describe themselves as glaciologists. Their work is quite different from glacier scientists. They publish in different journals, using different methods and addressing different questions. In popular usage, the term glaciology is therefore sometimes used more narrowly to include mainly the study of ice in glaciers. However, this narrow definition is incorrect. The World Data Centre for Glaciology that was established after the Geophysical Year of 1957–1958 has become the present-day National Snow and Ice Data Centre (NSIDC) and describes its area of interest as "the world's frozen realms: the snow, ice, glaciers, frozen ground, and climate interactions that make up Earth's cryosphere." (NSIDC, online). The major international organization for glaciology is the International Glaciological Society, which had its roots in the former "Association for the Study of Snow and Ice" and declares itself "open to all individuals who have a scientific, practical or general interest in aspects of snow and ice study" (IGS, online). Under the heading of glaciology it has published papers on topics ranging from ski design to ice on other planets, written by authors from disciplines as diverse as medical physics and marine dynamics. In the first issue of the Journal of Glaciology, the editor wrote

that it was partly in an endeavor to make the word "glaciology" universal and to combat the use of the word "cryology" for the scientific study of ice that the society adopted its title. He wrote: "It is argued by some that 'glaciology' has come to mean the study of glaciers, but the Latin *glacies* denotes ice and it cannot be right to appropriate the word for a single branch of the wide range of ice study. Neither do the Germans use *Glaziologie* nor the French *Glaciologie* in this restricted sense." (Seligman, 1947 p. 35). Technically, then, glaciology includes the study of ice in all its forms. In practice, however, some areas of glaciology are so strongly established as distinct subfields that they are rarely described under the heading of glaciology. These include not only the study of ice in specific environments (such as geocryology), but also the study of ice as a material in its own right: glaciology includes under its broad definition the interests of ice physicists, chemists, and materials scientists, but the course outlines for most postgraduate level courses entitled "glaciology" focus much more on ice in environmental settings, and on the responses of the cryosphere to environmental change, than on the atomic or molecular characteristics of the material. The primary focus of many scientists who currently describe themselves as glaciologists lies within the broad areas of snow (including avalanches), glaciers (including ice sheets and mountain glaciers), and sea ice. These are often combined with a broad interest in environmental change, the reconstruction of past environments, and the impact of glacial phenomena on landscapes. Definitions of the scope of glaciology are therefore somewhat contested, and the correct definition of the term is different from the use of the term that is frequently adopted in practice.

The history of glaciology

Glaciology is a relatively modern discipline. Clarke (1987), Walker and Waddington (1988), and Cunningham (1990) provide useful reviews of its early history. A major landmark was the publication in 1840 of Louis Agassiz' work drawing together a body of understanding that had been emerging over the previous decades and establishing clearly for the first time the idea that glaciers fluctuated over time, that they had previously been much more extensive than at present during a so-called ice age, and that their effects on the landscape could be identified in landforms and sediments in formerly glaciated areas (Agassiz, 1840). This "Glacial Theory" underpins our modern understanding of the subject. The majority of the core concepts in the study of glaciers were established relatively early in the development of the discipline. Lliboutry (1994) noted that all of the processes of glacial erosion that are known today had been recognized before the end of the nineteenth century, and Clarke (1987) argued that much of the progress that was made in the latter part of the twentieth century could have been made much earlier if modern technology had been available to nineteenth century science.

The role of technology in glaciology

Glaciology is a very technology-based discipline. Much of it is concerned with laboratory experimentation, field instrumentation, or computer-based numerical modelling. Huybrechts (2006) argued that the development of ice-sheet models able to describe the time-dependent flow and shape of ice sheets has closely followed technical progress in computer power, ice-drilling, remote sensing, and geophysical dating techniques. This close association of glaciology and technology was notable even in the early history of glaciology. Louis Agassiz used a mechanical drill to probe 60 m below the surface of Unteraargletscher in 1842, but as new technologies developed the depth to which glaciers could be drilled and the success with which ice cores could be extracted steadily improved. Recent work in Greenland and Antarctica has resulted in cores more than 3,000 m long being extracted from the ice sheets. Hot-water drilling has also opened up possibilities for accessing and instrumenting the bed beneath glaciers through boreholes. Fischer and Hubbard (2006) review a variety of instruments including water pressure sensors, sediment samplers, penetrometers, tiltmeters, and ploughmeters that can be emplaced in this way. Laboratory experimentation, as well as field research, has benefited from developing technologies. Glen's (1952, 1955) compression experiments on laboratory ice were another landmark in the history of glaciology. Iverson (2006) has argued that major progress in solving some longstanding glaciological problems could be made experimentally, and that an expansion of the experimental ethic would hasten progress in glaciology. It is partly the inaccessibility of many of the environments in which glaciological problems need to be addressed that has engendered this reliance on technology. Field observations can be supplemented, or sometimes replaced, by laboratory experimentation and computer-based numerical modelling, and where field observations are required they can be made more effectively within a better technical framework. Any review of the current status of the discipline is therefore closely tied not only to the dominant scientific questions but also to the available scientific technology.

Current issues in glaciology

As a broad and dynamic discipline, glaciology is concerned with a wide range of research topics. A great deal of modern glaciology is concerned with the interaction between the cryosphere and other components of the global environmental system, such as climate and sea level. The focus is partly on reconstructing ancient environments but largely on predicting the future responses of ice masses to climate change, and of sea-level to changes in ice volume. This area of research brings together scientists from many different areas of the discipline. For example, it involves both measuring and modeling ice dynamics, which require the coordination of fieldwork, remote sensing, and theoretically derived data.

It also involves the work of glacial geologists, geomorphologists, meteorologists, oceanographers, sea-ice specialists, and permafrost scientists in recognizing the impacts of climate change on the cryosphere and the impact of cryospheric changes on indicators such as landforms, ocean currents, atmospheric composition, and the sedimentary record.

Clarke (2005, p. 270) wrote that it "would be wrong to leave the reader with an impression that glaciology is a mature science, now dedicating itself to minor janitorial tasks. Glaciologists are inspired by the knowledge they have gained – much of it very recent – but they are challenged by what remains to be understood." Sugden (2006, p. 188) wrote that "a report card on the progress of glacial studies over the past 40 years or so might read 'encouraging progress, but surprisingly large gaps in knowledge remain'". Glaciologists are currently involved in addressing some of the biggest questions in Earth science, and we do not yet have the knowledge or understanding that we need to reach reliable answers. Even within one particular narrowly defined area of glaciology, the relationship between glaciers and climate change, it is easy to identify a large number of big unanswered questions and unsolved problems that go to the heart of the discipline. For example, we are only just beginning to make sufficiently accurate measurements of the mass balance of the world's ice sheets to be able to start making confident assertions about whether they are growing or shrinking, which will be a fundamental control on the future of global sea level. Measurement of ice-sheet dimensions and dynamics using both ground-based measurements and satellite remote sensing is crucial to progress in this area. Predicting future ice-sheet behavior will depend on a clear understanding of how glacier dynamics relates not only to climatic driving forces but also to subglacial conditions, especially thermal regime, hydrology, and bed mobility. Our knowledge in these areas remains far from complete. Sugden (2006) suggested that the lack of an effective theory of glacier sliding and the lack of basic data about the beds of current ice sheets brings into question the predictive power of any ice sheet model. Recent discussions about the role of glaciohydraulic supercooling in linking glacier dynamics, hydrology, sediment flux, and geomorphology (e.g., Alley et al., 2003) have highlighted the fact that there are very big questions in glaciology where new theory is still being developed and where our ability to make direct observations that would allow us to test those theories is limited. One of the most exciting prospects for the future is the development of new observation-based diagnostic criteria that can be used to ground-truth, test and calibrate theoretical and numerical models.

Conclusion: Prospects for the future

Several previous reviewers of the state of glaciology have drawn attention to the particular contributions of certain groups of scientists to the progress of the discipline. For example, Paterson (1994) in his keystone text book referred to the outstanding contributions of mathematical physicists. Iverson (2006) commended the value of laboratory experiments. Others have flagged up ice coring, numerical modelling, remote sensing, or geophysics as the next great hope for progress in glaciology. They are all right: each approach makes its own special contribution. However, the difficulty of defining and delimiting glaciology that emerged at the opening of this article gives us a clue as to what might in the end be the best way forward for the discipline as we attempt to address almost overwhelmingly large questions about the complex global system of which the cryosphere is a part. Glaciology draws together the efforts of scientists from a wide range of disciplines with a wide range of approaches, and the best hope for the discipline to address its outstanding problems lies in collaboration between different types of glaciologist and the coordinated application of a range of techniques. Sugden (2006) in outlining six Grand Challenges facing the discipline includes among them the challenge of reopening the kind of discussion among the wider cross-disciplinary community that proved its value in previous decades. Specifically, Sugden alludes to the link between glaciological theory and field-based empirical evidence. It is here, in conversations between numerical modellers and theoreticians on the one hand, and experimentalists and fieldworkers on the other, between those who collect empirical data and those who can (and must) use such data to calibrate and test their models and theory, that the most exciting parts of the near-term future of glaciology lie. For the longer term, where glaciology is required to go will continue to depend on what questions face the broader community of Earth and Environmental Scientists, what observations, experiments, and models are required to address them, and what technologies exist, or need to be developed, to carry out that work.

Bibliography

Agassiz, L., 1840. *Études Sur Les Glaciers, 2 vols*. Neuchâtel: H. Nicolet.Clarke.

Alley, R. B., Lawson, D. E., Larson, G. J., Evenson, E. B., and Baker, G. S., 2003. Stabilizing Feedbacks in Glacier-Bed Erosion. *Nature*, **424**, 758–760.

Clarke, G. K. C., 1987. A short history of scientific investigations on glaciers. *Journal of Glaciology* (special issue) 4–24.

Clarke, G. K. C., 2005. Subglacial processes. *Annual Review of Earth and Planetary Sciences*, **33**, 247–276.

Cunningham, F., 1990. *James David Forbes, Pioneer Scottish Glaciologist*. Edinburgh: Scottish Academic Press.

Fischer, U. H., and Hubbard, B. P., 2006. Borehole based subglacial instrumentation. In Knight, P. G. (ed.), *Glacier Science and Environmental Change*. Oxford: Blackwell, pp. 387–394.

Glen, J. W., 1952. Experiments on the deformation of ice. *Journal of Glaciology*, **2**(12), 111–114.

Glen, J. W., 1955. The creep of polycrystalline ice. *Proceedings of the Royal Society of London, Series A*, **228**, 519–538.

Huybrechts, P., 2006. Numerical modelling of polar ice sheets through time. In Knight, P. G. (ed.), *Glacier Science and Environmental Change*. Oxford: Blackwell, pp. 406–412.
IGS (International Glaciological Society) (online) http://www.igsoc.org (accessed May 2009).
Iverson, N. R., 2006. Laboratory experiments in glaciology. In Knight, P. G. (ed.), *Glacier Science and Environmental Change*. Oxford: Blackwell, pp. 449–456.
Lliboutry, L., 1994. Monolithologic erosion of hard beds by temperate glaciers. *Journal of Glaciology*, **40**(136), 433–450.
NSIDC (National Snow and Ice Data Centre) (online) http://www.NSIDC.com (accessed May 2009).
Paterson, W. S. B., 1994. *The Physics of Glaciers*, 3rd edn. Oxford: Pergamon.
Seligman, G., 1947. Cryology. *Journal of Glaciology*, **1**(1), 35.
Sugden, D. E., 2006. Changing glaciers and their role in earth surface evolution. In Knight, P. G. (ed.), *Glacier Science and Environmental Change*. Oxford: Blackwell, pp. 188–191.
Walker, J. C. F., and Waddington, E. D., 1988. Early Discoverers XXXV: descent of glaciers: some early speculations on glacier flow and ice physics. *Journal of Glaciology*, **34**(118), 342–348.

Cross-references

Geocryology
Glacial Geomorphology and Landforms Evolution
Glacier
Ice
Ice Sheet
Permafrost
Sea Ice
Snow

GLACIOMARINE

Amit Kumar
Department of Geology, Centre of Advanced Study in Geology, Panjab University, Chandigarh, India

The term glaciomarine refers to sediments and processes related to environments where marine water and glacial ice are in contact. Under this environment there is a possibility of action of glaciers and the sea, or the action of glaciers in the sea, which finally results in melting and deposition processes. In high latitude, icebergs produced by calving of large glaciers into the ocean often contain drift; as the icebergs drift in the ocean and melt, they release load in the form of sediment that has been transported to the oceans. Such sediments may contain large dropstones, transported by and dropped from icebergs, in the midst of fine-grained sediments.

Bibliography

Lisitzin, A. P., 2002. *Sea-Ice and Iceberg Sedimentation in the Ocean: Recent and Past*. Berlin: Springer. ISBN 3540679650.
Molnia, B. F., 1983. *Glacial-Marine Sedimentation*. New York/London: Plenum Press.

GLACIOSTATIC PRESSURE/STRESS

Divya Dudeja
Department of Geology, DBS College, Dehradun, Uttarakhand, India

A glacier flow in response to the stresses setup in the ice mass by the force of gravity. Each point within the glacier is subjected to stress as a result of the overlying ice. This stress can be divided into two components, namely, shear stress and vertical stress. Shear stress causes movement of the ice over its bed and is related to both the weight of the overlying ice and surface slope of the glacier called as glaciodynamic stress. Vertical stress due to static weight of the overlying ice column is called as glaciostatic stress or pressure.

Glaciostatic pressure increases with depth into the glacier as the overburden of ice increases. As it increases, shear stress also increases with respect to the bed. Glaciostatic pressure created by vertical load of ice on substratum is irrespective of ice movement. Assuming constant ice thickness over a level surface, the glaciostatic pressure would be equal and uniform in all directions.

Glaciostatic stress show variations over an irregular bed of a glacier. Undulations of the glacier bed will result in marked stress variations, because the magnitudes of the normal stress and shear stresses acting across a surface depend on its orientation relative to the applied force. Therefore, for a rough bed there will be areas where stresses are higher than average and others where they are lower than average. The pushing or pulling effect of the upstream and downstream ice also affects the stress. This effect is known as the longitudinal stress, which is compressive if the ice is slowing down and tensile if the ice is accelerating. Because the longitudinal stress is, by definition, approximately parallel to glacier flow and the surface slope, its principal effect is to modify the shear stress but if bed roughness is high, the longitudinal stress will also significantly affect the glaciostatic stress.

The gravity spreading model demonstrates that the total glaciotectonic stress needed to push glacial material from behind, permitting proglacial sediment failure and glaciotectonic thrusting, is obtained by the translation of compressive stress due to the weight of a spreading ice mass. Besides glaciodyanamic stress, the horizontal cumulative compressive stress transferred from the normal stress, that is, glaciostatic stress also forms one of the important components of the total glaciotectonic stress field. Failure can take place on a plane when the total glaciotectonic stress exceeds or equals the shear resistance.

Bibliography

Ber, A., 2007. *Glaciotectonism*. Amsterdam: Elsevier, 246 pp.
Paterson, W. S. B., 2000. *The Physics of Glaciers*, 3rd edn. Amsterdam: Elsevier, 481 pp.

GLACIOTECTONIC STRUCTURES, LANDFORMS, AND PROCESSES

James S. Aber[1], Andrzej Ber[2]
[1]Emporia State University, Emporia, KS, USA
[2]Polish Geological Institute – Polish Research Institute, Warszawa, Poland

Introduction

Glaciotectonics involves glacially induced deformations in the Earth's crust, which include all manner of folds, faults, and dislocations (Aber and Ber, 2007). Disturbed strata range from unconsolidated sediments, to well-indurated strata, to solid crystalline rocks. Glaciotectonism refers to the processes by which proglacial and subglacial deformations are created. The driving cause for these deformations is the combined weight of glacial ice and forward movement of the glacier or ice sheet, which together exert differential stress on the substratum. Such stress and changes in stress may be imposed in the advancing, maximal, and retreating phases of glaciation, during which the local direction of ice movement may shift substantially. The results in many cases are complex patterns and styles of superposed deformation (Pedersen, 2000).

Glaciotectonic structures and landforms were recognized and investigated beginning in the mid-nineteenth century at several classic sites: Norfolk, England (Lyell, 1863), Møns Klint, Denmark (Figure 1), and Martha's Vineyard, United States (Figure 2). Slater (1926) was the first person to specialize in the subject; he coined the term glacial tectonics, which is generally shortened to glaciotectonics (American) or glacitectonics (British)

Glaciotectonic Structures, Landforms, and Processes, Figure 1 Møns Klint, southeastern Denmark, as seen from the beach. Upper Cretaceous chalk masses are thrust up from below sea level. Sommerspiret, seen here, stands in vertical position >100 m high. Long known to geologists, the ice-shoved origin of the cliff structures was demonstrated first by Johnstrup (1874). The description and origin of Møns Klint continue to generate intense scientific interest and controversy (e.g., Pedersen, 2000). Photo by JSA.

Glaciotectonic Structures, Landforms, and Processes, Figure 2 Aquinnah Cliff and lighthouse on the island of Martha's Vineyard, Massachusetts, United States. The 40-m-high cliff displays upthrust Cretaceous and Cenozoic strata derived from ~20 m to >70 m below sea level. The glaciotectonic origin of Martha's Vineyard was determined in the late nineteenth century (Merrill, 1886). (Adapted from Aber and Ber, 2007.)

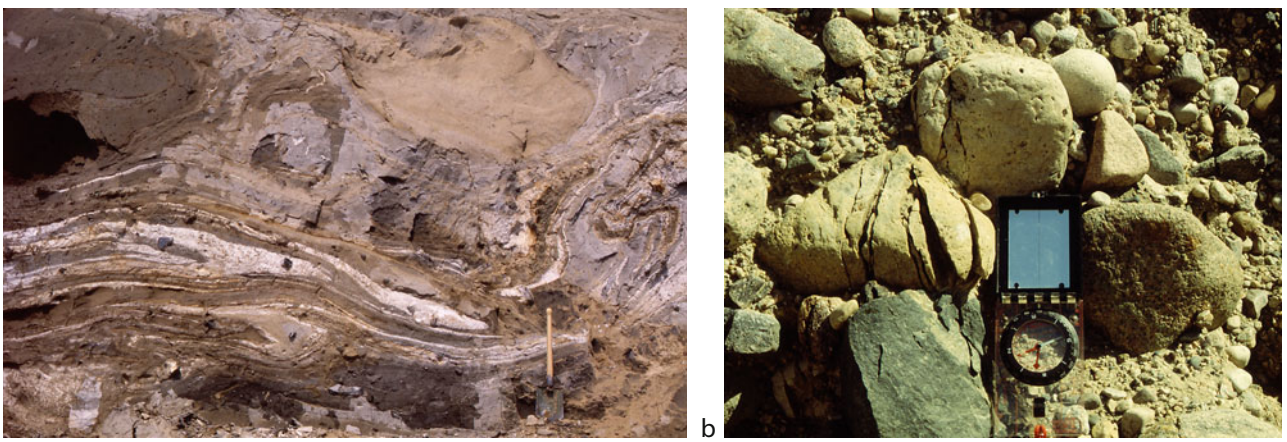

Glaciotectonic Structures, Landforms, and Processes, Figure 3 Typical ductile and brittle styles of glaciotectonic deformation. (**a**) Ductile deformation shown by strongly sheared and refolded chalk-till mélange exposed in cliff near Hvideklint on the island of Møn, Denmark. Small spade to right for scale. Adapted from Aber et al. (1989). (**b**) Brittle fracturing of hard cobbles in a drumlin at Dollard, Saskatchewan, Canada. Photo by JSA.

nowadays. The study of glaciotectonics expanded significantly in the middle twentieth century, primarily in Europe and North America, and by the late twentieth century had become an integrated part of glacial theory. Observations of glaciotectonics associated with modern glaciers played a key role for interpretation of ancient structures and landforms.

Most glaciotectonic disturbances are relatively shallow, typically <200 m deep, and include all manner of ductile and brittle styles of deformation (Figure 3). Ductile structures are most typical of unconsolidated or fine-grained strata that are deformed under high confining pressures. Common representatives of ductile structures are various folds, intrusions, diapirs, and contortions. Brittle deformations such as joints, faults, breccia, and fissures are most characteristic of well-consolidated or coarse-grained strata that are deformed under low confining pressure. Detailed structural analysis is applied for study of glaciotectonic

structures. This includes three stages: descriptive analysis (geometry, orientation, and structural patterns), kinematic analysis (measurements of strains and dislocations), and dynamic analysis (origin of the deformation).

The depth of deformation was often determined by a weak layer in the subsurface, such as a bed of shale, chalk, lignite, salt, clay, peat, or other soft material. Other weak zones or horizons include the lower limit of permafrost and position of a confined aquifer. Such weak layers represent décollements, above which strata were displaced and deformed, and below which no deformation took place. In some cases, even deeper deformation happened in which a décollement is situated 1 km or more beneath the surface. Glaciotectonic deformation within the substratum is often marked at the surface by distinctive landforms. In other cases, deformations may be completely concealed within the subsurface and have no morphologic expression in the landscape.

Glaciotectonic landforms

Considered broadly, glaciotectonic landforms may be largely constructional in nature, in other words, built up above the surrounding terrain, or destructive in origin as a result of removal of material. The former comprise various types of ice-shoved ridges, hills, and push moraines. The latter include ice-scooped basins, troughs, and depressions. The hill-hole pair is a basic glaciotectonic landform consisting of an ice-scooped depression and ice-shoved hill. Ideally, the size, shape, and volume of the ice-shoved hill correspond closely with dimensions of the adjacent basin, so that a direct genetic link is apparent (Figure 4). Large and small hill-hole pairs are found on land as well as the continental shelf as deep as 200–300 m below modern sea level (Sættem, 1990). At these depths, the glaciotectonic landforms were surely created when the ice sheet was marine based.

Ice-shoved ridges are commonplace in many formerly glaciated regions as well as in close proximity to modern glaciers, although distinct source basins cannot always be identified. Such composite ridges and push moraines range in size from >200 m in relief and thousands of square kilometers area to small, inconspicuous features. The latter often were overridden by subsequent ice advance, so were smoothed, reduced in size, and covered by till. The term cupola-hill is applied to such modified ice-shoved hills, which are in many cases streamlined into drumlin shapes.

Among the largest and best developed composite ridges are those found along the Missouri Coteau in southern Saskatchewan, Canada. The Dirt Hills and Cactus Hills are nearly ideal examples of late Wisconsin age (Figure 5). Cretaceous strata, mainly sandstone, mudstone, and lignite, are thrust upward >200 m above normal stratigraphic positions. Remarkable agreement exists between structural features, ridge trends, and the overall outlines of the Dirt Hills and Cactus Hills, which demonstrates that surface morphology is a direct expression of bedrock structures (Kupsch, 1962).

Hvideklint on the island of Møn represents a typical small cupola-hill, in which the internal structure is strongly disturbed, but the surface landform is indistinct (Aber, 1979). A cliff section reveals detached masses of upper Cretaceous chalk that are thrust, folded, and sheared

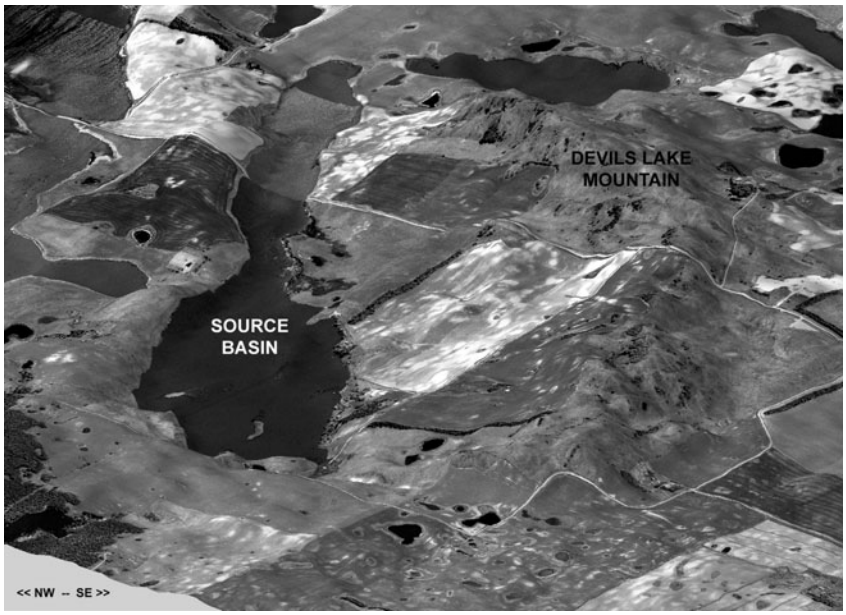

Glaciotectonic Structures, Landforms, and Processes, Figure 4 Perspective block diagram of Devils Lake Mountain as seen from the southwest, looking toward the northeast. The source basin lies to the left side of the ice-shoved ridge. Digital orthophoto image draped over digital elevation model. Large vertical exaggeration (Image courtesy of W. R. Jacobson, Jr.).

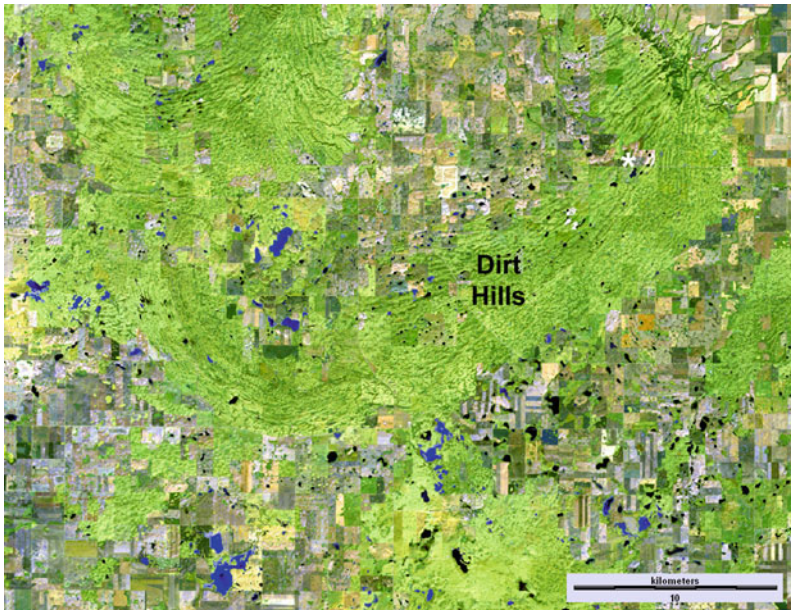

a

b

Glaciotectonic Structures, Landforms, and Processes, Figure 5 Dirt Hills, near Regina, Saskatchewan, Canada. (**a**) Ice-shoved ridges form large loops that outline the positions of ice lobes that pushed onto the Missouri Coteau upland from the north. The region south of the Dirt Hills is an outwash plain marked by numerous kettle holes. Landsat TM bands 2, 5 and 7 color coded as blue, green, and red; active vegetation appears in shades of green; September 2002. (**b**) View over the northern end of the Dirt Hills (* in part A). Highest ridges in center distance reach a maximum elevation of 880 m. Kite aerial photograph by JSA and S.W. Aber.

together with various Pleistocene strata (Figure 6). The disturbed section is overlain by two till layers. The lower till layer was deposited and deformed by the same ice advance that brought the chalk blocks from the northeast. The upper till layer is discordant and represents a later glacier readvance by an ice lobe coming from the east-northeast.

Elbląg Upland is an exceptionally large cupola-hill located on the margin of Gdańsk Bay in northern Poland. It covers nearly 400 km^2, stands almost 200 m above the surrounding lowlands, and has a volume of roughly 40 km^3. These dimensions place Elbląg Upland among the largest glaciotectonic landforms in the world (Aber and Ruszczyńska-Szenajch, 1997). The core of the upland consists entirely of disrupted, displaced, and uplifted Pleistocene strata, many of which were derived from below sea level beneath Gdańsk Bay (Figure 7). The upland was subjected to multiple ice advances, and primary glaciotectonic deformation may have taken place in an interlobate position between converging ice lobes.

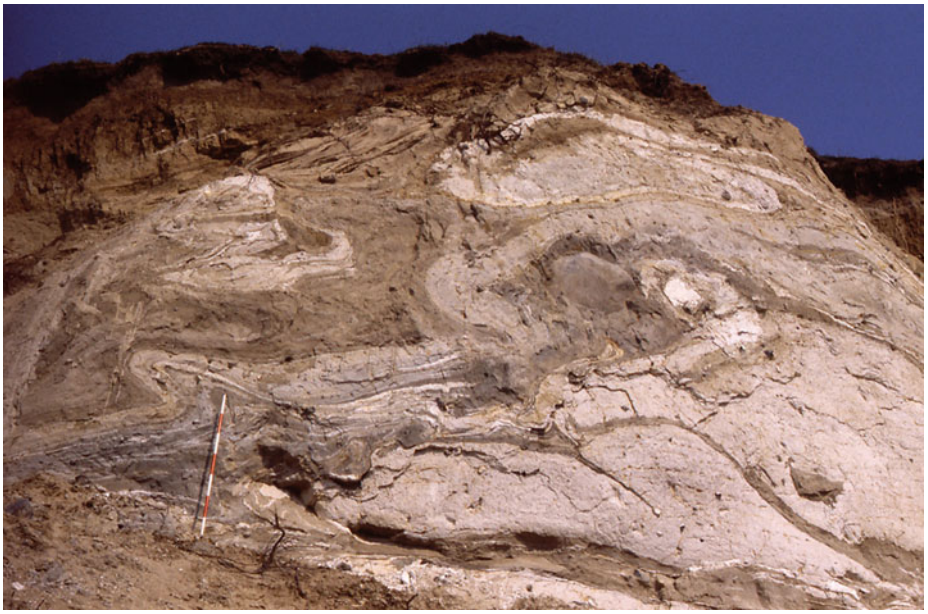

Glaciotectonic Structures, Landforms, and Processes, Figure 6 Cliff section at Hvideklint on the island of Møn, Denmark. Chalk, till, and sand are stretched, folded, and sheared into a glaciodynamic mélange. Note the overturned and "rolled" folds of chalk-banded till. Scale pole marked in 20-cm intervals. (Adapted from Aber and Ber, 2007.)

Glaciotectonic Structures, Landforms, and Processes, Figure 7 Exposure of dark Elbląg Clay standing in vertical position ~70–75 m above sea level in a clay mine at Kadyny, Poland. (Adapted from Aber and Ber, 2007.)

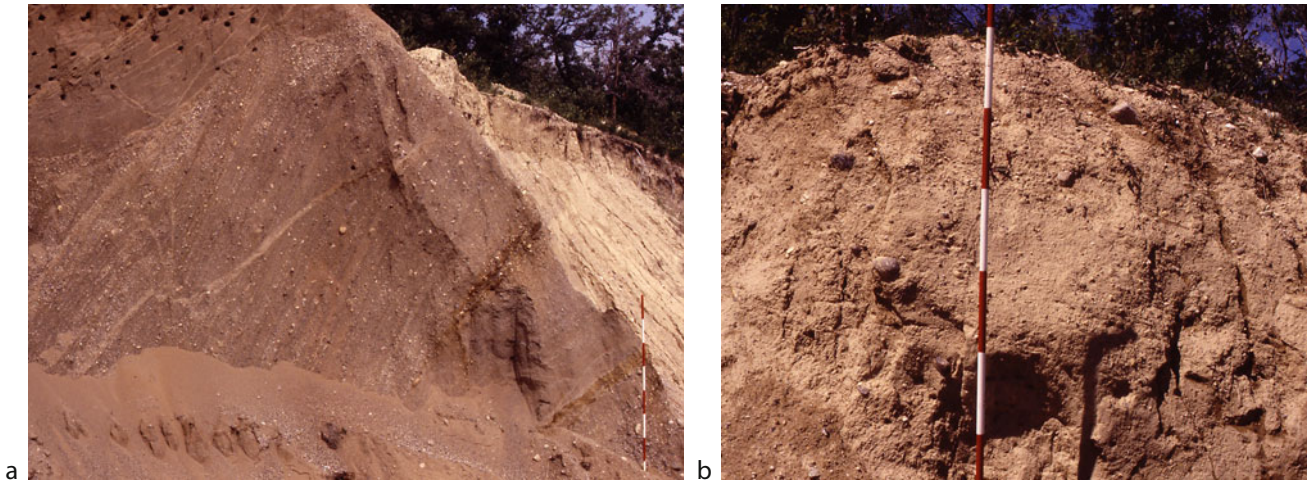

Glaciotectonic Structures, Landforms, and Processes, Figure 8 Photos of Brandon Hills. (**a**) Tilted, faulted, and folded sand and gravel in the core. (**b**) Discordant cap of sandy till with rounded pebbles and cobbles derived from underlying stratified drift. Scale pole marked in feet; photos by JSA.

A subsequent readvance overrode the upland, deposited a discordant cap of diamicton, and molded several dozen drumlins.

The term push moraine has been applied widely to many kinds of ice-shoved hills and ridges. The term is here restricted to those ice-shoved hills that are composed largely or completely of proglacial outwash and other glaciogenic strata into which the ice advanced (Aber and Ber, 2007). A prime example of this case is Brandon Hills in southwestern Manitoba, Canada. The internal structure of Brandon Hills consists of stratified drift blocks that are tilted, faulted, folded, and truncated below a cover of sandy till (Figure 8). Brandon Hills were created when a late Wisconsin readvance pushed up blocks of outwash sand and gravel left during a previous ice retreat. The readvance then overrode and eroded the ice-shoved ridges and laid down the discordant cap of till.

Most glaciotectonic structures and landforms are developed in relatively soft sedimentary strata. In some cases, however, well-consolidated bedrock was disturbed with the creation of distinctive landforms, as consequences of glacial loading and unloading. In northern Sweden, for example, the Pärve Fault was reactivated at the close of the last glaciation; it forms a continuous fault scarp 150 km long and up to 10 m high (Lundqvist and Lagerbäck, 1976).

Alpine glacial erosion, through overdeepening of valleys, may lead to structural collapse of the valley sides and mountain crest along normal faults, resulting in small, bedrock ridges and troughs. Sackung (plural: sackungen) is derived from the German word for "sagging," which describes the process of lateral spreading of the mountain side into the excavated glacial valley (Figure 9). Sackungen are commonly developed in crystalline rocks of the Alps and Rocky Mountains and also may form in well-consolidated sedimentary strata (Figure 10).

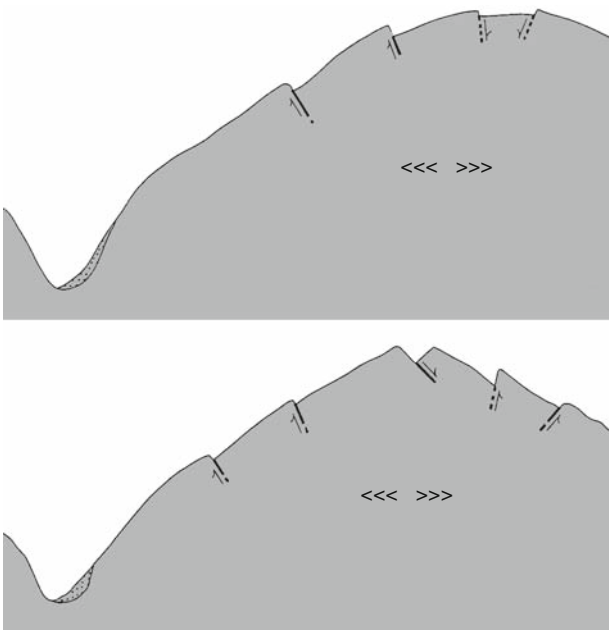

Glaciotectonic Structures, Landforms, and Processes, Figure 9 Idealized cross sections of sackungen on mountain sides and crests adjacent to a glacier-carved valley (on left). Small arrows indicate sense of fault displacement; large arrows show lateral spreading of mountain mass. (**a**) Ridge-top graben, (**b**) Double-crested ridge. Not to scale; (Adapted from Varnes et al., 1989.)

Concealed glaciotectonic structures

Glaciotectonic structures of diverse types and sizes underlie many glaciated plains without any morphologic expression at the surface (Figure 11). These structures may be produced in situ (autochthonous) within the

Glaciotectonic Structures, Landforms, and Processes, Figure 10 Sackung on the crest of the Culebra Range looking south toward Trinchera Peak (4,121 m) in the background. A deep cleft is marked by snow patches in the right foreground. Bedrock is well-consolidated arkosic and quartzose sandstone that is overturned and dips steeply toward the west (arrows in lower left corner). Sangre de Cristo Mountains, southern Colorado, United States. (Taken from Aber, 2008.)

substratum or within detached masses (allochthonous) during their transportation and deposition (Figure 12). Displaced megablocks, rafts and floes, various intrusions and diapirs, and basement structures may be attributed to the impact of glacial loading and movement (Aber and Ber, 2007). Stalker (1976) first applied the term megablock to large, relatively thin, slightly deformed masses of displaced bedrock in the Canadian Prairie region (Figure 13). Similar rafts are well known in many parts of central and eastern Europe. The largest known megablock is located at Esterhazy, Saskatchewan, Canada (Christiansen, 1971). The disrupted material consists of Cretaceous shale, claystone, and siltstone resting in places on till and covered with drift. The megablock covers $\sim$1,000 km^2 with an average thickness of 60 m.

A complete listing of concealed glaciotectonic structures is not possible, because so much variety exists in type, style, and size. Intrusions, diapirs, wedges, and other soft-sediment deformations are commonly found in glaciogenic sequences, but rarely give rise to distinctive landforms. They range from millimeter-sized features to structures hundreds of meters in extent. Diapirs typically form where clay or silt layers, buried beneath denser sand, gravel, or till, are mobilized by high-pressure pore water induced by overriding glacier ice (Figure 14). Among the deepest known glaciotectonic deformations are dislocations and folds in salt beneath the Finger Lakes region of New York (Figure 15). In the northern Finger Lakes, salt was displaced southward by repeated ice loading, which led to thickening of salt south of the Finger Lakes at depths $>$1 km (White, 1992). When the last glaciation retreated, salt flowed into anticlines beneath the longest and deepest of the ice-carved Finger Lakes troughs.

Poland contains several excellent examples of deeply buried basement structures that were reactivated during repeated glaciations and may have contributed to surficial glaciotectonic deformations as well. In North America, basement faults and seismic zones follow patterns of glaciation, wherein discrete crustal blocks responded differentially to glacial loading and unloading. This is

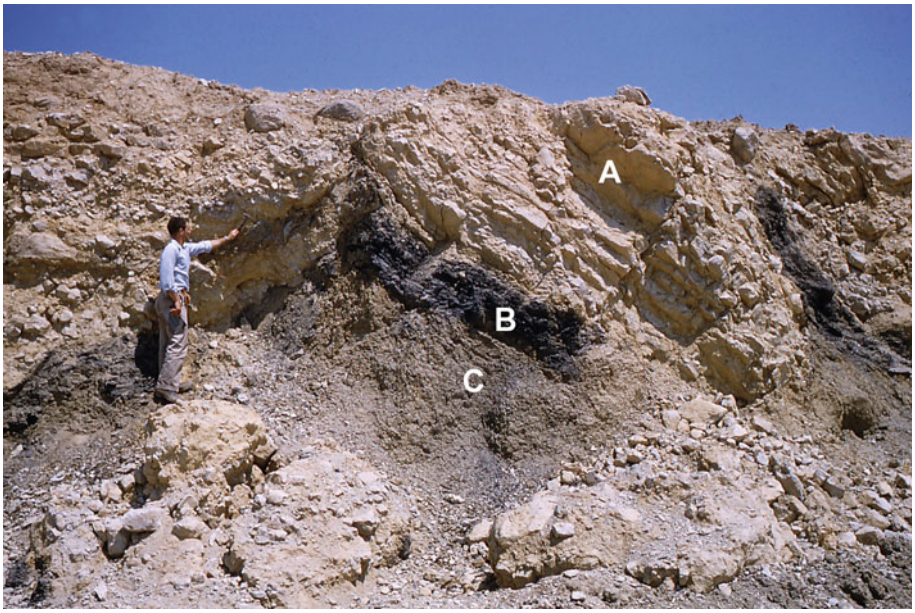

Glaciotectonic Structures, Landforms, and Processes, Figure 11 Folds in deformed upper Carboniferous limestone and shale, south-central Iowa, United States. A – Winterset Limestone Member and B – Stark Shale Member of the Dennis Limestone; C – Galesburg Shale. Notice angular fold limbs and piercing of shale upward along fold axial planes (Photo courtesy of L. F. Dellwig.)

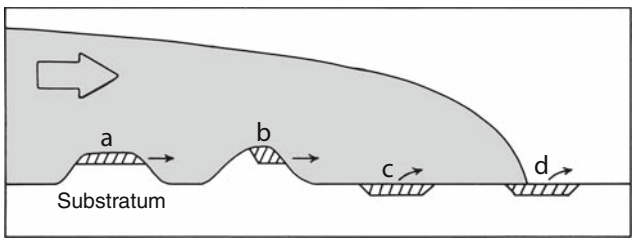

Glaciotectonic Structures, Landforms, and Processes, Figure 12 Possible means of detaching megablocks: a = beheading of butte, b = plucking from lee of hill, c = scooping from depression, d = proglacial thrusting. Vertical scale exaggerated; a, b, and c may occur anywhere under the ice. (Taken from Aber and Ber, 2007, Figure 7–4.)

especially apparent along the southern margin of the Laurentide Ice Sheet from the midcontinent to the Altantic continental shelf (Aber and Ber, 2007).

Distribution of glaciotectonics

Glaciotectonic structures and landforms are found throughout regions of former continental ice-sheet glaciation, but they are not randomly distributed. A distinct zonal pattern is found in both North America (Dyke and Prest, 1987; Aber et al., 1995) and Europe (Aber and Lundqvist, 1988; Ber, 2006). Three major geomorphic zones are developed (Figures 16 and 17):

- Outer zone – all manner of large and small glaciotectonic phenomena in drift and soft sedimentary bedrock on both land and continental shelves
- Intermediate zone – small, isolated glaciotectonic features found mainly in locally thick drift of the last glaciation
- Inner zone – widespread, small- and moderate-sized glaciotectonic features developed in older drift

The outer zone is underlain predominately by soft, poorly consolidated Mesozoic and Cenozoic sedimentary strata consisting mainly of Cretaceous, Paleogene, or Neogene bedrock. Thick and nearly continuous Pleistocene strata mantle the bedrock. Large looped end moraines, drumlin fields, older drift, and multiple till sequences are abundant. All kinds of large and small glaciotectonic features are commonplace; most of the examples given above come from the outer zone of glaciation.

The intermediate zone in Europe includes the Fennoscandian Shield of southern Sweden and Finland and the Caledonian Mountains of Norway and western Sweden, and in North America the Canadian Shield and northern Appalachians make up the intermediate zone. Drift cover is thin and patchy, and scoured crystalline rocks crop out over vast areas. Small glaciotectonic structures are occasionally found, and faults in crystalline bedrock are common. In both North America and Europe, the outer and intermediate zones are separated by transitional belts of varying width and lateral continuity. These transitional belts are underlain by consolidated Paleozoic sedimentary bedrock.

Within the inner zones of glaciation, drift is again moderately thick and continuous with drumlins and Rogen moraine common. Exposures of Precambrian and

Glaciotectonic Structures, Landforms, and Processes, Figure 13 Megablock of Cretaceous strata (light tone) exposed within thick glacial strata along the bluff of the Oldman River, near Taber, south-central Alberta, Canada. The upland surface is a nearly flat glacial plain. Note people standing at the base of the megablock, which is a shear zone in the underlying glacial sediment. Another megablock can be seen in the background. (Adapted from Aber and Ber, 2007.)

Glaciotectonic Structures, Landforms, and Processes, Figure 14 Independence Formation stratotype at Atchison, Kansas, United States. Upper (*brown*) and lower (*gray*) tills are separated by glaciolacustrine sand. Large diapir of gray till intrudes into the sand (person above ladder). (Adapted from Aber et al., 1989.)

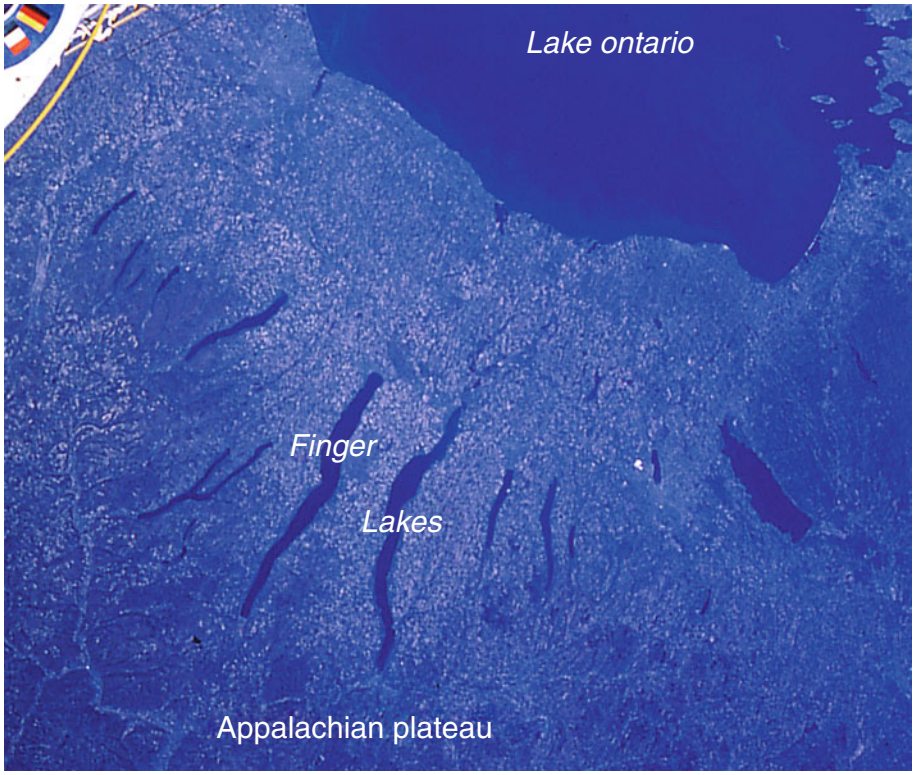

Glaciotectonic Structures, Landforms, and Processes, Figure 15 Near-vertical space-shuttle photograph of the Finger Lakes district of central New York, United States. Ice flow southward from the Ontario lowland into the Appalachian Plateau cut deep valleys that resemble inland fjords. Image adapted from NASA Johnson Space Center, STS 51B-33-028, 4/85.

Paleozoic bedrock make up only a small part of the landscape. Interstadial and interglacial sediments are found in many places below till of the last glaciation, and multiple Weichselian till sequences are known. Glaciotectonic structures are common within such overridden deposits (Figure 18), and even small ice-shoved hills are found.

The distribution, types, and sizes of glaciotectonic phenomena are related in a general way to availability of erodible or deformable strata, namely thick Pleistocene deposits or soft sedimentary bedrock. The three zones are the results of multiple Pleistocene glaciations and represent long-term, cumulative modifications of the continental substratum by ice sheets.

For the outer zone, glaciotectonic features are so abundant that their pattern of distribution may be compared with other glacial phenomena. Two basic regional patterns are recognized for glaciotectonic features.

- Sporatic distribution of megablocks, rafts, diapirs, and other features that have little or no morphologic expressions, along with small cupola hills and drumlins. These features presumably were created in subglacial settings well behind ice margins or were overridden and substantially modified by later glaciation.
- Ice-marginal position of morphologically prominent hill-hole pairs, composite ridges, and large cupola hills. These features were created at or near active ice margins, and their locations are closely related to development of ice lobes or tongues. Associated melt-water features include tunnel valleys, eskers, spillways, and outwash plains.

The Muskau Arc in eastern Germany and southwestern Poland is a particularly good example of glacier shoving around the margin of an ice lobe (Figure 19). Thrust slices of Neogene strata, including brown coal, form the primary core of the structure along with overturned folds and dikes. Highest ridges exceed +140 m elevation, and the basal décollement may reach −50 m. Deformation took place in multiple stages at the maximum advance of the Neiße ice lobe during the Elsterian glaciation, ~350,000 years ago (Kupetz and Kupetz, 2009). The Muskau Arc resembles other large composite ridges such as the Dirt Hills in Saskatchewan (see Figure 5).

Model for Glaciotectonism

A general model for glaciotectonism is based on observations of structures and landforms from many ancient and

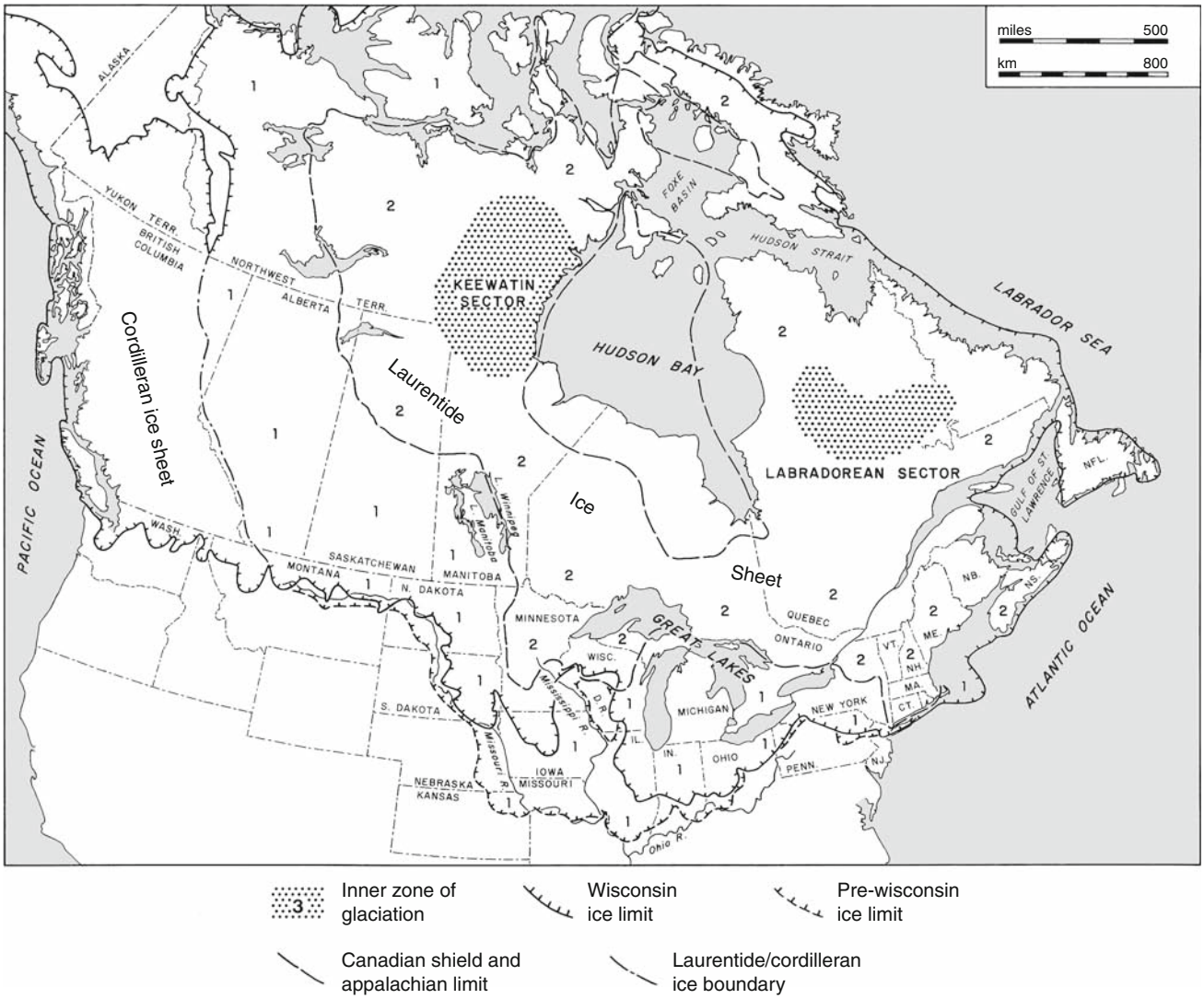

Glaciotectonic Structures, Landforms, and Processes, Figure 16 Major glacial landscape zones of North America: 1 – outer zone of predominant glacial deposition, glaciotectonism, and constructional morphology, 2 – intermediate zone of strong erosion, 3 – inner zones of lesser glacial modification. (Adapted from Aber and Ber, 2007.)

modern ice-shoved hills around the world. The model includes three main phases (Figure 20).

- Initial thrusting and uplift of a composite ridge take place in front of the ice and above a décollement. The décollement may be controlled by several features: lower boundary of permafrost, lithologic contact, position of confined aquifer, or buried hard-rock obstacle. High ground-water pressure is presumably developed along the décollement.
- A prominent ice-shoved hill begins to build up with continued deformation of the substratum at the ice margin. Meanwhile, a source basin is created beneath the glacier by removal of material behind the ice-thrust hill. Glacial deposits and melt-water features also develop simultaneously with continued deformation.
- Continued glacier advance eventually may overrun the ice-shoved hill, at which point a penetrative, highly sheared, metamorphic style of deformation may develop under the ice. Erosion of the hill provides reworked sediment for a discordant till cover, and gradually a cupola-hill morphology develops.

The driving force for these deformations is the pressure or stress difference between the advancing ice margin and the unloaded glacial foreland. The differential pressure

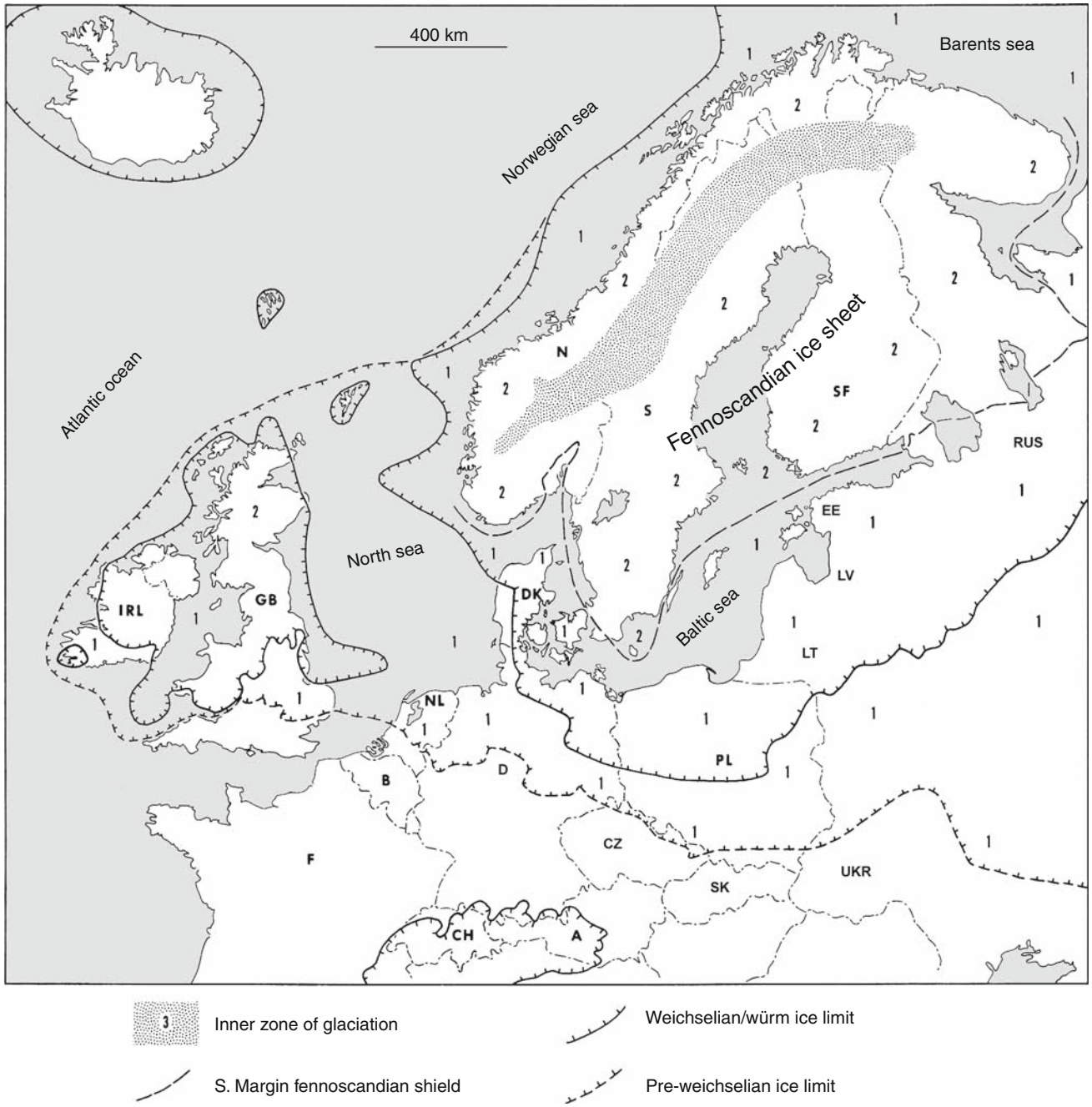

Glaciotectonic Structures, Landforms, and Processes, Figure 17 Major glacial landscape zones of northern Europe. Zone 1 includes the continental shelves, and it extends eastward across northern Russia including continental shelves of the Barents Sea and Kara Sea. (Modified from Aber and Ber, 2007.)

exerted by the ice mass results in shear stress within the substratum. Deformation takes place when the shear stress exceeds the shear strength of soft strata, which may be further weakened by high ground-water pressure. Rapid change in stress during ice-lobe surging over confined aquifers in soft substratum enhances the potential for creating large ice-shoved hills. This mechanism of glacier thrusting is identical, although smaller in scale, to plate-tectonic creation of major thrust mountain systems (Berthelsen, 1979; Figure 21).

Glaciotectonic Structures, Landforms, and Processes, Figure 18 Thrust fault with drag folds in pre-late Weichselian stratified drift at Grytan near Östersund, central Sweden; field of view ~10 m across. (Photo courtesy of J. Lundqvist.)

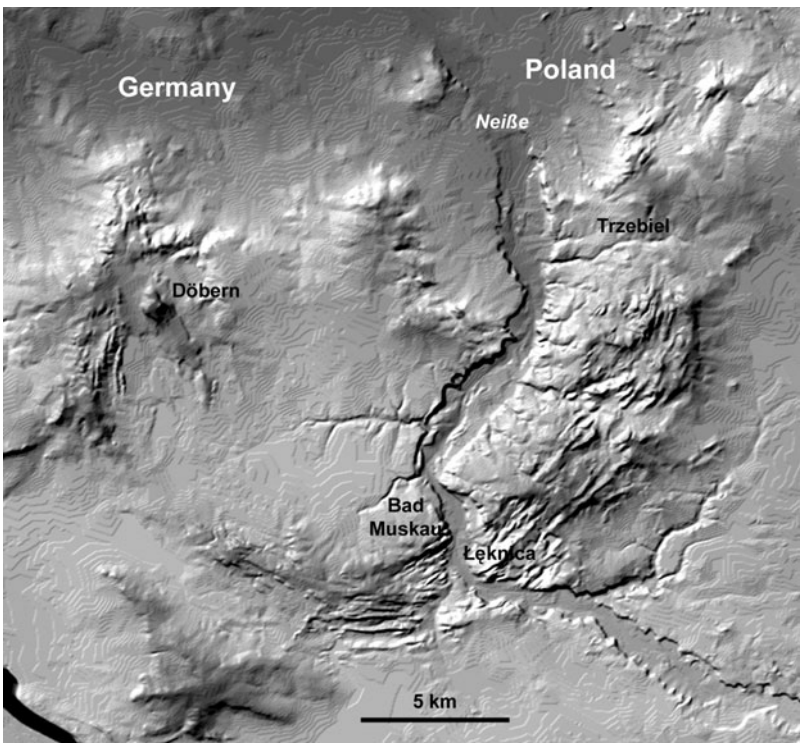

Glaciotectonic Structures, Landforms, and Processes, Figure 19 Shaded-relief digital elevation model for the Muskau Arc in eastern Germany and southwestern Poland. The composite ridges form a large loop bisected by the Neiße River, which marks the national border. (Modified from Aber and Ber, 2007.)

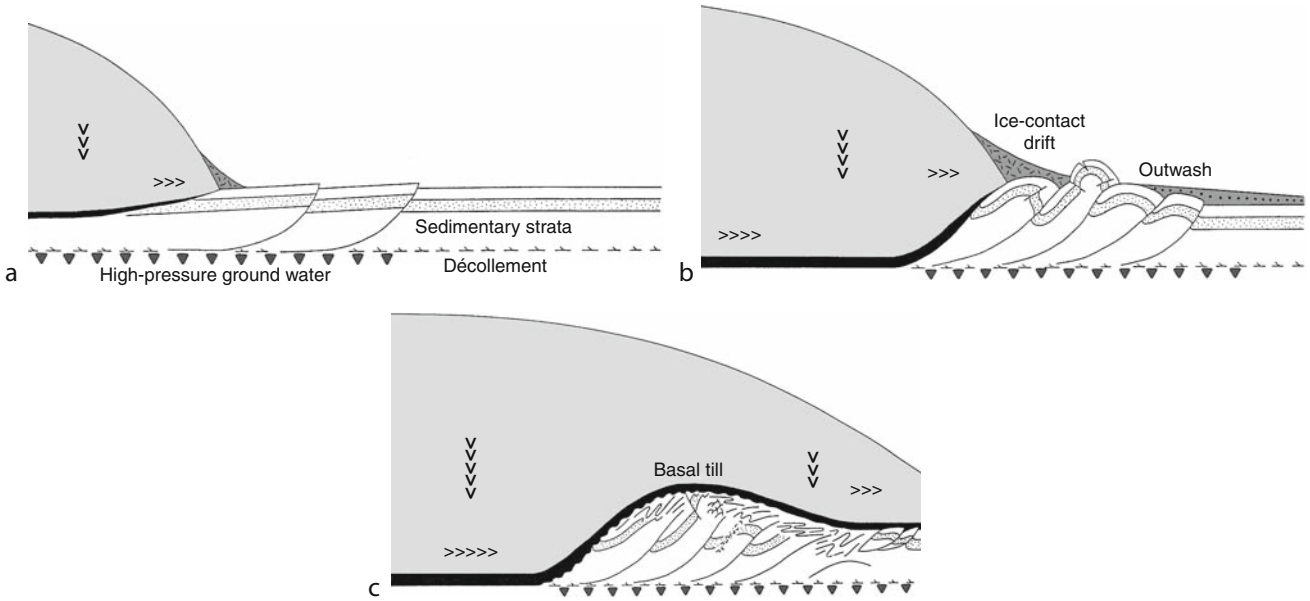

Glaciotectonic Structures, Landforms, and Processes, Figure 20 Generalized model for proglacial thrusting and subglacial modification of an ice-shoved hill during ice-lobe advance. (**a**) Initial proglacial thrusting, (**b**) Building ice-marginal composite ridge, (**c**) Overriding and smoothing cupola hill. Magnitude of vertical (gravitational) loading (V) and ice motion (>) indicated schematically. Note creation of ice-scooped basin (hole) behind the ice-shoved hill. Not to scale; subglacial melt-water features not shown. (Modified from Aber and Ber, 2007) with additions from (Kupetz and Kupetz, 2009.)

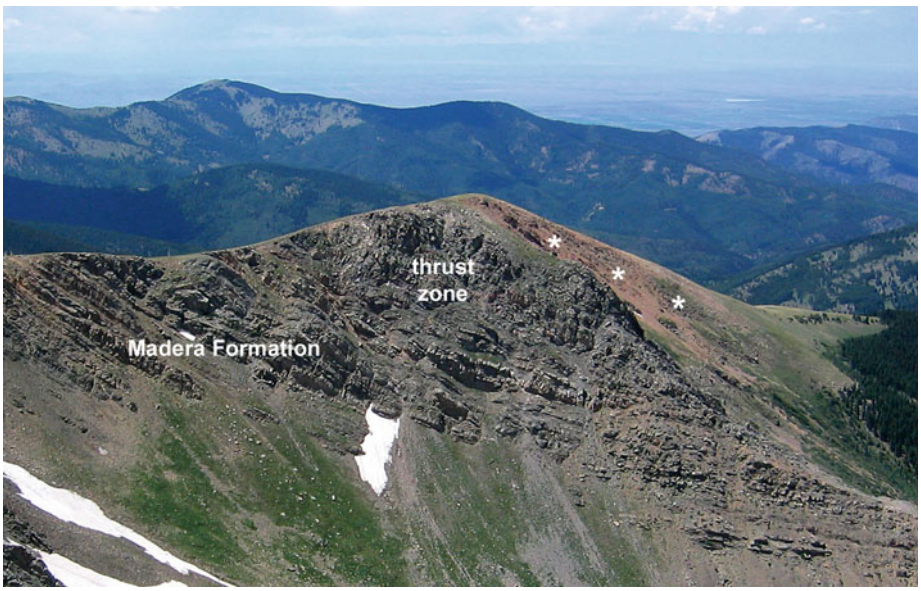

Glaciotectonic Structures, Landforms, and Processes, Figure 21 Tilted sedimentary strata of the Madera Formation (middle Pennsylvanian) are capped by early Proterozoic crystalline rocks (*). Rocks of the Madera Formation are contorted and brecciated in the fault zone, which marks the Culebra Thrust Fault. View from Trinchera Peak looking westward, Sangre de Cristo Mountains, southern Colorado, United States. (Photo by JSA.)

Summary

Glaciotectonic structures and landforms were created throughout zones of former and modern glaciation as a result of glacier loading and movement on the crust. These structures are mostly shallow (<200 m deep), but some extend a kilometer or more below the surface. Distinctive landforms comprise hill-hole pairs, ice-shoved hills, push moraines, cupola hills, and many drumlins. Concealed glaciotectonic structures include megablocks and rafts, diapirs and wedges, and deep-seated deformation of salt, as well as basement faults and seismic zones. On a regional scale, glaciotectonic features are closely related to ice lobes; on a continental basis glaciotectonic phenomena display a distinct distribution within the outer, intermediate, and inner zones of ice-sheet coverage.

Bibliography

Aber, J. S., 1979. Kineto-stratigraphy at Hvideklint, Møn, Denmark and its regional significance. *Geological Society Denmark, Bulletin*, **28**, 81–93.

Aber, J. S., 2008. Glacier-induced bedrock deformation in the Culebra Range, southern Colorado. *Transactions of the Kansas Academy of Science*, **111**, 29–38.

Aber, J. S., and Ber, A., 2007. *Glaciotectonism*. Developments in Quaternary Science, 6th edn. Amsterdam: Elsevier, p. 246.

Aber, J. S., Bluemle, J. P., Brigham-Grette, J., Dredge, L. A., Sauchyn, D. J., and Ackerman, D. L., 1995. *Glaciotectonic Map of North America, 1:6,500,000*. Geological Society of America, Maps and Charts Series, MCH079.

Aber, J. S., Croot, D. G., and Fenton, M. M., 1989. *Glaciotectonic landforms and structures*. Dordrecht, Netherlands: Kluwer, 200 p.

Aber, J. S., and Lundqvist, J., 1988. Glaciotectonic structures in central Sweden and their significance for glacial theory. *Géographique Physique et Quaternaire*, **42**, 315–323.

Aber, J. S., and Ruszczyńska-Szenajch, H., 1997. Origin of Elbląg Upland, northern Poland, and glaciotectonism in the southern Baltic region. *Sedimentary Geology*, **111**, 119–134.

Ber, A., 2006. *Glaciotectonic map of Poland, 1:1, 000, 000*. Warsaw, Poland: Panstwowy Instytut Geologiczny.

Berthelsen, A., 1979. Recumbent folds and boudinage structures formed by sub-glacial shear: an example of gravity tectonics. In van der Linden, W. J. M. (ed.), *Van Bemmelen and his search for harmony*. Geologie en Mijnbouw 58, pp. 253–260.

Christiansen, E. A., 1971. *Geology and groundwater resources of the Melville Area (62 K, L) Saskatchewan*. Saskatchewan Research Council, Geology Division, Map No. 12.

Dyke, A. S., and Prest, V. K., 1987. *Late Wisconsinan and Holocene history of the Laurentide Ice Sheet*. Géographie physique et Quaternaire XLI, pp. 237–263.

Johnstrup, F., 1874. Ueber die Lagerungsverhaltnisse und die Hebungs-phänomene in den Kreidefelsen auf Moen und Rügen. *Zeitschrift der Deutschen Geologischen Gesellschaft*, **1874**, 533–585.

Kupetz, A., and Kupetz, M. (eds.), 2009. Der Muskauer Faltenbogen. Wanderungen in die Erdgeschichte 24. Verlag Dr. Friedrich Pfeil, München, Germany, 224 p.

Kupsch, W. O., 1962. Ice-thrust ridges in western Canada. *Journal of Geology*, **70**, 582–594.

Lundqvist, J., and Lagerbäck, R., 1976. The Pärve Fault: a late-glacial fault in the Precambrian of Swedish Lapland. *Geologiska Föreningens i Stockholm Förhandlingar*, **98**, 45–51.

Lyell, C., 1863. *The geological evidences of the antiquity of man*, 3rd edn. London: John Murray.

Merrill, F. J. H., 1886. On some dynamic effects of the icesheet. *American Association for the Advancement of Science Proceedings*, **35**, 228–229.

Pedersen, S. A. S., 2000. Superimposed deformation in glaciotectonics. *Geological Society of Denmark Bulletin*, **46**, 125–144.

Sættem, J., 1990. Glaciotectonic forms and structures on the Norwegian continental shelf: Observations, processes and implications. *Norsk Geologisk Forening, Tidsskrift*, **70**, 81–94.

Slater, G., 1926. Glacial tectonics as reflected in disturbed drift deposits. *Geologists' Association Proceedings*, **37**, 392–400.

Stalker, A. M., 1976. Megablocks, or the enormous erratics of the Albertan Prairies. Geological Survey Canada, Paper 76-1C, pp. 185–188.

Varnes, D. J., Radbruch-Hall, D. H., and dSavage, W. Z., 1989. Topographic and structural conditions in areas of gravitational spreading of ridges in the western United States. US Geological Survey, Professional Paper 1496, 28 p.

White, W. A., 1992. Displacement of salt by the Laurentide ice sheet. *Quaternary Research*, **38**, 305–315.

GLOBAL CLIMATE MODELING IN CRYOSPHERIC ASSESSMENT

Jeffrey Ridley
Met Office, Hadley Centre, Exeter, UK

Definition

Global climate models (GCMs) are under continuous development. It has now become routine to verify the performance of all sub-models against global datasets, whenever a major change in the GCM is enacted (e.g., McLaren et al., 2006). In addition, sub-models themselves are verified, perhaps against more specialized regional datasets, whenever they undergo a physics upgrade (e.g., Pedersen et al., 2009; Vancoppenollea et al., 2009). Finally, parameterizations within sub-models can be assessed against specialized observations from focused field campaigns (e.g., Pomeroy et al., 1998). The retrieval of observations from measurements involves approximations and assumptions and whenever used to evaluate GCMs an observational uncertainty is required. The GCM component evaluated is deemed satisfactory if it lies within the range of observational uncertainty.

Sea ice

When verifying sea ice characteristics in a GCM, it is essential, due to regional differences in driving mechanisms, to do so separately for each hemisphere. The enclosed nature of the Arctic Ocean means that atmospheric variability plays a major role in sea ice variability. The ocean plays a dominant role in the Antarctic. Most sea ice model components of climate models are thermomechanical models, that is, they include components that simulate both the thermal and dynamical properties of sea ice.

Ice areal coverage

Satellite measurements of microwave radiances, available since 1979, are used to estimate the sea ice coverage. A wide range of instrumental and geophysical corrections and assumptions are needed before a geophysical retrieval can be extracted from the measurements. Estimates of the observational error may be obtained through comparing different methodologies. Such analysis shows that ice area retrievals are not accurate at low or high ice concentrations or during summer months when ice melt ponds are present.

Mean seasonal cycle

The hemispherically integrated monthly ice area fraction identifies if the phase of the GCM seasonal cycle is correct. An early melt may indicate that the GCM sea ice albedo parameterization, often a function of surface temperature and ice thickness, may be in error. Alternatively, it may be that the GCM generates a too high seasonal ocean heat transport.

Spatial distribution

Biases in the spatial patterns of ice area fraction will aid in the diagnoses of GCM mechanisms. For example, distinctive sea ice anomalies may be related to biases in the GCM sea-level pressure systems (North Atlantic Oscillation or Southern Annular Mode).

Interannual variations

A failure of the GCM to reproduce the interannual variations in ice extent may indicate a poor oceanic or atmospheric forcing. Alternatively, the ice may be responding too weakly to wind drag or too strongly to ocean drag.

Ice thickness and volume

Obtaining a good representation of the time-averaged ice thickness in a GCM is the best indicator that the combination of wind-forced dynamics and radiation-forced thermodynamics is well balanced. A further test is to verify the model against the equatorward ice transport. In the Arctic, this is characterized by the Fram Strait export. Changes in ice thickness (and volume) are a more sensitive indicator of climate change than changes in ice area.

Ice thickness

The primary source of thickness data for the Arctic is from the declassified sonar measurements of military submarines. The measurements of ice draft are converted to ice thickness following an assumption of snow depth and density. Submarine measurements, although dense along the submarine track, provide a sparse and incomplete coverage of the Arctic basin. Consequently, an ice thickness climatology requires considerable spatial interpolation (Bourke and Garrett, 1987).

Satellite altimetry can provide measurements of ice freeboard, which is then converted to ice thickness through assumptions about snow depth and density. Altimetry provides a temporally and spatially regular coverage but, because of the inclination of the satellite's polar orbit, coverage of the central Arctic is lacking. Considerable temporal and spatial averaging is required to reduce the measurement "noise." Satellite altimetry (from laser and radar), is a relatively new measurement system and the time series of observations has only been continuous since 1991 (Giles et al., 2008).

A compilation of in situ measurements and estimates from ship-borne observers provides a climatological ice thickness in the Antarctic (Worby et al., 2008). Efforts have been made to reduce systematic biases due to ship navigation practices, but the dataset suffers from poor spatial and temporal sampling.

Ice volume

The storage and release of freshwater in Arctic sea ice has important consequence for North Atlantic oceanography. In GCMs, we see that Arctic ice volume varies on a timescale of order a decade, while ice area varies over 2–3 years. Ice volume is a combination of ice thickness and ice area. The lack of full-hemisphere ice thickness observations in the Arctic, or regular observations in the Antarctic, precludes a validation of GCM ice volume.

Sea ice mass balance

Fixed buoys that continuously monitor the ice surface and basal changes provide a mass balance of sea ice (until the ice melts and the buoys are lost). Data from these buoys provides an assessment of the seasonal cycle of snow and ice melt and growth.

Ice thickness distribution

Many sea ice models include a depiction of the statistical distribution of ice thickness, in each GCM grid cell, through the use of ice thickness categories. The high-resolution spatial sampling of ice thickness by submarines and laser satellite altimetry allow these data to be compared with the modeled thickness distribution. The technique provides an estimate of the seasonal balance of multiyear and first-year ice, complementing mass balance measurements.

Ice drift

Sea ice drift is a balance of wind drag, ocean drag, Coriolis force, internal ice stresses, and ocean surface slope. A verification of ice drift against observations is primarily focused on tuning the sea ice sub-model wind and ocean drag coefficients. A poor GCM depiction of regional atmospheric surface pressure may compromise this process.

Multiple overpasses of a surface imaging satellite can be used to track the motion of features in the ice cover. When optimally merged with buoy drift vectors, a regional map of ice drift may be configured (e.g., Fowler, 2003).

Drift patterns

Ice convergence and divergence are determined by the drift patterns. In the Antarctic, the patterns of drift are

associated with strong ice formation in latent heat polynas at the front of the major ice shelves. Ice is then exported northward and is eventually entrained in the Antarctic Circumpolar Current. Elsewhere around the continent offshore winds and Coriolis force drive the ice westward in a coastal current until it encounters the northward flow from the polynas. In the Arctic, the polar winter atmospheric high-pressure system drives the ice around the Beaufort Gyre. Too strong a GCM gyre will result in a thickening of ice in the Beaufort Sea. Winds off the Russian coast result in strong formation in the East Siberian and Laptev seas driving a transpolar drift. This results in ice export from the Arctic, into the Atlantic, through the Fram Strait.

Fram strait export

The ice export through the Fram Strait is well monitored by fixed upward-looking sonar arrays and satellite observations. Steady-state ice formation in the Arctic will be balanced by in situ melt and export. A GCM that reproduces the annual cycle of ice area and the Fram Strait export will have the correct impact from the Arctic sea ice on the climate system.

Snow

Snow has a high albedo and is a good thermal insulator, thus its presence delays the onset of ice melt during summer and reduces ice thickness growth during winter. In the Antarctic, it is rare for snow to complete its melt in summer, and so progressive accumulation can result in ice thickness growth through snow to ice conversion. Observational data of snow depth on sea ice is available with the most reliable being in situ measurements (Konstantinov and Grachev, 2000; Massom et al., 2001). Reproducing realistic snow behavior in a GCM is partially dependent on the snow precipitation rates, but its accumulation can be controlled by tuning the GCM snow albedo.

Albedo

The annual cycle of sea ice produces changes in albedo. Snowmelts and bare ice develops in summer, followed by the formation of melt-ponds and their eventual refreeze, then more snow in winter. Although satellite observations can be used to derive summer albedo time series, these observations contain some cloud contamination and cannot distinguish between leads and melt ponds, presenting an area mean albedo rather than ice surface albedo. Field campaign measurements of albedo (e.g., Wyser et al., 2008) are the source of data for versification of sea ice albedo schemes (e.g., Pedersen et al., 2009).

Terrestrial snow

A robust feature of the response of climate models to increases in the atmospheric concentration of greenhouse gases is the poleward retreat of terrestrial snow, and the amplification of atmospheric temperature rise in the polar regions.

Many GCMs show biases against the observed seasonal cycle of land snow cover (especially the spring melt). Such biases are closely related to the large variations in GCM snow albedo feedback strength (Hall and Qu, 2006). A new result found independently by Winton (2006) and Qu and Hall (2005) is that surface processes are the main source of divergence in climate simulations of surface albedo feedback, rather than simulated differences in cloud fields in cryospheric regions.

The snow sub-models in GCMs are known to perform poorly, during the melt season, in regions where the snow energy budget is complex, such as under vegetated canopies and in mountainous regions. An additional complexity is that much of the snowmelt season is characterized by a patchy surface, unresolved at GCM scales. Differential heating of the snow and snow-free surfaces results in a significant horizontal transport of energy that affects and contributes to the snowmelt. The calculation of the rate of energy advection requires some knowledge of the behavior of the thermal boundary layer over the patches of snow and snow-free surfaces.

Verification of the snow models themselves occurs at a number of well-instrumented field sites (Pomeroy et al., 1998). Observations of snow cover can be retrieved from satellite, with global coverage and high temporal and spatial resolution. Currently, the most widely used satellite-derived snow cover product for model verification is the Interactive Multisensor Snow and Ice Mapping System (Ramsay, 1998).

Climate models parameterize snow as a water equivalent depth, SWE. The mapping of satellite-derived snow area SWE, requires a functional form that accounts for spatial inhomogeneities in topography and vegetation cover. An example might be

$$\mathrm{SWE} = (-\ln(1 - f_c))/D$$

where f_c is the snow fractional coverage and D is a characteristic masking depth of vegetation ($\sim$0.2 m globally).

Glaciers

There are currently no GCMs that incorporate interactive glaciers. This is partially because glaciers have almost no feedback with the climate system. Consequently, the contribution of glaciers to river runoff can be handled in off-line land surface schemes. The evaluation of GCM river runoff against observed river flow can reveal a missing summer component in some rivers that may be attributed to a lack of glaciers in the GCM.

Ice Sheets

All climate models treat ice sheets as static considering surface mass balance only. Various techniques are employed to ensure that global ocean mass does not drift under preindustrial climatic conditions. The simple expedient of having all snow fall, on ice sheets, instantly runoff to the ocean is commonly used. There are presently no climate models that routinely simulate ice sheet dynamics.

However, several climate models have experimentally coupled high-resolution (~20 km) ice sheet models (dynamics and thermodynamics) to the low-resolution (~200 km) climate components (Huybrechts et al., 2002; Fichefet et al., 2003; Ridley et al., 2005).

Surface mass balance
Estimates of ice sheet surface mass balance are derived from observations of snow accumulation and melt. Accumulation is derived from a combination of ice cores, snow stakes, satellite observations, and synoptic model reanalysis. Surface ablation is derived from empirical relationships between near-surface air temperature and direct runoff of snowmelt. The uncertainty in these methodologies is large, but they provide bounds with which to assess the surface mass balance in GCMs.

Conclusions

The validating of regional processes in climate models requires sources of observational data that are spatially homogeneous, of sufficient duration to incorporate decadal variability (i.e., at least 30 years), and well characterized biases and errors. The cyrosphere is not well provided for with long data series, but recently a wide variety of in situ and remote measurements have become available. A significant effort is required to intercompare the measurements and assess the quality and sampling issues. A recent focus on Arctic sea ice has provided a wealth of measurements to validate specific processes and feedback mechanisms. An example of combined satellite observations is that of sea ice area, drift, and thickness. Since these characteristics are intimately linked in sea ice model physics, the combination is a powerful tool to diagnose the performance of sea ice in climate models.

Bibliography

Bourke, R. H., and Garrett, R. P., 1987. Sea ice thickness distribution in the Arctic Ocean. *Cold Regions Science and Technology*, **13**, 259–280.

Fichefet, T., Poncin, C., Goosse, H., Huybrechts, P., Janssens, I., and Le Treut, H., 2003. Implications of changes in freshwater flux from the Greenland ice sheet for the climate of the 21st century. *Geophysical Research Letters*, **30**, Art. No. 1911.

Fowler, C., 2003. Polar Pathfinder daily 25 km EASE-Grid sea ice motion vectors, Natl. Snow and Ice Data Cent., Boulder, Colo, (available at http://nsidc.org/data/nsidc-0116.html.)

Giles, K. A., Laxon, S. W., and Worby, A. P., 2008. Antarctic sea ice elevation from satellite radar altimetry. *Geophysical Research Letters*, **35**, L03503.

Hall, A., and Qu, X., 2006. Using the current seasonal cycle to constrain snow albedo feedback in future climate change. *Geophysical Research Letters*, **33**, L03502, doi:10.1029/2005GL025127.

Huybrechts, P., Janssens, I., Poncin, C., and Fichefet, T., 2002. The response of the Greenland ice sheet to climate changes in the 21st century by interactive coupling of an AOGCM with a thermo-mechanical ice-sheet model. *Annals of Glaciology*, **35**, 409–415.

Massom, R. A., Eicken, H., Haas, C., Jeffries, M. O., Drinkwater, M. R., Sturm, M., Worby, A. P., Wu, X. R., Lytle, V. I., Ushio, S., Morris, K., Reid, P. A., Warren, S. G., and Allison, I., 2001. Snow on Antarctic Sea ice. *Reviews of Geophysics*, **39**, 413–445.

McLaren, A. J., et al., 2006. Evaluation of the sea ice simulation in a new coupled atmosphere-ocean climate model (HadGEM1). *Journal of Geophysical Research*, **111**, C12014, doi:10.1029/2005JC003033.

Pedersen, C. A., Roeckner, E., Lüthje, M., and Winther, J.-G., 2009. A new sea ice albedo scheme including melt ponds for ECHAM5 general circulation model. *Journal of Geophysical Research*, **114**, D08101, doi:10.1029/2008JD010440.

Pomeroy, J. W., Gray, D. M., Shook, K. R., Toth, B., Essery, R. L. H., Pietroniro, A., and Hedstrom, N., 1998. An evaluation of snow accumulation and ablation processes for land surface modelling. *Hydrological Processes*, **12**, 2339–2367.

Qu, X., and Hall, A., 2005. Surface contribution to planetary albedo variability in cryosphere regions. *Journal of Climate*, **18**, 5239–5252.

Ramsay, B. H., 1998. The interactive multisensor snow and ice mapping system. *Hydrological Processes*, **12**, 1537–1546.

Ridley, J. K., Huybrechts, P., Gregory, J. M., and Lowe, J. A., 2005. Elimination of the Greenland ice sheet in a high CO_2 climate. *Journal of Climate*, **18**, 3409–3427.

Vancoppenollea, M., Fichefet, T., Goosse, H., Bouillona, S., and Madec, G., 2009. Simulating the mass balance and salinity of Arctic and Antarctic sea ice. 1. Model description and validation. *Ocean Modelling*, **27**, 53.

Winton, M., 2006. Surface albedo feedback estimates for the AR4 climate models. *Journal of Climate*, **19**, 359–365.

Worby, A. P., Geiger, C. A., Paget, M. J., Van Woert, M. L., Ackley, S. F., and DeLiberty, T. L., 2008. Thickness distribution of Antarctic sea ice. *Journal of Geophysical Research*, **113**, C05S92, doi:10.1029/2007JC004254.

Wyser, K., et al., 2008. An evaluation of Arctic cloud and radiation processes during the SHEBA year: simulation results from eight Arctic regional climate models. *Climate Dynamics*, **30**, 203–223.

Cross-references

Antarctica
Arctic Hydroclimatology
Glacier Mass Balance
Global Outlook of Snowcover, Sea Ice, and Glaciers
Greenland Glaciers Outside the Ice Sheet
Greenland Ice Sheet
Ice Core
Ice Sheet
Sea Ice
Snow Water Equivalent

GLOBAL OUTLOOK OF SNOWCOVER, SEA ICE, AND GLACIERS

Mauri Pelto
Department of Environmental Science, Nichols College, Dudley, MA, USA

Definition

This article focuses on the broad issue of recent change in the extent of the principal cryospheric earth surface features, snowcover, sea ice, and glaciers.

Snowcover

An examination of Northern Hemisphere snowcover extent monthly anomalies provides a useful overview of recent changes in snowcover. Snowcover extent for the months of December–February as evidenced by the winter season anomaly has had no evident trend during the 2000–2009 period (Rutgers Global Snow, 2009). Of the 30 possible months, positive anomalies of greater than 1 million km^2 have occurred 11 times and negative anomalies of this magnitude three times. The spring season beginning with March is dominated by negative anomalies (Figure 1). In March, 6 of the last 10 years have had a negative anomaly of greater than 1 million km^2, no year had a positive anomaly of greater than 1 million km^2. In both April and May, 8 of the last 10 years have had a negative anomaly of greater than 1 million km^2, no year had a positive anomaly of greater than 1 million km^2. For the summer season, in June 9 of the last 10 years, in July and August all 10 of the years have a negative anomaly of greater than 1 million km^2. The fall season, September–November, as a whole does have an evident decline (Figure 1). This is almost entirely due to seven consecutive years 2002–2008 of negative snow cover anomalies in September. October and November have an equal balance of significant snowcover positive and negative anomalies. The key Northern Hemisphere snowcover change is the substantial spring and summer season negative seasonal trends in snowcovered area. That this has occurred despite winter snowcover extents anomalies tending to be positive from 2000 to 2009, indicates the important role that increased global temperatures are having. It is exclusively the melt season, March–September, snowcover extent that is being negatively impacted.

Examination of mountains snowcover records identifies some similar trends, both temperature and precipitation increases to date have impacted mountain snowpacks simultaneously on the global scale (Stewart, 2008). Warmer temperatures at mid-elevations have decreased snowpack and resulted in earlier melt in spite of precipitation increases, more rain events have also been observed reducing the snow water equivalent snowpack–precipitation ratio (Pelto, 2006). Higher elevations

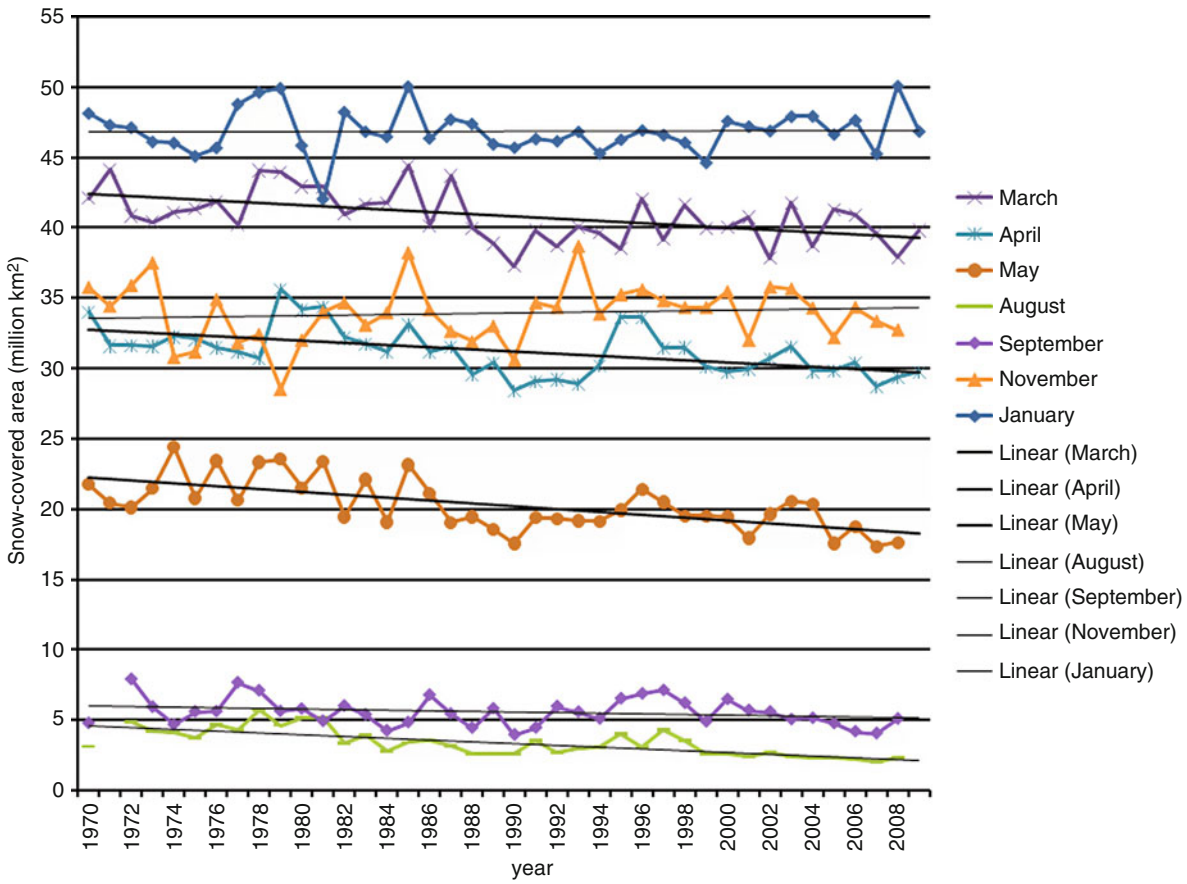

Global Outlook of Snowcover, Sea Ice, and Glaciers, Figure 1 Northern Hemisphere snowcover extent for selected months from 1970 to early 2009. November and January do not have a negative trend. The rate of decline increases from March through May, the spring melt season. The declining snowcover persists through September. Data source: Rutgers University Global Snow Lab.

have not been as affected as they remain well below freezing during winter. At high elevations, precipitation increases have resulted in increased snowpack in some cases (Stewart, 2008).

Arctic sea ice

Passive microwave satellite data have been reliably available since 1979. In the Arctic winter, sea ice extent has decreased about 4.2% per decade (Meier et al., 2005) and summer sea ice extent has declined at 8–10% per decade depending on which year is used as the end date from 2004 to 2008 (NSIDC, 2009). That the trend is consistently this large regardless of the end year argues for the robustness of the trend. The observed thinning of the pack is largely an indication of the reduced amount of multiyear ice (Nghiem et al., 2007). Both the 2008 and 2009 winters have recovered to a substantial percentage of normal cover; however, the amount of this cover being first year ice has been at unprecedented levels. The amount of perennial ice in the March ice cover has decreased from approximately 4.2 to 3.0 million km^2 over the period 1998–2007, this loss equals the areal decline from 1957 to 1997 (Nghiem et al., 2007). There has not been a single month since 2003 where Arctic sea ice cover has reached the long-term monthly average (Figure 2). In 2008 and 2009, sea ice older than 2 years comprised less than 10% of the sea ice cover at the end of February. The long-term average, 1981–2000, is older ice comprising 30% of the total sea ice cover at this time of the year (NSIDC, 2009). The thinner young ice is then more prone to summer melting as well as the impact of winds and currents (Maslanik et al., 2007; Serreze et al., 2007). The rapid loss of Arctic sea ice has along with glacier retreat been the most visible impact of global warming to date. The outlook is for continued declines in sea ice extent, with increasing seasonality to sea ice extent, with forecasts for the near-complete loss of summer Arctic Ocean sea ice, ranging from 2015 to 2060. Holland et al. (2006) ran a series of seven CCSM3 climate simulations, each suggested that abrupt increases in the summer Arctic sea ice cover loss are quite likely and are likely to occur early in the twenty-first century. The earliest date was 2015 with 2024 for being the mean date. The result was a nearly ice-free Arctic in September by 2040. The surface albedo feedback is the key factor in sea ice loss acceleration, as more solar radiation is absorbed in the surface ocean, increasing ice melt (Holland et al., 2006). Wang and Overland (2009) used the observed 2007/2008 September sea ice extents as a starting point for 23 simulations of ice extent using six different models. The expected time for a nearly sea ice-free Arctic in September is 2037. The increased open water is influencing climate beyond the melt season, delaying onset of freeze up and impact winter climate (Ford et al., 2009; Serreze et al., 2007).

Antarctic sea ice

The Antarctic Ocean has a much larger annual cycle in sea ice extent, with an average maximum and minimum of 18 million and 3 million km^2, respectively (NSIDC, 2009). The area covered by Antarctic sea ice has shown a small (not statistically significant) increasing trend from 1978 to 2009 of +1% per decade (Cavalieri et al., 2003). In

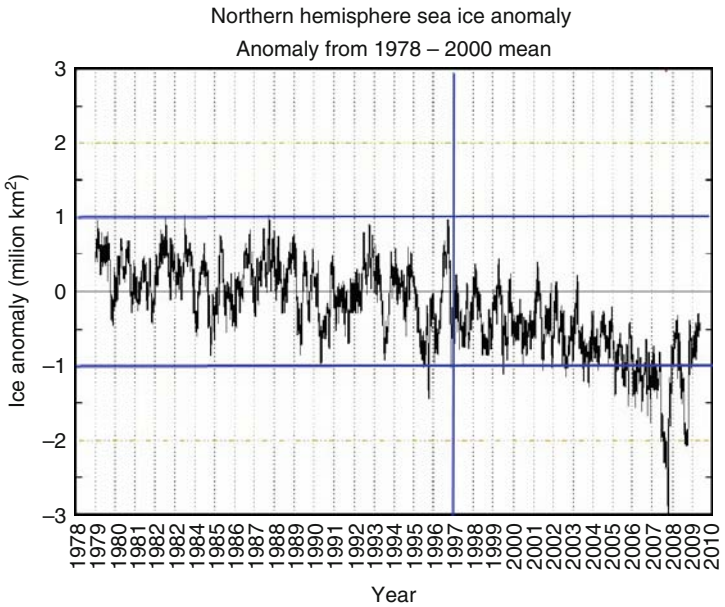

Global Outlook of Snowcover, Sea Ice, and Glaciers, Figure 2 Sea ice extent anomalies in the Arctic from 1979 to 2009. Beginning in 1997, Arctic sea ice cover does not approach a positive anomaly of 1 million km^2. Since 2003, there has not been a single month with a positive sea ice extent anomaly. Data source: National Snow and Ice Data Center.

the last decade there is no evident trend, mainly as a result of the dramatic annual and seasonal changes in the extent. The greatest minimum extent anomaly interval of the 1990–2009 period was 2002 and 2003 and the maximum period in the Austral summer of 2007–2008, followed by a decline to below normal extent anomalies by the Austral winter 2008 (NSIDC, 2009). There is an asymmetric trend with the largest increase in sea ice being in the Ross Sea region and the largest decrease in the Bellinghausen-Amundsen Sea region. Given the variability in Antarctic sea ice extent temporally and spatially, there is not a clear forecast for near-future sea ice trends around Antarctica.

Alpine glaciers

Glaciers have been studied as sensitive indicators of climate for more than a century and are now part of the Global Climate Observing System (Haeberli et al., 2000). The worldwide retreat of mountain glaciers is one of the clearest signals of ongoing climate change (Oerlemans, 2005; Haeberli and Hoelzle, 1995). The retreat is a reflection of strongly negative mass balances over the last 30 years (WGMS, 2007). Mass balance is the most sensitive climate parameter for glaciers, because it is a direct response to local weather conditions for a year (Pelto and Hedlund, 2001). The change in glacier length is a smoothed and delayed response to the mass balance changes (Haeberli and Hoelzle, 1995). The recent rapid retreat and prolonged negative balances have led to glaciers disappearing (Pelto, 2006).

Glacier mass balance is the difference between accumulation and ablation (melting and sublimation). Climate change may cause variations in temperature and snowfall, altering mass balance. A glacier with a sustained negative balance is out of equilibrium and will retreat. A glacier with sustained positive balance is out of equilibrium, and will advance to reestablish equilibrium. Glacier advance increases the area of a glacier at lower elevations where ablation is highest, offsetting the increase in accumulation. Glacier retreat results in the loss of the low-elevation region of the glacier. Since higher elevations are cooler, the disappearance of the lowest portion of the glacier reduces total ablation, increasing mass balance and potentially reestablishing equilibrium. If a glacier lacks a consistent accumulation zone, it is in disequilibrium, the accumulation zone will thin and the glacier will melt away without a change to a cooler-wetter climate (Pelto, 2010; Paul et al., 2007).

In 2007, mean mass balance of all the WGMS reporting glaciers was -528 mma^{-1}, and -673 mma^{-1} for the 30 reference glaciers, the 17th consecutive year of negative mass balance (Figure 3). WGMS preliminary data from 2008 indicate an 18th consecutive year of negative mass balance. Mass balance is reported in water equivalent thickness changes. A loss of 0.9 m of water equivalent is the same as the loss of 1.0 m of glacier thickness, since ice is less dense than water. The trend of consistent and substantial mass losses demonstrates why alpine glaciers are currently retreating. The cumulative loss of the last 30 years is the equivalent of cutting a 12–14 m thick slice off of the average glacier (Figure 2). The trend is remarkably consistent from region to region (WGMS, 2007).

The second parameter reported by WGMS is terminus behavior. The values are generally for glaciers examined annually. The number of advancing versus retreating glaciers reported to the WGMS shows a 2005 minimum in the percentage of advancing glaciers in Europe, Asia, and North America. In 2005, there were 442 glaciers examined, 26 advancing, 18 stationary, and 398 retreating. That is 90% retreating. Of the 26 advancing glaciers, 15 were in New Zealand. Overall, there has been a substantial volume loss of 11% of New Zealand glaciers from 1975 to 2005 (Chinn et al., 2005). More than 90% of the glaciers reported to the WGMS have retreated each year since 1990 (WGMS, 2008). In 1980, WGMS reported that more than 50% of the glaciers were advancing. This indicates that the ongoing retreat of the last 2 decades is in response to the warming global temperatures of the same time period, not part of a long-term trend of glacier retreat. The trend of negative mass balances indicates that glacier retreat will continue in the short term. The outlook for alpine glaciers is continued retreat and negative mass balances with the continued warm global temperatures.

For some glaciers, the forecast is for disappearance (Pelto, 2010). For a glacier to survive, it must have a persistent accumulation zone. If the upper reaches of a glacier where the accumulation zone becomes a frequent ablation-dominated area, the glacier cannot survive. The occurrence of this is evident by recession of the margin of the glacier in the accumulation zone or emergence of new rock outcrops (Pelto, 2010; Paul et al., 2007). Quantitative simulations of future perspectives for all glaciers in the European Alps are given by Haeberli and Hoelzle (1995). In both, the Swiss Alps and Pacific Northwest, numerous glaciers currently exhibit marginal recession or outcrop emergence in the accumulation zone (Pelto, 2010; Paul et al., 2007). The net result of glacier retreat will be reduced summer-water supply for irrigation, drinking water, aquatic life, and hydropower. The change in glacier extent for the twentieth century is from 25% to 40% in the Tien Shan, Pamir, Rocky Mountains, and Alps (WGMS, 2008), with a sharp increase in the rate noted in several of these areas (Paul et al., 2007; Pelto, 2010; Chinn et al., 2005).

Ice sheets and ice shelves

For the Greenland Ice Sheet, the two recent key changes have been changing melt extent and the acceleration of outlet glaciers. In 2005, melt extent reached a record area of 10.2 million km^2 (Tedesco, 2007). In 2007, the extent and magnitude of the melt was a record in southwest Greenland. In 2008, northern Greenland ice melt lasted 18 days longer than usual leading to 528 km^3 of runoff

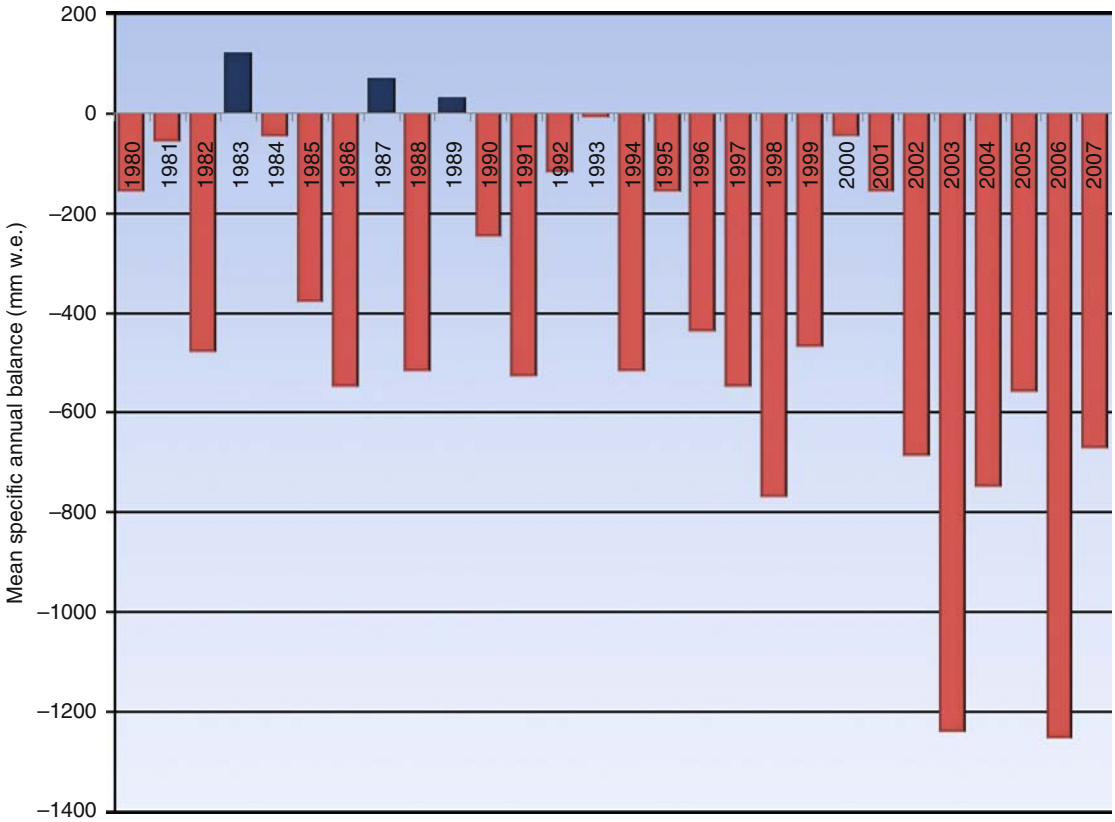

Global Outlook of Snowcover, Sea Ice, and Glaciers, Figure 3 Annual glacier mass balance reported to the World Glacier Monitoring Service. The negative mass balance of 2007 is the 17th consecutive year of negative mass balance.

(Tedesco et al., 2008). The record amount of ablation in northern Greenland reflected warm temperatures that led to the breakup of 29 km^2 of the floating terminus lobe of Petermann Glacier.

Two mechanisms have been utilized to explain the change in velocity of the Greenland ice sheets outlet glaciers. The first is the enhanced meltwater effect, which relies on additional surface melting, funneled through moulins reaching the glacier base and reducing the friction through a higher basal water pressure. The continued large extent of ice melt has provided additional meltwater. A brief seasonal acceleration of up to 20% occurred on the Jakobshavn Glacier in 1998 and 1999 at Swiss Camp (Zwally et al., 2002). The acceleration lasted 2–3 months and was less than 10% in 1996 and 1997. The additional meltwater has fueled a limited acceleration from enhanced lubrication from increased meltwater reaching the ice sheet base (Joughin et al., 2008). The acceleration has been short-lived even during the summer melt season and is less than 10%. Examination of recent rapid supraglacial lake drainage documented short-term modest velocity changes due to such events, but they had little significance to the annual flow of the large glaciers outlet glaciers (Joughin et al., 2008).

The second mechanism for Greenland outlet glacier acceleration is due to a force imbalance at the calving front (Thomas, 2004). Thinning causes the glacier to be more buoyant, reducing frictional backstress, which increases calving and velocity as larger areas of the glacier are afloat near the calving front. The reduced friction due to greater buoyancy allows for an increase in velocity. The reduced resistive force at the calving front is then propagated up-glacier via longitudinal extension because of the backstress reduction (Thomas, 2004).

Helheim Glacier, East Greenland had a stable terminus from the 1970s to 2000. In 2001–2005, the glacier retreated 7 km and accelerated from 20 m day^{-1} to 33 m day^{-1}, while thinning up to 130 m in the terminus region. Kangerdlugssuaq Glacier, East Greenland had a stable terminus history from 1960 to 2002. The glacier velocity was 13 m day^{-1} in the 1990s. In 2004–2005, it accelerated to 36 m day^{-1} and thinned by up to 100 m in the lower reach of the glacier. On Jakobshavn, the acceleration began at the calving front and spread up-glacier 20 km in 1997 and up to 55 km inland by 2003 (Joughin et al., 2004). On Helheim, the thinning and velocity propagated up-glacier from the calving front. In each case, the major outlet glaciers accelerated by at least 50%, much

larger than the impact noted due to summer meltwater increase. On each glacier, the acceleration was not restricted to the summer, persisting through the winter when surface meltwater is absent.

An examination of 32 outlet glaciers in southeast Greenland (Howat et al., 2008) indicates that the acceleration is significant only for marine terminating outlet glaciers. That is, glaciers that calve into the ocean. Thinning of the ice sheet is most pronounced for marine terminating outlet glaciers (Rignot and Kanagaratnam, 2006).

As a result of the above, Luckman et al. (2006) and Howat et al. (2008) concluded that the only plausible sequence of events is that increased thinning of the terminus regions, of marine terminating outlet glaciers, ungrounding the glacier tongues and subsequently allowing acceleration, retreat, and further thinning. Enhanced meltwater-induced acceleration does exist, but is of a notably smaller magnitude and duration. If the enhanced meltwater effect is key than since meltwater is a seasonal input, velocity would have a seasonal signal all glaciers would experience this effect, and the acceleration would begin inland and propagate toward the ice sheet margin. The force imbalance effect would be key if the velocity propagated from the terminus up-glacier, there was no seasonal velocity cycle, and the acceleration is focused on calving glaciers. The latter is the case indicating that force imbalance effects are the key to outlet glacier acceleration, not meltwater lubrication.

The primary cause of Greenland ice sheet acceleration has been a change in the balance of forces at the calving front of outlet glaciers. The key factor to Greenland's marine terminating outlet glacier acceleration has been dynamic thinning of the terminus zone of the marine terminating outlet glacier reducing the effective bed pressure, allowing acceleration. Terminus retreat reduces backstress, as does the resulting decrease in glacier thickness. The reduced backstress allows acceleration and increased calving. The acceleration was first reported from Helheim Glacier and Jakobshavn Isbrae. The acceleration began at the ice front and spread inland accompanied by large thinning and retreat. This acceleration has been noted to be present on all outlet glaciers. The widespread nature of this phenomenon indicates its importance and its likelihood of being a consistent and important part of Greenland ice sheet dynamics in a warmer world.

In 2000, six ice shelves remained along the north coast of Ellesmere Island (Mueller et al., 2003). Of the six remaining ice shelves, two have disappeared since 2000: Markham in 2008 and Ayles in 2005 (Copland et al., 2007; Mueller, 2008). Ward Hunt suffered an extensive breakup in 2003 and 2008. Serson experienced extensive breakup in 2008. Petersen has lost 30% of its area since 2005. Only Milne has not experience substantial volume loss in the last decade. On August 2005, almost the entire Ayles Ice Shelf (87.1 km^2) calved off reducing total Arctic Ice Shelf area by 8% (Copland et al., 2007). In 2008, extensive regional warmth that led to record melting in northern Greenland led to the breakup of Arctic ice shelves on the north coast of Ellesmere Island. Ward Hunt lost 22 km^2, Serson Ice Shelf lost 122 km^2, 60% of its area, and Markham lost all 50 km^2 of its area (Mueller, 2008). This system of ice shelves is almost gone.

A similar story has unfolded on the Antarctic Peninsula due to regional warming. The recent collapse of Wordie Ice Shelf, Mueller Ice Shelf, Jones Ice Shelf, and Larsen-A and Larsen-B Ice Shelf on the Antarctic Peninsula has made us aware of how dynamic Antarctic ice shelve systems are (Vaughan et al., 2003). After their loss, the reduced buttressing of feeder glaciers has allowed the expected speedup of inland ice masses after shelf ice breakup (Rignot et al., 2004). In Antarctica, Wilkins Ice Shelf lost 400 km^2 during a rapid February 2008 collapse. Humbert and Braun (2008) noted ongoing thinning preconditioned the ice shelf for collapse, and that existing rifts in February 2008 suggested an additional 2,000 km^2 was in imminent danger of collapse. During the Austral winter an additional 1,350 km^2 has been lost, and in April 2009 the final buttressing connection to Charcot Island failed, which led to additional ice losses.

The other significant change in Antarctica has been the acceleration, thinning, and retreat of Pine Island Glacier (Rignot et al., 2002; Shepherd et al., 2003). This glacier has been considered the weak underbelly of the West Antarctic Ice Sheet since it has only a small buttressing ice shelf and drains 10% of the ice sheet (Shepherd et al., 2003). Thinning and acceleration have reached 200 km behind the calving front and rates of thinning and acceleration increasing velocity from 26% to 42% (Scott et al., 2009). Pine Island Glacier has the largest mass loss of any outlet glacier in the world at present (Scott et al., 2009). This is a similar magnitude as the acceleration of the Greenland outlet glaciers. Wingham et al. (2009) reported that the 5,400 km^2 central trunk of the glacier had experienced a quadrupling in the average rate of volume loss quadrupled from 2.6 km^3 a year in 1995 to 10.1 km^3 a year in 2006. At present, the acceleration has not been noted beyond Pine Island and its neighboring Thwaites Glacier. The cause of the thinning that reduces backstress is thought to be increased basal melting of the floating ice shelf.

Conclusion

We have a consistent theme emerging from long-term records of glaciers, ice sheets, snowcover, ice shelves, and sea ice. The theme is enhanced melting, due to rising temperatures. This has led to: (1) Reduced glacier ice volume with 18 consecutive years of mean negative mass balance for alpine glaciers. (2) A failure of ice shelf systems in the Arctic and Antarctic Peninsula. (3) Substantial acceleration and retreat of marine terminating outlet glaciers in Greenland. (4) Reduced spring and summer snowcover extent in the Northern Hemisphere. (5) A large reduction in Arctic sea ice extent, particularly in summer and fall.

Bibliography

Chinn, T., Heydenrych, C., and Salinger, J., 2005. Use of the ELA as a practical method of monitoring glacier response to climate in New Zealand's Southern Alps. *Journal of Glaciology*, **51**, 85–95, doi:10.3189/172756505781829593.

Cavalieri, D. J., and Parkinson, C. L., 2008. Antarctic sea ice variability and trends, 1979–2006. *Journal of Geophysical Research*, **113**, C07004, doi:10.1029/2007JC004564.

Cavalieri, D. J., Parkinson, C. L., and Vinnikov, K. Y., 2003. 30-year satellite record reveals contrasting Arctic and Antarctic decadal sea ice variability. *Geophysical Research Letters* doi:10.1029/2003GL018031.

Copland, L., Mueller, D., and Weir, L., 2007. Rapid loss of the Ayles Ice Shelf, Ellesmere Island, Canada. *Geophysical Research Letters*, **34**, L21501, doi:10.1029/2007GL031809.

Fettweis, X., van Ypersele, J.-P., Gallée, H., Lefebre, F., and Lefebvre, W., 2007. The 1979–2005 Greenland ice sheet melt extent from passive microwave data using an improved version of the melt retrieval XPGR algorithm. *Geophysical Research Letters*, **34**, L05502, doi:10.1029/2006GL028787.

Ford, J., Gough, W. A., Laidler, G. J., MacDonald, J., Irngaut, C., and Qrunnut, K., 2009. Sea ice, climate change, and community vulnerability in northern Foxe Basin, Canada. *Climate Research*, **38**, 137–154, doi:10.3354/cr00777.

Haeberli, W., and Hoelzle, M., 1995. Application of inventory data for estimating characteristics of and regional climate-change effects on mountain glaciers: a pilot study with the European Alps. *Annals of Glaciology*, **21**, 206–212.

Haeberli, W., Cihlar, J., and Barry, R., 2000. Glacier monitoring within the Global Climate Observing System. *Annals of Glaciology*, **31**, 241–246.

Holland, M. M., Bitz, C. M., and Tremblay, B., 2006. Future abrupt reductions in the summer Arctic sea ice. *Geophysical Research Letters*, **33**, L23503, doi:10.1029/2006GL028024.

Howat, I., Joughin, I., Fahnestock, M., and Smith, B., 2008. Synchronous retreat and acceleration of southeast Greenland outlet glaciers 2000–06: ice dynamics and coupling to climate. *Journal of Glaciology*, **54**.

Humbert, A., and Braun, M., 2008. Wilkins Ice Shelf – break-up along failure zones. *Journal of Glaciology*, **55**(188), 943–944.

Joughin, I., Abdalati, W., and Fahenstock, M., 2004. Large fluctuations in speed on Greenlands Jakobshavn Isbrae glacier. *Nature*, **432**, 608–610.

Joughin, I., Das, S., King, M., Smith, B., Howat, I., and Moon, T., 2008a. Seasonal Speedup along the Western Flank of the Greenland Ice Sheet. *Science*, **320**, 781–783.

Joughin, I., Howat, I., Alley, R., Ekstrom, G., Fahenstock, M., Moon, T., Nettles, M., Truffer, M., and Tsai, V., 2008b. Ice-Front Variation and Tidewater Behavior on Helheim and Kangerdlugssuaq Glaciers, Greenland. *Journal of Geophysical Research*, **113**, F01004, doi:10.1029/2007JF000837.

Luckman, A., Murray, T., de Lange, R., and Hanna, E., 2006. Rapid and synchronous ice-dynamic changes in East Greenland. *Geophysical Research Letters*, **33**(3), L03503, doi:10.1029/2005GL025428.

Maslanik, J. A., Fowler, C., Stroeve, J., Drobot, S., Zwally, J., Yi, D., and Emery, W., 2007. A younger, thinner Arctic ice cover: Increased potential for rapid, extensive sea-ice loss. *Geophysical Research Letters*, **34**, L24501, doi:10.1029/2007GL032043.

Meier, W., Stroeve, J., Fetterer, F., and Knowles, K., 2005. Reductions in Arctic sea ice cover no longer limited to summer. *Eos, Transactions of the American Geophysical Union*, **86**(36), 326, doi:10.1029/2005EO360003.

Mueller, D., 2008. http://www.people.trentu.ca/~dmueller/iceshelfloss2008/.

Mueller, D., Vincent, W., and Jeffries, M., 2003. Break-up of the largest Arctic ice shelf and associated loss of an epishelf lake, *Geophysical Research Letters,* **30**(20), doi:10.1029/2003GL017931.

National Snow and Ice Data Center, 2009. http://nsidc.org/arcticseaicenews/index.html.

Nghiem, S. V., Rigor, I. G., Perovich, D. K., Clemente-Colon, P., Weatherly, J. W., and Neumann, G., 2007. Rapid reduction of Arctic perennial sea ice. *Geophysical Research Letters*, **34**, L19504, doi:10.1029/2007GL031138.

Oerlemans, J., 2005. Extracting a climate signal from 169 glacier records. *Science*, **308**, 675–677, doi:10.1126/science.1107046.

Overland, J. E., and Wang, M., 2007. Future regional sea ice declines. *Geophysical Research Letters*, **34**, L17705, doi:10.1029/2007GL030808.

Paul, F., Kääb, A., and Haeberli, W., 2007. Recent glacier changes in the Alps observed by satellite: consequences for future monitoring strategies. *Global and Planetary Change*, **56**, 102–111.

Pelto, M. S., 2006. The current disequilibrium of North Cascade glaciers. *Hydrological Processes*, **20**, 769–779.

Pelto, M. S., 2010. Forecasting temperate alpine glacier survival from accumulation zone observations. *The Cryosphere*, **4**, 67–75.

Pelto, M. S., and Hedlund, C., 2001. The terminus behavior and response time of North Cascade glaciers. *Journal of Glaciology*, **47**, 497–506.

Rignot, E., and Kanagaratnam, P., 2006. Changes in the velocity structure of the Greenland Ice Sheet. *Science*, **311**, 986–990.

Rignot, E., Gogineni, S., Krabill, W., and Ekholm, S., 1997. North and North East Greenland Ice Discharge from Satellite Radar Interferometry. *Science*, **276**, 934–937.

Rignot, E., Vaughan, D., Schmeltz, M., Dupont, T., and MacAyeal, D., 2002. Acceleration of Pine Island and Thwaites Glaciers, West Antarctica. *Annals of Glaciology*, **34**, 189–193.

Rignot, E., Casassa, G., Gogineni, P., Krabill, W., Rivera, A., and Thomas, R., 2004. Accelerated ice discharge from the Antarctic Peninsula following the collapse of Larsen B Ice Shelf. *Geophysical Research Letters*, **31**, L18401, doi:10.1029/2004GL020697.

Rutgers Global Snow Lab, 2009. http://climate.rutgers.edu/snowcover/.

Scott, J., Gudmundsson, G. H., Smith, A. M., Bingham, R. G., Pritchard, H. D., and Vaughan, D. G., 2009. Increased rate of acceleration on Pine Island Glacier strongly coupled to changes in gravitational driving stress. *The Cryosphere*, **3**, 125–131.

Serreze, M. C., Holland, M. M., and Stroeve, J., 2007. Perspectives on the Arctic's shrinking sea-ice cover. *Science*, **315**, 1533–1536.

Shepherd, A., Wingham, D., and Mansley, J., 2003. Inland thinning of the Amundsen Sea sector, West Antarctica. *Geophysical Research Letters*, **29**, 1364, doi:10.1029/2001GL014183.

Stewart, I., 2008. Changes in snowpack and snowmelt runoff for key mountain regions. *Hydrologic Processes*, **23**, 78–84.

Tedesco, M., 2007. Snowmelt detection over the Greenland ice sheet from SSM/I brightness temperature daily variations. *Geophysical Research Letters*, **34**, L02504, doi:10.1029/2006GL028466.

Tedesco, M., Fettweis, X., van den Broeke, M., van de Wal, R., and Smeets, P., 2008. Extreme Snowmelt in Northern Greenland During Summer 2008, *Eos Trans. AGU*, **89**(41), doi: 10.1029/2008EO410004.

Thomas, R. H., 2004. Force-perturbation analysis of recent thinning and acceleration of Jakobshavn Isbrae, Greenland. *Journal of Glaciology*, **50**(168), 57–66.

Vaughan, D. G., Marshall, G. J., Connolley, W. M., Parkinson, C., Mulvaney, R., Hodgson, D. A., King, J. C., Pudsey, C. J., and Turner, J., 2003. Recent rapid regional climate warming on the Antarctic Peninsula. *Climate Change*, **60**, 243–274.

Wang, M., and Overland, J. E., 2009. A sea ice free summer Arctic within 30 years? *Geophysical Research Letters*, **36**, L07502, doi:10.1029/2009GL037820.
WGMS, 2007. Glacier Mass Balance Bulletin No. 9 (2004–2005). Haeberli, W., Zemp, M., and Hoelzle, M. (eds.) (World Glacier Monitoring Service, Zurich, Switzerland, 2007).
WGMS, 2008. Global Glacier Changes: facts and figures. (UNEP-World Glacier Monitoring Service, Zurich, Switzerland, 2008).
Wingham, D. J., Wallis, D. W., and Shepherd, A., 2009. Spatial and temporal evolution of Pine Island Glacier thinning, 1995–2006. *Geophysical Research Letters*, **36**, L17501, doi:10.1029/2009GL039126.
Zhang, X., and Walsh, J. E., 2006. Toward a seasonally ice-covered Arctic Ocean: Scenarios from the IPCC AR4 model simulations. *Journal of Climate*, **19**, 1730–1747.
Zwally, H., Abdalati, W., Herring, T., Larson, K., Saba, J., and Steffen, K., 2002. Surface melt-induced acceleration of Greenland ice sheet flow. *Science*, **297**, 218–222.

Cross-references

Glacier Mass Balance
Ice Sheet Mass Balance
Retreat/Advance of Glaciers
Sea Ice
Thinning of Arctic Sea Ice
Thinning of Glaciers

GLOBAL WARMING AND ITS EFFECT ON SNOW/ICE/GLACIERS

Stephen J. Déry
Environmental Science and Engineering Program, University of Northern British Columbia, Prince George, BC, Canada

Synonyms

Impact of climate change on the cryosphere

Definition

Global warming. Rising air temperatures on a global scale.
Global warming and its effect on snow/ice/glaciers. Rising air temperatures on a global scale that are modifying components of the cryosphere, including snow, ice, and glaciers.

Introduction

One of the most notable manifestations of global warming is its impact on snow, ice, and glaciers. The cryosphere, defined as the portion of the earth system where water, soils, and other natural materials occur in the frozen form, is a prominent indicator and integrator of climate change as a contraction in its spatial extent, volume, and duration is particularly sensitive to rising air temperatures. Components of the cryosphere such as snow, ice, and glaciers play a major role in the global climate system through their distinct characteristics such as their high albedo values that induce strong positive feedbacks on warming (Déry and Brown, 2007) and their insulating properties that decouple the atmosphere with the underlying land surface or water (Stieglitz et al., 2003). Further, the cryosphere forms important and reliable reservoirs of freshwater, contributing water resources to a large fraction of the global population (Barnett et al., 2005).

Observational evidence of change

There is mounting observational evidence that global warming is leading to modifications in the state of the cryosphere. For instance, Déry and Brown (2007) report a 5% decline in snow cover extent in the Northern Hemisphere between 1972 and 2006 based on satellite measurements. Brown (2000) reconstructs the snow cover extent data prior to the satellite era and finds a decreasing trend in Northern Hemisphere snow cover extent over the period 1915–1997. Brown and Braaten (1998) find declining snow depths across most of Canada during the twentieth century. Mote et al. (2005) document a widespread decline in snow mass in the North American Cordillera from 1925 to 2000 in response to rising surface air temperatures. Ye et al. (1998) report decreasing (increasing) snow depths in the zonal band 50–60°N (60–70°N) in Eurasia from 1936 to 1983. Stone et al. (2002) document a twentieth-century trend toward earlier snowmelt in Alaska whereas Vaganov et al. (1999) observe an opposite trend in northern Eurasia.

Global warming also influences the different forms of ice found in oceans, lakes, or rivers. Observational records point to later freezing (trend of 5.8 days per century) and earlier breakup (trend of 6.5 days per century) of lake and river ice across the Northern Hemisphere from 1846 to 1995 (Magnuson et al., 2000). Sea ice in the Arctic declined in extent by about 3% per decade whereas sea ice in the Antarctic increased spatially by 1.3% per decade over 1978–1996 (Cavalieri et al., 1997). This observed asymmetric response of sea ice extent to global warming is consistent with global climate model (GCM) simulations. The annual minimum in Arctic sea ice extent, typically reached in mid-September, attained an unprecedented low value of 4.2×10^6 km^2 in 2007 (Maslanik et al., 2007). The rapid retreat in Arctic sea ice is outpacing all of the scenarios predicted by GCMs (Stroeve et al., 2007). Submarine measurements reveal a 42% decline in Arctic sea ice draft thickness over a period of 40 years ending in the 1990s (Rothrock et al., 1999).

In response to rising air temperatures and changing precipitation regimes, glaciers worldwide are experiencing a general trend toward negative mass balances (Oerlemans, 2005). Regional declines in glacier extent and volume include the Rockies and Coast Mountains of North America, the Andes of South America, the European Alps, and the Asian Himalayas. Glaciers are particularly sensitive to changes in summertime air temperatures that drive ablation and wintertime precipitation that forms accumulation. Strong modifications in either

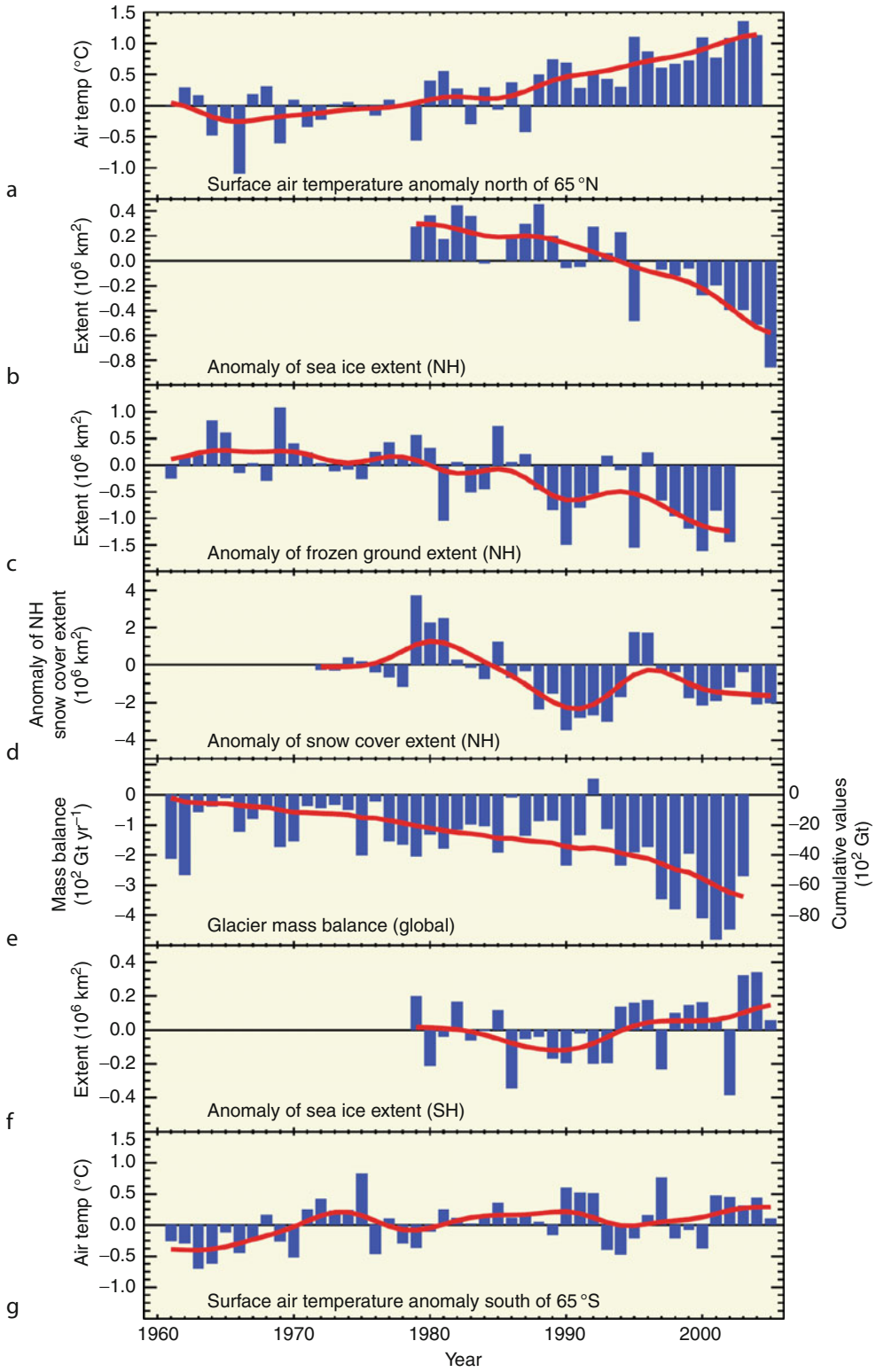

Global Warming and its Effect on Snow/Ice/Glaciers, Figure 1 Anomaly time series (departure from the long-term mean) of polar surface air temperature (**a**, **g**), arctic and Antarctic sea ice extent (**b**, **f**), Northern Hemisphere (NH) frozen ground extent (**c**), NH snow cover extent (**d**), and global glacier mass balance (**e**). The solid line in **e** denotes the cumulative global glacier mass balance; in the other panels, it shows decadal variations (Lemke et al., 2007).

of these seasonal quantities may alter the mass budget of glaciers. Discharge of ice from outlet glaciers of Greenland doubled in the period 1996–2005 (Rignot and Kanagaratnam, 2006) while surface melt and ablation expanded to record levels in response to global warming (Tedesco et al., 2008). In the Southern Hemisphere, global warming has not affected the overall mass balance of the Antarctic ice sheet owing in part to its colder environment than the Greenland ice sheet. However, the collapse of the Larsen ice shelf near the Antarctic Peninsula in January 1995 along with the subsequent acceleration of ice discharge and calving provide some evidence of a growing importance of climate change in the area (Rignot et al., 2004).

Future projections

A number of studies have examined the impacts of global warming on the potential future state of the cryosphere. In general, simulations of twenty-first century climate by GCMs project decreases in the spatial extent, volume, and duration of many components of the cryosphere. Déry and Wood (2006) project declines in the extent and duration of the Northern Hemisphere snow cover. They also report potential reductions in the seasonal accumulation of snow, particularly in the mid-latitudes whereas high-Arctic regions may experience increases in seasonal snow mass. Simulations of the future state of the global climate system project abrupt declines in sea ice extent and thickness, with the potential of an ice-free Arctic Ocean by the middle of the twenty-first century (Holland et al., 2006). Rising summertime air temperatures suggest that glaciers may disappear altogether in the Alps by 2100 and contribute substantially to rising sea levels (Zemp et al., 2006). Enhanced melting of the Greenland ice sheet and potentially the Antarctic ice sheet will further advance sea-level rise (Alley et al., 2005). Thus, global warming is anticipated to contribute to a shrinking cryosphere in the coming decades.

Repercussions of change

Changes in the cryosphere have profound environmental, biological, and societal repercussions (Barnett et al., 2005). As an example, mass wasting of glaciers has significant implications on downstream freshwater resources and hydrological processes. Glacier recession in western Canada has led to declines and phase shifts in late summer streamflow (Déry et al., 2009). This has important ramifications for populated downstream areas such as the arid Canadian Prairies that are now subject to an impending water crisis (Schindler and Donahue, 2006). Furthermore, glacier and ice sheet melt contributes to rising sea levels and potential changes in ocean currents (Alley et al., 2005).

Modifications in snowpack characteristics also affect ecological processes such as the duration of the growing season (Vaganov et al., 1999), and on plant productivity, density, and distribution. Changes in snowpack accumulation influence prey–predator relationships (Stenseth et al., 2004) and the feeding habits of mountain caribou and other ungulates (Kinley et al., 2007). The potential collapse in the populations of polar bears in the Arctic (Durner et al., 2009), emperor penguins in Antarctica (Jenouvier et al., 2009), and other species forms another potential consequence of a shrinking cryosphere.

Furthermore, cryospheric changes influence socioeconomic and recreational activities. The potential opening of the Northwest Passage in the Canadian Archipelago may lead to increased shipping activity in the high Arctic. Warmer winters have led to shorter periods with river ice covers in northern Canada, impeding commercial transport on ice roads. Tourism may suffer from the degradation of glaciers in many regions including Waterton National Park in the Canadian Rocky Mountains (Scott et al., 2007). Outdoor recreational activities such as skiing and ice skating may also be curtailed owing to reduced or unreliable snow/ice packs (Elsasser and Bürki, 2002).

Summary

Rising air temperatures are inducing dramatic changes in the state of the cryosphere. Global warming has led to a general decline in the presence of snow, ice, and glaciers over the past decades (Figure 1). Future projections of climate suggest that changes in the cryosphere will intensify and accelerate over the twenty-first century in response to continued global warming. The disappearance of snow, ice, and glaciers will reduce freshwater storage on the land surface, leading to diminishing water resources in many areas. Given the increasing demands for freshwater, changes in the cryosphere driven by global warming may pose serious challenges to humans and ecosystems in the twenty-first century.

Bibliography

Alley, R. B., Clark, P. U., Huybrechts, P., and Joughin, I., 2005. Ice sheet and sea-level changes. *Science*, **310**, 456–460.

Barnett, T. P., Adam, J. C., and Lettenmaier, D. P., 2005. Potential impacts of a warming climate on water availability in snow-dominated regions. *Nature*, **438**, 303–309.

Brown, R. D., 2000. Northern Hemisphere snow cover variability and change, 1915–97. *Journal of Climate*, **13**, 2339–2355.

Brown, R. D., and Braaten, R. O., 1998. Spatial and temporal variability of Canadian monthly snow depths. *Atmosphere-Ocean*, **36**, 37–54.

Cavalieri, D. J., Gloersen, P., Parkinson, C. L., Comiso, J. C., and Zwally, H. J., 1997. Observed hemispheric asymmetry in global sea ice changes. *Science*, **278**, 1104–1106.

Déry, S. J., and Brown, R. D., 2007. Recent Northern Hemisphere snow cover extent trends and implications for the snow-albedo feedback. *Geophysical Research Letters*, **34**, L22504, doi:10.1029/2007GL031474.

Déry, S. J., and Wood, E. F., 2006. Analysis of snow in the 20th and 21st century Geophysical Fluid Dynamics Laboratory coupled climate model simulations. *Journal of Geophysical Research*, **111**, D19113, doi:10.1029/2005JD006920.

Déry, S. J., Stahl, K., Moore, R. D., Whitfield, P. H., Menounos, B., and Burford, J. E., 2009. Detection of runoff timing changes in

pluvial, nival and glacial rivers of western Canada. *Water Resources Research*, **45,** doi: 10.1029/2008WR006975.
Durner, G. M., Douglas, D. C., Nielson, R. M., Amstrup, S. C., McDonald, T. L., Stirling, I., Mauritzen, M., Born, E. W., Wiig, O., DeWeaver, E., Serreze, M. C., Belikov, S. E., Holland, M. M., Maslanik, J., Aars, J., Bailey, D. A., and Derocher, A. E., 2009. Predicting 21st century polar bear habitat distribution from global climate models. *Ecological Monographs*, **79**, 25–58.
Elsasser, H., and Bürki, R., 2002. Climate change as a threat to tourism in the Alps. *Climate Research*, **20**, 253–257.
Holland, M. M., Bitz, C. M., and Tremblay, B., 2006. Future abrupt reductions in the summer Arctic sea ice. *Geophysical Research Letters*, **33**, L23503, doi:10.1029/2006GL028024.
Jenouvier, S., Caswell, H., Barbraud, C., Holland, M., Stroeve, J., and Weimerskirch, H., 2009. Demographic models and IPCC climate projections predict the decline of emperor penguin population. *Proceedings of the National Academy of Sciences of the United States of America*, **106**, 1844–1847.
Kinley, T. A., Goward, T., McLellan, B. N., and Serrouya, R., 2007. The influence of variable snowpacks on habitat use by mountain caribou. *Rangifer*, **17**, 1–10.
Lemke, P., Ren, J., Alley, R. B., Allison, I., Carrasco, J., Flato, G., Fujii, Y., Kaser, G., Mote, P., Thomas, R. H., and Zhang, T., 2007. Observations: changes in snow, ice and frozen ground. In Solomon, S., Qin, D., Manning, M., Chen, Z., Marquis, M., Averyt, K. B., Tignor, M., and Miller, H. L. (eds.), *Climate Change 2007: The Physical Science Basis. Contribution of Working Group I to the Fourth Assessment Report of the Intergovernmental Panel on Climate Change*. Cambridge, New York: Cambridge University Press.
Magnuson, J. J., Robertson, D. M., Benson, B. J., Wynne, R. H., Livingstone, D. M., Arai, T., Assel, R. A., Barry, R. G., Card, V., Kuusisto, E., Granin, N. G., Prowse, T. D., Stewart, K. M., and Vuglinski, V. S., 2000. Historical trends in lake and river ice cover in the Northern Hemisphere. *Science*, **289**, 1743–1746, doi:10.1126/science.289.5485.
Maslanik, J. A., Fowler, C., Stroeve, J., Drobot, S., Zwally, J., Yi, D., and Emery, W., 2007. A younger, thinner Arctic ice cover: increased potential for rapid, extensive sea-ice loss. *Geophysical Research Letters*, **34**, L24501, doi:10.1029/2007GL032043.
Mote, P. W., Hamlet, A. F., Clark, M. P., and Lettenmaier, D. P., 2005. Declining mountain snowpack in western North America. *Bulletin of the American Meteorological Society*, **86**, 39–49.
Oerlemans, J., 2005. Extracting a climate signal from 169 glacier records. *Science*, **308**, 675–677.
Rignot, E., and Kanagaratnam, P., 2006. Changes in the velocity structure of the Greenland Ice Sheet. *Science*, **311**, 986–990, doi:10.1126/science.1121381.
Rignot, E., Casassa, G., Gogineni, P., Krabill, W., Rivera, A., and Thomas, R., 2004. Accelerated ice discharge from the Antarctic Peninsula following the collapse of Larsen B ice shelf. *Geophysical Research Letters*, **31**, L18401, doi:10.1029/2004GL020697.
Rothrock, D. A., Yu, Y., and Maykut, G. A., 1999. Thinning of the Arctic sea-ice cover. *Geophysical Research Letters*, **26**, 3469–3472.
Schindler, D. W., and Donahue, W. F., 2006. An impending water crisis in Canada's western prairie provinces. *Proceedings of the National Academy of Sciences of the United States of America*, **103**, 7210–7216.
Scott, D., Jones, B., and Konopek, J., 2007. Implications of climate and environmental change for nature-based tourism in the Canadian Rocky Mountains: A case study of Waterton Lakes National Park. *Tourism Management*, **28**, 570–579.
Stenseth, N. C., Shabbar, A., Chan, K.-S., Boutin, S., Rueness, E. K., Ehrich, D., Hurrell, J. W., Lingjærde, O. C., and Jakobsen, K. S., 2004. Snow conditions may create an invisible barrier for lynx. *Proceedings of the National Academy of Sciences of the United States of America*, **101**, 10632–10634.
Stieglitz, M., Déry, S. J., Romanovsky, V. E., and Osterkamp, T. E., 2003. The role of snow cover in the warming of arctic permafrost. *Geophysical Research Letters*, **30**, 1721, doi:10.1029/2003GL017337.
Stone, R. S., Dutton, E. G., Harris, J. M., and Longenecker, D., 2002. Earlier spring snowmelt in northern Alaska as an indicator of climate change. *Journal of Geophysical Research*, **107**, 4089, doi:10.1029/2001JD000677.
Stroeve, J., Holland, M. M., Meier, W., Scambos, T., and Serreze, M., 2007. Arctic sea ice decline: faster than forecast. *Geophysical Research Letters*, **34**, L09501, doi:10.1029/2007GL029703.
Tedesco, M., Fettweis, X., van den Broeke, M., van de Wal, R., and Smeets, P., 2008. Extreme snowmelt in northern Greenland during summer 2008, *EOS Transactions AGU*, **89**(41), doi:10.1029/2008EO410004.
Vaganov, E. A., Hughes, M. K., Kidyanov, A. V., Schweingruber, F. H., and Silkin, P. P., 1999. Influence of snowfall and melt timing on tree growth in subarctic Eurasia. *Nature*, **400**, 149–151.
Ye, H., Cho, H. R., and Gustafson, P. E., 1998. The changes in Russian winter snow accumulation during 1936–83 and its spatial patterns. *Journal of Climate*, **11**, 856–863.
Zemp, M., Haeberli, W., Hoelzle, M., and Paul, F., 2006. Alpine glaciers to disappear within decades? *Geophysical Research Letters*, **33**, L13504, doi:10.1029/2006GL026319.

Cross-references

Climate Change and Glaciers
Deglaciation
Depletion of Snow Cover
Impacts of Snow and Glaciers on Runoff
Retreat/Advance of Glaciers
Sea Ice
Streamflow Trends in Mountainous Regions
Thinning of Arctic Sea Ice
Thinning of Glaciers

GPS IN GLACIOLOGY, APPLICATIONS

Matt A. King
School of Civil Engineering and Geosciences, Newcastle University, Newcastle upon Tyne, UK

Definition

GPS: Global Positioning System (GPS), the now-standard name applied to the NAVSTAR GPS of the U.S. Department of Defense, and used in glaciology to measure ice motion. One of several Global Navigation Satellite Systems (GNSS) in operation today.

Background

Glaciologists adopted GPS as early as the mid-1980s (Hinze and Seeber, 1988; Moller and Ritter, 1988) as it overcame line-of-sight restrictions from traditional survey techniques and reduced or eliminated the time spent in traversing from known locations. Despite the small size of the satellite constellation and complications with receiver signal tracking, memory and power consumption,

positions with precisions of several meters were reported. Completion of the satellite constellation and advances in receiver and power technology now mean that GPS receivers can be deployed year-round without user intervention, and position precisions of several millimeters may be obtained (e.g., Bindschadler et al., 2003).

Geodetic GPS relies on tracking carrier phase signals broadcast by the satellites on both the L1 and L2 frequencies. With a carrier phase tracking precision of ~1 mm, the complexity of obtaining precise positions rests with determining the positions of the GPS satellites and in correcting for signals in the atmosphere, signal multipath, and unwanted solid earth geophysical signal. As an interferometric system, GPS carrier observations suffer from an integer cycle ambiguity (N). A simplified equation for an observation Φ between receiver i and satellite k is

$$\Phi_i^k(t) = \rho_i^k - I_i^k + T_i^k + c\left(\mathrm{d}t_i - \mathrm{d}t^k\right) + \lambda N_i^k - \epsilon_i^k \quad (1)$$

where ρ is the geometric distance, c is the vacuum speed of light, λ is the signal wavelength, and ε are random errors (e.g., signal multipath). Receiver and satellite clock errors ($\mathrm{d}t_i$ and $\mathrm{d}t^k$, respectively) dominate and are double-differenced in relative positioning. Alternatively, previously computed satellite clock errors may be fixed and receiver clock errors treated as unknowns as is done in precise point positioning (*PPP*; Zumberge et al., 1997). A similar equation may be given for the less precise, but unambiguous, pseudo-range observations modulated on each carrier.

Satellite orbit errors are generally regarded as negligible when using precise ephemerides from the International GNSS Service (Dow et al., 2005). Atmospheric errors consist of ionospheric delay (I), essentially reduced to negligible levels by forming an ionosphere-free linear combination of the L1 and L2 carrier observations, and tropospheric delay (T), which cancels over short (<10 km length, <100 m height difference) baselines, but otherwise must be modeled with some imprecision, or the residual treated as an unknown for precise applications. Carrier phase multipath reaches up to 0.25λ (~0.05 m), with its magnitude depending on locations and characteristics of reflectors in the antenna proximity. In coordinate time series, multipath is evident through periodic signal repeating approximately once per sidereal day. Geophysical signals, such as solid earth tides or ocean tide or atmospheric loading displacements, cancel over short baselines, but not over longer baselines or in PPP and must be modeled.

Less-precise positions may be obtained using a subset of the dual frequency observables. The main advantages are the reduced power requirements and observation processing complexity and lower cost of receiver equipment purchase. The principal disadvantage is the much reduced positioning precision. Two such approaches are differential GPS (dGPS) positioning that uses pseudo-range data only or single frequency positioning that uses L1 carrier phase observations only. dGPS positioning is limited to precisions of a few decimeters to meters. Single frequency positioning is limited by ionospheric effects that quickly reach decimeters over baselines of a few tens of kilometers, although for long-term studies the precision may be sufficient (e.g., van de Wal et al., 2008).

Dual frequency carrier phase GPS data processing involves least squares estimation of three-dimensional coordinates, receiver clocks (in PPP), real-valued ambiguities, and possibly zenith-mapped tropospheric delays. In a kinematic environment new coordinates are estimated every observation epoch. For kinematic positioning, it is critical that ambiguities are fixed to correct integers and then removed from the solution. When using a Kalman Filter/Smoother solution it is also possible to retain real-valued, but precisely determined, ambiguity estimates with minor degradation in coordinate precision. Integer ambiguity fixing is a statistical process, and is not always possible to confidently fix ambiguities due to observation noise, such as multipath. Integer ambiguity fixing has only a small effect on static positioning (Blewitt, 1989).

Glaciological applications of derived coordinates or coordinate time series are diverse, with examples below.

Ice velocity and strain rates

Glacier and ice shelf velocities and strain rates were an early glaciological target application of GPS (Hulbe and Whillans, 1994). Velocity measurements were used in obtaining estimates of ice mass balance. In some early cases, GPS was used to determine absolute position, but conventional approaches used to determine strain rate (Determann et al., 1990). Ice shelf rift formation has been studied more recently (Bassis et al., 2005) and GPS velocities are now being used to detect change in ice velocity over many decades (Joughin et al., 2005; King et al., 2007), seasonally (Joughin et al., 2008) or nearly instantaneously (Das et al., 2008).

Tides and tidal modulation of flow

GPS observations have been made of ocean tides on sea ice (Aoki et al., 2000), ice shelves (Riedel et al., 1999), and of subglacial lake tides (Wendt et al., 2005). Measurements of tidal flexure in ice shelf grounding lines have also been made (Vaughan, 1995). Horizontally, tidal modulation of flow has been identified on ice streams (Anandakrishnan et al., 2003; Bindschadler et al., 2003; Gudmundsson, 2006) and ice tongues and shelves (Doake et al., 2002; Legresy et al., 2004). However, the GPS satellite constellation repeat period is not optimal for tidal studies, since it repeats very close to the K1 and K2 tidal frequencies, producing systematic errors of the order of a few millimeters over short baselines and up to ~10 mm using PPP (King et al., 2008).

Mass balance

The difference between the vertical velocity of markers anchored in firn and the long-term rate of snow accumulation reveals the local ice mass balance. Precise vertical

velocities have been determined using GPS to achieve this (Hamilton and Whillans, 2000). Satellite geometry and tropospheric errors, however, mean the vertical coordinate in GPS is less precise than the horizontal, and vertical velocities are subject to reference frame uncertainties and/or bias. Nevertheless, these tend to be too small (<1–2 mm/year) to be relevant to most glaciological studies.

Indirect measurements of ice mass change

GPS mounted adjacent to glaciers is sensitive to contemporaneous ice mass changes through elastic rebound (e.g., Grapenthin et al., 2006; Khan et al., 2007). The Earth's response to ice unloading since the last glacial maximum, known as glacial isostatic adjustment, may also be studied using GPS and therefore provide constraints on ice history and Earth rheology (Milne et al., 2001). Since the velocities of interest are generally small, advanced analysis techniques are required.

Digital elevation models

GPS antenna mounted on snowmobiles or aircraft may be used to determine position for generation of digital elevation models (e.g., Krabill et al., 1995). In airborne applications, GPS positions the LIDAR or photogrammetric camera. Examples of subsequent use include surface elevation change (e.g., King et al., 2009) and satellite calibration/validation (Phillips et al., 1998). Errors and uncertainties can be assessed by designing crossovers into the sampling strategy.

Data analysis

Different GPS data processing software may be divided along lines of their main audiences: the mass-market (commercial) and/or research geodesists. All GPS hardware manufacturers provide high-quality software that is designed to produce robust solutions over generally short (<30–80 km) baselines. Scientific software allows greater flexibility in parameterization, such as in the estimation of tropospheric parameters, or in solution control, such as site motion constraints via process noise settings in a Kalman Filter.

Incorrect processing of GPS data in glaciological environments may yield substantial spurious signal that could be interpreted as real (King, 2004). In particular, processing data from a moving site as if it were static, even for short periods, will likely produce erroneous results.

Several online services now exist, allowing open access to research quality software. Caution should be exercised, however, as to which observation level model options have been applied, including, for example, loading displacements and antenna phase centers. Except for almost stagnant ice, kinematic processing should be adopted.

GPS coordinate formal errors produced by all current GPS processing software do not reflect the true formal error, and are typically overoptimistic as they are based on somewhat arbitrary observation uncertainties and neglect between-epoch and between-observation correlations, which can be substantial. While receiver sampling at least every 30 s is vital, coordinate time series will be correlated over several minutes, especially for a slow-moving site. Scale factors for the reported formal errors may be obtained by examining coordinate time series repeatability (see King, 2004). For kinematic surveys, an examination of crossovers yields useful information (Borsa et al., 2007).

For long baseline or PPP studies of slowly moving ice, the present-day state-of-the-art is likely to yield epoch-to-epoch repeatability in the range 0.01–0.02 m for horizontal positions and 0.03–0.05 m for vertical positions. Multipath effects may be reduced through sidereal filtering (Choi et al., 2004). Errors relating to mounting the GPS antenna robustly in the ice may now dominate the GPS positioning error in many cases.

Conclusions

The GPS has revolutionized point-wise measurements in glaciology, complementing the wide spatial sampling available from interferometric SAR. As precision has improved and as observations switched from campaign style to continuous, new insights have been gained. In the near future multiple GNSS will be available, reducing both random and systematic errors in coordinate time series. Surveys in kinematic environments, such as in glaciology, will be among the greatest beneficiaries.

Bibliography

Anandakrishnan, S., Voigt, D. E., Alley, R. B., and King, M. A., 2003. Ice stream D flow speed is strongly modulated by the tide beneath the Ross ice shelf. *Geophysical Research Letters*, **30**(7), 1361, doi:10.1029/2002GL016329.

Aoki, S., Ozawa, T., Doi, K., and Shibuya, K., 2000. GPS observation of the sea level variation in Lutzow-Holm Bay, Antarctica. *Geophysical Research Letters*, **27**(15), 2285–2288.

Bassis, J. N., Coleman, R., Fricker, H. A., and Minster, J. B., 2005. Episodic propagation of a rift on the Amery Ice Shelf, East Antarctica. *Geophysical Research Letters*, **32**(6), L06502.

Bindschadler, R., King, M. A., Alley, R. B., Anandakrishnan, S., and Padman, L., 2003. Tidally controlled stick-slip discharge of a west Antarctic ice stream. *Science*, **301**(5636), 1087–1089.

Blewitt, G., 1989. Carrier phase ambiguity resolution for the global positioning system applied to geodetic baselines up to 2000 km. *Journal of Geophysical Research*, **98**(B8), 10187–10203.

Borsa, A. A., Minster, J.-B., Bills, B. G., and Fricker, H. A., 2007. Modeling long-period noise in kinematic GPS applications. *Journal of Geodesy*, **81**(2), 157–170, doi:10.1007/s00190-006-0097-x.

Choi, K. H., Bilich, A., Larson, K. M., and Axelrad, P., 2004. Modified sidereal filtering: Implications for high-rate GPS positioning. *Geophysical Research Letters*, **31**(22), L22608, doi:10.1029/2004GL021621.

Das, S. B., Joughin, I., Behn, M. D., Howat, I. M., King, M. A., Lizarralde, D., and Bhatia, M. P., 2008. Fracture propagation to the base of the Greenland ice sheet during supraglacial lake drainage. *Science*, **320**(5877), 778–781.

Determann, J., Grosfeld, K., and Ritter, B., 1990. Melting rates at the bottom of Filchner-Ronne Ice Shelf, Antarctica, from short-term mass-balance studies. *Polarforschung*, **60**(1), 25–32.

Doake, C. S. M., Corr, H. F. J., Nicholls, K. W., Gaffikin, A., Jenkins, A., Bertiger, W. I., and King, M. A., 2002. Tide-induced lateral movement of Brunt Ice Shelf, Antarctica. *Geophysical Research Letters*, **29**(8), doi:10.1029/2001GL014606.
Dow, J. M., Neilan, R. E., and Gendt, G., 2005. The international GPS service: celebrating the 10th anniversary and looking to the next decade. *Advances in Space Research*, **36**, 320–326.
Grapenthin, R., Sigmundsson, F., Geirsson, H., Árnadóttir, T., and Pinel, V., 2006. Icelandic rhythmics: annual modulation of land elevation and plate spreading by snow load. *Geophysical Research Letters*, **33**(24), L24305.
Gudmundsson, G. H., 2006. Fortnightly variations in the flow velocity of Rutford Ice Stream, West Antarctica. *Nature*, **444**(7122), 1063–1064.
Hamilton, G. S., and Whillans, I. M., 2000. Point measurements of mass balance of the Greenland Ice Sheet using precision vertical Global Positioning System (GPS) surveys. *Journal of Geophysical Research*, **105**(B7), 16295–16301.
Hinze, H., and Seeber, G., 1988. Ice-motion determination by means of satellite positioning systems. *Annals of Glaciology*, **11**, 36–41.
Hulbe, C. L., and Whillans, I. M., 1994. Evaluation of strain rates on Ice Stream B, Antarctica, obtained using GPS phase measurements. *Annals of Glaciology*, **20**, 254–262.
Joughin, I., Bindschadler, R. A., King, M. A., Voigt, D., Alley, R. B., Anandakrishnan, S., Horgan, H., Peters, L., Winberry, P., Das, S. B., and Catania, G., 2005. Continued deceleration of Whillans Ice Stream. *West Antarctica. Geophysical Research Letters*, **32**, L22501, doi:10.1029/2005GL024319.
Joughin, I., Das, S. B., King, M. A., Smith, B. E., Howat, I. M., and Moon, T., 2008. Seasonal speedup along the western flank of the Greenland ice sheet. *Science*, **320**(5877), 781–783.
Khan, S. A., Wahr, J., Stearns, L. A., Hamilton, G. S., van Dam, T., Larson, K. M., and Francis, O., 2007. Elastic uplift in southeast Greenland due to rapid ice mass loss. *Geophysical Research Letters*, **34**, L21701, doi:10.1029/2007GL031468.
King, M., 2004. Rigorous GPS data processing strategies for glaciological applications. *Journal of Glaciology*, **50**(171), 601–607.
King, M. A., Coleman, R., Morgan, P. J., and Hurd, R. S., 2007. Velocity change of the Amery Ice Shelf, East Antarctica, during the period 1968–1999. *Journal of Geophysical Research*, **112**, F01013, doi:10.1029/2006JF000609.
King, M. A., Watson, C. S., Penna, N. T., and Clarke, P. J., 2008. Subdaily signals in GPS observations and their effect at semiannual and annual periods. *Geophysical Research Letters*, **35**, L03302, doi:10.1029/2007GL032252.
King, M. A., Coleman, R., Freemantle, A., Fricker, H. A., Hurd, R. S., Legrésy, B., Padman, L., and Warner, R., 2009. A 4-decade record of elevation change of the Amery Ice Shelf. *East Antarctica. Journal of Geophysical Research*, **114**, F01010, doi:10.1029/2008JF001094.
Krabill, W. B., Thomas, R. H., Martin, C. F., Swift, R. N., and Frederick, E. B., 1995. Accuracy of airborne laser altimetry over the Greenland ice-sheet. *International Journal of Remote Sensing*, **16**(7), 1211–1222.
Legresy, B., Wendt, A., Tabacco, I., Remy, F., and Dietrich, R., 2004. Influence of tides and tidal current on Mertz Glacier, Antarctica. *Journal of Glaciology*, **50**(170), 427–435.
Milne, G. A., Davis, J. L., Mitrovica, J. X., Scherneck, H. G., Johansson, J. M., Vermeer, M., and Koivula, H., 2001. Space-geodetic constraints on glacial isostatic adjustment in Fennoscandia. *Science*, **291**(5512), 2381–2385.
Moller, D., and Ritter, B., 1988. Glacial geodetic contributions to the mass balance and dynamics of ice shelves. *Annals of Glaciology*, **11**, 89–94.
Phillips, H. A., Allison, I., Coleman, R., Hyland, G., Morgan, P. J., and Young, N. W., 1998. Comparison of ERS satellite radar altimeter heights using GPS-derived heights on the Amery Ice Shelf, East Antarctica. *Annals of Glaciology*, **27**, 19–24.
Riedel, B., Nixdorf, U., Heinert, M., Eckstaller, A., and Mayer, C., 1999. The response of the Ekstromisen (Antarctica) grounding zone to tidal forcing. *Annals of Glaciology*, **29**, 239–242.
van de Wal, R. S. W., Boot, W., van den Broeke, M. R., Smeets, C., Reijmer, C. H., Donker, J. J. A., and Oerlemans, J., 2008. Large and rapid melt-induced velocity changes in the ablation zone of the Greenland Ice Sheet. *Science*, **321**(5885), 111–113.
Vaughan, D., 1995. Tidal flexure at ice shelf margins. *Journal of Geophysical Research*, **100**(B4), 6213–6224.
Wendt, A., Dietrich, R., Wendt, J., Fritsche, M., Lukin, V., Yuskevich, A., Kokhanov, A., Senatorov, A., Shibuya, K., and Doi, K., 2005. The response of the subglacial Lake Vostok, Antarctica, to tidal and atmospheric pressure forcing. *Geophysical Journal International*, **161**(1), 41–49.
Zumberge, J. F., Heflin, M. B., Jefferson, D. C., Watkins, M. M., and Webb, F. H., 1997. Precise point positioning for the efficient and robust analysis of GPS data from large networks. *Journal of Geophysical Research*, **102**(B3), 5005–5017.

Cross-references

Dynamics of Glaciers
Formation and Deformation of Basal Ice
Glacier Motion/Ice Velocity
Glacioisostasy
Ice Sheet Mass Balance
Ice Shelf
LIDAR in Glaciology
Subglacial Lakes, Antarctic
Topographic Normalization of Multispectral Satellite Imagery

GRACE IN GLACIOLOGY

John Wahr
Department of Physics and CIRES, University of Colorado, Boulder, CO, USA

Definition

GRACE: The Gravity Recovery and Climate Experiment. A satellite mission launched in March, 2002 by NASA and the German Space Agency that maps out the Earth's global gravity field every month.

GIA: Glacial Isostatic Adjustment. The viscoelastic response of the Earth to past changes in ice mass; especially those associated with the disappearance of ice since the last glacial maximum, ~20,000 years ago.

Introduction

The long-term evolution of an ice sheet or glacier is largely determined by its mass balance: the difference between the mass added through precipitation, and the mass removed through, for example, sublimation, melting, and ice discharge into the ocean. But monitoring mass balance is not easy. Measurements of ice velocities, of changes in surface elevations, and of precipitation and other meteorological variables can all help. But they can provide only part of the mass balance picture, and must

ultimately be combined with models and assumptions of various types to obtain a complete estimate.

But there is now a satellite mission, called GRACE (The Gravity Recovery and Climate Experiment) that is capable of directly monitoring the total mass balance of the polar ice sheets and of large glacier systems, on a month-to-month basis. GRACE was launched in March, 2002 by NASA and DLR (the German Space Agency). As of this writing, the mission is expected to last through ~2014. Every month, GRACE provides a global map of the Earth's gravity field at scales of a few hundred kilometers and more. The gravity field changes from one month to the next because the Earth's mass distribution is constantly varying. The GRACE data allow users to learn about those mass variations and the processes that cause them. Results from GRACE have been used to study changes in the volume of groundwater stored in large aquifers, regional fluctuations in sea-floor pressure (sea-floor pressure is proportional to the amount of mass in the overlying ocean/atmosphere column), and glacial isostatic adjustment (GIA) in the Earth's interior (see below). But arguably, the most important results to come out of GRACE to-date have been estimates of mass loss from polar ice sheets and continental glacier systems.

Grace

GRACE consists of two satellites in identical near-polar orbits (89° inclination) about the Earth (an altitude of ~500 km), one satellite following the other at a distance of ~220 km (Tapley et al., 2004). As they orbit, they use microwaves to monitor their separation distance. That distance is constantly changing as they move through gravity highs and lows, and measurements of those changes can be used to determine the gravity field. Accelerometers on-board each spacecraft are used to detect nongravitational accelerations caused, for example, by atmospheric drag; and the results are used to remove those nongravitational effects from the satellite-to-satellite distance measurements before solving for the gravity field.

The monthly gravity solutions are typically represented as a set of spherical harmonic global expansion coefficients, determined by fitting to all the available GRACE data for that month. Those coefficients can be combined to obtain monthly estimates of mass variability averaged across specific regions of the Earth's surface, including over the ice sheets. Because the satellites are at 500 km altitude, they can provide accurate results only over regions with scales of a few hundred kilometers or greater. The resolution at higher latitudes is better than at lower latitudes, because the satellites' ground tracks are denser at high latitudes. The strengths of GRACE for mass recovery are that (1) it provides what are basically direct estimates of mass; no supplementary data or models are required (strictly speaking, GRACE measures gravity rather than mass, but mass variability can be inferred by a straightforward application of Newton's Law of Gravity); and (2) it inherently averages over an entire region; it does not miss small sub-regions, and does not require interpolation or extrapolation of point measurements. The weaknesses of GRACE are (1) it cannot resolve small-scale spatial variability; and (2) it has no vertical resolution. That is, a gravity signal across a region can be used to determine the total mass integrated vertically below that region; but it cannot determine the depth-dependence of that mass distribution. This latter point is important for the ice sheets, primarily because of the GIA process. At the last glacial maximum, some 20,000 years ago, large ice sheets covered northern Canada and Scandinavia, and the Greenland and Antarctic ice sheets were much larger than they are at present. That additional ice has since melted, but because the Earth is viscous it is still uplifting in response to the removal of that load. The resulting mass transport within the Earth's interior contributes to the mass estimate recovered by GRACE. And so, it is necessary to model and remove this GIA contribution before interpreting the GRACE results in terms of present-day ice sheet mass variability. The GIA signal appears as a linear trend, and so an error in the GIA model would cause secular errors in the apparent ice sheet mass.

A number of GRACE-based estimates of mass loss have been published for Antarctica (e.g., Velicogna and Wahr, 2006a; Chen et al., 2006a), Greenland (e.g., Luthcke et al., 2006; Chen et al., 2006b; Velicogna and Wahr, 2006b), and the Alaskan coastal glacier system (e.g., Tamisiea et al., 2005; Luthcke et al., 2008). Each of these published estimates shows significant mass loss, with the exact numerical values depending on the time span considered in the analysis. For instance, the mass loss rates for Antarctica and Greenland appear to have increased over the last few years; whereas the rate for the Alaskan coastal glaciers appears to have decreased. Figure 1 shows smoothed time series for the mass changes of Antarctica, Greenland, and coastal Alaskan glaciers as inferred from monthly GRACE gravity fields produced at the Center for Space Research at the University of Texas (results computed as described by Velicogna and Wahr, 2006a, b). Steady mass loss is apparent in the results for each region. To put these results in perspective, a 100 Gton mass loss causes a ~0.28 mm rise in global sea level.

The results shown in Figure 1 have been corrected for GIA, using model results based on the ICE-5G ice deglaciation history and VM2 viscosity profile of Peltier (2004). The Greenland and Alaskan results are not significantly changed by removing the GIA model. For example, applying the GIA correction has increased the Greenland mass loss estimate by only 5 Gton/year; an insignificant fraction of the Greenland trend evident in Figure 1. But the Antarctic numbers are critically dependent on the GIA correction. Applying the GIA correction has increased the mass loss estimate by an amount in excess of 180 Gtons/year, which is of the same order as the trend evident in the Antarctic figure. In fact, if no GIA correction had been made, the GRACE results would show virtually no trend at all. This implies that errors in the GIA model could have a significant impact on the

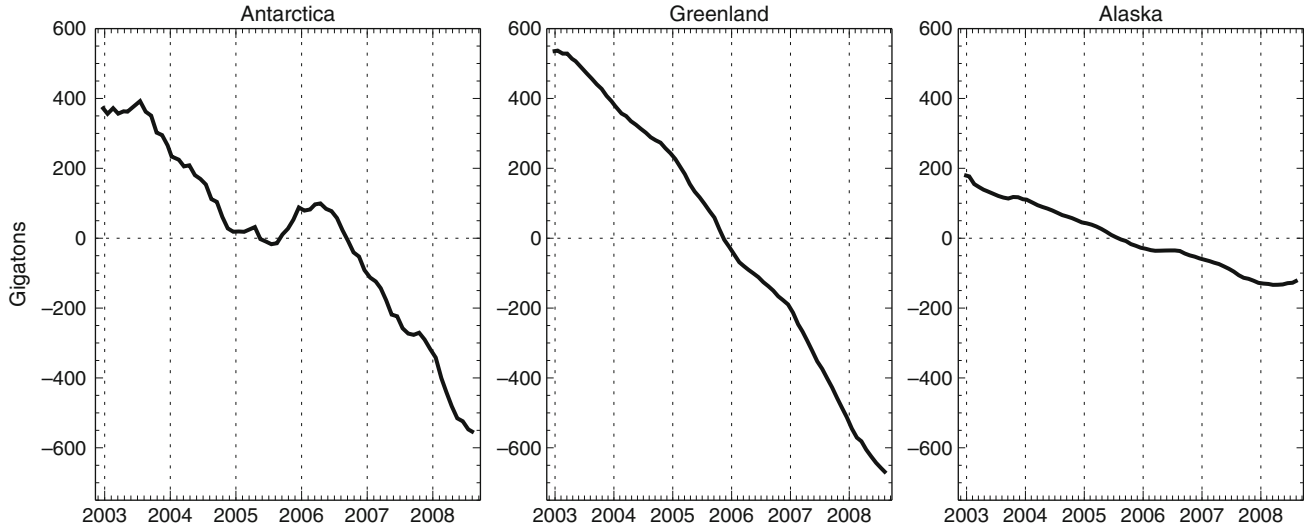

GRACE in Glaciology, Figure 1 Time series showing mass variability (in Gigatons) for the Antarctic and Greenland ice sheets, and for the coastal Alaskan glacier system, as inferred from monthly GRACE gravity fields produced by the Center for Space Research at the University of Texas. The method of analysis is as described in Velicogna and Wahr (2006a, b). Contributions from glacial isostatic adjustment, the ongoing viscoelastic response of the earth to the removal of ice loads after the last glacial maximum, have been removed using a model based on the ICE-5G ice deglaciation history (Peltier, 2004). The results shown in these figures have been smoothed to remove the seasonal cycle and other short-period variability. For reference, a 100 Gton mass loss causes a ∼0.28 mm rise in global sea level.

GRACE Antarctic estimates. GIA model results for different plausible viscosity profiles and for two Antarctic deglaciation histories (ICE-5G from Peltier, 2004; and IJ05 from Ivins and James, 2005) give GIA corrections for Antarctica that vary from 100 to 220 Gton/year, suggesting that until knowledge of the GIA process has improved, the uncertainty in GRACE Antarctic trends is on the order of ±60 Gton/year.

Summary

The recently launched GRACE satellite gravity mission is providing glaciologists with a powerful technique for estimating the mass balance of polar ice sheets and continental glacier systems. Results from GRACE show that the combined mass loss of Greenland, Antarctica, and the coastal Alaskan glacier system was probably in excess of 2,000 Gtons between 2003 and 2009.

Bibliography

Chen, J. L., Wilson, C. R., Blankenship, D. D., and Tapley, B. D., 2006a. Antarctic mass rates from GRACE. *Geophysical Research Letters*, **33**(11), L11502.

Chen, J. L., Wilson, C. R., and Tapley, B. D., 2006b. Satellite gravity measurements confirm accelerated melting of Greenland ice sheet. *Science*, **313**, 1958–1960.

Chen, J. L., Tapley, B. D., and Wilson, C. R., 2006c. Alaskan mountain glacial melting observed by satellite gravimetry. *Earth and Planetary Science Letters*, **248**(1–2), 368–378.

Ivins, E. R., and James, T. S., 2005. Antarctic glacial isostatic adjustment: a new assessment. *Antarctic Science*, **17**(4), 541–553.

Luthcke, S. B., Zwally, H. J., Abdalati, W., Rowlands, D. D., Ray, R. D., Nerem, R. S., Lemoine, F. G., McCarthy, J. J., and Chinn, D. S., 2006. Recent Greenland ice mass loss by drainage system from satellite gravity observations. *Science*, doi:10.1126/science.1130776.

Luthcke, S. B., Arendt, A. A., Rowlands, D. D., McCarthy, J. J., and Larson, C. F., 2008. Recent glacier mass changes in the Gulf of Alaska region from GRACE mascon solutions. *Journal of Glaciology*, **54**(188), 767–777.

Peltier, W. R., 2004. Global Glacial Isostasy and the Surface of the Ice-Age Earth: The ICE-5G(VM2) model and GRACE. *Annual Review of Earth and Planetary Sciences*, **32**, 111–149.

Tamisiea, M. E., Leuliette, E. W., Davis, J. L., and Mitrovica, J. X., 2005. Constraining hydrological and cryospheric mass flux in southeastern Alaska using space-based gravity measurements. *Geophysical Research Letters*, **32**, L20501.

Tapley, B. D., Bettadpur, S., Watkins, M., and Reigber, C., 2004. The gravity recovery and climate experiment: Mission overview and early results. *Geophysical Research Letters*, **31**(9), L09607.

Velicogna, I., and Wahr, J., 2006a. Measurements of time variable gravity shows mass loss in Antarctica. *Science*, **311**, 1754–1756.

Velicogna, I., and Wahr, J., 2006b. Significant acceleration of Greenland ice mass loss in spring, 2004. *Nature*, doi:10.1038/nature05168.

Cross-references

Alaskan Glaciers
Antarctica
Greenland Glaciers Outside the Ice Sheet
Greenland Ice Sheet
Ice Sheet Mass Balance
ICESat Data in Glaciological Studies
Optical Remote Sensing of Alpine Glaciers
Sea-Level

GRANULOMETRY

Amit Kumar
Department of Geology, Centre of Advanced Study in Geology, Panjab University, Chandigarh, India

It is defined as the measurement of sediment grain size in a granular material as a proportion by weight of particles of different sizes. Granulometric analysis involves the sieving of material and subsequent weighing of individual fractions as combined into mainly three groups. The smallest fraction, clay, has a diameter of less than 75 μm. The sand fraction contains all grains with diameters between 75 μm and 2 mm, and the gravel fraction consists of all grains with a diameter greater than 2mm. It should be noted that the names of these three groups do not correspond with the international geological classification of unconsolidated sediments, which includes all particles with diameters up to 200 μm in the clay fraction.

The grain size is only one of several parameters used to classify unconsolidated sediments. Methodology by Folk and Ward (1957) is mostly used for granulometry study. Parameters such as mean, standard deviation, skewness, and kurtosis are calculated for the sediment samples.

Bibliography

Bates, R. L., and Jackson, J. A., 1987. *Glossary of Geology*. Alexandria, VA: American Geological Institute.
Folk, R. L., and Ward, W. C., 1957. Brazos river bar: A study in the significance of grain size parameters. *Journal of Sedimentary Petrology*, **27**, 3–27.
Krinsley, D. H., and Takahashi, T., 1978. Sand surface textures. In Fairbridge, R. W., and Bourgeois, J. (eds.), *Encyclopedia of sedimentology*. Stroudsberg: Dowden.

GRAVEL SHEET

Amit Kumar
Department of Geology, Centre of Advanced Study in Geology, Panjab University, Chandigarh, India

Gravel sheets deposits are the Pleistocene meltwater deposits that originated during the Quaternary period (1.8 million years). Except of the erosion, transportation, and deposition by glaciers, glaciers lose ice to melting at lower reaches and produce meltwater, which becomes an important component of the glacial system. Meltwater produces several distinctive landforms and sediments from boulder to clay sizes. These widespread deposits of silt and sand and material were subsequently either scoured out by the advancing ice or covered with gravels. Usually gravel sheet covers a large extent of area to define it as sheet.

Bibliography

Benn, D. I., and David, J. A. E., 1998. *Glaciers and Glaciation*. London: Arnold.
Hambrey, M., and Jürg, A., 2004. *Glaciers*, 2nd edn. Cambridge: Cambridge University Press.

GRAVITATIONAL MASS MOVEMENT DEPOSITS

D. P. Dobhal
Wadia Institute of Himalayan Geology, Dehradun, Uttarakhand, India

"Gravitational mass movement" is a geologic term that encompasses the rapid downhill movement of rocks and fine particles due to the force of gravity. One of the most common and generic types of mass movement features on Earth are landslides, but there are many others such as rock falls, debris flows, soil creep, and snow/ice avalanches. The topographic factor such slope and type of terrain play a vital role in gravitational mass movement deposits.

GRAVITY FLOW (MASS FLOW)

Rajesh Kumar
Remote Sensing Division, Birla Institute of Technology, Extension Centre Jaipur, Jaipur, Rajasthan, India

The original form of Bernoulli's equation valid at any point along a streamline flow is

$$\frac{v^2}{2} + gz + \frac{p}{\rho} = \text{Constant}$$

v is the fluid flow speed at a point on streamline.
g is the acceleration due to gravity.
z is the elevation of the point above a reference plan, with the positive Z direction upward.
p is the pressure at the point.
ρ is the density of fluid at all points in the fluid.

If the pressure term is omitted from the above equation, it shows a balance between the velocity and gravity force and such type of flows are termed as gravity flow.

Hence, any material that flows due to the forces of gravity alone and not to an applied pressure will be under the gravity flow. A glacier flow also obeys this principle as the glacier is an accumulation of ice, air, water, and rock debris or sediment in a terrain of differential slope or the slope is created by the differential accumulation of ice mass over a region. Once the mass of compressed ice reaches a critical thickness, it becomes so heavy that it begins to deform and move downward. The sheer restraint of the ice, combined with gravity's influence, causes glaciers to flow downward very slowly due to its extraordinary weight.

GRAY-WHITE ICE

Chelamallu Hariprasad
Centre for Studies in Resource Engineering, IITB, Powai, Mumbai, India

Gray-white ice is a category of young ice (15–30 m thick). Young ice is an ice in the transition stage between nilas and first-year ice. The depth of the young ice varies between 10 and 30 cm. Based on its color, young ice classifies into two types namely, gray ice and gray-white ice (Figure 1).

GREENLAND GLACIERS OUTSIDE THE ICE SHEET

Jacob C. Yde
Center for Geomicrobiology, University of Aarhus, Aarhus C, Denmark

Synonyms

Local glaciers

Definition

Greenland Ice Sheet. The continental ice sheet occupying the central area of Greenland. It is often referred to as the Inland Ice or abbreviated as GIS.
Local glaciers. A term used to address all peripheral glaciers outside a continental ice sheet. In the context of Greenland, the term covers all glaciers in Greenland except the Greenland Ice Sheet.

Introduction

The local glaciers in Greenland can easily be overlooked in the presence of the vast Greenland Ice Sheet (GIS) (see entry *Greenland Ice Sheet*). This is probably the main reason why relatively limited research has been conducted on these glaciers; despite they cover about 5–10% of the total ice cap and minor glacier area of the world (Weidick and Morris, 1998). Another reason for the lack of research may be the remoteness of many local glaciers, which can be logistically and economically challenging for small research operations.

Gray-White Ice, Figure 1 Thingray-white ice showing the effects of ridging and rafting. (Photo courtesy of the Antarctic Sea-Ice Processes and Climate program (ASPeCt).)

The definition of a local glacier is not equivocal because some local glaciers merge with an ice sheet along a large distance of their margins and their ice dynamics may be strongly dependent on the ice dynamics of the adjacent ice sheet. According to Weidick and Morris (1998), three types of local glaciers can be identified: (1) local coastal glaciers, which exist independent from GIS or merge with GIS along a short distance up to about 50 km; (2) local fringing glaciers, which largely merge with GIS along a considerable distance; and (3) local glaciers within the ice sheet zone (e.g., marginal ice domes or glaciers on nunataks). Type 1 local glaciers are traditionally considered as "true" local glaciers, whereas Type 2 and 3 local glaciers often are formed as a consequence of ice thinning and deglaciation along the ice sheet margins. This gradual transition from being part of the ice sheet to become a local glacier is most obvious in East Greenland (termed the Blosseville Ice Cap) and Southeast Greenland (termed the Ammassalik Ice Cap) (Weidick and Morris, 1998). Attempts to delineate these transitional types are still lacking, and these local glaciers are therefore generally included in the GIS.

Very little is known about the number, size, and volume of the local glaciers. Estimations of the area covered by local glaciers range from 48,599 km^2 (Weng, 1995) to 76,000 km^2 (Holtzscherer and Bauer, 1954), but these figures must be considered as minimums as they are based on large-scale mapping and omit most minor glaciers and ice caps that merge with the GIS. Higher and more speculative estimates up to 163,200 km^2 have been presented by Sharp (1956) and references herein.

The most detailed glacier inventory (Weidick et al., 1992) covers the area from Kap Farvel (South Greenland) to Nuussuaq Peninsula (West Greenland) and comprises about 5,000 local glaciers (14,574 km^2). It is primarily based upon relatively old aerial photographs from between 1948 and 1964, and the local glaciers are classified according to a glacier identification code (Müller et al., 1977) based upon a hydrological basin code (Weidick and Olesen, 1980). The identification code system has been extended to cover parts of North Greenland (Weidick, 2001). Although not yet fully implemented to cover the entire Greenland, this glacier identification system provides very useful references as only a small proportion of the local glaciers have been given official names. However, due to the general glacier recession throughout the twentieth century some tributary glaciers have separated from their main glacier, while other glaciers have relocated their drainage routing to neighboring hydrological basins, causing discrepancies to the original inventory system.

The research on local glaciers in Greenland has generally focused on: (1) Pleistocene and Holocene glacier fluctuations, (2) mass balance and glacier velocity, (3) glacier surging, and (4) glacier hydrology and hydrochemistry.

Glacier distribution

Local glaciers occur in all regions surrounding the GIS, and they exist in all glacier morphological types from ice caps to glacierets and snow fields. Here follows an overview of local glacier extent in different regions of Greenland (Figure 1).

South Greenland

The landscape in South Greenland is alpine and constitutes of many islands and cross-cutting fjords. The second-largest ice cap in Greenland, Julianehåb Ice Cap (6,500 km^2), is confluent with the southern part of the GIS. The delineation between Julianehåb Ice Cap and the GIS is generally defined by the ice stream Qorqup Sermia draining westward and an ice stream draining eastward to the fjord Anoritup Kangerlua. Along the western and southern part of Julianehåb Ice Cap many minor ice caps, valley glaciers, and cirque glaciers exist, and especially the peninsula between Lindenows Fjord (Kangerlussuatsiaq) and Prins Christian Sund (Ikerasassuaq) is heavily glacierized.

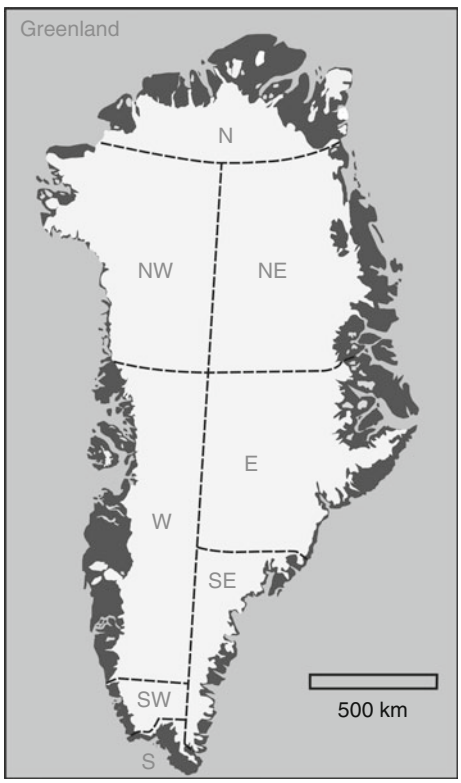

Greenland Glaciers Outside the Ice Sheet, Figure 1 Map showing the regions of Greenland.

Southwest Greenland

Cirque glaciers and glacierets occur on the highest mountains in the southern part of Southwest Greenland and in the alpine region between the GIS outlet glaciers Sermiligarssuk Bræ and Sermilik Bræ (Ukassorssuaq Sermia).

West Greenland

In southern West Greenland, there are primarily three glacierized regions: (1) the alpine region between Frederikshåb Isblink and Godthåbsfjorden containing ice caps such as Isortuarssuk Ice Cap (177 km^2) and Sermilik Ice Cap (117 km^2) and many valley and cirque glaciers (Figure 2); (2) the high plateau region between the village Kangamiut and the GIS, which comprises ice caps such as Qarajugtoq Ice Cap (2,010 km^2; Figure 3), Sukkertoppen Ice Cap (1,983 km^2), Perserajoq Ice Cap (692 km^2), Amitsuloq Ice Cap (193 km^2), and Qapiarfiup Sermia Ice Cap (116 km^2); and (3) the coastal alpine region near the fjord Nordre Isortoq. Along a 430 km section from Amitsuloq Ice Cap to Nuussuaq Peninsula, there are no local glaciers close to the GIS. In central West Greenland, Disko Island is 19% glacierized and contains about 1,070 glaciers and snow fields including Sermersuaq Ice Cap (918 km^2) and Bræpasset Ice Cap (254 km^2). On Nuussuaq Peninsula, there are about 600 glaciers and snow fields including Makitarigssagaq Ice Cap (379 km^2) and Qilertinguit Ice Cap (116 km^2). Further north, alpine islands and peninsulas such as Upernavik Ø and Svartenhuk Peninsula are relatively heavily glacierized with minor ice caps, valley glaciers, and cirque glaciers.

Northwest Greenland

Along the coast from Svartenhuk Peninsula to Melville Bugt, only a narrow fringe of land is ice-free. Minor ice caps, valley glaciers, and cirque glaciers occur on the larger islands and peninsulas. The area from Melville Bugt to Humboldt Gletscher is characterized by several ice caps.

North Greenland

This dry, sparsely vegetated plateau landscape features many ice caps such as Flade Isblink (c. 9,000 km^2) and Hans Tausen Ice Cap (4,208 km^2). The northernmost area, Johannes V. Jensen Land, has a more alpine landscape with valley glaciers and cirque glaciers.

Northeast Greenland

The low coastal plains are mainly ice-free (e.g., on Shannon Island and Hochstetters Forland). Further inland the landscape becomes alpine with outlet glaciers from ice caps and valley glaciers terminating in generally ice-free U-shaped valleys.

Greenland Glaciers Outside the Ice Sheet, Figure 2 Degrading cirque glaciers near Nuuk, southern West Greenland (photo: Jacob Yde, August 2008).

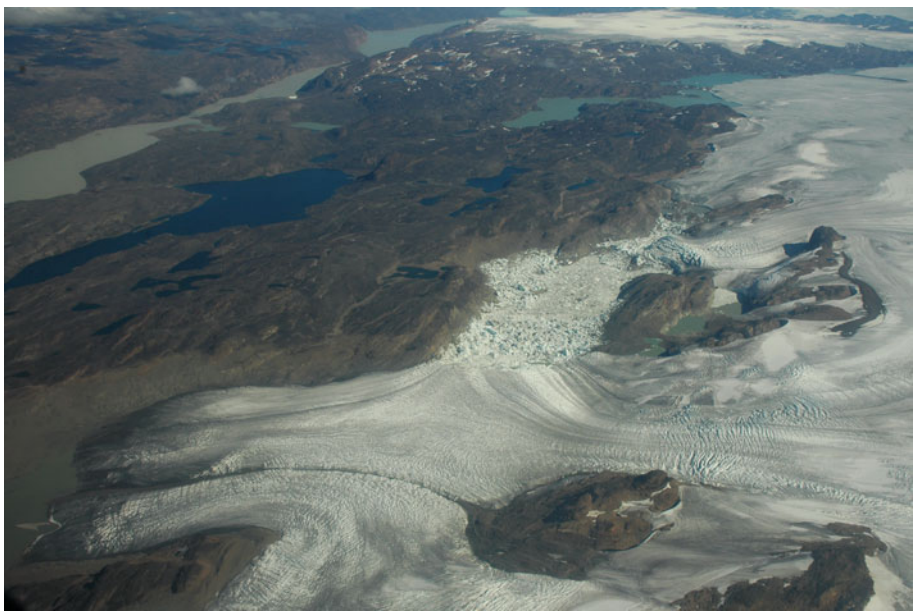

Greenland Glaciers Outside the Ice Sheet, Figure 3 Outlet glaciers descending from the northern margin of Qarajugtoq Ice Cap, West Greenland, looking east. A recent jökulhlaup from an ice-dammed lake (*c.* 6 km^2) caused calving by pressure-release and distribution of ice blocks over the lake floor (see entry *Glacier Lake Outburst Floods*). Amitsuloq Ice Cap is seen in the background, and Lake Tasersiaq, the largest lake in Greenland, is seen in the *upper left corner* (photo: Jacob Yde, August 2008).

East Greenland

In central East Greenland, north of Scoresby Sund, the alpine landscapes on Liverpool Land and Stauning Alper are characterized by valley glaciers and minor ice caps, whereas the intervening terrain on Jameson Land is mainly deglaciated. Closer to the GIS major ice caps dominate Nathorsts Land, Renland, Milne Land, and Gåseland, and adjacent to the GIS other ice caps merge with the GIS. South of Scoresby Sund the ice-free area is restricted to nunataks and both GIS outlet glaciers and

Greenland Glaciers Outside the Ice Sheet, Figure 4 Characteristic landscape along the Blosseville Coast, East Greenland, with large tidewater outlet glaciers receiving ice from ice-filled valleys (photo: Jacob Yde, July 2008).

local glaciers calve into the sea and fjords (Figure 4). The distinction between the GIS and confluent local ice caps is transitional and difficult to delineate (Weidick et al., 1992).

Southeast Greenland

North of the Sermilik Fjord the landscape consists of ice-filled valleys separated by mountain ridges with tributary cirque glaciers. On Ammassalik Island and nearby coastal islands minor ice caps and cirque glaciers dominate. Further south the landscape is characterized by fjords with calving glaciers emanating from the GIS and the eastern sector of Julianehåb Ice Cap and intervening glacierized peninsulas and islands.

Glacier fluctuations and mass balances

As argued by Weidick (1985), the Late Pleistocene and Early Holocene history of glacier variations in Greenland is nearly identical to our current knowledge of the deglaciation of the GIS margins. There is only sporadic information on deglaciation and rebuilding of coastal local glaciers and on detachment from and re-coupling to the GIS of local glaciers (see review by Kelly and Lowell, 2009). Radiocarbon datings from ice caps such as Hans Tausen Ice Cap, North Greenland (Landvik et al., 2001), and Mittivakkat Gletscher, Southeast Greenland (Figure 5; Knudsen et al., 2008), indicate that many local glaciers disappeared during the Holocene Climatic Optimum (8,500–6,000 BP), reformed as the temperature gradually declined and reached their Holocene maximum extent at the end of the Little Ice Age (1150–1920 AD).

Observations and measurements of glacier velocities and frontal fluctuations received significant attention in the pioneering years of systematic glaciological research on local glaciers. The most detailed information is from outlet glaciers descending from Lyngmarksbræ Ice Cap, Disko Island (e.g., Chamberlin, 1894; Steenstrup, 1901), and reports on local glacier fluctuations from other parts of Greenland are abundant (see review by Weidick, 1968).

Mass balance measurements based on stake networks and snow accumulation probing are scarce in Greenland and generally restricted to cover short periods (Weidick, 1984a). The longest record is from Mittivakkat Gletscher (formerly Mitdluagkat Gletscher), Southeast Greenland, where mass balance measurements have been conducted in 1986/1987 and from 1995/1996 onwards (Hasholt, 1988; Knudsen and Hasholt, 2004). Except for 1995/1996 (equilibrium) and 2002/2003 (positive mass balance), the annual net balance has been negative (N. Tvis Knudsen, pers. comm. 2009). Short-term mass balance records obtained at other local glaciers show both positive and negative mass balances for Qapiarfiup Sermia and Amitsuloq Ice Cap, West Greenland, during the period 1981–1985 (Olesen, 1986), and a slightly negative trend in 1994/1995 for Hare Glacier, an outlet glacier from Hans Tausen Ice Cap, North Greenland (Reeh et al., 2001).

Surge-type glaciers

In Greenland, there are two recognized surge clusters (see entry *Glacier Surging*), the Disko-Nuussuaq surge cluster (Weidick, 1988; Yde and Knudsen, 2007, 2009) and the

Greenland Glaciers Outside the Ice Sheet, Figure 5 Mittivakkat Gletscher, Southeast Greenland, is the most examined local glacier in Greenland. It has experienced recession since the end of the Little Ice Cap (photo: Jacob Yde, August 2007).

East Greenland surge cluster (Weidick, 1988; Jiskoot et al., 2003). In addition, confirmed or indicative surge activity has been reported from tidewater-terminating outlet glaciers from the GIS such as Harald Moltke Bræ, Northwest Greenland (Mock, 1966; Rignot and Kanagaratnam, 2006); Brikkerne Gletscher and Ryder Gletscher, North Greenland (Higgins and Weidick, 1988; Joughin et al., 1996); Storstrømmen, Northeast Greenland (Reeh et al., 1994); and Eqalorutsit Kitdlît Sermiat, South Greenland (Weidick, 1984b). Surge activity in Greenland is characterized by some of the longest frontal advances even recorded (about 10 km) and relatively long surge periodicities (i.e. the time interval between active surge events) compared to other surge clusters in the world (at least 100 years). There are indications of a decline in the frequency in surge events throughout since the termination of the LIA. Both Greenlandic surge clusters are primarily located in Tertiary basalt provinces with widespread occurrence of homothermal springs, indicating that the geothermal heat flux may be enhanced in these regions.

The Disko-Nuussuaq surge cluster comprises an estimated number of 75 surge-type glaciers on Disko Island (Yde and Knudsen, 2007, 2009) and two surge-type glaciers on Nuussuaq Peninsula (Weidick, 1988). In addition, there are signs of surge activity on at least two glaciers on Svartenhuk Peninsula (Yde, unpublished data). Most research has been focused on the 1995–1998 surge event of Kuannersuit Glacier, central Disko Island, which advanced 10.5 km down-valley with a maximum velocity of at least 70 m/day (Gilbert et al., 2002; Yde and Knudsen, 2005a; Yde et al., 2005a; Roberts et al., 2009).

The estimated number of surge-type glaciers included in the East Greenland surge cluster range from 71 (Jiskoot et al., 2003) to about 200 (Weidick, 2000). Particular in the Stauning Alper, surge-type glaciers are very common and include glaciers such as Løberen, Bjørnbo Gletscher, Roslin Gletscher, Schuchert Gletscher, Sirius Gletscher, and Østre Gletscher. On the Blosseville Kyst, the best-documented surge event is the 1992–1995 surge of Sortebræ, which advanced 10 km (e.g., Jiskoot et al., 2001; Murray et al., 2002).

Glacier hydrology and hydrochemistry

Measurements of runoff, sediment, and solute transport from local glaciers in Greenland are relatively sporadic (see entries *Glacier Hydrology*; *Sediment Yield* and *Solute in Glacial Meltwaters*).

The most intensive studies on glacier hydrology and suspended sediment transport are from the forefield of Mittivakkat Gletscher. In this coastal granitic-gneissic catchment, frequent runoff measurements have been conducted since 1958 (Larsen, 1959) and combined with sediment sampling, indicating a specific transport rate of about 1,000 $t\,km^{-2}\ year^{-1}$ (e.g., Hasholt, 1976). The solute yield has been estimated to 18 $t\,km^{-2}\ year^{-1}$ (Yde, unpublished data) and 32 $t\,km^{-2}\ year^{-1}$ (Hagedorn and Hasholt, 2004).

At the surge-type glacier Skelbræ, East Greenland, large irregular fluctuations in runoff have been related to precipitation events and ice-block damming events

(Stott and Grove, 2001). The suspended sediment yield has been estimated to 732 t km^{-2} year^{-1}.

At Zackenberg, Northeast Greenland, runoff, sediment, and solute monitoring has been conducted since 1996–1997 (Rasch et al., 2000). The distance from the hydrometric station to the local glaciers in A. P. Olsen Land is more than 30 km, suggesting that the periglacial area has a significant influence on water quality. The suspended sediment yield varies between 29 and 255 t km^{-2} year^{-1}, whereas the solute yield ranged between 5 and 22 t km^{-2} year^{-1} (Hasholt et al., 2008).

The 1995–1998 surge event of Kuannersuit Glacier, Disko Island, West Greenland, caused evacuation of extreme amounts of sediment from the overridden area. The sediment yield in 1999 has been estimated to 49,100 t km^{-2} year^{-1}, and it gradually decreased to about 7,700–13,400 t km^{-2} year^{-1} in 2001 (Knudsen et al., 2007). The solute yield and atmospheric CO_2 drawdown in 2001 was 76–98 t km^{-2} year^{-1} and 8,500–13,700 kg C km^{-2} year^{-1} (Yde et al., 2005b). Surge events on Disko Island have been related to the formation and occurrence of glacier-derived naled assemblages (Yde and Knudsen, 2005b).

In front of Kitdlerssuaq Gletscher, an outlet glacier from Amitsuloq Ice Cap, West Greenland, water level and conductivity measurements were conducted in 1982, showing that conductivity varied inversely with water level and ablation (Andreasen, 1984).

Summary

The local glaciers surrounding the GIS constitute a significant proportion (5–10%) of the global ice masses besides ice sheets. Nevertheless, they have not yet received much attention. The actual size of local glaciers in Greenland is difficult to determine because there is a gradual transition from dynamically dependence to independence from the GIS. This interrelationship along parts of the GIS margin may have fluctuated throughout the Holocene. Many coastal local glaciers diminished or disappeared during the Holocene Climatic Optimum (8,500–6,000 BP) and reformed to have a maximal Holocene extent at the end of the Little Ice Age (1150–1920 AD). Current mass balance measurements are in concordance with the global negative trend. Two areas with widespread surge activity exist in Greenland: the East Greenland surge cluster and the Disko-Nuussuaq surge cluster. Both clusters are mainly located on Tertiary basaltic rocks and have surge cycle periodicity of more than 100 years. The contribution from local Greenlandic glaciers to global sea-level rise derives mainly from meltwater runoff rather than marine calving, but a total contribution has not been thoroughly estimated due to the problems with the definition of local glaciers. The specific contribution of suspended sediments and solutes from glacierized areas is highest from the basaltic regions in West and East Greenland.

Bibliography

Andreasen, J.-O., 1984. Glacier meltwater chemistry at two subpolar glaciers in West Greenland. *Rapport. Grønlands Geologiske Undersøgelse*, **120**, 105–108.

Chamberlin, T. C., 1894. Glacial studies in Greenland II. *Journal of Geology*, **2**(8), 768–788.

Gilbert, R., Nielsen, N., Möller, H., Desloges, J. R., and Rasch, M., 2002. Glacimarine sedimentation in Kangerdluk (Disko Fjord), West Greenland, in response to a surging glacier. *Marine Geology*, **191**, 1–18.

Hagedorn, B., and Hasholt, B., 2004. Hydrology, geochemistry and Sr isotopes in solids and solutes of the meltwater from Mittivakkat Gletscher, SE Greenland. *Nordic Hydrology*, **35**, 369–380.

Hasholt, B., 1976. Hydrology and transport of material in the Sermilik area 1972. *Geografisk Tidsskrift*, **75**, 30–39.

Hasholt, B., 1988. Massbalance studies of the Mitdluagkat glacier, eastern Greenland. *Geografisk Tidsskrift*, **88**, 82–85.

Hasholt, B., Mernild, S. H., Sigsgaard, C., Elberling, B., Petersen, D., Jakobsen, B. H., Hansen, B. U., Hinkler, J., and Søgaard, H., 2008. Hydrology and transport of sediment and solutes at Zackenberg. *Advances in Ecological Research*, **40**, 197–221.

Higgins, A. K., and Weidick, A., 1988. The world northernmost surging glacier? *Zeitschrift für Gletscherkunde und Glazialgeologie*, **24**, 111–123.

Holtzscherer, J.-J., and Bauer, A., 1954. *Contribution à la Connaissance de l'Inlandsis du Groenland*. Paris: IAHS Publications 39, pp. 244–296.

Jiskoot, H., Pedersen, A. K., and Murray, T., 2001. Multi-model photogrammetric analysis of the 1990 s surge of Sortebræ, East Greenland. *Journal of Glaciology*, **47**(159), 677–687.

Jiskoot, H., Murray, T., and Luckman, A., 2003. Surge potential and drainage-basin characteristics in East Greenland. *Annals of Glaciology*, **36**, 142–148.

Joughin, I., Tulaczyk, S., Fahnestock, M., and Kwok, R., 1996. A mini-surge on the Ryder glacier, Greenland, observed by satellite radar interferometry. *Science*, **274**, 228–230.

Kelly, M. A., and Lowell, T. V., 2009. Fluctuations of local glaciers in Greenland during latest Pleistocene and Holocene time. *Quaternary Science Reviews*, **28**, 2088–2106.

Knudsen, N. T., and Hasholt, B., 2004. Mass balance observations at Mittivakkat Gletscher, southeast Greenland 1995–2002. *Nordic Hydrology*, **35**(4–5), 381–390.

Knudsen, N. T., Yde, J. C., and Gasser, G., 2007. Suspended sediment transport in glacial meltwater during the initial quiescent phase after a major surge event at Kuannersuit glacier, Greenland. *Danish Journal of Geography*, **107**, 1–7.

Knudsen, N. T., Nørnberg, P., Yde, J. C., Hasholt, B., and Heinemeier, J., 2008. Recent marginal changes of the Mittivakkat glacier, southeast Greenland and the discovery of remains of reindeer (Rangifer tarandus), polar bear (Ursus maritimus) and peaty material. *Danish Journal of Geography*, **108**, 141–146.

Landvik, J. Y., Weidick, A., and Hansen, A., 2001. The glacial history of the Hans Tausen Iskappe and the last glaciation of Peary Land, North Greenland. *Meddelelser om Gronland. Geoscience*, **39**, 27–44.

Larsen, H. V., 1959. Runoff studies from the Mitdluagkat Gletscher in SE-Greenland during the late summer 1958. *Geografisk Tidsskrift*, **58**, 54–65.

Mock, S. J., 1966. Fluctuations of the terminus of the Harald Moltke Bræ, Greenland. *Journal of Glaciology*, **6**(45), 369–373.

Müller, F., Caflisch, T., and Müller, G., 1977. *Instructions for Compilation and Assemblage of Data for a World Glacier Inventory: Temporary Technical Secretariat for World Glacier*

Inventory. Zürich: International Commission on Snow and Ice, Swiss Federal Institute of Technology (ETH), p. 28.
Murray, T., Strozzi, T., Luckman, A., Pritchard, H., and Jiskoot, H., 2002. Ice dynamics during a surge of Sortebræ, East Greenland. *Annals of Glaciology*, **34**, 323–329.
Olesen, O. B., 1986. Fourth year of glaciological field work at Tasersiaq and Qapiarfiup Sermia, West Greenland. *Rapport. Grønlands Geologiske Undersøgelse*, **130**, 121–126.
Rasch, M., Elberling, B., Jakobsen, B. H., and Hasholt, B., 2000. High-resolution measurements of water discharge, sediment, and solute transport in the river Zackenbergelven, Northeast Greenland. *Arctic, Antarctic, and Alpine Research*, **32**, 336–345.
Reeh, N., Bøggild, C. E., and Oerter, H., 1994. Surge of Storstrømmen, a large outlet glacier from the Inland Ice of North-East Greenland. *Rapport. Grønlands Geologiske Undersøgelse*, **162**, 201–209.
Reeh, N., Olesen, O. B., Thomsen, H. H., Starzer, W., and Bøggild, C. E., 2001. Mass balance parameterisation for Hans Tausen Iskappe, Peary Land, North Greenland. *Meddelelser om Gronland. Geoscience*, **39**, 57–69.
Rignot, E., and Kanagaratnam, P., 2006. Changes in the velocity structure of the Greenland ice sheet. *Science*, **311**, 986–990.
Roberts, D. H., Yde, J. C., Knudsen, N. T., Long, A. J., and Lloyd, J. M., 2009. Ice marginal dynamics and sediment delivery mechanisms during surge activity, Kuannersuit glacier, Disko island, West Greenland. *Quaternary Science Reviews*, **28**, 209–222.
Sharp, R., 1956. Glaciers in the Arctic. *Arctic*, **9**, 78–117.
Steenstrup, K. J. V., 1901. Beretning om en undersøgelsesrejse til øen Disko i sommeren 1898. *Meddelelser om Grønland*, **24**, 249–306 [in Danish].
Stott, T. A., and Grove, J. R., 2001. Short-term discharge and suspended sediment fluctuations in the proglacial Skeldal river, North-East Greenland. *Hydrological Processes*, **15**, 407–423.
Weidick, A., 1968. Observations on some Holocene glacier fluctuations in West Greenland. *Meddelelser om Grønland*, **165**(6), 192.
Weidick, A., 1984a. Studies of glacier behaviour and glacier mass balance in Greenland – a review. *Geografiska Annaler*, **66A**, 183–195.
Weidick, A., 1984b. Location of two glacier surges in West Greenland. *Rapport. Grønlands Geologiske Undersøgelse*, **120**, 100–104.
Weidick, A., 1985. Review of glacier changes in West Greenland. *Zeitschrift für Gletscherkunde und Glazialgeologie*, **21**, 301–309.
Weidick, A., 1988. Surging glaciers in Greenland – a status. *Rapport. Grønlands Geologiske Undersøgelse*, **140**, 106–110.
Weidick, A., 2000. Det Østgrønlandske højland og dets isdækker. In Jakobsen, B. H., Böcher, J., Nielsen, N., Guttesen, R., Humlum, O., and Jensen, E. (eds.), *Topografisk Atlas Grønland*. Copenhagen: C. A. Reitzels Forlag, pp. 84–87 [in Danish].
Weidick, A., 2001. Neoglacial glaciations around Hans Tausen Iskappe, Peary Land, North Greenland. *Meddelelser om Gronland. Geoscience*, **39**, 5–26.
Weidick, A., and Morris, E., 1998. Local glaciers surrounding the continental ice sheets. In Haeberli, W., Hoelzle, M., and Suter, S. (eds.), *Into the Second Century of World Glacier Monitoring – Prospects and Strategies*. Paris: UNESCO. UNESCO Studies and Reports in Hydrology, 56, pp. 167–176.
Weidick, A., and Olesen, O. B., 1980. Hydrological basins in West Greenland. *Rapport. Grønlands Geologiske Undersøgelse*, **94**, 51.
Weidick, A., Bøggild, C. E., and Knudsen, N. T., 1992. Glacier inventory and atlas of West Greenland. *Rapport. Grønlands Geologiske Undersøgelse*, **158**, 194.
Weng, W. L., 1995. Letter to the editor. *Arctic*, **40**, 206.
Yde, J. C., and Knudsen, N. T., 2005a. Glaciological features in the initial quiescent phase of Kuannersuit glacier, Greenland. *Geografiska Annaler*, **87A**, 473–485.
Yde, J. C., and Knudsen, N. T., 2005b. Observations of debris-rich naled associated with a major glacier surge event, Disko island, West Greenland. *Permafrost and Periglacial Processes*, **16**, 319–325.
Yde, J. C., and Knudsen, N. T., 2007. 20th-century glacier fluctuations on Disko island (Qeqertarsuaq), Greenland. *Annals of Glaciology*, **46**, 209–214.
Yde, J. C., and Knudsen, N. T., 2009. Surge-type glaciers on Disko island, Greenland. In Krugger, M. I., and Stern, H. P. (eds.), *New Permafrost and Glacier Research*. New York: Nova Science, pp. 283–297.
Yde, J. C., Knudsen, N. T., Larsen, N. K., Kronborg, C., Nielsen, O. B., Heinemeier, J., and Olsen, J., 2005a. The presence of thrust-block naled after a major surge event: Kuannersuit glacier, West Greenland. *Annals of Glaciology*, **42**, 145–150.
Yde, J. C., Knudsen, N. T., and Nielsen, O. B., 2005b. Glacier hydrochemistry, solute provenance, and chemical denudation at a surge-type glacier in Kuannersuit Kuussuat, Disko island, West Greenland. *Journal of Hydrology*, **300**, 172–187.

Cross-references

Calving Glaciers
Cirque Glaciers
Dynamics of Glaciers
Fjords
Glacier Hydrology
Glacier Surging
Greenland Glaciers Outside the Ice Sheet
Greenland Ice Sheet
Holocene Glacier Fluctuations
Ice Caps
Outlet Glacier
Retreat/Advance of Glaciers
Sediment Yield
Solute in Glacial Meltwaters

GREENLAND ICE SHEET

Poul Christoffersen
Scott Polar Research Institute, University of Cambridge, Cambridge, UK

Synonyms

Greenland ice cap

Introduction

The Greenland Ice Sheet covers 80% of the Greenland land surface area of 2.2 million km^2. The volume of ice in the ice sheet is 2.8 million km^3. The geographical position of the ice sheet ranges from 59° to 83° North and from 73° to 110° West. Each year, snow accumulation provides the equivalent of 680 km^3 of ice and if the ice sheet was in a steady state it would lose the same amount by surface meltwater runoff and iceberg discharge.

The Greenland Ice Sheet is thought to have formed approximately 3 million years ago when glaciations in the northern hemisphere became extensive. The cause of

Northern hemisphere glaciations is not fully established. It is possible that tectonic processes such as the uplift of Tibet and closure of the Panama sea way caused global cooling (e.g., Haug and Tiedemann, 1998), but Earth system modeling shows that a decline in atmospheric carbon dioxide could have triggered the most recent era of glaciations in Greenland (Lunt et al., 2008).

Ice cores and paleoclimate

Paleo-environmental records of a very high quality have been established from ice cores drilled on the Greenland Ice Sheet (Andersen et al., 2004; Dansgaard et al., 1993; Grootes et al., 1993). These records are established from the composition of stable isotopes and various types of gasses trapped in air bubbles that formed when snow transformed into firn and ice. Ice cores also contain atmospheric dust, which yields information about storminess. Salt is an indicator of the distance to open ocean and ash layers can be traced to known volcanic eruptions. The Greenland ice cores have shown that Earth's climate can change abruptly (e.g., Dansgaard et al., 1993). During the last glacial period temperatures rose by more than 10°C in recurring warm periods known as Dansgaard-Oeschgar events.

The first ice core to reach the base of the Greenland Ice Sheet was drilled at Camp Century in 1966. Additional deep ice cores were subsequently collected through the Greenland Ice Sheet Project (GISP), the Greenland Ice-Core Project (GRIP), and the North Greenland Ice Core Project (NGRIP). The North Greenland Eemian Ice Drilling Project (NEEM), which aims to determine the paleoclimate of the last interglacial period, began in 2008.

Ice sheet mass balance

The mass balance of ice sheets is the difference between the net accumulation of snow and the combined loss of snow and ice by melt processes, sublimation and iceberg discharge. Measuring the mass balance of the Greenland Ice Sheet is a scientific challenge because of its large size and remote position, but estimates can be made in a number of different ways. In the mass budget approach, snow accumulation rates are typically inferred from ice cores or meteorological models while surface meltwater runoff is assessed in energy balance models (e.g., Bougamont et al., 2007). Estimates of the discharge of ice into fjords and other coastal environments require knowledge of the speed and thickness of marine-terminating outlet glaciers (Figure 1). Speeds can be determined from surface displacements measured in situ using global positioning systems (van de Wal et al., 2008) or from satellite remote sensing methods such as radar interferometry and repeat pass tracking of surface features (e.g., Howat et al., 2007; Joughin et al., 2004; Luckman et al., 2006). The thickness of ice is measured by radio-echo sounding at the surface or from aircraft (Gogineni et al., 2001). Using the mass budget approach, Rignot et al. (2008) estimate the mass balance of

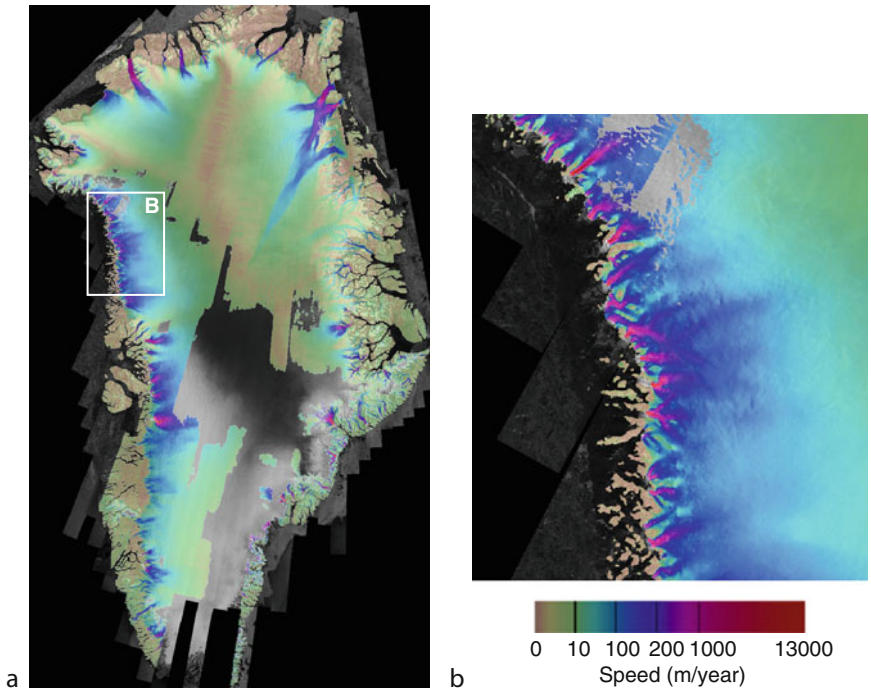

Greenland Ice Sheet, Figure 1 Velocity map of the Greenland Ice Sheet for winter 2006 derived from synthetic aperture radar imagery. The color scale illustrates surface speed, which is particularly high for marine-terminating outlet glaciers. (Courtesy of I. Joughin, Applied Physics Laboratory, University of Washington.)

the Greenland Ice Sheet to have deteriorated from a steady state in the 1970s to a state of rapid and sustained ice-mass loss of several hundred gigaton per year in the 2000s. Other approaches to measuring ice sheet mass balance include altimetry from satellites and aircraft (e.g., Krabill et al., 2000). Satellites in the Gravity Recovery and Climate Experiment (GRACE) can detect changes in gravitational attraction and this method also gives valuable information about short-term changes in ice sheet mass (e.g., Velicogna and Wahr, 2006). The various approaches used to measure ice sheet mass balance have different strengths and weaknesses and mass loss estimates are not always identical (Shepherd and Wingham, 2007). The relatively short timescale of satellite observations makes it difficult to accurately determine the magnitude of decadal variability in snowfall, surface ablation, and iceberg calving. This uncertainty is becoming less significant because mass-balance measurements are becoming longer and supported by new and complementary investigative techniques. Today, there is a clear consensus that the Greenland Ice Sheet is losing mass at a pace of at least a hundred gigaton of ice per year.

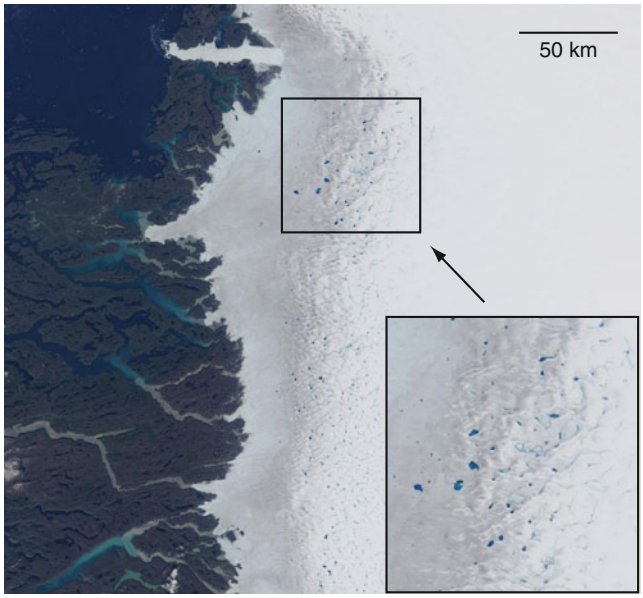

Greenland Ice Sheet, Figure 2 MODIS satellite image showing large and abundant supraglacial lakes on the surface of the western margin of the Greenland Ice Sheet.

Atmospheric or oceanic forcing?

The rapid loss of ice from the Greenland Ice Sheet since the mid-1990s coincides with a period where atmospheric temperatures were high. The seasonal extent of surface meltwater, which has been monitored by satellites since 1979, shows a variable, but progressive increase culminating with record high ablation in 2002, 2005, and 2007. Hanna et al. (2008) use meteorological observations and a surface energy–balance model to estimate meltwater runoff from the Greenland Ice Sheet during summers in the period 1958–2006. According to this model, the five record years were 1993, 1995, 1998, 2002 and 2006. Expanding the simulations by one more year showed that 2007 was yet another record year in terms of the magnitude of surface meltwater runoff (Rignot et al., 2008). The year 2010 was yet another year with record melt extent in Greenland.

Zwally et al. (2002) measured surface displacements with global positioning systems installed 35 km inland of the western margin of the ice sheet and over 1,175 m of ice. They identified possible relationships between changes in surface velocity and the timings and intensities of surface melting. It was proposed that short-term changes in surface velocity occur because surface meltwater drains to the bed and lubricates the basal motion of the ice sheet. The proposed link between ice flow and seasonal production of surface meltwater has been examined closely because satellite remote imagery show that glacial lakes on the surface of the Greenland Ice Sheet are numerous and widespread in the ablation zone (Figure 2). A direct response of the Greenland Ice Sheet to atmospheric forcing is of crucial significance because it may influence contemporary rates of sea-level change. If surface lowering occurs in response to surface-melt-induced ice-flow perturbations, it may trigger a precarious positive feedback mechanism whereby an increase in surface meltwater production increases the surface melt extent, which lead to yet more surface meltwater and so forth. Atmospherically coupled hydrological systems in ice sheets may accelerate the pace of ice moving from the interior toward lower and warmer elevations and this effect can potentially cause a fast demise of the ice sheet.

Recent studies have confirmed the occurrence of short-term velocity fluctuations in response to penetration of surface meltwater to the bed of the Greenland Ice Sheet (e.g., Das et al., 2008; Shepherd et al., 2009). However, the impact of the mechanism remains uncertain (van de Wal et al., 2008) and its influence seems restricted to the relatively slow-moving, land-terminating part of the ice sheet (Joughin et al., 2008). Surface-melt-induced basal lubrication does not appear to be an important driver of the fast flow of marine-terminating outlet glaciers, which exert a key control on the mass balance through discharge of icebergs to fjords and other coastal environments (Figure 3). Land-terminating glaciers have not changed significantly in recent years, at least not compared to the widespread and synchronous retreat reported for outlet glaciers terminating in seawater (Moon and Joughin, 2008). This suggests that the cause of recent rapid change may be oceanic. The exact nature of the oceanic forcing is not yet known, but it has been suggested that warm subsurface waters has triggered glacial recession of marine-terminating outlet glaciers because oceanic warming increases rates of submarine melting, thereby increasing rates of iceberg calving (Holland et al., 2008). It is possible that warming of subsurface waters occurs from

Greenland Ice Sheet, Figure 3 Aerial photograph of the marine-terminating Daugaard-Jensen Glacier in East Greenland. (From Christoffersen and Hambrey, 2006.)

air–ocean exchange of heat within the fjords or because warm Atlantic water enter fjords via coastal currents.

Fast-flowing outlet glaciers

Outlet glaciers in Greenland are steep and fast and they contribute to sea-level rise in a significant way despite their modest widths of approximately 5 km or less (Figure 3). Dynamic processes associated with fast glacier flow and iceberg discharge may have caused about two-thirds of the current rate of ice-mass loss (Rignot and Kanagaratnam, 2006). Approximately half of the icebergs discharged from the Greenland Ice Sheet in 2005 came from a dozen glaciers. Of their collective discharge, almost half came from the largest three. These glaciers are Jakobshavn Isbræ on the West Coast and Kangerdlugssuaq and Helheim glaciers on the East Coast.

Jakobshavn Isbræ was one of the first glaciers where major contemporary changes in flow dynamics were detected. The calving front of the glacier was in a relatively stable position from the 1950s to the 1990s. In 1998, the front retreated by 5 km and this caused flow speeds to increase from 5 km/year to 9 km/year. More dramatic changes followed between 2001 and 2003 as the majority of a floating ice tongue collapsed and caused the calving ice front to retreat several kilometers. This caused speeds to increase to 13 km/year (Joughin et al., 2004). Similar, although not identical events occurred in Kangerdlugssuaq and Sermilik fjords on the eastern side of the ice sheet. The front of Helheim Glacier retreated 7 km between 2001 and 2005. Subsequently, the speed of the glacier increased from 7 km/year to 11 km/year. Kangerdlugssuaq Glacier experienced an abrupt retreat of 5 km between 2004 and 2005 and its flow speed almost doubled from 7 km/year to about 13 km/year (Howat et al., 2007).

Jakobshavn Isbræ is currently capable of maintaining the accelerated pace set by the near-total disintegration of its floating ice tongue (Joughin et al., 2008). The response of Kangerdlugssuaq and Helheim Glaciers has been different. Both glaciers stopped retreating in 2005 and they have subsequently slowed down. The excess discharge caused by the speed-up events was about 30–50 Gt per glacier (Howat et al., 2007). The cumulative ice loss associated with excess discharge from numerous outlet glaciers experiencing retreat and flow acceleration in the early 2000s account for a considerable part of the volume loss identified across the ice sheet as a whole (e.g., Velicogna and Wahr, 2006).

Climate change

The Greenland Ice Sheet was in the past perceived to be in a relatively stable position and its demise was thought to require thousands of years of melting under warm climatic conditions. This premise has been questioned in light of the recent abrupt changes. Assessing the sensitivity and response of the Greenland Ice Sheet to the current warming of Earth's oceans and atmosphere is today an issue of tremendous scientific, societal, and political significance. The Greenland Ice Sheet contains enough ice to raise global sea levels by approximately 7 m. Gregory et al. (2004) forced an ice sheet model with outputs from a global climate model and the results suggest that global warming of 3°C is a critical threshold that could lead to a complete demise of the ice sheet. This threshold will

most likely be exceeded before 2100 unless emissions of carbon dioxide and other greenhouse gasses are stabilized and reduced to the level of year 2000 before 2050 (IPCC, 2007). This level of greenhouse gas reduction will require an economic outlook consistent with greenhouse gas emissions scenario with a global emphasis on resource-efficient technologies and global solutions to economic, social, and environmental sustainability. The alternative is less rapid economic development with emphasis on local solutions and environmental protection. So far, global economic growth remains fossil-fuel intensive, and this economic outlook is not consistent with a sustainable long-term presence of an ice sheet in Greenland.

The onset of a demise of the Greenland Ice Sheet may be tied to a predictable magnitude of global warming, but there is currently no consensus about the rate of demise. A demise controlled by surface melting mainly could take several thousand years (e.g., Ridley et al., 2005), but this scenario has been questioned on the basis of recent rapid change of the flow of outlet glaciers (Pfeffer et al., 2008). The main reason for this crucial lack of information is problems associated with the representation of dynamical processes in ice sheet models. Whereas assessments of surface mass balance are in good agreement with observational constraints, there are still major uncertainties associated with retention and runoff of surface meltwater in snow pack and on icy surfaces. The greatest problem, however, is the sheer lack of representation of outlet glaciers in ice sheet models. The available computational power currently limits the size of grid cells in ice sheet models to 5 km or more. This is obviously a major limitation because the widths of outlet glaciers are less than a single grid cell. Even with fast progress in the computer development industry, accurate quantitative predictions of sea-level rise from ice sheet models will require precise understanding of dynamic processes and representation of fast-flowing outlets in high spatial resolution.

Summary

The Greenland Ice Sheet is not in balance; it is losing mass at a rapid rate. The mass loss in some recent years was as high as 200 gigaton. This rate of ice-mass loss is equivalent to global sea-level rise of 0.6 mm per year. Approximately a third of this ice loss was in 2005 caused by runoff from increased surface melt. Two-thirds were attributed increased discharge from accelerated flow in outlet glaciers (Rignot and Kanagaratnam, 2006), although the dynamic contribution to the net mass loss is less (~50%) when losses are averaged over the period 2003–2008 (van den Broeke et al., 2009). Flow dynamics are thus a key control on ice-sheet and sea-level changes. It is well known that snowfall and surface melting in Greenland vary from year to year. Superimposed on these annual variations are seasonal as well as interannual variations in the speed and discharge of outlet glaciers. As a consequence, it is difficult to measure and understand variations in the mass of the Greenland Ice Sheet. However, new techniques and longer records have improved the understanding of the variability and decadal trends of ice sheet mass balance.

Rapid ice loss caused by increased discharge from outlet glaciers is likely to influence future rates of sea-level rise. The dynamic processes associated with fast glacier flow are nonetheless excluded from the projections in the IPCC Fourth Assessment Report (IPCC, 2007) because their potential magnitude is highly uncertain. The serious nature of dynamic contributions to sea-level rise is clearly demonstrated by rapid and widespread glacial recession followed by speed-up, thinning, and enhanced discharge. In recent years a dozen glaciers were responsible for approximately half of the ice that was discharged to the Greenland seas. Retreat and speed-up of the three largest glaciers, i.e., Jakobshavn, Kangerdlugssuaq, and Helheim, was associated with ice losses of around 60 gigaton per year. The three large glaciers have responded similarly to retreats of their calving ice fronts, but whereas Jakobshavn Isbræ is maintaining the accelerated pace of 13 km/year, the enhanced speeds of Kangerdlugssuaq and Helheim have dropped to levels more or less consistent with the state of flow prior to retreat.

The fact that recent abrupt changes occurred on glaciers terminating in fjords suggests an oceanic cause, but this does not exclude potentially significant impacts from atmospheric warming, which occurs at a faster rate in the Arctic than the global mean. These implications may include expansion of atmospherically coupled hydrological systems inside and beneath the Greenland Ice Sheet. Scientific focus is nonetheless also directed toward a better understanding of variations in the intensity and direction of ocean currents in the Arctic and the North Atlantic. It is well known that discharge of ice from the northern hemisphere ice sheets reduced the intensity of thermohaline circulation during the last glacial period (e.g., Dokken and Jansen, 1999), but it is possible that currents in the Arctic Ocean and the sub-Arctic seas in turn also influence the discharge of ice from the Greenland Ice Sheet.

Bibliography

Andersen, K. K., Azuma, N., Barnola, J. M., Bigler, M., Biscaye, P., Caillon, N., Chappellaz, J., Clausen, H. B., DahlJensen, D., Fischer, H., Fluckiger, J., Fritzsche, D., Fujii, Y., Goto-Azuma, K., Gronvold, K., Gundestrup, N. S., Hansson, M., Huber, C., Hvidberg, C. S., Johnsen, S. J., Jonsell, U., Jouzel, J., Kipfstuhl, S., Landais, A., Leuenberger, M., Lorrain, R., Masson-Delmotte, V., Miller, H., Motoyama, H., Narita, H., Popp, T., Rasmussen, S. O., Raynaud, D., Rothlisberger, R., Ruth, U., Samyn, D., Schwander, J., Shoji, H., Siggard-Andersen, M. L., Steffensen, J. P., Stocker, T., Sveinbjornsdottir, A. E., Svensson, A., Takata, M., Tison, J. L., Thorsteinsson, T., Watanabe, O., Wilhelms, F., White, J. W. C.,

and Project, N. G. I. C., 2004. High-resolution record of Northern Hemisphere climate extending into the last interglacial period. *Nature*, **431**, 147–151.
Bougamont, M., Bamber, J. L., Ridley, J. K., Gladstone, R. M., Greuell, W., Hanna, E., Payne, A. J., and Rutt, I., 2007. Impact of model physics on estimating the surface mass balance of the Greenland ice sheet. *Geophysical Research Letters*, **34**, L17501, doi:10.1029/2007GL030700.
Christoffersen, P., and Hambrey, M. J., 2006. Is the Greenland ice sheet in a state of collapse? *Geology Today*, **22**, 99–104.
Dansgaard, W., Johnsen, S. J., Clausen, H. B., Dahljensen, D., Gundestrup, N. S., Hammer, C. U., Hvidberg, C. S., Steffensen, J. P., Sveinbjornsdottir, A. E., Jouzel, J., and Bond, G., 1993. Evidence for general instability of past climate from a 250-Kyr Ice-core record. *Nature*, **364**, 218–220.
Das, S. B., Joughin, I., Behn, M. D., Howat, I. M., King, M. A., Lizarralde, D., and Bhatia, M. P., 2008. Fracture propagation to the base of the Greenland Ice Sheet during supraglacial lake drainage. *Science*, **320**, 778–781.
Dokken, T. M., and Jansen, E., 1999. Rapid changes in the mechanism of ocean convection during the last glacial period. *Nature*, **401**, 458–461.
Gogineni, S., Tammana, D., Braaten, D., Leuschen, C., Akins, T., Legarsky, J., Kanagaratnam, P., Stiles, J., Allen, C., and Jezek, K., 2001. Coherent radar ice thickness measurements over the Greenland ice sheet. *Journal Of Geophysical Research, Atmospheres*, **106**, 33761–33772.
Gregory, J. M., Huybrechts, P., and Raper, S. C. B., 2004. Climatology – threatened loss of the Greenland ice-sheet. *Nature*, **428**, 616–616.
Grootes, P. M., Stuiver, M., White, J. W. C., Johnsen, S., and Jouzel, J., 1993. Comparison of oxygen-isotope records from the Gisp2 and Grip Greenland ice cores. *Nature*, **366**, 552–554.
Hanna, E., Huybrechts, P., Steffen, K., Cappelen, J., Huff, R., Shuman, C., Irvine-Fynn, T., Wise, S., and Griffiths, M., 2008. Increased runoff from melt from the Greenland Ice Sheet: a response to global warming. *Journal of Climate*, **21**, 331–341.
Haug, G. H., and Tiedemann, R., 1998. Effect of the formation of the Isthmus of Panama on Atlantic Ocean thermohaline circulation. *Nature*, **393**, 673–676.
Holland, D. M., Thomas, R. H., De Young, B., Ribergaard, M. H., and Lyberth, B., 2008. Acceleration of Jakobshavn Isbrae triggered by warm subsurface ocean waters. *Nature Geoscience*, **1**, 659–664.
Howat, I. M., Joughin, I., and Scambos, T. A., 2007. Rapid changes in ice discharge from Greenland outlet glaciers. *Science*, **315**, 1559–1561.
IPCC, 2007. *Climate Change 2007: The Physical Science Basis*. Contributions of working group 1 to the fourth assessment report of the intergovernmental panel on climate change. Cambridge and New York: Cambridge University Press, p. 996.
Joughin, I., Abdalati, W., and Fahnestock, M., 2004. Large fluctuations in speed on Greenland's Jakobshavn Isbrae glacier. *Nature*, **432**, 608–610.
Joughin, I., Das, S. B., King, M. A., Smith, B. E., Howat, I. M., and Moon, T., 2008. Seasonal speedup along the western flank of the Greenland Ice Sheet. *Science*, **320**, 781–783.
Krabill, W., Abdalati, W., Frederick, E., Manizade, S., Martin, C., Sonntag, J., Swift, R., Thomas, R., Wright, W., and Yungel, J., 2000. Greenland ice sheet: high-elevation balance and peripheral thinning. *Science*, **289**, 428–430.
Luckman, A., Murray, T., de Lange, R., and Hanna, E., 2006. Rapid and synchronous ice-dynamic changes in East Greenland. *Geophysical Research Letters*, **33**, L07503, doi:10.1029/2006GL025758.
Lunt, D. J., Foster, G. L., Haywood, A. M., and Stone, E. J., 2008. Late Pliocene Greenland glaciation controlled by a decline in atmospheric CO_2 levels. *Nature*, **454**, 1102-U41.
Moon, T., and Joughin, I., 2008. Changes in ice front position on Greenland's outlet glaciers from 1992 to 2007. *Journal of Geophysical Research, Earth Surface*, **113**, F02022, doi:10.1029/2007JF000920.
Pfeffer, W. T., Harper, J. T., and O'Neel, S., 2008. Kinematic constraints on glacier contributions to 21st-century sea-level rise. *Science*, **321**, 1340–1343.
Ridley, J. K., Huybrechts, P., Gregory, J. M., and Lowe, J. A., 2005. Elimination of the Greenland ice sheet in a high CO_2 climate. *Journal of Climate*, **18**, 3409–3427.
Rignot, E., Box, J. E., Burgess, E., and Hanna, E., 2008. Mass balance of the Greenland ice sheet from 1958 to 2007. *Geophysical Research Letters*, **35**, L20502, doi:10.1029/2008GL035417.
Rignot, E., and Kanagaratnam, P., 2006. Changes in the velocity structure of the Greenland ice sheet. *Science*, **311**, 986–990.
Shepherd, A., Hubbard, A., Nienow, P., King, M., McMillan, M., and Joughin, I., 2009. Greenland ice sheet motion coupled with daily melting in late summer. *Geophysical Research Letters*, **36**, L01501, doi:10.1029/2008GL035758.
Shepherd, A., and Wingham, D., 2007. Recent sea-level contributions of the Antarctic and Greenland ice sheets. *Science*, **315**, 1529–1532.
van den Broeke, M., Bamber, J., Ettema, J., Rignot, E., Schrama, E., van de Berg, W. J., van Meijgaard, E., Velicogna, I., and Wouters, B., 2009. Partitioning recent Greenland mass loss. *Science*, **326**, 984–986.
van de Wal, R. S. W., Boot, W., van den Broeke, M. R., Smeets, C., Reijmer, C. H., Donker, J. J. A., and Oerlemans, J., 2008. Large and rapid melt-induced velocity changes in the ablation zone of the Greenland Ice Sheet. *Science*, **321**, 111–113.
Velicogna, I., and Wahr, J., 2006. Acceleration of Greenland ice mass loss in spring 2004. *Nature*, **443**, 329–331.
Zwally, H. J., Abdalati, W., Herring, T., Larson, K., Saba, J., and Steffen, K., 2002. Surface melt-induced acceleration of Greenland ice-sheet flow. *Science*, **297**, 218–222.

Cross-references

Ice Core
Ice Sheet Mass Balance

GROUND ICE

D. P. Dobhal
Wadia Institute of Himalayan Geology, Dehradun, India

At temperatures below 0°C almost all soil moisture remains in the form of ground ice. In permafrost regions, ground ice is one of the most important attributes of the terrain. Ground ice occurs in two main forms: (1) a structure-forming ice and (2) a large body of more or less pure ice. The structure-forming ice comprises segregated ice, intrusive ice, reticulate vein ice, ice crystals, and icy coatings on soil particles. The large bodies of more or less pure ice exist mainly in the upper part of the ground representing massive icy beds and ice wedges.

GROUND PENETRATING RADAR MEASUREMENTS OVER GLACIERS

David C. Nobes
Department of Geological Sciences, University of Canterbury, Christchurch, New Zealand

Synonyms

Georadar (primarily in Europe; géoradar in France); GPR; Ground probing radar; Subsurface interface radar (SIR)

Definition

Ground penetrating radar. GPR is a near-surface geophysical technique that uses the propagation of a shaped pulse or wavelet of radio-frequency electromagnetic energy (radar) into the subsurface and measures the radar echoes returned to yield *radargrams* or profiles of the physical property variations in the subsurface.

Radargram. A plot of individual GPR traces, one next to the other, to yield a cross-section of the subsurface structure and stratigraphy as expressed in the subsurface physical property variations.

Radar. An acronym for radio detection and ranging, the term RADAR has become so widespread and well known that the standard acronym capitalization long ago disappeared.

Ground penetrating radar

Ground penetrating radar (GPR) has been in widespread use for only a matter of decades, but its origins extend back much further (Leimbach and Löwy, 1910a, b, cited in Lampe, 2003). By the middle of the twentieth century, radar was being proposed as a means for determining glacier ice thickness (Steenson, 1951, cited in Evans, 1963, and in Daniels, 1996). In what may be an apocryphal story, it was reported that flights over Greenland and Antarctica during and immediately after World War II recorded errors in their radar altimetry, errors attributed to the radar transparency of ice (Waite and Schmidt, 1962; Evans, 1963; see *Antarctica*; *Greenland Ice Sheet*; *Radar Application in Snow, Ice, and Glaciers*). Subsequent experiments confirmed that radar could be used to determine glacier and ice sheet thicknesses (Evans, 1963; Waite, 1966; Rinker and Mock, 1967; Walker et al., 1968; Evans, 1969 and the accompanying papers). A P38 fighter bomber that crashed on the Greenland ice was found using radar (Fildes and Williams, 2001). The reasons for the crash are not mentioned, however.

Thus radar, specifically ground penetrating radar (GPR), can successfully provide images of ice sheets and glaciers, as shown by the example from the Garwood Glacier, a cold-based glacier (Figure 1, and see *Antarctica*; *Cold-Based Glaciers*). What distinguishes GPR from other radio-frequency techniques, such as radio echo sounding (RES), is that GPR antennas are constructed as an array of impedance-balanced wires that generate short-duration pulses (e.g., Annan, 1973; Arcone et al., 1995) that have better and more direct resolution of both englacial and basal glacial features. A more recent term has come into use – ice penetrating radar (IPR) – but IPR can mean either RES or GPR specifically applied to glacier measurements, and thus caution should be exercised in the use of the term IPR.

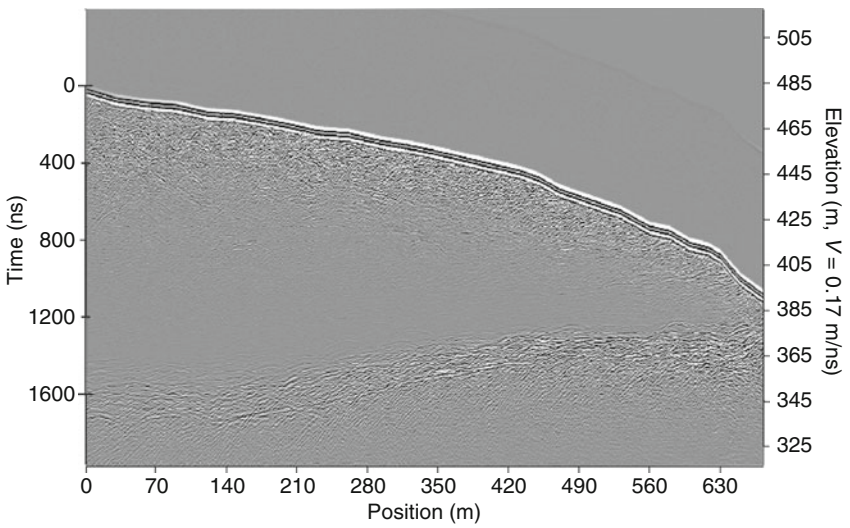

Ground Penetrating Radar Measurements Over Glaciers, Figure 1 GPR profile of the Garwood Glacier. An example of a ground penetrating radar profile of a glacier, in this case the cold-based Garwood Glacier in Antarctica. (Profile courtesy of Sean Fitzsimons, University of Otago.)

Basic GPR principles

Introduction

A GPR system usually comprises a set of two antennas, one an antenna that transmits a pulse of radio-frequency electromagnetic energy into the ground and the other a receiving antenna that detects the subsequent echoes that return from subsurface layers and structures (Figure 2a). The time it takes for an echo to return can be converted to the depth or distance to the reflecting surface if, and only if, the average radar velocity is known. The signal is then transferred through a console into a visual display and recording device. Sometimes the console and visual display and recording unit are one; sometimes the display and recording unit is a laptop. The record of voltage in the receiving antenna is stored and displayed; the record at each location – the trace – is typically plotted beside the previous trace so that time is on the vertical (down) axis and the position scrolls across the top of the display. Then any echoes that are spatially and temporally coherent are aligned, and the resulting radargram is a cross-section representation of the subsurface physical properties. These physical property changes frequently, but not always, correlate with the underlying geological and glaciological structure and stratigraphy (e.g., Davis and Annan, 1989; Annan and Cosway, 1992; Jol and Bristow, 2003).

The antennas are moved to cover the survey site: by shifting the individual antennas by hand – if for example the surface is rough as when there is significant debris cover; using a hand-towed sled (Figure 2b) for detailed imaging of a small area (e.g., Jol et al., 2004); or by towing an antenna sled using a vehicle such as a snowmobile or a tracked vehicle (Figure 2c).

Electromagnetic radiation pattern

GPR works because of an interesting effect. The electric and dielectric properties of a given material vary with frequency, except within the frequency range from about 1 to 1,000 megahertz (MHz). In this "radar range," the propagation of radio-frequency electromagnetic energy is dominated by the polarization properties of the material; the dielectric permittivity, ε, is a measure of how easily a material is polarized by the passage of a pulse of electromagnetic energy (Davis and Annan, 1989; Daniels, 1996).

A GPR antenna is composed of a set of regularly-spaced wires that have regularly-spaced resistors that, when properly constructed, yield a symmetrical oblate

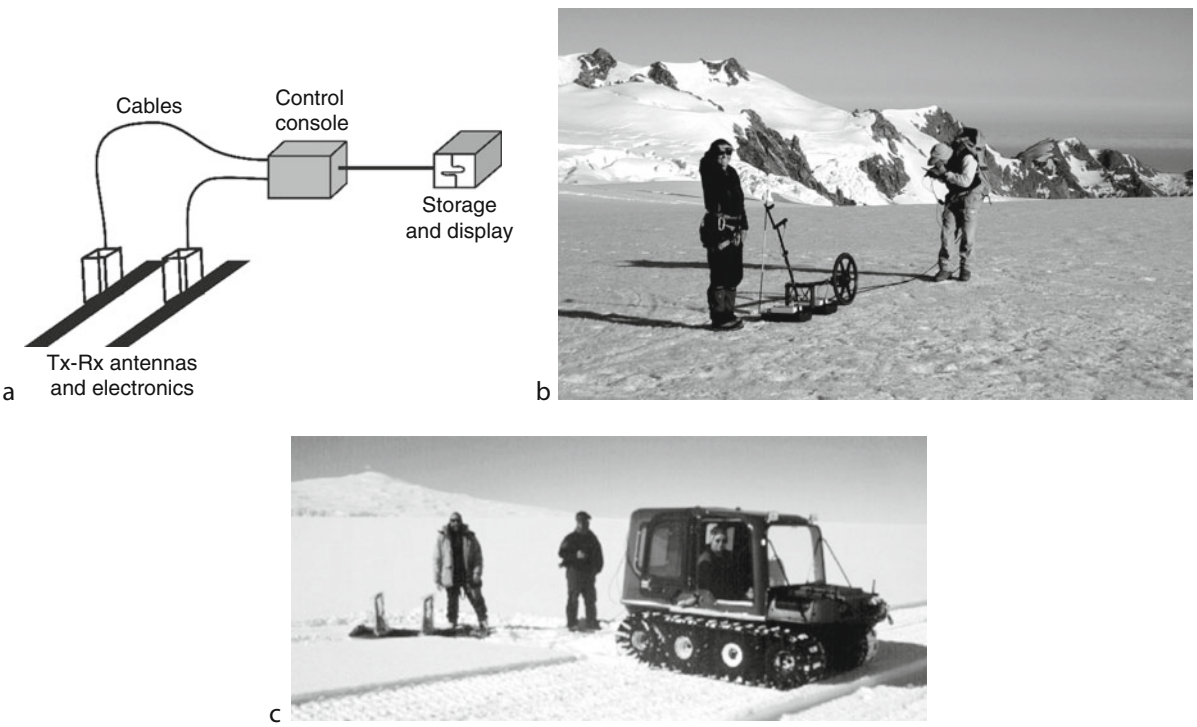

Ground Penetrating Radar Measurements Over Glaciers, Figure 2 GPR system schematic. (**a**) Schematic representation of a "typical" GPR system, showing: the transmitting–receiving antenna pair (Tx–Rx at lower left) with the electronics used to generate and measure the signal and its echoes; the cables connecting the Tx–Rx to the control console (center), where the cables may instead be an infrared remote communications system; and the storage and display unit, which may be incorporated into the main control console. (**b**) A hand-towed sled with high-frequency antennas was used for detailed imaging of the snowpack on the névé of the Franz Josef Glacier (Jol et al., 2004). (**c**) A vehicle towed sled with lower frequency antennas was used for imaging of the McMurdo Ice Shelf (Davis, 2003). (Photographs by the author.)

radiation pattern (Annan, 1973; Olsson et al., 1987; Annan and Cosway, 1992; Arcone, 1995). The energy radiates primarily in a direction perpendicular to the long axis of the antenna (Figure 3a) in what is called the H-mode (Arcone, 1995; Daniels, 1996). This has also been called the "broadside" mode in the applied literature (e.g., Nobes and Annan, 2000), but this terminology differs from that used in the electrical engineering literature. Conversely, the energy off the ends of the antenna (Figure 3a) is called the E-mode (Arcone, 1995; Daniels, 1996), or, in the applied literature, the "end-fire" mode. When in contact with the ground, the radiation pattern is bow-shaped (Figure 3b) from the long-edge of the GPR antenna when it is in contact with a material surface, such as the ground or the surface of a glacier. The pattern is different from the ends of the antenna (Figure 3c), where "nulls" or areas of little or no energy occur.

The radar pulse has a compact shape in time (Figure 4a). The length of the pulse or wavelet depends on the frequency content of the signal (Figure 4b). GPR antennas are in general characterized by their central frequencies, f_C, e.g., 50, 100, or 200 MHz, which usually has the peak amplitude. In many if not most cases, the bandwidth, f_B, is equal to the central frequency, so that the 100 MHz antenna has a 100 MHz bandwidth, from 50 to 150 MHz. The bandwidth determines how compact the pulse will be, and thus the resolution of the pulse in time and depth. The relationship between frequency, resolution, and depth of penetration will be discussed in more detail later.

GPR velocity and the dielectric permittivity

The velocity at which radar energy travels depends on the dielectric properties, ε, of the medium in which it is travelling. In particular, the velocity is determined by the relative dielectric permittivity, ε_r, which is frequently called the dielectric constant, a misnomer as it is not a constant.

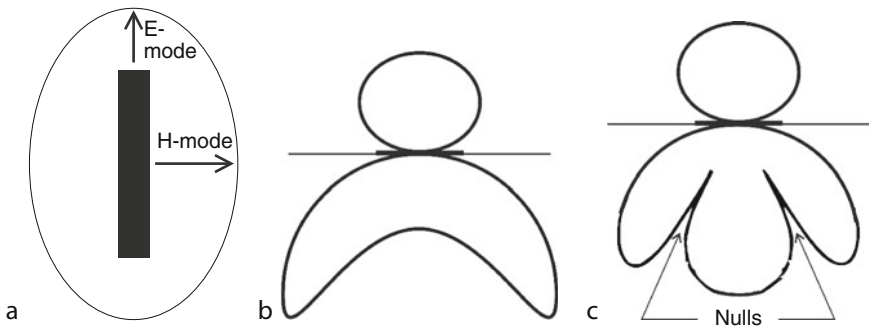

Ground Penetrating Radar Measurements Over Glaciers, Figure 3 GPR radiation pattern. Schematic diagram showing the radar radiation pattern for a GPR antenna in contact with the ground. In plan view (**a**), the radiation has two modes: the H-mode which is often in field applications called the broadside (BD) mode, and the E-mode which is sometimes called the end-fire (EF) mode. (**b**) The radiation pattern from the H-mode has a clearly lobate pattern with most of the energy directed into the ground. (**c**) In contrast, the E-mode has "nulls" which are at discrete angles dependent on the material properties of the subsurface.

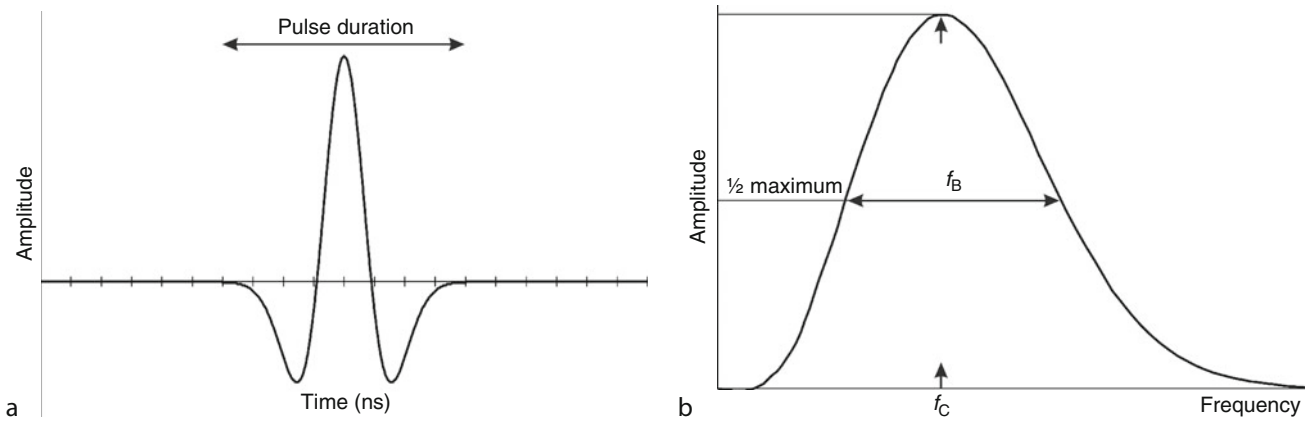

Ground Penetrating Radar Measurements Over Glaciers, Figure 4 GPR pulse. The GPR pulse or wavelet is relatively compact (**a**). The pulse duration depends on the frequency content (**b**), which is defined by the center frequency (f_C) and the bandwidth (f_B), that is the width of the amplitude versus frequency at half of the maximum amplitude.

In the absence of any significant amounts of magnetic material, the radar velocity, v, is equal to:

$$v = c/\sqrt{\varepsilon_r}, \quad (1)$$

where c is the speed of light in air, 300 metres per microsecond (m/μs). Table 1 lists the relative dielectric permittivities and radar velocities for some common materials, in particular water, snow, and ice. Note that these material velocities are those for "pure" materials. In the field, the velocity is rarely "pure," and is in general an average of the all of the materials between the antenna pair at the surface and the reflecting boundary at depth.

A quick glance at Table 1 shows that the presence or absence of water dominates the radar velocity. If water is present in any material to any extent, then the radar velocity of that material will be less, often significantly less, than it would be if it were dry or frozen. The way the dielectric properties, and hence the velocity, depend on various parameters, such as the water content, has been widely studied, and numerous relationships have been proposed, such as effective medium theories and the empirical Topp equation (Topp et al., 1980) which is still one of the more commonly used and robust equations for estimating the effect of the water content on the dielectric properties.

Because of the significant influence of water on the dielectric properties, and thus the radar velocity, then the thermal and hydrological state of a glacier can be estimated using the variations in the velocity (e.g., Macheret et al., 1993; Moorman and Michel, 2000; Copland and Sharp, 2001; Irvine-Fynn et al., 2006; Barrett et al., 2007; Murray et al., 2007; and see *Polythermal Glaciers*; *Subglacial Drainage System*; *Temperate Glaciers*). Similarly the imaging of internal structures can be related to changes in the radar velocities that in turn are related to changes in water content (e.g., Stevens et al., 2008; Watanabe et al., 2008; and see *Englacial Conduit*; *Englacial Processes*; *Meltwater Channels*; *Meltwater Conduit*; *Subglacial Drainage System*).

Ground Penetrating Radar Measurements Over Glaciers, Table 1 Dielectric properties and radar velocities for some common materials

Material	Relative dielectric permittivity, ε_r	Velocity (m/μs)
Air	1	300
Water	~80[a]	~33
Snow	2–3	200
Ice	3–4	160
Dry sand	3–5	150
Wet sand	20–30	60
Dry salt	5–6	130
Granite	4–6	130

[a]The dielectric properties, particularly for water, are temperature-dependent.

In the absence of water, the dielectric permittivity is related to the density of the material (Keller, 1982), and in particular the change in density from snow to firn to ice (Pearce and Walker, 1967; Tiuri et al., 1984; and see *Firn*; *Ice*; *Physical Properties of Snow*; *Snow Density* and *Transformations of Snow at the Earth's Surface and its Climatic and Environmental Consequences*) which gives rise to a corresponding increase in ε, the dielectric permittivity, and an associated decrease in the velocity (Equation 1). When the radar pulse encounters a boundary between layers with different dielectric properties, between firn and ice, for example, the velocity changes as well, and part of the signal is reflected back towards the surface. The reflection coefficient, r, is:

$$\begin{aligned} r &= (v_2 - v_1)/(v_2 + v_1) \\ &= (\sqrt{\varepsilon_1} - \sqrt{\varepsilon_2})/(\sqrt{\varepsilon_1} + \sqrt{\varepsilon_2}). \end{aligned} \quad (2)$$

where p_1 is the value of the parameter (velocity, v, or dielectric permittivity, ε) for layer 1, i.e., above the boundary, and p_2 is the value for layer 2, i.e., below the reflecting boundary. The amount of energy reflected is r^2, and the amount of energy that is transmitted through the boundary is:

$$t^2 = 1 - r^2. \quad (3)$$

The strength of the radar echo depends on the contrast in the dielectric properties between the layers; alternatively, it can be thought of as the contrast in the radar velocities. A velocity increase generates a positive radar echo, whereas a velocity decrease, as occurs at the water table, yields a negative radar echo. A single trace (Figure 5) will have a direct air wave arrival which serves as a time reference, a direct ground wave arrival which serves as a ground surface reference, and any reflection echoes.

The reflectivity associated with changes in density can be used to obtain a radar stratigraphy of snow and ice, especially high-resolution stratigraphy (e.g., Arcone, 1996; Jol et al., 2004; Kanagaratnam et al., 2004; Jacobel and Welch, 2005; see *Layering of Snow*; *Mapping of Internal Glacial Layers*; *Stratigraphy of Snowpacks*), determination of snow accumulation rates (Kohler et al., 1997; Pälli et al., 2002; Spikes et al., 2005; Machguth et al., 2006; Dunse et al., 2008; see *Scandinavian Glaciers*, *Snow Depth*; *Snow Drift*), near-surface structures in ice-rich permafrost (Hinkel et al., 2001; Munroe et al., 2007; Godfrey et al., 2008; Stevens et al., 2008; Watanabe et al., 2008; see *Alaskan Glaciers*; *Antarctica*; *Permafrost*), and processes at glacier margins (e.g., Fitzsimons, 2008). Seasonal freeze and thaw cycles will of course cause temporal changes in the reflectivity as well, specifically in polythermal glaciers (Irvine-Fynn et al., 2006; see *Climate Change and Glaciers*; *Polythermal Glaciers*), and in the Antarctic Dry Valleys permafrost (Godfrey et al., 2008; see *Antarctica*; *Permafrost*; *Permafrost and Climate Interactions*).

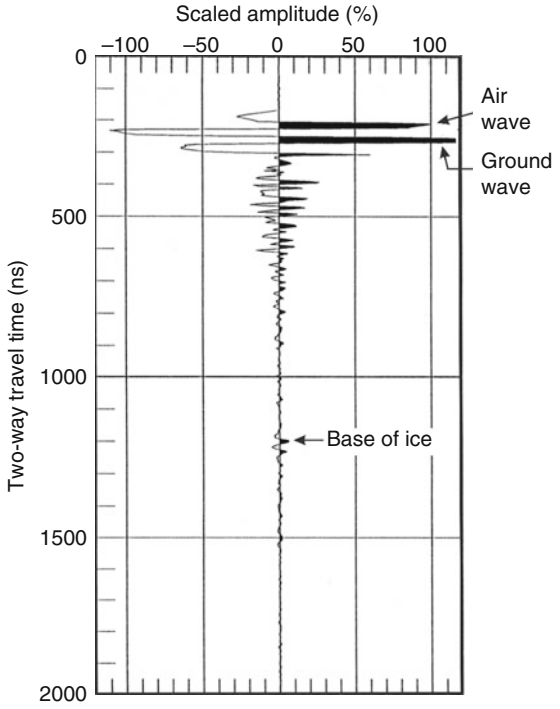

Ground Penetrating Radar Measurements Over Glaciers, Figure 5 Sample GPR trace. An example raw radar trace, without any gains (amplification), showing the relative amplitudes of the air wave, the ground wave and the reflection from the base of the ice. The air wave arrives first, and serves as a time reference for alignment of successive traces. The ground wave arrives immediately after the air wave, and represents a ground level reference. The basal reflection appears to be small, but is large when corrected for geometrical spreading. (Adapted and modified from Leary, 1993, and from Nobes et al., 1994.)

Monostatic versus bistatic GPR systems and survey design

The radar pulse is sent from a transmitting antenna. The receiving antenna can either be the same antenna as was used as the transmitter (a monostatic GPR system), or a separate and independent receiving antenna (a bistatic system). In a monostatic system, the pulse is transmitted and then the antenna is turned into a receiving antenna, listening for the radar echoes to return from reflecting boundaries and objects. The advantage of a monostatic system is that only one antenna is required. However, there are more advantages to bistatic systems, and so bistatic systems are the norm whereas monostatic systems are the exception. A separate receiving antenna allows the researcher to record the character of the transmitted signal as it appears entering the ground. A bistatic system also allows us to determine the subsurface velocity, v, which is needed for: (1) conversion of the two-way travel time, T, to depth, d:

$$d \cong vT/2, \tag{4}$$

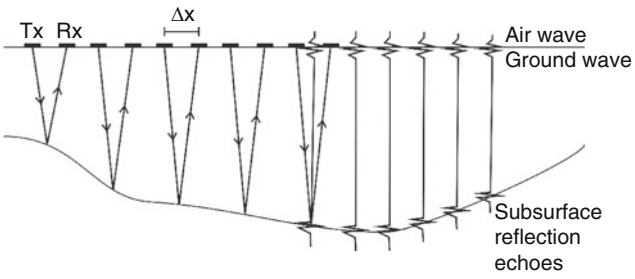

Ground Penetrating Radar Measurements Over Glaciers, Figure 6 Common offset geometry. The common offset mode of GPR data acquisition is illustrated. On the left, the transmitter–receiver (Tx–Rx) pair is shown stepped along at constant step sizes (offsets), Δx. At each location, a record of the radar echoes is recorded (shown on the *right*). The first arrival is the direct air wave, which serves as a time reference, followed by the direct ground wave, and at later times the subsurface reflection echoes (*bottom right*). Each successive trace (radar echo record) is plotted beside previous traces to form a radar profile or radargram that has the appearance of a subsurface cross-section.

which is valid when d is much greater than the antenna separation and (2) estimating the subsurface physical properties. The velocity is also needed for one of the final steps in the prevalent processing protocols, migration, which will be discussed later.

GPR surveys are normally conducted in what is called common offset mode (Figure 6). The antennas are separated by a constant distance, which will depend on the antenna frequency, and then stepped along at regular spatial increments, Δx. Those increments should be less than or equal to the minimum resolution required to "see" an object of a size Δx or greater (e.g., Annan and Cosway, 1992; Jol and Bristow, 2003). Alternatively, Δx is set equal to the resolution, R, at the ground surface for a given antenna, which is a function of the velocity of the material, v, and the antenna frequency, f:

$$R \approx \lambda/4 = v/4f, \tag{5}$$

where λ is the wavelength, which equals v/f. Equation 5 is the limiting case as the depth approaches zero for the first Fresnel scattering zone (Sheriff, 2002), which is that portion of a subsurface reflector that constructively scatters energy back to the receiving antenna. The size of the Fresnel scattering zone as a function of the wavelength, λ, and the depth, h, is:

$$R^2 = \lambda^2/16 + h\lambda/2 \tag{6}$$

Thus the design of a survey, including the step size and antenna frequency, can be based on the size of object the researcher wishes to target; alternatively the researcher designs the survey for the optimal step size as determined by the antenna frequency and the ground conditions. Frequently, the determining factor in survey design is not the

desired resolution but rather the depth of penetration needed to detect, for example, bedrock beneath a glacier (see *Bed (Bottom) Topography*). In general, as the antenna frequency is lowered, the depth of penetration increases.

The alternative survey mode is the wide-angle reflection and refraction (WARR) survey (e.g., Davis and Annan, 1989), which is commonly conducted in common mid-point (CMP) mode (Figure 7). The CMP involves stepping the transmitting and receiving antennas in equal steps out from a central survey point. The travel paths in the air and in the uppermost layer of the ground increase linearly with increasing antenna separation, and so therefore does the travel time for the signal to travel between antennas. The path of the signal that travels to and from a buried reflective surface, however, increases as the square root of the squares of the depth and separation, and thus so too does the two-way travel time (TWT), i.e., the travel time to and from the reflective boundary, T, depends on the depth, h, and antenna separation, s, as:

$$h^2 = x^2 + d^2 = s^2/4 + d^2 = V^2(T/2)^2 = V^2T^2/4, \quad (7)$$

where V is the velocity of the radar signal. By rearranging terms, we find that the travel time depends on depth and separation as:

$$T^2 = s^2/V^2 + 4d^2/V^2 = ms^2 + T_0^2. \quad (8)$$

The relationship between the TWT and the separation defines a parabola, whose curvature (shape), represented by the parameter m in equation (8), depends on the velocity of the radar wave in the subsurface above the reflective boundary, or conversely given the plot of T^2 versus s^2, then $V = \sqrt{m}$. Thus the curvature of the reflection parabola determines the subsurface velocity above the reflecting boundary. The time intercept, T_0, in turn depends on the depth and the velocity as:

$$T_0 = 2d/V. \quad (9)$$

The CMP survey thus yields the velocity structure and the depth to the reflecting boundary. The WARR style of survey cannot be done using a monostatic system, only with a bistatic system where the antennas can be operated independently.

The CMP geometry yields velocity information that allows us to construct a model of the dielectric layering (see *Mapping of Internal Glacial Layers* and *Stratigraphy of Snowpacks*) and to convert travel time to depth, as well as provide some information about water content (Murray et al., 2007). However, CMP acquisition must be carefully done, as even small errors in the survey geometry can cause errors in the calculated velocities and thus in the subsequent ice water content estimates (Barrett et al., 2007). It should also be noted that the velocity to a given reflector is the root-mean-square *weighted average* of the velocities of all of the overlying layers (e.g., Reynolds, 1997; Sheriff, 2002). The weights are the travel times spent in each layer. Hence although the radar velocity in ice is 160 m/ms, the observed field velocity is often greater due to the overlying layers of firn and snow, which have faster radar velocities (Table 1).

Advanced GPR principles and specific aspects of glacier GPR

WARR variants

A variation of the CMP is where one of the antennas, either the transmitter or receiver, is placed at the central point and the other antenna is systematically stepped out first to one side and then to the other. The result, once merged, yields a curve similar to that in Figure 7, but double-sided.

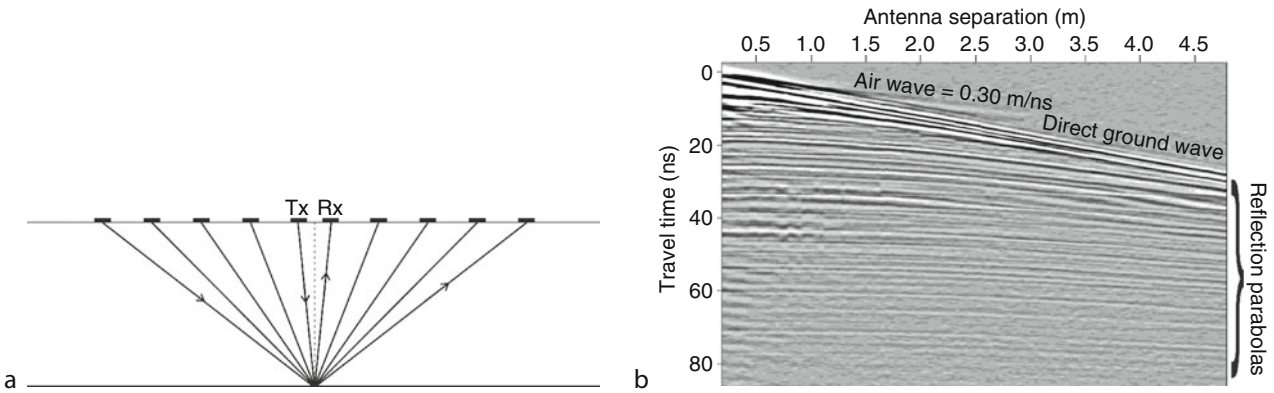

Ground Penetrating Radar Measurements Over Glaciers, Figure 7 CMP geometry. (**a**) The common mid-point (CMP) geometry uses a Tx–Rx pair stepped out from a common central point (*dashed vertical line*). (**b**) A CMP from the Franz Josef névé (Jol et al., 2004) illustrates the CMP concepts. The air wave is the first arrival, travelling at 0.30 m/ns (300 m/μs), followed by the direct ground wave which travels along the top surface of the ground. The reflections from subsurface reflective boundaries yield a set of parabolas, as the travel time squared is a function of the square of the antenna separation. The curvature is then used to determine the subsurface radar velocity down to the reflective boundary.

This is sometimes called a common depth point (CDP), because in the case of a flat-lying layer the reflections originate from a common depth. Such surveys are also called by their seismic analogues: If the receiver is the antenna fixed at the central point, then the survey is called a common receiver point or common receiver gather, whereas if the transmitter is fixed, it is called a common shot point or common shot gather. The advantage of a CDP-style survey is that if the reflecting boundary is not horizontal but dipping, then the dip of the layer can be determined in addition to the velocity (Nobes, 1999). Using a CMP geometry yields an apparent velocity that is instead a mix of the real velocity and a correction factor proportional to the sine of the dip of the layer. If the dip is small, then so is the effect of the dip on the velocity determinations.

Directionality and anisotropy

The radar radiation pattern, as shown schematically in Figure 3, leads to an obvious directionality in the radar response in almost all situations, whether structural or textural: schistosity or crystal orientation (Tillard, 1994; Matsuoka et al., 2003; see *Cryogenic Fabric*); sedimentary structures (van Overmeeren, 1994); or glacial structures (Watts and Wright, 1981; Nobes, 1999; Matsuoka et al., 2007; see *Crevasses*; *Englacial Conduit*; *Meltwater Conduit*; *Structural Glaciology*). This directionality is incorporated into the survey design by using different antenna orientations (e.g., Jol and Bristow, 2003; Figure 8). To optimize the overall survey design, in particular the survey line direction and antenna orientation, the overall structural and textural directions and their orientations relative to the antennas should, if possible, be known. The combination of the angle of the nulls in the "end-fire" response (Figure 3) with the dip of structural features can give rise to dramatic differences in the reflection energies; the broadside energy can be much greater, as has been observed on the Franz Josef Glacier in New Zealand (Nobes, 1999; Nobes and Annan, 2000; see *Temperate Glaciers*), in Antarctica (Matsuoka et al., 2003; see *Antarctica*), and in Iceland (Matsuoka et al., 2007; see *Iceland Glaciers*). Nobes (1999) ascribed the change in reflection energy with antenna orientation to structural alignment of glacial features (see *Crevasses* and *Structural Glaciology*), whereas Matsuoka et al. (2003, 2007) ascribe the change in reflection energy to the preferential orientation of ice crystal fabric (see *Cryogenic Fabric*). Thus, in designing a glacier GPR survey, the particular target must be kept clearly in mind. Is the internal structure the target, in particular ring fractures and associated crevasses? In that case, the antennas should be oriented perpendicular to the direction of glacier flow to yield maximum reflection energy from the internal structures. Is the ice–bedrock interface the target? Then the antennas should be parallel to the glacier flow direction so that the energy from the internal structure is minimized and the bedrock surface is the primary reflective boundary.

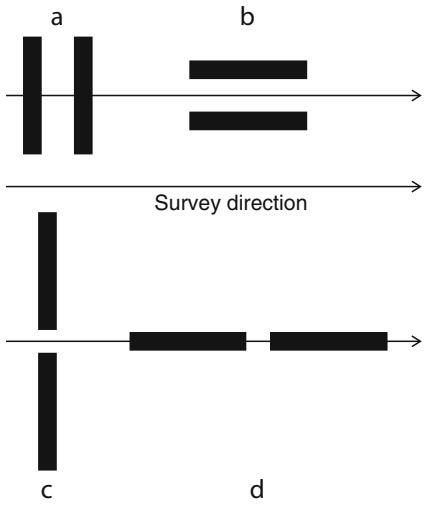

Ground Penetrating Radar Measurements Over Glaciers, Figure 8 Antenna geometries. Illustration of the most common antenna survey configurations. (**a**) The most commonly used antenna geometry is with the antennas in a broadside mode (i.e., the long edges of the Tx–Rx antennas aligned) and perpendicular to the survey line direction (*long arrow*). (**b**) The second most common geometry has the antennas in broadside mode but parallel to the survey direction. Less common are the "end-fire" geometries (**c**, **d**). As for a and b (*top*), the antennas are either perpendicular (**c**) or parallel (**d**) to the survey line direction. Geometry d is easy for towing large antennas, but at the expense of the maximum coupling of the signal strength between the antennas. That is why geometries a and b are the most commonly used.

In addition to structural and textural directionality, the GPR velocity can be inherently anisotropic (Rigsby, 1960; Kovacs and Morey, 1978; see *Cryogenic Fabric*). That is, the velocity differs depending on the orientation of the ice crystals. If they are preferentially aligned, as can happen in a flow environment where the forces acting can orient the crystals in the flow direction, then the velocity has maximum and minimum values in the *c*-axis direction (Kovacs and Morey, 1978; Matsuoka et al., 2003). However, while a change in reflection energy is noted, a change in velocity (and thus in travel times) is not always observed.

Larger scale structures, such as crevasses, can be difficult to detect (see *Crevasses* and *Structural Glaciology*). Nearly vertical features rarely generate direct reflections; the energy is not reflected back to the receiving antenna on the surface. However, either a lack of signal return or a disruption or sudden lack of layering, can allow for the detection of crevasses (Glover and Rees, 1992; Delaney et al., 2004). Similarly, features such as englacial and subglacial channels and water flow pathways can be detected (Moorman and Michel, 2000; Copland and Sharp, 2001; Stuart et al., 2003; see *Base Flow/Groundwater Flow*; *Englacial Conduit*; *Glacier Hydrology*; *Meltwater Channels*; *Meltwater Conduit*; *Scandinavian Glaciers*;

Subglacial Drainage System), often because they cause terminations of layers which in turn generate diffractions (e.g., Figure 9).

Diffractions

In addition to obtaining velocity estimates from WARR surveys, the subsurface velocity can be obtained from diffractions (Figure 9). Diffractions are the result of the scattering of the GPR signal by features such as truncated beds, boulders, englacial channels, etc. that have dimensions that are of the order of but smaller than the signal resolution, i.e., of the order of ¼ of the radar signal wavelength in the material. The shape of the diffraction – the steepness of the curvature – depends on the velocity between the surface and the feature causing the diffractions. This alternative way for estimating the velocity provides an independent check on the WARR velocity, if available, and its spatial homogeneity. In many cases, the surface of a glacier may be too rough and rugged for a WARR survey to be completed, especially in the case of debris-covered, debris-laden, and rock glaciers (see *Debris*; *Debris-Covered Glaciers*, and *Rock Glaciers*). In such cases, the diffractions may be the only means available to obtain velocity estimates. An example is shown in Figure 9b. Note the clear diffraction hyperbolas apparent at the base of the surface debris layer, and at depth arising from buried englacial channels (see *Englacial Conduit*; *Meltwater Channels*; *Meltwater Conduit*).

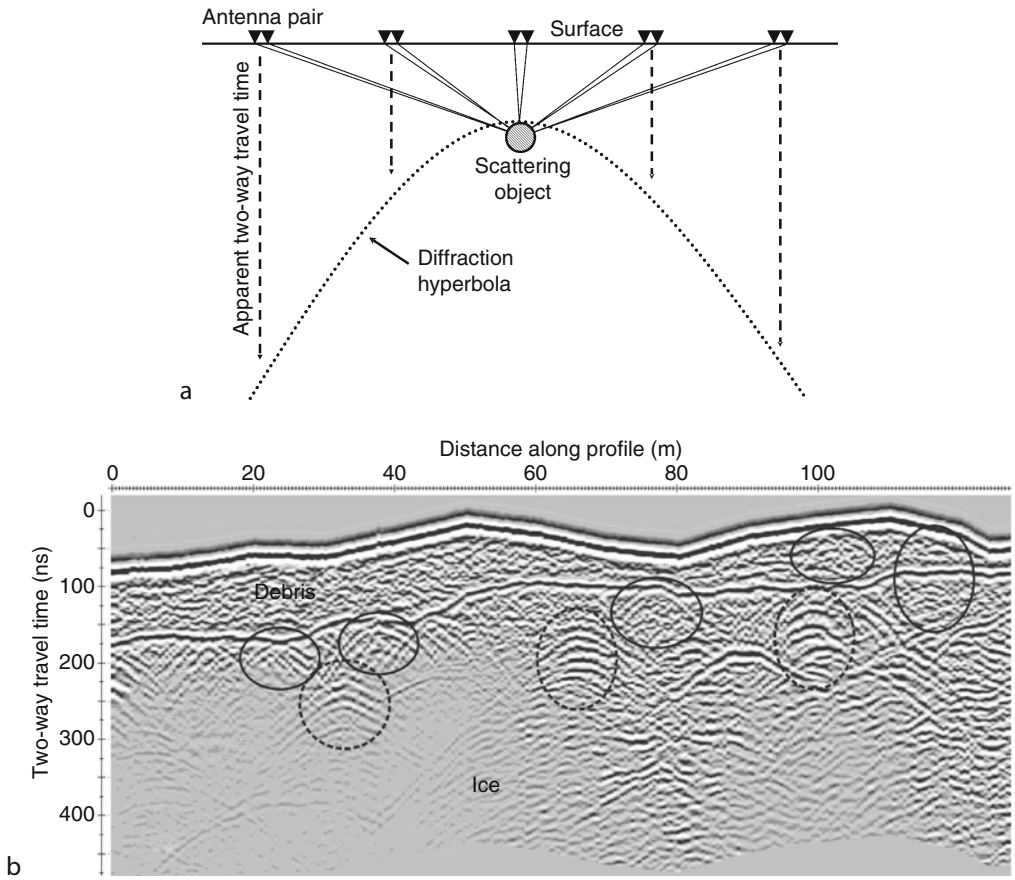

Ground Penetrating Radar Measurements Over Glaciers, Figure 9 Source of diffractions and sample radargram. (**a**) Schematic illustration of the cause of diffraction hyperbolae. A subsurface object or feature such as a boulder, englacial channel, etc., which is of the order of but smaller than 1/4 of a wavelength, will generate scattering as shown. As the antenna Tx–Rx pair approach the object, reflected energy is observed, but is plotted always as if the energy is directly below the antennas. As the antennas get closer to the object, the travel time decreases, reaching a minimum immediately above the object that is causing the scattering of the energy, and then increasing again as the antennas move away. The curvature of the resultant diffraction hyperbola is diagnostic of the velocity between the antennas and the object, and can be used as an alternative means of estimating the velocity. (**b**) Example of a GPR profile targetted at the shallow debris-covered portion of a glacier. Diffractions from boulders beneath and within the debris are clear – a few are circled – as are strong diffractions that appear to be stacked one above the other (*dashed circles*). The latter sets of diffractions are likely due to englacial channels that have small horizontal extent but substantial vertical extent. Vertical profile scale is about 30 m. (Profile courtesy of Natalya Reznichenko.)

Signal loss, attenuation and scattering

In addition to the simple propagation of a pulse of electromagnetic energy that is involved in GPR, we must consider attenuation of the signal (Davis and Annan, 1989; Daniels, 1996). There are many contributions to the loss of signal, the most important of which, for our purposes, are:

- Geometrical spreading: loss of energy as it spreads out across a volume of the subsurface
- Conductive losses (attenuation): loss of energy due to electric current induced to flow in the ground by the radar wave, in which case the attenuation, α, is:

$$\alpha \cong \sigma/\omega\varepsilon \tag{10}$$

where σ is the electrical conductivity, ω is the angular frequency, equal to $2\pi f$, and ε is, as before, the dielectric permittivity and

- Scattering losses or clutter: loss of energy because the high-frequency radar waves are scattered by boulders, fractures, etc. that are of the scale of the resolution of the signal.

As the signal travels through a medium, it spreads out geometrically as the inverse square of the distance. It is straightforward to correct for geometrical spreading, and some radar processing programmes do what is called spreading and exponential compensation (SEC). The signal is also attenuated, that is energy is lost from the pulse at an exponential rate:

$$e^{-\alpha z} \tag{11}$$

where α is the rate of signal loss. In contrast to geometrical spreading, the correction for attenuation is largely empirical, adjusted from an initial informed guess until the profile appears to be balanced between too much and too little amplification of echo strength. This serves to preserve, as much as possible, the relative strengths of the echoes from reflective boundaries, and serves to aid interpretation.

Alternatively, we frequently use automatic gain control (AGC) which amplifies the signal using a gain factor that is in essence equal to the inverse of the signal strength. Thus all echoes are amplified to the point where they are effectively equal. AGC is well suited for showing all of the stratigraphy in the subsurface, even subtle stratigraphy, without regard to how massive a bed might be (Nobes et al., 2001). Disadvantages of AGC are that it also amplifies any noise present, both random and coherent "noise," and also does not preserve the relative strengths of the radar echoes.

The electrical conductivity of almost all snow and ice, and thus of almost all glaciers, is negligible. The exception is sea ice, which can incorporate sea water into pores that gradually freeze and isolate pockets of hypersaline water, and ice shelves, where brine can infiltrate in a layer some kilometers inland from the sea (Heine, 1968; Morse and Waddington, 1984; see *Ice Shelf* and *Sea Ice*). Sea ice and ice shelves are thus special cases. The brine layer has such a large change in the physical properties, especially the electrical conductivity, that it can behave like a mirror that almost completely reflects radar signals (Nobes et al., 2005).

With the exception of sea ice and ice shelf brine layers, then, geometrical spreading, which is well constrained, and clutter or scattering are the most noteworthy contributions to loss of signal in glacier GPR. Clutter will be highly dependent on the degree of breakup of the ice, the nature and amount of debris, both surface debris and that incorporated into the mass of the glacier, especially rock glaciers (see *Debris*; *Debris-Covered Glaciers*; *Rock Glaciers*). The scattering of signals will often yield diffractions (as in Figure 9), and thus an abundance of diffractions will be diagnostic of a high degree of scattering and thus of loss of signal. Higher frequency signals will be more susceptible to clutter, but yield more detail (e.g., Figure 9b); lower frequency signals will suffer less from the effects of clutter, and have greater penetration, but at the expense of detail. Scattering and clutter will have the greatest detrimental effect on GPR across debris-covered, debris-laden, and rock glaciers. Nonetheless, GPR has been shown to work well on all such glaciers (e.g., Nobes et al., 1994; Degenhardt and Giardino, 2003; Degenhardt et al., 2003; Musil et al., 2006; Maurer and Hauck, 2007).

Frequency versus resolution

As noted earlier, there is a fundamental trade-off between the frequency and resolution, or to put it another way, depth versus detail. For example, higher frequency antennas will yield greater detail but that does not necessarily equate with greater information. In fact, the greater detail may well obscure the very features that we are trying to detect.

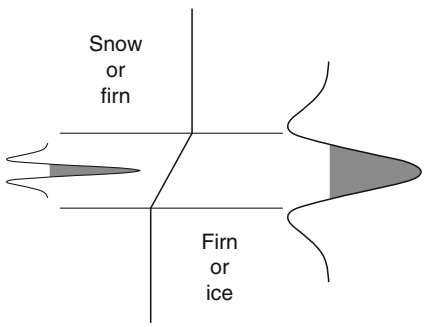

Ground Penetrating Radar Measurements Over Glaciers, Figure 10 A representation of the radar velocity at the boundary between snow and firn, or firn and ice. The change in velocity may be transitional, as shown by the near-vertical line. A sharp, high-frequency pulse (*left*) will see the transition as a separate layer with slowly changing properties, and no reflection will occur. A low-frequency pulse, in contrast, will see the transition as a sharp boundary between the layer above and the layer below.

For observing the base of a glacier, a lower frequency (e.g., 50 MHz or lower) might normally be used (e.g., Nobes et al., 1994, and Hochstein et al., 1995, on the Tasman Glacier terminus; see *Temperate Glaciers*), whereas a high-frequency system (e.g., higher than 200–250 MHz) would be used to provide images of layering in snow and ice (e.g., Jol et al., 2004, on the Franz Josef névé; and Kanagaratnam et al., 2004, in Greenland; see *Greenland Ice Sheet*; *Layering of Snow*; *Mapping of Internal Glacial Layers*). This is a good general rule of thumb, but there are other considerations.

Arcone and Laatsch (2004) observed that high frequency signals (400 MHz) yielded a clearer image of the base of the McMurdo Ice Shelf, whereas low to moderate frequency signals (100 MHz) yielded a clearer image of the stratigraphy (see *Antarctica*; *Ice Shelf*; *Mapping of*

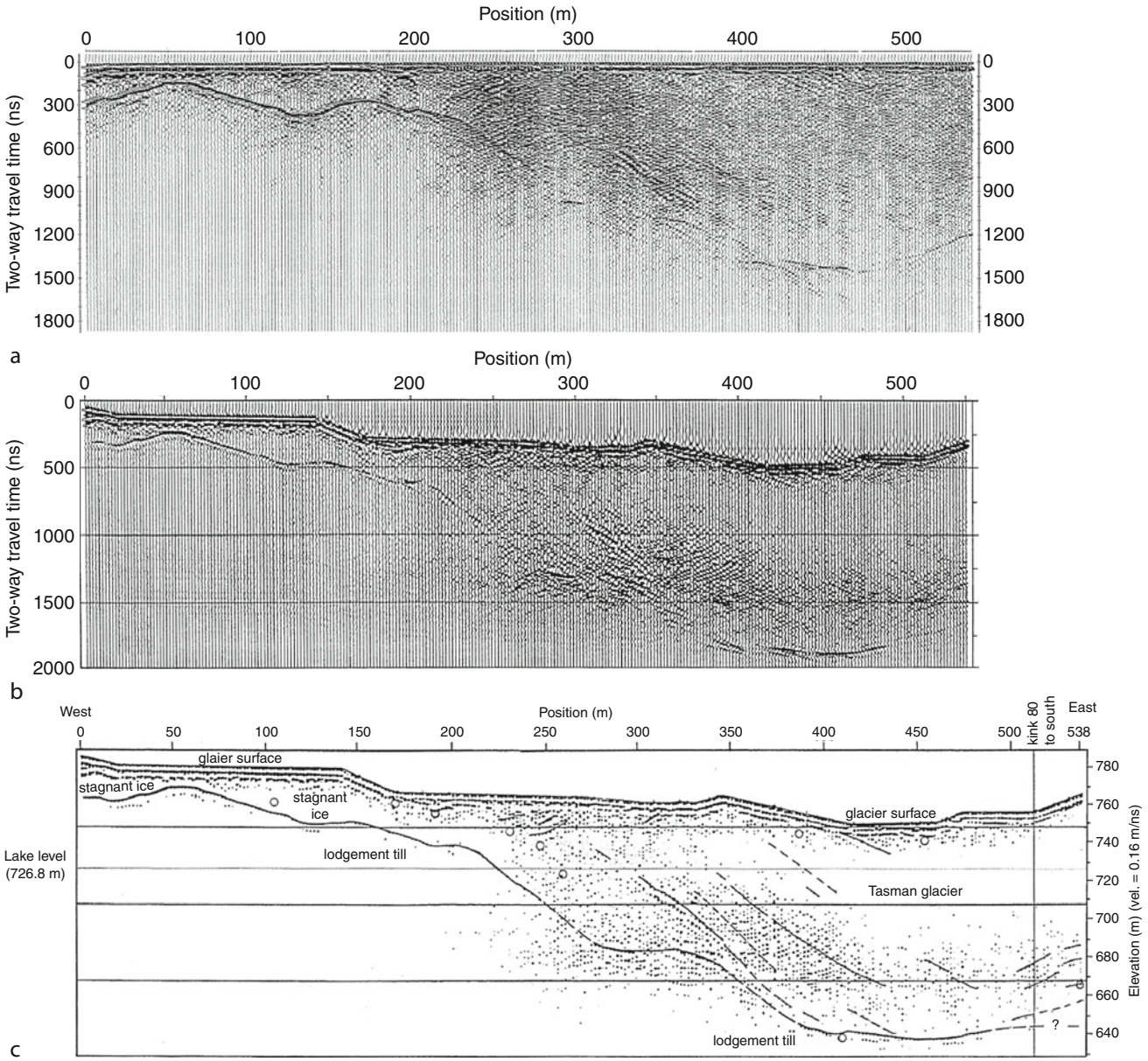

Ground Penetrating Radar Measurements Over Glaciers, Figure 11 Example raw, migrated and interpreted profiles. GPR profiles from the terminus of the Tasman Glacier showing the effects of processing, especially of migration. (**a**) The raw profile has significant energy from diffractions, and the basal reflection appears to be discontinuous. (**b**) When the profile is migrated and corrected for topography, the dipping bed in the centre becomes steeper and deeper. Where the dip shallows, the basal reflection becomes continuous, as it should be. The major diffractions have been collapsed, as they will if the correct velocity is used. (**c**) The migrated profile can then be interpreted. (Adapted and modified from Leary, 1993, and from Nobes et al., 1994.)

Internal Glacial Layers). This is at first glance counter-intuitive. Upon closer examination of the basic principles, this apparent contradiction can be explained.

First of all, the base of the ice shelf is rough (see *Bed Roughness*). The scale of the roughness is of the order of the resolution of the 100 MHz signal at that depth, of the order of 145 m. Thus the basal response appears as a set of diffractions. In contrast the high frequency signal shows a relatively continuous reflection from the ice shelf base. The attenuation of the radar signal in the ice of the McMurdo Ice Shelf is so low that even high-frequency signals are able to penetrate relatively large depths.

The lower frequency signal (100 MHz) showed more information about the layering because the transitions from one layer to the next are not sharp enough to cause high-frequency reflections. The reasons for this are illustrated in Figure 10. The high-frequency pulse simply refracts, or bends, at the boundary between the layers because the physical properties change slowly across a transition zone, whereas the low-frequency pulse "sees" the transition zone as a sharp boundary. Thus, in this case, the low-frequency signal yields more information on the layering. This is not uncommon, and has been observed, for example, in seismic surveys (e.g., Nobes and Schneider, 1996). The conclusion is that every site and the conditions present are unique, and the antennas and survey designs to use must be adapted to each site.

Migration and imaging

One of the last steps in the processing of GPR data is migration. Migration in essence is a mathematical inversion process that uses the velocity obtained from CMP, WARR, and diffraction analyses to collapse diffractions to their sources and place reflecting boundaries in their correct geometric positions (Sheriff, 2002, and Figure 11). Dipping boundaries, in particular, are steeper and deeper than they appear in raw radar profiles (compare Figure 11a and b). The migrated profile can then be properly interpreted, especially when topography is added to the top surface (Figure 11c). The velocity is used to convert the time to depth. However, we cannot always check that the velocities and thus the depths are correct, but when such tests have been done (e.g., Hochstein et al., 1995), the depths have often been confirmed, so long as the velocity determination has been completed correctly.

There are many ways to carry out migration (see Sheriff, 2002), but the traditional methods usually have an implicit assumption that the surface topography is small relative to the depth to the basal layers. This assumption is often false in glacier GPR; the topography can serve to significantly focus and de-focus the signal energy. In such instances, the topography becomes part of the migration process; the result is more effective at imaging layering and properly focussing reflections (Lehmann and Green, 2000).

Reflections of course do not occur in simple two-dimensional planes, but originate from complex three-dimensional (3D) beds and structures (see "*Bed (Bottom) Topography*" and "*Bed Load/Bedrock*"). The migration process, again, needs to take into account such complexities when they are present (Moran et al., 2003).

3D imaging provides additional information on subsurface structures and the continuity of layers and structures, including bedforms and basal hydrology (Moran et al., 2003; see also *Base Flow/Groundwater Flow*; *Bed Roughness*; *Glacier Hydrology*; *Subglacial Drainage System*), accumulation layers, the transition to firn, and englacial hydrological features (Jol et al., 2004; see *Firn*; *Mapping of Internal Glacial Layers*; *Temperate Glaciers*), and Antarctic permafrost polygonal patterned ground (Godfrey et al., 2008; see *Antarctica* and *Permafrost*). The logical extension to time lapse, or 4D (four-dimensional) imaging allows us to see whether the subsurface features we observe are evolving and changing with time, and to what extent (Godfrey et al., 2008; see also *Permafrost* and *Climate Change and Glaciers*).

Mars

No discussion on glacier GPR is complete without mention of Mars. The search for water or water ice on Mars necessarily involves radar methods, especially in permafrost environments on Earth (see *Antarctica* and *Permafrost*). The Antarctic Dry Valleys are a natural terrestrial analogue for the Martian environment, and have thus been a focus or at least a motivation for many such studies (Arcone et al., 2002; Berthelier et al., 2005; Godfrey et al., 2008), all of which show that radar has some promise in determining the presence and extent of Martian permafrost.

Summary

Ground penetrating radar is one of the predominant techniques to determine the thickness and internal structure of glaciers and other ice-rich environments, including layering and snow accumulation. The electric and dielectric properties which govern the propagation of radar signals allow radar to travel easily and far in snow and ice, even when laden with debris as in debris-covered and rock glaciers, or in mixtures of soil and ice as in permafrost. The directionality of the radar response tells us something about the structure and dynamics of the glacier, and the layering apparent in GPR profiles can be tied to accumulation rates and to particular isochrones for studies of paleoclimate. GPR imaging is providing not just 3D views of the subsurface, but time lapse imaging is allowing us to see those subsurface features change and evolve. The successful application of GPR on Earth will allow us to extend it to the search for water and water ice on Mars.

Bibliography

Annan, A. P., 1973. Radio interferometry depth sounding: Part l – Theoretical discussion. *Geophysics*, **38**, 557–580.

Annan, A. P., and Cosway, S., 1992. Ground penetrating radar survey design. In *Proceedings of the 4th Annual Symposium on*

Applications of Geophysics to Engineering and Environmental Problems (SAGEEP). Chicago, IL, pp. 329–351.

Arcone, S. A., 1995. Numerical studies of the radiation patterns of resistively loaded dipoles. *Journal of Applied Geophysics*, **33**, 39–52.

Arcone, S. A., 1996. High resolution of glacial ice stratigraphy; a ground-penetrating radar study of Pegasus Runway, McMurdo Station, Antarctica. *Geophysics*, **61**, 1653–1663.

Arcone, S. A., and Laatsch, J. E., 2004. Reversing the roles of high and low frequency to profile the dynamics of an ice shelf. In Slob, E., Yarovoy, A., and Rhebergen, J. (eds.), *GPR 2004: Proceedings of the 10th International Conference on Ground Penetrating Radar*, Delft, The Netherlands, pp. 781–784.

Arcone, S. A., Lawson, D. E., and Delaney, A. J., 1995. Short-pulse radar wavelet recovery and resolution of dielectric contrasts within englacial and basal ice of Matanuska Glacier, Alaska, USA. *Journal of Glaciology*, **41**, 68–86.

Arcone, S. A., Prentice, M. L., and Delaney, A. J., 2002. Stratigraphic profiling with ground-penetrating radar in permafrost; a review of possible analogs for Mars. *Journal of Geophysical Research*, **107**, 5108, doi:10.1029/2002JE001906.

Barrett, B. E., Murray, T., and Clark, R., 2007. Errors in radar CMP velocity estimates due to survey geometry, and their implication for ice water content estimation. *Journal of Environmental and Engineering Geophysics*, **12**, 101–111.

Berthelier, J. J., Bonaime, S., Ciarletti, V., Clairquin, R., Dolon, F., Le Gall, A., Nevejans, D., Ney, R., and Reineix, A., 2005. Initial results of the Netlander imaging ground-penetrating radar operated on the Antarctic ice shelf. *Geophysical Research Letters*, **32**, L22305, doi:10.1029/2005GL024203.

Bristow, C. S., and Jol, H. M. (eds.), 2003. *Ground Penetrating Radar in Sediments*. London: The Geological Society.

Copland, L., and Sharp, M., 2001. Mapping thermal and hydrological conditions beneath a polythermal glacier with radio-echo sounding. *Journal of Glaciology*, **47**, 232–242.

Daniels, D. J., 1996. *Surface-Penetrating Radar*. London: Institute of Electrical Engineers.

Davis, E. F., 2003. *Geophysical Investigation of the Pram Point Folds, McMurdo Ice Shelf, Antarctica*. M.Sc. thesis (Engineering Geology), Department of Geological Sciences, University of Canterbury, Christchurch, New Zealand.

Davis, J. L., and Annan, A. P., 1989. Ground penetrating radar for high-resolution of soil and rock stratigraphy. *Geophysical Prospecting*, **37**, 531–551.

Degenhardt, J. J., Jr., and Giardino, J. R., 2003. Subsurface investigation of a rock glacier using ground-penetrating radar; implications for locating stored water on Mars. *Journal of Geophysical Research*, **108**, 8036, doi:10.1029/2002JE001888.

Degenhardt, J. J., Jr., Giardino, J. R., and Junck, M. B., 2003. GPR survey of a lobate rock glacier in Yankee Boy Basin, Colorado, USA. In Bristow, C. S., and Jol, H. M. (eds.), *Ground Penetrating Radar in Sediments*. London: The Geological Society, pp. 167–179.

Delaney, A. J., Arcone, S. A., O'Bannon, A., and Wright, J., 2004. Crevasse detection with GPR across the Ross Ice Shelf, Antarctica. In *GPR 2004: Proceedings of the 10th International Conference on Ground Penetrating Radar*, Delft, The Netherlands, pp. 777–780.

Dunse, T., Eisen, O., Helm, V., Rack, W., Steinhage, D., and Parry, V., 2008. Characteristics and small-scale variability of GPR signals and their relation to snow accumulation in Greenland's percolation zone. *Journal of Glaciology*, **54**, 333–342.

Evans, S., 1963. Radio techniques for the measurement of ice thickness. *Polar Record*, **11**, 406–410.

Evans, S., 1969. Glacier sounding in the polar regions: A symposium. *The Geographical Journal*, **135**, 547–548, and the accompanying papers.

Fildes, J., and Williams, C., 2001. Glacier girl flies again. *New Scientist*, **172**, 58–61.

Fitzsimons, S. J., 2008. Sedimentary processes and landform formation at the margins of polar glaciers. *33rd International Geological Congress Abstracts*, **33**, Abstract 1360414.

Glover, J. M., and Rees, H. V., 1992. Radar investigations of firn structures and crevasses. In Pilon, J. (ed.), *Ground Penetrating Radar*, Geological Survey of Canada, Paper 90-4, pp. 75–84.

Godfrey, M. J., Bannister, M. T., Nobes, D. C., and Sletten, R. S., 2008. 3D time-lapse imaging of polygonal patterned ground in the McMurdo dry valleys of Antarctica. In *Proceedings of GPR2008: 12th International Conference on Ground Penetrating Radar*, Paper O12-6.

Heine, A. J., 1968. Brine in the McMurdo Ice Shelf, Antarctica. *New Zealand Journal of Geology and Geophysics*, **11**, 829–839.

Hinkel, K. M., Doolittle, J. A., Bockheim, J. G., Nelson, F. E., Paetzold, R., Kimble, J. M., and Travis, R., 2001. Detection of subsurface permafrost features with ground-penetrating radar, Barrow, Alaska. *Permafrost and Periglacial Processes*, **12**, 179–190.

Hochstein, M. P., Claridge, D., Henrys, S. A., Pyne, A., Nobes, D. C., and Leary, S. F., 1995. Downwasting of the Tasman Glacier, South Island, New Zealand; changes in the terminus region between 1971 and 1993. *New Zealand Journal of Geology and Geophysics*, **38**, 1–16.

Irvine-Fynn, T. D. L., Moorman, B. J., Williams, J. L. M., and Walter, F. S. A., 2006. Seasonal changes in ground-penetrating radar signature observed at a polythermal glacier, Bylot Island, Canada. *Earth Surface Processes and Landforms*, **31**, 892–909.

Jacobel, R. W., and Welch, B. C., 2005. A time marker at 17.5 kyr BP detected throughout West Antarctica. *Annals of Glaciology*, **41**, 47–51.

Jol, H. M., and Bristow, C. S., 2003. GPR in sediments: advice on data collection, basic processing and interpretation, a good practice guide. In Bristow, C. S., and Jol, H. M. (eds.), *Ground Penetrating Radar in Sediments*. London: The Geological Society, pp. 9–27.

Jol, H. M., Goodsell, B., Nobes, D. C., Finnemore, M., Cussins, T., de Passille, B., and Tealby, J., 2004. Preliminary results from high frequency GPR surveys and a 3D grid: Davis Snowfield, Franz Josef Glacier, New Zealand. In Slob, E., Yarovoy, A., and Rhebergen, J. (eds.), *GPR 2004: Proceedings of the 10th International Conference on Ground Penetrating Radar*, Delft, The Netherlands, pp. 773–776.

Kanagaratnam, P., Gogineni, S. P., Ramasami, V., and Braaten, D., 2004. A wideband radar for high-resolution mapping of near-surface internal layers in glacial ice. *IEEE Transactions on Geoscience and Remote Sensing*, **42**, 483–490.

Keller, G. V., 1982. Electrical properties of rocks and minerals. In Carmichael, R. S. (ed.), *Handbook of Physical Properties of Rocks*. Boca Raton, FL: CRC Press, pp. 217–293.

Kohler, J., Moore, J., Kennett, M., Engeset, R., and Elvehoy, H., 1997. Using ground-penetrating radar to image previous years' summer surfaces for mass-balance measurements. *Annals of Glaciology*, **24**, 355–360.

Kovacs, A., and Morey, R. M., 1978. Radar anisotropy of sea ice due to preferred azimuthal orientation of the horizontal c axes of ice crystals. *Journal of Geophysical Research C*, **83**, 6037–6046.

Lampe, B., 2003. Finite-difference time-domain modeling of ground-penetrating radar antenna systems. PhD dissertation, Institute of Geophysics, Swiss Federal Institute of Technology (ETH), Zurich, Switzerland.

Leary, S. F., 1993. Ground penetrating radar profiles of the Tasman and Mueller Glaciers. Unpublished B.Sc. (Honours) dissertation, Department of Geology, University of Canterbury, Christchurch, New Zealand.

Lehmann, F., and Green, A. G., 2000. Topographic migration of georadar data; implications for acquisition and processing. *Geophysics*, **65**, 836–848.

Leimbach, G., and Löwy, H., 1910a. Verfahren zur systematischen Erforschung des Erdinnern grösserer Gebiete mittels elektrischer Wellen. German patent 237944.

Leimbach, G., and Löwy, H., 1910b. Verfahren zum Nachweis unterirdischer Erzlager oder von Grundwasser mittels elektrischer Wellen. German patent 246836.

Macheret, Yu. Ya., Moskalevsky, M. Yu., and Vasilenko, E. V., 1993. Velocity of radio waves in glaciers as an indicator of their hydrothermal state, structure and regime. *Journal of Glaciology*, **39**, 373–384.

Machguth, H., Eisen, O., Paul, F., and Hoelzle, M., 2006. Strong spatial variability of snow accumulation observed with helicopter-borne GPR on two adjacent Alpine glaciers. *Geophysical Research Letters*, **33**, L13503, doi:10.1029/2006GL026576.

Matsuoka, K., Furukawa, T., Fujita, S., Maeno, H., Uratsuka, S., Naruse, R., and Watanabe, O., 2003. Crystal orientation fabrics within the Antarctic ice sheet revealed by a multipolarization plane and dual-frequency radar survey. *Journal of Geophysical Research*, **108**, 2499, doi:10.1029/2003JB002425.

Matsuoka, K., Thorsteinsson, T., Bjornsson, H., and Waddington, E. D., 2007. Anisotropic radio-wave scattering from englacial water regimes, Myrdalsjokull, Iceland. *Journal of Glaciology*, **53**, 473–478.

Maurer, H., and Hauck, C., 2007. Geophysical imaging of alpine rock glaciers. *Journal of Glaciology*, **53**, 110–120.

Moorman, B. J., and Michel, F. A., 2000. Glacial hydrological and system characterization using ground-penetrating radar. *Hydrological Processes*, **14**, 2645–2667.

Moran, M. L., Greenfield, R. J., and Arcone, S. A., 2003. Modeling GPR radiation and reflection characteristics for a complex temperate glacier bed. *Geophysics*, **68**, 559–565.

Morse, D. L., and Waddington, E. D., 1984. Recent survey of brine infiltration in the McMurdo Ice Shelf, Antarctica. *Annals of Glaciology*, **20**, 215–218.

Munroe, J. S., Doolittle, J. A., Kanevskiy, M. Z., Hinkel, K. M., Nelson, F. E., Jones, B. M., Shur, Y., and Kimble, J. M., 2007. Application of ground-penetrating radar imagery for three-dimensional visualisation of near-surface structures in ice-rich permafrost, Barrow, Alaska. *Permafrost and Periglacial Processes*, **18**, 309–321.

Murray, T., Booth, A., and Rippin, D. M., 2007. Water-content of glacier-ice; limitations on estimates from velocity analysis of surface ground-penetrating radar surveys. *Journal of Environmental and Engineering Geophysics*, **12**, 87–99.

Musil, M., Maurer, H., Hollinger, K., and Green, A. G., 2006. Internal structure of an Alpine rock glacier based on crosshole georadar traveltimes and amplitudes. *Geophysical Prospecting*, **54**, 273–285.

Nobes, D. C., 1999. The directional dependence of the ground penetrating radar response on the accumulation zones of temperate alpine glaciers. *First Break*, **17**, 249–259.

Nobes, D. C., and Annan, A. P., 2000. "Broadside" versus "End-fire" radar response: Some simple illustrative examples. In Noon, D. A., Stickley, G. F., and Longstaff, D. (eds.), *GPR 2000: Proceedings of the 8th International Conference on Ground Penetrating Radar*, Society of Photo-Optical Instrumentation Engineers (SPIE), Vol. 4084, pp. 696–701.

Nobes, D. C., and Schneider, G. W., 1996. Results of downhole geophysical measurements and vertical seismic profile from the Canandaigua borehole of New York state Finger Lakes. In Mullins, H. T., and Eyles, N. (eds.), *Subsurface Geologic Investigations of New York Finger Lakes: Implications for Late Quaternary Deglaciation and Environmental Change*, Geological Society of America Special Paper 311:51–63.

Nobes, D. C., Leary, S. F., Hochstein, M. P., and Henrys, S. A., 1994. Ground penetrating radar profiles of debris-covered glaciers: Results from the Tasman and Mueller Glaciers of the Southern Alps of New Zealand. In *Annual Meeting Program and Expanded Abstracts*, Society of Exploration Geophysicists, Vol. 64, pp. 826–829.

Nobes, D. C., Ferguson, R. J., and Brierley, G. J., 2001. Ground-penetrating radar and sedimentological analysis of Holocene floodplains: insight from the Tuross valley, New South Wales. *Australian Journal of Earth Sciences*, **48**, 347–355.

Nobes, D. C., Davis, E. F., and Arcone, S. A., 2005. "Mirror-image" multiples in ground penetrating radar. *Geophysics*, **70**, K20–K22.

Olsson, O., Falk, L., Forslund, O., Lundmark, L., and Sandberg, S., 1987. *Crosshole Investigations – Results from Borehole Radar Investigations*. Stripa Project Report 87-11, Stockholm: SKB.

Pälli, A., Kohler, J. C., Isaksson, E., Moore, J. C., Pinglot, J. F., Pohjola, V. A., and Samuelsson, H., 2002. Spatial and temporal variability of snow accumulation using ground-penetrating radar and ice cores on a Svalbard glacier. *Journal of Glaciology*, **48**, 417–424.

Pearce, D. C., and Walker, J. W., 1967. An empirical determination of the relative dielectric constant of the Greenland Ice Cap. *Journal of Geophysical Research*, **72**, 5743–5747.

Reynolds, J. M., 1997. *An introduction to applied and environmental geophysics*. West Sussex, England: Wiley.

Rigsby, G. P., 1960. Crystal orientation in glacier and in experimentally deformed ice. *Journal of Glaciology*, **3**, 589–606.

Rinker, J. N., and Mock, S. J., 1967. *Radar Ice Thickness Profiles Northwest Greenland*. Corps of Engineers, U.S. Army, Cold Regions Research and Engineering Laboratory (CRREL), Special Report 103.

Sheriff, R. E., 2002. *Encyclopedic dictionary of applied geophysics*, 4th edn. Tulsa, OK: Society of Exploration Geophysicists.

Spikes, V. B., Hamilton, G. S., Arcone, S. A., Kaspari, S., and Mayewski, P. A., 2005. Variability in accumulation rates from GPR profiling on the West Antarctic plateau. *Annals of Glaciology*, **39**, 238–244.

Steenson, B. O., 1951. *Radar Methods for the Exploration of Glaciers*. PhD thesis, California Institute of Technology, Pasadena, CA.

Stevens, C. W., Moorman, B. J., and Solomon, S. M., 2008. Detection of frozen and unfrozen interfaces with ground penetrating radar in the nearshore zone of the Mackenzie Delta, Canada. In *Proceedings of the 9th International Conference on Permafrost (ICOP)*, Fairbanks, Alaska, USA, pp. 1711–1716.

Stuart, G., Murray, T., Gamble, N., Hayes, K., and Hodson, A., 2003. Characterization of englacial channels by ground-penetrating radar; an example from austre Broggerbreen, Svalbard. *Journal of Geophysical Research*, **108**, 2525, doi:10.1029/2003JB002435.

Tillard, S., 1994. Radar experiments in isotropic and anisotropic geological formations (granite and schists). *Geophysical Prospecting*, **42**, 615–636.

Tiuri, M. E., Sihvola, A. H., Nyfors, E. G., and Hallikaiken, M. T., 1984. The complex dielectric constant of snow at microwave frequencies. *IEEE Journal of Oceanic Engineering*, **OE-9**, 377–382.

Topp, G. C., Davis, J. L., and Annan, A. P., 1980. Electromagnetic determination of soil water content: measurements in coaxial transmission lines. *Water Resources Research*, **16**, 574–582.

van Overmeeren, R. A., 1994. High speed georadar data acquisition for groundwater exploration in the Netherlands. In *GPR'94: Proceedings of the 5th International Conference on Ground Penetrating Radar*, Waterloo, Ontario, Canada, Vol. 3, pp. 1057–1073.

Waite, A. H., 1966. International experiments in glacier sounding, 1963 and 1964. *Canadian Journal of Earth Sciences*, **3**, 887–892.
Waite, A. H., and Schmidt, S. J., 1962. Gross errors in height indication from pulsed radar altimeters operating over thick ice or snow. *Proceedings of the Institute of Radio Engineers (IRE)*, **50**, 1515–1520.
Walker, J. W., Pearce, D. C., and Zanella, A. H., 1968. Airborne radar sounding of the Greenland Ice Cap: Flight 1. *Bulletin of the Geological Society of America*, **79**, 1639–1646.
Watanabe, T., Matsuoka, N., Christiansen, H. H., and Ikeda, A., 2008. Sounding ice and soil wedge structures with ground-penetrating radar. In *Proceedings of the 9th International Conference on Permafrost (ICOP)*, Fairbanks, Alaska, USA, pp. 1933–1938.
Watts, R. D., and Wright, D. L., 1981. Systems for measuring thickness of temperate and polar ice from the ground and from the air. *Journal of Glaciology*, **27**, 459–469.

Cross-references

Base Flow/Groundwater Flow
Bed (Bottom) Topography
Climate Change and Glaciers
Cold-Based Glaciers
Crevasses
Cryogenic Fabric
Debris
Debris-Covered Glaciers
Englacial Conduit
Englacial Processes
Firn
Greenland Ice Sheet
Ice
Iceland Glaciers
Mapping of Internal Glacial Layers
Meltwater Channels
Permafrost
Permafrost and Climate Interactions
Physical Properties of Snow
Radar Application in Snow, Ice, and Glaciers
Rock Glaciers
Scandinavian Glaciers
Sea Ice
Stratigraphy of Snowpacks
Structural Glaciology
Subglacial Drainage System
Temperate Glaciers
Transformations of Snow at the Earth's Surface and its Climatic and Environmental Consequences

H

HEAT AND MASS TRANSFER IN SEA ICE

Daniel J. Pringle
Arctic Region Supercomputing Center and Geophysical Institute, University of Alaska, Fairbanks, AK, USA

Definition

Heat and mass transfer in sea ice refers to the transport of, respectively, thermal energy and matter within and through sea ice.

Introduction

Sea ice is a boundary layer that mediates interactions between high-latitude oceans and the overlying atmosphere (Sea Ice). Heat and mass transport in sea ice underpin two well-known effects of sea ice: the ice-albedo feedback (Albedo, Energy Exchange over Snow and Ice Surfaces) and the effect of brine exclusion on thermohaline circulation (Dieckmann and Hellmer, 2003).

We here concentrate on the underlying mechanisms of the heat and mass transfer and the relevant ice properties. This short article is by no means exhaustive; for discussion of the connections with large-scale forcing and impacts, good starting points are the books of Wadhams (2000) and Thomas and Dieckmann (2003). Related processes not discussed here include sediment entrainment and transport by sea ice (e.g., Eicken et al., 2005) and the deposition of particulate matter from melting sea ice (Leventer, 2003).

The transfer of heat in sea ice is relevant to ice formation, persistence and decay, and, through the net surface energy balance, on the response of sea ice to changes in climate forcing (Thinning of Arctic Sea Ice). Mass transfer in sea ice relates mainly to the retention and passage of salts, gases, meltwater, pollutants, and biomass. The transfer of heat and mass are coupled. Sea ice is a porous medium with thermohaline equilibrium between pore-space brine and the surrounding ice. Brine, meltwater, and seawater may all flow through the pore space, transferring both heat and mass, and in the process changing the very properties of the ice that control these flows and transfers (Meltwater Fluxes due to Heat Fluxes, Meltwater Percolation).

Connection with sea ice structure, growth, and melt

The ability of heat and mass flow to flow through sea ice depends strongly on the salinity- and temperature-dependent structure. In general, sea ice is a porous, composite medium composed primarily of brine and gas inclusions within a matrix of pure ice (Sea Ice). Sea ice transport properties depend strongly on the volume fraction of brine and the pore space connectivity, which both depend on salinity and temperature (Weeks and Ackley, 1986; Eicken, 2003; Golden et al., 2007).

Brine motion may transfer both heat and mass. Given a temperature profile in the ice, there is a corresponding profile of equilibrium brine salinity given by the salinity–freezing point relationship. Brine motion due to drainage, flushing, or convective overturning may disturb this equilibrium (Weeks and Ackley, 1986; Eicken, 2003). Heat diffuses much faster than salt, so thermohaline equilibrium is restored as the ice around the inclusions either freezes, which releases latent heat, or melts, which absorbs latent heat.

Such changes to the pore space geometry of brine (and air) inclusions alter the fluid permeability, with feedbacks on fluid flow itself. Additional coupling of heat and mass transfer comes from the temperature-driven changes in the pore space permeability, and from the hydrology of surface melt ponds (Pringle and Ingham, 2009).

During sea ice growth, salts are excluded from the crystal lattice of ice and sea water is incorporated as intra-crystalline

Vijay P. Singh, Pratap Singh & Umesh K. Haritashya (eds.), *Encyclopedia of Snow, Ice and Glaciers*, DOI 10.1007/978-90-481-2642-2,

layers and in-grain boundaries. This brine exclusion makes sea ice less saline than sea water and has strong oceanographic impacts. Ice formation, typically in autumn and winter, therefore constitutes a salt flux into the upper ocean. Likewise, melt in spring and summer represents a flux of fresh water or a negative flux of salt. The overall effect is a delayed mass transfer, with significant effects on physical and biogeochemical aspects of polar oceanography (e.g., Dieckmann and Hellmer, 2003).

The desalination of warming sea ice leads to the important distinction between first year (FY) ice and multi-year (MY) ice. MY ice has undergone at least one melt season during which brine drainage and flushing significantly reduce the bulk sea ice salinity. This process is strongly coupled to the thermal evolution of the ice, and therefore heat transfer. As it warms, sea ice "rots from the inside out." The volume and connectivity of brine inclusions both increase, allowing drainage of internal brine layers, pockets, and channels. This increase in permeability also allows percolation through the ice of surface melt ponds formed from melted snow and ice (e.g., Freitag and Eicken, 2003).

Heat transfer and sea ice thermal properties

Sea ice growth involves the conduction to the atmosphere of latent heat released during freezing. Growth rates and thermal evolution are controlled by oceanic and atmospheric heat fluxes, the thermal conductivity, specific heat, and enthalpy of the ice (Weeks and Ackley, 1986; Eicken, 2003) (Physical Properties of Snow). Heat flow in sea ice is generally dominated by conduction, that is, molecular diffusive heat transfer. As air and brine have lower thermal conductivities than pure ice, effective medium models have been developed for various inclusion geometries to predict the bulk sea ice conductivity as a function of salinity, density, and temperature (Yen, 1981; Pringle et al., 2007). Conductivity measurements are difficult to make but in good general agreement with predictions. Specific heat measurements are in excellent agreement with predictions. The conductivity k (W m^{-1} K^{-1}) and specific heat c (J kg^{-1} K^{-1}) can be calculated by (Pringle et al., 2007).

$$k = \frac{\rho}{\rho_i}\left(2.11 - 0.011\,T + 0.09\frac{S}{T} - 0.01(\rho - \rho_i)\right),$$

$$c = 2113 + 7.5 - 3.4\,S + 0.08ST + 18040\frac{S}{T^2},$$

where ρ is sea ice bulk density (kg m^{-3}), S is sea ice bulk salinity (ppt, i.e., parts per thousand by weight), T is temperature (°C), and the subscript i indicates fresh ice.

The thermal conductivity of snow is an order of magnitude less than ice, meaning 10 cm of snow has an insulating effect of about 1 m of sea ice, and even thin snow cover can strongly reduce conductive heat flow (Sturm et al., 2002). Direct radiative heating of near-surface ice can occur in spring and summer (Eicken, 2003; Ehn et al., 2008).

Heat flow may be enhanced by convective and advective heat transport caused by fluid flow. If down-flowing, cold, saline brine is replaced with lower-salinity brine from below, there is a net transfer of sensible and (through refreezing) latent heat from ocean to atmosphere. The size of this contribution depends on location and ice type. In land-fast FY ice, the convective contribution to the spring/winter heat flux has been estimated as a few percent of the total winter heat flow (Pringle et al., 2007). In cold, low-salinity MY ice, the contribution will be less. Observations in FY Antarctic ice show significant heat flow associated with upwelling sea water when the high snow loading suppresses the ice/snow interface below sea level (Lytle and Ackley, 1996). Surface flooding can here lead to the formation of superimposed ice with the release of latent heat.

Mass transfer, fluid flow, and permeability

In general, mass transfer in sea ice is a by-product of fluid flow. Brine motion in a porous medium like sea ice is described by Darcy's law (e.g., Freitag and Eicken, 2003). The volumetric specific discharge q (m^3 s^{-1} m^{-2}) along a pressure gradient ∇P (Pa m^{-1}) is

$$q = -\frac{\Pi}{\mu}\nabla P,$$

where μ (kg m^{-1} s^{-1} = Pa s) is fluid dynamic viscosity and Π (m^2) is ice permeability. At sufficiently fast flow, turbulence occurs, resulting in energy dissipation and less flow than predicted by Darcy's law. The transition between laminar and turbulent flow occurs for a critical value of the dimensionless Reynolds number: $Re_c = \rho$ U l/μ , were ρ is density, μ dynamic viscosity, U mean fluid velocity, and la characteristic length scale. For complex porous media like sea ice, l is an average pore diameter and Re_C = 1–10 (Freitag and Eicken, 2003). Both laminar and turbulent flows have been observed and analyzed in sea ice permeability measurements (Freitag and Eicken, 2003). The origin of pressure gradients driving fluid flow include the hydraulic head of dense cold brine in ice above the freeboard, surface melt ponds, and density instabilities in brine inclusions and networks.

The fluid permeability depends on the pore-space connectivity and hence, the brine volume fraction, v_b. The permeability spans six orders of magnitude from 10^{-13} to 10^{-6} m^2, nearly half the range of all geological materials. Various parameterizations of permeability are presented in Petrich et al. (2006), Golden et al. (2007), and Pringle and Ingham (2009). Sea ice exhibits threshold behavior, being essentially impermeable for $v_b < 5\%$ (e.g., Freitag and Eicken, 2003; Petrich et al., 2006). For typical FY ice with S = 5 ppt, this threshold corresponds to about −5°C, easily remembered as the "rule of fives" (Golden et al., 1998).

Percolation theory has been applied to both the bulk permeability and connectivity of intracrystalline brine inclusions (Golden et al., 2007; Pringle et al., 2009).

The wide range in permeability is due to permeability scaling with the radius squared of restrictions in the flow path. Drainage of surface melt ponds can be greatly accelerated by seal breathing holes (up to a meter in diameter), or inhibited by impermeable "superimposed ice" formed early in the melt season by refreezing snowmelt (Refreezing of Meltwater). The detailed heat and mass budgets of melt ponds remains an area of active research.

Outlook: ecological and environmental aspects

Sea ice supports large communities of microorganisms in the thin, high-porosity skeletal layer at the ice base (Thomas and Papadimitriou, 2003). For these communities, there are beneficial and harmful mass transfers. First, they rely on the ongoing delivery of nutrients from the ocean. Modeling shows the advective volume flux F_V through the skeletal layer (the volume of water per time and interface area) to be 1–100 times the ice growth rate dh/dt, and to scale as $F_V \propto (dh/dt)^{1/2}$ (Chris Petrich, personal communication, 2008).

Second, under-ice pollutants may also enter through the skeletal layer (Pfirman et al., 1995). Recent renewed interest in Arctic oil development raises the potential for the under-ice spills. With a density of about 800 kg m^{-3}, crude oil is buoyant in water and ice, and will migrate up into sea ice as allowed by pore-space connectivity and surface tension constraints.

Bibliography

Dieckmann, G. S., and Hellmer, H. H., 2003. The importance of sea ice: an overview. In Thomas, D. N., and Dieckmann, G. S. (eds.), *Sea Ice, An Introduction to its Physics, Chemistry, Biology and Geology*. Oxford: Blackwell, pp. 1–21.

Ehn, J. K., Papakyriakou, T. N., and Barber, D. G., 2008. Inference of optical properties from radiation profiles within melting landfast sea ice. *Journal of Geophysical Research*, **113**, C09024, doi:10.1029/2007JC004656.

Eicken, H., 2003. From the microscopic, to the macroscopic, to the regional Scale: growth, microstructure and properties of sea ice. In Thomas, D. N., and Dieckmann, G. S. (eds.), *Sea Ice, An Introduction to its Physics, Chemistry, Biology and Geology*. Oxford: Blackwell, pp. 22–81.

Eicken, H., Gradinger, R., Graves, A., Mahoney, A., and Rigor, I., 2005. Sediment transport by sea ice in the Chukchi and Beaufort Seas: Increasing importance due to changing ice conditions? *Deep-Sea Research II*, **52**, 3281–3302.

Freitag, J., and Eicken, H., 2003. Melt water circulation and permeability of Arctic summer sea ice derived from hydrological field experiments. *Journal of Glaciology*, **49**, 349–358.

Golden, K. M., Ackley, S. F., and Lytle, V. I., 1998. The percolation phase transition in sea ice. *Science*, **282**, 2238–2241.

Golden, K. M., Eicken, H., Heaton, A. L., Miner, J. E., Pringle, D. J., and Zhu, J., 2007. Thermal evolution of permeability and microstructure in sea ice. *Geophysical Research Letters*, **34**, L16501, doi:10.1029/2007GL030447.

Leventer, A., 2003. Particulate flux from sea ice in polar waters. In Thomas, D. N., and Dieckmann, G. S. (eds.), *Sea Ice, An Introduction to its Physics, Chemistry, Biology and Geology*. Oxford: Blackwell, pp. 303–332.

Lytle, V. I., and Ackley, S. F., 1996. Heat flux through sea ice in the western Weddell Sea: Convective and conductive transfer processes. *Journal of Geophysical Research*, **101(C4)**, 8853–8868.

Petrich, C., Langhorne, P. J., and Sun, Z. F., 2006. Modelling the interrelationships between permeability, effective porosity and total porosity in sea ice. *Cold Regions Science and Technology*, **44**, 131–44, doi:10.1016/j.coldregions.2005.10.001.

Pfirman, S. L., Eicken, H., Bauch, D., and Weeks, W. F., 1995. The potential transport of pollutants by Arctic sea ice. *The Science of the Total Environment*, **159**, 129–146.

Pringle, D. J., and Ingham, M., 2009. Thermal, electrical and hydraulic properties of sea ice. In Eicken, H. et al. (eds.), *Field techniques for Sea Ice Research*. Fairbanks: University of Alaska Press, pp. 141–179.

Pringle, D. J., Eicken, H., Trodahl, H. J., and Backstrom, L. G. E., 2007. Thermal conductivity of landfast Antarctic and Arctic sea ice. *Journal of Geophysical Research*, **112**, C04017, doi:10.1029/2006JC003641.

Pringle, D. J., Miner, J. E., Eicken, H., and Golden, K. M., 2009. Pore space percolation in sea ice single crystals. *Journal of Geophysical Research*, **114**, C12017, doi:10.1029/2008JC005145.

Sturm, M., Perovich, D. K., Holmgren, J., 2002. Thermal conductivity and heat transfer through the snow on the ice of the Beaufort Sea. *Journal of Geophysical Research*, **107**, C10, SHE 19-1, doi:10.1029/2000JC000409.

Thomas, D. N., and Dieckmann, G. S. (eds.), 2003. *Sea Ice, An Introduction to its Physics, Chemistry, Biology and Geology*. Oxford: Blackwell, pp. 22–81.

Thomas, D. N., and Papadimitriou, S., 2003. Biogeochemistry of sea ice. In Thomas, D. N., and Dieckmann, G. S. (eds.), *Sea Ice, An Introduction to its Physics, Chemistry, Biology and Geology*. Oxford: Blackwell, pp. 267–302.

Wadhams, P., 2000. *Ice in the Ocean*. Amsterdam: Gordon Breach.

Weeks, W. F., and Ackley, S. F., 1986. The growth, structure of sea ice. In Untersteiner, N. (ed.), *The Geophysics of Sea Ice*. NATO ASI Series B: Physics, 146. New York: Plenum, pp. 9–16.

Yen, Y. -C., 1981. Review of thermal properties of snow, ice and sea ice. *CRREL Report 81–10*, U.S. Army Cold Reg. Res. and Eng. Lab., Hanover, NH.

Cross-references

Albedo
Meltwater Conduit
Sea Ice
Surface Energy Balance
Thinning of Arctic Sea Ice

HIGH ELEVATION GLACIO-CLIMATOLOGY

Vladimir Aizen
College of Science, University of Idaho, Moscow, ID, USA

Definition

Scientific study of the complex processes of climate and cryosphere interaction at high elevation (HE) mountains over a period of time ranging from months to thousands or millions of years. Reconstruction of past and modeling of modern and future climate variations are generally based on isotope-geochemistry and micro-biological analysis of HE ice-cores, borehole ice temperatures, modern meteorological observations, and remote sensing information.

Introduction

The HE glacio-climatology emphasizes on the statistical description in terms of the mean and variability of numerous glacio-meteorological and actinometrical elements and detail studies of the processes of interaction between snow/ice land-surface and atmosphere at HE environment and its feedback to climate and atmosphere circulation. The results of HE glacio-climatological investigations improve the regional and local energy balance/atmosphere circulation models and assist in study of the modern and past climate variability and water resources changes. The information from HE glacio-meteorological observations (Figure 1) delivers essential contribution to study alpine climate, alpine hydrology, and to estimate precisely the freshwater resources in regions where water demand has been projected to continuously rise, but where seasonal snow cover, glaciers, and permafrost cannot continue indefinitely to waste away. Our knowledge of HE glacio-climatology at alpine environment is limited by both difficulties to access HE areas and the paucity of observations, short records that seldom span lesser than 100 years, and a sparse station network and insufficient scientific attention given to the complex interaction of spatial scales in weather and climate phenomena in HE mountains.

Climate

Climate controls the cryosphere processes in HE area, that is, surface energy balance, snow and glacier ice accumulation and ablation, extension of seasonal snow covered areas, glacier mass balance and glacier dynamics, depth of permafrost active layer, permafrost dynamics, and land surface geomorphic activity. Glaciers grow and shrink in response to climatic changes and, therefore, glaciers are considered as sensitive indicators of climate change. The rise of global air temperature (IPCC, 2001) for the last century caused the mountain glaciers around the world to generally decrease in area and volume. From the standpoint of geographical determination, there are three factors that control the HE glacier climate, that is, latitude, topography, and level of continentality. There is a wide range of glacio-climate conditions that exist over the glaciers of Alaska to subtropical/tropical Himalayas to equatorial Andes' to Scandinavian marine areas to Central Asian/Tibetan areas.

Atmosphere is sensitive to physical changes at its low boundary, that is, at the earth surface. Snow cover and extended glacierized massive/caps are recognized as important factors influencing the climate both at the regional and local scales. The large HE glacier massifs deform air masses flows, barometric waves, and pressure field. There is a jump in energy/radiation balance, air temperature, and relative humidity between glacial/snow and non-glacial/non-snow surfaces. At HE, where there is snow/glacier cover, the sharp increased albedo (up to 85% of fresh snow; Gray and Male, 1981) causes reduction in absorbed short wave radiation and, consequently, net radiation decreases (20–30%; Barry, 1992). During ablation season, the amount of energy used to melt snow is of the same order as the combination of other components of the heat budget (e.g., heat associated with atmospheric advection, radiation balance, and turbulent heat exchange) (Aizen et al., 2000). The difference in air temperature between glacier and non-glacier surfaces is about 1–2°C (Krenke, 1982) in summer at the equilibrium line altitude. The cooling of atmosphere over glacier depends on glacier size, albedo, air temperature, latitude, and cloudiness. For example, the air balloon meteorological observations over one of the world's largest Fedchenko Glacier (Pamir) exhibits 1.5°C summer air temperature lower than at 5,000 m a.s.l. over the Pamir plains (Djodjio et al., 1962).

High Elevation Glacio-Climatology, Figure 1 High elevation glacio-climatological monitoring, Gongga Glacier, South-Eastern Tibet (photo by V. Aizen, 1990).

Over the glaciers, the radiation contributes more energy in the heat balance than the turbulent heat. Evaporation process is typical for the ablation zone of glaciers, while the condensation is a prevailing process over the accumulation field of glaciers. In regions with dry climate, glaciers evaporate moisture and wet the atmosphere, while in regions with humid climate, glaciers condensate moisture on their surface. HE glaciers catch the solid precipitation for decades, sometimes for thousands of years from global water cycle.

Cooling of atmosphere from extended glaciers develop continuous cold katabatic winds over the large glacierized massif that could decrease turbulent exchange, which results in minor contribution from sensible heat transfer in the heat balance of glaciers. Strong katabatic winds suppress precipitation, but favor evaporation reducing glacier melt even in the ablation zone. Human life and society are strongly depending on the heterogeneous precipitation distribution and weather changes due to this water and energy cycle processes.

Snow

Snow cover in HE mountains is the most important source of meltwater and heat exchange between surface and near surface atmosphere in HE areas. Seasonal snow contributes up to 60% of snowmelt runoff in non-glacial catchments (Aizen et al., 1996). Over the Tien Shan HE mountains, energy used for snowmelt amounted to 3×10^{13} MJ year^{-1} with a maximum from the end of spring to the middle of summer. The annual air volume cooled 5°C by snowmelt amounted, on average, to 10^7 km^3 year^{-1}. Heating of the air would have been three times higher if snowmelt had not occurred. Over the mountains, energy used for snowmelt amounted to about one third of heat loss in the continental plains. The difference in the proportions occurred as a result of lesser air thickness in mountains than over plains that allowed cooling a larger air volume in mountains under the same amounts of heat losses. The process of snow ablation and atmospheric cooling in mountains due to snowmelt occurs more slowly and without abrupt changes observed on the plains, and energy losses in mountains smooth the general processes of atmospheric cooling prolonging it until the beginning of autumn, that is, appearing new snow (Aizen et al., 2000). The feedback of the spring and summer snow ablation can explain the long-term rise in air temperatures, which is more pronounced from June to August (Aizen et al., 1997) when maximum energy losses from snowmelt occurs over the mountainous areas. The study of seasonal snow cover extension and the energy spent during the snowmelt are important in developing the regional and global climatic models.

Glaciers

Glacier ice at HE mountains presently covers approximately 3% of the Earth's total land surface or 500,000 km^2 and stores about 180,000 km^3 of the world's freshwater (Benn and Evans, 1998). Large HE glacierized areas, such as the Fedchenko Glacier in Pamir, Inylchek Glacier in Tien Shan, or Siachen Glacier in Karakoram are supplying water and generating river flow, which is vital not only for the millions of people living downstream, but also for forestry, agriculture, industry, and urban areas in adjacent lowlands. The glacier meltwater is particularly important when the lower courses flow through semi-arid and arid regions with high evaporation rates and high demands for irrigation water during the vegetation period in many mid-latitude areas adjacent to mountain systems, such as Alps, Andes, the mountains of central Asia and western China. Rapid glacier recession in mid- low-latitude mountain regions is a major concern in assuring freshwater resources for the future. A decrease in glacial and seasonal snow-covered areas reduces the portions of water in total river runoff, increasing the proportion of precipitation runoff. Although it has been demonstrated that total water quantity from glacier wastage is relatively small, the timing of release of those waters are critical. It is in years of generally low flow that glacier wastage contributes most and it is in late summer (when evaporation rates are high and when demand for water is also high) that glaciers make their biggest contributions to stream flow. Changes in seasonal precipitation, snow cover, and glacier melt regimes in HE mountains are already causing concern for water supply, agriculture, and hydropower in central Asian countries. Furthermore, study of high elevation glaciers allow to integrate climate variations over a wide range of time scales, making them natural sensors of climate variability and providing a visible expression of climate changes preserving climatic signatures, which can be used to reconstruct past climatic and environmental records in mid- low-latitudes through the glacier deep ice-cores isotope-geochemical analyses. The ice-coring research, paleo-climatic and environmental reconstructions at mid- low- latitudes, is the important part of high elevation glacio-climatology.

Conclusion

Glacio-climatological studies are an important part of geoscience that links global system involving global energy sources, the hydrological cycle, the atmospheric circulation, climate and physics of snow, glaciers, and permafrost.

Bibliography

Aizen, V. B., Aizen, E. M., and Melack, J., 1996. Precipitation, melt and runoff in the Northern Tien Shan. *Journal of Hydrology*, **186**, 229–251.

Aizen, V. B., Aizen, E. M., Melack, J., and Dozier, J., 1997. Climatic and hydrologic changes in the Tien Shan, Central Asia. *Journal of Climate*, **10**, 1393–1404.

Aizen, E. M., Aizen, V. B., Melack, J. M., and Krenke, A. N., 2000. Heat exchange during snow ablation in plains and mountains of Eurasia. *Journal of Geophysical Research-Atmospheres*, 105, D22: 22,013-27,022.

Barry, R. G., 1992. *Mountain Weather and Climate*. Routledge: London and NY, pp. 1–402.

Benn, D. I., and Evans, D. J. A., 1998. *Glaciers and glaciations*. London: Arnold.
Djodjio, V. A., Kolesnikova, V. N., Petrosyance M. A., 1962. Nekotorie cherty climate visokogornih raionov po nabludeniyam na lednike Fedchenko (High elevation Some climatic characteristics of high elevation areas by observations on the Fedchenko Glacier). 2, MGD, M., pp. 144–160.
Gorbunov, A. P., Marchenko, S. S., Severskiy, E. V., and Titkov, S. N., 1997. Geocryological condition changes in the Northern Tien Shan in connection with global climate warming. *Hydrometeorology and Ecology*, **3**, 97–109 (in Russian).
Gray, D. M., and Male, D. H. (eds.), 1981. *Handbook of Snow*. Pergamon: Toronto, pp. 1–751.
Krenke, A. N., 1982. Mass-exchange of glacier systems on USSR territory. Leningrad: Hydrometeo, pp. 1–288 (Russ.).
Satomura, T., 2000. Diurnal variation of precipitation over the Indo-China peninsula: Two dimensional numerical simulation. *Journal of the Meteorological Society of Japan*, **78**, 461–475.
Tucker, D. F., and Crook, N. A., 1999. The generation on a mesoscale convective system from mountain convection. *Monthly Weather Review*, **127**, 1259–1273.
Vilesov, E. N., and Belova, I. V., 1989. Reserves of Ice and General Features of Modern Glaciation of the Tien Shan Geocryological Research in the Mountains of USSR, Yakutsk, pp. 117–130 (in Russian).
Yanai, M., and Li, C., 1994. Mechanism of heating and the boundary layer over the Tibetan Plateau. *Monthly Weather Review*, **122**, 305–323.

HIMALAYA

John F. Shroder
Department of Geography and Geology, University of Nebraska at Omaha, Omaha, NE, USA

Introduction

The term "Himalaya" is a Sanskrit word that means "abode of snow." As the highest mountains in the world, the Himalaya are the so-called water towers of Asia whose snow and ice meltwaters provide essential irrigation, hydroelectricity, potable water, and other uses to billions of people downstream. The Himalaya are the product of plate tectonic collision of an Indian plate that broke from the Southern Hemisphere supercontinent of Gondwanaland in Mesozoic time, to eventually push inexorably north into the Asian plate during the Cenozoic. The mountain uplift of the Himalaya resulted from this slow upward thrusting of the mighty ranges as the two plates became progressively sutured together. The ongoing collision, which continues today at about the rate that fingernails grow, has resulted in more >7,000 and >8,000 m high peaks than anywhere else in the world. Where these peaks effectively trap moisture from the wintertime westerly winds and the summertime monsoon, the precipitation at such altitudes accumulates as snow and ice, with the result that the Himalaya host glacier stores of accumulated frozen water that is released later when it melts.

Himalayan orography is complex because of the long history of uplift and the diversity of geological mountain-building mechanisms that have occurred there. The result is a vast sweep of ranges from the so-called Pamir knot on the west to the complex of approximately north–south-trending, parallel ranges and rivers in south China, some 2,600 km to the east. In general, the Himalaya are marked at both the west and east ends by geological syntaxial bends in rock structures wherein the tight, fault-bounded, "trapdoor" or "pop-up" uplifts of Nanga Parbat on the west and Namche Barwa on the east have occurred in the past few million years. In the most modern *tectonic aneurysm model* of these uplifts (Zeitler et al., 2001a, b), the geomorphic diversion of the great Indus River and the Tsangpo-Brahmaputra by headward erosion of small rivers that undercut and captured these huge river discharges is thought to have so rapidly eroded the upper surfaces of the rocks that the crust of the Earth was thereby weakened at those locations and rose rapidly upward in a highly localized fashion. But in spite of the syntaxial uplifts that more or less mark the ends of the Himalaya, especially on the wider west end, a number of other ranges also occur somewhat further away that are included in Table 1.

In fact if one observes a map of the overall planimetric shape of the Himalaya without including the Tibetan Plateau as well, it is immediately apparent that the mountain range is wider on its western end than it is on the east. This is in large part an accident of the geometry of the way the crustal plates of the Earth became sutured together, with more crustal plate fragments being incorporated on the west over a longer time than on the east. Thus, the simplest organization of the geography of the Himalaya is one of the older subdivisions by Burrard and Hayden (1907–1908). This was done at the time, for example, wherein the main points for consideration of subdivision of the mountain range were done only in a weak topographic sense (river locations and general peak altitudes), and not in any true topographic or geologic sense. In some cases mountain range names were carried erroneously from the west (Ladakh Range) far into the east where clearly few would use that terminology.

In addition certain unusual regions at the east and west ends of the Himalaya came to be what is now known as the western syntaxis in Pakistan where the Indus River gorge incises into the Nanga Parbat – Haramosh massif uplift, and the eastern syntaxis in China where the Tsangpo-Brahmaputra cuts through the Namche Barwah – Gyala Pelri massif uplift. This division by syntaxes as to what constitutes the Himalaya may make some limited sense, especially at the wetter and more forest covered east end in China where less is known geologically, but not at the drier and more exposed west end in Pakistan. Here ending the Himalaya at the syntaxial bend is a topographic and geologic oversimplification because it entirely neglects directly contiguous and connecting ranges that are genetically linked to the main Himalaya. A further problem arises in that the topographic and geologic complexities at both ends of the Himalaya are of quite high altitude as well,

Himalaya, Table 1 Physical divisions of the Himalaya mountains (*sensu lato*), extending from Pakistan on the west, through northwest India, Nepal, and Chinese Tibet in the middle to northeast India and China on the east, with emphasis on mountains high enough to support past glaciation or present-day glacierization (after Burrard and Hayden, 1907–1908; Mason, 1955; Grötzbach, 1990; Neate, 1978; Neate, 1989; Bolinder et al., 1990; Bhutan, 2006; Bhutan Himalaya, 1996; Bossart, 1981; Karan, 1969; National Atlas of India, 1964; Verlag, 2008). Individual mountain massifs >7,000 m are named (after Neate, 1989). A number of directly peripheral ranges in Chinese Tibet are included in this table, although they are not considered further as part of the Himalaya

Western (Punjab) Himalaya (Pakistan, India, China)

1.0 Hindu Raj — Can be considered a part of a Lesser Himalaya of the west, although that term generally is not used in this region.
2.0 Kohistan ranges
- 2.1 Dir Kohistan
- 2.2 Swat Kohistan
- 2.3 Indus Kohistan

3.0 Pir Panjal — Occurs in both the western and central Himalaya.
4.0 Great Himalaya
- 4.1 Nanga Parbat massif
  - Nanga Parbat (8,126 m)
  - Raikot (7,070 m)
  - Mazeno
- 4.2 Pangi range
- 4.3 Nun Kun massif
  - Nun (7,135 m)
  - Kun (7,086 m)

5.0 Inner Himalaya
- 5.1 Deosai mountains
- 5.2 Zanskar range — Occurs in both western and central Himalaya.
- 5.3 Ladakh range — Occurs in both western and central Himalaya.

6.0 Lesser (South) Karakoram Himalaya of the trans-Himalaya
- 6.1 Naltar range
- 6.2 Rakaposhi range-Haramosh range (including Spantik-Sosbun Mtns)
  - Rakaposhi (7,788 m)
  - Diran (Minapin) (7,257 m)
  - Malubiting (7,458 m)
  - Haramosh (7,409 m)
  - Spantik (Ghenish Chhish, Pyramid peak, Golden Parri) (7,027 m)
- 6.3 Masherbrum (7,821 m) range
  - Baltistan peak (K6) (7,821 m)
  - Link Sar (7,041 m)
  - Chogolisa (Bride peak) (7,665 m)
  - Baltoro Kangri (Golden Throne) (7,240 m)
  - Yermanendi Kangri (7,260 m)
- 6.4 Saltoro range
  - Saltoro Kangri (7,742 m)
  - Sherpi Kangri (7,380 m)
  - Depak (7,150 m)
  - K12 (7,428 m)

7.0 Greater Karakoram Himalaya of the trans-Himalaya
- 7.1 Lupghar mountains
- 7.2 Batura Muztagh
  - Batura (7,795)
  - Kampire Dior (Karambar Sar) (7,143 m)
  - Muchu Chhish (7,453 m)
  - Pasu (7,284 m)
  - Shispare (7,611 m)
  - Bojohagur Duanasir (Ultar) (7,329 m)
- 7.3 Hispar Muztagh
  - Lupghar Sar (7,200 m)
  - Momhil Sar (7,343 m)
  - Trivor (7,728 m)
  - Malangutti Sar (7,025 m)
  - Disteghil Sar (7,885 m)
  - Bularung Sar (7,200 m)
  - Yazghil (7,559 m)
  - Khunyang Chhish (7,852 m)
  - Pumari Chhish (7,492 m)
  - Yukshin Gardan Sar (7,530 m)
  - Yutmaru Sar (7,330 m)
  - Kanjut Sar (7,760 m)
- 7.4 Panmah Muztagh
  - Baintha Braak (Ogre) (7,285 m)
  - Latok (7,145 m)
  - Changtok (Chiring) (7,091 m)
- 7.5 Baltoro Muztagh
  - Muztagh tower (7,273 m)
  - Chongtar (7,370 m)
  - Skil Brum (7,360 m)
  - K2 (8,611 m)
  - Skyang Kangri (Staircase peak) (7,544 m)
  - Broad peak (8,047 m)
  - Gasherbrum (Hidden peak) (8,068 m)
  - Urdok (7,300 m)
- 7.6 Siachen Muztagh
  - Sia Kangri (7,422 m)
  - Singhi Kangri (7,202 m)
  - Teram Kangri (7,462 m)
  - Apsarasas (7,245 m)
- 7.7 Rimo (7,385 m) Muztagh
  - Chong Kumdan (7,069 m)
  - Mamostong Kangri (7,516 m)
- 7.8 Saser Muztagh
  - Saser Kangri (7,672 m)

8.0 Lesser (North) Karakoram Himalaya of the trans-Himalaya
- 8.1 North Ghujerab mountains
- 8.2 South Ghujerab mountains
  - Karun Kuh (7,350 m)
- 8.3 Wesm mountains
  - Crown (Huang Guan Shan) (7,265 m)
- 8.4 Aghil range
- 8.5 Mushin-Ta-Ko-Shan
- 8.6 Mustagh Ata range (not on map)

9.0 Pangong range (Tibetan highlands of China)
10.0 Chang Chenmo range (Tibetan highlands of China)
11.0 Kailas range (Gangdise Shan) (Tibetan highlands of China – not on map)

Central (Garhwal or Kumaun [Kumaon], and Nepal) Himalaya (India, China, Nepal)

12.0 Lesser Himalaya (Garhwal and Nepal)
- 12.1 Dhauladhar range
- 12.2 Nag Tibba range
- 12.3 Mahabharat range

13.0 Great Himalaya (Garhwal)
- 13.1 Gangotri group
  - Chaukamba (7,138 m)
  - Satopanth (7,075 m)

Himalaya, Table 1 (Continued)

- 13.2 Kamet group
  - Abi Gamin (7,355 m)
  - Kamet (7,756 m)
  - Mana (7,272 m)
  - Makut Parbat (7,242 m)
- 13.3 Nanda Devi group
  - Dunagiri (7,066 m)
  - Hardeol (Tirisuli South) (7,151 m)
  - Tirisuli (East) (7,074 m)
  - Nandi Devi (7,816 m)
  - Trisul (7,120 m)

14.0 Great Himalaya (Nepal)

- 14.1 Karnali section
  - 14.1.1 Kubi Kangri
  - 14.1.2 Nalakankar Himal
    - Gurla Mandhata (7,728 m)
    - Api (7,132 m)
    - Saipal (7,031 m)
  - 14.1.3 Byasrikh Himal
  - 14.1.4 Changla Himal
  - 14.1.5 Punga Range
  - 14.1.6 Sisne Himal
  - 14.1.7 Kanji Roba Himal
  - 14.1.8 Dhaulagiri Himal
    - Churen Himal (7,371 m)
    - Dhaulagiri (8,167 m)
    - Gurja Himal (Sauwala) (7,193 m)
- 14.2 Gandaki section
  - 14.2.1 Annapurna Lamjung
    - Annapurna (8,091 m)
    - Gangapurna (7,455 m)
    - Khangsar Kang (7,485 m)
  - 14.2.2 Nilgiri North (7,061 m)
    - Tarke Kang (7,193 m)
    - Tilitso (7,134 m)
    - Varah Shikar (7,647 m)
  - 14.2.3 Peri Himal
    - Himlung (7,126 m)
    - Ratna Chuli (7,035 m)
    - Kang Guru (7,010 m)
  - 14.2.4 Larkya Himal
    - Manaslu (8,163 m)
    - Himal Chuli (7,893 m)
  - 14.2.3 Kutang Himal
  - 14.2.4 Ganesh Himal
    - Ganesh (7,406 m)
- 14.3 Kosi section
  - 14.3.1 Langtang Himal
    - Gang Benchen (Kangpenqing) (7,211 m)
    - Langtang Lirung (Ganchen Ledrub) (7,234 m)
  - 14.3.2 Jugal Himal
    - Lonpo Gang (7,080 m)
    - Risum (7,050 m)
  - 14.3.3 Lapche Kang
  - 14.3.4 Rolwaling Himal
    - Gaurishankar (7,134 m)
    - Menlungtse (7,181 m)
    - Nyanang Ri (7,071 m)
    - Phola Gangchen (7,661 m)
    - Porong Ri (7,284 m)
  - 14.3.5 Mahalungur Himal (Barun section)
    - Baruntse (7,129 m)
    - Chamlang (7,319 m)

Himalaya, Table 1 (Continued)

  - 14.3.6 Mahalungur Himal (Makalu section)
    - Kangchungtse (7,678 m)
    - Chomolönzo (7,790 m)
  - 14.3.7 Mahalungur Himal (Khumbu section, or Kumbhakarna Himal)
    - Pumori (7,161 m)
    - Cho Oyu (8,201 m)
    - Everest (8,848 m)
    - Nuptse (7,855 m)
    - Makalu (8,462 m)
    - Pumori (7,161 m)
    - Cho Aui (Nangpai Gosum II) (7,350 m)
    - Jasamba (7,351 m)
    - Nangpai Gosum III (7,110 m)
    - Gyachung Kang (7,952 m)
    - Hungchi (7,036 m)
    - Ngojumba Kang I (7,916 m)
    - Kharta Changri (7,056 m)
    - Khartaphu (7,227 m)
    - Palung Ri (7,013 m)
  - 14.3.8 Umbak Himal

Eastern Himalaya (India, Bhutan, China)

15.0 Lesser Himalaya (Sikkim)

16.0 Great Himalaya (Sikkim)

- 16.1 Kangchenjunga Himal (Singalila range)
  - Pathibara (Pyramid peak) (7,123 m)
  - Kanchenjunga (8,586 m)
  - Kabru (7,353 m)
  - Talung (7,349 m)
  - Zemu (7,780 m)
  - Dome Kang (7,442 m)
  - Janak (7,035 m)
  - Jongsong peak (7,483 m)
- 16.2 Chorten Nyima range
- 16.3 Janak Himal (Dongkya ridge)

17.0 Bhutan Himalaya

- 17.1 Lesser Himalaya (<∼4,000 m)
- 17.2 Chomolhari-Laya group (>∼4,000 m)
  - Chomolhari (Jomolhari) (7,315 m)
  - Gangchen Tag (Kangcheta) (7,000 m)
  - Matsa Gang (Masa Gang, Masang Gang) (7,200 m)
- 17.3 Luana group (>∼4,000 m)
  - Tsenda (7,100 m)
  - Teri Kang (7,000 m)
  - Jeje Khangphu (7,300 m)
  - Kangphu Gang (7,200 m)
  - Zongophu Gang (Table Mountain) (7,000 m)
  - Gang Chen (Kang Chen) (7,200 m)
  - Chomolhari Gang (Chomolhari Kangri) (7,000 m)
- 17.4 Bumthang group (>∼4,000 m)
  - Gangkar Puensum (Kangkar Pünzum Rinchita) (7,541 m)
  - Kula Kangri (Künla Kangri, Gula Kangri) (7,554 m)
  - Karjiang (7,221 m)
  - Melunghi Kang (7,000 m)
  - Chumhari Gang (7,000 m)
  - Chura Gang (7,000 m)
- 17.5 Trashi Yangtse Himalaya

18.0 Assam Himalaya

- 18.1 Lesser Himalaya (<∼4,000 m)
  - 18.1.1 Dafla hills
  - 18.1.2 Arbor hills
  - 18.1.3 Miri hills
  - 18.1.4 Mishmi hills

Himalaya, Table 1 (Continued)

18.2 Great Himalaya (>∼4,000 m)
Kangtö (7,090 m)
Nyegyi Kangsang (7,047 m)
Namche Barwa (Namjag Barwa Feng) (7,782 m)
Nai Peng (7,043 m)
Gyala Peri (Jialabiali Feng) (7,150 m)
19.0 Hengduan Shan (Tibetan highlands of China – not on map)
20.0 Nyenchen Tangla Shan (north of Lhasa) (Tibetan highlands of China – not on map)
Nyenchen Tangla (Nyingêntangla Feng) (7,162 m)

which requires sorting them out as much as possible in this classification.

Nonetheless then, with a careful ordering of all these ranges, and a reasonable subdivision of the Himalaya into its constituent parts, some semblance of order can be assigned to the widespread and complex region. In general only some of the ranges of the Tibetan Plateau were included if they were reasonably close to the main ranges of the Himalaya. Thus overall, we can subdivide the Himalaya into the Western or Punjab Himalaya, the Central Himalaya, and the Eastern Himalaya (Mason, 1955). These three master divisions are then further subdivided into subsections. The Western (Punjab) Himalaya is therefore mapped most easily into a series of as many as six northwest–southeast-trending subparallel ranges extending from Tibet across the main range axis and south into the foothills of the Himalaya. Fewer known or named separate ranges occur to the east, however. This reduction in number of ranges eastward occurs in part because several ranges join together successively in areas of the Central Himalaya in what Burrard and Hayden (1907–1908) termed as "bifurcations." Furthermore, the subdivision of the less extensive Central and Eastern parts of the Himalaya has also been done somewhat arbitrarily by drawing it into sections drawn transverse or perpendicularly to the main range axis, and even using somewhat random political boundaries (Mason, 1955). The resulting sections tend to be of rather arbitrary width, generally named for political boundaries coinciding in some cases with accessibility of drainage basins from the south, which is not an ideal situation but must suffice for now.

There are many ways to organize, subdivide, and classify mountain areas so that physical aspects of geology, geomorphology, orography, hydrology, or topography are featured, or so that cultural, political, and other such human-related aspects are also part of the consideration if that is desired. In the course of doing this work, we have become aware of certain assumptions, inconsistencies, lack of knowledge, out-of-date usages, and differences of opinion as to exactly where certain areas or mountain groups are located. In addition, a further complication occurs where various mountain ranges have been designated or named differently by different ethnic groups or nationalities, and on different sides of mountains. Accordingly it is the intention here to investigate what has been written and mapped in the past, with an eye toward reconciling where possible and reordering where necessary. With pervasive satellite imagery at all scales now so readily available, it would seem timely therefore to make a new map of the entire area from the Hindu Kush on the west to the farthest Himalaya on the east in order to bring some order to the apparent miscellany of ranges and peaks. We concentrated our efforts on the areas of the Himalaya of direct interest, but generally not on the more northern ranges of central Asia radiating out from the so-called Pamir Knot, an orographic designation that intrigued many 19th and early 20th century geographers. We did, however, incorporate a few of the trans-Himalayan ranges in Tibet because in many cases they had been ignored by scientists in the British Raj who were more or less unaware of them, or who had an imperfect understanding of their attributes in the early days of exploration and mapping, and because some or all of them have been directly involved in the geologically recent Himalayan uplift.

This map of the Himalaya was made with an ASTER-satellite-image-derived digital elevation model (DEM), with an emphasis on mountains high enough to support past glaciation or present-day glacierization, but some lower mountains have been included where continuity of classification was enhanced. Burrard and Hayden (1907–1908) classified the mountains of Asia according to an altitude hierarchy of first through a seventh order. First-order peaks are those >∼7,600 m, second-order >∼6,700 m, third-order >∼5,800 m, fourth-order >∼4,600 m, fifth-order >∼3,300 m, sixth-order >∼2,100 m, and seventh-order >∼910 m. These designations are used in a few cases herein where such designations were deemed useful. In several cases in the eastern Himalaya (Sikkim, Bhutan, Assam) DEM altitudes were used to crudely define the division between the Greater and Lesser Himalaya.

In general we tried to maintain all the existing and mutually compatible classifications of which we were aware, although in a few cases we had to change prior designations for various reasons having mostly to do with issues dealing with past or present glaciers. Several problems that emerged have to do with the older techniques of linking high mountain peaks into a geographically designated mountain range even across major river valleys, and a newer desire to designate ranges by circumscribing them in their valley bottoms using the pervasive new satellite imagery and DEMs. A further problem with this can be that large glaciers generally occupy valley bottoms in some places that mark borders between adjacent mountain ranges, so in those cases a glacier can, of course, have source areas in several different places.

One of the most recognized schemes of this sort of mountain range division is the work of Burrard and Hayden (1907), who initially subdivided the Himalaya based mainly upon main drainages to the south, coupled with political boundary delineations based on the government of the British Raj. In some cases they carried

geographic names from the far west to the far eastern parts of the Himalaya, which was not valid and is suppressed herein. Mason (1955) maintained these east-to-west designations of the Punjab Himalaya in the west, then the Karakoram, Kumaun Himalaya, and Nepal Himalaya with its Karnali, Gandaki, and Kosi sections, as well as the Sikkim and Assam Himalaya to the east. In a number of cases, Mason's designations of mountain divisions followed political boundaries set along river bottoms (India–Nepal border along the Kali River), which was convenient, but in other cases the division was at the ridge line (Sikkim Himalaya), which was not. Neate (1989) also followed these basic prior subdivision plans in her assessment of the 7,000 m peaks in the region. Statistics on names, heights, locations, and climbing histories are kept by a variety of people and organizations, but Neate's (1978) book is one of the more succinct versions up to the time of its publication. With these primary sources we have established our subdivisions of high south Asia, as well as the general locations of all the fourteen >8,000 m peaks, and many of the >400 examples of the >7,000 m ones as well. Where a great many peaks of similar height were too close together to plot separately, we did not consider them all (Table 1). In several cases in Nepal we listed large numbers of named "Himal" that occurred on a number of maps (United Kingdom Ministry of Defense, 1967, 1969; Nelles Maps, 2008) but were discussed in no other texts.

Western (Punjab) Himalaya

The Western Himalaya (Figure 1), considered as the Punjab Himalaya by Mason (1955), begins somewhat arbitrarily in western Pakistan close to the border with Afghanistan, and extends well into India where it terminates approximately along the Sutlej River and the old summer capital of Simla (now "Shimla") of the British Raj. The Western Himalaya is the widest in latitude of the Himalayan chains, extending >500 km north to south, if the Aghil and Kun Lun of Tibet are included, together with the Lesser and Greater Karakoram, and the Great and Lesser Himalaya.

Hindu Raj

These mountains in northern Pakistan between Chitral and Gilgit occur just south of the Wakhan Pamir and east of the East Hindu Kush of Afghanistan and the Pakistan border, and west of the Karakoram and Great Himalaya of Pakistan. The mountains of the Hindu Raj have no 7,000 m peaks but instead consist mainly of 5,000–6,000 m peaks so they are mountains primarily only of the third and fourth magnitudes (Burrad and Hayden, 1907–1908). The highest peak, Koyo Zom, is 6,872 m, and is near the head of the Yarkand River valley where the Baroghil Pass leads into Pakistan from the Wakhan Corridor of Afghanistan. The Chiantar Glacier is the largest ice mass in this area of the Hindu Raj.

Kohistan ranges

South of the Hindu Raj in Pakistan, the ranges of Dir, Swat, and the Indus Kohistan extend from northeast of the Kunar River at the Afghanistan–Pakistan border, across the Swat Valley area, to both sides of the Indus River valley and the Kaghan Valley where they meet the Great Himalaya at Nanga Parbat and the Pir Panjal of the Kashmir–Indian border. Although a very few peaks in the Kohistan Ranges make it over 6,000 m, most are only 4,000–5,000 m and the glaciers are all small. The mountains of the Lesser Himalaya here are even less consequential.

Punjab lesser Himalaya

The Pir Panjal and the Dhauladhar ranges occur as two lesser ranges in the front or the southernmost side of the Himalaya and both start at about the Pakistan–India border. The Pir Panjal mountains form the southernmost barrier to the Kashmir Valley and their highest peak, Tatticooti (~4,700 m), has glaciers around it. Numerous other small glaciers, moraines, and rock glaciers occur along the range top. The Pir Panjal extend from their start on the Pakistan–India border to the southeast into India, where they finally join with the Great Himalaya at about the point where the Sutlej (Satluj) River cuts through the ranges just upstream from the old Simla summer capital in India. Similarly the Dhauladhar range begins at the Himalayan front at about the Ravi River, extending past Dharmsala where lives the Dhali Lama, and across the Beas and Sutlej rivers to join the Great Himalaya near the Gangotri Glacier and the main source of the Ganges River. South of this mountain junction, the Nag Tibba constitutes the frontal range upon which Shimla is located.

Great Himalaya

The Great Himalaya extends across much of the Himalaya from west to east. The 7,000–8,000 m peaks of this part of the Himalaya in Pakistan and India are notable by the massiveness and considerable height of the Nanga Parbat massif in Pakistan and the Nun Kun massif in India. Nanga Parbat, at 8,126 m with the Indus River at its foot some 6,000 m lower, is one of the highest relief places on the planet and has an exceptionally unusual uplift history caused by rapid erosion from mass movement, glaciers, and rivers that unroofed the crust so rapidly that it developed into a tectonic aneurysm (Shroder and Bishop, 2000; Zeitler et al., 2001a, b), now ringed by a series of glaciers. The Nun Kun area in India is not such a dramatic structural feature but it also has several important glaciers around it.

Inner Himalaya

North of the Great Himalaya are the Deosai Mountains just south of Skardu, Pakistan, and the Pangi Range between them and the Kashmir Basin under Indian control. Numerous small glaciers occur in the Deosai and

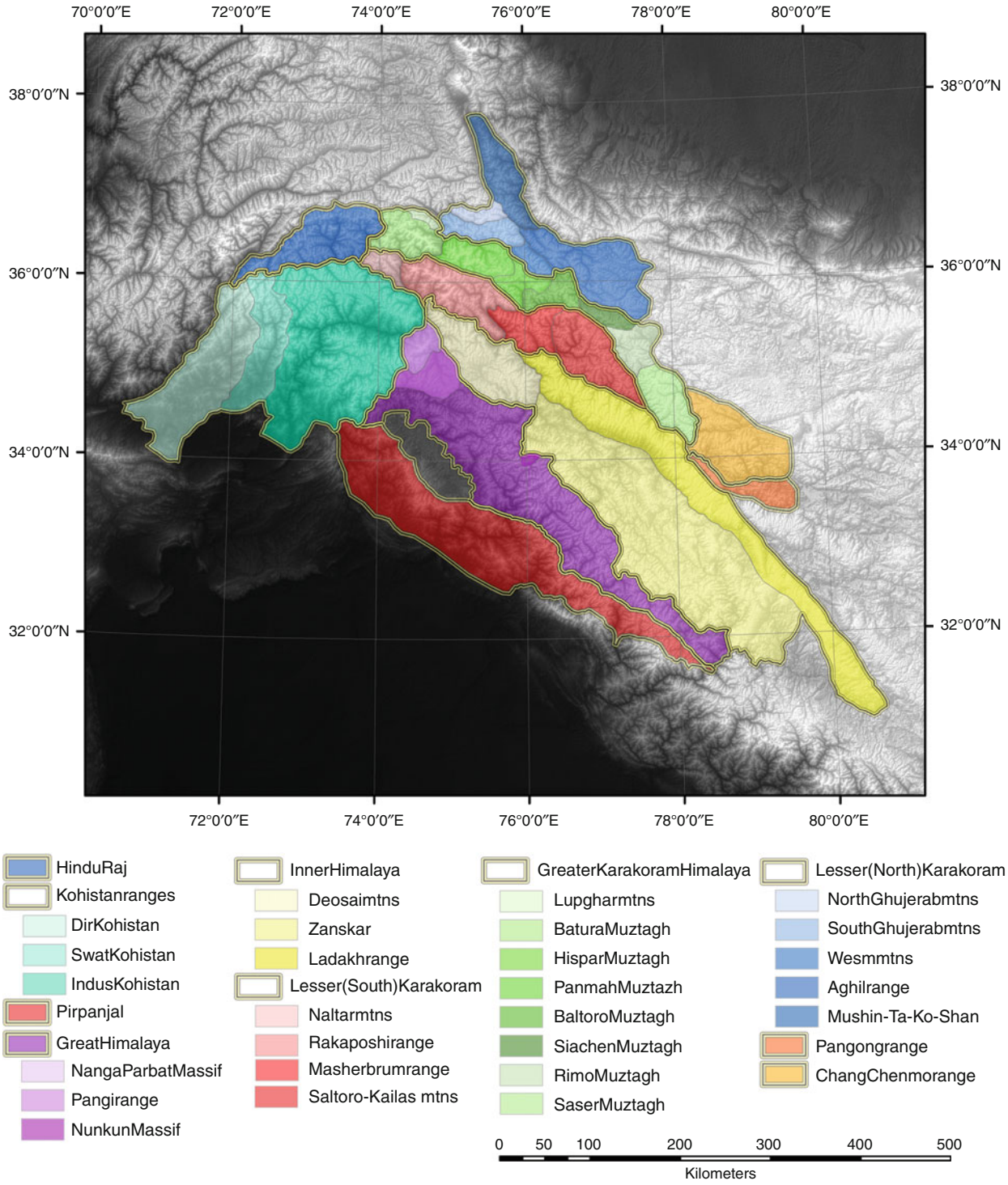

Himalaya, Figure 1 Ranges of the Western Himalaya.

a few in the Pangi Range. The continuations of these mountain ranges into India are the Ladakh Range and Zanskar (Zaskar) Range of the Inner Himalaya. The more northerly Ladakh Range extends across the Punjab Himalaya to the Sutlej River in the Kumaun Himalaya of India and Tibet. The Zanskar Range extends to at least the Sutlej River in the Kumaun Himalaya of India, and some would extend it at least as far as the Karnali section

of the Central or Nepal Himalaya where it joins with the Great Himalaya at the Karnali River.

Lesser (south) Karakoram Himalaya of the trans-Himalaya

This group of mountains and ranges extends from the Naltar and Rakaposhi mountains in Hunza, Pakistan, through the Haramosh and Spantik-Sosbun mountains just north of Nanga Parbat, to the Mango-Gusar and Shimshak mountains and the Masherbrum Range from Skardu north along the Baltoro Glacier, all under Pakistani control. From there the zone extends to the southeast into the Saltoro Range and the Kailas or South Saltoro mountains where the armies of India and Pakistan are looking down on the Siachen Glacier to their northeast, over which they have been fighting for decades.

Greater Karakoram Himalaya of the trans-Himalaya

This main part of the Karakoram Himalaya starts in the Batura area of Hunza and extends east and southeast through the Hispar, Panmah, and Baltoro regions under Pakistan control, the Siachen Glacier area under Indian control, and into the Rimo and Saser Kangri areas under Chinese control in some of the highest mountains and longest midlatitude glaciers of the world. Some 33 > 7,000 m peaks and 3 > 8,000 m peaks occur in this region that serve as great traps for arriving moisture so that profuse glaciers descend from the peaks in this militarily contentious area.

Lesser (north) Karakoram Himalaya of the trans-Himalaya

The northern Karakoram in Pakistan and China, which is largely an arid rain-shadow below the main Karakoram to the south, has only a few major peaks >7,000 m but a number of large glaciers from the greater Karakoram do terminate in this area. Several of the lesser peak areas trail off into various ranges in Tibet (Aghil, Mushin-Ta-Ko-Shan) that are not generally considered to be part of the Karakoram.

Kun Lun

These ranges that stand above the great Taklamakhan Depression start just north of the Karakoram and extend to the east to constitute the northern rim of the Tibetan (Xixang) Plateau. They are not mapped or considered further here.

Pangong range of the trans-Himalaya

This small group of mountains mapped in Figure 1 occurs at the southwest edge of Pangong Tso (lake) in Indian territory at the edge of the Aksai Chin, which is the territory claimed by India but taken by China in the war of 1962.

Chang Chenmo range of the trans-Himalaya

This small range is included with the Pangong in Figure 1 but is not further discussed or mapped.

Kailas range (Gangdise Shan) of the trans-Himalaya

This large range is included here but not mapped further.

Central Himalaya

This designation of the Central Himalaya (Figure 2) is not introduced here as being an entirely new designation, having been used by some recent workers (Singh et al., 2007) to combine Mason's subdivisions of the Kumaun Himalaya with his three subsections of the Nepal Himalaya. Nonetheless it is a useful designation and includes some of the most extensively glacierized portions of the Indian Himalaya, as well as all of the Nepal Himalaya.

Lesser Himalaya of the Garhwal and Nepal Himalaya

The irregularly faulted and dissected lower ranges on the south side of the Himalaya are diversely aggregated into the Pir Panjal that extends from Pakistan past the southern margins of the Kashmir Basin into India, and the Dhauladahar Range and Nag Tibba Range that extend to the Nepalese border. From there, the Mahabharat Range in several sections constitutes the main lower part of the Lesser Himalaya throughout Nepal.

Garhwal (Kumaun) Himalaya

Originally these two names hark back to the old administrative subdivisions of the British Raj that ruled India before 1947 that described slightly different regions, but nowadays the terms refer to basically the same mountainous areas of the Indian State of Uttar Pradesh. Mason (1955) drew his boundaries of this region across the ranges from the Tibetan Highlands to the lowlands of India, on its west side approximately through the Sutlej River and the old summer capital of Simla (Shimla), and on its east side along the western India–Nepal political border in the Himalaya. Beginning in Tibet first occurs the Nganglong Kangri range. Directly south of this occurs the Shiquan He (Sengge Khamba) tributary to the Indus River, which rises on the northern slopes of Kailas Range (Gangdise Shan). South of that range is the valley of the Gar Zangbo tributary of the Indus River, and then the southeast end of the Ladakh Range, before dropping down again into the upper valley of the Sutlej River as it passes over the Chinese–Tibet border and into India where an extension of the Zanskar Range forms the border range with the Kamet Group of mountain peaks along it. Directly south of the Zanskar Range, and partly connected to it by ridges between peaks, is the Great Himalaya, which includes such peaks as the Gangotri Group and the Nanda Devi Group.

Nepal Himalaya

The political entity of Nepal was divided by Mason (1955) into three large mountain-ringed drainage basins, from west to east the Gogra (Seti, Karnali, Bheri), Gandak, and Kosi rivers that define the Karnali, Gandaki, and Kosi sections of the Nepal Himalaya. These three sections with

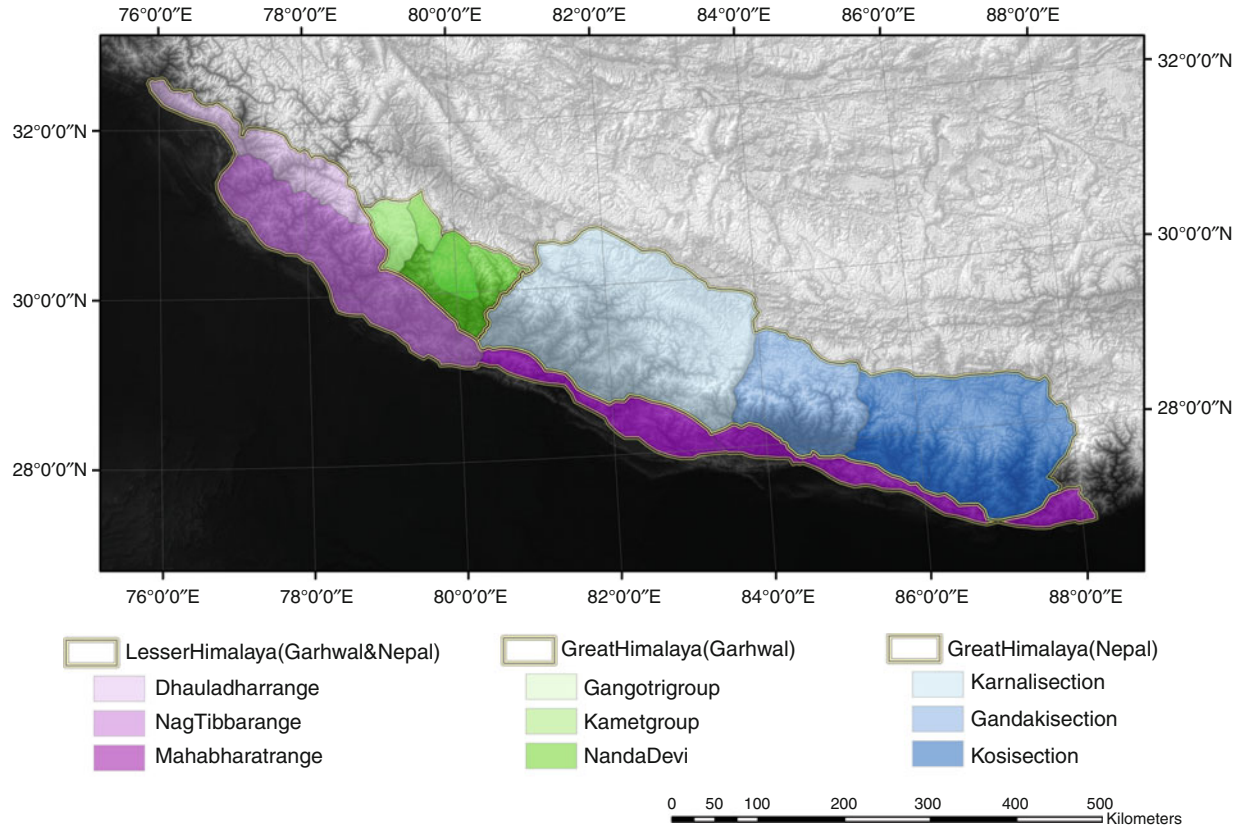

Himalaya, Figure 2 Ranges of the Central Himalaya.

their master drainages, all pass down through a number of subparallel ranges, on their way to being tributary to the Ganges River of India.

Karnali Section: The west part of this section is directly south of the famous and sacred religious site of Mount Kailas in the Kailas (Gangdise) Range, and the well-known lakes of Rakshastal and Manasarovar of the Tibetan Plateau. The well-known east-flowing Tsangpo River of the Tibetan Plateau heads in the Kubi Kangri and Kailas Ranges directly north of this section. The Karnali River system also heads in the Kubi Kangri (Changla Himala) ranges of the Nepal Tibet border region, before breaking south through wall of the Great Himalaya, which is represented by the Byasrikh Himal on the west and the Sisne Himal or Kanj Roba Himal on the east. Several other river tributaries join the Karnali, including to the southeast, the Thuli Bheri from the north side of the heavily glaciated Dhaulagiri massif. The Karnali and its tributaries all pass through the Mahabharat Range, which is only a sixth-order range of the Lesser Himalaya, and finally through the Churia Range of the Siwalik rocks in the foothills.

Gandaki Section: This section is characterized by the numerous tributaries of the Great Gandakhi River that rise from a number of ranges spread across the upper part of the section. For example, the Kali Gandaki tributary heads in the remote Mustang region before passing out of the Damodar Himal and between the Dhaulagiri and Annapurna Himals. To the east of this extensively glacierized region occur the Peri Himal, Larkya Himal, Kutang Himal, and Ganesh Himal, to the Langtang Himal on the far eastern side of the section that is also the beginning of the Kosi section.

Kosi Section: This extensively glaciated section in eastern Nepal is dominated by the peaks of the Great Himalaya, including Cho Oyu, Everest, Makalu, and Kanchenjunga on the east border with the Sikkim Himalaya, and is drained by the tributaries of the Sapt Kosi. The great 8,027 m peak of Shisenpangma occurs in southern Tibet just northeast of the Ganesh Himala and northeast of the Cho Oyu massif. The Langtang and Jugal Himals occur on the west side of this section, with the Lapche Kang and Rolwaling Himal constituting part of the well-glacierized ridge lines up to the Mahalungur or Khumbhakarna Himal in the middle. The chief drainage, which begins on the Tibetan Plateau north of the main ranges, is the Arun River, which begins on the Tibetan Plateau around the Nyonno Ri massif. This river then flows between the Khumbhakarna Himal (Mahalungur) with Everest as the highest peak and the Umba Himal and Singahila Range with Kanchenjunga as the highest peak on the far eastern side of the section.

Eastern Himalaya

The Eastern Himalaya (Figure 3) is less precisely defined than the Central and Western Himalaya, especially because national borders tend to be the most precise determinative factor of division. Nonetheless, all three regions are basically divided into areas of Lesser and great Himalaya.

Sikkim Himalaya: The state of Sikkim in the central part of extreme northern India is bounded on the west by Nepal and the east by a southward projection of Tibet. The N-S-trending Singalila Range extends up to the high Kangchenjunga (Kangchendzonga) massif and constitutes the western border area. Similarly, the Donkya Ridge does the same on the east where the Yadong valley forms a reentrant south, or projecting "parrots beak" of Tibetan territory between Sikkim on the west and Bhutan on the east.

The Sikkim Himalaya is thus a quite narrow (∼75 km) strip of the higher Great Himalaya that is really only the upper watershed of the Tists River and its tributaries. The Singalila Range of the western border with Nepal, and the eastern Dongkya Ridge both pass north into the more or less W-E-trending, high Himalaya of crystalline gneisses, which form most of the W-E-trending, Chortan Nyima Range and the Janak Himal of the Tibetan border with Sikkim.

Bhutan Himalaya: The independent country of Bhutan is an approximately rectangular-shaped mountain kingdom drained to the south by 3–4 main drainages (Torsa Chu, Raigve Chu, or Wang [Raichak], Mo Chu or Sankosh, and Manas Chu) that dissect the crystalline rocks of the country into many mountains. These rivers drain south through the peaks of the Lesser Himalaya there, that are generally <∼4,000 m altitude. The higher peaks along the border with Tibet of the Greater Himalaya include the Chomolhari – Laya, Luana, and Bumthang groups that are all extensively glacierized.

Assam Himalaya: The Himalayan ranges in the Assam state of India are not well studied, in part because of the more common jungle and difficult physical and cultural terrains of the region. The Himalayan ranges here are a Lesser Himalaya (<∼4,000 m) constituted by the lower Dafla Hills and Abor Hills and Miri Hills to the west of the Brahmaputra, and the Mishmi Hills east of the river and close to the border with China. To the north of the State of Assam in Chinese Tibet the Yarlung Tsangpo River

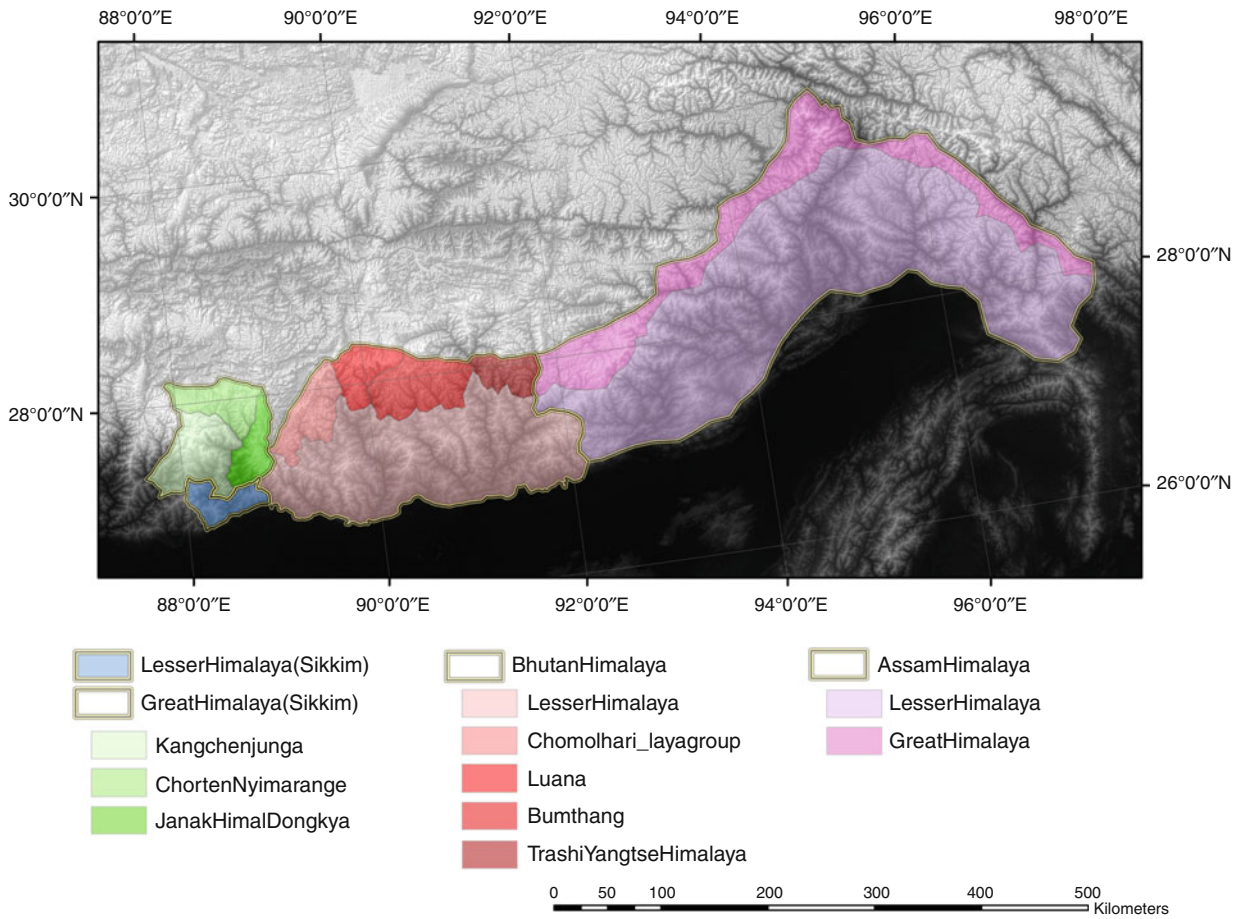

Himalaya, Figure 3 Ranges of the Eastern Himalaya.

makes a great loop to the north before bending abruptly back S and then SW through the Great Gorge where it becomes the lowland Brahmaputra River. This is the site of the eastern syntaxis where the capture of the Yarlung Tsangpo and diversion southward occurred when the higher altitude river of the Tibetan Plateau spilled over into the lower altitude Brahmaputra. The subsequent rapid erosional unroofing of the bedrock formed a tectonic aneurysm that caused the geologically rapid uplift of the peaks of Namche Barwa (Namjagbarva Feng) (7,756 m) on the inside of the bend, and Gyala Pelri (7,294 m), just outside the bend to the NW, both with plentiful glaciers.

Hengduan mountains

As this eastern syntaxial bend of rocks continued to be forced into Asia by the inexorable forces of plate tectonics over the past few tens of millions of years, not only did the Namche Barwa – Gyala Pelri massifs rise like a trapdoor or pop-up structure in the rock, but other ranges and rivers to the north and east also became crushed upward. They were dragged into the tightly constrained, topographically crumpled, Hengduan ranges, of southeast China, as well as the parallel rivers between the ranges that wrapped around the uplifted highlands, to cut deep parallel canyon twice as deep as the Grand Canyon in USA (Jenkins, 2009). Between the Nu and Lancang rivers and latitudes 28°–29° N, Mt. Kwagebo (Meili) rises some 6,740 m and hosts a number of strong glaciers on its slopes. Thus the Nu (Nak Chu or Salween in SE Asia), Lancang (Ngom Chu or Mekong in SE Asia), and Dri Chu or Jinsha Jiang (Yangtze) all rise on the eastern Tibet Plateau and all force their way through this farthest extent of the extreme Eastern Himalaya within a few tens of km of each other before escaping the uplands and making their way to the lowlands and out to the sea.

Nyenchen Tangla Shan (Nyainqenanglha)

Just north of the Yarlung Tsangpo and Lhasa, the capital of Tibet, the heavily glaciated ranges of Nyenchen Tangla Shan (Nyainqenanglha or Ninchin-Thang-La) Range also wrap around the syntaxial bend and constitute the last vestiges of Himalayan-style mountains in this region. Directly NW of Lhasa at that end of this range, only one peak is higher than 7,000 m, Nyenchen Tangla at 7,162 m. All of the others are lower, with several around 6,400 m and most being in the >5,000 m range as they curve around to the south at the far eastern ends of the Himalaya.

Overall, the many ranges of the Himalaya, as well as its collateral offshoots, constitute a geologically and topographically diverse series of peaks that are the highest altitude places anywhere on this planet. Because these peaks are so broad and tall, they serve as ideal traps for snow and ice, which over time become strong glaciers. As a result, the Himalaya has the longest and largest midlatitude glaciers on Earth.

Summary

The Himalaya, or "abode of snow" in the ancient Sanskrit language are the highest mountains on our planet, and as such constitute a huge repository of snow and ice, the meltwaters of which nourish many millions of Asian people. The Himalayan mountains are subdivided into the Western or Punjab Himalaya, the Central Garhwal or Kumaun Himalaya, and the Eastern Himalaya. Each one of these Himalayan divisions is further subdivided in separate ranges or groups of ranges, all of which are now located on a new digital elevation model derived from ASTER satellite imagery in Figures 1–3.

Bibliography

Bhutan (Scale 1:250,000), 2006. International Institute for Geo-Information Science and Earth Observation (ITC), Enschede, The Netherlands (2 maps – 100 m contour interval & satellite image).

Bhutan Himalaya (Scale 1:500,000), 1996. Swiss Foundation for Alpine Research, Zurich, Switzerland.

Bolinder, A., Wala, J., and Kowalewski, Z., 1990. Karakoram: Orographical Sketch Map. Sheet 1; Sheet 2; Scale 1:250,000. Swiss Foundation for Alpine Research, Zurich, Switzerland.

Bossart, H. F., 1981. Sikkim Himalaya (Scale 1:150,000; contour interval 100 m), Swiss Foundation for Alpine Research, Zurich, Switzerland.

Burrard, S. G. and, Hayden, H. H., 1907–1908. A sketch of the Geography and Geology of the Himalaya Mountains and Tibet. Survey of India, 359 p.

Grötzbach, E., 1990. *Afghanistan: Eine geographische Landeskunde*. Wissenschaftliche Länderkunde Bd. 37. Damstadt: Wissenschaftliche Buchgesellschaft.

Jenkins, M., 2009. Searching for Shangri-la. *National Geographic*, **215**(5), 56–83.

Karan, P. P., 1969. The Kingdom of Sikkim (1:150,000). Map Supplement Number 10, Annals Association American Geographers, 59(1).

Mason, K., 1955. *Abode of snow: a history of Himalayan exploration and mountaineering*. Dutton: R. Hart-Davis. 372 p.

National Atlas of India, 1964. Physiographc Regions (Plate 41).

Neate, J., 1978. *High Asia*. Seattle: The Mountaineers, 213 p.

Neate, J., 1989. *High Asia: An illustrated history of the 7,000 metre peaks*. Seattle: The Mountaineers.

Nelles Maps, 2008. Himalaya; including Tibet, Kashmir, Nepal, Sikkim, Bhutan. Scale 1:1,500,000.

Shroder, J. F., Jr., and Bishop, M. P., 2000. Unroofing the Nanga Parbat Himalaya. In Khan, M. A., Treloar, P. J., Searle, M. P., and Jan, M. Q. (eds.), *Tectonics of the Nanga Parbat syntaxis and the Western Himalaya*. Bath: Geological Society of London Special Publication 170, pp. 163–179.

Singh, P., Haritashya, U. K., and Kumar, N., 2007. Meteorological study for Gangotri glacier and its comparison with other high altitude meteorological stations in central Himalaya region. *Nordic Hydrology*, **38**(1), 59–77.

United Kingdom Ministry of Defense, 1967. Nepal 1:506,880 West Sheet, U462 (formerly U431).

United Kingdom Ministry of Defense, 1969. Nepal 1:506,880 East Sheet, U462 (formerly U431).

Verlag, N., 2008. *Himalaya (1:1, 1, 500, 000)*. München: Nelles.

Zeitler, P. K., Koons, P. O., Bishop, M. P., Chamberlain, C. P., Craw, D., Edwards, M. A., Hamidullah, S., Jan, M. Q., Khan, M. A., Khattak, M. U. K., Kidd, W. S. F., Mackie, R. L., Meltzer, A. S., Park, S. K., Pecher, A., Poage, M. A., Sarker, G., Schneider, D. A., Seeber, L., and Shroder, J. F., 2001a. Crustal reworking at

Nanga Parbat, Pakistan: metamorphic consequences of thermal-mechanical coupling facilitated by erosion. *Tectonics*, **20**, 712–728.
Zeitler, P. K., Meltzer, A., Koons, P. O., Craw, D., Hallet, B., Chamberlain, C. P., Kidd, W. S. F., Park, S. K., Seeber, L., Bishop, M., and Shroder, J. F., Jr., 2001b. Erosion, Himalayan geodynamics, and the geomorphology of metamorphism. *GSA Today*, **11**, 4–9.

HIMALAYAN GLACIERS IN 2010 AND 2035

J. Graham Cogley
Department of Geography, Trent University,
Peterborough, ON, Canada

Introduction

The aim here is to narrate the evolution of a mistaken but often-seen claim that Himalayan glaciers might disappear by 2035, to correct it by providing glaciological and climatic context, and to attempt a more realistic preliminary assessment of how Himalayan glaciers might evolve in the 25 years up to 2035.

Narrative

Early in 1999, S.I. Hasnain gave an interview to a magazine reporter (Chettri, 1999), and was quoted to have said "Glaciers in the Himalaya are receding faster than in any other part of the world and, if the present rate continues, the likelihood of them disappearing by the year 2035 is very high.... There won't be any glaciers left in the central and eastern Himalaya by 2035 if they continue to recede at the present rate." Chettri (1999) also quotes Kotlyakov (1996) as saying "Its total area will shrink from the present 500,000 to 100,000 km^2 by the year 2035."

A prominent science journalist then published another news story (Pearce, 1999) based upon Chettri (1999). Pearce too interviewed Hasnain, but apparently without cross-checking with any other glaciologist. Pearce reports statements similar to those in Chettri (1999). A photo caption above Pearce's text reads "Trouble at the top: Himalayan glaciers will vanish by 2035."

A study mentioned by both Chettri and Pearce was submitted to the International Commission of Snow and Ice (ICSI) by its Working Group on Himalayan Glaciology in July 1999, but remained unpublished until November 2009 when a copy was made available online by the International Association of Cryospheric Sciences, the successor of ICSI (Hasnain, 1999).

The claim that Himalayan glaciers might disappear by 2035 did not become widespread until it was repeated by Cruz et al. (2007), citing an overview prepared by the World Wildlife Fund (WWF, 2005), which in turn cited Pearce (1999).

Without citing Cruz et al. (2007), Raina (2009) challenged the by-then current idea that Himalayan glaciers were wasting abnormally. Bagla (2009) publicized Raina's report and contrasted its findings with statements in Cruz et al. (2007). This prompted investigations, which led to further coverage in the media and to Cogley et al. (2010), a correction that was published online on the same day as a formal retraction by the Intergovernmental Panel on Climate Change of Cruz et al.'s assessment of Himalayan glaciers (IPCC, 2010). The most prominent media report was a story by Pearce (2010), which triggered a spate of public comment and criticism lasting some weeks.

Clarification

Kotlyakov (1996) was not writing specifically about Himalayan glaciers but about all glaciers outside the polar regions and outside basins of internal drainage. He described his estimate of a decrease of total glacier area from 500,000 km^2 to 100,000 km^2 as "rough," noting that it was based on mass-balance records from the 1960s to the 1980s for six Norwegian glaciers. Further, Kotlyakov noted that the Himalaya would be among the regions

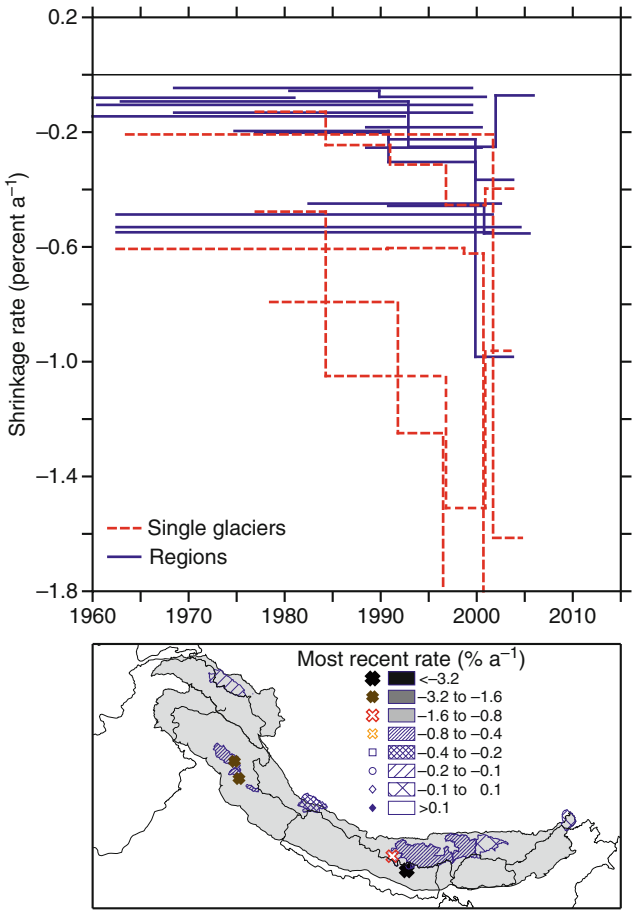

Himalayan Glaciers in 2010 and 2035, Figure 1 Measured shrinkage rates of Himalayan glaciers and glacierized regions. In the map, shading illustrates the most recent rate from the graph for each glacier or region; the Himalaya and (in the northwest) the Karakoram are defined by the thick lines, and thin lines are national borders.

retaining glaciers after a decrease to 100,000 km^2. Most strikingly, Kotlyakov's date for decrease to 100,000 km^2 is 2350, not 2035.

It is all but certain that those who cited Hasnain (1999) before November 2009 had not seen it. If they had, its irrelevance to the claim of disappearance by 2035 would have been obvious, for it does not contain any of the statements attributed to it in Chettri (1999) and Pearce (1999). In fact, all of the restatements of the 2035 claim seen by this author are either copies of text from one of those sources or variants that introduce new mistakes.

The publicly available first and second drafts of Cruz et al. (2007) show that the citation of WWF (2005) was added at a later stage to an originally unreferenced paragraph, and to the wrong sentence in that paragraph. Moreover, collation of Cruz et al. and Chettri (1999) shows that Cruz et al. copied from Chettri rather than from WWF. WWF (2005) is not entirely free from criticism, however, for like others it simply followed Chettri (1999) and Pearce (1999).

Recent state of Himalayan glaciers

The area occupied by Himalayan glaciers is not known with great accuracy. Dolgushin and Osipova (1989) give 33,050 km^2 while von Wissmann (1959), a source for some later estimates, gives 31,530 km^2. For the Karakoram these two sources give 15,400 km^2 and 15,145 km^2, respectively. The differences may be due partly to different definitions of

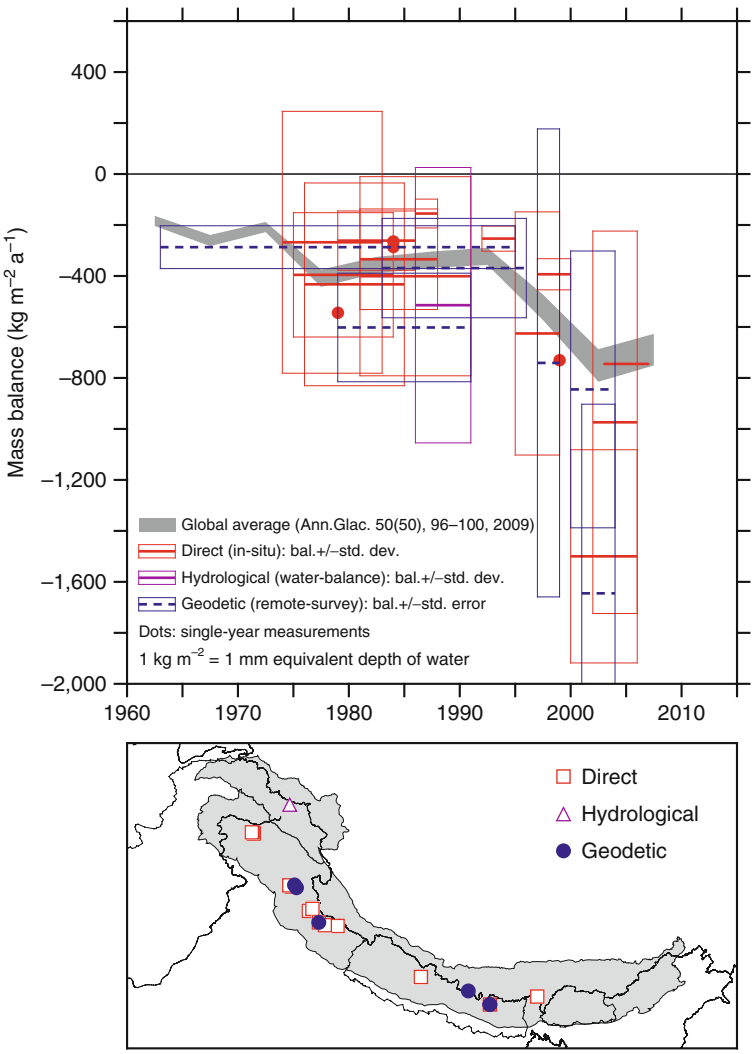

Himalayan Glaciers in 2010 and 2035, Figure 2 Measured mass balances of glaciers in the Himalaya and the Karakoram. Direct measurements are made in situ on the glacier surface, while hydrological measurements solve the glacier's water balance using estimates of precipitation, evaporation, and runoff; each series average is drawn as a horizontal line contained in a box representing ±1 standard deviation. Geodetic measurements compare a later map to an earlier one, the mean change of elevation being multiplied by glacier area to yield volumetric change and by a suitable density (usually 900 kg m^{-3}) to yield mass change. The box containing each geodetic balance represents the standard error.

the regions. It is not possible at present to assess the contribution of glacier shrinkage, discussed below, to uncertainty in the total glacierized areas.

Total volumes of ice are uncertain, not only because of uncertainty in the areal extent but also because there are only a handful of measurements of glacier thickness. Average thicknesses obtained by volume-area scaling (with the coefficients of Radić and Hock, 2010), relying on glacier areas in the inventory of Cogley (2009b), are 86 m for the Himalaya and 172 m for the Karakoram. The uncertainty in these estimates is large but unknown.

Contrary to the assertions reported by Chettri (1999), measured rates of terminus retreat (e.g., Cruz et al., 2007; Raina, 2009) are comparable to, not faster than, rates elsewhere. This can be verified readily by inspection of the standard compilation (WGMS, 2008), which appears on a 5-yearly basis and in which reports vary from a few tens of m a^{-1} of retreat to a few m a^{-1} of advance, with a clear majority of retreating glaciers. Advancing and stable termini appear to be common in the Karakoram (Hewitt, 2005).

Measurements of rates of shrinkage (reduction of area; Figure 1) are too few for generalization, although there is a suggestion that shrinkage is faster in the central and western Himalaya than in the east or the Karakoram. There are no instances of growth. The graph shows signs of accelerated shrinkage, but it must be interpreted cautiously. Smaller glaciers tend to shrink more rapidly, in percentage terms, than larger ones. Thus, differences between the rates of different regions may be influenced strongly by differences in their glacier size distributions as well as by variations in climatic or other factors.

That said, the arithmetic average of shrinkage measurements whose spans contain the year 1960, weighting each measurement by the initial size or extent, is –0.10% a^{-1}. For 1980, the equivalent figure is –0.18% a^{-1}, and for 2000 it is –0.45% a^{-1}. For context, Cogley (2008) estimated that the global average over the past 50 years has been about –0.10% to –0.20% a^{-1}.

There are no long-term, continuous series of mass-balance measurements from the Himalayan region (Figure 2). This is unfortunate. Because successive annual measurements are uncorrelated, the number of degrees of freedom is equal to the number of measurements, which means that the uncertainty in a multi-annual average decreases with the square root of the length of the series. The longest series of annual measurements is only 10 years long, but there are also some measurements by geodetic methods. Few as they are, the measurements taken together suggest firstly that average mass balance has been negative for the past several decades; and secondly, that the rate of loss has been greater after 1995 than before.

Evolution of Himalayan glaciers to 2035

The future evolution of Himalayan glaciers has not been modeled thoroughly. However, we can extrapolate on two simple assumptions: more conservatively, that the recent average mass-balance rate will remain unchanged; and, perhaps more plausibly, that the recent acceleration of the rate will remain unchanged. Both assumptions are risky, because they neglect concurrent changes in glacier geometry. In particular, they do not account for net shrinkage or for retreat to higher, colder elevations.

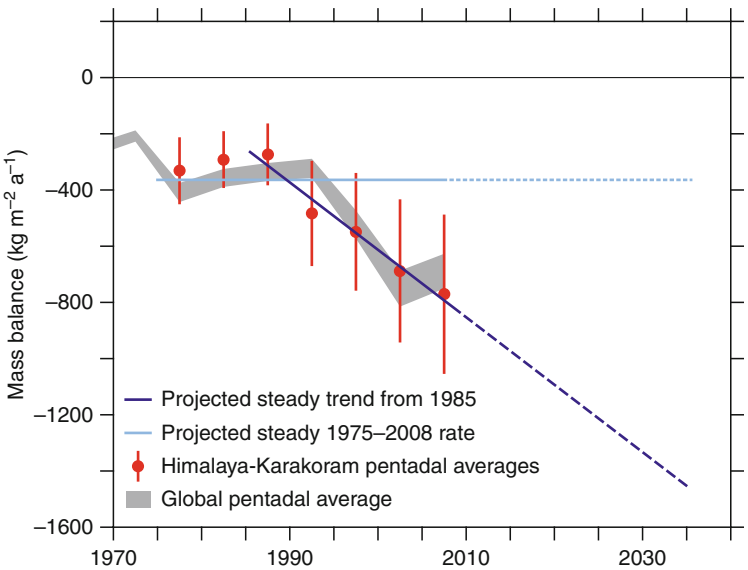

Himalayan Glaciers in 2010 and 2035, Figure 3 Five-yearly average mass balance of Himalaya and Karakoram glaciers, as measured and interpolated (*dots* with error bars) and as projected to 2035. Horizontal line (*dotted* in the future) shows the 1975–2008 average. Sloping line (*dashed* in the future) represents the trend fitted to pentadal averages between 1985 and 2008. The interpolated global average is as in Figure 2.

Figure 3 shows estimates of the Himalaya–Karakoram average mass balance for 1975–1976 to 2007–2008, extracted from the calculations of Cogley (2009a). These calculations draw on information from distant glaciers, discounted by a distance-decay function, to supplement local records, and place the beginning of accelerating mass loss somewhat earlier than the local measurements. The average rate is -364 ± 55 kg m^{-2} a^{-1} (1 kg m^{-2} = 1 mm water equivalent, w.e.); the more uncertain recent pentads have less weight, so the average is closer to the pentadal estimates before 1990. If the average were sustained, the glaciers would thin by 9 m w.e. between 2010 and 2035. The trend fitted to the estimates from 1985–1986 onward is –24 kg m^{-2} a^{-2}. If this acceleration were sustained, the thinning between 2010 and 2035 would be 28 m w.e.

These estimates are tentative, and oversimplify the complexity of glacier responses to forcing, but they rest on all of the available information. Although many small glaciers have present-day thicknesses of only 10–30 m, they account for little of the total mass and there is no reason for believing that all Himalayan glaciers might disappear by 2035.

Summary

The assertion that Himalayan glaciers might disappear as early as 2035 is unfounded. Although information is scanty, and does not allow accurate assessment of the total mass of ice, measurements of retreat and shrinkage suggest that Himalayan glaciers are evolving at rates comparable with those observed elsewhere. This does not justify complacency. Extrapolation of the limited measurements of mass balance suggests that mass loss from 2010 to 2035 will be of the order of 10–30 m of water-equivalent thickness. The larger of these numbers represents continuation of the recent trend and may be more probable. A more accurate assessment must await a detailed analysis of the response of the glaciers to projected radiative forcing, but such an analysis will be difficult without more, and more continuous, basic observations.

Bibliography

Bagla, P., 2009. No sign yet of Himalayan meltdown, Indian report finds. *Science*, **326**, 924–925. 13 November 2009.

Chettri, M., 1999. Glaciers beating retreat. *Down To Earth*, **7**(23). http://web.archive.org/web/20020827195937/www.cseindia.org/html/dte/dte990430/dte_analy.htm.

Cogley, J. G., 2008. Measured rates of glacier shrinkage. *Geophysical Research Abstracts*, **10**, EGU2008-A-11595. Paper presented at Annual General Assembly, European Geosciences Union, Vienna, 14 April 2008. http://www.cosis.net/abstracts/EGU2008/11595/EGU2008-A-11595.pdf.

Cogley, J. G., 2009a. Geodetic and direct mass-balance measurements: comparison and joint analysis. *Annals of Glaciology*, **50**(50), 96–100.

Cogley, J. G., 2009b. A more complete version of the World Glacier Inventory. *Annals of Glaciology*, **50**(53), 32–38.

Cogley, J. G., Kargel, J. S., Kaser, G., and van der Veen, C. J., 2010. Tracking the source of glacier misinformation. *Science*, **327**(5965), 522.

Cruz, R. V., Harasawa, H., Lal, M., Wu, S., Anokhin, Y., Punsalmaa, B., Honda, Y., Jafari, M., Li, C., and Huu Ninh, N., 2007. Asia. In Parry, M. L., Canziani, O. F., Palutikof, J. P., van der Linden, P. J., and Hanson, C. E. (eds.), *Climate Change 2007: Impacts, Adaptation and Vulnerability. Contribution of Working Group II to the Fourth Assessment Report of the Intergovernmental Panel on Climate Change.* Cambridge: Cambridge University Press, pp. 469–506.

Dolgushin, L. D., and Osipova, G. B., 1989. *Ledniki*. Moscow: Mysl' Publishing, 447 p.

Hasnain, S. I., 1999. Report on Himalayan glaciology. Appendix 6, unpublished minutes of the July 1999 meeting, ICSI Bureau. http://www.cryosphericsciences.org/docs.html.

Hewitt, K., 2005. The Karakoram anomaly? Glacier expansion and the "elevation effect," Karakoram Himalaya. *Mountain Research and Development*, **25**(4), 332–340.

IPCC, 2010. IPCC statement on the melting of Himalayan glaciers, http://www.ipcc.ch/pdf/presentations/himalaya-statement-20january2010.pdf.

Kotlyakov, V. M., 1996. The future of glaciers under the expected climate warming, pp. 61–66. In Kotlyakov, V. M. (ed.), Variations of Snow and Ice in the Past and at Present on a Global and Regional Scale, *Technical Documents in Hydrology*, Vol. 1. UNESCO, Paris (IHP-IV Project H-4.1), 78 p. http://unesdoc.unesco.org/images/0010/001065/106523e.pdf.

Pearce, F., 1999. Flooded out. *New Scientist*, **162**(2189), 18.

Pearce, F., 2010. Debate heats up over IPCC melting glaciers claim. *New Scientist*, **205**(2743), 11. http://www.newscientist.com/article/mg20527434.300–debate-heats-up-over-ipcc-melting-glaciers-claim.html.

Radić, V., and Hock, R., 2010. Regional and global volumes of glaciers derived from statistical upscaling of glacier inventory data. *Journal of Geophysical Research*, **115**, F01010, doi:10.1029/2009JF001373.

Raina, V. K., 2009. *Himalayan Glaciers: A State-of-Art Review of Glacial Studies, Glacial Retreat and Climate Change*, Discussion Paper, Ministry of Environment and Forests, Government of India, New Delhi, 56 p. http://moef.nic.in/downloads/public-information/MoEF%20Discussion%20Paper%20_him.pdf.

von Wissmann, H., 1959. *Die heutige Vergletscherung und Schneegrenze in Hochasien. Abhandlungen der Mathematisch-naturwissenschaftliche Klasse*. Mainz: Akademie der Wissenschaften und der Literatur, Vol. 14, pp. 1101–1407.

WGMS, 2008. *Fluctuations of Glaciers 2000–2005 (Vol. IX)*, World Glacier Monitoring Service, Zurich.

WWF, 2005. *An Overview of Glaciers, Glacier Retreat, and Subsequent Impacts in Nepal, India and China*. WWF Nepal Program. 67 p. http://assets.panda.org/downloads/an_overview_of_glaciers__glacier_retreat_and_its_subsequent_impacts_in_the_nepal__india_.pdf.

HINDU KUSH

John F. Shroder
Department of Geography and Geology, University of Nebraska at Omaha, Omaha, NE, USA

Introduction

The Hindu Kush is the group of ranges that occur dominantly in Afghanistan and northwestern Pakistan. With the pervasive satellite imagery at all scales now so readily available, it is possible to make new maps of entire

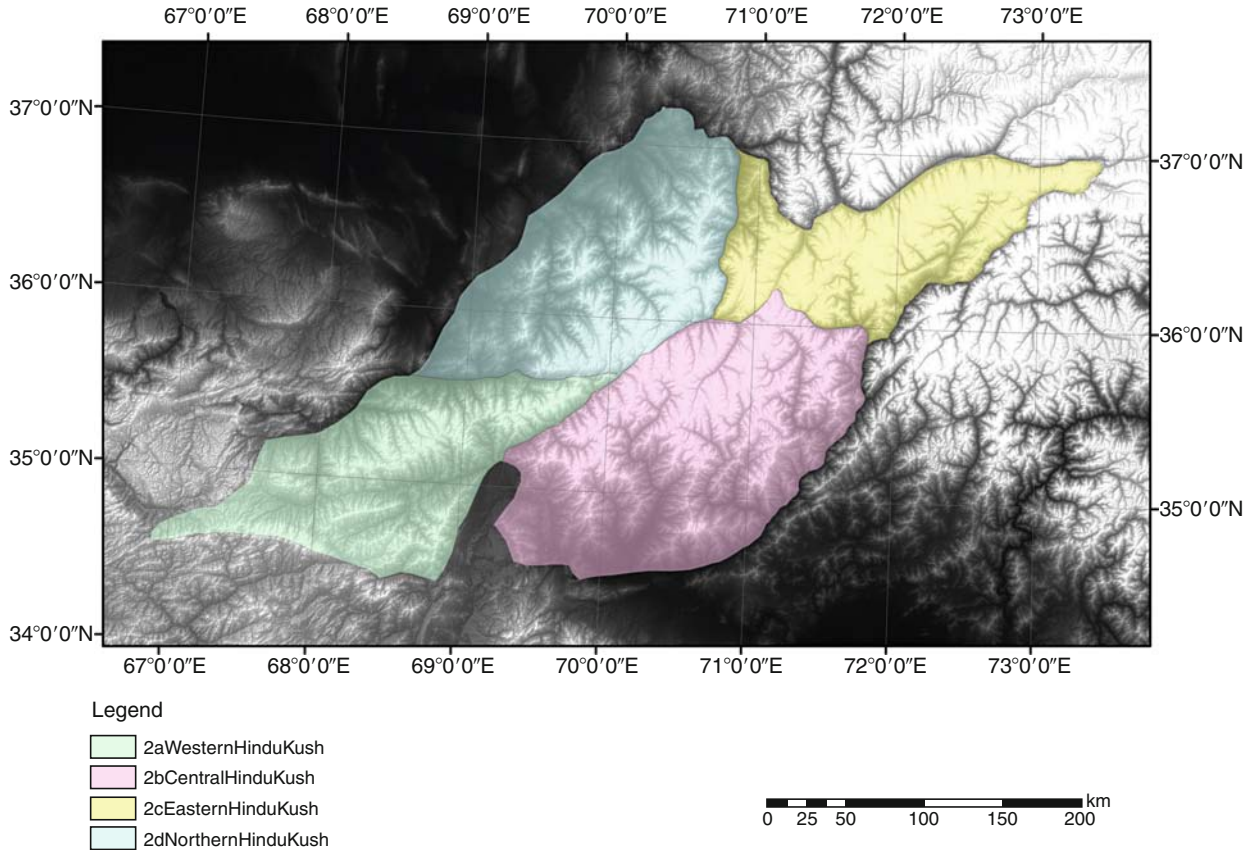

Hindu Kush, Figure 1 The Hindu Kush mountains of Afghanistan and northwestern Pakistan. The mountains to the southeast in Pakistan are the Hindu Raj and the ranges of Kohistan. To the north of the Hindu Kush are the Pamir ranges of Afghanistan and Tajikistan.

complex regions of mountains, to increase understanding of glacier formation and location (Figure 1). Among the complex regions in the mountains of central and south Asia are those that radiate out from the "Pamir Knot," an orographic designation that intrigued many nineteenth and early twentieth century geographers (Burrard and Hayden, 1907). The Hindu Kush ranges constitute the southwest and south parts of this Pamir Knot.

The main glacierized and glaciated mountain chain of Afghanistan is the Hindu Kush, although a number of other smaller ranges are satellite to it, and several others also have glaciers (Afghanistan Pamirs to the north in Badakshan), or have had glaciers in the past (Spin Ghar or Safed Koh to the south; Hesar Range to the west). The Hindu Kush Mountains are dominantly in Afghanistan, although an easternmost extension occurs also in Pakistan that constitutes part of the border along the southern edge of the Wakhan Corridor. A number of different people have subdivided all or parts of the Hindu Kush, but the work of Ervin Grötzbach (1990) is based on his familiarity with the ground, is the best thought out, and the most complete. He divided the Hindu Kush into four basic parts: (1) Western Hindu Kush; (2) Middle or Central Hindu Kush; (3) Eastern Hindu Kush; and (4) the Khwaja Mohammed Mountains, which can be considered as a northern Hindu Kush (Figure 1).

Western Hindu Kush

This region occurs to the north and northwest of the Kabul Basin. The border of this mountain area stretches from the Surkhab and Andarab gorges in the north, and the Khawak Pass in the northeast, south over the main peaks into the upper parts of the Panshir Valley of the Anjuman Pass, and east down the Panshir Valley to the north point of the Kabul Basin, thence southwestward along the edge of the Paghman Range and the Kabul Basin, before turning east again up the headwaters of the Kabul River and the Wonay Pass and into the Helmand headwaters.

The westernmost edge of the Hindu Kush has been placed in different places because of the lack of definitive breaks in the topography there. We find it useful to include the Koh-i-Baba Range where occur the few, southwesternmost ice masses remaining in south Asia, but not the Hesar Range on the west edge of the Yakawlang graben valley where also occurs the northwestern-most cirques and

a possible few small stagnant ice masses or semipermanent snowfields remaining after years of drought and melting.

Middle or Central Hindu Kush

This region occurs to the northeast and east of the Kabul Basin, and includes all of the mountains of Nuristan south and east of the Panjshir Valley and over the Anjuman Pass to the Dorah Pass into Pakistan near Chitral, down to the Kunar River Valley, all of which are in the Kabul River drainage basin. The Mir Samir glacierized area near the Panshir Valley (Gilbert et al., 1969) is important to any study because it received some of the first glaciological work ever done in Afghanistan (Shroder and Bishop, 2009).

Eastern Hindu Kush

This mountainous region extends east from its Kokcha River border with the Khawaja Mohammed Range, and east to the Ab-i-Panj river border of the Wakhan Corridor, as well as from the Anjuman to Dora Pass valley route to Chitral, as far as Baroghil Pass along the Afghanistan–Pakistan border in the Wakhan where it terminates. The Eastern Hindu Kush therefore includes all the high peaks along the Afghanistan–Pakistan border, including Noshak (7,492 m), the highest peak in Afghanistan, as well as Tirich Mir (7,706 m) above Chitral in Pakistan. In the west, close to the Kokcha River border with the Khwaja Mohammed Range, occurs the Koh-i-Bandaka area of glaciers that have been mapped and studied recently (Shroder and Bishop, 2010). The Keshnikhan Glacier in Afghanistan a few km NNE of the Noshaq and Tirich Mir peaks was first mapped and studied by an Austrian Expedition of 1970 (Braslau, 1974), and is again the focus of recent attention (Shroder and Bishop, 2009).

Khwaja Mohammed Range

This northernmost of the main Hindu Kush ranges extends northward from the southern boundary along the line of the Andarab–Khwak Pass–Anjuman Pass, between the Kokcha River on the east and the Surkhab–Kunduz River on the west.

North of the Hindu Kush and still inside Afghanistan are the Pamir ranges of Badakshan and the Wakhan Corridor. Outside of Afghanistan to the north in Tajikistan and neighboring states occur many more ranges of the Pamir, as well as the Pamir Knot.

Collectively the diverse sets of Hindu Kush ranges are characterized by ~3,000 small glaciers in Afghanistan that are almost nowhere more than a few kilometers in length. The glaciers of the Hindu Kush are dominantly nourished by winter westerly precipitation, although those in the southeast of Afghanistan can receive some summer snows from monsoonal augmentation from moisture sources in the Indian Ocean. In fact, the largest glaciers of the Hindu Kush actually occur on the south side of the Eastern Hindu Kush of northwest Pakistan where the Tirich Mir (7,690 m) and Noshaq (7,492 m) massifs tower high enough to intercept sufficient monsoonal moisture to produce a very few glaciers up to 24 km in length.

Summary

The Hindu Kush ranges of Afghanistan and the Pakistan border region can be subdivided into a Western, Central, and Eastern Hindu Kush, as well as a Northern or Khwaja Mohammed Range. Collectively the Hindu Kush ranges have many small glaciers that are dominantly only a few km in length. Meltwater from these glaciers constitutes a vital late season supply of critical irrigation that is threatened with climate change in this chronically drought-torn region.

Bibliography

Braslau, D., 1974. The glaciers of Keshnikhan. In Gratzal, K. (ed.), *Hindukusch; Österreichische Forschungsexpedition in den Wakhan 1970*. Graz: Akademische Druck-u. Verlagsanstalt, pp. 112–116.

Burrard, S. G., and Hayden, H. H., 1907. A sketch of the Geography and Geology of the Himalaya Mountains and Tibet. Survey of India, 359 pp.

Gilbert, O., Jamieson, D., Lister, H., and Pendlington, A., 1969. Regime of an Afghan glacier. *Journal of Glaciology*, **8**(52), 51–65.

Grötzbach, E., 1990. Afghanistan: Eine geographische Landeskunde (Wissenschaftliche Landerkunden). Darmstadt: Wissenschaftliche Buchgesellschaft, 449 pp.

Shroder, J. F., Jr., and Bishop, M. P., 2010. Glaciers of Afghanistan. In Williams, R. S., Jr., and Ferrigno, J. G. (eds.), *Satellite Image Atlas of Glaciers of the World*. U.S. Geological Survey Professional Paper 1386-F-3, F-167-F199.

HOLOCENE GLACIER FLUCTUATIONS

Johannes Koch
Department of Earth Sciences, Simon Fraser University, Burnaby, BC, Canada

Definition

Holocene is the most recent geological Epoch spanning the past 10,000–12,000 years.
Glacier fluctuations are advance and retreat phases of individual glaciers due to changes in their mass balance.

Introduction

Glacier extent during the Holocene was limited compared to the Pleistocene, but recent studies point to significant, rapid fluctuations of climate throughout the Holocene (e.g., Mayewski et al., 2004). One proxy of Holocene climate variability that has long been used is alpine glacier fluctuations (e.g., Denton and Karlén, 1973). Most alpine glaciers react rapidly to changes in their mass balance and thus to changes in temperature and precipitation, and studies of past glacier fluctuations allow reconstruction of climate variability on centennial and decadal timescales.

Reconstruction of Holocene glacier fluctuations is compromised by the fact that glacier advances in the Northern Hemisphere during the last millennium were generally the most extensive of the Holocene and obliterated or obscured most of the evidence of previous advances. Older moraines have been identified at few of the sites that have been investigated (e.g., Ryder and Thomson, 1986; Bakke et al., 2005), but dating control of these moraines is often poor. More complete Holocene histories have been inferred from sediments in lakes downvalley of glaciers (e.g., Karlén, 1988; Bakke et al., 2005), but these records can be complicated by nonclimatic factors. The most direct evidence for glacier advances that predate the last millennium is found in areas deglacierized in the twentieth century. Remnants of forests in these forefields include in situ tree stumps and detrital logs and branches. In addition, organic soils and detrital wood are exposed in composite lateral moraines. High-quality data on Holocene glacier fluctuations have been retrieved from many of these forefields and moraines (e.g., Luckman, 2000; Nicolussi and Patzelt 2000; Glasser et al., 2004; Holzhauser et al., 2005; Koch et al., 2007; Barclay et al., 2009).

This entry summarizes Holocene glacier fluctuations in mountainous areas around the world in chronological order. The summary benefits from recent regional reviews (Barclay et al., 2009; Briner et al., 2009; Geirsdóttir et al., 2009; Hall, 2009; Ivy-Ochs et al., 2009; Kelly and Lowell, 2009; Menounos et al., 2009; Nesje, 2009; Owen, 2009; Rodbell et al., 2009). Data presented here cover western North America, the North Atlantic region (Baffin Island, Greenland, Iceland), Europe (Scandinavia, Alps), Asia (Tibet, Himalaya, Tian Shan, Pamir-Alai, Altai, Caucasus, Polar Urals, Yakutia, and Kamtchatka), Africa, South America, New Zealand, and Antarctica. Chronological control for most of these studies was provided by dendrochronology, lichenometry, radiocarbon dating of fossil wood in moraines, cosmogenic surface exposure dating, proglacial lake sediments, tephras, and radiocarbon dating of basal organics in pits, bogs, and lakes that provide minimum limiting ages.

Global Holocene glacier fluctuations

There is evidence for broadly synchronous periods of glacier advance around the world at 8.6–8.1, 7.3–5.9, 5.1–4.2, 4.2–1.9, 1.9–0.9 ka (ka is used here instead of cal. years BP), and during the past millennium. The broad age ranges of the six periods of more extensive glaciation are the result of large uncertainties introduced by calibrating radiocarbon ages. Glacier extent at the end of each of the six periods, however, was much greater than at the beginning of the following advance period. Several areas presented here were still heavily glaciated in the early Holocene as glaciers retreated from their Last Glacial maxima, and there is strong evidence that glaciers might have disappeared completely prior to about 6 ka in some Northern Hemisphere locations.

Early Holocene advances

Evidence for glacier advances prior to the 8.2 ka event is sparse. A few glaciers in western Canada advanced slightly between 9.5 and 8.5 ka (Koch et al., 2007). Alpine glaciers in western Greenland advanced between 9 and 10 ka (Kelly and Lowell, 2009), and glaciers in Norway advanced around 9.7 and 9.2 ka, but this evidence has been questioned by more recent interdisciplinary studies (Nesje, 2009). Nicolussi and Patzelt (2000) report a short-lived advance in the Austrian Alps about 10.1 ka, while data from the central Swiss Alps indicate smaller than present glaciers about 9.7 ka (Hormes et al., 2001). In Tibet glaciers advanced 9.4–8.8 ka, and continental glaciers in northwestern China around 9.3 ka (Owen, 2009). Glaciers in the Southern Hemisphere appear to have been as extensive or more extensive in the early Holocene than during the past millennium with two advances recorded in the Patagonian Precordillera and New Zealand (Röthlisberger, 1986; Gellatly et al., 1988; Wenzens, 1999).

The 8.2 ka event

Evidence for this event is also sparse. Detrital wood along with an increase in clastic sediment in proglacial lakes in the Coast Mountains indicate a minor advance coeval with this event (Menounos et al., 2009). Alpine glaciers on Baffin Island advanced (Briner et al., 2009), and glacier expansion in Scandinavia was widespread (Nesje, 2009), with some glaciers likely more extensive at this time than during the past millennium. Brief advances of limited extent occurred in Austria (Nicolussi and Patzelt, 2000), but Hormes et al. (2001), argue for less extensive glaciers in the central Swiss Alps. Glaciers advanced in the Himalaya and Karakoram (Owen, 2009), as well as in Kamtchatka (Yamagata et al., 2002). Moraines well beyond the past millennium extent were deposited in the Patagonian Precordillera (Wenzens, 1999) and near the Northern Patagonian Icefield (Rodbell et al., 2009).

7.3–5.9 ka events

Evidence for these events is widespread in both hemispheres. Glaciers in the Coast and Rocky Mountains in western Canada advanced during this time (Menounos et al., 2009), and the data indicates that glaciers advanced two or three times and reached positions within 1 km of their Holocene maximum extent (Koch et al., 2007). Hubbard Glacier in coastal Alaska advanced and remained extensive for the next millennium (Barclay et al., 2009). Glaciers in the Brooks and Alaska Ranges advanced, and some may have attained greater extents than at later times (Calkin, 1988). Evidence from the European Alps also indicates three advances (Nicolussi and Patzelt, 2000), with less extensive glaciers than today between advances (Hormes et al., 2001). Glaciers in western Greenland and Scandinavia underwent two minor advances (Karlén, 1988; Kelly and Lowell, 2009; Nesje, 2009), while

glaciers in Iceland, on Baffin Island, in Kamtchatka, in continental northwestern China, and on Mount Kenya advanced once (Karlén et al., 1999; Savoskul, 1999; Briner et al., 2009; Geirsdóttir et al., 2009; Owen, 2009). Evidence for two advances comes from the central and the southern Andes (Rodbell et al., 2009), the Northern Patagonian Icefield (Rodbell et al., 2009), the Patagonian Precordillera (Wenzens, 1999), and the central Andes near Mendoza (Espizua, 2002), where moraines were deposited well beyond the past millennium moraines. Glaciers on the Antarctic Peninsula and South Atlantic islands fluctuated (Hall, 2009), and in New Zealand moraines were deposited (Schaefer et al., 2009).

5.1–4.2 ka events

Evidence for one or more advances during this time is widespread in both hemispheres. Glaciers in the Coast and Rocky Mountains in western Canada advanced twice (Menounos et al., 2009). Similarly, glaciers in Alaska appear to have advanced one or two times (Calkin, 1988; Barclay et al., 2009), and there is evidence for an advance in the Cascades (Davis, 1988). Moraines were deposited in Iceland (Geirsdóttir et al., 2009), and glaciers in Scandinavia expanded in some cases to positions outside maximum past millennium limits (Karlén, 1988; Nesje, 2009), while in northern Folgefonna glaciers reformed (Bakke et al., 2005). Glaciers in Austria advanced twice (Nicolussi and Patzelt, 2000), while glaciers in the central Swiss Alps appear to have been less extensive than today (Hormes et al., 2001). Glacier advances are recorded in the Himalaya and Karakoram, in northwestern China, in the former USSR, and on Mount Kenya (Serebryanny and Solomina, 1996; Karlén et al., 1999; Owen, 2009). Glaciers in the tropical and Patagonian Andes advanced (Glasser et al., 2004; Rodbell et al., 2009), and some deposited moraines well outside their past millennium margins (Wenzens, 1999). Evidence from New Zealand also indicates two advances during this time (Gellatly et al., 1988), while evidence in Antarctica is poorly constrained (Hall, 2009).

4.2–1.9 ka events

Glacier advances during this time have been identified in both hemispheres. Many glaciers in Canada achieved extents only slightly smaller than during the past millennium, with evidence that some were even more extensive (Ryder and Thomson, 1986). Multiple advances, up to three, are evident in the Canadian Rockies and Coast Mountains (e.g., Koch et al., 2007). Three advances deposited nearly synchronous moraines in the Brooks and the Alaska ranges (Calkin, 1988). Many glaciers in coastal Alaska as well as the Wrangell Mountains also expanded at this time, but the advances were less extensive than those of the past millennium (Barclay et al., 2009). Moraines were deposited in Iceland by two advances (Geirsdóttir et al., 2009), up to three advances are recorded on Baffin Island (Briner et al., 2009), and there is some evidence for glacier advances in Greenland (Kelly and Lowell, 2009). Multiple advances, up to five, occurred in the European Alps (Nicolussi and Patzelt, 2000; Holzhauser et al., 2005), with glaciers being possibly less extensive than today between some of these advances (Hormes et al., 2001). Glaciers in Scandinavia expanded several times, in some cases to limits beyond those of the past millennium (Karlén, 1988; Bakke et al., 2005; Nesje, 2009). Glaciers advanced several times in the Himalaya and Karakoram, in Tibet, in the former USSR, and on Mount Kenya (Serebryanny and Solomina, 1996; Karlén et al., 1999; Owen, 2009). Glaciers in the tropical Andes advanced once, and possibly twice in the Patagonian Andes, the Patagonian Precordillera, the Cordillera Darwin on Tierra del Fuego, and the south-central Andes (Wenzens, 1999; Espizua, 2002; Glasser et al., 2004; Rodbell et al., 2009). Glaciers in South America were generally more extensive at this time than during the past millennium (Espizua, 2002; Glasser et al., 2004). Three separate advances that deposited moraines have been identified in New Zealand (Gellatly et al., 1988; Schaefer et al., 2009), and glaciers in Antarctica advanced (Hall, 2009).

1.9–0.9 ka events

Glacier advances during this time have been identified in both hemispheres, and numerous sites show evidence for multiple phases. Evidence for this event is widespread in western Canada (Menounos et al., 2009), but glacier extent generally appears to have been smaller than during the previous and following events. In the Brooks and Alaska Ranges moraines indicate up to three advances (Calkin, 1988), and glaciers in maritime Alaska show a peak of activity around AD 600–650 (Barclay et al., 2009). Some glaciers on Baffin Island, in Greenland, and in Iceland advanced in the first millennium AD (Briner et al., 2009; Geirsdóttir et al., 2009; Kelly and Lowell, 2009). Ice cover in Scandinavia expanded twice (Karlén, 1988; Bakke et al., 2005; Nesje, 2009), and some glaciers were more extensive then than during the past millennium (Karlén, 1988; Nesje, 2009). Up to three advances are well documented in the European Alps, each separated by significant recession (Nicolussi and Patzelt, 2000; Hormes et al., 2001; Holzhauser et al., 2005). Maritime-influenced glaciers in southeastern Tibet advanced once, while glaciers in the Himalaya and Karakoram advanced twice (Owen, 2009). Glaciers also advanced in the former USSR and on Mount Kenya (Serebryanny and Solomina, 1996; Karlén et al., 1999). Glaciers in the tropical and Patagonian Andes advanced (Glasser et al., 2004; Rodbell et al., 2009), and moraines were deposited in the Patagonian Precordillera (Wenzens, 1999) and the tropical Cordillera Blanca (Rodbell et al., 2009). On the Antarctic Peninsula and on South Atlantic islands glaciers advanced (Hall, 2009), and moraines in New Zealand provide evidence for three separate advances (Gellatly et al., 1988; Winkler, 2004).

0.9–0.1 ka events

Evidence for these events is ubiquitous in both hemispheres, and the period is generally referred to as the Little Ice Age (Grove, 1988). Abundant evidence for several advances has been reported from numerous glaciers in Canada, and most reached their maximum Holocene extent during this interval. The Little Ice Age here began about AD 1050 and lasted until the early twentieth century (Luckman, 2000; Menounos et al., 2009). Evidence suggests that glaciers fluctuated significantly throughout this time period, but generally were more extensive than they were in the late twentieth century. Similarly, the Little Ice Age in Alaska began as early as AD 1100 (Barclay et al., 2009) and continued until the late nineteenth century (Calkin, 1988; Barclay et al., 2009). Most glaciers in Alaska achieved their maximum Holocene extent during the Little Ice Age. In the Cascade Range, Olympic Mountains, and Montana Rocky Mountains early advances occurred before the thirteenth century and continued until the early twentieth century (Davis, 1988). Glacier advances on Baffin Island, in Greenland, and in Iceland are generally the most extensive since late-glacial time (Briner et al., 2009; Geirsdóttir et al., 2009; Kelly and Lowell, 2009), but moraines deposited at Langjökull ice field in Iceland indicate smaller extents than during earlier advances (Geirsdóttir et al., 2009). Little Ice Age fluctuations of glaciers in the European Alps have been reconstructed in detail back to AD 1100, and indicate several distinct advances, which were the most extensive in the Holocene (Nicolussi and Patzelt, 2000; Holzhauser et al., 2005). Historical records for many glaciers date back to the mid-seventeenth century (Nicolussi and Patzelt, 2000; Holzhauser et al., 2005). The Little Ice Age in Scandinavia began about AD 1080, and lasted until the early twentieth century, with most Scandinavian glaciers attaining their maximum Holocene extent (Karlén, 1988; Bakke et al., 2005; Nesje, 2009). Glaciers in the former USSR and in Tibet and surrounding areas provide evidence for Little Ice Age advances, but those advances were generally less extensive than earlier advances (Serebryanny and Solomina, 1996; Owen, 2009). Glaciers in the tropical Andes advanced as early as the twelfth century, and moraines were formed between AD 1600 and 1900 (Rodbell et al., 2009), while on Mount Kenya advances occurred between AD 1400 and 1600 (Karlén et al., 1999). Moraine-building advances in Patagonia occurred as early as the mid-thirteenth century, but generally the Little Ice Age culminated sometime in the seventeenth century (Koch and Kilian, 2005). In New Zealand advances started around AD 1150, and lasted until the early twentieth century (Gellatly et al., 1988; Schaefer et al., 2009), and glacier expansion in Antarctica is evident at all sites (Hall, 2009).

Twentieth century

Glacier fluctuations during the twentieth century have been documented from photographic and historical evidence, and detailed reconstructions are available for many glaciers. Most glaciers throughout the world receded during the twentieth century, but some tidewater and surging glaciers in Alaska and Patagonia are at or near their Holocene maxima, while some glaciers in Scandinavia and New Zealand advanced late in the twentieth century. Most records show slow recession between 1900 and about 1910, followed by stillstands and minor readvances in the second and third decades of the century. Recession was most rapid between about 1930 and the 1950s, followed by another period of stillstands and minor readvances in the 1950s, 1960s, and 1970s. Most glaciers have receded rapidly since the mid-1980s.

Conclusions

Holocene glacier advances in both hemispheres are broadly synchronous at timescales of centuries and occurred during six periods: 8.6–8.1, 7.3–5.9, 5.1–4.2, 4.2–1.9, 1.9–0.9 ka, and the last millennium. Recent studies provide evidence that most of these events were marked by glacier behavior as complex as that of the past millennium. Synchronicity implies that one or more mechanisms have operated on a global scale to force Holocene glacier fluctuations. Early Holocene glacier advances in the Southern Hemisphere were generally more extensive than late Holocene advances, but dates are minimum ages and dating control is often not well constrained. In contrast, early Holocene advances in the Northern Hemisphere were generally less extensive than those of the late Holocene, with the latter, however, often wiping out evidence of previous events. A more complete and complex picture of glacier behavior since the Last Glacial Maximum in many places has only surfaced in the past decade and one can expect further advances on timing and extent of events around the globe due to new techniques.

Bibliography

Bakke, J., Lie, O., Nesje, A., Dahl, S. O., and Paasche, O., 2005. Utilizing physical sediment variability in glacier-fed lakes for continuous glacier reconstructions during the Holocene, northern Folgefonna, western Norway. *Holocene*, **15**, 161–176.

Barclay, D. J., Wiles, G. C., and Calkin, P. E., 2009. Holocene glacier fluctuations in Alaska. *Quaternary Science Reviews*, **28**, 2034–2048.

Briner, J. P., Davis, P. T., and Miller, G. H., 2009. Latest Pleistocene and Holocene glaciation of Baffin Island, Arctic Canada: key patterns and chronologies. *Quaternary Science Reviews*, **28**, 2075–2087.

Calkin, P. E., 1988. Holocene glaciation of Alaska (and adjoining Yukon Territory, Canada). *Quaternary Science Reviews*, **7**, 159–184.

Davis, P. T., 1988. Holocene glacier fluctuations in the American cordillera. *Quaternary Science Reviews*, **7**, 129–158.

Denton, G. H., and Karlén, W., 1973. Holocene climatic variations – their pattern and possible cause. *Quaternary Research*, **3**, 155–205.

Espizua, L. E., 2002. Late Pleistocene and Holocene glacier fluctuations in the Mendoza Andes, Argentina. In Casassa, G., Sepúlveda, F., and Sinclair, R. (eds.), *The Patagonian Icefields:*

a Unique Natural Laboratory for Environmental and Climate Change Studies. New York: Kluwer Academic/Plenum, pp. 55–66.
Geirsdóttir, Á., Miller, G. H., Axford, Y., and Ólafsdóttir, S., 2009. Holocene and latest Pleistocene climate and glacier fluctuations in Iceland. *Quaternary Science Reviews*, **28**, 2107–2118.
Gellatly, A. F., Chinn, T. J. H., and Röthlisberger, F., 1988. Holocene glacier variations in New Zealand: a review. *Quaternary Science Reviews*, **7**, 227–242.
Glasser, N. F., Harrison, S., Winchester, V., and Aniya, M., 2004. Late Pleistocene and Holocene palaeoclimate and glacier fluctuations in Patagonia. *Global and Planetary Change*, **43**, 79–101.
Grove, J. M., 1988. *The little ice age*. New York: Routledge.
Hall, B. L., 2009. Holocene glacial history of Antarctica and the sub-Antarctic islands. *Quaternary Science Reviews*, **28**, 2213–2230.
Holzhauser, H., Magny, M., and Zumbühl, H. J., 2005. Glacier and lake-level variations in west-central Europe over the last 3500 years. *Holocene*, **15**, 789–801.
Hormes, A., Müller, B. U., and Schlüchter, C., 2001. The Alps with little ice: evidence for eight Holocene phases of reduced glacier extent in the Central Swiss Alps. *Holocene*, **11**, 255–265.
Ivy-Ochs, S., Kerschner, H., Maisch, M., Christl, M., Kubik, P. W., and Schlüchter, C., 2009. Latest Pleistocene and Holocene glacier variations in the European Alps. *Quaternary Science Reviews*, **28**, 2137–2149.
Karlén, W., 1988. Scandinavian glacial and climate fluctuations during the Holocene. *Quaternary Science Reviews*, **7**, 199–209.
Karlén, W., Fastook, J. L., Holmgren, K., Malmstroem, M., Matthews, J. A., Odada, E., Risberg, J., Rosqvist, G., Sandgren, P., Shemesh, A., and Westerberg, L.-O., 1999. Glacier fluctuations on Mount Kenya since similar to 6000 cal. years BP: Implications for Holocene climatic change in Africa. *Ambio*, **28**, 409–418.
Kelly, M. A., and Lowell, T. V., 2009. Fluctuations of local glaciers in Greenland during latest Pleistocene and Holocene time. *Quaternary Science Reviews*, **28**, 2088–2106.
Koch, J., and Kilian, R., 2005. Little Ice Age glacier fluctuations at Gran Campo Nevado, southernmost Chile. *Holocene*, **15**, 20–28.
Koch, J., Osborn, G., and Clague, J. J., 2007. Pre-little ice age glacier fluctuations in Garibaldi Provincial Park, southern Coast Mountains, British Columbia, Canada. *Holocene*, **17**, 1069–1078.
Luckman, B. H., 2000. Little ice age in the Canadian rockies. *Geomorphology*, **32**, 357–384.
Mayewski, P. A., Rohling, E. E., Stager, J. C., Karlén, W., Maasch, K. A., Meeker, L. D., Meyerson, E.-A., Gasse, F., van Kreveld, S., Holmgren, K., Lee-Thorp, J., Rosqvist, G., Rack, F., Staubwasser, M., Schneider, R. R., and Steig, E. J., 2004. Holocene climate variability. *Quaternary Research*, **62**, 243–255.
Menounos, B., Osborn, G., Clague, J. J., and Luckman, B. H., 2009. Latest Pleistocene and Holocene glacier fluctuations in western Canada. *Quaternary Science Reviews*, **28**, 2049–2074.
Nesje, A., 2009. Latest Pleistocene and Holocene alpine glacier fluctuations in Scandinavia. *Quaternary Science Reviews*, **28**, 2119–2136.
Nicolussi, K., and Patzelt, G., 2000. Untersuchungen zur holozänen Gletscherentwicklung von Pasterze und Gepatschferner (Ostalpen). *Zeitschrift für Gletscherkunde und Glazialgeologie*, **36**, 1–87.
Owen, L. A., 2009. Latest Pleistocene and Holocene glacier fluctuations in the Himalayas and Tibet. *Quaternary Science Reviews*, **28**, 2150–2164.
Rodbell, D. T., Smith, J. A., and Mark, B. G., 2009. Glaciation in the Andes during the Lateglacial and Holocene. *Quaternary Science Reviews*, **28**, 2165–2212.
Röthlisberger, F., 1986. *10 000 Jahre Gletschergeschichte der Erde*. Aarau: Verlag Sauerländer.
Ryder, J. M., and Thomson, B., 1986. Neoglaciation in the southern Coast Mountains of British Columbia: chronology prior to the late Neoglacial maximum. *Canadian Journal of Earth Sciences*, **23**, 273–287.
Savoskul, O. S., 1999. Holocene glacier advances in the headwaters of Sredniaya Avacha, Kamtchatka, Russia. *Quaternary Research*, **52**, 14–26.
Schaefer, J. M., Denton, G. H., Kaplan, M., Putnam, A., Finkel, R. C., Barrell, D. J. A., Andersen, B. G., Schwartz, R., Mackintosh, A., Chinn, T., and Schlüchter, C., 2009. High-frequency Holocene glacier fluctuations in New Zealand differ from the northern signature. *Science*, **324**, 622–625.
Serebryanny, L. R., and Solomina, O. N., 1996. Glaciers and climate of the mountains of the former USSR during the Neoglacial. *Mountain Research and Development*, **16**, 157–166.
Wenzens, G., 1999. Fluctuations of outlet and valley glaciers in the southern Andes (Argentina) during the past 13, 000 years. *Quaternary Research*, **51**, 238–247.
Winkler, S., 2004. Lichenometric dating of the Little Ice Age maximum in Mt Cook National Park, southern Alps, New Zealand. *Holocene*, **14**, 911–920.
Yamagata, K., Sone, T., Sawagaki, T., and Muravyev, Y. D., 2002. Holocene fluctuations of the Bilchenok Glacier, Kamtchatka Peninsula. *Journal of Geography*, **111**, 509–518.

Cross-references

Alaskan Glaciers
Alps
Andean Glaciers
Antarctica
Arctic Hydroclimatology
Canadian Rockies and Coast Mountains of Canada
Climate Change and Glaciers
Dating Glacial Landforms
Glaciers of the Karakoram Himalaya
Global Warming and its Effect on Snow/Ice/Glaciers
Greenland Glaciers Outside the Ice Sheet
Himalaya
Iceland Glaciers
Moraine
New Zealand Glaciers
Pamirs
Patagonia
Retreat/Advance of Glaciers
Rocky Mountains
Scandinavian Glaciers
Tibetan Plateau
Tien Shan Glaciers
Tree-Ring Indicators of Glacier Fluctuations

HORIZONTAL COMPONENT OF ABLATION

Rijan B. Kayastha
Himalayan Cryosphere, Climate and Disaster Research Center (HiCCDRC), Kathmandu University, Dhulikhel, Kavre, Nepal

Horizontal component of ablation is the ablation which removes ice from a glacier margins. This is the main component which determines advance or retreat of glaciers.

Glacier terminus retreat will occur when the horizontal component of ablation is greater than the horizontal component of velocity of the glacier. Glacier margin will remain in the same position when the horizontal component of ablation equals the horizontal component of velocity, that is, when

$$U_{tx} = a_b/\tan\alpha$$

where U_{tx} is the horizontal component of velocity, a_b is the ablation rate, α is the glacier surface slope, and $(a_b/\tan\alpha)$ is the horizontal component of ablation (Boulton, 1986). Although the terminus position is stationary in this case, the ice itself is in motion but is removed from the leading edge at a rate equal to the velocity.

Bibliography

Boulton, G. S., 1986. Push moraines and glacier contact fans in marine and terrestrial environments. *Sedimentology*, **33**, 677–698.

HORIZONTAL COMPONENT OF VELOCITY

Rijan B. Kayastha
Himalayan Cryosphere, Climate and Disaster Research Center (HiCCDRC), Kathmandu University, Dhulikhel, Kavre, Nepal

Horizontal component of velocity represents the rate of movement of glacier horizontally. This component of velocity varies widely depending upon on the amount of surface melt water available and its pressure at the interface between ice and bed rock. The water pressure increases the sliding velocity of glacier. Mathematically, the horizontal component of velocity U_{tx} can be written as:

$$U_{tx} = a_b/\tan\alpha$$

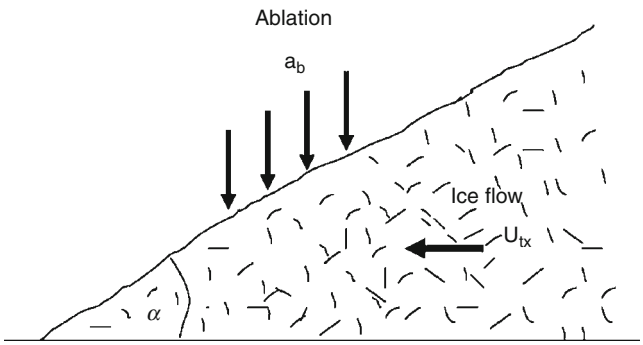

Horizontal Component of Velocity, Figure 1 Schematic diagram showing the influence if velocity, ablation rate and ice surface on glacier retreat and advance.

where a_b is the ablation rate, α is the glacier surface slope, and $(a_b/\tan\alpha)$ is the horizontal component of ablation (Boulton, 1986). The relation will be valid when the glacier margin remains in the same position (Figure 1). Iken and Bindschadler (1986) measured both horizontal velocity and subglacial water pressure on Findelegletscher and found the high horizontal velocity at high water pressure.

Bibliography

Boulton, G. S., 1986. Push moraines and glacier contact fans in marine and terrestrial environments. *Sedimentology*, **33**, 677–698.
Iken, A., and Bindschadler, R. A., 1986. Combined measurements of subglacial water pressure and surface velocity of Findelegletscher, Switzerland: conclusion about drainage system and sliding mechanism. *Journal of Glaciology*, **32**, 101–119.

HUMMOCKS (PEAT)

Subhajit Sinha
DBS College, Dehradun, Uttarakhand, India

Hummocks, small earth or peat mounds, are widely distributed in the arctic and develop as a consequence of biomass accumulation and cryoturbation in the active layer and in general the boreal peatlands is frequently hummocky. The hummocks and hollows develop from the peat and remain stable over long periods of time, even while climate and other environmental conditions change. The processes leading to the formation of these hummocks are not clearly understood. However, many types of simulation have generated satisfactory results of their formation. Recent studies have brought up a general consensus that the type of vegetation covering peat hummocks may alter the accumulation rate of organic material and thus hummock growth and local carbon sink dynamics.

HYDROCHEMICAL CHARACTERISTICS OF SNOW, ICE, AND GLACIERS

Jacob Clement Yde
Center for Geomicrobiology, University of Aarhus, Århus C, Denmark
Bjerknes Centre for Climate Research, University of Bergen, Bergen, Norway

Introduction

Studies on hydrochemical characteristics of snow, ice, and glaciers have traditionally been motivated by an interest in the role of chemical weathering in the regulation of atmospheric CO_2 on long time scales (>10,000 years) (Meltwater Quality as an Indicator of Subglacial

Processes). For instance, tectonic uplift has been suggested as a principal mechanism for increasing silicate weathering and thus enhancing atmospheric CO_2 drawdown and thereby causing global cooling (Raymo et al., 1988; Raymo and Ruddiman, 1992), but this theory remains controversial (Blum and Erel, 1995; Blum et al., 1998; Kump et al., 2000). Also, the shifting glacial–interglacial climate throughout the Quaternary has caused changes in the silicate weathering rate, but model results are still inconclusive (Gibbs and Kump, 1994, 1996; Kump and Alley, 1994; Tranter, 1996; Jones et al., 1999; Ludwig et al., 1999; Foster and Vance, 2006; Vance et al., 2009).

Mineral dissolution is strongly dependent on temperature, which theoretically will be reflected in the chemical composition of natural cold waters such as snowmelt, icemelt, and bulk meltwater emanating from glaciers (Chemical Composition of Snow, Ice, and Glaciers). However, in the field the temperature signal related to chemical erosion is often obscured by other factors related to climate (e.g., precipitation, runoff, continentality), lithology, tectonics (e.g., mechanical weathering, sediment transport, bedrock exposure and age), biomass effects, and anthropogenic effects (e.g., pollution, emission of greenhouse gasses, urbanization, land use, infrastructural effects). In glacial waters, the primary control is considered to be runoff, whereas lithology is a significant secondary control (Anderson et al., 1997; Hodson et al., 2000). Extensive reviews on hydrochemical characteristics of snow, ice, and glaciers can be found in Tranter (1991, 2003, 2006), Tranter and Jones (2001), and Brown (2002).

Meltwater characteristics

The primary characteristic of meltwater quality is that it generally is very dilute compared to other pathways in the hydrochemical cycle. In glacierized catchments, an inverse correlation exists between runoff and concentration so that low discharge waters are concentrated and high discharge waters are dilute (Tranter, 2006). This is reflected in solute concentration variations on diurnal and seasonal scales due to fluctuations in the intensity of ablation and retention time (Chemical Composition of Snow, Ice, and Glaciers and Solute in Glacial Meltwaters). For instance, preferential leaching of ions from snowpacks may cause large fluctuations in ion concentrations and ion ratios (e.g., Johannesen and Henriksen, 1978; Goto-Azuma et al., 1993; Raben and Theakstone, 1998). As a consequence of the low solute content of meltwater, concentration-derived parameters such as electric conductivity and ion strength are relatively low as well.

Another characteristic feature of glacial meltwater is the high suspended sediment concentration (Suspended Sediment Dynamics and Suspended Sediment Load) due to subglacial mechanical weathering (Mechanical Weathering, Physical Weathering, Subglacial Weathering, and Meltwater Quality as an Indicator of Subglacial Processes). Chemical weathering of the suspended sediments continue all the way from-source-to-sink and even after deposition. Therefore, the total glacier-derived solute yield is not only restricted to the solute flux from glacierized catchments (i.e., based on measurements at a station near a glacier portal), but is a result of biogeochemical processes all along water and airborne sediment transport trajectories to the suspended sediment sinks (Anderson, 2007).

Elemental ratios

The chemical composition of meltwater is closely related to solute provenance and governing controls. Therefore, the application of chemical mass balance budgets has become the standard approach in discriminating solute provenances in bulk meltwater (Sharp et al., 1995; Hodgkins et al., 1997; Hodson et al., 2000, 2002; Krawczyk et al., 2003; Yde et al., 2005, 2008, Krawczyk and Bartoszewski, 2008). Solute sources include sea-salts, acid aerosols, atmospheric sequestration, crustal denudation, organic sources, geothermal emission, and anthropogenic pollution.

While solute fluxes are important in studies on solute yield to the oceans and elemental cycles, they are not very useful in water quality and chemical weathering studies. Hence, elemental ratios are used as they are more conservative than absolute concentrations and permit comparisons between streams with high and low runoff (Négrel et al., 1993; Gaillardet et al., 1999). The molar K/Na, Ca/Si, and HCO_3/SO_4 ratio distributions in glacial waters have been reported to deviate from non-glacial waters and are therefore considered as distinctive hydrochemical characteristics of glacial waters. The K/Na ratio is suggested to be distinctly higher than in non-glacial runoff due to preferential weathering of K-mica minerals, resulting in high K concentrations (Anderson et al., 1996, 1997). The Ca/Si ratio is postulated to be higher in glacial waters due to preferential weathering of carbonates and slow weathering of silicates (Tranter, 2006), whereas the HCO_3/SO_4 ratio is proposed to be lower due to preferential weathering of sulfides (Tranter, 2006).

While elemental ratios allow comparisons between catchments with different runoff, they do not compensate for temperature effects due to cold waters. Also, coastal regions receive more marine-derived Na deposition than more continental regions such as the Alps and the Himalayas, affecting the K/Na ratio. Reference to global river chemistry may also be compromised by significantly anthropogenic pollution such as urban sewerage and salinization, and industrial and agricultural effluxes in non-glacial waters (Meybeck, 2005), and natural factors such as the global distribution of evaporites, which causes a strong bias because only a few glacierized regions are located on evaporitic outcrops, whereas on a global scale halite weathering delivers about 55% of the crustal-derived Na in rivers (Meybeck, 1987).

Summary

Despite many years of research, our understanding of hydrochemical characteristics of snow, ice, and glaciers and their controls remain unclear. The present impact on solute fluxes from glacial water on global geochemical cycles is limited, but this may have been different during periods of intense deglaciation such as during the Late Pleistocene. It must be recognized that we will always have very limited knowledge on the temporal and spatial variations in the hydrochemistry of snow, ice, and glaciers. The low number of sampling sites in glacierized regions may cause biased elemental ratios as they may not be representative as global average values. Also, the sampling frequency is often restricted to a short period during the ablation season or monthly sampling. Nevertheless, future hydrochemical modeling should change the scale from catchment to a regional or global perspective using careful extrapolations in order to provide more holistic views on the role of meltwater in the hydrochemical cycle (Anderson, 2007). Studies on minor and trace ion concentrations (Mitchell et al., 2001, 2006; Mitchell and Brown, 2007) and combining ion ratios with isotopic ratios (Isotopic Characteristics of Ice, Snow, and Glaciers) will provide new insights into the dominant control mechanisms of meltwater characteristics. Recent studies have focused on ecological aspects of nutrient characteristics in snow, ice, and glaciers (e.g., Hodson et al., 2005, 2008). It has been hypothesized that microbial processes significantly contribute to annual solute fluxes from glaciers (Skidmore et al., 2005), but it remains to be demonstrated (Chemical and Microbial Records in Snow and Ice, Glacial Ecosystems, and Microorganisms Associated with Glaciers).

Bibliography

Anderson, S. P., 2007. Biogeochemistry of glacial landscape systems. *Annual Review of Earth and Planetary Sciences*, **35**, 375–399.

Anderson, S. P., Drever, J. I., and Humphrey, N. F., 1996. Glacial chemical weathering regimes in relation to the continental norm. In Bottrell, S. H. (ed.), *Proceedings of the Fourth International Symposium on the Geochemistry of the Earth's Surface*, pp. 529–533.

Anderson, S. P., Drever, J. I., and Humphrey, N. F., 1997. Chemical weathering in glacial environments. *Geology*, **25**, 399–402.

Blum, J. D., and Erel, Y., 1995. A silicate weathering mechanism linking increases in marine $^{87}Sr/^{86}Sr$ with global glaciation. *Nature*, **373**, 415–418.

Blum, J. D., Gazis, C. A., Jacobson, A. D., and Chamberlain, C. P., 1998. Carbonate versus silicate weathering in the Raikhot watershed within the High Himalayan Crystalline Series. *Geology*, **26**, 411–414.

Brown, G. H., 2002. Glacier meltwater hydrochemistry. *Applied Geochemistry*, **17**, 855–883.

Foster, G. L., and Vance, D., 2006. Negligible glacial-interglacial variation in continental chemical weathering rates. *Nature*, **444**, 918–921.

Gaillardet, J., Dupré, B., Louvat, P., and Allègre, C. J., 1999. Global silicate weathering and CO_2 consumption rates deduced from the chemistry of large rivers. *Chemical Geology*, **159**, 3–30.

Gibbs, M. T., and Kump, L. R., 1994. Global chemical weathering at the last glacial maximum and the present: Sensitivity to changes in lithology and hydrology. *Paleoceanography*, **9**, 529–543.

Gibbs, M., and Kump, L., 1996. Global chemical weathering during deglaciation. In Bottrell, S. H. (ed.), *Proceedings of the Fourth International Symposium on the Geochemistry of the Earth's Surface*, pp. 733–737.

Goto-Azuma, K., Enomoto, H., Takahashi, S., Kobayashi, S., Kameda, T., and Watanabe, O., 1993. Leaching of ions from the surface of glaciers in western Svalbard. *Bulletin of Glacier Research*, **11**, 39–50.

Hodgkins, R., Tranter, M., and Dowdeswell, J. A., 1997. Solute provenance, transport and denudation in a High Arctic glacierized catchment. *Hydrological Processes*, **11**, 1813–1832.

Hodson, A. J., Tranter, M., and Vatne, G., 2000. Contemporary rates of chemical denudation and atmospheric CO_2 sequestration in glacier basins: an arctic perspective. *Earth Surface Processes and Landforms*, **25**, 1447–1471.

Hodson, A. J., Porter, P., Lowe, A., and Mumford, P., 2002. Chemical denudation and silicate weathering in Himalayan glacier basins: Batura Glacier, Pakistan. *Journal of Hydrology*, **262**, 193–208.

Hodson, A. J., Mumford, P. N., Kohler, J., and Wynn, P. M., 2005. The High Arctic glacial ecosystem: new insights from nutrient budgets. *Biogeochemistry*, **72**, 233–256.

Hodson, A. J., Anesio, A. M., Tranter, M., Fountain, A., Osborn, M., Priscu, J., Laybourn-Parry, J., and Sattler, B., 2008. Glacial ecosystems. *Ecological Monographs*, **78**, 41–67.

Johannesen, M., and Henriksen, A., 1978. Chemistry of snow meltwater: Changes in concentration during melting. *Water Resources Research*, **14**, 615–619.

Jones, I. W., Munhoven, G., and Tranter, M., 1999. Comparative fluxes of HCO_3^- and Si from glaciated and non-glaciated terrain during the last deglaciation. *IAHS*, **256**, 267–272.

Krawczyk, W. E., and Bartoszewski, S. A., 2008. Crustal solute fluxes and transient carbon dioxide drawdown in the Scottbreen Basin, Svalbard in 2002. *Journal of Hydrology*, **362**, 206–219.

Krawczyk, W. E., Lefauconnier, B., and Pettersson, L.-E., 2003. Chemical denudation rates in the Bayelva catchment, Svalbard, in the fall of 2000. *Physics and Chemistry of the Earth*, **28**, 1257–1271.

Kump, L. R., and Alley, R. B., 1994. Global chemical weathering on glacial time scales. In *Studies in geophysics: Material fluxes on the surface of the Earth*. Washington: National Research Council, National Academy, pp. 46–60.

Kump, L. R., Brantley, S. L., and Arthur, M. A., 2000. Chemical weathering, atmospheric CO_2, and climate. *Annual Review of Earth and Planetary Sciences*, **28**, 611–667.

Ludwig, W., Amiotte-Suchet, P., and Probst, J.-L., 1999. Enhanced chemical weathering of rocks during the last glacial maximum: a sink for atmospheric CO_2? *Chemical Geology*, **159**, 147–161.

Meybeck, M., 1987. Global chemical weathering of surficial rocks estimated from river dissolved loads. *American Journal of Science*, **287**, 401–428.

Meybeck, M., 2005. Looking for water quality. *Hydrological Processes*, **19**, 331–338.

Mitchell, A. C., and Brown, G. H., 2007. Diurnal hydrological - physicochemical controls and sampling methods for minor and trace elements in an Alpine glacial hydrological system. *Journal of Hydrology*, **332**, 123–143.

Mitchell, A., Brown, G. H., and Fuge, R., 2001. Minor and trace element export from a glacierized Alpine headwater catchment (Haut Glacier d´Arolla, Switzerland). *Hydrological Processes*, **15**, 3499–3524.

Mitchell, A. C., Brown, G. H., and Fuge, R., 2006. Minor and trace elements as indicators of solute provenance and flow routing in a subglacial hydrological system. *Hydrological Processes*, **20**, 877–897.
Négrel, P., Allègre, C. J., Dupré, B., and Lewin, E., 1993. Erosion sources determined by inversion of major and trace element ratios and strontium isotopic ratios in river water: The Congo Basin case. *Earth and Planetary Science Letters*, **120**, 59–76.
Raben, P., and Theakstone, W. H., 1998. Changes of ionic and oxygen isotopic composition of the snowpack at the glacier Austre Okstindbreen, Norway, 1995. *Nordic Hydrology*, **29**, 1–20.
Raymo, M. E., and Ruddiman, W. F., 1992. Tectonic forcing of late Cenozoic climate. *Nature*, **359**, 117–122.
Raymo, M. E., Ruddiman, W. F., and Froelich, P. N., 1988. Influence of late Cenozoic mountain building on ocean geochemical cycles. *Geology*, **16**, 649–653.
Sharp, M. J., Tranter, M., Brown, G. H., and Skidmore, M., 1995. Rates of chemical denudation and CO_2 drawdown in a glacier-covered alpine catchment. *Geology*, **23**, 61–64.
Skidmore, M., Anderson, S. P., Sharp, M., Foght, J., and Lanoil, B. D., 2005. Comparison of microbial community compositions of two subglacial environments reveals a possible role for microbes in chemical weathering processes. *Applied and Environmental Microbiology*, **71**, 6986–6997.
Tranter, M., 1991. Controls on the composition of snowmelt. *NATO ASI Series*, **G28**, 241–271.
Tranter, M., 1996. Glacial runoff as a sink for atmospheric CO_2 during the last glacial-interglacial transition. In Bottrell, S. H. (ed.), *Proceedings of the Fourth International Symposium on the Geochemistry of the Earth's Surface*, pp. 709–713.
Tranter, M., 2003. Geochemical weathering in glacial and proglacial environments. In Drever, J. I. (ed.), *Surface and Ground Water, Weathering, and Soils*. Treatise on Geochemistry: Elsevier, pp. 189–205.
Tranter, M., 2006. Chemical weathering, runoff composition and solute fluxes. In Knight, P. G. (ed.), *Glacier Science and Environmental Change*. Malden: Blackwell, pp. 71–75.
Tranter, M., and Jones, H. G., 2001. The chemistry of snow: processes and nutrient cycling. In Jones, H. G., Pomeroy, J. W., Walker, D. A., and Hoham, R. W. (eds.), *Snow Ecology – An Interdisciplinary Examination of Snow-Covered Ecosystems*. Cambridge: Cambridge University Press, pp. 127–167.
Vance, D., Teagle, D. A. H., and Foster, G. L., 2009. Variable Quaternary chemical weathering fluxes and imbalances in marine geochemical budgets. *Nature*, **458**, 493–496.
Yde, J. C., Knudsen, N. T., and Nielsen, O. B., 2005. Glacier hydrochemistry, solute provenance, and chemical denudation at a surge-type glacier, Disko Island, West Greenland. *Journal of Hydrology*, **300**, 172–187.
Yde, J. C., Riger-Kusk, M., Christiansen, H. H., Knudsen, N. T., and Humlum, O., 2008. Hydrochemical characteristics of bulk meltwater from an entire ablation season, Longyearbreen, Svalbard. *Journal of Glaciology*, **54**, 259–272.

Cross-references

Chemical and Microbe Records in Snow and Ice
Chemical Composition of Snow, Ice, and Glaciers
Chemical Processes in Snow and Ice
Geochemistry of Snow and Ice
Glacial Erosion
Glacier Hydrology
Isotopic Characteristics of Ice, Snow, and Glaciers
Sediment Entrainment, Transport, and Deposition
Solute in Glacial Meltwaters
Solutes in Glacier Ice
Subglacial Weathering

HYDROGEN ISOTOPES

Bhishm Kumar
Hydrological Investigations Division, National Institute of Hydrology, Roorkee, Uttarakhand, India

Definition

Hydrogen is the first element of the periodic table. It has three isotopes, two stable, that is, ^{1}H (protium) and ^{2}H (deuterium), and one radioactive ^{3}H (tritium). It is a very important component of atmosphere as it is present in water. The combinations of water like $^{1}H^{1}H^{16}O$, $^{1}H^{2}H^{16}O$ or $^{1}HD^{16}O$, $^{1}HD^{18}O$, $^{1}H^{1}H^{17}O$, and $^{1}HD^{17}O$ are considered important. Tritium (^{3}H) has very low abundance (around one part in 10^{18} parts of total hydrogen). It is a radioactive isotope of hydrogen with a half-life of 12.32 years. The natural occurrence of few very important types of water molecules is given below:

$H_2{}^{16}O \sim 997{,}640$ ppm (99.7640%)
$H_2{}^{18}O \sim 2{,}040$ ppm (0.204%)
$HD^{16}O \sim 320$ ppm (0.032%)

Origin

Hydrogen and deuterium occur naturally, while the tritium can be cosmogenic, lithogenic, or anthropogenic. Natural production of tritium in the atmosphere is very low. Due to the advent of thermonuclear technology, this production in the atmosphere has been supplemented by anthropogenic production. All atmospheric tritium, whether cosmogenic or anthropogenic, is rapidly incorporated into water molecules and falls in meteoric precipitation to enter the hydrologic cycle.

Uses

The $\delta^{2}H$ or $\delta^{18}O$ values offer the possibility for detecting the accumulation rates in an ice core of past periods and separation of runoff components. Climate change causes a shift of the ^{2}H or ^{18}O contents in precipitation, which can be preserved in old polar ice. Thus, it can be used to study the paleoclimates (Payne, 1983). Tritium is mainly used for dating the age of recent groundwater recharge. High levels of tritium (>∼30 TU) indicate water that was recharged during the late 1950s or early 1960s; moderate concentrations indicate modern recharge; levels close to detection (∼1 TU) are likely submodern or paleogroundwaters that have mixed with shallow modern groundwaters (Clark and Fritz, 1997).

Bibliography

Clark, I., and Fritz, P., 1997. *Environmental Isotopes in Hydrogeology*. Boca Raton and New York: Lewis.
Payne, B. R., 1983. Guidebook on nuclear techniques in hydrology, Technical report series no. 91, International Atomic Energy Agency, Vienna.

HYDROGRAPHS

Ian C. Willis
Department of Geography, Scott Polar Research Institute, University of Cambridge, Cambridge, UK

Definition

Hydrograph. A chart or graph showing changes in water quantity in a stream or river over time (Singh and Singh, 2001). Water quantity may be in units of stage (height above some datum), velocity, or Discharge. The time interval may be minutes, hours, days, months, years, or decades. Typically a hydrograph is depicted as discharge measured in cubic meters per second ($m^3\ s^{-1}$) sometimes abbreviated to cumecs.

Introduction

In snow and ice covered catchments, scientists and water resources managers are particularly interested in *diurnal hydrographs* (the change in discharge over a 24 h period, which typically increases during the day and decreases at night in response to diurnal variations in solar radiation and air temperature) (Diurnal Cycle of Runoff), *storm hydrographs* (the change in water quantity associated with a precipitation event), *flood hydrographs* (which may be associated with particularly high snow and ice melt or rainfall, but may also be due to the sudden release of water stored in the catchment) (Peak Flood Glacier Discharge), and *seasonal* or *annual hydrographs* (the variation in water quantity over a season, typically the "melt season" of late spring, summer, and early autumn, or a whole year).

The shape of a catchment hydrograph is a function of the patterns of water inputs to the catchment (from snow or ice melt or rainfall) (Melting of Snow/Ice and Meteorological Conditions) and the nature of the flow pathways (Catchment Routing) as the water travels through it (which will be affected by patterns of vegetation, soil type, extent of snow and ice cover, geology, and the overall size, shape, and altitude distribution – Hypsometry – of the catchment).

Diurnal, storm and flood hydrographs posses several characteristics, notably a *peak* (the highest point on the hydrograph when there is the greatest amount of water), the *rising limb* (the part of the hydrograph up to the peak), and a *falling limb* (the part after the peak). Under certain conditions, diurnal, storm, and flood hydrographs may possess *multiple peaks*. These could arise in a simple catchment where there are multiple water sources (e.g., a rainstorm following peak radiation-driven melt rates) or in a complex catchment where there are multiple water pathways (e.g., one containing both impermeable and permeable bedrock). Another important hydrograph characteristic is its *lag time*, the length of time between peak rainfall or peak melt rate and peak discharge.

Seasonal hydrographs

Figure 1a shows a typical seasonal hydrograph from a snow and ice covered catchment in Switzerland. Discharge is negligible during the winter and starts to increase in spring in response to greater radiation receipts and air temperatures causing snow melt (Melting Processes), especially in the lower part of the catchment (DeWalle and Rango, 2008; Jordan et al., 2008). Discharge increases during the summer as radiation receipts and air temperatures rise. It also increases due to the overall decrease in catchment Albedo as the snow melts exposing the underlying ground (thereby increasing air temperatures further) and underlying glacier ice (thereby increasing net shortwave radiation fluxes). It is for these reasons that seasonal discharges typically peak in late summer, several weeks after the summer solstice and maximum radiation receipts.

Diurnal hydrographs

Another key aspect of the snow/ice covered catchment hydrograph is the changing shape and lag times of the *diurnal hydrographs* during the season (Figure 1). They gradually evolve from low amplitude, fairly symmetrical hydrographs peaking many hours after solar noon (Figure 1b) to more peaky, high amplitude hydrographs with maximum values shortly after solar noon (Figure 1c). These changes reflect not only the changing sources of water in the catchment but also its routing. In spring, the dominant source is snow melt across the lower catchment, which is routed relatively slowly to the outlet as it moves vertically through the snowpack (Meltwater Percolation) and laterally across sediment and rock surfaces and as groundwater flow (Base Flow/Groundwater Flow). In late spring/early summer, snowmelt on the glacier is also retarded as it moves through firn. Snow/ice melt on the glacier is delayed as it moves across ice, and within constricted englacial (Englacial Conduit) and subglacial (Subglacial Drainage System) pathways, which have typically shrunk during the winter in response to Formation and Deformation of Basal Ice. By late summer, the dominant water source is glacier ice melt, which is routed quickly across the glacier surface to the edge and in ice marginal streams, or through large englacial and subglacial passageways that have enlarged in response to melting by the flowing water.

Storm hydrographs

Storm hydrographs are common in snow and ice covered catchments in the summer in response to frontal or convective rainfall, and are especially common in areas affected by monsoon rains. Figure 1d shows a storm rain-generated hydrograph, which disrupts the normal diurnal melt-generated hydrograph producing a bigger peak and longer duration hydrograph than usual. In the catchment of the Dokriani Glacier, Garhwal Himalaya (Himalaya), the ability of Summer Monsoon storms to affect diurnal and daily hydrographs depends on the

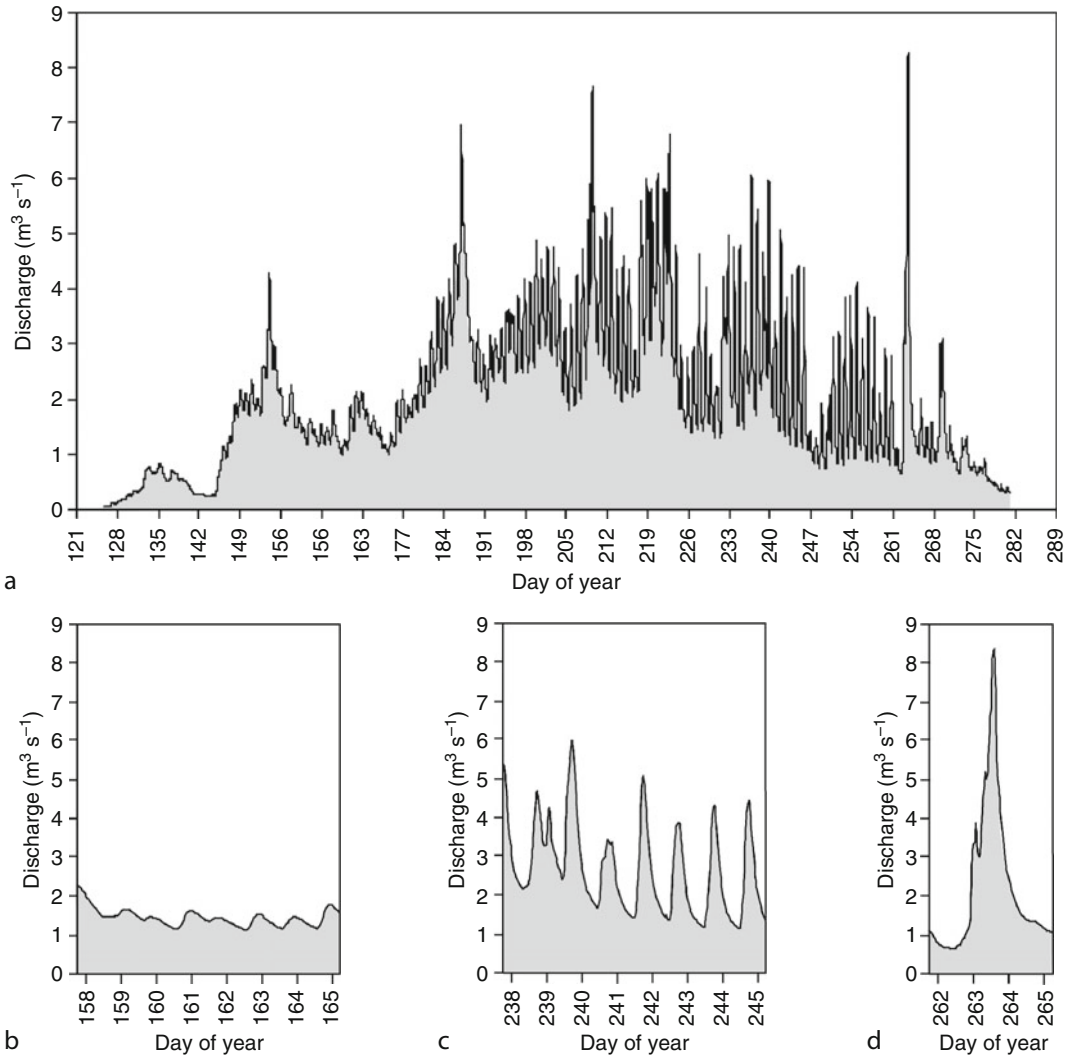

Hydrographs, Figure 1 (**a**) Hydrographs for the catchment of Haut Glacier d'Arolla, Switzerland. (**a**) Melt seasonal hydrograph from early May to mid-October 1999; diurnal hydrographs for (**b**) 7–14 May, and (**c**) 26 August–2 September; (**d**) storm hydrograph for 19–22 September. Note the multiple peaks on 27 August (Day 239); the first peak is the diurnal melt peak and the second is due to a rainstorm. Data kindly provided by Grande Dixence S.A.

season, intensity, duration, and distribution characteristics of the storm (Thayyen et al., 2005). Monsoon storms typically affect diurnal stream hydrographs early in the summer when the contribution from snow and ice melt is low, but later in the summer comparable rainstorms often have little or no influence as the higher discharges from snow/ice melt mask the effects. Rainstorms with intensities >30 mm day^{-1} always affect daily hydrographs. Those with intensities between 20 and 30 mm day^{-1} sometimes influence daily hydrographs depending on their duration and the time of year; those between June and August are more likely to affect daily hydrographs, whereas those in May or October are not, due to the influence of snow cover or reduced area experiencing liquid precipitation at these times. Intensities from 10 to 20 mm day^{-1} typically have negligible effect on diurnal hydrographs as the associated radiation and air temperature reduction lowers the melt contribution, compensating for the extra rain contribution. Intensities $<$10 mm day^{-1} typically reduce the daily discharge hydrograph due to the associated melt reduction.

Flood hydrographs

Flood hydrographs may be synonymous with storm hydrographs but may also be caused by the sudden release of water from ice marginal, supraglacial, or subglacial locations in what are often referred to as Glacier Lake Outburst Floods (GLOFs) or by their Icelandic name, jökulhlaups (Tweed and Russell, 1999). Ice marginal floods may be generated from moraine dammed lakes

where either the moraine dam fails or is overtopped, precipitating rapid incision and lake drainage. Similarly, floods may be released from ice dammed supraglacial or ice marginal lakes where either the Ice Dams is eventually overtopped leading to incision, or the lake level floats the adjacent ice and escapes underneath. Hydrographs from such floods are rarely recorded but some have been reconstructed from eyewitness accounts and empirical hydraulic formulae. For example, in 1985 a moraine-dammed lake in the Khumbu area of east Nepal was breached following a large ice avalanche into the lake (Vuichard and Zimmermann, 1987). The resulting flood caused massive destruction to infrastructure and valuable arable land over a distance of ~40 km downstream. The reconstructed flood hydrograph was asymmetrical with a steep rising limb and gentle falling limb, a peak discharge of ~1,500 $m^3 s^{-1}$, and a duration of ~5 h. The magnitude and frequency of such ice marginal floods may be expected to rise as glaciers continue to retreat rapidly from their Little Ice Age moraines (Haeberli and Beniston, 1998; Richardson and Reynolds, 2000). Subglacial floods occur when water builds up in a lake beneath an ice mass and eventually reaches a critical depth, allowing it to start escaping. Initially the escape route is small and hydraulically inefficient, but once water starts to flow, the frictional heat is able to melt an increasingly bigger and more hydraulically efficient drainage pathway allowing more and more water to drain. Consequently, the flood hydrographs typically possess a rising limb that gets progressively steeper up to the peak, reflecting the progressive enlargement of the drainage pathway, followed by a very steep falling limb as the water supply ceases or the drainage pathway closes due to the reduced water pressure. The best-documented subglacial floods are from Iceland Glaciers due to high geothermal heat fluxes and Subglacial Volcanism, especially those from the Grímsvötn caldera beneath Vatnajökull, which recur with a periodicity of around 5 years (Björnsson, 2003).

Floods are recognized as being an important feature of ice sheets, as well as many glaciers and ice caps. Flood hydrographs of surface lakes draining via hydrofracture into the Greenland Ice Sheet have been reconstructed from the monitoring of surface lake levels. These suggest that floods lasting a few hours with peak discharges of the order of 10^3–10^4 $m^3 s^{-1}$ (greater than the average flow rate of Niagara falls) may not be uncommon (Das et al., 2008). GPS monitoring of ice surface speed and elevation changes during the floods suggest the water is soon dissipated as it flows beneath the ice sheet to the margin. Subglacial floods have also been inferred from repeat satellite altimetry measurements of the Antarctic ice sheet, which show the rapid movement of water between Subglacial Lakes, Antarctic (Wingham et al., 2006; Fricker et al., 2007). Flood hydrographs have been constructed from the application of physics-based models fitted to the available data and suggest a progressively steepening rising limb lasting for several years reaching peaks of the order 10^2–10^3 $m^3 s^{-1}$ (Carter et al., 2009; Peters et al., 2009).

Climate and hydrograph analysis

Since hydrographs change their characteristics in response to changes in catchment processes, hydrographs and meteorological data from snow and ice covered catchments can be analyzed through time in an attempt to infer changing patterns of water sources and water routing. A variety of time domain statistical techniques (e.g., regression, cross-correlation, autoregressive integrated moving average, and transfer function-noise models) have been applied to climatic and hydrological time series from snow and ice covered catchments. These have been used to infer changing catchment processes through time, for example, switch from snowmelt to ice melt dominated; evolution from slow attenuated water transfer through a thick largely unsaturated snowpack to more rapid transfer through a thinner, more saturated snowpack; and change from moderately slow transfer through a distributed subglacial drainage system to rapid transfer through a channelized, hydraulically efficient subglacial drainage system (Gurnell et al., 1992; Hannah et al., 2000; Hodgkins, 2001). A problem with these time domain techniques is that the 24 h discharge cycle is not static, and the temperature–runoff relationships are highly dynamic. Several steps of data preparation are required prior to analysis and the time series need to be subdivided into periods of similar behavior before seasonal changes in the hydrograph characteristics can be evaluated. For these reasons, continuous spectral (Fourier Transform) analysis has also been used to investigate the meteorological – runoff relationships in nival and glacial catchments. For example, continuous wavelet analyses of hourly time series of air temperature, precipitation, and stream discharge were used to examine how seasonal and inter-annual variations in water sources and flow routing differed between the two main catchments upstream of Bow Lake, Alberta: the glacial stream draining the Wapta Icefields, and the snowmelt-fed Bow River (Lafrenière and Sharp, 2003). Several characteristics were identified, including: (i) rainfall had a bigger influence on stream hydrographs and followed quicker flow paths in the nival catchment than in the glacial catchment; (ii) snowpack thickness and catchment size were the primary controls on the phase relationship between diurnal temperature variations and diurnal hydrographs; and (iii) the diurnal glacial hydrograph signal was orders of magnitude higher in 1998 than in other years, suggesting that the 1997–1998 El Niño caused lower winter snowfall, greater summer ice exposure, and therefore the development of channelized hydraulically efficient glacial drainage.

Hydrograph separation

In addition to the analysis of climate and runoff hydrographs, several studies have attempted to separate a bulk hydrograph from a catchment into two (or more) component parts on the basis of stream chemical (Solute in Glacial Meltwaters) or isotope characteristics. Such "mixing models" make several assumptions. The first is that

there are two (or more) distinct flow pathways within a catchment, such as a "quick flow" and a "delayed flow" pathway that may be equated with specific types of drainage route (e.g., englacial/subglacial channelized flow and subglacial distributed flow within a glacierized catchment, or overland, soil water, and groundwater flow within a nival catchment). Second, that the water in the different flow pathways has unique and constant chemical or isotopic compositions. Third, that the flow components merge close to the catchment outlet monitoring station and that mixing is conservative, that is, there are no post-mixing chemical reactions. Collins (1979) was the first to use chemically based mixing models in glacial catchments and using stream electrical conductivity (a surrogate for total solute concentration) separated the bulk hydrographs of the adjacent glaciers Findelengletscher and Gornergletscher, Switzerland, into dilute "quick flow" and more chemically enriched "delayed flow" components. Interestingly, both hydrographs varied in phase with bulk flow at Findelengletscher, but at Gornergletscher the delayed flow hydrograph was out of phase with both the quick flow and bulk flow. This suggested that the two glaciers were dominated by distributed and channelized subglacial drainage systems, respectively. Since Collins's (1979) pioneering work, detailed hydrochemical analysis of waters in glacierized catchments, including in situ waters collected from the base of boreholes, together with laboratory dissolution experiments, have shown that the three key assumptions for chemically based hydrograph separation are questionable (Sharp et al., 1995; Brown, 2002). The second and third assumptions are more valid for isotopes. These may be used, therefore, to examine the proportion of bulk runoff that is derived from snow and ice ("recent" and "old," respectively), since snow and ice typically have distinct isotopic compositions (e.g., Wagnon et al., 1998). See *Hydrogen Isotopes* for more details.

Summary

Hydrographs depict the changes in water quantity, usually expressed as discharge, in a stream or river over time. In snow and ice covered catchments, discharge varies over a range of scales and it is possible to identify diurnal, storm, flood, and seasonal hydrographs. Since catchment hydrographs vary in response to variations in water inputs (from snow and ice melt or rainfall) and water routing, the analysis of hydrograph characteristics can be used to infer a variety of catchment processes. Increasingly, hydrologists and water resource planners are adopting a more conceptual or physics-based approach to modeling catchment hydrographs that may be used for predictive purposes (Hydrological Response in Glacierized Basins).

Bibliography

Björnsson, H., 2003. Sub glacial lakes and jökulhlaups in Iceland. *Global and Planetary Change*, **35**, 255–271.

Brown, G. H., 2002. Review: glacier meltwater hydrochemistry. *Applied Geochemistry*, **17**, 855–883.

Carter, S. P., Blankenship, D. D., Young, D. A., Peters, M. E., Holt, J. W., and Siegert, M. J., 2009. Dynamic distributed drainage implied by the flow evolution of the 1996–1998 Adventure Trench subglacial lake discharge. *Earth and Planetary Science Letters*, **283**, 24–37.

Collins, D. N., 1979. Quantitative determination of the subglacial hydrology of two Alpine glaciers. *Journal of Glaciology*, **23**, 347–362.

Das, S. B., Joughin, I., Behn, M. D., Howat, I. M., King, M. A., Lizarralde, D., and Bhatia, M. P., 2008. Fracture propagation to the base of the Greenland Ice Sheet during supraglacial lake drainage. *Science*, **320**, 778–781.

DeWalle, D. R., and Rango, A., 2008. *Principles of Snow Hydrology*. Cambridge, UK: CUP. 420 pp.

Fricker, H. A., Scambos, T., Bindschadler, R., and Padman, L., 2007. An active subglacial water system in West Antarctica mapped from space. *Science*, **315**, 1544–1546.

Gurnell, A. M., 1993. How many reservoirs? An analysis of flow recessions from a glacier basin. *Journal of Glaciology*, **39**, 409–414.

Gurnell, A. M., Clark, M. J., and Hill, C. T., 1992. Analysis and interpretation of patterns within and between hydroclimatological time series in an alpine glacier basin. *Earth Surface Processes and Landforms*, **17**, 821–839.

Haeberli, W., and Beniston, M., 1998. Climate change and its impacts on glaciers and permafrost in the Alps. *Ambio*, **27**, 258–265.

Hannah, D. M., Smith, B. P. G., Gurnell, A. M., and McGregor, G. R., 2000. An approach to hydrograph classification. *Hydrological Processes*, **14**(317), 338.

Hodgkins, R., 2001. Seasonal evolution of meltwater generation, storage and discharge at a non-temperate glacier in Svalbard. *Hydrological Processes*, **15**, 441–460.

Jordan, R. E., Albert, M. R., and Brun, E., 2008. Physical processes within the snow cover and their parameterization. In Armstrong, R. L., and Brun, E. (eds.), *Snow and Climate: Physical Processes*. UK: Surface Energy Exchange and Modeling. CUP. Cambridge, pp. 12–69.

Lafrenière, M., and Sharp, M., 2003. Wavelet analysis of interannual variability in the runoff regimes of glacial and nival stream catchments, Bow Lake, Alberta. *Hydrological Processes*, **17**, 1093–1118.

Peters, N., Willis, I., and Arnold, N., 2009. A numerical analysis of rapid water transfer beneath Antarctica. *Journal of Glaciology*, **55**(192), 640–650.

Richardson, S. D., and Reynolds, J. M., 2000. An overview of glacial hazards in the Himalayas. *Quaternary International*, **65**(66), 31–47.

Sharp, M., Brown, G. H., Tranter, M., Willis, I. C., and Hubbard, B., 1995. Comments on the use of chemically based mixing models in glacier hydrology. *Journal of Glaciology*, **41**, 241–246.

Singh, P., and Singh, V. P., 2001. Snow and Glacier Hydrology. Water Science and Technology Library, Vol. 37. Dordrecht/Boston/London: Kluwer Academic, 742 pp.

Thayyen, R. J., Gergan, J. T., and Dobhal, D. P., 2005. Monsoonal control on glacier discharge and hydrograph characteristics, a case study of Dokriani Glacier, Garhwal Himalaya, India. *Journal of Hydrology*, **306**, 37–49.

Tweed, F. S., and Russell, A. J., 1999. Controls on the formation and sudden drainage of glacier-impounded lakes: implications for jökulhlaup characteristics. *Progress in Physical Geography*, **23**, 79–110.

Vuichard, D., and Zimmermann, M., 1987. The 1985 catastrophic drainage of a moraine-dammed lake, Khumbu Himal, Nepal: cause and consequences. *Mountain Research and Development*, **7**, 91–110.

Wagnon, P., Ribstein, P., Schuler, T., and Francou, B., 1998. Flow separation on Zongo Glacier, Cordillera Real, Bolivia. *Hydrological Processes*, **12**, 1911–1926.
Wingham, D. J., Siegert, M. J., Shepherd, A., and Muir, A. S., 2006. Rapid discharge connects Antarctic subglacial lakes. *Nature*, **440**, 1033–1036.

Cross-references

Albedo
Base Flow/Groundwater Flow
Diurnal Cycle of Runoff
Formation and Deformation of Basal Ice
Glacier Lake Outburst Floods
Hydrographs
Hydrological Response in Glacierized Basins
Melting Processes
Meltwater Conduit
Monsoonal Records Observed from Snow/Ice/Glacier
Solute in Glacial Meltwaters
Subglacial Drainage System

HYDROLOGIC CYCLE AND SNOW

Ronald P. Daanen[1], Debasmita Misra[2], Anita M. Thompson[3]
[1]Geophysical Institute, University of Alaska Fairbanks, Fairbanks, AK, USA
[2]Geological Engineering, College of Engineering and Mines, University of Alaska Fairbanks, Fairbanks, AK, USA
[3]Department of Biological Systems Engineering, University of Wisconsin-Madison, Madison, WI, USA

Synonyms

Water cycle; Precipitation; Snow hydrology

Definition

Hydrologic cycle. Hydrologic cycle is the continuous movement of water through the atmosphere and on and below the earth's surface.
Precipitation. Any of the forms of water particles, whether liquid or solid, that fall from the atmosphere and reach the ground. The forms of precipitation are: rain, drizzle, snow, snow grains, snow pellets, diamond dust, hail, and ice pellets. (Source: National Snow and Ice Data Center, http://nsidc.org/arcticmet/glossary/precipitation.html.)
Snow. Precipitation in the form of crystalline water ice.
Interception. The component of precipitation that is intercepted by plants that evaporates or sublimates back to the atmosphere without reaching the earth's surface.
Runoff. The component of precipitation that moves across the land surface or through surface channels.
Snowmelt. The runoff that results from melting snow.
Evaporation. The physical process by which a liquid or solid substance is transformed to the gaseous state. In meteorology, evaporation usually is restricted in use to the change of water from liquid to gas. (Source: National Snow and Ice Data Center, http://nsidc.org/arcticmet/glossary/precipitation.html.)
Sublimation. The transition of a substance from the solid phase directly to the vapor phase, or vice versa, without passing through an intermediate liquid phase. Snow would sublime when exposed to solar radiation and at certain atmospheric pressure regimes. (Source: National Snow and Ice Data Center, http://nsidc.org/arcticmet/glossary/precipitation.html.)
Snow Hydrology. The hydrologic study of composition, dispersion, and movement of snow and ice.

Introduction

During the winter period, precipitation falls predominantly in the form of snow when the air temperature is below freezing ($<0°C$). In the hydrological cycle, this means that water is temporarily stored at the soil surface after which it is released in the form of meltwater (snowmelt). In many mountainous regions in the world, this water is of vital importance as a drinking water supply. During the summer, warm temperatures release this stored water as meltwater from higher elevation regions. Often, these regions have a small subsurface catchment volume and steep gradients, which support only limited groundwater storage.

Snow climatology and generation

Snow hydrology impacts the hydrologic processes in higher altitude and latitudes of the earth. Hence, understanding of the processes that lead to snowfall and its distribution is critical. According to McKay and Gray (1981), "The occurrence of snowfall in a region is generally dependent on several geographic and climatic factors: latitude, altitude, the distance from major water bodies, and the nature of regional air mass circulation." Snowfall does not occur in lower latitudes because the heat balance at the earth's surface renders air temperatures well above the freezing temperature during winter. Air temperature decreases with altitude; hence, higher altitudes experience more snowfall than lower areas. Both proximity to large water bodies and atmospheric circulation needed to transfer water vapor affect the moisture supply needed for snowfall when temperatures are low enough at the earth's surface. So, given cold air and an adequate supply of moisture, the local and regional snowfall climatology is governed by the atmospheric circulations (DeWalle and Rango, 2008).

Snow precipitates by the type of mechanism associated with its formation (Singh and Singh, 2001; DeWalle and Rango, 2008). There are four distinguished mechanisms of snow formation and each has characteristics that have important hydrologic consequence. These mechanisms of formation are (1) convective, (2) cyclonic, (3) orographic, and (4) turbulence. Heavy snowfall is mostly associated with cyclonic or orographic mechanisms, while turbulence in the atmosphere might produce fine snowfall.

Convective precipitation is usually limited to the tropics and is not a mechanism for snowfall.

Distribution of snow

Mountains have a strong impact on spatial distribution of precipitation (Singh and Singh, 2001). The knowledge of spatial distribution of snow is critical in planning and management of water resources, runoff simulations, and assessment of precipitation in a region. Singh and Singh (2001, Table 2.4, p. 79) have provided a summary of world-wide precipitation distribution studies in which they specifically conclude that snowfall increases linearly with altitude. They also conclude that the ratio of snowfall to annual precipitation varies linearly with altitude and that more than 60% of annual precipitation is in the form of snow in the regions that are above 2,000 m in altitude.

Another mechanism of distribution of snow is by lake-effect snowfall (DeWalle and Rango, 2008). Lake-effect snowfalls can cause some of the highest snowfall intensities from large water bodies such as the great lakes of the USA. The contrast in temperature between the air and the water and the evaporation rates from the unfrozen lakes are generally very high during the early winter period resulting in greater lake-effect snowfall, downwind from the lake. The factors that control the lake-effect snowfall are increase in ground elevation downwind of the lake and rough shoreline terrain causing *turbulence* in the atmosphere.

According to DeWalle and Rango (2008), "The Southern Oscillation which gives rise to El Niño conditions, or its counterpart La Niña conditions, is now known to have far-reaching effects on global climate and snowfall." They further state, "Snowfall totals in moderate to strong La Niña years averaged higher than in moderate to strong El Niño years, while neutral years generally had intermediate snowfall totals." Besides the Southern Oscillation, snow is also transported and distributed over large distances by the wind before it sublimates or comes to rest in a snowpack. Sublimation of blowing snow results in more than 50% of the loss in winter precipitation. Such magnitude of loss in regions of low precipitation and without supplemental irrigation can have significant impact in spring soil moisture levels and agricultural productivity. The blowing snow is usually transported by turbulent suspension, saltation, and creep (DeWalle and Rango, 2008). Such transport and distribution render uneven snowpack distribution that results in uneven meltwater delivery in spring.

Interception of snow

Snowfall often interacts with the vegetation prior to forming a snowpack. DeWalle and Rango (2008) define two important processes that are components of the hydrologic cycle:

> Snow that is lodged within the canopies of plants is referred to as intercepted snow, while snow that falls or drips to the ground from or through the canopy is termed throughfall. Throughfall from intercepted snow can be in the form of ice particles dislodged by the wind that filter through the canopy during cold, windy conditions or in the form of large masses of intercepted snow that slide from the plant branches during warm, melting conditions or as branches bend under the weight of intercepted snow. Meltwater from intercepted snow that reaches the ground by flowing down the stems of plants is called stemflow. Stemflow is a minor pathway for intercepted water to reach the ground (Brooks et al., 1997; Johnson, 1990), especially in winter when melt rates from intercepted snow are often much less than rainfall rates. Intercepted snow can be sublimated or evaporated from the canopy before reaching the ground and the mass lost to the atmosphere is referred to as interception loss. Interception loss can occur while the snow is stored within the canopy or as the intercepted snow is being redistributed within and over the landscape by the wind. Knowledge of the distribution and type of vegetation across a watershed is essential in successfully modeling effects of interception on snowmelt runoff.

Snowmelt runoff

The study of snowmelt runoff is complex. Understanding the generation of streamflow from snowmelt involves integration of processes that produce meltwater within the snowpack, processes that delay and store liquid water in the snowpack, and processes that direct the flow of meltwater through watersheds to stream channels (DeWalle and Rango, 2008). Once the outflow from the snowpack reaches the land surface, active hydrologic flow paths can cause such outflows to rapidly transition into streamflow depending on existing conditions such as soil frost, permafrost, or saturated subsurface. Flow paths for meltwater may be channels, overland flow, interflow, or groundwater recharge. Snowpack outflow onto frozen, impermeable ground may result in rapid streamflow response through overland flow while a portion of it might be stored or intercepted in surface ditches. Such rapid delivery of meltwater poses considerable problems in the arctic and sub-arctic watersheds. Micrometeorology determines energy supply on scales of meters due to canopy shading and unsaturated fingered flow in the snowpack controls' heterogeneous liquid water distribution in time and space over scales of centimeters (Waldner et al., 2004). Many of these processes equilibrate over watershed scales and multiple years, which make simulation of snowmelt runoff possible at these scales with intensive calibration. These models are not very transferable to other regions due to a lack of data and physical input required for model simulation. Besides, the prediction of the depth of soil frost, the infiltration capacity of the frozen ground becomes critical in modeling streamflow from snowmelt.

In arctic watersheds with low-relief and windy conditions, snow dams can alter the downstream delivery of meltwater (Woo and Sauriol, 1980; Woo, 1983). Streamflow in the arctic generally ceases in the winter due to the freezing of the active layer. The redistribution due to blowing snow in these watersheds fills the topographic depressions. During the spring melt, these

deposits act as dams and are responsible for slow downslope migration of meltwater. These deposits often become saturated with meltwater causing slush flows, tunneling in the snowpack, or surface flow over the saturated snow layers. Ponding may also occur in such snow dam conditions thus delaying the movement of meltwater downstream by several days. Snow damming presents special problems for modeling the movement of meltwater along slopes through the snow and prediction of snowmelt runoff in such basins (Hinzman and Kane, 1991).

Effect of uneven snowpack distribution and snow cover on hydrologic cycle

Small scale variations in snow depth affect the terrestrial ecosystem due to its effect on freezing rates. These heterogeneous freezing rates can result in a non-sorted circle environment, where water drives seasonal heaving and subsiding of the ground surface (Daanen et al., 2008a; Daanen et al., 2008b). Spring snowmelt can infiltrate more readily due to this heterogonous freezing because organic material, which is most often found underneath the greatest snow accumulation, dries out as the active layer freezes. This reduces overland snowmelt runoff in tundra regions.

Climate change effects on the hydrological cycle of snow

Seasonal snow cover has a major effect on the earth's climate system due to an increase in albedo when snow is present. This climate effect causes the hydrologic cycle to slow down during the winter over vast regions of the earth. The implications and feedbacks between climate and snow cover are currently a major topic of research. A reduction of snow cover extent results in a major positive feedback to climate warming due to increased absorption of radiation by the earth's surface. Climate warming in cold regions leads to a longer draining and evapotranspirating season with a drying result at the soil surface. Snowfall is, however, projected to increase as a result of increased moisture content in the atmosphere at lower latitudes. The two scenarios of increased input of snow and increased drainage may result in a net water balance with a greater through put of water. Currently, however, the tundra is experiencing dryer conditions and the increased snowfall has not been observed.

Seasonal snow cover also has a major effect on permafrost temperatures. Increase of snow depth insulates the ground more and can in some cases prevent the active layer (seasonally thawed ground on top of permafrost) from freezing (Yoshikawa and Hinzman, 2003). This thawed layer is also called a talik and depending on its location, it can contribute to increased drainage of permafrost affected regions. Increased drainage affects the whole hydrologic system from terrestrial ecosystems to salt concentrations in the Arctic Ocean.

Human impact on the hydrological cycle of snow

Human impact on the hydrological cycle of snow is small when viewed over the globe. However, in cities there is a major effect due to impervious surfaces and the removal of snow from highways and roads. Transportation and stock piling of snowmelts is slower than that of a regular snowpack, but the use of salt and gravels on the streets results in earlier and reduced snowmelt peaks. Air pollution also affects the hydrological cycle of snow, because ice crystals are more efficient in removing pollution from the air than rain droplets. These pollutants are released during the early snowmelt period.

Summary

Snow as a precipitate is a significant component of the hydrologic cycle especially in watersheds of high latitude or higher altitudes. The processes that are responsible for the timing and quantity of snowfall are reasonably well understood. However, estimation of basic liquid input from precipitation and snowpacks for modeling has been a challenge due to blowing snow and interception. Meltwater from snow as runoff has been difficult to model due to ice damming conditions and lack of direct measurements and physical input required for model simulation. Snowfall has considerable effect on landscape changes, global climate, and the hydrologic cycle.

Bibliography

Brooks, K. N., Ffolliott, P. F., Gregersen, H. M., and DeBano, L. F., 1997. *Hydrology and the Management of Watersheds*, 3rd edn. Ames, IA: Iowa State University Press.

Daanen, R. P., Romanovsky, V. E., Walker, D. A., and LaDouceur, M., 2008a. High Resolution, Surface and Subsurface, Survey of a Non-sorted Circle System. *Ninth International Confererence on Permafrost*, **1**, 321–326.

Daanen, R. P., Misra, D., Epstein, H., Walker, D., and Romanovsky, V., 2008b. Simulating nonsorted circle development in arctic tundra ecosystems. *Journal of Geophysical Research – Biogeosciences*, **113**, G03S06.

DeWalle, D. R., and Rango, A., 2008. *Principles of Snow Hydrology*. Cambridge: Cambridge University Press.

Hinzman, L. D., and Kane, D. L., 1991. Snow hydrology of a headwater Arctic basin 2. Conceptual analysis and computer modeling. *Water Resource Research*, **27**, 1111–1121.

Johnson, R. C., 1990. The interception, throughfall and stemflow in a forest in Highland Scotland and the comparison with other upland forests in the U.K. *Journal of Hydrology*, **118**, 281–287.

McKay, G. A., and Gray, D. M., 1981. Chapter 5: The distribution of snow cover. In Gray, D. M., and Male, D. H. (eds.), *Handbook of Snow, Principles, Processes, Management and Use*. Toronto: Pergamon, pp. 153–190.

Singh, P., and Singh, V. P., 2001. *Snow and Glacier Hydrology*. Dordrecht, The Netherlands: Kluwer Academic.

Waldner, P. A., Schneebeli, M., Schultze-Zimmermann, U., and Flühler, H., 2004. Effect of snow structure on water flow and solute transport. *Hydrological Processes*, **18**, 1271–1290.

Woo, M.-K., 1983. Hydrology of a drainage basin in the Canadian high Arctic. *Annals of the Association of American Geographers*, **73**, 577–596.

Woo, M.-K., and Sauriol, J., 1980. Channel development in snow-filled valleys, Resolute, N. W. T., Canada. *Geografiska Annaler*, **62A**, 37–56.
Yoshikawa, K., and Hinzman, L. D., 2003. Shrinking thermokarst ponds and groundwater dynamics in discontinuous permafrost near Council, Alaska. *Permafrost and Periglacial Processes*, **14**, 151–160.

HYDROLOGICAL RESPONSE IN GLACIERIZED BASINS

Ian C. Willis
Scott Polar Research Institute, Department of Geography, University of Cambridge, Cambridge, UK

Introduction

A basin's hydrological response refers to the ways in which its water pathways, stores, and outputs respond to water inputs (Singh and Singh, 2001). Glacierized basins have a different hydrological response to non-glacierized basins due largely to the presence of snow and ice and the lack of vegetation and soil. Inputs are in the form of Melting of Snow/Ice and rainfall. Pathways and stores may be supraglacial (Snow, Firn, Lakes), englacial (Crevasses, Moulins, Englacial Conduit), subglacial (Subglacial Drainage System, Subglacial Lakes, Antarctic), ice marginal lakes, or groundwater. Outputs are usually defined as stream or river runoff at the catchment outlet. The hydrological response of glacierized basins changes rapidly through time, especially during the spring and summer due to variations in snow and ice melt, rainfall, and the evolution of the glacier's hydrological system. Glacierized basins are also prone to flooding following high melt rates or intense rainstorms, changes in the glacier's drainage system, or lake outbursts.

Year to year variations in hydrological response

Glaciers are natural reservoirs, increasing in mass by storing water as snow and ice during wet, cool years; losing mass by releasing meltwater in dry, warm years. Climate ultimately controls the mass balance of a glacier. Year to year fluctuations in climate will affect a catchment's hydrological response depending on how radiation, temperature, and rainfall are affected. A dry, warm year will increase runoff from glacier melt, but decrease it from rainfall – the "compensating effect." Whether total annual runoff goes up or down depends on the relative importance of melt and rain inputs to the catchment, and the ways in which these inputs are affected by climate variability. Year to year runoff fluctuations depend, therefore, on the percentage of the catchment that is glacierized (Röthlisberger and Lang, 1987). Variability is high for catchments that are 0% or 100% glacierized but reaches a minimum for catchments that are ~40% glacierized (Willis, 2005, Figure 1). The "compensating effect" is greatest where catchment runoff is controlled approximately equally by rainfall and glacier melt.

Year to year runoff variability not only depends on the magnitude of annual radiation, temperature, and rainfall changes, but also their timing during the year. For example, in eight glacierized basins in western China between 1953 and 1993 both mean annual temperatures and precipitation were higher after the late 1970s than before (Liu et al., 1999). However, annual stream flow decreased over time, as although precipitation increases occurred throughout the year, temperature rises were concentrated in the winter. This increased winter accumulation and decreased summer melt.

Year to year climate variability not only affects river flows directly, but a long-term climate trend affects them indirectly through its effects on glacier mass balance, geometry, and the relative proportions of snow, firn, and ice area. Summer temperature increases may increase runoff in the short-term, but decrease it due to glacier shrinkage in the long-term (Pelto, 1996). This is particularly true if climate change increases the area of ice compared to firn and snow, since ice melts faster than snow or firn for a given climate due to its lower Albedo.

Season to season variations in hydrological response

Seasonal runoff regime depends largely on the annual distribution of water inputs and depends largely, therefore, on patterns of radiation, temperature, and precipitation throughout the year. Catchments in mid-latitudes have marked variations in radiation and temperature, and relatively small variations in precipitation. The year is divided into a winter accumulation season and a summer ablation season. Here, glaciers are "winter accumulation type" (see Benn and Evans, 1998), storing water as snow and ice during the winter and releasing it during the summer. Mid-latitude glacierized basins are characterized by a long summer melt season, a large annual variation in runoff, and a delay in the timing of maximum annual flow compared to that in an equivalent non-glacierized basin. This is due to meltwater production peaking in mid-summer and the temporary storage of spring meltwater (Willis, 2005, Figure 3a).

High latitude catchments have even greater annual radiation and temperature variations than those in mid-latitudes, with long periods of sub-zero temperatures. They also have moderate annual precipitation variations with lower precipitation totals than the mid-latitudes. High latitude glaciers in maritime areas are "winter accumulation type," but those in continental regions may be thought of as "summer accumulation type." The hydrology of such basins is characterized by a shorter melt season and a lower annual runoff variation compared to mid-latitude basins (Willis, 2005, Figure 3b and c).

Low latitude catchments have small annual radiation and temperature variations, but large fluctuations in humidity, cloudiness, and precipitation. Low latitude

glaciers are either "summer accumulation type," or "year round ablation type." The former occur in high altitude regions, with dry cold winters and high summer precipitation maxima, such as the monsoon-dominated parts of the Outer and Middle Himalayas, Pamirs, Altai, Karakoram, Tien Shan, Kunlun, Qilian, and the high Andes. Here, there is little winter precipitation, with precipitation falling mostly in summer as snow at high elevations, and rain at lower elevations. Annual ablation variations are caused largely by variations in cloudiness and humidity, with sublimation dominating in the winter and melting in the summer. Glaciers tend not to store and release water over annual timescales as they do in mid-latitude basins. Catchments are still subject to large annual runoff variations, with high runoff in the wet season when both melting and rainfall are high (Willis, 2005, Figure 3d). Year round ablation type glaciers occur in high altitude areas in the inner tropics where precipitation occurs throughout the year, although concentrated into one or two wet seasons. Glaciers have fairly even rates of accumulation and ablation throughout the year, although, as with summer accumulation type glaciers, both may be slightly higher during the wetter months. Glaciers do not store and release water over annual timescales and runoff occurs fairly evenly over the year.

Seasonal changes in the hydrological response of glacierized basins depend not only on geographical setting, but also catchment size, hypsometry, and, importantly, percentage glacier cover (Röthlisberger and Lang, 1987; Willis, 2005). Annual runoff variation is at a minimum for catchments with ~30–40% glacier cover, with a higher variation in basins with both lower and higher percentage glacier cover. Catchments with a high percentage glacier cover are small upland catchments with a low elevation range, and, especially in the mid-latitudes and high latitudes, low water inputs in the winter (as precipitation falls as snow and there is little melt), and high inputs during summer (due to rainfall and melt). Conversely, catchments with a low percentage glacier cover tend to be large, have a high elevation range, and extend to the lowlands. Here, liquid water inputs are highest in the winter and lowest in the summer (as most precipitation falls across the catchment as rain and the effects of glacier accumulation and melt high in the catchment are relatively insignificant). Thus, annual runoff variability is again high, but with maximum and minimum discharges in the winter and summer respectively. In catchments with ~30–40% glacier cover, high melt in the upper catchment compensates for low rain in the lower catchment during the summer, and vice versa in the winter. The net result is a fairly even distribution of runoff throughout the year.

Spring to summer variations in hydrological response

Mid-latitude and high latitude glacierized basins undergo large hydrological changes during the spring and summer due to rapid changes in melt inputs and water routing (Catchment Routing). Melt inputs increase as the summer snowline migrates up glacier lowering surface albedo and increasing its roughness, thereby increasing the fluxes of net solar radiation and turbulent heat (Hock, 2005). Water transfer rates increase as the snowpack warms, becomes more saturated, thins, and eventually disappears (Depletion of Snow Cover) (Willis et al., 2002). Firn becomes more saturated (Jansson et al., 2003), surface lakes fill, coalesce and may cause hydrofracture so that water can flow across or into the ice (Boon et al., 2003). Additionally, the englacial and subglacial drainage systems enlarge and become more hydraulically efficient (Fountain and Walder, 1998; Nienow and Hubbard, 2005; Sharp, 2005). Seasonal changes in water inputs and routing cause major changes to the shape, peak magnitude, and lag times of proglacial stream diurnal discharge Hydrographs (Diurnal Cycle of Runoff).

Low latitude glaciers tend not to experience big hydrological changes during the spring and summer, as accumulation and ablation occur more evenly through the year, and annual variations in water inputs and routing are therefore small.

Flooding

Floods are a common occurrence in glacierized basins. The biggest are Glacier Lake Outburst Floods also known as jökulhlaups caused by the rapid drainage of either ice-dammed subglacial lakes or of moraine- or ice-dammed ice-marginal lakes (Tweed and Russell, 1999).

The most documented subglacial lake floods are from Grimsvötn beneath Vatnajökull, Iceland. Floods recur every 1–10 years releasing 0.5–4 km^3 of water over 2–30 days with maximum proglacial discharges of 0.6–50 $\times$ 10^3 m^3 s^{-1} (Björnsson, 2003). Less predictable floods occur during volcanic eruptions such as that at Gjalp, just north of Grimsvötn in 1996 where 3.2 km^3 of water drained from the lake within 40 h with maximum lake exit discharges of 40 $\times$ 10^3 m^3 s^{-1} (Björnsson, 2003). Grimsvötn floods are typically initiated when lake levels approach the ice overburden pressure, allowing water to escape. However, the unusual 1996 flood occurred once flotation pressures were reached. The flood Hydrographs have an increasingly steep rising limb, as the flowing water melts a drainage pathway between the lake and the snout at an accelerating rate, followed by a rapid termination as the lake level drops to a threshold level sealing off the outlet.

Ice-dammed ice-marginal lakes form in the following three locations: (a) where a main valley glacier blocks the drainage of a glacier free side valley; (b) where a side valley glacier extends across a glacier free main valley; and (c) at the confluence of two valley glaciers (Benn and Evans, 1998). GLOFs are initiated when the lake level overtops the ice, cutting a spillway across the ice or between the ice and the valley side, or when it approaches local ice overburden pressure allowing water to escape underneath. Floods along supraglacial spillways or

ice-marginal channels typically possess a more symmetrical steep rise to, and fall from, the hydrograph peak compared to subglacial conduit floods.

GLOFs from moraine-dammed lakes mostly occur by mechanical failure of the moraine dam, or by the lake water overtopping part of the dam initiating rapid and accelerating incision (Richardson and Reynolds, 2000). Recorded hydrographs from moraine-dammed lake GLOFs are rare but one measured ~100 km downstream of a flood from Luggye Tsho, Bhutan in 1994 shows a rapid 1 h rise to peak followed by a moderate fall, and then a more gradual fall with the entire flood lasting ~22 h (Richardson and Reynolds, 2000).

In addition to large floods associated with catastrophic lake drainage, smaller floods may be generated by high melt rates or rainfall (e.g., Davies et al., 2003), or by the sudden release of water stored within the glacier's englacial/subglacial drainage system, particularly in the spring or early summer. On Temperate Glaciers, such floods appear to be related to a switch in the dominant type of subglacial drainage, from distributed to more channelized, and are often associated with glacier uplift and acceleration, and the purging of sediment; they are termed "spring events" (e.g., Anderson et al., 1999). On Polythermal Glaciers, floods are associated with the release of water stored subglacially beneath the warm-based core of the glacier in the upper ablation area. The water eventually breaks through the "thermal dam" and is able to flow beneath the cold-based lower ablation area to the terminus (e.g., Rippin et al., 2003).

Modelling hydrological response

There is increasing need to model the hydrological response of ice-covered basins for scientific investigation of catchment processes and for practical water resource management purposes (Singh and Singh, 2001; Hock and Jansson, 2005; DeWalle and Rango, 2008). Early models in the 1960s and 1970s were stochastic and involved the use of statistical regression equations to predict proglacial stream hydrographs from nearby climate data. They made reasonably accurate predictions, but lacked a conceptual basis, required long data series to fix model parameters, remained site specific, and could not readily be transferred to other catchments, or used to predict runoff under different climatic regimes in the future.

Since the 1980s, conceptual models have increasingly been used to predict catchment runoff. The catchment is typically treated as a series of linear reservoirs, linked in series, parallel, or some combination, each with a different storage constant to represent, e.g., snow, firn, glacier ice, groundwater. Examples include the single reservoir HYMET model, the two-reservoir UBC model or the three-reservoir "Hock" or "Escher-Vetter" models (Hock and Jansson, 2005). Such models are widely used in operational forecasting, and because they have a conceptual basis, they are more transferable between catchments and climatic regimes.

Although physically based models are increasingly being used in glacierized catchments, they are mainly used for scientific rather than practical purposes. One such model has been developed for glaciers dominated by flow in channels (Arnold et al., 1998) and another for glaciers underlain by thick sediment layers where porous, macroporous (sheet) and groundwater flow dominate (Flowers and Clarke, 2002). The latter model has been adapted to allow channel flow and the transfer of water between a channel and sheet (Flowers et al., 2004). Because the models are complex and require extensive data sets to both set boundary conditions and parameterise and test them, they have been applied only to specific glaciers so far (Haut Glacier d'Arolla, Switzerland, Trapridge Glacier, Yukon, Canada and Vatnajökull, Iceland). Models were able to reproduce key features of measured subglacial water pressure fluctuations and/or proglacial stream hydrographs. Additionally, the "channel" model could simulate measured moulin to snout throughflow velocities determined from dye-tracing experiments (Arnold et al., 1998).

Modelling studies are increasingly concerned with quantifying the effects of climate change on the hydrological response of glacierized basins. A variety of models in a range of geographical settings show that in a warmer climate: (a) spring/summer runoff will be enhanced, with annual maximum flows occurring earlier in the year; (b) flood risk will be greater; and (c) over time, as glaciers shrink, annual runoff will decrease (Singh and Kumar, 1997; Hagg and Braun, 2005; Hagg et al., 2007).

Summary

A glacierized basin's supraglacial, englacial, subglacial, ice marginal, and groundwater pathways and stores, modify the inputs from melt and rain producing its characteristic hydrological response, measured as basin water output. A basin's response varies through time at a variety of timescales in response to variations in water inputs, pathways, and stores. Some of the most notable changes occur in mid-latitude and high latitude catchments during the spring and summer. Less predictable changes are associated with flooding due to high melt rates or intense rainstorms, changes in the glacier's drainage system, or lake outbursts.

Bibliography

Anderson, S. P., Fernald, K. M. H., Anderson, R. S., and Humphrey, N. F., 1999. Physical and chemical characterization of a spring flood event, Bench Glacier, Alaska, U.S.A.: evidence for water storage. *Journal of Glaciology*, **45**, 177–189.

Arnold, N., Richards, K., Willis, I., and Sharp, M., 1998. Initial results from a semi-distributed, physically-based model of glacier hydrology. *Hydrological Processes*, **12**, 191–219.

Benn, D. I., and Evans, D. J. A., 1998. *Glaciers and Glaciation*. London: Edward Arnold, 734 pp.

Björnsson, H., 2003. Subglacial lakes and jökulhlaups in Iceland. *Global and Planetary Change*, **35**, 255–271.

Boon, S., Sharp, M., and Nienow, P., 2003. Impact of an extreme melt event on the runoff and hydrology of a high Arctic glacier. *Hydrological Processes*, **17**, 1051–1072.
Davies, T. R. H., Smart, C. C., and Turnbull, J. M., 2003. Water and sediment outbursts from advanced Franz Josef Glacier, New Zealand. *Earth Surface Processes and Landforms*, **28**, 1081–1096.
DeWalle, D. R., and Rango, A., 2008. *Principles of Snow Hydrology*. Cambridge, UK: CUP, 420 pp.
Flowers, G. E., and Clarke, G. K. C., 2002. A multicomponent coupled model of glacier hydrology. 2. Application to Trapridge Glacier, Yukon, Canada. *Journal of Geophysical Research*, **107B**(11), 2288, doi:10.1029/2001JB001124.
Flowers, G. E., Björnsson, H., Pálsson, F., and Clarke, G. K. C., 2004. A coupled sheet-conduit mechanism for jökulhlaup propagation. *Geophysical Research Letters*, **31**, L05401, doi:10.1029/2003GL019088.
Fountain, A. G., and Walder, J. S., 1998. Water flow in glaciers. *Reviews of Geophysics*, **36**, 299–328.
Hagg, W., and Braun, L. N., 2005. The influence of glacier retreat on water yield from high mountain areas: Comparison of Alps and Central Asia. In De Jong, C., Ranzi, R., and Collins, D. (eds.), *Climate and Hydrology in Mountain Areas*. Chichester: Wiley, pp. 263–275.
Hagg, W., Braun, L. N., Kuhn, M., and Nesgaard, T. I., 2007. Modelling of hydrological response to climate change in glacierized Central Asian catchments. *Journal of Hydrology*, **332**, 40–53.
Hock, R., 2005. Glacier melt: a review of processes and their modelling. *Progress in Physical Geography*, **29**, 362–391.
Hock, R., and Jansson, P., 2005. Modelling glacier hydrology. In Anderson, M. G., and McDonnell, J. (eds.), *Encyclopedia of Hydrological Sciences.* Wiley, Chichester, Vol. 4, Chap. 170, pp. 2647–2655.
Jansson, P., Hock, R., and Schneider, T., 2003. The concept of glacier storage: a review. *Journal of Hydrology*, **282**, 116–129.
Liu, J., Fukushima, Y., and Hiyama, T., 1999. Hydrological response of meltwater from glacier covered mountain basins to climate change in northwest China. In Interactions Between the Cryosphere, Climate and Greenhouse Gases. *IAHS Publication,* **256**, 193–207.
Nienow, P., and Hubbard, B., 2005. Englacial drainage of glaciers and ice sheets. In Anderson, M. G., and McDonnell, J. (eds.), *Encyclopedia of Hydrological Sciences.* Wiley, Chichester, Vol. 4, Chap. 166, pp. 2575–2586.
Pelto, M. S., 1996. Changes in glacier and alpine runoff in the North Cascade Range, Washington, USA 1985–1993. *Hydrological Processes*, **10**, 1173–1180.
Richardson, S. D., and Reynolds, J. M., 2000. An overview of glacial hazards in the Himalayas. *Quaternary International*, **65**(66), 31–47.
Rippin, D., Willis, I., Arnold, N., Hodson, A., Moore, J., Kohler, J., and Björnsson, H., 2003. Changes in geometry and subglacial drainage of Midre Lovénbreen, Svalbard determined from digital elevation models. *Earth Surface Processes and Landforms*, **28**, 273–298.
Röthlisberger, H., and Lang, H., 1987. Glacial Hydrology. In Gurnell, A. M., and Clark, M. J. (eds.), *Glacio-fluvial Sediment Transfer, an Alpine Perspective*. Chichester: Wiley, pp. 207–284.
Sharp, M., 2005. Subglacial drainage. In Anderson, M. G., and McDonnell, J. (eds.), *Encyclopedia of Hydrological Sciences.* Wiley, Chichester, Vol. 4, Chap. 167, pp. 2587–2600.
Singh, P., and Kumar, N., 1997. Impact assessment of climate change on the hydrological response of a snow and glacier melt runoff dominated Himalayan river. *Journal of Hydrology*, **193**, 316–350.
Singh, P., and Singh, V. P., 2001. *Snow and Glacier Hydrology. Water Science and Technology Library*. Dordrecht/Boston/London: Kluwer, Vol. 37, 742 pp.
Tweed, F. S., and Russell, A. J., 1999. Controls on the formation and sudden drainage of glacier-impounded lakes: implications for jökulhlaup characteristics. *Progress in Physical Geography*, **23**, 79–110.
Willis, I. C., 2005. Hydrology of glacierized basins. In Anderson, M. G., and McDonnell, J. (eds.), *Encyclopedia of Hydrological Sciences.* Wiley, Chichester, Vol. 4, Chap. 168, pp. 2601–2631.
Willis, I. C., Arnold, N. S., and Brock, B. W., 2002. Effect of snowpack removal on energy balance, melt and runoff in a small supraglacial catchment. *Hydrological Processes*, **16**, 2721–2749.

Cross-references

Albedo
Catchment Glacier
Crevasses
Depletion of Snow Cover
Diurnal Cycle of Runoff
Firn
Glacier Lake Outburst Floods
Hydrographs
Melting Processes
Moulins
Subglacial Drainage System
Subglacial Lakes, Antarctic

HYDROLOGY OF JÖKULHLAUPS

Fiona Tweed
Department of Geography, Staffordshire University, Stoke-on-Trent, Staffordshire, UK

Synonyms

Glacial outburst floods

Definition

"Jökulhlaup" is an Icelandic term derived from the words jökull (Glacier) and hlaup (meaning sprint or burst). A jökulhlaup is a sudden and often catastrophic release of meltwater from a *glacier* or a moraine-dammed lake, resulting in a significant increase in meltwater discharge over a period of minutes to several weeks (e.g., Young, 1980; Roberts, 2005).

Jökulhlaups can originate from meltwater stored in ice-marginal, subglacial, englacial, and supraglacial locations (Ice-Dammed Lakes) although volcanogenic and rainfall-induced floods in glaciated environments can occur without significant water storage (see Tweed and Russell, 1999; Roberts, 2005). The release of meltwater during the termination of glacier surges can also result in jökulhlaups (e.g., Kamb et al., 1985).

Estimates of maximum peak flow range from 1.5×10^6 m^3s^{-1} for historic floods (e.g., Maizels, 1995) to 1×10^7 m^3s^{-1} for jökulhlaups in the late Pleistocene (e.g., O'Connor and Baker, 1992). There is a substantial body of work devoted to the modeling of jökulhlaups

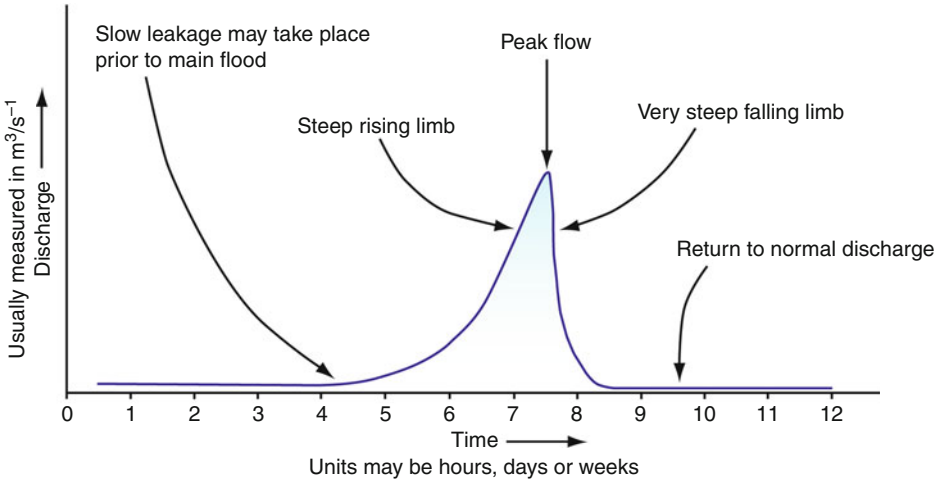

Hydrology of Jökulhlaups, Figure 1 Idealized jökulhlaup hydrograph adapted from Young (1980). The differences in hydrograph shape reflect different mechanisms of water flow through glaciers during jökulhlaups.

(e.g., Nye, 1976; Spring and Hutter, 1981; Clarke, 1982; Björnsson, 1992; Walder and Costa, 1996; Roberts, 2005). The most widely used model of peak discharge estimation was developed by Clague and Mathews (1973) and links maximum instantaneous discharge to maximum water volume thus:

$$Q_{\max} = 75\ V_{\max}^{0.67}$$

where Q_{max} is the maximum instantaneous discharge ($m^3 s^{-1}$) and V_{max} is available water storage ($m^3 \times 10^6$). This model has been modified, but still forms the basis of peak discharge estimation for jökulhlaups generated from *ice-dammed lakes*.

Jökulhlaup *hydrographs* are varied (e.g., Young, 1980; Roberts, 2005); a generalized jökulhlaup hydrograph is illustrated in Figure 1. Some floods generate exponentially rising limbs and others are characterized by a sharp, linear rise to peak discharge. Hydrograph shape is strongly influenced by the flood generating mechanism, subglacial water pressure, and floodwater routing. Floodwater can drain supraglacially, englacially, ice-marginally, or subglacially, via single conduits or multiple floodwater outlets (see Tweed and Russell, 1999; Roberts, 2005). In the case of jökulhlaups generated from moraine-dammed lakes, common drainage initiators include overtopping and concomitant downcutting of the moraine dam or seepage of water through the moraine (e.g., Richardson and Reynolds, 2000). The routing of floodwater during outbursts from glaciers is heavily influenced by the flood trigger mechanism and the nature of the damming *glacier* and its drainage system (Tweed and Russell, 1999; Roberts, 2005).

Jökulhlaups exert a significant potential for landscape change in glaciated environments; they can erode deep canyons, streamline landforms, and create scour marks around obstacles. Jökulhlaups frequently transport large quantities of sediment, depositing boulders, gravel bars, and large gravel and sand dunes with megaripples (e.g., Russell and Knudsen, 1999; Carling et al., 2002; Rudoy, 2002). Evidence of jökulhlaups can be deduced from the sedimentary record on the basis of diagnostic features (e.g., Maizels, 1997; Marren, 2005).

Bibliography

Björnsson, H., 1992. Jökulhlaups in Iceland: prediction, characteristics and simulation. *Annals of Glaciology*, **16**, 95–106.

Carling, P. A., Kirkbride, A. D., Parnachov, S., Borodavko, P. S., and Berger, G., 2002. Late Quaternary catastrophic flooding in the Altai Mountains of south-central Siberia: a synoptic overview and an introduction to flood deposit Sedimentology. In Martini, P., Baker, V., and Garzón, G., (eds.), *Flood and Megaflood Processes and Deposits: Recent and Ancient Examples*. International Association of Sedimentologists, Special publication, **32**, pp. 17–35.

Clague, J. J., and Mathews, W. H., 1973. The magnitude of jökulhlaups. *Journal of Glaciology*, **12**, 501–504.

Clarke, G. K. C., 1982. Glacier outburst floods from "Hazard Lake", Yukon Territory, and the problem of flood magnitude prediction. *Journal of Glaciology*, **28**, 3–21.

Kamb, B., Raymond, C. F., Harrison, W. D., Engelhardt, H., Echelmeyer, K. A., Humphrey, N., Brugman, M. M., and Pfeffer, T., 1985. Glacier Surge Mechanism: 1982–1983 Surge of Variegated Glacier, Alaska. *Science*, **227**, 469–479.

Maizels, J. K., 1995. Sediments and landforms of modern proglacial terrestrial environments. In Menzies, J. (ed.), *Modern Glacial Environments*. Oxford: Butterworth-Heinemann, pp. 365–416.

Maizels, J., 1997. Jökulhlaup deposits in proglacial areas. *Quaternary Science Reviews*, **16**, 793–819.

Marren, P. M., 2005. Magnitude and frequency in proglacial rivers: a geomorphological and sedimentological perspective. *Earth-Science Reviews*, **70**, 203–251.

Nye, J. F., 1976. Water flow in glacier – jökulhlaups, tunnels and veins. *Journal of Glaciology*, **17**, 181–188.

O'Connor, J. E., and Baker, V. R., 1992. Magnitudes and implications of peak discharges from glacial Lake Missoula. *Geological Society of America Bulletin*, **104**, 267–279.

Richardson, S. D., and Reynolds, J. M., 2000. An overview of glacial hazards in the Himalayas. *Quaternary International*, **65**(66), 31–47.

Roberts, M. J., 2005. Jökulhlaups: a reassessment of floodwater flow through glaciers. *Reviews of Geophysics*, **43**, RG1002, doi:10.1029/2003RG000147.
Rudoy, A. N., 2002. Glacier-dammed lakes and geological work of glacial superfloods in the Late Pleistocene, southern Siberia, Altai Mountains. *Quaternary International*, **87**, 110–140.
Russell, A. J., and Knudsen, Ó., 1999. Controls on the sedimentology of the November 1996 jokulhlaup, Skeidararsandur, Iceland. In Smith, N. D., and Rogers, J. (eds.), *Fluvial Sedimentology VI*, Special Publication of the International Association of Sedimentologists, **28**, pp. 315–329.
Spring, U., and Hutter, K., 1981. Numerical studies of jökulhlaups. *Cold Regions Science and Technology*, **4**, 227–244.
Tweed, F. S., and Russell, A. J., 1999. Controls on the formation and sudden drainage of glacier-impounded lakes: implications for jökulhlaup characteristics. *Progress in Physical Geography*, **23**, 79–110.
Walder, J. S., and Costa, J. E., 1996. Outburst floods from glacier-dammed lakes: the effect of mode of drainage on flood magnitude. *Earth Surface Processes and Landforms*, **21**, 701–723.
Young, G. J., 1980. Monitoring glacier outburst floods. *Nordic Hydrology*, **11**, 285–300.

Cross-references

Glacier Lake Outburst Floods
Glacier
Hydrographs
Ice-Dammed Lakes

HYDROPOWER: HYDROELECTRIC POWER GENERATION FROM ALPINE GLACIER MELT

Mauri S. Pelto
Department of Environmental Science, Nichols College, Dudley, MA, USA

Definition and introduction

Alpine glaciers act as natural reservoirs storing water in a frozen state instead of behind a dam. Glacier's modify streamflow releasing the most runoff during the warmest, driest periods when all other sources of water for hydropower are at a minimum (Stenborg, 1970; Fountain and Tanborn, 1985). This seasonal variation characteristic mitigates low flow intervals and the dependability helps make glacier runoff a valuable water resource for hydropower (Fountain and Tangborn, 1985). Annual glacier runoff is highest in warm, dry summers and lowest during wet, cool summers, further providing a balance to alpine summer runoff, this is the glacier compensation effect (Lang, 1986). Dependable and consistent glacier runoff allows for run of river hydropower and smaller reservoir storage in glaciated basins. For long range planning minimum flows are greater and maximum flows less in glacier fed basins (Fountain and Tangborn, 1985). At the same time that glacier extent has been rapidly declining, the use glacier runoff for hydropower has been expanding (Table 1). This highlights the importance of understanding and quantifying the role of glacier runoff for hydropower.

The amount of runoff provided by a glacier is the product of its surface area and ablation rate. Glacier runoff does not increase or decrease the long term runoff for a basin, total runoff over a period of several years is determined largely by annual precipitation. Glacier runoff peaks at the height of the melt season July and August in the Northern Hemisphere, greatly enhancing summer runoff (Hock et al., 2005). Runoff from non-glacier alpine basins peaks in May and June in all but the monsoon fed alpine regions (Figure 1). The loss of a glacier does not necessarily reduce annual runoff, annual precipitation changes are the key for annual runoff changes. Glacier retreat results in the reduction of runoff in the summer, when other sources are also depleted. The increase in flow will be in the spring when water supply is already high in alpine regions. Glacier retreat results in reduced spatial extent for melting and reduced reservoir capacity. The retreat can initially offset runoff reduction due to the loss in area though increased ablation rate, but quite quickly the reduced melt area overtakes the enhanced ablation rate. Unlike non-glacier runoff, glacier runoff correlates better with temperature than precipitation, due to the dominant role of glacier melt compared to precipitation in summer

Hydropower: Hydroelectric Power Generation from Alpine Glacier Melt, Table 1 The glacier area in selected river basins with hydropower facilities operating and proposed.

Region	Glacier area km^2	Hydropower production	Under construction
Rio Santo, Peru	387	1,540 MW	
Cachapoal and Tinguiririca, Chile	328	76 MW	423 MW
Zongo Valley, Bolivia	25	205 MW	
Bhagirathi, India	286	2,400 MW	520 MW
Alaknanda	100+		140 MW
Parbati-Saltuj, India	4,000	1,200 MW	800 MW
Vaksh River, Tajikistan	11,600	3,000 MW	
Skagit River, United States	126	530 MW	
Columbia River, British Columbia-WA	3,000	24,000 MW	
Rhone River, France	1,150	3,000 MW	
Styggevatnet, Norway	12	288 MW	
Hardanger, Norway	40	620 MW	

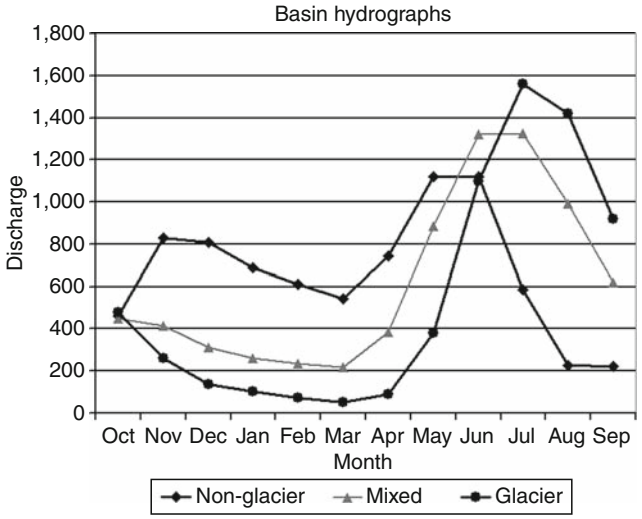

Hydropower: Hydroelectric Power Generation from Alpine Glacier Melt, Figure 1 The timing of discharge from non-glacier and glacier streams is highlighted by this comparison of neighboring drainage basins. Non-glacier basin runoff peaks in May and June. Glacier basin runoff in July and August.

runoff from glacierized basins. This is also the reason for the strong diurnal nature of glacier runoff.

There are two changes in glacier runoff that occur as a result of warming and enhanced glacier melt. The initial response is an increase in glacier melt rate enhancing glacier runoff, while the glacier extent is still substantial in comparison to previous size. The initial enhance glacier runoff has been observed in several regions (Andreassen et al., 2005; Braun et al., 2000; Zhang et al., 2008). Eventually the resulting decline in glacier extent reduces the area available for melting causing a decrease in glacier runoff. In several basins a decline of more than 20% in glacier area has led to a decrease in glacier runoff (Pelto, 2008; Stahl and Moore, 2006). There is a threshold of glacier extent reduction dependent on the magnitude of ablation rate increase, where glacier runoff declines, the few examples suggest this is in the 10–20% areal extent loss. In the long run glacier retreat simply results in the reduction of runoff in the summer, when other runoff sources are also depleted. The increase in streamflow will be in the winter and spring when water supply is already high in most alpine regions. Examination of recent changes in glacier runoff indicate several frequent responses, highlighted by comparison of glaciated and unglaciated basins in North America (Fountain and Tangborn, 1985; Fleming, 2005; Pelto, 2008). A specific example is between neighboring basin unglaciated Newhalem Creek and Thunder Creek 14% glacier cover (Pelto, 2008).

1. Streamflow has risen 18% in Newhalem Creek and 19% in Thunder Creek despite only a slight increase, 2% in winter precipitation at Diablo Dam, within 5 km of both basins. Alpine runoff throughout the Pacific Northwest is increasing in the winter (November–March), as more frequent rain on snow events enhance melting and reduce snow storage.
2. Spring runoff (April–June) has increased in both basins by 5–10% due to earlier alpine snowpack melting.
3. Summer runoff has decreased markedly, 27%, in the non-glacier Newhalem Basin with the earlier melt of reduced winter snowpack. In Thunder Basin runoff has in contrast decreased negligibly, 4%. The difference is accounted for in part by enhanced glacier melting. The observed net loss of −0.52 m/a in glacier mass spread over the melt season is equivalent to 2.45 m^3/s in Thunder Basin, which is 10% of the mean summer streamflow.

Selected glacier-dependent hydropower projects

South America

A number of South American countries are highly dependent upon glaciers and glacial runoff for energy production. In the Andes region, hydropower supplies 81% of Peru's electricity, 73% of Colombia's, 72% of Ecuador's, and 50% of Bolivia's, in each country glaciers contribute a significant portion of this runoff. In the Cordillera Blanca, Peru glacial cover has been shrinking since the 1970s, decreasing by 15% over a 25 year span. In the Rio Santa Basin of Peru glacier runoff comprises 35% of the total runoff (Vergara et al., 2008). The Canon del Plato hydropower project would experience a decrease from 1,540 to 1,250 Gwh for a 50% glacier runoff reduction and decline to 970 Gwh for a 100% glacier loss (Vergara et al., 2008). The energy lost from glacier extent loss would be $5.7–$11.5 million $USD. Pacific Hydro has recognized the potential of glacier fed alpine streams for hydropower in Chile and has built a facility on the glacier fed Cachapoal River and is developing projects on the Tinguiririca River. The combination of snow melt, glacial melt and rainfall water sources provides for reliable runoff in these basins. Zongo Glacier is a small valley glacier located north-east of La Paz, Boliva and its runoff is directed to an important hydropower station which supplies La Paz. From 1956 to 1975 the Zongo Glacier was near equilibrium, since it has lost mass. From 1991 to 2005 the glacier has lost 5 m of thickness and retreated substantially (Soruco et al., 2009). A continuing trend in glacier loss will seriously decrease the water reserves stored as ice, reducing melt season runoff.

Asia

In India, 50% of hydroelectric power is generated by runoff from Himalayan glaciers. A key component of India's energy self-sufficiency is more hydropower. Most of the hydropower is from northern India on streams draining Himalayan glaciers. The Alaknanda River headwater is the Satopanth and Bhagirath Kharak Glaciers. India has applied to the World Bank for run of river hydropower along this glacier fed river. In 2005 the Tehri Dam was finished on the Bhagirathi River, it is a 2,400 mw facility that

began producing hydropower in 2006. At the headwaters of the Bhagirathi River are the Gangotri and Khatling Glacier, Garhwal Himalaya. Gangotri Glacier has retreated 1 km in the last 30 years, and with an area of 109 km^2 provides up to 190 m^3/s (Singh et al., 2006). The Himalayan glaciers have one unique aspect, the wet season is the summer monsoon, which coincides with the primary melt season. Thus, the loss of glacier area does not cause as large a change in summer runoff as in other glaciated alpine regions. Parbait Glacier retreated 52 m/a from 1990 to 2003 (Kulkarnil et al., 2005). This is one of 36 glacier feeding the Beas River and the currently under construction Parbati Hydropower Project, slated to provide 800 MW in the Himachal Pradesh.

Nepal is beginning to turn to hydropower, with run of river hydropower development on the glacier fed Arun River opening in 2003. In China glaciers occupy a total area of 59,406 km^2. Runoff from these glaciers yield some 60 billion m^3 annually. On the Yangtze 14 additional dams to the Three Gorges project are proposed that would take advantage of the existing glacier runoff time and again. To date glacier runoff has increased due to increased melt (Zhang et al., 2008). Glacier runoff is forecast to decrease markedly as retreat progresses in China.

Pakistan generates about 45% of its electricity from hydropower on the Indus River. The headwaters of the Indus River are the large glaciers of the Karokoram Range. The Biafo and Baltura are two or the largest. Both glaciers have experience rapid retreat and loss of area in the last 2 decades. The Indus River flows have also declined. Most of the rivers in Tajikistan originate from glaciers. On Vakhsh river, there are already five hydroelectric plants, among which is the largest in Central Asia – the Nurek hydroelectric power station, with a production of 3 Gwh (Normatov and Petrov, 2006). Glaciers provide about 13 km^3 of water during the summer peak melt period and the Abramov and Fedchenko glacier are at the headwaters of the Vaksh River (Normatov and Petrov, 2006). Tajikistan has plans to increase hydropower by several 100%, increasing the importance of glacier runoff.

Europe

Glacial runoff supplies hydropower for 50% of Switzerland's electricity as well (Paul et al., 2007). In Switzerland, 84 out of 85 glaciers under observation retreated in 2006 (WGMS, 2008). Between 1850 and 1973 Swiss glaciers lost 27% of their area. Based on satellite observation, a sample of 270 glaciers also lost 20% of their area between 1973 and 1998. This loss in melt extent is reducing glacier runoff and summer alpine streamflow. The Grand Dixence Dam is situated on the relatively small Dixence River, but collects a large amount of water thanks to a system of water supply tunnels over 100 km long bringing water from other rivers and valleys. Most of the water comes from glaciers providing meltwater during the summer. The lake is usually full of water by late September, and is emptied during the winter, reaching its lowest point by April.

Austria generates 70% of its electricity from hydropower, with many of the larger projects being glacier fed such as Kaprun. The Kaprun power station produces 700 MW, 60% of its water supply is from Pasterze Glacier, which is transferred through a 12 km long tunnel to Mooserboden Reservoir. Pasterze Glacier has been retreating at a rate of 15 m/a, which will reduce melt season runoff.

The Rhone River has 19 hydropower plants supplying 25% of France's hydropower and 4% of the total energy supply. The Rhone River begins at the Rhone Glacier, Switzerland and is fed by the largest glacier in the Alps Gross Aletsch. The Rhone River is also fed by the glaciers of Mont Blanc and the Matterhorn region.

In Norway, 98% of the electricity comes from hydroelectric power, and 15% of the exploited water flow comes from glacier melt. Because a large share of the runoff in the glacial water systems comes from melting, most of this runoff, up to 80%, takes place in the summer. In dry and warm summers, glacial melting helps maintain a substantial water flow. The summer of 2002 had unusually high temperatures resulting in unusually little water flow in rivers without glaciers in their catchment area. The high temperatures provided large amounts of runoff from the glaciers. In the Nigardsbreelva watershed in Jostedalen, where 75% of the catchment area is covered by glacier, water flow approached flood levels throughout much of August. Austdalsbreen outlet of Jostedalsbreen the glacier terminates in Austdalsvatnet, which has been part of the hydropower reservoir Styggevatnet since 1988. Glaciological investigations at Austdalsbreen started in 1986 in connection with the hydropower project have recorded a 459 m retreat since 1988 (Andreassen et al., 2005). In northern Norway, the Svartisen ice cap and smaller ice caps and glaciers in the same watershed cover about 50% of the drainage area that is utilized by the Svartisen hydropower plant in northern Norway (Andreassen et al., 2005). Statkraft runs the Sima Power Station that is fed from Rembesdalsvatnet Reservoir and the larger Sysenvatn fed by the southern glaciers of Hardanger Ice Cap. This system produces 620 Mw of hydropower. The largest glacier draining the western side of the ice cap is the Rembesdalsskaka with an area of 17 km^2. Since the LIA maximum Rembesdalsskaka has retreated almost 2 km.

North America

British Columbia, Canada hydropower accounts for approximately 90% of the electiricity. In dry years glacier runoff constitutes most of later summer inflows to several large reservoirs. In the Columbia River Basin 10–20% of annual flow and 50% of summer flow are from glaciers. In the Columbia River Basin, Mica (1,740 MW), and Revelstoke (1,840 MW) hydroelectric plants are principally glacier fed during the summer (Fleming and

Hydropower: Hydroelectric Power Generation from Alpine Glacier Melt, Figure 2 Dams along the Columbia River that provide hydropower from Mica Dam, BC to Bonneville, WA; there are 14 major dams.

Clark, 2005) (Figure 2). Downstream of these stations are 14 additional dams on the Columbia River each tapping this same glacier runoff for hydropower. British Columbia rivers had a statistically significant decrease in August streamflow from 1976 to 1996, partly due to earlier snow melt (Stahl and Moore, 2006).

Volume loss of BC glaciers over the 1985–1999 was found to be occurring at a rate of 22.48 ± 5.53 km^3/year. Covering an area of 30,000 km^2 and 48% of BC's gaged systems, glacier melt moderates inter-annual variability in streamflow and helps to maintain higher runoff volume in times of extreme warm and dry conditions. Glacier melt also supports ecosystem functions by maintaining cooler water temperatures. However, a large majority of streams in glaciated basins in BC showed a statistically significant decrease in August streamflow during 1976–1996, which suggests that these glaciers even with increased melt rates are providing less runoff (Stahl and Moore, 2006).

North Cascades, Washington currently support approximately 700 glaciers. These glaciers store as much water as all of the states lakes, rivers, and reservoirs combined. North Cascade Glaciers release approximately 800 million m^3 of water during the summer. This water is nearly fully utilized for irrigation, salmon fisheries and power generation.

Hydropower: Hydroelectric Power Generation from Alpine Glacier Melt, Figure 3 Mount Baker's glacier feed Baker Lake, which is impounded by the Baker Dam hydropower facility.

With recent warming in the area all 47 monitored glaciers have been retreating (Pelto and Hedlund, 2001). The loss in glacier volume in the last 25 years has been 20–40%. In the Baker Lake Basin glaciers provide critical water runoff for hydropower at Upper Baker Dam and Lower Baker Dam (Figure 3). These two Puget Sound Energy projects provide 170 MW. The glaciated area in the basin draining is 29.8 km^2. From July 1 to October 1 the average glacier loses 2.7 m of water equivalent thickness from melting. This represents 80 million m^3 of water. The flow in the Baker River in Concrete (USGS) is 520 million m^3 during this period. Glacier runoff then represents 16% of the total flow during this period, peaking at 24% in August. However, the contribution is larger during dry summers and is higher for Baker Lake, which has a smaller basin area. In a dry year such as 1998 glaciers yielded 110 million m^3 of runoff to Baker Lake, 45% of the basin's total flow (Pelto, 2008). The Skagit River drains the heart of the North Cascades and has Seattle City Light hydropower projects at Diablo Dam and Gorge Dam provide 360 MW and are fed substantially by glacier runoff (Fountain and Tangborn, 1985; Pelto, 2008). In both basins glacier area has been declining significantly since 1979 (Pelto, 2008).

Conclusion

It is apparent that the demand for hydropower is increasing in most alpine region. In many alpine regions glaciers are an important contributor of runoff during the melt season when other water sources are typically at a minimum. This led Canada, Switzerland, and Norway in particular to develop this resource over the last century. Today we see Tajikistan, India, Nepal, Pakistan, Chile, Boliva, Peru and China looking to take further advantage of what has over the last century been a dependable supply of glacier runoff. As glacier area is lost there will be a long term decline in glacier runoff and alpine streamflow during the melt season. This will reduce the hydropower output during the melt season. There is also an expansion in the demand for microhydropower and run of river hydropower projects (Paish, 2002). Both types avoid the issue of large reservoirs, but rely on consistent and dependable flow, which glaciers help foster.

Bibliography

Andreassen, L. M., Elvehøy, H., Kjøllmoen, B., Engeset, R., and Haakensen, N., 2005. Glacier mass balance and length variation in Norway. *Annals of Glaciology*, **42**, 317–325.

Bradley, R. S., Vuille, M., Diaz, H. F., and Vergara, W., 2005. Threats to water supplies in the tropical andes. *Science*, **312**(5781), 1755–1756.

Braun, L. N., Weber, M., and Schulz, M., 2000. Consequences of climate change for runoff from Alpine regions. *Annals of Glaciology*, **31**, 19–25.

Brugman, M. M., Raistrick, P., and Pietroniro, A., 1997. Glacier related impacts of doubling atmospheric carbon dioxide concentration on British Columbia and Yukon (Chap. 6). Environment Canada and BC Ministry of Environment, Lands, and Parks.

Chen, J., and Ohmura, A., 1990. On the influence of Alpine glaciers on runoff. In Lang, H., and Musy, A. (eds.), *Hydrology of Mountainous Regions I. Proceedings of two Lausanne Symposia*, IAHS, Vol. 193, pp. 117–126.

Collins, D. N., and Taylor, D. P., 1990. Variability of runoff from partially-glacierised Alpine basins. In Lang, H., and Musy, A. (eds.), *Hydrology of Mountainous Regions I. Proceedings of two Lausanne Symposia*, IAHS, Vol. 193, pp. 365–372.

Fleming, S. W., 2005. Comparative analysis of glacial and nival streamflow regimes with implications for biotic habitat quantity and fish species richness. *River Research and Applications*, **21**, 363–379.
Fleming, S., and Clark, G. K. C., 2005. Attenuation of high-frequency interannual streamflow variability by watershed glacial cover. *ASCE Journal of Hydraulic Engineering*, **131**, 615–618.
Fountain, A. G., and Tangborn, W. V., 1985. The effect of glaciers on streamflow variations. *Water Resources Research*, **21**, 579–586.
Hock, R., Jansson, P., and Braun, L., 2005. Modelling the response of mountain glacier discharge to climate warming. In Huber, U., Bugmann, M., and Reasoner, M. (eds.), *Global Change and Mountain Regions*. Dordrecht: Springer, pp. 243–252.
Hopkinson, C., and Young, G., 1998. The effect of glacier wastage on the flow of the Bow river at Banff, Alberta, 1951–1993. *Hydrological Processes*, **12**, 1745–1762.
Kulkarnil, A., Rathorel, B., Mahajan, S., and Mathur, P., 2005. Alarming retreat of Parbati glacier, Beas basin, Himachal Pradesh. *Current Science (IAS)*, **88**(11), 1844–1550.
Lang, H., 1986. Forecasting meltwater runoff from snow-covered areas and from glacier basins. In Kraijenhoff, D. A., and Moll, J. R. (eds.), *River Flow Modelling and Forecasting. Reidel Publishing*. Dordrecht, pp. 99–127.
Moore, R. D., Fleming, S. W., Menounos, B., Wheate, R., Fountain, A., Stahl, K., Holm, K., and Jakob, M., 2009. Glacier Change in Western North America: Influences on Hydrology, Geomorphic Hazards and Water Quality. *Hydrologic Processes*, **23**, 42–61.
Normatov, I., and Petrov, G., 2006. Reservoirs and their role in social and economical development in Tajikistan and Central Asia. In *Dams and Reservoirs, Societies and Environment in the 21st Century*. London: Taylor Francis Books.
Paish, O., 2002. Small hydro power: technology and current status. *Renewable & Sustainable Energy Reviews*, **6**(6), 537–556.
Paul, F., Kääb, A., and Haeberli, W., 2007. Recent glacier changes in the Alps observed by satellite: consequences for future monitoring strategies. *Global and Planetary Change*, **56**, 102–111.
Pelto, M. S., 2008. Impact of climate change on north cascade alpine glaciers, and alpine runoff. *Northwest Science*, **82**, 65–75.
Pelto, M. S., and Hedlund, C., 2001. The terminus behavior and response time of North Cascade glaciers. *Journal of Glaciology*, **47**, 497–506.
Singh, P., Haritashya, U., Kumar, N., and Singh, Y., 2006. Hydrological characteristics of the Gangotri Glacier, central Himalayas, India. *Journal of Hydrology*, **327**, 55–67.
Soruco, A., Vincent, C., Francou, B., Ribstein, P., Berger, T., Sicart, J. E., Wagnon, P., Arnaud, Y., Favier, V., and Lejeune, Y., 2009. Mass balance of Glaciar Zongo, Bolivia, between 1956 and 2006, using glaciological, hydrological and geodetic methods. *Annals Glaciology*, **50**(50), 1–8, doi:10.3189/172756409787769799.
Stahl, K., and Moore, R., 2006. Influence of watershed glacier coverage on summer streamflow in British Columbia, Canada. *Water Resources Research*, **42**, W06201, doi:10.1029/2006WR005022.
Stenborg, T., 1970. Delay of runoff from a glacier basin. *Geografi ska Annaler*, **52A**, 1–30.
Vergara, W., Deeb, A., Valencia, A., Bradley, R., Francou, B., Zarzar, A., GrÜnwaldt, A., and Haeussling, S., 2008. Economic impact of rapid glacier retreat in the Andes. *EOS*, **88**(25), 261–262.
WGMS, 2007. In Haeberli, W., Zemp, M., and Hoelzle, M. (eds.), *Glacier Mass Balance Bulletin No. 9 (2004–2005)*. (World Glacier Monitoring Service, Zurich, Switzerland).
WGMS, 2008. In Zemp, M., Roer, I., Kääb, A., Hoelzle, M., Paul, F., and Haeberli, W. (eds.), *Global Glacier Changes: facts and figures*. (World Glacier Monitoring Service, Zurich, Switzerland).
Zhang, Y., Liu, S., Xu, J., and Shangguan, D., 2008. Glacier change and glacier runoff variation in the Tuotuo River basin, the source region of Yangtze River in western China. *Environmental Geology*, **56**, 59–68.

Cross-references

Global Outlook of Snowcover, Sea Ice, and Glaciers

HYPSOMETRY

Andrés Rivera[1,2,3], Fiona Cawkwell[4], Camilo Rada[1], Claudio Bravo[1]
[1]Centro de Estudios Científicos, CECS, Valdivia, Chile
[2]Universidad de Chile, Santiago, Chile
[3]Centro de Ingeniería de la Innovación, CIN, Valdivia, Chile
[4]Department of Geography, University College Cork, Cork, Ireland

Definition

Hypsometry describes the distribution of elevation of land with respect to sea level within an area of interest, with positive values being above sea level and negative values below sea level.

Quantifying hypsometry graphically

One approach to analyzing hypsometry is to produce a histogram of the frequency of different elevation bins. This simple approach requires a compromise between having bins that are too large such that insufficient detail can be extracted, and too small such that an underlying signal is obscured by noise. Alternatively, a graph of cumulative area (0–100%) with altitude can be plotted to show the relative proportion of a region at a specific elevation, known as the hypsometric curve. The elevations may be normalized relative to the range of elevations in the study area (value-minimum)/(maximum-minimum), and the area under this normalized curve is the hypsometric integral, which by definition lies between 0 and 1. The concept of a hypsometric curve has been widely used in geomorphological studies for many years to characterize drainage basins, with differently shaped hypsometric curves associated with different landscape forming processes and stages of landscape evolution. Hypsometry can be defined over a range of scales from a single drainage basin to the whole planet.

Glacier hypsometry

The same principle can be applied to the distribution of the area of an ice mass with altitude, that is, the glacier hypsometry. One of the first people to describe the hypsometry of glaciers and provide a typology for

hypsometric curves was Ahlmann (in Lliboutry, 1956), who defined several types of curves: one for ice sheets, four types for valley glaciers, one for cirque glaciers, and one for piedmont glaciers. These classes were generated by manually calculating glacier areas based upon contour lines.

As an increasing amount of information on surface elevation has become available in digital form, for example from radar and laser altimetry, the construction of hypsometric curves has become more straightforward and they have been derived for many glaciers. One recent source of worldwide (60°N to 56°S) topographic information is the Shuttle Radar Topography Mission (SRTM), available at 90 m resolution outside the USA. This data set is the most recent detailed topographic information for many mountain regions with glaciers, for example, South America, the Himalayas.

Classifying glaciers by their hypsometric curves

From SRTM data, hypsometric curves for glaciers can be digitally derived. In order to classify these curves, they are compared to a theoretical linear hypsometry defined as a model. In this way, three main families of curves are obtained (Figure 1): glaciers with hypsometries above the model (dashed line), glaciers with similar distributions above and below the model (solid line), and glaciers with hypsometries below the model (dotted line). The first type of hypsometric curve (dashed lines) is typical of glaciers with large accumulation areas, located at plateaus surrounded by peaks, from where tongues flow down the valleys, that is, glaciers with predominantly high altitude areas (Figure 2). The second curve (solid line) is associated with glaciers that have similar widths from top to bottom, for example, those located on the flanks of cone-shaped volcanoes. The third curve (dotted line) is associated with piedmont glaciers or glaciers fed by more than one accumulation area whose tongues join at low altitude, yielding a large area at low altitude (Figure 2).

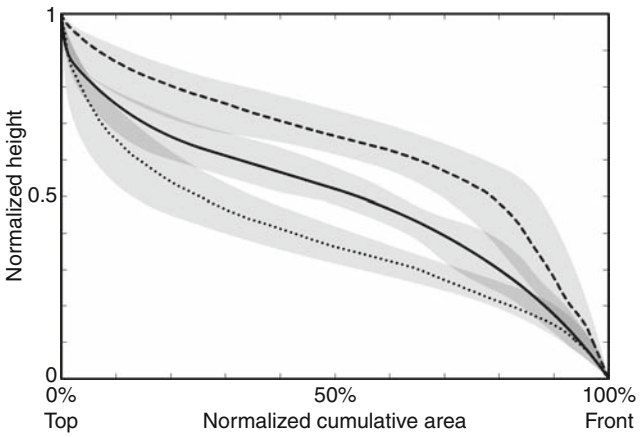

Hypsometry, Figure 1 Main types of hypsometric curves derived from Shuttle Radar Topography Mission (SRTM) data of tens of glaciers with a wide range of areas and types measured in Chile.

Relationship between hypsometric curve and Equilibrium Line Altitude

The above shapes reveal little about the glacier behavior if they are not analyzed together with the position of the Equilibrium Line Altitude (ELA) of each glacier within the hypsometric curve. Depending on the geometry of the glacier, a small change in the elevation of the ELA might result in a marked change in the areas of accumulation and ablation if a large portion of the glacier is at an elevation similar to the ELA. Conversely if there is only a small area at the ELA even a large change in its height may have little effect. Moreover, two glaciers with an identical ELA may exhibit very different behavior if one has a wide accumulation area with a narrow snout and another has a narrow upper basin and a broad tongue (Furbish and Andrews, 1984). By plotting the ELA on the hypsometric curve, the percentage area in the accumulation and ablation zones of the glacier can be easily calculated, and changes with time constructed. The derived ratio between the accumulation area and the total area of a glacier (accumulation area ratio) is one of the parameters often used to describe a glacier.

Examples of glacier hypsometric curves

Figure 3 illustrates the hypsometric curve for Pío XI glacier in the Southern Patagonian Icefields of Chile based on a digital terrain model derived from aerial photographs (Rivera and Casassa, 1999). This curve shows a steep slope for altitudes over 2,200 m and less than 1,000 m, indicating relatively small areas of land within these elevation bands. The majority of the Pío XI glacier lies at intermediate heights, especially in the 1,100–1,300 m region where the curve is much flatter (45.2% of the area of the glacier lies between 1,000 and 1,500 m). The ELAs from 5 dates, ranging from 800 m in 1962 to 1,100 m in 1995, are superimposed on the curve showing a general tendency for an increase in elevation over time. For much of this period, the ELA has been confined to the steeper section of the curve (below 1,100 m) so the change in area from accumulation to ablation zone has been small, with minimal impact on frontal behavior. This is one of the reasons why this glacier has been steady or even advancing in recent decades (Rignot et al., 2003). However, regional warming may in the future raise the ELA to a critical position, whereby a small further increase in the ELA may result in a significant loss of accumulation area, with a notable effect on the overall behavior of the glacier.

Comparing the behavior of the Upsala and Moreno Glaciers, also in the Southern Patagonian Icefields, further illustrates the importance of the position of the ELA with respect to the area-altitude distribution. The Upsala Glacier, where the ELA is located in a flat region of the hypsometric curve, has experienced significant retreat in recent decades, with a small increase in ELA due to

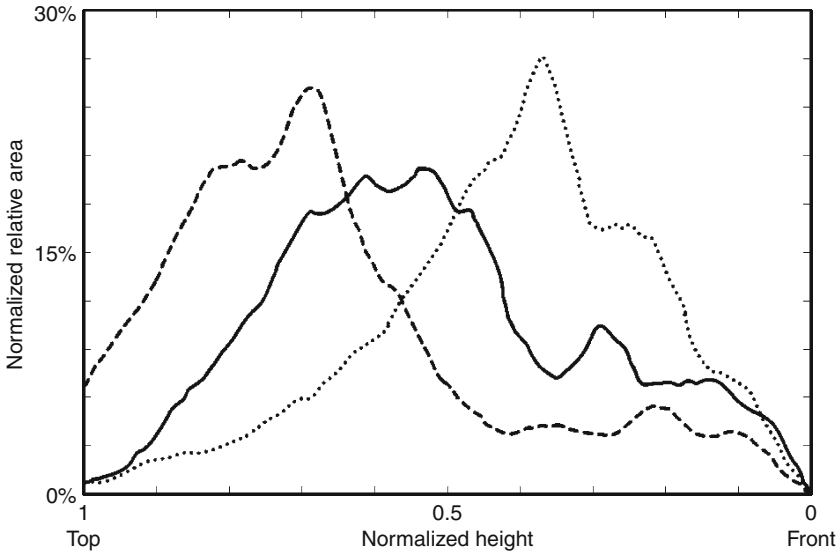

Hypsometry, Figure 2 Typical histograms for each main hypsometric curve.

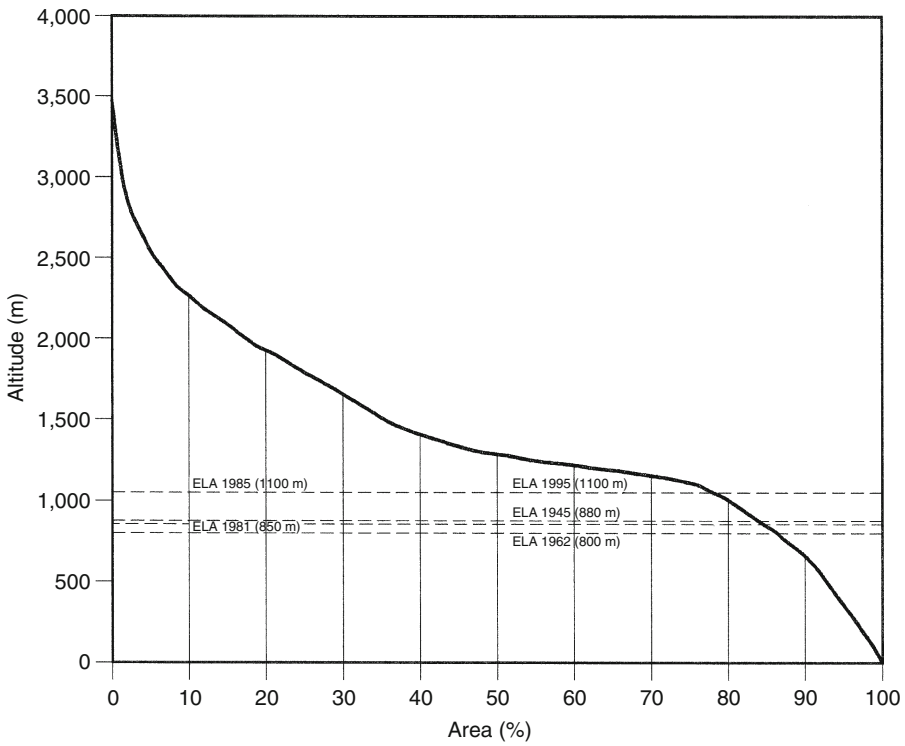

Hypsometry, Figure 3 Hypsometric curve and Equilibrium Line Altitude changes for Pío XI Glacier, Chile (From Rivera and Casassa, 1999).

atmospheric warming resulting in a large decrease in the accumulation area. Moreno Glacier however, with a much steeper hypsometric curve, experienced only small variations in frontal position during the twentieth century and is thus relatively insensitive (up to now) to a rise in ELA (Naruse et al., 1995).

Similar results have been shown by studies on glaciers globally. Oerlemans (1992) illustrated how the large fluctuations, on the order of 4 km, in the front of Nigardsbreen in Norway can be attributed to relatively small climatic changes because of the glacier's geometry, with a narrow tongue fed by a large accumulation area which decreases

markedly in size for a small increase in ELA. On Svalbard, Nuth et al. (2007) found that the glaciers of Prins Karls Forland, with a generally low hypsometric distribution, are generally downwasting, whereas those in Brøggerhalvøya and Oscar II Land with a higher hypsometric weighting are able to maintain their accumulation area.

Oerlemans et al. (1998) further demonstrated the importance of a glacier's hypsometry in understanding its response to climate change by modeling 12 glaciers and ice caps under different climate change scenarios. The authors found that no straightforward relationship between glacier size and fractional change of ice volume was apparent for any given climate scenario, which they attributed to the impact of the hypsometry of individual ice masses on their response.

Reconstructing past glacial conditions from hypsometric curves

The concept of hypsometry is also used to try and reconstruct past glacial limits from estimates of the ELA. Brozovic et al. (1997) postulate that during the Last Glacial Maximum, ELAs in the north-western Himalayan region could have been 600–1,000 m lower than at present, therefore, based on the geomorphological hypsometry, the area above the snowline would have been between 2 and 4 times greater than today, with many areas that are currently unglaciated being under a layer of ice. The hypsometry of glaciated regions can also be used to infer how rates of glacial erosion compare with those of tectonic uplift. Brozovic et al. (1997) showed that the hypsometries of glaciated landscapes around Nanga Parbat are correlated with the snowline elevation and independent of rates of rock uplift, thus indicating that glacial erosion rates can match, and exceed, uplift with climate dominating the evolution of the landscape.

Conclusion

By definition, hypsometry is a single statistic or curve which attempts to quantify a region, and this can be an effective way in which to assess the impact of glaciers on the landscape and their response to change. As concluded by Beedle et al. (2008), using accurate glacier outlines and hypsometries is essential for understanding glacier mass balance, volumetric change, the contribution of ice masses to sea level rise, and relationships between ice masses and climate. However, the hypsometric curve alone cannot explain ice dynamics, the impacts of volcanic activity, and the role of other localized features within individual basins, such as hanging valleys, narrow outlet gorges, or nunataks (rock outcrops surrounded by ice), all of which may also affect the behavior of a glacier. Thus, it is recommended by Brocklehurst and Whipple (2004) that hypsometry should not be used in isolation when assessing glaciers and glaciated landscapes.

Bibliography

Beedle, M. J., Dyurgerov, M., Tangborn, W., Khalsa, S. J. S., Helm, C., Raup, B., Armstrong, R., and Barry, R. G., 2008. Improving estimation of glacier volume change: a GLIMS case study of Bering Glacier system, Alaska. *The Cryosphere*, **2**, 33–51.

Brocklehurst, S. H., and Whipple, K. X., 2004. Hypsometry of glaciated landscapes. *Earth Surface Processes and Landforms*, **29**, 907–926.

Brozovic, N., Burbank, D. W., and Meigs, A. J., 1997. Climatic limits on landscape development in the northwestern Himalaya. *Science*, **276**, 571–574.

Furbish, D. J., and Andrews, J. T., 1984. The use of hypsometry to indicate long-term stability and response of valley glaciers to changes in mass transfer. *Journal of Glaciology*, **30**, 199–211.

Lliboutry, L., 1956. *Nieves y glaciares de Chile. Fundamentos de Glaciología*. Santiago: Ediciones de la Universidad de Chile, p. 471.

Naruse, R., Aniya, M., Skvarca, P., and Casassa, G., 1995. Recent variations of calving glaciers in patagonia, South America, revealed by ground surveys, satellite-data analyses and numerical experiments. *Annals of Glaciology*, **21**, 297–303.

Nuth, C., Kohler, J., Aas, H. F., Brandt, O., and Hagen, J. O., 2007. Glacier geometry and elevation changes on Svalbard (1936–1990): a baseline dataset. *Annals of Glaciology*, **46**, 106–116.

Oerlemans, J., 1992. Climate sensitivity of glaciers in southern Norway: application of an energy balance model to Nigardsbreen, Hellstugubreen and Alfotbreen. *Journal of Glaciology*, **38**(129), 223–232.

Oerlemans, J., Anderson, B., Hubbard, A., Huybrechts, P., Johannesson, T., Knap, W. H., Schmeits, M., Stroeven, A. P., van de Wal, R. S. W., Wallinga, J., and Zuo, Z., 1998. Modelling the response of glaciers to climate warming. *Climate Dynamics*, **14**, 267–274.

Rignot, E., Rivera, A., and Casassa, G., 2003. Contribution of the Patagonia icefields of South America to global sea level rise. *Science*, **302**, 434–437.

Rivera, A., and Casassa, G., 1999. Volume changes on Pio XI Glacier, Patagonia, 1975–1995. *Global and Planetary Change*, **22**, 233–244.

Cross-references

Equilibrium-Line Altitude (ELA)
Patagonia

HYSTERESIS

Vijay Kumar
National Institute of Hydrology, Roorkee, India

Hysteresis is a phenomenon in which the response of a physical system to an external influence depends not only on the present magnitude of that influence, but also on the previous history of the system. Expressed mathematically, the response to the external influence is a doubled-valued function; one value applies when the influence is increasing, the other applies when the influence is decreasing. It is derived from the Greek word "husteros" which means slow, lagging behind or delayed.

In hydrology, the river discharge, soil moisture tension, solute concentration, and suspended sediment concentrations experience the hysteresis phenomenon. Hysteresis in river discharge occurs during unsteady flow when the water surface slope changes due to either rapidly rising or rapidly falling water levels in a channel control reach. Hysteresis is most pronounced in flat sloped streams. On rising stages, the water surface slope is significantly steeper than for steady flow conditions, resulting in greater discharge than indicated by the steady flow rating. The reverse is true for falling stages. When a flood wave passes down a river channel and through a given cross section, the effect of the wave front when upstream of the cross section is to increase the velocity of approach at the cross section. When the flood peak passes into the reach downstream of the cross section, the rear of the wave increases the backwater conditions and so reduces the velocity at a given discharge at the cross section. Consequently, for the same stage, the discharge is higher during rising stage than during falling stage.

The relationship between soil water content and soil water tension also exhibits hysteresis. Soil water tension at a given soil moisture content depends on the sequence of events of wetting and drying by which the current water content of the soil is attained. For the same soil water content, the soil moisture tension of a drying soil is greater than that of a wetting soil.

Solute concentration tends to be higher on the rising than on the falling limb of a flood wave as a result of the mobilization of soluble material that has accumulated during the pre-storm period, producing a looped trend or clockwise hysteresis in the relationship between concentration and discharge (Walling and Webb, 1988).

Suspended sediment concentrations generally show clockwise or positive hysteresis loops. Suspended sediment concentrations on the rising limb of a storm hydrograph are higher than those measured at equivalent flows on the falling limb. Hence, sediment concentrations typically reach their maximum prior to the hydrograph peak. This effect is caused by, among other factors, sediment depletion in the channel system or the increased portion of the baseflow during the recession limb. However, anti- or counterclockwise hysteresis can occur. This is probably due to bank collapse or sediment originating from distant sources (Baca, 2008).

Bibliography

Baca, P., 2008. Hysteresis effect in suspended sediment concentration in the Rybárik basin, Slovakia. *Hydrological Sciences Journal*, **53**(1), 224–235.

Walling, D. E., and Webb, B. W., 1988. The reliability of rating curve estimates of suspended sediment yield: some further comments. In Bordas, M. P., and Walling, D. E. (eds.), *Sediment Budgets*. Proceedings of Porto Alegre Symposium, IAHS Publ. 174. Wallingford, UK: IAHS, pp. 337–350.

ICE

Yoshinori Furukawa
Research Group for Phase Transition Dynamics of Ice, Institute of Low Temperature Science, Hokkaido University, Sapporo, Japan

Definition

Solid phase of water.

Introduction

Natural behaviors on the surface region of the Earth depend on the abundance of solid, liquid, and vapor phases of water and the dynamic variations of Earth's environments involving the phase transitions. When the liquid water is frozen under usual atmospheric conditions or water vapor is deposited at temperatures below 0°C and above about −80°C, the water molecules are arranged in orderly repetitive positions to form a crystalline solid with hexagonal symmetry, which is referred to as normal hexagonal ice, namely ice Ih. Though the ice Ih is only one of at least 13 crystalline phases, which have been observed under different conditions of pressure and temperature, it is the most important and popular phase appearing in the terrestrial and planetary conditions.

The properties of ice should be recognized into two stages, because of the wide scale of the molecular-level to the terrestrial-level ice substance. The crystallographic structure of ice links to the arrangements of water molecules and the properties of single crystals, but on a large scale, ice is always a polycrystalline substance and the mechanical properties of ice are dependent on this polycrystalline structure.

Many books have been published to describe the general information of ice physics (Fletcher, 1970; Hobbs, 1974; Petrenko and Whitworth, 1999; Lock, 1990). The International Conference on Physics and Chemistry of Ice have been held every 4^5 years since 1962. The last conference was held in Japan in 2010 after the conference at Germany in 2006. The next conference will be held in Hanover, New Hampshire, USA in 2014.

Structures and physical properties of ice Ih

The water molecules are arranged in orderly repetitive positions to form a crystalline structure with hexagonal symmetry, which is referred as hexagonal ice, ice Ih, or simply ice. Figure 1 shows the crystalline structure of ice Ih. The oxygen atoms, shown by the open circles, are arranged on a hexagonal lattice with a structure named after the mineral Wurtzite, which is the hexagonal form of ZnS. Each oxygen atom has four nearest neighbors at the corners of a tetrahedron and are covalently connected to each other by a hydrogen bond. The hydrogen atoms, shown as a dark spots, are located on the alternative site of two possible hydrogen sites on each bond to form H_2O molecules in the crystal lattice. A statistical model for the disordered arrangement of the hydrogen atoms in the crystalline lattice of ice Ih is ruled by the assumptions referred as the Bernal–Fowler rules (or ice rule), which are (1) there are two hydrogens adjacent to each oxygen; (2) there is only one hydrogen per bond. As a result, the disordered structures for the orientations of water molecules are realized in three dimensions.

The phase diagram for the equilibrium between ice Ih and the liquid and vapor phases is illustrated in Figure 2. The triple point, where the three phases coexist in equilibrium, is at 273.16 K and 611.7 Pa. As an unusual feature, the ice melting point curve (the boundary between ice and water phases) has a negative slope with increasing pressure and the melting point reach 273.15 K at atmospheric pressure, and this value is taken as the zero degree of the Celsius scale of temperature. The negative slope of the melting curve conduces to the fact that ice floats on water

Vijay P. Singh, Pratap Singh & Umesh K. Haritashya (eds.), *Encyclopedia of Snow, Ice and Glaciers*, DOI 10.1007/978-90-481-2642-2,

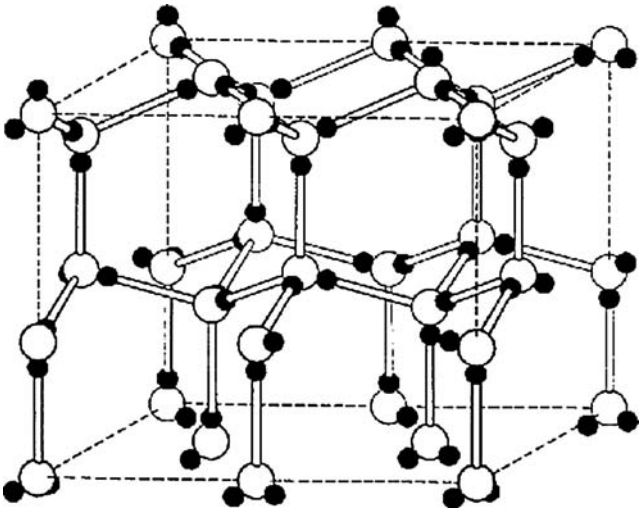

Ice, Figure 1 The crystal structure of ice Ih, showing a particular disordered arrangement of the water molecules. Open and solid circles indicate the oxygen atoms and hydrogen atoms, respectively (Fletcher, 1970).

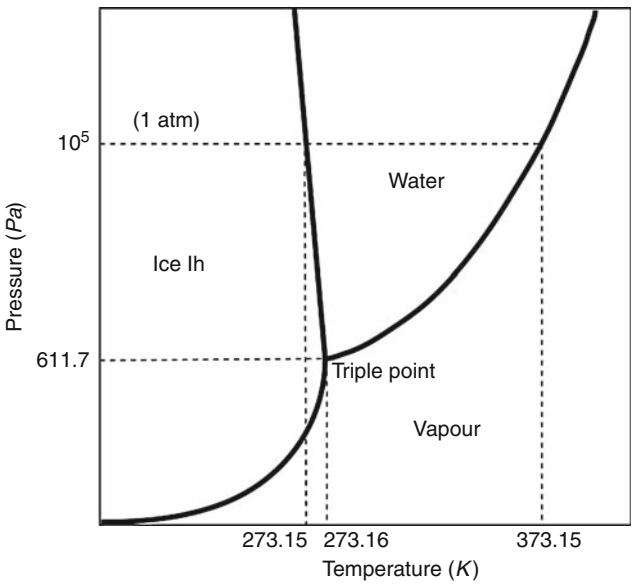

Ice, Figure 2 Schematic phase diagram of water around the triple point (not to scale).

and vessel and pipe are broken by freezing of ice, the pressurized wire goes through the ice (so-called regelation), etc. This expansion is also very important for the special benefit of the birth and evolution of the terrestrial creatures.

Ice indicates the dielectric and conductive properties and which are unusual and strongly relate how water molecules turn round or protons flow through the crystalline lattice, rather than the molecular arrangement and lattice vibrations of ice crystal. For example, ice exhibits a high static relative permittivity that is comparable to that of liquid water. To explain the electric properties of ice, we have to assume the deviation from the simple ice rules for the proton positions and various types of defects included in the ice crystal lattices.

Ice crystalline structure contains many kinds of point defects, dislocations, and planer defects. For the point defects, there are several categories in ice: molecular defects, impurity defects, electronic defects protonic defects, and combined defects. Dislocations in the ice structure are formed during the growth and the plastic deformation of ice crystal and can be directly observed by X-ray topography. Since the crystal structure of ice consists of (0001) planes of molecules stacked above one another, the stacking fault can be easily introduced as a planer defect normally lying on a (0001) plane.

Many of the mechanical properties of ice are determined by line defects or dislocations in common with other crystalline materials. It is well known as the most typical property that the ductile to brittle transition with increasing strain rate is observed. Plastic deformation of single ice crystal mainly occurs by the slip on basal planes. Furthermore, the plastic deformation of polycrystalline ice is also very important in relation to the glacier flow, the Antarctic ice flow, and so on.

Surface properties of ice crystal

It is well known that the ice surface is covered by the thin melted liquid film, which is so-called the quasi-liquid layer or the liquid-like layer, at the temperature range close to the melting point. This phenomenon relates to the surface melting (a kind of first-order phase transition) commonly occurring on the surfaces of various crystalline materials. The process of surface melting begins at a temperature below the melting point of bulk ice. It is due to the weaker binding of the surface water molecules, which are thus more susceptible to thermal disorder than the bulk interior. Further temperature increases lead to breakdown of the surface layers and an increase in the defect density; hence, the water molecule mobility increases. This mobility eventually becomes the same as in the bulk liquid phase, and finally the liquid film thickness becomes arbitrarily large at the melting point. The existence of the melting layer on ice surface relates to various phenomena that occur in the cold climate on the Earth, such as the snow crystal formation, the thunderstorm lightning, the frost heaving, the chemical reaction on ice surface, and so on.

Ices under the nonequilibrium conditions

Ice crystals grow or melt under the nonequilibrium environments of temperature or saturation. Especially the crystal growth of ice is very important in relation to the formations of snowflakes, sea ice, and lake ice. Beautiful patterns of snowflakes with the hexagonal symmetry are formed by their continuous growth from the supersaturated

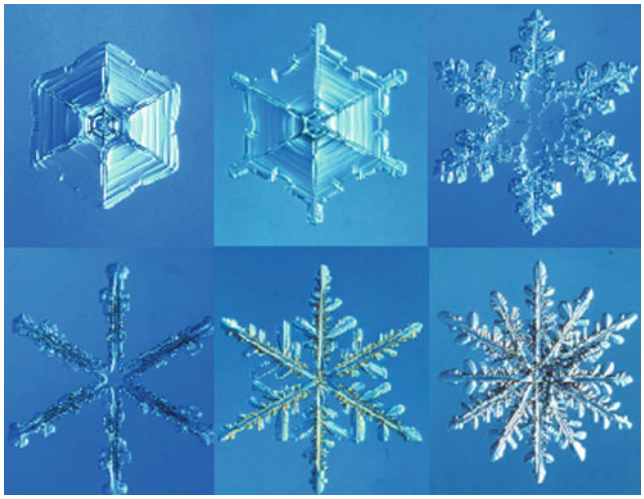

Ice, Figure 3 Pictures of natural snowflakes.

Ice, Figure 4 A picture of ice crystal grown from supercooled water (D_2O) under the microgravity condition in the International Space Station (ISS). Only three branches of a hexagonal dendrite can be formed, because the crystal is grown at the tip of thin glass capillary (*right edge*).

water vapor in the atmosphere. Figure 3 shows some pictures of natural snowflakes that were taken in central area of Hokkaido, Japan. Ukichiro Nakaya of Hokkaido University, Sapporo was led to start his research of snowflakes in 1932. He classified the snowflakes in about 40 categories of morphology by observing more than 3,000 natural snowflakes within several years, and subsequently succeeded in producing almost all natural snowflake morphologies in the laboratory (Nakaya, 1954). As a result, he elucidated the relationship between the snowflake morphologies and the atmospheric conditions, i.e., the temperature and the supersaturation of atmosphere. His results are summarized in the so-called Nakaya diagram, which allows one to "read" the meteorological information "written" on a snow crystal, because we can infer the weather conditions in the upper air by observing snow crystal morphologies on the ground. In this sense, Nakaya was often quoted referring the snow crystal as "a letter from the sky." The growth of snowflakes is strongly controlled by the surface kinetics, which is the incorporation process of water molecules from the vapor phase to solid phase at the surface. The habit change of snowflake morphology (change between the plate-like and prism-like morphologies) occurring as a function of temperature relates to anisotropic surface melting of ice and the secondary change (from the stable to unstable growth modes) can be explained as the morphological instability. A beautiful review about the formation of snowflakes was given by Kobayashi and Kuroda (1987).

An ice crystal growing in supercooled water changes from circular disk to perturbed disk and finally to developed dendrite with the hexagonal symmetry. Properties of pattern formation are completely different from those of snowflake. The morphological instability occurs at the edge plane on ice disk immediately after its thickness reaches a critical value and then continues to the development of perturbation along the edge plane. Understanding the pattern formation mechanism of ice crystal with these discriminative properties is a new perspective for the general studies of pattern formation and morphological instability based on the anisotropic kinetic effects between the basal and edge planes. In the period from December 2008 to March 2009, microgravity experiments of ice crystal growth in supercooled water were carried out in the International Space Station (ISS) to clarify the mechanism of morphological instability of ice. Figure 4 shows a picture of dendritic ice crystal grown in the KIBO module of ISS. These pictures are very useful to discuss the growth and pattern formation mechanisms of ice.

Summary

Ice is the most important material in relation to the various phenomena in the cryosphere. The physical properties of ice were summarized briefly in this article. Especially, it is to be emphasized that the phase transition dynamics among the vapor, liquid, and solid was important to understand the mechanisms of natural phenomena in the cryosphere.

Bibliography

Fletcher, N. H., 1970. *The Chemical Physics of Ice*. Cambridge: Cambridge University Press.

Furukawa, Y., and Wettlaufer, J. S., 2007. Snow and ice crystals. *Physics Today*, **60**(12), 70–71.

Hobbs, P. V., 1974. *Ice Physics*. Oxford: Clarendon.

Kobayashi, T., and Kuroda, T., 1987. Snow crystals. In Sunagawa, I. (ed.), *Morphology of Crystals*. Tokyo: Tera Scientific Publication, p. 645.

Lock, G. S. H., 1990. *The Growth and Decay of Ice*. Cambridge: Cambridge University Press.
Nakaya, U., 1954. *Snow Crystals-Natural and Artificial*. Boston: Harvard University Press.
Petrenko, V. F., and Whitworth, W., 1999. *Physics of Ice*. Oxford: Oxford University Press.

Proceedings for the International Conferences on Physics and Chemistry of Ice

Proceedings for the International Conferences on Physics and Chemistry of Ice. In Maeno, N., and Hondoh, T. (ed.), 1992. *Physics and Chemistry of Ice*. Sapporo: Hokkaido University Press (Conference held in 1991, Sapporo, Japan).
Proceedings for the International Conferences on Physics and Chemistry of Ice. In *Journal of Physical Chemistry*, 1997, **101**(32), 6079–6312. (Conference held in 1996, Hanover, New Hampshire, USA).
Proceedings for the International Conferences on Physics and Chemistry of Ice. In *Canadian Journal of Physics*, 2003, **81**(1/2), 1–544. (Conference held in 2002, St. John's, Canada).
Proceedings for the International Conferences on Physics and Chemistry of Ice. In Kuhs, W. F. (ed.), 2006. *Physics and Chemistry of Ice*. Cambridge: RSC Publishing. (Conference held in 2006, Bremerhaven, Germany.)

Cross-references

Atmosphere-Snow/Ice Interactions
Frost
Ice Core
Lake Ice
Melting Processes
Recrystallization of Ice
Sea Ice
Snow Crystal Structure

ICE AGE

Matthias Kuhle
Department of Geography and High Mountain Geomorphology, University of Göttingen, Göttingen, Germany

Synonyms

Glacial epoch; Glacial period; Glacial time; Pleistocene epoch; Pleistocene (ice ages); Period of global Pleistocene glaciations; Quaternary period; Quaternary (ice ages)

Definition

Period of the earth history with global cooling (climatic deterioration) and a vast extent of the glacier cover. An Ice Age Era is a period of time with alternating changes between cold glacials and warm interglacials, that is, rhythmic glaciations.

Within an Ice Age, relatively short climatic oscillations can be evidenced by glacier stagnations, small ice retreats, or small advances called interstadials (interglacials), that is, stages (stades).

Introduction

The term "Ice Age" refers mainly to the era of the earth previously called Diluvium, namely to the Pleistocene, that is, the Quaternary ice age. Up to now the beginning of the Quaternary ice age has not been established definitely by a paleontological, that is, biogenetic limit. In consideration is the time mark of the sudden global trend toward increased ice volume that set in about c. 3–2.6 million years BP (Ehlers and Gibbard, 2003) or the beginning of the period with a maximum ice volume before c. 1 (1.3–0.8) million years (Tiedemann et al., 1994). The cooling, however, started already in the Pliocene. For the Last Ice Age (W-ice age: Würm, Weichsel, Waldai (or Valdai), Wisconsin), a maximum ice extent of at least 45 million km² is accepted; for the previous to Last Ice Age, the Riss Glacial, the ice extent was at least 50 million km². These ice extents are roughly three times as great than the current glacier face of c. 15.3 million km² of which the Antarctic alone is 82%. This corresponds to c. 89% of the ice mass on the earth (~25–30 million km³ ice: c.f. Ingólfsson, 2004). During the Würm ice age, these glacier faces covered at least 29% and during the Riss ice age at least 33% of the mainland, while at present only c. 10% is ice-covered (see Figure 1).

Würm ice age

Because of the short interval and the combined best preservation of glaciogeomorphological- and -geological evidences, the Last Ice Age, the Würm ice age, is best known. It is dated to MIS (Marine Oxygen Isotope Stage) 4– or 3–2 (cf. Ehlers and Gibbard, 2003). There existed a north-European inland ice sheet that reached down from the Scandes, the High Mountains of Scandinavia, up to the northern Middle Europe to the south (Ehlers et al., 2004). The glacier ice flowed down to the northwest, to the Norwegian coast forming fjords there. To the south, the inland ice filled and crossed the basin of the Baltic Sea up to north Germany, Poland, and Russia (among others, Boulton et al., 2004). During the Brandenburger Stage, that is, about 20–18 Ka, the Würm, that is, Weichsel ice reached its greatest extent in the north-German lowland. For comparison: on its S-margin, the Riss ice (= Saale ice age) in Germany was still further extended, namely up to the low mountain ranges (among others, Liedtke, 1981). In the basin of the current North Sea, there existed a controversial glacier confluence of the Scandinavian inland ice with that of the British Isles, built up from the mountains of Scotland, Great Britain, Ireland, and Wales (Clark et al., 2004). In the east of Scandinavia, the exact measurement of the extent of the North-Siberian inland ice was still in progress. It was connected through the Barents Sea part of the Kara ice sheet. Thus, it stretched from the Kola Peninsula in the west up to approximately the Wrangel Isle and the Bering Strait in the east (Arkhipov, 1998; Astakhov, 1998; Grosswald, 1998) (see Figure 1). In the older literature before 1984, only mountain glaciations, for example, in the Verkhoyansk

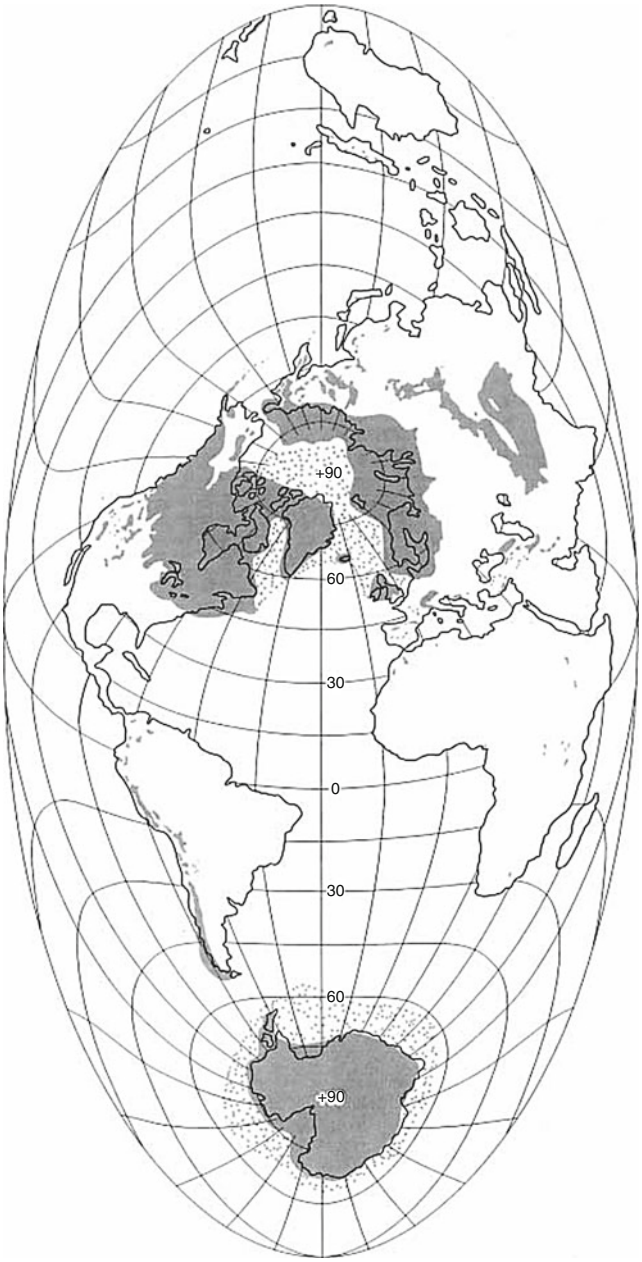

Ice Age, Figure 1 Maximum extent of glaciated areas during the LGM, based on an equal-area projection. Continental ice is indicated by a dense, marine ice by a sparse signature. Based on Broecker and Denton (1990), modified after Kuhle (among others, 1974, 1987, 2004a, b).

mountains (Kolpakov and Belova, 1980), the Koryak highlands, and the eastern Chukotka (Degtyarenko, 1984), were considered as being certain (Zamoruyev, 2004). From the North Cape in Scandinavia, a uniform ice surface across a connected ice shelf up to the ice cap of Spitsbergen at 80°N is under discussion (Svendsen et al., 2004) (see Figure 1). In several European high mountains, as, for example, the Alps, valley glacier systems have developed that converged into ice stream networks. Their lowest ice margins even left the mountain valleys and – for example, in the north- and west-foreland of the Alps – formed a connected, lobe-shaped piedmont glaciation (Penck and Brückner, 1901–1909; Fiebig et al., 2004; Buoncristiani and Campy, 2004). But also, other lower mountains of Europe showed ice caps or valley and single glaciers, for example, the Pyrenees and further mountains of the Iberian Peninsula, the Cévennes, Corsica, the Durmitor Mountains, the Vosges, the Black Forest, the Harz, the Riesengebirge, and many others.

From south Siberia at c. 53°N, with the Sayan and Transbaikal Mountains, a bridge of mountain glaciations existed in Central Asia, for example, in the Altai and Tienshan, as well as greater ice caps in Mongolia and on the Tienshan Plateau between Kungey Alatau and Terskey Alatau as far as high Asia (Kuhle, 2004a; Sheinkman, 2004). The ice stream networks of Pamir, Hindukush, Altun Shan, and Nanshan were connected to the Tibetan inland ice. In the north, the Tibetan ice sheet was connected over a length of c. 2,000 km with the ice stream network of the Kuenlun. In the south up to the southwest, it was fringed by the 2,500 m-long cornice of the connected ice stream networks of the Himalaya and Karakorum. On this highest and largest global mass uplift that currently shows permafrost and the still today greatest non-arctic glaciation, a subtropic glacier face of c. 2.4 million km² existed during glacial times (Kuhle, 1987, 2004a; Zhou et al., 2004).

In North America, the Laurentide ice sheet was built up from Labrador facing southwest. This inland ice merged with the ice stream network of the Rocky Mountains situated to the west and reached c. 37°30′N with the S-margin (see Figure 1) (among others, Dyke, 2004; Hughes, 1998). From the Greenland inland ice – which was not enlarged compared to the current ice on a large scale (Funder et al., 2004) – a broad ice bridge led via Ellesmere Island to the North American ice sheet (see Figure 1).

Numerous mountain systems in the tropics and subtropics, for example, the Andes, wore ice caps or had ice stream networks and dendritic valley glacier systems, for example, the Aconcagua group and adjacent massifs in the Mendoza Andes (Kuhle, 2004b); but in addition to the larger glaciers, there were also hanging glaciers, for example, in Ecuador, Peru, Bolivia, Colombia, Costa Rica, Guatemala, Chile, and México (Mark et al., 2004; Heine, 2004; Lachniet, 2004; Helmens, 2004; Harrison, 2004; Vázquez-Selem and Heine, 2004). Also glaciated were Malaysia and Indonesia (Hope, 2004), Papua New Guinea (Peterson et al., 2004) as well as the Iraq mountains (Wright, 2004), and the southeast Iranian mountains in the Zagros (Kuhle, 1974, 1987, 2007). In spite of semi-arid conditions, even a small piedmont glaciation occurred there. Smaller valley glaciers and larger and smaller hanging glaciers developed in the northwest- and east-African mountains, as, for example, in the Mount Kenya massif (Mahaney, 2004), on Kilimanjaro, Ruwenzori (Osmaston, 2004), and in the

Ethiopian mountains (Umer et al., 2004). Apart from those cited above, large LGM-ice faces of the outer tropics (ektropics) have been reconstructed in Patagonia (Coronato et al., 2004), on Iceland (Geirsdóttir, 2004), and on South Island in New Zealand (Suggate, 2004). Also important is the strong Ice Age valley glaciation of the Caucasus with glaciers up to 70 km in length and an ELA-depression of 1,200–1,300 m (Gobejishvili, 2004). Mountain glaciations up to the dimensions of valley glaciers are also reconstructed for Japan (Sawagaki et al., 2004). Obviously, the Antarctic Last Glacial Maximum ice sheet was much larger and the peripheral domes were 500–1,000 m thicker than at present. The grounding line positions during the LGM and later in the initial ice retreat during the Late Glacial were probably eustatically controlled (Ingólfsson, 2004).

Glacier traces as evidences of a past ice cover

The glacier cover left a lasting effect that has changed and modified the surface forms of the respective sections of continents and mountains. The whole glacier reconstruction and evidence of the Ice Age extent of glaciation is based on this observation. In many places, the debris abraded in the catchment, and source areas of the Ice Age glaciers were transported far away and deposited at a great distance from the place of erosion as accumulation of clast, that is, as moraine. In the areas of removal that in many places are mountainous, cirques, trough valleys with polishings (smoothings and glacier striae), and other characteristic traces of exaration in the rock can be observed; also, polish basins and polish thresholds, roches moutonnées, and glacially streamlined hills, as well as truncated spurs etc., are key forms of glacial erosion. As for the accumulation areas far below the snowline (ELA), flat plates of ground moraine (influenced by permafrost) or drumlins and drumlin fields (in ground moraine areas in the permanent thawing layer) are characteristic; further key forms are tongue basins lined by lateral and end moraines in which dead ice kettles (Sölle) may occur. The development of meltwater that already sets in subglacially led to meltwater channels and eskers (osar), as well as outside of the glaciers to meltwater lakes. In the lateral valleys between glacier margins and valley flanks, kames have been heaped up and within them, between lateral moraines and valley flanks, lateral sanders were accumulated. Marginally, as well as downward and increasingly outside the lowest glacier margins and end moraines, sanders have accumulated and Pleistocene watercourses (Urstromtäler) formed by the meltwaters coming out of the glacier snouts. The sanders canalized by the mountain valleys, as well as those accumulated on a large scale in form of a fan in the mountain forelands and flat lands, developed during the climax of the ice ages when the precipitation was less prevalent, because at that time the meltwater rivers were overloaded by the supply of moraine debris. Towards the end of the Ice Age, in the Late Glacial, the meltwaters cut up the sanders, whereby terrace landscapes were developed. In many places of the High Glacial glacier tongue basins, lakes formed in the still water of which the meltwaters from the already back-melted Late Glacial glacier tongues deposited rhythmically layered banded clays (varved clays). All of these indicators can unambiguously be diagnosed and are arranged in a compelling physical-functional position to one another (Kuhle, 1990). Only the isolated instances, as well as their spatial connection could render the reconstruction of the Ice Age glacier cover possible.

Characteristic of the further vicinity of the Ice Age glaciers and inland ices are phenomena that can be classified as periglacial occurrences, such as permafrost, frost debris, patterned (polygonal) grounds, cryoturbation, rock glaciers, block fields, solifluction (gelifluction) etc. The development of eolian forms as, for example, loess is also typical of the fringe area of Ice Age glaciers.

The Cold Ages in the non-glaciated areas of the earth

The subtropic arid areas, as well as the varying-humidity tropics were more extended than today, so that the areas of the tropic rainforest were heavily reduced. Only in a few regions such as North Africa, was precipitation clearly higher than nowadays. In the Sahara, this led to pluvial periods.

In contrast to the terrestrial deposits, which due to discordances are full of gaps, absolute datings by means of deep-sea sediments have been attempted. According to at least some regions, a complete sequence exists to which the variations of the $^{16}O/^{18}O$-relation in the calcareous shells of sedimented marine fossils can be assigned. It is not so much the life conditions of those organisms (sea animals) that allow us to draw conclusions as to the accompanying climate conditions, but rather the temperature-dependent abundance ratio of the stable oxygen isotope ^{16}O and ^{18}O in the sea water and in the calcareous shells of mostly foraminifers according to the Emiliani-curve. In connection with other dating techniques, evidence for the change of more than 20 interglacial and glacial ages have been obtained from this isotope relation. For the inland ices of the Antarctic and Greenland, comparable courses of the temperature have been extracted for the last c. 100 Ka by means of bore samples. Today, however, they can only partly be parallelized with the global terrestrial incidents.

During the Würm Ice Age, the development of terrestrial ice masses led to a eustatic depression of sea level of 80–130 m (among others, Flint (1971). For the Riss Ice Age, up to 200 m are quoted. The interference of eustatic uplift of the sea level during the Late- and Postglacial with a glacio-isostatic, as well as primarily tectonic elevation of land, led to the emergence of various high shore terraces on the graded shores and river deltas, as well as steep coasts worldwide.

Ice Age climate

The lowering of the average annual temperature on the continent compared to today was 4–15°C, but also values of 18°C – and in extreme continental regions still higher values of lowering – are indicated. The surface temperature of the oceans was about 4–7° lower. The depression of the snow-line (ELA) reached c. 1,000–1,200 m worldwide and locally, as in the today arid areas of the Andes, for example, in the Aconcagua massif, or on the northern hemisphere in the Zagros mountains and in the Karakorum (Kuhle, 1974, 2004a, b; Wright, 2004), and also in the European Alps 1,300–1,500 m (Penck and Brückner, 1901–1909). On the Himalayan south side, the Würmian ELA-depression even amounted up to 1,630 m. According to the specific humid conditions of that time, this corresponds to a depression of the average annual temperature of c. 8–10°C (Kuhle, 2005). For the Last Glacial, the temperatures of January at the Ice Age sea level in Central Europe have been calculated to be −14 to −22°C; for the temperatures of July, between +5°C and +10°C have been deduced. The basis of reconstructions like these is the shifting of the northern limit of forest growth to the south of the European Alps. Between the Alps and the southern margin of the inland ice, there existed the dwarf shrub vegetation of a frost debris tundra. It was occupied by the typical cold-accustomed Ice Age fauna with mammoth, woolly rhinoceros, bison, cave bear, Arctic fox, and lemming (among others, Woldstedt, 1961–1965; Kahlke, 1994). According to the vegetation, the interglacial climate largely corresponded with the current conditions. In the course of the Quaternary, however, it became somewhat cooler and drier.

Homo sapiens

The influence of the Ice Age on the Paleolithic (Old Stone Age) man and its cultures is evident. The deterioration of the climate led to a shifting of his habitat. While in northern Europe the ice cover restricted the usable land, the depression of sea level and the dewatered shelf areas widened the possibilities of man to use sea-animals near to the coast-like mussels and sea mammals, but also fishes. Due to the land bridges created by the depression of sea level, the settlement of America via the Bering-Street and of the southeast-Asian islands, as well as Australia was made feasible.

Pre-quaternary Ice Age eras

The oldest traces of glaciation evidenced by glacier polishings and abrasions, as well as tillites date from the older Precambrian system (c. 2.3 billion years BP) from North America and South Africa. c. 2 billion years ago (Eokambrium), a further longer glaciation period existed with a greater extent of ice. Again for South Africa but also in North Africa (Sahara), an Ordovician-Silurian glaciation has been proved. Known by the largest glaciation surfaces that have been evidenced is the Permo-Carboniferous glaciation (among others, the Dwyka-group), which coincided with the beginning breakage of the Gondwana-continent.

Beginnings of the history of research

About 1815 J.-P. Perraudin, a Swiss mountaineer from the Val de Bagnes, expressed his conviction that in past ages the alpine glaciers were extended up to clearly beyond their current termini. About 1818, the highway engineer I. Venetz, whom Perraudin met in the Val de Bagnes (Imbrie and Imbrie, 1979), and later on also J. G. de Charpentier during a mountain trip in the Walliser Alps (Kahlke, 1994), heard about Perraudin's interpretation of an earlier glacier extent reaching at least 5 km further down-valley. On a meeting of the Swiss Society of Natural Sciences in Luzern, 1834, de Charpentier reported about the opinion of Perraudin, which he had completed in the meantime (Kahlke, 1994). In 1836, during field excursions from the Alps up to its forelands, Venetz and de Charpentier convinced L. Agassiz that numerous forms in the field must have been shaped by past glaciers, even in the flatland. In 1937, Agassiz lectured on "The Theory of a Great Ice Age" during the meeting of the Swiss Society of Natural Sciences in Neuchâtel (Imbrie and Imbrie, 1979). In his publication 3 years later (Agassiz, 1840), he extended this theory to all regions in which erratic boulders had been observed, thus postulating an Ice Age for northern Europe. Later, he postulated an ice filling of the Amazon basin.

Summary

The (Quaternary) Ice Age was a period of global cooling of the climate with large areas of glaciation that were approximately three times more extended on the continent than the current terrestrial ice areas. Due to the chronological nearness and the modification of older glacier traces during the Last Glacial, the reliable state of knowledge as to the Last Ice Age is the most extensive, so that the findings of the Würmian glacier extent provide a valid example for the Ice Age glaciation on the whole. The geomorphological and Quaternary-geological method, that is, the decoding of the arrangements of the positions of landforms (topography) and sediments caused by glacier ice and its dynamics, is the scientific basis of Ice Age reconstruction. The Ice Age climate has been primarily deduced from the reconstructed past glaciation. The climate changes associated with synchronous cold ages in the non-glaciated areas of the earth are also understandable by the secondary global cooling that was strengthened by the feedback of the glaciations.

Bibliography

Agassiz, L., 1840. Études sur les glaciers: Neuchâtel: privately published, plates, atlas, 1–346.

Arkhipov, S. A., 1998. Stratigraphy and Paleogeography of the Sartan Glaciation in West Siberia. *Quaternary International*, **45**(46), 29–42.

Astakhov, V., 1998. The Last Ice Sheet of the Kara Sea: Terrestrial Constraints on its Age. *Quaternary International*, **45**(46), 19–28.

Boulton, G. S., Dongelmans, P., Punkari, M., and Broadgate, M., 2004. Evidence of European ice sheet fluctuation during the last glacial cycle. *Development in Quaternary Science* 2c (In Ehlers, J., and Gibbard, P. L. (eds.), Quaternary Glaciations – Extent and Chronology, Part I: Europe) Amsterdam: Elsevier B.V., pp. 441–460.

Broecker, W. S., and Denton, G. H., 1990. What drives glacial cycles? *Scientific American*, **1**, 48–56.

Buoncristiani, J.-F., and Campy, M., 2004. The palaeogeography of the last two glacial episodes in France: the Alps and Jura. *Development in Quaternary Science* 2c (In Ehlers, J., and Gibbard, P. L. (eds.), Quaternary Glaciations – Extent and Chronology, Part I: Europe) pp. 101–110.

Clark, C. D., Gibbard, P. L., and Rose, J., 2004. Pleistocene glacial limits in England, Scotland and Wales. *Development in Quaternary Science* 2c (In Ehlers, J., and Gibbard, P. L. (eds.), Quaternary Glaciations – Extent and Chronology, Part I: Europe) pp. 47–82.

Coronato, A., Martinez, O., and Rabassa, J., 2004. Glaciations in Argentine Patagonia, southern South America. *Development in Quaternary Science* 2c (In Ehlers, J. and Gibbard, P. L. (eds.), Quaternary Glaciations – Extent and Chronology, Part III: South America, Asia, Africa, Australia, Antarctica) Amsterdam: Elsevier B.V., pp. 49–67.

Degtyarenko, Y. P., 1984. Extent of modern and Quaternay glaciations of the Koryak Highlands and Eastern Chokotka. In Bespaly, V. G. (ed.), *Pleistocene glaciations of Eastern Asia*. Magadan: North-East Complex Research Institute, pp. 66–76 (in Russian).

Dyke, A. S., 2004. An outline of North American deglaciation with emphasis on central and northern Canada. *Development in Quaternary Science* 2c (In Ehlers, J., and Gibbard, P. L. (eds.), Quaternary Glaciations – Extent and Chronology, Part II: North America) Amsterdam: Elsevier B.V., pp. 337–424.

Ehlers, J., and Gibbard, P., 2003. Viewpoint extent and chronology of glaciations. *Quaternary Science Reviews*, **22**(5–17), 1561–1568.

Ehlers, J., Eissmann, L., Lippstreu, L., Stephan, H.-J. and Wansa, S., 2004. Pleistocene glaciations of North Germany. *Development in Quaternary Science* 2c (In Ehlers, J., and Gibbard, P. L. (eds.), Quaternary Glaciations – Extent and Chronology, Part I: Europe) pp. 135–146.

Fiebig, M., Buiter, S. J. H., and Ellwanger, D., 2004. Pleistoce glaciations of South Germany. *Development in Quaternary Science* 2c (In Ehlers, J., and Gibbard, P. L. (eds.), Quaternary Glaciations – Extent and Chronology, Part I: Europe) pp. 147–154.

Flint, R. F., 1971. *Glacial and Quaternary Geology*. New York: Wiley, pp. 1–892.

Funder, S., Jennings, A., and Kelly, M., 2004. Middle and late Quaternary glacial limits in Greenland. *Development in Quaternary Science* 2c (In Ehlers, J., and Gibbard, P. L. (eds.), Quaternary Glaciations – Extent and Chronology, Part II: North America) pp. 425–430.

Geirsdóttir, À., 2004. Extent and chronology of glaciations in Iceland: a brief overview of the glacial history. *Development in Quaternary Science* 2c (In Ehlers, J., and Gibbard, P. L. (eds.), Quaternary Glaciations – Extent and Chronology, Part I: Europe) pp. 175–182.

Gobejishvili, R., 2004. Late Pleistocene (Würmian) glaciation of the Caucasus. *Development in Quaternary Science* 2c (In Ehlers, J., and Gibbard, P. L. (eds.), Quaternary Glaciations – Extent and Chronology, Part I: Europe) 129–134.

Grosswald, M., 1998. Late-Weichselian ice sheet in Artic and Pacific Siberia. *Quaternary International*, **45**(46), 3–18.

Harrison, S., 2004. The Pleistocene glaciations of Chile. *Development in Quaternary Science* 2c (In Ehlers, J., and Gibbard, P. L. (eds.), Quaternary Glaciations – Extent and Chronology, Part III: South America, Asia, Africa, Australia, Antarctica) pp. 89–103.

Heine, K., 2004. Late Quaternary glaciations of Ecuador. *Development in Quaternary Science* 2c (In Ehlers, J., and Gibbard, P. L. (eds.), Quaternary Glaciations – Extent and Chronology, Part III: South America, Asia, Africa, Australia, Antarctica) pp. 165–169.

Helmens, K. F., 2004. The Quaternary glacial record of the Colombian Andes. *Development in Quaternary Science* 2c (In Ehlers, J., and Gibbard, P. L. (eds.), Quaternary Glaciations – Extent and Chronology, Part III: South America, Asia, Africa, Australia, Antarctica) pp. 115–134.

Hope, G. S., 2004. Glaciation of Malaysia and Indonesia, excluding New Guinea. *Development in Quaternary Science* 2c (In Ehlers, J., and Gibbard, P. L. (eds.), Quaternary Glaciations – Extent and Chronology, Part III: South America, Asia, Africa, Australia, Antarctica) pp. 211–214.

Hughes, T. J., 1998. *Ice Sheets*. New York: Oxford University Press, pp. 1–343.

Imbrie, J., and Imbrie, K. P., 1979. *Ice Ages – Solving the Mystery*. New Jersey: Enslow, pp. 1–224.

Ingólfsson, O., 2004. Quaternary glacial climate history of Antarctica. *Development in Quaternary Science* 2c (In Ehlers, J., and Gibbard, P. L. (eds.), Quaternary Glaciations – Extent and Chronology, Part III: South America, Asia, Africa, Australia, Antarctica) pp. 3–43.

Kahlke, H. D., 1994. Die Eiszeit. 3., korr. Aufl. Leipzig; Jena; Berlin; Urania-Verlag, 1–192.

Kolpakov, V. V., and Belova, A. P., 1980. Radiocarbon dating in glaciated part of the Verkhoyansk Range and its vicinity. In Ivanova, I. K., and Kind, N. V. (eds.), *Quaternary Geochronology*. Moscow: Nauka, pp. 230–235 (in Russian).

Kuhle, M., 1974. Vorläufige Ausführungen morphologischer Feldarbeitsergebnisse aus den SE-Iranischen Hochgebirgen am Beispiel des Kuh-i-Jupar. *Zeitschrift für Geomorphologie N.F*, **18**(4), 472–483.

Kuhle, M., 1987. Subtropical Mountain- and Highland-Glaciation as Ice Age Triggers and the Waning of the Glacial Periods in the Pleistocene. *GeoJournal*, **14**(4), 393–421.

Kuhle, M., 1990. The Probability of Proof in Geomorphology – an Example of the Application of Information Theory to a New Kind of Glacigenic Morphological Type, the Ice-marginal Ramp (Bortensander). *GeoJournal*, **21**(3), 195–222.

Kuhle, M., 2004a. The High Glacial (Last Ice Age and LGM) ice cover in High and Central Asia. *Development in Quaternary Science* 2c (In Ehlers, J., and Gibbard, P. L. (eds.), Quaternary Glaciation – Extent and Chronology, Part III: South America, Asia, Africa, Australia, Antarctica) pp. 175–199.

Kuhle, M., 2004b. The Last Glacial Maximum (LGM) glacier cover of the Aconcagua group and adjacent massifs in the Mendoza Andes (South America). *Development in Quaternary Science* 2c (In Ehlers, J., and Gibbard, P. L. (eds.), Quaternary Glaciations – Extent and Chronology, Part III: South America, Asia, Africa, Australia, Antarctica) pp. 75–81.

Kuhle, M., 2005. The maximum Ice Age (Würmian, Last Ice Age, LGM) glaciation of the Himalaya – a glaciogeomorphological investigation of glacier trim-lines, ice thicknesses and lowest former ice margin positions in the Mt. Everest-Makalu-Cho Oyu massifs (Khumbu and Khumbakarna Himal) including informations on late-glacial, neoglacial and historical glacier stages, their snow-line depressions and ages. *GeoJournal* **62**(3–4) (Tibet and High Asia(VII): Glaciogeomorphology and Former Glaciation in the Himalaya and Karakorum) pp. 191–650.

Kuhle, M., 2007. The Pleistocene Glaciation (LGP and pre-LGP, pre-LGM) of SE-Iranian Mountains exemplified by the

Kuh-i-Jupar, Kuh-i-Lalezar and Kuh-i-Hezar Massifs in the Zagros. *Polarforschung*, **77**(2–3), 71–88.
Lachniet, M. S., 2004. Late Quaternary glaciation of Costa Rica and Guatemala, Central America. *Development in Quaternary Science* 2c (In Ehlers, J., and Gibbard, P. L. (eds.), Quaternary Glaciations – Extent and Chronology, Part III: South America, Asia, Africa, Australia, Antarctica) pp. 135–138.
Liedtke, H., 1981. Die nordischen Vereisungen in Mitteleuropa, 2nd edn. *Forschungen zur deutschen Landeskunde*, Vol. 204, 307pp.
Mahaney, W. C., 2004. Quaternary glacial chronology of Mt. Kenya massif. *Development in Quaternary Science* 2c (In Ehlers, J., and Gibbard, P. L. (eds.), Quaternary Glaciations – Extent and Chronology, Part III: South America, Asia, Africa, Australia, Antarctica) pp. 227–231.
Mark, B. G., Seltzer, G. O., and Rodbell, D. T., 2004. Late Quaternary glaciations of Ecuador, Peru and Bolivia. *Development in Quaternary Science* 2c (In Ehlers, J., and Gibbard, P. L. (eds.), Quaternary Glaciations – Extent and Chronology, Part III: South America, Asia, Africa, Australia, Antarctica). pp. 151–163.
Osmaston, H., 2004. Quaternary glaciations in the East African mountains. *Development in Quaternary Science* 2c (In Ehlers, J., and Gibbard, P. L. (eds.), Quaternary Glaciations – Extent and Chronology, Part III: South America, Asia, Africa, Australia, Antarctica) pp. 139–150.
Penck, A., and Brückner, E., 1901–1909. Die Alpen im Eiszeitalter. Vol. 1–3, pp. 1–1199, Leipzig.
Peterson, J. A., Chandra, S., and Lundberg, C., 2004. Landforms from the Quaternary glaciation of Papua New Guinea: an overview of ice extent during the Last Glacial Maximum. *Development in Quaternary Science* 2c (In Ehlers, J., and Gibbard, P. L. (eds.), Quaternary Glaciations – Extent and Chronology, Part III: South America, Asia, Africa, Australia, Antarctica) pp. 313–319.
Sawagaki, T., Aoki, T., Hasegawa, H., Iwasaki, S., Iwata, S., and Hirakawa, K., 2004. Late Quaternary glaciations in Japan. *Development in Quaternary Science* 2c (In Ehlers, J., and Gibbard, P. L. (eds.), Quaternary Glaciation – Extent and Chronology, Part III: South America, Asia, Africa, Australia, Antarctica) pp. 217–225.
Sheinkman, V. S., 2004. Quaternary glaciation in the High Mountains of Central and North-east Asia. *Development in Quaternary Science* 2c (In Ehlers, J., and Gibbard, P. L. (eds.), Quaternary Glaciations – Extent and Chronology, Part III: South America, Asia, Africa, Australia, Antarctica) pp. 325–336.
Suggate, R. P., 2004. South Island, New Zealand; ice advances and marine shorelines. *Development in Quaternary Science* 2c (In Ehlers, J., and Gibbard, P.L. (eds.), Quaternary Glaciation – Extent and Chronology, Part III: South America, Asia, Africa, Australia, Antarctica) pp. 285–291.
Svendsen, J. I., Gataullin, V., Mangerud, J., and Polyak, L., 2004. The glacial History of the Barents and Kara Sea Region. *Development in Quaternary Science* 2c (In Ehlers, J., and Gibbard, P.L. (eds.), Quaternary Glaciations – Extent and Chronology, Part I: Europe) pp. 369–378.
Tiedemann, R., Sarnthein, M., and Shackleton, N. J., 1994. Astronomic timescale for the Pliocene Atlantic O_{18} and dust flux records of Ocean Drilling Program Site 659. *Paleoceanography*, **9**(4), 619–638.
Umer, M., Kebede, S., and Ostmaston, H., 2004. Quaternary glacial activity on the Ethiopian mountains. *Development in Quaternary Science* 2c (In Ehlers, J., and Gibbard, P. L. (eds.), Quaternary Glaciation – Extent and Chronology, Part III: South America, Asia, Africa, Australia, Antarctica) pp. 171–174.
Vázquez-Selem, L., and Heine, K., 2004. Late Quaternary glaciation of México. *Development in Quaternary Science* 2c (In Ehlers, J., and Gibbard, P. L. (eds.), Quaternary Glaciation – Extent and Chronology, Part III: South America, Asia, Africa, Australia, Antarctica) pp. 233–242.
Woldstedt, P., 1961–1965. Das Eiszeitalter, Grundlinien einer Geologie des Quartärs. 3 Bände, 3. unveränderte Aufl., Stuttgart, Ferdinand Enke Verlag; **1**, 1961: 1–374; **2**, 1958: 1–438; **3**, 1965: 1–328.
Wright, H. E., 2004. Pleistocene Glaciation of Iraq. *Development in Quaternary Science* 2c (In Ehlers, J., and Gibbard, P. L. (eds.), Quaternary Glaciation – Extent and Chronology, Part III: South America, Asia, Africa, Australia, Antarctica) pp. 215–216.
Zamoruyev, V., 2004. Quaternary glaciation of north-eastern Asia. *Development in Quaternary Science* 2c (In Ehlers, J., and Gibbard, P. L. (eds.), Quaternary Glaciation – Extent and Chronology, Part III: South America, Asia, Africa, Australia, Antarctica) pp. 321–323.
Zhou, S. Z., Li, J., Zhang, S. Q., Zhao, J. D., and Cui, J. X., 2004. Quaternary glaciations in China. *Development in Quaternary Science* 2c (In Ehlers, J., and Gibbard, P. L. (eds.), Quaternary Glaciation – Extent and Chronology, Part III: South America, Asia, Africa, Australia, Antarctica) pp. 105–114.

Cross-references

Albedo
Cirque Glaciers
Glacial Striations
Glaciofluvial
Ice Age Development Theory
Last Glacial Maximum Glaciation (LGM/LGP) in High Asia (Tibet and Surrounding Mountains)
Moraine
Palaeoclimate and Past Glaciations
Periglacial
Permafrost
Quaternary Glaciation
Rock Glaciers
Tibetan Plateau

ICE AGE CYCLES: DATA, MODELS, AND UNCERTAINTIES

Donald Rapp
South Pasadena, CA, USA

Definition

Measurements that indicate the occurrence of alternating cycles of heavy glaciation and deglaciation on Earth, theories that attempt to explain such occurrences, and uncertainties remaining in these explanations.

This chapter is based on the book by Rapp (2009), which includes several hundred relevant references.

Introduction

Polar ice core data and ocean sediment data provide convincing evidence that Earth has experienced periodic heavy glaciation (ice ages) a number of times over the past few million years. While we tend to think of the present

climate as "normal" and ice ages as deviant, the data suggest that over the past million years, ice ages had longer durations than interglacials. Hence, it might make sense to think of the ice age as a "normal" climate for Earth at this juncture, and an interglacial as a deviation from normalcy.

During the last glacial maximum some 20,000 years ago, Canada and the Northern U.S. were blanketed by huge ice sheets up to 4 km in thickness. In addition, there was a large ice sheet covering Scandinavia that reached down into Northern Europe. The Antarctic ice sheet was somewhat more extensive than today. Local glaciations existed in mountainous regions of North America, Europe, South America, and Africa driving the tree line down by up to 700–800 m. The temperature of Greenland was lower by up to 20°C, but the climate was only a few degrees colder than normal in the tropics.

These ice sheets tied up so much of the Earth's water that the oceans were as much as 120 m shallower. As a result, the shorelines of the continents moved outward by a considerable distance.

The sharp temperature discontinuity at the edges of the ice sheets created convection currents producing violent vertical winds that swept up dust and dirt from dry regions, filling the atmosphere with dust.

This ice age began to wane around 15,000 years ago, and dissipated through a series of gyrating climate oscillations, ending in a comparatively benign period that has lasted for the past ~10,000 years, called the Holocene.

Evidence indicates that the ice sheets did not originate near the North Pole. Formation of ice sheets requires moisture and a land base on which snow and ice can accumulate. Thus the centers of ice sheet generation occurred at upper-middle latitudes, typically around 60–70°N (see Figure 1).

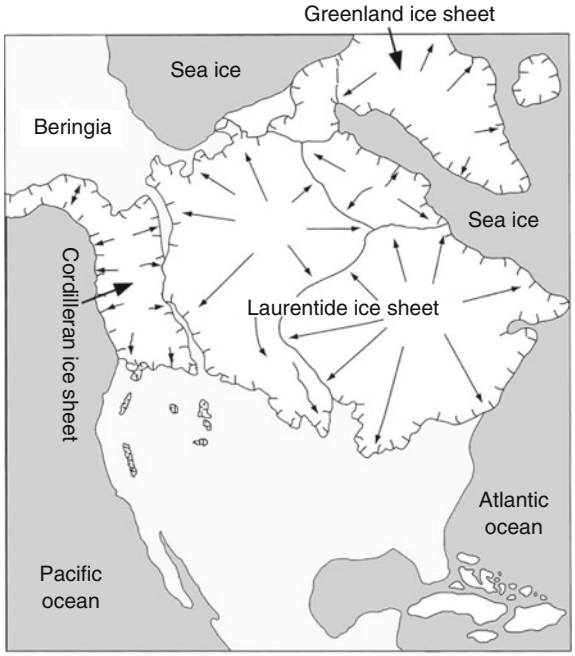

Ice Age Cycles: Data, Models, and Uncertainties, Figure 1 Formation of ice sheets at upper latitudes during the last ice age (Rapp, 2009).

Data

Geological evidence

A few geologists of the nineteenth century noted the presence of large boulders with characteristic scratch marks in the Swiss Alps, as well as scratch marks on the walls of rock in mountains, and suggested that these may have been generated by huge ancient glaciers that covered the mountains. The three main sources of evidence were: (1) grooves and scratches on rocks in place, and on boulders shoved along under the ice, (2) extensive unstratified deposits known as "till" traceable to glacier action, and (3) transported material (typically large rocks) that could only have been delivered by ice (not water).

Louis Agassiz was the principal proponent of the ice age theory, but it took many years to gain acceptance. Imbrie and Imbrie (1979) described this history in their classic book. Prior to the implementation of ice core drilling and use of sediments to infer historical temperatures tens or hundreds of thousands of years ago, geologists had to rely on their observations of rocks and strata for guidance. Wright (1920) discussed the geological evidence for ice ages in great detail. He provided Figures 2 and 3 that are just two of many examples of the effects of the gigantic ice sheets. By the latter part of the nineteenth century, it was well established that ice ages had occurred, and scientists were already conjecturing on possible causes.

Polar ice core isotopic evidence

Willi Dansgaard is a Danish scientist who is credited with the original idea for using ice cores for probing temperature changes over the past thousands of years. His book provides a very interesting history of the early evolution of this technique (Dansgaard, 2005).

While 99.99% of water is $H_2{}^{16}O$, other forms, particularly $H_2{}^{18}O$ and the $HD^{16}O$ occur in concentrations of about 2,000 and 320 ppm (parts per million), respectively. When water evaporates, a higher concentration of the lighter form of water appears in the water vapor, and conversely, when water vapor condenses, there is an increase in the concentration of the heavier form in the product liquid compared to the original vapor. These processes are temperature-dependent.

Dansgaard developed the model shown in Figure 4 for northern climes. Water evaporates from the sea with depleted ^{18}O. As the clouds move toward the shore they cool, and as rain continues to fall, the remaining water vapor in the clouds is further depleted in ^{18}O. Thus as the water-bearing clouds move inland, they cool ever

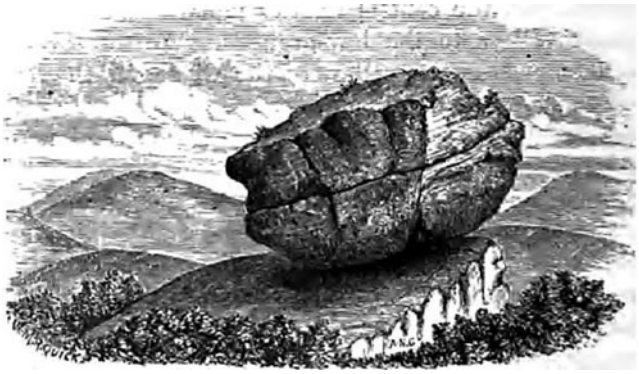

Ice Age Cycles: Data, Models, and Uncertainties, Figure 2 Erratic stone (Wright, 1920).

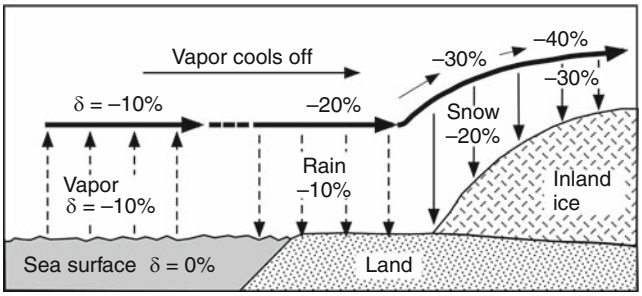

Ice Age Cycles: Data, Models, and Uncertainties, Figure 4 δ-changes (isotopic fractionation) in vapor and precipitation by evaporation from the sea and precipitation from a cooling air mass during its move toward higher latitudes and/or higher altitudes (adapted from Dansgaard, 2005).

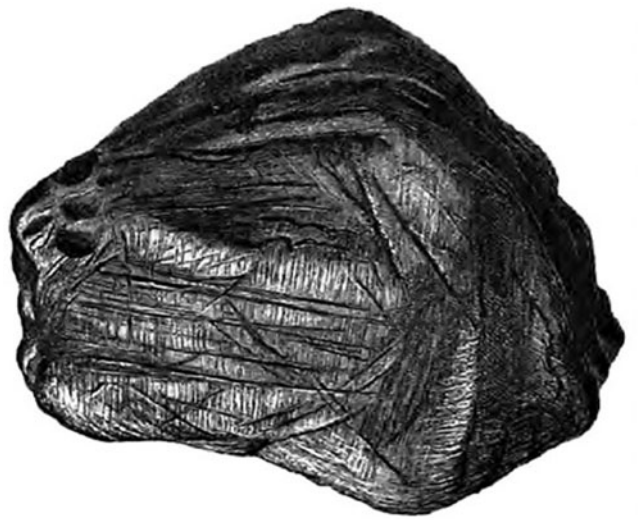

Ice Age Cycles: Data, Models, and Uncertainties, Figure 3 Scratched stone (Wright, 1920).

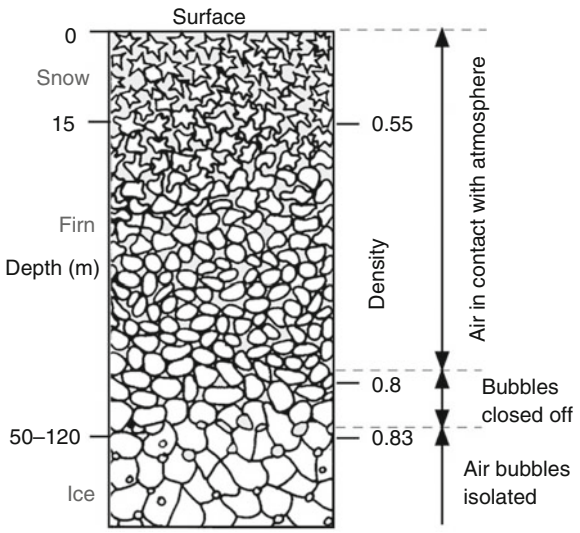

Ice Age Cycles: Data, Models, and Uncertainties, Figure 5 The sintering process as snow is converted to firn and then on to ice with bubbles of air entrapped (Adapted from: http://www.csa.com/discoveryguides/icecore/review.php).

more, and the depletion of ^{18}O continues. The snow that accumulates on the ice sheet above the land is depleted in ^{18}O in proportion to the general climatic temperatures prevailing.

The accumulated past snowfall in the polar caps and ice sheets provides a basis for paleoclimatic reconstruction. These are referred to as ice cores even though strictly speaking there is typically a combination of snow and ice. Somewhat compressed old snow is called a firn. The transition from snow to firn to ice occurs as the weight of overlying material causes the snow crystals to compress, deform, and recrystallize in a more compact form. When firn is buried beneath subsequent snowfalls, the density is increased as air spaces are compressed due to mechanical packing, as well as plastic deformation. Interconnected air passages may then be sealed and appear as individual air bubbles. See Figure 5. At this point, the firn becomes ice. Paleoclimatic information derived from ice cores is obtained from four principal mechanisms: (1) analysis of stable isotopes of hydrogen and atmospheric oxygen; (2) analysis of other gases in the air bubbles in the ice; (3) analysis of dissolved and particulate matter in the firn and ice; and (4) analysis of other physical properties such as thickness of the firn and ice. The firn-ice transition usually occurs at a depth of around 70–100 m, typically deeper in Antarctica than in Greenland.

The ice presently buried at depth in polar caps and ice sheets was once water vapor that condensed out and became incorporated into the firn, and ultimately the ice core of the ice sheet. The isotope ratios contained in this buried ice contain an implicit historical record of the

temperatures prevailing when precipitation occurred, perhaps many thousands of years ago. In addition to the relative heavy/light isotope ratios, the trapped bubbles in ice cores provide a record of atmospheric concentrations of trace gases including greenhouse gases such as carbon dioxide, methane, and nitrous oxide. Furthermore, the ice cores contain records of aerosols and dust content resulting from volcanic eruptions and other changes in particulate content in the atmosphere. The relative atmospheric concentrations of greenhouse gases, as well as aerosol and particulate content coupled with other climate information can provide insight into both the importance of these as causes and the effects of temperature change.

A series of ice core studies at Greenland has provided a wealth of information on historical temperatures. Ice cores from Greenland have the advantage that annual layers are relatively thick due to relatively high precipitation, and can be visually observed in many cases. However, the Greenland ice cores only cover a maximum time range of up to about 150,000 YBP. Antarctica cores comprise up to 800,000 years.

Two major issues in deriving historical data from ice cores are:

1. Developing date-to-depth relationship that provides a chronology of the ice core measurements at any depth.
2. Developing algorithms for proxies contained in the cores (typically based on isotope ratios) that reveal temperature, ice accumulation, or other historical climatological data.

The actual procedures used in dating ice cores typically involve a number of intricately woven factors. Dating of Greenland ice cores is greatly enhanced by the ability in many cases to visually discern annual layers, although these tend to blur below a moderate depth. Visual layers are not discernible at Antarctica.

Typical long-term ice core data are shown in Figure 6.

As polar snow is transformed to ice, atmospheric air is trapped in bubbles. By extracting the gases contained in ice cores, data can be obtained on the composition of the atmosphere in the past. Closure of ice pores proceeds at a slow pace: in Central East Antarctica, this process may take as much as 4,000 years, during which time some exchange of air between the pores and the free atmosphere takes place. Consequently, the air extracted from polar ice cores is younger than the accompanying snow. Present-day analytical procedures enable us to extract some gases from the ice – carbon dioxide (CO_2) and methane (CH_4) – and measure them with great accuracy.

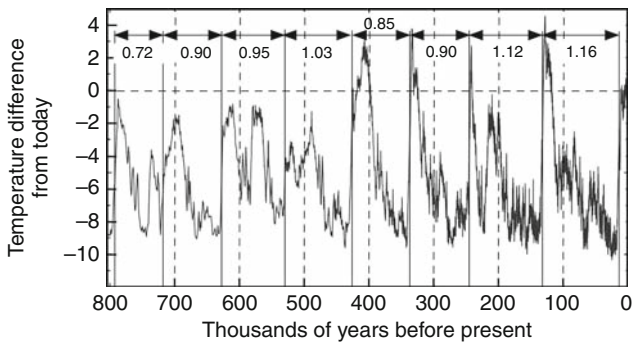

Ice Age Cycles: Data, Models, and Uncertainties, Figure 6 Temperature history (°C) derived from Antarctica ice cores (EPICA, 2004).

Ocean sediment data

Forams are shelled microorganisms found in aquatic and marine environments. There are both planktic (floating in the water column) and benthic (bottom dwelling) forms. Foram shells are made up of calcium carbonate ($CaCO_3$). These organisms record evidence of past environmental conditions in their shells. Remains of foram and diatom shells can be found by taking sediment cores from lakes and oceans, since their shells get buried and preserved in sediments as they die. The chemical makeup of these shells reflects water chemistry at the time of shell formation. Stable oxygen isotope ratios contained in the shell can be used to infer past water temperatures. Warmer water tends to evaporate off more of the lighter isotopes, so shells grown in warmer waters will be enriched in the heavier isotope. Measurements of stable isotopes of planktic and benthic foram and diatom shells have been taken from hundreds of deep-sea cores around the world to map past surface and bottom isotope variations. Planktic (surface dwelling) forams provide estimates of sea temperature, whereas Benthic (bottom dwelling) forams provide estimates of global ice volume. Water that evaporates from ocean is about 4% depleted in ^{16}O. At a glacial maximum, about 2.6% of the former oceans are stored as glacial ice. The remaining ocean waters are thereby enriched in ^{18}O by $0.04 \times 0.026 = 0.1\%$. Benthic forams provide a means of estimating the historical variability of ice volume. A great deal of analysis has focused on benthic data. However, deriving the chronology of this data presents significant challenges.

Initially, objective dating of sediment cores was limited to radiocarbon dates on the sediments younger than about 30,000 years. In addition, a notable marker point in the records was the last interglacial high temperature, which other evidence now suggests was about 135,000 YBP. An additional time marker point was added by measuring the position of a polarity change (due to reversal of the Earth's geomagnetic field) in deep-sea cores and assigning an age to this point based on radiometric (K/Ar) age estimation of the polarity change in lava flows as 780,000 years. Ice core data discontinuities have been used to provide "markers." However, most chronological assignments have been made on the basis of comparison with solar variability to high latitudes – assuming the astronomical theory is correct; this process is known as "tuning." This has led to some circular reasoning in testing astronomical theory. In a few cases, the deposition rate appears

to be constant in time – linear dependence of time on depth. In most cases, reports of ocean sediment data combine data from many oceanic sites, in which the belief is that there is a common temperature signal obfuscated by differing amounts of noise at various sites. By averaging the data over many sites, the hope is that the noise will cancel out, leaving a truer signal. Such a combination of sediment site data is known as a "stack."

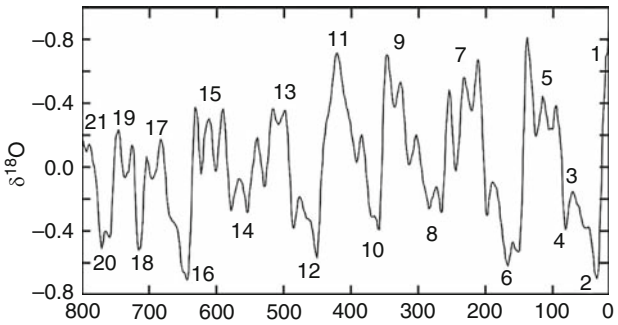

Ice Age Cycles: Data, Models, and Uncertainties, Figure 7 Ocean sediment stack data (Rapp, 2009).

End results of stack data are shown in Figures 7 and 8. The data suggest that over the past few million years, the amplitude and period of climate oscillations has increased significantly.

Comparison of ocean sediment data with ice core data

There are some striking parallels between ocean sediment data and ice core data as shown in Figure 9. However, it appears that the chronologies of these data were "fudged" to some extent and may not be independent of common assumptions, particularly regarding tuning. If the ice core data represent regional temperatures and the ocean sediment data represent ice sheet volume, presumably there should be a sizable time lag in the ocean sediment data. The fact that the two sets of data appear to have common timescales is a problem, not a virtue. It is also noteworthy that the ocean sediment data show less short-term variability, since they are more dependent on slowly varying global ice volume than rapidly fluctuating regional temperatures.

Other data sources

There are a number of other sources of data on the past climate over several hundred thousand years. Devil's Hole,

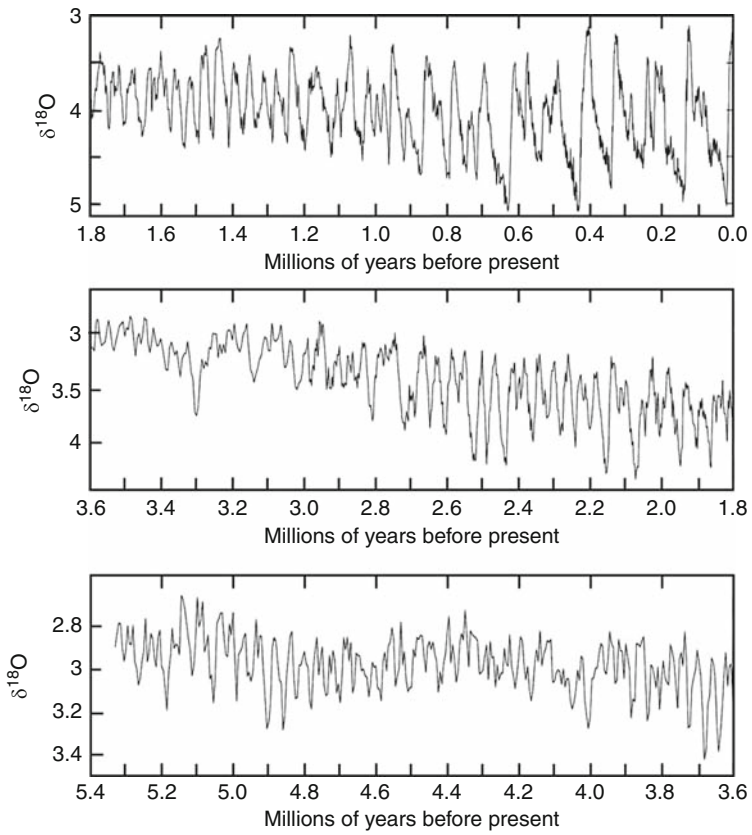

Ice Age Cycles: Data, Models, and Uncertainties, Figure 8 Ocean sediment data over several million years (Rapp, 2009).

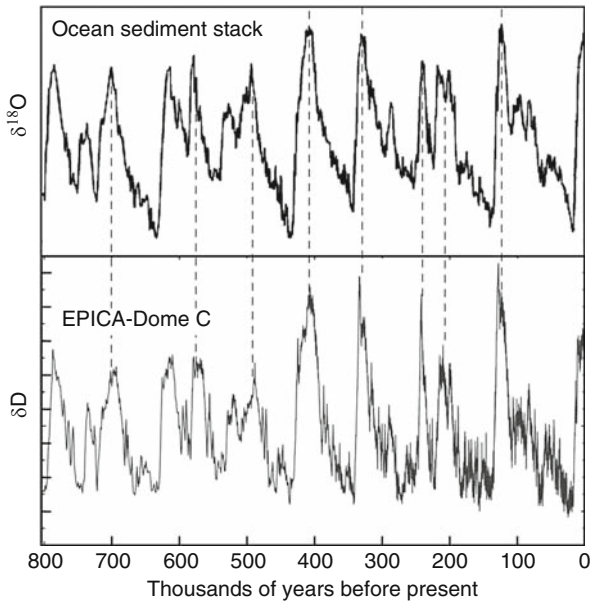

Ice Age Cycles: Data, Models, and Uncertainties, Figure 9 Comparison of ocean sediment data and ice core data (Rapp, 2009).

Nevada calcite deposits provide a 500,000-year temperature estimate with good chronology based on the ratios of radioactive isotopes of uranium and thorium. While these results qualitatively resemble those from ocean sediments, there are several important discrepancies between the Devil's Hole data and the predictions of astronomical theory. This generated considerable controversy in the literature. Since the dating of the Devil's Hole data was independent of the astronomical theory, it provided an independent check without the concern that "tuning" might have led to circular reasoning.

Other sources of data include speleothem formed in limestone or dolostone caves, pollen acting as climate proxies, ice sheet moraines, mountain glacier markings, Red Sea sediments, and coral terraces.

Theories on the cause of ice ages

They were pretty smart in the nineteenth century

More than 100 years ago, G. Frederick Wright (1896) asked: "What were the causes of the accumulation of the ice sheets of the Glacial period?" and concluded that "Two classes of theories have been presented in answer to these questions."

> In one class, ... are the explanations of the climate of the ice age through astronomic or cosmic causes, comprising all changes in the Earth's astronomic relationship to the heat of space and of the Sun.
>
> The second class embraces terrestrial or geologic causes, as changes of areas of land and sea, of oceanic currents, and altitudes of continents, while otherwise the Earth's relations to external sources of heat are supposed to have been practically as now, or not to have entered as important factors in the problem.

Wright identified nine possible causes of ice age cycles. These included shifting of the polar axis, a former period of greater moisture in the atmosphere at higher latitudes, depletion of carbon dioxide in the atmosphere, variations in the heat radiated by the Sun, changes in the Earth's orbit, and changes in the distribution of land and water, as well as changes in land elevation.

Potential causes of ice age cycles

The following list summarizes the major concepts that have been suggested as a possible cause of ice ages:

1. *Solar*: Variability of the Sun – variations in the innate solar intensity due to structural variations within the Sun.

Unfortunately, there are no reliable estimates of historical solar variability, and there is no reason to suspect a quasi-periodic pattern in such variability, even if it occurs.

2. *Astronomical Theory*: Variability of Earth orbital parameters – quasi-periodic variations in eccentricity, obliquity, and precession of the equinoxes produce changes in sequencing of solar intensity to higher latitudes.

This is the most favored theory of ice ages. We shall discuss this theory further in the section on Astronomical Theory given below.

3. *Volcanism*: The occurrence or absence of high levels of volcanism cause temporary changes in the Earth's response to the Sun that may trigger initiation of longer-term glacial-interglacial cycles.

Volcanic eruptions have had a significant, but not sustained effect on climate – their effects tend to die out in less than 3 years. The gigantic Toba eruption of $\sim$ 71,000 years ago may be an exception – models suggest that this may have significantly amplified the budding ice age that was forming at that time.

4. *Greenhouse Gases*: Variability of concentrations of greenhouse gases (particularly CO_2 and CH_4) induced by unspecified forcings have been conjectured to be a cause of glacial-interglacial cycles via changes in the greenhouse effect.

There is no innate reason why greenhouse gas concentrations should change on their own according a quasi-periodic timetable. Furthermore, the data suggest that changes in greenhouse gas concentrations lag temperature changes during ice age cycles by about 1,000 years. Thus, changes in greenhouse gas concentrations are likely to be an effect, not a cause of ice ages.

5. *The Oceans*: Variability in the thermohaline circulation of the oceans producing large changes in heat delivered to higher latitudes.

It has been theorized that variability of the thermohaline circulation (which delivers heat from equatorial regions to higher latitudes) might be involved in ice age cycles, and indeed, there is evidence that such variability does occur. However, there is no basis for the observed long-term quasi-periodic variability. In addition, 90% of heat delivered to polar areas is from the atmosphere, not the oceans.

6. *Extraterrestrial Interactions*: Several models are based on effects due to quasi-periodic accretion of extraterrestrial dust or penetration of cosmic rays in the Earth's atmosphere as the primary forcing that induces changes in cloud cover that in turn, affects the climate.

This topic is discussed in greater detail in the section on Extraterrestrial Interactions given below.

7. *Ocean–Atmosphere Interactions*: In this model, the primary factor that controls large-scale variations in the Earth's climate is the albedo of the Earth, which in turn, is controlled by the degree of cloudiness which is hypothesized to go through repetitive cycles due to ocean–atmosphere interactions.

This topic is discussed in greater detail in Ocean–Atmosphere Interactions Theory.

Ocean–atmosphere interactions theory

Bell and Eng (2007) expounded their theory on the origin of ice ages and interglacial cycles as an alternative to the astronomical theory. Orbital variations have been around for many millions of years, but ice ages have only been around for about 3 million years – which suggests that the origin of ice ages does not lie in orbital variations.

In their model, the primary factor that controls large-scale variations in the Earth's climate is the albedo of the Earth, which in turn, is controlled to a considerable degree by the amount of cloudiness. Cloudiness affects the Earth's albedo, and since the average solar input to Earth is about 342 W/m^2, a change of only 1% or 2% in overall albedo can produce an effective forcing of 3.4–6.8 W/m^2, which would produce a significant impact on the climate. Actually, the solar input to the tropics is considerably higher, and variability of cloudiness in the tropics could have a dramatic effect on net solar input to Earth.

Consider a cold glacial period. With the Earth colder than average, cloudiness is assumed to be subnormal because the vapor pressure of water is reduced. As a result, solar penetration to Earth increases above normal, instigating a warming trend in the atmosphere. Gradually, this heat is transferred to the oceans, but that may require many thousands of years. As the Earth warms up and enters an interglacial period, the oceans slowly warm up with a considerable time lag. By the time the Earth is well into the interglacial period, the oceans have warmed up enough to significantly increase world cloudiness by evaporation. This process reduces the net solar input to Earth, instigating a cooling trend. Now the process reverses. High levels of cloudiness cool the atmosphere quickly and the oceans follow slowly. By the time the Earth has entered a glacial state, the oceans have not lost all their excess heat. As the glacial state persists, the oceans eventually cool off, reducing cloudiness. Now, the warming cycle begins again.

This theory has some attractive features. A cyclic climate history falls out naturally from the facts that the warming or cooling of the oceans lags the warming or cooling of the surface, and warming produces clouds, which in turn, produces cooling via increased albedo. However, Bell and Eng did not seem to include the greenhouse effect of water vapor, which is likely to be very significant, in opposition to the putative cloud effect. Furthermore, when one traces out multiple cycles of surface temperature, ocean temperature, cloud formation, and ice formation, it is difficult to obtain a result with long glacial periods and comparatively short interglacials.

Extraterrestrial interactions

As we pointed out in the previous section, cloud cover is an important factor that controls the way that radiation is absorbed and reflected by the Earth. Increases in cloudiness enhance global albedo, thus cooling the surface but increased cloudiness also traps thermal radiation leading to warming. Overall, the cooling effect is believed to be dominant but this is a function of cloud height and type with thin high clouds causing a net warming. Any factor tending to modify cloud cover will thus have an impact on climate so that it is important to understand the natural variability in cloud climate forcing.

If there are forces acting on the Earth that produce quasi-periodic changes in cloud cover, these forces could produce alternating periods of glaciation interspersed by deglaciation periods. Two such models have been developed. One model has to do with interplanetary dust acting to affect the stratospheric conductivity, and thereby affecting cloud formation via a complex process. Another is based on quasi-periodic changes in cosmic ray penetration of the Earth's atmosphere producing ions that act as nuclei for cloud formation.

Benestad (2005) provides an extended discussion of a theory that cosmic rays, controlled by the Sun's magnetic field, produce changes in cloud formation that affect the Earth's climate. He provides many references. Only a brief report is given here. The theory here is that as variations in solar activity take place, the solar wind changes, and the solar wind controls the amount of galactic cosmic rays from deep space that enter our solar system and penetrate the Earth's atmosphere. The solar wind thus acts like a control grid on an old-fashioned triode vacuum tube where the cosmic rays provide the "current to the anode." The theory then claims that cosmic rays enhance cloud formation by producing charged atmospheric aerosols that act as nuclei for cloud formation. Thus, according to this model, an increased flux of cosmic rays due to lower solar activity produces a cooling effect on the Earth. So, it is claimed that a putative correlation of solar activity with climate is an indicator of solar wind effects that in turn

affect cosmic ray penetration, which affects cloud formation, which in turn produces cooling. Several versions of this concept have been proposed.

Svensmark (2000) showed that the production of radiocarbon-14 in the Earth's atmosphere was inversely related to the pattern of Earth temperature over the past 1,000 years, with low production of ^{14}C during warmer periods and high production during cold periods. The production of ^{14}C decreased sharply in the twentieth century as the Earth warmed. Svensmark said:

> In 1900 the cosmic rays were generally more intense than now and most of the warming during the 20th Century can be explained by a reduction in low cloud cover. Going back to 1700 and the even higher intensities of cosmic rays, the world must have seemed quite gloomy as well as chilly, with all the extra low-level clouds.

Lockwood and Fröhlich (2007) published a rebuttal to Svensmark's theory. Svensmark and Friis-Christensen (2007) published a response to Lockwood and Fröhlich (2007).

Most recently, the world experienced a significant downturn in global temperature in years 2007–2008. At the same time, there was a serious diminution of sunspot activity accompanied by a notable lack of solar magnetic activity. Archibald (2009) presented an interesting analysis of solar cycle 23 and its comparison to earlier sunspot cycles. Solar cycle 23 has been a very long cycle with low sunspot numbers at its tail end, and it appears to be a progenitor of a period of reduced solar activity. A number of papers have predicted an era of low solar activity after sunspot cycle 23.

In a recent prediction update released May 8, 2009, a NOAA panel of experts predicted a peak of about 90 sunspots in May 2013 for solar cycle 24, which would make it the weakest cycle in a very long time. If low solar activity is associated with enhanced cloud formation, this could suggest a cooling effect.

Astronomical theory

The astronomical theory of ice age cycles originated in the nineteenth century and has evolved over the past century and a half. Quasi-periodic variations in the Earth's orbital parameters change the solar energy input to higher latitudes with periods of multiple tens of thousands of years. The fact that solar inputs to high latitudes and data on past climate variations are both subject to quasi-periodic variations over similar time periods suggests the two may be coupled. Spectral analysis supports this viewpoint to some extent.

This variability of solar input to higher latitudes has a significant effect on the ability of surface and sea ice at higher northern latitudes to withstand the onslaught of summer. Thus, according to this theory, variability of the Earth's orbit about the Sun is a primary factor in determining the timing of glacial–interglacial cycles.

The three key factors in the Earth's orbit that affect solar input to higher latitudes are the eccentricity (*elongation*, period ~100,000 years), the obliquity (*tilt of the spin axis*, period ~41,000 years), and the precession of the equinoxes (*the change in season when the Earth is closest to the Sun*, period ~22,000 years). As a result of variability of these parameters, the solar input to high northern latitudes changes with time as shown in Figure 10. The variation of the precession acts like a "carrier wave" whose amplitude is modulated by the eccentricity and obliquity.

According to this concept, ice will spread at high northern latitudes during years with low summer solar input, and retract when summer solar input is high. Despite the many published papers on the astronomical theory, there is an appalling lack of modeling of specifically how solar variations produce extreme climate change. Perhaps that can be excused to some extent because of the extreme complexity of the problem, but that being the case, how can so many scientists reach firm conclusions on the veracity of the astronomical theory? In actual fact, the astronomical theory is basically a high-level intuition that solar variations affect climate. Exactly how these variations affect climate remains uncertain. A few models have been developed but none of these are very detailed.

While credible mechanisms for the processes by which solar variability affects climate are not available, nevertheless one may hope to gain wisdom by comparing the solar curves (from Figure 10) with isotope data from ice cores and ocean sediments. Here, the situation is somewhat akin to that of a detective trying to solve a crime by examining clues. Two approaches have been taken.

In one approach, the solar variability and the isotope data are both analyzed spectrally, and to the extent that the two have important frequency components that agree, there is an implication that the two are coupled. That is somewhat in the realm of "circumstantial evidence" – for example, the suspect was known to be in the vicinity where the crime was committed – but it does not lead to direct cause-effect conclusions.

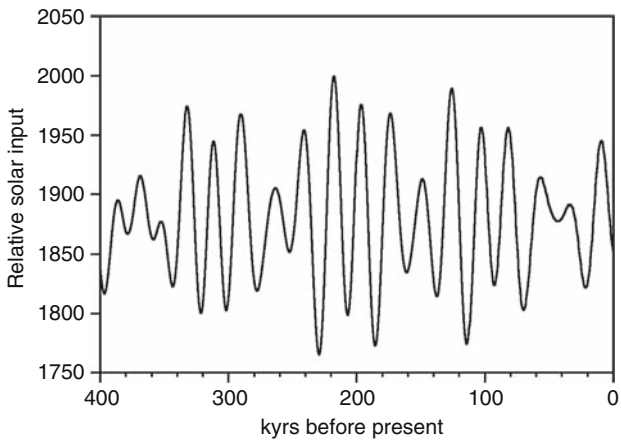

Ice Age Cycles: Data, Models, and Uncertainties, Figure 10 Calculated yearly solar input (kWh/m^2) to 65°N over 400,000 years (Rapp, 2009).

The second approach involves comparing the detailed time series of isotope data with the solar data over hundreds of thousands (or even millions) of years to determine consonance between trends in the two datasets. However, there is a difficulty here because it is obvious that solar variability due to precession of the equinoxes involves more rapid variations than the long-term trends in global ice volume.

Assuming that the astronomical theory is fundamentally sound, it seems likely that the buildup and decay of gigantic ice sheets is a slow process that depends on the integral of solar variations over long periods – perhaps tens of thousands of years. Therefore, an integrative model is needed to estimate the slow buildup and decay of ice sheet volume as a function of more rapidly varying solar input. One can then compare either the rate of change of ice volume with the solar variations, or an integral of solar variations with the measured time series for ice volume versus time. There does not seem to be a single a priori model based entirely on physics that has no adjustable parameters, that allows unequivocal comparison of theory with data. Unfortunately, all models developed to date have been limited by their simplicity, as well as the obvious bias of many scientists determined to "validate" the astronomical theory via curve fitting. The combination of fixing the chronology of isotope data fixed by "tuning" to astronomical theory and using adjustable parameters to fit simplistic models to the "tuned" data raises questions of circular reasoning. However, one could argue that the models provide a framework for connecting theory with data, and the curve fitting process fills in quantitative parameters that are too difficult to estimate from fundamental principles in the real world. But the degree of elasticity in the models creates doubt as to where such procedures fit between the extremes of determination of physical parameters, or mere mathematical curve fitting.

The "bottom line" seems to be that the astronomical theory may well be correct to some extent in principle – that is, there appears to be a solar influence on glacial/interglacial cycles – but translating this into a detailed quantitative comparison of theory and experiment is not simple.

Comparison of theory and experiment

Comparison of astronomical theory with data

In Figure 11, we compare the solar input to high latitudes with the estimated temperature from an Antarctic ice core over 800,000 years. There is considerable agreement with

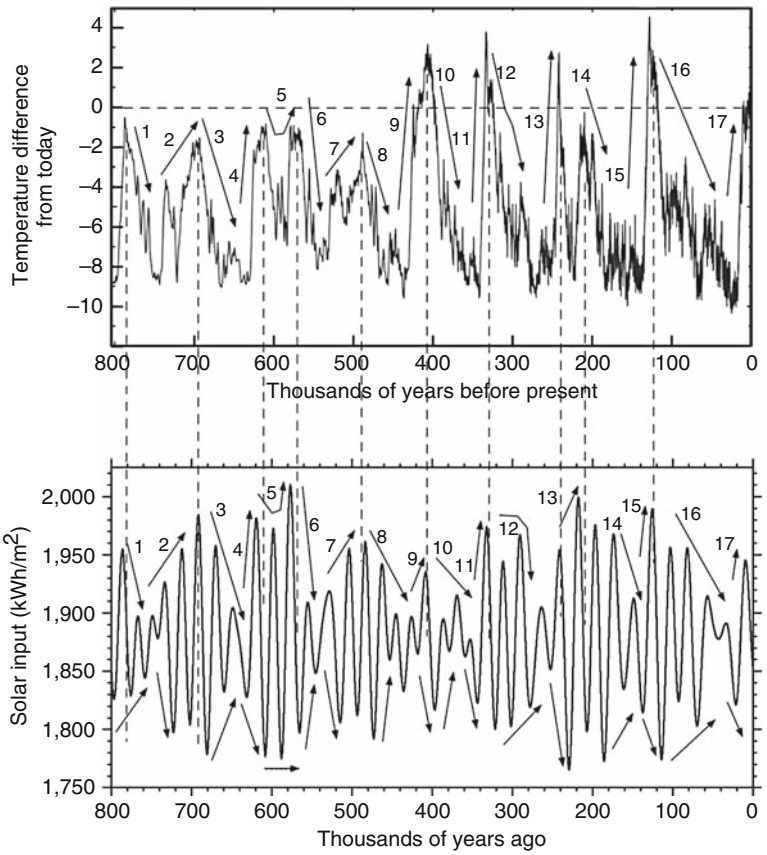

Ice Age Cycles: Data, Models, and Uncertainties, Figure 11 Comparison of the solar input to high latitudes with the estimated temperature from an Antarctic ice core over 800,000 years (Rapp, 2009).

trends if we ignore rapid oscillations of the solar input and concentrate on the envelope of the solar variability. However, Trend #9 is a major difficulty ("the 400 kyr problem").

One possible interpretation of Figure 11 (perhaps amongst many) is this:

According to this interpretation, the Earth naturally tends toward an ice age (at least over the past several hundreds of thousand years). Ice sheets build more slowly than they disintegrate. The "natural" state of the Earth's climate may be glacial. During those periods of the order of perhaps ~50,000 to 60,000 years, when oscillations in solar input are minimal, the solar input never gets high enough to melt summer ice, the climate cools, and ice sheets build up. However, during those periods when oscillations of solar input are large, the solar input gets high enough during the up-lobes of the oscillations to melt summer ice, the ice sheets diminish, and the climate warms. Even though there are also steep downward oscillations in solar input, the down lobes are insufficient to rebuild ice sheets lost in the previous upward oscillation, probably due to albedo effects and the likelihood that ice sheets build slowly and disintegrate more rapidly. When the amplitude of the solar oscillations is high, there is a tendency toward reducing global ice and heading into an interglacial period. When the amplitude is small, ice volume tends to increase and the ice age deepens. However, the warm period around 400,000 years ago remains a contradiction.

In order to compare the astronomical theory with ocean sediment data that represents ice volume, we require a model that relates ice volume to solar input to higher latitudes. Imbrie and Imbrie (1980) developed a simple model as described next.

During ice sheet decay, the rate of change of volume of the ice sheet is given by

$$\frac{dy}{dt} = -\frac{1+B}{T}(x+y) \qquad \text{if}(x+y) > 0$$

and during ice sheet buildup, the rate is given by

$$\frac{dy}{dt} = -\frac{1-B}{T}(x+y) \qquad \text{if}(x+y) > 0$$

in which

y = ice volume

x = solar input to high northern latitudes

T = time constant for lag between solar and ice volume buildup

B = constant to assure ice buildup is slower than ice decay

It is not immediately clear why y should appear on the right side of equation – this term reduces the rate of ice volume growth as the ice sheet volume increases.

Integration of the Imbrie's equations leads to a consistent timeline but the amplitude of oscillations can be adjusted with parameters. The Imbries chose $B = 0.6$ and $T = 17{,}000$ years to get a "best fit" to ocean sediment data over 600,000 years. Time constants for buildup and decay of ice sheets are then 42,500 years and 10,600 years, respectively (ice sheet decay is four times faster than ice sheet buildup when $B = 0.6$). More recently, Raymo adjusted B and T to be time-dependent to fit data over wider time span (3 million years) – T must decrease as the data go back further in time. The comparison of the model with data is shown in Figure 12. The degree of agreement lies in the eye of the beholder.

The primary cycle periods that characterize variability of the precession of the equinoxes, obliquity, and eccentricity are roughly 22,000, 41,000, and ~100,000 years, respectively. The spectral analysis of the Vostok and ocean sediment data indicate a strong peak with a period of roughly 100,000 years and a smaller spectral peak at 41,000 years. This should be tempered by the fact that since some tuning was used to assign the chronology for Vostok data, one might expect that elements of the astronomical model will appear in the spectrum for Vostok temperatures.

Summary

About 2.7 million years ago, the Earth entered an enhanced cooling phase that has continued unabated to the present day. Since then, the Earth has undergone a large number of climate cycles ranging from ice ages with large ice sheets in the northern hemisphere and a general cooling of the entire Earth, to interglacial periods that were comparable or perhaps warmer than the present climate. These cycles have become lengthier and of greater amplitude in the most recent million years.

Data are available from ice cores and ocean sediments, as well as other sources that reveal aspects of past climates dating back hundreds of thousands and even millions of years. These data indicate that there has typically been a long-term secular pattern of very roughly repeatable cycles, whereby great ice sheets have slowly built up over many tens of thousands of years culminating in a glacial maximum, followed shortly by a rather abrupt end of the ice age with rapid global warming leading to an interglacial period of perhaps 10,000 or more years.

The interglacial periods seem to end with abrupt climatic cooling to start a new ice age that gradually expands over many tens of thousands of years. This pattern is actually quite variable, but the outline described here seems to roughly describe the last four ice age cycles.

Ice core and ocean sediment data are couched in terms of isotope ratios. Converting these data into specific climatological variables (e.g., global average temperature, global ice volume, etc.) is not straightforward. Greenland and Antarctic isotope ratio data are believed to represent regional temperature conditions even if the absolute conversion to temperature is uncertain.

Ocean sediment data from benthic sources are believed to represent mainly global ice volume, although Lisiecki, Raymo, and Curry (2008) recently concluded: "Generating a robust age model for benthic $\delta^{18}O$ or ice volume without the assumptions of orbital tuning remains an important, unsolved problem."

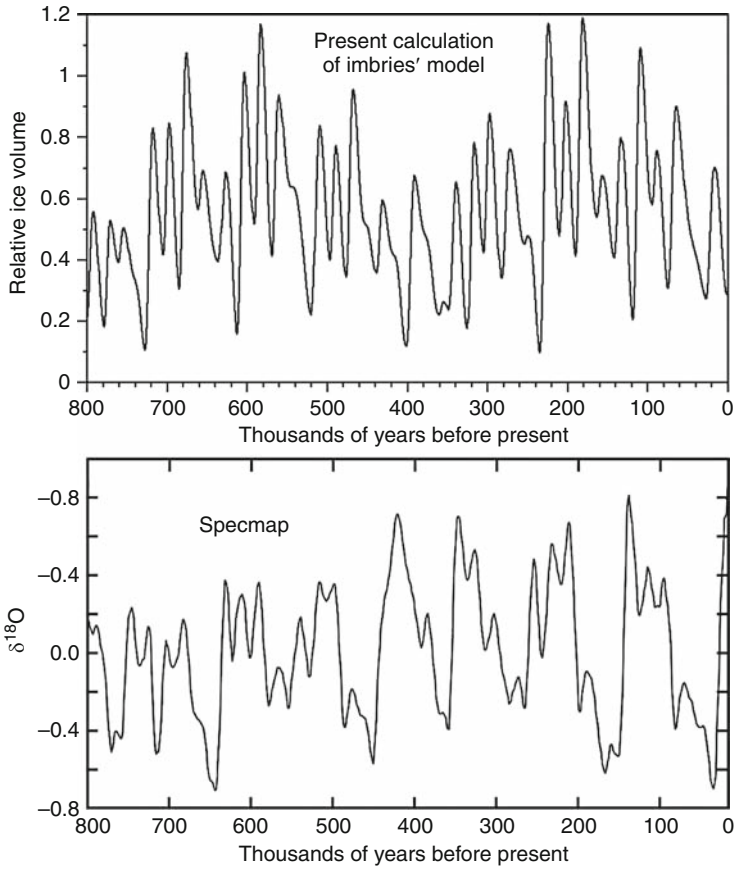

Ice Age Cycles: Data, Models, and Uncertainties, Figure 12 Comparison of Imbries' model with ocean sediment data.

In attempting to compare the astronomical theory with data, one must first clarify what the data represent.

- Isotope ratio data at Greenland and Antarctica are believed to represent local temperatures. These interpretations of isotope ratios are far from ironclad, and involve a number of uncertainties. Nevertheless, accepting these assumptions regarding the interpretation of ice core data, we still face the problem of how to compare ice core data with variability of solar intensity from year to year.
- If increased solar intensity raises temperatures, is there a time lag and does it depend on other factors as well?
- If the main driver for climate change is Northern Hemisphere solar intensity, how does this relate to Antarctica climate and temperature?
- Isotope data from marine sediments are typically believed to primarily represent ice volume – however, ice volume models are notoriously simplistic. Comparisons of theory with data are often compromised by use of "tuning" to set chronology.

In most cases, the time periods with higher amplitude solar oscillations appear to be associated with higher temperatures, and the periods during which solar oscillations are weak seem to be associated with lower temperatures. This would be the case if

- There is a fundamental tendency toward glaciation.
- Ice sheets grow slowly and disintegrate rapidly.

In that case, ice sheets would disintegrate and not recover when solar oscillations were large, but would grow when solar oscillations were small. All of this is very tenuous and represents a somewhat subjective interpretation of the data. However, the fact that the frequency spectrum shows the frequencies for eccentricity and obliquity but not precession, suggests that it is the amplitude of solar oscillations that matters, and the precession frequency does not directly contribute to climate change but rather, only the eccentricity and obliquity determine the amplitude of precession oscillations.

There are problems with this interpretation:

- The change from ~41,000 years spacing to ~100,000 years spacing of ice ages
- The occurrence of an ice age around 400,000 YBP when solar oscillations were minimal

And while there are innumerable books, reports, and published articles claiming that the astronomical theory is proven, the basis for such claims is not ironclad.

Bibliography

Archibald, D. C., 2009. Solar Cycle 24: Expectations and implications. *Energy and Environment*, **20**, 1–10.
Bell, L. G., and Eng, P., 2007. *Ice Age Mystery: A Proposed Theory for Climate Change*. Bloomington, IN: Author House.
Benestad, R. E., 2005. *Solar Activity and Earth's Climate*, 2nd edn. UK: Praxis.
EPICA Community Members, 2004. Eight glacial cycles from an Antarctic ice core. *Nature*, **429**, 623–628.
Dansgaard, W., 2005. *Frozen Annals*. Copenhagen, Denmark: Niels Bohr Institute.
Geike, J., 1894. *The Great Ice Age*.
Imbrie, J., and Imbrie, J. Z., 1980. Modeling the climatic response to orbital variations. *Science*, **207**, 943–953.
Imbrie, J., and Imbrie, K. P., 1979. *Ice Ages*. Harvard: Harvard University Press.
Lisiecki, L. E., Raymo, M. E., and Curry, W. B., 2008. Atlantic overturning responses to Late Pleistocene climate forcings. *Nature*, **456**, 85–88.
Lockwood, M., and Fröhlich, C., 2007. Recent oppositely directed trends in solar climate forcings and the global mean surface air temperature. *Proceedings of the Royal Society A*, **463**, 2447–2460.
Rapp, D., 2009. *Ice Ages and Interglacials*. UK: Springer/Praxis.
Svensmark, H., 2000. Cosmic Rays and Earth's Climate. Space Science Reviews 93, 155–166. www.junkscience.com/Greenhouse/influence-of-cosmic-rays-on-the-earth.pdf
Svensmark, H., and Friis-Christensen, E., March 2007. Reply to Lockwood and Fröhlich – The persistent role of the Sun in climate forcing. Danish National Space Center Scientific Report. www.space.dtu.dk/upload/institutter/space/research/reports/scientific%20reports/dnsc-scientific_report_3_2007.pd
William Dawson, J., 1893. *The Canadian Ice Age*, Montreal.
Wright, G. F., 1896. *Greenland Ice Fields and Life in the North Atlantic*, New York: D. Appleton & Co.
Wright, G. F., 1920. *The Ice Age in North America and its Bearing on the Antiquity of Man*, 6th edn, New York: Appleton & Co.

ICE AGE DEVELOPMENT THEORY

Matthias Kuhle
Department of Geography and High Mountain Geomorphology, University of Göttingen, Göttingen, Germany

Synonyms

Onset of the Pleistocene Ice Age Era and its rhythmic glaciations

Definition

Theory on the development and course of the Quaternary ice ages.

Introduction

Several theories on the development of ice ages are under discussion. They state extraterrestrial causes or the CO_2-household, ocean currents, and the closure of the Panamanian seaway.

The $\delta^{18}O$ records of planktonic foraminifera (Shackleton et al., 1988; Tiedemann et al., 1994) have shown that the Quaternary ice age began at about 2.75 Ma BP; from ~1 Ma BP onwards, its intensity (ice volume) and the length of its glacial phases approximately doubled (Figure 2b). It is now recognized that the explanation of these events cannot be fully exhausted by the variations of the Earth's orbital parameters (Berger et al., 1999). Insolation variations (Figure 2a) – which have displayed the same patterns for tens of millions of years (Berger and Loutre, 1991) – account for the waxing and waning of global ice volumes to a limited degree (Hays et al., 1976), but to explain why ice ages occur at all and why they increased so rapidly during the past 1 Ma, we must look for an additional, terrestrial cause.

In recent years, the continuous decline in levels of the greenhouse gas CO_2 in the atmosphere and a concomitant global cooling have been considered to be the most likely cause (Broecker, 1995; Ruddiman et al., 1997). Computer simulations by Berger et al. (1999) show that, to trigger ice ages in this way, atmospheric CO_2 must have decreased from more than 320 ppm by volume (ppmv) to 200 ppmv during the past 3 Ma. However, the latest alkenone-based CO_2 estimates (Pagani et al., 1999) have shown that, in spite of high temperatures, CO_2 levels during the Tertiary were by no means higher – sometimes even lower – than the preindustrial value of 270 ppmv in postglacial times or >300 ppmv during the Eem Interglacial (Fischer et al., 1999). So there is still no evidence for a general decrease in atmospheric CO_2 concentration since the Tertiary/Quaternary transition that may have caused temperatures to fall. Furthermore, the fine-scale records of the GRIP ice core confirm that during the last three glaciations the decrease of the CO_2 values lagged climatic change by as much as several thousands of years (Fischer et al., 1999). This reverses the previously accepted causal nexus: evidently, atmospheric CO_2 concentrations decreased in the wake of glacial-interglacial transitions, rather than promoting them.

The hypothesis that the closure of the Panamanian seaway and the resulting North Atlantic deep water formation were responsible for the onset of the ice ages (Haug and Tiedemann, 1998) is still inconclusive. Closure occurred 4.6–3.6 Ma ago, that is, 1 Ma too soon. The argument that increasing obliquity amplitudes between 3.1 and 2.5 Ma BP caused the ice to build up contradicts the fact that the decrease in obliquity amplitudes between 1 and 0.8 Ma does not coincide with ice retreat; on the contrary, it corresponds in time with an intensification of global glaciation (Figure 2a, b). Long-term global climatic changes may also have been caused by Cenozoic plateau uplift (especially of the Himalaya-Tibetan and the North American plateaux), inducing a change of zonal wind and precipitation patterns and a steepening of the climatic south-north gradient (Ruddiman and Kutzbach, 1992). However, uplift of the Tibetan plateau started 20 Ma BP

ago (Harrison et al., 1992) and, as the onset of the summer monsoon suggests, it began to act as a climate-effective barrier some 8 Ma ago (Prell and Kutzbach, 1992; Tiedemann et al., 1994; De Menocal, 1995) – too early for the start of the ice ages.

As an alternative a terrestrial Ice Age development theory will be introduced here. It is the relief-specific model of the Ice Age on the basis of uplift-controlled glacier areas in Tibet and the corresponding albedo increase as well as their positive climatological feedback by means of the global radiation geometry. It explains the onset of the Pleistocene glaciation as an autocycle on the basis of a 2.4 million km² ice sheet on the Tibetan Plateau (Kuhle, a.o., 1985, 1987, 1988, 2002).

The beginning of the winter monsoon c.2.75 Ma BP ago is evidence of the start of a restricted glaciation on the Tibetan Plateau, i.e., the height of the plateau reached the snow-line (ELA) for the first time. At that time the global cooling began. Since c.1 Ma BP Tibet has exceeded the ELA on a large scale and the distinct stages of glaciation led to the breakdown of the summer monsoon. The alternation with intercalated interglacials results from glacial-isostatic lowerings and rebounds. It overlaps with the amplifying or weakening efficacy of the variations of the Earth's orbital parameters.

Empirical induction

1. Observations of standard forms of glacial accumulation and erosion are evidence of a large-scale Pleistocene glacier cover of the Tibetan highland. Marginal sites at 2,000–2,460 m a.s.l. in all of the surrounding mountains of Tibet are evidence of an equilibrium line

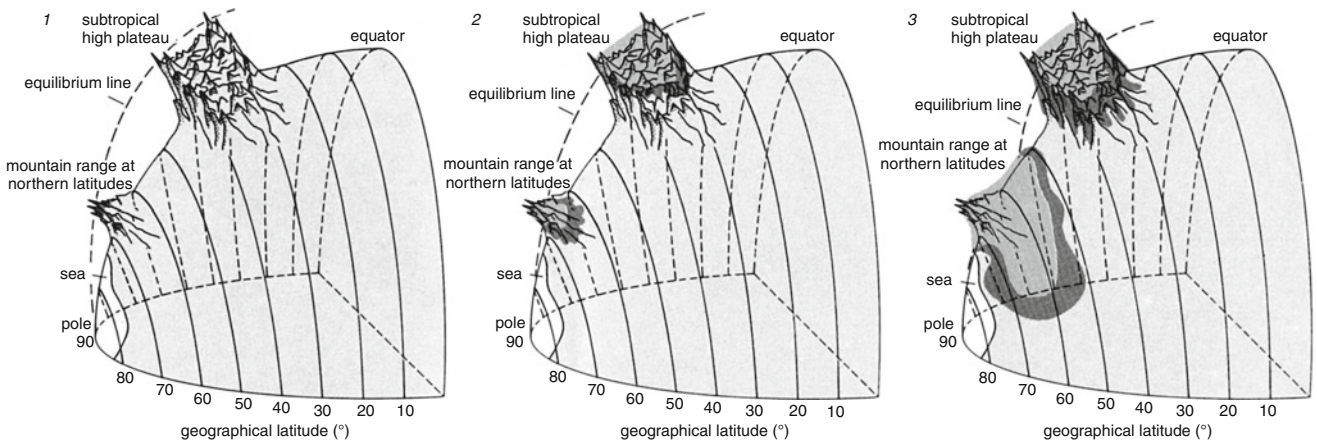

Ice Age Development Theory, Figure 1 Schematized presentation of the principle of the relief-related origin and termination of ice ages. The causative intensification of the cooling-down process emanates from a subtropical high plateau (such as the Tibetan Plateau) due to the fact that the initial lowering of the equilibrium line by approximately 500 m leads to the glacier's descent by 1,000 m from the mountains, thus suddenly glaciating large plateau areas (*step 1 to 2*). Mountain chains at higher latitudes experience the same amount of equilibrium line lowering as a result of the cooling down by 3.5°C during a change in the parameters of the earth's orbit. Since the altitudinal distance of the present glaciation to the height of the foreland areas is too great, glaciation has had little effect on area and thus on reflection (2). As the subtropical high plateau has undergone large-scale glaciation, with the transformation of a formerly very effective "heating panel" into an area of reflection, the further cooling down of the atmosphere caused in this way leads to a renewed lowering of the equilibrium line. The consequence is a chain-reaction-like worldwide enlargement of glacier areas. This advanced particularly fast in all those places where the lowering of the glaciation line reaches the flat mountain forelands (*step 2 to 3*). The sequence of additions of mountain foreland glaciation depends on the particular altitudinal distance of pre-ice-age hanging glacier ends from the altitudinal level of the foreland. Although, due to the conditions of radiation, the cooling effect per glacier area is greatest in the subtropics, the areal gain of glaciers increases significantly with the decreasing equilibrium line at higher latitudes (3). The reason for this is the fact that the equilibrium line dips toward the polar regions, and that the starting point of equilibrium line heights becomes progressively lower toward the lowlands. In the end the ice areas of the high latitudes outnumber those of subtropical high plateaus and mountains by approximately 8:1, by which time their cooling effect has increased around twofold. Nonetheless, such far-reaching glaciation would not have occurred without the impact of the subtropical inland ice. The cooling, which reacts upon the impact of the subtropical plateau ice as well, can hardly result in any further increase of the area of ice there because the glaciers cannot reach the lowlands when flowing over the edge of the plateau (*step 2 to 3*). In a reverse process (*steps 3 to 1*) the end of the Ice Age begins in the N and S lowland plains: on the return to normal values of solar radiation and a rise in temperatures by those initial 3.5°C the corresponding rise in the equilibrium line by 500 m with a rise in the glacier ends by 1,000 m becomes particularly effective for areas of flat lowland glaciation (*step 3 to 2*). Whilst lowland ice areas experience extreme reductions, thus forcing a global warming, the surface areas of the subtropical highland ice will remain almost constant, because only the steeply descending outlet of glacier tongues on the margins will become shorter on the initial upward move of the equilibrium line, whereas the reduction in glaciation is far from reaching the flat plateau ice proper (*step 3 to 2*). Only when the further warming of the earth has been initiated and has progressed through the disappearance of lowland ice, will the subtropical highland areas also be freed from ice (*step 2 to 1*); (Kuhle, 1987).

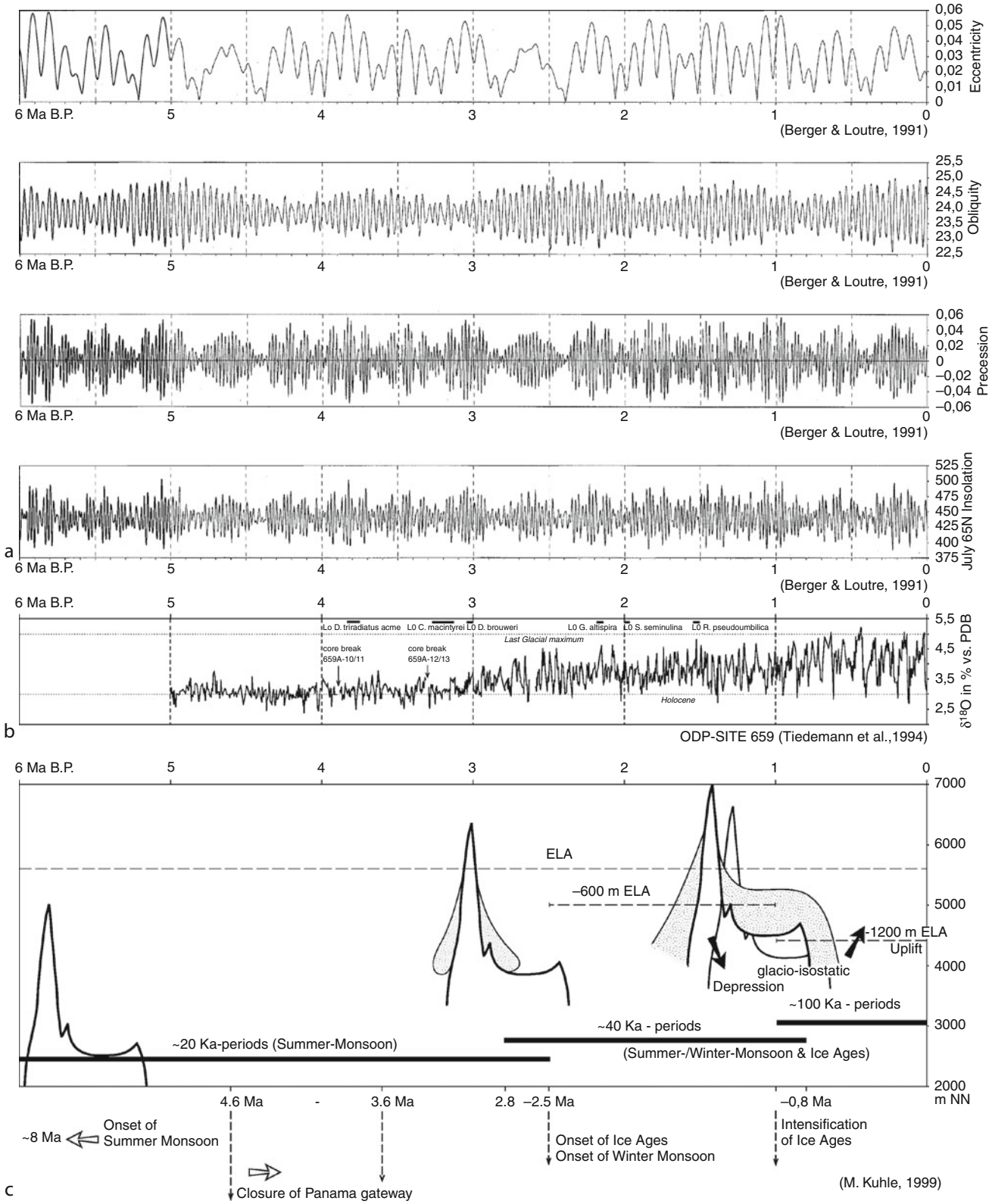

Ice Age Development Theory, Figure 2 (Continued)

depression of 1,100–1,660 m to 4,720–3,250 m a.s.l. The Ice Age equilibrium line thus ran up to 600 m below 85% of the Tibetan surface. This resulted in a 2.4 million km² inland ice mass with a thickness of 700–2,000 m (up to 2,700 m), (cf. Last Glacial Maximum Glaciation (LGM/LGP) in High Asia (Tibet and Surrounding Mountains), in this volume). Its volume was the equivalent of an approximately 5.4–6.5 m drop in sea level.
2. 14C ages substantiate the formation of inland ice at a date more recent than ∼50 ka and older than 9 ka (MIS 3–2, Würm).
3. Amounts of uplift of Central Tibet of more than 10–521 mm per annum are far in excess of the tectonically younger Himalaya, and are consequently interpreted as glacio-isostatic.
4. Presently consisting of 99% rock and scree, the Tibetan surface reflects only 15–20% of the high subtropical radiation coming from space. This results in a global heating effect of the atmosphere. Covering 97% of Tibet and reflecting 85–90% of the radiation, inland ice achieved a global cooling effect that is four times greater than at the latitudes of Nordic inland ice.

Theoretical deduction

1. Even an uplift of the Tibetan Plateau of 500 m or an equilibrium line depression of 500 m (=3.5°C drop in temperature) as a result of cyclical changes in the parameters of the earth's orbit was bound to lead to the formation of larger glacier areas in Tibet. According to this the highland necessarily was a pacemaker for the Ice Age (Figures 1, 2). The initial glacier cover of one third of Tibet caused further autocyclic equilibrium line depressions, aided by the 85% albedo of high subtropical incoming radiation. The resulting ice increase in Tibet aided global cooling and led to an approximately 46 million km² global High Ice Age glacier area, 26.3 million km² of which is Nordic inland ice (Figure 1), without the uncertain Siberian ice.
2. Milankovic radiation anomalies operated during the Pre-Pleistocene, without giving rise to an ice age (Figure 2). The glaciation of a subtropical energy-effective high plateau appears to trigger the Ice Age proper (see above).
3. In accordance with insolation being four times higher than at Nordic glaciated areas, the Tibetan ice was a much more influential global climatic body. Only 15% of the energy that previously heated the atmosphere before glaciation remained available for ablation. The reversal from a heating to cooling surface was also four times more effective and implies a corresponding increase in the self-intensification of glaciation from high to low latitudes.
4. In Tibet even a net precipitation of 200 mm/year would lead to an ice cover having an average thickness of 1,100 m within a little less than 10,000 years. This shows that in terms of time – from 90 to 60 ka, for instance – Tibetan ice would have been able to fulfill its role as a pacemaker.
5. An alimentation model is based on an analogy for the Antarctic ice: a depression that drew in humidity lay above a cold and shallow anticyclone situated over the ice cap.
6. With four times less cloud cover in the subtropics than at high latitudes, a subtropical inland ice sheet was bound to exert a particularly large global cooling effect.
7. The termination of the ice age cycle originated from the Nordic lowland ice. The end of extraterrestrial cooling (Milanković cycle) led to a rise of the equilibrium line by 500 m. The marginal and steep high plateau ice was initially not reduced during this ELA rise. By contrast, the vast lowland ice was bound to undergo an extreme loss of area. A lowland albedo loss led to global rewarming and an interglacial period.
8. In their role of pacemakers the uplift of a subtropical plateau above the ELA as well as its glaciation were triggers of the Ice Age on condition of the relief-specific Ice Age mechanism. This mechanism is

Ice Age Development Theory, Figure 2 (**a**) Astronomical parameters of the earth's orbit and rotation and corresponding insolation values for 65°N for the last 6 Ma according to Berger and Loutre (1991). (**b**) Benthic oxygen isotope records from Ocean Drilling Program Site 659 according to Tiedemann et al. (1994). The fluctuations in the $\delta^{18}O$ content of the foraminifera reflect the fluctuations of the global ice volume, with high values corresponding to the glacials and low values to the interglacials. Neither the beginning nor the intensification of the Quaternary glaciation period is correlated with the insolation (**a**). (**c**) Synopsis of the uplift and glaciation of the Tibetan plateau in their relation to other geoecological events. Comparison between (**a**) and (**b**) shows that an additional factor apart from orbital variations is required to explain both the start of the ice ages about 2.8 Ma and their increasing intensity from 1 Ma onwards. The closure of the Panama gateway occurred too early to be the terrestrial cause. The uplift of the Tibetan plateau, as far as it can be reconstructed from the onset of the summer- and winter monsoons, and, derived from this, the begin of an autochthonous glaciation of Tibet from ∼2.5 Ma BP onwards, were synchronous with the onset of the global ice ages. Evidence that variations of the summer- and winter monsoon intensity documented by marine dust flux records and loess-palaeosol sequences on the Chinese loess plateau occurred in phase not with the insolation variation but with glacial-interglacial cycles (40 ky and ∼100 ky periods) is a strong pointer to the existence of a Tibetan glaciation. Gradual uplift of the Tibetan Plateau toward the ELA (equilibrium line) level enabled an ice sheet of 2.4 million km to grow from ∼1 Ma BP onwards; the resulting cooling effect permitted a maximum expansion of the Nordic lowland ice sheets (−1,200 m ELA). The now beginning glacio-isostatic depression, deglaciation, and following rebound of the plateau were responsible for the occurrence and duration of interglacial-glacial cycles (∼100 ky periods).

based on global radiation geometry. The spherical geometry of the earth and the position of the Earth's axis are the necessary requirements for the formation of large lowland ice sheets at high latitudes, while subtropical glaciers occur at extreme elevations and are therefore restricted to small areas. Their small extent is compensated by a very high radiation energy, so that a minimal area of ice cover triggers the Ice Age (Figures 1, 2). A small rise in the equilibrium line is all that is needed to begin global rewarming through loss of glacier surface area. Proven moraines from that time, plus the reconstructions of their positions, will certainly permit a later corroboration of the kind of orogeny that extended up into the vicinity of the equilibrium line during the Permo-Carboniferous glaciation, for instance.

9. Extraterrestrial cooling is not needed to trigger the ice ages. The Tibetan Plateau would only require an uplift of an additional 500–1,000 m for a glaciation to occur without this cooling. An uplift of this kind could occur within 50–100 ka, so that a renewed Ice Age – accelerated extraterrestrially – might take place in a few dozen millennia. The denudation of the Tibetan High Plateau will terminate the Ice Age of the Pleistocene Era.
10. The uplift of Tibet came to its Early Pleistocene end as a result of the loading of inland ice. This ensured the deglaciation of the plateau as a continuation of the wasting begun by the lowland ice. The present extreme uplifts in Tibet are to be regarded as compensatory glacio-isostatic movements. Altitudes of plateaus and highlands of earth are climatically controlled by the position of the equilibrium line. The greatest possible plateau altitudes are found in subtropical latitudes.

Confirmations of the relief-specific ice age theory

The central role of the Tibetan plateau for the understanding of the Quaternary climatic changes is undeniable (Hughes, 1998). This is also derivable from the increasing importance of a Tibetan inland ice for all climate simulations (cf. Last Glacial Maximum Glaciation (LGM/LGP) in High Asia (Tibet and Surrounding Mountains), in this volume). The ecological consequences of a subtropical inland ice of c.2.4 million km² are of utmost importance (Lautenschlager and Santer, 1991). The albedo of snow-covered ice surfaces reaches from 75% to 95%. This means that this portion of global radiation is reflected and thus lost for the atmosphere. Regionally the ice cover of the plateau is especially important, because today (interglacially) Tibet is one of the most significant heating faces of the Earth. Energy balance calculations suggested that during the LGM/LGP 70.5% of the albedo-induced energy loss was caused by the Nordic lowland ices, but solely 20.5% was due to the ice on the Tibetan plateau (Bielefeld, 1997).

Sensitivity experiments with a general circulation model (Felzer et al., 1998) show that the Nordic lowland ices caused a cooling of −2.8°C of the altogether −6.5°C ice age decrease in GMT (Global Mean Temperature), whilst the Tibetan ice caused a GMT drop of at least −0.8°C. This is a minimum value, because the energy loss due to the Tibetan glaciation amounts to even 32% instead of 20.5% when the changed infra-red emission is taken into account (Bielefeld, 1997).

Synchronism of Tibetan uplift and the ice ages

In the opinion (Kuhle, 1987, 1988, 2002) that the reaching of the plateau's elevation of 4,600–5,000 m a.s.l is the cause of the intensification of global glaciation between 1 and 0.8 Ma before today along with the change to a 100,000 years rhythm (Shackleton et al., 1988; Tiedemann et al., 1994), geological indicators confirm the Tibetan uplift during this interval at the beginning of the Pleistocene (Ding et al., 1995; Chen Zhiliang, 1999). This chronology of Tibetan uplift and start of the High Glacials is proved by the change of the intensity of summer- and winter monsoon (Figure 2) which sets in. Under modern orographic conditions the intensity of monsoon circulation is controlled by insolation in low latitudes (Prell and Kutzbach, 1992; Felzer et al., 1998) and thus should follow the 21,000 years rhythm of precession. However, there is only evidence for a dominant 20,000 years rhythm prior to 2.8 Ma before today (De Menocal, 1995). Afterwards, up to c.1 Ma before present, a 41,000 year rhythm followed and then the current glacial 100,000 year rhythm where glacials have a weak summer- and strong winter monsoon, and interglacials vice versa (Tiedemann et al., 1994; De Menocal, 1995; Emeis et al., 1995; Xiao et al., 1995; Ding et al., 1995) (cf. Last Glacial Maximum Glaciation (LGM/LGP) in High Asia (Tibet and Surrounding Mountains), in this volume.)

Development of loess

The worldwide most important loess sedimentation on the Chinese loess plateau as a secondary deposit of glacial genesis is a hard indicator for the rhythmical inland glaciation of the Tibetan plateau since 2.75 Ma with a maximum extension since 1 Ma. This cannot be explained by an insignificant mountain glaciation but is dependent on inland ices (Kuhle, 1985, 1987, 1988, 2007).

Summary

The onset of the ice age era at ∼2.75 Ma BP and its increasing intensity from ∼1 Ma BP onwards cannot be explained by variations of the Earth's orbit. Evidence

supporting a 2.4 million km² ice sheet on the Tibetan plateau during the Last Glacial Maximum has led to the hypothesis that the resulting albedo-induced heat loss in the Earth's atmosphere may have triggered global ice ages. Recent data obtained from marine and terrestrial sediment records now confirm the climatic ecological impact of a Tibetan glaciation; they also show that the development of Tibet's ice sheet was synchronous with the onset and intensification of global ice ages.

Bibliography

Berger, A., and Loutre, M. F., 1991. Insolation values for the climate of the last 10 million years. *Quaternary Science Reviews*, **10**, 297–317.

Berger, A., Li, X. S., and Loutre, M. F., 1999. Modelling northern hemisphere ice volume over the last 3 Ma. *Quaternary Science Reviews*, **18**, 1–11.

Bielefeld, B., 1997. Investigation into albedo-controlled energy loss during the last glaciation. In Kuhle, M. (ed.), *GeoJournal*, *Tibet and High Asia IV*, **42**(2–3), 329–336.

Broecker, W. S., 1995. Chaotic climate. *Scientific American*, **11**, 44–50.

De Menocal, P. B., 1995. Plio–Pleistocene African climate. *Science*, **270**, 53–59.

Ding, Ling, Zhong, Dalai, Pan, Yusheng, Huang, Xuan, and Wang, Qinglong, 1995. Evidences of fission track dating on the rapid uplift of east Himalaya Mountains since Pliocene. *Chinese Science Bulletin*, **40**(16), 1497–1500.

Emeis, K-Ch, Anderson, D. M., Doose, H., Kroon, D., and Schulz-Bull, D., 1995. Sea-surface temperatures and the history of monsoon upwelling in the northwest Arabian Sea during the last 500,000 years. *Quaternary Research*, **43**, 355–361.

Felzer, B., Webb, T., III, and Oglesby, R. J., 1998. The impact of ice sheets, CO_2, and orbital insolation on late quaternary climates: sensitivity experiments with a general circulation model. *Quaternary Science Reviews*, **17**, 507–534.

Fischer, H., Wahlen, M., Smith, J., Mastroianni, D., and Deck, B., 1999. Ice core records of atmospheric CO_2 around the last three glacial terminations. *Science*, **283**, 1712–1714.

Harrison, T. M., Copeland, P., Kidd, W. S. F., and An, Y., 1992. Raising Tibet. *Science*, **255**, 1663–1670.

Haug, G. H., and Tiedemann, R., 1998. Effect of the formation of the Isthmus of Panama on Atlantic Ocean thermohaline circulation. *Nature*, **393**, 673–676.

Hays, J. D., Imbrie, J., and Shackleton, N. J., 1976. Variations in the earth's orbit: pacemaker of the ice ages. *Science*, **194**, 1121–1132.

Hughes, T. J., 1998. *Ice sheets*. New York: Oxford University Press, p. 343.

Kaufmann, G., and Lambeck, K., 1997. Implications of Late Pleistocene Glaciation of the Tibetan Plateau for present-day uplift rates and gravity anomalies. *Quaternary Research*, **48**, 267–279.

Kuhle, M., 1985. Glaciation research in the Himalayas: a new ice age theory. *Universitas*, **27**(4), 281–294.

Kuhle, M., 1987. Subtropical mountain- and highland-glaciation as ice age triggers and the waning of the glacial periods in the Pleistocene. *GeoJournal*, **14**(4), 393–421.

Kuhle, M., 1988. The Pleistocene glaciation of Tibet and the onset of ice ages – An autocycle hypothesis. *GeoJournal*, 17(4) Tibet and High-Asia. Results of the Sino-German Joint Expeditions (I),581–596.

Kuhle, M., 2002. A relief-specific model of the ice age on the basis of uplift-controlled glacier areas in Tibet and the corresponding albedo increase as well as their positiv climatological feedback by means of the global radiation geometry. *Climate Research*, **20**, 1–7.

Kuhle, M., 2007. The past ice stream network in the Himalayas and the Tibetan ice sheet during the last glacial period and its glacial-isostatic, eustatic and climatic consequences. *Tectonophysics*, **445**(1–2), 116–144.

Lautenschlager, M., and Santer, B. D., 1991. Atmospheric response to a hypothetical Tibetan ice sheet. *Journal of Climate, AMS*, **4**(4), 386–394.

Pagani, M., Freeman, K. H., and Arthur, M. A., 1999. Late Miocene atmospheric CO_2 concentrations and the expansion of C4 grasses. *Science*, **285**, 876–879.

Prell, W. L., and Kutzbach, J. E., 1992. Sensitivity of the Indian monsoon to forcing parameters and implications for its evolution. *Nature*, **360**, 647–652.

Ruddiman, W. F., Raymo, M. E., Prell, W. L., and Kutzbach, J. E., 1997. The uplift-climate connection: a synthesis. In Ruddiman, W. F. (ed.), *Tectonic uplift and climate change*. New York: Plenum Press, pp. 471–515.

Ruddiman, W. F., and Kutzbach, J. E., 1992. Plateau uplift and climatic change. *Scientific American*, **3**, 42–50.

Shackleton, N. J., Imbrie, F. R. S., and Pisias, N. G., 1988. The evolution of oxygen-isotope variability in the North Atlantic over the past three million years. *Philosophical Transactions of the Royal Society of London. Series B*, **318**, 679–688.

Tiedemann, R., Sarnthein, M., and Shackleton, N. J., 1994. Astronomic timescale for the Pliocene Atlantic O18 and dust flux records of ocean drilling program site 659. *Paleoceanography*, **9**(4), 619–638.

Xiao, J., Porter, S. C., An, Z., Kumai, H., and Yoshikawa, S., 1995. Grain size of quartz as an indicator of winter monsoon strength on the loess plateau of central China during the last 130,000 year. *Quaternary Research*, **43**, 22–29.

Zhiliang, Chen, 1999. The extending plateau: late Cenozoic uplift of the northern Tibetan plateau. *Terra Nostra*, **2**, 27.

Cross-references

Himalaya
Ice Age
Ice Age Cycles: Data, Models, and Uncertainties
Last Glacial Maximum Glaciation (LGM/LGP) in High Asia (Tibet and Surrounding Mountains)

ICE APRON

Mahendra R. Bhutiyani
Hazard Assessment and Forecasting Division, Snow and Avalanche Study Establishment, Chandigarh, India

Definition

Ice aprons are small accumulations of snow and ice masses that stick to the topography of the glacierized basin (Figure 1). They are generally found above the equilibrium line.

Ice Apron, Figure 1 Ice aprons in the cirque of a glacier in the Karakoram Himalaya.

Origin

Ice aprons are formed in snow-bound glacierized basins as some parts of the snowcover stay put in smaller depressions on moderately inclined slopes, even after avalanches have brought down most of the snow. With accumulation of residual snow, these ice patches grow in size and undergo metamorphism with each passing year. They may undergo movement by internal plastic deformation due to shear stresses imposed by a component of gravitational force.

Significance

Ice aprons at some places develop into smooth icy slopes, which may facilitate triggering of loose snow avalanches. At a few places where conditions favor their growth into comparatively larger ice patches, they may develop into overhangs as a result of ice-deformation and may become potential sites of dangerous ice avalanches.

ICE CAPS

Mahendra R. Bhutiyani
Hazard Assessment and Forecasting Division, Snow and Avalanche Study Establishment, Chandigarh, India

Definition

Ice caps can be defined as large masses of ice covering the Polar Regions with a surface area less than 50,000 km^2. They are essentially the huge glacier masses that almost submerge the topography beneath. At places the peaks of the covered terrain protrude through the ice mass, giving rise to the formation of "nunataks." On the periphery, the ice caps spread out into number of polar glaciers occupying the valleys. These glaciers, being at subzero temperatures, unlike their counterparts in the temperate regions, do not generate high amount of runoff. The examples of ice caps are the high-latitude continental ice sheets covering Antarctica and Greenland (see the Figure 1), where their growth is limited by the surrounding oceans. They are also found in regions such as the Canadian Rockies and Patagonia where altitudes are higher.

Origin

Ice caps generally form in regions where polar to subtemperate climatic conditions prevail throughout the year. Accumulation generally exceeds the ablation as subzero temperatures inhibit melting and the glaciers grow on the tops of individual mountains. They may merge together, forming an icy band around the mountain. If the conditions favor, this may grow until it covers the mountain's summit. Ice caps from nearby mountains can merge to form really big ice caps.

Significance

The ice caps served as the cores of many continental ice sheets that formed during Ice Ages in the past. When the ice sheets melted, the core ice caps may have survived.

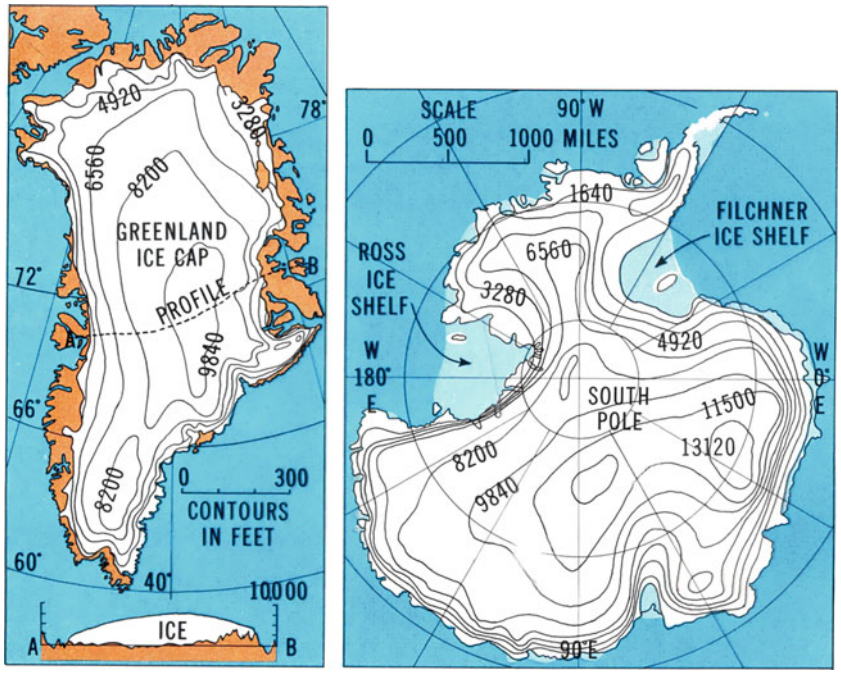

Ice Caps, Figure 1 Ice caps of Greenland and Antarctica(From Ward's Natural Science Establishment, Inc. 1964).

ICE CAVES

Mahendra R. Bhutiyani
Hazard Assessment and Forecasting Division, Snow and Avalanche Study Establishment, Chandigarh, India

Definition

Caves formed within the glacier body or at its base (ice-rock interface) are often called ice caves or glacier caves. They are generally found in those glaciers where temperatures remain subzero for large parts of the year.

Origin

They are mostly formed by surficial melting on the glacier surface during ablation season. The supraglacial meltwater channels thus formed (Figure 1) enter the glacier body either through the crevasses or vertical shaft like holes called "moulins" or "mills" (Figure 2). Full-depth crevasses or moulins may guide this water to the base of the glacier. Subglacial cavities or channels are thus formed due to hydrostatic pressure exerted and enlargement of cavities facilitated by heat transfer from the water by its whirling action and the air to the ice mass. These meltwater channels ultimately exit at the glacier snout (Figure 3). Some subglacial ice caves are formed by geothermal heat from the earth and also from volcanic vents or hot springs beneath the ice. Sometimes, water falling through half-depth crevasses or moulins may carve its own englacial meltwater cave and a channel by similar process.

Ice Caves, Figure 1 Supraglacial meltwater channel on the glacier surface.

The ice cave thus formed may get enlarged through melting in summer. They are very dynamic and change from year to year. They may disappear as glaciers melt and retreat in response to the rising temperatures.

Ice Caves, Figure 2 A typical glacier "mill" or "moulin."

Ice Caves, Figure 3 Ice cave of Zemu Glacier in Sikkim Himalaya, India.

Significance

These ice caves help the glaciologists to study the interior of glaciers. The study of glacier caves themselves is sometimes called glaciospeleology.

ICE CORE

Nancy A. N. Bertler
Joint Antarctic Research Institute, Victoria University of Wellington and GNS Science, Wellington, New Zealand

Definition

An ice core is drilled from glaciers or ice sheets. It represents, like tree rings, an often sub-annual record of snow accumulation through time. Geochemical analyses of the ice, gas bubbles, and particulates can be used to reconstruct a detailed view of environmental conditions at the time of the snow precipitation. This includes reconstruction of local temperature, snow accumulation, humidity and temperature at the source region of the moisture, as well as atmospheric circulation pattern and vigor, storminess, sea-ice extent, ocean productivity, and greenhouse gas concentrations.

Introduction

As snow precipitates and accumulates to create glaciers and ice sheets, it captures and preserves a realm of information on the climatic and environmental conditions at the time of precipitation. As the snow is buried by subsequent snow fall, it forms isochrones (layers of same age) that can be read like pages of a detailed diary of past climate variability with near instrumental quality (Alley, 2000; Mayewski and White, 2002). Depending on annual snow accumulation and the seasonal distribution of snow fall, ice cores can provide climate records with sub-annual to decadal resolution for hundreds of millennia. The longest ice core record to date has been recovered by the European Programme for Ice Coring in Antarctica (EPICA) at Dome C in East Antarctica and spans almost 1 million years (EPICA Community Members, 2004). The deepest ice core record is 3,623 m long and has been recovered from Russian Vostok Station in Antarctica, which contains a record of the past 460,000 years (Petit, 1999) and lies above the largest lake in Antarctica, Lake Vostok. However, ice cores have been recovered from many places, including Greenland (Mayewski et al., 1993; O'Brien et al., 1995; Sigfus J. Johnsen et al., 2001; Steffensen et al., 2008) and Antarctica (EPICA Community Members, 2004; Jouzel et al., 1987; Mayewski et al., 2004; Mayewski et al., 2005; Petit et al., 1999; Wolff et al., 2009), and also from mountainous regions outside the polar regions, such as the Himalayas (Kang et al., 2004; Kaspari et al., 2008), Rocky Mountains (Osterberg et al., 2008), European Alps (Preunkert et al., 2000; Schwikowski et al., 1999), South American Andes (Aristarain and Delmas, 1993), and even the tropics (Stager and Mayewski, 1997; Thompson et al., 2003), such as Mt Kilimanjaro (Thompson et al., 2002) (Figure 1).

Structure of an ice core

As snow is compressed under the weight of new snow accumulating above, snowflakes turn into firn and eventually ice (Figure 2). The transition between those stages is defined by density. Snow is defined as lighter than 0.55 g/cm^3, while ice has the density of 0.83 g/cm^3, and firn lies in between. While snow and firn is permeable to air, below the bubble close off depth that lies between 0.80 and 0.83 g/cm^3, the ice becomes impermeable and the crystals trap pockets of atmospheric gases in tiny bubbles between crystal boundaries. As the bubbles are not closed off above the firn-ice transition, the gas in the bubbles is younger than the surrounding ice by the time it takes the ice to reach the bubble close off depth from the surface. This age difference depends on annual snow

Ice Core, Figure 1 Danish Hans Tausen Drill containing an ice core from Greenland from about 400 m depth. (Picture taken by Nancy Bertler.)

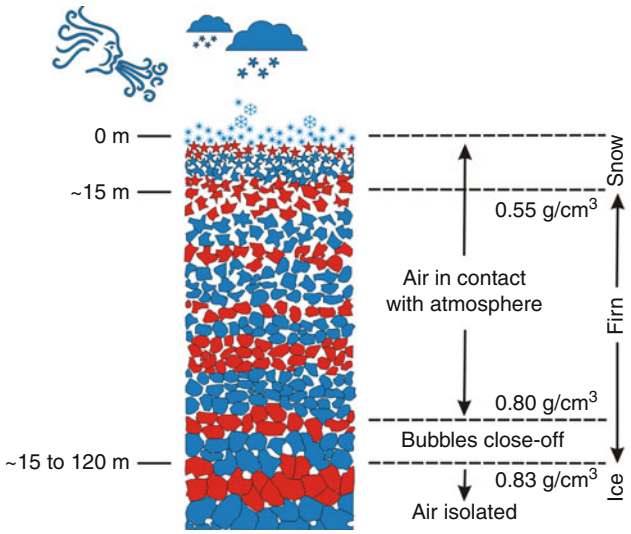

Ice Core, Figure 2 Schematic model of snow densification to firn and ice as defined by density. The depth of these transitions is highly dependent on site-specific characteristics such as average annual temperature and snow accumulation.

accumulation (the higher the annual snow accumulation the smaller the age difference) and annual average temperature (the warmer the temperature the smaller the age difference). For this reason the age difference does not stay constant even at a particular site, but is larger, for example, during glacial than during interglacial periods.

Resolution and length of an ice core record

In general, three types of ice cores are distinguished: shallow, intermediate depth, and deep ice cores. While shallow ice cores are in the order of a few meters to perhaps 100 m depth (e.g., the ITASE project), intermediate depth ice cores can be up to ~1,500 m deep (e.g., Berkner Island and Law Dome ice cores), and deep ice core projects have recovered cores of 3–4 km length (e.g., Vostok, EPICA, Dome F, Byrd, NGRIP, GISP2, GRIP ice cores). The logistical challenge of drilling intermediate or deep ice core limits the number of projects to a few, very large international efforts. While intermediate drilling projects might require 10–20 personnel on site, deep drilling projects are multi-year deployments with ~50 or more personnel on site. These projects often target long ice core records for many millennia in both high (WAIS, Greenland) and low snow accumulation (Vostok, EPICA) sites. Shallow ice cores can be obtained by a small team of 2–5 people and are often used for site reconnaissance, to reconstruct the recent past (perhaps the last 50–200 years), and to quantify geographical variability by obtaining a large grid of ice cores from different places, such as achieved by the International Trans Antarctic Scientific Expedition (ITASE) programme in Antarctica (Mayewski et al., 2005).

Types of information derived from ice cores

Ice cores provide three general types of proxies: (a) geochemical characteristics of the ice, (b) content and isotopic composition of gas bubbles enclosed in the ice, and (c) particulates.

Geochemical characteristics of ice

The ice is routinely measured for stable isotopes signature and geochemical composition.

Stable isotopes: The melted water of ice cores is commonly analyzed for stable isotope ratios of oxygen ($\delta^{18}O$) and hydrogen (δD) and measured against an international standard (V-SMOW – Standard Mean Ocean Water supplied from Vienna office of the International Atomic Energy Agency). Either isotope record (oxygen or hydrogen) can be used to reconstruct past temperature variability at the sampling site (Jouzel et al., 1997). Depending on the time resolution and length of the record, the data can reflect the seasonal change and/or longer-term temperature variability, such as glacial–interglacial cycles. To convert the stable isotope record into a temperature record, the data require site-specific calibration, which takes into account potential changes in moisture source, precipitation height over the surface (e.g., inversion layer), and site elevation changes (e.g., as ice sheets grow and shrink) (Jouzel et al., 1997). Over longer time periods (glacial/interglacial time scale) changes in the ocean composition have also to be taken into account, as the ice core record combines the signal of two effects (a) cooler temperatures and (b) a trend toward isotopically heavier ocean water during glacial time periods as

preferentially more and more isotopically lighter water is stored in the expanding ice sheets.

When both isotope ratios are measured, deuterium excess (d excess) can be calculated using the formula:

$$\text{d excess} = \delta\text{D} - 8 \times \delta^{18}\text{O}$$

Dansgaard (1964) observed for the first time that deuterium excess, or the deviation of the measured sample from the global meteoric water line, is sensitive to the sea surface temperature and absolute humidity at the moisture source region. When plotting global stable isotope measurements of meteoric water creates a linear correlation between oxygen and hydrogen isotope data, with a graph that intercepts with a value of 10 and a slope of approximately 8. While the slope is a result of the different diffusivity of deuterium and hydrogen, the intercept of 10 represents a global mean of deuterium excess. Deuterium excess is sensitive to kinetic fractionation of the water isotopes, which is primarily sensitive to phase changes such as evaporation and snow formation, providing a powerful proxy for sea surface temperature and humidity over the ocean, as well as air mass origin (Petit et al., 1991; Vimeux et al., 2002).

Geochemical analyses: The melted water is commonly measured for concentration of major ions, in particular Na, Cl, K, Mg, Ca, NO_3, SO_4, and methane sulfonate (Bertler et al., 2005). Together they represent a substantial proportion of all soluble aerosols in the atmosphere (Legrand and Mayewski, 1997) and provide a comprehensive view of the geochemical composition of the atmosphere and its circulation pattern. Circulation pattern can be reconstructed by identifying sources and transport mechanism of these aerosols, which indicate, for example, marine air-mass influences (e.g., Na and Cl), stratospheric air-mass input (e.g., NO_3), and volcanic events (e.g., SO_4). In addition, Boutron and colleagues developed methods to measure extremely low concentrations of trace and rare earth elements to provide preindustrial background levels (Boutron and Lorius, 1979). Today, the focus has shifted toward understanding their source and sinks as well as transport characteristics by using concentrations as well as isotopic ratios of these elements (Osterberg et al., 2008; Rothlisberger, 2000) as well as organic acids (Legrand et al., 1992).

Gas bubbles

Since 1958 AD atmospheric measurements at Mount Mauna Loa Observatory monitor the concentration of carbon dioxide (CO_2) in the atmosphere (Keeling et al., 1976). Prior to the onset of the observational record, ice core records have been used to extend the record of greenhouse gas concentration back to almost 1 million years (EPICA Community Members, 2006; Luthi et al., 2008; Petit et al., 1999). As snow compacts under the overlaying burden of new snow precipitation, it changes into firn and eventually ice. At the firn-ice transition, tiny bubbles are closed off between the ice crystals. Those bubbles contain a sample of the atmosphere at the time of bubble close off and hence can provide a detailed record of past variability of greenhouse gas concentrations, such as carbon dioxide (CO_2), methane (CH_4), and nitrous oxide (N_2O). The available resolution of the gas records depends on the depth and age of the bubble close off layer and the mixing ratio of the gas in the firn. While the firn is permeable, it is more vented at the top than toward the firn-ice transition. The gradual capture and gravitational fractionation of the gases has to be taken into account. One of the highest available greenhouse gas records has been derived from Law Dome in Antarctica. There the age difference between the gas and the ice at the modern firn-ice transition is only 60 ± 2 years and the diffuse mixing time of the gas down to the bubble close off is 8 years (Morgan et al., 2002). At colder, lower snow accumulation sites, for example, Vostok, the age difference is well over 1,000 years; however, the records are significantly longer (Petit et al., 1999).

Ice cores have shown for the first time that greenhouse gas concentration and temperature covaried in the past. The Vostok ice core was the first core to show the close relationship between carbon dioxide and methane and temperature over the last four glacial/interglacial time periods (Petit et al., 1999). The EPICA Dome C core record extended that record and showed that carbon dioxide and methane remained in a narrow range over the past 800,000 years, not exceeding 300 ppm (Luthi et al., 2008) and 800 ppb (Loulergue et al., 2008), respectively, during past warm periods. These records provide a baseline to compare modern concentrations and show that over the past 250 years during the industrial revolution, greenhouse gas concentration in the atmosphere increased significantly – about 35% for carbon dioxide, 150% for methane, and 16% for nitrous oxide (IPCC, 2007).

Particulates

Through predominantly dry deposition, dust and other particulate material is trapped in porous snow and firn, which provides a detailed record of past atmospheric particulate loading. Dust is an important driver of global climate, and appears to be the first indicator to change over glacial–interglacial time periods (Broecker, 2000; Delmonte, 2004; Lambert et al., 2008; Steffensen, 1997; Wolff et al., 2006). Dust particulates effect the climate system through iron fertilization of the ocean (Blain et al., 2007; Boyd et al., 2000), the influence of aerosols and dust particles on nuclei formation and drop size in clouds, and on the residence time of water molecules in the atmosphere (Broecker, 2000). Global dust particulates are characterized by modal grain size between 2 and 6 μm (Delmonte et al., 2004). The transport of particulates to snow surfaces is dependent on weathering of crustal sources, the proximity of the source region, wind speed, wind turbulence, and snow accumulation (Delmonte et al., 2004). In addition, studies of black carbon particulates in ice cores provide records of past forest fires and anthropogenic pollution (McConnell et al., 2007).

Dating ice cores

The most common dating technique of ice cores is by counting seasonal variability, which can be expressed in stratigraphy (e.g., denser winter and lighter summer layers), stable isotope variance (low oxygen or hydrogen isotope values for winter and higher values for summer), geochemical differences (e.g., sodium often peaks during winter, while MS peaks during autumn), etc. (Alley, 2000; Mayewski and White, 2002). In addition, time markers from volcanic eruptions are often used to evaluate the accumulative dating error of annual layer count and to adjust the annual layer count to absolute ages back in time. Rarely is tephra found as evidence of the volcanic eruption, instead sulfate or SO_4 is used, which shows large peaks for many eruptions, such as Tambora and Krakatau (Dixon et al., 2005; Kurbatov et al., 2006; Zielinski et al., 1997). In addition, radioactive isotopes such as 10Be, 14C, 36Cl, and Tritium are used as radioactive clocks (Beer et al., 1988; Muscheler et al., 2005; Petrenko et al., 2006). Long ice core records, covering many glacial–interglacial records, are often dated using age models which are based and tuned to Milankovitch cycles (Parrenin et al., 2004; Schwander et al., 2001).

The future of ice core research efforts: the International Partnership on Ice Coring Sciences (IPICS)

To coordinate the science efforts of the ice core community of the next decades, the International Partnerships on Ice Coring Sciences, or IPICS, was established. IPICS is a group that represents 18 nations (Australia, Belgium, Brazil, Canada, China, Denmark, Estonia, France, Germany, India, Italy, Japan, Korea, Netherlands, New Zealand, Norway, Russia, Sweden, Switzerland, United Kingdom, and the United States) and is composed of ice core scientists and drilling engineers. IPICS identified four scientific and one technical focus area for the ice community for the next 10–20 years. These are (http://www.pages.unibe.ch/ipics/documents.html):

- The Oldest Ice (at least 1.4 million years and beyond)
  This focus group investigates the characteristics and cause of the transition from 40,000-year cycles to 100,000-year cycles in the late Pleistocene. One of the main contributions of such an ice core would be to reconstruct greenhouse gas concentrations during the 40,000-year cycle period in comparison to the last 1 million years that was dominated from 100,000-year cycles.
- The IPICS 40,000-year array: A bipolar record of climate forcing and response
  The behavior and timing of the last deglaciation shows large geographical variability in the available ice core records. This focus group aims to obtain more intermediate deep ice cores that will help to understand these geographical differences and correlate records from the Northern and Southern Hemispheres.
- Northwest Greenland Eemian
  The extent of the Greenland during the last interglacial, the Eemian, is still unknown. The North Eemian Ice Core Project, or NEEM, is anticipating to find Eemian ice in Greenland, which will provide proof that the Greenland ice sheet existed during this warmer-than-today time period, and will provide new insights of the climate and environmental conditions in Greenland and globally.
- The IPICS 2,000 year array
  This focus group investigates the geographical variability of ice core records from Antarctica and Greenland to help interpret deeper records and to understand current climate variability, such as interhemispheric relationships and the timing and expression of the Little Ice Age. The suggested work is based on the efforts of the International Trans Antarctic Scientific Expedition, or ITASE, programme, which focuses on the past 200 years.
- New Drilling Technology
  Ice core research is a rapidly growing science branch that necessitates new technology to cater for new sampling requirements, such as directional drilling, drilling of the ice-bedrock interface, clean drilling technology, etc. This focus group provides a platform to share new developments and to prioritize technological needs.

Summary and conclusions

"Ice Cores provide the most direct and highly resolved records of (especially) atmospheric parameters for the last 1,000,000 years" (EPICA Community Members, 2004). Major scientific contributions of ice core research linked atmospheric temperature and greenhouse gas concentrations (Petit et al., 1999), and provided evidence that major climate swings can occur within less than 2.5 years (Steffensen et al., 2008). Large international collaborations, such as ITASE and IPICS, started to integrate ice core records from across the world and to prioritize the most important work for the ice core community. With new drilling and analytical technological developments and ever more new proxies and higher resolution records, ice cores have yet big stories to tell for the decades to come.

Bibliography

Alley, R. B., 2000. *The Two-Mile Time Machine*, 1st edn. Princeton: Princeton University Press, p. 229.

Alley, R. B., et al., 1997. Visual-stratigraphic dating of the GISP2 ice core: basis, reproducibility, and application. *Journal of Geophysical Research*, **102**(C12), 26, 367–326,381.

Aristarain, A. J., and Delmas, R. J., 1993. Firn-core study from the southern Patagonia ice cap, South America. *Journal of Glaciology*, **39**(132), 249–254.

Beer, J., et al., 1988. Information on past solar activity and geomagnetism from 10Be in the Camp Century ice core. *Nature*, **331**(6158), 675–679.

Bertler, N., et al., 2005. Snow chemistry across Antarctica. *Annals of Glaciology*, **41**, 167–179.

Blain, S., et al., 2007. Effect of natural iron fertilization on carbon sequestration in the Southern Ocean. *Nature*, **446**(7139), 1070–1074.
Boutron, C., and Lorius, C., 1979. Trace metals in Antarctic snows since 1914. *Nature*, **277**, 551–554.
Boyd, P. W., et al., 2000. A mesoscale phytoplankton bloom in the polar Southern Ocean stimulated by iron fertilization. *Nature*, **407**(6805), 695–702.
Broecker, W. S., 2000. Abrupt climate change: causal constraints provided by the paleoclimate record. *Earth Science Reviews*, **51**, 137–154.
Dansgaard, W., 1964. Stable isotopes in precipitation. *Tellus*, **16**, 436–468.
Delmonte, B., 2004. Dust size evidence for opposite regional atmospheric circulation changes over east Antarctica during the last climatic transition. *Climate Dynamics*, **23**, 427–438.
Delmonte, B., et al., 2004. Comparing the Epica and Vostok dust records during the last 220, 000 years: stratigraphical correlation and provenance in glacial periods. *Earth Science Reviews*, **66** (1–2), 63–87.
Dixon, D., et al., 2005. A 200 year sulfate record from 16 Antarctic ice cores and associations with Southern Ocean sea-ice extent. *Annals of Glaciology*, **41**, 155–166.
EPICA Community Members, 2004. Eight glacial cycles from an Antarctic ice core. *Nature*, **429**, 623–628.
EPICA Community Members, 2006. One-to-one coupling of glacial climate variability in Greenland and Antarctica. *Nature*, **444**, 195–198.
IPCC, 2007. *Climate Change 2007: The Physical Science Basis. Contribution of Working Group I to the Third Assessment Report of the Intergovernmental Panel on Climate Change. Summary for Policymakers*. Cambridge: Cambridge University Press, p. 21.
Johnsen, S. J., et al., 2001. Oxygen isotope and palaeotemperature records from six Greenland ice-core stations: Camp Century, Dye-3, GRIP, GISP2, Renland and NorthGRIP. *Journal of Quaternary Science*, **16**(4), 299–307.
Jouzel, J., et al., 1987. Vostok ice core: a continuous isotope temperature record over the last climatic cycle (160, 000 years). *Nature*, **326**, 403–408.
Jouzel, J., et al., 1997. Validity of the temperature reconstruction from water isotopes in ice cores. *Journal of Geophysical Research*, **102**(C12), 26, 471–426, 487.
Kang, S., et al., 2004. Seasonal differences in snow chemistry from the vicinity of Mt, Everest, central Himalayas. *Atmospheric Environment*, **38**(18), 2819–2829.
Kaspari, S., et al., 2008. Snow accumulation rate on Qomolangma (Mount Everest), Himalaya: synchroneity with sites across the Tibetan Plateau on 50100 year timescales. *Journal of Glaciology*, **54**, 343–352.
Keeling, C. D., 1997. Climate change and carbon dioxide: an introduction. *Proceedings of the National Academy of Sciences of the United States of America*, **94**, 8273–8274.
Keeling, C. D., and Whorf, T. P., 1994. Atmospheric CO_2 concentrations (ppmv) derived from in situ air samples collected at Mauna Loa Observatory, Hawaii. In Boden, T. A. et al. (eds.), *A compendium of Data on Global Change*. Oak Ridge: Carbon Dioxide Information Analysis Center, update. Available from http://cdiac.esd.ornl.gov/ndps/ndp001.html
Keeling, C. D., et al., 1976. Atmospheric carbon dioxide variations at Mauna Loa Observatory, Hawaii. *Tellus*, **28**, 538.
Kurbatov, A. V., et al., 2006. A 12, 000 year record of explosive volcanism in the Siple Dome Ice Core, West Antarctica. *Journal of Geophysical Research*, **111**.
Lambert, F., et al., 2008. Dust-climate couplings over the past 800, 000[thinsp) years from the EPICA Dome C ice core. *Nature*, **452**(7187), 616–619.
Legrand, M., and Mayewski, P. A., 1997. Glaciochemistry of polar ice cores: a review. *Reviews of Geophysics*, **35**(3), 219–243.
Legrand, M., et al., 1992. Large eruptions of ammonium and organic acids content in the Summit-Greenland Ice core. Fingerprint from Forest Fires? *Geophysical Research Letters*, **19**, 473–475.
Loulergue, L., et al., 2008. Orbital and millennial-scale features of atmospheric CH_4 over the past 800, 000(thinsp)years. *Nature*, **453**(7193), 383–386.
Luthi, D., et al., 2008. High-resolution carbon dioxide concentration record 650, 000–800, 000(thinsp)years before present. *Nature*, **453**(7193), 379–382.
Mayewski, P. A., and White, F., 2002. *The Ice Chronicles*. Hanover: University Press of New England, p. 233.
Mayewski, P. A., et al., 1993. Greenland ice core "signal" characteristics: an expanded view of climate change. *Journal of Geophysical Research*, **98**(D7), 12, 839–812, 847.
Mayewski, P. A., et al., 2004. Holocene climate variability. *Quaternary Research*, **62**(3), 243–255.
Mayewski, P. A., et al., 2005. The International Trans-Antarctic Scientifc Expedition (ITASE) – an overview. *Annals of Glaciology*, **41**(1), 180–185.
McConnell, J., et al., 2007. 20th-century industrial black carbon emissions altered Arctic climate forcing. *Science*, **317**(5843), 1381–1384.
Morgan, V., et al., 2002. Relative timing of deglacial climate events in Antarctica and Greenland. *Science*, **297**, 1862–1864.
Muscheler, R., et al., 2005. Geomagnetic field intensity during the last 60, 000 years based on 10Be and 36Cl from the Summit ice cores and 14C. *Quaternary Science Reviews*, **24**(16–17), 1849–1860.
O'Brien, S. R., et al., 1995. Complexity of holocene climate as reconstructed from a Greenland ice core. *Science*, **270**(5244), 1962–1964.
Osterberg, E., et al., 2008. Ice core record of rising lead pollution in the North Pacific atmosphere. *Geophysical Research Letters*, **35**.
Pales, J. C., and Keeling, C. D., 1965. The concentration of atmospheric carbon dioxide in Hawaii. *Journal of Geophysical Research*, **70**(24), 6053–6076.
Parrenin, F., et al., 2004. New modeling of the Vostok ice flow line and implication for the glaciological chronology of the Vostok ice core. *Journal of Geophysical Research*, **109**.
Petit, J. R., 1999. Climate and atmospheric history of the past 420, 000 years from the Vostok ice core, Antarctica. *Nature*, **399**, 429–436.
Petit, J. R., et al., 1991. Deuterium excess in recent Antarctic snow. *Journal of Geophysical Research*, **96**, 5113–5122.
Petit, J.-R., et al., 1999. Climate and atmospheric history of the past 420, 000 years from the Vostok ice core, Antarctica. *Nature*, **399**, 429–436.
Petrenko, V. V., et al., 2006. Gas records from the West Greenland ice margin covering the Last Glacial Termination: a horizontal ice core. *Quaternary Science Reviews*, **25**(9–10), 865–875.
Preunkert, S., et al., 2000. Col du Dôme (Mt Blanc Massif, French Alps) suitability for ice-core studies in relation with past atmospheric chemistry over Europe. *Tellus B*, **52**(3), 993–1012.
Rothlisberger, R., 2000. Technique for continuous high-resolution analysis of trace substances in firn and ice cores. *Environmental Science & Technology*, **34**, 338–342.

Schwander, J., et al., 2001. A tentative chronology for the EPICA dome Concordia ice core. *Geophysical Research Letters*, **28**, 4243–4246.
Schwikowski, M., et al., 1999. A high-resolution air chemistry record from an Alpine ice core: Fiescherhorn Glacier, Swiss Alps. *Journal of Geophysical Research*, **104**, 13709–13719.
Stager, J. C., and Mayewski, P. A., 1997. Abrupt early to mid-holocene climatic transition registered at the Equator and the Poles. *Science*, **276**(5320), 1834–1836.
Steffensen, J. P., 1997. The size distribution of microparticles from selected segments of the Greenland Ice Core Project ice core representing different climatic periods. *Journal of Geophysical Research*, **102**, 26755–26763.
Steffensen, J. P., et al., 2008. High-resolution Greenland ice core data show abrupt climate change happens in few years. *Science*, **321**(5889), 680–684.
Thompson, L. G., et al., 1995. Late glacial stage and holocene tropical ice core records from Huascaran, Peru. *Science*, **269**(5220), 46–50.
Thompson, L. G., et al., 2002. Kilimanjaro ice core records: evidence of Holocene climate change in tropical Africa. *Science*, **298**, 589–593.
Thompson, L. G., et al., 2003. Tropical glacier and ice core evidence of climate change on annual to millennial time scales. *Climatic Change*, **59**(1), 137–155.
Vimeux, F., et al., 2002. New insights into Southern Hemisphere temperature changes from Vostok ice cores using deuterium excess correction. *Earth and Planetary Science Letters*, **203** (3–4), 829–843.
Wolff, E. W., et al., 2006. Southern Ocean sea-ice extent, productivity and iron flux over the past eight glacial cycles. *Nature*, **440**(7083), 491–496.
Wolff, E. W., et al., 2009. Glacial terminations as southern warmings without northern control. *Nature Geosci*, **2**(3), 206–209.
Zielinski, G., et al., 1997. Volcanic aerosol records and tephrochronology of the Summit, Greenland, ice cores. *Journal of Geophysical Research*, **102**(C12), 26, 625–626, 640.

ICE COVERED LAKES

Lars Bengtsson
Department of Water Resources Engineering, Lund University, Lund, Sweden

Definition

Ice on lakes grows in a static way. Ice is produced as black ice, when heat is lost to the cold atmosphere from the water underneath the ice, or as snow ice, when the ice is suppressed under the water surface by heavy snow and water freezes in the slush layer in the snow on top of the ice.

Lakes at high latitudes or high altitudes are ice covered part of the year; typically from November through April and in the very north sometimes from October to early June. Arctic lakes may be ice covered throughout the year. When there is a regular ice cover for several months, the ice thickness reaches more than ½ m, as shown in the example in the figure from Luleå, Sweden. At mid-latitudes, occasional ice cover may appear for short periods several times during a winter. Where there is a stable ice cover, ice roads are prepared. Fishing is done also at commercial scale. Ice covered lakes are used for recreation.

Ice on a small lake is formed rather quickly after the surface water is cooled down to the freezing point – most often after a cold night with no wind. It takes much longer time for a large lake to freeze over than a small lake, since relatively warm water is brought to the surface during the more intense mixing in a large lake. Once ice is formed, it grows rather quickly the first weeks until the ice cover insulates itself and snow on the ice insulate the water from the atmosphere and the rate of ice growth is slowed down. The heat lost from the water to the atmosphere must be taken from the latent heat released when ice is formed, since the water just below the ice is at the freezing point. Balancing the ice formation at the underside of the ice cover and the heat conduction through the ice leads to the degree-day method, which well determines the ice thickness:

$$h = CS^{1/2}$$

$$S = \text{accumulated negative degree} - \text{days after the first thin ice is formed}$$

where the coefficient C is about 2 cm/(°C-day)$^{1/2}$, when there is snow on the ice and 3.5 cm/(°C-day)$^{1/2}$ for snow-free ice. As an example, after 1 month with −10°C and snow on the ice, the ice thickness should be 35 cm, and after 5 months with −10°C, 77 cm. The snow thickness on the ice is limited by the lifting force from the ice. From Archimedes' principle, the maximum snow cover is seen to be one third of the ice thickness, when the snow density is 0.3 relative that of water (common on ice some time after the snowfall) and half the ice thickness when the relative snow density is 0.2.

An example of ice growth is shown in Figure 1 from a bay in the Luleå archipelago (almost fresh water). The computed ice thickness using a degree-day approach is also shown.

Ice formed from the underside of the ice sheet has crystals with columnar structure; it is possible to see through the ice. Such ice is called black ice. Ice can also be formed in a slush layer between the snow and the top of the ice. When the weight of the snow is more than the lifting force from the ice, the ice cover is forced under the water surface and water enters into the snow, which becomes saturated with water. When this slush layer freezes, snow ice or white ice is formed. The crystals in this kind of ice are randomly distributed. The ice is like milk; it is not transparent.

The ice on a lake has ecological consequences. The water is insulated from the atmosphere. Due to heat flux from the sediments, the heat content of the water in an ice-covered lake slowly increases during winter. A warm bottom layer of close to 4°C is becoming thicker and

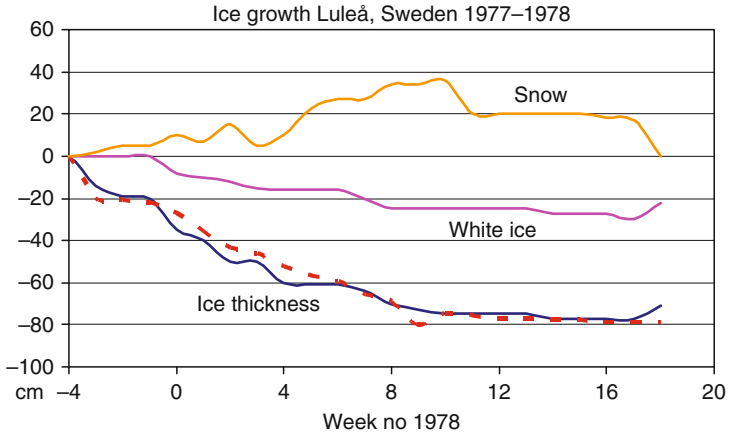

Ice Covered Lakes, Figure 1 Observed ice growth in the inner archipelago in Luleå, Sweden. Snow depth on the ice is shown and, separately, the snow ice growth. The *dotted line* is the computed ice thickness using a degree-day approach. Measurements by the author.

thicker. Since there is no exchange with the atmosphere, the oxygen content of the water decreases and the bottom layers may be completely depleted. The circulation in an ice covered lake is very much reduced as compared to ice-free conditions. There is no wind-driven circulation. However, slow back and forth seiche movements are initiated by the wind acting on the ice cover giving rise to some dispersion near the ice. The heat flux from the sediments causes large-scale very slow convection. In spring, when the ice is free from snow, solar radiation may penetrate through the ice and induce convective mixing of the top few meters.

Man's impact on lake ice is mainly from release of oxygen consumption substances, which increases the rate at which the lake water is depleted in oxygen. All releases from industries and waste water treatment plants and also the increased winter flows in regulated rivers have local effects on the ice cover.

Bibliography

Adams, W. P., 1981. Snow and ice on lakes. In Gray, D. M., and Male, D. H. (eds.), *Handbook of Snow*. Canada: Pergamon, pp. 437–474.

Korhonen, J., 2006. Long-term changes in lake ice cover in Finland. *Nordic Hydrology*, **37**, 347–363.

Lepparanta, M., 1983. A growth model for black ice, snow ice and snow thickness on subarctic basins. *Nordic Hydrology*, **14**, 59–70.

Cross-references

Circulation and Mixing in Ice-Covered Lakes
Heat and Mass Transfer in Sea Ice
Physical Properties of Snow
Thermal Regime of Ice-Covered Lakes

ICE DAMS

Mahendra R. Bhutiyani
Hazard Assessment and Forecasting Division, Snow and Avalanche Study Establishment, Chandigarh, India

Definition

Ice dams are the temporary reservoirs of impounded meltwater formed in glacierized river basins.

Origin

They owe their origin to either the "retreating" glaciers or the "surging" glaciers (with abnormally high velocities). Smaller glaciers with narrow valleys while retreating in response to warming climate leave behind large mounds of inactive end or terminal moraines in the valley. They act as a barrier or a wall resembling a dam to the flow of the glacier stream. Meltwater accumulates and gradually a reservoir builds up in the upstream direction (Figures 1 and 2), exerting significant hydrostatic pressure on the structure. Failure of such fragile dams may sometimes lead to disastrous flash floods (Figure 3). Depending upon the situation, such floods are also known as glacier lake outburst flood (GLOF). There have been many incidences of such floods in the Himalayas. Similar dams are also formed when smaller "surging" glaciers in the transverse valleys move rapidly to such an extent that they block the main longitudinal valley and obstruct the flow of its meltwater stream (Figure 4). An ice dam thus formed is also subjected to large hydrostatic forces due to the buildup of a large reservoir upstream.

Ice Dams, Figure 1 A typical retreating glacier with a formation of an ice dam.

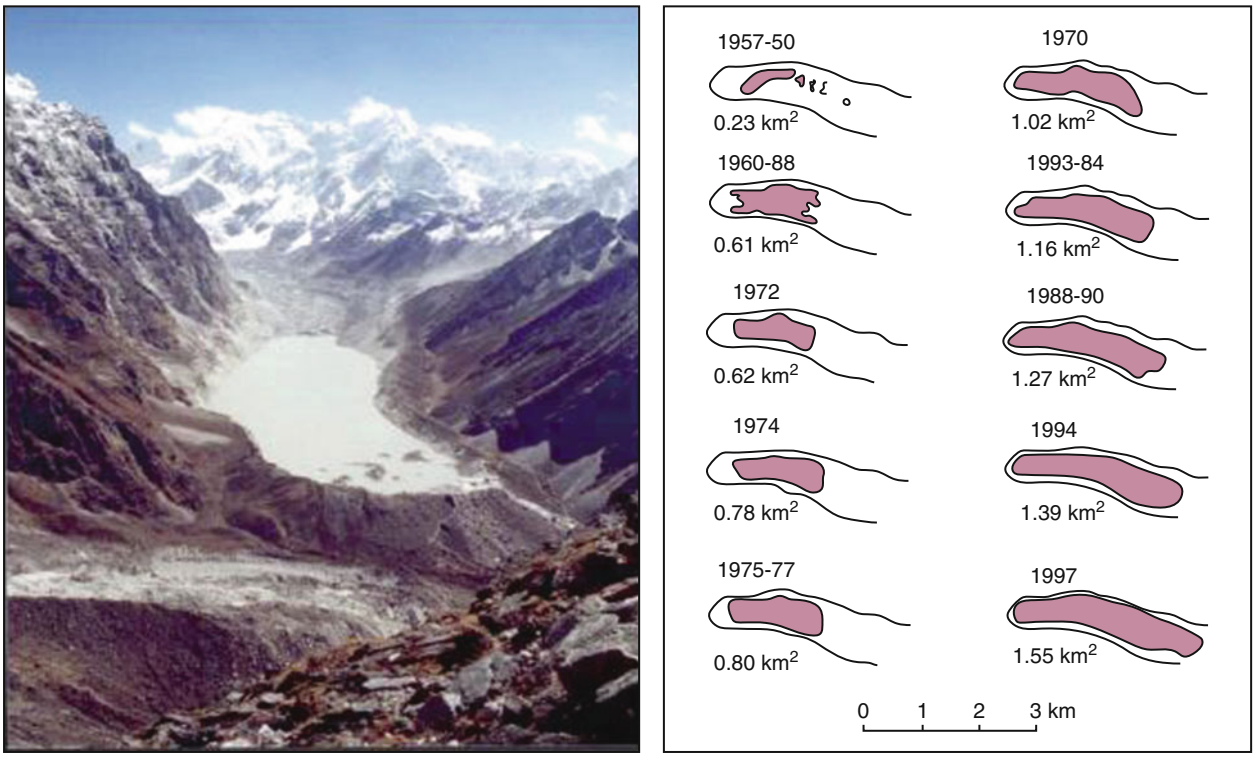

Ice Dams, Figure 2 This NASA image shows the formation of numerous glacial lakes at the termini of receding glaciers in Bhutan Himalaya.

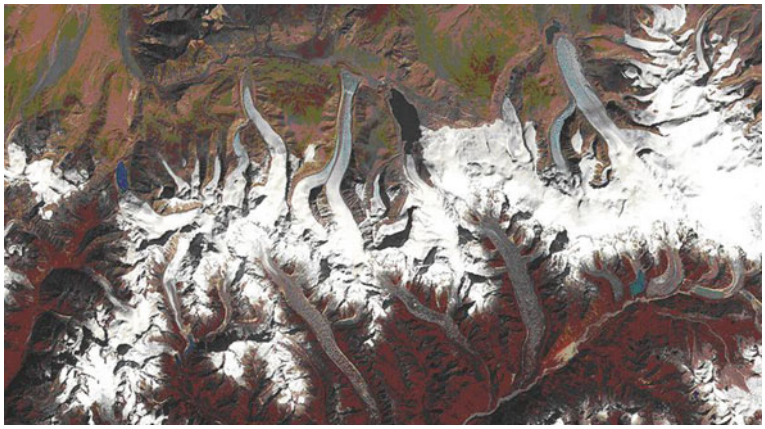

Ice Dams, Figure 3 Growth of potentially dangerous ice dam in Nepal Himalaya.

Ice Dams, Figure 4 Google Earth (2007) slanted view of Thangman Glacier – a "surging" glacier in the Karakoram Himalaya with a potential to form an ice dam upstream.

Significance

Failure of these dams has given rise to number of disastrous glacier meltwater flash floods in the Himalayas, the Alps, and the Rocky Mountains.

ICE SHEET

Alastair G. C. Graham
Ice Sheets Programme, British Antarctic Survey, Cambridge, UK

Definition

Ice Sheet. A perennial mass of glacier ice, and snow, that covers surrounding terrain and that has an area greater than 50,000 km^2 (19,305 miles^2) (after Armstrong et al., 1973).

Introduction

The two remaining polar ice sheets are the largest single bodies of ice and snow on the planet, covering 3% of the Earth's surface – the surface areas of Greenland and Antarctica measure 1,710,000 and 14,000,000 km^2, respectively (Figure 1). They act as important stores for over 80% of the world's fresh water (Bamber et al., 2007). The water trapped in Antarctica's ice sheet alone would fill Lake Superior 2,000 times over, and has the capacity to raise global sea level by up to ~61 m, if it were to melt fully.

Both the Antarctic and the Greenland ice sheets have, however, a longevity that belies their fragile composition. Ice has been present in some form at the poles for at least 5 Ma, with a year round ice cover on East Antarctica since at least 14 Ma, and has survived many periods of global change – even periods when the Earth was

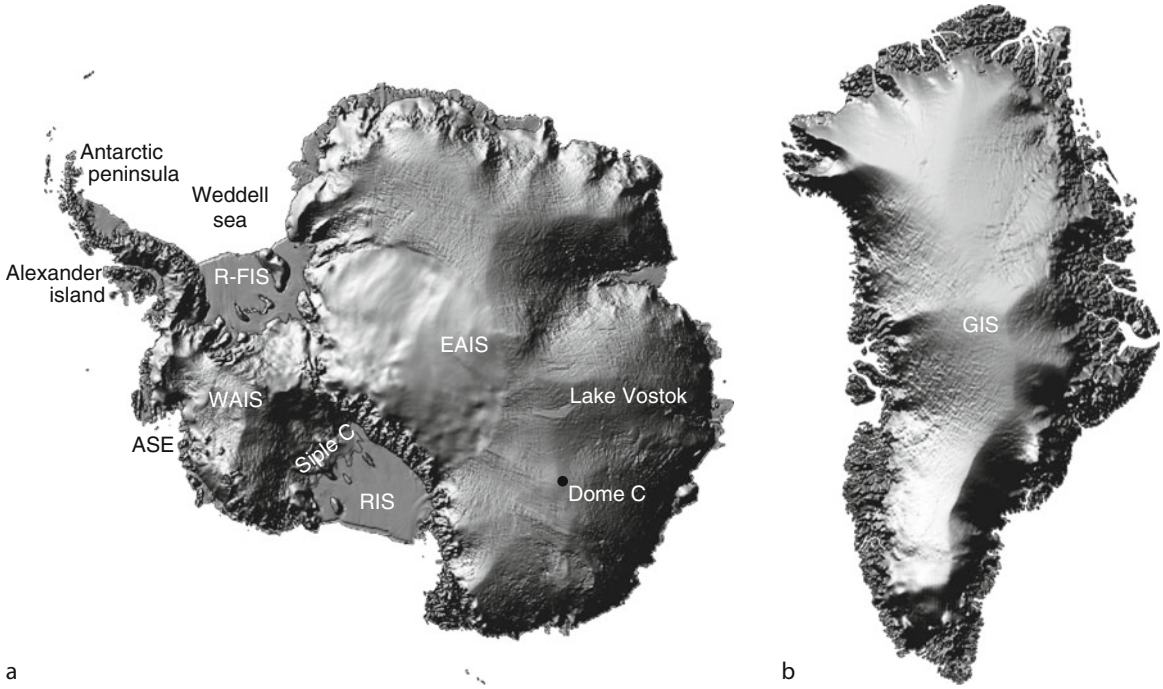

Ice Sheet, Figure 1 Digital elevation models (DEMs) of the two remaining polar ice sheets, shaded to highlight their topography and form. (**a**) Antarctic surface topography DEM from Liu et al. (1999). (**b**) Greenland surface topography DEM extracted from the ETOPO2v2 2-min gridded global relief dataset (http://www.ngdc.noaa.gov/mgg/fliers/01mgg04.html). Key locations discussed in the text are labelled: *ASE* – Amundsen Sea Embayment; *RIS* – Ross Ice Shelf; *Siple C* – Siple Coast ice streams; *R-FIS* – Ronne Filchner Ice Shelf.

warmer than it is at present. Despite this proven resilience and their truly "glacial" rates of response, ice sheets are surprisingly dynamic on the geological-timescale, responsive to their external environment over both long timeframes; for example, the tens of thousands of years over which the orbit of the Earth around the Sun alters; and the rather shorter timescales; for example, the daily cycles manifested in the tides of Earth's oceans. Ice sheets are important features within the global climate and ocean systems and with the potential to produce widely felt impacts well outside the polar regions. An improved understanding of their behavior and interactions is, therefore, urgently required by those scientists involved in trying to predict the future climate of Earth.

Indeed, in the last decade, observations of change in both ice sheets, made possible by a new generation of sophisticated Earth-observing satellites, has demonstrated that ice sheets may be more sensitive to change in their surroundings than previously thought. This implies that particularly vulnerable parts of both ice sheets may be threatened by even relatively small perturbations in climate. The future increase in mean global temperature, caused by anthropogenic warming, which is projected to rise an average of 3°C by the end of the twenty-first century (the Intergovernmental Panel on Climate Change [IPCC], 2007), may have severe and irrevocable consequences for polar ice masses. Indeed, the past 30 years have already seen major and apparently rapid changes occurring in the polar ice sheets, perhaps as a consequence of the "greenhouse effect." In response to this warming, the demise of polar ice sheets would have damaging repercussions, not only for the environment, but for society and the economy (Stern, 2006). As a result, understanding the physical processes in polar ice sheets, their geological setting, the potential for their future change, and possible collapse, have become leading questions for climate policymakers (IPCC, 2007), the media and society (e.g., Gore, 2006), and polar scientists alike.

This entry provides an overview on the subject of ice sheets and ice sheet change, offering an introduction to their physical and glaciological character from an Earth Science perspective. This entry introduces some concepts of growth, flow, and loss, before describing the form and features of ice sheets. We consider the shift in focus of ice sheet research over the years, and illustrate some of the changes underway in the polar ice sheets today. We frame these against evidence for changes in former ice masses from the geological record, and conclude by discussing the future of the modern ice sheets on the planet.

Physical and glaciological character

Ice sheets describe the vast, contiguous masses of ice that form the Earth's two largest glacial bodies (Figure 1): the Greenland Ice Sheet (GIS), and the Antarctic Ice Sheet, which in itself comprises three unique provinces: the West Antarctic Ice Sheet (WAIS), Antarctic Peninsula Ice Sheet (APIS), and East Antarctic Ice Sheet (EAIS). In their broadest context, the ice sheets are linked to the climate of Earth through a complex and intricate ice–ocean–atmosphere circulation system, which regulates the movement of heat, water, and ice in both hemispheres, and at both poles (Figure 2). Our understanding of the physical changes in ice sheets (and indeed in any glacier or ice cap) is built around these climate systems and specifically the concept of steady-state ice flow (see also *Atmosphere-Snow/Ice Interactions*).

Each year, ~7–8 mm of water from the surface of the world's oceans enters the polar ice sheets as snowfall. If this buildup of ice was not returned to the ocean in some way, sea levels would fall by ~8 cm every decade, while the ice sheets would continue to grow to impracticable sizes. Glacial flow is the mechanism that regulates the size of the ice sheets, ensuring the amount of ice gained is compensated by ice lost. A "steady state" is achieved, in principle, where the input and output of ice is exactly equal. The fine balance that exists between this input and output – known as mass balance (see also *Glacier Mass Balance*) – ultimately influences whether an ice sheet grows or shrinks (Figure 2). In today's polar ice sheets, the repeated growth and loss of ice has resulted in the ice sheets achieving a sensitive balance between their input and outflow; almost to the point of "steady" equilibrium. However, the many billions of tons of ice that enters and leaves the AIS and GIS each year results in parts of the ice sheets being surprisingly responsive, and to even the smallest of imbalances. Assessments of the state of the ice sheets, both now and in the future, are important because mass balance and thus

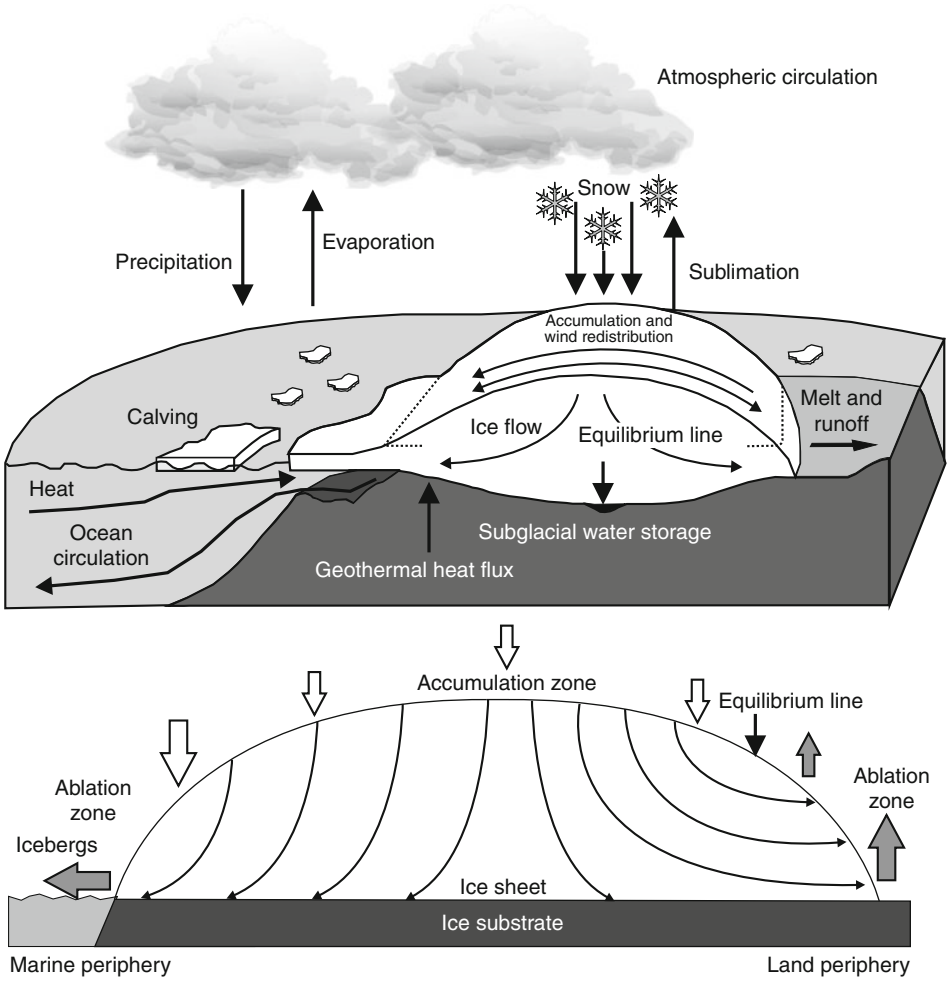

Ice Sheet, Figure 2 Schematic illustrations of the Earth's ice–ocean–climate system, and the various components involved in determining ice sheet mass balance. *Top* schematic redrawn and modified from US Global Change Research Program (http://www.usgcrp.gov; last visited 20/04/2009), *bottom* schematic redrawn and modified from Siegert (2007).

ice volume is a major control on global sea level. The growth, flow, and loss in ice sheets are the fundamental mechanisms for understanding how imbalances may occur.

Ice sheet growth, flow, and loss

An ice sheet builds mass at its surface by deposits of snowfall and frost, which, because of the persistent cold environment, do not melt but amass year-on-year in the accumulation zone (Figure 2). Gradual compression and packing of surface snows, as they are buried by the weight of new snowfall, eventually transforms them into solid ice, at depth (see *Transformations of Snow at the Earth's Surface and its Climatic and Environmental Consequences*). At a critical mass, gravitational forces lead the ice sheet to move, which it does so as an ultra-viscous fluid. The general domed topography of ice sheets dictates that most of this ice is driven toward the ice sheet exterior, where it is lost in the ablation zone, or at the ice margin where the ice sheet meets the ocean (Figure 2). The flow of ice is initiated because of differences in pressure caused mainly by the ice-surface slopes, which result in the ice sheet being held under permanent strain, in response to applied stress. Normal and shear stresses cause motion in the ice sheet, through a combination of deformation of the ice, deformation of the ice substrate, and sliding at the ice-bed interface. Other conditions impart a resistance against ice flow, and include physiographic factors such as roughness at the bed, as well as glaciological factors; for example, through buttressing from floating ice shelves.

The Equilibrium Line Altitude (ELA) is the boundary dividing the areas of net growth and net loss in the ice sheets (Figure 2). Its position is an important gauge of ice sheet balance and therefore "state." Ice accumulates in the area of the ice sheet above the ELA, where the precipitation rates, elevation, and surface area of the ice sheet determine net growth. The great size, cold conditions, and overall form of the ice sheets help create unique microclimates in their inland centers, which allow them to continually regulate their mass balance. In contrast, expanses of the ice sheet beneath the ELA are exposed to greater melting and to net loss. Forced changes in the position of the ELA, whether natural or human-induced, can tip the balance in favor of ice growth or decay accordingly.

In both polar ice sheets, fringing glaciers provide the main outlets for ice flow to drain to the exterior, and most mass loss can be attributed to these arterial drainage components (Figure 3). In marine ice sheets such as the WAIS that have margins terminating straight into the ocean, when the flow of glacial ice eventually reaches the sea it either calves off as icebergs or melts directly into coastal waters (Figures 2 and 3). Melting at the ice sheet fringes can be enhanced externally, by the heat transfer from ocean waters feeding the underside of the floating portions of the ice sheet (ice shelves), and delivering warmer water to the ice sheet grounding line (the line or zone at which an ice mass entering a water body begins to float). The contrasting example is a terrestrial ice sheet, like that of Greenland, where most of the ice is grounded upon dry land, and where most ice loss occurs by a combination of melt-out, runoff, and surface ablation (Figure 2).

Marine and terrestrial ice sheets

The way mass balance changes are manifested in an ice sheet, and the resulting dynamics of that ice, are both strongly influenced by the physiography of the bed buried beneath several hundreds of meters or kilometers of ice. Indeed, the flow and stability of an ice sheet grounded in a marine versus a terrestrial setting is quite different e.g., (Figure 2).

The beds of the WAIS and parts of the EAIS lie well below sea level today, meaning the ice sheet above is marine-based (Figure 4). With a base below sea level, the WAIS is anchored to its sole only because it is too thick to float off. Marine ice sheets are thus inherently unstable

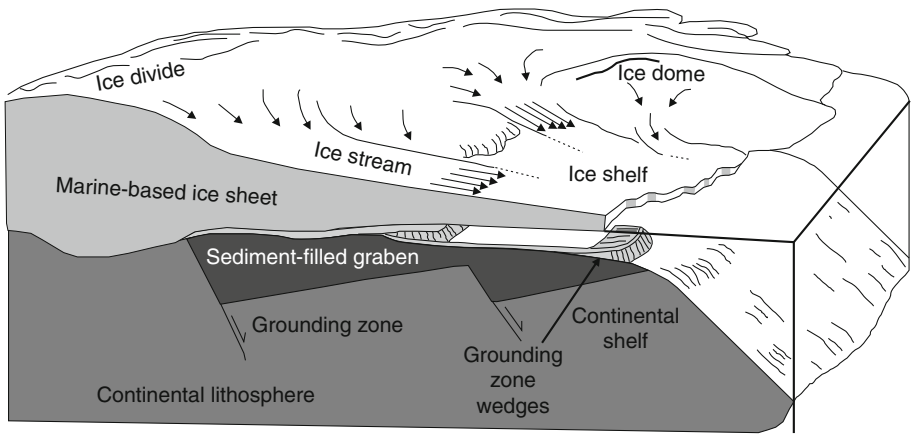

Ice Sheet, Figure 3 Schematic illustration of the geological setting and glaciological components of a marine-based ice sheet, such as the West Antarctic Ice Sheet. Note the ice centers and ice domes drained by well-defined ice streams, which in turn, feed floating ice shelves at the ice sheet periphery. After http://icesat.gsfc.nasa.gov/science.php (last visited 20/04/2009).

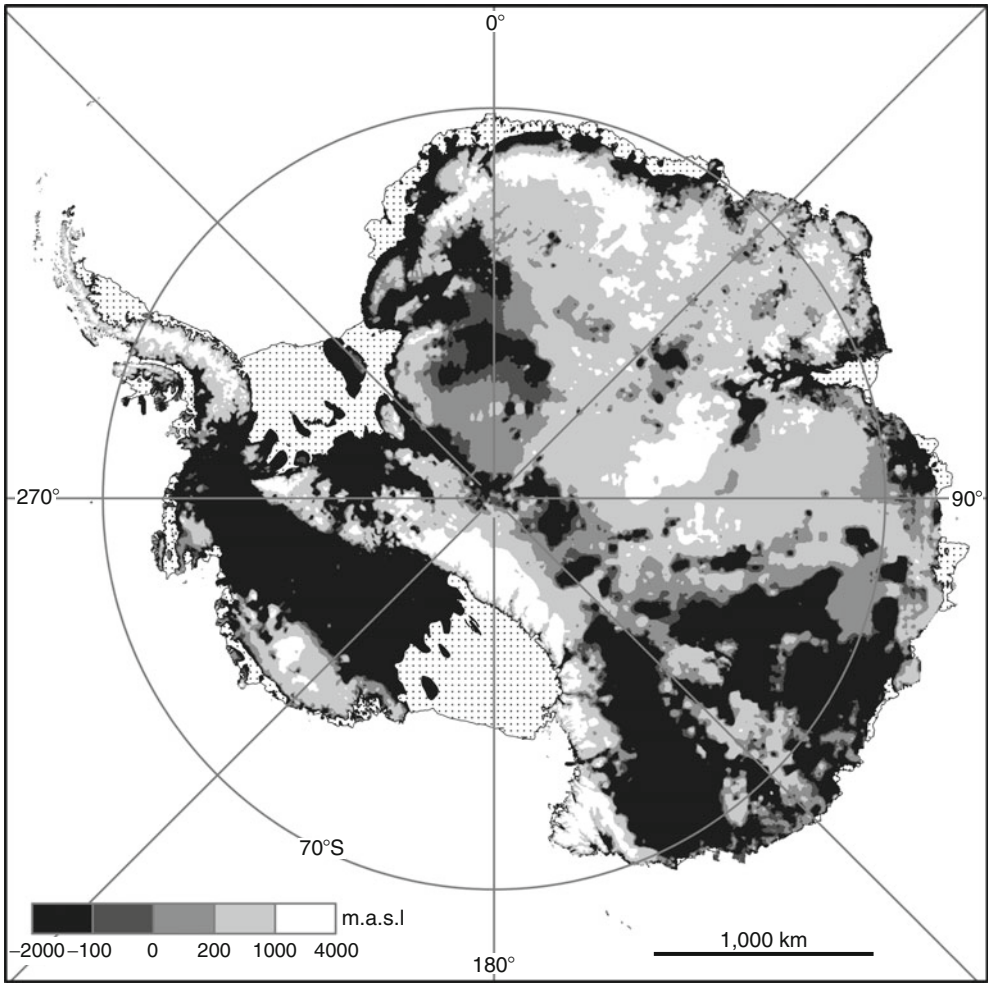

Ice Sheet, Figure 4 Map of the bed topography beneath the Antarctic Ice Sheet in relation to modern-day sea level. The basins of West and East Antarctica shaded black have a bed well below sea level and are therefore susceptible to rapid deglaciation. M.a.s.l. (meters above sea level). Drawn from the BEDMAP dataset (Lythe et al., 2001). Ice shelves are denoted by stippled shading.

as they come into direct contact with the ocean, and because changes in their mass can effect their buoyancy.

Marine ice is especially unstable where the ice sheets have beds that slope inland. On a back-sloping base, even small amounts of ice thinning or increases in outlet-glacier velocity can trigger a positive feedback in retreat of the grounding line. Initial retreat inevitably leads to further flow enhancement and loss because, while the ice sheet may be retreating, the thickness of the ice at the grounding line and the gradient of its surface profile both increase inland (Schoof, 2007; Vaughan and Arthern, 2007). The increasing negative imbalance resulting from this feedback far outweighs the ability for the ice sheet to be replenished by new snowfall, and runaway "collapse" (i.e., rapid deglaciation) of the marine parts of the ice sheet is therefore possible under these conditions.

A terrestrial ice sheet has few areas of ice grounded below sea level at its margins meaning the ice sheet is essentially buffered against a similar marine collapse. Instead, warming from the atmosphere above, or from the substrate beneath the ice sheet, are the most important controls on terrestrial ice sheet balance. These factors influence the position of the ELA on the ice sheet, and the conditions of ice flow within it. Unlike marine ice, rapid deglaciation of terrestrial ice sheets is really only achievable where warming raises the ELA sufficiently so that growth of the ice sheet is no longer possible without significant global cooling.

Form and features

Whether marine- or terrestrial-based, ice sheets can usually be considered in terms of a number of unifying glaciological components. The drainage characteristics described herein are important for ice flow and form, and for assessing ice sheet changes (Figure 3).

Inland ice sheet: slow-moving centers

The centers, or inland parts of the polar ice sheets are amongst the driest, coldest, and most inhospitable places on Earth. They are also the slowest moving and most stable parts of an ice sheet. Major ice divides characterize this zone, segregating individual ice domes, and delineating the first-order ice drainage basins (see also Figure 5). The surface character of the inland ice sheet is generally flat and featureless over vast expanses, although in places wind-blown dunes (sastrugi) form ridge-troughs in the direction of prevailing winds, causing small-scale roughness elements in the upper layers of the snow cover (Figure 6a).

Beneath parts of the Antarctic interior, vast mountain ranges have been imaged and mapped (e.g., the Gamburtsev mountain range), which serve as major obstacles for ice flow, and which strongly influence the broad-scale ice dynamics of the overlying ice sheet. These ranges offer insight into how the ice on Antarctica was first conceived, and have been the targets of recent pioneering, multidisciplinary survey campaigns in inland East Antarctica.

Recent observations beneath these interior zones have also identified the importance of ice sheet centers for subglacial hydrology. Pools of trapped water beneath the ice – subglacial lakes – imaged by radar, exist toward the center of ice sheets, often near to ice divides, and exploit topographic lows or tectonic boundaries. These form key components within an interconnected network of channels and isolated basins that make up a complex subglacial hydrologic system. Water is now known to move between these pools and along ice-flow pathways abruptly and in massive quantities, demonstrating a dynamic side to ice sheets that was previously unknown. More important to ice sheet change perhaps, is the recent realization that subglacial lakes can significantly alter the dynamics of overlying ice by enhancing ice flow in the upstream reaches of ice sheet drainage outlets (e.g., Bell et al., 2007). The lakes can instigate acceleration in downstream ice because, above the lake, the basal stress of the ice sheet is reduced to zero. Lakes can also alter the subglacial thermal regime of ice sheets by warming the ice over the lake, due to the heat released during processes of accretion. Both processes may cause ice to remain unfrozen to its bed downflow.

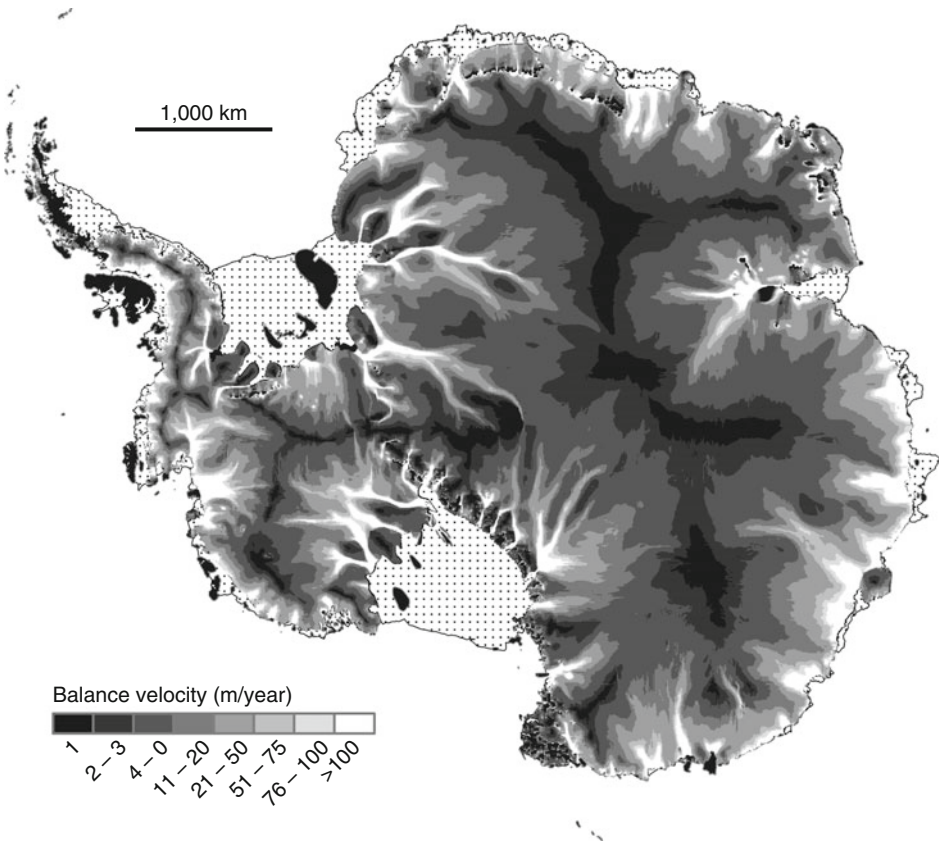

Ice Sheet, Figure 5 Balance velocity map for the Antarctic Ice Sheet inferred from satellite datasets (after dataset in Bamber et al., 2000). The map shows the distribution of ice divides as areas of low velocity (black to dark-gray), and inter-fingering networks of high-flux, faster-flowing ice streams (light-gray to white). Ice shelves are denoted by stippled shading.

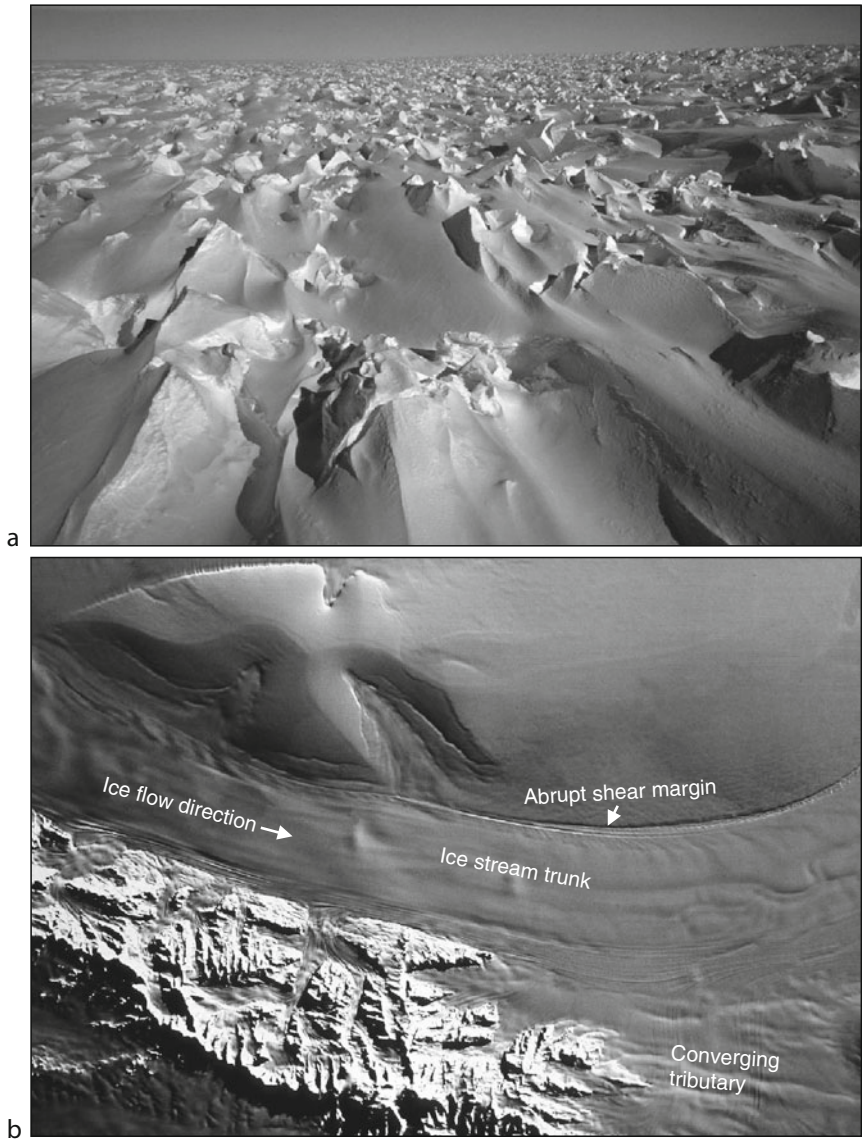

Ice Sheet, Figure 6 (**a**) Photograph of the inland part of the Antarctic Ice Sheet, showing wind-blown dunes (sastrugi) on the ice surface (image from BAS photo database), (**b**) A Landsat image of the Rutford ice stream, illustrating its fast-flow trunk, distinct shear margin, and converging tributaries at onset (image from BAS photo database). Width of the main ice stream trunk is c. 26 km.

The largest known subglacial lake, today, is Lake Vostok in East Antarctica (Figure 1; c. 14,000 km^2 in area). Vostok lies beneath one of the thickest parts of the ice sheet – as thick as the largest peaks of the Rocky Mountains are high. The lake is associated with a rather prominent morphological surface feature in that the ice sheet surface over the lake is flat and featureless, resembling the upper plain of an ice shelf. Up to 280 subglacial lakes have now been recognized beneath the AIS based on similar surface observations (Siegert et al., 2005; Wingham et al., 2006; Smith et al., 2009), as well as detailed characterization and classification of the ice sheet bed from airborne and satellite datasets. It is likely that many more subglacial lakes remain to be discovered at the poles.

Ice streams: outlets of fast flow

Whether enhanced by an underlying subglacial lake, or simply driven by the force of gravity, the transfer of ice from the "static" interior to the ice exterior is a key process in all ice sheets. Calculations of the polar ice sheets' balance velocity – the velocity required to maintain ice sheet steady state at each given point on the ice sheet – show

that this process is not uniform around ice sheet edges (Figure 5; Bamber et al., 2000). Indeed, more than 50% of the outflow from the AIS passes through just 40 of its largest outlets – pathways of restricted, faster glacier flow, termed ice streams (Figures 3, 5, and 6b). These streams represent the transition from interior flow to marginal or ice-shelf spreading, and serve to focus ice drainage (as well as water and sediment drainage) toward the coasts or ice sheet periphery, acting as large conveyer belts that deliver ice from centers of accumulation to areas of loss (Figures 3, 5, and 6b).

Maps of the balance flux of the ice sheets also show that ice streams originate from the ice sheet cores, and gradually increase in velocity downstream along their length (Figure 5). Flow speeds in the main trunks of some of the major Antarctic ice streams have been measured in a range from about 100 to more than 2,000 m year^{-1} (e.g., Pine Island Glacier), faster than the surrounding ice in which they are emplaced by a factor of 100 or more (Truffer and Echelmeyer 2002). As a result, the highest ice flux rates focus along these pathways (Figure 5), and it is of little surprise that they have been described as the arteries of an ice sheet (Figures 5 and 6b; Bennett, 2003). Accountable for 90% of drainage in the AIS, ice streams are, therefore, inextricably linked to the amount of ice lost and thus an ice sheet's mass balance.

Ice flow within ice sheets, let alone within their ice streams, cannot be explained by gravitational force alone. The flow of ice streams is therefore made possible, and enhanced, by their flow within sediment-filled subglacial valleys or across regions of subglacial meltwater (Bell et al., 1998; Studinger et al., 2003; Peters et al., 2006). The latest observations have demonstrated that many of the changes in ice sheets originate in, and radiate from, channelized ice streams or outlet glaciers. Hence, ice streams have received a lot of recent attention as the regulators of flow in ice sheets. A case in point are the extensive field campaigns that have taken place, in recent years, along the Siple Coast of West Antarctica (Figure 1; Alley and Binschadler, 2001), aimed at better understanding the role of ice streams in ice sheet change. Ice streams in this region appear to be capable of rapid changes, including migration within the ice sheet (Fahnestock et al., 2000), and abrupt "switch off," as observed in the case of Ice Stream C (Rose, 1979). An interesting conclusion stemming from the Siple coast studies is that ice stream behavior may be nonlinear, in so much that ice streams may be difficult to predict and more prone to rapid change than current estimates suggest.

Borne out of these detailed studies, much of the nonlinearity observed in ice streams in recent times (e.g., rapid changes) may have its roots in the operating conditions at the ice-bed interface. Investigations into the rheology of ice stream beds and the basal conditions beneath ice streams have become major research emphases because our current knowledge of subglacial processes and drainage is poor.

Through methods of bed characterization (e.g., from seismic data), direct sampling (e.g., from boreholes), and state-of-the-art computer modelling, there is now a general consensus that ice streams flow via a combination of traction and sliding over a thin (meters-thick) layer of deformable debris, which is water-saturated at the bed. Physical measurements on the till – the mixed carpet-like layer of mud and debris commonly found at the base of glaciers – beneath Antarctica's ice streams, showed low yield stress associated with a high pore pressure in the sediments (Boulton and Hindmarsh, 1987; Kamb, 1991). The physical character of this "weak" dilated subglacial layer is now known to enable the ice to flow faster in ice streams than over surrounding terrain, and may also contribute to their unstable behavior.

Ice shelves: floating margins

A final component of flow occurs exclusively at the mouths of marine ice streams or outlet glaciers, where it is common to find an adjoining tongue of floating ice, an ice shelf, that remains permanently attached to the grounded ice sheet (Figures 2, 3, and 5; see *Ice Shelf*). Vast plateaus of flat, floating shelf ice are well developed today in Antarctica, in the Ross Sea and Weddell Sea, while smaller ice shelves fringe the glaciers that drain much of East Antarctica, and along both coasts of the Antarctic Peninsula (Figure 5, stippled shading). While physically dissimilar to much of the grounded part of the ice mass, ice shelves are best considered as part of this system, because they play an important role in an ice sheet's flow configuration. We shall examine the exact reasons for this a little later.

History of measuring change in ice sheets

The interiors, ice streams, and ice shelves of the polar ice sheets have not always been so well understood however. Although ice sheets have been centers of scientific investigation since the late eighteenth century, the early explorers of the high latitudes were intent on exploration, and it is only the more recent generation of targeted survey and measurement that has led to a better understanding of ice sheet processes and their ability to change.

A scientific focus on the polar territories did not emerge until the 1957–1958 International Geophysical Year, which directed science questions at ice sheets for the first time. Even so, up until about 30 years ago, measurements on the ice sheets themselves were still few, confined to only a limited number of traverses across the ice interiors. Even in the 1970s, large parts of the poles remained uncharted and still appeared as empty white space on maps.

The major difficulty in filling these white spaces was that the ice sheets could still only be mapped using in situ data and represented local measurements at single points in time (e.g., seismic shots for ice-thickness soundings; Behrendt, 1998). In monitoring the ice itself, these methods offered little in the way of appreciation for

how the ice sheets might be changing over the years. Furthermore, with a ground perspective rather than a continent-wide view of the ice sheets, it remained virtually impossible to connect observations in one part of an ice sheet with those in another.

Recent improvements in the way ice sheets and their various changes can be measured, both upon and within the ice sheets today, and offshore from the geological records of the past, have vastly improved knowledge of ice sheets and their climate links. The last decades, in particular, have witnessed the birth of new technologies, which allow remote sensing of ice sheets from the air and from the space (Figure 7). Coupled with rapidly improving logistical access to the poles, this capability has revolutionized our understanding of ice sheets and their response to future change.

New technologies for studying ice sheets

Satellite radar interferometry is perhaps the most surprising and innovative tool that has been directed toward ice sheet understanding. It has revolutionized knowledge of ice motion in the polar regions (Figure 7) and is capable of detecting ice-flow rates, and even the subtle transition from grounded to floating ice. With the launch of ERS-1 in 1992, ERS-2 in 1995, and Radarsat-1 in 1997, maps of ice motion on Greenland and Antarctica have been produced with a coverage that makes ice-sheet-wide interpretations now possible. Similar to interferometric technology, satellite altimeters, which measure changes in the surface elevation of the ice sheets, are now so precise that they can yield maps of even the very small changes in ice-surface profile, to as little as 1 cm year^{-1}. By tracking changes in both elevation and dynamics over time, changes in the "state" of the ice sheets can be measured in detail.

Prior to these satellite capabilities however, and as late as the early 1990s, assessments of input versus output of ice from the polar ice sheets, based on direct measurements of snow accumulation and rudimentary calculations of ice loss, revealed no measurable "imbalance" in their state. In other words, until very recently, the ice sheets did not appear to be changing appreciably – if anything, the ice sheet in Antarctica appeared to be slowly gaining net mass (Bentley, 1993). However, these older assessments contained some significant uncertainties, with the smaller coastal systems of the ice sheets specifically understudied.

More recently, near-complete maps of the velocity of Greenland glaciers were assembled using Radarsat-1 data, and employed to calculate ice discharge and mass balance of the entire GIS. Results were surprising, indicating that the mass loss from the GIS had actually doubled in the decade between 1996 and 2006 (Rignot and Kanagaratnam, 2006). In Antarctica, both ERS-1/2 and Radarsat-1 data were also used to map ice velocity across ~85% of the coastline. A picture of dynamic and rapidly changing sectors of Antarctica emerged, revealing slow rates of thickening in some parts of the ice sheet, as predicted, but unexpected rapid rates of thinning in others. Particular focus in these studies was directed at the coastal areas, and it is here where the ice sheets' changes now appear to be most significant (Pritchard et al., 2009).

As well as satellite datasets of surface change and flow rates, advanced over-snow and airborne methods have made it possible to quickly and accurately derive a range of detailed ice-flow parameters, including ice thickness and flow velocity (Figure 7). These methods have offered a new way to analyze the bed of ice sheets that were impenetrable by more conventional methods, and have led to a much-improved understanding of processes

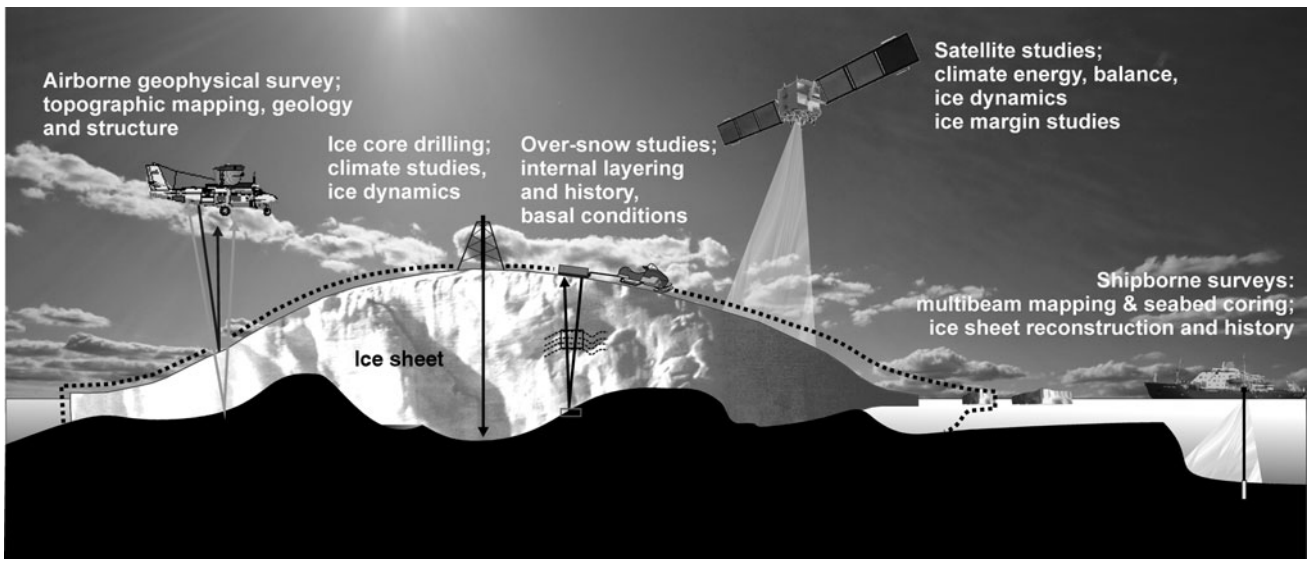

Ice Sheet, Figure 7 Cartoon illustrating the various technologies employed in modern-day ice sheet surveys.

occurring at the ice-bed. Radio-echo sounding (RES) constitutes a main technique by which glaciologists have investigated the subsurface properties of the polar ice sheets (Bingham and Siegert, 2007). Using RES, the internal layering of the ice sheets can be imaged to resolve local dynamics, helping to understand englacial and subglacial processes, and the histories of change in flow configuration. Ice-penetrating radar and seismic data have also been used widely to derive information on basal mechanics in different parts of the ice sheet, showing the presence of water or saturated sediments at the bed, and characterizing the mechanics of ice motion over its substrate (e.g., Smith and Murray, 2009). These are important components in understanding the processes of ice flow and the mechanisms that might lead to ice sheet change, at the scales witnessed by the satellites.

Better shipboard mapping and sampling techniques have also revealed a greater understanding of the history of ice sheets, from the offshore geological record. Shipborne multibeam echo sounders have replaced single depth-soundings as the most effective way of mapping the seafloor (Figure 7). These sonars measure bathymetry from a large footprint of the seabed allowing now-submerged former ice-beds to be mapped in near real-time, and at a high resolution. Coring of seabed deposits from ships capable of breaking sea-ice in areas once covered by, or which lay adjacent to, past ice sheets enables archives of glacial change to be obtained from the stratigraphic records of sediments that have accumulated slowly through time (Figure 7).

Around Antarctica, geomorphological features generated by ice sheets and sediments deposited at their base provide insights into former ice-bed conditions and flow directions. They act as indicators of past ice retreat that show how paleo-ice sheets once behaved and how they have changed through geological history.

Recent advances in the dating methods applied to samples and sediment sequences recovered from these environments have also significantly improved our ability to date long-term, geological-timescale changes in ice sheets. These include new radiocarbon techniques on marine sediment cores, designed to date histories of ice retreat while removing the problems that commonly arise from the reworking of older carbon-bearing sediments by glaciers (Schrum et al., 2006; see *Dating Glacial Landforms*). Independent records of relative paleomagnetic intensity are also being used to date stratigraphic sequences that lack carbonate material suitable for radiocarbon analysis. Most recently, land-based cosmogenic isotope dating has emerged as a key tool in calculating the length of exposure time since glacial erratics and regions of bedrock last became ice-free. Cosmogenic dating is now an essential technique for assessing rates of long-term thinning in presently glaciated areas. Importantly, the information from paleo-records has been influential in framing the recently observed twentieth- and twenty-first-century ice sheet changes against a picture of long-term geological rates of ice sheet retreat; the two are clearly at odds with one another, as we will go on to show.

Ice-age theory to polar meltdown: the shift in rationale

The rapid progress in these methods, and the growth in knowledge that has inevitably followed, has led to some recent notable changes in the foci of ice sheet investigations. The last 30 years, in particular, has witnessed a complete reversal in the rationale for investigating the polar ice sheets – shifting from one focused previously on "ice-age theory" to one centered on the possibility of future ice sheet collapse.

During the 1970s, the imperative for most ice sheet research revolved around the Earth descending into a "new ice age," with the polar ice sheets growing to their former large extent, and new ice sheets forming in the mid-to-high latitudes. More recently, this idea has been dispelled by predictions from the eccentricity of Earth's orbit, which suggest that interglacial conditions (i.e., natural continued warming) will persist over the next 5–50 kyr (Loutre and Berger, 2000). Moreover, the impact of anthropogenic warming is such that it may drive further widespread warming over a number of decades to come (IPCC, 2007). Worryingly, this warming may be contributing to or even instigating some dramatic changes that are currently taking place in the AIS and GIS, as hinted at by the satellites, and particularly in their fringing outlet glacier systems where fast ice margin recession, thinning of parts of the ice sheets, and rapid acceleration of glaciers have occurred. Recent changes in ice sheets and the potential for their future retreat have therefore become a focus for the large majority of modern-day ice sheet investigation.

These same recent observations have also led to a general consensus that ice sheets are able to operate over timescales that were once not thought possible for large ice masses. Within the observational window afforded by continuous satellite monitoring, glaciers along the WAIS, Antarctic Peninsula, and Greenland margins have displayed ever-greater change year-on-year. Some changes have been abrupt, and with clear triggers, demonstrating the short response time of ice sheets to external conditions. Together, they support a general picture of ice sheets being complex and dynamic landscapes with changes taking place much faster than previously anticipated.

The corollary of a future characterized by both increased warming and rapidly responding ice sheets is such that, rather than renewed onset of glacial conditions, further glacial retreat in the major ice sheets seems likely – and may be possible over the timescale of only a few lifetimes. Sea-level rise, estimated at 7.2 and 61.1 m for a "polar meltdown" (a complete rapid deglaciation of the GIS and AIS) is the obvious hazard associated with such retreat (IPCC, 2007) and thus forms the imperative for a large majority of today's polar science.

Drivers of ice sheet change

Before examining some specific recent changes in the Antarctic and Greenland ice sheets, we first consider

why ice sheet changes occur – be they the extremes of a polar meltdown or simply a minor thickening over a number of years – and the processes driving ice sheet variations.

The dominant controls on mass balance, and the climate systems discussed previously, are external to the ice sheets and operate at varying timescales. They dictate that ice sheet equilibrium – we have referred to it as "steady state" – is never truly reached.

The most important of these relates to the Earth's orbit around the Sun. Climate records of the past 2 million years attest to periods of past warming: interglacial periods; separated by lengthy times of cooling: glacial periods, with changes in global ice volume correlating with sea level, with oceanic and atmospheric conditions, and global temperature changes. The generally accepted view is that large fluctuations in ice sheet size, in the form of expansions during glacials and deglaciations during interglacials, are forced by orbital variations – the Milankovitch cycles – and that the polar ice sheets therefore pulse to a "natural" (geological) rhythm over tens of thousands of years (see *Glaciations and Groundwater Flow Systems*; *Ice Age*).

Other ice sheet drivers operate subordinately to the Milankovitch cycles leading to local or short-term deviations from steady-state conditions that are a perpetual characteristic of the "changing" ice sheets. The range of these is vast and complex, including, for example, tidal oscillations, which influence diurnal to fortnightly velocities in Antarctica's glaciers, through to seasonal solar forcing effects that exert a strong control over ice flow and discharge in the GIS. Sea-level changes, variations in surface albedo, ice sheet elevation, and ocean salinity are just a few of the many other drivers and feedbacks that help to comprise sensitive ice sheet systems, and that cause ice sheets to be, naturally, predisposed to change (Siegert, 2007).

But it is not only the natural drivers that effect changes in the ice sheet state. There is now a growing body of literature, which suggests that the past ~200 years of human activity is being reflected, indirectly, through ice sheet changes at the poles.

In the Amundsen Sea region of West Antarctica, late-twentieth-century changes in glacier flow appear to be connected to ocean warming, where Pacific waters bathe the marine outlet glaciers. There, the process of warm Circumpolar Deep Water upwelling onto the continental shelf is probably responsible for the thinning of the ice sheet and its ice shelves, the advanced rate of retreat in the grounding line, as well as a marked increase in glacier acceleration in the sector (Jacobs et al., 1992; Thoma et al., 2008). High basal melt rates noted at the fringes of other parts of West Antarctica in recent decades are also likely to be linked to oceanic warming where the warmer ocean comes into contact with the grounding line. We can be certain that ocean circulation and heat transfer are linked to the atmospheric climate (Figure 2). As a result, it is quite plausible that the changes seen in places like the Amundsen Sea, and elsewhere across the marine parts of polar ice sheets are in fact the result of warming through increased anthropogenic greenhouse emissions.

Another example comes from Greenland, where the ice margins are predominantly terrestrial, so that the effects of ocean warming on ice sheet change are not as apparent. However, even in the GIS, mechanisms exist whereby small climate perturbations are still observed to influence ice motion. One particular study by Zwally et al. (2002) showed that meltwater, pooled in lakes on the Greenland ice surface, periodically drained through cavities in the ice sheet, infiltrating the cracks that connect the ice surface to its bed and leading to enhance rates of glacier flow only a short time later. Perhaps more significant than the process itself was the finding that periods of higher melting at the ice surface correlated positively to larger increases in flow acceleration. An indisputable link between warming and climate change at the ice surface, and motion in the ice sheet beneath, was therefore established for the first time. Such rapid feedbacks have led to a recent conclusion that the GIS is highly responsive to environmental and anthropogenic change and, like the ice in the Antarctic, is also more capable of rapid changes than once expected.

Evidence for recent changes in ice sheets

Driven by the complex cycles of the planet, or by greenhouse warming, the evidence for recent and dramatic changes in the polar ice sheets is now clear, and certainly not restricted to the two examples given above. Indeed, there is now widespread proof that major changes are afoot in all parts of the ice sheets, but particularly noticeable in two of the most sensitive gauges of their state: in ice streams, and in ice shelves.

Changes in ice streams

Recent maps of ice sheet change have successfully highlighted those areas that are fast-flowing as ice streams e.g., (Figure 5). They have also highlighted that the parts of Antarctica and Greenland where the largest changes are taking place, and which pose the greatest risk in terms of contributions to future sea-level rise, are concentrated in those areas drained by ice streams (Rignot et al., 2008).

In Antarctica, the Amundsen Sea Embayment (ASE) appears to be the one area where ice stream changes are most dramatic (Vaughan, 2008). Two major ice streams have outlets into the ASE – the Pine Island and Thwaites Glaciers. The first time-series maps of Antarctic ice-thickness change produced about a decade ago, including the Pine Island–Thwaites system, seemed to show the majority of the ice sheet at or near its expected balance. One exception, however, was noted in a prominent surface thinning of ~10 cm year^{-1} in the Pine Island and Thwaites Glaciers. While an anomaly on its own, at the same time and over roughly the same period, the grounding line of Pine Island Glacier was found to have been retreating inland at an alarming rate (~1 km year^{-1}). These early results seemed to suggest that the oceanic warming of

ice shelves noted several years earlier was leading to advanced retreat in these ice streams of the WAIS.

Since that time, other observations have revealed further evidence for dramatic changes; short-term thinning and periods of acceleration that have led to the Pine Island glacier to speed up by ~34% over the past decade. Time-series analyses of satellite images of Pine Island Glacier have shown that its ice shelf had, in one part, been thinning for almost three decades (at a rate of 4.8 m year^{-1}) up to 2002, even though the position of the ice-shelf front had not shown any clear trend over the last 50 years (Vaughan, 2008). Thinning in the main body of the glaciers has also occurred in their fastest-flowing portions, and other surveys have concluded that neighboring glaciers – the Smith and Kohler glaciers – have also been undergoing similar changes.

The most recent calculation of ice flux in the basins of Pine Island and Thwaites Glaciers showed the net mass balance to be -33 ± 10 km^3 ice year^{-1}, meaning the glaciers are almost certainly losing mass in response to their increased flow acceleration (Rignot et al., 2008). Surface elevation change, the rate of flow acceleration, and rate of grounding-line retreat in Pine Island Glacier are all greater now than at any time since measurements began (Scott et al., 2009). The drainage area captured by these major ice streams, alone, contains the potential to raise sea level by ~1.2–1.5 m. Fast-flowing outlets that drain the ASE therefore appear to be responding to a common forcing and are able to alter rapidly enough to make a significant addition to the rate of sea-level rise (Bamber et al., 2007; Rignot et al., 2008).

Changes in ice shelves

Seaward of the ice streams, the evidence for very recent climate changes reflected in Antarctica's ice shelves is both explicit and dramatic. Many of the Antarctic Peninsula ice shelves have been lost in recent years, during phases of rapid and catastrophic collapse: a long-predicted result of climate warming along the Peninsula spine (Mercer, 1978). The most publicized of these events occurred in 2002, involving the breakup of the Larsen B ice shelf, on the northeastern Antarctic Peninsula (Figure 8a, b). The retreat of Larsen B, and other ice shelves on the Peninsula, is understood as a devastating response to a combination of long-term thinning and decomposition, coupled with a recent trend of oceanic and atmospheric warming across the whole of West Antarctica (Steig et al., 2009).

At first, many glaciologists suspected that these types of collapses were part of a natural cycle of shelf-ice growth, evacuation, and regrowth – similar to the cyclic shedding of large icebergs from floating glacier tongues. Surprisingly however, historical records of ice-shelf conditions, as shown in sediment cores collected from areas several kilometers away from the Larsen B coast, confirmed a long-term stability of the ice shelf. The cores revealed that the 2002 collapse was actually unprecedented over the past 11,000 years, indicating that twentieth-century changes in the maritime Antarctic were adverse on millennial timescales, and without a Holocene analogue (Domack et al., 2003).

However, this picture is not so clear in the sediment archives for other ice shelves on the west of the Antarctic Peninsula. Here, ice shelves appear to have collapsed and reformed periodically over the last 10,000 years. Sediments on Alexander Island, for example, show that the neighboring George VI Ice Shelf collapsed ~9,600 years ago following a phase of climatic warming but then reformed from ~7,700 years ago, and has survived in its

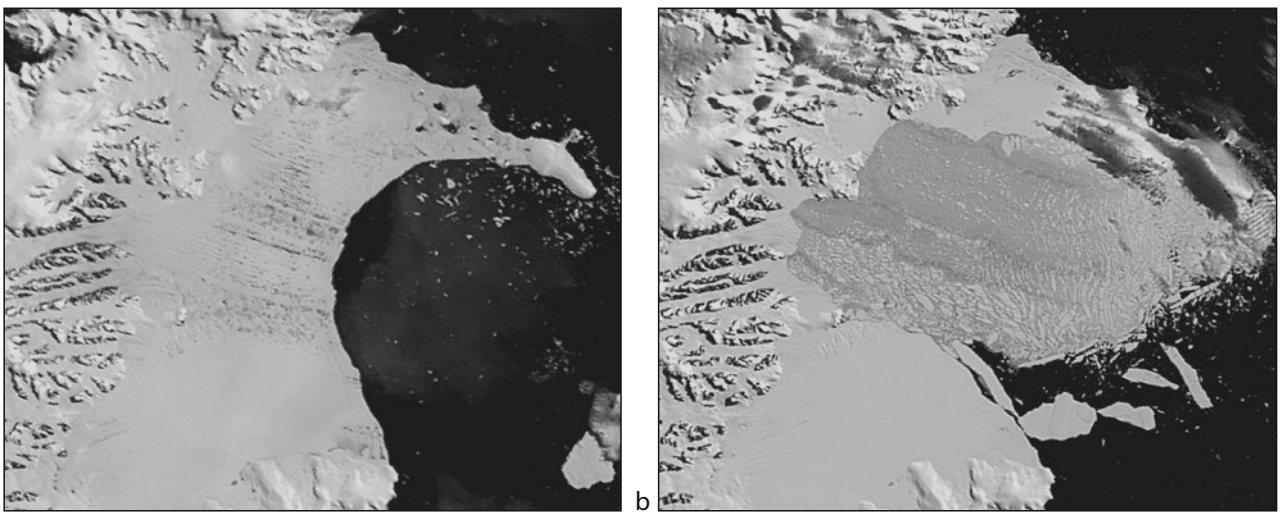

Ice Sheet, Figure 8 (**a** and **b**) MODIS satellite imagery of the breakup of Larsen B Ice Shelf, Antarctic Peninsula. Full-resolution, grayscaled images: (**a**) at the start of the collapse on January 31, 2002, and (**b**) after the collapse on March 7, 2002. The area of ice lost between the two images is approximately 3,250 km^2. Source: http://svs.gsfc.nasa.gov/vis/a000000/a002400/a002421/index.html (last visited 27/05/2009).

current state through to the present (Smith et al., 2007). Some ice shelves therefore appear sensitive, not only to warming, but also to short-term, centennial-to-millennial climate cooling trends. Past influxes of warmer water and concomitant atmospheric warming are believed to be causal factors in the past collapse of Antarctica's ice shelves, and may be comparable to the conditions driving renewed ice-shelf retreat today.

In fact it may be because of this warming that over the past 20 years, ~14,000 km^2 of ice shelf has been lost along the Antarctic Peninsula. While some parts of the ice sheet have not been seen to respond to ice-shelf disintegration in terms of velocity variation, elsewhere significant acceleration has been observed in glaciers once supported by ice shelves, following their breakup (e.g., De Angelis and Skvarca, 2003; Rignot et al., 2004; Scambos et al., 2004). Ice shelves work to exert an important back pressure on the ice sheet behind it, effectively putting the brakes on the ice sheet advancing forward. Without these fringing shelves, the glaciers behind are vulnerable to the intrusion of warm oceanic waters, which may lead to increases in their flow-rate, and increased mass loss via calving at the grounding line.

The timing and duration of glacier change in response to ice-shelf breakup remains an uncertainty at present. However, new models of one Antarctic ice stream system, with a presently intact floating tongue, have shown that it would take up 150 years for the glacier's velocity and flow conditions to stabilize, if its ice shelf should collapse. While floating ice is, therefore, not a direct contributor to sea-level rise, the loss of buttressing ice shelves on the Antarctic Peninsula, and at the periphery of a warming West Antarctica (Steig et al., 2009), may serve to destabilize ice streams, leading to enhanced retreat and sea-level contributions from the ice sheet, with lasting effects felt over several centuries.

Lessons from the past: long-term records of ice sheet change

While the recent changes in ice stream and ice-shelf systems have occurred over short timeframes, the greatest changes in ice sheets occur across timescales of glacial–interglacial cycles, over tens of thousands of years. During past glaciations, ice sheets covered up to 30% of Earth's surface, extending well beyond currently glaciated terrain (Ehlers and Gibbard, 2004). A major advance in our understanding of ice sheets has therefore come from the ability to draw lessons from the disappearance of past ice masses to inform current and future scenarios of deglaciation (see Siegert et al., 2008 for a review).

Major ice sheets have existed on Antarctica since at least Oligocene times, approximately 34 million years ago. Records of ice sheet state over the last 1 million years remain the most instructive however, because these ice sheets witnessed cycles of glacial–interglacials most similar to the present, with major oscillations in climate coincident with the regular growth and decay of continental ice (see also *Pleistocene Epoch*; *Quaternary Glaciation*). The archives of change from this period are also the most well preserved in the geological record. Within this 1 million year window, in each glacial cycle, deglaciations form the most rapid events in the climate record, and are probably the most suitable analogues for present ice-climate scenarios at the poles.

For the most recent deglaciation, the short-term changes observed in ice sheets over the past decades overprint a much longer-term trend of ice retreat that began immediately prior to, and continued through the Holocene, c. 11,000 years ago (e.g., Conway et al., 1999; Anderson et al., 2002, Siegert et al., 2008). The fact that ice sheets survive within the current warm period, but appear only partially deglaciated at present, makes deciphering current-and-future natural ice retreat from human-induced ice sheet change particularly difficult. However, by understanding the size and timing of previous glacial cycles, the configuration of ice during these past glacial transitions, and the forcing behind such changes, questions regarding future ice sheet change may become clearer.

Marine and terrestrial archives of past ice sheet change

Marine sediments provide one important archive for assessing changes in ice sheet configuration through time (Figure 7). Drift accumulations resting on the continent at the ice sheet fringes (i.e., on the continental shelf, slope, or continental rise) reveal a natural succession of sediments that record the depositional environments in the deep ocean and shallow glacial seas over millions of years. The varying sediment types and structures, their organic, heavy-mineral and isotopic content, the provenance of the grains within the sediments, and the rate at which sediments were deposited, all provide useful indicators of the state of the ice sheet and the neighboring ocean at time slices through recent history. The archive of ice sheet changes held in sediment cores can be used to show environmental conditions during periods of past ice loss, and to date the speed and timing of withdrawal of ice sheets from the polar continental shelves after the last major glaciation (the Last Glacial Maximum [LGM], c. 25–19,000 years ago).

Onshore, a new and promising method for assessing how longer-term ice sheet change may be underwriting the short-term measured record of change has come from the terrestrial rock record. The abundance of cosmogenic 10Be and 26Al in quartz-bearing rocks is directly related to the duration of their exposure following the onset of deglaciation, and can be measured to give an exposure date. In this way, geological surfaces can be prescribed a minimum age indicating when an ice sheet last covered them.

One recent example of this method applied to ice sheet change was carried out by Johnson et al. (2008) who collected a small suite of glacially derived boulders for cosmogenic isotope analysis from four sites surrounding Pine Island Bay, in order to establish a geological record of ice thinning in the ASE since the LGM. Exposure ages

from these samples yielded results that suggest that the rapid ice sheet thinning rates observed in the Amundsen sector over the past decade (e.g., Thomas et al., 2004) are unusual when placed against the longer-timescale pattern of Antarctic ice retreat, by at least one order of magnitude – a thinning of ~2–4 cm year^{-1} over the last 15 kyr, compared against a thinning rate of ~3.5 m year^{-1} measured on Pine Island Glacier for 2007 (Scott et al., 2009). These ages support similar studies, which show that the magnitude and rates of current changes in some parts of the polar ice sheets are highly extraordinary in the context of the recent geological past.

Ice cores

Another archive is found in the ice cores through layers of ice that have accumulated through time (Figure 7). In Antarctica, the oldest ice core recovered dates back ~800,000 years (EPICA core at Dome C; Figure 1), but ice older than 1 million years probably exists in areas of particularly low accumulation. During the slow compaction of snowfall to ice, interconnected air bubbles in the near-surface ice remain open to the atmosphere. Over time, the air and associated impurities (dust and particulates) captured in these pockets are sealed off, and eventually pushed by the weight of the overlying ice into the crystalline structure of the ice itself. The sample air preserved within the ice structure can be released and captured for analysis by sampling ice from different levels in cores.

The history of past climates available from ice cores is one of the most important sources of information about how the climate on Earth has changed through time. The chemical composition of the air samples that can be obtained from the cores reveals how the important greenhouse gases have changed through glacial–interglacial cycles. Relative concentrations of different isotopes of oxygen and hydrogen also provide an indication of variation in the global ratio of seawater to ice volume, and serve as a "natural thermometer" that shows how the temperature of the planet has fluctuated through the past.

The most recent ice core extracted from Dome C shows that current levels of greenhouse gases in the atmosphere are higher now than at any time in the past 650,000 years. Carbon dioxide is about 30% higher than at any time, and methane 130% higher than at any time. Furthermore, the rates of increase are exceptional: 200 times faster than rates of natural change over the same period. Because variations in Antarctic temperature and atmospheric carbon dioxide follow each other closely, such changes may cause global climate and its related ice sheet systems to alter rapidly.

Ice sheet "collapse": geological precedents for future rapid deglaciation?

From the changes in the ice core and geological records, and those observed in the ice sheets themselves, it appears that a combination of natural and anthropogenic warming could trigger the future collapse of the polar ice sheets. Mercer (1978) was the first to argue the hypothesis that anthropogenic climate warming could instigate a rapid loss of much of the WAIS. Though unsupported at the time, recent ice sheet models have confirmed Mercer's original fears that even small amounts of warming could lead to positive feedback in WAIS retreat where ice is grounded on an inland-sloping base (Schoof, 2007). In particular, major evacuation of marine basins seems to be possible in situations where the ice may be close to becoming ungrounded from pinning points and where the bed slope is monotonic toward the ice interior – and several of the major Antarctic glacier catchments currently meet the criteria for this unstable situation (e.g., the Thwaites glacier).

Indeed, the instability of marine ice sheets is no mere hypothesis. The rapid and widespread collapse of former marine ice sheets is likely to have occurred in the past, such as in the rapid steps of deglaciation in the Laurentide Ice Sheet, between ~14,600 and 7,500 years ago. For Antarctica, compelling evidence for past WAIS collapse was first presented in the late 1990s, in samples recovered from the muddy bed beneath the ice sheet. In four separate samples, sediment yielded fossils of microscopic marine plants along with isotopes showing that the fossils were deposited under open water conditions. It is widely regarded that these deposits provide evidence that the ice sheet collapsed at some point during the Late Quaternary (in the last 1.3 Myrs, probably during Marine Isotope Stage [MIS] 11), and that the ice sheet interior formed a seaway where it was inundated by marine waters.

Deep-marine sediment cores recovered on the continental rise offshore of the ASE also record anomalies in the state of the ice sheet through the Late Quaternary, with one notable period dating back to about 620 to 500 ka. Sedimentological proxies for climate in the cores from this time slice display indicators for an unusually prolonged interglacial period, within an otherwise rhythmic pattern of glacial–interglacial cycles. This climate anomaly also appears to coincide with perturbations observed in paleoclimate records from both hemispheres (Hillenbrand et al., 2009); suggesting this "event" had global significance. Although further work is needed to test the hypothesis, it seems quite likely that these deposits relate to a time of reduced glacial activity, and may record a large drawdown of the WAIS during MIS 13–15.

The presence of thick diatomite sequences, interbedded with glacial diamictons, drilled from beneath the McMurdo ice shelf has also been used to argue the evidence for repeated loss of the WAIS through the Pliocene and Pleistocene (Naish et al., 2009). The criteria for a West Antarctic collapse from these deposits appear somewhat contentious at present – especially given that thick sequences of diatomaceous mud have accumulated in glacial marine basins through the Holocene, while the WAIS and EAIS have remained mainly intact. Nevertheless, ice sheet model outputs support the inferences from the rock record, predicting a dynamic oscillation of the AIS over

the past 5 Myrs, with punctuated collapse and growth. Large collapses are inferred during the early Pliocene and during the warm "superinterglacial" of MIS 31, at c. 1 Ma years ago (Naish et al., 2007).

Independent of the geological archives, sea-level "fingerprinting" has also shown abrupt rises in global sea level in the past, and there is a strong suggestion that these events must relate to massive discharges of meltwater from at least a partial collapse of the polar ice sheets (Clark et al., 2002). Taking these data alongside the above geological evidence for former ice sheet collapse, it appears that regardless of exactly when, a future widespread deglaciation of the ice sheets has at least one geological precedent.

The future of the polar ice sheets

Although the evidence for potentially rapid retreat of marine ice sheets existing in the geological archives and the record of global sea level is difficult to ignore, the general instability of marine ice sheets is not universally accepted, and several researchers have argued that complete collapse of WAIS may be unlikely within a few centuries (Vaughan and Spouge, 2002; Vaughan, 2008) – although this still allows for significant and substantial rates of sea-level rise. Indeed, the current contribution from the Amundsen Sea alone is sufficient to raise sea level by more than 0.2 mm year^{-1} (Thomas et al., 2004).

Yet, it remains to be seen how far the current changes are precursors of a major ice sheet loss, with ongoing difficultly in predicting the future of the polar ice masses (Vaughan and Arthern, 2007). The shortfall in present understanding is likely a result of a lack of knowledge in the mechanisms of ice sheet change, but also an inability for observed rapid changes to be successfully reproduced in ice sheet models (IPCC, 2007). Some areas of the science require further improvements in "skill" before qualified predictions of ice sheet response to external forcing can be made. Amongst these, the dynamics of sub-ice stream processes, their stability on back-sloping surfaces (Schoof, 2007), and the physics of grounding-line–ice-shelf interactions, remain major research emphases.

Summary

The two remaining polar ice sheets are the cornerstone of the global cryosphere and climate systems. They are sensitively balanced through processes of growth, flow, and loss, and comprise a number of glaciological components that are key to maintaining this balance (including inland centers, ice streams, and ice shelves). However, the ice sheets may be threatened by future warming of the planet, which is projected to rise significantly over coming centuries. Indeed, whether driven by humans, or by the natural cycles of the Earth, there is evidence that parts of the polar ice sheets are already undergoing major changes. Geological clues from the past hint at times when ice sheets were completely disintegrated, and demonstrate that the current rates of change are unusual in the context of longer-term ice dynamics. However, while we know much about the history of ice sheets and their present-day operating mode, their future behavior remains a continual uncertainty. Thus, many lines of enquiry form an ongoing programme of research into ice sheets, their past, present, and future changes.

Bibliography

Alley, R. B., and Binschadler, R. A., 2001. The west Antarctic ice sheet and sea-level change. In Alley, R. B., and Binschadler, R. A. (eds.), *The West Antarctic Ice Sheet: Behavior and Environment*. Washington, DC: American Geophysical Union, pp. 1–11.

Anderson, J. B., Shipp, S. S., Lowe, A. L., Wellner, J. S., and Mosola, A. B., 2002. The Antarctic ice sheet during the last glacial maximum and its subsequent retreat history: a review. *Quaternary Science Reviews*, **21**, 49–70.

Armstrong, T., Roberts, B., and Swithinbank, C., 1973. *Illustrated Glossary of Snow and Ice.* Cambridge, UK: Scott Polar Research Institute, Special Publication No. 4.

Bamber, J. L., Vaughan, D. G., and Joughin, I., 2000. Widespread complex flow in the interior of the Antarctic ice sheet. *Science*, **287**, 1248–1250.

Bamber, J. L., Alley, R. B., and Joughin, I., 2007. Rapid response of modern day ice sheets to external forcing. *Earth and Planetary Science Letters*, **257**, 1–13.

Behrendt, J. C., 1998. *Innocents on the Ice: A Memoir of Antarctic Exploration, 1957*. Boulder: University Press of Colorado.

Bell, R. E., Blankenship, D. D., Finn, C. A., Morse, D. L., Scambos, T. A., Brozenal, J. M., and Hodge, S. M., 1998. Influence of subglacial geology on the onset of a West Antarctic ice stream from aerogeophysical observations. *Nature*, **394**, 58–62.

Bell, R. E., Studinger, M., Shuman, C. A., Fahnestock, M. A., and Joughin, I., 2007. Large subglacial lakes in East Antarctica at the onset of fast-flowing ice streams. *Nature*, **445**, 904–907.

Bennett, M. R., 2003. Ice streams as the arteries of an ice-sheet: their mechanics, stability and significance. *Earth-Science Reviews*, **61**, 309–339.

Bentley, C. R., 1993. Antarctic mass balance and sea level change. *Eos*, **74**, 585–586.

Bingham, R. G., and Siegert, M. J., 2007. Radio-echo sounding over polar ice masses. *Journal of Environmental and Engineering Geophysics*, **12**, 47–62.

Boulton, G. S., and Hindmarsh, R. C. A., 1987. Sediment deformation beneath glaciers: rheology and geological consequences. *Journal of Geophysical Research*, **92**, 9059–9082.

Clark, P. U., Mitrovica, J. X., Milne, G. A., and Tamisiea, M. E., 2002. Sea-level fingerprinting as a direct test for the source of global meltwater pulse IA. *Science*, **295**, 2438–2441.

Conway, H., Hall, B. H., Denton, G. H., Gades, A. M., and Waddington, E. D., 1999. Past and future grounding-line retreat of the west Antarctic ice sheet. *Science*, **286**, 280–283.

De Angelis, H., and Skvarca, P., 2003. Glacier surge after ice shelf collapse. *Science*, **299**, 1560–1562.

Domack, E., Duran, D., Leventer, A., Ishman, S., Doane, S., McCallum, S., Amblas, D., Ring, J., Gilbert, R., and Prentice, M., 2003. Stability of the Larsen B ice shelf on the Antarctic peninsula during the Holocene epoch. *Nature*, **436**, 681–685.

Ehlers, J., and Gibbard, P. L., 2004. *Quaternary Glaciations – Extent and Chronology.* Amsterdam: Elsevier.

Fahnestock, M. A., Scambos, T. A., Bindschadler, R. A., and Kvaran, G., 2000. A millennium of variable ice flow recorded by the Ross Ice Shelf, Antarctica. *Journal of Glaciology*, **46**, 652–664.

Gore, A., 2006. *An Inconvenient Truth: The Planetary Emergency of Global Warming and What We Can Do about It*. London: Bloomsbury.
Hillenbrand, C.-D., Kuhn, G., and Frederich, T., 2009. Record of a Mid-Pleistocene depositional anomaly in West Antarctic continental margin sediments: an indicator for ice-sheet collapse? *Quaternary Science Reviews*, **28**, 1147–1159.
Intergovernmental Panel on Climate Change, 2007. Climate Change 2007: The Physical Science Basis–Summary for Policymakers. Geneva, Switzerland: IPCC Secretariat. Available at http://www.ipcc.ch/SPM2feb07.pdf.
Jacobs, S. S., Hellmer, H. H., Doake, C. S. M., Jenkins, A., and Frolich, R. M., 1992. Melting of ice shelves and the mass balance of Antarctica. *Journal of Glaciology*, **38**, 375–387.
Johnson, J. S., Bentley, M. J., and Gohl, K., 2008. First exposure ages from the Amundsen Sea Embayment, West Antarctica: the Late Quaternary context for recent thinning of Pine Island, Smith and Pope Glaciers. *Geology*, **36**, 223–226.
Kamb, B., 1991. Rheological nonlinearity and flow instability in the deforming bed mechanism of ice stream motion. *Journal of Geophysical Research*, **96**, 16585–16595.
Loutre, M. F., and Berger, A., 2000. No glacial-interglacial cycle in the ice volume simulated under a constant astronomical forcing and variable CO_2. *Geophysical Research Letters*, **27**, 783–787.
Lythe, M. B., Vaughan, D. G., BEDMAP Consortium, Lambrecht, A., Miller, H., Nixdorf, U., Oerter, H., Steinhage, D., Huybrechts, P., et al., 2001. BEDMAP: a new ice thickness and subglacial topographic model of Antarctica. *Journal of Geophysical Research*, **106**, 11335–11351.
Mercer, J. H., 1978. West Antarctic ice sheet and CO_2 greenhouse effect: a threat of disaster. *Nature*, **271**, 321–325.
Naish, T., Powell, R., Levy, R., Henrys, S., Krissek, L., Niessen, F., Pompilio, M., Scherer, R., Wilson, G., and The ANDRIL-MIS Science Team, 2007. Synthesis of the initial scientific results of the MIS Project (AND-1B Core), Victoria Land Basin, Antarctica. *Terra Antarctica*, **14**, 317–327.
Naish, T., Powell, R., Levy, R., et al., 2009. Obliquity-paced Pliocene West Antarctic ice sheet oscillations. *Nature*, **458**, 322–328.
Peters, L., Anandakrishnan, S., Alley, R. B., Winberry, J. P., Voigt, D. E., Smith, A. M., and Morse, D. L., 2006. Subglacial sediments as a control on the onset and location of two Siple Coast ice streams, West Antarctica. *Journal of Geophysical Research*, **111**, 1–14.
Pritchard, H. D., Arthern, R. J., Vaughan, D. G., and Edwards, L. A., 2009. Extensive dynamic thinning on the margins of the Greenland and Antarctic ice sheets. *Nature*, **461**, 971–975.
Rignot, E., and Kanagaratnam, P., 2006. Changes in the velocity structure of the Greenland ice sheet. *Science*, **311**, 986–990.
Rignot, E., Thomas, R. H., Kanagaratnam, P., Casassa, G., Frederick, E., Gogineni, P., Krabill, W., Rivera, A., Russell, R., Sonntag, J., Swift, R., and Yungel, J., 2004. Improved estimate of the mass balance of glaciers draining into the Amundsen Sea of West Antarctica from CECS/NASA 2002 campaign. *Annals of Glaciology*, **39**, 231–237.
Rignot, E., Bamber, J., van den Broeke, M., Davis, C., Li, Y., van de Berg, W. J., and van Meijgaard, E., 2008. Recent Antarctic ice mass loss from radar interferometry and regional climate modelling. *Nature Geoscience*, **1**, 106–110.
Rose, K. E., 1979. Characteristics of ice flow in Marie Byrd Land Antarctica. *Journal of Glaciology*, **24**, 63–74.
Scambos, T. A., Bohlander, J. A., Shuman, C. A., and Skvarca, P., 2004. Glacier acceleration and thinning after ice shelf collapse in the Larsen B embayment Antarctica. *Geophysical Research Letters*, **31**, L18402.
Schoof, C., 2007. Ice sheet grounding line dynamics: Steady states, stability and hysteresis. *Journal of Geophysical Research*, **112**, 1–14.
Schrum, H., Hayes, J., and Domack, E., 2006. Refining the radiocarbon dating of Antarctic marine sediments via stepped combustion. *Eos Transactions*, *AGU*, 87, Abstract OS25H-06.
Scott, J. B. T., Gudmundsson, G. H., Smith, A. M., Bingham, R. G., Pritchard, H. D., and Vaughan, D. G., 2009. Increased rate of acceleration on Pine Island Glacier strongly coupled to changes in gravitational driving stress. *The Cryosphere*, **3**, 125–131.
Siegert, M. J., 2007. Glacial landforms, ice sheets: growth and decay. In Elias, S. A. (ed.), *Encyclopedia of Quaternary Science*. Amsterdam: Elsevier.
Siegert, M. J., Carter, S., Tabacco, I., Popov, S., and Blankenship, D., 2005. A revised inventory of Antarctic subglacial lakes. *Antarctic Science*, **17**, 453–460.
Siegert, M. J., Barrett, P., DeConto, R., Dunbar, R., Ó Cofaigh, C., Passchier, S., and Naish, T., 2008. Recent advances in understanding Antarctic climate evolution. *Antarctic Science*, **4**, 313–325.
Smith, A. M., and Murray, T., 2009. Bedform topography and basal conditions beneath a fast-flowing West Antarctic ice stream. *Quaternary Science Reviews*, **28**, 584–596.
Smith, B. E., Fricker, H. A., Joughin, I. R., and Tulaczyk, S., 2009. An inventory of active subglacial lakes in Antarctica detected by ICESat (2003–2008). *Journal of Glaciology*, **55**, 573–595.
Smith, J. A., Bentley, M. J., Hodgson, D. A., Roberts, S. J., Verleyen, E., Leng, M. J., Lloyd, J. M., Barrett, M. J., and Sugden, D. E., 2007. Oceanic and atmospheric forcing of early Holocene ice shelf retreat, George VI Ice Shelf, Antarctic Peninsula. *Quaternary Science Reviews*, **26**, 500–516.
Steig, E. J., Schneider, D. P., Rutherford, S. D., Mann, M. E., Comiso, J. C., and Shindell, D. T., 2009. Warming of the Antarctic ice-sheet surface since the 1957 International Geophysical Year. *Nature*,**457**,459–462.
Stern, N., 2006. Stern Review on the Economics of Climate Change: Executive Summary. http://news.bbc.co.uk/1/shared/bsp/hi/pdfs/30_10_06_exec_sum.pdf. Last visited, 2 April 2009.
Studinger, M., Bell, R. E., Karner, G. D., Tikku, A. A., Holt, J. W., Morse, D. L., Richter, T. G., Kempf, S. D., Peters, L. E., Blankenship, D. D., Sweeney, R. E., and Rystrom, V. L., 2003. Ice cover, landscape setting, and geological framework of Lake Vostok, East Antarctica. *Earth and Planetary Science Letters*, **205**, 195–210.
Thoma, M., Jenkins, A., Holland, D., and Jacobs, S., 2008. Modelling circumpolar deep water intrusions on the Amundsen Sea continental shelf, Antarctica. *Geophysical Research Letters*, **35**, L18602.
Thomas, R., Rignot, E., Casassa, G., et al., 2004. Accelerated sea-level rise from West Antarctica. *Science*, **306**, 255–258.
Truffer, M., and Echelmeyer, K. A., 2002. Of isbrae and ice streams. *Annals of Glaciology*, **36**, 67–72.
Vaughan, D. G., 2008. West Antarctic ice sheet collapse – the fall and rise of a paradigm. *Climatic Change*, **91**, 65–79.
Vaughan, D. G., and Arthern, R., 2007. Why is it hard to predict the future of ice sheets? *Science*, **315**, 1503–1504.
Vaughan, D. G., and Spouge, J. R., 2002. Risk estimation of collapse of the West Antarctic sheet. *Climatic Change*, **52**, 65–91.
Villa, G., Lupi, C., Cobianchi, M., Florindo, F., and Pekar, S. F., 2008. A Pleistocene warming event at 1 Ma in Prydz Bay, East Antarctica: evidence from ODP Site 1165. *Palaeogeography, Palaeoclimatology, Palaeoecology*, **260**, 230–244.
Wingham, D. J., Siegert, M. J., Shepherd, A., and Muir, A. S., 2006. Rapid discharge connects Antarctic subglacial lakes. *Nature*, **440**, 1033–1036.
Zwally, H. J., Abdalati, W., Herring, T., Larson, K., Saba, J., and Steffen, K., 2002. Surface melt-induced acceleration of Greenland ice-sheet flow. *Science*, **297**, 218–222.

Cross-references

Antarctica
Atmospheric Circulation and Glaciochemical Records
Blue Ice
Deglaciation
Firn
Formation and Deformation of Basal Ice
Glacial Drainage Characteristics
Glacial Geomorphology and Landforms Evolution
Glacier Mass Balance
Glacier Motion/Ice Velocity
Glaciology
Greenland Ice Sheet
Ice
Ice Caps
Ice Sheet Mass Balance
Ice Shelf
Lake Vostok
Marine Ice Sheet
Outlet Glacier
Palaeo-Ice Stream
Quaternary Glaciation
Radar Application in Snow, Ice, and Glaciers
Sea-Level
Sediment Core and Glacial Environment Reconstruction
Subglacial Drainage System
Subglacial Processes

ICE SHEET MASS BALANCE

Eric Rignot
Department of Earth System Science, University of California Irvine, Irvine, CA, USA
Jet Propulsion Laboratory, Pasadena, CA, USA

Definition

Ice sheet mass balance refers to the balance between additions to and losses of mass from an entire ice sheet. It is expressed as a mass per unit of time, positive if the ice sheet is gaining mass, negative if the ice sheet is losing mass. The term is often used loosely to mean either the surface mass balance or the total mass balance. Surface mass balance, however, signifies the addition of mass to the surface of the specified region. It does not include processes such as the advection of ice by glaciers and ice streams or the melting of ice at the underside of ice streams or floating ice shelves. Total mass balance or mass balance signifies the balance between all additions (snow, advection of ice from upstream, basal freezing, etc.) and all losses (ice motion, ice melt, basal melting) from the region of ice under investigation.

Introduction

Ice sheets have a large impact on global sea level. At the last glacial maximum, global sea level was 120 m lower than today. If all ice in Greenland and Antarctica were to melt to sea today, it would raise sea level by another 65–70 m. In the early part of the twentieth century, sea level was rising at a rate of 1.8 mm/year. At present, it is rising at 3 mm/year and the rate is expected to increase in the coming centuries with the melting of ice sheets, mountain glaciers, and ice caps, and the thermal expansion of the oceans. To determine the contribution to sea level rise of ice sheets, we need to determine their state of mass balance, that is, the rate at which they are gaining or losing mass to the ocean with time. For every 360 Gt/year of loss in mass of an ice sheet, sea level increases by 1 mm/year.

Until the 1990s, the state of mass balance of the ice sheets in Greenland and Antarctica was virtually unknown. Significant progress has been made since due to the advent of satellite missions and the deployment of modern instruments onboard airborne platforms. There are at present three major techniques to measure the continent-wide mass balance of ice sheets:

1. The mass budget method, comparing perimeter losses with interior accumulation, to infer the net change in mass of the ice sheet
2. The gravity method, utilizing time series of time-variable gravity data, to infer mass changes directly, except on floating ice tongues and ice shelves
3. The altimetry method, which uses repeated altimetry surveys of the ice sheet surface elevation to infer volume changes, which are subsequently converted into mass changes

All three techniques have been applied to the entire ice sheets. The mass balance values obtained from these independent techniques do not all agree perfectly, for various reasons, but the level of agreement is improving with time as processing errors and uncertainties associated with the spatial and temporal variations of the signal are more fully understood and resolved. Most important, all three techniques bring a piece of puzzle on how the ice sheets are changing and why.

Mass budget

Interior accumulation of mass is essentially equivalent to the surface mass balance of the ice sheet. It includes snow accumulation minus ablation from processes such as melting, evaporation, sublimation, and wind transport. Snow accumulation may be inferred in situ from ice cores, stake measurements, snow pits, or ground-penetrating radars, but such data are difficult to extrapolate for characterizing total snow accumulation on areas as large as Greenland (1.7 M km^2) or Antarctica (14 M km^2). Interpolation of these data has been performed using satellite passive microwave data or meteorological information or large-scale atmospheric modeling, with mixed level of success, especially along wet, coastal sectors where surface measurements are lacking. More recently, regional atmospheric climate models constrained by global climate reanalysis data have made significant improvements in estimating net snow accumulation over ice sheets. Models such as the Regional Atmospheric Climate Model 2 (RACMO2) resolve interior accumulation accurately and capture coastal gradients realistically for the first time.

These models employ in situ measurements to evaluate their absolute level of precision instead of using them for calibration (van de Berg et al., 2006; Ettema et al., 2009). The results reveal higher-than-expected accumulation along wet coastal sectors and higher total snowfall overall (Van den Broeke et al., 2006). The level of precision of these models is about 9% total accumulation in Greenland, 5% in dry sectors of Antarctica, degrading to 30% in its wet coastal sectors. Expressed in Gt (gigatons = 10^{12} kg = 10^{9} metric tons) per year, these uncertainties translate into surface mass balance known within ±41 Gt/year in Greenland and ±102 Gt/year in Antarctica.

Measurements of perimeter losses improved drastically as well. Early characterizations of perimeter losses were based on a few velocity data points and limited knowledge of ice thickness. Surface velocity of ice is now measured with satellites, mainly synthetic-aperture radar interferometry (Insert), over the entire periphery of ice sheets, with a precision of a few meters per year, at a spatial sampling of a few hundred meters. For ice flux calculations, these surface velocities must be translated into depth-averaged velocities. Because the largest dischargers of ice are also the fastest glaciers, this is not a major issue because most of these glaciers are sliding almost entirely on their bed and numerical models indicate that the difference between surface and depth-averaged velocity is typically less than 2%. Similarly, ice velocity is often measured at one time during the year, typically in winter in Greenland, hence must be corrected for seasonally variations. In Antarctica, seasonal variations are negligible. In Greenland, ice motion accelerates by 8–10% on average during the summer months, independent of latitude (Rignot and Kanagaratnam, 2006). This translates into an underestimation of the annual velocity from the winter velocities by about 2%. Overall, the underestimation from the seasonality and the approximation of depth-averaged flow nearly compensate each other, so that in Greenland the error in depth-averaged velocity is at the sub-percent level is one uses winter surface velocities instead. In Antarctica, the error should be much less than 2%.

Ice thickness is measured using airborne radio echo sounders over a growing share of the coastal sectors, at a precision of about 10 m in the interior, degrading to a few 10 m in outlet glaciers. These measurements are limited in spatial extent to the flight tracks of the airborne platform, but new techniques of two-dimensional mapping are now emerging. Historical data did not systematically cover the grounding line region, either because the grounding line position was not well known or the radar instrument did not operate well over that type of ice (in Wilkes Land, East Antarctica, for instance, historical data typically have no bed echoes over main glacier troughs) or the data were not acquired with sufficient precision (no GPS location, no digital recording of radar echoes). In Greenland, modern radars have difficulties in obtaining bed returns in warm, deeply entrenched coastal troughs occupied by outlet glaciers. In these areas, a new approach based on airborne gravity measurements at the sub-milligal level is being explored, with a precision of 100 m vertical and 3–5 km horizontal. Otherwise, ice fluxes have to be calculated farther upstream and changes in speed and thickness at the glacier grounding line are employed to estimate grounding line fluxes required in the mass budget calculation (Rignot and Kanagaratnam, 2006).

In places where such modern data are not available and ice reaches floatation in seawater, ice thickness may be deduced from ice surface elevation assuming hydrostatic equilibrium of ice with seawater (Rignot et al., 2008). Ice surface elevation is measured with satellite laser or radar or laser/radar combined altimetry (Bamber et al., 2009), that is, ERS-1 in 1994 and ICESAT-1 in the year 2000. These data yield estimates of ice shelf elevation with a submeter precision, and translate into grounding line thicknesses with a precision of 80 m, degrading to 120 m in more complex settings (Rignot et al., 2008). For small glaciers entrenched in narrow valleys, the current surface elevation data derived from satellites is difficult to use.

All thickness data must be corrected from the depth of the firn layer, so that all ice thicknesses represent an equivalent thickness of solid ice, instead of a total thickness of ice and firn. Firn depth correction may be calculated as a by-product of Regional Atmospheric Climate Models. In Antarctica, the correction varies from 0 to 10–25 m (Van den Broeke, 2006).

Quadruple difference interferometry has been used to detect the position of the grounding line of glaciers, where ice detaches from its bed to become afloat, at a horizontal precision better than 100 m (Rignot, 1996). This transition boundary is the natural boundary where to measure ice fluxes into the ocean since the resulting fluxes represent the discharge of ice, hence of mass, into the ocean, independent of the melting of floating glacier ice downstream of the grounding line. This boundary may be inferred from aerial or satellite photographs of the surface reflectance at visible wavelengths, with uncertainties of the order of 10–100 km, from radio echo sounding as a transition from a dim ice-bed interface to a bright ice-seawater interface, also with uncertainties of the order of many kilometers, or from GPS, laser altimetry, and tilt meter instruments typically at a precision of 1 km (Vaughan, 1995). In Greenland, floating extensions of glaciers are only found in the north.

The ice fluxes, obtained from the integration of ice thickness times the depth-averaged velocity across the glacier width, are converted to mass using a solid ice density of 917 kg/m^3.

The mass budget compares two large numbers, perimeter losses with snow accumulation, with large uncertainties (Rignot and Thomas, 2002). It is critical to minimize these uncertainties to below a level of about 10%. This requires complete inventories of the ice sheets with the highest precision measurements and high-quality regional atmospheric climate models. At present, the

largest source of uncertainty remains the surface mass balance component, so that current estimates of the mass balance are no better than 9% precision in Greenland or about 50 Gt/year and no better than 5% in Antarctica or 100 Gt/year. The precision of the measurements in Antarctica is largely biased by the vast extent of dry East Antarctica. In the rapidly changing sectors of West Antarctica and the Antarctic Peninsula, our knowledge of net accumulation is indeed no better than 10%.

Time-variable gravity

Since April 2002, the GRACE satellite has been measuring the Earth's gravity field and its temporal variability. After removing the effects of ocean tides, atmospheric loading, variable pressure fields, and other effects, high-latitude data contain information on temporal changes in the mass distribution of the ice sheets and underlying rock. Because of its relatively high altitude aboveground, GRACE only collects coarse-resolution measurements (200–400 km) of the gravity field and its changes with time. The chief advantage of this technique is to yield a direct measurement of mass changes that does not require knowledge of its different components, the density at which the surface elevation changes, the fluxes of ice, or the position of the grounding line. Floating ice is not influencing the gravity field because floating ice is isostatically compensated, so gravity data does not include the contribution from floating ice.

Error sources include processing errors, leakage of gravity signal from regions surrounding the ice sheets, and causes of gravity changes other than ice-sheet changes. Of these, the largest uncertainty is the gravity change associated with vertical bedrock motion. Velicogna and Wahr (2006) estimated a mass-balance correction of 5 ± 17 Gt/year for bedrock motion in Greenland, and 173 ± 71 Gt/year for Antarctica (Velicogna and Wahr, 2006). As more constraints are established on the magnitude of postglacial rebound, for instance using the GPS data collected by POLNET, the gravity technique will provide high-precision measurements of mass balance and continental-scale maps of mass changes. On the other hand, these data do not provide direct information on the components of change, that is, whether they are due to a change in snowfall, ice melt, or glacier discharge. It is an integrated method.

Another source of uncertainty affecting these data is the short duration of the GRACE mission. During that short duration, the signal is influenced not only by the long-term evolution of the mass of ice sheets but also by the seasonal, interannual to decadal variability in surface mass balance. This is especially significant in Antarctica where total surface mass balance is nearly seven times larger than in Greenland but the total mass losses are comparable in magnitude. A number of studies have examined the average mass loss over short periods. The results are biased by the evolution of surface mass balance during that time period, which may not reflect long-term changes. In addition, it is well established that the mass loss of these ice sheets is not constant, but is increasing with time. Time averages calculated over different periods of time therefore naturally disagree.

In terms of absolute mass loss, the gravity technique is capable of a precision of 20–30 Gt/year in Greenland and 70–90 Gt/year in Antarctica, which is better than the mass budget method. In terms of changes with time, or the second-order derivative of mass, $M(t)$, with respect to time, or d^2M/dt^2, it is important to note that the GRACE data is not affected by the precision of postglacier rebound since this signal is constant over the timescale under consideration. Hence the technique is even more reliable to detect changes in mass loss with time than to quantify absolute losses.

Repeated altimetry survey

Rates of surface-elevation change reveal changes in ice-sheet mass after correction for changes in depth/density profiles and bedrock elevation, or for hydrostatic equilibrium and tides if the ice is floating. Satellite radar altimetry has been widely used (e.g., Shepherd et al., 2002; Davis et al., 2005; Johannessen et al., 2005; Zwally et al., 2005), together with laser altimetry from airplanes (Krabill et al., 2000), or NASA's ICESat (Zwally et al., 2002a; Thomas et al., 2007). Modeled corrections for isostatic changes in bedrock elevation (e.g., Peltier, 2004) are small (few mm/year) but with errors comparable to the correction. Those for near-surface snow density changes (Arthern and Wingham, 1998) are larger (1 or 2 cm/year) and also uncertain. Historically, this technique has the longest time record, which is critically valuable for examining the interior regions of ice sheets, which are dominated by a strong interannual variability in surface mass balance. This is also the first technique proposed historically to monitor ice sheets.

Radar altimetry employs beams of 20 km or more, designed primarily for the surface of the nearly flat ocean. Radar returns are far more complex over the sloping and undulating ice-sheet surfaces with spatially and temporally varying dielectric properties. Radar range measurements are generally off nadir, and return-waveform information is biased toward the earliest reflections (i.e., highest regions) within the large footprint, and depends on radar penetration into near-surface snow. On glaciers and ice streams, ice flows in surface depressions that can be narrower than the radar footprint, so that elevation changes are weighted toward slower-moving ice along the glacier sides. At high elevation, climate warming affects the depth of the reflecting horizon of ice sheets, and those changes may be misinterpreted as volume change, especially Greenland (Thomas et al., 2007). This makes the interpretation of radar altimetry data on a melting surface challenging to interpret.

Laser altimetry provides data that is easier to interpret: footprints are small (1 m for airborne, 60 m for satellite)

and there is negligible penetration of laser into snow and ice. However, cloud cover, atmospheric conditions, and laser pointing errors limit the precision of the technique to 20–30 cm vertical, versus 10–20 cm vertical from an airplane platform. Existing laser data are sparse compared to radar altimetry data because of the orbit selection for ICESAT-1, and the limited range of aircrafts. Laser altimetry has been operating from 1993 on airplanes in Greenland, from 2002 in Antarctica, and from 2002 on satellites.

Both laser and radar altimetry operate in profiling mode with a narrow swath that does not allow a comprehensive survey of the entire ice sheet. This introduces biases in regions where changes are concentrated and high, for example, for a rapidly thinning glacier. Most often, this may result in an underestimation of the glacier loss or of the glacier thickening. Once this issue is solved, changes in volume must then be converted into changes in mass. This requires knowledge of the density at which these changes are taking place, for example, snow (density of 0.3) versus pure ice (density of 0.917), and corrections from temporal variations in the depth of the firn layer, or firn compaction. Overall, the issues of steep slopes in the coastal regions, coarse track spacing, unknown density, and firn compaction have limited the potential of altimetry at providing reliable estimates of total mass loss. This technique has however been important and critical to outline regions of change, to document the pattern of thinning of glaciers and ice streams, and to detect decadal trends in interior accumulation. This technique has clearly demonstrated the importance of losses from ice dynamics by mapping out areas of ice thinning corresponding to areas of fast flow. It has also revealed sharp transition in mass balance across ice divides (Krabill et al., 1999). The continuing record of altimetry data is extending in time and improving with each additional year on record.

Results

Ice locked in the Greenland and Antarctic ice sheets has long been considered immune to change, protected by the extreme cold of the polar regions. Global climate models suggested that climate warming would enhance precipitation in the interior, increased melting from coastal regions, yielding a small loss in mass from Greenland and a gain in mass from Antarctica for an overall modest contribution to sea level. Observations from the last 2 decades and recent advances in regional climate modeling however show a different story.

In terms of precipitation on ice sheets, regional climate models show no significant change in precipitation, but large interannual to decadal variability, which, taken over short time periods of a few years to a decade reveal growth or shrinkage, but analyzed over the last 25–50 years show no evidence for change, except for the western flanks of the Antarctic Peninsula where precipitation has increased (Monaghan et al., 2006; Van den Broeke et al., 2006). In Greenland, the results are similar but models and in situ data indicate a marked increase in ice melt, at a rate of 14 ± 4 Gt/year^2 in 1992–2008 (Ettema et al., 2009). As a result, the surface mass balance of Antarctica exhibits no long-term trend, while in Greenland it has decreased steadily since the 1990s.

Airborne observations indicated that the Greenland ice sheet is thinning along its edges and near balance in the interior (Krabill et al., 2000). Thinning at the coast is concentrated along narrow channels occupied by outlet glaciers and is therefore not indicative of a change in snowfall but of a change in ice dynamics. In Antarctica, changes are concentrated along the coast in narrow channels occupied by ice streams and glaciers. Glacier acceleration is confirmed using InSAR and other measurements of ice stream motion (Rignot and Kanagaratnam, 2006; Rignot et al., 2008). The dynamic response of the glaciers is complex, however, and not fully understood. Even though we know that it is affected by the geometry of the glaciers, their depth below sea level, the makeup of the glacier beds, ocean water heat fluxes, surface runoff, and other effects, the complex interactions between these processes are poorly documented, understood, and modeled.

In Greenland, the results from the three mass balance techniques do not agree perfectly in terms of absolute losses, but they all indicate a similar trend in increasing mass losses. For the mass budget method, the results will improve as the survey of glaciers becomes more complete and accurate, and regional atmospheric climate models operated at higher resolution gain in precision. For the time-variable gravity method, it is now possible to detect the increase in mass loss from ice sheets (Velicogna, 2009). For radar altimetry, we have a long record of glacier and ice shelf changes.

Some of the differences between measurement techniques are directly explainable. For instance, areas not surveyed by airborne laser altimetry were estimated using a melt model. Mass losses were therefore systematically estimated in places where losses from ice dynamics are significant. Similarly, the GRACE results do not always address the same time periods, hence includes periods where surface mass balance – the dominant term of the signal – behaves differently. For the mass budget method, recent surface mass balance has shown large disagreements with earlier estimates based on interpolation of in situ data.

To improve upon these results, more ice thickness data are needed on the outlet glaciers, regional climate models must be operated at a higher spatial resolution and compared to additional field data, and time-variable gravity, altimetry, and ice motion must be collected systematically and almost continuously for many decades to come. Such observations are critical to help numerical models of ice sheet flow become more reliable and more practical for prediction. In addition to these satellite measurements and associated field program, we need to continue

documenting surface climate with weather stations, and collect critical data about processes taking place at the bed and occluded from the view of satellites. In the case of ice–ocean interactions and their impact on ice sheet balance, multidisciplinary efforts going well beyond the field of glaciology are required to circumvent our current limitations and make great strides at improving the predictability of ice sheets.

Bibliography

Arthern, R. J., Winebrenner, D. P., and Vaughan, D. G., 2006. Antarctic snow accumulation mapped using polarization of 4.3-cm wavelength microwave emission. *Journal of Geophysical Research*, **111**, D06107, doi:10.1029/2004JD005667.

Bamber, J. L., Gomez-Dans, J. L., and Briggs, J. A., 2009. A new 1 km digital elevation model of the Antarctic derived from combined satellite radar and laser data. Part 1: data and methods. *The Cryosphere Discuss.*, **2**, 811–841.

Chen, J. L., Wilson, C. R., and Tapley, B. D., 2006. Satellite gravity measurements confirm accelerated melting of Greenland Ice Sheet. *Science*, doi:10.1126/science.1129007 (Published Online: *Science Express*, August 10, 2006).

Davis, C. H., Li, Y., McConnell, J. R., Frey, M. M., and Hanna, E., 2005. Snowfall-driven growth in East Antarctic ice sheet mitigates recent sea-level rise. *Science*, **308**(5730), 1898–1901.

Ettema, J., van den Broeke, M. R., van Meijgaard, E., van de Berg, W. J., Bamber, J. L., Box, J. E., and Bales, R. C., 2009. Higher surface mass balance of the Greenland ice sheet revealed by high-resolution climate modeling. *Geophysical Research Letters*, **36**, L12501, doi:10.1029/2009GL038110.

Helsen, M. M., van den Broeke, M. R., van de Wal, R. S. W., van de Berg, W. J., van Meijgaard, E., Davis, C. H., Li, Y., and Goodwin, I., 2008. Elevation changes in Antarctica mainly determined by accumulation variability. *Science*, **320**, 1626–1629, doi:10.1126/science.1153894.

Holland, D. M., Thomas, R. H., deYoung, B., Ribergaard, M. H., and Lyberth, B., 28 September 2008. Acceleration of Jakobshavn Isbrae triggered by warm subsurface ocean waters. *Nature Geoscience*, **1**, 659–664, doi:10.1038/ngeo316.

Howat, I. M., Joughin, I., Tulaczyk, S., and Gogineni, S., 2005. Rapid retreat and acceleration of Helheim Glacier, east Greenland. *Geophysical Research Letters*, **32**, 22, doi:10.1029/2005GL024737.

Johannessen, O. M., Khvorostovsky, K., Miles, M. W., and Bobylev, L. P., 2005. Recent ice-sheet growth in the interior of Greenland. *Science*, **310**(5750), 1013–1016.

Joughin, I., Abdalati, W., and Fahnestock, M., 2004. Large fluctuations in speed on Greenland's Jakobshavn Isbrae glacier. *Nature*, **432**, 608–610.

Krabill, W., et al., 2000. Greenland ice sheet: high-elevation balance and peripheral thinning. *Science*, **289**(5478), 428–430.

Krabill, W., et al., 2004. Greenland Ice Sheet: increased coastal thinning. *Geophysical Research Letters*, **31**, L24402.

Luckman, A., and Murray, T., 2005. Seasonal variation in velocity before retreat of Jakobshavn Isbræ, Greenland. *Geophysical Research Letters*, **32**, L08501, doi:10.1029/2005GL022519.

Nick, F. M., Vieli, A., Howat, I. M., and Joughin, I., 2009. Large-scale changes in Greenland outlet glacier dynamics triggered at the terminus. *Nature Geoscience*, **2**, 110–114, doi:10.1038/NGEO394.

Peltier, W. R., 2004. Global glacial isostasy and the surface of the ice-age earth: the ice-5G (VM2) model and grace. *Annual Review of Earth and Planetary Sciences*, **32**, 111–149.

Rignot, E., 1996. Tidal motion, ice velocity and melt rate of Petermann Gletscher, Greenland, measured from radar interferometry. *Journal of Glaciology*, **42**(142), 476–485.

Rignot, E., 2008. Changes in West Antarctic ice stream dynamics observed with ALOSPALSAR data. *Geophysical Research Letters*, **35**, L12505, doi:10.1029/2008GL033365.

Rignot, E., and Kanagaratnam, P., 2006. Changes in the velocity structure of the Greenland Ice Sheet. *Science*, **311**, 986–989.

Rignot, E., and Thomas, R. H., 2002. Mass balance of Polar Ice Sheets. *Science*, **297**, 1502–1506.

Rignot, E., Casassa, G., Gogineni, P., Krabill, W., Rivera, A., and Thomas, R., 2004. Accelerated ice discharge from the Antarctic Peninsula following the collapse of Larsen B ice shelf. *Geophysical Research Letters*, **31**, L18401.

Rignot, E., et al., 2008a. Recent Antarctic ice mass loss from radar interferometry and regional climate modelling. *Nature Geoscience*, **1**, 106–110.

Rignot, E., Box, J. E., Burgess, E., and Hanna, E., 2008b. Mass balance of the Greenland ice sheet from 1958 to 2007. *Geophysical Research Letters*, **35**, L20502, doi:10.1029/2008GL035417.

Rignot, E., Koppes, M., Velicogna, I., in press. Rapid melting of the calving faces of Greenland's tidewater glaciers. *Nature Geoscience*.

Shepherd, A., Wingham, D., and Mansley, A., 2002. Inland thinning of the Amundsen Sea Sector, West Antarctica. *Geophysical Research Letters*, **29**(10), Art. No. 1364.

Thomas, R. H., 2004. Force-perturbation analysis of recent thinning and acceleration of Jakobshavn Isbrae, Greenland. *Journal of Glaciology*, **50**, 57–66.

Thomas, R. H., et al., 2007. A comparison of Greenland ice-sheet volume changes derived from altimetry measurements. *Journal of Glaciology*, **54**, 203–212.

Van de Berg, W. J., van den Broeke, M. R., and van Meijgaard, E., 2006. Reassessment of the Antarctic surface mass balance using calibrated output of a regional atmospheric climate model. *Journal of Geophysical Research*, **111**, D11104, doi:10.1029/2005JD006495.

Van den Broeke, 2006. Towards quantifying the contribution of the Antarctic ice sheet to global sea level change. *Journal de Physique IV France*, **139**, 179–187.

Van den Broeke, M. R., van de Berg, W. J., and van Meijgaard, E., 2006. Snowfall in coastal West Antarctica much greater than previously assumed. *Geophysical Research Letters*, **33**, L02505, doi:10.1029/2005GL025239.

Vaughan, D. G., 1995. Tidal flexure at ice shelf margins. *Journal of Geophysical Research*, **100**(B4), 6213–6224.

Vaughan, D. G., Bamber, J. L., Giovinetto, M., Russell, J., and Cooper, A. P. R., 1999. Reassessment of net surface mass balance in Antarctica. *Journal of Climate*, **12**, 933–946.

Velicogna, I., 2009. Increasing rates of ice mass loss from the Greenland and Antarctic Ice Sheets revealed by GRACE. *Geophysical Research Letters*, **36**, L19503.

Velicogna, I., and Wahr, J., 2006. Acceleration of Greenland ice mass loss in spring 2004. *Nature*, **443**(7109), 329–331.

Velicogna, I., and Wahr, J., 24 March 2006. Measurements of time-variable gravity show mass loss in Antarctica. *Science*, **311**, 1754–1756.

Velicogna, I., Wahr, J., Hanna, E., and Huybrechts, P., 2005. Short term mass variability in Greenland, from GRACE. *Geophysical Research Letters*, **32**, L05501.

Wingham, D. J., Wallis, D. W., and Shepherd, A., 2009. Spatial and temporal evolution of Pine Island Glacier thinning, 1995–2006. *Geophysical Research Letters*, **36**, L17501, doi:10.1029/2009GL039126.

Zwally, H. J., et al., 2005. Mass changes of the Greenland and Antarctic ice sheets and shelves and contributions to sea-level rise: 1992–2002. *Journal of Glaciology*, **51**(175), 509–527.

ICE SHELF

Adrian Jenkins
British Antarctic Survey, Natural Environment Research Council, Cambridge, UK

Definition

Ice shelf. Part of an *ice sheet* that floats on the ocean while remaining attached to grounded ice.

General characteristics

Ice shelves form at the margins of an *ice sheet*, where the ice becomes thin enough to float free of a bed that lies below sea level. Ice shelf-like features also form in the interior of ice sheets where the ice floats on subglacial lakes. Most of the ice shelves that currently exist on Earth are found in *Antarctica*. In particular, ice shelves almost completely surround the *marine ice sheet* of West Antarctica. The larger ice shelves are fed by multiple glaciers, the outflows from which coalesce to form a distinct glaciological feature, but the smaller ones are generally the floating termini of single *tidewater glaciers*. Although any ice that exists between the grounding line and the calving front of a tidewater glacier is formally an ice shelf, these features are often not accorded an identity distinct from their parent glaciers.

Ice shelves range in thickness from less than 100 to over 2,000 m and individually cover areas of up to 0.5 million km^2 (Vaughan et al., 1999). In Antarctica, the combined area of all the ice shelves is only 14% of that of the grounded ice sheet, but around 80% of the snow that falls over the grounded ice drains into them before being lost to the oceans (Vaughan et al., 1999). The processes of mass loss from the ice shelves are therefore critical in determining the overall mass balance of the ice sheet. Their level and largely crevasse-free surfaces gave the great ice shelves of Antarctica historical significance as providers of relatively safe routes to the interior of the ice sheet for the earliest exploratory expeditions.

Ice shelf dynamics

Ice shelves are distinct from other parts of the ice sheet in that they rest on a frictionless substrate. The flow of an ice shelf is therefore controlled entirely by the tendency of the ice to spread horizontally and the degree to which this tendency is opposed by the lateral confinement provided by surrounding ice or land masses (see Paterson, 1994 for a review of the mathematics).

The tendency to spread is a result of the density difference between the ice and the water in which it floats. The lower density ice has a freeboard, with between 10% and 20% of its thickness being supported above the waterline. As a consequence the pressure at any point within the ice shelf, resulting from the weight of overlying ice, exceeds the pressure at the same level within the ocean, resulting from the weight of overlying seawater. Only at the level of the ice shelf base does the pressure within the ocean equal that within the ice; this is the floatation condition. The ice shelf response to the excess pressure is lateral spreading, the speed of which is controlled by the effective viscosity of the ice. The forces that drive spreading increase with the thickness of the ice shelf, so lateral spreading and the consequent thinning of the ice shelf are more rapid where the ice thickness is greater. As a result variations in thickness tend to decay over time, and this gives rise to one of defining characteristics of ice shelves; the near absence of surface topography.

For an ice shelf that is bounded on more than one side by ice or land masses, additional processes need to be considered. Spreading of the ice is restricted by the lateral barriers, so that for an ice shelf occupying an embayment with near-parallel sides the spreading is predominantly unidirectional, parallel to the bay walls. Importantly, there is also a frictional resistance to ice flow parallel to the walls. This means that even in the direction that the ice is free to spread there is a force opposing the spreading generated by the need to push all the ice downstream past the bay walls. The magnitude of this force is related to the degree of confinement of the ice and is greater for ice in the interior of the ice shelf than for ice near the seaward edge.

By a similar argument, ice flowing across the grounding line of an ice shelf must push the entire ice shelf past its confining obstructions, but how far inland this effective restraint on the flow of the grounded ice sheet is felt has been the subject of much debate. The *ice streams* feeding the ice shelves are themselves closely confined by lateral shear margins, and flow over a bed where additional frictional resistance is generated. Inland these local forces will eventually dominate, but the distance over which the restraint of the ice shelf plays a role in controlling the ice stream flow is a critical parameter, since it determines the extent to which the flow of grounded ice can be influenced by changes in the ice shelf.

Mass balance

Ice shelves are fed by the flow of ice from the grounded ice sheet and by the *accumulation* of snowfall on the upper surface. In some places accumulation of mass also occurs at the lower surface, through the *freezing* on of seawater. In most cases, the flow of ice from inland is the dominant input. Mass loss occurs by the *calving* of *icebergs* from the seaward edge, and by the *melting* of ice from the underside. More rarely, some mass loss occurs by surface melting or sublimation.

Calving from ice shelves tends to produce massive tabular icebergs, the largest of which can exceed 10,000 km^2 in area. The process is quasiperiodic, with long stages of steady ice front advance, lasting anywhere from a few years to many decades, interspersed with major calving events. A stable ice front will generally have its location determined by the arrangement of confining ice or land features. Periods of advance will take the ice front beyond the influence of the confining features, then calving will

eventually remove the less well constrained ice. If calving removes ice from parts of the ice shelf where the flow is controlled by lateral confinement, it has been suggested that the configuration is then unstable and further rapid retreat of the ice front is probable (Doake et al., 1998). However, our understanding of the processes by which fractures in ice initiate and propagate remains insufficient at present to formulate a physically based calving law, and the long timescales involved complicate the collection of the observational data required to validate such a model.

Their strong interaction with the seawater beneath them is a defining feature of ice shelves, and the processes that drive melting and freezing beneath ice shelves have been the subject of much research over the past 3 decades (see Jacobs et al., 1992 and Williams et al., 1998 for general discussions). One critical point is the pressure dependence of the freezing point of seawater. Seawater that is cooled through contact with the atmosphere cannot be made colder than about −1.9°C. At this temperature ice begins to form. However, the temperature at which the phase change occurs falls by about 0.75°C for every 1,000 m of water depth. Seawater that is cooled through contact with the base of an ice shelf can therefore attain a temperature lower than the surface freezing point. Water that has such a property is referred to as Ice shelf water (ISW).

When seawater that is warmer than its depth-dependent freezing point comes into contact with the base of an ice shelf, it gives up some of its heat to melt ice. Melting the ice shelf freshens the seawater, lowering its density. The less dense water rises toward the surface, constrained by the sloping ice shelf base. The reduction in pressure as the water ascends means that its freezing point rises, a process that would tend to reduce its potential to drive further melting, but the outflowing water gains heat continuously by turbulent mixing. If the heat supplied to the outflow is sufficient to maintain its temperature above the freezing point, melting will persist. The continued input of meltwater leads to a further increase in the buoyancy of the outflow, sustaining its motion along the ice shelf base. If the input of heat from turbulent mixing is insufficient to maintain the temperature above the freezing point, the water becomes *supercooled*, and melting will give way to freezing. Ice will be deposited in the form of *frazil ice* crystals on the ice shelf base and the loss of freshwater from the outflow will decrease its buoyancy, eventually halting its rise toward the sea surface.

Seawater temperatures observed near ice shelves range from the surface freezing point (−1.9°C) to about 3.5°C above the freezing point, while inferred mean melt rates range from a few tens of centimeters per year to several tens of meters per year.

Ice shelves in a changing climate

Being in contact with both the atmosphere above and the ocean below, ice shelves are seen as sensitive indicators of climate change. The retreat and disintegration of ice shelves along the Antarctic Peninsula appear to be linked to regional atmospheric warming and were among the earliest and most dramatic indicators of change in the Antarctic Ice Sheet (Vaughan and Doake, 1996). The most significant changes in surface elevation that have been revealed by radar altimetry since the early 1990s have occurred over the ice shelves of the Amundsen Sea, where thinning rates of several meters per year have been inferred (Shepherd et al., 2004). The magnitude of the thinning suggests that the cause is a change in the basal melt rate of the ice shelves, brought about by some change in the ocean.

There are several reasons why the Peninsula ice shelves have been the ones most dramatically affected by changes in surface air temperature. One is the fact that air temperatures along the Peninsula have been rising faster over the last 50 years than elsewhere in Antarctica, where little change has occurred (Turner et al., 2005). However, even a rapid change in surface temperature would have little impact on an ice shelf if the temperatures remained below freezing year-round. The warming has been critical because it has increased the area where summer temperatures rise above the freezing point, causing the surface of the ice shelves to melt. Wet snow and liquid water have a lower albedo than dry snow, so once melting starts the surface absorbs more shortwave radiation, which contributes toward further melting in a positive feedback cycle.

The lack of surface topography on ice shelves means that meltwater ponds locally. Runoff can only occur if drainage pathways open up through the ice shelf to the underlying ocean. This can happen when sufficient meltwater is generated to fill surface crevasses. The pressure within a water-filled crevasse exceeds that in the surrounding ice shelf, driving the crevasse open. Penetration of multiple fractures through the ice by this mechanism is thought to be the process behind the catastrophic breakup of the Peninsula ice shelves (Scambos et al., 2000). The vulnerability of ice shelves to surface melt imposes a strict climatic limit on their existence. If the summers become warm enough to generate significant surface melt, the ice shelf is no longer viable in the long term and its eventual demise appears to be inevitable.

In the Amundsen Sea, surface air temperatures remain below freezing even in summer, so despite suggestions that this region may also have warmed over the past 50 years (Steig et al., 2009), those changes have had little impact on the ice shelves. However, along the Amundsen Sea coast, subsurface water temperatures are more than 3°C above the pressure freezing point throughout the year (Hellmer et al., 1998). The warm water is a derivative of Circumpolar Deep Water (CDW), a water mass that circles Antarctica within the Circumpolar Current, but that only reaches the ice shelves in the Amundsen and Bellingshausen seas. Understanding the reasons for its presence close to the ice shelves and the possible causes of variability in its flow are critical steps in defining the cause of the observed ice shelf thinning. One possibility is that variability in the wind forcing of the Amundsen

Sea circulation is a source of variability in the flow of CDW toward the ice shelves (Thoma et al., 2008).

Links with the global climate system

Changes in the size of the ice shelves affect global sea level by two processes. Contrary to popular belief there is a small affect on sea level when floating ice is converted to meltwater (Jenkins and Holland, 2007). Since the meltwater is fresh it has a lower density than saltwater and hence occupies a volume that is about 2.5% greater than that of the seawater that was displaced by the ice. The density of seawater is an approximately linear function of its salinity, so the total volume of the ocean and fresh meltwater remains fixed as the two are mixed together. The net result of a reduction in the volume of the ice shelves is therefore a slight freshening and consequent expansion of the ocean. A further contribution to sea level that is generally more significant is related to the dynamical coupling between the ice shelves and the inland ice sheet discussed earlier. A reduction in the size of the ice shelves reduces the restraint they exert on the flow of the inland ice, allowing the outlet glaciers to accelerate and discharge more grounded ice into the ocean. Although the scale and rapidity of the inland changes that could result is still the subject of debate, the impacts have been observed. Following the disintegration of the northern peninsula ice shelves, the glaciers that fed them experienced marked accelerations, at least at their downstream ends (Rignot et al., 2004), while the ongoing changes in the flow of the main Amundsen Sea glaciers (Rignot, 2008) have generally been attributed to thinning of the floating ice shelves.

Around most of the Antarctic coastline outside of the Amundsen and Bellingshausen seas the winters are sufficiently cold that all the waters close to the ice shelves are cooled to the surface freezing point. Thus, further cooling beneath an ice shelf inevitably produces ISW, as described above. The production of ISW has implications for the global ocean circulation (Foldvik and Gammelsrød, 1988), since ISW is one ingredient in the densest form of Antarctic Bottom Water (AABW). AABW is found at the bottom of the ocean throughout most of the world, and its formation around Antarctica is one component of the global overturning circulation that regulates the Earth's climate.

Summary

Ice shelves are ubiquitous features of marine-terminating ice sheets. They form where the ice sheet margins are thin enough to float free of the seabed. Their flow is characterized by lateral spreading, and critically controlled by the degree of lateral confinement. They interact both with the atmosphere and, particularly strongly, with the ocean, which through melting the ice shelf base and transporting icebergs away exerts the primary controls on the thickness and extent of the ice shelves. Changes in the ice shelves have implications for global sea level, because of the control exerted by the ice shelves on the flow of the grounded ice sheet, and for the global ocean circulation, because of the role played by ISW in the formation of AABW.

Bibliography

Doake, C. S. M., Corr, H. F. J., Rott, H., Skvarca, P., and Young, N. W., 1998. Breakup and conditions for stability of the northern Larsen Ice Shelf, Antarctica. *Nature*, **391**, 778–780.

Foldvik, A., and Gammelsrød, T., 1988. Notes on Southern Ocean hydrography, sea-ice and bottom water formation. *Palaeogeography, Palaeoclimatology, Palaeoecology*, **67**, 3–17.

Hellmer, H. H., Jacobs, S. S., and Jenkins, A., 1998. Oceanic erosion of a floating Antarctic glacier in the Amundsen Sea. In *Ocean, Ice and Atmosphere: Interactions at the Antarctic Continental Margin*. Antarctic Research Series, 75. Washington: American Geophysical Union, pp. 83–99.

Jacobs, S. S., Hellmer, H. H., Doake, C. S. M., Jenkins, A., and Frolich, R. M., 1992. Melting of ice shelves and the mass balance of Antarctica. *Journal of Glaciology*, **38**, 375–387.

Jenkins, A., and Holland, D., 2007. Melting of floating ice and sea level rise. *Geophysical Research Letters*, **34**, L16609.

Paterson, W. S. B., 1994. *The Physics of Glaciers*, 3rd edn. Oxford: Elsevier Science.

Rignot, E., 2008. Changes in West Antarctic ice stream dynamics observed with ALOS PALSAR data. *Geophysical Research Letters*, **35**, L12505.

Rignot, E., Casassa, G., Gogineni, P., Krabill, W., Rivera, A., and Thomas, R., 2004. Accelerated ice discharge from the Antarctic Peninsula following the collapse of Larsen B ice shelf. *Geophysical Research Letters*, **31**, L18401.

Scambos, T., Hulbe, C., Fahnestock, M., and Bohlander, J., 2000. The link between climate warming and break-up of ice shelves in the Antarctic Peninsula. *Journal of Glaciology*, **46**, 516–530.

Shepherd, A., Wingham, D., and Rignot, E., 2004. Warm ocean is eroding West Antarctic ice sheet. *Geophysical Research Letters*, **31**, L23402.

Steig, E. J., Schneider, D. P., Rutherford, S. D., Mann, M. E., Comiso, J. C., and Shindell, D. T., 2009. Warming of the Antarctic ice-sheet surface since the 1957 international geophysical year. *Nature*, **457**, 459–462.

Thoma, M., Jenkins, A., Holland, D., and Jacobs, S., 2008. Modelling Circumpolar Deep Water intrusions on the Amundsen Sea continental shelf, Antarctica. *Geophysical Research Letters*, **35**, L18602.

Turner, J., Colwell, S. R., Marshall, G. J., Lachlan-Cope, T. A., Carleton, A. M., Jones, P. D., Lagun, V., Reid, P. A., and Iagovkina, S., 2005. Antarctic climate change during the last 50 years. *International Journal of Climatology*, **25**, 279–294.

Vaughan, D. G., and Doake, C. S. M., 1996. Recent atmospheric warming and retreat of ice shelves on the Antarctic Peninsula. *Nature*, **379**, 328–331.

Vaughan, D. G., Bamber, J. L., Giovinetto, M., Russell, J., and Cooper, A. P. R., 1999. Reassessment of net surface mass balance in Antarctica. *Journal of Climate*, **12**, 933–946.

Williams, M. J. M., Jenkins, A., and Determann, J., 1998. Physical controls on ocean circulation beneath ice shelves revealed by numerical models. In *Ocean, Ice and Atmosphere: Interactions at the Antarctic Continental Margin*. Antarctic Research Series, 75. Washington: American Geophysical Union, pp. 285–299.

Cross-references

Antarctica
Calving Glaciers
Frazil

Freezing Bottom (Ice Shelf)
Ice Sheet
Supercooled Water
Tidewater Glaciers

ICE-CORED MORAINES

Sven Lukas
Department of Geography, Queen Mary University of London, London, UK

Synonyms

Buried ice; Dead-ice zone; Hummocky moraine; Ice-collapse landscape; Kame-and-kettle terrain; Kettle moraine

Definition

Ice-cored moraines are ice-marginal landforms that comprise a discrete body of glacier ice buried underneath sediment. These landforms are transitional because any incorporated ice needs to melt out before the final resulting landform, e.g. a stable moraine, is formed.

Introduction

The term "ice-cored moraine" was introduced into the scientific literature by Østrem (1959, 1965) to describe the frequently observed occurrence of bodies of ice within sediment accumulations at or near ice fronts. Such landforms are widespread in modern glacier forelands and have been investigated in numerous settings over the past five decades.

Usually, ice-cored moraines evolve through a chain of processes involving: (a) the isolation of a body of glacier ice through the establishment of a sediment/debris cover near the margin which, if sufficiently thick, shields the ice from melting, resulting in (b) differential melting of protected sediment-covered ice and clean ice upglacier. At some point (c) the sediment-covered ice will be cut off from supply of active ice upglacier, leading to a transition to either stagnant or dead ice. From this point onwards (d) the body of sediment-covered ice, especially if ridge- or mound-like in appearance and occurring along the ice margin, can be regarded as an ice-cored moraine sensu stricto. Such landforms occur as individual mounds or ridges (Lukas et al., 2007; Figure 1) or constitute broad belts or zones up to several kilometers wide that are unconnected to a glacier (e.g., Kjær and Krüger, 2001). However, some authors prefer to use the term much more loosely to include moraine-like ridges in supraglacial sediment underlain by ice, irrespective of the fact that the ice is still flowing (active) and/or continuous underneath the sediment cover (e.g., Lønne and Lyså, 2005; Evans, 2009).

Ice-Cored Moraines, Figure 1 Photograph showing an ice-cored moraine at the margin of Gornergletscher, Switzerland, June 2007. The ice core was still in contact with the ice margin at the time this photograph was taken, illustrating the process of cutoff from a formerly coherent body of glacier ice.

Ice-core formation

There are three ways in which buried ice can be formed. Firstly, active glacier ice near the ice-margin can be covered by sediment and thus be cut off from supply of active ice upglacier during periods of negative mass balance. Secondly, continued delivery of material to the same spots (depocenters) can lead to thickening of the supraglacial debris cover and thus differential ablation. Thirdly, dead ice can remain in situ and be incorporated where a glacier advances over older dead-ice terrain.

The physical principle behind dead ice formation is that clean or debris-free glacier ice has a much higher albedo than dirty ice. While a thin cover of debris will lead to enhanced ablation (e.g., Adhikary et al., 2000), thicker layers will insulate underlying ice from melting; several decimeters to meters of debris may be required, depending on local factors. Uneven clean ice-debris distribution leads to differential ablation, and thicker layers of debris may lead to the cutoff of glacier ice near the margin and ultimately to the formation of ice-cored moraines.

This debris can be either derived from rockfall or reach the glacier surface through englacial debris septa in the ablation area. Supraglacial load tends to be concentrated near the margins by longitudinal compressive flow, leading to the establishment of thick supraglacial debris layers (Anderson, 2000). Englacial debris septa can either result from incremental adfreezing of meltwater and sediment (e.g., Alley et al., 1997) or folding, shearing, and thrusting near the margin (e.g., Glasser and Hambrey, 2003). They frequently occur as a result of flow compression at the transition between temperate and cold-based ice near the margins of polythermal glaciers. However, such debris septa have also been described from temperate glaciers in the Alps (Lukas et al., 2011).

If material from an englacial debris septum melts out at the glacier surface, it will mix with meltwater and slowly move down the glacier surface as a debris flow (Figure 2a). If the glacier surface lowers under negative glacier mass balance, the material along the top of the debris septum, as well as that relocated downslope, will protect the underlying ice and lead to the formation of an initial debris cone or ridge; this will subsequently be transformed into an isolated mound or ridge of debris overlying a conical or linear ice structure and may be classed as an ablation-dominant medial moraine (Figure 2b; Anderson, 2000).

If this process occurs in a setting where a number of debris septa are closely spaced (Figure 2c), a more uniform layer of supraglacial sediment may be created by lateral redistribution through debris flows, which may eventually lead to the isolation of wider tracts of glacier ice (Figure 2d) and the formation of controlled moraines where englacial structures of the parent ice are inherited (cf. Evans, 2009).

In permafrost environments, nivation and aeolian deposition are potentially significant extraglacial sources of supraglacial material (Lukas et al., 2005; Schomacker and Kjær, 2007). Additional sources are the meltout of material from englacial conduits or crevasse fills and collapse of preexisting material in the foreland onto the ice during glacier advance and bulldozing.

De-icing processes

Characteristic redistribution processes transform ice-cored moraines during de-icing. Two types of melting, classified according to the location of the melting front, have been described: downwasting and backwasting (cf. Kjær and Krüger, 2001).

Downwasting refers to a horizontally orientated melting front. Top-melt occurs where the debris cover is insufficiently thick to prevent conduction of thermal energy to the underlying ice. While the threshold thickness, above which melting ceases, varies in non-permafrost environments, it corresponds to the active layer thickness in permafrost environments. Bottom-melt is usually more limited than top-melt and may only equal or exceed the latter in areas with high geothermal gradients.

Backwasting is by far the dominant process in de-icing landscapes leaving a clear geomorphological imprint. It refers to all melting processes occurring on slopes and comprises the melting of free ice-cliffs and sediment-covered slopes.

De-icing processes include debris flows, gravity sorting, and melt pond formation. In humid, non-permafrost environments like Iceland, debris is redistributed in wider zones of dead-ice terrain, with debris being transferred from ice-cored moraines into depressions. Over time, topographic highs (ice-cored moraines) are lowered while

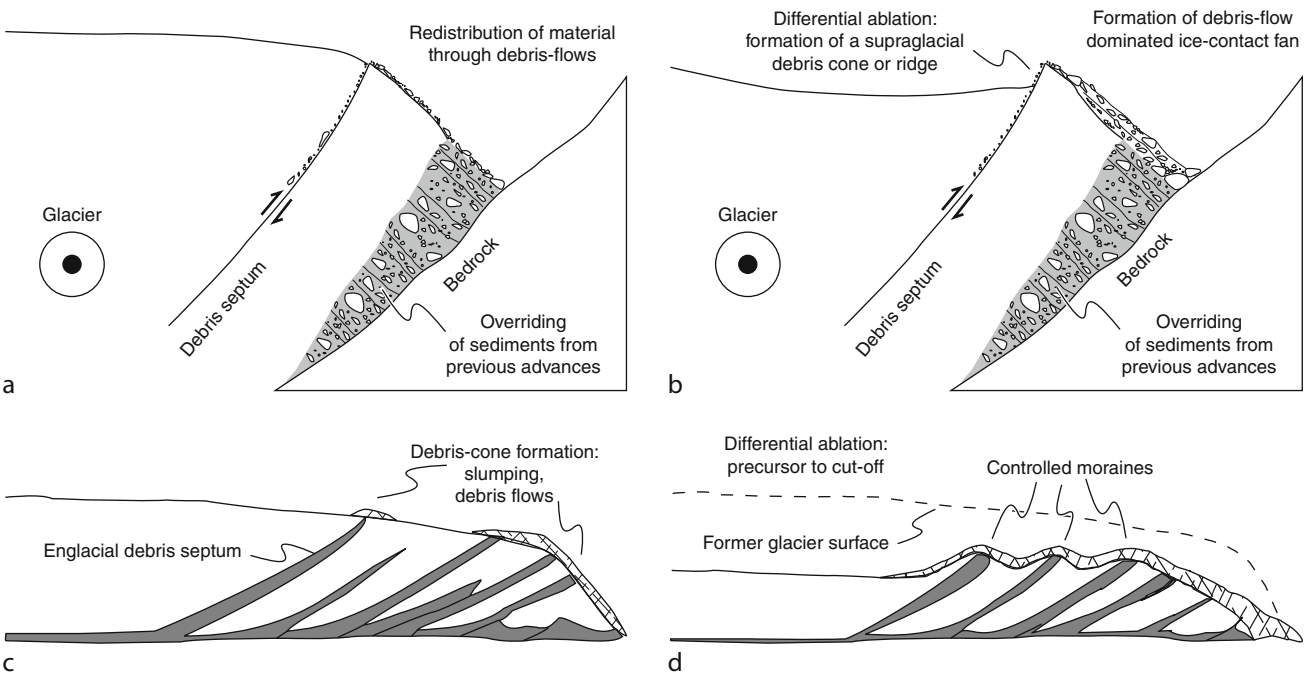

Ice-Cored Moraines, Figure 2 Schematic diagrams illustrating (**a**) the effect of emerging supraglacial debris along a debris septum and (**b**) the formation of a debris cone or ridge (cross-sectional view with ice flow away from the viewer). (**c**) Longitudinal view of the effect of a number of englacial debris septa emerging near a glacier margin and the effect of this (**d**) on the formation of a continuous debris cover and "controlled moraines."

former low-points (depressions) are infilled, resulting in relief inversion, but also an overall lowering of the relative heights within such dead-ice terrain.

In permafrost environments such as Svalbard debris flows have been reported to be by far the dominant process (Lukas et al., 2005; Schomacker and Kjær, 2008). This is probably because debris mostly exceeds the thickness of the active layer; therefore, any melt is limited to topographically unstable settings (slopes) where redistribution processes are active and expose buried ice.

Sedimentologically, the meltout of buried ice will leave an imprint that can help decipher the presence of paleo-dead ice in Quaternary sediments. Kjær and Krüger (2001) list a number of diagnostic criteria, such as de-stratification and openwork boulder accumulations within sediments. Benn (1992) and Lukas (2005) show how such structures can be used to reconstruct the presence of paleo-dead ice.

Implications

Ice-cored moraines (and other landforms containing buried ice) will be altered upon de-icing. However, the degree of alteration, and thus the preservation potential of an ice-cored moraine, will depend on the ice–debris ratio. If the latter is high, preservation potential will be low and vice versa. This is because (a) melting ice will release meltwater and cause redistribution of material (see above) and (b) dead ice occupies space that will be replaced with sediment during de-icing. Hence, any landscape containing buried ice cannot be taken as the final landscape. Consequently, any models that use such landscapes as modern analogues for interpreting paleo-glacier dynamics during the Pleistocene need to take this into account.

Some recent discussions on work in Svalbard have centered on precisely this problem: Some authors (e.g., Graham et al., 2007) have suggested that modern Svalbard glaciers, the forelands of which contain significant amounts of ice-cored moraines (termed "moraine-mound complexes" by those authors), can be used as one-to-one analogues of Younger Dryas glacial conditions in Upland Britain. However, the Svalbard landform assemblages used are largely transitional as outlined above, and thus this comparison ought to be viewed with caution (cf. Lukas, 2007; Evans, 2009). This debate illustrates the need to take into account the de-icing dynamics of ice-cored moraines.

Ice-cored moraines occur in a landscape which has, by definition, not completed deglaciation. Thus, while the glacier may have visibly retreated from a zone of apparently stable moraines, it needs to be considered that dead ice may still be present. De-icing can take decades to millennia (Everest and Bradwell, 2003); Dyke and Savelle (2000) even report an extreme case where ice-cored moraines have survived the entire Holocene under continuous permafrost conditions.

Therefore, the presence of dead-ice has profound implications on dating glacial landforms on Quaternary timescales. Any dead ice and its associated meltout will delay surface stabilization. This time lag means that any ages obtained, no matter by which dating method, represent minimum ages that are not a true reflection of the time of primary deglaciation. Therefore, any study using formerly ice-cored terrain in paleo-glacier and paleoclimate reconstruction needs to take great care to establish whether dead ice may have been present. This can best be achieved by using an integrated approach of geomorphology and sedimentology.

Conclusions

Ice-cored moraines are important features in glacial environments, because they occur in many ice-marginal settings under a wide range of glacier thermal regimes and alter significantly during de-icing. They are thus transitional landforms that cannot be used for glacier and palaeoclimate reconstruction or numerical dating in as straightforward a manner as de-iced, stable moraines. Likewise, any study using ice-cored moraines in conceptual models of ice-marginal dynamics and landform genesis needs to take into account de-icing processes in order to make robust predictions of future foreland evolution.

The term ice-cored moraine has been used rather widely in the literature to refer to quite different phenomena. It is suggested here that the term ice-cored moraine should be reserved for a landform (moraine) that (a) is disconnected from the active ice margin and (b) contains a discrete body of ice that is surrounded by sediment. This way, any overlaps with other parts of the ice-marginal/supraglacial debris-ice continuum, such as debris-covered ice margins, can be avoided.

Bibliography

Adhikary, S., Nakawo, M., Seko, K., and Shakya, B., 2000. Dust influence on the melting process of glacier ice: experimental results from Lirung Glacier, Nepal Himalayas. In Nakawo, M., Raymond, C. F., and Fountain, A. (eds.), *Debris-Covered Glaciers*. Wallingford: IAHS Press, pp. 43–52. IAHS-AISH Publication 264.

Alley, R. B., Cuffey, K. M., Evenson, E. B., Strasser, J. C., Lawson, D. E., and Larson, G. J., 1997. How glaciers entrain and transport basal sediment: physical constraints. *Quaternary Science Reviews*, **16**, 1017–1038.

Anderson, R. S., 2000. A model of ablation-dominated medial moraines and the generation of debris-mantled glacier snouts. *Journal of Glaciology*, **46**, 459–469.

Benn, D. I., 1992. The genesis and significance of 'hummocky moraine': evidence from the Isle of Skye, Scotland. *Quaternary Science Reviews*, **11**, 781–799.

Dyke, A. S., and Savelle, J. M., 2000. Major end moraines of Younger Dryas age on Wollaston Peninsula, Victoria Island, Canadian Arctic: implications for palaeoclimate and for formation of hummocky moraine. *Canadian Journal of Earth Sciences*, **37**, 601–619.

Evans, D. J. A., 2009. Controlled moraines: origins, characteristics and palaeoglaciological implications. *Quaternary Science Reviews*, **28**, 183–208.
Everest, J. D., and Bradwell, T., 2003. Buried glacier ice in southern Iceland and its wider significance. *Geomorphology*, **52**, 347–358.
Glasser, N. F., and Hambrey, M. J., 2003. Ice-marginal terrestrial landsystems: Svalbard polythermal glaciers. In Evans, D. J. A. (ed.), *Glacial Landsystems*. London: Arnold, pp. 65–88.
Graham, D. J., Bennett, M. R., Glasser, N. F., Hambrey, M. J., Huddart, D., and Midgley, N. G., 2007. A test of the englacial thrusting hypothesis of "hummocky"moraine formation: case studies from the northwest Highlands, Scotland: Comments. *Boreas*, **36**, 103–107.
Kjær, K. H., and Krüger, J., 2001. The final phase of dead-ice development: processes and sediment architecture, Kötlujökull, Iceland. *Sedimentology*, **48**, 935–952.
Lønne, I., and Lyså, A., 2005. Deglaciation dynamics following the Little Ice Age on Svalbard: implications for shaping of landscapes at high latitudes. *Geomorphology*, **72**, 300–319.
Lukas, S., 2005. A test of the englacial thrusting hypothesis of 'hummocky' moraine formation - case studies from the northwest Highlands, Scotland. *Boreas*, **34**, 287–307.
Lukas, S., 2007. Englacial thrusting and (hummocky) moraine formation: a reply to comments by Graham et al. (2007). *Boreas*, **36**, 108–113.
Lukas, S., Nicholson, L. I., Ross, F. H., and Humlum, O., 2005. Formation, meltout processes and landscape alteration of high-arctic ice-cored moraines - examples from Nordenskiöld Land, central Spitsbergen. *Polar Geography*, **29**, 157–187.
Lukas, S., Nicholson, L. I., and Humlum, O., 2007. Comment on Lønne and Lyså 2005: Deglaciation dynamics following the Little Ice Age on Svalbard: Implications for shaping of landscapes at high latitudes, Geomorphology 72, 300–319. *Geomorphology*, **84**, 145–149.
Lukas, S., Coray, S., Graf, A., and Schlüchter, C., 2011. The influence of clast lithology and fluvial reworking on the reliability of clast shape measurements in glacial environments – a case study from a temperate Alpine glacier. In Bridgland, D. R. (ed.), *Clast Lithological Analysis. Technical Guide*. London: Quaternary Research Association, in press.
Østrem, G., 1959. Ice melting under a thin layer of moraine, and the existence of ice cores in moraine ridges. *Geografiska Annaler*, **51**, 228–230.
Østrem, G., 1965. Problems of dating ice-cored moraines. *Geografiska Annaler*, **47A**, 1–38.
Schomacker, A., and Kjær, K. H., 2007. Origin and de-icing of multiple generations of ice-cored moraines at Brúarjökull, Iceland. *Boreas*, **36**, 411–425.
Schomacker, A., and Kjær, K. H., 2008. Quantification of dead-ice melting in ice-cored moraines at the high-Arctic glacier Holmströmbreen, Svalbard. *Boreas*, **37**, 211–225.

Cross-references

Dating Glacial Landforms
Debris-Covered Glaciers
Deglaciation
Ice-Marginal Deposition
Ice-Marginal Processes
Moraine
Permafrost
Polythermal Glaciers
Sediment Gravity Flow
Supra-Glacial Debris Entrainments
Temperate Glaciers
Younger Dryas

ICE-DAMMED LAKES

Fiona Tweed
Department of Geography, Staffordshire University, Stoke-on-Trent, Staffordshire, UK

Definition

An ice-dammed lake is best defined as "a substantial body of standing water, located in, on, under or at the margin of a *glacier*, such that its existence is in some way dependent on damming by *glacier* ice" (Blachut and Ballantyne, 1976, p. 1).

The occasional or recurrent release of the water stored within ice-dammed lakes can effect significant geomorphic change in glaciated environments (Hydrology of Jökulhlaups). Ice-dammed lakes can form supraglacially, subglacially, or ice-marginally and can be classified by their position in relation to the damming *glacier* and the surrounding landscape (e.g., Hutchinson, 1957; Tweed and Russell, 1999). Figure 1 illustrates the range of topographic settings in which ice-dammed lakes form, identifying the type of lake and likely flood routing (after Tweed and Russell, 1999). In most settings, ice-dammed lake formation is a gradual process, linked to *glacier* mass balance and, ultimately, climate forcing (Evans and Clague, 1994). However, independently of climate, sudden glacial advance during surging can block drainage channels and create ice-dammed lakes (e.g., Clague, 1979; Clarke and Mathews, 1981; Mayo, 1989).

Ice-dammed lake drainage occurs when a lake exceeds a critical threshold, the triggering mechanism for any given lake depending on lake-basin topography and ice-dam characteristics (e.g., Tweed and Russell, 1999). Some ice-dammed lakes exhibit temporal changes in their drainage behavior in response to fluctuations in the nature of the ice dam (Evans and Clague, 1994). As glaciers recede, ice dams become thinner resulting in progressively decreasing depths of lake water being required to initiate floods. Under these circumstances, outbursts usually decrease in magnitude, but become more frequent. Conversely, under advancing conditions, a thickening glacial dam can impound lake water at increasingly higher levels and floods tend to increase in magnitude and decrease in frequency. Floods from ice-dammed lakes are part of a wider spectrum of floods generated by the failure of a range of natural dams, including the breaching of moraine dams (e.g., Vuichard and Zimmerman, 1987; Richardson and Reynolds, 2000), dams formed by landslide debris (e.g., Costa and Schuster, 1988; Korup, 2002), and snow dams (e.g., Gore, 1992).

The existence of ice-dammed lakes is documented for most presently glaciated areas. Alaskan and Canadian ice-dammed lakes are well reported (e.g., Stone, 1963; Mathews, 1965; Clarke, 1982; Sturm and Benson, 1985) and drainage of ice-dammed lakes in South America (e.g., Nichols and Miller, 1952; Bruce et al., 1987) and Asia (e.g., Gunn et al., 1930; Hewitt, 1982; Ives, 1986) is

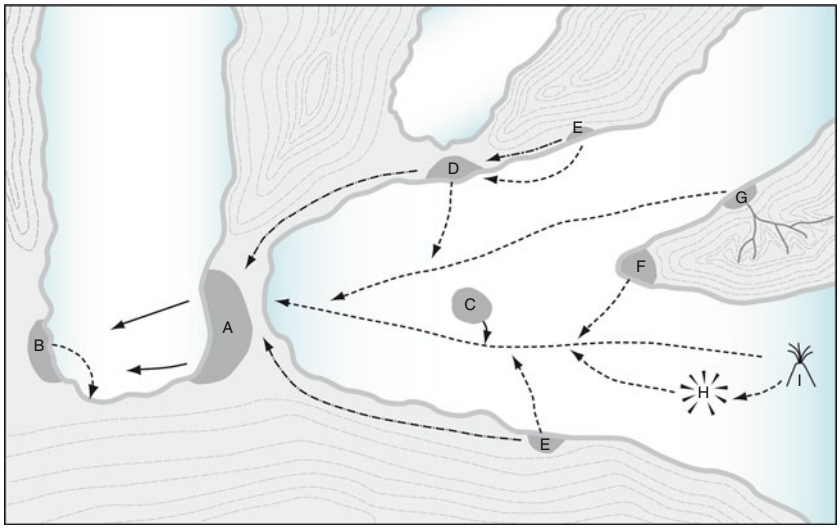

Letter	Ice-dammed lake type
A	Tributary glacier water dammed in trunk valley
B	Water dammed proglacially
C	Supraglacial water
D	Water dammed between tributary and trunk glacier
E	Ice-marginally dammed water
F	Water dammed by converging glaciers
G	Stream valley blocked by trunk glacier
H	Subglacial caldera
I	Volcanic waters (usually no storage)

Ice-Dammed Lakes, Figure 1 The topographic settings of ice-dammed lakes and indicative floodwater routing (Adapted from Tweed and Russell, 1999). The key identifies the principal ice-dammed lake types illustrated.

also described. Ice-dammed lakes in Norway (e.g., Liestøl, 1956; Knudsen and Theakstone, 1988), Greenland (e.g., Dawson, 1983; Sugden et al., 1985; Russell et al., 1990), Iceland (e.g., Thorarinsson, 1939; Björnsson, 1976, 2002), and the European Alps (e.g., Haeberli, 1983) have been the subject of research; however, Arctic and Antarctic ice-dammed lakes are less frequently discussed (e.g., Blachut and McCann, 1981; Siegert et al., 1996). The sudden drainage of ice-dammed lakes during the last stages of the *Pleistocene Epoch* caused some of the largest floods on Earth (e.g., Bretz, 1928; Baker, 1973; Baker et al., 1993; Rudoy, 2002; Carling et al., 2002; O'Connor and Costa, 2004). Given the backdrop of climate change, the ability to monitor and predict the formation of ice-dammed lakes and the likely location, timing, magnitude, and impact of resultant outburst floods will be vital to the management of glaciated regions (Evans and Clague, 1994; Korup and Tweed, 2007).

Bibliography

Baker, V. R., 1973. Paleohydrology and Sedimentology of Lake Missoula flooding in eastern Washington. *Geological Society of America Special Paper*, **144**, 1–79.

Baker, V. R., Benito, G., and Rudoy, A. N., 1993. Paleohydrology of late Pleistocene superflooding Altay Mountains, Siberia. *Science*, **259**, 348–350.

Björnsson, H., 1976. Marginal and supraglacial lakes in Iceland. *Jökull*, **26**, 40–50.
Björnsson, H., 2002. Subglacial lakes and jökulhlaups in Iceland. *Global and Planetary Change*, **35**, 255–271.
Blachut, S. P., and Ballantyne, C. K., 1976. Ice-dammed lakes: a critical review of their nature and behaviour. Discussion paper no. 6, Department of Geography, McMaster University, Hamilton, Ontario.
Blachut, S. P., and McCann, S. B., 1981. The behaviour of a polar ice-dammed lake, Ellesmere Island, N.W.T., Canada. *Arctic and Alpine Research*, **13**, 63–74.
Bretz, J. H., 1928. The Channeled Scabland of eastern Washington. *Geographical Review*, **18**, 446–477.
Bruce, R. H., Cabrera, G. A., Lenia, J. C., and Lenanzo, L. E., 1987. The 1987 surge and ice dam of Glacier Grande del Nevado del Plomo, Argentina. *Journal of Glaciology*, **33**, 131–132.
Carling, P. A., Kirkbride, A. D., Parnachov, S., Borodavko, P. S., and Berger, G., 2002. Late Quaternary catastrophic flooding in the Altai Mountains of south-central Siberia: a synoptic overview and an introduction to flood deposit Sedimentology. In Martini, P., Baker, V., and Garzón, G. (eds.), *Flood and Megaflood Processes and Deposits: Recent and Ancient Examples*. International Association of Sedimentologists, Special publication, **32**, pp. 17–35.
Clague, J. J., 1979. An assessment of some possible flood hazards in Shakwak Valley, Yukon Territory. Current Research, Part B, Geological Survey of Canada Paper, 79-1B:63–70.
Clarke, G. K. C., 1982. Glacier outburst floods from "Hazard Lake", Yukon Territory, and the problem of flood magnitude prediction. *Journal of Glaciology*, **28**, 3–21.
Clarke, G. K. C., and Mathews, W. H., 1981. Estimates of the magnitude of glacier outburst floods from Lake Donjek, Yukon territory, Canada. *Canadian Journal of Earth Sciences*, **18**, 1452–1463.
Costa, J. E., and Schuster, R. L., 1988. The formation and failure of natural dams. *Geological Society of America Bulletin*, **100**, 1054–1068.
Dawson, A. G., 1983. Glacier-dammed lake investigations in the Hullet Lake area, south Greenland. *Meddelelser om Grønland Geoscience*, **11**, 3–22.
Evans, S. G., and Clague, J. J., 1994. Recent climatic change and catastrophic geomorphic processes in mountain environments. *Geomorphology*, **10**, 107–128.
Gore, D. B., 1992. Ice-damming and fluvial erosion in the Vestfold Hills, East Antarctica. *Antarctic Science*, **4**, 227–234.
Gunn, J. P., Todd, H. J., and Mason, K., 1930. The Shyok flood, 1929. *Himalayan Journal*, **2**, 35–47.
Haeberli, W., 1983. Frequency and characteristics of glacier floods in the Swiss Alps. *Annals of Glaciology*, **4**, 85–90.
Hewitt, K., 1982. Natural dams and outburst floods of the Karakoram Himalaya. In Glen, J. W., (ed.), Hydrological aspects of alpine and high-mountain areas. International Association of Hydrological Sciences publication, 138, pp. 259–269.
Hutchinson, G. E., 1957. *A Treatise on Limnology.* New York: Wiley, Vol. 1.
Ives, J. D., 1986. Glacial lake outburst floods and risk engineering in the Himalaya. International Centre for Integrated Mountain Development Occasional paper 5.
Knudsen, N. T., and Theakstone, W. H., 1988. Drainage of the Austre Okstindbreen ice-dammed lake, Okstindan, Norway. *Journal of Glaciology*, **34**, 87–94.
Korup, O., 2002. Recent research on landslide dams - a literature review with special attention to New Zealand. *Progress in Physical Geography*, **26**, 206–235.
Korup, O., and Tweed, F. S., 2007. Ice, moraine and landslide dams in mountainous terrain. *Quaternary Science Reviews*, **26**, 3406–3422.
Liestøl, O., 1956. Glacier dammed lakes in Norway. *Norsk Geografisk Tidsskrift*, **15**, 122–149.
Mathews, W. H., 1965. Two self-dumping ice-dammed lakes in British Columbia. *Geographical Review*, **55**, 46–52.
Mayo, L. R., 1989. Advances of Hubbard Glacier and the 1986 outburst of Russell Fjord, Alaska, U.S.A. *Annals of Glaciology*, **13**, 189–194.
Nichols, R. L., and Miller, M. M., 1952. The Moreno Glacier, Lago Argentina, Patagonia, advancing glaciers and nearby simultaneously retreating glaciers. *Journal of Glaciology*, **2**, 41–50.
O'Connor, J. E., and Costa, J. E., 2004. The world's largest floods, past and present – their causes and magnitudes. U.S. Geological Survey Circular 1254.
Richardson, S. D., and Reynolds, J. M., 2000. An overview of glacial hazards in the Himalayas. *Quaternary International*, 65/66, 31–47.
Rudoy, A. N., 2002. Glacier-dammed lakes and geological work of glacial superfloods in the Late Pleistocene, southern Siberia, Altai Mountains. *Quaternary International*, **87**, 110–140.
Russell, A. J., Aitken, J. F., and de Jong, C., 1990. Observations on the drainage of an ice-dammed lake in West Greenland. *Journal of Glaciology*, **36**, 72–74.
Siegert, M. J., Dowdeswell, J. A., Gorman, M. R., and McIntyre, N. F., 1996. An inventory of Antarctic subglacial lakes. *Antarctic Science*, **8**, 281–286.
Stone, K. H., 1963. Alaskan ice-dammed lakes. *Annals of the Association of American Geographers*, **53**, 332–349.
Sturm, M., and Benson, C. S., 1985. A history of jökulhlaups from Strandline Lake, Alaska, U.S.A. *Journal of Glaciology*, **31**, 272–280.
Sugden, D. E., Clapperton, C. M., and Knight, P. G., 1985. A jökulhlaup near Søndre Strømfjord, West Greenland, and some effects on the ice sheet margin. *Journal of Glaciology*, **31**, 366–368.
Thorarinsson, S., 1939. The ice-dammed lakes of Iceland, with particular reference to their value as indicators of glacier oscillations. *Geografiska Annaler*, **21A**, 216–242.
Tweed, F. S., and Russell, A. J., 1999. Controls on the formation and sudden drainage of glacier-impounded lakes: implications for jökulhlaup characteristics. *Progress in Physical Geography*, **23**, 79–110.
Vuichard, D., and Zimmermann, M., 1987. The 1985 catastrophic drainage of a moraine-dammed lake, Khumbu Himal, Nepal: causes and consequences. *Mountain Research and Development*, **7**, 91–110.

Cross-references

Glacier
Hydrology of Jökulhlaups
Pleistocene Epoch

ICE-MARGINAL DEPOSITION

Mahendra R. Bhutiyani
Hazard Assessment and Forecasting Division, Snow and Avalanche Study Establishment, Chandigarh, India

Definition

An undulating hilly belt consisting of an unsorted mixture of clay, silt, boulders, cobbles, and pebbles that was brought by the moving ice in traction on the surface and

accumulated beneath the ice margin (Figures 1 and 2). They are also termed as "glacier till" deposits or "moraines" and are exposed after the ice mass has disappeared. Melting of small ice blocks in this hilly belt, which is also described as "knob and kettle landscape," gives rise to the formation of kettles and may contain small lakes and ponds.

Origin

Outermost deposits at the periphery of a moving ice mass are "terminal moraines"; the moraine that is formed between two ice lobes is an "interlobate" moraine. Where the ice margin temporarily holds a fixed marginal position during its period of general retreat, a "recessional moraine" is formed. Behind the terminal moraine are commonly found "eskers" – the long, narrow ridges of gravels and cobblestones that were formed as deposits on the floors of ice tunnels. Eskers may be 30–70 m in height and may extend for tens of kilometers across the country. There may also be present numerous "drumlins" that are rounded hills of glacier till, shaped by moving ice as it dragged the till over the ground surface. At certain points the till was plastered in successive layers upon small knobs, eventually forming the drumlins, which resemble a shape of an inverted bowl of a teaspoon with the long dimension paralleling the ice motion. Drumlins are about 400 meters to about 1.5 km in length and 30–70 m in height.

Over the entire region previously covered by the ice, there may be found a layer of till, varying in thickness

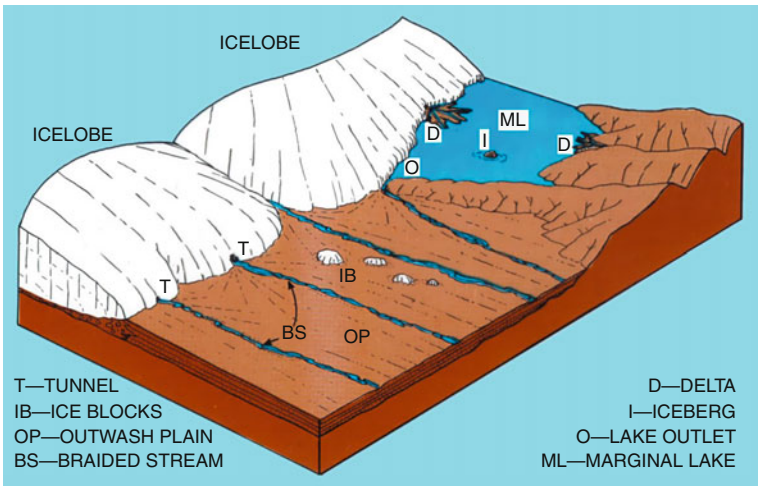

Ice-Marginal Deposition, Figure 1 Marginal deposits of ice sheets before deglaciation.

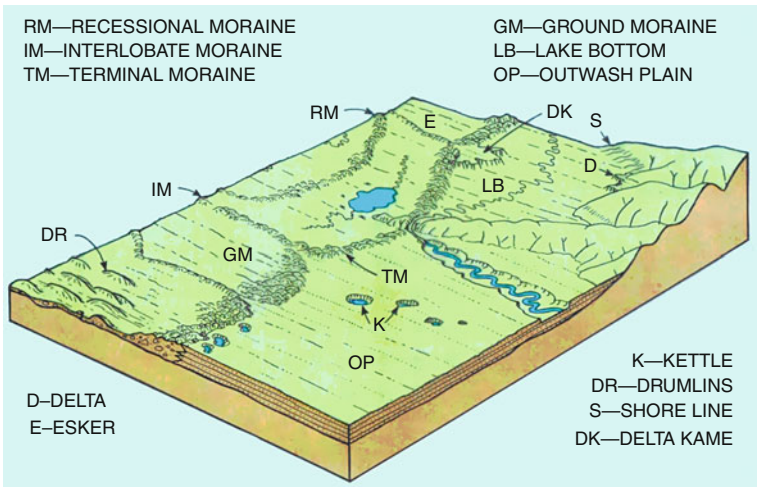

Ice-Marginal Deposition, Figure 2 Marginal deposits of ice sheets after deglaciation.

from a few meters to about few tens of meters. This irregular blanket of till is known as "ground moraine." Because of uneven deposition, ground moraine has many areas of swamps and lakes.

The marginal lake shown in Figure 1 has now disappeared, but there remain various evidences of its existence. A small delta produced in front of the ice now stands as a flat-topped "delta kame." Along the hillsides are seen a "delta" and a "shoreline." On the lake bed are found alternating thin layers of clay and silt known as "varved" clays. On the outwash plain are "kettles," which are ice-block depressions with steep sides that give rise to lakes.

Significance

Ice-marginal deposits present excellent geomorphological evidences for the study of geographical coverage of past glaciation and paleoclimates in the region.

Bibliography

Ward's Natural Science Establishment, Inc. Rochester, N.Y 1964.

ICE-MARGINAL PROCESSES

Matthew R. Bennett
School of Applied Sciences, Bournemouth University
Talbot Campos, Dorset, UK

Definition

Ice margin. The interface between ice and the glacier foreland or pro-glacial zone.
Pro-glacial. Area beyond the ice margin.
Glaciotectonic. Deformation of ice and/or sediment by glacier ice.
Décollement. Slip surface along which deformation is concentrated.

Introduction

Ice-marginal processes are extensive in scope and nature. At its simplest, the *ice margin* is the interface between ice and the glacial foreland, or *pro-glacial* zone. It is a zone of sediment transfer associated with the phase change of ice to water. As such, it can be seen as a transfer system with an input of glacial sediment, an output of sediment, an internal storage (landforms & sediments), and a range of transfer mechanisms that facilitate the movement of sediment within this system. Figure 1 provides a simple conceptual model of a terrestrial ice-marginal zone based on this idea. The input of sediment to the ice-marginal zone is determined by the debris content of the ice, the rate of delivery which is a function of ice velocity and ablation, the rate (if present) of subglacial sediment deformation and associated sediment advection, as well as the sediment discharged within glacial meltwater wherever it be located – supraglacial, englacial, subglacial, or as groundwater. The output of sediment from the glacial foreland is via meltwater discharge and in some cases by aeolian processes. Within the ice-marginal zone and immediate foreland, sediment is stored and/or transferred via a range of processes with a variety of residence times from a few hours to millennia depending on the geometry of the ice margin and the foreland basin in which it terminates along with the degree of "connectivity" between the glacial and non-glacial realms. We can recognize five major process families at work in transferring sediment within this ice-marginal system, they are: (1) mass movement; (2) fluvial; (3) glaciotectonic; (4) aeolian; and (5) groundwater.

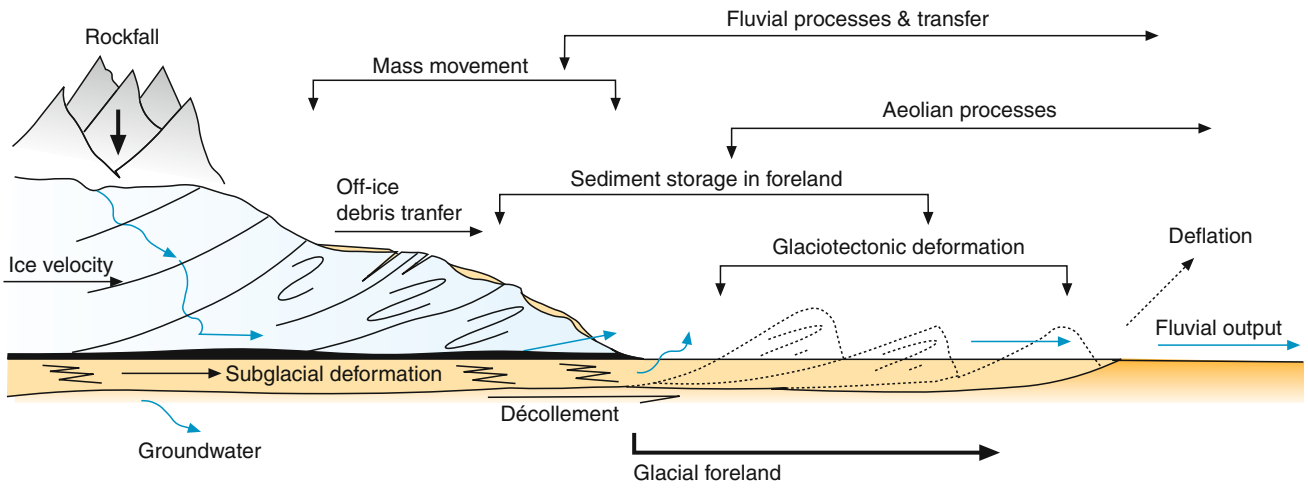

Ice-Marginal Processes, Figure 1 Schematic model of a terrestrial ice margin based on the idea that it is a transfer system for water and ice at the interface between the glacial & pro-glacial zones.

Mass movement

Mass movement processes involve the transfer of sediment from the ice margin and may involve everything from rockfall and granular avalanches, to cohesive debris flows. Debris emerges on the ice surface both as a result of surface ablation revealing englacial debris in high-level transport and via direct rock fall onto the ice surface in the ablation zone. In addition, subglacial (low-level transport) debris may outcrop on the ice surface where it has been elevated to a supraglacial position via rising debris bands, stratification, thrusts, and folds associated with compressive flow in the terminal zone of a glacier. The ice-marginal debris supply of any given glacier is a function of the sediment load within the ice, the rate of surface ablation, and ice velocity which determines the rate of sediment delivery. As debris first melts out of the ice, it will darken the ice surface leading to enhanced melting, since dark surfaces absorb more solar radiation; however, as the debris thickens, it will begin to inhibit melting as it insulates the ice surface. The stability of this caprice of supraglacial debris in the ice-marginal zone depends on the ice surface gradient as well as the grain-size distribution of the debris and therefore its ability to hold moisture. Coarse debris on a steep ice surface will fall or move as a dry granular flow accumulating at the base of the slope as a talus- or scree-like deposit. In contrast, fine-grained sediment on a gentler ice slope may become water saturated and fail as a cohesive debris flow. Where the ice-marginal geometry is relatively smooth and steep, sediment will be transferred efficiently to the ice margin accumulating as a linear accumulation along the ice margin, either as a dump moraine, or as an ice-marginal debris fan. If the debris transfer is less efficient, or there is strong spatial variation in debris load within the ice, it will result in an ice-cored topography of ridges and mounds on the ice surface. In this scenario, debris may have a much longer residence time within the ice-marginal zone, being reworked repeatedly as the ice-cored topography changes over time. This re-working of sediment generates flow tills whose properties will reflect the debris sources (glacial transport pathway) from which the debris is blended as well as the fluidity of the debris flow via which the sediment was emplaced. Fluvial re-working may also be a feature of such a complex ice-marginal zone.

Fluvial

Fluvial processes are also important both in the ice-marginal and foreland zones. Supraglacial water flow helps transfer debris from the ice margin and is common where the ice is cold-based, meltwater production is high, and there are few crevasses. Sediment transfer will also take place where water flow occurs within or below the ice. Size sorting may occur in some cases, although, in most cases, the high discharge rates and rapid discharge fluctuations will tend to lead to massive and poorly sorted deposits. Surface flow may also be dominant in a complex ice-marginal zone with large amounts of buried ice leading to the deposition of glaciofluvial sediments in association with flow tills thereby creating "kame and kettle" topography as the ice melts.

As water emerges from meltwater portals in the ice margin, the velocity falls with the loss of confining water pressure and rapid deposition of coarse bed load may occur close to the portal entrance favoring the formation of outwash fans (Hochsander Fans). These may build up over the ice margin burying it and thereby blurring the location of the true ice margin. The degree of fluvial re-working at a given ice margin depends on the temporal stability of the meltwater portals at the ice margin as it fluctuates over time and with any advance or retreat of the ice margin. A stable routing of meltwater will limit re-working to a clearly defined fluvial corridor, whereas instability involving regular switching of meltwater portals along an ice margin will lead to more widespread re-working of sediment along the margin. Away from the ice margin in a distal direction, the meltwater route may become more stable and a braided river system will develop.

Storage of sediment within the pro-glacial zone depends on the degree of "connectivity" between the ice margin and the fluvial system. Connectivity in this context refers to the ease with which sediment is transferred from one process system to the next – in this case, glacial to fluvial. At glacier margins with a high meltwater discharge and good connectivity, sediment will be re-worked rapidly by the fluvial system and transferred efficiently away from the ice margin. The system is essentially supply limited and the pro-glacial zone will be dominated by fluvial rather than glacial landforms; the preservation potential, for example, of ice-marginal moraines will be limited. In comparison, where meltwater discharge is less or the degree of connectivity between the glacial and fluvial system is more limited, sediment storage will be the norm. In this case, the system and ice-marginal zone is transport limited and ice-marginal landforms of glacial original will be dominant. Connectivity is determined by a complex range of variables, including such things as the rate of sediment supply; the geometry of the ice margin; its temporal dynamics; the geometry of the foreland basin; meltwater discharge; and the spatial and temporal stability of the drainage routes along an ice margin. It is important to note that connectivity is also scale dependent and may change laterally along an ice margin as well as through time.

Glaciotectonics

Glaciotectonic processes may also be important within the ice-marginal zone both in terms of sediment supply via subglacial deformation and via the mass-transfer of sediment within the ice-marginal zone through the formation of glaciotectonic moraines. If an ice margin is advancing, whether in a sustained fashion or seasonally, and is well coupled to its foreland, it has the capacity to either compress part of the foreland and/or move it in a distal

direction. Ice-marginal to foreland coupling is aided by things such as a reverse bedrock slope at the ice margin, or an ice-marginal outwash fan against which the ice can push as it advances. Of equal importance at thin ice margins is the potential for the seasonal "freezing-on" of a subglacial sediment layer within the ice-marginal zone.

Glaciotectonic deformation, especially the distal movement of a thin slab of foreland, is facilitated by the presence of a basal décollement horizon, perhaps in the form of a more ductile sediment layer or one with elevated pore-water pressures, over which the foreland slab may slide. The nature of the deformation – folds versus thrust, for example – and the degree of distal movement will depend on the relative strength of the foreland slab with respect to the frictional properties of the décollement. A rigid slab resting on a weak décollement will favor distal movement of the slab, whereas a weak foreland resting on a stronger décollement will lead to in situ compression. The former may also be associated with a more brittle deformation regime (e.g., thrusts and faults) than the latter which will favor ductile deformation (e.g., folds). The interplay of the factors will determine the nature of the ice-marginal glaciotectonic landforms produced along the ice margin and also their size and internal tectonic architecture.

Groundwater

Groundwater and the hydrogeological properties within an ice-marginal zone may also be key processes especially in determining the nature of glaciotectonic deformation. They also provide a potential transfer route for dissolved or fine-grained sediment. For completeness, we should also include aeolian processes within this review of ice-marginal processes since in certain situations, they may assist with the export of fine-grained sediment from a pro-glacial zone.

Summary

In summary, therefore, it is possible to see the ice-marginal zone as the interface between the glacial and non-glacial process domains. It is a zone characterized by sediment transfer and storage and the degree of connectivity between the two process domains is critical in determining whether the ice-marginal zone is dominated by glacial or by fluvial processes. It is important to note that this discussion has focused on terrestrial ice-marginal environments, but the basic principles also apply in aquatic ice-marginal environments.

Bibliography

Bennett, M. R., and Glasser, N. F., 2009. *Glacial Geology: Ice Sheets & Landforms*, 2nd edn. Chichester: Wiley.

Cross-references

Englacial Processes
Glacial Geomorphology and Landforms Evolution
Ice-Marginal Deposition

ICE-VOLCANO INTERACTIONS

Hugh Tuffen
Lancaster Environment Centre, Lancaster University, Lancaster, UK

Synonyms

Glaciovolcanism; Volcano-ice interactions

Definition

Ice–volcano interactions. The interplay between the activity of volcanoes and ice sheets or valley glaciers. This includes how individual eruptions interact with ice and meltwater, how basal melting in volcanic areas affects ice sheets, and how changes in ice thickness influence longer-term patterns of volcanism.

Glaciovolcanism. The interactions between magma and ice in all its forms (snow, firn, ice, and meltwater), on Earth and other planets.

Key localities

Iceland, West Antarctic Ice Sheet, Antarctic Peninsula, Andes, British Columbia, Alaska, Mars

Interactions between magma, ice, snow, and meltwater during eruptions

The interactions between volcanic eruptions and ice and snow cover a broad spectrum from eruptions beneath ice sheets hundreds of meters thick to the melting of smaller bodies of ice or snow on volcanoes by pyroclastic deposits or lava flows (Major and Newhall, 1989; Smellie, 2000; Subglacial volcanism). A common feature of all interactions is the transfer of heat from magma to ice or snow, which leads to the production of meltwater.

Eruptions beneath ice sheets

During eruptions beneath ice sheets magma rises to the base of the ice either at a point source or a fissure (Wilson and Head, 2002; Tuffen, 2007), leading to the construction of a volcanic edifice and the generation of meltwater. In general, eruptions beneath thick ice begin with the gentle effusion of pillow lavas, which give way to increasingly explosive interactions between magma and meltwater as the edifice grows upward toward the ice surface within an ice-confined meltwater lake and the confining pressure decreases (Smellie, 2000). This phase of activity generates hyaloclastites. If the eruption is sufficiently sustained, it may pierce the ice surface and terminate with the effusion of subaerial lava flows (Figure 1); this is termed a tuya-building eruption. The products of such eruptions may thus approximately record past ice sheet thicknesses (Subglacial volcanism).

Observations of the 1996 Gjálp eruption, which occurred beneath 450–650 m of ice at the Vatnajökull ice sheet in Iceland, have greatly advanced our understanding of eruptions beneath ice sheets (Guðmundsson

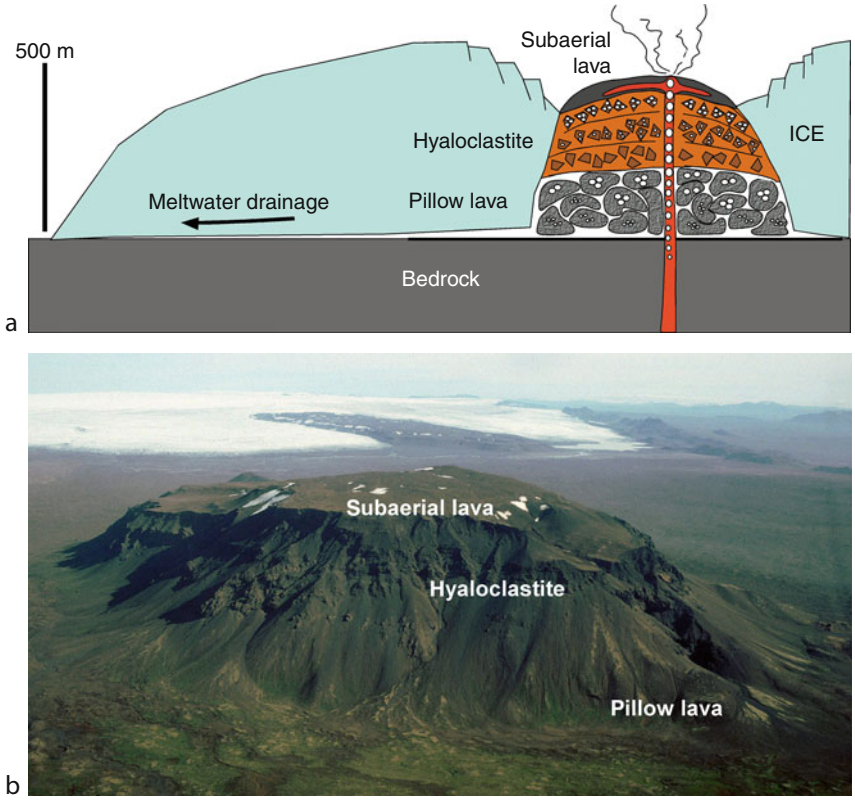

Ice-Volcano Interactions, Figure 1 (**a**) Cartoon showing the products of a basaltic tuya-building eruption beneath an ice sheet, where the ice surface has been breached. The transition from hyaloclastites to subaerial lavas therefore provides a minimum estimate of the palaeo-ice thickness. (**b**) Aerial photograph of Hlodufell tuya (1,188 m) in western Iceland, which was formed in a basaltic tuya-building eruption during the last glacial period. Photograph by Prof. John Smellie.

et al., 1997; Smellie, 2000). Key observations include the astonishing rapidity of the melting (>450 m of ice was melted in only 36 h) and that local subglacial hydrology controls whether meltwater collects or escapes from the eruption site, and thus the pressure at the vent area and the style of eruption (Guðmundsson et al., 2005). Meltwater from Gjálp gathered in the nearby Grímsvötn caldera for several weeks before being discharged in a catastrophic jökulhlaup (jökulhlaup) with a peak discharge of 45,000 m^3s^{-1}.

Melting of snow and ice on stratovolcanoes

Many stratovolcanoes, particularly in the Andes, are mantled by permanent snow and ice both on their upper flanks and in their summit craters. This creates a major natural hazard as melting of ice or snow during eruptions may trigger meltwater floods (lahars) that inundate valleys on the volcano flanks, with devastating consequences (Major and Newhall, 1989; Natural hazards associated with glaciers and permafrost). The 1985 eruption of Nevados del Ruiz, a 5,300-m high stratovolcano in Columbia, triggered lahars that claimed the lives of 23,000 people (Lowe et al., 1986; Major and Newhall, 1989). The geological record of such volcano–ice interactions includes lahar deposits and ice-contact lava flows (Lescinsky and Fink, 2000; Subglacial volcanism).

Models of ice–volcano interactions

Several aspects of the complex processes that occur during ice–volcano interactions have recently been modeled mathematically, guided by observations of recent eruptions and the geological record of past eruptions. These include calculations of the volume and pressure changes during subglacial eruptions (Hoskuldsson and Sparks, 1997), the propagation of dykes and sills into ice sheets (Wilson and Head, 2002), the rate of heat transfer from magma to ice during eruptions (Guðmundsson, 2004), and the interplay between melting and deformation of ice (Tuffen, 2007). Nonetheless, many major uncertainties remain, including whether eruptions may fracture ice sheets or prise them from the bedrock, and which factors control the explosivity of eruptions under ice.

The geological record of past ice sheets and glaciers

The products of past eruptions that have interacted with ice and snow record a wealth of information about the extent, thickness, and nature of past ice sheets and glaciers

(Smellie et al., 2008). This is particularly valuable as many volcanic rocks can be readily dated, thus providing unique insight into the timing of palaeoenvironmental changes. When eruptions have pierced the ice surface, the transition from subglacial to subaerial formations roughly indicates the palaeo-ice thickness (Figure 1; Mathews, 1947; Smellie, 2000; Subglacial volcanism). The recognition of distinctive fracture patterns in lava flows that have contacted ice, snow, and meltwater allows precise reconstruction of ice and snow extents on stratovolcanoes (Lescinsky and Fink, 2000; Mee et al., 2006). The concentration of volcanic gasses dissolved in volcanic deposits may even record the pressure when they quenched beneath the ice and thus palaeo-ice thicknesses (Schopka et al., 2006), but there are currently uncertainties in this technique. Researchers are currently using these methods to record and unravel the history of ice sheet fluctuations in Antarctica, Iceland, and elsewhere.

Effects of changing ice thicknesses on volcanic activity

Fluctuations in the thickness of ice covering volcanic zones may strongly affect the amount of magma that is erupted. As an ice sheet, hundreds of meters thick, abruptly receded from the Northern Volcanic Zone in Iceland during the last deglaciation at about 11 ka, the rate of volcanism increased thirtyfold (Maclennan et al., 2002). This is because the removal of ice led to rapid decompression of the mantle and greatly enhanced melting and magma production. Crustal decompression can also open the fracture pathways that help magma to rise to the surface.

On a shorter timescale, thinning of the Vatnajökull icecap in Iceland by tens of meters during the twentieth century is thought to have increased magma production by over 1 km^3 (Pagli and Sigmundsson, 2008), although this increase is modest compared to the acceleration during the last deglaciation. On a still shorter timescale of hours to days, drainage of tens of meters of meltwater from the Grímsvötn caldera during jökulhlaups can trigger minor eruptions, showing that some volcanic systems are very sensitive to modest pressure changes at the base of the ice.

Changes in eruptive activity due to ice sheet fluctuations are not confined to Iceland, as deglaciation is also known to have accelerated rates of Quaternary volcanism in other volcanic areas, including the western USA, France, and Germany.

Effects of volcanic activity on ice sheets and glaciers

The mass balance of glaciers and ice sheets is strongly influenced by basal melting due to geothermal heat (Bell, 2008; Basal melting). As subglacial volcanoes are regions with exceptionally high geothermal heat fluxes they may therefore have a significant impact on the local mass balance. Enhanced basal melting in volcanic zones coincides with the presence of poorly consolidated volcanic rocks, thus encouraging basal sliding and, potentially, the formation of ice streams (Blankenship et al., 1993).

According to current knowledge, an individual eruption may affect an ice sheet or glacier in three principal ways. Firstly, volcanically produced meltwater may inundate the existing subglacial drainage system, encouraging glacier surging (Björnsson, 1998). Secondly, melting and fracturing at the eruption site may drastically change the ice surface topography (Guðmundsson et al., 1997). Thirdly, deposition of volcanic ash onto ice, which occurs if the eruption melts through the ice, may affect ablation rates (Wilson and Head, 2009).

Ice–volcano interactions and life on Mars

There is increasing evidence that widespread interactions between rising magma and the Martian cryosphere have occurred through much of the planet's history, creating a wide variety of landforms associated with meltwater movement and ice-contact volcanic deposits (e.g., Head and Wilson, 2007). This has generated considerable interest as areas of geothermal heating and meltwater production are the most probable environments where life may have developed on Mars. Current research includes documenting the landforms generated (Head and Wilson, 2007), modeling ice–volcano interactions in the Martian environment (Wilson and Head, 2002), and investigating whether the microbial ecosystems that develop at terrestrial ice-covered volcanoes may survive the harsh conditions on Mars (Cousins et al., 2009).

Outlook: current investigations, controversies, and gaps in current knowledge

As the study of ice–volcano interactions is still in its infancy, a number of fundamental questions remain unanswered. These include:

- Can enhanced volcanism during deglaciation play an important role in the destruction of ice sheets and glaciers?
- Will the current thinning of glaciers on Andean stratovolcanoes trigger more frequent eruptions and greater hazards?
- Is current thinning of Antarctic ice likely to trigger enhanced volcanism in the near future?

In order to address these issues, volcanologists and glaciologists need to look into the geological record to see how ice and volcanoes have interacted during previous episodes of climate change. Our understanding of the complex physical processes involved will improve with further field, experimental, and modeling studies of ice–volcano interactions.

Bibliography

Bell, R. E., 2008. The role of subglacial water in ice-sheet mass balance. *Nature Geoscience*, **1**, 297–304.

Björnsson, H., 1998. Hydrological characteristic of the drainage system beneath a surging glacier. *Nature*, **395**, 771–774.

Blankenship, D. D., Bell, R. E., Hodge, S. M., Brozena, J. M., Behrendt, J. C., and Finn, C. A., 1993. Active volcanism beneath the West Antarctic Ice Sheet and implications for ice-sheet stability. *Nature*, **361**, 526–529.
Cousins, C. R., Smellie, J. L., Jones, A. P., and Crawford, I. A., 2009. A comparative study of endolithic microborings in basaltic lavas from a transitional subglacial–marine environment. *International Journal of Astrobiology*, doi:10.1017/S1473550408004369.
Guðmundsson, M. T., Sigmundsson, F., and Björnsson, H., 1997. Ice-volcano interaction of the 1996 Gjálp subglacial eruption, Vatnajökull, Iceland. *Nature*, **389**, 954–957.
Head, J. W., and Wilson, L., 2007. Heat transfer in volcano-ice interactions on Mars: synthesis of environments and implications for processes and landforms. *Annals of Glaciology*, **45**, 1–13.
Höskuldsson, A., and Sparks, R. S. J., 1997. Thermodynamics and fluid dynamics of effusive subglacial eruptions. *Bulletin of Volcanology*, **59**, 219–230.
Lescinsky, D. T., and Fink, J. H., 2000. Lava and ice interaction at stratovolcanoes: use of characteristic features to determine past glacial events and future volcanic hazards. *Journal of Geophysical Research*, **105**, 23711–23726.
Lowe, D. L., Williams, S. N., Leigh, H., Connor, C. B., Gemmell, J. B., and Stoiber, R. E., 1986. Lahars initiated by the 13 November 1985 eruption of Nevado del Ruiz, Colombia. *Nature*, **324**, 51–53.
Maclennan, J., Jull, M., McKenzie, D. P., Slater, L., and Gronvold, K., 2002. The link between volcanism and deglaciation in Iceland. *Geochemistry, Geophysics, Geosystems*, doi:10.1029/2001GC000282.
Major, J. J., and Newhall, C. G., 1989. Snow and ice perturbation during historical volcanic eruptions and the formation of lahars and floods. *Bulletin of Volcanology*, **52**, 1–27.
Mathews, W. H., 1947. "Tuyas." Flat-topped volcanoes in northern British Columbia. *American Journal of Science*, **245**, 560–570.
Mee, K., Tuffen, H., and Gilbert, J. S., 2006. Snow-contact volcanic facies at Nevados de Chillan volcano, Chile, and implications for reconstructing past eruptive environments. *Bulletin of Volcanology*, **68**, 363–376.
Pagli, C., and Sigmundsson, F., 2008. Will present day glacier retreat increase volcaninc activity? Stress induced by recent glacier retreat and its effect on magmatism at the Vatnajökull ice cap. *Iceland. Geophysical Research Letters*, **35**, L09304, doi:10.1029/2008GL033510.
Schopka, H. H., Guðmundsson, M. T., and Tuffen, H., 2006. The formation of Helgafell, SW-Iceland, a monogenetic subglacial hyaloclastite ridge: sedimentology, hydrology and ice-volcano interaction. *Journal of Volcanology and Geophysical Research*, **152**, 359–377.
Smellie, J. L., 2000. Subglacial eruptions. In Sigurðsson, H., Houghton, B. F., McNutt, S. R., Rymer, H., and Stix, J. (eds.), *Encyclopaedia of Volcanoes*. London: Academic Press, pp. 403–418.
Smellie, J. L., Johnson, J. S., McIntosh, W. C., Esser, R., Guðmundsson, M. G., Hambrey, M. J., and van Wyk de Vries, B., 2008. Six million years of glacial history recorded in the James Ross Island Volcanic Group, Antarctic Peninsula. *Palaeogeography Palaeoclimatology Palaeoecology*, **260**, 122–14.
Tuffen, H., 2007. Models of ice melting and edifice growth during subglacial basaltic eruptions. *Journal of Geophysical Research*, **112**, doi:10.1029/2006JB004523.
Wilson, L., and Head, J. W., 2002. Heat transfer and melting in subglacial basaltic volcanic eruptions: implications for volcanic deposit morphology and meltwater volumes. In Smellie, J. L., and Chapman, M. G. (eds.), *Ice-volcano interaction on Earth and Mars*. London, Geological Society of London Special Publication 202, pp. 5–26.
Wilson, L., and Head, J. W., 2009. Tephra deposition on glaciers and ice sheets on Mars: Influence on ice survival, debris content and flow behaviour. *Journal of Volcanology and Geothermal Research*, doi:10.1016/j.jvolgeores.2008.10.003.

Cross-references

Antarctica
Bottom Melting or Undermelt (Ice Shelf)
Glacier Lake Outburst Floods
Iceland Glaciers
Natural Hazards Associated with Glaciers and Permafrost
Subglacial Drainage System
Subglacial Volcanism

ICEFALL

Mahendra R. Bhutiyani
Hazard Assessment and Forecasting Division, Snow and Avalanche Study Establishment, Chandigarh, India

Definition

Icefall is that portion of the glacier body where it gets vertically broken down into number of half-depth to full-depth crevasses across its flow, giving rise to a messy and rugged topography consisting of sharp ice columns and ridges called "seracs." An area where tributary glacier meets the main trunk glacier may also have an icefall if there is a sudden change in the gradient. A classic example is the Khumbu Icefall of the Khumbu Glacier (Figure 1) on the way to Mount Everest at an altitude of about 5,500 meters above sea level.

Origin

Glacier moves by basal sliding to some extent but largely by plastic deformation of ice under the influence of gravity, because of the gradient in its subglacial valley profile. Shear stress along the slope direction, caused by the gravitational pull, far exceeds the shear strength of the glacier ice. Consequent plastic deformation may fail to keep pace with such higher velocities, giving rise to multiple failures and formation of number of transverse crevasses. Once the gradient becomes normal, glacier-flow velocities slow down and crevasses close, making the glacier surface smoother.

Significance

Mountaineers, on their way to the summit, have to traverse highly crevassed treks of the glaciers in the icefall regions, with the help of ladders (Figure 2) or confining their movements to areas where the crevasses narrow down or on lateral moraines (Figure 3) or at times, on the steep valley escarpments. Although glacier-flow velocities in the icefall region are abnormally high on the yearly scale, they

Icefall, Figure 1 The Khumbu Icefall located in the Khumbu region of northeastern Nepal on the southern slopes of Mount Everest. (*Source* – Wikipedia, the free encyclopedia.)

Icefall, Figure 2 A "roped–up" mountaineer crossing a serac in the Khumbu Icefall region. (*Source* – Wikipedia, the free encyclopedia.)

are barely visible on hourly or daily basis and may cause sudden collapse of a serac without warning. Mountaineers are extremely vulnerable to such unpredictable behavior as moving ice columns may weaken/disturb the anchors/abutments of the ladders on both sides. A cautious approach employing a "roping-up" technique while crossing such areas, whereby the members of the team, are suitably roped up with adequate distance between two successive members, may mitigate the danger to a large extent.

Icefall, Figure 3 Trekkers traversing an icefall on a glacier (seen on the *left* portion of the photograph) in Karakoram Himalaya on the lateral moraine.

ICELAND GLACIERS

Oddur Sigurðsson
Veðurstofu Íslands, Icelandic Meteorological Office, Reykjavík, Iceland

Introduction

Although, according to tradition, Iceland is named for sea ice, the glaciers of the country are very prominent. Glaciers covered 11,048 km^2 at the turn of the twenty-first century, i.e., 11% of the total area of the country (Figure 1) and add immensely to the scenery in most districts because they are generally on the highest mountains. Moreover, glaciers have had a considerable impact on the history of the nation from the very beginning, particularly as a result of the hazards associated with explosive, subglacial eruptions in ice-capped volcanoes and the glacierized part of the neovolcanic zone.

The largest ice caps are found where the precipitation is greatest in the southern and southeastern part of the country and the central highlands. One is situated on the northwest peninsula. Of ca. 280 glaciers in Iceland, about 190 are found in the northern highlands. All of those are quite small mountain glaciers, primarily facing north (Figure 2). About 40 similar mountain glaciers are distributed throughout the mountains of the eastern fjords. The highest mountains in the country are active volcanoes. All of them have ice caps. Of the glaciers and outlet glaciers in Iceland 269 have modern, documented place-names (Sigurðsson and Williams, 2008). Björnsson and Pálsson (2008) and Björnsson (2009a) summarized information about the glaciers of Iceland.

Oscillations of glaciers

During the last glaciation, Iceland was almost entirely covered by glacier ice. After the sudden end of the last glaciation glaciers more or less disappeared about 7000 years ago (Geirsdóttir et al., 2009), leaving only the very highest mountains with ice caps. The early manuscripts mention the presence of glaciers and the turbid water of the glacial rivers at the time of settlement 1,100 years ago. The word *jökull* (glacier) is commonplace in the oldest place-names which indicates the presence of glaciers during the time of settlement more or less in the same places as they are at the present time.

According to contemporary documents glaciers have advanced more or less continuously at least since the seventeenth century and probably since the thirteenth century. Grazing areas, forests, and inhabited districts were overrun by glaciers, which indicates that this was the greatest advance of glaciers since the last glaciation (Sigurðsson, 2005).

In Iceland the Little Ice Age ended about 1890. The retreat of glaciers, however slow, was obvious during the first decades of the twentieth century (Björnsson, 1998). In the 1920s considerable climate warming resulted in high rate of retreat of all glaciers in the country so that by 1960 all glaciers within the country had retreated from their 1930 position (Sigurðsson, 1998). This retreat continued at a moderate pace until about 1970. During the period 1970–1995 glaciers advanced almost continuously due to a cooler climate in an area extending from Labrador and across southern Greenland to Iceland (Hanna et al., 2004). During the first years of the twenty-first century glaciers have retreated faster than at any time since 1930, when meteorologist Jón Eyþórsson began monitoring

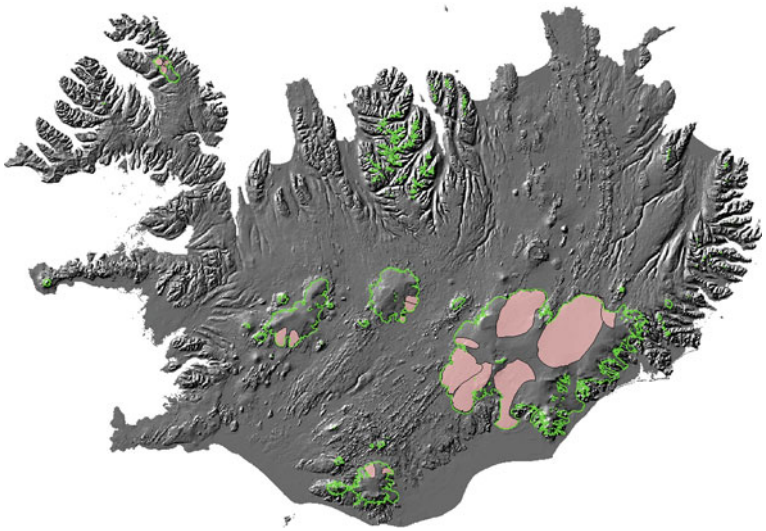

Iceland Glaciers, Figure 1 Location map of Iceland with glacier outlines. Identified surge-type glaciers are shaded.

Iceland Glaciers, Figure 2 Two surge-type cirque glaciers, Teigardalsjökull (quiescent) and Búrfellsjökull (surging) in Northern Iceland. (Photo by Oddur Sigurðsson).

glacier front variations, a project that was continued by the Iceland Glaciological Society since it was founded in 1950 (Figures 3 and 4) (Eythorsson, 1963; Sigurðsson, 1998; Jóhannesson and Sigurðsson, 1998; Sigurðsson, 2006). During the first decade of the twenty-first century the glacier surface area has decreased on the average by about 20–30 km^2 (0.2–0.3%) per year, and by about 0.4% in thickness according to mass balance measurements (Sigurðsson, 2006). According to models of mass balance Icelandic glaciers will essentially disappear during the next two centuries if global warming continues as expected. The discharge of glacial rivers will increase accordingly (Jóhannesson et al., 2007).

Outlines of all Icelandic glaciers have been traced recently from conventional vertical aerial photographs, Landsat 7 and SPOT-5 images (http://gullhver.os.is/website/hpf/orkustofnun_english/viewer.htm) and the interpretation of the location of the outlines has been verified by oblique aerial stereo photographs.

The terminus of non-surge-type glaciers in Iceland usually reacts to change in mass within 1–3 years (Figure 3) (Sigurðsson, 2006). This is independent of the glacier size

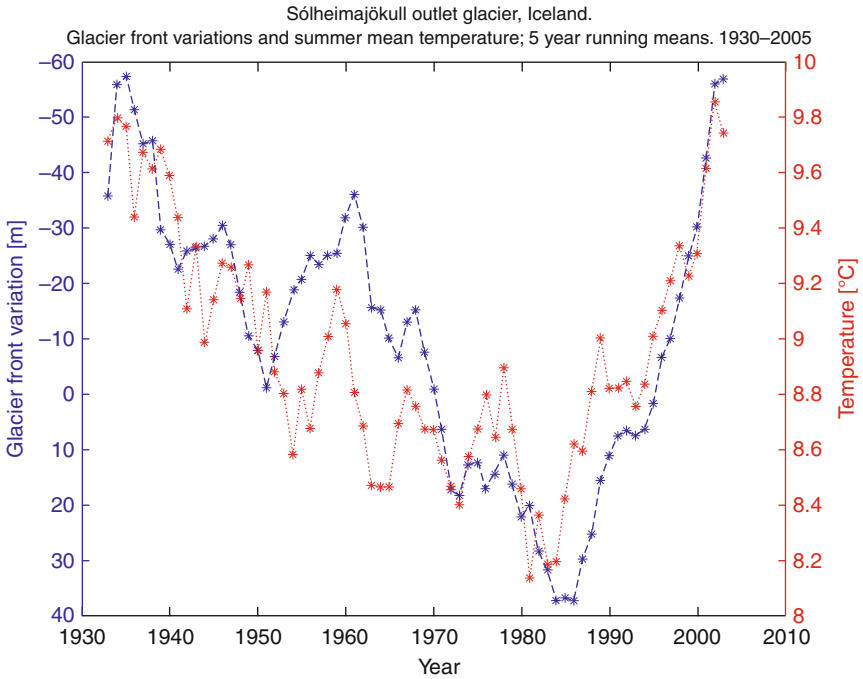

Iceland Glaciers, Figure 3 Annual variations of the terminus of Sólheimajökull outlet glacier compared with mean summer temperature in Stykkishólmur, western Iceland (5-year running mean). (Updated from Sigurðsson, 2006).

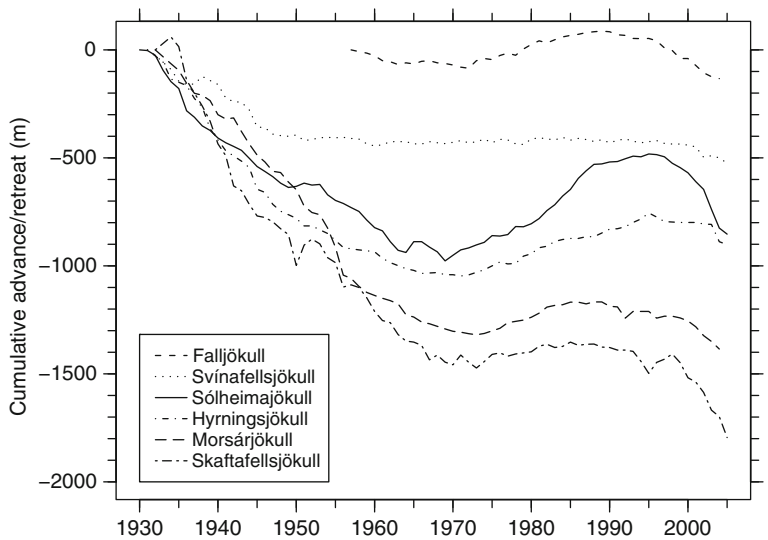

Iceland Glaciers, Figure 4 Cumulative front variations of six non-surge-type outlet glaciers since 1930. (Courtesy of International Glaciological Society).

(Sigurðsson et al., 2007). Surge-type glaciers react in a different way as explained below.

During the twentieth century glaciers in Iceland retreated approximately as far as they advanced from 1600–1900 (Sigurðsson, 2005). Glaciers retreat in proportion to their length. The largest glaciers have retreated about 4–5 km during the twentieth century but the small mountain glaciers of northern Iceland have retreated only on the order of 100 m. Cirque glaciers that are covered by debris in the ablation area have decreased very little in length. A few of the smallest glaciers have disappeared entirely, leaving only remnants of ice-cored moraines.

Surge-type glaciers

Inherent differences among individual glaciers or outlet glaciers may affect the reaction of glacier termini to mass balance. In particular, it is important to distinguish between non-surge-type glaciers and surge-type glaciers. The common feature of surge-type glaciers is that they do not maintain balance velocity for steady state transport sufficient to stay in balance. This results in a gradually increasing surface gradient which inevitably results in a period of faster flow. This may evolve into a surge. Why some glaciers do not maintain balance velocity has not yet been adequately explained.

Quite a number of glaciers in Iceland have been identified as surge-type (Figure 1). They range in size from small cirque glaciers less than 1 km^2 in area (Figure 2) up to the largest outlet glaciers in Iceland, which measure about 1,500 km^2. Their average surface slope ranges from 1° to 13° (Björnsson et al., 2003).

The surges seem to have very little relation to climate changes and, therefore, surge-type glaciers cannot be used as an indicator of climatic conditions.

Climatic and non-climatic factors that affect mass balance

The two principal climatic factors governing the waxing and waning of glaciers are:

- Precipitation during the winter
- Temperature during the summer

In addition to surges several non-climatic factors can affect the mass balance of glaciers. In many locations onset of calving into lakes formed at a retreating ice margin ablates a substantial volume of ice in addition to the climate-related ablation. While calving, glaciers may not reach equilibrium with the climate or the equilibrium is offset.

Glacier surfaces in Iceland can become covered with debris by several means:

- Medial moraines
- Debris from the head wall of cirque glaciers that melt out in the ablation area (Figure 5)
- Landslides or rockslides from the side slopes
- Volcanic eruptions

Except when this layer is very thin (a couple of mm) the debris inhibits melting and thus affects the mass balance and the variations of the terminus.

Subglacial volcanic eruptions in Iceland occur on the average about 10 times per century (Larsen et al., 1998). The melting that results from such an event can be anything from negligible to huge in comparison with the volume of the glacier. Some of the historic eruptions of Katla volcano in Mýrdalsjökull ice cap are assumed to have melted several cubic kilometers of glacier ice in one eruption (Tómasson, 1996). This equates to several years of greatly negative mass balance, which has led to substantial retreat of the glacier terminus.

Iceland Glaciers, Figure 5 Kvarnárjökull northern Iceland is a cirque glacier covered by debris in the ablation area. (Photo by Oddur Sigurðsson).

Geothermal activity has considerable effect on the mass balance of several glaciers in Iceland. In some cases the geothermal activity creates a permanent cauldron in the glacier surface that funnels all precipitation in its vicinity through a sinkhole to the base of the glacier (Figure 6). From there the water discharges subglacially to the margin of the glacier. The area around the cauldron, confined by ice divides on all sides, can be considered as a glacier without terminus and exceeds 100 km^2 in the case of Grímsvötn (Björnsson, 1988).

Mass balance of glaciers

Continuous monitoring of mass balance of glaciers in Iceland started in 1988 (Björnsson et al., 2002; Sigurðsson, 2006). The measured glaciers have had negative mass balance every year since 1995. These measurements show that the variations of the summer balance are much greater than the variations of the winter balance. Therefore, the mean summer temperature, which is the main driver of summer balance, is mostly responsible for the annual variations of glaciers in the country.

During the measurement period glaciers in Iceland have on the average lost 0.5 m or more of their thickness per year. The highest net balance value for a single ice flow basin was positive ~1.7 m for Dyngjujökull outlet glacier in the year 1991–1992 and the lowest value was negative

Iceland Glaciers, Figure 6 Geothermal cauldrons in Vatnajökull ice cap by Pálsfjall nunatak. (Photo by Oddur Sigurðsson).

2.2 m for Eyjabakkajökull outlet glacier in 1996–1997 (Björnsson et al., 2002).

Airfall of volcanic ash on a glacier surface will in most cases increase ablation considerably due to decreased albedo but only during 1 year. This is because in the accumulation area snow will quickly bury the ash layer and in the ablation area the layer will be washed away.

Historical information contained in the glaciers of Iceland

Precipitation is heavy in Iceland, making the turnover of the glacier mass particularly high. The oldest ice in an Icelandic glacier is about 1,000 years old (Larsen et al., 1998); glaciers therefore contain material deposited continuously through the nation's entire history and they can shed light on how climate has varied during that time. The volcanic history is also well preserved in the stratigraphy of the ice. All glaciers in Iceland are temperate, which means that they are at the pressure-freezing point from bottom up. As a result, liquid water is to be found throughout. All soluble chemicals are, therefore, dispersed through the glacier body. However, dust layers, which form every summer on the glacier surface, and layers of volcanic airfall will keep their place in the stratigraphy.

The chemical fingerprint of volcanic tephra layers can be analyzed and traced to the volcano of origin (Figure 7). Through historical records, many of the volcanic eruptions can be dated to a specific year (Larsen et al., 1998). Thus, the age of the ice containing the tephra layers can be determined.

Jökulhlaup

Ice-dammed lakes, either subglacial or at the glacier margin, are common in Iceland. Periodically these ice dams fail, either suddenly or with a gradual exponential increase (Björnsson, 1988; Björnsson, 2009b). In either case, the result is a dramatic release of water from behind the dam, called *jökulhlaup* in Icelandic. As the phenomenon is more common in Iceland than any other place in the world, "jökulhlaup" has been adopted into the international terminology of glaciology. On the average about 5–10 jökulhlaups will occur each year in Iceland. On the order of 10 jökulhlaups per century will exceed 10,000 m^3s^{-1} in discharge and usually at least one per century will exceed 100,000 m^3s^{-1} (Sigurðsson and Einarsson, 2005).

The most catastrophic jökulhlaups are induced by subglacial volcanic eruptions. Substantial parts of the neovolcanic zone in Iceland are covered by thick glaciers so eruptions can occur at places with several hundreds of meters of ice overburden. The jökulhlaup associated with the 1996 Gjálp eruption within Vatnajökull is a prime example (Snorrason, et al., 2002). The energy required to melt the 3.2 km^3 of ice during the eruption was 10^{18} J or equivalent to 10,000 atomic bombs like the one that exploded in Hiroshima in 1945. The maximum discharge of the resulting jökulhlaup amounted to about 50,000 m^3/s, which is roughly the same as the discharge of the second largest river in the world, the Congo River. About 750 km^2 were inundated during the jökulhlaup. Katla volcano, which lies beneath the Mýrdalsjökull ice cap, usually produces the largest and most devastating jökulhlaups. In historical time it has averaged two eruptions per century. The maximum discharge of Katla jökulhlaups has exceeded that of the Amazon River, which is the largest river in the world. Katla last erupted in 1918; statistically the next eruption should be expected any time.

Summary

Glaciers constitute 11% of the area of Iceland. About 20% of the total precipitation falls on the glaciers. The outlines

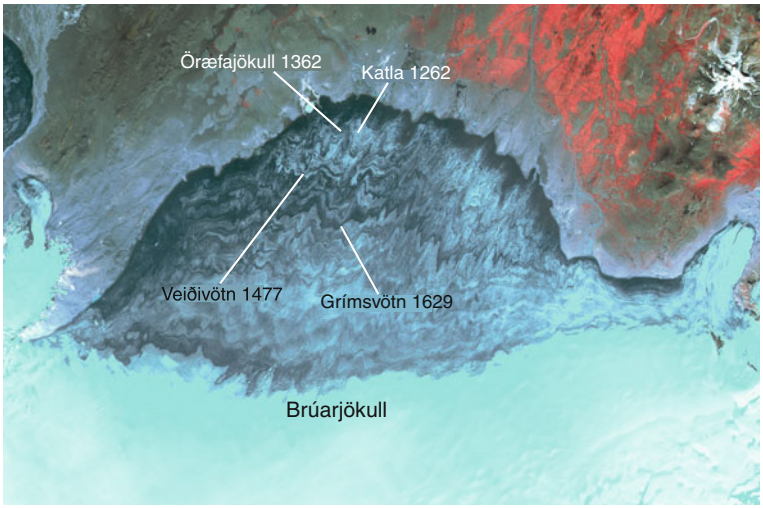

Iceland Glaciers, Figure 7 Undulating lines of volcanic tephra (information from Larsen et al., 1998) can be identified even on satellite images. IRS satellite image of Brúarjökull outlet glacier in Vatnajökull ice cap 1998.

of about 280 glaciers have been identified and mapped in the country, most of them mountain glaciers in the northern districts but the main area and volume lies in the five major ice caps. Glaciers have posed great hazards to human populations historically by advancing over inhabited districts and causing jökulhlaups (glacier outburst floods) that have inundated hundreds of square kilometers in various districts of the country. In postglacial time glaciers had their minimum about 7000 BP when they were limited to the very highest mountains. Records of advancing glaciers go back to the fourteenth century and they advanced more or less continuously to about 1890. During the last century, glaciers have lost volume and retreated accordingly particularly during the second quarter of the twentieth century and again, even faster, at the turn and the beginning of the twenty-first century. The glacial discharge has increased as a result. Rivers have gathered in fewer courses as glaciers retreated. A few small mountain glaciers have vanished entirely during the last century. The vast majority of Icelandic glaciers are expected to disappear during the next two centuries if current warming trends continue.

Bibliography

Björnsson, H., 1988. Hydrology of ice caps in volcanic regions. Vísindafélag Íslendinga, Societas Scientarium Islandica, Rit XLV, Reykjavík, 139 p. + maps.

Björnsson, F., 1998. Samtíningur um jökla milli Fells og Staðarfjalls. (Glacier variations between Fell and Staðarfjall, southeastern Iceland.). *Jökull*, **46**, 49–61.

Björnsson, H., 2009a. Jökulhlaups in Iceland:sources, release and drainage. In Burr, D. M., Carling, P. A., and Baker, V. R. (eds.), *Megaflooding on Earth and Mars*. Cambridge: Cambridge University Press, pp. 50–64.

Björnsson, H., 2009b. *Jöklar á Íslandi (Glaciers in Iceland)*. Reykjavík: Bókaútgáfan Opna, p. 479.

Björnsson, H., and Pálsson, F., 2008. Icelandic glaciers. *Jökull*, **58**, 365–386.

Björnsson, H., Pálsson, F., and Haraldsson, H. H., 2002. Mass balance of Vatnajökull (1991–2001) and Langjökull (1996–2001), Iceland. *Jökull*, **51**, 75–78.

Björnsson, H., Pálsson, F., Sigurðsson, O., and Flowers, G. E., 2003. Surges of glaciers in Iceland. *Annals of Glaciology*, **36**, 82–90.

Eythorsson, J., 1963. Variation of Iceland glaciers. *Jökull*, **13**, 31–33.

Geirsdóttir, Á., Miller, G. H., Axford, Y., and Ólafsdóttir, S., 2009. Holocene and latest Pleistocene climate and glacier fluctuations in Iceland. *Quaternary Science Reviews*, **28**, 2107–2118.

Hanna, E., Jónsson, T., and Box, J. E., 2004. An analysis of Icelandic climate since the nineteenth century. *International Journal of Climatology*, **24**, 1193–2004.

Jóhannesson, T., and Sigurðsson, O., 1998. Interpretation of glacier variations in Iceland 1930–1995. *Jökull*, **45**, 27–33.

Jóhannesson, T., Aðalgeirsdóttir, G., Björnsson, H., Crochet, P., Elíasson, E.B., Guðmundsson, S., Jónsdóttir, J. F., Ólafsson, H., Pálsson, F., Rögnvaldsson, O., Sigurðsson, O., Snorrason, A., Sveinsson, O. G. B., and Thorsteinsson, T., 2007. Effect of climate change on hydrology and hydro-resources in Iceland. OS-2007/011, National Energy Authority, Reykjavík, 91 p.

Larsen, G., Guðmundsson, M. T., and Helgi, B., 1998. Eight centuries of periodic volcanism at the center of the Iceland hotspot revealed by glacier tephrostratigraphy. *Geology*, **26**(10), 943–946.

Sigurðsson, O., 1998. Glacier variations in Iceland 1930–1995 - From the database of the Iceland Glaciological Society. *Jökull*, **45**, 3–25.

Sigurðsson, O., 2005. Variations of termini of glaciers in Iceland in recent centuries and their connection with climate. In Caseldine, C., Russel, A., Harðardóttir, J., and Knudsen, E. I. (eds.), *Iceland – Modern Processes and Past Environments*. London: Elsevier, pp. 241–255, 335–397 (references), 408 (map).

Sigurðsson, O., 2006. Jöklabreytingar 1930–1970, 1970–1995, 1995–2004 og 2004–2005 (Glacier variations 1930–1970, 1970–1995, 1995–2004 og 2004–2005.) Jökull, **56**, 85–91.

Sigurðsson, O., and Bergur E., 2005. Jökulhlaupaannáll 1989–2004. (Annals of jökulhlaups 1989–2004), Report OS-2005/031, National Energy Authority, Reykjavík, 46 p.

Sigurðsson, O., and Williams, R.S., Jr., 2008. Geographic names of Iceland's glaciers: Historic and modern. U.S. Geological Survey Professional Paper 1746, 225 p. (w/8 p. in appendix) (http://pubs.usgs.gov/pp/p1746/).
Sigurðsson, O., Jónsson, T., and Jóhannesson, T., 2007. Relation between glacier-termini variations and summer temperature in Iceland since 1930. *Annals of Glaciology*, **46**, 170–176.
Snorrason, Á., Jónsson, P., Sigurðsson, O., Pálsson, S., Árnason, S., Víkingsson, S., and Kaldal, I., 2002. Jökulhlaup on Skeiðarársandur outwash plain, Iceland. In Martini, P., Baker, V. R., and Garzón, G. (eds.), *Flood and Megaflood Processes and Deposits: Recent and Ancient Examples*. London: Blackwell Science, pp. 55–65.
Tómasson, H., 1996. The jökulhlaup from Katla in 1918. *Annals of Glaciology*, **22**, 249–254.

ICESAT DATA IN GLACIOLOGICAL STUDIES

Thomas A. Neumann[1], H. J. Zwally[1], Bob E. Schutz[2]
[1]NASA Goddard Space Flight Center, Greenbelt, MD, USA
[2]Center for Space Research, University of Texas at Austin, Austin, TX, USA

The ICESat mission

The Ice, Cloud, and land Elevation Satellite (ICESat) mission, launched in January 2003, has been an exceptional new tool for laser exploration of the planet – measuring the Earth's surface and atmosphere in unprecedented three-dimensional detail. ICESat's measurements have proven the unique capability of spaceborne laser altimetry for a variety of advances in Cryospheric and Earth Sciences.

ICESat's instrumentation was designed to make accurate measurements of surface and near-surface elevations with a 1,064-nm laser channel. Return signals are digitized to provide unprecedented detail of the height distributions of the surface and near-surface (e.g., trees) and vertical distribution of backscatter from the atmosphere. ICESat is in a 600-km orbit with an inclination of 94°. The agile spacecraft control system directs the laser beam to reference ground tracks over the ice sheets to within 100 m, enabling close repeat tracks for elevation change detection, and to targets of special interest up to 5° off-nadir.

Although initially intended to run continuously for 3–5 years along a 91-day repeat orbit, unforeseen manufacturing defects caused significant reduction in the laser lifetime. A revised operation plan called for 33-day observation periods conducted three times per year. In 2007, this strategy was further revised to twice-yearly 33-day campaigns in March/April and October/November. To date, ICESat has completed 16 operations periods.

The 2-cm precision of ICESat's satellite-to-surface range is five times better than designed, making it very valuable for monitoring sea ice and for other applications. The accuracy of radial orbit determinations is about 2–3 cm. The achieved accuracy of ice surface elevations is 10 cm for individual point measurements over surfaces with low slopes, increasing to 20 cm over surfaces with 2° slopes.

Glaciological research highlights include mapping elevation changes of the Greenland and Antarctic ice sheets and mass-loss estimation; discovery of subglacial water drainage/transfer under West Antarctic ice streams; precision mapping of ice-shelf grounding lines; and seasonal and interannual changes in sea-ice thickness distribution. ICESat data is used to derive important information about the interactions between ice sheets and climate that is needed to develop models to assess ice sheet behavior as the climate changes as well as the associated sea-level contributions from this change. The ability to do this is greatly enhanced by measurements over a long duration.

Elevation change and mass balance of the Greenland ice sheet

Using knowledge of the precise location of ICESat and the laser footprint on the Earth's surface, the elevation of the surface can be determined. Elevation changes (dH/dt) presented here are derived from 12 sets of 33-day repeat tracks over 4 years (October 2003 to November 2007). The along-track analysis techniques to obtain reliable dH/dt results are described elsewhere (Zwally et al., Journal of Glaciology). Briefly, the elevation change along each ground track depends on the surface slope and the cross-track separation of the repeated passes (nominally 100 m), as well as the change in surface elevation with time ($H(t)$). This requires solution of the equation $H(X, \alpha, t) = X \tan \alpha + t\ (dH/dt)$ for dH/dt and the surface slope (α). Because of the limited number of passes, it is necessary to assume that dH/dt is constant with time and that there is no seasonal cycle. At each along-track point (separated by 172 m), at least four passes of the 12 repeats are needed to solve for both α and dH/dt. Error analysis (Zwally et al., Journal of Glaciology) demonstrates that the accuracy improves to about ~20 cm/year over surface slopes less than about 2° with data from 10 or more passes. Some data gaps are due to the higher frequency of clouds near the edges of the ice sheet, which prevent the transmission of the laser pulse. Continuing ICESat's 33-day repeat tracks in campaigns through winter of 2011 will provide five more opportunities for additional coverage and eliminating these gaps. Here, we highlight studies of mass loss from the Greenland ice sheet.

ICESat ice-thickness change (dI/dt) results for the Greenland ice sheet from 2003 to 2007 are shown in Figure 1 along with the derived estimates of mass change (dM/dt) from major drainage systems (Zwally et al., Journal of Glaciology). To obtain dI/dt, the measured dH/dt is adjusted for bedrock motion and the time–variable firn compaction (dC/dt). The firn compaction adjustment (Li et al., 2007) has become critically important because of increasing temperatures in Greenland that are increasing the rate of compaction. The dI/dt map shows detailed patterns of thickening and thinning, with thickening occurring most at the higher inland elevations. Although the

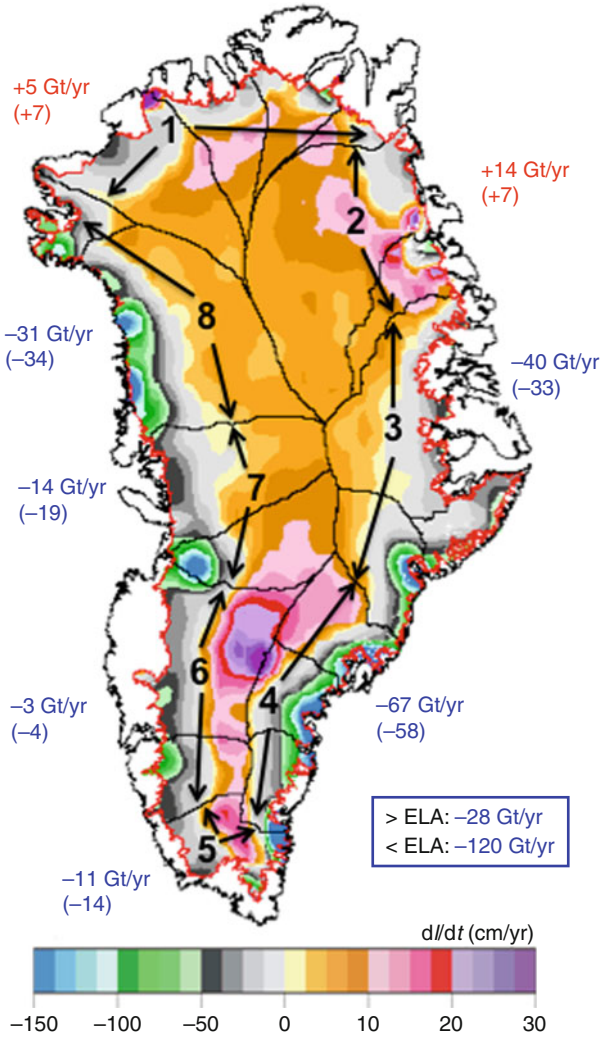

ICESat Data in Glaciological Studies, Figure 1 Mass loss estimates of the Greenland ice sheet are obtained from this ICESat-derived map of ice-thickness change (d*l*/d*t*) for 2003–2007. Mass gains and losses for each of the major drainage basins 1–8 (indicated by *black arrows*) are shown, along with the changes (in *parenthesis*) relative to values for the period 1992–2002 obtained from ERS radar altimetry and aircraft laser measurements. The ice sheet continues to thicken inland, as it did in the 1990s, but thinning at the margins has increased significantly due to increased summer melting and acceleration of outlet glaciers (Zwally et al., Journal of Glaciology).

lower elevations along the coast have a mixed pattern of thickening and thinning, areas of thinning are dominant. Compared to results for the 1990s from a combination of airborne laser surveys (Krabill et al., 2000) and satellite radar altimetry (Davis and Sun, 2004), the inland thickening at elevations above ~2,200 m has not changed. However, at lower elevations, the thinning has increased markedly, especially below the equilibrium line altitude (ELA). Zwally et al. (Journal of Glaciology) derive d*M*/d*t* by determining the average density associated with the elevation change; it is a combination of ice loss and change in firn compaction through time. The net mass loss has increased to 148 Gt/year from close to zero loss in the 1990s, with the loss below the ELA increasing from only 42 Gt/year to 120 Gt/year due to increased melting near the margins and accelerating outflow of some glaciers. Increasing losses are largest in the southeast and along the western margin, with small increases in the north perhaps indicative of increasing precipitation. The net contribution to global sea-level rise from the Greenland ice sheet is now about 0.4 mm/year.

Subglacial hydrology

To study "active" subglacial lakes, ICESat exploits surface deformation that occurs as the ice surface above the lake rises and falls in response to water moving at the glacier bed. ICESat data along repeated tracks were used to reveal an active subglacial system in the Whillans, Mercer, and MacAyeal ice streams, East Antarctica (Fricker et al., 2007). This study showed the subglacial system is composed of several "active" lakes connected by inferred channels, with water rapidly transferring between reservoirs.

Using 4.5 years (2003–2008) of ICESat laser altimeter data, Smith et al. (2009) made a comprehensive study of active subglacial lakes for the entire Antarctic ice sheet and detected 124 active lakes during this period. They determined that ICESat-detected lakes not only exist under the ice divides in the slow moving parts of the ice sheets, but are also present under most of the largest outlet drainage systems that transport ice from the continent to the ice shelves and, ultimately, deliver it to the ocean. Lakes sometimes appear to transfer water from one to another, but also often exchange water with distributed sources invisible to ICESat, suggesting that the lakes may provide water to or withdraw water from the reservoirs that lubricate glacier flow. This proves the significance of the subglacial water system throughout Antarctica, which affects ice flow rates and can alter Antarctica's mass balance and contribution to sea-level rise (Fricker, 2008).

Ice shelves

Recent studies have depended on ICESat's sampling characteristics to improve our understanding of ice shelf variability and the processes affecting ice motion and stability, especially at the critical juncture of grounded and floating ice near the grounding line (GL). Science teams have used ICESat elevation data in a multi-instrument study of long-term trends and shorter-term (interannual) variability in the surface height of the Amery Ice Shelf (King et al., 2009). The time series spanned 4 decades and used datasets acquired through optical leveling, GPS, ERS-1, and ERS-2 satellite radar altimetry, and ICESat. Fricker and Padman (2006) used ICESat altimetry at crossovers on ice shelves to measure time variability of ice shelf surface height, including high-frequency

contributions from the tide and dH/dt trends from processes such as surface accumulation and basal melt. ICESat altimetry acquired along repeat tracks across the grounding zone (GZ) at different phases in the tidal cycle identified both the landward and seaward limits of this tidal flexure zone.

Knowledge of GZ extent and ice sheet thickness at the GL is required for ice sheet mass balance studies and to model ice-shelf/ocean interactions. ICESat is currently the only satellite capable of precisely locating the limits of flexure, by virtue of its high along-track resolution, and accurate ground track repetition. ICESat also provides accurate surface elevation data at the GL, from which ice thickness can be estimated. Comparisons between the landward flexure limit (the GL) and surface topography from MODIS imagery facilitates development of a detailed grounding-line data set beyond the intermittent coverage of the GL obtained from Interferometric Synthetic Aperture Radar (InSAR) (Fricker and Padman, 2006).

Smith and Joughin (2008) used an Antarctic DEM (Bamber et al., 2008) to calculate offshore ice mass flux and basal melt rate in the region of the GZ of northern Dronning Maud Land. Accurate knowledge of the surface elevation is critical in these areas, because the surface height of floating ice is used in calculating the ice thickness. This, combined with measurements of surface velocity, gives the rate of ice discharge into the ocean and the basal melt rate at the grounding line. Because of ICESat's small footprint, the data are uniquely able to resolve the sharp change in surface slope that is frequently found near the GL. The ICESat profiles revealed a systematic bias in the 5-km region around the GL in the DEM, which would have led to errors in the ice discharge rate of up to 15%, and severe overestimates of the basal melt rate near the GL.

ICESat data have been used to study processes related to ice shelf break-up. Elevation profiles across drifting icebergs were used to look at iceberg calving and ice shelf break-up processes by proxy (Scambos et al., 2008). A fortuitous acquisition along a ground track across Wilkins Ice Shelf on February 28, 2008, during the period of active break-up (Scambos et al., 2009), provided quantitative information about the disintegration mechanism.

Sea ice

Farrell et al. (2009) used data from ICESat to analyze sea ice freeboard in the Arctic Ocean. Using knowledge of the local sea surface height and sea ice elevation, they estimated sea ice freeboard and presented a time series of Arctic freeboard spanning 5 years between 2003 and 2008. ICESat data from fall (October–November) and winter (February–March) illustrate the seasonal and interannual

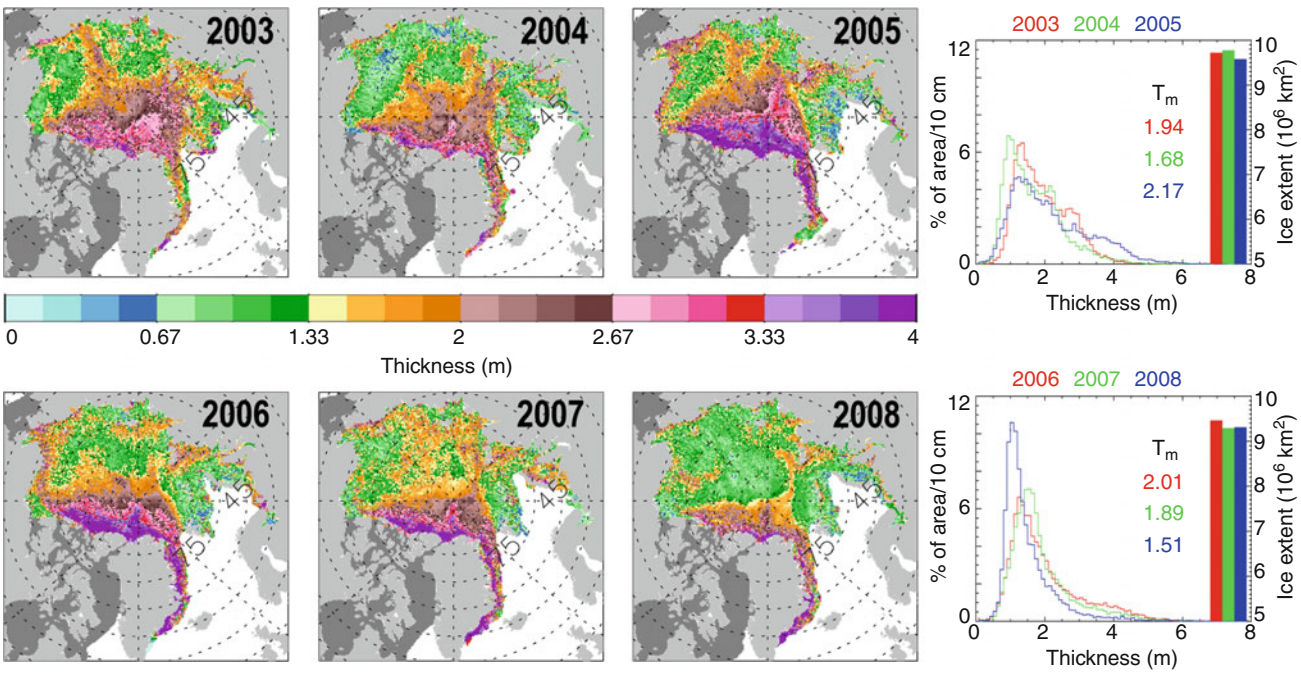

ICESat Data in Glaciological Studies, Figure 2 A significant decrease in the average wintertime thickness from about 2–1.5 m is derived from ICESat's measurements of sea ice freeboard heights for the February–March observation periods from 2003 to 2008. Much of the thicker multiyear (MY) ice located north of Canada and Greenland has disappeared. In October after the summer melt season, the average ice thickness decreased by about 25% while the areal extent decreased by a similar amount giving a volume loss of about 50% in only 5 years. Measurements of ice thickness changes are critical to understanding when the Arctic Ocean may become ice free in summer (based on Kwok et al., 2009).

variations in freeboard. Following the September 2007 record minimum sea ice extent, the fall 2007 and winter 2008 spatially averaged freeboards were below the seasonal means at −4.5 cm, and −6.8 cm, respectively. Over the observation period, mean freeboard has declined at a rate of approximately −1.8 cm/year during the fall period and approximately −1.6 cm/year during the winter period. Due to the short 5-year observation period, it is unclear whether these results represent a long-term, downward trend in Arctic freeboard or are part of a natural variability.

Kwok et al. (2009) present an estimate of the thickness and volume of the Arctic Ocean ice cover from ten ICESat campaigns that span a 5-year period between 2003 and 2008. Along with a more than 42% decrease in multiyear (MY) ice coverage since 2005, there was a remarkable thinning of ∼0.6 m in MY ice thickness over 4 years. In contrast, the average thickness of the seasonal ice in midwinter (∼2 m), which covered more than two thirds of the Arctic Ocean in 2007, exhibited a negligible trend. Average winter sea ice volume over the period, weighted by a loss of ∼3,000 km^3 between 2007 and 2008, was ∼14,000 km^3. The total MY ice volume in the winter has experienced a net loss of 6,300 km^3 (>40%) in the 4 years since 2005 while the FY ice cover gained volume due to increased overall area coverage (Figure 2). The overall decline in volume and thickness is explained almost entirely by changes in the MY ice cover. Combined with a large decline in MY ice coverage over this short record, there is a reversal in the volumetric and areal contributions of the two ice types to the total volume and area of the Arctic Ocean ice cover. In this period, seasonal ice became the dominant ice type. It seems that the near zero replenishment of the MY ice cover after the summers of 2005 and 2007 has played a significant role in the loss of Arctic sea ice volume over the ICESat record.

Summary

The Ice, Cloud, and land Elevation Satellite (ICESat) mission, launched in January 2003, has been an exceptional new tool for laser exploration of the planet – measuring the Earth's surface and atmosphere in unprecedented three-dimensional detail. ICESat's measurements have proven the unique capability of spaceborne laser altimetry for a variety of advances in Cryospheric and Earth Sciences. Glaciological research highlights include mapping elevation changes of the Greenland and Antarctic ice sheets and mass-loss estimation; discovery of subglacial water drainage/transfer under West Antarctic ice streams; precision mapping of ice-shelf grounding lines; and seasonal and interannual changes in sea-ice thickness distribution. ICESat data is used to derive important information about the interactions between ice sheets and climate that is needed to develop models to assess ice sheet behavior as the climate changes as well as the associated sea-level contributions from this change.

Bibliography

Bamber, J. L., Gomez-Dans, J. L., and Griggs, J. A., 2008. A new 1 km digital elevation model of the Antarctic derived from combined satellite radar and laser data Part 1: data and methods. *The Cryosphere Discussion*, **2**, 811–841.

Davis, C. H., and Sun, S., 2004. Long-term thinning of the southeast Greenland Ice Sheet from Seasat, Geosat and GFO satellite radar altimetry. *IEEE Geoscience and Remote Sensing Letters*, **1**(2), 47–50.

Farrell, S. L., Laxon, S. W., McAdoo, D. C., Yi, D., and Zwally, H. J., 2009. Five years of Arctic sea ice freeboard measurements from ICESat. *Journal of Geophysical Research–Oceans*, **114**, C04008, doi:10.1029/2008JC005074.

Fricker, H. A., 2008. Glaciology: water slide. *Nature Geoscience*, **1**, 809–810.

Fricker, H. A., and Padman, L., 2006. Ice shelf grounding zone structure from ICESat laser altimetry. *Geophysical Research Letters*, **33**, L15502, doi:10.1029/2006GL026907.

Fricker, H. A., Scambos, T., Bindschadler, R., and Padman, L., 2007. An active subglacial water system in West Antarctica mapped from space. *Science*, **315**, 1544–1548.

King, M. A., Coleman, R., Freemantle, A. J., Fricker, H. A., Hurd, R. S., Legrèsy, B., Padman, L., and Warner, R., 2009. A 4-decade record of elevation change of the Amery Ice Shelf. East Antarctica. *Journal of Geophysical Research*, **114**, F01010, doi:10.1029/2008JF001094.

Krabill, W., Abdalati, W., Feredrick, E., Manizade, S., Martin, C., Sonntag, J., Swift, R., Thomas, R., Wright, W., and Yungel, J., 2000. Greenland ice sheet: high-elevation balance and peripheral thinning. *Science*, **289**, 428–430.

Kwok, R., Cunningham, G. F., Wensnahan, M., Rigor, I., Zwally, H. J., and Yi, D., 2009. Thinning and volume loss of the Arctic Ocean sea ice cover: 2003–2008. *Journal of Geophysical Research*, **114**, C07005, doi:10.1029/2009JC005312.

Li, J., Zwally, H. J., and Comiso, J. C., 2007. Ice-sheet elevation changes caused by variations of the firn compaction rate induced by satellite-observed temperature variations (1982-2003). *Annals of Glaciology*, **46**, 8–13.

Scambos, T., Ross, R., Bauer, R., Yermolin, Y., Skvarca, P., Long, D., Bohlander, J., and Haran, T., 2008. Calving and ice shelf break-up investigated by proxy: Antarctic tabular iceberg evolution during northward drift. *Journal of Glaciology*, **54**(187), 579–591.

Scambos, T., Fricker, H. A., Liu, C., Bohlander, J., Fastook, J., Sargent, A., Massom, R., and Wu, A., 2009. Ice shelf disintegration by plate bending and hydro-fracture: satellite observations and model results of the 2008 Wilkins ice shelf break-ups. *Earth and Planetary Science Letters*, doi:10.1016/j.epsl.2008.12.027.

Smith, B. E., and Joughin, I. R., 2008. Weddell Sea and Dronning Maud Land ice shelf mass balance from satellite altimetry and velocity measurements. *Eos Transactions, Fall Meeting Supplement*, abstract C41D-07.

Smith, B. E., Fricker, H. A., Joughin, I. R., and Tulaczyk, S., 2009. An inventory of active subglacial lakes in Antarctica detected by ICESat (2003–2008). *Journal of Glaciology*, **55**(192), 573–595.

Zwally, H. J., Li, J., Brenner, A. C., Beckley, M., Cornejo, H. G., DiMarzio, J., Neumann, T. A., Robbins, J., Saba, J. L., Yi, D., and Wang, W. Greenland ice sheet mass balance: distribution of increased mass loss with climate warming. *Journal of Glaciology*.

Cross-references

Antarctica
Greenland Ice Sheet
Ice Shelf
Sea Ice
Subglacial Lakes, Antarctic

ICICLE

P. Pradeep Kumar
Department of Atmospheric and Space Sciences, Pune University, Pune, India

An icicle is a spike of ice formed when water dripping or falling from an object freezes. Typically, icicles will form when ice or snow is melted by either sunlight or some other heat source (such as heat leaking from the interior of a heated building), and the resulting melted water runs off into an area where the ambient temperature is below the freezing point of water (0°C), causing the water to refreeze. Icicles are mostly observed as hanging spike. They can form off building roof, from branches of trees, rocks near waterfalls, water seepage points, etc.

Bibliography

http://en.wikipedia.org/wiki/Icicle

ICING

P. Pradeep Kumar
Department of Atmospheric and Space Sciences, Pune University, Pune, India

In general, the freezing of water on exposed surface can be called as icing. In the atmosphere, icing is usually associated with aviation. It occurs when the aircraft fly through clouds containing supercooled drops in clouds above freezing level. The rain striking the frame of the aircraft freezes on it and forms glace ice. Icing can also occur at seas when sea spray can freeze on the body of ships and boats.

Bibliography

Lankford, T. T., 1999. *Aircraft Icing: A Pilot's Guide*. New York, USA: McGraw-Hill, ISBN 0071341390, 9780071341394, 336 pp.

IMPACTS OF SNOW AND GLACIERS ON RUNOFF

Sarah Boon
Department of Geography, University of Lethbridge, Lethbridge, AB, Canada

Synonyms

Nival and glacial runoff regimes

Definition

Effect of seasonal melt, water storage, and runoff from snow and glacier ice on discharge from snow-covered and/or glacierized basins.

Snow and ice extent

Seasonal snow cover has a maximum areal extent of 9% of the earth's surface, while glaciers cover ~10% (15×10^6 km^2) of the Earth's surface (NSIDC, 2008). In the Northern Hemisphere, peak snowpack extent occurs in January, north of 50° (Stewart, 2009). In the Southern Hemisphere, snowpack outside of Antarctica is confined to alpine regions of South America, Africa, and New Zealand. Glaciers and ice sheets are distributed at high latitudes and in lower latitude alpine regions of both hemispheres (Figure 1), and store >70% of global freshwater. Runoff production in mid- and high-latitude mountain ranges is influenced largely by seasonal snow cover, while glaciers are the dominant water source in low-latitude mountain ranges during the dry season (Hock et al., 2005). In arid and semiarid regions, snow- and icemelt can contribute more than 80% of annual streamflow (Viviroli et al., 2003). Approximately one-sixth of the global population lives in basins fed predominantly by snow- and icemelt (Barnett et al., 2005).

The water balance in snow- and glacier-covered regions can be written as:

$$Q_{tot} = Q_s + Q_p + Q_i + Q_g + Q_l - Q_e \quad (1)$$

where Q_{tot} is the total potential runoff, Q_s is the snowmelt from ice-free areas, Q_p is the rainfall runoff, Q_i is the glacial contribution to discharge (including snowmelt from ice-covered areas), Q_g is groundwater discharge, Q_l is condensation of water vapor and Q_e is evaporation (Hagen et al., 2003). The latter three terms are often considered negligible.

The majority of research on snow and glacier runoff has been conducted in North America and Europe (Meier, 1969; Henoch, 1971; Krimmel and Tangborn, 1974; Fountain and Tangborn, 1985; Demuth et al., 2009), with far fewer studies in Central Asia (Hewitt and Young, 1993) and the Andes (Kaser et al., 2003; Casassa et al., 2009). Research in the Upper Colorado basin indicates that river flow is driven largely by seasonal SWE, with maximum discharge occurring in May or June (Fassnacht, 2006). Studies in the subarctic mountains of northwestern North America also note that snowmelt drives the majority of annual and peak runoff. In South America, tropical glaciers have been shown to provide the majority of dry season (May–September) runoff (Kaser et al., 2003). On Svalbard, north of mainland Europe, surface runoff from glacier snow and icemelt is slightly greater than that from snow accumulation alone, at 680 ± 140 mm/year (Hagen et al., 2003).

Snow- and icemelt

In contrast to pluvial systems, where runoff is a function of precipitation and evaporation, runoff production from snow- and ice-covered (nival and glacial, respectively) regions is a function of the net energy available for melt. This energy is derived mainly from incoming radiation. Radiative fluxes vary with latitude and altitude: for

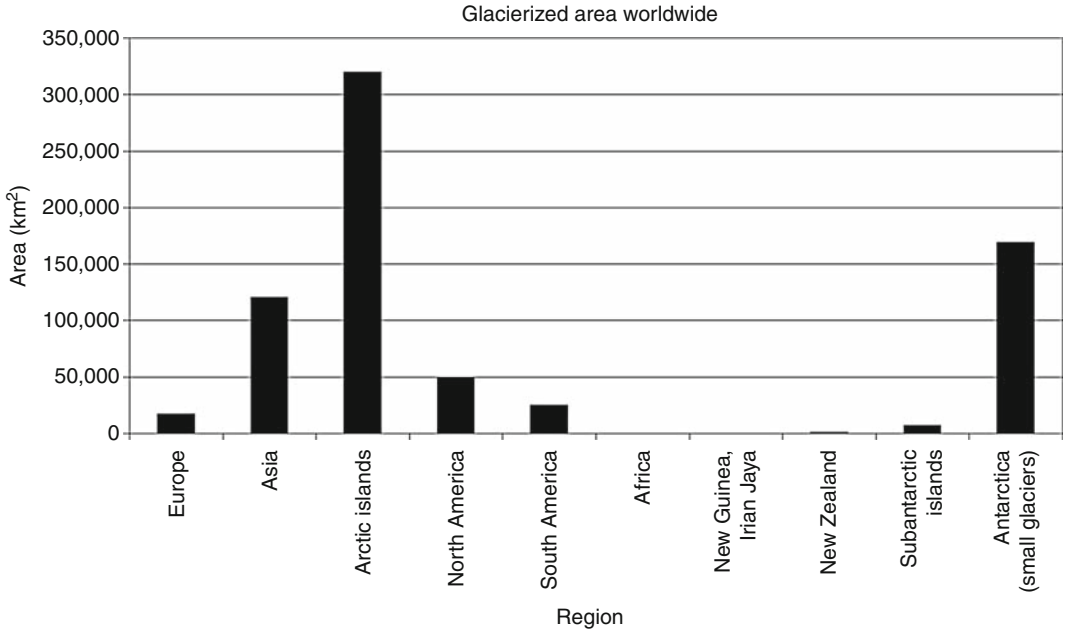

Impacts of Snow and Glaciers on Runoff, Figure 1 Global glacier cover, by region. (Data from Dyurgerov and Meier, 2004.)

example, high latitude/low altitude (Arctic) basins receive continuous incoming radiation during the summer months, and thus have much different runoff response than low latitude/high altitude basins, which receive a diurnal cycle of incoming radiation (Hodson et al., 1998). The energy balance at the glacier surface is thus strongly affected by peak shortwave radiation inputs in midafternoon, resulting in subsequently high melt production. In tropical regions, however, low latitude/high altitude basins experience a fairly constant air temperature throughout the year, with changes only in precipitation (snow accumulation during the wet season, October–April) and sublimation (maximum during the dry season, May–September) (Kaser et al., 2003).

While shortwave radiation is the main driver of snow- and icemelt, melt energy is also derived from advection of heat from weather systems. For example, rain-on-snow events can accelerate snowmelt by transferring latent and sensible heat to the snowpack, reducing the snowpack cold content, and enhancing spring runoff peaks. Although this has largely been observed in maritime climates (e.g., Kattelmann, 1997), it can also occur in continental climates dominated by orographic precipitation generation (e.g., López-Moreno and García-Ruiz, 2004). The frequency and magnitude of regional pressure systems is thus highly significant for snow- and icemelt: high pressure systems with high air temperatures, clear skies, and high incoming radiation result in rapid melt and greater likelihood of rapid meltwater transfer to surface streams. Alternatively, low pressure systems with lower air temperatures and cloudy skies can reduce melt and delay runoff production. In some mountainous regions, föhn (chinook) events during the winter season, with their associated high wind speeds, high air temperatures, and steep vapor pressure gradients, can result in midwinter melt events and the possibility of melt contribution to winter streamflow (Hayashi et al., 2005).

Melt production is also strongly affected by the hypsometry (area-altitude distribution) of both the watershed and the glacier surface. In watersheds with relatively flat topography, melt is highly spatially synchronized given similar meteorological conditions across large spatial extents (Eaton and Moore, 2008). Melt is more desynchronized in watersheds with steep terrain, where air temperature and precipitation lapse rates are steeper and snowmelt at higher elevations is delayed. Melt production is greatest on relatively flat glaciers with high proportions of their mass in the ablation zone, as it is more likely that the annual snowline will retreat to the top of the glacier given this morphology. On steep glaciers, however, the corresponding steep temperature and precipitation lapse rates limit snowline retreat to the lower parts of the glacier except in years with above average energy inputs. Thus, these glaciers have a small proportion of their mass in the ablation zone and produce less melt.

Snow and ice runoff

Runoff generation from nival and glacial catchments is a function of basin hypsometry, total water available for melt, and the interaction between melt and intermediate storage locations prior to reaching the basin outlet (Young, 1982).

Flat watersheds with synchronized melt response can produce a large freshet peak of short duration. In steep terrain, the freshet peak may be of lower magnitude but

attenuated over a longer time period. As snowline retreats, runoff contributing area decreases and less permeable surfaces with lower albedos are exposed (Hodson et al., 1998), reducing hydrologic response.

Runoff volume from nival catchments is positively correlated with the water equivalent of snow (SWE) stored in the basin at the onset of melt, and the air temperature during the melt period. Snowpack is a natural storage reservoir for cold-season precipitation, releasing water to streamflow during the warmer months as a spring runoff peak, or freshet. As the melt season progresses and snowline retreats, the amplitude of the diurnal signal decreases and runoff becomes less responsive to temperature (Lafrenière and Sharp, 2003). SWE amounts drive the timing and magnitude of freshet: low SWE produces an earlier runoff peak than high SWE, and can result in faster melt and increased likelihood of flooding (Stewart, 2009). Research to measure spring snowpack for downstream flood management has been under way since 1909, when engineers in Nevada correlated water levels in Lake Tahoe with snow water content on nearby Mount Rose (Male and Gray, 1981). Further research by the US Army Corps of Engineers (1956) and Kuzmin (1961) forms the basis for current studies of snowmelt and runoff. In mountainous watersheds, up to 90% of snowmelt goes to runoff, indicating that upland snowpacks are critical to downstream systems. For example, in the western USA, spring/early summer snowmelt runoff accounts for 50–80% of the total annual runoff for snowmelt-dominated basins (Stewart et al., 2004).

While runoff from non-glacierized basins is correlated with precipitation (snow or rainfall) and evaporation (Collins, 2008), runoff from glacierized basins is highly correlated with summer air temperature and net radiation: as percent glacier cover in a watershed decreases, the correlation between runoff and annual precipitation increases (Meier, 1969; Krimmel and Tangborn, 1974; Meier and Tangborn, 1961; Meier, 1973; Chen and Ohmura, 1990). The glacial outflow hydrograph is similar to that of nival basins given the effect of significant snow cover. However, snow cover persists longer on glacier surfaces than on surrounding terrain, resulting in delayed snowmelt contributions to streamflow, followed by late-season glacier melt once the ice surface is exposed (Collier, 1958). Glacial runoff regimes are therefore characterized by a later maximum runoff peak than nival catchments (Figure 2) (Fountain and Tangborn, 1985) followed by augmentation of late summer streamflow (August/September), with higher winter baseflows (Fleming and Clarke, 2005). As the percentage of ice-covered area in a watershed increases, the proportion of runoff occurring during May–September increases (Figure 3). Interannual (2–3 years) variability in glacial runoff decreases with increasing fractional glacier cover (up to ~30–40% cover) given the mutual buffering of runoff variability between ice-free and glacierized portions of the catchment (Figure 4) (Henshaw, 1933; Collins and Taylor, 1990; Fleming and Clarke, 2005). Warm/dry years with low snow accumulation result in earlier snowline retreat and glacier ice exposure, leading to increased glacier melt that compensates for reduced snowmelt from ice-free areas. During cold/wet years, glacier melt decreases and snowmelt runoff from ice-free areas increases given greater precipitation amounts and reduced evaporation, maintaining total streamflow but reducing the proportion of glacial contributions.

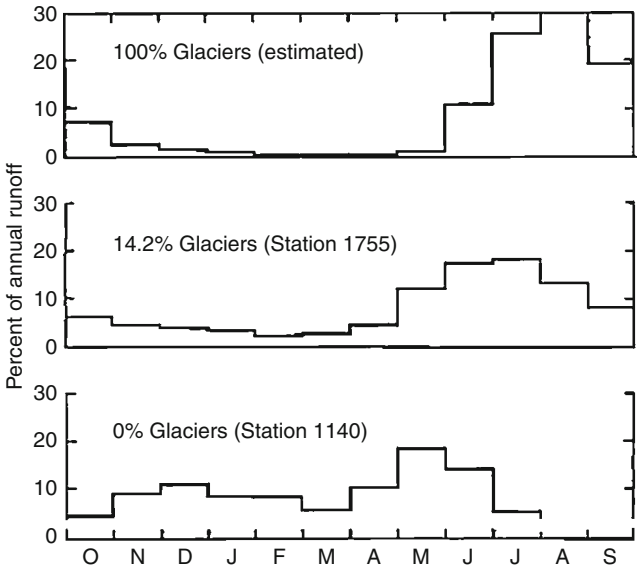

Impacts of Snow and Glaciers on Runoff, Figure 2 Monthly fraction of annual specific runoff for basins of various glacier covers. (Modified from Fountain and Tangborn, 1985.)

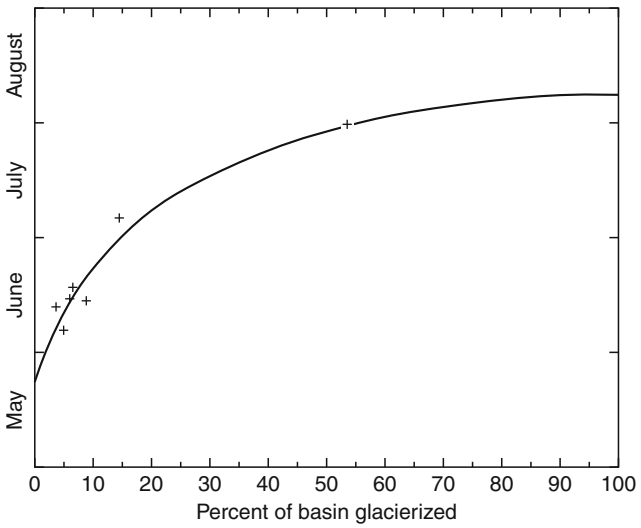

Impacts of Snow and Glaciers on Runoff, Figure 3 Time of peak specific runoff as a function of glacier cover for basins in the North Cascades, Washington. (From Fountain and Tangborn, 1985.)

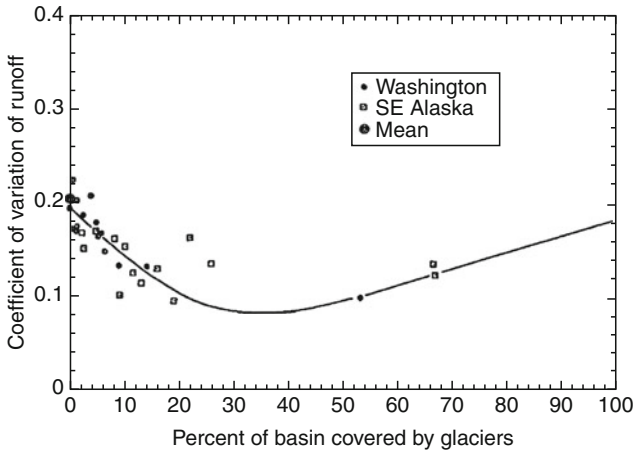

Impacts of Snow and Glaciers on Runoff, Figure 4 Coefficient of variation of annual specific runoff values versus percent of basin glacierized. (From Fountain and Tangborn, 1985.)

Basin outflow hydrographs integrate the physiographic, climatic, and storage characteristics of basins fed by snow- and glacier melt. During the melt season, the rising limb of the hydrograph is driven by the melt rate while the recession limb is a function of basin storage characteristics. Recession analysis of discharge hydrographs over time can thus explain the storage characteristics of snow- and glacier melt-dominated basins.

In nival watersheds and the snow-covered portions of glacial watersheds, the lag between snowmelt onset and runoff production is initially a function of meltwater storage within the pore spaces of the snowpack. Once the snowpack cold content has been removed and its liquid water holding capacity maximized (US Army Corps of Engineers, 1956), meltwater is released to runoff. The time delay between meltwater production and release from the snowpack is a function of snow depth, and to a lesser extent the slope of the underlying terrain – steeper slopes allow for faster runoff than shallower slopes (Male and Gray, 1981). Meltwater runoff from the snowpack is then routed to soil moisture storage. If the soil is either frozen or saturated, the time lag for snowpack runoff to reach the stream is fairly short. However, the presence of unsaturated, unfrozen soils requires several days to reach saturation, thus increasing the time required for snowpack runoff to reach the stream. The final storage location is in-stream, as runoff from the snow-covered contributing area is transported to the watershed outlet (Male and Gray, 1981). This storage is a function of the standard in-stream water balance including bank flow, hyporheic exchange, and groundwater recharge.

In glacial watersheds, recession trends in the outflow hydrograph following exposure of glacier ice by the retreating snowline are caused by the presence of internal glacier structures delaying meltwater release. Glacial runoff is affected by storage processes at three temporal scales: daily, seasonal, and annual to decadal (Jansson et al., 2003). At the daily scale, short-term storage produces diurnal fluctuations in runoff. Short-term storage locations include the supraglacial snowpack and the glacier firn layer, which is a highly effective meltwater reservoir that affects the timing of runoff throughout the year, but has a minimal impact on total runoff (Fountain, 1996; de Woul et al., 2006).

At the seasonal scale, intermediate storage affects discharge patterns as melt is routed to runoff through the glacier drainage system. The effect of en- and subglacial storage is a function of the character of both glacier geometry and the glacier bed (Flowers, 2008). Adverse bed slopes, very thick or very thin ice, and short glaciers result in slow meltwater transport to runoff, as do the presence of many surface depressions and ice seams where meltwater can collect in glacier surface storage prior to flowing to runoff. Subglacially, a hard bed routes meltwater to runoff more quickly than a porous bed. These storage locations can reduce glacier contributions to streamflow during critical late summer low flow periods in high melt years (Hopkinson and Young, 1998). Meltwater stored over winter often contributes to the next summer's discharge (Tangborn et al., 1975), representing a lengthy delay between melt production and runoff generation.

At the annual to decadal scale, long-term storage changes control the net basin water balance. This is largely related to glacier mass balance fluctuations in response to large-scale atmospheric circulation, which are driven by precipitation and air temperature (Moore and Demuth, 2001). For example, the shift in the Pacific Decadal Oscillation (PDO) in 1976–1977 from a negative to a positive phase significantly affected streamflow in six southeastern Alaskan streams (Neal et al., 2002). The nival streams saw an increase in winter flows and a decrease in summer flows, as a greater proportion of winter precipitation fell as rain and thus contributed to streamflow during winter rather than being stored in the snowpack and contributing to spring streamflow. The glacial stream, however, showed an increase in all seasonal flows, likely due to an increase in glacier melt. Broadly similar responses have been found in relation to the effects of the Arctic Oscillation (AO) and the El Niño-Southern Oscillation (ENSO). In northwestern North America, positive AO years are associated with warmer spring–summer conditions, resulting in an earlier freshet in nival rivers with little change in the annual mean flow, but higher melt production in glacial rivers yielding overall yearly flow increases (Fleming et al., 2006). In the Western Cordillera, the 1997–1998 El Niño event caused increased flow in a glacier-fed river and decreased flow in a nearby nival river due to both low snow accumulation and enhanced glacier melt resulting from early snow disappearance (Lafrenière and Sharp, 2003).

Glacier runoff is also affected by episodic discharge events such as jökulhlaups, which occur when glacier runoff forms unstable lakes behind ice- or moraine dams (Clarke, 1982; Blown and Church, 1985). When these dams fail, the flood wave moves downstream, causing

significant destruction. Glacial outburst floods are an annual occurrence in catchments in northwestern British Columbia, southwestern Yukon and southeastern Alaska, and occur frequently in the Andes and Central Asia.

Climate change impacts

Climate change in snow- and icemelt-dominated regions is expected to result in increased air temperatures, particularly in the late winter and early spring, and increased precipitation, with a greater proportion at low- to mid-elevations falling as rain than snow (Mote et al., 2005). Global snow-covered area will also decline. These changes have already advanced the timing of spring freshet and reduced its magnitude in several regions of North America and Europe (e.g., Burn and Hag Elnur, 2002), thus reducing streamflow during the later part of the summer season. The opposite is seen in glacial flow regimes, where climate change increases glacier contributions to runoff during the summer season, due largely to glacier thinning. Climate change also reduces the extent of the glacier firn reservoir, reducing diurnal storage of meltwater. Once glacier thinning shifts to reductions in glacier extent, however, the glacier often becomes too small to contribute significantly to runoff – at which point runoff begins to decline. Glacierized basins in British Columbia and Alberta (North America), and basins with moderate to low glacierization in the European Alps have already passed this critical threshold extent, thus negating their ability to attenuate late-season streamflows (Stahl and Moore, 2006; Collins, 2008; Casassa et al., 2009). Others in the Yukon and Alaska (North America), Central Asia, the Andes, and highly glaciated basins in the Alps are still in the stage of increasing contributions to streamflow (Fleming and Clarke, 2005; Casassa et al., 2009), and will begin to reduce their contributions over the next few decades.

New directions

Groundwater/melt interactions

Recent research has shown that Q_g may be more important in the mountain water balance than previously thought, indicating the importance of quantifying the role of groundwater (subglacial, talus/moraine, subsurface) in snow and glacier melt-dominated systems. Results challenge the widely held assumption that runoff from mountain landscapes is initially snowmelt dominated, followed by glacial- and then groundwater-dominated flow (Liu et al., 2004; Brown et al., 2006b; Hood et al., 2006; Flowers, 2008; Roy and Hayashi, 2009). Flow separation has indicated that both quick flow and groundwater recharge are fed by snowmelt, resulting in runoff signatures from snowmelt in both rapid and slow response waters (Brown et al., 2006a). Groundwater may therefore play an important role in modulating streamflow response to snow- and icemelt, thus reducing variability in the melt signal and reducing effects on downstream systems.

Ecology and snow/glacier-melt dominated streamflow

New research is under way to assess the effects of snow- and glacier melt on river ecology. Results suggest that seasonal fluctuations in meltwater production and storage affect stream temperature and associated ecological processes, and are thus critical in maintaining between-site and regional biodiversity of macroinvertebrates in melt-dominated rivers (Brown et al., 2007).

Summary

Snow and glaciers have a significant impact on runoff. Melt produced from snow and glaciers is a function of the energy available for melt from radiative and advective fluxes and basin hypsometry. This melt is routed to runoff through a range of short-, intermediate-, and long-term storage locations within the snowpack, within the glacier, and within the watershed itself. Nival flow regimes are characterized by a spring runoff peak (freshet), with glacial flow augmenting runoff in the late summer (August–October). Nival and glacial basins have opposing responses to changing climate and atmospheric circulation, as glaciers constitute a larger storage than the snowpack on a seasonal timescale. Continuing climate changes are leading to shifts in the timing and magnitude of runoff from nival and glacial basins, with subsequent concerns regarding impacts on groundwater and ecohydrology in these regions.

Bibliography

Barnett, T. P., Adam, J. C., and Lettenmaier, D. P., 2005. Potential impacts of a warming climate on water availability in snow-dominated regions. *Nature*, **438**, 303–309.

Blown, I., and Church, M., 1985. Catastrophic lake drainage within the Homathko River basin, British Columbia. *Canadian Geotechnical Journal*, **22**, 551–563.

Brown, L. E., Hannah, D. M., and Milner, A. M., 2006a. Hydroclimatological influences on water column and streambed thermal dynamics in an alpine river system. *Journal of Hydrology*, **325**, 1–20.

Brown, L. E., Hannah, D. M., Milner, A. M., Soulsby, C., Hodson, A. J., and Brewer, M. J., 2006b. Water source dynamics in an alpine glacierized river basin (Taillon-Gabiétous, French Pyrénées). *Water Resources Research*, **42**, W08404, doi:10.1029/2005WR004268.

Brown, L. E., Hannah, D. M., and Milner, A. M., 2007. Vulnerability of alpine stream biodiversity to shrinking glaciers and snowpacks. *Global Change Biology*, **13**, 958–966.

Burn, D. H., and Hag Elnur, M. A., 2002. Detection of hydrologic trends and variability. *Journal of Hydrology*, **255**, 107–122.

Casassa, G., López, P., Pouyaud, B., and Escobar, F., 2009. Detection of changes in glacial run-off in alpine basins: examples from North America, the Alps, central Asia and the Andes. *Hydrological Processes*, **23**, 31–41.

Chen, J. Y., and Ohmura, A., 1990. On the influence of alpine glaciers on runoff hydrology in mountain regions. I. Hydrological measurements: the water cycle. *IAHS Publication*, **193**, 117–125.

Clarke, G. K. C., 1982. The 1978 outburst flood from "Hazard Lake", Yukon Territory and the problem of flood magnitude prediction. *Journal of Glaciology*, **28**(98), 3–21.

Collier, E. P., 1958. Glacier variation and trends in runoff in the Canadian Cordillera. *IAHS Publication*, **4**, 344–357.
Collins, D. N., 2008. Climatic warming, glacier recession and runoff from Alpine basins after the Little Ice Age maximum. *Annals of Glaciology*, **48**, 119–124.
Collins, D. N., and Taylor, D. P., 1990. Variability of runoff from partially-glacierised alpine basins. *IAHS Publication*, **193**, 365–373.
de Woul, M., Hock, R., Braun, M., Thorsteinsson, T., Jóhannesson, T., and Halldórsdóttir, S., 2006. Firn layer effect on glacial runoff – a case study at Hofsjökull, Iceland. *Hydrological Processes*, **20**, 2171–2185.
Demuth, M., Pinard, V., Pietroniro, A., Luckman, B., Hopkinson, C., Dornes, P., and Comeau, L., 2009. Recent and past-century variations in the glacier resources of the Canadian Rocky Mountains: Nelson River system. *Terra Glacialis*, Special Issue: Mountain Glaciers and Climate Changes of the Last Century: 27–52.
Dyurgerov, M. B., and Meier, M. F., 2004. Glaciers and the changing earth system: a 2004 snapshot. *Occasional Paper 58, Institute of Arctic and Alpine Research*, University of Colorado, 117 pp.
Eaton, B. C., and Moore, R. D., 2008. Regional hydrology. In *Compendium of Forest Hydrology and Geomorphology in British Columbia*. Published online at: http://www.forrex.org/program/water/PDFs/Compendium/Compendium_Chapter04.pdf, Forest Research and Extension Partnership.
Fassnacht, S. R., 2006. Upper versus Lower Colorado River subbasin streamflow: characteristics, runoff estimation and model simulation. *Hydrological Processes*, **20**, 2187–2205.
Fleming, S. W., and Clarke, G. K. C., 2005. Attenuation of high-frequency interannual streamflow variability by watershed glacial cover. *ASCE Journal of Hydraulic Engineering*, **131**, 615–618.
Fleming, S. W., Moore, R. D., and Clarke, G. K. C., 2006. Glacier-mediated streamflow teleconnections to the Arctic Oscillation. *International Journal of Climatology*, **26**, 619–636.
Flowers, G. E., 2008. Subglacial modulation of the hydrograph from glacierized basins. *Hydrological Processes*, **22**, 3903–3918.
Fountain, A., and Tangborn, W. V., 1985. The effect of glaciers on streamflow variations. *Water Resources Research*, **21**, 579–586.
Fountain, A.G., 1996. The effect of snow and firn hydrology on the physical and chemical characteristics of glacial runoff. Hydrological Processes, **10**, 509–521.
Hagen, J. O., Kohler, J., Melvold, K., and Winther, J. G., 2003. Glaciers in Svalbard: mass balance, runoff and freshwater flux. *Polar Research*, **22**, 145–159.
Hayashi, M., Hirota, T., Iwata, Y., and Takayabu, I., 2005. Snowmelt energy balance and its relation to foehn events in Tokachi, Japan. *Journal of the Meteorological Society of Japan*, **83**(5), 783–798.
Henoch, W. E. S., 1971. Estimate of glacier's secular (1948–1966) volumetric change and its contribution to the discharge in the upper North-Saskatchewan River Basin. *Journal of Hydrology*, **12**, 145–160.
Henshaw, F. F., 1933. Notes on variation of runoff on the Pacific slope. *Transactions of the American Geophysical Union*, **14**, 431–435.
Hewitt, K., and Young, G. J., 1993. The snow and ice hydrology project: a Pakistan–Canada research and training program. *IAHS Publication*, **218**, 49–58.
Hock, R., Jansson, P., and Braun, L., 2005. Modelling the response of mountain glacier discharge to climate warming. In Huber, U. M., Reasoner, M. A., and Bugmann, H. (eds.), *Global Change and Mountain Regions. A State of Knowledge Overview*. Dordrecht: Kluwer, pp. 243–252.
Hodson, A. J., Gurnell, A. M., Washington, R., Tranter, M., Clark, M. J., and Hagen, J. O., 1998. Meteorological and runoff time-series characteristics in a small, high-Arctic glaciated basin, Svalbard. *Hydrological Processes*, **12**, 509–526.
Hood, J. L., Roy, J. W., and Hayashi, M., 2006. Importance of groundwater in the water balance of an alpine headwater lake. *Geophysical Research Letters*, **33**(13), L13405, doi:10.1029/2006GL026611.
Hopkinson, C., and Young, G., 1998. The effect of glacier wastage on the flow of the Bow River. *Hydrological Processes*, **12** (10–11), 1745–1763.
Jansson, P., Hock, R., and Schneider, T., 2003. The concept of glacier storage – a review. *Journal of Hydrology*, **282**(1–4), 116–129.
Kaser, G., Juen, I., Georges, C., Gomez, J., and Tamayo, W., 2003. The impact of glaciers on the runoff and the reconstruction of mass balance history from hydrological data in the tropical Cordillera Blanca, Peru. *Journal of Hydrology*, **282**, 130–144.
Kattelmann, R., 1997. Flooding from rain-on-snow events in the Sierra Nevada. *IAHS Publication*, **239**, 59–65.
Krimmel, R. M., and Tangborn, W. V., 1974. South Cascade Glacier – the moderating effect of glaciers on runoff. In *Proceedings of the 42nd Western Snow Conference*, Anchorage, Alaska, pp. 9–13.
Kuzmin, P., 1961. The process of snowpack melting. *L. Hydrometeoizdat*, 345 pp.
Lafrenière, M., and Sharp, M., 2003. Wavelet analysis of inter-annual variability in the runoff regimes of glacial and nival stream catchments, Bow Lake, Alberta. *Hydrological Processes*, **17**, 1093–1118.
Liu, F., Williams, M. W., and Caine, N., 2004. Source waters and flow paths in an alpine catchment, Coloardo Front Range, United States. *Water Resources Research*, **40**, W09401, doi:10.1029/ 2004WR003076.
López-Moreno, J. I., and García-Ruiz, J. M., 2004. Influence of snow accumulation and snowmelt on streamflow in the central Spanish Pyrenees. *Hydrological Sciences Journal*, **49**(5), 787–802.
Male, D. H., and Gray, D. M., 1981. Snowcover ablation and runoff. In Gray, D. M., and Male, D. H. (eds.), *Handbook of Snow. Principles, Management & Use*. Toronto: Pergamon, pp. 360–430.
Meier, M., 1969. Glaciers and water supply. *Journal of the American Water Works*, **61**(1), 8–12.
Meier, M. F., 1973. Hydraulics and hydrology of glaciers. *IAHS Publication*, **107**, 353–369.
Meier, M. F., and Tangborn, W. V., 1961. Distinctive characteristics of glacier runoff. *USGS Professional Paper*, **424B**, 14–16.
Moore, R. D., and Demuth, M. N., 2001. Mass balance and stream flow variability at Place Glacier, Canada, in relation to recent climate fluctuations. *Hydrological Processes*, **15**, 3473–3486.
Mote, P. W., Hamlet, A. F., Clark, M. P., and Lettenmaier, D. P., 2005. Declining mountain snow pack in western North America. *Bulletin of the American Meteorological Society*, **86**, 39–49.
National Snow and Ice Data Centre (NSIDC), 2008. *State of the Cryosphere*. Accessed 27 June at http://nsidc.org/sotc/snow_extent.html.
Neal, E. G., Walter, M. T., and Coffeen, C., 2002. Linking the pacific decadal oscillation to seasonal stream discharge patterns in Southeast Alaska. *Journal of Hydrology*, **263**, 188–197.
Roy, J. W., and Hayashi, M., 2009. Multiple, distinct groundwater flow systems of a single moraine-talus feature in an alpine watershed. *Journal of Hydrology*, **373**, 139–150.
Stahl, K., and Moore, R. D., 2006. Influence of watershed glacier coverage on summer streamflow in British Columbia, Canada. *Water Resources Research*, **42**, W06201, doi:10.1029/2006WR005022.
Stewart, I. T., 2009. Changes in snowpack and snowmelt runoff for key mountain regions. *Hydrological Processes*, **23**, 78–94.
Stewart, I. T., Cayan, D. R., and Dettinger, M. D., 2004. Changes in snowmelt runoff timing in western North America under

a 'Business as Usual' climate change scenario. *Climatic Change*, **62**, 217–232.
Tangborn, W. V., Krimmel, R. M., and Meier, M. F., 1975. A comparison of glacier mass balance by glaciological, hydrological and mapping methods, South Cascade Glacier, Washington. *IAHS Publication*, **104**, 185–196.
United States Army Corps of Engineers, 1956. *Snow Hydrology: Summary Report of the Snow Investigations*. Portland: US Army Corps of Engineers, North Pacific Division.
Viviroli, D., Weingartner, R., and Messerli, B., 2003. Assessing the hydrological significance of the world's mountains. *Mountain Research and Development*, **23**, 32–40.
Young, G. J., 1982. Hydrological relationships in a glacierized mountain basin. *IAHS Publication*, **138**, 51–59.

Cross-references

Characteristics of Snow and Glacier Fed Rivers in Mountainous Regions with Special Reference to Himalayan Basins
Direct Surface Runoff
Discharge/Streamflow
Diurnal Cycle of Runoff
Frozen Soil Hydrology
Glacial Drainage Characteristics
Glaciations and Groundwater Flow Systems
Glacier Hydrology
Glacier Lake Outburst Floods
Glacier Mass Balance
Global Outlook of Snowcover, Sea Ice, and Glaciers
Hydrographs
Hydrological Response in Glacierized Basins
Hydropower: Hydroelectric Power Generation from Alpine Glacier Melt
Little Ice Age
Melt Runoff Modeling
Melting Processes
Runoff Generation
Runoff Observations
Snow Hydrology
Snow Ripening
Snow Water Equivalent
Specific Melt Rate
Streamflow Trends in Mountainous Regions
Subglacial Drainage System
Water Balance in the Glacierized Region

INTERCEPTION OF SNOW

Manmohan Kumar Goel
Water Resources System, National Institute of Hydrology, Roorkee, Uttarakhand, India

Definition

When snow falls over a catchment, the whole of it does not fall directly on to the ground and contributes to runoff. A part of it may be caught by the vegetation. This part of snowfall is known as interception.

Precipitation falling on the vegetation may be retained on the leaves or blades of grass and evaporated back to the atmosphere (interception loss), may flow down the stem of trees to the ground (stem flow), or may fall off the leaves (through fall). Interception loss is solely due to evaporation and does not include transpiration, through fall, or stem flow.

The amount of interception in a basin during a storm is a function of the storm character, species, age and density of plants, and season of the year. Interception loss is large for small precipitation amounts and reaches to a constant minimum value for large storms. The total interception loss during a storm may be related to the storage capacity of the vegetation and the evaporation rate as:

$$L_i = S_v + R_i E t$$

where L_i is the total interception loss for the projected area of the canopy (mm), S_v is the storage capacity of vegetation for projected canopy area (mm), R_i is the ratio of the vegetal surface area to the projected area, E is the evaporation rate from the vegetal surface (mm/h), and t is the duration of precipitation (h). Interception process has significant impact on the water balance of a region. Usually, 10–20% of precipitation during the growing season is intercepted and returned to the hydrologic cycle through evaporation (Subramanya, 1991). Under very dense forest conditions, it may even be as high as 25% of the total precipitation.

Interception of snowfall by a vegetative canopy plays a major role in the snow hydrology processes. When snowflakes fall from the sky, small bridges form at narrow openings of the tree leaves and branches that increase the interception area of a tree. After the maximum holding capacity of a tree is reached, subsequent snow retention on a tree is roughly balanced by the loss of intercepted snow falling to the ground.

Snow interception by vegetation is affected by its mass, surface area, age, density, strength and flexure of branches, and configuration and orientation of leaves (Gray and Prowse, 1992). Since deciduous forests shed their leaves in winter, interception by coniferous forests is much greater than by deciduous forests. Meteorological factors also play an important role in the amount of snow interception. Subzero temperatures favor higher interception rates during storms. High winds reduce the amount of snow interception by disrupting the bridging process, vibrating the vegetation, eroding the intercepted snow, and by retaining snow particles in suspension.

The amount of intercepted snow continuously changes because of wind erosion, evaporation, sublimation, melting, and avulsion. It is difficult to quantify various components of the intercepted snow because of measurement problems and particular site-specific conditions (Gray and Prowse, 1992).

Bibliography

Gray, D. M., and Prowse, T. D., 1992. Snow and floating ice. In Maidment, D. R. (ed.), *Handbook of Hydrology*. New York: McGraw-Hill.
Subramanya, K., 1991. *Engineering Hydrology*. New Delhi: Tata McGraw-Hill Publishing Company Limited.

INTERFLOW

Manmohan Kumar Goel
Water Resources System, National Institute of Hydrology, Roorkee, Uttarakhand, India

Synonyms

Quick return flow; Storm seepage; Subsurface storm flow; Through flow

Definition

Interflow refers to that part of precipitation that infiltrates into the surface soil, moves laterally through the upper crusts of soil, and returns to the surface at some distance away from the point of entry into the ground.

When precipitation starts falling on a catchment area, some part of it is evaporated back to the atmosphere; some part is intercepted by the buildings, trees, shrubs, and other objects (known as interception); some part is infiltrated into the ground (known as infiltration); while some part finds its way to numerous depressions filling them to their overflow level (depression storage). Precipitation in excess of these storages starts building up on the ground before it can move laterally over the surface (detention storage). The runoff from precipitation commences after satisfying the evaporation, interception, infiltration, and depression and detention storage requirements of a catchment.

Interflow moves at shallow depths and reaches the surface channels in a relatively short time. Therefore, it is commonly considered as a part of the direct surface runoff. Depending upon the time delay between the infiltration and outflow, the interflow is also classified as prompt interflow and delayed interflow. Temporal distribution of interflow in a storm hydrograph is characterized by a slowly increasing rate up to the end of precipitation, followed by a gradual recession that terminates at the intersection of surface flow and base flow components.

The amount of interflow in a catchment depends on its geological conditions. If a pervious soil layer is underlain by a rock or hard surface in a catchment, then a large amount of interflow is expected. On the other hand, uniform permeable soil favors vertical passage of infiltrated water to the groundwater.

INTERNATIONAL POLAR YEAR 2007–2008

Ian Allison
Australian Antarctic Division and Antarctic Climate and Ecosystems CRC, Hobart, Tasmania, Australia

Synonyms

IPY 2007–2008

Definition and introduction

The international polar year (IPY) 2007–2008 was an intensive, internationally coordinated campaign of research and observations in both polar regions that took place mostly between March 1, 2007 and March 1, 2008. A large part of this research dealt with the ice and snow cover of the Arctic and Antarctica. IPY was cosponsored by the International Council for Science (ICSU) and the World Meteorological Organization (WMO). It included over 160 endorsed science projects assembled from the ideas of researchers in more than 60 countries and was supported by substantial new funding (estimated at more than US$400 million). This was coordinated with and supplemented the ongoing polar research and monitoring programs in many nations.

Previous International Polar Years

The IPY 2007–2008 built on more than a century of internationally coordinated study of the polar regions. The first IPY 1882–1883 was sponsored by the International Meteorological Organization (IMO), a predecessor of the WMO. The scientific goals of this program addressed geophysical phenomena that were beyond the capabilities of one nation alone. Twelve nations carried out 15 expeditions: 13 to the Arctic and 2 to Southern Ocean islands, resulting in important scientific advances and the exploration of new terrain. The first IPY set a precedent for international cooperation in natural science.

The second IPY was held in 1932–1933, also with the sponsorship of the IMO. It accomplished significant advances in meteorology, magnetism, atmospheric science, and the understanding of ionospheric phenomena. Forty nations participated in spite of the economic constraints of the 1930s Depression.

The International Geophysical Year (IGY), held between July 1, 1957 and December 31, 1958, was modeled on the earlier Polar Years, but covered the global domain. It was sponsored jointly by the ICSU and WMO, and brought together 67 nations. There was a considerable focus during IGY on Antarctic science and exploration, including establishment of a number of permanent Antarctic stations, the first estimates of the size of the Antarctic ice sheet, and the eventual negotiation of the Antarctic Treaty, a major geopolitical advance. Other accomplishments of IGY include the discovery of the Van Allen Radiation Belts encircling the Earth and confirmation of the theory of continental drift. The IGY took place at the height of the Cold War, but demonstrated that even in such tense times, scientists could collaborate internationally on projects of global significance.

Early development of IPY 2007–2008

An IPY 2007–2008, on the 50th anniversary of the IGY, was suggested independently by a number of scientists and organizations. In June 2003, the Executive Board of the ICSU established an IPY Planning Group charged with developing an IPY 2007–2008 science plan and

implementation strategy. This Planning Group consulted widely with the international research community in developing a framework for IPY (Rapley et al., 2004). The WMO, independently of the initial ICSU effort, also approved the concept of an IPY in 2003. In February 2004, it was agreed to merge interests and WMO became the cosponsor of IPY 2007–2008 (Figure 1).

The IPY Planning Group set four major goals for the program. These were:

- To make major advances in polar knowledge and understanding
- To leave a legacy of new or enhanced observational systems, facilities, and infrastructure
- To enthuse a new generation of polar scientists and engineers
- To elicit exceptional interest and participation from polar residents, schoolchildren, the general public, and decision-makers worldwide.

Scientific themes of IPY 2007–2008

The scientific issues that defined the themes of IPY 2007–2008 were determined by the broad polar science community in a process that was largely driven from the "bottom up." From this process, the IPY planning committee set six broad themes which were:

1. *Status*: To determine the present environmental status of the polar regions
2. *Change*: To quantify and understand, past and present natural environmental and social change in the polar regions; and to improve projections of future change
3. *Global linkages*: To advance understanding on all scales of the links and interactions between polar regions and the rest of the globe, and of the processes controlling these
4. *New frontiers*: To investigate the frontiers of science in the polar regions
5. *Vantage point*: To use the unique vantage point of the polar regions to develop and enhance observatories from the interior of the Earth to the Sun and beyond the cosmos
6. *Human dimension*: To investigate the cultural, historical, and social processes that shape the sustainability of circumpolar human societies, and to identify their unique contributions to global cultural diversity and citizenship.

International Polar Year 2007–2008, Figure 1 The logo of the International Polar Year (IPY) 2007–2008. The polar regions are clearly highlighted on the representation of the globe, a symbolic satellite orbit draws connection with the logo of the International Geophysical Year (IGY), and the human figure represents the inclusion of social and human science issues in IPY.

In November 2004, an ICSU/WMO Joint Committee for IPY was established with responsibility for overall scientific planning, coordination, guidance, and oversight of the program. This committee was supported by the IPY International Programme Office, based at Cambridge, UK. Over 900 expressions of intent were submitted as proposed IPY activities and, with guidance from the Joint Committee and the Programme Office, these were clustered into over 160 endorsed science projects and over 50 endorsed education and outreach activities. Effective data management leading to free and unrestricted data availability and education and outreach activities were two essential components of projects accepted as part of IPY. The scope of IPY defined by the endorsed science projects is described by Allison et al. (2007).

Endorsed IPY projects were required to obtain their own funding and logistic support and to be self-managed. While not all endorsed projects were eventually funded, there was considerable new support that resulted in a very substantial surge in polar science during the IPY.

IPY 2007–2008 activities and achievements

The full scientific legacy of IPY will evolve in the years and decades after the completion of the observational program. Already however, significant advances in scientific knowledge and understanding have begun to emerge.

New assessments of the state of the Greenland and Antarctic ice sheets were made which reinforced evidence that both the Greenland and the Antarctic ice sheets are losing mass and thus raising sea level, and that the rate of ice loss from at least Greenland is increasing. In both Greenland and Antarctica, a large part of the loss is due to increased ice outflow, and the potential for these ice sheets to undergo further rapid increase in ice discharge remains the largest unknown in projections of the rate of sea level rise. An internationally coordinated circum-Arctic survey also investigated the dynamics of the glaciers in that region that are decreasing in size in response to global warming.

International traverses across the interior of Antarctica resurveyed regions not visited for 50 years and collected ice cores for the study of climate change over periods from centuries to millennia. Collaborative airborne surveys, using sophisticated ice-penetrating radar and other geophysical systems, were used on a scale not seen since the 1970s to map characteristics of the ice and underlying bedrock over vast areas of Antarctica and Greenland. These new images of the ice sheet and the underlying terrain highlighted the presence of liquid water at the bed of the ice sheets and will be essential for producing accurate models to predict future changes to the ice sheets.

Intensive multi-ship surveys of both the Arctic and the Southern Oceans were made in support of IPY studies of oceanography, marine biodiversity, marine geophysics, and sea ice. During IPY, the summer minimum extent of Arctic perennial sea ice decreased by about a million square kilometers to its minimum extent since satellite records began. IPY expeditions recorded an unprecedented rate of ice drift across the Arctic basin, providing compelling evidence of changes in the Arctic ice–ocean–atmosphere system.

New evidence of the rate of global warming also came from the oceans. Data from robotic ocean profiling floats, instrumented marine mammals, and IPY research vessels confirmed that the Southern Ocean, and particularly the southern flank of the Antarctic Circumpolar Current, had warmed more rapidly than the global ocean average. In addition, the dense bottom water formed near Antarctica had freshened in some locations and warmed in others. The freshening is consistent with increased melt from the Antarctic ice shelves and ice sheet.

Pools of carbon stored in permafrost, which are larger than previously estimated, were identified during broad-scale IPY observations. These are perhaps more likely to reach the atmosphere as additional greenhouse gases as warming continues, although the patterns of permafrost change vary widely across the Arctic. Modeling studies completed during the IPY suggest that terrestrial permafrost degrades much faster than expected, and that gas hydrates in the seafloor can escape more easily to the atmosphere with decreasing sea ice extent. IPY research cruises along the Siberian coast observed substantial outgassing of methane from ocean sediments.

Summary

IPY 2007–2008 took place during a period of significant planetary change, change particularly evident in polar regions. It eventuated as the largest internationally coordinated planetary research effort in the past 50 years, engaging the intellectual resources of thousands of scientists, often from "nonpolar" countries. The IPY was a truly international and interdisciplinary endeavor that laid the foundation for major scientific advances in knowledge and understanding of the polar regions and their role in the functioning of our planet. New observational and analysis technologies (including both in situ and remote sensing) and novel system-level approaches were fundamental features of IPY science.

The rapid pace of scientific advance and our increasing awareness of mankind's impact on the Earth system as a whole suggest that research and data from this IPY will leave a lasting legacy in many fields of science, particularly in providing a clearer picture of what future changes may occur and what effects they may have.

Bibliography

Allison, I., Béland, M., and the ICSU/WMO Joint Committee for IPY., 2007. *The Scope of Science for the International Polar Year 2007–2008*. WMO/TD-No. 1364, World Meteorological Organization, Geneva, 79 pp.

Rapley, C., Bell, R., and the ICSU IPY 2007–2008 Planning Group., 2004. *A framework for the International Polar Year 2007–2008*. Paris: ICSU, 58 pp.

Cross-references

Antarctica
Climate Change and Glaciers
Greenland Ice Sheet
Ice Core
Ice Sheet Mass Balance
Permafrost
Sea Ice
Sea-Level

INTERSTITIAL ICE

P. Pradeep Kumar
Department of Atmospheric and Space Sciences, Pune University, Pune, India

When ice is formed in narrow spaces between rocks or sediments in soil, it is called as interstitial ice. Interstitial ice zones are important in the permafrost in the cold regions. Interstitial means that it lies in between any two things or spaces.

Bibliography

Smithson, P., Addison, K., Atkinson, K., 2002. *Fundamentals of the Physical Environment*. London: Routledge, ISBN 0415232945, 9780415232944, 627 pp.

INTRUSIVE ICE

Chelamallu Hariprasad
Centre for Studies in Resource Engineering, IITB, Powai, Mumbai, Maharashtra, India

Intrusive ice is defined as the ice formed from water injected into soils or rocks. Intrusive ice may form layers up to several meters in thickness as a result of pressurized water flow toward the freezing zone. The pressurized water

may be derived from groundwater flow beneath permafrost (open system), or arise from pore water expulsion ahead of a penetrating freezing front in saturated coarse sands and gravels. Expulsion of water results from the expansion that occurs as pore water changes phase from water to ice.

INVENTORY OF GLACIERS

Frank Paul
Department of Geography, University of Zurich, Zurich, Switzerland

Synonyms

Glacier inventory; Inventory of perennial snow and ice

Definition

An inventory of glaciers is a detailed compilation of topographic and morphometric data (e.g., size, length, elevation, aspect) about the individual glaciers in a larger region.

Historic background

An inventory of glaciers should provide quantitative information about the overall area covered by glaciers in a certain region (e.g., an entire country) as well as topographic details on individual glaciers. The latter implies that a glacier is defined in a physical sense, that its extent has been mapped in a cartographic sense, and that the perimeter of individual entities can be determined in a topological sense (ice divides, tributaries). These constraints imply that the compilation of glacier inventories is closely related to the state of cartographic and topographic surveying in a country as well as to the available knowledge on the physical nature of glaciers. For these reasons, initial assessments of overall glacier coverage had been made in the Alps. For the eastern part of the Alps, such a first inventory of overall glacier coverage was compiled by Richter (1888) and for Switzerland by Jegerlehner (1903). For some smaller regions, special glaciological maps exist from earlier times, but their limited cartographic quality limits possibilities to interpret them in a quantitative way (e.g., Kinzl, 1955; Kretschmer, 2002). However, for some individual glaciers or parts of them high-quality maps exist from the mid-nineteenth century (Brunner, 1988).

The main impetus for a worlwide inventory of glaciers came from hydrology. Large differences in the estimated total area of glaciers outside the two continental ice sheets Greenland and Antarctica were recognized in the 1960s. At a symposium on glacier mapping in 1965 this deficit was addressed and "the necessity of a new world inventory of glaciers based on recently surveyed maps" (Hoinkes, 1968) was discussed. The Commission on Snow and Ice decided one year later to establish a working group led by Fritz Müller to prepare guidelines for a "world inventory of perennial ice and snow masses on and beneath land surfaces" (Hoinkes, 1968) and a global effort to create a new glacier inventory was launched as part of the International Hydrological Decade (1965–1974). This initiative resulted in a set of guidelines (UNESCO, 1970; Müller et al., 1977) and a status report on the World Glacier Inventory (WGI) was published in 1989 (WGMS, 1989). The main purpose of the WGI was to obtain information on the distribution of surface area and ice volume of all glaciers outside the two ice sheets and to repeat a similar effort after a few decades to detect changes. However, it was realized that the original inventory method using aerial photography, topographic maps, and planimetry was too time consuming to keep up with the rapid changes that glaciers are experiencing.

The use of satellite imagery for glacier inventory creation was proposed by Howarth and Ommanney (1986). With the availability of 30 m resolution data from the Thematic Mapper (TM) sensor (launched in 1982), automated mapping of glaciers from multispectral bands became possible and related methods were developed (Automated Glacier Mapping). In combination with geographic information systems (GIS) and digital elevation models (DEMs), automated procedures allow the extraction of glacier inventory data (Paul et al., 2002). Within the framework of the Global Land Ice Measurements from Space (GLIMS) initiative a global network of regional centers was established, which map the glaciers in specified regions and provide the digital vector outlines and related further inventory information to the GLIMS glacier database (Raup et al., 2007). This database is steadily growing, all data are freely available, and change assessment from multitemporal datasets become possible. Several guideline documents have been created that help the analysts with the interpretation and delineation of glaciers (e.g., Rau et al., 2005; Raup and Singh Khalsa, 2007).

The World Glacier Inventory

The objectives of the WGI were threefold (cf. Müller and Scherler, 1980):

1. To increase the knowledge about the local, regional and global water cycle and balance
2. To serve as a database for practical purposes (e.g., fresh water resources, hydropower, irrigation, disaster prevention, and recreational facilities)
3. To provide data for the study of climatic processes and for monitoring climatic change

To fulfil the above objectives, it is required to compile a standardized dataset for each glacier that can be analyzed. Because the WGI was compiled during the 1970s and 1980s, data storage and processing was based on the possibilities of that time, i.e., Fortran and punch cards. As a consequence, the entries in the WGI have been organized in a fixed syntax of machine readable codes (Müller et al., 1977) and look-up tables provide the code for each attribute to be translated. The entries listed for each glacier include (cf. Hoelzle and Trindler, 1998): A unique code,

name, location (lon./lat., country), year of map/photo, size, length, aspect, various elevations (minimum/maximum/median), a classification scheme (type, front, profile, nourishment, activity, moraine) and, where available, additional data on the snow line (elevation, accuracy, date) or glacier thickness. From these entries a large number of additional glacier characteristics can be calculated using simplified schemes (Haeberli and Hoelzle, 1995) and assessments on a global scale were possible (e.g., Raper and Braithwaite, 2006).

However, the detailed information in the WGI is spatially incomplete and some highly glacierized regions have information about total area only (WGMS, 1989). An overview of the regions covered in the WGI with detailed information is shown in Figure 1. In some regions like Arctic Canada, the data were compiled but not entirely forwarded to the world data centers (Ommanney, 2009). In an attempt to fill some of these data gaps in the WGI and to extend, standardize and better describe the attributes, Cogley (2009) has prepared an extended version of the WGI called WGI-XF. This data set is closely related to the original WGI as the reference period (1970s to 1980s) and the way of geographic notation (coordinates of label points) is the same. As it is difficult or even impossible to use the point information for change assessment, the GLIMS glacier database also stores glacier outlines.

The GLIMS glacier database

The GLIMS glacier database can be seen as an update of the WGI regarding the temporal frame, but it is more an update of available technology as it is open to store also the information of the WGI when the data are made available in the required digital format, i.e., GIS compatible vector outlines (Raup et al., 2007). In principal, the source of the glacier outlines does not matter, but the use of satellite derived products is strongly encouraged (e.g., Haeberli, 2006) and the Advanced Spaceborne Thermal Emission and reflection Radiometer (ASTER) on-board the Terra satellite was specially programmed for glacier mapping (Raup et al., 2000).

The entries in the GLIMS database are comparable to those from the WGI, but the organization is somewhat more complex and special emphasis is given to consider the remote sensing nature of most data sets (see the webpage glims.org for details). When glacier inventory data are calculated automatically from digital sources (e.g., intersection of outlines with a DEM), they have a slightly different interpretation than in the WGI (Paul et al., 2009). For example, mean aspect refers in the WGI to the direction of the central flowline rather than to the mean of all cells a glacier is composed of. Moreover, the GIS-based calculations are reproducible and they can be standardized to a high degree. Apart from this, two further advantages of the digitally available datasets in the GLIMS glacier database are: a sound change assessment is possible as the calculation can be related to exactly the same glacier entities and corrections can more easily be applied to parts of the data when errors are detected.

Challenges

The main challenge for creating a glacier inventory is related to the correct interpretation of the available imagery (either from space-borne or aerial sources). This issue has a methodological component (e.g., which parts belong to a certain glacier?) and a practical part, which is related to the interpretation of regions with clouds, seasonal snow, debris cover, and low contrast (cf. Automated

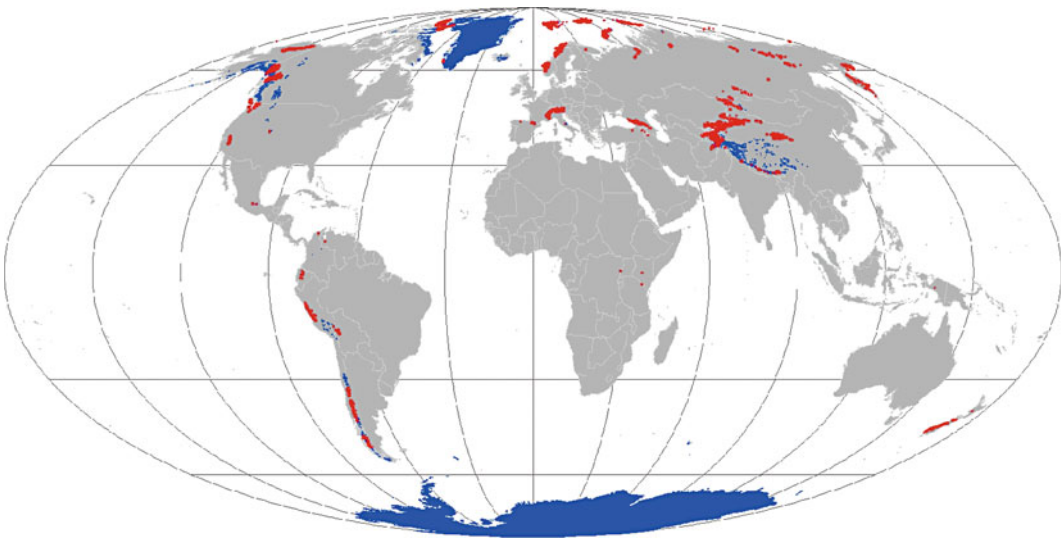

Inventory of Glaciers, Figure 1 Data holdings in the WGI (*red*) compared to the ice cover (*blue*) in the digital chart of the world (DCW). The map was provided by M. Zemp from WGMS.

Glacier Mapping). These are the major sources of uncertainty and require careful consideration and expert knowledge during processing (e.g., Paul and Andreassen, 2009). When a direct comparison with a previous inventory is attempted, two issues have to be considered: At first, the used ice divides must be identical and secondly, the classified objects (glaciers versus perennial snow) should be the same.

The guidelines for the WGI state that all perennial snow and ice should be included in the inventory as the main purpose at that time was a hydrologic one (Müller et al., 1977). Today, an important purpose is a climatic one (i.e., glacier changes as indicators of climate change) and there is thus a focus on change assessment. As the location and extent of perennial snow is often controlled by local topography (e.g., avalanche deposits) rather than climate, they tend to be unchanged for decades (e.g., DeBeer and Sharp, 2009). This requires that they are treated separately in the inventory and have to be identified properly. Due to the difficulties in distinguishing seasonal from perennial snow, this is hardly feasible and it is recommended to map glaciers only, that is, with visible bare ice. Of course, this also decreases the comparability with previous data sets. Baseline imagery without seasonal snow would be optimal, but they are only rarely acquired in most parts of the world.

Outlook

The current entries in the GLIMS database already complement the WGI in previously uncovered regions (see glims.org for the recent coverage). It is expected that it might take some further years to have a globally complete and detailed glacier inventory. Existing and upcoming opportunities of globally available DEM data will help to make this dataset particular valuable. For instance, hypsographic information (area-elevation distribution of the ice cover) can be appended to each glacier which will greatly improve the calculation of the glacier contribution to global sea-level rise (e.g., Raper and Braithwaite, 2006; Hock et al., 2009).

Bibliography

Brunner, K., 1988. Exakte großmaßstäbige Karten von Alpengletschern Ein Säkulum ihrer Bearbeitung. *Petermanns Geographische Mitteilungen*, **132**(2), 129–140.

Cogley, J. G., 2009. A more complete version of the World Glacier Inventory. *Annals of Glaciology*, **50**(53), 8–14.

DeBeer, C. M., and Sharp, M. J., 2009. Topographic influences on recent changes of very small glaciers in the Monashee Mountains, British Columbia, Canada. *Journal of Glaciology*, **55**(192), 691–700.

Gross, G., 1987. Der Flächenverlust der Gletscher in Österreich 1850–1929–1969. *Zeitschrift für Gletscherkunde und Glazialgeologie*, **23**(2), 131–141.

Haeberli, W., 2006. Integrated perception of glacier changes: a challenge of historical dimensions. In Knight, P. G. (ed.), *Glacier Science and Environmental Change*. Oxford: Blackwell, pp. 423–430.

Haeberli, W., and Hoelzle, M., 1995. Application of inventory data for estimating characteristics of and regional climate-change effects on mountain glaciers: a pilot study with the European Alps. *Annals of Glaciology*, **21**, 206–212.

Hock, R., de Woul, M., Radic, V., and Dyurgerov, M., 2009. Mountain glaciers and ice caps around Antarctica make a large sea-level rise contribution. *Geophysical Research Letters*, **36**, L07501.

Hoelzle, M., and Trindler, M., 1998. Data management and application. In Haeberli, W., Hoelzle, M., and Suter, S. (eds.), *Into the Second Century of World Glacier Monitoring: Prospects and Strategies. Studies and Reports in Hydrology*. Paris: UNESCO, pp. 53–72.

Hoinkes, H. C., 1968. Presidental Address. *IAHS*, **79**, 7–16.

Howarth, P., and Ommanney, C. S., 1986. The use of Landsat digital data for glacier inventories. *Annals of Glaciology*, **8**, 90–92.

Jegerlehner, J., 1903. Die Schneegrenze in den Gletschergebieten der Schweiz. *Gerland's Beitragen zur Geophysik*, **5**(3), 486–566.

Kinzl, H., 1955. Die Darstellung der Gletscher im Atlas Tyrolensis von Peter Anich und Blasius Hueber (1774). *Mitteilungn der Geologischen Gesellschaft in Wien*, **48**, 89–104.

Kretschmer, I., 2002. Carl Sonklars «Atlas» der Ötztaler Gebirgsgruppe – ein früher Gletscheratlas der Ostalpen. *Cartographica Helvetica*, **25**, 11–20.

Müller, F., and Scherler, K., 1980. Some comments on the Swiss glacier inventory. *IAHS*, **126**, 185–194.

Müller, F., Caflisch, T., and Müller, G. (eds.), 1977. Instructions for the compilation and assemblage of data for a world glacier inventory. IAHS(ICSI)/UNESCO report, Temporal Technical Secretariat for the World Glacier Inventory (TTS/WGI), ETH Zurich, Switzerland: 19 pp + Appendix.

Ommanney, C. S. L., 2009. Canada and the World Glacier Inventory. *Annals of Glaciology*, **50**(53), 5–10.

Paul, F., and Andreassen, L. M., 2009. A new glacier inventory for the Svartisen region, Norway, from Landsat ETM+ data: challenges and change assessment. *Journal of Glaciology*, **55**(192), 607–618.

Paul, F., Kääb, A., Maisch, M., Kellenberger, T. W., and Haeberli, W., 2002. The new remote sensing derived Swiss glacier inventory Methods. *Annals of Glaciology*, **34**, 355–361.

Paul, F., Barry, R. G., Cogley, J. G., Frey, H., Haeberli, W., Ohmura, A., Ommanney, C. S. L., Raup, B., Rivera, A., and Zemp, M., 2009. Recommendations for the compilation of glacier inventory data from digital sources. *Annals of Glaciology*, **50**(53), 119–126.

Raper, S. C. B., and Braithwaite, R. J., 2006. Low sea level rise projections from mountain glaciers and icecaps under global warming. *Nature*, **439**, 311–313.

Rau, F., Mauz, F., Vogt, S., Singh Khalsa, S. J., and Raup, B., 2005. Illustrated GLIMS glacier classification manual. NSIDC: 36 pp. Online at: http://www.glims.org/MapsAndDocs/assets/ GLIMS_Glacier-Classification-Manual_V1_2005-02-10.pdf.

Raup, B. H., and Singh Khalsa, S. J., 2007. GLIMS analysis tutorial. NSIDC: 15 pp. Online at: http:// www.glims.org/MapsAndDocs/assets/GLIMS_Analysis_Tutorial_a4.pdf.

Raup, B. H., Kieffer, H. H., Hare, T. M., and Kargel, J. S., 2000. Generation of data acquisition requests for the ASTER satellite instrument for monitoring a globally distributed target: glaciers. *IEEE Transactions on Geoscience and Remote Sensing*, **38**(2), 1105–1112.

Raup, B., Racoviteanu, A., Singh Khalsa, S. J., Helm, C., Armstrong, R., and Arnaud, Y., 2007. The GLIMS geospatial glacier database: a new tool for studying glacier change. *Global and Planetary Change*, **56**, 101–110.

Richter, E., 1888. Die Gletscher der Ostalpen. Handbücher zur Deutschen Landes und Volkskunde, Bd. 3, Engelhorn, Stuttgart: 306 pp.

Sonklar, Carl von, 1860. Die Oetzthaler Gebirgsgruppe mit besonderer Rücksicht auf Orographie und Gletscherkunde. Gotha: 292 pp.
UNESCO, 1970. Perennial ice and snow masses: a guide for compilation and assemblage of data for the World Glacier Inventory. *Technical Papers in Hydrology*, **1**, 54 pp.
WGMS, 1989. World glacier inventory – Status 1988. Haeberli, W., Bösch, H., Scherler, K., Østrem, G., and Wallén, C. C. (eds.), IAHS (ICSI)/UNEP/UNESCO, World Glacier Monitoring Service, Zurich, Switzerland: 458 pp.

Cross-references

Aerial Photogrammetry for Glacial Monitoring
Alps
Arctic Hydroclimatology
Climate Change and Glaciers
Deglaciation
Digital Elevation Model Generation Over Glacierized Region
Glacier
Ice Caps
Ice Sheet
Impacts of Snow and Glaciers on Runoff
Moraine
Sea Level Rise
WGMS (World Glacier Monitoring Service)

INVERSE METHODS IN GLACIOLOGY

G. Hilmar Gudmundsson
British Antarctic Survey, Cambridge, UK

Definition

Inverse methods deal with the indirect estimation of parameters. When set of measurements (y) can be linked to the parameters to be estimated (x) through a function f, i.e., $y = f(x)$, then the inverse problem is that of estimating x given the measurements y and the function f. In the terminology of inverse methods, the function f is commonly referred to as the forward model, x as the system state, and y as the measurement vector.

Introduction

Inverse methods are routinely used in glaciology to estimate model parameters. Examples of such inverse problems include the estimation of basal conditions from surface measurements on glaciers (e.g., MacAyeal, 1992, 1993; Vieli and Pane, 2003; Thorsteinsson et al., 2002; Joughin et al., 2004; Gudmundsson, 2004; Truffer, 2004; Maxwell et al., 2008; Gudmundsson and Raymond, 2008; Raymond and Gudmundsson, 2009; Joughin et al., 2009), the determination of geothermal heat flux from englacial temperature measurements (e.g., Dahl-Jensen et al., 2003; Buchardt and Dahl-Jensen, 2007), dating of ice cores (Parrenin et al., 2001), and the inference of spatial pattern of surface snow accumulation from the distortion of layers within a glacier (Martín et al., 2006; Waddington et al., 2007; Eisen, 2008).

Inverse problems typically share a number of features that complicate their solution. There is, in general, no guarantee that such a problem has a unique solution for a given set of measurements. Solutions to inverse problems are also often sensitive to small changes in the measurement data. One of the consequences is that even when two sets of measurements are in some sense "similar," the solutions of the two corresponding inverse problems may not be "similar." Measurements are never completely free of errors and we can therefore, in general, expect that a given inverse problem has not one but an infinite number of possible solutions, and that some of these solutions differ greatly. If the number of unknown parameters is limited, some trial-and-error techniques can often be used for parameter estimation. However, in many inverse problems, the number of parameters is large and some systematic approach is needed.

There are, broadly speaking, two different approaches commonly used to deal with such illposed problems involving large number of unknowns: regularization and statistical inference. The idea behind regularization is to introduce some additional constraints on possible solutions. For example, one might select a solution that is in some sense "smooth" while at the same time giving a reasonably good fit to measurements. The most commonly used statistical inference approach is Bayesian inference where one calculates the conditional probability $P(x|y)$ of the system state x for given set of measurements y.

Most nonlinear inverse methods involve a repeated minimization or maximization of some objective function. In a regularization method, the objective function to be minimized might be written as $|x|_a + |y - f(x)|_b$ for some function norms $|.|_a$ and $|.|_b$, while in Bayesian inference the quantity to be maximized is the conditional probability $P(x|y)$ as a function of x. Due to the large number of unknown variables typically involved in inverse problems, solving such problems is often only feasible if either the forward model is computationally inexpensive or if an effective way of maximizing/minimizing the objective function can be found. Most efficient minimization algorithms require estimates of the gradient of the cost function with respect to the model parameters. The gradients are in turn often difficult to estimate. Adjoint methods, first introduced in glaciology by MacAyeal (1993), are commonly used to speed up the calculation of the gradient of the objective function.

Inverse modeling is often performed as a part of a model validation exercise. The inverse modeling step delivers the best possible values for model parameters, i.e., the parameter values that minimize/maximize the objective function, given some statistical estimates about data errors and the propagation of errors from system state to measurement state through the forward model. Model validation involves determining if both the size and distribution of the model residuals are in accord with those statistical error estimates. If not, either the forward model, or the error description used, is lacking in some sense. If successful, model

validation provides some confidence that the forward model is capable of simulating the physical situation under study.

Main uses of inverse modeling in glaciology to date

The inverse problem that has received the greatest attention in glaciology to date is that of determining basal conditions of glaciers using surface measurements of velocities and topography. There are a number of reasons why glaciologists are interested in mechanical conditions at the base of ice streams and ice sheets. On fast-flowing ice streams, most of the forward movement is due to basal motion as opposed to internal deformation of ice. Without a good understanding of what controls the basal motion, our understanding of ice streams dynamics is severely lacking and the possibility of predicting future behavior limited. In most flow modeling work of glaciers, the modeler is also often faced with the practical problem of initializing the model parameters to ensure good fit with surface measurements. Such an initialization is often needed before any transient runs and perturbations experiments can be conducted. For glaciers where large part of the forward movement is due to basal motion, the most important model parameters tend to be those defining the mechanical properties of the lower boundary. Basal motion is often parameterized using a sliding law that relates the basal sliding velocity to the forces acting on the glacier. Inverse methods can be used to systematically determine the spatial variation of the parameters in the sliding law.

The first systematic approach to determine basal conditions using surface data was given by MacAyeal (1992, 1993). He showed how adjoint methods could be used to efficiently calculate the gradient of an objective function describing the misfit between surface data and the output from a forward model. One of the earlier uses of this method was to calculate spatial distribution of basal friction on Ice Stream E (MacAyeal, 1992) (Ice Stream E was later renamed to MacAyeal Ice Stream). This method can currently be considered the standard method for inverting surface data on ice streams. A recent application of this method is that of Joughin et al. (2009) who determined the basal stress distribution of Pine Island and Twhaites Glaciers, West Antarctica, using extensive data sets of surface velocities and surface topography (Figure 1).

Recently several new methods of determining basal conditions on glaciers have been proposed. Maxwell et al. (2008) suggest using an iterative method where two different well-posed forward problems are solved in sequence. One forward problem uses an estimate of basal stresses and measured surface data as boundary conditions (N step). Another forward problem, the D step, uses as boundary conditions the previously calculated basal velocities from the N step, together with the free surface condition. A series of alternating N and D steps is calculated until a stopping criterion based on the misfit between measured and modeled surface velocities from the D step is met. Maxwell et al. (2008) used their method to estimate basal velocities of Athabasca and Perito Moreno glaciers using a full Stokes forward model.

Arthern and Gudmundsson (2010) proposed a further new method of calculating the basal drag coefficient and the effective ice viscosity from surface data. Similar to the approach of Maxwell et al. (2008) the only

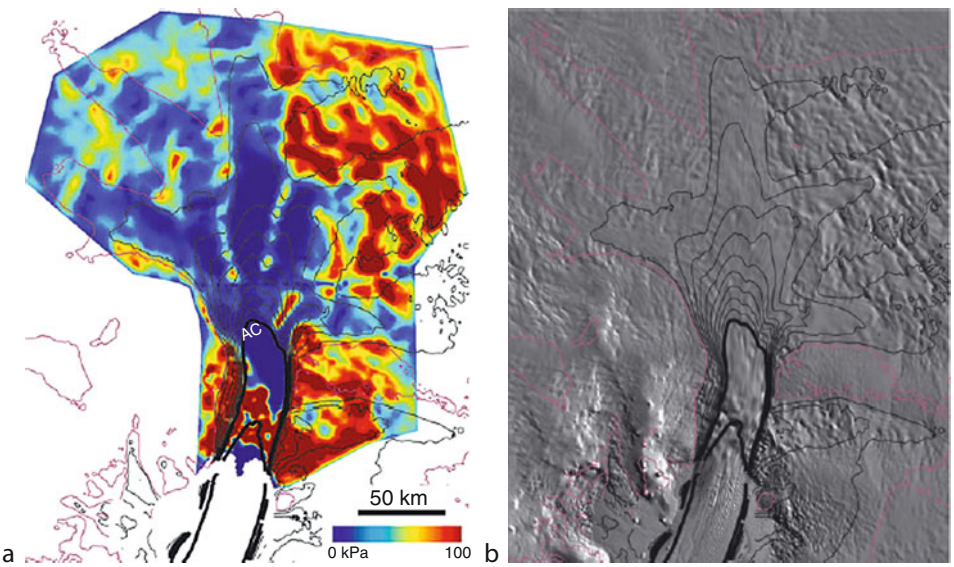

Inverse Methods in Glaciology, Figure 1 Example of an estimate of basal shear stress distribution of a glacier obtained from inverse modeling of surface data (Joughin et al., 2009). The area shown is Pine Island Glacier, West Antarctica. *Contour lines* show surface flow velocities. (**a**) Basal shear stress distribution. (**b**) Satellite image (MOA) from the same area.

requirement that the method places upon the forward solver is that the Newman, Dirichlet, and Robin type boundary conditions can all be implemented. One of the advantages of the methods of Arthern and Gudmundsson (2010) and Maxwell et al. (2008) is the ease by which they can be implemented given a forward model. Arthern and Gudmundsson (2010) give an example of a three-dimensional flow problem where the basal drag coefficient is extracted from surface data using a commercial Stokes solver.

One of the difficulties associated with estimating basal stresses and basal velocities for glaciers is the fact that the geometry of the glacier bed is only known approximately. Gudmundsson (2004) suggested solving simultaneously for both bedrock geometry and basal slipperiness using Bayesian inverse methods. An application of the method to a flow line down Rutford Ice Stream, West Antarctica (Raymond-Pralong and Gudmundsson, 2010), showed all short scale (<10 ice thicknesses) spatial variability in surface ice speed to be caused by variations in bedrock geometry rather than to variations in basal slipperiness.

A further use of inverse methods in glaciology is the determination of spatial variations in effective viscosity of ice in flow models. The rheology of ice is nonlinear and the effective viscosity of ice a function of stress. In addition, temperature strongly affects the effective viscosity. Calculating englacial temperatures in ice sheets is, in principle, a fairly straightforward task given accurate boundary data such as geothermal heat fluxes. However, such data is often lacking and the reliability of calculated temperature distributions therefore sometimes limited. A way of circumventing this problem is to calculate ice flow using spatially variable viscosity distribution that has been indirectly determined from surface data using inverse methods. As ice rheology is not expected to change markedly in a short span of time, having reliable estimates of the effective viscosity distribution greatly enhances the potential to make short-term (decadal time scale) predictions about future ice sheet behavior. Examples of this approach include the determination of the effective viscosity distribution of ice Ronne and the Larsen B Ice Shelves, West Antarctica (Larour et al., 2005; Vieli et al., 2006; Khazendar et al., 2007).

Determining the effective viscosity from surface data prior to conducting perturbation experiments with the forward model is an example of a model initialization. To date, the number of such forward model initializations studies in glaciology using formal inverse models is rather limited, but this shortcoming can be expected to change in the future. One of the attractive aspects of this methodology is that after initialization, and once the level of confidence in the forward model has been established through forward model validation, predictions about future development of the ice sheet can be made together with an estimate of the forecast error. Arthern and Hindmarsh (2006) discuss how the future contribution of Antarctica to sea-level change can be estimated in this fashion.

Layers within glaciers and ice sheets reflect spatial and temporal variations in surface snow accumulation and the effects of ice flow. Extracting information about patterns of surface accumulation from internal layers using a flow model that calculates internal layering for given spatial and temporal variations in surface mass balance, is an example of an inverse problem. Various approaches to this inverse problem have been proposed (Martín et al., 2006) applied control method to optimally match modeled and measured internal layers using parameters describing spatial variability in surface accumulation as control variables while Eisen (2008) used inverse methods to determine the velocity field from the spatial structure of dated firn layers. Recently, Waddington et al. (2007) showed how spatial patterns in surface snow accumulation can be inferred from deep layers in glaciers using a formal geophysical inverse modeling approach.

Because of steady increase in computer power and ongoing development in the design of inverse algorithms, it can be expected that in the future even greater use will be made of inverse modeling techniques in glaciology. Increasingly, modelers of large ice masses have at their disposal large and high-quality data sets obtained from both in situ geophysical measurements and remote sensing. Inverse modeling methods provide a systematic way of exploiting the potential of models and of extracting information from such data sets.

Summary

Inverse methods are ideally suited for the indirect estimation of a large number of model parameters. Such problems arise naturally in many types of glaciological modeling work, the prime example being the indirect estimation of basal boundary parameters on ice streams using surface data. In the future, inverse methods can be expected to play an increasing role in glaciological modeling work. In particular, the use of inverse methods for model initialization when forecasting the near-future (several decades) behavior of ice sheets is an interesting prospect.

Bibliography

Arthern, R. J., and Gudmundsson, G. H., 2010. Initialisation of ice sheet forecasts viewed as an inverse Robin problem. *Journal of Glaciology*, **56**(197), 527–533.

Arthern, R. J., and Hindmarsh, R. C., 2006. Determining the contribution of Antarctica to sealevel rise using data assimilation methods. *Philosophical Transactions of the Royal Society A: Mathematical, Physical and Engineering Sciences*, **364**(1844), 1841–1865.

Buchardt, S. L., and Dahl-Jensen, D., 2007. Estimating the basal melt rate at northgrip using a Monte Carlo technique. *Annals of Glaciology*, **45**, 137–142.

Dahl-Jensen, D., Gundestrup, N., Gorgineni, S. P., and Miller, H., 2003. Basal melt at northgrip modeled from borehole, ice-core and radio-echo sounder observations. *Annals of Glaciology*, **37**, 207–212.

Eisen, O., 2008. Inference of velocity pattern from isochronous layers in firn, using an inverse method. *Journal of Glaciology*, **54**, 613–630.

Gudmundsson, G. H., 2004. *Glaciers and Earth's Changing Environment, chapter Estimating Basal Properties of Glaciers from Surface Measurements*. Blackwell.
Gudmundsson, G. H., and Raymond, M., 2008. On the limit to resolution and information on basal properties obtainable from surface data on ice streams. *The Cryosphere*, **2**(2), 167–178.
Joughin, I., MacAyeal, D. R., and Tulaczyk, S., 2004. Basal shear stress of the Ross ice streams from control method inversions. *Journal of Geophysical Research*, **109**, B09405.
Joughin, I., Tulaczyk, S., Bamber, J. L., Blankenship, D., Holt, J. W., Scambos, T., and Vaughan, D. G., 2009. Basal conditions for Pine Island and Thwaites Glaciers, West Antarctica, determined using satellite and airborne data. *Journal of Glaciology*, **55**, 245–257.
Khazendar, A., Rignot, E., and Larour, E., 2007. Larsen B ice shelf rheology preceding its disintegration inferred by a control method. *Geophysical Research Letters*, **34**, L19503.
Larour, E., Rignot, E., Joughin, I., and Aubry, D., 2005. Rheology of the Ronne Ice Shelf, Antarctica, inferred from satellite radar interferometry data using an inverse control method. *Geophysical Research Letters*, **32**(L05503), 1–4.
MacAyeal, D. R., 1992. The basal stress distribution of Ice Stream E, Antarctica, inferred by control methods. *Journal of Geophysical Research*, **97**(B1), 596–603.
MacAyeal, D. R., 1993. A tutorial on the use of control methods in ice-sheet modeling. *Journal of Glaciology*, **39**(131), 91–98.
Martín, C., Hindmarsh, R., and Navarro, F., 2006. Dating ice flow change near the flow divide at Roosevelt Island, Antarctica. *Journal of Geophysical Research*, **111**, F011011.
Maxwell, D., Truffer, M., Avdonin, S., and Stuefer, M., 2008. An iterative scheme for determining glacier velocities and stresses. *Journal of Glaciology*, **54**, 888–898.
Parrenin, F., Jouzel, J., Waelbroeck, C., Ritz, C., and Barnola, J.-M., 2001. Dating Vostok ice core by an inverse method. *Journal of Geophysical Research*, **106**, 31837–31851.
Raymond, M. J., and Gudmundsson, G. H., 2009. Estimating basal properties of ice streams from surface measurements: a nonlinear bayesian inverse approach applied to synthetic data. *The Cryosphere*, **3**(2), 265–278.
Raymond-Pralong, M., and Gudmundsson, G. H., 2010. Bayesian estimation of basal properties of Rutford Ice stream, West Antarctica, from surface data. *Journal of Glaciology*. submitted.
Thorsteinsson, T., Raymond, C. F., Gudmundsson, G. H., Bindschadler, R. B., Vornberger, P., and Joughin, I., 2002. Bed topography and lubrication inferred from surface measurements on fast flowing ice streams. *Journal of Glaciology*, **49**(167), 481–490.
Truffer, M., 2004. The basal speed of valley glaciers: an inverse approach. *Journal of Glaciology*, **50**(169), 236–242.
Vieli, A., and Pane, A. J., 2003. Application of control methods for modelling the flow of Pine Island Glacier, West Antarctica. *Annals of Glaciology*, **36**, 197–204.
Vieli, A., Payne, A. J., Du, Z., and Shepherd, A., 2006. Numerical modelling and data assimilation of the Larsen B ice shelf, Antarctic Peninsula. *Philosophical Transactions of the Royal Society Series A*, **364**, 1815–1839.
Waddington, E. D., Neumann, T. A., Koutnik, M. R., Marshall, H.-P., and Morse, D. L., 2007. Inference of accumulation-rate patterns from deep layers in glaciers and ice sheets. *Journal of Glaciology*, **53**, 694–712.

Cross-references

Bed (Bottom) Topography
Dynamics of Glaciers
Glacier Motion/Ice Velocity
Glacier Sliding

INVERSION LAYERS

Mahendra R. Bhutiyani
Hazard Assessment and Forecasting Division, Snow and Avalanche Study Establishment, Chandigarh, India

Definition

Under normal atmospheric conditions in the troposphere, temperature generally decreases with altitude at the rate of about 6.5° km^{-1}. This gradient is called as the temperature lapse rate in meteorology. However, under certain conditions, a deviation occurs and temperature is seen to increase with altitude, giving rise to an inversion layer where the air is colder near the ground surface than higher elevations.

Origin

Inversion layer generally occurs at night when the ground cools more rapidly than the air above it, because of radiative, or direct, cooling from the earth's surface. The effects of an inversion are thus greatest during early morning hours, usually the coolest part of the day. Inversions also occur as a result of subsidence (sinking) of air in an anticyclone, or high pressure system, where the descending air warms adiabatically, that is, within itself, while the ground remains cool. In the Polar and high altitude mountainous regions such as the Alps, Rockies, and the Himalayas, inversions are quite common in winters during clear, cloud-free nights and early morning hours. As the sun rises, the valley sides warm up gradually; creating local eddies along the valley walls and the convection currents within the inversion layer destroy the inversion layer in a few hours.

Significance

In urban and plain areas, inversion layers block the upward movement of air, trapping moisture and natural and man-made pollutants near the ground, resulting in fog and smog.

INVERTED CUP DEPTH HOAR CRYSTALS

Mahendra R. Bhutiyani
Hazard Assessment and Forecasting Division, Snow and Avalanche Study Establishment, Chandigarh, India

Definition

These are large-grained, faceted, cup-shaped crystals (up to 10 mm in diameter) that resemble the sugar granules. They are also called as temperature-gradient or TG crystals. Layers of such crystals are generally found in early winter when clear sky conditions along with cold air temperatures prevail for a very long duration and the snowpack is thin. They are also found in areas where

snowpack remains in the shady condition for long, particularly on slopes with the northern aspect in the North Hemisphere.

Origin

They are formed because of strong temperature gradient ($>0.25°C\ cm^{-1}$) in the layers of the snowpack when the ground is warmer and the snow-surface temperatures are lower (−2 to −15°C). As a result of vapor transfer (sublimation), snow crystals occurring at the base of a snowpack grow bigger at the cost of smaller grains as uprising water vapor freezes at their base and they ultimately acquire an inverted cup shape.

Significance

Because of the absence of intergranular bonds, the layers with TG or inverted cup depth hoar crystals have very weak shear strength. They are likely to fail easily and lead to catastrophic collapse of the layer. Fractures commonly propagate long distances and around corners. Almost all catastrophic, hard wind slab climax avalanches (involving the entire season's snow cover) are triggered due to the failure of snow layer with inverted cup depth hoar crystals.

IRREDUCIBLE WATER

Mahendra R. Bhutiyani
Hazard Assessment and Forecasting Division, Snow and Avalanche Study Establishment, Chandigarh, India

Definition

Like in a soil, liquid water occurs in a snowpack in three different forms: the hygroscopic water, the capillary water, and gravitational water. Irreducible water or "hygroscopic water" occurs as a thin film of water molecules around the snow grains.

Origin

Meltwater on the snow surface, which is produced as a result of complex heat transfer process at the snow-atmosphere interface, percolates down in the snowpack. Water holding capacity of snow depends primarily upon the temperature regime of the snowpack and its physical properties such as porosity, permeability, and particle size and saturation level. Hygroscopic or irreducible water is held by a strong adhesive force between the water molecules and the ice molecules in the snow grains, against the force of gravity. Moist snowpack that is isothermal at 0°C and at a very low saturation level is likely to have irreducible or hygroscopic water. It is generally less than 3% (by pore volume) of the snow. It is not available for generation of melt-runoff unless the whole crystal melts.

Bibliography

Colbeck, S. C., 1973. *A theory of metamorphism of wet snow.* CREEL, Hanover, New Hampshire Report.
Singh, P., and Singh, V. P., 2001. Snow and Glacier Hydrology. Dordrecht: Kluwer Academic Publishers.

ISOTOPE ANALYSIS

Tandong Yao, Wusheng Yu, Huabiao Zhao, Yongqin Liu
Laboratory of Tibetan Environment Changes and Land Surface Processes (TEL), Institute of Tibetan Plateau Research, Chinese Academy of Sciences, Haidian District, Beijing, China

Introduction

Naturally occurring oxygen includes three stable isotopes, ^{16}O, ^{17}O, and ^{18}O, with the relative abundances of 99.763%, 0.0375%, and 0.1995%, respectively. Isotopic analysis does not consider the absolute abundances of the isotope, but rather, the ratios of ^{18}O to ^{16}O relative to one of the two standards: Vienna Standard Mean Ocean Water (VSMOW) or Vienna Pee Dee Belemnite (VPDB). Isotope mass spectrometry measures oxygen and hydrogen stable isotopic ratios (Craig, 1961). Carbon dioxide that has equilibrated with water at a constant temperature provides the oxygen for analysis (Epstein and Mayeda, 1953).

Numerous papers and books have discussed environmental isotopes in hydrology and stable isotope paleoclimatology over the past 50 years. Some of the more common in the key theme areas of stable isotope in water include: the Handbook of Environmental Isotope Geochemistry series, edited by Fritz and Fontes in the 1980s, as well as reviews by Fontes and Edmunds (1989), Coplen (1993), and Gat (1996); textbooks by Mazor (1997), Clark and Fritz (1997), and Cook and Herczeg (2000); and some excellent research papers delivered by Dansgaard (1964), Epstein et al. (1965), Gat (1996), Johnsen et al. (1972), Jouzel et al. (1987), Rozanski et al. (1992), and Thompson et al. (2000).

Stable isotopes are widely used to reconstruct paleoclimate variations preserved in ice core records (Lorius et al., 1985; Jouzel et al., 1987; Dansgaard et al., 1993; Cuffey et al., 1994; Johnsen et al., 1972, 1995; Thompson et al., 1997, 2000). However, the interpretation of stable isotope records in ice cores must be based on the knowledge of temporal and spatial variations of stable isotopes in precipitation and their relationships with meteorological conditions. The precipitation isotopic compositions ($\delta^{18}O$) represent an integrated climatic parameter, reflecting the evaporation and condensation history of an air mass (Dansgaard, 1964; Merlivat and Jouzel, 1979; Rozanski et al., 1982, 1992; Jouzel and Merlivat, 1984; Schoch-Fischer et al., 1984; White et al., 1997).

Since 1961, the International Atomic Energy Agency (IAEA), in cooperation with the World Meteorological

Organization (WMO), has set up 550 meteorological stations for measuring the isotopic composition of monthly precipitation (the Global Network of Isotopes in Precipitation, GNIP). However, few of these stations lie on the Tibetan Plateau, limiting studies on stable isotope ratios in precipitation in this region. The difficulty in accessing such high-altitude sites strongly limits the ability to maintain continuous precipitation sampling, especially during the monsoon season. However, high-altitude Tibetan glaciers offer unique archives of past tropical precipitation and several ice cores have been successfully retrieved (e.g., Thompson et al., 1995). One must have some knowledge of the seasonal and spatial distributions of isotopic compositions in modern Tibetan Plateau precipitation in order to interpret past changes in the isotopic compositions. The isotopic composition of precipitation also offers an opportunity to distinguish between different water sources and therefore better define the northward limits of the monsoon influence. Beginning in 1991, the Chinese Academy of Sciences (CAS) launched a project to establish a new observation network (Third Pole Regions Environment Observation & Research Platform, TORP) to continually survey stable isotope variations in individual precipitation events on the Tibetan Plateau and adjacent regions. In 2007, launched an even larger network, titled as China Network of Isotopes in River and Precipitation (CNIRP), to observe stable isotope variations in river water and precipitation in China. Many scientists have investigated various climatic factors, especially regarding how the Asian monsoons influence the $\delta^{18}O$ composition in precipitation (Aizen et al., 1996; Hoffmann and Heimann, 1997; Posmentier et al., 2004; Johnson and Ingram, 2004; Vuille et al., 2005). In China, Yao et al. (1995, 1996, 1999) and Zhang et al. (1995) analyzed the correlation between $\delta^{18}O$ in precipitation and air temperatures at Urumqi, Delingha, and Tuotuohe, and found that a good linear relationship exists between $\delta^{18}O$ in precipitation and air temperature, indicating that temperature effects control $\delta^{18}O$ in precipitation. As scientists began to take interest in the variations of stable isotopes in precipitation at Lhasa on the southern Tibetan Plateau, their studies showed that stable isotopes in precipitation reflected an apparent precipitation "amount effect" (Araguás-Araguás et al., 1998; Tian et al., 2001a, b, 2003).

Understanding stable isotope variations in precipitation over this large region and a longer time scale can provide insight and a theoretical basis for interpreting observations of stable isotopes in ice cores. Based on the above-mentioned references, precipitation samples were collected continuously at Nyalam, Lhasa, Nagqu, Tuotuohe, and Delingha (from south to north on the Tibetan Plateau) from the 1990s to 2008 (Figure 1). More recently, observations initiated on stable isotope variations on the eastern and western Tibetan Plateau have also contributed to an understanding of these effects (Yu et al., 2006, 2007; Tian et al., 2007).

Our study sampled each precipitation event. The precipitation sampling program recorded the duration of each

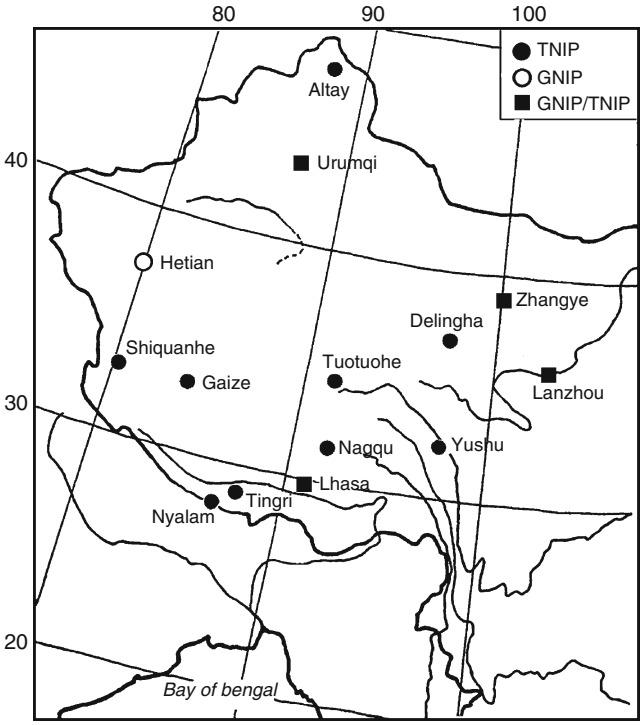

Isotope Analysis, Figure 1 Map of the precipitation sampling sites.

precipitation event, rainfall amount, and surface air temperatures before and after each precipitation event. Rainfall samples were collected and immediately sealed in plastic bottles. Snow and other solid precipitation were collected on clean porcelain plates, put into clean plastic bags, and sealed. After the samples melted at room temperature, they were processed the same as rainfall. All the samples were stored below freezing in a cold laboratory until analyzed. The State Key Laboratory of Cryospheric Science, Chinese Academy of Sciences, Lanzhou, China, measured oxygen isotope compositions of all the precipitation samples using a MAT-252 mass spectrometer with a precision of ±0.2‰. The measured $\delta^{18}O$ in precipitation samples is expressed as parts per mil (‰) of their deviation relative to the Vienna Standard Mean Ocean Water (VSMOW). The Laboratory of Ecological Research Center of Kyoto University, Japan, also measured oxygen isotope ratios in some of the samples using a MAT-252 mass spectrometer, for quality assurance.

$\delta^{18}O$ in precipitation from north to south on the Tibetan Plateau

Temperature dependence of $\delta^{18}O$ in precipitation

Figure 2 shows the relationships between $\delta^{18}O$ values of individual precipitation events and air temperatures at the four stations across the Tibetan Plateau: Delingha, Tuotuohe, Nagqu, and Lhasa. A significant positive

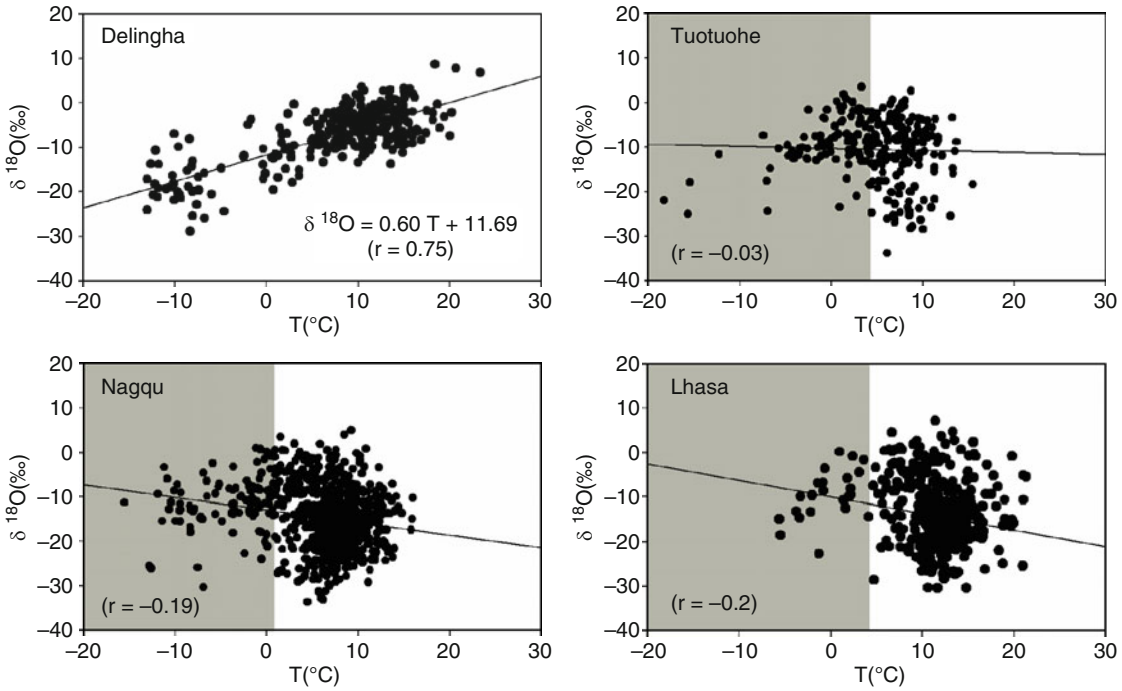

Isotope Analysis, Figure 2 Relationships between $\delta^{18}O$ and air temperature in recent precipitation events at four meteorological stations on the Tibetan Plateau.

relationship between $\delta^{18}O$ in precipitation and air temperature exists at the Delingha station, on the northern Plateau. The correlation coefficient is 0.75, within a 0.01 confidence limit. This demonstrates a significant temperature effect on $\delta^{18}O$ in precipitation during the sampling period from the seasonal variations at Delingha. However, from the middle to the south of the transect, the oxygen isotopic compositions of precipitation at the Tuotuohe, Nagqu, and Lhasa stations show a weak *inverse correlation* between $\delta^{18}O$ values and air temperatures in individual precipitation events. Moreover, the *inverse correlation* weakens with increasing latitude from Lhasa to Tuotuohe (Yu et al., 2008).

Compared with the relationship for individual precipitation events, the correlations improve between monthly amount-averaged $\delta^{18}O$ values and monthly-averaged air temperatures (during precipitation events) at the Delingha and Tuotuohe stations (Equations 1 and 2). Moreover, the monthly-averaged $\delta^{18}O$ – T correlation at Delingha, in the northern Tibetan Plateau, is more significant than that at Tuotuohe, in the north-central Tibetan Plateau.

$$\text{Delingha}: \delta^{18}O = 0.56\overline{T} - 11.16\,(r = 0.84,\ n = 36,\ p < 0.01) \quad (1)$$

$$\text{Tuotuohe}: \delta^{18}O = 0.33\overline{T} - 11.71\,(r = 0.51,\ n = 24,\ p < 0.05) \quad (2)$$

Temperature effects still appear to largely control the $\delta^{18}O$ values in precipitation at the Tuotuohe station, although the influence of air temperature upon individual precipitation events at the synoptic scale is very weak. Siegenthaler and Oeschger (1980) have demonstrated that the temperature effects are best analyzed on an averaged basis rather than from individual events.

Temporal and spatial variations of $\delta^{18}O$ in precipitation

From north to south, the seasonal distribution of $\delta^{18}O$ in individual precipitation events at the four stations across the Tibetan Plateau shows a continuous change (Figure 3). At Delingha, on the northern Tibetan Plateau, $\delta^{18}O$ values and air temperature trends correlate strongly with high values in summer and low values in winter. The occurrences of high $\delta^{18}O$ values in summer precipitation and low $\delta^{18}O$ values in winter precipitation at the Delingha station match the temporal distributions of oxygen isotopes in precipitation in other inland areas of central Asia (Araguás-Araguás et al., 1998). On the other hand, the $\delta^{18}O$ values in precipitation remain low in summer precipitation at both Lhasa on the southern Plateau and Nagqu on the south-central Plateau. Compared with the low $\delta^{18}O$ values in summer precipitation at Nagqu and Lhasa, most of the $\delta^{18}O$ values in summer precipitation at Tuotuohe, north-central Tibetan Plateau, are less negative.

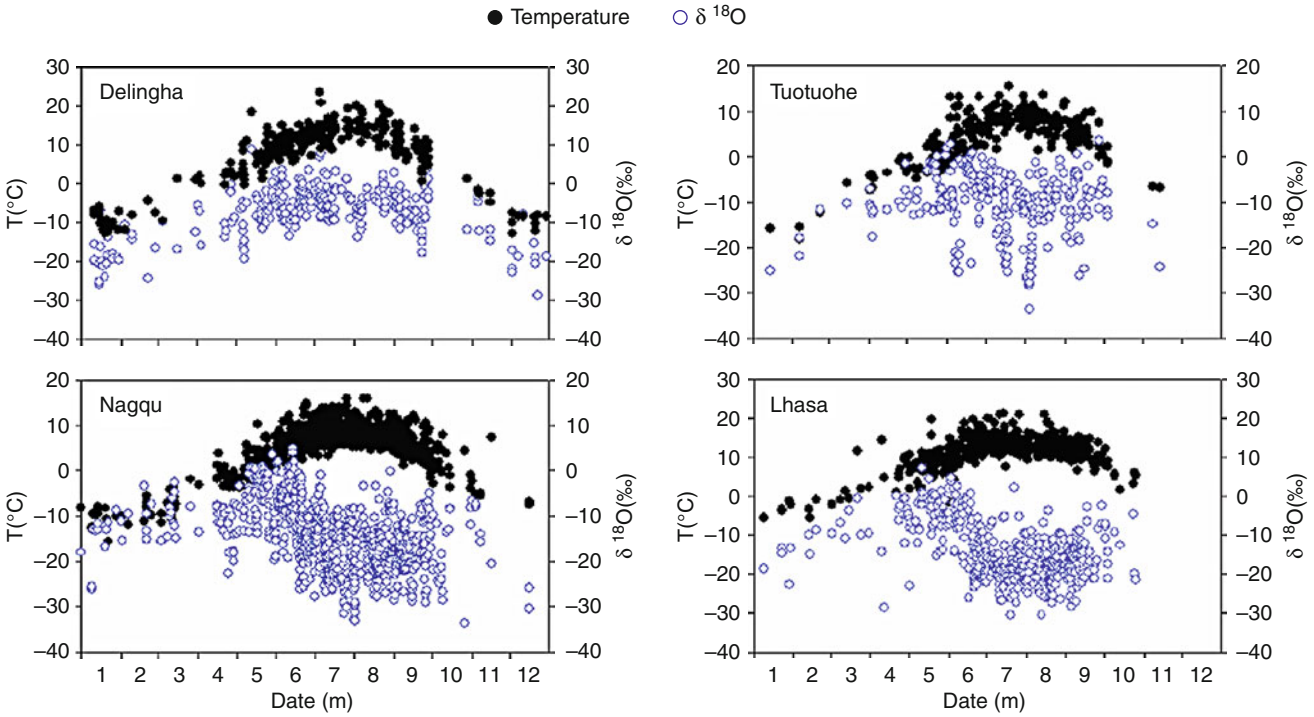

Isotope Analysis, Figure 3 Seasonal distribution of air temperatures and $\delta^{18}O$ in precipitation events at four meteorological stations on the Tibetan Plateau: Delingha, Tuotuohe, Nagqu, and Lhasa.

Figure 3 also shows that from January to May, before the onset of the southwest monsoon, the $\delta^{18}O$ values increased gradually at all four stations, in sync with their air temperature trends. We therefore calculated the correlations between $\delta^{18}O$ values and air temperature before the monsoon onset at the four stations (Table 1), and found that these correlations are more significant than those for individual precipitation events over the entire year. Furthermore, the correlations weaken gradually from north to south across the Tibetan Plateau (Table 1). This shows that temperature effects on $\delta^{18}O$ in precipitation during the pre-monsoon period along this transect exceed those in the entire year. It was also found that from January to May, the slopes ($d\delta^{18}O/dT$) and correlation coefficients (r) of the regression result between $\delta^{18}O$ and air temperature at Tuotuohe resemble those at Delingha. On the other hand, the slope and correlation coefficient at Nagqu appear similar to those at Lhasa (Table 1).

Figure 4 displays the temporal variations of monthly weighted mean $\delta^{18}O$ values in precipitation and air temperature at each of the four stations on the transect. The air temperature trends for the four stations vary similarly, with temperatures high in summer and low in winter. However, the trends of the corresponding $\delta^{18}O$ values in precipitation exhibit obvious differences. From January to May, all the $\delta^{18}O$ trends increase gradually, paralleling those of air temperature. The $\delta^{18}O$ values in precipitation at the Lhasa, Nagqu, and Tuotuohe stations rise to their maxima in May. Beginning in June, the $\delta^{18}O$ values of precipitation at both Lhasa and Nagqu fall rapidly to relatively low values in July. During this period, the $\delta^{18}O$ values in precipitation at the Tuotuohe station decrease more moderately, reaching a minimum in August. In contrast, after the $\delta^{18}O$ values at the Delingha station continue to increase from January to May, rising to a maximum in July, they then begin a slow decrease. The tendency for low $\delta^{18}O$ values during the mid-summer precipitation progressively strengthens from north to south (Figure 4).

Several factors may affect the relationship between $\delta^{18}O$ in precipitation and air temperature. Spatial variations of $\delta^{18}O$ may be a factor at stations exposed to homogenous moisture origin (Tian et al., 2003). Figure 5 shows the spatial variations of mean air temperature and the weighted mean of $\delta^{18}O$ for the separate periods, January–May (solid lines), June–September (dotted lines), and the entire year (dash-dotted lines) at the four Plateau stations. The bar graphs at the bottom of Figure 5 show elevation (filled bars) and annual precipitation (open bars).

Between January and May, the spatial variations of $\delta^{18}O$ values in precipitation positively correlate with air temperature at the two southern stations (Lhasa, Nagqu). That is, the mean $\delta^{18}O$ values and mean air temperatures both decrease with increasing latitude and altitude. However, between the two northern stations (Tuotuohe and Delingha), although the elevation is lowering and the corresponding mean air temperature increases, the mean $\delta^{18}O$ value decreases (Figure 5a and b). The observed variation of $\delta^{18}O$ values results from the rainout effect due to

Isotope Analysis, Table 1 Comparison of the regression results between $\delta^{18}O$ and temperature at the four stations on the Tibetan Plateau prior to the monsoon

Station	Period	$d\delta^{18}O/dT$	r	n
Delingha	January–May	0.68	0.78	77
Tuotuohe	January–May	0.78	0.73	44
Nagqu	January–May	0.57	0.51	128
Lhasa	January–May	0.50	0.38	74

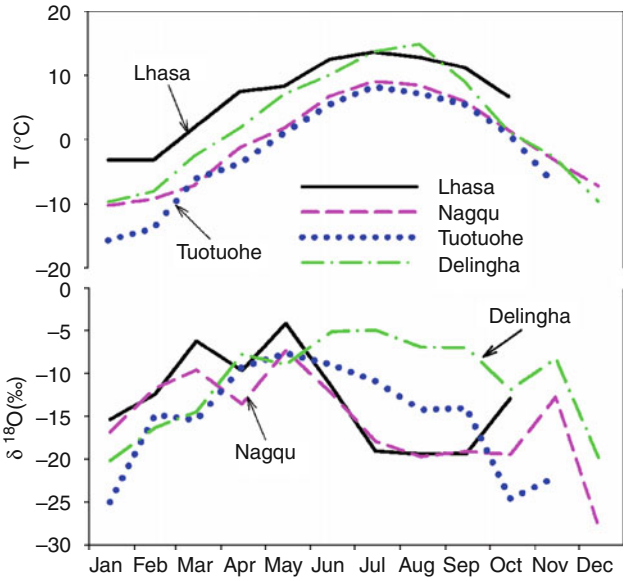

Isotope Analysis, Figure 4 Temporal variations of monthly weighted mean $\delta^{18}O$ in precipitation and air temperature for the four stations on the Tibetan Plateau.

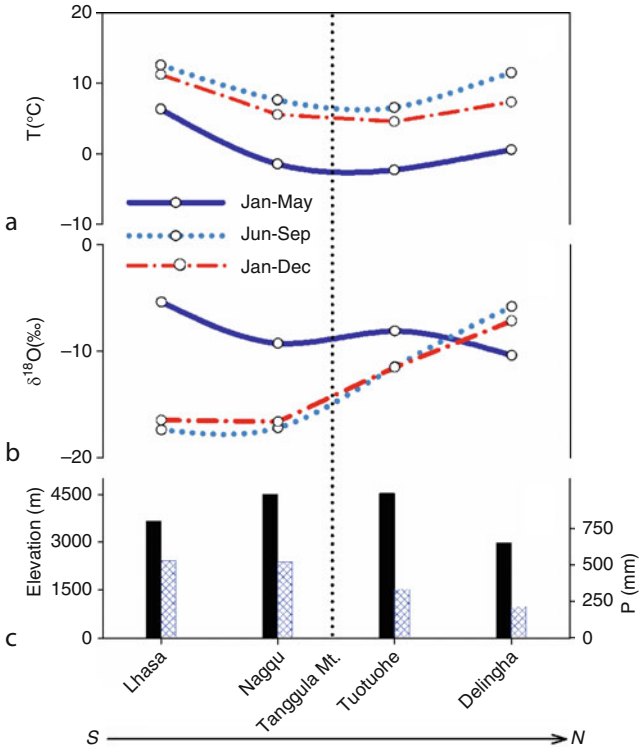

Isotope Analysis, Figure 5 South to north spatial variations during three periods of air temperature (**a**), and weighted mean $\delta^{18}O$ values (**b**). *Solid lines* indicate weighted monthly means for January–May; and *dotted lines* indicate weighted monthly means for June–September; and the *dash-dotted lines* stand for weighted annual means for the entire year. For reference, (**c**) shows the elevations (*filled bars*) and annual precipitation (*open bars*) at the four stations.

increasing continentality. In winter, the westerlies mostly control the moisture on the Tibetan Plateau and adjacent regions. Because of the greater distance to Delingha from west or south, the rainout effect at Delingha is more intensive than that at the other three stations, resulting in low $\delta^{18}O$ values.

Between June and September, the mean $\delta^{18}O$ values increase gradually from Lhasa to Tuotuohe, but the corresponding mean air temperatures decrease gradually. As seen at Delingha on the other hand, to the north of Tuotuohe, the mean $\delta^{18}O$ values increase further, but the corresponding air temperature increases (Figure 5a and b).

The trends of averaged air temperature and weighed-averaged $\delta^{18}O$ values for the entire year appear similar to those for June–September (Figure 5a and b). This results from the summer season from June to September capturing about 80% of the annual precipitation at the four stations. Accordingly, the variations of $\delta^{18}O$ in summer precipitation at the four stations generate the main trends of $\delta^{18}O$ for the entire year. As discussed above, the southwest monsoon impacts $\delta^{18}O$ in summer precipitation in the middle and the southern portions of the Tibetan Plateau. That probably causes the poor correlation between air temperature and $\delta^{18}O$ in precipitation for the entire year at the Lhasa, Nagqu, and Tuotuohe stations.

The temporal and spatial variations of $\delta^{18}O$ in precipitation on the Tibetan Plateau indicate the period around late May or early June to be an important time, and the Tanggula Mountains an important boundary. A major limitation exists for discussing the correlations between $\delta^{18}O$ in precipitation and air temperature in this study, namely that the air temperatures come from ground measurements, and not temperatures at the condensation levels in the cloud. This limitation significantly impacts this study. Findings indicate that temperature differences between the ground and the condensation levels (in the cloud) during convective storms in the winter and spring are likely much smaller than during summer monsoon events. Moreover, the convection within winter storms is far less intense than that in summer over the Plateau. Furthermore, during periods of low ground-level air temperature, the temperature difference between ground and the condensation level remains small. Accordingly, before late May or early June,

the correlations between $\delta^{18}O$ in precipitation and air temperature are very significant.

Other recent studies also conclude that the region of the Tanggula Mountain range, extending from west to east between the Nagqu and Tuotuohe stations, forms an important climatic divide (Yao et al., 1991; Tian et al., 2001b, 2003; Yu et al., 2006). These massive mountains block the flow of the southwest monsoon from the south. As a result, the southwest monsoon prevails at the Lhasa station during summer, south of the Tanggula Mountains, but without the monsoon influence in winter, the westerlies provide most of the moisture to Lhasa. At the Delingha station, north of the Tanggula Mountains the westerlies and continental air masses provide the dominant influence all year round. Hence, temperature effects control $\delta^{18}O$ in precipitation in the north (such as at Delingha), whereas the "amount effect" plays an important role for the $\delta^{18}O$ values related to the monsoon precipitation in the south (such as at Lhasa).

Because of the intense convection in the south, oceanic moisture coming from the Indian Ocean via the Bay of Bengal onto the Tibetan Plateau rises to very high altitudes, with accompanying very low temperatures. Accordingly, oxygen isotope ratios in precipitation are low, resulting in a weakening of the correlation between $\delta^{18}O$ and ground-level air temperatures in the southern and the middle portions of the Plateau during the monsoon. Moreover, because of the blocking action of the massive mountains at the southernmost Tibetan Plateau (e.g., the Himalayas), oceanic moisture rises to higher altitudes. Hence, the orographic uplift effect accentuates the lower $\delta^{18}O$ in precipitation in the southern and the middle portions of the Plateau. However, the monsoon precipitation causes the summer rainfall to be considerably higher than that in winter. An inverse correlation exists between $\delta^{18}O$ in summer precipitation and rainfall, accounting for an "amount effect" on $\delta^{18}O$ in summer precipitation in the south.

The Tuotuohe and Nagqu stations lie within a climatic divide, located at the northern and southern edges of the Tanggula Mountains. Accordingly, the Tuotuohe and Nagqu stations sit in a transition zone between the regions in the south dominated by the monsoon and the regions in the north dominated by the westerlies and the continental air masses. In this transition zone, the westerlies, the southwest monsoon, and continental air masses intermingle with the southwest monsoon dominating in summer and the westerlies prevailing in winter. Consequently, both air temperatures and moisture sources impact the variations of $\delta^{18}O$ in precipitation at the Tuotuohe and Nagqu stations. Furthermore, the decreasing influence of monsoon precipitation in summer from south to north not only results in gradually decreasing annual precipitation (P) (Figure 5c), but also results in increasing $\delta^{18}O$ values in summer precipitation (June–September) from south to north. Accordingly, the $\delta^{18}O$ variations in precipitation correlate both with air temperatures, and with moisture trajectories. Before the onset of the southwest monsoon, the westerlies provide most of the moisture at all four stations, and result in very similar trends of $\delta^{18}O$ and air temperature, with temperatures and $\delta^{18}O$ values increasing gradually from January to May (Figure 4). At the onset of the monsoon, $\delta^{18}O$ values in precipitation at the Lhasa and Nagqu stations decrease rapidly. During the rainy season between June and September, the monsoon activities are very strong on the southern Tibetan Plateau. These two stations located there exhibit lower $\delta^{18}O$ values in summer precipitation, while summer air temperatures remain high (Tian et al., 2001a, 2003). Because weaker convection and precipitation occur during the monsoon period at the Tuotuohe station than at Lhasa and Nagqu, the $\delta^{18}O$ values decrease only slightly after June, and the values in summer precipitation remain higher than those at Lhasa and Nagqu.

The Delingha station lies on the northern Tibetan Plateau, beyond the influence of the southwest monsoon activities. Accordingly, with little the monsoon influence, $\delta^{18}O$ values in precipitation show a strong temperature dependence (Zhang et al., 1995, Tian et al., 2003). The $\delta^{18}O$ values and air temperatures both rise in summer and drop in winter (Figure 4). Considerable evidence, based on (a) the trends of $\delta^{18}O$ values at the four stations, (b) the slopes ($d\delta^{18}O/dT$), and (c) the correlation coefficients (r) of the regressions between pre-monsoon $\delta^{18}O$ and air temperature, shows that the $\delta^{18}O$ variations at Nagqu resemble those at Lhasa, whereas the $\delta^{18}O$ variations at Tuotuohe parallel those at Delingha. We find that the $\delta^{18}O$ values in summer precipitation increase from south to north (Figure 5b). This results from the weakening of the southwest monsoon activities and the strengthening of the westerlies from south to north on the Plateau.

Based on this study, the characteristics of $\delta^{18}O$ in recent precipitation events on the south of the Tibetan Plateau (such as at the Lhasa and Nagqu stations) can explain the changes of $\delta^{18}O$ records in the Dasuopu and Far East Rongbuk ice core records from the Himalayas. According to the results from Thompson et al. (2000) and Kang et al. (2001), some short-term $\delta^{18}O$ records show that high $\delta^{18}O$ values in these two ice cores correspond to low precipitation, and low $\delta^{18}O$ values correspond to high precipitation. This inverse correlation between ice core $\delta^{18}O$ and precipitation may result from variations in the influence of monsoon precipitation. However, the changes in long-term $\delta^{18}O$ records from the two ice cores correspond directly with temperature changes over the Northern Hemisphere, and the $\delta^{18}O$ records can still be used as a proxy for temperature (Thompson et al., 2000; Kang et al., 2001).

$\delta^{18}O$ in precipitation from west to east on the Tibetan Plateau

Temperature dependence of $\delta^{18}O$ in precipitation

A positive correlation exists between $\delta^{18}O$ and air temperature for recent precipitation events at the Shiquanhe, Gaize, and Yushu stations (see Figure 1 for location).

The correlations between monthly mean $\delta^{18}O$ and monthly mean temperature at Shiquanhe, Gaize, and Yushu are stronger than those for individual precipitation events. These results suggest that temperature influences $\delta^{18}O$ values in precipitation at Shiquanhe, Gaize, and Yushu. The relationship between monthly mean $\delta^{18}O$ and air temperature for individual precipitation events at Gaize is weaker than that at Shiquanhe.

The close proximity to the monsoon region at Nagqu results in the variations of $\delta^{18}O$ in precipitation being similar to the $\delta^{18}O$ variations on the southern Tibetan Plateau (Tian et al., 2003; Yu et al., 2008). Hence, we also analyzed isotopic data from Nagqu, south-central Tibetan Plateau, and found an *inverse correlation* between $\delta^{18}O$ in precipitation and air temperature. However before the monsoon onset, a positive correlation still exists between $\delta^{18}O$ and air temperature for recent precipitation events at Nagqu; and air temperature remains the controlling factor for the variations of $\delta^{18}O$ in this area.

Temporal and spatial variations of $\delta^{18}O$ in precipitation

As mentioned above, the region of 32°N–33°N (the west to east extending Tanggula Mountain range) forms an important climatic divide. The Shiquanhe, Gaize, Tuotuohe, and Yushu stations lie within this climatic divide. All these stations fall in the transition belt between the regions dominated by the "temperature effect" in the north and the "amount effect" in the south. Hence, all these stations experience similar variation patterns of $\delta^{18}O$ in precipitation. In this zone, the westerlies and monsoon intermingle with the monsoon dominating in summer. The rest of the year, the westerlies mainly control the moisture sources at the four stations. Consequently, $\delta^{18}O$ in precipitation shows a temperature dependence at the annual scale. The monsoon activities in summer weaken the correlations between $\delta^{18}O$ and air temperature. Except at Nagqu, $\delta^{18}O$ variations in precipitation relate closely to the variations of temperature on an annual basis, despite the $\delta^{18}O$ values being low in summer as a result of the monsoon precipitation (Tian et al., 2003; Yu et al., 2004). As mentioned above, the closer the proximity to the monsoon region, the more similar the results in the variations of $\delta^{18}O$ in precipitation at Nagqu become to the $\delta^{18}O$ variations on the southern Tibetan Plateau. However, before the monsoon onset, air temperature remains the dominant factor that controls the variations of $\delta^{18}O$ in this area (see Table 2). Table 2 also shows that the correlations of $\delta^{18}O$ and air temperature at these stations before the monsoon onset are more significant than those on an annual basis. Furthermore, the slopes ($d\delta^{18}O/dT$) are also higher for the pre-monsoon period than those for the entire year. Clearly, the monsoon activities in summer have an impact upon the relationships between $\delta^{18}O$ in precipitation and air temperature in the transition zone.

Figure 6 shows the seasonal variations of $\delta^{18}O$ in precipitation with air temperature at the Shiquanhe, Gaize, Nagqu, and Yushu stations. Before the onset of the southwest monsoon, the $\delta^{18}O$ values increase gradually, consistent with the trends of air temperature. Apparently, temperature effects control the $\delta^{18}O$ values in precipitation in this area before the monsoon onset, when the westerlies control the moisture origins, the frequency of precipitation events remains very low, and precipitation events yield little rainfall (Figure 6).

During the rainy season between late May and August, strong monsoon conditions exist at all four stations, and $\delta^{18}O$ values decrease (the $\delta^{18}O$ values fall to a minimum at the end of July or early August), while summer air temperatures remain high. The southwest monsoon in summer causes the frequency of precipitation events to increase rapidly. Compared with the pre-monsoon period, rainfall amounts increase significantly during the monsoon (Figure 6).

With the retreat of monsoon precipitation, temperature remains the dominant factor controlling the variation of $\delta^{18}O$. With air temperatures lowering gradually, the $\delta^{18}O$

Isotope Analysis, Table 2 Relationships between $\delta^{18}O$ in precipitation and air temperature before the summer monsoon

Station	Period	$d\delta^{18}O/dT$	R	n
Yushu	January–May	0.47	0.70	46
Nagqu	January–May	0.57	0.51	128
Gaize	January–June[a]	0.74	0.75	25
Shiquanhe	January–June[a]	0.77	0.72	21

[a]The rainy season starts around July at the Gaize and Shiquanhe stations.

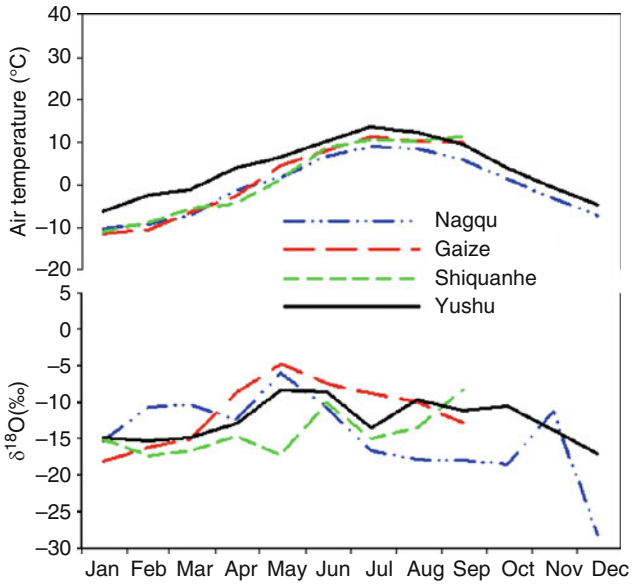

Isotope Analysis, Figure 6 Seasonal changes in weighted-averaged $\delta^{18}O$ and air temperature at the Nagqu, Gaize, Shiquanhe, and Yushu stations.

values decrease correspondingly. Furthermore, $\delta^{18}O$ reaches its lowest value in December, when air temperatures also attain their lows at Nagqu and Yushu. After the monsoon retreat, the westerlies mainly control the moisture sources in the area and the content of atmospheric water vapor rapidly decreases, resulting in sparse precipitation in this region.

Overall, the temperature effect controlled the variation of $\delta^{18}O$ over the measurement period at the four stations. However, the southwest monsoon transports oceanic moisture with low $\delta^{18}O$ into the regions in summer, especially from June to August, resulting in the lower $\delta^{18}O$ values than would be predicted from air temperature alone. Accordingly, the monsoon activities weaken the correlation between $\delta^{18}O$ and air temperature. Before the monsoon onset and after the monsoon retreat, the periods when the westerlies dominate the moisture sources, the $\delta^{18}O$ values correlate significantly with air temperatures.

Bibliography

Aizen, V., Aizen, E., Melack, J., et al., 1996. Isotopic measurements of precipitation on central Asian glaciers (southeastern Tibet, northern Himalayas, central Tien Shan). *Journal of Geophysical Research*, **101**(D4), 9185–9198.

Araguás-Araguás, L., Froehlich, K., and Rozanski, K., 1998. Stable isotope composition of precipitation over Southeast Asia. *Journal of Geophysical Research*, **103**(D22), 28721–28742.

Clark, I., and Fritz, P., 1997. *Environmental Isotopes in Hydrology*. Boca Raton, FL: Lewis.

Coplen, T. B., 1993. Uses of environmental isotopes. In Alley, W. M. (ed.), *Regional Groundwater Quality*. New York: Van Nostrand Reinhold, pp. 227–254.

Craig, H., 1961. Isotopic variations in meteoric waters. *Science*, **133**, 1702–1703.

Cuffey, K. M., Alley, R. B., Grootes, P. M., et al., 1994. Calibration of the $\delta^{18}O$ isotopic palaeothermometer for central Greenland, using borehole temperature: results and sensitivity. *Journal of Glaciology*, **40**, 341–349.

Dansgaard, W., 1964. Stable isotopes in precipitation. *Tellus*, **16**(4), 436–468.

Dansgaard, W., Johnsen, S. J., Clausen, H. B., et al., 1993. Evidence for general instability of past climate from a 250-kyr ice-core record. *Nature*, **364**, 218–220.

Epstein, S., and Mayeda, T. K., 1953. Variations of the $^{18}O/^{16}O$ ratio in natural waters. *Geochimica Cosmochimica Acta*, **4**, 213.

Epstein, S., Sharp, R. P., and Gow, A. J., 1965. Six-year record of oxygen and hydrogen isotope variations in South Pole firn. *Journal of Geophysical Research*, **70**(8), 1809–1814.

Fontes, J. C., and Edmunds, J. N., 1989. The use of environmental isotope techniques in arid zone hydrology. IHP-III project 5.2 UNESCO, Paris.

Gat, J. R., 1996. Oxygen and hydrogen isotopes in the hydrologic cycle. Annu. Rev. Earth Planet. *Annual Review of Earth and Planetary Sciences*, **24**, 225–262.

Hoffmann, G., and Heimann, M., 1997. Water isotope modeling in the Asian monsoon region. *Quaternary International*, **37**, 115–128.

Johnsen, S. J., Dansgaard, W., Clausen, H. B., et al., 1972. Oxygen isotope profiles through the Antarctic and Greenland ice sheets. *Nature*, **235**, 429–434.

Johnsen, S. J., Dahi-Jensen, D., Dansgaard, W., et al., 1995. Greenland palaeotemperatures derived from GRIP bore hole temperature and ice core isotope profiles. *Tellus*, **47B**, 624–629.

Johnson, K. R., and Ingram, B. L., 2004. Spatial and temporal variability in the stable isotope systematics of modern precipitation in China: implications for paleoclimatic reconstructions. *Earth and Planetary Science Letters*, **220**, 365–377.

Jouzel, J., and Merlivat, L., 1984. Deuterium and oxygen 18 in precipitation: modeling of the isotopic effects during snow formation. *Journal of Geophysical Research*, **89**(D7), 11749–11757.

Jouzel, J., Lorius, C., Petit, J. R., et al., 1987. Vostok ice core: a continuous isotope temperature record over the last climatic cycle (160,000 years). *Nature*, **329**, 403–407.

Kang, S. C., Qin, D. H., Paul, A. M., et al., 2001. Climatic and environmental records from the Far East Rongbuk ice core, Mt. Qomolangma (Everest). *Episodes*, **24**(3), 176–181.

Kendell, C., and Coplen, T. B., 1985. Multisample conversion of water to hydrogen by zinc for stable isotope determination. *Analytical Chemistry*, **57**, 1437–1440.

Lorius, C., Jouzel, J., Ritz, C., et al., 1985. A 150,000-year climatic record from Antarctic ice. *Nature*, **316**, 591–596.

Mazor, E., 1997. *Chemical and isotopic groundwater hydrology: the applied approach*. New York: Marcel Dekker. 413 pp.

Merlivat, L., and Jouzel, J., 1979. Global climatic interpretation of the deuterium oxygen-18 relationship for precipitation. *Journal of Geophysical Research*, **84**(8), 5029–5033.

Posmentier, E. S., Feng, X., and Zhao, M., 2004. Seasonal variations of precipitation $\delta^{18}O$ in eastern Asia. *Journal of Geophysical Research*, **109**, D23106, doi:10.1029/2004JD004510.

Rozanski, K., Araguás-Araguás, L., and Gonfiantini, R., 1992. Relation between long-term trends of oxygen-18 isotope composition of precipitation and climate. *Science*, **258**, 981–985.

Schoch-Fischer, H., Rozanski, K., Jacob, H., et al., 1984. Hydrometeorological factors controlling the time variation of D, ^{18}O and ^{3}H in atmospheric water vapour and precipitation in the northern westwind belt. In: Isotope Hydrology 1983. Vienna/Austria: IAEA-publications, pp. 3–30.

Siegenthaler, U., and Oeschger, H., 1980. Correlation of ^{18}O in precipitation with temperature and altitude. *Nature*, **285**, 314–317.

Thompson, L. G., Mosley-Thompson, E., Davis, M. E., et al., 1995. A 1000 year climatic ice-core record from the Guliya ice cap, China: its relationship to global climate variability. *Annals of Glaciology*, **21**, 175–181.

Thompson, L. G., Yao, T. D., Davis, M. E., et al., 1997. Tropical climate instability: the last glacial cycle from a Qinghai-Tibetan ice core. *Science*, **276**(5320), 1821–1825.

Thompson, L. G., Yao, T. D., Mosley-Thompson, E., et al., 2000. A high-resolution millennial record of the South Asian Monsoon from Himalayan ice cores. *Science*, **289**, 1916–1919.

Tian, L. D., Yao, T. D., Numaguti, A., et al., 2001a. Stable isotope variations in monsoon precipitation on the Tibetan Plateau. *Journal of the Meteorological Society of Japan*, **79**(5), 959–966.

Tian, L. D., Masson-Delmotte, V., Stievenard, M., et al., 2001b. Tibetan Plateau summer monsoon northward extent revealed by measurements of water stable isotopes. *Journal of Geophysical Research*, **106**(D22), 28,081–28,088.

Tian, L. D., Yao, T. D., Schuster, P. F., et al., 2003. Oxygen-18 concentrations in recent precipitation and ice cores on the Tibetan Plateau. *Journal of Geophysical Research*, **108**(D9), ACH 16-1–ACH 16-10.

Tian, L. D., Yao, T. D., MacClune, K., et al., 2007. Stable isotopic variations in West China: a consideration of moisture sources. *Journal of Geophysical Research* 112(D10112), doi:10.1029/2006JD007718.

Vuille, M., Werner, M., Bradley, R. S., et al., 2005. Stable isotopes in precipitation in the Asian monsoon region. *Journal of Geophysical Research*, **110**, D23108, doi:10.1029/2005JD006022.

White, J. W. C., Barlow, L. K., Fisher, D., et al., 1997. The climate signal in the stable isotopes of snow from Summit, Greenland:

results of comparisons with modern climate observations. *Journal of Geophysical Research*, **102**(C12), 26425–26439.
Yao, T. D., Ding, L. F., Pu, J. C., et al., 1991. Characteristic of $\delta^{18}O$ in snow and its relation with moisture sources in Tanggula Mountains, Tibetan Plateau (in Chinese). *Chinese Science Bulletin*, **36**(20), 1570–1573.
Yao, T. D., Thompson, L. G., Jiao, K. Q., et al., 1995. Recent warming as recorded in the Qinghai-Tibetan cryosphere. *Annals of Glaciology*, **21**, 196–200.
Yao, T. D., Thompson, L. G., Mosley-Thompson, E., et al., 1996. Climatological significance of $\delta^{18}O$ in north Tibetan ice cores. *Journal of Geophysical Research*, **101**(D23), 29531–29537.
Yao, T. D., Masson, V., Jouzel, J., et al., 1999. Relationships between $\delta^{18}O$ in precipitation and surface air temperature in the Urumqi River Basin, east Tianshan Mountains, China. *Geophysical Research Letters*, **26**(23), 3473–3476.
Yu, W. S., Yao, T. D., Tian, L. D., et al., 2006. Oxygen-18 isotopes in precipitation on the eastern Tibetan Plateau. *Annals of Glaciology*, **43**, 263–268.
Yu, W. S., Yao, T. D., Tian, L. D., et al., 2007. Stable isotope variations in precipitation and moisture trajectories on the western Tibetan Plateau, China. *Arctic Antarctic and Alpine Research*, **39**(4), 688–693.
Yu, W. S., Yao, T. D., Tian, L. D., et al., 2008. Relationships between $\delta^{18}O$ in precipitation and air temperature and moisture origin on a south-north transect of the Tibetan Plateau. *Atmospheric Research*, **87**(2), 158–169.
Zhang, X. P., Shi, Y. F., and Yao, T. D., 1995. Variational features of precipitation $\delta^{18}O$ in Northeast Qinghai-Tibet Plateau. *Science in China Series B*, **38**(7), 854–864.

ISOTOPIC CHARACTERISTICS OF ICE, SNOW, AND GLACIERS

Bhism Kumar
Hydrological Investigation Division, National Institute of Hydrologyl, Uttarakhand, India

Definition and introduction

The isotopic methods are based mainly on analyses of environmental isotope contents (primarily ^{2}H, ^{3}H, ^{18}O). The stable isotopes particularly deuterium and oxygen-18 are useful as tracers in hydrologic systems. They are naturally present as part of the water molecules and their concentration is influenced by physical processes operating within the hydrologic cycle. In many cases the isotopic profile of snow cover gives information about the isotopic variation of those snowfalls that have contributed to snow cover accretion.

Historical background

Dansgaard (1954) first proposed that the ^{18}O content in glacier ice might reflect climatic conditions of the past. Since then, extensive work has been carried out in this field, on both of the large polar ice sheets. The most successful work that has been done in this field is undoubtedly the establishment of the $\delta^{18}O$ profile for the camp century ice core that is 1,390 m deep (Dansgaard and Johnsen, 1969). Another deep ice core, approximately 2,000 m long, has been obtained by drilling through the Antarctic ice sheet at Byrd Station (Ueda and Garfield, 1969) and its $\delta^{18}O$ content measured through its entire length (Johnsen et al., 1972). Although the physical conditions of Byrd Station core are considerably better than those for Greenland (no core pieces were lost or broken), the Byrd Station ice core is much more difficult to interpret due to low accumulation rate, absence of seasonal isotope variation that made it difficult to date. Deuterium profiles in sea-ice cores are rarely described in the literature. Friedman et al. (1961) explained the negative δD values (−2 to −14‰) of ice samples collected on Ice Island T3 and on Drift Station Alpha by the presence of a relatively thin layer of deuterium-depleted water on parts of the surface of the Arctic Ocean during the summer. Gow and Epstein (1972) reported on deuterium concentrations connected with a special sea-ice growth situation in McMurdo Sound, Antarctica.

Such long climatic records as those obtained from the two polar ice cores have two main applications: the study of climatic changes as far back in the earth's history as possible and the use of this information for predicting possible climatic changes of the future.

Isotopic characteristics

The important aspect is that the heavier water tends to evaporate slower and condense faster than the lighter ones. Thus, the ratio of the heavy isotopes to the light isotopes is not constant, but changes during condensation and evaporation processes.

In ice cores, usually the ratio of ^{18}O to ^{16}O is measured. Deuterium profiles in ice cores are rarely described in the literature. Gow and Epstein (1972) reported on deuterium concentrations connected with a special sea-ice growth situation in McMurdo Sound, Antarctica. To study these isotopes in glaciers, the best method is the measurement of stable isotopic ratio (Isotopic Fingerprinting). Some other isotopes that have been found important are ^{210}Pb, ^{36}Cl, ^{10}Be, ^{39}Ar, and ^{32}Si. From the decrease in ^{210}Pb activity, firn profiles can be dated. Successful measurements have been performed in Antarctica (Picciotto et al., 1968) and in an Alpine cold Glacier (Gaggler, 1977), which have been used for determining accumulation rates for the last 80–90 years. ^{36}Cl can be detected relatively in small samples if accelerators are used. This study was first conducted in Antarctica (Nishizumi et al., 1979).

During ice ages, the oceans had a higher stable isotope ratio than today (1–2‰ for $\delta^{18}O$), because additional water depleted in ^{18}O was contained in the ice sheets. This has to be taken into account for ice core interpretation. However, for one climate period it may be assumed to be constant. On expeditions that led from the coast of Greenland or Antarctica to the interior of the continent, the mean annual air temperature and the $\delta^{18}O$ of the snow were measured. Since the altitude of the ice sheets increases toward the interior, the air temperature and the $\delta^{18}O$ decrease. It was found that there is a simple linear relationship between

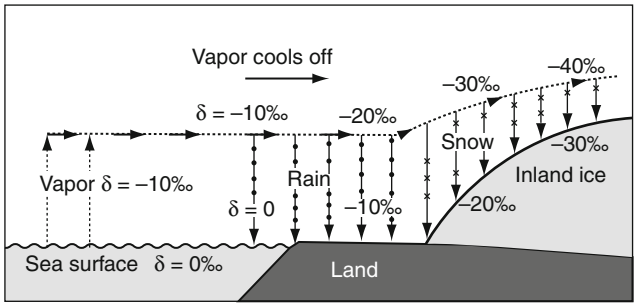

Isotopic Characteristics of Ice, Snow, and Glaciers,
Figure 1 Changes in $\delta^{18}O$ from the first evaporation to the final snow fall (Payne, 1983).

the two variables. To understand this, we have to follow the path of the precipitation from the beginning to the final snowfall. This is shown in Figure 1.

During the first evaporation from the ocean, the heavier isotopes are slower to evaporate than the lighter ones, thus the first water vapor is relatively light compared to the ocean water. The air and thus the water vapor is raised and cooled until the first condensation takes place and clouds are formed. Now the heavier molecules condensate earlier than the light ones, thus the process is reversed and the first raindrops from the clouds may have the same isotope ratio as the ocean water. Now the air mass and thus the cloud is moved, let us say, in case of Antarctica, southward, the heavier isotopes condense earlier, thus the rain or snowfall contains heavier water, whereas the remaining moisture in the cloud gets lighter and lighter. At the edge of the continent, the air is raised due to the increasing altitude of the ice sheet surface, and thus cooled even stronger. (The air temperature decreases both with altitude and latitude.) The farther inland the snow falls, the lower is the isotope ratio, since most of the heavier isotopes have fallen out already at lower latitudes. Thus, we get a relationship between the stable isotope ratio and the temperature, the air had when the precipitation was formed. Figure 2 shows the $\delta^{18}O$ profile of a "shallow" core that has been drilled close to the German Antarctic wintering base "Neumayer." It can be seen that the $\delta^{18}O$ oscillates: we find high values in summer and low values in winter. Thus, one can find the annual layers in the core. The red lines mark the borders between two annual layers. By counting the annual layers, one can determine the age of the ice. This method works only until a certain depth, because, as mentioned above, the ice is compressed under its own weight, and at some point the annual layers become so thin that it is impossible to distinguish single annual layers. Some other dating methods are used for these parts of ice cores, for example:

- Identifying horizons of known age, such as acid layers from dated volcano eruptions.
- Matching features of the $\delta^{18}O$ record with another dated climatic record, such as ocean or lake sediments.
- Radiocarbon dating of CO_2 extracted from air bubbles in the ice.

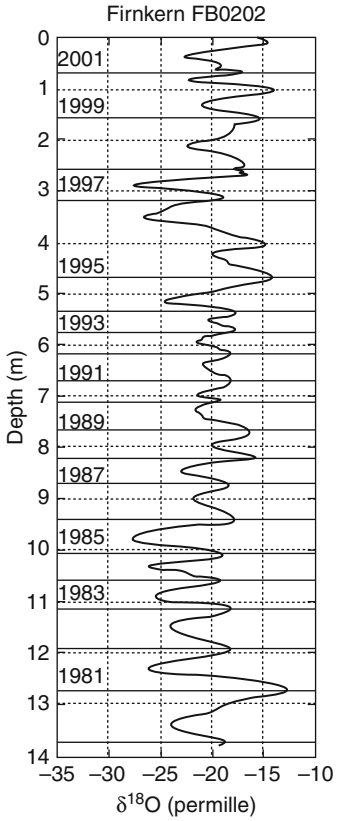

Isotopic Characteristics of Ice, Snow, and Glaciers,
Figure 2 $\delta^{18}O$ profile of a "shallow" core (Payne, 1983).

Although it is clear, that there is a strong relationship between temperature and isotope ratio, the quantitative conversion of $\delta^{18}O$ to air temperature is still a problem.

There are many different reasons for the persistent uncertainty. The $\delta^{18}O$ is influenced by many other factors apart from air temperature, such as the original isotope ratio of the ocean water (which was different from today during ice ages), the origin of precipitation and the seasonal distribution of snowfall events. Additionally to these meteorological factors, there are glaciological influences. It has to be taken into account, that the ice flows and thus the ice in the core might come from areas of higher altitude, which are cooler than the drilling site. Also, during glacial periods the altitude of the ice sheet was higher than today, thus the ice in the core might originate from a cooler area than today. Scientists have also measured today's temperature in the bore holes of the ice cores. Although the signal is considerably attenuated, one can still find the colder ice ages and warmer interglacial in the cores, and by using physical laws, the scientists can calculate the original temperature profiles, which especially for Greenland, yielded results different from the ones retrieved by measuring stable isotope ratios. So the discussion about this is still going on at present.

Applications of isotope data in glaciology

Accumulation rates

One of the most important parameters for the study of the mass balance of the glacier is the determination of the accumulation rates. The determination of the accumulation rates by the stable isotope method is relatively simple, as far as the firn and the uppermost part of the glacier are concerned. One need only count to the summer maxima down the ice profile and determine the density of the ice. At greater depths, the thickness of the annual layers must be corrected for vertical strain since the time of deposition. Since the strain also depends upon the temperature history and the thickness and slope of the ice sheets, such corrections can be quite complicated. Therefore, the stable isotope method for determining accumulation rate is mainly of importance on the uppermost part of the glaciers, where reliable results are obtained because of the simplicity of the method. The isotopic composition of snow falling in the accumulation area of glacier will differ from place to place and from time to time for the following reason: the altitude effect causes snow falling higher in the accumulation area to have a relatively lower O^{18}/O^{16} ratio. Preliminary studies show that the magnitude of this effect in terms of per mil variation for each 1,000 ft of altitude is 1.8 in Greenland, 1.7 on the west slope of the Sierra Nevada of California, and 0.6 on the Saskatchewan Glacier, Canada (Gat and Gonfiantini, 1981).

On temperate glaciers where the seasonal δ-variations are strongly modified by percolation of meltwater and where there is intensive homogenization, the stable isotope method does not work unless the conditions are favorable.

Runoff ratio

The runoff ratio indicates which part of the precipitation escapes as accumulation and is consequently an important parameter in mass balance studies of temperate glaciers. The validity of isotopic method for determining the runoff ratio rests on the fact that it only requires information about the isotopic composition of the snowpack, after the homogenization is completed, and information about the isotope content of the total precipitation. The isotopic composition of the snowpack can be measured easily in the firn.

Dating of the ice core

Dating of the ice core is closely related to determining the accumulation rate. In both cases, the results are based on counting the summer maxima of the annual *d*-variations. The stable isotope method is valid when the difference between the summer and winter δ-values is not less than 2‰ for ^{18}O and not less than 20‰ for deuterium. Thus, the method works particularly well on the high-polar glaciers where the seasonal amplitude has been found to be preserved in the ice for thousands of years.

According to Dansgaard et al. (1973), Johnsen et al. (1972), and Hammer et al. (1978), the mean thickness (λ) of annual layers depends on the distance from the bottom, that is, $(y)\lambda = f(y)$. The age, t, of a respective ice layer in years can be calculated from the equation,

$$t = \tau \int_{H}^{H-y} \frac{dy}{fy}$$

where τ being 1 year and H the total thickness of the ice sheet. Thus, the determination of λ by stable isotope measurements in different spaced increments of the core gives the age of the ice at the respective increment (Gat and Gonfiantini, 1981).

Paleoclimates

One of the dominating parameters determining the stable isotope ratio of a given precipitation is the temperature of its formation. This is reflected in the seasonal variation of the isotope content. In a similar way, it is to be expected that long-term climatic variations are reflected in the isotope content of the precipitation of the past and should be detectable in ice profiles. The use of stable isotope profiles of glacier ice to record past climatic changes is mainly of interest in relation to polar glaciers. Temperate glaciers are of less interest for this field, mainly for two reasons. First, the ice at the bottom of the temperate glaciers is very young compared with that of the polar glaciers; such a record therefore only spans a very short time period under favorable conditions possible for 2,000 years. Second, the percolating water is found to obliterate the seasonal variations and in some cases strongly to change the original isotopic content of the accumulation (Gat and Gonfiantini, 1981).

Summary

Isotopic studies have been proved useful for solving many environment-related problems. It has several applications in snow, ice, and glaciology. The methods are mainly based on the isotopes ^{2}H, ^{3}H, and ^{18}O because seasonal variations of these isotopes in snowfall can be preserved within the snow cover for a considerable time, especially in polar regions. Several studies have been conducted in this field. But there is still a great scope in studying the seasonal fluctuations and reconstruction of past climatic changes.

Bibliography

Dansgaard, W., 1954. The ^{18}O abundance of fresh water. *Geochimica et Cosmochimica Acta*, **6**, 241.

Dansgaard, W., and Johnsen, S. J., 1969. A flow model and a time scale for the ice core from camp century, Greenland. *Journal of Glaciology*, **8**, 215.

Dansgaard, W., Johnsen, S. J., Clausen, H. B., and Gundestrup, H. G., 1973. Stable isotope glaciology. *Medd Greoland*, **197**(2), 1.

Friedman, I., Schoen, B., and Harris, J., 1961. The deuterium concentration in arctic sea ice. *Journal of Geophysical Research*, **66**, 1861–1864.

Gaggler, H., 1977. 210Pb dating on the Colle Gnifetti core 1976. *Z Gletscherkde Glazialgeol*, **13**, 204.
Gat, J. R., and Gonfiantini, R., 1981. Stable isotope hydrology: Deuterium and oxygen-18 in the water cycle, IAEA Technical Report Series No. 210.
Gow, A. J., and Epstein, S., 1972. On the use of stable isotopes to trace the origins of ice in a floating ice tongue. *Journal of Geophysical Research*, **77**, 6552–6557.
Hammer, C. U., Clausen, H. B., Dansgaard, W., Gundestrup, N., Johnsen, S. J., and Reeh, N., 1978. Dating of Greenland ice cores by flow models, isotopes, volcanic debris and continental dust. *Journal of Glaciology*, **20**, 3.
Johnsen, S. J., Dansgaard, W., Clausen, H. B., and Langway, C. C., Jr., 1972. Oxygen isotope profiles through the Antarctic and Greenland ice sheets. *Nature*, **235**, 429.
Nishizumi, K., Arnold, J. R., Elmore, D., Ferraron, R. D., Grove, H. E., Finkel, R. C., Beukens, R. P., Chang, K. H., and Kilius, L. R., 1979. Measurement of 36Cl in Antarctic meteorites and Antarctic ice using a van de Graaff accelerator. *Earth and Planetary Science Letters*, **45**, 285.
Payne, B. R., 1983. Guidebook on nuclear techniques in hydrology, Technical report series no. 91, International Atomic Energy Agency, Vienna.
Picciotto, E., Cameron, R., Crozaz, C., Deutsch, S., and Wilgain, S., 1968. Determination of the rate of snow accumulation inaccessibility, Eastern Antartica. A comparison of glaciological and isotopic methods. *Journal of Glaciology*, **7**, 273.
Ueda, H. T., and Garfield, D. E., 1969. Core drilling through Antarctic ice sheets, US army cold region and research lab, Technical Report No. 231.

Cross-references

Isotope Analysis

ISOTOPIC FRACTIONATION OF FREEZING WATER

Martyn Tranter
School of Geographical Sciences, University of Bristol, Bristol, UK

Definition

Isotopic behavior of water molecules during freezing.

Isotopic composition of water

Water molecules with different molecular weights behave differently during freezing, with the heavier molecules showing a slight preference to enter ice, whereas the lighter molecules have a slight preference to remain as a liquid. The molecular weights of water molecules differ because hydrogen and oxygen have a number of isotopes. Hydrogen has two stable isotopes, ^{1}H and ^{2}H (or deuterium, D), and one radioactive isotope, ^{3}H (or tritium). Oxygen has three stable isotopes, ^{16}O, ^{17}O, and ^{18}O. There are nine possible molecular weights, and isotopic configurations, for water molecules, but almost all water molecules are of three molecular weights because of the low abundance of the heavier isotopes. For example, the D content of a typical water is only 0.0156% of the H content, and the typical relative ratios of ^{16}O : ^{17}O : ^{18}O are of the order of 99.763 : 0.037 : 0.2 (Greenwood and Earnshaw, 1984). The different molecular weights impart slightly different physical properties to the molecules because the vibrational energies of their bonds differ slightly (Table 1). This in turn means that the water molecules fractionate differently between ice and water during freezing. In general, the lighter molecules have bonds that vibrate more quickly, and tend to fractionate or remain in the liquid slightly more that the heavier molecules, whose bonds vibrate slightly less and have a slight preference for the solid ice.

Nomenclature of isotope fractionation

The degree to which the water isotopes fractionate into ice is defined by the Fractionation Factor, α (Equation 1):

$$\alpha = \frac{R_i}{R_w} \tag{1}$$

where R is the ratio of the heavy to light isotope (e.g., $^{18}O/^{16}O$ and $D/^{1}H$) in ice, i, and water, w (Faure, 1986; Hoefs, 2004). Values of α are dependent on the rate of freezing in particular, and are quite close to 1 see (Table 2), showing that there is only a slight fractionation of the isotopes between ice and water. However, these small changes are relatively easy to measure both accurately and precisely by mass spectrometry. The values of R usually differ only slightly between many different ices and waters, and so their R values are expressed by the δ notation to make comparison of the R values easier. The δ value is defined by reference to the R value of Vienna standard

Isotopic Fractionation of Freezing Water, Table 1 Some physical properties of the three most common isotope combinations of water (Hoefs, 2004)

Property	$^{1}H_2{}^{16}O$	$^{2}H_2{}^{16}O$	$^{1}H_2{}^{18}O$
Density @ 20°C (g/cm^3)	0.997	1.0151	1.1106
Boiling Point (°C)	100.0	101.42	100.14
Temperature of maximum density (°C)	3.89	11.24	4.30

Isotopic Fractionation of Freezing Water, Table 2 Typical values for the fractionation factors (α) of the stable isotopes of hydrogen and oxygen in water and ice during freezing

Comment	α D	$\alpha^{18}O$	Source
Equilibrium values	1.0171–1.0235	1.0026–1.0031	(Ferrick et al., 2002)
Fast – slow freezing rates	1.007–1.015	1.0005–1.0027	(Ferrick et al., 2002)
River ice values	1.0212	1.00291	(Ferrick et al., 2002)
Subglacial lake Vostok values	1.0208	1.00310	(Jouzel et al., 1999)

mean ocean water (SMOW), as shown in Equation 2, and gives rise to positive or negative values. Positive values denote samples enriched in the heavier isotope and are often referred to as "heavy" values, whereas negative values denote samples enriched in the lighter isotope and are often referred to as "light" values (Faure, 1986).

$$\delta_{\text{sample}} = \frac{(R_{\text{sample}} \div R_{\text{SMOW}}) - 1}{1000} \quad (2)$$

Isotope fractionation during freezing

The heavier isotopes fractionate into ice during freezing, and so the remaining water becomes enriched in lighter isotopes. At equilibrium, the ice has δD and $\delta^{18}O$ values which are +17.1‰ to +23.5‰ and +2.6 to +3.1 more positive or "heavier," respectively, than the water. These differences can be derived from the first line of Table 2, using Equation 3, which is derived from Equations 1 and 2.

$$\delta_i - \delta_w = 1000(\alpha - 1) \quad (3)$$

The extent of fractionation critically depends on the rate of freezing. Rapid rates of freezing prohibit the fractionation, so giving rise to the smaller α values given in the second line of Table 2, whereas slower rates of freezing give rise to α values that approach equilibrium values (Ferrick et al., 2002).

The $\delta^{18}O$ and δD of most natural precipitation, including snow, have values that lie on or near to the Global Meteoric Water Line (GMWL), defined as (Craig, 1961)

$$\delta D = 8\delta^{18}O + 10 \quad (4)$$

The values of the mean annual $\delta^{18}O$ of precipitation are positively associated with mean annual air temperature, and hence snow typically has relatively low (or light) values, particularly at high latitude (Dansgaard, 1964). A particular consequence of the progressive freezing of a closed body of water, such as at the bed of a glacier, is that the water and ice samples have an isotope composition that moves off the GMWL (Jouzel et al., 1999). The slope of the association is lower (i.e. <8) because condensation processes in clouds determine the slope of the GMWL, which enhance the fractionation effects of water molecules with different molecular weights more so than freezing does (Faure, 1986). Finally, progressive freezing of a closed water body drives the isotopic composition of the remaining water increasingly lighter, and very light isotope values can be produced in the residual waters. This process is called Rayleigh Fractionation (Faure, 1986; Hoefs, 2004).

Bibliography

Craig, H., 1961. Isotopic variations in meteroic waters. *Science*, **133**, 1702–1703.

Dansgaard, W., 1964. Stable isotopes in precipitation. *Tellus*, **16**, 436–468.

Faure, G., 1986. *Principles of Isotope Geology*. New York: Wiley.

Ferrick, M. G., Calkins, D. J., Perron, N. M., Cragin, J. H., and Kendall, C., 2002. Diffusion model validation and interpretation of stable isotopes in river and lake ice. *Hydrological Processes*, **16**(4), 851–872.

Greenwood, N. N., and Earnshaw, A., 1984. *Chemistry of the Elements*. Oxford: Pergamon, p. 1542.

Hoefs, J., 2004. *Stable Isotope Geochemistry*. Berlin: Springer, p. 340.

Jouzel, J., et al., 1999. More Than 200 Meters of Lake Ice Above Subglacial Lake Vostok, Antarctica. *Science*, **286**(5447), 2138–2141.

Cross-references

Geochemistry of Snow and Ice

ISOTOPIC SIGNATURES

Bhishm Kumar
Hydrological Investigations Division, National Institute of Hydrology, Uttarakhand, India

Synonyms

Isotopic fingerprinting

Definition

An isotopic signature (also isotopic fingerprint) is a ratio of stable or unstable isotopes of particular elements found in an investigated material. The atomic mass of different isotopes affects their chemical kinetic behavior, leading to natural isotopic separation process.

Expression

Stable isotope ratios are normally reported as δ values in units of parts per thousand (denoted as ‰, i.e., per mill) relative to a standard of known composition.

$$\delta = \left(R_{\text{sample}} - R_{\text{reference}}\right)/R_{\text{reference}}$$

where R's are the ratios of the $^{18}O/^{16}O$ and D/H isotopes in case of water.

The difference between samples and references are usually quite small, δ values are, therefore, expressed in per mille differences (‰), that is, per thousand, δ(‰) = δ × 1,000.

$$\delta(‰) = [(R_s - R_r)/R_r] \times 10^3 = [(R_s/R_r) - 1] \times 10^3$$

If δ value is positive, it refers to the enrichment of the sample in the heavy-isotope species with respect to the reference whereas negative value corresponds to the sample depleted in the heavy-isotope species. The reference standards normally considered are SMOW (Standard Mean Oceanic Water) and VSMOW (Vienna Standard Mean Ocean Water).

Bibliography

Clark, I., and Fritz, P., 1997. *Environmental Isotopes in Hydrogeology*. Boca Raton, New York: Lewis.

K

KAME AND KETTLE TOPOGRAPHY

Amit Kumar
Department of Geology, Centre of Advanced Study in Geology, Panjab University, Chandigarh, India

Definition

A kame is a stratified geomorphologic feature which is created by deposition action of glacier meltwater, an irregularly shaped hill or mound composed of sand, gravel, and till, commonly associated with end moraine. A kame may occur as an isolated hill but in general each kame is one mound in a low-lying terrain of many hummocks, terraces, ridges, and hollows. Kames are often associated with kettle holes. Kettles are depressions in the outwash plains, which formed due to the melting of large ice blocks and this is referred to as kame and kettle topography. Kame and kettle topography is an indicator of a high-discharge supraglacial and englacial drainage system of a glacier in the final stages of melt, and large quantities of glacially derived debris associated with meltwater.

Origin

Glacier meltwater that exists in the ablation area of glaciers during the melting season flows down on the glacier surface, in the ice, or on the bedrock, making complex systems of drainage channels. Deformation of ice, movement of glacier, freezing, and melting processes influence on the position and form of channels. Meltwater escapes through numerous small and temporary streams. These streams carry sediments for longer distances and deposit them in various forms. Sometimes, these streams also carry some ice. Thus, the deposition of sediments after the ablation (melting of glacier) is called glaciofluvial deposits and the landforms resulting from such deposits are called glaciofluvial landforms. The sediments are deposited in the form of low alluvial fans (if deposited on land) or deltas (if deposited in standing water).The glaciofluvial landform include kame, kame terrace, kettle, kettle holes, outwash plains, etc.

Bibliography

Benn, D. I., and Evans, D. J. A., 1998. *Glaciers and Glaciation*. London: Arnold.
Hambrey, M., and Alean, J., 2004. *Glaciers*, 2nd edn. Cambridge: Cambridge University Press.

Cross-references

Glaciofluvial
Glaciogenic Deposits

KATABATIC WIND: IN RELATION WITH SNOW AND GLACIERS

Amit Kumar
Centre of Advanced Study in Geology, Department of Geology, Panjab University, Chandigarh, India

Synonyms

Drainage wind; Fall winds; Piteraq and williwaw

Definition

Katabatic wind (Greek: *katabaino* – to go down) is the common name for downslope winds flowing from high elevations of mountains, plateaus, and glacier down their slopes to the valleys or planes underneath. Such winds are sometimes also called fall winds. Particularly, it is a wind that carries high density air from a higher elevation down a slope under the force of gravity. This occurs on the largest scale as the outflowing winds from Greenland and Antarctica. In Greenland these winds are called Piteraq

Vijay P. Singh, Pratap Singh & Umesh K. Haritashya (eds.), *Encyclopedia of Snow, Ice and Glaciers*, DOI 10.1007/978-90-481-2642-2,

and in South America as well as in Alaska, it is wind known as a Williwaw.

Alpine valleys produce their own local wind systems as a result of thermal differences. The cold air slides down the slope under gravity during night. The radiative cooling of the ground surface under clear and calm conditions during night provides colder air near the surface. The nighttime downslope movement of the colder air is referred to as katabatic winds. The anabatic wind is developed prior to the daytime, whereas katabatic drainage is developed in the night. The katabatic winds usually flow gently downslope with low speed, but greater speeds are also experienced when the depth of cold air is large and the slope is higher.

Bibliography

Benn, D. I., and Evans, D. J. A., 1998. *Glaciers and Glaciation*. London: Arnold.

Bennett, M. R., and Glasser, N. F., 1996. *Glacial Geology: Ice Sheets and Landforms*. Chichester: Wiley.

Colbeck, S., 1980. *Dynamics of Snow and Ice Masses*. London: Academic.

Defant, F., 1949. Zur Theorie der Hangwinde, nebst Bemerkungen zur Theorie der Berg- und Talwinde. (On the theory of slope winds, along with remarks on the theory of mountain and valley winds.). *Archiv für Meteorologie Geophysik und Bioklimatologie*, **A1**, 421–450.

Singh, P., and Singh, V. P., 2001. *Snow and Glacier Hydrology*. Dordrecht: Kluwer.

KILIMANJARO

Douglas R. Hardy
Climate System Research Center and Department of Geosciences, University of Massachusetts, Morrill Science Center, Amherst, MA, USA

Definition

Kilimanjaro is Africa's highest mountain (5,895 m), located in northern Tanzania just south of the Kenya border (3°4′S; 37°21′E). At the seasonally snow-covered summit, the extent of glacier ice is now less than 2 km^2, roughly half of that remaining on the continent.

Overview

The cryosphere is sparsely represented in Africa, primarily on a small handful of the continent's highest mountains. Among these is Kilimanjaro, the "white roof of Africa," whose glaciers have achieved notoriety far out of proportion to their size (miniscule), importance as a water resource (negligible), or potential contribution to sea-level rise (zero). Yet, Kilimanjaro's summit mantle of *Snow* (qv) and *Ice* (qv) is starkly beautiful, and thus among the mountain's most fascinating, distinctive, and best-known attributes. Thousands of international visitors are attracted annually, bringing valuable tourism revenue to Tanzania.

Geographic setting

Kilimanjaro is a massive, dormant volcano in Tanzania, built up of both lava flows and pyroclastic material, situated roughly equidistant (~300 km) south of the Equator and west of the Indian Ocean. Three primary volcanic centers are thought to have been active sequentially since the Pleistocene, which together form the Kilimanjaro massif: Shira (4,005 m), Mawenzi (5,140 m), and Kibo (5,895 m). At the apex of Kibo is a relatively flat caldera measuring 1.9 by 2.7 km (Figure 1); Uhuru Peak is the highest point along the southern scarp, ~180 m above the caldera floor.

History of cryospheric research on Kilimanjaro

The earliest scientific discussion of snow and ice on Kilimanjaro began with the initial European "discovery" of the snowcap by Johannes Rebmann in 1848. English Geographers were incredulous, and dismissed Rebmann's report for more than a decade (Meyer, 1891). Hans Meyer climbed nearly to the crater rim in 1887, reaching the summit 2 years later on 6 October 1889 (Meyer, 1891). Additional European scientists soon reached the summit area and published their qualitative findings. Logistical constraints rendered ascents and fieldwork considerably more difficult than at present, yet virtually every account describes features and processes not unlike those of today. Most also discuss the decreasing extent of ice, and many predict disappearance – within decades – of either individual glaciers or all of the mountain's ice.

Mid-twentieth-century perspectives on Kibo's summit and slope glaciers were provided by Humphries (1959), Downie and Wilkinson (1972), and Hastenrath (1984). Henry Osmaston (1989) then published an analysis of glacier *Moraine* (qv) as mapped from aerial photographs, which for the first time quantified the nineteenth century extent of glaciers on the mountain. Hastenrath and Greischar (1997) built upon Osmaston's work and provided the first cartographic documentation of ice recession. Thereafter, a resurgence of research on Kibo began in February 2000 with *Ice Core* (qv) drilling, aerial photography, and installation of an automated weather station (AWS) on the Northern Icefield (Hardy, 2002; Thompson et al., 2002). A *Network of Stakes* (qv) has expanded steadily since 2000 to represent most of the glacierized area at the summit, and two additional AWS are now operating on summit glaciers (Mölg et al., 2008).

Today, as during the nineteenth century, snow and ice on Kilimanjaro are again controversial. A new ice-extent map released in 2001 was accompanied by a prediction that the glaciers could disappear within 20 years (Irion, 2001). Kilimanjaro was quickly employed to symbolize the impacts of global warming (e.g., Greenpeace, 2001). However, cautious statements by scientists such as Kaser et al. (2004, p. 337) that ". . . mass loss on the summit . . . is little affected by air temperature," or Mote and Kaser (2007, p. 325) that ". . . loss of ice on Mount Kilimanjaro cannot be used as proof of global warming," were eagerly

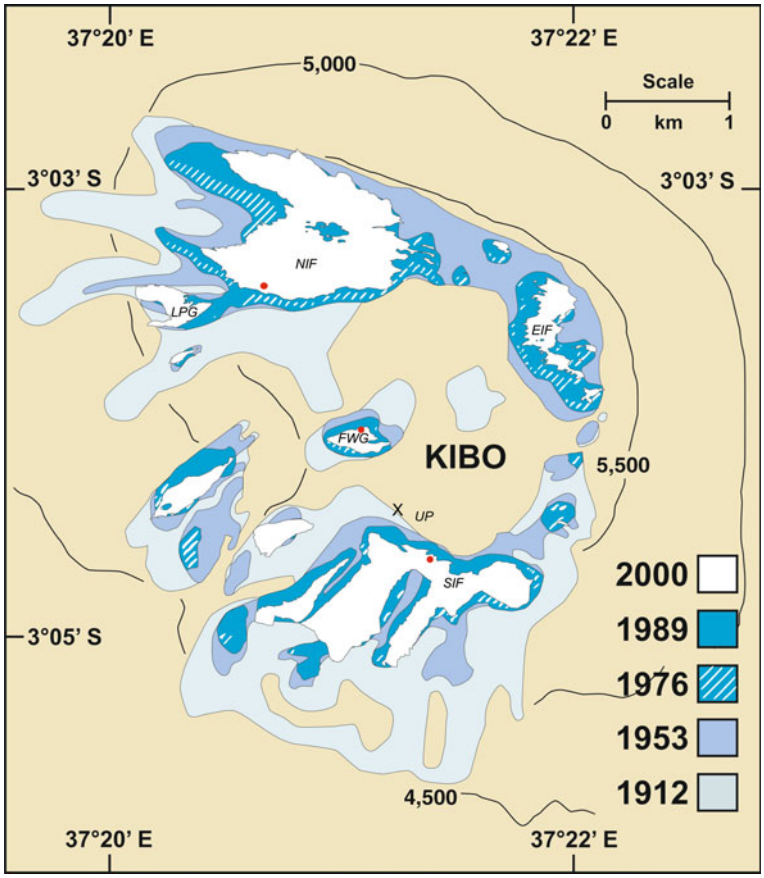

Kilimanjaro, Figure 1 Kibo peak of Kilimanjaro, with remnants of the *ice cap* (qv) that once encircled the summit. The crater is the area surrounded by ice and labeled "KIBO." Contours are in meters. Solid circle symbols indicate location of 2000 ice-core drilling sites (Thompson et al., 2002), and the ice extent is shown for five epochs (1912–1989 after Hastenrath and Greischar (1997), 2000 after Thompsen et al. (2002)). NIF, EIF, and SIF are the former Northern, Eastern, and Southern Ice Fields (respectively), *FWG* Furtwängler Glacier, *UP* Uhuru Peak (5,895 m), and *LPG* Little Penck Glacier. Automated weather stations currently operate near the NIF and SIF drill sites.

embraced by those seeking to cast doubts about global warming (e.g., GES, 2004). Resolution of the modern-time controversy awaits a comprehensive understanding of how Kilimanjaro's summit climate has been impacted by large-scale atmospheric circulation changes; this effort is well underway (Mölg et al., 2009; Thompson et al., 2009; Winkler et al., 2010).

Climate

Kilimanjaro rises 5,000 m above the surrounding plains, extending halfway through the tropical atmosphere to ~506 hPa. Climate varies dramatically and sharply with elevation, causing the mountain's dramatic ecological zonation. Whereas air temperature drops steadily and uniformly with elevation, the annual precipitation amount increases and then decreases with elevation. Southern and southwestern slopes reach a maximum annual total at ~2,200 m (Hemp, 2006), but northern slopes are drier (Coutts, 1969; Hemp, 2006). This precipitation pattern accounts in part for the asymmetrical distribution of glaciers on Kilimanjaro.

Precipitation at the summit annually totals only ~10% of that received by the forest below, and snow is the predominant form of precipitation at elevations above the mean annual freezing-level altitude, roughly 4,700 m (Hastenrath, 1984). Snowfall can occur at any time of year, but is primarily associated with northern Tanzania's two seasonally-wet periods, the November–December "short rains," and the "long rains" of March to May. Summit climate is thus best defined by seasonal humidity fluctuations, and by strong diurnal cycles driven largely by the tremendous daily fluctuation in incoming solar radiation; the following synopsis is based on AWS measurements made on the Northern Ice Field (NIF) since 2000 (Hardy, in prep.).

Summit climate is most stable through an extended dry season centered on July and August. This interval is

characterized by annual minima of humidity, snowfall, air temperature, and wind speed, and by increasing solar irradiance after the solstice minima.

By the middle of September, the beginning of an important seasonal change is marked by rapidly increasing wind speed, and an increase in air temperature. Solar irradiance gradually reaches an annual maximum as the sun moves into the southern hemisphere. Humidity increases slowly during September, rapidly into October, and continues climbing steadily into December. The "short rains" typically begin in mid-October, although the timing and magnitude vary from year to year – with important implications for glacier mass balance. For example, September and October (and even November) can be a time of considerable ablation (e.g., Hardy, 2003), when net solar irradiance remains high in the absence of snowfall, accompanied by increasing turbulent energy transfer as wind speed, air temperature, and humidity are increasing.

By mid-January the short rains are usually ending, with both humidity and snowfall dropping quickly to early February minima and a brief secondary dry period. The long rains then typically begin in early March, with humidity and snowfall continue increasing into April, and snow accumulation typically continues into May. Then, air temperature decreases rapidly, wind direction backs slightly from east toward north, and humidity drops drastically. By June, another dry season is beginning.

Mean annual temperature at the summit is approximately −7°C, with monthly means ranging only 1.3°C. On the NIF, daily temperature ranges between an average low of −9° and an average maximum of −4°C. Thus, air temperature on the glaciers is consistently below freezing; extreme radiational cooling at night brings surfaces temperatures below −15°C (to −27°), so a considerable cold content must be overcome each day before ablation of the snow or ice surface can occur.

Kilimanjaro glaciers

Currently, there are roughly eight glaciers on Kibo, some distinct and some in clusters as formerly larger bodies break up (Figure 1). These are all remnants of a once tenfold larger *ice cap* (*Ice Caps* qv) that encircled the volcano's summit in the mid-nineteenth century, filling at least portions of the crater itself while also spilling outward and down the slopes. The areal extent of this earlier ice cap – likely the maximum *Holocene* (*Holocene Glacier Fluctuations* qv) extent – was 20 km^2, as determined by mapping moraines (Osmaston, 1989). Subsequent ice recession through the twentieth century was "dramatic and monotonic" (Hastenrath and Greischar, 1997, p. 459), based on four area determinations averaging 26 years apart and with unknown errors; updated maps show continuing retreat (Figure 1; Thompson et al., 2002; Cullen et al., 2006; Thompson et al., 2009).

By the beginning of the twentieth century, many of the ice cap's broad lobes had been named after early explorers (see Hastenrath, 1984 for list). These names remain in use, despite morphological changes. On the south-facing slope below the crater's sharp southern rim, a Southern Ice Field has encompassed what are now or will soon be separate entities, the Heim, Kersten, Decken, and Rebmann Glaciers. Within the crater, the Furtwängler Glacier has been the only ice entity for several decades, splitting into two parts by 2007. Straddling the crater rim's north side, the Northern Ice Field (NIF) comprised slightly more than half of Kibo's total ice area until the 1970s, when an Eastern Ice Field (EIF) became distinct. Although the EIF has since broken into numerous entities, the NIF remains Kibo's largest body of ice. Extending down north- and northwest-facing slopes below the NIF are what remains of the Credner, Drygalski, and Great Penck Glaciers. The Little Penck Glacier, prominently visible today from western ascent routes, separated from the NIF during the 1990s (Figure 1) and has considerably decreased in area since 2000.

All ice masses on Kibo are here termed glaciers for discussion purposes, although most ice is now static and some entities are just tiny fragments. Ice thickness is poorly known due to limited measurements, with a probable maximum of ∼50 m for the Northern Ice Field.

Little was known of energy and mass balance details on Kibo's glaciers until 2000, other than that the total ice area had been decreasing for over a century. However, early observations were astute; Geilinger (1936, p. 9), for example, recognized that glaciers on the outer slopes and those of the crater behaved differently "... with regard to the melting process." Building upon this distinction, Kaser et al. (2004) subdivided summit glaciers into (1) horizontal glacier surfaces, the typical glacier regime studied; (2) slope glaciers; (3) near-vertical margins; and (4) basal surfaces.

Horizontal glacier surfaces

Most glaciers on Kibo's summit have horizontal or nearly horizontal upper surfaces, unbroken by crevasses. At times the surfaces are flat and smooth, but this changes from year to year. On a whole-glacier scale, the surfaces are often comprised of "massive steplike features" (Gillman, 1923, p. 17); at smaller scales one sometimes sees "fantastic ice-shapes" (Sampson, 1965, p. 121) or ice "honeycombed in many places to a depth of over 6 ft, and weathered into countless grooves and ruts and pointed spikes" (Meyer, 1891, p. 147; see also Figure 2). Since 2000 this regime has been the focus of measurements and modeling (e.g., Mölg and Hardy, 2004; Mölg et al., 2008), and is today the best known of the four regimes. Mass balance here governs glacier thickness, and balance fluctuations are largely independent of ice area, in the absence of flow. Although details of mass exchange at this surface remained unknown until 2000, historical accounts suggest that twentieth century ice thickness probably never averaged more than about twice that of today.

Kilimanjaro, Figure 2 Three views of Kibo summit glaciers, taken: (**a**) September 28, 2008, (**b**) January 30, 2009, and (**c**) October 7, 2007. Note fluting of vertical walls (**a**, **b**) and horizontal-surface penitentes (bottom of image **a**, **c**). For scale, note people in image (**b**) and ablation stake at ice surface in image (**c**) (~0.5 m visible; upper right-hand corner of image).

Horizontal and slope glacier surfaces on Kibo are typically comprised of hard glacier ice, appearing and behaving as expected for ablation-zone ice of density approaching 900 kg/m^3. A thin mantle of *Seasonal Snow Cover* (qv) blankets the ice during most wet seasons. Snow – or snow transitioning to superimposed ice – persists from one wet season to the next when snowfall is above average.

In the current climate at Kibo's summit, the horizontal surface, multiyear mass balance is negative – and the glaciers are thinning (Figure 3). Indeed, the hypothetical ELA has probably been above summit-level for some time (Humphries, 1959; Kaser and Osmaston, 2002). Nonetheless, speculation continues as to whether the ELA might be lower on the south slopes (e.g., Kaser and Osmaston, 2002; Mölg et al., 2009), despite little evidence.

Mass loss on horizontal surfaces is resulting from a predominance of negative energy balance, due to net radiation receipt as controlled by *Albedo* (qv; Mölg and Hardy, 2004; Mölg et al., 2008). Field measurements of mass balance support these modeling results. Mass is being lost from surfaces through both *sublimation* (*Sublimation from Snow and Ice* qv) and *melting* (*Melting Processes* qv); for a 1-year period March 2001 through February 2002, sublimation accounted for 86% of mass loss at the NIF AWS site. Yet, some areas clearly experience a higher proportion of melting, as a high degree of both spatial and temporal variability exists in surface characteristics and processes (Figure 3). Accordingly, simple generalizations based on point-scale modeling (e.g., Mote and Kaser, 2007) are questionable.

One important suggestion of recent field measurements is that the rate of mass loss from horizontal surfaces may be increasing (Thompson et al., 2009), even without a demonstrable change in forcing. Continuing ablation is concentrating particulate matter (i.e., dust) on an increasingly older surface, decreasing albedo and thus increasing net radiation receipt and accelerating ablation. Indeed, in the vicinity of the NIF weather station and *Ice Core* (qv) sites, the glacier surface is almost certainly older than 57 years, a figure based on ^{36}Cl measurements in the ice cores (Thompson et al., 2002). More recent ^{14}C-dating of organic material indicates that the surface could be over 300 years old (D. Hardy, 2004, 2009), although it is unlikely that the surface age is uniform, given the considerable spatial variability in accumulation and ablation patterns (e.g., Figure 3).

Understanding horizontal-surface processes and mass balance is important, because these control what is revealed by ice cores penetrating through layers of accumulation, and previously exposed ablation surfaces. Six cores were drilled on Kibo through three different ice entities (see Figure 1). In the absence of reliable ^{14}C dates from the core, the resulting chronology was developed – necessarily – by assuming an invariant accumulation rate

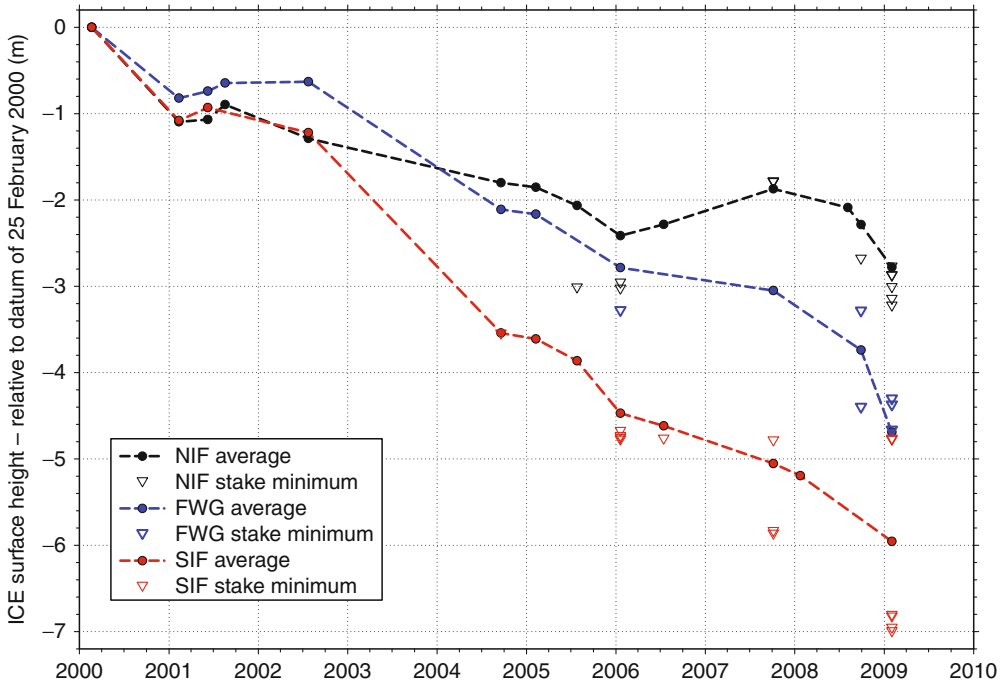

Kilimanjaro, Figure 3 Ice surface height change on three Kibo summit glaciers, from measurements at mass balance stakes. In general, only one stake per glacier was monitored through 2004, and 3–19 stakes each subsequently; average values shown. Triangles symbolize minimum height change at individual stakes that ablated out and fell over between measurements (values were used in averages). Punctuating the overall thinning trend are intervals of positive mass balance due to superimposed ice formation. Resolution of height fluctuations between these discrete stake measurements is not possible.

(Thompson et al., 2002). This record, however uncertain (e.g., Gasse, 2002; Kaser et al., 2010), will endure until an alternative chronology is provided by better dating.

Slope glaciers

Glaciers currently extend down from Kibo's crater rim in only a few cases (Figure 1). These include the Kersten and Decken Glaciers on the south side, along with the Rebmann Glacier to a minor extent, all inclined at 30–40° and all remnants of the former Southern Ice Field. The Credner Glacier still extends down the northwest flank. Additional glaciers and small ice bodies remain on the slopes but are no longer connected to ice at the crater rim. These include the Heim and Great Barranco Glaciers on the southwest flank, and the Little Penck remnant on the west side. Even by the mid-1930s, Geilinger (1936, p. 12) referred to such ice as "... independent dead glaciers of the outer slopes."

At their late-nineteenth century maximal extent, revealed by moraines, slope glaciers extended down as low as 4,400 m (Osmaston, 1989), and as recently as 1971 there were seven tongues reaching below 4,870 m (Messerli, 1980). Today, glacier ice is scarce below 5,000 m, likely with an increasing proportion buried under a mantle of debris (Humphries, 1959; Downie and Wilkinson, 1972; Young and Hastenrath, 1991; Kaser et al., 2004).

To an even greater extent than for horizontal ice surfaces at the summit, some slope glacier surfaces are today quite dirty, due to deposition of wind-blown dust (e.g., Figure 2c). This inorganic matter is being concentrated, due to a prolonged period of negative mass balance, and is accelerating mass loss by changing the energy balance.

Slope glacier meteorological measurements begun in 2005 have allowed energy balance modeling for these surfaces. To date, energy and mass balance characteristics appear similar to those on the NIF horizontal surface, with even a slightly higher proportion of mass loss to sublimation (Mölg et al., 2008).

Near-vertical ice margins

Vertical or near-vertical margins are a special characteristic of Kilimanjaro's summit glaciers (Figure 2; Winkler et al., 2010). Typically, the vertical surfaces are fluted, and "sometimes slightly undercut at the base" (Downie and Wilkinson, 1972, p. 40). Such margins have been reported since the earliest observations (e.g., Meyer, 1891; Gillman, 1923).

Ablation at the vertical margins is driving the areal recession revealed by mapping (e.g., Hastenrath and Greischar, 1997). Although ice retreat is probably the best-documented environmental change occurring high on the mountain, our understanding of vertical-wall ablation processes remains incomplete, despite the important

contribution of Mölg et al. (2003) confirming early speculation that retreat is governed by energy from direct solar radiation (e.g., Geilinger, 1936). Melting is the primary mechanism by which vertical walls retreat (lose mass), and measurements confirm that the ice temperature often reaches 0°C during the day when seasonally irradiated (Winkler et al., 2010). In addition, collapse features (calving) can be observed around most summit glacier margins, and must also be considered a mechanism of vertical margin ablation, as speculated by Downie and Wilkinson (1972).

Vertical ice exposures on Kibo nicely illustrate stratification, or the sedimentary banding associated with accumulation over time, and these can often be traced laterally for considerable distances. Notably, especially from the perspective of ice-core interpretation, some bands appear to represent buried surfaces that suggest a break in snow accumulation (i.e., missing time intervals), or at which ". . .there appears to have been marked erosion of the ice surface before further accumulations of snow" (Humphries, 1959, p. 477). Such unconformities are sometimes marked by dirt bands, which Downie and Wilkinson (1972, p. 42) described as locally common but "almost nonexistent" on a larger scale. Especially at the upper end of the southern glaciers, unconformities sometimes illustrate an angular discordance with the overlying stratigraphy, a phenomenon awaiting explanation.

Basal surfaces

Kibo glaciers rest primarily on volcanic sand, and to a lesser extent on bedrock. During February 2000 ice-core drilling (Thompson et al., 2002), the NIF basal temperature was −0.4°C, and 0°C was measured within the SIF. The NIF 10-m-depth temperature of −1.2°C suggests that meltwater is transporting heat energy into the glacier, given the −7°C mean annual air temperature.

Little is known about the spatial variability and magnitude of geothermal heat flux on Kilimanjaro, especially relative to that beneath the glaciers. However, fumeroles are present within the inner crater, and even prior to their first observation by W.H. Tilman in 1933, Jäger (1909), Gillman (1923), and Geilinger (1936) all speculated that volcanic heat might be influencing ice recession. Local-scale glacier impacts, apparently due to steam venting, have been observed and reported (e.g., Kaser et al., 2004).

Kilimanjaro snow

Snow on Kibo is ephemeral, meaning that within a relatively short period of time (i.e., minutes to months) it either ablates and disappears, or is transformed into glacier ice. Here, the term snow refers exclusively to solid precipitation, or that which has accumulated as snow cover on either glacier or crater surfaces. Although glaciers are a perennial and long-term feature of Kilimanjaro, snow cover is not – and the historical literature indicates that snow has always come and gone at high frequency (∼annual).

Few early explorers or mountaineers made snow depth measurements, but a seasonal absence of snow has been noted since the first observations. For example, Meyer (1891, p. 316) remarked that in October ". . .when all the snowfields had disappeared, there was likewise comparatively little snow to be met with on the ice-cap." Sampson (1965, p. 123) wrote that from August to October "the chances of finding any snow patches. . . are very poor at heights over ∼4,000 m." Additional evidence for the seasonal absence of snow in the past comes from historical photographs, which cannot easily quantify snow depth but nicely document times when snow is absent.

Snowfall events can be brief, such as those associated with afternoon convection (e.g., graupel), or can persist for multiple days. Wet-season events are typically of longer duration and yield the greatest accumulation. Within the past decade, seasonal snow accumulation on the glaciers of ∼1 m has been noted at least twice (early in 2001, 2007; D. Hardy, 2004, 2009), with lesser accumulations on unglacierized portions of the crater. Anecdotal accounts from guides suggest that snowfall magnitude has diminished in recent decades, although no reliable long-term station data for precipitation exist from above ∼1,800 m on Kibo. The greatest documented accumulation is that reported for the 1961–1962 combined wet seasons, involving "snowfall of over six feet," much of which ". . .was still present more than a year later" (Segal, 1965, p. 126). The extent to which this interval was unusual remains unknown, as summit visitation is much less frequent during the wet seasons.

Once deposited, ablation of snow cover from glacier and crater surfaces involves both melting and sublimation, based on observations and energy balance modeling (Mölg and Hardy, 2004; Kaser et al., 2004; Mölg et al., 2008, 2009). Of these two processes, melting is the more readily observable, both on and off the glaciers. Although sometimes difficult to distinguish from ice melt, evidence for snowmelt includes icicles, supraglacial meltwater ponds, areas of thin, water-saturated snow, and rarely, meltwater runoff. Melting at the summit is not a recent development, for Humphries (1959, p. 477) observed "melting ice and pools of melt water at the summit during the day." Sublimation of snow is often indicated by the presence of penitentes (Figure 2a, c), which form over both ice and crater surfaces in the intense radiation environment on Kibo (cf. Lliboutry, 1954). With fully developed penitentes, melting ice or wet crater sand may be present between the spikes. Although present recently in sufficient density and height to impede glacier travel, penitentes are transient features, today and in the past. Gillman (1923, p. 18) for example, did "not come across penitents" on his single trip to the summit, yet their presence in 1929 was noted by Geilinger (1936). As with other aspects of the cryosphere on Kibo, spatial and temporal variability render generalizations difficult.

Lastly, recent research highlights the extreme sensitivity of horizontal glacier surfaces to the variability of snowfall frequency and amount. By governing albedo

variability, and thus net receipt of solar radiation, snowfall has emerged as the key atmospheric variable controlling ablation and mass balance (Hardy, 2003; Mölg and Hardy, 2004; Mölg et al., 2008, 2009). Figure 3 illustrates that the system is especially sensitive to the interannual variability of snowfall during the short rains (November–December).

Summary

Currently, there are ~8 distinct ice entities on Kibo, together covering a total area of less than 2 km^2 and all remnants of a once larger ice cap. The summit glaciers are relatively flat, with near-vertical margins, and the slope glaciers today are concentrated on the mountain's southwest- and northwest-facing flanks. Glaciers on Kilimanjaro are a product of climatic conditions at the summit that no longer exist, as no area of accumulation has existed for many decades and perhaps since the current recession began. Today, as in the past, snow cover on the mountain is seasonal and subject to considerable interannual variability. Measurements and modeling in recent years have demonstrated that the mass and energy balances on horizontal ice surfaces are very sensitive to the magnitude and frequency of snowfall events – perhaps increasingly so as dirt concentration increases on exposed, ablating ice surfaces.

Acknowledgments

This material is based upon work supported by the National Science Foundation (NSF), and NOAA Office of Global Programs, Climate Change Data and Detection Program, under Grant No. 0402557, and NSF ATM-9909201 (Paleoclimate Program) to the University of Massachusetts. Additional support was provided by NOAA U.S. Global Climate Observing System.

Bibliography

Coutts, H. H., 1969. Rainfall in the Kilimanjaro area. *Weather*, **24**, 66–69.

Cullen, N. J., Mölg, T., Kaser, G., Hussein, K., Steffen, K., and Hardy, D. R., 2006. Kilimanjaro glaciers: recent areal extent from satellite data and new interpretation of observed 20th century retreat rates. *Geophysical Research Letters*, **33**, L16502, doi:10.1029/2006GL027084.

Downie, C., and Wilkinson, P., 1972. *The Geology of Kilimanjaro*. Sheffield: Geology Deparment, University of Sheffield.

Gasse, F., 2002. Kilimanjaro's secrets revealed. *Science*, **298**, 548–549.

Geilinger, W., 1936. The retreat of the Kilimanjaro glaciers. *Tanganyika Notes and Records*, **2**, 7–20.

Gillman, C., 1923. An ascent of Kilimanjaro. *Geographical Journal*, **61**, 1–27.

Greening Earth Society, 2004. Snow fooling. Newsletter of 7 March 2004. Available from http://www.worldclimatereport.com/index.php/2004/03/07/snow-fooling/, accessed 27 April 2009.

Greenpeace, 2001. Press release: "Kilimanjaro set to lose its ice field by 2015 due to climate change." Availbale from http://archive.greenpeace.org/pressreleases/climate/2001nov6.html, accessed 27 April 2009.

Hardy, D. R., 2002. Eternal ice and snow? In Salkeld, A. (ed.), *Kilimanjaro: To the Roof of Africa*. Tampa: National Geographic Society, pp. 224–225.

Hardy, D. R., 2003. Kilimanjaro snow. In Waple, A. M., and Lawrimore, J. H. (eds.), *State of the Climate in 2002*. Boston: Bulletin of the American Meteorological Society, Vol. 84, p. S48.

Hastenrath, S., 1984. *The Glaciers of Equatorial East Africa*. Dordrecht: D. Reidel Publishing Company.

Hastenrath, S., and Greischar, L., 1997. Glacier recession on Kilimanjaro, East Africa, 1912–1989. *Journal of Glaciology*, **43**, 455–459.

Hemp, A., 2006. Vegetation of Kilimanjaro: hidden endemics and missing bamboo. *African Journal of Ecology*, **44**, 305–328.

Humphries, D. W., 1959. Preliminary notes on the glaciology of Kilimanjaro. *Journal of Glaciology*, **3**, 475–479.

Irion, R., 2001. The melting snows of Kilimanjaro. *Science*, **291**, 1690–1691.

Jäger, F., 1909. Forschungen im den Hochregionen des Kilimandscharo. *Mitteilungen aus den Deutschen Schutzgebieten*, **22**, 113–197.

Kaser, G., and Osmaston, H., 2002. *Tropical Glaciers. International Hydrology Series*. Cambridge, UK: UNESCO/Cambridge University Press, 207p.

Kaser, G., Hardy, D. R., Mölg, T., Bradley, R. S., and Hyera, T. M., 2004. Modern glacier retreat on Kilimanjaro as evidence of climate change: observations and facts. *International Journal of Climatology*, **24**, 329–339, doi:10.1002/joc.1008.

Kaser, G., Mölg, T., Cullen, N. J., Hardy, D. R., and Winkler, M., 2010. Is the decline of ice on Kilimanjaro unprecedented in the Holocene? *The Holocene*, **20**, 1079–1091, doi:10.1177/0959683610369498.

Lliboutry, L., 1954. The origin of penitentes. *Journal of Glaciology*, **2**, 331–338.

Messerli, B., 1980. Mountain glaciers in the Mediterranean and in Africa. In *Proceedings of the Riederalp Workshop*, September 1978. IAHS-AISH Publ. no. 126, pp. 197–211.

Meyer, H., 1891. *Across East African glaciers*. London: George Philip & Son.

Mölg, T., and Hardy, D. R., 2004. Ablation and associated energy balance on a horizontal glacier surface on Kilimanjaro. *Journal of Geophysical Research-Atmospheres*, **109**, D16104, doi:10.1029/2003JD004338.

Mölg, T., Hardy, D. R., and Kaser, G., 2003. Solar-radiation-maintained glacier recession on Kilimanjaro drawn from combined ice-radiation geometry modeling. *Journal of Geophysical Research-Atmospheres*, **108**, 4731, doi:10.1029/2003JD003546.

Mölg, T., Cullen, N. J., Hardy, D. R., Kaser, G., and Klok, L., 2008. Mass balance of a slope glacier on Kilimanjaro and its sensitivity to climate. *International Journal of Climatology*, **28**, 881–892, doi:10.1002/joc.1589.

Mölg, T., Cullen, N. J., Hardy, D. R., Winkler, M., and Kaser, G., 2009. Quantifying climate change in the tropical mid troposphere over East Africa from glacier shrinkage on Kilimanjaro. *Journal of Climate*, **22**, 4162–4181.

Mote, P. W., and Kaser, G., 2007. The shrinking glaciers of Kilimanjaro: can global warming be blamed? *American Scientist*, **95**, 318–325.

Osmaston, H., 1989. Glaciers glaciations and equilibrium line altitudes on Kilimanjaro. In Mahaney, W. C. (ed.), *Quaternary and Environmental Research on East African Mountains*. Rotterdam: Balkema, pp. 7–30.

Sampson, D. N., 1965. The geology, volcanology, and glaciology of Kilimanjaro. *Tanganyika Notes and Records*, **64**, 118–124.

Segal, D., 1965. Expedition ramonage – ten days in the Crater of Kibo. *Tanganyika Notes and Records*, **64**, 125–130.

Thompson, L. G., Mosley-Thompson, E., Davis, M. E., Henderson, K. A., Brecher, H., Zagorodnov, V. S., Lin, P.-N., Mashiotta, T., Mikhalenko, V. N., Hardy, D. R., and Beer, J., 2002. Kilimanjaro ice core records: evidence of Holocene climate change in tropical Africa. *Science*, **298**, 589–593.

Thompson, L. G., Brecher, H. H., Mosley-Thompson, E., Hardy, D. R., and Mark, B. G., 2009. Glacier Loss on Kilimanjaro Continues Unabated. *Proceedings of the National Academy of Science*, **106**, 19770–19775, doi:10.1073/pnas.0906029106.

Winkler, M., Kaser, G., Cullen, N. J., Mölg, T., Hardy, D. R., and Tad Pfeffer, W., 2010. Land-based marginal ice cliffs: focus on Kilimanjaro. *Erdkunde*, **64**, 179–193, 10.3112/erdkunde.2010.02.05.

Young, J. A. T., and Hastenrath, S., 1991. Glaciers of Africa. Satellite image atlas of glaciers of the worlds: glaciers of the Middle East and Africa. US Geological Survey Professional Paper 1386-G-3. US Geological Survey, Washington: DC, pp G49–G70.

Cross-references

Albedo
Holocene Glacier Fluctuations
Ice
Ice Caps
Ice Core
Melting Processes
Moraine
Sublimation from Snow and Ice

KUNLUN MOUNTAINS

Jingshi Liu
Institute of Tibetan Plateau Research, Chinese Academy of Sciences, Haidian district, Beijing, China

Definition

Kunlun Mountains extend about 2,500 km from the Pamirs/China in the west to the Mount Yuzhu in Sichuan, China, in the east, and have an average elevation of 5,000 m. Their highest mount, Muztag, is 7,723 m. In this region there are 6,580 glaciers with a total area of 10,844 km^2, and an ice volume of 1,175 km^3, which corresponds to about 72% of the glacier area in the whole Kunlun (Liu, 2000). The West Kunlun Mountains lies in the western part of the Tibetan Plateau; the largest glaciers mostly 20–30 km long are distributed in the high mounts between Tianshuihai Pass and the southern Yurunkax River basin; and the alpine type glaciers are usually developed on the West Kunlun where the lands are severely cut and highly shadowed. Ice cap (flat-topped glacier), slope glaciers, and the valley glaciers are mainly developed on the south slope due to advantageous topographical and climatic conditions.

Introduction

Researchers have estimated increasing greenhouse gases which can cause change in regional temperature and precipitation. The change in climate may have affected the hydrological cycle, such as precipitation form, snow accumulation and meltwater, evapotranspiration, streamflow, and its recharge to groundwater as well (IPCC, 2007).

The landform of the southern Tarim basin is characterized by the three huge mountains: the Pamirs/China, the West Kunlun, and Karakoram Mountains; all rivers originate from the mountains and drain into their basins (Figure 1). Typical snow and glacier-fed rivers, the Hotan and Keriya, are from the glaciated center at the largest icecap, and Guliya from the West Kunlun flow into the Tarim basin.

The land surface on the upstream of the watersheds is characterized by snow and glacier cover and a little grassland, and on the downstream by Gobi and desert where rainfall seldom produces runoff due to strong evaporation except for storm rainfall. Since their upper streams are covered by a great number of glaciers and snowpacks where there is much precipitation in summer, stream flow occurs also in the summer (June–September), and there is a close linear relationship between summer flow and air temperature, as the former contributes 70–90% of stream water annually. With the rise in temperature and increase in rainfall, the maximum monthly runoff in July contributes about 30% of the annual runoff, and the minimum in February or March contributes only 1.2–1.8%. Eighty percent of their drainage areas are over an altitude of 3,000 m; it means streamflow is closed to the exchange between heat and water within the glacier system in the high mountains. Meanwhile, due to hot weather and rainy season in July and August annually, their combined role causes annual maximum floods. According to hydrological records, more than 90% of the maximum floods occur during the period of late July to early August.

The Hotan River basin is the largest basin in the west Tibet Plateau and includes parts of the Karakoram and the south territories of the Tarim basin in the west China. The basin covers an area of approximately 34,558 km^2, which encompasses a wide variety of climatic conditions, including the periglacial, the alpine permafrost, and desert zones. Glaciers, snow cover, and patterned ground features associated with continuous and discontinuous permafrost are found in the south, while agriculture and stock raising are important economic activities in the northern part. Figure 1 shows the features of permafrost regions in west China and in the Hotan River basin. The drainage area is located in the seasonal frozen ground and alpine permafrost region. The elevation ranges from 1,860 to 7,167 m with an average altitude of 4,200 m estimated by the DEM, and the low limit of alpine permafrost is about 4,400 m, thus approximately 45% of the basin lies within the continuous and discontinuous mountain permafrost zones (Zhou et al., 2000).

The Hotan River consists of two large subbasins: the Yurungkax in the east and the Karakax in west. There are a great number of glaciers in the upstream above 4,800 m, with a total area of 5,127.15 km^2 (Yang and An, 1990). Hydrometeorological records indicate a simple

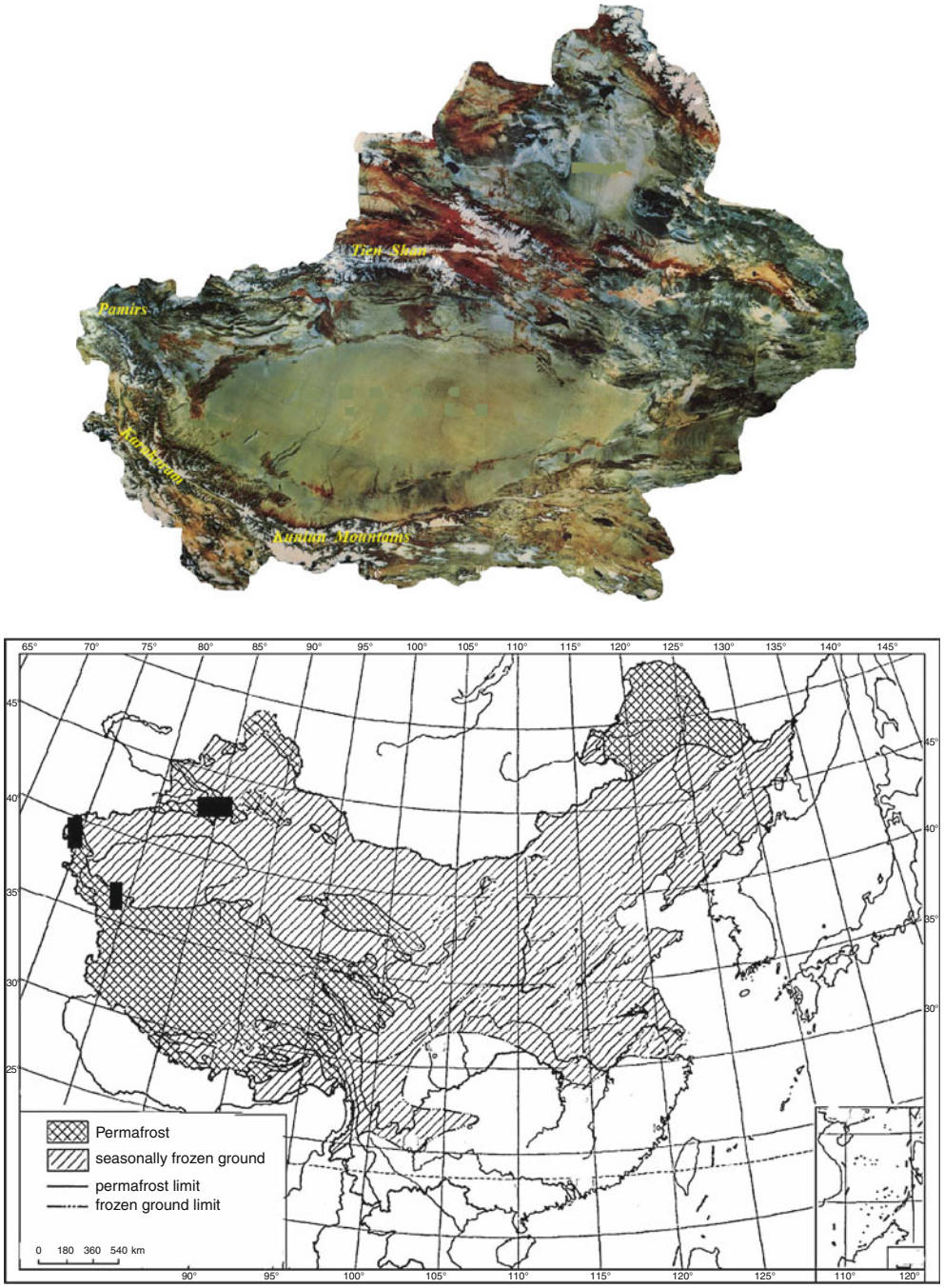

Kunlun Mountains, Figure 1 Snow and glacier distribution in the Kunlun Mountains (*top graph*) and Permafrost regions in the west China (*bottom graph*).

pattern of streamflow under an extreme continental climate. During mild and rainy summer, weather is influenced by the westerlies, the streamflow from snow and glacier meltwater is the main supply to the oasis. The precipitation distribution in the mountains is extremely heterogeneous ranging from 70 mm in the valleys to 350 mm of the glaciated areas up to 5,800 m (Nakawo et al., 1990). The annual mean air temperature at 1,860 m is 7.9°C, the estimated annual air temperature over the alpine permafrost is below −2.7°C, and ranges from −5.6°C to −14.6°C according to a lapse rate of air temperature with −0.75°C/100 m in cold season from

observations for 6 years along an eastern neighboring valley (Abe and Wang, 2004).

The ablation period of the glacier is about 120 days from June to September according to an investigation on the glacier Gozha (5,200 m) in the headwaters, and shorter and shorter eastward due to higher glacier terminus (Cao and Aseit, 1992). The seasonal distribution of runoff, therefore, is quite variable as recharged mainly by summer meltwater and the monsoonal rainfall accounting for about 80% of the annual runoff, and the maximum is 34% of the annual in July, and the minimum is only 0.95% in February (Liu et al., 1999).

In long and cold winter from October to March, periodic events of soil freeze and thaw frequently occur. Meanwhile snow cover exists from November to May and increases snow thickness in high mountains. The river in winter, therefore, drains into the recessive period recharged only by groundwater, which is greatly affected by the freeze–thaw cycle of both the seasonally frozen ground and the active layer of permafrost.

Glaciers in the West Kunlun develop at the elevation over 5,200 m. Only individual large glaciers can extend downward at a lower elevation below 4,800 m on a southern slope. The glacier coverage and meltwater contribution, being mainly hydrological index for such rivers recharged by meltwater in China, can reflect the role of meltwater and floods to streamflow.

Change in air temperature and precipitation

Climate in the West Kunlun indicates period of both cold and warm temperature (Figure 2). The annual and winter temperature has been consistently fluctuating from the mid-1950s to the mid-1980s, and then it shows an abrupt rise after the late 1980s, the annual average in two recent decades since 1987 is 0.8°C higher than that of the previous 40 years. The highest annual temperature during 53 years was recorded in 2006 and 1994. However, the rise in monthly temperature is nonuniform – the greatest rise in winter. The monthly temperature in December to February has increased about 1.8–1.9°C since the 1980s; whereas, the summer temperature since the 1950s has kept consistent, although it is warming since 1990s.

Precipitation during the 1950s–1970s had been gradually decreasing in the mountains; however, it has started increasing since the 1980s. The maximum precipitation has increased by 10–30% more than that for the previous 40 years, a little increase in at Keriya, the maximum before 1980, for example, was 188.5 mm (1963), now once exceeded 200 mm. Precipitation might have a more dramatic increase in the high mountains.

It is interesting to note that the annual and summer flow did not respond to the climate warming since the 1980s as above. River flow only in Keriya, however, indicated a little increase by 9% after 1985 with a delay of 5–6 years to the increasing precipitation, but meltwater in Hotan River still kept rather stable or decreased a little. It is not coincidental with favorable water and heat both for rainfall and meltwater runoff since the 1980s.

Winter streamflow

The change in winter streamflow is related to permafrost degradation in cold regions (Liu et al., 2003; Qin et al., 2005). Graphical and numerical analyses of winter monthly discharges are given in Figure 3, where winter streamflow during October to March showed a strongly upward trend since 1997, the monthly flow increased by 47.4%, 32.2%, 18.8%, 32.7%, 33.5%, and 31.5%, respectively. The remaining months generally did not exhibit any significant trend. For example, an insignificant number of trends were found for the summer flow from June to September. According to the detection of the change point for monthly temperature, there was a statistically significant upward year (change point) after 1986. For winter streamflow, a statistically significant upward year was observed since 1995, but the earliest one was in January 1985. Winter streamflow in all 6 months were much more sensitive than the seasonal air temperature; trend changes were found in 4 monthly discharges with a significance

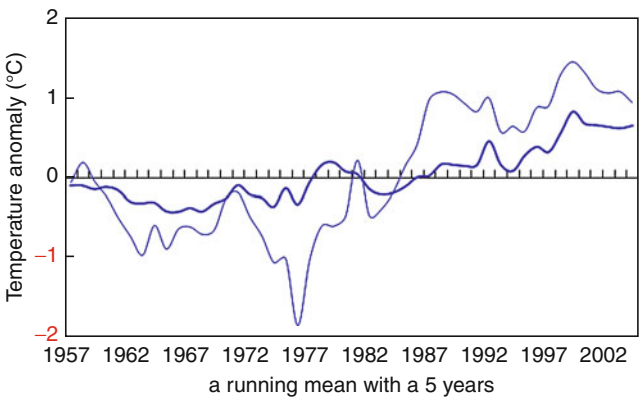

Kunlun Mountains, Figure 2 The annual (*bold line*) and winter (October–March) (*fine line*) air temperature at Yurungkax station in the west Kunlun.

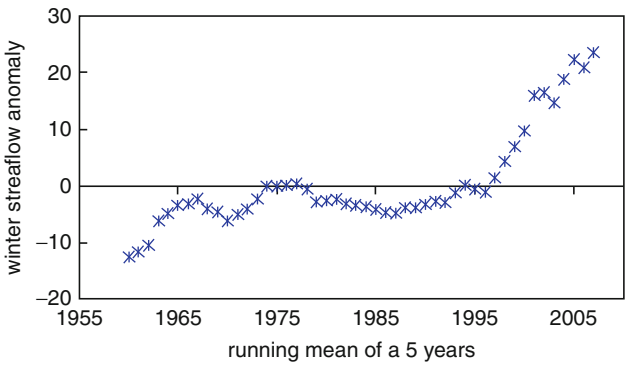

Kunlun Mountains, Figure 3 Increase in winter flow (October–March) of Hotan River in the west Kunlun.

level at 99%, the most sensitive with the maximum variability was in January discharge (Huang et al., 2008; Liu et al., 2009).

Summary

In the Kunlun Mountains, snow cover, glacier, and permafrost are the various reservoirs of water. The seasonal meltwater from this region supplies most important resources for the oasis life along the downstream area in the extremely arid desert basin, but the annual flood can cause loss of human life and property and eco-environment as well. From the point of the hydrological scale, the response to the climate fluctuations from snow and glacier-fed drainage basins with less glacier cover and in lower elevation seems to be more sensitive to the change in precipitation and air temperature than that with more glacier cover at higher elevations. The hydrological regime of these rivers in the Kunlun is developing in an advantageous direction in winter to the local economy and eco-environment of the oases.

Bibliography

Abe, O., and Wang, L., 2004. Meteorological characteristics in upstream regions of the Qira river, West Kunlun Mts., China. *Bulletin of Glaciological Research, Japanese Society of Snow and Ice*, **21**, 17–22.

Cao, Z. T., and Aseit, A., 1992. Runoff characteristics in Gozha glacier region on the southern slope of the West Kunlun, China. *Journal of Glaciology and Geocryology*, **15**(2), 156–161.

Huang, Y. Y., Liu, J. S., Shang, S. C., Ding, Y. J., and Liu, S. Y., 2008. Study on monthly runoff in winter, frozen earth and climate change in the Keriya river basin in the Kunlun mountains. *Arid Zone Research*, **25**(2), 174–178.

IPCC, 2007. Summary for policymakers. In Solomon, S., Qin, D., Manning, M., Chen, Z., Marquis, M., Averyt, K. B., Tignor, M., and Miller, H. L. (eds.), *Climate Change: The Physical Science Basis. Contribution of Working Group I to the Fourth Assessment Report of the Intergovernmental Panel on Climate Change*, Cambridge University Press, Cambridge, UK and New York.

Liu, C. H., 2000. *Qaidam inland drainage basin, Glacier inventory of China*. Beijing: Science Press.

Liu, J. S., Fukusima, Y., and Hiyama, T., 1999. Hydrological response of meltwater from glacier covered watersheds to the climatic change in the Northwest China. *IHAS Publication*, **256**, 193–207.

Liu, J. S., Hayakawa, N., Lu, M. J., Dong, S. H., and Yuan, J. Y., 2003. Winter streamflow, ground temperature and active-layer thickness in Northeast China. *Permafrost and Periglacial Processes*, **14**(1), 11–18.

Liu, J. S., Wei, W. S., Huang, Y. Y., and Shang, S. C., 2006. Hydrological response of winter stream- flow to climate change and permafrost degradation in Manas watershed, Tienshan Mts. *Journal of Glaciology and Geocryology*, **28**(5), 656–662.

Nakawo, M., Ageta, Y., and Han, J. K., 1990. Climatic information from Chongce ice cap, the West Kunlun, China. *Annals of Glaciology*, **14**, 205–207.

Qin, D. H., Chen, Y. Y., and Li, X. Y., 2005. *Climate and Environmental Changes in China*. Beijing: Science Press, pp. 104–181.

Yang, and An, 1990. *Hotan river basin, Tarim inland drainage basin, Glacier inventory of China*. Beijing: Science Press.

Zhou, Y. W., Guo, D. X., Qiu, G. Q., Cheng, G. D., and Li, S. D., 2000. *Geocryology in China*. Beijing: Science Press, pp.108–118.

L

LAKE ELLSWORTH

John Woodward[1], Martin J. Siegert[2], Andy M. Smith[3], Neil Ross[4]
[1]Division of Geography, School of Applied Sciences, Northumbria University, Newcastle upon Tyne, UK
[2]School of GeoSciences, University of Edinburgh, Grant Institute, Edinburgh, UK
[3]British Antarctic Survey, High Cross, Cambridge, UK
[4]School of Geosciences, University of Edinburgh, Geography Building, Edinburgh, UK

Introduction

Subglacial Lake Ellsworth is located near the Ellsworth Mountains in West Antarctica at 78.9°S 90.6°W. The lake basin is in the center of the West Antarctic Ice Sheet (WAIS) in the Pine Island Glacier drainage basin, 20 km from the ice divide with the Institute Ice Stream. The lake is approximately 15 km long and over 3 km across at its widest point. Seismic surveys have revealed that the lake is over 100 m deep in places. The ice sheet above the lake is between 2.9 and 3.3 km thick, with the lake surface over 1 km beneath present sea level within a distinct topographic hollow, ~1.5 km deeper than the surrounding subglacial bed. The basin is fjord-like in its topographic setting, and is one of a series of fjord-like over-deepenings on the western flank of the Ellsworth Subglacial Highlands.

This summary of our current knowledge will document the series of radio-echo sounding (RES) transects and field campaigns from which the lake has been identified. Basal thermal regime and ice-flow conditions, which are believed to control the lake will then be described. The final section will describe future plans for the exploration of Lake Ellsworth (Lake Ellsworth Consortium, 2007).

Radio-echo sounding data

Subglacial lakes can be identified on radio-echo sounding (RES) records. RES utilizes VHF radio-waves to measure the thickness of ice sheets and suggests the presence of subglacial lakes in three ways: (1) reflections from a water surface beneath the ice are at least an order of magnitude stronger than from ice-rock contacts; (2) reflections are of constant strength across the lake, rather than the more common variable strength that returns from bedrock; (3) the surface of a subglacial lake is smooth and flat compared with the rough surrounding topography. Using these criteria enables the identification of subglacial lakes and, where more than one RES transect is available, their surface extents to be measured. Two independent airborne and two ground-based RES campaigns have identified Lake Ellsworth:

1. The first knowledge of Lake Ellsworth is reported in Siegert et al. (2004), and is restricted to one RES line, acquired in 1977–1978 (Figure 1a and b). Later RES profiles (described below) suggest that the sounding line is near-parallel to the lake long-axis, and is also near parallel to ice flow over the lake. Preliminary modeling of the lake environment suggests that the mean gradient of the lake surface reflector is 0.02, about ~11 times the ice surface slope, suggesting the lake is in hydrostatic equilibrium with the overriding ice. The slope of the ice base across Lake Ellsworth is not entirely constant; being concave over the lake's upstream side and convex across its downstream side. In other words, the ice sheet "sags" as it flows onto the lake, and buckles against the sidewall as it re-grounds. The same features have been identified over Lake Vostok and are an expected characteristic of deep-water subglacial lakes. In the cases of both lakes, the strength of the reflections from the ice-water

Vijay P. Singh, Pratap Singh & Umesh K. Haritashya (eds.), *Encyclopedia of Snow, Ice and Glaciers*, DOI 10.1007/978-90-481-2642-2,

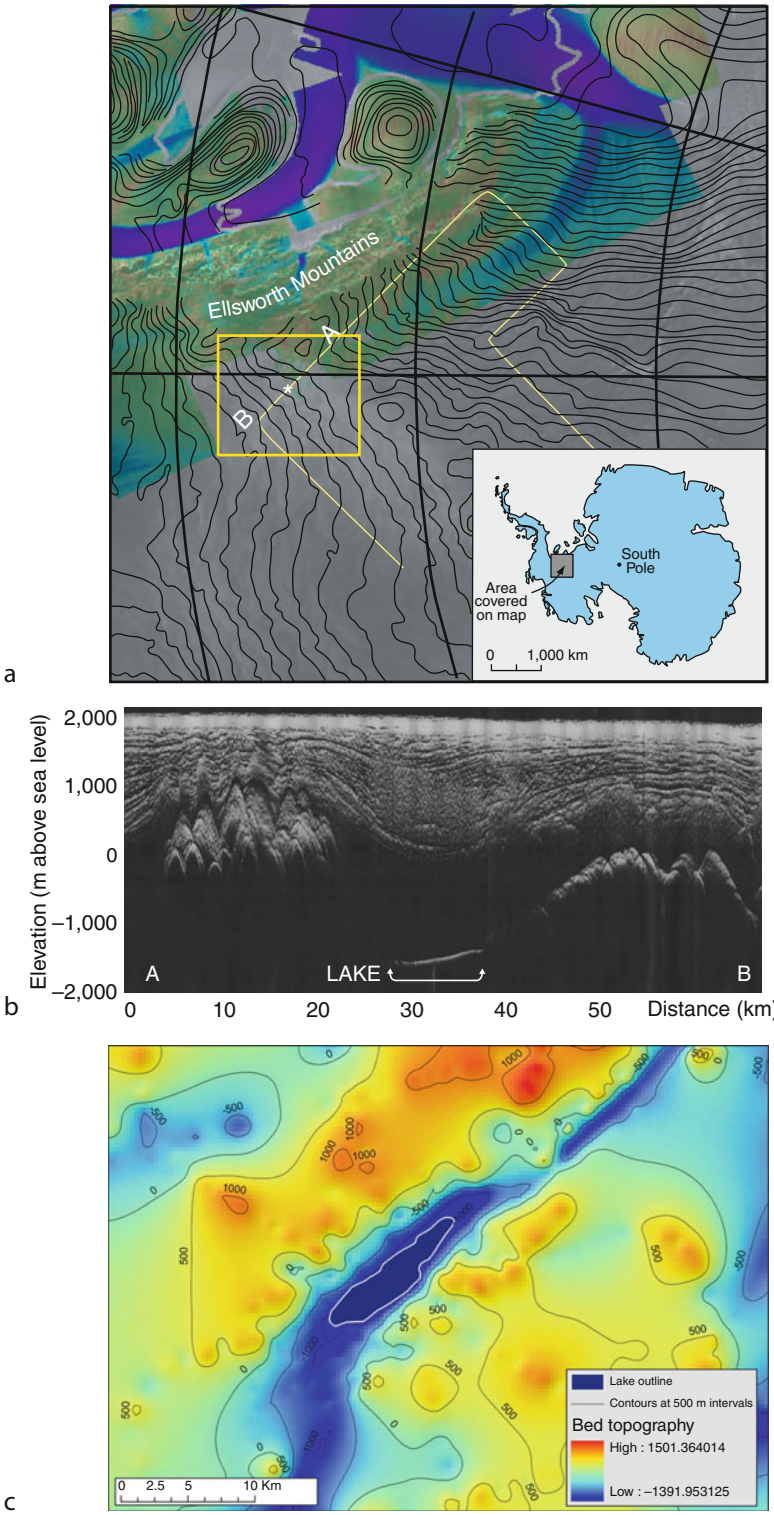

Lake Ellsworth, Figure 1 (**a**) The location of Lake Ellsworth. *Background colors* represent satellite-derived ice surface velocities (*green* = low, *purple* = high, *grey* = no data). The *yellow box* denotes bed information given in (**c**). Transect AB is provided in (**b**); (**b**) Raw 1977–1978 RES transect. The subglacial lake is located between 28 and 38 km (indicated by *arrowed line*). The pronounced slope of the lake surface is accentuated by the vertical exaggeration of the image; (**c**) Basal topography of the immediate area of Lake Ellsworth. Elevation (in meters) relative to the WGS-84 ellipsoid. Adapted from Siegert et al. (2004).

interface varies near the shores, as a consequence of the reflector's shape (Siegert et al., 2004).

2. In austral summer 2004–2005, the British Antarctic Survey flew a sounding line, using a 150 MHz ice-sounding radar, across Lake Ellsworth in the form of a bow. Part of a 35,000 km grid pattern being collected over Pine Island Glacier also crossed the lake, and identified other lake-like reflectors in the surrounding area (Vaughan et al., 2007). This suggests the lake is part of a wider subglacial drainage system. The new radar lines confirm the bright specular nature of the reflector and show a much shorter reflector than the 1977–1978 survey, of between 1.5 and 2.3 km in length. This suggests that the lake is long relative to its cross-profile, occupying a fjord-like basin on the flanks of the Ellsworth Subglacial Highlands (Figure 1c). Analysis of the RES data suggests that the ice is floating on a fluid whose density is 950–1,013 kg m^{-3}, possibly indicating that the lake is composed of fresh water (Vaughan et al., 2007).
3. In January 2006, a ground-based Chilean expedition traversed the Institute Ice Stream to Lake Ellsworth and acquired several RES transects over the lake (Vaughan et al., 2007). A 150 MHz RES system was used to collect nine lines, totaling 15 km over the lake-like reflector (Rivera et al., 2006). These lines bound the lake to the north and west, though do not constrain its upstream margins to the south and east. Here, transitional zones indicated by Rivera et al. (2006) show areas around the lake where off-line radar reflections from steep bedrock surfaces prevent the lake surface being imaged.
4. In 2007/2008 a 3-month field season, using ground-based RES and seismics, revealed the lake to be in excess of 100 m deep and confirmed it as an ideal candidate for in situ measurement and sampling. An over-snow 1 MHz ice-penetrating radar was used to acquire new radar data from Lake Ellsworth and its surroundings during 2007/2008. The survey was designed to acquire data in a grid pattern, to allow: (1) the refinement of the lake outline mapped by Vaughan et al. (2007); (2) the imaging of internal layering within the ice; and (3) the development of a digital elevation model (DEM) of the lake and the surrounding subglacial terrain. The new radar and seismic data confirms the general form of the lake outline established by Vaughan et al. (2007), but shows that Lake Ellsworth is wider and slightly longer at its downstream end than previously mapped. Internal layering is apparent within the topmost 2 km of the ice sheet overlying the lake. Localized buckling of these layers can be used to infer the direction of long-term ice flow over the lake as these structures can be traced, through a sequence of radar profiles, back to their point of origin; an area of high subglacial topography identified up-flow. Internal layering data have been integrated with the DEM of the subglacial bed to facilitate 3D numerical modeling of ice flow and basal melting over Lake Ellsworth, work that is currently in progress.

Basal thermal conditions and ice flow modeling

The basal heat flux calculated in West Antarctica from temperature gradients in boreholes is around 70 mW m^{-2} (e.g., Hulbe and MacAyeal, 1999). Numerical thermodynamic evaluations suggest that the subglacial environment above Lake Ellsworth is warm, that is, at the pressure melting point (Siegert et al., 2004). Due to increased ice thickness at the last glacial maximum (LGM), it is expected that the ice sheet was also warm based at the LGM. This indicates that Ellsworth may have existed during both the present interglacial and the LGM.

Preliminary ice flow modeling of the lake environment using internal layer architecture to invert for basal melting also suggests that the dominant process at the basal boundary condition is one of melting (Siegert et al., 2004). The model predicts that as ice flows over the lake, basal melting is expected at a rate comparable to the surface accumulation rate (which near the ice divide is $\sim$17 cm $year^{-1}$) (Siegert et al., 2004). This melt rate is significantly greater than that calculated for Lake Vostok, though is comparable to the situation in Lake Vostok in terms of its value as a proportion of the surface accumulation rate. As melting is the driving force behind water circulation (Mayer et al., 2003), the enhanced rates of melting predicted by the model may lead to circulation in Lake Ellsworth being stronger than Lake Vostok (and many other subglacial lakes). Upstream of Lake Ellsworth, a small region of basal accretion is modeled at a rate of 20 cm $year^{-1}$. It is not yet known whether this freezing rate is real, or whether three-dimensional flow of ice (not accounted for in the model) complicates ice flow upstream of the lake and influences the internal layer structures. As the rate of water supplied to the lake is considerable, it is likely that Ellsworth is part of a wider subglacial hydrological network, feeding water into the basal environment of the Pine Island catchment.

Exploration of Lake Ellsworth

It is a well-established hypothesis that Antarctic subglacial lakes house unique forms of life and hold detailed sedimentary records of past climate change. Testing this hypothesis requires in situ examination. Of the >145 subglacial lakes known in Antarctica, Lake Ellsworth stands out as a candidate for first exploration for the following reasons (Lake Ellsworth Consortium, 2007):

- The base of the West Antarctic Ice Sheet has been accessed, sampled, and measured. Accessing Ellsworth would, therefore be less environmentally sensitive compared to accessing an East Antarctic subglacial lake.
- Lake Ellsworth is located close to the ice divide, so drilling from the ice surface into the lake will not be complicated by ice flow.

- Lake Ellsworth has been meaningfully characterized by geophysical methods.
- The sediments across the floor of Lake Ellsworth may contain a record of West Antarctic Ice Sheet history.
- The geological setting of the lake is better understood than any other Antarctic subglacial lake, as there is substantial outcrop of rock in the nearby Ellsworth Mountains.
- The ice-sheet surface elevation over Lake Ellsworth is 2,000 m above sea level; more than a kilometer lower than the ice surface over East Antarctic subglacial lakes. Altitude related problems encountered by scientists at the center of the East Antarctic Ice Sheet would not be an issue during the study of Lake Ellsworth.

A consortium of over twenty scientists from eleven institutions has been assembled to plan the exploration of Lake Ellsworth. Lake Ellsworth will be accessed using clean technology hot water drilling. Once lake access is achieved, a sterile probe will be lowered down the borehole and into the lake. The probe will contain a series of instruments to measure the lake water and sediments, and will be tethered to the ice surface through which power, communication, and data will transmit. The probe will be dropped down the water column to the lake floor. The probe will then be pulled up and out of the lake, measuring its environment continually as this is done. Once at the ice surface, any samples collected will be taken from the probe for laboratory analysis. The duration of the science mission, from deployment of the probe to its retrieval, is likely to be between 24 and 36 h. Measurements to be taken by the probe include: depth, pressure, conductivity, and temperature; pH levels; biomolecules (using life marker chips); anions (using a chemical analyzer); nitrogen isotopes (using a tuned laser diode); visualization of the environment (using cameras and light sources); dissolved gases (using chromatography); and morphology of the lake floor and sediment structures (using sonar). After the probe has been retrieved, a sediment corer will be dropped into the lake to recover material from the lake floor. The consortium plans to access Lake Ellsworth in 2012–2013.

Acknowledgments

Funding was provided by UK NERC grants NER/D008751/1, NE/D009200/1 and NER/D008638/1.

Bibliography

Hulbe, C. L., and MacAyeal, D. R., 1999. A new numerical model of coupled inland ice sheet, ice stream, and ice shelf flow and its application to the West Antarctic Ice Sheet. *Journal of Geophysical Research*, **104**(25), 25,349–25,366.

Lake Ellsworth Consortium, 2007. Exploration of Ellsworth Subglacial Lake: a concept paper on the development, organisation and execution of an experiment to explore, measure and sample the environment of a West Antarctic subglacial lake. *Reviews in Environmental Science and Biotechnology*, **6**, 161–179.

Mayer, C., Grosfeld, K., and Siegert, M. J., 2003. The effect of salinity on water circulation within subglacial Lake Vostok. *Geophysical Research Letters*, **30**(14), 1767, doi:10.1029/2003GL017380.

Oswald, G. K. A., and Robin, G. de Q., 1973. Lakes beneath the Antarctic Ice Sheet. *Nature*, **245**, 251–254.

Rivera, A., et al., 2006. Expedicion al lago subglacial Ellsworth, *Boletin Antarctico Chileno*, **25**(1), 7–11.

Siegert, M. J., Dowdeswell, J. A., Gorman, M. R., and McIntyre, N. F., 1996. An inventory of Antarctic sub-glacial lakes. *Antarctic Science*, **8**, 281–286.

Siegert, M. J., Hindmarsh, R., Corr, H., Smith, A. M., Woodward, J., King, E. C., Payne, T., and Joughin, I., 2004. Subglacial Lake Ellsworth: a candidate for in situ exploration in West Antarctica. *Geophysical Research Letters*, **31**, L23403.

Vaughan, D. G., Rivera, A., Woodward, J., Corr, H. F. J., Wendt, J., and Zamora, R., 2007. Topographic and hydrological controls on Subglacial Lake Ellsworth, West Antarctica. *Geophysical Research Letters*, **34**, L18501, doi:10.1029 /2007GL030769.

LAKE ICE

Rajesh Kumar
School of Engineering and Technology, Sharda University, Greater Noida, NCR, India

The lake ice formation takes place when the daily temperature is below the freezing point. Lake ice cover is normally

Lake Ice, Figure 1 Synoptic view of the lake ice formed on the upper surface of lake water in the Baralacha La region of Himachal Pradesh, India.

Lake Ice, Figure 2 Close view of above lake showing liquid water underneath the thin lake ice.

a seasonal phenomenon and once formed the lake ice gets thicker and thicker over the course of the winter as the temperature gets colder and colder. It starts melting in spring. The surface water of the lake freezes at 0°C while the bottom layer of water maintains at above freezing temperature.

The occurrence of lake ice is primarily a function of air temperature. Once meteorological conditions provide colder breeze over warmer water, it forms ice on the surface of water due to advection cooling. But the water below the surface of ice is not much cooled so it exists in liquid phase. Hence the lake ice is found at the lake surface only (Figures 1 and 2).

LAKE VOSTOK

Malte Thoma
Bavarian Academy and Sciences, Commission for Glaciology, Munich, Germany
Alfred Wegener Institute for Polar and Marine Research, Bremerhaven, Germany

Definition

Subglacial Lake. A lake covered by an ice sheet or glacier.

Introduction

Subglacial Lake Vostok is the largest of at least 370 (Wright and Siegert, 2010) subglacial lakes in Antarctica, and it was the first to be discovered. A lot of our knowledge about Antarctica, about the Earth's climate history, and about the subglacial lakes has been descended from the research station built at this location. This contribution summarizes some of the knowledge gained after more than 50 years of research in the heart of Antarctica, on top of, within, and below the ice.

On top of the ice: discovery

During the *International Geophysical Year*, the *Second Soviet Antarctic Expedition* encountered a quite plain area in the center of Antarctica. For the intended permanently manned station far away from any human settlement, airborne transport is indispensable, and hence this location was chosen to establish *Vostok Station*, on December 16, 1957. It is located close to the *Southern Pole of Inaccessibility* and the *South Geomagnetic Pole*. Many scientific experiments have been carried out at Vostok Station. Analyzing the results of seismic soundings, Soviet scientists had speculated about water beneath the 3,750 m thick ice sheet even in the 1960s. Further evidence of the existence of a lake was provided by radio echo sounding in the 1970s, which was confirmed later by satellite altimetry and seismic sounding (Kapitsa et al., 1996).

Subglacial Lake Vostok's area of about 16,000 km^2 can be estimated from airborne measurements and satellite imagery (Figure 1). The lake is surrounded by a bedrock-based ice sheet, and the ice flow approaches Subglacial Lake Vostok from Ridge B in the west, but is deflected southward over the lake (Figure 2). As the lake's surface is flat, it is reasonable to assume an isostatic equilibrium, that is, the ice floats on the water like an ice shelf. The observed ice surface slope over the lake is only 0.02%, leading to an elevation difference of about 50 m. However, because of the density differences between water and ice, surface ice slopes are enhanced approximately ten times at the lake–ice interface. This results in a lake surface elevation difference between the northern and southern tip of about 500 m.

In the ice: drilling and indications of life

In the 1970s, Soviet scientists started to drill ice cores in the vicinity of their station. These early boreholes were less than 1,000 m deep, but nevertheless they provided a unique climate archive. Deeper cores were drilled in 1984 and in the 1990s. The deepest core reached a depth of 3,623 m and penetrated the boundary between meteoric ice and refrozen lake ice at 3,539 m. From this ice core, a climate archive dating back 420,000 years was revealed. According to the seismic soundings, the water interface below Vostok Station is about 3,750 m deep, which means that below Vostok Station a layer of about 210 m refrozen lake water exists (e.g., Jouzel et al., 1999). Today, the deepest borehole is less than 100 m away from the lake's surface.

Subglacial Lake Vostok is an oligotrophic environment: Temperatures of about −3°C, permanent darkness, low nutrient supply, and a supersaturated oxygen level provide a hostile environment, which has been separated from any atmospheric influence since the Antarctic Ice Sheet formed millions of years ago. However, analyses of the refrozen water reveal that potential nutrients and even viable microorganisms exist in Subglacial Lake Vostok (e.g., D'Elia et al., 2009). If this is verified in the future, a so far undiscovered ecosystem on Earth can be explored. Subglacial Lake Vostok may be an extraordinary example of how life may develop under such extreme

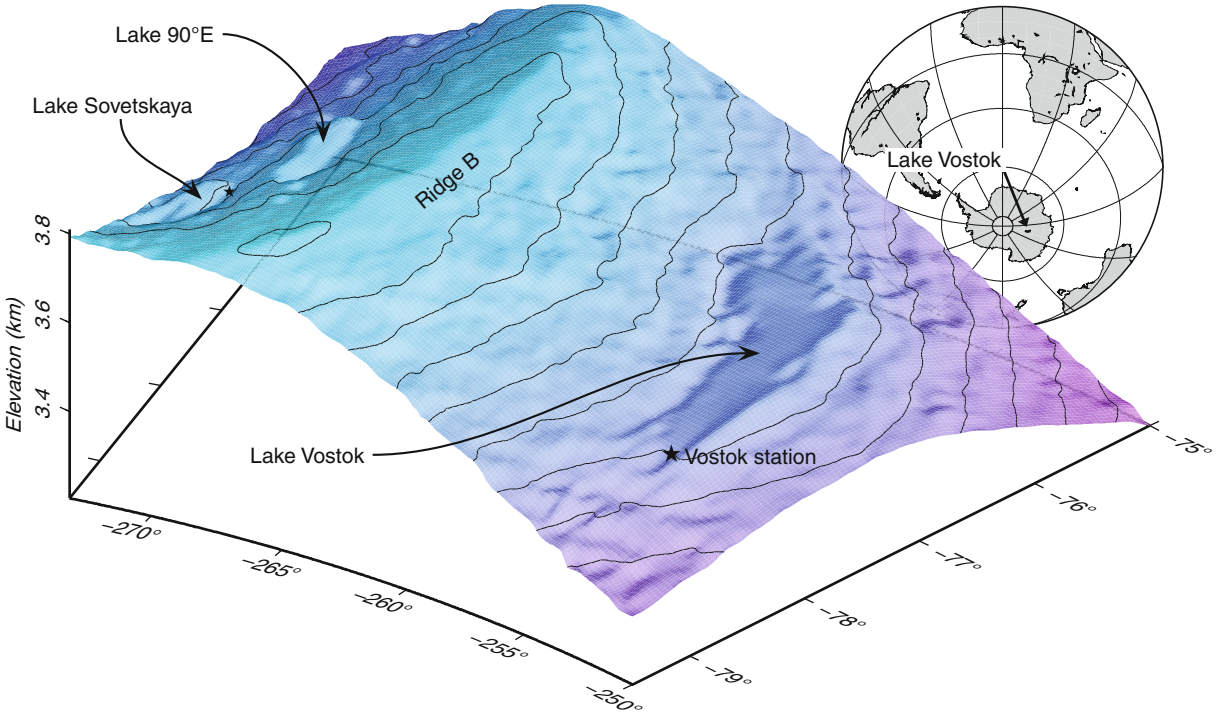

Lake Vostok, Figure 1 Lake Vostok, East Antarctica. Subglacial lakes can easily be identified by means of their flat ice sheet surface. Vostok Station is located in the southern tip of Lake Vostok. Two other major lakes can be identified across Ride B in central Antarctica: Lake 90°E and Lake Sovetskaya, named after another Russian Research station.

conditions, and this nourishes speculations about extraterrestrial life on the ice-covered Jovian moon Europa in our planetary system.

Besides life in the lake water itself, remnants of preglacial life might be stored within the sediments at the lake's bottom – at least if the lake did exist before the ice sheet formed, which is still a matter of debate (Siegert et al., 2004). After the ice formed over the preglacial lake, the supply of light, oxygen, and nutrients from the atmosphere was intercepted, leading to mass extinction. If the sediments at the lake's ground are probed, a new climate archive will be opened and information about life million years before present will be available. However, it will be problematic to probe Lake Vostok without contaminating it. According to the *observer effect*, it is impossible to sample something without changing it. In the closed subglacial system, any contamination released by a drilling equipment will permanently and irreversibly modify the lake's composition. In this sense, Lake Vostok can be interpreted as a macroscopic example of the uncertainty principle.

Because of these well-founded worries of the scientific community against a probing, Russia agreed in the late 1990s to delay the penetration of the lake until further risk assessments have been made. It is undisputed that the Russians' drilling project does not violate the *Antarctic Treaty*. Therefore, they already have filed an *Initial Environmental Evaluation*, and only the obligatory *Comprehensive Environmental Evaluation* is pending. Hence, the drilling will be legitimate. The Russians are not the only ones who have interest in probing Lake Vostok. The American Space Agency NASA has announced that they would like to test their equipment to be used on missions to other planets and moons on Earth beforehand, and that Lake Vostok would be an ideal location for this. Meanwhile, a British consortium of scientists has launched an already accepted proposal to explore and penetrate a subglacial environment at the much more accessible and tiny Antarctic Subglacial Lake Ellsworth (e.g., Woodward et al., 2010) This has stirred the somewhat calmed plans to unlock Lake Vostok again: Despite the worries and protests of scientists (e.g., Hobbie et al., 2007) and the *Antarctic and Southern Ocean Coalition* (ASOC, an environmental organization), Russian scientists reinitialized drilling during the field season 2005/2006 with an overhauled equipment and stopped the drilling only a few tens of meters close to the lake. The Russian scientists claim that they are capable of sampling lake water without infecting it with modern microbes. However, this will be quite a task as their drilling hole is filled with kerosene and other noxious fluids necessary to prevent the borehole from refreezing or from closing due to pressure forces. Technical and legal reasons have postponed the penetration of the lake so far, but the Russians have announced that after 2010 they plan to go where no man has gone before (Schiermeier, 2008).

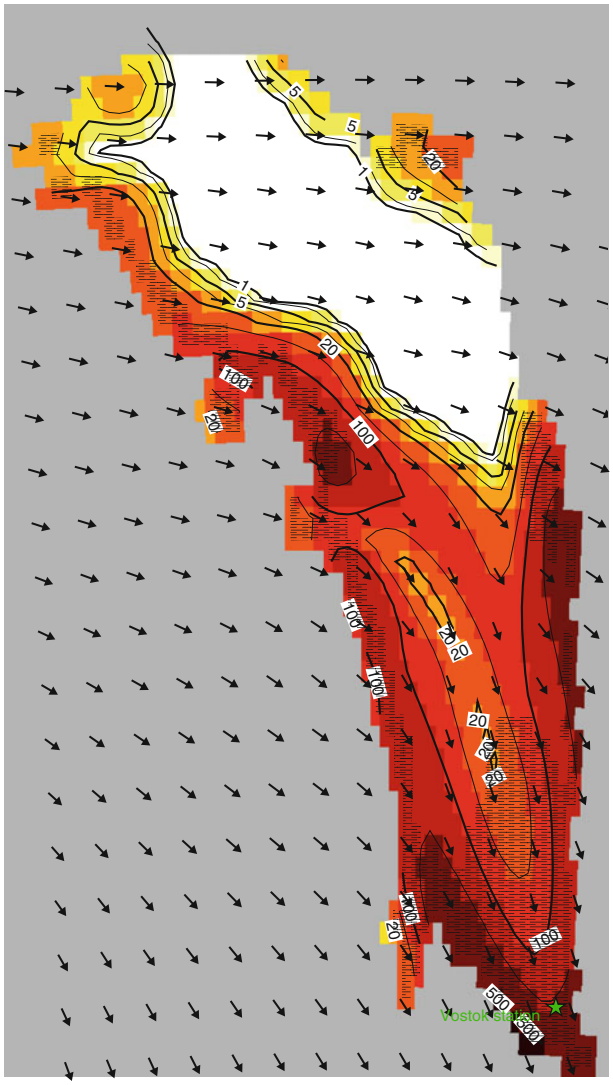

Lake Vostok, Figure 2 Modelled accreted ice distribution and its thickness (m) at the lake–ice interface (indicated by *color*) and areas where freezing takes place (*white shaded*). The surface ice flow direction (After Tikku et al., 2004) is indicated by *black arrows*.

Below the ice: modeling

The lake's area can be estimated from the surface topography, and a lot of valuable information about Lake Vostok can be gathered from the accreted refrozen lake water in the ice core. But until the lake is directly probed, detailed information about circulation and water mass exchange under the ice can only be derived from numerical modeling. From airborne gravity data and assumptions about the densities of ice, water, sediment, and rock, the lake's geometry and its water depth can be estimated (Studinger et al., 2004). In addition, seismic sounding can be used to constrain the derived geometry model (Filina et al., 2008). According to these studies, the lake's largest depth exceeds 1,000 m, the volume is about 5,000 km^3, and a sedimentary layer at the lake's bottom is several hundred meters thick.

The surface temperatures in central Antarctica are, on average, about −65°C during winter, and even in the brief summer, they barely reach −35°C. This is well below the freezing point of water, and hence ice never melts in this region of the Earth – at least not at the ice sheet's surface. Nevertheless, water does exist in its liquid form below about 4,000 m of ice. At this depth, the freezing point of fresh water is about −3°C. A small geothermal heat flux of about 50 mW/m^2, as estimated for the area of Lake Vostok, is therefore responsible (and sufficient) for melting the ice's base. Additional hydrothermal energy sources are not expected to provide energy for the melting. The meltwater is collected in the topographic basin (a rift valley according to Bell et al., 2006) forming Lake Vostok.

With this valuable information, a lake-flow model can be set up to calculate the average water circulation, the basal mass (im)balance, and the distribution of melting and freezing at the lake–ice interface (Thoma et al., 2008). These simulations show a ceaseless melting-induced ice loss of about 5×10^{-2} km^3/a, which is not balanced by freezing, and a horizontal (vertical) water velocity on the order of 1 mm/s (10 μm/s). However, the modeled low vertical velocity is a spatial average; heating from below results in upwelling of plumes that rise significantly faster (about 0.3 mm/s) to the lake's surface (Wells and Wettlaufer, 2008). The combination of the modeled basal mass balance and ice flow information allows for estimating the distribution and thickness of the accreted ice at the ice sheet base from which samples have been drilled at Vostok Station. According to Thoma et al. (2010), about 65% of the lake–ice interface is covered with accreted ice (Figure 2).

Most probably, Lake Vostok is not an isolated lake but is connected to other lakes via a subglacial network like other lakes have proven to be before (Wingham et al., 2006; Fricker et al., 2007). The water collected in the Lake Vostok basin will finally reach the Southern Ocean. The age of the lake water is estimated to be between a few thousand years and more than 100,000 years, and a more recent model-based study (Thoma et al., 2010) indicates a mean water age of about 50,000 years. However, these timescales are short compared to the Antarctic Ice Sheet's age of several million years, which means that the lake water has been replaced several times since its inception.

Conclusions

After more than 50 years of research in the heart of Antarctica, some of Lake Vostok's mysteries are revealed (like the dimension of the lake), some are depreciated (like the theory of an isolated, sealed environment), but a lot is still unknown about the massive water basin beneath the 4,000 m thick Antarctic Ice Sheet. Within the next few years, we can expect more insights to be gained from the subglacial environment, perhaps by direct sampling through an access hole.

Bibliography

Bell, R. E., Studinger, M., Fahnenstock, M. A., and Shuman, C. A., 2006. Tectonically controlled subglacial lakes on the flanks of the Gamburtsev Subglacial Mountains, East Antarctica. *Geophysical Research Letters*, **33**, L02504, doi:10.1029.2005GL025207.

D'Elia, T., Veerapaneni, R., Theraisnathan, V., and Rogers, S. O., 2009. Isolation of fungi from Lake Vostok accretion ice. *Mycologia*, **101**(6), 751–763, doi:10.3852/08-184.

Filina, I. Y., Blankenship, D. D., Thoma, M., Lukin, V. V., Masolov, V. N., and Sen, M. K., 2008. New 3D bathymetry and sediment distribution in Lake Vostok: implication for pre-glacial origin and numerical modeling of the internal processes within the lake. *Earth and Planetary Science Letters*, **276**, 106–114, doi:10.1016/j.epsl.2008.09.012.

Fricker, H. A., Scambos, T., Bindschadler, R., and Padman, L., 2007. An active subglacial water system in west Antarctica mapped from space. *Science*, **315**(5818), 1544–1548, doi:10.1126/science.1136897.

Hobbie, J. E., Baker, A., Clarke, G., Doran, P. T., Karl, D., Methe, B., Miller, H., Mukasa, S. B., Race, M., Vincent, W., Walton, D., White, J. W., and Uhle, M., 2007. *Exploration of Antarctic subglacial aquatic environments: environmental and scientific stewardship*. Washington, DC: National Academy.

Jouzel, J., Petit, J. R., Souchez, R., Barkov, N. I., Lipenkov, V. Y., Raynaud, D., Stieve-nard, M., Vassiliev, N. I., Verbeke, V., and Vimeux, F., 1999. More than 200 meters of lake ice above subglacial Lake Vostok, Antarctica. *Science*, **286**, 2138–2141, doi:10.1126/science.286.5447.2138.

Kapitsa, A. P., Ridley, J. K., Robin, G. d. Q., Siegert, M. J., and Zotikov, I. A., 1996. A large deep freshwater lake beneath the ice of central East Antarctica. *Nature*, **381**, 684–686, doi:10.1038/381684a0.

Schiermeier, Q., 2008. Russia delays Lake Vostok drill, Antarctica's hidden water will keep its secrets for another year. *Nature*, **454**, 258–259, doi:10.1038/454258a.

Siegert, M. J., 2004. Comment on "A numerical model for an alternative origin of Lake Vostok and its exobiological implications for Mars" by N. S. Duxbury, I. A. Zotikov, K. H. Nealson, V. E. Romanovsky, and F. D. Carsey. *Journal of Geophysical Research*, **109**(E02007), 1–3, doi:10.1029/2003JE002176.

Studinger, M., Bell, R. E., and Tikku, A. A., 2004. Estimating the depth and shape of subglacial Lake Vostok's water cavity from aerogravity data. *Geophysical Research Letters*, **31**(L12401), doi:10.1029/2004GL019801.

Thoma, M., Mayer, C., and Grosfeld, K., 2008. Sensitivity of Lake Vostok's flow regime on environmental parameters. *Earth and Planetary Science Letters*, **269**(1–2), 242–247, doi:10.1016/j.epsl.2008.02.023.

Thoma, M., Grosfeld, K., Smith, A. M., and Mayer, C., 2010. A comment on the equation of state and the freezing point equation with respect to subglacial lake modelling. *Earth and Planetary Science Letters*, **294**(1–2), 80–84.

Tikku, A. A., Bell, R. E., Studinger, M., and Clarke, G. K. C., 2004. Ice flow field over Lake Vostok, East Antarctica inferred by structure tracking. *Earth and Planetary Science Letters*, **227**, 249–261, doi:10.1016/j.epsl.2004.09.021.

Wells, M. G., and Wettlaufer, J. S., 2008. Circulation in Lake Vostok: a laboratory analogue study, *Geophysical Research Letters*, **35**(L03501), 1–5, doi:10.1029/2007GL032162.

Wingham, D. J., Siegert, M. J., Shepherd, A., and Muir, A. S., 2006. Rapid discharge connects Antarctic subglacial lakes. *Nature*, **440**(C6), 1033–1036, doi:10.1038nature04660.

Woodward, J., Smith, A. M., Ross, N., Thoma, M., Corr, H. F. J., King, E. C., King, M. A., Grosfeld, K., Tranter, M., and Siegert, M., 2010. Location for direct access to subglacial Lake Ellsworth: An assessment of geophysical data and modeling. *Geophysical Research Letters* **37**(L11501).

Wright, A., and Siegert, M. J., 2010. The identification and physiographical setting of Antarctic subglacial lakes: an update based on recent geophysical data. In: Siegert, M. J., Kennicutt, C., and Bindschadler, B., (eds.), Subglacial Antarctic Aquatic Environments, AGU Monograph, accepted.

Cross-references

Antarctica
Bed (Bottom) Topography
Formation and Deformation of Basal Ice
Ice Core
Ice Sheet
Ice Shelf
Lake Ice
Melting Processes
Subglacial Drainage System
Subglacial Lakes, Antarctic

LAMINATED SEDIMENTS

Rajesh Kumar
School of Engineering and Technology, Sharda University, Greater Noida, NCR, India

The laminated sediments have traditionally been considered by geologists as strata with a thickness of about less than 1 cm (Berthault, 1988). This is one of the characteristic features in the sedimentary rocks. The deposition of sediments for several years or at different geological time might have slight difference in their mineralogical composition. This exhibits different shades of colors even if they are belonging to the same area. After consolidation, these depositions in the sedimentary rocks exhibit them in the form of thin layers. Each laminated sediments or the thin layer/band represents a different phase of deposition. Lamination clusters together signify all the structures characterizing sedimentary rocks within a bed or stratum. One of the most common examples for the laminated sediments is the medium-grained reddish sandstone that possesses thin bands of red shades due to difference in iron content at each depositional phase. The ticker laminated sediments are called as bedding planes.

Bibliography

Berthault, G., 1988. Experiments on lamination of sediments. EN Technology Journal, **3**, 25–29.

LANDFORMS OF GLACIAL DEPOSITION

John F. Shroder
Department of Geography and Geology, University of Nebraska at Omaha, Omaha, NE, USA

Definition

Glacial erosion occurs in the upper, dominantly accumulation area whereas farther down near the terminus

the ice produces areas and landforms of deposition. This entry describes some of the common depositional landforms under one umbrella. For detailed description of Jökulhlaups, Moraine, and Till, please see the respective entries *Hydrology of Jökulhlaups*; *Moraine*; *Till* in this Encyclopedia.

Landforms produced by deposition of glacier materials are mainly differentiated on the basis of whether or not they are primarily ice contact or meltwater in origin. Ice contact generally means that the landform is composed dominantly of unsorted, unstratified tills, which are generally mixtures of all clast sizes from clay, silt, and sand, to cobbles and boulders. Till deposits form as *lodgement tills* through the pressure of overlying ice that consolidates them and plasters them onto the substrate beneath; the under-melt and over-melt *ablation tills* that melt out both beneath and above the ice; and *flow tills* that form from any prior tills that become water saturated and flow over other deposits and landforms. Meltwater deposits tend to be sorted and stratified. In the waning phases of the Pleistocene ice age many glaciers melted away to leave complex mixtures of various kinds of tills and glaciofluvial sediments and landforms that are collectively known as *kettle and kame topography.*

Moraine is the general term used for almost all of the landforms composed of till, and there are many kinds of moraines, depending upon where the moraine occurs in relation to the original ice that formed it and how it was formed. Thus *lateral moraines* are the long ridges that develop alongside glacier edges where sub-, en-, and supra-glacial till debris accumulates. At the terminus or front of the glacier where the mass balance of accumulation versus wastage has allowed the glacier front to remain in place for a while, some of the same processes pile up masses of till in arcuate ridges that become the *end* or *terminal moraine*. As the glacier retreats back from its farthest extent, it can form recessional moraines where the terminus holds its position for a few years. The common medial moraines that form on the surface and down inside glacier ice commonly does not hold its long, commonly sinuous landform shape once the ice melts away; instead together with other miscellaneous sources of sub-, en-, and supra-glacial debris, it becomes undifferentiated *ground moraine* that tends to be scattered about formerly glaciated landscapes. Some ground moraines become *fluted moraine* where the basal tills are scraped, squeezed, and streaked out into lineations known as "flutes."

Push moraines form where a thick glacier terminus overrides preexisting tills or glaciofluvial sediments and forces the materials bulldozer-like, up into apparent morainal forms in front of the glacier, even where some are not made only of till. Other types of moraines that are formed transverse to ice flow are *ribbed* or *Rogen moraines* that are rather irregular in shape. They can form as the result of pushing or overriding of materials reactivated by the ice, or perhaps as a transition between streamlined features up-ice and transverse forms down-ice, or where thermal transitions occur in deglaciation along the sub-ice line that can perhaps migrate on some temporally controlled basis between cold-based ice frozen to its bed and warm-based ice further toward the terminus.

De Geer moraines are much more fine or more delicate than the Rogen type and are successions of discrete narrow ridges, thought possibly to be the result of till sediments dropped out along an ice-contact sublacustrine grounding line where icebergs calved off into a lake or the sea, or where till was squeezed up. Similar *Kalixpinmo hills* or *moraines* also may be where subglacial materials are squeezed up into cavities or deformed by glacier flow.

Smooth *drumlin* forms can form from prior deposited tills that are swept over by a new ice advance that selectively erodes away surrounding tills to leave the streamlined hills behind. Drumlins are thought to form when sub-glacial meltwaters also erode the streamlined shape. Some drumlins can also have internal glaciofluvial deposits that are sorted and stratified. Together with erosional rock drumlins, it is clear that drumlin landforms are polygenetic. Finally, various crag and tail forms can occur where a glacially overridden hill can have a mass of streamlined debris drawn out behind it down-ice in a streamlined form.

Kames are a common glacial hill or ridge landform composed dominantly of glaciofluvial sediments that are deposited in a variety of meltwater environments, such as englacial, supraglacial, and proglacial environments where conditions are appropriate for accumulation of sediment. Supraglacial lakes, crevasses, the bottoms of moulin (glacial water mills), and other miscellaneous depressions are all possible localities for establishment of kames. No particular shape is implied in the designation of the polygenetic term, although those flat-topped ones that form along the margins of glaciers or across the top of the glacier by meltwater streams or lakes, commonly become *kame terraces*.

Eskers are polygenetic also and can form as long, winding ridges of glaciofluvial sediments, commonly as a result of deposition in linear subglacial and englacial streams in tunnels, as well as in supraglacial streams. In some cases, however, the depositional processes can involve deposition of glaciofluvial sediment in a series of deltas into ice-contact lakes, which as the ice front retreats, allows the delta to retreat as well, leaving behind a series of long- or short-beaded eskers.

Glacier-fed deltas associated directly with meltwaters are classified on the basis of water depth and gradients of the feeder river. Shoal or shallow water types form Hjulström types of deltas with gently sloping fronts. Steeper and slightly deeper forms are the "classic" Gilbert-type deltas with clear topset, foreset, and bottomset bedding forms. As the water deepens and the slopes vary, various subaqueous debris cones, submarine ramps, and lobes develop, commonly as a result of subaqueous mass movement.

The regions out in front of glaciers that are washed over extensively by braided meltwater streams are replete with widespread fluvioglacial sediments that in mountainous regions form *valley trains,* and in more open regions spread out as *outwash plains* or *sandars* (singular – *sandur*).

Such regions may be the product of the slow melt of glaciers in the region, or the more spectacular breakout floods due to breakage of an ice dam or because of subglacial volcanic eruptions that result in abrupt, high-discharge floods or *jökulhlaups*. Valley trains and outwash plains are commonly pocked with kettle holes result where blocks of ice melted out leaving a remnant, commonly water-filled, depression behind.

Cross-references

Glacier Lake Outburst Floods
Hydrology of Jökulhlaups
Moraine
Sediment Entrainment, Transport, and Deposition
Till

LANDFORMS OF GLACIAL EROSION

John F. Shroder
Department of Geography and Geology, University of Nebraska at Omaha, Omaha, NE, USA

Definition

Landforms produced by the glacial erosion. Glacial erosion occurs in the upper, dominantly accumulation regions beneath the ice of glacierized valleys and ice sheets and ice caps. For detailed description of various aspects, please see the following entries: *Glacial Erosion*; *Landscapes of Glacial Erosion*; *Sediment Entrainment, Transport, and Deposition*.

The characteristics of glacially eroded landforms are primarily classified into four main categories of bedrock, topography, glacial processes, and time. Bedrock controls include the actual lithologies themselves, the character and spacing of the joints, the degree of preglacial weathering, and the overall rock structure. Topographic controls of glacial erosion are constituted by the relative relief, the shape of the relief, its alignment in relation to ice flow, and the overall altitudes involved. The morphology of the ice mass and its thickness help to control landform production, as does the direction of the ice flow, the velocity of the basal ice, and the character and amount of glacial debris. The temperature of the basal ice is essential because cold-based glaciers frozen to their beds do not erode their substrates, whereas warm-based ice in association with plentiful meltwater is a highly effective erosive agent. Change of any of these factors over time will affect the character of the eroded landforms, just as does the overall length of time that the region is glacierized.

Glacial erosion occurs by a number of processes that commonly generate sequences of scale-dependent landforms as a result of direct ice contact through crushing and fracturing, plucking or quarrying, and abrasion, as well as through fluvial erosion beneath the ice. The processes of *crushing* and *fracture* of the rock beneath a glacier produce chattermarks and crescentic fractures. *Plucking* or *quarrying* occurs during regelation slip wherein meltwater migrates to the downglacier side of an obstruction and refreezes to also incorporate fractured rock into the regelation layer that the glacier then carries away. *Abrasion* occurs where small to large grains of rocks and minerals are held by the ice and dragged over the substrate to grind away at it. At the very smallest level, fine clastic abrasives beneath the ice cover can polish the rock; at slightly larger scales, *striae* or scratches result, and above that even larger grooves are cut into the rock. *Plastically molded surfaces* or *P-forms* are eroded into bedrock as sinuous rounded forms possibly formed by the action of water-saturated tills, which are forced out under pressure beneath the ice. Fluvial erosion occurs beneath warm-based glaciers that are not frozen to their beds where meltwaters can be under pressure and where they can entrain large quantities of clastic particles that act as effective erosive tools. *Subglacial channels* and *potholes* can be developed, as well as large *tunnel valleys* that can be kilometers in width and tens of kilometers in length.

Glacially eroded valleys are easy to recognize because they so commonly have a U-shaped cross section, in contrast to the more V-shaped valleys produced by running water alone. *Glacial troughs* most closely conform to a caternary curve that forms primarily through plucking and abrasion on the lower sidewalls and bottoms of the valleys. In the course of its movement down valley, the glacier commonly exploits valley-wall constrictions, differences in rock hardness, closer joint spacing directly below where a tributary glacier added to the ice discharge to enhance its erosional ability.

Glacial troughs can be carved out of winding river valleys that have interlocking spurs, in which case they will be eroded away to leave *ice-faceted spurs* or *truncated spurs* that align between the lateral valleys. Where tributary ice streams have joined the trunk ice stream, the floors of these smaller glacier troughs are generally above the floor of the main glacier valley and *hanging troughs* or *hanging valleys* form, commonly with waterfalls once the ice has melted away.

As glacial troughs are blocked by moraines, they can fill with *glacial trough lakes* that drown the valley floor. Similarly, where glaciers descended close to or below sea level, a subsequent postglacial rise in sea level has generated *glacial fiords* invaded by an arm of the sea into the submerged glacial trough.

At the head of a glacial trough commonly exists a steep-headed, half-bowl-shaped basin or *cirque* scooped out of the bedrock that forms as a consequence of intense frost action and nival processes adjacent to the ice. The flow lines in the ice in the zone of accumulation carry rock fragments down to the bedrock beneath the glacier where it becomes deeply abraded and even overdeepened through abrasion and plucking. Once the ice has melted away, a *tarn* lake can result where the water is dammed up behind the rock sill at the lip of the cirque.

As cirques and glacial troughs dissect a mountain range, the upland remnants between three or more back-to-back

cirques erode rectilinear glacial monuments, generally in flat-lying rocks, or triangularly faced *horns* in other rocks or in places where the monuments have been reduced by headward erosion from the opposing cirques. A saw-toothed ridge or divide between cirques or glacier troughs consists of low *cols* and sharp knife-edged ridges that can form an *arête*. Multiple cirques along a mountain range can form a *scalloped upland* or *biscuit-board topography*, in analogy to a layer of prepared bread dough on a pastry board with arcuate pieces cut out for biscuits that leave the cirque shape behind.

Landform eminences produced primarily by plucking and quarrying at the smaller end of the scale form streamlined *roche moutonnée* of a few meters to a few decimeters in size that tend to be plucked and rough and jagged on the down-ice or lee side, and rounder, smoother, and abraded on the up-ice or stoss side. At the large end of the scale, the same sort of streamlined landform is hundreds of meters in size and generally stands as an isolated and asymmetric rocky crag or mountain *flyggbirge*. In a few cases of completely streamlined erosional forms, *whalebacks* or larger *rock drumlins* can form. Finally, jagged mountain peaks that protrude through a surrounding ice sheet are *nunataks*, which is an Inuit word for "place of refuge."

Summary

Glacial erosion occurs most prominently in association with warm-based ice that is not frozen to its bed and in abundant association with meltwaters. Glacial erosion is accomplished primarily by subglacial abrasion from other rock fragments entrained in the moving ice, as well as by plucking in which basal meltwater refreezes beneath the ice to pull off blocks of bedrock. A wide variety of small-scale and large landforms are produced in the bedrock.

Bibliography

Benn, D. I., and Evans, D. J. A., 1998. *Glaciers and Glaciation*. London: Arnold, p. 743.

Menzies, J., 2002. *Modern and Past Glacial Environments*. Oxford: Butterworth Heinmann, p. 543.

Cross-references

Glacial Erosion
Landscapes of Glacial Erosion
Sediment Entrainment, Transport, and Deposition

LANDFORMS OF GLACIAL TRANSPORTATION

John F. Shroder
Department of Geography and Geology, University of Nebraska at Omaha, Omaha, NE, USA

Definition

Landforms produced due to the movement of glacier.

All glacial deposits were transported from other sources but landforms specific only to transportation can be considered where the mechanism of motion and its results are the most important factors to be considered. Thus features such as *erratics*, *boulder trains*, or glacial erratic *indicator fans* or *dispersal fans* are the chief landforms of glacial transportation. Such landforms are commonly recognized as exotic blocks far from their original source that will reveal paleo-flow directions of the ice once the course of transport is determined by finding the original outcrop from which they were derived.

For an erratic to be incorporated within a glacier, it is necessary either for the ice to exert enough tractive force on a block to pick it up from the bed over which it is flowing, or for the block to fall from high cliffs to the glacier surface and be carried along passively thereafter. Small blocks are brought into ice streams both ways constantly but very large blocks require unusual sets of circumstances in order to become transported landforms. A possibility can be that huge erratic blocks might be moved by cold-based glaciers if the 0°C isotherm moves down reasonably close to the glacier bed so that the block is frozen onto the overlying ice. Then, if the friction at the frozen ice/rock interface exceeds that occurring on the lower unfrozen plane of weakness in the rock or that of the substrate below, the whole block can be picked up and dragged along. Subsequently as is characteristic of cold-based glaciers, the block can rise in the ice stream as ever more material and ice is added underneath it by regelation refreezing at the glacier base.

A huge such erratic in Germany measures 4 km by 2 km by 120 m thick. Elsewhere large quartzite blocks of the Foothills Erratic Train occur on the prairie underlain by Cretaceous bedrock in Alberta, Canada, more than 375 km from their source in the mountains of Jasper National Park. The largest of these erratic blocks, the Okotoks erratic near Calgary, is thought to weigh about 16,000 t.

Erratic trains can be divided into two chief types: the *Dubawnt type* in which erratic blocks are spread as a plume down-ice from a relatively restricted source outcrop; and the *Boothia type*, which on the other hand is a boulder train characterized by erratic plumes that extend out from small parts of large source areas by ice streams of more rapid flow within an ice sheet. In general, no matter which type of erratic train is involved, the dispersal patterns of the erratics can be used to reconstruct former ice transportation pathways. Care must be exercised in interpretation, however, because debris transport histories may involve several cycles of glaciations during which time ice divides and ice-flow vectors may shift altogether from one direction to another, even as much as 90° or more. In general, most boulder trains are fan-shaped down-ice, although some may be rather rectilinear in the shape of their edges.

In those rare cases where a medial moraine from a glacier is preserved on the ground after the glacier has melted away, a clear transportation landform results.

For example, in the case of medial moraines that derive from a nunatak mountain that projects through an ice sheet, the erratic debris spread out from that nunatak while the ice is in place will form a more-or-less vertical debris septum within the ice that exists as a medial moraine on the surface of the ice. If the ice melts away without too much meltwater removal of the debris, a linear pile of boulders and moraine hills will show the original transportation direction.

Summary

All glacial deposits were transported from somewhere else but only a few show clear evidence of transportation that sets them apart from the others. Thus, glacial landforms of transportation include single erratics, boulder trains of erratics, and indicator fans or dispersal fans. More rarely, medial moraines may be preserved.

Bibliography

Benn, D. I., and Evans, D. J. A., 1998. *Glaciers and Glaciation*. London: Arnold, p. 743.

Menzies, J., 2002. *Modern and Past Glacial Environments*. Oxford: Butterworth Heinmann, p. 543.

Cross-references

Glacier Motion/Ice Velocity

LANDSCAPES OF GLACIAL EROSION

Martin P. Kirkbride
Geography, School of the Environment, University of Dundee, Dundee, Scotland, UK

Definition

A landscape of glacial erosion is one in which a large part of the landscape comprises exposed glacially molded bedrock, evidence of the net removal of rock by glacier abrasion and quarrying. Landscapes comprise erosional landforms at scales from centimeters to kilometers. This entry discusses the significance of these landscapes and their role in landscape evolution beneath ice sheets and alpine glaciers. For detailed description about landforms and glacier erosion, please see following entries: *Glacial Erosion*; *Landforms of Glacial Erosion*, etc.

A new realization of the significance of glacial erosional landscapes

Glaciers have been recognized as potent agents of landscape modification since the earliest days of classical Glacial Theory. At the landscape scale, understanding glacial topography was for many decades limited to sterile descriptions of form, because a physical understanding of subglacial erosion processes was insufficiently advanced to explain landform assemblages at landscape scales. Furthermore, the impossibility of deriving direct chronological information from denuded bedrock landscapes precluded any empirical attempt to construct evolutionary models of erosion-dominated landscape development. All this changed in the late twentieth century due to advances in four areas of science: (1) the development of powerful numerical models of glacier and ice sheet behavior; (2) application of new techniques for estimating denudation rates in eroded landscapes, notably thermochronometry and cosmogenic isotope analysis; (3) better understanding of subglacial erosion, notably the integration of basal water pressure variations into explanatory models, and (4) high-resolution proxy records of global climate history from ice cores and marine sediments, which could be used to drive computer models of glacier and ice sheet behavior. Recent research attempts to integrate glaciological and geomorphological models to "recreate" glacial erosional landscapes. Their outputs can then be measured against real landscapes and empirically calculated rates of glacial erosion and topographic change. These advances allow long-standing questions in glacial geomorphology finally to be addressed, such as:

What do the preserved landscapes of former ice sheet beds tell us about the life cycles of ice sheets?
How long does it take for glacial topography to form on a previously unglaciated landscape?
What are the relative rates of fluvial and glacial erosion at landscape scales of space and time?
What role do glaciations play in the uplift and evolution of mountain ranges?

Modeling glacial landscape evolution using coupled ice-bedrock models takes two approaches. Forward modeling shows how an initial unglaciated landscape is modified by ice cover (e.g., Jamieson et al., 2008): reverse modeling starts with current terrain models and works backward to "recreate" the preglacial landscape (e.g., Jamieson et al., 2005). Armed with these techniques, studies of glacial landscape evolution are now contributing to wider debates involving the roles of ice sheets and of alpine mountain building in global climate change.

Classification and origins of erosional landscapes under ice sheets

Sugden and John (1976) classified glacial erosional landscapes at continental scales according to the role of thermal regime in promoting or inhibiting erosion, and to the consequent character of the deglaciated terrain (Table 1). The main landscape types of areal scouring, selective linear erosion, and little or no erosion, are primarily related to spatial variations in thermal regime (Sugden, 1974, 1978). Areal scouring creates distinctive landscapes of exposed bedrock in the form of rock basins, roches moutonées, and other more-or-less streamlined forms reflecting former ice flow. Though often limited to low-relief landscapes, areal scouring of uplands (including summits) should also be included in the landscape type where the terrain was inundated by an ice sheet moving across the area from a distant source.

Landscapes of Glacial Erosion, Table 1 Classification of landscapes of glacial erosion (After Sugden, 1974; Sugden and John, 1976; Summerfield, 1991; Benn and Evans, 1998)

Landscape type	Thermal regime	Topography	Examples
Areal scouring	Warm-based	Landscape dominated by exposed, plucked, and abraded bedrock forms whose scale depends on joint and fault density. Rock basins, roche moutonées, streamlined erosional forms, and striated pavements. Negligible glacial sediment cover and disorganized post-glacial drainage. Erosion aided by impermeable bedrock.	NW Scotland W Baffin Island, Canada
Selective linear erosion	Warm-based over valleys, cold-based over interfluves	Glacial modification of pre-existing fluvial valleys into troughs. Largely unmodified plateaux and interfluves may retain delicate non-glacial landforms (patterned ground, regolith)	Cairngorm Mountains, Scotland Trollaskagi Peninsula, N Iceland Beartooth Mts, Montana, USA E Greenland
Little or no erosion	Cold-based	Preglacial slope forms survive with regolith cover. Presence of former glacier cover may itself be contentious. Limited evidence of meltwater activity during deglaciation. Erosion may partly be suppressed by permeable bedrock.	NE Scotland W Sweden E Baffin island (Canada)
Alpine landscapes	Warm-based in valleys	Cirques line sharp-crested mountain ranges above glacially modified troughs, with periglacial morphogenesis on high ice-free slopes. Predominance of steep terrain with avalanche couloirs supplying much glacial accumulation.	Southern Alps (New Zealand) European Alps Southern Alaskan coast ranges

Landscapes of selective linear erosion are specific to mixed-regime ice sheets under which thin ice over uplands remains cold-based while thick ice over valleys slides under a warm-based regime, often aided by flow convergence from surrounding uplands. Valleys are deepened and reshaped to "U"-shaped trough forms, often exploiting geological weaknesses. Landscapes of little or no erosion may be controversial, because evidence of former cold-based glaciation may be elusive, and preservation of preglacial landforms and sediments may suggest ice-free conditions throughout the Quaternary.

This classic partitioning of glacial landscapes underpins all the more recent research exploring the thermomechanical controls on glacial erosion at large spatial scales. The modern challenge is to upscale process explanations of abrasion and plucking (Boulton, 1979; Hallet, 1979, 1996) to provide models of landscape evolution under ice sheets at continental scales. The challenge has been approached both empirically (Sugden, 1978; Li et al., 2005; Phillips et al., 2006; Swift et al., 2008) and theoretically, using coupled ice-sheet-erosion computer models (Hildes et al., 2004; Jamieson et al., 2008). An up-to-date summary of the fundamental controls on glacial erosion is provided by Jamieson et al. (2008). In summary, effective abrasion and quarrying require that ice is moving over the glacier bed, in turn requiring water to be present at the bed. This requires a temperate thermal regime, due to an excess heat supply to basal ice from some combination of geothermal heat flux (especially under insulating very thick ice), frictional heating by flowing ice, and heat advection by flow convergence. How effectively the resulting basal water then promotes sliding depends on another set of factors including substrate properties, water pressure variations, bed permeability, and the connectivity of the subglacial drainage network and its seasonal evolution. These factors interact on glacier beds of widely differing lithology and topography to give a challenging modeling environment. Thus, empirical observations of former ice sheet beds are vital for defining boundary conditions and geomorphological outcomes.

Former ice sheet beds show strong patterns in the distribution of glacial erosion, evidenced by landscape types, and indicative of past ice sheet thermal regime and flow structure. Earlier representations of ice sheets as defining first-order radial zones of thermal regime, erosion, and deposition (Sugden and John, 1976; Sugden, 1978) have been refined to integrate the role of dynamic ice streams evacuating ice from ice-drainage basins within ice sheets. These operate, perhaps intermittently, when thermal, substrate and hydrological conditions combine to provide conditions facilitating optimum sliding and erosion. Such palaeo-ice streams are now being recognized from their distinct geomorphological signatures. For example, in Scotland, the late Pleistocene Minch ice stream drained much of NW Scotland out to the continental shelf edge (Stoker and Bradwell, 2005) and the Strathmore ice stream concentrated ice discharges from the south and east Highlands (Golledge and Stoker, 2006). The erosional landscapes of the hinterlands and main axes of such ice streams are important evidence of their significance for the dynamics of Pleistocene ice sheets.

Alpine glacial erosion and the height of mountains

Alpine landscapes of glacial erosion are assemblages of familiar (though sometimes poorly understood) forms

including cirques, horns, arêtes, and troughs, with the common characteristic of local accumulation sources and erosion by partly or entirely warm-based cirque and valley glaciers. As a result, alpine landscapes are best developed in mid-latitude mountain ranges.

The significance of alpine erosional topography for tectonic-isostatic modeling of mountain uplift highlights another example of a renewed scientific interest in "old-fashioned" glacial landscapes. Molnar and England (1990) highlight the feedbacks between the glacial denudation of mountain ranges and their uplift. Isostasy compensates for the majority of the crustal thickness lost to erosion of the mountains. Thus, removing 60 m of crust from range crests would lower the mountains by only c. 10 m. Molnar and England provocatively suggest that if the erosion was focused along valleys, and the isostatic response was areally distributed, this could lead to an increase in summit elevations, greater ice cover, and more erosion. Paradoxically, deepening of glacial troughs during glacial cycles could thereby increase the maximum height of alpine mountains even if average relief did not change. They hint that the initiation of Quaternary glaciations could thereby have accelerated mountain-building processes due to climatic change.

This controversial idea has been countered by the "glacial buzzsaw" hypothesis (Brozović et al., 1997). This depends on a premise that glacial erosion in alpine terrain is more effective than fluvial erosion, as several authors including Montgomery (2002) have argued. As a mountain massif is uplifted above the glaciation threshold, trough cutting will accelerate mass loss from the uplifting crust while cirque development and periglacial slope mass-wasting will "shave off" the summits to limit range heights. Where summits intersect the glaciation limit by only enough to produce cirque glaciers, cirque evolution primarily by lengthening more than by deepening or widening (Brook et al., 2006a) means that retreating headwalls on opposing slopes may lower the ridgelines. A negative feedback is hypothesized, in which the taller and steeper the mountains, the more erosive the glaciers, so that the height of mountain ranges becomes self-limiting. This mechanism has been suggested to explain range hypsometry and/or long-term sediment yields in the Himalaya (Brozović et al., 1997) the Andes (Montgomery et al., 2001), Alaska (Spotila et al., 2004), and the Western Cordillera of North America (Mitchell and Montgomery, 2006; Foster et al., 2008). Evidence for the buzzsaw also includes systematic relationships between both equilibrium-line altitudes and range crests (Porter 1964), and between ELA and maximum ice flux and erosion (Foster et al., 2008). The buzzsaw hypothesis can be criticized for an overreliance on the hypsometric (area-altitude) distribution of relief. In the European Alps, for example, uplifted preglacial valley floors below glacially modified peaks could be mistaken for "buzzsaw" planation. The applicability of the buzzsaw hypothesis to different tectonic and climatic settings is an area for further research.

Landscape modification over multiple glacial cycles

How long does it take to establish a glacial erosional landscape on initially unglaciated terrain? Modeling of trough cross-sectional development showed that a mature "U"-shaped valley can develop within a single glacial cycle of c. 10^5 years (Harbor et al., 1988). In New Zealand's Southern Alps, empirical verification for this estimate is provided by examining the erosional geomorphology of mountains in which trough-and-arête topography evolved on uplifting ranges exposed to glaciations for only the last 200,000 years of glacial duration (Kirkbride and Matthews, 1997; Brook et al., 2006b). These studies imply that mature troughs can be established early in a succession of glacial cycles in tectonically active maritime mountain ranges, where glacial erosion rates are of the order of at least several millimeters per year. Glacial landscape evolution would be correspondingly slower where low erosion rates (c. 0.01–0.1 mm/year) occur in dry climates and on durable crystalline rocks. On geological timescales, erosive alpine glaciers can impose glacial landscapes on the Earth's crust very rapidly. Later glaciations presumably contribute little to further topographic evolution once valley cross sections are adjusted to efficiently evacuate ice discharges. Long-term feedbacks between glacial landscape evolution and ice extent are suggested by Kaplan et al.'s (2009) observation that Patagonian glaciations were of successively smaller magnitude over the last 1.1 million years, in spite of favorable climate, as glacial erosion reduced potential ice accumulation areas and provided a topography favoring low-gradient fast ice flow.

Conclusions

Glacial modification of topography is important in two main respects. First, understanding how glacial erosion operates at landscape scales allows reconstruction of past basal processes beneath continental ice sheets, helping to understand ice sheet evolution and response to climate change. Second, erosional landscapes in alpine mountain ranges have a characteristic hypsometry and elevated sediment yield that feeds into models of mountain uplift and denudation. The study of landscapes of glacial erosion has progressed remarkably over several decades from bland description of form and topography to being an integral component of modeling climate-tectonic interactions in Earth system science.

Bibliography

Benn, D. I., and Evans, D. J. A., 1998. *Glaciers and Glaciation*. London: Arnold, p. 734.

Boulton, G. S., 1979. Processes of glacial erosion on different substrata. *Journal of Glaciology*, **23**, 15–37.

Brook, M. S., Kirkbride, M. P., and Brock, B. W., 2006a. Cirque development in a steadily uplifting range: rates of erosion and long-term morphometric change in alpine cirques in the Ben Ohau Range, New Zealand. *Earth Surface Processes and Landforms*, **31**, 1167–1175.

Brook, M. S., Kirkbride, M. P., and Brock, B. W., 2006b. Quantified timescale for glacial valley cross-profile evolution in alpine mountains. *Geology*, **34**, 637–640.
Brozović, N., Burbank, D. W., and Meigs, A. J., 1997. Climatic limits on landscape development in the northwestern Himalaya. *Science*, **276**, 571–574.
Foster, D., Brocklehurst, S. H., and Gawthorpe, R. L., 2008. Small valley glaciers and the effectiveness of the glacial buzzsaw in the northern Basin and Range, USA. *Geomorphology*, **102**, 624–639.
Golledge, N. R., and Stoker, M. S., 2006. A palaeo-ice stream of the British ice sheet in eastern Scotland. *Boreas*, **35**, 231–243.
Hallet, B., 1979. A theoretical model of glacier abrasion. *Journal of Glaciology*, **23**, 39–50.
Hallet, B., 1996. Glacial quarrying, a simple theoretical model. *Annals of Glaciology*, **22**, 1–8.
Harbor, J. M., Hallet, B., and Raymond, C. F., 1988. A numerical model of landform development by glacial erosion. *Nature*, **333**, 347–349.
Hildes, D. H. D., Clarke, G. K. C., Flowers, G. E., and Marshall, S. J., 2004. Subglacial erosion and englacial sediment transport modelled for the North American ice sheets. *Quaternary Science Reviews*, **23**, 409–430.
Jamieson, S. S. R., Hulton, N. R. J., Sugden, D. E., Payne, A. J., and Taylor, J., 2005. Cenozoic landscape evolution of the Lambert basin, East Antarctica: the relative role of rivers and ice sheets. *Global and Planetary Change*, **45**, 35–49.
Jamieson, S. S. R., Hulton, N. R. J., and Hagdorn, M., 2008. Modelling landscape evolution under ice sheets. *Geomorphology*, **97**, 91–108.
Kaplan, M. R., Hein, A. S., Hubbard, A., and Lax, S. M., 2009. Can glacial erosion limit the extent of glaciation? *Geomorphology*, **103**, 172–179.
Kirkbride, M., and Matthews, D., 1997. The role of fluvial and glacial erosion in landscape evolution: the Ben Ohau Range, New Zealand. *Earth Surface Processes and Landforms*, **22**, 317–327.
Li, Y., Harbor, J., Stroeven, A. P., Fabel, D., Klemen, J., Fink, D., Caffee, M., and Elmore, D., 2005. Ice sheet erosion patterns in valley systems in northern Sweden investigated using cosmogenic nuclides. *Earth Surface Processes and Landforms*, **30**, 1039–1049.
Mitchell, S. G., and Montgomery, D. R., 2006. Influence of a glacial buzzsaw on the height and morphology of the Cascade Range in central Washington State, USA. *Quaternary Research*, **65**, 96–107.
Molnar, P., and England, P., 1990. Late Cenozoic uplift of mountain ranges and global climate change: chicken or egg? *Nature*, **346**, 29–34.
Montgomery, D. R., 2002. Valley formation by fluvial and glacial erosion. *Geology*, **30**, 1040–1050.
Montgomery, D. R., Balco, G., and Willett, S. D., 2001. Climate, tectonics, and the morphology of the Andes. *Geology*, **29**, 579–582.
Phillips, W. M., Hall, A. M., Mottram, R., Fifield, L. K., and Sugden, D. E., 2006. Cosmogenic ^{10}Be and ^{26}Al exposure ages of tors and erratics, Cairngorm Mountains, Scotland: timescales for the development of a classic landscape of selective linear glacial erosion. *Geomorphology*, **73**, 222–245.
Porter, S. C., 1964. Composite Pleeistocene snowline of Olympic mountains and Cascade range, Washington. *Geological Society of America Bulletin*, **75**, 477–482.
Spotila, J. A., Buscher, J. T., Meigs, A. J., and Reiners, P. W., 2004. Long-term glacial erosion of active mountain belts: example of the Chugach-St.Elias ranges, Alaska. *Geology*, **32**, 501–504.
Stoker, M., and Bradwell, T., 2005. The Minch palaeo-ice stream, NW sector of the British-Irish ice sheet. *Journal of the Geological Society*, **163**, 425–428.
Sugden, D. E., 1974 Landscapes of glacial erosion in their relationships to ice, topographic and bedrock conditions. *Institute of British Geographers, Special Publication* 7, pp. 177–195.
Sugden, D. E., 1978. Glacial erosion by the Laurentide ice sheet. *Journal of Glaciology*, **20**, 367–391.
Sugden, D. E., and John, B. S., 1976. *Glaciers and Landscape*. London: Arnold.
Summerfield, M. A., 1991. *Global Geomorphology*. Longman: Harlow, p. 537.
Swift, D. A., Persano, C., Stuart, F., Gallagher, K., and Whitham, A., 2008. A reassessment of the role of ice sheet glaciations in the long-term evolution of the East Greenland fjord region. *Geomorphology*, **97**, 109–125.

Cross-references

Alps
Andean Glaciers
Cirque Glaciers
Glacial Erosion
Glacial Geomorphology and Landforms Evolution
Himalaya
Landforms of Glacial Erosion
Subglacial Processes
Temperate Glaciers

LAST GLACIAL MAXIMUM GLACIATION (LGM/LGP) IN HIGH ASIA (TIBET AND SURROUNDING MOUNTAINS)

Matthias Kuhle
Department of Geography and High Mountain Geomorphology, Geographical Institute, University of Göttingen, Göttingen, Germany

Synonyms

Pleistocene glaciation of High Asia during the last ice age; Quarternary glaciation of High Asia during the MIS 3-2

Definition

Reconstruction of the maximum extent of the ice cover in High Asia.

Introduction: The state of research up to 1973

A synopsis of older results and views on the Pleistocene glacier cover in High- and Central Asia has been provided by Wissmann's (1959) compilation. Glacier cover of Tibet is discussed in the Chinese literature by Shi and Wang (1979), and has also been reproduced by CLIMAP (Cline, 1981, entitled "Last Glacial Maximum"). These authors speak of a 10% to maximum 20% ice cover of the mountains and plateaus of Tibet. Even in the "Quaternary Glacial Distribution Map of Qinghai-Xizang (Tibet) Plateau" (Shi et al., 1991), this opinion is to a great extent repeated and supported. However, there was a first restriction: Zhou Shangzhe, a member of this group, agreed with the author's reconstruction of an inland ice as for the Tibetan plateau area on Animachin (cf. Figure 1) (Kuhle, 1987, 1988a). In this map, he put down a plateau glacier area of still 400 × 300 km in size. But time and time again, from as long ago as the turn of the nineteenth to twentieth

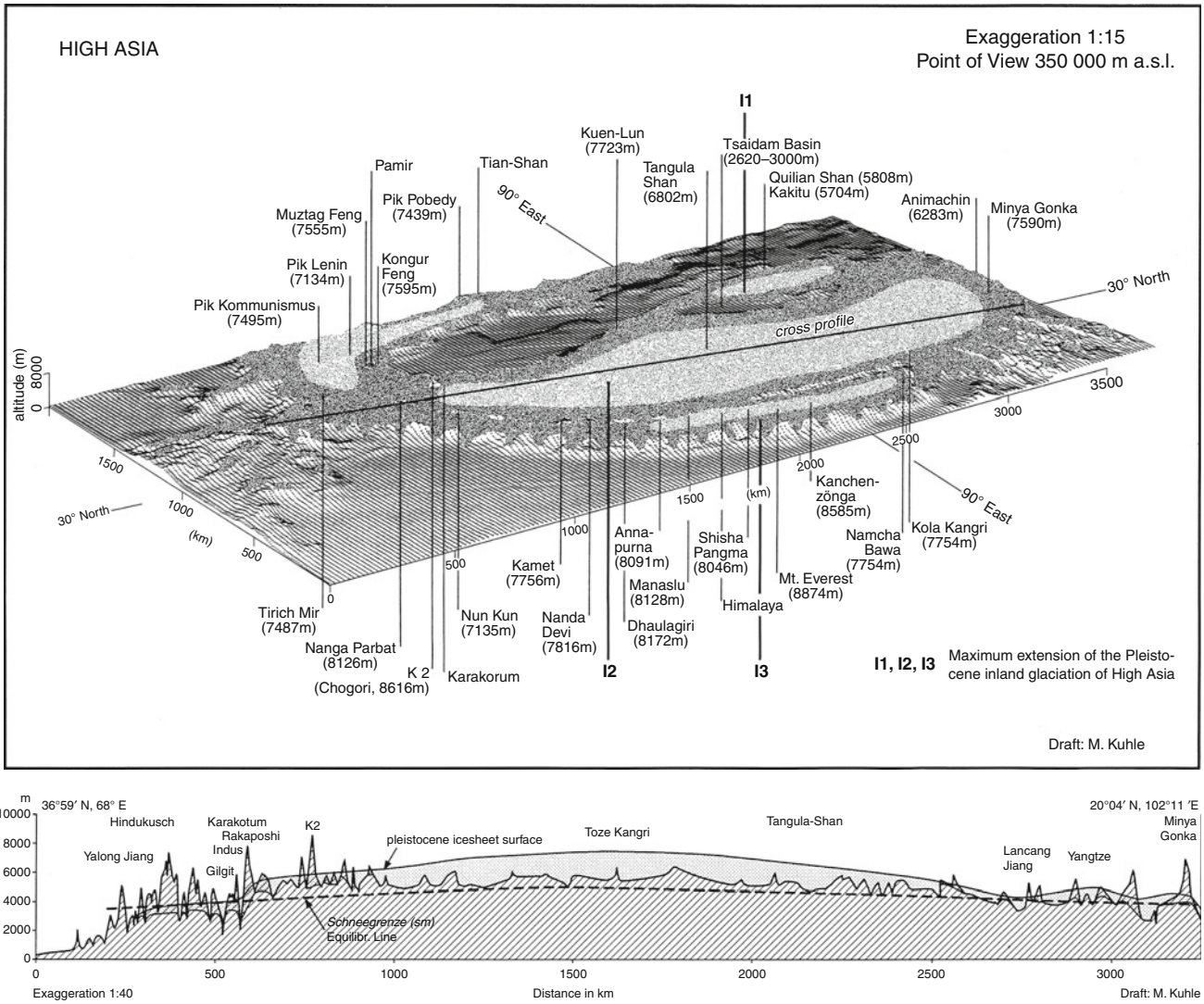

Last Glacial Maximum Glaciation (LGM/LGP) in High Asia (Tibet and Surrounding Mountains), Figure 1 *Top*: The reconstructed 2.4 million square kilometres ice sheet or ice stream network covering the Tibetan plateau (Kuhle, 1987, 1988a, b, 1989, 1995, 1998, 2001, 2004, 2005, 2007, 2011), with the three centers I 1, I 2, I 3. Only peaks higher than 6,000 m rise above the ice surface. *Figure 1. Bottom*: Cross profile of the central ice sheet from Hindu Kush in the west to Minya Gonka in the east.

century, there have been single investigators, such as Oestreich (1906), Dainelli and Marinelli (1928), Norin (1932), and others (see Kuhle, 1988b:416–417), who described ancient ice margin sites scattered throughout the high regions of Asia. According to the author's calculations, the above work represents ELA (equilibrium line altitude) depressions of more than 1,000 m and indicates, locally, significantly more glacier cover than the Wissmann scheme had acknowledged. However, these authors neither drew nor gave voice to such conclusions. Other early researchers, such as Huntington (1906), Tafel (1914), Trinkler (1932), Zabirov (1955), and others (see Kuhle, 1988b: 416–417), making more or less direct use of the data they obtained by observation, reconstructed larger glacier areas which, depending on the altitude of the mountains of plateaus, had built up only a few hundred meters of ELA depression.

The author has been fortunate in being able to carry out about 37 expeditions and research visits since 1973, some of which extended to 7 months, with the purpose of reconstructing the extent of glaciers in Asia during the glacial periods. The location and large number of areas under investigation permit reconstuction of the glacier areas to be made for the whole Tibet and parts of Central Asia. Reconstructions are supported by data from some earlier authors (see above) and are in glaring contrast to the negligible ice cover published by CLIMAP as late as 1981 (Cline, 1981) and the "Quaternary Glacial Distribution Map of Qinghai-Xizang (Tibet) Plateau" (Shi Yafeng et al., 1991). For example, the extent of glaciation of Tibet

during the Last Ice Age is given as approximately 2.4 million km² and is estimated to include a central thickness of about 2 km. Breaking up on the edges, ice discharged through the surrounding mountains as steep outlet glaciers (a.o., Kuhle, 1989, 1998, 2005).

Synopsis of the extent of the inland-ice in Tibet since the earliest Last Glacial Period (LGP)

Figure 1 shows the reconstruction of the maximum glaciation in Tibet, with an area of about 2.4 million km². In the central part, it formed a compact inland ice sheet with outflows that descended through the surrounding mountains and terminated at the steep edges of the high plateau.

To err on the safe side, the 50–70 m high, glaciofluvial gravel terraces east of 84°–85°E, which lie there on a valley floor at 3,800–3,900 m a.s.l, are classified as High Glacial deposits (Kuhle, 1989, 1998, 2004). They indicate a glacier-free Tsangpo section, which separates glacier complexes I3 and I2 as far west as 84°E (Figure 1, top).

Further in the west, the complexes I2 and I3 join again during the maximum of the Last Glacial Period (LGP) (Figure 1, top). With an equilibrium line as low as 600 m below the average plateau altitude (Figure 1, bottom), glaciation seems likely, even in the case of the more easterly Tsangpo section. This would place the gravel terraces and varved clays of the deepest parallel valleys in the late Last Glacial Period (LGP). Thus until now, at least for one time-interval during the LGP, this valley section is regarded as free of ice. A precise dating of the terraces is to be done (Figure 1, top, from north of Shisha Pangma to near Kola Kangri; cf. Kuhle, 2004). The second ice free area is the Tsaidam Depression. In the block diagram of Figure 1 (top), it shows up as narrow strip below I1 (cf. Kuhle, 2004).

Dates of lake sediments in the area of the former ice sheet are all younger than 13,000 years old because they developed only after the glaciers had melted (Gasse et al., 1996, and others). By contrast, lakes in nearby, nonglaciated areas such as the Tsaidam basin (Figure 1) and the Gobi desert display continuous sediment records going back more than 40,000 years (Pachur and Wünnemann, 1995; and others).

In a north-westerly direction from Mt. Everest to K2 (Figure 1), and from Dhaulagiri to the western Kuen Lun (Figure 1), the cross section shows that the Last Glacial Period (LGP) Equilibrium Line Altitude (ELA) runs parallel to the present ELA (in the area of southern Central Tibet the ELA attained an altitude of over 4,700 m a.s.l. (Figure 1, bottom)) (Kuhle, 1998, 2004). Nonetheless, a Last Glacial Period (LGP) Equilibrium Line Altitude (ELA) depression of at least 1,200 m means that 83–86% of the plateau surface was above the ELA. The accumulating ice necessarily led to the filling of valleys that incised the Tibet plateau. The remainder accounts for the remaining 14–17%.

Last Glacial Period (LGP) glaciers attained an approximate thickness of 2,700 m. Glacier thicknesses, ascertained by means of abrasions, polishings, and erratics, reach 1,600–2,000 m in the Himalaya and 700–1,200 m in Central and North Tibet. In the northern, southern, and western Karakorum, thicknesses of 1,750–2,600 m have been observed (Kuhle, 1987, 1988a, b, 1989, 2004, 2005) and in some places confirmed by Hewitt (2009a, b). However, these are probably minimum values. The ice may well have risen to 2,500–3,000 m in Central Tibet owing to a compact ground plan that extended over 1,500 × 3,000 km. The high viscosity of cold, continental glacier ice with annual temperatures of around −6°C to −10°C at the ELA (Kuhle, 1998) supports the build-up of ice, provided that there is sufficient precipitation. An average thickness for all of the Tibet ice of approximately 1,000 m implies that 2.2 million km³ of water was bound in the ice sheet of Tibet. This corresponds to a lowering of sea level of about 5.4–6.5 m (Kuhle, 1998).

Earlier it has been shown (cf. Kuhle, 1998, Figure 22) how the glaciated area in Tibet and in the Karakorum relates to an ELA depression or an uplift of the plateau- and mountain relief of only 500 m. At the same time, it permits an estimation of conditions if the equilibrium line drops by 1,200 m and makes the cupola-shaped build-up of the inland ice to a considerable thickness plausible. With the ice held back by mountain barriers, build-up was assisted by the low run-off, and initially by freezing to the subsurface. At a later stage, due to ice build-up, the pressure-induced melting point was reached. Run-off from the central inland ice sheet gradually increased until an equilibrium had been achieved. This was the end of ice build-up.

Meanwhile the Tibetan ice is confirmed by different disciplines. This will be shown by only three selected items

Breakdown of the summer monsoon, strengthening of the winter monsoon, and pioneering role of the subtropical inland ice

A Tibetan inland ice must have prevented the development of a low-pressure cell, a heat low, as it exists today over the heated debris covers of Tibet. Accordingly, the summer monsoon weakened. In the meantime, deep-sea cores from the Arabian Sea prove the glacial breakdown of the SW-Indian summer monsoon via dust fall (Sirocko et al., 1993). Loess-palaeosol sequences in China showing the fluctuations of the East-Asian monsoon also confirm the dramatical weakening of the summer monsoon during glacial phases (Rutter and Ding, 1993). At the same time, however, the winter monsoon strengthens during the ice ages like a mirror image of the summer monsoon. The winter monsoon was the result of differences in temperature, in this case between cold continental and catabatic winds of the Tibetan ice and the relatively warm air over the Pacific and Indian oceans. The resulting cold/dry anticyclonic wind blew loess out of the Inner-Asian glaciolimnical meltwater pits and deposited it on the Chinese loess plateau. Due to grain-size measurements in loess–palaeosol sequences, evidence was provided of

monsoonal variations and a special intensity of the winter monsoon during the glacial period (Xiao et al., 1995). Modeling has shown that the Nordic inland ices have nearly no effect on monsoon circulation whose intensity is primarily controlled by direct insolation at low altitudes (Felzer et al., 1998). Hence, the weakening of the summer monsoon and simultaneous strengthening of the winter monsoon is a clear pointer to a large-scale subtropical glaciation on the Tibetan plateau (Anderson and Prell, 1993). At the same time, this enormous climate-ecological influence on the monsoon makes clear that the Tibetan inland ice must have had a central influence on the global atmospheric circulation and energy balance. Probably, this climate-ecological signal is even strong enough to recognize a decisive influence on the global tendency towards glaciation. Tibet may have been the pacemaker and trigger for the ice ages (Kuhle, 1988a; cf. Ice age development theory, in this volume). Tibet's key role is confirmed by computer models showing that the Tibetan ice sheet is not only the first to be built up at the onset of a glacial cycle, but that when the build-up of the Tibetan inland ice had already come to an end, only half of the Nordic lowland ices were built up, i.e., that they develop much more slowly. The global ice volume then measured only 50% of the maximum ice volume during the LGM (Marsiat, 1994).

Glacial isostasy

Glacial-isostatic rebound during inter- and postglacial periods is an indicator of a High Glacial inland ice cover. The very high uplift rate of 12 mm per year measured on the Tibetan plateau (Hsu et al., 1998) is such a glacio-isostatic indicator because its value lies far above that of normal tectonic uplift. Just within the short Pleistocene period (1,000,000 years), it would lead to an unrealistic uplift of 12 km. These measurements confirm corresponding uplift calculations of the applicant due to meanwhile self-glaciated end moraines N of Shisha Pangma (S-Tibet) (Kuhle, 1995). The thickness of the inland ice of 2,000 m led to a glacio-isostatic lowering of the plateau by 600–700 m down to c. 4,300 m a.s.l. At the same time, this is the cause of the interglacial deglaciation of Tibet (Kuhle, 1995). On the basis of changes of geoid anomaly in relation to gravity anomaly – a method that allows to distinguish glacio-isostatic from tectonic uplift – also Kaufmann and Lambeck (1997) and Wang (2001) have shown a glacio-isostatic uplift of Tibet and thus have confirmed a Tibetan glaciation (Nesje and Dahl, 2001:127). Obviously, the effects of an up to 2,000 m thick ice sheet on the height of the plateau are so profound that the satellite missions CHAMP and GRACE were able to identify them (Kuhle, 2001).

Computer models and tests of general circulation models

Up to now, the general circulation models made up and tested by computer modeling were based on the global inland ice configurations of CLIMAP (1981) and COHMAP (1988), i.e., they did not include the glaciation of Tibet. These climate models unanimously show the tendency of Tibet to develop a permanent snow cover and thus to form a large-scale glaciation of the Tibetan plateau (Kutzbach et al., 1998). All sensitive experiments also indicate the growth of an ice sheet in Central Tibet which is much more likely and the development of which must have set in much earlier than that of the more northern Laurentide- and Fenno-Scandinavian ice sheets (Verbitsky and Oglesby, 1992; Marsiat, 1994). Marsiat also shows that on conditions of a reduced glaciation of Tibet, the development of the Nordic lowland ices is insignificant, too (Marsiat, 1994). This independent modeling result has been considered to be an unexpected mistake of these climate models (Verbitsky and Oglesby, 1992; Marsiat, 1994; Kutzbach et al., 1998). Actually, however, it is a clear confirmation of the terrestrial field data (Kuhle, 1987, 1988a, b, 1989, 1995, 1998, 2001, 2004, 2005, 2007, 2011).

Dating

In the area of the Tsangpo bend in SE Tibet (Figure 1, left-hand side of Namcha Bawa), a last strong glacier advance is proved about or after 9.820+/−350 YBP. In addition, seven datings of trees from an 80 m high opening (1989) have been analyzed (Kuhle, 1998:83 Table 2: 99; 2004: 190 Figure 37). The eight ^{14}C-samples stem from the lower 32 m of the opening. These limnic basal sands, in which the trunks were embedded, have been overlain by 8 m thick varved clays. They provide evidence of an ice-dammed lake in this lower section of the Tsangpo valley at merely c. 3,000 m a.s.l. Accordingly, this ice-dammed lake is of the same age or younger than 48.580–9.820 YBP. Therefore, it is classified as being of the Last Glacial Maximum up to Late Glacial. The counting out of the varves yielded that the lake existed c. 1,000 years. It was situated between the ice complexes I2 and I3 (Figure 1, left-hand side of Namcha Bawa) and was dammed up by the Nyang Qu Glacier. The Nyang Qu Glacier, which was an outlet glacier of the ice complex I2, followed the Nyang Valley, reaching the Tsangpo Valley 17.5 km down-valley from the opening. Ground and lateral moraines confirm that the glacier bended into the Tsangpo Valley, and thus the ice-dammed lake came into being. These are several of the datings which establish an immediate genetic connection to the inland glaciation of Central Tibet and thus provide evidence of the Ice Sheet during the Last Glacial Period (LGP).

Discussion of datings

For several years, TCN-dating in High Asia has been carried out by some authors. However, a methodically fundamental mistake is that the astrophysical metric of cosmic radiation has not been sufficiently explored so far, and that the TCN-dating method therefore is not considered to be a reliable dating technique. In the critical remark (Kuhle and Kuhle, 2010), however, it is referred to the, at least up to now, unsolved astrophysical problem which states that one cannot assume constancy of cosmic radiation; the constancy assumption is, however, the indispensably

most important prerequisite for both TCN- and OSL-dating techniques.

As has been shown in other areas of the Himalaya, Karakoram, and Tibet, up to now, only ^{14}C-datings are glaciogeomorphologically safe, while the OSL- and TCN-datings carried out so far because of the high sea level are fourfold to tenfold overestimated, i.e., they led to too old ages. Thus, by means of ^{14}C-datings of moraines in the Khumbu Himal, a snowline (ELA)-depression up to 500 m has been evidenced during the Neoglacial period c. 2.1 and 4.2 ka ago; while the same ELA-depressions according to OSL- and TCN-ages were dated to c. 16–23 ka, i.e., they were overestimated by a factor 6.5. More OSL- and TCN-overestimations are evidenced for S- and Central Tibet and the Karakoram (Kuhle and Kuhle, 2010).

Probably the age of the TCN-data that so far have not been calibrated with regard to the high sea level of High Asia has been overestimated on the following grounds:

1. Obviously, the correction factors underestimate the amount of cosmic rays that really hit the surfaces of very high altitudes.
2. Due to magnetic field excursions, the amount of cosmic rays (CR) was additionally strengthened during the Late and High Glacial. This must have had a special effect at high altitudes, so that the age overestimation exponentially increases with moraine age.

This means that the Late Glacial moraine stages can already be extremely overestimated as to their age and thus differ from the Holocene stages in a clear age leap, while the glaciogeological findings do not confirm this great difference in age.

Actually there are already several independent proofs with regard to an "age leap" like this of the TCN-dating in High Asia (ibid. and Kuhle, 2011).

With regard to this deficiency of TCN-dating – that unfortunately has come into fashion – it is scientifically extremely important to take the complete glaciogeological and glaciogeomorphological setting into consideration and give to it the primary importance it deserves (Kuhle and Kuhle, 2010).

Summary

Since 1973, new data were obtained on the maximum extent of glaciation in High Asia. Evidence for an ice sheet covering Tibet during the Last Glacial Period means a radical rethinking about glaciation in the Northern Hemisphere. The ice sheet's subtropical latitude, vast size (2.4 million km²), and high elevation (6,000 m a.s.l.) are supposed to have resulted in a substantial, albedo-induced cooling of the Earth's atmosphere and the disruption of summer monsoon circulation. Moraines were found to reach down to 460 m a.s.l. on the southern flank of the Himalayas and to 2,300 m a.s.l. on the northern slope of the Tibetan Plateau, in the Qilian Shan region. On the northern slopes of the Karakoram, Aghil, and Kuen Lun mountains, moraines occur as far down as 1,900 m a.s.l. In southern Tibet, radiographic analyses of erratics suggest a former ice thickness of at least 1,200 m. Glacial polish and roches moutonnées in the Himalayas and Karakoram suggest former glaciers as thick as 1,200–2,700 m. On the basis of this evidence, an 1,100–1,600 m lower equilibrium line (ELA) has been reconstructed, resulting in an ice sheet of 2.4 million km², covering almost all of Tibet. ^{14}C ages classify this glaciation as MIS 3-2 in age (Würmian = Last Glacial Period (LGP), c. 60.000–18.000 years ago).

Bibliography

Anderson, D. M., and Prell, W. L., 1993. A 300 KYR record of upwelling off Oman during the late quaternary: evidence of the Asian southwest monsoon. *Paleoceanography*, **8**, 193–208.

Cline, R. (ed.), 1981. *Climap Project: Seasonal Reconstructions of the Earth's Surface at the Last Glacial Maximum*. New York: Geological Society of America, pp. 1–18.

COHMAP, 1988. Climatic changes of the last 18, 000 years: observations and model simulations. *Science*, **241**, 1043–1052.

Dainelli, G., and Marinelli, O., 1928. Le condizione fisiche attuali. Risultati Geologici e Geografici, Relazione scientifiche della Speditizione Italiana De Filippi nell'Himalaya, Caracorum e Turchestan Cinese (1913–1914), Ser.II, Vol. IV, Bologna.

Felzer, B., Webb, T., and Oglesby, R. J., 1998. The impact of ice sheets, CO², and orbital insolation on late quaternary climates: sensitivity experiments with a general circulation model. *Quaternary Science Reviews*, **17**, 507–534.

Gasse, F., Fontes, J Ch, Van Campo, E., and Wei, K., 1996. Holocene environmental changes in Bangong Co basin (Western Tibet). Part 4: Discussion and conclusions. *Palaeogeography, Palaeoclimatology, Palaeoecology*, **120**, 79–92.

Hewitt, K., 2009a. Catastrophic rock slope failures and late quaternary developments in the Naga Parbat – Haramosh Massif, Uper Indus basin, northern Pakistan. *Quaternary Science Reviews*, doi:10.1016/j.quascirev.2008.12019.

Hewitt, K., 2009b. Glacially conditioned rock-slope failures and disturbance-regime landscapes, Upper Indus Basin, northern Pakistan. *Geological Society, London, Special Publications*, **320**, 235–255, doi:10.1144/SP320.15.

Hsu, H., Zhang, C., and Wang, Y., 1998. Study on crustal movements of Tibetan plateau and its mechanism by geodetic methods. *"International Symposium on the Qinghai-Tibet Plateau"* 4, Xining, China.

Huntington, A., 1906. Pangong, a glacial lake in the Tibetan plateau. *Journal of Geology*, **14**, 599–617.

Kaufmann, G., and Lambeck, K., 1997. Implications of Late Pleistocene glaciation of the Tibetan plateau for present-day uplift rates and gravity anomalies. *Quaternary Research*, **48**, 267–279.

Kuhle, M., 1987. The problem of a Pleistocene Inland glaciation of the Northeastern Qinghai-Xizang-Plateau. In Hövermann, J., and Wenjing, W. (eds.), *Reports on the Northeastern Part of Quinghai-Xizang (Tibet)-Plateau by the Sino-German Scientific Expedition 1981*. Beijing: Science Press, pp. 250–315.

Kuhle, M., 1988a. Subtropical mountain- and highland-glaciation as ice age triggers and the waning of the glacial periods in the Pleistocene. *Chinese Translation Bulletin of Glaciology and Geocryology*, **5**(4), 1–17. in Chinese language.

Kuhle, M., 1988b. Zur Geomorphologie der nivalen und subnivalen Höhenstufe in der Karakorum-N-Abdachung zwischen Shaksgam-Tal und K2 Nordsporn: Die quartäre Vergletscherung und ihre geoökologische Konsequenz. In Becker, H. (ed.), *Tagungsbericht und wissenschaftliche Abhandlung des* 46. Deutschen Geographentag 1987 München. Steiner: Stuttgart, pp. 413–419.

Kuhle, M., 1989. Die Inlandvereisung Tibets als Basis einer in der Globalstrahlungsgeometrie fußenden, reliefspezifischen Eiszeittheorie. In *Petermanns Geographische Mitteilungen*. Justus Perthes Verlag: Gotha, Vol.133 (4), pp. 265–285.
Kuhle, M., 1995. Glacial isostatic uplift of tibet as a consequence of a former ice sheet. *GeoJournal*, **37**(4), 431–449.
Kuhle, M., 1998. Reconstruction of the 2.4 million qkm Late Pleistocene ice sheet on the Tibetan plateau and its impact on the global climate. *Quaternary International*, **45/46**, 71–108. Erratum: Vol. 47/48:173-182 (1998) included.
Kuhle, M., 2001. The Tibetan ice sheet; its impact on the palaeomonsoon and relation to the Earth's oribatal variations. *Polarforschung*, **71**(1/2), 1–13.
Kuhle, M., 2004. The high glacial (last ice age and LGM) ice cover in high and Central Asia. In Ehlers, J., Gibbard, P. L. (eds.), *Development in Quaternary Science*, 2c (Quaternary Glaciation – Extent and Chronology, Part III: South America, Asia, Africa, Australia, Antarctica), Amsterdam: Elsevier B.V, pp. 175–199.
Kuhle, M., 2005. Glacial geomorphology and ice ages in Tibet and surrounding mountains. *The Island Arc*, **14**(4), 346–367. Blackwell Publishing Asia Pty Ltd.
Kuhle, M., 2007. Critical approach to the methods of glacier reconstruction in High Asia (Qinghai-Xizang(Tibet) plateau, West Sichuan plateau, Himalaya, Karakorum, Pamir, Kuenlun, Tienshan) and discussion of the probability of a Qinghai-Xizang (Tibetan) inland ice. *Journal of Mountain Science (JMS)*, **4**(2), 91–123.
Kuhle, M., 2011. The High Glacial (LGP, LGM, MIS 3-2) southern outlet glaciers of the Tibetan inland ice through Mustang into the Thak Khola as further evidence of the Tibetan ice. *Journal of Nepal Geological Society*, submitted 14th November 2010.
Kuhle, M., and Kuhle, S., 2010. Review on dating methods: numerical dating in the quaternary of High Asia. *Journal of Mountain Science*, **7**, 105–122.
Kutzbach, J., Gallimore, R., Harrison, S., Behling, P., Selin, R., and Laarif, F., 1998. Climate and biome simulations for the past 21, 000 years. *Quaternary Science Reviews*, **17**, 473–506.
Marsiat, I., 1994. Simulation of the northern hemisphere continental ice sheets over the last glacial-interglacial cycle: experiments with a latitude-longitude vertically integrated ice sheet model coupled to a zonally averaged climate model. *Palaeoclimates*, **1**, 59–98.
Nesje, A., and Dahl, S., 2001. Glaciers and environmental change. Key Issues in *Environmental Change*: 1–200.
Norin, E., 1932. Quaternary climatic changes within the Tarim Basin. *Geographical Review*, **22**, 591–598. New York.
Oestreich, K., 1906. Die Täler des nordwestlichen Himalaya. *Petermanns Geographische Mitteilungen, Ergänzungsband*, **155**, 1–106.
Pachur, H.-J., and Wünnemann, B., 1995. Lake evolution in the Tengger desert, northwestern China, during the last 40, 000 years. *Quaternary Research*, **44**, 171–180.
Rutter, N., and Ding, Z., 1993. Paleoclimates and monsoon variations interpreted from micromorphogenic features of the Baoji Paleosols, China. *Quaternary Science Reviews*, **12**(10), 853–862.
Sirocko, F., Sarnthein, M., and Erlenkeuser, H., 1993. Century-scale events in monsoonal climate over the past 24, 000 years. *Nature*, **364**, 322–324.
Tafel, A., 1914. Meine Tibetreise. Eine Studienreise durch das nordwestliche China und durch die innere Mongolei in das östliche Tibet. 2 Bde., Karte, Stuttgart.
Trinkler, E., 1932. Geographische Forschungen in westlichen Zentralasien und Karakorum-Himalaya. *WissenschaftlicheErgebnisse der Dr. Trinklerschen Zentralasien-Expedition*. Berlin, pp. 1–133.
Verbitsky, M. Y., and Oglesby, R. J., 1992. The effect of atmospheric carbon dioxide concentration on continental glaciation of the northern hemisphere. *Journal of Geophysical Research*, **97**(D5), 5895–5909.
Wang, H., 2001. Effects of glacial isostatic adjustment since the late Pleistocene on the uplift of the Tibetan plateau. *Geophysical Journal International*, **144**, 448–458.
Wissmann, Hv., 1959. Die heutige Vergletscherung und Schneegrenze in Hochasien mit Hinweisen auf die Vergletscherung der letzten Eiszeit. *Akad Wiss Lit Abh Math-Natwiss Kl*, **14**, 1103–1407.
Xiao, J., Porter, S. C., An, Z., Kumai, H., and Yoshikawa, S., 1995. Grain size of quartz as an indicator of winter monsoon strength on the loess plateau of central China during the last 130, 000 yr. *Quaternary Research*, **43**, 22–29.
Yafeng, S., and Jing-Tai, W., 1979. The fluctuations of climate, glaciers and sea level since Late Pleistocene in China: Sea level, ice and climatic change. *Proceedings Canberra Symposium.* Canberra.
Yafeng, S., Binyuan, L., Jijun, L., Zhijiu, C., Benxing, Z., Qingsong, Z., Fubao, W., Shangzhe, Z., Zuhui, S., Keqin, J., and Jiancheng, K. (eds.), 1991. *Quaternary Glacial Distribution Map of Qinghai-Xizang (Tibet) Plateau, Scale 1:3, 000, 000*. Beijing: Science Press.
Zabirov, R. D., 1955. Oledenenie Pamira (Glaciations of the Pamir Mountains), Moscow, Geografgiz.

Cross-references

Climate Variability and High Altitude Temperature and Precipitation
Glacioisostasy
Himalaya
Ice Age
Ice Age Development Theory
Monsoonal Records Observed from Snow/Ice/Glacier
Quaternary Glaciation
Reconstruction of the Last Glaciations in the Whole of Asia
Sea-Level
Tibetan Plateau

LATENT HEAT OF CONDENSATION

Prem Datt
Research & Design Center (RDC), Snow and Avalanche Study Establishment, Himparishar, Chandigarh, India

The condensation is the opposite process of evaporation. Latent heat of condensation is energy released when water vapor condenses to form liquid droplets. The latent heat of condensation is defined as the heat released when one mole of the substance condenses. The temperature does not change during this process, so heat released goes directly into changing the state of the substance. It is expressed as kg/mol or kJ/kg. The energy released in this process is called heat of condensation. The heat of condensation of water is about 2,260 kJ/kg, which is equal to 40.8 kJ/mol. The heat of condensation is numerically exactly equal to the heat vaporization, but has the opposite sign. In the case of evaporation, the energy is absorbed by the substance, whereas in condensation heat is released by the substance. For example, as moist air is lifted and cooled, water vapor eventually condenses, which then allows for huge amounts of latent heat energy to be released, feeding the storm.

Bibliography

Armstrong, R. L., and Brun, E., 2008. *Snow and Climate: Physical Processes, Surface Energy Exchange and Modeling*. Cambridge: Cambridge University Press. ISBN 978-0-521-85454-2.
Jones, E. R., and Childers, R. L. *Contemporary College Physics.* Addison Wesley.
McClung, D., and Schaerer, P., 1993. *The Avalance Hand Book.* Seattle, WA: The Mountaineers.
The international classification for seasonal snow on the ground prepared by the ICSI-UCCS-IACS Working Group on Snow Classification, IHP-VII Technical Documents in Hydrology, IACS Contribution, UNESCO, Paris, 2009.

LATENT HEAT OF FUSION/FREEZING

Prem Datt
Research and Design Center (RDC), Snow and Avalanche Study Establishment, Himparishar, Chandigarh, India

Fusion is a physical process in which a solid converts into a liquid. The latent heat of fusion at a particular temperature is the amount of heat required to convert a unit mass of solid into liquid. For example, when ice melts into water the amount of heat required at 0°C is estimated equal to 334 kJ/kg, which is the latent heat of fusion of ice at 0°C. *This process is opposite to the process of freezing.* In a natural snowpack the fusion process generates melt-freeze polycrystals and melt-freeze clusters of the small rounded grains. A hard crust within snow results after multiple melt-freeze processes.

Bibliography

Armstrong, R. L., and Brun, E., 2008. *Snow and Climate: Physical Processes, Surface Energy Exchange and Modeling*. Cambridge: Cambridge University Press. ISBN 978-0-521-85454-2.
Jones, E. R., and Childers, R. L. *Contemporary College Physics.* Addison Wesley.
McClung, D., and Schaerer, P., 1993. *The Avalance Hand Book.* Seattle, WA: The Mountaineers.
The international classification for seasonal snow on the ground prepared by the ICSI-UCCS-IACS Working Group on Snow Classification, IHP-VII Technical Documents in Hydrology, IACS Contribution, UNESCO, Paris, 2009.

LATENT HEAT OF SUBLIMATION

Prem Datt
Research and Design Center (RDC), Snow & Avalanche Study Establishment, Himparishar, Chandigarh, India

Sublimation is a physical process in which a solid directly converts into a gaseous (vapor) state without going through a liquid state. The latent heat of sublimation at a particular temperature is the amount of heat required to convert a unit mass of solid into gas. For example, when ice sublimates into vapor, the amount of heat required at 0°C is estimated equal to 2,838 kJ/kg, which is the latent heat of sublimation of ice at 0°C. In the crystal growth of ice and snow in atmosphere, this process plays a dominant role. This process is opposite to the process of deposition.

Bibliography

Armstrong, R. L., and Brun, E., 2008. *Snow and Climate: Physical Processes, Surface Energy Exchange and Modeling*. Cambridge: Cambridge University Press. ISBN 978-0-521-85454-2.
Jones, E. R., and Childers, R. L. *Contemporary College Physics.* Addison Wesley.
McClung, D., and Schaerer, P., 1993. *The Avalance Hand Book.* Seattle, WA: The Mountaineers.
The international classification for seasonal snow on the ground prepared by the ICSI-UCCS-IACS Working Group on Snow Classification, IHP-VII Technical Documents in Hydrology, IACS Contribution, UNESCO, Paris, 2009.

LATENT HEAT OF VAPORIZATION/CONDENSATION

Prem Datt
Research and Design Center (RDC), Snow and Avalanche Study Establishment, Himparishar, Chandigarh, India

When a substance changes phase, the arrangement of its molecules changes, but its temperature does not change. If the new arrangement has a higher amount of thermal energy, then the substance absorbs thermal energy from its environment in order to make the phase change. If the new arrangement has a *lower* amount of thermal energy, the substance releases thermal energy to its environment.

Latent heat of vaporization is a physical property of a substance. It is defined as the heat required to change one mole of liquid at its boiling point under standard atmospheric pressure. It is expressed as kg/mol or kJ/kg. When a material in liquid state is given energy, it changes its phase from liquid to vapor; the energy absorbed in this process is called heat of vaporization. The heat of vaporization of water is about 2,260 kJ/kg, which is equal to 40.8 kJ/mol.

The vaporization is the opposite process of condensation. The heat of condensation is defined as the heat released when one mole of the substance condenses at its boiling point under standard pressure.

Bibliography

Armstrong, R. L., and Brun, E., 2008. *Snow and Climate: Physical Processes, Surface Energy Exchange and Modeling*. Cambridge: Cambridge University Press. ISBN 978-0-521-85454-2.
Jones, E. R., and Childers, R. L. *Contemporary College Physics.* Addison Wesley.
McClung, D., and Schaerer, P., 1993. *The Avalance Hand Book.* Seattle, WA: The Mountaineers.
The international classification for seasonal snow on the ground prepared by the ICSI-UCCS-IACS Working Group on Snow Classification, IHP-VII Technical Documents in Hydrology, IACS Contribution, UNESCO, Paris, 2009.

LATEROGLACIAL

Lasafam Iturrizaga
Geography/High Mountain Geomorphology, Institute of Göttingen, University of Göttingen, Göttingen, Germany

Synonyms

Ice-marginal

Definition

The term "lateroglacial" defines the ice-marginal areas along the lateral sides of the glacier. The lateroglacial environments grade downglacier into the latero-frontal and proglacial environments. They are composed of specific geomorphological and glaciological landform assemblages, such as ablation depressions, lateral moraines, breach lobes or earth pyramids. Lateroglacial landforms are mostly developed between the glacier and the adjacent valley flank in high mountain landscapes. However, they occur as well in the mountain forelands, especially along dam glaciers or outlet glaciers (e.g., in Iceland), but to a more limited extent. Relict lateroglacial sediments may serve as important geomorphological evidence for reconstructing the extent and ice thickness of former glaciations.

Bibliography

Iturrizaga, L., 2001. Lateroglacial valleys and landforms in the Karakoram Mountains (Pakistan). *GeoJournal*, **54**(2–4), 397–428. Tibet and high Asia (VI), Glacio-geomorphology and prehistoric glaciation in the Karakorum and Himalaya.

Iturrizaga, L., 2003. The distribution and genesis of lateroglacial valleys in the Karakoram Mountains (Pakistan). *Zeitschrift für Geomorphologie N.F.*, **130**(Suppl. Bd), 51–74.

Cross-references

Ablation Depression
Lateroglacial Landform Systems

LATEROGLACIAL LANDFORM SYSTEMS

Lasafam Iturrizaga
Geography/High Mountain Geomorphology, Institute of Göttingen, University of Göttingen, Göttingen, Germany

Synonyms

Ice-marginal landforms

Definition

Lateroglacial landforms are located at the lateral margins of the glaciers and belong to the glacial landscape systems. Down glacier they pass over into the laterofrontal and proglacial sediment environments. Lateroglacial landforms show characteristic landform sequences and assemblages (i.e., lateroglacial valleys, ablation depressions, earth pyramids) and are classified as a specific geomorphologic unit of the glacial environment.

Distribution

Lateroglacial landforms may occur at any glacier, preferentially at valley glaciers in mountain regions with sufficient debris supply areas and their associated forelands (i.e., in the European Alps, the Andes, and the Himalayas). They are best developed in the Karakoram Mountains (72°–79°E; 35°–36°N), where they have been investigated systematically as a specific geomorphological unit along 53 glaciers in regard to their distribution, evolution, and morphodynamics (Iturrizaga, 2001, 2003, 2007). The Karakoram shows the highest concentration of large valley glaciers outside of the polar regions with glacier lengths of up to 72 km. In combination with a surrounding high mountain relief of over 8,000 m, the Karakoram provides large-sized debris supply areas for the formation of a heterogeneous lateroglacial environment. Lateroglacial sediment complexes may attain a length of up to several to tens of kilometers and can be referred to as lateroglacial valleys. Besides their large horizontal distribution, they are spread over a considerable vertical range in the Karakoram and occur between altitudes of about 2,500–5,000 m. The upper limit of lateroglacial sediments deriving from the glacier is theoretically given by the altitude of the snow line. Due to the fact that a major part of the glaciers are avalanche-fed glaciers and therefore show steep inclined head walls of up to 3,000 m in absolute height, the distribution of lateroglacial sediments starts usually 1,000–1,500 m lower than the snow line.

Types of lateroglacial landforms and their processes of formation

The transition from the valley flank to the glacier emerges in different morphological variations. One of the most well-known and prominent landforms are the lateroglacial valleys, which are ice-marginal depressions between the glacier and the valley flank and may be filled with sediments. They even show in some cases an own drainage system over short distances. They are not true valleys in sensu stricto, but rather glacier-marginal discontinuous depressions. Where mountain spurs stand out against the glaciated main valley, the lateroglacial valleys may be interrupted. The topographical depression can be filled up with a wide range of different types of sediments or the sediments themselves may even be the trigger for the formation of the lateroglacial valleys. One of the main characteristics of the lateroglacial sediment regime is the damming effect by the glacier, which results in a large-scaled sediment storage along the glacier margins. The lateroglacial sediments are highly polygenetic landforms.

A characteristic type of lateroglacial valleys is the *lateral moraine valley*. It is a mostly linear depression or sediment assemblage between the lateral moraine and the valley flank (Oestreich, 1906). It had been erroneously often referred to as "*ablation valley*." Visser (1938) carried

out the first systematic investigation on these landforms and postulated an insolation-controlled distribution of all lateroglacial landforms. This terminology has been widely criticized by many authors (v. Klebelsberg, 1938; Hewitt, 1993) as the lateroglacial depressions show various formation processes. Consequently, the nongenetical expression "lateroglacial valleys" has been introduced (Iturrizaga, 2001). However, the formation of a lateroglacial valley might be triggered by the presence of an ablation depression as it can provide initial sediment traps.

The formation of lateral moraine valleys is mainly a result of (a) dumping processes of the lateral moraine against the valley flank, especially during times of a comparatively smaller extent of the glacier, and (b) different type of debris inputs from the adjacent tributary valleys and valley slopes. Their width attains a size of up to 1 km. The great dimension already indicates that ablation processes only play a subordinated role in their formation. The *lateral moraine* is the most distinct depositional landform in lateroglacial environments. It may attain a height of about 250 m. Its large size has been attributed to repetitive glacier advances and accordingly to various deposition processes. The lateral moraine is often composed of an older moraine core, which has been superimposed by younger moraine layers and/or processes of moraine accretion. The time period of their formation goes in general back to the Neoglacial and Little Ice Age. Once the lateral moraine has been built up, it prevents the direct debris transfer from the glacier to the interior of the lateroglacial valleys. Consequently, the sedimentary system in the lateroglacial depression is well protected from glacial activities, unless some overspilling or breakthrough of the lateral moraine takes place. The lateral moraine also impedes the drainage of the tributary rivers into the glacier system.

The lateral moraine valleys are distinguished into two principal types: (a) The V-shaped lateral moraine valley, in which the lateral moraine is directly connected with the adjacent valley flank. Its origin goes mainly back to dumping processes occurring at the glacier margin (Figure 1). (b) The lateral moraine valley with a valley bottom floor (Figure 2). The incorporated sediments are composed of heterogeneous debris sources (Figure 3):

1. Primary processes of rock disintegration such as ice avalanches and freeze-thaw processes as well as glaciofluvial sediments from the main and tributary glaciers provide debris for the formation of lateroglacial sediments, especially for the formation of the lateral moraine.
2. A considerable part of the debris supply for the lateroglacial sediment complexes derives from the tributary valleys, in particular at glaciers framed by highly dissected mountain relief (Figure 1). The sediment cones, such as alluvial fans, debris flow cones, and avalanche cones, drain toward the glacier either into an existent ice-marginal depression or even onto the glacier. Especially large-sized, catastrophic debris flows can even initiate the formation of a lateroglacial valley. Rockslides, debris flows, and snow avalanches deposited into a lateroglacial valley frequently dam lateroglacial rivers and cause the deposition of lacustrine sediments. As a result, a considerable proportion of the lateroglacial sediments is of non-glacial origin. This fact has to be taken into consideration regarding glacier reconstruction in recent non-glaciated

Lateroglacial Landform Systems, Figure 1 V-shaped lateral moraine valley at the Pumari Chhish glacier in 4,100 m. Photo: L. Iturrizaga (1999).

Lateroglacial Landform Systems, Figure 2 Lateral moraine valley (◊) at the almost 2 km broad Batura glacier in S-aspect. Debris supply derives mainly from the tributary valleys (←) and the resedimentation of slope moraines (Δ). In the background the Batura massiv (7,885 m) is visible. Photo: L. Iturrizaga (2000).

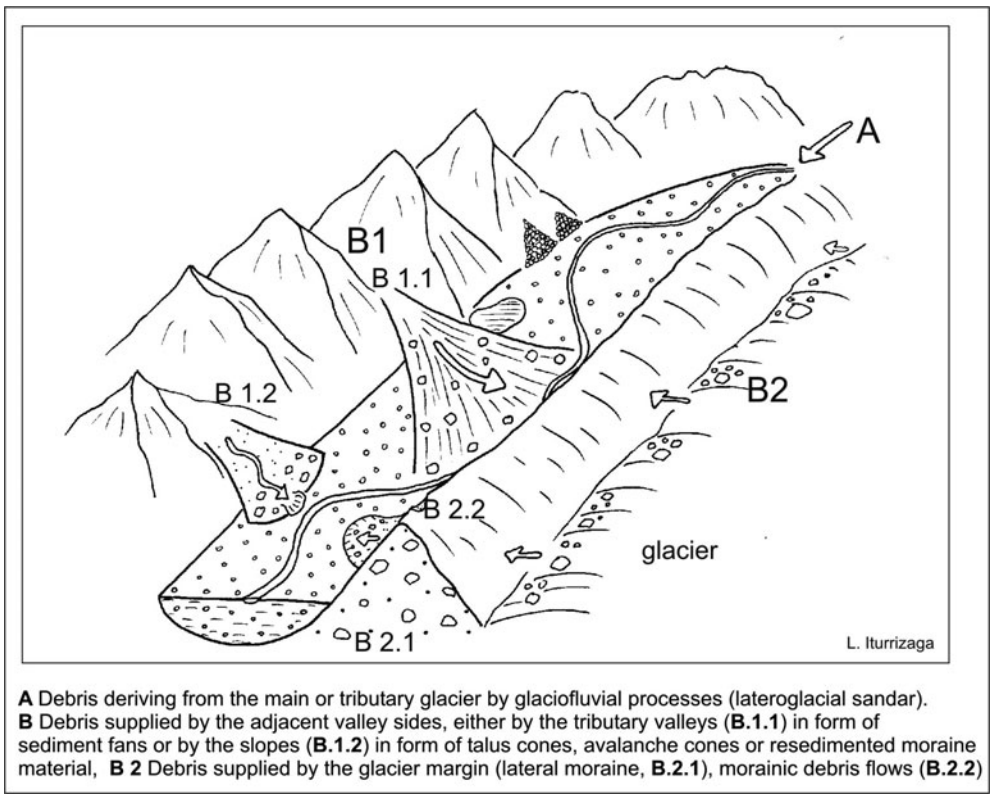

A Debris deriving from the main or tributary glacier by glaciofluvial processes (lateroglacial sandar).
B Debris supplied by the adjacent valley sides, either by the tributary valleys (**B.1.1**) in form of sediment fans or by the slopes (**B.1.2**) in form of talus cones, avalanche cones or resedimented moraine material, **B 2** Debris supplied by the glacier margin (lateral moraine, **B.2.1**), morainic debris flows (**B.2.2**)

Lateroglacial Landform Systems, Figure 3 Source areas of debris supply for lateroglacial valleys.

mountain valleys. Dendritic glaciers in which the individual tributary glaciers recede and loose the contact to the main glacier are prone to the formation of lateroglacial sediment complexes.

3. The lateroglacial sediment landscape is built up to a great extent by the secondary debris supply in form of the reworking of older glacigenic deposits mantling the valley flanks (Figure 4). Many glaciers show a close interfingering of Late Glacial slope moraines and younger lateroglacial landforms. After the gradual down-melting of the Pleistocene glacier surface, moraine deposits remain along the lateroglacial margins, partly as terraces, partly as amorphous deposits and are dislocated into the lateroglacial valley by different types of mass movements.
4. In some parts, the sediments are deposited in the form of small-scaled *lateroglacial sandar*. These are glaciofluvial deposits which originate directly from the melt waters of the main or the tributary glacier. They are located between the glacier and the valley flank or the lateral moraine. After the deglaciation, these sediments are preserved as kame terraces.

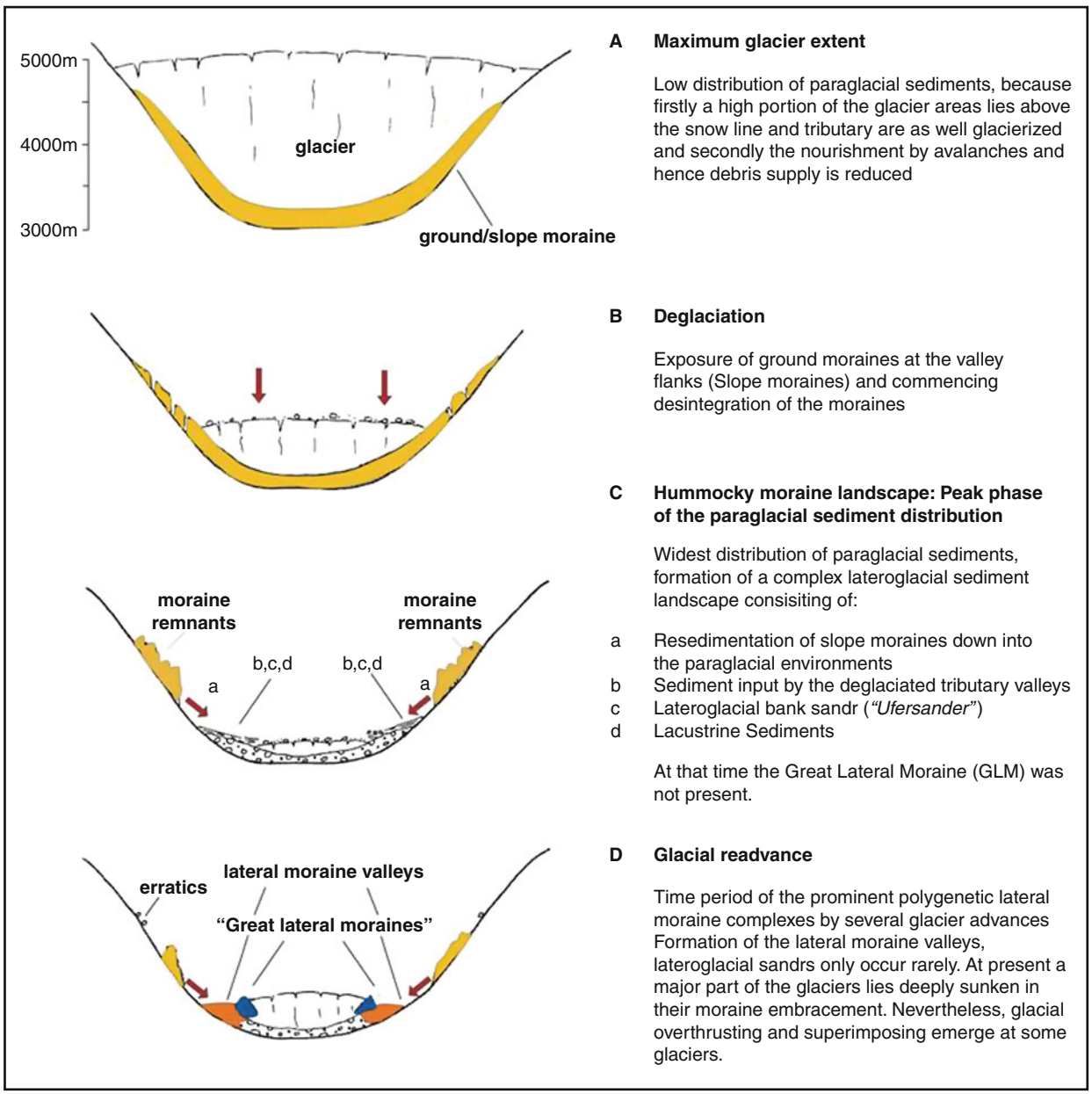

L. Iturrizaga

Lateroglacial Landform Systems, Figure 4 Genesis of the lateroglacial valleys deduced from the glacial history.

Relict lateroglacial valleys occur as high as 1,000 m above the present glacier surfaces and are important landforms for reconstructing the Pleistocene glacier thickness.

Summary

Lateroglacial landforms are composed of a large variety of different sediment types. The higher and more spaciously the surrounding mountain relief of the glacier in general is, the more complex are the lateroglacial landform systems. In many mountain areas, i.e., the European Alps, the Canadian Rocky Mountains, and also the Himalayas, lateral moraine valleys represent rather stable landforms. However, at many locations, they are in the stage of destruction due to glacier surface lowering and the missing abutment of the glacier. In the Karakoram, lateral moraine valleys may also be destroyed by present glacier advances or lateral widening as those glaciers are even today highly dynamic in the form of short-term glacier advances or surges. Lateroglacial valleys are a major location for temporary settlements and their pasture areas. Changes in the settlement situation are valuable indicators for glacier dynamics along the lateroglacial margins.

Bibliography

Hewitt, K., 1993. Altitudinal oranization of Karakoram geomorphic processes and depositional environments. In Shroder, J. F., jr (ed.), *Himalaya to the Sea. Geology, Geomorphology and the Quaternary.* London: Routledge, pp. 159–183.

Iturrizaga, L., 1999. Typical debris accumulation forms and formations in High Asia. A glacial-history-based concept of the origin of postglacial debris accumulation landscapes in subtropical high mountains with selected examples from the Hindu Kush, the Karakoram and the Himalayas. In Kuhle, M. (ed.), Tibet and High Asia (V), *GeoJournal*, **47**(1–2), 277–339.

Iturrizaga, L., 2001. Lateroglacial valleys and landforms in the Karakoram mountains (Pakistan). In Kuhle, M. (ed.), Tibet and High Asia (VI), Special Volume, *GeoJournal*, **54**(2–4), 397–428.

Iturrizaga, L., 2003. The distribution and genesis of lateroglacial valleys in the Karakoram mountains (Pakistan). *Zeitschrift für Geomorphologie N.F*, **130**, 51–74.

Iturrizaga, L., 2007. Die Eisrandtäler im Karakorum: Verbreitung, Genese und Morphodynamik des lateroglazialen Sedimentformenschatzes. In *Geography International*. Aachen: Shaker Verlag, Vol. 2, p. 389.

Iturrizaga, L., 2008. Post-sedimentary transformation of lateral moraines: the tributary tongue basins of the Kvíárjökull (Iceland). *Journal of Mountain Sciences*, **5**(1), 1–16.

Oestreich, K., 1906. Die Täler des nordwestlichen Himalaya. In *Petermanns Geographische Mitteilungen*, Vol. 155, 106 pp.

Visser, P. C., 1938. Glaziologie. In Visser, Ph. C., and Visser-Hooft, J. (eds.) Wissenschaftliche Ergebnisse der Niederländischen Expeditionen in den Karakorum und die angrenzenden Gebiete in den Jahren 1922, 1925 und 1929/30. vol. 2, 215 pp.

von Klebelsberg, R., 1938. Visser's Karakorum-Glaziologie. *Zeitschrift für Gletscherkunde*, **26**(3/4), 307–320.

Cross-references

Ice-Marginal Deposition
Ice-Marginal Processes

LAURENTIDE ICE SHEET

John T. Andrews
Institute of Arctic and Alpine Research and Department of Geological Sciences, University of Colorado, Boulder, CO, USA

Definition

Laurentide Ice Sheet (LIS) – refers to an Antarctic-size ice sheets that extended from the general area of the Great Lakes in the USA northward to the Canadian Arctic coast, and westward from the uplands and fjords of Baffin Island and Labrador to the foot of the Rocky Mountains (Figure 1). In the west, it was at times contiguous with the Cordilleran Ice Sheet, and in the NE merged with the Innuitian Ice Sheet.

Introduction

The LIS had an area of approximately 12×10^6 km^2, a central thickness estimated to be in the range of 3–4 km, and sufficient mass to cause a worldwide fall in sea level of around 70± m, out of a total global sea level extraction of ~120–130 m due to expansion of ice sheets and glaciers worldwide (Figure 2). The term LIS should strictly be only applied to the last great ice sheet of the Wisconsinian Glaciation (Figure 2), but it is frequently used to cover a broader span of Quaternary time. Because of its area, height, and volume the LIS has to be considered a major component in the late Quaternary climate of our planet, seriously influencing ice sheet/ocean/atmospheric interactions. Waters from the ice sheet debouched into three marine basins – drainage from the Great Lakes westward were directed into the Gulf of Mexico, waters from the long eastern margin entered Baffin Bay, the Labrador Sea and the western North Atlantic, whereas the northern margin drained to the Arctic Ocean (Figure 1). The input of meltwater into the oceans has been called upon as having a significant impact of the thermohaline circulation of the oceans. Tidewater outlets and ice streams also injected icebergs into the North Atlantic and Arctic oceans. Ice-rafted debris (IRD) from the North American continent has been traced across the Arctic Ocean and in the North Atlantic as far east as the Portugal margin.

A brief history of concepts about the LIS

By the 1890s, a good deal of research had been carried out in the glaciated area of the USA and in southern Canada. In 1898, Tyrrell produced a map of the former North America ice sheets. This map is remarkably similar in many ways to present-day concepts of the LIS, that is, an ice sheet that like the Antarctic Ice Sheet, had several dispersal center with ice divides over Labrador, Foxe Basin, Keewatin, and the Patrician Center off SW Hudson Bay. This notion prevailed until the 1940s when Flint argued for the growth of an ice sheet from the mountains of the eastern Canadian Arctic to finally form a massive

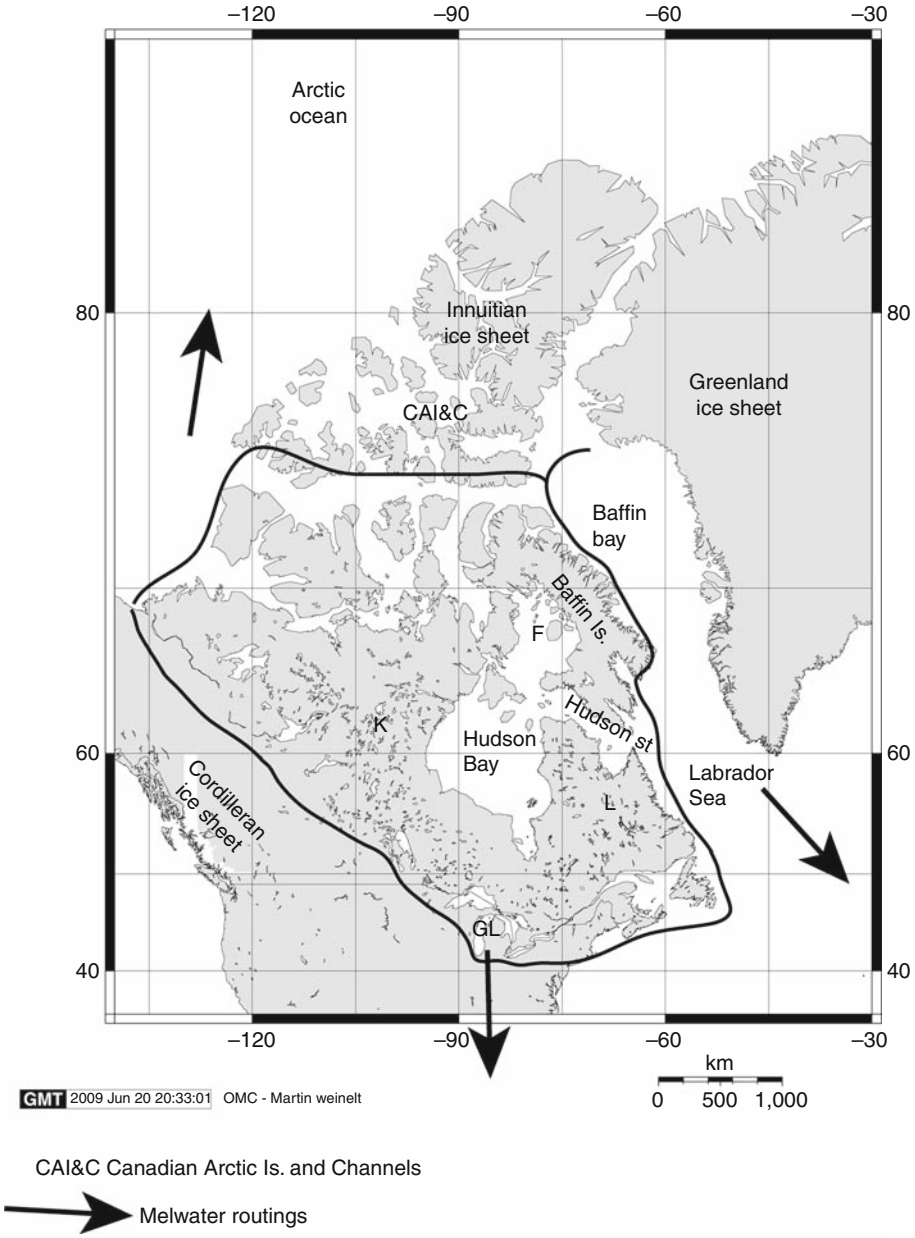

Laurentide Ice Sheet, Figure 1 North American showing the outline of the Laurentide Ice Sheet during the last glacial maximum. K = Keewatin ice divide, L = Labrador ice divide, F = Foxe Basin ice divide.

single-domed ice sheet centered over Hudson Bay. Flint's model was based on a conceptual model for the growth and development of the ice sheet. This model continued to have adherents into the 1970s and 1980s but is now largely abandoned.

Wide-ranging field observations in the Eastern Canadian Arctic in the late 1950s and 1960s, combined with adequate topographic maps, aerial photographs, satellite imagery, and increased knowledge of the tectonic evolution of the North Atlantic region during the Tertiary, resulted in an appreciation of the role that the high rolling uplands of the Eastern Canadian Arctic played in the onset of glaciation, and in the overall complex pattern of shifts in flow regimes during the Wisconsinian Glaciation.

Onset of glaciation

Our knowledge of the growth and buildup of the LIS during the interstadials of marine isotope stage (MIS) 5, namely 5d and 5b, is limited (Figure 2). The last full interglacial over North America (MIS 5e) was warmer than present, and it is possible that many of the smaller ice caps

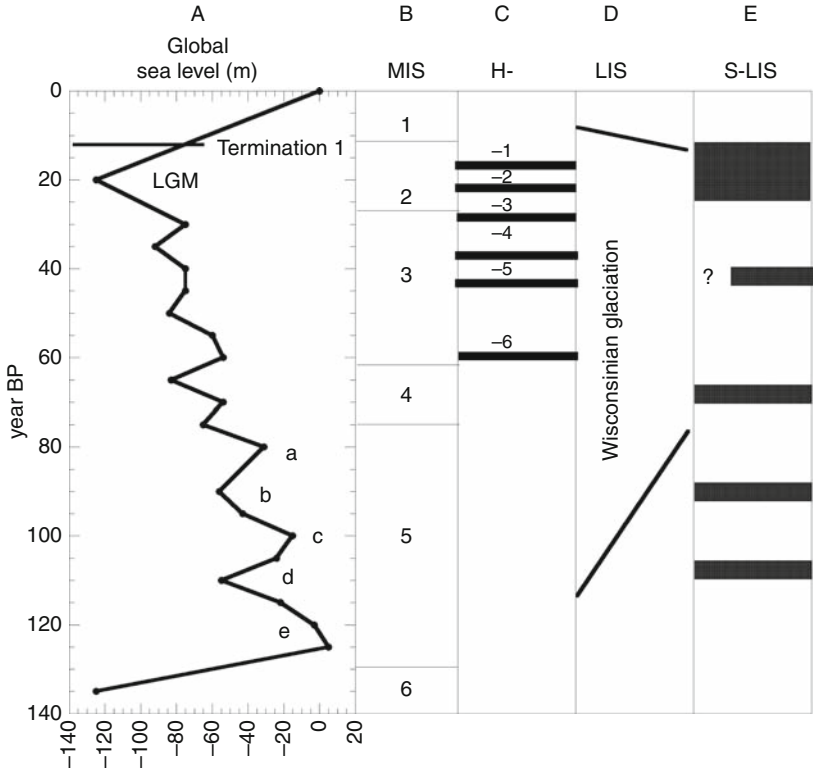

Laurentide Ice Sheet, Figure 2 Evolution of global sea level during the last glacial (Wisconsinian) cycle. (**a**) global sea level (Shackleton 1987); (**b**) marine isotope stages (MIS); (**c**) Heinrich (H-) events; (**d**) age span of the Wisconsinian Glaciation; (**e**) glacial episodes of the Laurentide Ice Sheet (LIS) in the area of the Great Lakes (Figure 1) (Karrow et al., 2000).

and glaciers in the Eastern Canadian Arctic disappeared. On the global level, the relationship between ice volume and $\delta^{18}O$ of marine foraminifera indicate that the growth of ice sheets during MIS 5d was remarkably rapid as global sea level fell to –55 m in ~10,000 years. What fraction of this global extraction of water for ice sheet buildup is associated with the LIS is largely unknown, but on general climatic grounds it seems reasonable that a considerable fraction of the 55 m of global sea level was locked into the initial growth of the LIS.

The global pattern of changes in sea level, a proxy for ice sheet growth and decay, has been successfully linked to changes in insolation, which in turn has been linked to the orbital variations of the Earth relative to the Sun – the so-called Milankovitch orbital variations. Spectral analysis of $\delta^{18}O$ time series covering the last 700,000 years shows that the variations in sea level, hence ice sheet mass, have 100,000, 41,000, and 25,000 periodicities, and this gives an initial template for evaluating the history of the LIS. However, subsequent research has shown that the LIS is also marked by much shorter periodic events, such as Heinrich (H-) events (Figure 2).

The uplands of the Eastern Canadian Arctic, that is the largely undissected Precambrian shield that lies to the west of the Tertiary rift-margin along the Labrador and Baffin Island coast, have a large fraction of their elevation >500 m asl. Imagery and fieldwork indicate that during the Little Ice Age (LIA) ca. AD 1400–2000 large fraction of these uplands were covered with permanent snow beds or small ice caps, thus demonstrating the sensitivity of these areas to relatively small changes in net mass balance. Hence, virtually all attempts to model the development and growth of the LIS over the last 120,000 years, show the initial growth of the ice sheet over the uplands of Labrador and Baffin Island. As conditions cooled, it is also probable that ice sheets developed over the somewhat lower plateaus terrain of Keewatin, west of Hudson Bay, and an ice sheet may have developed across the High Canadian Arctic islands and Channels. Thus, the initial movement of the various accumulation centers would have been from the uplands through the fiords of Labrador and Baffin Island, and toward the large interior seas of Hudson Bay and Foxe Basin. A critical question is whether the advancing ice sheets based over Labrador and Baffin Island merged across Hudson Strait prior to glacial inundation of Hudson Bay – if that did not happen then a large glacially dammed lake would have been ponded within the Bay.

At some point, possibly in MIS 4, Hudson Bay, and Foxe Basin were filled and the LIS then became a marine-based ice sheet, somewhat similar in that respect

to the West Antarctic Ice Sheet today. Because of the mass of the LIS the bedrock under the ice sheet would be isostatically depressed – thus meaning a large fraction of the ice sheet was grounded below the sea level, and linked to the North Atlantic via the deep graben of Hudson Strait (Figure 1). Hudson Bay, Foxe Basin, and Hudson Strait are floored with Paleozoic carbonates composed of calcite and dolomite, and these rocks provide powerful tracers of ice sheet activity in the adjoining deep-sea basins of the Labrador Sea and Baffin Bay.

Glacial landscapes

The extension of the LIS along its eastern margin is limited by the presence of the adjacent ocean basins, and it is in these areas that some trace of the history of the ice sheet can be recovered in piston cores through marine sediments. The deep water connections between the ice sheet (~450 m at the Hudson Strait sill, without isostatic depression) and the Labrador Sea represent one major potential point of instability; others exist in other deep marine embayments, such as the Gulf of St Lawrence. However, on the grand scale of the LIS there is also another large spatial difference, that is between the "hard bed," glaciological speaking, of the sediments produced by erosion of the Precambrian granites and gneisses, versus the "soft-bed" younger sedimentary rocks that flank the shield rocks along the southern flank. Reconstruction of profiles of the ice sheet and its outlets in the areas of the Canadian Prairies, Iowa, and in the Great Lakes indicate that the basal shear stress was much lower and the ice much thinner than where the ice sheet was moving across the shield bedrock. Thus the configuration of the LIS and its potential response to climate and other changes are quite different from the neighboring Greenland Ice Sheet.

The effect of the combination of bedrock, elevation, and tectonics on the large-scale patterns of glacial erosion is evident on satellite imagery. The uplifted eastern rim of the Shield is dissected by fiords, and large-scale grabens extend into or toward the center of the ice sheet. On the flanks of Foxe Basin and Hudson Bay where the eastward flowing ice attained thicknesses of 2 km or more the Shield rocks have been glacially eroded along joint and fracture planes to form a landscape of glacial scour, with limited thickness of glacially derived sediments (till). Between the fiord landscape and the scoured areas there is frequently an area (usually >400 m asl) with little or no scour; this is interpreted as an area that was covered by thinner ice with basal temperatures below the pressure melting point (i.e., cold-based ice). In the flanking region along the southern margin of the ice sheet the thickness of till is greater and the underlying bedrock is masked by glacial and glaciofluvial sediments. Contrary to some theories, the area at the geographic center of the LIS, the western Hudson Bay lowlands, has a thick sequence of preserved non-glacial and glacial sediments that are a critical record of the LIS.

The LIS and Wisconsinian glaciation

The marine isotope records form a template for global changes in ice sheet volumes acting on multi-millenial scales (Figure 2). How far does the stratigraphic record from the area of the LIS match this master template, indeed how far can we express the history of the LIS in a single description versus regional differences in glacial history? This question faces several major problems. First is the fact that the stratigraphic record within the margins of the LIS is largely an intermittent record of temporal events at the best; in addition, the ice sheet has also the potential to erode evidence of past oscillations. Secondly, to place the history of the LIS into a time perspective to match with the $\delta^{18}O$ record requires (a) materials that can be dated, and (b) dating methods that span, ideally, 120,000 years or so. It should be noted that the marine time series are not without problems, in-so-far-as the main "absolute" dating method is radiocarbon dating of foraminifera, which only extends back 40,000–50,000 years BP. Thus, the chronology for MIS 4 and 5 is largely derived from a process of correlation with the astronomical (insolation) variations with links to U-series dates on raised coral reefs. Within or at the margins of the LIS implications for ice sheet growth or retreat are based on the stratigraphic sequence (including the nature of the sediments and paleobiological data) with ^{14}C dates being derived from wood, peat, shells, whalebone, or other organic materials. Often exposed sections have no material for dating or events are dated at >40,000 BP. In the last 10–20 years, a dating revolution has occurred with the advent of cosmogenic exposure age dating. This method allows, for the first time, moraines and eroded surfaces to be directly dated. This approach has shed new light on the LIS history, especially in Arctic areas, where materials for ^{14}C dating were scarce or absent, but where large surface boulders and exposed bedrock are abundant.

The LIS probably grew from its inception grounds during the interglacials of MIS 5 and expanded across the Gulf of St. Lawrence and into the Great Lakes during MIS 4 ca. 75,000 years ago (Figure 2). The history of the ice sheet during MIS 3 is proving difficult to unravel but the ice sheet may have been largely confined to the "hard bed" of the PreCambrian shield. Whether the glaciologically sensitive area of the interior basin of Hudson Bay was ever deglaciated is debatable and hinges on issues involved with dating marine sediments in the Hudson Bay lowlands and the interpretation of sediments in the Labrador Sea.

Heinrich events and LIS instability

The relatively smooth intervals of growth and retreat of ice sheets that are implied in the ocean ^{18}O records were infact punctuated by massive instabilities of the marine-based LIS. Heinrich (H-) events (Figure 2) record massive outbreaks of meltwater and icebergs into the North Atlantic, with the major source being the ice

stream in Hudson Strait. H-events have been documented in the Labrador Sea eastward toward Europe due to their distinctive mineralogical composition, mainly detrital carbonate (DC) grains. Similar, but temporally offset DC events occur in Baffin Bay, representing collapse of the LIS and Innuitian ice sheets across the Canadian Arctic channels that lead into Baffin Bay. Detrital carbonate events also occur in Arctic Ocean sediments and represent events along the Arctic margin of the LIS and Innutian ice sheets. The massive thickness of DC sediments associated with H-4 in the Labrador Sea argues that Hudson Bay was not ice-free during MIS 3.

The last glacial maximum (LGM) and deglaciation of the LIS

The LIS expanded from its more restricted, more largely unmapped, extent during MIS3 to reach its maximum last glacial extent ~20,000 years BP (Figure 1). Note that the LGM is also marked by a major H-event (Figure 2). Given the geographic and climatic extent of the LIS during the LGM, it is unlikely that every margin of the ice sheet reached its maximum extent at exactly the same time. Indeed, for much of the eastern flank of the ice sheet the exact location of the margin at ~20,000 years BP is unknown and does not appear to be marked by large moraine systems, possibly because the ice sheet was cold-based.

The deglaciation of the LIS has now been mapped and dated across thousands of sites. Viewed in the light of the previous 120,000 years the deglaciation is relatively abrupt and is termed, globally, Termination I (Figure 2). Briefly the LIS retreats asymmetrically with initial high rates of ice retreat along the southern and western margins, with little change along the long eastern margin. As summer insolation increased, meltwaters were directed into adjacent oceans (Figure 1). The stability of the ice sheet was weakened by a massive collapse through Hudson Strait during H-1 (16,000 years ago). As the ice sheet retreated in the south and west at some point the continental drainage divide was revealed and a series of large, glacially dammed lakes were formed – these lakes are often lumped under the name Glacial Lake Agassiz. The final demise of much of the LIS occurred ca 8.4 years ago when waters from the Labrador Sea, penetrating through Hudson Strait, breached the remaining ice over Hudson Bay and connected with and drained glacial lakes that had been dammed south of the ice sheet. This outburst event and earlier meltwater events impacted the thermohaline circulation.

In subsequent years, the ice retreated and disappeared from the Labrador plateaus but the last remnants of the LIS still exist across central Baffin Island in the form of the Barnes Ice Cap.

Summary

The Laurentide Ice Sheet was the largest ice sheet in the Northern Hemisphere, comparable in size to the present Antarctic Ice Sheet. Growth and retreat were controlled by periodic changes in insolation but its marine-based nature made it susceptible to major collapses with massive outflows of meltwater and icebergs.

Bibliography

Andrews, J. T., 1998. Abrupt changes (Heinrich events) in late Quaternary North Atlantic marine envrionments: a history and review of data and concepts. *Journal of Quaternary Science*, **13**, 3–16.

Andrews, J. T., Kirby, M. E., Aksu, A., Barber, D. C., and Meese, D., 1998. Late Quaternary Detrital Carbonate (DC-) events in Baffin Bay (67°–74° N): Do they correlate with and contribute to Heinrich Events in the North Atlantic? *Quaternary Science Reviews*, **17**, 1125–1137.

Briner, J. P., Miller, G. H., Davis, P. T., Bierman, P. R., and Cafee, M., 2003. Last Glacial Maximum ice sheet dynamics in Arctic Canada inferred from young erratics perched on ancient tors. *Quaternary Science Reviews*, **22**, 437–444.

Clark, P. U., and Walder, J. S., 1994. Subglacial drainage, eskers, and deforming beds beneath the Laurentide and Eurasian ice sheets. *Geological Society of America Bulletin*, **106**, 304–314.

Clark, P. U., Licciardi, J. M., MacAyeal, D. R., and Jenson, J. W., 1996. Numerical reconstruction of a soft-bedded Laurentide Ice Sheet during the last glacial maximum. *Geology*, **24**, 679–682.

Denton, G. H., and Hughes, T. J., 1981. *The Last Great Ice Sheets*. New York: Wiley, p. 484.

Dyke, A. S., 2004. An outline of North American deglaciation with emphasis on central and northern Canada. In *Quaternary Glaciations – Extent and Chronology*, Part II. New York: Elsevier, pp. 373–424.

Dyke, A. S., Andrews, J. T., Clark, P. U., England, J. H., Miller, G. H., Shaw, J., and Veillette, J. J., 2002. The Laurentide and Innuitian ice sheets during the Last Glacial Maximum. *Quaternary Science Reviews*, **21**, 9–31.

Fulton, R. J. (ed.), 1989. *Quaternary Geology of Canada and Greenland*, Geological Survey of Canada, Geology of Canada No. 1, Queens Printer, Ottawa, 839 pp.

Hesse, R., Klaucke, I., Ryan, W. B. F., et al., 1997. Ice-sheet sourced juxtaposed turbidites systems in labrador sea. *Geoscience Canada*, **24**, 3–12.

Karrow, P. F., Dreimanis, A., and Barnett, P. J., 2000. A proposed diachronic revision of Late Quaternary time-stratigraphic classicagtion in the Easterrn and Northern Great Lakes area. *Quaternary Research*, **54**, 1–12.

Marshall, S. J., and Clarke, G. K. C., 1999. Ice sheet inception: subgrid hypsometric parameterization of mass balance in an ice sheet model. *Climate Dynamics*, **15**, 533–550.

Marshall, S. J., Teller, J. S., and Clarke, G. K. C., 2002. North American ice sheet reconstructions at the Last Glacial Maximum. *Quaternary Science Reviews*, **21**, 175–192.

Matthews, W. H., 1974. Surface profiles of the Laurentide Ice Sheet in its marginal areas. *Journal of Glaciology*, **13**, 37–43.

Miller, G. H., Wolfe, A. P., Steig, E. J., Sauer, P. E., Kaplan, M. R., and Briner, J. P., 2002. The Goldilocks dilemma: big ice, little ice, or "just-right" ice in the Eastern Canadian Arctic. *Quaternary Science Reviews*, **21**, 33–48.

Shackleton, N. J., 1987. Oxygen isotopes, ice volume and sea level. *Quaternary Science Reviews*, **6**, 183–190.

Stokes, C. R., Clark, C. D., Darby, D. A., and Hodgson, D. A., 2005. Late Pleistocene ice export events into the Arctic Ocean from the M'Clure Strait Ice Stream, Canadian Arctic Archipelago. *Global and Planetary Change*, **49**, 139–162.

Sugden, D. E., 1977. Reconstruction of the morphology, dynamics and thermal characteristics of the Laurentide Ice Sheet at its maximum. *Arctic and Alpine Research*, **9**, 21–47.
Teller, J. T., Leverington, D. W., and Mann, J. D., 2002. Freshwater outbursts to the oceans from glacial Lake Aggassiz and their role in climate change during the last deglaciation. *Quaternary Science Reviews*, **21**, 879–888.
Thorliefson, L. H., Wyatt, P. H., and Warman, T. A., 1993. Quaternary stratigraphy of the severn and winisk drainage basins, Northern Ontario. *Geological Survey of Canada*, **Bulletin 442**, 59.

Cross-references

Deglaciation
Ice Age
Sea-Level

LAYERING OF SNOW

Rajesh Kumar
School of Engineering and Technology, Sharda University, Greater Noida, NCR, India

Snow layers are formed as a tabular body of snow with younger at top and oldest at the bottom having well defined boundaries of their precipations if at certain gaps (AGI, 1960). The layers are differentiated from the surrounding one due to unique deposition and post-deposition processes. Each layer of snow forms a snow packs which differs in physical and microstructural properties from those above and below. The layering sequence and its characteristics govern thermal, physical, and mechanical properties of the snow pack. The strength of the snow pack and the transport of air, water, and heat through it are also dependent on layer's characteristics. Under natural conditions they exhibit irregular boundaries and a wide range of grain and bond characteristics when traced laterally.

The definition focuses on the fact that the microstructure (grain size, shape, and arrangement and nature of bonds) differs from one layer to another. Though the layering seems simple, the real snow layers can be complex (Matthew and Carl, 2004). The knowledge about snow mechanics is very crucial in dealing with the snow avalanche formation and hazard mitigation measures. Snow stability depends on the layering of snow. The most relevant mechanical properties like compressive, tensile, and shear strength of the individual snow layers within the snow cover vary significantly in space and time. Local observations of snow layers are used as the basis for spatial extrapolation of snow properties and for establishing a time record of snow deposition.

Bibliography

AGI (American Geological Institute), 1960. *Dictionary of Geologic Terms*. Garden City, NY: Anchor Books, 472 pp.
Matthew, S., and Carl, B., 2004. Scales of spatial heterogeneity for perennial and seasonal snow layers. *Annals of Glaciology*, **38**, 253–260.

LIDAR IN GLACIOLOGY

Michael N. Demuth
Glaciology Section, Geological Survey of Canada, Earth Sciences Sector Program on Climate Change Geoscience, Natural Resources Canada, Ottawa, ON, Canada

Synonyms

Laser altimetry; Laser radar (considered misleading); Laser swath mapping as used in *Airborne Laser Swath Mapping* (ALSM); Laser terrain mapping as used in *Airborne Laser Terrain Mapping* (ALTM)

Definition

LiDAR. Coined from "**L**ight **D**etection **A**nd **R**anging"
Glaciology. The study of glaciers
LASER. Coined from "**L**ight **A**mplification by **S**timulated **E**mission of **R**adiation"

Introduction

The study of the Earth's glaciers and ice sheets is of tremendous importance as their fluctuation has consequences on sea level, river flow, ecosystem functioning, ocean circulation, and climate stability. Recent studies have shown that the Earth's small glaciers are in measurable decline on account of secular atmospheric warming (Kaser et al., 2006; UNEP/WGMS, 2009), and whose environmental services (e.g., hydrological regulation) vary regionally – from short-term flow augmentation to long-term decline (Bonardi, 2008; Casassa et al., 2008; Sauchyn et al., 2008). There is considerable concern regarding the state and evolution of the Earth's larger glacier systems and the ice sheets, and their effect on global sea levels (Abdalati et al., 2002; Arendt et al., 2004; Zwally et al., 2002b; Rignot and Thomas, 2002; Thomas et al., 2006; Bamber et al., 2007; van de Wal et al., 2008; Alley et al., 2009; Thomas et al., 2009; Vinther et al., 2009).

Increasingly, remote sensing tools have been used to study and understand in a more comprehensive, regional manner, the sign, magnitude, rate, and causality of the Earth's glacier and ice sheet mass balance changes. Reflecting on the Greenland ice sheet, Reeh (1999) suggested that modern observation methods in combination with trimline observations, large-scale snow accumulation and mass flux estimates, and ice sheet modeling could reduce the uncertainty associated with understanding its mass balance variation. It has also been recognized for some time that the worldwide glacier surveillance strategy has historically been biased to relatively small glacier sizes, with large glacier systems being relatively underrepresented (Haeberli et al., 1998). The application of laser-based detection and ranging strategies, including the support they provide for glacier and ice sheet mass and energy balance studies, plays a key role in addressing

these thematic concerns, methodological opportunities, and surveillance biases.

The following reviews the principle of lidar, its integration as an instrument in typical glacier surveillance applications, and important error considerations. The capability of lidar is illustrated with numerous examples from the available literature. Survey planning considerations and specific technical challenges are also discussed.

Lidar ranging/swath mapping principles

Lidar for range finding has been in use since the 1970s (e.g., Measures, 1984), and provides long-distance ranging capability to ascertain the position of planetary satellites and moons as applied to geodesy and related fields. This entry concerns laser ranging and detection of the surface of the Earth's glaciers and ice sheets from fixed points, aircraft or artificial satellites, with an emphasis on swath mapping from aircraft.

Lidar-operating principles are generally similar to those of microwave-based RaDAR (**Ra**dio **D**etection **A**nd **R**anging) systems, but instead make use of "light." This light is commonly in the form of near-infrared radiation pulses emitted by a laser. This laser energy interacts with surface features and upon scattering may then return back to a coincident detector, enabling "time of flight" (t) measurement. The range is simply:

$$r = c\frac{t}{2} \tag{1}$$

where c is the velocity of light.

In a typical scanning or swath mapping configuration, laser pulses are directed toward the Earth's surface by employing an oscillating or nutating mirror. This results in a scanning pattern of measurements. In an airborne deployment, this pattern repeats itself along-track. The ground measurement locations are in fact of finite size, and so the matter of laser beam divergence determines the effective illuminated footprint dimensions over which the detection and ranging occurs. Terrain orientation and target range are chief factors, with the spatial coherence of the light over the target surface being a function of the quality of the laser light and the influence of the atmosphere between the source and the target. While usually described as some fraction of a probability density function, aspects of the positional probability and the terrain orientation can complicate defining the footprint dimension.

A key element in a lidar-based topographic mapping system is locating the reference axes of the lidar boresite/detector relative to a spatial reference system for the Earth. For an airborne application, for example, this is enabled by continuously measuring the attitude (pitch, roll, yaw) and position of the aircraft (Figure 1). The former is generally determined with an "inertial measurement unit" (IMU) or outputs from a suitably equipped "inertial navigation system" (INS), while the later is derived from measurements obtained with the aid of Global Navigation Satellite Systems (GNSS; e.g., GPS and/or, GLONASS). Simultaneous GNSS data is collected over a known ground control point within the survey baseline to enable differential correction of the platform position data. "Mechanical offset" measurements between the reference axes, the IMU sensor and the GNSS receiver antenna phase center must also be made (Figure 1). In some systems, the entire laser sensor head is stabilized with gimbals, while other systems use attitude and position data to feedback to and control the scanner mirror directly so that the generated swath remains stable regardless of changes in the aircraft orientation.

Software is used to extract ground-point positions relative to the spatial reference system. The platform velocity, scanner rate, laser pulse repetition frequency (PRF), and IMU data rate for most airborne applications will also require the use of software to project the position of the measurement platform between those determined with the low data rate GNSS measurements (typically 1–2 Hz).

Typical laser scanning systems may employ "first-pulse" and "last-pulse" measurement modes, where the former measures the range between the initial outgoing pulse and the first return pulse detected, while the latter measures the range between the initial outgoing pulse and the last return pulse detected. This may prove useful for "surfaces" having a complex vertical structure. In many systems, the power of the laser return pulse is recorded in the form of an intensity measurement, usually expressed as a function of the percent reflectance of the measured surface. This data can be used to assess the quality of the range measurements as well as give an indication of surface properties.

In the case of a lidar mounted onboard an artificial satellite (e.g., the Global Laser Altimeter System, GLAS, aboard the NASA/EOS Ice Cloud and Elevation Satellite, ICESat; Zwally et al., 2002a), precision orbit determination, timing and geo-location are enabled with GNSS measurements, while "star trackers" are utilized to effect platform pointing and stability control.

A comprehensive treatment of lidar ranging practice can be found in Wehr and Lohr (1999).

Error considerations

Critical to assessing the total survey error budget and the uncertainty associated with, for example, a digital elevation model (DEM) are two major sources of error in lidar data: (1) the forward propagation of individual system component errors and (2) the backward propagation of external contributions such as those manifested by terrain slope.

Starting with Favey et al. (1999) there began a number of efforts where error considerations were discussed with increasing thoroughness (e.g., Krabill et al., 2002;

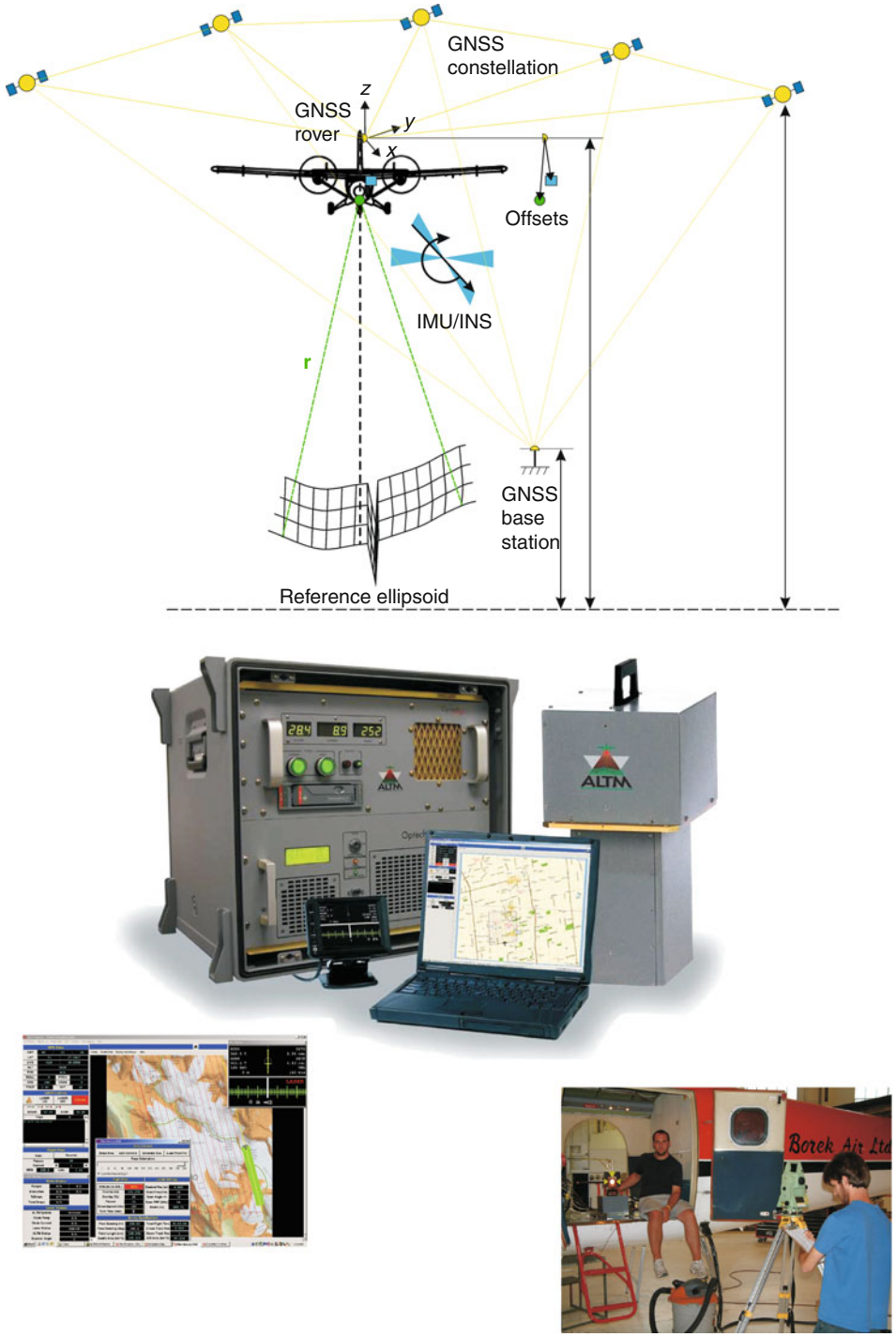

LIDAR in Glaciology, Figure 1 *Top*: Schematic of the measurement and reference framework for airborne lidar mapping; *Middle*: Typical ALTM system components including, clockwise from *top left*: console containing the control module, data storage, IMU and GNSS system interface and laser power supply; laser/mirror assembly; notebook computer/operator interface; pilot display; *Bottom*: Surveying mechanical offsets for an installation in a de Havilland Canada Twin Otter (System photograph courtesy Optech Inc., Toronto Canada; photograph of mechanical offset measurement courtesy Chris Hopkinson and the Canadian Consortium for Lidar Environmental Applications Research, C-CLEAR).

Lutz et al., 2003; Hodgson and Bresnahan, 2004). This was in response to the problems associated with steep terrain, detecting small changes over large areas, GNSS ambiguity resolution, and long survey baselines. Work in other fields (e.g., Davenport et al., 2004) has benefited error assessment considerations for glaciological applications, particularly as it concerns to high point-density and surface morphology studies. Goulden (2009) provides a comprehensive treatment of terrain slope errors in which initial errors are first estimated by propagating the error of the individual measurement systems in the LiDAR system using the General Law of Propagation of Variances. These are then cast in terms of the effect of the local slope to produce a "worst-case scenario" of the actual terrain. For a variety of heights above ground level (AGL) and scan angles, Goulden and Hopkinson (2010) provide a thorough treatment of forward error propagation as it concerns the laser beam divergence, and IMU and GNSS subsystems specifically.

Vibration modes having their origin in the measurement platform can also impart errors through the nature of gimbal or scanner mechanical structures, though most of these problems can be ameliorated through control system design and structural tuning. For installations on aircraft where the location of various system components may be dictated by cable routing, power supplies, structural bulkheads, and aperture and antenna locations, aeroelastic resonance may impart particularly troublesome consequences on the final data. These can include the manifestation of surface roughness where there is none, or noise that precludes the study of surface roughness (personal communication, Robert Gurney).

A better understanding of the error budgets associated with the application of lidar has manifested the broader utility of lidar as a tool in glaciology, including determining survey expectations a priori, assessing specifications provided by commercial lidar manufacturers, establishing lidar data acquisition/mission planning standards, and the development of some novel applications.

Lidar in practice

Almost all field glaciologists, young and not so young, will be familiar with laser range finding as part of simple trigonometric "theodolite" surveys or with "total station" instruments. Range measurements are made by discrete, manual repositioning of a reflector prism, though there are motorized total station systems that can follow the reflector prism continuously. Techniques employing GNSS have largely replaced this method of topographic mapping.

More recently, ground-based scanning lidar has been used to automatically map surfaces with sub-centimeter range and positional accuracy over ranges spanning several meters to more than 1 km (e.g., Intelligent Laser Ranging and Imaging System or ILRIS; www.optech.ca). Typical deployments involve locating the system over several established ground control points, with the resulting scanner data ingested by software to produce 3-D models of exceptional quality. ILRIS and similar systems are used primarily for engineering applications requiring high tolerances, but have also seen use in periglacial geomorphology studies. Because engineering applications dominate the commercial ILRIS market, and therefore must operate as "eye-safe" (e.g., urban environments), 1,550 ηm laser light is employed. For snow and ice, particularly in the presence of any melting, 1,550 ηm is considered unsuitable; because both transmission and specular reflection occur, laser return dropout rates are extremely high (personal communication, Chris Hopkinson). As such, they have not seen much use in the glaciological community. Nevertheless, the author is aware of one proof-of-concept effort that included a quantitative assessment of the range capability of an ILRIS instrument over glacier ice and snow-covered surfaces (Hopkinson, 2004).

Airborne lidar applications are now common despite the high instrument and software costs associated with commercially available systems, and the high aviation costs associated with typical surveys. Garvin (1997) reviewed the contemporary efforts of the 1990s, including the preeminent work of Krabill et al. (1995) who measured surface elevation change over the Greenland ice sheet and its outlet glaciers using the NASA Wallops Flight Facility, Airborne Topographic Mapper (ATM). This and subsequent missions have contributed to much of the Greenland ice sheet literature quoted in the introduction (Figure 2). In 1995, NASA's ATM team collaborated with the Glaciology Group of the Geological Survey of Canada (GSC) to begin repeat altimetry measurements over all of the major ice caps of the Canadian Arctic Islands (Abdalati et al., 2004), a collaborative effort that continues to this day. Echelmeyer et al. (1996) utilized a "pencil" lidar over the extensive glacier systems of Alaska, and in subsequent efforts, expanded the investigation to include the numerous accumulation areas located in the Yukon Territory, Canada that feed some of the Alaskan glaciers. With this data, Arendt et al. (2002) reported on the significant sea level contributions from this relatively little studied region. Notably, this effort was enabled by assembling a system "off-the-shelf" and installing it in a private light aircraft flown by Echelmeyer.

Smaller-scale efforts to map surface topography were initiated over a single small glacier in Norway by Kennet and Eiken (1997) using an early-generation commercial scanner system. They compared their results to those derived from the application of traditional stereo photogrammetry. Favey et al. (1999) reported on the utility of repeat scanning lidar surveys for estimating volume changes over a small glacier in Switzerland, as did Hopkinson et al. (2001) and Hopkinson and Demuth (2006) for a large ice field in the Canadian Rocky Mountains and its outlet glaciers (Figure 2).

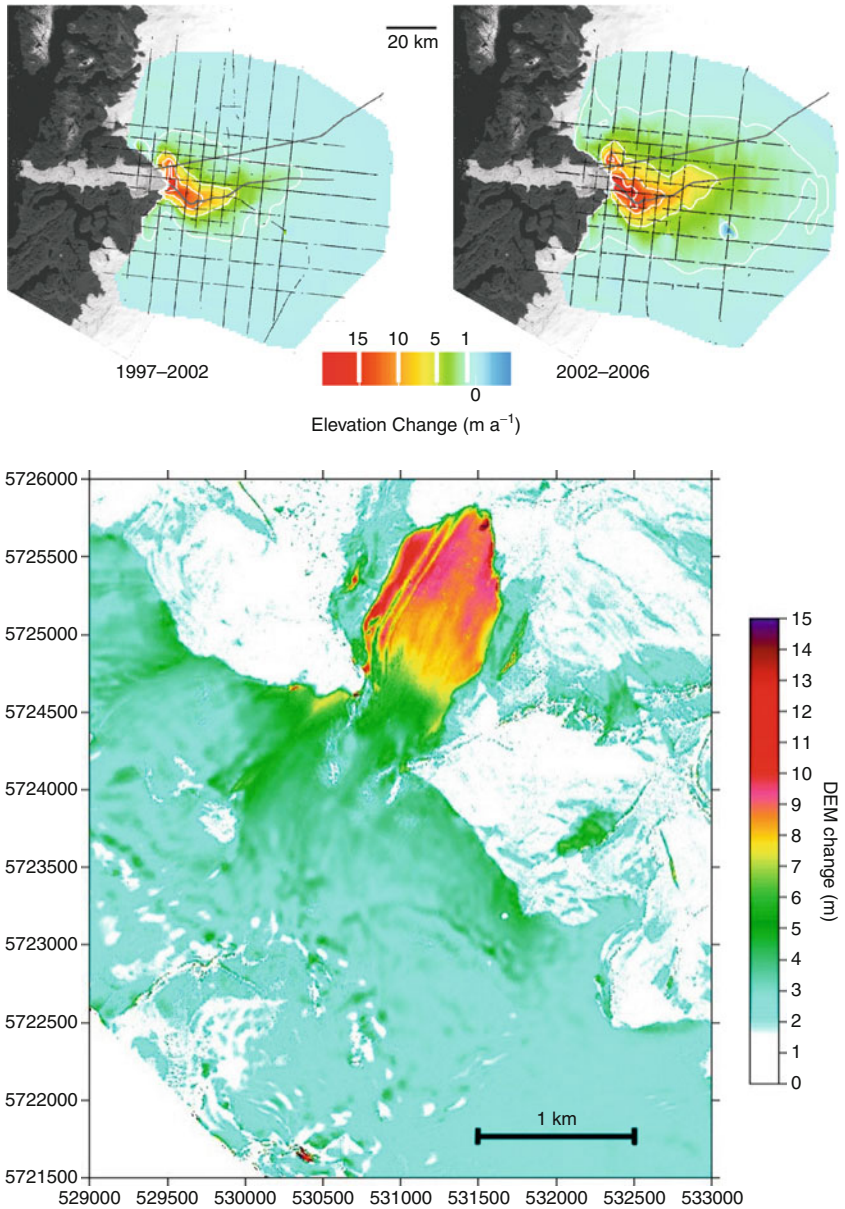

LIDAR in Glaciology, Figure 2 Inferred surface elevation change determined from repeat laser altimetry. *Top*: Jakobshavn Isbræ, Greenland, 1997–2002–2006, to a point where it converges into its rapidly flowing outlet (After Thomas et al., 2009; with permission International Glaciological Society); *Bottom*: Peyto Glacier, Canadian Rocky Mountains, 2000–2002 (After Hopkinson and Demuth, 2006; with permission Canadian Aeronautical and Space Institute).

If surveys are conducted with a high enough point measurement density, mapping surface features such as meltwater channels, moulins, and other thermal or mechanical surface manifestations is possible e.g., (Figure 3; see also Hopkinson et al., 2001; Arnold et al., 2006). Repeat surface mapping can enable surface feature tracking in support of glacier motion studies (Abdalati and Krabill, 1999; Arnold et al., 2006; Hopkinson and Demuth, 2006; Hopkinson et al., 2009). Several investigators have utilized return pulse intensity values to map the distribution of seasonal snow, firn, and ice over the glacier surface e.g., (Figure 4; see also Lutz et al., 2003; Arnold et al., 2006; Hopkinson and Demuth, 2006).

Airborne lidar has enabled detailed investigations in regions that are, for the most part, very difficult to access due to weather and terrain. These "hurry up and wait"

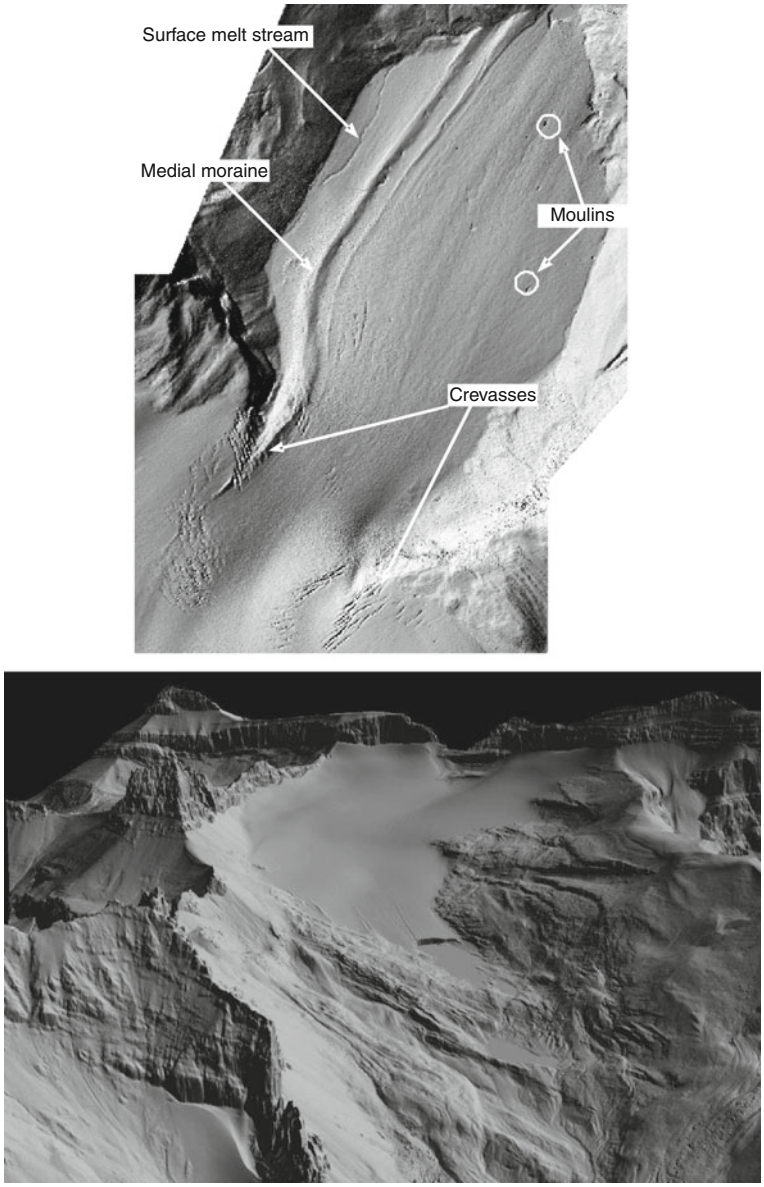

LIDAR in Glaciology, Figure 3 *Top*: Shaded-relief rendering of last-pulse data (gridded at 2 m resolution) collected over the terminus of Peyto Glacier, Canadian Rocky Mountains, 2002. Crevasses, meltwater streams, moulins and medial moraine forms are clearly evident. *Bottom*: Oblique rendering of the Ram River Glacier and the upper Ram River Valley, Canadian Rocky Mountains, 2002. The glacier has retreated out of an over deepened basin resulting, in this instance, in a calving terminus. Surface meltwater streams are also evident. (Data courtesy of C-CLEAR, Optech Inc. and the Geological Survey of Canada).

scenarios, where taking advantage of brief periods of fair weather is key, include studies of glacier elevation change in Patagonia (Keller et al., 2007), and assessing the mechanism and volumes of material involved in ice and rock avalanche events in the Icefield Ranges of Canada's Saint Elias Mountains (Lipovsky et al., 2008).

High-resolution ALTM has also been used in support of glacier energy-balance modeling and hydrology (Chasmer and Hopkinson, 2001; Arnold and Rees, 2003; Hopkinson and Demuth, 2006; Hopkinson et al., 2010). Lidar-derived DEMs can support satellite-based glaciological studies including the terrain-correction of SAR imagery (e.g., Wivell et al., 1992), and removing the topography effect necessary in the application of InSAR for glacier motion studies. Satellite altimetry cal/val campaigns routinely utilize lidar. For example, the CryoSat-2 (e.g., Wingham et al., 2006) calibration/validation effort will utilize ICESat low-slope crossovers, and under-flights with the NASA ATM. Lidar has also been used in the validation of glacier DEMs derived from the Shuttle Radar (SRTM)

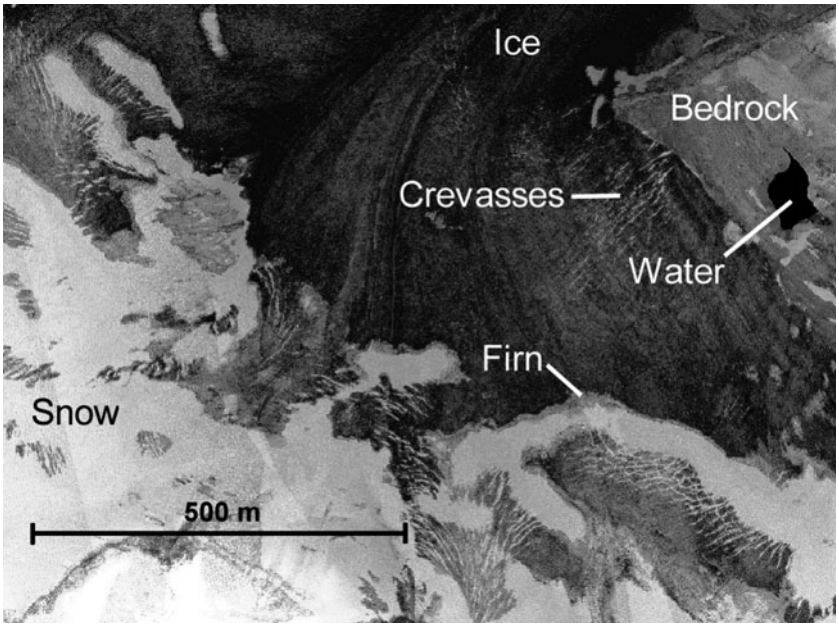

LIDAR in Glaciology, Figure 4 Return pulse intensity image from a portion of Peyto Glacier near its equilibrium line, demarcating regions of snow, firn, and ice. (After Hopkinson and Demuth, 2006; by permission Canadian Aeronautical and Space Institute).

and the Advanced Spaceborne Thermal Emission Radiometer (ASTER) instrument aboard NASA's EOS/Terra spacecraft.

Lidar-based altimetry from artificial satellites is currently the realm of ICESat's GLAS instrument (Zwally et al., 2002a), which has seen service over both ice sheet interiors, their margins and ice streams, ice shelves, and the large glacier systems of Alaska and Svalbard (e.g., Csatho et al., 2005; and overview by Zwalley, 2005).

Mission planning

Returning again to airborne swath mapping, a few salient points related to mission planning are now provided.

Survey goals and aviation resources will, to a large degree, dictate the ground-point measurement density, which is in turn realized by adjusting survey system parameters: laser PRF, scanner angle/field of view, scanner rate; and flight variables: height AGL and ground speed. Estimating the nominal point-spacing will also vary according to the type of scanner/mirror configuration employed. High point-densities may be desirable for glacier morphological and surface facies studies, whereas, lower point-densities may be acceptable for DEM generation so long as topographic noise does not confound the survey goals. It should also be noted that due to the finite speed of light, the laser PRF will be height limited; and that "eye-safe" laser range may impose minimum flying heights in regions where, for example, recreational alpine ski touring is popular.

Notwithstanding aviation and meteorological considerations, mission planning for swath mapping typically involves determining the number of flight lines (fl) for a given width ($\overleftrightarrow{Y}$) of the planned survey area (perpendicular to the flightline direction), and the desired swath overlap fraction (olp):

$$fl = \frac{\overleftrightarrow{Y}}{sw(1 - olp)} \tag{2}$$

where sw is the swath width given by:

$$sw = 2h \tan\left[\frac{\theta_{sc}}{2}\right] \tag{3}$$

and where h is the height above ground and θ_{sc} is the scanner angle/field of view. Overlap is desirable for error checking and stitching swath data for contiguous mapping.

"Terrain following" is often employed to maintain a nominal height AGL, resulting in a more uniform swath and overlap widths and generally results in fewer laser return dropouts. Aviation considerations include flying the aircraft within gimbal and IMU tolerances and making rudder turns that prevent the loss of signal lock with the GNSS.

Challenges

Several additional technical challenges confront the user of lidar-derived terrain information, particularly as it concerns the detection and interpretation of height change data. In many glaciological applications, we are concerned with detecting small changes over large areas. Notwithstanding what has already been discussed with respect to coupled system and terrain errors, attention must be paid to the vertical reference systems used in precision height

measurement. A good overview is provided by Töyrä et al. (2003), albeit confined to the Canadian Spatial Reference System. A more general overview describing the representation of the Earth's surface undulations can be found at: http://www.kartografie.nl/geometrics/Reference%20surfaces/body.htm.

While repeat lidar mapping can lead to relatively straightforward estimates of surface elevation change, deriving surface mass balances over the accumulation area will require additional information describing the contribution to elevation change of snow densification, accumulation, and ice flow/divergence. For example, densification alone can manifest thinning, while in actuality there may have been zero mass change. Conversely, thickening may be the result of changing ice flow conditions – for example, as possibly manifested by a delayed Little Ice Age cooling having stiffened the ice near the glacier bed, therefore retarding the flow of ice (personal communication, Martin Sharp).

While alluded to previously, instrument and aviation costs are likely the largest challenge to the systematic use of lidar in the study of glaciers. To date this has been ameliorated by developing research consortia such as the Canadian-based C-CLEAR, and international cooperation founded by NASA's Wallops Flight Facility and the Geodynamics Department of the Danish National Space Centre. Indeed, these entities have been the means to developing research applications in both Hemispheres. In many jurisdictions, national aviation laboratory facilities cannot be seen to compete with the private sector airborne survey industry, and so valuable surveillance capacity may sit underutilized. C-CLEAR regularly conducts national-scale, multi–theme survey missions where all research stakeholders share the aviation costs. Other groups have endeavored to construct integrated systems by assembling off-the-shelf components and installing them in private light aircraft (Geophysical Institute, University of Alaska Fairbanks) or coordinating installations with air force or navy assets (Centro de Estudios Científicos, Chile).

Despite these challenges, the literature suggests that lidar-based surveys of glacier surface elevation change and other variables will assist differentiating interannual variability from long-term trends – a critical aspect of glaciological study in a water resources and sea level context.

Summary

This entry has presented a brief review of the principle of light detection and ranging, and a description of a variety of laser-based systems used in glaciological studies. A discussion of error considerations has been provided, and the capability of lidar was illustrated with numerous examples from the available literature. Basic survey planning considerations and some of the specific challenges of using lidar in the study of glaciers and ice sheets were discussed. A bibliography for further study and reference accompanies this text.

Bibliography

Abdalati, W., and Krabill, W., 1999. Calculation of ice velocities in the Jakobshavn Isbrae area using airborne laser altimetry. *Remote Sensing of Environment*, **67**, 194–204.

Abdalati, W., Krabill, W., Frederick, E., Manizade, S., Martin, C., Sonntag, J., Swift, R., Thomas, R., Yungel, J., and Koerner, R., 2004. Elevation changes of ice caps in the Canadian Arctic Archipelago. *Journal of Geophysical Research*, **109**, F04007, doi:10.1029/2003JF000045.

Alley, R. B., Andrews, J. T., Clarke, G. K. C., Cuffey, K. M., Funder, S., Marshall, S. J., Mitrovica, J. X., Muhs, D. R., and Otto-Bleisner, B., 2009. Past extent and status of the Greenland ice sheet. In *Past Climate Variability and Change in the Arctic and at High Latitudes*. U.S. Climate Change Program and Subcommittee on Global Change Research. U.S. Geological Survey, Reston, VA, pp. 303.357.

Arendt, A. A., Echelmeyer, K. A., Harrison, W. D., Lingle, C. S., and Valentine, V. B., 2002. Rapid wastage of Alaska glaciers and their contribution to rising sea level. *Science*, **297**, 382.

Arnold, N. S., and Rees, W. G., 2003. Self-similarity in glacier surface characteristics. *Journal of Glaciology*, **49**, 547–554.

Arnold, N. S., Rees, W. G., Devereux, B. J., and Amable, G. S., 2006. Evaluating the potential of high-resolution airborne LiDAR data in glaciology. *International Journal of Remote Sensing*, **27**(6), 1233–1251, doi:10.1080/01431160500353817.

Bamber, J. L., Alley, R. B., and Joughin, I., 2007. Rapid response of modern day ice sheets to external forcing. *Earth and Planetary Science Letters*, **257**, 1–13.

Bonardi, L. (ed.), 2008. Mountain glaciers and climate changes in the last century. *Terra Glacialis*, Special Issue, 239 pp.

Casassa, G., López, P., Pouyaud, B., and Escobar, F., 2008. Detection of changes in glacial run-off in alpine basins: examples from North America, the Alps, central Asia and the Andes. *Hydrological Processes*, **23**(1), 31–41.

Chasmer, L., and Hopkinson, C., 2001. Using airborne LASER altimetry and GIS to assess scale-induced radiation-loading errors in a glacierized basin. In *Proceedings of the 58th Eastern Snow Conference*, May 17–19, 2001, Ottawa, Canada, pp. 195–205.

Csatho, B., Ahn, Y., Yoon, T., van der Veen, C. J., Vogel, S., Hamilton, G., Morse, D., Smith, B., and Spikes, V. B., 2005. ICESat measurements reveal complex pattern of elevation changes on Siple Coast ice streams, Antarctica. *Geophysical Research Letters*, **32**, L23S10, doi:doi:10.1029/2005GL024306.

Davenport, I. J., Holden, N., and Gurney, R. J., 2004. Characterizing errors in airborne laser altimetry data to extract soil roughness. *IEEE Transactions on Geoscience and Remote Sensing*, **42**, 2130–2141.

Echelmeyer, K. A., Harrison, W. D., Larsen, C. F., Sapiano, J., Mitchell, J. E., Demallie, J., Rabus, B., Adalgeirsdottir, G., and Sombardier, L., 1996. Airborne surface profiling of glaciers: a case study in Alaska. *Journal of Glaciology*, **42**, 538–547.

Favey, E., Geiger, A., Gudmundsson, G. H., and Wehr, A., 1999. Evaluating the potential of an airborne laser-scanning system for measuring volume changes of glaciers. *Geografiska Annaler*, **81A**, 555–561.

Garvin, J. B., 1997. *Monitoring glaciers with airborne and spaceborne laser altimetry.* United States Geological Survey Open-file Report, 98-31, Williams Jr., R. S., and Ferrigno J. G. (eds.): URL: http://pubs.usgs.gov/of/1998/of98-031/index.htm.

Goulden, T., 2009. *Prediction of Error Due to Terrain Slope in Lidar Observations*. Unpublished Master of Science in Engineering thesis, Canada, The University of New Brunswick, 144 pp.

Goulden, T., and Hopkinson, C., 2010. The forward propagation of integrated system component errors within airborne lidar

data. *Photogrammetric Engineering and Remote Sensing*, **76**, 589–601.
Haeberli, W., Hoelzle, M., and Suter, S. (eds.), 1998. *Into the Second Century of Worldwide Glacier Monitoring: Prospects and Strategies*. Paris: UNESCO. Studies and Reports in Hydrology, Vol. 56, p. 227.
Hodgson, M., and Bresnahan, P., 2004. Accuracy of airborne LiDAR-derived elevation: empirical assessment and error budget. *Photogrammetric Engineering and Remote Sensing*, **70**, 331–339.
Hopkinson, C., 2004. *Place Glacier Terrain Modeling and 3D Laser Imaging*. Contract Report No. TSD051603X. Prepared for the National Glaciology Program of the Geological Survey of Canada, M.N. Demuth, Scientific Authority, 22 pp + digital files on CD.
Hopkinson, C., Chasmer, L., Munro, D. S., and Demuth, M. N., 2010. The influence of DEM resolution on simulated solar radiation-induced glacier melt. *Hydrological Processes*, **24**(6), 775–788.
Hopkinson, C., and Demuth, M. N., 2006. Using airborne lidar to assess the influence of glacier downwasting on water resources in the Canadian Rocky Mountains. *Canadian Journal of Remote Sensing*, **32**(2), 212–222.
Hopkinson, C., Demuth, M., Sitar, M., and Chasmer, L., 2001. Applications of lidar mapping in a glacierised mountainous terrain. In Stein, T. I. (ed.), *IGARSS'01: Proceedings of the International Geoscience and Remote Sensing Symposium*, July 9–14, Sydney, Australia. CDROM. IEEE, New York.
Hopkinson, C., Demuth, M. N., Barlow, J., Sitar, M., Young, G., Pomeroy, J., and Munro, D. S., 2009. Investigating glacier dynamics using temporal air photo, LiDAR and oblique thermal imagery at Peyto Glacier; an overview. In *Proceedings of the Canadian Symposium on Remote Sensing*, June 22–25, Lethbridge, Alberta. Canadian Aeronautical and Space Institute.
Kaser, G., Cogley, J. G., Dyurgerov, M. B., Meier, M. F., and Ohmura, A., 2006. Mass balance of glaciers and ice caps: consensus estimates for 1961-2004. *Geophysical Research Letters*, **33**, L19501, doi:10.1029/2006GL027511.
Keller, K., Casassa, G., Rivera, A., Forsberg, R., and Gundestrup, N., 2007. Airborne laser altimetry survey of Glacier Tyndall, Patagonia. *Global and Planetary Change*, **59**, 101–109, doi:10.1016/j.gloplacha.2006.11.039 DOI:dx.doi.org.
Kennet, M., and Eiken, T., 1997. Airborne measurement of glacier surface elevation by scanning laser altimeter. *Annals of Glaciology*, **24**, 235–238.
Krabill, W. B., Thomas, R., Jezek, K., Kuivinen, K., and Manizade, S., 1995. Greenland ice sheet thickness changes measured by laser altimetry. *Geophysical Research Letters*, **22**, 2341–2344.
Krabill, W. B., Abdalati, W., Frederick, E. B., Manizade, S. S., Martin, C. F., Sonntag, J. G., Swift, R. N., Thomas, R. H., and Yungel, J. G., 2002. Aircraft laser altimetry of elevation changes of the Greenland ice sheet: technique and accuracy assessment. *Journal of Geodynamics*, **34**, 357–376.
Lipovsky, P. S., Evans, S. G., Clague, J. J., Hopkinson, C., Couture, R., Bobrowsky, P., Ekström, G., Demuth, M. N., Delaney, K. B., Roberts, N. J., Clarke, G. K. C., and Schaeffer, A., 2008. The July 2007 rock and ice avalanches at Mount Steele, St. Elias Mountains, Yukon, Canada. *Landslides*, doi:10.1007/s10346-008-0133-4.
Lutz, E., Geist, T., and Stotter, J., 2003. Investigations of airborne laser scanning signal intensity on glacial surfaces – utilizing comprehensive laser geometry modelling and orthophoto surface modelling (a case study: Svartisheibreen, Norway). In Mass, H.-G., Vosselman, G., and Streilein, A. (eds.), *Proceedings of the ISPRS Workshop on 3D Reconstruction from Airborne Laser Scanner and InSAR Data*, October 8–10, Dresden, Germany, pp. 101–106.
Measures, R. M., 1984. *Laser Remote Sensing*. New York: Wiley.
Reeh, N., 1999. Mass balance of the Greenland ice sheet: can modern observation methods reduce the uncertainty? *Geografiska Annaler*, **81A**, 735–742.
Rignot, E., and Thomas, R. H., 2002. Mass balance of Polar ice sheets. *Science*, **297**, 1502–1506.
Sauchyn, D., Demuth, M. N., and Pietronrio, A., 2008. Upland watershed management and global change: Canada's Rocky Mountains and western plains. In Garrido, A., and Dinar, A. (eds.), *Managing Water Resources in a Time of Global Change: Mountains, Valleys and Floodplains*, Contributions from the Rosenberg International Forum on Water Policy, Vaux Jr. H. (series ed.). London: Routledge, pp. 49–66.
Thomas, R., Frederick, E., Krabill, W., Manizade, S., and Martin, C., 2006. Progressive increase in ice loss from Greenland. *Geophysical Research Letters*, **33**, L10503, doi:10.1029/2006GL026075.
Thomas, R., Frederick, E., Krabill, W., Manizade, S., and Martin, C., 2009. Recent changes on Greenland outlet glaciers. *Journal of Glaciology*, **55**(189), 147–162.
Töyrä, J., Pietroniro, A., Hopkinson, C., and Kalbfleisch, W., 2003. Assessment of airborne scanning laser altimetry (lidar) in a deltaic wetland environment. *Canadian Journal of Remote Sensing*, **29**(6), 718–728.
UNEP/WGMS, 2009. Global Glacier Changes – Facts and Figures: www.grid.unep.ch/glaciers/.
van de Wal, R. S. W., Boot, W., van den Broeke, M. R., Smeets, C. J. P. P., Reijmer, C. H., Donker, J. J. A., and Oerlemans, J., 2008. Large and rapid melt-induced velocity changes in the Ablation Zone of the Greenland Ice Sheet. *Science*, **321**, 111–113.
Vinther, B. M., Buchardt, S. L., Clausen, H. B., Dahl-Jensen, D., Johnsen, S. J., Fisher, D. A., Koerner, R. M., Raynaud, D., Lipenkov, V., Andersen, K. K., Blunier, T., Rasmussen, S. O., Steffensen, J. P., and Svensson, A. M., 2009. Holocene thinning of the Greenland ice sheet. *Nature*, **461**, 385–388, doi:10.1038/nature08355.
Wehr, A., and Lohr, U., 1999. Airborne laser scanning — an introduction and overview. *ISPRS Journal of Photogrammetry and Remote Sensing*, **54**, 68–82.
Wingham, D. J., Francis, C. R., Baker, S., Bouzinac, C., Brockley, D., Cullen, R., de Chateau-Thierry, P., Laxon, S. W., Mallow, U., Mavrocordatos, C., Phalippou, L., Ratier, G., Rey, L., Rostan, F., Viau, P., and Wallis, D. W., 2006. CryoSat: A mission to determine the fluctuations in Earth's land and marine ice fields. *Advances in Space Research*, **37**, 841–871.
Wivell, C. E., Steinwand, D. R., Kelly, G. G., and Meyer, D. J., 1992. Evaluation of terrain models for the geocoding and terrain correction of synthetic aperture radar (SAR) images. *IEEE Transactions on Geoscience and Remote Sensing*, **30**(6), 1137–1144.
Zwalley, H. J., 2005. Overview of scientific advances from the ICESat mission. *EOS Transactions, American Geophysical Union*, **86**(52), Fall Meeting Supplement, Abstract C33A-01.
Zwally, H. J., Schutz, B., Abdulati, W., Abshire, J., Bentley, C., Brenner, A., Bufton, J., Dezio, J., Handcock, D., Harding, D., Herring, T., Minster, B., Quinn, K., Palm, S., Spinhirne, J., and Thomas, R., 2002a. ICESat's laser measurements of polar ice, atmosphere, ocean and land. *Journal of Geodynamics*, **34**, 405–445.
Zwally, H. J., Abdalati, W., Herring, T., Larson, K., Saba, J., and Steffen, K., 2002b. Surface melt-induced acceleration of Greenland ice-sheet flow. *Science*, **297**, 218–222.

Cross-references

Automated Glacier Mapping
Digital Elevation Model Generation Over Glacierized Region

Equilibrium-Line Altitude (ELA)
Glacier Mass Balance
Glacier Motion/Ice Velocity
Glaciology
GPS in Glaciology, Applications
Ice Sheet Mass Balance
ICESat Data in Glaciological Studies
Optical Remote Sensing of Alpine Glaciers
Synthetic Aperture Radar (SAR) Interferometry for Glacier Movement Studies

LITTLE ICE AGE

Rajesh Kumar
School of Engineering and Technology, Sharda University, Greater Noida, NCR, India

There is no agreed beginning year to the Little Ice Age when the world experienced relatively cooler temperatures compared to the present, but it is conventionally defined as a period extending from the sixteenth to the nineteenth centuries when there was expansion of mountain glaciers (http://www.meteo.psu.edu/~mann/shared/articles/littleiceage.pdf; Lamb, 1972; http://earthobservatory.nasa.gov/Glossary/?mode=alpha&seg=l&segend=n). During this period, glaciers in many parts of the world expanded and came down to the lower altitude. It is speculated that the amount of solar radiation emitted by the Sun was low at that time as a periodical phenomenon. Volcanic eruption is accounted for an unexpected blockage of sunlight, leading to worldwide cooling.

Bibliography

http://www.meteo.psu.edu/~mann/shared/articles/littleiceage.pdf
http://earthobservatory.nasa.gov/Glossary/?mode=alpha&seg=l&segend=n
Lamb, H. H., 1972. *The cold Little Ice Age climate of about* 1550 to 1800. *Climate: present, past and future*. London: Methuen, p. 107, ISBN 0-416-11530-6. (noted in Grove 2004:4).

LOBE

Rajesh Kumar
School of Engineering and Technology, Sharda University, Greater Noida, NCR, India

A rounded projection of glacier is known as lobe. Ice lobes are dynamic features within large ice sheets that reflect glacier accumulation and ablation, ice temperature, bedrock topography, ice topography, marginal seas, and ice flow. The ice lobes are the more active parts of the uniform ice sheet. They represent parts that had bordered on each other in different directions or on more passive portions of the ice (Punkari, 1980). Marginal extension of ice stream along broad bedrock trough or valley may be hundreds of kilometers long often terminating in large ice lobes. With the increasing water pressure near the bed of ice lobe, the area of an ice lobe increases while its thickness decreases (Hughes, 1981). The ice is thickest near the central lines of lobe and thinnest near the marginal zone that gives rise to a fan-shaped directions of glacial flow (Reeh, 1982). At the ice margins, thrust moraines and hummocky stagnation topography are more common than single-crested, simple moraines if the ice lobes had repeated advances. Normally terminal moraines are formed at the farthest extent of ice lobe. In the boundary zones of the different ice lobes, there occur exceptionally large glaciofluvial forms and moraines.

Bibliography

http://cgrg.geog.uvic.ca/abstracts/JenningsTerrestrialThe.html.
Hughes, T. J., 1981. Numerical reconstructions of paleo-ice sheets. In The Last Great Ice Sheets, eds *G. H. Denton and T. J. Hughes*, pp. 222–274. John Wiley, New York.
Punkari, M., 1980. The ice lobes of the Scandinavian ice sheet during the deglaciation in Finland. *Boreas*, **9**, 307–310.
Reeh, N., 1982. A Plasticity theory approach to the steady-state shape of a three-dimensional ice sheet. *Journal of Glaciology*, **28**, 431–455.

M

MAPPING OF INTERNAL GLACIAL LAYERS

David A. Braaten
Department of Geography, Center for Remote Sensing of Ice Sheets, University of Kansas, Lawrence, KS

Synonyms

Isochronous layers

Definition

Internal glacial layer: A change in structure or composition of glacial ice that may be observed with remote sensing instrumentation, such as ice penetrating radar.

Introduction

Internal layers preserved within glacial ice are generally considered to be former deposition surfaces that became entombed in the ice, and therefore the age of a particular layer is equal or isochronous. Internal layers hold a wealth of information about glacier behavior and past climate, and may be detected and tracked with radio-echo sounding (RES) from both the surface and the air (Gogineni et al., 2007; Kanagaratnam et al., 2004). Internal glacial layers have been detected with RES on most polar glaciers, polar ice sheets, and high alpine glaciers, and these layers can often be mapped over great distances. RES detects internal layers, because a small portion of a transmitted electromagnetic radar pulse is reflected back from the layer and is detected by the radar receiver. A radar reflection from an internal layer is caused by a local change in the dielectric constant of the snow or ice, which can be due to an abrupt change in snow or ice density, acidity, or ice crystal fabric orientation (Hempel et al., 2000). If internal layers in glacial ice can be dated using ice core records or a depth-age model (Fahnestock et al., 2001), the layers can be used to understand the formation history of an ice mass, provide temporal information on snow accumulation, and provide input data for numerical ice sheet models, constraints for the model, and data for verification of the model results (Parrenin et al., 2006).

Near-surface internal layers

In the upper few hundred meters of glacial ice, abrupt vertical density changes are the primary cause of RES-detected internal layers. These density changes are related to seasonal changes in solar insolation, with the lower density layers forming during the summer, and high density layers forming during winter. These density contrasts remain intact until depths of several hundred meters (Fujita et al., 2002). Hence, near-surface internal layers can often be interpreted as annual layers, and along with a representative density profile, used to assess the temporal and spatial distribution of snow accumulation, which is a critical parameter in assessing ice sheet and glacier mass balance. By mapping internal layers with RES, an area average accumulation rate may be determined to compliment and reduce the uncertainty of a point measurement of accumulation rate from an ice core.

Deep layers

For RES-detected internal glacial layers at depths beyond a few hundred meters, the radar reflections generally result from acidity and/or ice crystal fabric changes, since the overburden has compressed the ice to a nearly homogeneous density at these depths. Annual layers are no longer detected, and the deep internal layers represent events that deposited acidic material on the glacial surface (e.g., from volcanic activity) or caused a realignment in the crystal

Vijay P. Singh, Pratap Singh & Umesh K. Haritashya (eds.), *Encyclopedia of Snow, Ice and Glaciers*, DOI 10.1007/978-90-481-2642-2,

fabric orientation. However, these deep internal glacial layers are isochronous, and reveal information about long-term climate patterns, long-term ice flow dynamics, and interactions of the glacial ice with the bed (Waddington et al., 2007; Eisen, 2008). The age of deep internal layers can be determined from the analysis of an ice core, and subsequently tracked over hundreds of kilometers (Siegert and Payne, 2004).

Summary

The ability to detect and track internal glacial layers at many different ice depths with RES has provided unique insights that have greatly benefited glaciologists and climate scientists. These internal layers are isochrones and their three-dimensional structure provides critical information on the flow history of glacial ice, changes in accumulation rates, and interactions with the underlying terrain. This information has provided critical inputs for numerical ice sheet models and serves to validate ice sheet model results (Waddington et al., 2007).

Bibliography

Eisen, O., 2008. Inference of velocity pattern from isochronous layers in firn, using an inverse method. *J. Glaciol.,* **54**, 613.

Fahnestock, M., Abdalati, W., Luo, S., and Gogineni, S., 2001. Internal layer tracing and age-depth accumulation relationships for the northern Greenland ice sheet. *J. Geophys. Res.,* **106**, 33,789.

Fujita, S., Maeno, H., Furukawa, T., and Matsuoka, K., 2002. Scattering of VHF radio waves from within the top 700m of the Antarctic ice sheet and its relation to the depositional environment: a case-study along the Syowa-Mizuho-Dome Fuji traverse. *Ann. Glaciol.,* **34**, 157.

Gogineni, S., Braaten, D., Allen, C., Paden, J., Akins, T.; Kanagaratnam, P., Jezek, K., Prescott, G., Jayaraman, G., Ramasami, V., Lewis, C., Dunson, D., 2007. Polar Radar for Ice Sheet Measurements (PRISM). *Remote Sensing of Environment - Special Issue: Cryosphere,* **111**, 204.

Hempel, L., Thyssen, F., Gundestrup, N., Clausen, H. B., and Miller, H., 2000. A comparison of radio-echo sounding data and electrical conductivity of the GRIP ice core. *J. Glaciol.,* **46**, 369.

Kanagaratnam, P., Gogineni, S. P., Ramasami, V., and Braaten, D., 2004. A wideband radar for high-resolution mapping of near-surface internal layers in glacial ice. *IEEE Trans. Geosci. Remote Sens.,* **42**, 483.

Parrenin, F., Hindmarsh, R. C. A., and Remy, R., 2006. Analytical solutions for the effect of topography, accumulation rate, and lateral flow divergence on isochrone layer geometry. *J. Glaciol.,* **52**, 191.

Siegert, M. J., and Payne, A. J., 2004. Past rates of accumulation in central West Antarctica. *Geophys. Res. Lett.,* **31**, L12403.

Waddington, E. D., Neumann, T. A., Koutnik, M. R., Marshall, H. P., and Morse, D. L., 2007. Inference of accumulation-rate patterns from deep layers in glaciers and ice sheets. *J. Glaciol.,* **53**, 694.

Cross-references

Bottom Melting or Undermelt (Ice Shelf)
Dynamics of Glaciers
Ice Core
Radar Application in Snow, Ice, and Glaciers

MARGINAL CHANNEL (LATERAL MELTWATER CHANNEL)

Amit Kumar
Department of Geology, Center of Advanced Study in Geology, Panjab University, Chandigarh, India

The marginal channels in the glacierized area are categorized as follows:

Ice marginal channel: It is a channel cut by flowing water along the ice margin. These channels are often left dry, or with remnant lakes, after the ice melts away. Parallel sets of ice marginal channels may form when the ice margin retreats down a slope.

Meltwater channel: It is a channel or a valley formed or followed by a glacial meltwater stream; according to their position, they are divided into ice-marginal (lateral) channels, subglacial channels, etc. Some lateral meltwater channels have only one side and form a step or terrace on the hillside. Others form meander-shaped gouges in the hillside, with both sides of the channel floor left hanging.

Lateral meltwater channels in general form along or just beneath and roughly parallel to margin of the ice. They occur in groups or single channels oriented subparallel to the contour of the land.

MARGINAL ICE ZONES

Rajesh Kumar
School of Engineering and Technology, Sharda University, Greater Noida, NCR, India

The region of solid ice cover near the edge of the sea ice pack where the ice breaks up and drifts away from or back to the ice cap under the action of waves or wind is known as the marginal ice zone (MIZ). It is an area of broken ice field between the interfacial region of frozen oceans and open oceans. The formation and dynamics of marginal ice zone is mainly governed by ocean wave interaction with the ice cover, wind and the strong temperature gradients in the atmosphere and ocean. Once formed, the broken ice scatters wave energy and protects the interior of the ice from further breaking (Squire et al., 1995). The wind blowing away from the ice pack can extend the marginal ice zone significantly while wind blowing towards the ice pack can squeeze the marginal ice zone to a relatively smaller width. These are very common in polar region and may extend hundreds of kilometers from the ice edge, and in some regions right to the coast.

Bibliography

Squire, V. A., Dugan, J. P., Wadhams, P., Rottier, P. J., and Liu, A. J., 1995. Of ocean waves and sea ice. *Annual Review of Fluid Mechanics*, **27**, 115–168.

MARINE GLACIERS

Rajesh Kumar
School of Engineering and Technology, Sharda University, Greater Noida, NCR, India

The glaciers, like floating slabs of ice that deform under their own weight and terminate in ocean or lakes, are termed "marine glaciers." They often end in an ice shelf. They are relatively small, independent streams of ice that travel from the higher altitudes to the sea level. Their fronts either ground and calve icebergs into the ocean, or push out into the water as a floating "tongue." In spite of being solid in appearance, glaciers are constantly flowing under the force of gravity. The average velocity of most of the glaciers are of the order of few metres per year but the marine glaciers (like Antarctic 'ice streams' and 'outlet glaciers') are capable of draining ice from the ice sheet interiors to the ocean with substantially larger velocity. Like other glaciers, marine glaciers are also under the retreating phase. Due to increase in the ocean temperature under global warming, the melting rate of marine glaciers will also increase, speeding the flow of outlet glaciers.

MARINE ICE SHEET

Rajesh Kumar
School of Engineering and Technology, Sharda University, Greater Noida, NCR, India

Marine ice sheets are continental ice masses resting on bedrock below sea level (Schoof, 2007). Large portions of its ice rest on the ocean floor well below sea level and its edges flow into floating ice shelves for miles out into the sea. The importance of the transition zone between grounded and floating ice in controlling the dynamics of marine ice sheets was pointed out in seventies by Weertman (1974). Dynamics of marine ice sheets are similar to those of land-based ice sheets except that they must couple with the surrounding floating ice shelves at the grounding line, where the ice reaches a critical flotation thickness. Marine ice sheets can lose mass not only through melting, but also through outflow of ice into the surrounding ice shelves. The stability of a marine ice sheet strongly depends on the basal slope and/or changes in the cross-sectional area. The transition from ice-sheet to ice-shelf flow takes place in case of rapidly sliding ice sheets.

Marine ice sheets are inherently unstable; whereby small changes in climate could trigger irreversible retreat of the grounding line (a location along the coast where the ice is no longer ground supported and begins to float) (Hughes, 1973; Thomas and Bentley, 1978; Weertman, 1974). During the last glacial period, which reached its peak about 20,000 years ago, large marine ice sheets existed in both the Northern and Southern Hemispheres. Due to the gradual warming that followed, they all disappeared by about 6,000 years ago, except for the West Antarctic Ice Sheet and some minor marine ice sheets of East Antarctica (e.g., that of the Lambert Glacier).

Bibliography

Hughes, T. J., 1973. Is the West Antarctic ice-sheet disintegrating. *Journal of Geophysical Research*, **78**, 7884–7910.
Schoof, C., 2007. Marine ice-sheet dynamics. Part1 – The case of rapid sliding. *Journal of Fluid Mechanics*, **573**, 27–55, doi:10.1017/S0022112006003570.
Thomas, R. H., and Bentley, C. R., 1978. A model for holocene retreat of the West Antarctic ice sheet. *Quaternary Research*, **10**, 150–170.
Weertman, J., 1974. Stability of the junction between an ice sheet and an ice shelf. *Journal of Glaciology*, **13**, 3–11.

MECHANICAL WEATHERING

Rajesh Kumar
School of Engineering and Technology,
Sharda University, Greater Noida, NCR, India

Mechanical weathering is a special type weathering that works by physical means. It is related with the physical degeneration or breakdown of materials which are exposed to the natural environment. Under this process the larger rocks or minerals are gradually broken into smaller pieces. The important activities that cause the mechanical weathering are frost action, root action, water pressure, rain and wind. Mechanical weathering can be divided into following categories.

Exfoliation: The solar heating on the materials (rocks and minerals) can cause differences in temperature between the surface and the interior of materials. This differential temperature causes a loosening of the surface of the materials and break in sheets along the joints parallel to the earth surface. This process of weathering is known as exfoliation. This process is mostly occurring on the large rock masse brought on the surface as a result of tectonic activities.

Abrasion: It is the type of mechanical weathering which occurs under the action of wind, running water, waves and gravity. The frictional force of wind, running water and waves removes the upper layer of the rock and make them smaller. The rock fall under the gravitational pulls break the bigger rock into pieces.

Mechanical Weathering, Figure 1 Example of mechanical weathering in the Kumaon Himalaya, India (photograph by Rajesh Kumar).

Freeze and Thaw Weathering: It is the type of weathering which is common in places where the night temperature goes down below freezing point. Water that infuses into a rock fracture grows as crystals under the freezing temperature. The volume of frozen water is higher than the liquid water that exerts pressure on the rock and expands the cracks for the further attack and in due course of time it breaks the rock. Also the changing temperature in the day and night cause unequal expansion and contraction of rock materials (especially different minerals expands and contracts at different rates), which give rise to the development of cracks. Under this process, rocks are deformed into smaller sizes. Plant root growth also helps in expanding the cracks to further expand, making them more vulnerable to frost expansion and breaking of the rocks.

MEDIAN ELEVATION OF GLACIERS

D. P. Dobhal
Wadia Institute of Himalayan Geology, Dehradun, India

The median elevation is mean of total elevation extent of a glacier (arithmetic mean value of highest and lowest elevations of a glacier) and used value as elevation parameter in glacier inventory. In earlier studies it was often used for quick Equilibrium-line altitudes (ELA) estimation, but geometry and empirical evidence from modern glaciers suggests that this method overestimates the ELAs. In addition, in the modern glaciers median elevation of a glacier is found far away from the ELA as ablation area exceeds the accumulation area.

MEDITERRANEAN GLACIERS AND GLACIATION

Philip D. Hughes
Geography, School of Environment and Development, The University of Manchester, Manchester, UK

Definition

Mediterranean. Lands surrounding the Mediterranean Sea
Glaciers. Dynamic body of ice
Glaciation. The action of glaciers in shaping the land surface

The Mediterranean region: physical characteristics

The Mediterranean Sea lies between 35°N and 45°N and is almost surrounded by mountains – the only exception being the southeastern shores in North Africa (and of course, the Straits of Gibraltar). The climate of the Mediterranean is distinct and is characterized by pronounced seasonality with hot and dry summers and cool and wet winters. This seasonal climate produces large snowfalls in many mountain areas, and in some places this snow lasts all year round, even sustaining glaciers today (Figure 1).

Modern glaciers in the Mediterranean mountains

Small temperate glaciers, like those in the Mediterranean mountains, are extremely sensitive indicators of climate and their behavior provides important insight into climatic changes in this important climatic region. The modern-day glaciers are described below.

Iberia (Spain/France)

Until recently, the southernmost glacier in Europe existed in the Sierra Nevada, Spain (37°N, 3°E). Here, a glacier survived in the Corral Veleta cirque until it disappeared during the first decades of the twentieth century. Further north, in the Picos de Europa, four ice patches still survive. The only "true" remaining glaciers in Iberia are present in the Pyrenees where 21 glaciers were present at the beginning of the twentieth century covering a total area of 495 ha; of which less than 260 ha are on the Spanish side and 235 ha are on the French side (González Trueba et al., 2008). The highest peak in the Pyrenees, Pico de Aneto (3,404 m), supports the largest glaciers in these mountains. However, as with most other areas of the Pyrenees, glaciers retreated dramatically through the twentieth century and glaciers had shrunk by 530 ha between 1894 and 2001 (González Trueba et al., 2008).

Maritime Alps (France/Italy)

Fifteen small glaciers are present in the Maritime Alps on the border of France and Italy (Federici and

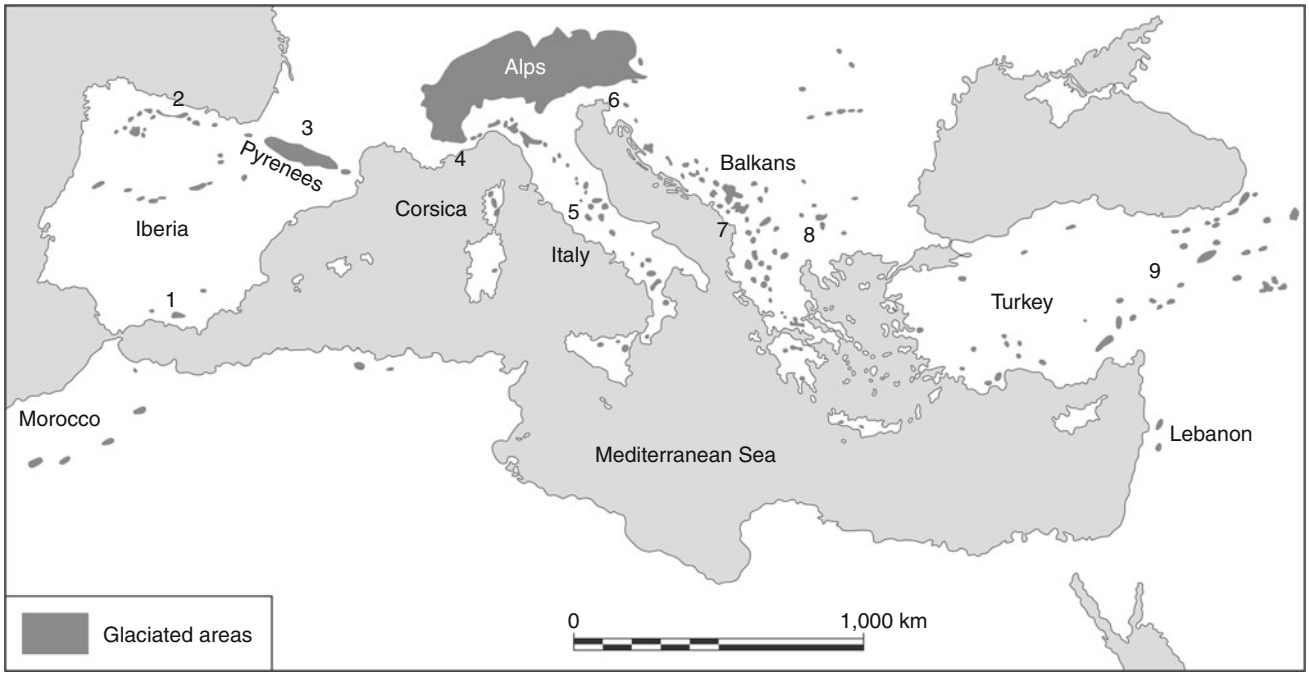

Mediterranean Glaciers and Glaciation, Figure 1 The extent of past Pleistocene glaciers in the Mediterranean mountains showing the locations of surviving (or recently extinct) modern-day glaciers and ice patches. **1**: Sierra Nevada, Spain – Corral Veleta glacier disappeared in twentieth century (González Trueba et al., 2008); **2**: Picos de Europa – 4 ice patches (González Trueba et al., 2008); **3**: Pyrenees – (21 glaciers González Trueba et al., 2008); **4**: Maritime Alps – 15 glaciers (Federici and Pappalardo, 1995); **5**: Italian Apennines – 1 glacier (D'Orefice et al., 2000); **6**: Julian Alps – 2 glaciers; **7**: Dinaric and Albanian Alps – 5 glaciers (Hughes, 2007; Hughes, 2009); **8**: Pirin Mountains, Bulgaria – 2 glacierets (Grunewald et al., 2006); **9**: Turkey – >40 glaciers (Kurter and Sungur, 1980; Kurter, 1991).

Pappalardo, 1995). These glaciers are the most southerly in the European Alps and some are situated less than 50 km from the Mediterranean Côte d'Azur. The rest of the European Alps are excluded here, despite draining into the Mediterranean Sea, since given the scale of these mountains they are best described as a separate geographical entity. Thirteen of the glaciers are found in the Argentera Massif, which contains the highest peaks of the Alpes Maritimes. The equilibrium line altitude (ELA) of the six largest Argentera glaciers is currently c. 2,800 m a.s.l. (Fisinger and Ribolini, 2001). In common with other parts of the Mediterranean, all of these glaciers have retreated during the last century and ELAs during the Little Ice Age were 100–150 m lower than in the late twentieth century (Federici and Pappalardo, 1995; Pappalardo, 1999).

Apennines (Italy)

A small glacier is present in a north-facing cirque below the highest peak of the Italian Apennines, Corno Grande (2,912 m). The glacier retreated through the twentieth century and between 1916 and 1990, and over this period the volume of the glacier is estimated to have been reduced by about 90% and the area by about 68% (Gellatly et al., 1994; D'Orefice et al., 2000). In recent years, the glaciers split into two portions and the remaining ice is rapidly shrinking (Pecci et al., 2008).

Julian Alps (Slovenia)

In Slovenia, two small glaciers exist below the peaks of Triglav (2,864 m a.s.l.) and Skuta (2,532 m a.s.l.). On Triglav, the Zeleni Sneg glacier is situated on the northern slopes between c. 2,550 and 2,400 m a.s.l. This glacier has undergone dramatic retreat throughout the second half of twentieth century. In 1995, the glacier covered an area of only 3.3 ha (Gabrovec, 1998). By 2003, the glacier area had reduced to only 0.7 ha. The Skuta glacier has also suffered from rapid retreat (Pavšek, 2004).

Dinaric and Albanian Alps (Montenegro/Albania)

In the Dinaric Alps of Montenegro, a small glacier exists at Debeli Namet in the Durmitor massif. This glacier survives in a north-facing hollow below the mountain of Sljëme (2,455 m) (Figure 2). In 2005, this glacier covered an area of c. 5.0 ha (Hughes, 2007). The glacier has suffered only minor retreat since the late nineteenth century and the glacier front in 2006 was only 25–50 m up-valley of moraines dated at c. 1878 and 1904 AD using lichenometry (Hughes, 2007). In northern Albania, several small glaciers also survive in the

Mediterranean Glaciers and Glaciation, Figure 2 The Debeli Namet glacier, Montenegro. (Photograph by Philip Hughes, September 2006.)

Prokletije Mountains (North Albanian Alps). At least four glaciers are present around the highest peak, Maja Jezerce (2,694 m), the largest covering an area of c. 5.4 ha (Milivojević et al., 2008; Hughes, 2009). The Montenegrin and Albanian glaciers survive at a very low altitudes for this latitude as a result of avalanching and windblown snow in addition to shading, with snow accumulation of more than 4,000 mm (water equivalent) required to balance summer melting (Hughes, 2008, 2009).

Pirin Mountains (Bulgaria)

In the Pirin Mountains of Bulgaria, Grunewald et al. (2006) noted two glacierets (mikrogletscher) and several perennial snow patches. The largest of these, the Sneschnika glacier, was found below the northern cliffs of Vihren (2,914 m) and covered an area of just 1 ha in 2005. This Bulgarian glacieret is currently the southernmost such feature in Europe.

Turkey

At least 40 glaciers are present in the mountains of Turkey and the largest Mediterranean glaciers occur in the mountains of eastern Turkey (Akçar and Schlüchter, 2005). In 1980, glaciers covered a total area of c. 22.9 km^2 (Kurter and Sungur, 1980), although almost everywhere glaciers are in retreat (Çiner, 2004). Mount Ararat, a dormant stratovolcano situated in the easternmost Taurus Mountains, is the highest peak in Turkey (5,137 m) and is covered by an ice cap of about 10 km^2. However, the recent state of this ice cap is unclear. Glaciers are also found on other Turkish volcanoes, including Mount Süphan (4,058 m) and Mount Erciyes (3,917 m). The southeastern Taurus contains the greatest concentration of modern glaciers in Turkey. These are also the most southerly glaciers in the Mediterranean basin and owe their existence to the high altitude of these mountains (>4,000 m) (Kurter, 1991). The largest occur on Mount Cilo (4,135 m) where the Uludoruk glacier is nearly 4 km long and covers an area of 8 km^2. In common with many other glaciers in Turkey, it has retreated throughout the twentieth century and the altitude of the glacier front rose approximately 400 m between 1937 and 1991 (Çiner, 2004). Smaller glaciers occur in the central Taurus, further to the west on the mountains of Aladag (3,756 m) and Bolkardag (3,524 m). The snowline in these areas is situated at c. 3,450 m and glacier survival in such marginal conditions is controlled by local climatological and physiographic conditions (Kurter, 1991). Further north, at least 12 small glaciers exist in the Pontic Mountains on mountains such as Kaçkar (3,932 m) and cover a total area of about 2.54 km^2 with ELAs between 3,100 and 3,400 m (Çiner, 2004).

Pleistocene glaciations in the Mediterranean mountains

Most of the Mediterranean mountains supported glaciers during the Pleistocene – from Morocco in the west to the Lebanon in the east (Hughes et al., 2006a). The largest ice caps formed over the Pyrenees and the Maritime Alps.

Mediterranean Glaciers and Glaciation, Figure 3 Pleistocene cirque moraines in the High Atlas Mountains, Morocco. (Photograph by Philip Hughes, January 2007.)

In the case of the latter, Pleistocene ice caps were contiguous with the main Alpine ice sheet that covered a total area of 126,000 km^2 during the last cold stage (Ehlers, 1996). Ice caps also formed over the mountains of northwest Iberia (Vieira, 2008; Cowton et al., 2009) and also over large areas of the Balkans (Hughes et al., 2006a) while large ice fields formed in northern Greece. The consequences of these glaciations are clearly seen in the Mediterranean mountains where glaciers have shaped the landscape to form cirques, U-shaped valleys, arêtes, roche moutonees, glacial lakes, and moraines (Figure 3).

In many areas, glacial deposits record glaciations during multiple Pleistocene cold stages. The oldest and most extensive glaciations occurred during the Middle Pleistocene. In northwest Spain, this has been shown using cosmogenic nuclide analyses (Fernandez Mosquera et al., 2000), while in Greece Middle Pleistocene glacial deposits have been recognized using Uranium-series dating (Hughes et al., 2006b). Elsewhere, in Turkey and Corsica, cosmogenic nuclide analyses suggest that the most extensive recorded glaciation occurred during the last cold stage of the Pleistocene. It appears that the timing of glacier advances was asynchronous across the Mediterranean and the extent of glaciations also varied between regions during different Pleistocene cold stages (Hughes and Woodward, 2008).

Summary

Glaciers exist today in the mountains of the Mediterranean. Some survive at very low altitudes (2,000–2,500 m) for this latitude as a result of high levels of winter precipitation and also avalanching and windblown snow. However, many Mediterranean glaciers have retreated significantly since the nineteenth century and many have vanished completely over the last 100 years. During the Pleistocene cold stages, glaciers were much larger and existed in mountains all over the Mediterranean region and glaciation has been a major contributor to landscape development in this region.

Bibliography

Akçar, N., and Schlüchter, C., 2005. Paleoglaciations in Anatolia: a schematic review and first results. *Eiszeitalter und Gegenwart*, **55**, 102–121.

Çiner, A., 2004. Turkish glaciers and glacial deposits. In Ehlers, J., and Gibbard, P. L. (eds.), *Quaternary Glaciations – Extent and Chronology. Part I: Europe*. Amsterdam: Elsevier, pp. 419–429.

Cowton, T., Hughes, P. D., and Gibbard, P. L., 2009. Palaeoglaciation of Parque Natural Lago de Sanabria, northwest Spain. *Geomorphology*, **108**, 282–291.

D'Orefice, M., Pecci, M., Smiraglia, C., and Ventura, R., 2000. Retreat of Mediterranean glaciers since the Little Ice Age: case study of Ghiacciaio del calderone, Central Apennines, Italy. *Arctic, Antarctic, and Alpine Research*, **32**, 197–201.

Ehlers, J., 1996. *Quaternary and Glacial Geology*. Chichester: Wiley, p. 578.

Federici, P. R., and Pappalardo, M., 1995. L'evoluzione recente dei ghiacciai delle Alpi Maritime. *Geografia Fisica e Dinamica Quaternaria*, **18**, 257–269.

Fernandez Mosquera, D., Marti, K., Vidal Romani, J. R., and Weigel, A., 2000. Late Pleistocene deglaciation chronology in the NW of the Iberian Peninsula using cosmic-ray produced 21 NE in quartz. *Nuclear Instruments and Methods in Physics Research*, **B172**, 832–837.

Fisinger, W., and Ribolini, A., 2001. Late glacial to Holocene deglaciation of the Colle Del Vei Bouc-Colle Del Sabbione area Argentera massif, Maritime Alps, Italy – France. *Geografia Fisica e Dinamica Quaternaria*, **24**, 141–156.
Gabrovec, M., 1998. The Triglav glacier between 1986 and 1998. *Geografski zbornik*, **38**, 89–110.
Gellatly, A. F., Smiraglia, C., Grove, J. M., and Latham, R., 1994. Recent variations of Ghiacciaio del Calderone, Abruzzi, Italy. *Journal of Glaciology*, **40**, 486–490.
González Trueba, J. J., Martín Moreno, R., Martínez de Pisón, E., and Serrano, E., 2008. Little Ice Age' glaciation and current glaciers in the Iberian Peninsula. *Holocene*, **18**, 551–568.
Grunewald, K., Weber, C., Scheithauer, J., and Haubold, F., 2006. Mikrogletscher im Piringebirge (Bulgarien). *Zeitschrift für Gletscherkunde und Glazialmorphologie*, **39**, 99–114.
Hughes, P. D., 2007. Recent behaviour of the Debeli Namet glacier, Durmitor, Montenegro. *Earth Surface Processes and Landforms*, **32**, 1593–1602.
Hughes, P. D., 2008. Response of a Montenegro glacier to extreme summer heatwaves in 2003 and 2007. *Geografiska Annaler*, **192**, 259–267.
Hughes, P. D., 2009. Twenty-first century glaciers and climate in the Prokletije Mountains, Albania. *Arctic, Antarctic and Alpine Research*, **41**(4), 455–459.
Hughes, P. D., and Woodward, J. C., 2008. Timing of glaciation in the Mediterranean mountains during the last cold stage. *Journal of Quaternary Science*, **23**, 575–588.
Hughes, P. D., Woodward, J. C., and Gibbard, P. L., 2006a. Glacial history of the Mediterranean mountains. *Progress in Physical Geography*, **30**, 334–364.
Hughes, P. D., Woodward, J. C., Gibbard, P. L., Macklin, M. G., Gilmour, M. A., and Smith, G. R., 2006b. The glacial history of the Pindus Mountains, Greece. *Journal of Geology*, **114**, 413–434.
Kurter, A., and Sungur, K., 1980. Present glaciation in Turkey. *International Association of Hydrological Sciences*, **126**, 155–160.
Kurter, A., 1991. Glaciers of the Middle East and Africa – glaciers of Turkey. In Williams, R. S., and Ferrigno, J. G., (eds.), *Satellite Image Atlas of Glaciers of the World*. United States Geological Survey Professional Paper, 1386-G-1. Washington: United States Government Printing Office, pp. 1–30.
Milivojević, M., Menković, L., and Ćalić, J., 2008. Pleistocene glacial relief of the central part of Mt. Prokletije (Albanian Alps). *Quaternary International*, **190**, 112–122.
Pappalardo, M., 1999. Remarks on the present-day condition of the glaciers in the Italian Maritime Alps. *Geografia Fisica e Dinamica Quaternaria*, **22**, 79–82.
Pavšek, M., 2004. The Skuta glacier. *Geografski obzornik*, **51**, 11–17.
Pecci, M., Agata, C., and Smiraglia, C., 2008. Ghiacciaio del Calderone (Apennines, Italy): the mass balance of a shrinking Mediterranean glacier. *Geografia Fisica e Dinamica Quaternaria*, **31**, 55–62.
Vieira, G. T., 2008. Combined numerical and geomorphological reconstruction of the Serra da Estrela plateau icefield, Portugal. *Geomorphology*, **97**, 190–207.

Cross-references

Cirque Glaciers
Equilibrium-Line Altitude (ELA)
Glacieret
Ice Caps
Little Ice Age
Moraine
Quaternary Glaciation

MELT RUNOFF MODELING

Pratap Singh
Tahal Consulting Engineers Ltd, New Delhi, India

Synonyms

Glacier melt runoff modeling; Snowmelt runoff modeling

Definition

The melt runoff is modeled using a watershed hydrological model which has an option of computing melt runoff. The model attempts to mathematically represent each component of the total melt process. The basic difference between the various models is the mathematical relationships which they use for each component. The simulation models are relatively recent innovations and offer a great potential as both a forecasting tool and a means to improve the understanding of snowmelt processes. Such a model can be used to provide hydrologic simulations of basin required for the planning, design, and operation of hydropower and water resources projects.

Introduction

Snow is an important part of the hydrologic cycle and considered as a dominant source of streamflow in many parts of the World. The geographical distribution of snow indicates a general increase in both snowfall and snow cover with an increase in latitude and altitude.

Accurate estimates of the volume of water stored in the basin in the form of snow in winter and its rate of release due to melting in summer are needed for many purposes, including streamflow and flood forecasting, reservoir operation, watershed management, water supply, and design of hydraulic structures. The planning of new multipurpose projects further emphasizes the need for reliable estimates from rain, snow, and glacier runoff. For purposes of melt runoff modeling, a thorough understanding of the relationships between meteorological variables and snow and glacier melt processes is needed for seasonal and short-term water yield forecasting.

The worldwide status of data collection, and climatic and physiographic characteristics are not uniform. In some countries, the network in the mountainous regions is dense or reasonably good providing adequate hydrometeorological data, whereas in many countries, such as Asian countries, it is very poor or sparse with very limited data. Therefore, development, selection, or application of models is not the same for each region. A number of hydrological models with snowmelt component have been developed worldwide.

Types of models

Snowmelt models are categorized on the basis of approach adopted for snow or ice melting computation. There are

two basic approaches generally adopted for the computation of snowmelt from a snowpack. The first approach is known as energy budget or the energy balance approach (see entry *Surface Energy Balance*) and the second is the temperature index or degree-day approach (see entry *Degree-Days*). Hydrological models either use an energy balance approach or a temperature index approach for melt computation. Thus snowmelt models are divided into two types of models, namely, index models and energy budget models. Broadly, energy balance models require information on radiant energy, sensible and latent heat, energy transferred through rainfall over snow and heat conduction from ground to the snowpack. Several meteorological parameters are to be monitored to obtain this information over the snowpack. An understanding of the basic energy transfer processes and their role in melting of snowpack helps in improving the performance of the operational snowmelt models.

Index models use one or more variables in an empirical expression to estimate snow cover energy exchange. Air temperature is the most commonly used index, but other variables, such as net radiation, wind speed, vapor pressure, and solar radiation, are also used. The studies have been made to assess the relative importance of meteorological variables in snowmelt and found that if only one meteorological variable is available for snowmelt prediction, average temperature is the best predictor. The degree-day method is more popular, because temperature represents reasonably the energy flux and at the same time it is relatively an easy parameter to measure, extrapolate, and probably to forecast. However, snowmelt prediction can be significantly improved by using vapor pressure, net radiation, and wind rather than the temperature variable alone.

Consideration of limited variables in an index model is preferred; otherwise it becomes difficult to correctly account for the interdependency between the variables when a large number of variables are considered. If data for a number of parameters are available for use, it is probably much more logical to use a theoretically based energy balance model to ensure that the variables are combined in a reasonable manner. Techniques need to be devised to account for the effect of factors like slope, aspect, elevation, and forest cover on various input parameters.

Energy budget models

The physics of melting of snow and ice and transformation of meltwater into runoff is well represented in such models. The melting of snow is an overall result of the different heat transfer processes in the snowpack. Sun is the ultimate source of energy that is responsible for the melting of the snowpack, but there is a complex interaction between the incoming solar radiation, earth's atmosphere, and the terrain surface. Hence, a number of intermediate steps in the process of energy transfer to the snow surface have to be considered to understand the process of snowmelt and also to make quantitative estimates of the melt.

Energy balance or heat budget of a snowpack governs the production of meltwater. This method involves accounting of the incoming energy, outgoing energy, and the change in energy storage for a snowpack for a given period of time. The net energy is then expressed as equivalent of snowmelt. The seasonal variability in the energy inputs available for melt, in general, increases toward the poles. The energy balance of the snowpack for any time interval can be expressed as

$$Q_m = Q_{nr} + Q_h + Q_e + Q_p + Q_g + Q_q \quad (1)$$

where Q_m, the energy available for melting of snowpack; Q_{nr}, the net radiation; Q_h, the sensible or convective heat gained from the air; Q_e, the latent heat of evaporation, condensation or sublimation; Q_g, the heat gained through conduction from underground; Q_p, the heat content of rainwater; and Q_q, the change of internal energy of the snowpack.

In the above energy balance equation, different components of energy are considered in the form of energy flux, which is defined as the amount of energy received on a horizontal snow surface of unit area over a unit time. The positive value of Q_m will result in the melting of snow.

The relative importance of the various heat transfer processes involved in the melting of a snowpack depends on time and local conditions. For example, radiation melting dominates in the weather conditions when wind is calm. Melting due to sensible heat flux dominates under warm weather conditions. When all the components of energy balance equation are known, the melt rate due to the energy flux can be expressed as

$$M = Q_m/[\rho_w L \beta] \quad (2)$$

where M is the depth of meltwater (m/day), L is the latent heat of fusion (333.5 kJ/kg), ρ_w is the density of water (1000 kg/m^3), and β is the thermal quality of snow. The thermal quality of snow depends on the amount of free water content (generally 3–5%) and temperature of the snowpack. For a snow that is thermally ripened for melting and contains about 3% of free water content, the value of β is 0.97.

Temperature index models

The specific type of data required for the energy budget method is rarely available for carrying out snowmelt studies. This is particularly true for the Himalayan basins where the network for data collection is very poor. The most generally available data are daily maximum and minimum temperatures, humidity measurements, and surface wind speed. That is why temperature indices are widely used in the snowmelt estimation, because it is generally considered to be the best index of heat transfer processes

associated with snowmelt. Air temperature expressed in degree-days is used in snowmelt computations as an index of the complex energy balance tending to snowmelt. This method is also known as the degree-day method. A degree-day, in a broad sense, is a unit expressing the amount of heat in terms of persistence of a temperature for 24 h period of 1°C departure from a reference temperature. The simplest and the most common expression relating daily snowmelt to the temperature index is

$$M = D_f(T_i - T_b) \quad (3)$$

where M, the melt produced in cm of water in a unit time; D_f, the degree-day factor (cm $°C^{-1}day^{-1}$); T_i, the index air temperature (°C); and T_b, the base temperature (usually 0°C).

Daily mean temperature is the most commonly used index temperature for snowmelt. There are several methods of dealing with the index temperature used in calculating the degree-day value. When using the maximum–minimum approach, the most common way is to use the temperature as it is recorded and calculate the average daily temperature. In many parts of the Western US mountainous areas, the drop in minimum temperature is so much that the daily mean temperature comes to below 0°C, thereby indicating no degree-days, whereas snowmelt conditions have prevailed during part of the day when air temperature was much above the freezing point. The inclusion of minimum temperature at an equal weight with the maximum temperature gives undue emphasis to this effect. On the other hand, the use of maximum temperature only excludes this effect entirely. Figure 1 shows a comparison of observed and computed daily runoff in the Gangotri Glacier basin (Indian Himalayas), which has snow and ice melt dominated runoff in the river.

Application of melt runoff modeling

Efficient management of water resources, including water availability, flood forecasting, reservoir operation, and design of hydraulic and hydrologic structures, requires best estimates of available resources. Keeping in view the importance of water generated from snow and glaciers, the modeling of melt runoff becomes an important tool for various applications such as:

1. Forecasting of the volume of water to be released from snow and glaciers
2. Simulation/forecasting of streamflow, including floods caused by high-intensity rainfall, combination of rainfall and intense melting, and glacier–lake outburst flood (GLOF)
3. Better estimates of water availability and design flood for the planning and designing of hydropower projects on snow and glacier-fed rivers
4. Simulation of continuous supply of meltwater for ground water reservoirs and in turn the contribution of ground water as base flow during the lean season for operation of hydropower projects
5. Impact assessment of climate change on different hydrological variables

Some important snowmelt models

Several simulation models accounting for snow accumulation and melting processes have been developed

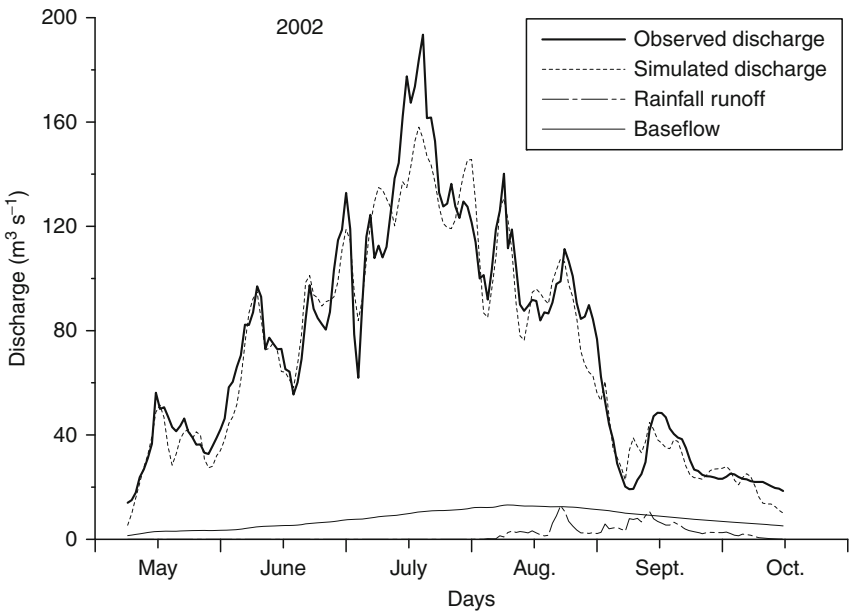

Melt Runoff Modeling, Figure 1 Comparison of observed and simulated discharge for Gangotri glacier basin in the Himalayan region using snowmelt model (SNOWMOD).

worldwide. Hydrologic simulation models that include snow are generally divided into three basic components, namely, snow cover, precipitation–runoff relationship, and runoff distribution and routing procedures. Most simulation models simulate the entire snow accumulation and melt season. Some of the models simulate only the snowmelt processes, whereas other models are used in conjunction with models of soil moisture accounting.

Snowmelt models that simulate runoff can be classified using a number of model characteristics. It begins with the division of the basin model into two major components, namely, a snowmelt model and a transformation model. The snowmelt model simulates the processes of snow accumulation and snowmelt, while the distribution and routing is accomplished by the transformation model which relates the snowmelt and rainfall-runoff volumes to discharge hydrographs. The most common transformation function is the unit hydrograph. For downstream channel reaches, the routing may be accomplished by a number of hydrologic routing techniques.

Singh and Singh (2001) have described snowmelt and ice melt modeling processes as well as concerned models in detail. Some of the important snowmelt runoff simulation models are listed below:

1. Snowmelt Model (SNOWMOD), India
2. Streamflow Synthesis and Reservoir Regulation (SSARR), USA
3. Snowmelt Runoff Model (SRM), Switzerland
4. University of British Columbia Watershed Model (UBC), Canada
5. Hydrologic Engineering Center (HEC-1) Model, USA
6. National Weather Service Snow Accumulation and Ablation Model, USA
7. HBV Model, Sweden

Summary

Modeling of melt runoff generated from snow and glaciers in a basin involves an understanding of snow accumulation, depletion, water percolation through snowpack, and routing of generated runoff up to the point of interest. In melt computation, mostly temperature index methods are used simply because of the availability of temperature data as compared to radiation data. Although there are a number of models available to simulate and forecast melt runoff, there is still much scope for improving modeling of melt runoff focusing on accurate estimation of spatial distribution of melt rate.

Bibliography

Singh, P., and Singh, V. P., 2001. *Snow and Glacier Hydrology*. Dordrecht: Kluwer.

Cross-references

Degree-Days
Surface Energy Balance

MELTING PROCESSES

Luke Copland
Department of Geography, University of Ottawa, Ottawa, ON, Canada

Definition

Melting refers to the change of state from solid to liquid, such as the change from ice to water. It occurs at 0°C for pure ice/snow at surface atmospheric pressures, although both changes in pressure and impurities (e.g., salt) can change the melting point. This review describes melting processes as they relate to ice and snow, with a focus on processes that contribute to both surface and basal melting on glaciers.

Surface melting

The main controls on surface melting of ice and snow are air temperature and solar radiation, although other factors such as surface albedo, rainfall, humidity, and wind can also be important (Hock, 2005). The importance of these factors has long been researched (e.g., Ångström, 1933), and is illustrated by discharge records from alpine glaciers, which show strong diurnal variability in the summer. Surface melting is usually the main way by which snow and ice bodies lose mass in temperate climates, although in cold climates (e.g., Antarctica) mass losses from iceberg calving and sublimation often dominate. In terms of surface melting, there are three main factors that control rates on ice and snow:

1. Net radiation
   The net radiation at the surface describes the difference between incoming and outgoing energy (Hock, 2005). Incoming energy is provided by:
   (a) Direct, diffuse, and reflected shortwave radiation that originates from the sun. On clear days, most shortwave radiation reaches the surface as direct sunshine, but on cloudy days diffuse radiation dominates due to the effectiveness of atmospheric water vapor, dust, and aerosols in scattering shortwave radiation (Paterson, 1994; Hock, 2005).
   (b) Longwave radiation emitted by objects such as clouds and surrounding mountain slopes after they have been heated, typically by incoming shortwave radiation.

   Outgoing energy occurs in the form of longwave radiation. Net melting occurs if there is less energy emitted than absorbed once the ice/snow has reached 0°C. Surface albedo is one of the most important factors in controlling how much shortwave radiation is absorbed by a surface and variations in albedo can produce dramatic differences in surface melt rates. For example, an old (firn) snow surface with an albedo of ~0.45 will melt approximately twice as fast as a new snow surface with an albedo of ~0.90 for the same

amount of incoming solar radiation (albedo values from Paterson, 1994, Table 4.1).

In a study of melt patterns on a glacier on Ellesmere Island, Canada, Arendt (1999) found that the absorbed shortwave radiation flux accounts for 96–99% of the energy available for melt. In a summary of 16 studies by Hock (2005), it was similarly found that net radiation provides the majority of energy for melt, averaging 65.1%.

2. Sensible heat
   Sensible heat refers to heat that is transferred between the atmosphere and an ice/snow surface, and is primarily supplied by warm air masses (Benn and Evans, 1998; Paterson, 1994). In general, it is less important than net radiation, with the review of Hock (2005) finding that it contributed an average of 26.4% of the total melt energy. However, the proportion of glacier melt that originates from sensible heat is very sensitive to wind, with the sensible flux sometimes dominating over net radiation on windy days (Holmgren, 1971). A rough ice surface also encourages wind turbulence and the transfer of sensible heat to the surface. Rain also produces a sensible heat flux, but is generally an insignificant factor for the annual surface energy balance of most glaciers (Hock, 2005). However, it can be locally important during heavy rain events on glaciers in temperate climates such as New Zealand, where Hay and Fitzharris (1988) found that it contributed 37% of the daily ablation during one prolonged event.
3. Latent heat
   Energy from latent heat is produced from a change in state, and can warm an ice/snow surface when there is condensation of water vapor (e.g., dew) or the freezing of rainwater. It can also significantly raise temperatures where there is refreezing of percolating meltwater within a snowpack. It can be locally important, but in general it is the least significant source of energy for surface melt, with the review by Hock (2005) indicating that it accounted for an average of 7.8% of total melt energy.

Seasonal characteristics and snowpack processes

In the spring, melting and runoff from snow and ice bodies typically occur several days to weeks after air temperatures reach 0°C as energy is initially expended on warming the snow and ice to the melting point. Once melt begins, surface runoff from the lower (ablation) area of glaciers typically occurs via supraglacial streams as ice is essentially impermeable. These streams can enter crevasses and moulins, which enable the movement of meltwater to the interior or base of glaciers through englacial and subglacial streams. Direct measurements of melt rates on alpine glaciers record typical surface losses of ~50–100 mm day^{-1} in summer. For example, Purdie and Fitzharris (1999) recorded average summer surface melt rates of 96 mm day^{-1} on bare ice over the terminus of the Tasman Glacier, New Zealand, with a variation between 30 and 175 mm day^{-1}. However, surface debris had a significant insulating effect, with melt rates averaging only ~7 mm day^{-1} where the debris was 1.1 m thick.

In snowpacks and snow-covered parts of glaciers (mainly their accumulation areas), meltwater will not directly runoff the surface but will instead percolate vertically and refreeze where there are internal cold layers and irregularities in the snowpack. This creates internal ice lenses that can lead to retardation and vertical and horizontal channeling of meltwater. The percolation and refreezing process warms the snow via the release of latent heat, and is typically the dominant method by which snow in the accumulation area of many glaciers is warmed. Indeed, it is common for polythermal glaciers in locations such as Svalbard to have high altitude accumulation zones, which are warmer (i.e., typically at 0°C) than their low altitude ablation zones due to this process (Björnsson et al., 1996).

On polythermal glaciers, the refreezing of surface meltwater within and at the base of a snowpack can produce significant quantities of superimposed ice. In this situation, the melting process does not result in a net loss of mass, but the redistribution of it within the existing snow/ice body. Superimposed ice typically occurs at the boundary between the accumulation and ablation zones, and has the net effect of moving the equilibrium line altitude to a lower level.

Basal melting

Significant melting can occur at the base of glaciers and ice sheets if energy is available from sources such as geothermal heat, frictional heat due to ice flow, and sensible heat from meltwater that originated from the surface. The relative importance of these heat sources varies between ice masses, with surface-derived meltwater likely dominating on temperate glaciers (due to the predominance of crevasses and moulins), and geothermal heat dominating in the center of the large ice sheets (where there is little basal motion and no surface meltwater). The inaccessibility of the glacier bed makes it difficult to directly measure the importance of these processes, although the recent discovery of a large number of subglacial lakes beneath the Antarctic Ice Sheet (Siegert et al., 2005) indicates that basal meltwater can persist for a long time once formed.

The influence of pressure on the melting point can be a significant factor for thick ice masses, depressing it at a rate of 0.072°C per million Pascal (MPa) (Benn and Evans, 1998). A 1 km thick glacier has a basal pressure of ~8.8 MPa, which means that the pressure melting point at the base of the ~4 km thick Antarctic Ice Sheet is approximately −2.5°C. The change in pressure melting point with depth means that a body of ice that is solid near

the surface can melt at its base without any change in temperature. In addition, if all ice is at the pressure melting point (e.g., in a temperate glacier) then local variations in pressure can be expected to cause local melting. This regelation process can result in melting on the upstream side of bedrock bumps where pressures are higher than average, and refreezing on the downstream side where pressures are reduced. This explains how water can be produced at the glacier bed without a change in temperature.

Summary

In summary, surface melt processes on ice and snow are strongly tied to climatic conditions, with net radiation typically providing the main source of energy for melt. Internal factors such as geothermal heat fluxes are more important for determining basal melt rates and processes, although climate conditions are also important where surface meltwater is able to reach the bed of a glacier via moulins or crevasses.

Bibliography

Ångström, A., 1933. On the dependence of ablation on air temperature, radiation and wind. *Geografiska Annaler*, **15**, 264–271.
Arendt, A., 1999. Approaches to modelling the surface albedo of a high arctic glacier. *Geografiska Annaler*, **81A**, 477–487.
Benn, D. I., and Evans, D. J. A., 1998. *Glaciers and Glaciation*. London: Arnold.
Björnsson, H., Gjessing, Y., Hamran, S.-E., Hagen, J. O., Liestøl, O., Pálsson, F., and Erlingsson, B., 1996. The thermal regime of sub-polar glaciers mapped by multi-frequency radio-echo sounding. *Journal of Glaciology*, **42**, 23–32.
Hay, J. E., and Fitzharris, B. B., 1988. A comparison of the energy-balance and bulk-aerodynamic approaches for estimating glacier melt. *Journal of Glaciology*, **34**, 145–153.
Hock, R., 2005. Glacier melt: a review of processes and their modeling. *Progress in Physical Geography*, **29**(3), 362–391, doi:10.1191/0309133305pp453ra.
Holmgren, B., 1971. Climate and energy exchange on a sub-polar ice cap in summer. *Arctic Institute of North America Devon Island Expedition 1961–1963*. Uppsala: Meteorologiska Institutionen, Uppsala Universitet. Meddelande 107 Part A–E.
Paterson, W. S. B., 1994. *The Physics of Glaciers*, 3rd edn. New York: Elsevier Science.
Purdie, J., and Fitzharris, B., 1999. Processes and rates of ice loss at the terminus of Tasman Glacier, New Zealand. *Global and Planetary Change*, **22**, 79–91.
Siegert, M. J., Carter, S., Tabacco, I., Popov, S., and Blankenship, D., 2005. A revised inventory of Antarctic subglacial lakes. *Antarctic Science*, **17**, 453–460.

Cross-references

Albedo
Bottom Melting or Undermelt (Ice Shelf)
Calving Glaciers
Equilibrium-Line Altitude (ELA)
Refreezing of Meltwater
Subglacial Drainage System
Sublimation from Snow and Ice
Surface Energy Balance

MELTWATER CHANNELS

Cliff Atkins
School of Geography, Environment, and Earth Sciences, Victoria University of Wellington, Wellington, New Zealand

Definition

Channels eroded by glacial meltwater into bedrock or sediment beneath or near the margins of glaciers and other ice masses.

Introduction

Meltwater channels encompass a wide variety of erosional channel features formed by flowing water sourced from melting glacier ice. They form either beneath the ice (subglacial), along the margins of the ice (ice marginal), or immediately in front of the ice (proglacial). Meltwater channels may be single, discrete channels or branching networks and range in size from small (meter scale) channels (e.g., Hambrey, 1994) to large-scale tunnel channels, hundreds of meters deep and kilometers wide (e.g., Jorgensen and Sandersen, 2006). However, most references to meltwater channels refer to channels that range from meters to tens of meters width and depth and range from tens of meters to kilometers in length.

Meltwater channels are one of the most obvious features of past and present glacial environments and provide a complex but powerful means of delineating past ice limits, glaciological conditions, and deglaciation trends for glaciers and ice sheets. The majority of studies regarding meltwater channels have focused on the Pleistocene ice sheets of the Northern Hemisphere. For example, the recognition of different channel types, combined with mapping of channel distribution have allowed detailed meltwater flow patterns and deglaciation histories to be constructed for the Pleistocene British Ice Sheet (e.g., Glasser and Sambrook Smith, 1999; Evans et al., 2005; Greenwood et al., 2007), Fennoscandian Ice Sheet (e.g., Kleman et al., 1997), and Laurentide Ice Sheet (e.g., Dyke, 1993). However, meltwater channels have been described from many other regions and from various intervals of earth history. For example, Lewis et al. (2006) described meltwater channels formed by subglacial drainage from beneath the East Antarctic Ice Sheet during the Miocene and Williams (2005) reported channels thought to have formed by subglacial meltwater 1.8 billion years ago in what is now the arid northwest of Australia.

Temperature, glacier thermal regime, and meltwater

The amount of meltwater generated in a glacial system varies according to the regional climate and associated thermal regime of glaciers (Eyles, 2006). The thermal

regime controls how the water can move in, under, and around the glacier and therefore influences the types of channels that are formed.

Temperate glaciers, sometimes called "wet-" or "warm"-based glaciers are those that have ice at melting point throughout and generate large amounts of meltwater. The water can move on the surface (supraglacial), within (englacial), or at the bottom of the glacier (subglacial). Where the meltwater reaches the base of the glacier, subglacial channels form. Meltwater draining along the flanks of the glacier may produce marginal channels and water draining away from the glacier margin form proglacial meltwater channels. Subglacial and proglacial meltwater channels are a particularly common feature of past and present temperate glacial environments.

For subpolar (polythermal) and polar (cold-based) glaciers, the margins of the glacier are frozen to the substrate. Subglacial channels do not form because supraglacial meltwater is prevented from moving downward to the bed. Instead, it is deflected and concentrated along the margins of the glacier, producing distinctive lateral meltwater channels. Despite the generally low volume of meltwater, lateral channel formation often constitutes the dominant geomorphic process occurring along cold-based margins (O'Cofaigh et al., 1999; Atkins and Dickinson, 2007) and may be the only evidence left by predominantly or fully cold-based glaciers and ice caps (Benn and Evans, 1998).

Subglacial meltwater channels

Subglacial channels are most commonly associated with temperate glaciers and form where meltwater under pressure erodes into the substrate beneath a glacier. Where the substrate is bedrock, they are often referred to as Nye Channels (N-channels) following the work of Nye (1973). The channels represent subglacial drainage systems and occur both as single channels and networks of channels typically aligned with the glacier flow, although they sometimes wind around subglacial topography (Benn and Evans, 1998). These channels often have abrupt terminations and sometimes show undulating long profiles indicating that meltwater was under pressure allowing it to flow "uphill." These channels reflect the hydraulic conditions beneath the glacier, and have therefore been widely used to reconstruct glacier surface slopes and subglacial drainage histories (e.g., Benn and Evans, 1998).

A variety of small-scale (cm–m) erosional features known as "P-forms" or "S-forms" such as muschelbruche, sichelwannen, flutes, furrows, and potholes are also widely considered to be the result of scour by pressurized subglacial meltwater flow (e.g., Shaw, 1994; Benn and Evans, 1998). However, despite some of these features reaching several meters in length (Hambrey, 1994), they are not usually classified as meltwater channels.

Large subglacial channels are referred to as tunnel channels or tunnel valleys and have been described in many areas that have formerly been covered with ice sheets. They are typically elongated, sinuous troughs that may form anastomosing networks and can be up to hundreds of meters deep and several kilometers wide (Beaney, 2002). They form in both bedrock and sediment substrates and are thought to form by subglacial drainage under high hydrostatic pressure or from catastrophic meltwater flows (Jorgensen and Sandersen, 2006). An example of these is the impressive network of channels known as the Labyrinth in front of the Upper Wright Glacier at the margin of the East Antarctic Ice Sheet in the Antarctic Dry Valleys (Denton and Sugden, 2005; Lewis et al., 2006).

Lateral meltwater channels

Lateral meltwater channels are incised into bedrock or sediment along the margins of glaciers. They are particularly common along the flanks of cold-based and polythermal glaciers where meltwater is concentrated in ice marginal streams (Skidmore and Sharp, 1999). However, they can also form along the margins of temperate glaciers in some situations and care is required when using the presence of lateral meltwater channels as an indication of glacier thermal regime (Syverson and Mickelson, 2009). Lateral meltwater channels can occur in contact with ice or lie between an ice-cored lateral moraine and valley side or in some cases, actually erode into the glacier ice rather than the permafrozen ground, forming submarginal channels (Hambrey, 1994; Benn and Evans, 1998). Lateral meltwater channels are typically short (tens to hundreds of meters) and shallow (<20 m) and often occur oblique to topographic contour lines (Hattestrand and Stroeven, 2002). Where topography is suitable, sets of nested lateral channels are formed (e.g., O'Cofaigh et al., 1999) and these have been used to delineate the retreat of cold-based or polythermal ice sheet margins, sometimes with successive closely spaced channels providing very fine temporal resolution (Dyke, 1993). Nested lateral meltwater channels along the margins of fully cold-based glaciers in hyperarid regions, such as the Dry Valleys of Antarctica are often the most obvious and persistent geomorphological signature of cold-based glacier activity. In this setting, the glacier may be able to advance and retreat over older channels and relict surfaces without necessarily destroying them, resulting in a potentially complex record of glacial events and channel formation (Atkins and Dickinson, 2007).

Proglacial meltwater channels

Proglacial meltwater channels are not in direct contact with the ice and typically drain downslope away from the glacier margin. These are most common in front of temperate glaciers where the volume of meltwater is generally high but variable on diurnal and seasonal timescales (Benn and Evans, 1998). Therefore, proglacial channels are subject to widely fluctuating flows, including catastrophic outburst floods known as jökulhlaups, which can cause rapid and dramatic channel changes and deposit large blocks of ice downstream from the glacier.

The meltwater in proglacial channels usually contains a high volume of sediment and although the channels may occupy and accentuate Nye channels exposed by glacial retreat, they typically grade into a network of shallow, sediment-floored channels separated by gravel bars that collectively make up an outwash plain or sandar (Benn and Evans, 1998). The channels tend to shift rapidly and share many processes and features of braided fluvial channels.

Meltwater channels on Mars?

There is a growing body of literature describing a wide variety of gully and channel features on the surface of Mars. Several studies have compared the channels to meltwater channels in the Canadian Arctic (e.g., Lee and Rice, 1999) and Antarctica (e.g., Marchant and Head, 2007). The similarity in channel characteristics has led to the interpretation of the Martian channels as subglacial, ice marginal, and proglacial channels formed by meltwater sourced from ground ice and glaciers. Ongoing study of these channels is likely to provide further insight into the glacial history of Mars.

Summary

Channels eroded by glacial meltwater vary widely in shape and size. The characteristics of the channels depend on the availability of meltwater, thermal regime of the glacier, and also the substrate conditions. They constitute one of the most obvious and persistent features of glacial landscapes and are useful for interpreting past glacial conditions. Ongoing research into meltwater channels includes new descriptions of modern meltwater channels (e.g., Atkins and Dickinson, 2007; Syverson and Mickleson, 2009) and paleo meltwater channels (e.g., Evans et al., 2005), combined with refinement of diagnostic geomorphological criteria used to classify and interpret meltwater channel origin (Greenwood et al., 2007). This continues to improve the use of meltwater channels in reconstructing past glacial events on earth and beyond.

Bibliography

Atkins, C. B., and Dickinson, W. W., 2007. Landscape modification by meltwater channels at margins of cold-based glaciers, Dry Valleys, Antarctica. *Boreas*, **36**, 47–55.

Beaney, C. L., 2002. Tunnel channels in southeast Alberta, Canada: evidence for catastrophic channelized drainage. *Quaternary International*, **90**(1), 67–74.

Benn, D. I., and Evans, D. J. A., 1998. *Glaciers and Glaciation*. Arnold: London, 734 pp.

Denton, G. H., and Sugden, D. E., 2005. Meltwater features that suggest Miocene ice-sheet overriding of the Transantarctic Mountains in Victoria Land, Antarctica. *Geografiska Annaler*, **87A**, 67–85.

Dyke, A. S., 1993. Landscapes of cold-centred Late Wisconsinan ice caps, Arctic Canada. *Progress in Physical Geography*, **17**, 223–247.

Evans, D. J. A., Clark, C. D., and Mitchell, W. A., 2005. The last British Ice Sheet: a review of the evidence utilised in the compilation of the Glacial Map of Britain. *Earth Science Reviews*, **70**, 253–312.

Eyles, N., 2006. The role of meltwater in glacial processes. *Sedimentary Geology*, **190**, 257–268.

Glasser, N. F., and Sambrook Smith, G. H., 1999. Glacial meltwater erosion of the Mid-Cheshire Ridge: implications for ice dynamics during the Late Devensian glaciation of northwest England. *Journal of Quaternary Science*, **14**(7), 703–710.

Greenwood, S. L., Clark, C. D., and Hughes, A. L. C., 2007. Formalising an inversion methodology for reconstructing ice-sheet retreat patterns from meltwater channels: application to the British Ice Sheet. *Journal of Quaternary Science*, **22**, 637–645.

Hambrey, M. J., 1994. *Glacial Environments*. University College London Press: London, 296 p.

Hattestrand, C., and Stroeven, A. P., 2002. A relict landscape in the centre of Fennocsandian glaciation: geomorphological evidence of minimal Quaternary glacial erosion. *Geomorphology*, **44**, 127–148.

Jorgensen, F., and Sandersen, P. B. E., 2006. Buried and open tunnel valleys in Denmark-erosion beneath multiple ice sheets. *Quaternary Science Reviews*, **25**, 1339–1363.

Kleman, J., Hattestrand, C., Borgstrom, I., and Stroeven, A., 1997. Fennoscandian palaeoglaciology reconstructed using a glacial geological inversion model. *Journal of Glaciology*, **43**, 283–299.

Lee, P., and Rice, J. W., Jr., 1999. Small Valleys Networks on Mars: The Glacial Meltwater Channel Networks of Devon Island, Nunavut Territory, Arctic Canada, as Possible Analogs. The Fifth International Conference on Mars, July 19–24, 1999, Pasadena, California, abstract no. 6237.

Lewis, A. R., Marchant, D. R., Kowalewski, D. E., Baldwin, S. L., and Webb, L. E., 2006. The age and origin of the Labyrinth, western Dry Valleys, Antarctica: evidence for extensive middle Miocene subglacial floods and freshwater discharge to the Southern Ocean. *Geology*, **34**(7), 513–516.

Marchant, D. R., and Head, J. W., 2007. Antarctic dry valleys: Microclimate zonation, variable geomorphic processes, and implications for assessing climate change on Mars. *Icarus*, **192**, 187–222.

Nye, J. F., 1973. The motion of ice past obstacles. In Whalley, E., Jones, S. J., and Gold, L. W. (eds.), *The Physics and Chemistry of Ice*. Ottowa: Royal Society of Canada, pp. 387–394.

O'Cofaigh, C., Lemmen, D. S., Evans, D. J. A., and Bednarski, J., 1999. Glacial landform-sediment assemblages in the Canadian High Arctic and their implications for late Quaternary glaciation. *Annals of Glaciology*, **28**, 195–201.

Shaw, J., 1994. Hairpin erosional marks, horseshoe vortices and subglacial erosion. *Sedimentary Geology*, **91**, 269–283.

Skidmore, M. L., and Sharp, M. J., 1999. Drainage system behaviour of a High-Arctic polythermal glacier. *Annals of Glaciology*, **28**, 209–215.

Syverson, K. M., and Mickelson, D. M., 2009. Origin and significance of lateral meltwater channels formed along a temperate glacier margin, Glacier Bay, Alaska. *Boreas*, **38**, 132–145.

Williams, G. E., 2005. Subglacial meltwater channels and glaciofluvial deposits in the Kimberley Basin, Western Australia: 1.8 Ga low-latitude glaciation coeval with continental assembly. *Journal of the Geological Society*, **162**, 111–124.

Cross-references

Glacier Hydrology
Hydrology of Jökulhlaups
Ice-Marginal Processes
Marginal Channel (Lateral Meltwater Channel)
Meltwater Erosion
Nye (N) Channels
Palaeo-Channel
Subglacial Drainage System

MELTWATER CONDUIT

D. P. Dobhal
Wadia Institute of Himalayan Geology, Dehradun, Uttarakhand, India

Once the snow or ice is melted it can take several pathways over the ice bed in the form of supraglacial, englacial, and subglacial channels. Water carrying channel flows through narrow, tubular chute and cylindrical hollows and that connects to glacier beds or margins is called meltwater conduit.

MELTWATER EROSION

Rajesh Kumar
School of Engineering and Technology, Sharda University, Greater Noida, NCR, India

Landscapes that experience glaciations undergo considerable modification as a result of the erosion caused by the moving masses of ice. The direct glacial erosion is accomplished by three processes, namely, abrasion, crushing, and plucking. Another important, but indirect erosion

Meltwater Erosion, Figure 1 Erosion by Gangotri glacier meltwater, observed few kilometers down to snout.

Meltwater Erosion, Figure 2 Bed erosion visible at the cave type terminus of a glacier in Suru Basin, India.

process is meltwater erosion. The production of water through melting of ice that undergoes erosional process like loosening, dissolving, and removing action on debris or rock material in a glacial environment is called as meltwater erosion. Glacial meltwater is a very effective agent of mechanical erosion as well as chemical erosion because of the high water pressure that flows through tunnels in the ice and emerges at the end as a meltwater stream. The meltwater inside the glacier may be under hundreds of feet of ice and is under great pressure. The release of this water under high pressure mixed with the sediment carves rock on the way like a saw and enhances the rate of erosion.

If there are large amounts of meltwater under the glacier, it lubricates the ice and may allow the glacier to slide more rapidly down its bedrock valley hence enhancing the erosion of the bedrock. In addition, the meltwater streams that flow along the base of glacier has strong erosive potential and erode rocks in the same way as surface streams. Water at the base of a glacier is squeezed by the enormous weight of ice above (hydrostatic pressure) and causes meltwater stream to flow much faster. This combined effect makes meltwater stream a stronger erosive agent than surface rivers (Figures 1 and 2).

The broader relevance of meltwater erosion in glaciology can be used in estimating the depth of ice sheets, dating glaciers and ice sheets, as well as in tracking their seasonal movements.

MELTWATER PRESSURE

Rajesh Kumar
School of Engineering and Technology, Sharda University, Greater Noida, NCR, India

Meltwater flows through tunnels in the ice and may emerge at the end as a meltwater stream. Beneath the glacier, the water may be under hundreds of feet of ice and is under great pressure. If it can escape, the water pressure plus the sediment in the water can carve rock like a saw. If there are large amounts of meltwater under the glacier, it lubricates the ice and may allow the glacier to slide more rapidly down its bedrock valley. However the surface meltwater streams will be influenced by overall relief of the glacial surface. The sliding eventually halts when the moving glacier opens up spaces in its bed that can accommodate some of the excess water, helping to relieve the water pressure. In addition, high rates of water flow eventually enlarge the conduits and control the outburst flood of meltwater by decreasing the water pressure.

Meltwater pressure influences the glacier hydrology and impacts sediment yields in two ways. First, high water pressure beneath the glacier enhances the rate that the ice can slide over its bed and more rapid sliding results in faster bedrock erosion rates. Second, the ability of water flowing through the glacier system to transport sediment is dictated by water pressure that governs the rate of water flowing through the system. In general, subglacial conduits have high capacity and competence to transport sediment due to their large water pressure and relatively rapid water speeds (Riihimaki et al., 2005).

In some temperate glaciers, the seasonal changes in the amount of meltwater influence the meltwater pressure in the hydrologic system. The conduits tend to form or enlarge near the terminus in the spring, and extend further upglacier as the melt season proceeds. With the onset of winter, the melt rates slow down and conduits collapse. Seasonal changes in the transport of sediment out of the glacier system are strongly controlled by the evolution of this subglacial drainage and the meltwater pressure in the drainage system (http://serc.carleton.edu/vignettes/collection/25438.html).

Bibliography

Riihimaki, C. A., MacGregor, K. R., Anderson, R. S., Anderson, S. P., and Loso, M. G., 2005. Sediment evacuation and glacial erosion rates at a small alpine glacier. *Journal of Geophysical Research*, **110**, F03003, doi:10.1029/2004JF000189.

MELTWATER STORAGE

Pratap Singh
Tahal Consulting Engineers Ltd,
New Delhi, India

Definition

The meltwater storage is defined as storage of the part of meltwater generated during the day time over the glacier surface. This happens when the upper surface of glacier is covered by snow/firn. Thermal characteristics of the available snowpack control the passage of water through snowpack. At times, like in the beginning of melt season, meltwater passing through the snowpack is frozen within the snowpack as the lower part of snowpack has sub-zero temperatures. Meltwater is not stored in the exposed ice surface of glacier because ice is impermeable to water.

Snow and glaciers exhibit meltwater storage characteristics. During the summer period, in the glacier fed streams only a portion of the meltwater produced each day emerges as runoff from the snout of the glacier on the same day. The remaining meltwater is stored within the glacier. Thus a considerable contribution to streamflow is received from the meltwater stored in the glacier. Even at diurnal cycle, the runoff also contains a part of this stored meltwater. Evidently, the streamflow of a glacier fed stream is controlled by storage characteristics of the glacier and determined by delayed response of the basin. The size of the glacier, extent of snow cover, depth of snow over the glacier, and drainage network of the glacier are important factors that control the

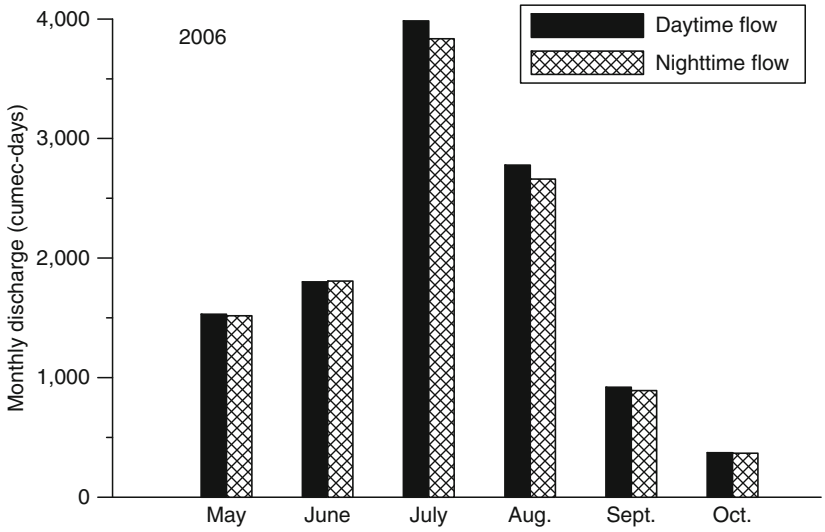

Meltwater Storage, Figure 1 Monthly distribution of daytime and nighttime observed discharge near the snout of Gangotri Glacier (Indian Himalayas) for summer 2006.

flow rate and volume of the water emerging as runoff. The discharge time response is also a function of the ablation and accumulation area ratio. Runoff dominated by meltwater from the accumulation area has a longer time of concentration as compared to the meltwater generated in the ablation area. The runoff generated from the melting of snow and glaciers plays a vital role in the runoff generated in the rivers. In some case, like the Himalayas, contribution from snow and glaciers makes the rivers perennial and ensures the continuous availability of streamflow. The presence of snow and glaciers act as natural frozen reservoirs in the basin and provide flows in a regulated manner for the operation of hydropower and water resources schemes. In case of polar regions, where extent and depth of snow and ice cover is very large, meltwater storage characteristics are very strong.

The meltwater storage characteristics of snow and glacier fed river can be demonstrated by analyzing hourly data of streamflow. Daily (24 h) streamflow records are sub-divided into daytime flow (0900–2000 h) and nighttime flow (2100–0800 h). Monthly daytime and nighttime discharges for summer months for Gangotri Glacier (Indian Himalayas) are shown in Figure 1. The magnitude of the streamflow during daytime and nighttime indicates that the volume of the nighttime flow is comparable with the daytime flow. As such, very little or no melting takes place on the glacier surface during the night period, but still a high amount of discharge is observed in the stream during the nighttime. It shows that meltwater produced during the daytime is partly stored in the glacier and released later, while such trends in the rain fed rivers do not exist.

This analysis suggests that meltwater storage characteristics of the glacier are much stronger in the early part of the melt season and reduces as the melt season develops. Trends of variations in the ratio of daytime flow to nighttime flow with melt season can be explained on the basis of availability of snow cover on the glacier body and progressive development of the drainage network in the glacier. The greater extent of snow cover in the early part of the melt season along with a poorly developed drainage network amounts to a more delayed response of the meltwater from the basin to the outlet, resulting in reduced difference between daytime and nighttime streamflows. Reduction in the extent of snow cover area and progressive development of a drainage network with melt season also attribute to a faster response of meltwater in mid- or late-melt season, which also increases the difference in the daytime and nighttime flows. Singh et al. (2004, 2005) have provided useful information by carrying out detailed studies of meltwater storage behavior of glaciers. They have suggested that such behavior of glaciers play an important role in runoff delaying characteristics of the glaciers.

Bibliography

Singh, P., Haritashya, U. K., and Kumar, N., 2004. Seasonal melt water storage and drainage characteristics of the Dokriani Glacier, Garhwal Himalayas (India). *Nordic Hydrology*, **35**(1), 15–29.

Singh, P., Haritashya, U. K., Ramasastri, K. S., and Kumar, N., 2005. Diurnal variations in discharge and suspended sediment concentration including runoff delaying characteristics of the Gangotri Glacier in Garhwal Himalayas. *Hydrological Processes*, **19**, 1445–1457.

MICROORGANISMS ASSOCIATED WITH GLACIERS

Vanya I. Miteva
Department of Biochemistry and Molecular Biology, The Pennsylvania State University, University Park, PA, USA

Definition

Microorganisms. Microscopic forms of life (bacteria, archaea, fungi, small protists, viruses) which are ubiquitous in the environment, found virtually everywhere on Earth, and play important roles in natural processes and biogeochemical cycles.

Introduction

Permanently frozen environments such as the polar *Ice Sheets* (qv) and the nonpolar high-altitude *Glaciers* (qv) on all continents are characterized by extremely hostile conditions for living organisms. However, they contain an enormous microbial reservoir (9.61×10^{25} bacterial cells in the Antarctic and Greenland ice sheets according to Priscu and Christner (2004)) and provide a unique low-temperature habitat that preserves diverse microbial life chronologically for hundreds of thousands of years. Therefore, similarly to the historic trace gas records used to reconstruct past climates, microbial populations entrapped in glaciers may yield valuable information about the biological history on Earth and potentially augment paleoclimatic data. Furthermore, glacier ice is considered the best analogue of possible extraterrestrial life. Glacial microorganisms also provide ideal models for studying the mechanisms of cold adaptation and survival. These exciting possibilities spurred a significant recent interest in microbiological studies of glaciers.

Microbial origin, chronological deposition, and variable distribution

Microbial cells associated with dust particles, aerosol droplets, pollen grains, plant debris, insects, etc., are carried by atmospheric circulations from geographically close and distant places, deposited with snow on the ice surface, and gradually compressed and embedded in the deeper ice layers. Major sources of microbial cells are terrestrial dust, marine surface aerosols, and volcanic ashes with varying dominance at different periods and in different glaciers. Isotopic and mineralogical measurements have provided excellent in-depth geochemical records used to estimate the dust and aerosol geographic origins, for example, eastern Asian deserts are the main source of dust (microbes) deposited over Greenland, while dust in Antarctic ice originates mostly from Patagonia.

Microbial cells have been found on the glacier surface, in deeper ice reaching 3–4 km at the poles and in subglacial terrestrial and liquid water environments. Their number varies with depths, glacier altitudes, and among glaciers, ranging from less than 100 to 10^6–10^7 cells/mL. The pioneering work of Abyzov (1993) in Antarctica showed that these quantitative fluctuations are directly proportional to the dust load and aerosol content in annual snow precipitation and depend on the climate conditions with higher cell numbers deposited during colder climates. Similar correlations were reported in Tibetan and Greenland ice (Xiang et al., 2005; Yao et al., 2006; Zhang et al., 2007; Miteva et al., 2009). Local and global environmental factors also shape the composition of the microbial populations and determine the variable distribution of distinct microbial types within ice.

Glacial ice as a microbial habitat: microbial survival and metabolic activity

Despite reports of microorganisms having been observed and isolated from glaciers since the beginning of the twentieth century, many considered this extreme environment devoid of life or a mere repository of dormant cells. It was only recently that glacier ice was viewed as a habitat for living, and possibly metabolizing, microbial cells. Price (2000, 2009) suggested three habitats within the polycrystalline ice: (1) the liquid veins at the triple junctions of ice crystals that can provide water, energy, and carbon in sufficient quantities to maintain a small population (10–100 cells/cm^3) for up to 400,000 years; (2) the thin liquid layer coating the mineral grains, and (3) the interior of individual ice crystals, where cells can metabolize by redox reactions with ions from the grains or dissolved gases diffusing through the ice lattice. This hypothesis was supported experimentally by microscopic observations of cells partitioned in veins (Mader et al., 2006) and demonstrations of microbial activity at subfreezing temperatures down to −39°C (reviewed in Miteva, 2008). The spatial limitations and other specific factors within ice may restrict microbial activity to survival or basic maintenance to repair molecular damage with increased metabolic potential under suitable conditions, for example, near the glacier surface or in basal ice. The *Cryoconite* (qv) holes, which cover up to 10% of the glacial surface are known as "hot spots" of microbial activity and geochemical cycling by bacteria, algae, and viruses (Hodson et al., 2008; Anesio et al., 2009). The deep subglacial habitats have drawn strong attention recently due to their ecological variability (frozen terrestrial sediment, melt waters, or lakes), significant microbial content and potentially diverse microbial processes (Christner et al., 2008). Certainly, *Lake Vostok* (qv) and the accretion ice above it has been and still is the focal point of numerous studies (Christner et al., 2001; Priscu et al., 2007; D'Elia et al., 2008).

Although the conditions within glaciers are considered extreme for most living organisms due to subfreezing temperatures ranging from −56°C to −10°C, high hydrostatic pressure, low nutrient and water availability, darkness, etc., these special habitats are also superior for long-term

microbial survival and ancient DNA preservation (Willerslev and Cooper, 2005). Earth glaciers provide an excellent model system to study cold adaptation and to refine strategies for searching for life on icy extraterrestrial bodies.

Detection of microorganisms in glaciers

Modern microbiological studies of glaciers use a variety of methods and instrumentation to reveal the microbial abundance, diversity, and activity in relationship to climate history and to advance our understanding of the mechanisms of survival at the lowest temperature limits of life. These investigations are performed on specifically drilled shorter (up to 100 m) *Ice Cores* (qv) or on previously drilled deep polar ice cores (3–4 km) stored in special facilities such as the US National Ice Core Laboratory (http://nicl.usgs.gov). The detection of glacier microorganisms is methodologically challenging for several reasons: (1) Decontamination of each sample is needed to eliminate any accidental microbial contamination during ice core retrieval and storage and to validate the authenticity of the detected and cultivated microorganisms as truly indigenous to the corresponding sample. Existing procedures (rinsing with disinfectants, physical removal of the outer surface, aseptic sub-coring) are efficient but not yet standardized among laboratories. (2) The limited volume of ice core samples, often with extremely low cell numbers, significantly hampers obtaining sufficient quantity and quality DNA for molecular analyses. Novel methods for whole genome amplification are then required to increase DNA yields; (3) Cultivation of individual organisms from environmental samples and glacier ice in particular is especially difficult because of the well-established phenomenon of nonculturability. Over 99% of the otherwise viable environmental microorganisms cannot be cultivated on conventional laboratory media due to temporal dormancy, cell damage, or unknown growth requirements. Nontraditional cultivation strategies have proven promising for recovery of novel organisms. Another related problem is the assessment of the viability status of nonculturable microbial cells, which often depends on the method used.

Recent methodological advances have significantly improved the detection of individual cells and microbial populations in glaciers and the determination of their abundance, viability, metabolic activity, and diversity. Approaches can be divided in three groups: (a) direct observations using modern high-resolution microscopic, spectroscopic, and flow cytometric techniques that are often combined with selective staining or molecular and isotopic biomarkers; (b) culture-independent methods based on analyses of nucleic acids extracted directly from melted ice; and (c) cultivation of complex enrichments or individual organisms on laboratory media with the addition of labeled substrates in some cases.

Microbial diversity associated with glaciers

Microbial diversity defines the variability of all types of microorganisms. Based on genetic, morphological, and physiological characteristics, microorganisms are classified hierarchically in taxonomic groups with the species as the lowest systematic unit. The accepted phylogenetic classification system, commonly used to determine microbial diversity, reflects genetic similarity and evolutionary relatedness based on sequence analyses of universal genes for ribosomal RNA. The relationships are expressed as branched diagrams referred to as trees (Figure 1). New microbial sequences obtained by polymerase chain reaction (PCR) are identified through comparisons with sequence databases (http://www.ncbi.nlm.nih.gov)

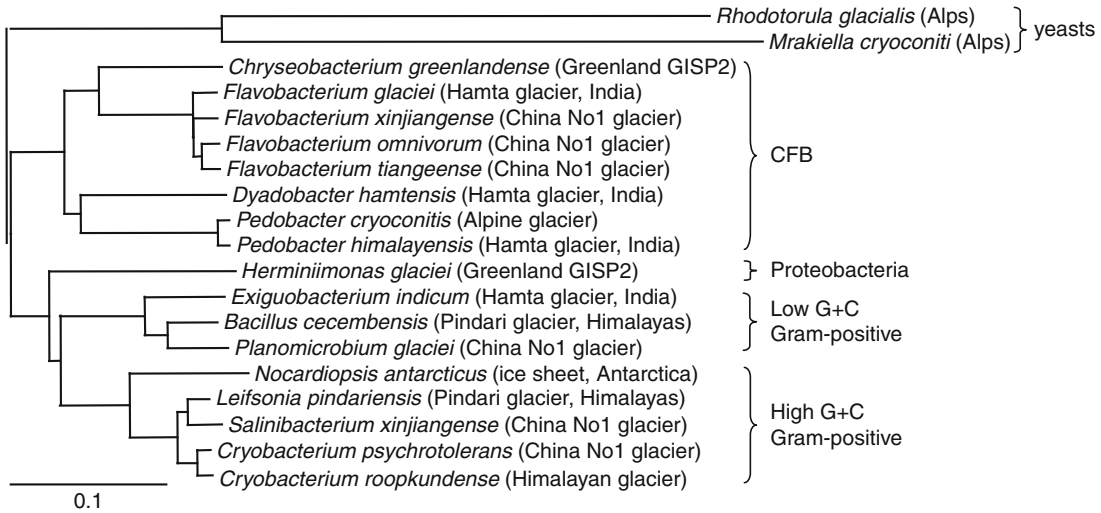

Microorganisms Associated with Glaciers, Figure 1 Phylogenetic tree of validly named novel glacial isolates designated with genus and species name (*italics*) and origin (*in parenthesis*). Clusters show major phylogenetic groups.

representing the three major domains of life: Bacteria, Archaea, and Eukarya.

The recently intensified microbiological studies of glaciers have revealed microbial populations with widely diverse morphological, physiological, and phylogenetic representation. Some general findings from studies of polar and nonpolar glaciers are:

- Smaller microbial cells are more likely to occupy the thin liquid veins within glacial ice.
- Diversity results obtained by culture-independent and cultivation methods are complementary rather than overlapping, which helps create a better picture of the microbial populations.
- Glacial microorganisms represent all major bacterial phylogenetic groups: Proteobacteria, high and Low G + C Gram-positives, and CFB (Cytophaga-Flavobacteria-Bacteroides). Bacteria possess enormous structural, genetic, and physiological diversity indicating significant metabolic potential and nutrient versatility. Examples of such features differentiating bacterial groups and species include formation of spores, oxygen tolerance, use of simple inorganic or complex organic nutrients, etc. In addition to bacteria, many cold-adapted eukaryotic microorganisms (fungi, yeasts) are often detected in glacial environments (Abyzov, 1993; Ma et al., 2005, Butinar et al., 2007). Interestingly, the plant and bacterial viruses found in glaciers (Castello et al., 2005) were suggested to control microbial population size. Very few Archaea have been detected up to date mostly due to methodological issues.
- The relative distribution of these groups at different ice depths or in geographically distant glaciers has shown specific patterns that may be related to deposition climate characteristics or origin. At the same time, the consistent finding of several common genera and species in different glaciers has triggered the question whether these organisms are cosmopolitan or specific only for particular habitats. At present, the worldwide distribution of related glacial microorganisms has been explained by similar strategies for cold adaptation and survival. Further bipolar and among glacier comparisons of diversity and novel methodologies are needed to solve this problem.

Recovery of microbial isolates from glaciers

Obtaining isolates is important for describing new species, complete genomes sequencing, and identifying physiological properties of the organisms, which cannot be found by sequence analysis alone. Recently the recovery of isolates from glaciers has been fairly successful. The application of innovative cultivation strategies, mostly by mimicking the specific glacier environment, has increased the number of culturable organisms and resulted in obtaining hundreds of individual microorganisms. A common observation is the very long period of initial growth (colony formation), which is explained with the need for repair of cell injuries or transition of cellular structure and metabolism from dormant, nonculturable state that may have lasted for thousands of years. Many isolates originated from ancient ice core samples such as 120,000-year-old Greenland ice (Miteva and Brenchley, 2005), 420,000-year-old Vostok accretion ice, and 750,000-year-old ice from the Guliya ice cap in Tibet (Christner et al., 2001, 2003). This suggests that microbial cells have adapted and remained alive at extremely stressful conditions. Common physiological and cellular features related to cold adaptation include colony pigmentation (Figure 2), formation of exopolymeric substances as cryoprotectants, ability to grow at low temperatures with low nutrients, specific membrane structure, and synthesis of cold-shock proteins and cold-active enzymes. Numerous studies have suggested unique molecular mechanisms of cold adaptation and their potential for biotechnological applications (reviewed in Margesin et al., 2008).

At present, about 10,000 microbial species isolated from all environments have been officially named and described whereas their estimated number in nature ranges from 3 to 100 million (for updates see http://www.bacterio.cict.fr). Similarly, the number of novel validly described species from glaciers is still very limited

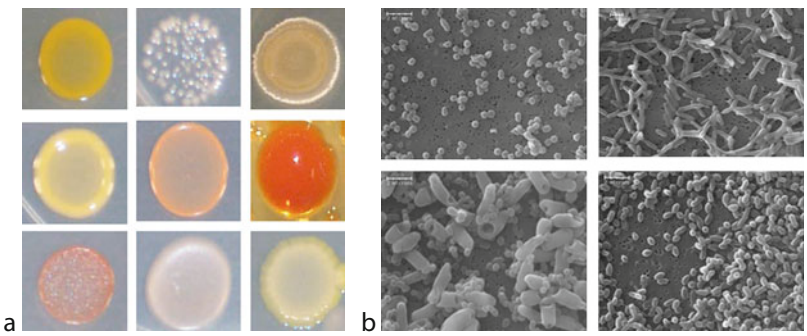

Microorganisms Associated with Glaciers, Figure 2 Examples of pigmented colonies of glacial isolates (**a**) and scanning electron microscopy of microbial cells of different sizes and shapes (**b**).

although phylogenetic analyses of isolates have detected many novel organisms (Figure 1). Each of these organisms has been subjected to a set of required morphological, physiological, biochemical, and genetic analyses in order to be validated as a new species that is sufficiently different from closest relatives. Further efforts in this direction will fill this gap and provide new model organisms for genomic and functional studies.

Summary

Recent important findings from microbiological studies of glaciers include: (a) an estimated significant microbial content in polar and nonpolar ice, (b) detection of viable and diverse microbial populations in ancient ice, (c) evidence for microbial activity at subfreezing temperatures, and (d) correlations between microbial composition and deposition climates. Employing advanced technologies and interdisciplinary approaches will allow the analyses of genomic and cellular components of individual cells and the exploration of the composition and functioning of complex microbial populations in their natural environment enhancing our understanding of the diversity and ecological role of microorganisms dwelling in one of the harshest environments on Earth.

Bibliography

Abyzov, S., 1993. Microorganisms in the Antarctic ice. In Friedman, E. I. (ed.), *Antarctic Microbiology*. New York: Willey, pp. 265–295.

Anesio, A., Hodson, A., Fritz, A., Psenner, R., and Sattler, B., 2009. High microbial activity on glaciers: importance to the global carbon cycle. *Global Change Biology*, **15**, 955–960.

Butinar, L., Spencer-Martins, I., and Gunde-Cimerman, N., 2007. Yeasts in high Arctic glaciers: the discovery of a new habitat for eukaryotic microorganisms. *Antonie van Leeuwenhoek*, **91**, 277–289.

Castello, J., Rogers, S., Smith, J., Starmer, W., and Zhao, Y., 2005. Viruses in Greenland ice. In Castello, J., and Rogers, S. (eds.), *Life in Ancient Ice*. Princeton, NJ: Princeton University Press, pp. 196–207.

Christner, B., Mosley-Thompson, E., Thompson, L., and Reeve, J., 2001. Isolation of bacteria and 16S rDNAs from Lake Vostok accretion ice. *Environmental Microbiology*, **3**, 570–577.

Christner, B., Mosley-Thompson, E., Thompson, L., and Reeve, J., 2003. Bacterial recovery from ancient glacial ice. *Environmental Microbiology*, **5**, 433–436.

Christner, B., Skidmore, M., Priscu, J., Tranter, M., and Foreman, C., 2008. Bacteria in subglacial environments. In Margesin, R., Schinner, F., Marx, J.-C., and Gerday, C. (eds.), *Psychrophiles: From Biodiversity to Biotechnology*. Berlin: Springer-Verlag, pp. 51–71.

D'Elia, T., Veerapaneni, R., and Rogers, S., 2008. Isolation of microbes from Lake Vostok accretion ice. *Applied and Environmental Microbiology*, **74**, 4962–4965.

Hodson, A., Anesio, A., Tranter, M., Fountain, A., Osborn, M., Priscu, M., Laybourn-Parry, J., and Sattler, B., 2008. Glacial ecosystems. *Ecological Monographs*, **78**, 41–67.

Ma, L., Catranis, C., Starmer, W., and Rogers, S., 2005. The significance and implications of the discovery of filamentous fungi in glacial ice. In Castello, J., and Rogers, S. (eds.), *Life in Ancient Ice*. Princeton, NJ: Princeton University Press, pp. 159–181.

Mader, H., Pettitt, M., Wadham, J., Wolff, E., and Parkes, R., 2006. Subsurface ice as a microbial habitat. *Geology*, **34**, 169–172.

Margesin, R., Schinner, F., Matx, J.-C., and Gerday, C. (eds.), 2008. *Psychrophiles: From Biodiversity to Biotechnology*. Berlin: Springer-Verlag, pp. 177–333.

Miteva, V., 2008. Bacteria in snow and glacier ice. In Margesin, R., Schinner, F., Marx, J.-C., and Gerday, C. (eds.), *Psychrophiles: From Biodiversity to Biotechnology*. Berlin: Springer-Verlag, pp. 31–50.

Miteva, V., and Brenchley, J., 2005. Detection and isolation of ultrasmall microorganisms from a 120, 000 years old Greenland glacier ice core. *Applied and Environmental Microbiology*, **71**, 7806–7818.

Miteva, V., Teacher, C., Sowers, T., and Brenchley, J., 2009. Comparison of microbial diversity at different depths of the GISP2 Greenland ice core in relation to deposition climate. *Environmental Microbiology*, **11**, 640–656.

Price, B., 2000. A habitat for psychrophiles in deep Antarctic ice. *Proceedings of the National Academy of Sciences of the United States of America*, **97**, 1247–1251.

Price, P., 2009. Microbial genesis, life and death in glacial ice. *Canadian Journal of Microbiology*, **55**, 1–11.

Priscu, J., and Christner, B., 2004. Earth's icy biosphere. In Bull, A. (ed.), *Microbial Diversity and Bioprospecting*. Washington, DC: ASM Press, pp. 130–145.

Priscu, J., Christner, B., Foreman, C., and Royston-Bishop, G., 2007. Biological material in ice cores. In Elias, S. A. (ed.), *Encyclopedia of Quaternary Sciences*. Amsterdam: Elsevier, pp. 1156–1167.

Willerslev, E., and Cooper, A., 2005. Ancient DNA. *Proceedings of the Royal Society B: Biological Sciences*, **272**, 3–16.

Xiang, S., Yao, T., An, L., Xu, B., and Wang, J., 2005. 16S rRNA sequences and difference in bacteria isolated Muztag Ata Glacier at increasing depths. *Applied and Environmental Microbiology*, **71**, 4619–4627.

Yao, T., Xiang, S., Zhang, X., and Wang, N., 2006. Microorganisms in the Malan ice core and their relation to climatic and environmental changes. *Global Biogeochical Cycles* 20, GB1004, doi:10.1029/2004GB002424.

Zhang, S., Hou, S., Qin, D., and Chen, T., 2007. Culturable bacteria in Himalayan glacial ice in response to atmospheric circulation. *Biogeosciences*, **4**, 1–9.

Cross-references

Antarctica
Cryoconite
Greenland Ice Sheet
Ice Core
Ice Sheet
Lake Vostok
Subglacial Lakes, Antarctic

MONITORING AND WARNING SYSTEMS

Markus Konz
Hydrologie und Wasserwirtschaft, ETH Zürich, Institut für Umweltingenieurwissenschaften, Zürich, Switzerland

Glaciers are sensitive to the impacts of climate change. The glacier mass balance, as the direct response to

Monitoring and Warning Systems, Table 1 Glaciers and mass-balance series in the World Glacier Monitoring data basis (taken from Zemp et al., 2009)

Region	Ice area (km^2)	No of mass-balance series	Reference glaciers	First survey	Last survey	Average observation duration
Africa, New Guinea, Irian Jaya	9	1	0	1979	1996	18.0
New Zealand	1,160	1	0	2005	2006	2.0
European Alps, Pyrenees, Caucasus	3,785	43	10	1948	2006	20.2
Sub-Antarctic Islands	7,000	0	0	–	–	–
South America	25,000	11	1	1976	2006	8.6
Scandinavia, Iceland, West Arctic Islands	50,809	59	10	1946	2006	15.7
Northern Asia, Siberia, East Arctic Islands	59,279	9	0	1973	2000	6.0
Around Greenland	76,200	5	0	1979	2006	3.5
High Mountain Asia, Japan	116,180	40	5	1957	2006	15.0
North America (US + CD + MX), Alaska	124,260	45	4	1953	2006	16.3
Canadian Arctic Archipelago	151,433	13	0	1960	2006	13.3
Around Antarctica	169,000	1	0	2002	2006	5.0
Global	**784,115**	**228**	**30**	**1948**	**2006**	**15.3**

climatic-system fluctuations, is an essential variable for quantifying impacts of climate change. Reliable monitoring of glacier systems requires long-term measurements of mass balances, changes in volume, area, or length with time. Such data are valuable indices of long-term climate change. Worldwide glacier surveys were initiated in 1894 at the 6th International Geological Congress in Zurich, Switzerland. Since then the World Glacier Monitoring Service (WGMS) and its predecessor organizations have monitored dimensions and magnitudes of glaciers around the world. In cooperation with the US National Snow and Ice Data Center (NSIDC) in Boulder and the Global Land Ice Measurements from Space (GLIMS) initiative, the WGMS is in charge of the Global Terrestrial Network for Glaciers (GTN-G) within the Global Climate/Terrestrial Observing System (GCOS/GTOS).

Today, WGMS collects standardized observations on glacier fluctuations obtained by direct glaciological and geodetic methods around the globe (WGMS, 2008; Zemp et al., 2009), with 30 glaciers that have continuous in situ measurements going back to 1976 and earlier based on ablation stakes and snow pits (Zemp et al., 2009). Data collection is done annually through the collaboration network of national investigators. Preliminary data are published on the WGMS website (www.wgms.ch) and every 2 years in the "Glacier Mass Balance Bulletins," as well as every 5 years, in full detail, in "Fluctuations of Glaciers." All data are available digitally on request and free of charge. However, the mass-balance observations are unequally distributed around the globe, with about 90% of the mass-balance series coming from the Northern Hemisphere and about 40% from Europe (Table 1).

Besides the monitoring of glacier fluctuations, the early warning of potential hazards related to, e.g., rapid melting or outbursts of moraine-dammed glacier lakes (GLOFS) is an important task. Mountainous regions are prone to such hazards and therefore flood warning systems, that monitor the water level of the glacier lakes, are installed, and engineering approaches to lower the lake level have been operating in order to mitigate the risk. An interesting example for an early warning system is the Tsho Rolpa glacier lake in Nepal. It is one of the best monitored lakes in the Himalayas, and it is expected that the intensive monitoring and engineering works reduces the risk of GLOF by about 20% (Rana et al., 2000).

Bibliography

Global Climate Observing System (GCOS): www.wmo.ch/pages/prog/gcos

Global Land Ice Measurements from Space (GLIMS): www.glims.org

Global Terrestrial Network for Glaciers (GTN-G): www.fao.org/gtos/gt-netGLA.html

Global Terrestrial Observing System (GTOS): www.fao.org/gtos

Rana, B., Shrestha, A. B., Reynolds, J. M., Aryal, R., Pokhrel, A. P., and Budhathoki, K. P., 2000. Hazard assessment of the Tsho Rolpa Glacier Lake and ongoing remediation measures. *Journal of Nepal Geological Society*, **22**, 563–570.

WGMS, 2008. Global Glacier Changes: facts and figures. In Zemp, M., Roer, I., Kääb, A., Hoelzle, M., Paul, F., and Haeberli, W. (eds.), *UNEP, World Glacier Monitoring Service*, Zurich, Switzerland, pp. 88 (available online at http://www.grid.unep.ch/glaciers).

World Glacier Monitoring Service: www.wgms.ch

Zemp, M., Hoelzle, M., and Haeberli, W., 2009. Six decades of glacier mass-balance observations: a review of the worldwide monitoring network. *Annals of Glaciology*, **50**, 101–111.

MONSOONAL RECORDS OBSERVED FROM SNOW/ICE/GLACIER

Shichang Kang
Key Laboratory of Tibetan Environment Changes and Land Surface Processes, Institute of Tibetan Plateau Research, Chinese Academy of Sciences, Haidian District, Beijing, China
State Key Laboratory of Cryospheric Sciences, Chinese Academy of Sciences, Lanzhou, China

Definition

Monsoonal records: Indices monsoonal strength from different records such as ice cores, lake sediments, loess sediments, stalagmite, and tree rings.

The monsoon is a seasonal reversal of wind patterns and precipitation on Earth. The primary cause of monsoon is the much greater annual variation of temperature over large land areas compared with neighboring ocean surfaces, causing an excess of pressure over the continents in winter and a deficit in summer (Glickman, 2000). The monsoon regions include North America, South America, Sub-Saharan Africa, Australia, East Asia, and South Asia. In particular, the monsoons are strongest on the southern and eastern sides of Asia, affecting 60% of the Earth's population via the availability of water.

The formation of the Asia Monsoon has been linked to the uplift of the Tibetan Plateau after the collision of India and Asia around 50 million years ago (Ye and Wu, 1998; An et al., 2001). Now the monsoonal strength varies significantly under the influence of global climate change. For example, the variation in the strength of the South Asia monsoon has been suggested to be linked to the variation of soil moisture (Douville, 2002), Eurasian snow cover (Wu and Qian, 2003), ElNino-Southern Oscillation (ENSO) (Davis et al., 2005), and tropical sea surface temperatures (Cole et al., 2000). However, the relatively short period of most instrumental climate records restricts the study of South Asian monsoon variability over longer time periods. The Himalayas mark the boundary between the South Asia monsoon and continental climate of central Asia. The glaciers located at very high elevation (usually more than 5,500 m) receive most of the moisture from Indian subcontinent and thus records summer monsoon rainfall. Therefore, the ice cores drilled from the Himalayas and the Tibetan Plateau are special interest for the information they contain to depict the variation of the monsoonal strength in the past with the help of proxy data (such as snow accumulation and oxygen isotopic ratios, $\delta^{18}O$).

According to a study carried out at Dasuopu, central Himalayas with elevation over 7,000 m, the seasonal variations of $\delta^{18}O$ values and major ion concentrations indicate the summer monsoon and dust signals in the firn core (Kang et al., 2000). Annual variations in the $\delta^{18}O$ values are controlled by the amount effect, with more negative $\delta^{18}O$ representing summer monsoon precipitation from tropical regions (Kang et al., 2000). Meanwhile, the variability of snow accumulation (monsoon precipitation) could be deduced from an ice core also drilled at Dasuopu, which covers the last 295-year record. The record shows the monsoon in central Himalayas had weakened in eighteenth century and strengthened throughout much of nineteenth and early twentieth century, and then weakening again from early 1920s to the present (Duan et al., 2004).

At Mt. Qomolangma (Everest), the summit of the world, similar works on ice cores were also conducted (Kaspari et al., 2007, 2008). Annual-layer thickness data, spanning AD 1534–2001, from an ice core from East Rongbuk Col yield an age-depth profile. The profile shows that the mean accumulation rate has changed every 50–100 years. The mean annual accumulation rate decreased from ~0.8 m ice equivalent in the 1500s to ~0.3 m in the mid-1800s. From ~1880 to ~1970 the rate increased. However, it has decreased since ~1970. Comparison with six other records from the Himalaya and the Tibetan Plateau shows that the changes in accumulation in East Rongbuk Col are broadly consistent with a regional pattern over much of the Tibetan Plateau. However, the record from Dasuopu, 125 km northwest of Qomolangma and 700 m higher than East Rongbuk Col, shows a maximum in accumulation during the 1800s, a time during which the East Rongbuk Col and the Tibetan Plateau ice core and tree-ring records show a minimum. This difference may be due to altitudinal or seasonal differences in monsoon versus westerly moisture sources or complex mountain meteorology (Kaspari et al., 2008).

Summary

Generally, ice cores from the mid-latitudes provide an extended record of the monsoon variability in a densely inhabited part of the globe where instrumental records are short and other proxy records sparse, despite more work still needed in the future.

Bibliography

An, Z., Kutzbach, J. E., Prell, W. L., and Porter, S. C., 2001. Evolution of Asian monsoons and phased uplift of the Himalaya-Tibetan Plateau since Late Miocene times. *Nature*, **411**, 62.

Cole, J. E., Dunbar, R. B., McClanahan, T. R., and Muthiga, N. A., 2000. Tropical Pacific forcing of decadal SST variability in the western Indian Ocean over the past two centuries. *Science*, **287**, 617.

Davis, M. E., Thompson, L. G., Yao, T., and Wang, N., 2005. Forcing of the Asian monsoon on the Tibetan Plateau: Evidence from high-resolution ice core and tropical coral records. *Journal of Geophysical Research*, **110**, D04101, doi:10.1029/2004JD004933.

Douville, H., 2002. Influence of soil moisture on the Asian and African monsoons. Part II: Interannual variability. *Journal of Climate*, **15**, 701.

Duan, K., Yao, T., and Thompson, L. G., 2004. Low-frequency of southern Asian monsoon variability using a 295-year record from the Dasuopu ice core in the central Himalayas. *Geophysical Research Letters*, **31**, L19209, doi:10.1029/2004GL020015.

Glickman, T. S., 2000. *Glossary of Meteorology*. Boston: American Meteorological Society.
Kang, S., Wake, C. P., Dahe, Q., Mayewski, P. A., and Tandong, Y., 2000. Monsoon and dust signals recorded in Dasuopu glacier, Tibetan Plateau. *Journal of Glaciology*, **46**, 222.
Kaspari, S., Mayewski, P., Kang, S., Sneed, S., Hou, S., Hooke, R., Kreutz, K., Introne, D., Handley, M., and Maasch, K., 2007. Reduction in northward incursions of the South Asian monsoon since 1400 AD inferred from a Mt. Everest ice core. *Geophysical Research Letters*, **34**, L16701, doi:10.1029/2007GL030440.
Kaspari, S., Hooke, R. L., Mayewski, P. A., Kang, S., Hou, S., and Qin, D., 2008. Snow accumulation rate on Qomolangma (Mount Everest), Himalaya: synchroneity with sites across the Tibetan Plateau on 50100 year timescales. *Journal of Glaciology*, **54**, 343.
Wu, T. W., and Qian, Z. A., 2003. The relation between the Tibetan winter snow and the Asian summer monsoon and rainfall: an observational investigation. *Journal of Climate*, **16**, 2038.
Ye, D. Z., and Wu, G. X., 1998. The role of the heat source of the Tibetan Plateau in the general circulation. *Meteorology and Atmospheric Physics*, **67**, 181.

Cross-references

Geochemistry of Snow and Ice
Glacier
Himalaya
Ice Core
Oxygen Isotopes

MORAINE

Anders Schomacker
Institute of Earth Sciences, University of Iceland, Reykjavík, Iceland
Department of Geology, Norwegian University of Science and Technology, Trondheim, Norway

Synonyms

The term "moraine" was previously used both to describe glacigenic sediments (diamict, till) and glacial landforms. The current use of the term should be restricted to descriptions of glacial landforms, i.e., moraines.

Definition

"Moraine" is a genetic term for a landform or landscape formed by deposition and/or deformation in a glacial environment. Most commonly "moraine" is used to describe ridge-shaped glacial landforms, i.e., moraine ridges, although the term also covers landforms of large spatial extent, such as subglacial till plains (ground moraines) and hummocky moraines formed by melt-out of large areas of stagnant, debris-covered glacier ice. The interior of moraines consists of unconsolidated sediments, deposited or deformed by glaciers.

Introduction

The term "moraine" covers an extremely wide range of glacial landforms, both in modern and past glacial environments. Spatially, moraines span from small (~1-m wide and ~1-m high) annual moraine ridges (Krüger, 1995; Matthews et al., 1995; Krüger et al., 2010a) to vast till plains or ground moraine, covering thousands of kilometers, e.g., in North America and Canada (Dyke and Prest, 1987; Stokes and Clark, 2002; Ross et al., 2009). Moraines form in almost all glacial environments; end moraines and other ice-marginal moraines form at the margins of glaciers, ground moraines or till plains form in subglacial environments, and hummocky moraines form in dead-ice environments. In addition, a number of other less-abundant moraines form in such environments or a combination of them. This broad category comprises, but is not restricted to, ribbed moraines, rim ridges, controlled moraines, and morainal banks (e.g., Lagerbäck, 1988; Hättestrand and Kleman, 1999; Mollard, 2000; Dunlop and Clark, 2006; Todd et al., 2007; Lindén et al., 2008; Evans, 2009).

Moraines in past glaciated areas are important features for palaeoenvironmental reconstructions. End moraines or terminal moraines indicate the extent of former glaciers and ice sheets. In alpine landscapes, lateral moraines additionally aid in deciphering past ice thickness. The distribution of ground moraine or till plains indicate deposition by warm-based glaciers and are thus an important key to understanding past glacier dynamics. Similarly, hummocky moraines suggest deposition from stagnant, debris-covered ice in dead-ice environments.

Moraines consist of unconsolidated sediments, directly deposited by glaciers or deformed and accumulated by glaciers. Marginal moraines may contain sediment dumped, squeezed, pushed, or thrusted by a glacier (Price, 1970; Boulton et al., 1999; Krüger et al., 2002; Bennett, 2001; Benediktsson et al., 2008, 2009, 2010). This implies that such moraines are either built up of glacial sediments or of preexisting sediments deformed by a glacier. Thus, the interior of many moraines are of non-glacial material such as seen in many prominent push moraines in modern and past glacial environments (Aber and Ber, 2007; Benediktsson et al., 2008, 2010). The spectacular push moraine in front of Holmströmbreen, Svalbard, for instance, consists mainly of glaciotectonically deformed fine-grained marine and tidal sediments (Boulton et al., 1999).

Ground moraines (till plains) are formed subglacially by actively flowing ice (Stewart et al., 1988; Evans and Twigg, 2002; Kjær et al., 2008; Schomacker et al., 2010). They therefore consist of subglacial sediments, typically basal till. Basal till is a diamict sediment with diagnostic subglacial characteristics: strong clast fabric, striated clasts, stoss-lee-shaped clasts, and often with subglacial surface landforms such as drumlins, flutes, and other glacial lineations (e.g., Krüger, 1979; Piotrowski et al., 2004; Evans et al., 2006). Hummocky moraines, on the other hand, form in dead-ice environments and contain more chaotic sediments. Often, they are composed of resedimented diamicts and sorted meltwater-deposited sediments (e.g., Boulton, 1972; Ham and Attig, 1996; Schomacker, 2008).

This paper briefly reviews the most important moraine types, with respect to geomorphology, sedimentology, genesis, and palaeoenvironmental significance. Focus is directed both toward moraines recently formed or currently forming in modern glacial environments and toward Pleistocene moraines.

Ice-marginally formed moraines

Ice-marginally formed moraines are ridges mirroring the ice-marginal shape and position at the time of formation (Figure 1). Ice-marginal moraines range from minor single-crested ridges, around 1 m or less in height and width, to large multi-crested ridge complexes up to ca. 10-km width and ca. 200-m height (e.g., Benn and Evans, 1998; Bakker, 2004; Aber and Ber, 2007). The material in marginal moraine ridges might either be of glacial origin with direct deposition at the ice margin (dumping) or consist of non-glacial or preexisting glacial material as seen when older sediments are pushed and thrusted by marginal glaciotectonism. Minor moraine ridges may also form by squeezing-out of sediment at the margin due to the ice load and the pressure gradient directed toward the margin (Price, 1970; Benn and Evans, 1998). Ice-marginal moraines are known from the margins of modern and past glaciers, from ice sheets to cirque glaciers, at temperate, polythermal, and cold-based glaciers, and during retreat, advance, surge, and stationary phases. The morphology and sedimentary architecture of such ridges reflects the depositional environment and glacier dynamics. The nongenetic terms "ice-marginal moraine," "end moraine," and "terminal moraine" all refer to marginal moraine

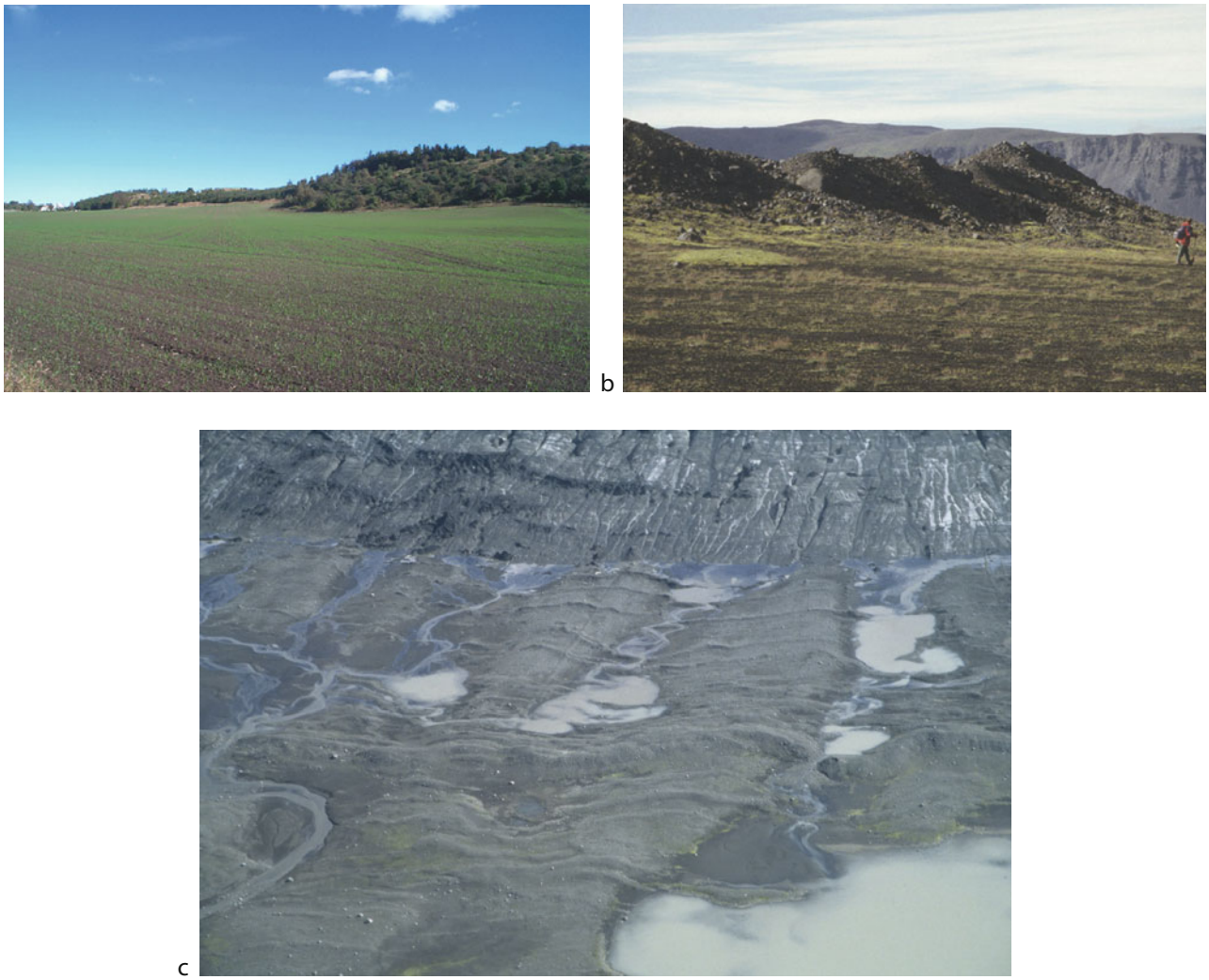

Moraine, Figure 1 **(a)** Late Weichselian end-moraine ridge, Bjergsted, Denmark. An outwash plain slopes gently away from the moraine ridge, September 2002. **(b)** Single-crested end moraine formed by dumping of sediment at the margin of the Kötlujökull glacier, South Iceland. Ice flow was from left toward right. (Photo courtesy by J. Krüger, August 1997.) **(c)** A series of annual moraine ridges deposited during the retreat of the Sléttjökull glacier, South Iceland, August 2001.

ridges, although "terminal moraine" is used to describe a moraine ridge marking the maximum extent of a glacier advance both in Pleistocene and modern settings.

Push moraines form when an advancing glacier transfers stress to sediments in its forefield. When the applied stress exceeds the shear strength of the forefield sediments, they deform into a push moraine (Figure 2). This deformation can either be ductile, brittle, or a combination of both, and each process leaves characteristic structures in push moraines. Ductile deformation produces folds and brittle deformation produces (thrust) faults. The surface morphology of push moraines depend on the style and magnitude of deformation during formation and of the nature of the deformed material. Typically, folding forms smooth ridges with washboard morphology, whereas thrust faulting forms series of imbricated slabs with steeper slopes (e.g., Benediktsson et al., 2010). However, multi-crested push moraines might appear with washboard morphology in both cases. Degradation of the surface makes it hard to determine the style of deformation, only based on the geomorphology. Internal sedimentary structures are better preserved and often provide an excellent view of the deformations either directly from geological sections or from geophysical investigations (e.g., Boulton et al., 1999; Bennett, 2001; Jakobsen and Overgaard, 2002; Aber and Ber, 2007; Benediktsson et al., 2010).

A certain type of annual push moraines might form when receding or stationary glaciers re-advance shortly during winter and spring (Figure 1c; Boulton, 1986; Krüger, 1993). At the peak of these winter re-advances, a small frozen-on slab of the forefield is pushed up at the margin (Krüger, 1993, 1995; Krüger et al., 2010a). As seen in Figure 1c, series of annual moraines form during multi-year periods of glacier retreat. These landforms are, however, too small to be preserved and have not been described from Pleistocene glacial landscapes.

Moraine, Figure 2 Oblique aerial view from 1936 of the prominent push moraine in front of the Holmströmbreen glacier, central Spitsbergen, Svalbard. Ice flow was from left toward right. (Aerial photograph number S36 1382, © Norwegian Polar Institute. Published with permission.)

Ice-marginal dump moraines are ridges consisting of en- and supraglacial material that melts out and flows down a stationary ice margin (Figure 1b; Boulton and Eyles, 1979; Krüger et al., 2002). Frontal dump moraines might continue as lateral moraines along the sides of valley glaciers. Most commonly, they consist of diamict with coarse-grained, passively transported material, although parts of the debris might have experienced a subglacial transport prior to dumping at the ice margin (Boulton and Eyles, 1979; Benn and Ballantyne, 1994). The size of dump moraines depends on the duration of the glacier standstill and the debris flux to the margin (Benn and Evans, 1998; Spedding and Evans, 2002). In alpine environments and at debris-covered glaciers, the debris flux is high, and frontal dump moraines might reach considerable heights. The spectacular ice-marginal dump moraine in front of Kvíarjökull, Iceland, for instance, is more than 100-m high (Spedding and Evans, 2002; Iturrizaga, 2008). This moraine ridge might, however, be the result of more than one glacier advance and stillstands at the same position.

Subglacially formed moraines

Ground moraine

Ground moraines, or basal till plains, are low-relief glacial landscapes commonly with a surface of ice-flow parallel subglacial landforms such as drumlins, flutes, or mega-scale lineations (Figure 3). They are well known both from past glaciated areas and modern glacier forefields. In North America, vast areas of ground moraine formed by the Laurentide Ice Sheet dominates the landscape for hundreds of kilometers, e.g., in the Great Lakes region and Ontario (Boyce and Eyles, 2001; Jennings, 2006). On a smaller spatial scale (1–10 km), many till plains are being exposed during the current retreat of the broad lowland glacier lobes of the Icelandic ice caps (Evans and Twigg, 2002; Kjær et al., 2003, 2008; Schomacker et al., 2010) and at many other glaciers (e.g., Eklund and Hart, 1996; Larsen et al., 2006).

As the synonymous genetic term "basal till plain" indicates, ground moraines consist of basal till. Basal till is a diamict deposited by a glacier sole that slides over and/or deforms its substratum, and sediment accumulates from pressure-melt-out from the glacier sole, lodgement, and deformation of the bed (e.g., Boulton and Hindmarsh, 1987; Benn and Evans, 1996; Piotrowski et al., 2004; Nelson et al., 2005; Evans et al., 2006). Thus, basal till displays many features characteristic for deposition in a subglacial environment such as strong clast fabrics, striated and bullet-shaped clasts, and shear structures (Krüger, 1979; Kjær et al., 2003; Larsen and Piotrowski, 2003). Because ground moraines are deglaciated by a frontal retreat, very little or no supraglacial debris overlies the basal till.

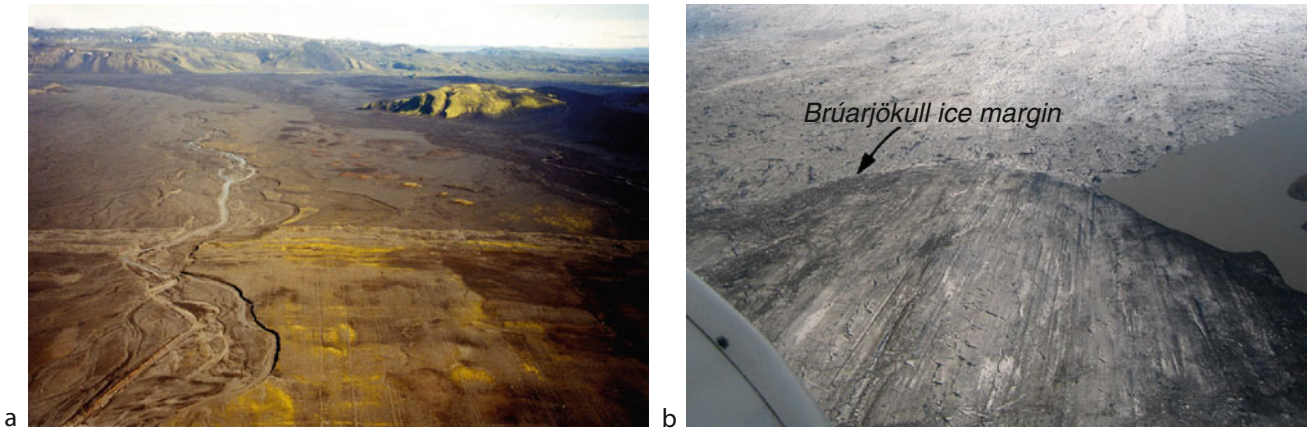

Moraine, Figure 3 **(a)** Fluted ground moraine in the forefield of the Sléttjökull glacier, South Iceland. The Mælifellssandur outwash plain is seen in the background, distal to the end-moraine ridges, August 2001. **(b)** Fluted ground moraine appearing during the retreat of the Brúarjökull glacier, East Iceland, September 2008.

Although ground moraines generally have a low relief, they might display a prominent subglacially streamlined surface of flutes, drumlins, or mega-scale glacial lineations. Flutes are elongate ice-flow parallel ridges with a length much longer than the width (Figure 3). They rarely exceed 1 m in height or width, whereas the length might exceed 2 km (Gordon et al., 1992; Evans and Twigg, 2002; Kjær et al., 2008). Flutes are small-scale landforms, and their preservation potential is low. They therefore occur mainly in modern glacier forefields, whereas drumlins and mega-scale lineations are better preserved and well known from Pleistocene glacial landscapes.

The large basal till plains in North America host many spectacular drumlin fields, e.g., in New York State with ca. 10,000 individual landforms (Menzies, 1979; Briner, 2007). Drumlins are subglacially streamlined, ice-flow parallel hills with a steep, blunt stoss side and a gentle, tapering lee side (Menzies, 1979; Menzies and Rose, 1987; Jørgensen and Piotrowski, 2003). Mega-scale glacial lineations (MSGLs) also belong to the group of subglacial landforms that might cover the surface of ground moraines. MSGLs are much larger than flutes and drumlins; in length they might extend up to 100 km and in width up to 200–1,300 m (Clark and Stokes, 2003). They are indicative of fast ice flow, i.e., ice streams. In terrestrial settings, MSGLs are well described from the paleo-ice streams of the Laurentide Ice Sheet in North America (e.g., Stokes and Clark, 2001, 2002; de Angelis and Kleman, 2007).

Supraglacially formed moraines

Lateral moraine

Lateral moraines are ridges of supraglacially deposited debris located along the sides of valley and cirque glaciers (Figure 4a; Boulton and Eyles, 1979; Spedding and Evans, 2002). Where debris accumulation is high, they can reach heights of more than 100 m (e.g., Iturrizaga, 2008). In modern glacial environments, lateral moraines might be ice cored. Typically, the material in lateral moraines is angular and coarse-grained supraglacial debris, originating from the valley sides, although they might also contain debris that has experienced sub- and englacial transport before deposition in the lateral moraine (Benn and Ballantyne, 1994). Lateral moraines form only below the equilibrium line altitude (ELA), where debris accumulates due to net ablation. The maximum elevation of lateral moraines is therefore an important indicator of the ELA, both in modern and ancient glacial environments (Nesje, 1992). Because lateral moraines occur on unstable valley sides, they generally have a low preservation potential. However, some Pleistocene lateral moraines exist, in particular, where valley glaciers have expanded out of their confining valleys (Clark et al., 2003; Easterbrook et al., 2003).

Medial moraine

Medial moraines are ice-flow parallel debris ridges on the surface of glaciers (Figure 4c). They are very striking features in the supraglacial environment, giving an impressive visualization of the ice-flow dynamics. Similar to the lateral moraines, they only occur below the ELA. Medial moraines can extend for tens of kilometers but usually only consist of a thin layer of supraglacial debris. Medial moraines are the surface expression of englacial debris septa, sometimes extending to the glacier bed (Hambrey et al., 1999). The debris might therefore contain a component of en- and subglacially transported material, although coarse-grained, angular supraglacial material is most common. “Ablation-dominant medial moraines” occur in the ablation area by the melt-out of debris entrained further upglacier (Eyles and Rogerson, 1978). “Ice-stream interaction medial moraines,” such as shown in Figure 4c, occur downglacier of the confluence of two

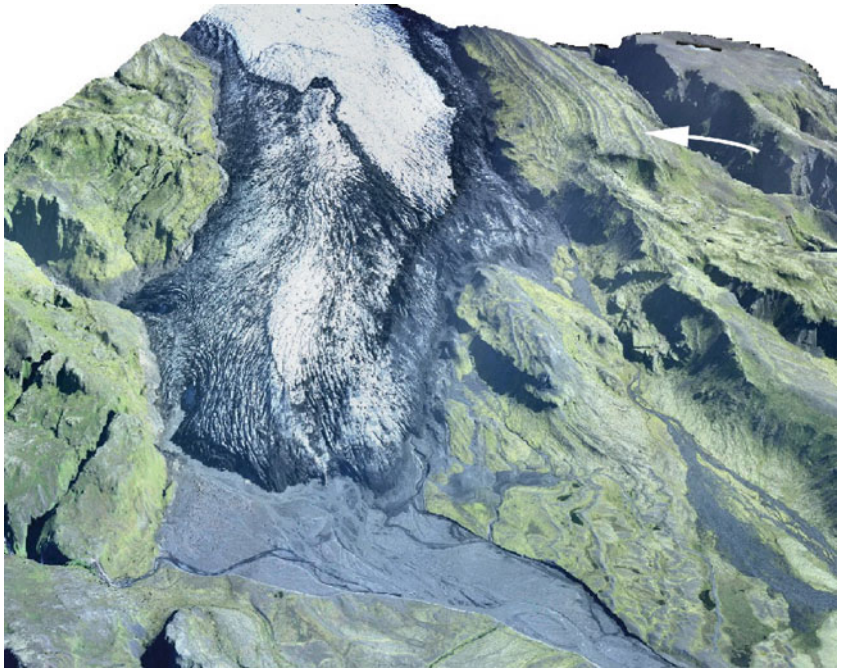

a

b

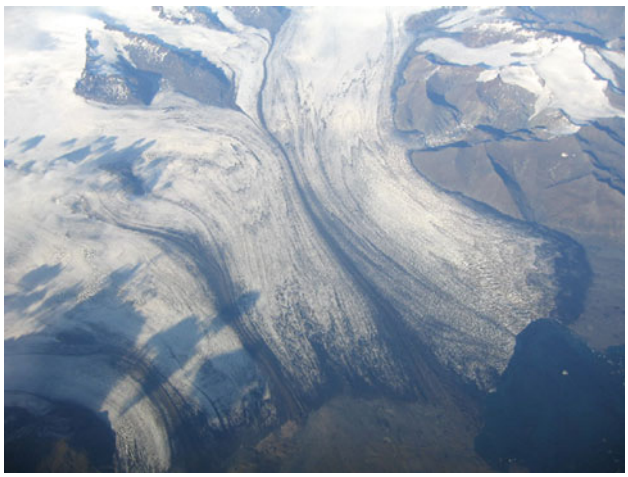

c

Moraine, Figure 4 Distinct set of lateral moraines (*arrow*) along the sides of the Sólheimajökull glacier, southern Iceland. Aerial photograph from 2001 draped over a digital elevation model with 1.5× vertical exaggeration. **(b)** Hummocky moraines in the Kviárjökull forefield, southeastern Iceland, May 2009. **(c)** Medial moraines at the surface of the Breiðamerkurjökull glacier, southeastern Iceland. The medial moraines originate where individual ice flow units merge downstream of the Esjufjöll nunataks, September 2009.

individual ice-flow units. Such medial moraines are often the continuation of two merged lateral moraines from each flow unit. When supraglacial rock avalanches are transported downglacier, they might get stretched out and appear as "avalanche-type medial moraines" on glacier surfaces.

A certain type of medial moraines, looped medial moraines, appears on surge-type glaciers. When a main trunk glacier surges, it advances so rapidly that medial moraines from tributary glaciers are detached or extended into a loop or a drop-shaped supraglacial feature. Looped medial moraines on a glacier are easily identified and strongly suggest that the main glacier has surged (Meier and Post, 1969).

Medial moraines from Pleistocene glaciations are not common due to the low preservation potential and the small volumes of sediment in such landforms. Prominent Pleistocene medial and lateral moraines have been described from the eastern Sierra Nevada, California, USA (Easterbrook et al., 2003).

Hummocky moraine

Hummocky moraine (also known as dead-ice moraine or moraine mounds) is a chaotically appearing glacial landscape consisting of many individual hummocks, with no preferred orientation or organization of landforms, size, spacing, or slope. Controlled moraines and rim ridges (circular moraine ridges) are described separately below. Depressions, usually referred to as sinkholes or dead-ice hollows, are abundant in such landscapes. Hummocky moraines occur both in lowlands glaciated in the Pleistocene and in the forefields of past and present valley glaciers. Other landforms characteristic of deposition in dead-ice environments, such as ice-walled-lake plains, kames, and flat-topped eskers, commonly occur in association with hummocky moraines (Clayton et al., 2008; Krüger et al., 2010b). Individual hummocks may range from a few meters in diameter (e.g., Spedding and Evans, 2002) to several hundreds of meters (e.g., Johnson and Clayton, 2003). The relief and hummock height often varies significantly both within the same hummocky moraine and between different localities. Hummocks just a few meters in height are known from, e.g., Kvíarjökull, Iceland (Figure 4b), whereas hummocks up to 60 m originating from the last Laurentide Ice Sheet have been described from North America (Ham and Attig, 1996).

The sediments within hummocky moraines are normally dominated by diamicts (Benn, 1992; Kjær and Krüger, 2001; Lukas, 2005; Schomacker and Kjær, 2007, 2008). Diamicts in hummocky moraines are often heterogeneous and associated with sediment gravity-flow deposits and meltwater-deposited sediments (e.g., Kjær and Krüger, 2001; Lukas, 2005).

Most depositional models for hummocky moraines suggest that they form in dead-ice environments by melt-out and resedimentation of debris from stagnant glacier ice. Thus, the hummocky topography originates from the resedimentation of an unevenly distributed supraglacial debris cover and topographical inversion cycles during dead-ice melting. The models are often supported by the observations from modern glacial environments, where the genesis of hummocky moraines has been monitored (e.g., Boulton, 1972; Clayton and Moran, 1974; Hambrey et al., 1999; Schomacker and Kjær, 2007, 2008). For instance, Krüger and coworkers closely followed the dead-ice melting and hummocky moraine development at Kötlujökull, Iceland over a 30-year period and were able to link the sedimentary processes to the products left in the geological record (Krüger and Kjær, 2000; Kjær and Krüger, 2001; Krüger et al., 2010b). Alternative models for hummocky moraines have suggested formation by sinking of stagnant ice into a soft subglacial bed (Boone and Eyles, 2001) or even by erosion by subglacial meltwater (Munro and Shaw, 1997). These models are, however, mainly of local interest and should not be viewed as general explanations for the genesis of hummocky moraines.

Controlled moraine

Controlled moraines also form in dead-ice environments and are characterized by inherited linear ridges, originating from debris-rich thrust planes in the parent dead ice (Boulton, 1972; Bennett et al., 1998; Evans, 2009). Supraglacial linear outcrops of debris-filled thrusts are often seen in early stages of melt-out of ice-cored moraines (Schomacker and Kjær, 2008; Krüger et al., 2010b). Although such thrusts are very exposed to resedimentation in the dead-ice environment, the occurrence of controlled moraines in Pleistocene landscapes and recently deglaciated forefields indicates that the debris-rich thrusts can survive as ridges after deicing (Bennett et al., 1998; Lukas, 2005; Evans, 2009). Based primarily on studies of modern glaciers in Svalbard, it has been suggested that controlled moraines form at polythermal glacier snouts, where marginal debris entrainment and thrusting is particularly likely to occur (e.g., Bennett et al., 1996; Hambrey et al., 1999; Evans, 2009).

Polygenetic moraines and other important moraine types

Ribbed moraine

Ribbed moraines are ice-flow transverse ridges, occurring in fields with ridges arranged in a subparallel pattern (e.g., Hättestrand and Kleman, 1999; Lindén and Möller, 2005; Dunlop and Clark, 2006; Möller, 2006; Todd et al., 2007; Lindén et al., 2008). The ridges are usually curved and some types have "horns" pointing downice. They might reach heights of 10–30 m and widths of 150–300 m. Ribbed moraines are located in the core areas of former ice sheets (Dunlop and Clark, 2006). This broad category of moraines spans over ridges formed in many different glacial environments, and there is no single unifying model of formation for "ribbed moraine," rather they represent a group of moraine ridges with morphological similarities.

De Geer moraines are transverse moraines found below the highest shoreline, e.g., in areas glaciated by the Scandinavian Ice Sheet and the Laurentide Ice Sheet (Lindén and Möller, 2005; Todd et al., 2007). Based on the detailed sedimentological and morphological studies of De Geer moraines in North Sweden, Lindén and Möller (2005) suggested that the De Geer moraines formed submarginally in a glacioaquatic environment at the grounding line of the retreating ice sheet. Moraine ridges built up due to subglacial sediment advection in a deforming bed and deposition of sediment gravity flow material at their distal side.

"Rogen moraines" are probably the most striking type of ribbed moraine (Figure 5). Many highly differing models of formation have been suggested, some involving reshaping of earlier glacial landforms, subglacial extensional fracturing of sediments, or shearing and stacking of basal debris-rich ice (e.g., Hättestrand and Kleman, 1999; Dunlop and Clark, 2006; Finlayson and Bradwell, 2008).

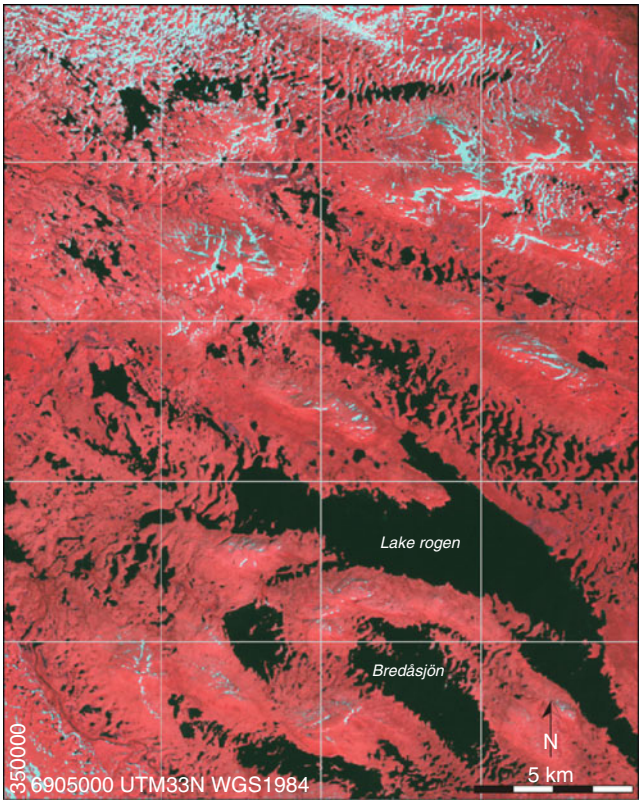

Moraine, Figure 5 Ribbed moraine landscape in the Lake Rogen area, western Sweden. This is the type locality of "Rogen moraines." Individual moraine ridges are up to ca. 1,000-m long, ca. 50–200-m wide, and ca. 20-m high. The ribbed moraine ridges appear in a pattern transverse to the local ice-flow direction of the Scandinavian Ice Sheet during the Weichselian glaciation. The "horns" usually point in a downglacier direction. False-color Landsat ETM7+ imagery recorded May 19, 2002. Coordinates are in meters, UTM WGS 1984.

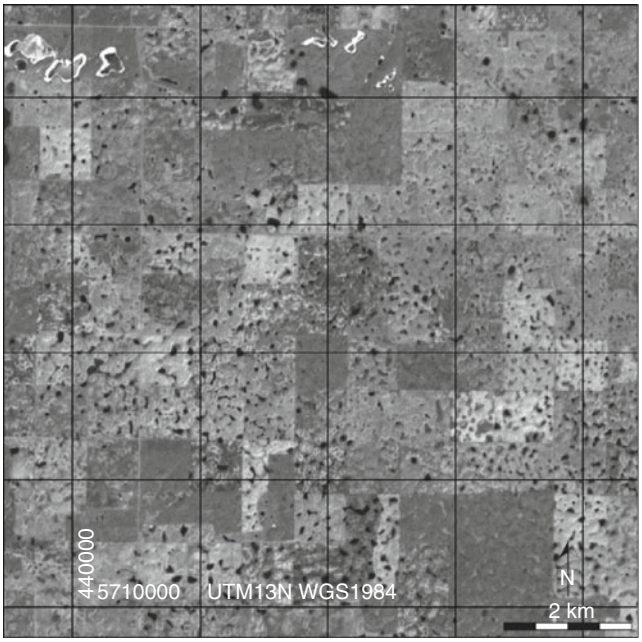

Moraine, Figure 6 Circular moraine ridges ca. 30 km East of Kenaston, Saskatchewan, Canada. The ring forms are up to ca. 200 m across and are located in a low-relief glacial landscape formed by the Laurentide Ice Sheet during the Wisconsinan glaciation. Landsat 7ETM+ imagery recorded May 24, 2001. Coordinates are in meters, UTM WGS 1984.

Most studies have focused on the geomorphology of Rogen moraines, and only recently sufficiently detailed sedimentological investigations have added to the understanding of these landforms (Möller, 2006). Based on studies in central Sweden, Möller (2006) suggested that Rogen moraines form in a two-stage manner. According to his model, preexisting transverse moraine ridges deposited in dead-ice environments survived below cold-based ice until the Preboreal deglaciation, where the ice sheet turned warm-based and became more dynamic. It is in this final phase that the "horns" formed and the precursor transverse landforms were re-moulded into Rogen moraines.

Rim ridges or circular-shaped moraines

Rim ridges are ring-shaped moraines, with an outer ridge surrounding a central depression (Figure 6; Mollard, 2000; Johnson and Clayton, 2003). They have mainly been described from the Great Plains of North America, although ring-shaped moraines and ice-walled lake plains also occur in Scandinavia (e.g., Lagerbäck, 1988; Lidmar-Bergström et al., 1991). Rim ridges usually occur in clusters of hundreds or thousands of low-relief landforms, each one sized up to 200 m in diameter (Johnson and Clayton, 2003). Most conceptual models suggest that they form by a topographical inversion in the last melt-out phase of individual buried ice blocks in dead-ice environments (Clayton and Moran, 1974; Ham and Attig, 1996; Johnson and Clayton, 2003). Despite their organized appearance in clusters, they might therefore be considered as a type of hummocky moraine.

Conclusions

The geomorphology, sedimentology, and genesis of most moraines described here are generally well understood. However, the variety between moraines in the same area and between the same types of moraines in different areas is immense. This also explains why moraines of similar type are often termed with local names. In particular, studies of processes in modern glacial environments have provided important depositional models for ancient moraines. Although this approach has been very valuable, there are still many research questions to be answered. One of the largest challenges is the lack of suitable modern analogs. For instance, the vast areas and large sediment volumes

of the hummocky moraines and ground moraines in North America are hard to understand from the studies on modern glaciers, which are orders-of-magnitude smaller than the Pleistocene ice sheets. Because most modern ice sheets terminate in marine environments or in alpine terrain, it is still very challenging to understand the deposits and palaeodynamics of past ice sheets terminating in lowlands and resting on soft sediment beds.

Bibliography

Aber, J. S., and Ber, A., 2007. *Glaciotectonism*. Developments in Quaternary Science 6. Amsterdam: Elsevier.

de Angelis, H., and Kleman, J., 2007. Palaeo-ice streams in the Foxe/Baffin sector of the Laurentide Ice Sheet. *Quaternary Science Reviews*, **26**, 1313–1331.

Bakker, M. A. J., 2004. *The Internal Structure of Pleistocene Push Moraines. A Multidisciplinary Approach with Emphasis on Ground-Penetrating Radar*. Ph.D thesis, Queen Mary University of London, TNO and Geological Survey of the Netherlands.

Benediktsson, Í. Ö., Möller, P., Ingólfsson, Ó., van der Meer, J. J. M., Kjær, K. H., and Krüger, J., 2008. Instantaneous end moraine and sediment wedge formation during the 1890 glacier surge of Brúarjökull, Iceland. *Quaternary Science Reviews*, **27**, 209–234.

Benediktsson, Í. Ö., Ingólfsson, Ó., Schomacker, A., and Kjær, K. H., 2009. Formation of submarginal and proglacial end moraines: implications of ice-flow mechanism during the 1963-64 surge of Brúarjökull, Iceland. *Boreas*, **38**, 440–457.

Benediktsson, Í. Ö., Schomacker, A., Lokrantz, H., and Ingólfsson, Ó., 2010. The 1890 surge end moraine at Eyjabakkajökull, Iceland: a re-assessment of a classic glaciotectonic locality. *Quaternary Science Reviews*, **29**, 484–506.

Benn, D. I., 1992. The genesis and significance of "hummocky moraine": evidence from the Isle of Skye, Scotland. *Quaternary Science Reviews*, **11**, 781–799.

Benn, D. I., and Ballantyne, C. K., 1994. Reconstructing the transport history of glacial sediments: a new approach based on the co-variance of clast form indices. *Sedimentary Geology*, **91**, 215–227.

Benn, D. I., and Evans, D. J. A., 1996. The interpretation and classification of subglacially-deformed materials. *Quaternary Science Reviews*, **15**, 23–52.

Benn, D. I., and Evans, D. J. A., 1998. *Glaciers and Glaciation*. London: Arnold.

Bennett, M. R., 2001. The morphology, structural evolution and significance of push moraines. *Earth-Science Reviews*, **53**, 197–236.

Bennett, M. R., Huddart, D., Hambrey, M. J., and Ghienne, J. F., 1996. Moraine development at the high-arctic valley glacier Pedersenbreen, Svalbard. *Geografiska Annaler*, **78A**, 209–221.

Bennett, M. R., Hambrey, M. J., Huddart, D., and Glasser, N. F., 1998. Glacial thrusting & moraine-mound formation in Svalbard & Britain: the example of Coire a' Cheud-chnoic (Valley of Hundred Hills), Torridon Scotland. *Quaternary Proceedings*, **6**, 17–34.

Boone, S. J., and Eyles, N., 2001. Geotechnical model for great plains hummocky moraine formed by till deformation below stagnant ice. *Geomorphology*, **38**, 109–124.

Boulton, G. S., 1972. Modern Arctic glaciers as depositional models for former ice sheets. *Journal of the Geological Society of London*, **128**, 361–393.

Boulton, G. S., 1986. Push-moraines and glacier-contact fans in marine and terrestrial environments. *Sedimentology*, **33**, 677–698.

Boulton, G. S., and Eyles, N., 1979. Sedimentation by valley glaciers: a model and genetic classification. In Schlüchter, C. (ed.), *Moraines and Varves*. Rotterdam: Balkema, pp. 11–23.

Boulton, G. S., and Hindmarsh, R. C. A., 1987. Sediment deformation beneath glaciers: rheology and geological consequences. *Journal of Geophysical Research*, **92**, 9059–9082.

Boulton, G. S., van der Meer, J. J. M., Beets, D. J., Hart, J. K., and Ruegg, G. H. J., 1999. The sedimentary and structural evolution of a recent push moraine complex: Holmströmbreen, Spitsbergen. *Quaternary Science Reviews*, **18**, 339–371.

Boyce, J., and Eyles, N., 2001. Architectural element analysis applied to glacial deposits: internal geometry of a Late Pleistocene till sheet, Ontario, Canada. *Geological Society of America Bulletin*, **112**, 98–118.

Briner, J. P., 2007. Supporting evidence from the New York drumlin field that elongate subglacial bedforms indicate fast ice flow. *Boreas*, **36**, 143–147.

Clark, C. D., and Stokes, C. R., 2003. Palaeo-ice stream landsystem. In Evans, D. J. A. (ed.), *Glacial Landsystems*. London: Arnold, pp. 204–227.

Clark, D., Gillespie, A. R., Clark, M., and Burke, B., 2003. Mountain glaciations of the Sierra Nevada. In Easterbrook, D. J. (ed.), *Quaternary Geology of the United States, INQUA 2003 Field Guide Volume*. Reno, NV: Desert Research Institute, pp. 287–311.

Clayton, L., and Moran, S. R., 1974. A glacial process-form model. In Coates, D. R. (ed.), *Glacial Geomorphology*. Binghamton: State University of New York, pp. 89–119.

Clayton, L., Attig, J. W., Ham, N. R., Johnson, M. D., Jennings, C. E., and Syverson, K. M., 2008. Ice-walled-lake plains: implications for the origin of hummocky glacial topography in middle North America. *Geomorphology*, **97**, 237–248.

Dunlop, P., and Clark, C. D., 2006. The morphological characteristics of ribbed moraine. *Quaternary Science Reviews*, **25**, 1668–1691.

Dyke, A. S., and Prest, V. K., 1987. Late Wisconsinan and Holocene history of the Laurentide Ice Sheet. *Géographie physique et Quaternaire*, **41**, 237–263.

Easterbrook, D. J., Pierce, K., Gosse, J., Gillespie, A., Evenson, E., and Hamblin, K., 2003. Quaternary geology of the western United States. In Easterbrook, D. J. (ed.), *Quaternary Geology of the United States, INQUA 2003 Field Guide Volume*. Reno, NV: Desert Research Institute, pp. 19–79.

Eklund, A., and Hart, J. K., 1996. Glaciotectonic deformation within a flute from the Isfallsglaciären, Sweden. *Journal of Quaternary Science*, **11**, 299–310.

Evans, D. J. A., 2009. Controlled moraines: origins, characteristics and palaeoglaciological implications. *Quaternary Science Reviews*, **28**, 183–208.

Evans, D. J. A., and Twigg, D. R., 2002. The active temperate glacial landsystem: a model based on Breiðamerkurjökull and Fjallsjökull, Iceland. *Quaternary Science Reviews*, **21**, 2143–2177.

Evans, D. J. A., Phillips, E. R., Hiemstra, J. F., and Auton, C. A., 2006. Subglacial till: formation, sedimentary characteristics and classification. *Earth-Science Reviews*, **78**, 115–176.

Eyles, N., and Rogerson, R. J., 1978. A framework for the investigation of medial moraine formation: Austerdalsbreen, Norway, and Berendon Glacier, British Columbia, Canada. *Journal of Glaciology*, **20**, 99–113.

Finlayson, A. G., and Bradwell, T., 2008. Morphological characteristics, formation and glaciological significance of Rogen moraine in northern Scotland. *Geomorphology*, **101**, 607–617.

Gordon, J. E., Whalley, W. B., Gellatly, A. F., and Vere, D. M., 1992. The formation of glacial flutes: assessment of models with evidence from Lyngsdalen, North Norway. *Quaternary Science Reviews*, **11**, 709–731.

Ham, N. R., and Attig, J. W., 1996. Ice wastage and landscape evolution along the southern margin of the Laurentide Ice Sheet, north-central Wisconsin. *Boreas*, **25**, 171–186.
Hambrey, M. J., Bennett, M. R., Dowdeswell, J. A., Glasser, N. F., and Huddart, D., 1999. Debris entrainment and transfer in polythermal valley glaciers. *Journal of Glaciology*, **45**, 69–86.
Hättestrand, C., and Kleman, J., 1999. Ribbed moraine formation. *Quaternary Science Reviews*, **18**, 43–61.
Iturrizaga, L., 2008. Post-sedimentary Transformation of Lateral Moraines – the Tributary Tongue Basins of the Kviárjökull (Iceland). *Journal of Mountain Science*, **5**, 1–16.
Jakobsen, P. R., and Overgaard, T., 2002. Georadar facies and glaciotectonic structures in ice marginal deposits, northwest Zealand, Denmark. *Quaternary Science Reviews*, **21**, 917–927.
Jennings, C. E., 2006. Terrestrial ice streams – a view from the lobe. *Geomorphology*, **75**, 100–124.
Johnson, M. D., and Clayton, L., 2003. Supraglacial landsystems in lowland terrain. In Evans, D. J. A. (ed.), *Glacial Landsystems*. London: Arnold, pp. 228–258.
Jørgensen, F., and Piotrowski, J. A., 2003. Signature of the Baltic Ice Stream on Funen Island, Denmark during the Weichselian glaciation. *Boreas*, **32**, 242–255.
Kjær, K. H., and Krüger, J., 2001. The final phase of dead-ice moraine development: processes and sediment architecture, Kötlujökull, Iceland. *Sedimentology*, **48**, 935–952.
Kjær, K. H., Krüger, J., and van der Meer, J. J. M., 2003. What causes till thickness to change over distance? Answers from Mýrdalsjökull, Iceland. *Quaternary Science Reviews*, **22**, 1687–1700.
Kjær, K. H., Korsgaard, N. J., and Schomacker, A., 2008. Impact of multiple glacier surges – a geomorphological map from Brúarjökull, East Iceland. *Journal of Maps*, **2008**, 5–20.
Krüger, J., 1979. Structures and textures in till indicating subglacial deposition. *Boreas*, **8**, 323–340.
Krüger, J., 1993. Moraine-ridge formation along a stationary ice front in Iceland. *Boreas*, **22**, 101–109.
Krüger, J., 1995. Origin, chronology and climatological significance of annual-moraine ridges at Mýrdalsjökull, Iceland. *The Holocene*, **5**, 420–427.
Krüger, J., and Kjær, K. H., 2000. De-icing progression of ice-cored moraines in a humid, subpolar climate, Kötlujökull, Iceland. *The Holocene*, **10**, 737–747.
Krüger, J., Kjær, K. H., and van der Meer, J. J. M., 2002. From push moraine to single-crested dump moraine during a sustained glacier advance. *Norsk Geografisk Tidsskrift*, **56**, 87–95.
Krüger, J., Schomacker, A., and Benediktsson, Í. Ö., 2010a. Ice-marginal environments: Geomorphic and structural genesis of marginal moraines at Mýrdalsjökull. In Schomacker, A., Krüger, J., and Kjær, K. H. (eds.), *The Mýrdalsjökull Ice Cap, Iceland. Glacial Processes, Sediments and Landforms on an Active Volcano*. Developments in Quaternary Science 13. Amsterdam: Elsevier, pp. 79–104.
Krüger, J., Kjær, K. H., and Schomacker, A., 2010b. Dead-ice environments: a landsystems model for a debris-charged, stagnant lowland glacier margin, Kötlujökull. In Schomacker, A., Krüger, J., and Kjær, K. H. (eds.), *The Mýrdalsjökull Ice Cap, Iceland. Glacial Processes, Sediments and Landforms on an Active Volcano*. Developments in Quaternary Science 13. Amsterdam: Elsevier, pp. 105–126.
Larsen, N. K., and Piotrowski, J. A., 2003. Fabric pattern in a basal till succession and its significance for reconstructing subglacial processes. *Journal of Sedimentary Research*, **73**, 725–734.
Larsen, N. K., Piotrowski, J. A., Christoffersen, P., and Menzies, J., 2006. Formation and deformation of basal till during a glacier surge; Elisebreen, Svalbard. *Geomorphology*, **81**, 217–234.
Lagerbäck, R., 1988. The Veiki moraines in northern Sweden – widespread evidence of an Early Weichselian deglaciation. *Boreas*, **17**, 469–486.
Lidmar-Bergström, K., Elvhage, C., and Ringberg, B., 1991. Landforms in Skåne. South Sweden. Preglacial and glacial landforms analysed from two relief maps. *Geografiska Annaler*, **73A**, 61–91.
Lindén, M., and Möller, P., 2005. Marginal formation of De Geer moraines and their implications to the dynamics of grounding-line recession. *Journal of Quaternary Science*, **20**, 113–133.
Lindén, M., Möller, P., and Adrielsson, L., 2008. Ribbed moraine formed by subglacial folding, thrust stacking and lee-side cavity infill. *Boreas*, **37**, 102–131.
Lukas, S., 2005. A test of the englacial thrusting hypothesis of "hummocky" moraine formation: case studies from the north-west Highlands, Scotland. *Boreas*, **34**, 287–307.
Matthews, J. A., McCarroll, D., and Shakesby, R. A., 1995. Contemporary terminal-moraine ridge formation at a temperate glacier: Styggedalsbreen, Jotunheimen, southern Norway. *Boreas*, **24**, 129–139.
Meier, M. F., and Post, A., 1969. What are glacier surges? *Canadian Journal of Earth Sciences*, **6**, 807–817.
Menzies, J., 1979. A review of the literature on the formation and location of drumlins. *Earth-Science Reviews*, **14**, 315–359.
Menzies, J., and Rose, J. (eds)., 1987. Drumlin Symposium. Rotterdam: Balkema.
Mollard, J. D., 2000. Ice-shaped ring-forms in Western Canada: their airphoto expressions and manifold polygenetic origins. *Quaternary International*, **68–71**, 187–198.
Möller, P., 2006. Rogen moraine: an example of glacial reshaping of pre-existing landforms. *Quaternary Science Reviews*, **25**, 362–389.
Munro, M., and Shaw, J., 1997. Erosional origin of hummocky terrain in south-central Alberta, Canada. *Geology*, **25**, 1027–1030.
Nelson, A. E., Willis, I. C., and Cofaigh, C., 2005. Till genesis and glacier motion inferred from sedimentological evidence associated with the surge-type glacier, Brúarjökull, Iceland. *Annals of Glaciology*, **42**, 14–22.
Nesje, A., 1992. Topographical Effects on the Equilibrium-Line Altitude on Glaciers. *GeoJournal*, **27**, 383–391.
Piotrowski, J. A., Larsen, N. K., and Junge, F. W., 2004. Reflections of soft subglacial beds as a mosaic of deforming and stable spots. *Quaternary Science Reviews*, **23**, 993–1000.
Price, R. J., 1970. Moraines at Fjallsjökull, Iceland. *Arctic and Alpine Research*, **2**, 27–42.
Ross, M., Campbell, J. E., Parent, M., and Adams, R. S., 2009. Palaeo-ice streams and the subglacial landscape mosaic of the North American mid-continental prairies. *Boreas*, **38**, 421–439.
Schomacker, A., 2008. What controls dead-ice melting under different climate conditions? A discussion. *Earth-Science Reviews*, **90**, 103–113.
Schomacker, A., and Kjær, K. H., 2007. Origin and melt-out of multiple generations of ice-cored moraines at Brúarjökull, Iceland. *Boreas*, **36**, 411–425.
Schomacker, A., and Kjær, K. H., 2008. Quantification of dead-ice melting in ice-cored moraines at the high-Arctic glacier Holmströmbreen, Svalbard. *Boreas*, **37**, 211–225.
Schomacker, A., Kjær, K. H., and Krüger, J., 2010. Subglacial environments, sediments and landforms at the margins of Mýrdalsjökull. In Schomacker, A., Krüger, J., and Kjær, K. H. (eds.), *The Mýrdalsjökull Ice Cap, Iceland. Glacial Processes, Sediments and Landforms on an Active Volcano*. Developments in Quaternary Science 13. Amsterdam: Elsevier, pp. 127–144.
Spedding, N., and Evans, D. J. A., 2002. Sediments and landforms at Kviárjökull, southeast Iceland: a reappraisal of the glaciated valley landsystem. *Sedimentary Geology*, **149**, 21–42.
Stewart, R. A., Bryant, D., and Sweat, M. J., 1988. Nature and origin of corrugated ground moraine of the Des Moines lobe, Story County, Iowa. *Geomorphology*, **1**, 111–130.

Stokes, C. R., and Clark, C. D., 2001. Palaeo-ice streams. *Quaternary Science Reviews*, **20**, 1437–1457.
Stokes, C. R., and Clark, C. D., 2002. Are long subglacial bedforms indicative of fast ice flow? *Boreas*, **31**, 239–249.
Todd, B. J., Valentine, P. C., Longva, O., and Shaw, J., 2007. Glacial landforms on German Bank, Scotian Shelf: evidence for Late Wisconsinan ice-sheet dynamics and implications for the formation of De Geer moraines. *Boreas*, **36**, 148–169.

Cross-references

Dating Glacial Landforms
Debris-Covered Glaciers
Dynamics of Glaciers
Glacial Geomorphology and Landforms Evolution
Glacier Surging
Glaciogenic Deposits
Glaciotectonic Structures, Landforms, and Processes
Ice-Marginal Deposition
Landforms of Glacial Deposition
Landforms of Glacial Transportation
Sediment Entrainment, Transport, and Deposition
Subglacial Processes
Supra-Glacial Debris Entrainments
Till

MOULINS

Umesh K. Haritashya[1], Vijay P. Singh[2], Pratap Singh[3]
[1]Department of Geology, University of Dayton, Dayton, OH, USA
[2]Department of Biological and Agricultural Engineering, Texas A&M University, College Station, TX, USA
[3]Tahal Consulting Engineers Ltd, New Delhi, India

Synonyms

Glacier mill; Glacier sinkholes

Definition

Moulins are narrow, tubular shafts that allow surface meltwater to enter a glacier (Figure 1).

In order to form, a moulin requires crevasses, enough availability of melt water, and relatively flat area. It normally forms at the tip of a crevasse, when it starts accumulating supraglacial meltwater. When a new moulin is formed upstream, it restricts water movement downstream and ultimately abandons the old moulin. It is a big part of the glacier system and can be found in almost all type of glaciers. In many ways moulins are one of the most complex yet stunning features to view. They can be several meters wide and can go all the way to the bed of the glacier, linking supraglacial system of the glacier with the subglacial system. Although most moulins stop somewhere in between and link the supraglacial system with the englacial system. Moulins can be used to inject a fluorescent dye which is one of the widely used methods to study glacial drainage networks and channel systems. Moulins also lower supraglacial and englacial debris to the glacier bed and plays a major role in sediment entrainment and transport. In the last two decades, our understanding about moulins has been widely enhanced by major research initiatives that have drawn conclusions about their importance in the distribution of water within a glacier, glacier's ability to store water, glacier velocity, and pressurizing the subglacial system. Efforts are underway to use moulins as a pathway to study the linkage between glacial water flow from the ice sheets to the sea.

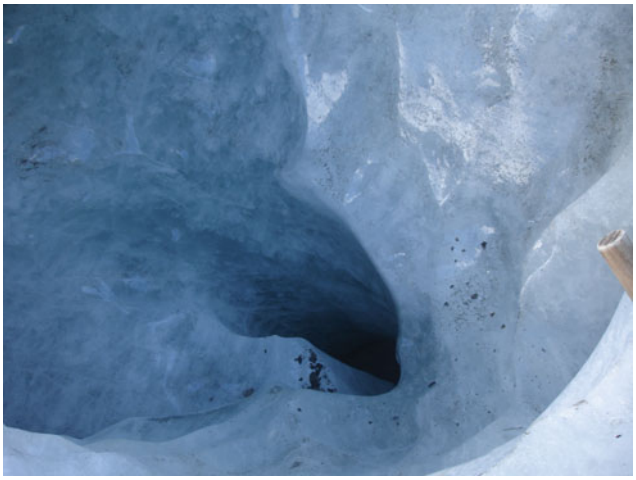

Moulins, Figure 1 Moulin on Fox Glacier in New Zealand. Photo by Umesh Haritashya May 21, 2010.

Cross-references

Crevasses
Englacial Processes
Subglacial Processes

MOUNT EVEREST

Rijan B. Kayastha
Himalayan Cryosphere, Climate and Disaster Research Center (HiCCDRC), Kathmandu University, Dhulikhel, Kavre, Kathmandu, Nepal

Synonyms

Chomolungma (in Tibetan); Sagarmatha (in Nepali); Zhumulangma Feng (in Chinese)

Definition

Mount Everest is the highest mountain on Earth. The height of its summit is 8848 m above mean sea level and its coordinates are 27°59′17″N, 86°55′31E″. It is located on the border between Sagarmatha Zone, Nepal and Tibet, China. It is a part of the Mahalangur Himal in the

Himalaya Range in Asia. Since there was no local Nepali name of this highest mountain of the world, it was officially named Mount Everest by the Royal Geographical Society after the Surveyor General of India, George Everest, in 1865. In the early 1960s, the Nepalese Government gave its official name as Sagarmatha (सगरमाथा *meaning Head of the Sky*). It lies in the Sagarmatha National Park which was declared as the World Heritage Site by UNESCO in 1981. The first successful ascent of the Everest was made by the New Zealander Edmund Hillary and Tenzing Norgay from Nepal on May 29, 1953, via South Col Route. Since then, many climbers have reached the summit. By the end of the 2008 climbing season, there had been 4,109 ascents to the summit by 2,700 individuals. Appa Sherpa, on May 22, 2010, climbed the Everest for the 20th time breaking his own record for the highest number of successful summits.

Mount Everest, Figure 1 Mount Everest.

Mount Everest, Figure 2 Khumbu Icefall.

Geologists have subdivided the rocks comprising Mount Everest into three units called formations: the Qomolungma Formation, the North Col Formation, and the Rongbuk Formation (Yin and Kuo, 1978; Sakai et al., 2005). The Qomolungma Formation is from its summit to the top of the Yellow Band, about 8600 m above sea level. It consists of grayish to dark gray or white, parallel laminated and bedded limestone interlayered with subordinate beds of recrystallized dolomite with argillaceous laminae and siltstone. The North Col Formation consists of the bulk of the Mount Everest, between 7000 and 8600 m, of which the Yellow Band forms its upper part between 8200 and 8600 m. The Yellow Band consists of intercalated beds of diopsite-epidote-bearing marble, which weathers a distinctive yellowish brown, and muscovite-biotite phyllite and semischist. The lower part of the North Col Formation exposed between 7000 and 8200 m consists of interlayered and deformed schist, phyllite, and minor marble. The Rongbuk Formation below 7000 m consists of sillminite-K-feldspar grad schist and gneiss intruded by numerous sills and dikes of leucogranite.

The Khumbu Glacier and Rongbuk Glacier are on the southern and northern slopes of Mount Everest. The Khumbu Glacier is located on the Khumbu region and flows down from the Khumbu Icefall on the southern slopes of the Everest. The ablation area of the Khumbu Glacier ranges in elevation from 5400 m immediately below the icefall to 4900 m at the terminus. Within this ablation area, the ice thickness varies from about 20 m near the terminus to 450 m near the icefall (Gades et al., 2000). The Rongbuk Glacier is located in the Himalaya of southern Tibet. It is formed by two large tributary glaciers, the East and West Rongbuk Glaciers. It flows north and forms the Rongbuk Valley north of the Mount Everest.

Bibliography

Gades, A., Conway, H., Nereson, N., Naito, N., and Kadota, T., 2000. Radio echo-sounding through supraglacial debris on Lirung and Khumbu glaciers, Nepal Himalayas. In Nakawo, M., Raymond, C. F., and Fountain, A. (eds.), *Debris-Covered Glaciers (Proceedings of a Workshop Held at Seattle, Washington, USA, September 13–15, 2000)*. Oxfordshire: IAHS Publ. No. 264, pp. 13–22.

Sakai, H., Sawada, M., Takigami, Y., Orihashi, Y., Danhara, T., Iwano, H., Kuwahara, Y., Dong, Q., Cai, H., and Li, J., 2005. Geology of the summit limestone of Mount Qomolangma (Everest) and cooling history of the Yellow Band under the Qomolangma detachment. *Island Arc*, **14**(4), 297–310.

Yin, C. H., and Kuo, S. T., 1978. Stratigraphy of the Mount Jolmo Lungma and its north slope. *Scientia Sinica*, **5**, 630–644.

MOUNT KENYA

William C. Mahaney
Quaternary Surveys, Thornhill, ON, Canada

Definition and introduction

Mount Kenya, one of the principal high mountains of East Africa, rises to 5,199 m a.s.l. As a recorder of Quaternary glacial events, the massif contains documented tills reaching beyond the Olduvai subchron, nearly to the Plio-Pleistocene boundary. Surfaced with the oldest documented tills in the tropical mountains it is one of the most studied mountains in the tropics. Mount Kenya stands alone, not only as a major mountain, exceeded in altitude only by Kilimanjaro, which is much younger; but much higher than its nearest rivals in Kenya – Elgon and the Aberdares – and closer in elevation to the Virungas and the Ruwenzori in Central Africa. Mount Kenya has undergone six glaciations since the crystallization of the main volcanic plug 2.64 Ma (Everden and Curtis, 1965), and contains a wealth of interglacial paleosols that have provided important information on paleoenvironments between glaciations.

For just over a century, Mount Kenya has attracted the attention of glacial geologists keen to refine the chronology of episodic glaciation and climatic change (Gregory, 1894; Baker, 1967; Hastenrath, 1984; and Mahaney, 1990), which are the underpinnings of ecological change, dispersal of remnant flora and fauna

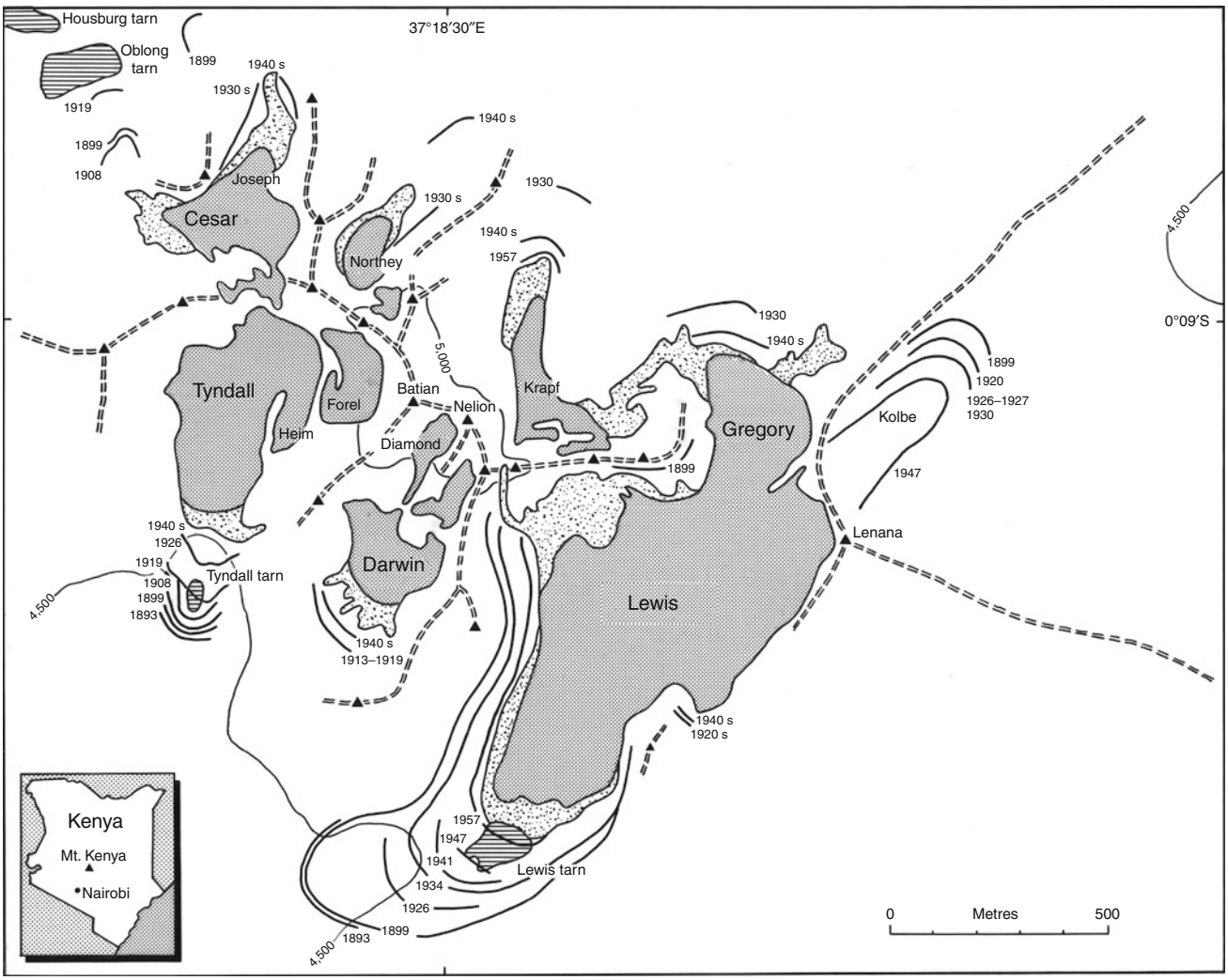

Mount Kenya, Figure 1 Central Peaks of Mount Kenya. Moraine ages are based on historical documentation to 1960 and ice limits (ca. 2009) are much reduced owing to global warming.

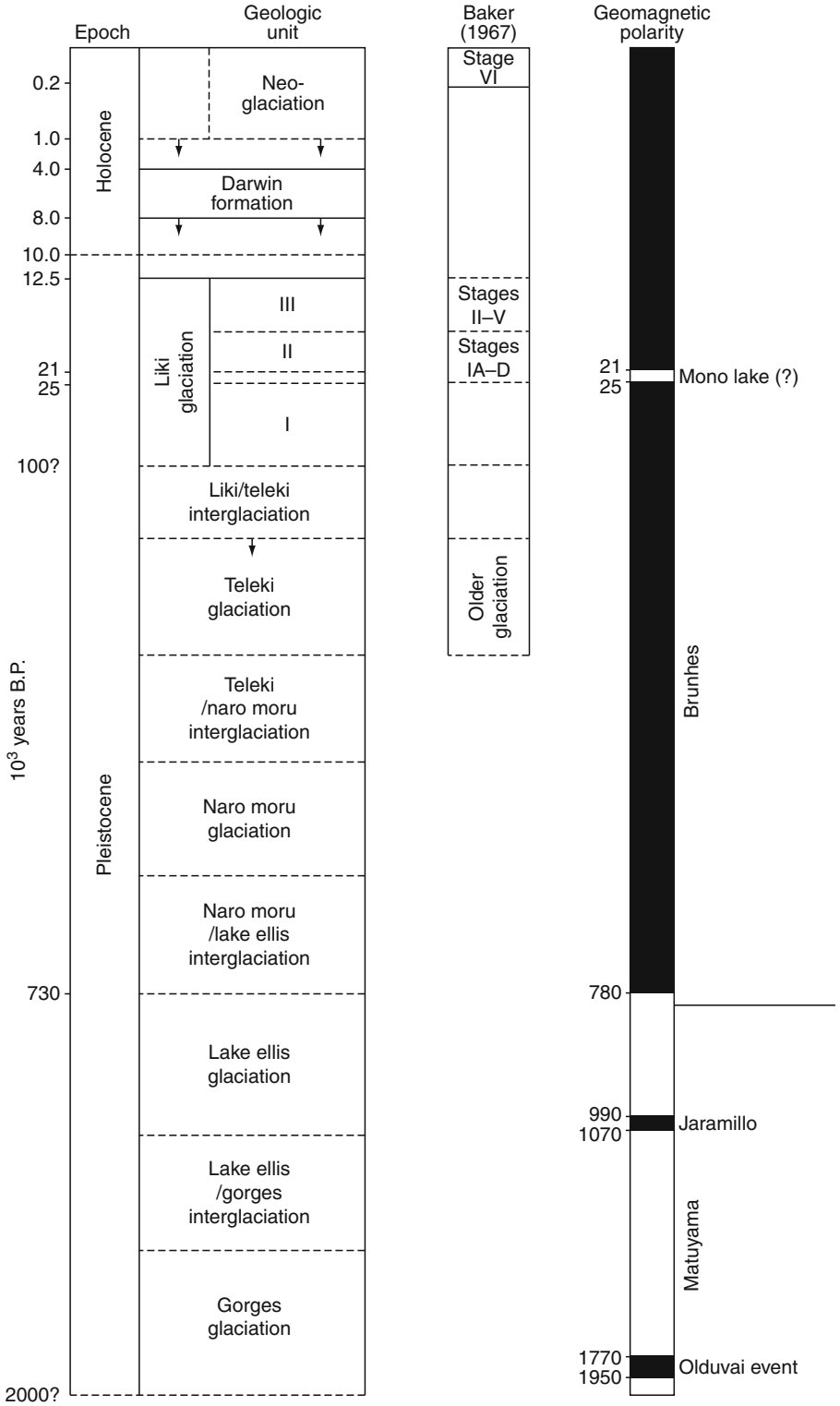

Mount Kenya, Figure 2 Chronology of Mount Kenya showing geological climatic units. Ages of glacial and interglacial deposits are based on radiocarbon dates (Liki Glaciation and younger) and paleomagnetic polarity. The Last Glacial Maximum (LGM) and Late Glacial stages of Baker (1967) are inclusive in Liki stades II and III, respectively.

(Coe, 1967; Harmsen, 1989), and genesis of soils and paleosols. After Gregory, Mackinder (1900) offered new insights into the biogeography of the mountain, but unfortunately lost most of his specimens on the way home. After several years of scientific inactivity, Eric Nilsson, in 1927 and 1932, mapped moraines in Gorges Valley near the Nithi Waterfall (Liki moraines of Mahaney, 1990); his observations (Nilsson, 1931) of an "early till," below the 3,200 m contour in the Nithi Catchment on the eastern flank, were followed up by Mahaney (1990) who carried out detailed investigations starting in 1983.

Nilsson's observations are particularly important because he was the first to describe the moraine sequence around Harris Tarn, on the northeastern flank of the mountain (Figure 1), into which the Kolbe Glacier descended in the first few decades of the twentieth century. The Kolbe Glacier has since melted away and will soon be followed by many of the other small glaciers on the mountain (Mahaney, 1990).

Moreover, Nilsson was the first to surmise that since the moraine sequence on Mount Kenya correlated closely with Mount Kilimanjaro, Mount Elgon, and the Ruwenzori Mountains, it was quite likely that all resulted from the same climatic change. Nilsson's maps of the eastern flank of the mountain are among the most accurate ever made on any of the East African summits.

At about the same time (1934), Carl Troll and K. Wien began glaciological investigations on Mount Kenya which resulted in a photogrammetric survey and flow measurements (Troll and Wien, 1949). Just after WWII, P.C. Spink (1945, 1949) began monitoring glacier recession, a series of observations that have continued on and off (Hastenrath, 1984) up to the present day. In 1947, F.E. Zeuner (1949) studied soil-frost structures and loess on the mountain, focusing attention on needle-ice development, a peculiar process involving diurnal freezing in the tropical mountains. Mahaney (1990) showed not only that loess is present in the surface of almost all soils on Mount Kenya, but that it is represented by quartz-rich horizons in the epipedons (surface horizons) of interglacial paleosols. The tills are represented principally by ferromagnesian minerals.

During the IGY, a number of reconnaissance studies in glaciology and glacial geology were undertaken in various catchments on the mountain, all briefly documented by Baker (1967) who also published the first detailed bedrock map of the mountain.

Mount Kenya is part of the Central Plateau of East Africa, an area of intense tectonic activity that has waxed and waned since the Early Miocene (Mahaney, 1990). Following fractures as old as Cretaceous, a system of rift valleys formed in the Late Tertiary with enormous lakes; major faulting led to down dropping of several rift valleys while others remained several hundred meters above sea level. Immense lava flows, including Mt. Kenya and Mt. Kilimanjaro, erupted through and were aligned with deep fractures in the crust, all dating from the Pliocene and Pleistocene. Not all mountain massifs are volcanic, as some formed as erosional remnants (Cherangani Hills, north of Mt. Kenya) and others from regional faulting of metasedimentary rocks (Mount Elgon on the Uganda–Kenya border, a prime example).

A full discussion of the climate on Mount Kenya is given by Mahaney (1990). While not known with precision, the MAT at 3,000 m a.s.l. is estimated at close to 10°C; at 4,000 m a.s.l., +3°C, which conforms to a lapse rate of 6.5°C/km (International Standard Atmosphere). Data on precipitation collected during the IGY show the wettest drainages to be on the west and south, all fed by thunderstorms. The eastern flank of the mountain is dry above 3,000 m altitude, whereas, below the 3,000-m contour, the climate becomes wet with precipitation well over 1 m/year; and during the monsoon (April–July), the lower reaches are exceedingly humid. The northern slopes are often under anticyclonic activity and very dry. In effect, this climatic distribution led to the development of the largest modern glaciers on the western flank (Figure 1) where they would be least starved of moisture. The ancient Pleistocene climatic regime was quite different, with the largest glaciers on the eastern side of the mountain, in Gorges and Hobley valleys. Presumably, during each glaciation, there may have been an upward shift in the monsoon which fed moisture in much greater quantity onto the upper eastern slopes, giving rise to a partial ice cap that covered Point Lenana (4,985 m a.s.l.; Mahaney, 1990).

Moraine positions, outlined on the Mount Kenya map shown in Mahaney (1990; Plates 1–5), are based on geologic mapping and stratigraphic data compiled into the chronology shown in Figure 2.

Bibliography

Baker, B. H., 1967. *Geology of the Mount Kenya area*. Geological Report NO. 79, Kenya Geological Survey, Nairobi, 78 p.

Coe, M. J., 1967. *The Ecology of the Alpine Zone of Mount Kenya*. The Hague: Junk, p. 136.

Coetzee, J. A., 1967. Pollen analytical studies in East and Southern Africa. *Palaeoecology of Africa*, **3**, 146.

Everden, J. F., and Curtis, G. H., 1965. The potassium-argon dating of late Cenozoic rocks in East Africa and Italy. *Current Anthropology*, **6**, 343–385.

Gregory, J. W., 1894. The glacial geology of Mount Kenya. *Quarterly Journal Geological Society*, **56**, 205–222.

Harmsen, R., 1989. Recent evolution and dispersal of insects on the East African mountains. In Mahaney, W. C. (ed.), *Quaternary and Environmental Research on East African Mountains*. Balkema: Rotterdam, pp. 245–256.

Hastenrath, S., 1984. *The Glaciers of Equatorial East Africa*. Dordrecht: Reidel, p. 353.

Mackinder, H. J., 1900. A journey to the summit of Mount Kenya, British East Africa. *Geographical Journal*, **15**, 453–486.

Mahaney, W. C., 1990. *Ice on the Equator*. Ellison Bay: Wm Caxton, p. 386.

Nilsson, E., 1931. Quaternary glaciation and pluvial lakes in British East Africa and Abyssinia. *Geografiska Annaler*, **H13**, 241–248.

Nilsson, E., 1935. Traces of ancient changes of climate in East Africa. *Geografiska Annaler*, **1–2**, 1–21.

Spink, P. C., 1945. Further notes on the Kibo inner crater and glaciers of Kilimanjaro and Mount Kenya. *Geographical Journal*, **106**, 210–216.
Spink, P. C., 1949. The equatorial glaciers of East Africa. *Journal of Glaciology*, **1**, 277–283.
Troll, C., and Wien, K., 1949. Der Lewisgletcher am Mount Kenya. *Geografiska Annaler*, **31**, 257–274.
Zeuner, F. E., 1949. Frost soils on Mount Kenya and the relation of frost soils to aeolian deposits. *Journal of Soil Science*, **1**, 20–30.

Cross-references

Alps
Cirque Glaciers
Climate Change and Glaciers
Dating Glacial Landforms
Deglaciation
Glacial/Interglacial Cycles
Holocene Glacier Fluctuations
Ice Age
Kilimanjaro
Last Glacial Maximum Glaciation (LGM/LGP) in High Asia (Tibet and Surrounding Mountains)
Little Ice Age
Moraine
Palaeoclimate and Past Glaciations
Quaternary Glaciation
Rock Glaciers
Stratigraphy of Snowpacks
Younger Dryas

MOUNTAIN GEOMORPHOLOGY

David R. Butler
Mountain GeoDynamics Research Group, Department of Geography, Texas State University-San Marcos, San Marcos, TX, USA

Definition

Mountain. Although no universally accepted definition of *mountain* exists, it is generally accepted that a mountain is a large landform that rises abruptly from the surrounding level and attains a high elevation, typically in the form of a peak that is separated from the surrounding lower elevations and adjacent peaks.
Geomorphology. The study of landforms and the processes by which they are created.

Introduction

Mountains have long been a central focus in the discipline of Geomorphology (Harbor, 2004; Kennedy, 2006), and "their steep surface gradients, and rapid spatial and temporal changes in biophysical variables that control geomorphic processes" (Harbor, 2004, p. xix) offer a diverse landscape for geomorphologists. The study of mountain geomorphology has been the focus of several edited books (Slaymaker, 1972; Butler et al., 2003; Bishop and Shroder, 2004; Owens and Slaymaker, 2004), but no recent text has focused specifically on mountain geomorphology. Price (1986) surveyed the range of geomorphic processes that occur in mountain environments, but his work was not specific to mountain geomorphology.

Geomorphic processes in mountains

The high energy of alpine environments produces a suite of geomorphic processes that result in often unique landforms, many of which are associated with the presence of snow, ice, and/or glaciers. Glacial and periglacial conditions, past and current, typify most high mountain environments, and hazardous mass movements such as snow avalanches and a range of landslides are widespread (Giardino et al., 1987; Benn and Evans, 1997; Kalvoda and Rosenfeld, 1998). Quaternary glaciations sculpted many mountain ranges, leaving behind signature landforms such as U-shaped valleys. Smaller mountain glaciers reformed during the Little Ice Age, imparting their own legacy on the landscape. Active and relict rock glaciers (Giardino et al., 1987) are also found in mountain landscapes around the world, and geocryological processes associated with the presence of permafrost and/or seasonal ground ice are also widespread (Price, 1986). Twentieth- and twenty-first-century climate change associated with global warming has caused drastic recession, and in many cases disappearance, of alpine glaciers. Climate change has also affected geocryological processes and landforms in alpine regions, allowing tree seedling establishment and upward advance of upper tree line into alpine tundra (Butler et al., 2009).

Summary

Mountain geomorphology is a subfield of geomorphology focused on the geomorphic processes currently and recently operating in mountain environments. Mountains provide sensitive natural laboratories for the study of geomorphic processes, and mountain geomorphologists are actively involved in studies of climate change in the twenty-first century.

Bibliography

Benn, D. I., and Evans, D. J. A., 1997. *Glaciers and Glaciation*. London: Hodder Arnold.
Bishop, M. P., and Shroder, J. F., Jr. (eds.), 2004. *Geographic Information Science and Mountain Geomorphology*. Heidelberg: Springer Praxis Books.
Butler, D. R., Malanson, G. P., Walsh, S. J., and Fagre, D. B. (eds.), 2009. *The Changing Alpine Treeline*. Amsterdam: Elsevier.
Butler, D. R., Walsh, S. J., and Malanson, G. P. (eds.), 2003. *Mountain Geomorphology - Integrating Earth Systems*. Amsterdam: Elsevier.
Giardino, J. R., Shroder, J. F., Jr., and Vitek, J. D. (eds.), 1987. *Rock Glaciers*. Unwin Hyman: London.
Harbor, J., 2004. Foreword (geomorphology perspective). In Bishop, M. P., and Shroder, J. F., Jr. (eds.), *Geographic Information Science and Mountain Geomorphology*. Heidelberg: Springer Praxis Books, pp. xix–xxi.
Kalvoda, J., and Rosenfeld, C. L. (eds.), 1998. *Geomorphological Hazards in High Mountain Areas*. Heidelberg: Springer.
Kennedy, B. A., 2006. *Inventing the Earth*. Oxford: Blackwell.

Owens, P. N., and Slaymaker, O., 2004. *Mountain Geomorphology.* London: Hodder Arnold.
Price, L. W., 1986. *Mountains and Man*. Berkeley: University of California Press.
Slaymaker, O. (ed.), 1972. *Mountain Geomorphology: Geomorphological Processes in the Canadian Cordillera*. Tantalus Research: Vancouver.

Cross-references

Little Ice Age
Natural Hazards Associated with Glaciers and Permafrost
Periglacial
Quaternary Glaciation
Rock Glaciers

N

NATURAL HAZARDS ASSOCIATED WITH GLACIERS AND PERMAFROST

Andreas Kääb
Department of Geosciences, University of Oslo, Oslo, Norway

Introduction and definitions

Glacier and permafrost hazards are related to *glacial*, *paraglacial*, and *periglacial phenomena and processes*. Though usually defined more narrowly, we subsume here in the context of hazards any perennial land surface ice body as *glacier*. The glacial, paraglacial, and periglacial environment is defined, respectively, as the zone of glaciers or their action, the non-glacial zone directly conditioned by glaciation or deglaciation, and the non-glacial zone in cold regions with frost action being the predominant geomorphic process. Often, the periglacial zone is characterized by *permafrost* (lithospheric material with negative temperatures throughout 2 or more years). Glacier and permafrost hazards are, thus, connected to glaciers and their present or past actions, and to year-round negative ground temperatures and related processes. Hazards associated to glaciers and permafrost are best treated together in an integrative way, because the environments they origin from are often in direct contact and the relevant processes interact.

Disasters associated to the glacial, paraglacial, and periglacial environment can cause thousands of casualties in one event. Related damages or mitigation costs are on the order of several hundred million EUR as a long-term annual average global sum (Kääb et al., 2005b). Glacier and permafrost-related problems and threats include glacier- and permafrost-related floods, stable and unstable glacier length changes as well as glacier fluctuations, glacier- and permafrost-related mass movements, permafrost thaw settlement and frost heave, and threats from glacier-clad volcanoes. Often, combinations of these (and other) processes lead to the most severe glacier- and permafrost-related catastrophes. While the above direct glacier and permafrost threats are very palpable, so too are indirect threats, such as changes in dry-season river flows, adverse effects on land use, and related socioeconomic consequences.

In this contribution, the following terms are used (JTC1, 2004): *threat* is a "natural phenomenon that could lead to damage, described in terms of its geometry, mechanical and other characteristics. The threat can be an existing one (such as a creeping slope) or a potential one (such as a rockfall)." *Susceptibility* is the spatial distribution of threats (sometimes referred to as hazard disposition). *Hazard* is the "probability that a particular threat occurs within a given period of time." Threat therefore describes the process and magnitude of a dangerous event, susceptibility includes its spatial distribution, and hazard its temporal frequency. *Vulnerability* is the "degree of loss to a given element, or to a set of elements within the area affected by a hazard," or to a "set of conditions and processes resulting from physical, social, economic, and environmental factors." *Risk* is a "measure of the probability and severity of an adverse effect to life, health, property, or the environment."

In this contribution we do not treat natural threats associated with temporary land ice (seasonal ice or shorter), river, lake and sea ice, and snow (e.g., avalanches, snow melt floods).

Glacier-related floods

Generally, glacier floods represent the glacial threat with the highest potential for disaster and damages. Glacier floods occur in most glacierized mountains of the world and are triggered by the outburst of water reservoirs in, on, underneath, and at the margins of glaciers

Vijay P. Singh, Pratap Singh & Umesh K. Haritashya (eds.), *Encyclopedia of Snow, Ice and Glaciers*, DOI 10.1007/978-90-481-2642-2,

(Figures 1, 2, and 3). Most reservoir types develop slowly and can be identified at the surface, a precondition that favors the application of remote sensing techniques for monitoring glacial and periglacial lakes (Kääb et al., 2005a; Quincey et al., 2005; Kääb, 2008). Floods from ice-dammed lakes and proglacial moraine-dammed lakes, in particular, represent a recurring and severe danger. Different outburst mechanisms are involved in glacier floods.

Breaching of moraine dams

Retrogressive erosion at the outer slope of a moraine dam or collapse of parts of a moraine dam may lead to a progressively enlarging breach through which large parts or the entire moraine lake may empty (Figure 1; Haeberli, 1983; Costa and Schuster, 1988; Clague and Evans, 1994; Clague and Evans, 2000; Richardson and Reynolds, 2000; Haeberli and Burn, 2002). Trigger for such processes are usually enhanced runoff into the glacial lake (e.g., heavy snow and ice melt), impact waves (e.g., from ice, rock or snow avalanches), temporary damming/jamming at the lake outlet (e.g., lake ice jams, snow drift), or progressive groundwater flow and erosion in the moraine (piping). A moraine lake outburst may stop before the entire lake has emptied when large blocks, which are large enough to not be washed away by the flood, are eroded out of the moraine and deposited at the breach bottom so that the breach is not further incised and stabilizes. As a consequence, typical maximum breach cross-section areas can be found for some regions, depending on the lake volumes and the composition of the moraine materials.

In cold conditions, ground thermal conditions in moraines are often important to the stability of moraine-dammed lakes. Permafrost or near-permafrost conditions cause the long-term preservation of dead-ice bodies, which leave behind cavities when they melt (Haeberli, 1992a; Haeberli et al., 2001; Kääb, 2008). Occurrence of such cavities may drastically reduce the stability of a moraine dam.

Failure or overtopping of ice dams

Natural ice dams may fail mechanically, hydraulically, or be overtopped. For permanent ice dams, the disasters often repeat because the ice dam may recover after an outburst. Related outbursts stem from ice-marginal lakes, supraglacial lakes, and from temporary ice dams formed by ice avalanche deposits or glacier surges (Figure 2). A sudden mechanical breach of an ice dam causes the highest peak discharges of glacier floods (Clague and Mathews, 1973; Clarke, 1982; Walder and Costa, 1996; Tweed and Russel, 1999; Ng et al., 2007). It happens in particular when the ice dam is composed by insufficiently coherent ice

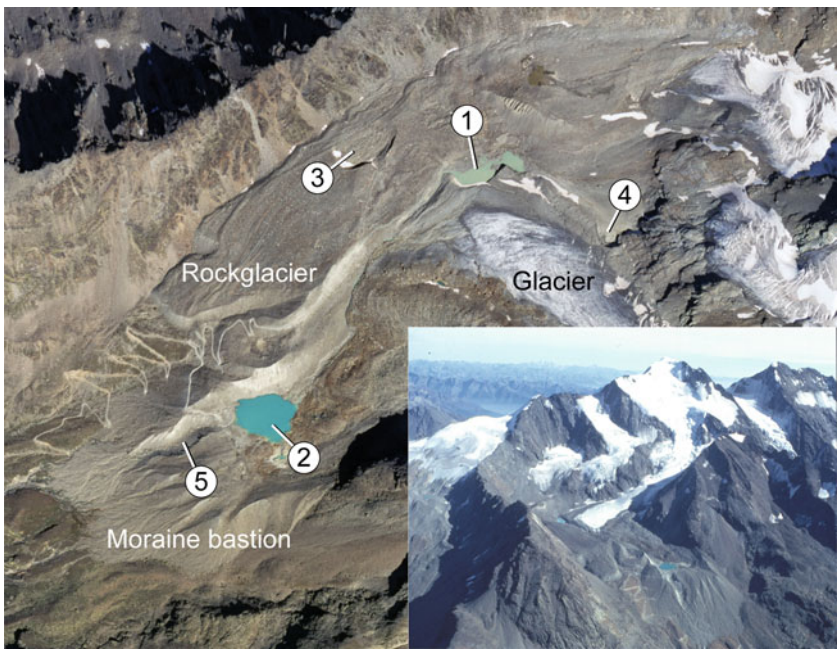

Natural Hazards Associated with Glaciers and Permafrost, Figure 1 Gruben area, Saas valley, Valais, Swiss Alps (latitude 46.172°, longitude 7.976°). Ice-dammed lake (*1*), moraine lake (*2*), former thermokarst lake (*3*), former ice-dammed lake (*4*), and moraine breach (*5*). In 1968 and 1970 the ice-dammed lake *1* burst out, presumably triggered by extraordinary water influx from the ice-dammed lake *4*. The resulting flood reached the moraine lake *2*, causing dam overtopping, erosion of the moraine dam (breach *5*), and debris flow. Mitigation measures taken after these events performed well until the mid-1990s when a newly developed thermokarst lake (*3*) had to be emptied artificially, the ice-dammed lake *1* lowered, and the outflow of the moraine lake *2* toward the breach *5* stabilized (Haeberli et al., 2001; airphoto of 1999: swisstopo).

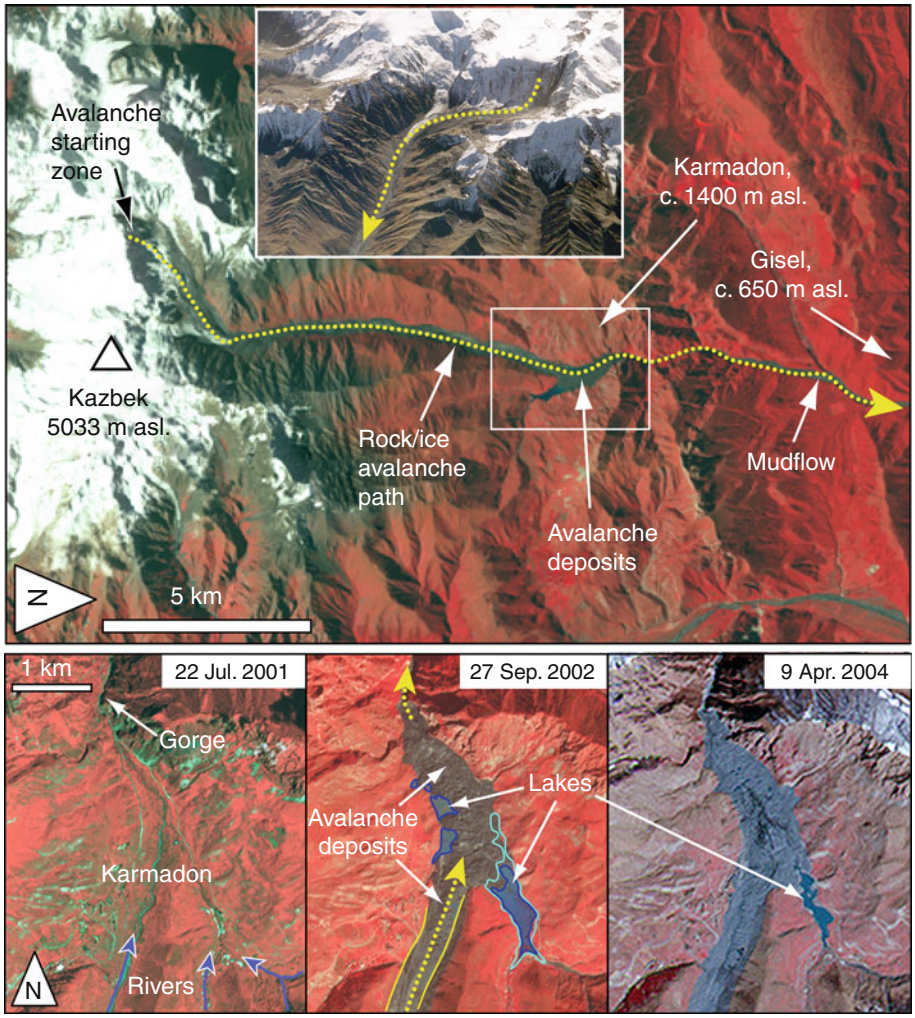

Natural Hazards Associated with Glaciers and Permafrost, Figure 2 Kolka/Karmadon area, North Ossetia, Russian Caucasus (latitude 42.84°, longitude 44.52°). On September 20, 2002, the break-off of the entire Kolka glacier, presumably triggered by repeat rock avalanches from the rock wall to its south (International Space Station image shortly after the event in the upper middle inset), caused a huge ice/rock avalanche that reached and partially destroyed the village of Karmadon 18 km downstream (overview on ASTER satellite image in upper panel; ASTER image details of Karmadon area of different times before and after the event in lower panels). A mud flow resulted immediately from the impact of the avalanche deposits at Karmadon and travelled another 15 km to the village of Gisel. The blue arrows in the lower *left* panel indicate the rivers that were dammed by the ice avalanche and formed lakes that changed size over time (*light blue* and *blue outlines* in *middle lower* panel). The *yellow dotted line* indicates the avalanche and mud flow path (Kääb et al., 2003).

fragments or highly crevassed ice, such as ice avalanche deposits or glacier ice under surge conditions.

Hydraulic failure of an ice dam happens through the (partial) floatation of the ice mass and leads to the progressive development of sub- and intraglacial channels due to the heat capacity and advection of the water bursting out (Clague and Mathews, 1973; Nye, 1976; Spring and Hutter, 1981; Clarke, 2003; Ng and Bjornsson, 2003; Roberts, 2005).

Overtopping of an ice dam happens when the level of the water reservoir rises, but the ice dam is stable enough not to burst and its density large enough to prevent floatation (e.g., through debris content or cover). Also, supraglacial permafrost conditions, that is, when the ice dam is frozen to its bed, may prevent from ice-dam floatation. The speed and magnitude of ice incision, and with that the discharge of a lake outburst through overtopping, depends much on the length and slope of the outburst channel over ice, and if supra- and intraglacial debris stabilize the channel bottom after a while.

Breaching of thermokarst and supraglacial lakes

Thermokarst and supraglacial lakes can develop on ice-rich permafrost or glacier ice, in particular stagnant ice (Figure 1; Benn et al., 2000; Reynolds, 2000; Kääb and Haeberli, 2001). Thermal convection leads to progressive

Natural Hazards Associated with Glaciers and Permafrost, Figure 3 Belvedere Glacier, Monte Rosa, Italian Alps (latitude 45.953°, longitude 7.911°). Connected to a surge-type acceleration that started in 2001, a large temporary lake developed on *top* of the Belevedere glacier posing a severe outburst threat to the villages downvalley, in particular Macugnaga. An outburst of the moraine lake to the right caused already severe damage in 1979 (Kääb et al., 2004).

lake growth. Outburst causes are similar to breaching of moraine and ice dams, and, in addition, progressive melt of the ice or permafrost dam. The development of such lakes is often slow, that is, over several years and can thus well be monitored. Permafrost thermokarst lakes are particularly common in Arctic low lands and breach regularly (Hinkel et al., 2007). But they may also develop in mountainous terrain (Figure 1; Kääb and Haeberli, 2001).

Glacier outbursts

For some cases, catastrophic water discharge from the en- or subglacial drainage systems is reported (Haeberli, 1983; Walder and Driedger, 1994, 1995; Bjornsson, 1998, 2003). Causes may be geothermal or volcanic activity, temporary en- or subglacial water storage and sudden release, or catastrophic water release connected to surge termination.

Displacement waves

Displacement waves impact on people, natural and artificial lake dams, and other installations (Tinti et al., 1999). Those displacement waves have been the trigger for a number of lake outburst events. They originate from the impact of snow-, ice-, rock-avalanches, landslides, debris flows, etc. into the lake, or from break-off and floatation of icebergs. Once such displacement waves create a tsunami they can run up the lake shores and create damage. If the waves overrun moraine or ice dams they may cause erosion at the airside slopes and eventually retrogressive dam breaching (see above sections) (Walder et al., 2003). Artificial dams are usually not designed to withstand forces from wave overtopping and might be damaged or even break.

Glacier length and volume changes

Advancing and retreating glaciers can pose a direct threat to infrastructures. From a global point of view, the prediction of glacier length variations is complicated by the fact that glaciers can vary in a continuous (stable) or unstable way (i.e., glacier surges).

Glacier surges

Glacier surges are a temporary instability of large glacier parts with ice velocity increased by an order of magnitude (or more) (Raymond, 1987; Harrison and Post, 2003). Usually, glacier surges are accompanied by drastic glacier advance. Surging glaciers are able to rapidly destroy installations or induce other threats, such as icefalls or falling rocks from supraglacial debris, for example, if they advance into steeper terrain (Haeberli et al., 2002; Kääb et al., 2004). They can temporarily dam lakes, which, when these dams fail, produce some of the largest known outburst floods (Bruce et al., 1987). Due to the crevassing and low cohesion of ice sections and ice debris within a surging glacier, there is a high probability that such temporary dams fail through sudden mechanical burst leading to particularly high flood peak discharges. Often, glacier surges are accompanied by enhanced englacial water storage, which is possibly released at the surge end in a catastrophic way (Figure 3).

Stable glacier advance and retreat

Advancing glaciers may inundate land, override installations (e.g., hydropower installations), dam rivers and form lakes, cause ice break-offs when the glacier advances over a cliff, etc. (Tufnell, 1984; Grove, 1987; Mayo, 1988; Yamada and Sharma, 1993). Glacier retreat forms usually no direct threat but is able to trigger a number of secondary threats such as various slope instabilities and ice avalanches (see below). Causes for such stable glacier length changes are changes in mass balance and/or in ice dynamics.

Changes in glacier runoff and seasonality

Glacier mass loss leads to reduction of water resources as stored in glaciers and to changes in dry-season river flows. The short-term perspective is increasing discharge due to enhanced melt; the long-term perspective is decreasing discharge when the glaciers in a basin become substantially smaller or disappear. These processes have consequences for drinking water supply, irrigation, hydropower production, industrial water use, fishery, water quality, etc. Arid and semiarid regions like parts of the Andes or Central Asia are particularly vulnerable to reduction of dry-season river flows (Wagnon et al., 1999; Francou and Coudrain, 2005).

Glacial and paraglacial mass movements

Compared to the distances covered by glacier floods, ice and rock avalanches often affect much smaller areas. Corresponding disasters are generally restricted to densely populated high-mountain regions. However, in combination with other processes, ice and rock avalanches have the potential for far-reaching disasters. In zones with high seismic activity and geothermal heat flow, the probability of major ice break-offs is greatly increased, as was demonstrated dramatically by one of the most destructive glacier catastrophes, the Huascarán disaster in 1970, with a loss of over 18,000 lives. Also, the extraordinary September 20, 2002, rock/ice avalanche at Kolka/Karmadon (Caucasus), a combination of rock and ice destabilization killing over 100 people, drastically underlines the devastating potential of ice/rock avalanches (Figure 2). A widespread hazard in high mountains is related to accumulations of loose sediments on steep slopes, which represent potential sources of debris flows. Such debris accumulations can occur in the form of moraines, moraine dams, or steep valley flanks uncovered by retreating glaciers.

Ice fall and ice avalanches

Steep glaciers (or glacier parts) are a common source of ice break-offs and subsequent ice avalanches (Alean, 1985; Margreth and Funk, 1999; Pralong and Funk, 2006). Ice break-offs are a usual form of ablation for steep glaciers, in particular at high elevations where melt ablation is not sufficient to keep a glacier in balance. In general, a discrimination between glaciers in cliff and ramp situations is useful. The break-off volumes from glaciers that flow from a flat part over a steep cliff are usually restricted to individual ice lamellas. Glaciers that lie on a steep ramp exist in such situations usually only because their entire bed or at least their frontal parts are frozen to the rock (i.e., permafrost conditions). For such ramp-type glaciers the break-off volumes can be larger or even include the entire glacier. The thermal conditions of the glacier front are crucial for the stability of ramp-type glaciers. Changes of these conditions, for instance through atmospheric warming, can therefore drastically alter stability conditions.

In rare cases also the detachment of complete flat glaciers seems possible (See for instance the 2002 Kolka/Karmadon event; Haeberli et al., 2005; Figure 2). Ice avalanches are particularly dangerous in winter with reduced basal friction, extended runout, and mass gain from snow. Glacier parts can also fail due to a failure of the underlying rock (e.g., the 1970 Huascaran event). Ice avalanches can be triggered by earthquakes. Ice avalanches itself can trigger lake outbursts, dam rivers, or transform into mud/debris flows.

Rock fall and rock avalanches

Glacier retreat uncovers and debuttresses rock flanks. The related change in thermal, hydrologic, hydraulic, and mechanic conditions can lead to rock fall and rock avalanches (fast mass movement) (Plafker and Erikson, 1978; Evans and Clague, 1988; Haeberli et al., 1997; Barla et al., 2000; Deline, 2001; Giani et al., 2001; Huggel et al., 2008). Rock avalanches can carry parts of overlaying glaciers. Rock avalanches can be of increased magnitude in glacial environments. The runout of such avalanches is extended on glaciers due the reduced friction on ice compared to other surface types. In addition, the rock mass may be combined with ice that was additionally released during the break-off (detachment of glacier parts overlying the failing rock mass), or entrained on the avalanche path (e.g., rip-off of crevasses). Such entrainment increases the volume of the avalanche and leads to partial liquefaction of the included ice through impact and friction energy (Evans and Clague, 1988; van der Woerd et al., 2004; Haeberli et al., 2005). Through processes not yet fully understood the slope angle of such combined rock-ice can be surprisingly low (Figure 2). Rock avalanches can be triggered by earthquakes.

Landslides and rock slides

Among other causes, glacier retreat or slope undercutting by floods uncovers and debuttresses rock and debris flanks. The related change in hydrologic, hydraulic, and mechanic conditions can lead to mass movements (slow mass movement) (Figure 4; Ballantyne, 2002; Holm et al., 2004; Kääb, 2005). These can create secondary hazards such as river dams, potentially causing outbursts and floods when these dams fail.

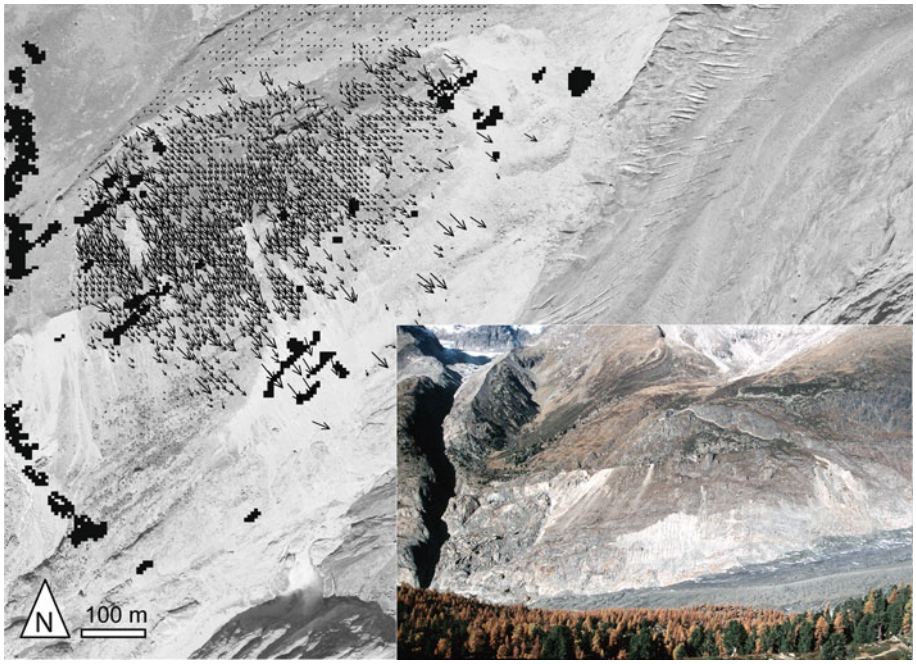

Natural Hazards Associated with Glaciers and Permafrost, Figure 4 Tongue of Aletsch Glacier, Swiss Alps (latitude 46.403°, longitude 8.027°). Glacier retreat and thickness loss of up to 300 m since the Little Ice Age caused debutressing and subsequent destabilization (rock sliding) of parts of the valley flanks. The main panel shows photogrammetrically derived surface displacements on the order of 10 cm a^{-1} superimposed on an aerial orthophoto. The inset is a view on the instable valley flank from the opposite side of the glacier (Kääb, 2005; airphoto of 2006: swisstopo).

Debris flows

Glacier retreat leaves behind unprotected and unconsolidated moraine material that is particularly prone to enhanced erosion and debris flows (Zimmermann and Haeberli, 1992; Rickenmann and Zimmermann, 1993; Chiarle et al., 2007). Furthermore, glacier and permafrost floods are often accompanied by debris flows when erodible material is available in steep parts of the flood path.

Interaction between volcanic activity and glaciers

Interactions between volcanic activity and glaciers are potentially among the most devastating disasters with glacier involvement (Brugmann and Post, 1981; Pierson et al., 1990; Thouret, 1990; Aguilera et al., 2004; Julio Miranda et al., 2005; Julio-Miranda et al., 2008). Enhanced geothermal activity, geometric and mechanic changes, deposition of hot eruptive materials, or albedo change by volcanic ash can lead to drastic melt of ice or ice break-off on ice-clad volcanoes and to volcanic landslides or lahars. Ash layers thicker than some millimeters or centimeters insulate the underlying ice.

Permafrost-related problems and hazards

Permafrost influences the stability and hydrology of debris and rock slopes. While the trigger mechanisms of frequently unexpected debris flows and rock avalanches from permafrost zones often remain unclear (melting dead ice, permafrost-hydrology interactions, etc.) and are therefore difficult to predict in individual cases, the respective hazard potential seems to be connected to the presence of permafrost and its changes. Changes in the thermal regime of cold rock walls and related effects on rock stability are still poorly understood processes but are of increasing concern in view of some recent catastrophes.

Adverse effects of permafrost creep

Permafrost creep, exemplified by the creep of rockglaciers, may have adverse effects such as inundation of land, destabilization of construction, and rockfall from the rockglacier front. Permafrost creep can transport debris into locations from which debris flows or landslides originate (Figure 5; Burger et al., 1999; Kääb and Reichmuth, 2005; Kääb et al., 2007).

Thaw settlement and frost heave

Changes in ground ice content from ice-lense accumulation or thermokarst processes may result in changes in permafrost surface geometry. Such changes can affect constructions or trigger the development of thermokarst lakes (Nelson et al., 2001, 2002). Thaw and frost heave processes may also be caused by constructions, for instance, when they change the local snow cover regime or through basement heating.

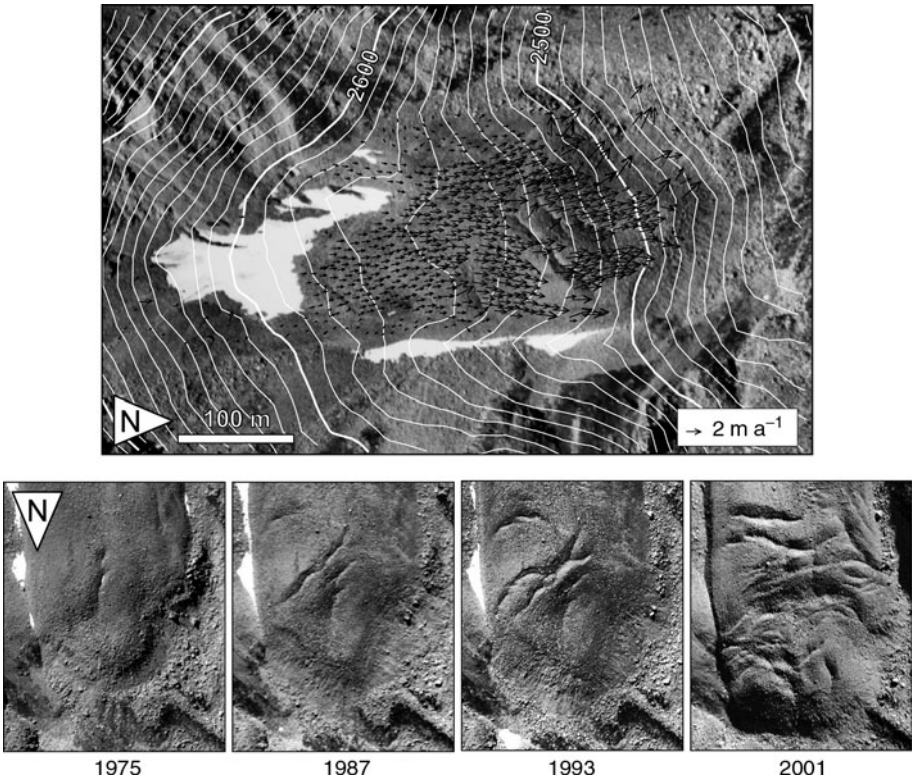

Natural Hazards Associated with Glaciers and Permafrost, Figure 5 Destabilizing rockglacier, Turtmann valley, Swiss Alps (latitude 46.202°, longitude 7.723°). *Upper* panel: photogrammetrically derived surface velocities on the rockglacier. *Lower* panel: series of airphotos showing the decay of the rockglacier tongue causing rock fall and landslide hazards (Kääb et al., 2007; airphotos: swisstopo and university of Bonn; processing I. Roer).

Debris flows from permafrost

Permafrost thaw changes the mechanical and hydrological conditions in frozen material. While frozen debris can reach very steep slope angles through the strong cohesion by its ice content, thawing debris has to adjust to much lower friction angles. In addition, the water content of such thawing ice-containing materials is comparably high. As a consequence the hazard from periglacial debris flows may increase (Haeberli, 1992b, a; Zimmermann and Haeberli, 1992; Kneisel et al., 2007). Temporary runoff concentration and ground saturation is, thereby, often involved as trigger.

Destabilization of frozen debris slopes

In rare cases entire sections of rockglaciers or frozen debris slopes might destabilize (Figure 5; Kääb et al., 2007). Reasons for such processes are largely unknown (dynamics, ground warming?). Such destabilization can lead to rock fall, debris flows, inundation of land, and destruction of infrastructure.

Rockfall and rock avalanches from frozen rock faces

The thermal regime and ground ice in frozen rock faces have complex thermal, mechanical, hydraulic, and hydrological effects on rock stability (Figure 2; Haeberli et al., 1997; Wegmann et al., 1998; Fischer et al., 2006; Noetzli et al., 2006).

Runoff concentration at the permafrost table

There are cases reported where runoff concentration at the permafrost table has triggered debris flows and other mass movements.

Active layer detachments, thaw slumps, and permafrost-related landslides

In areas of continuous permafrost or large patches of discontinuous permafrost even small disturbances or changes in the active layer, for instance by river bank erosion, may trigger, often progressive, active layer detachments, thaw slumps, or landslides (Burn, 2000; Lantuit and Pollard, 2005; Lewkowicz and Harris, 2005a, b; Lyle and Hutchinson, 2006; Wei et al., 2006).

Erosion of frozen river banks, lake shores, and sea coasts

Frozen river banks, lake shores, and sea costs are vulnerable to thermally driven and mechanical erosion. Thereby both atmospheric heat and heat advection from the water may lead to fast and large-scale erosion and retreat of the

coast line that endangers coastal settlements and installations (Johnson et al., 2003; Mars and Houseknecht, 2007).

Hazard interactions and integral assessment

The glacier- and permafrost-related processes listed above represent relevant hazard potentials on an individual basis. However, combinations and interactions between these or other hazard types are of similar or even greater importance. In fact, many of the largest known glacier catastrophes are characterized by threat combinations and/or process chains. The assessment of glacier and permafrost hazards requires, therefore, systematic and integrative approaches. Concentration on just one obvious threatening process may easily lead to misjudgment of a situation and its full consequences.

Climate change, human activities, and related shifts of hazard zones

Mountain and polar regions are particularly sensitive to climate change. Changes in glaciers, snow and permafrost, and corresponding impacts on natural threats are among the most directly visible signals of global warming and may seriously affect human activities (Haeberli and Beniston, 1998; Haeberli and Burn, 2002; Kääb et al., 2005b). For example, in the Himalayas in Nepal and Bhutan, glacier lake outburst floods occurred at a frequency of roughly one flood per decade in the 1950s; this rate has since increased to one flood every 3 years in the 1990s and it is anticipated that event frequency could further increase (Richardson and Reynolds, 2000). It is predicted that both the number and size of glacial lakes will increase as climate changes and atmospheric warming causes through negative glacier mass balances most glaciers worldwide to retreat and possibly leave behind glacier lakes.

Coupled with increasing rural development and investments in infrastructure, particularly in hydropower, the vulnerability of mountain communities to outburst floods is growing rapidly. Furthermore, for those rivers fed largely by ice melt, reduction in glacier volumes will have a particularly strong impact on dry-season river flows, and on the provision of downstream water for hydropower, irrigation, and potable water supplies. In some regions, most noticeably in Pakistan, climate change will increase environmental, economic, and social vulnerability for tens of millions of people. While catastrophic floods (too much water too quickly) are a very palpable hazard, so too are "soft" threats, such as reduced glacier water during the dry season. Consequently, threats in high mountains must be considered in relation to water resource management and cannot be seen in isolation. As an example, in Peru, hazards associated with high altitude glacial lakes are being mitigated, using methods that control the lake water volume and ensure safe water reservoirs.

Marked changes in glacier extent due to climate change may be accompanied by both the formation and disappearance of ice- and moraine-dammed lakes, and steep hanging glaciers may become less stable. On the other hand, steep glacier tongues with their present-day potential for large ice avalanches could disappear. Revegetation of deglaciated terrain is slow and leaves morainic deposits unprotected against erosion over extensive time periods of several decades and more. On steep slopes, freshly exposed or thawing non-consolidated sediments can become unstable, resulting in debris flows and landslides of varying magnitudes. Once one event has occurred in a particular valley, the remaining slopes may become destabilized even further. In places of pronounced glacier retreat, changes in stress distribution and surface conditions of rock walls in deeply cut glacier troughs could induce large mass instabilities. The general tendency is thus toward a shifting of hazard zones with considerable changes in the processes involved and a widespread decrease in the stability of slopes. Special measures are needed to ensure the structural stability and durability of installations for tourism, transportation, and telecommunication in permafrost areas. Similarly, detailed hazard assessments must be undertaken routinely and regularly to avoid damage to hydropower installations due to the impact of glacier-derived floods, which can cost many tens of millions of Euros. With the evolvement of environmental conditions in high-mountain and polar regions beyond the range of historical variability, hazard assessments become increasingly difficult because estimates of hazard potential based on empirical data from the past (historical documents, statistics, geomorphological evidence) will not be directly applicable under new conditions.

Hazard assessment

Historical data on glacier and permafrost hazards can be used to test spatial models based on new earth-observation and geo-informatics techniques. Such modern methodologies provide powerful tools to assist hazard assessments in complex mountain or polar systems, which are experiencing increasing change and divergence from equilibrium conditions.

The assessment of glacier and permafrost hazards requires systematic and integrative approaches. Presently, the most successful strategy is based on the combination of remote sensing, modelling with geographical information systems (GIS), geophysical soundings, and other local field surveys. These methods are best structured in a downscaling approach from area-wide first-order assessments for systematically detecting hazard potentials (i.e., the domain of space-borne remote sensing and GIS techniques) to detailed ground-based or air-borne local investigations in high-risk areas (i.e., the domain of geophysics, surveying, and air-borne and close-range remote sensing).

The application of earth-observation techniques is particularly important for a number of reasons:

- Typically, related threat source areas are situated in remote regions, often difficult to access physically for topographic, political, and/or security reasons.

- The remote location of most threat sources, the potential process interactions and chain reactions, and the far reach of some of the threats require remote sensing sensors capable to cover large areas at once.
- Climate change induces disturbance in glacier and permafrost equilibrium and can shift hazard zones beyond historical knowledge. In addition, human settlements and activities increasingly extend toward endangered zones in many regions. As a result, historical data alone are not sufficient any more for hazard assessments and have to be combined with new observation and modelling approaches (see above).
- Due to the current rapid change of high-mountain environments, hazard assessments shall be undertaken routinely and regularly, combined with continuous monitoring. Remote sensing is particularly suited for both regular and rapid observation.

Air- and space-borne optical and microwave data can be applied to automatically classify glaciers, lakes, debris, and other terrain types relevant to glacier and permafrost hazards (Kääb et al., 2005a; Quincey et al., 2005; Kääb, 2008). Furthermore, some of this data can be used to derive digital terrain models (DTM), an invaluable prerequisite for analyzing hazard potential in high mountains and for related GIS-modelling. Even ice flow and terrain displacements can be measured with high accuracy from repeated remote sensing data. With these methods, the terrain cover, geometry, and dynamics of an area can be fully investigated without direct access. This can be especially beneficial in areas where the potential sources of glacial hazards lie in geopolitically unstable regions (e.g., Kashmir, Afghanistan) but where the principal impact zones lie significantly downstream. Remote sensing can also be of great use in assessing glacial hazards across international borders where glaciers in an inaccessible part of a country extend their impact into a neighboring country (e.g., China into Bhutan, India, and Nepal).

A further step toward an integrative hazard assessment consists in the application of GIS and other numerical models for simulating processes that are too complex or undetectable by remote monitoring. Glacier lake outburst floods, ice avalanches, or debris flows can be modelled with a GIS. Also, permafrost distribution, approximate ground-, firn-, and ice-temperatures, or various other terrain parameters that have an impact on natural hazards can be computed. Especially the fusion of remote sensing results with numerical process models provides a promising base for the assessment of hazard potentials.

A more detailed analysis of the hazard sources detected by remote sensing often involves ground-based methods. Geophysical investigations, employing electrical resistivity tomography and ground penetrating radar, in particular, have been used to develop three-dimensional maps of geological structures and have provided information on instability zones such as buried ice bodies within moraine dams, which could lead to breaches in the dam if the ice were to melt. Furthermore, the use of geophysical methods can provide information about the prevalent physical processes behind glacial and periglacial hazards and can lead to a better understanding of the behavior of natural dams and their potential to fail. Terrestrial surveying, using laser ranging or global positioning systems (GPS), is needed for accurate mapping and detection of terrain dynamics with high spatial and temporal resolution.

While many glacial and periglacial hazards may develop into major potential threats, if left unchecked, there are many examples in the Alps, in Nepal, Bhutan, and especially Peru, where lakes with high hazard potential have been remediated very successfully. The remote monitoring of changes in glacial lakes is crucial in order to help prioritize which lakes should be remediated first and when it would be most expedient.

Mitigation

Once a threatening situation is recognized and assessed, it might be necessary to undertake mitigation measures. Such measures can be *active* or *passive*, and *temporary* or *permanent.*

Typical *temporary passive* mitigation measures are to control and limit access to the endangered area, closing down infrastructure that brings people to critical areas, or to temporarily evacuate population living or staying in such areas. Typical *permanent passive* measures are land planning and hazard zoning that lead to, for instance, a permanent prohibition of building construction or access. The application and success of such passive measures depends a lot on specific regional socioeconomic factors, such as the civil protection, political, police, and legal system, culture, religion, economic dependencies, etc., that have to be taken into account when developing such measures.

Passive measures can be much less described in general terms but are rather very specific to the process and threat type. In general measures can be undertaken at the threat source and in the runout zone.

Ice fall and avalanches. In case of ice fall and avalanches, explosives might be used at the steep glacier for controlled triggering of impending events. In the runout zones deflection or retention dams can prevent an avalanche reaching critical zones. In case a potential ice avalanche would reach a river it might be useful to situate the river within the critical zone in a tunnel or tube in order to prevent the ice debris to dam up the river and cause a flood threat. In case a potential ice avalanche would reach an artificial or natural lake, where displacement waves could overtop the dam and cause an outburst, it might be necessary to temporarily or permanently increase the freeboard by lowering the lake level or heighten the dam, or to secure the dam in order to prevent erosion in case of dam overtopping (see below for lakes).

Glacial and periglacial lakes. The major goal at dangerous temporary or permanent glacial and periglacial lakes is to lower the lake level and reduce the lake volume.

This can be achieved by pumping or siphons. These measures are effective only for a limited time and are thus mainly used as rapid response or in order to prepare construction of more permanent measures. Such more permanent measures can be open channels and spillways, or tubes and tunnels either through the lake dam itself or through the surrounding bedrock or debris. Additionally, and possibly in combination with the above measures, parts of the lake can be filled up by debris and thus its volume reduced. Glacial and periglacial environments are very prone to, sometimes fast, changes such as lake changes or dam settlement. It is therefore crucial to integratively monitor the site, regularly control the functioning of the constructions, and possibly adapt the measures to environmental changes (Haeberli et al., 2001).

Lake outbursts in a glacial and periglacial environment often lead to debris flows due to the large amounts of erodible material available. Active permanent measures in the runout zone of a potential lake outburst can be deflection or retention dams. Channel constructions may prevent or reduce the bed erosion and debris uptake by the flood, or the flooding and inundation of surrounding terrain. Sediment traps can separate parts of the water and debris content of the debris flow. Reduction of the water content of a debris flows is an established measure to bring it to a stop.

Glacier advance. Few possibilities exist to mitigate threats related to a glacier advance. Endangered installations might be moved or changed, for instance converted from surface to subsurface type. The latter measures are, for example, applied in case of water intakes for hydropower purposes. In case a glacier advance increases the ice avalanche disposition or creates a dangerous lake, the above-listed measures can be necessary.

Periglacial debris flows. Few possibilities exist to remediate potential starting zones of periglacial debris flows, possibly influencing the ground thermal or hydrological regime. In the runout zone measures as listed above for debris flows from glacial lake outbursts are applied.

Rock fall/rock avalanches. Steel nets on parts of a rock face can prevent rock falls to break off. Explosives can be used to trigger rock avalanches of limited volume in a controlled way. The adverse effects of rock avalanches or combined ice-rock avalanches of limited size can be reduced by deflection or retention dams, and steel nets or barriers.

Summary and outlook

Threats related to glacier and permafrost are usually characterized by the involvement of surface or subsurface ice. As such they are highly sensitive to climatic changes and other changes in boundary conditions. Environmental changes can thus rapidly change hazard conditions. Furthermore, glacier and permafrost disasters are often characterized by complex and sometimes far-reaching process combinations and chain reactions. These can be particularly difficult to assess. These special challenges for the detection and management of glacier and permafrost threats require systematic and frequent observation and modelling work.

The expertise about handling of glacier and permafrost threats is worldwide highly scattered, among others due to the temporally and spatially highly scattered occurrence of the related disasters. An improved common understanding of such threats among involved scientists, civil protection agencies, and engineers should thus be a major aim of coordinated activities – on local, national, and international levels. Particularly little developed is the account for socioeconomic and cultural aspects of glacier and permafrost threats and their management.

Bibliography

Aguilera, E., Pareschi, M. T., Rosi, M., and Zanchetta, G., 2004. Risk from Lahars in the northern valleys of Cotopaxi Volcano (Ecuador). *Natural Hazards*, **33**(2), 161–189.

Alean, J., 1985. Ice avalanche activity and mass balance of high-altitude hanging glaciers in the Swiss Alps. *Annals of Glaciology*, **6**, 248–249.

Ballantyne, C. K., 2002. Paraglacial geomorphology. *Quaternary Science Reviews*, **21**, 1935–2017.

Barla, G., Dutto, F., and Mortara, G., 2000. Brenva glacier rock avalanche of January 18, 1997 on the Mont Blanc range, NW Italy. *Landslide News*, **13**, 2–5.

Benn, D. I., Wiseman, S., and Warren, C. R., 2000. Rapid growth of a supraglacial lake, Ngozumpa glacier, Khumbu Himal, Nepal. In Nakawo, M., Raymond, C. F., and Fountain, A. (eds.), *Debris-Covered Glaciers*. Wallingford: IAHS Publications No. 264, pp. 177–185.

Bjornsson, H., 1998. Hydrological characteristics of the drainage system beneath a surging glacier. *Nature*, **395**(6704), 771–774.

Bjornsson, H., 2003. Subglacial lakes and jokulhlaups in Iceland. *Global and Planetary Change*, **35**(3–4), 255–271.

Bruce, R., Cabera, G. A., Leiva, J. C., and Lenzano, L. E., 1987. The 1985 surge and ice dam of Glaciar Grande del Nevado del Plomo, Argentina. *Journal of Glaciology*, **33**(113), 131–132.

Brugmann, M. M., and Post, A., 1981. *Effects of Volcanism on the Glaciers of Mount St. Helens*. Reston: US Geological Survey Circular. 850-D. p. 11.

Burger, K. C., Degenhardt, J. J., and Giardino, J. R., 1999. Engineering geomorphology of rock glaciers. *Geomorphology*, **31** (1–4), 93–132.

Burn, C. R., 2000. The thermal regime of a retrogressive thaw slump near Mayo, Yukon territory. *Canadian Journal of Earth Sciences*, **37**(7), 967–981.

Chiarle, M., Iannotti, S., Mortara, G., and Deline, P., 2007. Recent debris flow occurrences associated with glaciers in the Alps. *Global and Planetary Change*, **56**(1–2), 123–136.

Clague, J. J., and Evans, S. G., 1994. *Formation and Failure of Natural Dams in the Canadian Cordillera*. Ottawa: Geological Survey of Canada, Bulletin, p. 464.

Clague, J. J., and Evans, S. C., 2000. A review of catastrophic drainage of moraine-dammed lakes in British Columbia. *Quaternary Science Reviews*, **19**(17–18), 1763–1783.

Clague, J. J., and Mathews, W. H., 1973. The magnitude of jökulhlaups. *Journal of Glaciology*, **33**(113), 501–504.

Clarke, G. K. C., 1982. Glacier outburst floods from "Hazard Lake," Yukon territory, and the problem of flood magnitude prediction. *Journal of Glaciology*, **28**(98), 3–21.

Clarke, G. K. C., 2003. Hydraulics of subglacial outburst floods: new insights from the Spring-Hutter formulation. *Journal of Glaciology*, **49**(165), 299–313.

Costa, J. E., and Schuster, R. L., 1988. The formation and failure of natural dams. *Geological Society of America Bulletin*, **100**, 1054–1068.

Deline, P., 2001. Recent Brenva rock avalanches (Valley of Aosta): new chapter in an old story? *Supplementi di Geografia Fisica e Dinamica Quaternaria*, **5**, 55–63.

Evans, S. G., and Clague, J. J., 1988. Catastrophic rock avalanches in glacial environment., In Bonnard, C. (ed.), *Proceedings of the Fifth International Symposium on Landslide*, Balkema, Vol. 2, pp. 1153–1158.

Fischer, L., Kääb, A., Huggel, C., and Noetzli, J., 2006. Geology, glacier retreat and permafrost degradation as controlling factors of slope instabilities in a high-mountain rock wall: the Monte Rosa east face. *Natural Hazards and Earth System Sciences*, **6**(5), 761–772.

Francou, B., and Coudrain, A., 2005. Glacier shrinkage and water resources in the Andes. *EOS. Transactions of the American Geophysical Union*, **86**(43), 415.

Giani, G. P., Silvano, S., and Zanon, G., 2001. Avalanche of January 18, 1997 on Brenva glacier, Mont Blanc Group, western Italian Alps: an unusual process of formation. *Annals of Glaciology*, **32**, 333–338.

Grove, J. M., 1987. Glacier fluctuations and hazards. *Geographical Journal*, **153**, 351–369.

Haeberli, W., 1983. Frequency and characteristics of glacier floods in the Swiss Alps. *Annals of Glaciology*, **4**, 85–90.

Haeberli, W., 1992a. Construction, environmental problems and natural hazards in periglacial mountain belts. *Permafrost and Periglacial Processes*, **3**(2), 111–124.

Haeberli, W., 1992b. Possible effects of climatic change on the evolution of Alpine permafrost. In Boer, M., and Koster, E. (eds.), *Greenhouse-Impact on Cold-Climate Ecosystems and Landscapes: Selected Papers of the European Conference on Landscape Ecological Impact of Climate Change, Lunteren, the Netherlands, December 3–7, 1989*. Cremlingen-Destedt: Catena. Catena Supplement, pp. 23–35.

Haeberli, W., and Beniston, M., 1998. Climate change and its impacts on glaciers and permafrost in the Alps. *Ambio*, **27**(4), 258–265.

Haeberli, W., and Burn, C. R., 2002. Natural hazards in forests: glacier and permafrost effects as related to climate change. In Sidle, R. C. (ed.), *Environmental Change and Geomorphic Hazards in Forests*. Wallingford/New York: CABI. IUFRO Research Series, pp. 167–202.

Haeberli, W., Wegmann, M., and Vonder Mühll, D., 1997. Slope stability problems related to glacier shrinkage and permafrost degradation in the Alps. *Eclogae Geologicae Helvetiae*, **90**, 407–414.

Haeberli, W., Kääb, A., Vonder Mühll, D., and Teysseire, P., 2001. Prevention of debris flows from outbursts of periglacial lakes at Gruben, Valais, Swiss Alps. *Journal of Glaciology*, **47**(156), 111–122.

Haeberli, W., Kääb, A., Paul, F., Chiarle, M., Mortara, G., Mazza, A., and Richardson, S., 2002. A surge-type movement at Ghiacciaio del Belvedere and a developing slope instability in the east face of Monte Rosa, Macugnaga, Italian Alps. *Norwegian Journal of Geography*, **56**(2), 104–111.

Haeberli, W., Huggel, C., Kääb, A., Oswald, S., Polvoj, A., Zotikov, I., and Osokin, N., 2005. The Kolka-Karmadon rock/ice slide of September 29, 2002 – an extraordinary event of historical dimensions in North Ossetia (Russian Caucasus). *Journal of Glaciology*, **47**(156), 111–122.

Harrison, W. D., and Post, A. S., 2003. How much do we really know about glacier surging? *Annals of Glaciology*, **36**, 1–6.

Hinkel, K. M., Jones, B. M., Eisner, W. R., Cuomo, C. J., Beck, R. A., and Frohn, R., 2007: Methods to assess natural and anthropogenic thaw lake drainage on the western Arctic coastal plain of northern Alaska. *Journal of Geophysical Research-Earth Surface,***112**(2), F02S16. doi:10.1029/2006JF000584.

Holm, K., Bovis, M., and Jakob, M., 2004. The landslide response of alpine basins to post-Little Ice Age glacial thinning and retreat in southwestern British Columbia. *Geomorphology*, **57**(3–4), 201–216.

Huggel, C., Wessels, R., and Caplan-Auerbach, J., 2008. Recent extreme avalanches: triggered by climate change? *EOS. Transactions of the American Geophysical Union*, **89**(47), 469–470.

Johnson, K., Solomon, S., Berry, D., and Graham, P., 2003. Erosion progression and adaptation strategy in a northern coastal community. In Phillips, Springman, and Arenson (eds.), *Proceedings of the Eighth International Conference on Permafrost*. Lisse: Swets and Zeitlinger, Vol. 1, pp. 489–494.

JTC1, 2004 ISSMGE, ISRM and IAEG Joint Technical Committee on Landslides and Engineered Slopes (JTC1): ISSMGE TC32 – Technical Committee on Risk Assessment and Management. Glossary of Risk Assessment Terms – Version 1, July 2004

Julio Miranda, P., Gonzales-Huesca, A. E., Delgado Granados, H., and Kääb, A., 2005. Glacier melting and lahar formation during January 22, 2001 eruption, Popocatépetl volcano (Mexico). *Zeitschrift für Geomorphologie*, **N.F. Suppl.140**, 93–102.

Julio-Miranda, P., Delgado-Granados, H., Huggel, C., and Kaab, A., 2008. Impact of the eruptive activity on glacier evolution at Popocatepetl Volcano (Mexico) during 1994–2004. *Journal of Volcanology and Geothermal Research*, **170**(1–2), 86–98.

Kääb, A., 2005. *Remote Sensing of Mountain Glaciers and Permafrost Creep*. Zurich: University of Zurich. Schriftenreihe Physische Geographie. Glaziologie und Geomorphodynamik, Vol. 48.

Kääb, A., 2008. Remote sensing of permafrost-related problems and hazards. *Permafrost and Periglacial Processes*, **19**(2), 107–136.

Kääb, A., and Haeberli, W., 2001. Evolution of a high-mountain thermokarst lake in the Swiss Alps. *Arctic, Antarctic, and Alpine Research*, **33**(4), 385–390.

Kääb, A., and Reichmuth, T., 2005. Advance mechanisms of rockglaciers. *Permafrost and Periglacial Processes*, **16**(2), 187–193.

Kääb, A., Wessels, R., Haeberli, W., Huggel, C., Kargel, J. S., and Khalsa, S. J. S., 2003. Rapid ASTER imaging facilitates timely assessment of glacier hazards and disasters. *EOS. Transactions of the American Geophysical Union*, **84**(13), 117, 121.

Kääb, A., Huggel, C., Barbero, S., Chiarle, M., Cordola, M., Epifani, F., Haeberli, W., Mortara, G., Semino, P., Tamburini, A., and Viazzo, G., 2004. Glacier hazards at Belvedere glacier and the Monte Rosa east face, Italian Alps: processes and mitigation. Internationales Symposium Interpraevent 2004, Riva/Trient, pp. 67–78.

Kääb, A., Huggel, C., Fischer, L., Guex, S., Paul, F., Roer, I., Salzmann, N., Schlaefli, S., Schmutz, K., Schneider, D., Strozzi, T., and Weidmann, W., 2005a. Remote sensing of glacier- and permafrost-related hazards in high mountains: an overview. *Natural Hazards and Earth System Sciences*, **5**, 527–554.

Kääb, A., Reynolds, J. M., and Haeberli, W., 2005b. Glacier and permafrost hazards in high mountains. In Huber, U. M., Bugmann, H. K. M., and Reasoner, M. A. (eds.), *Global Change and Mountain Regions (A State of Knowledge Overview). Advances in Global Change Research*. Dordrecht: Springer, pp. 225–234.

Kääb, A., Frauenfelder, R., and Roer, I., 2007. On the response of rockglacier creep to surface temperature increase. *Global and Planetary Change*, **56**(1–2), 172–187.

Kneisel, C., Rothenbuhler, C., Keller, F., and Haeberli, W., 2007. Hazard assessment of potential periglacial debris flows based

on GIS-based spatial modelling and geophysical field surveys: a case study in the Swiss Alps. *Permafrost and Periglacial Processes*, **18**(3), 259–268.

Lantuit, H., and Pollard, W. H., 2005. Temporal stereophotogrammetric analysis of retrogressive thaw slumps on Herschel Island, Yukon territory. *Natural Hazards and Earth System Sciences*, **5**(3), 413–423.

Lewkowicz, A. G., and Harris, C., 2005a. Morphology and geotechnique of active-layer detachment failures in discontinuous and continuous permafrost, northern Canada. *Geomorphology*, **69**(1–4), 275–297.

Lewkowicz, A. G., and Harris, C., 2005b. Frequency and magnitude of active-layer detachment failures in discontinuous and continuous permafrost, northern Canada. *Permafrost and Periglacial Processes*, **16**(1), 115–130.

Lyle, R. and Hutchinson, D. J., 2006. Influence of degrading permafrost on landslide processes: Little Salmon Lake, Yukon Territory, Canada. ECI Conference on Geohazards. Paper 4.

Margreth, S., and Funk, M., 1999. Hazard mapping for ice and combined snow/ice avalanches – two case studies from the Swiss and Italian Alps. *Cold Regions Science and Technology*, **30**(1–3), 159–173.

Mars, J. C., and Houseknecht, D. W., 2007. Quantitative remote sensing study indicates doubling of coastal erosion rate in past 50 year along a segment of the Arctic coast of Alaska. *Geology*, **35**(7), 583–586.

Mayo, L. R., 1988. Advance of Hubbard glacier and closure of Russel Fjord, Alaska – environmental effects and hazards in the Yakutat area. In Galloway, J. P., and Hamilton, T. D. (eds.), *Geological Studies in Alaska by the U.S. Geological Survey During 1987*. Washington: US GPO. US Geological Survey Circular, pp. 4–16.

Nelson, F. E., Anisimov, O. A., and Shiklomanov, N. I., 2001. Subsidence risk from thawing permafrost – the threat to man-made structures across regions in the far north can be monitored. *Nature*, **410**(6831), 889–890.

Nelson, F. E., Anisimov, O. A., and Shiklomanov, N. I., 2002. Climate change and hazard zonation in the circum-Arctic permafrost regions. *Natural Hazards*, **26**(3), 203–225.

Ng, F., and Bjornsson, H., 2003. On the Clague-Mathews relation for jokulhlaups. *Journal of Glaciology*, **49**(165), 161–172.

Ng, F., Liu, S., Mavlyudov, B., and Wang, Y., 2007. Climatic control on the peak discharge of glacier outburst floods. *Geophysical Research Letters*, **34**(21), L21503. doi:10.1029/2007GL031426.

Noetzli, J., Huggel, C., Hoelzle, M., and Haeberli, W., 2006. GIS-based modelling of rock-ice avalanches from Alpine permafrost areas. *Computational Geosciences*, **10**(2), 161–178.

Nye, J. F., 1976. Water flow in glaciers: Jökulhlaups, tunnels and veins. *Journal of Glaciology*, **17**, 181–207.

Pierson, T. C., Janda, R. J., Thouret, J. C., and Borrero, C. A., 1990. Perturbation and melting of snow and ice by the November 13, 1985 eruption of Nevado del Ruiz, Colombia, and consequent mobilization, flow and deposition of lahars. *Journal of Volcanology and Geothermal Research*, **41**, 17–66.

Plafker, G., and Erikson, F. E., 1978. Nevados Huascaran avalanches, Peru. In Voight, B. (ed.), *Rockslides and Avalanches: Natural Phenomena*. Amsterdam: Elsevier, pp. 277–314.

Pralong, A., and Funk, M., 2006. On the instability of avalanching glaciers. *Journal of Glaciology*, **52**(176), 31–48.

Quincey, D., Lucas, R. M., Richardson, S. D., Glasser, N. F., Hambrey, M. J., and Reynolds, J. M., 2005. Optical remote sensing techniques in high-mountain environments: application to glacial hazards. *Progress in Physical Geography*, **29**(4), 475–505.

Raymond, C. F., 1987. How do glaciers surge. A review. *Journal of Geophysical Research*, **92**(B9), 9121–9134.

Reynolds, J. M., 2000. On the formation of supraglacial lakes on debris-covered glaciers. In Nakawo, M., Raymond, C. F., and Fountain, A. (eds.), *Debris-Covered Glaciers: Proceedings of an International Workshop Held at the University of Washington in Seattle, Washington, DC, September 13–15, 2000*. Willingford: IAHS Publications No. 264, pp. 153–161.

Richardson, S. D., and Reynolds, J. M., 2000. An overview of glacial hazards in the Himalayas. *Quaternary International*, **65/66**, 31–47.

Rickenmann, D., and Zimmermann, M., 1993. The 1987 debris flows in Switzerland: documentation and analysis. *Geomorphology*, **8**, 175–189.

Roberts, M. J., 2005. Jokulhlaups: a reassessment of floodwater flow through glaciers. *Reviews of Geophysics*, **43**(1), 1–21.

Spring, U., and Hutter, K., 1981. Numerical-studies of Jokulhlaups. *Cold Regions Science and Technology*, **4**(3), 227–244.

Thouret, J. C., 1990. Effects of the November 13, 1985 eruption on the snow pack and ice cap of Nevado del Ruiz volcano, Colombia. *Journal of Volcanology and Geothermal Research*, **41**, 177–201.

Tinti, S., Maramai, A., and Cerutti, A. V., 1999. The Miage Glacier in the Valley of Aosta (western Alps, Italy) and the extraordinary detachment which occurred on August 9, 1996. *Physics and Chemistry of the Earth. Part A: Solid Earth and Geodesy*, **24**(2), 157–161.

Tufnell, L., 1984. *Glacier Hazards*. London: Longman.

Tweed, F. S., and Russel, A. J., 1999. Control on the formation and sudden drainage of glacier-impounded lakes: implications for jökulhlaup characteristics. *Progress in Physical Geography*, **23**(1), 79–110.

van der Woerd, J., Owen, L. A., Tapponnier, P., Xu, X. W., Kervyn, F., Finkel, R. C., and Barnard, P. L., 2004. Giant, similar to M8 earthquake-triggered ice avalanches in the eastern Kunlun Shan, northern Tibet: characteristics, nature and dynamics. *Geological Society of America Bulletin*, **116**(3–4), 394–406.

Wagnon, P., Ribstein, P., Kaser, G., and Berton, P., 1999. Energy balance and runoff seasonality of a Bolivian glacier. *Global and Planetary Change*, **22**, 49–58.

Walder, J. S., and Costa, J. E., 1996. Outburst floods from glacier-dammed lakes: the effect of mode of lake drainage on flood magnitude. *Earth Surface Processes and Landforms*, **21**, 701–723.

Walder, J. S., and Driedger, C. L., 1994. Rapid geomorphic change caused by glacial outburst floods and debris flows along Tahoma Creek, Mount Rainier, Washington, USA. *Arctic and Alpine Research*, **26**(4), 319–327.

Walder, J. S., and Driedger, C. L., 1995. Frequent outburst floods from South Tahoma glacier, Mount-Rainier, USA – relation to debris flows, meteorological origin and implications for subglacial hydrology. *Journal of Glaciology*, **41**(137), 1–10.

Walder, J. S., Watts, P., Sorensen, O. E., and Janssen, K., 2003. Tsunamis generated by subaerial mass flows. *Journal of Geophysical Research, Solid Earth*, **108**(B5), 2236–2255.

Wegmann, M., Gudmundsson, G. H., and Haeberli, W., 1998. Permafrost changes in rock walls and the retreat of alpine glaciers: a thermal modelling approach. *Permafrost and Periglacial Processes*, **9**(1), 23–33.

Wei, M., Niu, F. J., Satoshi, A., and An, D. W., 2006. Slope instability phenomena in permafrost regions of Qinghai-Tibet plateau, China. *Landslides*, **3**(3), 260–264.

Yamada, T., and Sharma, C. K., 1993. Glacier lakes and outburst floods in the Nepal Himalaya. In Young, G. J. (ed.), *Snow and Glacier Hydrology*. Wallingford, Oxfordshire: IAHS Publ. No. 218, pp. 319–330.

Zimmermann, M., and Haeberli, W., 1992. *Climatic Change and Debris Flow Activity in High-Mountain Areas – a Case Study in the Swiss Alps*. Cremlingen-Destedt: Catena Supplement. 22, pp. 59–72.

Cross-references

Catastrophic Rock Slope Failures and Mountain Glaciers
Debris
Glacier Lake Outburst Floods
Glacier Surging
Permafrost
Retreat/Advance of Glaciers

NEGATIVE TEMPERATURE GRADIENT (IN ICE)

Rajesh Kumar
Remote Sensing Division, Birla Institute of Technology, Extension Center Jaipur, Jaipur, Rajasthan, India

When the temperature at the top layer of ice is lower than the temperature at the bottom layer, it creates a negative temperature gradient. The temperature gradient is a function of the depth of the snow and ice, and the temperature at the top and bottom of the snow and ice. The relationship of the variations of temperature with depth in snow and ice can be expressed as:

$$dT/dZ = (T_s - T_b)/Z$$

where T = temperature, T_s = surface temperature, T_b = bottom temperature, and Z = depth of the ice.

The ice is a good insulator to heat. The atmospheric cooling easily reduces the surface temperature of ice but it does not affect so easily the vertically downward profile of ice due to very less conductivity. Hence the upper surface has low temperature than bottom and creates negative temperature gradient. The rise in the temperature of the ice generally shows an exponential rate of increase with depth in glacier.

NEOGLACIATION

Rajesh Kumar
Remote Sensing Division, Birla Institute of Technology, Extension Centre Jaipur, Jaipur, Rajasthan, India

The neoglaciation is the Earth's climatic phase characterized by rebirth and/or growth of glaciers associated with a readvance of ice sheets between the postglacial phase and the present. It basically describes the cooling trend in the Earth's climate during the Holocene period. It has no well marked beginning but a period of general expansion of glaciers variously defined approximately as spanning from 3,000 to 2,000 years ago or covering the last 4,000–5,000 years.

The neoglaciation period was the return of cool moist condition from the warming of Holocene period. The cooling was accompanied by increased precipitation and moisture which helped in the renovation of the glaciers that had not existed since the last ice age.

Neoglaciation is also said to have started with the fluctuations of ice field in response to the climatic oscillations of the little ice age cycle. The most severe part of the neoglacial period seems to have been at its end, in the Little Ice Age. The neoglacial period is ending in present times and appears to be partially due to natural cycles and partially to man-made global warming.

NETWORK OF STAKES

Pratap Singh
Tahal Consulting Engineers Ltd, New Dehli, India

Snow stakes are used to determine the depth of snow accumulation in a basin. They are fixed at a representative site which can be easily inspected and read from a distance. Stakes represent a point value of snow depth. Snow stakes are used where a large accumulation of snow occurs. Stakes are painted white to minimize undue melting of snow in their immediate surroundings. Larger snow stakes, called aerial snow depth marker, are used for monitoring of snow depth using a low flying aircraft.

The variability of water equivalent and other associated parameters is established through a snow surveying network where stakes are installed. The network of stakes is designed in such a way that reliable index of water stored as snow over the entire basin is represented by the data obtained through the stakes. An appropriate network of stakes is also required for the mass balance studies of glaciers. For this purpose, stakes are installed over the glacier surface and read to know accumulation or depletion of snow over the glacier.

NEW ZEALAND GLACIERS

Wendy Lawson
Department of Geography, University of Canterbury, Christchurch, New Zealand

Definition

The *glaciers of New Zealand* are the valley and alpine glaciers of the mountain ranges of the tectonically active Southern Hemisphere mid-latitude island nation of New Zealand.

Overview

There are more than 3,000 glaciers in New Zealand – *Aotearoa*. Most of the glaciers are clustered in the Southern Alps of the South Island, in the latitudinal range of 42°–46° south, within a 100 km radius of *Aoraki* Mt Cook (3,754 m asl, Figure 1). In the North Island, there are a handful of rapidly retreating glaciers on the slopes of the active volcano Mt Ruapehu in the central volcanic plateau. A late twentieth

New Zealand Glaciers, Figure 1 The locations of glaciers of New Zealand (from McSaveney, 2009).

century glacier inventory reported that the 3,144 glaciers covered approximately 1,160 km^2, with a total ice volume of 53km^3 at that time (Chinn, 1989).

New Zealand's mid-latitude position and island topography is such that the glaciers are temperate, and the climate regime ultra maritime, characterized by high precipitation and very steep precipitation gradients. Annual precipitation exceeds 12 m in the wettest parts of the Southern Alps (Griffiths and McSaveney, 1983), and there is a strong west-east gradient of precipitation across the main divide, which in places is located within 35 km of the western coastline.

The best known, frequently visited, and most widely studied glaciers in New Zealand – the Franz Josef Glacier, the Fox Glacier, and the Tasman Glacier – share a basin boundary along the main divide of the Southern Alps, with the Franz and the Fox lying to the west of the main divide, and the Tasman to the east. The Tasman Glacier is the longest glacier in New Zealand, at 29 km in length, and its debris-covered tongue is rapidly retreating inside substantial late-glacial moraines. A rapidly enlarging lake that is currently more than 4 km long has formed in the last 20 or so years.

Mass balance of New Zealand's glaciers

Direct measurement of mass balance in New Zealand has been limited to short periods of study at individual glaciers. The most comprehensive direct record of mass balance to date is from the Ivory Glacier (43.13°S, 170.92°E), and was obtained between 1969 and 1975 when the Ivory was selected as New Zealand's glaciated representative basin for the International Hydrological Decade. Over those 6 years of measurement, the Ivory Glacier experienced dramatic retreat, lake formation at the terminus, and a cumulative negative mass balance of nearly 15 m w.e. (Anderton and Chinn, 1978).

Most mass balance information in New Zealand is derived indirectly, based on an annual oblique aerial survey. This method yields proxy information on annual mass balance, in the form of an elevation difference between the annual end-of-summer snowline for a series of 50 index glaciers, and an assumed equilibrium line altitude (ELA_o) for each glacier (Chinn et al., 2005a). The method is affected by a series of uncertainties, not least of which is the assumptions necessary to determine ELA_o. Nevertheless, the value of the data has been recognized by the World Glacier Monitoring Service (WGMS, 2008).

For 21 of the last 33 years (1977–2009), the average mass balance for the 50 index glaciers inferred from this indirect method has been positive (Figure 2). The recent positive mass balances, like those of Scandinavia's coastal glaciers, are a result of precipitation delivered by increased westerly airflow associated with a change in the Interdecadal Pacific Oscillation (Chinn et al., 2005b). The predominantly positive mass balance state of New Zealand's in the last few decades follows a period of significant loss since the middle of the nineteenth century: between 1850 and 1977, for example, New Zealand glaciers lost 49% of their surface area (Hoelzle et al., 2007).

At the Brewster Glacier (44.05°S, 169.44°E), where mass balance has been measured directly since 2004, the results of direct measurements coincide in direction with the results of indirect analysis (Figure 3). In balance year 2005/2006, the Brewster Glacier was one of only 7 of the 104 WGMS glaciers that experienced positive balance (WGMS, 2008, 2009). A spatially distributed surface energy–balance model suggests that the temperature sensitivity of mass balance at the Brewster is −2.0 m w.e. $a^{-1}\,°C^{-1}$, one of the highest sensitivities reported globally (Anderson et al., 2010).

Franz Josef glacier Ka Roimata O Hine Hukatere

The Franz Josef Glacier is the best known of New Zealand's glaciers to scientists and tourists alike, with 100s of tourist walking on the glacier each day during the summer months. The Franz Josef Glacier is 11 km long, 35 km^2 in area, and ranges in elevation from 2,900 m asl to a few hundred meters asl (Figure 4). Annual rates of ablation at the terminus can reach 20 m w.e., and annual accumulation lies in the range 4–8 m w.e. in the upper

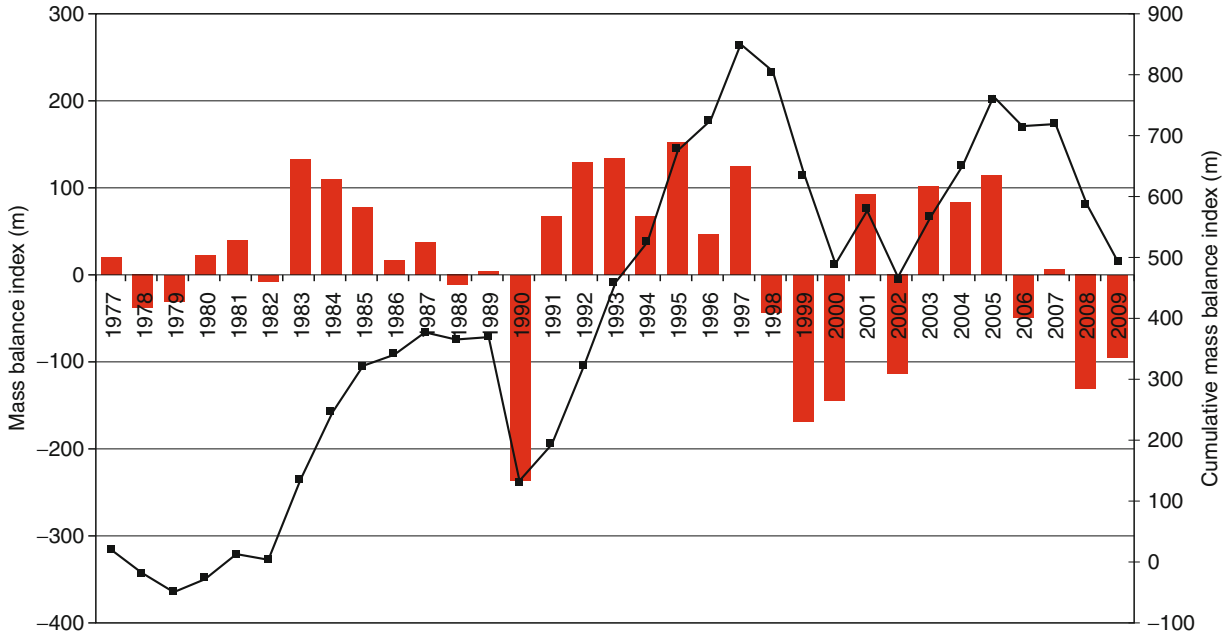

New Zealand Glaciers, Figure 2 Annual mean mass balance index and cumulative mass balance index for 50 index glaciers in New Zealand 1977–2009. The mass balance index is the difference in elevation between the ELA and the end-of-summer snowline, where positive values indicated positive mass balance.

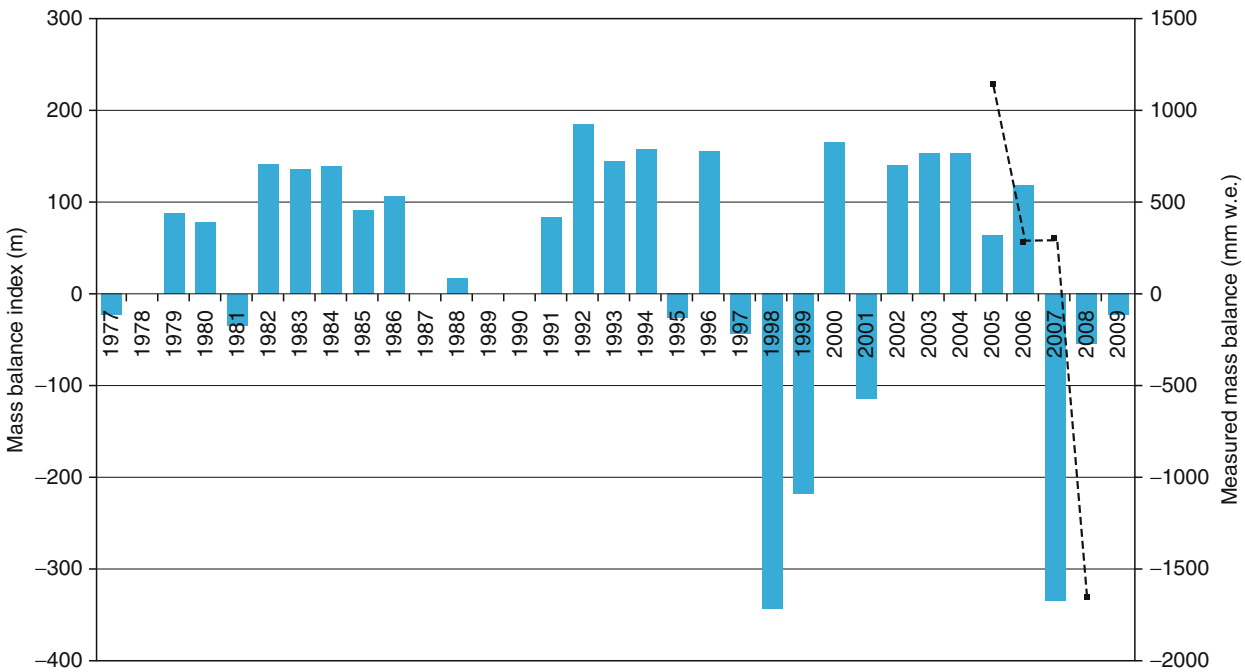

New Zealand Glaciers, Figure 3 Mass balance index and directly measured mass balance for the Brewster glacier 1977–2009.

glacier, although up to 15 m w.e. of precipitation may be received (Anderson et al., 2006).

Between 1894 and 2005, the Franz Josef Glacier lost mass at an annual rate of 0.02 m a^{-1} w.e.. Between 2000 and 2005, the annual mass balance ranged from −0.75 to +1.5 m w.e., with only one of those years (2000/2001) experiencing negative balance. Modeling indicates that the climate sensitivity of mass balance at Franz Josef is −1.9 m w.e. a^{-1} $°C^{-1}$ (Anderson et al., 2006), and that regional climate change under a mean warming scenario

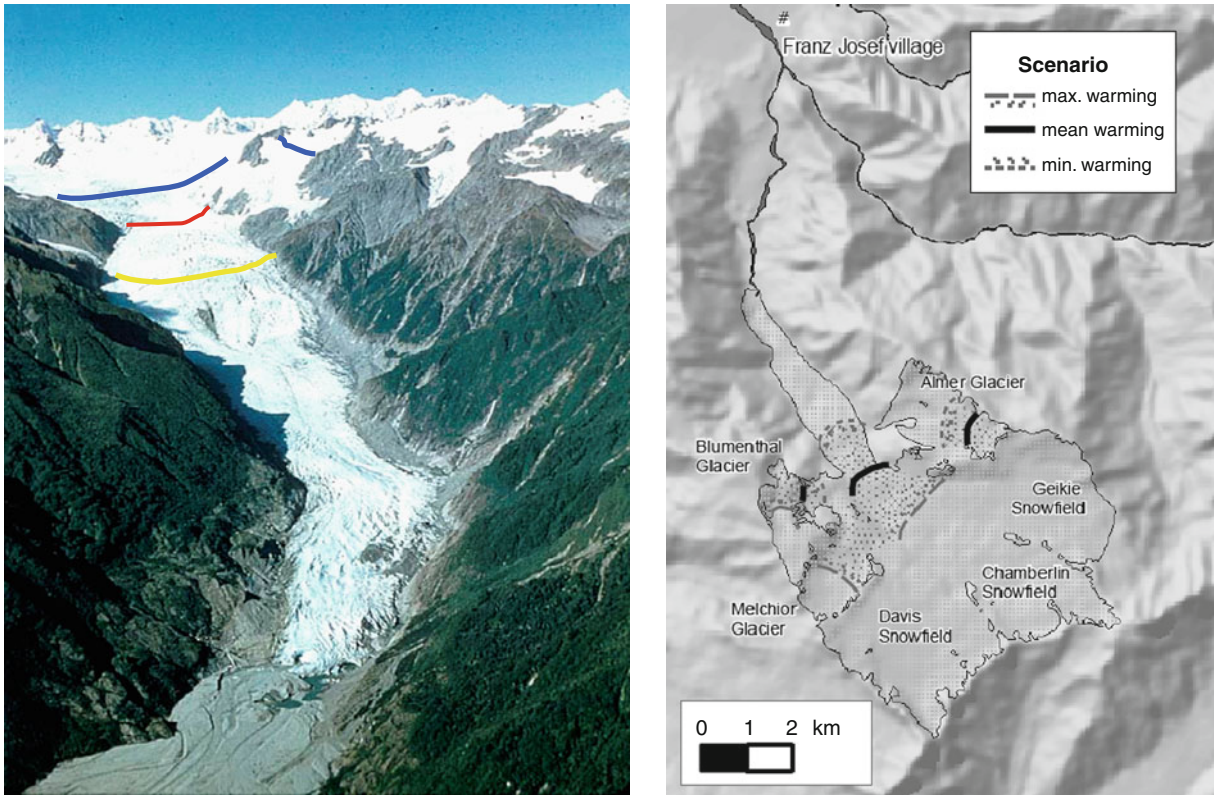

New Zealand Glaciers, Figure 4 Franz Josef Glacier Ka Roimate o Hine Hukatere, showing the approximate location of the terminus in 2100 under various warming scenarios (Source: diagram on *right* Anderson et al., 2008). In the photograph on the *left*, the *blue*, *red*, and *yellow lines* indicate the position of the terminus under maximum, mean, and minimum warming scenarios, respectively.

will cause terminus retreat of 5 km and mass loss of 40% by 2100 (Figure 4; Anderson et al., 2008).

Temperature exerts a stronger control than precipitation at the Franz Josef Glacier at a range of timescales (Anderson et al., 2006, Anderson and Mackintosh, 2006). The increase in glacier extent necessary to form the well-known Waiho Loop moraine (~13,000 year b.p.), which is 10 km downstream of the current glacier terminus, requires a cooling of 3–4°C. It is possible, in this highly tectonically active environment, that non-climatic factors have an important role in historical changes in extent of the Franz Josef Glacier (Tovar et al., 2008).

Summary

New Zealand's glaciers contain a relatively small volume of ice, but are highly sensitive to climate, with modeling suggesting some of the highest temperature sensitivities of the global glaciers. Proxy data indicate that the glaciers have experienced positive mass balance for most of the last 4 decades because of increasingly westerly air flow. Comparable environments are found in western Scandinavia, and Patagonia. The tectonically active landscape in New Zealand means that non-climatic factors also have a significant influence on terminus behavior.

Bibliography

Anderson, B., and Mackintosh, A., 2006. Temperature change is the major driver of late-glacial and Holocene glacier fluctuations in New Zealand. *Geology*, **34**(2), 121–124.

Anderson, B., Lawson, W., and Owens, I., 2008. Response of Franz Josef Glacier Ka Roimata o Hine Hukatere to climate change. *Global and Planetary Change*, **63**, 23–30.

Anderson, B., Lawson, W., Owens, I., and Goodsell, B., 2006. Past and future mass balance of Ka Roimata o Hine Hukatere Franz Josef Glacier. *New Zealand Journal of Glaciology*, **52**(179), 597–607.

Anderson, B., Mackintosh, A., Stumm, D., George, L., Kerr, T., Winter-Billington, A., and Fitzsimons, S., 2010. Climate sensitivity of a high-precipitation glacier in New Zealand. *Journal of Glaciology*, **56**(195), 114–128.

Anderton, P. W., and Chinn, T. J., 1978. Ivory glacier, New Zealand, an IHD representative basin study. *Journal of Glaciology*, **20**, 67–84.

Chinn, T., 1989. Glaciers of New Zealand. In Williams, R., and Ferrigno, J. (eds.), *Satellite Image Atlas of Glaciers of the World, USGS Professional Paper 1386H*. Washington, DC: United States Printing Office.

Chinn, T., Heydenrych, C., and Salinger, J., 2005a. Use of the ELA as a practical method of monitoring glacier response to climate in New Zealand's Southern Alps. *Journal of Glaciology*, **51**(172), 85–95.

Chinn, T., Winkler, S., Salinger, M. J., and Haakensen, N., 2005b. Recent glacier advances in Norway and New Zealand; a comparison of their glaciological and meteorological causes. *Geografiska Annaler*, **87**(A), 141–157.

Griffiths, G. A., and McSaveney, M. J., 1983. Distribution of mean annual precipitation across some steepland regions of New Zealand. *New Zealand Journal of Science*, **26**, 197–209.
Hoelzle, M., Chinn, T., Stumm, D., Oaul, F., Zemp, M., and Haeberli, W., 2007. The application of glacier inventory data for estimating past climate change effects on mountain glaciers: a comparison between the European Alps and the Southern Alps of New Zealand. *Global and Planetary Change*, **56**, 69–82.
McSaveney, E., 2009. Glaciers and glaciation – glaciers in New Zealand. In Te Ara – The Encyclopedia of New Zealand, Updated March 1, 2009. URL: http://www.TeAra.govt.nz/en/glaciers-and-glaciation
Tovar, D., Shulmeister, J., and Davies, T. R., 2008. Evidence for a landslide origin of New Zealand's Waiho Loop moraine. *Nature Geoscience*, **1**(8), 524–526.
World Glacier Monitoring Service (WGMS), 2008. Fluctuations of glaciers 2000–2005, Volume IX. In Haeberli, W., Zemp, M., Kaab, A., Paul, F., and Hoelzle, M. (eds.), *ICSU(FAGS)/IUGG (IACS)/UNEP/UNESCO/WMO*. Zurich: World Glacier Monitoring Service.
World Glacier Monitoring Service (WGMS), 2009. Glacier mass balance bulletin No.10 (2006–2007). In Haeberli, W., Gartner-Roer, I., Hoelzle, M., Paul, F., and Zemp, M. (eds.), *ICSU (WDS)/IUGG(IACS)/UNEP/UNESCO/WMO*. Zurich: World Glacier Monitoring Service. pp. 96.

Cross-references

Climate Change and Glaciers
Debris-Covered Glaciers
Patagonia
Scandinavian Glaciers

NICHE GLACIER

D. P. Dobhal
Wadia Institute of Himalayan Geology, Dehradun, Uttarakhand, India

Niche glaciers are very small in size. Such glaciers occupy gullies and hollow on the slopes and appear as little more than large snow fields. They do not make image of a typical glacier. A niche glacier may develop into a corrie/cirque glacier if conditions are favorable, and it is common in glaciated areas to finds small niche glaciers between larger corrie/cirque glaciers.

NORMALIZED-DIFFERENCE SNOW INDEX (NDSI)

Dorothy K. Hall[1], George A. Riggs[2]
[1]Crysopheric Sciences Branch, Code 614.1, NASA/Goddard Space Flight Center, Greenbelt, MD, USA
[2]SSAI, Lanham, MD, USA

Definition

Normalized-Difference Snow Index (NDSI) – normalized difference of two bands (one in the visible and one in the near-infrared or short-wave infrared parts of the spectrum) is used to map snow. Snow is highly reflective in the visible part of the EM spectrum and highly absorptive in the near-infrared or short-wave infrared part of the spectrum, whereas the reflectance of most clouds remains high in those same parts of the spectrum, allowing good separation of most clouds and snow.

Introduction

The NDSI has a long history. The use of ratioing visible (VIS) and near-infrared (NIR) or short-wave infrared (SWIR) channels to separate snow and clouds was documented in the literature beginning in the mid-1970s by Valovcin (1976, 1978) and also by Kyle et al. (1978). A considerable amount of work on this subject was conducted at, and published by, the Air Force Geophysics Laboratory (AFGL) (e.g., see Bunting and d'Entremont, 1982). The objective of the AFGL work was to discriminate snow cover from cloud cover using an automated algorithm to improve global cloud analyses. Later, automated methods that relied on the VIS/NIR ratio were refined substantially using satellite data, by Crane and Anderson (1984), Dozier (1989), and Rosenthal and Dozier (1996) for regional scales, and by Riggs et al. (1993), Hall et al. (1995, 2002), and Hall and Riggs (2007) for global snow-cover mapping. In this section, we provide a brief history of the use of the NDSI for mapping snow cover.

Band ratios used to discriminate snow and clouds

Results of an investigation of snow reflectance characteristics using data from Skylab Earth Resources Experiment Package (EREP) S192 multispectral scanner are presented by Barnes and Smallwood (1975). For the first time, satellite study of snow from the spectral range extending from the VIS to the IR (0.41–12.5 μm) was possible, and this paved the way for automated snow-cover mapping. Shortly thereafter, Valovcin (1976) at AFGL introduced the idea of using the ratio of radiance values in the VNIR (0.68–0.76 μm) and NIR or SWIR (1.55–1.75 μm) to provide a method to discriminate between snow cover and clouds. Kyle et al. (1978) used the ratio of the 1.6–0.754 μm channels to distinguish snow and clouds using a cloud physics radiometer with 0.754–1.64 μm channels. They also used an IR band to test for surface temperature further distinguished snow and clouds.

Additional work done at AFGL by Bunting and d'Entremont (1982) employed a 1.6 μm sensor flown on the Defense Meteorological Satellite Program (DMSP) Special Sensor C (SSC) to separate snow and clouds. They also used 11% reflectance to define the lower bound of reflectance for snow cover. Crane and Anderson (1984) reviewed the previous work, mainly conducted at AFGL, and employed the DMSP Operational Linescan System (OLS), which operated in the 0.4–1.0 μm and 8–13 μm range, along with SSC data (1.51–1.63 μm). They

employed reflectances derived from the various sensors to map snow using a threshold technique.

More-sophisticated use of band ratios as applied with Landsat Thematic Mapper TM data was developed by Dozier (1987, 1989). The normalized difference of TM bands 2 (0.52–0.60 μm) and 5 (1.55–1.75 μm) was introduced in Dozier (1989). Dozier and Marks (1987) discuss automated snow mapping and threshold tests for shadowed snow, cloud, vegetation, and soil in sunlit areas.

With the anticipated launch of the Moderate Resolution Imaging Spectroradiometer (MODIS) at the end of the 1990s, a global snow-mapping algorithm needed to be developed that would perform automatically and not be computationally intensive. Using the heritage algorithms discussed above, Hall et al. (1995) coined the term normalized-difference snow index and outlined a snow-mapping algorithm that would be the basis of the MODIS standard snow-mapping product. The prototype algorithm, called Snowmap, used a normalized difference between MODIS band 4 (5.45–5.65 μm) and 6 (1.628–1.652 μm), as was done in Bunting and d'Entremont (1982), Crane and Anderson (1984), and Dozier (1989) using TM bands 2 and 5. The prototype MODIS algorithm also employed several spectral tests. A planetary reflectance $\leq$11% was a threshold test in which values $<$11% were mapped as "not snow," determined not to be snow.

The prototype MODIS snow-mapping algorithm was improved with additional spectral tests. One key modification is that the NDSI threshold was changed in forested areas based on results of a canopy reflectance model (Klein et al., 1998), using both the Normalized Difference Vegetation Index (NDVI) and NDSI in densely forested areas as determined from the NDVI test. A thermal mask was also included to remove erroneous "snow" in locations where snow is considered to be impossible. Small specks of erroneous snow that show up on an image may be due to sand. If the band 31 (10.780–11.280 μm) temperature is >283 K, then a pixel is considered "not snow." This type of thermal test of surface temperature had previously been used by Kyle et al. (1978) and Romanov and Gutman (2000). The standard MODIS cloud mask is also employed as an input to the snow algorithm.

Following the 1999 launch of the MODIS on the Terra spacecraft, the snow algorithm was modified several times, but the NDSI has remained the basis of the algorithm. The current algorithm is Version 005 (see Riggs et al., 2006).

Summary

The term normalized-difference snow index (NDSI) was coined by Hall et al. (1995), but the NDSI technique already had nearly a 20-year heritage as similar methods using various visible and near-infrared bands had been used since the mid-1970s to map snow and separate snow from most clouds. Following the launch of the MODIS in 1999, the NDSI approach to mapping snow cover became automated using an algorithm that utilizes the NDSI along with a variety of threshold tests.

Bibliography

Barnes, J. C., and Smallwood, M. D., 1975. Synopsis of current satellite snow mapping techniques with emphasis on the application of near-infrared data. In Rango, A. (ed.), *Operational Applications of Satellite Snowcover Observations*. NASA Special Publication SP-391, pp. 199–213.

Bunting, J. T., and d'Entremont, R. P., 1982. Improved cloud detection utilizing Defense Meteorological Satellite Program near infrared measurements, Air Force Geophysics Laboratory, Environmental Research Papers, No. 765, AFGL-TR-82-0027, 27 January 1982, 91 pp.

Crane, R. G., and Anderson, M. R., 1984. Satellite discrimination of snow/cloud surfaces. *International Journal of Remote Sensing*, **5**(1), 213–223.

Dozier, J., 1987. Remote sensing of snow characteristics in the southern Sierra Nevada, "Large Scale Effects of Seasonal Snow Cover," *Proceedings of the Vancouver Symposium,* August 1987, IAHS, 166, pp. 305–314.

Dozier, J., 1989. Spectral signature of alpine snow cover from the Landsat Thematic Mapper. *Remote Sensing of Environment*, **28**, 9–22.

Dozier, J., and Marks, D., 1987. Snow mapping and classification from Landsat Thematic Mapper data. *Annals of Glaciology*, **9**, 1–7.

Hall, D. K., and Riggs, G. A., 2007. Accuracy assessment of the MODIS snow-cover products. *Hydrological Processes*, **21**, 1534–1547.

Hall, D. K., Riggs, G. A., and Salomonson, V. V., 1995. Development of methods for mapping global snow cover using Moderate Resolution Imaging Spectroradiometer (MODIS) data. *Remote Sensing Environment*, **54**, 127–140.

Hall, D. K., Riggs, G. A., Salomonson, V. V., DiGirolamo, N. E., and Bayr, K. J., 2002. MODIS snow-cover products. *Remote Sensing of Environment*, **83**, 181–194.

Klein, A. G., Hall, D. K., and Riggs, G. A., 1998. Improving snow-cover mapping in forests through the use of a canopy reflectance model. *Hydrological Processes*, **12**, 1723–1744.

Kyle, H. L., Curran, R. J., Barnes, W. L., and Escoe, D., 1978. A cloud physics radiometer, Third Conference on Atmospheric Radiation, American Meteorological Society, 28–30 June 1978, Davis, Calif., p. 107.

Riggs, G. A., Hall, D. K., Barker, J. L., and Salomonson, V. V., 1993. *The Developing Moderate Resolution Imaging Spectroradiometer (MODIS) Snow Cover Algorithm, Proceedings of the 50th Annual Eastern Snow Conference. 8–10 June*. Quebec, Canada: Quebec City, pp. 51–58.

Riggs, G. A., Hall, D. K., and Salomonson, V. V., 2006. *MODIS Snow Products User Guide*. http://modis-snow-ice.gsfc.nasa.gov/sugkc2.html.

Romanov, P., and Gutman, G., 2000. Automated monitoring of snow cover over North America with multispectral satellite data. *Journal of Applied Meteorology*, **39**, 1866–1880.

Rosenthal, W., and Dozier, J., 1996. Automated mapping of montane snow cover at subpixel resolution from the Landsat Thematic Mapper. *Water Resources Research*, **32**(1), 115–130.

Valovcin, F. R., 1976. Snow/cloud discrimination, AFGL-TR-76-0174, ADA 032385.

Valovcin, F. R., 1978. Spectral radiance of snow and clouds in the near infrared spectral region, AFGL-TR-78-0289, ADA 063761.

NOVAYA ZEMLYA

Chris R. Stokes
Department of Geography, Durham University, Durham, UK

The Russian islands of Novaya Zemlya ("New Land") are situated in the *Arctic* Ocean between 70.5–77°N and E51–69°E. There are numerous small islets but the archipelago primarily consists of the South (Yuzhny) and North (Severny) Islands, separated by the narrow Matochkin Strait. They form an elongated arc stretching for almost 1,000 km and narrowing from 150 km in the southwest to 40 km in the northeast. Geologically, they are a northern extension of the *Ural Mountains*, characterized by a rugged terrain (maximum elevation: 1,547 m above sea level) and with large parts of the coastline incised by *fjords*. They represent a major orographic barrier between the Barents Sea to the west and the Kara Sea to the east.

The archipelago covers an area about of 90,000 km^2 of which ~24,400 km^2 is covered by *glacier ice* (Dowdeswell and Williams, 1997), dominated by a large *ice cap* on the North Island. The Catalogue of Glaciers of the USSR (Kotlyakov, 1978) lists 685 glaciers, most of which are relatively small *mountain/cirque glaciers*. There are, however, 60–70 large *tidewater glaciers* that drain the *ice caps* and *ice fields* in the north and *calve icebergs* along both the east and west coasts. Further south, smaller glaciers terminate at much higher elevations. Indeed, glacier *equilibrium line altitudes* (ELA), which broadly range from 300 to 700 m a.s.l., increase from north to south, concomitant with an increase in mean annual temperature of ~5°C (Kotlyakov, 1978; Zeeberg and Forman, 2001). ELAs also increase in a west-to-east direction, reflecting a decrease in precipitation away from the more maritime climate of the Barents Sea, which is heavily influenced by advection of warm North Atlantic water. *Sea ice* is also less persistent along the west coast, which can remain ice-free for much of the year. Interestingly, the different climatic regimes appear to influence the location *surging glaciers*, which are far more common in the west (Grant et al., 2009).

In the past, ice extent on Novaya Zemlya has been far more extensive. During the *Last Glacial Maximum*, for example, the archipelago was covered by the Barents Sea *Ice Sheet* (Svendsen et al., 2004). Following its *deglaciation* by the early Holocene (~9,500 cal year BP), there was a period of relatively high sea level between 7,500 and 6,000 cal year BP that created shorelines ~13 m above the present coastline (Forman et al., 1999). More recently, several relatively minor glacier fluctuations have taken place, with the latest readvance linked to "Little Ice Age" cooling in the second half of the nineteenth century (Zeeberg and Forman, 2001). Subsequent warming during the first half of the twentieth century resulted in rapid glacier recession (>300 m a^{-1}: Zeeberg and Forman, 2001). Perhaps surprisingly, mean annual temperatures appear to have decreased in the latter half of the twentieth century and, in addition to increased winter precipitation, some glaciers are thought to have stabilized, whereas others have continued to retreat (Zeeberg and Forman, 2001). However, more recent data from a sample of 692 glaciers suggests that widespread retreat has occurred in response to a marked increase in summer temperatures since the 1980s (Grant, 2010).

Bibliography

Dowdeswell, J. A., and Williams, M., 1997. Surge-type glaciers in the Russian High Arctic identified from digital satellite imagery. *Journal of Glaciology*, **43**(145), 489–494.

Forman, S., Lubinski, D., Zeeberg, J., Polyak, L., Miller, G., Matishov, C., and Tarasov, G., 1999. Postglacial emergence and Late Quaternary glaciation on northern Novaya Zemlya, Arctic Russia. *Boreas*, **28**, 134–145.

Grant, K. L., Stokes, C. R., and Evans, I. S., 2009. Identification and characteristics of surge-type glaciers on Novaya Zemlya, Russian Arctic. *Journal of Glaciology*, **55**(194), 960–972.

Grant, K. L., 2010. Change in glacier extent since the Little Ice Age and links to 20th/21st Century climatic variability on Novaya Zemlya, Russian Arctic. Unpublished Ph.D. Thesis, The University of Reading, UK.

Kotlyakov, V. (Ed.)., 1978. Catalogue of Glaciers USSR: Novaya Zemlya. Leningrad, Hydrometeoizdat. [In Russian].

Svendsen, J., Alexanderson, H., Astakhov, V. I., Demidov, I., Dowdeswell, J. A., Funder, S., Gatullin, V., Henriksen, M., Hjort, C., Houmark-Nielsen, M., Hubberton, H. W., Ingólfson, O., Jakobsson, M., Kjær, K., Larsen, E., Lokrantz, H., Lunkka, J. P., Lysså, A., Mangerud, J., Matiouchkov, A., Murray, A., Möller, P., Niessen, F., Nikolskaya, O., Polayk, P., Saarnisto, M., Siegert, C., Siegert, M., Spielhagan, R., and Stein, R., 2004. Late Quaternary ice sheet history of northern Eurasia. *Quaternary Science Reviews*, **23**, 1229–1271.

Zeeberg, J., and Forman, S. L., 2001. Change in glacier extent on north Novaya Zemlya in the twentieth century. *The Holocene*, **11**(2), 161–175.

NYE (N) CHANNELS

D. P. Dobhal
Wadia Institute of Himalayan Geology, Dehradun, India

N-channels are the product of discrete or consolidated base flow which transports large volumes of meltwater. It is basically a subglacial melt water channel. Subglacial meltwater flow can occur in distributed or discrete system, and it includes sheet flow or linked cavity network. Nye channel cuts into bedrock or consolidated sediments and leaves the imprint on the land surface once the glacier is retreated.

O

OGIVES

Divya Dudeja
Department of Geology, DBS College, Dehradun, Uttarakhand, India

Synonyms

Alaskan bands; Forbes bands; Wave ogives

Ogives are surface features exposed on the surface of glaciers as repetitive dark and light arcs or waves. They are regarded as the indicators of glacier flow. Ogives attracted the attention of glaciologists in the mid-nineteenth century, when the fundamentals of glacier flow were first being established.

Ogives are of mainly two types: wave ogives and band/concealed ogives. In wave ogives, alternate light and dark bands are thick in width having wave-like structure and are convex in downflow side. Such wave ogives are observed in Sunder Bamak glacier, a tributary of Chatrungi Glacier of Uttarakhand, India (Raina and Srivastava, 2008). Concealed/band ogives have alternate dark and light bands in the shape of semicircular ring, instead of wavy structure. Similar to wave ogives, they also show convexity in the direction of glacier flow.

Bibliography

Goodsell, B., Hambrey, M. J., and Glasser, N. F., 2002. Formation of band ogives and associated structures at Bas Glacier d'Arolla, Valais, Switzerland. *Journal of Glaciology*, **48**(161), 287–300.
Posamentier, H. W., 1978. Thoughts on ogive formation. *Journal of Glaciology*, **20**(82), 218–220.
Raina, V. K., and Srivastava, D., 2008. Glacier Atlas of India, Geological Society of India, Pragati Graphics, Bangalore, p. 311.
Waddington, E. D., 1986. Wave Ogives. *Journal of Glaciology*, **32**(112), 325–334.

OPTICAL REMOTE SENSING OF ALPINE GLACIERS

Duncan J. Quincey[1], Michael P. Bishop[2]
[1]Institute of Geography and Earth Sciences, Penglais Campus, Aberystwyth University, Aberystwyth, Wales, UK
[2]Department of Geography and Geology, University of Nebraska-Omaha, Omaha, NE, USA

Definition

Optical remote sensing. The measurement of surface reflectance in the visible, near-infrared, middle-infrared, and thermal-infrared regions of the electromagnetic spectrum.
Spatial resolution. The effective ground dimensions in meters (x,y) of each picture element (pixel) within a remote sensing image.
Spectral resolution. The ability of a sensor to detect fine spectral differences.
Image classification. The labeling of pixels within a remote sensing image into a thematic scheme (e.g., land cover), usually based upon their spectral reflectance characteristics.
Stereo-pair. A pair of remote sensing images of the same ground area, acquired from different satellite or aircraft positions, from which elevation data can be extracted.
Orthorectified. A planimetrically correct image (i.e., with geometric and topographic distortions removed).

Introduction

Concerns over greenhouse-gas forcing and warmer temperatures have prompted investigations into climate forcing and Earth-system responses. There is considerable scientific debate regarding climate forcing and system response, as complex geodynamics regulate feedback mechanisms that couple atmospheric, geologic, and hydrologic processes. A significant component in the

Vijay P. Singh, Pratap Singh & Umesh K. Haritashya (eds.), *Encyclopedia of Snow, Ice and Glaciers*, DOI 10.1007/978-90-481-2642-2,

coupling of Earth's systems involves the cryosphere, as glaciological processes govern atmospheric, hydrospheric, and lithospheric responses (Meier and Wahr, 2002). Consequently, scientists have recognized the significance of understanding glacier fluctuations and their use as direct and indirect indicators of climate change.

The international scientific community is actively engaged in assessing ice sheet and glacier fluctuations at the global scale (Bishop et al., 2004; Kargel et al., 2005). Glaciological, remote sensing, and geographic information system (GIS) studies indicate that recent glacier retreat and wastage appear to be global in nature (Dyurgerov and Meier, 2005; Paul et al., 2004a). It is essential that we identify and characterize those regions that are changing most rapidly and that are having the most significant impact on sea level, water resources, economics, and geopolitics. Many regions have not been adequately studied, however, and detailed information on the number of ice masses, land-ice distributions, glacier-length changes, ice-volume changes, glacier sensitivity to forcing factors, mass balance, dynamic response time, ice-flow dynamics, and other important glaciological parameters and processes are required to better understand climate forcing and climate-glacier fluctuations.

Optical remote sensing data have provided information on alpine glaciers (Alpine) and how they have changed for more than 30 years, first through the use of aerial photography and, later, satellite sensors. Early satellite sensor imagery was limited by its coarse *spatial* and *spectral resolutions*, but as sensor technologies advanced, image data became increasingly detailed, and information extraction techniques and approaches evolved to generate an ever-increasing amount of land surface information. Contemporary satellite sensor measurements are commonly made at spatial resolutions comparable to aerial photographs but with wide swaths, on a repeat basis, and across many narrow spectral bands, offering quantitative biophysical information about the glacial environment that may not be available through field investigation alone. Fieldwork measurements can be further limited in high-mountain areas by their remoteness, harsh conditions, and, occasionally, restricted access for political reasons. Satellite remote sensing has therefore become an essential part of alpine glacial studies.

The availability of new satellite data, however, does not directly translate into accurate information extraction. There are numerous techniques and approaches that can be used to extract quantitative and thematic information, but the issue of producing accurate high-quality information is very dependent on the choice of algorithms and the analytical approach. Problems exist in ensuring the quality of input image data, as the level and exact nature of preprocessing is often not transparent. In addition, processing protocols have not been established, and many techniques are un-validated, meaning results can vary widely between analysts, even when employing the same data. Despite these information extraction issues, remote sensing has provided some of the greatest advances in our understanding of alpine glacial processes at a range of spatial scales, contributing to predictions of global sea-level rise (Meier et al., 2007), regional assessment of water resources (Singh and Bengtsson, 2005), and local monitoring of glacial hazards (Huggel et al., 2005).

We provide an overview of such advances and discuss the key optical remote sensing instruments and their characteristics that are of relevance in alpine glacier studies. Specifically, we present details of how remote sensing can be routinely used to analyze glacier areal fluctuations, the distribution of surface features and structures, glaciers flow rates, the degree to which they are melting or accumulating mass and, given atmospheric warming, the increasing emergence of glacial hazards. With issues of data quality and measurement accuracy in mind, we also summarize some of the major issues and concerns in remote sensing of alpine glaciers.

Optical remote sensing – key instruments for alpine glacier measurements

Optical remote sensing is defined as the measurement of surface reflectance at optical wavelengths, specifically at visible (0.4–0.7 μm), near-infrared (0.7–1.3 μm), shortwave infrared (1.3–3.0 μm) and thermal infrared (3.0–14.0 μm) wavelengths. Early satellite sensors collected measurements in a limited number of discrete spectral ranges that were characterized by coarse *spatial and spectral resolution*, such that small features on the ground were not discernible and broad wavelength ranges generalized spectral reflectance measurements. For example, the Landsat Multispectral Scanner (MSS) was one of the earliest satellite sensors available for nonmilitary purposes, and measured reflectance in the green, red, and near-infrared (two bands) regions of the electromagnetic spectrum, at 68 m × 82 m spatial resolution. Modern day satellite sensors collect data in many more, and narrower, spectral bands, and at increasingly fine spatial resolution. Some satellite sensors (e.g., Quickbird) even offer imagery at a spatial resolution comparable to aerial photography (<1 m), but generally with less spectral information than those coarser spatial resolution sensors.

A number of key optical sensors are useful for alpine glacier studies (Figure 1). The Landsat series of sensors provides a long archive of images acquired at various spatial resolutions (15–60 m), which since early 2009, have been available free of charge through the United States Geological Survey (USGS; http://www.glovis.usgs.gov). A similarly long archive of data is available from the Systeme pour Observation de la Terre (SPOT) series of sensors, with spatial resolution improving with time; currently, 2.5 m resolution images are available for most alpine areas. The data archive is available to browse at http://www.sirius.spotimage.fr and academic institutions can gain access to reduced cost imagery through the ISIS scheme (http://www.isis-cnes.spotimage.fr). Since 2000, the Advanced Spaceborne Thermal Emission and Reflection Radiometer (ASTER) has measured surface

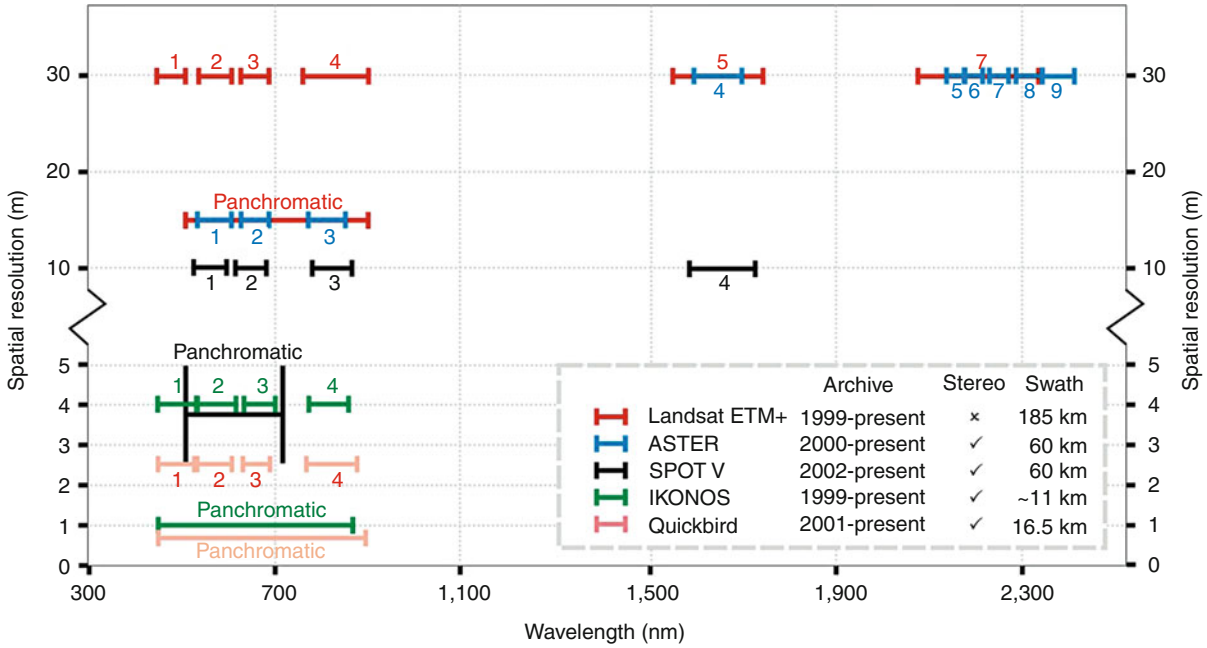

Optical Remote Sensing of Alpine Glaciers, Figure 1 Key satellite sensors operating at optical wavelengths and commonly used in glaciological studies.

reflectance in 14 bands throughout the visible and infrared wavelengths, with a second sensor pointing backward to acquire a *stereo-pair*, facilitating the extraction of digital elevation data. ASTER data may be purchased through the Earth Remote Sensing Data Analysis Center (ERSDAC) at http://www.gds.aster.ersdac.or.jp, or acquired free of charge under a recognized researcher agreement with NASA. Most alpine glacier studies make use of one or more of these image sources because of their comprehensive archives, their low cost relative to other sensors, and the detailed information content they provide, which is well suited for assessing the surface characteristics of small to large glaciers.

As with ASTER, a number of other satellite sensors collect *stereo-pairs*, which can be used to extract the surface elevation value of every pixel in the image. The resulting image, which represents the surface topography (altitude field) of the area covered by the stereo-pair, is called a Digital Elevation Model (DEM; Digital Elevation Model Generation Over Glacierized Region). The process of deriving surface elevation data from satellite imagery in this way relies on recreating the geometry between the sensor and the terrain at the exact time of image acquisition. The user supplies approximate data relating to the aircraft location and the average terrain height above sea level in addition to accurate statistics on the camera geometry and image dimensions. Using "least squares" regression, it is possible to reduce the errors in the approximations and arrive at a stereo model that realistically represents the position and orientation (in three dimensions) of the sensor(s) at the time(s) of image acquisition. In much the same way that humans generate three-dimensional perspectives using information from both eyes, a spatial ray is generated from the first image that intersects in three dimensions with the corresponding point on the second image, thus giving a surface elevation value for each modeled pixel. The errors associated with producing DEMs from satellite imagery can be quite high; however, an increasing number of studies are therefore employing elevation measurements made by laser altimeter (see, for example, http://www.csr.utexas.edu/glas). These data, which are extremely accurate but currently limited in swath width, promise to be of great benefit to geomorphology and glaciology as they become more widely available.

Deriving glacier characteristics

Glacier outlines (debris-covered and non-debris covered)

Perhaps the most basic information that is required for assessing alpine glaciers is their spatial extent and the nature of temporal fluctuations. Its primary applications are in the local- to regional-scale measurement of glacier fluctuations in response to climatic warming, and in the regional- to global-scale mapping of ice and snow distributions for inclusion in global databases, with which both past and future comparisons can be made (Inventory of Glaciers; World Glacier Inventory (WGI): http://nsidc.org/data/g01130.html; Global Land Ice Measurements from Space (GLIMS): www.glims.org; and GlobGlacier: http://globglacier.ch).

The distinct spectral properties of snow and ice permit accurate semiautomatic delineation of debris-free glaciers using a variety of techniques. A simple example is using thresholded ratio images from Landsat TM bands 4 and 5 (TM4/TM5), as topographic effects (Topographic Normalization of Multispectral Satellite Imagery) are reduced, which facilitates mapping. Classification of debris-covered ice is more complex however (Bishop et al., 2001; Paul et al., 2004b), because of the spectral similarities between the supraglacial debris cover and the rocks and sediment in the ablation and proglacial valleys. This issue has often been addressed by using manual digitization as the predominant technique for delineating the glacier boundary for small samples.

It is important to note that the use of traditional statistical-based *image classification* algorithms to classify glaciers rely upon the concept of statistical separability in *n*-dimensional feature space to be able to distinguish between classes. In general, it is difficult to effectively utilize multispectral imagery and spectral features to permit spectral differentiation. Consequently, researchers are investigating other classification algorithms, which are based on fuzzy logic, and can incorporate inaccurate sensor measurements, vague class descriptions, and imprecise modeling into the analysis, by assigning values to each pixel representing the pixel's degree or probability of membership in each class. This method removes a large part of the error associated with mixed pixels, but does not necessarily provide a solution to distinguishing between spectrally identical materials. Artificial intelligence techniques such as neural networks and expert systems can also be employed, although researchers have recognized that additional information such as geomorphometric land surface parameters, texture, context, and spatial topology must be utilized (Bishop et al., 2001, 2004; Paul et al., 2004b). It is widely recognized that many approaches are empirical and require thresholding, which may not be universally applicable, and also require manual editing to ensure a satisfactory level of accuracy.

Several approaches can be used to address this problem that range in levels of sophistication and accuracy. Paul et al. (2004b) proposed an approach that followed five major steps: (1) the identification of clean ice using a TM4/TM5 ratio; (2) the classification of vegetation-free areas using the hue component of an intensity-hue-saturation image transformation; (3) the identification of flat ($<24°$) terrain, characteristic of low-angle debris-covered glacier tongues; (4) the removal of noise using a median filter; and (5) the removal of all pixel clusters not connected to classified clean ice. The authors concluded that the method could be rapidly applied to hundreds of glaciers, and that the accuracy obtained can be equal to pixel resolution (Figure 2).

Bishop et al. (2001) developed an automated approach that makes use of geomorphometry and object-oriented analysis of land surface parameters such as terrain slope angle, slope azimuth, curvature, and relief to diagnostically map and delineate debris-covered glaciers. They were able to accurately delineate the ablation zone of the heavily debris-covered Raikot Glacier in the Nanga Parbat Himalaya. Terrain-object properties were found to be diagnostic of glacier processes representing glacierization, thereby differentiating glacier topography from other surfaces governed by other surface processes. The approach has tremendous potential although it requires the use of high-quality DEMs, which may not always be available.

In general, studies of changes in alpine glacier extent indicate accelerated decline in recent decades, although glaciers in some regions of the world have been expanding (Hewitt, 2005). Small glaciers are disappearing, and in many places around the world large glaciers are fragmenting into a number of smaller glaciers. Recession has been shown to be particularly strong in the European Alps, where glaciers between 0.1 and 1 km^2 in area comprise approximately 25% of all glacierized area (Kääb et al., 2002). Here, wastage has been particularly strong since the 1970s, with a reduction in glacierized area of 22% from 1973 to 1999 being measured using digitized inventory data and Landsat TM imagery, respectively. Measurements of change in glacier area are not always representative of glacier recession, however, as the extent may remain relatively constant even though down-wasting (surface lowering) is rapidly occurring. This is the case with many debris-covered glaciers of Central and eastern Asia, where surface lowering is the major symptom of wastage, and multi-temporal measurements of surface topography (Glacier Elevation Changes) can give the most accurate indication of recession rates (Bolch et al., 2008).

Glacier geomorphology

Mountain topography is the result of complex interactions involving tectonism, climate, and surface processes. Glacier geomorphology refers to the influence of glaciers and glacier processes on landform development and landscape evolution (Evans, 2006). Mapping and assessing landforms and erosion in mountain environments is essential in order to understand landscape denudation and complex feedback mechanisms (Bishop et al., 2003).

Satellite imagery and digital elevation models can be used to obtain information about landforms, erosion potential, and tectonic impact on the topography. Traditional geomorphological mapping is conducted in the field, using an *orthorectified* satellite image or aerial photograph as a base layer, to aid interpretation and to provide a spatial reference for observations made in the field. The choice of scale and level of detail may be restricted by the spatial resolution of the base layer, which may also determine the locational accuracy of features placed on the resulting map. As a rule of thumb, the geomorphologist working on a 1:10,000-scale base should aim for a locational accuracy of 1 mm on the map, equivalent to 10 m on the ground.

With the advent of GIS, it is possible to conduct terrain analysis to segment the topography into functional units (e.g., drainage basins), generate a drainage network, and map a variety of glacial features and landforms (e.g., ice

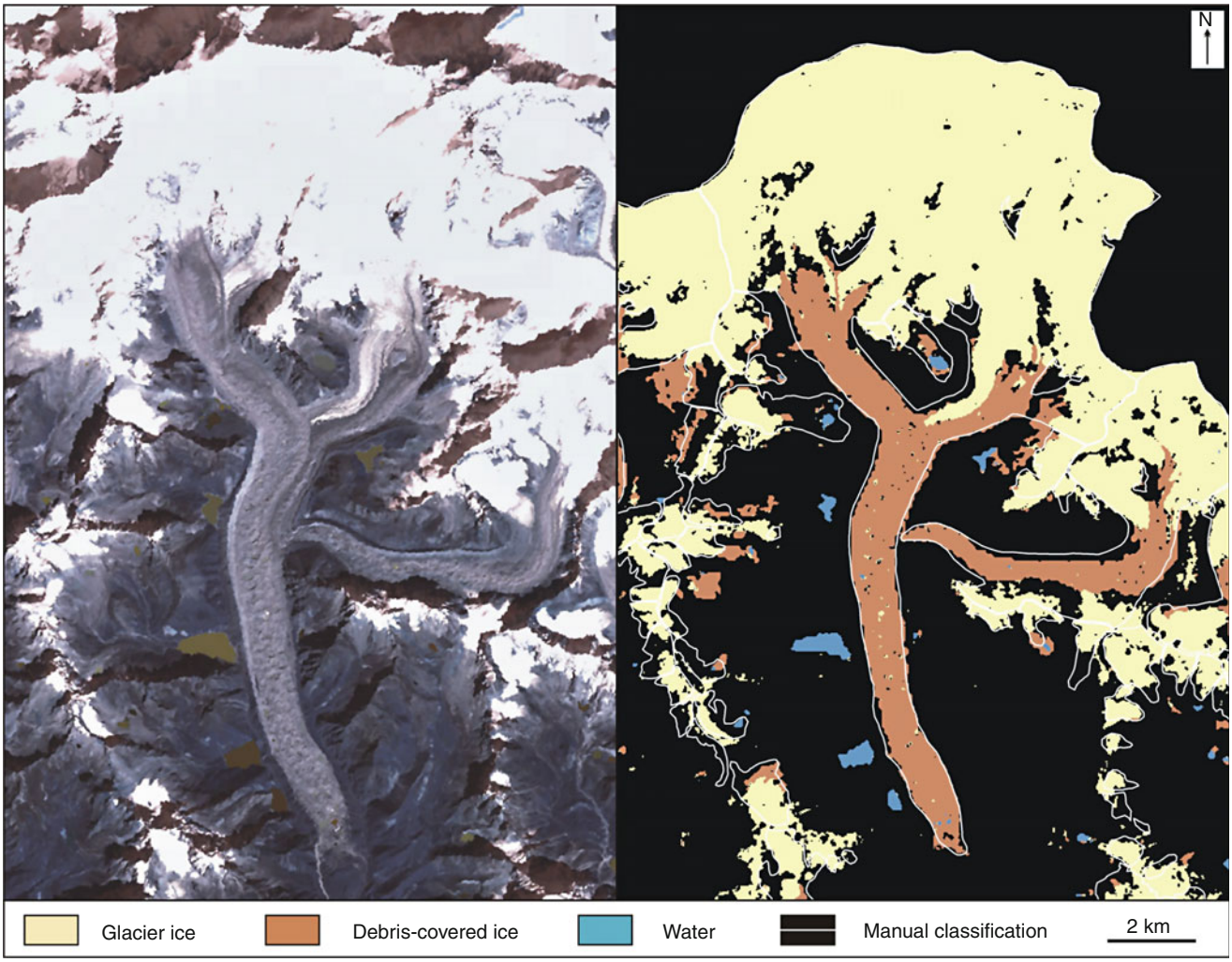

Optical Remote Sensing of Alpine Glaciers, Figure 2 Semiautomatic classification of the Ngozumpa Glacier, Nepal Himalaya, following the method of Paul et al. (2004b).

cliffs, medial moraines, and lateral moraines). Terrain analysis combined with multispectral image analysis permits an assessment of the surface biophysical conditions. Hypsometric analysis of the topography and other geomorphometric techniques (see below) can facilitate an assessment of landscape dissection and erosion, thereby depicting the influence of glacial erosion in relation to relief production. Research indicates that glacier erosion reduces relief at intermediate altitudes, although the hypsometric integral may be relatively low. Other surface processes such as river incision and mass movement increase local relief and generate a relatively low integral value. Furthermore, object-oriented analysis of the morphology of drainage basins and valley profiles reveal those portions of the landscape that currently exhibit rapid uplift rates. Collectively, this information generated from satellite imagery permits geomorpholgical assessment and evaluation of the polygenetic nature of landscape evolution.

Glacier geomorphometry

Glacier geomorphometry refers to the three-dimensional topographic characteristics of the glacier surface including its size, shape, hypsometry, orientation, and position. Numerous geomorphometric parameters govern microclimatic conditions and have been shown to influence glacier fluctuations (Gellatly et al., 1986; Warren, 1991), ELA positions (Equilibrium-Line Altitude (ELA)) on a subregional scale (Allen, 1998), ablation rates, velocity gradients, supraglacial lake development, and possibly glacier surging (Barrand and Murray, 2006; Glacier Surging). Consequently, geomorphometric analysis is fundamental for understanding glacier form–process relationships and estimating glacier mass balance.

Digital elevation models of a glacier surface can be generated using terrestrial laser-scanning equipment; however, DEMs derived from airborne and satellite sensors are critical for synoptic coverage. Geomorphometric

analysis can be used to generate a large number of glacier surface parameters, although the accuracy of these parameters is dependent on the accuracy and level of detail represented in the DEM. Accuracy and uncertainties are governed by the image sources (aerial photography and satellite imagery) used to derive the DEM, as well as the quality of the input ground control and tie-point data. Land surface parameters can be used for glacier mapping, or as input into numerical models to simulate glacier dynamics.

Quantifying surface dynamics

Glacier ice-flow velocity fields

Multitemporal aerial and satellite imagery are useful for detecting glacier surface changes and the movement of surface features caused by ice flow. Although the surface ice-flow speed of a glacier is not, strictly speaking, the same as glacier velocity (ice velocity profiles change significantly with depth (Glacier Motion/Ice Velocity)), it provides a useful surrogate for velocity where detailed field investigations are not possible. Early measurements of surface velocity were made using co-registered optical images and measuring the displacement of prominent features (e.g., large boulders, crevasses, and supraglacial ponds) over the imaged period, by hand. This resulted in a sparse, point-based velocity field, derived with a maximum accuracy of ± 1 pixel.

Improved methods for co-registering multi-temporal data and increased computational power has led to the emergence of automated feature tracking, which relies on the same fundamental principle as manual feature tracking – the identification of the same feature across an image pair – but provides a dense coverage of matched features with a reported sub-pixel accuracy (Scherler et al., 2008; LePrince et al., 2007; Figure 3). The first stage in feature tracking is to finely co-register the two images. This is achieved by selecting features known to be stationary (e.g., bedrock outcrops) and matching the images to sub-pixel accuracy using cross-correlation only in these stationary areas. In this way, ground control for zero velocities is provided, against which glacier movement can be compared, and velocities retrieved from stationary areas can provide a measure of error associated with the technique. Subsequently, cross-correlation is applied to the whole image (i.e., to both stationary and nonstationary areas). Robust correlations are accepted on the strength of their signal-to-noise ratio and by rejecting matches in regions of shadow. Errors in the technique arise from changes in the crevasse patterns through time and space, geometric transformations of the data, and errors in zero displacement reference points. The longer the time delay between images, the lower the error related to measured displacement but the larger the error in finding an exact match for a surface pattern that may have changed through time.

Glacier elevation changes

Many alpine glacier snouts are partially or completely debris-mantled (Debris-Mantled Glacier Snouts), and

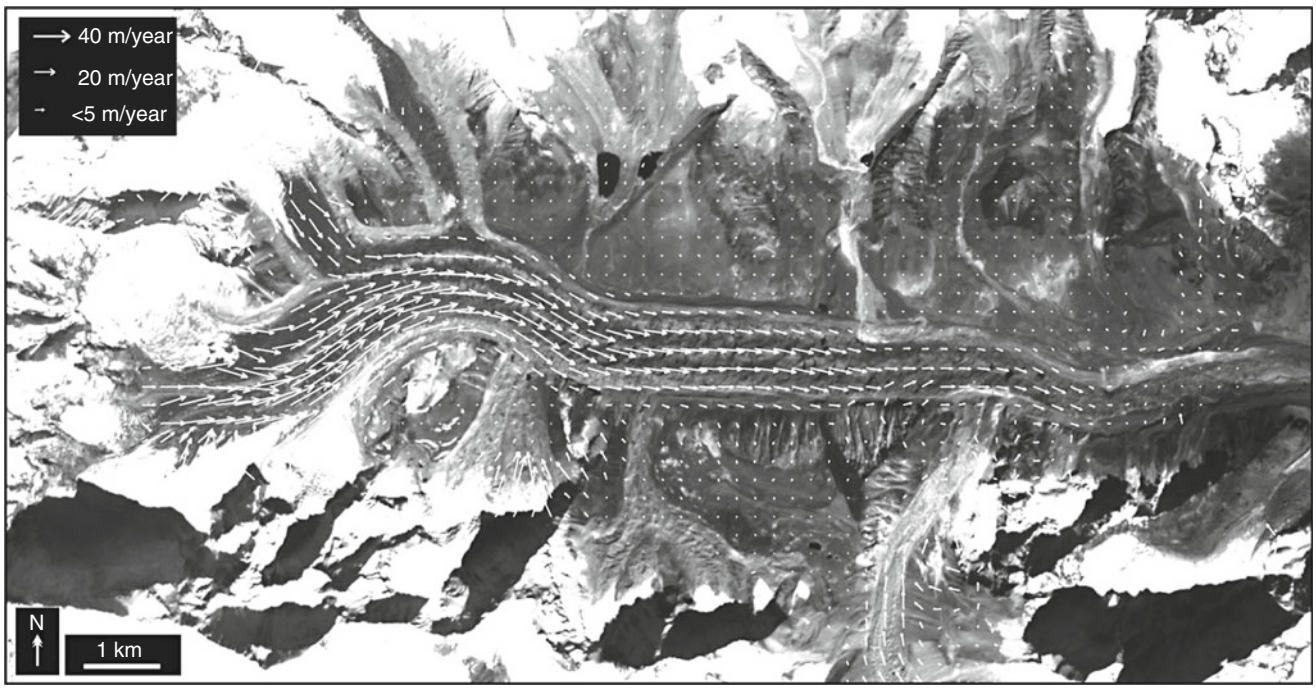

Optical Remote Sensing of Alpine Glaciers, Figure 3 Glacier velocity field for the Kangshung Glacier, Nepal Himalaya, using multi-temporal ASTER imagery from October 2004 and December 2005.

sustained periods of negative mass balance result in extensive down-wasting and stagnation of low elevation glacier tongues. In such cases, frontal recession can be a poor indicator of glacier health, and measurements of volumetric change are thus required. Multi-temporal DEM data have been widely used to make assessments of glacier surface lowering (or thickening) and, consequently, calculations of mass wastage (or accumulation).

A major difficulty in using stereo satellite imagery to generate elevation data over glacier surfaces is that snow and ice often do not provide sufficient spectral variation to correlate image pairs. In such areas, the automatic extraction of elevation data can fail, or be subject to large error. Debris-covered glaciers normally exhibit a wide range of features on which tie points can be placed, but again problems can occur in accumulation areas where snow and ice make the surface cover homogeneous. Such problems can often be overcome by employing imagery acquired toward the end of the ablation season, when snow cover is at a minimum, and by choosing low-sun illumination angles, to enhance the sensitivity of the reflectivity to micro-topography (Berthier and Toutin, 2008). Large errors can also occur on sharp mountain peaks with steep slopes, narrow moraine ridges, and deep stream channels (Kääb, 2002), but can often be identified and rectified by manual editing of the resultant DEM.

Distortions between multi-temporal products can be minimized by processing all images within a single image block (Kääb, 2002). This is done by connecting multi-temporal stereo models to each other by a large number of tie points, the absolute coordinates of which do not need to be known. Model ground control points (GCPs; features identified on imagery with known x, y and z coordinates) introduce a second-order error that is small (in the order of a few percent) for the final vertical displacements, which is consistent between the two DEMs providing they are bundle adjusted as a single image block. Therefore, the technique can, in theory, be used without any ground control at all, while still producing accurate vertical displacement results from the relative image orientation alone.

Digital elevation data derived from separate sources can also be employed to measure glacier surface elevation displacements, but usually with reduced accuracy. Some of the oldest imagery available for DEM extraction comes from the CORONA satellite series (1960–1972), originally collected for American intelligence but recently declassified. The absolute errors associated with a single DEM extraction from CORONA data can be relatively high, but if surface changes are measured over a sufficiently long time period, the magnitude of displacement can still exceed any uncertainty in the combined datasets (Bolch et al., 2008). Contemporary DEM data are most often provided by the ASTER and SPOT HRS and HRG sensors, at a spatial resolution of ~15–30 m, much coarser than those available from IKONOS and Quickbird (~5–10 m), but at lower cost. In particular, the SPOT HRS sensor is capable of producing elevation data using only the sensor acquisition parameters (position and attitude), removing the requirement of a priori knowledge of ground-based feature locations (GCPs), which is of particular value for the study of remote glaciers, or those with limited accessibility (Berthier and Toutin, 2008).

Assessing accumulation and ablation

Snow grain size and albedo

Using sensor measurements in the visible and near-infrared portions of the electromagnetic spectrum, it is possible to derive information on snow grain size, from which albedo (Albedo) can also be estimated.

Snow grain size can crudely be estimated using reflectance data collected in the near-infrared and shortwave infrared portions of the spectrum, but the most accurate quantifications of grain size are available using reflectance data specifically collected in the range 1.0–1.3 μm. In particular, a prominent ice absorption feature exists at 1.03 μm, and reflectance measurements made in a continuum across this wavelength are most robust.

Albedo is primarily determined by snow grain size at near-infrared wavelengths, and by absorbing impurities in the visible portion of the spectrum. Albedo is the single most important input parameter for determining the surface energy balance of a glacier, which, in turn, can be used to model ablation, ultimately contributing to mass balance estimates (see below).

ELA assessment

The ELA (Equilibrium-Line Altitude (ELA)) marks the position where, over a period of 1 year, accumulation of snow is exactly balanced by ablation (Benn and Lehmkuhl, 2000). Measurements of the ELA over multiple years can provide an indication of glacier response to climate change, as well as allow reconstructions of former climates and the prediction of future glacier behavior. Remote sensing imagery can be useful for determining the transient snowline altitude (SLA – Transient Snowline), which itself is a reasonable proxy for ELA at the end of the ablation season (Clare et al., 2002).

The SLA can be defined as the boundary between snow and ice and can be delineated using, for example, the Normalized Difference Snow Index (NDSI). The NDSI exploits the high-reflectance properties of snow and ice in visible wavelengths and their high-absorption properties at shortwave infrared wavelengths:

$$\mathrm{NDSI} = (B_{\mathrm{Blue}} - B_{\mathrm{SWIR}})/(B_{\mathrm{Blue}} + B_{\mathrm{SWIR}})$$

In addition to the specific boundary between snow and ice, different snow facies may also be observed using the NDSI, for input to snowmelt runoff modeling simulations.

Mass balance

Local scale (i.e., single glacier) observations of mass balance (Glacier Mass Balance) are most commonly carried out using repeat measurements of accumulation and ablation at stakes and snow pits on the glacier surface to

determine summer and winter balances. This glaciological approach, however, does not account for the high spatial variability of ablation as controlled by debris cover, glacier surface topography, and mesoscale topographic variations. Consequently, remote sensing offers the only practical approach to address such high spatial variability and assessment of multiple glaciers within a region.

The simplest method for estimating glacier mass balance relies upon the successful identification of the AAR (Accumulation Area Ratio), which can be calculated when the ELA is known (see above) and the glacier extent is accurately delineated. Where measurements of AAR from remote sensing are combined with field measurements of mass balance, remote quantification of changes in the glacier mass balance becomes possible by observing changes in AAR. This method is locally specific, however, primarily because of the requirement for in situ calibration data, but also because the ELA may change from glacier to glacier due to the strong influence of avalanching, debris cover, and topographic effects on patterns of accumulation and ablation.

Similarly, observed changes in areal glacier extent may be used as a proxy for mass balance, but interpretation should be made with caution. Terminus recession is often taken as an indication of negative mass balance, but may not be truly reflective of mass changes across the glacier as a whole. A stable glacier terminus does not necessarily indicate equilibrium either; many glaciers, particularly those that are debris-covered, react to changes in mass by thickening or thinning. It has been suggested that for debris-covered glaciers in the Himalaya, the surface topographic profile may indicate an increasing or decreasing mass, with thickening/advancing glaciers indicated by a convex surface profile, and thinning/receding glaciers depicting a concave surface profile (Quincey et al., 2009).

The geodetic approach to measuring mass balance also uses glacier surface topography as an indication of long-term accumulation and ablation trends (e.g., Berthier et al., 2007). Glacier elevation changes (see above) are typically measured over multiple years, or even decades, to ensure short-term variabilities in accumulation and ablation do not bias the data, and also to ensure the errors in the technique do not exceed the magnitude of change to be measured. The change in elevation can then be translated into a change in mass assuming the surrounding terrain is stable (i.e., not tectonically active) and the density of the ice mass has not changed significantly between image acquisitions. For a more complete treatment of remote sensing methods for determining glacier mass balance, refer to Bamber and Rivera (2007).

Debris-cover assessment

Supraglacial debris characteristics are known to play a significant role in governing glacier dynamics (Kirkbride, 2000). Specifically, the supraglacial lithologies, coverage, and debris cover thickness regulate ablation and the availability of meltwater. Consequently, remote sensing of supraglacial debris parameters is vital for (1) the assessment of surface energy-balance and estimation of ablation rates, (2) runoff modeling in mountain catchments, (3) the assessment of glacier lake development and catastrophic flooding, (4) understanding glacier response to climate forcing, and (5) estimating the magnitude of sea-level rise caused by alpine glaciers.

Supraglacial debris lithology dictates thermal properties and heat flux that control ablation beneath the debris. This supraglacial parameter can frequently be assessed using satellite imagery acquired from the visible, near-infrared, and middle-infrared regions of the spectrum. Igneous, sedimentary, and metamorphic lithologies can often be differentiated and mapped, given spectral variations caused by felsic versus mafic minerals. This capability is significantly improved when using hyperspectral data, such that diagnostic mineral spectral absorption features can be utilized. The ability to uniquely map supraglacial lithologies is highly dependent upon the spatial, spectral, and radiometric characteristics of the sensor. In general, dominant lithologies and debris-cover estimates can be generated using a variety of methodological approaches.

The most significant supraglacial debris parameter related to ablation is debris-cover thickness. The relationship between debris thickness and ablation is nonlinear, as a thin layer of debris enhances ablation, while thick debris reduces ablation. Empirical studies indicate hyperbolic trends exist between debris-cover thickness and ablation (Figure 4), although different magnitudes and gradients in the relationship are common due to geographic location and many other variables (Mattson et al., 1993).

Assessing this variable via remote sensing can be complex, as numerous processes regulate the debris thickness

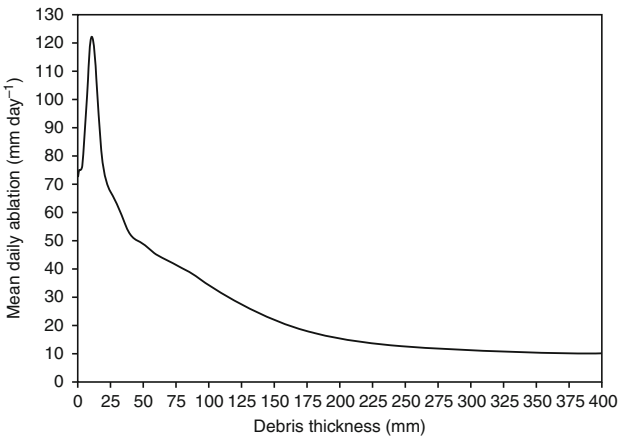

Optical Remote Sensing of Alpine Glaciers,
Figure 4 Relationship between debris-cover thickness and ablation for the Raikot Glacier, located in the Nanga Parbat Himalaya, Pakistan. The general nonlinear trend in ablation has been reported on other debris-covered glaciers. Ablation data for the period June 22 to August 8, 1986. From Mattson et al. (1993).

and the amount of energy available to melt ice. The geographic location (x,y,z) and local topographic parameters (i.e., slope and slope azimuth) govern solar geometry and the magnitude of incident shortwave and long-wave radiation. Lithological differences influence the surface albedo and net radiation flux. Sediment transfer due to ice motion and slopes alters sediment depth and compressive ice flow results in a thickening of the debris layer. Thinning and thickening of the debris can also result from sediment settling and englacial-load meltout. Supraglacial debris is also transported and deposited via meltwater, while variations in debris moisture content alter the surface albedo and the thermal conductivity. Differential ablation also exhibits feedbacks with topography and sediment transport. Consequently, glaciers can exhibit extreme spatiotemporal variability in debris-cover thickness, making this a complex parameter to accurately estimate.

Nevertheless, thermal imagery can be used to estimate debris-cover thickness and thermal resistivity (Suzuki et al., 2007; Mihalcea et al., 2008). The approach is based upon using the thermal resistance of a debris layer as an index for ice melting, where thermal resistance (R) is defined as

$$R = \frac{h}{k}$$

where R is in units of m^2 K W^{-1}, h is debris thickness (m), and k is thermal conductivity (m^{-1} K^{-1} W). The thermal resistance can be estimated assuming a linear trend in the temperature profile within the debris layer given an ice temperature of 0°C such that

$$Q_m = \frac{T_s}{R}$$

where Q_m is the amount of energy available for melting (conductive heat flux, W m^{-2}), and T_s is the surface temperature of the debris (°C). Field measurements can be used to derive empirical equations for computing the effective thermal resistance (e.g., Mihalcea et al., 2008), and Q_m can be estimated using field weather station data or distributed models that account for the net radiation, sensible, latent, and turbulent energy fluxes. Furthermore, researchers have found linear and nonlinear relationships between T_s and h (Mihalcea et al., 2008). Consequently, surface temperature estimates generated from thermal imagery can be used to map debris depths and thermal resistance.

Ultimately, the ablation rate beneath a debris layer can be computed as

$$A = \frac{Q_m}{\rho_i L_f}$$

where A is the ablation rate (m s^{-1}), ρ_i is the density of ice (900 kg m^{-3}), and L_f is the latent heat of fusion (334 kJ kg^{-1}).

Hazard evaluation – glacial lakes

Glacial lake formation

Glacier-related floods occur when water is released from the glacial drainage system (subglacially, englacially, or supraglacially) or from lakes dammed behind glacier ice or moraine material (Richardson and Reynolds, 2000). Supraglacial lakes tend to form on debris-covered (rather than clean ice) glaciers, and begin as a number of small, supraglacial ponds where insulating debris cover is absent because of crevassing or sink holes. These small ponds expand rapidly because of subaerial melt and then by subaqueous calving, increasing in size until they coalesce with adjacent water bodies, or intercept an englacial conduit and drain. Rapid lake growth follows once hydrological base level is reached and the ponds cease to be ephemeral (Benn et al., 2001).

Remote sensing can be used to rapidly identify existing glacial lake locations, lake sizes, and rates of expansion. Water has particularly low spectral reflectance at near-infrared wavelengths, so the automatic delineation of supraglacial ponds and streams is a relatively straightforward task. The NDWI (cf. Huggel et al., 2002) is commonly applied:

$$\mathrm{NDWI} = (B_{\mathrm{NIR}} - B_{\mathrm{Blue}})/(B_{\mathrm{NIR}} + B_{\mathrm{Blue}})$$

Predicting future lake development is a more complex task. It has been shown that lakes commonly form on flat glacier tongues, the identification of which is possible using digital elevation data, derived from overlapping remote sensing images. Other factors such as dam characteristics and trigger mechanisms also play an important role on lake development and outburst potential and can sometimes be identified or discounted by remote sensing image analysis where the imagery is sufficiently detailed.

Dam characteristics

The existence of a moraine dam to impound water represents one of the more important factors for predicting lake formation. However, automatic delineation of dam structures from remote sensing data can be problematic, because they usually comprise materials very similar or even identical to glacier debris and also the surrounding environment. Visual inspection is often the most appropriate method for detecting a dam structure although the integration of elevation data allows more detailed and precise information to be derived regarding (1) the height of the dam from the valley floor and (2) the dam crest relative to the glacier or lake surface. DEM data can also highlight the presence of any low points on the dam that could be exploited as a point of weakness should a lake-outburst occur (Figure 5).

The geometry and composition of a dam are the two most important parameters related to its stability and thus the susceptibility of a lake to overtopping or breaching. The height-to-width ratio of the moraine dam is an indicator of its ability to withstand displacement waves and can be determined from fine-resolution elevation data.

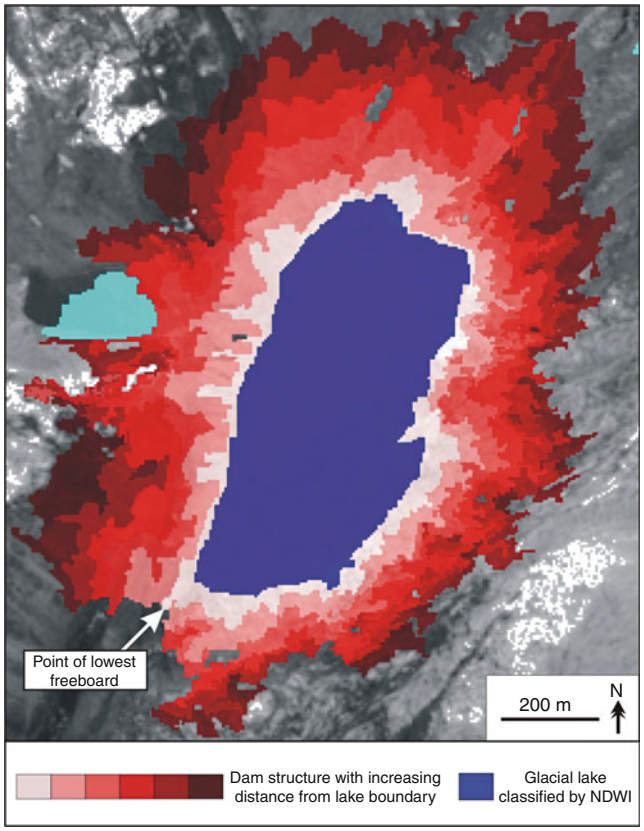

Optical Remote Sensing of Alpine Glaciers, Figure 5 Automatic delineation of a natural dam structure impounding a glacial lake in the Nepal Himalaya, and the identification of the point of lowest freeboard where overtopping is most likely to occur. Measurements were made using eCognition segmentation-based software and an ASTER-derived DEM.

Similarly, freeboard height can be determined once a lake has developed providing reliable elevation data can be extracted from the (usually featureless) water surface.

Trigger mechanisms

Ice avalanches are the most common source of displacement waves in many of the high-mountain ranges of the world. Where receding glaciers exist upstream of a large glacial lake, the possibility of displacement-wave generation from ice avalanching is substantially heightened. The positive identification of ice and rock avalanche sources is also difficult with current remote sensing imagery, however. Digital elevation models can aid in the identification of ice and rock slopes above a certain threshold (Salzmann et al., 2004), but their susceptibility to failure is difficult to assess without detailed fieldwork.

Issues and concerns

While optical remote sensing can provide a useful range of data at various spatial, spectral, and temporal scales for mapping and characterizing alpine glacial environments, analyses based solely on remote sensing can be limited by specific sensor system characteristics. First, fine spatial resolution data remain too costly for most users. Aerial photographs have been shown to provide very fine-resolution data on microscale glacial processes, but overflights are expensive to commission, and, although historical photography often exists, locating and purchasing the imagery can be difficult, particularly in politically sensitive regions. Even where data are available, their usefulness can be limited by missing or incomplete calibration parameters, poor reproduction, and an absence of coincident field data. Where fine-spatial resolution satellite data are available, swath widths are generally narrow (e.g., 60 km), limiting analyses to single, or at best a small number of glaciers. Given the scale of extensive mountain ranges around the world, the limited spatial coverage is problematic for glacier inventory compilation, as full coverage over a large area is not always available.

Second, many satellite sensors are limited to measuring spectral reflectance in a relatively small (often <10) number of discreet spectral bands that are not always appropriate for a given application. Hyperspectral satellite data are becoming increasingly available, but their value for glacial studies is yet to be fully evaluated and validated, particularly as these sensors may exhibit a relatively low spatial resolution (e.g., 60 m for the proposed HYSPIRI sensor). Regardless of spectral resolution, all optical sensors are hampered by atmospheric effects including aerosols and clouds. In areas with extreme relief (i.e., the majority of glacierized alpine terrain) this can be particularly problematic, with persistent cloud cover masking large areas for long periods. Where coincident data are collected in the SWIR part of the spectrum (e.g., by ASTER), cloud cover can be easily identified and removed from an image, although surface reflectance data are unavailable. Furthermore, the complex topography of mountain environments produces differential illumination and cast shadows, which limits selected areas from being analyzed. Therefore, most satellite imagery contains a topographic effect, such that surface reflectance variations are caused by multi-scale topographic effects and do not entirely represent surface matter biophysical conditions. Given these issues, the imagery must be carefully radiometrically calibrated to account for anisotropic reflectance variations caused by topography. This issue is usually addressed by utilizing spectral features such as image ratios and principal component images that reduce, but do not eliminate topographic variation.

Finally, for satellite sensor data to be used routinely for glacier observations, a range of temporal overpass frequencies is required. For example, the end of the ablation season (August/September for Northern Hemisphere) is usually the optimum time for extracting glacier-related information, but at midlatitudes satellite overpass frequency is lower than toward the poles and therefore coverage of an exact time period is not always possible. Optimum times even differ between regions, based upon

climate dynamics, for example (e.g., monsoon season). Furthermore, change detection studies usually require systematic time frames, and for many regions of the world the multi-temporal coverage is inadequate.

In addition to sensor system characteristics, problems exist in the methods used to process satellite imagery for information extraction. Scientists employ a wide range of analytical tools, algorithms and processing approaches when studying the glacial environment, but the exact methods followed are highly empirical, such that the accuracy of the derived information is highly dependent upon the analyst. This means that it can be difficult for remote sensing scientists to repeat analysis efforts presented elsewhere, and even more difficult to take existing methods and apply them to new areas. Standardization and protocols for information extraction are required if the quality of data, the accuracy of published results, and the validity of comparing measurements across different studies (and study areas), is to be assured.

Summary

The increasing availability of optical data (often without charge) and the range of potential applications in glaciological studies have made remote sensing an essential part of glaciology. It provides the only realistic means of conducting glaciological work over large areas, which is quite often necessary as an event, change, or feature in one part of the glacial system can be a product of processes interacting many kilometers away. Human interpretation of optical satellite imagery remains an important method of information extraction, although computer-assisted analysis and the development of new algorithms and processing procedures are increasingly improving our ability to accurately generate "higher-level" quantitative information that is not directly apparent from visualizations (e.g., surface velocity fields and debris-depth maps). While a number of limitations still exist in the use of remote sensing data for glaciological studies, remote sensing, terrain analysis, and GIS-based numerical modeling can be effectively utilized to generate a wealth of information about glacierized terrain that complements, and even in some cases improves upon, field investigations. Continuing advances in sensor technology, processing methods, and numerical models are expected to overcome the most significant of these limitations in coming years, and therefore yield even more detailed assessments of glacier characteristics and processes.

Bibliography

Allen, T. R., 1998. Topographic context of glaciers and perennial snowfields, Glacier National Park, Montana. *Geomorphology*, **21**, 207–216.

Bamber, J. L., and Rivera, A., 2007. A review of remote sensing methods for glacier mass balance determination. *Global and Planetary Change*, **59**, 138–148.

Barrand, N. E., and Murray, T., 2006. Multivariate Controls on the Incidence of Glacier Surging in the Karakoram Himalaya. *Arctic, Antarctic, and Alpine Research*, **38**(4), 489–498.

Benn, D. I., and Lehmkuhl, F., 2000. Mass balance and equilibrium-line altitudes of glaciers in high-mountain environments. *Quaternary International*, **65**(66), 15–29.

Benn, D. I., Wiseman, S., and Hands, K. A., 2001. Growth and drainage of supraglacial lakes on debris-mantled Ngozumpa Glacier, Khumbu Himal, Nepal. *Journal of Glaciology*, **47**, 626–638.

Berthier, E., and Toutin, T., 2008. SPOT5-HRS digital elevation models and the monitoring of glacier elevation changes in North-West Canada and South-East Alaska. *Remote Sensing of Environment*, **112**, 2443–2454.

Berthier, E., Arnaud, Y., Kumar, R., Ahmad, S., Wagnon, P., and Chevallier, P., 2007. Remote sensing estimates of glacier mass balances in the Himachal Pradesh (Western Himalaya, India). *Remote Sensing of Environment*, **108**, 327–338.

Bishop, M. P., Bonk, R., Kamp, U., and Shroder, J. F. Jr., 2001. Terrain analysis and data modeling for alpine glacier mapping. *Polar Geography*, **25**, 182–201.

Bishop, M. P., Shroder, J. F. Jr., and Colby, J. D., 2003. Remote sensing and geomorphometry for studying relief production in high mountains. *Geomorphology*, **55**, 345–361.

Bishop, M. P., Barry, R. G., Bush, A. B. G., Copland, L., Dwyer, J. L., Fountain, A., Haeberli, W., Hall, D. K., Kaab, A., Kargel, J. S., Molnia, B. F., Olsenholler, J. A., Paul, F., Raup, B. H., Shroder, J. F., Trabant, D. C., Shroder, J. F., and Wessels, R., 2004. Global Land-Ice Measurements from Space (GLIMS): remote sensing and GIS investigations of the Earth's cryosphere. *Geocarto International*, **19**(2), 57–84.

Bolch, T., Buchroithner, M., Pieczonka, T., and Kunert, A., 2008. Planimetric and volumetric glacier changes in the Khumbu Himalaya since 1962 using Corona, Landsat TM and ASTER data. *Journal of Glaciology*, **54**(187), 592–600.

Clare, G. R., Fitzharris, B. B., Chinn, T. J. H., and Salinger, M. J., 2002. Interannual variation in end-of-summer snowlines of the Southern Alps of New Zealand, and relationships with Southern Hemisphere atmospheric circulation and sea surface temperature patterns. *International Journal of Climatology*, **22**, 107–120.

Dozier, J., and Painter, T. H., 2004. Multispectral and hyperspectral remote sensing of Alpine snow properties. *Annual Review of Earth and Planetary Sciences*, **32**, 465–494.

Dyurgerov, M. B., and Meier, M. F., 2005. Glaciers and the changing earth system: A 2004 snapshot. Occasional paper 58. Institute of Arctic and Alpine Research, University of Colorado, Boulder.

Evans, D. J. A., 2006. Glacial landsystems. In Knight, P. G. (ed.), *Glacier Science and Environmental Change*. Oxford: Blackwell, pp. 83–88.

Gellatly, A. F., Whalley, W. B., and Gordon, J. E., 1986. Topographic control over recent glacier changes in southern Lyngen Peninsula, North Norway. *Norsk Geografisk Tidsskrift*, **40**, 211–218.

Hewitt, K., 2005. The Karakoram Anomaly? Glacier Expansion and the 'Elevation Effect,' Karakoram Himalaya. *Mountain Research and Development*, **25**(4), 332–340.

Huggel, C., Kääb, A., Haeberli, W., Teysseire, P., and Paul, F., 2002. Remote sensing based assessment of hazards from glacier lake outbursts: a case study in the Swiss Alps. *Canadian Geotechnical Journal*, **39**(2), 316–330.

Huggel, C., Zgraggen-Oswald, S., Haeberli, W., Kääb, A., Polkvoj, A., Galushkin, I., and Evans, S. G., 2005. The 2002 rock/ice avalanche at Kolka/Karmadon, Russian Caucasus: assessment of extraordinary avalanche formation and mobility, and application of Quickbird satellite imagery. *Natural Hazards and Earth System Sciences*, **5**, 173–187.

Kääb, A., 2002. Monitoring high-mountain terrain deformation from repeated air- and spaceborne optical data: examples using digital aerial imagery and ASTER data. *ISPRS Journal of Photogrammetry and Remote Sensing*, **57**, 39–52.

Kääb, A., Paul, F., Maisch, M., Kellenberger, T., and Haeberli, W., 2002. The new remote sensing derived Swiss glacier inventory: II. First results. *Annals of Glaciology*, **34**, 362–366.
Kargel, J. S., Abrams, M. J., Bishop, M. P., Bush, A., Hamilton, G., Jiskoot, H., Kääb, A., Kieffer, H. H., Lee, E. M., Paul, F., Raui, F., Raup, B., Shroder, J. F., Soltesz, D., Stainforth, D., Stearns, L., and Wessels, R., 2005. Multispectral imaging contributions to global land ice measurements from space. *Remote Sensing of Environment*, **99**(1–2), 187–219.
Kirkbride, M. P., 2000. Ice marginal geomorphology and Holocene expansion of debris-covered Tasman Glacier, New Zealand. In Nakawo, M., Raymond, C., and Fountain, A. (eds.), *Debris-Covered Glaciers*, 264th edn. Oxfordshire, UK: IAHS, pp. 211–217.
LePrince, S., Barbot, S., Ayoub, F., and Avouac, J-P., 2007. Automatic and precise orthorectification, coregistration, and subpixel correlation of satellite images, application to ground deformation measurements. *IEEE Transactions Geoscience Remote Sensing*, **45**(6), 1529–1558.
Mattson, L. E., Gardner, J. S., and Young, G. J., 1993. Ablation on Debris Covered Glaciers: an Example from the Rakhiot Glacier, Punjab, Himalaya. Snow and Glacier Hydrology (Proceedings of the Kathmandu Symposium, November 1992). *IAHS*, **218**, 289–296.
Meier, M. F., and Wahr, J. M., 2002. Sea level is rising: do we know why? *Proceedings of the National Academy of Science*, **99**(10), 6524–6526.
Meier, M. F., Dyurgerov, M. B., Rick, U. K., O'Neel, S., Pfeffer, W. T., Anderson, R. S., Anderson, S. P., and Glazovsky, A. F., 2007. Glaciers dominate eustatic sea-level rise in the 21st century. *Science*, **317**, 1064–1067.
Mihalcea, C., Mayer, C., Diolaiuti, G., D'Agata, C., Smiraglia, C., Lambrecht, A., Vuillermoz, E., and Tartari, G., 2008. Spatial distribution of debris thickness and melting from remote-sensing and meteorological data, at debris-covered Baltoro glacier, Karakoram, Pakistan. *Annals of Glaciology*, **48**, 49–57.
Paul, F., Kääb, A., Maisch, M., Kellenberger, T., and Haeberli, W., 2004a. Rapid disintegration of Alpine glaciers observed with satellite data. *Geophysical Research Letters*, **31**, L21402.
Paul, F., Huggel, C., and Kääb, A., 2004b. Combining satellite multispectral image data and a digital elevation model for mapping debris-covered glaciers. *Remote Sensing of Environment*, **89**, 510–518.
Quincey, D. J., Luckman, A., and Benn, D., 2009. Quantification of Everest region glacier velocities between 1992 and 2002, using satellite radar interferometry and feature tracking. *Journal of Glaciology*, **55**(192), 596–606.
Richardson, S. D., and Reynolds, J. M., 2000. An overview of glacial hazards in the Himalayas. *Quaternary International*, **65**(66), 31–47.
Salzmann, N., Kääb, A., Huggel, C., Allgöwer, B., and Haeberli, W., 2004. Assessment of the hazard potential of ice avalanches using remote sensing and GIS-modelling. *Norsk Geografisk Tidsskrift*, **58**, 74–84.
Scherler, D., Leprince, S., and Strecker, M. R., 2008. Glacier-surface velocities in alpine terrain from optical satellite imagery - Accuracy improvement and quality assessment. *Remote Sensing of Environment*, **112**(10), 3806–3819.
Singh, P., and Bengtsson, L., 2005. Impact of warmer climate on melt and evaporation for the rainfed, snowfed and glacierfed basins in the Himalayan region. *Journal of Hydrology*, **300**, 140–154.
Suzuki, R., Fujita, K., and Ageta, Y., 2007. Spatial distribution of thermal properties on debris-covered glaciers in the Himalayas derived from ASTER data. *Bulletin of Glaciological Research*, **24**, 13–22.
Warren, C. R., 1991. Terminal environment, topographic control and fluctuations of West Greenland glaciers. *Boreas*, **20**, 1–15.

OROGRAPHIC PRECIPITATION

Justin R. Minder[1], Gerard H. Roe[1,2]
[1]Department of Atmospheric Science, University of Washington, Seattle, WA, USA
[2]Department of Earth and Space Sciences, University of Washington, Seattle, WA, USA

Definition

Precipitation that has been generated or modified by topography, typically through the forcing of vertical atmospheric motions.

Introduction

The influence of mountains upon rain and snowfall is often profound, creating some of the Earth's wettest places (e.g., Cherrapunji in India, where monsoon flow encounters the southern Himalayas, has received 26.5 m in 1 year) and driest places (e.g., the central valleys of the Atacama desert, shielded by surrounding mountains, can go for decades without rainfall). Orographic effects on precipitation are also responsible for some of the planet's sharpest climatic transitions. The classic example is the so-called rain shadow; for a mountain range oriented perpendicular to the prevailing winds, precipitation is greatly enhanced on the windward side and suppressed in the lee. However, the full gamut of orographic influences is much broader than this: precipitation can be enhanced in the lee, over the crest, or well upwind of a mountain.

The mass balance of Earth's snow and ice is strongly affected by orographic precipitation. Orographic snowfall is the source of mass that maintains mountain snowpacks and glaciers. The Greenland and Antarctic Ice sheets are themselves substantial topographic features responsible for orographic effects on precipitation. Avalanches are sensitive to the detailed stratigraphy of the snowpack, which is partly determined by the sequence of orographic graupel, rain, ice, and various snow crystals that fall during storms.

This article will focus on the important physical processes controlling orographic precipitation, and the observational and modeling techniques that have been used to characterize and understand it. More complete reviews may be found in Smith (1979), Roe (2005), and Smith (2006).

Fundamentals

Orographic precipitation is shaped by myriad nonlinear processes operating on scales ranging from the 1,000 km size of storms and major mountains to the sub-micron size of cloud droplets. Still, the most fundamental of these processes are thermodynamic in nature and are well understood. Almost all orographic influences on precipitation occur due to rising and descending atmospheric motions forced by topography. These motions can be forced mechanically, as air impinging on a mountain is lifted over it, or thermally, as heated mountain slopes trigger

buoyancy-driven circulations. Rising motion causes the air to expand and cool, which is important since the amount of water that may exist as vapor in air is an approximately exponential function of temperature (described by the Clausius Clayperon equation). Thus, if cooling is sufficient, air saturates and the water vapor condenses into cloud droplets or forms cloud ice crystals. These droplets and crystals grow by various processes until they become large enough to fall as rain and snow. It is important to emphasize that moist ascent over topography alone is typically insufficient to generate precipitation: these orographic effects mainly modify precipitation during preexisting storms (e.g., Browning et al., 1974; Smith, 2006). Conversely, when air descends it warms and dries, and both cloud and precipitation evaporate.

A useful tool for understanding some of the basic controls on orographic precipitation is the "upslope" model (e.g., Smith, 1979, 2006). This idealized and physically based model predicts the water condensed when flow with a given surface-specific humidity (q_v, expressed as a mixing ratio), density (ρ), and uniform wind velocity ($\bar{U}$) impinges upon topography (with height: $h(x,y)$). The model assumes saturated air, an idealized temperature profile, and flow that parallels the topography at all heights. Under these assumptions the vertically integrated source of condensed water per unit time is:

$$S(x,y) = \rho q_v \bar{U} \cdot \nabla h(x,y) \tag{1}$$

This is also the precipitation rate at the surface if it is further assumed that conversion of cloud condensate to precipitation and fallout of precipitation are instantaneous. This model reveals some key controlling parameters: the moisture flux ($\rho\, q_v \bar{U}$), which determines the vapor available for condensation, and the topographic slope (∇h) in the direction of the airflow, which determines the rate of the forced vertical motion.

Airflow dynamics

Actual flow over topography during precipitation is seldom as simple as that assumed in the upslope model. Atmospheric density and temperature stratification strongly control the flow, since the typically stable stratification of the atmosphere means that a parcel of air displaced upwards becomes negatively buoyant (since it is cooler and denser than its surroundings) and is pulled back downwards. The strength of this effect may be quantified by the Brunt-Vaisala buoyancy frequency:

$$N^2 = \frac{g}{T}(\gamma - \Gamma) \tag{2}$$

with γ representing the observed atmospheric lapse rate (i.e., the rate of decrease of temperature with height), and Γ the theoretical dry adiabatic lapse rate for a rising air parcel (-9.8 K km^{-1}). When stratification is stable ($N^2 > 0$) the buoyancy restoring force causes airflow over mountains to take the form of waves, which oscillate with frequency N. These wave motions cause orographic uplift to be displaced upstream by varying degrees (enhancing precipitation ahead of the mountain) or decay with height (limiting precipitation enhancement) depending on the strength of the incoming flow and stratification relative to the mountain width (Smith, 1979; Smith and Barstad, 2004).

Under conditions where N^2 is large and positive, the incoming flow is weak, and/or the mountain is high, the effects of stratification can be overwhelming and the low-level flow may be unable to surmount the mountain. In such cases the flow is said to be blocked, and air is forced to deflect around the mountain, stagnate, or even reverse (e.g., Smith, 1979; Marwitz, 1987). This can result in orographic enhancement that is limited or forced to occur further upstream (e.g., Houze and Rotunno, 2007). A parameter useful for predicting the onset of blocking is the nondimensional mountain height:

$$M = \frac{hN}{\bar{U}} \tag{3}$$

where $\bar{U}$ is the incoming flow speed and h is the mountain height. When M exceeds unity blocking is favored.

When the atmosphere is unstably stratified ($N^2 < 0$) convective overturning motions may be triggered. Convective cells embedded within a storm are a common feature in orographic precipitation (e.g., Browning et al., 1974). When the atmosphere is strongly unstable orographic thunderstorms may be triggered.

As air rises and moisture condenses latent heat is released. This heating effectively reduces the stratification. As a result, many flows that would be blocked are able to flow over mountains when condensation occurs, leading to important impacts on precipitation distributions (e.g., Jiang, 2003).

Microphysics

Conversion of water from vapor to cloud to precipitation is a substantial task. Typical cloud particles must grow about one-billion-fold in volume before they are large enough to fall as precipitation. The evolution of cloud and precipitation particles occurs on scales from millimeter to micron, earning it the term cloud microphysics. Cloud droplets initiate and grow on fine particulates known as cloud condensation nuclei or ice nuclei, the concentration of which determines the size and number of cloud drops. The growth of cloud particles to the size of rain and snow occurs by the diffusion of vapor onto cloud particles and by the collision, coalescence, and aggregation of droplets and crystals. These growth processes depend on temperature, humidity, and the character of the airflow.

Hobbs et al. (1973) demonstrated the importance of microphysical processes by simulating a winter orographic storm with varying initial ice crystal concentrations. For small concentrations of cloud ice, snow grew quickly and fell to the ground over the windward slopes, whereas for large concentrations growth was slow and

snow was blown nearly 100 km into the lee. Precipitation phase is also crucial, as snow falls much more slowly than rain (roughly 0.5–2 m s^{-1} vs 7–10 m s^{-1}), and snow rimed with super-cooled water (graupel) falls at intermediate speeds. These fall speeds determine how far downwind precipitation drifts as it falls.

The melting level

Knowing the melting level – the elevation at which snow turns to rain as it falls – is important for studies of mountain snow and glaciers. Characterizing the melting level over topography is not as simple as just measuring it upstream since orographic effects may modify melting levels during storms. The lifting of air on the upwind side of the mountain leads to expansion and cooling, while the phase change of orographic snow falling through the melting level causes latent cooling, both of which are responsible for observed depression of the melting level over windward slopes that can amount to 0.5 km or more (e.g., Marwitz, 1987). The thermal inertia of the land, cold air trapped in valleys, and the degree of turbulent mixing near the surface may all influence the melting level as well.

Observations

The most direct observations characterizing orographic precipitation come from rain and snow gauges that measure accumulation at mountain sites. For example, the Cascade and Olympic Mountains (Figure 1a), located in the northwestern USA, receive plentiful orographic rain and snow from the mid-latitude cyclones of the Pacific storm track. Rain and snowfall varies greatly over the Cascades, but fully characterizing these variations with gauges alone is quite challenging due to the paucity of observations located within the mountains away from the populated valleys and foothills (Figure 1a). The high concentration of gauges needed to characterize orographic precipitation is highlighted by observations from a dense gauge network in the southwestern Olympics (Figure 1a, Minder et al., 2008). These observations show large differences in annual mean precipitation over scales of a few kilometers, maximizing on ridge-tops (Figure 1e). This pattern of precipitation is distinct from the rain shadow predicted by the upslope model. It arises because precipitation from aloft falls through low-level orographic clouds and grows by colliding with and collecting cloud droplets, in what is termed the "seeder-feeder" mechanism (Bergeron, 1968).

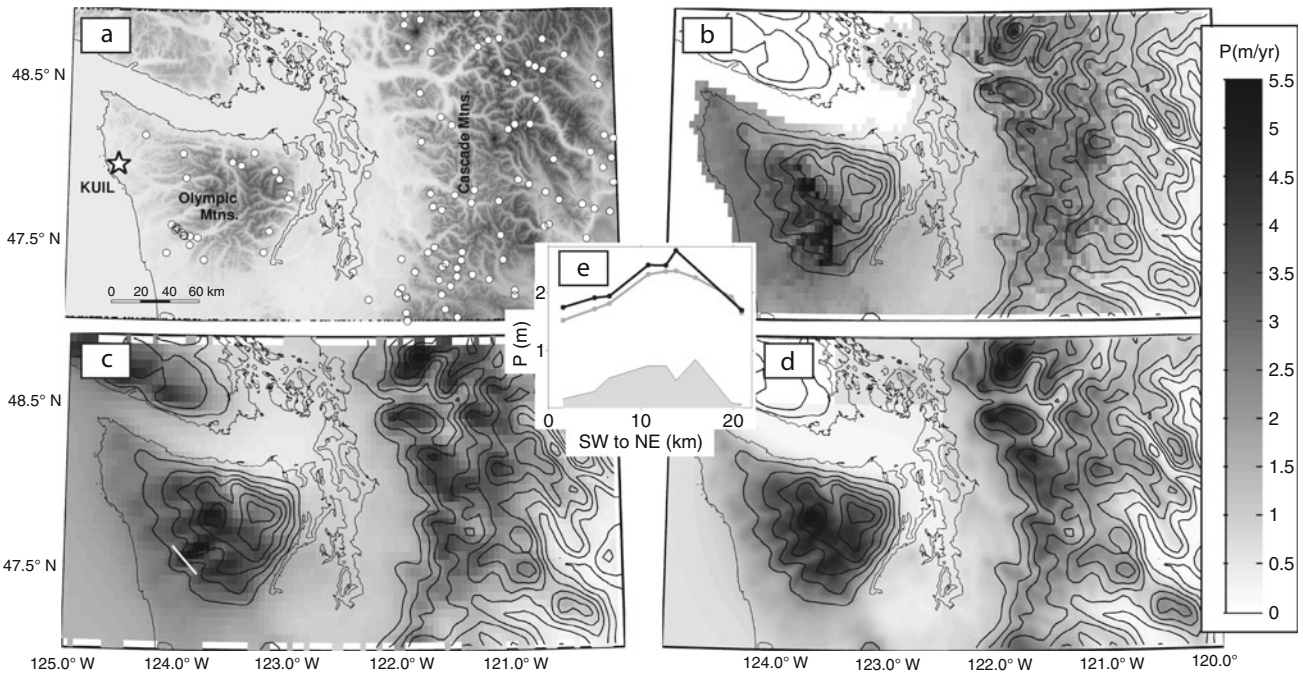

Orographic Precipitation, Figure 1 Topography and precipitation for the Olympic and Cascade Mountains of northwestern Washington, USA. (**a**) Shows elevation in grayscale (*black* corresponds to 3.5 km) and the location of regularly reporting precipitation gauges located above 150 m elevation (*white dots*). (**b**–**d**) Shows precipitation from October 2000 – September 2007 in *gray* shading, and smoothed contours of elevation every 250 m. (**b**) Is the PRISM analysis of gauge observations (Daly et al., 1994; data from PRISM Group, Oregon State University, http://www.prismclimate.org). (**c**) Is from the operational MM5 numerical weather predictions (e.g., Minder et al., 2008; http://www.atmos.washington.edu/mm5rt/). (**d**) Is from the model of Smith and Barstad (2004) forced with data taken from atmospheric soundings at KUIL (shown in **a**). (**e**) Compares the observed (*gray*) and MM5 (*black*) precipitation for a gauge transect in the southwestern Olympics (location shown with *white line* in **c**) for the winter of 2004–2005. The topographic profile (peak elevation of 800 m) is shaded (Modified from Minder et al. (2008) and reproduced with permission from Wiley-Blackwell).

Statistical techniques can fill in gaps in observational networks. For example, the Parameter Regression on Independent Slopes Method (PRISM; Daly et al., 1994) uses localized regressions of elevation and precipitation to interpolate between observations. PRISM output is shown for the Cascades and Olympics in Figure 1c. Other gridded gauge analyses from the well-instrumented European Alps (Frei and Schär, 1998) reveal more complex large-scale patterns than shown in Figure 1c. The Alps receive storms arriving from a much wider range of directions, erasing any simple rain shadow and producing precipitation maxima on both sides of the range.

Remote sensing offers an alternative method for studying orographic precipitation. Satellite methods are particularly useful for remote, poorly instrumented regions. For example, the Tropical Rainfall Measuring Mission (TRMM) satellite operates by emitting pulses of microwave radiation, which are reflected by precipitation. Data from TRMM have been used to characterize the pattern of precipitation over the Himalayas at 10 km scales (Anders et al., 2006), revealing a broad double-band of maximum precipitation along the southern slopes and local enhancements within windward valleys relative to the 4-km-high flanking ridges where the moisture content is quite low (Anders et al., 2006). Additional remotely sensed data come from ground-based radars, a great number of which are deployed for weather forecasting. These can be used to make detailed observations of precipitation, including precipitation phase, with high spatial and temporal resolution. In a classic study, Browning et al. (1974) used radar over the coastal hills of Wales to show that intense periods of mountain precipitation occur when rainfall cells from upwind of the mountains are advected over the mountains and enhanced as instability is released and the seeder-feeder mechanism acts. Unfortunately, radar can be challenging to use in mountainous terrain where the beam is often blocked by topography.

Both in situ and remote observations from aircraft have been a central component of several field projects devoted to better understanding orographic precipitation. The most expansive of these efforts to date, the Mesoscale Alpine Programe (MAP), focused on the southern slopes of the European Alps. Results from MAP revealed "that detailed knowledge of the orographically-modified flow is crucial for predicting the intensity, location, and duration of orographic precipitation" (Houze and Rotunno, 2007, p. 811), and that this flow is a strong function of the low-level stratification. Furthermore, under different flow regimes contrasting microphysical growth mechanisms become important, influencing the enhancement and distribution of precipitation (Houze and Rotunno, 2007).

Models

A vast array of models, each with their own advantages and drawbacks, have been used to characterize and understand orographic precipitation. The most basic of these are statistical in nature, relying upon empirical relations to estimate precipitation as is done for PRISM. Such models can be quite quantitatively successful, but need adequate data for calibration and can fail dramatically when observations are sparse or when anomalous atmospheric conditions occur.

The upslope model, described above, is an example of a class of simple physically based models that rely upon a series of idealizing assumptions to estimate precipitation with only minimal information about the incoming flow. Such models can illuminate fundamental processes and make ballpark estimates of precipitation, but a neglect of airflow dynamics and cloud microphysics severely limits their physical realism.

Another class of models is intermediate in complexity, maintaining simplicity while incorporating more governing physics than the upslope model. An example of this is the linear theory model put forth by Smith and Barstad (2004), which builds on the upslope model to include linearized mountain wave airflow dynamics, microphysical conversion, and fallout timescales, and lee side evaporation of precipitation. Such models are useful for the same reasons as the upslope model, but offer a much more complete physical representation and better performance. Still, these models neglect important nonlinear processes such as airflow blocking and microphysical collection and must be calibrated to perform well. An application of Smith and Barstad (2004)'s model to the Cascades and Olympics is shown in Figure 1d.

Mesoscale numerical weather prediction models are the most sophisticated modeling tool used in the study of orographic precipitation. They solve the full time-dependent equations of atmospheric motion and thermodynamics numerically on a three-dimensional grid and use schemes that simulate the interactions occurring on the microphysical scale between vapor, clouds, and precipitation. These models are capable of realistically representing transient interactions between large-scale storms and mountains, and nonlinear effects of blocking and microphysics. Yet, this physical realism comes at a computational cost, and these models can take substantial time to run even on fast computers with parallelization. Precipitation from the MM5 mesoscale model, used for operational weather forecasting, is shown in Figure 1c over the Olympics and Cascades. For some regions the model performance is excellent even on small scales, as shown in Figure 1e. However, these models cannot be taken for truth as they can be configured in a multitude of ways that give differing results. Even the best models can still have major errors, for individual storms and climatological averages, due to the challenges of simulating microphysical processes as well as inherent limits that exist on atmospheric predictability.

Climate change and variability

The sensitivity of orographic precipitation to large-scale climate variability and climate change is an active area of research. It is well known that year-to-year variations

in mountain rain and snowfall for ranges such as the Cascades are largely due to variations in the intensity and location of the mid-latitude storminess, with some of those variations related to large-scale patterns of climate variability such as the El Nino Southern Oscillation. Understanding how orographic precipitation will be altered due to anthropogenic climate change requires understanding the temperature sensitivity of orographic precipitation processes, as well as knowledge of how storm tracks and large-scale circulation will change.

The temperature dependence of orographic precipitation was investigated in depth by Kirshbaum and Smith (2008) using a mesoscale model. They found that while precipitation increases with the temperature and humidity of the atmosphere, these increases are buffered since orographic precipitation becomes less efficient at extracting moisture from the flow, due both to thermodynamic and microphysical effects. Salathé et al. (2008) used a mesoscale model to downscale global climate model projections over the Cascade and Olympic mountains and showed that possible changes in the direction of airflow during storms may alter the intensity and distribution of precipitation over the region. Generally, orographic snowfall is very likely to decrease with climate warming as melting levels during storms rise and a larger fraction of precipitation falls as rain. Some loss may be offset by orographic precipitation rate increases, but for mountains like the Cascades and Olympics, where temperatures are not typically far below freezing during storms, this compensation can be only modest due to the substantial loss of snow accumulation area.

Summary

Orographic precipitation processes strongly shape the climate in and around mountainous regions. Orographic influences can be pronounced on spatial scales ranging from the size of individual hills to the scale of major mountain ranges, and on temporal scales from the duration of a brief snow squall to the long-term climatology. Almost all orographic influences are fundamentally caused by topographically driven ascending and descending atmospheric motions that force condensation and evaporation. However, these basic forcings combine with a wide range of dynamical and microphysical processes to shape the precipitation distribution. Since different physical processes can be important for different storms and for different mountain ranges, orographic precipitation influences may take many forms.

Characterizing and understanding the effects of topography on precipitation remains an active field of research. Current research questions include: How does orographic precipitation change with climate? How do turbulent atmospheric motions affect orographic enhancement? What are the limits on predictability of orographic precipitation? Synthesis of new theories, models, and observational techniques continues to aid us in trying to answer these and other important questions.

Bibliography

Anders, A. M., Roe, G. H., Hallet, B., Montgomery, D. R., Finnegan, N. J., and Putkonen, J., 2006. Spatial patterns of precipitation and topography in the Himalaya. In Willett, S. D., Hovius, N., Brandon, M., and Fisher, D. M. (eds.), *Tectonics, Climate, and Landscape Evolution: GSA Special Paper 398*. Boulder: Geological Society of America, pp. 39–53.

Bergeron ,T., 1968. On the low-level redistribution of atmospheric water caused by orography. Presented at the International Cloud Physics Conference, Toronto.

Browning, K. A., Hill, F. F., and Paradoe, C. W., 1974. Structure and mechanism of precipitation and the effect of orography in a wintertime warm sector. *Quarterly Journal Royal Meteorological Society*, **100**, 309–330.

Daly, C., Neilson, R. P., and Phillips, D. L., 1994. A statistical-topographic model for mapping climatological precipitation over mountainous terrain. *Journal of Applied Meteorology*, **33**, 11–38.

Frei, C., and Schär, C., 1998. A precipitation climatology of the Alps from high-resolution rain-gauge observations. *International Journal of Climatology*, **18**, 873–900.

Hobbs, P. V., Easter, R. C., and Fraser, A. B., 1973. A theoretical study of the flow of air and fallout of solid precipitation over mountainous terrain: part II microphysics. *Journal of Atmospheric Sciences*, **30**, 813–823.

Houze, R. A., and Rotunno, R., 2007. Lessons on orographic precipitation from the Mesoscale Alpine Programme. *Quarterly Journal Royal Meteorological Society*, **133**, 811–830.

Jiang, Q., 2003. Moist dynamics and orographic precipitation. *Tellus. Series A*, **55**, 301–316.

Kirshbaum, D. J., and Smith, R. B., 2008. Temperature and moist-stability effects on midlatitude orographic precipitation. *Quarterly Journal Royal Meteorological Society*, **134**, 1183–1199.

Marwitz, J. D., 1987. Deep orographic storms over the Sierra Nevada part I: thermodynamic and kinematic structure. *Journal of Atmospheric Sciences*, **44**, 159–173.

Minder, J. M., Durran, D. R., Roe, G. H., and Anders, A. M., 2008. The climatology of small-scale orographic precipitation over the Olympic Mountains: patterns and processes. *Quarterly Journal Royal Meteorological Society*, **134**, 817–839.

Roe, G. H., 2005. Orographic precipitation. *Annual Review of Earth and Planetary Sciences*, **33**, 645–671.

Salathé, E. P., Steed, R., Mass, C. F., and Zahn, P. H., 2008. A high-resolution climate model for the US Pacific Northwest: Mesoscale feedbacks and local responses to climate change. *Journal of Climate*, **21**, 5708–5726.

Smith, R. B., 1979. The influence of mountains on the atmosphere. *Advances in Geophysics*, **21**, 87–230.

Smith, R. B., 2006. Progress on the theory of orographic precipitation. In Willett, S. D., Hovius, N., Brandon, M., and Fisher, D. M. (eds.), *Tectonics, Climate, and Landscape Evolution: GSA Special Paper 398*. Boulder: Geological Society of America, pp. 1–16.

Smith, R. B., and Barstad, I., 2004. A linear theory of orographic precipitation. *Journal of Atmospheric Sciences*, **61**, 1377–1391.

Cross-references

Atmosphere-Snow/Ice Interactions
Frequency Analysis of Snow Storms

Global Warming and its Effect on Snow/Ice/Glaciers
Permanent/Perpetual Snow Line
Precipitation

OUTLET GLACIER

Monohar Arora
National Institute of Hydrology (NIH), Roorkee, UA, India

The outlet glacier is confined to the narrow valley by the neighboring cliffs, and by lateral moraines deposited during a geologically recent period of glacier expansion. During that expansion, the outlet glacier reached the valley floor, pooled, and formed a piedmont lobe confined only by its own terminal moraine. In other words, it is a tongue of ice that extends radially from an ice dome. It may be identified within the dome as a rapidly moving ribbon of ice (an "ice stream"), while beyond the dome it typically occupies a shallow, irregular depression. The 700 km long Lambert Glacier, Antarctica, is one of the world's largest outlet glaciers.

OVERBURDEN PRESSURE

Prem Datt
Research and Development Center (RDC), Snow and Avalanche Study Establishment, Himparisar, Chandigarh, India

The compressive load imposed by overlying material on a layer of snow, ice, soil, or rock is called overburden pressure. If a snowpack is lying on a slope, the vertical component of the load is responsible for the densification which increases the cohesion and may increase snowpack strength. In glaciers, overburden pressure causes pressure melting from the basal plane. The overburden pressure at a depth z is given by

$$p(z) = p_0 + g\int_0^Z \rho(z)\,\mathrm{d}z$$

where $\rho(z)$ is the density of the overlying snow/ice at depth z and g is the acceleration due to gravity. p_0 is the datum pressure, like the pressure at the surface.

Bibliography

Jones, E. R., and Childers, R. L., Contemporaray College Physics, University of South Carolina; Addison Wesley.
The Avalance Hand book, David McClung and Peter Schaerer; The Mountaineers. 1001 SW Klickitat Way, Seattle, Washington, 98–134.

OXYGEN ISOTOPES

Bhishm Kumar
Hydrological Investigation Division, National Institute of Hydrology, Roorkee, Uttarakhand, India

Definition

Oxygen is the eighth element of the periodic table. Oxygen has 11 isotopes, ^{12}O, ^{13}O, ^{14}O, ^{15}O, ^{16}O, ^{17}O, ^{18}O, ^{19}O, ^{20}O, ^{21}O, and ^{22}O, but except ^{16}O, ^{17}O, and ^{18}O all other isotopes are radioactive and their existence in nature is very small (half life vary from 150 s to few femoseconds – of the order 10^{-15} s); therefore, we normally talk about only three isotopes of oxygen, that is, ^{16}O, ^{17}O, and ^{18}O.

Analytical principal

As the different isotopes have different masses, it is possible to separate them by passing a stream of the ionized sample (usually in a gas form) through a powerful magnetic field in a mass spectrometer. The heavier ions have greater momentum than the lighter ones, and hence are deflected to a lesser extent than the lighter ones. This splits the stream of ions into its heavy and light components – each of which can be measured using a Faraday collector. The abundance of the ^{18}O isotope is expressed as a percentage of the ^{18}O isotope relative to ^{16}O. For oxygen, on average, the natural abundance of ^{18}O relative to ^{16}O is 0.204% (Clark and Fritz, 1997).

Uses

$\delta^{18}O$ and $\delta^{2}H$ can be used to trace the hydrological cycle from evaporation in the oceans to local precipitation and groundwater. Because $\delta^{18}O$ and $\delta^{2}H$ values have a strong positive correlation with temperature, their measurements in ice cores are valuable indicators of climate variability. $\delta^{18}O$ and $\delta^{2}H$ values can be used to date snow and determine average snow accumulation rates. Dansgaard (1954) proposed that the ^{18}O content in glacier might reflect climatic conditions of the past. The most successful work that has been done in this field is undoubtedly the establishment of the ^{18}O profile of the Camp Century ice core which is 1,390 m deep (Dansgaard et al., 1969).

Bibliography

Clark, I., and Fritz, P., 1997. *Environmental Isotopes in Hydrogeology.* Boca Raton and New York: Lewis.
Dansgaard, W., 1954. The ^{18}O-abundance of fresh water. *Geochimica et Cosmochimica Acta*, **6**, 241.
Dansgaard, W., Johnsen, S. J., Moller, J., and Langway, C. C., 1969. One thousand centuries of climate record from camp century on the Greenland ice sheet. *Science*, **166**, 377.

P

PALAEO GLACIOFLUVIAL SEDIMENT SYSTEMS

Norm R. Catto
Department of Geography, Memorial University of Newfoundland, St. John's, NL, Canada

Definition

Palaeo-glaciofluvial sediment systems are defined as those that indicate the former presence of glaciofluvial activity but which are not associated with a modern or active glacier.

Introduction

Recognition and analysis of palaeo-glaciofluvial sediment systems provides details concerning the extent and nature of former glaciation. In many areas, glaciofluvial landforms are well preserved, forming distinct indications of both former ice-frontal positions and drainage patterns influenced by glaciation. Palaeo-glaciofluvial features can be both depositional and erosional.

Depositional features

Depositional features include all types of glaciofluvial landforms that can be found adjacent to modern glaciers, including eskers, kames, and outwash plains (also called sandur). In many instances, preservation of landforms has been affected by subsequent erosion. In addition, deposition in the glaciofluvial environment also commonly involves inclusion of blocks of detached glacial ice. Outwash discharged from a glacier may also be deposited on snow or winter ice. Subsequent melting of ice and snow will result in disruption of the sediment and landforms. Common internal sedimentary features include loading and collapse deformations, load casts, and diapers (Figure 1). Normal faulting is also common, as a result of differential melting or subsidence of trapped blocks of ice. Compaction structures can result as water-saturated glaciofluvial sediments are dewatered over time.

Cross-bedding and ripples initially deposited over ice can be displaced by subsequent melting. Displaced beds will exhibit angles of inclination substantially in excess of the critical angle of repose or the normal depositional attitude of the sediments, producing cross-strata inclined at angles in excess of 45° in some instances (Figure 2). Sand and gravel deposits showing anomalously high angles of cross-strata are considered an indicative of glaciofluvial deposition.

Eskers

Preservation of eskers is influenced by the degree of erosion by running water, both penecontemporaneous with deposition and in the period following glacial retreat. Subglacially formed eskers are more likely to be preserved than are supraglacial features. Individual segments of a subglacially formed esker may exceed 20 m in height and 20 km in length. Adjacent segments indicate the direction of subglacial meltwater flow. Connection and correlation of adjacent segments, facilitated by an analysis of the mineralogy of sediments within the esker deposits, indicates that eskers can represent the remnants of river systems extending hundreds of kilometers. Eskers develop sequentially over time, however, so that not all segments were formed simultaneously. They may be single ridges or may be aligned in a braided or reticulate pattern. Eskers served as passage routes for animals through forests and are commonly used as sources of gravel and sand aggregate for road construction.

Kame complexes

Palaeo-glaciofluvial kame complexes also mark former ice-front positions (Figure 3). A kame is a deposit of stratified material adjacent to, within, or upon a glacier, formed by meltwater. Kame complexes develop where

Vijay P. Singh, Pratap Singh & Umesh K. Haritashya (eds.), *Encyclopedia of Snow, Ice and Glaciers*, DOI 10.1007/978-90-481-2642-2,

Palaeo Glaciofluvial Sediment Systems, Figure 1 Deformation structures in palaeo-glaciofluvial deposit, Ragged Harbor area, Newfoundland and Labrador, Canada.

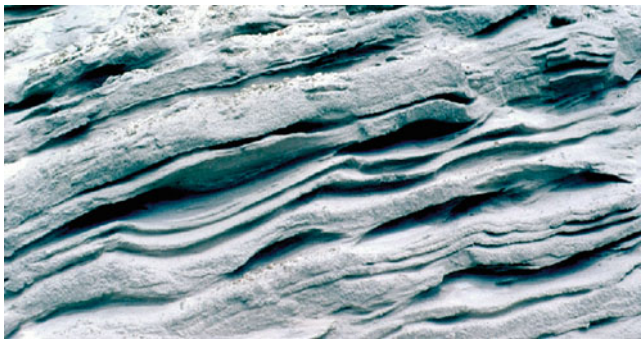

Palaeo Glaciofluvial Sediment Systems, Figure 2 Inclined ripples indicate displacement as a result of melting of underlying ice. Terra Nova, Newfoundland and Labrador, Canada.

glaciofluvial sediments are accumulated during relatively prolonged stands of glacial ice, commonly tens to hundreds of years. Most large moraines contain substantial quantities of glaciofluvial deposits, as the original tills and debris flow deposits are reworked by running water from the melting ice. Mixed assemblages of glaciofluvial and glaciomarine (or glaciolacustrine) deposits form where the glacial front rested in relatively shallow marine (or lacustrine) waters. Typical frontal kame moraines consist of segmented ridges aligned parallel to the former ice frontal position, with interspersed glacial, glaciomarine, or glaciofluvial sediments, situated in the belts of several kilometers width.

Crevasse fills

Crevasse fills also are indicative of palaeo-glaciofluvial activity. Crevasse fills are elongate ridges formed by the infilling of crevasses by glaciofluvial sediment. Crevasse fills often are characterized by angular bends and wide, level tops. The infill material may be sand, gravel, diamicton, or a combination of all the three. Crevasse fills commonly occur in groups. Preservation depends upon melting of glacial ice predominantly from below, coupled with minimal reworking subsequent to formation.

Palaeo Glaciofluvial Sediment Systems, Figure 3 Kame Complex, Carrot Creek, Alberta, Canada.

Erosional features

Palaeo-glaciofluvial erosional features are also indicative of former glacial activity. Meltwater channels represent drainage routes that formerly were occupied by meltwater derived from glacial ice but which have subsequently been partially or totally abandoned. Meltwater channel orientations indicate the effects of disruption and blockage of drainage by glacial ice. Channels which developed adjacent to an ice front may be carved into the sides of hills, with one bank having been formerly supported by an adjacent glacial ice.

Summary

Palaeo-glaciofluvial sediment features and landforms are frequently the best-preserved remnants of glaciation. Depositional features include all types of glaciofluvial landforms that can be found adjacent to modern glaciers, including eskers, kames, crevasse fills, and outwash deposits. Erosional features formed by running water in glacial environments, including meltwater channels, also indicate the former presence of glaciers.

Cross-references

Bed Forms (Fluvial)
Crevasses
Discharge/Streamflow
Glaciofluvial
Kame and Kettle Topography
Meltwater Channels

PALAEO-CHANNEL

Vijay Kumar
National Institute of Hydrology, Roorkee, India

The word paleo-channel is formed from the words "paleo" or "old," and channel; i.e., a paleo-channel is an old channel. Paleo-channels are deposits of unconsolidated sediments or semi-consolidated sedimentary rocks deposited in ancient, currently inactive river and stream channel systems. These are typical riverine geomorphic features in a location representing drainage streams, rivers, rivulets which were flowing either ephemeral or perennial during the past time and now stands either buried or lost or shifted due to tectonic, geomorphologic, anthropogenic process/activities, as well as climatic changes. When a channel ceases to be part of an active river system, it becomes a paleo-channel. Paleo-channels are also identified as remnants of stream channels cut in older rocks/sediments and filled by younger overlying sediments, representing the distribution of valley systems as these existed at a given geological time in the past (Bates and Jackson, 1980). Paleo-channel is synonymous with paleo-river, paleo-drainage, lost river, buried river, buried channel, or buried valley. Paleo-channels vary greatly in age. Those from the recent geological past (perhaps tens to hundreds of years old) include meander cut-offs and longer reaches. A paleo-channel is distinct from the overbank deposits of currently active river channels, including ephemeral water courses which do not regularly flow. A paleo-channel is distinct from such watercourses because the river bed is filled with sedimentary deposits which are unrelated to the normal bed load of the current drainage pattern.

The water-bearing rock characteristics of paleo-channels are highly porous gravel, coarse-medium sand (in the alluvial fan area), medium fine sand, fine silt (in the river channel zones), and silt (in the delta). The paleo-channels are potential sources of recharge, as they commonly serve as flood channels or aqueducts. They have good paths of infiltration as they have usually sandy soil or sandy loam on the surface. The main features which govern the hydrology and recharge of paleo-channels are the size (spatial extent and depth) of the feature and the stratigraphy (layering of soil properties) within the profile. Most of the paleo-channels are interlinked with present rivers or canals, which is beneficial to lateral recharge of the groundwater. Relict fluvial channels that are filled with high permeability sediments act as preferred pathways for groundwater flow and solute transport. In coastal regions, such paleo-channels can provide a hydraulic connection between freshwater aquifers and the sea, resulting in saltwater intrusion landward or freshwater discharge offshore.

Paleo-channels have long attracted scientific and practical interest. Where paleo-channels are well preserved they provide valuable information about past flow regimes. They can also provide information about the response of catchments and rivers to past climatic changes, with implications for projected changes to climate in the future. Paleo-channels are important in geology for understanding the movements of faults; for preserving the old and recent sediments and fossils within them; and for preserving sedimentary records useful for understanding climatic conditions, including various isotopic indicators of past rainfall, temperature, and climates. Amongst other things, these abandoned channels are economically important because they often contain deposits of Tin, Tungston, Uranium, Lignite, Gold, Platinum, Silver, and Diamonds besides permeable fills which form excellent aquifers. The presence of paleo-channel can pose serious threats to engineering projects within the region. A large number of geophysical methods – electrical resistivity, electromagnetic potential, seismic refraction, and reflection – are being successfully used in delineating and exploiting paleo-channel.

Bibliography

Bates, R. L., and Jackson, J. A. (eds.), 1980. *Glossary of Geology*. Falls Church: American Geological Institute.

PALAEO-ICE STREAM

Chris R. Stokes
Department of Geography, Durham University, Durham, UK

Introduction

An *ice stream* is a region in a grounded ice sheet that flows at an order of magnitude faster than the slow-flowing ice that borders it. The term *paleo-ice stream* is used to describe ice streams that no longer exist as a result of deglaciation. Ice streams have been referred to as the "arteries" of an ice sheet (Bennett, 2003) because their high velocities are responsible for the vast majority of ice sheet discharge, despite representing a relatively small component of their surface area (Bamber et al., 2000). It is for this reason that they are viewed as a critical component of ice sheet mass balance and have important implications for sea-level change (Shepherd and Wingham, 2007). The dynamic nature of ice streams is further emphasized by the relatively recent discoveries that they are capable of accelerating, decelerating, migrating, and shutting down over very short timescales (e.g., Joughin et al., 2004; Conway et al., 2002).

Perhaps surprising, given their undoubted importance, is that ice streams are a relatively recent discovery. They were formally defined in the 1950s (Swithinbank, 1954) but only began to be intensively studied as late as the 1970s (e.g., Rose, 1979). Since that time, however, their identification in modern ice sheets has been enhanced by remote sensing techniques that enable a large-scale view of the flow features on the ice sheet surface (e.g., flow-stripes, crevasse patterns) and, more recently, the calculation of ice velocities

and elevation (e.g., Joughin et al., 2004). These studies reveal that ice streams are typically large features (100s km long; 10s km wide) and possess very abrupt lateral shear margins, where intense crevassing is generated at the border with slow-flowing ice. Their rapid velocity is a defining characteristic and observations of their bed, whilst logistically very difficult, suggests that their motion is facilitated by a layer of saturated, deformable sediments that deform beneath the ice and offers minimal frictional resistance to basal sliding (Alley et al., 1986; Engelhardt and Kamb, 1998). Where subglacial sediment deformation is pervasive, high sediment transport rates are known to produce "till" wedges at the terminus of the ice stream (Anandakrishnan et al., 2007).

Identification of paleo-ice streams

Ice streams are a fundamental property of the flow structure of modern-day continental ice sheets and it can be assumed that they played a similar role in past (paleo-) ice sheets. It was the recognition of their significance to ice sheet dynamics in the late 1970s and 1980s (e.g., Rose, 1979; Alley et al., 1986) that prompted several workers to attempt to reconstruct their location and behavior in paleo-ice sheets (e.g., Denton and Hughes, 1981; Dyke and Prest, 1987). These pioneering workers recognized that ice streams should leave behind geological/geomorphological evidence of their activity that would be very different from the slow-flowing regions of the ice sheet, and cited evidence of distinctive erratic dispersal trains with abrupt lateral margins (Hicock, 1988; Dyke and Morris, 1988). The discovery of highly elongated subglacial bedforms on paleo-ice sheet beds, known as mega-scale glacial lineations (cf. Clark, 1993), was also linked to paleo-ice stream activity. Despite these important advances, the identification of paleo-ice streams was somewhat subjective, with a wide variety of evidence used to infer their location in former ice sheets (e.g., see review in Stokes and Clark, 2001).

Mathews (1991) highlighted the need for some objective criteria to identify paleo-ice streams and Stokes and Clark (1999) later proposed some "geomorphological" criteria based on the characteristics of modern-day ice streams. These criteria are listed in Table 1 and, where several are identified together on a paleo-ice sheet bed, are likely to indicate robust evidence of ice streaming.

The criteria, listed in Table 1, can be grouped together into a glacial landsystem, which represents the unique imprint (or 'footprint') of paleo-ice stream activity (see Stokes and Clark, 2001). Indeed, numerous paleo-ice stream imprints have now been recognized from all of the major paleo-ice sheets from the last ice age (e.g., Laurentide, Scandinavian-Barents Sea, British-Irish; see special issue introduced by Clark et al., 2003) and even those from more ancient glaciations 100s of millions of years ago (Moreau et al., 2005). Paleo-ice stream imprints have also been reported from predominantly bedrock terrain (e.g., Roberts and Long, 2003), including in mountainous areas (cf. Evans, 1996), based on the morphometry and pattern of streamlined erosional landforms.

Palaeo-Ice Stream, Table 1 Geomorphological criteria for identifying paleo-ice streams (From Stokes and Clark, 1999)

Contemporary ice stream characteristic	Proposed geomorphological signature
A. Characteristic shape and dimensions	1. Characteristic shape and dimensions (>20 km wide and >150 km long)
	2. Highly convergent flow patterns
B. Rapid velocity	3. Highly attenuated subglacial bedforms
	4. Boothia-type erratic dispersal trains (see Dyke and Morris, 1988)
C. Sharply delineated shear margins	5. Abrupt lateral margins (<2 km)
	6. Ice stream marginal moraines
D. Deformable bed conditions	7. Glaciotectonic and geotechnical evidence of pervasively deformed till
E. Focused sediment delivery	8. Submarine accumulation of sediment, e.g., "trough mouth fan" or "till delta," (only marine-terminating ice streams)

Arguably, the best preserved paleo-ice stream imprints have been identified on the sea-floor of the continental shelf surrounding modern-day ice sheets (e.g., in Antarctica) and associated with paleo-ice sheets. Figure 1 shows an exceptionally well-preserved submarine paleo-ice stream bed off the coast of northern Norway in Malangsdjupet. This ice stream 'footprint' contains many of the geomorphological criteria shown in Table 1.

Paleo-ice streams in marine settings (e.g., see Figure 1) have been shown to exhibit a characteristic evolution of subglacial bedforms along their length (Wellner et al., 2001; Ó Cofaigh et al., 2002). The inner shelf is usually characterized by bedrock drumlins, crag-and-tails, and meltwater channels, which progress downstream into more elongated drumlins and highly attenuated mega-scale glacial lineations in major cross-shelf troughs. Significantly, the deglaciation signature may also be superimposed on this pattern, offering crucial insights into the style of ice stream retreat (Ó Cofaigh et al., 2008). Where ice retreat was slow and steady, a series of closely spaced transverse recessional ridges are found superimposed on top of the mega-scale glacial lineations. Major still-stand positions are marked by the intermittent building of 'grounding zone wedges' (GZWs), and a series of such features, with no recessional ridges in between, is thought to represent episodic retreat. Other imprints have been identified with very few recessional features (GZWs or recessional moraines) and with only a thin veneer of deglacial sediments. Such an imprint is thought to represent a rapid retreat of the ice stream (Ó Cofaigh et al., 2008).

The other broad approach to reconstructing paleo-ice streams is through the use of numerical ice sheet models (e.g., Tarasov and Peltier, 2004). Incorporating ice stream processes into ice sheet models represents a major scientific and computational challenge, which has been described as "one of the key goals of theoretical glaciology" (Hindmarsh, 2009). The challenge for numerical

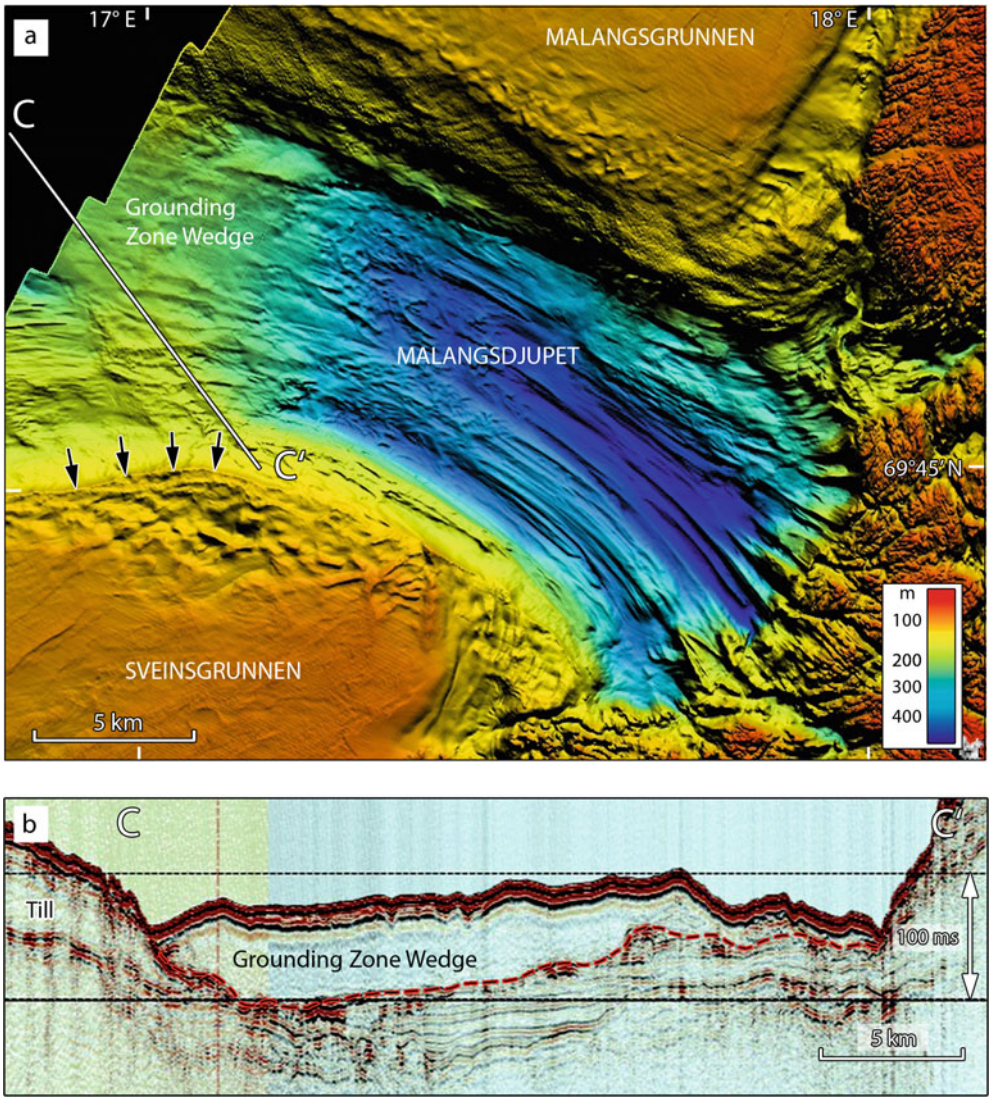

Palaeo-Ice Stream, Figure 1 (**a**) Malangsdjupet paleo-ice stream from the former Fennoscandian Ice Sheet. This ice stream bed contains almost all of the geomorphological criteria for a paleo-ice stream imprint (see Table 1), including the characteristic shape and dimensions with a convergent onset zone, highly attenuated mega-scale glacial lineations on the floor of the trough, and abrupt lateral margins with lateral shear margin moraines (identified with *black arrows*). The trough also contains evidence of focused sediment delivery in the form of a grounding zone wedge, shown in a seismic profile in (**b**) (transect C to C′ shown in (**a**)) Sun illumination from NE (From Ottesen et al., 2008).

ice sheet models is to be able to incorporate the physics of ice streaming and reproduce the 'known' location of paleo-ice streams identified from geological/geomorphological evidence. This is a robust way in which the success of ice sheet models can be evaluated and tested (e.g., Stokes and Tarasov, 2010). Furthermore, there may be some paleo-ice streams where evidence is either scarce, obscured, or yet to be discovered. Numerical ice sheet models have the potential to predict these paleo-ice stream locations and guide the search for new discoveries.

Once identified, paleo-ice streams hold huge potential for advancing our understanding of past ice sheet dynamics and their links to the ocean-climate system. If we can reproduce a robust reconstruction of paleo-ice stream activity, it is possible to learn about their behavior over much longer timescales than present-day observations permit and their links to paleoceanography and abrupt climate change. Moreover, the exposed beds of paleo-ice streams permit access to the basal environment and facilitate investigation of subglacial sedimentary processes beneath ice streams, which is logistically very difficult beneath modern ice streams. The following sections briefly highlight the importance of paleo-ice stream research in each of these key areas.

Paleo-ice streams and past ice sheet dynamics

Any attempt to reconstruct the behavior of a paleo-ice sheet that ignores ice streaming is likely to be unrealistic. The large ice flux of ice streams has a profound impact on ice sheet configuration (e.g., thickness, margin extent, and ice divide locations) and so it is important to know where and when they operated in order to reconcile ice sheet reconstructions with their geological evidence. A good example to illustrate this point is the former North American Laurentide Ice Sheet (LIS).

Several workers reconstructed the low-surface profile of the LIS in many of its marginal areas, particularly where the underlying geology was characterized by relatively 'soft,' fine grained sediments (e.g., Mathews, 1974). These areas of thin ice were in conflict with models of the LIS that required a thick, single-domed ice sheet, centered over Hudson Bay (e.g., Denton and Hughes, 1981). However, the low surface slopes of the ice sheet are easily explained by the presence of ice streams whose rapid velocity was induced by the deformation of soft water-saturated sediments (Fisher et al., 1985). Indeed, the higher velocities of these ice streams can also explain the lobate nature of the ice sheet margin and subsequent work has reported clear evidence of paleo-ice stream imprints associated with such lobes (Patterson, 1998).

It has also been suggested that, once the LIS margin retreated back on to the more resistant ('hard') Canadian Shield rocks, ice stream activity was inhibited and ice sheet retreat was more stable (Clark, 1994). This geological control on ice streaming (which, incidentally, has also been suggested from work on modern-day ice streams: Winsborrow et al., 2010) has since been questioned; because robust evidence for ice streaming during deglaciation has been found on the Canadian Shield (Stokes and Clark, 2003). This discovery demonstrates that the spatial controls on ice streaming may be more complex than previously thought and highlights the importance of paleo-ice stream research in contributing to our overall understanding of their behavior. Indeed, a recent review by Winsborrow et al. (2010) identified seven potential controls on ice stream activity: topographic focusing, topographic steps, macroscale bed roughness, calving margins, 'soft' subglacial geology, geothermal heat flux, and subglacial meltwater routing.

Reconstruction of paleo-ice stream histories is also an excellent approach to understanding the temporal controls on ice streaming. Modern-day observations of their behavior are often limited to several decades, but reconstructions of paleo-ice streams are capable of spanning thousands of years of activity. For example, whilst much research is focused on the mass balance of ice streams draining into the Ross Ice Shelf in West Antarctica, examination of the paleo-ice stream tracks in their foregrounds indicates that they have been receding since the early Holocene and could continue to retreat even in the absence of further external forcing (Conway et al., 1999). Thus, paleo-ice stream research can provide a useful context in which to assess the significance of relatively small changes in their behavior that have been and will continue to be observed in modern-day ice sheets. Moreover, whilst it is known from contemporary ice stream research that ice streams are capable of switching positions and shutting down, research on paleo-ice streams has revealed equally dramatic switches in ice stream position from one glacial cycle to the next (e.g., Dowdeswell et al., 2006) and even during deglaciation of a single glacial cycle (e.g., Stokes et al., 2009).

Paleo-ice streams and subglacial processes

Although great progress has been made in understanding the subglacial environment beneath ice streams and the mechanisms that lead to their rapid flow (e.g., Alley et al., 1986; Engelhardt and Kamb, 1998), most information from the bed of modern-day ice streams is limited by the spatial and temporal resolution (e.g., indirect geophysical studies or borehole investigation). For this reason, many workers have recognized the potential that the now-exposed beds of paleo-ice streams hold for understanding their basal processes. The sediments and landforms they have left behind preserve important information regarding their basal processes and operation.

As noted above, the arrangement and morphometry of subglacial bedforms on paleo-ice stream beds has been used to hypothesize that highly elongate bedforms are associated with fast ice flow (e.g., Clark, 1993; Stokes and Clark, 2002). Due to the inaccessibility of modern-day ice stream beds, this hypothesis has been difficult to test. However, advances in geophysical techniques have led to their recent discovery beneath Rutford Ice Stream in West Antarctica, providing the first conclusive evidence of this relationship (King et al., 2009). Moreover, because ice streaming results in such a distinct subglacial landscape (characterized by elongated subglacial bedforms), it should be possible to identify and investigate the nature of localized 'sticky spots,' which are known to be important from studies of modern-day ice streams (e.g., Alley, 1993) but which, to date, have been very difficult to observe and characterize. Sticky spots should interrupt the predictable pattern of landforms that characterize a paleo-ice stream bed and be easily recognizable (cf. Stokes et al., 2007). They should also be manifest in the sediments preserved on the paleo-ice stream bed, which may even provide a 'smoking gun' of the mechanisms that led to ice stream shutdown. For example, Christoffersen and Tulaczyk (2003) reported an unusual till sequence from beneath the Baltic Ice Stream in southern Scandinavia, consisting of a strong and well-consolidated till crust, underlain by weak and poorly consolidated till. They hypothesized that this sequence could be associated with the processes of basal freeze-on, whereby meltwater is extracted from the subglacial till and accreted to the base of the ice stream. Such a process can starve the ice stream of its layer of lubricating water, leading ice stream shutdown.

Paleo-ice stream sediment transport and deposition

Paleo-ice streams can be extremely powerful erosional agents, especially those that extend across continental shelves and operate over soft, deformable, marine sediments (Vorren and Laberg, 1997). These ice streams can be very efficient at eroding and transporting subglacial sediment, and their sediment flux is comparable to the largest fluvial systems, despite their far shorter duration of operation. Moreover, the focused sediment discharge toward the shelf edge can create huge depocentres, known as 'trough mouth fans' (Vorren and Laberg, 1997; Vorren et al., 1998). Significantly, investigation of the architecture of these trough mount fans has enabled investigators to reconstruct past sediment fluxes and the long-term record of ice stream activity (ice discharge, velocity), sometimes extending back through several glacial cycles (Vorren et al., 1998). For example, the Norwegian Channel paleo-ice stream in southern Norway is thought to have transported $>3.2 \times 10^4$ km^3 of sediment on to the North Sea Fan during the last 0.5 million years, with extreme and punctuated sediment discharges as high as 1.1 Gt a-1 during the last glacial cycle (Nygård et al., 2007).

The extreme sedimentation rates associated with paleo-ice stream trough mouth fans also holds implications for geohazards, such as submarine debris slides and flows. It is known that the high sediment supply can lead to unstable deposits and an increased likelihood of slope failures in these areas, particularly after seismic activity and/or decomposition of gas hydrates (Vorren et al., 1998).

Paleo-ice streams, paleoceanography, and abrupt climate change

Finally, the large ice flux of paleo-ice streams also holds important implications for the delivery of icebergs and freshwater fluxes into the ocean. Ocean circulation (e.g., the North Atlantic thermohaline circulation) is highly sensitive to such influxes of freshwater and perturbation of these systems can lead to major and abrupt climatic changes (Broecker, 1994). Because ice streams have the capacity to drain large portions of an ice sheet relatively rapidly, they have the potential to deliver huge amounts of icebergs into the ocean and represent a key link in the coupling of the ice sheet and ocean systems. Episodes of ice streaming in Hudson Strait, for example, are thought to be responsible for several large iceberg export events into the North Atlantic between 60 and 10 ka (Broecker et al., 1992). Evidence for these events comes from bands of ice-rafted debris in ocean cores, known as Heinrich layers, which have been specifically linked to sedimentary rocks beneath a paleo-ice stream in Hudson Strait (Andrews and Tedesco, 1992). The influx of freshwater resulting from these events was sufficient to cause changes in sea surface temperature and salinity, which had a considerable impact on ocean circulation and northern hemisphere climate (Broecker, 1994). Although the trigger for these episodes of ice streaming remain unclear, it is now recognized that they can be instrumental in driving abrupt changes in mid-high latitude climate and oceanography.

Elsewhere in the LIS, paleo-ice streams have been implicated in similar iceberg discharge events, particularly at the northwestern margin in the Canadian Arctic Archipelago (e.g., Stokes et al., 2005). Significantly, the timing of these events is similar to those issued from the Hudson Strait ice stream, hinting at the possibility that they were part of a pan-ice sheet destabilization. The large marine-terminating ice streams at the northern margin of the Laurentide Ice Sheet are also thought to have contributed to the development of a thick (>1,000 m) Arctic ice shelf, which may have occupied the Arctic Ocean several times during the Late Pleistocene (Polyak et al., 2001), further emphasizing their important role in the ice sheet-ocean-atmosphere system.

Bibliography

Alley, R. B., 1993. In search of ice stream sticky spots. *Journal of Glaciology*, **39**(133), 447–454.

Alley, R. B., Blankenship, D. D., Bentley, C. R., and Rooney, S. T., 1986. Deformation of till beneath ice stream B, West Antarctica. *Nature*, **322**, 57–59.

Anandakrishnan, S., Catania, G. A., Alley, R. B., and Horgan, H. J., 2007. Discovery of till deposition at the grounding line of Whillans ice stream. *Science*, **315**, 1835–1838.

Andrews, J. T., and Tedesco, K., 1992. Detrital carbonate-rich sediments, northwestern Labrador Sea: implications for ice-sheet dynamics and iceberg-rafting events in the North Atlantic. *Geology*, **20**, 1087–1090.

Bamber, J. L., Vaughan, D. G., and Joughin, I., 2000. Widespread complex flow in the interior of the Antarctic ice sheet. *Science*, **287**, 1248–1250.

Bennett, M. R., 2003. Ice streams as the arteries of an ice sheet: their mechanics, stability, and significance. *Earth Science Reviews*, **61**(3–4), 309–339.

Broecker, W., 1994. Massive iceberg discharges as triggers for global climate change. *Nature*, **372**, 421–424.

Broecker, W., Bond, G., Klas, M., Clark, E., and McManus, J., 1992. Origin of the northern Atlantic's Heinrich events. *Climate Dynamics*, **6**, 265–273.

Christoffersen, P., and Tulaczyk, S., 2003. Signature of palaeo-ice stream stagnation: till consolidation induced by basal freeze-on. *Boreas*, **32**, 114–219.

Clark, C. D., 1993. Mega-scale glacial lineations and cross-cutting ice flow landforms. *Earth Surface Processes and Landforms*, **18**, 1–29.

Clark, P. U., 1994. Unstable behaviour of the Laurentide ice sheet over deforming sediment and its implications for climate change. *Quaternary Research*, **41**, 19–25.

Clark, C. D., Evans, D. J. A., and Piotrowski, J. A., 2003. Palaeo-ice streams: an introduction. *Boreas*, **32**(1), 1–3.

Conway, H., Hall, B. L., Denton, G. H., Gades, A. M., and Waddington, E. D., 1999. Past and future grounding line retreat of the West Antarctic Ice Sheet. *Science*, **286**, 280–283.

Conway, H., Catanina, G., Raymond, C. F., Gades, A. M., and Waddington, E. D., 2002. Switch in flow direction of an Antarctic ice stream. *Nature*, **419**, 465–467.

Denton, G. H., and Hughes, T. J., 1981. *The Last Great Ice Sheets*. New York: Wiley.

Dowdeswell, J. A., Ottesen, D., and Rise, L., 2006. Flow switching and large-scale deposition by ice streams draining former ice sheets. *Geology*, **34**, 313–316.

Dyke, A. S., and Morris, T. F., 1988. Drumlin fields, dispersal trains, and ice streams in Arctic Canada. *Canadian Geographer*, **32**, 86–90.
Dyke, A. S., and Prest, V. K., 1987. Palaeogeography of northern North America, 18,000-5,000 years ago. Geological Survey of Canada Map, 1703A, scale 1:12,500,000.
Engelhardt, H., and Kamb, B., 1998. Basal sliding of ice stream B, West Antarctica. *Journal of Glaciology*, **44**, 223–230.
Evans, I. S., 1996. Abraded rock landforms (whalebacks) developed under ice streams in mountain areas. *Annals of Glaciology*, **22**, 9–16.
Fisher, D. A., Reeh, N., and Langley, K., 1985. Objective reconstructions of the Late Wisconsinan Laurentide ice sheet and the significance of deformable beds. *Géographie Physique et Quaternaire*, **39**(3), 229–238.
Hicock, S. R., 1988. Calcareous till facies north of Lake Superior, Ontario: implications for Laurentide ice streaming. *Géographie Physique et Quaternaire*, **42**(2), 120–135.
Hindmarsh, R. C. A., 2009. Consistent generation of ice-streams via thermo-viscous instabilities modulated by membrane stresses. *Geophysical Research Letters*, **36**, L06502, doi:10.1029/2008GL036877.
Joughin, I., Abdalati, W., and Fahnestock, M., 2004. Large fluctuations in speed on Greenland's Jakobshavns Isbrae glacier. *Nature*, **432**, 608–610.
King, E. C., Hindmarsh, R. C. A., and Stokes, C. R., 2009. Formation of mega-scale glacial lineations observed beneath a West Antarctic ice stream. *Nature Geoscience*, **2**, 585–588.
Mathews, W. H., 1974. Surface profiles of the Laurentide ice sheet in its marginal areas. *Journal of Glaciology*, **13**, 37–43.
Mathews, W. H., 1991. Ice sheets and ice streams: thoughts on the Cordilleran ice sheet symposium. *Géographie Physique et Quaternaire*, **45**, 263–267.
Moreau, J., Ghienne, J.-F., Le Heron, D. P., Rubino, J.-L., and Deynoux, M., 2005. 440 Ma ice stream in North Africa. *Geology*, **33**, 753–756.
Nygård, A., Sejrup, H. P., Haflidason, H., Lekens, W. A. H., Clark, C. D., and Bigg, G. R., 2007. Extreme sediment and ice discharge from marine-based ice streams: new evidence from the North Sea. *Geology*, **35**, 395–398.
Ó Cofaigh, C., Pudsey, C. J., Dowdeswell, J. A., and Morris, P., 2002. Evolution of subglacial bedforms along a paleo-ice stream, Antarctic peninsula continental shelf. *Geophysical Research Letters*, **29**, 41.1–41.4.
Ó Cofaigh, C., Dowdeswell, J. A., Evans, J., and Larter, R. D., 2008. Geological constraints on Antarctic paleo-ice stream retreat. *Earth Surface Processes and Landforms*, **33**(4), 513–525.
Ottesen, D., Stokes, C. R., Rise, L., and Olsen, L., 2008. Ice-sheet dynamics and ice streaming along the coastal parts of northern Norway. *Quaternary Science Reviews*, **27**, 922–940.
Patterson, C. J., 1998. Laurentide glacial landscapes: the role of ice streams. *Geology*, **26**(7), 643–646.
Polyak, L., Edwards, M. H., Coakley, B. J., and Jakobsson, M., 2001. Ice shelves in the Pleistocene Arctic Ocean inferred from Glaciogenic deep-sea bedforms. *Nature*, **410**, 453–457.
Roberts, D. H., and Long, A. J., 2003. Streamlined bedrock terrain and fast ice flow, Jakobshavns Isbrae, West Greenland: implications for ice stream and ice sheet dynamics. *Boreas*, **34**(1), 25–42.
Rose, K. E., 1979. Characteristics of flow in Marie Byrd Land, Antarctica. *Journal of Glaciology*, **24**, 63–75.
Shepherd, A., and Wingham, D., 2007. Recent sea level contributions of the Antarctic and Greenland ice sheets. *Science*, **315**, 1529–1532.
Stokes, C. R., and Clark, C. D., 1999. Geomorphological criteria for identifying Pleistocene ice streams. *Annals of Glaciology*, **28**, 67–75.
Stokes, C. R., and Clark, C. D., 2001. Palaeo-ice streams. *Quaternary Science Reviews*, **20**, 1437–1457.
Stokes, C. R., and Clark, C. D., 2002. Are long subglacial bedforms indicative of fast ice flow? *Boreas*, **31**, 239–249.
Stokes, C. R., and Clark, C. D., 2003. Laurentide ice streaming on the Canadian Shield: a conflict with the soft-bedded ice stream paradigm? *Geology*, **31**, 347–350.
Stokes, C. R., Clark, C. D., and Storrar, R., 2009. Major changes in ice stream dynamics during deglaciation of the north-western margin of the Laurentide Ice Sheet. *Quaternary Science Reviews*, **28**, 721–738.
Stokes, C. R., and Tarasov, L., 2010. Ice streaming in the Laurentide Ice Sheet: a first comparison between data-calibrated numerical model output and geological evidence. *Geophysical Research Letters*, **37**, L01501, doi:10.1029/2009GL040990, 2010.
Stokes, C. R., Clark, C. D., Darby, D. A., and Hodgson, D. A., 2005. Late Pleistocene ice export events into the Arctic Ocean from the M'Clure Strait ice stream, Canadian Arctic Archipelago. *Global and Planetary Change*, **49**, 139–162.
Stokes, C. R., Clark, C. D., Lian, O. B., and Tulaczyk, S., 2007. Ice stream sticky spots: a review of their identification and influence beneath contemporary and palaeo-ice streams. *Earth Science Reviews*, **81**, 217–249.
Swithinbank, C. W. M., 1954. Ice streams. *Polar Record*, **7**, 185–186.
Tarasov, L., and Peltier, W. R., 2004. A geophysically constrained large ensemble analysis of the deglacial history of the North American ice-sheet complex. *Quaternary Science Reviews*, **23**, 359–388.
Vorren, T. O., and Laberg, J. S., 1997. Tough mouth fans – palaeoclimate and ice-sheet monitors. *Quaternary Science Reviews*, **16**, 865–881.
Vorren, T. O., Laberg, J. S., Bluame, F., Dowdeswell, J. A., Kenyon, N. H., Mienert, J., Rumohr, J., and Werner, F., 1998. The Norwegian-Greenland Sea continental margins: morphology and Late Quaternary Sedimentary processes and environment. *Quaternary Science Reviews*, **17**, 273–302.
Wellner, J. S., Lowe, A. L., Shipp, S. S., and Anderson, J. B., 2001. Distribution of glacial geomorphic features on the Antarctic continental shelf and correlation with substrate: implications for ice behaviour. *Journal of Glaciology*, **47**(158), 397–411.
Winsborrow, M. C. M., Clark, C. D., and Stokes, C. R., 2010. What controls the location of ice streams? *Earth Science Reviews*, **103**, 45–59.

Cross-references

Climate Change and Glaciers
Elongation Ratio
Glacial Grooves
Ice Age
Outlet Glacier
Quaternary Glaciation
Subglacial Processes

PALAEOCLIMATE AND PAST GLACIATIONS

Philip D. Hughes
Geography, School of Environment and Development, The University of Manchester, Manchester, UK

Definition

Palaeoclimate: climates of the past
Past glaciations: the presence and action of glaciers in the past

Past glaciations

Glaciers have been considerably larger in the recent geological past and regular fluctuations in global ice volume characterized the Pleistocene (2.6 million years to 11,700 years ago), as well as during much earlier episodes in Earth history. The effect of Pleistocene glaciations on land has left characteristic landforms and sediments and these can be used to reconstruct former glaciers and their associated climates. Many areas have experienced multiple glaciations and, since the 1970s, it has been widely accepted that the quasi-regular changes in global ice volume during the Pleistocene were paced by cyclical variations in the Earth's orbit (Hays et al., 1976). However, the best-preserved glacial landforms and sediments are typically those formed during the Middle and Late Pleistocene. Glaciers have also fluctuated in size during the Holocene too, and moraine positions can be used to reconstruct even very recent climates, such as during the Little Ice Age (Grove, 2004).

Reconstructing former glaciers

Glaciers leave their mark by eroding, transporting, and depositing rock and sediment leaving a characteristic imprint on the landscape: glaciation. While glaciations have occurred on numerous occasions at different times through the geological column, the clearest evidence of glaciation is the product of the Quaternary glaciations: especially during the last cold stage and through the Holocene to the present day.

Geomorphological evidence of glaciation includes, among others, classic features such as cirques, arêtes, moraines, glacial lakes, and hanging valleys. The basis of glacier reconstruction rests on the accurate depiction of glacial features on a geomorphological map. The most important elements of glacial geomorphology for glacier reconstruction are features that mark the lateral, terminal, and vertical limits of former glaciers such as moraine crests and trimlines. Moraine crests mark the margins of former glaciers during ice advance or ice front stabilization while trimlines mark the transition on land surfaces between subglacial erosional processes and subaerial periglacial weathering.

The limits of former glaciers marked on geomorphological maps can be used to build the former ice surface. This is done by drawing ice-surface contours on to the former glaciers. The shape of ice contours should follow that observed on modern glaciers, whereby ice-surface contours are concave toward the top of the glacier and convex toward the snout.

Once the ice surface is reconstructed, the equilibrium line altitude (ELA) can be reconstructed. The ELA is crucial for palaeoclimate reconstruction. The ELA of a glacier is the altitude at which accumulation and ablation are equal. It is a critical concept in the understanding of glacier dynamics and there is a very close relationship between the ELA and the local climate (Ohmura et al., 1992). Several methods have been applied to calculate the ELA on former glaciers and the choice of method depends on the former glacier morphometry, former climate regime, and the nature of the geomorphological evidence (Benn and Lehmkuhl, 2000). These methods are outlined in Table 1.

Reconstructing palaeoclimate using former glaciers

Empirical curved or linear relationships

The relationship between glaciers and climate is fundamental toward understanding glacier behaviour. There are well-established relationships between annual precipitation, or accumulation, and summer mean temperature at the equilibrium line altitude (ELA) on glaciers around the world (Ohmura et al., 1992 and references therein) (see Figure 1). Various forms of this relationship have been applied to reconstructions of Pleistocene glaciers and the relationship provides one of the most useful approaches for palaeoclimate reconstruction using glacial evidence. However, the utility of the relationship between annual precipitation, or accumulation, and summer mean temperature at the equilibrium line altitude (ELA) for palaeoclimate work is constrained by the need to isolate one of these variables in order to derive the other. In particular, it is frequently very difficult to isolate summer temperatures for palaeoglaciological work and it is even more difficult to isolate values of precipitation in mountainous regions.

Degree-day modelling

A degree-day model can be used to calculate the amount of accumulation required to sustain the glaciers. The degree-day model is based upon the notion that glacier melting occurs when air temperatures 1–2 m above the glacier surface are above the melting point (0°C). The total melt over a period at some point is therefore proportional to the sum of positive temperatures at the same point, i.e., the positive degree-day total. The annual accumulation required at the equilibrium line altitude to balance melting equals the sum of daily snowmelt, using a degree-day factor. Braithwaite (2008) found that degree-day factors for snow on 66 glaciers worldwide had averages of 3.5 ± 1.4 and 4.6 ± 1.4 mm day^{-1} K^{-1} in low- and high-accumulation conditions, respectively, with an overall mean of 4.1 ± 1.5 mm day^{-1} K^{-1}.

The degree-day model is widely used for modelling the mass balance of the Greenland ice sheet, but has also been applied to mountain glaciers and ice caps (Braithwaite et al., 2003). While the degree-day model has been used widely used in modern glacier-climate research, it has been utilized less so in palaeoglacier-climate research. However, degree-day modelling has been applied to reconstruct past climates associated with former glaciers in the USA (Brugger, 2006) and Greece (Hughes and Braithwaite, 2008).

Braithwaite (2008) used a degree-day model to demonstrate that the data underlying the single empirical curve of

Palaeoclimate and Past Glaciations, Table 1 Methods available for reconstructing palaeoglacier equilibrium line altitudes (ELAs). Sources are examples only and do not necessarily represent first usage

Method	Sources	Advantages	Disadvantages
Maximum elevation of lateral moraines	Benn and Lehmkuhl (2000, and references therein)	Simple, quick, and easy to apply in the field or using aerial photographs/satellite imagery	Inaccurate. Does not take into account lateral moraine formation during glacier recession
Toe-to-headwall altitude ratio (THAR)	Benn and Lehmkuhl (2000, and references therein)	Simple, quick, and easy to apply	Crude and takes no account of glacier hypsometry or climatic considerations. Requires some assumption on a suitable ratio
Toe-to-summit altitude method	Benn and Lehmkuhl (2000, and references therein)	Simple, quick, and easy to apply	Crude and takes no account of glacier hypsometry or climatic considerations
Median glacier elevation	Braithwaite and Müller (1980)	Appropriate for small cirque glaciers with even area/altitude distributions	Rarely applied on palaeoglaciers. Theoretically equivalent to an AAR of 0.5. Inflexible for different settings
Area-weighted mean altitude	Sissons (1974)	Appropriate for small cirque glaciers with even area/altitude distributions	Assumes a linear mass balance curve. Calculated ELA values tended to overestimate the real ELA
Accumulation area ratio (AAR)	Benn and Lehmkuhl (2000, and references therein)	Rigorously empirically tested. For modern mid- and high-latitude glaciers, steady state AARs generally lie in the range 0.5–0.8 with typical values lying in the range 0.6 ± 0.05	Does not take into account variations in glacier shape, particularly the distribution of glacier area over its altitudinal range, or hypsometry. AARs can be affected strongly by debris-covered glacier surfaces
Accumulation area ratio/ standard deviation	Kaser and Osmaston (2002, pp. 149–192)	Avoids problems of glacier hypsometry and defines a balance ratio by using standard deviation to isolate a statistical "best-fit" for the ELA	Not yet rigorously tested for accuracy on modern glaciers
Balance ratio	Furbish and Andrews (1984)	Takes into account both glacier hypsometry and the shape of the mass balance curve	Problems in defining analogous balance ratios

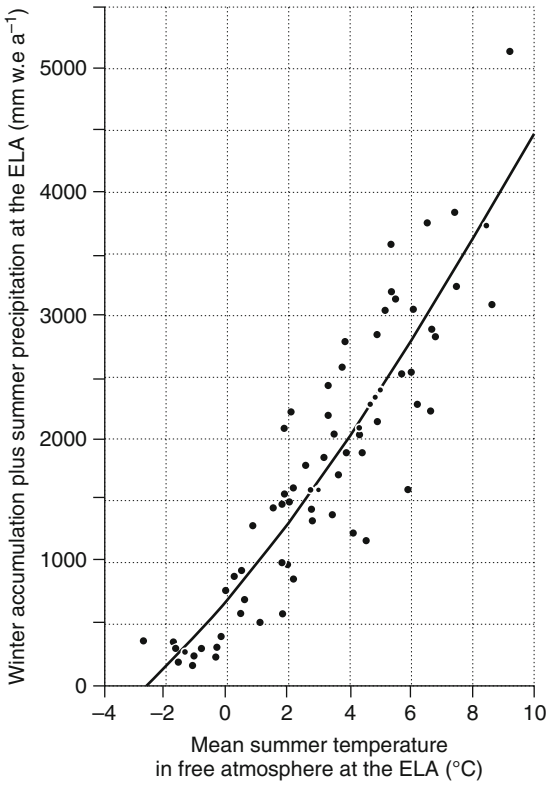

Palaeoclimate and Past Glaciations, Figure 1 Empirical curve relating mean summer temperature and winter accumulation + summer precipitation at 70 glaciers around the world (Redrawn using data from Ohmura et al. (1992)).

Ohmura et al. (1992) relating summer temperature and winter balance + summer precipitation is in fact better described by multiple curves, depending on the region. These different regional relationships are effectively determined by different annual temperature ranges (see Figure 2).

Energy balance modelling

This approach tends to be more complex than the previous two approaches and involves computation of different energy fluxes at the reconstructed glacier surface. Plummer and Phillips (2003) used a simple energy balance model to calculate the effects of topography on shortwave radiation, the largest component of the surface energy balance. Their model calculates the distribution of snow accumulation using a surface mass and energy balance approach and calculates the resultant glacier shapes with a two-dimensional flow model. However, this approach remains less widely used than simpler relationships between air temperature and mass balance, such as the Ohmura et al. (1992) regression. This is probably because of problems of complexity and uncertainties involved when reconstructing the former energy balance on palaeoglaciers.

Summary

Former glaciation can be interpreted using the geomorphological and geological record and used to reconstruct palaeoglaciers. In addition to glacier shape and form, the former equilibrium line altitude (ELA) can be reconstructed for past glaciers. The ELA of glaciers has a close relationship with climate and this fact can be utilized to reconstruct

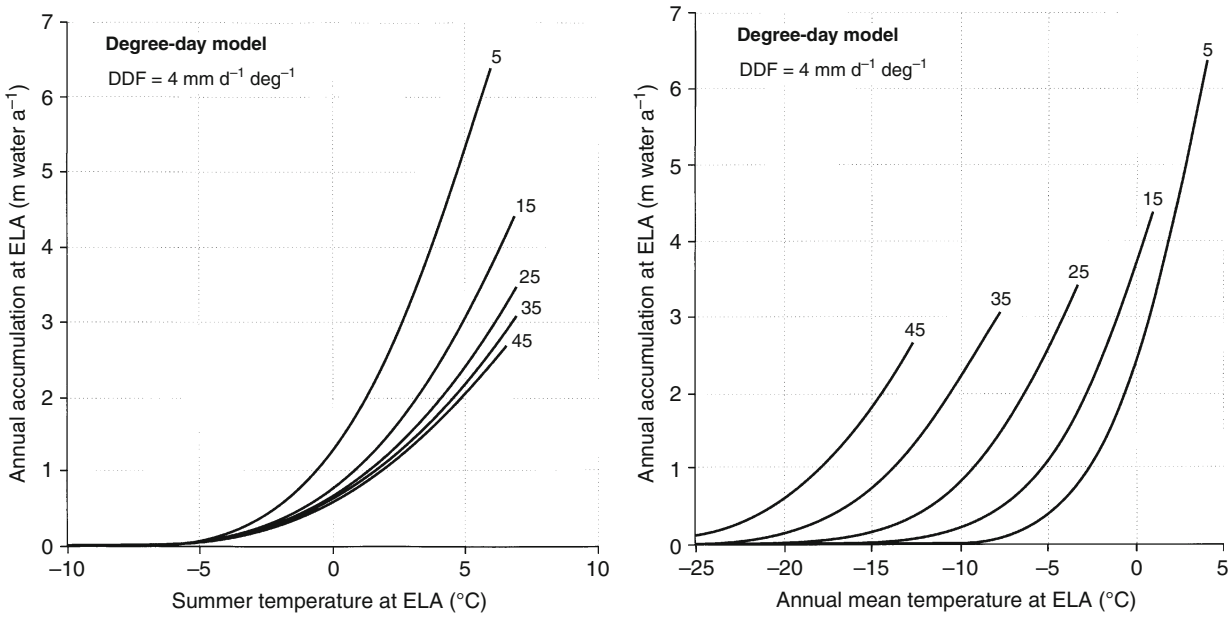

Palaeoclimate and Past Glaciations, Figure 2 Annual accumulation at the equilibrium line altitude (ELA) as a function of summer mean temperature (June–August) and mean annual temperature (January–December). The degree-day model was applied assuming a sinusoidal temperature variation throughout the year with annual temperature ranges of 5, 15, 25, 35, and 45°C (Based on an approach described in Hughes and Braithwaite, 2008).

palaeoclimate on former glaciers. Three main approaches can be used: (1) empirical curved or linear relationships; (2) degree-day modelling; and (3) energy balance modelling. The first two are more widely used than energy balance – largely because of their simplicity, requiring relatively few inputs in order to model palaeoclimate.

Bibliography

Benn, D. I., and Lehmkuhl, F., 2000. Mass balance and equilibrium-line altitudes of glaciers in high mountain environments. *Quaternary International*, **65**(66), 15–29.

Braithwaite, R. J., Zhang, Y., and Raper, S. C. B., 2003. Temperature sensitivity of the mass balance of mountain glaciers and ice caps as a climatological characteristic. *Zeitschrift für Gletscherkunde und Glazialgeologie*, **38**, 35–61.

Braithwaite, R. J., 2008. Temperature and precipitation climate at the equilibrium-line altitude of glaciers expressed by the degree-day factor for melting snow. *Journal of Glaciology*, **54**, 437–444.

Braithwaite, R. J., and Müller, F., 1980. On the parameterization of glacier equilibrium line altitude. *IAHS-AISH Publication*, **126**, 263–271.

Brugger, K. A., 2006. Late Pleistocene climate inferred from the reconstruction of the Taylor River glacier complex, southern Sawatch Range, Colorado. *Geomorphology*, **75**, 318–329.

Furbish, D. J., and Andrews, J. T., 1984. The use of hypsometry to indicate long-term stability and response of valley glaciers to changes in mass transfer. *Journal of Glaciology*, **30**, 199–211.

Grove, J. M., 2004. *Little Ice Ages: Ancient and Modern*, 2nd edn. London: Routledge, Vol. I and II.

Hays, J. D., Imbrie, J., and Shackleton, N. J., 1976. Variations in the Earth's orbit: pacemaker of the Ice Ages. *Science*, **194**, 1121–1132.

Hughes, P. D., and Braithwaite, R. J., 2008. Application of a degree-day model to reconstruct Pleistocene glacial climates. *Quaternary Research*, **69**, 110–116.

Kaser, G., and Osmaston, H., 2002. *Tropical Glaciers*. Cambridge: Cambridge University Press, pp. 149–192.

Ohmura, A., Kasser, P., and Funk, M., 1992. Climate at the equilibrium line of glaciers. *Journal of Glaciology*, **38**, 397–411.

Plummer, M., and Phillips, F. M., 2003. A 2-D numerical model of snow/ice energy balance and ice flow for paleoclimatic interpretation of glacial geomorphic features. *Quaternary Science Reviews*, **14**, 1389–1406.

Sissons, J. B., 1974. A Late-glacial ice-cap in the central Grampians, Scotland. *Transactions of the Institute of British Geographers*, **62**, 95–114.

Cross-references

Equilibrium-Line Altitude (ELA)
Glacier Mass Balance
Quaternary Glaciation
Surface Energy Balance

PALAEOHYDROLOGY

Vijay Kumar
National Institute of Hydrology, Roorkee, India

Paleohydrology is the science of the waters of the earth, their composition, occurrences, distribution, and movement on ancient landscapes from the occurrence of the first precipitation to the beginning of continuous historic hydrological records. Paleohydrology provides a link between the scientific hydrology of the present with the sciences of Earth history and past environments (Schumm, 1967). The term "paleohydrology" was first used by Leopold and Miller (1954) in a study of alluvial chronology of valleys in Wyoming.

The major reason for the development of paleohydrology was to improve knowledge about hydrological conditions by providing information about events, conditions, and hydrological situations in periods prior to the availability of continuous records (Gregory, 1996). Paleohydrology enhances understanding of the impacts of human activity on the hydrological cycle, water balance, sediment yield, river channel morphology, and basin characteristics. A further purpose of paleohydrology has been to make a contribution to the understanding of the impacts of global climate change. As major impacts of global climate change are felt through the hydrological cycle, paleohydrology has a very important role to play in understanding these impacts.

Paleohydrology applies the knowledge of contemporary hydrology to information derived from geomorphological evidences, such as ancient channels and sediments. Paleohydrology involves several disciplines like meteorology and climatology, hydrology, hydrogeology, paleoecology, dendrochronology, archaeology, geomorphology, sedimentology, etc. to provide information about hydrological events prior to continuous hydrological records. Paleohydrological speculations and conclusions depend on existing knowledge of the effects of climatic, vegetational and geologic controls on runoff, sediment concentration and yield, water chemistry, groundwater and lake water levels, and the nature of flood events. There are three general modes of paleohydrological inferences. First, the general theories of hydrology are used to infer specific effects that can then be discerned in evidence of past hydrological processes. Second mode of paleohydrological inference uses empirical relationships that are developed from numerous observations of related hydrological phenomenon. Third mode of reasoning, which is used extensively in paleohydrology, is retro-deductive or abductive inferences (Baker, 1998).

Bibliography

Baker, V. R., 1998. Palaeohydrology and the hydrological sciences. In Benito, G., Baker, V. R., and Gregory, K. J. (eds.), *Palaeohydrology and Environmental Change*. Wiley: Chichester, pp. 1–10.

Gregory, K. J., 1996. Definition and development of palaeohydrology. In Branson, J. (ed.), *Palaeohydrology: Context, Components and Application*, BHS Occasional Paper No. 7, British Hydrological Society.

Leopold, L. B., and Miller, J. P., 1954. Post-glacial chronology for alluvial valleys in Wyoming. *US Geological Survey Water-Supply Paper*, **1**(261), 61–85.

Schumm, S. A., 1967. Palaeohydrology: application of modern hydrologic data to problems of the ancient past. *In Proceedings of the International Hydrology Symposium.* Fort Collins, Vol. 1, pp. 161–180.

PAMIRS

Vladimir Aizen
College of Science, University of Idaho, Moscow, USA

Synonyms

Alpine glaciers; Glaciers of central Asia; Glaciers of Kyrgyzstan, Tajikistan, China, Afghanistan; Glaciers of mid-latitudes; Pamir

Definition

The alpine glaciers of the mid-latitudes that exist in the Pamir Mountains in sub-continental and arid continental climate.

The Pamir is one of the largest and highest mountain systems in Asia. It occupies the territory of Tajikistan, north-eastern Afghanistan, and the north-western part of China between 36° N and 40° N and 66° E and 76° E, 450 km from north to south and 850 km from west to east. The Pamir elevation and terrain is very diverse, ranging from 300 m at the lower Amu Dariya River to 7,700 m at the eastern Pamir in China. The Pamir Mountains are situated between the Aralo-Caspian and Tarim endorheic basins and the Indian Ocean. By 1990, Pamir glaciers covered approximately 12,000 km^2 (13,000 glaciers, 1,300 km^3 volume of ice) (Glacier Inventory of the USSR, 1979; Glacier Inventory of China. IV, 1987, Dolgushin and Osipova, 1989). Many Pamir glaciers including the giant Fedchenko Glacier are surging glaciers (Zabirov, 1955; Dolgushin and Osipova, 1989). Glaciers of the Pamir high mountains supply water to over 60 million people in Tajikistan, Uzbekistan, Turkmenistan, Afghanistan, and Xinjiang province of the PR of China. The Amu Dariya River is the largest central Asian river (2,400 km long, 534,739 km^2 total basin area), which originates in the Pamir Mountains of Tajikistan and Afghanistan. The Amu Dariya River provides 65% of inflow to the Aral Sea. The main moisture delivered to Pamir glaciers are from the Westerlies (southwestern cyclones). Indian monsoon occasionally reaches south eastern Pamir in summer (Aizen et al., 2009). Two thirds of annual precipitation occurred in the winter and spring seasons.

By glacio-climatic regime and landscape, Pamirs are divided into five major regions: Pamir-Alai, Western Pamir, Central Pamir, South-Eastern, and Eastern Pamir (Figure 1).

Western Pamir receives highest rate of annual precipitation (up to 2,000–2,500 mm) but only one fourth of precipitated snow gets accumulated and transferred to firn and ultimately to ice. Elevations of mountain ridges in the western Pamir are no more than 5,000 m. The Equilibrium Line Altitude (ELA) in this region ranges between 3,600 and 4,000 m a.s.l. and over 70% glacier covered area spread between 3,400 and 4,200 m a.s.l. Glaciers in western Pamir largely fed by avalanches and accumulation areas characterized by warm infiltration-recrystallization type of ice formation. Glaciers in western Pamir exist mainly at the northern slopes in deep high elevated valley, cirques, and niches.

Central Pamir represents glacierized massifs with large dendrite glaciers and accumulation zone reaching 7,400 m a.s.l and ELA rises to 4,400–4,800 m a.s.l. Fedchenko Glacier in central Pamir is the world's largest alpine glacier outside of the polar regions, 72 km long, 714 km^2 total area and 900–1,000 m ice thickness at elevation over 5,000 m. Surface ice velocity of the Fedchenko glacier may reach 150–200 m a year. Annual precipitation in central Pamir varies between 800 and 1,500 mm. The cold infiltration-recrystallization zones of ice formation largely spread at the high elevated accumulation areas in central Pamir. Ten to fifteen percent of glacier tongues were surface covered by moraine debris in the western and central Pamir (Schetinnikov, 1998). Central Pamir has many surging glaciers including most

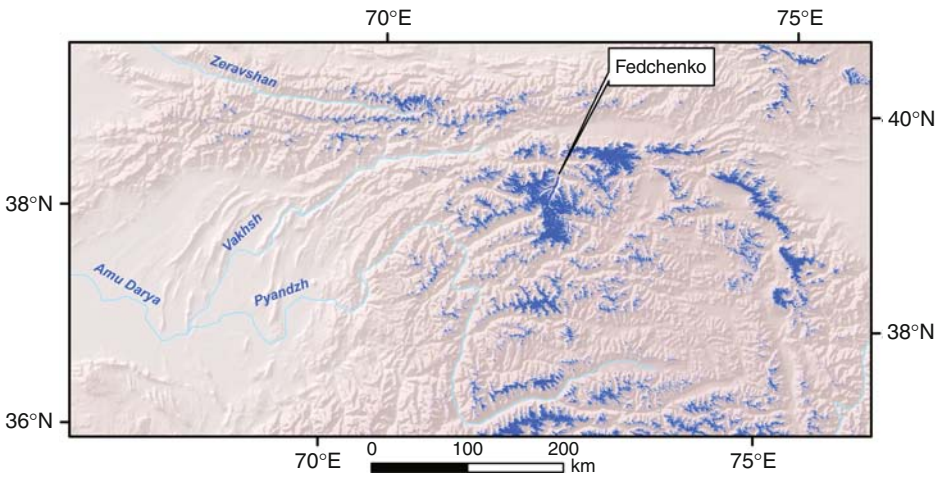

Pamirs, Figure 1 Glaciers of the Pamir Mountain system.

known Medvejiy Glacier, which has 12–15 years interval between the surges.

Eastern Pamir high elevation plateau spread over 4,000 m a.s.l. occupying approximately 100,000 km^2 and has extremely arid climate with annual precipitation between 50 and 150 mm similar to Tibetan Plateau. Glaciers in this area dispersed and existed mainly along high elevated ridges over 5,000 m. Glaciers in the eastern Pamir represented by ice-caps and slope niche glaciers, with small numbers of valley glaciers in eastern part of Zaalaiskiy Ridge at the eastern edge of Pamir and particularly in the Muztagata-Kongur glacierized massifs with the highest elevations in Pamir (7,500–7,700 m a.s.l.). ELA in eastern Pamir ranges between 4,800 and 5,200 m a.s.l. During summer, meltwater saturates through thin winter accumulation layers, refreezes, and forms ice during 1–2 years. Extremely dry air and high solar radiation create an ideal condition for moisture evaporation from

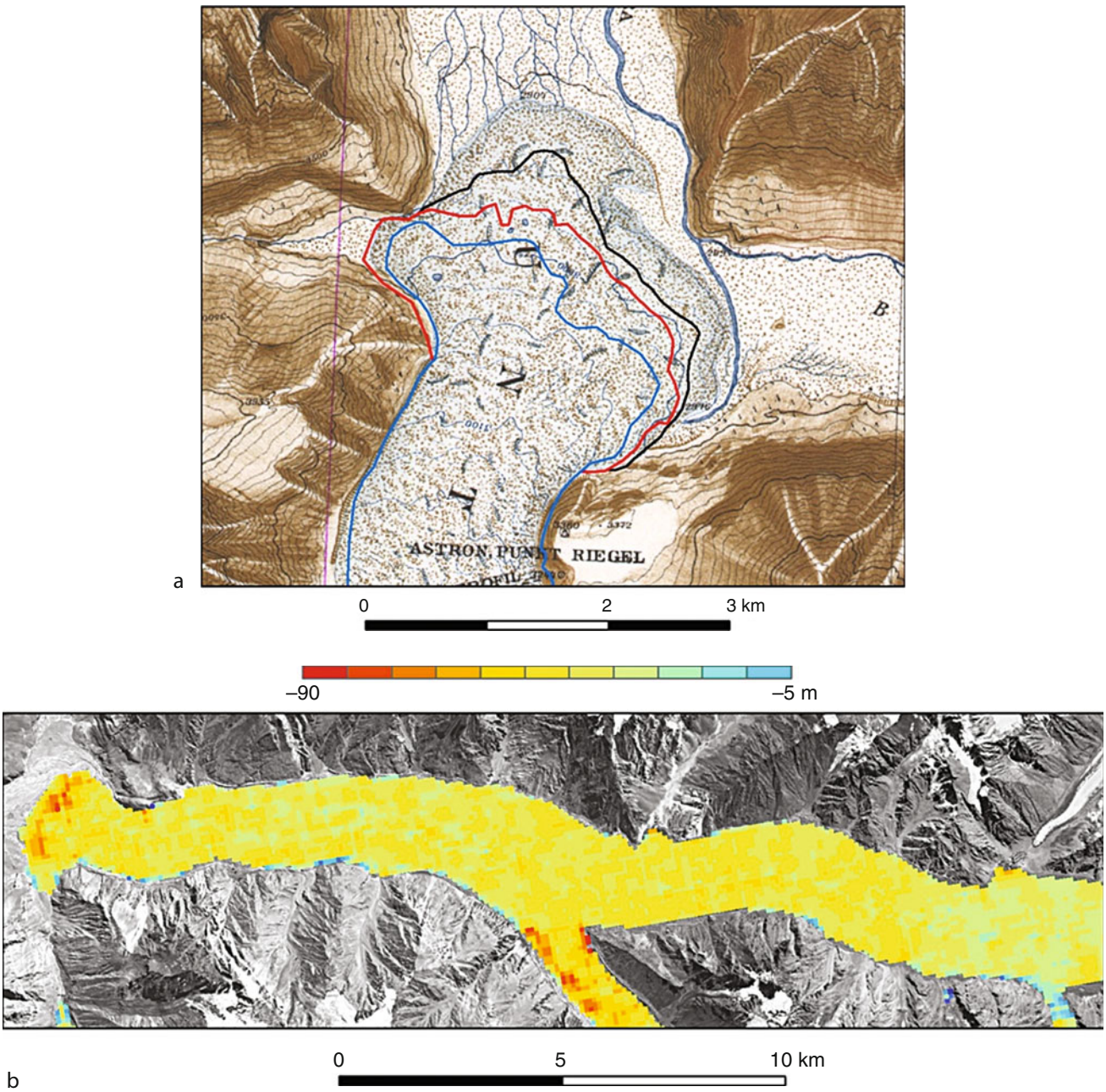

Pamirs, Figure 2 Glacier Fedchenko area changes between 1928 (*map in background*) and 1958 (*black line*), 1980 (*red line*) and 2009 (*blue line*) (**a**), and the glacier surface lowered between 1958 and 2009 (**b**) (Aizen et al., 2010b).

snow surface during ablation period. The eastern Pamir glaciers are covered very little by moraine debris in contrary to the western and central Pamir glaciers.

Since the end of Little Ice Age (LIA), glaciers of Pamir continue to retreat but the rate of glacier recession is different even within each of the regions that are described above. The largest recession (15%), during the last 50 years, was observed in western Pamir in Gissaro-Alai ridges and smallest in the central and eastern Pamir regions (3–5%). The largest Fedchenko Glacier retreated 1,131 m during the last 80 years (755 m from 1958 to 2000). The total area loss was 2 km^2 from 1958 to 2009 of the total 716.1 km^2 in 1958. However, the surface of this glacier melted and lowered to 90 m on the glacier tongue area at 2,896 m a.s.l. and 40 m at elevation of 4,000 m (Figure 2) (Aizen et al., 2010a). The river runoff in Pamir rivers increased by 2% during the last 10–20 years due to increase of air temperature and glacier ice melt and precipitation in high Pamir Mountains.

Bibliography

Aizen, V. B., Mayewski, P. A., Aizen, E. M., Joswiak, D. R., Kaspari, S., Sneed, S., Surazakov, A. B., Grigholm, B., and Finaev, A., 2009. Stable-isotope and chemical time series from fedchenko glacier firn core (pamir). *Journal of Glaciology*, **55**(190), 275–291.

Aizen, V. B., Aizen, E. M., Surazakov, A. B., and Nikitin, S. A., 2010a. Climate, snow, glaciers and river runoff changes in Pamir in the last 80 years. *Journal of Climate* (*in preparation*).

Aizen, V. B., Aizen, E. M., Surazakov, A. B., Nikitin, S. A., and Khang, Z., 2010b. LCLUC NASA Annual Report, Grant # NNX08AL68G: Collaborative Research: Diagnosis of changes in alpine water storages and land surface degradation in Pamir mountains and Amu Dar'ya River basin.

Dolgushin, L. D., and Osipova, G. B., 1989. Ledniki (Glaciers), M., Mysle Publishing, 447p (in Russ.).

Glacier Inventory of China. IV, 1987. Pamir Mountains (Interior Drainage Area of Tarim Basin), Lanzhou Institute of Glaciology and Geocryology. *China Science Press*.

Glacier Inventory of the USSR. 1979. *Catalogue of Glaciers in the USSR. Middle Asia and Kazakhstan*. Leningrad: Hydrometeo, 1970–1978 (Russ.).

Schetinnikov, A. C., 1998. Morfologiya i Regime Lednikov Pamiro-Alaya (Morphology and Regime of the Pamir-Alai Glaciers), CANIGMI, Tashkent, 219p (in Russ.).

Zabirov, R. D., 1955. Oledenenie Pamira (Pamir Glaciers). Geograph-GIZ, M., 372p (in Russ.).

PANCAKE ICE

Chelamallu Hariprasad
Centre for Studies in Resource Engineering, Indian Institute of Technology, Bombay Powai, Powai, Mumbai, Maharashtra, India

Pancake ice is a form of ice that consists of round pieces of ice with diameters ranging from 30 cm to 3 m, depending on the local conditions that affect ice formation. It may have upto 10 m thickness. Pancake ice features elevated rims with a nearly uniform height of a few centimeters. These rims are the first indication of the onset of the formation of the pancake ice from less consolidated forms of ice.

Pancake Ice, Figure 1

Pancake ice may be formed in two ways. It may be formed on water covered to some degree in slush, shuga, or grease ice.

Bibliography

http://iceglaces.ec.gc.ca/app/WsvPageDsp.cfm?Lang=eng&lnid=3&ScndLvl=yes&ID=10992

PAPUA

Ian Allison
Australian Antarctic Division and Antarctic Climate and Ecosystems CRC, Hobart, Tasmania, Australia

Definition

Papua is the official Indonesian and internationally recognized name for the province. After Indonesian annexation in 1969, the province became known as "West Irian" or "Irian Barat" until 1973, and thereafter was renamed "Irian Jaya" by the Suharto administration. The official name "Papua" was adopted in 2002.

Introduction

The only present-day equatorial glaciers in the Asian region are in the Indonesian province of Papua (formerly Irian Jaya) on the western part of the island of New Guinea. These small glaciers lie at elevations of over 4,400 m around the highest part of the Central Cordillera of New Guinea, Puncak Jaya (formerly Carstenz Pyramid or Mt. Carstensz). Located at 4°05′ S, 137°10′ E, the glaciers are only about 450 km south of the Equator.

Puncak Jaya Glaciers

Although native hunters have been active in the Puncak Jaya area for more than 5,000 years, the first westerner to report sighting these glaciers was the Dutch explorer, Jan Carstenz, sailing in the Arafura Sea to the south in 1623. It was not until 1936 that a European party, led by A.H. Colijn, reached the main glacier area with support from aircraft reconnaissance and food depots. During this visit, the geologist J.J. Dozy marked the location of the glacier snouts and obtained oblique aerial photographs of the glaciers. Expeditions from a consortium of Australian Universities made two visits to the area (December 1971 to March 1972 and January to February 1973) and undertook the first comprehensive scientific investigations of the glaciers and the surrounding region.

In 1972, there were five main glacier masses in the region, covering a total area of about 7 km^2 and an estimated total ice volume of about 0.25 km^3 (Allison and Peterson, 1976). These were the western and eastern portions of the Northwall Firn (3.6 km^2), divided by ice-free New Zealand Pass; two westward flowing valley glaciers, the Meren Glacier (2.2 km^2), and the Carstensz Glacier (1.4 km^2); and the Southwall Hanging Glacier (0.1 km^2) on the steep south face of Puncak Jaya (Figure 1). The Meren Glacier, which was contiguous with the eastern portion of the Northwall Firn, was so-called because of the large number of small englacial lakes that covered its ablation zone. The area for the Carstensz Glacier includes two small contiguous ice masses, the Wollaston and Van de Water glaciers that flow southward from the ice divide at the top of the Carstensz Glacier.

The Meren Glacier and the Carstensz Glacier have the morphology of classical valley glaciers. The centerline length of the Meren and Carstensz glaciers in 1972 were about 1.9 and 1.7 km respectively. The Meren Glacier had a mean ice thickness of 40 m, a maximum measured ice thickness of 81 m, an average of 25 m/year and a maximum measured surface velocity of 34 m/year. The Carstensz Glacier had a mean ice thickness of 38 m and a maximum measured ice thickness of 74 m. Because it was slightly thinner, and less steep than the Meren, ice movement was slower, with an average centerline surface velocity of 15 m/year and a maximum measured surface velocity of 18 m/year. The ablation zones of both glaciers were temperate. The morphology and dynamics of these glaciers are described by Allison (1975, 1976).

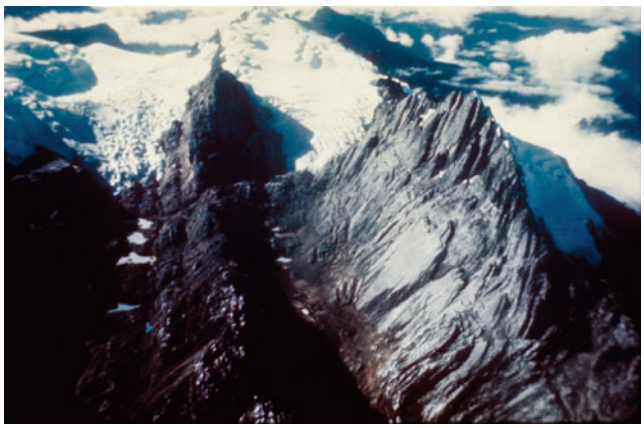

Papua, Figure 1 1972 oblique aerial photograph looking east and showing, from left to right, eastern portion of the Northwall Firn, Meren Glacier flowing into the Yellow Valley, Carstensz Glacier flowing into Carstensz Valley, and Southwall Hanging Glacier on the back of Puncak Jaya. (Photograph: Australian Universities' Carstensz Glaciers Expedition.)

Seasonal climatic variations on the Puncak Jaya massif are slight, and the monthly mean temperatures vary by less than 0.5°C over the year. There appears to be no marked seasonal variation in precipitation, radiation, or cloud cover (Allison and Bennett, 1976). Hence the net surface mass balance of the glaciers is relatively uniform over the year. Ablation tends to occur year round below the equilibrium line and accumulation occurs year round above it. Surface mass balance measurements over 1972 indicated an equilibrium line altitude of 4,580 m, with an accumulation area ratio of 0.59 for the Meren, and 0.66 for the Carstensz. The net annual balance in 1972 varied between +1 m/year water equivalent (w.e.) at 4,800 m elevation, near the top of the glaciers, and −5 m/year w.e. at 4,400 m, near the termini. Both the Meren and Carstensz Glaciers had a negative mass budget, consistent with their observed retreat.

Retreat of the Puncak Jaya glaciers since the mid-nineteenth Century

Peterson et al. (1973) estimated the mid 19th Century (approx. 1850) neoglacial extent of the Puncak Jaya ice masses from moraines and other geomorphologic features as 19.3 km^2. Since then a steady retreat of the glaciers has been recorded from cairns left by various expeditions to mark the glacier fronts, from aerial photographs, and more recently from satellite images. By 1942 the total ice area had reduced to 9.9 km^2 (Allison and Peterson, 1976); by 1972 it had reduced further to 7.3 km^2 (Allison and Peterson, 1989); and by 2002 there was only 2.1 km^2 of ice-covered area remaining (Klein and Kincaid, 2006). Allison and Kruss (1977) used a simple 2-D flow-line model of glacier dynamics to show that the retreat of the Meren and Carstensz glaciers between 1850 and 1972 was most likely due to a temperature increase of 0.6°C over the period, rather than to changes in snowfall.

Between 1992 and 2000 the Meren Glacier disappeared completely, the western Northwall Firn fragmented into several small remnants, and the Carstensz Glacier reduced to half its 1972 extent (Klein and Kincaid, 2006).

Other ice masses in Papua

As well as the glaciers of Puncak Jaya, the high peaks of Papua have supported other ice areas in the recent past. These have been rarely visited, but high resolution satellite monitoring provides a sketchy record of their retreat. On Ngga Pilimsit (Idenburg-top; 4°03′ S, 137°02′ E; 4,717 m), about 12 km west of Puncak Jaya, a small ice cap on the summit (several hundred meters in diameter) and a slightly

smaller glacier on an adjoining ledge existed until at least 1983 (Allison and Peterson, 1989), but had disappeared by 2003 (Klein and Kincaid, 2006). An ice cap on Puncak Trikora (Wilhelmina-top; 4°15′ S, 138°45′ E; 4,730 m) disappeared sometime between 1939 and 1962 (Peterson et al., 1973), and the small ice cap on Puncak Mandala (Juliana-top; 4°48′ S, 140°20′ E; 4,640 m) disappeared between 1989 and early 2003 (Klein and Kincaid, 2008).

Summary

All the small ice caps on the high mountains of Papua have disappeared over the last century, and only remnants of the larger ice fields in the Puncak Jaya area remain. Even here, by 2002 the total ice area had reduced to about 11% of its mid-nineteenth century extent, and one of the two valley glaciers, the Meren, had disappeared by 2003 (Klein and Kincaid, 2006). The retreat rate of the Papuan glaciers appears to be fairly uniform since ~1850, although Klein and Kincaid (2006) do report periods of more rapid retreat in total ice extent in the late 1930s and in the 1970s. With continuing retreat at the average rate over the last century, no significant ice masses will remain in Papua beyond the middle of the twenty-first century.

Bibliography

Allison, I., 1975. Morphology and dynamics of the tropical glaciers of Irian Jaya. *Zeitschrift für Gletscherkunde und Glazialgeologie*, **10**, 129–152.

Allison, I., 1976. Glacier regimes and dynamics. In Hope, G. S., Peterson, J. A., Radok, U., and Allison, I. (eds.), *The equatorial glaciers of New Guinea*. Rotterdam: A.A. Balkema, pp. 39–59.

Allison, I., and Bennett, J., 1976. Climate and microclimate. In Hope, G. S., Peterson, J. A., Radok, U., and Allison, I. (eds.), *The equatorial glaciers of New Guinea*. Rotterdam: A.A. Balkema, pp. 61–80.

Allison, I., and Kruss, P., 1977. Estimation of recent climate change in Irian Jaya by numerical modeling of its tropical glaciers. *Arctic and Alpine Research*, **9**, 49–60.

Allison, I., and Peterson, J. A., 1976. Ice areas on Mt. Jaya: their extent and recent history. In Hope, G. S., Peterson, J. A., Radok, U., and Allison, I. (eds.), *The equatorial glaciers of New Guinea*. Rotterdam: A.A. Balkema, pp. 27–38.

Allison, I., and Peterson, J. A., 1989. Glaciers of Irian Jaya, Indonesia. In Williams, R. S.Jr., and Ferrigno, J. G. (eds.), *Satellite Image Atlas of Glaciers*. U.S. Geological Survey Professional Paper 1386-H, pp. H1–H20.

Klein, A. G., and Kincaid, J. L., 2006. Retreat of glaciers on Puncak Jaya, Irian Jaya, determined from 2000 and 2002 IKONOS satellite images. *Journal of Glaciology*, **52**, 65–79.

Klein, A. G., and Kincaid, J. L., 2008. On the disappearance of the Puncak Mandala ice cap, Papua. *Journal of Glaciology*, **54**, 195–197.

Peterson, J. A., Hope, G. S., and Mitton, R., 1973. Recession of snow and ice fields of Irian Jaya, Republic of Indonesia. *Zeitschrift für Gletscherkunde und Glazialgeologie*, **9**, 73–87.

Cross-references

Equilibrium-Line Altitude (ELA)
Glacier Mass Balance
Moraine
Snow Water Equivalent
Temperate Glaciers

PARAGLACIAL LANDSCAPE TRANSFORMATIONS

Lasafam Iturrizaga
Geography/High Mountain Geomorphology, Institute of Geography, University of Göttingen, Göttingen, Germany

Synonyms

Glacially conditioned; Transglacial

Definition

The term paraglacial ("para" (prefix) from Greek, alongside, beyond, altered, contrary to) means literally "beyond the glacier" (Slaymaker, 2004) and has been defined as non-glacial processes, which are directly conditioned by glaciation (Church and Ryder, 1972).

Paraglacial landforms are formed during and after the deglaciation in the course of the readjustment toward an assumed environmental equilibrium stage. Besides its general meaning, the term "paraglacial" has been used in a temporal way ("paraglacial period," "paraglaciation") as well as in a spatial context.

Introduction: evolution of a geomorphological concept

The term "paraglacial" has been employed by Ryder (1971) for explaining the formation of alluvial fans by the fluvial redeposition of glacigenic till following the Wisconsinan deglaciation in the Fraser and Thompson Rivers (British Columbia) (Figure 1). In order to evaluate the findings, comparative studies have been carried out in a presently glaciated area in Baffin Island (Canadian Arctic) where paraglacial sedimentation supposed to be highly active (Church and Ryder, 1972). Subsequently "paraglacial" has been defined as "non-glacial processes, which are directly conditioned by glaciation" and referred "both to proglacial processes, and to those occurring around and within the margins of a former glacier that are the direct result of the earlier presence of the ice" (Church and Ryder, 1972). Even though this definition is already rather broad, its interpretation became in the following decades considerably extended beyond the application for the glacially conditioned formation of fluvial landforms.

Ballantyne (2002a) has compiled the main research studies concerned with the adaptation of the landscape after deglaciation and introduced an overall concept for "paraglacial geomorphology." It includes the study of earth-surface processes, sediments, landforms, landsystems, and landscapes that are directly conditioned by non-glacial earth-surface processes triggered by the former glaciation and deglaciation. Since then, research topics on paraglacial geomorphology increased significantly in number (Mercier and Étienne, 2008), especially in the light of global warming and the associated landscape response to deglaciation (André, 2009). The dominant glacier shrinkage since the Little Ice Age resulted in

Paraglacial Landscape Transformations, Figure 1 Paraglacial valley fill in the Fraser Valley (British Columbia). Photo: L. Iturrizaga Sept. 1999.

deglaciated terrain in the order of several kilometers in length and some hundred meters in absolute height which offers an excellent landscape setting to investigate the historical and most recent paraglacial geomorphological activity (e.g., Harrison and Winchester, 1997; Curry et al., 2006, Figure 2). Besides that, the overall landscape development after the Lateglacial deglaciation has been a major concern of paraglacial morphology challenging especially conventional periglacial landform interpretations.

Key issues of the paraglacial concept

In principle, the term "paraglacial" is not linked to a specific process, but includes a variety of non-glacial processes which might be conditioned directly by the former glaciation and occur during the adjustment of the landscape after deglaciation. The paraglacial concept cannot be pinpointed by processes (Ballantyne, 2003), even though the expression of "paraglacial processes" has been now in common use (André, 2009). It rather focuses on conditions of accelerated geomorphological activity after glacier retreat. A common feature of deglaciated landscape is the supply of additional sediment sources, such as unstable rock walls or glacigenic sediment storages, which are prone to further erosional processes. The paraglacial effect is materialized by the extraordinary sediment supply which exceeds by far the rate of debris produced by weathering. In turn, high sediment transfer rates result in different landforms of temporary storage. These landforms may often be identical with fluvial or mass movement landforms. Enhanced sediment transport continues as long as sediment supply areas remain accessible to fluvial activity. Therefore the paraglacial imprint can by far outlast the actual period of deglaciation.

Paraglacial sediment yield and sediment cycle

One of the key results of the study of Ryder (1971) is that the sedimentation of the alluvial fans in British Columbia River took place soon after deglaciation in the Early Holocene proved by a volcanic ash layer (Mazama ash, 6,000 years B.P.) in the top part of the alluvial fans. Thus, it was assumed that the rate of sediment yield is higher immediately after ice retreat, but later declines towards the regional average rate. (Church and Ryder, 1972).

Church and Slaymaker (1989) investigated the specific sediment yield of drainage basins of different sizes in British Columbia. In contrast to previous models, in which the specific sediment yield declines with increasing drainage basin area, they showed that the sediment yield increases for larger basins. The reason supposed to be that most of the sediment yield derives from reworked valley fill deposits from the Quaternary glaciation. Thus, they concluded that the rivers still respond to the deglaciation and extended the paraglacial period from some one thousand years as proposed earlier to more than 10,000 years. The crucial quintessence of this assumption is that the recent sediment yield does not reflect the erosion rate for the prevailing climatic and regional geology setting in the Holocene, but it is still influenced by the effects of the Quaternary glaciation. During the deglaciation occurs a shift from the redistribution of sediment material from the upland toward the major valleys, which was termed

Paraglacial Landscape Transformations, Figure 2 The Bualtar valley (Karakoram) has been deglaciated in the mid of the twentieth century. The slopes are covered with paraglacial talus cones of different ages. Photo: L. Iturrizaga Aug. 2000.

as paraglacial sediment cycle (Church and Slaymaker, 1989). This fact supposed to explain the downstream increase in sediment yield in river basins in British Columbia.

Jordan and Slaymaker (1991) considered perturbations of the paraglacial sedimentation cycle in form of volcanic activity and associated debris flows and human impacts. Harbour and Warburton (1993) have reflected the variation of catchment size in the paraglacial model and came up with varying relaxation times, which depend on the scale of the catchment. They proved that the different catchment sizes may show identical sediment yield. Moreover, the peaks in specific sediment yield may vary in time for different catchment sizes.

The glacially conditioned sediment release has been formalized by a sediment exhaustion model Ballantyne (2002b), which is based on steady-state conditions and the precondition that sediment sources are not replenished. Assuming that the rate of sediment release is dependent only on sediment availability, it declines approximately exponentially through time. New approaches have been undertaken to quantify the paraglacial sediment storage in order to allow conclusions on the sediment flux rates and finally on the landscape evolution (Otto, 2009).

Paraglacial period

The "paraglacial period" was originally referred to as the "time during which paraglacial processes occur" (Church and Ryder, 1972). Ballantyne (2003) has suggested a redefinition as "the timescale over which a glacially conditioned sediment source either becomes exhausted or attains stability in relation to particular reworking processes." The paraglacial period covers a time span of only 10–100 years up to more than several ten thousand years (Ballantyne, 2002a). The readjustment of sediments in recently deglaciated glacier forefields counts to the more short-term readjustments (Curry, 2000), whereas the valley flanks in solid rock may need a longer time for relaxation.

The time scale of the paraglacial period depends among others on the topographical setting, the intensity of the erosion and the occurrence of temporary storage areas. Vegetation is also a controlling factor in terms of the duration of paraglacial activity (Church and Ryder, 1972). Lakes, such as the suite of glacial lakes in the Tasman valley (New Zealand), may significantly delay the paraglacial influence on the lowlands. Here the rivers are still responding on the Quaternary glaciation, and the Canterbury Plains with their extensive braided river systems may be considered as the result of the Lateglacial ice retreat. However, intra-catchment variability has to be taken into account with respect to the magnitude-frequency regime in regard for the prediction of sediment fluxes in response to hydro-climatic forcing (Carrivick and Rushmer, 2009).

The paraglacial period supposed to start with the beginning with the glacial sedimentation. The effective duration of the paraglacial period may vary considerably, and its end is difficult to determine precisely, especially when including the secondary paraglacial systems. In general, it may extend the glaciation phase and ensue into the non-glacial interval (Slaymaker, 2004). A stratigraphical differentiation of this transitional period is not possible.

Paraglacial landsystems

Ballantyne (2002a) has extended the paraglacial concept so far, that it should become suitable for an own subdivision of geomorphology. Thus, paraglacial geomorphology encompasses landsystems, landforms, and associated processes as well as the paraglacial period, in which paraglacial processes take place. Using the landsystem approach, six paraglacial landsystems are distinguished: rock slopes, drift-mantled slopes, glacier foreland, alluvial, lacustrine and coastal systems.

Primary paraglacial systems are those in which the released sediment has been directly conditioned by glaciers. Secondary paraglacial systems includes the reworking of paraglacial sediment stores (Ballantyne, 2002b). Ballantyne (2003) has also proposed a paraglacial sediment cascade differentiating between (a) sediment sources (rockwalls, drift-mantled slopes, valley floor glacigenic deposits, and coastal glacigenic deposits), (b) primary sediment stores (i.e., talus cones, debris flow deposits, alluvial fans, barrier beaches), (c) secondary sediment stores (i.e., alluvial valley fill deposits, lacustrine deposits, coastal deltas), and (d) sediment sinks (alluvial valley fill deposits, lacustrine deposits, coastal and nearshore deposits, shelf and offshore deposits). The transport from the sediment source to the sediment sink is not linear, but may involve several cycles of deposition and resedimentation. External perturbations may complicate significantly the process succession in this simplified model. Besides the paraglacial fluvial landforms, Ballantyne (2002a) highlights among others the importance of the adjustment of rock slopes after deglaciation (Wyrwoll, 1977; Augustinus, 1995; Ballantyne, 2008). He distinguished the rock slope system by the mode of failure (catastrophic rock slope failure, rock mass creep and progressive small-scale rock fall activity). Rock slope failure at the glacially oversteepened valley flanks may be caused by debutressing and unloading processes in association with stress release after deglaciation (Cossart et al., 2008). The inclusion of coastal landsystems into the paraglacial concept has been one of the major extensions of glacially conditioned landscape transformation (Forbes and Syvitski, 1994). Therewith, the paraglacial concept has extended its focus from the mountainous areas toward the final sediment sink, the ocean, and made the model even more a holistic landscape approach.

Distribution of paraglacial landsystems and landforms

Paraglacial landforms occur in proglacial as well as in lateroglacial environments, i.e., in valley-side locations at the lateral margins of the glaciers. Paraglacial landscape transformation is most obvious in mountainous areas, where steep slopes provide the necessary relief energy for enhanced geomorphological processes. During the paraglacial period, an intensification of non-glacial processes takes place.

Each mountain region around the world possesses a specific paraglacial landform assemblage depending on the geological, topographical, and climatic setting (especially during the deglaciation); ice thickness; glacier type (topographical and thermal regime); and ratio of accumulation–ablation area. Thus, the individual mountain regions show in particular major differences in the distribution in moraine-mantled slopes.

The greatest altitudinal range of paraglacial landforms is achieved in High Asia, especially in the Karakoram (Iturrizaga, 1999a). The Karakoram represents a classical example of moraine-mantled slope environments (Li et al., 1984; Owen and Derbyshire, 1989). The topographical setting and therefore the glacier type and the ice thickness determine to some extent the availability of moraine-mantled valley slopes. Ice thicknesses of up to 2,900 m have been reconstructed in this mountain range (Kuhle, 2001). Despite the extensive glaciation, high amounts of relief still surmounted the ice stream network and delivered a large amount of debris into the lateroglacial environments (Iturrizaga, 2003). The vast sediment availability is a result of an ice stream network which disintegrated gradually into individual glaciers and which were still themselves dendritic glaciers types.

Tributary glaciers became disconnected with the main glacier and supplied sediment material mainly by glaciofluvial activity. Moreover, the immense ice thickness and increased stress pattern on the valley flanks resulted in major rock slope failures after deglaciation, especially in large-sized rock avalanches (Hewitt, 1999), but as well in the formation of glacially induced talus cones (Iturrizaga, 1999a).

The local ice thickness controls the center-to-periphery change of the distribution of paraglacial landforms. Ice thickness may generally be the highest in the upper middle part of the glacier stream. Thus, a reduced vertical relief amplitude has been transformed by glacial processes toward the mountain interior and the former glacier terminus. The glacially induced talus cones are replaced upvalley by talus cones originating from weathering processes on the parent rock.

A glacially history-based concept of the development of debris accumulations in High Asia (Hindukush, Karakoram, Himalayas) has been proposed by Iturrizaga (1999a, b). In this regard, the term "transglacial" has been introduced to address to landforms, which have been formed by the transformation of the glacially stressed valley flanks as well as by the postsedimentary transformation of slope moraines after the deglaciation in mountain areas (Iturrizaga, 2006, Figures 3 and 4). These transglacial landforms may be used in their topographical relationship as geomorphological indicators for the reconstruction of the former glacier extent. Moreover, high magnitude-low frequency events play an important role in the sediment transfer in this mountain region.

Some new insights of paraglacial geomorphology

An interesting issue is the interfingering and coexistence of periglacial and paraglacial landscape environments,

Paraglacial Landscape Transformations, Figure 3 Alluvial fan composed partly of fluvially reworked till in the Mastuj valley (Hindukush). The valley flanks are covered with slope moraines up to several hundred meters above the valley floor. Photo: L. Iturrizaga Aug. 2004.

Paraglacial Landscape Transformations, Figure 4 Talus cones composed of reworked slope moraines at the Yazghil glacier (Karakoram). Photo: L. Iturrizaga July 2001.

particularly, in regard to time frames for the occurrence of periglacial processes (Coleman and Carr, 2008; Knight and Harrison, 2009). In the British upland, valley bottom drift was conventionally considered as periglacial solifluction deposits. They supposed to have been formed during the Loch Lomond Stadial, where favorable conditions occurred for permafrost environments. Harrison (1996) has proposed that the sediments are the result of debris flows which occurred shortly after the deglaciation during warm climatic conditions. The paraglacial hypothesis would imply a much older age of those deposits. Poorly investigated until now is the relationship between contemporary periglacial weathering regimes and those that prevailed during paraglaciation (Thorn, 2004).

Talus cones and talus slopes have been previously classified as key forms of the periglacial landscape environment assuming that frost-weathering processes are the principal form of mechanical rock disintegration. However, the rate of frost-weathering turned out to be much too low to account for the formation of talus cones in various high-mountain regions of the world (Rapp, 1960; Luckman and Fiske, 1997). Thus a paradigm shift takes place concerning the development of talus cones as they are no longer considered only as wholly climatic-controlled landforms, but also as paraglacial landforms or composite landform of periglacial and paraglacial origin (Iturrizaga, 1999b, 2008; Wilson, 2009, Figure 4).

A further trend of reassessment is recognizable in regard to terminal moraines. Some of them have been reinterpreted as deposits of rock avalanches (i.e., in the Andes, Abele, 1981, and in the Himalayas, Fort and Peulvast, 1995). In recent times, these large-sized mass movements have also been partly considered in a paraglacial context in the Karakoram and were linked to oversteepening by glaciation and debutressing of rock walls during deglaciation (Hewitt, 2009).

Critics and reassessment

The paraglacial concept has undergone a critical review in the last years (Knight and Harrison, 2009) and is therefore in a stage of reassessment (Wilson, 2009). On the one hand side, there is the argument that the term "paraglacial" should not only be referred to glacial processes but also to transitional forms in general (Slaymaker, 2009). It supports more the concept of a transient landscape which responds to environmental disturbances in general. On the other hand, as vague as the term "paraglacial" itself is, it has been applied in so many ways (spatially, temporally, genetically) in regard to the glacially conditioned landscape transition that the term faces almost to become redundant (Slaymaker, 2007). There is an apparent problem in referring the term "paraglacial" to processes, as "paraglacial processes" are identical with processes operating outside of glaciated areas, only in an accelerated way. Paraglacial geomorphology is a concept without distinctive processes.

Moreover, geomorphology is concerned about the explanation of distinct landforms and, in this respect, a lack of characteristic "paraglacial landforms" can be noticed. Looking at the individual landsystems (rock slopes, drift-mantled slopes, glacier foreland, alluvial, lacustrine and coastal systems) and the according landforms (i.e., catastrophic failure, mass movement, frost action), it is apparent that they are overlapping with existent landsystems, such as purely coastal, fluvial, or periglacial, and are rather unspecific. The use of "paraglacial" as an all-round term for landscape transformation conditioned by glaciation may be thus sometimes rather confusing.

Conclusions

The introduction of "paraglacial geomorphology" as a new proposed subdivision of geomorphology has been an important step in order to unify previous and current research studies concerned with the geomorphological adjustment of the landscape after deglaciation into one overall concept. The immense impact of glaciation and deglaciation on the geomorphological landscape evolution has been investigated before in different respects, but it has been mainly focused either on the transformation of the bedrock morphology, i.e., the transition from a V-shaped to an U-shaped valley, and associated rock slope failures, or on the deposition of specific glacigenic sediments. The paraglacial concept stresses the importance of the transformation of the landscape after the glaciations in terms of glacially conditioned sediment supply, sediment storage, and sediment flux. Thereby, one key element of this approach is that the landforms are not treated as individual landforms, but in their interconnectedness. These results have provided some reinterpretation of landforms, which have formerly considered as periglacial in origin. However, there exists a close interlinkage between glaciation, paraglaciation, and periglaciation, and many landforms may have faced a polygenetic origin.

On the whole, the paraglacial concept needs some basic reevaluation of its principal definition (e.g., differentiation between paraglacial and proglacial, inclusion of glacioisostatic rebound effects) and a clearer limitation in its application (Slaymaker, 2007). It remains to be seen whether paraglacial geomorphology will be only a temporal concept in an attempt to link glacial and periglacial landscape (Dixon and Thorn, 2005).

Bibliography

Abele, G., 1981. Trockene Massenbewegungen, Schlammströme und rasche Abflüsse. Dominante morphologische Formen in den chilenischen Anden. Mainzer Geographische Studien, Heft 23, 102 pp.

André, M. F., 2009. From climatic to global change geomorphology: contemporary shifts in periglacial geomorphology. *Geological Society Special Publications (London)*, **320**, 5–28.

Augustinus, P. C., 1995. Glacial valley cross-profile development: the influence of in situ rock stress and rock mass strength, with examples from Southern Alps, New Zealand. *Geomorphology*, **11**, 87–97.

Ballantyne, C. K., 2002a. Paraglacial geomorphology. *Quaternary Science Reviews*, **21**(18–19), 1935–2017.

Ballantyne, C. K., 2002b. A general model of paraglacial landscape response. *Holocene*, **12**(2), 371–376.

Ballantyne, C. K., 2003. Paraglacial landsystems. In Evans, D. J. (ed.), *Glacial Landsystems*. London: E. Arnold, pp. 432–461.

Ballantyne, C. K., 2008. After the ice: Holocene geomorphic activity in the Scottish highlands. *Scottish Geographical Journal*, **124**(1), 8–52.

Carrivick, J. L., and Rushmer, E. L., 2009. Inter- and intra-catchment variations in proglacial geomorphology: an example

from Franz Josef glacier and Fox glacier, New Zealand. *Arctic, Antarctic, and Alpine Research*, **41**(1), 18–36.
Church, M., and Ryder, J. M., 1972. Paraglacial sedimentation: a consideration of fluvial processes conditioned by glaciation. *Geological Society of America Bulletin*, **83**, 3059–3071.
Church, M., and Slaymaker, O., 1989. Disequilibrium of Holocene sediment yield in glaciated British Columbia. *Nature*, **337**, 452–454.
Coleman, C. G., and Carr, S. J., 2008. Complex relationships between Younger Dryas glacial, periglacial and paraglacial landforms, Brecon Beacons, South Wales. *Proceedings of the Geologists' Association*, **119**(3–4), 259–276.
Cossart, E., Braucher, R., Fort, M., Bourles, D. L., and Carcaillet, J., 2008. Slope instability in relation to glacial debuttressing in alpine areas (Upper Durance catchment, southeastern France): evidence from field data and 10Be cosmic ray exposure ages. *Geomorphology*, **95**(1–2), 3–26.
Curry, A. M., 2000. Observations on the distribution of paraglacial reworking of glacigenic drift in western Norway. *Norsk Geografisk Tidsskrift*, **54**, 139–147.
Curry, A. M., Cleasby, V., and Zukowskyj, P., 2006. Paraglacial response of steep, sediment-mantled slopes to post-little Ice Age glacier recession in the central Swiss Alps. *Journal of Quaternary Science*, **21**, 211–225.
Dixon, J. C., and Thorn, C. E., 2005. Chemical weathering and landscape development in mid-latitude alpine environments. *Geomorphology*, **1–2**, 127–145.
Forbes, D. L., and Syvitski, J. P. M., 1994. Paraglacial coasts. In Carter, R. W. G., and Woodroffe, C. D. (eds.), *Coastal Evolution: Late Quaternary Shoreline Morphodynamics*. Cambridge: Cambridge University Press, pp. 373–424.
Fort, M., and Peulvast, J.-P., 1995. Catastrophic mass-movements and morphogenesis in the Peri-Tibetan ranges: examples from West Kunlun, East Pamir and Ladakh. In Slaymaker, O. (ed.), *Steepland Geomorphology*. New York: Wiley, pp. 171–198.
Harbor, J., and Warburton, J., 1993. Relative rates of glacial and nonglacial erosion in Alpine environments. *Arctic and Alpine Research*, **25**(1), 1–7.
Harrison, S., 1996. Paraglacial or periglacial? The sedimentology of slope deposits in upland Northumberland. In Anderson, M. G., and Brooks, S. M. (eds.), *Advances in Hillslope Processes*. Chishister: Wiley, pp. 1197–1218.
Harrison, S., and Winchester, V., 1997. Age and nature of paraglacial debris cones along the margins of the San Rafael Glacier, Chilean Patagonia. *Holocene*, **7**(4), 481–487.
Hewitt, K., 1999. Quaternary Moraines vs Catastrophic Rock avalanches in the Karakoram Himalaya, northern Pakistan. *Quaternary Research*, **51**(3), 220–237.
Hewitt, K., 2009. Glacially conditioned rock-slope failures and disturbance-regime landscapes, Upper Indus Basin, northern Pakistan. *Geological Society Special Publications (London)*, **320**(2009), 235–255.
Iturrizaga, L., 1999a. Die Schuttkörper in Hochasien – Eine geomorphologische Bestandsaufnahme und Typologie postglazialer Hochgebirgsschuttkörper im Hindukusch, Karakorum und Himalaya. In: Göttinger Geographische Abhandlungen, Band 106, 326 pp.
Iturrizaga, L., 1999b. Typical debris accumulation forms and formations in high Asia. A glacial-history-based concept of the origin of postglacial debris accumulation landscapes in subtropical high mountains with selected examples from the Hindu Kush, the Karakoram and the Himalayas. In Kuhle, M. (ed.), Tibet and High Asia Special volume (V), *GeoJournal*, **47**, 277–339.
Iturrizaga, L., 2003. The distribution and genesis of lateroglacial valleys in the Karakoram Mountains (Pakistan). *Zeitschrift für Geomorphologie N.F.*, **130**, 51–74.
Iturrizaga, L., 2006. Transglacial sediments in the Karakoram (Pakistan) – a case study from the Shimshal valley. In Kreutzmann, H. (ed.), *Karakoram in Transition*. Oxford: Oxford University Press, pp. 96–108.
Iturrizaga, L., 2008. Paraglacial landform assemblages in the Hindu Kush and Karakoram Mountains. *Geomorphology*, **95**(1–2), 27–47.
Jordan, P., and Slaymaker, O., 1991. Holocene sediment production in Lillooet River, British Columbia: a sediment budget approach. *Géographie Physique et Quaternaire*, **45**, 45–57.
Knight, J., and Harrison, S., 2009. Periglacial and paraglacial environments: a view from the past into the future. *Geological Society Special Publications (London)*, **320**, 1–4.
Kuhle, M., 2001. The maximum Ice Age (LGM) glaciation of the Central- and South Karakorum: an investigation of the heights of its glacier levels and ice thicknesses as well as lowest prehistoric ice margin positions in the Hindukush, Himalaya and in East-Tibet on the Minya Konka-massif. In Kuhle, M. (Ed.), *Tibet and High Asia VI, Glacio-Geomorphology and Prehistoric Glaciation in the Karakorum and Himalaya GeoJournal*, **54**(2–4), 109–396.
Li, J., Derbyshire, E., and Xu, S., 1984. Glacial and paraglacial sediments of the Hunza valley North–West Karakoram, Pakistan: a preliminary analysis. In Miller, K. J. (ed.), *The International Karakoram Project*. Cambridge: Cambridge University Press, Vol. 2, pp. 496–535.
Luckman, B. H., and Fiske, C. J., 1997. Holocene development of coarse debris landforms in the Canadian Rocky Mountains. In Matthews, J. A., Brunsden, D., Frenzel, B., Gläser, B., and Weiß, M. M. (eds.), *Rapid Mass Movement as a Source of Climatic Evidence for the Holocene*. Stuttgart: Gustav Fischer, pp. 283–298.
Mercier, D., and Étienne, S., 2008. Paraglacial geomorphology: processes and paraglacial context. *Geomorphology*, **95**, 1–102.
Owen, L. A., and Derbyshire, E., 1989. The Karakoram glacial depositional system. *Zeitschrift für Geomorphologie*, **76**, 33–73.
Otto, J. C., 2009. Paraglacial sediment storage quantification in the Turtmann valley, Swiss Alps. In *Bonner Geographische Abhandlungen*, Heft Nr. 124, 130 pp.
Rapp, A., 1960. Recent development of mountain slopes in Kärkevagge and surroundings, northern Scandinavia. *Geografiska Annaler*, **XLII**, 60–200.
Ryder, J. M., 1971. The stratigraphy and morphology of paraglacial alluvial fans in south-central British Columbia. *Canadian Journal of Earth Sciences*, **8**, 279–298.
Slaymaker, O., 2004. Paraglacial. In Goudie, A. S. (ed.), *Encyclopedia of Geomorphology*. London: Routledge, Vol. 2, pp. 759–762.
Slaymaker, O., 2007. Criteria to discriminate between proglacial and paraglacial environments. *Landform Analysis*, **5**, 72–74.
Slaymaker, O., 2009. Proglacial, periglacial or paraglacial? *Geological Society Special Publications (London)*, **320**, 71–84.
Thorn, C. E., 2004. Whither, or wither, periglacial weathering studies? *Polar Geography*, **28**(1), 4–12.
Wilson, P., 2009. Rockfall talus slopes and associated talus-foot features in the glaciated uplands of Great Britain and Ireland: periglacial, paraglacial or composite landforms? *Geological Society Special Publications (London)*, **320**, 133–144.
Wyrwoll, K.-H., 1977. Causes of rock-slope failure in a cold area: Labrador-Ungava. *Geological Society of America. Reviews in Engineering Geology*, **3**, 59–67.

Cross-references

Catastrophic Rock Slope Failures and Mountain Glaciers

PATAGONIA

Stephan Harrison
School of Geography, Archaeology and Earth Resources, University of Exeter, Penryn, Cornwall, UK

Definition

Patagonia forms the southern regions of Argentina and Chile south of 40° S. The western sector of Patagonia is dominated by the southern Andes mountains and associated ice masses and fringes the Pacific Ocean. To the east, the land becomes increasingly arid, low-lying, and rolling.

Current knowledge of the Patagonian Ice Caps

Two major ice masses (the North and South Patagonian Icefields [NPI and SPI]) and numerous snow- and ice-capped volcanoes and mountain icefields currently exist in the region. The North Patagonian Icefield, called in Spanish, Hielo Patagónico Norte, (47°00′ S, 73°39′ W) is some 120-km long and 40–60-km wide, capping the Andean Cordillera between altitudes of 700 and 2,500 m above sea level. The icefield covers some 3,953 km^2 (Rivera et al., 2007). Much of the icefield is a plateau 1,100–1,500 m in elevation with mountains up to 4,000 m rising above it. Around 30 glaciers drain the icefield. The main ones draining the western sector into the Pacific Ocean are Glaciar San Rafael (the lowest latitude tidewater glacier in the world and the only tidewater glacier of the icefield) and Glaciar San Quintín (the largest outlet of the icefield and one which forms a piedmont lobe). With the largest catchment areas being on the west, these glaciers are the major ice discharge routes from the icefield. Draining the northern sector are Glaciars Exploradores and Grosse (the latter being one of the few debris-covered glaciers on the icefield). A strong west–east precipitation gradient exists across the region, and glaciers on the eastern side of the icefield are smaller than those on the west. Major glaciers here include Glaciars Nef and Leones (both of which calve into lakes) and Colonia which delivers ice from Glaciar Arenales into Rio Baker. The main outlet glaciers of the southern part of the ice field are Glaciar Benito and three unnamed glaciers that flow to the west (HPN 1–3) and Glaciar Steffen and Glaciares Pared (Norte and Sur) that flow to the south.

Annual precipitation on the western side of the icefield increases from 3,700 mm at sea level to an estimated maximum of 6,700 mm at 700 m a.s.l. before decreasing sharply on the eastern side (Escobar et al., 1992).

Other independent ice masses exist in the region. Cerro Hudson is an active volcano at latitude 45°55′ S, with a 10-km-wide icefield and several debris-covered outlet glaciers. To the southwest of the icefield is the glacierized mountain massif of Cerro San Lorenzo (3,700 m, latitude 47°36′ S, long 72°19′ W) with several large outlet glaciers.

The South Patagonian Icefield (Hielo Patagónico Sur in Spanish) covers an area of ca. 13,000 km^2 (Aniya, 1999) and runs north–south for 360 km between 48°50′ S and 51°30′ S, with a mean width of 40 km. North of latitude 49°S, most of the ice field is a uniform plateau with only a few mountains rising above it (Lliboutry, 1999). The main outlet glaciers are Glaciar Jorge Montt (with a surface area of around 464 km^2), flowing northward to Fiordo Calén; Glaciar Bernardo (536 km^2), flowing westward to Fiordo Bernardo; Glaciar Greve (438 km^2), flowing westward and then southward; and Glaciar O'Higgins (820 km^2). The largest glaciers are Glaciar Perito Moreno (255 km^2), which has a calving front in Lago Argentino (fig. 39), and Glaciares Grey (269 km^2) and Tyndall (331 km^2).

South of the SPI the elevation of the mountains drops. However, small mountain glaciers and icefields exist in many places. The largest of these is found on Tierra del Fuego. Here the Cordillera Darwin rises to 2,469 m at Monte Shipton and the glaciers form an icefield of around 2,300 km^2.

Pleistocene and Holocene behavior of the icefields

During much of the Quaternary, the NPI and SPI combined to form the Patagonian Icesheet (PI) and its fluctuations to the east throughout this time is recorded by a remarkable set of moraines and associated deposits, which constrain the eastern margin of large lakes such as Lago General Carrera/Buenos Aires and Lago Argentino (Caldenius, 1932; Coronato et al., 2004). Dating of the outermost moraine system shows it to have been formed between 1.1 and 2.3 Ma ago. The Last Glacial Maximum in Patagonia is dated to around 30–18 ka BP and marked by the innermost moraines in this moraine belt. Closer to the present icefields, glacier fluctuations during the Lateglacial are marked by moraines recording climate cooling during the Antarctic Cold Reversal (14.5 ka BP) and there are also moraines associated with glacier expansion during Younger Dryas times (12.8–11.5 ka BP). The geographical extent of these events, their climatic significance, and aspects of their chronology are the subjects of considerable debate. Further moraine systems close to the present ice fronts are dated to the mid and late Holocene (Harrison et al., 2007, 2008).

Contemporary glacier behavior

Until quite recently, fundamental glaciological data on the Patagonian icefields have been lacking; largely, the result of difficult access in this remote region. However, over the last decade, significant advances have been made in assessing the behavior of the icefields and their outlet glaciers over time using a variety of remote sensing techniques. Initial work using Synthetic Aperture Radar (SAR) analyzed glacier velocities surface topography and strain rates (e.g., Rignot et al., 1996). Subsequent research has used Advanced Spaceborne Thermal Emission Radiometers (ASTER) imagery to map the

glacial geomorphology of the icefields and surrounding areas (e.g., Glasser et al., 2005, 2008).

Many of the outlet glaciers from the icefields have calving margins. Warren and Aniya (1999) report that 76% of the major glaciers on the NPI calve into water bodies and 96% on the SPI. Remote sensing has allowed systematic investigations to be made of the behavior of these glaciers. As a result, velocity measurements from several calving glaciers are now available and show considerable short-term variability although, over seasonal timescales, the fluctuations in velocity are low. For instance, Shuttle Imaging radar has been used to assess glacier velocity on Glaciar Perito Moreno, which drains part of the eastern flank of the SPI (Michel and Rignot, 1999). They showed a flow rate of 800 m/year at the calving front and half of this in its terminal valley – comparable velocities to those measured in the 1980s. Similarly, at Glaciar Pío XI, a westward-flowing calving glacier on the SPI showed short-term velocities ranging from 15.2 to 36.8 m/day during 14–17 November 1995, although such high velocities do not appear to be maintained over long time periods. In contrast, sustained flow velocities at the rate of 17 m/day have been observed at Glaciar San Rafael on the NPI, making it one of the world's fastest non-surging glaciers (Warren and Aniya, 1999).

Recession

Recent work has used Digital Elevation Models of the NPI and SPI derived from the 2000 Shuttle Radar Topography Mission (SRTM) to assess the ice loss from the largest 63 glaciers of icefields since 1968 (Rignot et al., 2003). Most of the glaciers underwent considerable ice loss and frontal retreat over this period. The authors estimated that the NPI lost around 3.2 km^3 volume of ice per year throughout this time, whilst the SPI lost around four times this amount (around 13.5 km^3/year). The total combined volume loss from the icefields amounts to nearly 17 km^3/year, equivalent to a contribution to sea level rise of 0.042 ± 0.002 mm/year. Data from a restricted part of the SPI since 1995 showed an accelerated ice loss from both icefields at around 42 km^3/year, which is equivalent to a sea level rise (SLR) of 0.105 ± 0.011 mm/year.

The authors attributed this ice loss to negative mass balance caused by climate change associated with a temperature increase of 0.4–1.4°C south of 46°S during the twentieth century. However, rates of glacier thinning are larger than those that would be expected from the observed rise in regional temperatures. Rignot et al. (2003) suggest that the influence of calving processes on many of the glacier termini explains much of this anomalous behavior with calving glaciers having undergone rapid recession once pushed out of equilibrium by rising temperatures. They compare the behavior of Patagonian glaciers with those of Alaska and conclude that the contribution of Patagonian glaciers to sea level rise is disproportionately larger by a factor of around 1.5 than that indicated by their areas. They attribute this to the relatively low ELAs of Patagonian glaciers, their high ice fluxes, and the dominance of calving fronts.

Summary

The Patagonian icefields are the largest temperate ice masses on Earth and their outlet glaciers are also some of the most dynamic. Maintained by the southern Westerlies, the icefields have undergone considerable fluctuations throughout the Quaternary and over the past few decades, there has been a major research initiative to reconstruct this behavior and relate it to the climate change in the midlatitudes of the southern hemisphere. Modeling studies have also shown that the glaciers are likely to be highly responsive to continued global warming throughout this century, although accurate estimates of their behavior have not been worked out in detail.

Bibliography

Aniya, M., 1999. Recent glacier variations of the Hielos Patagonicos, South America, and their contribution to sea-level change. *Arctic, Antarctic and Alpine Research*, **31**, 165–173.

Caldenius, C. C., 1932. Las glaciaciones cuaternarios en la Patagonia y Tierra del Fuego. *Geografiska Annaler*, **14**, 1–164 (English summary, pp. 144–157).

Coronato, A., Martinez, O., and Rabassa, J., 2004. Glaciations in Argentine Patagonia, Southern South America. In Ehlers, J., and Gibbard, P. L. (eds.), *Pleistocene Glaciations: Extent and Chronology*. INQUA Working Group 5. Amsterdam: Elsevier, pp. 49–67.

Escobar, F., Vidal, F., Garin, C., and Naruse, R., 1992. Water balance in the Patagonian Icefield. In Naruse, R., and Aniya, M. (eds.), *Glaciological Researches in Patagonia, 1990*. Nagoya: Japanese Society of Snow and Ice, pp. 109–119.

Glasser, N. F., Jansson, K. N., Harrison, S., and Rivera, A., 2005. Geomorphological evidence for variations of the North Patagonian Icefield during the Holocene. *Geomorphology*, **71**, 263–277.

Glasser, N. F., Jansson, K. N., Harrison, S., and Kleman, J., 2008. The glacial geomorphology and Pleistocene history of South America between 38°S and 56°S. *Quaternary Science Reviews*, **27**, 365–390.

Harrison, S., Winchester, V., and Glasser, N. F., 2007. The timing and nature of recession of outlet glaciers of Hielo Patagónico Norte, Chile, from their Neoglacial IV (Little Ice Age) maximum positions. *Global and Planetary Change*, **59**, 67–78.

Harrison, S., Glasser, N. F., Winchester, V., Haresign, E., Warren, C. R., Duller, G. A. T., Bailey, R., Ivy-Ochs, S., Jansson, K., and Kubik, P., 2008. Glaciar León, Chilean Patagonia: late-Holocene chronology and geomorphology. *The Holocene*, **18**, 643–652.

Lliboutry, L., 1999. The glaciers of Chile and Argentina. In Williams, R. S. Jr., and Ferrigno, J. G. (eds.), *Satellite Image Atlas of Glaciers of the World*. U.S. Geological Survey Professional Paper 1386-I.

Michel, R., and Rignot, E., 1999. Flow of Glaciar Moreno, Argentina, from repeat-pass Shuttle Imaging Radar images: comparison of the phase correlation method with radar interferometry. *Journal of Glaciology*, **45**(149), 93–100.

Rignot, E., Forster, R. R., and Isacks, B. L., 1996. Interferometric radar observations of Glaciar San Rafael, Chile. *Journal of Glaciology*, **42**(141), 279–291.

Rignot, E., Rivera, A., and Cassassa, G., 2003. Contribution of the Patagonia icefields to sea level rise. *Science*, **302**, 434–437.

Rivera, A., Benham, T., Casassa, G., Bamber, J., and Dowdeswell, J. A., 2007. Ice elevation and areal changes of glaciers from the Northern Patagonia Icefield, Chile. *Global and Planetary Change*, **59**, 126–137.
Warren, C. R., and Aniya, M., 1999. The calving glaciers of southern South America. *Global and Planetary Change*, **22**, 59–77.

Cross-references

Calving Glaciers
Climate Change and Glaciers
Deglaciation
Little Ice Age
Neoglaciation
Quaternary Glaciation

PATERNOSTER LAKES

Umesh K. Haritashya[1], Vijay P. Singh[2], Pratap Singh[3]
[1]Department of Geology, University of Dayton, Dayton, OH, USA
[2]Department of Biological and Agricultural Engineering, Texas A&M University, College Station, TX, USA
[3]Tahal Consulting Engineers Ltd, New Delhi, India

Synonyms

Staircase lakes; String of beads

Definition

A series of lakes that are formed in the low depression of a U-shaped valley.

Paternoster lakes are erosional landforms formed by scouring a valley bed that contains rocks of varying resistance. When a glacier advances and moves downhill, it encounters all types of rocks, rocks that are softer and less resistant get eroded deeper than those that are more resistant, thus forming a depression on the valley bed. The scouring power of a glacier also depends on the basin relief, type of flow (extensive or compressive), and subglacial temperature and water availability. These eroded depressions later get filled with water as glacier starts receding and produces a series of lakes (Figure 1). These lakes are characteristics of alpine glaciation and show advancement and subsequent retreat of glaciers. Lakes are beaded together by a river running between them, which can be a part of single stream or a braided stream system. The number of lakes in any particular U-shaped valley depends mainly on the geological and structural characteristics of the bed material. Lake sediment can be extremely helpful in understanding the glaciation history of any basin, depending on the depth of the lake. In most cases, they are not deep enough to do any meaningful analysis.

Cross-references

Glacial Erosion
Landscapes of Glacial Erosion

Paternoster Lakes, Figure 1 Series of the paternoster lakes in the U-shaped valley as seen from the Mount Evans, highest auto road (14,260 ft) in North America. Four lakes are visible in this photograph. Photo by Umesh Haritashya August 9, 2009.

PEAK FLOOD GLACIER DISCHARGE

Monohar Arora
National Institute of Hydrology (NIH), Roorkee, UA, India

Sudden release of glacially impounded water causes catastrophic floods (sometimes called by the Icelandic term "jôkulhlaup"), known as outburst floods, and occasionally spawn debris flow that pose significant hazards in mountainous areas. Commonly, the peak flow of an outburst flood may substantially exceed local conventional benchmarks, such as the 100-year flood peak, but predicting the peak discharge of these subglacial outburst floods is a very difficult task. Increasing human habitation and recreational use of alpine regions has significantly increased the hazard posed by such floods. Outburst floods released in steep, mountainous terrain commonly entrain loose sediment and transform into destructive debris flows.

PERCOLATION ZONE

Prem Datt
Research and Development Center (RDC),
Snow and Avalanche Study Establishment, Himparisar, Chandigarh, India

The area on a glacier or ice sheet or in a snowpack where a meltwater percolates are known as percolation zone. In case of glaciers, the upper part of the glacier (accumulation zone) where ice is covered by snow represents the percolation zone. As such water percolates through the snowpack because snow behaves like a porous media, while in the lower part of glacier (ablation zone) water flows over the ice because ice is not permeable and hardly allows any percolation. This is the reason the water channels are found in the ablation part of the glaciers where exposed ice surface is available.

PERENNIALLY FROZEN GROUND

Monohar Arora
National Institute of Hydrology (NIH), Roorkee, UA, India

Perennially frozen ground occurs wherever the ground temperatures remain continuously below 0°C for 2 or more years. Most permafrost is located in high latitudes (i.e., land in close proximity to the North and South poles), but alpine permafrost may exist at high altitudes in much lower latitudes. The extent of permafrost can vary as the climate changes. Permafrost, or perennially frozen ground, is a critical component of the cryosphere and the Arctic system. Permafrost regions occupy approximately 24% of the terrestrial surface of the Northern Hemisphere. Today, a considerable area of the Arctic is covered by permafrost (including discontinuous permafrost).

PERIGLACIAL

H. M. French
University of Ottawa (retired), North Saanich, BC, Canada

Synonyms

Cryogenic

Definition

"Periglacial": an adjective used to refer to cold, nonglacial landforms, climates, geomorphic processes, or environments.
"Periglaciation": the degree or intensity to which periglacial conditions either dominate or affect a specific landscape or environment.

Origin

The term *periglacial* was first used by a Polish geologist, Walery von Łozinski, in the context of the mechanical disintegration of sandstones in the Gorgany Range of the southern Carpathian Mountains, a region now part of central Romania. Łozinski described the angular rock-rubble surfaces that characterize the mountain summits as *periglacial facies* formed by the previous action of intense frost (Łozinzki, 1909). Following the XI Geological Congress in Stockholm in 1910 and the subsequent field excursion to Svalbard in 1911 (Łozinzki, 1912), the concept of a *periglacial zone* was introduced to refer to the climatic and geomorphic conditions of areas peripheral to Pleistocene ice sheets and glaciers. Theoretically, this was a tundra zone that extended as far south as the tree-line. In the mountains, it was a zone between timberline and snow line (Figure 1).

Today, Łozinski's original definition is regarded as unnecessarily restricting; few, if any, modern analogs exist (French, 2000). There are two main reasons. First, frost action phenomena are known to occur at great distances from both present-day and Pleistocene ice margins. In fact, frost action phenomena can be completely unrelated to ice-marginal conditions. For example, parts of central Siberia and interior central Yukon remained unglaciated during the Pleistocene, yet these are regions in which frost action was, and is, very important. Second, although Łozinski used the term to refer primarily to areas rather than processes, the term has increasingly been understood to refer to a complex of cold-dominated geomorphic processes. These include not only unique frost action and permafrost-related processes but also the range of azonal processes, such as those associated with snow, running

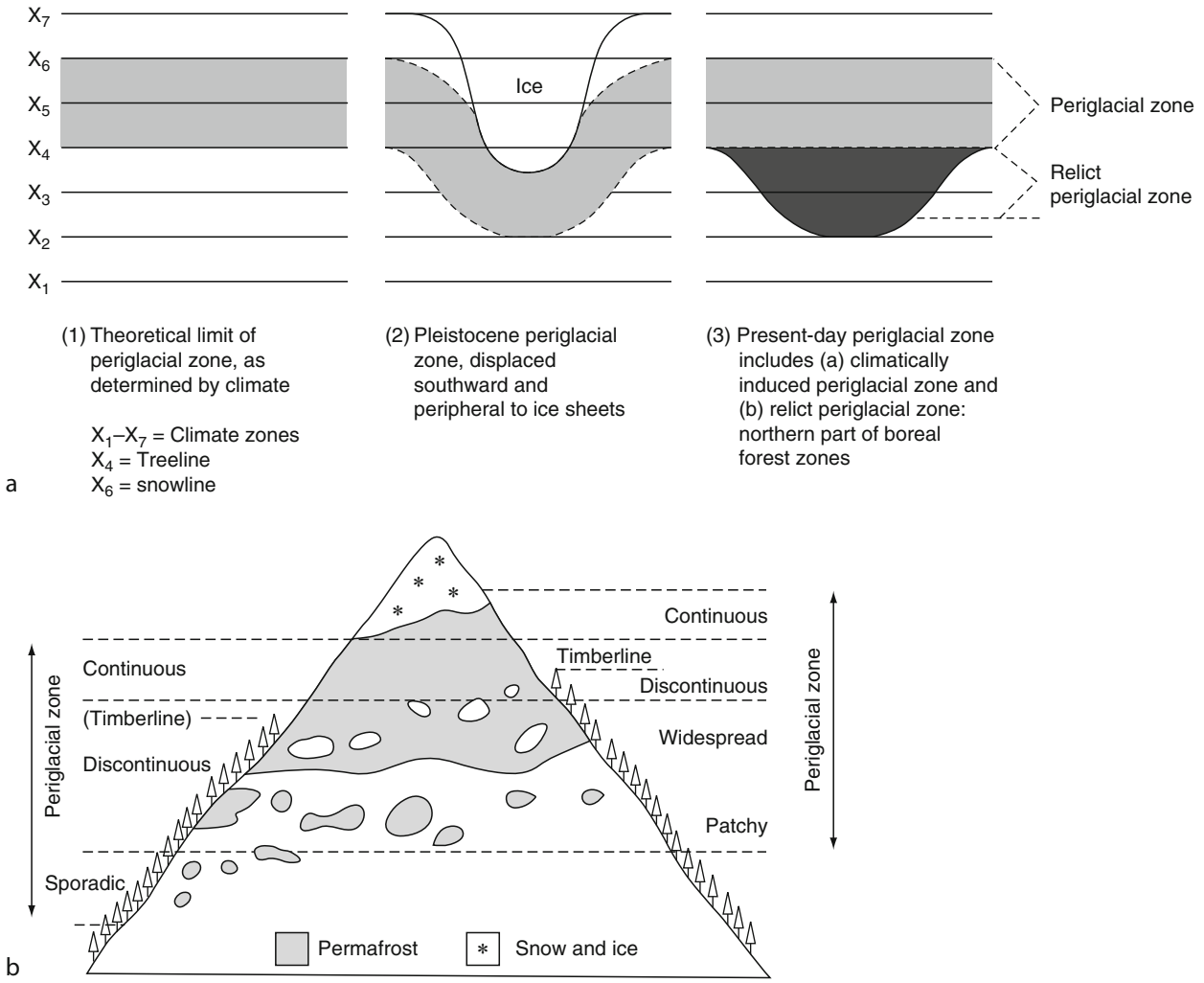

Periglacial, Figure 1 Schematic diagram illustrating the concept of the periglacial zone in (**a**) high-latitude and (**b**) high-altitude (alpine) areas. (From French, 2007.)

water and wind, which demand neither a peripheral ice-marginal location nor excessive cold. Instead, they assume distinctive or extreme characteristics under cold, non-glacial (i.e., periglacial) conditions.

Historical context

Periglacial geomorphology developed in a relatively rapid fashion in the 2 decades after 1945 as a branch of a European-dominated, but somewhat unscientific, climatic geomorphology. It was aimed largely at Late-Pleistocene paleo-climatic reconstruction. This changed in the latter half of the twentieth century when isotopic dating techniques and the explosion of the Quaternary sciences came to dominate paleo-environmental reconstruction. At the same time, the growth of permafrost studies in Arctic North America and the emergence of Russian geocryology liberated periglacial geomorphology from its Pleistocene heritage.

Modern periglacial geomorphology is a branch not only of mainstream geomorphology but also of permafrost science or geocryology (Washburn, 1979; Romanovskii, 1980; Williams and Smith, 1989; Yershov, 1990; Zhou et al., 2000). Periglacial areas are regarded as cold-climate "zones" in which seasonal and perennial frost, snow, and normal azonal processes are all present to greater or lesser degrees (French, 2007). The reality is that many so-called periglacial landscapes inherit the imprint, in varying degrees, of previous glacial conditions.

Extent and significance of periglacial environments

Periglacial environments are restricted to areas that experience cold, but essentially non-glacial, climates. They occur not only as tundra zones in the high latitudes, as defined by Łozinski`s concept, but also as forested areas south of tree-line and in the high-altitude (i.e., alpine) regions of

mid-latitudes (Figure 2). They include (a) the polar deserts and semi-deserts of the High Arctic, (b) the extensive tundra zones of high northern latitudes, (c) the northern parts of the boreal forests of North America and Eurasia, and (d) the alpine zones that lie above timberline and below snowline in mid-latitude and low-latitude mountains. To these must be added: (a) the ice-free areas of Antarctica, (b) the high-elevation montane environments of central Asia, the largest of which is the Qinghai-Xizang (Tibet) Plateau of China, and (c) small oceanic islands in the high latitudes of both Polar Regions.

Periglacial environments occur over approximately one quarter of the Earth's land surface. During the Pleistocene glacial periods, large areas of now-temperate mid-latitude experienced reduced temperatures because of their proximity to the continental ice sheets and glaciers. Permafrost and/or intense frost action would have characterized an additional 20–25% of the earth's land surface at some time during the Pleistocene.

As regards human occupance, the periglacial environments are relatively sparsely populated. A reasonable estimate is just seven to nine million people, mostly living in Russia, or only 0.3% of the world's population. Thus, the larger importance of periglacial environments lies not in their spatial extent, their snow and ice, or their proximity to glaciers but in their environment and their natural resources. For example, the Precambrian basement rocks that outcrop as huge tablelands in both Canada and Siberia contain precious minerals, such as gold and diamonds, and sizable deposits of lead, zinc, and copper, while the sedimentary basins of western Siberia, northern Alaska, and the Canadian High Arctic contain large hydrocarbon

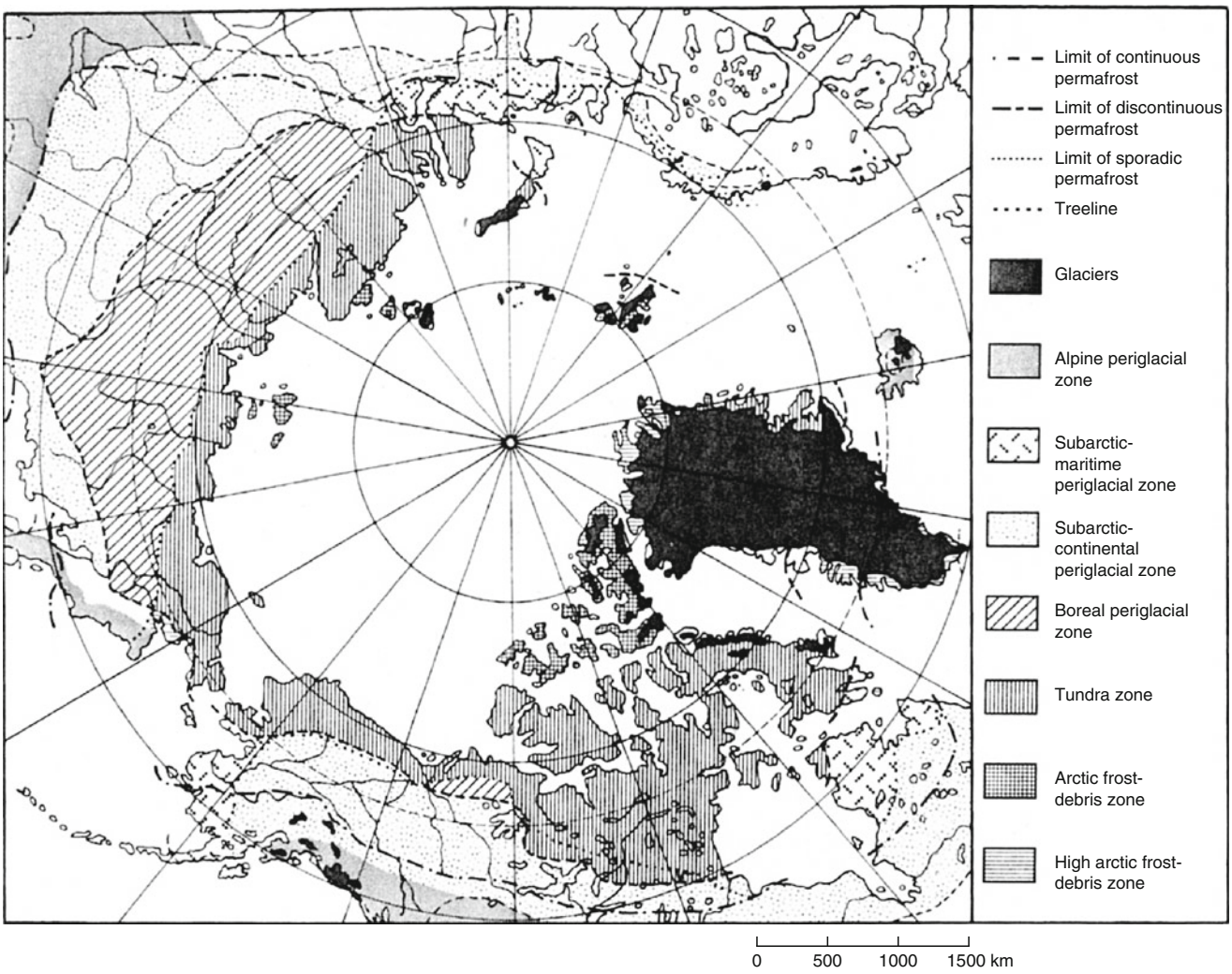

Periglacial, Figure 2 Map showing the extent of the current periglacial domain in the northern hemisphere. Not included are the alpine areas of mid-latitude mountains and the high-altitude montane environment of central Asia. (From Karte and Liedtke, 1981. Reproduced in French, 2007.)

reserves. In the more distant future, the exploitation of gas hydrates that occur within permafrost and the freshwater resources associated with the large northern lakes and rivers will become important. A second reason why periglacial environments are of significance is their place within the cryosphere (snow, ice, frozen ground, sea ice) and the critical role which the cryosphere plays in the global climate system.

Periglacial climates

Periglacial environments experience mean annual air temperatures of less than +3°C. They can be subdivided by the −2°C mean annual air temperature into environments in which frost action dominates (mean annual air temperature less than −2°C) and those in which frost action occurs but does not necessarily dominate (mean annual air temperature between −2°C and +3°C). Fundamental to most periglacial environments is the freezing of water and its associated frost heaving and ice segregation.

Based upon temperature and solar radiation characteristics, the majority of periglacial environments can be categorized as being either (1) High Arctic (polar), (2) Continental, or (3) Alpine in nature. In both High Arctic and Continental environments, temperatures are dominated by a seasonal rhythm; summer temperatures range between 10°C and 30°C and winter temperatures may fall as low as −30°C. Perennially frozen ground (permafrost) is widespread. By contrast, the Alpine mid-latitude environment experiences both diurnal and seasonal rhythms. Permafrost may, or may not, be present.

Periglacial environments that do not fit the above classification are (1) the extensive high-altitude montane environments of central Asia that experience a mix of both seasonal and continental temperature rhythms, (2) Iceland, and other smaller islands in the subarctic oceans of both polar regions such as Jan Mayen, Kerguelen, and South Georgia that experience diurnal, seasonal and/or perennial frost, and (3) the high elevations and summits of mountains in South America and Africa that, lying near the equator, experience low annual temperature range and strong diurnal rhythms. The freezing and thawing conditions experienced by these different periglacial environments are summarized in Figure 3.

In terms of periglacial landscape dynamics, ground temperature is probably more important than air temperature. Typically, the depth of ground freezing varies from as little as 10–20 cm beneath organic materials to over 500 cm in areas of exposed bedrock. It is important to stress that relatively few freeze-thaw cycles occur at depths in excess of 30 cm; there, only the annual temperature cycle usually occurs. It is important to differentiate between the mean annual air temperature (MAAT) and the mean annual ground surface temperature (MAGST) that results in the so-called *surface offset* and the mean annual ground surface temperature (MAGST) and the temperature at the top of permafrost (TTOP) that results in the so-called *thermal offset* (Smith and Riseborough, 2002). The surface offset reflects primarily the influence of snow cover and vegetation, while the thermal offset is conditioned largely by the physical properties of the active layer (thermal conductivity and moisture content).

Periglacial ecosystems

Periglacial environments contain a range of ecosystems. The most extensive are those of the high northern latitudes. They can be regarded as being either arctic or subarctic in nature (Table 1). The boundary between the two approximates the northern limit of trees, the so-called tree-line. This is a zone, 30–150 km in extent, north of which trees are no longer able to survive. Ecologists refer to the barren, treeless Arctic as tundra. The tundra progressively changes into polar desert at extreme high latitude as climate becomes increasingly colder and drier. The tree-line also approximates the southern boundary of the zone of continuous permafrost; i.e., north of the tree-line, the terrain is perennially frozen and the surface thaws for a period of only 2–3 months each summer (see above).

The mid-latitude alpine environments are a localized and specialized periglacial environment. They are dominated by both diurnal and seasonal climatic effects, by steep slopes, tundra (alpine) plants, rocky outcrops, and snow and ice. In such environments, the timberline constitutes the boundary between the alpine and sub-alpine. The montane environments of central Asia are also distinct and consist of extensive steppe grasslands and intervening desert-like uplands. Finally, the ice-free areas of Antarctica and northeast Greenland are essentially polar deserts or rock-rubble surfaces.

The tundra and polar desert regions of both North America and Eurasia contain a surprisingly large number of plant and animal species. Plant cover varies from 5% in the polar deserts to over 60–75% in meadow tundra terrain (Figure 4a). In the western Canadian Arctic Archipelago, the diversity of flora and vascular plants is especially well documented (e.g., Porsild, 1957). Large mammals such as the polar bear, musk-oxen, and fox all manage to survive in the extreme high northern latitudes.

In the subarctic, two major ecological zones can be recognized. Near the tree-line is a zone of transition from tundra to forest, consisting of either open woodland or forest-tundra. Here, the trees are stunted and deformed, often being less than 3–4-m high (Figure 4b). Woodland caribou and grizzly bear replace polar bear and musk-oxen. This zone merges into the boreal forest, or *taiga*, an immense zone of almost continuous coniferous forest extending across both North America and Eurasia. It is regarded as a fire climax community (Figure 4c). In North America, the dominant tree is spruce (*Picea glauca* and *Picea mariana*) and in central Siberia, both pine (*Pinus silvestris*) and tamarack (*Larix dahurica*) are dominant. In northern Scandinavia, on account of the warm Gulf Stream, stunted birch forest (*Betula nana*) forms the tree-line (Figure 4d). The southern boundary of the subarctic is less clearly defined than its northern boundary;

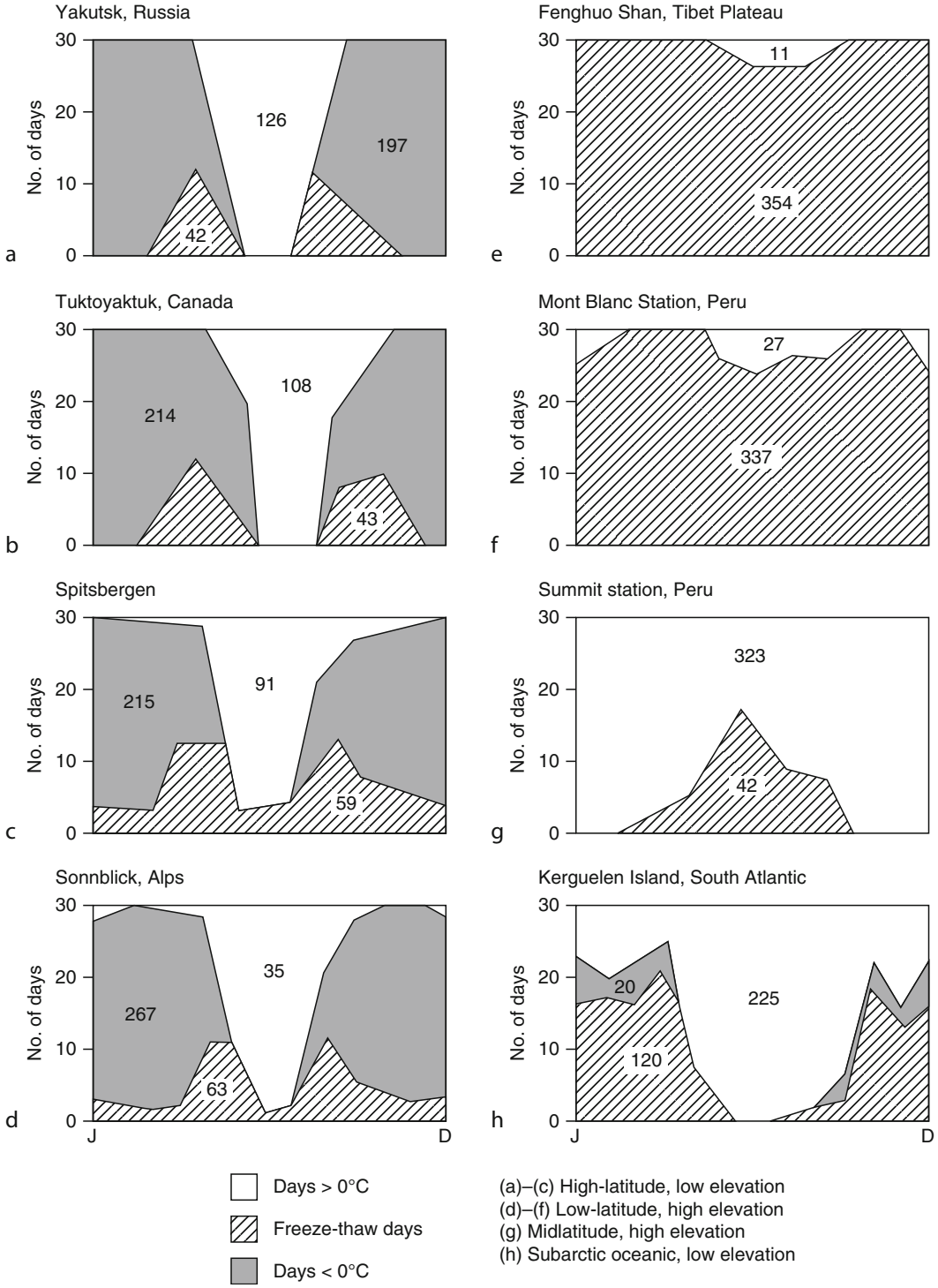

Periglacial, Figure 3 Freezing and thawing conditions in various periglacial environments of the world. (From French, 2007.)

typically, coniferous species begin to be replaced by others of either local or temperate distribution, such as oak, hemlock, and beech, or by steppe, grassland, and semi-arid woodland in more continental areas. Ungulates such as bison and yak take advantage of these grasslands. Because these ecosystems experience deep seasonal frost, they represent the outer spatial extent of the periglacial environment.

Periglacial, Table 1 Summary characteristics of high-latitude periglacial ecosystems

	Arctic		Antarctic
	Low Arctic	High Arctic	Continent, not Peninsula
Climate:	Very cold winters, cold summers, low precipitation, 3.5–5 months >0°C	Very cold winters, cold summers, very low precipitation, 2–3 months >0°C	Extremely cold, short summers, very low precipitation, strong winds ~ 1 month >0°C
Snow-free period	~3–4 months	~1–1.5 months	~1–2 months
Length of growing season	~3.5–5 months	~1–2 months	Negligible
Permafrost:	Continuous: temperature is ~−3 to −4°C at 10–30-m depth	Continuous: temperature is ~−10 to −14°C at 10–30-m depth	Continuous: temperature is ~−8 to −18°C at 10–30-m depth
Active-layer depth	~30–50 cm in silt/clay ~2–5m in sand	~30–50 cm in silt/clay ~70–120 cm in sand	30–50 cm in gravel and ablation till ~1–2 m in bedrock
Vascular plants:	400–600 species	50–350 species	Hair-grass, pearlwort
Mosses	Sphagnum common	Sphagnum minor	30+ types
Lichens	Foliose species abundant	Fruticose and crustose species common	125+ types
Total plant cover	80–100%	1–5% polar deserts 20–100% polar semi-deserts 80–100% sedge-moss tundra	<5% in most areas
Total plant production	200–500 g/m²	0.5 g/m² polar deserts 20–50 g/m² polar semi-deserts 150–300 g/m² sedge-moss tundra	0.5 g/m² in most areas
Vegetation:	Tundra types dominate Tall shrubs, 2.4 m Low shrubs, 0.5 m Cottongrass tussock- Dwarf shrub heath Dwarf shrub heath wet-edge sedge	Tundra types minor Polar semi-desert common Cushion plant – moss Cushion plant – lichen Herb-moss Polar desert common Herb-moss	Mosses, lichens
Mammals:	10–15 species	8 species	(1) Terrestrial: none (2) Southern Ocean: numerous marine mammals
Nesting Birds:	30–60 species	10–20 species	Penguins, skuas
Large herbivores:	Barren-ground caribou, musk-oxen, moose, Polar bear, fox, wolf	Peary's caribou, musk-oxen, Polar bear, wolf	None
Fishes: (lakes and rivers)	4–6+ species	1–2 species (Arctic char, trout)	(1) Rivers: none (2) Southern Ocean: numerous

The harsh, climatic environments of the ice-free areas of Antarctica support little life. However, these areas are adjacent to a highly productive marine ecosystem that results from the nutrients associated with upwelling of water along the Antarctic Divergence. Not surprisingly, a number of marine mammals (e.g., Antarctic elephant seal, southern fur seal) and birds (e.g., penguins, wondering albatross) use the ice-free areas for critical breeding purposes. However, the terrestrial flora and fauna are few; mainly mosses and lichens. There are no land mammals in Antarctica.

Periglacial landscapes

The geomorphic footprint of periglacial environments is not always achieved and most periglacial landscapes possess some degree of inherited paraglacial or proglacial characteristics. The reality is that periglacial landscapes range between those in which the entire landscape is fashioned by permafrost and frost-action processes and those in which frost-action processes are subservient to others. This diversity is accentuated by the fact that (1) certain rock types are more prone to frost weathering than others and (2) many regions currently experiencing periglacial conditions have only recently emerged from beneath continental ice sheets and are largely glacial landscapes. For example, certain areas of western Siberia and the northwestern Canadian Arctic possess large bodies of relict glacier ice, of Pleistocene age, partially preserved beneath ablation till (e.g., Astakov et al., 1996; Murton et al., 2005). It is clear that these so-called periglacial landscapes are largely relict and that periglacial processes are slowly modifying the landscape.

The only periglacial landscapes that are probably in geomorphic equilibrium are those that have protracted histories of cold non-glacial conditions. In the northern

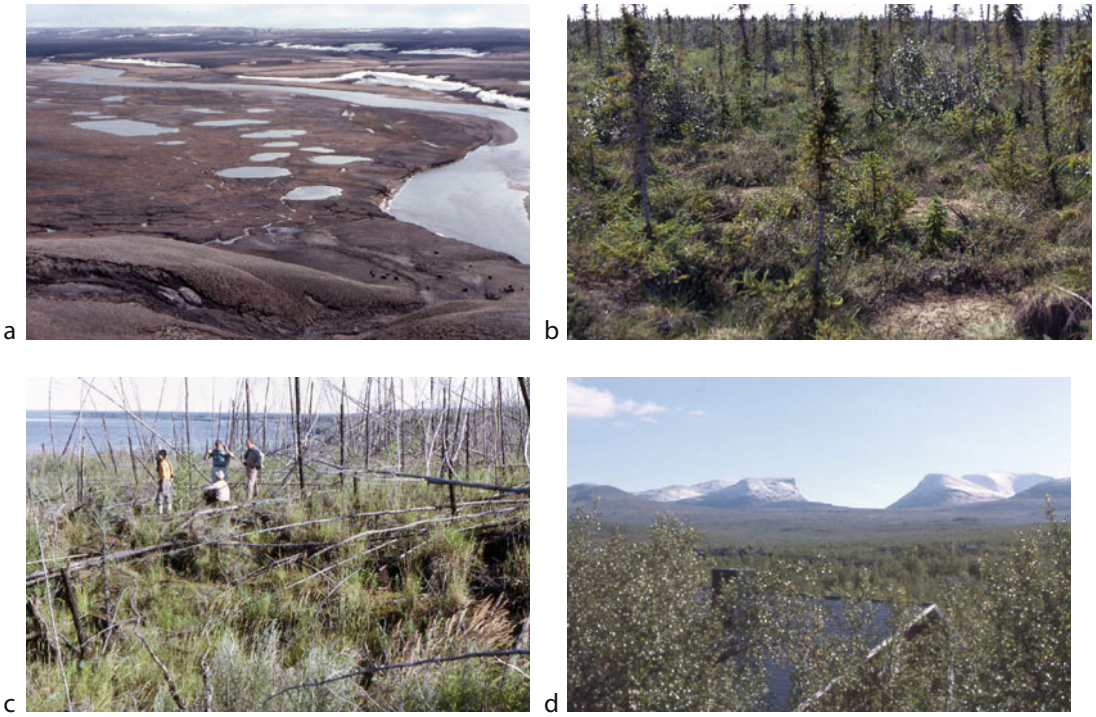

Periglacial, Figure 4 Examples of typical periglacial ecosystems: (**a**) Lowland tundra, Kellett River, southern Banks Island, Canada, showing ice-wedge polygon terrain, thaw lakes, an active-layer detachment (in foreground) and grazing muskoxen; (**b**) Northern boreal forest near the tree-line, just south of Inuvik, NWT, Canada, showing stunted black spruce with non-sorted circles (mud/earth hummocks); (**c**) A recently burned area of taiga forest, Lena River valley, central Siberia, now subject to thermokarst erosion and willow/shrub revegetation; (**d**) Birch trees constitute the northern boreal forest in northern Finland.

hemisphere, these include (1) parts of central Alaska and interior Yukon, (2) much of central and eastern Siberia, and (3) much of the montane and steppe environments on, and surrounding, the Qinghai-Xizang (Tibet) Plateau. In the southern hemisphere, some of the ice-free areas of Victoria Land are thought to have been free of ice for several million years.

In all these areas, it is clear that geological structure and lithology largely control the macroscale periglacial landscape. For example, in areas of resistant igneous, metamorphic and sedimentary bedrock, the higher elevations consist of structurally-controlled rock outcrops. Everywhere, the upland surfaces and upper valley-side slopes are covered by angular rock-rubble accumulations (variously termed "mountain-top detritus," blockfields, or kurums). Bedrock is frequently disrupted by joint and fissure widening, the frost-jacking of blocks, and by brecciation. Typically, uplands are bordered by low-angle, pediment-like surfaces. In many ways, these landscapes resemble those of the hot deserts of the world. By contrast, areas of poorly-lithified bedrock and unconsolidated Tertiary- and Quaternary-age sediments form more undulating, poorly-drained, lowland terrain. Typically, the landscape is characterized by large-scale tundra polygons, thaw lakes and depressions, and widespread mass-wasting and patterned-ground phenomena.

Frost action and cold-climate weathering

The weathering of bedrock in periglacial areas is generally assumed to be mechanical in nature and the result of freezing and thawing of water within rock or mineral soil. Rates of cold-climate rock weathering are usually assumed to be as great, if not greater, than those in warmer environments but this has yet to be convincingly demonstrated.

Rock disintegration by frost action is generally assumed to be the result of either (1) volumetric expansion of ice or (2) ice segregation.

Volumetric expansion

The freezing of water is accompanied by a volumetric expansion of approximately 9%. In theory, this can generate pressures as high as 270 MPa inside cracks in a rock strong enough to withstand such pressures. While volumetric expansion was probably the mechanism that Łozinski envisaged when he talked of "periglacial facies," the dominant role attributed to simple volumetric expansion is probably incorrect. This is because the conditions necessary for frost weathering by volumetric expansion are somewhat unusual. Not only must the rock be water saturated but also freezing must occur rapidly from all side. On the other hand, there is no doubt that volumetric expansion of water within existing joints and other lines

of weakness within bedrock outcrops can lead to bedrock heave and joint widening, and that near-surface frost wedging in fissile sedimentary rocks is a common occurrence (Figure 5a).

A related mechanism is hydrofracturing, in which rock disintegration results from pressures generated by pore-water expulsion. For this to happen, the water-saturated rock must possess large interconnected pores, the expelled pore water is unable to drain away as quickly as it is expelled, and pore-water pressures must rise sufficiently to deform or "hydrofracture" the rock. Rapid inward freezing is the ideal circumstance; for example, there have been occasional instances where Arctic field observations indicate that boulders or rocks on the ground surface have burst or "exploded" during periods of rapid temperature drop during midwinter.

A third possible mechanism relates to the breakup of individual mineral particles by the wedging effect of ice formed in micro-cracks or by the freezing of water within gas–liquid inclusions at cryogenic (i.e., subzero) temperatures. For example, certain Russian laboratory experiments (e.g., Konishchev and Rogov, 1993) indicate that, during repeated freeze-thaw cycles, quartz sand breaks down more readily than feldspar and produces finer particles; this may also reflect the increasing brittleness of quartz at very low temperatures when compared to other minerals.

Ice segregation

There is increasing acceptance that the progressive growth of ice lenses as liquid water migrates to the freezing plane is the most likely cause of the widespread fracture of moist porous rocks (Walder and Hallet, 1986). This is because it is now understood that moisture migrates within freezing or frozen ground. It is the result of a temperature gradient-induced suction (dP_w) that affects the unfrozen water held in capillaries and adsorbed on the surfaces of mineral particles. In theory, a temperature drop of 1°C induces a cryosuction of 1.2 MPa (12 atm). According to Williams and Smith (1989):

$$dP_w = dTl/VT \quad (1)$$

where, dT is the lowering of the freezing point, l is the latent heat of fusion, V is the specific volume of water, and T is the absolute temperature.

The conditions needed for ice segregation are slow rates of freezing and sustained subzero temperatures. These are relatively common in most periglacial environments. In frost-susceptible sedimentary bedrock, long-continued ice segregation can lead to the brecciation of bedrock to a depth of several meters (Figure 5b). Ice segregation and rock fracture has also been verified in laboratory experiments that simulate natural uni- and bi-directional freezing; the most susceptible rock types

Periglacial, Figure 5 Examples of frost action and cold-climate rock weathering: (**a**) In situ bedrock disintegration and frost jacking of Devonian-age siltstone and sandstone, Rea Point, Melville Island, Arctic Canada; (**b**) An exposure of Late-Cretaceous shale in the wall of a drilling sump illustrates near-surface brecciation due to ice lensing, Sabine Peninsula, Melville Island, Arctic Canada; (**c**) Fractured, fine-grained diorite boulder lying on ablation till surface ("Younger Drift"), Simpson Crags, northern Victoria Land, Antarctica; (**d**) Taffoni weathering of coarse-grained monzogranite boulder, Terra Nova Bay, northern Victoria Land, Antarctica.

appear to be fine-grained porous rocks such as chalk and shale (Murton et al., 2006).

Other mechanisms

A number of other weathering mechanisms are also thought to operate in periglacial environments. These are briefly discussed below.

First, insolation weathering, or spalling, refers to cracking in bedrock thought to be caused by temperature-induced volume changes such as expansion and contraction. For many years these thermally-induced stresses were thought more appropriate for rock weathering in hot arid regions than for cold regions. However, laboratory studies suggest the threshold value for thermal shock approximates to a rate of temperature change of 2°C/min and experimental studies, using cold room facilities, have established that different minerals have varying coefficients of linear thermal expansion in the range of +10 to −10°C. These parameters certainly apply to many periglacial environments. For example, in parts of Antarctica, field studies document daily temperature ranges of 40°C–42°C, and rates of heating and cooling of 0.8°C/min and of 15–20°C/h. These measurements suggest that thermal stress, or fatigue, may be a viable rock-weathering process (Hall, 1999) (Figure 5c). Unfortunately, until further field, laboratory, and experimental studies are undertaken, this important mechanism is still largely speculative.

Second, equally perplexing is the relationship between salt, present in the snow in areas adjacent to marine environments and the granular disintegration of coarse-grained igneous rocks that results in cavernous weathering in the ice-free polar deserts of Antarctica (French and Guglielmin, 2000) (Figure 5d). These phenomena are similar to the more well-known "taffoni" of mediterranean and tropical regions.

Third, the efficacy of chemical weathering at low temperatures is unclear, despite a number of recent detailed studies in northern Scandinavia (e.g., Dixon and Thorn, 2005), while the nature of the biological and biochemical weathering processes associated with rock-colonizing organisms and the formation of phenomena such as rock varnish are extremely poorly understood (e.g., Guglielmin et al., 2005; Etienne, 2002).

It would appear that cold-climate weathering is complex, frost action takes many forms, certain processes act alone, others in combination, and some may be physico-chemical in nature.

Frozen ground

Periglacial environments experience either seasonally frozen or perennially frozen ground. The latter, if it persists for more than 2 years, is termed permafrost (Muller, 1943) (Permafrost). In areas underlain by permafrost, the active layer refers to the near-surface layer of ground which thaws during summer. Where discontinuous permafrost is present, the active layer may be separated from underlying permafrost by an unfrozen layer (tálik), or by a residual thaw layer if permafrost is relict. If no permafrost is present, the active layer no longer exists and the near-surface layer is one of seasonal freezing and thawing.

The typical ground thermal regime of an area underlain by permafrost is illustrated in Figure 6. Thawing begins in early summer and the depth of thaw reaches a maximum in late summer at which point, freeze-back occurs. The freeze-back is slower than the thaw because the release of latent heat offsets the temperature drop. This gives rise

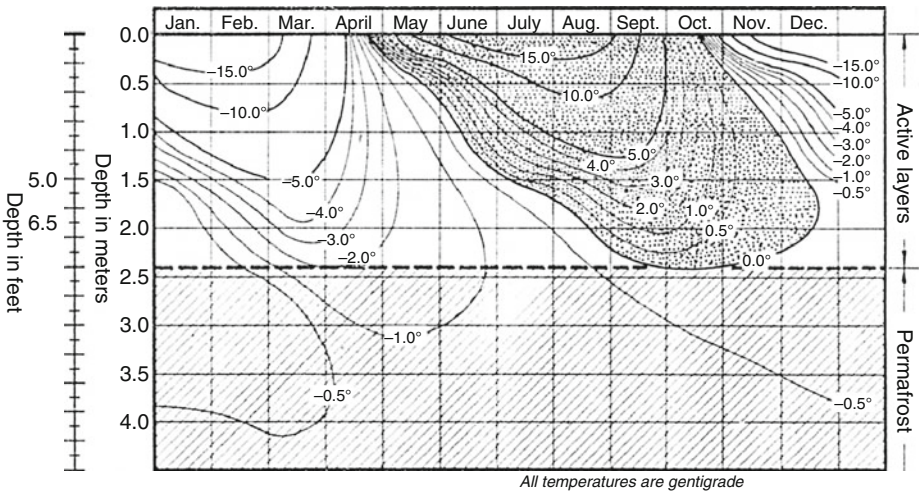

Periglacial, Figure 6 Diagram illustrating the typical ground thermal regime of a permafrost area, Skovorodino, Siberia, 1928–1930. (From Muller, 1943.)

to the so-called zero-curtain effect, in which near isothermal conditions persist in the active layer for several weeks. Both thawing and freezing are one-sided processes, from the surface downward. However, if permafrost was present, freezing is a two-sided process, occurring both downward from the surface and upward from the perennially frozen ground.

The Stefan equation is sometimes used to approximate the thickness of the active layer:

$$Z = \sqrt{2TKt/Q_i} \quad (2)$$

where Z = thickness of the active layer (m or cm), T = ground surface temperature during thaw season (°C), K = thermal conductivity of unfrozen soil (W/m K or kcal/m °C h), t = duration of the thawing season (day, h, s), and Q_i = volumetric latent heat of fusion (kJ/m³). The Stefan equation can also be used to calculate the depth of seasonal frost penetration. In this case, time t is the duration of the freezing season ($T <$ °C) and K represents the thermal conductivity of frozen soil.

The base of the active layer represents an unconformity between frozen and unfrozen earth material. Because the annual depth of thaw may vary from year to year, depending upon the variability of summer climate, the concept of the transient layer recognizes the different periodicities at which near-surface permafrost cycles through 0°C (Shur et al., 2005). The active-layer permafrost interface is commonly ice-rich. This is because, in summer, as the active layer thaws, moisture migrates downward and refreezes at the base while, during winter, unfrozen water migrates upward in response to the colder temperatures at the surface. Thus, the active layer not only limits the depth to which freeze-thaw action occurs but also its base acts as a slip plane for solifluction and other gravity-induced near-surface movements such as active-layer detachments and for slope instability.

Ground ice is an important component of permafrost. Many of the human occupance problems of periglacial environments relate to either frost heaving of the ground or thaw subsidence (thermokarst) of ice-rich material. Pore and segregated ice are the most widespread forms of ground ice but other types include vein ice and intrusive ice. In parts of western Siberia and the western North American Arctic, massive icy bodies of either an intra-sedimental (i.e., segregated ice) or glacier-ice origin are present (Astakov et al., 1996; Mackay and Dallimore, 1992). In general, fine-grained materials are often ice rich and frost-susceptible, whereas coarse-grained materials are ice poor and generally regarded as non-frost-susceptible. Typically, the base of the active layer and the upper 1–3 m of permafrost contain the highest amounts of ice, often exceeding 50% by volume. Ground ice is discussed more fully under Permafrost.

Periglacial processes and landforms

Geomorphological processes clearly unique to periglacial environments are those related to the formation and degradation of perennially frozen ground. Other processes, not necessarily restricted to periglacial environments, are important on account of their high magnitude or frequency in cold environments. They relate to the presence of snow, or lake and river ice. Other azonal processes, such as fluvial, eolian, and coastal processes, assume special characteristics in cold environments.

Permafrost-related processes

Permafrost-related processes include (1) the aggradation of permafrost and ground-ice bodies, (2) thermal contraction cracking of frozen ground, (3) thawing of permafrost (thermokarst), and (4) the creep of ice-rich permafrost. All are intimately related to the presence of ice within permafrost.

Much of our understanding of permafrost-related landforms and geomorphic processes is derived from the 50 years of field investigations undertaken by J. R. Mackay in the Mackenzie Delta region of the western Canadian Arctic (e.g., Mackay, 1963, 1998, 2000; Mackay and Burn, 2002).

Frost mounds, reflecting the growth of ground ice bodies, are aggradational permafrost features. A range of forms exists. The largest and most dramatic is the pingo, a perennial ice-cored mound. Pingos are of two types: either hydaulic (open) or hydrostatic (closed) in nature. Both cases require specific hydrologic conditions for their formation. Pingos are relatively rare in the majority of periglacial landscapes; however, the largest concentration of closed-system pingos, over 1,350, occurs in the Mackenzie Delta region of Canada (Figure 7a), while more isolated open-system pingos are found in central Yukon and interior Alaska, Svalbard, and central and northern Siberia. In many subarctic areas, the preferential growth of permafrost beneath organic material results in the formation of peat plateaus and palsas. A number of smaller frost mounds, mostly seasonal in nature, also occur.

The most widespread surface feature that is characteristic of permafrost is a network of thermal-contraction cracks, typically 15–30 m in dimensions, which divide the ground surface up into orthogonal or random-orthogonal patterns or polygons (Figure 7b). The cracks are caused by thermal contraction cracking of the ground during winter. In summer, the cracks fill with water from snow melt that subsequently freezes to form wedge-shaped bodies of foliated ice (Figure 7c). In lowland tundra terrain, ice-wedge ice may constitute between 10% and 20% by volume of the upper 5–10 m of permafrost.

The thaw of ice-rich permafrost gives rise to distinct features. These, and the complex of processes associated with thawing permafrost, are generally termed thermokarst. For example, snowmelt-induced runoff in spring results in gully erosion along the lines of ice wedges and where massive icy bodies become exposed, as along riverbanks and at coastal locations, retrogressive ground-ice slumps may develop (Figure 7d). On terrain underlain

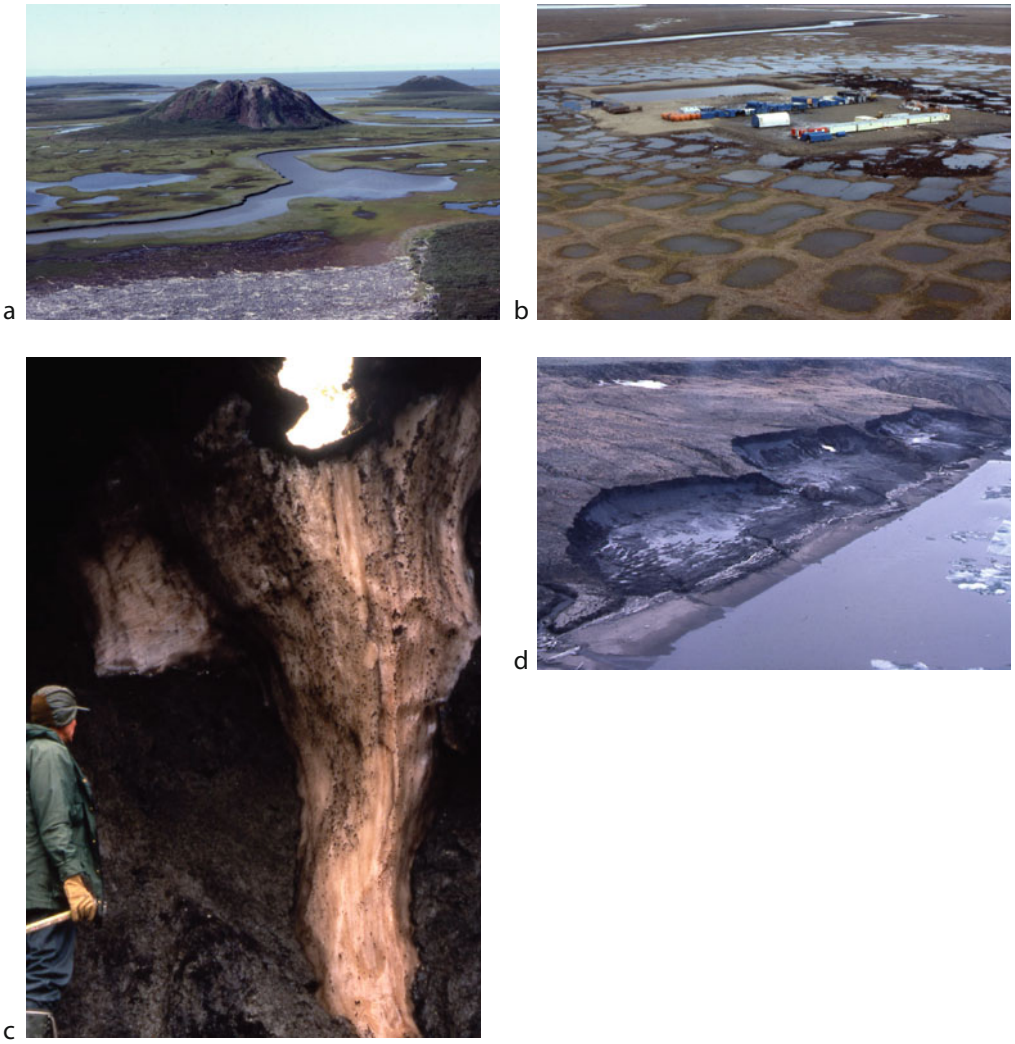

Periglacial, Figure 7 Features of permafrost terrain: (**a**) Closed-system pingo near Tuktoyaktuk, NWT, Canada; (**b**) Poorly drained tundra lowland, northern Alaska, showing low-centered ice-wedge polygons; (**c**) Epigenetic ice wedge, southern Banks Island, Arctic Canada; (**d**) Ground- ice slump, northern Yukon coast, Canada.

by fine-grained and ice-rich sediments, numerous shallow ponds or thaw lakes can develop (see Figure 4a). On gentle slopes, active-layer-detachment failures may occur in years of enhanced summer thaw (see Figure 4a). On bedrock outcrops, the thaw of ice within joints can lead to instability and enhanced rockfall activity.

The creep of permafrost refers to the long-term deformation of frozen ground under the influence of gravity. Fine-grained frozen sediments, such as silt and clay, which contain large unfrozen water content amounts, are especially suitable to frozen creep deformation. Rates of movement are slow, usually less than 0.5 cm/year. The most rapid creep deformation is recorded in rock glaciers, especially those that occur in mid-latitude mountains. For example, the Muragle rock glacier in Switzerland is reported to be deforming at a rate of 50 cm/year (Kaab and Kneisel, 2006).

Azonal processes

Mass-wasting processes are not unique to cold environments but can assume distinctive characteristics and enhanced importance. For example, in non-permafrost regions in summer there is slow mass wasting of the water-saturated thawed layer. This is termed solifluction. Where it occurs in permafrost regions, the process is called gelifluction (Figure 8a). The result is heterogeneous slope deposits, or diamicts, that mantle gentle and lower valley-side slopes. These may form lobes and terraces, usually with risers between 0.5 and 3 m in height (Figure 8b). More rapid movements involve rockfalls, debris flows, and avalanches. These are particularly common in humid alpine environments where steep bedrock outcrops are present. Frost-induced movements within the active layer, or in the zone of seasonal frost, leads to the formation of stone nets that, as slope angle increases, turn into stone

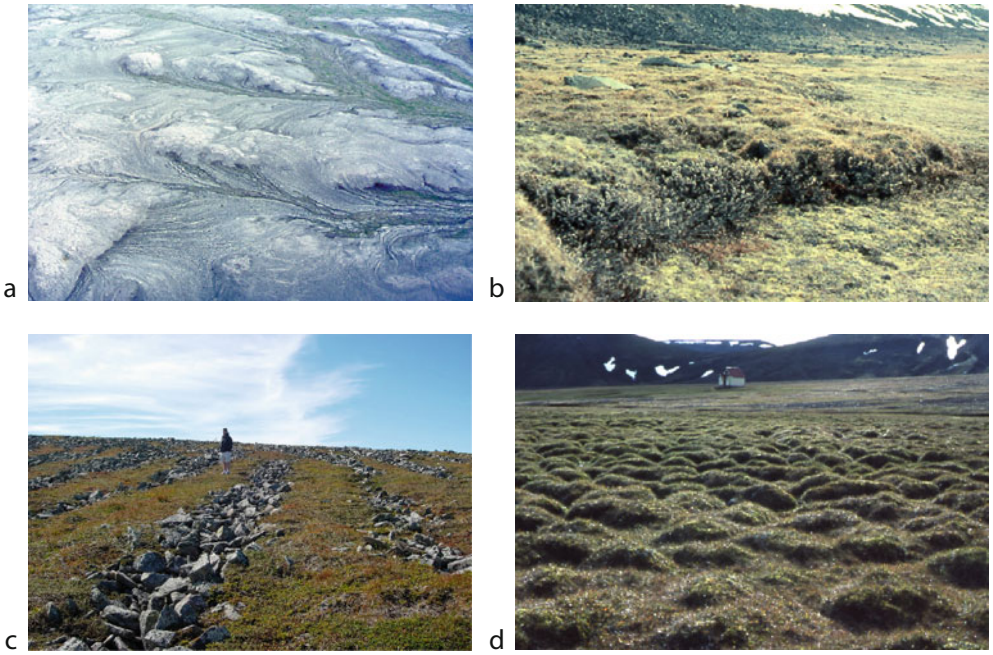

Periglacial, Figure 8 Examples of periglacial patterned-ground phenomena: (**a**) Oblique air view of mass wasting (non-sorted stripes) and gelifluction movement, Sachs Harbour, Banks Island, Canada; (**b**) Turf-banked gelifluction lobe, Holman, Victoria Island, Arctic Canada; (**c**) Stone stripes on low angled slopes (3–7°) are separated from each other by vegetated stripes of finer material; the patterned ground is relict, Mont Jacques-Cartier, Gaspésie, Québec, Canada; (**d**) Small earth or frost hummocks (thufur), central Iceland.

stripes (Figure 8c). Even in non-permafrost environments, frost action and ice segregation within the seasonally frozen layer gives rise to the formation of small-scale sorted and non-sorted patterned ground (circles, nets, stripes), frost heaving of bedrock, and the formation of small hummocks or frost mounds (thufurs, earth hummocks) (Figure 8d).

Wind plays an especially important geomorphic role in the tundra and polar desert environments (Seppala, 2004). For example, the depth and coverage of snow is determined by the prevailing wind regime. Typically, upland surfaces are blown clear of snow, while lee slopes and lower valley-side slopes are sites of snow-bank accumulation. In spring, the melt of snow banks promotes runoff or surface wash that transports sediment down slope. Solifluction or gelifluction is enhanced immediately below snow banks because of the saturated near-surface thaw layer. In some regions, preferential snow distribution results in enhanced solifluction on lee slopes and the development of asymmetrical valleys, with streams being progressively "pushed" toward the windward (steeper) slope. Elsewhere, localized wind erosion can occur in weakly consolidated sedimentary bedrock and deflation operates on fine-grained sediments.

In the absence of vegetation, deflation assumes local importance in many periglacial environments (Figure 9a). In more continental periglacial environments, loess and cover-sand deposition is widespread. For example, in parts of northwestern North America, long-continued mass wasting of loessic materials has led to the partial infilling of valleys with heterogenous organic-rich and ice-rich sediments known locally as "muck" while in parts of central Siberia, similar mass wasting combined with long-continued aggradation of alluvial sediments has created similar ice-rich sediments known locally as "Yedoma complex."

A special characteristic of periglacial areas immediately adjacent to the Antarctic and Greenland ice sheets, and to a lesser degree, the ice-marginal areas peripheral to all glaciers, is the presence of persistent and strong gravity-driven (katabatic) winds that flow outward from the ice. At extremely low temperatures, snow crystals become effective abrasive agents with MOH hardness values exceeding 4 at −40°C; as a result, wind-polished and fluted rocks and bedrock outcrops and wind-abraded cobbles (ventifacts) are common (Figure 9b). In the dry valleys of southern Victoria land and Antarctica, these winds promote sublimation to such an extent that perennial snow and ice is unable to form.

In spite of apparent aridity, fluvial activity is another important component of periglacial environments. This is because losses through evaporation and infiltration are minimized by low temperatures and frozen ground, respectively. The result is a highly seasonal discharge regime, dominated by a nival (snowmelt) peak in early spring. The fluvial dynamics are no different to other

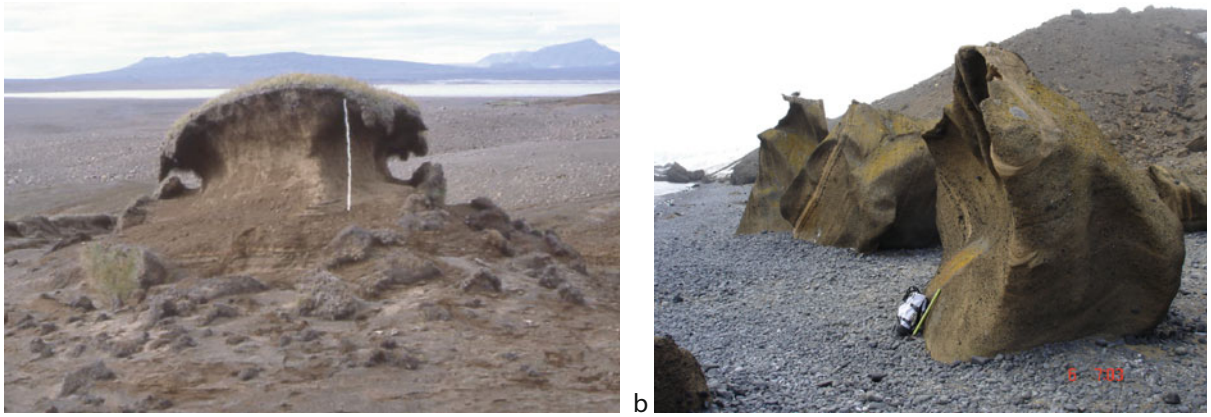

Periglacial, Figure 9 Examples of wind action in periglacial environments: (**a**) Deflation caused by strong winds and an absence of surface vegetation, central Iceland; (**b**) Wind-sculpted bedrock blocks of welded volcanic ash, Brown Bluffs, Antarctic Peninsula.

environments, but high sediment loads and highly variable seasonal discharges lead to a dominance of braided channels as opposed to straight, meandering, and anastomozing patterns. In fact, the well-developed drainage networks and large-scale organization of periglacial landscapes are not dissimilar to those elsewhere. River and lake ice persists for several months of the year; at spring melt, ice jams may develop, causing flooding and damage to structures such as bridges. Where powerful perennial springs emerge, the freezing of discharge in the downstream direction forms tabular ice bodies (river icings) that may cover several square kilometers.

In the northern hemisphere, periglacial coasts experience wave action for a restricted period of the year and are often protected from erosion by an ice foot. Ice pushing is a common feature of many arctic coastlines. Where the coast is formed in ice-rich unconsolidated sediments, as along much of the Beaufort, Laptev, and East Siberian Seas, wave action and thermal erosion result in coastal retreat of several meters per year. The rapid formation of spits and offshore bars is characteristic. In Antarctica, wave action and coastal processes are relatively unimportant on account of the hard bedrock that forms the coastline and the extremely short open-water season.

Periglacial environments, environmental challenges, and global climate change

Periglacial environments constitute part of the cryosphere. As such, they play a critical role in global climate change (Lemke et al., 2007). It is now understood that the hydrological cycle of the big northern rivers of North America and Eurasia links snowmelt and precipitation with river runoff, sea ice, and ocean circulation in a single system. This influences deep water formation in the Arctic basin and the corresponding global thermohaline circulation of the oceans (Peterson et al., 2002). At the same time, any reduction in the extent of sea ice or snow cover reduces albedo, or reflectivity, of land or ocean surface and allows more solar radiation to be absorbed.

Periglacial environments are thought to act, therefore, as a positive feedback mechanism for climate warming. Already, there is speculation that this is the cause of recent reductions in snow cover and sea-ice extent. In the future, any thaw of the organic-rich upper layers of permafrost, especially in the subarctic, will release significant quantities of carbon dioxide and methane, both of which are important greenhouse gases. Finally, the significance of gas hydrates, which exist frozen within permafrost, is still not widely recognized. Yet, their eventual potential release to the atmosphere will lead to a dramatic increase in greenhouse gases and this could further accelerate any climate warming.

If climate warming proceeds as predicted, periglacial environments will be among the first to be affected. Warming will be enhanced because of (1) increased methane flux due to decomposition of organic matter frozen in near-surface permafrost and release of methane hydrates as permafrost bodies degrade, (2) increased biomass production and decay in tundra and taiga zones, and (3) decreased surface albedo as snow-cover extent and duration decrease. Already, there is evidence that warming of permafrost has been ongoing for over 30 years (e.g., Osterkamp, 2008; Brown and Romanovsky, 2008). This may lead to long-term changes. For example, at the southern (warm) limits of the discontinuous permafrost zone, permafrost bodies will progressively disappear, the tree-line will advance northward, and the active-layer thickness will increase. The latter, monitored by the CALM program of the International Permafrost Association (Brown et al., 2000), will probably lead to an increase in the frequency of active-layer detachment failures and slope instability, to changing snow-melt and hydrological regimes, and to enhanced mass wasting and landscape modification in high-latitude permafrost environments. In alpine periglacial environments, thawing permafrost

may lead to instability of rock outcrops that could threaten the foundations of ski lifts and other recreational installations at high elevation (Gruber and Haeberli, 2007; Haeberli, 1992).

A number of environmental concerns relate to global climate change and the impact of human activity in periglacial environments. Many centre around the various problems associated with natural resource management, exploitation, and ownership (e.g., Young, 2009; Tin et al., 2009). For example, the marine and terrestrial ecosystems are increasingly being subject to environmental stress. In the arctic, the marine food chain is linked to sea ice, nutrient availability, and water density. Any changes to these may induce changes to the marine ecosystem and the associated biochemical cycling of essential nutrients. The terrestrial food chain is limited by the short growing season, low temperatures, and low rates of nutrient cycling. Thus, climate warming in high latitudes will change plant and animal communities. This will affect the hunting and harvesting of animals and plants by northern indigenous peoples in Canada, Greenland, and northern Scandinavia. A second environmental concern for the northern high latitudes is the recent increase in industrial air pollution from mid-latitudes. Small particles, such as sulfur dioxide, are transported by atmospheric circulation toward high latitudes where they appear as "arctic haze." The harsh reality is that the northern high latitudes act as an atmospheric "sink" for industrial pollutants generated in the mid-latitudes, especially those of northern Europe and European Russia. Third, in Antarctica, the increasing number of cruise ships and related tourism activities will soon inadvertently impact upon certain of the critical marine- and bird-breeding localities in South Georgia and the Antarctic Peninsula. There is also the possibility of a major marine environmental disaster if a cruise ship were to hit an iceberg and sink in Antarctic waters. Finally, Chinese upgrading of the Qinghai-Xizang (Tibet) Highway in recent years and completion of the Qinghai-Tibet Railway in 2003 has opened the large montane periglacial environment of the Tibet Plateau to a potential increase in human occupancy and economic activity with, as yet, unknown consequences.

Bibliography

Astakov, V. I., Kaplyanskaya, F. A., and Tarnogradski, V. D., 1996. Pleistocene permafrost of West Siberia as a deformable glacier bed. *Permafrost and Periglacial Processes*, **7**, 165–191.

Brown, J., and Romanovsky, V. E., 2008. Report from the International Permafrost Association: State of permafrost in the first decade of the 21st century. *Permafrost and Periglacial Processes*, **19**, 255–260.

Brown, J., Hinkel, K. M., and Nelson, F. E., 2000. The Circumpolar Active Layer Monitoring (CALM) program. Research design and initial results. *Polar Geography*, **24**, 165–258.

Dixon, J. C., and Thorn, C. E., 2005. Chemical weathering and landscape development in mid-latitude alpine environments. *Geomorphology*, **67**, 85–106.

Etienne, S., 2002. The role of biological weathering in periglacial areas: a study of weathering rind in south Iceland. *Geomorphology*, **47**, 75–86.

French, H. M., 2000. Does Łozinzki's periglacial realm exist today? A discussion relevant to modern usage of the term "periglacial". *Permafrost and Periglacial Processes*, **11**, 35–42.

French, H. M., 2007. *The Periglacial Environment*, 3rd edn. Chichester: Wiley, 458 pp.

French, H. M., and Guglielmin, M., 2000. Cryogenic weathering of granite, Northern Victoria Land, Antarctica. *Permafrost and Periglacial Processes*, **11**, 305–314.

Guglielmin, M., Cannone, N., Strini, A., and Lewkowicz, A. G., 2005. Biotic and abiotic processes on granite weathering landforms in a cryotic environment, Northern Victoria Land, Antarctica. *Permafrost and Periglacial Processes*, **16**, 69–85.

Gruber, S., and Haeberli, W., 2007. Permafrost in steep bedrock slopes and its temperature-related destabilization following climate change. *Journal of Geophysical Research*, **112**, F02S18, doi:10.1029/2006JF000547.

Haeberli, W., 1992. Construction, environmental problems and natural hazards in periglacial mountain belts. *Permafrost and Periglacial Processes*, **3**, 111–124.

Hall, K., 1999. The role of thermal stress fatigue in the breakdown of rock in cold regions. *Geomorphology*, **31**, 47–63.

Kaab, A., and Kneisel, C., 2006. Permafrost creep within a recently deglaciated glacier forefield: Muragl, Swiss Alps. *Permafrost and Periglacial Processes*, **17**, 79–85.

Karte, J., and Liedtke, H., 1981. The theoretical and practical definition of the term "periglacial" in its geographical and geological meaning. *Biuletyn Peryglacjalny*, **28**, 123–135.

Konishchev, V. N., and Rogov, V. V., 1993. Investigations of cryogenic weathering in Europe and Northern Asia. *Permafrost and Periglacial Processes*, **4**, 49–64.

Lemke, P., Ren, J., Alley, R. B., Allison, I., Carrasco, J., Flato, G., Fujii, Y., Kaser, G., Mote, P., Thomas, R. H., and Zgang, T., 2007. Observations: changes in snow, ice and frozen ground. In Solomon, S., Qin, D., Manning, M., Chen, Z., Marquis, M., Averyt, K. B., Tignor, M., and Miller, H. L. (eds.), *Climate Change 2007: The Physical Science Basis. Contribution of Working Group 1 to the Fourth Assessment Report of the Intergovernmental Panel on Climate Change*. Cambridge, UK/New York: Cambridge University Press.

Łozinzki, Walery von, 1909. Über die mechanische Verwitterung der Sandsteine im gemässigten klima. *Bulletin International de l'Academie des Sciences de Cracovie, Classe des Sciences Mathematiques et Naturelles*, **1**, 1–25. (English translation: Mrozek, T., 1992. On the mechanical weathering of sandstones in temperate climates. In Evans, D. J. A. (ed.), *Cold Climate Landforms*, Chichester, UK: Wiley, pp. 119–134).

Łozinzki, Walery von, 1912. Die periglaziale fazies der mechanischen Verwitterung. *Comptes Rendus, XI Congrès Internationale Geologie*, Stockholm 1910, 1-39-1053.

Mackay, J. R., 1963. The Mackenzie Delta area. *Geographical Branch Memoir*, No 8, Ottawa, 202 pp.

Mackay, J. R., 1998. Pingo growth and collapse, Tuktoyaktuk Peninsula area, western Arctic coast, Canada: a long-term field study. *Géographie physique et Quaternaire*, **52**, 271–323.

Mackay, J. R., 2000. Thermally-induced movements in ice-wedge polygons, western Arctic coast. *Géographie physique et Quaternaire*, **54**, 41–68.

Mackay, J. R., and Burn, C. R., 2002. The first 20 years (1978-1979 to 1998-1999) of active-layer development, Illisarvik experimental drained lake-site, western Arctic coast, Canada. *Canadian Journal of Earth Sciences*, **39**, 1657–1674.

Mackay, J. R., and Dallimore, S. R., 1992. Massive ice of the Tuktoyaktuk area, western Arctic coast, Canada. *Canadian Journal of Earth Sciences*, **29**, 1235–1249.

Muller, S. W., 1943. *Permafrost or permanently frozen ground and related engineering problems.* Special Report, Strategic Engineering Study, Intelligence Branch Chief of Engineers,

No 62, 136 pp. Second printing, 1945, 230 pp. (reprinted in 1947, J. W. Edwards, Ann Arbor, MI, 231 pp).
Murton, J. B., Peterson, R., and Ozouf, J.-C., 2006. Bedrock fracture by ice segregation in cold regions. *Science*, **314**, 1127–1129.
Murton, J. B., Whiteman, C. A., Waller, R. I., Pollard, W. H., Clark, I. D., and Dallimore, S. R., 2005. Basal ice facies and supraglacial melt-out till of the Laurentide ice sheet, Tuktoyaktuk Coastlands, western Arctic Canada. *Quaternary Science Reviews*, **24**, 681–708.
Osterkamp, T. E., 2008. Thermal state of permafrost in Alaska during the fourth quarter of the Twentieth Century. In Kane, D. E., and Hinkel, K. M. (eds.), *Volume Two: Proceedings, Ninth International Conference on Permafrost, June 29-July 3, 2008*. Fairbanks, AK: University of Alaska Fairbanks, Institute of Northern Engineering, pp. 1333–1338.
Peterson, B. J., Holmes, R. M., McClelland, J. W., Vorosmarty, C. J., Lammers, R. B., Shiklomanov, A. I., Shiklomanov, I. A., and Rahmstorf, S., 2002. Increasing river discharge to the Arctic Ocean. *Science*, **298**, 2171–2173.
Porsild, A. E., 1957. Illustrated flora of the Canadian Arctic Archipelago. *National Museum of Canada*, Bulletin No 146, 209 pp.
Romanovskii, N. N., 1980. *The Frozen Earth*. Moscow: Moscow University Press, 188 pp (in Russian).
Seppala, M., 2004. Wind as a geomorphic agent in cold climates. Cambridge University Press: Cambridge, 368 pp.
Shur, Y., Hinkel, K. M., and Nelson, F. E., 2005. The transient layer: implications for geocryology and climate-change science. *Permafrost and Periglacial Processes*, **16**, 5–18.
Smith, M. W., and Riseborough, D. W., 2002. Climate and the limits of permafrost: a zonal analysis. *Permafrost and Periglacial Processes*, **13**, 1–15.
Tin, T., Fleming, Z. L., Hughes, K. A., Ainley, D. G., Convey, P., Moreno, C. A., Pfeiffer, S., Scott, J., and Snape, I., 2009. Impacts of local human activities on the Antarctic environment. *Antarctic Science*, **21**, 3–33.
Walder, J. S., and Hallet, B., 1986. The physical basis of frost weathering: toward a more fundamental and unified perspective. *Arctic and Alpine Research*, **18**, 27–32.
Washburn, A. L., 1979. *Geocryology: A Survey of Periglacial Processes and Environments*. London: Edward Arnold, 406 pp.
Williams, P. J., and Smith, M. W., 1989. *The Frozen Earth. Fundamentals of Geocryology*. Cambridge: Cambridge University Press, 306 pp.
Yershov, E. D., 1990. *Obshcheya Geokriologiya*. Nedra, Moscow (English translation: Williams, P. J., 1998, *General Geocryology*, Cambridge: Cambridge University Press, 580 pp).
Young, O. R., 2009. Whether the Arctic? Conflict or cooperation in the circumpolar north. *Polar Record*, **45**, 73–82.
Zhou, Y., Dongxin, G., Guodong, C., and Shude, L., 2000. *Geocryology in China*. Lanzhou: Cold and Arid regions Environmental and Engineering Research Institute (CAREERI), Chinese Academy of Sciences, 450 pp (in Chinese).

PERMACRETE

Ashok Kumar Verma
Department of Geography and Environmental Studies, Cold Regions Research Center, Wilfrid Laurier University, West Waterloo, ON, Canada

Synonyms

Duracrete

Definition

Permacrete is a versatile and unique resurfacing material that can be applied to concrete, masonry, foam, steel, stucco, and aggregate surfaces. Permacrete is an architectural, chemical-concrete with twice the strength of standard concrete (What is Permacrete, 2009). Permacrete is a very strong and heat-resistant material that can be used in a variety of applications.

Formation

Permacrete is a three part, acrylic polymer cementations system with strength of over 6,000 PSI (pounds force per square inch). These three parts include a matrix mix (early-strength concrete mixture), chemical bonding additive, and a stain sealer. It is sealed and nonporous, resists chemicals, and withstands freeze-thaw cycles as well as intense heat and ultraviolet rays (What is Permacrete, 2009; Kirk, 1998).

Thermal disturbance and exposure to solar heat considerably affect the physical and mechanical properties of the permafrost. Preservation of the thermal properties in the permafrost is the major challenge in building the engineering and construction work (Jumikis, 1983). Since the permacrete has the high insulating and heat-resistant properties, it is extensively used in permafrost regions to build the residential properties (houses) and commercial properties (oil, gas pipelines, and tunnels) in combination of soil and ice material.

The ancient form of similar material can be compared with use of snow by Eskimos where they used the block of ice to build the igloos for their shelters in high arctic environment. The application of permacrete as building material can be found when the US Army developed the artificial aggregates by mixing silicates and aluminum-silicate with snow to form "permacrete" while performing experiments in Greenland (Kirk, 1998).

Bibliography

Kirk, R., 1998. *Snow*. University of Washington Press: Seattle, p. 150.
Jumikis, A. R., 1983. *Rock Mechanics*. Trans Tech: Clausthal, pp. 87–88.
Permacrete, 2009. http://www.permacrete.com/commercial/faq.php
What is Permacrete, 2009. http://www.bulifant.com/HFBulifant/permacrete.htm

PERMAFROST

Yuri Shur[1], M. Torre Jorgenson[2], M. Z. Kanevskiy[1]
[1]Department of Civil and Environmental Engineering, University of Alaska Fairbanks, Fairbanks, AK, USA
[2]Alaska Ecoscience, Fairbanks, AK, USA

Synonyms

Perennially cryotic ground

Definition

Permafrost. Ground (soil or rock and included ice and organic material) that remains at or below 0°C for at least 2 consecutive years.
Perennially cryotic ground. Soil or rock at or below 0°C for at least 2 consecutive years, but the material may not be frozen because of freezing-point depression.
Active layer. The layer of ground that is subject to annual thawing and freezing in areas underlain by permafrost.
Ice-rich permafrost. Thaw-sensitive permafrost containing excess ice.
Ground ice. Pore, segregated and/or massive ice that occurs in frozen ground.
Permafrost aggradation. A naturally or artificially caused increase in the thickness and/or areal extent of permafrost.

Permafrost definition

The term "*permafrost*" was introduced into the English literature by Muller (1947) as an abbreviation of the original Russian term "*Permanently frozen ground (soil)*" (Sumgin et al., 1940). North American and Russian concepts, however, have differed in how the terms differentiate the presence of frozen water in relation to cold temperatures. Both Muller and Sumgin defined permafrost as soil, bedrock, or other earth materials, whose temperature remains below 0°C for at least 2 consecutive years. This definition has been accepted by The Multi-language Glossary of Permafrost and Related Ground-ice Terms developed by the International Permafrost Association (van Everdingen, 1998). In contemporary Russian permafrost literature, however, permafrost is defined as soil which remains frozen (has ice as its component) for years. "The temperature alone is not a sufficient characteristic of ground to be considered as permafrost" (Baulin and Murzaeva, 2003). Thus, the main difference between Russian and English definitions of permafrost is the occurrence of ice in ground. In Russian permafrost science, permafrost is the perennially frozen ground. Ground can have temperatures below 0°C and not have ice because it does not contain water (usually bedrock) or its freezing point is below its temperature (e.g., saline ground).

To include soil or other earth materials with temperature at or below 0°C, with and without ice, Russian permafrost science uses the term "cryolithozone" (Baulin and Murzaeva, 2003). The permafrost glossary also has a term "*cryotic ground*," which defines soil or rock at temperature 0°C or lower. It also recommends a term "*perennially cryotic ground*," which is synonymous to permafrost. In the Glossary, perennially frozen ground differs from permafrost. "Permafrost is synonymous with perennially cryotic ground; it is defined on the basis of temperature. It is not necessarily frozen, because the freezing point of included water may be depressed several degrees below 0°C; moisture in the form of ice may or may not be present. In other words, perennially frozen ground is permafrost, but not all permafrost is perennially frozen" (van Everdingen, 1998). In the last definition, the word "*permafrost*" lost its origin as a short form for permanently (perennially) frozen ground.

Permafrost distribution

Permafrost regions occupy almost 25% of global land area (Baranov, 1959; French, 2007; Washburn, 1980), about one half of Canada, and almost two thirds of Russia. Permafrost occurs also in China, USA (mostly Alaska), Mongolia, Greenland, Antarctica, and at high elevations in many mountain regions in Eurasia, Africa, and South America. Permafrost occurrence in the Northern hemisphere is shown in Figure 1.

Terrestrial permafrost includes four zones with different distribution of areas with and without permafrost: (1) continuous permafrost, where permafrost exists everywhere and can be interrupted by taliks under big water bodies (deep lakes and rivers); (2) discontinuous permafrost, where permafrost is interrupted or alternates with areas of unfrozen soil; (3) sporadic permafrost, where permafrost occurs as separate masses surrounded by unfrozen soil; (4) isolated permafrost, which occurs mainly in peat mounds and ridges surrounded by unfrozen bogs. The circumarctic map of permafrost and ground ice conditions (Brown et al., 1997) divides the permafrost region in four zones, based on the percentage of the area underlain by permafrost as continuous, 90–100%; discontinuous, 50–90%; sporadic, 10–50%; and isolated patches of permafrost, 0–10%. Figure 2 shows typical permafrost distribution in different permafrost zones. Similar classes of permafrost are often used for small areas. For example, the Copper River Lowland in Alaska is located in the discontinuous permafrost zone, but permafrost there is widespread and shown as continuous on permafrost maps (Ferrians, 1965). It is common to describe permafrost at construction sites located in the discontinuous permafrost zone as continuous, if permafrost underlies the entire site.

Continuous permafrost depends entirely on climate and the impact of local conditions on which permafrost distribution is minimal (except taliks beneath large water bodies). In the continuous permafrost zone, permafrost exists everywhere beneath the land surface and under shallow water, and it takes only 1 year to start permafrost formation after soil is newly exposed in drained lake basins. Impacts on the soil surface from disturbance, such as fire and development, increase the thickness of the active layer and trigger permafrost-related processes (e.g., thermokarst and thermal erosion), but do not lead to degradation of continuous permafrost. The permafrost table usually merges with the bottom of the active layer. Permafrost temperature in this zone varies widely and greatly depends on snow thickness and water depth.

Distribution of discontinuous and sporadic permafrost is affected by both climate and local factors (Shur and Jorgenson, 2007). In the Northern hemisphere south of the continuous permafrost zone, the effects of climate on permafrost decrease and permafrost temperature and distribution become more dependent on topography, soil

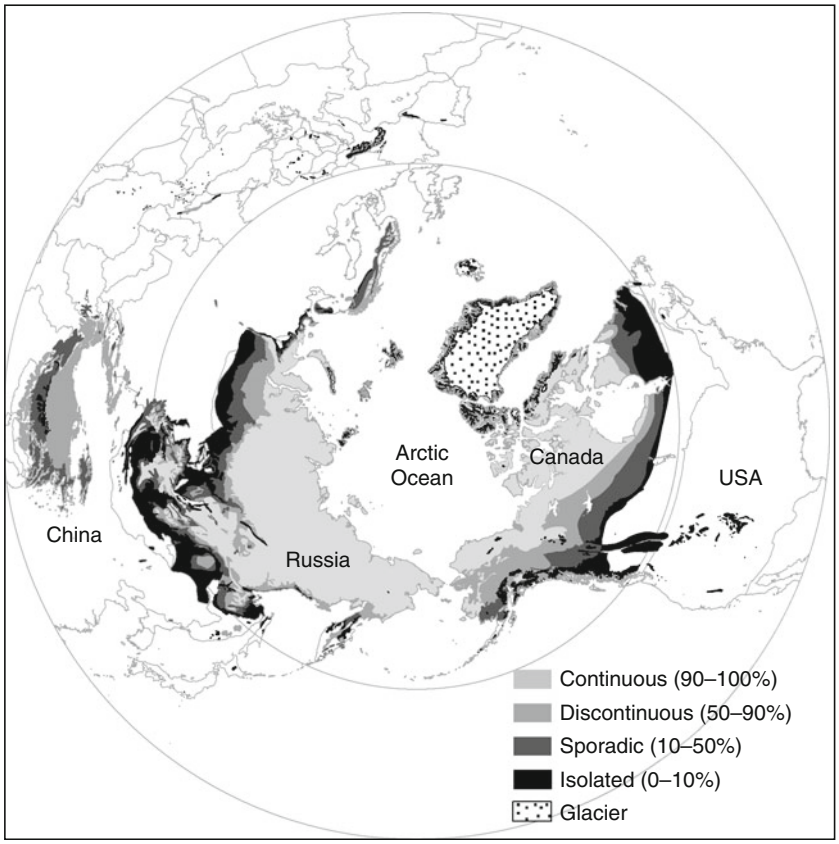

Permafrost, Figure 1 Permafrost occurrence in the Northern hemisphere (Based upon Brown et al., 1997).

properties, snow depth, and vegetation. Conditions of permafrost formation vary from favorable to unfavorable in a sequence of ground types involving peat, clay, silt, sand, and gravel. Transition from permafrost to unfrozen ground in the northern part of the discontinuous permafrost zone occurs first in gravel. At the southern boundary of the permafrost region, permafrost exists only in peat mounds, under dense coniferous forest with thick moss and peat layer on the soil surface, or in clay-rich glaciolacustrine sediments. For permafrost existence, composition and properties of the active layer are more important than composition and properties of underlying soil.

Vertical extent of permafrost sequences

The upper boundary of permafrost is called the permafrost table. It is located at the base of the active layer (if it merges with the bottom of the active layer) or can be isolated from the bottom of the active layer by a layer of unfrozen soil (if the depth of seasonal freezing does not reach the upper boundary of permafrost). In the continuous permafrost zone, the lowered permafrost table often occurs beneath lakes and rivers, and also in areas with a very thick snow cover. In the discontinuous permafrost zone, the lowered permafrost table is often a sign of permafrost degradation.

Sequences of perennially cryotic ground (Figure 3) can be presented completely by perennially frozen ground; by perennially frozen ground underlain or overlaid by cryotic unfrozen ground; by perennially frozen ground overlaid by unfrozen ground (perennially frozen ground with lowered permafrost table); completely by cryotic unfrozen ground, and by several layers of perennially frozen ground alternating with unfrozen or cryotic ground.

Active layer

The upper layer of ground in permafrost areas seasonally thaws and freezes. This layer is termed the "*active layer*" (Muller, 1947), after the Russian term "*deyatel'nyi sloy.*" In Russian permafrost science, the active layer is differentiated into a "*seasonally thawed layer*" if the bottom of this layer merges with the permafrost table and a "*seasonally frozen layer*" if the layer of seasonal freezing does not merge the permafrost table or if permafrost at a site is absent.

The active-layer thickness (maximum depth reached in the end of summer before freezing) greatly depends on local conditions, such as vegetation and soil composition. Local factors often have greater impact on the thickness of the active layer than regional ones. The impact of climate on active-layer depth is greater in areas with a thin organic layer. In the high Arctic, the thickness of the active layer

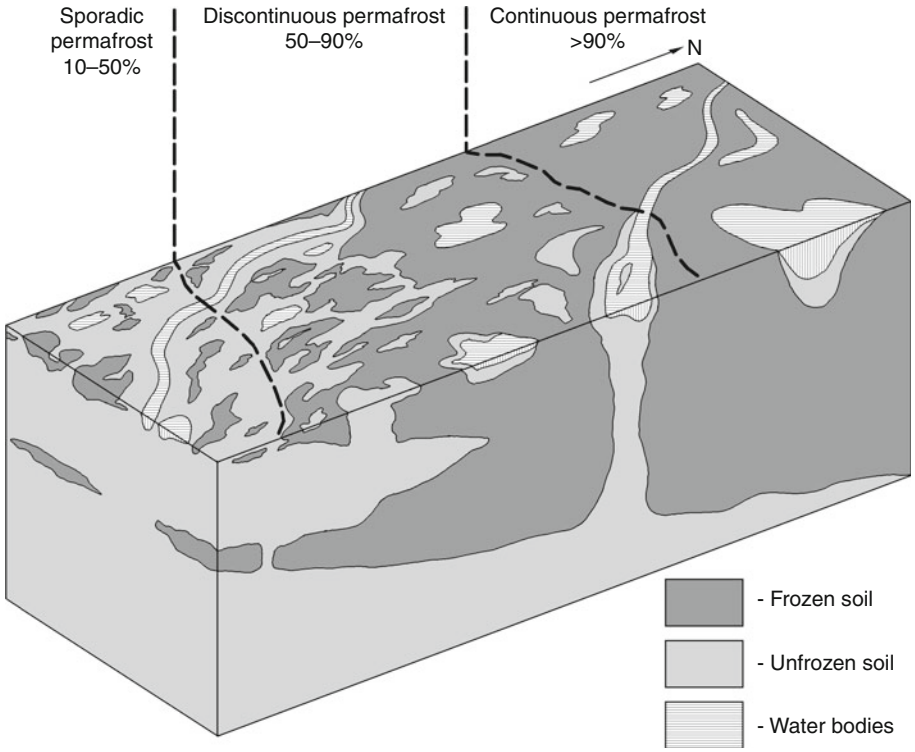

Permafrost, Figure 2 Typical permafrost distribution in continuous, discontinuous, and sporadic permafrost zones.

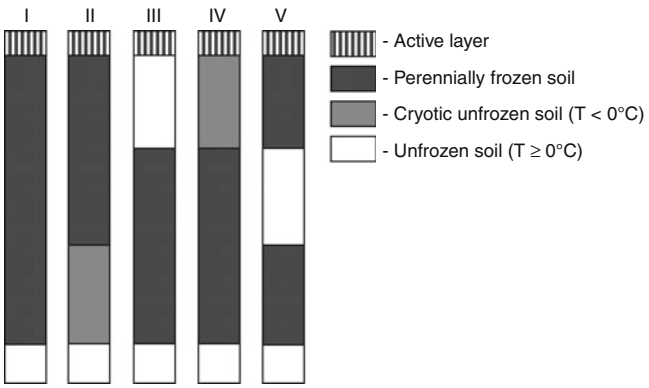

Permafrost, Figure 3 Main sequences of the perennially cryotic ground. *T* = soil temperature.

varies from about 1 m in coarse mineral ground to about 0.2 m in peat. In the discontinuous and sporadic permafrost zones, the thickness of the active layer in areas with a thick organic layer typically varies from 0.3 to 0.7 m. Active-layer depth is greatest for unvegetated or highly disturbed areas with coarse ground located near the southern boundary of the continuous permafrost zone. In the discontinuous permafrost zone, such areas are either free of permafrost or have degrading permafrost with the lowered table. In the continuous permafrost zone, active-layer thickness is determined by summer factors and about 80% of the active-layer depth can be reached in the first half of the summer. In the discontinuous permafrost zone, the thickness of the active layer is determined by winter factors. The lower part of the active layer can remain unfrozen in warm winters and winters with high snowfall (especially when significant snow accumulation happens in the first part of winter).

The thickness of the active layer varies in space and time. For example, a large-scale map of active-layer thickness within a 7 by 6 m grid located in the forest tundra zone of West Siberia (Moskalenko et al., 1978) shows thickness varying from 20 to 100 cm over short distances (Figure 4). It creates an irregular relief of the permafrost table, which is often more prominent than a local relief of the soil surface at the site. Such relief affects lateral water flow in the active layer, with accumulation of water in depressions of the permafrost table.

Active-layer thickness varies from year to year even in stable climate conditions. In mineral soils, variations are usually about 10–15% of the annual mean, but they can be as much as 30%. In organic soils, they can reach about 40% of the annual mean. A layer of soil that belongs to permafrost for several years and joins the active layer in other years is called "*transient layer*." It has a profound impact on the processes in the upper permafrost, on the formation of soil, and the thermal stability of permafrost in the face of climatic variations (Shur et al., 2005).

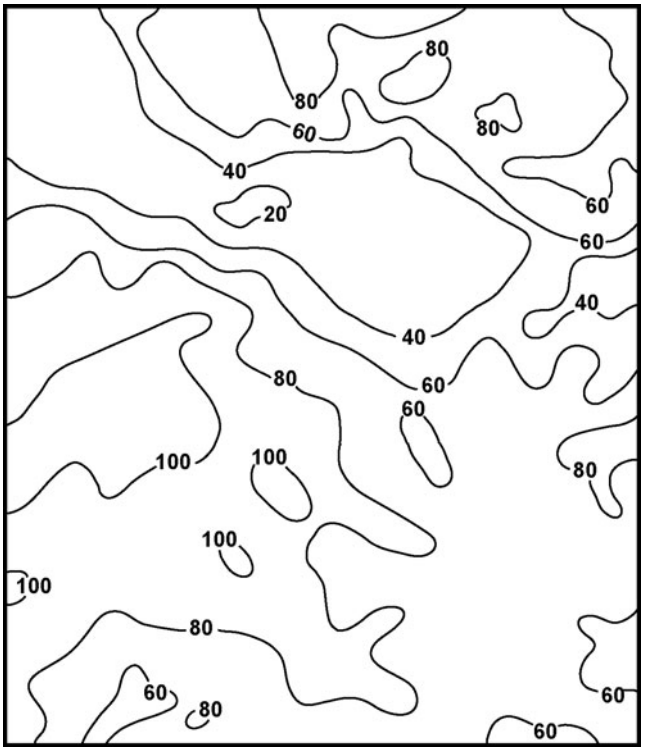

Permafrost, Figure 4 Thickness (cm) of the active layer at the transect 7 by 6 m in forest tundra zone of West Siberia (Based upon Moskalenko et al., 1978) .

Permafrost, Figure 5 Ataxitic (suspended) cryostructure of the intermediate layer, Northern Alaska.

Active-layer thickness usually decreases along with development of an ecosystem, mainly because of accumulation of organic matter on the soil surface. During this process, the bottom part of an initial active layer joins permafrost. This layer of permafrost is termed the "*intermediate layer*" (Shur, 1988). It is usually extremely ice-rich and has a unique cryostructure (pattern of ice inclusions in soil) called "*ataxitic*" or "*suspended*" (Figure 5).

Permafrost, Table 1 Classification of frozen ground due to visible ice content (based on GOST 25100-95)

	Visible ice (part of volume)	
Soil category	Bedrock	Soil
Ice-poor	<0.01	<0.20
Moderately ice-rich	0.01–0.05	0.20–0.40
Ice-rich	>0.05	0.40–0.60
Extremely ice-rich		>0.60

Ground ice

The volume and type of ground ice is important in determining thaw settlement characteristics and the sensitivity of permafrost to disturbance and thawing. Ice-rich permafrost is defined as thaw-sensitive permafrost containing excess ice (van Everdingen, 1998). It means that perennially frozen ground contains ice in excess of the ice volume required to fill pore space in unfrozen state. Thaw sensitivity of permafrost is subjective and site specific. Thaw strain (thaw settlement divided by initial thickness of a soil in frozen state) as much as 2% is not sufficient to affect structural integrity, while thaw strain of 3% or more can cause settlement damaging to most structures, but practically negligible for most of natural processes. The circumpolar map of permafrost and ground ice (Brown et al., 1997) classifies content of visible segregated ice (percent of its volume in the upper 10 m of permafrost) >20% as high; 10–20% as medium, and <10% as low (for areas with thick overburden cover). For areas of generally thin overburden cover, only two classes of ground ice are mapped, medium to high (>10%) and low (<10%). Russian frozen ground engineering defines four categories of frozen soil on the basis of visible ice content (Table 1). Visible ice content can be evaluated by measurement of thickness of ice inclusions in field or from photographs. The approach can be misleading for syngenetic permafrost, however, because abundant, very thin ice lenses are nearly invisible and often overlooked. The other approach is to define frozen soil by its thaw strain.

Ground ice can be highly variable with many distinctive forms that affect both ice volume and stability of permafrost.

Permafrost aggradation

Permafrost aggradation is a naturally or human-caused increase in the thickness and/or areal extent of permafrost (van Everdingen, 1998). Permafrost aggradation is a synonym to permafrost formation. It can be driven by climate or by change in local conditions (Shur and Jorgenson, 2007). Increase in the permafrost thickness occurs as a downward advance in epigenetic permafrost (forms after sediments have been deposited) and an upward advance in syngenetic permafrost (forms at the same time that sediments are deposited).

A special type of permafrost aggradation is associated with thinning of the active layer during ecosystem development due to changes in vegetation and accumulation of organic matter with low thermal conductivity on the soil surface. This process is widespread in continuous and discontinuous permafrost zones. It leads to a decrease in the thickness of the active layer and formation of a special layer of upper permafrost termed the "*intermediate layer*" (Shur, 1988) (Figure 6). Formation of the intermediate layer is "*quasi-syngenetic*" because permafrost is growing upward, similar to syngenetic permafrost formation, but without accumulation of new sediment on the soil surface. Transformation of the lower part of the active layer into the extremely ice-rich intermediate layer is accompanied by accumulation of aggradational ice (Mackay, 1972; Shur, 1988). Its formation is accompanied by perennial frost heave that can raise the ground surface by as much as 2 m. Formation of the intermediate layer is important to the formation of frost boils and earth hummocks (Shur et al., 2008). Accumulation of aggradational ice near the soil surface makes permafrost vulnerable to thaw subsidence on flat surfaces and to slumping on sloping terrain. Thawing of the intermediate layer is usually associated with an increase in active-layer depth, which can be caused by wildfire, stripping vegetation, or construction works. Relic intermediate layers, which initially formed during periods of decreasing sedimentation and temporal stabilization of the soil surface, can be evident at depth in syngenetic Pleistocene permafrost (Kanevskiy, 2003).

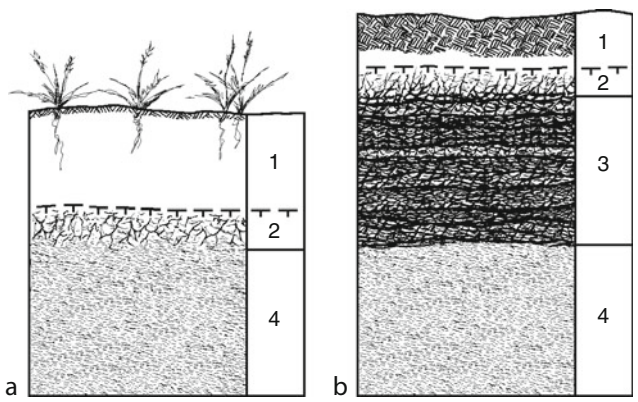

Permafrost, Figure 6 Structure of the upper permafrost before (**a**) and after (**b**) intermediate layer formation. Ice is black. Decrease in the active-layer thickness is related to accumulation of organic matter at the surface. 1 – active layer; 2 – transient layer; 3 – intermediate layer with aggradational ice; 4 –permafrost sequence before formation of the intermediate layer (Based upon Shur, 1988; French and Shur, 2010).

Permafrost landforms

A great variety of periglacial landforms can develop on permafrost terrain in response to the aggradation and degradation of permafrost. Some prominent features associated with ground ice aggradation include low-centered polygons, palsas, and pingos. In contrast, features associated with collapse of ice-rich terrain include thermokarst lakes, thaw slumps, collapse-scar bogs, and high-centered polygons (Jorgenson and Osterkamp, 2005). These landforms are useful in mapping permafrost distribution and in assessing the amount and type of ground ice present.

Palsa

Palsas are peat and peat-mineral soil mounds formed by frost heave due to accumulation of segregated ice. They rise above unfrozen bogs in the discontinuous and sporadic permafrost zones and usually form isolated patches of permafrost. Palsas occur separately or in clusters as rounded mounds and ridges. In some areas, they form large fields of tightly neighboring mounds.

The height of separate palsas varies from dozens of centimeters to 10 m, and they occupy area from a few to thousands of square meters. Palsa is the best example of the ecosystem-driven permafrost (Shur and Jorgenson, 2007). It is also the most sophisticated permafrost feature. It forms in wide range of climatic conditions of the discontinuous and sporadic permafrost zones. Both climate and vegetation succession participate in their formation. Palsas develop in the conditions most unfavorable to permafrost formation in the permafrost region. Accumulation of organic matter including sphagnum moss and peat are essential to palsa formation (Seppälä, 1986). Palsa formation cannot be explained only by an impact of physical factors such as temperature and snow depth.

Development of palsas includes pre-permafrost and permafrost stages. At the pre-permafrost stage, ecological succession prepares conditions favorable to perennial soil freezing. In the discontinuous and sporadic permafrost zones, bogs with water on the surface are free of permafrost. To be susceptible to perennially freezing, vegetation succession and accumulation of peat in bogs should reach the stage at which the surface of the bog rises above the water level. In West Siberia, for example, this stage is presented by a dwarf shrub-sphagnum association. Accumulation of sphagnum and a rise of bog ridges and hummocks create conditions in which the difference between thermal properties of peat in frozen and unfrozen state becomes an important modifier of soil climate that can be compared with increase in the winter freezing index and decrease in summer thawing index. The thickness of snow on the locally elevated surface is smaller than on

surrounding terrain, which is also a factor stimulating perennial freezing of soil in palsas (Seppälä, 1990). Initial formation creates a positive feedback to further permafrost aggradation because of natural snow removal by wind from the elevated surfaces surrounded by lower flat terrain.

Palsas are typical features of a poorly drained terrain in discontinuous and sporadic permafrost zones. They widely occur in Fennoscandia, Russian European North, West Siberia, Russian Far East, and Kamchatka. West Siberia is the greatest region of palsa development where the area of their occurrence is about 500 km by 1,000 km. Its southern boundary coincides with the southern boundary of the permafrost area and its northern boundary is the southern boundary of the continuous permafrost zone. The range of mean annual air temperature in this area varies from about −1°C to −7°C. Although palsas are mostly features of discontinuous and sporadic permafrost zones, small palsas can be observed sometimes in the continuous permafrost zone where they develop as a result of expansion of aquatic marsh vegetation in lakes and ponds.

The age of palsas varies from a few years to thousands of years. In the discontinuous permafrost zone of West Siberia, the formation of palsas is a contemporary process on lacustrine-fluvial plains and flood plains in the northern taiga and southern forest-tundra. During the last 30 years, height of some palsas has increased from 30 to 200 cm with a maximum rise occurring in the coldest winters (Ponomareva and Shur, 2008). This process can be occasionally reversed by settlement due to thawing of the ice-rich core of a palsa from its base. Surface of palsas is often affected by dilation cracks with a possible impact of thermal cracking.

Engineering design for permafrost

Knowledge of the permafrost characteristics described above is essential to the proper engineering design of structures in permafrost terrain. Two main factors for designing structures on permafrost ground are the thaw settlement of thawing permafrost and frost heave associated with soil freezing. The first step for designing structures in permafrost regions is to answer the question: "can a structure tolerate a possible thaw settlement if permafrost thaws beneath it?" The answer to this question determines the appropriate design approach shown in Figure 7. The two main approaches, "*passive*" and "*active*" were developed in Russia by the 1930s (Muller, 1947) and are also known as Principle I (use of soil in the base of structures in its permanently frozen state) and Principle II (use of soil in thawing or thawed state).

Passive method – maintain frozen state of soil

The passive method of maintaining soil in a frozen state is typically used in permafrost regions. In general, it is easier to protect continuous permafrost than discontinuous. There are different engineering means to protect permafrost from thawing. They usually take advantage of the cold climate and are based on two simple principles: (1) separation of the floor of a structure from the soil surface; and (2) chilling soil in winter and/or protecting it from warming and thawing in summer. Combining these principles brings the best results.

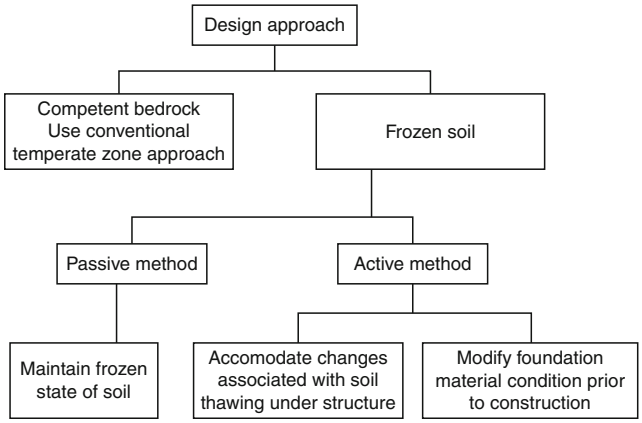

Permafrost, Figure 7 Design approaches for permafrost regions.

Open naturally ventilated air space (crawl space) beneath a building erected on piles or posts is a very effective and widely used mean of permafrost protection. Flow of cold winter air and absence of snow under a building effectively chills soil in winter and the shade from a building protects the soil surface under it from direct solar radiation. Well-designed and operated open air space reduces permafrost temperature and increases its bearing capacity. This method has limitations, however, and cannot be used for large buildings with heavy floor loads. To protect permafrost under such buildings, use of ventilated ducts next to foundations has been implemented with mixed success. Ice blockage in ducts often impairs this method and compromises integrity of foundations. Foundations with ventilated air space and ducted foundations have been used for decades.

Thermosyphons are relatively new systems for providing permafrost stability. Vertical or inclined, they can be designed as parts of foundations (thermal piles) or can be located close to foundations as freestanding chilling devices. There are two types of thermosyphons: one phase and two phases. In one-phase thermosyphons, liquid circulates in winter due to its different density along the thermosyphon – cold and heavier liquid in the aboveground part moves downward and replaces warmer and lighter liquid in the underground part of a thermosyphon. One-phase thermosyphons have been widely used in Russia in combination with open air ventilated foundations to chill warm permafrost under multistory buildings and support frozen cores of dams. In two-phase thermosyphons, heat exchange between soil and ambient air occurs through a cycle of phase transitions, first from liquid to vapor in the embedded part (a radiator) and then from vapor to liquid in aboveground part (a condenser).

First implemented by E. Long (1963) in Alaska, two-phase thermosyphons have been widely used everywhere in the permafrost regions.

Active method

Accommodate changes associated with permafrost thawing under structure

If permafrost under heated buildings is not protected by special means, it will lead to the formation of a thaw bulb. In thaw-sensitive permafrost, which has excess ice and settles upon thawing, thawing can lead to differential settlement and have severe impact on structures. Most buildings cannot tolerate settlement greater than about 20 cm. The settlement is a product of both depth of permafrost thawing and thaw strain of ground. Thaw strain of thawing permafrost varies from almost zero to about 0.8–0.9 and most permafrost ground have a thaw strain greater than 0.2. Application of the active method to accommodate changes associated with permafrost thawing requires detailed information on soil properties and accurate prediction of thaw depth and potential thaw settlement. Unexpected factors can make structures more vulnerable to thaw settlement than originally predicted.

Modify foundation material conditions prior to construction

The active method of modifying ground conditions prior to construction can be applied if ground is generally thaw-stable. A thin layer of thaw-unstable permafrost over bedrock or over thaw-stable soil can be replaced with thaw-stable soil. Preliminary thawing is the other method of soil modification prior to construction. Initially developed for mining in permafrost, this method also has been used for civil engineering projects. It is effective in coarse-grained ground, but preliminary thawing of ice-rich, fine-grained ground can create big problems. Steam, water, and electricity are used for thawing.

Bibliography

Baranov, I. Y., 1959. Geographical distribution of seasonally frozen ground and permafrost. In Shvetsov, P. F., and Dostovalov, B. A. (eds.), *General Geocryology (Permafrost Studies)*. Moscow: USSR Academy of Sciences, pp. 193–218 (in Russian).

Brown, J., Ferrians, O. J., Heginbottom, J. A., and Melnikov, E. S., 1997. *Circum-Arctic Map of Permafrost and Ground-Ice Conditions*. Reston: U.S. Geological Survey.

Baulin, V. V., and Murzaeva, V. E. (eds.), 2003. *Dictionary of Geocryology*. Moscow: Geos, p. 140.

Ferrians, O. J., 1965. *Permafrost Map of Alaska*. U.S. Geological Survey Misc. Inv. Series Map I-455, scale 1:2,500,000.

French, H. M., 2007. *The Periglacial Environment*, 3rd edn. Chichester: Wiley.

French, H., and Shur, Y., 2010. The principles of cryostratigraphy. *Earth-Science Reviews*, **101**, 190–206.

GOST 25100-95, 1995. *Classification of Soils. International Standard*. Moscow (in Russian).

Jorgenson, M. T., and Osterkamp, T. E., 2005. Response of boreal ecosystems to varying modes of permafrost degradation. *Canadian Journal of Forest Research*, **35**, 2100–2111.

Kanevskiy, M., 2003. Cryogenic structure of mountain slope deposits, northeastern Russia. In *Proceedings of the Eights International Conference on Permafrost*, July 21–25, 2003, Zurich, Switzerland. Vol. 1, pp. 513–518.

Long, E. L., 1963. The Long thermopile. In *Proceedings Permafrost International Conference*, November 11–15, 1963, Lafayette, pp. 487–491.

Mackay, J. R., 1972. The world of underground ice. *Annals of the Association of American Geographers*, **62**, 1–22.

Moskalenko, N., Slavin-Borovsky, V. B., and Shur, Y. L., 1978. Detailed study of terrain units in northwestern Siberia. In Malevskiy, S. P., and Shur, Y. L. (eds.), *Processes of Natural Heat Exchange in Permafrost Environment, Transactions of Main Geophysical Observatory*. Leningrad: Hydrometeoizdat, Vol. 402, pp. 94–105 (in Russian).

Muller, S. W., 1947. *Permafrost or Permanently Frozen Ground and Related Engineering Problems*. Ann Arbor: J.W. Edwards.

Ponomareva, O., and Shur, Y., 2008. Long-term monitoring of frost heave and thaw settlement in the northern taiga of West Siberia. In *Proceedings of the Ninth International Conference on Permafrost*, June 29–July 3, 2008, Fairbanks. Vol. 2, pp. 1439–1444.

Seppälä, M., 1986. The origin of palsas. *Geografiska Annaler. Series A, Physical Geography*, **68**(3), 141–147.

Seppälä, M., 1990. Depth of snow and frost on a palsa mire, Finnish Lapland. *Geografiska Annaler. Series A, Physical Geography*, **72**(2), 191–201.

Shur, Y. L., 1988. *Upper Horizon of the Permafrost Soils and Thermokarst*. Novosibirsk: Nauka, Siberian Branch (in Russian).

Shur, Y., and Jorgenson, M. T., 2007. Patterns of permafrost formation and degradation in relation to climate and ecosystems. *Permafrost and Periglacial Processes*, **18**, 7–19.

Shur, Y., Jorgenson, T., Kanevskiy, M., and Ping, C.-L., 2008. Formation of frost boils and earth hummocks. In *Proceedings of the Ninth International Conference on Permafrost, extended abstracts*, June 29–July 3, 2008, Fairbanks, pp. 287–288.

Shur, Y., Hinkel, K. M., and Nelson, F. E., 2005. The Transient layer: implications for geocryology and climate-change science. *Permafrost and Periglacial Processes*, **16**, 5–18.

Sumgin, M. I., Kachurin, S. P., Tolstikhin, N. I., and Tumel, V. F., 1940. *General Permafrost Science*. Moscow: USSR Academy of Sciences (in Russian).

Sumgin, M. I., 1927. *Permafrost in the USSR Boundary*. Vladivostok: Far-East Geophysical Observatory (in Russian).

van Everdingen, R. O. (ed.), 1998. *Multi-Language Glossary of Permafrost and Related Ground-ice Terms*. International Permafrost Association. The Arctic Institute of North America, University of Calgary, Calgary, 268 pp.

Washburn, A. L., 1980. *Geocryology*. New York: Wiley.

Cross-references

Permafrost and Climate Interactions
Permafrost Modeling

PERMAFROST ON ASTEROIDS

William C. Mahaney
Quaternary Surveys, Thornhill, ON, Canada

Definition

Asteroids, especially Near Earth Objects (NEOs), are considered to be dry, barren piles of rock, either C-, E, S-, or

M-type bodies (Asphaug, 2007). A recent engineering feat carried out by the Japanese Aerospace Agency (JAXA) resulted in the successful rendezvous (2005) of the Hayabusa Space Craft with Asteroid 25143-Itokawa, located some 320 million kilometers from Earth. Itokawa is small by comparison to Ceres and Eros, two much larger stony asteroids; Eros was imaged by Near-Shoemaker (2000), orbiting 50 km above the surface (Asphaug, 2007) and showing considerably greater relief than is present on Itokawa. Imagery of Eros from orbit and controlled descent to the surface is available at *nssdc.gsfc.nasa.gov/planetary/near.html*. The presence of universally segregated rubble on Itokawa (Mahaney, 2009; Mahaney and Kapran, 2009; Mahaney et al., 2009) approximating polygonal ground, talus, stone-banked lobes, and debris flows on Earth should come as no surprise as similar features have been observed on Eros. When NASA's Dawn Mission reaches 4-Vesta in 2011, and Ceres in 2015, it may well record a surface geology rife with periglacial landforms requiring the presence of permafrost. The existence of permafrost should also come as no surprise since all asteroids are thought to have encountered comets since the dawn of the solar system.

Permafrost and asteroids

Imagery of asteroid 25143-Itokawa (Figure 1) released by the JAXA Science Team (2007) reveals prominent cold environment mass wastage landforms similar to those on Earth, including debris flows, patterned ground, stone-banked lobes, and talus. These geomorphological features, not previously recognized in the published literature from the Hayabusa Mission to Itokawa, are of significance because in the terrestrial environment they indicate the presence of permafrost and periodic release of meltwater. The existence of periglacial landforms suggests periodic, if not episodic, changes in surface thermal characteristics of sufficient magnitude to melt permafrost caused by orbital changes and high variation in aphelion and perihelion of Itokawa. The presence of landforms requiring moisture further suggests that Itokawa may have a detailed paleohydrological record, and with it, the possibility of either extant or fossil microbial life. Indeed, similar periglacial features on the surface of Eros (NASA, Near-Shoemaker Mission 2000; Figure 2) suggest permafrost may be far more prevalent on asteroids than previously thought. Future sampling missions to asteroids should consider targeting evidence for water release and associated large macroscale landforms.

The assumption that impacts on asteroids result in vibrational sorting of fines and coarse debris producing near uniform and universally continuous sheets of regolith (Miyamoto et al., 2007), has been reassessed (Mahaney, 2009; Mahaney and Kapran, 2009; Mahaney et al., 2009) after the recent release of imagery from the Hayabusa Mission to Itokawa (http://www.jaxa.jp). Regolith is used in the same sense as on Earth, referring to unconsolidated, undifferentiated, and largely incoherent loose rock material mantling bedrock, often partly weathered with a surface soil in terrestrial environments. In the case of Itokawa (Miyamoto et al., 2007; Asphaug, 2007), the entire mass is a loose assemblage of mineral debris, of basaltic composition (Abell et al., 2007), ostensibly indurated with a high porosity of 30–40% (Abe et al., 2006; Cheng et al., 2007). Analysis of regolith evolution at the asteroid surface, however, reveals landform distributions similar to periglacial areas on Earth.

At the end of November, 2005, the Hayabusa spacecraft carried out a series of remarkable engineering feats,

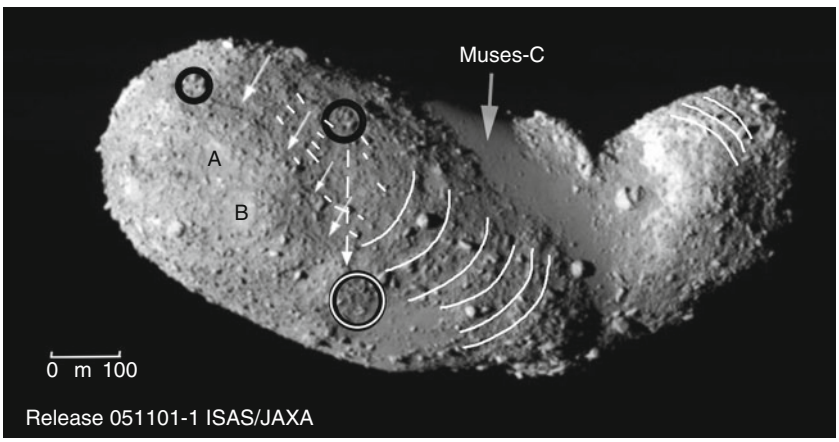

Permafrost on Asteroids, Figure 1 Image of Itokawa taken by the Hayabusa Mission (JAXA-2005) showing the rubble-strewn surface. Arcuate-shaped lobes are identified in white, hydrological sources with black rings, prominent debris flow trough by arrows, meltwater trough by *dashed arrow*, hydrological sink by *black/white circle*, and talus by individual clasts marked in *white* with orientation on an artificial horizon to the southeast. The Muses-C is a fine-grained accumulation of sediment from topographically higher adjoining areas. Sites A and B are impact craters. The surface channel system to the right of Muses-C may be slope wash from meltwater release at the top. Tonal contrast is a measure of nanophase secondary Fe accumulation: white is young; varying shades of gray are old (Hiroi et al., 2006). (Credit: ISAS/JAXA released image 051101–1.)

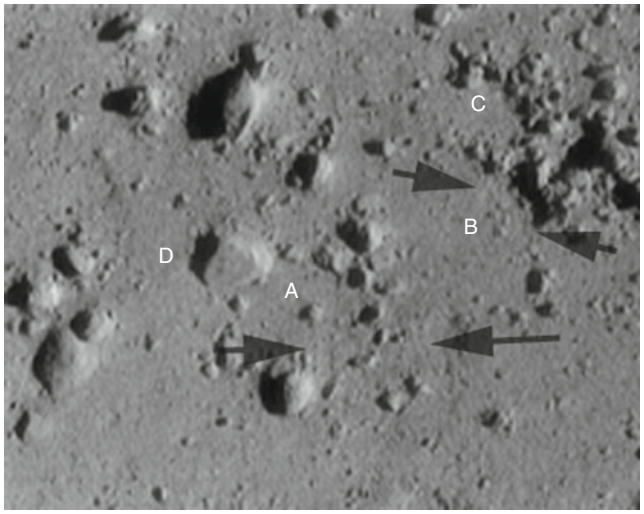

Permafrost on Asteroids, Figure 2 Surface of Eros (NASA Web site; Near-Shoemaker's descent image 0157417133) – 12 m across, taken at 250 m; rock cluster upper right is 1.4 m across showing debris flow features (*arrows*) complete with source areas, troughs with levees and sinks. Circular accumulations of clasts could be borders of polygons (*capital letters* show polygon centers) and nested clasts in upper right might signify a boulder-cored frost boil feature (Harris and Matthews, 1984). (Credit: NASA.)

including precise navigation tests and two touchdowns on the asteroid surface, the latter sufficient to collect a small sample for return to Earth (Miyamoto et al., 2007) by 2010. While the resolution of imagery taken by the cameras aboard the spacecraft is at a scale only sufficient to identify major and some minor landforms amidst the collection of rubble on the asteroid surface, some of the regolith is well segregated into distinct landform assemblages as shown below in Figure 1. Earth analogue examples of these landforms are illustrated in Mahaney (2009) and Mahaney et al. (2009).

Grain-size calculations carried out by Miyamoto et al. (2007) indicate that Itokawa is covered with unconsolidated gravels, distributed across the surface by vibrational effects giving rise, in part, to an imbricated sheet mass in some instances. Fines are either electrostatically elevated and lost to space by solar radiation pressure, ejected following impact, and/or taken up by filling holes created by enveloping larger gravels. The three major "smooth terrains" identified on Itokawa, the largest being the Muses-C region (Figure 1), act as topographic lows for the accumulation of fine-grade size material, with slopes $<8^{o}$. Above these depressions, the larger size gravels, consisting of pebble through boulder size clasts, are aligned with directions parallel to local slope and gravity, their present spatial pattern compatible with vibrations caused by meteorite impact and response to local microgravity. Granular convection models (Miyamoto et al., 2007), which explain gravel distributions on Itokawa, are supported by laboratory experiments on vibration tables and models of global shaking from meteorite collisions (Bruzzone et al., 2008). All these experiments and models rely on smaller particles descending along a slope angle that falls within the friction angle of the particles. Despite the higher inclination of coarse terrain (Scheeres, et al., 2004), such particles remain in areas of higher gravitational potential (Fujiwara et al., 2006) until a future impact event results in their movement or until they are disturbed by movement with a hypothesized active permafrost layer (Mahaney, 2009; Mahaney et al., 2009).

Despite the coarse accumulation of gravels into mounds and ridges, as shown in Figure 1, there are also areas with pebble debris and finer matrix material including sand and possibly finer silts and clays. As indicated, not all fine material escapes into convection cells below the asteroid surface. The corollary of rough terrain with imbricated gravel surfaces on Earth, as proposed by Miyamoto et al. (2007), matches only part of the surface jumble of clastic debris shown in Figure 1. The remainder, where strong long-axis clast orientations match the slope, is more analogous with talus accumulations on Earth (although the slope angle is $<27^{o}$ [Scheeres, et al., 2004]), where gravity-induced migrations of clasts are clearly shown. Some of the chaotic terrain on Itokawa is presumably in areas recovering from the last vibration event as proposed by Miyamoto et al. (2007), while others are partially sorted in response to a small microgravity component that redirects the downslope movement of clasts toward local depressions.

Coarse accumulations of large gravels into mounds and ridges on Itokawa is in places chaotic, as indicated above, while in others clasts group into forms resembling stone-banked lobes, i.e., landforms often observed in periglacial areas on Earth (Mahaney and Spence, 1984). Additionally, the presence of polygonal ground on Itokawa (and on Eros; Figure 2) argues for an active layer in permafrost, complete with segregated ice lenses capable of sorting clastic material. Similar features are reported on Mars near the equator from analysis (Balme et al., 2008) of HIRISE (High Resolution Imagery Science Experiment) imagery. On Earth, these landforms owe their origin to a source of coarse and fine clastic debris, sourced either from moraine material or from mass-wasting processes, such as frost riving and solifluction (Mahaney and Spence, 1984; Vieira and Ramos, 2003). Similar structures, although with less relief, are present in the Dry Valleys of Antarctica (Mahaney et al., 2001) and all bear a close similarity to ridges on Itokawa. Given the close correspondence between mean surface temperatures on Itokawa (−73°C) and in Antarctica (−65°C), it is plausible that similar forms may equate to similar processes, the cold dry climate of Antarctica (Mahaney et al., 2001) being not that different from the cold, barren, ice-choked worlds of Itokawa and Eros. While permafrost likely assists in the development and evolution of stone-banked lobes in the middle latitude mountains of Earth, and polar areas as well, current models of asteroid evolution do not consider the possibility of permafrost, or that of an associated active

layer, occasionally forming due to a minor or major change in incoming radiation.

Close examination of Figure 1 shows chaotic mounds of large gravels. In the upper left of Figure 1, a debris-flow trough is observed, following a circuitous route approximately 250 m from northwest to southeast – direction on the figure is calculated using an artificial horizon to navigate from the source to termination. The boulder mound might owe its relief to fine material atop permafrost with the active layer accumulating moisture and heaving, much as in boulder-cored frost boils (Harris and Matthews, 1984) and polygons on Earth. Branching off the chaotic boulder mound, levee ridges on either side of the main drainage trough, outlined in the figure show a distinctly finer texture than the terrain through which the debris flow channel is cut, thus suggesting lower-flow regime clast-charged meltwater discharge. The very fact that debris flows exist on Itokawa indicates the presence of permafrost, a frozen sediment bed over which meltwater could flow suggesting at least one cycle of warming that produced sufficient discharge of meltwater to send a charged liquid mass downslope for a considerable distance. Even if the debris-flow channel bed were to thaw, meltwater could flow easily over terrain shown in the close-up imagery of Figure 2A, E, and F in Miyamoto et al. (2007), where bulk density of the sediment appears high enough to retain moisture, not unlike debris flows in the tropical mountains of Earth (Mahaney, 1990; Figure 6A). The fact that the levees remain in place argues for a recent age, as meteorite bombardment would have rearranged clasts into random or semi-oriented clast distributions on the slope.

From another boulder mound to the north of the debris flow system shown in Figure 1, a series of longitudinal ridges and troughs lie oriented south toward the near-termination area of the debris flow at site C. These forms resemble channels cut by water, and their orientation indicates the termination zone may be a sink area, where moisture generated by changes in the surface thermal regime of the asteroid is channeled.

The evidence for the presence of water in isolated areas on Itokawa suggests something of a puzzle as to what produced the melting. The albedo of the asteroid at 0.19 is low, which implies that solar absorption is high when orbital variations take it across Earth's orbit nearer to the sun. The wide variation in perihelion (0.9533) and aphelion (1.6948) (http://NEODyS25143-Itokawa) leads to variable radiation receipt, possibly strong enough when accompanied by solar radiation outbursts to melt underlying permafrost, thereby providing sufficient moisture to initiate mass-wasting events. Even if the asteroid has a paleohydrological record, it is necessarily short-lived, as seismic/vibration events will lead eventually to the redistribution of spatial networks of clasts, either randomly dispersed or aligned with the regional slope, i.e., talus-like bodies (Mahaney et al., 2009).

Because water is the only geologic agent capable of producing debris flows, and in addition the asteroid is of insufficient mass to generate liquid methane, meltwater may well be an agent that assists in the minor lubrication of stone-banked lobes in other areas on the surface (Figure 1). Moreover, the presence of liquid water on what is considered to be a barren, dry world opens up the possibility of the presence of microbes (Mahaney et al., 2001), either extant or fossil, the probability of which is enhanced by the asteroid lithology where Fe exists in ample supply. As indicated by optical measurements (Hiroi et al., 2006), which show higher amounts of nanophase-Fe on darker patches of Itokawa relative to lighter surfaces, the chondrite olivine-pyroxene composition is a lithology conducive to the development of microbes. As microbe physiology requires water in liquid form, together with iron for respiration processes, it might behoove asteroid researchers working on Itokawa to focus on the chemical composition of light-toned surfaces to determine if salts are present. Adsorption of water to surface clasts in the vacuum of space might be explained by recourse to surface particle energy, mineral orientation, pore presence, crystal defects and dislocations, and chemisorption (de Leeuw et al., 2000; Stimpfl et al., 2006). Much as in the Dry Valleys of Antarctica (Mahaney et al., 2001), concentrations of salts in the near-surface environment of Itokawa would lower the freezing temperature of water to a point where microbial colonies might evolve and persist.

Given the prevalence of periglacial landforms on Itokawa and Eros, future sampling missions to asteroids (i.e., NASA's Dawn Mission) should consider targeting evidence for permafrost and meltwater release.

Summary

Near Earth Objects (NEOs), long considered to be dry, barren rock piles, either C, E, S, or M (i.e., carbonaceous, enstatite-achondrite, stony, metal) type bodies often reveal universally segregated clast distributions of landforms approximating periglacial environments on Earth. If permafrost exists on asteroids such as Eros and Itokawa it may well be present on other asteroids and these bodies may carry a hydrological record that reflects their ancient histories and encounters with comets over the lifespan of the solar system. With the arrival of NASA's Dawn Mission at 4-Vesta in 2011 and Ceres in 2015, we may have new clues about the presence/absence of periglacial landscapes. Imagery from 21-Lutetia, a probable M type asteroid will be available in 2010 from the Rosetta Space Probe (European Space Agency, ESA), launched in 2004, which also returned (2008) imagery from 2867-Steins, an E type asteroid. The Steins imagery from 800-km distance showed numerous craters, large-scale surface ruptures, numerous scalloped-shaped depressions, round raised mounds that could be periglacial in origin, and long raised ridges of unknown origin.

Bibliography

Abe, S., et al., 2006. Mass and local topography measurements of Itokawa by Hayabusa. *Science*, **312**(5778), 1344–1347.

Abell, P. A., Vilas, F., Jarvis, K. S., Gaffey, M. J., and Kelley, M. S., 2007. Mineralogical composition of 25143 Itokawa 1998 SF_{36} from visible and near-infrared reflectance spectroscopy: evidence for partial melting. *Meteoritics and Planetary Science*, **42**, 2035–2182.
Asphaug, E., 2007. The shifting sands of asteroids. *Science*, **316**, 993–994.
Balme, M. R., Gallagher, C. J., Page, D. P., Murray, J. B., and Muller, J.-P., 2008. Sorted stone circles in Elysium Planitia, Mars: implication for recent martian climate. *Icarus*, **200**, 30–38.
Bruzzone, J. S., Roland, S., Tancredi, G., and Favre, S., 2008. Itokawa: a global shaken and fractured asteroid with Brazilian nut effect. *Asteroids, Comets and Meteors*, 8271. pdf.
Cheng, A. F., Barnouin-Jha, O., Hirata, N., Miyamoto, H., Nakamura, R., and Yano, H., 2007. Fundamentally distinct outcomes of asteroid collisional evolution: Itokawa and Eros. *Geophysical Research Letters*, **34**, L09201, doi:10.1029/2007GL029559.
de Leeuw, N. H., Parker, S. C., Catlow, R. A., and Price, G. D., 2000. Proton-containing defects at forsterite 010 tilt grain boundaries and stepped surfaces. *American Mineralogist*, **85**(9), 1143–1154.
Fujiwara, A., et al., 2006. The rubble-pile asteroid Itokawa as observed by Hayabusa. *Science*, **312**(5778), 1330–1334.
Harris, C., and Matthews, J. A., 1984. Some observations on boulder-cored frost boils. *The Geographical Journal*, **150**(1), 63–73.
Hiroi, T., Abe, M., Kitazato, K., Abe, S., Clark, B., Sasaki, S., Ishiguro, M., and Barnouin-Jha, O. S., 2006. Developing space weathering on the asteroid 25143-Itokawa. *Nature*, **443**, 56–58.
Mahaney, W. C., 1990. *Ice on the Equator*. Ellison Bay: Wm Caxton. 386 pp.
Mahaney, W. C., 2009. Geomorphological analysis of Asteroid 25143-Itokawa indicates presence of meltwater processes, IAG-Planetary Working Group, http://www.psi.edu/pgwg/images/oct09image.html.
Mahaney, W. C., and Spence, J., 1984. Late Quaternary deposits, soils, chronology and floristics, Jaw Cirque Area, Central Teton Range, Western Wyoming. *American Journal of Science*, **284**, 1056–1081.
Mahaney, W. C., and Kapran, B., 2009. Landforms on Asteroid 25143-Itokawa: a geomorphological perspective on periglacial origin and meltwater history. *Geomorphology*, **108**, 321–323.
Mahaney, W. C., Dohm, J. M., Baker, V. R., Newsom, H. E., Malloch, D., Hancock, R. G. V., Campbell, I., Sheppard, D., and Milner, M. W., 2001. Morphogenesis of Antarctic paleosols: martian analogue. *Icarus*, **154**, 113–130.
Mahaney, W. C., Kalm, V., Kapran, B., and Hewitt, K., 2009. Clast fabric and mass wasting on Asteroid 25143-Itokawa: correlation with talus and other periglacial features on Earth. *Sedimentary Geology*, **219**, 44–57.
Miyamoto, H., Yano, H., Scheeres, D. J., Abe, S., Barnaouin-Jha, O., Cheng, A. F., Demura, H., Gaskell, R. W., Hirata, N., Ishiguro, M., Michikami, T., Nakamura, A. M., Hakamura, R., Saito, J., and Sasaki, S., 2007. Regolith migration and sorting on Asteroid Itokawa. *Science*, **316**, 1011–1014.
Scheeres, D. J., Broschart, S., Ostro, S. J., and Benner, L. A., 2004. The dynamical environment about Asteroid 25143 Itokawa: target of the Hayabusa Mission. In *AIAA/AAS Astrodynamical Specialist Conference and Exhibit,* August 16–19*,* Providence, pp. 1–12.
Stimpfl, M., de Leeuw, N. H., Deymier, P., Drake, M. J., and Walker, A. M., 2006. In the beginning there was water and dust: a look into adsorption as a mechanism to explain water in the inner solar system. In *Lunar and Planetary Science XXXVII Conference*, 1395 pdf.
Vieira, G., and Ramos, M., 2003. Geographic factors and geocryological activity in Livingston Island, Antarctica: Preliminary results. In: M. Philips, S. M. Springman and L. U. Arenson (eds.) Proceedings of 8th International Conference on Permafrost, 21–25 July, Swets and Zeitlinger, Lisse, pp. 1183–1188.

Cross-references

Albedo
Antarctica
Chemical and Microbial Records in Snow and Ice
Ice
Periglacial
Permafrost
Solifluction

PERMAFROST AND CLIMATE INTERACTIONS*

Sharon L. Smith, Margo M. Burgess
Geological Survey of Canada, Natural Resources Canada, Ottawa, ON, Canada

Definition

Permafrost and active layer – see entry *Permafrost*

Introduction

Permafrost is defined as a thermal condition in which the temperature of the ground (soil or rock) remains continuously below 0°C for 2 years or more (Brown and Pewe, 1973). Most permafrost, however, has existed for much longer and under the cold climates of the Arctic can extend to thicknesses of up to several hundred meters. The upper part of the ground above the permafrost that thaws each summer and refreezes in the winter is called the active layer.

Factors influencing permafrost–climate relationships

The atmospheric climate is the main factor controlling the formation and existence of permafrost (Brown and Pewe, 1973). Although a general relationship exists between air and ground temperatures, local environmental factors play an important role in determining the heat transfer between the ground and the air. These conditions include aspect, elevation, snow cover, vegetation, the presence or absence of an organic layer, surficial materials, soil moisture content, and drainage (French, 2007). These factors determine the ground surface temperature on which the spatial distribution, thickness, and temperature of permafrost are highly dependent. A change in climate may result in changes in ground temperature and permafrost distribution but the magnitude and the rate at which these changes occur will vary depending on the site characteristics.

Snow is an effective insulator due to its low thermal conductivity. During the winter, the snow acts to reduce

the energy exchanges between the air and ground surface so that warmer winter ground temperatures will exist beneath deeper snowpacks. In the discontinuous permafrost zone, snow depth can be an important factor determining the existence of permafrost (Brown and Pewe, 1973). Studies done by Nicholson and Granberg (1973) at Schefferville, Quebec, Canada, where mean annual air temperature is warmer than −5°C, suggest that where the snow depth is greater than 75 cm the ground is well insulated from winter air temperatures and generally not underlain by permafrost. Recent observations at York Factory Manitoba, Canada, show that open, windswept areas with minimal snow cover are underlain by permafrost while the ground in adjacent areas where thick snow covers may build up may not be frozen (Sladen et al., 2009).

In the discontinuous permafrost zone, vegetation has an important influence on the permafrost distribution (Brown and Pewe, 1973). Vegetation provides shade in the summer and in the case of coniferous trees, reduces the amount of snow on the ground in the winter, leading to lower ground temperatures in forested areas compared to treeless areas. Permafrost may therefore be thin or nonexistent in treeless areas compared to forested areas within the discontinuous zone. Above the tree line, warmer permafrost conditions are often found where shrubs, such as willows, are present (Figure 1) as they tend to trap snow during the winter in contrast to open areas where the wind may remove the snow (e.g., Burn and Kokelj, 2009).

The presence and nature of organic material or peat at the ground surface is also an important factor controlling permafrost occurrence and persistence especially at the southern margins of the permafrost zone where mean annual ground temperatures are close to 0°C (e.g., Vitt et al., 1994). The thermal conductivity of peat varies during the year. Peat becomes a good insulator in the summer when it is dry and a good conductor in the fall and winter when it is wet. This characteristic enables permafrost to persist in organic terrain although it may be absent in adjacent mineral soils with no significant peat cover (Figure 2; e.g., Burgess and Smith, 2000). This insulation offered by the peat can therefore act to buffer the ground thermal regime from the effects of long-term climate change as well as reduce the response to shorter-term climate variability (e.g., Halsey et al., 1995; Woo et al., 2007).

The thermal properties of the underlying soil or rock also play a role in determining the relationship between climate and the ground thermal regime. Fine-grained soils such as clay and silt will generally have a low thermal conductivity while sand and bedrock with a higher quartz content will generally have a higher thermal conductivity. The ground ice content is also important. For ice-rich material, the latent heat effects of thawing are important in determining the rate of permafrost degradation (Riseborough, 1990). The thermal regime of fine-grained soils having high ice contents would therefore be expected to respond more slowly to changes in climate especially as temperatures approach 0°C.

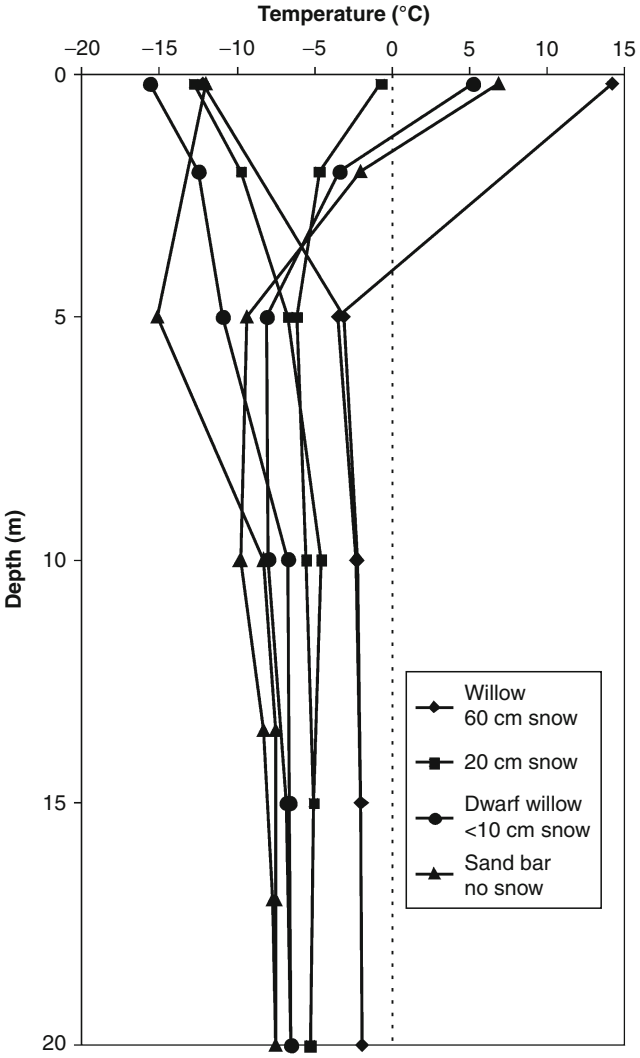

Permafrost and Climate Interactions, Figure 1 Ground temperatures at a site in the Mackenzie Delta, Canada. For each site, the March and July 1992 temperature profile is shown. Where vegetation is able to trap snow, permafrost is warmer than sites where the wind removes the snow (from Burgess and Smith, 2000).

Changes in permafrost conditions over time

Changes in both areal extent and thickness of permafrost have occurred in the past in response to changes in climate occurring at scales of decades to centuries to millennia. Under a cooling climate, permafrost becomes thicker and more extensive regionally while a warming climate results in thickening of the active layer and thinning or even complete disappearance of permafrost. In Canada, for example, warmer conditions existed during the mid-Holocene, 6,000–9,000 years ago with the southern limit of permafrost north of its present position and active layers generally thicker (e.g., Burn et al., 1986; Zoltai, 1995). Cooler conditions followed the mid-Holocene

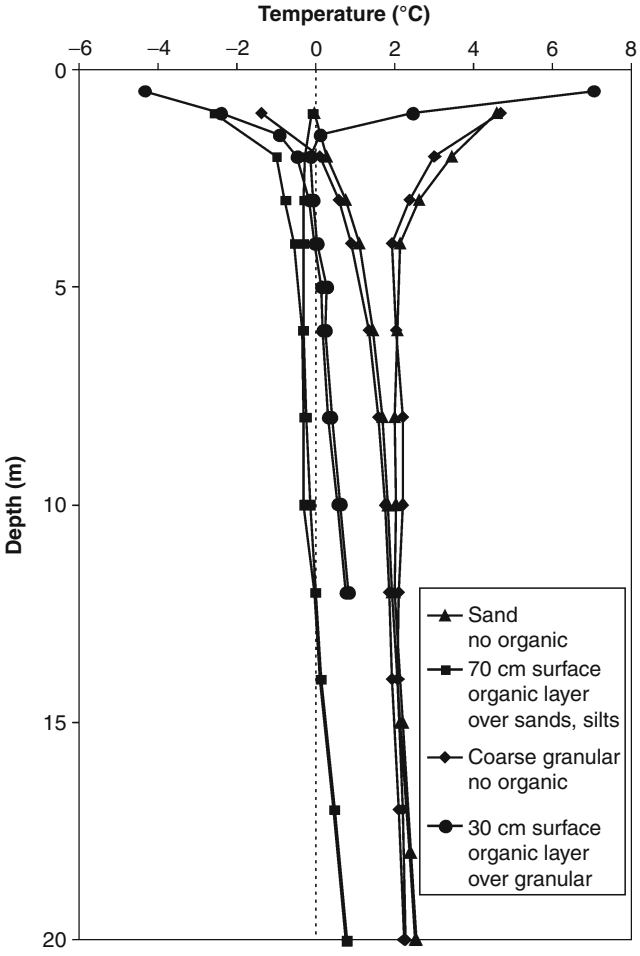

Permafrost and Climate Interactions, Figure 2 Ground temperature envelopes (maximum and minimum annual ground temperature for 1986) for four sites in the discontinuous permafrost zone near Fort Simpson, NWT, Canada. Although the climate is similar at all sites, permafrost is absent from sites lacking a significant organic layer (from Burgess and Smith, 2000).

Warm Period about 3,700–5,000 years ago and this was accompanied by an increase in permafrost extent (e.g., Zoltai, 1993; Vardy et al., 1998). During the Little Ice Age between 1550 AD and 1850 AD, air temperatures were colder and permafrost occurred farther south than at present (e.g., Vitt et al., 1994). At the southern fringes of the discontinuous permafrost zone, some of this permafrost still persists in organic terrain (frozen peatlands) at temperatures close to the thawing point due to the insulation provided by a thick layer of peat, while in mineral soils it has largely disappeared (Halsey et al., 1995; Smith et al., 2008). Similar fluctuations in permafrost extent have occurred over the last 20,000 years in northern Eurasia (Lisitsyna and Romanovskii, 1998). Relic permafrost bodies 100–200 m thick, that were formed during colder climates of the Pleistocene, have been mapped in central and southern Siberia (Ananjeva et al., 2003). The top of this relic permafrost can be more than 80 m below the ground surface which indicates that permafrost has been degrading in response to Holocene warming. Relict permafrost of Pleistocene age that has been in existence for at least 125,000 years is also found in central Alaska (French, 2007).

Subsea permafrost also exists which is a relic from periods of lower sea level during the glacial maxima of the Quaternary Period. In the Beaufort Sea, for example, large areas of the continental shelf were above sea level during the Quaternary and thus were exposed to air temperatures which were as much as 18°C lower (Allen et al., 1988) than those currently occurring at the seabed, allowing permafrost up to 700 m thick to form. During interglacial periods and in postglacial time as sea levels increased, these exposed areas were covered by Arctic Ocean water, having bottom water temperatures between 0°C and −2°C, which has gradually warmed the sediments and led to slow degradation of subsea permafrost (Taylor, 1991). Similar bodies of relic subsea permafrost also exist in the Laptev and eastern Siberian Seas (Danilov et al., 1998; Delisle, 1998; Overduin et al., 2008).

More recently, over the past two to three decades, there has been a general warming of permafrost across the circumpolar permafrost region (Romanovsky et al., 2007; Lemke et al., 2007). Observations from permafrost monitoring sites throughout the northern hemisphere, including North America (e.g., Smith et al., 2010), Russia (e.g., Romanovsky et al., 2010), the Arctic and alpine areas of Europe (Harris and Isaksen, 2008), and plateau of central Asia (e.g., Sharkhuu et al., 2008; Zhao et al., 2008), generally indicate that permafrost temperatures have increased though the rate and magnitude of this increase varies regionally. A few examples are provided below.

In northwestern North America, in Alaska and the Mackenzie valley region of NWT Canada, for example, a region which has experienced an increase in air temperature of about 1.5°C over the last century, permafrost temperatures at depths of 10–20 m have increased by a few tenths of degree per decade in the south and central area (Figure 3) to about 1°C/decade in the north (e.g., Arctic Coastal Plain, Mackenzie Delta region) since the 1980s (Kanigan et al., 2008; Smith et al., 2010). Smaller increases in permafrost temperature have been observed in the more southerly, warmer and thinner permafrost as there is greater buffering from air temperature changes by the forest cover and also due to the latent heat required to thaw ground ice as temperatures approach 0°C.

In the high Arctic tundra where mean annual ground temperatures can be as low as −15°C, the ground temperatures are more responsive to changes in air temperature due to the lack of a buffer layer (little vegetation, thin snow cover) and because the cold permafrost conditions mean phase changes are not occurring and therefore the presence of unfrozen water does not obscure the climate signal. At Alert Nunavut (latitude 82.5°N), for example,

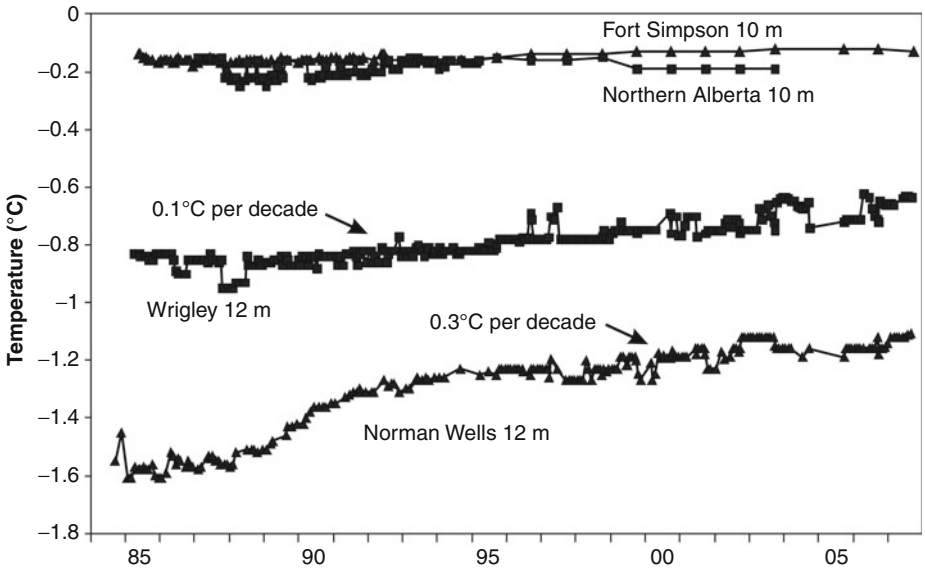

Permafrost and Climate Interactions, Figure 3 Trends in permafrost temperatures between 1984 and 2007 at depths of 10–12 m, at sites in the south and central Mackenzie Valley, NWT, Canada. The rate of ground temperature increase is greater for sites having colder thicker (greater than 30 m) permafrost (Norman Wells, 65°52′N 126°26′W and Wrigley, 63°13′N 123°26′W) than those located further south (Fort Simpson, 61°52′N 121°21′W and Northern Alberta, 59°32′N 119°37 W) where permafrost is at temperatures near 0°C and less than 15 m in thickness (updated from Romanovsky et al., 2007).

permafrost at a depth of 15 m warmed by about 0.1°C/year over the last two to three decades (Smith et al., 2010). Similar recent increases in shallow ground temperatures have also been observed in other Arctic regions such as Scandinavia and Svalbard (Harris and Isaksen, 2008).

Observed changes in permafrost temperature are generally consistent with trends in air temperature. However, snow cover variations are also an important factor. Osterkamp (2008), for example, found that warming of permafrost in the late 1980s and early 1990s in Alaska may be primarily a response to a series of thicker snow covers. Similarly, Taylor et al. (2006) suggest that in the high Arctic, changes in snow cover may counteract changes in air temperature so that permafrost temperatures may increase during periods of higher snow cover but lower air temperature.

Changes in active layer thickness have also been observed over the past 10–20 years. However, these changes in active layer often reflect shorter-term fluctuations in climate (compared to the deeper permafrost temperatures) and therefore the record shows a great deal of interannual variability making it difficult to characterize longer-term trends from the shorter records. Russian observations between 1956 and 1990 indicate an average increase in active layer thickness of 21 cm (Frauenfeld et al., 2004) with more recent observations at a limited number of sites indicating a general deepening of thaw (Mazhitova et al., 2008). While there is some evidence of increases in thaw depths in other regions since the 1990s, there is much variation with maximum thaw depths being observed in extreme warm years such as 1998 in Alaska and northwestern Canada (e.g., Osterkamp, 2008; Smith et al., 2009), consistent with responses in other cryospheric components (Atkinson et al., 2006), and in the warm summers of 2002 and 2003 in Europe (Harris et al., 2003).

There is also evidence of permafrost degradation and in some cases complete loss of permafrost in the southern portion of the permafrost zone since the mid-twentieth century (Lemke et al., 2007). Degradation of frozen peatlands has been observed in the southern Canadian permafrost zone in the southern Mackenzie valley, northern Saskatchewan, Manitoba, and Quebec (e.g., Beilman et al., 2001; Beilman and Robinson, 2003; Camill, 2005; Vallée and Payette, 2007; Fortier and Aubé-Maurice, 2008; Smith et al., 2008). Loss of permafrost is also occurring on the Tibetan Plateau, with the lower altitudinal limit of permafrost moving upward by 25 m since 1975 in the Kunlun Mountains (Nan et al., 2003).

The various interactions between climate and permafrost discussed above need to be considered in the development of models to predict how permafrost conditions may change in the future in response to climate change. A variety of empirical, physically based, deterministic and probabilistic models have been developed to predict future permafrost conditions at local, regional, and circumpolar scales (Riseborough et al., 2008). These models are generally driven by the temperature and precipitation outputs from global circulation models. Although the various modelling studies generally predict warmer ground conditions and increased active layer thickness (e.g., Romanovsky et al., 2007; Woo et al., 2007; Riseborough

et al., 2008), the accuracy of results is largely limited by the availability of information on the various environmental factors (e.g., vegetation, organic layer thickness, snow cover, and soil conditions) which influence the relationship between changes in air temperature and the ground thermal regime.

Changes in permafrost conditions can have impacts on both natural and human systems. Warming and thawing of permafrost especially if it is ice-rich can lead to ground instability, such as differential settlement or slope movements, which can have implications for the performance and integrity of infrastructure (e.g., Romanovsky et al., 2007; Prowse et al., 2009). For several years, engineers have developed several risk management approaches and design, construction, and operational techniques to deal with the challenges presented by the permafrost environment including warming and thawing of the ground resulting from construction and operation of infrastructure. These techniques (possibly with modification) along with an understanding of how permafrost conditions may change in response to a changing climate will be required to adapt to future conditions (e.g., Prowse et al., 2009).

Summary

The existence of permafrost and its thermal condition depend largely on the atmospheric climate. However, this relationship between permafrost and climate is modulated by a number of local factors which influence the microclimate at a particular site. Variations in permafrost thickness, temperature, and lateral extent have occurred in the past and will continue in the future, over periods of several decades to centuries to millennia, in response to changes in climate across the entire permafrost region. The magnitude and rate of these permafrost changes will vary regionally, as a function of the regional climatic changes, as well as the regional soil, ground ice, and microclimatic conditions.

Bibliography

Allen, D., Michel, F., and Judge, A., 1988. Paleoclimate and permafrost in the Mackenzie Delta. In *Proceedings of the Fifth International Conference on Permafrost*, 2–5 August 1988, Trondheim, Norway. Norway: Tapir, pp. 33–38.

Ananjeva, G. V., Melnikov, E. S., and Ponomareva, O. E., 2003. Relict permafrost in the central part of western Siberia. In Phillips, M., Springman, S. M., and Arenson, L. U. (eds.), *Proceedings of Eight International Conference on Permafrost*. Zurich: A.A. Balkema, pp. 5–8.

Atkinson, D. E., Brown, R., Alt, B., Agnew, T., Bourgeois, J., Burgess, M., Duguay, C., Henry, G., Jeffers, S., Koerner, R., Lewkowicz, A. G., McCourt, S., Melling, H., Sharp, M., Smith, S., Walker, A., Wilson, K., Wolfe, S., Woo, M.-K., and Young, K., 2006. Canadian cryospheric response to an anomalous warm summer: a synthesis of the Climate Change Action Fund Project "The state of the Arctic Cryosphere during the extreme warm summer of 1998". *Atmosphere-Ocean*, **44**, 347–375.

Beilman, D. W., and Robinson, S. D., 2003. Peatland permafrost thaw and landform type along a climate gradient. In Phillips, M., Springman, S. M., and Arenson, L. U. (eds.), *Proceedings of Eighth International Conference on Permafrost*. Zurich: A.A. Balkema, pp. 61–65.

Beilman, D. W., Vitt, D. H., and Halsey, L. A., 2001. Localized permafrost peatlands in western Canada: definition, distributions, and degradation. *Arctic, Antarctic, and Alpine Research*, **33**, 70–77.

Brown, R. J. E., and Pewe, T. L., 1973. Distribution of permafrost North America and its relationship to the environment: a review, 1963–1973. In *Proceedings Second International Conference on Permafrost, North American Contribution, 13–28 July 1973, Yakutsk*. Washington, DC: National Academy of Sciences, pp. 71–100.

Burgess, M. M., and Smith, S. L., 2000. Shallow ground temperatures. In Dyke, L. D., and Brooks, G. R. (eds.), *The Physical Environment of the Mackenzie Valley, Northwest Territories: a Baseline for the Assessment of Environmental Change*. Geological Survey of Canada Bulletin, Vol. 547, pp. 89–103.

Burn, C. R., and Kokelj, S. V., 2009. The environment and permafrost of the Mackenzie Delta area. *Permafrost and Periglacial Processes*, **20**(2), 83–105.

Burn, C. R., Michel, F. A., and Smith, M. W., 1986. Stratigraphic isotopic, and mineralogical evidence for an early Holocene thaw unconformity at Mayo, Yukon Territory. *Canadian Journal of Earth Sciences*, **23**, 794–803.

Camill, P., 2005. Permafrost thaw accelerates in boreal peatlands during late-20th century climate warming. *Climatic Change*, **68**, 135–152.

Danilov, I. D., Komarov, I. A., and Vlasenko, A. Y., 1998. Pleistocene-Holocene permafrost of the East Siberian Eurasian Arctic Shelf. In Lewkowicz, A. G., and Allard, M. (eds.), *Proceedings of the Seventh International Conference on Permafrost, 23–27 June 1998, Yellowknife*. Québec: Université Laval, Collection Nordicana, No.57, pp. 207–212.

Delisle, G., 1998. Numerical simulation of offshore permafrost development in the Laptev sea, Siberia. In Lewkowicz, A. G., and Allard, M. (eds.), *Proceedings of the Seventh International Conference on Permafrost, 23–27 June 1998, Yellowknife*. Québec: Université Laval, Collection Nordicana, No.57, pp. 213–219.

Fortier, R., and Aubé-Maurice, B., 2008. Fast permafrost degradation near Umiujaq in Nunavik (Canada) since 1957 assessed from time-lapse aerial and satellite photographs. In Kane, D. L., and Hinkel, K. M. (eds.), *Proceedings Ninth International Conference on Permafrost*. Fairbanks: Institute of Northern Engineering, University of Alaska Fairbanks, pp. 457–462.

Frauenfeld, O. W., Zhang, T., Barry, R. G., and Gilichinsky, D., 2004. Interdecadal changes in seasonal freeze and thaw depths in Russia. *Journal of Geophysical Research*, **109**(D05101), 12, doi:10.1029/2003JD004245.

French, H. M., 2007. *The Periglacial Environment*, 3rd edn. West Sussex: Wiley, p. 458.

Halsey, L. A., Vitt, D. H., and Zoltai, S. C., 1995. Disequilibrium response of permafrost in Boreal Continental Western Canada to climate change. *Climatic Change*, **30**, 57–73.

Harris, C., and Isaksen, K., 2008. Recent warming of European permafrost: evidence from borehole monitoring. In Kane, D. L., and Hinkel, K. M. (eds.), *Proceedings Ninth International Conference on Permafrost*. Fairbanks: Institute of Northern Engineering, University of Alaska Fairbanks, pp. 655–661.

Harris, C., Muhll, D. V., Isaksen, K., Haeberli, W., Sollid, J. L., King, L. H., Holmlund, P., Dramis, F., Guglielmin, M., and Palacios, D., 2003. Warming permafrost in European mountains. *Global and Planetary Change*, **39**, 215–2254.

Kanigan, J. C. N., Burn, C. R., and Kokelj, S. V., 2008. Permafrost response to climate warming south of treeline, Mackenzie Delta, Northwest Territories, Canada. In Kane, D. L., and Hinkel, K. M. (eds.), *Proceedings Ninth International Conference on*

Permafrost. Fairbanks: Institute of Northern Engineering, University of Alaska Fairbanks, pp. 901–906.

Lemke, P., Ren, J., Alley, R. B., Allison, I., Carrasco, J., Flato, G., Fujii, Y., Kaser, G., Mote, P., Thomas, R. H., and Zhang, T., 2007. Observations: changes in snow, ice and frozen ground. In Solomon, S., Qin, D., Manning, M., Chen, Z., Marquis, M., Averyt, K. B., Tignor, M., and Miller, H. L. (eds.), *Climate Change 2007: The Physical Science Basis. Contribution of Working Group 1 to the Fourth Assessment Report of the Intergovernmental Panel on Climate Change*. Cambridge, UK and New York, USA: Cambridge University Press.

Lisitsyna, O. M., and Romanovskii, N. N., 1998. Dynamics of permafrost in northern Eurasia during the last 20,000 years. In Lewkowicz, A. G., and Allard, M. (eds.), *Proceedings of the Seventh International Conference on Permafrost, 23–27 June 1998, Yellowknife*. Québec: Université Laval, Collection Nordicana, No.57, pp. 675–681.

Mazhitova, G., Malkov, G., Chestnykh, O., and Zamolodchikov, D., 2008. Recent decade thaw-depth dynamics in the European Russian Arctic, based on Circumpolar Active Layer Monitoring (CALM) data. In Kane, D. L., and Hinkel, K. M. (eds.), *Proceedings Ninth International Conference on Permafrost*. Fairbanks: Institute of Northern Engineering, University of Alaska Fairbanks, pp. 1155–1160.

Nan, Z., Gao, Z., Li, S., and Wu, T., 2003. Permafrost changes in the northern limit of permafrost on the Qinghai-Tibet plateau in the last 30 years. *Acta Geographica Sinica*, **58**, 817–823.

Nicholson, F. H., and Granberg, H. B., 1973. Permafrost and snow cover relationships near Schefferville, In *Proceedings of the Second International Conference on Permafrost, North American Contribution, 13–28 July 1973, Yakutsk*. Washington, DC: National Academy of Sciences, pp. 151–158.

Osterkamp, T. E., 2008. Thermal state of permafrost in Alaska during the fourth quarter of the twentieth century. In Kane, D. L., and Hinkel, K. M. (eds.), *Proceedings Ninth International Conference on Permafrost, 29 June–3 July 2008, Fairbanks*. Fairbanks: Institute of Northern Engineering, University of Alaska Fairbanks, Vol. 2, pp. 1333–1338.

Overduin, P. P., Rachold, V., and Grigoriev, M. N., 2008. The state of subsea permafrost in the western Laptev nearshore zone. In Kane, D. L., and Hinkel, K. M. (eds.), *Proceedings Ninth International Conference on Permafrost, 29 June–3 July 2008, Fairbanks*. Fairbanks: Institute of Northern Engineering, University of Alaska Fairbanks, pp. 1345–1350.

Prowse, T. D., Furgal, C., Chouinard, R., Melling, H., Milburn, D., and Smith, S. L., 2009. Implications of climate change for economic development in Northern Canada: energy, resource, and transportation sectors. *Ambio*, **38**, 272–281.

Riseborough, D. W., 1990. Soil latent heat as a filter of the climate signal in permafrost. In *Proceedings of the Fifth Canadian Permafrost Conference, 5–9 June 1990*, Québec. Québec: Université Laval, Collection Nordicana No. 54, pp. 199–205.

Riseborough, D., Shiklomanov, N., Etzelmuller, B., Gruber, S., and Marchenko, S., 2008. Recent advances in permafrost modelling. *Permafrost and Periglacial Processes*, **19**, 137–156.

Romanovsky, V. E., Gruber, S., Instanes, A., Jin, H., Marchenko, S. S., Smith, S. L., Trombotto, D., and Walter, K. M., 2007. Frozen ground, Chap. 7. In UNEP (ed.), *Global Outlook for Ice & Snow*. Nairobi: United Nations Environment Program, pp. 181–200.

Romanovsky, V. E., Drozdov, D. S., Oberman, N. G., Malkova, G. V., Kholodov, A. L., Marchenko, S. S., Moskalenko, N. G., Sergeev, D. O., Ukrainsteva, D. G., Abramov, A. A., and Vasiliev, A. A., 2010. Thermal state of permafrost in Russia. *Permafrost and Periglacial Processs*, **21**, 106–116.

Sharkhuu, N., Sharkhuu, A., Romanovsky, V. E., Yoshikawa, K., Nelson, F. E., and Shiklomanov, N. I., 2008. Thermal state of permafrost in Mongolia. In Kane, D. L., and Hinkel, K. M. (eds.), *Proceedings Ninth International Conference on Permafrost, 29 June–3 July 2008, Fairbanks*. Fairbanks: Institute of Northern Engineering, University of Alaska Fairbanks, pp. 1633–1638.

Sladen, W., Dyke, L. D., and Smith, S. L., 2009. Permafrost at York Factory National Historic Site of Canada, Manitoba, Canada. *Geological Survey of Canada Current Research*, **2009–4**, 10 p.

Smith, S. L., Burgess, M. M., and Riseborough, D. W., 2008. Ground temperature and thaw settlement in frozen peatlands along the Norman Wells pipeline corridor, NWT Canada: 22 years of monitoring. In Kane, D. L., and Hinkel, K. M. (eds.), *Proceedings Ninth International Conference on Permafrost, 29 June–3 July 2008, Fairbanks*. Fairbanks: Institute of Northern Engineering, University of Alaska Fairbanks, pp. 1665–1670.

Smith, S. L., Wolfe, S. A., Riseborough, D. W., and Nixon, F. M., 2009. Active-layer characteristics and summer climatic indices, Mackenzie Valley, Northwest Territories, Canada. *Permafrost and Periglacial Processes*, **20**, 201–220.

Smith, S. L., Romanovsky, V. E., Lewkowicz, A. G., Burn, C. R., Allard, M., Clow, G. D., Yoshikawa, K., and Throop, J., 2010. Thermal state of permafrost in North America – a contribution to the International Polar Year. *Permafrost and Periglacial Processes*, **21**, 117–135.

Taylor, A. E., 1991. Marine transgression, shoreline emergence: evidence in seabed and terrestrial ground temperatures of changing relative sea levels, Arctic Canada. *Journal of Geophysical Research*, **96**(B4), 6893–6909.

Taylor, A. E., Wang, K., Smith, S. L., Burgess, M. M., and Judge, A. S., 2006. Canadian Arctic Permafrost Observatories: detecting contemporary climate change through inversion of subsurface temperature time-series. *Journal of Geophysical Research*, **111**(B02411), 14, doi:10.1029/2004JB003208.

Vallée, S., and Payette, S., 2007. Collapse of permafrost mounds along a subarctic river over the last 100 years (northern Québec). *Geomorphology*, **90**, 162–170.

Vardy, S. R., Warner, B. G., and Aravena, R., 1998. Holocene climate and the development of a subarctic peatland near Inuvik, Northwest Territories, Canada. *Climatic Change*, **40**, 285–313.

Vitt, D. H., Halsey, L. A., and Zoltai, S. C., 1994. The bog landforms of continental western Canada in relation to climate and permafrost patterns. *Arctic and Alpine Research*, **26**, 1–13.

Woo, M.-K., Mollinga, M., and Smith, S. L., 2007. Climate warming and active layer thaw in the boreal and tundra environments of the Mackenzie Valley. *Canadian Journal of Earth Sciences*, **44**, 733–743.

Zhao, L., Wu, T., Ding, Y., and Xie, C., 2008. Monitoring permafrost changes on the Qinghai-Tibet plateau. In Kane, D. L., and Hinkel, K. M. (eds.), *Proceedings Ninth International Conference on Permafrost, 29 June–3 July 2008, Fairbanks*. Fairbanks: Institute of Northern Engineering, University of Alaska Fairbanks, pp. 2071–2076.

Zoltai, S. C., 1993. Cyclic development of permafrost in the peatlands of Northwestern Alberta, Canada. *Arctic and Alpine Research*, **25**, 240–246.

Zoltai, S. C., 1995. Permafrost distribution in peatlands of west-central Canada during the Holocene warm period 6,000 years BP. *Géographie Physique et Quaternaire*, **49**, 45–54.

Cross-references

Perennially Frozen Ground
Permafrost
Permafrost Modeling
Thermokarst

PERMAFROST MODELING

Daniel Riseborough
Geological Survey of Canada, Ottawa, ON, Canada

Definition

Permafrost modeling is the use of quantitative methods (analytical, numerical, or empirical) to predict the thermal condition of the ground (temperature or frozen state) in environments where permafrost may be present. Permafrost models may be used to predict the presence or absence of permafrost or to predict ground temperature in one, two, or three dimensions, including changes over time.

Introduction

Permafrost occurs where atmospheric processes and earth material thermal properties combine to permit the ground to remain at or below 0°C for at least 2 years. Existing beneath a ground surface layer that undergoes thawing and freezing annually (the *active layer*), permafrost cannot be detected directly at the surface. Determining the distribution of permafrost in many settings requires extensive field work. Permafrost models are used to predict permafrost conditions where direct field evidence is lacking, or in hypothetical cases such as under a future climate or altered environment.

Models

Permafrost models can be classified as process-based (*analytical* or *numerical*) or *empirical* models. Permafrost models are usually formulated as point or one-dimensional models, often used within spatial models to map permafrost distribution at local to continental and global scales. While most analytical and empirical permafrost models assume a static relationship between permafrost conditions and model parameters, the transient response of permafrost to change is usually studied using numerical models.

Permafrost models link atmospheric climate to ground temperature. The simplest empirical models make a direct link between mean annual air and the presence of permafrost. Many models divide the year into freezing and thawing seasons, using season-long degree-day totals above or below 0°C (freezing and thawing indices) to summarize the annual regime. Models of intermediate complexity may require several parameters to account for the various influences on ground surface temperature. For example, field-based empirical relationships between freezing and thawing indices in the air and at the ground surface (e.g., *n* factors) allow surface temperature to be estimated for areas with similar surface characteristics. The most complete numerical models calculate ground surface temperature by solving the surface energy balance, including snow cover in winter, requiring extensive meteorological inputs; this surface temperature drives calculations of temperature below the surface.

Analytical models

Analytical permafrost models are mathematical functions based on the physics of heat transfer, especially conduction with phase change (freezing and thawing). While real-world environments do not meet the conditions of the few exact analytical models describing the thermal state of the ground when freezing or thawing occurs, several approximate analytical models have been developed using simplifying assumptions. Several permafrost models (e.g., Frost Index, Kudriavtsev, and TTOP models) employ simple models of freezing and thawing to predict the presence or the temperature of permafrost in equilibrium conditions. Models that ignore phase change can be useful, especially in environments with low soil moisture.

Numerical models

Numerical (geothermal) permafrost models can represent relatively complex conditions with relatively small errors. Numerical models divide continuous time into finite time steps and continuous space into finite pieces, creating an array of much simpler conditions that can be solved approximately (Zhang et al., 2008). Numerical models can be implemented in one, two, or (rarely) three dimensions. Earth materials are represented by an array of elements (or nodes) and continuous temperature is represented by temperatures at discrete points, truncated at the model boundaries. Numerical schemes that can solve freezing and thawing problems must deal with the latent heat of fusion. In mountain environments with low porosity rock, the direct effects of freezing and thawing can be small enough to ignore in some conditions. Nonconductive processes such as convection are often ignored due to the low permeability of frozen soil.

Once initial ground temperature conditions and thermal properties are specified, numerical simulations proceed by specifying the temperature (or heat flow) conditions at the model boundaries for each time step. Snow cover may be treated as a distinct layer, or treated as a seasonal transfer function such as the *n* factor. The geothermal heat flux is typically assumed for the lower boundary.

Empirical models

Empirical permafrost models use field-based relationships between permafrost conditions and measurable environmental parameters (such as mean annual air temperature, elevation, potential solar radiation, vegetation type, snow cover, soil and moisture conditions, etc.) to predict permafrost presence or absence. Empirical permafrost models are commonly used in mountainous terrain where large variations in conditions over relatively short distances make it difficult to model using process-based approaches (Harris et al., 2009). Empirical models are developed for particular locations, so their predictive relationships may not give accurate predictions in other regions.

Models based on the BTS (Basal Temperature of Snow) method are widely used in mountain environments, based on the correlation between the ground surface temperature beneath deep snow cover measured late in winter and the presence of permafrost (Lewkowicz and Bonnaventure, 2008). While the correlation between BTS values and permafrost conditions is only moderately strong, BTS is easy to measure, allowing many point measurements can be taken quickly, allowing development of statistically significant relationships with environmental conditions.

Spatial models

Spatial permafrost models aggregate the results of analytical, empirical, or numerical models to predict permafrost distribution at regional to global scales. Spatial models rely on map-based and remote sensing data to supply the model input parameters, and may use climate data from a meteorological network or from climate simulation results. Early spatial models used simple analytical permafrost models, but numerical models are becoming more common within spatial models as they allow for simulation of the transient behavior of permafrost in response to a changing environment.

Summary

Permafrost models include a range of approaches that are capable of predicting the current distribution and future evolution of permafrost conditions at local to global scales, useful for local to global environmental assessments. The past decade has seen the development of spatial models capable of predicting the transient response of permafrost to changing climate. As models and the data necessary to work with them continue to improve, future advancements may integrate permafrost dynamics with environmental evolution.

Bibliography

Harris, C., Arenson, L. U., Christiansen, H. H., Etzelmüller, B., Frauenfelder, R., Gruber, S., et al., 2009. Permafrost and climate in Europe: monitoring and modelling thermal, geomorphological and geotechnical responses. *Earth Science Reviews*, **92**(3–4), 117–171.

Lewkowicz, A. G., and Bonnaventure, P. P., 2008. Interchangeability of mountain permafrost probability models, northwest Canada. *Permafrost and Periglacial Processes*, **19**(1), 49–62.

Riseborough, D., Shiklomanov, N., Etzelmüller, B., Gruber, S., and Marchenko, S., 2008. Recent advances in permafrost modelling. *Permafrost and Periglacial Processes*, **19**(2), 137–156.

Zhang, Y., Carey, S. K., and Quinton, W. L., 2008. Evaluation of the algorithms and parameterizations for ground thawing and freezing simulation in permafrost regions. *Journal of Geophysical Research, D: Atmospheres*, **113**(17), D17116.

Cross-references

Permafrost
Permafrost and Climate Interactions
Surface Energy Balance

PERMANENT/PERPETUAL SNOW LINE

Monohar Arora
National Institute of Hydrology (NIH), Roorkee, UA, India

The altitude above which or the latitude beyond which snow does not melt even during summer is usually called the permanent snow line. Factors that affect the location of the snow line are prevailing weather conditions, particularly solid precipitation and temperature. In the Himalayan region, the permanent snow line varies from west to east, but can be considered as 4,500 m above mean sea level. Beyond the tropics, the snow line becomes progressively lower as the latitude increases, to just below 3,000 m in the Alps and falling all the way to sea level itself at the ice caps near the poles.

PHYSICAL PROPERTIES OF SNOW

Florent Domine
Laboratoire de Glaciologie et Géophysique de l'Environnement, CNRS, Saint Martin d'Hères, France

Definition

Snow Crystal Structure (qv). Ice crystals formed in the atmosphere by the condensation of water vapor or the freezing of water droplets (i.e., riming).
Snow cover or snow pack or snowpack. The accumulation of snow crystals on the ground.
Snow (qv). Can refer either to snow crystals in the atmosphere or to snow on the ground. Here snow means snow on the ground, and the discussion is limited to dry seasonal snow.
Physical properties of snow. The range of values that characterize the physical behavior of snow.

Introduction

Dry snow on the ground is a porous medium formed of air, ice crystals, small amounts of chemical impurities, and sometimes also containing microorganisms and macroscopic impurities in the form of vegetal and geological debris. Falling snow crystals have a wide range of shapes such as plates, dendritic crystals, columns, and irregular crystals, and their deposition conditions are affected by variables such as temperature, wind speed, and state of the surface. The density of snow as it deposits onto the ground is therefore highly variable, and usually in the range 10–200 kg m^{-3}, with the result that other physical properties also show wide ranges of values.

Because ice has a high vapor pressure (165 Pa at −15°C, 610 Pa at 0°C), the vertical temperature gradient that forms within the snowpack generates sublimation of crystals and condensation of water vapor that modify the size and shape of snow crystals, resulting in changes

in macroscopic physical variables such as *Snow Density* (qv), albedo, thermal conductivity, permeability, and hardness. These physical changes have formed the basis for the definition of *Snow Metamorphism* (qv) (Colbeck, 1982). One further distinguishes "dry metamorphism" that takes place at $T < 0°C$ from "wet metamorphism" that takes place at 0°C and where the presence of liquid water is observed.

Impurities contained in snow can be chemically inert such as mineral dust particles, but *Chemical Processes in Snow and Ice* (qv) such as the photolysis of impurities can produce changes in the *Chemical Composition of Snow, Ice, and Glaciers* (qv). These chemical processes are affected by the physical properties of the snow. We review here the ranges of values of selected snow physical properties, how they are affected by climatic variables, and briefly discuss how they in turn affect snow chemical properties.

Snow metamorphism and climatic variables

As detailed by Sturm et al. (1995), climatic variables, and especially wind speed, temperature, and the amount of precipitation determine the conditions of snow metamorphism, and especially the temperature gradient in the snowpack. At the beginning of the winter season, the ground is at 0°C, and the atmosphere may have already cooled down to −30°C, so that temperature gradients in excess of 100°C m^{-1} can exist in the thin early season snowpack. These generate large water vapor fluxes that produce sublimation and condensation of snow crystals, leading to the formation of faceted crystals that turn into depth hoar crystals once their size exceeds about 1–2 mm (Akitaya, 1974). This process is especially efficient in the boreal forest, where snow is sheltered from wind and remains of low density, therefore facilitating water vapor transport and the growth of large crystals (Sturm and Benson, 1997; Taillandier et al., 2006). In the Arctic tundra, the process also takes place but less efficiently because the higher wind speeds result in denser snow. In late winter and spring, temperature gradients have decreased because the snowpack is thicker and the ground has cooled, with the result that depth hoar cannot form anymore on the tundra, and the basal depth hoar layer is then topped by a hard windpack formed of small highly sintered rounded grains (Dominé et al., 2002).

In midlatitude regions, conditions are very different with warmer temperatures and more abundant precipitation. Depth hoar forms less frequently, small rounded grains predominate, and melt-freeze structures are common (Sturm et al., 1995). Figure 1 illustrates the layering structure for three different snowpack types that form in the boreal forest (taiga), tundra, and maritime regions. Figure 2 shows clusters of crystals sampled in fresh snow, layers of small rounded grains and Arctic depth hoar. The

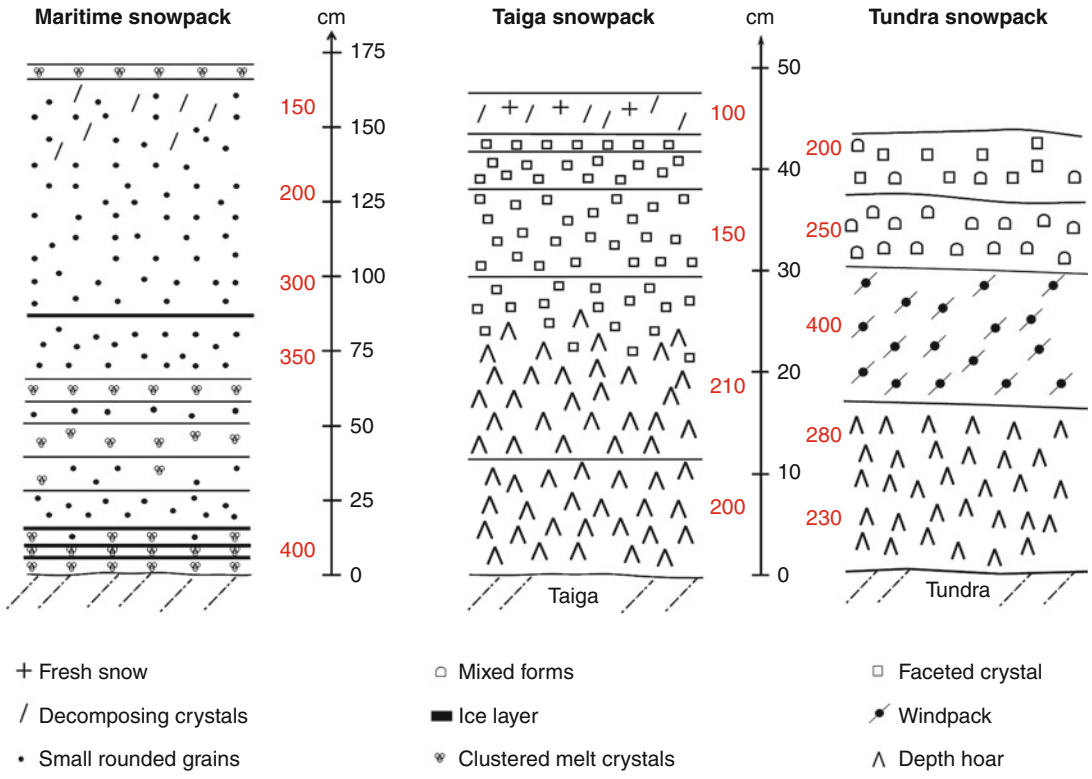

Physical Properties of Snow, Figure 1 Typical stratigraphies of the maritime, taiga, and tundra snowpacks. Bold numbers next to the stratigraphies are density values, in kg m^{-3}.

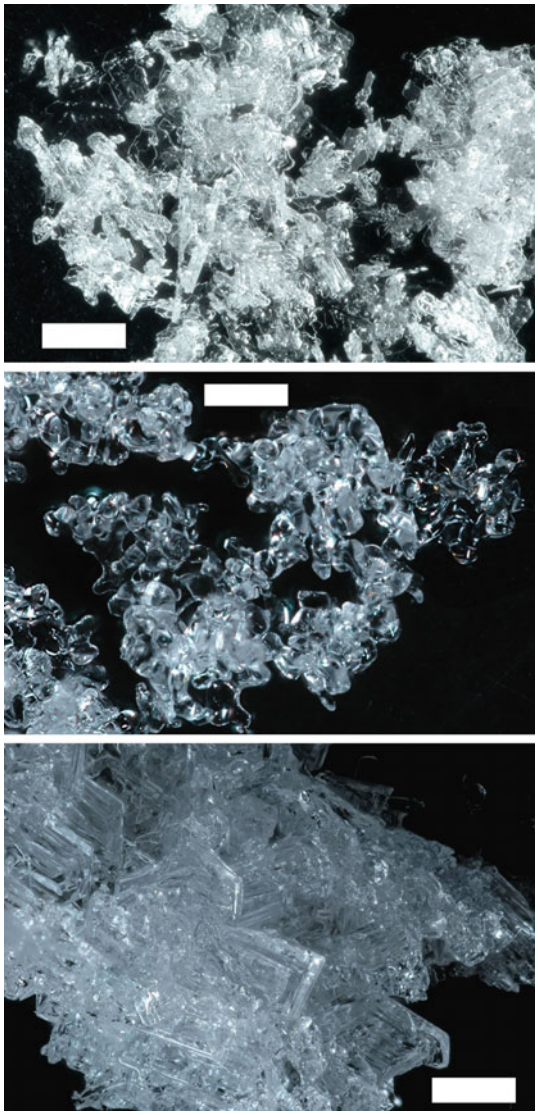

Physical Properties of Snow, Figure 2 Photomicrographs of clusters of snow crystals sampled on the ground. *Top*: Fresh Arctic snow comprised of dendritic crystals and columns, deposited under windy conditions. *Middle*: 2-weeks old snow sampled in a low elevation area of the French Alps, 2 weeks after deposition, in a snowpack classified as maritime. Precipitating particles cannot be recognized; grains are rounded and have started to sinter. *Bottom*: Arctic depth hoar crystals, of density 300 kg m^{-3}, about 3 months old. In this high density depth hoar, grains have remained small and the sample is unusually cohesive for depth hoar. Scale bars: 1 mm.

structures of these snow layers are quite dissimilar, and very different physical properties are expected in snow, as determined by climatic conditions.

Physical properties of snow

Variables such as density, albedo, light *e*-folding depth, specific surface area (SSA), crystal size and shape, thermal conductivity, permeability, diffusivity, and shear resistance are required for a complete physical description of the snowpack. These are reviewed in several publications such as Domine et al. (2008) and Petrovic (2003). This entry will only discuss density, SSA, albedo, and thermal conductivity.

Snow density

Density is the most widely studied snow physical property. It is defined as the mass per unit volume, and it is usually measured in the field or the laboratory by weighing a sample of known volume. Even though density is a very intuitive concept and many attempts have been made to correlate most physical properties to density, it is clear that density alone cannot be used as a descriptor of other snow properties.

Snow density shows a wide range of values: from less than 10 kg m^{-3} for fresh cold dendritic snow to more than 600 kg m^{-3} for very hard windpacks and snow subjected to numerous melt-freeze cycles. Physical processes producing density changes include compaction by the weight of subsequent layers, wind-drifting, and dry and wet metamorphism. Precipitated snow (density in the range 10–200 kg m^{-3}) is subject to settling and compaction. Wind-drifted snow often forms thick layers of small rounded grains that subsequently sinter well to form hard windpacks with densities 300–600 kg m^{-3}. High temperature gradient metamorphism produce upward water vapor fluxes that compensate the effects of densification, so that density in the boreal forest snowpack is vertically fairly constant around 200 kg m^{-3} (Sturm and Benson, 1997; Taillandier et al., 2006). The appearance of liquid water usually leads to crystal rounding, compaction, and density increase. The range of snow density for a variety of snow types are reported in Table 1.

Specific surface area and grain size

Another intuitive snow property is grain size. However, the definition is unclear and observer-dependent. For example, what is the size of a dendritic crystal 5 mm in diameter but 40 μm in thickness? Likewise, what is the size of a 10 mm hollow depth hoar crystal with 200 μm thick walls? At present, it is more and more accepted that specific surface area (SSA) is physically more meaningful and should be used preferentially to grain size. SSA is the surface area per mass unit. Snow SSA values range from over 150 m^2 kg^{-1} for fresh snow to less than 2 m^2 kg^{-1} for melt-freeze crusts (Domine et al., 2007). If snow crystals are assumed to be spheres, then SSA = $6/\rho_{ice}\, d$, where d is the sphere diameter and ρ_{ice} is the density of pure ice (917 kg m^{-3} at 0°C). Thus, the above SSA range translates to sphere diameters of 44 μm to 3.2 mm. This diameter is called the *effective grain size*, it is objective and should be used preferentially to cursory intuitive observations. Snow SSA usually decreases during metamorphism, and adsorbed impurities are therefore released to the gas

Physical Properties of Snow, Table 1 Typical ranges of values of selected physical variables for the most frequent snow crystal types in surface snow (top 50 cm). Data from Domine et al. (2008) and references therein

Physical variable	Fresh snow	Rounded grains, maritime snowpack	Rounded grains, windpack	Depth hoar	Melt-freeze layers
Density (kg m^{-3})	10–200	150–350	300–600	150–320	150–450
Specific surface area (m^2 kg^{-1})	35–160	11–30	15–38	7–22	2–5
Visible albedo (0.38–0.78 μm) pure snow	0.98–0.99	0.96–0.975	0.965–0.978	0.95–0.97	0.94
Thermal conductivity (W m^{-1} K^{-1})	0.025–0.12	0.08–0.3	0.2–0.6	0.03–0.15	0.1–0.6

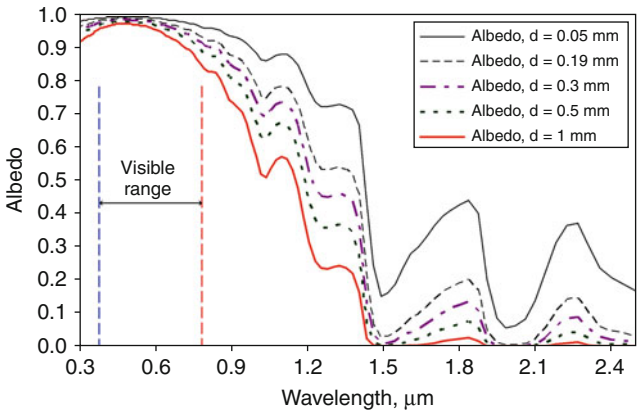

Physical Properties of Snow, Figure 3 Spectral albedo of snow calculated for samples made of spheres of diameter d: 0.05, 0.19, 0.3, 0.5, and 1 mm, corresponding to SSAs of 131, 34.4, 21.8, 13.1, and 6.5 m^2 kg^{-1}. The range used to obtain the visible albedo values in Table 1 is shown. Calculations were made using the DISORT code of Stamnes et al. (1988), with diffuse light conditions.

phase, so that their concentration in snow decreases (Taillandier et al., 2006).

Snow albedo

SSA, or effective grain size, is useful to evaluate snow optical properties. In particular, the calculation of snow albedo, that is, the hemispherical reflectance, requires the knowledge of snow SSA (Grenfell and Warren, 1999). Snow albedo is determined by scattering and absorption. In the visible, ice is a very weak absorber: its absorption coefficient is very difficult to measure but could be lower than 10^{-3} m^{-1} at 390 nm (Warren et al., 2006). As a result, absorption of visible radiation by snow is determined by impurities such as soot particles, whose concentrations in snow are highly variable (Flanner et al., 2007). Figure 3 shows calculated albedos for pure snow. It is obvious that in the visible, albedo depends little on effective grain size. This is because the probability that an incident photon is absorbed by ice is so low that it can undergo a long and tortuous path in the snow until it is reflected. This will almost not be influenced by the number of reflections onto snow crystals. In the IR where absorption by ice becomes important, a strong dependence of albedo on SSA appears, because photons are absorbed after a short pathlength in ice, and smaller grains increase the number of reflections and the probability that the photon will exit the snow. The albedo dependence on SSA in the IR is used to infer effective grain size from remote sensing measurements of snow, for example using satellites (Kokhanovsky and Schreier, 2009).

The difference is often made between spectral albedo, that is, the hemispherical reflectance at a given wavelength, and broad-band albedo, that is, the hemispherical reflectance over a given spectral range, usually the visible range or the range of the solar spectrum. Table 1 shows the visible albedo of several snow types, assumed to be free of absorbing impurities.

Thermal conductivity of snow

The thermal conductivity of snow, k_T, is an essential environmental and climatic variable. Snow insulates sea ice from the cold atmosphere and limits sea ice growth (Fichefet et al., 2000). Likewise, snow limits ground freezing and permafrost extent (Zhang, 2005). Snow k_T is very strongly dependent on snow structure, because diffusive thermal transport mostly takes place through the network of interconnected ice crystals (Sturm et al., 1997). Fresh snow k_T can be as low as 0.025 W m^{-1} K^{-1}, that is, more insulating than styrofoam, while very hard windpacks or melt-freeze layers have values as high as 0.65 W m^{-1} K^{-1} (Sturm et al., 1997), similar to light concrete. In models of sea ice growth, an average value k_T = 0.31 W m^{-1} K^{-1} is often used (Fichefet et al., 2000). Values of k_T for different snow types are shown in Table 1.

The value of snow k_T determines the temperature gradient in the snowpack, and therefore the rate of chemical reactions. It also determines the temperature gradient, and therefore the intensity of sublimation-condensation cycles that can release dissolved impurities to the gas phase. This further illustrates that physical and chemical properties of snow are coupled.

Summary

Snow is a porous medium made mostly of air and ice, whose *transformation at the Earth's surface* (qv *Transformations of Snow at the Earth's Surface and its Climatic and Environmental Consequences*) is greatly affected by climatic variables. Because a snow cover is present in

a wide range of climates, from temperate to polar, the physical properties of snow show wide ranges of values: density values varies by a factor of 60, thermal conductivity values by a factor of 25, specific surface area (and effective grain size) by a factor of 80. These properties in turn also affect the reactivity of impurities contained in snow, so that snow physical and chemical properties are linked. Snow therefore interacts with environmental chemistry and climate. It is an environmental compartment that deserves detailed description for complete studies in natural sciences.

Bibliography

Akitaya, E., 1974. Studies on depth hoar. *Contributions from the Institute of Low Temperature Science, Series A*, **26**, 1–67.

Colbeck, S. C., 1980. Thermodynamics of snow metamorphism due to variations in curvature. *Journal of Glaciology*, **26**, 291–301.

Colbeck, S.C., 1982. An overview of seasonal snow metamorphism. *Reviews of Geophysics*, **20**, 45–61.

Domine, F., Taillandier, A.-S., and Simpson, W. R., 2007. A parameterization of the specific surface area of snow in models of snowpack evolution, based on 345 measurements. *Journal of Geophysical Research*, **112**, F02031, doi:10.1029/2006JF000512.

Domine, F., Albert, M., Huthwelker, T., Jacobi, H.-W., Kokhanovsky, A., Lehning, M., Picard, G., and Simpson, W. R., 2008. Snow physics as relevant to snow photochemistry. *Atmospheric Chemistry and Physics*, **8**, 171–208.

Dominé, F., Cabanes, A., and Legagneux, L., 2002. Structure, microphysics, and surface area of the Arctic snowpack near Alert during ALERT 2000. *Atmospheric Environment*, **36**, 2753–2765.

Fichefet, T., Tartinville, B., and Goosse, H., 2000. Sensitivity of the Antarctic sea ice to the thermal conductivity of snow. *Geophysical Research Letters*, **27**, 401–404.

Flanner, M. G., Zender, C. S., Randerson, J. T., and Rasch, P. J., 2007. Present-day climate forcing and response from black carbon in snow. *Journal of Geophysical Research*, **112**, D11202, doi:10.1029/2006JD008003.

Grenfell, T. C., and Warren, S. G., 1999. Representation of a nonspherical ice particle by a collection of independent spheres for scattering and absorption of radiation. *Journal of Geophysical Research*, **104**, 31697–31709.

Kokhanovsky, A., and Schreier, M., 2009. The determination of snow specific surface area, albedo and effective grain size using AATSR space-borne measurements. *International Journal of Remote Sensing*, **30**, 919–933.

Petrovic, J. J., 2003. Mechanical properties of ice and snow. *Journal of Materials Science*, **38**, 1–6.

Stamnes, K., Tsay, S. C., Wiscombe, W., and Jayaweera, K., 1988. Numerically stable algorithm for discrete-ordinate-method radiative transfer in multiple scattering and emitting layered media. *Applied Optics*, **27**, 2502–2509.

Sturm, M., and Benson, C. S., 1997. Vapor transport, grain growth and depth hoar development in the subarctic snow. *Journal of Glaciology*, **43**, 42–59.

Sturm, M., Holmgren, J., and Liston, G. E., 1995. A seasonal snow cover classification system for local to global applications. *Journal of Climate*, **8**, 1261–1283.

Sturm, M., Holmgren, J., König, M., and Morris, K., 1997. The thermal conductivity of snow. *Journal of Glaciology*, **43**, 26–41.

Taillandier, A.-S., Domine, F., Simpson, W. R., Sturm, M., Douglas, T. A., and Severin, K., 2006. Evolution of the Snow Area Index (SAI). of the subarctic snowpack in central Alaska over a whole season. Consequences for the air to snow transfer of pollutants. *Environmental Science & Technology*, **40**, 7521–7527, doi: 10.1021/es060842j.

Taillandier, A.-S., Domine, F., Simpson, W. R., Sturm, M., and Douglas, T. A., 2007. The rate of decrease of the specific surface area of dry snow: isothermal versus temperature gradient conditions. *Journal of Geophysical Research*, **112**, F03003, doi:10.1029/2006JF000514.

Warren, S. G., Brandt, R. E., and Grenfell, T. C., 2006. Visible and near-ultraviolet absorption spectrum of ice from transmission of solar radiation in snow. *Applied Optics*, **45**, 5320–5334.

Zhang, T., 2005. Influence of the seasonal snowcover on the ground thermal regime: an overview. *Reviews of Geophysics*, **43**, RG4002, doi: 10.1029/2004RG000157.

Cross-references

Chemical Composition of Snow, Ice, and Glaciers
Chemical Processes in Snow and Ice
Snow
Snow Crystal Structure
Snow Density
Snow Grains
Snow Metamorphism
Transformations of Snow at the Earth's Surface and its Climatic and Environmental Consequences

PIEDMONT GLACIERS

Monohar Arora
National Institute of Hydrology (NIH), Roorkee, UA, India

Piedmont glaciers form where valley glaciers exit from the mountains and meet flat ground. There they spread out in a fan or lobe shape. Piedmont glaciers commonly are a merger of several valley glaciers. Glaciers of this kind are especially common in Alaska. The lower portion of this glacier is almost flat and covered with so much soil and rock debris that it supports a thick forest. The Malaspina Glacier in Alaska is one of the most famous examples of this type of glacier. It is the largest piedmont glacier in the world.

PINGO

Himali Panthri
Department of Geology, D.B.S (P.G) College, Dehradun, Uttarakhand, India

Synonyms

Cryolaccolith; Hydrolaccolith

Definition

Pingos (Eskimo word *pingurayung* = low hill) also called *bulganniakh* are low mounds and cones covered with soils or mantle deposits having cores of massive ice. Pingos often support vegetation at their top.

Generally 10–70 m high, they may go as high as 90 m and 20–400 m in diameter.

Location

They are generally found in the continuous as well as discontinuous permafrost areas of Canada, Alaska, Greenland, and Siberia. Modern pingos are generally restricted to 65°–75° north latitude. They usually occur in drained lake basins and former fluvial channels.

Origin and growth

Pingos develop when hydrostatic pressure of water causes upheaval of a layer of frozen ground. This upward growth causes dilation and radial cracks which may form fractures, trenches, and gullies. In general, small pingos have closed tops while large ones have open tops often with a crater sometimes accommodating a shallow lake in summers.

On the basis of their mode of formation, pingos are divided into following two categories:

(a) Hydrostatic or closed system pingos
(b) Hydraulic or open system pingos

Hydrostatic or closed system pingos generally found in low lying areas like thermokarst and thaw lakes where permafrost is continuous. During summer months, melting often causes overflow along the banks causing draining of lakes which results into formation of a layer of permafrost above talik; the unfrozen bottom of the lake. Now this permafrost surrounding talik advances into it. Water within the talik gets pressurized due to expansion and freezing of newly forming ice and therefore moves upwards (direction of least resistance) making the ground above it to rise into a dome like, or elongated shape. Hydrostatic system pingos shape.

Hydraulic or open system pingos also known as Greenland type generally occur in valley bottoms, mostly in the areas of discontinuous permafrost. They are called open system pingos because of water flows into permafrost from an outside source (e.g., an aquifer). An ice core develops as the continuously infiltrating water is frozen by permafrost. This expanding ice forces the overlying surface upwards ultimately creating the dome-like form of pingo.

However, formation process of hydraulic pingos is still not completely understood.

Pingos generally grow with the rate of a few centimeters per year. They follow a growth cycle and eventually break down and collapse leaving water filled hollow (known as *ognip*). After a while, another cycle of pingo formation may take place in the same site.

Pingo ice may help in finding past climatic conditions.

Bibliography

Gurney, S. D., 1998. Aspects of the genesis and geomorphology of pingos: perennial permafrost mounds. *Progress in Physical Geography*, **22**(3), 307–324.
Mackay, J. R., 1978. Sub-pingo water lenses, Tuktoyaktuk Peninsula area, Northwest Territories. *Canadian Journal of Earth Sciences*, **15**(1), 219–1227.
Mackay, J. R., 1998. Pingo growth and collapse, Tuktoyaktuk Peninsula area, western arctic coast, Canada: a long term field study. *Geographie physique et Quternaire*, **52**, 271–323.
Waltham, T., 2003. Pingos of Tuk. *Geology Today*, **19**(6), 212–215.

PLASTIC DEFORMATION

A. K. Singh
DIAT (Deemed University), Girinagar, Pune, Maharashtra, India

Plastic deformation is a permanent change in shape or size of a solid body without fracture resulting from the application of sustained stress beyond the elastic limit.

Mechanically, snow exhibits viscoelastic properties. The viscous qualities of snow allow it to deform slowly, in some cases, without fracture. The elastic properties of snow allow energy to be stored and this sets the stage for the brittle type fracture. Many materials have well-defined failure criteria but snow does not. How snow reacts to the application of stress is determined by its complex and interrelated physical properties, as well as, the rate of stress application. When snow lies on a slope, the relationship between strength and stress becomes important. In general, the stress condition is simply related to the mass of snow on the slope and the slope angle, but strength is controlled by the complex properties of numerous individual layers. Thus, the process of ice and snow deformation should be divided into stages, each with its peculiar deformation mechanism, depending on the state of the snow, that is, on its structure, density, and temperature. Researchers have shown that the deformation of snow is accompanied by an increase in the number and areas of contacts between individual crystals. The growth of contact areas results in the increase of adhesion. In due time, the mechanically joined but initially separate crystals freeze together. On the other hand, deformation of snow is associated with breaking of structural connections.

Glide and diffusional processes play significant roles in the plastic deformation of polycrystalline ice (glacial ice considered as polycrystalline). Ice deformation is strongly dependent on temperature (factor A in Glen's flow law). Compression experiments show that polycrystalline ice deforms instantly when a stress is applied suddenly.

PLASTIC FLOW

A. K. Singh
DIAT (Deemed University), Girinagar, Pune, Maharashtra, India

Plastic flow is a rheological phenomenon in which flowing behavior of the material occurs after the applied

stress reaches a critical value (yield). The viscosity of the ice (related to the ice temperature), and the nature of the bed over which it flows and the ice/bed coupling mechanisms, all interact to control ice flow rate. Glacier flow is a classical example of plastic flow and is a simple consequence of the weight and creep properties of ice. As ice tends to build up in the accumulation area of a glacier, a surface slope towards the ablation zone is developed. This slope and the weight of the ice induce a shear stress throughout the mass. When subjected to a shear stress over time, ice will undergo creep, or plastic deformation. The rate of plastic deformation under constant shear stress is initially high but tapers off to a steady value. This illustrates what is known as the flow law or constitutive law of ice called Glen flow law by glaciologists: the rate of shear strain is approximately proportional to the cube of the shear stress. It is the basis for all analysis of the flow of ice sheets and glaciers. Ice deformation is strongly dependent on temperature (factor A in Glen's flow law).

Glacier movement occurs by basal sliding and plastic flow of the lower part of the glacier, and passive riding along an overlying rigid zone. Due to friction between the glacial ice and the valley sides and floor, valley glacier flow is fastest at the top center of a glacier and slowest along its margins.

Other studies have suggested that many glaciers and ice sheets do not slide on a rigid bed but ride on a deforming layer of water-charged sediment. This phenomenon is difficult to analyze because the sediment layer may thicken or thin, and thus its properties may change, depending on the history of deformation. In fact, the process may lead to an unsteady, almost chaotic, behavior over time.

PLEISTOCENE EPOCH

Amit Kumar
Department of Geology, Centre of Advanced Study in Geology, Punjab University, Chandigarh, India

Synonyms

Glacial epoch; Pleistocene epoch

Definition

The term "Pleistocene" (Gr. pleistos, "most"; kainos, "recent") was introduced by the British geologist Charles Lyell in 1839. In the geological time scale, it followed the Pliocene epoch and preceded the Holocene epoch of Quaternary period. The Pleistocene covers a period from about 1.8 million years ago to about 11,800 years ago, according to the time scale released by the International Commission on Stratigraphy in 2004.

Pleistocene (Pleistocene epoch, Glacial epoch), also commonly referred to as the Ice Age, represents the extensive glaciation of the northern hemisphere. During that time, there were a number of advances and retreats of the glaciers, which are termed as glacial and interglacial stages, respectively. It was when the world's temperate zones were alternately covered by glaciers during cool periods and uncovered during the warmer interglacial periods that the glaciers retreated. The glaciers of Greenland and Antarctica are leftovers of the last glacial advance, and we presently reside in an interglacial stage termed the Holocene epoch. At the ending of Pleistocene (and the beginning of the Holocene) about 11,000 years ago, the Ice Age ended. It is to be expected that the Earth will experience another glacial advance, perhaps in the next 10,000–20,000 years, and that the glacial/interglacial cycles will continue.

Bibliography

Flint, R. F., 1971. *Glacial and Quaternary Geology.* New York: Wiley, xiv, 892 p.
Sharp, R. P., 1991. *Living Ice: Understanding Glaciers and Glaciation*. Cambridge: Cambridge University Press, xii, 228 p.

PLUCKING

Amit Kumar
Department of Geology, Centre of Advanced Study in Geology, Panjab University, Chandigarh, India

Glaciers have played an important role in the development of landscapes in the middle, high latitudes and also in alpine environments. Glaciers have ability to erode soil and rock mass, and transport of sediment. As a glacier flows downwards hill, there may be an obstruction which causes a development of high-pressure zone on the up-ice side and a low-pressure zone on the down-ice side. Basal ice melts in the high-pressure area and the resulting meltwater infiltrates through cracks present in the bedrock. It results in removal of relatively large fragments of bedrock by direct glacial action, which is known as plucking.

Bibliography

Benn, D. I., and Evans, D. J. A., 1998. *Glaciers and Glaciation*. London: Arnold.

POLYTHERMAL GLACIERS

Neil F. Glasser
Centre for Glaciology, Institute of Geography and Earth Sciences, Aberystwyth University, Aberystwyth, UK

Synonyms

Sub-polar glaciers; Thermally complex glaciers

Definition

Polythermal glacier. A glacier that has a mixed basal thermal regime, consisting of both warm ice (at 0°C) and cold ice (below 0°C).

Introduction

Glaciers are commonly divided into three types according to their basal thermal regime: cold-based, warm-based, and polythermal. Polythermal glaciers are glaciers that have a mixed basal thermal regime. These glaciers have warm ice (at 0°C) in their interior where the ice is thick and is warmed to the pressure melt point, and cold ice (below 0°C) around their margins where ice is thin and on their surface. Typically, it is the thicker, higher-level ice in the accumulation area that is warm-based and it is the snout, lateral margins and surface layer of the glacier that are below the pressure-melting point.

Geographical distribution of polythermal glaciers

Polythermal glaciers are widely distributed around the world. They are particularly a feature of the Arctic: they occur widely on Svalbard and throughout the Canadian Arctic. They also occur in other regions of the world, including the European Alps, the Caucasus, the Polar Urals, and Altai. Polythermal glaciers are probably also common on the Antarctic Peninsula, although there are few specific measurements to substantiate this. In different geographical regions, polythermal glaciers may have markedly different proportions of warm and cold ice. For example, Canadian high-arctic polythermal glaciers typically consist predominantly of cold ice with only a thin area of warm basal ice. Conversely, Svalbard-type polythermal glaciers typically consist predominantly of warm ice with a smaller, thin layer of cold basal ice around the margins and on the surface.

Dynamics of polythermal glaciers

This mix of thermal regimes makes the dynamics of polythermal glaciers complex. The typical polythermal glacier moves by sliding on its bed or subsole deformation where warm-based ice dominates, and moves only by internal deformation where it is cold-based, for example, at the snout and lateral margins. Meltwater tends to follow supra- and englacial routes and well-developed basal hydrological networks are rare. As a result, polythermal glaciers tend to carry a high basal debris load, with debris-rich basal ice zones between 1 and 3 m thick, and debris concentrations of up to 50%. Their surfaces rarely have a substantial cover of debris, although medial moraines are commonly observed in their lower ablation areas.

Superimposed ice (formed by the refreezing of melted snow) is common on the surface of polythermal glaciers. This superimposed ice forms on the glacier surface if there are short periods of positive air temperatures in early winter, often coinciding with rainfall, which cause rapid glacier-wide melting. Percolating water then refreezes to form superimposed ice on the lower half of the glacier, and wetted-refrozen snow and ice lenses at higher altitudes. The formation of superimposed ice has significant implications for the mass balance of polythermal glaciers, because it locally comprises up to 20% of the winter balance and accounts for between 16% and 25% of the annual accumulation. The contribution from superimposed ice to glacier mass balance is therefore potentially very significant on many polythermal glaciers. The equilibrium line, which is not a physically marked feature on many polythermal glaciers, is often somewhere in the superimposed ice zone on these glaciers.

Svalbard, which contains numerous polythermal glaciers, is also famous for its high proportion of surge-type glaciers. An estimated 35% of the glaciers on Svalbard are surge-type. These glaciers are prone to dramatic increases in velocity, often accompanied by rapid frontal advances, followed by periods of quiescence during which velocities are generally low. Surge-type glaciers in Svalbard typically have relatively long quiescent phases (10–200 years) between short-lived surge events (1–5 years). It is not clear why these polythermal glaciers should be prone to surge-type behavior.

Sediments and landforms associated with polythermal glaciers

Field observations of the sediments and landforms produced by polythermal glaciers on Svalbard indicate that these glaciers are strongly influenced by structural glaciological controls on debris entrainment and transport. For example, moraine-mound complexes in front of receding Svalbard glaciers are formed by proglacial and englacial thrusting, folding, and deformation of the ice during glacier flow, particularly during rapid advances or glacier surges. On a smaller scale, a range of glacier structures arrange debris into foliation-parallel ridges, supraglacial debris stripes, and geometrical ridge networks.

Deformation of permafrost is also important in the formation of ice-cored moraines and push moraines in front of polythermal glaciers. Stresses beneath the advancing glaciers are transmitted to the proglacial sediments and can be sufficient to cause proglacial deformation of the permafrost layer. Folding, thrust-faulting, and overriding of proglacial sediments are also possible under these conditions. The nature of the deformation is controlled by the mechanical properties of the sediment, which is influenced by the water content and thermal condition, and whether it is frozen or unfrozen.

Summary

Polythermal glaciers are those glaciers that have a mixed basal thermal regime. They have warm ice (at 0°C) in their interior where the ice is thick and is warmed to the pressure melt point, and cold ice (below 0°C) around their margins where ice is thin and on their surface. They have a restricted geographical range and are particularly common in the Arctic, suggesting that there are climatic controls on their distribution. Proglacial and englacial thrusting, folding, and deformation of the ice are common during glacier flow, as is the deformation of permafrost in proglacial areas.

Bibliography

Boulton, G. S., Van der Meer, J. J. M., Hart, J., Beets, D., Ruegg, G. H. J., Van der Wateren, F. M., and Jarvis, J., 1996. Till and moraine emplacement in a deforming bed surge – an example from a marine environment. *Quaternary Science Reviews*, **15**, 961–987.

Boulton, G. S., Van der Meer, J. J. M., Beets, D. J., Hart, J. K., and Ruegg, G. H. J., 1999. The sedimentary and structural evolution of a recent push moraine complex: Holmstrømbreen, Spitsbergen. *Quaternary Science Reviews*, **18**, 339–371.

Copland, L., and Sharp, M., 2001. Mapping thermal and hydrological conditions beneath a polythermal glacier with radio-echo sounding. *Journal of Glaciology*, **47**, 232–242.

Copland, L., Sharp, M. J., and Nienow, P. W., 2003. Links between short-term velocity variations and the subglacial hydrology of a predominantly cold polythermal glacier. *Journal of Glaciology*, **49**, 337–348.

Etzelmüller, B., Hagen, J. O., Vatne, G., Ødegård, R. S., and Sollid, J. L., 1996. Glacial debris accumulation and sediment deformation influenced by permafrost: examples from Svalbard. *Annals of Glaciology*, **22**, 53–62.

Glasser, N. F., and Hambrey, M. J., 2001. Styles of sedimentation beneath Svalbard valley glaciers under changing dynamic and thermal regimes. *Journal of the Geological Society of London*, **158**, 697–707.

Glasser, N. F., and Hambrey, M. J., 2003. Ice-marginal terrestrial land systems: Svalbard polythermal glaciers. In Evans, D. J. A. (ed.), *Glacial Land Systems*. London: Arnold, pp. 65–88.

Hambrey, M. J., Bennett, M. R., Dowdeswell, J. A., Glasser, N. F., and Huddart, D., 1999. Debris entrainment and transfer in polythermal glaciers. *Journal of Glaciology*, **45**, 69–86.

Ó Cofaigh, C., Evans, D. J. A., and England, J., 2003. Ice-marginal terrestrial land systems: sub-polar glacier margins of the Canadian and Greenland High Arctic. In Evans, D. J. A. (ed.), *Glacial Land Systems*. London: Arnold, pp. 44–64.

Wadham, J. L., and Nuttall, A.-M., 2002. Multiphase formation of superimposed ice during a mass-balance year at a maritime high-Arctic glacier. *Journal of Glaciology*, **48**, 545–551.

Cross-references

Arctic Hydroclimatology
Canadian Rockies and Coast Mountains of Canada
Cold-Based Glaciers
Dynamics of Glaciers
Englacial Processes
Glacier Motion/Ice Velocity
Glacier Surging
Glaciology
Scandinavian Glaciers
Structural Glaciology

PRECIPITATION

Donna F. Tucker
Department of Geography, University of Kansas, Lawrence, KS, USA

Definition

Precipitation: Solid or liquid phase water particles that are formed in the atmosphere and that fall and reach the earth's surface. The quantity of such particles that have reached the earth's surface at a given location over a given period of time.

Introduction

Precipitation may take a variety of forms including rain, snow, sleet, and hail. The form depends on whether the water is frozen and also on the formation mechanism of the precipitation. The quantity of precipitation is generally measured in linear units of liquid water (e.g., millimeters or inches) – with an assumption that this measurement is per unit area. Snow accumulation is also measured as depth above the surface.

Formation of precipitation

Condensation of water vapor in the atmosphere may take place when the air is saturated. Air is typically brought to saturation by cooling and this cooling is generally accomplished by upward motion and the resulting adiabatic expansion of the air. The saturation vapor pressure over a curved surface is much higher than that over a flat surface. To form a stable water droplet would require much larger supersaturations than are observed in the atmosphere unless the water condensed on some other substance. Condensation on another substance reduces the radius of curvature of the water droplet. Thus, water vapor requires solid and liquid particles known as condensation nuclei on which to condense. The concentrations of these nuclei vary greatly in the atmosphere from the order of 10–1,000 cm^{-3} (Pruppacher et al., 1997). Larger values are found over the continents and urban areas and these appear due to human influence (Andreae and Rosenfield, 2008). Some condensation nuclei, known as hygroscopic nuclei, have a particular affinity for water and water may condense on them at relative humidities that are less than 100% (with respect to a flat surface of pure water).

Deposition of ice in the atmosphere requires that the atmosphere be saturated and also that the temperature be below the freezing point of water. At temperatures above −40°C, deposition requires, in addition, that suitable particles known as ice nuclei are present. The exact properties that make a substance a suitable ice nuclei are not well known (Cantrell and Heymsfield, 2005). The number of ice nuclei in the atmosphere varies with temperature – more ice nuclei activate at lower temperatures – but averages about 1/L at −20°C. Thus, ice nuclei are considerably scarcer than condensation nuclei.

Water droplets and ice crystals fall under the influence of gravity but their fall is impeded by air resistance. Therefore, they do not continue to accelerate indefinitely but reach a terminal velocity. Cloud droplets are typically 2–50 μm in diameter. To reach the earth's surface in a reasonable period of time, their volume must increase about a million times (Wallace and Hobbs, 2006). Ice crystals must grow larger still.

Water droplets can grow larger by additional condensation. Condensation is favored on larger droplets as well as

on droplets containing dissolved substances. Water droplets can also grow by encountering and merging with other cloud droplets in a process known as collision and coalescence, which also favors the growth of larger droplets as opposed to smaller ones. Precipitation can and does develop in clouds whose temperatures are not low enough for ice crystals to form. Such conditions are more likely to occur in the tropics and subtropics than in middle or polar latitudes.

Ice crystals can also grow larger by additional deposition of water vapor. But since there are relatively few ice nuclei in the atmosphere, ice crystals and supercooled water droplets often coexist in clouds whose temperature is below freezing. The saturation vapor pressure over water is greater than that over ice. Thus, conditions can exist where the water droplets are subsaturated and the ice crystals are supersaturated. The ice crystals grow at the expense of the water droplets in what is known as the Bergeron process. The Bergeron process is responsible for the vast majority of precipitation (including rain) in middle and higher latitudes as well as in tropical thunderstorms. Ice crystals are always six sided but may take a variety of forms: columns, needles, plates, and the elaborate branching structures, known as dendrites, of the stereotypical snowflake. The structure of the ice crystal is dependent on the temperature and humidity of the air in which it forms (Rogers and Yao, 1989). Ice crystals may collide and merge in a process called aggregation. In addition, ice crystals may encounter water droplets that freeze on impact with the ice crystal. This process is known as riming. Aggregation efficiency depends on temperature but riming efficiency is close to one (Houze, 1993).

Types of precipitation

Precipitation in the liquid form when it reaches the earth's surface may be divided into two categories: rain and drizzle. The distinction between them is entirely based on size–drizzle drops are less than 0.5 mm in diameter and raindrops are at least 0.5 mm in diameter. Drizzle typically falls from fog or low stratus clouds and generally produces small quantities of precipitation. Rain will fall from nimbostratus or cumulonimbus clouds.

Likewise, frozen precipitation that has experienced a little or no riming and has not previously melted may come in the form of snow or snow grains. Snow is larger in size having often experienced aggregation, especially if the temperature is near freezing. Snow grains are the frozen equivalent of drizzle and typically fall from fog or low stratus clouds. They are small, white, and opaque with diameters less than 1 mm. Snow crystals that are moderately rimed are called graupel, snow pellets, or soft hail. They are white due to their core, which was formed by deposition. They are typically 2–5 mm in diameter and may bounce when they hit the ground.

When ice crystals fall though a thick enough layer that is above freezing they will melt. If they then fall through another fairly thick layer that is below freezing before they reach the ground, they will refreeze. The resulting precipitation is called ice pellets or sleet (in the USA). (In British English, sleet refers to a mixture of rain and snow [Sumner, 1988].) Ice pellets are transparent or translucent because they were formed by freezing liquid and not deposition of vapor. They are less than 5 mm in diameter. If the layer that is below freezing next to the earth's surface is very thin, a falling water drop may not have time to freeze before it hits the ground. In this case, the liquid water drop will freeze on contact with the ground creating a thin sheet of ice. The precipitation is then known as a freezing rain. Figure 1 illustrates the environment in which the various types of precipitation form. Freezing rain (and to a lesser extent, ice pellets) can be extremely hazardous to ground transportation because friction with a surface coated with freezing rain is even less than for a surface coated with snow. Freezing rain can also coat trees and power lines, unlike snow, which will fall off both if accumulations are high enough. Heavy coatings can break tree branches and power lines resulting in substantial damage.

Hail may be considered an extreme case of rimed ice crystals. Hail is greater than 5 mm in diameter. Hail typically has had several coatings of liquid water freeze on it. On larger hailstones, these layers can be seen if the hailstone is cut open. To collect enough water to grow to even minimum size, the embryo hailstone must remain in the cloud longer than other types of precipitation. Although there is some disagreement as to all the processes involved in forming a hailstone, it is generally agreed that the storm must have at least a moderately strong updraft to prevent the precipitation from falling out too soon. Thus, hail falls almost exclusively from cumulonimbus clouds. The shape and thickness of the thunderstorm updraft may be important factors as well as its orientation with respect to the downdraft.

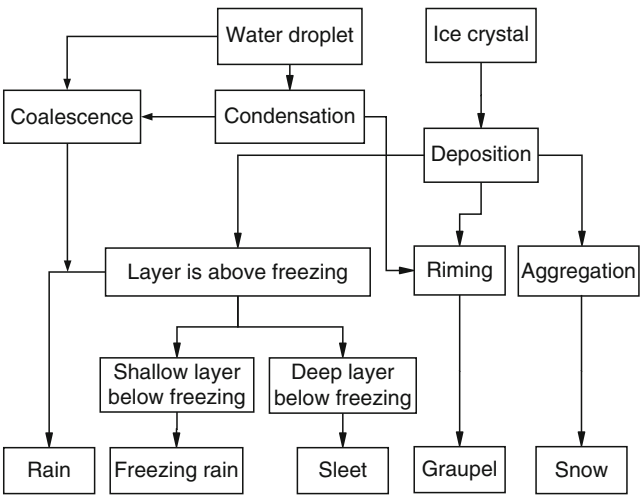

Precipitation, Figure 1 Processes forming different types of precipitation.

Measurement of precipitation

Precipitation has traditionally been measured directly at the earth's surface with a container into which the precipitation falls. Snow drifts easily, so depth measurements (generally over a flat board) must be taken at multiple locations (Sumner, 1988). The water equivalent of snow varies greatly and the depth of snow changes depending on the length of time since the snow fell. Therefore, the liquid equivalent of the frozen precipitation has typically been a more useful measurement.

The standard rain gauge has a wide, usually circular, opening converging to a narrower inner tube. The cross-sectional area of the inner tube is generally one tenth that of the outer opening. The depth of precipitation is measured manually with a specially calibrated ruler. This method can be economically advantageous because of the low cost and durability of the equipment. Its disadvantage lies in the difficulty of determining the rate at which the precipitation fell.

A weighing gauge can record the rate of precipitation accumulation. It measures the change in weight as liquid accumulates in a container. The liquid equivalent of frozen precipitation can also be measured if a known weight of antifreeze solution is in the container. The antifreeze can also reduce evaporative losses of accumulated precipitation. The minimum amount of precipitation recorded depends on the sensitivity of the gauge. This type of gauge is more costly and needs to be calibrated often.

Remote readings of precipitation accumulation are easier with the tipping bucket type of rain gauge. This instrument has a small container that is divided in two. The container pivots around its center in a seesaw manner such that only one side of the container accumulates precipitation at a time. When a known weight of precipitation accumulates in one side of the container, it will tip, empty its load, and allow the other side to accumulate precipitation. The number of tips is recorded electronically. This type of gauge makes no record of less than some minimum precipitation accumulation – less than one tip's worth. It may have difficulty keeping up in very heavy rain and it tends to have more splash errors than other types of direct measurements.

Overall, these direct measurements are subject to a number of errors. One is that precipitation in the gauge may evaporate before it is recorded. Another is that moisture may adhere to the collecting tube and not be measured. The most serious errors occur because catch decreases with increasing wind speed. Gauges are usually mounted as close to the earth's surface as possible to minimize this error. Some gauges may be fitted with a windshield to help reduce this bias. It should be kept in mind that places with high average wind speeds may have precipitation measurements, which are consistently lower than the actual amount that fell (Strangeways, 2007). Even outside of windy areas, errors in gauge measurements trend more toward underestimating rather than overestimating the amount of precipitation that actually fell.

Sensors have also been developed to infer precipitation amounts from detection of individual drops. Drops may be detected optically or by measuring the impact of the drops on a surface. These instruments are relatively expensive and dependent on an algorithm to translate drops detected to rainfall amounts.

Precipitation displays extreme areal variability and it is not usually feasible to have enough gauges to measure most of the variability. Generally, the horizontal resolution of observations is very uneven. Thus, there is considerable incentive to estimate precipitation amounts with techniques yielding more spatial resolution.

Satellite measurements of infrared radiation (IR) in a narrow wavelength band have been related to precipitation. These estimates have been based on the assumption that higher clouds emitting less IR are more likely to be generating precipitation. This method works better in regions, such as the tropics, where most precipitation is convective in nature (New et al., 2001). The total outgoing IR radiation (i.e., wide band of wavelengths) has also been related to precipitation as it is also sensitive to soil moisture. Microwave radiation is more sensitive to cloud water and ice and thus easier to relate to precipitation directly. But the best algorithm for doing so varies by location and season (Kidd, 2001).

Radar reflectivity has also been used to estimate precipitation amounts. To use this technique a drop size distribution must be assumed. Estimates of precipitation may be poor if drop size distribution in a particular storm is unusual. This method cannot directly determine how much of the precipitation in the air will reach the ground without evaporating. This technique is more difficult to apply to frozen precipitation as radar is less sensitive to it. Obviously, it is only applicable in parts of the world with reliable radar measurements.

Perhaps the most promising way of determining how much precipitation has fallen is to combine remotely sensed and gauge data. These methods use the gauge data to reduce the impact of the assumptions, which must be made in remote sensing estimates. They are therefore able to take advantage of the high resolution of the remotely sensed data as well as the greater (but not perfect) accuracy of the gauge data (Young et al., 2000).

Summary

Precipitation takes a variety of forms. We have learned much about how precipitation forms but many unknowns remain. Although precipitation measurement is conceptually simple, in practice, precipitation varies greatly over small areas and doubts concerning accuracy are always present.

Bibliography

Andreae, M. O., and Rosenfield, D., 2008. Aerosol–cloud–precipitation interactions. Part 1. The nature and sources of cloud-active aerosols. *Earth Science Reviews*, **89**, 13–41.

Cantrell, W., and Heymsfield, A., 2005. Production of ice in tropospheric clouds. *Bulletin of the American Meteorological Society*, **86**, 795.
Houze, R. A., 1993. *Cloud Dynamics*. San Diego: Academic.
Kidd, C. K., 2001. Satellite rainfall climatology. *International Journal of Climatology*, **21**, 1041.
New, M., Todd, M., Hulme, M., and Jones, P., 2001. Precipitation measurements and trends in the twentieth century. *International Journal of Climatology*, **21**, 1899–1922.
Pruppacher, H. R., and Klett, J. D., 1997. *Microphysics of Clouds and Precipitation*, 2nd edn. Dordrecht: Kluwer.
Rogers, R. R., and Yao, M. K., 1989. *A Short Course in Cloud Physics*. New York: Pergamon.
Strangeways, I., 2007. *Precipitation: Theory, Measurement and Distribution*. Cambridge: Cambridge University Press.
Sumner, G., 1988. *Precipitation Process and Analysis*. New York: Wiley.
Wallace, J. M., and Hobbs, P. V., 2006. *Atmospheric Science: An Introductory Survey*. New York: Academic.
Young, C. B., Bradley, A. A., Krajewski, W. F., Kruger, A., and Morissey, M. L., 2000. Evaluating NEXRAD multisensor precipitation estimates for operational hydrologic forecasting. *Journal of Hydrometeorology*, **1**, 241.

Cross-references

Artificial Production of Snow
Cloudburst
Condensation Nuclei
Slush and Sleet of Snow
Snow
Snow Pellet
Snow Storm
Snowboard

PROGLACIAL LAKES

Brenda L. Hall
Department of Earth Sciences and Climate Change Institute, Bryand Global Sciences Center, University of Maine, Orono, ME, USA

Definition

Proglacial lake. Ice-contact lake occurring adjacent to the frontal margin of a glacier.

Introduction

A proglacial lake abuts and extends beyond the glacier terminus. Many proglacial lakes are moraine-dammed, whereas others form in basins created by isostatic depression near the ice margin. These latter lakes commonly are buttressed by the ice itself. Not all ice-dammed lakes, however, are proglacial, so these terms are not strictly synonymous. Some ice-dammed lakes, for instance, form laterally, such as when a glacier dams river flow in a side valley. Possibly the best-known ice-dammed lake was Glacial Lake Missoula, which occupied thousands of square kilometers of western Montana and Idaho before draining catastrophically (many times) to the Pacific.

Proglacial lakes can be ephemeral in nature or persist hundreds, if not thousands of years. The transient nature of some lakes results from several processes, including drainage (catastrophic or otherwise) caused by breaching of the moraine dam or by gradual isostatic uplift. Proglacial lakes also infill with sediment over time and can be replaced by outwash plains or bogs.

The sometimes catastrophic nature of proglacial lake drainage presents a significant problem to society. Rapid outbursts caused by moraine failure or tectonic activity lead to property destruction and loss of life (i.e., Lliboutry et al., 1977; Richardson and Reynolds, 2000; Allen et al., 2009). Even without complete drainage, the surface-level of proglacial lakes tends to vary, because of the changing elevation of outlets (i.e., due to moraine degradation or isostatic rebound), advance or retreat of glaciers, and periods of large recharge (such as the summer melt season or rainfall events).

Proglacial lakes are a product of both glacial and interglacial times. For example, rapid ice recession over the past century has led to the development of new, commonly moraine-dammed proglacial lakes (Figure 1) associated with retreating alpine glaciers. During the last deglaciation, large proglacial lakes abutted the melting ice sheets in both North America and Europe. One of the most famous, Glacial Lake Agassiz, covered more than half a million square kilometers and occupied basins that sloped down toward the retreating Laurentide Ice Sheet over central Canada. Catastrophic drainage of this lake at ~8,200 years before present (Barber et al., 1999) occurred when lake water was able to float the remnant ice sheet and flow out through Hudson Strait. Some have argued that large injections of fresh meltwater into the climatically sensitive North Atlantic Ocean from lakes such as Agassiz caused shutdowns of thermohaline circulation and consequent cooling of the Northern Hemisphere several times during the last deglaciation (i.e., Teller, 2004; Teller and Leverington, 2004; although see Lowell et al., 2005 for an alternate interpretation).

Sedimentation

Proglacial lakes affect both the adjacent glacier and its sedimentation. Calving is a significant ablation process in proglacial lakes, with rates increasing as water deepens (Warren and Kirkbride, 2003). Thus, glaciers attached to proglacial lakes may retreat more rapidly than those terminating on land. Conversely, readvances occur more slowly, because the glaciers must overcome ice loss caused by calving.

Proglacial lakes can produce thick sedimentary sequences. Commonly, the sediments consist of rock flour, fine-grained glacial silt produced by subglacial abrasion. Such flour gives many proglacial lakes a characteristic milky or blue color. Strong seasonal differences in meltwater and sediment input lead to the formation of varves or other rhythmic bedding in some proglacial lakes. The sediments also can include ice-rafted dropstones. In

Proglacial Lakes, Figure 1 Photograph of Ventisquero Holanda (54° 56′S, 69° 07′W), Cordillera Darwin, Chile, with proglacial lake. This lake, which formed over the past several decades, is dammed by a moraine complex at its distal end.

polar regions, rare types of proglacial lakes, known as "proglacial lake-ice conveyors" can transport glacial till on their perennial ice cover kilometers beyond the actual glacier margin (Hendy et al., 2000) and deposit it in seasonally open water near the lake edge.

Proglacial lake sediments afford an opportunity for reconstructing glacier mass balance and climate (i.e., Leemann and Niessen, 1994). Different proxies, such as sediment grain size, preserved in annual layers, can be used to estimate changes in meltwater volume and glacier proximity. In some well-constrained cases, it is possible to estimate not only ice-marginal fluctuations, but (potentially) former equilibrium-line and temperature changes (i.e., Nesje et al., 2001; Shakesby et al., 2007; Thomas and Briner, 2009).

Summary

Proglacial lakes are common features of glacial landscapes. Drainage of large lakes that formed during the last deglaciation alongside the southern margin of the Laurentide Ice Sheet in North America have been implicated in abrupt climate change, although this is an area of ongoing research. The long records preserved in many proglacial lakes are receiving increasing attention as researchers look for high-resolution, continuous proxies of past glacier and climate fluctuations.

Bibliography

Allen, S., Schneider, D., and Ovens, I., 2009. First approaches towards modelling glacial hazards in the Mount Cook region of New Zealand's Southern Alps. *Natural Hazards and Earth System Sciences*, **9**, 481–499.

Barber, D., Dyke, A., Hillaire-Marcel, C., Jennings, A., Andrews, J., Kerwin, M., Bilodeau, G., McNeely, R., Southon, J., Morehead, M., and Gagnon, J.-M., 1999. Forcing of the cold event of 8200 years ago by catastrophic drainage of Laurentide lakes. *Nature*, **400**, 344–348.

Hendy, C. H., Sadler, A. J., Denton, G. H., and Hall, B. L., 2000. Proglacial lake-ice conveyors: a new mechanism for deposition of drift in polar environments. *Geografiska Annaler*, **82A**, 249–270.

Leemann, A., and Niessen, F., 1994. Holocene glacial activity and climatic variations in the Swiss Alps – reconstructing a continuous record from proglacial lake sediments. *The Holocene*, **4**, 259–268.

Lliboutry, L., Morales Arnao, B., Pautre, A., and Schneider, B., 1977. Glaciological problems set by the control of dangerous lakes in Cordillera Blanca, Peru. I: historic failure of moraine dams, their causes and prevention. *Journal of Glaciology*, **18**, 239–254.

Lowell, T., Fisher, T., Comer, G., Hajdas, I., Waterson, N., Glover, K., Loope, H., Schaefer, J., Rinterknecht, V., Broecker, W., Denton, G., and Teller, J., 2005. Testing the Lake Agassiz meltwater trigger for the Younger Dryas. *EOS. Transactions of the American Geophysical Union*, **86**(40), 365, 372.

Nesje, A., Matthews, J., Dahl, S., Berrisford, M., and Andersson, C., 2001. Holocene glacier fluctuations of Flatebreen and winter-precipitation changes in the Jostedalsbreen region, western Norway, based on glaciolacustrine sediment records. *The Holocene*, **11**, 267–280.

Richardson, S., and Reynolds, J., 2000. An overview of glacial hazards in the Himalayas. *Quaternary International*, **65**(66), 31–47.

Shakesby, R. A., Smith, J. G., Matthews, J. A., Winkler, S., Dresser, P. Q., Bakke, J., Dahl, S. O., Lie, Y., and Nesje, A., 2007. Reconstruction of Holocene glacier history from distal sources: glaciofluvial stream-bank mires and a glaciolacustrine sediment core near Sota Søter, Breheimen, southern Norway. *The Holocene*, **17**, 729–745.

Teller, J. T., 2004. Controls, history, outbursts, and impact of large late-Quaternary proglacial lakes in North America. In Gillespie, A., Porter, S., and Atwater, B. (eds.), *The Quaternary Period in the United States*. Amsterdam: Elsevier, pp. 45–61.

Teller, J. T., and Leverington, D. W., 2004. Glacial Lake Agassiz: a 5000-year history of change and its relationship to the $\delta^{18}O$ record of Greenland. *Geological Society of America Bulletin*, **116**, 729–742.

Thomas, E., and Briner, J., 2009. Climate of the past millennium inferred from varved proglacial lake sediments on northeast Baffin Island, Arctic Canada. *Journal of Paleolimnology*, **41**, 209–224.

Warren, C., and Kirkbride, M., 2003. Calving speed and climatic sensitivity of New Zealand lake-calving glaciers. *Annals of Glaciology*, **36**, 173–178.

Cross-references

Glacier Lake Outburst Floods
Natural Hazards Associated with Glaciers and Permafrost

Q

QUATERNARY GLACIATION

Jürgen Ehlers[1], Philip Gibbard[2]
[1]Geologisches Landesamt, Hamburg, Germany
[2]Quaternary Palaeoenvironments Group, Cambridge Quaternary, Department of Geography, University of Cambridge, Cambridge, UK

Synonyms

Ice age; Last glacial maximum; Pleistocene

Definition

The Quaternary is the youngest Period/System division of the Geological Time Scale and represents 2.6 million years of geological time. It spans the Pleistocene (2.6–0.11 Ma) and Holocene (0.11–0 Ma) Series and includes the present day. It is essentially the "Ice Age" of popular terminology.

The term Last Glacial Maximum or LGM is widely used to refer to the maximum global ice volume during the last glacial cycle corresponding with the trough in the marine isotope record centered on ca. 18 ^{14}C Ka BP (Martinson et al., 1987) and the associated global eustatic sea-level low also dated to 18 ^{14}C Ka BP (Yokoyama et al., 2000).

Introduction

Since the recognition in the mid-nineteenth century that glaciers had been considerably more extensive than at present, the Quaternary has been synonymous with glaciation of the mid-latitudes. Today evidence from both the land and ocean-floor sediment sequences demonstrates that the major continental glaciations occurred repeatedly over what are now temperate regions of the Earth's surface. Knowledge about the number of glaciations has increased, and also knowledge about the extent of the Pleistocene ice sheets. Recent progress can be seen in a comparison between the glacial limits of the northern European ice sheets as summarized by Flint (1971) and by the INQUA Work Group 5 project "Extent and Chronology of Quaternary Glaciations" (2004) (Figure 1). While the maximum extent has undergone comparatively few changes, the Late Weichselian ice sheet has changed fundamentally. Today, a single ice sheet is envisioned instead of Flint's three major glaciation centers. Major differences include the (1) glaciation of the Bering Sea, (2) non-glaciation of the North Sea, (3) non-glaciation of the northern Urals, and (4) limitation of glaciation in Siberia to the Putorana Massif and the Taimyr coast. Extensive ice-rafting, an indication that glaciers had reached sea-level, is found from the earliest cold stage (2.6–2.4 Ma) in both the North Atlantic and North Pacific oceans (cf. Haug et al., 2005). The initiation of conditions that resulted in glaciation are a consequence of the long-term declining cooling trend in world climates that began early in the previous Tertiary Period. Apart from some limited activity in the Eocene, significant glaciation began in the late Oligocene (*c*. 35 Ma) in eastern Antarctica. It was followed by mountain glaciation through the Miocene (23–5.3 Ma) in Alaska, Greenland, Iceland and Patagonia, and later in the Pliocene (5.3–2.6 Ma) in the Alps, the Bolivian Andes and possibly in Tasmania. From the Neogene, glacially derived ice-rafted debris is found in ocean-sediment cores from the North Atlantic region, including the Barents Sea, and areas adjacent to Norway, N and SE Greenland, Iceland and northern North America, and in the Southern Ocean off-Antarctica.

Glaciation during the Quaternary

The climatic variation that characterizes the Earth's climate during the late Cenozoic, and indeed before, is controlled by variations of the Earth's orbit around the Sun that therefore controlled the receipt of solar energy at the Earth's surface. These Milankovitch variations, named

Vijay P. Singh, Pratap Singh & Umesh K. Haritashya (eds.), *Encyclopedia of Snow, Ice and Glaciers*, DOI 10.1007/978-90-481-2642-2,

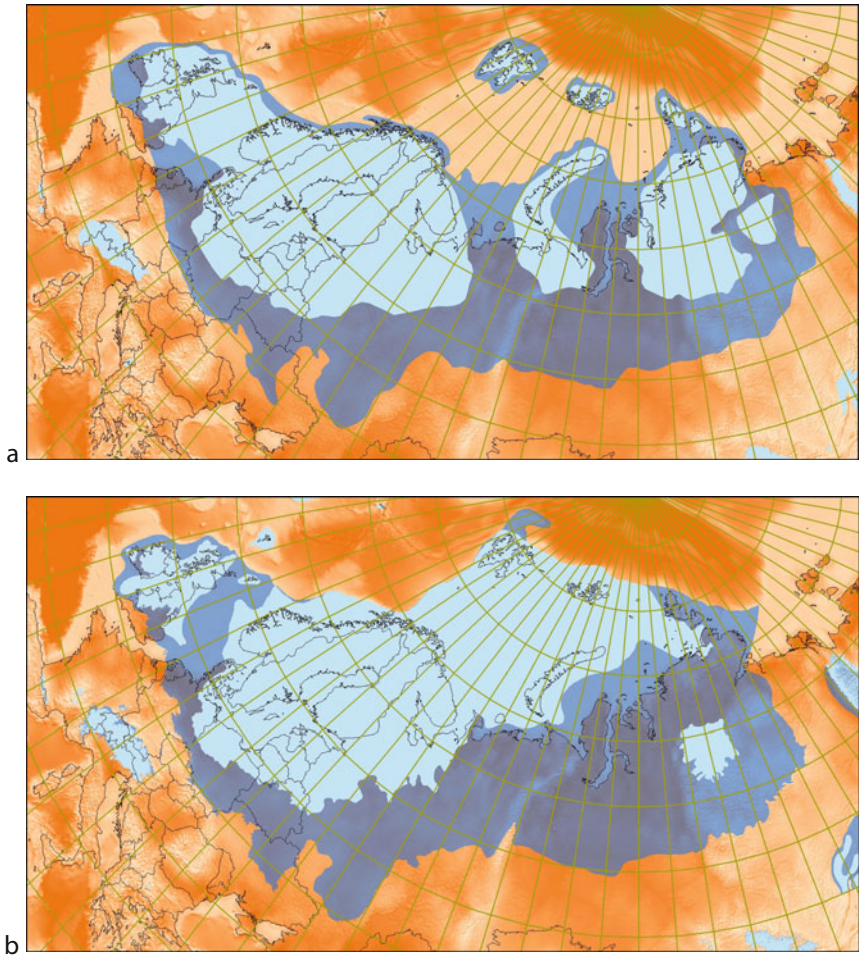

Quaternary Glaciation, Figure 1 Overview map showing the difference of the Eurasian ice sheet between Flint (1971) and "Extent and Chronology" to illustrate the changes that have occurred in the last 40 years.

after their discoverer, are responsible for the cyclic climate changes that characterize the Quaternary and indeed much of Earth's history. One of the most critical ways they are expressed is through the development of "Ice Ages" or periods when glaciation extended across large areas of the Earth. The Early Pleistocene (2.6–0.8 Ma) was characterized by climatic fluctuations dominated by the 41 Ka precession cycle, during which relatively few cold periods were sufficiently cold and long to allow the development of substantial ice sheets. Only 14 of the 41 cold stages of that period currently show evidence of major glaciation. They include the Plio-Pleistocene boundary events Marine Isotope Stage (MIS) 104, 100, and 98, together with Early Pleistocene MIS 82, ?78, 68, 60, 58, 54, 52, 36, 34, ?30, and 26 which reach δ18O ocean‰ of *c*. 4.6–5. It is not until the transition in dominant orbital cyclicity to the 100 Ka cycles, which began *c*. 1.2 Ma and was fully established by about 800 Ka ("middle Pleistocene transition"), that the cold periods (glacials) were regularly cold and long enough to allow ice-sheet development on a continental scale, outside the polar regions. However, it is during MIS 22 (*c*. 870–880 Ka) that the first of the "major" cold events that reached critical values of *c*. 5.5 or above δ18O ocean‰ equivalent to substantial ice volumes that typify glaciations of the later Pleistocene (i.e., MIS 16, 12, 10, 6, 4–2). Potentially therefore, it is likely that there were a minimum of 20 periods during which extensive glaciation could have developed during the last 2.6 Ma, with the most extensive (*c*. 5–6 periods) being limited to the last 900 Ka (Tables 1–3).

Precisely where these glaciations occurred and how far they extended is very difficult to determine, given that the remnants of less extensive early glaciation tend to be obliterated and mostly removed by later, more extensive advances. Although this is so in all terrestrial areas, it is especially difficult in mountain regions where the preservation potential of older sequences rapidly diminishes with time and subsequent glaciation. However, examination of the frequency of glaciation through the Cenozoic indicates that glaciation in the Southern Hemisphere having been established first, principally in Antarctica and southern South America, occurred continually from the

Quaternary Glaciation, Table 1 Occurrence of glaciation in Europe through the Cenozoic based on numbers of observations presented in contributions to the INQUA project "Extent and Chronology of Quaternary Glaciations" (Ehlers and Gibbard, 2004a)

Stage/age		MIS (approx)	Austria	Belarus	Croatia	Czechia	Denmark	Great Britain	Estonia	Finland	Alps/Jura/Massif central	Pyrennes	North Germany	South Germany	Greece	Iceland	Ireland	North Italy	Italian Alps/Appenines	Latvia	Lithuania	Netherlands	Norway	Poland	European Russia	Eastern European Russia	Siberia	Sweden	Barents Sea	Slovenia	Spain	Switzerland	Ukraine	North Sea	North Atlantic
Weichselian		2	Δ	Δ	Δ	Δ	Δ	Δ	Δ	Δ	Δ	?Δ	Δ	Δ	Δ	Δ	Δ	Δ	Δ	Δ	Δ		Δ	Δ	Δ	Δ	Δ	Δ	Δ	Δ	?	Δ	Δ	Δ	Δ
		3					Δ			?Δ	Δ					Δ							Δ				Δ	Δ	?			?Δ		Δ	
		4			Δ		Δ	Δ	Δ	Δ		Δ	?Δ			Δ	?Δ	Δ		?Δ			Δ	Δ	?	?Δ	Δ	Δ	Δ		Δ	Δ		Δ	Δ
Saalian		6	Δ	Δ	Δ	Δ	Δ	Δ	Δ	Δ		Δ		Δ	Δ	Δ	Δ	Δ	Δ	Δ	Δ	Δ	Δ	Δ	Δ	Δ	Δ	Δ	Δ	Δ		Δ	Δ	Δ	
		8		?Δ									Δ			?Δ	?Δ	?Δ			?Δ		Δ	Δ				?Δ	?						
Elsterian		?12	Δ	Δ	Δ	Δ	Δ	Δ	Δ	?Δ		Δ	Δ	?Δ	Δ	?Δ	?	?Δ	??	?Δ	Δ	Δ	?Δ	Δ	Δ	Δ		?Δ	?	Δ	?Δ	Δ	Δ	Δ	Δ
Cromerian		?14	Δ	Δ			?Δ									Δ		Δ				Δ			Δ							Δ			
		16					?Δ	?Δ								Δ		Δ	?	?			?	Δ	?Δ	Δ			Δ	Δ	?Δ	Δ	?Δ	?		
	B	?18 or 20					Δ									Δ									?Δ	Δ			?Δ			Δ			
	M	22+												Δ		Δ		Δ					Δ						Δ						
Early Pleistocene		34–38														Δ		?Δ				Δ Δ	Δ						Δ			?		Δ	
		60																																	
		64–72														Δ		?Δ			Δ		?Δ						?Δ			?			Δ
		?78–82												Δ		Δ		Δ					Δ						?Δ						Δ
Plio-Pleistocene		*c*.98–104												Δ		Δ		?Δ					?Δ						Δ			Δ			Δ
Pliocene	G	Upper														Δ													Δ			Δ			Δ
		Lower														Δ							?Δ						Δ						Δ
Miocene		Upper														Δ													Δ						Δ
		Lower														Δ							?Δ						Δ						Δ

Quaternary Glaciation, Table 2 Occurrence of glaciation in North America through the Cenozoic based on numbers of observations presented in contributions to the INQUA project "Extent and Chronology of Quaternary Glaciations" (Ehlers and Gibbard, 2004b)

Stage/age		MIS (approx)	Northern Canada and Alaska	Alberta	British Columbia	California	Great Basin	Illinois	Minnesota	Montana and North Dakota	New England	New Brunswick	New York	Nova Scotia	Ohio	Ontario	Pennsylvania	Québec	Rocky Mountains**where?	Washington	Wisconsin	Greenland
Wisconsinan		2	Δ	Δ	Δ	Δ	Δ	Δ	Δ	Δ	Δ	Δ	Δ	Δ	Δ	Δ	Δ	Δ	Δ	Δ	Δ	Δ
		3	Δ		?Δ	Δ						?Δ		?		Δ		Δ	Δ	?Δ	?	Δ
		4	Δ	?Δ	Δ	Δ	Δ				?Δ	Δ	?Δ	?Δ		Δ		Δ	Δ	Δ	Δ	Δ
Illinoian		6	Δ	Δ	Δ	Δ	Δ	Δ	Δ	Δ	Δ	?		Δ	Δ	Δ	Δ	?	Δ	?Δ	Δ	Δ
Pre-Illinoian A		8	Δ		?Δ																	Δ
Pre-Illinoian B		?12	Δ	?Δ	Δ			?Δ	Δ	?Δ							Δ					Δ
Pre-Illinoian C		?14	Δ																			Δ
Pre-Illinoian D		16	Δ			Δ		?Δ	Δ	Δ							Δ		Δ			Δ
Pre-Illinoian E	B	?18 or 20	Δ		Δ					Δ												Δ
Pre-Illinoian F	M	22+	Δ		Δ	Δ			?Δ	Δ		Δ			Δ		?Δ		Δ	?Δ	Δ	Δ
Pre-Illinoian G		34–38	Δ		?Δ	?Δ			?Δ	?Δ										?Δ		Δ
Re-Illinoian H		60	Δ			Δ			?Δ	Δ											Δ	Δ
Pre-Illinoian I, J		64–72	Δ						?Δ													Δ
		?78–82	Δ			?Δ			?Δ	Δ									?Δ		Δ	Δ
Plio-Pleistocene (pre-Illinoian K)		*c*.98–104	Δ		?Δ	Δ			?Δ	Δ							Δ					Δ
Pliocene	G	Upper	Δ		?Δ					Δ												Δ
		Lower	?Δ		Δ																	Δ
Miocene		Upper																				Δ
		Lower	Δ																			

Quaternary Glaciation, Table 3 Occurrence of glaciation in the rest of the World through the Cenozoic based on numbers of observations presented in contributions to the INQUA project "Extent and Chronology of Quaternary Glaciations" (Ehlers and Gibbard, 2004c)

Stage/age		MIS (approx)	Antarctica and Southern Ocean	Argentina	Patagonia	Bolivia	Chile	China–Tibet	China–Tianshu	Columbia	E.African mountains	Equador	Mexico	New Zealand	Tasmania
Weichselian/Wisconsinan		2	Δ	Δ	Δ		Δ	Δ	Δ	Δ	Δ	Δ	Δ	Δ	Δ
		3	Δ				Δ	Δ	Δ	Δ					
		4	Δ				Δ	Δ	Δ	Δ				Δ	
Saalian/Illinoian		6	Δ	Δ	Δ		Δ	Δ	Δ	Δ	Δ	Δ	Δ	Δ	
		8	Δ				Δ	Δ	Δ	Δ		?Δ			
Elsterian/pre-Illinoian B		?12	Δ	Δ	Δ		Δ	Δ	Δ	Δ	Δ	?Δ	?Δ	Δ	
Early middle Pleistocene		?14	Δ				Δ			Δ					
		16	Δ				Δ	?Δ	?Δ	Δ					?Δ
	B	?18 or 20	Δ		Δ		Δ			Δ					
Early Pleistocene	M	22+	Δ	Δ	Δ		Δ			?Δ	Δ				
		34–38	Δ	Δ			Δ								
		60	Δ				Δ								
		64–72	Δ	Δ			Δ								
		78–82	Δ			Δ	Δ				Δ	Δ		Δ	
Plio-Pleistocene		*c*.100–104	Δ				Δ			?Δ		Δ		Δ	
Pliocene	G	Upper	Δ			Δ	Δ					Δ		Δ	?Δ
		Lower	Δ	Δ			Δ								
Miocene		Upper	Δ				Δ								
		Lower	Δ	Δ			Δ								
Palaeogene		Palaeogene	Δ												

early Neogene to the present day. By contrast, Northern-Hemisphere glaciation, although initially somewhat restricted, increased markedly at the beginning of the Quaternary, increasing again in frequency in the latest Early Pleistocene and reaching very high levels in the Middle–Late Pleistocene. While this pattern is not unexpected, the striking increase in ice sheets through the Quaternary clearly emphasizes that worldwide glaciation is in effect a northern-hemispheric phenomenon.

Examination of the evidence accumulated in the INQUA project "Extent and Chronology of Quaternary Glaciations" (Ehlers and Gibbard, 2004a, b, c), supported by other published sources, demonstrates the current state of knowledge. When examining the resulting tables (Tables 1–3), it is important to bear in mind that the stratigraphical control between regions, beyond the range of radiocarbon dating, is weaker than might be desired. This is particularly a problem outside Europe where biostratigraphy is less well developed and the sheer extent of the unexplored regions makes future discoveries likely. Thus, the presentation below can only be a first step toward a comprehensive overview. The correlations applied here are based on the Global Correlation Chart (Gibbard and Cohen, 2008).

Plio-Pleistocene glaciation

Evidence of glaciation is widespread from throughout the Quaternary and indeed the Neogene in the northern hemisphere. The longest sequences are restricted to Alaska, and the adjacent North-West Territories of Canada which, together with Greenland and the Rockies, preserve evidence of glaciation from the Neogene to the present. In northern Canada and Alaska, the oldest till and accompanying ice-rafted detritus in marine settings dates from the Early Miocene, with regionally widespread glaciation occurring in the Pliocene and regularly throughout the Pleistocene (cf. Haug et al., 2005). In adjacent British Columbia, a comparable sequence is found, particularly in the north. Similarly, in Greenland and Iceland, glaciation began in the Miocene, occurring regularly through the Pliocene and onward to the present day in the mountains. Likewise, in Norway, its adjacent offshore and the neighboring Barents Sea, glaciation is recorded from the Early Miocene, Early Pliocene, and Plio-Pleistocene. By the late Miocene, inland ice shields were periodically present in Greenland, especially in the mountainous east, with ice reaching the sea in SE Greenland, while contiguous ice sheets have occurred since the earliest Pleistocene (*c*. 2.3 my) (Funder, personal communication, 2003). In the eastern Rockies of the USA, a much shorter glacial sequence occurs. Here Plio-Pleistocene-aged till is known from Montana, North Dakota, and California. On Mount Kilimanjaro, in East Africa, the first glaciation is recognized at *c*. 2.0 my (*c*. MIS 68). In Europe, glaciation before the Middle Pleistocene glaciation is represented only by ice-rafted material, outside the mountain regions (e.g., in the Netherlands, lowland Germany, European Russia, and Britain). Substantial glaciation of the Baltic region late in the Early Pleistocene is indicated by erratic materials in the Netherlands (1–1.2 Ma; MIS 34–36). Glaciation is also established in the Alps from the Plio-Pleistocene.

In the southern hemisphere, glaciation is much longer established, as noted above. Here the ice already formed in the Late Eocene – Early Oligocene in East Antarctica and built up in a step-like pattern through the Neogene. The present polar conditions were already established by the Early Pleistocene after 2.5 Ma. A similar history is known from the Piedmont areas of Argentina and Chile, where substantial ice caps were established by 14 Ma. Widespread lowland glaciation occurred here between 2.05 and 1.86 Ma (*c*. MIS 68–78), followed by the "Great Patagonian Glaciation" that took place at 1.15–1.00 Ma (*c*. MIS 30–34). Further north, the earliest glaciation recorded in the Bolivian Andes dates from 3.27 Ma, with extensive events at 2.2 Ma (*c*. MIS 82). In Columbia, the record also begins at 2.5 Ma. The earliest records in Australiasia are found in Tasmania and New Zealand from the Plio-Pleistocene (2.6 Ma: MIS 98–104). Only slightly younger is New Zealand's oldest known glacial event (the Porika Glaciation).

The 'glacial' Pleistocene

The 'glacial' Pleistocene effectively begins with ice sheets spreading over vast lowland areas, particularly around the North Atlantic region, and the intensification of global cold period (glacial) climates, in general. It coincides with the 'Middle Pleistocene transition' (1.2–0.8 Ma) when the transition from the dominant 41–100 Ka Milankovitch orbital cyclicity resulted in periods sufficiently cold and long to allow the development of continental-scale ice sheets.

The till sheets of the major glaciations of the 'glacial Pleistocene' are found throughout major parts of Europe and North America, and especially in the lowlands and under the sea. Widespread lowland glaciation began in the early Middle Pleistocene shortly after the Brunhes/Matuyama palaeomagnetic reversal (780 Ka). In Europe, the phases represented include the Weichselian (Valdaian, MIS 4–2), Saalian (Dniepr and Moscovian, MIS 6, 8 and 10), Elsterian (Okan, MIS 12), and the Donian (Narevian, MIS 16). More limited glaciation may also have occurred in the circum-Baltic region during the latest Early Pleistocene (MIS 20 and 22). Curiously, evidence for early Middle Pleistocene glaciation is absent from the North Atlantic and Norway, while it is certainly present in Denmark, the Baltic region, and European Russia. In the Italian Dolomites, glaciation becomes established in MIS 22 (Muttoni et al., 2003). Comparable evidence is also found from north of the Alps in Switzerland and southern Germany. Further to the west, in the Pyrenees, the oldest glaciation identified is of late Cromerian age (MIS 16 or 14). Widespread lowland glaciation again is first seen throughout North America in MIS 22. From this

point onward, major ice sheets covered large regions of the continent during the Middle Pleistocene pre-Illinoian events MIS 16, 12, 8 and 6 (Illinoian *s.s.*) and the Late Pleistocene MIS 2–4 (Wisconsinan). In Mexico, the oldest moraines on volcanoes have been dated to 195 Ka and probably relate to a pre-MIS 6 glaciation. Evidence from East Greenland suggests that its quasi-permanent ice sheet may have almost disappeared during the Eemian Stage interglacial (*c*. MIS 5e) (Funder, personal communication, 2003). Glaciation of Tibet and Tianshu is not recorded before the Middle Pleistocene, of which MIS 12 was the most extensive. In Tainshu, older glaciation (?MIS 16) may have also occurred. This apparently delayed glaciation of the Himalayan chain might reflect late uplift of high Asia. Subsequent events took place during MIS 8, 6 and 4–2, and continue today in the highest peaks.

As in Europe and North America, glaciation increased in intensity throughout the Andean chain from 800 Ka to the present day, but in the south, it was less extensive than during the Early Pleistocene events. In Australasia, following a 1 Ma break, the glacial record continues in MIS 12, followed by MIS 6, 4, and 3. In Tasmania, an early Middle Pleistocene event, possibly during MIS 16, is followed by glaciations during MIS 6 and 3. The glacial record during this time in Africa is restricted to the East African mountains Mount Kilimanjaro, Mount Kenya, and the High Atlas, where glaciations appear to be broadly equivalent to those elsewhere, i.e., during MIS 12, 6, and 2.

Last glaciation

The term Last Glacial Maximum or LGM is widely accepted as referring to the maximum global ice volume during the last glacial cycle corresponding to the trough in the marine isotope record centered on ca. 18 ^{14}C Ka BP (Martinson et al., 1987) and the associated global eustatic sea-level low also dated to 18 ^{14}C Ka BP (Yokoyama et al., 2000). It has also been assigned chronozone status (23–19 or 24–18 Ka cal BP dependent on the dating applied) by Mix et al. (2001) who consider the event should be centered on the calibrated date at 21 Ka cal BP (i.e., LGM sensu stricto). However, since the last maximum glaciation after MIS 5 occurred much earlier in some areas than in others, the term LGM should be used with care.

During the LGM, the extent of the glaciation of the Southern Hemisphere differed very little from that of the Pleistocene glacial maximum. Glaciers in Antarctica still reached to the shelf edge, and on New Zealand, Tasmania, and in South America, the glacier tongues were only slightly smaller than during earlier events (Andersen et al., 1999; Coronato et al., 2004a, b). On mainland Australia, local mountain glaciation occurred (Barrows et al., 2001, 2002). It seems that the LGM in the Southern Hemisphere began earlier than in the Northern Hemisphere, probably around 27 Ka (Suggate and Almond, 2005). The high mountains of East Africa were glaciated (Osmaston, 2004). There is no unequivocal evidence of glaciation in South Africa, although minor glaciers have been postulated by various authors (Borchert and Sänger, 1981; Hall, 1994). However, it must be borne in mind that South Africa is located relatively close to the equator to the North. Were it in the Northern Hemisphere, Cape Town would be situated at the same latitude as Atlanta in Georgia, USA or, if placed relative to the European ice sheet, it would be south of Tunis. Consequently, sea-ice cover did not reach the southern end of Africa (Figure 2b).

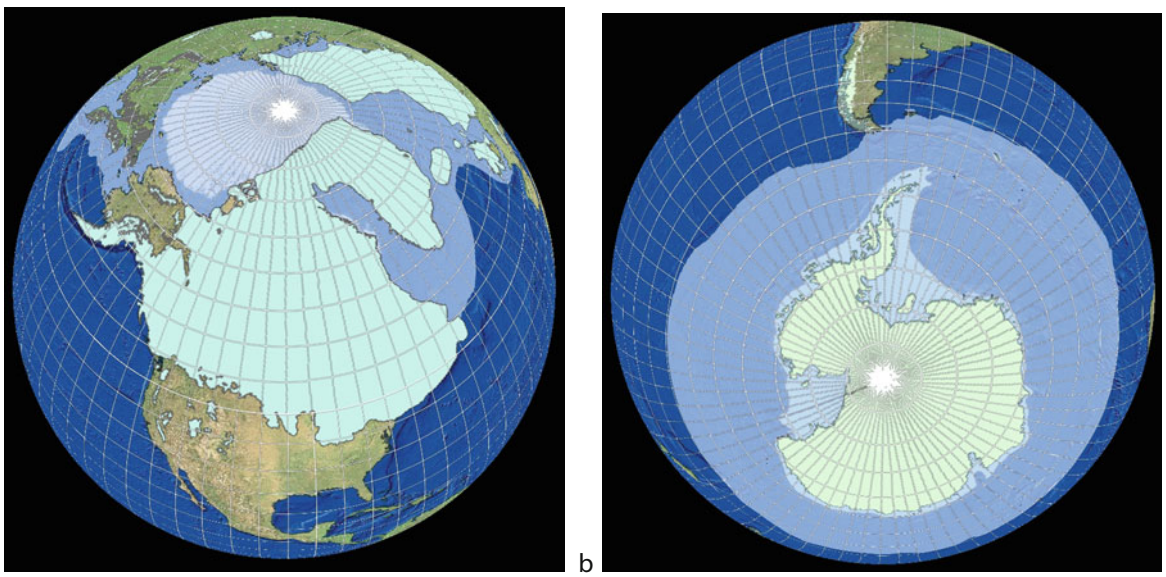

Quaternary Glaciation, Figure 2 Distribution of glaciers and sea ice in the Northern and Southern Hemispheres during the Last Glacial Maximum.

During the LGM, ice in many parts of the Northern Hemisphere reached an extent very similar to the Quaternary glacial maximum. In North America, the differences are very small. Again, most parts of Canada were ice covered, including the shelf areas (Dyke, 2004). It is the same in Greenland (Funder et al., 2004; Weidick et al., 2004). The map of global ice distribution (Figure 2a) shows that while sea-ice cover went very far south, most parts of the land areas of Beringia remained ice free.

In Europe, however, the situation was different. New evidence suggests that the North Sea was not fully glaciated during the Weichselian glacial maximum but slightly earlier (Sejrup et al., 1994, 2009; Carr, 2004). An ice sheet covered the Barents Sea and extended well into the Kara Sea but hardly touched the Russian mainland (Svendsen et al., 1999; Svendsen et al., 2004a, b). The ice sheet was markedly smaller than during the Quaternary glacial maximum. It seems that the northwards drainage of the Ob and Yenisei rivers was not impeded (Lambeck et al., 2006). Not only the glaciation of the Alps has been mapped in great detail (Figure 3), but also knowledge of the mountain glaciations has increased considerably. In glaciated mountain areas outside the major ice sheets, such as in Italy and Greece, the maximum Middle Pleistocene glaciations were much bigger than the local last glacial maxima (Giraudi, 2004; Woodward et al., 2004). This is attributed to a change in equilibrium-line altitude (ELA) because it has a much bigger impact on glacier size in areas characterized only by mountain glaciation than in areas where ice covered the lowlands during multiple glaciations.

There were major ice sheets or mountain glacier systems in the Siberian mountains further to the east. Because of the lack of detailed investigations to date, in most cases, it is not possible to differentiate between the extent of the LGM and earlier glaciations (Glushkova, 2001; Zamoruyev, 2004). Likewise, the age and extent of the glaciers in Iran and the mountain ranges and high plateaux further to the east, and especially the extent of glaciation on the Tibetan Plateau, are still matters of debate (Owen et al., 2003; Klinge and Lehmkuhl, 2004; Kuhle, 2004; Lehmkuhl and Owen, 2005; Abramowski et al., 2006). In contrast, the small mountain glaciers of Japan are well mapped and dated and, unlike those of the adjoining Asian mainland, the maximum ice advance of the last glaciation occurred in MIS 4 (Sawagaki et al., 2004). The same date for the maximum extent is found in New Zealand (Suggate, 1990; Preusser et al., 2005).

Summary

The Quaternary is synonymous with extensive glaciation of Earth's mid- and high-latitudes. Although there were

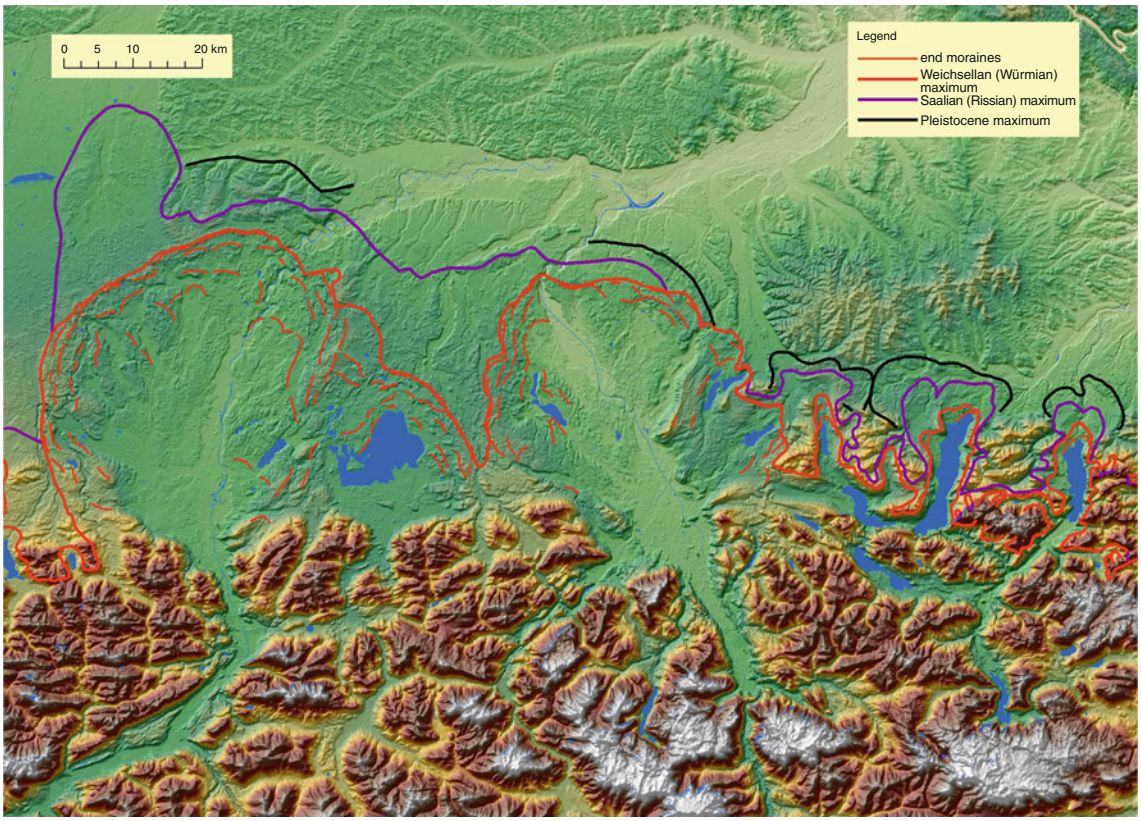

Quaternary Glaciation, Figure 3 Northern margin of the Alpine ice sheet draped on the SRTM terrain model.

local precursors, significant glaciation began in the Oligocene in eastern Antarctica. It was followed by glaciation in mountain areas through the Miocene (in Alaska, Greenland, Iceland, and Patagonia), later in the Pliocene (e.g., in the Alps, the Bolivian Andes, and possibly in Tasmania) and in the earliest Pleistocene (New Zealand, Iceland and Greenland). Today evidence from both the land and the ocean floors demonstrates that the major continental glaciations, outside the polar regions, rather than occurring throughout the 2.6 Ma of the Quaternary, were markedly restricted to the last 1 Ma to 800 Ka or less. Marine Isotope Stage (MIS) 22 (*c*. 870–880 Ma) included the first of the 'major' world-wide events with substantial ice volumes that typify the later Pleistocene glaciations (i.e., MIS 16, 12, 10, 6, 4–2).

Bibliography

Abramowski, U., Bergau, A., Seebach, D., Zech, R., Glaser, B., Sosin, P., Kubik, P. W., and Zech, W., 2006. Pleistocene glaciations of Central Asia: results from ^{10}Be surface exposure ages of erratic boulders fromthe Pamir (Tajikistan), and the Alay-Turkestan range (Kyrgyzstan). *Quaternary Science Reviews*, **25**, 1080–1096.

Andersen, B. G., Denton, G. H., and Lowell, Th V., 1999. Glacial geomorphologic maps of Llanquihue Drift in the area of the southern Lake District, Chile. *Geografiska Annaler*, **81A**, 155–166.

Barrows, T. T., Stone, J. O., Fifield, L. K., and Cresswell, R. G., 2001. Late Pleistocene glaciation of the Kosciuszko Massif, Snowy Mountains, Australia. *Quaternary Research*, **55**, 179–189.

Barrows, T. T., Stone, J. O., Fifield, L. K., and Cresswell, R. G., 2002. The timing of the Last Glacial Maximum in Australia. *Quaternary Science Reviews*, **21**, 159–173.

Borchert, G., and Sänger, H., 1981. Research findings of a Pleistocene glaciation of the Cape mountain-ridge in South Africa. *Zeitschrift für Geomorphologie*, **25**, 222–224.

Carr, S. J., 2004. The North Sea basin. In Ehlers, J., and Gibbard, P. L. (eds.), *Quaternary Glaciations – Extent and Chronology, Part I: Europe*. Amsterdam: Elsevier. Developments in Quaternary Science, Vol. 2a, pp. 261–270.

Coronato, A., Martínez, O., and Rabassa, J., 2004a. Glaciations in Argentine Patagonia, southern South America. In Ehlers, J., and Gibbard, P. L. (eds.), *Quaternary Glaciations – Extent and Chronology, Part III: South America, Asia, Africa, Australasia, Antarctica*. Amsterdam: Elsevier. Developments in Quaternary Science, Vol. 2c, pp. 49–67.

Coronato, A., Meglioli, A., and Rabassa, J., 2004b. Glaciations in the Magellan Straits and Tierra del Fuego, southernmost South America. In Ehlers, J., and Gibbard, P. L. (eds.), *Quaternary Glaciations – Extent and Chronology, Part III: South America, Asia, Africa, Australasia, Antarctica*. Amsterdam: Elsevier. Developments in Quaternary Science, Vol. 2c, pp. 45–48.

Dyke, A., 2004. An outline of North American deglaciation with emphasis on central and northern Canada. In Ehlers, J., and Gibbard, P. L. (eds.), *Quaternary Glaciations – Extent and Chronology, Part II: North America*. Amsterdam: Elsevier. Developments in Quaternary Science, Vol. 2b, pp. 1–7.

Ehlers, J., and Gibbard, P. L., 2003. Extent and chronology of glaciations. *Quaternary Science Reviews*, **22**, 1561–1568.

Ehlers, J., and Gibbard, P. L. (eds.), 2004a. *Quaternary Glaciations – Extent and Chronology, Part I: Europe*. Amsterdam: Elsevier. Developments in Quaternary Science, Vol. 2a.

Ehlers, J., and Gibbard, P. L. (eds.), 2004b. *Quaternary Glaciations – Extent and Chronology, Part II: North America*. Amsterdam: Elsevier. Developments in Quaternary Science, Vol. 2b.

Ehlers, J., and Gibbard, P. L. (eds.), 2004c. *Quaternary Glaciations – Extent and Chronology, Part III: South America, Asia, Africa, Australasia, Antarctica*. Amsterdam: Elsevier. Developments in Quaternary Science, Vol. 2c.

Ehlers, J., and Gibbard, P., 2008. Extent and chronology of Quaternary glaciation. *Episodes*, **31**(No.2), 211–218.

Flint, R. F., 1971. *Glacial and Quaternary Geology*. John Wiley, New York.

Funder, S., Jennings, A., and Kelly, M., 2004. Middle and late Quaternary glacial limits in Greenland. In Ehlers, J., and Gibbard, P. L. (eds.), *Quaternary Glaciations – Extent and Chronology, Part II: North America*. Amsterdam: Elsevier. Developments in Quaternary Science, Vol. 2b, pp. 425–430.

Gibbard, P. L., and Cohen, K. M., 2008. Global chronostratigraphical correlation table for the last 2.7 million years. *Episodes*, **31**, 243–247.

Giraudi, C., 2004. The Apennine glaciations in Italy. In Ehlers, J., and Gibbard, P. L. (eds.), *Quaternary Glaciations – Extent and Chronology, Part I: Europe*. Amsterdam: Elsevier. Developments in Quaternary Science, Vol. 2a, pp. 215–223.

Glushkova, O. Y., 2001. Geomorphological correlation of Late Pleistocene glacial complexes of Western and Eastern Beringia. *Quaternary Science Reviews*, **20**, 405–417.

Hall, K., 1994. Cutbacks in the Natal Drakensberg Escarpment: an hypothesis on their origin. *South African Journal of Science*, **90**, 263–264.

Haug, H. H., Ganopolski, A., Sigman, D. M., Rosell-Mele, A., Swann, G. E. A., Tiedemann, R., Jaccard, S. L., Bollman, J., Maslin, M. A., Leng, M. J., and Eglinton, G., 2005. North Pacific seasonality and the glaciation of North America 2.7 million years ago. *Nature*, **433**, 821–825.

Klinge, M., and Lehmkuhl, F., 2004. Pleistocene glaciations in southern and eastern Tibet. In Ehlers, J., and Gibbard, P. L. (eds.), *Quaternary Glaciations – Extent and Chronology, Part III: South America, Asia, Africa, Australasia, Antarctica*. Amsterdam: Elsevier. Developments in Quaternary Science, Vol. 2c, pp. 361–369.

Kuhle, M., 2004. The High Glacial (Last Ice Age and LGM) ice cover in High and Central Asia. In Ehlers, J., and Gibbard, P. L. (eds.), *Quaternary Glaciations – Extent and Chronology, Part III: South America, Asia, Africa, Australasia, Antarctica*. Amsterdam: Elsevier. Developments in Quaternary Science, Vol. 2c, pp. 175–199.

Lambeck, K., Purcell, A., Funder, S., Kjær, K. H., Larsen, E., and Möller, P., 2006. Constraints on the Late Saalian to early Middle Weichselian ice sheet of Eurasia from field data and rebound modelling. *Boreas*, **35**, 539–575.

Lehmkuhl, F., and Owen, L., 2005. Late Quaternary glaciation of Tibet and the bordering mountains: a review. *Boreas*, **34**, 87–100.

Martinson, D. G., Pisias, N. G., Hays, J. D., Imbrie, J., Moore, T. C., and Shackleton, N. J., 1987. Age dating and the orbital theory of the ice ages: development of a high resolution 0–300,000 year chronostratigraphy. *Quaternary Research*, **27**, 1–29.

Mix, A. C., Bard, E., and Schneider, R., 2001. Environmental processes of the ice age: land, oceans, glaciers (EPILOG). *Quaternary Science Reviews*, **20**, 627–657.

Muttoni, G., Carcano, C., Garzanti, E., Ghielmi, M., Piccin, A., Pini, R., Rogledi, S., and Sciunnach, D., 2003. Onset of Pleistocene glaciations in the Alps. *Geology*, **31**, 989–992.

Osmaston, H., 2004. Quaternary glaciations in the East African mountains. In Ehlers, J., and Gibbard, P. L. (eds.), *Quaternary Glaciations – Extent and Chronology, Part III: South*

America, Asia, Africa, Australasia, Antarctica. Amsterdam: Elsevier. Developments in Quaternary Science, Vol. 2c, pp. 139–150.

Owen, L. A., Haizhou, M., Derbyshire, E., Spencer, J. Q., Barnard, P. L., Nian, Z. Y., Finkel, R. C., and Caffee, M. W., 2003. The timing and style of Late Quaternary glaciation in the La Ji Mountains, NE Tibet: evidence for restricted glaciation during the latter part of the Last Glacial. *Zeitschrift für Geomorphologie*, **130**, 263–276. Supplement band.

Preusser, F., Andersen, B. G., Denton, G. H., and Schlüchter, Ch., 2005. Luminescence chronology of Late Pleistocene glacial deposits in North Westland, New Zealand. *Quaternary Science Reviews*, **24**, 2207–2227.

Sawagaki, T., Aoki, T., Hasegawa, H., Iwasaki, Sh, Iwata, Sh, and Hirakawa, K., 2004. Late Quaternary glaciations in Japan. In Ehlers, J., and Gibbard, P. L. (eds.), *Quaternary Glaciations – Extent and Chronology, Part III: South America, Asia, Africa, Australasia, Antarctica*. Amsterdam: Elsevier. Developments in Quaternary Science, Vol. 2c, pp. 217–225.

Sejrup, H. P., Nygård, A., Hall, A. M., and Haflidason, H., 2009. Middle and Late Weichselian (Devensian) glaciation history of south-western Norway, North Sea and eastern UK. *Quaternary Science Reviews*, **28**, 370–380.

Sejrup, H. P., Haflidason, H., Aarseth, I., Forsberg, C. F., King, E., Long, D., and Rokoengen, K., 1994. LateWeichselian glaciation history of the northern North Sea. *Boreas*, **23**, 1–13.

Suggate, R. P., 1990. Late Pliocene and Quaternary glaciations of New Zealand. *Quaternary Science Reviews*, **9**, 175–197.

Suggate, R. P., and Almond, P. C., 2005. The Last Glacial Maximum (LGM) in western South Island, New Zealand: implications for the global LGM and MIS 2. *Quaternary Science Reviews*, **24**, 1923–1940.

Svendsen, J. I., Astakhov, V. I., Bolshiyanov, D. Y., Demidov, I., Dowdeswell, J. A., Gataullin, V., Hjort, C., Hubberten, H. W., Larsen, E., Mangerud, J., Melles, M., Möller, P., Saarnisto, M., and Siegert, M. J., 1999. Maximum extent of the Eurasian ice sheets in the Barents and Kara Sea region during the Weichselian. *Boreas*, **28**, 234–242.

Svendsen, J. I., Gataullin, V., Mangerud, J., and Polyak, L., 2004a. The glacial history of the Barents and Kara Sea Region. In Ehlers, J., and Gibbard, P. L. (eds.), *Quaternary Glaciations – Extent and Chronology, Part I: Europe*. Amsterdam: Elsevier. Developments in Quaternary Science, Vol. 2a, pp. 369–378.

Svendsen, J. I., Alexanderson, H., Astakhov, V. I., Demidov, I., Dowdeswell, J. A., Funder, S., Gataullin, V., Henriksen, M., Hjort, C., Houmark-Nielsen, M., Hubberten, H. W., Ingolfsson, O., Jakobsson, M., Kjær, K. H., Larsen, E., Lokrantz, H., Lunkka, J. P., Lysså, A., Mangerud, J., Matiouchkov, A., Murray, A., Möller, P., Niessen, F., Nikolskaya, O., Polyak, L., Saarnisto, M., Siegert, C., Siegert, M. J., Spielhagen, R. F., and Stein, R., 2004b. Late Quaternary ice-sheet history of northern Eurasia. *Quaternary Science Reviews*, **23**, 1229–1271.

Weidick, A., Kelly, M., and Bennike, O., 2004. Late Quaternary development of the southern sector of the Greenland Ice Sheet, with particular reference to the Qassimiut lobe. *Boreas*, **33**, 284–299.

Woodward, J. C., Macklin, M. G., and Smith, G. R., 2004. Pleistocene glaciation in the mountains of Greece. In Ehlers, J., and Gibbard, P. L. (eds.), *Quaternary Glaciations – Extent and Chronology, Part I: Europe*. Amsterdam: Elsevier. Developments in Quaternary Science, Vol. 2a, pp. 155–173.

Yokoyama, Y., Lambeck, K., DeDeckker, P., Johnston, P., and Fifield, K., 2000. Timing of the Last Glacial Maximum from observed sea-level minima. *Nature*, **406**, 713–716.

Zamoruyev, V., 2004. Quaternary glaciation of north-eastern Asia. In Ehlers, J., and Gibbard, P. L. (eds.), *Quaternary Glaciations – Extent and Chronology, Part III: South America, Asia, Africa, Australasia, Antarctica*. Amsterdam: Elsevier. Developments in Quaternary Science, Vol. 2c, pp. 321–323.

Cross-references

Antarctica
Isotopic Fractionation of Freezing Water
Pleistocene Epoch

R

RADAR APPLICATION IN SNOW, ICE, AND GLACIERS

G. Venkataraman, Gulab Singh
Centre of Studies of Resources Engineering, Indian Institute of Technology Bombay, Mumbai, Bombay, India

Synonyms

Radar and glaciology

Definition

Radar. The term RADAR is an acronym for "RAdio Detection And Ranging." Radar is a system that uses electromagnetic waves to determine range, speed, direction, and physical properties of any target. Typically, a radar system has a transmitter and a receiver. The transmitter transmits the electromagnetic waves. The transmitted waves are reflected back by the target and are sensed using the receiver. The amplitude, phase, and the frequency shift of the received waves with respect to the transmitted waves give a measure of the properties of the target.
Snow. Dry snow is the mixture of ice and air whereas wet snow is the mixture of ice, air, and contents of free liquid water (wetness).
Ice. A mass of frozen water.
Glacier. A large mass of ice, which is moving very slowly through a valley or spreading outward from a center. Glaciers form over many years from packed snow in areas where snow accumulates faster than it melts.

Introduction

This entry elucidates the recent developments in the application of Microwave Remote Sensing techniques particularly space borne synthetic aperture RADAR (SAR) systems for snow, ice, and glacier studies. SAR is an active system imaging the earth's surface in day and night, in all weather, through cloud or haze, and their spatial resolution is compatible with the topographic variations in the Himalayan region. Currently space borne synthetic aperture RADAR data are widely used to map glacier-covered area in alpine and Himalayan regions and also to develop algorithms to infer geophysical parameters. Backscatter image of RADAR is extremely useful for the quantitative estimation of snowpack characteristics like snow wetness, snow grain size, snow density, and snow water equivalence, which are essential for hydrologic applications.

SAR data can also be useful to map snow cover and also identify different types of snow. Multi-temporal SAR data have great potential in mapping glacier facies which has distinct advantage in the glacier mass balance estimation. Various satellite SAR systems available in the past and present are presented in Table 1.

Radar data processing methodology

Calculation of backscattering coefficient
For any meaningful and quantitative analysis of Radar images, it is necessary to convert the DN values of these intensity images into their corresponding radar backscattering coefficient (σ^o) values. A variety of factors influence backscatter strength including satellite ground-track, incidence angle, radar polarization, surface roughness, and the dielectric properties of the surface. Different objects having same digital number are likely to correspond to different backscatter values. Hence, more accurate analysis on microwave remote sensing image can be done on backscatter value images. For example, Advanced Synthetic Aperture Radar data processing methodology is given in this entry.

Vijay P. Singh, Pratap Singh & Umesh K. Haritashya (eds.), *Encyclopedia of Snow, Ice and Glaciers*, DOI 10.1007/978-90-481-2642-2,

Radar Application in Snow, Ice, and Glaciers, Table 1 Present and past space borne SAR systems

Sensor	Band/Frequency (GHz)	Polarization capability	Incidence angle (°)	Pixel resolution in m	Available time frame
ERS-1/2	C	VV	Fixed at 23°	3.8–12.5	Since 1991/1995
SIR-C/X-SAR	L,C & X/1.25, 5.3 & 9.6	HH + HV + VH + VV VV	Varying with date takes (17°–63°)	6–27	April and October, 1994
JERS-1	L/1.27	HH	Fixed at 35°	18	1994–1997
RADARSAT-1	C/5.3	HH	Varying with mode (10°–58°)	8–100	Since 1997
ASAR	C/5.6	HH or VV HH + HV HH + VV VV + VH	varying with mode (15°–45°)	3.8–150	Since 2002
PALSAR	L/1.27	(HH + HV + VH + VV) (HH + HV) HH	Varying with mode (8°–60°)	10–100	Since January 2006
TerraSAR-X	X/9.6	VV/HH (HH + HV) (VV + VH) (HH + VV) (HH + HV + VH + VV Experimental Mode only)	Varying with mode (20°–55°)	1–16	Since June 2007
RADARSAT-2	C/5.4	(HH + HV + VH + VV) (HH + VH) (VV + VH) HH	Varying with mode (10°–60°)	3–100	Since December 2007

As described in ESA document Rosich and Meadows (2004), the backscattering coefficient (σ^o) values of ASAR are obtained by combining the radar average pixel intensity and the incidence angle (I_j) at each pixel location, where the angle of incidence is obtained from the ASAR header data using interpolation method.

Radar average pixel intensity was then converted into backscatter coefficient (σ^0) using the following equation Rosich and Meadows (2004):

$$\sigma_j^{\,0} = \frac{< DN^2 >}{K} \times \left(\frac{R_{\mathrm{d}}}{R_{\mathrm{ref}}}\right)^4 \times \left(\frac{1}{G^2}\right) \times \mathrm{Sin}(\mathrm{I}_j) \qquad (1)$$

where I_j is the incidence angle at the j^{th} range pixel (the angle between radar line of sight and vertical when assuming a flat earth or it is equivalent to look angle), K is the absolute calibration constant, $<DN^2>$ is average pixel intensity, G^2 is two-way antenna gain at distributed target look angle, R_{d} is distributed target slant range distance, and R_{ref} is reference slant range distance. All images were multi-looked five times in azimuth and one time in range direction. Originally the image size is 24,886 lines by 6,033 pixels. After multi-looking and also removing nonoverlapping portion of the image, the size of the image is 4,997 lines by 6,033 pixels. The final spatial resolution is about 19.5 m in azimuth and 7.8 m in range. All the images were subjected to speckle suppression using Frost filter (Frost et al., 1982) with window size 3 × 3, and coefficient of variation and smoothing parameter using ERDAS Imagine radar module. The backscatter intensity images were converted into backscattering coefficient by taking $10.\mathrm{Log}_{10}\,(\sigma_{\mathrm{j}}^{\,0})$.

Slant-to-ground range correction

Using slant-to-ground range correction tool, the satellite data are projected into ground distance. Each pixel represents a specific area on the ground. Multi-look images are projected from slant-to-ground range. The input (slant range) pixel size 7.8 m is converted into given output (ground range) pixel size 19.5 m using satellite parameters like near range look angle, satellite height, slant range pixel size, and near slant range. After slant-to-ground range correction, finally spatial resolution of image is about 19.5 m in azimuth and 19.5 m in ground range and the size of the image is 4,983 lines by 3,685 pixels.

Due to the oblique incidence of SAR beam the terrain features become distorted in the image. This terrain distortion correction is performed by relating each pixel in the SAR image into cartographic reference system using high precision digital elevation model (DEM) and knowledge of the imaging and processing geometry. Among the above parameters geometric structure of the target plays an important role to correct the radar backscatter coefficient values. The topographic effect can be removed from the backscatter coefficient values by considering the local incidence angle. Finally, real-time snow parameters collected on these dates at different locations have been considered for calculating snow parameters, and

corresponding backscattering values were obtained from the corrected SAR backscattering images. The data processing steps are shown in Figure 1.

Radar applications in snow

Microwave interaction with snow

Microwave interaction with snow depends on dielectric and geometric properties of the object. Sensor properties also influence the target response to incident wave. In the case of snow-covered terrain, the total backscattered signal is the sum of scattering from air-snow, volume scattering in the snow layer, and scattering from the snow-ground attenuated by snow layer (Ulaby et al., 1986):

$$\sigma^0(\theta) = \sigma^0{}_{\mathrm{s}}(\theta) + \sigma^0{}_{\mathrm{v}}(\theta') + \frac{\gamma^2{}_{\mathrm{s}}(\theta')}{L^2(\theta')}\sigma^0{}_{\mathrm{g}}(\theta') \tag{2}$$

where $\sigma^0{}_{\mathrm{sa}}(\theta)$is surface scattering by the air/snow interface, $\sigma^0{}_{\mathrm{s}}(\theta')$is the volume backscattering by the snow layer, $\gamma_{\mathrm{s}}(\theta')$ is the power transmission coefficient for the air/snow boundary, $L^2(\theta')$is the one-way loss factor of the snow layer, $\sigma^0{}_{\mathrm{g}}(\theta')$is the scattering coefficient of the ground surface, and θ' is the transmission angle in the snow layer.

Information about the extension and the properties of snow-covered areas are very important for climatological and hydrological investigations. Because the physical mechanisms governing the backscattering from natural snow cover are complicated, unequivocal relationships between snowpack properties and SAR observations do not exist (Strozzi and Matzler, 1998). Hence, an intensive study is required for proper understanding of the interaction between microwaves and snow cover. These studies can proceed in two different ways.

For dry snow cover the backscattering from the snow surface may be neglected and the total backscattering is a combination of volume scattering from snow and surface scattering from the ground. In *wet snow*, the absorption loss is high and the scattering from the snow/ground interface may be neglected. The presence of liquid water content increases the absorption coefficient. Therefore, the volume scattering albedo is inversely correlated to snow wetness and snow density. At constant wetness and density, the volume scattering albedo increases as the size of the scatterers or their size variation increases, because, as Rayleigh scattering theory explains, the scattering coefficient is proportional to the third power of the scatterer's radii for a given volume fraction (Shi and Dozier, 1995).

Snowpack characteristics

Empirical relations

On the experimental side, in situ backscattering measurements of a homogeneous scene are made and the snow cover characteristics are collected simultaneously (Strozzi and Matzler, 1998). These measurements can be used in developing empirical models for snow parameters.

Backscattering from a snow-covered terrain depends on (1) sensor parameters, which include frequency, polarization, and viewing geometry, and (2) snowpack and ground parameters, which include snow density, liquid water content, ice particle size and shape, surface roughness parameters, and stratification also.

Inversion algorithms

Inversion model for dry snow density. Microwave interaction with snow depends on dielectric and geometric properties of the snow. Sensor properties also influence the target response to incident wave. In the case of snow-covered terrain, different processes contribute to the total backscattered signal: (1) scattering at the air/snow interface, (2) scattering inside the snow layer due to ice particles and at density boundaries, and (3) scattering at the snow/ground interface.

Total backscattering from the snow is sum of scattering from air-snow, volume scattering in the snow layer, and scattering from the snow-ground attenuated by snow layer (Ulaby et al., 1986). Due to large penetration (approximately 10 m at 200 kg/m^3 snow density) at C-band, in dry snow layer and small contribution of air/snow interface scattering in total backscattering from dry snow, we can neglect the air/snow interface scattering contribution from the total backscattering coefficient (Shi et al., 1990). Therefore total backscattering coefficient for dry snow is the sum of two main components, that is, snow volume backscattering and snow-ground backscattering.

Under an assumption that snow surface has no significant air/snow interface scattering and angle of refraction remains constant in dry snowpack, total backscattering from the dry snowpack can be defined as

$$\sigma_{\mathrm{t}}{}^{\mathrm{pp}}(k,\theta) = \sigma_{\mathrm{v}}{}^{\mathrm{pp}}(k_1,\theta_{\mathrm{r}}) + \sigma_{\mathrm{sg}}{}^{\mathrm{pp}}(k_1,\theta_{\mathrm{r}}) \tag{3}$$

In Equation 3, σ_{t}, σ_{v}, and σ_{sg} are total backscattering, volume backscattering, and snow/ground interface backscattering coefficients, respectively. pp is either VV or HH. k and k_1 are the incident wave numbers in the air and in snowpack, respectively. θ is incident angle and θ_{r} is angle of refraction.

The incident angle at air/snow interface and the angle of refraction in the snow layer and snow/ground interface can be related by the Snell's law. The observable change of wavelength at different densities in snow layers is found at L-band (Shi and Dozier, 2000) by comparing the difference between incident angle at air/snow interface and at snow/ground interface with different snow density (100–500 kg/m^3). For a given snow density, incident angle at the snow surface causes the change in the incident angle in the snow layer. These changes are observed at L-band propagation wavelength by Shi and Dozier (Shi and Dozier, 2000). Therefore, these changes can also be considered at C-band because C-band has lower penetration capability as compared to L-band. Hence C-band is more sensitive for above mentioned changes as compared to L-band. Since both the angle of refraction and wavelength

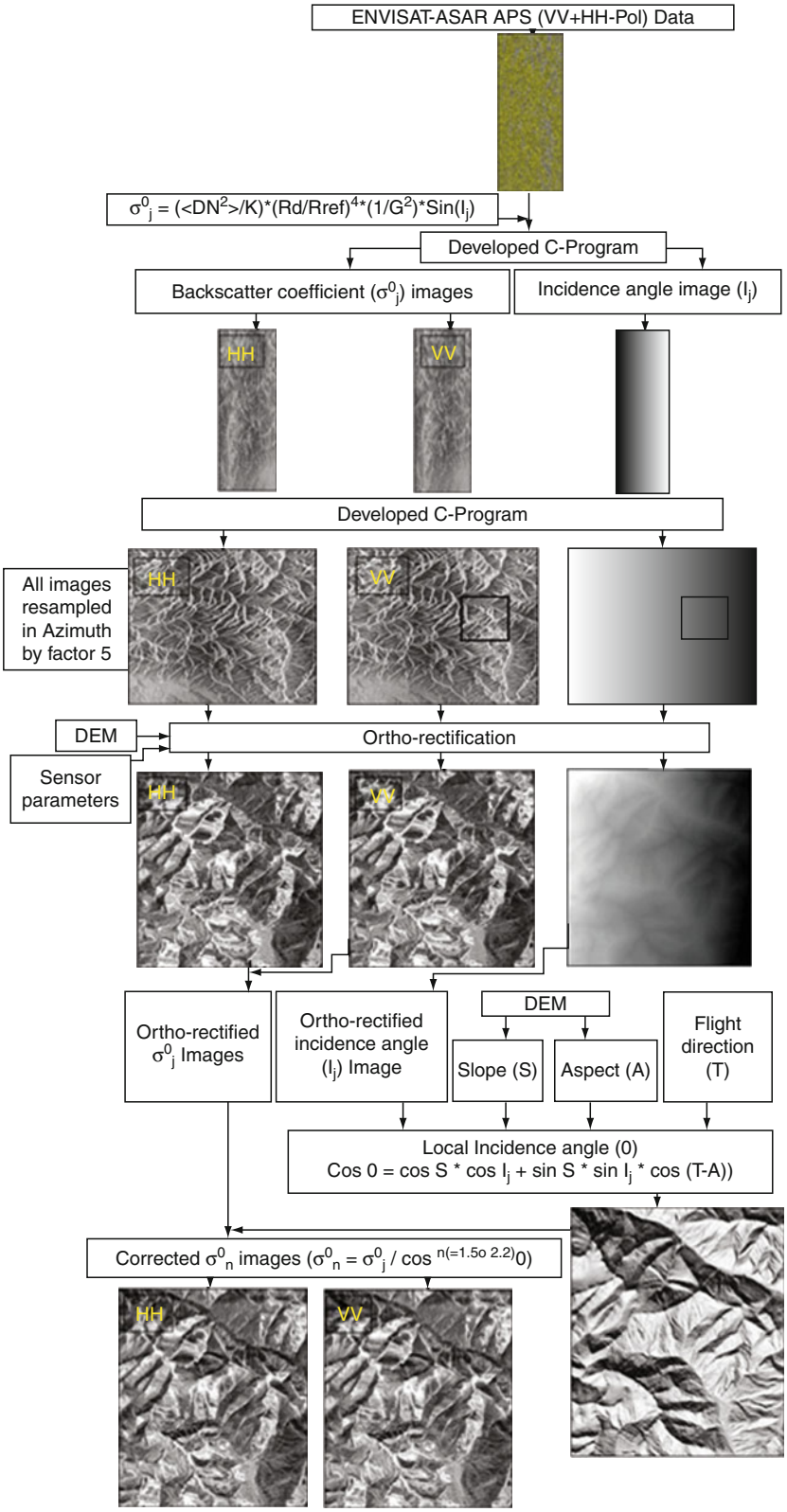

Radar Application in Snow, Ice, and Glaciers, Figure 1 Data processing steps in details.

shifts are only a function of the snow dielectric constant, which is mainly governed by the snow density, it is possible to estimate snow density by using C-band ASAR data.

For developing an algorithm for snow density estimation, the first order volume scattering model and the integral equation method with an exponential correlation function for the surface backscattering contribution from the snow/ground interface could be used. Both models depend on the four unknown functions, namely, dielectric constant, incident angle, volume scattering albedo, and root mean square height and surface correlation length. In case of snow/ground interface, using best pair of polarization, the unknown can be reduced to only dielectric constant and incident angle. In the case of volume backscattering, using volume backscattering ratios, the unknown can be reduced to only dielectric constant and incident angle. In the final term combining both volume backscatter and snow-ground scattering, only two functions, namely, incident angle and dielectric constant, remain (Singh and Venkataraman, 2009):

$$\sigma_t^{AP(vvhh)} = \frac{\sigma_t^{hh} \times \left(\frac{|T_{vv}|^2}{|T_{hh}|^2}\right) \times \left(\frac{|\alpha_{vv}|}{|\alpha_{hh}|}\right) + \sigma_t^{vv}}{\left(\frac{|T_{vv}|}{|T_{hh}|}\right) \times \left[\left(\frac{|\alpha_{vv}|}{|\alpha_{hh}|}\right) + 1\right]} \tag{4}$$

where

$$\begin{cases} \alpha_{hh} = \dfrac{\cos\theta - \sqrt{\varepsilon_s - \sin^2\theta}}{\cos\theta + \sqrt{\varepsilon_s - \sin^2\theta}} \\ \alpha_{vv} = (\varepsilon_s - 1)\dfrac{\sin^2\theta - \varepsilon_s(1 + \sin^2\theta)}{\left[\varepsilon_s \cos\theta + \sqrt{\varepsilon_s - \sin^2\theta}\right]^2} \end{cases} \tag{5}$$

T_{vv} and T_{hh} are Fresnel transmission coefficients, θ is incidence angle and it can be replaced by Snell's law, that is, $\sin^2\theta = \varepsilon_s \sin^2\theta_r$ in Equation 5. By knowing the incident angle, Equation 4 can be used to estimate the dielectric constant of the snow, which can be directly related to snow density using Looyenga's semiempirical formula given by (Looyenga, 1965)

$$\varepsilon_s = 1 + 1.5995\rho_s + 1.861\rho_s^3 \tag{6}$$

Integral equation method based algorithm is given which has been developed for retrieval of snow density from polarimetric data at C-band. An algorithm is also applied on radar backscattering coefficient for the estimation of snow permittivity and snow density in Himalayan region. ASAR estimated values for snow density have been validated by in situ measurements recorded concurrently with ENVISAT ASAR pass in the study region. The ground truth data are the average value from the top to bottom of snow layers of each snow pit. The field measured and estimated snow densities are given in Table 2. The comparison of snow density between field measured and ASAR estimated at seven snow pits has been done.

Radar Application in Snow, Ice, and Glaciers, Table 2 Measured and estimated snow density

Estimated ρ_s (kg/m^3)	Measured ρ_s (kg/m^3)	Absolute error $\|\Delta\|$ (kg/m^3)	Mean absolute error
204	242	38	21.2 kg/m^3
217	252	35	
240	247	7	
258	266	8	
280	268	12	
308	274	34	
321	306	15	

The absolute error was observed to be 21.2 kg/m^3. It indicates that the algorithm works well for the seasonal fresh snow cover. At higher elevation to moderate elevation, calculated snow density is observed to be 400–500 kg/m^3, increasing to <100–400 kg/m^3 at moderate to lower elevation (Figure 2).

At the lower altitudes area, snow is fresh and thin. On the other hand, due to permanent snow cover at higher altitudes or over glaciers, there is a recrystallization process which results in the density increase. The spatial distribution of estimated snow density agrees well with regional condition.

The model does not require roughness properties. This investigation shows that this algorithm can be used for estimating dry snow density. The model can be applied to the seasonal snow cover when the snow is dry where the subsurface is soil or rock. The mean absolute error between measured and estimated snow density was found to be 21.2 kg/m^3 where subsurface is soil without vegetation cover but it may not be useful where the subsurface is dominated by volume scattering, for example, in snow-covered firn area.

Furthermore, effect of vegetation cover on snow density mapping may be included for accurate mapping of snow cover in vegetated area. Best range of incident angle will be found out for this model because this model is dependent on incident angle.

Inversion model for wetness estimation. For this entry, authors have demonstrated Integral Equation Method based inversion model, which has been developed (Shi and Dozier, 1995) for retrieval of snow wetness from polarimetric data at C-band. This model includes two main scattering components (snow volume backscatter and surface backscatter from air/snow interface) for wet snow.

The first order volume scattering and surface scattering models depend on the four unknown functions, namely, dielectric constant, incident angle, volume scattering albedo, and root mean square height and surface correlation length. In the case of surface backscattering through simplified nonlinear regression equations and also using best pair of polarization, the unknown can be reduced to only dielectric constant. In the case of volume backscattering, using volume backscattering ratios, the unknown can

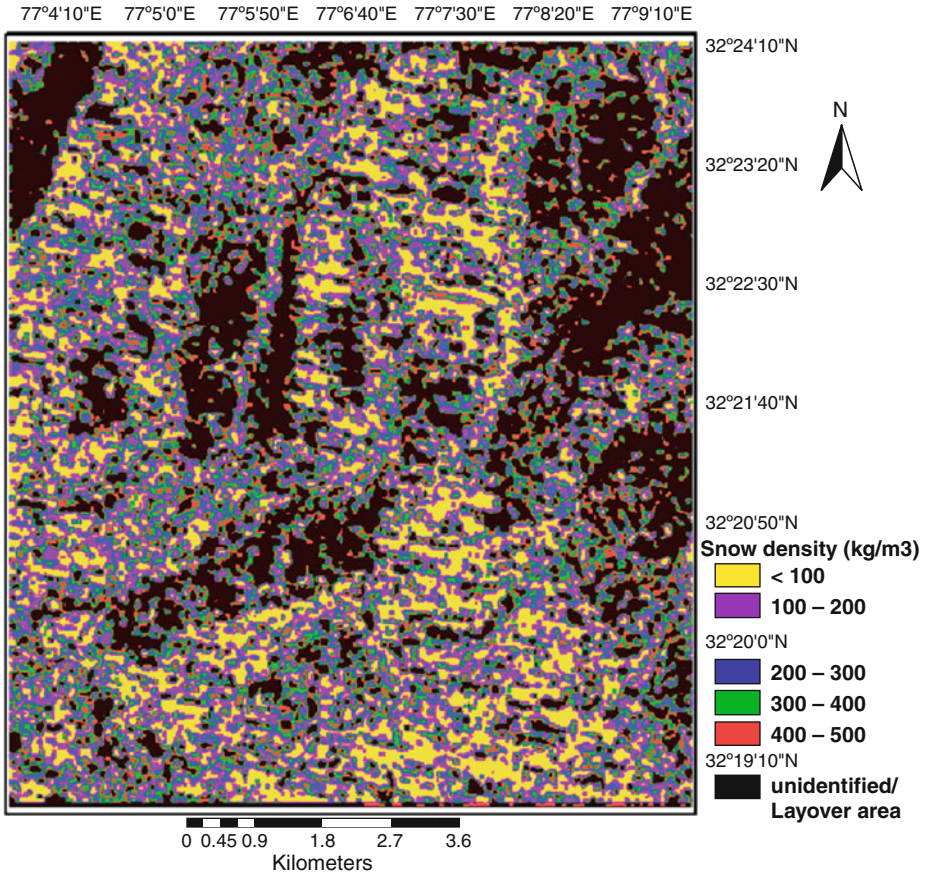

Radar Application in Snow, Ice, and Glaciers, Figure 2 Snow density map of 24 Dec. 2007.

be reduced to only dielectric constant and incident angle. In the final term combining both surface and volume backscatter, only two functions, namely, incident angle and dielectric constant, will remain. Knowing the incident angle, one can solve snow permittivity which can be directly related to snow wetness.

Equation 7 can be used to estimate the permittivity of the snow:

$$M_1[a_{vx}\mathrm{Re}[\alpha_{vv}\alpha^*{}_{hh}](a_{vhx}D_{RS}-D_{TS})+b_{vx}M_2] = M_2\left[a_{vx}(\theta_i)\mathrm{Re}[\alpha_{vv}\alpha^*{}_{hh}] + \frac{b_{vx}M_2}{a_{vhx}D_{RS}-D_{TS}} - D_{Tv}|\alpha_{vv}|^2\right] \quad (7)$$

where

$$M_1 = \sigma_t{}^{vvhh} - D_{TV}\sigma_t{}^{vv} \quad (8)$$

$$M_2 = \sigma_t{}^{vv} + \sigma_t{}^{vv} - D_{TS}\sigma_t{}^{vvhh} \quad (9)$$

$$D_{TS} = \frac{D_{TV}+D_{TH}}{D_{TV}D_{TH}} \quad (10)$$

$$D_{RS} = \frac{|\alpha_{vv}|^2+|\alpha_{hh}|^2}{\mathrm{Re}[\alpha_{vv}\alpha^*{}_{hh}]^2} \quad (11)$$

$$D_{TV} = \frac{\sigma_v{}^{vvhh}}{\sigma_v{}^{vv}} = \frac{\mathrm{Re}[T_{vvhh}]^2}{T^2{}_{vv}} \quad (12)$$

$$D_{TH} = \frac{\sigma_v{}^{vvhh}}{\sigma_v{}^{hh}} = \frac{\mathrm{Re}[T_{vvhh}]^2}{T^2{}_{vv}} \quad (13)$$

$$\sigma_v{}^{vvhh} = \mathrm{Re}\left[S_v{}^{vv}S_v{}^{hh*}\right] \quad (14)$$

and the coefficient $a_{vx}(\theta_i), b_{vx}(\theta_i)$ and $a_{vhx}(\theta_i)$ are provided in the appendix of Shi and Dozier (1995). Figure 3 shows ASAR estimated snow wetness image based on the modified Shi and Dozier (1995) inversion model.

Model for grain size estimation. A dry snow layer is a heterogeneous medium composed of ice particles with different size and microstructures. When snow is dry, the principle mechanism is volume scattering from the snowpack, and the most important variables are density and grain size. Backscattering increases as the snow grain size

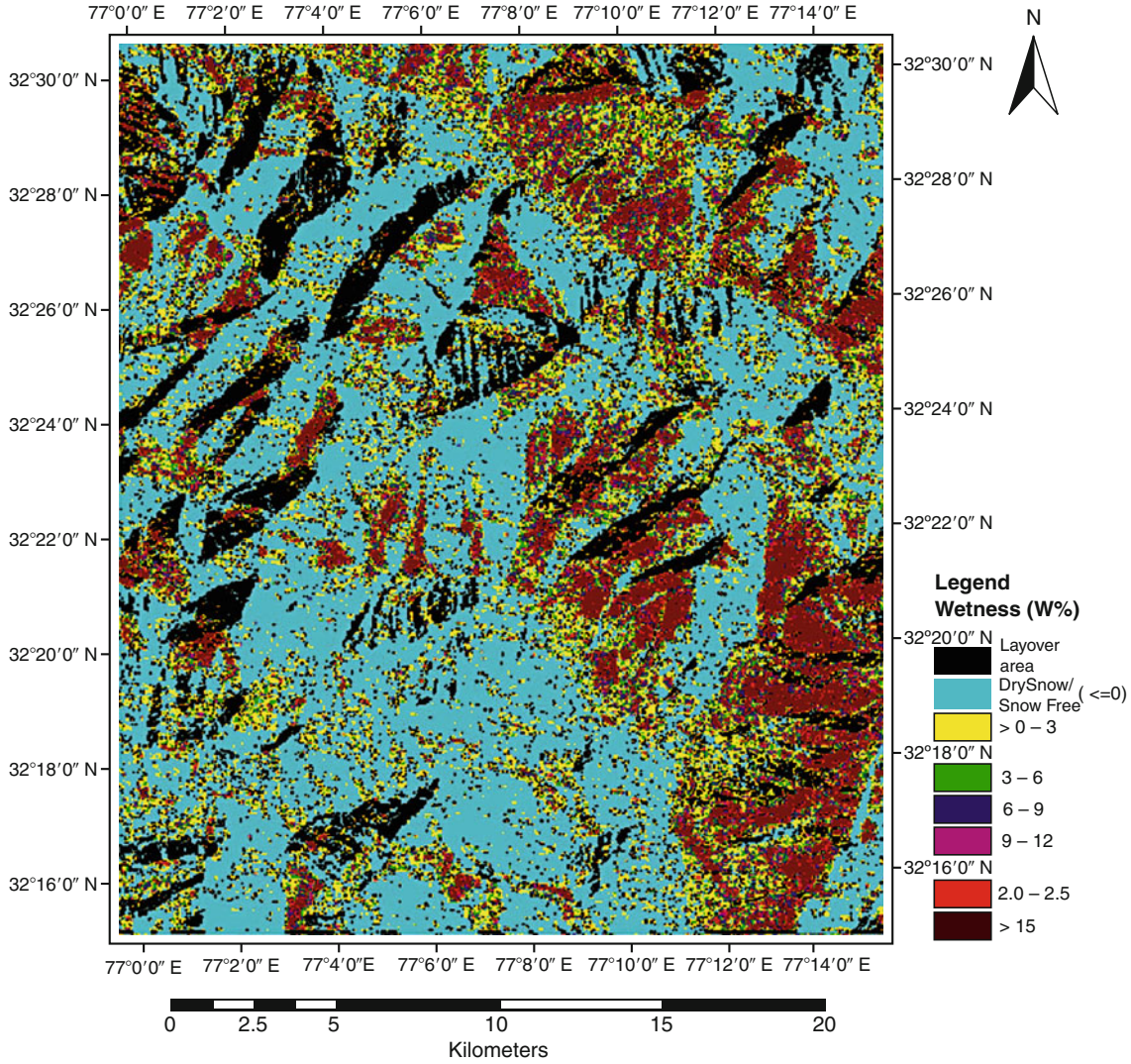

Radar Application in Snow, Ice, and Glaciers, Figure 3 Snow wetness map of 27 Feb. 2006.

increases. Based on Rayleigh scattering, the backscattering coefficients for dry snow can be written as

$$\sigma^0{}_{\mathrm{ds}} = \frac{4\pi^3 r^3 \left|\frac{\varepsilon-1}{\varepsilon+2}\right|^2 \cos\theta'}{\lambda^3 \left|\mathrm{Im}\left\{\frac{\varepsilon-1}{\varepsilon+2}\right\}\right|} \tag{15}$$

For example, λ is C-band ASAR wavelength (λ= 0.056 m, and incidence angle varies from 15° to 45°) and measured average dielectric constant is 1.76–0.00029j. Grain size can be estimated using Equation 15.

The color-coded grain size value image is shown in Figure 4. The ASAR estimated snow grain sizes agree well with the field measurements. The comparison of ASAR C-band estimated value with field grain size measurement shows an absolute error of 0.045 mm and relative error 9.6%. Backscattering coefficient increases as the grain size increases.

Seasonal snow cover mapping

Snow mapping using single polarization SAR images

Rott et al. (1988) developed a snow mapping procedure in which actual image and simulated image are used. The simulated image is generated using local incidence angle map of the area using DEM and some constant parameters which depends on surface type. Rott et al. (1988) used the following equation for the simulation of (σ^0):

$$\sigma^0(\theta_{\mathrm{i}}) = a\,\exp\left(\frac{\theta_{\mathrm{i}}}{\varphi}\right) + c\,\sqrt{\cos\theta_{\mathrm{i}}} \tag{16}$$

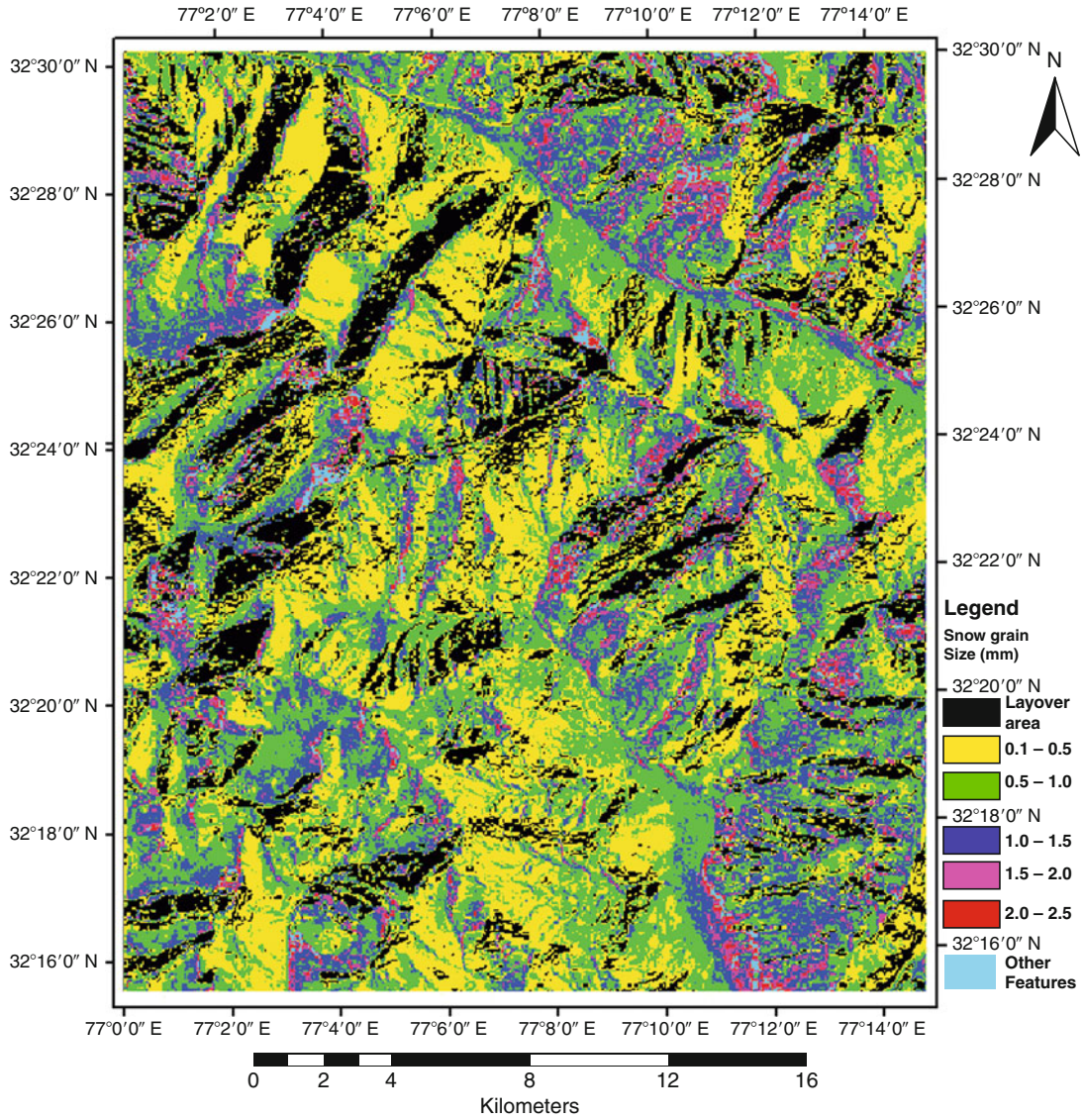

Radar Application in Snow, Ice, and Glaciers, Figure 4 Snow grain size map.

where σ^0 is the radar cross section in units per m^2, θ_i is the local incidence angle of the radar beam, and a, c, and φ are constant values for a particular surface type. For moraine and rock surfaces, the values $a = 0.35$, $c = 0.55$, and $\varphi = 10°$ were used by Rott et al. Rott et al. used C-HH polarized data and simulated data with the following conditions to map snow-covered area.

for	σ^0hh/σ^0sim	≤ 1.8	snow- and ice-free
for	$1.8 < \sigma^0$hh/σ^0sim	< 3.5	glacier ice
for	$3.5 \leq \sigma^0$hh/σ^0sim		snow

Rott et al., compared SAR classified results with that of TM and found that snow surface was underestimated in the SAR classification.

Shi and Dozier (1993) and Shi et al. (1994) used a different function for snow mapping using single polarized data. The normalized σ_n^0 is given by

$$\sigma^0{}_n = \sigma^0(\theta_i)/f(\theta_i) \tag{17}$$

where $f(\theta_i) = \cos^n(\theta_i)$, and n takes different values depending on frequency and polarization. The snow classification is performed by applying threshold of $\sigma^0{}_n$. The classification based on $\sigma^0{}_n$ at C-band VV gave an

overall agreement of 66% when compared with Landsat TM classification.

Snow mapping using multifrequency and polarimetric data

Rott et al. (1992) used polarimetric data for snow cover mapping. Based on the depolarization properties of the radar signal, they used the following equation for mapping snow cover. If the backscattering power satisfies the following condition,

$$P_{HV}/P_{VV} > m \quad \text{snow covered} \tag{18}$$

where $m = 0.04$ was used, P_{HV} is received power of cross-polarization, and P_{VV} is co-polarization data at C-band. Shi et al. (1994) also used the same procedure and their results are in agreement with Rott et al. (1992).

Snow mapping using repeat-pass SAR observations (single polarization)

This method was developed by Rott and Nagler (1992) and Rott and Nagler (1993) and used with ERS-1 SAR data. It is based on the fact that dry snow is not discriminated against snow-free ground during winter as the dry snow is transparent at C-band. Images acquired during snow-free conditions are usually taken as reference image. However, wet snow strongly reduced the backscattered signal. Images acquired during wet conditions are usually known as wet snow images. The change in σ^0 between snow and reference images leads to the detection of wet snow. By combining ascending and descending pass data, they could map snow cover even in layover and shadow areas.

Nagler and Rott (2000) used threshold value -3 dB for wet snow mapping after comparing the results with snow classification using TM data. This procedure has been modified for snow cover mapping in our study and the modified procedure is shown in Figure 5.

Koskinen et al. (1997) suggested an algorithm which is optimized to detect snow in forested areas. By conducting a pixel-wise comparison between the two reference images and the current image, the equation for the relative fraction of snow-free ground is given by

$$F_g = 100\frac{\sigma_i^0 - \sigma_w^0}{\sigma_g^0 - \sigma_w^0}\% \tag{19}$$

where σ_i^0, σ_w^0, and $\sigma_g^0$are the backscattering during snow melt, and at the beginning of the snow melt period, and for snow-free ground, respectively.

Luojus et al. (2006) demonstrated a two-step technique for mapping wet snow cover over Boreal forest in Finland using ERS-2 multi-temporal data sets. The first step is the forest canopy compensation. This is done by nonlinearly fitting ERS-2 measured data with a semiempirical forest-backscattering model (Pulliainen et al., 2003) and information with forest stem volume to estimate

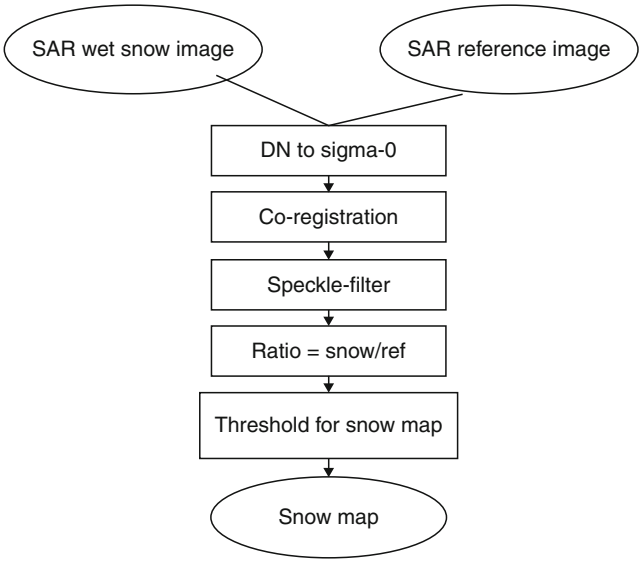

Radar Application in Snow, Ice, and Glaciers, Figure 5 Flow chart of wet snow cover mapping.

the backscattering signal at ground surface and the volume backscattering signals, the two-way transitivity of the forest canopy. In the second step, the fraction of wet snow-covered area (SCA) is calculated as

$$\text{SCA} = \frac{\sigma_{surf}^0 - \sigma_{ground-ref}^0}{\sigma_{snow-ref}^0 - \sigma_{ground-ref}^0}100\% \tag{20}$$

where σ_{surf}^0 is the estimated backscattering coefficient at ground surface, $\sigma_{ground-ref}^0$ is the reference signal from the snow-free ground, and $\sigma_{snow-ref}^0$ is the reference signal from the wet snow ground. One reference image describes the signal with fully wet snow cover situation and the other describes the snow-free at the end of the snow melting season. In addition to these two reference images, this method requires forest stem volume distribution.

Snow mapping using repeat-pass interferometric techniques

An Interferometry SAR technique for topographic mapping of surface does not only produce a high resolution DEM but also gives the information about changes on the surface during the repeat-pass cycle of satellite from the correlation properties of the radar echo. The measurement of interferometer correlation provides the information of changes during the timescale of the satellite repeativity and size scale on the order of a SAR wavelength. The coherence measurement between two repeat passes provides another useful measurement for snow cover mapping over large area. Strozzi et al. (1999) analyzed the ERS-1/2 tandem data and observed that coherence can help separate wet snow from other

surface where backscatters do not discriminate snow from other surface.

The basis of InSAR is phase comparison over many pixels. This means that the phase between scenes must be statistically similar. The coherence is a measure of the phase noise of the interferogram. The interferometric coherence is defined as the absolute value of the normalized complex cross-correlation between the two signals. The correlation will always be a number between 0 and 1. If the pixels are similar this will result in a high correlation and good results. If the pixels are not similar, that is, not correlated at a certain degree, then the phase will vary greatly and the result will be noise.

Theoretical and experimental studies have shown that coherence is determined by the spatial baseline of the interferometric pair, the time separation of the images, topographic effects, and noise sources. The change of backscattering characteristic at surface will cause the change of coherence degree at the separate time. Integrating the backscattering intensity, one can make classification using the difference of coherence degree for different surface type.

The technique is based on coherence between two images acquired at different dates. The coherence may vary depending on the melting of snow, forest growth, precipitation, soil moisture, and movement of the glaciers. Through this technique, wet snow-covered areas can be identified through coherence change. Rao et al. (2008) observed poor coherence in most of the areas if the interval between two dates is more than 30 days. Shi et al. (1997) processed SIR-C data at L-band for the analysis of interferometric coherence and thereby executed snow mapping. The limitation of this technique is that two images are to be acquired in a short interval with same viewing angle and swath mode. Presently, almost all satellites give data in the interval of 25–35 days.

Coherence measurement using repeat-pass SAR observations indicate low values for both wet and dry snow covers. The radar echoes get decorrelated for measurements between wet snow cover and bare ground. This happens mainly because radar signal can penetrate few centimeters in wet snow cover and hence the radar senses two different targets. In case of dry snow the dominant scattering is from the interface of snow and ground. Decorrelation occurs in dry snow mainly due to volume scattering from the snow layer and changes the local incidence angle.

The coherence was measured between several pairs repeat-pass ERS-1/2 and ENVISAT image data. Data analysis was performed using Gamma SAR and interferometric processing software. The coherence degrees of interferometric pair were calculated for different types of surface at different time interval. However, the amount of decorrelation is expected to be relatively smaller because radar senses same target with same scattering mechanism (only change in magnitude). The glacier has varied coherence degree according to the moving state. The correlation of snow is relatively lower due to the change of snow surface and roughness caused by snow and snow melting.

Coherence images of Gangotri glacier were obtained using ERS-1&2 tandem data of March 25 and 26, 1996, in ascending mode; ENVISAT ASAR 35-day interval data of July 9 and August 13, 2003, in descending pass; and ENVISAT ASAR 70-day interval data of May 19, 2004, and July 28, 2004. Authors acquired the nearest IRS – LISS III image to verify the classification accuracy.

Coherence images of Siachen glacier with April 1 and 2, 1996, ERS-1 and 2 tandem pair; May 2 and 3, 1996, tandem pair; and ASAR 70-day interval and ASAR 350-day interval data indicate that the coherence degrees of objects are high in the ERS SAR pairs due to short time interval and relatively short baseline. For snow and glacier region, snow melting and glacier movement will result in large decorrelation.

The wet snow cover over the glacier and non-glacier area can be discriminated from other targets using degree of coherence because wet snow metamorphism changes the scattering geometry, and therefore coherence is lost. But the decorrelation of time and baseline should be reasonable. Short time interval pair between snow and non-snow cover is better for separating snow from other targets.

Radar application in land ice and glacier studies

Glaciated terrain classification using full polarimetric SAR data

SAR Polarimetry is a very active area of research in Radar Remote Sensing and Classification using fully polarimetric SAR images (van Zyl et al., 1987; Novak and Burl, 1990; Ulaby and Elachi, 1990; Lee et al., 1991; Zebker et al., 1991; Rignot et al., 1992; van Zyl and Burnette, 1992; Novak et al., 1993; Boerner et al., 1998). SAR polarimetry can be important to snow study and to prepare the POLSAR data analysis and to develop methodology to snow parameters retrieval. Hence, an urgent need exists for establishing an approach for monitoring, modeling, and planning of snow parameters retrieval. However, such a systematic approach is still lacking. There is a need to explore the potential of Polarimetric SAR data, incorporating state-of-art scattering mechanism and polarimetric techniques based processing in formulating snow cover monitoring, snow wetness, snow density, etc. World over, there is no proven methodology/algorithms readily available, which can be directly applied for snow parameter studies in Himalayas. Hence, suitable methodology/algorithms are required to be developed for Himalayas for snow cover related studies. Hence, in this study, full polarimetric L-band ALOS-PALSAR data have been analyzed for snow cover classification of glaciated terrain in and around Badrinath region in Himalaya. ALOS-AVNIR-2 image was also used to provide assistance in the selection of different training classes. PALSAR data has been classified based on various components scattering mechanism models, namely, Entropy-Anistropy-Alpha by Cloude and

Pottier, Three components by Freeman and Durden (1998), and Four components by Yamaguchi et al. (2006). And all model results have been compared.

The Cloude–Pottier (1996) target decomposition is the most popular method used for snow cover classification. This method is based on eigenvalues of coherency matrix.

A three-component (surface, double bounce, and volume) scattering model based on the covariance matrix has been successfully applied by Freeman and Durden (1998) to decompose scattering mechanisms in POLSAR image analysis under the reflection symmetry condition. In this study, a four-component model (Yamaguchi et al., 2006; Yajima et al., 2008) has been used for snow cover study using ALOS-PALSAR data of May 12, 2007, over the Badrinath region in Himalaya. A four-component (surface, double bounce, volume and helix) scattering model is the extension of three-component scattering model, which deals with nonreflection symmetric scattering cases. There are problems in the implementation of the four-component algorithm on full polarimetric data because some negative powers occur in the decomposed image. This negative power occurrence problem is contradictory with physical conditions. In this entry, authors have demonstrated both old (Yamaguchi et al., 2006) and modified (Yajima et al., 2008) four-component decomposition procedures applied on PALSAR data, taking care of the negative powers occurrence problem and that the algorithm should be applicable to all areas in a general way.

In literature, both coherent and incoherent target decomposition theorems are available, namely, coherent decomposition: Pauli and Krogager decomposition and incoherent decomposition: decomposition of Freeman and Durden (1992, 1998), Cloude and Pottier (1996), and Yamaguchi et al. (2006).

The scattering matrix [S] is only able to characterize the coherent or pure scatterers. On the contrary, this matrix cannot be employed to characterize the distributed scatterers. This type of scatterers can only be characterized statistically, due to the presence of speckle noise.

The coherency matrix is given as

$$[T] = k.k^{*T} \tag{21}$$

where *T denotes complex conjugation and transposition and **k** denotes the target vector.

Target vector is obtained by vectorization V (.) of the scattering matrix **S** in each pixel:

$$k = V(s) = (1/2)\mathrm{Trace}\{S[\Psi]\} \tag{22}$$

Ψ is a set of 2 by 2 complex basis matrices.

Using Pauli basis matrix, target vector is defined as

$$k = (1/\sqrt{2})\begin{bmatrix} S_{\mathrm{hh}} + S_{\mathrm{vv}} \\ S_{\mathrm{hh}} - S_{\mathrm{vv}} \\ 2S_{\mathrm{hv}} \end{bmatrix} \tag{23}$$

where S_{hh}, S_{vv}, and S_{hv} are the elements of scattering matrix **S**.

The incoherent decomposition theorems can be expressed as

$$[T] = q_1[T_1] + q_2[T_2] + q_3[T_3] + \cdots + q_k[T_k] \tag{24}$$

In this work, *H/A/Alpha* (Cloude and Pottier, 1996), three-component scattering power decomposition (3-CSPD) model (Freeman and Durden, 1998), and 3-CSPD model extension a four component scattering power decomposition model (Yamaguchi et al., 2006) have been studied.

The $H/A/\alpha$ decomposition technique is based on the three eigenvalues (λ_1, λ_2, and λ_3 with decreasing magnitude) of the coherence matrix $<T>$, and defines the entropy H, the anisotropy A, and the α angle.

The degree of randomness of each target or the degree of statistical disorder of each target is known as the entropy. The entropy (H) can be defined in the Von Neumann sense from the logarithm sum of the eigenvalues of $[T]$:

$$H = -P_1\log_3 P_1 - P_2\log_3 P_2 - P_3\log_3 P_3 \tag{25}$$

$$0 \le P_i = \frac{\lambda_i}{\sum_{i=1}^{3}\lambda_i} \le 1 \tag{26}$$

The entropy indicates depolarization of the target. If entropy is low then target is weakly depolarized; when entropy is high then the target is depolarized.

The anisotropy A is the linear combination ratio of the second and third eigenvalues of $[T]$. Thus anisotropy can be defined as

$$A = \frac{\lambda_2 - \lambda_3}{\lambda_2 + \lambda_3}; \quad 0 \le A \le 1 \tag{27}$$

The mean scattering angle (α) is an angle between incident and return radar beam. It varies from 0° to 90°.

$$\bar{\alpha} = P_1\alpha_1 + P_2\alpha_2 + P_3\alpha_3 \tag{28}$$

With the three-component scattering mechanism model based decomposition theorem, presented by Freeman and Durden (1998), the coherency matrix can be decomposed into

$$[T] = f_{\mathrm{s}}[T_{\mathrm{s}}] + f_{\mathrm{d}}[T_{\mathrm{d}}] + f_{\mathrm{v}}[T_{\mathrm{v}}] \tag{29}$$

With the four-component scattering mechanism model based decomposition theorem, presented by Yamaguchi et al. (2006), similarly the coherency matrix can be decomposed into

$$[T] = f_s[T_s] + f_d[T_d] + f_v[T_v] + f_c[T_h] \tag{30}$$

where f_s, f_d, f_v, and f_c are surface, double bounce, volume, and helix scattering coefficients, respectively.

For supervised classification Wishart complex distribution (Lee and others, 1994) has been applied for snow cover classification. The Wishart distribution is expressed as

$$P(\langle T\rangle/T_m) = \frac{L^{Lp}|\langle T\rangle|^{L-P}e^{-LTr\left([T_m]^{-1}\langle T\rangle\right)}}{\pi^{\frac{p(p-1)}{2}}\Gamma(L)...\Gamma(L-p+1)[T_m]} \quad (31)$$

where L is number of looks and p is polarimetric dimension. Using the complex Wishart distribution of the coherency matrix **T**, an appropriate distance measure, d, can then be calculated according to Bayes maximum likelihood classification as

$$d_m(\langle T\rangle) = LTr\left([T_m]^{-1}\langle T\rangle\right) + L\ln([T_m]) - \ln(P([T_m])) + K \quad (32)$$

thus leading to a minimum distance classification independent of the number of looks used to form the multilooked coherency matrix $<\mathbf{T}>$:

$$\langle[T]\rangle \in [T_m] if d_m(\langle[T]\rangle) < d_j(\langle[T]\rangle)\forall j \neq m \quad (33)$$

In this investigation, H/Alpha Wishart and H/A/Alpha Wishart approaches have been attempted for the classification of PALSAR images. The flowchart of the H/A/Alpha Wishart unsupervised classification scheme is shown in Figure 6.

The decomposition schemes were applied on L-band PALSAR data set over the Badrinath region, which includes snow, forest, glacier, rocks, etc.

AVNIR-2 image of May 6, 2007, is used for analysis. Some part of this image covered by cloud and in other part, snow cover and non-snow cover area can be easily visually interpreted. Pauli RGB was made using diagonal element of coherency matrix which gives the clear information about single scattering (Snow cover area over glacier and non-glacier), double bounce (dihedral features) and volume scattering (Vegetation) in the study area. The H, A, and α parameters are decomposed from polarimetric PALSAR data over Badrinath area using H/A/Alpha

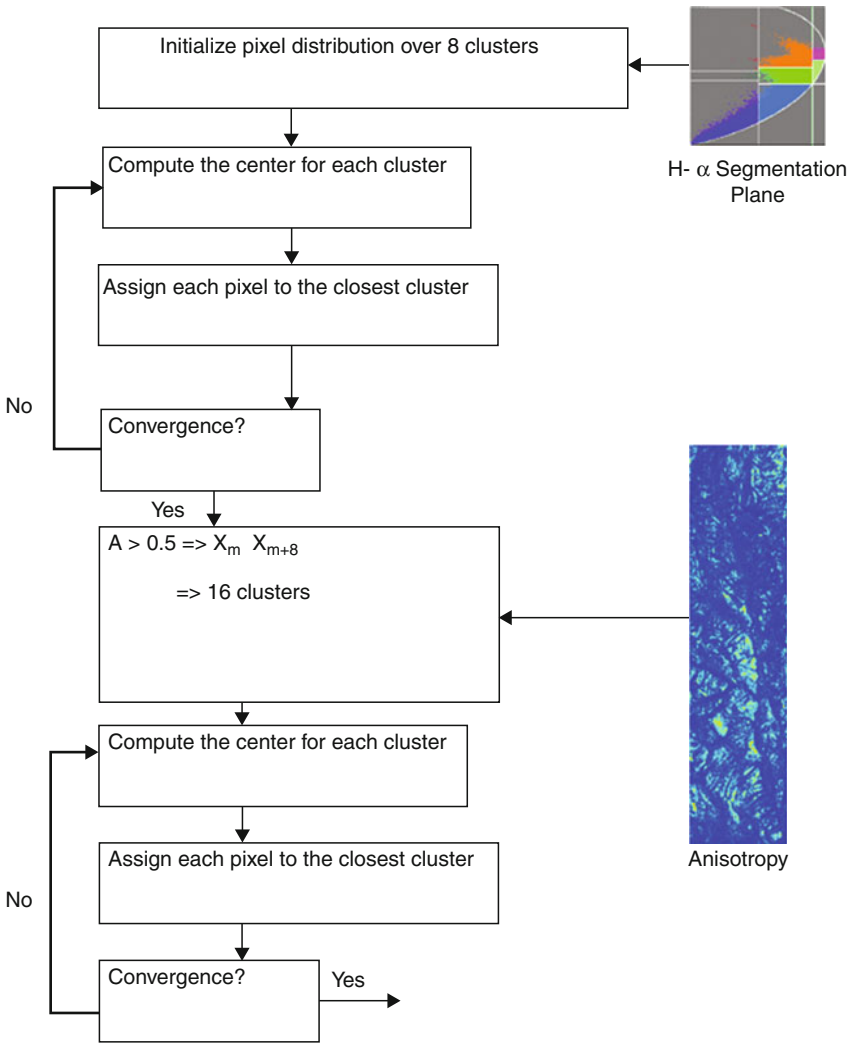

Radar Application in Snow, Ice, and Glaciers, Figure 6 Flow chart of the H/A/Alpha Wishart unsupervised classification scheme.

decomposition technique. The images were classified using H/A/Alpha Wishart unsupervised classifier (Entropy, anisotropy, and alpha angle corresponding to scattering mechanism). Results show that most of the pixels fall in single scattering and roughness scattering regions of the Entropy (H)/Alpha plane. The area has some small villages and forest and hence, the corresponding pixels have the content of multiple (dihedral and double bounce) scattering. The H/Alpha Wishart classifier classified the total image into eight different classes and after introducing anisotropy (A), number of different classes becomes 16. The classified images show that H/A/Alpha Wishart unsupervised classified images (Figure 7b) are better than those obtained using H/Alpha Wishart unsupervised classifier (Figure 7a). With the help of AVNIR-2 images, field information and Survey of India topography map, legend has been given to classified images and it was also identified that the H/A/Alpha Wishart unsupervised classifier has classified snow cover area into five classes whereas H/Alpha Wishart combination classified into two classes. After that, all snow classes have been merged and made one class for total snow cover mapping. H/A/Alpha Wishart classifier classified more pixels under snow classes as compared to H/Alpha-Wishart classifier.

Entropy-Anistropy-Alpha-Wishart classifier for training the samples provides better classification results according to region of interest. Classification technique was applied on Entropy-Anistropy-Alpha combination images, which are generated by speckle filtered data. Speckle filter (Sheng and Xia, 1996) for reducing the noise from the polarimetric data provides better accuracy. Also previous work shows that classification accuracy increases as refined Lee filter window size increases (Singh et al., 2008). Speckle is suppressed by refined Lee filter with window size 7×7. Using H/A/Alpha Wishart classifier, ALOS-PALSAR data was classified into six major classes (e.g., snow, non-snow, and unidentified/layover). Snow cover area was classified into one single class. When two training samples for snow-covered area (snow Class 1 and Class 2) were used, then classified image gives information about seven distinct classes. And user accuracy for snow class is higher as compared to single snow class

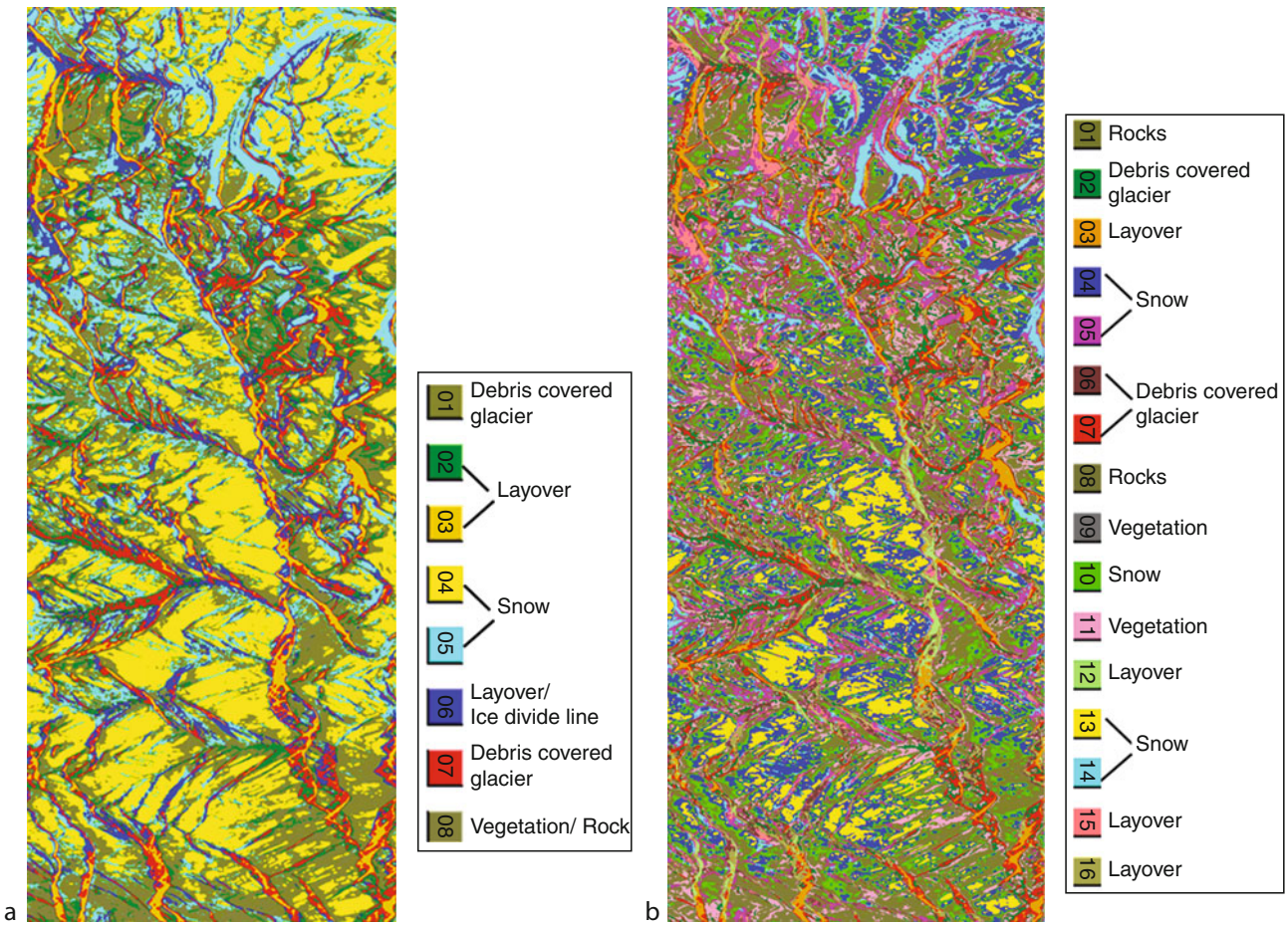

Radar Application in Snow, Ice, and Glaciers, Figure 7 (**a**) H/Alpha Wishart classified image (**b**) H/A/Alpha Wishart classified image.

classified image. Similarly, three different training samples for snow class were assigned, and it provides better user accuracy for snow classes as compared to classified image with one and two snow training samples for classification (the confusion matrix of the classified classes based on given training sample are shown in Tables 3a, 3b, and 3c). Classified image with eight (three snow and five non-snow) classes shows that more pixels were classified as snow compared to classified image with six and seven classes.

For this entry, authors also compared the visual interpretation of all decomposed FCC with the Pauli RGB and AVNIR-2 image. It was found that updated four-components scattering decomposition FCC seems better compared to three-components and old four-components FCC. Figure 8a, b shows the classified PALSAR image using 4- scattering component model and Wishart distribution.

Using old four-component and Wishart classifier, ALOS-PALSAR data was classified into major classes (e.g., snow, non-snow, and unidentified/layover, Figure 8a and b). Snow cover area was classified as one single class (Figure 8a) and as two classes (snow Class 1 and Class 2, Figure 8b). Supervised Wishart classification technique was applied on coherency matrix, and training samples were taken from four-component color composite image with the help of visual interpretation of ALOS AVNIR-2 image and field information. Four-scattering component model Wishart supervised classified images are shown in Figure 8a and Figure 8b. With the help of 4-component scattering component decomposition, snow can be easily classified into two classes using supervised methods but with the help of H/A/Alpha decomposition it can be classified into three classes. Tables 3a, 3b, 3c, 3d, and 3e reveal higher user accuracy for snow classes. This means that L-band PALSAR data are good for snow mapping.

Radar Application in Snow, Ice, and Glaciers, Table 3a Confusion matrix for H/A/Alpha Wishart supervised classified seven classes in PALSAR image

	Snow	Rock	Debris covered glacier (DCG)	Settlement	Vegetation	Layover
Snow	**95.26**	0.00	0.43	0.00	0.00	4.31
Rock	0.25	**78.07**	14.42	0.00	3.33	3.93
DCG	1.19	5.82	**81.70**	0.00	6.77	4.51
Settlement	0.00	2.42	0.97	**92.97**	3.15	0.48
Vegetation	0.00	6.10	18.09	0.00	**75.81**	0.00
Layover	0.00	16.69	10.69	0.00	0.00	**72.62**

Radar Application in Snow, Ice, and Glaciers, Table 3b Confusion matrix for H/A/Alpha Wishart supervised classified seven classes in PALSAR image

	Snow1	Snow2	Rock	DCG	Settlement	Vegetation	Layover
Snow1	**96.03**	0.84	2.26	0.00	0.00	0.00	0.77
Snow2	0.50	**99.23**	0.00	0.28	0.00	0.00	0.00
Rock	0.40	0.61	**80.48**	6.02	0.00	2.56	9.94
DCG	0.39	0.90	7.80	**68.92**	0.00	21.27	0.72
Settlement	0.00	0.00	3.52	0.00	**91.52**	3.27	1.70
Vegetation	0.00	0.00	2.07	17.1	0.00	**73.85**	6.96
Layover	0.00	0.00	3.53	0.00	0.00	2.12	**94.35**

Radar Application in Snow, Ice, and Glaciers, Table 3c Confusion matrix for H/A/Alpha Wishart supervised classified eight classes in PALSAR image

	Snow1	Snow2	Snow3	Rock	DCG	Settlement	Vegetation	Layover
Snow1	**96.07**	3.93	0.00	0.00	0.00	0.00	0.00	0.00
Snow2	0.22	**99.56**	0.00	0.00	0.00	0.00	0.00	0.22
Snow3	1.91	0.05	**97.51**	0.00	0.51	0.00	0.01	0.00
Rock	0.00	1.16	0.00	**70.88**	3.04	0.00	8.69	16.23
DCG	0.00	0.47	2.72	11.91	**78.22**	0.00	6.57	0.11
Settlement	0.00	0.00	0.00	2.52	0.93	**90.77**	4.38	1.40
Vegetation	0.00	0.04	0.00	1.28	28.36	0.00	**70.31**	0.00
Layover	0.00	0.40	0.00	27.13	0.00	0.00	8.91	**63.56**

Radar Application in Snow, Ice, and Glaciers, Table 3d Confusion matrix for 4-scattering component model Wishart supervised classified six classes in PALSAR image

	Snow	Rock	Debris covered glacier (DCG)	Settlement	Vegetation	Layover
Snow	**98.55**	0.33	0.36	0.00	0.43	0.32
Rock	5.26	**79.25**	0.00	1.45	14.04	0.00
DCG	0.00	0.00	**86.58**	0.00	2.24	11.18
Settlement	0.00	8.75	0.00	**89.96**	1.28	0.00
Vegetation	0.00	12.60	5.91	0.00	**81.14**	0.35
Layover	0.00	0.00	4.14	0.00	0.00	**95.86**

Radar Application in Snow, Ice, and Glaciers, Table 3e Confusion matrix for 4-scattering component model Wishart supervised classified seven classes in PALSAR image

	Snow1	Snow2	Rock	DCG	Settlement	Vegetation	Layover
Snow1	**97.51**	0.00	0.00	0.00	0.00	0.07	2.41
Snow2	0.00	**100.00**	0.00	0.00	0.00	0.00	0.00
Rock	0.00	0.00	**77.78**	0.00	7.97	14.25	0.00
DCG	0.00	0.00	0.05	**93.52**	0.00	0.56	5.87
Settlement	0.00	0.00	9.30	0.00	**87.89**	2.81	0.00
Vegetation	0.00	0.00	11.99	2.96	0.00	**84.96**	0.10
Layover	0.00	0.00	0.00	0.26	0.00	0.00	**89.74**

In addition, the higher user accuracy snow class was found for 4-scattering component model Wishart supervised classified image (Table 3e). Based on the quantitative comparison and other analysis it seems that H/A/Alpha Wishart unsupervised classified images are better than the images obtained using H/Alpha Wishart unsupervised classifier.

Glacier facies mapping

Glacier facies are distinct zones in the surface layer of an ice sheet or glacier. The concept of glacier facies developed as a result of physical measurements made in Greenland on repeated traverses that went inland from the west coast at two latitudes and north to south along the crest of the ice sheet. Snow pits and shallow cores showed discontinuities in physical characteristics that defined the facies boundaries (Partington, 1998).

The dry-snow zone, where there is no surface melt, is located at the highest elevations of the ice sheet. The percolation zone, where some melt occurs but meltwater percolates into the snowpack and refreezes, is immediately below the dry-snow zone in elevation. It is not easily distinguished from the wet-snow zone, where the complete annual accumulation of snow may experience meltwater percolation and refreezing. However, at the lower elevations of the wet-snow zone numerous melt ponds form and there are large areas of slush. Lower still is the superimposed ice zone, where meltwater has refrozen onto the colder glacier ice surface. Because superimposed ice is created by melting and refreezing of the current year's snow, this zone is still considered part of the ice sheet accumulation area. The lowest elevation zone is the bare ice zone, which represents the ablation region. The equilibrium line is defined as the boundary between the regions of net accumulation and net ablation, that is, the lower boundary of the superimposed ice zone. The snow (or firn) line is the lowermost elevation where, at the end of the ablation season, snow (or firn) remains on the glacier surface, that is, the upper boundary of the superimposed ice zone. Firn is densified snow that survives at least one melt season.

Radar glacier facies and zones can be identified on glaciers and ice fields on the basis of backscatter variations in multi-temporal SAR images (Partington, 1998). These glacier zones have backscatter signatures related to the structure of the snowpack, which varies, with the balance of accumulation and melt at various elevations (Fahnestock et al., 1993). It has been observed that (1) backscatter is sensitive to the near-surface temperature in the dry-snow zone, (2) backscatter coefficient is totally dominated by the ice structure in the percolation zone, and (3) the presence of thick ice layer leads to different spectral responses in the wet snow zone and a higher backscatter value is observed at higher frequencies.

Terrain corrected backscatter coefficient (σ_i^0) images of winter, late summer, and early summer have been obtained using the aforesaid processing procedure. These three multi-temporal images were merged together through layer stack program of ERDAS. Imagine by assigning winter image as Layer 1, late summer image as Layer 2, and early summer image as Layer 3. DEM was also merged with the SAR composite. This combination helps to obtain the elevation value as well as backscatter coefficient values for any particular pixel to carry out quantitative analysis.

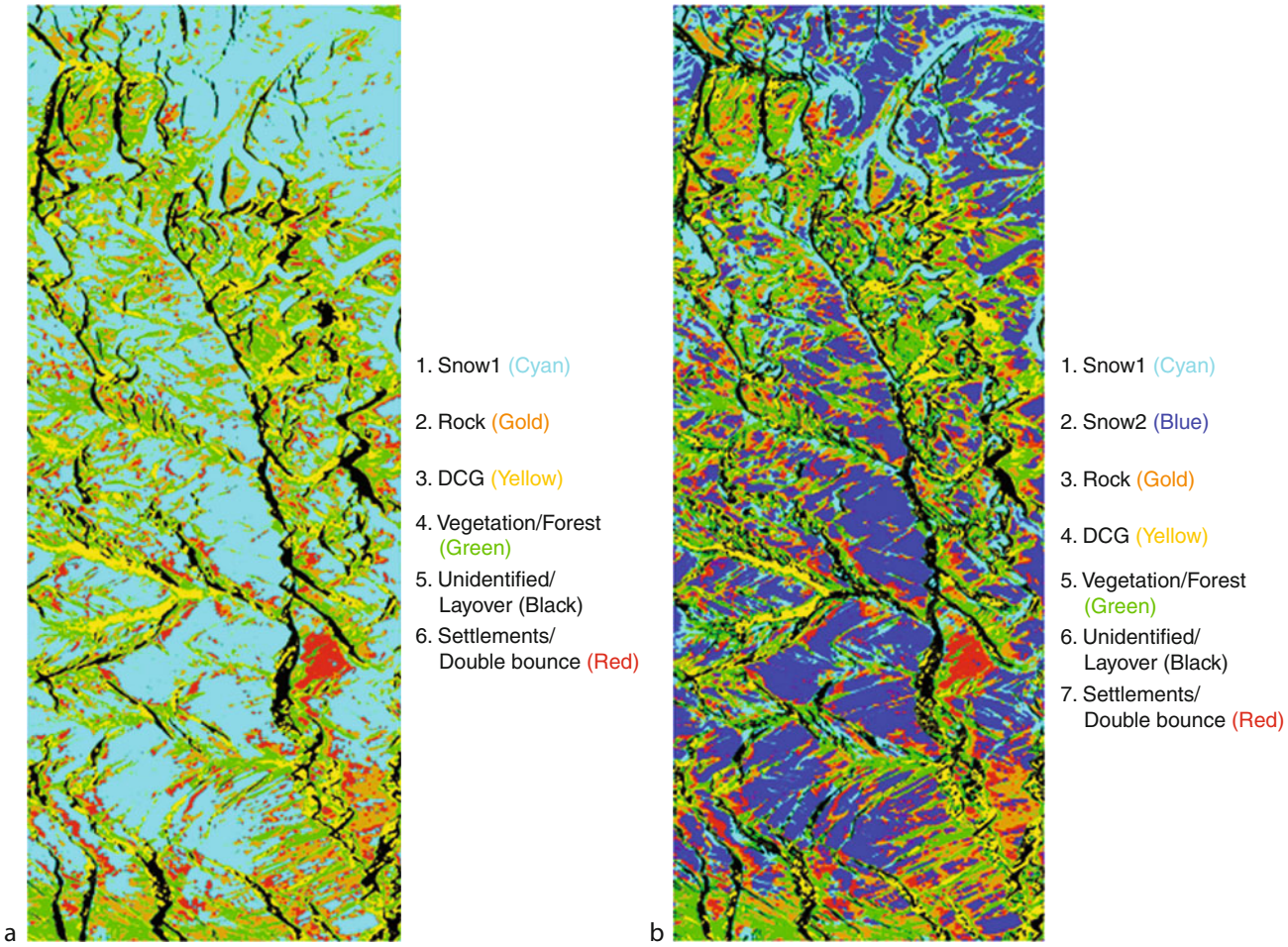

Radar Application in Snow, Ice, and Glaciers, Figure 8 (**a**) 4- scattering component model -Wishart supervised classified image with 1 snow classes (**b**) 4- scattering component model - Wishart supervised classified image with 2 snow classes.

From this combined image, the study area has been extracted displaying Layer 1 in Blue channel, Layer 2 in Green channel, and Layer 3 in Red channel. This color combination SAR image is useful to identify different glacier zones due to tonal variations based on SAR composite image interpretation key (Table 4).

Further, for quantitative analysis the difference image showing the difference in backscatter coefficient values between September and January season was also generated. Generally, the winter image defines maximum freeze conditions and the late summer image defines maximum melt conditions. In addition to the generation of combined SAR images as composite, the backscatter coefficient value along with corresponding elevation data have been extracted along a profile cutting across various glacier zones separately for all these three SAR images. The analysis and plotting of these values and the interpretation of the combined SAR composite help in delineation of various glacier zones and this is discussed in the following.

Two parameters considered in combination to give the best positioning for the snow line and dry snow line are winter backscatter coefficient and the difference between the end of ablation and winter backscatter coefficient (Partington, 1998). Figure 9 shows the plot of January backscatter and September minus January backscatter vs. elevation data extracted along a profile (Figure 10) for Beaskund glacier. This plot shows very clearly the delineation of Percolation/Wet snow facies and Ice facies and thus helps to clearly define the snow line. However, the separation between percolation facies and wet snow facies is not distinct. From this figure, it is clear that ice facies goes below 4,000 m. Above the altitude of 4,000 m lies the percolation facies together with wet snow facies. Dry snow facies is absent in Beaskund glacier. These findings need confirmation through field observations.

Further, for quantitative analysis of the difference image showing the difference in backscatter coefficient values between September and January season was also generated. Generally, the winter image defines maximum freeze

Radar Application in Snow, Ice, and Glaciers, Table 4 Key for SAR composite image interpretation

Satellite data from seasons	Assigned in channel
Winter	Blue
Late summer	Green
Early summer	Red

Glacier Facies		Winter	Late summer	Early summer	Final appearance
Dry snow facies		Low	Low	Low	Dark grey
Percolation/	Highest	Moderate	High	Moderate	Green
Wet snow	Upper	High	High	High	White
Facies	Middle	High	Moderate	High	Purple/Pink
	Lower/wet snow	High	Low	Low	Green
Ice facies		Low	High	Low	Green

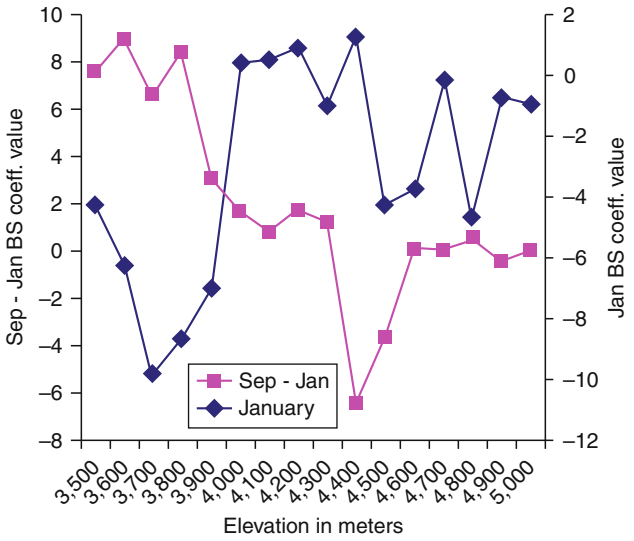

Radar Application in Snow, Ice, and Glaciers, Figure 9 September Minus January and January Backscatter Vs. Elevation.

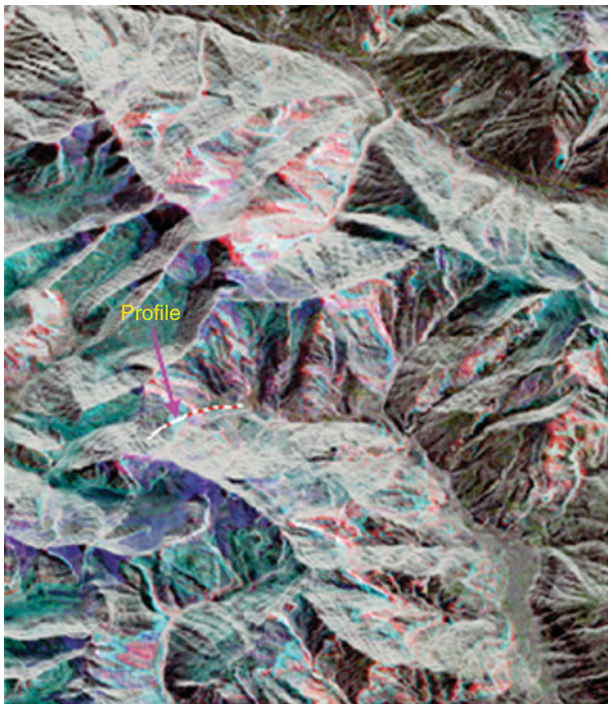

Radar Application in Snow, Ice, and Glaciers, Figure 10 Multitemporal Radarsat Image combining winter, late summer and Early Summer Images.

conditions and the late summer image defines maximum melt conditions. In addition to the generation of combined SAR images as composite, the backscatter coefficient value along with corresponding elevation data have been extracted along a profile cutting across various glacier zones separately for all these three SAR images. The analysis and plotting of these values and the interpretation of the combined SAR composite help in delineation of various glacier zones and this is discussed in the following.

The region beyond the elevation of 4,000 m is the region with comparatively bright returns. This region has been identified as percolation zone together with wet snow zone. In percolation zone backscatter increases due to scattering from ice lenses and vertical ice pipes formed due to the freezing of percolating meltwater. According to Baumgartner et al. (1999), in the percolation zone, the backscatter coefficient is independent of the frequency, and the angular response is controlled by the ice structures such as surface roughness, lenses, and pipes. In wet snow zone the snow has reached the melting point as a result of latent heat released by extensive refreezing of meltwater (Fahnestock et al., 1993). In this zone backscatter is of intermediate intensity. In the wet snow zone the backscatter coefficient is temporally dependent as the temperature variations affect the moisture content and modifies the spectral backscatter energy. The snow and ice surface roughness determine the angular response (Baumgartner et al., 1999). In the present study it was not possible to clearly distinguish between percolation zone and wet

snow zone. Hence, it is grouped as a single unit called percolation/wet snow zone. This zone extends from altitude 4,000 up to > 5,000 m. This zone shows generally higher backscatter coefficient value and the values range between 10.667 and 2.590 dB. Further, this zone can be subdivided into four small zones as seen in the multi-temporal color image. At higher levels of percolation facies white zone is observed in the multi-temporal SAR image. White color zone is quite natural as the percolation facies has higher backscatter values in all three seasons. This is because there is no melt in any of the three seasons. At some higher altitude also green color is found somewhere in the multi-temporal color image. However, the appearance of green color in the higher altitude of percolation facies is somewhat anomalous and unusual. This indicates higher backscatter in September than in January or May. As there is no ground truth to validate an interpretation, Partington (1998) has suggested three possible explanations for future investigations. These include summer depth hoar development, rime-frost development, and high winter accumulation over percolation facies. Further down, the zone appears purple, as the backscatter will be uniformly high during winter and early summer and low in late summer. In this region melt is present in the late summer image but not in the early summer or winter image. Finally, toward the lowest altitude in the percolation/wet snow facies, the zone appears blue, as the backscatter would be high in the winter data and low in both summer images. In this region melt is associated with both early and late summer images. This blue color zone is a narrow zone of intermediate brightness.

The lowest zone is the bare ice zone which is a combination of glacier ice produced by compaction of snow at higher elevations and superimposed ice that forms by freezing of meltwater at the base of the firn (Fahnestock et al., 1993). This zone extends from terminus of the glacier to firn line, which is the highest elevation to which the annual snow cover recedes during the melt season. Compared to wet snow zone, the bare ice zone appears smooth with low backscatter in winter image. However, in late summer image this is inverted (Fahnestock et al., 1993). The ice facies lies below the equilibrium line, which is at 4,000 m altitude. The ablation region can be seen to lie below the "blue" lower zone of the percolation/wet snow facies (Figure 11). The backscatter coefficient values of the ice facies vary from 15.068 to 3.219 dB. It has been observed that the late summer backscatter values are higher than winter and early summer backscatter values. Because of this, it appears as having a green tint in the multi-temporal image (Figure 11). Bare ice exists at the end of the ablation season but earlier in the season there remains snow cover.

Glacier mass balance

Mass balance can be defined as the algebraic sum of the accumulation and ablation at any time. Accumulation includes all processes by which material is added to the glaciers, whereas ablation includes all processes by which snow and ice are lost from the glaciers. The measurement of the net balance can be determined using direct glaciological measurements. However, in terrains where the field measurements are impossible, indirect photogrammetric methods are useful to estimate net balance (Paterson, 1994).

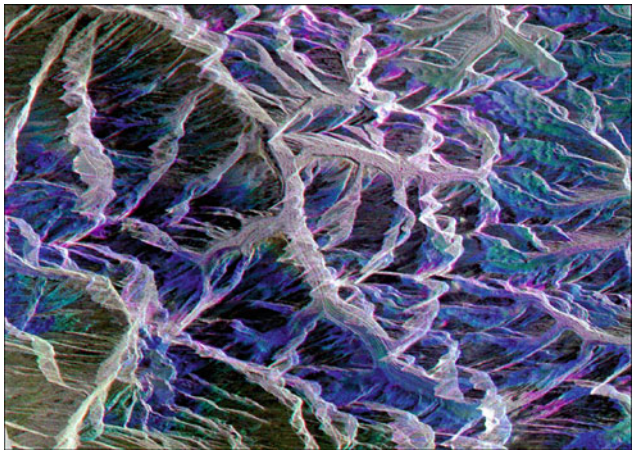

Radar Application in Snow, Ice, and Glaciers, Figure 11 SAR FCC image over Gangotri glacier combining Winter (Blue), Late summer (Green) and Early summer (Red).

Radar application in mass balance estimation

SAR interferometry DEM

Volume change estimation of mountain glaciers can be done using high resolution multi-temporal digital elevation model (DEM) and extent measurement of glacier. Shuttle Radar Topography Mission (SRTM) C-band data and a digital elevation model (DEM) generated from topographic maps have been used for measuring the change in height. ERS-1/2 data TanDEM is very useful for generation of DEM of the glaciated terrain. Multi-temporal DEM derived from ERS-1/2 TanDEM data can be used for estimating the volume change in glacier or ice. High resolution InSAR DEM can be generated using spotlight mode SAR interferometric pairs of TerraSAR-X. Change in glacier height can be deciphered using differencing two DEMs after resampling them on the same spatial resolution. Change in area of the glacier and change in height generally give the information of change in total volume of glacier/ice.

Cryosat-2 elevation

In near future, Cryosat-2 Elevation can be used to obtain variation in the glacier elevations and relate these variations to gain or loss in mass balance. The study of the mass balance of glaciers can be estimated using data sets of SAR Interferometric mode of SAR Interferometric Radar Altimeter (SIRAL) onboard CryoSat-2, which is intended to provide improved elevation estimates over ice sheets with variable topography. The change in the elevation

can be related to mass balance study. The details about Cryosat-2 can be obtained from the following link: http://www.esa.int/esaLP/LPcryosat.html

TanDEM-X

TanDEM-X (*T*erraSAR-X *a*dd-o*n* for *D*igital *E*levation *M*easurement) opens a new era in space borne radar remote sensing. The first bistatic SAR mission is formed by adding a second, almost identical spacecraft, to TerraSAR-X and flying the two satellites in a closely controlled formation with typical distances between 250 and 500 m. Primary mission objective is the generation of a consistent global digital elevation model. The scientific use of the data can be divided into three areas: new quality Digital Elevation Models, along-track interferometry, and new bistatic applications. The mission has been approved for full implementation by the German Space Agency with a planned launch in fall 2009 (for more details see this link: http://www.dlr.de/hr/desktopdefault.aspx/tabid-2317/3669_read-5488). This mission will be very useful for glacier mass balance study.

ELA method based on SAR FCC

Glaciers often lie in remote areas that are difficult to access, and they can have vast surface areas. This makes it difficult and costly to collect in situ data at regular time intervals, be it for direct measurements of the mass balance or for meteorological measurements. Satellite based remote sensing with its characteristics such as synoptic view, repetitive coverage, and uniformity over large areas is an important tool for glacier monitoring and mapping. Here the use of satellite instruments for measuring only the mass balance related glaciological parameters are discussed. The mass balance cannot be presently established using remote sensing alone. In case of small and medium sized alpine glaciers there are possibilities to determine the equilibrium line altitude (ELA) by analyzing the multi-temporal high resolution satellite data. The ELA is assumed to coincide with the snow line altitude at the end of ablation season (Kulkarni et al., 2004).

Since several obstacles like presence of cloud cover for optical remote sensing techniques and difficulties in field work for mass balance change detection using ground based measurement method. Hence synthetic aperture radar (SAR) can be used to detect the changes in mass balance and glacier facies using SAR FCC. The annual position of the equilibrium line can be retrieved from backscatter observation due to composite contribution to the backscatter variation in the equilibrium zone.

Once the theoretical snowline is obtained the same snowline can be used in the existing algorithm to estimate the mass balance and the difference can be studied. One such algorithm is developed by Rabatel et al. (2005) which can be used to find the mass balance calculation.

Summary

In this entry, application of synthetic aperture radar (SAR) for snow, ice, and glacier are discussed. Empirical as well as inversion models for estimation snowpack characteristics are described with case study. Various algorithms and techniques involving single pass SAR data with fixed polarization, repeat-pass InSAR coherence technique, and polarimetric SAR techniques are elucidated for mapping snow cover. Multi-temporal SAR data have great potential for identification and delineation of glacier facies, which helps to map equilibrium line. New emerging radar satellite for development of high precision DEM are also included which have direct application for glacier mass balance study. In the beginning of the entry a comprehensive methodology for SAR data processing is enclosed specially for glacier application scientists.

Bibliography

Baumgartner, F., Jezek, K., Forster, R. R., Gogineni S. P., and Zabel, I., 1999. Spectral and Angular Ground-Based Radar Backscatter Measurements of Greenland Snow Facies, IGARSS'99, June 28 – July 2, Hamburg, Germany, pp. 1053–1055.

Bell, D., Menges, C., Ahmad, W., and Van Zyl, J. J., 2001. The application of dielectric retrieval algorithms for mapping soil salinity in a tropical coastal environment using airborne polarimetric SAR. *Remote Sensing of Environment*, **75**, 375–384.

Benediktsson, J. A., and Swain, P. H., 1989. A method of statistical multisource classification with a mechanism to weight the influence of the data source. *Proceedings of the IEEE Symposium Geoscience Remote Sensing (IGARSS)*, Vancouver: Canada, pp. 517–520.

Benson, C. S., 1996. *Start graphic studies in the snow and firn of green land ice sheet*, SIPRE Research Report 70.

Boerner, W. M., Mott, H., Luneburg, E., Livingstone, C., Brisco, B., Brown, R. J., and Paterson, J. S., 1998. Polarimetry in radar remote sensing: basic and applied concepts. In Herderson, F. M., and Lewis, A. J. (eds.), *Principles and Applications of Imaging Radar, The Manual of Remote Sensing*, 3rd edn. New York: American Society of Photogrammetry and Remote Sensing. Chapter 5.

Cloude, S. R., and Pottier, E., 1996. A review of target decomposition theorems in radar polarimetry. *IEEE Transactions on Geoscience and Remote Sensing*, **34**(2), 498–518.

Cloude, S. R., and Pottier, E., 1998. A review of target decomposition theorems in radar polarimetry. *IEEE Transactions on Geoscience and Remote Sensing*, **34**(2), 498–514.

Denoth, A., 1989. Snow dielectric measurements. *Advances in Space Research*, **9**(1), 233–243.

Denoth, A., 1994. An electronic device for long term snow wetness recording. *Annual of Glaciology*, **19**, 104–106.

Einstein, T. H., 1982. *Effect of frequency averaging on estimation of clutter statistics used in setting CFAR detection thresholds*. MIT Lincoln Laboratory project report. TT-60, AD A131947, November 1982.

Fahnestock, M., Binschadler, R., Kwok, R., and Jezek, K., 1993. Greenland ice sheet surface properties and ice dynamics from ERS -1SAR imagery. *Science*, **262**(5139), 1530–1534.

Frankot, R. T., and Chellappa, R., 1987. Lognormal random-field models and their applications to radar image synthesis. *IEEE Transactions on Geoscience and Remote Sensing*, **GE 25**(2), 195–207.

Freeman, A., and Durden, S. L., 1998. A three-component scattering model for polarimetric SAR data. *IEEE Transactions on Geoscience and Remote Sensing*, **36**(3), 936–973.

Frost, V. S., Stiles, J. A., et al., 1982. A model for radar images and its application to adaptive digital filtering of multiplicative noise.

IEEE Transactions on Pattern Analysis and Machine Intelligence, **PAMI-4**, 157–166.

Fung, A., 1994. *Microwave Scattering and Emission Models and Their Applications*. Boston: Artech House. 573 p.

Fung, A., Lee, Z., and Chen, K. S., 1992. Backscattering from a randomly rough dielectric surface. *IEEE Transactions on Geoscience and Remote Sensing*, **30**(2), 356–369.

Hallikainen, M., Ulaby, F. T., and Abdelrazik, M., 1986. Dielectric properties of snow in the 3–37 GHz range. *IEEE Transactions on Antennas and Propagation*, **34**(11), 1329–1340.

Kendra, J., Sarabandi, K., and Ulaby, F., 1998. Radar measurements of snow: experiments and analysis. *IEEE Transactions on Geoscience and Remote Sensing*, **36**(3), 864–879.

Koskinen, J. T., Pulliainen, J. T., and Hallikainen, M. T., 1997. The use of ERS-1 SAR data in snow melt monitoring. *IEEE Transactions Geoscience and Remote Sensing*, **35**(3), 601–610.

Kulkarni, A. V., Rathore, B. P., and Alex, S., 2004. Monitoring of glacial mass balance in the Baspa basin using accumulation area ratio method. *Current Science*, **86**(1), 185–190.

Leconte, R., 1995. Exploring the behaviour of microwaves in a snowpack using modelling techniques. *Canadian Journal of Remote Sensing*, **22**(1), 23–35.

Lee, J.S., Grues, M.R., and Kwok, R., 1994. Classification of multilook polarimetric SAR imagery based on complex Wishart distribution. *International Journal of Remote Sensing*, **15**, 2299–2311.

Lee, J. S., Grunes, M. R., and Mango, S. A., 1991. Speckle reduction in multipolarization, multifrequency SAR imagery. *IEEE Transactions on Geoscience and Remote Sensing*, **29**(4), 535–544.

Li, Z., and Shi, J., 1995. Snow mapping with SIR-C multipolarization SAR in Tienshan Mountain. *IEEE International Symposium on Geoscience and Remote Sensing (IGARSS'95),* Florence, Italy, pp. 136–138.

Lillesand, T. M., and Kiefer, R. W., 2000. *Remote Sensing and Image Interpretation*, 4th edn. Singapore: Wiley, p. 724.

Looyenga, H., 1965. Dielectric constant of heterogeneous mixtures. *Physica*, **21**, 401–406.

Luojust, K., Puliiainen, J. T., Metsamaki, S., and Hallikainen, M. T., 2006. Accuracy assessment of SAR data based snow-covered area estimation method. *IEEE Transactions on Geoscience and Remote Sensing*, **44**(2), 277–287.

Nagler, T., 1995. Methods and analysis of SAR data from ERS-1 and X-SAR for snow and glcier applications, Ph.D. thesis, University of Innsbruck, September 1996.

Nagler, T., and Rott, H., 2000. Retrieval of wet snow by means of multi-temporal SAR data. *IEEE Transactions on Geoscience and Remote Sensing*, **38**(2), 754–765.

Novak, L. M., and Burl, M. C., 1990. Optimal speckle reduction in polarimetric SAR imagery. *IEEE Transactions on Aerospace and Electronic Systems*, **26**(2), 293–305.

Novak, L. M., Burl, M. C., and Irving, W. W., 1993. Optimal polarimetric processing for enhanced target detection. *IEEE Transactions on Aerospace and Electronic Systems*, **29**(1), 234–244.

Partington, K. C., 1998. Discrimination of glacier facies using multi-temporal SAR data. *Journal of Glaciology*, **44**(146), 480–488.

Partington, K. C., and Hanna, M., 1994. Modelling radar sea ice backscatter in support of ERS-1 SAR. *EARSeL Advances in Remote sensing*, **3**(2), 42–53.

Paterson, W. S. B., 1994. *The Physics of Glaciers*, 3rd edn. Oxford: Pergamon.

Pulliainen, J. T., Engdabi, M., and Hallikainen, M. T., 2003. Feasibility of multitemporal interferometric SAR data for stand-level estimation of boreal forest stem volume. *Remote Sensing of Environment*, **85**, 397–409.

Rabatel, A., Dedieu, J. P., and Vincent, C., 2005. Using remote-sensing data to determine equilibrium-linealtitude and mass-balance time series: validation on three French glaciers, 1994–2002. *Journal of Glaciology*, **51**(175), 539–546.

Raney, R. K., 2006. Dual-polarized SAR and stokes parameters. *IEEE Geoscience and Remote Sensing Letters*, **3**(3), 317–319.

Rao, Y. S., Kumar, V., Singh, G., Venkataraman, G., and Mani, S., 2008. The loss of coherence in the InSAR images of Himalayan Glaciers. *Proceedings of international workshop on Snow, Ice, Glacier and Avalanches*, held at IIT Bombay during January 7–9, 2008, pp. 232–239.

Rignot, E., Chellappa, G., and Dubois, P., 1992. Unsupervised segmentation of polarimetric SAR data using the covariance matrix. *IEEE Transactions on Geoscience and Remote Sensing*, **30**(4), 697–705.

Rosich, B., and Meadows, P., 2004. Absolute calibration of ASAR Level 1 products generated with PFASAR. *ESA/ESRIN, Technical Note ref. ENVI-CLVL-EOPG-TN-03-0010*, Issue 1, Rev. 4, January 2004.

Rott H., 1991. Multi-parameter SAR experiments on snow and glacier application, *Proceedings of the 11th EARSeL symposium*. EARSeL, pp. 79–91.

Rott H., and Nagler, T., 1992. Snow and glacier investigations by ERS-1 SAR, First results in *Proceedings of the 1st ERS-1 symposium*, ESA SP-359, November 4–6, 1992, ESA, pp. 577–582.

Rott, H., and Nagler, T., 1993. Capabilities of ERS-1 SAR for snow and glacier monitoring in Alpine areas, *Proceedings of the 2nd ERS-1 Symposium*, 11–14 October 1993, Hamburg, ESA pp. 965–970.

Rott H., Matzler N., Strobi D., Bruzzi S., and Lenhart K., 1988. *Study on SAR land applications for snow and glacier monitoring*, Contact Report 6618/85/F/FL(SC), ESA, 1988.

Rott J., Davis R., and Dozier J., 1992. Polarimetric and multifrequency SAR signatures of wet snow. *Proceedings of IGARSS'92*, Houston, pp. 1658–1660.

Sheng Y., Xia, Z., 1996. A Comprehensive Evaluation of Filters for Radar Speckle Suppression. *Proceedings of IGARSS'*96, Vol. 3, Lincoln, pp. 1559–1561.

Shi, J., and Dozier, J., 1993. Measurements of snow and glacier-covered areas with single polarization. *Annals of Glaciology*, **17**, 72–76.

Shi, J., and Dozier, J., 1995. Inferring snow wetness using C-band data from SIR-C's polarimetric synthetic aperture radar. *IEEE Transactions on Geoscience and Remote Sensing*, **33**, 905–914.

Shi J., and Dozier J., 1996. Estimation of snow water equivalence using SIR C/X SAR. *Proceedings of the IEEE Geoscience and Remote Sensing Symposium (IGARSS'96)*, Lincoln, pp. 2002–2004.

Shi, J., and Dozier, J., 1997. Mapping seasonal snow with SIR-C/X-SAR in mountainous areas. *Remote Sensing of Environment*, **59**(2), 294–307.

Shi, J., and Dozier, J., 2000. Estimation of snow water equivalence using SIR-C/X-SAR – part I. inferring dry snow density and subsurface properties. *IEEE Transactions on Geoscience and Remote Sensing*, **38**(6), 2465–2474.

Shi J., Dozier J., and Davis R. E., 1990. Simulation of snow-depth estimation from multi-frequency radar. *Proceedings of the IGARSS'90*, Institute of Electrical and Electronic Engineering: New York, pp. 1129–1132.

Shi J., Dozier J., and Rott H., 1993. Deriving snow water equivalence using C-band polarimetric SAR. *Proceedingsof the IEEE*

*International Symposium on Geoscience and Remote Sensing (IGARSS'93),*Tokyo: Japan, pp. 1038–1041.
Shi, J., Dozier, J., and Rott, H., 1994. Snow mapping in alpine regions with synthetic aperture radar. *IEEE Transactions on Geoscience and Remote Sensing*, **32**(1), 152–158.
Shi, J., Hensley, S., and Dozier, J., 1997. Mapping snow cover with repeat pass synthetic aperture radar. In: *Proceedings of the International Geoscience and Remote Sensing Symposium 1997*, II, 628–630.
Gulab, S., and Venkataraman, G., 2009. Snow density estimation using polarimetric ASAR data. *Proceedings Micowave08*, Jaipur, India, pp.463–466.
Singh, G., Venkataraman, G., Kumar, V., Rao, Y. S., and Mani, S., 2008. The H/A/Alpha polarimetric decomposition theorem and complex wishart distribution for snow cover monitoring. *Proceedings IGRASS'08*, Vol. 4, Jaipur, pp. 1081–1084.
Singh, G., and Venkataraman, G., 2009. Snow density estimation using polarimetric ASAR data. *Proceedings Micowave08*. Jaipur, India, pp. 463–466.
Strozzi, T., and Matzler, C., 1998. Backscattering measurements of alpine snow covers at 5.3 and 35 GHz. *IEEE Transactions Geoscience Remote Sensing*, **36**, 838–848.
Strozzi, T., Wegmuller, U., and Matzler, C., 1999. Mapping wet snow covers with SAR interferometry. *International Journal of Remote Sensing (series No. 12)*, **20**, 2395–2403.
Ulaby, F. T., and Elachi, C., 1990. *Radar Polarimetry for Geoscience Applications*. Norwood: Artech House.
Ulaby, F. T., and Stiles, W. H., 1980. The active and passive microwave response to snow parameters 2. Water equivalent of dry snow. *Journal of Geophysical Research*, **85**(C2), 1045–1049.
Ulaby, F., Moore, R., and Fung, A., 1981. *Microwave Remote Sensing, Active and Passive*. Norwood: Artech House, Vol. I.
Ulaby, F. T., Moore, R. K., and Fung, A. K., 1982. *Microwave Remote Sensing, Active and Passive*. Reading: Addison-Wesley, Vol. II, pp. 457–1064.
Ulaby, F. T., Moore, R. K., and Fung, A. K., 1986. *Microwave Remote Sensing, Active and Passive*. Dedham: Artech House, Vol. III.
van Zyl, J. J., and Burnette, F., 1992. Bayesian classification of polarimetric SAR images using adaptive a priori probabilities. *International Journal of Remote Sensing*, **13**(5), 835–840.
van Zyl, J. J., Zebker, H. A., and Elachi, C., 1987. Imaging radar polarization signatures: theory and observations. *Radio Science*, **22**(4), 29–543.
Yajima, Y., Yamaguchi, Y., Sato, R., Yamada, H., and Boerner, W. M., 2008. Polsar image analysis of wetlands using a modified four-component scattering power decomposition. *IEEE Transactions on Geoscience and Remote Sensing*, **46**(6), 1667–1673.
Yamaguchi, Y., Yajima, Y., and Yamada, H., 2006. A four-component decomposition of POLSAR images based on the coherency matrix. *IEEE Geoscience and Remote Sensing Letters*, **3**(3), 292–296.
Zebker, H. A., van Zyl, J. J., Durden, S. L., and Norikane, L., 1991. Calibrated imaging radar polarimetry: techniques examples and applications. *IEEE Transactions on Geoscience and Remote Sensing*, **29**(6), 942–961.

Cross-references

Digital Image Information Extraction Techniques for Snow Cover Mapping from Remote Sensing Data
Optical Remote Sensing of Alpine Glaciers
Synthetic Aperture Radar (SAR) Interferometry for Glacier Movement Studies

RADIATIVE TRANSFER MODELING

Jie Cheng[1], Shunlin Liang[2]
[1]College of Global Change and Earth System Science, Beijing Normal University, Beijing, China
[2]Department of Geography, University of Maryland, College Park, MD, USA

Definition

Albedo. The total fraction of light scattered into the upward hemisphere by a surface.
Emissivity. Emissivity is defined as the ratio of the actual radiance emitted by a given surface to that emitted by a blackbody at the same temperature. It is a measure of surface radiation ability.

Introduction

Radiative transfer (RT) is the radiant energy transported through a medium in the form of an electromagnetic wave. The interactions between electromagnetic waves and media are complex physical processes that include absorption, scattering, and emission. These interactions can be described mathematically with the radiative transfer equation, in which energy is always represented by the spectral radiance or intensity:

$$\frac{\mathrm{d}I(s)}{\mathrm{d}s} = -K(I - J),$$

where $I(s)$ represents the spectral radiance (I) at a specific direction (S), K is the volume extinction coefficient, and J is the source function.

The radiative transfer equation has been widely used in astronomy, atmospheric science, and remote sensing. However, the radiative transfer equation is a differential integral equation (Liang, 2004), and it is preferable to use the radiation at fixed locations in a medium in actual applications. Thus, we should determine the solution to the radiative transfer equation, given the optical properties of the medium and their boundary conditions. Generally, there are two types of solutions: approximate solutions (also called *analytical solutions*) and numerical solutions. Both of these solution types characterize the behavior of radiation in the medium.

In remote sensing, satellite sensors measure the radiation signal attenuated by the intervening atmosphere between the satellites and the surface. The measured radiation signal and the surface parameters are primarily linked by surface and atmospheric radiative transfer models. Therefore, radiative transfer models are essential for satellite radiation signal interpretation and the inversion of surface parameters.

Importance of RT modeling

Snow, ice, and glaciers are important land surface types. They have high albedos in the visible and near-infrared

spectrum (Figure 1), and substantially reflect solar radiation. They also have high emissivities in the thermal infrared spectral region (Figure 2). Furthermore, these land surface types have pronounced effects on the energy budget of the Earth-atmosphere system. They determine the amount of water that will be released during spring runoff, and are the primary water sources for almost all of the major river systems across the world. Therefore, snow, ice, and glaciers are very important for hydrological applications and water resource management.

In situ measurements of the physical properties of snow, ice, and glaciers are extremely difficult, due to spatial and temporal representations and expenses, and can even be dangerous. Remote sensing has the advantage of global coverage at high temporal frequencies, and is an ideal tool for studying these land surface types at the regional and global scales. Additionally, the satellite remote sensing of snow, ice, and glaciers often requires a radiative transfer model to simulate and invert their radiation properties.

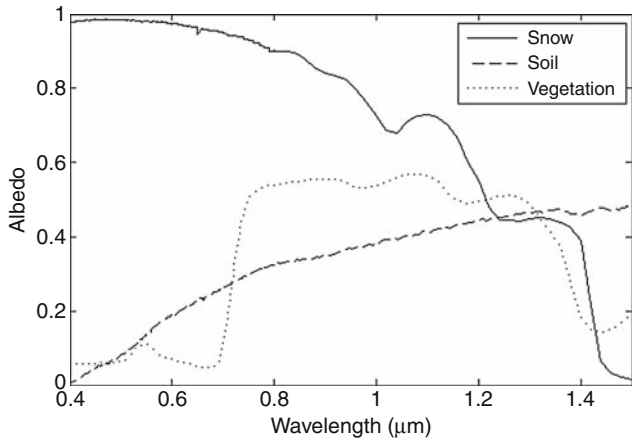

Radiative Transfer Modeling, Figure 1 Spectral albedo values of snow, soil, and vegetation in the visible and near-infrared spectral region.

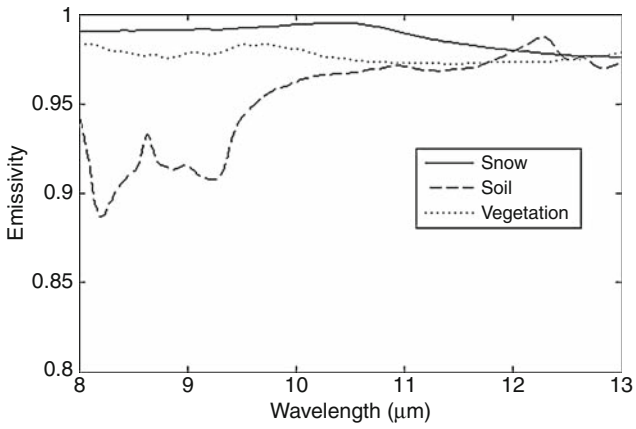

Radiative Transfer Modeling, Figure 2 Spectral emissivities of snow, soil, and vegetation in the thermal infrared spectral region.

The basic physical components of snow, ice, and glaciers are irregular ice crystals, air in porosity, liquid water production when melting, and impurities when contaminated by aerosols and other pollutants. The ice crystal is the basic scattering, absorbing, and emitting agent in snow, ice, and glacial media. In the optical region, the factors of greatest concern are the albedos and emissivities of these land surfaces types. The former determines how much incident solar radiation is reflected back into the sky by snow, ice, and glacier surfaces, and the latter determines how much radiation is emitted; both influence the radiation budgets of these surface types. Microwave remote sensing can be used to determine the snow cover, snow depth, and snow water equivalent (SWE), which are indicators of global climate change, particularly the glacial ablation resulting from global warming.

Surface albedo and emissivity modeling

Snow can be considered a layered particulate medium. To model the albedo and emissivity of a snow surface cover, it is necessary to begin with the known single-scattering properties of snow particles, which govern the ensemble properties of the snow medium (Nolin and Liang, 2000). The single-scattering properties needed as inputs for radiative transfer models are the extinction cross section, single-scattering albedo (ratio of scattering to extinction cross section), particle scattering phase function, and asymmetry factor (the cosine of the average of the particle scattering phase function). Calculating the scattering properties of a snow particle requires the optical constants, $m = n + ik$ (also referred to as the *complex refractive index*), where n is the usual refractive index that determines the phase speed and k is related to the absorption coefficient, as well as the size parameter, $x = 2\pi r/\lambda$, where r is the sphere radius and λ is the wavelength. A compilation of the optical constants of ice, from the ultraviolet to the microwave spectrum, is now available (Warren and Brandt, 2008). Figure 3 shows the complex refractive index of ice.

There are numerous light scattering theories and computational codes available to calculate the single-scattering parameters for a single particle (Wriedt, 2009). One of the most popular theories is the Mie theory (Mie, 1908) for optically homogeneous spherical particles. Although realistic snow particles are nonspherical and tend to be spheroidal, randomly oriented "equivalent spheres" with the same volume-to-surface ratios are commonly used to represent snow grains. These "equivalent spheres" allow the Mie theory to be used for the computation of the single-scattering parameters of snow particles. Previous studies have shown that the "equivalent spheres" assumption is a feasible surrogate. For example, Mugnai and Wiscombe (1987) demonstrated that their scattering results were the same as those for ensembles of nonspherical

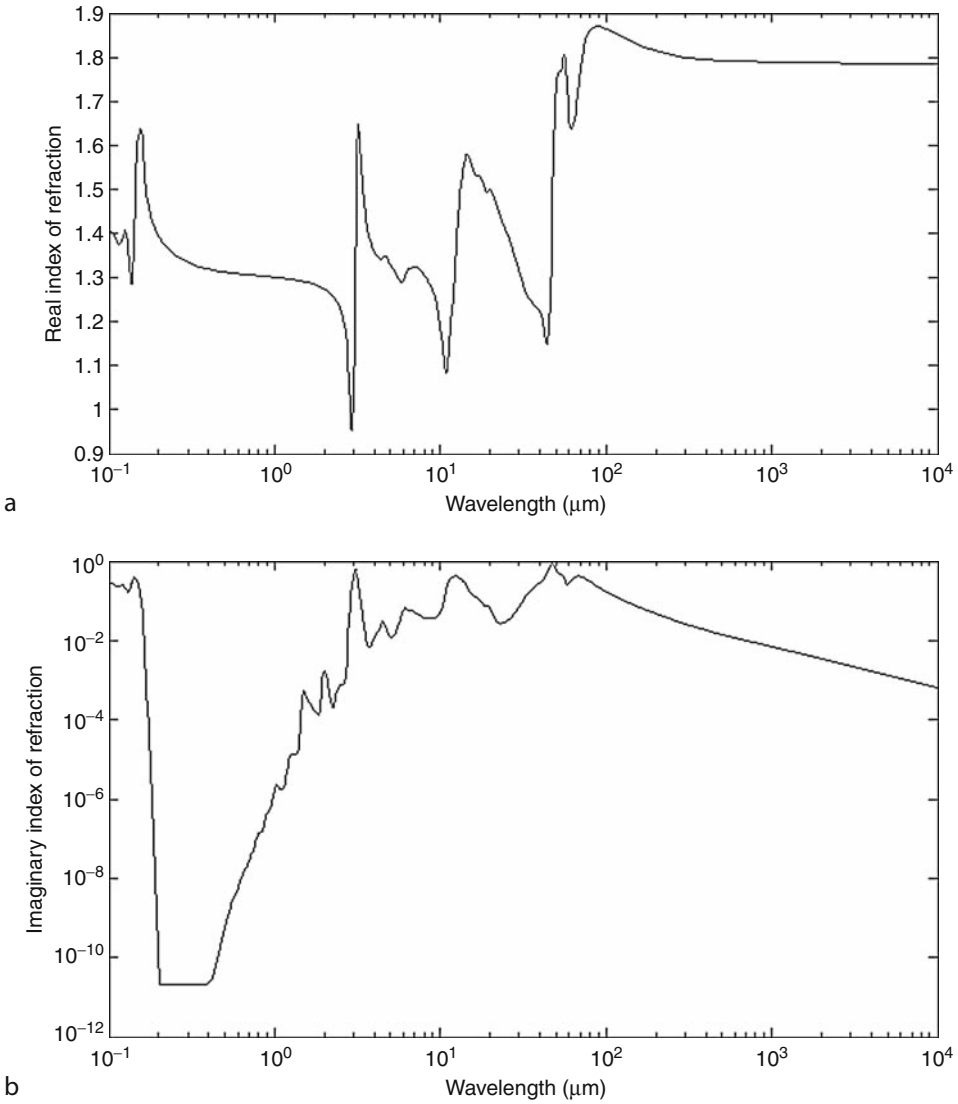

Radiative Transfer Modeling, Figure 3 Complex refractive index of ice: (**a**) Real part, (**b**) Imaginary part.

particles. Other studies (Dozier, 1989; Grenfell and Warren, 1999) have shown that the volume-to-surface area ratio of an ice particle can be used to represent an optically equivalent grain size for ensembles of nonspherical ice particles. Thus, snow particles are often represented by "equivalent spheres" in radiative transfer models.

In the past, there were several limited snow albedo models (Dunkle and Bevans, 1956; Giddings and La Chapelle, 1961; Barkstrom, 1972; Bohren and Barkstrom, 1974) available to the scientific community. Unfortunately, these models are now obsolete due to their obvious shortcomings, because no single model is valid for all wavelengths in the solar spectrum, or for an arbitrary combination of diffuse and direct incidence. To address this issue, a practical snow spectral albedo analytical model was put forward by Wiscombe and Warren (1980). In the Wiscombe and Warren model, the extinction cross section, single-scattering albedo, and asymmetry factor are calculated by the Mie theory using known snow optical constants and size parameters. The δ-Eddington approximation is used for multiple scattering (Joseph et al., 1976). The formulations of direct-beam and diffuse albedos are presented. Figure 4 depicts semi-infinite direct-beam and diffuse albedos calculated by the Wiscombe and Warren formulation. The snow effective radius is 50 μm and the solar zenith angle is 30°. Snow is always contaminated by desert dust and carbon soot aerosols, which absorb in the visible and near-infrared spectral regions, and have pronounced effects on snow albedo modeling in the visible spectral region. Warren and Wiscombe (1980) extended their previous snow albedo model to incorporate the optical constant of these impurities into the snow optical constant to allow for aerosol contamination.

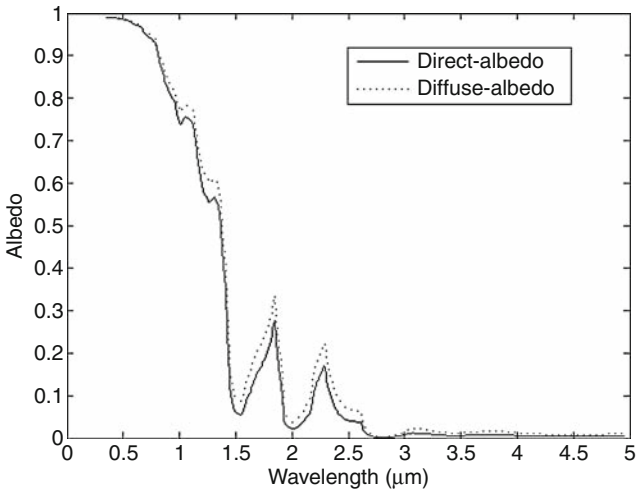

Radiative Transfer Modeling, Figure 4 Semi-infinite direct-beam and diffuse albedo values calculated by Wiscombe and Warren model. Snow effective radius is 50 μm and solar zenith angle is 30°.

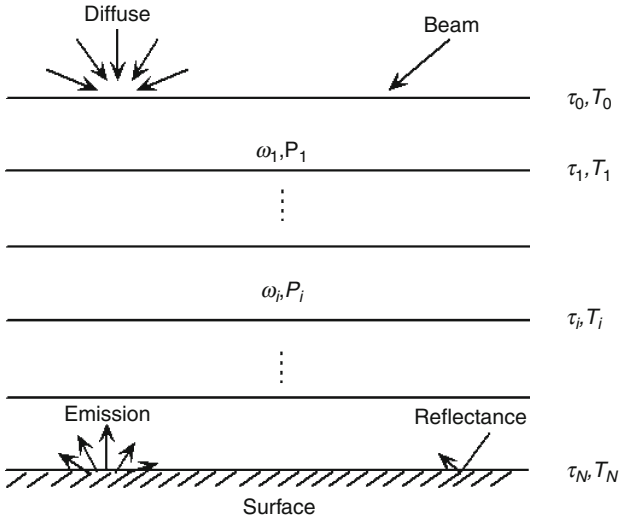

Radiative Transfer Modeling, Figure 5 Schematic illustration of optical medium stratification for numerical calculation of radiative transfer. Each layer has single-scattering albedo ω, phase function P, and temperature T. They are defined as layer averages.

Several analytical radiative transfer models were originally designed for other semi-infinite media such as quartz, soil, and the planetary surface. These models can also be used for snow. Conel (1969) developed a cloudy atmosphere model of the condensed powder emission spectrum in which the Mie theory is used to calculate single-scattering parameters, and multiple scattering is modeled with a two-stream approximation. Hapke (1981, 1993) developed a series of analytical bidirectional reflectance models for a semi-infinite particulate medium. In Hapke's reflectance models, the single-scattering properties of a particle are calculated with the geometric optical method, and multiple scattering is approximated with the two-stream method. In Hapke's emittance model, the directional emissivity of a semi-infinite medium is derived through the embedded invariance theory (Hapke, 1993). Moersch and Christensen (1995) used the Mie theory to replace the geometric optical method for single-scattering parameters, and evaluated the Mie/Hapke hybrid model using laboratory-measured quartz emissivity spectra. Liang and Townshen (1996) developed a modified Hapke model for a soil bidirectional reflectance simulation by dividing the original multiple-scattering parameters into those for double scattering and higher-order scattering. The modified Hapke model demonstrates higher accuracy than the original. In these models, particles are treated as independent and do not impact each other. In actuality, particles in semi-infinite media, like snow and soil, touch each other and are sometimes densely packed. As pointed out by Van de Hulst, the neighboring particles must be separated by three particle radii for the independent scattering approximation to be valid (Hulst, 1957). Thus, the independent scattering approximation is not valid for such media. Wald (1994) questioned the rationality of an independent scattering approximation and put forward a diffraction subtraction method to correct the Mie theory in relation to the single-scattering albedo and asymmetry factor. Mishchenko also developed a method to correct the Mie theory (Mishchenko and Macke, 1997). He used a static structure factor based on the filling factor – an index to characterize packing conditions. The static structure factor has a strong physical foundation, and is based on solving Maxwell's equation for light scattering and the statistical mechanics for dense packing. Pitman et al. (2005) used these two correction methods to modify the Mie single-scattering parameters and drive several radiative transfer models of silicate surface emissivity. Comparisons using measured silicate surface emissivities show that radiative transfer models cannot replicate observations, even if the Mie single-scattering parameters are modified using these correction methods.

In addition to analytical radiative transfer models, numerical models are also widely used in snow albedo modeling, including the discrete ordinates radiative transfer (DISORT) model, adding-doubling model, and spherical-harmonic model. The DISORT model was introduced by Wick (1943) and further developed by Chandrasekhar to model the radiative transfer of planetary atmospheres (Chandrasekhar, 1960). Liou (1973) extended the DISORT model for aerosols and cloudy atmosphere conditions, and demonstrated that it is an effective and powerful tool. A numerical DISORT computational code was introduced by Stamnes et al. (1988). DISORT assumes that the medium consists of multiple adjacent homogeneous layers. For each layer, the single-scattering albedo and phase function are assumed to be constant, but these can vary from layer to layer (Figure 5). Given the single-scattering properties, DISORT can be used to calculate the reflective characteristics (e.g., surface albedo and

bidirectional reflectance) of snow. Because it is a highly accurate model, DISORT is often used as a benchmark to evaluate the performance of other analytical radiative transfer models. The adding-doubling model was introduced by Hansen for the interpretation of the intensity and polarization of sunlight reflected from clouds (Hansen, 1971). It starts with a thin cloud layer with a known single-scattering albedo and phase matrix, and then adds a layer with a double optical depth. This process is repeated until the total optical depth is achieved. The reflectance and transmittance of the layered medium can be calculated by adding the values of each individual thin layer. Leroux et al. (1999) used the adding-doubling model to develop the polarized bidirectional reflection distribution function (BRDF). Aoki et al. (2000) used this model to simulate the spectral albedo and bidirectional reflectance of the snow surface. The spherical-harmonic model was developed by Mishchenko et al. (1999), and is an efficient model for calculating the bidirectional reflectance of a semi-infinite homogeneous particulate medium.

Based on Kirchhoff's law, the directional emissivity can be calculated by subtracting the directional-hemispherical reflectance. Thus, the radiative transfer models used to calculate snow albedo can also be used for calculating the directional emissivity of snow. Dozier and Warren (1982) derived a formulation of the directional emissivity of snow based on Kirchhoff's law and the Wiscombe and Warren snow spectral albedo analytical model, with the assumption that snow is a semi-infinite scattering medium. Their studies showed that the directional emissivity of snow can result in a 3 K difference between the thermodynamic temperature and brightness temperature in the 12–14 μm spectral region. Wald used the single-scattering parameters corrected by diffraction subtraction as inputs for the Wiscombe and Warren model (Wiscombe and Warren, 1980), Hapke emittance model (Hapke, 1993) and doubling model (Wiscombe, 1976) to investigate their feasibility for snow emissivity modeling. This method quantitatively predicts the directional hemispheric reflectance of disaggregated snow samples with particle radii greater than 50 μm. Cheng et al. (2010) investigated the abilities of three analytical radiative transfer models (Conel model, Dozier and Warren model, and Hapke emittance model) and one numerical (DISORT) radiative transfer model to determine the directional emissivity of snow, and compared the simulation results with actual in situ measurements of the directional emissivity of snow. The most suitable hybrid RT model was identified. For modeling the directional emissivity of snow, the Mie-corrected/Hapke model is the best choice. The root mean square error (RMSE) of the Mie-Mishchenko/Hapke model is less than 0.005 for r = 35 μm in the 8–11 μm spectra region; the RMSE of the Mie-Wald/Hapke model is less than 0.009 for r = 400 μm in the 8–11 μm spectra region; the RMSE is less than 0.006 for r = 300 in the 8–13 μm spectra region; and the RMSE is less than 0.006 for r = 550 μm in the 8–11 μm spectra region – except for the 60 and 75° view angles.

Ice can be treated as a smooth surface. Its bidirectional reflectance can be calculated with the Fresnel reflectance theory given the relative refractive index and emittance angle. The directional emissivity of ice can be derived with the Fresnel reflectance theory and Kirchhoff's Law. Hori et al. (2006) calculated the directional emissivity of bare ice using the Fresnel reflectance theory and compared the result with field and laboratory measured values. They obtained consistent results with absolute differences on the order of 0.01, which is the desired accuracy for remote emissivity sensing devices. Figure 6 shows the measured nadir and 15° emissivities of ice, as well as the values calculated by the Fresnel reflectance theory.

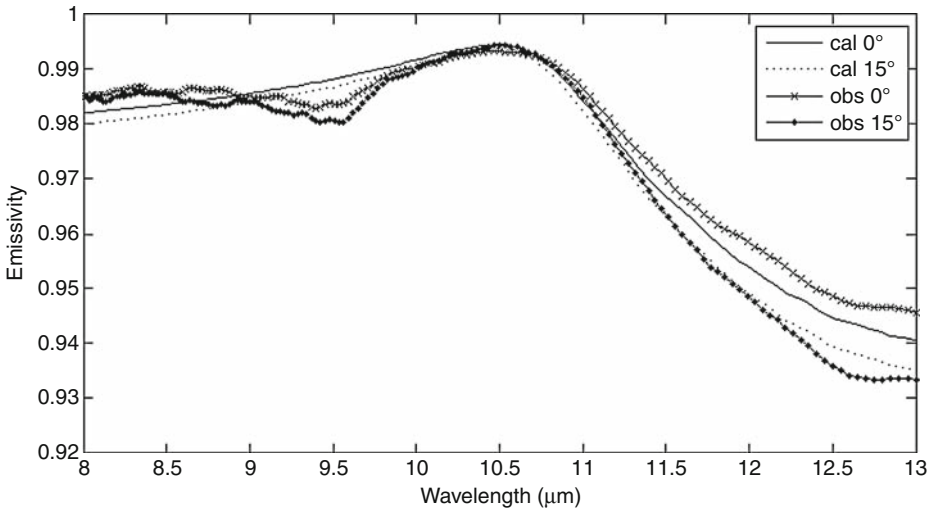

Radiative Transfer Modeling, Figure 6 Comparison of measured directional emissivity of ice with that calculated by the Fresnel reflectance theory.

Microwave emission modeling

In the microwave spectral region, snow is a dense particulate medium, and the interactions between microwave signals and snow include surface and volume scatterings. Snow volume scattering is composed of coherent and incoherent multiple scatterings. Microwaves can penetrate the snow surface and interact with the underlying ground. The microwave emissions from a snowpack come from the snow itself and from the underlying ground. These two emissions are governed by the extinction and emission properties of the snow layer, and by the transmission and reflection properties of the air-snow and snow-ground interfaces. The ground emission, and the interactions at the snow-ground boundary, must be considered in a snow-microwave emission model.

There are many models for surface scattering, including the small perturbation method (SPM), Kirchhoff approximation (KA) (Ulaby et al., 1982; Fung, 1994), small slope approximation (SSA) (Broschat, 1993), and integral equation model (IEM) (Fung et al., 1992). These models have individual applicabilities and are similar under specific conditions. For example, the SPM is valid for slightly rough surfaces, while the KA can be used for surfaces with greater roughness. SSA and SPM produce the same simulation results for emissivity. The IEM has demonstrated its applicability for a wide range of surface roughness parameters through comparisons with Monte Carlo simulations and laboratory-controlled measurements. However, it cannot achieve satisfactory emissivity simulation results for very rough surfaces because of several weak assumptions adopted by the model. Chen et al. (2003) extended the original IEM model by removing these weak assumptions, and subsequent comparisons of the surface emission simulation results of AIEM with those of three-dimensional Monte Carlo simulations for Gaussian rough surfaces indicate that AIEM is accurate and applicable for a wide range of surface dielectrics, roughness values, and sensor frequencies. These achievements have produced a fundamentally improved understanding of the measured microwave signals for snow.

In recent years, significant progress has been made in the theoretical modeling of microwave emissions from snow. Several microwave snow emission models have been published to describe the relationships between snow parameters and electromagnetic quantities (e.g., brightness temperature). These include the microwave emission model of layered snowpacks (MEMLS) model (Wiesmann and Matzler, 1999), the model developed by the Helsinki University of Technology (HUT) (Pulliainen et al., 1999), the dense medium radiative transfer (DMRT) model (Chuah et al., 1996; Tsang and Kong, 2001), and the slab multiple-scattering microwave emission model (also referred to as the DRRT-AIEM-MD model, Jiang et al., 2007). Microwave emission models can be classified as empirical, semiempirical, and theoretical. The DMRT model is one of the theoretical models, which are based solely on physical theory, without the use of any experimental data. The MEMLS, HUT, and DRRT-AIEM-MD are semiempirical models, which are developed by combining theory with measured results. For example, the HUT model was developed from the radiative transfer theory, and the extinction coefficient in the model was derived from experimentation. Because of the different approaches used to model physical processes, characterize the electromagnetic properties of snow, and solve the radiative transfer equations, each kind of model has its own application limitations. The DMRT model can be used to validate semiempirical models, and as a forward simulation tool to provide the data used to establish the empirical relationships in empirical models. However, it cannot be included in an operational inversion methodology due to its complexity. The MEMLS model is a multilayer and multi-scattering snow emission radiative transfer model, and although it is not suitable for the direct retrieval of snow variables, it can be used to validate a retrieval algorithm. The HUT model only considers one homogeneous snow layer, which includes the soil, vegetation, and atmosphere, and is widely used to determine the SWE or snow depth from remote sensing data because of its simplicity (Figure 7). The influence of internal layering in a snowpack is not considered in the HUT model. Such internal layering will increase the scattering in the snowpack and change the spectral gradient. It should be pointed out that there is no single algorithm that yields good estimates for the SWE at the global scale.

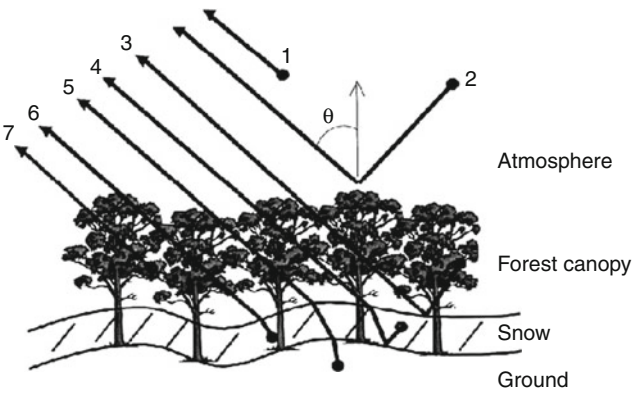

Radiative Transfer Modeling, Figure 7 Major contributions to spaceborne observed scene brightness temperature. All of these contributions are included in the Helsinki University of Technology (HUT) snow emission model: (1) upward emitted atmospheric radiation; (2) downward emitted reflected atmospheric radiation; (3) downward emitted reflected forest canopy emission contribution; (4) downward emitted reflected snowpack emission contribution; (5) upward emitted reflected emission contribution; (6) upward emitted snowpack emission contribution; (7) upward emitted forest canopy emission contribution [From Pulliainen and Hallikainen (2001), Remote Sensing of Environment. Copyright © 2001 with permission from Elsevier.]

Complementary modeling techniques

In addition to the analytical and numerical radiative transfer models, geometrical optical models and Monte Carlo methods can also be used to simulate the radiation properties of snow, ice, and glaciers. These are complementary to the analytical and numerical radiative transfer models, and can be treated as a part of radiative transfer modeling. When the particles are very large relative to the wavelength of the incident light, the geometrical optics approach can be used to model the surface reflectance. Leroux et al. (1998) used a photometric roughness model based on a model developed by Roujean et al. (1992) that used vertical protrusions arranged on a flat scattering surface to investigate the snow surface roughness effects on the albedo. They found that the sastrugi caused by wind erosion have a darkening effect that can reduce the albedo by as much as 10%. Leroux and Fily (1998) modified the model by orienting the regularly spaced identical protrusions along the same direction, ignoring the inter-facet multiple scattering, and assigning an appropriate bidirectional reflectance to the underlying flat snow surface. They found that there was still a quantitative disagreement between the simulations and measurements. Two factors are thought to be responsible for this disagreement: the imperfections of the roughness model and uncertainties in the experimental data. Clearly, more measurements and model refinements should be carried out in the future.

In the analytical or numerical radiative transfer models, a basic scattering unit is assumed to be homogeneous and have the same properties, such as the commonly used plane-parallel assumption. The scatters in each optical thin plane are assumed to have the same properties, even though these are miscellaneous. When considering the radiation distribution calculation for a complex dense medium, these approaches sometimes have limited domains of validity.

The Monte Carlo method is effective at solving mathematical problems by random sampling (Kim et al., 2004). It consists of simulating the behavior of each individual photon using probabilistic methods. In order to get satisfactory results, it is essential to produce a large number of photons in the simulations. The wave scattering problem has been a hot topic of continued study for many years because of its broad applications (Li et al., 1999). Fortunately, the advent of modern computers and more efficient computation methods makes it possible to model microwave scattering with the Monte Carlo method (Chan et al., 1998). Two kinds of microwave scattering problems can be solved with the Monte Carlo method – the rough surface and discrete scatter problems (Zurk et al., 1996). In the rough surface scattering problem, the bi-static scattering coefficients can be derived by directly solving Maxwell's equation using the Monte Carlo method. For a dense medium problem, a large number of photons are needed to perform Monte Carlo simulations of the extinction, phase matrix, and absorption coefficients. These parameters are then used in either analytical or numerical radiative transfer models to calculate the bi-static scattering properties of a dense medium.

Nieto-Vesperinas and Soto-Crespo (1987) simulated the scattered intensities of a one-dimensional perfectly conductive random surface with the Monte Carlo method. Tsang et al. (1992) iteratively solved Maxwell's equation in multiple scattering form, and used the Monte Carlo method to compute the extinction rates for fractional volumes of up to 25%. Zurk et al. (1995) used the Monte Carlo method to simulate the extinction rates for densely packed spheres with clustered and non-clustered geometries. Zurk et al. (1996) used the Monte Carlo method to derive the phase matrix, effective permittivity, and scattering coefficients for a densely packed medium composed of up to 5,000 spheres. The simulated parameters were used as inputs to a second-order radiative transfer model to predict the backscattering of a layer of snow. These results were compared with those calculated using DMRT and the independent scattering assumption. Different results were obtained due to the assumption used in the calculation of the extinction coefficient, phase matrix, and effective permittivity. Three-dimensional method-of-moment Monte Carlo simulations of microwave emissions from lossy dielectric random rough surfaces were made possible by fast computation methods (Li et al., 2000). Chen et al. (2003) used Monte Carlo simulations of the three-dimensional solutions of Maxwell's equations to study the frequency dependence of the scattering by dense media.

Primary applications

Radiative transfer models have been used (Liang, 2004, 2008): (1) to directly calculate surface albedo and emissivity given the basic surface physical parameters, and (2) to invert the surface physical parameters from remote sensing data.

Surface albedo and emissivity calculation

The albedo of a snow, ice, or glacier surface determines how much incident solar energy is absorbed and reflected by the surface. The emissivity of a snow, ice, or glacier surface characterizes its ability to emit radiation, and can be used to estimate the surface temperature. The albedo and emissivity are two critical parameters in estimating the surface energy budget, which is highly related to the physical state of the surface, such as one involving snowmelt and runoff. The Wiscombe and Warren (1980) snow spectral albedo model has been embedded in land surface and global circulation models to calculate the snow surface albedo (Dai et al., 2003; Schmidt et al., 2006). Dozier and Warren (1982) derived a formulation for the directional emissivity of snow from the Wiscombe and Warren (1980) directional-hemispherical reflectance equation using Kirchhoff's law. They used this formulation to study the directionality of snow emissivity from its brightness temperature. The formulation of Dozier and Warren (1982) was used to calculate the directional emissivity of

a snow-covered surface, and the calculated directional emissivity was used to determine the surface temperature from satellite data (Key and Haefliger, 1992; Key et al., 1997). Snyder et al. (1998) used the formulation of Dozier and Warren (1982) to consider the angular effect of snow surface emissivity. Even though the formulation of Dozier and Warren (1982) has been widely used in calculating snow surface emissivity because of its reliable temperature determination, it cannot reflect the radial dependence of snow emissivity (i.e., the decrease in snow emissivity with an increase in particle radius). Cheng et al. (2010) investigated the ability of radiative transfer models to determine the directional emissivity in snow modeling, and compared the simulation results with in situ measurements of the directional emissivity of snow. They found that the hybrid Mie-corrected/Hapke model is the best choice for determining the directional emissivity in snow modeling.

Surface physical parameters retrieval

The surface physical parameters derived from remote sensing data can be used in many applications such as forecasting avalanches, validating metamorphism models, and obtaining snow data in remote areas (Brun et al., 1989; Bourdelles and Fily, 1993; Nolin and Stroeve, 1997). Therefore, many studies have focused on determining the snow grain size, emissivity, SWE, or snow depth from remote sensing data. While the previous discussion focused on the details of the spectral albedo and emissivity calculations, we will now focus primarily on estimating: (1) the snow grain size, and (2) the SWE or snow depth.

Snow grain size retrieval

Dozier et al. (1981) investigated the effects of the snow grain size on the visible and near-infrared reflectance using the Advanced Very High Resolution Radiometer (AVHRR) data. Their results indicate the dependence of the snow reflectance on the snow grain size and snow water equivalent. Dozier and Marks (1987) showed that it was possible to retrieve the snow grain size by combining the Wiscombe and Warren (1980) model and AVHRR data. Nolin and Dozier (1993) estimated the snow grain size from the Airborne Visible/Infrared Imaging Spectrometer (AVIRIS) data, using an exponential relationship between the snow grain size and 1.04-μm reflectance derived with the DISORT model. Fily et al. (1997) retrieved the snow grain size from the Landsat data for highly mountainous terrain in the French Alps based on the forward radiative transfer DISORT model. Nolin and Dozier (2000) discovered that, in spectral snow reflectance, the scaled band area of absorption by ice centered at 1.03 μm depends on the snow grain size, and developed a new algorithm for grain size retrieval. Their retrieval experiments indicated that this new algorithm is both robust and accurate. In their algorithm, the relationship between the snow grain size and scaled band area is derived with DISORT. Li et al. (2001) compared the snow grain sizes retrieved from four AVIRIS channels using a logarithmic expression derived from DISORT simulations, obtaining different snow grain sizes from the same pixel. The different penetration depths for different wavelengths are thought to be responsible for this phenomenon. It could be used to retrieve the average snow grain size for different snow layers. Painter et al. (2003) used a bidirectional reflectance model based on the Mie theory and DISORT model, in conjunction with a spectral mixture analysis based on the endmember reflectances for different snow grain sizes, to simultaneously retrieve the snow grain size and snow cover. Stamnes et al. (2007) developed an algorithm to determine the snow grain size and impurity concentration from the Advanced Earth Observing Satellite II (ADEOS-II) Global Imager (GLI) data utilizing the Mie theory and DISORT model. Aoki et al. (2007) validated the algorithm using the GLI and Moderate Resolution Imaging Spectrometer (MODIS) data.

SWE or snow depth retrieval

The penetration depth of the visible, near-infrared, and thermal-infrared wavelengths is very limited, while microwaves can always penetrate the snow surface and reach the underlying ground. Microwave remote sensor data are always used for determining the SWE or snow depth, especially passive microwave remote sensing data. Pulliainen and Hallikainen (2001) explored the use of the HUT snow emission model to retrieve the SWE of dry snow cover from spaceborne Special Sensor Microwave/Imager (SSM/I) observations. The derived SWE values were compared with those derived with an empirical regression algorithm. The comparison results showed that the overall accuracy of the algorithm based on the HUT snow emission model was substantially better than that of the empirical regression algorithm. The algorithm based on the HUT snow emission model could estimate the regional SWE under dry snow conditions with an overall RMSE of about 30 mm, without using any training reference data on the SWE. Roy et al. (2004) investigated the feasibility of using the HUT snow emission model for the estimation of the SWE in a Canadian boreal forest environment. They first compared the snow-covered ground brightness temperatures modeled with the HUT snow emission model to those measured by an airborne radiometer. Large biases were discerned, which they ascribed to the extinction coefficient modeling in the HUT snow emission model. They proposed a new semiempirical function for the extinction coefficient. The modified HUT snow emission model can now obtain a more accurate brightness temperature in a boreal forest environment. The modified HUT snow emission model was used to retrieve the SWE based on an iterative inversion technique. The retrieval results showed that a mean error of ± 10 mm could be achieved,

with a negligible bias. Pulliainen (2006) proposed a novel assimilation technique based on the modeling of observed brightness temperatures as a function of snowpack characteristics. They mapped the SWE and snow depth in boreal and subarctic zones by assimilating spaceborne microwave radiometer (SSM/I and AMSR-E) data and ground-based observations. Their results show that assimilation techniques can substantially improve the SWE and snow depth retrieval accuracy. Parde et al. (2007) used the HUT snow emission model to estimate the SWE from airborne and satellite data, and validated their retrieval results with ground-based SWE measurements. These validation results showed that the accuracy of the retrieved SWE could meet the requirements of seasonal snow pack evolution, interannual variation, and hydrological applications. Vachon et al. (2010) developed a method to monitor the SWE using a modified HUT model. In their method, the model was first calibrated by incorporating in situ measurements (snow depth and density) to find optimized initial assumptions for the model parameters, including the extinction coefficients. The SWE was then retrieved from the satellite observations. The validation results showed that model calibration before SWE retrieval could improve the accuracy of the SWE estimation.

Bibliography

Aoki, T., Aoki, T., Fukabori, M., Hachikubo, A., Tachibana, Y., and Nishio, F., 2000. Effects of snow physical parameters on spectral albedo and bidirectional reflectance of snow surface. *Journal of Geophysical Research*, **105**(D8), 10219–10236.

Aoki, T., Hori, M., Motoyoshi, H., Tanikawa, T., Hachikubo, A., Sugiura, K., Yasunari, T. J., Storvold, R., Eide, H. A., Stamnes, K., Li, W., Nieke, J., Nakajima, Y., and Takahashi, F., 2007. ADEOS-II/GLI snow/ice products – Part II: validation results using GLI and MODIS data. *Remote Sensing of Environment*, **111**, 274–290.

Barkstrom, B. R., 1972. Some effects of multiple scattering on the distribution of solar radiation in snow and ice. *Journal of Glaciology*, **11**, 357–368.

Bohren, C. F., and Barkstrom, B. R., 1974. Theory of the optical properties of snow. *Journal of Geophysical Research*, **79**, 4527–4535.

Bourdelles, B., and Fily, M., 1993. Snow grain size determination from Landsat imagery over Terre-Adelie, Antarctica. *Annals of Glaciology*, **17**, 86–92.

Broschat, S. L., 1993. The small slope approximation from a "Pierson-Moskowitz" sea surface. *IEEE Transactions on Geoscience and Remote Sensing*, **31**(5), 1112–1114.

Brun, E., Martin, E., Simon, V., Gendre, C., and Coleou, C., 1989. An energy and mass model of snow cover suitable for operational avalanche forecasting. *Journal of Glaciology*, **35**(121), 333–342.

Chan, C. H., Tsang, L., and Li, Q., 1998. Monte Carlo simulations of large-scale one-dimensional random rough-surface scattering at near-grazing incidence: penetrable case. *IEEE Transactions on Geoscience and Remote Sensing*, **46**(1), 142–149.

Chandrasekhar, S., 1960. *Radiative Transfer*. New York: Dover.

Chen, K. S., Wu, T.-D., Tsang, L., Li, Q., Shi, J., and Fung, A. K., 2003. Emission of rough surfaces calculated by the integral equation method with comparison to three-dimensional moment method simulations. *IEEE Transactions on Geoscience and Remote Sensing*, **41**(1), 90–101.

Cheng, J., Liang, S., Wang, J., and Li, X., 2010. Comparison of radiative Transfer models for simulating snow surface thermal infrared emissivity. *IEEE Journal of Selected Topics in Earth Observations and Remote Sensing*, **3**, 323–336.

Chuah, H.-T., Tjuatja, S., Fung, A. K., and Bredow, J. W., 1996. A phase matrix for a dense discrete random medium: evaluation of volume scattering coefficient. *IEEE Transactions on Geoscience and Remote Sensing,* **34**(5), 1137–1143.

Conel, J. E., 1969. Infrared emissivities of silicates: experimental results and a cloudy atmosphere model of spectral emission from condensed particulate mediums. *Journal of Geophysical Research*, **74**, 1614–1634.

Dai, Y., Zeng, X., Dickinson, R. E., Baker, I., Bonan, G. B., Bosilovich, M. G., Denninig, A. S., Dirmeyer, P. A., Houser, P. R., Niu, G., Oleson, K. W., Schlosser, C. A., and Yang, Z.-L., 2003. The common land model. *Bulletin of the American Meteorological Society*, **84**, 1013–1023.

Dozier, J., and Marks, D., 1987. Snow mapping and classification from Landsat Thematic Mapper data. *Annals of Glaciology*, **9**, 97–103.

Dozier, J., and Warren, S. G., 1982. Effect of viewing angle on the thermal infrared brightness temperature of snow. *Water Resources Research*, **18**, 1424–1434.

Dozier, J., Schneider, S. R., David, F., and Mcginnis, J., 1981. Effect of grain size and snowpack water equivalent on visible and near-infrared satellite observations of snow. *Water Resources Research*, **17**(4), 1213–1221.

Dozier, J., 1989. Spectral signature of alpine snow cover from the landsat thematic mapper. *Remote Sensing of Environment*, **28**, 9–22.

Dunkle, R. V., and Bevans, J. T., 1956. An approximation analysis of the solar reflectance and transmittance of a snow cover. *Journal of Meteorology*, **74**, 212–216.

Fily, M., Bourdelles, B., Dedieu, J. P., and Sergent, C., 1997. Comparison of in situ and Landsat Thematic mapper derived snow grain characteristics in the Alps. *Remote Sensing of Environment*, **59**, 452–460.

Fung, A. K., Li, Z., and Chen, K. S., 1992. Backscattering from a randomly rough dielectric surface. *IEEE Transactions on Geoscience and Remote Sensing*, **30**(2), 356–369.

Fung, A. K., 1994. *Microwave Scattering and Emission Models and their Applications*. Norwood, MA: Artech House.

Greenfell, T. C., and Warren, S. G., 1999. Representation of a nonspherical ice particle by a collection of independent spheres for scattering and absorption of radiation. *Journal of Geophysical Research*, **104**, 31697–31709.

Giddings, J. C., and La Chapelle, E. R., 1961. Diffusion theory applied to radiant energy distribution and albedo of snow. *Journal of Geophysical Research*, **66**, 181–189.

Griggs, M. (1968). Emissivities of natural surfaces in the 8- to 14-micron spectral region. *Journal of Geophysical Research*, **73** (7545–7551).

Hansen, J. E., 1971. Multiple scattering of polarized light in planetary atmospheres. Part II. Sunlight reflected by terrestrial water clouds. *Journal of the Atmospheric Science*, **28**, 1400–1426.

Hapke, B., 1981. Bidirectional Reflectance Spectroscopy 1. Theory. *Journal of Geophysical Research*, **86**(B4), 3039–3054.

Hapke, B., 1993. *Theory of Reflectance and Emittance Spectroscopy*. New York: Cambridge University Press.

Hori, M., Aoki, T., Tanikawa, T., Motoyoshi, H., Hachikubo, A., Sugiura, K., Yasunari, T. J., Eide, H., Storvold, R.,

Nakajima, Y., and Takahashi, F., 2006. In-situ measured spectral directional emissivity of snow and ice in the 8-14 um atmospheric window. *Remote Sensing of Environment*, **100**, 486–502.

Hulst, Vd, 1957. *Light Scattering by Small Particles*. New York: Dover.

Jiang, L., Shi, J., Tjuatja, S., Dozier, J., Chen, K., and Zhang, L., 2007. A parametized multiple-scattering model for microwave emission from dry snow. *Remote Sensing of Environment*, **111**, 357–366.

Joseph, J. H., Wiscombe, W. J., and Weinman, J. A., 1976. The delta-Eddington approximation for radiative flux transfer. *Journal of Atmospheric Science*, **33**, 2452–2459.

Key, J., and Haefliger, M., 1992. Arctic ice surface temperature retrieval from AVHRR thermal channels. *Journal of Geophysical Research*, **97**, 5885–5893.

Key, J., Collins, J., Fowler, C., and Stone, R., 1997. High-latitude surface temperature estimating from thermal satellite data. *Remote Sensing of Environment*, **61**, 302–309.

Kim, M.-J., Skofronick-Jackson, G. M., and Weinman, J. A., 2004. Intercomparison of millimeter-wave radiative transfer models. *IEEE Transactions on Geoscience and Remote Sensing*, **42**(9), 1882–1890.

Leroux, C., and Fily, M., 1998. Modeling the effect of sastrugi on snow reflectance. *Journal of Geophysical Research*, **103**, 25779–25788.

Leroux, C., Deuze, J.-L., Goloup, P., Sergent, C., and Fily, M., 1998. Ground measurements of the polarized bidirectional reflectance of snow in the near-infrared spectral domain: comparisons with model results. *Journal of Geophysical Research*, **103**, 19721–19731.

Leroux, C., Lenoble, J., Brogniez, G., Hovenier, J. W., and Hann, J. E. D., 1999. A model for the bidirectional polarized reflectance of snow. *Journal of Quantitative Spectroscopy and Radiative Transfer*, **61**, 273–285.

Li, Q., Chan, C. H., and Tsang, L., 1999. Monte Carlo simulations of wave scattering from lossy dielectric random rough surfaces using the physicas-based two-grid method and the canonical-grid method. *IEEE Transactions on Geoscience and Remote Sensing*, **47**(4), 752–763.

Li, Q., Tsang, L., Pak, K. S., and Chan, C. H., 2000. Bistatic scattering and emissivities of random rough dielectric lossy surfaces with the physics-based two-grid method in conjunction with the sparse-matrix canonical grid method. *IEEE Transactions on Geoscience and Remote Sensing*, **48**(1), 1–11.

Li, W., Stamnes, K., and Chen, B., 2001. Snow grain size retrieved from near-infrared radiances at multiple wavelengths. *Geophysical Research Letters*, **28**(9), 1699–1702.

Liang, S., 2004. *Quantitative Remote Sensing of Land Surface*. New Jersey: Wiley and Sons, Inc.

Liang, S. (ed.), 2008. *Advances in Land Remote Sensing: System, Modeling, Inversion and Application.* Berlin: Springer.

Liang, S., and Townshen, J. R. G., 1996. A modified hapke model for soil bidirectional reflectance. *Remote Sensing of Environment*, **55**, 1–10.

Liou, K. N., 1973. A numerical experiment on Chandrasekhar's discrete-ordinates method for radiative transfer: application to cloudy and hazy atmospheres. *Journal of Atmospheric Science*, **30**, 1303–1326.

Mie, G., 1908. Beitrage zur optik truber medien speziell kolloidaler metrllosungen (Contribution to the optics of turbid media, particularly of colloidal metal solutions). *Annals of Physics*, **25**, 377–445.

Mishchenko, M. I., and Macke, A., 1997. Asymmetry parameters for the phase function for isolated and densely packed spherical particles with multiple internal inclusions on the geometric optics limit. *Journal of Quantitative Spectroscopy and Radiative Transfer*, **57**(6), 767–794.

Mishchenko, M. I., Dlugach, J. M., Yanovitskij, E. G., and Zakharova, N. T., 1999. Bidirectional reflectance of flat optically thick particulate layers-an efficient radiative transfer solution and applications to snow and soil surfaces. *Journal of Quantitative Spectroscopy and Radiative Transfer*, **63**, 409–432.

Moersch, J. E., and Christensen, P. R., 1995. Thermal emission from particulate surfaces: a comparison of scattering models with measured spectra. *Journal of Geophysical Research*, **100**, 7465–7477.

Mugnai, A., and Wiscombe, W. J., 1987. Scattering of radiation by moderately nonspherical particles. *Journal of the Atmospheric Science*, **37**, 1291–1307.

Nieto-Vesperinas, M., and Soto-Crespo, J. M., 1987. Monte Carlo simulations for scattering of electromagnetic waves from perfectly conductive random rough surfaces. *Optics Letters*, **12**(12), 979–981.

Nolin, A. W., and Dozier, J., 1993. Estimating snow grain size using AVIRIS data. *Remote Sensing of Environment*, **44**, 231–238.

Nolin, A. W., and Dozier, J., 2000. A hyperspectral method for remotely sensing the grain size of snow. *Remote Sensing of Environment*, **74**(207–216).

Nolin, A. W., and Liang, S., 2000. Progress in bidirectional reflectance modeling and applications for surface particulate media: Snow and Soils. *Remote Sensing Reviews*, **18**, 307–342.

Nolin, A. W., and Stroeve, J. C., 1997. The changing albedo of the Greenland ice sheet: implications for climate change. *Annals of Glaciology*, **25**, 51–57.

Painter, T. H., Dozier, J., Roberts, D. A., Davis, R. E., and Green, R. E., 2003. Retrieval of subpixel snow-covered area and grain size from imaging spectrometer data. *Remote Sensing of Environment*, **85**, 64–77.

Parde, M., Goita, K., and Royer, A., 2007. Inversion of a passive microwave snow emission model for water equivalent estimation using airborne and satellite data. *Remote Sensing of Environment*, **111**, 346–356.

Pitman, K. M., Wolff, M. J., and Clayton, G. C., 2005. Application of modern radiative transfer tools to model laboratory quartz emissivity. *Journal of Geophysical Research*, **110**(E08003): doi:10.1029/2005JE002428.

Pulliainen, J., and Hallikainen, M., 2001. Retrieval of regional snow water equivalent from space-borne passive microwave observations. *Remote Sensing of Environment*, **75**, 76–85.

Pulliainen, J. T., Grandell, J., and Hallikainen, M. T., 1999. HUT snow emission model and its applicability to snow water equivalent retrieval. *IEEE Transactions on Geoscience and Remote Sensing*, **37**(3), 1378–1390.

Pulliainen, J., 2006. Mapping of snow water equivalent and snow depth in boreal and sub-arctic zones by assimilating space-borne microwave radiometer data and ground-based observations. *Remote Sensing of Environment*, **101**, 257–269.

Roujean, J.-L., Leroy, M., and Deschamps, P.-Y., 1992. A bidirectional reflectance model of the earth's surface for the correction of remote sensing data. *Journal of Geophysical Research*, **97**(D18), 20455–20468.

Roy, Y., Goita, K., Royer, A., Walker, A. E., and Goodison, B. E., 2004. Snow water equivalent retrieval in a Canadian boreal environment from microwave measurements using the HUT snow emission model. *IEEE Transactions on Geoscience and Remote Sensing*, **42**(9), 1850–1859.

Schmidt, G. A., Ruedy, R., and Hansen, J. E., 2006. Present-day atmospheric simulations using GISS ModelE: comparison to in situ satellite, and reanalysis data. *Journal of Climate*, **19**, 153–192.

Snyder, W. C., Wan, Z., Zhang, Z., and Feng, Y.-Z., 1998. Classification-based emissivity for land surface temperature

measurement from space. *International Journal of Remote Sensing*, **19**, 2753–2774.
Stamnes, K., Tsay, S.-C., Wiscombe, W. J., and Jayaweera, K., 1988. Numerically stable algorithm for discrete-ordinate-method radiative transfer in multiple scattering and emitting layered media. *Applied Optics*, **27**, 2502–2509.
Stamnes, K., Li, W., Eide, H., Aoki, T., Hori, M., and Storvold, R., 2007. ADEOS-II/GLI snow/ice products-Part I: Scientific basis. *Remote Sensing of Environment*, **111**, 258–273.
Tsang, L., and Kong, J. A., 2001. *Scattering of Electromagnetic Waves. Advanced Topics*. New York: Wiley-Interscience.
Tsang, L., Mandt, C. E., and Ding, K. H., 1992. Monte Carlo simulations of the extinction rate of dense media with randomly distributed dielectric spheres based on solution of Maxwell's equation. *Optics Letters*, **17**(5), 314–316.
Ulaby, F. T., Moore, R. K., and Fung, A. K., 1982. *Microwave remote sensing, active and passive*. Norwood, MA: Artech House.
Vachon, F., Goita, K., Seve, D. D., and Royer, A., 2010. Inversion of a snow emission model calibrated with in situ data for snow water equivalent monitoring. *IEEE Transactions on Geoscience and Remote Sensing*, **48**(1), 59–71.
Wald, A. E., 1994. Modelling thermal infrared (2–14 um) reflectance spectra of frost and snow. *Journal of Geophysical Research*, **99**(B12).
Warren, S. G., and Brandt, R. E., 2008. Optical constants of ice from the ultraviolet to the microwave: a revised compilation. *Journal of Geophysical Research*, **113**(D14220): doi: 10.1029/2007JD009744.
Warren, S. G., and Wiscombe, W. J., 1980. A model for spectral albedo of snow. II. Snow containing atmospheric aerosols. *Journal of Atmospheric Science*, **37**, 2734–2745.
Wick, G. C., 1943. Uber ebene diffusionprobleme. *Zeitschrift für Physik A*, **121**, 702.
Wiesmann, A., and Matzler, C., 1999. Microwave emission model of layered snowpacks. *Remote Sensing of Environment*, **70**, 307–316.
Wiscombe, W. J., 1976. Extension of the doubling method to inhomogeneous sources. *Journal of Quantitative Spectroscopy and Radiative Transfer*, **16**, 477–489.
Wiscombe, W. J., and Warren, S. G., 1980. A model for the spectral albedo of snow. I. Pure snow. *Journal of Atmospheric Science*, **37**, 2712–2733.
Wriedt, T., 2009. Light scattering theories and computer codes. *Journal of Quantitative Spectroscopy and Radiative Transfer*, **110**, 833–843.
Zurk, L. M., Tsang, L., Ding, K. H., and Winebrenner, D. P., 1995. Monte Carlo simulations of the extinction rate of densely packed spheres with clustered and nonclustered geometries. *Journal of the Optical Society of America*, **12**(8), 1772–1781.
Zurk, L. M., Tsang, L., and Winebrenner, D. P., 1996. Scattering properties of dense media from Monte Carlo simulations with application to active remote sensing of snow. *Radio Science*, **31**(4), 803–819.

Cross-references

Albedo
Geochemistry of Snow and Ice
Global Outlook of Snowcover, Sea Ice, and Glaciers
Ice
Optical Remote Sensing of Alpine Glaciers
Snow
Snow Density
Snow Depth
Snow Water Equivalent
Surface Energy Balance

RADIOACTIVE FALLOUT

Bhishm Kumar
Hydrological Investigation Division, National Institute of Hydrology, Roorkee, Uttarakhand, India

Synonyms

Nuclear fallout

Definition

Fallout is the residual radiation hazard from a nuclear explosion, so named because it "falls out" of the atmosphere into which it is spread during the explosion. It commonly refers to the radioactive dust created when a nuclear weapon explodes. This radioactive dust, consisting of hot particles, is a kind of radioactive contamination. It can lead to contamination of the food chain (Simon et al., 2006).

Effects

A wide range of biological changes may follow the irradiation of animals. These vary from rapid death following high doses of penetrating whole-body radiation, to essentially normal lives for a variable period of time until the development of delayed radiation effects, in a portion of the exposed population, following low dose exposures.

Unit

The unit of actual exposure is the Roentgen which is defined in ionizations per unit volume of air, and all ionization-based instruments (including Geiger counters and ionization chambers) measure exposure. However, effects depend on the energy per unit mass, not the exposure measured in air. A deposit of 1 J/kg has the unit of 1 gray. For 1 MeV energy gamma rays, an exposure of 1 Roentgen in air will produce a dose of about 0.01 gray (1 centigray, cGy) in water or surface tissue. Because of shielding by the tissue surrounding the bones, the bone marrow will only receive about 0.67 cGy when the air exposure is 1 Roentgen and the surface skin dose is 1 cGy. Some of the lower values reported for the amount of radiation which would kill 50% of Population (the "LD_{50}") refer to bone marrow dose, which is only 67% of the air dose.

Bibliography

Simon, S. L., Bouville, A., and Land, C. E., 2006. Fallout from nuclear weapons tests and cancer risks. *American Scientist*, **94**, 48–57.

RADIOACTIVE ISOTOPES

Bhishm Kumar
Hydrological Investigation Division, National Institute of Hydrology, Roorkee, Uttarakhand, India

Synonyms

Radioisotopes; Radionuclides; Unstable isotopes

Radioactive Isotopes, Table 1

Isotope	Half-life (years)	Decay mode	Principal sources	Commonly measured phases
^{3}H	12.43	β^-	Cosmogenic, weapons testing	H_2O, CH_2O
^{14}C	5730	β^-	Cosmogenic, weapons testing	DIC, DOC, CO_2, $CaCO_3$, CH_2O
^{36}Cl	301,000	β^-	Cosmogenic and subsurface	Cl^-, surface Cl-salts
^{39}Ar	269	β^-	Cosmogenic and subsurface	Ar
^{85}Kr	10.72	β^-	Nuclear fuel processing	Kr
^{81}Kr	2,10,000	ec	Cosmogenic and subsurface	Kr
^{129}I	1.6×10^7	β^-	Cosmogenic, subsurface, nuclear reactors	I^- and I in organics
^{222}Rn	3.8 days	α	Daughter of ^{226}Rn in ^{238}U decay series	Rn gas
^{226}Ra	1,600	α	Daughter of ^{230}Th in ^{238}U decay series	Ra^{2+}, carbonate, clays
^{230}Th	75,400	α	Daughter of ^{234}U in ^{238}U decay series	Carbonate, organics
^{234}U	2,46,000	α	Daughter of ^{234}Pa in ^{238}U decay series	UO_2^{2+}, carbonate, organics
^{238}U	4.47×10^9	α	Primordial	UO_2^{2+}, carbonate, organics

β^- – beta emission; α – alpha emission; ec – electron capture

Definition

Radioactive isotopes are the atoms with unstable nucleus which decay with time by emitting different types of particles or radiations such as neutrons, electrons (beta particles), etc. or gamma radiations (see *Radioactivity*).

Origin

Naturally occurring radionuclides fall into three categories: primordial radionuclides, secondary radionuclides, and cosmogenic radionuclides. Primordial radionuclides originate mainly from the interiors of stars and, like uranium and thorium, are still present because their half-lives are so long that they have not yet completely decayed. Secondary radionuclides are radiogenic isotopes derived from the decay of primordial radionuclides. They have shorter half-lives than primordial radionuclides. Cosmogenic isotopes, such as carbon-14, are present because they are continually being formed in the atmosphere due to cosmic rays. Artificially produced radionuclides can be produced by nuclear reactors, particle accelerators, or radionuclide generators. The details of various radioisotopes with their half-lives, decay mode, principle sources, etc. are given in Table 1.

Uses

The radioisotope of hydrogen (tritium) in the form of water molecule (^3H_2O) and denoted by symbol ^3H or T is still widely used for various hydrological studies. There are other variety of artificially produced radioisotopes like ^{60}Co, ^{82}Br, ^{131}I, ^{137}Cs, ^{198}Au, ^{226}Ra, ^{241}Am, etc. that are used for various hydrological investigations. Radioisotopes are used to study the movement of surface water, and to measure water runoffs from rain and snow, as well as the flow rates of streams and rivers. Natural radionuclides are used in geology, archaeology, and paleontology to measure ages of rocks, minerals, and fossil materials.

Dangers

If radioisotopes are released into the environment, through accident, poor disposal, or other means, they can potentially cause harmful effects of radioactive contamination.

Bibliography

Clark, I., and Fritz, P., 1997. *Environmental Isotopes in hydrogeology*. Boca Raton: Lewis.

RADIOACTIVITY

Bhishm Kumar
Hydrological Investigation Division, National Institute of Hydrology, Roorkee, Uttarakhand, India

Definition

The process of decay of an unstable atom in order to attain a stable nuclear configuration by giving out α, β particles and γ or x rays is known as radioactivity (See *Radioactive Isotopes*).

The process of radioactivity may complete in a fraction of second or it may continue for millions of years depending upon the type of decaying atom. During the process of radioactivity, an unstable atom may be converted into a different type of stable atom in one stroke or there may be a series of chain of daughter nuclei before finally stable nuclide is formed. The decaying atom is called the parent nuclide, while the intermediate transformations and finally stable nuclide are called daughter and granddaughter nuclides, respectively.

Radioactive decay

The rate of decay of any radioisotope obeys the following exponential law:

$$N = N_o * \exp(-\lambda t),$$

where N is the number of radioactive atoms present at time t, N_o is the number of radioactive atoms present t = 0, and λ is the decay constant, which is a unique property for each isotope. Usually, the rate of decay is defined by the half-life ($T_{1/2}$), where

$$T_{1/2} = \ln(2)/\lambda$$

which is the time required for half of the radioactive nuclei to disintegrate. Half-life values for radioisotopes vary from fractions to a second to millions of years.

Unit

The unit of radioactivity is the Becquerel (Bq), which is defined as the quantity of any radioisotope that decays at the rate of one disintegration per second (dps). Earlier the unit was the curie (Ci), which is equal to 3.7×10^{10} Bq. Specific activity is defined as the amount of radioactivity of a given radioisotope per gram of a compound or element (Payne, 1983).

Bibliography

Payne, B. R., 1983. *Guidebook on Nuclear Techniques in Hydrology*. Technical report series no. 91. Vienna: International Atomic Energy Agency.

RAIN-INDUCED SNOWMELT

Delphis F. Levia, Daniel J. Leathers
Department of Geography, University of Delaware, Newark, NJ, USA

Synonyms

Rain-on-snow event

Definition

Rain-induced snowmelt. Liquid water generated within a melting snowpack by rain heat flux and turbulent atmospheric fluxes.
Rain-on-snow. A hydrometeorological event occurring when rain infiltrates an existing snowpack.

Introduction

Net radiative and sensible, latent, and rain heat fluxes constitute the major energy sources that result in snowmelt. The importance of each of these fluxes to the generation of snowmelt depends on the local context and varies with time and space. Rain-induced snowmelt contributes to meltwater movement in forests (Levia and Underwood, 2004), runoff (Ishii and Fukushima, 1994), and streamflow (Ikebuchi et al., 1986). Rain-induced snowmelt is, however, of greatest importance with regard to rain-on-snow events. Rain-on-snow events are not uncommon in alpine and temperate regions of the world (Gray and Male, 1981; Singh et al., 1997). In the western United States, for example, over 380 cooperative weather station sites reported > 100 rain-on-snow events and another 86 cooperative weather stations reported >200 rain-on-snow events in a 55-year period from 1949 to 2003 (McCabe et al., 2007). Early season rain-on-snow events are of societal importance as they have been reported to create persistent weak layers (i.e., facet–crust combinations) in seasonal snowpacks that can lead to avalanches (Hägeli and McClung, 2003). Rain-on-snow events also have been documented to lead to catastrophic flooding (Leathers et al., 1998; Marks et al., 2001) and slushflows (Tomasson and Hestnes, 2000; Hestnes and Bakkehoi, 2004) that result in widespread property damage and loss of life.

Snowmelt energetics

Rain-induced snowmelt is an important component of the hydroclimatology of regions with ephemeral seasonal snow cover. The prevailing meteorological situation and the condition of the snowpack are two major factors in determining the intensity of rain-induced melt and the energy fluxes responsible for snowpack ablation. The total energy gained by a snowpack during a rain-induced melt event can be expressed using the formula:

$$Q = Q_n + Q_h + Q_e + Q_r + Q_g$$

where Q is the total energy gained by the snowpack, Q_n is the net radiation, Q_h is the sensible heat flux, Q_e is the latent heat flux, Q_r is the rain heat flux, and Q_g is the ground heat flux (Singh et al., 1997). The net radiation (Q_n) can be broken into its components and expressed as:

$$Q_n = S_n + L_n = S\downarrow(1-\alpha) + (L\downarrow - L\uparrow)$$

where S_n is the net shortwave radiative flux, L_n the net longwave radiative flux, $S\downarrow$ the incoming shortwave radiation, α albedo, $L\downarrow$ the incoming longwave radiation, and $L\uparrow$ the outgoing longwave radiation (King et al., 2008).

Meteorological effects on rain-induced snowmelt

During rain-induced melt events, the most important energy fluxes to the pack are generally the sensible (Q_h), latent (Q_e), and rain heat (Q_r) fluxes. By definition, the meteorological situations that result in significant rainfall occur in association with thick cloud cover. Thus, net radiation is commonly small during rain events as is the ground heat flux, at least in comparison to the turbulent fluxes and energy transfer by the rain itself. Sensible and latent heat fluxes can be estimated in diverse ways (King et al., 2008). Sensible heat flux is dependent upon the temperature difference between the snowpack and the atmosphere, and the wind speed, and can be expressed as:

$$Q_h = \rho C_a C_H w(T_a - T_o)$$

where ρ is the density of the atmosphere, C_a is the specific heat of the atmosphere at constant pressure, C_H is the bulk

transfer coefficient for sensible heat, w is the wind speed, and T_a and T_o are the air and snow surface temperatures, respectively. From this equation, it is obvious that greater differences in temperature between the snowpack and the atmosphere lead to larger sensible heat fluxes. Moreover, an increase in the wind speed also increases the magnitude of the sensible heat flux into the snowpack.Similarly, the flux of latent heat can be expressed as:

$$Q_e = L_v C_E w(q_a - q_s)$$

where L_v is the latent heat of vaporization, C_E is the bulk transfer coefficient for latent heat, w is the wind speed, and q_a and q_s are the water vapor densities of the atmosphere and snow surface, respectively. This equation suggests that the value of the latent heat flux is primarily dependent upon the water vapor density difference between the atmosphere and the snow surface, and the wind speed. The vapor density difference over a melting snowpack is a function of the atmospheric dew point temperature, and hence a characteristic of the overlying atmosphere (higher dew point temperatures lead to larger vapor density differences).

Consideration of the equations for both sensible and latent heat fluxes indicates that the magnitude of the turbulent fluxes is dependent on the meteorological conditions. The snow surface/atmosphere temperature differences that drive the sensible heat flux depend upon the characteristics of the air mass in contact with the ablating snowpack, as do the water vapor density differences that drive the latent heat flux. Both equations are also highly sensitive to the wind speed. Thus, the temperature and dew point temperature of the overlying air mass and the wind speed associated with the meteorological situation drive the magnitude of the turbulent energy fluxes. Because most rainfall situations are accompanied by temperature and dew points above 0°C, and often high wind speeds, these atmospheric characteristics generally lead to large fluxes of energy into the snowpack.

Energy transfer from rainfall to the snowpack can also be important in the ablation of snow cover. The flux of energy from liquid precipitation to the pack can be expressed as:

$$Q_r = 0.001 \times \rho_w \times C_{pw} \times (T_r - T_s) \times R$$

where ρ_w is the density of water (1,000 kg m^{-3}), C_{pw} is the specific heat of water (4.2 kJ kg^{-1} °C^{-1}), T_r is the temperature of the rain, T_s is the temperature of the snow surface, and R is the rainfall rate (Singh et al., 1997). Thus, the amount of energy transferred to the pack by rainfall depends upon the temperature difference between the liquid precipitation and the snow surface, and the rate at which the precipitation is falling (Figure 1). Therefore, in most rain-induced snowmelt events, the meteorological situation is of primary importance. As an air mass with temperatures and dew point temperatures above 0°C overspreads a snow-covered region, large sensible and latent heat fluxes are directed into the pack. It is important to note that the dew point temperature of the air mass is critically important in the melt process. Condensation of water vapor will occur on the snowpack whenever the dew point temperature of the air mass is above 0°C. The condensation releases latent heat directly into the pack, either warming the pack or supplying energy for melt. The rain heat flux is governed by the temperature of the liquid precipitation and rainfall rate, which is also dependent on the specific meteorological context. The combination of these three energy fluxes (sensible, latent, and rain heat) can cause very rapid melt of a snowpack, resulting in flash floods and slushflows.

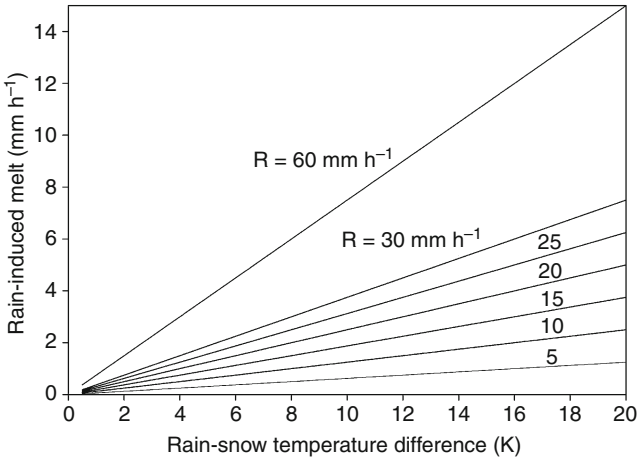

Rain-Induced Snowmelt, Figure 1 Rain-induced snowmelt (mm h^{-1}) for various rainfall rates (R, mm h^{-1}) and rainfall/snowpack temperature differences (K).

It should be clear that rain-induced snowmelt will differ both spatially and temporally as a function of land cover type. The precipitation partitioning of incident rainfall by a forest canopy would exhibit marked spatial and temporal variability of snowmelt as a result of interception and the channeling of throughfall and stemflow at localized points on the forest floor. Thus, the routing of snowmelt (rain-induced or otherwise) in the subcanopy would be spatially heterogeneous (Bründl et al., 1999). The complex three-dimensional geometry of a forest canopy also would lead to pronounced temporal heterogeneity of melt of intercepted snow due (partly) to shading by neighboring trees and the lower albedo of intercepted snow compared to fresh snow on the earth's surface (Leonard and Eschner, 1968). As such, a prairie would be expected to have a more homogeneous melt signature as it lacks the tall vegetation of a forest canopy and its coincident geometric irregularities that complicates energy balances, heat fluxes, and snowmelt patterns.

Snowpack characteristics and rain-induced snowmelt

The condition of the snowpack also affects the timing and intensity of melt during a rainfall event (Gray and Male, 1981). Snowpacks can fall into one of two very

general categories. In many cases, the snowpack may have temperatures below 0°C throughout. In this case, liquid precipitation will freeze as it enters the pack, releasing its latent heat of fusion, helping to warm the snowpack temperature. This process will continue until the pack has warmed enough for melt to begin. Rain that falls on a melting snowpack will add energy to the pack proportional to its temperature and the rainfall rate. In this case, the energy can go directly into the melt process. Thus, a cold snowpack (pack temperature <0°C) will delay the onset of melt as energy from liquid precipitation and turbulent fluxes warm the pack to a temperature of 0°C.

Rain-on-snow events and severe flooding

An excellent example of the potential for destruction associated with rain-induced snowmelt can be seen by consideration of the January 1996 event that occurred in the mid-Atlantic region of the United States (Leathers et al., 1998). During this event, the rapid ablation of a snowpack of nearly 1-m depth and heavy rainfall combined to cause catastrophic flooding across north-central Pennsylvania. This event resulted in as many as 30 fatalities, many injuries, and approximately $1.5 billion in damages. A strong meteorological disturbance moved across the region on January 18th and 19th with temperatures and dew point temperatures that, in many cases, rose above 15°C. Rainfall in excess of 7.0 cm fell in many locations over a 24-h period with corresponding wind speeds reaching 12 m s^{-1}. The meteorological conditions resulted in large values of sensible, latent, and rain energy fluxes into the pack, with total flux values greater than 500 W m^{-2} during much of the event. In this case, the combination of the fluxes described above led to maximum melt rates of greater than 12 cm h^{-1}.

Summary

Rain-induced snowmelt engendered by rain-on-snow events is of hydrologic importance in many areas of the world. The primary energy fluxes accounting for rain-induced snowmelt include turbulent (sensible and latent heat) and rain heat fluxes. The magnitude of these fluxes is dependent upon meteorological conditions particular to a specific event. Antecedent snowpack conditions also affect the timing and intensity of rain-induced snowmelt. A comprehensive understanding of rain-induced snowmelt fluxes is critical to the hydroclimatology of regions with frequent rain-on-snow events that can cause flooding and slushflows.

Bibliography

Bründl, M., Schneebeli, M., and Flühler, H., 1999. Routing of canopy drip in the snowpack below a spruce crown. *Hydrological Processes*, **13**, 49–58.

Gray, D. M., and Male, D. H., 1981. *Handbook of Snow: Principles, Processes, Management and Use*. Toronto: Pergamon.

Hägeli, P., and McClung, D. M., 2003. Avalanche characteristics of a transitional snow climate – Columbia Mountains, British Columbia, Canada. *Cold Regions Science and Technology*, **37**, 255–276.

Hestnes, E., and Bakkehoi, S., 2004. Slushflow hazard prediction and warning. *Annals of Glaciology*, **38**, 45–51.

Ikebuchi, S., Takebayashi, S., and Tomomura, T., 1986. Snow accumulation, melting and runoff in the warm climate of Japan. In Morris, E. M. (ed.), *Modelling Snowmelt-Induced Processes*. Wallingford: IAHS, Publication No. 155, pp. 175–192.

Ishii, T., and Fukushima, Y., 1994. Effects of forest coverage on snowmelt runoff. In Jones, H. G., Davies, T. D., Ohmura, A., and Morris, E. M. (eds.), *Snow and Ice Covers: Interactions with the Atmosphere and Ecosystems*. Wallingford: IAHS, Publication No. 223, pp. 237–245.

King, J. C., Pomeroy, J. W., Gray, D. M., Fierz, C., Föhn, P. M. B., Harding, R. J., Jordan, R. E., Martin, E., and Plüss, C., 2008. Snow-atmosphere energy and mass balance. In Armstrong, R. L., and Brun, E. (eds.), *Snow and Climate: Physical Processes, Surface Energy Exchange and Modeling*. Cambridge: Cambridge University Press, pp. 90–124.

Leathers, D. J., Kluck, D. R., and Kroczynski, S., 1998. The severe flooding event of January 1996 across north-central Pennsylvania. *Bulletin of the American Meteorological Society*, **79**, 785–797.

Leonard, R. E., and Eschner, A. R., 1968. Albedo of intercepted snow. *Water Resources Research*, **4**, 931–935.

Levia, D. F., and Underwood, S. J., 2004. Snowmelt induced stemflow in northern hardwood forests: a theoretical explanation on the causation of a neglected hydrological process. *Advances in Water Resources*, **27**, 121–128.

Marks, D., Link, T., Winstral, A., and Garen, D., 2001. Simulating snowmelt processes during rain-on-snow over a semi-arid mountain basin. *Annals of Glaciology*, **32**, 195–202.

McCabe, G. J., Clark, M. P., and Hay, L. E., 2007. Rain-on-snow events in the western United States. *Bulletin of the American Meteorological Society*, **88**, 319–328.

Singh, P., Spitzbart, G., Hübl, H., and Weinmeister, H. W., 1997. Hydrological response of snowpack under rain-on-snow events: a field study. *Journal of Hydrology*, **202**, 1–20.

Tomasson, G. G., and Hestnes, E., 2000. Slushflow hazard and mitigation in Vesturbyggd, northwest Iceland. *Nordic Hydrology*, **31**, 399–410.

Cross-references

Melting Processes
Meltwater Conduit

RAM RESISTANCE

Prem Datt
Research and Design Center (RDC), Snow and Avalanche Study Establishment, Himparishar, Chandigarh, India

Ram resistance is the resistance offered by snow while driving a ram penetrometer (ramsonde) vertically within it. The ram resistance is an index of the relative hardness. A graphical profile that exhibits ram resistance with depth is called a Ram profile. The ram is a tube or rod with a centimeter scale for depth and a standard cone-shaped tip (diameter 40 mm, apex angle 60°). Ram index $R = T + H + nHf/p$, where n is the number of blows, f is the vertical fall height of the hammer, T is the weight of

tube, H is the weight of the hammer and guide rod, and p is the penetration depth.

Bibliography

Jones, E. R., and Childers, R. L., *Contemporaray College Physics*. Carolina: University of South Carolina, Addison Wesley.

McClung, D., and Schaerer, P., The Avalance Hand book. The Mountaineers. 1001 SW Klickitat Way, Seattle, Washington 98134.

RATING CURVE

Ian C. Willis
Department of Geography, Scott Polar Research Institute, University of Cambridge, Cambridge, UK

Definition

A *rating curve* is a relationship between two stream or river variables, usually its Discharge (m^3 s^{-1}) and a related variable such as water stage (depth of water above a local datum, m). A suspended sediment rating curve is a relationship between Suspended Sediment Concentration (kg m^{-3} or g l^{-1}) and discharge. A solute rating curve is a relationship between solute concentration (typically in mg l^{-1}) and discharge. If more than one solute (Solute in Glacial Meltwaters) is considered at a time, concentrations are usually expressed in equivalent units (meq l^{-1}). Rating curves are usually constructed using linear or nonlinear (log–normal or log–log) regression, where parameters are fitted by the least squares method. Rating curves are used to calculate or predict a variable that is difficult to measure continuously, from another variable that is easier to determine. The aim is to produce a continuous time-series of discharge, or suspended sediment or solute concentration.

Generating a rating curve

Rating curves are needed, as water discharge is the fundamental unit of measurement in most hydrological studies or for water resource planning purposes, and yet it is difficult to measure continuously. Since discharge is the product of mean channel width, depth, and velocity, it may be determined at a weir or other gauging device where velocity variations are kept to a minimum, as water builds up behind the weir, so that discharge varies mostly with cross-section area (width × depth). If the weir geometry is known, the head of water above the weir crest can be converted directly to discharge via a mathematically defined rating curve. Often a V-notch weir is used, where an arithmetic change in stage produces a geometric change in discharge defined by a logarithmic rating relation between the two variables. Weir construction is costly, requires maintenance, and is potentially environmentally damaging. Therefore in places where this is not possible or desirable, for example, for a short-term study in an upland mountain catchment, an alternative method of determining discharge is required.

An empirically defined rating curve may be constructed at a natural stable river cross section, preferably where the channel depth to width ratio is high. Stage may be measured continuously at a point in a channel (see below). Several instantaneous discharge measurements are made over the range of stage values recorded and used together with the associated stage measurements to define the rating curve. The curve is then used together with the stage records to synthesize a continuous discharge Hydrographs for the catchment.

Measuring variables needed to construct a rating curve

Constructing a rating curve requires various attributes of a stream or river to be measured (Hubbard and Glasser, 2005). Continuous measurements of stage can be made using an analogue chart recorder. The simplest method involves a float and counterweight housed within a stilling well. The float moves up and down with the water level and activates a pen, which draws a line on a rotating drum. The drum rotates via a mechanically or electrically driven clockwork device. A complete revolution of the drum can take a week or a month or even a year, depending on the data resolution required and the resources available for changing the chart paper. Digital data loggers, which record calibrated electronic voltage or current inputs from a pressure transducer or transmitter, have now largely replaced chart recorders as a means of obtaining continuous stage measurements.

Instantaneous measurements of discharge are typically made using either the "velocity-area technique" or by dilution gauging (Hubbard and Glasser, 2005). The former involves measuring average cross-section area and velocity and multiplying these together to produce discharge. Often, the cross section is divided into smaller segments of known width. The depths marking the ends of each segment are measured and averaged. Similarly, the depth-averaged velocities at the ends of each segment are measured and averaged to give the average velocity of the segment. Velocity is measured using a flow (current) meter (sometimes called a velocimeter). This may be a mechanical propeller device, where the number of revolutions per unit time is recorded and converted to velocity using a calibration equation. Alternatively, an ultrasonic flow meter may be used of which there are two main types: transit-time flow meters or Acoustic Doppler Velocimeters (ADVs). Since the velocity measured at 40% of the distance up from the bed is typically representative of the depth-averaged velocity, a single measurement using a flow meter at this depth is often sufficient. Having determined the average depth and velocity of each segment, they can be multiplied together with the segment width to give the discharge for each segment. Cumulating across all segments gives the total discharge for the channel.

Dilution gauging involves the injection into the stream of a known quantity of salt or dye solution, of known concentration, and the monitoring of salt or dye concentrations at high temporal resolution some distance downstream as the salt or dye cloud passes. The distance between the injection and monitoring sites (the mixing length) must be of the order of 10 channel widths for turbulent streams, and up to 100 channel widths for more gently flowing streams. This is so that the distance is great enough to ensure that the initial solution is completely mixed in the water as it passes the monitoring site but not too great for concentrations to fall below the detection level as the cloud passes. The product of the initial solution concentration and volume (kg m^{-3} m^3) divided by the integral of the monitored breakthrough curve concentration, with respect to time (kg m^{-3} s), gives the total discharge of the stream.

Uses of rating curves

Rating curves have been constructed in many snow- and ice-covered catchments in order to generate continuous catchment outlet hydrographs that can be used to investigate snow/ice Melting Processes and Catchment Routing. For example, Willis et al. (1990) constructed rating curves on two streams draining Midtdalsbreen, Norway and were able to construct continuous discharge hydrographs for the streams over two summer melt seasons (Figure 1a). This then enabled them to interpret the results of dye tracing experiments and infer the characteristics of the glacier drainage system (Willis et al., 1990) to calculate water storage variations within the catchment (Willis et al., 1993) and to explain sediment dynamics in the proglacial stream and identify the influence of glacier movement on sediment evacuation from the catchment (Willis et al., 1996).

Rating curves are not only useful for generating hydrographs from catchment outlets but have also been used to generate hydrographs at specific points within catchments. For example, Kohler (1995) and Willis et al. (2002) produced stage discharge curves for supraglacial streams feeding Moulins. Kohler (1995) used a "moulin bag," a large fabric funnel connected to a section of open pipe at its lower end. The bag was suspended in a moulin and as the flow of water into the moulin varied, the water level in the bag rose and fell and was recorded continuously using a pressure transducer and logger. Seventeen discharge measurements were made in the supraglacial stream feeding the moulin (Figure 1b). A comparison of moulin input discharges and proglacial stream outflow discharges enabled Kohler (1995) to model the proportion of pressurized and non-pressurized flow in the englacial/subglacial drainage system (Englacial Conduit). Willis et al. (2002) used a pressure transducer at the base of a hole drilled into a supraglacial stream and six measurements of discharge from which to construct a stage discharge curve (Figure 1c). The resultant hydrograph enabled the testing of a glacier surface melt and routing model.

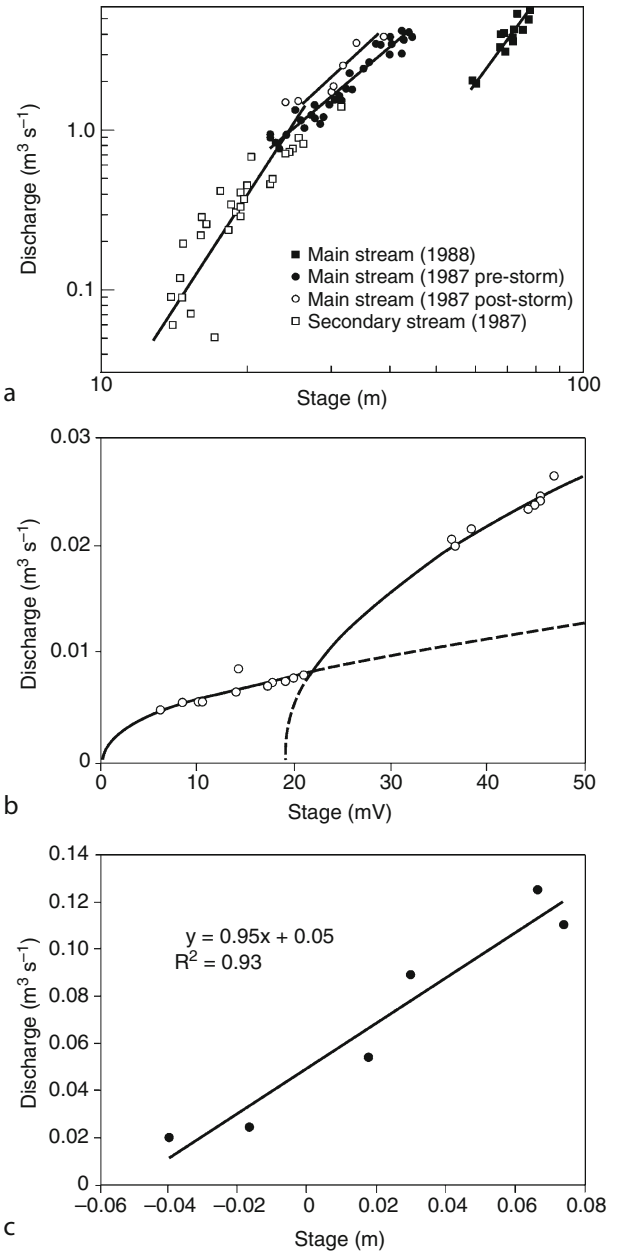

Rating Curve, Figure 1 Stage discharge rating curves developed for: (**a**) Proglacial streams at Midtdalsbreen, Norway (Willis et al., 1990); and supraglacial streams feeding moulins at (**b**) Storglaciären, Sweden (Kohler, 1995) and (**c**) Haut Glacier d'Arolla, Switzerland (Willis et al., 2002). Note that for (**a**), there are separate rating curves for a main stream and a secondary stream, for the main stream for two different years, and for the main stream in one year but before and after a flood, which dislodged the stage recorder. For (**b**), two rating curves are defined, one for low flows and one for high flows as the "moulin bag" contained a main outlet, which operated all the time but a secondary outlet that operated only at high flows. Also note that the stage units are in pressure transducer raw millivolt output. For (**c**), the stage records have been de-trended to remove the effects of surface melt on the pressure transducer records, so units are deviations from this trend.

Suspended sediment rating curve

Suspended sediment rating curves are often constructed in order to calculate catchment Sediment Yield (weight or volume of sediment transported in a given time period, kg a^{-1} or m^3 a^{-1}) or Erosion Rate (sediment yield divided by catchment area, m a^{-1}). This is of interest from a scientific and practical standpoint. Scientifically it is of interest for understanding short- medium- and long-term erosion, transport and depositional processes within a catchment (Sediment Entrainment, Transport, and Deposition; Sediment Routing). It is of practical interest for the design of hydroelectric power or for water supply or irrigation purposes since sediment will fill reservoirs, abrade turbines and silt up artificial channels and tunnels. Suspended sediment yield can be calculated by integrating instantaneous calculations of Suspended Sediment Load over time, where load (in units of kg s^{-1}) is the product of sediment concentration (kg m^{-3}) and discharge (m^3 s^{-1}). If hourly measurements of suspended sediment concentration (SSC) and discharge are known, their product will give hourly values of instantaneous suspended sediment load. Multiplying this by 3,600 (the number of seconds in an hour) will give hourly values of yield, and cumulating these over, say, a year will give the annual catchment suspended sediment yield. Unfortunately, with very few exceptions, continuous long-term measurements of suspended sediment concentrations are rarely made in snow- or ice-covered catchments, and so alternative methods must be adopted to calculate yields.

The usual method is to monitor discharge continuously (or generate a continuous hydrograph using a rating curve approach described above), obtain several measurements of suspended sediment concentration over the range of discharges observed, define an empirical relationship between the measurements of SSC and the contemporaneous measures of discharge – the suspended sediment rating curve – and use this relationship to estimate SSC from discharge, thereby producing a continuous SSC time-series. Often there is a logarithmic relationship between the two variables. If this is the case, SSCs and therefore suspended sediment yields will be underestimated due to statistical bias and a correction factor may be used to improve the estimates (Ferguson, 1986). The bias increases with the degree of scatter on the bivariate rating plot. Scatter exists due to: (1) seasonal variations in sediment availability, (2) Hysteresis effects associated with variations in sediment supply on the rising and falling limbs of diurnal hydrographs and with a downstream kinematic wave effect, (3) transient flushes of sediment in the absence of discharge variations due to snow bridge or bank collapse or glacier movement (Basal Sediment Evacuation by Subglacial Drainage System), and (4) sediment supply processes associated with rainstorms (Fenn et al., 1985). For these reasons, multiple regression and time-series techniques may be used in favor of a simple rating curve to improve the accuracy of estimating SSC and load in nival and glacial streams (Gurnell and Fenn, 1984; Willis et al., 1996). Figure 2a shows a suspended sediment rating curve constructed for 6 years of summer data for a glacierized (Glacierization) catchment in Switzerland.

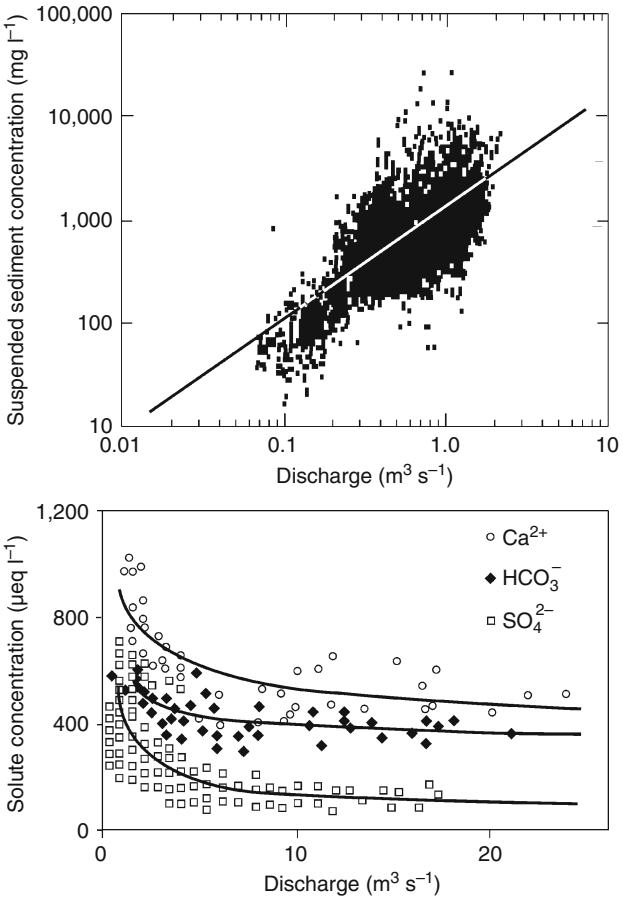

Rating Curve, Figure 2 (**a**) Suspended sediment rating curve for 6 years of data collected in the catchment draining Glacier de Tsidiore Nouve, Switzerland (Fenn, 1988). (**b**) Solute rating curves for three of the major ions in a meltwater stream draining Finsterwalderbreen, Svalbard (Wadham et al., 1997).

A recent study has used continuous stage records together with empirically derived stage–discharge rating curves and suspended sediment rating curves to calculate discharges and suspended sediment loads in ten remote catchments in Nepal (Gabet et al., 2008). The catchments range in size from 7 km^2 to 3,217 km^2 and are between 0% and 21% glacierized. Instantaneous sediment loads varied over four orders of magnitude (10^1–10^4 kg s^{-1}), mostly due to large variations in discharge and rainfall. Accounting also for solute and Bed Load contributions enabled the calculation of total yields and erosion rates across Nepal. Erosion rates varied between ~0.1 and ~2.0 mm a^{-1} and were higher in the wetter southern catchments than in the drier northern ones. These fall within the range found in a large review of erosion rates in glacierized catchments, which vary over four orders of magnitude

from 0.01 mm a^{-1} for polar glaciers and thin temperate plateau glaciers on crystalline bedrock to 0.1 mm a^{-1} for temperate valley glaciers on crystalline bedrock in Norway, to 1.0 mm a^{-1} for temperate glaciers on a variety of rock types in Switzerland to 10–100 mm a^{-1} for large fast-flowing temperate glaciers in the tectonically active southeast Alaska (Hallet et al., 1996).

Solute rating curve

A few studies have attempted to construct solute rating curves for snow or ice fed catchments in an attempt to determine catchment solute yields (weight or volume of dissolved material transported in a given time period). As with suspended sediment yields described above, this is of interest scientifically for determining catchment denudation rates. Ideally, separate regression-based rating curves should be constructed for each major chemical species (Figure 2b), although many studies concentrate solely on the main cations. Additionally, most studies fail to account for solutes derived from sea salt and the snowpack, and attribute all dissolved material to crustal weathering. Typically, due to dilution effects, strong negative correlations exist between stream discharge and individual solute species. Exceptions may occur for Cl^- and NO_3^- due to particularly high concentrations at low discharges associated with solute flushing from the snowpack in spring, and so corrections may need to be made to account for this (Sharp et al., 1995). As with suspended sediment rating curves, bias will occur if the timing of solute sampling is not representative of the range of discharges measured. For example, a 15-year study in the Swiss Alps showed that the weekly bulked discharge-proportional sampling was vastly preferable to grab (instantaneous) samples taken every 2 weeks at reproducing unbiased yields of major cations and anions (Schleppi et al., 2006).

A comparison of a few studies in snow- and ice-covered catchments shows that cationic weathering rates are of the order 500–1,000 meq m^{-2} a^{-1}, significantly higher than estimates for continents as a whole, and that the total solute denudation rate measured in a Swiss Alps catchment is about three times higher than a global average estimate (Sharp et al., 1995). Comparisons between catchments suggest that those with higher discharges also have the highest solute fluxes. However, comparisons within an individual catchment between years with contrasting climatic conditions suggest that the increased discharge is offset by decreased solute concentrations (due to reduced residence time between rock/sediment and water), so that solute flux remains fairly constant from year to year (Collins et al., 2002).

Summary

Rating curves are widely used in catchment hydrology studies and for water resource planning and management. Stage–discharge rating curves (Stage–Discharge Relationship) are used to produce continuous records of stream or river discharge, i.e., catchment or sub-catchment Hydrographs. Suspended sediment and solute rating curves are used to generate continuous time-series of suspended sediment or solute concentration from a discharge series, which are often used, together with the discharge series, to estimate catchment sediment and solute yields and thereby denudation rates. Such studies suggest that snow- and ice-covered catchments generally have higher denudation rates than their snow- and ice-free counterparts. As most rating curves are empirically derived using statistical regression, they have errors associated with them and they can only be used within the catchment for which they were designed and within the range of stage or discharge values that were used to define them.

Bibliography

Collins, D. N., Harrison, J., and Kitcher, J. M. S., 2002. Climatic variation and solute concentration and flux in meltwaters draining from an alpine glacier. *Water, Air & Soil Pollution*, **2**, 191–207.

Fenn, C. R., 1988. Quantifying the errors involved in transferring suspended sediment rating equations across ablation seasons. *Annals of Glaciology*, **13**, 64–68.

Fenn, C. R., Gurnell, A. M., and Beecroft, I. R., 1985. An evaluation of the use of suspended sediment rating curves for the prediction of suspended sediment concentration in a proglacial stream. *Geografiska Annaler*, **67A**, 71–82.

Ferguson, R. I., 1986. River loads underestimated by rating curves. *Water Resources Research*, **22**, 74–76.

Gabet, E. J., Burbank, D. W., Pratt-Sitaula, B., Putkonen, J., and Bookhagen, B., 2008. Modern erosion rates in the High Himalayas of Nepal. *Earth and Planetary Science Letters*, **267**, 482–494.

Gurnell, A. M., and Fenn, C. R., 1984. Box-Jenkins transfer function models applied to suspended sediment concentration-discharge relationships in a proglacial stream. *Arctic and Alpine Research*, **16**, 93–106.

Hallet, B., Hunter, L., and Bogen, J., 1996. Rates of erosion and sediment evacuation by glaciers: a review of field data and their implications. *Global and Planetary Change*, **12**, 213–235.

Hubbard, B., and Glasser, N., 2005. *Field Techniques in Glaciology and Glacial Geomorphology*. Chichester, UK: Wiley, 400 pp.

Kohler J., 1995. Determining the extent of pressurized flow beneath Storglaciären, Sweden, using results of tracer experiments and measurements of input and output discharge. *Journal of Glaciology*, **41**(138), 217–231.

Schleppi, P., Waldner, P. A., and Stähli, M., 2006. Errors of flux integration methods for solutes in grab samples of runoff water, as compared to flow-proportional sampling. *Journal of Hydrology*, **319**, 266–281.

Sharp, M., Tranter, M., Brown, G. H., and Skidmore, M., 1995. Rates of chemical denudation and CO_2 drawdown in a glacier-covered alpine catchment. *Geology*, **23**, 61–64.

Wadham, J. L., Hodson, A. J., Tranter, M., and Dowdeswell, J. A., 1997. The rate of chemical weathering beneath a quiescent, surge-type, polythermal based glacier, southern Spitsbergen. *Annals of Glaciology*, **24**, 27–31.

Willis, I. C., Sharp, M. J., and Richards, K. S., 1990. Configuration of the drainage system of Midtdalsbreen, Norway as indicated by dye-tracing experiments. *Journal of Glaciology*, **36**, 89–101.

Willis, I. C., Sharp, M. J., and Richards, K. S., 1993. Studies of the water balance of Midtdalsbreen, Hardangerjokulen, Norway. II. Water storage and runoff prediction. *Zeitschrift für Gletscherkunde und Glazialgeologie*, **27/28**, 117–138.

Willis, I. C., Richards, K. S., and Sharp, M. J., 1996. Links between proglacial stream suspended sediment dynamics, glacier hydrology and glacier motion at Midtdalsbreen, Norway. *Hydrological Processes*, **10**, 629–648.
Willis, I. C., Arnold, N. S., and Brock, B. W., 2002. Effect of snowpack removal on energy balance, melt and runoff in a small supraglacial catchment. *Hydrological Processes*, **16**, 2721–2749.

Cross-references

Alps
Catchment Glacier
Discharge/Streamflow
Hydrographs
Hysteresis
Melting Processes
Moulins
Sediment Entrainment, Transport, and Deposition
Sediment Yield
Solute in Glacial Meltwaters
Stage-Discharge Relationship
Suspended Sediment Concentration
Suspended Sediment Load

RECESSION COEFFICIENT

Manmohan Kumar Goel
Water Resources System, National Institute of Hydrology, Roorkee, Uttarakhand, India

A hydrograph has three major components: direct surface runoff, interflow, and groundwater flow. The rising limb extends from the time of beginning of surface runoff to the first inflection point on the hydrograph and represents the increase in discharge due to increase in storage in the basin. The crest segment of a hydrograph is in-between the inflection point on the rising limb to a corresponding point on the recession limb and represents the arrival of flow from that portion of the basin which receives the highest concentration of runoff volume. The point of inflection on the falling side of a hydrograph marks the beginning of recession limb which represents the withdrawal of water from various storages built up in the basin. The shape of recession curve depends entirely on the basin characteristics and it is mathematically represented as:

$$q_t = q_0 K^t \tag{1}$$

where "q_o" is specific initial discharge, "q_t" is discharge after time "t" (both "q_o" and "q_t" are within the same straight segment), and "K" is the recession coefficient. Taking $t = 1$, we get:

$$K = q_1/q_0 \tag{2}$$

In the recession limb of a hydrograph, the recession coefficient represents the ratio of the discharge after a unit time step of some specific initial discharge to the specific initial discharge, provided both the discharges are along the same straight segment.

Recession coefficient increases as the discharge hydrograph stabilizes. After the cessation of precipitation, various basin storages that contribute to the recession curve include surface storage (surface detention and channel storage), interflow storage, and groundwater storage. Recession coefficient is considered to be made up of three components (K_s for surface storage, K_i for interflow storage, and K_g for groundwater storage) to take care of the three types of storages as:

$$K = K_s.K_i.K_g \tag{3}$$

Different recession coefficients can be determined by analyzing the recession curve for a long time. When Equation 1 is plotted on a semi-log paper with discharge on the log-scale, its plots as a straight line and recession coefficients for different flow components can be found. Initial rough estimates of these coefficients (when t is in days) could be: K_s (0.05–0.50), K_i (0.50–0.85), and K_g (0.85–0.99).

Recession coefficients depend on the units of time and the area of catchment. Smaller time units tend to increase the values of K. Similarly, larger basins may also indicate higher values of K.

RECESSION OF DISCHARGE

Manoj K. Jain
Department of Hydrology, Indian Institute of Technology, Uttarakhand, Roorkee, India

Synonyms

Streamflow recession

Definition

Recession of discharge. The gradual depletion of discharge during periods with little or no precipitation constitutes the recession of discharge. A recession period lasts until streamflow begins to increase again due to subsequent precipitation. Depending on the source of flow in the recession period, the recession is further classified as recession of quick flow, recession of interflow, and recession of baseflow.

Recession curve. The specific part of discharge hydrograph after the crest (and the precipitation event), where streamflow diminishes during a rainless or dry period is called the flow recession curve, at a specific river cross section of the basin. Hence, recession curves are the part of the hydrograph that are dominated by the release of water from natural storages.

Introduction

Streamflow recession represents withdrawal of water from natural storages with no inflow (Singh, 1989). Therefore, it is more or less independent of time variation in rainfall and infiltration; it may be slightly dependent, however,

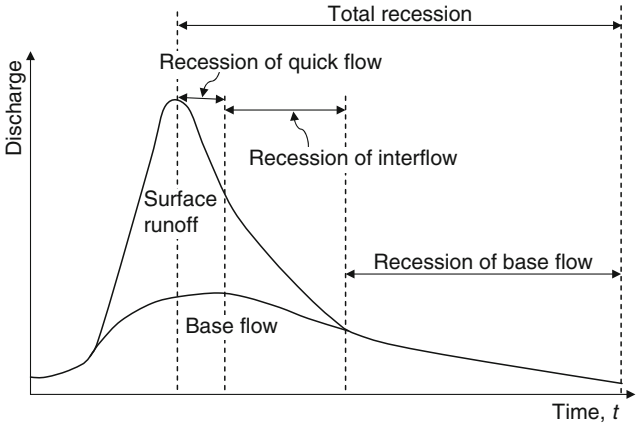

Recession of Discharge, Figure 1 Typical hydrograph showing recession of individual components of runoff.

on rainfall distribution and heavily dependent on ground conditions (Chow, 1964). It constitutes the falling limb of a hydrograph to the right after the crest where streamflow diminishes during a dry period. Its analysis yields information on retention characteristics of the basin and of groundwater storage and depletion. Streamflow recession rates and consequently, the shape of recession curves depend primarily on catchment topography and geology. Individual components of runoff: quick flow, interflow, and baseflow have their own distinct recession characteristics and rates (Barnes, 1939). The ranges of these rates may overlap, which reflect the fact that the distinctions between surface flow and interflow and between interflow and baseflow are not always clear (Klaassen and Pilgrim, 1975; Nathan and McMohan, 1990). A typical hydrograph showing recession of individual components of runoff is shown in Figure 1. As can be seen from Figure 1, initially the recession curve is steep as quick flow leaves the basin. It flattens out with delayed flow supply from deeper subsurface stores and may eventually become nearly constant if sustained by outflow from a glacier or from groundwater storage.

Analysis of recession

Analysis of recession of discharge has long been a subject of considerable interest (Barnes, 1939; Knisel, 1963; Hall, 1968, 1982; Nathan and McMohan, 1990; Tallaksen, 1995; Chapman, 1999; Wittenberg, 1999; Singh et al., 2000; Sujono et al., 2004; Hammond and Han, 2006). It has many practical applications in many areas of hydrological research, water resources assessment, planning, and management. Analysis of recession of discharge is also important in snowmelt runoff studies (Garstka et al., 1958; Martinec, 1965; Singh et al., 2000), glacier runoff studies (Meier, 1964), mass balance, and melt water delay characteristics of different parts of the glacier (Singh, 1994; Singh et al., 1995). The recession characteristics of a snowmelt hydrograph contain substantial information about snow water storage and can be considered as an index of snow water storage (Singh et al., 2000). A comprehensive review of streamflow recession analysis and its various applications have been compiled by Hall (1968), Anderson and Burt (1980), Singh (1989), and Tallaksen (1995).

Many methods are available in literature to model recession. These include methods based on use of basic flow equations, reservoir outflow, autoregressive processes, empirical relations, wavelet transform analysis, etc. (Singh, 1989; Wittenberg, 1994, 1999; Tallaksen, 1995; Chapman, 1999; Sujono et al., 2004). The most commonly used method for modeling recession is to use linear and nonlinear stores. Use of linear stores for recession analysis can be traced back in literature to studies by Boussinesq in 1877 and Millet in 1905. The method however became popular after Barnes (1939) analyzed the structure of discharge recession curves. In linear store method, the flow during recession is linearly related to storage, S.

$$S = kQ \tag{1}$$

This leads to relation between flow at time t, Q_t to flow at time $t = 0$, Q_0 as

$$Q_t = Q_0 e^{-kt} \tag{2}$$

where, Q_0 = initial discharge at start of recession, Q_t = discharge after time t and k = a constant known as recession constant or depletion factor. A plot of $\log(Q_t)$ against time should show a straight line if the storage–outflow relation is linear. A best-fit line is drawn through the plotted points and the slope is determined. This slope represents the value of the recession coefficient, k. A higher value of k results in faster draining of water from the basin, whereas a lower value of k represents slower drainage from the basin. The typical ranges of daily recession constants for streamflow components, namely quick flow (0.2–0.8), interflow (0.7–0.94), and groundwater flow (0.93–0.995) do overlap (Nathan and McMohan, 1990). However, high recession constants (e.g., >0.9) tend to indicate dominance of baseflow in streamflow. A curved semi-logarithmic plot for recessions means that the storage–outflow relationship is nonlinear and may be analyzed using appropriate nonlinear relations (e.g., Wittenberg, 1999).

Time variability of recession

A considerable variability is observed in recession behavior of a stream for most catchments with time. This is reflected in variations, in the shape of the recession segments found in a stream hydrograph. Variations in recession rates are caused by difference in climate during the time of recession; variability in areal distribution of rainfall, residual storage in connected surface water bodies, catchment wetness, and conditions prevailing prior to the start of recession. In large catchments, spatial variability in storm patterns cause differences in the distribution of flow paths in the catchment, which in turn may influence

the drainage pattern (Laurenson, 1961). Climate influences the recession rate during the time of recession by recharge from precipitation or snow melt, or by loss from evapotranspiration (Tallaksen, 1995). High evaporation rates during warm weather of active growing season can significantly influence low flows and recession dynamics particularly in shallow water table regions.

Conclusion

The recession segment of streamflow hydrograph contains information on retention characteristics of the basin and of groundwater storage and depletion. Analysis of recession can provide valuable information needed for hydrological research, water resources assessment, planning and management, snow melt, glacier melt, glacier mass balance, etc. Many models of varying complexities have been developed in the past to understand dynamism in recession characteristics of a stream. Further research, however, is required to understand better physical processes governing recession of discharge and its variability with time.

Bibliography

Anderson, M. G., and Burt, T. P., 1980. Interpretation of recession flow. *Journal of Hydrology*, **46**, 89–101.

Barnes, B. S., 1939. The structure of discharge-recession curves. *Transactions of the American Geophysical Union*, **20**, 721–725.

Boussinesq, J., 1877. Essai sur la theorie des eaux courantes. Memoires presentes par divers savants a l'Academie des Sciences de l'Institut National de France, Tome XXIII, No. 1. (Cited by Hall (1968).)

Chapman, T., 1999. A comparison of algorithms for stream flow recession and base flow modelling. *Hydrological Processes*, **13**, 701–704.

Chow, V. T., 1964. *Handbook of applied hydrology*. New York, NY: McGraw-Hill.

Garstka, W. U., Love, L. D., Goodell, B. C., and Bertle, F. A., 1958. Factors affecting snowmelt and streamflow. U.S. Bureau of Reclamation and US Forest Service.

Hall, F. R., 1968. Baseflow recession – a review. *Water Resources Research*, **4**, 973–983.

Hall, F. R., 1982. Subsurface water contribution to stream flow. In Singh, V. P. (ed.), *Rainfall–runoff relationship*. Littleton, CO: Water Resources, pp. 237–244.

Hammond, M., and Han, D., 2006. Recession curve estimation for storm event separation. *Journal of Hydrology*, **330**, 573–585.

Klaassen, B., Pilgrim, D. H., 1975. Hydrograph recession constants for New South Wales streams. Inst. Engng. Civil Engng. Trans., CE17, 43–49.

Knisel, W. G., 1963. Baseflow recession analysis for comparison of drainage basin and geology. *Journal of Geophysical Research*, **68**, 3649–3653.

Laurenson, B. E., 1961. A study of hydrograph recession curves of an experimental catchment. *Journal of the Institute of Engineers (Austrlia)*, **33**, 253–258.

Maillet, E., 1905. Essai d'hydraulique souterraine et fluviale. Libraire Sci., A. Herman, Paris. (Cited by Hall (1968).)

Martinec, J., 1965. A representative watershed for research of snowmelt-runoff relation. IAHS Symposium on representative and experimental watersheds. Budapest. pp. 494–501.

Meier, M. F., 1964. Ice and glaciers. In Chow, V. T. (ed.), *Handbook of Applied Hydrology*. New York, NY: McGraw Hill, pp. 16-16–16-21.

Nathan, R. J., and McMohan, T. A., 1990. Evaluation of automated techniques for baseflow and recession analysis. *Water Resources Research*, **26**, 1465–1474.

Singh, V. P., 1989. *Hydrologic Systems – Vol. II. Watershed Modeling*. Englewood Cliffs, NJ: Prentice Hall, pp. 172–179.

Singh, P., 1994. Glacier mass balance and recession trends of hydrographs. In International Symposium on Snow and its Manifestations. 26–28 September 1994, Snow and Avalanch Establishment, Manali (H.P.), India.

Singh, P., Ramasastri, K. S., Singh, U. K., Gergan, J. T., and Dobhal, D. P., 1995. Hydrological characteristics of Dokriani glacier in Garhwal Himalayas. *Hydrological Processes*, **40**, 243–257.

Singh, P., Huebl, H., and Weinmeister, H. W., 2000. Use of recession characteristics of snowmelt hydrographs in assessment of snow water storage in a basin. *Hydrological Processes*, **14**, 91–101.

Sujono, J., Shikasho, S., and Hiramatsu, K., 2004. A comparison of techniques for hydrographic recession analysis. *Hydrological Processes*, **18**, 403–413.

Tallaksen, L. M., 1995. A review of baseflow recession analysis. *Journal of Hydrology*, **165**, 349–370.

Wittenberg, H., 1994. Nonlinear analysis of low flow recession curves. FRIENDS: Flow Regimes from International and Experimental Network Data. IAHS Publ. No 221:61

Wittenberg, H., 1999. Baseflow recession and recharge as nonlinear process. *Hydrological Processes*, **13**, 715–726.

RECONSTRUCTION OF THE LAST GLACIATIONS IN THE WHOLE OF ASIA

Matthias Kuhle
Department of Geography and High Mountain Geomorphology, University of Göttingen, Göttingen, Germany

Synonyms

Pleistocene glaciation of Asia during the last Ice Age (Würm, Weichsel); Quaternary glaciation of Asia during the MIS 4-2

Definition

Reconstruction of the maximum former extent of the ice cover in Asia.

Introduction

The current state of ice age research suggests to confine this overview of the reconstruction of the past glaciation in High Asia to the Last Ice Age, the Würm-Ice Age (Weichsel-Ice Age MIS 4-2), i.e., to the last maximum ice extent and at most to a somewhat earlier ice extent during the early to middle Würm-Ice Age – if at all there is a reliable possibility to differentiate these two advances regionally, considering the data obtained so far. With regard to the method this restriction suggests itself because of the chronological nearness of the LGM-advance, so that naturally the indicators might be best

preserved. The former extents of the ice – as far as they have not been overthrust by the last advance and thus underwent a Quaternary-geological reshaping, i.e., destruction – could only be preserved by still more extended glacier traces beyond those of the LGM. However, due to the several times higher age, this ought to have led to much clearer solifluidal and erosive traces of modification, i.e., blurrings. The resulting uncertainties as to the diagnosis of the older glaciations lead to this restriction to the youngest maximum extent of the ice.

Detailed explanations with regard to the Weichsel-(Würm Ice Age) glaciation in Asia

N-Asia, Siberia

According to the climate zones the largest LGM-glacier faces can be assumed to be in the Siberian Arctic region. Indeed, there exist relevant investigations showing an eastward continuation of the European ice sheet with its center in Scandinavia up to beyond the Urals, i.e., up to the area of the Kara Sea (Grosswald, 1998; Astakhov, 1998; Arkhipov, 1998). However, the interpretations as to the extent of the LGM-Kara-ice sheet are different: Grosswald (ibid. pp. 16–17) assumes a continuous N-Siberian ice sheet that has dammed up the rivers discharging interglacially and currently to the N. This led to the development of large proglacial lakes which were integrated into a transcontinental system of meltwater drainage. Here, the existence of these ice-dammed lakes – evidenced by correlating lake sediments, lake terraces, overflow channels and spillways – is put forward as independent finding of a continuous ice sheet in the Siberian Arctis. So, in the Turgay Valley of SW-Siberia, Grosswald recognizes the Quaternary-geologically provable function of a Late-Würm spillway that led the Siberian ice sheet meltwater into the Aralo-Caspian basin. This interpretation is contradictory to that of Astakhov (1992). The later analysis of space images with strong resolution by V.R. Baker (Grosswald, 1998) supports the opinion that geomorphologically young features of erosion are concerned here as they can only derive from the turbulent and powerful streamflow of a W-Siberian ice-dammed lake. A confirmation is seen in a second valley, the Manych valley, as a major spillway which connected the Khvalyn meltwater basin, i.e., the ancient Caspian Sea, with the Black Sea (V.R. Baker; personal communication after Grosswald, 1998, p. 16). Obviously this is also a geomorphologically young form.

As far as the Kara ice sheet is concerned, Astakhov (1998, p. 26) follows the reconstruction of Grosswald (1980) especially with regard to the extent of the S-ice margin, which similar to Scandinavia, is supposed to have been located 500–1,000 km away from the ice divide. Later comments with regard to a Kara ice sheet reaching even further southward (Grosswald and Goncharov, 1991; Grosswald, 1994), however, are not in agreement with Astakhov (1998). The maximum ice thickness is estimated at 2–3 km, whereby the great Pleistocene thickness of permafrost is considered to be an indication of very cold ice and, accordingly, a rather greater ice thickness. The soft underground of Cretaceous, Palaeogene, and Quaternary very clayey sediments, however, rather might have flattened the ice dome (ibid.). According to Arkhipov et al. (1980) the reconstructed ice thickness of still 400–500 m very close to the ice margin in the Polar Urals is a further indication of very cold and therefore thick glacier ice. Anyway, due to a thick ice like this and the very cold conditions, the possibility of mountainous ice dispersal centers has to be ruled out, particularly since the Urals are only 50–80 km wide. Dibner (1970) mapped a submerged hummocky relief and the ice directional features and erratics prove an advance of the Kara ice sheet from the W-Kara Sea basin not only to the S and W (see above), but also to the E up to the Yamal Peninsula (Astakhov, 1979; Gataullin, 1988). The sparse 14C-datings limit the corresponding ice advance in the area of Novaya Zemlya to older than 15 Ka. This chronological classification, which has to be understood as minimum age, is confirmed by loess-like silts with syngenetic wedges, lying on youngest tills, that in the area of the Yamal peninsula are dated to 13–14 Ka (Bolikhovskaya and Bolikhovsky, 1992). Because the uppermost till contains large fields of fossil glacial ice (isolated masses of dead ice are still buried in the drift: Astakhov and Isayeva, 1988) that would not have survived the very warm Eemian transgression, the oldest time-period of the Kara ice sheet that has been proposed is MIS 4 (110–50 Ka) (Astakhov, 1998).

As for the eastern continuation of the proposed connected N-Siberian ice sheets the reports of the Pole Star-Expedition 1993 (Fütterer, 1994) are important. Here the opinion is expressed, that the observed erosive incision into the shelf of the Laptev Sea E of the Taimyr Peninsula gives evidence of the Ice Age existence of the Lena River which eroded the glacially dewatered shelf. Thus, the synchronous existence of an E-Siberian ice sheet was also refuted. Grosswald and Spektor (1993) and Grosswald and Hughes (1995), however, think that this erosion form is the result of one or several floods of a Lena paleo-lake dammed up by the E-Siberian ice sheet and broken out during the Late Glacial.

According to the comments above, also a northern continuation of the terrestrial Pleistocene Siberian ice sheet in the shape of a marine ice sheet in the Arctic Ocean is presented (Vogt et al., 1994). To this point findings at a depth of the ocean of 500–850 m and perhaps up to 2,000 m in the form of detected plowmarks on the Yermak Plateau. These speak at least for huge icebergs and thus thick calving ice fronts, if not for a crushed ice shelf. The existence of this marine ice sheet on the N-margin of Siberia is also supported by investigations of box core sediments for evidence of biological life in the Arctic Ocean which did not show any traces of life between 13 and 26 Ka. This suggests the covering of the area by an ice shelf with a thickness of several hundreds of meters, so that in the water underneath an abiotic zone had developed, as shown by Travis (1994). These findings are in

contradiction to those of Zubakov and Borzenkova (1990) who plead for an uninterrupted, continuous evolution of organic life in the Arctic Ocean against the existence of a whole Arctic ice sheet and also an ice shelf.

Again further to the E the mapping of oriented tundra landforms and oriented lakes shows a radial structure of outline. They run from the environment of the New Siberian Island to the S diverging in a fan-like pattern up to the Yana-Indigirka Lowland and adjacent areas including the ridge- and lake complex. These forms – taken from space images and air photographs – that received their shape from drumlinization as well as large-scale fluting produced by a marine ice sheet are also interpreted as indicators of the Late Weichsel continuation of the inland ice in excess of 145°E (Grosswald, 1998, Figures 9 and 19). For Grosswald and Hughes (1995) these flowlines, derived from both the ice-shoved features and oriented tundra forms, at the same time were the basis for the reconstruction of another great ice sheet connected to the E, the so-called "Beringian ice sheet." Corresponding indicators, but also push moraines, are stated by those authors for the lower Kolyma basin, Karchyk Peninsula, and the adjacent Ayon Island. The accompanying ice-spreading center was situated NE of the Kolyma Delta. Furthermore, appropriate evidences of till sheets and accumulations of glacial erratics or "Lapland-style" geomorphology are stated for the Chukchi Peninsula, Cap Serdtse Kamen, and the Wrangel Island (Laukhin et al., 1989; Grosswald, 1998). With regard to a connected S- to SE-ice extent as far as into the Bering Strait and across the Chukchi Range evidences are given by, e.g., truncated spurs and huge masses of coarse debris accumulated on the lee (southern) side of the 700-m-high steep flank of the mountains up to high up to Cape Dezhnev, as well as numerous U-shaped valleys oriented in a N–S-direction up to down to the S at 60°N at Cape Oljutorskij (Grosswald, 1998, Figure 12). The extent of the Bering ice sheet along meridian 167°E to the S up to 55°N is supported by findings as, e.g., glacial troughs and striations on the Bering Island (Erlich and Melekestsev, 1974).

Last the recently discussed question with regard to a possible ice sheet in the Sea of Ochotsk as an additional center of the Siberian ice sheet has to be approached. The area is surrounded by mountain ranges (Kolymsky, Suntar Khayata, and Koryak Ranges) that due to ELA-depressions up to near to sea level of the – according to the Kara Sea – cold Sea of Ochotsk were heavily glaciated (Grosswald, 1998). Geomorphological investigations of Udintsev (1957) show that the Ice Age margins of the mountain glaciers in a seaward direction have reached up to the sea. Terrestrial outlet glaciers like these enter the Penzhina- and Gizhiga inlets and have filled the Shelikhov Bay at least up to 59°N. Accompanying chains of parallel end moraines, eskers, and drainage channels are described by Grosswald (1998, p. 15) for the W-coast of the Kamchatka Peninsula. As for forms of the U-shaped basin bottom of the Sea of Ochotsk, situated at a water depth about 1,000 m, a variety of explanations have advanced (Udintsev, 1957; Volnev, 1983), so, e.g., tectonic faulting and folding of the crust. Grosswald (1998) tends to the opinion that these are glacigenic forms, and further to the S, at 47°–49°N, he postulates a geomorphologically diagnosable area of an ice shelf break. This can be supported by coarse sediments, including boulders (Bezrukov, 1960), found at several places of the sea floor, so, e.g., off the coast of SW Kamtchatka, where a 3–8-m-thick lodgement till was cored (Kuzmina and Yeremeeva, 1990). Up to now it is unexplored how far this still hypothetical Ochotsk ice sheet, as an additional center of the Siberian glaciation, has reached the SE. Possibly in the SE the ice sheet changed into an ice shelf that was buttressed by the submarine ridge of the Kuril (Grosswald, 1998).

The Siberian mountains

Zamoruyev (2004) thinks that in NE-Asia no large ice sheets have existed like in Europe or North America, but that the glaciation was restricted to the mountains N of the Stanowoi mountains up to the Werchojansk mountains in the N and up to the Korjaken mountains in the E. Thereby cirque and hanging glaciers up to large dendritic glaciers with piedmont glacier tongues were concerned. A mountain ice cap of a few 100 km in diameter developed as largest glacier type in the S-Werchojansk mountains (ibid. p. 321). According to this opinion only glaciers from the Chukotka Peninsula reached the ocean and covered the modern shelf. While the extent of the recent glacier surface in the NE-Asian mountains is not much greater than 560 km², that of the Pleistocene glaciation was still 500,000 km². After Kind et al. (1971), Velichko (1973), Svitoch (1978) and Degtyarenko (1984) the period of the Late Pleistocene (Weichsel, LGM) was that of the greatest extent. Among others this has been proved by 14C-data about 33–35 Ka and by means of glacial deposits which in the W-slope of the Werchojansk mountains reached down up to the Lena River. According to Zamoruyev (2004) the Ice Age glaciation of the Werchojansk mountains and its chronology is representative for the other mountain regions in NE-Asia. But also the ice cover – as far as it derives from the mountains – is still seen controversially. So, e.g., Svitoch et al. (1980) even are of the opinion that the inner lowland of Chukotka has never been reached by the mountain glaciers.

Sheinkman (2004) in principle agrees with the summarized vergency of Zamoruyev (2004) as to a mountain climate for Central- and NE-Asia that during the Pleistocene ice age was colder, but with respect to the precipipitation similar to the current climate. Compared with Europe – he explains – the LGM-glaciation was rather insignificant. As well directly as indirectly this contradicts the findings as to an extended N-Siberian inland glaciation summarized above (see Section N-Asia, Siberia). Indirectly, because the very large proglacial

lakes, dammed up by the inland ice, and their transcontinental meltwater drainage system must have brought an enormous humidity in the currently rather semiarid continental areas. Thus, much greater ELA-depressions as suggested by the last-mentioned authors would become probable for the local mountain glaciations.

As for the Altai mountains Sheinkman (2004) found out a maximum length of the valley glaciers of 70 km during the Late Pleistocene, while for the NE-Siberian glaciers (see above) he supposes extents of twice this size (about 150 km in length) in the past, though the current glaciers in the Altai are the greater ones. An Ice sheet glaciation is ruled out. However, local piedmont glaciations, i.e., ice fields at the foot of the mountains are stated as maximum advances (ibid. p. 334).

The mountains to the S and E outside of Siberia

Not only the large past ice surfaces are paleoclimatically important, but also the comparatively minor high mountain glaciations. These make possible to reconstruct the Ice Age increase of the ELA (uplift of the snowline) from the Siberian Arctis via the temperate latitudes and the high-continental- semiarid subtropics as far as to the monsoon-humid tropics of S-Asia. Therefore, exemplary findings of glaciation are to be described from several further high mountains of Asia.

In the Japanese Alps, altogether five glacier advances occurred during the Last Glaciation, i.e., here since MIS 4; to these belong advances just before 24 Ka, 20–18 Ka, 11–10 Ka, and in the early Holocene (Sawagaki et al., 2004); in the Hidaka Mountains this has also taken place during MIS 3 and 2, here stated by tephrochronological investigations. The whole glacier surface is determined to be c. 800 km² large and the glaciated areas decrease from 2,500 m asl at 35°N to 1,000 m asl at 45°N (ibid. p. 217). However, for the Japanese Alps between 34° and 37°N and at c. 137–139°E, Iozawa (1979) describes besides cirques between 2,400 and 2,700 m asl, also U-shaped valleys extending to below of 1,000 m asl. This speaks in favor of a clearly minor sea-level of the corresponding lowest ice margins than 1,000 m asl, also in the Japanese Alps. For the Northern and Central Japanese Alps, Sawagaki et al. (2004, Figure 2) settle the lowest ice margins about 1,100 m asl. Information as to the S-Alps is lacking, so that obviously the lowest positions of the ice margins are situated noticeably below 1,000 m. In general, however, the N-Japanese Alps are supposed to have been heavier glaciated than the Central and S-Alps (ibid.). Due to the lack of current glaciers, a minimum depression of the ELA of 1,200 m has to be considered according to these data. In the Hidaka mountains (42°–43°N) with heights of 1,500–2,000 m asl, which are seen as second key-area of the past Japanese glaciation, the lowest, c. 40 Ka old positions of the glacier termini reached down to c. 800 m asl (Sawagaki et al., 2004, Figure 2). This proves an LGP (Last Glacial Period) height of the snowline at a maximum of c. 1,400 m asl and corresponds to an ELA-depression of at least 1,000–1,200 m.

The Würm-glaciation of Taiwan (22°–25°N) with its highest elevation, the 3,952 m-high Yu Shan, reconstructed since 1934 (Tanaka and Kano, 1934; Panzer 1935), has been described by youngest papers of Böse and Hebenstreit (2001) as a still provisional interim report; (Böse, 2004,"studies are in progress", p. 351). This much is certain: there existed a cirque- and hanging valley glaciation during MIS 2 that, e.g., has led to concave longitudinal valley profiles as far as down to 3,350 m asl. From these and further findings an ELA-depression of at least 3,300 m asl (Yu Shan) has been extracted according to an ELA-depression of at least 600–700 m asl (ibid.).

In Malaysia we find the highest mountain between the monsoon-tropical Himalaya and the equatorial peaks of New Guinea: Mt. Kinabalu (4,101 m asl, 6°05′N 116°33′E) on the N-tip of Kalimantan. For the LGM Koopmans and Stauffer (1967) reconstructed a 5.5 km² large ice cap on the highest E-plateau and a thicker one on the lower W-plateau. The plateau-ice was at least 80 m thick. In addition, small valley glaciers had developed. In the main valley one of them has created a U-shaped cross-profile inset up to 1,000 m deep; at 2,900 m asl moraines are left behind. A further moraine is described from the N-slope near Paka Cave at 3,100 m asl (Hope, 2004). Accordingly, snowline altitudes about 3,500 m asl are verified. Smith and Lowry (1968) describe several cirques at different positions. In any case, the ELA must have run below 3,600 m, i.e., below the glaciated summit plateau. Hope (2004), however, raises objections, because the rock forms led back to a past glaciation, as, e.g., stripping of the summit plateau, smoothing and plucking, etc., might also be a result of the rock structure of the granite and its weathering, like exfoliation which creates smooth slabs. However, on the basis of his knowledge of literature, i.e., without knowing the field himself, he supposes the glaciation to be the probable cause of the forms concerned. As test area in Indonesia, Mount Leseur in N-Sumatera (3°45′N) is approached. For this massif van Beek (1982) indicates a glaciated surface of about 100 km² and a Pleistocene ELA at 3,100 m asl. As for the highest summit of Sumatera, the centrally situated 3,805 m-high Mount Kerinci, Hope (2004) quotes an ELA at 3,450 m and an Ice Age glacier nourishing area of 2.4 km² situated above. To sum up, one may assume a height of the snowline of c. 3,500 m for Malaysia and Indonesia during the LGP.

As an example from the arid SW of Asia a reconstruction of the glaciation in the Iraq mountains is approached by Wright (2004). Among others he describes for the Algurd Dag in the NW Zagros, the ridges of which reach 3,000–3,500 m asl, that "extensive Pleistocene glaciers formed on the N-slopes and flowed through gaps southward down-valley tributary to the greater Zab River to elevations as low as 1,100 m" (ibid., p. 215). On subsidiary ridges also exposed to the N, cirques with bottoms about 1,500 m asl have been met; they were also classified as belonging to the Late Pleistocene. This corresponds with an ELA-depression in excess of 1,700 m against today (ibid., p. 215). Evidence has also been provided of

a mountain glaciation in the 4,135 m-high, currently non-glaciated Kuh-i-Jupar massif in the semiarid SE-Zagros (S of Kerman) during the LGP (Würm glaciation, MIS 4-2:60-18 Ka) (Kuhle, 1974, 2007a). During the LGP glaciation, the glaciers reached a maximum of 10–12 km in length. They flowed down into the mountain foreland as far as 2,160 m. The thickness of the valley glaciers reached 350 m. The glacier termini mostly remained separated in the mountain foreland. The climatic ELA ran at c. 3,050 m asl, that is 1,500 m below the current theoretical snowline. Thus, a temperature depression of c. 10–15°C must be assumed for the SE-Iranian highland. The recessional moraines, which are preserved in the high valleys, document a Late Glacial glacier retreat in four stages (I–IV). These four Late Glacial stages can be identified at many places in the mountains of High and Central Asia. Additional evidence of a Late Pleistocene glaciation was found on the adjacent massifs of the Kuh-i-Lalezar and Kuh-i-Hezar (ibid.).

High Asia

Between Siberia and High Asia, i.e., from Central- to S-Asia, Last Ice Age mountain glaciers mediated, e.g., in the E-Sayan mountains, the Transbaikalian mountains, the Altai (see above The Siberian mountains) as well as the Tianshan with their in part relatively large high plateau glacier areas, so on the Tienshan plateau, up to the Tibetan inland ice area and the high mountains surrounding Tibet with their icestream networks (Kuhle, 2004; Sheinkman, 2004 and others).

Published up to 1973, but also even later, the synopsis of older results and views on the Pleistocene glacier cover in High Asia provided by Wissmann's 1959 compilation, was considered as being accepted. This concept of a very insignificant glacier cover of Tibet and its mountains was also pursued in the recent Chinese literature by Shi and Wang (1979); it has also been reproduced by CLIMAP (Cline, 1981, entitled "Last Glacial Maximum"). These authors speak of a 10% to a maximum of 20% ice cover of the mountains and plateaus of Tibet. Since 1973 new data were obtained on the maximum extent of glaciation in High Asia. Evidence for an ice sheet covering Tibet during the Last Glacial period means a radical rethinking about glaciation in the Northern Hemisphere. The ice sheet's subtropical latitude, vast size (2.4 million km²), and high elevation (6,000 m asl) are supposed to have resulted in a substantial albedo-induced cooling of the Earth's atmosphere and the disruption of summer monsoon circulation. Moraines were found to reach down to 460 m asl on the S-flank of the Himalayas and to 2,300 m asl on the N-slope of the Tibetan plateau, in the Qilian Shan region. On the N-slopes of the Karakoram, Aghil, and Kuen-Lun mountains moraines occur as far down as 1,900 m asl. According to the arrangement of the positions of their morphological and sedimentological elements they were classified. Samples have been analyzed as to their grain size distribution, lime- and humus content, as well as sorting coefficient. Additionally, petrographical and morphoscopical analyses of quartz grains were carried out. Thus, ground-, lateral-, and end moraines could be differentiated and subglacial or subaerial fluvial reshaping was diagnosed. Radiographic analyses of erratics suggest a former ice thickness of at least 1,200 m. Glacial polish and roches moutonnées in the Himalayas and Karakoram suggest former glaciers as thick as 1,200–2,700 m. On the basis of this evidence, a 1,100–1,600 m lower equilibrium line altitude (ELA) has been reconstructed, resulting in an ice sheet of 2.4 million km², covering almost all of Tibet. 14C-ages classify this glaciation as MIS 4-2 in age (Würmian = LGP, c. 60,000–18,000 years ago) (Kuhle, 1998, 2004).

As for the reconstruction of the Ice Age glaciation of the mountains, evidences have to be quoted of a farthest and lowest glacier extension from the Karakoram, from S-Tibet up to the Himalaya-S-slope and on the E-margin of Tibet: so, e.g., in the Shaksgam-, Shimshal-, Hunza-, Hispar-, Barpu-, Hassanabad-, Bar-, Braldu-, Bassna-, Indus valley, etc., and connected massifs; in the Zanskar-, Bhagirathi (Gangotri)-, Nandakini-, and Alaknanda valleys in the Garhwal Himal; in the Kanjiroba-, Dhaulagiri-, Annapurna-, Damodar-, Manaslu-, Langtang-, Rolwaling-, Everest-, and Kangchendzönga massifs with accompanying valley systems; in the Minyang valley, the Konka Shan, and in the Anymachin (Kuhle, 1982, 2007b).

Glacial horns, roches moutonnées, flank polishings, abraded mountain spurs, glacially streamlined hills, etc., but also high erratics prove a large-scale ice cover. Important ice thicknesses do occur according to transfluences: e.g., in the Hunza valley system a 2,000-m-thick Hunza glacier reached down from the Khunjerab-pass as far as into an Indus trunk glacier. The joint glaciers flowed up to Sazin and then 20 km down the lower Indus valley up to below 870 m asl (35°32′N/73°18′E). This glacier was part of a continuous ice stream network. In the N, via the Khunjerab-pass, it was connected to the ice of the E-Pamir, via the Shimshal-, Hispar-, and Barpu glaciers to the Shaksgam-, Basna-, and Shigar glaciers (Kuhle, 1997, 2001, 2006).

In the Nanda Devi-Kamet group, in the Alaknanda valley, the lowest ice margin was near Pipalkoti (30°26′N/79°25′40″E) at 1,000–1,100 m asl. In the Mandakini valley it was at c. 1,300 m, in the Nandakini valley at 1,200–1,400 m, and in the Bhagirathi valley at 1,050 m asl, 3 km downward from Uttarkashi (Kuhle, 2005, Figure 2, 2007b).

LGP-glacier traces (Würm) reached down to at most 460 m asl, i.e., to Dumre near the exit of the Marsyandi Khola or to Thuma at 890 m in the Tamur Khola. This corresponds to ELA-depressions of c. 1,660 m (Kuhle, 1997, 1998).

The LGM-Minyang glacier was one of the larger E-Tibetan outlet glaciers flowing down to c. 1,040 m asl. It came to an end c. 45 km S of Wenchuan. The Ice Age

Hailuogou- and Yantsöko glaciers flowed down from the Minya Konka SE- and NE-flanks into the Dadu main glacier, which had still a thickness of c. 300 m. Accordingly, the lowest LGM ice margin of this E-outlet glacier of the Tibetan inland ice must have been situated at c. 1,150 m asl at 29°30′N/102°11′30″E below Wantung (Kuhle, 2001, 2007b).

In the S-slopes of the Mt. Everest-Makalu-Cho Oyu massifs (Khumbu and Khumbakarna Himal) an ice stream network has been reconstructed for the last glacial period (MIS 4-2) (Kuhle, 2005). It has communicated across transfluence passes with the neighboring ice stream networks toward the W and E. The ice stream network has also received inflow from the N, from a Tibetan ice stream network, by the Kyetrak-Nangpa-Bote Koshi Drangka in the W, by the W-Rongbuk- into the Ngozumpa Drangka, by the Central Rongbuk- into the Khumbu Drangka, and by the Arun transverse-valley in the E of the investigation area. The ice thickness of the glacier sections above the snowline was 1,000–1,450 m. The most extended parent glaciers have measured 70 km in length (Dudh Koshi-glacier), 67 km (Barun-Arun-glacier) and 80 km (Arun-glacier). The Arun-glacier flowed down to 500 m asl and the Dudh Koshi-glacier to 900 m asl. The current climatic glacier snowline in the research area runs about 5,500 m asl. The snowline depression of the last glacial period calculated by four methods has run about 3,870 m asl so that an ELA-depression of 1,630 m has been determined. This corresponds to a lowering of the annual temperature by 8–10°C.

From this most important past glacier extension up to the current glacier margins 13 glacier stages have been differentiated and in part 14C-dated. They were four glacier stages of the late glacial-, three of the neoglacial-, and six of the historical period. By means of 130 glaciers the corresponding ELA-depressions have been calculated in comparison with the current courses of the orographic snowline. The number of glacier stages since the maximum glaciation agrees with that in many other mountain systems on globe since the last glacial period. Accordingly, this is an indication of the Würm-age of the lowest ice margin positions.

As to the 11–13 glacier positions met also in the further test areas (see above), which can be differentiated from the current glacier tongues up to the lowest Last Glacial end moraines, and also with regard to a global snowline depression about 1,200–1,500 m as against the current snowline altitude, High Asia corresponds with the global glacier reconstructions as they have been established, e.g., in the Alps, the Rocky mountains, New Zeeland, and the Andes (ibid.).

A recently formulated alternative position as to the outlined extensive LGP glaciation of High Asia is represented by Seong et al. (2008) and Owen et al. (2008) on the basis of OSL- and TCN datings. However, these datings are inconsistent and contradictory; moreover, in comparison with the conventional radiocarbon data, they are overrated. The factor of overrating lies between c. 4 and 10 (Kuhle, 2008).

A possible reason for this chronological overrating of the datings goes back to the calculation of the scaling factors for the Ice Age High Asia which is insufficient so far. But due to the atmospheric cosmogenic isotope chronology, it is certain that the intensity of the cosmic ray flux during the cold phases in general was higher than today. However, since the age determination is dependent on the local cosmic ray intensity, the modulation of which during the past was determined by the complex interrelations between the solar and terrestrial magnetic fields and their secular excursions, a reliable calibration of the OSL- and TCN-techniques for High Asia is not yet possible. The overrating of the age determinations might indicate that the scaling models so far underrate the Ice Age radiation and thus produce age determinations that are too high. In case minima of the terrestrial and solar magnetic field overlie each other – as this must have happened several times during the past – the TCN-productivity is at least by the factor 4.5 higher than today (Beer, 2000, Figures 2 and 4; Lifton et al., 2005; Pigati and Lifton, 2004) and an irradiation of 1 Ka is enough to simulate an age of 4.5 Ka. A wrong calibration like this cannot be identified by the datings itself. Therefore the CRONUS-Earth project recommends the search for "Production Rate Calibration Sites," that are made safe by conventional radiocarbon data. Even more important is the fact that a calibration of the TCN-technique can only proceed from the basis of an already existing Quaternary-geological chronology and not the other way round. The papers concerning High Asia, which contain OSL- and TCN-datings (ibid.), are not able to cope with this procedure. However, all these papers contain the following circular argument: if a moraine, situated at an insignificant distance from the recent glacier tongues, is dated by OSL- or TCN-techniques as being of a High Glacial (LGM) age, indications to a more extensive glaciation either are ignored or shifted to an older glacial period, without providing a further argument that is independent of the dating.

Accordingly, here a non-calibrated scale (namely, the OSL- and TCN-data) is interpreted to be an absolute scale and at the same time the scale of the indispensable glacio-geological method is given up.

The comprehensively documented Quaternary-geological indicators of the LGM-glaciation in High Asia described above, which indicates an ELA-depression between 1,200 and 1,500 m asl that is coherent with the N-hemispheric glaciation and shows a parallel chronological period of time, are not defeated so far. In the contrary, in the meantime regional findings and their glacio-geologically establised classification into the LGM have been confirmed among others by Hewitt (2009). Their paleoclimatic acceptability is evidenced by the relative chronology of the stages as well as state and extent of the preservation of the glacigenic indicators and 14C-datings.

Summary

It is not easy to summarize the current state of knowledge of the Asian ice cover during the Last Ice Age in a map, because up to now the interpretations of the ice-age researchers are contradictory as to this largest continent. In spite of that the author refers to a presentation of the then ice cover which seems to him to be the temporarily best compromise between the positions of a minimum and maximum glaciation (see Kuhle, 2010, Figure 1 (in chapter "*Ice Age*" in this volume)). Besides this cartographic summary of the glacier areas during the Weichsel-period, the extracted heights of the snowline (ELA) are especially appropriate guidelines that present the product of past temperature and precipitation in summary. Thus they make possible to get a Paleoclimatic overview over Asia during the Ice Age: According to the glacier reconstruction (see above N-Asia, Siberia) the ELA in the Siberian Arctis ran at sea-level (0 m asl); toward the middle- up to S-Siberian mountains (see above The Siberian mountains) it was uplifted to 1,250–1,450 m asl (E-Sayan- and Khama Darban Mountains, 53°–52°N); to the S, to the Altai and Tienshan (44°–40°N) it increased to 2,200–2,900 m asl; from the N-margin of Tibet (Kuenlun 36°N) up to the Himalaya (28°N) (see above High Asia) it was uplifted from 3,600 to 3,700 m up to 4,000–4,300 m and then decreased again to 3,600 m asl in the Himalaya-S-slope. From here further to the S (see above The mountains to the S and E outside of Siberia) the ELA drops as far as close to the equator to 3,500–3,100 m asl (Malaysia and Indonesia). On the E-margin of Asia in the Japanese Hidaka Mountains (42°–43°N), the maritime influence led to an altitude of the snowline about max. 1,400 m asl, that has increased toward the equator via Taiwan (3,300 m asl at 22°–25°N). The most astonishing climatic depressions of the snowline to only ELA = 2,500–3,050 m asl have been reconstructed in the currently semiarid SW-Asia (Zagros, 29°–37°N).

Bibliography

Arkhipov, S. A., 1998. Stratigraphy and paleogeography of the Sartan glaciation in West Siberia. *Quaternary International*, **45/46**, 29–42.

Arkhipov, S. A., Astakhov, V. I., Volkov, I. A., Volkova, V. S., and Panychev, V. A., 1980. *Paleogeografia Zapadno-Sibirskoi ravniny y maksimum pozdnezyryanskogo oledeneniya (Palaeogeography of the West Siberian Plain at the Late Zyryanka glaciation maximum)*. Novosibirsk: Nauka, p. 109. in Russian.

Astakhov, V. I., 1979. *New data on the latest activity of Kara shelf glaciers in West Siberia*. IGGR Project 73/1/24. Quaternary glaciations in the Northern Hemisphere, Report 5 Prague, pp. 22–31.

Astakhov, V. I., 1992. The last glaciation in West Siberia. *Sveriges Geologiska Undersökning, Ser. Ca*, **81**, 21–30.

Astakhov, V. I., 1998. The last ice sheet of the Kara sea: terrestrial constraints on its age. *Quaternary International*, **45/46**, 19–28.

Astakhov, V. I., and Isayeva, L. L., 1988. The 'Ice Hill': an example of 'retarded deglaciation' in Siberia. *Quaternary Science Reviews*, **7**, 29–40.

Beer, J., 2000. Neutron monitor records in broader historical context. *Space Science Reviews*, **93**, 107–119.

Bezrukov, P. L., 1960. Bottom sediments in the Sea of Okhotsk. In Bezrukov, P. L. (ed.), Geologicheskiye issledovaniya v Dalnevostochnykh moriakh (Proceedings Institute of Oceanology). Moscow: Academy of Science Publishers, Vol. 32, pp. 15–95.

Bolikhovskaya, N. S., and Bolikhovsky, V. F., 1992. The radiocarbon chronology and palynostratigraphy of the Yedoma sediments of West Siberia. In *Geokhronologia Chetvertichnogo Perioda*. Moscow (in Russian): Nauka, pp. 102–111.

Böse, M., 2004. Traces of glaciation in the high mountains of Taiwan. In Ehlers, J., and Gibbard, P. L. (eds.), *Development in Quaternary Science 2c. Quaternary Glaciation – Extent and Chronology, Part III: South America, Asia, Africa, Australia, Antarctica*. Amsterdam: Elseveir, pp. 347–352.

Böse, M., and Hebenstreit, R., 2001. Geomorphic evidence of late Pleistocene glaciation in the high mountains of Taiwan. Abstract. *Transactions, Japanese Geomorphological Union*, **22**(4), C 28, Tokyo 1.

Cline, R. (ed.), 1981. *Climap Project: Seasonal Reconstructions of the Earth's Surface at the Last Glacial Maximum*. New York: Geological Society of America, pp. 1–18.

Degtyarenko, Y. P., 1984. Extent of modern and quaternay glaciations of the Koryak Highlands and Eastern Chokotka. In Bespaly, V. G. (ed.), *Pleistocene Glaciations of Eastern Asia*. Magadan: North-East Complex Research Institute, pp. 66–76 (in Russian).

Dibner, V. D., 1970. Geomorphology. In *Sovietskaya Arktika*. Moscow: Nauka, pp. 59–64 (in Russian).

Erlich, E. N., and Melekestsev, I. V., 1974. Commander islands. In Luchitsky, I. V. (ed.), *Kamchatka, Kurilskiye I Komandorskiye ostrova*. Moscow: Nauka, pp. 327–337.

Fütterer, D. K. (ed.), 1994. The expedition ARCTIC"93, Leg ARK-IX/4 of RV 'Polarstern' 1993. (Berichte zur Polarforschung 149'94). AWI, Bremerhaven.

Gataullin, V. N., 1988. *The Upper Quaternary Sediments of the Western Coast of the Yamal Peninsula*. Ph.D. thesis, VSEGEI, Leningrad (in Russian).

Grosswald, M. G., 1980. Late Weichselian ice sheet of northern Eurasia. *Quaternary Research*, **13**, 1–32.

Grosswald, M. G., 1994. Drumlin fields of the Novaja Zemlja, Uralian Upland and their bearing on the Kara Sea center of glaciation. *Geomorphology*, **1**, 40–53 (in Russian).

Grosswald, M. G., 1998. Late-Weichselian ice sheet in Artic and Pacific Siberia. *Quaternary International*, **45/46**, 3–18.

Grosswald, M. G., and Goncharov, S. V., 1991. On the southern limit of the last Kara ice dome. *Institute of Geography of the Russian Academy of Sciences*, **71**, 154–159. Materialy glatsiologicheskikh issledovaniy (in Russian).

Grosswald, M. G., and Hughes, T. J., 1995. Paleoglaciology's grand unsolved problem. *Journal of Glaciology*, **41**, 313–332.

Grosswald, M. G., and Spektor, V. B., 1993. The glacial relief of the Tiksi region (west shore of Buor-Khaya Inlet, North Yakutia). *Polar Geography and Geology*, **17**, 154–166.

Hewitt, K., 2009. Catastrophic rock slope failures and late Quaternary developments in the Naga Parbat – Haramosh Massif, Uper Indus basin, northern Pakistan. *Quaternary Science Reviews*, doi:10.1016/j.quascirev.2008.12019.

Hope, G. S., 2004. Glaciation of Malaysia and Indonesia, excluding New Guinea. In Ehlers, J., and Gibbard, P. L. (eds.), *Development in Quaternary Science 2c. Quaternary Glaciations – Extent and Chronology, Part III: South America, Asia, Africa, Australia, Antarctica*. Amsterdam: Elseveir, pp. 211–214.

Iozawa, T., 1979. *Bird's Eye View of the Japanese Alps*. Tokyo: Kodansha, p. 190. in Japanese.

Kind, N. V., Kolpakov, V. V., and Sulerzhitskiy, L. D., 1971. To the problem of age of the glaciations in the Verkhoyan'ye (upper reaches of the Yana River) destrict. *Proceedings of the USSR Academy of Sciences, Geological Series*, **10**, 135–144 (in Russian).

Koopmans, B. N., and Stauffer, P. H., 1967. Glacial phenomena on Mount Kinabalu, Sabah, Borneo Region. *Malaysia Geological Survey Bulletin*, **8**, 25–35.

Kuhle, M., 1974. Vorläufige Ausführungen morphologischer Feldarbeitsergebnisse aus den SE-Iranischen Hochgebirgen am Beispiel des Kuh-i-Jupar. *Zeitschrift für Geomorphologie NF*, **18**(4), 472–483.

Kuhle, M., 1982. Der Dhaulagiri- und Annapurna-Himalaya. Ein Beitrag zur Geomorphologie extremer Hochgebirge. *Zeitschrift für Geomorphologie,* supplement 41 (Suppl. Bd.), Bd. I (Text): 1–229; Bd. II (Abb.): 1–183 und Geomorph. Karte 1:85 000 (English summary).

Kuhle, M., 1997. New findings concerning the Ice Age (last glacial maximum) glacier cover of the East-Pamir, of the Nanga Parbat up to the central Himalaya and of Tibet, as well as the age of the Tibetan Inland Ice. *GeoJournal*, **42**, (2–3, Tibet and high Asia. Results of investigations into high mountain geomorphology, paleo- glaciology and climatology of the Pleistocene (Ice Age Research) IV, 87–257.

Kuhle, M., 1998. Reconstruction of the 2.4 million qkm Late Pleistocene ice sheet on the Tibetan plateau and its impact on the global climate. *Quaternary International*, **45/46**, 71–108. Erratum: Vol. 47/48:173-182 (1998) included.

Kuhle, M., 2001. The maximum Ice Age (LGM) glaciation of the Central- and South Karakorum: an investigation of the hights of its glacier levels and ice thickness as well as lowest prehistoric ice margin positions in the Hindukush, Himalaya and in East-Tibet on the Minya Konka-massif. *GeoJournal*, **54** (1–4), **55** (1 Glaciogeomorphology and prehistoric glaciation in the Karakorum and Himalaya. Tibet and high Asia (VI)), 109–396. Kluwer.

Kuhle, M., 2004. The high glacial (last Ice Age and LGM) ice cover in high and central Asia. In Ehlers, J., and Gibbard, P. L. (eds.), *Development in Quaternary Science 2c Quaternary Glaciation – Extent and Chronology, Part III: South America, Asia, Africa, Australia, Antarctica*. Amsterdam: Elsevier, pp. 175–199.

Kuhle, M., 2005. The maximum Ice Age (Würmian, last Ice Age, LGM) glaciation of the Himalaya – a glaciogeomorphological investigation of glacier trim-lines, ice thicknesses and lowest former ice margin positions in the Mt. Everest-Makalu-Cho Oyu massifs (Khumbu and Khumbakarna Himal) including informations on late-glacial, neoglacial and historical glacier stages, their snow-line depressions and ages. *GeoJournal*, **62**(3–4, Tibet and high Asia(VII): glaciogeomorphology and former glaciation in the Himalaya and Karakorum), pp. 191–650.

Kuhle, M., 2006. The Past Hunza glacier in connection with a Pleistocene Karakorum ice stream network during the last Ice Age (Würm). In Kreutzmann, H., and Saijid, A. (eds.), *Karakoram in Transition*. Karachi: Oxford University Press, pp. 24–48. ISBN ISBN-13: 978-0-19-547210-3.

Kuhle, M., 2007a. The Pleistocene glaciation (LGP and pre-LGP, pre-LGM) of SE-Iranian Mountains exemplified by the Kuh-i-Jupar, Kuh-i-Lalezar and Kuh-i-Hezar Massifs in the Zagros. *Polarforschung*, **77**(2–3), 71–88.

Kuhle, M., 2007b. The past ice stream network in the Himalayas and the Tibetan ice sheet during the last glacial period and its glacial-isostatic, eustatic and climatic consequences. *Tectonophysics*, **445**(1–2), 116–144.

Kuhle, M., 2008. Correspondence to on-line-edition (doi.101016/jj. quascirev.2007.09.015 Elsevier) Quaternary Science Reviews article "Quaternary glacier history of the Central Karakorum" by Seong, Y. B., Owen, L. A., Bishop, M. P., Bush, A., Clendon, P., Copland, L., Finkel, R., Kamp, U., and Shroder, Jr. J. F., *Quaternary Science Reviews*, **27**, 1655–1656.

Kuhle, M., 2010. Ice Age. *Encyclopedia of Snow, Ice and Glaciers*. Springer Verlag (in print).

Kuzmina, N. N., and Yeremeeva, G. P., 1990. New data on the origin and age of boulder clay from the shelf of West Kamchatka. *Doklady Akademii Nauk SSSR*, **310**, 1425–1428.

Laukhin, S. A., Drozdov, N. I., Panychev, V. A., and Velichko, S. V., 1989. The age of the last glaciation in northern East Chukotka. *Izvestiya Akademii Nauk SSSR Seriya Geologicheskaya*, **N3**, 136–140.

Lifton, N. A., Bieber, J. W., Clem, J. M., Duldig, M. L., Evenson, P., Humble, J. E., and Pyle, R., 2005. Addressing solar modulation and long-term uncertainties in scaling secondary cosmic rays for in situ cosmogenic nuclide applications. *Earth and Planetary Science Letters*, **239**, 140–161.

Owen, L. A., Caffee, M. W., Finkel, R. C., and Seong, Y. B., 2008. Quaternary glaciation of the Himalayan-Tibetan orogen. *Journal of Quaternary Science*, **23**, 513–531.

Panzer, W., 1935. Eiszeitspuren auf Formosa. *Zeitschrift für Gletscherkunde*, **XXIII**, 81–91.

Pigati, J. S., and Lifton, N. A., 2004. Geomagnetic effects on time-integrated cosmogenic nuclide production with emphasis on in situ ^{14}C and ^{10}Be. *Earth and Planetary Science Letters*, **226**, 193–205.

Sawagaki, T., Aoki, T., Hasegawa, H., Iwasaki, S., Iwata, S., and Hirakawa, K., 2004. Late quaternary glaciations in Japan. In Ehlers, J., and Gibbard, P. L. (eds.), *Development in Quaternary Science 2c. Quaternary Glaciation – Extent and Chronology, Part III: South America, Asia, Africa, Australia, Antarctica*. Amsterdam: Elseveir, pp. 217–225.

Seong, Y. B., Owen, L. A., Bishop, M. P., Bush, A., Clendon, P., Copland, L., Finkel, R., Kamp, U., and Shroder, J. F. Jr., 2008. Quaternary glacier history of the Central Karakoram. *Quaternary Science Reviews*, **26**, 3384–3405.

Sheinkman, V. S., 2004. Quaternary glaciation in the high Mountains of Central and North-east Asia. In Ehlers, J., and Gibbard, P. L. (eds.), *Development in Quaternary Science 2c Quaternary Glaciation – Extent and Chronology, Part III: South America, Asia, Africa, Australia, Antarctica*. Amsterdam: Elseveir, pp. 325–336.

Smith, J. M. B., and Lowry, J. B., 1968. Further exploration and observations on Mount Kinabalu East. *Malay Naturalist Journal*, **22**, 29–40.

Svitoch, A. A., 1978. Quaternary paleogeography of Southeastern Chukotka. In Gorbarenko, S. A., and Gasanov, S. S. (eds.), *Pleistocene Paleogeography of the Far East and its Seas*. Vladivostok: Far East Scientific Center of the USSR Academy of Sciences, pp. 21–27 (in Russian).

Svitoch, A. A., Basilevskaya, L. I., and Boyarskaya, T. D., 1980. *Quaternary Deposits and Paleogeography of Chukotka*. Moscow: Nauka Publishing House, p. 295. in Russian.

Tanaka, K., and Kano, T., 1934. Glacial topograhies in the Nankotaizan Mountain group in Taiwan. *Geographical Review*, **X**(3), 169–190. Tokyo (in Japanese).

Travis, J., 1994. Taking a bottom-to-sky 'slice' of the Arctic Ocean. *Science*, **266**, 1947–1948.

Udintsev, G. B., 1957. Geomorphology of the sea of Okhotsk floor. In Bezrukov, P. L. (ed.), *Geologicheskiye issledovaniya v Dalnevostochnykh moryakh*, Proceedings of Institute of Oceanology. Moscow: Academy of Science Publishers, Vol. 22, pp. 3–76.

van Beek, C. G. G., 1982. A geomorphological and pedological study of the Gunung Leuser National Park, North Sumatera, Indonesia. Wageningen, Wageningen Agricultural University. *Utrechtse Geografische Studies*, **26**, 187.

Velichko, A. A., 1973. *The Natural Process in Pleistocene*. Moscow: Nauka Publishing House, p. 256. in Russian.

Vogt, P. R., Crane, K., and Sundvor, E., 1994. Deep Pleistocene iceberg plowmarks on the Yermak Plateau: sidescan and 3.5 kHz evidence for thick calving ice fronts and a possible marine ice sheet in the Arctic Ocean. *Geology*, **22**, 403–408.

Volnev, V. M., 1983. On the origin of the ridgy topography in the Tinro Basin, the Sea of Okhotsk. *Geomorphologiya*, **N3**, 66–75.
von Wissmann, H., 1959. Die heutige Vergletscherung und Schneegrenze in Hochasien mit Hinweisen auf die Vergletscherung der letzten Eiszeit. *Akademie der Wissenschaften und der Literatur in Mainz, Abhandlungen der Mathematisch-Naturwissenschaftlichen Klasse*, **14**, 121–123.
Wright, H. E., 2004. Pleistocene glaciation of Iraq. In Ehlers, J., and Gibbard, P. L. (eds.), *Development in Quaternary Science 2c. Quaternary Glaciation – Extent and Chronology, Part III: South America, Asia, Africa, Australia, Antarctica*. Amsterdam: Elseveir, pp. 215–216.
Yafeng, S., and Jing-Tai, W., 1979. The fluctuations of climate, glaciers and sea level since Late Pleistocene in China: sea level, ice and climatic change. *Proceedings of the Canberra Symposium*, December 1979, Canberra.
Zamoruyev, V., 2004. Quaternary glaciation of north-eastern Asia. In Ehlers, J., and Gibbard, P. L. (eds.), *Development in Quaternary Science 2c. Quaternary Glaciation – Extent and Chronology, Part III: South America, Asia, Africa, Australia, Antarctica*. Amsterdam: Elseveir, pp. 321–323.
Zubakov, V. A., and Borzenkova, I. I., 1990. *Global Palaeoclimate of the Late Cenozoic*. Amsterdam: Elsevier.

Cross-references

Equilibrium-Line Altitude (ELA)
Himalaya
Ice Age
Ice Age Cycles: Data, Models, and Uncertainties
Ice Age Development Theory
Ice Shelf
Last Glacial Maximum Glaciation (LGM/LGP) in High Asia (Tibet and Surrounding Mountains)
Palaeoclimate and Past Glaciations
Permafrost
Pleistocene Epoch
Quaternary Glaciation
Siberia
Tibetan Plateau

RECRYSTALLIZATION OF ICE

Ashok Kumar Verma
Department of Geography and Environmental Studies, Cold Regions Research Center, Wilfrid Laurier University, Waterloo, ON, Canada

Recrystallization of ice refers to the formation and deposition of the large ice particle on the expense of smaller ice particles. The process of recrytallization occurs through when the deformed form of the crystal behaves as the nuclei for the new crystal formation and this process continues till the original nucleus is totally consumed.

This process governs by the two major events such as nucleation and grain size growth. Each event is highly dependent on the temperature and supersaturation (Rogers and Yau, 1989). Nucleation is the first step toward the crystal formation which solely depends on the solute concentration and temperature condition of the underlying environment. Once the formation of the stable nuclei accomplished, the clustering of the nuclei begins to reach the critical size that enhance the recrytallization process toward the growth of ice particles.

In glaciers, the process of the recrystallization is continuous. This process of recrystallization primarily depends on the temperature, the melting point, and stress on the ice. Recrystallization always tends to increase the size of the crystal. The new size was directly proportional to temperature and inversely proportional to stress (Paterson, 1981). Ice near the melting point recrystallizes rapidly but recrystallizations tend to stop below −10°C (Rigsby, 1960). Collectively all these factors decide the metamorphism of the ice (Lock, 1990). The process of recrystallization helps to understand the development of creep and fracture within the glacial systems which result due to deformation in glacial ice (Evans and Benn, 1998).

Bibliography

Evans, D. J. A., and Benn, D. I., 1998. *Glaciers and Glaciation*. London: Arnold, pp. 148–149.
Lock, G. S. H., 1990. *The Growth and Decay of Ice*. New York: Cambridge University Press, p. 244.
Paterson, W. S. B., 1981. *The Physics of Glaciers*, 2nd edn. Oxford: Pergamon, pp. 231–236.
Rigsby, G. P., 1960. Crystal orientation in glacier and in experimentally deformed ice. *Journal of Glaciology*, **3**, 273–278.
Rogers, R. R., and Yau, M. K., 1989. *A Short Course in Cloud Physics*, 3rd edn. Amsterdam: Elsevier.

REFREEZING OF MELTWATER

Ashok Kumar Verma
Department of Geography and Environmental Studies, Cold Regions Research Center, Wilfrid Laurier University, Waterloo, ON, Canada

Refreezing of the meltwater occurs through the release of latent heat from the meltwater. These processes are important in describing the glacier accumulation in the temperate regions (Benn and Evans, 1998).

Processes: The melting from snow/ice occurs in the day time when the surface air temperature at the snowpack is higher than 0°C. The meltwater produced in day time percolates at the base of snowpack. In night time when snow–surface temperatures are below 0°C, the percolated meltwater in the snowpack refreezes in the night releasing the latent heat (Dingman, 2002).

Bibliography

Benn, D. I., and Evans, D. J. A., 1998. *Glaciers and Glaciation*. New York: Oxford University Press, pp. 157–158.
Dingman, S. L., 2002. *Physical Hydrology*, 2nd edn. New Jersey: Prentice Hall, pp. 187–188.

Cross-references

Regelation

REGELATION

Ashok Kumar Verma
Department of Geography and Environmental Studies, Cold Regions Research Center, Wilfrid Laurier University, Waterloo, ON, Canada

Regelation is a process of generation of melt water from ice which is subjected to higher pressure. Higher pressure of ice mass lowers the melting point and causes to melt the ice. The ideal example that demonstrates this phenomenon would be the melting from the glacier ice. The huge mass of glacier ice can exert a sufficient amount of pressure on its lower surface (glacier base) to lower the melting point of its ice. The melting of the ice at the glacier's base allows it to move from a higher elevation to a lower elevation due to ice movement within the course of glacier advancement and retreat.

Regelation related with formation of melt arises from the subglacial systems in the form of a water film. The principle role of water film is to transfer the water from high-pressure areas of glacier bed to the areas of regelation (often described as low-pressure area). These forms of water film are described as *regelation water films*. The regelation can be identified as a possible mechanism for transferring ice past obstacle which is known as *regelation sliding* (Benn and Evans, 1998). In this process, there is an occurrence of melting on the upglacier side of obstacle and refreezing on the downside of glacier followed by the glacier ice movement (sliding) over the rough glaciers terrain. This process provides the resistance to the glacier movement which results in developing the local high pressure and consequently lowering of melting temperature. Regelation process found important in explaining the glacier sliding (Clarke, 1987).

Bibliography

Benn, D. I., and Evans, D. J. A., 1998. *Glaciers and Glaciation*. New York: Oxford University Press, pp. 157–158.
Clarke, G. K. C., 1987. A short history of scientific investigations on glaciers. *Journal of Glaciology*, Special Issue, 4–24.
Regelation, 2009. *Encyclopaedia Britannica*. Encyclopaedia Britannica Online: http://www.britannica.com/EBchecked/topic/495857/regelation.

REMOBILIZATION (OF DEBRIS)

Renoj J. Thayyen
Western Himalayan Regional Centre, National Institute of Hydrology, Jammu (J&K), India

Debris produced in a glacial system undergo several cycles of movement and remobilization before final deposition.

Remobilization debris in a glacial system occurs through supraglacial, englacial, and subglacial environments. Two important processes of remobilization of debris in a glacial system are gravitational mass movement and transport by water. Supraglacial zone of the glacier receives debris from exposed rock faces and walls adjacent to the glacier ice margins, released by freeze – thaw weathering. The surface relief of the glacier undergoes continuous change and the gravitational remobilization of debris occurs along the sloping glacier surfaces and characteristics of such mass flows are strongly depended on the water content and other factors such as mean grain size, maximum flow thickness, shear strength, porosity, and bulk density (Boulton 1968, 1971; Lawson, 1982). Remobilization, which occurs in supraglacial and englacial zones, is considered as passive transport as the original characteristics of the sediment such as particle size and shape are retained during the movement. However, debris movement through the subglacial system is subjected to modification by rolling, sliding, crushing, and abrasion. Entrainment of englacial sediment mainly occurs at firn zone of the glacier. It also occur through crevasses and moulin, fed by the supraglacial debris and moved through "high level" sediment transport pathways in a englacial system. It is also possible that the sediment movement across the glacier occurs from subglacial zone to supraglacial zone. Such movement occurs close to the glacier snout, where under compression flow-lines turn upward or thrust-faulting is developed in the glacial system. Remobilization of debris by meltwater flow can take place in supraglacial, englacial, and subglacial zones and its margins.

Bibliography

Boulton, G. S., 1968. Flow tills and related deposits on some Vestspitsbergen glaciers. *Journal of glaciology*, **7**, 391–412.
Boulton, G. S., 1971. Till genesis and fabric in Svalbard, Spitsbergen. In Goldthwait, R. P. (ed.), *Till: A Symposium*. Columbus: Ohio State University Press, pp. 41–72.
Lawson, D. E., 1982. Mobilisation, movement and deposition of subaerial sediment flows, Matanuska Glacier, Alaska. *Journal of Geology*, **90**, 279–300.

RESEDIMENTATION

Subhajit Sinha
DBS College, Dehradun, Uttarakhand, India

Sediments are any particulate matter that forms by the breakdown of pre-existing igneous, metamorphic, and sedimentary rocks and the process by which these broken particulates are deposited is called sedimentation process. There are three main processes operating in a sedimentary system: erosion, transportation, and deposition. Resedimentation is a process whereby these previously deposited sediments are moved from its original place of deposition through a process generated by the mechanical behavior of flow. For example, the term

"sediment gravity flow" was introduced to describe the major flow types involved in resedimentation processes and was defined as the flow of sediments or sediment–fluid mixture in which the interstitial fluid is driven by the grains moving under the action of gravity. Instability of the earlier sediments is the prerequisite for generation of flows involved in resedimentation processes. Such instability normally comes into existence either due to oversteepening of the parent deposit or through some process of liquidization including seismogenic slumping and storm wave-induced landslide.

RETREAT/ADVANCE OF GLACIERS

Luke Copland
Department of Geography, University of Ottawa, Ottawa, ON, Canada

Definition

The retreat and advance of glaciers traditionally refers to changes in the position of a glacier terminus over time. More recently, quantification of the retreat/advance of glaciers has been extended to include measurement of ice thickness changes, which provides a more direct picture of how ice volume is changing as it is directly related to mass balance. These measures are the most common way in which the response of glaciers to climate change is monitored, as conditions favorable for positive glacier mass balance (e.g., increasing snowfall, lower temperatures) typically result in glacier advance, while negative mass balance conditions (e.g., lower snowfall, higher temperatures) typically result in glacier retreat (Figure 1).

Controls on glacier terminus advance/retreat patterns

The position of a glacier terminus is primarily defined by the balance between two factors: ice motion that is driving the ice front forward, and melt/calving that results in loss of the ice front. Changes in either, or both, of these factors control the ultimate terminus position. For example, the terminus of a glacier will retreat if surface melt is greater than the rate of forward ice motion, even if there is still substantial ice flow along the lower glacier. In another example, a glacier will advance if surface melt rate stays constant but ice velocity increases.

The initial reaction time of a change in terminus position to a climate perturbation can be asymmetric as an increase in air temperature can lead to a rapid retreat via immediate melting at the terminus, whereas an increase in snowfall can take years or longer to produce a terminus change due to the time it takes for ice to flow from the top to bottom of a glacier. The reaction time differs from the response time, which is defined as the time it takes for a glacier to completely adjust to a climate perturbation (Haeberli and Hoelzle, 1995). The response time and total change in terminus position for a given climate forcing depends to a large extent on the original size of the glacier, with larger glaciers experiencing larger terminus changes due to the requirement for mass conservation (Nye, 1965; Johannesson et al., 1989). When combined with models of ice dynamics, this enables reconstruction of past mass balances from glacier length changes (e.g., Hoelzle et al., 2003) and the prediction of future glacier advance/retreat patterns for given climate forcings (Oerlemans et al., 1998). The change in terminus position for the same external forcing will also vary between glaciers depending on the geometry of the valley in which they lie. Glaciers which have a large, broad accumulation area that feeds into a narrow valley will undergo large changes in terminus position in response to changes in mass balance. Conversely, ice masses that have broad ablation areas (e.g., ice caps) would see much less variation in terminus position for the same change in mass balance.

Given the above considerations, the relationship between the retreat/advance of glacier termini and climate is rarely straightforward. Glaciers are always adjusting to their surrounding conditions, since weather and climate can and do vary on much shorter timescales than glaciers. Glacier terminus changes typically reflect a low-frequency response to external forcing (UNEP, 2007), with short-term climate variations being averaged out over timescales of a few years to decades for glaciers in wet, maritime climates where there is high mass turnover and relatively fast flow (e.g., New Zealand Alps, Patagonia, Alaska; Paterson, 1994; Raper and Braithwaite, 2009). In contrast, glaciers in drier, more continental climates (e.g., Arctic Canada) have a lower mass turnover and flow relatively slowly, which means that it can take them decades to centuries or longer to respond to changes in climate.

As techniques for monitoring glaciers have developed (e.g., airborne laser altimetry; Hopkinson and Demuth, 2006), it is clear that measurement of the position of a glacier terminus over time provides an imperfect measure of how the glacier is responding to external factors such as climate. Measurements of changes in ice thickness provide a more direct measure of these effects, as the response time of glacier surface height changes to external forcing is typically much shorter than the response time of changes in terminus position (UNEP, 2007). Increases in surface elevation typically mean that a glacier is healthy and gaining mass (e.g., due to increasing snowfall and/or reduced melt), while decreases in surface elevation typically indicate that a glacier has a negative mass balance and is wasting away. These techniques are discussed in more detail elsewhere in this volume (e.g., see under "*Glacier Mass Balance*").

Historical terminus advance/retreat patterns

Despite the limitations and uncertainties in interpreting the causes of changes in glacier terminus position, they are

Retreat/Advance of Glaciers, Figure 1 Photo illustrating retreat of the terminus position of the Easton Glacier, North Cascade Mountains, USA, between 1985 and 2003. (Source and copyright: http://en.wikipedia.org/wiki/File:Eastonterm.jpg).

still one of the most widely used measures of glacier health. This is because glacier terminus position is one of the most visible and easily measured glaciological indicators, both in historical sources (e.g., paintings, photography) and modern satellite imagery. For example, the longest known record of changes in glacier length is provided by the Untere Grindelwaldgletscher, Switzerland (Oerlemans, 2005), whose cumulative length changes have been reconstructed since 1534 (Zumbühl, 1980). Over long time periods, air temperature provides the dominant control on terminus position as it provides the main control on glaciologically important climate parameters such as the long-wave radiation balance, the ratio of solid to liquid precipitation, and turbulent heat exchange (WGMS, 2008).

It can be problematic to connect climate changes to the advance/retreat pattern of a single glacier, but consistent changes across many glaciers in the same region increases confidence that air temperature is providing a dominant control. For example, widespread advance of glaciers in the European Alps during the Little Ice Age between ~1650 and 1850 occurred as a response to cooler conditions during this time (Grove, 1988). Since then, there has been widespread glacier retreat in this region as a response to climate warming. For example, the terminus of the Rhonegletscher has retreated dramatically between 1870 and the present day (Figure 2). Useful comparisons of glacier changes over time are available at http://www.swisseduc.ch/glaciers/index-en.html.

Complicating controls on terminus advance/retreat patterns

Interpretation of the terminus retreat/advance pattern of glaciers as an indicator of climate change can be complicated in situations where morphological and internal processes provide a strong control on glacier changes. In particular, there are three types of glaciers where this can be a factor (WGMS, 2008):

1. Surging glaciers: on these ice masses, dramatic changes in terminus position and surface height are mainly related to periodic redistribution of mass within the glacier due to changes in internal flow dynamics. For example, the terminus of the Kutiàh Glacier, Pakistan, advanced by 12 km over an approximately 3-month period in 1953 due to a surge (Desio, 1954). These changes are largely unrelated to external climate conditions, which means that surge-type glaciers are usually omitted from inventories that use glacier advance/retreat patterns to assess the impacts of climate change.
2. Tidewater glaciers: glaciers that end in freshwater or marine locations have floating termini, which can display complex terminus responses defined by relationships between factors such as water depth, pinning points, ice dynamics, tides, and climate forcing (Benn and Evans, 1998). Consequently, advance/retreat patterns of individual tidewater glaciers are often problematic to interpret in terms of climate forcing, particularly over short timescales. However, tidewater

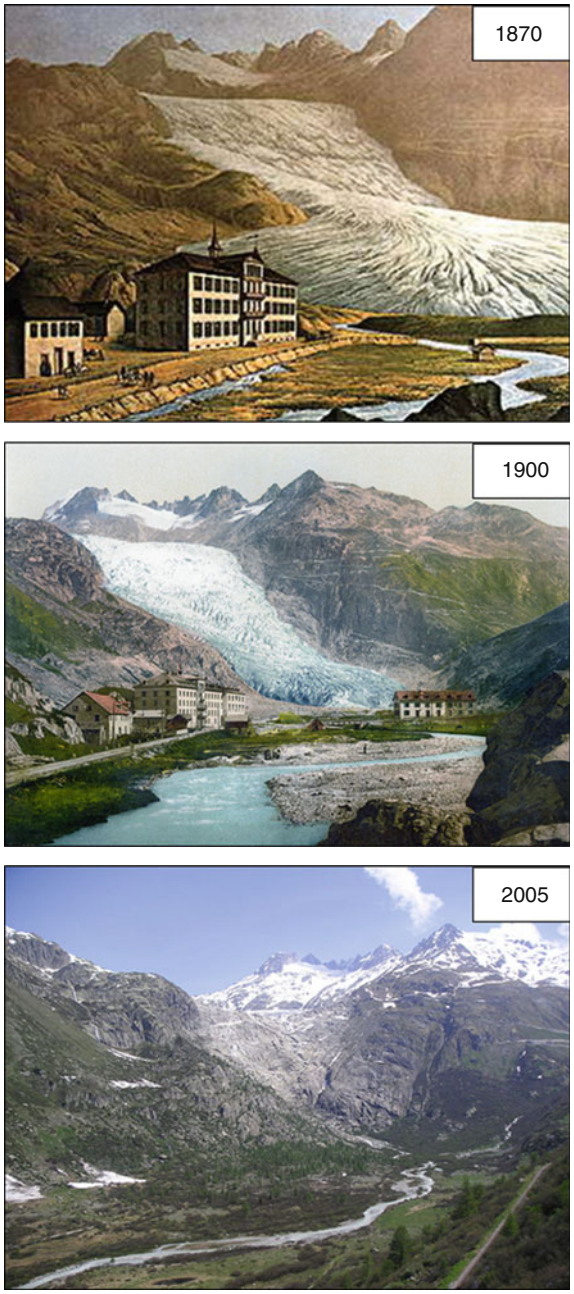

Retreat/Advance of Glaciers, Figure 2 Retreat of Rhonegletscher, Switzerland, from the end of the Little Ice Age (1870) to the present day. (Source and copyright: http://de.wikipedia.org/wiki/Rhonegletscher).

glaciers can provide useful information on climate changes if they display consistent terminus advance/retreat patterns over large areas and for long periods (e.g., Joughin et al., 2008). The tidewater advance/retreat pattern is typically asymmetric, with advances occurring over long periods (centuries) and retreats occurring relatively rapidly (decades). Consequently, a majority of calving glaciers would be expected to be advancing in a constant climate.

3. Debris-covered glaciers: glaciers in tectonically active mountain ranges (e.g., Himalayas) are frequently heavily debris covered over their lower ablation areas, with debris thicknesses of >1 m common (Shroder et al., 2000). This debris is effective at protecting the ice from melting, which means that their terminus advance/retreat patterns are commonly muted compared to nearby non-debris covered glaciers (WGMS, 2008). Negative mass balance on these ice bodies often results in downwasting of the glacier in situ, rather than a distinct retreat of the terminus.

World glacier monitoring service

The World Glacier Monitoring Service (http://www.geo.unizh.ch/wgms/), based at the University of Zurich, Switzerland, maintains the main global database of the advance/retreat patterns of glaciers. Researchers from around the world are encouraged to provide standardized annual measurements of parameters such as glacier mass balance, volume, area, and length that are inventoried by WGMS. Since the late 1950s, they have published the "Fluctuations of Glaciers" series every 5 years that provides the main record of these parameters and how they are changing over time. This information is used by agencies such as the Intergovernmental Panel on Climate Change in the compilation of their reports on the impacts of climate change (e.g., IPCC, 2007). In addition, WGMS/UNEP also recently published the book on "Global Glacier Changes: Facts and Figures" that provides a valuable summary of glacier advance/retreat patterns around the world (WGMS, 2008).

The WGMS assesses the advance/retreat patterns of glaciers within a hierarchy of measures of glacier health under the auspices of the Global Terrestrial Network for Glaciers (http://www.geo.unizh.ch/wgms; Haeberli et al., 2000). Within this strategy, detailed monitoring of glacier mass balance and flow dynamics on an annual basis is limited to a relatively small number of sites ($\sim 10^1$–10^2) where access and logistical cost allows. These locations provide the most direct measure of glacier health, but are limited by their lack of spatial coverage. To expand on this coverage, monitoring of changes in glacier length is completed at a much larger number of glaciers ($\sim 10^2$–10^3) on a less regular basis (approx. every 5–10 years). This provides a global picture of how glaciers are changing over time, and monitoring over longer time periods increases confidence that changes in terminus position represent long-term trends rather than annual anomalies.

Recent advance/retreat patterns of glaciers and ice caps

One of the most comprehensive analyses of glacier terminus advance/retreat patterns is provided by Oerlemans (2005), who compiled mean length variations of 169 glaciers over the period 1700–2000 (Figure 3). The spatial

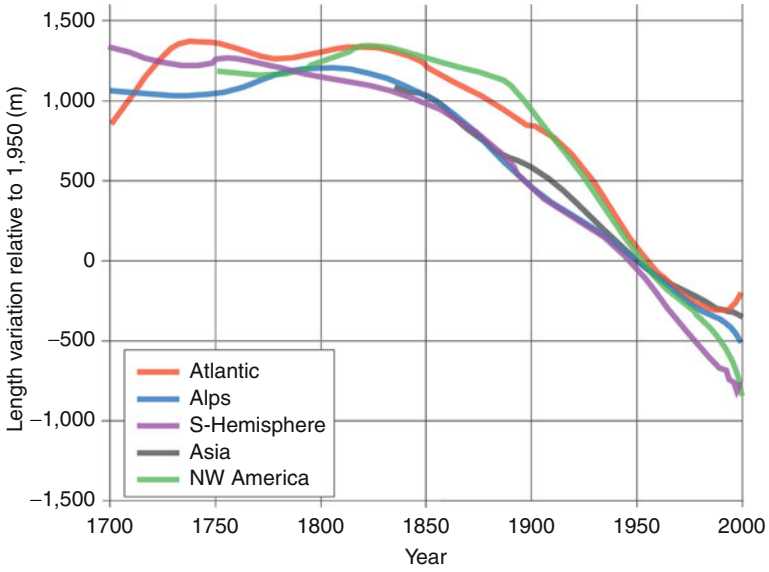

Retreat/Advance of Glaciers, Figure 3 Large-scale regional mean length variations of glacier tongues (Oerlemans, 2005). The raw data are all constrained to pass through zero in 1950. The curves shown are smoothed with the Stineman (1980) method . Glaciers are grouped into the following regional classes: SH (tropics, New Zealand, Patagonia), northwest North America (mainly Canadian Rockies), Atlantic (South Greenland, Iceland, Jan Mayen, Svalbard, Scandinavia), European Alps and Asia (Caucasus and central Asia). (Source: IPCC 2007, their Fig. 4.13). (Source and copyright: http://www.ipcc.ch/publications_and_data/publications_and_data_figures_and_tables.htm).

and temporal coverage of these records is incomplete due to the lack of continuous long-term monitoring of glaciers, but the changes are still remarkably similar from many different regions around the world. In the early period (1700–1850), glacier lengths were largely stable during the Little Ice Age, when mean temperatures were approximately 1.0°C cooler than at present (Oerlemans, 2005). Consistent retreat began around 1850 and has continued up to the present day, with glacier fronts on average ~2 km further back in 2000 than in 1850. In the European Alps, this has coincided with a loss of approximately two third of glacier volume between 1850 and the early 2000s (Zemp et al., 2006).

Glacier terminus retreats have accelerated since the early to mid-1980s in many parts of the world (Solomina et al., 2008; WGMS, 2008). In single very warm and dry summers, such as 2003, losses of up to 5–10% of the total remaining ice volume of the European Alps have been observed. This has lead to concerns that the remaining glaciers may almost entirely disappear within the next few decades (Zemp et al., 2006). Similar dramatic reductions have been recorded in North America, with widespread glacier area and volume losses in the Rocky Mountains (De Beer and Sharp, 2007; Demuth et al., 2008) and Alaska/Yukon (Arendt et al., 2002; Larsen et al., 2007), particularly at low elevations. Similar changes have also occurred in the Patagonia Icefields (which hold most of the ice in South America), with the majority of outlet glaciers dramatically retreating since the mid-1900s (Lopez et al., 2010), including a doubling of ice thinning rates over 1995–2000 compared to 1968/1975–2000 (Rignot et al., 2003).

Many high-altitude tropical glaciers in locations such as New Guinea and Africa have completely disappeared during the latter part of the twentieth century (Cullen et al., 2006; Klein and Kincaid, 2008), with a poor outlook for the remaining ice bodies in these areas (WGMS, 2008).

While most glaciers and ice caps have undergone widespread retreat over the past century, there are a few areas where glacier advances have been observed. In particular, glaciers on the west coast of New Zealand and Norway showed marked advances between the early 1980s and 2000 (WGMS, 2008). These areas are climatologically similar, being dominated by westerly atmospheric circulation across open ocean that produces very high precipitation amounts (>10,000 mm yr^{-1} in some parts of New Zealand). Their recent advances have been linked to increases in the strength of this circulation, with an increase in El Niño/Southern Oscillation (ENSO) events corresponding to increased precipitation in New Zealand, and a strongly positive North Atlantic Oscillation (NAO) corresponding to increased precipitation and a seasonal shift to more winter precipitation in Norway (Chinn et al., 2005). Recent glacier advances and velocity increases have also been reported for the Karakoram Himalaya, again as a response to increases in precipitation (Hewitt, 2005; Quincey et al., 2009).

To put these recent changes in context, it is also useful to consider the changes in glacier extent that have occurred since the end of the last glacial period. At the peak of the last glaciation (21 ka), ice covered approximately one third of the land surface on Earth (Paterson, 1994), with most of North America and Northern Europe

covered by the Laurentide and Eurasian Ice Sheets, respectively. Available field evidence indicates that warming during the Early Holocene caused dramatic glacier retreats in most mountainous areas such as the Alps, with glaciers reaching similar extents ~11–10 ka as those at the end of the twentieth century (WGMS, 2008). These retreats were punctuated by temporary readvances, such as one at 8.2 ka that appears to be related to changes in thermohaline circulation of the oceans (Alley and Agustsdottir, 2005). However, glaciers in most parts of the world continued their general retreat and reached their minimum extents ~4–6 ka (Solomina et al., 2008). Minor advances and retreats have occurred since then, with the most recent glacier advances occurring during the Little Ice Age that ended around 1850.

The above examples highlight the complexity of glacier responses to climate change over different time periods. The vast majority of glaciers and ice caps around the world have undergone dramatic retreat since the end of the Little Ice Age, but these patterns have been occasionally punctuated by local advances, particularly in response to increases in precipitation. These local increases appear to be largely temporary in nature, however, and are insufficient to counteract the dramatic losses that have occurred elsewhere. Glacier retreat patterns during most of the Holocene appear to be largely driven by natural changes in incoming solar radiation caused by changes in the Earth's orbit (Solomina et al., 2008). In contrast, glacier length changes in the past couple of decades have occurred at rates that cannot be explained by natural variability, making it highly likely that human-induced forcing (e.g., due to increased atmospheric CO_2 levels) is the primary cause (IPCC, 2007).

Summary

In summary, advance/retreat patterns of glacier termini provide one of the most easily measured and recognizable indicators of climate change. Advancing glaciers typically indicate positive mass balance conditions and a healthy glacier, while terminus retreat is usually indicative of negative mass balance. There are many factors that can complicate interpretation of the causes of changes in terminus position, but in general similar advance or retreat patterns across many glaciers in the same region can be interpreted in terms of changes in climate. Air temperatures typically provide the primary control, although precipitation can also be important in some locations (e.g., maritime regions). Modern satellite imagery now enables the monitoring of glacier terminus positions over large areas, which has revolutionized understanding of the spatial patterns of recent changes.

Bibliography

Alley, R. B., and Agustsdottir, A. M., 2005. The 8 k event: cause and consequences of a major Holocene abrupt climate change. *Quaternary Science Reviews*, **24**, 1123–1149.

Arendt, A. A., Echelmeyer, K. A., Harrison, W. D., Lingle, C. S., and Valentine, V. B., 2002. Rapid wastage of Alaska glaciers and their contribution to rising sea level. *Science*, **297**(5580), 382–386, doi:10.1126/science.1072497.

Benn, D. I., and Evans, D. J. A., 1998. *Glaciers and Glaciation*. London: Hodder.

Chinn, T., Winkler, S., Salinger, M. J., and Haakensen, N., 2005. Recent glacier advances in Norway and New Zealand: a comparison of their glaciological and meteorological causes. *Geografiska Annaler*, **82A**, 141–157.

Cullen, N. J., Mölg, T., Kaser, G., Hussein, K., Steffen, K., and Hardy, D. R., 2006. Kilimanjaro glaciers: recent areal extent from satellite data and new interpretation of observed 20th century retreat rates. *Geophysical Research Letters*, **33**(L16502), doi:10.1029/2006gl027084.

De Beer, C. M., and Sharp, M., 2007. Recent changes in glacier area and volume within the southern Canadian Cordillera. *Annals of Glaciology*, **46**, 215–221.

Demuth, M. N., Pinard, V., Pietroniro, A., Luckman, B. H., Hopkinson, C., Dornes, P., and Comeau, L., 2008. Recent and past-century variations in the glacier resources of the Canadian Rocky Mountains – Nelson River System. *Terra Glacialis*, **11**, 27–52.

Desio, A., 1954. An exceptional glacier advance in the Karakoram-Ladakh region. *Journal of Glaciology*, **2**(16), 383–385.

Grove, J. M., 1988. *The Little Ice Age*. London: Routledge.

Haeberli, W., and Hoelzle, M., 1995. Application of inventory data for estimating characteristics of and regional climate-change effects on mountain glaciers: a pilot study with the European Alps. *Annals of Glaciology*, **21**, 206–212.

Haeberli, W., Cihlar, J., and Barry, R. G., 2000. Glacier monitoring within the global climate observing system. *Annals of Glaciology*, **31**, 241–246.

Hewitt, K., 2005. The Karakoram anomaly? Glacier expansion and the 'Elevation Effect', Karakoram Himalaya. *Mountain Research and Development*, **25**(4), 332–340.

Hoelzle, M., Haeberli, W., Dischl, M., and Peschke, W., 2003. Secular glacier mass balances derived from cumulative glacier length changes. *Global and Planetary Change*, **36**, 77–89.

Hopkinson, C., and Demuth, M., 2006. Using airborne lidar to assess the influence of glacier downwasting to water resources in the Canadian Rocky Mountains. *Canadian Journal of Remote Sensing*, **32**(2), 212–222.

IPCC, 2007. In Solomon, S., Qin, D., Manning, M., Chen, Z., Marquis, M., Averyt, K. B., Tignor, M., and Miller, H. L., (eds.), *Climate Change 2007: The Physical Science Basis. Contribution of Working Group I to the Fourth Assessment Report of the Intergovernmental Panel on Climate Change.* Cambridge: Cambridge University Press.

Johannesson, T., Raymond, C. F., and Waddington, E. D., 1989. Time-scale for adjustment of glaciers to changes in mass balance. *Journal of Glaciology*, **35**, 355–369.

Joughin, I., Howat, I., Alley, R. B., Ekstrom, G., Fahnestock, M., Moon, T., Nettles, M., Truffer, M., and Tsai, V. C., 2008. Ice-front variation and tidewater behavior on Helheim and Kangerdlugssuaq Glaciers, Greenland. *Journal of Geophysical Research*, **113**, F01004, doi:10.1029/2007FJ000837.

Klein, A. G., and Kincaid, J. L., 2008. On the disappearance of the Puncak Mandala ice cap, Papua. *Journal of Glaciology*, **54**, 195–197.

Larsen, C. F., Motyka, R. J., Arendt, A. A., Echelmeyer, K. A., and Geissler, P. E., 2007. Glacier changes in southeast Alaska and northwest British Columbia and contribution to sea level rise. *Journal of Geophysical Research*, **112**, F01007, doi:10.1029/2006JF000586.

Lopez, P., Chevallier, P., Favier, V., Pouyaud, B., Ordenes, F., and Oerlemans, J., 2010. A regional view of fluctuations in glacier length in southern South America. *Global and Planetary Change*, **71**, 85–108.

Nye, J. F., 1965. A numerical method of inferring the budget history of a glacier from its advance and retreat. *Journal of Glaciology*, **5**, 589–607.
Oerlemans, J., 2005. Extracting a climate signal from 169 glacier records. *Science*, **308**, 675–677.
Oerlemans, J., Anderson, B., Hubbard, A., Huybrechts, P., Johannesson, T., Knap, W. H., Schmeits, M., Stroeven, A. P., van de Wal, R. S. W., Wallinga, J., and Zuo, Z., 1998. Modelling the response of glaciers to climate warming. *Climate Dynamics*, **14**, 267–274.
Paterson, W. S. B., 1994. *The Physics of Glaciers*, 3rd edn. New York: Elsevier.
Quincey, D. J., Copland, L., Mayer, C., Bishop, M., Luckman, A., and Belo, M., 2009. Ice velocity and climate variations for the Baltoro Glacier, Pakistan. *Journal of Glaciology*, **55**, 1061–1071.
Raper, S. C. B., and Braithwaite, R. J., 2009. Glacier volume response time and its links to climate and topography based on a conceptual model of glacier hypsometry. *The Cryosphere*, **3**, 183–194.
Rignot, E., Rivera, A., and Casassa, G., 2003. Contribution of the Patagonia Icefields of South America to sea level rise. *Science*, **302**, 434–437.
Shroder, J. F., Bishop, M. P., Copland, L., and Sloan, V. F., 2000. Debris-covered glaciers and rock glaciers in the Nanga Parbat Himalaya, Pakistan. *Geografiska Annaler*, **82A**, 17–31.
Solomina, O., Haeberli, W., Kull, C., and Wiles, G., 2008. Historical and Holocene glacier-climate relations: general concepts and overview. *Global and Planetary Change*, **60**, 1–9.
Stineman, R.W., 1980. A consistently well-behaved method of interpolation. Creative Computing, July 1980, 54–57.
UNEP, 2007. *Global Outlook for Ice and Snow*. United Nations Environment Programme, EarthPrint, 235 pp.
WGMS, 2008. *Global Glacier Changes: Facts and Figures*. United Nations Environment Programme.
Zemp, M., Haeberli, W., Hoelzle, M., and Paul, F., 2006. Alpine glaciers to disappear within decades? *Geophysical Research Letters*, **33**, L13504, doi:10.1029/2006GL026319.
Zumbühl, H. J., 1980. *Die Schwankungen der Grindelwaldgletscher in den historischen Bild- und Schriftquellen des 12. bis 19. Jahrhunderts.* Basel: Birkhäuser Verlag.

Cross-references

Climate Change and Glaciers
Dynamics of Glaciers
Glacier Hydrology
Glacier Mass Balance
Glacier Motion/Ice Velocity
Glacier Surging
Global Warming and its Effect on Snow/Ice/Glaciers
Sea-Level

RIME ICE

Renoj J. Thayyen
Western Himalayan Regional Centre, National Institute of Hydrology, Jammu (J&K), India

The white, granular deposits of ice formed on cold surfaces by freezing of supercooled vapor or water droplets carried by the wind are known as rimed ice.

The rimed ice is formed on objects that are at a temperature below the freezing point. Rime occurs when supercooled water droplets (at a temperature lower than 0°C) come in contact with a surface that is also at a temperature below freezing. The droplets are so small that they freeze almost immediately upon contact with the object. Rime ice is commonly formed on windward upper slopes of mountains that are enveloped by supercooled clouds. These rime deposits generally take the form of long plumes of ice oriented into the direction of the wind. Rime is composed of small ice particles with air pockets between them and causes its typical white appearance and granular structure. Because of the rapid freezing of each individual supercooled droplet, there is relatively a poor cohesion between the neighboring ice particles, and the deposits may easily be shattered or removed from objects they form on. Rime ice can form on various surfaces like aircraft, glacier surface, trees, grass, etc.

Bibliography

Ahrens, C. D., 1991. *Meteorology Today*. St.Paul: West Publishing Company.
Benn, D. I., and Evans, D. J. A., 1998. *Glaciers and Glaciation*. New York: Wiley.

RIVER ICE HYDROLOGY

Hung Tao Shen
Department of Civil and Environmental Engineering, Clarkson University, Potsdam, NY, USA

Definition

Hydro-meteorological effects on river ice evolution and its effect on river hydrology.

Introduction

In cold and temperate regions of the world, wintertime operation of river systems is a key element in the management of surface water resources. River ice is known to affect many of the world's largest rivers. In the Northern Hemisphere, about 60% of rivers experience significant seasonal effects of river ice (Prowse, 2005). The formation and evolution of river ice is affected by the river discharge supplied by the catchment. The hydrological effect of river ice is mainly its influence on the river discharge and stages. In addition to ice-induced extreme flow events, river ice can also have serious environmental and ecological effects (e.g., Prowse, 2001a, 2001b). In the last couple of decades, significant progress has been made on river ice research. Several books and reviews on river ice processes and the state of research have been published (Ashton, 1986; Beltaos, 1995, 2008a; Beltaos and Prowse, 2009; Donchenko, 1987; Gerard, 1990; Prowse, 2005; Shen, 2003, 2006). An overview of river ice processes and its hydrological effects will be presented.

River ice processes

River ice phenomena include formation, evolution, transport, accumulation, deterioration, and dissipation of various forms of ice. These phenomena involve complex interactions between hydrodynamic, mechanical, and thermal processes, under the influence of meteorological and hydrological conditions.

Freeze up

In the beginning of winter, when the water temperature drops to the freezing point, further heat loss will lead to supercooling and frazil ice formation. Subsequently, various types of ice can form in the river depending on the flow intensity. In slow flowing areas, where the turbulence intensity is not strong enough to mix the water or frazil ice crystals from the surface over the depth, skim ice can form on the supercooled water surface even before the depth-averaged water temperature drops to the freezing point. In slow flowing shore zones, this appears in the form of border ice (Svensson et al., 1989). Further cooling will lead to thermal growth of skim ice and border ice, and supercooling of turbulent flow in the river.

When mixed in supercooled turbulent water, frazil crystals can grow in size, multiply in number, and agglomerate into flocs (Daly, 1984; Hammar and Shen, 1995; Osterkemp, 1978). Frazil crystals entrained to the bottom of the channel under supercooled conditions can attach to the bed and underwater objects to form anchor ice (Kerr et al., 2002). The presence of anchor ice can cause changes in flow resistance, water level, and discharge. As the frazil particles and flocs grow in size and quantity, the increase in buoyancy may overcome the vertical mixing to form a surface layer of moving ice. Depending on the turbulence condition and travel time in the river, the surface ice run could consist of ice pans or slush ice. Ice pieces on the river surface will grow in size and strength due to further accumulation of frazil ice from the suspension, freezing of interstitial water, and thermal thickening. Surface ice elements may either sinter into large floes while traveling along the river, or break into fragments when encountering rapid sections. Partial coverage of the water surface by surface ice floes will result in a reduction of the net ice production rate due to the insulating effect of the surface ice (Lal and Shen, 1991). In addition to thermal growth, lateral growth of border ice can occur due to the accumulation of surface ice along edges of existing border ice (Michel et al., 1982; Miles, 1993). This type of lateral growth of the ice cover is limited by the stability and strength of surface ice elements in contact with the existing edge of the border ice. Limited field observations showed that the border ice growth would cease when the local depth-averaged velocity exceeds a critical value of about 0.4 m/s (Matousek, 1990; Shen and Van DeValk, 1984). In rapid reaches, the high turbulent intensity of the flow will limit the size of flocs by turbulent shear and prevent them from rising to the surface. In this case, the frazil flocs in the supercooled water will evolve into frazil granules entrained in the flow to form a suspended frazil ice run. Shen (2006) described the evolution process of different types of ice runs. Matousek (1984) provided a useful empirical method for determining the occurrence of various types of ice formation, but a theoretical formulation still needs to be developed.

Ice cover evolution and ice jams

As more and more ice is produced and surface ice concentration increases, downstream transport of the surface ice will eventually lead to *bridging* or jamming of surface ice across the river (Shen et al., 2000). Jamming of the surface ice run by congestion initiates the accumulation of surface ice into an ice cover. Once an ice cover is initiated, it will progress upstream through the accumulation of the incoming surface ice (Pariset and Hausser, 1961). A cover formed under any hydraulic condition has to reach a thickness and strength so that it is capable of withstanding the forces acting on it. These forces include water drag, wind drag, weight of the cover, and bank resistance. The formation of a thin crust near the top of the newly formed cover due to freezing can significantly increase the strength of the cover. Surface ice jam formation is a part of this surface ice cover progression process. Ice jams appear as localized thick accumulations when subject to larger external forces (Beltaos, 1995; 2008b). As the cover progression encounters high velocity reaches, where incoming surface ice can underturn or become entrained at the leading edge, the cover progression will cease. The limiting condition for cover progression has been defined by the Froude number at the leading edge of the cover. This limiting Froude number is about 0.09 (Sun and Shen, 1988). The transport and deposit of the entrained ice on the underside of the cover can form thick accumulations commonly known as hanging dams. In addition, when the progression of an ice cover stops at a cross section due to the high flow velocity, the rapid reach upstream of the leading edge will remain open during the winter. This open water reach will continue losing heat through the water surface and produce frazil. Since the open water reach has relatively high velocity, the ice in the reach will likely be in the form of frazil granules entrained in the flow. When the frazil granules enter the ice-covered reach, they rise to the underside of the cover and transport and accumulate along the cover to form a frazil jam. The evolution of frazil jam is governed by the ice transport capacity similar to the bed load transport in alluvial rivers (Shen and Wang, 1995). Localized frazil jams have been viewed as another type of hanging dam.

The formation of surface ice, especially a stationary surface ice cover or jam, adds to the flow resistance and causes an increase in channel storage with the backwater effect. This will raise the water level in and upstream of the ice covered reach and reduce the discharge downstream. Ice jam accumulations often lead to severe flooding. The water level rises with the increase of ice

accumulation thickness. In the case of a frazil jam, the level rises gradually over the winter with the gradual increase in the size of the jam before it recedes with the erosion of the undercover accumulation. In the case of a surface jam, the water level could increase rapidly over a very short period due to the rapid jam formation process (e.g., Gerard, 1990; Beltaos, 2008b). Analytical formulations for the hydraulics of flow in rivers with moving or stationary surface ice have been developed (e.g., Lal and Shen, 1991; Shen et al., 1995, 2000). One difficulty in analyzing flow in the presence of ice is the determination of the hydraulic resistance of the ice. Some empirical guidelines exist for floating ice covers. It has been observed that the ice roughness diminishes with time due to thermal and hydraulic smoothing. This time dependent variation of cover roughness may be represented by an exponential decay function (Nezhikovskiy, 1964; Yapa and Shen, 1986). For surface ice jams, Beltaos (2001) and Shen et al. (2000) suggested that the roughness increases with the jam thickness.

As heat exchange continues through a consolidated ice cover, water-filled voids in the ice accumulation will freeze from the free surface downward. This thermal growth will continue beyond the initial thickness of the cover into the underlying river water (Shen and Chiang, 1984; Shen and Yapa, 1985; Shen et al., 1995).

Breakup

At the beginning of spring, or during a warm spell in the winter, decay of the ice cover occurs. The warm spring runoff can also significantly accelerate the thermal erosion process through the turbulent heat transfer between river water and the ice cover. The thermal erosion of ice cover and the deterioration of cover through internal melting by solar radiation lead to the reduction of cover strength (Ashton, 1985; Prowse et al., 1990). The weakening of ice cover makes it more susceptible to mechanical breakup. However, if the river discharge remains relatively steady, the ice cover will remain stable until the eventual meltout.

A mechanical breakup begins with a detachment of the cover from the banks with increasing river flow, followed by the formation of far-spaced transverse cracks (Beltaos, 1984). Beltaos (1990) defined the onset of the breakup as the time when sustained ice movement occurs at a particular site and formulated an empirical method for predicting its occurrence based on the boundary constraints of the river plane geometry in allowing the movement of the large ice plates. If a rapid increase in river discharge occurs, as the result of a runoff increase, an upstream ice jam release, or a surge produced by a hydropower station, the traveling river wave will produce a pressure disturbance underneath the cover. This disturbance may further crack and fragment the cover (Xia and Shen, 2002).

An ice run will occur after the fragmentization of the cover, if the water level rises further. The ice rubble moving along the river can incorporate additional ice fragments by breaking the stationary ice covers downstream. Intermittent stoppage and movement of the rubble field, accompanied by ice jam formation and release, can occur during the downstream progression of the ice run. The basic dynamics of breakup surface ice run and ice jam is essentially the same as those that occurred during the freeze up period. However, the breakup ice runs can be more abrupt and violent, especially if the breakup occurs early in the spring with a high water discharge.

Sudden release or failure of ice jams accompanied by the release of channel storage often generates surges of water with high water velocity and rapid increase in stage (Jasek, 2003). Liu and Shen (2004) showed that the ice resistance has significant effects on both stage and discharge hydrographs during an ice jam release. A flood wave produced by jam release propagates slower than a flood wave without ice. The ice resistance also lowers the peak discharge significantly.

Summary

River ice processes are affected by the ambient meteorological and hydrological conditions and interact in a complex manner with the river flow. River ice affects river hydrology mainly through its influence on the river flow by introducing additional hydraulic resistance. One of the most recognized effects of ice on river hydrology is the influence of ice cover and jams on the stage and discharge. Both the increase in wetted perimeter due to the presence of ice cover and the reduction in flow cross section by the cover or jam thickness contribute to the additional flow resistance. Other processes such as anchor ice growth, and the internal ice resistance in a surface ice run, can also affect the river flow. Significant progress has been made on river ice research in the last couple of decades. Further research to gain fundamental understanding on many of the individual ice processes, such as the evolution of the freeze up ice run and the development of methods for simulating breakup processes are needed.

Bibliography

Ashton, G. D., 1985. Deterioration of floating ice covers. *Journal of Energy Resources Technology*, **107**, 177–182.

Ashton, G. D. (ed.), 1986. *River and Lake Ice Engineering*. Littleton, CO: Water Resources.

Beltaos, S., 1984. A conceptual model of river ice breakup. *Canadian Journal of Civil Engineering*, **11**(3), 516–529.

Beltaos, S., 1990. Fracture and breakup of river ice cover. *Canadian Journal of Civil Engineering*, **17**(2), 173–183.

Beltaos, S. (ed.), 1995. *River Ice Jams*. Highlands Ranch, CO: Water Resources.

Beltaos, S., 2001. Hydraulic roughness of breakup ice jams. *Journal of Hydraulic Engineering, ASCE*, **17**(8), 650–656.

Beltaos, S. (ed.), 2008a. *River Ice Breakup*. Highlands Ranch, CO: Water Resources.

Beltaos, S., 2008b. Progress in the study and management of river ice jams. *Cold Regions Science and Technology*, **51**(1), 2–19.

Beltaos, S., and Prowse, T., 2009. River-ice hydrology in a shrinking cryosphere. *Hydrological Processes*, **23**, 122–144.

Daly, S. F., 1984. Frazil ice dynamics. *CRREL Monograph 84-1*, U.S. Army CRREL, Hanover, NH.
Donchenko, P. B., 1987. *River Ice Conditions in the U.S.S.R.* Chinese Translation, published in 1990, China Science and Technology Publisher, Beijing.
Gerard, R., 1990. Hydrology of floating ice. In Prowse, T. D., and Ommanney, C. S. L. (eds.), *Northern Hydrology – Canadian Perspective*. Saskatoon: National Hydrology Research Institute, pp. 103–134.
Hammar, L., and Shen, H. T., 1995. Frazil evolution in channels. *Journal of Hydraulic Research*, **33**(3), 291–306.
Jasek, M., 2003. Ice jam release surges, ice runs, and breaking fronts: field measurements, physical descriptions, and research needs. *Canadian Journal of Civil Engineering*, **30**, 113–127.
Kerr, D. J., Shen, H. T., and Daly, S. F., 2002. Evolution and hydraulic resistance of anchor ice on gravel bed. *Cold Regions Science and Technology*, **35**(2), 101–114.
Lal, A. M. W., and Shen, H. T., 1991. A mathematical for river ice processes. *Journal of Hydraulic Engineering*, **117**(7), 851–867.
Liu, L., and Shen, H. T., 2004. Dynamics of ice jam release surges. In *Proceedings, 17th International Symposium on Ice*, IAHR, pp. 244–250.
Matousek, V., 1984. Types of ice run and conditions for their formation. In *Proceedings, IAHR Ice Symposium.* pp. 315–327.
Matousek, V., 1990. *Thermal Processes and Ice Formation in Rivers.* Papers and Studies No. 180, Water Research Institute, Prague.
Michel, B., Marcotte, N., Fonseca, F., and Rivard, G., 1982. Formation of border ice in the St. Anne River. In *Proceedings, Workshop on Hydraulic of Ice-Covered Rivers*, Edmonton, pp. 38–61.
Miles, T., 1993. *A Study of Border Ice Growth on the Bruntwood River*. M.S. Thesis, Department of Civil Engineering, University of Manitoba.
Newbury, R. W., 1968. *Nelson River: A Study of Subartic River Processes*. Ph.D. Thesis, Baltimore, John Hopkins University.
Nezhikovskiy, R. A., 1964. Coefficients of roughness of bottom surface of slush ice cover. *Soviet Hydrology: Selected Papers*, 2, 127–148.
Osterkemp, T. E., 1978. Frazil ice formation: a review. *Journal of Hydraulics Division, ASCE*, **104**(HY9), 1239–1255.
Pariset, R., and Hausser, H., 1961. Formation and evolution of ice covers on rivers. *Transaction Engineering Institute of Canada*, **5**(1), 41–49.
Prowse, T. D., 2001a. River ice ecology: Part A) Hydrologic, geomorphic and water quality aspects. *Journal of Cold Regions Engineering*, **15**(1), 1–16.
Prowse, T. D., 2001b. River ice ecology: Part B) Biological aspects. *Journal of Cold Regions Engineering*, **15**(1), 1–16.
Prowse, T. D., 2005. River-ice hydrology. In Anderson, M. G. (ed.), *Encyclopedia of Hydrological Science*. West Sussex: Wiley, Vol. 4, pp. 2657–2677.
Prowse, T. D., Demuth, M. N., and Chew, H. A. M., 1990. The deterioration of freshwater ice under radiation decay. *Journal of Hydraulic Research*, **28**(6), 685–691.
Shen, H. T., 2003. Research on river ice processes: progress and missing links. *Journal of Cold Regions Engineering, ASCE*, **17**(4), 134–142.
Shen, H. T., 2006. A trip through the life of river ice – Progress of river ice research in the last thirty years. In *Proceedings, 18th IAHR Ice Symposium*, Sapporo.
Shen, H. T., and Chiang, L. A., 1984. Simulation of growth and decay of river ice cover. *Journal of Hydraulics Division, ASCE*, **110**(7), 958–971.
Shen, H. T., and Van DeValk, W. A., 1984. Field investigation of St. Lawrence River hanging ice dams. In *Proceedings, IAHR Ice Symposium*, Hamburg, pp. 241–249.
Shen, H. T., and Wang, D. S., 1995. Under cover transport and accumulation of frazil granules. *Journal of Hydraulic Engineering, ASCE*, **120**(2), 184–194.
Shen, H. T., and Yapa, P. D., 1985. A unified degree-day method for river ice cover thickness simulations. *Canadian Journal of Civil Engineering*, **12**, 54–62.
Shen, H. T., Wang, D. S., and Lal, A. M. W., 1995. Numerical simulation of river ice processes. *Journal of Cold Regions Engineering, ASCE*, **9**(3), 107–118.
Shen, H. T., Su, J., and Liu, L., 2000. SPH simulation of river ice dynamics. *Journal of Computational Physics*, **165**(2), 752–771.
Sun, Z. C., and Shen, H. T., 1988. A field investigation of frazil jam in Yellow River. In *Proceedings of Fifth Workshop on Hydraulics of River Ice/Ice Jams,* Winnipeg, pp. 157–175.
Svensson, U., Billfalk, L., and Hammar, L., 1989. A mathematical model for border ice formation. *Cold Regions Science and Technology*, **16**, 179–189.
Xia, X., and Shen, H. T., 2002. Nonlinear interaction of ice cover with shallow water wave in channels. *Journal of Fluid Mechanics*, **467**, 259–267.
Yapa, P. D., and Shen, H. T., 1986. Unsteady flow simulation for an ice-covered river. *Journal of Hydraulic Engineering, ASCE*, **112**(11), 1036–1049.

Cross-references

Anchor Ice
Discharge/Streamflow
Frazil
Pancake Ice
Stage–Discharge Relationship
Supercooled Water

ROCHE MOUTONNEES

Himali Panthri
Department of Geology, D.B.S (P.G) College, Dehradun, Uttarakhand, India

Roche moutonnees are asymmetrical mounds or hillocks having a gradual, smooth, and striated abraded slope on one side and a comparatively craggy and steep slope on the other side. Continental glaciers being several hundred kilometers long and thick exert tremendous amount of pressure upon the ground beneath while moving. As the ice advances, the onset or the stoss side is smoothened by combined mechanisms of abrasion and polishing, and the down flow or lee side is steepened due to greater intensity of plucking on this side. Roche moutonnees commonly occur in swarms, often with a common alignment that indicates the direction of the movement of the ice.

Bibliography

Tarbuck, E. J., and Lutgens, F. K., 2002. *Earth: An Introduction to Physical Geography*, 7th edn. Upper Saddle River: Prentice Hall.
Trenhaile, A., 2007. *Geomorphology: A Canadian Perspective*. Don Mills, Ontario: Oxford University Press.

ROCK GLACIERS

John R. Giardino, Netra R. Regmi, John D. Vitek
Department of Geology and Geophysics, Texas A&M University, College Station, TX, USA

Synonyms

Rockglacier; Rock streams; Rubble stream

Definition

A rock glacier is a lobate or tongue-shaped landform consisting of rock debris and either an ice core or an ice-cemented matrix. This landform is distinguished by its distinctive series of ridges and furrows on the surface, which give the form its characteristic "wrinkled" pattern. Rock glaciers serve as distinctive reservoir for debris and water in alpine drainage basins.

Introduction

The surface of Earth, a patchwork of landforms, is shaped by various geologic and geomorphic processes influenced by the various subsystems of Earth (Figure 1). Individual landforms on a continuous surface serve as magnifying glasses into the history of Earth by providing a record of how past climates and environments interacted with the surface through erosion and deposition. Rock glaciers, often spectacular landforms, are one of the most ambiguous forms regarding human understanding of the process(es) of formation. This essay will explain the form of rock glaciers and the processes associated with formation. Moreover, perspectives on the role of rock glaciers in landscape development will be advanced.

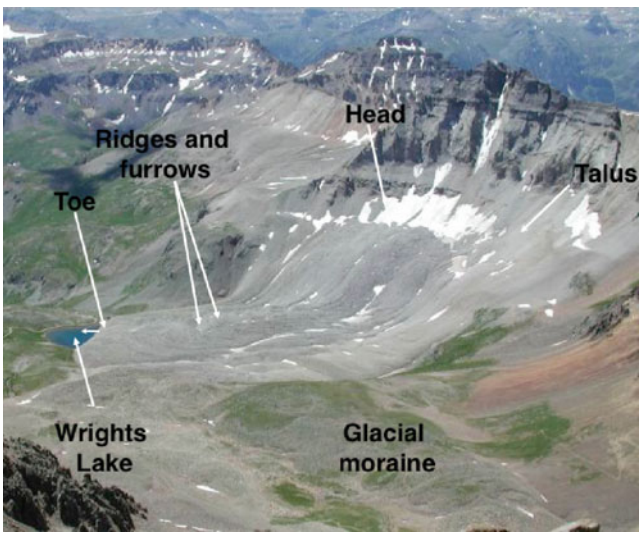

Rock Glaciers, Figure 1 Yankee Boy Basin Rock Glacier, Colorado. (Photograph taken by J. R. Giardino.)

What is a rock glacier?

A rock glacier, one form in the landscape continuum, has been mistakenly confused with other landforms (e.g., rock streams, talus flows, and rubble streams). It is separated from the surrounding terrain by a steep front and side slopes and exhibits a surface expression of ridges and furrows that are generally perpendicular to the direction of flow (Giardino et al., 1987). The "wrinkled" pattern of ridges and furrows influenced Capps (1910) to coin the term "rock glacier" for the forms that he observed in Alaska. The downslope movement or flow of this rock debris has been estimated to be between a few centimeters and decimeters per year. Research has shown that movement is the result of plastic deformation of ice contained within the blocky debris of the form. Simplicity, however, is not the norm because of the wide range of rock glaciers around the world. The mineralogy of the rock debris varies considerably as do the elevation and latitude of these forms, which influence debris transport. From hundreds of papers cited in the literature by the mid-1980s, the literature has exploded into thousands of investigations that have and continue to investigate all aspects of this interesting landform. Whereas citing even the majority of the research is not possible in this short essay, key articles will help readers uncover the rich literature that exists on the various topics addressed herein.

A rock glacier is a transitional phenomenon between glacial and non-glacial processes. Size, location, microrelief, and distribution are its distinguishing characteristics. The surface of the lower parts of the rock glacier commonly consists of parallel ridges and furrows that are arced in the downstream direction; the length and width of a rock glacier are controlled by local condition. The toe slope tends to be at or greater than the angle of repose for rock debris where the process of deformation is active, and the head of a rock glacier may merge smoothly with the talus cone.

The morphology of a rock glacier is controlled by lithology, geographic location and position, microclimate, aspect, and local conditions (Johnson and Thackray, 2008). A rock glacier is a deposit of poorly sorted, angular and blocky to tabular debris held together by massive ice or a matrix of ice-cemented fine clastics (Giardino and Vitek, 1988). The surface structures supported by the internal structures (Figure 2) can be best used to explain the mechanics of development and movement.

Process of formation

Whereas the term "glacier" is used to denote a landform and a process, a rock glacier is simply a form that moves in response to a variety of processes, many of which are poorly understood. Giardino and Vitek (1988) developed a conceptual diagram (Figure 3) to show the relationship between form and process and demonstrates that a rock glacier is a transitional form regardless of the process(es) that formed it. With the passage of time and processes

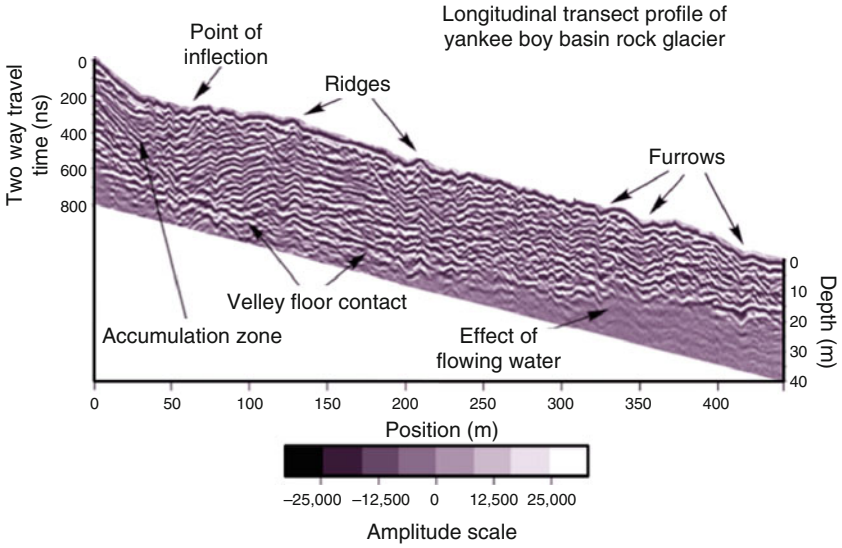

Rock Glaciers, Figure 2 Topographically corrected 25 MHz GPR profile of Yankee Boy Basin. (Adapted from Degenhardt and Giardino, 2003.)

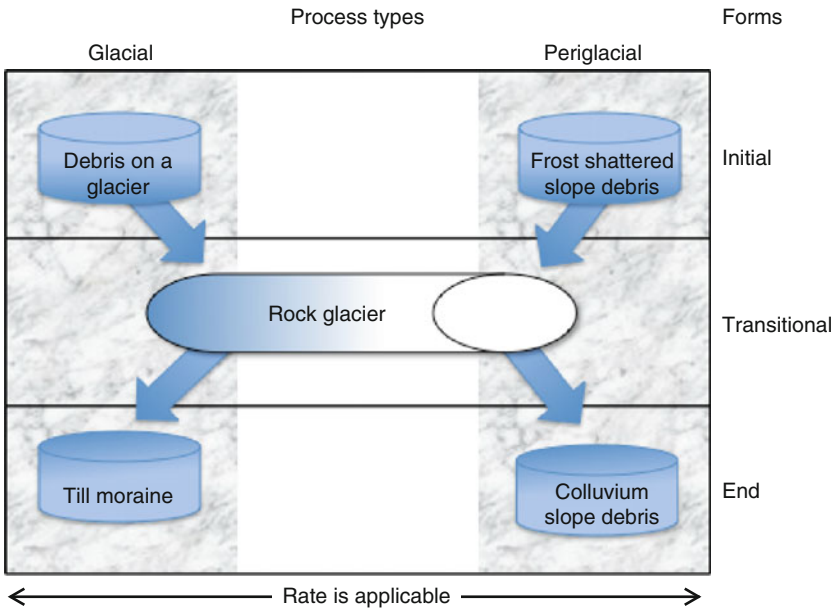

Rock Glaciers, Figure 3 Alpine landscape continuum. (Modified from Giardino and Vitek, 1988.)

operating on this accumulation of rocky debris, the rock glacier will cease to exist and will become a sedimentary deposit in the rock record.

Many authors incorrectly use the terms "fossil," "inactive," or "active," to describe a rock glacier. These terms should refer to the process rather than the form. The process may be "active" or "inactive" and subsequently the form will change although the rate of change can vary from imperceptible to observable. Sharp crested, cascading front slopes, sharp and defined surface features indicate recent movement and are the key characteristics to identify active processes in a rock glacier. Rounded crests at the toe and stable fronts with mature lichens on talus, which means debris is no longer supplied to the rock glacier, are related to inactive processes in the rock glacier. The movement of a rock glacier can also be defined in terms of the basal shear stress, although it is relatively difficult to calculate. Giardino and Vick (1987) determined that basal shear stress for active rock glaciers lies between 1.0 and 2.0 bars and Wahrhaftig and Cox (1959)

determined that basal shear stress for inactive rock glacier is less than 1.0 bar.

The basic components of a glacier, primarily ice with rock debris mixed in, contribute directly to the rate of motion and the effects of the glacier on the landscape. In contrast, the visible portion of a rock glacier consists of unsorted boulders and clasts and particles of various sizes. This material can be deposited over a former glacier, in which mechanics attributable to glacial processes may dominate surficial appearance and movement characteristics. Some rock glaciers, however, have formed in areas that have not been glaciated (Giardino and Vitek, 1985; Giardino and Vitek, 1988). In these locations, interstitial ice is the major factor of formation and change. Periglacial processes, therefore, are capable of developing rock glaciers with similar surficial characteristics like rock glaciers derived from glacial processes. In reality, rock glaciers in glacial environments experience periglacial conditions although the impact of these conditions on resulting forms and processes are difficult to assess.

Composition of rock glacier

The mechanics and the development of the rock glaciers can be best explained by internal structure. Two types of the rock glaciers, based on the internal structure near the landform surface and margins, can be distinguished. The first is the rock glacier having predominantly interstitial ice that consists of an accumulation of clasts from boulders to fines. The second type is the rock glacier that contains predominantly massive ice and plugs of ice that are covered by ice-saturated talus or landslide rock debris.

Classification of rock glacier

Shapes, various modes of origin, geomorphic position, and ice content, among other factors, are the major characteristics of a rock glacier. Several classification schemes for rock glaciers exist: some are genetic classifications and some are geometric classifications. In genetic classifications, rock glaciers are described as debris-covered glaciers, ice-cored rock glaciers, and ice-cemented rock glaciers. In geometric classifications, rock glaciers are categorized on length to width ratios. They also can be described as moraine rock glaciers, talus-derived rock glaciers, avalanche rock glaciers, and protalus rock glaciers.

Hydrology and climate warming

Rock glaciers have been identified and studied as unique features for over a hundred years (Cross and Howe, 1905), but the hydrological relationship between rock glaciers and watersheds has been more or less overlooked. Johnson (1981) examined the relationship between internal structure and water flow in rock glaciers in Canada. Giardino et al. (1992) examined the chemical aspects of rock glacier-fed streams in Colorado. Brenning (2005) studied the hydrological aspects of rock glaciers in the Andes.

The hydrological properties of the rock glacier are controlled by the local weather conditions, thermal properties of the debris layer, and the physical mechanisms that control the flow of meltwater through the rock glacier (Figure 4). Therefore, the seasonal variation of water supply controls the variation in the discharge through a rock glacier. During summer, water from thunderstorms and snowmelt increases the discharge from a rock glacier. Likewise during the summer, the water temperature of the rock glacier lies constantly below 1°C and the electrical conductivity remains low as a result of high amounts of meltwater derived from snow, ice melt, and precipitation. The electrical conductivity increases during cold weather and during autumn when discharge is very low and consists of mainly groundwater (Burger et al., 1999).

Giardino et al. (1992) suggested that the interior of a rock glacier can act as an aquifer and the hydrological characteristics of the rock glacier can be viewed as a system. In their model (Figure 5), water input to the rock glacier is directly from precipitation, runoff from adjacent slopes, avalanche, and groundwater, and water output as surface runoff, surface discharge, subsurface seepage, sublimation evaporation, and ice storage. This model considers water flow as near subsurface flow above the permafrost and as deep subsurface flow below the permafrost. A permafrost layer acts as an impermeable layer between these two layers. The hydrological cycle of a rock glacier is viewed as a cascading system to define the manner in which water moves through the landform (Giardino et al., 1992). Water in a rock glacier can occur in liquid and solid forms. The net change in the water storage is governed by the microclimate (Johnson, 1981) and the insulating nature of the rock mantle; the change in the net storage over a long period is very slow (Burger et al., 1999).

Rock Glaciers, Figure 4 Tongue-shaped rock glaciers in the Mount Sneffels Area, Colorado. (Photograph taken by J. R. Giardino.)

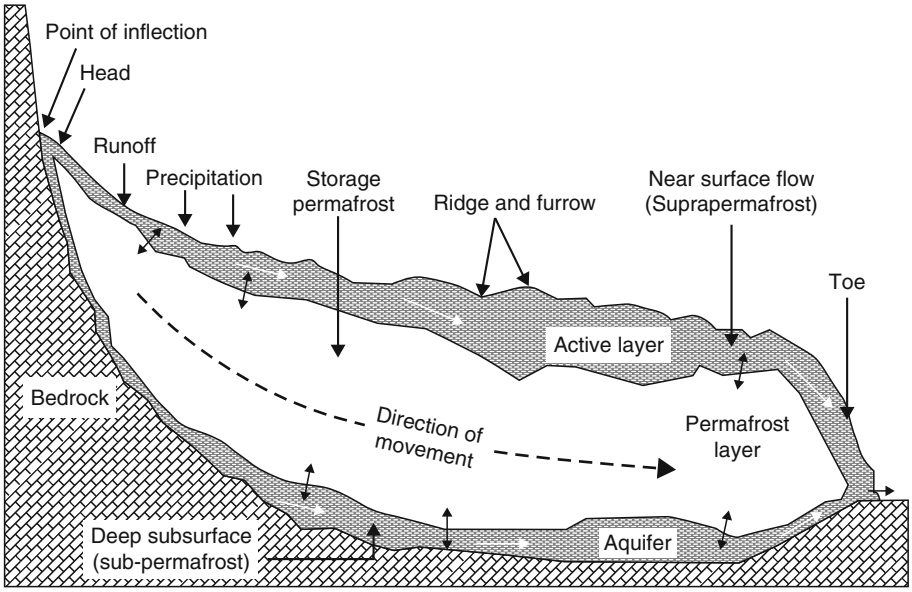

Rock Glaciers, Figure 5 A model of waterflow pathways through a rock glacier. (Modified from Giardino et al., 1992.)

The hydrologic cycle of a rock glacier can vary slowly with long-term climatic change and more rapidly with seasonal fluctuations in ambient temperatures (Johnson, 1981). Burger et al. (1999) described how water discharge through the rock glacier varies with the season. During late winter, water within the active layer is frozen and discharge originates entirely from ground water flow systems at the base of the rock glacier. During late spring/early summer, the thawing front moves downward toward the top of the perennial permafrost; melting snow and ice recharge the upper portion of the rock glacier and create a seasonal aquifer perched on top of the frozen core. During summer, free water within the upper portion of the rock glacier disappears and discharge originates from the base of the rock glacier. Meltwater from snow patches in depressions on the surface continue to melt throughout the summer. During late summer/early fall, falling temperatures create freezing fronts that move upward from the perennial permafrost and downward from the rock glacier surface, confining the remaining water in the central portion of the rock glacier. Seasonal thunderstorms replenish free water in the active layer.

Rock glaciers play an important role in the hydrological cycle of alpine watersheds. They provide both long-term and short-term water storage. Water is stored as ice cores and interstitial ice in the interior of the rock glacier. In addition, the contact of the ice in the rock glacier with underlying permafrost in many arctic locations provides a recharge pathway for groundwater in the watershed. From a short-term perspective, rock glaciers provide a pathway for meltwater from snow and avalanches to maintain stream flow during summer and fall. Many streams in alpine watersheds are fed from spring melt; flow is maintained through summer via melt from lingering snow patches, glaciers, and rock glaciers. Climate conditions, the past hundred years, have maintained the contributions from snow, glaciers, and rock glaciers to stream flows.

Global warming is negatively impacting glaciers and permafrost. The volume of glacial ice and permafrost is decreasing in many locations. This direct impact on glaciers occurs because the surface of the glacier is unprotected from direct incoming radiation. Permafrost, on the other hand, whereas having a covering of soil and vegetation several meters thick is not sufficient to retard melting. Ice cores and interstitial ice in rock glaciers are also negatively impacted by global warming, but to a lesser degree because of the insulating mantle of rock debris on the rock glacier.

Rock glaciers form an important part of the alpine sediment cascade. Because of a long persistence in the landscape, they play a vital role in sediment storage. Water contained in the ice of rock glaciers or rock-ice-features (RIFs) is protected from rising air temperatures by the insulating effect of the rock mantle. As a result, thaw of ice in rock glaciers significantly lags behind ice glaciers. For this reason, rock glaciers are likely to become increasingly critical alpine water reservoirs as temperatures rise. The role of rock glaciers is also of critical importance in arid mountain ranges as snowpack decreases and ice glaciers retreat and soon become the primary sources of persistent groundwater for high mountain regions. Global warming appears to be reducing summer stream flows and drying out meadows. Rock glaciers, therefore, are important water storage and water input systems.

Rock glaciers and paleoclimatic implication

Information about the climate (i.e., paleoclimate) can be deduced from the characteristics of rock glaciers. Evidence of past environments may be abundant if the complex relationship between form, process, and climate can be discerned.

Survival of the debris ice matrix in the rock glacier depends on the ambient temperature, precipitation, and the instability of the bedrock. Cooler climates are effective in debris production, formation of interstitial ice, and flow of a rock glacier (Refsnider and Brugger, 2007). An increase in temperature increases the rate of ice melt in a rock glacier and eventually increases the deformation and the velocity of the rock glacier (Patterson, 1994; Whalley and Azizi, 1994; Haeberli et al., 2006; Janke and Frauenfelder, 2008). Temperature and precipitation control the formation of rock glaciers because they control the amount of snowfall, which is an important component in the formation of a rock glacier. Generally, glaciers retreat because of a decrease in precipitation and an increase in temperature. Furthermore, glacier unloading and permafrost melting can promote catastrophic rockfalls and rock slides. Rock glaciers form within specific precipitation and temperature regimes (King, 1986) although low temperatures and high precipitation promote the growth of glaciers (Harrison et al., 2008). Research suggests that rock glaciers can form where temperatures and precipitation totals are relatively low (e.g., Haeberli, 1985; Barsch, 1988). The three factors (temperature, precipitation, and the availability of the debris source or the instability of the cliff) complicate the paleoclimatic signal of the rock glacier. Furthermore, the genetic types of rock glaciers probably reflect the environmental conditions of formation (Harrison et al., 2008) but at present, the knowledge to identify the climatic boundary is insufficient. Records from ice cores show that periods of rapid cooling occurred throughout the Late Pleistocene (Andrews, 1998; Alley et al., 2003), and the climatic conditions suitable for the formation of rock glaciers in many parts of the world may have prevailed during this time. Based on the study of the rock glaciers and RIFs in the Sierra Nevada, USA, Miller and Westfall (2008) estimated the temperature during the Pleistocene as 3.3–4.1°C colder than current (Holocene) temperatures.

Conclusions

Rock glaciers demonstrate that glacial and periglacial processes have been active on alpine slopes. Rock debris has been entrained and is moving, albeit slowly, to a lower and more stable elevation. Form and process are intertwined and care must be taken when using adjectives such as active, inactive, and fossil. The form demonstrates that processes have been involved but does not provide definitive answers about all of the processes that can be present. Because rock glaciers have never been found in the rock record, we have noted in our model that it is a transitional form to a moraine or colluvial deposit, material which has been identified in the rock record.

Variability in climate and weather can be detected in how water flows through this rock debris. New technology, including ground-penetrating radar and global positioning satellites, will enhance the quality of the data acquired and the interpretation of these forms relative to future change. Although the number of research papers has soared in recent years, researchers must be careful to clearly distinguish between the interactions of form and processes, including the use of terminology in how these interesting forms are described.

Bibliography

Alley, R. B., Marotzke, J., Nordhaus, W. D., Overpeck, J. T., Peteet, D. M., Pielke, R. A., Jr., Pierrehumbert, R. T., Rhines, P. B., Stocker, T. F., Talley, L. D., and Wallace, J. M., 2003. Abrupt climate change. *Science*, **299**, 2005–2010.

Andrews, J. T., 1998. Abrupt changes (Heinrich events) in Late Quaternary North Atlantic marine environments: a history and review of data and concepts. *Journal of Quaternary Science*, **13**, 3–16.

Barsch, D., 1988. Rock Glaciers. In Clark, M. J. (ed.), *Advances in Periglacial Geomorphology*. Chichester, NY: Wiley, pp. 69–90.

Barsch, D., 1996. *Rock Glaciers: Indicators for the Present and Former Geoecology in High Mountain Environments*. Berlin: Springer, p. 331.

Brenning, A., 2005. Geomorphological, Hydrological and Climatic Significance of Rock Glaciers in the Andes of Central Chile (33–35°S). *Permafrost and Periglacial Processes*, **16**(3), 231–240.

Burger, K. C., Degenhardt, J. J., and Giardino, J. R., 1999. Engineering geomorphology of rock glaciers. In *Proceedings of the 28th Binghamton Symposium in Geomorphology.* Giardino, J. R., Marston, R. A., and Morisawa, M. (eds.), *Changing the Face of Earth: Engineering Geomorphology.* New York: Elsevier Science, pp. 93– 132.

Capps, S. R., Jr., 1910. Rock Glaciers in Alaska. *Journal of Geology*, **18**, 359–375.

Cross, W., and Howe, E., 1905. Silverton Folio. *USGS*, Folio No. 120.

Degenhardt, J. J., and Giardino, J. R., 2003. Subsurface investigation of a rock glacier using ground-penetrating radar: implications for locating stored water on mars. *Journal of Geophysical Research*, **108**, 17 p.

Giardino, J. R., and Vick, S. G., 1987. Geologic engineering aspects of rock glaciers. In Giardino, J. R., Shroder, J. F., Jr., and Vitek, J. D. (eds.), *Rock Glaciers*. London: Allen and Unwin, pp. 265–287.

Giardino, J. R., and Vitek, J. D., 1985. A statistical study of the fabric of a rock glacier. *Arctic, Antarctic, and Alpine Research*, **17**(2), 165–177.

Giardino, J. R., and Vitek, J. D., 1988. The significance of rock glaciers in the glacial–periglacial landscape continuum. *Journal of Quaternary Science*, **3**(1), 97–103.

Giardino, J. R., Shroder, J. F., and Vitek, J. D., 1987. *Rock glaciers*. London: Allen and Unwin, p. 355.

Giardino, J. R., Vitek, J. D., and DeMorett, J. L., 1992. A model of water movement in rock glaciers and associated water characteristics. In Dixon, J. C., and Abrahams, A. D. (eds.), *Periglacial Geomorphology*. Chichester, MA: Wiley, pp. 159–184.

Haeberli, W., 1985. Creep of mountain permafrost: internal structure and flow of alpine rock glaciers. *Mitteilungen der*

Versuchsanstalt für Wasserbau, Hydrologie und Glaziologie, **77**, 1–142.
Haeberli, W., Hallet, B., Arenson, L., Elconin, R., Humlum, O., Kääb, A., Kaufmann, V., Ladanyi, B., Matsuoka, N., Springman, S., and Vonder Mühll, D., 2006. Permafrost creep and rock glacier dynamics. *Permafrost and Perigiacial Processes*, **17**, 189–214.
Harrison, S., Whalley, B., and Anderson, E., 2008. Relict rock glaciers and protalus lobes in the british isles: implications for late pleistocene mountain geomorphology and palaeoclimate. *Journal of Quaternary Science*, **23**(3), 287–304.
Janke, J., and Frauenfelder, R., 2008. The relationship between rock glacier and contributing area parameters in the front range of Colorado. *Journal of Quaternary Science*, **23**(2), 153–163.
Johnson, P. G., 1981. The structure of a talus-derived rock glacier deduced from its hydrology. *Canadian Journal of Earth Sciences*, **18**, 1422–1430.
Johnson, B. G., and Thackray, G. D., 2008. The effect of topography, latitude, and lithology on rock glacier distribution in the Lemhi Range, Central Idaho, USA. *Geomorphology*, **91**(1–2), 38–50.
King, L., 1986. Zonation and ecology of high mountain permafrost in Scandinavia. *Geografiska Annaler*, **68A**, 131–139.
Millar, C. I., and Westfall, R. D., 2008. Rock glaciers and related periglacial landforms in the Sierra Nevada, CA, USA; inventory, distribution and climatic relationships. *Quaternary International*, **188**(1), 90–104.
Patterson, W. S. B., 1994. *The physics of glaciers*. Oxford: Pergamon.
Refsnider, K. A., and Brugger, K. A., 2007. Rock glaciers in Central Colorado, U.S.A., as indicators of Holocene climate change. *Arctic, Antarctic, and Alpine Research*, **39**(1), 127–136.
Wahrhaftig, C., and Cox, A., 1959. Rock glaciers in the Alaska range. *Geological Society of America Bulletin*, **70**, 383–436.
Whalley, W. B., and Azizi, F., 1994. Models of flow of rock glaciers: analysis, critique and a possible test. *Permafrost and Periglacial Processes*, **5**, 37–351.

ROCKY MOUNTAINS

Eric M. Leonard
Department of Geology, Colorado College, Colorado Springs, CO, USA

Definition

The Rocky Mountains are a system of mountain ranges in western North America, extending about 3,000 km from north-central New Mexico (USA) in the south to northeastern British Columbia (Canada) in the north (Figure 1).

Location and topography

The Rocky Mountains comprise the easternmost ranges of the North American Cordillera, rising from the Great Plains to the east. To the west they are separated from the Pacific Ocean by a 500–1,000 km-wide region of generally high topography – an "intermontane" zone of valleys, mountain ranges, and plateaus, and further west the Pacific Mountain System, which includes the Coast and Insular Ranges of British Columbia, and the Cascade Range, Olympic Mountains, Sierra Nevada, and Coast Mountains of the western United States. The Rocky Mountains form the drainage divide for much of North America, separating Atlantic and Arctic Ocean drainage on the east from Pacific drainage on the west.

The United States portion of the Rocky Mountains generally consists of individual ranges separated by broad basins or "parks" (Figure 1). The Canadian Rockies, and their southward extension into northern Montana, are more topographically continuous. The highest terrain in the Rockies is located near their southern end, particularly in Colorado where approximately 600 summits exceed 4,000 m. The highest summit is 4,399 m Mount Elbert in the Colorado Sawatch Range. Overall altitude, but not relief or ruggedness, decreases northward. There are no 4,000 m peaks north of Wyoming, although Mount Robson in British Columbia reaches nearly that altitude and stands much higher above local tree line and snow line than summits in the U.S. Rockies.

Although the distinction between the U.S. and Canadian Rocky Mountains is an arbitrary one in terms of most environmental characteristics, this entry focuses on the former as the Canadian Rockies are covered in another entry (Canadian Rockies and Coast Mountains of Canada).

Climate

The Rocky Mountains have a continental climate with larger diurnal and seasonal temperature fluctuations and lower precipitation than the ranges further west. Moisture comes dominantly from the west, although southerly and southeasterly moisture sources are also significant, particularly along the eastern flank of the Rockies. Fall-through-spring precipitation is dominated by westerly cyclonic storms, summer precipitation by monsoonal flow and local convection (Mock, 1996). Nearly all fall-through-spring precipitation falls as snow, most summer precipitation as rain. Local precipitation patterns reflect orographic influences.

The storm track over the western U.S. is controlled by the position and intensity of the Pacific jet stream. This jet stream undergoes substantial subseasonal-to-interannual variability, and controls the frequency and location of cyclonic storms impinging upon the west coast. Storms associated with northwesterly flow into western North America bring fall-through-spring snowfall mainly to portions of the Rockies from central Colorado northward. Southwesterly flow, commonly associated with a southerly position of the jet, brings heavy snowfall to the southern Rockies (Changnon et al., 1993). These storms commonly also draw southeasterly moisture flow from Gulf of Mexico, leading to heavy "upslope" snowfall along the eastern margin of the southern Rockies, especially during spring and fall. When the jet is weakened or far to the south during the winter, polar air from the north and northeast may impinge on the eastern flank of the Rockies, bringing extremely low temperatures, but generally little snowfall. Interannual-to-multidecadal climate oscillations, including El Niño-Southern Oscillation (ENSO), the Pacific Decadal Oscillation (PDO), and the Pacific-North America Oscillation (PNA), influence

Rocky Mountains, Figure 1 Location map of the Rocky Mountains (*insert*). The western boundary of Rockies in the United States (*dashed line*) is not well defined. Some workers extend the term "Rocky Mountains" northward into the Yukon and Alaska. Main map identifies features of the U.S. Rockies mentioned in the text. L/GNP, Lewis Range/Glacier National Park; B, Beartooth Mountains; YP, Yellowstone Plateau; T, Teton Range; WR, Wind River Range; LB, Pleistocene Lake Bonneville; W, Wasatch Range; U, Uinta Mountains; F, Colorado Front Range; S, Sawatch Range; SJ, San Juan Mountains; SC, Sangre de Cristo Mountains.

the magnitude and distribution of Pacific-derived precipitation in the Rockies (Cayan, 1996; Clark et al., 2001; McCabe and Dettinger, 2002). El Niño conditions, for example, are statistically associated with higher-than-normal snowfall in the southern Rockies, lower-than-normal in the north. La Niña conditions tend to reverse these departures from normal.

In the U.S. Rockies summer precipitation is due primarily to local convection. Convection is particularly strong when associated with monsoonal flow involving northward advection of moist air from the eastern Pacific/Gulf of California area and/or the Gulf of Mexico, resulting from summer heating of the Great Basin and Colorado Plateau. Monsoonal flow commonly results in heavy summer precipitation in the southern U.S. Rockies.

Snowpack

Snowpack data are currently (2010) collected at more than 400 automated Snowpack Telemetry (SNOTEL) sites throughout the U.S. Rocky Mountains (http://www.wcc.nrcs.usda.gov/snow/). Historical data are available for more than 1,000 snow survey courses, many of which have been discontinued in recent years (http://www.wcc.nrcs.usda.gov/snowcourse/).

Snowpack is strongly controlled by elevation, although in many ranges it is asymmetric, with greater accumulation on the range flank facing the predominant winter moisture source and a "snow-shadow" on the opposite side. Typically more accumulation occurs on the west sides of ranges although in the Sangre de Cristo, and possibly other ranges along the eastern flank of the Rockies,

this pattern is reversed with more accumulation on the east, due to a prevalence of southeasterly "upslope" precipitation. Within-range patterns may be complex. The Colorado Front Range receives precipitation from both westerly winter cyclonic and southeasterly upslope storms, the latter primarily during the spring. Stations on the west side of the range and those at highest altitude on the east have winter snowfall maxima, reflecting westerly storms. Those lower on the east side have spring maxima, reflecting both a winter snow-shadow and spring upslope conditions (Barry, 2008). Regionally, snowpack generally decreases west-to-east reflecting the dominance of westerly-sourced winter precipitation, and north-to-south.

Wind redistribution of snow is important in the Rocky Mountains for several reasons including (1) low moisture content of the snow, (2) presence of large areas above tree line, and (3) presence in some ranges, especially the Colorado Front Range and Uinta Mountains of Utah, of broad, low-relief areas above tree line along topographic divides. Wind drift is critical to the preservation of modern glaciers in the Front Range (Outcalt and MacPhail, 1965). Wind loading, the prevalence of temperature-gradient snowpack metamorphism, and the episodic nature of heavy snowfall make Rocky Mountain snowpacks particularly susceptible to avalanching.

Over the last 50 years snowpack water-equivalent depth (SWE) has broadly decreased across the western United States, due to a combination of generally decreased winter precipitation and increased temperature (Mote et al., 2005). In the Rocky Mountains SWE has decreased from central Colorado northward. In southern Colorado and New Mexico, however, many sites show an increase in SWE, apparently due to an increase in winter precipitation that outweighs effects of warming.

Modern glaciers and permanent snow and ice

Modern glaciation in the U.S. Rocky Mountains is limited to cirque and niche glaciers, most with areas of less than 1 km^2, typically in topographically and microclimatically favored sites. The 3.3 km^2 Gannett Glacier in the Wind River Range is the largest in the U.S. Rockies (Fountain, 2006). Drawing primarily on Graf (1977), Krimmel (2002) identified 80.2 km^2 of glacier ice in the U.S. Rockies, largely in Montana (42.5 km^2 – primarily in the Lewis and Beartooth Ranges) and Wyoming (35.0 km^2 – primarily in the Wind River Range). A few very small glaciers exist in Colorado, Idaho, and Utah. Fountain (2006) identified 2,982 permanent ice or snow bodies covering 149.3 km^2 in the U.S. Rockies. Equilibrium-line altitudes of modern glaciers range from about 2,200 m in northern Montana (Locke, 1989) to about 3,700 m in Colorado.

No long-term glacier mass-balance data are available for the U.S. Rockies. Short-term studies have been undertaken in Montana, Wyoming, and Colorado (Mayo, 1984; Reardon et al., 2008). Glacier areas and volumes have decreased significantly over the last 100–150 years. More than 80% of the glaciers that existed in Glacier National Park in Montana in the mid nineteenth century have since disappeared (Reardon et al., 2008) and the remaining glaciers have lost on average about 60% of their area since 1900 (http://glaciers.research.pdx.edu/). Twentieth century loss of glacier area was slightly less in the Wind River Range and Colorado Front Range, around 40% (http://glaciers.research.pdx.edu/).

Quaternary glaciation

Rocky Mountain glacial history has long been a topic of study, recently reviewed by Pierce (2004). Working in the Wind River Range, Blackwelder (1915) established the current regional stratigraphic nomenclature, including the name "Pinedale Glaciation" for the last Pleistocene glaciation. Evidence for multiple earlier Pleistocene glaciations has also been found throughout the Rockies. In northwestern Montana and northern Idaho ice of the Cordilleran Ice Sheet flowed south from British Columbia along major valleys. Elsewhere only local alpine ice was present in the U.S. Rockies – valley and cirque glaciers in many ranges as far south as New Mexico, and mountain icecap/outlet glacier complexes in several highlands areas, notably northwestern Montana, the Yellowstone Plateau, and the San Juan Mountains (Porter et al., 1983; Locke, 1995). Pinedale equilibrium-line altitudes ranged from about 1,800 m in northwestern Montana and northern Idaho (Pierce, 2004) to about 3,700 m in parts of the San Juan and Sangre de Cristo ranges in Colorado (Refsnider et al., 2009). Estimates of Pinedale temperature depression from the present based on glacial and periglacial evidence range from about 6°C to 15°C, but it is difficult to disentangle effects of temperature and precipitation changes (Pierce, 2004; Leonard, 2007). Timing of the Pinedale maximum ice stand varies somewhat range-to-range, even valley-to-valley (Licciardi and Pierce, 2008; Thackray, 2008). These differences may reflect (1) changing regional synoptic climatology, (2) changing local moisture sources, and/or (3) different dynamics of ice bodies of different size and morphology. Pinedale advances in the southern and central Rockies, as far north as the Wind River Range, generally correspond closely in time with the global Last Glacial Maximum (LGM), about 21 ± 2 ka. In the Yellowstone region further north, Pinedale advances culminated several 1,000 years later (Licciardi and Pierce, 2008). Climate models generally suggest that at the global LGM northwesterly flow into the northern U.S. Rockies was weakened as a result of southward migration of the jet stream and/or of the development of easterly anticyclonic circulation associated with the Laurentide Ice Sheet to the northeast (Bartlein et al., 1998), changes that could explain the relatively limited LGM extent of Yellowstone glaciers and their post-LGM advances. Glaciers in the Wasatch and Uinta Ranges of Utah also reached their Pinedale maxima after the global LGM, likely responding to post-LGM expansion of Lake Bonneville, a significant local moisture source for those ranges (Munroe et al., 2006; Laabs et al., 2009).

At several sites in the U.S. and Canadian Rockies, moraines far upvalley from the LGM moraines have been attributed to small glacier readvances during the Younger Dryas interval (ca 13–11.5 ka; reviewed in Pierce, 2004). Valleys in many ranges contain multiple Holocene moraines, commonly suggesting a three-fold sequence of advances during the Neoglacial interval of the last 5,000 years, with the final advance during the Little Ice Age interval of the last several centuries (Davis, 1988).

Permafrost and periglacial processes

Discontinuous permafrost is present at higher elevations throughout the U.S. Rockies. At the Canadian border the lower limit of permafrost is at about 2,000 m, in New Mexico at about 3,500 m (Péwé, 1983). Relict Pleistocene periglacial features occur in the mountains as much as 600–1,000 m lower than modern permafrost (Péwé, 1983; Janke, 2005). Modeling by Janke (2005) indicates that warming of 2°C would cause a 94% reduction in the area of permafrost in the Colorado Front Range.

Rock glaciers, perhaps the most conspicuous active periglacial features in the Rockies, are found in most ranges. Rock glacier dynamics have been studied in Wyoming (Konrad et al., 1999) and Colorado (Leonard et al., 2005). Throughout the region many cirques occupied by true (ice) glaciers in the late Pleistocene supported only rock glaciers during the Holocene, likely only during the last 3–5,000 years. Limited data from Colorado suggest that rock glacier flow has slowed in response to post-Little Ice Age warming.

Summary

The Rocky Mountains are a system of ranges in the interior of western North America that form the hydrologic divide for much of the continent. Snowfall in the Rockies is derived from several sources, but primarily from westerly cyclonic storms whose tracks reflect the position and intensity of the Pacific Jet Stream. Local snowpack is strongly influenced by altitude, aspect, and wind. Modern glaciation in the U.S. Rockies is very limited, but there is abundant evidence of more extensive Pleistocene glaciers. Range-to-range differences in Pleistocene glacial history appear to reflect a combination of changing position of the jet stream and changes in local moisture sources. Discontinuous permafrost and active periglacial features are present at higher elevations throughout the Rockies.

Bibliography

Barry, R. G., 2008. *Mountain Weather and Climate*. Cambridge: Cambridge University Press.

Bartlein, P. J., Anderson, K. H., Anderson, P. M., Edwards, M. E., Mock, C. J., Thompson, R. S., Webb, R. S., Webb, T., III, and Whitlock, C., 1998. Paleoclimate simulations for North America over the past 21, 000 years: features of the simulated climate and comparisons with paleoenvironmental data. *Quaternary Science Reviews*, **17**, 549–585.

Blackwelder, E., 1915. Post-cretaceous history of the mountains of central western Wyoming. *Journal of Geology*, **23**, 97–117, 193–217, 307–340.

Cayan, D. R., 1996. Interannual climate variability and snowpack in the western United States. *Journal of Climate*, **9**, 928–948.

Changnon, D., McKee, T. B., and Doesken, N. J., 1993. Annual snowpack patterns across the Rockies: long term trends and associated 500-mb synoptic patterns. *Monthly Weather Review*, **121**, 633–647.

Clark, M. P., Serreze, M. C., and McCabe, G. J., 2001. Historical effects of El Nino and La Nina events on the seasonal evolution of the montane snowpack in the Columbia and Colorado River Basins. *Water Resources Research*, **37**, 741–757.

Davis, P. T., 1988. Holocene glacier fluctuations in the American Cordillera. *Quaternary Science Reviews*, **7**, 129–157.

Fountain, A. G., 2006. Glaciers online: glaciers of the American West. Available at: http://glaciers.research.pdx.edu (accessed August 18, 2010).

Graf, W. L., 1977. The distribution of glaciers in the Rocky Mountains of the United States. *Journal of Glaciology*, **18**, 325–328.

Janke, J. R., 2005. Modeling past and future alpine permafrost distribution in the Colorado Front Range. *Earth Surface Processes and Landforms*, **30**, 1495–1508.

Konrad, S. K., Humphrey, N. F., Steig, E. J., Clark, D. H., Potter, N., Jr., and Pfeffer, W. T., 1999. Rock glacier dynamics and paleoclimatic implications. *Geology*, **27**, 1131–1134.

Krimmel, R. M., 2002. Glaciers of the conterminous United States: glaciers of the Western United States. U.S. Geological Survey Professional Paper 13856-J-2. In Williams, R. S., and Ferrigno, J. G. (eds.), *Satellite Image Atlas of Glaciers of the World: North America*. US Geological Survey Professional Paper 1386-J, pp. J329–J381.

Laabs, B. J. C., Refsnider, K. A., Munroe, J. S., Mickelson, D. M., Applegate, P. J., Singer, B. S., and Caffee, M. W., 2009. Latest Pleistocene glacial chronology of the Uinta Mountains: support for moisture-driven asynchrony of the last deglaciation. *Quaternary Science Reviews*, **28**, 1171–1187.

Leonard, E. M., 2007. Modeled patterns of Late Pleistocene glacier inception and growth in the Southern and Central Rocky Mountains, USA: sensitivity to climate change and paleoclimatic implications. *Quaternary Science Reviews*, **26**, 2152–2166.

Leonard, E. M., Staab, P., and Weaver, S. G., 2005. Kinematics of the Spruce Creek rock glacier, Colorado. *Journal of Glaciology*, **51**, 259–268.

Licciardi, J. M., and Pierce, K. L., 2008. Cosmogenic exposure-age chronologies of Pinedale and Bull Lake glaciations in greater Yellowstone and the Teton Range, USA. *Quaternary Science Reviews*, **27**, 814–831.

Locke, W. W., 1989. Present climate and glaciation of western Montana, U.S.A. *Arctic and Alpine Research*, **21**, 234–244.

Locke, W. W., 1995. Modelling of icecap glaciation of the northern Rocky Mountains of Montana. *Geomorphology*, **14**, 123–130.

Mayo, L. R., 1984. Glacier mass balance and runoff research in the U.S.A. Geografiska Annaler. *Series A, Physical Geography*, **66A**, 215–227.

McCabe, G. J., and Dettinger, M. D., 2002. Primary modes and predictability of year-to-year snowpack variations in the western United States from teleconnections with Pacific Ocean climate. *Journal of Hydrometeorology*, **3**, 13–25.

Mock, C. J., 1996. Climatic controls and spatial variations of precipitation in the western United States. *Journal of Climate*, **9**, 1111–1125.

Mote, P. W., Hamlet, A. F., Clark, M. P., and Lettenmaier, D. P., 2005. Declining mountain snowpack in western North America. *Bulletin of the American Meteorological Society*, **86**, 1–39.

Munroe, J. S., Laabs, B. J. C., Shakun, J. D., Singer, B. S., Mickelson, D. M., Refsnider, K. A., and Caffee, M. W., 2006.

Latest Pleistocene advance of alpine glaciers in the southwestern Uinta Mountains, Utah, USA: evidence for the influence of local moisture sources. *Geology*, **34**, 841–844.
Outcalt, S. I., and MacPhail, D. S., 1965. A survey of neoglaciation in the Front Range of Colorado. University of Colorado Studies Series in Earth Science, 4.
Péwé, T. L., 1983. Alpine permafrost in the contiguous United States: a review. *Arctic and Alpine Research*, **15**, 145–156.
Pierce, K. L., 2004. Pleistocene glaciation of the Rocky Mountains. In Gillespie, A. R., Porter, S. C., and Atwater, B. F. (eds.), *The Quaternary Period in the United States*. Amsterdam: Elsevier, pp. 63–76.
Porter S. C., Pierce, K. L., and Hamilton, T. D., 1983. Late Wisconsin mountain glaciation in the western United States. In Porter, S. C. (ed.), *The Late Pleistocene*, Vol. 1, of Wright, H. E., Jr. (ed.) *Late Quaternary Environments of the United States*. Minneapolis: University of Minnesota Press, pp. 71–111.
Reardon, B. A., Harper J. T., and Fagre, D. B., 2008. Mass balance of a cirque glacier in the U.S. Rocky Mountains. In *Proceedings of the Mass Balance Measurement and Modeling Workshop*, Skeikampen: Norway, pp. 1–5.
Refsnider, K. A., Brugger, K. A., Leonard, E. M., McCalpin, J. P., and Armstrong, P. P. (2009). Last glacial maximum equilibrium-line altitude trends and precipitation patterns in the Sangre de Cristo Mountains, Southern Colorado, USA. *Boreas*, **38**, 663–678.
Thackray, G. D., 2008. Varied climatic and topographic influences on Late Pleistocene mountain glaciation in the western United States. *Journal of Quaternary Science*, **23**, 671–681.

Cross-references

Canadian Rockies and Coast Mountains of Canada
Climate Change and Glaciers
Equilibrium-Line Altitude (ELA)
Periglacial
Permafrost
Rock Glaciers
Snow Course
Snow Drift

RÖTHLISBERGER (R)-CHANNELS

Renoj J. Thayyen
Western Himalayan Regional Centre, National Institute of Hydrology, Jammu (J&K), India

Definition

Semicircular subglacial tunnels incised upwards from the glacier bed into the overlying ice are called Röthlisberger or R-channels. These channels were named after H. Röthlisberger who proposed the numerical frame work for such subglacial channels (Röthlisberger, 1972).

Description

Röthlisberger or R-channels are one of the two fundamental types of subglacial channels which are incised up into the glacier ice (other is the N-channels, which are incised down to bedrock or sediment). R-channels in a glacier are similar to the englacial conduit with an exception that they are floored by rock rather than completely surrounded by ice. R-channels are kept open by melting of the tunnel wall by frictional heat. Contraction of R-channel occurs by ice creep due to pressure difference between glacier ice and tunnel. Therefore, the size of these channels and water pressure within them reflects a balance between channel enlargement and closure by ice creep (Röthlisberger, 1972; Shreve, 1972). The path taken by the R-channel is governed by the hydraulic gradient at the glacier bed. At equilibrium conditions, most of the hydraulic gradient is due to the surface slope of the ice and a small component is contributed by the gradient of the bed. It suggests that R-channels need not follow the slope of the bed, but can flow across the slope or even uphill. Eskers are formed by infilling of R-channels.

Bibliography

Röthlisberger, H., 1972. Water pressure in intra- and sub-glacial channels. *Journal of Glaciology*, **11**, 177–203.
Shreve, R. L., 1972. Movement of water in glaciers. *Journal of glaciology*, **11**, 205–214.

RUNOFF COEFFICIENT

Manmohan Kumar Goel
Water Resources System, National Institute of Hydrology, Roorkee, Uttarakhand, India

Definition

Runoff coefficient is a dimensionless factor that is used to convert the rainfall amounts to runoff. It represents the integrated effect of catchment losses and hence depends upon the nature of land surface, slope, degree of saturation, and rainfall intensity. It is also affected by the proximity to water table, degree of soil compaction, porosity of soil, vegetation, and depression storage. Some of its probable values for different land uses (Mutreja, 1990; Subramanya, 1991) are presented in Table 1. The joint committee of the American Society of Civil Engineers and Water Pollution Control Federation has recommended values of runoff coefficient for a variety of land uses, soil types, and surface slopes (ASCE and WFCP, 1969).

In addition to various catchment factors as mentioned above, runoff coefficient also varies for different storm

Runoff Coefficient, Table 1 Usual values of runoff coefficient for different types of areas

Type of area	Runoff coefficient
Urban	0.30–0.50
Forest	0.05–0.20
Commercial and industrial	0.70–0.90
Parks and pastures	0.05–0.30
Pavements and roads	0.70–0.95
Flat agriculture	0.10–0.50
Hilly agriculture	0.30–0.70

events (from nearly zero [for small storms] to a relatively high value [for a major storm]) depending upon the initial moisture content. Considerable judgment and experience are required in selecting satisfactory values of runoff coefficient for design. Field inspection and aerial photographs can prove useful in estimating the nature of surface in a basin. A reasonable coefficient must be chosen to represent the integrated effects of various factors.

Runoff coefficient is used in the *rational method* which is one of the widely used methods for peak flow predictions in small catchments, urban drainage design, and design of small culverts and bridges. The rational method (described by statement $Q_p = C.I.A$) states that if rainfall intensity "I" over a catchment area "A" continues beyond the time of concentration "t_c," then the peak runoff "Q_p" would occur at time t_c when all the catchment will contribute to the flow at the outlet. The ratio of inflow rate in the catchment ($I.A$) to the peak runoff Q_p is termed as runoff coefficient "C". Because of its popularity, the method is sometimes also known as *runoff coefficient method*. Normally, runoff coefficient is applied to storm events, but it can also be used for monthly and annual rainfall and runoff values.

Bibliography

American Society of Civil Engineers and Water Pollution Control Federation, 1969. Design and Construction of Sanitary Storm Sewers. ASCE Manuals and Reports on Engineering Practice no. 37 and WPCF Manual of Practice no. 9.

Mutreja, K. N., 1990. *Applied Hydrology*. New Delhi: Tata McGraw-Hill.

Subramanya, K., 1991. *Engineering Hydrology*. New Delhi: Tata McGraw-Hill.

RUNOFF GENERATION

Anita M. Thompson[1], Debasmita Misra[2]
Ronald P. Daanen[3]
[1]Department of Biological Systems Engineering, University of Wisconsin-Madison, Madison, WI, USA
[2]Geological Engineering, College of Engineering and Mines, University of Alaska Fairbanks, Fairbanks, AK, USA
[3]Geophysical Institute, University of Alaska Fairbanks, Fairbanks, AK, USA

Synonyms

Effective snowmelt generation; Excess precipitation generation; Glacial melt runoff generation; Infiltration excess generation; Overland flow generation; Saturation excess generation; Surface runoff generation

Definition

Runoff. It is a major component of the hydrologic cycle and is generated when water from precipitation or snow and glacial melt flows over the land. It is often referred to as the surface runoff. It is the water that is not absorbed by the soil.

Introduction

Runoff is the portion of precipitation or snow and glacial melt that flows across the landscape until it reaches streams, rivers, and, ultimately, oceans. Surface runoff generation depends on rainfall or snowmelt characteristics (amount, duration, intensity, and time distribution) and landscape characteristics (vegetation, land use, topography, soil texture and structure, and antecedent soil moisture conditions).

Conditions of runoff generation

Runoff during non- or partially frozen ground conditions occurs as *infiltration excess* or *saturation excess* when surface water inputs (rainfall or snowmelt) exceed the infiltration capacity of the soil (also referred to as *Hortonian overland flow*; Horton, 1933) and when liquid precipitation falls on an already saturated soil (Hewlett and Hibbert, 1967; Dunne and Black, 1970). The critical controls for runoff generation are precipitation intensity, duration of precipitation, and infiltration/storage capacity (related to the permeability of the soil and the antecedent soil moisture pressure gradient) of the soil (e.g., Tindall and Kunkel, 1999). On an impermeable surface or completely frozen soil, runoff starts almost immediately and is equivalent to precipitation less abstractions due to vegetative interception and surface depressional storage. Additionally, return flow is subsurface water that returns to the surface and contributes to overland flow.

Runoff generation from direct precipitation

Runoff generation within a watershed is a dynamic process that varies in both space and time. According to Beven (2001), in many areas, particularly on vegetated surfaces, infiltration excess rarely occurs unless the soil becomes saturated, thereby decreasing the infiltration capacity. Infiltration capacities will first be exceeded in areas of low permeability soils and high initial water contents. Only a small portion of a watershed may contribute to infiltration excess, a concept known as the *partial-area* concept of infiltration excess overland flow (Betson, 1964). Areas of saturated soil tend to occur first where antecedent soil moisture is high (e.g., valley bottoms) or on areas where storage capacity is limited or in low permeability and low slope areas that tend to stay wet during recession periods (Beven, 2001). Areas of saturated soil tend to expand and contract during a precipitation event, leading to the concept known as *variable source area* runoff (Hewlett and Hibbert, 1967; Dunne and Black, 1970).

Runoff generated from snowmelt

Runoff generated as a result of snowmelt varies with landscape position since elevation and aspect affect air temperature and radiation inputs to the snow. According to Singh and Singh (2001), rainfall or snowmelt at the surface of

a snowpack will pass through the snowpack and flow as interflow after reaching the ground. When meltwater reaches the base of the snowpack, a thin saturated layer is formed over the ground surface due to the accumulation of percolating water. It is possible that water generated at the snow surface may not contribute to runoff. For example, at the beginning of the melt season, if there is a deficiency in the cold content or liquid water of the snowpack, water generated at the surface may be used in the ripening (the process by which a snowpack reaches a state where it can yield meltwater) of the snowpack (Singh and Singh, 2001). As the snowmelt season progresses and air temperatures increase, the depth and extent of snow-covered area decreases and melting rates increase. The main factors that influence snowmelt runoff generation are surface melt, stratigraphic features of the snowpack, movement of water through the snowpack, interaction of meltwater with underlying soil, and lateral flow at the base of the snowpack (Singh and Singh, 2001).

Runoff generated from glacial melt

Runoff from glaciers may occur as flow of ice sheets or as meltwater. Glaciers receive precipitation both in liquid and solid form, store water as ice, and release it when melted, depending upon the climatological factors (Jansson et al., 2003). These glaciers are often referred to as the temperate glaciers. In late spring, such glaciers are covered by a thick snowpack subjected to a melting temperature. The liquid precipitation and the melt water move through the snowpack, percolating at a slow rate, until they reach well-defined meltwater channels in the solid ice downstream. During the summer, the snowpack is thinner. Hence, there are well-defined drainage paths that migrate the liquid precipitation and the snowmelt rapidly through the glacier. During the winter, the snow accumulates rendering a frozen surface layer. Thus, migration of meltwater and precipitation is reduced or subsides at the surface. The ice reservoir, however, continues to drain.

Runoff generated in permafrost regions

Regions underlain by permafrost cover approximately a quarter of the land surface of the earth. These regions also suffer from sparse and extremely uneven distribution of hydrometeorological data network. However, recent increase in attention to studies associated with the global processes and the protection of the northern environment have diverted attention toward investigation of permafrost hydrological processes and especially the runoff generation from these areas (Kuchment et al., 2000). According to Kuchment et al. (2000), "the hydrology of the permafrost regions has several common well-expressed peculiarities which make it clearly distinguishable from the hydrology of other geographical zones." According to Woo (1990), these peculiarities are: (1) the frozen ground has limited permeability, (2) most hydrological activities are confined to the seasonally frozen and thawed zone above the permafrost table (the active layer), (3) energy and water fluxes are closely linked as water storage and redistribution are modified by freeze-thaw events, and (4) snow and ice storage on a seasonal or multi-annual basis affects the temporal distribution of water. Due to small permeability of the frozen ground, runoff generation is governed by evaporation, water storage in depressions, peat mats, and soils with high porosity. During snowmelt, overland flow is the major mechanism of runoff generation in these regions. According to Sokolov (1975) as cited in Kuchment et al. (2000), "a part of the melt water can refreeze in the snow, in the peat mats or in the ground during the nightly lowering of air temperature and because of the low ground temperatures. The water frozen in the surface basin storage and in the active layer of the ground can generate a significant portion of river runoff during the entire warm period. There are the river basins where floods occur as a result of *ice melting* after cessation of snowmelt. Subsurface flow starts after the beginning of the ice melt in the ground and can become the main mechanism of rainfall runoff generation on the mountainous slopes." Most of the annual runoff in permafrost regions is of ice and snowmelt origin but in the southern regions rainfall runoff can dominate (Kuchment et al., 2000).

Summary

Runoff generation occurs due to excess liquid precipitation, snowmelt, or glacial ice melt. The major difference between catchments fed by glaciers and those by precipitation is that the runoff from glacierized catchments is dominated by energy, while the other catchments are dominated by quantity of precipitation, soil moisture capacity, antecedent soil moisture, and other physical factors. Catchments that receive snow as precipitation are partially dominated by energy and partially by other physical conditions. Runoff generation in permafrost areas are governed by evaporation, water storage in depressions, peat mats, and soils with high porosity. Melting of ice in the permafrost regions can cause major floods in the streams of the region. Most of the annual runoff in permafrost regions is of ice and snowmelt origin but in the southern regions rainfall runoff can dominate.

Bibliography

Betson, R. P., 1964. What is watershed runoff? *Journal of Geophysical Research*, **69**(8), 1541–1552.

Beven, K. J., 2001. Rainfall-runoff modelling: the primer. New York, NY: J. Wiley & Sons.

Dunne, T., and Black, R. D., 1970. Partial area contributions to storm runoff in a small New England watershed. *Water Resources Research*, **6**(5), 1296–1311.

Hewlett, J. D., and Hibbert, A. R., 1967. Factors affecting the response of small watersheds to precipitation in humid areas. In: *International Symposium on Forest Hydrological Processes*. Pergamon, New York, NY, pp. 275–290.

Horton, R. E., 1933. The role of infiltration in the hydrologic cycle. *Transactions of the Americal Geophysical Union*, **14**, 446–460.

Jansson, P., Hock, R., and Schneider, T., 2003. The concept of glacier storage: a review. *Journal of Hydrology*, **282**, 116–129.

Kuchment, L. S., Gelfan, A. N., and Demidov, V. N., 2000. A distributed model of runoff generation in the permafrost regions. *Journal of Hydrology*, **240**, 1–22.
Singh, P., and Singh, V. P., 2001. *Snow and Glacier Hydrology*. Dordrecht, The Netherlands: Kluwer Academic.
Sokolov, B. L., 1975. *Naleds and River Runoff*. Leningrad, Russian: Hydrometeorological Publication.
Tindall, J. A., and Kunkel, J. R., 1999. *Unsaturated Zone Hydrology for Scientists and Engineers, Chapter 11*. New Jersey, USA: Prentice Hall.
Woo, M-K., 1990. Permafrost hydrology. In: Prowse, T. D., Ommanney, C. S. L. (Eds.), *Northern Hydrology: Canadian Perspectives*, NHRI Science Rep. No. 1. National Hydrology Research Institute, Environment Canada, Saskatoon, Saskatchewan, pp. 63–76.

Cross-references

Glacier Hydrology
Permafrost

RUNOFF OBSERVATIONS

Anita M. Thompson[1], Debasmita Misra[2], Ronald P. Daanen[3]
[1]Department of Biological Systems Engineering, University of Wisconsin – Madison, Madison, WI, USA
[2]Department of Mining and Geological Engineering, College of Engineering and Mines, University of Alaska Fairbanks, Fairbanks, AK, USA
[3]Geophysical Institute, University of Alaska Fairbanks, Fairbanks, AK, USA

Synonyms

Glacier-melt runoff; Runoff measurements; Snowmelt Observation; Streamflow characteristics

Definition

Runoff. The component of precipitation that moves across the land surface or through surface channels.
Observation. An act of recognizing and noting a fact or occurrence often involving measurement with instruments (weather observations); a record or description so obtained (source: Merriam-Webster's Online Dictionary).

Introduction

Runoff observations from precipitation events, snowmelt, or glacier-melt are critical in the planning of various hydrological projects in the basins. For example, Linacre (1992) has provided maximum daily snowmelt rates in various locations of the globe. Such data are useful in engineering planning and flood forecasting exercises. Melting of glaciers provides significant amounts of source water for many rivers and lakes around the globe. With the current discussion on climate warming resulting in increased glacial melting, runoff from those could result in global sea-level rise and spell disaster for coastal areas. Thus, observation of glacier-melt runoff needs significant attention and has been the focus of recent studies. The runoff observations from any source are usually recorded by a runoff hydrograph.

The runoff hydrograph

Runoff observations are represented graphically by a runoff hydrograph or plot of the time distribution of water discharge at a particular point of interest. A streamflow, or total, hydrograph represents the combined effects of direct runoff (surface runoff and short-term interflow) and baseflow (long-term interflow and groundwater discharge). The total runoff hydrograph represents the combined influence of physical characteristics of the drainage basin and rainfall, snowmelt, or ice melt characteristics. The depth and extent of snow cover in a basin affects the shape of the streamflow hydrograph. According to Singh and Singh (2001), "The availability of snow causes a much delayed response to rainfall or snowmelt because water available at the surface takes time to pass through the snowpack and flow as interflow after reaching the ground. In case rainfall occurs over snow, it is soaked in the snowpack like a sponge and the rain water behaves as snowmelt thereafter. Depending on the cold content and liquid water deficiency of the snowpack, as in the beginning of the melt season, it is also possible that water generated at the surface does not contribute to runoff at all. Under such conditions, the water generated either from rainfall or melting of surface is used up in the ripening of the snowpack. When cold content and liquid water deficiency are satisfied, rainfall or snowmelt moves through the snowpack and appear as delayed runoff . . .. As the snowmelt season progresses, both the depth and extent of snow-covered area of the basin decrease and melting occurs at a higher rate because of the increase in temperature. Therefore, a relatively faster response of the basin is obtained in the summer time." In shallow snowcovers (e.g., those encountered in Prairies), nighttime radiation losses can result in negative heat storage which must be satisfied before snowcover runoff occurs the following day, resulting in a diurnal cycle in the runoff hydrograph mainly during the early part of the melt season (Male and Gray, 1981). Measured meltwater from a snowpack follows a diurnal wave with maximum discharge decreasing with depth from the surface (Colbeck and Davidson, 1973). Delay and attenuation of runoff can occur as a result of storage in the snowpack. Drainage way obstructions from snow accumulation can impede runoff water and store snowcover runoff, delaying the time of peak streamflow occurrence.

In mountain regions, the precipitation temporarily stored within the snowpack is released during warm months. Over a large portion of the northern hemisphere, runoff from snowmelt contributes significantly to the annual water yield and spring flooding (Male and Gray, 1981). In the western United States, spring/early summer snowmelt runoff accounts for 50–80% of the total annual

runoff from snowmelt-dominated basins (Stewart et al., 2004). Rango (1995) reports that the snowmelt season in the mountainous areas is occurring progressively earlier. Slope aspect can have a large impact on snowmelt rates (e.g., Murray and Buttle, 2003). Snow on a south facing slope melts faster than snow on a north facing slope due to differences in the amount of solar radiation received. Snowmelt rates are generally enhanced under shrub canopies compared to open snowfields (Carey and Pomeroy, 2009). Snowmelt runoff rates vary depending on climate and vegetation; for example, Male and Gray (1981) summarize runoff rates ranging from 1.7 to 4.57 mm/(°C·d) for forested basins with deep snowpacks and average runoff rates of 3.9, 4.78, and 10.96 mm/(°C·d) for stubble, pasture, and fallow conditions, respectively.

In addition to meteorologic factors, snowmelt runoff depends on the depth, aerial extent, and snow water equivalent of the snowpack. Snow depth can be measured using snow stakes or optical snow depth meters. Snow water equivalent (SWE) is the vertical depth of water that is produced upon melting the snow cover. Instrumentation for measuring SWE includes snow pillows, snow surveys, and gamma-ray snow-gauges. Snow pillows typically have a flat stainless steel surface area. The pillow below the flat surface is filled with antifreeze solution and the pressure in the pillow is related to the water-equivalent depth of the snow on the platform (source: Webster's Online Dictionary). A gamma-ray snow-gauge determines snow water content by measuring the amount of gamma radiation absorbed by the snow overlying the transmitter that is placed at the surface (source: American Meteorologic Society Glossary of Meteorology). The aerial extent of snow can be measured using ground observations; however, visual and physical obstructions combined with travel to observation points render this method difficult. Methods with greater potential for studying runoff from large or remote areas include the use of aerial photography and satellite imagery.

Stewart (2009) discusses the intrinsic link between the timing, volume, and extent of mountain snowpack, and the associated snowmelt runoff, and seasonal climate variability and change. For example, warmer cold season temperatures reduce snow accumulation, while warmer spring temperatures hasten snowmelt. Therefore, runoff occurs earlier and later season flows are reduced. Also noted by Stewart (2009) is that the season in which precipitation occurs affects the amount stored as snow and consequently the volume of spring snowmelt.

"The changes in the extent and timing of the annual snowpack and melt have impacted the volume and timing of snowmelt-dominated streamflow on the continental to global scale," Stewart (2009).

Runoff measurement methods

Runoff can be measured using a variety of methods and instrumentation depending on the landscape position and the level of runoff information desired. Runoff can be measured or observed at the edge of a small plot or field or in a stream channel. Runoff measurement from a plot or field typically requires physical bounding of a contributing drainage area (i.e., runoff plot). Runoff generated from within the border is collected at the downslope edge and focused into a collection and flow measurement device. Flow measurement devices can be grouped into those that measure the total volume of runoff (e.g., a simple collection bucket) and those that measure the time varying rate of runoff (e.g., tipping bucket or hydraulic flume). Streamflow measurement or streamgaging requires continuous measurement of stream stage (or depth) combined with periodic measure of discharge to establish a relationship between stage and discharge. This relationship between stage and discharge is used to determine a continuous record of streamflow from the continuous measure of stage. Methods for measuring discharge in an open channel include dilution (flow is measured by how much of a known mass of tracer is diluted), area-velocity (cross-sectional area and velocity are measured and multiplied to determine discharge), and use of hydraulic controls (e.g., weirs, flumes). Streamflow monitoring sites are generally sparse at higher elevations and daily streamflow records (many of which are discontinuous) seldom exist for more than a few decades (Stewart, 2009).

Summary

With the global climate change in effect, runoff observations have become critical as increased runoff due to increased precipitation, snowmelt, and glacier-melt rates have impact on flooding, sea-level rise, and lake water volumes. As such, the observations of runoff from basins have been accomplished by recording streamflow stage-discharge changes along with other hydrological parameters that affect generation of surface runoff. Additional sites have been instrumented and remote sensing imagery tools are being deployed and used to provide continuous observation of runoff on a temporal scale. Glaciers have gained more focus due to their increased rate of receding in the recent years thus resulting in production of substantial quantity of runoff that has resulted in rise in the level of the sea in the world.

Bibliography

Carey, S. K., and Pomeroy, J. W., 2009. Progress in Canadian snow and frozen ground hydrology, 2003–2007. *Canadian Water Resources Journal*, **34**(2), 127–138.

Colbeck, S. C., and Davidson, G., 1973. Water percolation through homogeneous snow. In *The Role of Snow and Ice in Hydrology: Proceedings of the Banff Symposia, September, 1972*. Unesco-WMO-IAHS, Geneva-Budapest-Paris, ÎAHS Publ. no.106, Vol.1, pp. 242–257.

Linacre, E., 1992. *Climate Data and Resources*. London: Routledge.

Male, D. H., and Gray, D. M., 1981. Snowcover ablation and runoff. In Gray, D. M., and Male, D. H. (eds.), *Handbook of Snow*. Toronto: Pergamon.

Murray, C. D., and Buttle, J. M., 2003. Impacts of clearcut harvesting on snow accumulation and melt in a northern hardwood forest. *Journal of Hydrology*, **271**, 197–212.

Rango, A., 1995. Effects of climate change on water supplies in mountainous snowmelt regions. *World Resource Review*, **7**(3), 315–325.
Singh, P., and Singh, V. P., 2001. *Snow and Glacier Hydrology*. Dordrecht: Kluwer Academic.
Stewart, I. T., 2009. Changes in snowpack and snowmelt runoff for key mountain regions. *Hydrological Processes*, **23**, 78–94.
Stewart, I. T., Cayan, D. R., and Dettinger, M. D., 2004. Changes in snowmelt runoff timing in western North America under a "Business as Usual" climate change scenario. *Climatic Change*, **62**, 217–232.

Cross-references

Hydrographs
Snow Water Equivalent

RUNOUT DISTANCE

A. K. Singh
DIAT (Deemed University), Pune, Maharashtra, India

Landslides and avalanches occur on hilly slopes. A landslide takes place primarily during the wet season and occurs due to intensive rainfall. They may also occur during the dry season by earthquakes and volcanic eruptions. Essential elements for avalanche are deep snow and steep slopes. Due to variation in snow and terrain conditions, avalanche appears in various forms and sizes with 30–45° slopes experiencing maximum avalanche activity.

In the runoff zone, avalanches decelerate and stop on terrain with a low inclination. Topographic parameters that describe and predict avalanche runout are mean path, slope angle (which is a dependent variable that defines the runout distance), and slope of the path above the 10° profile point.

One of the main problems affecting the estimates of runout distance is the lack of information and uncertainties about the values of the friction coefficients, that is, friction coefficient (μ) which depends on snow properties and magnitude of flow depth (decreases considerably with flow depth) and a resistance due to ground roughness, (coefficient ξ) which is proportional to the square of the speed. Significant experience is needed to make realistic estimate of runout distance because selection of the beginning of the runout zone and the point from which runout distance should be measured is critical and difficult in terrain having a gentle change of slope.

Runout distance information is used in landslide and avalanche of debris movement as assessment of debris flow is essential for hazard/risk management.

Bibliography

Buser, O., Frutiger, H., 1980. Observed maximum runout distance of snow avalanches and the determination of the friction coefficients μ and ξ. *Journal of Glaciology*, **26**(94), 121–130.
Godison, B. E., Ferguson, H. L., and Mckay, G. A., 1981. Measurement and data analysis. In Grey, D. M., and Male, D. H. (eds.), *Handbook of snow*: *principles*, *processes*, *management and use*. Pergamon Press: Canada Ltd., Canada, pp. 191–274.
McClung, D., Schaerer, P., 1976. The avalanche handbook. US Forest Services, Seattle WA, USA
Mears, A. I., 1994. Regional variations in extreme avalanche runout distance. Proceedings of SNOWSYMP-94, Int. Symposium on Snow and Related Manifestations, 26–28 Sept, pp. 252–255.

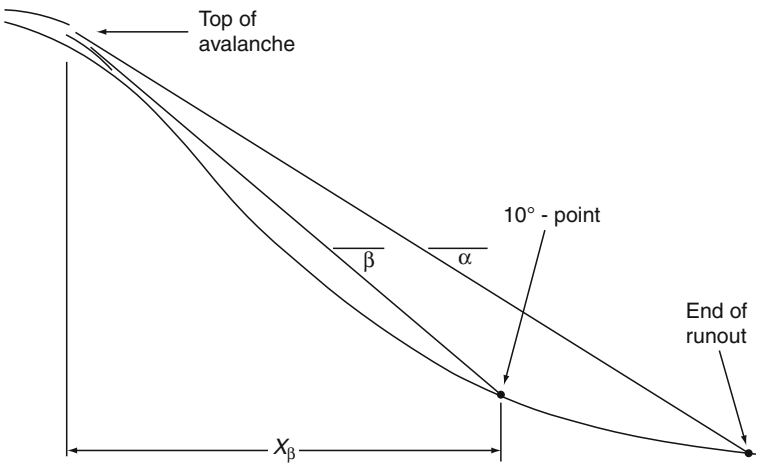

Runout Distance, Figure 1 Runout distance generic diagram with slope and length parameters (Mears, 1994).

S

SALINITY

C. K. Jain
National Institute of Hydrology, Centre for Flood Management Studies, Dispur, Guwahati, Assam, India

Synonyms

Brininess; Salinity; Salt; Saltiness

Definition

Concentration of dissolved salts found in a sample of water. It is measured as the total amount of dissolved salts in parts per 1,000. Seawater has an average salinity of about 35 parts/1,000.

Nearly all water contains dissolved chemicals, even rainwater. These dissolved chemicals are called salts. The salinity of normal ocean water is about 35 parts per 1,000, total dissolved solids. This is written as 35‰ or 35 ppth. A salinity of 35‰ is the same as 3.5%. The symbol resembles a percentage sign (%), but percent means per 100. But the symbol with two zeros on the bottom of the fraction (‰) means per 1,000.

Salinity varies slightly from place to place around the world, and also varies somewhat with the seasons (affected by temperature and precipitation). The salinity of seawater ranges from about 30‰ to 40‰. Warm temperatures and high evaporation rates (particularly in shallow seas) raise the salinity. Warmer waters will tend to have higher salinity than cooler waters.

Water of salinity between freshwater and seawater is called brackish. Brackish water can be found in estuaries. Water with salinity greater than normal seawater is called hypersaline. For example, the Great Salt Lake, Utah, and the Dead Sea are hypersaline. Hypersaline lakes tend to occur in arid areas. They are land-locked basins with no outlet for the waters to flow from the lake. The salts are concentrated as a result of evaporation. Evaporation is so extreme in some lakes (ephemeral lakes or playa lakes) that they dry up completely every few years, leaving a saltpan.

Freshwater input (rivers, precipitation, or melting ice) lowers the salinity. In polar areas where glaciers and ice caps are melting, the seawater has lower salinity.

SALTATION

C. K. Jain
National Institute of Hydrology, Centre for Flood Management Studies, Dispur, Guwahati, Assam, India

Saltation is a specific type of particle transport by fluids such as wind, or the denser fluid water. It occurs when loose material is removed from a bed and carried by the fluid, before being transported back to the surface. Examples include pebble transport by rivers, sand drift over desert surfaces, soil blowing over fields, or even now drift over smooth surfaces such as those in the Arctic or Canadian Prairies.

At low-fluid velocities, loose material rolls downstream, staying in contact with the surface. This is called *creep*. Here the forces exerted by the fluid on the particle are only enough to roll the particle around the point of contact with the surface. At higher speeds, the lift and moment exerted by the fluid on the particle is enough to pull it away from the surface and into the flow. Initially the particle moves quite rapidly compared to the flow and so has high lift, moving it away from the surface. As the particle moves into the faster flow away from the bed, the velocity difference between particle and flow decreases and so lift decreases. When the particle weight is greater than the lift force, the particle sinks back toward the

Vijay P. Singh, Pratap Singh & Umesh K. Haritashya (eds.), *Encyclopedia of Snow, Ice and Glaciers*, DOI 10.1007/978-90-481-2642-2,

surface. During its descent, the particle keeps some of the speed it picked up in the faster moving flow, and so returns to the surface at higher speed than the fluid near the surface. This gives the particle a parabolic trajectory through the fluid, which is the defining characteristic of saltation. Depending on the surface, more loose material could be dislodged by the impacting particle, the particle might disintegrate on impact, or the particle could continue bouncing downstream. In rivers, this process repeats continually, gradually eroding away the riverbed, but also transporting in fresh material from upstream.

SCANDINAVIAN GLACIERS

Juha P. Lunkka
Institute of Geosciences, University of Oulu,
Oulu, Finland

Definition

Scandinavia: Geographical area in northern Europe consisting Norway, Sweden, and northwestern part of Finnish Lapland.

Introduction

Scandinavia is located in northern Europe between latitudes 55–71° North (Figure 1). The mountains that run through mainland Scandinavia from south to north are not very high but in many places they are very steep. The highest peaks reach well over 2,000 m above the present sea level. Their northern location and moisture from the North Atlantic Ocean to the west of Scandinavia has caused the formation of many glaciers in the coastal areas as well as further inland several times, particularly during the past 2.6 million years. At present, the glaciers in Scandinavia are relatively small and cover mostly mountainous areas, occurring in a wide latitudinal range from ca. 60° N to 70°N. Although glaciated areas in Scandinavia consist of only 0.2% of the ice coverage in Arctic regions (Dowdeswell and Hagen, 2004), they have provided valuable records on the behavior of glaciers and proxy data for recent climate events in northwestern Europe.

History of the Scandinavian glaciers

The Fennoscandian Shield, including Scandinavia, has hosted glaciers many times throughout Earth's history, although its latitudinal position and topography has changed constantly in time as a result of plate tectonism. The geological record from Scandinavia, extending back to the Precambrian, includes metasedimentary rocks of glacial origin, for example, in Finnish North Karelia, on the Kola Peninsula, and on the Varanger Peninsula, Norway. This evidence indicates that glaciers covered Fennoscandia several times during the Early Proterozoic around 2.4–2.2 billion years ago and in the Neoproterozoic Era ca. 700–600 million years ago (cf. Siedlecka and Roberts, 1992; Melezhik, 2006). However, there is no geological evidence to indicate that any major glaciers existed in the Fennoscandian shield between the Palaeozoic and Mesozoic Era (540–65 million years ago).

Results from the central Arctic Ocean and Norwegian-Greenland Sea suggest that continental glaciers were present around the Arctic Basin during the Late Eocene as early as 35 million years ago (Moran and ACEX Members, 2006; Eldrett et al., 2007), but the distribution and extent of these ice masses are not known in detail. Ice-Rafted Detritus (IRD) in the deep-sea sediments west of Norway indicate that glaciers must have existed in Scandinavia already about 11 million years ago (Mangerud et al., 1996).

Glaciers in the Scandinavian mountains are thought to have been the nucleus of the Scandinavian Ice Sheet (SIS) that spread over the southern and eastern continental areas adjacent to Scandinavian mountains and was confluent with the Barents and British Ice Sheets several times during the Quaternary period (cf. Mangerud, 2004) (Figure 2). It has been estimated that during the past 2.6 million years, the Scandinavian mountains were covered by glacial ice ca. 90% of the time (cf. Holmlund, 2005). Geological evidence indicates the presence of an ice sheet over Scandinavia for most part of the Elsterian (ca. 500,000–450,000 years ago), Saalian (ca. 390,000–130,000 years ago), and Weichselian (115,000–11,500 years ago) glaciations (cf. Donner, 1995; Mangerud, 2004; Svendsen et al., 2004). During the last glacial maximum (LGM) ca. 20,000–18,000 years ago the Scandinavian Ice Sheet was at its largest for at least the past 130,000 years extending from the North Sea and the Norwegian shelf areas to the Russian Plain (Figure 2). At the LGM, the modelled thickness of the ice sheet over Scandinavia was ca. 2.5 km (Siegert and Dowdeswell, 2004) and during the Younger Dryas cold climate event (ca. 12,500–11,500 years ago) SIS still covered most of Fennoscandia (Figure 1). It is thought that glaciers started to melt relatively fast at the beginning of the Holocene and may have disappeared completely at least once during the period from 8,000–4,000 years ago (Nesje et al., 2008). After their disappearance most of the Scandinavian glaciers attained their largest extent during the Little Ace Age most likely about 1,750 A.D. (cf. Whalley, 2004).

Present glaciers in Scandinavia

At present the total number of glaciers in Scandinavia is ca. 1,900, of which slightly over 1,600 in Norway and ca. 300 in Sweden (Østrem and Haakensen, 1993; Schytt, 1993). The average sizes of the glaciers in Norway and Sweden are 2.6 km^2 and 1 km^2, respectively (cf. Holmlund, 2005). Morphologically the largest glaciers are categorized as ice caps and ice fields or plateau glaciers while the medium-size glaciers are valley glaciers and cirque glaciers. The largest glacier in Scandinavia, and also in mainland Europe, is Jostedalsbreen (487 km^2), which is located in Norway. Other sizeable

Scandinavian Glaciers, Figure 1 Location map of the glaciers in Scandinavia (*squares*) with names of the glaciers mentioned in text. The Younger Dryas ice limit (ca. 12,500–11,500 years ago) is also indicated.

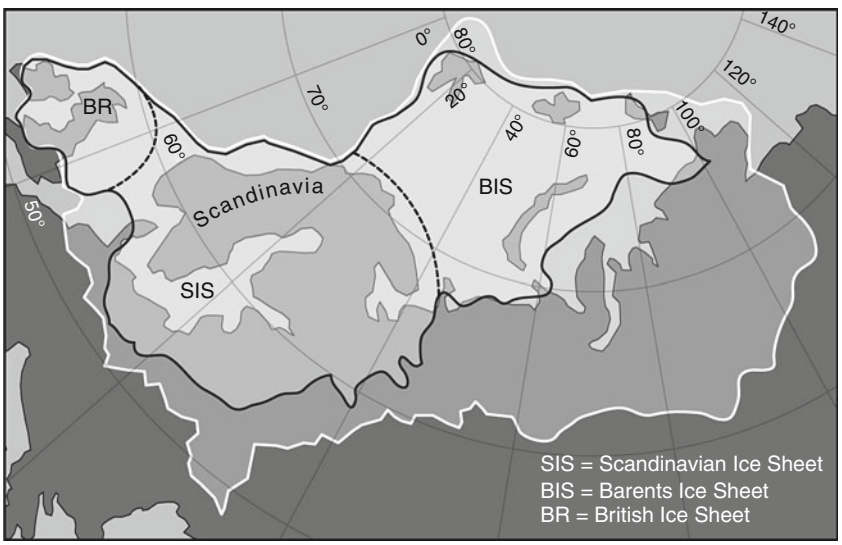

Scandinavian Glaciers, Figure 2 The reconstruction of the Eurasian ice sheet at the Saalian glaciation ca. 160,000–140,000 years ago (*white line*) and at the last glacial maximum ca. 20,000–18,000 years ago (*black line*).

glaciers in Norway are Svartisen West (221 km^2), Folgefonna South (168 km^2), and Svartisen East (148 km^2) (Figure 2). The total glacier volume of Norway is estimated to be 164 km^3 (Nesje et al., 2008). Glaciers in Sweden are relatively small compared to those in Norway. The largest glaciers in Sweden are Stourrajekna and Ålmaijekna both less than 12 km^2 (Schytt, 1993).

Glaciers in mainland Scandinavia cover an area of approximately 2,900 km^2 (cf. Whalley, 2004). In this area, glaciers occur mainly in mountainous areas, that is, in the Scandinavian Mountain range (Figure 2). Climate in the western part of the mountain range is locally maritime, becoming more continental on the eastern side of the mountains. In the maritime climatic areas, the glaciers on the mountains are normally fed by orographic precipitation while in the climatically more continental eastern part of the mountain range precipitation is lower and the glaciers here are fed by wind-driven snow accumulation (cf. Holmlund, 2005).

The largest glaciers are built up in the maritime climate of the Norwegian west coast between 60–62° N and 66–70° N latitudes within 180 km of the coast (Østrem and Haakensen, 1993; Grove, 2004). Annual accumulation in the glaciated areas close to the western coast of Norway is ca. 3–4 m (snow water equivalent), while the annual accumulation in the more easterly located glaciers in Sweden and Norway is less than 1 m (snow water equivalent) (cf. Holmlund, 2005). The glaciers in

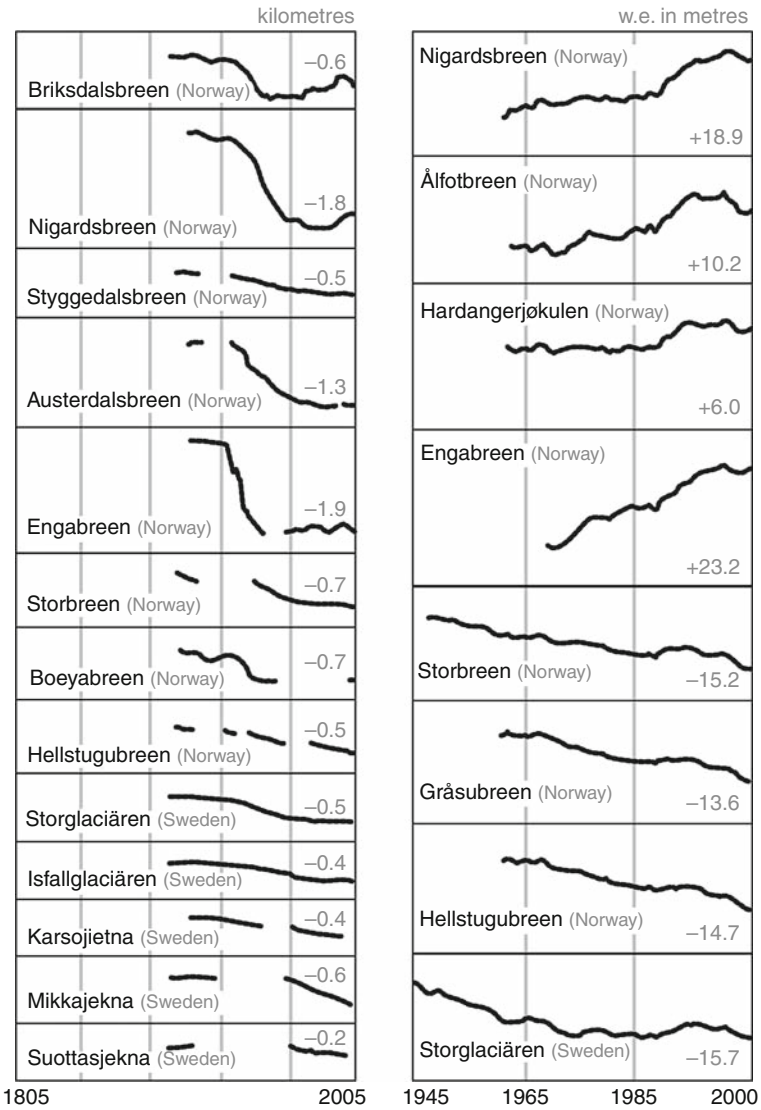

Scandinavian Glaciers, Figure 3 The diagram on the *left* shows glacier frontal changes and the total frontal change in kilometers of different Scandinavian glaciers (*left* panel) up to the year 2005. The diagram on the *right* panel shows the mass balance variations and the total mass balance change in water equivalent of different glaciers up to the year 2005 in Scandinavia.

Scandinavia are mainly warm-based but a few glaciers are polythermal and some glaciers on high mountain plateaux are cold-based (cf. Whalley, 2004 and references therein).

Glacier frontal position and mass balance

Systematic monitoring of the Scandinavian glaciers already began at the turn of the twentieth century with observations on the ice-marginal positions (the glacier change in length) in many glaciated areas. At present data on changes of ice-marginal position from around the world are reported in every fifth year by the World Glacier Monitoring Service (http://www.geo.uzh.ch/wgms/) in their report entitled *Fluctuations of Glaciers*. The ice-frontal position record of most outlet glaciers in Scandinavia indicates a clear overall receding trend of the glacial margins from the mid-1930s to the present (Figure 3). The ice-frontal position for the past ca. 70 years generally indicates a total retreat between 0.3 km and 2.4 km in most of the glaciers observed (Zemp and van Woerden, 2008). During the twentieth century the retreat of the ice margins has not been continuous. While most of the inland glaciers have retreated during the whole observation period starting at the turn of twentieth century, many maritime glacier margins have experienced several advance periods. Maritime glaciers have advanced particularly around 1910 and 1930, late 1970s and 1990s (cf. Andersen et al., 2005; Zemp and van Woerden, 2008). A relatively fast retreating trend has been observed in most glaciers in Scandinavia since 2001 (Andersen et al., 2005).

Mass balance measurements are highly important when studying and describing glacier behavior and their response to variations in climate. The first mass balance measurements of the Scandinavian glaciers were begun late in the 1940s (Schytt, 1959; Liestøl, 1967). The summer, winter, and net-mass balance record of Storglaciären in the Kebnekaise area, Sweden extends back to 1945 and that of Storbreen in Jotunheimen, Norway back to 1949. These two mass balance records are the longest records in the world. Nowadays mass balance data from a number of glaciers from around the world are reported every second year by World Glacier Monitoring Service (http://www.geo.uzh.ch/wgms/) in their *Glaciers Mass Balance Bulletin*.

The mass balance record from the Scandinavian glaciers indicates slight variation over time within individual glaciers depending on local climate conditions, such as the amount of precipitation, but the general trend over the past decades is relatively clear (Figure 3). In general, the maritime glaciers have had a positive mass balance trend from the beginning of the early 1960s. Mass balance became even more positive between the late 1980s and 2000. It has also been shown that there is a clear correlation between the North Atlantic Oscillation (NAO) index and the mass balance records of the maritime glaciers in southern Norway (Nesje et al., 2000; Reichert et al., 2001). In contrast, the mass balances of the more continental glaciers, such as Storglaciären and Storbreen, have had a negative trend over decades. However, all glaciers in Scandinavia have lost mass since 2001 (Anderssen et al., 2005).

Conclusion

Research on past and present Scandinavian glaciers has a long history. Datasets on past and present glaciers, compiled over a century, are one of the most extensive in the world. Despite this fact, the behavior of the past glaciers and ice sheets, their environmental impact, and the relationship between climate and glaciers are still not fully understood. It seems to be vital to seek more high resolution proxy data from terrestrial and marine archives and integrate that with ice sheet modelling in order to understand the causes and mechanisms of the past environmental and climate changes.

Extensive mass balance and other glaciological data on Scandinavian glaciers, together with climatic records, have formed a firm foundation for a detailed study of diverse range of glaciers throughout the region. In addition, reliable field data is essential to test models of glacier behavior. Research on mass balance variations of the Scandinavian glaciers and climate has already shown important results on glaciers' behavior under different climate conditions. Mass balance changes are strongly dependent on climate and therefore it is highly important to understand the mechanisms and response times behind glaciers' mass balance variations in different climate and glacial settings in order to predict glacial behavior in the future climate change.

Bibliography

Andreassen, L. M., Elvehøy, H., Kjøllmoen, B., Engeset, R. V., and Haakensen, N., 2005. Glacier mass balance and length variations in Norway. *Annals of Glaciology*, **42**, 317–325.

Donner, J., 1995. *The Quaternary History of Scandinavia*. Cambridge: Cambridge University Press.

Dowdeswell, J. A., and Hagen, J. O., 2004. Arctic ice masses. Chapter 15. In Bamber, J. L., and Payne, A. J. (eds.), *Mass Balance of the Cryosphere*. Cambridge: Cambridge University Press, pp. 527–557.

Eldrett, J. S., Harding, I. C., Wilson, P. A., Butler, E., and Roberts, A. P., 2007. Continental ice in Greenland during the Eocene and Oligocene. *Nature*, **446**, 176–179.

Grove, J. M., 2004. *Little Ice Ages: Ancient and Modern*. London/New York: Routledge, Vol. I–II.

Holmlund, P., 2005. Glaciers. In Seppälä, M. (ed.), *The Physical Geography of Fennoscandia*. Oxford: Oxford University Press, pp. 175–184.

Liestøl, O., 1967. Storbreen glacier in Jotunheimen, Norway. *Norsk Polarinstitut Skrifter*, **141**, 1–63.

Mangerud, J., 2004. Ice sheet limits in Norway and on the Norwegian continental shelf. In Ehlers, J., and Gibbard, P. L. (eds.), *Quaternary Glaciations – Extent and Chronology, Part I: Europe*. Amsterdam: Elsevier, pp. 271–294.

Mangerud, J., Jansen, E., and Landvik, J. Y., 1996. Late Cenozoic history of the Scandinavian and Barents sea ice sheets. *Global and Planetary Change*, **12**, 11–26.

Melezhik, V. A., 2006. Multiple causes of Earth's earliest global glaciation. *Terra Nova*, **18**, 130–137.

Moran, K., and ACEX Members, 2006. The Cenozoic palaeoenvironments of the Arctic ocean. *Nature*, **441**, 601–605.
Nesje, A., Lie, Ø., and Dahl, S. V., 2000. Is the North Atlantic oscillation reflected in Scandinavian glacier mass balance records? *Journal of Quaternary Science*, **15**, 587–601.
Nesje, A., Bakke, J., Dahl, S. O., Lie, Ø., and Matthews, J. A., 2008. Norwegian mountain glaciers in the past, present and future. *Global and Planetary Change*, **60**, 10–17.
Østrem, G., and Haakensen, N., 1993. Glaciers in Europe – glaciers in Sweden. In Williams, R. S., Jr., and Ferringo, J. G. (eds.), *Satellite Image Atlas of Glaciers of the World*. Washington: U.S. Geological Survey professional paper, 1386-E-3, pp. 63–109.
Reichert, B. K., Bengtsson, L., and Oerlemans, J., 2001. Mid latitude forcing mechanisms for glacier mass balance investigated using general circulation models. *Journal of Climate*, **14**, 3767–3784.
Schytt, V., 1959. The glaciers of the Kebnekaise-Massif. *Geografiska Annaler*, **41**, 213–227.
Schytt, V., 1993. Glaciers in Europe – glaciers in Sweden. In Williams, R. S., Jr., and Ferringo, J. G. (eds.), *Satellite Image Atlas of Glaciers of the World*. Washington: U.S. Geological Survey professional paper, 1386-E-3, pp. 111–125.
Siedlecka, A., Roberts, D., 1992. *The Bedrock Geology of Varanger Peninsula, Finnmark, North Norway: An Excursion Guide*. Trondheim, Norway: Norges Geologiske Undersøkelse Special Publication 5.
Siegert, M. J., and Dowdeswell, J. A., 2004. Numerical reconstructions of the Eurasian Ice Sheet and climate during the Late Weichselian. *Quaternary Science Reviews*, **23**, 1273–1283.
Svendsen, J. I., Alexanderson, H., Astakhov, V. I., Demidov, I., Dowdeswell, J. A., Funder, S., Gataullin, V., Henriksen, M., Hjort, C., Houmark-Nielsen, M., Hubberten, H. W., Ingólfsson, Ó., Jakobsson, M., Kjær, K. H., Larsen, E., Lokrantz, H., Lunkka, J. P., Lyså, A., Mangerud, M., Matiouchkov, A., Murray, A., Möller, P., Niessen, F., Nikolskaya, O., Polyak, L., Saarnisto, M., Siegert, C., Siegert, M. J., Spielhagen, R., and Stein, R., 2004. Late quaternary ice sheet history of northern Eurasia. *Quaternary Science Reviews*, **23**, 1229–1271.
Whalley, W. B., 2004. Glacier research in mainland Scandinavia. In Cecil, L. D., Green, J. R., and Thompson, L. G. (eds.), *Earth Paleoenvironments: Records Preserved in Mid- and Low-Latitude Glaciers*. Secaucus: Kluwer, pp. 121–143.
Zemp, M., and van Woerden, J., 2008. *Global Glacier Changes: Facts and Figures*. Zürich: World Glacier Monitoring Service. URL: http://www.grip.unep.ch/glaciers/.

SEA ICE

Matti Leppäranta
Department of Physics, University of Helsinki, Helsinki, Finland

Definition

Any form of ice found at sea that has originated from the freezing of seawater (WMO, 1970). Icebergs and ice islands, also found in the polar oceans, are *ice of land origin*.

Introduction

Sea ice occurs in about 10% of the surface of the world ocean. Perennial ice is found in high polar latitudes in the Central Arctic Ocean, in the East Greenland Current, and in the western Weddell Sea. The seasonal sea ice zone extends on average to 60° latitudes, not so low in the Northeast Atlantic Ocean but more south in subarctic shallow semi-enclosed seas. Sea ice renewal time is short due to ice melting and advection; perennial ice is mostly less than 10 years old. Solid sea ice lids are statically unstable and break into fields of ice floes, undergoing transport, as well as opening and ridging that altogether create the exciting sea ice landscape as it appears to a human eye (Figure 1).

The history of sea ice science initiated in the l800s with the polar expeditions constructing the geographical picture of the sea ice world (Weeks, 1998b). Microscale structural sea ice models were prepared in the 1950s, and sea ice thermodynamics problem and the closure of sea ice dynamics problem were completed. The modern era commenced in the 1970s based on new technological innovations. Satellite remote sensing revealed the character of time-space variations of sea ice conditions, computing technology made realistic sea ice models possible, and automatic monitoring systems were introduced. The present research focuses on scaling issues, ice thickness observation methods, and the climate problem, with applications to shipping, oil, and gas exploration and ecology of freezing seas.

Sea ice structure and properties

Sea ice physics covers a wide range of scales. *Microscale* includes individual grains and impurities extending from sub-millimeter size to 0.1 m. *Local scale*, 0.1–10 m, considers sea ice as a polycrystalline continuum, and *ice floe scale* extends from 10 m to 10 km, including ice floes and types such as pressure ridges. When the scale exceeds the floe size, the sea ice medium is called *drift ice*.

Microscale – crystal structure and impurities. The freezing point of seawater is $T_f = -1.8°C$. In calm weather, a thin primary ice layer forms first but in windy conditions frazil crystals are generated forming a solid sheet when their buoyancy overcomes the turbulence. Ice crystal platelets overlain together form macrocrystals. Due to constitutional supercooling in the molecular diffusion of salt and heat, cellular ice–water interface forms and encloses liquid brine pockets between the crystal platelets and the crystal boundaries become jagged (Weeks, 1998a). The salinity of new ice is 25–50% of the water salinity. The brine salinity always corresponds to the freezing point of the ambient temperature, that is, brine volume changes with temperature, and salts crystallize in their eutectic temperatures (Figure 2). In summer, the brine pockets expand into drainage network and much brine flows out. Brine pockets serve as biological habitats, for algae with primarily light-limited growth. The most active layer is the bottom layer or so-called skeleton layer.

Local scale – forms of sea ice. Sea ice formation is based on three main mechanisms resulting in *congelation ice*, *frazil ice*, and *superimposed ice* (Weeks, 1998a). Congelation ice crystals are columnar and grow down from the

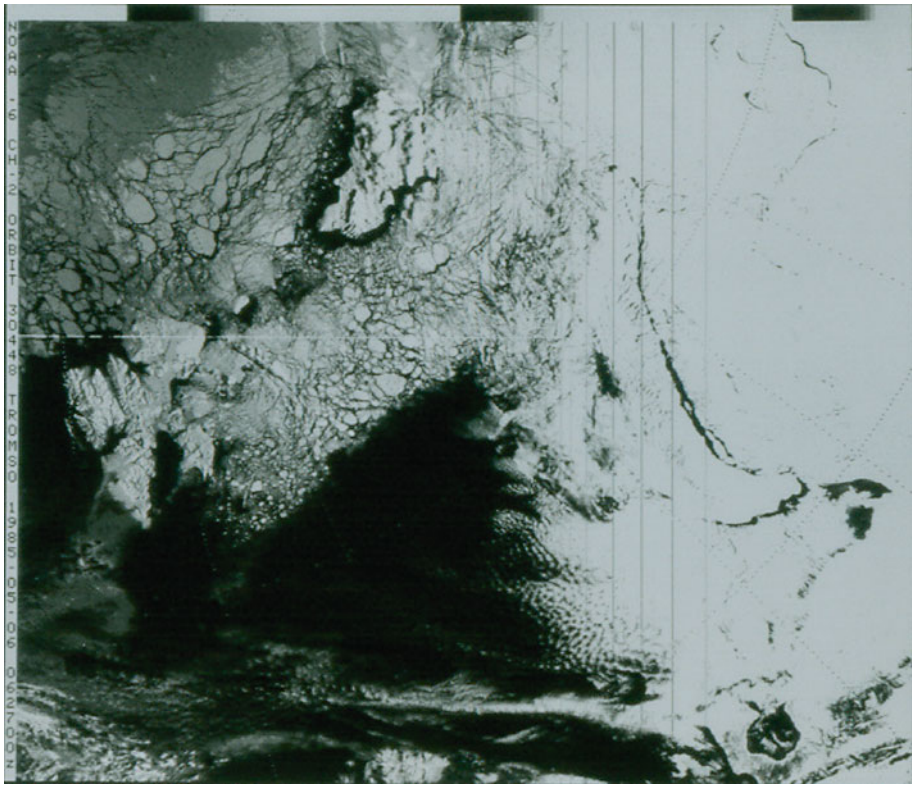
a


b

Sea Ice, Figure 1 Sea ice cover over the Barents Sea and part of the Central Arctic Ocean shown in a NOAA image and a field photograph.

ice–water interface; it is dominant type in the Arctic Ocean. Frazil ice forms in open water areas, with small crystal size; in Antarctica, this is the dominant type. In shallow waters, frazil may attach into the sea bottom to form anchor ice, which may rise up with bottom material. In superimposed ice formed of slush, the crystals are small. Sea ice contains gas bubbles, which have a major influence on scattering of electromagnetic waves, and sediment particles originating from the water body, sea bottom, or atmospheric fallout. Optical properties of sea ice

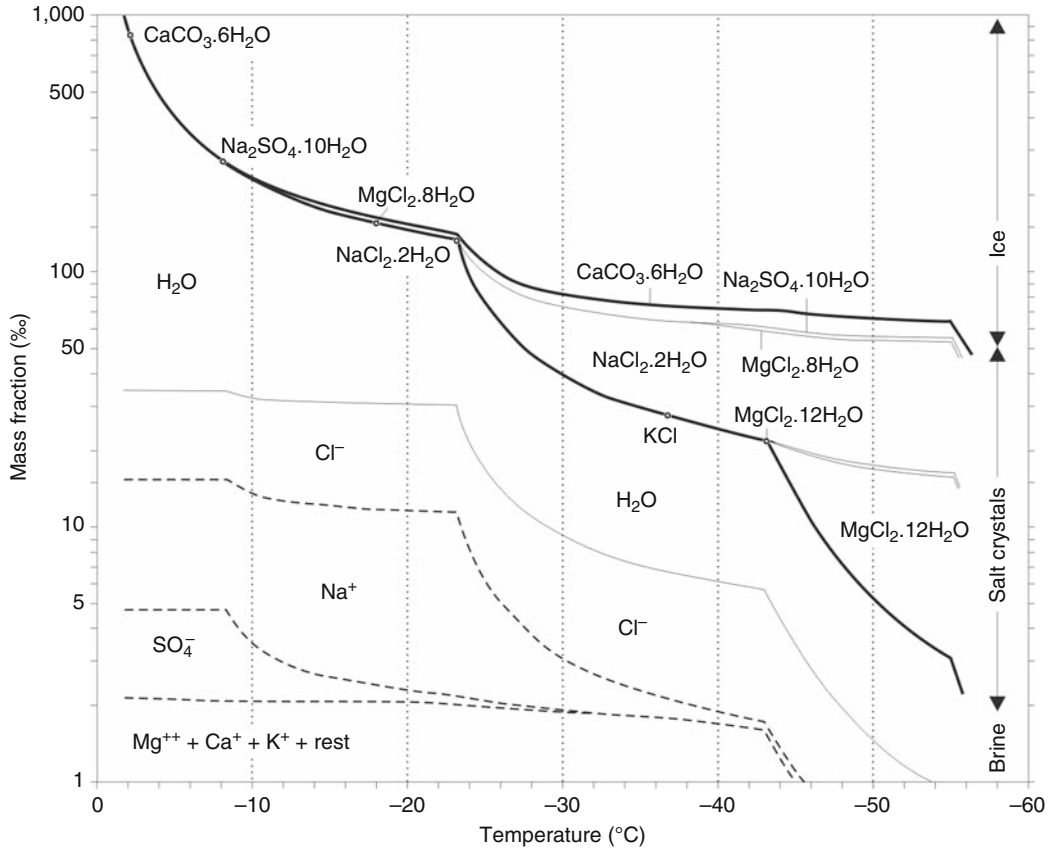

Sea Ice, Figure 2 Sea ice phase diagram with the proportions of ice, brine, and solid salts as a function of temperature. The chemical symbols show the eutectic points of the main salts. Redrawn from Assur (1958).

are influenced by the salt and gas content. Sea ice is less transparent than seawater, the attenuation coefficient being around 1 m^{-1} for normal sea ice.

Drift ice – fields of ice floes. A sea ice landscape consists of ice floes with ridges and other morphological features, as well as *leads* and *polynyas*. The central drift ice pack is free of influence from the boundaries, and the length scale is the size of the basin. (Land) fast ice extends from the shore to about 10–20 m depths. Further out is the shear zone (width 10–200 km), where the mobility of the ice is restricted by the boundary and strong deformation takes place. Marginal ice zone (100 km) lies along the boundary to open sea, characterized as the zone, which "feels the presence of the open ocean." Drift ice is a peculiar geophysical medium (Leppäranta, 2005). It is granular – ice floes are the basic elements – compressible, and highly nonlinear. For continuum models, the size of material particles D must be satisfied, $d << D << \Lambda$, where d is the floe size and Λ is the gradient length scale. The ranges are in nature $d \sim 10^1$–10^4 m, $D \sim 10^3$–10^5 m, and $\Lambda \sim 10^4$–10^6 m. An ice state is defined for the material description, usually taken as the ice thickness distribution (Thorndike et al., 1975), defined by the spatial density function $\pi = \pi(h)$ in a grid cell.

Sea ice growth and decay

In ice growth, latent heat is released and conducted through the ice to the atmosphere. The thicker the ice, the slower is the conduction and growth – mostly less than 5 cm/day for very thin ice and less than 1 cm/day for ice thicker than 1 m. Sea ice has no definite melting point, but always there is melting involved when sea ice warms to dilute the brine and vice versa. The melt rate is of the order of 1 cm/day, mainly due to the net radiation and oceanic heat flux. Where the summer melt is less than the winter growth, multi-year ice develops. First-year ice grows up to 2 m and multi-year ice to 3–4 m.

A simple, analytic approach for the ice growth problem is Zubov's model. The basic assumptions are to ignore solar radiation, oceanic heat flux, and snow. The thickness of ice is

$$h = \sqrt{aS + d^2} - d \tag{1}$$

where $a = 2\kappa/\rho L \approx 11$ cm $(°C \cdot day)^{-1}$, κ is thermal conductivity of ice, ρ is ice density, L is latent heat of freezing, $S = \int_o^t (T_f - T_a)dt'$, usually referred as the "sum of freezing-degree-days," T_a is air temperature ($T_a \leq T_f$), and $d \approx 10$ cm is the insulation efficiency of the atmospheric

surface layer. In the melting season, there is no conduction but the ice melts at the boundaries by the surface fluxes and inside by the solar radiation. Melting of ice goes into ice thickness and porosity ν:

$$\frac{\mathrm{d}\nu h}{\mathrm{d}t} = -\frac{Q}{\rho L} < 0 \tag{2}$$

where Q is the total heat flux into the ice. Snow protects the ice cover due to its high albedo and small optical depth. The equilibrium thickness of multiyear ice is obtained when the summer melt Δh equals the winter growth:

$$h_e = \frac{h_1^2}{2\Delta h} - \frac{\Delta h}{2} \tag{3}$$

where h_1 is the thickness of first-year ice; h_1 = 2 m, and Δh = ½ m gives h_e = 3.75 m. More detail level thermodynamics are examined by numerical modeling (Maykut and Untersteiner, 1971). The results show that the thickness of first-year ice is sensitive to snowfall and oceanic heat flux and the thickness of multi-year ice additionally to albedo.

Drift ice dynamics

Ice kinematics. Drift ice speed is 1–100 cm/s. In the Arctic Ocean, the Transpolar Drift Stream takes ice across the Eurasian side through the Fram Strait into the Greenland Sea, while in the American side ice rotates clockwise in the Beaufort Sea Gyre. Average velocities are 1–5 cm/s, higher toward the Fram Strait. In Antarctica, the governing features are westward flow zone close to the continent and eastward drift zone farther out, driven by the easterly and westerly winds. Meridional displacements interchange ice floes between the two annuli, in particular up along the Antarctic Peninsula in the Weddell Sea. Frequency spectra of ice velocity reach highest levels at the synoptic time scales, and secondary peaks appear at tidal and inertial periods. The ice–wind–ocean current correlation is usually good, but remarkable noncoherent changes appear due to the internal friction of the ice.

Conservation of ice. Ice conditions are modified by thermal and mechanical processes, dictated by the ice conservation law. Mechanical deformation occurs as opening and closing of leads, rafting, and ridging. The general form is (Thorndike et al., 1975)

$$\frac{\partial \pi}{\partial t} + u \cdot \nabla \pi = \psi - \pi \nabla \cdot u + \frac{\partial \phi(h)\pi}{\partial h} \tag{4}$$

where ψ is the mechanical ice thickness redistributor and ϕ is the growth rate of ice.

Drift ice rheology. The main mechanisms behind internal ice stress σ is friction between ice blocks in mechanical deformation (secondary, come floe collisions, floe breakage, and potential energy production). Stress level is negligible for compactness less than 0.7, but compact ice has significant yield strength. The rheological law is formally $\sigma = \sigma(\pi, \varepsilon, \dot{\varepsilon})$, where ε is strain and $\dot{\varepsilon}$ is strain-rate (Figure 3). At compactness more than 0.8 floe collisions

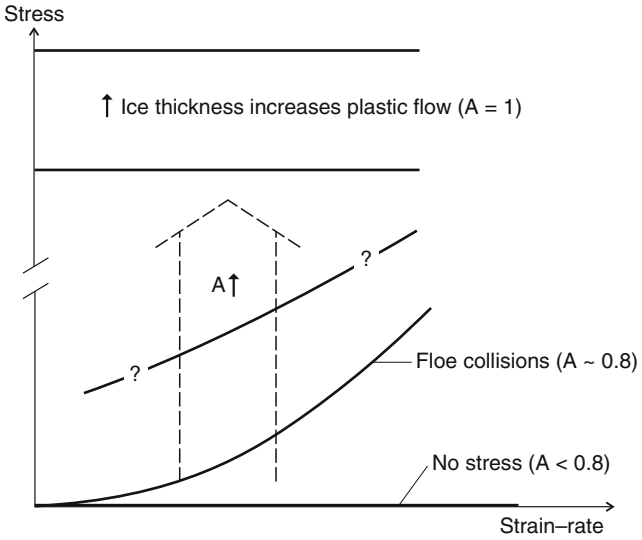

Sea Ice, Figure 3 Schematic presentation of the sea ice rheology as a function of ice compactness *A* and thickness *h*. The cut in the ordinate axis tells of a jump of several orders of magnitude (Leppäranta, 2005).

and shear friction between ice floes increase the stress and plastic flow results, yield strength increasing with ice thickness. Normally, compressive strength is taken twice the shear strength, and for changes in compactness the e-folding strength scale is taken as 5%.

Equation of motion. Integration through the thickness of ice gives the two-dimensional system as (e.g., Leppäranta, 2005)

$$\rho H\left(\frac{\partial u}{\partial t} + u \cdot \nabla u + f k \times u\right) = \nabla \cdot \sigma + \tau_a + \tau_w - \rho H g \beta \tag{5}$$

where ρ is ice density, f is the Coriolis parameter, g is acceleration due to gravity, and β is the sea surface slope. The air and water stresses are turbulent drag laws with drag coefficients and Ekman angles as their parameters. The sea ice dynamics solution is divided to three cases/categories. *Stationary ice cover* results when the forcing is below the yield level. In *free drift*, internal friction is absent and the solution is obtained as vector addition:

$$u = u_a + U_w \tag{6}$$

where U_w is the geostrophic surface current and u_a is the wind-driven ice drift, 2–3% of the wind speed and 20–40° to the right (left) of the wind direction in the northern (southern) hemisphere (Figure 4).

For *ice drift in the presence of internal friction*, numerical continuum models are employed (Hibler, 1979; Hibler and Bryan, 1987). A full model consists of four elements: ice state, rheology, equation of motion, and ice conservation law. The first and second elements constitute

the heart of the model. The primary geophysical parameters are the air and water drag coefficients and compressive strength of ice. The mean annual velocity comes out well from the simulation together with the mean thickness field, validated against submarine data (Figure 5). Models predict that there is always a small amount of open water or thin ice present in the Central Arctic, and further that the annual cycle of the mean thickness has about the same amplitude as in thermodynamic models but the level drops down by about one meter. The maximum ice thicknesses are 5–8 m due to mechanical deformation off the northern coast of Greenland.

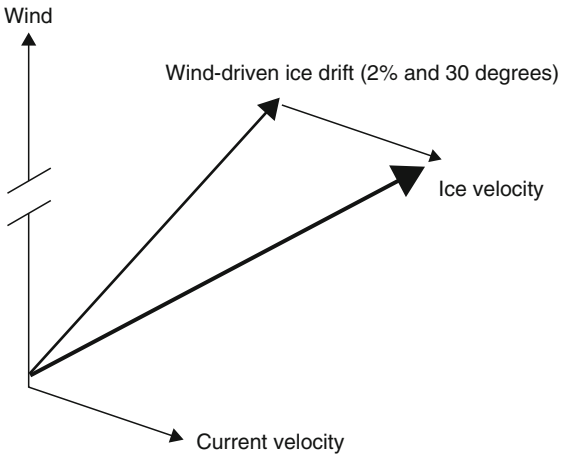

Sea Ice, Figure 4 The free drift solution as the vector sum of wind-driven ice drift and geostrophic ocean current.

Short-term modeling (1 h to 10 days) applications are in shipping and marine technology, while in long-term modeling (1 month to 100 years) the main objective is the climate problem. Sea ice drift transports latent heat and fresh water, modifies the ice boundary and air-sea interaction, and by freezing and melting the ice has a major influence on the hydrographic structure of the ocean. Differential ice drift opens and closes leads bringing major changes to the air-sea heat fluxes, and ridging accumulates ice blocks adding large amounts to the total volume of ice.

Sea ice literature is rather limited. Extensive lecture notes from summer schools are given in Untersteiner (1986) and Leppäranta (1998). Wadhams (2000) presented an excellent general book of the sea ice geophysics, Leppäranta (2005) focused on the drift of sea ice, and McPhee (2008) on the ice–ocean interaction.

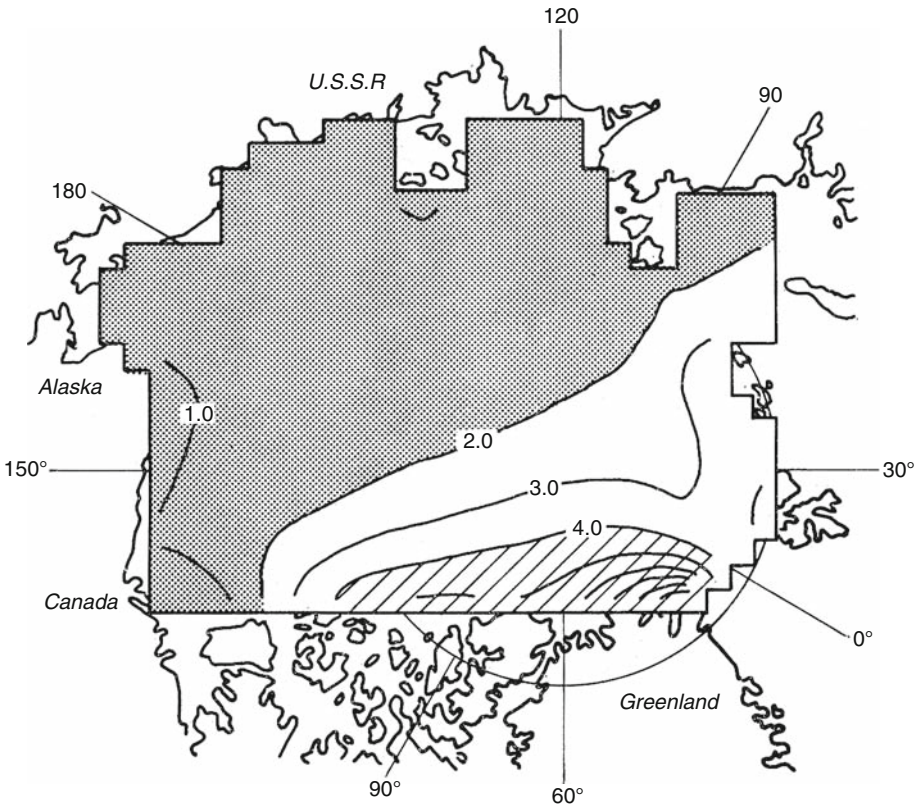

Sea Ice, Figure 5 Ice thickness field in April in the Arctic Ocean as produced by the Hibler (1979) model.

Bibliography

Assur, A., 1958. Composition of sea ice and its tensile strength. In Thurston, W. (ed.), *Arctic Sea Ice*. U.S. National Academy of Science/National Research Council: Publ. No 598, pp. 106–138.
Hibler, W. D., III, 1979. A dynamic-thermodynamic sea ice model. *Journal of Physical Oceanography*, **9**, 815–846.
Hibler, W. D., III, and Bryan, K., 1987. A diagnostic ice–ocean model. *Journal of Physical Oceanography*, **17**, 987–1015.
Leppäranta, M. (ed.), 1998. *Physics of Ice-Covered Seas*. Helsinki: Helsinki University Press, Vol. II, pp. 715–773.
Leppäranta, M., 2005. *The drift of sea ice*. Germany: Springer-Praxis.
Maykut, G. A., and Untersteiner, N., 1971. Some results from a time-dependent, thermodynamic model of sea ice. *Journal of Geophysical Research*, **76**, 1550–1575.
McPhee, M. G., 2008. *Air–Ice–Ocean Interaction: Turbulent Ocean Boundary Layer Exchange Processes*. New York: Springer. 215 p.
Thorndike, A. S., Rothrock, D. A., Maykut, G. A., and Colony, R., 1975. The thickness distribution of sea ice. *Journal of Geophysical Research*, **80**, 4501–4513.
Untersteiner, N. (ed.), 1986. *Geophysics of Sea Ice*. New York: Plenum.
Wadhams, P., 2000. *Ice in the Ocean*. Amsterdam, The Netherlands: Gordon and Breach Science.
Weeks, W. F., 1998a. Growth conditions and structure and properties of sea ice. In Leppäranta, M. (ed.), *Physics of Ice-Covered Seas, Vol. 1*. Helsinki: Helsinki University Press, pp. 25–104.
Weeks, W. F., 1998b. The history of sea ice research. In Leppäranta, M. (ed.), *Physics of Ice-Covered Seas, Vol. 1*. Helsinki: Helsinki University Press, pp. 1–24.
WMO, 1970. *WMO sea-ice nomenclature*. Terminology, codes and illustrated glossary. Edition 1970. Geneva, Secretariat of the World Meteorological Organization, 1970, 147 p. (WMO/OMM/BMO, No. 259, TP. 145.)

Cross-references

Albedo
Arctic Hydroclimatology
Atmosphere–Snow/Ice Interactions
Biogeochemistry of Sea Ice
Estuary Ice Cover
Fast Ice
Finger Rafting
Marginal Ice Zones
Pancake Ice
Thinning of Arctic Sea Ice

SEA-LEVEL

Anny Cazenave
Laboratoire d'Etudes en Géophysique et Océanographie Spatiales (LEGOS), LEGOS-CNES, Observatoire Midi-Pyrénées, Toulouse, France

Definition

Sea level is the height of the sea surface with respect to a given reference. Sea level variations are called "absolute" or "relative" depending in which reference frame (inertial or terrestrial) they are expressed. Absolute sea level variations generally represent change in the volume of water in ocean basins (either due to water density change or water mass change) while relative sea level variations designate sea surface height changes with respect to the ground (accounting thus for both "absolute" sea level variations plus ground motions).

Spatiotemporal scales of sea level variations

Sea level may vary globally or regionally depending on the causes. Global (uniform) variations are sometimes called eustatic. However this term should be avoided because it is sometimes misused and attributed to water mass change of the oceans only (by opposition to water density change). Superimposed to any global mean sea level change, regional variations may also occur (see below). Temporal sea level variations spread over a very broad spectrum. The largest global-scale sea level changes (10–100 m amplitude) occur on geological time scales (10–100 Myr) and depend primarily on tectonics processes (e.g., large-scale change in the shape of ocean basins associated with seafloor spreading and mid-ocean ridges expansion). Formation of long-live ice sheets (e.g., formation of the Antactica ice sheet about 30 Myr ago) is also able to produce >50 m global sea level variations. On shorter time scales (tens to hundred thousand years), quasiperiodic growth and decay of polar ice caps driven by changes of the Earth's obliquity and orbit around the sun represent another cause of global-scale sea level change, with amplitude on the order of 100 m. Century- to millenium-scale sea level fluctuations are mainly driven by climate change in response to natural forcing factors (e.g., solar radiation, volcanic eruptions) and internal variability of the climate system (related, for example, atmosphere-ocean perturbations such as El Nino-Southern Oscillation –ENSO, North Atlantic Oscillation –NAO, Pacific Decadal Oscillation-PDO, etc.).

Recent past and present-day sea level variations

For the last century and past few decades, sea level variations depend on global climate changes induced by natural climate variability and eventually anthropogenic forcing. The two main factors causing sea level change (globally and regionally) are thermal expansion of sea waters and fresh water mass exchange between land and oceans. For example, as the ocean warms in response to global warming, sea waters expand, and thus sea level rises. When mountain glaciers melt in response to increasing air temperature, sea level rises because of fresh water mass input to the oceans. Similarly, ice mass loss from the ice sheets causes sea level rise. Modification of the land hydrological cycle due to climate variability and direct anthropogenic forcing may lead to increased or decreased runoff, hence ultimately to sea level change.

Observations of recent past and present-day sea level variations

Twentieth century

Our knowledge of past century sea level change comes from tide gauge measurements located along continental coastlines and islands. The largest tide gauge database of monthly and annual mean sea level records is the Permanent Service for Mean Sea Level (PSMSL, www.pol.ac.uk/psmsl/) which contains data for the twentieth century from ~2,000 sites maintained by about 200 nations. The records are somewhat inhomogeneous in terms of data length and quality. For long-term sea level studies, only ~10% of this data set is useable because of data gaps and limited tide gauge distribution in the past. Tide gauges measure sea level relatively to the ground, hence monitor also ground motions. In active tectonic and volcanic regions, or in areas subject to strong ground subsidence due to natural causes (e.g., sediment loading in river deltas) or human activities (ground water pumping and oil/gas extraction), tide gauge data are directly affected by the corresponding ground motions. Post glacial rebound, the elastic response of the Earth crust to last deglaciation (also called Glacial Isostatic Adjustment), is another process that gives rise to vertical land movement.

After the ~120 m sea level rise associated with the last deglaciation that started about 15,000 years ago, geological and archeological observations indicate that the mean sea level remained almost stable during the last 2–3 millennia (Lambeck et al., 2010). But tide gauges available since the late nineteenth century have reported significant sea level rise during the twentieth century, especially since 1950, with a mean rate of ~1.7 mm/year over the past 50 years (Church et al., 2004).

Satellite altimetry era

Since the early 1990s, satellite altimetry has become the main tool for precisely and continuously measuring sea level with quasi global coverage and a few days revisit time. Compared to tide gauges which provide sea level relative to the ground, satellite altimetry measures "absolute" sea level variations. The concept of the satellite altimetry measurement is simple: the onboard radar altimeter transmits microwave radiation toward the sea surface which partly reflects back to the satellite. Measurement of the round-trip travel time of the signal provides the height of the satellite above the instantaneous sea surface (called "range"). The quantity of interest in oceanography is the sea surface height above a reference fixed surface (typically a conventional reference ellipsoid). It is obtained by the difference between the altitude of the satellite above the reference (deduced from precise orbitography) and the range measurement. The estimated sea surface height needs be corrected for various factors due to atmospheric delay and biases between the mean electromagnetic scattering surface and sea at the air–sea interface. Other corrections due to geophysical effects, such as solid Earth, pole, and ocean tides, are also applied. High-precision altimetry started with the launch of the Topex/Poseidon satellite in 1992. Its successors, Jason-1 and Jason-2, were launched in 2001 and 2008, respectively. The precision of an individual sea surface height measurement based on these missions has reached the 1–2 cm level, allowing a precision on the global mean rate of rise of ~0.4 mm/year (Ablain et al., 2009). The temporal evolution of the global mean sea level from satellite altimetry since early 1993 (Figure 1) shows an almost linear increase (except for two temporary anomalies associated with the 1997–1998 El Nino and the 2008 La Nina). Over this 18-year-long period, global mean sea level has been rising at a rate of ~3.3 $\pm$ 0.4 mm/year (Ablain et al., 2009; Nerem et al., 2010), a value significantly higher than the mean rate recorded by tide gauges over the past decades.

Sea level budget for the recent years/decades

Ocean warming

Analyses of in situ ocean temperature data collected over the past 50 years by ships and recently by profiling floats indicate that ocean heat content, and hence ocean thermal expansion, has significantly increased since 1950. Ocean warming explains about 25% of the observed sea level rise of the last few decades (Bindoff et al., 2007). This number is likely a lower bound, due to the lack of hydrographic data in remote regions of the southern hemisphere and in the deep ocean (below 1,000 m) (Dominguez et al., 2008). A steep increase is observed in thermal expansion over the decade 1993–2003 (Bindoff et al., 2007). Since about 2003, thermal expansion rate has reduced (Cazenave and Llovel, 2010) but this likely reflects short-term natural variability rather than a new long-term trend. On an average, over the satellite altimetry era (1993–2009), the contribution of ocean warming to sea rise accounts for ~30% (Cazenave and Llovel, 2010).

Glaciers melting

Being very sensitive to global warming, mountain glaciers and small ice caps have retreated worldwide during the recent decades, with significant acceleration during the 1990s. From mass balance studies of a large number of glaciers, estimates have been made of the contribution of glacier's ice melt to sea level (Lemke et al., 2007; Cogley, 2009). For the period 1993–2009, glaciers and ice caps have accounted for ~30% of sea level rise (Cazenave and Llovel, 2010).

Ice sheets

If totally melted, Greenland and West Antarctica would raise sea level by about 7 and 5 m, respectively. Thus, even a small amount of ice mass loss from the ice sheets would produce substantial sea level rise, with adverse societal and economical impacts on vulnerable low-lying coastal regions. Since the early 1990s, different remote sensing observations based on airborne laser and satellite

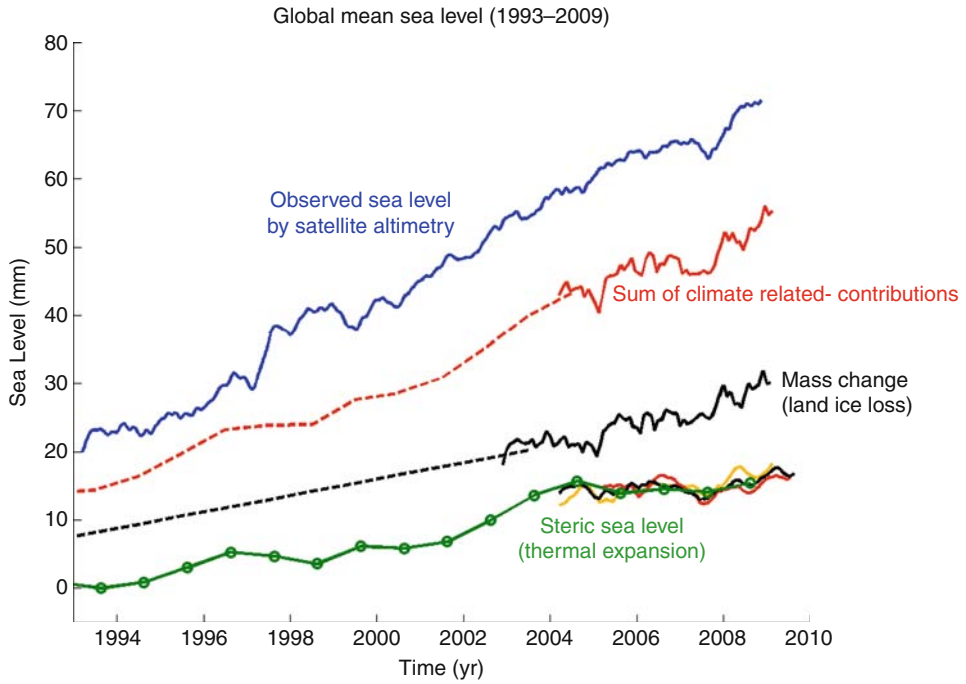

Sea-Level, Figure 1 Evolution of the global mean sea level observed by satellite altimetry (*upper blue curve*), thermal expansion (*botton green curve*), land ice contribution (*middle black curve*), and total climate contributions (*middle red curve*).

altimetry, as well as Synthetic Aperture Radar Interferometry (InSAR) technique and space gravimetry (GRACE space mission), have provided important observations of the mass balance of the ice sheets. These indicate accelerated ice mass loss in coastal regions of Greenland and West Antarctica (Allison et al., 2009; Velicogna, 2009; Steffen et al., 2010). For 1993–2003, <15% of the rate of global sea level rise was due to the mass loss of the ice sheets of Greenland and Antarctica (Lemke et al., 2007), but this contribution has clearly increased after 2003 (Velicogna, 2009) (Figure 2). On an average, over 1993–2009, the two ice sheets have contributed by 30% to sea level rise, with almost equal amount from Greenland and West Antarctica (Cazenave and Llovel, 2010).

Land water storage

Change in land water storage, due to natural climate variability and human activities (i.e., anthropogenic changes in the amount of water stored in soils, reservoirs and aquifers as a result from dam building, underground water mining, irrigation, urbanization, deforestation, etc.), is another potential contribution to sea level change. Model-based estimates of land water storage change caused by natural climate variability suggest no long-term contribution to sea level for the past few decades, although interannual/decadal fluctuations may have been significant. Since 2002, space gravimetry observations from the GRACE space mission now allow determination of the total (i.e., due to climate variability and human activities) land water contribution to sea level. The land water signal is dominated by interannual variability with only a modest contribution (<10%) to the trend (Cazenave and Llovel, 2010).

Sea level budget over the years 1993–2009

Although none of the climate factors discussed above change linearly with time, on an average over the 1993–2009 time span, ocean warming, glaciers melting, and ice sheet mass loss have each contributed by ~30% to global mean sea level rise (Cazenave and Llovel, 2010). Figure 1 compares the thermal expansion and total land ice loss contributions with observed sea level rise.

Regional variability in sea level trends

Satellite altimetry has revealed that sea level is not rising uniformly. In some regions (e.g., western Pacific), the rates of sea level rise are faster by a factor up to three times the global mean rate. In other regions rates are slower than the global mean (e.g., eastern Pacific). The regional variability in sea level trends is mainly due to large-scale changes in the density structure of the oceans and its interaction with the ocean circulation (Wunsch et al., 2007). The largest regional changes in sea level trends result from ocean temperature change (i.e., from non uniform thermal expansion), but in some regions, change in water salinity is also important (Wunsch et al., 2007). Observations of

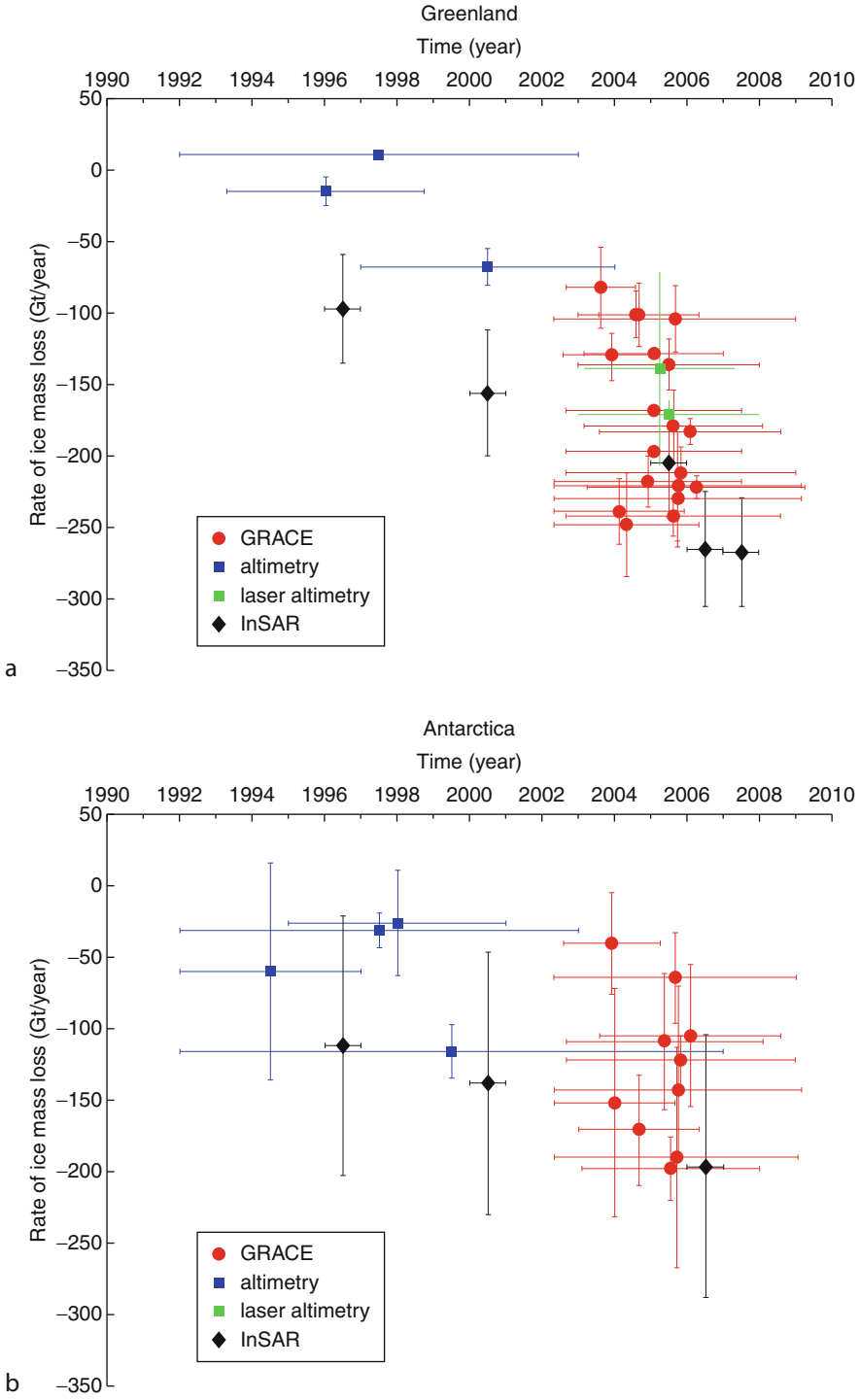

Sea-Level, Figure 2 Mass balance of the ice sheets estimated by remote sensing techniques; compilation of published results (see Cazenave and Llovel, 2010); *horizontal bars* correspond to the time span of data analysis and *vertical bars* represent uncertainty. (**a**) Greenland ice sheet; (**b**) Antarctica ice sheet.

ocean temperature over the past few decades show that trend patterns in thermal expansion are not stationary but fluctuate both in space and time in response to natural perturbations of the climate system such as ENSO (El Nino-Southern Oscillation), NAO (North Atlantic Oscillation), and PDO (Pacific Decadal Oscillation) (Bindoff et al., 2007). As a result, sea level trend patterns observed by satellite altimetry over the last 18 years may be different from those of the last 50 years.

Future sea level rise

IPCC AR4 projections based on coupled climate models indicate that sea level should be higher than today's value by ~38 cm by 2100 (within a range of ±15 cm due to model results dispersion and uncertainty on future greenhouse gases emissions) (Meehl et al., 2007). However this value is possibly a lower bound because AR4 projections only accounted for future ocean warming and glaciers melting. A large proportion of Greenland and West Antarctica ice mass loss results from coastal glacier flow into the ocean through complex dynamical instabilities (Allison et al., 2009; Steffen et al., 2010). Such processes have begun to be understood only recently and were not taken into account in the AR4 sea level projections.

Present-day sea level rise is not uniform; this is also expected for the future. The regional sea level map for 2090–2100 provided by IPCC AR4 (average of an ensemble of models) shows higher than average sea level rise in the Arctic Ocean and along a narrow band in the south Atlantic and south Indian ocean. However, as noticed in IPCC AR4 (Meehl et al., 2007), geographical patterns of sea level change from different models are not generally similar, reflecting current model deficiency in modeling regional changes, in particular those associated with decadal/multidecadal natural variability. This is a research area where improvements are crucially needed, in particular for assessing future coastal impacts of sea level rise. It is worth noticing that IPCC AR4 regional projections are different from present-day observed patterns of sea level rise, a result of spatiotemporal change in spatial trend patterns.

Impacts of sea level rise

Sea level rise is a major concern for populations living in low-lying coastal regions (about 25% of human beings) because it will give rise to inundation, wetland loss, shoreline erosion, saltwater intrusion in surface water bodies and aquifers, and will rise water tables (Nicholls, 2010). Moreover, in many coastal regions of the world, the effects of rising sea level act in combination with other natural and/or anthropogenic factors, such as decreased rate of fluvial sediment deposition in deltaic areas, ground subsidence due to tectonic activity or ground water pumping, and hydrocarbon extraction.

Besides factors that modify shoreline morphology (e.g., sediment deposition in river deltas, change in coastal waves and curren), what does matter in coastal regions is relative sea level rise, i.e., the combination of sea level rise and vertical ground motions. In many coastal regions of the world, these two factors are currently of the same order of magnitude and most often of opposite sign (sea level rises and ground subsides). Accelerated ground subsidence is reported in many regions, either because of local groundwater withdrawal or hydrocarbon extraction. Whatever the causes, ground subsidence directly interacts with and amplifies climate-related sea level rise (long-term trend plus regional variability). However, if sea level continues to rise at current rates and more likely accelerates, the climate factors (sea level rise) will become dominant. But as mentioned above, IPCC AR4 sea level projections could be underestimated. In addition climate models do not yet provide reliable regional variability projections (that superimposes to the global mean rise) for the next few decades. Hence, it is very difficult to quantify future sea level rise in specific regions where various factors interfer in a complex way.

Summary

Measuring sea level rise and understanding its causes has considerably improved in the recent years, essentially because new in situ and remote sensing observations have become available. Sea level is presently rising at a sustained rate and will continue in the future decades because of expected increased global warming. However, the exact amount of sea level rise by 2100 is presently an open question. The main source of uncertainty is the future behavior of the Greenland and Antarctica ice sheets in a changing climate. Ice mass loss in these regions has accelerated in the recent years but we do not know yet how fast and how much the ice sheets will continue to lose mass, hence how they will affect sea level in the future. Improved understanding and modeling of the complex dynamical response of the ice sheets to global warming is one of the priorities of current climate research.

Bibliography

Ablain, M., Cazenave, A., Valladeau, G., and Guinehut, S., 2009. A new assessment of the error budget of global mean sea level rate estimated by satellite altimetry over 1993–2008. *Ocean Science*, **5**, 193–201.

Allison, I., Alley, R. B., Fricker, H. A., Thomas, R. H., and Warner, R. C., 2009. Ice sheet mass balance and sea level. *Antarctic Science*, **21**, 413–426.

Bindoff, N., Willebrand, J., Artale, V., Cazenave, A., Gregory, J., Gulev, S., Hanawa, K., Le Quéré, C., Levitus, S., Nojiri, Y., Shum, C. K., Talley, L., and Unnikrishnan, A., 2007. Observations: oceanic climate and sea level. In Solomon, S., Qin, D., Manning, M., Chen, Z., Marquis, M., Averyt, K. B., Tignor, M., and Miller, H. L. (eds.), *Climate change 2007: The physical Science Basis: Contribution of Working Group I to the Fourth Assessment Report of the Intergovernmental Panel on Climate Change*. Cambridge/New York: Cambridge University Press.

Cazenave, A., and Llovel, W., 2010. Contemporary sea level rise. *Annual Review of Marine Science*, **2**, 145–173.

Church, J. A., White, N. J., Coleman, R., Lambeck, K., and Mitrovica, J. X., 2004. Estimates of the regional distribution of

sea-level rise over the 1950–2000 period. *Journal of Climate*, **17**(13), 2609–2625.
Cogley, J. C., 2009. Geodetic and direct mass balance measurements: comparison and joint analysis. *Annals of Glaciology*, **50**, 96–100.
Dominguez, C., Church, J., White, N., Glekler, P. J., Wijffels, S. E., Barker, P. M., and Dunn, J. R., 2008. Improved estimates of upper ocean warming and multidecadal sea level rise. *Nature*, **453**, 1090–1093, doi:10.1038/nature07080.
Lambeck, K., Woodroffe, C. D., Antonioli, F., Anzidei, M., Gehrels, W. R., Laborel, J., and Wright, A. J., 2010. Paleoenvoronmental records, geophysical modelling and reconstruction of sea level trends and variability on centennial and longer time scales. In Church, J. A., et al. (eds.), *Understanding Sea Level Rise and Variability*. Oxford: Wiley-Blackwell.
Lemke, P., et al., 2007. Observations: changes in snow, ice and frozen ground. In Solomon, S., Qin, D., Manning, M., Chen, Z., Marquis, M., Averyt, K. B., Tignor, M., and Miller, H. L. (eds.), *Climate Change 2007: The Physical Science Basis. Contribution of Working Group I to the Fourth Assessment Report of the Intergovernmental Panel on Climate Change*. Cambridge/New York: Cambridge University Press.
Meehl, G. A., et al., 2007. Global climate projections. In Solomon, S., Qin, D., Manning, M., Chen, Z., Marquis, M., Averyt, K. B., Tignor, M., and Miller, H. L. (eds.), *Climate Change 2007: The Physical Science Basis. Contribution of Working Group I to the Fourth Assessment report of the Intergovernmental Panel on Climate Change*. Cambridge/New York: Cambridge University Press.
Nerem, R. S., Chambers, D. P., Choe, C., and Mitchum, G. T., 2010. Estimating mean sea level change from the Topex and Jason altimeter missions. *Marine Geodesy*, **33**, 435–446.
Nicholls, R. J., 2010. Impacts of and responses to sea level rise. In Church, J. A., et al. (eds.), *Understanding Sea Level Rise and Variability*. Oxford: Wiley-Blackwell.
Steffen, K., Thomas, R. H., Rignot, E., Cogley, J. G., Dyugerov, M. B., Raper, S. C. B., Huybrechts, P., and Hanna, E., 2010. Cryospheric contributions to sea level rise and variability. In Church, J. A., et al. (eds.), *Understanding Sea Level Rise and Variability*. Oxford: Wiley-Blackwell.
Velicogna, I., 2009. Increasing rates of ice mass loss from the Greenland and Antarctica ice sheets revealed by GRACE. *Geophysical Research Letters*, **36**, L19503.
Wunsch, C., Ponte, R. M., and Heimbach, P., 2007. Decadal trends in sea level patterns: 1993–2004. *Journal of Climate*, **20**(24), 5889–5911, doi:10.1175/2007JCLI1840.1.

Cross-references

Calving Glaciers
Catastrophic Rock Slope Failures and Mountain Glaciers
Climate Change and Glaciers
Deglaciation
Glacioeustasy
Glacioisostasy
Glaciology
Global Warming and its Effect on Snow/Ice/Glaciers
Greenland Ice Sheet
Hydrologic Cycle and Snow
Ice Age
Ice Sheet Mass Balance
Impacts of Snow and Glaciers on Runoff
Last Glacial Maximum Glaciation (LGM/LGP) in High Asia (Tibet and Surrounding Mountains)
Quaternary Glaciation
Surface Energy Balance

SEASONAL FROST

Chelamallu Hariprasad
Centre for Studies in Resource Engineering, IITB Powai, Mumbai, Maharashtra, India

The occurrence of ground temperatures below 0°C for only part of the year is known as seasonal frost. This may occur in the regions where temperature prevails at subzero temperature for a period of time.

SEASONAL SNOW COVER

Amit Kumar
Department of Geology, Centre of Advanced Study in Geology, Punjab University, Chandigarh, India

During winter, when climate conditions do not allow melt of the deposited snow, a snow cover is formed by the deposition of successive snowfall events. Although highly stratified with many layers, the seasonal snow cover is often treated as a homogeneous medium. Each layer has its own physical properties due to the initial snow condition at the time of deposition on the previous surface layer and subsequent metamorphosis, which is mainly determined by the varying field conditions and load and arrangement of ice particles in the layer. Thus, a snow cover has a stratified structure because snowfall is deposited in a series of layers. Individual layers corresponding to different snowfall event may be thick or thin. Thick layers are the result of steady snowfall in calm weather, whereas thin layers occur due to ice crusts formed due to melting, freezing, and wind conditions on the surface of deposited snow cover depends on the topography and the presence of vegetation. A seasonal snow cover is deposited and melted within 1-year cycle, and is normally developed from a series of winter storm. In addition to being an important component of water considered it is also a major component of regional and global hydrology balance. Permanent snowfields, which turn into glacier gradually, are developed at high places where total accumulated snow is not melted away in the summer season.

The changes in snow cover depend upon the prevailing weather conditions such as temperature, precipitation radiation, and wind. In warm conditions, the snow may melt away or stay for a short period. Snow cover that stays only for a few days and then depleted due to climate conditions is known as temporary snow cover.

Snow cover constitutes the largest component of the cryosphere and plays a significant role in the global climate and climate response to global changes. The extent and variability of seasonal snow cover are important parameters in climate and hydrologic systems due to effects on energy and moisture budgets. Seasonal snow can cover more than 50% (50 million km^2) of the Northern

Hemisphere land surface during the winter, making it the largest single component of the cryosphere.

Bibliography

Benn, D. I., Evans, D. J. A., 1998. *Glaciers and glaciation*. Arnold: London.

Singh, P., Singh, V. P., 2001. Snow and glacier hydrology. *Water Science and Technology Library*, Kluwer Academic: Dordrecht.

SEDIMENT BUDGETS

Helen E. Reid, Gary J. Brierley
School of Environment, The University of Auckland, Auckland, New Zealand

Definition

A sediment budget is an account of sediment movement within a defined spatial unit (e.g., hillslope, river reach, or catchment) over a given time frame. It is measured as:

$$O - I \pm \Delta S = 0$$

where O = sediment output, I = sediment input, and ΔS refers to the change in sediment storage over a given time frame. If sediment inputs exceed outputs then net deposition (storage) has occurred within the system. If outputs exceed inputs, then net erosion has occurred.

Introduction

Sediment budgets are an integral part of geomorphic enquiry (Slaymaker, 2003). They can be applied to any situation where sediment is being transported, whether over land, within water bodies, or within the atmosphere (Thomas and Goudie, 2000). In terrestrial terms, sediment budgets can be performed over a wide range of spatial scales for differing compartments of a landscape. In general, however, they are applied at the (sub)catchment scale (Reid and Dunne, 1996), reflecting the primacy of the catchment as the fundamental geomorphic unit (Chorley, 1969). As drainage basins operate as closed systems, they are the ideal unit/spatial scale at which sediment budgets can be performed (e.g., Reid and Dunne, 1996). However, sediment budgets may be a useful tool at smaller scales, such as reach-scale analyses of sediment transfer along a river or plot-scale analyses of soil erosion on farms.

River systems act as conveyer belts that move sediments from source zones (hillslopes of headwater areas, where net erosion occurs) through transfer zones in mid-catchment where erosion and deposition are approximately in balance, to accumulation zones (i.e., oceans or inland basins; Schumm, 1977). Analysis of sediment budgets entails identification of sediment sources and erosion rates (whether primary erosion or reworking of sediment stores), measurement of sediment accumulation within landscape compartments (i.e., deposition and restorage of materials), and determination of sediment output at the outlet of the spatial unit that is being studied. Changes to relationships between sediment sources, storage elements, and pathways of sediment movement may bring about dramatic changes to landscape form and sediment flux.

Sediment yield refers to the quantity of sediment that reaches the outlet of a drainage basin (Thomas and Goudie, 2000). The primary difference between analysis of sediment yield and derivation of sediment budgets is consideration of the processes that fashion sediment storage, and the efficiency with which sediment stores are reworked. The sediment delivery ratio defines the "proportion of sediment leaving an area, relative to the amount of sediment eroded in that area" (Brown et al., 2009: 37). Residence times for sediment reworking vary markedly for differing sediment storage units, whether on hillslopes or along the valley floor (both channel and floodplain compartments). In a sense, the nature and pattern of sediment stores reflects spatial variability in accommodation space within a landscape (i.e., places where sediments may be stored, however effectively) and the nature of geomorphic processes that rework these sediments (i.e., the magnitude–frequency relationships of reworking processes, and the sequence of events that determine whether sediments in stores are eroded, or additional materials are added to that store). Meaningful differentiation can be made between short-term *stores* that are prone to reworking (e.g., mobile sediments that make up mid-channel bars in river systems) and long-term *sinks* that are spatially isolated from reworking processes (e.g., cohesive sediments that make up floodplain and/or terrace features; Fryirs and Brierley, 2001). Residence time for sediment storage within a unit reflects the effectiveness of erosion, transport, and deposition processes that fashion the behavior of that landscape compartment which, in turn, is affected by the position of that feature within the landscape, the surrounding topography, climatic conditions, and vegetation cover (Brown, 1987). Residence times usually increase downstream within a catchment, as slopes decrease and accommodation space increases (Fryirs et al., 2007a).

The nature and rate of sediment movement through a landscape reflects the connectivity of the system (Harvey, 2002; Fryirs et al., 2007b). In highly coupled systems, sediment from hillslopes is delivered directly to the channel. High gradient, headwater channels are highly coupled with their hillslopes, directly inputting materials into channels. High slopes generate high steam power; so competence-limited channels are able to flush all but the largest material. As a result, sediment stores are limited in these highly connected parts of landscapes. Once slope flattens in downstream reaches, accommodation space and sediment stores increase. Floodplain pockets disconnect hillslope-derived sediments from within-channel features such as mid-channel bars and benches. Terraces have even longer residence times than the contemporary floodplain, further acting to decouple the system. In general terms, the residence time of sediment stores tends to

increase with distance downstream. Indeed, as sediments are buried and the thickness of the basin fill increases, subsidence increasingly traps and compresses sediments, facilitating their incorporation into the rock record.

Buffers, barriers, and blankets impede sediment conveyance within a catchment (Fryirs et al., 2007a, b). Buffers restrict sediment transfer from hillslopes to the channel network, as sediments are stored within features such as intact valley fills, piedmont zones, alluvial fans, floodplain pockets, and terraces. Barriers inhibit downstream movement of sediment along channels, as features such as dams and bedrock steps induce base level controls along longitudinal profiles. Blankets smother landforms, protecting underlying sediments from reworking. The more connected the system, the more efficient the rate of sediment transfer.

Sediment movement is not uniform over time. Rather, pulses in sediment reflect stochastic inputs and transfer mechanisms, such as landslides, rainfall events, earthquakes, and fires (Benda and Dunne, 1997). The amount of sediment moved by a single event is linked to the magnitude and duration of the event, whereas the amount of sediment that is moved over a period of time reflects the frequency of events of different sizes. Each landscape compartment is subjected to a suite of processes that have their own magnitude–frequency domain (or spectra). The sediment budget reflects the synchronicity of these relationships across differing compartments of the landscape (i.e., sediments sourced from one unit may be flushed to the outlet, or become trapped elsewhere within the system). This is most readily exemplified by the transfer of sediments from hillslopes to a channel system. If sediment generation from hillslopes is too high, and the channel is unable to remove all sediments, aggradation occurs on the valley floor. Alternatively, if sediment supply from hillslopes is too low, the channel will incise into its bed. In both instances, the channel adjusts to mediate conditions operating on hillslopes. The relationship between hillslope and river processes determines the rate of sediment flux (and storage) in differing parts of river systems.

Using sediment budgets to place landscape responses to human disturbance in light of natural variability

Long-term changes in sediment flux must be understood before the imprint of human disturbance upon a system can be determined (Brierley and Fryirs, 2005; Houben et al., 2009). Sediment storage and movement reflect the interaction of geologic, climatic, and anthropogenic memory, highlighting how the imprint of the past upon sediment stores is key to predicting future sediment fluxes (Brierley, 2010). For example, Pleistocene glacial stores continue to influence contemporary sediment fluxes in some systems (Church and Slaymaker, 1989). In their modelling of sediment flux at the global scale, Syvitski and Milliman (2007) found that geological controls explained 65%, climate 14%, and anthropogenic factors 16% of the viability in sediment loads. Therefore, natural geologic characteristics including basin area, lithology (i.e., erodibility), relief (i.e., erosivity, as determined by potential energy), and ice erosion are major determinants on the amount of sediment a landscape generates.

As sediment movement is largely stochastic, large events may cause fundamental shifts in the functioning of the system, prospectively bringing about a change in system state as threshold conditions are exceeded (Schumm, 1977; Reid and Dunne, 1996; Brierley and Fryirs, 2005). For example, landslides may block a channel system from reworking sediments. Sediment budgets can be used to understand landscape responses to natural, commonly high magnitude events such as volcanic eruptions (Tagata et al., 2005), landslides (Peart et al., 2005), bush fires (Wallbrink et al., 2005), and system responses to climatic fluctuations (Aalto et al., 2003).

Human activities have had a profound impact upon sediment movement in landscapes, and sediment budgets are commonly used to analyze the nature and extent of system responses to human disturbance (Houben et al., 2009). Every system is unique, its functioning driven by landscape history and more contemporary patterns of anthropogenic activity (Brierley, 2010). Wilkinson and McElroy (2007) assert that reworking of sediment stores generated in response to forest clearance is testimony to the primacy of human disturbance as the greatest influence upon contemporary sediment budgets across the Earth's surface. Examples of the use of sediment budgets to analyze the impact of contemporary land uses include agricultural impacts (Trimble 1983, 2009), mining (Knighton, 1991), logging (Roberts and Church, 1986), dams (Bogen and Bonsnes, 2005), roads (Megahan et al., 1986; Ramos-Scharron and MacDonald, 2007), and urbanization (Nelson and Booth, 2002). Tracking of contaminants and heavy metal pollutants, and analyses of carbon, nitrogen, and phosphorus cycles can be a component of sediment budget analyses (e.g., Houghton et al., 1999; Prosser et al., 2001; Slaymaker et al., 2003). Vorosmarty et al. (2003) highlight the primary role of dams in storing sediments of river systems. Understanding how human activities have altered sediment flows between compartments of a system allows for targeted management, identifying and mitigating the areas that are having the most detrimental affect on the system.

What techniques are used to derive sediment budgets?

Any sediment budget must give careful consideration to the spatial scale at which it is to be applied. Typically, a trade-off must be made between scale and precision and the level of accuracy that is sought (Brown et al., 2009). Local scale studies tend to be more fieldwork intensive, involving in-depth investigation into the relationships among specific components that make up the system (e.g., Bartley et al., 2007; Trimble, 1983). In contrast, sediment budgets undertaken at national

(Hicks et al., 1996) or global (Syvitski and Milliman, 2007) scales tend to consider sediment yields (outputs) rather than identification of sources and stores.

Given the stochastic nature of the forcing elements that determine sediment movement and storage, timescale of analysis is a critical consideration in the derivation of sediment budgets. Long-term perspectives may incorporate changes in climatic periods, land use, and sea level whereas short-term, more contemporary analyses can be used to analyze system responses to a given event (or sequence of events), such as impacts of floods, fire, or land-use alterations. Seasonal changes may be an important driver of sediment flux (e.g., tropical wet-dry seasonality, or impacts of snowmelt). Sediment flux at any given time is greatly influenced by the amount of sediment that is available to be moved at that time, especially the availability of readily accessible stores. Conditions experienced at the time of measurement have major implications when extrapolating data over longer time periods.

Techniques used to derive and analyze sediment budgets range from simple qualitative conceptualizations used to examine process interactions to in-depth quantitative analyses that derive volumetric information about the rates at which sediment is entering and leaving landscape components (Reid and Dunne, 2003). Most budgets use a mixture of desk, field, and analytical techniques.

Conceptual models of sources, sinks, and the pathways of transfer are used to identify the primary processes and units that influence sediment flux within a system (Reid and Dunne, 1996; Bartley et al., 2007). Various analytical techniques are used to assess processes of erosion, transport, and deposition that affect different units. Aerial photographs and maps aid identification of erosion rates for differing surfaces such as erosion scarps or gully complexes (Reid and Dunne, 1996). Historical images can be used to interpret the types and magnitude of channel and hillslope change (e.g., differences in active versus vegetated bar surface areas over time (Ham and Church, 2000)). The availability of map, photograph, and archival sources makes it much easier to interpret human impacts upon natural systems in the New World than elsewhere (Brown et al., 2009).

Most small-scale sediment budgets have a fieldwork component applying repeat surveys such as cross section analysis, erosion pins, flumes, ground-penetrating radar, bed load transport, floodplain coring, or trenches to assess the level of floodplain deposition (Bartley et al., 2006, 2007; Brown et al., 2009; Trimble, 1983; Walling et al., 1998; Reid and Dunne, 1996). Sediment-rating curves can be derived from analyses of turbidity (suspended sediment loads) and bed load sampling at gauging stations. Fieldwork provides important contextual information with which to ground modelling applications. However, use of field techniques in isolation can be problematic, as getting accurate data is very expensive and time consuming, and issues always arise regarding reliability and representativeness (Brown et al., 2009). Ideally, modelling techniques are supported and verified using field-based evidence (e.g., Bartley et al., 2007). However, more ground can be covered with higher accuracy when computer-based techniques are used (Brown et al., 2009).

Advances in computer-based technology, remote sensing imagery, and Geographic Information Science (GIS) have aided the development of more detailed and complex sediment budgets, increasing what can be achieved in terms of speed, accuracy, and scale (Brooks et al., 2008; Brown et al., 2009). GIS allows large datasets to be overlayed with greater spatial accuracy (e.g., Ramos-Scharron and MacDonald, 2007). Repeat surveys using advanced remote sensing technologies such as light detection and ranging (LiDAR) can be applied to generate precise digital elevation models from which fine resolution sediment budgets can be derived (Brown et al., 2009).

Paleo-records can be used to interpret how sediment fluxes have changed over time, isolating responses to different forcing mechanisms such as different cycles in climate or extreme events. The further back that analysis is based, the more likely it is that changes in climate and morphology have driven the system, altering cause–response relationships (Houben et al., 2009). Applications of dating techniques to derive sediment age and source are an integral part of sediment budget analyses. While dating can be expensive and have a degree of error, it allows more accurate interpretation of the timescales and rates over which landscape evolution has occurred. Finally, sediment fingerprinting using environmental and fallout radionuclides and chemical sediment characteristics can be used to trace the sources and pathways of sediment movement and accumulation (Walling, 2003; Walling and Horowitz, 2005; Wallbrink et al., 2005).

Summary

Sediment budgets are an integral part of geomorphic investigations into sediment movement through landscapes. Recent conceptual and technological advances in sediment budgeting aid interpretations of landform development and responses to anthropogenic disturbance. Hence, sediment budgets are a key conceptual framework in the analysis of landscape systems, allowing researchers and managers to gain critical insights into how landscapes look and operate, aiding spatial prioritization of management applications.

Bibliography

Aalto, R., Maurice-Bourgoin, L., Dunne, T., Montgomery, D. R., Nittrouer, C. A., and Guyot, J. L., 2003. Episodic sediment accumulation on Amazonian flood plains influenced by El Niño/Southern Oscillation. *Nature*, **425**, 493–497.

Bartley, R., Roth, C., Ludwig, J., McJannet, D., Liedloff, A., Corfield, J., Hawdon, A., and Abbott, B., 2006. Runoff and erosion from Australia's tropical semi-arid rangelands: influence of ground cover for differing space and time scales. *Hydrological Processes*, **20**, 3317–3333.

Bartley, R., Hawdon, A., Post, D. A., and Roth, C. H., 2007. A sediment budget for a grazed semi-arid catchment in the Burdekin basin, Australia. *Geomorphology*, **87**, 5–28.

Benda, L., and Dunne, T., 1997. Stochastic forcing of sediment supply to channel networks from landsliding and debris flow. *Water Resources Research*, **33**(12), 2849–2863.

Bogen, J., and Bonsnes, T. E., 2005. The impact of hydropower development on the sediment budget of the river Beiarelva, Norway. In Horowitz, A. J., and Walling, D. E. (eds.), *Sediment Budgets 2*. Willingford, UK: IAHS Pub 292, pp. 214–222.

Brierley, G. J., 2010. Landscape memory: the imprint of the past on contemporary landscape forms and processes. *Area*, **42**(1), 76–85.

Brierley, G. J., and Fryirs, K. A., 2005. *Geomorphology and River Management: Applications of the River Styles Framework*. Oxford: Blackwell.

Brooks, A. P., Spencer, J., Shellberg, J. G., Knight, J., and Lymburner, L., 2008. Using remote sensing to quantify sediment budget components in a large tropical river-Mitchell River, Gulf of Carpentaria. In Schmidt, J., Cochrane, T., Philips, C., Elliott, S., Davies, T., and Basher, L. (eds.), *Sediment Dynamics in Changing Environments*. Willingford: IAHS Pub 325, pp. 225–236.

Brown, A. G., 1987. *Long-Term Sediment Storage in the Severn and Wye Catchments*. In Gregory, K. J., Lewin, J., and Thornes, J. B. (eds.), Palaeohydrology in Practice. John Wiley and Sons Ltd. Great Britain, pp. 307–332.

Brown, A. G., Carey, C., Erkens, G., Fuchs, M., Hoffmann, T., Macaire, J. J., Moldenhauer, K. M., and Walling, D. E., 2009. From sedimentary records to sediment budgets: multiple approaches to catchment sediment flux. *Geomorphology*, **108**, 35–47.

Chorley, R. J., 1969. The drainage basin as the fundamental unit. In Chorley, R. J. (ed.), *Water, Earth and Man: A synthesis of Hydrology*. Methuen, London: Geomorphology and Socioeconomic geography, pp. 77–99.

Church, M., and Slaymaker, O., 1989. Disequilibrium of Holocene sediment yield in glaciated British Columbia. *Nature*, **337**(6206), 452–453.

Fryirs, K., and Brierley, G. J., 2001. Variability in sediment delivery and storage along river courses in Bega catchment, NSW, Australia: implications for geomorphic river recovery. *Geomorphology*, **38**, 237–265.

Fryirs, K. A., Brierley, G. J., Preston, N. J., and Kasai, M., 2007a. Buffers, barriers and blankets: the (dis)connectivity of catchment-scale sediment cascades. *Catena*, **70**, 49–67.

Fryirs, K. A., Brierley, G. J., Preston, N. J., and Spencer, J., 2007b. Catchment-scale (dis)connectivity in sediment flux in the upper Hunter catchment, New South Wales, Australia. *Geomorphology*, **84**, 297–316.

Ham, D. G., and Church, M., 2000. Bed-material transport estimated from channel morphodynamics: Chilliwack river, British Columbia. *Earth Surface Processes and Landforms*, **25**, 1123–1142.

Harvey, A. M., 2002. Effective timescales of coupling within fluvial systems. *Geomorphology*, **44**, 175–201.

Hicks, M. D., Hill, J., and Shankar, U., 1996. Variation of suspended sediment yields around New Zealand: the relative importance of rainfall and geology. In Walling, D. E., and Webb, B. W. (eds.), *Erosion and Sediment Yield: Global and Regional Perspectives*. Willingford: IAHS Pub 236, pp. 149–156.

Houben, P., Wunderlich, J., and Schrott, L., 2009. Climate and long-term human impact on sediment fluxes in watershed systems. *Geomorphology*, **108**, 1–7.

Houghton, R. A., Hacker, J. L., and Lawrence, K. T., 1999. The U.S. carbon budget: contributions from land-use change. *Science*, **285**, 574–578.

Knighton, A. D., 1991. Channel bed adjustment along mine affected rivers of northeast Tasmania. *Geomorphology*, **4**(3/4), 205–219.

Megahan, W. F., Seyedbagheri, K. A., Mosko, T. L., and Ketcheson, G. L., 1986. Construction phase sediment budget for forest roads on granitic slopes in Idaho. In Hadley, R. (ed.), *Drainage Basin Sediment Delivery*. Willingford: IAHS Pub 159, pp. 31–39.

Nelson, E. J., and Booth, D. B., 2002. Sediment sources in an urbanizing, mixed land use watershed. *Journal of Hydrology*, **264** (1–4), 51–68.

Peart, M. R., King, J. P., and Ruse, M. E., 2005. Sediment production by landslides in Hong Kong: two case studies. In Walling, D. E., and Horowitz, A. (eds.), *Sediment Budgets 1*. Willingford: IAHS Pub 291, pp. 29–36.

Prosser, I. P., Rutherfurd, I. D., Olley, J. M., Young, W. J., Wallbrink, P. J., and Moran, C. J., 2001. Large-scale patterns of erosion and sediment transport in river networks with examples from Australia. *Marine and Freshwater Research*, **52**, 81–99.

Ramos-Scharron, C. E., and MacDonald, L. H., 2007. Development and application of a GIS-based sediment budget model. *Journal of Environmental Management*, **87**(2), 157–172.

Reid, L. M., and Dunne, T., 1996. *Rapid Evaluation of Sediment Budgets*. Germany: Catena.

Reid, L. M., and Dunne, T., 2003. Sediment budgets as an organising framework. In Kondolf, G. M., and Piegay, H. (eds.), *Tools in Fluvial Geomorphology*. Chichester: Wiley, pp. 463–500.

Roberts, R. G., and Church, M., 1986. The sediment budget in severely disturbed watersheds, Queen Charlotte Ranges, British Columbia. *Canadian Journal of Forest Research*, **16**, 1092–1106.

Schumm, S. A., 1977. *The Fluvial System*. New York: Wiley.

Slaymaker, O., 2003. The sediment budget as conceptual framework and management tool. *Hydrobiologia*, **494**, 71–82.

Slaymaker, O., Souch, C., Menounos, B., and Filippelli, G., 2003. Advances in Holocene mountain geomorphology inspired by sediment budget methodology. *Geomorphology*, **55**, 305–316.

Syvitski, J. P. M., and Milliman, J. D., 2007. Geology, geography and humans battle for dominance over the delivery of fluvial sediment to the coastal ocean. *Journal of Geology*, **115**, 1–19.

Tagata, S., Yamakoshi, T., Doi, Y., Sasahara, K., Nishimoto, H., and Nagura, H., 2005. Post-eruption sediment budget of a small catchment on the Miyakejima volcano, Japan. In Walling, D. E., and Horowitz, A. J. (eds.), *Sediment Budgets 1*. Willingford: IAHS Pub 291, pp. 37–45.

Thomas, D. S. G., and Goudie, A., 2000. *The Dictionary of Physical Geography*. Malden: Blackwell.

Trimble, S. W., 1983. A sediment budget for Coon Creek basin in the driftless area, Wisconsin, 1853–1977. *American Journal of Science*, **283**, 454–474.

Trimble, S. W., 2009. Fluvial processes, morphology and sediment budgets in the Coon Creek basin, WI, USA, 1975–1993. *Geomorphology*, **108**, 8–23.

Vorosmarty, C. J., Meybeck, M., Fekete, B., Sharma, K., Green, P., and Syvitski, J. P. M., 2003. Anthropogenic sediment retention: major global impact from registered river impoundments. *Global and Planetary Change*, **39**(1–2), 169–190.

Wallbrink, P., Blake, W., Doerr, S., Shakesby, R., Humphreys, G., and English, P., 2005. Using tracer based sediment budgets to assess redistribution of soil and organic material after severe bush fires. In Horowitz, A., and Walling, D. E. (eds.), *Sediment Budgets 2*. Willingford: IAHS Pub 292, pp. 223–230.

Walling, D. E., 2003. Using environmental radionuclides as tracers in sediment budget investigations. In Bogen, J., Fergus, T., and Walling, D. E. (eds.), *Erosion and Sediment Transport Measurements in Rivers: Technological and Methodological Advances*. Willingford: IAHS Pub 283, pp. 57–78.

Walling, D. E., and Horowitz, A. J., 2005. Preface. In Walling, D. E., and Horowitz, A. (eds.), *Sediment Budgets 1*. Willingford: IAHS Pub 291, pp. v–viii.

Walling, D. E., Owens, P. N., and Leeks, G. J. L., 1998. The role of channel and floodplain storage in the suspended sediment budget of the river Ouse, Yorkshire, UK. *Geomorphology*, **22**, 225–242.
Wilkinson, B. H., and McElroy, B. J., 2007. The impact of humans on continental erosion and sedimentation. *Geological Society of America Bulletin*, **119**(1–2), 140–156.

Cross-references

Glacial Erosion
Sediment Entrainment, Transport, and Deposition
Sediment Transfer Modeling
Sediment Yield

SEDIMENT CORE AND GLACIAL ENVIRONMENT RECONSTRUCTION

Jostein Bakke[1], Øyvind Paasche[2,3]
[1]Department of Geography/Bjerknes Centre for Climate Research, University of Bergen, Bergen, Norway
[2]Bjerknes Centre for Climate Research, University of Bergen, Bergen, Norway
[3]Department of Research Management, University of Bergen, Bergen, Norway

Synonyms

Glacier reconstructions

Definition

Sediment core and glacial environment reconstructions describe the methods used to reconstruct past glacier activity based on sediments deposited in distal glacier-fed lakes (Figure 1). By quantifying physical properties of glacial and extra-glacial sediments deposited in catchments, and in downstream lakes and fjords, it is possible to isolate and identify past glacier activity – size and production rate – that subsequently can be used to reconstruct changing environmental shifts and trends. Moreover, detailed glacier reconstructions can also be used to assess denudation rates, chemical and physical weathering, as well specific glaciological changes.

Introduction

Alpine glaciers are often located in remote and high-altitude regions of the world, areas that only rarely are covered by instrumental records. Understanding the behavior of glaciers and linking their activity to climate changes can therefore be challenging, but when successful glacier reconstructions can shed light on past and present climate variability on both shorter and longer time scales.

Few, if any, other proxies have responded in a more unambiguous way to global warming than glaciers, which now are receding in a hitherto unrecognized pattern.

Robust glacier reconstructions can thus be an important source of knowledge for a better understanding of not only natural climate variability, but also change induced by anthropogenic emissions of greenhouse gases. Producing glacier records is not straightforward and is frequently based on a blend of different methods, which occasionally is difficult to reconcile. This can, for instance, be due to the method applied for estimating the equilibrium-line-altitude (ELA) or even the preferred physical parameter that is interpreted to reflect glacier activity.

One major drawback with glacier reconstructions based solely on moraine chronologies – by far the most common – is that due to selective preservation of moraine

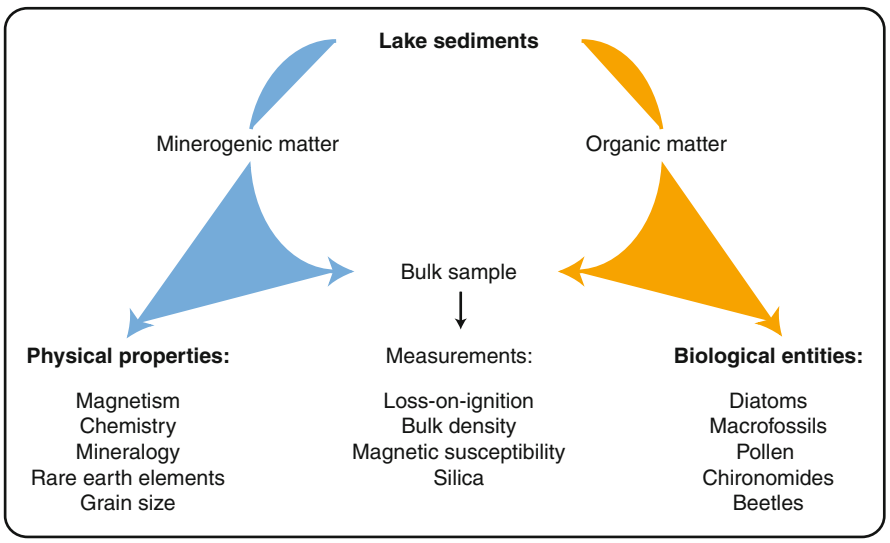

Sediment Core and Glacial Environment Reconstruction, Figure 1 Shows a simplified representation of different organic and minerogenic components making up the bulk sediments typically found in records retrieved from distal glacier-fed lakes. It is commonly the physical properties of the sediments that are used for glacier reconstructions.

ridges such records do not exclude the possibility of multiple Holocene glacier advances. This problem is true regardless of whether cosmogenic isotopes or lichenometry have been used to date the moraines, or also radiocarbon dating of mega fossils buried in till or underneath the moraines themselves.

To overcome this problem, Karlén (1976) initially suggested that glacial erosion and the associated production of rock-flour deposited in downstream lakes could provide a continuous record of glacial fluctuations, hence overcoming the problem of temporal incomplete reconstructions. Reading the glacial signal, as preserved in downstream lake sediments, now includes the application of various methods such as measuring the amount of minerogenic versus biologic matter (typically inferred from Loss-on-Ignition (LOI)), grain-size analysis (GSA), magnetic properties (MP), geochemical elements (GE), Rare-Earth Elements (REE), Bulk Sediment Density (BSD), but also other techniques (e.g., Bakke et al., 2009; Guyard et al., 2007; Leeman and Niessen, 1994; Leonard and Reasoner, 1999; Lie et al., 2004; Paasche et al., 2007).

Paleorecords of natural climate variability based on glacier reconstructions are arguably more reliable if separate events, like those that happened to produce individual moraines, can be compared relative to each other. Being able to do so requires knowledge not only about the conditions during the deposition of a single moraine, but also the conditions both prior and after the advance. It is not until such knowledge is made available through continuous glacier reconstructions that changing climate conditions adequately can be evaluated in terms of glacier response. Being able to do so is the main advantage with using sediment cores as basis for glacial environment reconstruction. Here we offer a brief review on prospects and problems associated with the employment of such an approach and also how continuous glacier reconstructions can be used as proxies for past climates.

Methods review

Changes in average sediment evacuation from alpine glaciers are mainly governed by glacier size and the mass turnover gradient, determining the deformation rate at any given time. The amount of solid precipitation (mainly winter accumulation) versus loss due to melting during the ablation-season (mainly summer temperature) determines the mass turnover gradient in either positive or negative direction. In this simplified world, a prevailing positive net balance will lead to higher sedimentation rates and vice versa, which in turn can be recorded in downstream lakes. To retrieve these glacial sediments it is necessary to collect sediment cores from the lake bottom. A range of coring equipment is now available, with different operating mechanisms and different levels of success in core recovery (see Table 1). A number of problems (often overlooked) are encountered during coring operations or during subsequent transport: (1) sediment disturbance/deformation due to coring, (2) cores not capturing all sedimentary units, (3) not enough cores retrieved, and (4) potential onsite pollution of the sediments in the cores.

To optimize the coring effort it is preferable to carry out seismic or similar investigations. New technology has made it possible to do advanced imaging of the soft sediments in glacial lakes using, for instance, Ground Penetrating Radar (GPR) or light-weighted Pinger or Kirp systems (see Moorman, 2001). With these tools it is possible to measure the actual sediment distribution within a basin, which can ensure that the selected coring sites indeed are representative for the overall sediment distribution.

Extra-glacial and also paraglacial sediment sources represent a source of error in glacier lakes because they may influence the way the bulk sediment samples are interpreted. Many are well-known and typically include debris flows, talus cones, dirty snow avalanches, subaquatic slumping, melt-out of permafrost, and so forth.

Sediment Core and Glacial Environment Reconstruction, Table 1 An overview of available coring devices, how they are operated, what maximum water coring depth they are suited for and what the maximum length of the retrieved core is expected to. The last column contains reference to some papers describing these devices

Coring device	Operation	Operating water depth	Core length (m)	References
Piston corers driven by rods (also modified with hammer or percussion)[a]	Hand operated and motorized	<100 m	40 m	(e.g., Livingstone, 1955; Nesje, 1992)
Cable-operated piston corers[a]	Motor, hydraulics	<500 m	40 m	(e.g., Kelts et al., 1986)
Box cores and dredges[a]	Hand operated	<10 m	10–20 cm	(e.g., Murdoch and Azcue, 1995)
Open-barrel and gravity corers[a]	Hand operated	<40–50 m	>1 m	(e.g., Renberg, 1991)
Chamber-type samplers[a]	Hand operated	<15 m	<15 m	(e.g., Russian peat corers, Hiller corers)
Vibracorers[a]	Motorized	<50 m	<15 m	(e.g., Thompson et al., 1991)
Freeze samplers	Hand operated	<50 m	<1 m	(e.g., Lotter et al., 1997)
Modified gravity corers[a]	Motorized for deep water	<500 m	2–4 m	(e.g., Cushing et al., 1997)
Pneumatic corers[a]	Motorized	<30 m	6 m	(e.g., Mackereth, 1969)

[a]Tube diameter varies between 30 and 200 mm

The shortcomings of many lake sediment studies are precisely that they do not distinguish different processes affecting lake sedimentation from each other (Bakke et al., 2005; Snowball and Sandgren, 1996). More recent studies build on multi-proxy approaches (Figure 2), taking advantage of the sediment's different physical qualities, which in due turn allows for the possibility of discriminating glacial flour produced at the sole of the glacier from extra-glacial and paraglacial sediments (Paasche et al., 2007; Rosqvist et al., 2004).

The landscape relief around lakes is also important as gentle slopes reduce the risk of snow avalanches and rock falls, which otherwise might impact the overall sediment budget of the lake (Dahl et al., 2003). Using lacustrine sediments retrieved from downstream glacier-fed lakes to reconstruct past glacier activity requires careful validation of the records in question since several sources of error are present. The bulk sediment composition, as seen from the lake-sedimentary archive, consists of extra-glacial components that need to be identified and isolated, as this would otherwise corrupt the glacier reconstruction. Being able to unmix bulk sediments is the most important research frontier in work dealing with glacial reconstructions based on continuous sedimentary records.

Methods that potentially can be used to distinguish different sedimentary components include rock magnetic properties (magnetic grain size, magnetic mineralogy, signal strength), XRF core scanning, and changes in physical grain-size composition (Bakke et al., 2005, 2010; Guyard et al., 2007; Paasche et al., 2007).

Sedimentary fingerprinting by means of magnetic properties usually requires a suit of measurements, which in sum might allow for a more accurate glacial reconstruction (Paasche et al., 2007; Rosenbaum and Reynolds, 2004). Variations in magnetic mineralogy are, for instance, widely used in environmental magnetism to ascertain contributions from different sediment sources, utilizing variations in provenance when erosion of different lithologies occurs. Not only will magnetic properties yield insight to provenance, it is also possible to identify chemical processes associated with transport and subsequent deposition. Magnetic measurements required to perform such a task typically involve bulk magnetic susceptibility (scrutinizing between paramagnetic susceptibility, diamagnetic susceptibility, and ferromagnetic susceptibility), saturation isothermal magnetization (sIRM), anhysteretic remanent magnetization (ARM), coercivity specters (IRM-H curves), first-order-reversal-curves (FORCS), and hysteresis loops.

XRF count rate of titanium in distal glacier-fed lakes have been employed with some success to detect glacier activity, as observed from lake sediments (Bakke et al., 2009, 2010). Other stable geochemical elements that also can be used – they are present in many lithologies – are Silicon, Potassium, and Rubidium (Guyard et al., 2007). Rubidium can, for instance, be used to monitor the amount of detrital clays (i.e., glacier flour), indicative of glacier erosion (Guyard et al., 2007). The relative new XRF scanning technology provides tools for further unmixing of the lake sediments derived from non-glacial processes.

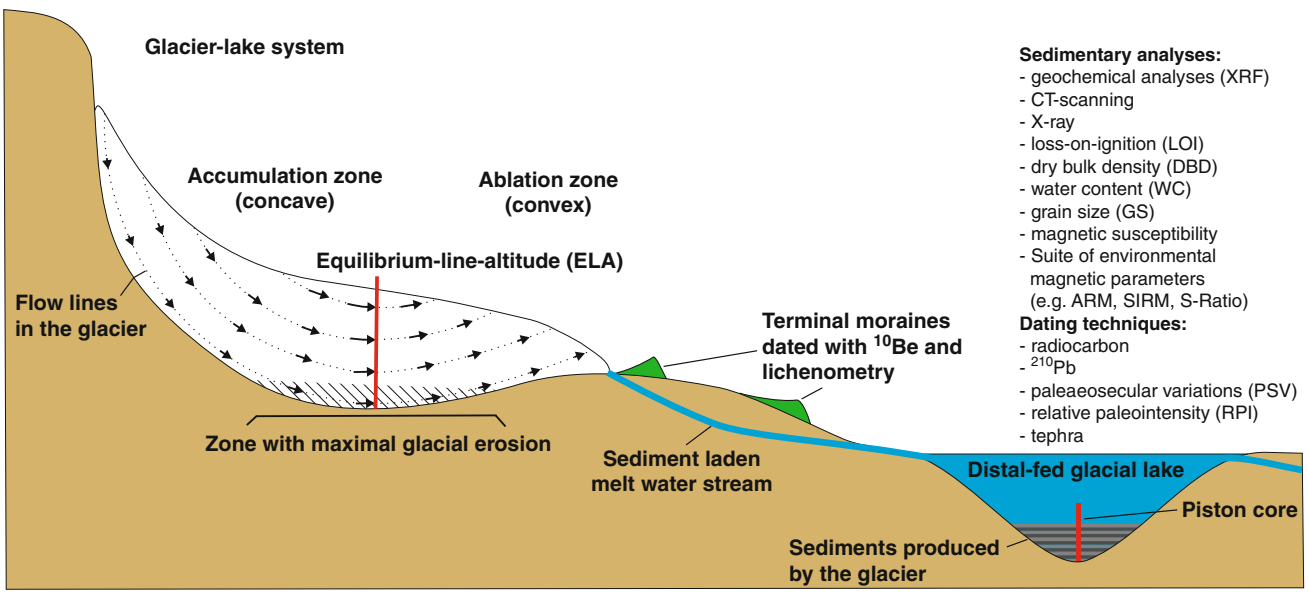

Sediment Core and Glacial Environment Reconstruction, Figure 2 Shows a conceptual illustration of an alpine glacier in relation to a distal glacial-fed lake that receives sediment-laden meltwater directly from the glacier through the glaciofluvial system. Possible sedimentary analyses that can be performed are listed together with the possible dating techniques that will make it possible to integrate the sedimentary records with, e.g., independently dated terminal moraines. Parts of this methodology have previously been used; however, few studies use all the available methods to validate the sedimentary records in question.

By employing different ratios such as Titanium/Iron and Titanium/Magnesium, which are metals assumed to be redox-sensitive and redox-insensitive, respectively, inferences about slope wash or paraglacial processes can be inferred.

X-rays and CT scanners can also be used to identify any sedimentological signatures that may indicate disturbance in the sedimentary records (e.g., erosional contact, drop stones, bioturbation, etc.).

A complementary approach is to use grain sizes that may reflect transport capacity of meltwater entering a lake. Given that this assumption is valid it may be possible to link variability in the distribution of grain sizes directly to variations in glacier runoff and hence indirectly to size (Bakke et al., 2009, 2010). The critical assumption here is that larger glaciers, on average, release more meltwater than smaller glaciers and that such changes do not also change the potential sediment contribution from other extra-glacial sources. On shorter time scales (annual) large deviations are likely, but on longer timescales (decadal to centennial) this assumption might be valid.

Paleoclimatic reconstructions based on sediment cores

Temperate glaciers respond both to temperature and solid winter precipitation. The importance of these two climatic parameters varies from glacier to glacier, but for maritime glaciers winter precipitation tends to be more important in explaining changes in the overall mass balance budget, whereas for continental glaciers temperature tends to be more important.

The potential of disentangling the climate forcing that plays such a crucial role in most glaciers 'health-state' is precisely the reason for them being sought after as proxies for past and present climate change. By reconstructing maritime glaciers along a certain transect it is, for instance, possible to assess changes of past atmospheric circulation anomalies (cf. Bakke et al., 2008) because such patterns govern the distribution of precipitation.

Over the last 30 years numerous glacial reconstructions based on sediments from distal glacier-fed lakes worldwide are published. They all provide important information about glacier and climate variations from regions often without any other paleoclimatic archives available. It is however critical that each glacier record is seen in the context of both local and regional climate before the results are upscaled.

Many reconstructions during the 1980s and 1990s were based on the pioneer work from Northern Sweden where Karlén (1976) used the organic content of lacustrine sediments (measured by loss-on-ignition, LOI) to quantify glacial erosion and its associated rock-flour production. From North America/Canada and Scandinavia several studies are based on this approach covering the time span from the deglaciation towards present day (e.g., Leonard and Reasoner, 1999). It is especially the Neo-glacial time period that is suited for the methods based on sediments from distal glacier-fed lakes because it is crucial to standardize the sedimentary archives when the boundary conditions are similar to present day. Also in the Alps several glacier reconstructions are based on sediments from distal glacier-fed lakes, such as from Lake Silvaplana (Leeman and Niessen, 1994) and Lake Bramant (Guyard et al., 2007). However, due to few lakes and high sedimentation rates the most important source for information about glacier variability in the Alps still comes from radiocarbon dating of mega fossils as well as historical sources.

State-of-the-art glacier reconstructions from distal glacier-fed lakes should aim for a quantitative-based reconstruction of the ELA. When sediment records are validated (i.e., intra-core comparison, stacking records, and/or establishing a masterstratigraphy), the next critical step involves connecting the continuous sediment record to corresponding shifts in ELA of the glacier in question. The ELAs (present and past) of dated glacier advances can be reconstructed with established methods such as, for instance, area-altitude balance ratio (AABR) (Osmaston, 2005).

In certain studies dry bulk density (DBD) or SIRM have been used for such a quantification (Bakke et al., 2010; Bakke et al., 2005). First step in this approach is, nevertheless, to integrate an independently dated moraine chronology with an independently dated sedimentary record. As evident from Figure 3, it is possible to establish a statistical relationship between the ELAs calculated from dated moraines and the corresponding sedimentary values obtained from sediment core analysis.

The second step is to use (if available) ^{210}Pb-dated sections in the sedimentary records to correlate sedimentary values to historical documented glacier-front positions recalculated to ELA. Taken together, this allows for a construction of a continuous record of ELA variations, which is based on two independently dated archives (Figure 3). The ELA reconstruction at hand must then be, if necessary, adjusted for potential land uplift before values are used for whatever reason. In Figure 3 the strong statistical relationship between ELA and winter precipitation suggests one area where such an ELA reconstruction can be valuable.

Holocene paleoclimatic trends and future prospects

Alpine glaciers located in the mid- to high latitudes in Northern Hemisphere is small or absent glaciers from 9,000 to 8,000 years BP until ca. 6,000 years BP, which possibly is the most characteristic trend for glacier records during the entire Holocene. After ca. 6,000 years BP the big picture gets more complicated and numerous advances are recorded several places, including South America, North America, Canada, the Alps, and Scandinavia (see Wanner et al., 2008). The major trend in the Holocene glacier variations in the NH seems to be connected to the gradually decreasing summer insolation due to orbital forcing.

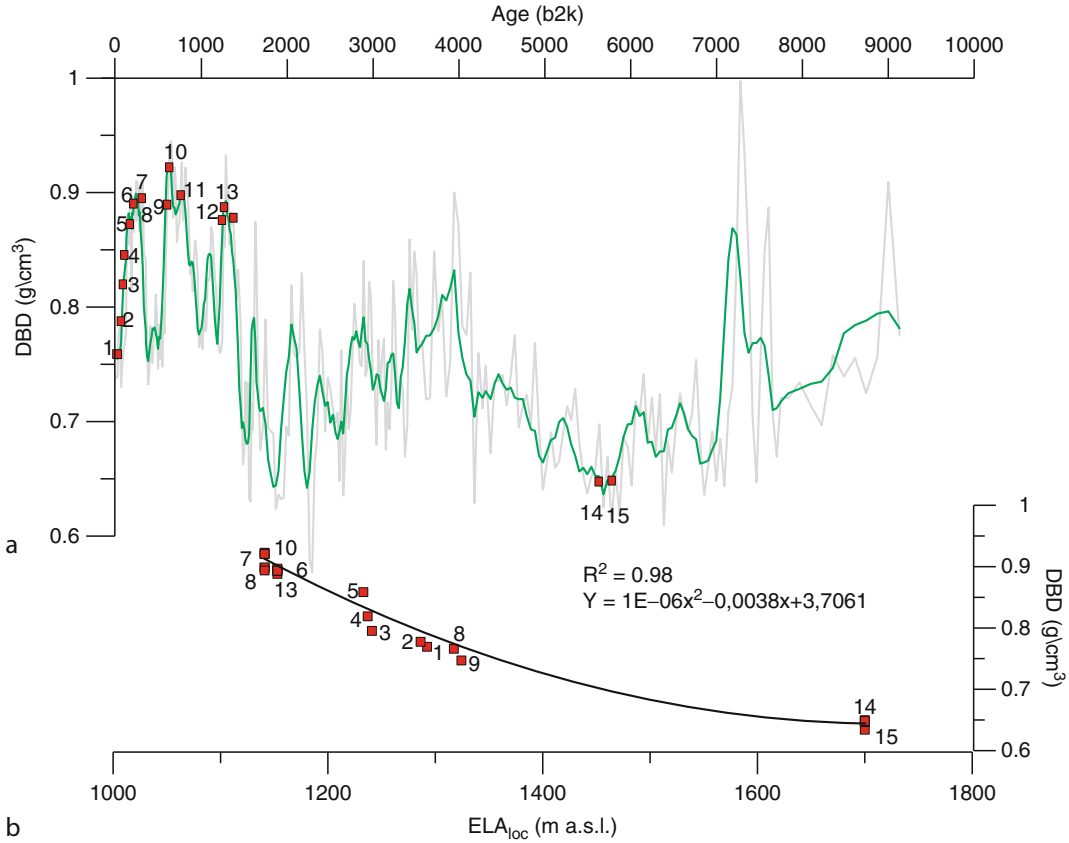

Sediment Core and Glacial Environment Reconstruction, Figure 3 (**a**) Diagram illustrating how it is possible to transform a sedimentary proxy into a continuously record of past ELA fluctuation. *Red dots* indicate periods when the ELA is known, either based on historical data, lichenometric data, and/or interpretation of lake sediments. (**b**) Shows the statistical relationship between periods with known ELA (meter above sea level) and dry bulk density (DBD) values. The regression model is used to model a continuous ELA_{loc} for Holocene. (Modified after Bakke et al., 2010).

Besides the 3,000-year period during the early Holocene when glaciers are small or even absent, another common feature for NH-glaciers is that many of them reach Holocene maximum advances during the Little Ice Age (LIA), occurring sometime between AD 1450 and AD 1910.

A challenge for future studies that seek to extract paleoclimatic information from continuous glacier sediment archives is to more actively use Earth System Models, and also modern meteorological observations. Such an approach can allow for positive identification of regions and areas where glaciers are (or are likely to be) most sensitive to changing climate conditions, and also to explore the critical number of glacier reconstructions required in order to adequately represent a particular region or weather system such as the North Atlantic Oscillation (NAO).

Another possibility for future studies is to aim for improving coring techniques by for instance combining the use of short and long cores in order to retrieve pristine sediment stratigraphies from lakes and fjords. Only when in possession of undisturbed top sediments, overlapping with the longer cores, can crucial calibration against modern processes and environment be carried out.

Overlapping time series with glacier mass-balance measurements are important for verifying and quantifying past ELAs. Using modern mass-balance data in combination with simple flow models can shed light on glacier behavior in both long and short perspectives, specifically when it comes to understanding sediment release from glaciers during advance and subsequent retreats.

Modern multi-proxy approaches, partly outlined here, have opened up new avenues for quantifying glacier process in alpine environments and linking them to changing environmental conditions. Furthermore, improving the accuracy of continuous glacier reconstructions hinges on our ability to better decipher lake sediments, i.e., connect the different sedimentary components to their factual source, and also to identify what processes that might have affected them during production, transport, and deposition. Unless we are able to improve the understanding of the glacier-lake system much of the paleoclimatic inferences will be hampered by noise. Distal glacier-fed lakes are, for instance, frequently perturbed by floods, which

can be difficult to recognize in lake-sedimentary cores, but by employing new methods such as XRF and CT scanning it is now possible to generate reconstructions for avalanche and flooding activity from the same lakes that earlier were only used for glacier reconstructions. This represents an optimization of the sediment core–based glacier reconstructions, but it also implies more accurate paleoclimatic reconstructions.

Bibliography

Bakke, J., Lie, Ø., Nesje, A., Dahl, S. O., and Paasche, Ø., 2005. Utilizing physical sediment variability in glacier-fed lakes for continous glacier reconstructions during the Holocene, northern Folgefonna, western Norway. *Holocene*, **15**(2), 161–176.

Bakke, J., Lie, Ø., Dahl, S. O., Nesje, A., and Bjune, A. E. 2008. Strength and spatial patterns of the Holocene wintertime westerlies in the NE Atlantic region. *Global and Planetary Change*, **60**(1–2), 28–41. doi:10.1016/j.gloplacha.2006.07.030.

Bakke, J., et al., 2009. Rapid oceanic and atmospheric changes during the Younger Dryas cold period. *Nature Geoscience*, **2**(3), 202–205.

Bakke, J., et al., 2010. A complete record of Holocene glacier variability at Austre Okstindbreen, northern Norway: an integrated approach. *Quaternary Science Reviews*, **29**, 1246–1262.

Cushing, S. J., Desjardins, S. J., and Fillion, J. M., 1997. Parachute-assisted gravity sediment corer (Algonquin Corer). *Journal of Paleolimnology*, **18**, 380–384.

Dahl, S. O., Bakke, J., Lie, O., and Nesje, A., 2003. Reconstruction of former glacier equilibrium-line altitudes based on proglacial sites: an evaluation of approaches and selection of sites. *Quaternary Science Reviews*, **22**(2–4), 275–287.

Guyard, H., et al., 2007. High-altitude varve records of abrupt environmental changes and mining activity over the last 4000 years in the Western French Alps (Lake Bramant, Grandes Rousses Massif). *Quaternary Science Reviews*, **26**, 2644–2660.

Karlén, W., 1976. Lacustrine sediments and tree-line variations as indikators of climatic fluctuations in Lappland, northern Sweden. *Geografiska Annaler*, **58A**, 1–34.

Kelts, Z., Briegel, K. G., and Husu, K., 1986. The limnology-ETH coring system. *Schweizerische Zeitschrift für Hydrologie*, **48**, 104–115.

Leeman, A., and Niessen, F., 1994. Holocene glacial activity and climatic variations in the Swiss Alps: reconstructing a continuous record from proglacial lake sediments. *Holocene*, **4**, 259–268.

Leonard, E. M., and Reasoner, M. A., 1999. A continuous Holocene glacial record inferred from proglacial lake sediments in Banff National Park, Alberta, Canada. *Quaternary Research*, **51**, 1–13.

Lie, O., Dahl, S. O., Nesje, A., Matthews, J. A., and Sandvold, S., 2004. Holocene fluctuations of a polythermal glacier in high-alpine eastern Jotunheimen, central-southern Norway. *Quaternary Science Reviews*, **23**(18–19), 1925–1945.

Livingstone, D. A., 1955. A lightweight piston sampler for lake depostis. *Ecology*, **36**, 137–139.

Lotter, A., Renberg, I., Hannsson, H., Stöckli, R., and Strum, M., 1997. A remote controlled freeze corer for sampling unconsolidated surface sediments. *Aquatic Sciences*, **59**, 295–303.

Mackereth, F. J. H., 1969. A short core sampler for sub-aqueous deposits. *Limnology and Oceanography*, **3**, 181–191.

Moorman, B. J., 2001. Ground-penetrating radar applications in paleolimnology. In Last, W. M., and Smol, J. P. (eds.), *Tracking Environmental Change Using Lake Sediments*. Dordrecht: Kluwer. Basin Analysis, Coring, and Chronological Techniques, Vol. 1, pp. 23–47.

Murdoch, A., and Azcue, J. M., 1995. *Manual of Aquatic Sediment Sampling*. Boca Raton: Lewis, p. 219.

Nesje, A., 1992. A piston corer for lacustrine and marine-sediments. *Arctic and Alpine Research*, **24**(3), 257–259.

Osmaston, H., 2005. Estimates of glacier equilibrium line altitudes by the Area × Altitude, the Area × Altitude Balance Ratio and the Area × Altitude Balance Index methods and their validation. *Quaternary International*, **138**, 22–31.

Paasche, O., Dahl, S. O., Bakke, J., Lovlie, R., and Nesje, A., 2007. Cirque glacier activity in arctic Norway during the last deglaciation. *Quaternary Research*, **68**(3), 387–399.

Renberg, I., 1991. The HON-Kajak sediment corer. *Journal of Paleolimnology*, **6**, 167–170.

Rosenbaum, J. G., and Reynolds, R. L., 2004. Record of Late Pleistocene glaciation and deglaciation in the southern Cascade Range: II. Flux of glacial flour in a sediment core from Upper Klamath Lake, Oregon. *Journal of Paleolimnology*, **31**, 235–252.

Rosqvist, G., Jonsson, C., Yam, R., Karlen, W., and Shemesh, A., 2004. Diatom oxygen isotopes in pro-glacial lake sediments from northern Sweden: a 5000 year record of atmospheric circulation. *Quaternary Science Reviews*, **23**(7–8), 851–859.

Snowball, I. F., and Sandgren, P., 1996. Lake sediment studies of Holocene glacial activity in the Kårsa valley, northern Sweden: contrasts in interpretation. *Holocene*, **6**, 367–372.

Thompson, T. A., Miller, C. S., Doss, P. K., Thompson, L. D. P., and Baedke, S. J., 1991. Land-based vibracoring and vibracore analysis: tips, tricks, and traps. Indiana Geological Survey Occasional Paper, vol. 58, 13 p.

Wanner, H., et al., 2008. Mid- to Late Holocene climate change: an overview. *Quaternary Science Reviews*, **27**(19–20), 1791–1828.

Cross-references

Atmospheric Circulation and Glaciochemical Records
Cirque Glaciers
Climate Change and Glaciers
Glacial Erosion
Glacier Mass Balance
Glacier Motion/Ice Velocity
Proglacial Lakes
Retreat/Advance of Glaciers
Scandinavian Glaciers
Suspended Sediment Concentration
Temperate Glaciers

SEDIMENT ENTRAINMENT, TRANSPORT, AND DEPOSITION

Michael J. Hambrey, Neil F. Glasser
Centre for Glaciology, Institute of Geography & Earth Sciences, Aberystwyth University, Aberystwyth, Ceredigion, Wales, UK

Definition

Sediment entrainment, transfer and deposition explains how debris is incorporated into the base or onto the surface of a glacier, then modified and deformed during glacier flow, and finally deposited beneath or in front of the glacier, including its subsequent reworking.

Introduction

Importance of glacial sediments

Glacial sediments provide a vital legacy for interpreting past climates of the Quaternary and earlier geological periods. Their importance can be gauged from the facts that 30% of the Earth's land surface was under ice during the last ice age, and that even today 10% of the land is still covered by glaciers and ice sheets. During the Quaternary Period, in addition to those that survive in Antarctica and Greenland, vast ice sheets grew over North America, Scandinavia and the British Isles, northern Russia, Tibet, and Patagonia. Smaller icefields grew over the Alps, New Zealand, and central Asian ranges, together with smaller ice masses in many other of the Earth's mountain ranges. Glacier ice has left a complex but often patchy record of deposition on land, but offshore has contributed substantially to the buildup of high-latitude continental shelves.

Glacial transport and deposition is intimately associated with a wide range of other processes, including ice deformational and glaciotectonic, fluvial, mass flowage, aeolian, lacustrine, and marine. The resulting sedimentary facies associations are highly variable, and even with detailed investigation can be interpreted in widely different ways. It is only within the last 4 decades that studies of glacial processes in modern settings have made it possible to develop plausible models of past glacial depositional environments.

Understanding the nature of Quaternary glacial sediments and their associated landforms is crucial in the glaciated areas of North America, Europe, and elsewhere. This is because sand and gravel extraction, notably from glaciofluvial sequences, is essential for construction purposes, as well as informed management of water resources and waste disposal. Some pre-Quaternary glacigenic facies are also economically important in some regions, such as in the Permo-Carboniferous and Neoproterozoic basins of the Middle East and South America, where they constrain the presence of petroleum resources.

Glacial sediments also have an important aesthetic appeal. In mountain regions, they add to the character of impressive glacial erosional landscapes, while in lowland regions they provide a rolling topography of lakes and hills, all of which underpin the tourism business.

The wider implications of focusing on glacial sediments and their associated landforms center on reconstructing past ice sheets. This topic, referred to as paleoglaciology, is of increasing importance as we seek to understand past response of ice masses to climate. Using this concept provides us with constraints on predictions of climate change.

This article is an updated version of that published in the *Encyclopedia of Sediments and Sedimentary Rocks* (Hambrey and Glasser, 2003).

Historical background

It is widely recognized today that the Earth experienced a series of ice ages. However, when the concept was first promoted in the early nineteenth century, it met with fierce opposition. At that time, most of the unconsolidated deposits (so-called drift) that were familiar to geologists were attributed to the biblical Noah's flood. Indeed, the flood concept was used to explain the presence of large boulders displaced from their source bedrock ("erratics") that were deposited from icebergs (Hambrey, 1994, Chap. 1 for review). The Swiss natural historian, Agassiz, became the chief protagonist of the "Ice Age Theory," and when he delivered his ideas in 1837, they had a Europe-wide impact. In the following decades, through Agassiz's influence, geologists in the UK and North America gradually accepted the theory as being also applicable to their regions. In the second half of the nineteenth century, "ancient" glacial deposits (*tillites*) were recognized in many parts of the world. However, even in the second half of the twentieth century, the glacial origin of supposed tillites was challenged, notably those of Neoproterozoic age. It has taken systematic sedimentological investigations, coupled with an appreciation of modern glacial processes, to settle these debates.

Glaciological aspects of debris entrainment and transport

To evaluate the processes whereby sediment is entrained and deposited, we need to understand a number of key glaciological phenomena; several of these are dealt with more thoroughly in this volume (see Section "Cross-references").

Mass balance

The state of health of a glacier and its capacity to carry debris is a reflection of its mass balance, and the supply of debris from surrounding headwalls and from the base. A positive mass balance allows rapid burial of supraglacial debris and transport through an englacial pathway, while a negative mass balance sees the exposure and emergence of greater quantities of debris at the surface. The basal conditions also vary, with a positive mass balance causing the glacier to flow more rapidly and erode the bed more intensely, and a negative mass balance allowing stagnation and rapid deposition of the sediment load (Figure 1).

Glacier dynamics

In order to interpret the origin of glacial sediments and landforms, it is necessary to understand the mechanisms of ice deformation and glacier flow. Glaciers flow by one or more of three main mechanisms: internal deformation, basal sliding, and movement over a soft, deformable bed (Paterson, 1994). In simple terms, *internal deformation* results in the slowest flow occurring at the margins and at the base of a glacier, but large-scale reorganization of preexisting structures, with or without debris, through folding and foliation development is also common. *Basal sliding* is important where rain or meltwater is able to lubricate the bed, and varies according to the season and

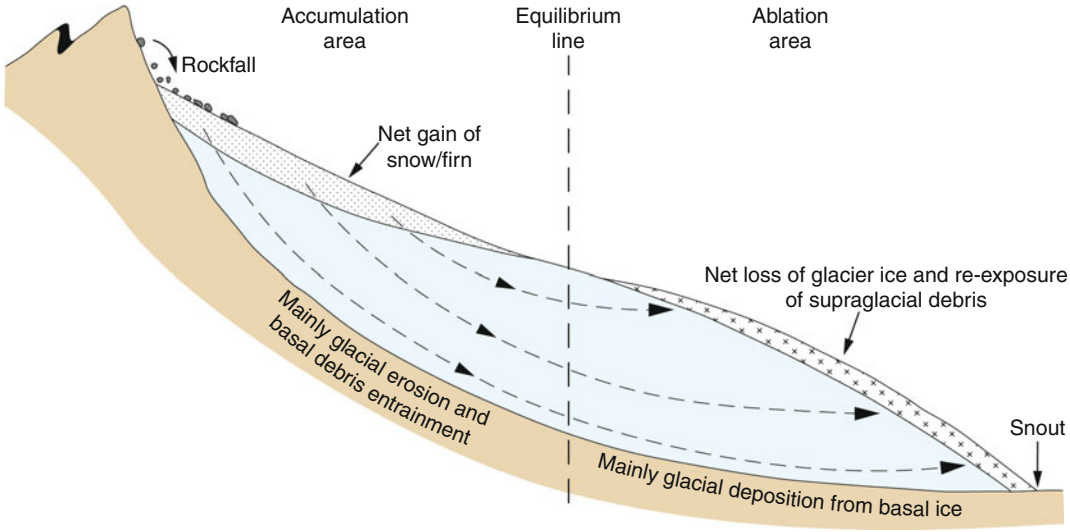

Sediment Entrainment, Transport, and Deposition, Figure 1 Longitudinal profile through a valley or cirque glacier, illustrating the relationship between mass balance, particle paths (*arrows*), and debris entrainment processes.

time of day or night. Frictional and geothermal heating may add to the availability of meltwater. All these factors control erosion and regelation at the glacier bed. Many glaciers flow over a *deformable bed* of unconsolidated sediment which, when saturated, can behave as a slurry that enhances the flow of the glacier. Deformable beds exist beneath modern fast-flowing ice streams in Antarctica and Greenland, as well as many ice caps and outlet glaciers. Much of the movement of the Quaternary ice sheets in North America has also been linked to deformation of the bed. The relative importance of these mechanisms is highly variable. In moist temperate regions as much as 80% of glacier flow is from sliding. Cold polar glaciers, which are frozen to their beds, flow almost entirely by internal deformation. Polythermal glaciers (with both cold and warm ice) have a combination of sliding and frozen bed conditions. Debris entrainment commonly occurs where there is a transition between the two modes of flow. Where a deformable bed exists, the bulk of movement may be within the sediment layer beneath the ice, while the sediment itself is transported in conveyor belt–like fashion. In *surge-type glaciers*, flow is unstable, with long periods (often decades) of quiescence punctuated by short bursts (several months to a few years) of high velocity (*surges*). During the most active phase of a surge, the velocity may reach several orders of magnitude above normal, and the glacier may advance rapidly, and redistribute large volumes of sediment.

Glacier structure

Glacier structures are principally the product of internal deformation, and are intimately associated with the transport of debris (Paterson, 1994; Hambrey and Lawson, 2000). Glacier ice is similar to any other type of geological material in that it comprises strata that progressively deform to produce a wide range of structures. Primary structures in glacier ice include stratification derived from snow and superimposed ice, and unconformities. Regelation layering, resulting from pressure melting and refreezing at the base of a glacier, the latter also sometimes being referred to as stratified ice, although not strictly in the geological sense. Secondary structures are the result of deformation, and include both brittle features (crevasses, crevasse traces, faults, and thrusts) and ductile features (foliation, folds, boudinage). All these structures are associated with debris, whether by direct accumulation as rockfall (as in stratification), or by concentration in foliation as in shear zones between two merging flow units. Typically, a glacier reveals a sequential development of structures as in deformed rocks, so that by the time the glacier snout is reached, ice may record several "phases" of deformation. Similarly, the cumulative strain which glacier ice has undergone commonly changes the original geometry of the structure and associated sediment out of all recognition.

Thermal regime

The temperature distribution or *thermal regime* of a glacier is fundamental to glacier flow, meltwater production and routing, and to styles of glacial erosion and deposition. *Temperate* or *warm* glaciers, in which the ice is at the pressure-melting point throughout, tend to slide rapidly on their beds and are highly erosive. These glaciers are typical of alpine regions. *Cold* glaciers are the end member at the opposite temperature extreme, the ice being below the pressure melting point throughout; they occur in high polar regions or at very high altitudes only. These glaciers have long been thought incapable of eroding their

bed, although evidence from Antarctica indicates that this is not strictly true. An intermediate type of glacier, found especially in the high Arctic, is referred to as *polythermal*. In such glaciers, it is typical for the snout, margins and surface layer of the glacier to be below the pressure-melting point, whereas thicker, higher-level ice is warm based.

Glacier hydrology

Glacial erosion and sediment transport would be much less effective were it not for the presence of meltwater within, beneath, and beyond the glacier. Water, derived from melting snow and ice, flows in supraglacial rills, channels, and canyons cut into the glacier surface. If structural weaknesses exist, the meltstreams commonly plunge into the interior or bed of the glacier via moulins, before emerging at the snout. Drainage routes, and therefore sediment transport paths, differ according to the thermal regime of the glacier. In cold and polythermal glaciers, meltwater tends to be forced toward the glacier margins, as subzero ice prevents surface water penetrating far below the glacier surface. In contrast, water flows in discrete channels at the bed in temperate glaciers, often emerging from the glacier at a single portal. Glaciers act as natural storage reservoirs, retaining water and sediment in winter and releasing them in summer. Thus discharge is markedly seasonal and diurnal. On a typical braided outwash plain, beyond the glacier, marked fluctuations in discharge result in rapid, continuous channel shifts, and deposition of both suspended and bed-load sediment. Meltwater and sediment also accumulates in ice-constrained lakes, including ice-dammed, proglacial, supraglacial, and subglacial types. Many of these are ephemeral, and those dammed by ice, which are most commonly associated with polythermal glaciers, are particularly prone to catastrophic failure, resulting in outburst floods called *jökulhlaups*. Moraine-dammed lakes, which typically grow behind Little Ice Age moraines are also prone to catastrophic failure, notably in the Andes and the Himalaya. Glacial meltwater is not only a powerful erosive agent, but is also responsible for among the most important sedimentary facies in glacierized regions.

Morphological controls on sediment transport

As documented elsewhere in this volume, glaciers range in size from ice masses only a few hundred meters across to the huge ice sheets that cover Antarctica and Greenland, and there are thus many different morphological types (Hambrey, 1994; Bennett and Glasser, 2009; Benn and Evans, 2010). Ice sheets and ice caps carry most of their sediment load in the bed, where regelation processes have entrained the debris. Conversely, they carry little supraglacial debris, other than dust, or where compressive flow causes upward movement of basal debris in the terminal region. Valley and cirque glaciers carry much more supraglacial debris as a result of rockfall, induced by freeze-thaw processes, especially in high-relief temperate zones. Dealing with the past record, one of the key roles of the glacial sedimentologist is to reconstruct the morphological characteristics of former ice masses, in order to constrain the interpretation of past climates and sea-level response.

Glacial erosion

The processes whereby a glacier or ice sheet picks up and transports rock fragments and sediment, and transfers this material to another location are referred to as glacial erosion. In summary, glacial erosion occurs by means of four main processes: *glacial abrasion*, *glacial plucking* (or *quarrying*), *glacial meltwater erosion*, and *subglacial sediment deformation*, and gives rise to a wide range of spectacular landforms (Figure 2). Since glacial erosion is the starting point for debris entrainment and transport by glaciers and ice sheets, an understanding of this topic is essential if we are to understand the sedimentary products of ice masses.

Glacial abrasion is the process by which particles entrained in the basal layer of a glacier are dragged across the subglacial surface. The scratching and polishing associated with glacial abrasion tends to create smoothed rock surfaces, commonly with striations or grooves.

Glacial quarrying (or *plucking*) is the process whereby a glacier removes and entrains large fragments of its bed. The processes of rock fracture are controlled by the density, spacing, and depth of preexisting joints in bedrock, together with the stresses applied by the glacier. Fracturing of bedrock is also aided by the presence of meltwater beneath the glacier, where bedrock is loosened by subglacial water-pressure fluctuations. Material ranging from quarried blocks to fine material is then entrained in basal ice by freezing-on (*regelation*), when surrounded by flowing ice, or when incorporated along thrusts. Entrainment is most pronounced in polythermal glaciers, especially where there is a transition from sliding-bed to frozen-bed conditions, and a complex layer several meters thick may develop (Figure 3a). In contrast, the abundance of meltwater precludes substantial entrainment of debris in temperate glaciers, and the basal debris layer may be less than a meter thick (Figure 3b). Although not noted for being erosional agents, cold glaciers can entrain blocks of frozen subglacial sediment and bedrock as a result of shear at the ice/substrate contact (Figure 3c).

Glacial meltwater erosion involves both mechanical and chemical processes. Mechanical erosion occurs primarily through fluvial abrasion by the transport of suspended sediment and bedload within meltwater at the base of the glacier. Locally, fluvial *cavitation* (the sudden collapse of bubbles within turbulent meltwater under high pressure) may also be important. In subglacial channels, chemical erosion involves the removal of rock and rock debris in solution, especially in areas of carbonate bedrock. Rates of chemical erosion beneath ice masses are high because of high flushing rates, the availability of large amounts of chemically reactive rock flour, and the enhanced solubility of CO_2 at low temperatures.

Sediment Entrainment, Transport, and Deposition, Figure 2 Glacially sculpted peaks of Piz Morteratsch and Piz Bernina, Graubünden, Switzerland, with the glacier Vadret da Tschierva in the center. The huge lateral moraines on either side of the valley and the hummocky moraine in the foreground date from the Little Ice Age.

Subglacial sediment deformation is a relatively new concept, and is believed to be a major component of glacier flow beneath ice streams and valley glaciers (Boulton, 1996). The process involves net removal of wet sediment in conveyor belt–like fashion and can contribute to the progradation of sediment aprons or wedges where there is a sharp break in slope, for example, at the edge of a continental shelf or in a lake.

Debris entrainment and transport

Debris is entrained within a glacier both at the bed as basal glacial debris and at the surface as supraglacial debris. In addition, there is transfer of debris from low to high level and vice versa by means of a range of processes related to deformation of the ice (Figure 4). The following discussion considers both low- and high-level transport and stages in between, but in effect entrainment is a continuum of processes at different levels within the glacier. Transport paths and textural character of glacial sediments are related to the dynamic and thermal characteristics of the glacier. Broadly speaking, polythermal glaciers tend to carry a high basal debris load (Figure 3a), and the surface rarely has a substantial cover of debris. In contrast, temperate glaciers, especially those in high-relief regions, normally carry relatively little basal debris (Figure 3b), but the surface commonly has an extensive cover of supraglacial debris. The resulting sedimentary products can thus be used to infer the thermal and topographic regimes of a former glacier regime.

Low-level debris entrainment and transport

Debris is entrained at the bed by a combination of pressure melting and refreezing (regelation). Freezing to the base of the glacier occurs when the 0°C isotherm migrates into the substrate, sometimes even allowing sediment or bedrock to be entrained en masse. The thickness of the basal ice layer can be increased by folding and thrusting, or concentration around obstacles. These complex processes create a basal debris layer that comprises a wide range of ice types (or facies), involving frozen meteoric water, glacier ice, different concentrations of debris, and even solid sediment (Knight, 1997; Hubbard et al., 2009), as is well known from studies of both temperate and polythermal glacier margins (Figure 5). Basally derived debris is subject to abrasion, fracturing, and crushing at the ice/bedrock interface. The resulting entrained sediment is dominated by clasts up to boulder-size, with subangular and subrounded shapes, faceted surfaces, and striations (if the lithologies are fine grained) (Figure 6). In addition, much clay- or silt-grade sediment is produced by abrasion. Together, on deposition, the resulting sediment is poorly sorted with a wide range of clast shapes and sizes.

A second mechanism of debris entrainment at the glacier bed, discovered in recent years at a temperate glacier in Alaska, is associated with glaciohydraulic supercooling. This involves sediment-laden supercooled water refreezing to the glacier sole on the upslope side of an overdeepening in the glacier bed. The process preferentially selects finer-grained sediment, and can lead to the buildup of a several-meters-thick basal ice layer.

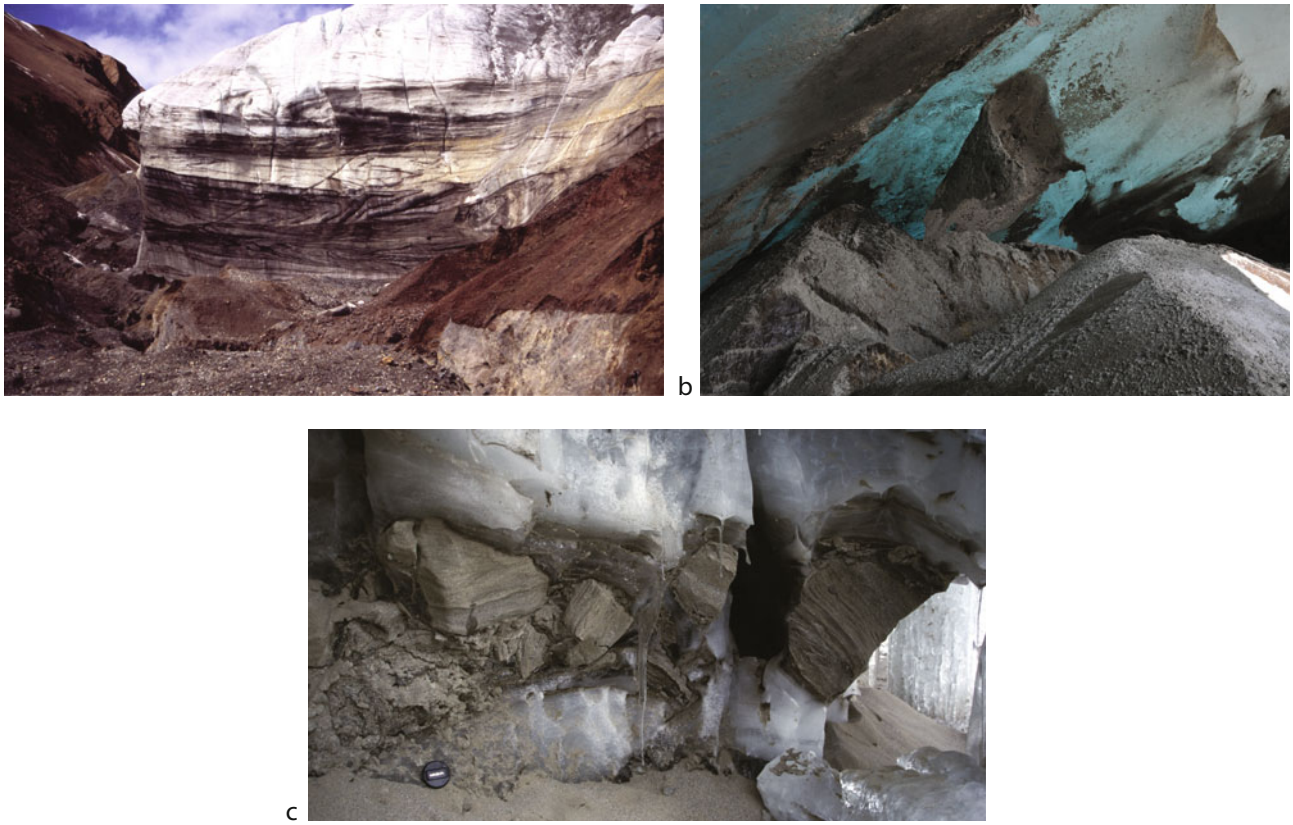

Sediment Entrainment, Transport, and Deposition, Figure 3 Debris entrainment compared in the base of thermally contrasting glaciers. (**a**) Several-meters-thick basal debris layer, repeated by folding in polythermal Trapridge Glacier, Yukon; the cliff is c. 10 m in height. (**b**) Minimal basal debris in a cave at the snout of temperate Rhonegletscher, Switzerland; a thin film of granitic sand mantles the bedrock, while a 1-m-wide folded layer of debris hangs from the roof. (**c**) Solid frozen blocks of glaciofluvial sand incorporated, boudinaged, and rotated in the base of cold Wright Lower Glacier, Dry Valleys, Antarctica.

High-level debris entrainment and transport

In high-relief areas, freeze-thaw processes on exposed bedrock in the accumulation area of a glacier result in rockfall onto the snowpack below, where it is buried as the layer of stratified snow, firn, and ice buildups. Similarly, along the flanks of the glacier in the ablation zone, rockfall allows debris to drape large areas of the glacier surface, sometimes covering it completely to a depth of several meters (Figure 7). Debris falling high in the accumulation area tends to take an englacial path and emerge near the snout, following the flow lines through the glacier, whereas debris falling close to the equilibrium line will follow a shallow englacial path and emerge a short distance down glacier (Figure 1). However, superimposed on this simple pattern are the complexities of folding, as discussed below. Supraglacial debris is generally dominated by gravel (pebble to boulder-sized) material, with few fines, and clast shapes are typically angular and very angular (Figure 7).

Debris on the surface of a glacier is commonly concentrated into flow-parallel ridges of debris, referred to as medial moraines, of which there are two types: *flow-unit interaction moraines* (also confusingly referred to as ice-stream interaction moraines) and *ablation-dominant moraines*. An understanding of structural glaciology is necessary to infer which is the correct mechanism involved. Flow-unit interaction moraines are formed by the confluence of two lateral moraines at the junction of two glacier flow units (Figure 8). The medial moraine consists of a debris-covered ridge that represents the surface expression of a vertical debris septum that may extend down to the bed of the glacier. The internal structure of the septum may be complex, consisting, for example, of anastomosing shears and isoclinal folding. Texturally, these moraines are highly variable; some consist of angular supraglacial debris, but others are mixed with sediment reworked at the ice/bed interface and so comprises more rounded material. *Ablation-dominant moraines* form

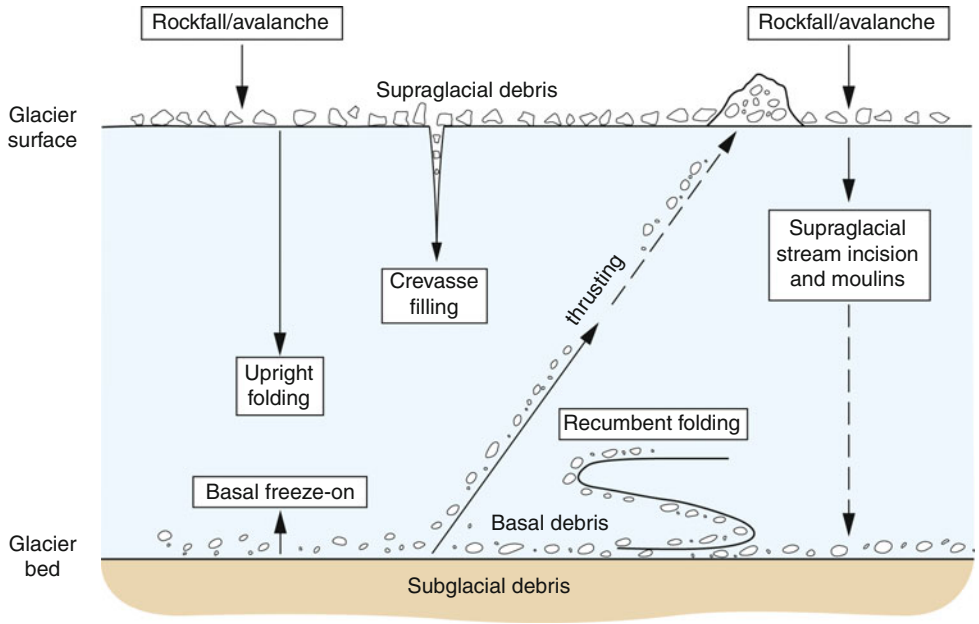

Sediment Entrainment, Transport, and Deposition, Figure 4 Schematic longitudinal cross section through a glacier, summarizing the various processes whereby debris is entrained and transported.

Sediment Entrainment, Transport, and Deposition, Figure 5 Deformed basal ice layer in a cave at the snout of Glacier de Tsanfleuron, Valais, Switzerland. The glaciologist (Bryn Hubbard) is standing on striated limestone bedrock, and there is a folded multilayered basal ice sequence to his right.

where ridges of englacial debris emerge from the ice surface in the ablation zone and extend to the snout. This type of moraine may form in two ways:

1. From a point source between two flow units in the accumulation area where the debris is initially buried and then takes an englacial path through the glacier. Structurally, these are similar to flow-unit interaction moraines.
2. Incorporation of angular rockfall material within the stratified sequence of snow and firn (Figure 9).

This debris takes an englacial path through the glacier, and becomes folded, especially in zones of lateral compression, such as where multiple accumulation basins feed into a narrow tongue. Fold styles range from the broad open "similar" type to isoclinal folds (with parallel limbs). In the ablation area, the debris emerges at the surface on the flow-parallel hinges and upper limbs of the folds, producing medial moraines that merge toward the snout. The resulting lines of debris are deposited on the proglacial area in the form of regular trains of angular debris, as the glacier recedes. This process has been inferred from several small valley glaciers in Svalbard and the Alps (Hambrey et al., 1999).

Sediment Entrainment, Transport, and Deposition, Figure 6 Striated and faceted clast of limestone on the proglacial basal till surface of Austre Lovenbreen, Svalbard.

The above mechanisms result in typical flow-parallel medial moraines than can be tracked long distances downglacier. However, perturbations in flow resulting from surging can distort the moraines into folds and loops (Figure 10). These contortions allow surge-type glaciers to be identified even when there is no historical record of a surge having taken place. Another situation where folded moraines develop is where narrow tongues spread out into piedmont lobes. In this case, the folds generate axes normal to the maximum compression that is parallel to the ice margin.

Debris transfer between low and high levels

An understanding of glacier structure is once again vital to appreciate how debris is redistributed within the glacier, especially where basal debris is uplifted to a higher-level position. In this context, glacier ice behaves no differently from any other geological material deforming where the Earth's crust is subject to lateral stresses. Debris in glaciers is transferred from the bed to an englacial and even a supraglacial position by three main glaciotectonic processes: thrusting, basal crevasse-filling, and incorporation within longitudinal foliation. Of these, the role of thrusting versus crevasse-filling has been much debated, and certainty of the mechanism cannot always be achieved.

Thrusts, typically inclined upglacier at angles ranging from a few to c. 40°, develop under longitudinal

Sediment Entrainment, Transport, and Deposition, Figure 7 Thick layer of largely angular avalanche-derived supraglacial debris draping the surface of Khumbu Glacier, Mt. Everest region, Nepal.

Sediment Entrainment, Transport, and Deposition, Figure 8 Medial moraines of the flow-unit interaction type on Kaskawulsh Glacier, Yukon.

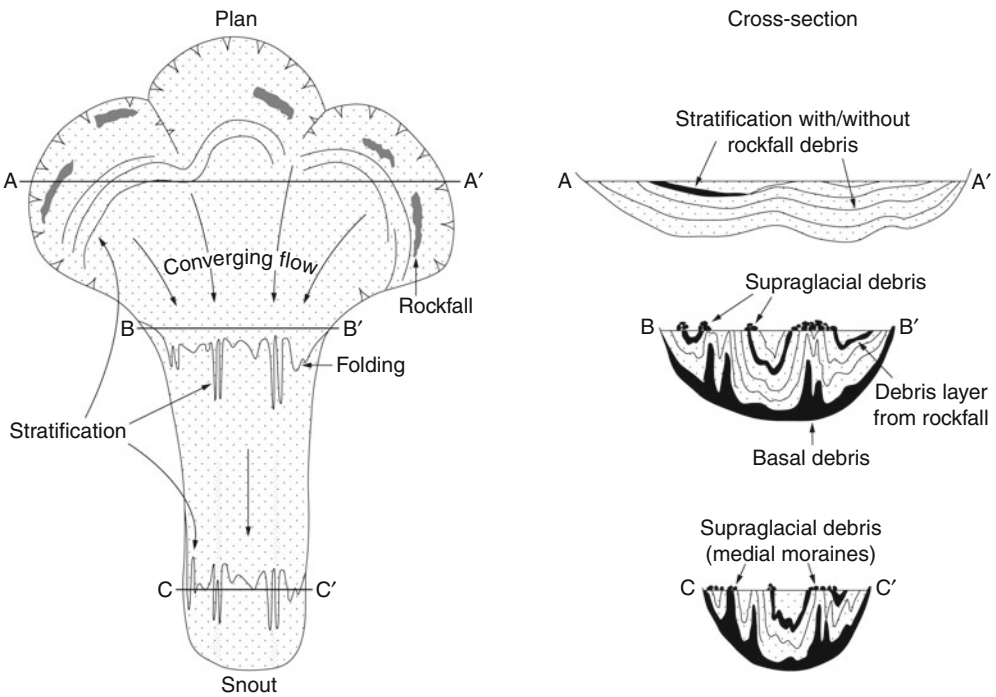

Sediment Entrainment, Transport, and Deposition, Figure 9 Conceptual models of debris entrainment and the development of ablation-dominant moraines, illustrating both high-level folding of supraglacial debris and low-level folding of basal debris. (After Hambrey et al., 1999; published with permission of the International Glaciological Society.)

Sediment Entrainment, Transport, and Deposition, Figure 10 Complex folding and looped moraines are characteristic features of surge-type glaciers, this example being Lowell Glacier in the Icefield Ranges, Yukon.

compression in three main situations: (1) where there is a downstream transition from a sliding to a frozen bed, as in polythermal glacier; (2) where ice flows against a reverse bedrock or sediment slope; and (3) in surging glaciers as the strongly compressive surge front moves down glacier. Thrusts carrying abundant debris are a feature of many polythermal and cold glaciers, but they also occur to a limited extent in temperate glaciers. Specifically, debris-rich basal ice (including regelation ice) and rafts of subglacial sediments are uplifted into an englacial position, sometimes emerging at the ice surface (Figure 11). This material is more varied than rockfall debris, and reflects the substrate lithologies: typically poorly sorted sediment (diamicton) with striated clasts (inferred to be basal till), sandy gravel (glaciofluvial sediment, and even laminated or stratified mud and sand (glaciolacustrine or glaciomarine sediment). The thrusts may extend upward to the ice surface and be associated with recumbent folding with lower limbs being sheared off at the thrust surface. Other so-called blind thrusts may terminate within the ice mass. As thrusts melt out at the glacier surface, groups of roughly aligned, commonly arcuate ridges and hummocks of basally derived sediment are formed.

Flowage of subglacial sediment into basal crevasses, followed by rotation during glacier flow, has also been inferred to explain the emergence of debris on inclined planes at the glacier surface. There are few direct sightings of basal crevasses, but such fractures are thought to occur especially when a glacier surges over a soft deformable bed of till. Once they attain a moderate angle, they resemble thrusts, and discrimination between the two processes relies on whether the feature is associated with basal ice, in which case the thrusting mechanism is most likely. The sedimentary product of incorporation of debris into basal crevasses is a suite of meter-scale landforms referred to as crevasse-fill ridges.

A third mechanism involves incorporation of debris of both supraglacial and basal character within longitudinal foliation. This process is particularly evident at the glacier margins and at flow-unit boundaries where the folding is commonly isoclinal. The folding has an axial planar relationship with the foliation. At depth, it is inferred (but not so far observed) that the lateral compressive regime that produces high-level folding, also induces folding is soft subglacial and basal sediments of the same geometry (Figure 9). As these features melt out, low (meter-scale) longitudinal ridges form that are similar to, but genetically different from, flutes; these are referred to as "foliation-parallel ridges."

Debris transfer between high and intermediate levels

In addition to burial and folding of supraglacial debris, described above, debris can enter an englacial position via crevasses. Crevasses generally do not penetrate to the bed, and in temperate glaciers are theoretically no more than 30 meters deep unless water filled. Structures commonly influence the pattern of supraglacial and englacial drainage. For example, a moulin that captures a supraglacial stream may form along a crevasse trace, which acts as a plane of weakness in the ice. Supraglacial sediment washed into the stream may tumble into the moulin and enter an englacial position or even reach the bed.

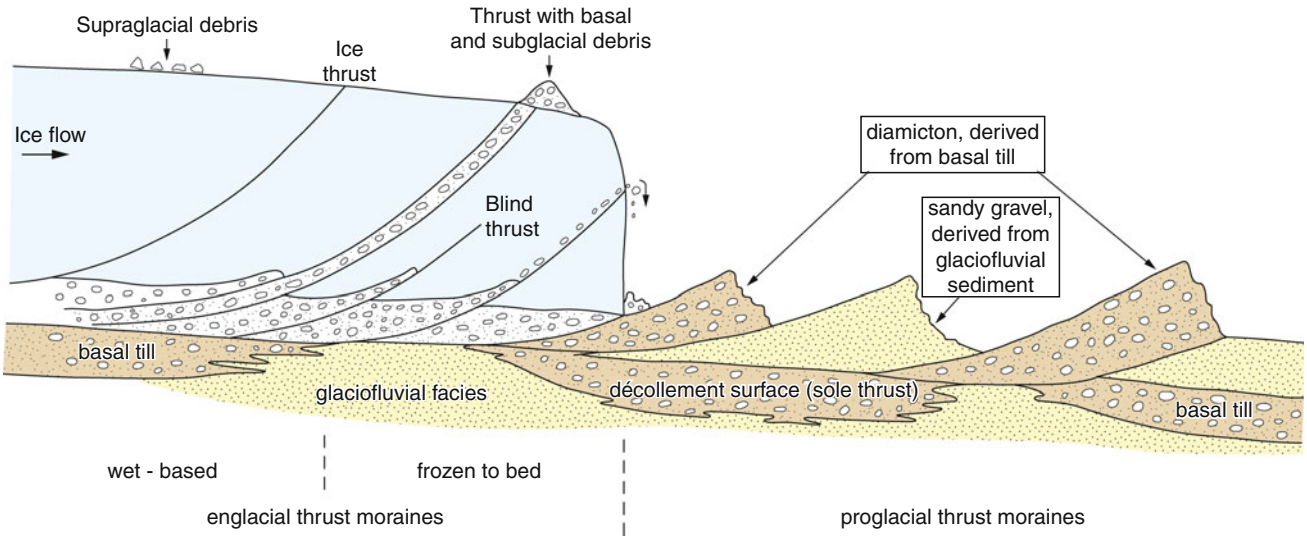

Sediment Entrainment, Transport, and Deposition, Figure 11 Simplified model of thrusting as exemplified by an advancing polythermal glacier, with thrusts propagating beyond the ice margin into frozen ground of the forefield.

Glacial depositional processes and facies

Glacial sedimentation involves the direct release of debris that has been transported on or within glacier ice. Debris is modified during transport primarily by basal processes (e.g., abrasion, crushing, and quarrying during intra-clast collision, subglacial sediment deformation), and by water in subglacial, englacial, and supraglacial stream channels. Debris that follows a passive transport path (supraglacially or englacially) tends to retain its primary characteristics.

Sediment may be deposited directly beneath the glacier or at its margins, or it can be transported significant distances from the glacier itself by other agents such as rivers or by iceberg calving. During release from the ice, numerous glacier-related processes, including reworking in marginal streams and lakes, debris flows, and aeolian activity, may modify sediment. Many glacigenic sediments may be related to specific glacial environments. For example, the temperate terrestrial glacier system is commonly regarded as being dominated by a mixture of basal (actively transported) and supraglacial (passively transported) sediment, with a strong element of glaciofluvial modification upon release (Figure 12a). Glaciers terminating in fjords produce a suite of sediments that is also dependent on thermal regime. Temperate and polythermal glaciers, such as those in Alaska and Greenland, respectively (Figure 12b), not only provide basal and supraglacial debris inputs, but also sediments released from subglacial streams emanating at or below water level close to the ice margin, sediment released from suspension over the whole depositional basin, and iceberg-rafted debris. The resulting sediment associations reflect thermal regime, which primarily controls the balance between direct glacial deposition and fluvial inputs. For the coldest glaciers, terminating as ice shelves on the continental shelf, as in Antarctica today, direct glacial deposition is restricted to the grounding line, while the volume of meltwater sediments is limited. Rather, biogenic sedimentation in the form of diatom ooze may become dominant (Figure 12c). Indeed, rather than releasing sediments, some ice shelves accrete saline ice at their base, trapping sediment, which is released only when the tabular icebergs, calved from the ice shelf, disintegrate.

Glaciotectonism

Glaciotectonic deformation is now recognized as a widespread phenomenon (Maltman et al., 2000). Commonly visible at the scale of entire moraine complexes (Figure 13), it is also widely recognized at the microscopic level and recent years have seen substantial advances in understanding the role played by deformation in the character of glacial sediments. Not only is deformation associated with internal processes, such as folding and thrusting, as noted above, but it is also transmitted subglacially and proglacially. Glaciotectonic deformation operates in any topographic setting, both during advancing and recessional phases, and involves all types of material, including frozen, saturated, and dry unconsolidated sediments, as well as bedrock. Deformation may detach blocks of rock and sediment, occasionally hundreds of meters across, incorporating them into the ice by thrusting or pushing them in front of the glacier. Faults and brecciated zones are common in such materials. Sediments may also be deformed in ductile fashion, especially if wet and fine grained. Beneath ice sheets, deformation may affect sediment and bedrock to depths of several hundred meters.

Reworking of glacigenic sediments

Glacigenic sediments are typically subject to syn-depositional and postdepositional modification by fluvial, mass-movement, and aeolian processes. In terrestrial settings, fluvial modification by proglacial streams is

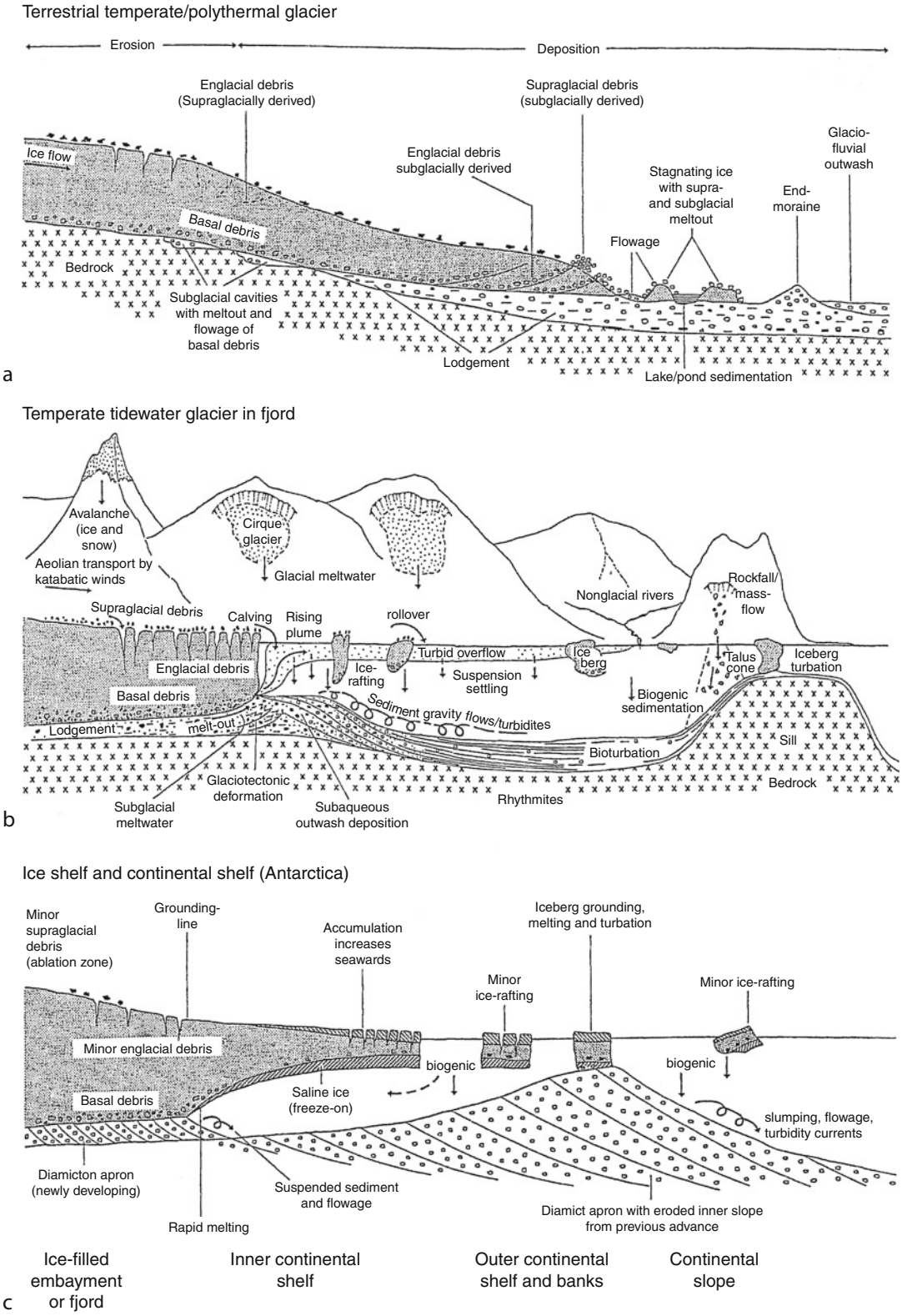

Sediment Entrainment, Transport, and Deposition, Figure 12 Depositional processes and products in a selection of glacial environments: (**a**) terrestrial, (**b**) fjord with temperate tidewater glacier, and (**c**) ice shelf on the Antarctic continental margin. (After Hambrey, 1999; published by permission of Terra Antartica, Museo Nazionale dell'Antartide, Siena.)

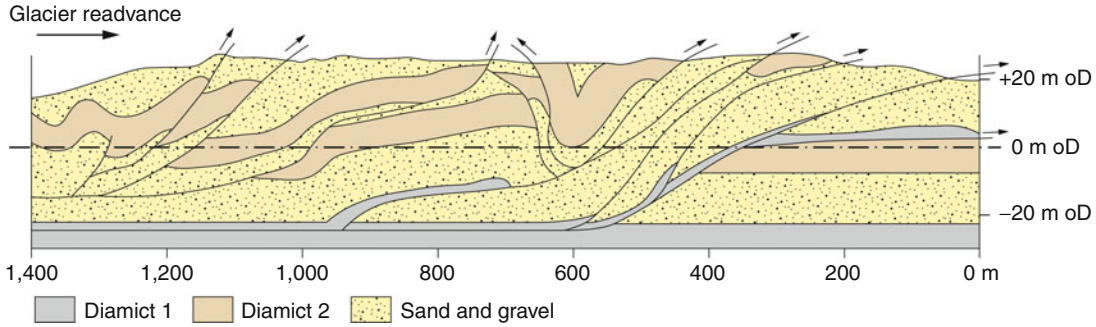

Sediment Entrainment, Transport, and Deposition, Figure 13 Glaciotectonic deformation exemplified by the push moraine complex at Dinas Dinlle, North Wales. The section is exposed in a coastal cliff and the subsurface geometry was revealed by a seismic survey. (Modified from Harris et al., 1997.)

particularly important in temperate climates, and many temperate glaciers terminate at the head of large *outwash* or *sandur* plains composed almost entirely of reworked glacial sediments. Resedimentation by mass-movement processes is common in ice-cored terrain where water, released by the melting of buried glacier ice or permafrost, mixes with sediment to create *glacigenic sediment flows*. Modification by wind, especially in cold arid environments such as Antarctica, involves the redistribution of sand and silt, creating *deflation surfaces* and *ventifacts*. The extent to which each of these processes operates is controlled to a great extent by the local topographic, meteorological, and climatological conditions. Resedimentation by subaqueous gravity flows is also important in glaciomarine and glaciolacustrine environments, where large volumes of sediment may accumulate on relatively steep ice-contact slopes that become unstable during recession.

Terminology of terrestrial glacigenic sediments

The terminology used to describe glacigenic sediment has always been in a state of flux, and the evolution of terms may be linked to progressive improvement of understanding glacial processes. For an objective study of glacigenic sediments, a nongenetic classification of poorly sorted sediments is required. The use of process-focused terms such as "till" should only follow from careful description of a wide range of attributes, including texture, clast-shape and surface characteristics, bed-geometry, and boundary relationships.

The terms *diamicton* (unlithified), *diamictite* (lithified), and *diamict* (both) are now well established for "a nonsorted or poorly sorted terrigenous sediment that contains a wide range of particle sizes" (Flint et al., 1960). However, this definition hides a vast range of textures, and the literature abounds with conflicting ideas about what constitutes a "diamicton." A textural classification, based on the relative proportions of sand and gravel, has subsequently been developed (Hambrey and Glasser, 2003) (Table 1).

The genetic terminology is perhaps even more confused. First, we need to define some widely used general terms:

Glacigenic sediment: "of glacial origin"; the term is used in the broad sense to embrace sediments that have been influenced by glacier ice.

Glacial debris: material being transported by a glacier and thus in contact with glacier ice.

Glacial drift: a general term embracing all rock material in transport by glacier ice, all deposits released by glaciers, and all deposits predominantly of glacial origin deposited in the sea by icebergs, or from glacial meltwater.

Till: sediment deposited directly by glacier ice that has not been subsequently disaggregated by flow or gravity. There are several subcategories of till, which are explained below.

Subglacial sedimentary processes

It is evident from the general nature of the above terms that texturally glacigenic sediments are exceedingly variable, and therefore a lack of consensus as to their appearance is apparent in the literature. Nevertheless, there are several processes which have been identified by which debris in transport is deposited: lodgement, meltout, flow, subglacial deformation, and sublimation. All these processes give rise to subcategories of till, and all are widespread except sublimation till, which is confined to the cold arid environment of Antarctica. This classification of till has traditionally been widely used and adopted by the International Quaternary Association (Dreimanis, 1989; Hambrey, 1994), but these distinctions have been challenged over the past decade following the development of microstructural (micromorphological) analysis of till in thin section. Indeed, most "tills" form by a combination of processes, especially in the subglacial environment, and they are thought by some to be the product of deformation rather than depositional processes; hence the new term *tectomict* (Bennett and Glasser, 2009 give an up-to-date synthesis of this issue).

Sediment Entrainment, Transport, and Deposition, Table 1 Textural classification of poorly sorted sediments (From Hambrey, 1994; modified from Moncrieff 1989). In order to derive sediment name, percent of gravel is first estimated (horizontal axis) and then the proportion or percent of sand in the matrix (vertical axis)

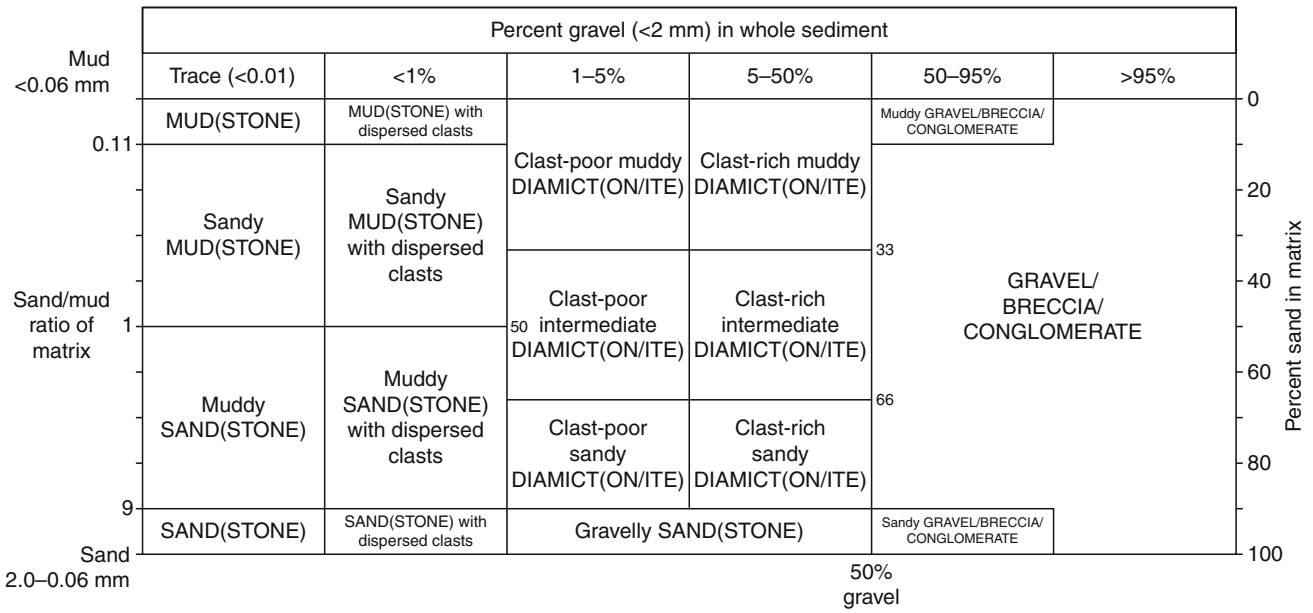

Supraglacial sedimentary processes

Debris on the glacier surface includes material that has fallen on the surface via rockfalls and passively transported as well as basally derived debris that originates where flow units combine, or where glaciotectonic processes have lifted basal sediments from the bed. This debris accumulates as a result of melting under the influence of solar radiation. A thin cover of debris will enhance melting, but as the debris accumulates, it retards melting, so debris-covered areas tend to be elevated compared with surrounding ice surfaces. Debris is concentrated into mounds and ridges, and as slopes increase in angle by the differential melting, it is prone to constant movement by sliding and slumping. Sediment thus accumulates in hollows which, when sufficiently thick, retards ablation so gradually becoming a new high point – a process known as topographic inversion.

Glaciomarine (or glacimarine) sedimentation

Glaciomarine sediments are much less studied than terrestrial glacigenic sediments, but nevertheless considerable strides in understanding have been made in recent years. Sediments are released into the ocean via several processes, giving rise to a distinctive suite of attributes that are subtly different from their terrestrial counterparts.

Ice-proximal glaciomarine sediment comprises debris that is released either from floating basal glacier ice or by continuous rain-out from icebergs, without subsequent winnowing by currents and waves.

Ice-distal glaciomarine sediment is debris that is released from icebergs, but in this case subject to winnowing and admixing with other marine sediment, including biogenic components. Texturally, this facies is sandy mud or muddy sand with dispersed clasts, and in modern environments is often rich in diatoms.

Iceberg turbate is sediment deposited on the sea floor that is subsequently reworked by grounded icebergs. The end product is commonly a massive diamicton with a heavily grooved upper surface.

Cyclopels (silt/mud couplets) and *cyclopsams* (graded sand/mud couplets) are rhythmically laminated sediments derived from turbid overflow plumes originating from subglacial discharge, especially in fjords, typically producing two couplets a day according to the tidal cycle.

Subaqueous sediment flows are the product of remobilization of all of the above sediment types. They range from massive uniform diamicton, resulting from down-slope creep or mobile flow, as on land, to well-graded beds of mud, sand and gravel where disaggregated in a turbidity flow.

Glaciolacustrine (or glacilacustrine) sedimentation

Glaciolacustrine sediments are similar to those in glaciomarine environments. In addition, lakes commonly have rhythmically laminated sand and mud called *varves*. They are similar to cyclopsams and cyclopels, but each couplet forms over 1 year.

Facies analysis of glacigenic sediments

The facies approach

For objective treatment of glacial sediments, and following other branches of sedimentology, the facies approach must be used. The first step is to describe the *lithofacies* (types of sediment) found in a vertical section or core, using a wide range of criteria (texture, sedimentary structures, bed geometry and boundary relations, clast characteristics), and avoiding genetic terms such as "till." Some authors use a formal lithofacies code (Eyles et al., 1983) which has been widely adopted, but this is thought by others (e.g., Hambrey, 1994; Miller, 1996) to be too inflexible and not totally objective as it includes interpretative elements.

The next step is to group the lithofacies into *facies associations* that contain a set of attributes that will allow the depositional setting to be determined, such as glacioterrestrial or glaciomarine. On a regional scale, given sufficient three-dimensional exposure on land, or extensive seismic and borehole stratigraphy offshore, derivation of the *facies architecture* is a desirable aim, allowing one to address larger issues, such as basin evolution, ice sheet–scale fluctuations and sea-level changes. Representative facies associations from terrestrial, lacustrine, and glaciomarine settings are illustrated in Figure 14.

Glacial sediment/landform associations

The concept of *glacial sediment/landform associations* (the "*landsystem*" approach) rests on the assumption that, at the large scale, it is possible to identify areas of land with common attributes, distinct from the surrounding areas, that can be related to the processes involved in their development (Benn and Evans, 2010; Evans, 2003). The landsystem approach was pioneered for glaciated terrain in an attempt to identify tracts of land created by similar till-forming processes and therefore of similar geotechnical properties. The *glacial landsystem* concept was then applied to former ice-sheet beds. Originally, three distinct landsystems were defined: (1) the *subglacial landsystem*, in which the dominant glacial sediment/landform associations are formed at the glacier bed; (2) the *supraglacial landsystem*, in which the dominant glacial sediment/landform associations are largely composed of a drape of supraglacial debris; and (3) the *glaciated valley landsystem*, in which the dominant glacial sediment/landform association is that formed by mountain glaciation.

As the concept has developed, other landsystems have been added to this simple list (Evans, 2003). These include landsystems formed in proglacial and glaciomarine environments, as well as those found in settings where surge-type glaciers are common. It is also possible to define landsystems according to glacier thermal regime. Thus we can identify landsystems related to warm-based ("temperate"), polythermal, and cold-based ("polar") glacier margins. A criticism of the landsystems approach is that it takes little account of spatial patterns of ice-sheet erosion and deposition, and how these vary during ice-sheet growth and decay.

Glacial depositional landforms

Glaciers and ice sheets produce a huge variety of depositional landforms that are commonly grouped according to their origin into ice-marginal and subglacial types (Hambrey, 1994; Menzies, 1995, 1996; Bennett and Glasser, 2009; Benn and Evans, 2010). Distinguishing between the different types of moraine is important for reconstructing the size, morphology, and dynamics of former ice masses.

Ice-marginal landforms. Ice-marginal landforms can be produced by advancing, stationary, or receding ice margins, as well as during seasonal fluctuations of the glacier terminus. These landforms include *glaciotectonic moraines, push moraines, dump moraines*, and *thrust-block moraines* (Figure 11).

Ablation moraines (sometimes referred to as *ice-cored moraines*) form wherever ice-melt is retarded beneath a cover of supraglacial debris (Figure 12). If the cover of insulating debris is irregular, irregular ridges and mounds of debris, referred to as *hummocky moraines* or *moraine-mound complexes*, will develop.

Subglacial landforms (sometimes referred to as *subglacial bedforms*) are produced beneath actively flowing ice. They provide information about former subglacial conditions, including ice-flow directions, thermal regime, and paleohydrology. The most common of these is a family of ice-molded landforms, all of which are parallel to ice flow. This includes *flutes, megaflutes, mega-scale glacial lineations*, and *drumlins.*

Ribbed moraines (also known as *Rogen moraines*) are large, regularly and closely spaced moraine ridges consisting of glacigenic sediment.

Geometric ridge networks and *crevasse-fill ridges* are subglacial landforms that are not generally ice-molded. They form by the squeezing of subglacial material into basal crevasses or former subglacial tunnels, commonly during surges, or beneath glaciers as a result of the intersection of foliation-parallel ridges and englacial thrusts.

Eskers are glaciofluvial landforms created by the flow of meltwater in subglacial, englacial, or supraglacial channels. *Concertina eskers* are deformed eskers, created by compression beneath overriding ice.

Outwash fans and *outwash plains* (or *sandar*, plural; *sandur*, singular) are formed as glacial meltwater emerges from the glacier and sediment is deposited at or beyond the ice margin. Outwash fans form at stationary ice margins where meltwater is concentrated at a particular point for a length of time. Outwash plains are much larger features, formed where individual fans coalesce away from the glacier to create a braided-river facies association. Characteristics of the glaciofluvial environment are braided river channels with rapidly migrating bars, terraces, frequent channel avulsions, and the formation of *kettle holes* where sediment is deposited over buried ice.

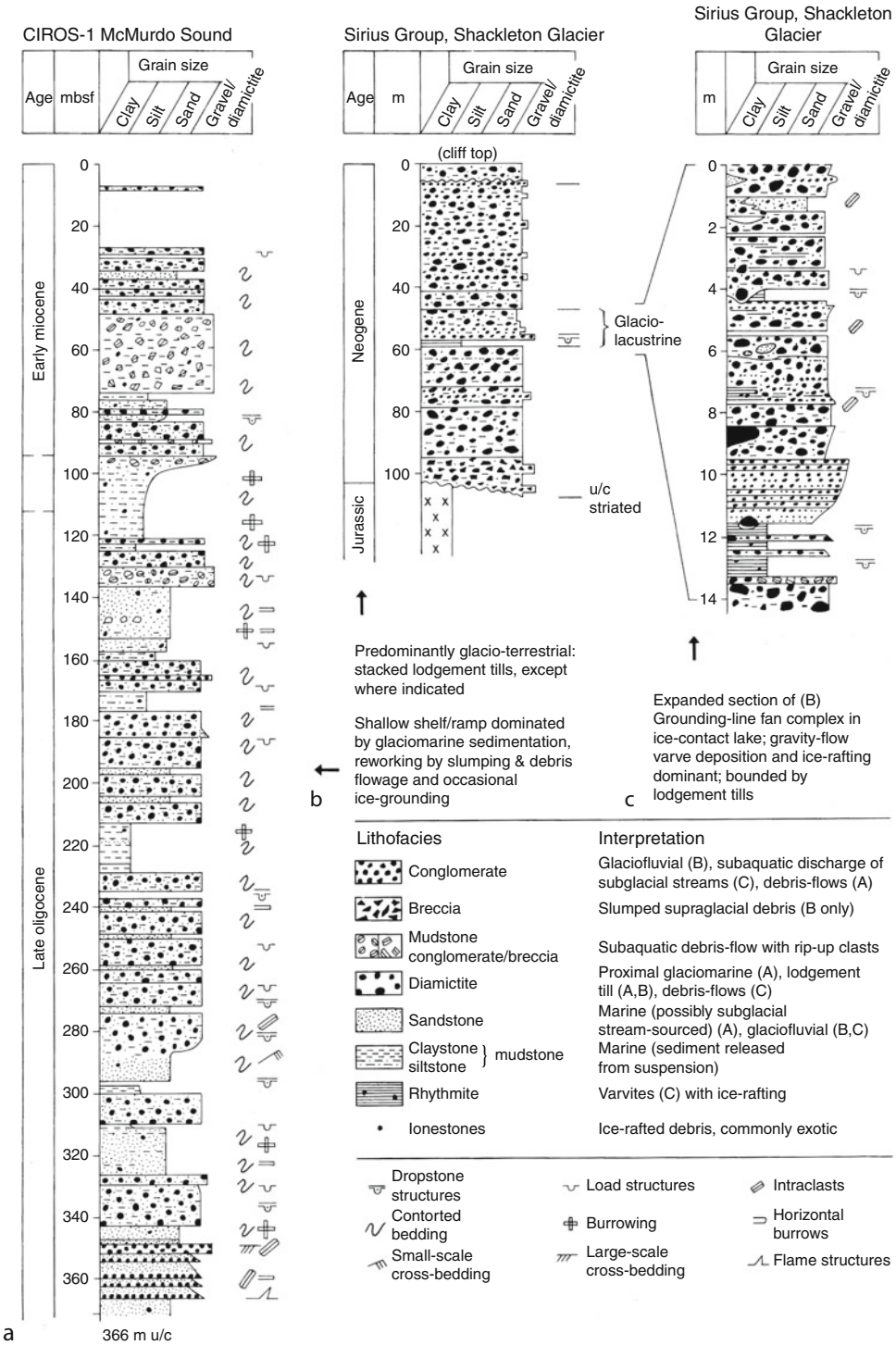

Sediment Entrainment, Transport, and Deposition, Figure 14 Characteristic glacigenic facies associations from marine and terrestrial settings in Antarctica. (**a**) Late Oligocene – Early Miocene proximal continental shelf facies association, upper part of CIROS-1 drill-core, McMurdo Sound, illustrating deposition in a subsiding rift-basin, with occasional ice-grounding events (after Barrett, 1989). (**b**) A terrestrial glacigenic facies association dominated by repeated lodgement till deposition, represented by stacked diamictites, but with a lacustrine phase of sedimentation in midsection: Sirius Group (Neogene), Shackleton Glacier, Transantarctic Mountains. (**c**) Enlargement of the glaciolacustrine facies association in B illustrating ice-proximal deposition dominated by slumping and debris flowage of rain-out diamictite and varve-sedimentation. (From Middleton, 2003 published with permission of Kluwer Publishers, Dordrecht.)

Kame terraces are formed when sediment is deposited by meltwater flowing laterally along an ice margin. *Kames* are more fragmentary features, formed in a similar manner, but often in ice-walled tunnels and against steep valley sides. *Kame-and-kettle topography* is the term used to describe the landform-sediment assemblage often found on glacier forefields where there was formerly a high proportion of buried ice.

Bathymetric forms resulting from glacial processes

Erosional forms

Various erosional phenomena, mainly associated with grounded ice or subglacial meltwater are found in marine settings. The larger-scale forms are filled by sediment and may be recognizable in seismic profiles (e.g., Anderson, 1999). *Submarine troughs* are found on continental shelves, and are genetically equivalent to fjords and other glacial troughs, but are generally much broader. Formed by ice streams, the largest occur in Antarctica where they attain dimensions of over 400 km in length, 200 km in width, and 1,100 m in depth. Where two ice streams merge, an *ice-stream boundary ridge* is formed. Steep-sided channels a few kilometers wide, carved out by subglacial meltwater and subsequently filled by sediment are known as *tunnel valleys*. These are well known from the NW European continental shelf around Britain, the Scotian Shelf off Canada, and in Antarctica. Icebergs can also cause considerable erosion as they become grounded on the sea floor. Large tabular bergs can scour the bed of the sea for several tens of kilometers, leaving impressions up to 100 m wide and several meters deep. *Slope valleys* are groups of gullies forming a dendritic pattern that develop just beyond the ice margin, on the continental slope, as a result of erosion by sediment gravity flows that emanate from sediment accumulation at the ice margin. On continental shelf areas, where the ice repeatedly becomes grounded, and then releases a large amount of rain-out sediment, alternations of diamicton and *boulder pavements* may be observed. The pavements build up by accretion of boulders around an obstacle, by subglacial erosion, or they represent a lag deposit from winnowing by bottom currents.

Depositional forms

The morphology and sediment composition of subaquatic features, particularly in fjords and on continental shelves are less well known than their terrestrial counterparts, but major strides have been made in identifying such features in the last 3 decades. As on land, depositional assemblages reflect the interaction of a wide range of processes and they comprise a diverse range of sediments.

Ice-contact features form when a glacier terminus remains almost stationary in water, particularly in fjords (Powell and Cooper, 2002). *Morainal banks* form by a combination of meltout from basal ice, dumping of englacial and supraglacial debris, push and squeeze processes, combined with glaciofluvial discharge. The end product is an assemblage of poorly sorted deposits with some evidence of glaciotectonically disturbed stratification (Figure 15). *Grounding-line fans* extend from a subglacial tunnel that discharges meltwater and sediment into the sea, and are typically composed of sand and gravel. A series of such fans may develop if glacier recession is interrupted. Developing out of grounding-line fans are *ice-contact deltas* that form when the terminus remains stable long enough for sediment to build up to the surface of the fjord. Where a glacier becomes disconnected from the water body, alluvial sediments may prograde to form *fluviodeltaic complexes*, which comprise sand and gravel. In addition to these large-scale forms (measured in hundreds of meters), there are small-scale features (measured in meters or less), found particularly on beaches, such as iceberg tool-marks, ridges, depressions from melting of buried ice, bounce-marks, chattermarks, and roll-marks. Icebergs can also churn up submarine sediment, particularly on shoals, producing *iceberg turbates*.

Depositional forms on continental shelves are best known from a combination of deep drilling and seismic profiling. Some, as in Alaska, are simply larger-scale analogues of fjordal features, such as delta-fan complexes, but others form under floating tongues that are typical of the colder ice of the polar regions. These include subglacial deltas, till tongues, diamicton aprons, and the immense (up to 400 km wide) trough-mouth fans, all of which are commonly associated with ice streams. Other features are similar to those on land, including shelf moraines, flutes, mega-scale glacial lineations, and transverse ridges.

Glacial sediments in the geological record

Identification of glaciation in the geological record

The recognition of glacigenic sediments and landforms in the rock record is of fundamental importance to the emerging field of paleoglaciology, which embraces paleoclimatological and paleoenvironmental reconstructions. Even where exposure is good, evidence for glaciation may be equivocal as, for example, in alpine regions where mass-movement and fluvial processes may overprint direct evidence for glacial deposition, or in those areas where tectonic deformation has overprinted depositional features. However, detailed analysis may yield sufficient criteria that, taken together, could form the basis of a glacial interpretation.

Preservation potential of glacigenic successions

Tectonic setting is the principal control on whether a glacial succession is preserved. Eyles (1993) provided a detailed review of the wide range of tectonic settings suitable for preservation. Intracratonic basins, rifts, forearc and backarc basins, and subsiding continental shelves are particularly suitable receptacles for accumulation and preservation of glacial sediments, especially if those sites are first buried and later uplifted and exposed. Except for deposits of Quaternary age, land areas are less likely to preserve glacial sediment, as continued erosion tends to

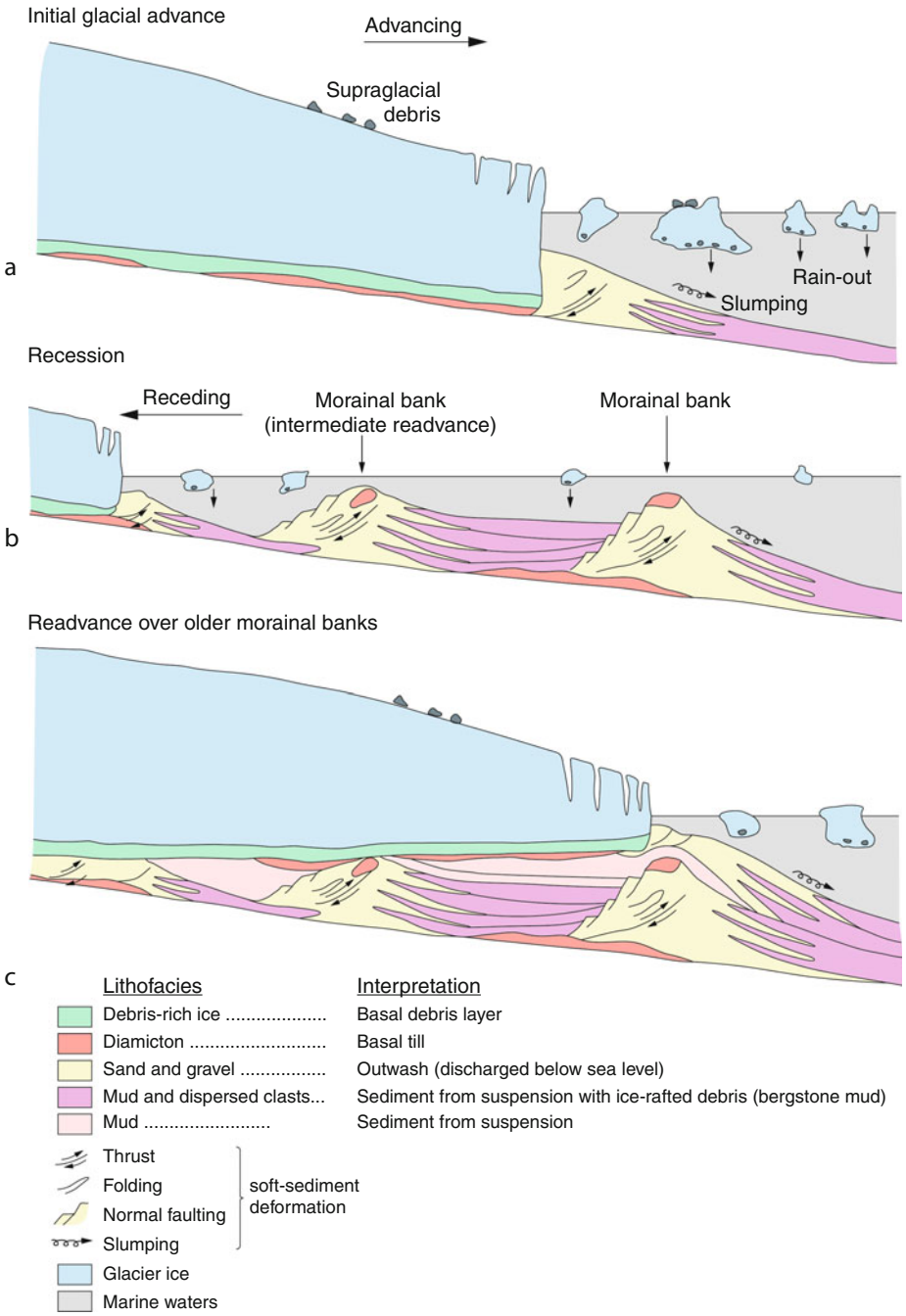

Sediment Entrainment, Transport, and Deposition, Figure 15 Conceptual model for the development of the morainal bank facies association, as exemplified by the succession recovered by the Cape Roberts Drilling Project, western McMurdo Sound, Antarctica. (Simplified from Powell and Cooper, 2002.)

remove traces of glaciation. There are, however, notable exceptions in the geological record.

Earth's glacial record

Far more is known about the Quaternary glaciations than all previous glaciations put together, even though some of those earlier events were equally dramatic in terms of scale. Since the International Geological Correlation Programme compiled an inventory of all known pre-Quaternary glacigenic sequences (Hambrey and Harland, 1981), several syntheses have been undertaken (e.g., Eyles, 1993; Deynoux et al., 1994; Crowell, 1999). For the Quaternary Period there is a vast literature from which to choose.

The oldest known glacigenic sediments are of late Archaean age (2,600–3,100 Ma) from South Africa. Extensive Paleoproterozoic (2,500–2,000 Ma) tillites are known from South Africa, Australia, and Finland. The most prolonged and globally extensive glacial era took place in Neoproterozoic time (1,000–550 Ma). Evidence for glaciation occurs on all continents, leading to the "snowball earth" hypothesis that envisages the Earth being totally ice covered, although this concept has proved highly controversial (Allen and Etienne, 2008). Sporadic Early Paleozoic glacial events are best represented by the late Ordovician to early Silurian deposits and erosional features of the supercontinent of Gondwana, notably in Africa. The most prolonged and extensive phase of glaciation during the Phanerozoic Eon spanned about 90 Ma of the Carboniferous and Permian Periods, affecting all Gondwana continents. Finally, after a phase of global warmth, with little evidence of ice on Earth, the Cenozoic glaciations began in Antarctica at the Eocene/Oligocene transition (c. 34 Ma). Northern Hemisphere glaciation followed, with minor ice-rafting events recorded in the North Atlantic from late Miocene time, until full-scale glaciations began in late Pliocene time (2.4 Ma) and continued through the Quaternary to the present day.

Summary

Sediment entrainment, transport, and deposition are important in understanding the legacy of former glaciers and ice sheets. The entrainment and transport processes depend primarily on glacier mass balance, dynamics, structure, thermal regime, hydrology, and morphology. Sediment entrainment takes place at the bed and the surface of a glacier, and there are transfers between both zones. Structural evolution plays a key role in defining the distribution of sediment through a glacier. Structural processes are also evident in the depositional environment, especially in terms of glaciotectonic deformation of sediments and landforms, for example, through folding and thrusting. Systematic analysis of the sedimentary record following deposition, through the facies approach, allows inferences to be made about the environments of deposition and paleoclimates, and approach which is valid not only for understanding the Quaternary record, but also that of ancient glaciations.

Bibliography

Allen, P. A., and Etienne, J. L., 2008. Sedimentary challenge to snowball Earth. *Nature Geoscience*, **1**, 817–825.

Anderson, J. B., 1999. *Antarctic Marine Geology*. Cambridge: Cambridge University Press, 297 p.

Barrett, P. J. (ed.), 1989. *Antarctic Cenozoic History from the CIROS-1 Drillhole, McMurdo Sound*. Wellington: DSIR Publishing. DSIR Bulletin 245.

Benn, D. I., and Evans, D. J. A., 2010. *Glaciers and Glaciation*, 2nd edn. London: Arnold.

Bennett, M. R., and Glasser, N. F., 2009. *Glacial Geology: Ice Sheets and Landforms*. Chichester: Wiley.

Boulton, G. S., 1996. Theory of glacial erosion, transport and deposition as a consequence of subglacial sediment deformation. *Journal of Glaciology*, **42**, 43–62.

Crowell, J. C., 1999. Pre-Mesozoic ice ages: Their bearing on understanding the climate system. Geological Society of American Memoir 192, pp. 1–106.

Deynoux, M., Miller, J. M. G., Domack, E. W., Eyles, N., Fairchild, I. J., and Young, G. M., 1994. *Earth's Glacial Record*. Cambridge: Cambridge University Press.

Dreimanis, A., 1989. Tills, their genetic terminology and classification. In Goldthwait, R. P., and Matsch, C. L. (eds.), *Genetic Classification of Glacienic Deposits*. Rotterdam: Balkema, pp. 17–84.

Evans, D. J. A. (ed.), 2003. *Glacial Landsystems*. London: Arnold.

Eyles, N., 1993. Earth's glacial record and its tectonic setting. *Earth Science Reviews*, **35**, 1–248.

Eyles, N., Eyles, C. H., and Miall, A. D., 1983. Lithofacies types and vertical profile models; an alternative approach to the description and environmental interpretation of glacial diamict and diamictite sequences. *Sedimentology*, **30**, 393–410.

Flint, R. F., Sanders, J. E., and Rodgers, J., 1960. Diamictite: a substitute term for symmictite. *Geological Society of America Bulletin*, **71**, 1809–1810.

Hambrey, M. J., 1994. *Glacial Environments.* Vancouver: University of British Columbia Press, and London: UCL Press.

Hambrey, M. J., 1999. The record of Earth's glacial history during the last 3000 Ma. In Barrett, P. J., and Orombelli, G. (eds.), *Geological Records of Global and Planetary Changes*. Terra Antartica Reports 3, Siena, Italy, pp. 73–107.

Hambrey, M. J., and Glasser, N. F., 2003. Glacial sediments: processes, environments and facies. In Middleton, G. V. (ed.), *Encyclopedia of Sediments and Sedimentary Rocks*. Dordrecht: Kluwer, pp. 316–331.

Hambrey, M. J., and Harland, W. B., 1981. *Earth's Pre-Pleistocene Glacial Record*. Cambridge: Cambridge University Press.

Hambrey, M. J., and Lawson, W. J., 2000. Structural styles and deformation fields in glaciers: a review. In Maltman, A. J., Hubbard, B., and Hambrey, M. J. (eds.), *Deformation of Glacial Materials*. London: Geological Society of London. Special Publication, 176, pp. 59–83.

Hambrey, M. J., Bennett, M. R., Dowdeswell, J. A., Glasser, N. F., and Huddart, D., 1999. Debris entrainment and transfer in polythermal valley glaciers. *Journal of Glaciology*, **45**, 69–86.

Harris, C., Brabham, P. J., Williams, G. D., and Eaton, G., 1997. The nature and significance of glaciotectonic structures at Dinas Dinlle, northwest Walesm UK. *Quaternary Science Reviews*, **18**, 109–127.

Hubbard, B., Cook, S., and Coulson, H., 2009. Basal ice facies: a review and unifying approach. *Quaternary Science Reviews*, **28**, 1956–1969.

Knight, P. G., 1997. The basal ice layer of glaciers and ice sheets. *Quaternary Science Reviews*, **16**, 975–993.

Maltman, A. J., Hubbard, B., and Hambrey, M. J. (eds.), 2000. *Deformation of Glacial Materials*. London: Geological Society of London. Special publication, 176.

Menzies, J. (ed.), 1995. *Modern Glacial Environments: Processes, Dynamics and Sediments*. Oxford: Butterworth-Heinemann.

Menzies, J. (ed.), 1996. *Past Glacial Environments: Sediments, Forms and Techniques*. Oxford: Butterworth-Heinemann.

Middleton, G. V. (ed.), 2003. *Encyclopedia of Sediments and Sedimentary Rocks*. Dordrecht: Kluwer.

Miller, J. M. G., 1996. Glacial sediments. In Reading, H. G. (ed.), *Sedimentary Environments: Processes, Facies and Stratigraphy,* 3rd edn. Oxford: Blackwell Science, Chap. 11, pp. 454–484.

O'Cofaigh, C., and Dowdeswell, J. A. (eds.), 2002. *Glacier-Influenced Sedimentation on High-Latitude Continental Margins*. London: Geological Society. Special publication, 203.

Paterson, W. S. B., 1994. *Physics of Glaciers*. Oxford: Pergamon.
Powell, R. D., and Cooper, J. M., 2002. A glacial sequence stratigraphic model for temperate, glaciated continental shelves. In O'Cofaigh, C., and Dowdeswell, J. A. (eds.), *Glacier-Influence Sedimentation on High-Latitude Continental Margins*. London: Geological Society, Special publication 203, pp. 215–244.

Cross-references

Cold-Based Glaciers
Debris
Debris-Covered Glaciers
Englacial Processes
Formation and Deformation of Basal Ice
Glacier Hydrology
Glacier Motion/Ice Velocity
Glacier Surging
Meltwater Channels
Moraine
Polythermal Glaciers
Retreat/Advance of Glaciers
Sediment Core and Glacial Environment Reconstruction
Structural Glaciology
Temperate Glaciers
Till
Transformations of Snow at the Earth's Surface and its Climatic and Environmental Consequences

SEDIMENT FLUX SOURCE-TO-SINK

Achim A. Beylich
Quaternary Geology and Climate Group, Geological Survey of Norway (NGU), Trondheim, Norway
Department of Geography, Norwegian University of Science and Technology (NTNU), Trondheim, Norway

Synonyms

Sediment transfer source-to-sink; Sediment transport source-to-sink

Definition

Erosion (mobilization), transport (transfer), and deposition (accumulation, storage) of sediment within a defined area (landscape unit).

Introduction

Geomorphologic processes, responsible for transferring sediments and affecting landform change, are highly dependent on climate, and it is anticipated that climate change will have a major impact on the behavior of Earth surface systems. Research on sedimentary fluxes from source to sink in a variety of different climatic environments is very well documented in the literature. Studies on source-to-sink fluxes generally refer to the development of sediment budgets. A sediment budget is an accounting of the sources and disposition of sediment as it travels from its point of origin to its eventual exit from a defined landscape unit like a drainage basin (e.g., Reid and Dunne, 1996). Accordingly, the development of a sediment budget necessitates the identification of processes of erosion, transport, and deposition within a defined area, and their rates and controls (Reid and Dunne, 1996; Slaymaker, 2000; Beylich and Warburton, 2007). The fundamental concept underpinning source-to-sink sediment flux and sediment budget studies is the basic sediment mass balance equation:

$$I = O + -\Delta S$$

where inputs (I) equal outputs (O) plus changes in net storage of sediment (ΔS). Source-to-sink study allows quantification of the transport and storage of sediment in a system. A thorough understanding of the current sediment production and flux regime within a system is fundamental to predict likely effects of changes to the system, whether climatic induced or human influenced. Source-to-sink sediment flux and sediment budget research therefore enables the prediction of changes to erosion and sedimentation rates, knowledge of where sediment will be deposited, how long it will be stored, and how much sediment will be remobilized (Gurnell and Clark, 1987; Reid and Dunne, 1996; Beylich and Warburton, 2007).

Sediment sources

Sediments are eroded and mobilized in source areas. Sediment sources are diverse and subject to variation in response to climate change. Global warming leads to the loss of glacial ice, which in turn increases slope instability caused by glacial de-buttressing, and flooding from glacial and moraine-dammed lakes (Evans and Clague, 1994; Ballantyne, 2002). All these processes redistribute sediments and operate at different rates as a result of change to the system. Glaciers and ice sheets exert strong controls on the supply of sediments. For example, Knight et al. (2002) identify the basal ice layer of a section of the Greenland ice sheet as the dominant source of sediment production. There is, however, only limited knowledge of debris fluxes from ice sheets and glaciers, and its variability. The main mechanisms of sediment production in source areas can be described in terms of contemporary environmental conditions. However, in order to fully understand sediment supply, a longer-term perspective is needed. Over the Quaternary, glacier fluctuations have had profound influences in depositing extensive mantles of sediments. More-widely, periglacial activity has altered the landscape under non-glacial cold climate conditions. The obvious imprint of this legacy is often reflected in contemporary sediment transfer rates where preexisting deposits are eroded by present-day processes (Ballantyne, 2002; Warburton, 2007).

Sediment transfers

Sediment transfers move eroded sediments from their source area to an area of temporal storage or long-term deposition in sinks. Rates of sediment transfer are not only conditioned by competence of geomorphic processes but

also by the availability of sediment for transport. Accordingly, in assessing sediment transfer, we need to quantify the forces that drive transport processes but equally account for the factors that control sediment supply (Warburton, 2007). Glacial fluxes are arguably the most significant processes for contemporary sediment flux (Harbor and Warburton, 1992). Small-scale process studies very often focus on sedimentary fluxes from areas of weathering and erosion to areas of storage within defined landscape units like drainage basins, whereas large-scale sediment systems couple headwaters to oceanic sinks. For example, Gordeev (2006), applying models developed by Morehead et al. (2003), estimates the increase in sediment load in Arctic rivers in response to a rise in surface temperature of the drainage basins. Based on this model, increases in river discharge lead to an increase in the sediment flux of the six largest Arctic rivers, predicted to range from 30% to 122% by the year 2100.

Sediment stores/sinks

The identification of storage elements and sinks is critical to the effective study and understanding of source-to-sink sedimentary fluxes (Reid and Dunne, 1996). The setting of a particular drainage basin defines the boundary conditions for storage within that landscape unit. In a defined landscape unit like a drainage basin, the slope and valley infill elements constitute the key storage units and storage volumes are important for addressing time-dependent sediment budget dynamics. Dating of storage in sedimentary source-to-sink flux studies is applied to determine or estimate the age and chronology of the storage components within the system. An understanding of the nature of primary stores, secondary stores, and the potential storage capacities of different types of drainage basins is important along with knowledge of sediment residence times. Of growing importance is the development of innovative field methods, such as geophysical techniques for estimating sediment storage volumes (Schrott et al., 2003; Sass, 2005; Hansen et al., 2009). Within large-scale sediment systems, oceanic sinks are most important and provide the opportunity to estimate rates of sediment production and delivery at long-term temporal as well as continental spatial scales (Rise et al., 2005; Dowdeswell et al., 2006).

Summary

Studies on sedimentary fluxes from source to sink are an accounting of the sources and deposition of sediment as it travels from its point of origin to its eventual exit from a defined area. The connected development of a sediment budget necessitates the identification of processes of erosion, transport, and deposition within this defined area, and their rates and controls. Within the scope of climate change research, knowledge on the contemporary sediment production and flux regime within a system enables the prediction of possible future changes to erosion and sedimentation rates. In addition, improved knowledge of where sediment will be deposited, how long it will be stored and how much sediment will be remobilized can be achieved. The main mechanisms of sediment production in source areas can be described in terms of contemporary environmental conditions. However, in order to fully understand sediment supply also a long-term perspective is required. Sediment transfers move eroded sediments from their source area to an area of temporal storage or long-term deposition in sinks, with glacial fluxes being arguably the most significant processes for sediment flux. An understanding of the nature of primary stores, secondary stores, and the potential storage capacities of different types of drainage basins is important along with knowledge of residence times. Within large-scale sediment systems oceanic sinks are most important and provide the opportunity to estimate rates of sediment production and delivery at large temporal and spatial (continental) scales.

Bibliography

Ballantyne, C. K., 2002. Paraglacial geomorphology. *Quaternary Science Reviews*, **21**, 1935–2017.

Beylich, A. A., and Warburton, J. (eds.), 2007. Analysis of source-to-sink-fluxes and sediment budgets in changing high-latitude and high-altitude cold environments: SEDIFLUX Manual. *NGU Report* 2007.053.

Dowdeswell, J. A., Ottesen, D., and Rise, L., 2006. Flow switching and large-scale deposition by ice streams draining former ice sheets. *Geology*, **34**, 313–316.

Evans, S. G., and Clague, J. J., 1994. Recent climate change and catastrophic geomorphic processes in mountain environments. *Geomorphology*, **10**, 107–128.

Gordeev, V. V., 2006. Fluvial sediment flux to the Arctic Ocean. *Geomorphology*, **80**, 94–104.

Gurnell, A. M., and Clark, M. J. (eds.), 1987. *Glacio-Fluvial Sediment Transfer: An Alpine Perspective*. Chichester: Wiley.

Hansen, L., Beylich, A. A., Burki, V., Eilertsen, R., Fredin, O., Larsen, E., Lysså, A., Nesje, A., Stalsberg, K., and Tønnesen, J.-F., 2009. Stratigraphic architecture and infill history of a deglaciated bedrock-valley based on georadar, seismic profiling and drilling. *Sedimentology*, **56**, 1751–1773.

Harbor, J., and Warburton, J., 1992. Glaciation and denudation rates. *Nature*, **356**, 751.

Knight, P. G., Waller, R. I., Patterson, C. J., Jones, A. P., and Robinson, Z. P., 2002. Discharge of debris from ice at the margin of the Greenland ice sheet. *Journal of Glaciology*, **48**, 192–198.

Morehead, M. D., Syvitski, J. P., Hutton, E. W., and Peckham, S. D., 2003. Modeling the temporal variability in the flux of sediment from ungauged river basins. *Global and Planetary Change*, **39**, 95–110.

Reid, L. M., and Dunne, T., 1996. *Rapid evaluation of sediment budgets*. Cremlingen: Catena.

Rise, L., Ottesen, D., Berg, K., and Lundin, E., 2005. Large-scale development of the mid-Norwegian margin during the last 3 million years. *Marine and Petroleum Geology*, **22**, 33–44.

Sass, O., 2005. Spatial patterns of rockfall intensity in the northern Alps. *Zeitschrift für Geomorphologie N.F. Suppl.-Bd*, **138**, 51–65.

Schrott, L., Hufschmidt, G., Hankammer, M., Hoffmann, T., and Dikau, R., 2003. Spatial distribution of sediment storage types and quantification of valley fill deposits in an alpine basin, Reintal, Bavarian Alps, Germany. *Geomorphology*, **55**, 45–63.

Slaymaker, O., 2000. Research developments in the hydrological sciences in Canada (1995–1998): Surface water – quantity, quality and ecology. *Hydrological Processes*, **14**, 1539–1550.
Warburton, J., 2007. Sediment budgets and rates of sediment transfer across cold environments in Europe: a commentary. *Geografiska Annaler*, **89A**(1), 95–100.

Cross-references

Climate Change and Glaciers
Glacial Erosion
Sediment Budgets
Sediment Yield

SEDIMENT GRAVITY FLOW

George Postma
Faculty of Geosciences, EUROTANK Laboratories, TA Utrecht, The Netherlands

Synonyms

Density currents; Gravity currents; Mass flows; Sediment flows

Definition

Sediment gravity flows are mixtures of water and sediment particles where the gravity acting on the sediment particles moves the fluid, in contrast to rivers, where the fluid moves the particles.

Introduction

Sediment gravity flows are catastrophic subaerial and subaqueous events that occur at various frequencies. An event can originate from sliding of unstable sediment mass on a slope, in which case the trigger is often by storm, tidal wave, seismic shock, or heavy rainfall. It can also originate from flood wave in a river that debouches onto the delta slope, where it, if denser than the basin water, first plunges down as hyperpycnal flow and continues as sediment gravity flow.

Sediment gravity flows have the ability to transport large masses of coarse-grained sediment into places, where otherwise only fines are deposited from suspension. Their deposits have been found in oceanic basins at 5 km depth at more than 2,000 km away from the continental slope, but also occur almost everywhere on land and in shallow seas and lakes and occur also in present-day glacial environments.

Since the rheology of sediment gravity flows varies and has great impact on the type of deposits, first an overview is given of this variation, which is followed by an impression of how rheology and flow characteristics (density, velocity) is reflected in the deposits. Finally, their occurrence in the glacial environments is highlighted.

Rheology of sediment gravity flows

The rheology of sediment gravity flows falls into two main classes of flow behavior that are fundamentally different and which difference is often reflected in the final deposit. The first class is characterized by fluidal behavior similar to Newtonian fluid, where shear stress is linearly related to strain according to

$$\sigma_s = \mu \,.\, \varepsilon_s \quad \left[\mathrm{N/m^2}\right] \tag{1}$$

where σ_s is the shear stress, μ is the apparent viscosity, and ε_s is rate of shear strain. In a fluid the shear strain is measured by the velocity gradient, hence dU/dz, where U is velocity at height z in the flow. Characteristic for waning, fluidal flow is that deposition occurs from the bed upward. Such depositional behavior is in sharp contrast with the second class of sediment gravity flow with plastic-viscous flow behavior. Such flows exhibit strength, while above the yield point viscous deformation occurs. Their rheology is described by the Coulomb-viscous model (Johnson, 1970, Figure 1):

$$\sigma_s = k + \mu_b.\varepsilon_s \quad \left[\mathrm{N/m^2}\right] \tag{2}$$

where k is the yield strength, μ_b is the Bingham viscosity, and ε_s rate of shear strain. The expression tells us that above the yield strength k the flow behaves viscous and has a linear viscosity called the Bingham or plastic viscosity. The apparent viscosity may be shear stress related and deformation above the yield strength is in such case non-Newtonian. Flow of plastic-viscous sediment mass is characterized by a nondeforming rigid plug which is riding on a viscously deforming basal layer, a behavior that

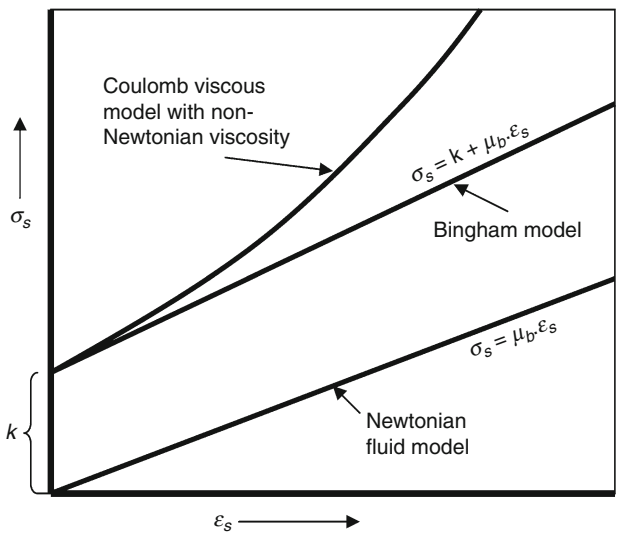

Sediment Gravity Flow, Figure 1 Diagram showing the Bingham rheological model: If strength $k = 0$, the flow experiences only Newtonian viscous deformation. In case of nonlinear viscous deformation, the viscosity is stress depended and non-Newtonian.

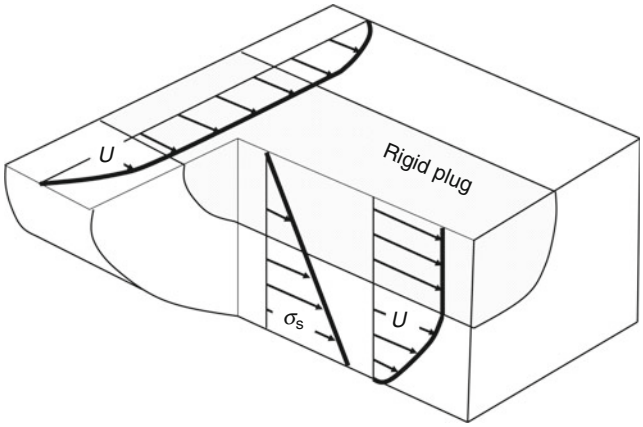

Sediment Gravity Flow, Figure 2 Plastic-viscous flow characterized by the formation of a rigid plug if the shear stress σ_s is equal or less than the shear strength k (see Eq. 2). The velocity gradient in the plug is zero.

is exemplified by the flow of concrete cement (Figure 2). The plug exists for $\sigma_s \leq k$.

The strength k within a debris flow mass is a function of the effective normal stress (σ') through the relationship

$$k = c' + \sigma \tan \Phi \quad [\mathrm{N/m^2}] \tag{3}$$

where c' is the effective cohesion and Φ' is the effective angle of internal friction (Rodine and Johnson, 1976). Extreme poor sorting reduces the internal friction; whereas the normal stress is reduced by

$$\sigma' = \sigma - p \quad [\mathrm{N/m^2}] \tag{4}$$

where σ is the total normal stress (the total weight of the debris and p is the pore pressure, which if positive (excess pressure) reduces the normal stress. Hence the excess pore pressure may locally (in most cases it is maximal at the base of the flow) significantly reduce the strength (up to 100%). The ability of the flow to trap pore pressure depends on the particle-size distribution (Rodine and Johnson, 1976). Very poorly sorted fabrics can maintain high excess pore pressure, because the narrow passageways (pore necks) hinder the fluid to escape upward. The presence of minimum amount of silt and clay (as little as 5%) appears to be important trapping the pore fluid and hinders draining of the flow, which greatly enhances its mobility.

Flow transformations

If a flow accelerates or decelerates, its behavior may change due to dilution or to deposition. Four types of flow transformations are feasible (Fisher, 1983): Body transformation, when the flow changes between laminar and turbulent; Gravity transformation, when initial turbulent, particle charged flows become gravitationally segregated into a 2-phase flow with a high-concentrated lower and a low-concentrated upper suspension layer; Surface transformation, when fluid becomes mixed or lost at flow boundaries resulting in dilution; Fluidization transformation, which develops by upward-moving fluids from the substrate or at the head of the flow also diluting the sediment gravity flow.

All types of transformations may play a role during the lifetime of a sediment gravity flow. Upon failure of a sediment mass on a slope, fluidization can make entire sediment slice on a slope unstable and initiate movement of the slice due to failure of, what can be, a thin weak layer where pore pressure could build up sufficiently to reduce its strength (e.g., Brunsden and Prior, 1984). At low rates of shear clast concentrations over 35–58 vol% still form a supporting framework of clasts in contact with each other (Rodine and Johnson, 1976) in which strength derives from both frictional resistance and cohesion. Hence, the slice can start to move as a rigid body riding on a thin shear zone behaving essentially as a plastic body, i.e., if its movement stops its original internal structure is still intact. If the slice accelerates it dilates by water intake from below (fluidization transformation), and from above (surface transformation). This may enhance body transformation, causing the sediment mass to move in either plastic-viscous or fluidal fashion depending on the remaining strength.

Experiments show that sustained, quasi-steady fluidal flows can have concentrations of up to 35 vol% (see Baas et al., 2004). In such highly concentrated fluidal flows, grains are held in suspension mainly by grain-to-grain collisions that cause an upward directed dispersive pressure (Bagnold, 1954). At concentrations less than 9 vol%, grains can be fully supported by turbulence of the fluid (Bagnold, 1954; Sohn, 1997). Flume experiments on high-concentration sandy to gravelly turbulent suspensions by Postma et al. (1988; Figure 3) show how behind the fully turbulent head of the flow the coarsest particles separated out into a highly concentrated basal layer by gravity transformation. The experiments reveal the presence of so-called traction carpets that are overridden by a low-concentrated turbulent suspension (2-phase suspension flows, see Postma et al., 2009).

Deposits of sediment gravity flows

Middleton and Hampton (1973) were the first to summarize a range of sediment gravity flow deposits based on sediment support mechanisms during flow. Later, Lowe (1982), Nemec and Steel (1984), Postma (1986), Nemec (1990), Mutti (1992), Kneller and Branney (1995), Sohn (1997), Russell and Arnott (2003), Postma et al. (2009), and many others addressed in detail the variety of deposits that stems from plastic-viscous and fluidal flow behavior of sediment mixtures. Although some controversies about whether to relate some structureless poorly sorted, coarse-grained deposits to plastic-viscous or to fluidal flow behavior still exist to date (and the just cited papers give a fair insight into these controversies), a fair overview of flow rheology and related deposits can be given, without

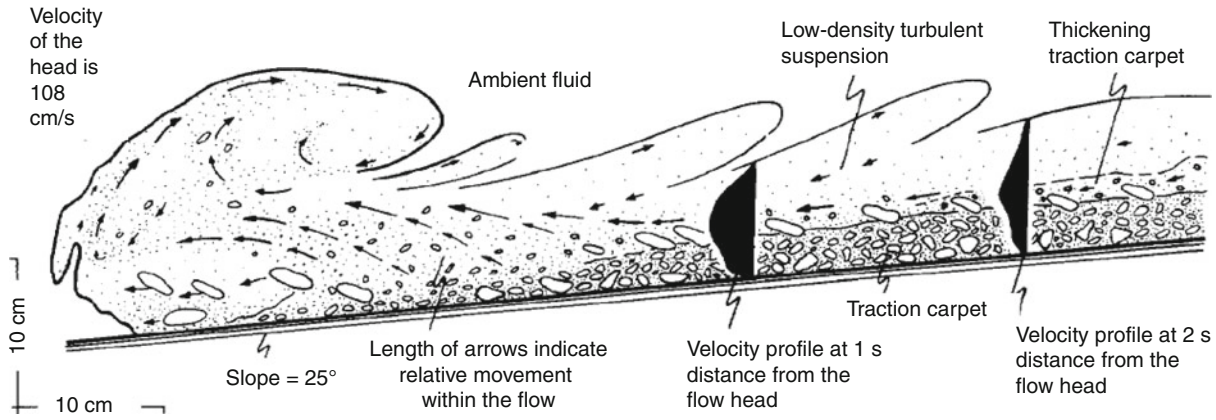

Sediment Gravity Flow, Figure 3 An initial high-concentration turbulent flow transforms by gravity transformation as observed through time (head of flow passes observer at 0 s). The passing head of the current is a fully turbulent 1-phase suspension flow and just before 1 s has passed, a density interface has developed separating the high-concentration traction carpet from the low concentration overriding suspension flow (2-phase flow). The drawing is traced from photographs with a high-speed film camera (70 frames per second (Slightly modified from Postma et al., 1988).

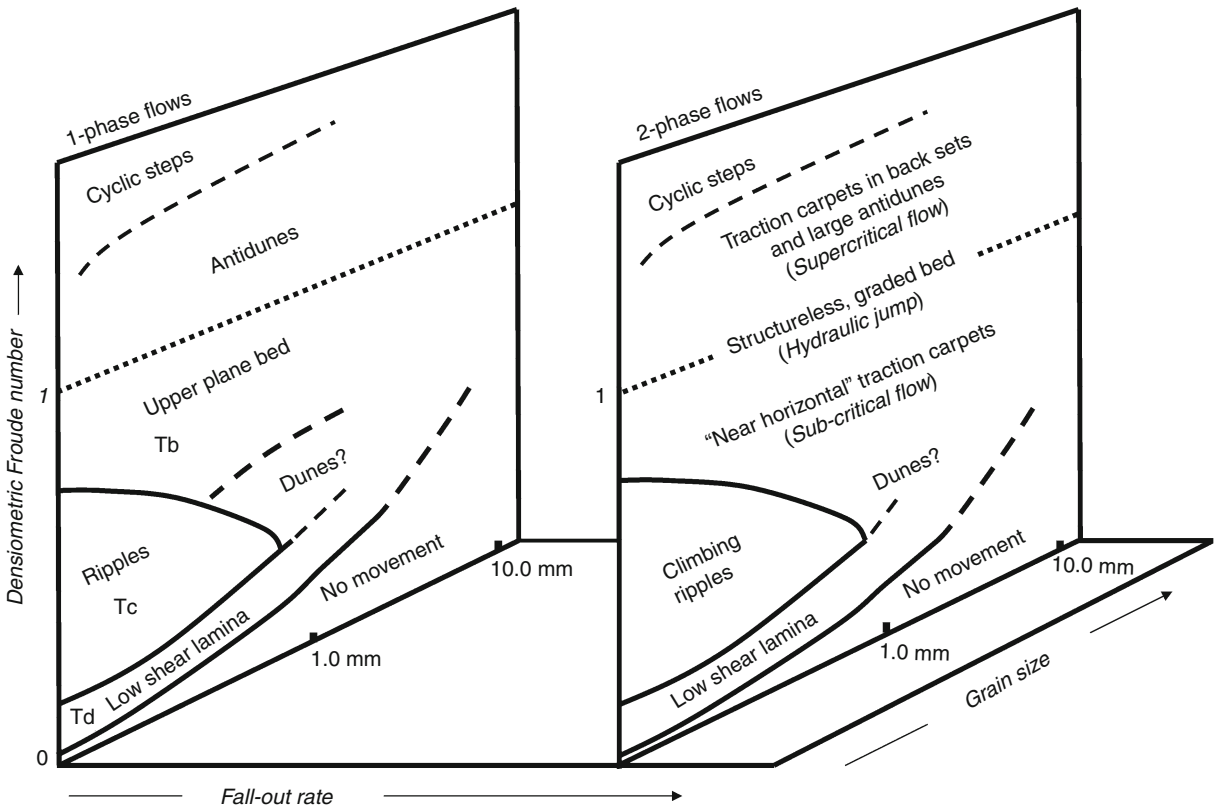

Sediment Gravity Flow, Figure 4 Three-dimensional bed-form stability diagram for 1- and 2-phase suspension flows. To illustrate the position of the hydraulic jump, the stability fields of the various bed forms are given relative to critical flow conditions ($Fr' = 1$). Hence, the boundaries of the stability feeds are only approximate (From Postma et al., 2009).

discussing extensively the right or wrong of certain interpretations.

Deposits of plastic-viscous sediment gravity flow

The deposit of a plastic-viscous flow is called debris flow deposit, or debrite. The basal layer of such deposit is often finer grained than its body and could have a "ropy" appearance representing the original shear zone underlying the rigid plug: The latter is often structureless and nongraded, with large clasts floating in a matrix (similar to *diamicton*). The strength of the debris flow is measured by its largest clast size (Hampton, 1975), and a good correlation between max particle size and bed thickness has been demonstrated in studies of Nemec and Steel (1984).

Deposits of fluidal sediment gravity flow

To fully understand the deposits of fluidal sediment gravity flows it is imperative to realize that deposition can take place under both supercritical, critical, and subcritical flow conditions as defined by the densimetric Froude number. The densiometric Froude number is determined by

$$\mathrm{Fr}' = \frac{U}{\sqrt{g' h}} \quad [-] \tag{5}$$

where U is the flow velocity, h is the flow thickness, and g' is the reduced gravity

$$g' = g\,\frac{\rho_{\mathrm{mix}} - \rho}{\rho} \quad \left[\mathrm{m/s^2}\right] \tag{6}$$

and where ρ_{mix} is the density of the flow, ρ is the density of the ambient water, and g is the gravity constant. For $\mathrm{Fr}' < 1$, the turbidity current is called subcritical, for $\mathrm{Fr}' > 1$ the flow is supercritical, and when $\mathrm{Fr}' \approx 1$ it is critical. When a supercritical flow switches to a subcritical flow it passes the hydraulic jump. Most fluidal sediment gravity flows are already supercritical on slopes of 0.001.

The various bed forms that may develop from a fluidal sediment gravity flow are depicted in the diagram of Figure 4, which illustrates that bed forms are different for 1-phase and 2-phase suspension flows. In 1-phase flows, suspension concentration is below 9 vol% criterion. In such flows fallout rate is low and bed-load transport is dominant, a flow behavior very similar to unidirectional water flow. In 2-phase suspension flows the fallout rate is sufficiently high to form traction carpets (gravity transformation). Various styles of traction-carpet deposits have been recognized as a function of the varying rheology of the layer during its deposition, as was discussed by Sohn (1997). Field and flume evidence indicate that traction

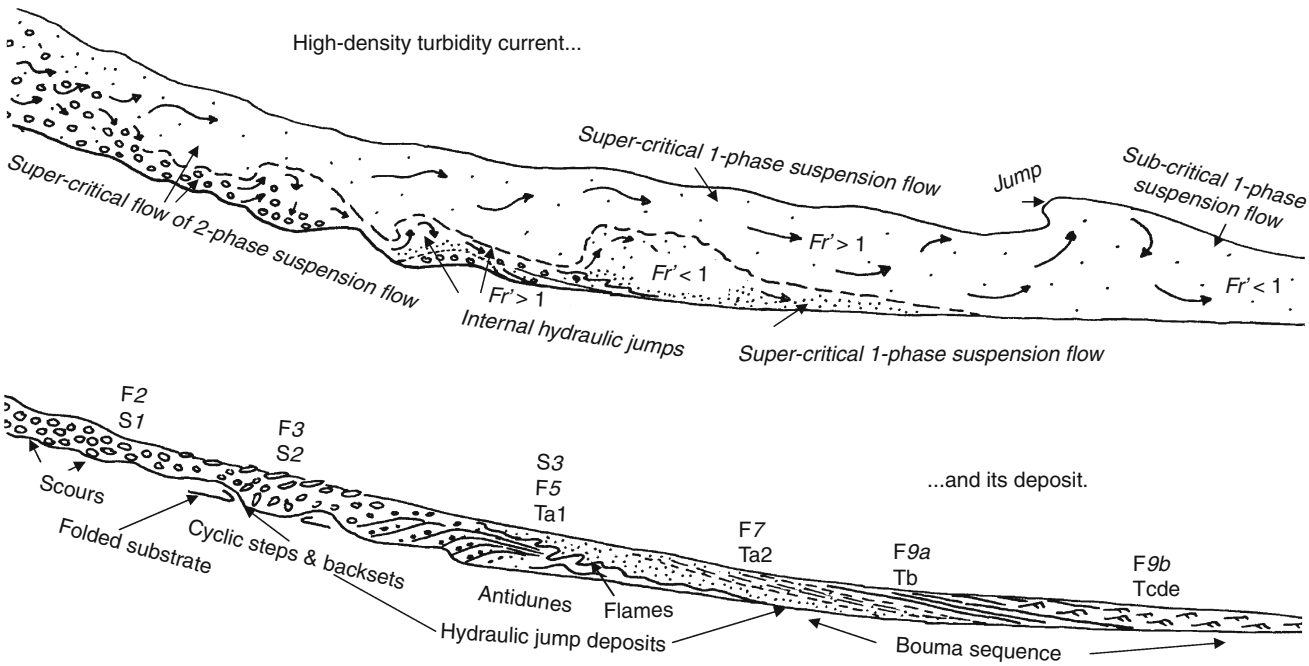

Sediment Gravity Flow, Figure 5 Flow transformation from supercritical to subcritical, with an internal hydraulic jump that leads to the development of Bouma Ta_1 (structureless coarse-tail graded gravelly sand) with flame structures at the base of the unit. In the supercritical region traction carpets deposit in back sets and large wavelength antidunes, whose deposits can be truncated by Bouma Ta_1. In the subcritical region, down slope of the internal jump, weakly stratified Bouma Ta_2 may develop truncated by Bouma Tbcd units of the subcritical flow regime.

carpets can form under both super and subcritical flows, as long as the required fallout rate is achieved.

The evolution of a decelerating high-concentration sediment gravity flow is depicted in Figure 5, together with the resultant deposits, a sketch inspired by Mutti (1992). The F numbers refer to detailed descriptions and illustrations of deposits by Mutti (1992), the S numbers refer to deposits described by Lowe (1982) and the T numbers refer to deposits described by Bouma (1962). The number addition for Ta1 and Ta2 gives the difference between structureless and weakly stratified deposits in the Bouma Ta unit (Postma et al., 2009).

Traction carpets formed under supercritical condition are deposited as large backsets, long-wave (>30 m) antidunes, and large sand and gravel waves (cyclic steps). Backsets and long-wave antidunes have been described from Gilbert-type deltas (see review by Nemec, 1990) and from ice-marginal lakes in deposits formed by subaqueous water jets occurring at the outlet of subaqueous tunnel valleys (e.g., Russell and Arnott, 2003). Traction carpets formed under subcritical conditions are straight and tabular often deposited in association with plane bed lamination (Bouma Tb) and climbing ripple sets (Bouma Tc, see Postma et al., 1983). The deposit of a waning, low concentration turbidity current is described in detail by the Bouma Ta–e sequence with coarse-tail graded basal unit (Ta) followed by plane bed lamination (Tb), small-scale ripple sets (Tc), and silt lamina formed by low shear and suspension fall out (Tde).

Sediment gravity deposits in the various glacigenic environments

Sediment gravity flows and their deposits occur in many present-day glacial environments, and have, for instance, been encountered in fjords in association with deltas (e.g., Bornhold and Prior, 1990), in glacial lakes (e.g., Postma et al., 1983; Gilbert and Crookshanks, 2008), and in many subaerial and subaqueous ice-contact environments. In the latter case, deposits are not necessarily from sediment gravity flows *sensu stricto*, because the high-concentration suspension is for great part driven by the subaqueous jet efflux originating from subglacial melt water drainage systems (tunnel valleys). Yet, their deposits show many close similarities with those of sediment gravity flows (Postma et al., 1983; Russell and Arnott, 2003; Hornung et al., 2007). At the terminus of glaciers, subaerial sediment gravity flows originate where sediment overlies the ice. The ablation of ice disaggregates the overlying sediment and mixes it with the melt water resulting in watery debris slurries. A beautiful example of debris flow deposits has been studied on James Ross Island (Antarctica). The debris flow deposits attain thicknesses of up to 150 m and extend over 4 km laterally. The high volume of glacigenic sediment delivery implicit in the James Ross Island successions indicates that a series of dynamic ice fronts crossed the region during the late Miocene and Pliocene epochs (Nelson et al., 2009). The highly fossiliferous glacigenic debris flows are well dated and signify episodes of ice expansion during relatively warm periods (interglacials).

Summary

The deposits of sediment gravity flows are common in both subaerial and subaqueous glacial environments. They are strongly related to the rheology of the suspension carrying flow and flow characteristics such as speed, densiometric Froude number, and particle concentration and size. The deposits of fluidal sediment gravity flow class are varied and have been organized here in a bedform stability diagram and a longitudinal cross-section.

Bibliography

Baas, J. H., Van Kesteren, W., and Postma, G., 2004. Deposits of depletive, quasi-steady high-density turbidity currents: a flume analogue of bed geometry, structure and texture. *Sedimentology*, **51**, 1053–1089.

Bagnold, R. A., 1954. Experiments on a gravity free dispersion of large solid spheres in a Newtonian fluid under shear. *Proceedings of the Royal Society of London. Series A*, **225**, 49–63.

Bornhold, B. D., and Prior, D. B., 1990. Morphology and sedimentary processes on the subaqueous Noeick River delta, British Columbia, Canada. In Colella, A., Prior, D. B. (eds.), *Coarse Grained Deltas*. International Association of Sedimentologists Special Publication 10. UK: Blackwell, pp. 160–184.

Bouma, A. H., 1962. *Sedimentology of Some Flysch Deposits: A Graphic Approach to Facies Interpretation*. Amsterdam: Elsevier, p. 168.

Brunsden, D., and Prior, D. B. (eds.), 1984. *Slope Instability*. New York: Wiley, p. 620.

Gilbert, R., and Crookshanks, S., 2008. Sediment waves in a modern high-energy glacilacustrine environment. *Sedimentology*, **56**, 645–659.

Fisher, R. V., 1983. Flow transformations in sediment gravity flows. *Geology*, **11**, 273–274.

Hampton, M. A., 1975. Competence of fine grained debris flows. *Journal of Sedimentary Petrology*, **49**, 753–793.

Hornung, J. J., Asprion, U., and Winsemannn, J., 2007. Jet-efflux deposits of a subaqueous ice-contact fan, glacial Lake Rinteln, north western Germany. *Sedimentary Geology*, **193**, 197–192.

Johnson, A. M., 1970. *Physical Processes in Geology*. San Francisco: Freeman, Cooper and Co, p. 577.

Kneller, B. C., and Branney, M. J., 1995. Sustained high-density turbidity currents and the deposition of thick massive sands:. *Sedimentology*, **42**, 607–616.

Lowe, D. R., 1982. Sedimentary gravity flows: II depositional models with special reference to the deposits of high density turbidity currents. *Journal of Sedimentary Petrology*, **52**, 279–297.

Middleton, G. V., and Hampton, M. A., 1973. Subaqueous sediment transport and deposition by sediment gravity flows. In Middleton, G. V., and Bouma, A. H. (eds.), *Turbidites and Deep Water Sedimentation*. Anaheim: Society of Economic Paleontologists Mineralogists, Short course 1, pp. 1–38.

Mutti, E., 1992. *Turbidite Sandstones*. Agip Special Publication, Istituto de geologia, Universita di Parma, p. 275.

Nemec, W., and Steel, R. J., 1984. Alluvial and coastal conglomerates: their significant features and some comments on gravelly mass-flow deposits. In Kosters, E. H., and Steel, R. J. (eds.), *Sedimentology of Gravels and Conglomerates*. Canada: Canadian Society of Petroleum Geologists, Galcary, pp. 1–32.

Nemec, W., 1990. Aspects of sediment movement on steep delta slopes. In Colella, A., and Prior, D. B. (eds.), *Coarse Grained*

Deltas. International Association of Sedimentologists Special Publication 10. UK: Blackwell, pp. 29–74.
Nelson, A. E., Smellie, J. L., Hambrey, M. J., Williams, M., Vautravers, M., Salzmann, U., McArthur, J. M., and Regelous, M., 2009. Neogene glacigenic debris flows on James Ross Island, northern Antarctic Peninsula, and their implications for regional climate history. *Quaternary Science Reviews*, **28**, 3138–3160.
Postma, G., Roep, Th. B., and Ruegg, G. J. H., 1983. Sandy gravelly mass flow deposits in an ice-marginal lake (Saalian, Leuvenumsche Beek Valley, Veluwe, The Netherlands), with emphasis on plug-flow deposits. *Sedimentary Geology*, **34**, 59–82.
Postma, G., 1986. Classification for sediment gravity-flow deposits based on flow conditions during sedimentation. *Geology*, **14**, 291–294.
Postma, G., Nemec, W., and Kleinspehn, K. L., 1988. Large floating clasts in turbidites – a mechanism for their emplacement. *Sedimentary Geology*, **58**(1), 47–61.
Postma, G., Cartigny, M., and Kleverlaan, K., 2009. Structureless, coarse-tail graded Bouma Ta formed by internal hydraulic jump of the turbidity current? *Sedimentary Geology*, doi:10.1016/j.sedgeo.2009.05.018.
Rodine, J. D., and Johnson, A. M., 1976. The ability of debris, heavily freighted with coarse material, to flow on gentle slopes. *Sedimentology*, **23**, 213–234.
Russell, H. A. J., and Arnott, R. W. C., 2003. Hydraulic-jump and hyperconcentrated-flow deposits of a glacigenic subaqueous fan: Oakridges moraine, southern Ontario, Canada. *Journal of Sedimentary Research*, **73**(6), 887–905.
Sohn, Y. K., 1997. On traction-carpet sedimentation:. *Journal of Sedimentary Research*, **67**, 502–509.

Cross-references

Glacier Lake Outburst Floods
Gravitational Mass Movement Deposits
Gravity Flow (Mass Flow)

SEDIMENT ROUTING

Subhajit Sinha
DBS College, Dehradun, Uttarakhand, India

Sediment is transported from areas of uplift and erosion into adjacent sedimentary basins. The relationship between transport processes and storage sites of the sediments is sediment routing. From its generation to its reaching the depozones, the position a sediment particle occupies, depends on its location at the time of deposition. Large sediment routing systems are among the largest geological features on earth, commonly spanning ocean–continent boundaries and occasionally crossing plate boundaries.

Basin models conventionally involve modeling of the filling of sedimentary basins is dependent on incorporating surface processes of weathering, sediment release and dispersal, and long-term burial in the basin. This integrated process system from source to sink is the sediment routing system. Tectonics and sediment routing systems are closely coupled. Dispersal of a mixed sediment supply into a basin with a certain spatial pattern of tectonic subsidence also controls the regional slope and downstream granulometric fining of the depositional system, the positioning of discontinuities such as the gravel front, and gross depositional facies. This offers the possibility that certain basin types may be occupied by particular styles of sediment routing system.

SEDIMENT TRANSFER MODELING

Richard Hodgkins
Department of Geography, Loughborough University, Leicestershire, UK

Synonyms

Sediment transport modeling

Definition

Simulation of rates of suspended-sediment transport in glacial meltwaters, by statistical or physical methods.

Introduction

Models of suspended-sediment transfer in glacially fed rivers have been developed in order to forecast sediment yields for engineering purposes (e.g., Bezinge et al., 1989; Bogen, 1989), to predict erosion rates for geomorphological purposes (e.g., Swift et al., 2002, 2005), to investigate fluvial processes (e.g., Church and Gilbert, 1975; Gurnell and Fenn, 1984), and to identify and interpret seasonal changes in suspended-sediment transfer from glacierized catchments (e.g., Gurnell et al., 1992, 1994; Hodgkins, 1996). Although sophisticated, computational fluid dynamics approaches are well established in hydraulic engineering, the modeling of sediment transfer in glacial environments is typically restricted by the perennial difficulties of acquiring continuous, high-quality hydrometric and sediment transport data at fine spatial and temporal resolutions, in unstable proglacial and inaccessible subglacial environments. Parameterizations of complex models require detailed data such as precise fluvial network topology, bed characteristics and velocity profiles that are usually impractical to obtain in proglacial locations, and even less so in subglacial ones.

Rating-curve approaches

Because of the difficulties of parameterizing physical models, statistical approaches to sediment transfer modeling are much more widespread. By far the most common model is a rating curve derived from linear regression of Suspended-Sediment Concentration (SSC), or sometimes (spuriously, from a statistical point of view) Suspended-Sediment Load (SSL), on discharge (e.g., Repp, 1988). Swift et al. (2005) used residuals from linear regressions of daily SSL on discharge to highlight important changes in the seasonal efficiency of sediment transfer, which were investigated further at a sub-seasonal scale using SSC as

the dependent variable. The popularity of the rating curve stems from its simplicity of construction and interpretation, with SSC deterministically predicted from discharge. However, the discharge-SSC relationship is far from simple in reality, and the performance of rating curves is frequently poor. For instance, Parks and Madison (1984) derived rating curves for glacierized basins in Alaska that had standard errors ranging from −50% to +100%, while Fenn (1989) found that rating curves developed for one season's data from the Glacier de Tsidjiore Nouve (Switzerland) predicted suspended loads from 34% to 278% of measured values when applied beyond that season. Such limitations arise because the bivariate discharge-SSC relationship is unstable over a range of temporal scales. Fenn et al. (1985) summarized the effects that limit the performance of sediment rating curves as follows:

1. Variations in sediment supply at the seasonal scale, such as from early-season flushing (Liestøl, 1967; Collins, 1989), late-season exhaustion (Østrem, 1975; Gurnell et al., 1992), or changing sediment sources (Gurnell et al., 1994; Hodgkins, 1996).
2. Variations in sediment supply at the diurnal scale, between the rising and falling limbs of the hydrograph, leading to diurnal hysteresis (Bogen, 1980; Hodgkins, 1996). This is a particular problem for forecasting SSC from discharge alone, since there are distinct, rising- and falling-limb values of SSC for any one value of discharge.
3. Transient SSC pulses, which are independent of discharge (Gurnell, 1982; Gurnell and Warburton, 1990).
4. Variable entrainment and deposition of sediment in the proglacial region (Maizels, 1979; Warburton, 1990; Hodgkins et al., 2003).
5. Variations in sediment supply associated with rainfall-induced events (Church, 1972; Richards, 1984).

Time-series (stochastic) approaches

The limitations of the rating curve are usually reflected in the presence of autocorrelation in the residual series. *Quasi-autocorrelation* results from shortcomings in the formulation of the model: nonlinearity, omission of relevant independent variables, the presence of response lags/leads, and hysteresis at different time scales (Fenn et al., 1985). *True-autocorrelation*, however, indicates that the SSC series is generated not through a linear dependence on discharge, but by a stochastic process in which the present value of SSC is not independent of previous values of SSC, but a probabilistic function of them and of present and previous random disturbances (Richards, 1979).

Gurnell and Fenn (1984) took advantage of true-autocorrelation, estimating a Box-Jenkins transfer function (Box and Jenkins, 1976) between discharge and SSC series from Glacier de Tsidjiore Nouve. AutoRegressive Integrated Moving-Average (ARIMA) stochastic time-series models of discharge and SSC series were developed for an estimation period, and the transfer function used to bring them into phase and apply a scaling factor. Predictions from the transfer-function model were far superior to those from rating curves, such that Gurnell and Fenn (1984) recommended a similar approach be used whenever possible. Fenn (1989) found that a transfer-function model gave predictions of SSL from 96% to 105% of measured values at Glacier de Tsidjiore Nouve, even when applied beyond the season in which it was developed. Nevertheless, despite the advantages of the transfer-function approach, it has not been widely adopted, because: (1) it requires an unbroken series of uniformly spaced observations for estimation, (2) it is sometimes difficult to place physical interpretations on the ARIMA parameters (Swift et al., 2005).

Simpler implementations of time-series approaches are available, however. Linear regression models for successive subperiods of an SSC time series acquired at Scott Turnerbreen (Svalbard), using discharge as the independent variable, accounted for between none (when not significant) and about 52% of the variance in SSC (Hodgkins, 1996). However, *autoregression* models, incorporating both discharge, Q, and an ARIMA (1,0,0) component ($SSC_t = aQ_t + bSSC_{t-1} + \varepsilon_t + c$, where a and b are regression coefficients, c the regression intercept, and ε is a random disturbance), indicate that the latter dominates the regression relationship, and is relatively constant with a value close to unity, throughout the melt season (Hodgkins, 1999). Likewise, Gurnell et al. (1994) found that a first-order autoregressive ARIMA model was largely sufficient to describe an SSC time series obtained at Austre Brøggerbreen (Svalbard), although a second-order autoregressive, or sometimes also a diurnal moving-average, model was required for series obtained at Haut Glacier d'Arolla (Switzerland): this is a temperate glacier with a seasonally evolving, multi-reservoired, subglacial drainage network (Gurnell et al., 1992) of greater complexity than the largely sub-serial networks of the essentially non-temperate Svalbard examples. Inferring the structure of the glacial drainage system was an early motivation of sediment transfer modeling, and remains important. For example, Swift et al. (2005) noted increasing sediment availability through a strong relationship between daily SSL and discharge amplitude at Haut Glacier d'Arolla, and inferred that increasing subglacial water pressure variation as a consequence of increasingly peaked diurnal run-off cycles was likely to have increased access to basal sediment, by encouraging extra-channel flow excursions and/or enhancing basal sediment deformation.

Subdivision of time series

Other attempts to improve rating-curve performance have involved subdividing the discharge and SSC series into shorter intervals of more uniform response, for which a linear relationship may be more valid. Collins (1979) estimated rating curves for individual rising and falling limbs of the diurnal hydrograph at Gornergletscher

(Switzerland). Hammer and Smith (1983) derived early- and late-season rating curves for Hilda Glacier (Canada). Richards (1984) obtained separate rating curves for periods of meltwater runoff and storm runoff at Storbreen (Norway). Gurnell et al. (1992) divided discharge and SSC series from Haut Glacier d'Arolla into five subperiods on the basis of variations in diurnal maximum and minimum discharge, prior to estimating regression and ARIMA models. Statistical hydrograph classification has also been used as a tool to trace the seasonal evolution of subglacial drainage configuration, which has in turn been used to define periods of consistent run-off sediment transfer response for further statistical analysis, e.g., Orwin and Smart (2004) and Swift et al. (2005) used principal components and hierarchical clustering analyses to classify hydrographs on the basis of shape and magnitude at Small River Glacier (Canada) and Haut Glacier d'Arolla, respectively. Orwin and Smart (2004) also applied these analyses to diurnal suspended-sediment cycles, and compared the resulting classes with discharge and meteorological data to analyze sediment transfer patterns. This approach showed that relatively low SSC and clear diurnal cycling were the norm, but that about 70% of the total seasonal sediment load occurred in "irregular," relatively high-SSC events associated with rainfall and enhanced snowmelt: the proglacial area was the source for up to 80% of the sediment yield of the glacier basin. Proglacial storage effects are particularly relevant to the modeling of sediment transfer in glacierized catchments, and careful field experimental design is required to distinguish the glacial sediment transfer signal from the proglacially modulated one, though it is not always possible to achieve this in intractable glacial locations.

Multivariate approaches

A further approach has been to develop multivariate rating curves incorporating additional explanatory variables, which may represent components of variability at different temporal scales. Richards (1984) introduced the *rate of change of discharge per hour*, positive during rising and negative during falling stages, to represent diurnal hysteresis. It was found that this variable was the main control on SSC variation during periods of meltwater runoff. Willis et al. (1996) found that the variables *discharge*, *rate of change of discharge,* and *days since discharge was equalled or exceeded* were all significant in a multivariate rating curve from Midtdalsbreen (Norway), although the improvement over a rating curve using discharge alone was slight, and the residuals were autocorrelated. Likewise, Swift et al. (2005) found that the variables *days since discharge was equalled or exceeded*, *rate of change of discharge* and *rainfall* were significant in multivariate regression models at Haut Glacier d'Arolla; again, autocorrelation, though reduced compared with bivariate models, was not removed. However, autocorrelation was absent from models that included the variable SSC_{t-1}, indicating true-autocorrelation arising either from a dependence of the current value of SSC on recent values of SSC (denoting sediment availability), from the settling velocity of fine particles being lower than that required for their entrainment (Hodson and Ferguson, 1999), or from some combination of these factors. In all models, SSC_{t-1} became the most significant explanatory variable at the expense of Q. Note that lagging an independent variable in a regression is not the same process as building an ARIMA (1,0,0) model: the former still uses the least-squares approach to estimate its parameters, while the latter takes a maximum-likelihood approach (Akaike, 1974). However, both methods can reduce autocorrelation. Hodgkins (1999) earlier noted that the dependence of SSC on the magnitude of discharge in time series from Scott Turnerbreen was weak and highly variable, whereas the dependence of current SSC on recent values of SSC, revealed through an ARIMA(1,0,0) term, was strong (an order of magnitude greater than Q) and relatively constant. The dominant control on SSC was therefore short-term sediment availability: a corollary of this is that forecasting becomes problematic in the absence of recent SSC data. The challenge is therefore presented of identifying and modeling processes that control sediment *availability.*

Physical approaches

Physical models of sediment transfer are far less developed than statistical ones. A notable contribution is that of Clarke (1996), who developed a lumped-element model of the subglacial hydraulic system. He related the sediment flux from the bed into suspension (erosion), $F_S^{\uparrow}$, to the porosity of the bed, n, the sediment density, ρ_S, and the bed shear stress, τ_0:

$$F_S^{\uparrow} = \rho_S(1-n)k_E(\tau_0 - \tau^*)^N \quad \tau_0 > \tau^*$$

where k_E is a constant relating to the character of the flow and the bed surface, τ^* is a threshold boundary shear stress for erosion and N is an experimentally derived constant. Clarke (1996) assumed an unlimited sediment supply, but this is not a necessary assumption of the model. τ^* depends on grain size, and can be approximately zero for silt particles. Assuming that Stokes' Law governs the processes of sedimentation, the sediment flux from suspension into the bed (deposition), $F_S^{\downarrow}$, can be written

$$F_S^{\downarrow} = c_S v_S = c_S \frac{(\rho_S - \rho)gD_P^2}{18\mu}$$

where c_S is SSC (essentially supplied from upstream), v_S is the settling velocity of grains of diameter D_P, and density ρ_S from a fluid of density ρ and viscosity μ. Mass conservation requires the flux of sediment per unit time from a drainage element of volume V and bed surface A to be equal to the flux in, plus erosion, minus deposition. Therefore a sediment balance can be written:

$$\frac{dc_S}{dt} = \frac{1}{V}\left[-c_S\frac{dV}{dt} + c_S^{in}Q^{in} - C_S^{out}Q^{out} = A\left[\rho_S(1-n)k_E(\tau_0-\tau^*)^N - \frac{c_S(\rho_S-\rho)gD_P^2}{18\mu}\right]\right]$$

Clarke (1996) notes astutely that the main limitations on subglacial hydraulic modeling are not in the mathematical treatment, but in our poor knowledge of drainage configurations and of sediment sources and sinks.

Jones and Arnold (1999) applied Clarke's (1996) equations to a subglacial water routing model (Arnold et al., 1998) and obtained reasonable results for the period when conduits were well established in the mid-to-late melt season, though not before. An observed reduction in peak diurnal SSCs toward very end of melt season was not seen in modeled data, which suggested it was not caused by any reduction in water discharge or velocity. Instead, it was suggested that sediment exhaustion was occurring, as at that point of the melt season the conduits had been established for some 30 days, with little headward expansion, and therefore without potential access to fresh sediment sources (though note Swift et al.'s (2005) interpretations, above). The diurnal range of SSC was more sensitive than the mean SSC to changing parameter values, and diurnal SSC maxima and minima tended to increase/decrease together. This suggested that, to improve model performance, it would probably be necessary to include additional physical processes, such as sediment exhaustion, hiding of grains, and the exposure of fine particles if and when larger particles become entrained. This is to reiterate the point that sediment availability is probably the key control of sediment transfer, and that while variations in availability can be identified by statistical analysis of SSC/SSL time series, there are currently no effective means to model it.

Summary

Sediment transfer rates in glacial meltwaters have so far mainly been modeled by statistical means, and the rating-curve approach has been the most important of these. However, while it can be improved by subdividing time series and incorporating independent variables other than runoff, the rating curve is essentially simplistic and fails to account for the true-autocorrelation that is pervasive in sediment transfer series. Stochastic methods, such as ARIMA, can model autocorrelation explicitly, but are more complex to estimate, more demanding of data, and more difficult to interpret. Autocorrelation at short lags shows that sediment availability is probably the key control of sediment transfer rates. An expanding range of statistical approaches, including the classification of hydrographs and sedigraphs by principal components and clustering analyses, have shed valuable light on temporal patterns of sediment availability, but a really effective means to model the availability of sediment in a predictive manner remains elusive. Physical models of sediment transfer are underdeveloped by comparison with statistical approaches, but they may become more widely adopted as our ability to parameterize complex hydrological processes improves.

Bibliography

Akaike, H., 1974. A new look at the statistical model identification. *IEEE Transaction on Automatic Control*, **AC-19**, 716–723.

Arnold, N., Richards, K., Willis, I., and Sharp, M., 1998. Initial results from a distributed, physically-based model of glacier hydrology. *Hydrological Processes*, **12**(2), 191–219.

Bezinge, A., Clark, M. J., Gurnell, A. M., and Warburton, J., 1989. The management of sediment transported by glacial melt-water streams and its significance for the estimation of sediment yield. *Annals of Glaciology*, **13**, 1–5.

Bogen, J., 1980. The hysteresis effect of sediment transport systems. *Norsk Geografisk Tidsskrift*, **34**, 45–54.

Bogen, J., 1989. Glacial sediment production and development of hydro-electric power in glacierized areas. *Annals of Glaciology*, **13**, 6–11.

Box, G. E. P., and Jenkins, G. M., 1976. *Time Series Analysis, Forecasting and Control*, rev. edn. San Francisco: Holden-Day.

Church, M. A., 1972. Baffin Island Sandurs: a study of Arctic fluvial processes. *Bulletin of the Geological Survey of Canada*, **216**, 208 pp.

Church, M. A., and Gilbert, R., 1975. Proglacial fluvial and lacustrine environments. In Jopling, A. V., and MacDonald, B. C. (eds.), *Glaciofluvial and Glaciolacustrine Sedimentation*. Tulsa, Oklahoma, USA: Society of Economic Palaeontologists and Mineralogists Special Publication, 23, pp. 22–100.

Clarke, G. K. C., 1996. Lumped-element model for subglacial transport of solute and suspended sediment. *Annals of Glaciology*, **22**, 152–159.

Collins, D. N., 1979. Sediment concentration in meltwaters as an indicator of erosion processes beneath an Alpine glacier. *Journal of Glaciology*, **23**(89), 247–257.

Collins, D. N., 1989. Seasonal development of subglacial drainage and suspended sediment delivery to melt waters beneath an Alpine glacier. *Annals of Glaciology*, **13**, 45–50.

Fenn, C. R., 1989. Quantifying the errors involved in transferring suspended sediment rating equations across ablation seasons. *Annals of Glaciology*, **13**, 64–68.

Fenn, C. R., Gurnell, A. M., and Beecroft, I. R., 1985. An evaluation of the use of suspended sediment rating curves for the prediction of suspended sediment concentration in a proglacial stream. *Geografiska Annaler*, **67A**(1–2), 71–82.

Gurnell, A. M., 1982. The dynamics of suspended sediment concentration in an Alpine pro-glacial stream network. In *Hydrological Aspects of Alpine and High Mountain Areas* (*Proceedings of the Symposium*), Exeter, July 1982. International Association of Hydrological Sciences Publication Number, 138, pp. 319–330.

Gurnell, A. M., and Fenn, C. R., 1984. Box-Jenkins transfer function models applied to suspended sediment concentration-discharge relationships in a proglacial stream. *Arctic and Alpine Research*, **16**, 93–106.

Gurnell, A. M., and Warburton, J., 1990. The significance of suspended sediment pulses for estimating suspended sediment load and identifying suspended sediment sources in alpine glacier basins. In *Hydrology in Mountainous Regions. I. Hydrological Measurements; the Water Cycle* (*Symposium*), Lausanne, 1990. International Association of Hydrological Sciences Publication Number, 193, pp. 463–470.

Gurnell, A. M., Clark, M. J., and Hill, C. T., 1992. Analysis and interpretation of patterns within and between

hydroclimatological time series in an Alpine glacier basin. *Earth Surface Processes and Landforms*, **17**, 821–839.
Gurnell, A. M., Hodson, A., Clark, M. J., Bogen, J., Hagen, J. O., and Tranter, M., 1994. Water and sediment discharge from glacier basins: an arctic and alpine comparison. In Variability in Stream Erosion and Sediment Transport (*Symposium*), Canberra, 1994. International Association of Hydrological Sciences Publication Number, 224, pp. 325–334.
Hammer, K. M., and Smith, N. D., 1983. Sediment production and transport in a proglacial stream: Hilda Glacier, Alberta, Canada. *Boreas*, **12**, 91–106.
Hodgkins, R., 1996. Seasonal trends in suspended-sediment transport at an Arctic glacier, and their implications for drainage system structure. *Annals of Glaciology*, **22**, 147–151.
Hodgkins, R., 1999. Controls on suspended-sediment transfer at a High-Arctic glacier, determined from statistical modelling. *Earth Surface Processes and Landforms*, **24**, 1–21.
Hodgkins, R., Cooper, R., Wadham, J., and Tranter, M., 2003. Suspended sediment fluxes in a High-Arctic glacierised catchment: implications for fluvial sediment storage. *Sedimentary Geology*, **165**, 105–117.
Hodson, A. J., and Ferguson, R. I., 1999. Fluvial suspended sediment transport from cold and warm-based glaciers in Svalbard. *Earth Surface Processes and Landforms*, **24**(11), 957–974.
Jones, H., and Arnold, N., 1999. Modelling the entrainment and transport of suspended sediment in subglacial hydrological systems. *Glacial Geology and Geomorphology*, http://boris.qub.ac.uk/ggg/papers/full/1999/rp091999/rp09.html.
Liestøl, O., 1967. *Storbreen glacier in Jotunheimen*. Norway: Norsk Polarinstitutt Skrifter, p. 141.
Maizels, J. K., 1979. Proglacial aggradation and changes in braided channel patterns during a period of glacier advance: an Alpine example. *Geografiska Annaler*, **61A**(1–2), 87–101.
Orwin, J. F., and Smart, C. C., 2004. Short-term spatial and temporal patterns of suspended sediment transfer in proglacial channels, Small River Glacier, Canada. *Hydrological Processes*, **18**, 1521–1542.
Østrem, G., 1975. Sediment transport in glacial meltwater streams. In Jopling, A. V., and MacDonald, B. C., (eds.), *Glaciofluvial and Glaciolacustrine Sedimentation*. Tulsa, Oklahoma, USA: Society of Economic Palaeontologists and Mineralogists Special Publication, 23, pp. 101–122.
Parks, B., and Madison, R. J., 1984. *Estimation of selected flow and water quality characteristics of Alaskan streams*. U.S. Geological Survey Water Resources Investigations Report 84-4247.
Repp, K., 1988. The hydrology of Bayelva, Spitsbergen. *Nordic Hydrology*, **19**, 259–268.
Richards, K. S., 1979. *Stochastic processes in one-dimensional series; an introduction*. Norwich: Geo-abstracts. Concepts and Techniques in Modern Geography, Vol. 23.
Richards, K. S., 1984. Some observations on suspended sediment dynamics in Storbregrova, Jotunheim. *Earth Surface Processes and Landforms*, **9**, 101–112.
Swift, D. A., Nienow, P. W., Spedding, N., and Hoey, T. B., 2002. Geomorphic implications of subglacial drainage configuration: rates of basal sediment evacuation controlled by seasonal drainage system evolution. *Sedimentary Geology*, **149**, 5–19.
Swift, D. A., Nienow, P. W., and Hoey, T. B., 2005. Basal sediment evacuation by subglacial meltwater: suspended sediment transport from Haut Glacier d'Arolla, Switzerland. *Earth Surface Processes and Landforms*, **30**(7), 867–883.
Warburton, J., 1990. An alpine proglacial sediment budget. *Geografiska Annaler*, **72A**(3–4), 261–272.
Willis, I. C., Richards, K. S., and Sharp, M. J., 1996. Links between proglacial stream suspended sediment dynamics, glacier hydrology and glacier motion at Midtdalsbreen, Norway. *Hydrological Processes*, **10**, 629–648.

Cross-references

Glacier Hydrology
Hydrographs
Hysteresis
Meltwater Erosion
Rating Curve
Sediment Budgets
Sediment Yield
Suspended Sediment Dynamics

SEDIMENT YIELD

Kelly MacGregor
Geology Department, Macalester College, Saint Paul, MN, USA

Synonyms

Annual sediment yield; Integrated sediment flux

Definition

Sediment yield: Total quantity of sediment, expressed in units of mass (or volume) per unit time. In the case of glacial or fluvial environments, sediment yield is typically the volume of sediment transported from a drainage basin over a given time period.
Annual sediment yield: Total quantity of sediment fluxed from a basin during an entire year, expressed in units of mass or volume per annum.

Introduction

Sediment yield is broadly understood in earth surface processes to mean the total volume or mass of sediment evacuated, transported, or deposited from a drainage basin. As the term yield implies, the amount of sediment removed is estimated or measured over a known period of time. Yield is then reported as mass per year (typically tons/year) or volume per year. Sediment yield refers to the inorganic fraction of sediment, ignoring organic material frequently in transport in fluvial systems.

Source of sediment in glacierized basins

Measurements of sediment yield are typically difficult to make, in part because of the large distribution in grain size produced by glacial processes. Accurate measurements of sediment yield consider the coarse-grained fraction (from headwall processes and subglacial quarrying) and the finer-grained material (produced during subglacial abrasion). Fine-grained sediments (silts and clays) are often carried to proglacial lakes and fjords in streams, while coarser material is transported more slowly and over shorter distances. The production of sediment is either subglacial (subglacial abrasion and quarrying) and therefore impossible to observe directly, or sourced from the valley walls but incorporated into glacier ice in the accumulation zone or from rockfall into the bergschrund or

crevasses. Some rockfall from the valley walls either falls or emerges in the ablation zone; this material is eventually moved to the proglacial zone and deposited in the form of moraines. While there may be a contribution of subglacial or proglacial fluvial bedrock erosion contributing to sediment yield, this is typically assumed to be many orders of magnitude less than the glacial contribution of sediment.

Measurement of sediment yield in glacierized basins

The variety of methods for quantifying sediment yield fall into three general categories: measurement of active suspended sediment and bedload flux in proglacial streams and ice proximal marine settings; mapping terrestrial deposits and landforms; and bathymetric, ground-penetrating radar, and/or coring studies of subaqueous sedimentary deposits.

A key study of sediment yield using measurements of sediment flux from an active glacier is Humphrey and Raymond (1994). Using measurements of suspended sediment at Variegated Glacier in Alaska, the authors constrained sediment yield from the glacier over a wide range of measured ice velocities. The techniques used to measure sediment flux in proglacial streams are well documented (e.g., Ostrem, 1975; Gurnell, 1987; Bogen, 1989). Measurement of the bedload fraction is difficult to constrain; examples of studies that have successfully quantified bedload contributions to sediment yield include Pearce et al. (2003) and Riihimaki et al. (2005). In addition to measuring sediment concentration and flux in proglacial streams, some studies of active glaciers utilize sediment traps to assess yield. Direct measurements of settling sediment in lakes have been used (e.g., Hunter, 1994); uncertainties can be high over daily to seasonal timescales.

Terrestrial measurements of moraine volume and debris cover have been used to estimate basin-wide sediment yield (e.g., Reheis, 1976; Heimsath and McGlynn, 2008). Calculations of sediment yield are made using mapping and estimates of moraine density. An important uncertainty with this technique is constraining the timescales over which the deposits were formed. The use of cosmogenic radionuclides (CRN) to determine sediment yield in non-glacierized basins has been used with good success (e.g., Blanckenburg, 2005; Kirchner et al., 2002), and is beginning to be used in alpine settings to constrain the timescales over which sediment accumulates on moraines (e.g., Heimsath and McGlynn, 2008). An important challenge for utilizing CRN in glacierized basins is the shielding of subglacial sediment and rock with ice and snow, as well as the extremely steep angles of valley walls, both of which complicate the estimated exposure and inheritance of basin surfaces (discussed in Bierman and Nichols, 2004).

Measurements of total sediment volume deposited in well-defined traps such as proglacial lakes, fjords, and debris fans in subaqueous ocean environments have been used with some good success (in addition to the summary provided in Hallet et al. (1996), Koppes and Hallet (2002) provide a new methodology for determining the time series of sediment yield from a retreating tidewater glacier). Ground-penetrating radar and bathymetric measurements have been used to image and constrain sediment volume and density in these areas. Lake coring has also been used to constrain sediment yields from glacierized basins; sediment accumulation rates from cores are converted to volume by averaging across the surface area of the lake (Foster et al., 1990) or an averaging technique using multiple cores (e.g., O'Hara et al., 1993; Evans and Church, 2000). Loso et al. (2004) quantified sediment yield by measuring the accumulation of fine and coarse-grained sediment in an ice-dammed lake that had drained. This work highlighted the uncertainties associated with measuring only suspended sediment yield as a proxy for total sediment flux.

Sediment yield is frequently converted to basin-averaged (or glacier-averaged) erosion rate. The effective erosion rate is simply the sediment yield divided by the basin area or glacier footprint. A key assumption in these calculations is that subglacial storage of sediment is either zero (i.e., the bed beneath the glacier is bare bedrock) or storage of sediment is steady (input of sediment into the glacier is equal to sediment output). It is difficult to assess the validity of this assumption in subglacial settings.

Sediment yields from glacierized basins

An excellent summary of sediment yield from glacierized basins can be found in Hallet et al. (1996). Typically, sediment yield is converted to basin-averaged erosion rate and reported in mm a^{-1}. Hallet et al. (1996) reported rates of erosion in glacierized basins exceed those in fluvial settings by an order of magnitude or more, with sediment yields increasing with greater ice cover. Sediment yields converted to erosion rates vary from 0.01 mm a^{-1} for polar glaciers, to 10–100 mm a^{-1} beneath fast-moving temperate glaciers (Hallet et al., 1996). Koppes and Hallet (2002) document variability in sediment yield and, therefore, erosion rate in Alaskan tidewater glaciers. Their work suggests the extremely high modern rates of erosion (greater than 30 mm a^{-1} in this region) are about five times greater than long-term erosion rates because of rapid ice motion and calving resulting from warming since the Little Ice Age.

Summary

Sediment yield from glacierized basins is a key measurement for constraining rates of glacial erosion. Models of exhumation and range-scale evolution are sensitive to the timing and distribution of rock removal, and quantifying sediment yield is an important aspect of constraining these models and their predictions. While measurements of sediment yield are difficult to make, they offer insight into basin-wide erosional dynamics in arctic and alpine systems.

Bibliography

Bierman, P. R., and Nichols, K. K., 2004. Rock to sediment, slope to sea with ^{10}Be; rates of landscape change. *Annual Review of Earth and Planetary Sciences*, **32**, 215–255.
Bogen, J., 2008. The impact of climate change on glacial sediment delivery to rivers; sediment dynamics in changing environments. *IAHS-AISH Publication*, **325**, 432–439.
Evans, M., and Church, M., 2000. A method for error analysis of sediment yields derived from estimates of lacustrine sediment accumulation. *Earth Surface Processes and Landforms*, **25**(11), 1257–1267.
Foster, I. D. L., Dearing, J. A., Grew, R., and Orend, K., 1990. The sedimentary database; an appraisal of lake and reservoir sediment based studies of sediment yield; erosion, transport and deposition processes. *IAHS-AISH Publication*, **189**, 19–43.
Gurnell, A. M., 1987. Fluvial sediment yield from alpine, glacierized catchments. In Gurnell, A. M., and Clark, M. J. (eds.), *Glacio-Fluvial Sediment Transfer; an Alpine Perspective*. Chichester, UK (GBR): Wiley.
Hallet, B., Hunter, L., and Bogen, J., 1996. Rates of erosion and sediment evacuation by glaciers; a review of field data and their implications. *Global and Planetary Change*, **12**(1–4), 213–235.
Heimsath, A. M., and McGlynn, R., 2008. Quantifying periglacial erosion in the Nepal High Himalaya. *Geomorphology*, **97** (1–2), 5–23.
Humphrey, N. F., and Raymond, C. F., 1994. Hydrology, erosion and sediment production in a surging glacier; Variegated Glacier, Alaska, 1982–83. *Journal of Glaciology*, **40**(136), 539–552.
Hunter, L. E., 1994. *Grounding-Line Systems of Modern Temperate Glaciers and Their Effects on Glacier Stability*. PhD thesis, De Kalb, IL, Northern Illinois University, 467 p.
Koppes, M. N., and Hallet, B., 2002. Influence of rapid glacial retreat on the rate of erosion by tidewater glaciers. *Geology (Boulder)*, **30**(1), 47–50.
O'Hara, S. L., Street-Perrott, F. A., and Burt, T. P., 1993. Accelerated soil erosion around a Mexican highland lake caused by pre-Hispanic agriculture. *Nature*, **362**, 48–51.
Ostrem, G., 1975. Sediment transport in glacial meltwater streams. In Jopling, A. V., and McDonals, B. C. (eds.), *Glaciofluvial and Glaciolacustrine Sedimentation, Vol 23*. Tulsa, OK: Society of Economic Paleontologists and Mineralogists (special publication), pp. 101–122.
Pearce, J. T., Pazzaglia, F. J., Evenson, E. B., Lawson, D. E., Alley, R. B., Germanoski, D., and Denner, J. D., 2003. Bedload component of glacially discharged sediment; insights from the Matanuska Glacier, Alaska. *Geology (Boulder)*, **31**(1), 7–10.
Reheis, M. J., 1975. Source, transportation and deposition of debris on Arapaho glacier, Front Range, Colorado, USA. *Journal of Glaciology*, **14**, 407–420.
Riihimaki, C. A., MacGregor, K. R., Anderson, R. S., Anderson, S. P., and Loso, M. G., 2005. Sediment evacuation and glacial erosion rates at a small alpine glacier. *Journal of Geophysical Research*, **110**(F3), 17.

Cross-references

Basal Sediment Evacuation by Subglacial Drainage System
Discharge/Streamflow
Glacial Erosion
Glacier Motion/Ice Velocity
Glaciofluvial
Sediment Budgets
Sediment Core and Glacial Environment Reconstruction
Sediment Entrainment, Transport, and Deposition
Subglacial Processes
Suspended Sediment Dynamics

SEM ANALYSIS OF GLACIAL SEDIMENTS

William C. Mahaney
Quaternary Surveys, Thornhill, ON, Canada

Definition

Microtextures studied by SEM are found on quartz and other mineral grains from different sedimentary environments, and these along with grains from bedrock release, are transported by glaciers which inflict the most extensive array of fracture and abrasion microfeatures. Anywhere from 10% to 20% of grains in glaciers may escape contact with other grains, and hence sojourn in the ice without suffering physical damage. The other 80–90% of glacial grains will exit the system with fractured and abraded surfaces some of which are diagnostic of the glacial environment. These grains record damage that, to a large extent, depends on the thickness of the ice and the distance of transport with temperatures close to pressure-melting (p-melting). While the distance of transport is nearly impossible to compute with total accuracy, it would seem that long-distance transport close to p-melting will yield a triangular faceted quartz grain totally reformed from its original shape and size, and with the greatest damage inflicted on it. No other geological agent is capable of this transformation and none have the damaging effect that glaciers can inflict on quartz and other minerals entrained in the ice.

SEM analysis of glacial sediments

Sand grain surface microtexture analysis, using the Scanning Electron Microscope (SEM), was initiated by Dave Krinsley and John Doornkamp (1973), who introduced the subject to sedimentology. The original atlas became a repository of sand grain imagery and provided the first attempt to collate microtextures on sands, specifically quartz sands, linking them to specific geologic agents and/or sedimentary environments. After five decades of research on sand grain morphometry/fractography, it is now known that only a few microtextures are unique to specific environments, or geologic processes. Many microtextures, previously believed to be unique signatures of a particular environment, are now known on sands emplaced by different geologic/geomorphic processes. Thus, microtextures ranging across many environments perfectly illustrate the *Principle of Equifinality*, that is, in open systems a given end state can be reached by many potential means (Mahaney, 2002). Beyond this, investigators need the power of a representative population of grains to definitively identify the conditions under which grains are sourced, transported, and emplaced. The initiation of SEM analysis of sediments was pioneered by Biederman (1962), Porter (1962), and Krinsley and Takahashi (1962), and has since undergone several modifications as equipment has evolved into the digital age. During the inception of SEM

investigations in the early 1960s, research emphasis focused on sedimentological and mineralogical applications. However, increasingly over the years, the method has been applied to other fields where SEM-EDS (Energy Dispersive Spectrometry) methods can be employed to build a database of microtextures, microstructures, and chemical spectra that help to answer questions related to weathering in paleoenvironments as well as generate new ones. For example, standard databases on precipitates and coatings, information lacking in the Krinsley and Doornkamp (1973) volume, are now frequently used to help solve questions related to weathering of glacial grains (Mahaney, 2002), the coating chemistry offering new insight into wetting depths and paleoleaching in paleosols (Mahaney, 1990a), all of which may provide valuable information on preweathering prior to glacial transport (Mahaney et al., 1991) and relative dating of sediments (Mahaney et al., 2009).

The 1973 volume on glacial grain surface microtextures, although long out of date, remains a basic reference for researchers interested in the application of the technique since that time. Additional work by Whalley (1978) and Marshall (1987) has added numerous case studies in the microtexture field since that time. The new SEM atlas by Mahaney (2002) contains additional case studies intended to complement and expand upon these earlier reference works; however, the intent here is to bring the reader up to date on current techniques used and the range of microtextures now recognized on sands from glacial environments. From the evidence discussed by Mahaney (2002), it is possible, for example, to separate till from glaciolacustrine and glaciofluvial grains within the glacial sedimentary environment. Similarly, while it has proved difficult to separate tills genetically (Mahaney et al., 2001), it is possible to generate information related to glacial thickness and differences between warm and cold-based ice (Mahaney et al., 1988), as well as the relative amount of water transport within the glacier system.

In general terms, the pathway of grains from initial bedrock release (Figure 1a; quarrying process) leads to the production of *fracture faces* (Mahaney, 2002), the one common, but by no means the only, microtexture resulting from mechanical weathering. The fracture face is undeniably the common microtexture found on grains entering alpine glacial systems (Mahaney et al., 1991) and one that is soon overridden by a complex of new signatures comprised of subparallel linear fractures, conchoidal fractures, arc-shaped steps, uplifted plates, deep grooves, and microstriations, the latter being the one unique glacial microtexture, just as striations can be taken as evidence of glacial movement. Hence, glacial signatures can only be assessed from individual samples of till if the ice responsible attained a minimum thickness (~50–100 m) and applied a minimum force (Mahaney et al., 1988). Indeed, SEM microtexture imagery of α-quartz grains grown in an ice column and subjected to uniaxial stress under controlled conditions has indicated the importance of greatly increased glacial crushing that occurs along a transition from cold-based to warm-based ice with a minimum thickness in excess of ~100 m. At temperatures close to p-melting, and with cryostatic pressures equal to 1- and 2-km thick ice sheets, stick–slip motions appear to induce an array of microtextures on quartz sand grains that closely resemble microtextures observed on grains in tills deposited by the thickest Pleistocene glaciers of Canada, Europe, and the Antarctic. Aside from striated surfaces, it is not the presence of individual microfeatures that identifies the mechanism of glaciation, but the range of microtextures associated with varying degrees of glacial crushing. With decreasing ice thickness the range of microfeatures diminishes until, with thin cirque ice, little damage appears on grains transported from source to end moraines (Mahaney et al., 1988).

Grains subjected to aeolian processes (Figure 1b) produce bulbous edges, rounding and frosting on larger grains due to abrasion, along with occasional upturned plates and the presence of numerous craters of variable geometry (abrasion fatigue). Aeolian grains may be subject to multiple turbulent collisions during transport and later subjected to glacial transport which adds a whole new array of microtextures. The very fact that aeolian and glacial grains were differentiated in an analysis of Saharan ergs (Mahaney and Andres, 1996), without any previous knowledge of sedimentary processes on the part of the SEM operator, should convince skeptics that there is, indeed, an advantage in using SEM imagery in sedimentological analyses of various kinds. Aeolian microtextures are generally limited to superficial "skin" disruption and damage to individual grains which distinguishes them from deeper, more linear oriented "Wallner lines" produced by glaciation (Mahaney, 1991, 2002). Grains subjected to aeolian transport may retain their windblown signatures after transport in glacial systems but most often deeply embedded glacial crushing microfeatures may completely obliterate the aeolian source markings.

The fluvial environment, like the aeolian one, produces an array of superficial fractures and abrasion microfeatures often superficially disrupting the surfaces of grains, all of which are fine-tuned in the glacial environment. However, for the most part, fluvial transport tends to produce severe rounding and abrasion correlated with the discharge and turbulence of river or tsunami wave flow, the latter with optimal geomorphological parameters often results in resurfacing of quartz with a high count of v-shaped percussion scars (Mahaney et al., 2010b). Overprinting of fluvial grains brings forceful grain collisions that produce v-shaped percussion scars (Figure 1c), the one microtexture exclusive to the fluvial and geothermal environments. Interpretive difficulties arise because similar microfeatures are also produced by meltwater transport within glaciers, as for instance, in moulin systems or in fast moving, turbulent subglacial and englacial meltwater channels. If such grains are fluvially overprinted upon leaving the glacial system, the origin of the grain may be difficult or impossible to decipher. Of course, in nonglacial areas, streams leave an indelible record of water transport on quartz and other mineral

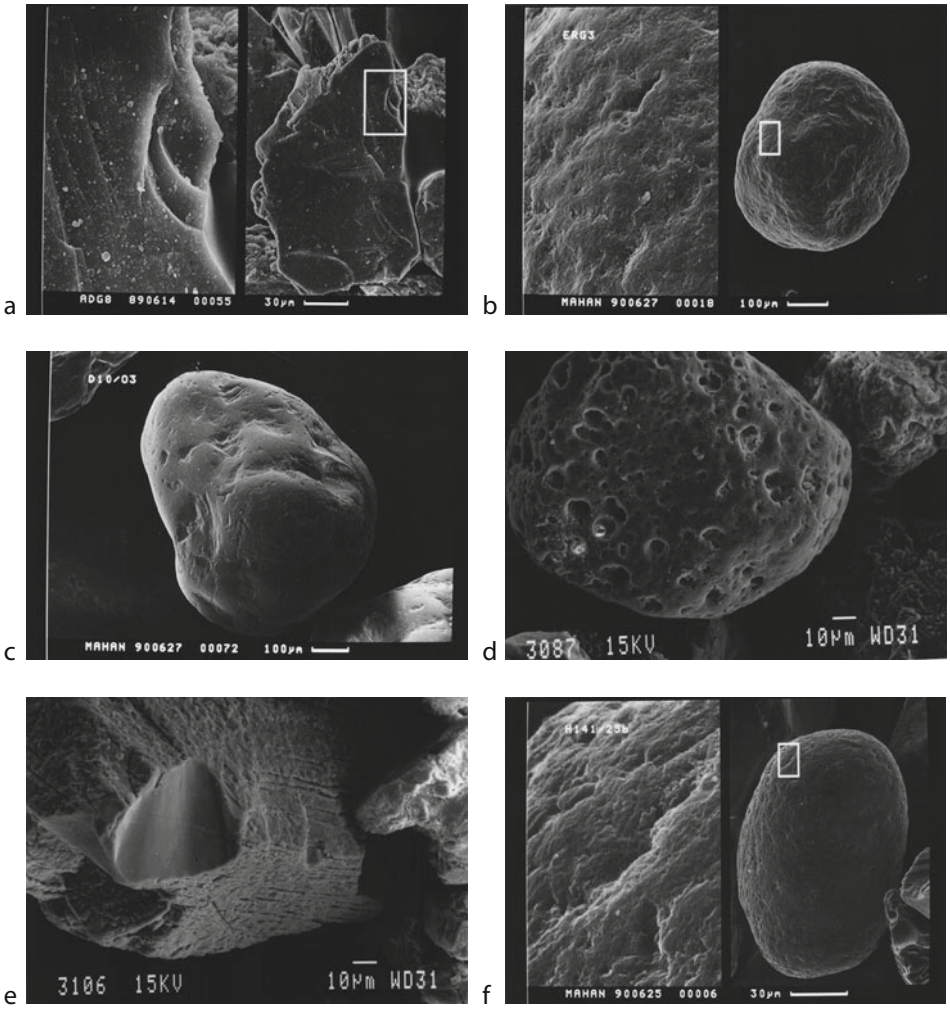

SEM Analysis of Glacial Sediments, Figure 1 (**a**) Mass wasted quartz grain, Adishy Glacier Area, Caucasus Mountains, Russia. The fracture face on the grain is typical of bedrock release accompanied by deep conchoidal fractures. The reverse side appears to be partly etched and covered with coating. Close up of the fractues is ×5. (**b**). Round quartz from Saharan ergs shows slight bulbous microfeatures (*right and top left facets*) and minor abrasion fatigue, a type of disrupted lattice formed from dry grinding. The disrupted lattice consists of broken surface structures of mm or micron size made up of small cracks, dislocations. The elongate depressions shown in the enlargement (×10) produce microrelief not seen with hand lens and probably result from saltation. (**c**), Aeolian grain with bulbous edges overprinted with v-shaped percussion cracks from transport in the Nile River; (**d**), Subround shock melted quartz with interconnecting melt cavities from Clear Creek, Colorado (K/T ejecta); (**e**), Shock lamellae on partially melted quartz, partially melted and annealed (From Mahaney, 2002, courtesy Oxford University Press). (**f**), Round quartz from lacustrine sand in the Thorncliffe Formation, Middle Wisconsinan age, Little Rouge Creek, Ontario, Canada. A plethora of v-shaped percussion scars attest to continual movement in Upper Flow Regime water masses (lacustrine or fluvial) prior to the ingress of Last Glacial Maximum ice in Southern Ontario.

fragments. Mass wasting, a neglected geologic agent in microtextural studies (Bull et al., 1987), initially leaves a record of bedrock release on grains just as in the glacial environment; however, fast or slow movement in gravitationally induced systems leads to the generation of new microtextures that involve grain packing and slickensides, microfeatures that are quickly erased in later glacial transport. The most distinctive microtexture in mass wasted sediments is the fracture face, a relatively clean break on the grain surface, often surrounded by varying degrees of chemical dissolution, microfeatures that survive transport in alpine glaciers, but are usually obliterated with long-distance transport in continental ice sheets. Thus, SEM investigations offer the chance to reconstruct source microtextures, followed by glacial, aeolian, and fluvial transport.

Some researchers (Oberbeck et al., 1993) consider that bolide (asteroid) impacts provide a plausible explanation for the occurrence of some tillites (ancient glacial deposits), characterized mainly by fragmented and

fractured quartz particles (Figures 1d and e). The tillites in question, however, are lacking in shock-melted quartz and planar deformation features (pdfs) which are the main product of extreme high-energy impacts ([15–25 km/s] [Boggs et al., 2001; Kennett et al., 2009; Firestone et al., 2007; Mahaney et al., 2010b]). Additional investigations of tillites are needed to determine if shock-melted quartz can be located in sufficient quantity to support the impact theory.

Glacial grains (Figures 2a–c and 3a–b) probably carry the greatest range of deeply embedded microtextures when compared with grains affected by other geologic agents. This includes the full range of fractures (Figures 2a–c and 3a–b), grooves, and abrasion microfeatures listed in Mahaney (2002), as well as solution-precipitation microfeatures and other coatings that may predate or postdate a glacial episode. Moreover, some grains (perhaps as many as 1 in 5) make the "glacial trip" unscathed by their sojourn in the ice and carry only microtextures related to previous environments. These fragments may carry a record of release from bedrock with unremarkable fracture faces, without the usual grain-to-grain contact in glacial systems that produce triangular faceted, sharp-edged grains with moderate to high relief, the latter usually well abraded with a multitude of fractures, grooves, and well-worn abrasion microfeatures.

As recorded in most studies, quartz is the ubiquitous and well-studied recorder of glaciation in many environmental settings (Krinsley and Doornkamp, 1973; Helland and Diffendal, 1993), major mineral suites, including all the plagioclase and orthoclase minerals, as well as many heavy minerals and gold, may also be analyzed to determine the degree of damage inflicted during glacial transport (Mahaney, 2002). This discussion, however, concentrates on quartz as the prime environmental recorder.

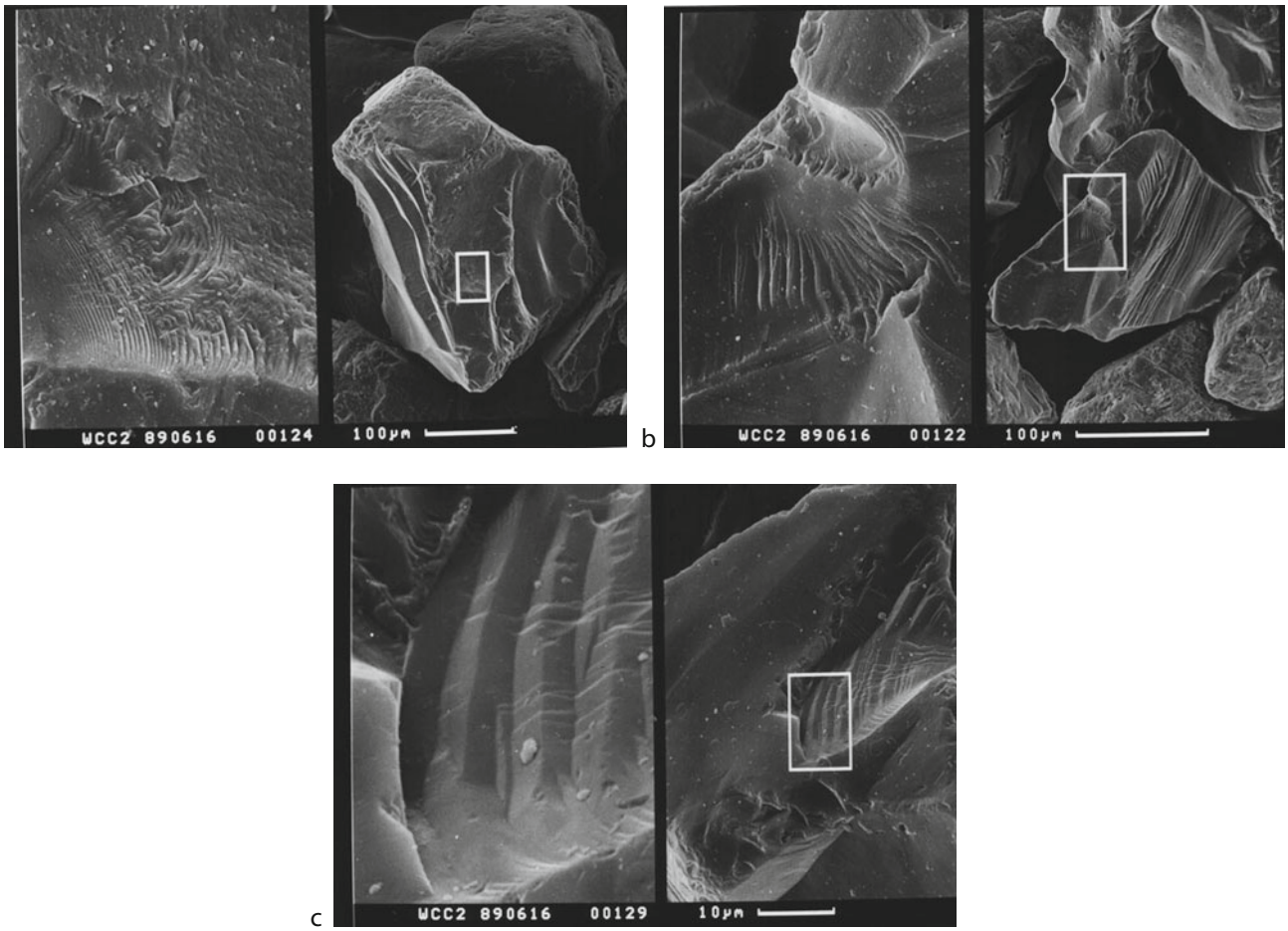

SEM Analysis of Glacial Sediments, Figure 2 (**a**), Deep troughs in subangular quartz from basal till, Wildcat Creek, Indiana. Linear troughs to left, curved troughs to right. Pseudo-chattermarks terminate on an upper ridge. See Folk (1975) for similar microfeatures on garnet. Upper grain is subrounded quartz and carries numerous v-shaped percussion scars from transport in meltwater. Crossed fractures, like crossed striae, depict typical high frequency younger fractures overprinting low frequency, higher wavelength microfeatures to the right in the enlargement (×10). (**b**), Quartz, heavily abraded and fractured; (**c**), Quartz with deep striations.

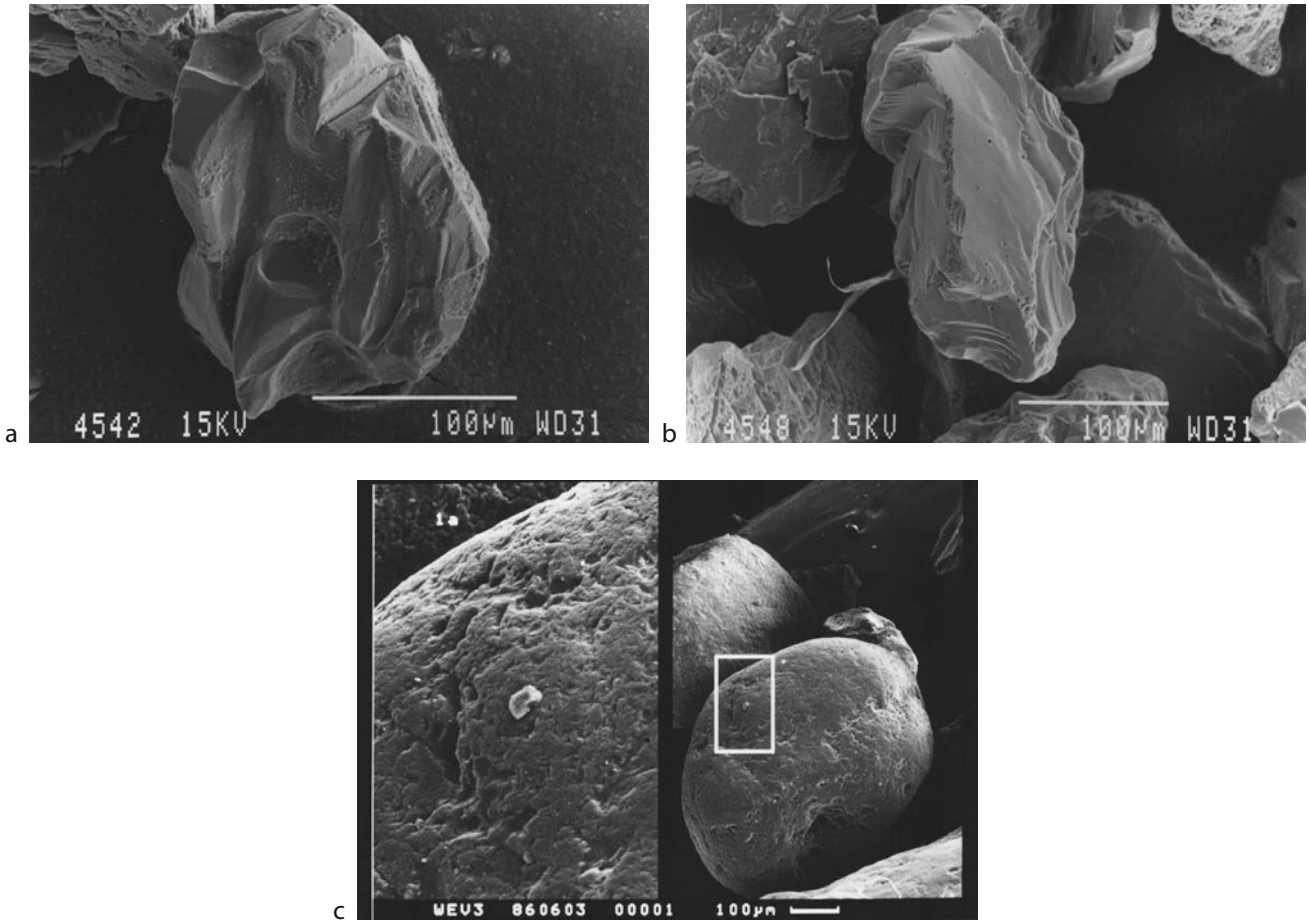

SEM Analysis of Glacial Sediments, Figure 3 (**a**) Angular quartz with partial abraded edges in Weichselian Till from sample TAR 3/3, Estonia. The sample shows deep grooves, multiple striations, deep cavities, well-abraded facets, and minor preweathering as indicated by minor etching; (**b**) from the same section, angular quartz with wavy, smoothed top and multiple grooves, striations and conchoidal fractures along the *c*-axis; (**c**) Two subround quartz grains with numerous v-shaped percussion cracks in the lowermost till, WEV3 Section, Wellsch Valley, Saskatchewan, Canada. The number of round grains with fluvial transport signatures depends on whether the till has a warm- or cold-based history. These grains have a warm-based history that becomes depleted up-section.

The relative hardness of quartz (7.0 on Mohs hardness scale) and its widespread occurrence in nearly every environment make it an ideal candidate for microtextural study. Grains are often unblemished, existing as colorless, hexagonal crystals, although sometimes colored by impurities. With an absence of cleavage, especially in the coarse fractions (2,000–50 µm), it is composed exclusively of silica-oxygen tetrahedra with oxygen atoms joined with silicon into a strong geometrical network (Frondel, 1962). Unlike weaker minerals, quartz is capable of transiting the glacier system many times and it is possible to examine complex quartz grains that have undergone many trips in the ice. Because quartz is subject to slow dissolution and precipitation, it is also an ideal mineral to record subaerial and diagenetic weathering events; moreover, it is possible to observe preweathered microfeatures overprinted with the fresh scars of glacial transport, followed by more recent weathering events. Hence, a single grain may carry evidence of several transport/weathering episodes (Mahaney, 2002).

Load

The load transported by ice ranges from clay to boulder and block sized material. It also includes a minor amount of aeolian-delivered grains as well as mass wasted material derived from nunataks and high-cirque walls. The supraglacial load may be light to heavy, depending on the nature of the source rocks and the climatic setting (tropical mountains to Arctic or Antarctic environments), and consist of material delivered by airfall influx and gravity to the glacier surface. There must be grain-to-grain contact even at pressures close to 1–2 atm to achieve sufficient stress in the basal ice to comminute mineral

material. The englacial environment, however, is relatively free of clastic load, although subsurface channels may move large volumes of meltwater that may occasionally carry clastic load. In these turbulent sluiceways grains may suffer heavy abrasion, giving overprints partially masking previously inherited weathering (e.g., preweathering) and other fractures and/or abrasion inflicted during the initial stage of ice transport.

The basal ice, containing the bulk of the clastic load in a glacier, together with variable amounts of water, provides the environment with the highest probability of grain-to-grain contact. Increasing water content tends to create hydrostatic pressures close to one bar and nearly equal in all directions. With decreasing water content, shear stress rises somewhat but falls far below the pressures that result from stick–slip processes (up to ~200 bars) where sudden slippage generates vibrations, the sudden convergence of kinetic energy to elastic energy. The vibrations produced by glacier movement are manifest in the array of fractures seen in great numbers on glacial grains. No other geologic agent can generate the strong vibrations, cones of energy that produce deeply embedded microfeatures in clasts nicely demonstrated by the multitude of fracture microfeatures often observed on glacial grains.

Of the many pathways by which clasts may enter, move through, and exit a glacier, grains of any description may: (a) sink into the ice from the glacial surface, (b) be carried by surface and subsurface meltwater streams to exit the terminal areas, (c) be forced to the surface by thrusting, and/or (d) be entrained from contact with underlying bedrock and/or till. This raises the question as to where to sample till, and whether it is best to concentrate on subglacial deposits where glacial grinding is apt to be at a maximum, or alternatively sample end or lateral moraines, which might likely contain a mix of material deposited directly in contact with ice or from meltwater.

Unlike aeolian and fluvial grains, glacial grains are generally held in bondage by the ice, or by other grains in rigid suspension, so that the ultimate amount of grinding occurs with movement down glacier. Aeolian and fluvial grains, as previously discussed, are capable of considerable turbulent random movement, and while they are capable of high-energy collisions, they are not subjected to the sustained and concentrated high-energy fields inflicted on glacial grains. While aeolian grains may produce scars somewhat reflecting microfeatures resulting from glaciation, the damage is far less deeply imbedded in the former grain surfaces.

As suggested by Barcilon and MacAyeal (1993) and Mahaney (1995, 2002) stick–slip motions at the base of glaciers tend to fracture and abrade particles in ice. Particle surface microtextures are governed partly by bedrock release (mechanical weathering), preweathering, resultant transport by different geologic agents and diagenesis/pedogenesis in a depositional environment. Within the ice body, quartz grains form inhomogeneous elastic inclusions with different strengths depending on preweathered states and these respond to variable stresses by forming fracture and abrasion microfeatures. If the particles are already weakened by chemical preweathering, and if they have fracture faces (Mahaney, 1995) derived from frost riving (Mahaney et al., 1991), they may easily comminute into smaller particles. This is particularly the case if they come into contact with one another in the basal ice layer where stick–slip processes produce high basal shear stresses and high strain rates (Barcilon and MacAyeal, 1993). Basal till, with meltwater lubrication, glides over bedrock and occasionally surges, subjecting particles carried as load to high fracture and abrasive stress, engendering low velocity impacts which impart microtextures onto quartz sand surfaces. While there are similar shallow, conchoidal and linear fractures on quartz from aeolian (Mahaney and Andres, 1996) and fluvial environments, the angular shape, deep entrenchment of conchoidal and linear fractures, and frequent directionality of troughs and grooves (striations) are unique to grains emplaced by glacial transport. As shown by Sweet and Soreghan (2010), Soreghan et al. (2008) and Strand et al. (2003) glacial microtextures may remain in the rock record for tens of millions of years.

Microtexture recognition

Almost all the microfeatures listed and discussed in Mahaney (2002) can be found on glacial grains. All dissolution and weathering microfeatures resulting from subaerial weathering and or diagenesis are presumably inherited from interstadial or interglacial climates having survived the damages inflicted on a large proportion of grains moving through glaciers.

Taking the array of microtextures as possible candidates for microfeatures likely observed on glacial grains, the researcher is faced with the question of how many grains to analyze and at what resolution. All microtextures should be logged by their frequency of occurrence, and it is necessary to analyze several samples and several fractions of each sample in order to arrive at a meaningful interpretation. A quick overview of each sample can be obtained by analysis of the fine and very fine sand fraction taking into account that angularity is often extreme in the finer fractions. This should be followed by analysis of at least 20 grains in the medium sand fraction (500–250 μm) and 20 grains in the coarse to very coarse fractions (2,000–500 μm). These grains should be collected as randomly as possible and studied under the light microscope prior to using the SEM.

The degree of relief is one of the first assessments to make when analyzing a sample suite. Because of heavy fracturing and abrasion, high relief often dominates on glacial grains. This needs to be assessed and given a percent frequency of occurrence. Next, among the population of grains studied, the degree of angularity, edge rounding, and all fracture and abrasion microfeatures need to be identified and frequency of occurrence tabulated. Last, all weathering, precipitation, and dissolution

features should be assessed in a similar fashion. Glacial grains should be compared and contrasted with grains resulting from the action of other geological agents, perhaps in the same section or between sections.

Continental glaciation

Wisconsinan and pre-Wisconsinan tills provide a wealth of information on glacial processes and preweathering that occurred prior to glacial entrainment (Mahaney, 1990a). One of the most striking microfeatures on grains from thick and extensive valley glaciers and continental glaciers are curved grooves, striations similar to those forms on bedrock or on pebble, and cobble clasts residing in tills (Figure 3a, b). Linear grooves may be glacial but they may also result from fault movement although with tectonic origins there is usually lattice distortion, very high abrasion, and uplifted surfaces that allow differentiation from glacial processes. Curvilinear grooves are unidirectional features that are as much an indisputable proof of the glacial environment as striations on rock. Whether these grains are frozen into the ice and dragged along the surface or affected by ice drag on particles, which eventually break off from bedrock; they are clearly the product of ice contact similar to macrofeatures that have been invoked to prove glaciation for nearly two centuries since the advent of the Glacial Theory proposed by Louis Agassiz.

Another microfeature typically observed on glacial grains is the v-shaped percussion crack (Figure 3c) that indicates the effect of water transport, presumably in this case, meltwater flow. Also with attrition along the edge of the grain some rounding appears to have been in progress when these grains were incorporated into till. Edge rounded grains, nearly equant, often carry surface scars of meltwater transport in somewhat greater abundance than is usual in fluvial systems. Often they are associated with grains showing directional grooves, steplike features, cirque-like amphitheater, overprinted with superficial radiating fractures less deeply inscribed and uplifted surface plates that have been lifted out leaving the amphitheater-like feature, the radiating fractures of which indicate plate removal may have come from a high-stress collision.

Antarctic tills

Grains in polar environments show heavily damaged surfaces representative of tills emplaced by continental ice. Often refashioned into triangular-shaped particles (Figure 4a–b), they exhibit deep fractures, upturned plate along the bottom of the grain, somewhat curved directional trough from top to mid region and steplike features on top right; much of the grain is extensively abraded. Considered to be the product of high stress fields, such microfeatures might be expected in thick continental ice with low water content where high local stick–slip motion might produce pressure capable of starting to dislocate the lattice. Polar grains display grains with high degrees of abrasion and directional troughs. While adhering particles are rather scarce on most of the sands shown here, they are more prevalent on the abraded grains.

The most intense crushing comes from the thickest ice as indicated by observations made by Mahaney et al. (1988) following a thorough examination of samples from Mount Kenya and southern Canada. Quartz sand grains in thick ice, such as the Antarctic Ice Sheet, are presumably subjected to transport over long distances with maximum stress generated by stick–slip mechanisms at the base of the ice.

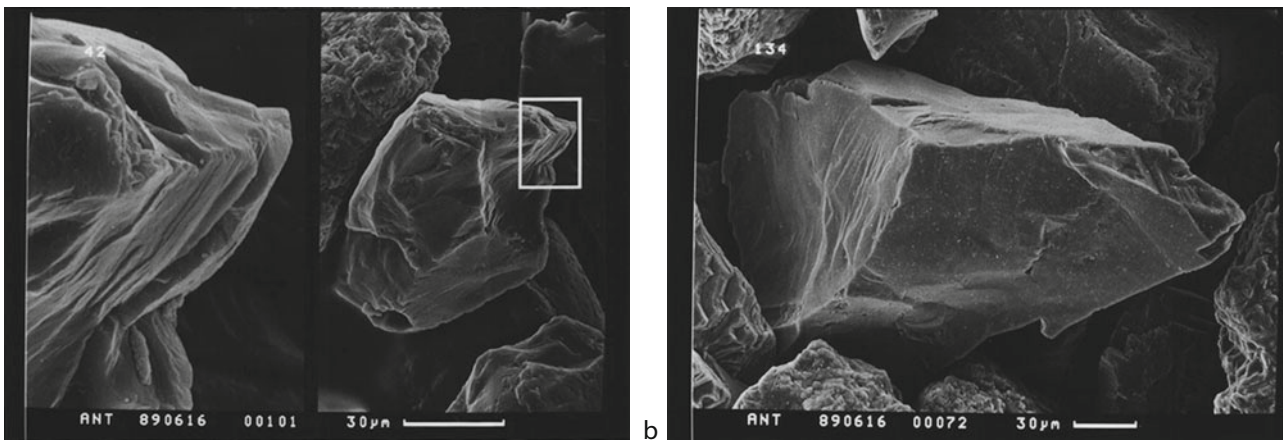

SEM Analysis of Glacial Sediments, Figure 4 (**a**) Angular quartz from till 42 (Mahaney et al., 1996) exhibiting multiple fractures, deposited by the Inland Ice Sheet, Antarctica. Edge of fractured quartz lower right; preweathered plagioclase in upper left; (**b**) Angular quartz with multiple fractures and minor preweathered etching in upper left surrounded by preweathered calcite and plagioclase.

Alpine glaciation

Quartz and other mineral grains, recovered from various tropical and middle latitude alpine areas (Figure 5a, b), show ranges of fracture microfeatures, striations, and abrasion that appear to be related to ice thickness and distance of transport (see Mahaney, 2002). Quartz and other minerals surviving transport in alpine ice carry a range of fractured and abraded preweathered grains showing varying degrees of *minor* subparallel linear fractures, conchoidal fractures, and abrasion that suggest low shear stress, low stress field conditions for stick–slip occurrences, and, of course, minimum transport distance. As previously discussed, many alpine subglacial tills are well lubricated with water giving them very low shear stress and high pore water pressure making it difficult to fracture grains carried as basal load. This condition must also affect stick–slip processes (Barcilon and MacAyeal, 1993; Mahaney, 1995) creating a situation where, even if stick–slip were to occur, the resulting shear stress would not overcome the shear resistance of the grain.

Reworking of grains from other environments through the glacial system is evidenced from several suites of samples from African massifs, the Andes, Tibet, Rocky Mountains, and the European Alps. The greatest ratio of preweathered to fresh grains is often observed in alpine areas for both Neoglacial and late Pleistocene tills studied to date. For example, the imagery indicates glacially crushed grains may carry extensive dissolution features, overprinted with a glacial signature followed by younger weathering and re-entrainment in an active glacier.

Experimental fractography

The theory of brittle and ductile fracture, the central canon of microtexture theory, requires the fracturing of quartz and other minerals to result from increasing stress until strain produces slow to catastrophic crack propagation. The resulting fractures may open along preexisting flaws in minerals (Griffith cracks) and/or generate new flaws extending across mineral surfaces, either as shallow or deeply embedded cracks. These fractures are predetermined by the stress–strain energy field, much as vibrational energy is released through the grain (Mahaney, 1995). In a glacier, large sand grains of very coarse to coarse (2,000–500 μm) grade size require less stress to fracture than smaller ones (500–50 μm), but much depends on the applied stress field, strength of the minerals undergoing strain, and particularly their weathered state. In general smaller grains require, on average, higher stress fields to induce failure leading to crack propagation. Put another way, the probability of fracture by breaking the weakest mineral increases with increasing size of fragments. Particularly susceptible are mineral intergrowths, as for example, quartz and biotite, with the latter mineral prone to rupture. Analysis of different grade sizes of glacial sands (Mahaney, 2002) within the same till sample reveals that coarse fractions exhibit about the same range of glacial microtextures as fine ones.

Analysis of different fragment grade sizes of sands in glacial sediment has shown that repeated fracturing results in increased fragmentation. Increased fragmentation, and hence smaller size material, requires increased stress to achieve continual fracturing as particle size diminishes from sand to silt. Small silt-size fragments (<50 μm) continually fragmented/comminuted and/or liberated from larger grains by grinding at the base of the ice lie at the end of their size reduction run (Dreimanis and Vagners, 1971), and are apt to be preserved intact in till after their sojourn in the ice. These smaller grains may carry the final range of microtextures from glacial crushing, the end product of a long series of grinding and fragmentation from very coarse sand to silt. Other small fragments of

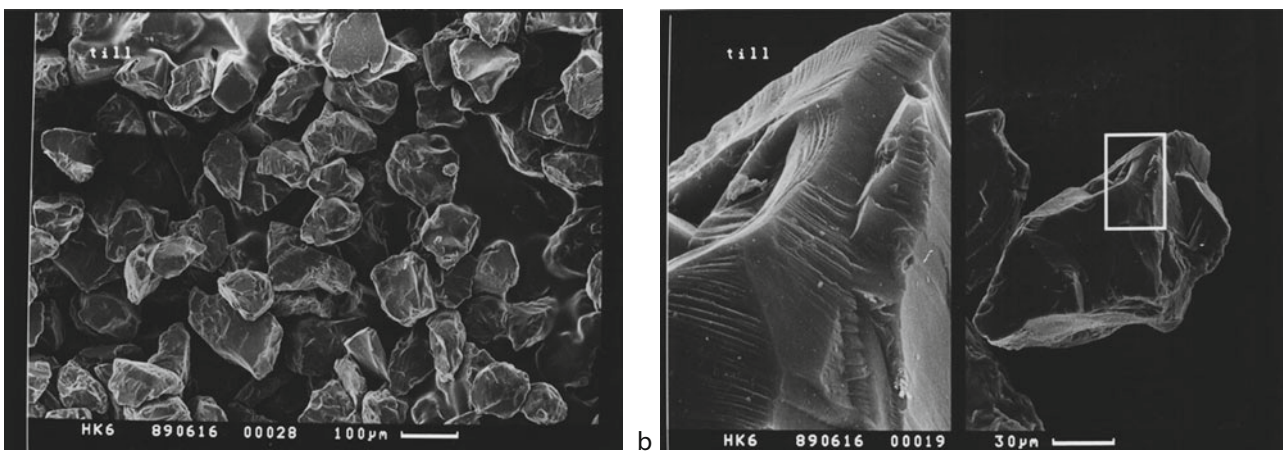

SEM Analysis of Glacial Sediments, Figure 5 (**a**) General frame showing angular and subangular grains, a mix of plagioclase, orthoclase, minor biotite, and quartz in till from section HK6, Zillertal Alps, Austria; (**b**) Angular quartz with multiple fractures and deep grooves.

the same size, subjected to low pressure mechanical action by either mass wasting, aeolian, and/or fluvial agencies long before they are added as load to a glacier, are likely to be little modified by the mechanical forces of an active glacier although they may be overprinted with a glacial signature. This is why fine sand–silt fractions are important to study with the objective of cataloging the range of microtextures at close to the final stage of comminution. Therefore, depending on grain-to-grain contact within the ice some of the grains in the fine and medium silt fractions may have a microtexture record entirely unrelated to travel in the ice; that is, some grains make the glacial trip in isolation, without contact with other grains.

Fractography, that is the identification and interpretation of fractures on particle surfaces (Krinsley and Donahue, 1968; Krinsley and Doornkamp, 1973; Margolis and Krinsley, 1974; Mahaney et al., 1988; Mahaney, 1990a, b, 1995; Marshall, 1987), has been pursued with the objective of analyzing individual fracture markings, and their frequency of occurrence, as a means to gain insight into glacial grain history. All attempts to target certain microtextures as "glacial" have made it necessary to pose several important questions: (1) Do characteristic mechanical damage microfeatures reside on grains subjected to glacial transport? (2) If glacial microfeatures exist, are they related to glacial dynamics? (3) If unique glacial microtextures exist, is it possible to deduce distance of transport and ice thickness from the fractography?

Many different minerals have been used to study crack propagation in glacial grains but quartz is the usual material selected as test material for stress–strain relationship tests because it is abundant in glacial deposits and its hardness ensures it to be an excellent long-lived recorder of damage inflicted on it. As a test, amorphous silica glass spheres have been utilized: (1) as an analog of quartz that could be subjected to low stress in a confined space, (2) using a spherical shaped object makes it possible to compare with crushed mineral grains, and (3) to determine the shape and number of fractured particles.

Since several previous fractographic studies were performed on till particles in the 50–500 μm range (Krinsley and Donahue, 1968), and on larger particles of 16–26.5 mm diameter (Iverson, 1990), it seemed logical to carry out laboratory experiments using quartz of a similar size. In the first three tests, particles were selected from fragments of a large single piece of optically translucent α-quartz (from Brazil), crushed by low velocity impact. After separating the particles into three size categories of 50–500 μm sizes, they were subjected to compression in a cylindrical volume of ice at 2,000 psi capacity (see Mahaney, 2002). Compression was achieved in a piston cylinder that contained a cooling agent maintained at a constant low-test temperature.

Mineral fragments were sprinkled widely on ice, which was grown by layer to insure particle segregation. Each layer was periodically subjected to a low vacuum of ~1 Torr to eliminate as much air as possible. The first three tests were run on quartz fragments. In Test 1 the ice temperature was below −10°C, thus similar to a cold glacier. Tests 2 and 3 were carried out using quartz (2) and silica glass (3) and with the temperature raised to p-melting simulating warm glacier conditions. The objective of the experiment was to determine the amount of fracturing that occurred in the charge before and after compression in ice.

Test 1 (Figure 6a) used the *fine* sand fraction (125–250 μm), selected as load with a maximum pressure of 2,000 psi or 17.5 Mpa on the ice cylinder, as before equating to an ice thickness of 1.98 km, applied for 30 min. Recovered grains showed several new fragments with sizes finer than the starting size. Original fragments with protrusions were subjected to considerable edge rounding and several flaky particles were likely due to physically induced spalling probably from lattice disruption.

In Test 2 (Figure 6b), the grain size and cylinder pressure were approximately the same as in Test 1. In this experiment, grains were subjected to similar pressure as in Test 2 for 40 min while temperature was brought up to p-melting. The imagery of the resultant charge shows considerable change in particle size and distribution. Here, several small fragments and fine fragments cling to larger ones, which survived compression. P-melting conditions in the test cylinder led to formation of meltwater; ice bridges melted, allowing particles to join. Particles at the base of the brass cylinder were subjected to high hydraulic pressure causing some quartz to become embedded in the brass base. In this third test, quartz grains were fractured into numerous particles brought into mutual contact under high load. These particles exhibited unmistakable arc-shaped steps with numerous and deeply imbedded conchoidal and subparallel linear fractures, with a sizable population of fine adhering particles.

Test 3 (Figures 6c and d), the concluding test in this series, was designed to study the effect of compression on a population of well-isolated, untouched, and perfectly spherical silica glass spheres. These were situated to represent inhomogeneous inclusions exactly as would occur with fresh quartz released from bedrock. Because of their sphericity, they represented a set of particles with equal geometric stress concentrating factors, easily amenable to theoretical analysis but different from what would occur in nature. Pressure was applied at 17.5 Mpa as in the previous tests, and after a short time, the temperature was raised to p-melting. Mechanical damage on this load was severe with four spheres totally shattered into small fragments of fine sand and silt size, others greatly reduced in diameter, and still others escaping with only a few craters produced. Apparently the nine spheres suffering the greater damage released fine particles simulating glacial grinding, the latter process originally postulated by Smalley (1966).

These experiments show that coarse silt inclusions in ice apparently unaffected escape compression. Sizes ranging from fine to medium sand are affected by compression depending on temperature. Clearly, the p-melting temperature is critical to produce the greatest degree of fragmentation as shown in Tests 2 and 3. Large particles of equal

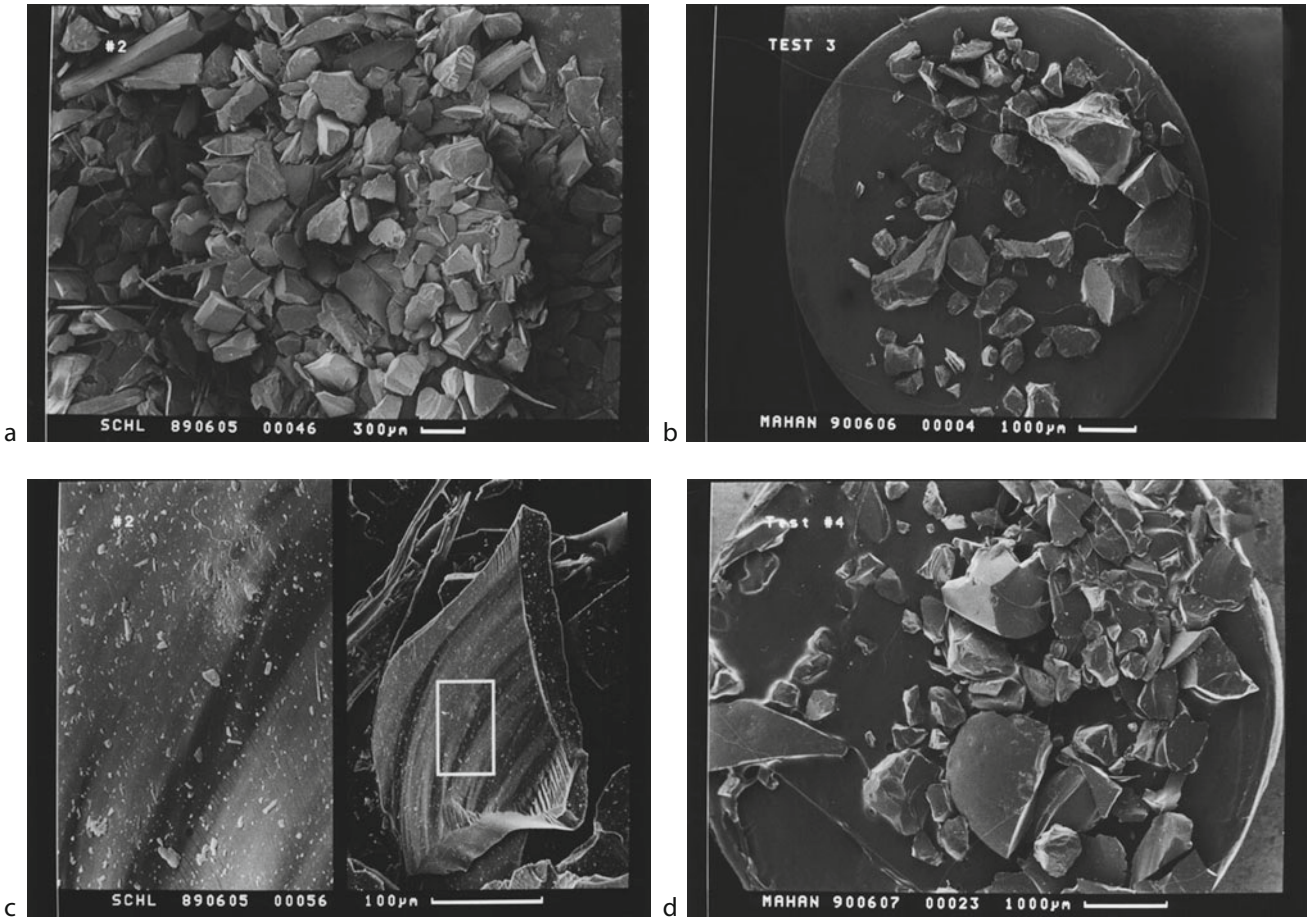

SEM Analysis of Glacial Sediments, Figure 6 (**a**) Recovered charge of fragmented sands originally sieved to medium and fine sand size (125–250 μm diameter). Approximately 25–30 grains of the sample were fragmented into smaller sizes; (**b**) Representative quartz fragments from Test 2 of approximately 125 μm diameter, with deeply imbedded conchoidal and subparallel linear fractures and sharp edges with numerous adhering particles; (**c**) Fragments of silica spheres, originally of 250–1,000 μm size recovered (Test 3) after compression in ice at simulated thickness of 1.98 km; (**d**) Recovered fragmented charge from Test 4. Original size of the silica spheres was 3.5 cm. Simulated ice thickness was 1.98 km. Experimental laboratory work compressing alpha quartz and silica spheres at simulated glacial crushing pressures was done in the laboratory of Prof. H. Schloessin, University of Western Ontario, London.

sphericity are subject to considerable comminution when temperature is raised to the p-melting point. The experimental data show that ice of varying thickness is capable of glacial crushing as originally postulated by Krinsley and Doornkamp (1973), but much depends on grain to grain contact, glacial overprinting on preweathered grains, and cold versus warm ice.

Conclusions

The triangular faceted "glacial grain," depicted in Krinsley and Doornkamp (1973), as a triangular faceted, refashioned quartz, with a multitude of fracture and abrasion features is one of the *common* particles found in the sand fraction of tills. As shown here it is by no means the only well-fractured and abraded particle in till, although depending on the ice thickness and distance of transport it could amount to 40% or 50% of grains observed. There are other grains including equant grains with minor damage, flake-shaped grains often with an abundance of abrasion and little fracture, partly streamlined abraded particles with variable damage, and preweathered grains. The preweathered grains often reach 30% of the total population of grains in till observed under the SEM, which means that perhaps as many as 1 in 3 of the grains analyzed might carry important information about preglacial weathering. Indeed, in some instances, the degree of preweathering might yield important information about paleoleaching and the strength of interglacial climates (see Mahaney, 1990a). Indeed, on Mount Kenya, plagioclase and quartz from the last interglacial carried coatings of fibrous and nodular gibbsite in considerable

quantity as determined by XRD and SEM/EDS, the product of aggressive leaching and removal of Si leading to meta-halloysite degradation (Mahaney, 1995).

Microtextures considered of unequivocal glacial origin include directional curved and straight grooves or troughs. Groove is a useful term for lightly imbedded striations, with troughs reserved for deeply embedded features, to the order of 5 μm or more. These are as much the exclusive product of the glacial environment as macrostriations that have been used for nearly two centuries as chief indicators of glaciation. In the microworld it may be that minerals harder than quartz (topaz, zircon, etc.), while of low mass in most tills, could, when in contact with quartz, leave directional troughs and grooves. Perhaps this leads to the production of pencil-shaped zircons commonly found in some tills (Mahaney and Milner, 1998).

Deeply inscribed fractures are common on glacial grains, but not exclusive to the glacial environment. Over a large population of grains, however, conchoidal and subparallel linear fractures would be expected to dominate as one of the most frequently occurring forms. Only thick valley glaciers and glaciers of continental proportions would be expected to produce deeply imbedded features of this type. Sharp edges, where grains have been worn away by abrasion, are also a hallmark of the glacial environment. They are not unequivocally glacial, but taken as a proportion of the whole in a large population of samples they can be expected to have a frequent occurrence.

Relief on glacial grains is often considered high but with extreme abrasion, common with thick ice, grain surfaces may be worn to produce minimum relief. Grains deposited by cirque ice and outlet glaciers often exhibit moderate to high relief, which may in fact mislead investigators into thinking considerable grain modification and reformation has been achieved.

Chattermarks (Folk, 1975; Peternecht and Tietz, 2010), often touted as the common glacial microtexture, are in reality extremely rare, despite infrequent observations that seem to attract attention. Trails of chattermarks forming rune-like grooves, while infrequently common on glacial grains, are now known to be the product of mechanically induced fractures that become visible after chemical etching, a process originally envisioned by Bull (1981). Experimental work carried out by Peternecht and Tietz (2010) confirms that collision of minerals leads to disruption of the internal crystal lattice, the fracture sites dissolving faster than the surrounding mineral fabric. Once the mechanically induced fractures are subjected to chemical weathering, the fracture sites become visible. Chattermarks are therefore considered to be part of a two-stage process; first, mechanical collision during transport followed by chemical weathering at a later stage.

Steplike features resulting from well placed and deeply embedded fractures are unequivocally glacial in origin (Mahaney, 2002). These mechanically induced microfeatures may result from larger grains blasting fragments off smaller grains as a result of their increased mass/energy relationships. Much depends on random events within the ice mass and the probability of grain-to-grain contact, impact angle, force (cone of energy), bulk mass, and hardness of the material.

The fact that so many preweathered grains make the glacial trip without damage means that not all glacial grains come into contact with one another. While preweathered grains provide important information on interglacial climates, their coatings can range from carbonate and silica to iron and manganese; even clay coats have been documented (Mahaney et al., 1996) from the Antarctic. As with other geologic agents, to prove a glacial origin requires a large number of samples from different size fractions (very coarse–coarse; medium; and fine–very fine sand), all documented with replicates.

Bibliography

Barcilon, V., and MacAyeal, D. R., 1993. Steady flow of a viscous ice stream across a no slip/free transition at the bed. *Journal of Glaciology*, **39**, 167–185.

Biederman, E., 1962. Destruction of shoreline environments in New Jersey. *Journal of Sedimentary Petrology*, **32**, 181–200.

Boggs, S., Krinsley, D. H., Goles, G. G., Seyedolali, A., and Dypvik, H., 2001. Identification of shocked quartz by scanning cathodoluminescence imaging. *Meteoritics and Planetary Science*, **36**, 783–791.

Bull, P. A., 1981. Environmental reconstruction by scanning electron microscopy. *Progress in Physical Geography*, **5**, 368–397.

Bull, P. A., Goudie, A. S., Price-Williams, D., and Watson, A., 1987. Colluvium: a Scanning Electron Microscopy analysis of a neglected sediment type. In Marshall, J. R. (ed.), *Clastic Particles*. New York: Van Nostrand Reinhold, pp.16–35.

Dreimanis, A., and Vagners, U. J., 1971. Bimodal distribution of rock and mineral fragments in basal tills. In Goldthwaite, R. P. (ed.), *Till-A Symposium*. Columbus: Ohio State University Press, pp. 237–250.

Firestone, R. B., West, A., Kennett, J. P., Becker, L., Bunch, T. E., Revay, Z. S., Schultz, P. H., Belgya, T., Kennett, D. J., Erlandson, J. M., Dickenson, O. J., Goodyear, A. C., Harris, R. S., Howard, G. A., Kloosterman, J. B., Lechler, P., Mayewski, P. A., Montgomery, J., Poreda, R., Darrah, T., Que Hee, S. S., Smith, A. R., Stich, A., Topping, W., Wittke, J. H., and Wolbach, W. S., 2007. Evidence for an extraterrestrial impact 12, 900 years ago that contributed to the megafaunal extinctions and the Younger Dryas cooling. *Proceedings of the National Academy of Sciences*, **104**, 16016–16021.

Folk, R. L., 1975. Glacial deposits identified by chattermark tracks in detrital grains. *Geology*, **3**, 475–479.

Frondel, C., 1962. *The System of Mineralogy, Vol. II, Silica Minerals*. New York: Wiley, 334 p.

Helland, P. E., and Diffendal, R. F., Jr., 1993. Probable glacial climatic conditions in source areas during deposition of parts of the Ash Hollow Formation, Ogallala Group (Late Tertiary), of western Nebraska. *American Journal of Science*, **293**, 744–757.

Iverson, N. R., 1990. Laboratory simulations of glacial abrasion: comparison with theory. *Journal of Glaciology*, **36**, 304–314.

Kennett, D. J., Kennett, J. P., West, A., Mercer, C., Que Hee, S. S., Bement, L., Bunch, T. E., Sellers, M., and Wolbach, W. S., 2009. Nanodiamonds in the Younger Dryas boundary sediment. *Science*, **323**(5910), 94.

Krinsley, D., and Donahue, J., 1968. Environmental interpretation of sand grain surface textures by electron microscopy. *Geological Society of America Bulletin*, **79**, 743–748.

Krinsley, D., and Doornkamp, J. C., 1973. *Atlas of Sand Grain Surface Textures*. Cambridge: University Press, p. 91.
Krinsley, D., and Takahashi, T., 1962. The surface textures of sand grains: an application of electron microscopy. *Science*, **135**, 923–925.
Mahaney, W. C., 1990a. *Ice on the Equator*, Ellison Bay, WI: William Caxton Ltd, 386 p.
Mahaney, W. C., 1990b. Macrofabrics and quartz microstructures confirm glacial origin of Sunnybrook drift in the Lake Ontario Basin. *Geology*, **18**, 145–148.
Mahaney, W. C., 1991. Two distinct particle types in the Lanzhou Loess. *Naturwissenschaften*, **78**, 167.
Mahaney, W. C., 1995. Pleistocene and Holocene glacier thicknesses, transport histories and dynamics inferred from SEM microtextures on quartz particles. *Boreas*, **24**, 293–304.
Mahaney, W. C., 2002. *Atlas of Sand Grain Surface Textures and Applications*. Oxford, UK: Oxford University Press. 237 p.
Mahaney, W. C., and Andres, W., 1996. Scanning electron microscopy of quartz sand from the north-central Saharan desert of Algeria. *Zeitschrift für Geomorphologie N.F, Suppl-BD.*, **103**, 179–192.
Mahaney, W. C., and Milner, M., 1998. Zircon microstriators in the sand of auriferous Andean tills: fine tools and noble metals. *Boreas*, **27**, 140–152.
Mahaney, W. C., Vortisch, W. A., and Julig, P., 1988. Relative differences between glacially crushed quartz transported by Mountain and continental ice-some examples from North America and East Africa. *American Journal of Science*, **288**, 810–826.
Mahaney, W. C., Vaikmae, R., and Vares, K., 1991. Scanning Electron Microscopy of quartz grains in surpraglacial debris, Adishy Glacier, Caucasus Mountains, USSR. *Boreas*, **20**, 395–404.
Mahaney, W. C., Claridge, G., and Campbell, I., 1996. Microtextures of quartz grains in tills from Antarctica. *Paleo-3*, **121**, 89–103.
Mahaney, W. C., Stewart, A., and Kalm, V., 2001. Quantification of SEM microtextures useful in sedimentary environmental discrimination. *Boreas*, **30**, 165–171.
Mahaney, W. C., Kalm, V., Kapran, B., Milner, M. W., and Hancock, R. G. V., 2009. Soil chronosequence, Humboldt Glacier, northwestern Venezuelan Andes. *Geomorphology*, **10**, 99–110.
Mahaney, W. C., Dohm, J., Costa, P., and Krinsley, D. H., 2010a. Tsunamis on Mars: Earth analogues of projected Martian sediment. *Journal of Planetary and Space Science* (in press).
Mahaney, W. C., Kapran, B., Milner, M. W., Kalm, V., Krinsely, D., Beukens, R., Boccia, S., and Hancock, R. G. V., 2010b. Evidence from the northwestern Venezuelan Andes for extraterrestrial impact. *Geomorphology* (in press).
Margolis, S., and Krinsley, D., 1974. Processes of formation and environmental occurrence of microfeatures on detrital quartz grains. *American Journal of Science*, **274**, 449–464.
Marshall, J. R., 1987. *Clastic Particles*. New York: Van Nostrand Reinhold Co. 346 p.
Oberbeck, V. R., Marshall, J. R., and Aggarwal, H., 1993. Impacts, tillites and the breakup of Gondwanaland. *Journal of Geology*, **101**, 1–19.
Peterknecht, K. M., and Tietz, G. F., 2010. Chattermark trails: surface features on detrital quartz grains indicative of a tropical climate. *Journal of Sedimentary Research* (In press).
Porter, J., 1962. Electron microscopy of sand surface textures. *Journal of Sedimentary Petrolgy*, **32**, 124–135.
Smalley, I. J., 1966. The properties of glacial loess and the formation of loess deposits. *Journal of Sedimentary Petrology*, **36**, 669–676.
Soreghan, G. S., Soreghan, M. J., Poulsen, C. J., Young, R. A., Eble, C. F., Sweet, D. E., and Davogustto, O. C., 2008. Anomalous cold in the Pangaean tropics. *Geology*, **36**, 659–662.
Strand, K., Passchier, S., Nasi, J., 2003. Implications of quartz grain microtextures for onset of Eocene/Oligocene glaciation in Prydz Bay, ODP Site 1166, Antarctica. *Palaeo*-3, **198**, 101–111.
Sweet, D. E., and Soreghan, G. S., 2010. Application of quartz sand microtextural analysis to infer cold-climate weathering for the equatorial Fountain Formation (Pennsylvanian-Permian, Colorado, USA). *Journal of Sedimentary Research*, **80**, 666–677.
Whalley, W. B. (ed.), 1978. *Scanning Electron Microscopy in the Study of Sediments*. Norwich: GeoAbstracts.

Cross-references

Alps
Andean Glaciers
Antarctica
Cirque Glaciers
Dynamics of Glaciers
Geocryology
Glacial Grooves
Glacial Striations
Glacier
Glacier System
Ice Age
Little Ice Age
Moraine
Quaternary Glaciation

SEPTA OF ENGLACIAL DEBRIS

Subhajit Sinha
DBS College, Dehradun, Uttarakhand, India

Debris input to glaciers occurs most commonly at ice margins and is thus concentrated along the base of cirques and in medial debris septa that ultimately become medial moraines. Proximal debris addition from rockfalls and increasing debris concentration from below by ice sublimation results in supraglacial debris mantles in the distal direction with great spatial variability in thickness and grain size. As ablation proceeds, debris accumulations represented by englacial septa emerge and form longitudinal or transverse debris ridges separated by areas of cleaner or bare ice.

SERAC

Markus Konz
ETH Zürich Institut für Umweltingenieurwissenschaften, Hydrologie und Wasserwirtschaft, Zürich, Switzerland

The word “serac” originated from the Swiss French sérac, which is a type of a crumbly white cheese. Seracs are needle-like towers, individual blocks, or columns of ice on the surface of a glacier. Their height varies between few meters to tens of meters. They can be found within icefalls or on the lower edge of hanging glaciers (e.g., Post

and Lachapelle, 2000). Seracs are commonly formed by intersecting crevasses where the glacier is periodically broken as it passes over a steep slope. They can cause disastrous hazards and are dangerous to mountaineers due to rapid toppling often with little advance warning time.

Bibliography

Post, A., and Lachapelle, E. R., 2000. Glacier ice. University of Washington Press, Seattle.

SIBERIA

Kazuyoshi Suzuki
Research Institute for Global Change, Japan Agency for Marine-Earth Science and Technology, Yokohama, Japan

Definition

Siberia: a region of northern Asia of Russia, stretching from the Ural Mountains to the Pacific Ocean.
Continental air mass: vast body of air that forms over the interior of a continent, excluding mountainous areas.
Anticyclone: weather phenomenon in which there is a descending movement of the air and a high pressure area over the part of the planet's surface affected by it.
Continental arctic air: air that are extremely cold and dry due to their continental source region between 60° and 90° north latitude.
Tundra: a biome in which tree growth is hindered by low temperatures and short growing seasons.
Taiga: a biome characterized by coniferous forests.

Introduction

Siberia has the largest area of permafrost in the world. Furthermore, the freshwater in the large Arctic rivers of Eurasia that flow from Siberia to the Arctic Ocean plays an important role in the control of the global thermohaline circulation by modifying salinity and sea-ice formation in the Arctic Ocean. In addition, snow and ice greatly affect the lives of the people inhabiting Siberia. This article discusses the characteristics of snow and ice in Siberia.

Geography and climate

Siberia occupies the Asian part of Russia and consists of three major subregions shown in Figure 1a. In the west, abutting the Ural Mountains, is the huge West Siberian Plain, drained by the Ob and Yenisey rivers. It varies little in relief and includes wide tracts of swampland. East of the Yenisey River is central Siberia, a vast area that consists mainly of plains and the central Siberian Plateau. Farther east, the basin of the Lena River separates central Siberia from the complex series of mountain ranges, upland massifs, and intervening basins that make up East Siberia.

According to *Climates of the U.S.S.R.* by Borisov (1965), there are four major climate zones in Siberia. The climate zones of West and East Siberia are each subdivided into two climate zones according to the dominant vegetation, tundra or taiga. Here, West Siberia as used here includes the central Siberian Plateau. West Siberia is characterized by many days dominated by continental arctic air and East Siberia by prevailing continental temperate climate and continental arctic air masses, which converge to form mainly extensive anticyclones, especially in winter. The taiga corresponds with regions of subarctic and cold continental climate with long, severe winters (up to 6 months with mean temperatures below freezing) and short summers as characteristic, as has a wide range of temperatures between the lows of winter and highs of summer. On the other hand, tundra corresponds with the regions of polar climate with extremely short growing season (6–10 weeks) and long, cold, dark winters. Tundra occupies the region between tree line and polar ice cap. Tundra–taiga boundary is corresponding to the arctic front (Bryson, 1966).

Figure 1b denotes the four major climate regions. The West Siberian tundra region is characterized by contrast in the intensity of solar radiation during the year and by a long, severe winter with frequent passage of low-pressure systems accompanied by violent gales and heavy snowstorms. In contrast, a high-pressure system typically develops over the East Siberian tundra region in winter, leading to stable winter weather and a negligible snow cover. Because of its great continentality, the region is characterized by contrasting conditions between summer and winter. The West Siberian taiga region is characterized by the active movement of air masses from the Atlantic and Arctic oceans with the continental air mass and anticyclones formed in Siberia. The East Siberian taiga region is characterized by marked continentality such as the prevalence of clear-cut anticyclonic weather conditions, very frosty and cold cloudless winter weather and hot summers with high solar radiation, and the sudden onset of seasons.

Frozen ground

Permafrost is the dominant component of the Siberian soil; about 80% of area in the subsurface in Siberia is composed of permafrost. Kondratjeva et al. (1993) showed that permafrost in Siberia mostly developed in the Late Pleistocene during the Sartanian glaciation (Late Wisconsinan/Weichselian, 18,000–27,000 years ago). The average air temperature at that time was 8–10°C lower than at present, and under these very cold conditions, permafrost spreads over Siberia, eventually extending its southern boundary to 48–49° N during the Sartanian glaciation. Subsequently, in the Holocene, the spatial extent of the permafrost was greatly reduced in West Siberia, where the southern permafrost border has been displaced northward to 60° N. Although in East Siberia the permafrost has retained almost the same spatial coverage as during the last glacial period, it has likely become reduced in thickness. Duchkov (2006) showed that permafrost reaches its greatest thickness (more than 1 km) in Yakutia, central Siberia, where it forms the lowest temperature block of

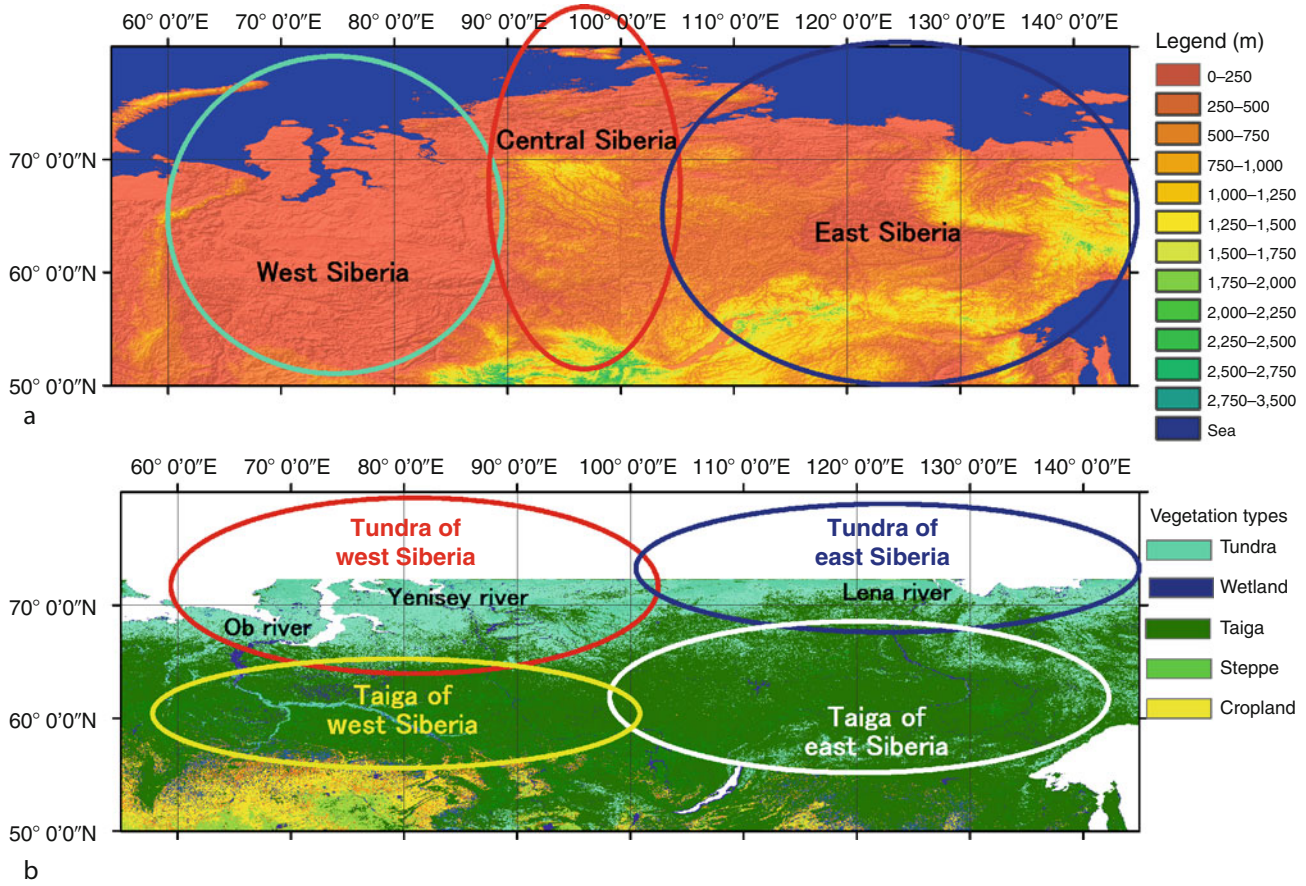

Siberia, Figure 1 Map of Siberia. (**a**) Topography map for geography indicated West, central, and East Siberia and (**b**) vegetation map for climate for tundra and taiga of West and East Siberia.

lithosphere in northern Eurasia. Terrestrial heat flow acts as one of the heat sources for permafrost to determine the lower limit of the permafrost depth. Terrestrial heat flow in the area of Yakutia does not exceed 30 mW m^{-2}, in contrast to other Siberian regions, where terrestrial heat flow is 50–70 mW m^{-2} and the permafrost is no more than 400–600-m thick.

The top layer of soil above the permafrost layer thaws seasonally and is called the active layer. The active layer affected direct runoff and peak flow in a small permafrost watershed, as shown by Yamazaki et al. (2006). Water within the active layer has a role of memory in previous years, because water within the active layer has a residence time of more than a half year and it affects snowmelt runoff due to the change of the capability of infiltration into frozen ground (Suzuki et al., 2006a) and transpiration due to recovering shortage of water for transpiration from the thawing ground water during the summer (Sugimoto et al., 2003). Rest of the parts of Siberia without permafrost are covered by seasonal frost, where the ground freezes in winter and thaws in summer. Zimov et al. (2006) showed that the permafrost stores a large amount of carbon, and if it were to thaw, a great deal of carbon would be released. One of the pathways for terrestrial carbon cycle in permafrost region is carbon transport in the rivers. Suzuki et al. (2006b) showed that a large quantity of dissolved organic matter is transported from the upper catchments of the Lena river to the Arctic Ocean.

Snow

During winter, snow covers all of Siberia. The snowpack structure in Siberia is characterized by a thick layer of depth hoar at the bottom, which forms as a result of the large temperature gradient between the relatively warm soil and cold air. Kitaev et al. (2005) analyzed the distribution of snow over Russia from 1936 to 2000. In East Siberia, the mean snow depth, snow cover days from 1936 to 2000, and snow water equivalent from 1966 to 1996 were 34 cm, 220 days, and 90 mm, respectively, and in West Siberia, they were 34 cm, 192 days, and 133 mm, respectively. In both West and East Siberia, snow depth and snow cover days generally increased from 1936 to 2000.

The presence of snow cover influences the depth of the active layer and of seasonal frost in Siberia. In addition,

snowmelt runoff contributes greatly to the discharge of Siberian Rivers, rather than rain. Tree growth as indicated by tree ring width is related to winter precipitation as snow, because recent tree growth is not only related to air temperature but also to the timing of snow disappearance (Vaganov et al., 1999). A few snow researches have been carried out in the southern mountain region of East Siberia, where Suzuki et al. (2006c) showed that sublimation accounts for nearly 10% of snow ablation beneath larch forest. Furthermore, Suzuki et al. (2006c) found that snow albedo is related to snow density. In the tundra region of East Siberia, Hirashima et al. (2004) developed a land surface model that incorporated blowing snow and estimated that about 40% of winter precipitation sublimated during blowing snow events. Tundra regions of Siberia are characterized by a shallow snowpack and a heterogeneous snow cover because of the small topographic relief, because strong wind induced blowing snow events occasionally, but taiga regions tend to have a uniform snow cover since forest canopy reduced wind speed and large snow-folding capacity.

Glaciers and river and lake ice

Ice in Siberia occurs in glaciers and as river and lake ice. The large volume of ice constitutes an important water resource and influences the inhabitants of Siberia. According to Kotlyakov et al. (1996) and UNEP (United Nations Environment Programme) (2007), from 1950 to 1970, Siberia's glaciers were widely dispersed on mountain ranges, from the Ural Mountains to Kamchatka, covering a total area of about 3,600 km^2 (USSR Glacier Inventory). Since 1970, Siberian glaciers have generally retreated, mainly from lower elevations and southern latitudes, and the amount of retreat has a wide variety in the places.

River and lake ice are of more importance to the people living in Siberia than glaciers because they are an important freshwater resource. The timing of the break-up or freeze-up of lake ice depends primarily on air temperature. Walter et al. (2006) reported that during thaws, a lake in northern East Siberia emits a large amount of methane.

The break-up of river ice in spring occasionally causes large floods in Siberia, especially in permafrost-dominated regions. By incorporating river ice into a river run-off model, Ma et al. (2005) showed that river ice volume greatly affects estimations of snowmelt run-off in the Lena River. Vuglinsky (2002) noted that the knowledge of river ice is important for understanding run-off processes, and the duration of river ice each year also greatly affects the use of large rivers for transporting cargo from or to the sea. Smith (2000) showed that the river ice in central and East Siberia is melt onset 1–3 weeks earlier since 1930s but found no trend in West Siberian river.

Thick icing is commonly observed in the permafrost regions of the northern hemisphere, including Siberia. Icing is often seen on the river in Siberia. In southern East Siberia, aufeis (icing) can be 5–10-m thick. Icing contributes about 10% of annual river discharge (Sokolov and Vuglinsky, 1997). Icing may be an important indicator of groundwater movement in permafrost regions of Siberia.

Summary

Because of the extremely cold winter climate of Siberia, the region is characterized by a thick and extensive winter snow cover and many frozen water bodies in winter. However, people in Siberia are more aware of global warming and its effects on snow and ice in Siberia are posing a threat to infrastructures due to thawing snow and ice. Warming air temperature by itself can cause the shorter periods or less volume of snow and ice in Siberia, but it cannot explain all of the observed changes such as the small changes of timing of river ice freeze-up or permafrost thawing. Vegetation characteristics also influence how warmer air temperatures affect snow and ice in Siberia. Most of Siberia is covered by taiga forest. In East Siberia, the taiga forests consist mainly of larch, which is a deciduous conifer, whereas West Siberia is characterized by wetlands and evergreen coniferous forest. Suzuki et al. (2007) showed that a moss layer protects the soil from heating by the atmosphere and helps to maintain a constant ground temperature and moisture content. Thus, the vegetation type affects snow and ice in Siberia and complicates our understanding of snow and ice cover changes in Siberia. In the future, this subject should be studied by a multidisciplinary approach.

Bibliography

Borisov, A. A., 1965. *Climates of the U.S.S.R.* Chicago: Aldine.

Bryson, R. A., 1966. Airmasses, streamlines and the boreal forest. *Geographical Bulletin (Canada)*, **8**, 228–269.

Duchkov, A. D., 2006. Characteristics of permafrost in Siberia. In Lombardi, S., Altunina, L. K., and Beaubien, S. E. (eds.), *Advances in the Geological Storage of Carbon Dioxide*. New York: Springer, pp. 81–91.

Hirashima, H., Ohata, T., Kodama, Y., Yabuki, H., Sato, N., and Georgiadi, A., 2004. Nonuniform distribution of tundra snow cover in eastern Siberia. *Journal of Hydrometeorology*, **5**, 373–389.

Kitaev, L., Forland, E., Razuvaev, V., Tveito, O. E., and Krueger, O., 2005. Distribution of snow cover over Northern Eurasia. *Nordic Hydrology*, **36**, 311–319.

Kondratjeva, K. A., Khrutzky, S. F., and Romanovsky, N. N., 1993. Changes in the extent of permafrost during the late quaternary period in the territory of the former Soviet Union. *Permafrost and Periglacial Processes*, **4**, 113–119.

Kotlyakov, V. M., et al., 1996. *Glaciation in North and Central Eurasia at present time*. Moscow: Nauka.

Ma, X. Y., Yasunari, T., Ohata, T., and Fukushima, Y., 2005. The influence of river ice on spring runoff in the Lena river, Siberia. *Annals of Glaciology*, **40**, 123–127.

Smith, L. C., 2000. Trends in Russian Arctic river-ice formation and breakup, 1917 to 1994. *Physical Geography*, **21**, 46–56.

Sokolov, B. L., and Vuglinsky, V. S., 1997. *Energy and water exchange in mountain Taiga in the south of east Siberia*. St. Petersburg: State Hydrological Institute, pp. 1–90.

Sugimoto, A., Naito, D., Yanagisawa, N., Ichiyanagi, K., Kurita, N., Kubota, J., Kotake, T., Ohata, T., Maximov, T. C., and Fedorov, A. N., 2003. Characteristics of soil moisture in permafrost

observed in East Siberian taiga with stable isotopes of water. *Hydrological Processes*, **17**, 1073–1092.
Suzuki, K., Konohira, E., Yamazaki, Y., Kubota, J., Ohata, T., and Vuglinsky, V., 2006a. Transport of organic carbon from the Mogot Experimental Watershed in the southern mountainous taiga of eastern Siberia. *Nordic Hydrology*, **37**, 303–312.
Suzuki, K., Kubota, J., Ohata, T., and Vuglinsky, V., 2006b. Influence of snow ablation and frozen ground on spring runoff generation in the Mogot Experimental Watershed, southern mountainous taiga of eastern Siberia. *Nordic Hydrology*, **37**, 21–29.
Suzuki, K., Kubota, J., Zhang, Y. S., Kadota, T., Ohata, T., and Vuglinsky, V., 2006c. Snow ablation in an open field and larch forest of the southern mountainous region of eastern Siberia. *Hydrological Sciences Journal*, **51**, 465–480.
Suzuki, K., Kubota, J., Yabuki, H., Ohata, T., and Vuglinsky, V., 2007. Moss beneath a leafless larch canopy: influence on water and energy balances in the southern mountainous taiga of eastern Siberia. *Hydrological Processes*, **21**, 1982–1991.
UNEP, 2007. *Global Outlook for Ice & Snow*. Birkeland: Birkeland Trykkeri A/S.
Vaganov, E. A., Hughes, M. K., Kirdyanov, A. V., Schweingruber, F. H., and Silkin, P. P., 1999. Influence of snowfall and melt timing on tree growth in subarctic Eurasia. *Nature*, **400**, 149–151.
Vuglinsky, V. S., 2002. Peculiarities of ice events in Russian Arctic rivers. *Hydrological Processes*, **16**, 905–913.
Walter, K. M., Zimov, S. A., Chanton, J. P., Verbyla, D., and Chapin, F. S., 2006. Methane bubbling from Siberian thaw lakes as a positive feedback to climate warming. *Nature*, **443**, 71–75.
Yamazaki, Y., Kubota, J., Ohata, T., Vuglinsky, V., and Mizuyama, T., 2006. Seasonal changes in runoff characteristics on a permafrost watershed in the southern mountainous region of eastern Siberia. *Hydrological Processes*, **20**, 453–467.
Zimov, S. A., Schuur, E. A. G., and Chapin, F. S., 2006. Permafrost and the global carbon budget. *Science*, **312**, 1612–1613.

Cross-references

Icing
Inverted Cup Depth Hoar Crystals
Lake Ice
Permafrost
River Ice Hydrology
Snow Hydrology

SLUSH AND SLEET OF SNOW

A. K. Singh
DIAT (Deemed University), Girinagar, Pune, Maharashtra, India

Snow that partially melts upon reaching the ground, to the point that it accumulates in puddles of partially frozen water, is slush, whereas sleet is snow falling mixed with rain, that is, rain containing snow. Slush is slurry, mixture of liquid and solid forms of water. A slushy layer of snow also results when rain or meltwater percolates downward from the snow surface but cannot penetrate an icy layer or the ground surface beneath. Because of its low binding strength, slush that forms in hilly terrain, can sometimes pose a hazard by releasing wet snow avalanches. These avalanches can occur even on very gentle slopes where, though they are unable to gather much speed, the large mass of slush can make avalanches destructive. In the natural environment, slush forms as ice and snowmelts. This often mixes with dirt and other materials, resulting in a gray or muddy brown color. Solid ice or snow often blocks the drainage of liquid water from slushy areas and slush goes through multiple freeze/thaw cycles before disappearing completely.

In dry snow crystal growth rate is limited by the rate at which water vapor diffuses across the pores from smaller particles to larger ones. However, in slush, the pores between the ice crystals are occupied by liquid water rather than air and hence the crystal growth rate is driven by thermal diffusion between particles through the water filled pores.

As raindrops pass through layers of air at varying temperatures, while passing through a layer with temperature below the freezing point, they turn into sleet, that is, precipitation of small, partially melted grains of ice. Snowflakes that have melted by passing through a warm layer will turn into sleet if they happen to pass through a freezing layer. Sleet often falls together with snow and rain. It occurs only during the winter, while hail, a different form of icy precipitation, may fall at any time of the year. Sleet is less prevalent than freezing rain and is more difficult to forecast as it develops under specialized atmospheric conditions.

SNOW

A. K. Singh
DIAT (Deemed University), Girinagar, Pune, Maharashtra, India

Snow is a form of precipitation, measured using snow gauge, in the form of ice crystals, usually flakes of star-like crystals that can be in a variety of shapes and sizes. Snow stakes and simple scales can be used to determine the depth of the snow pack. Snow is less dense than liquid water by a factor of $\approx$10 (fresh and dry snow). By the time flakes reach the ground they undergo transformations resulting from growth, disintegration, or agglomeration. Highly branched or dendrite crystals occupy more space between the arms of ice that form the snowflake and this snow will therefore have a lower density, referred to as dry snow and is highly reflective (0.9 and higher albedo). Conditions that create columnar or plate-like crystals will have much less air space within the crystal and will therefore be denser. When all the snow does not melt in the summer it evolves into firn, where individual granules become more spherical in nature, evolving into glacier ice.

Snow is a thermodynamically active material, exhibiting strange behavior near the melting temperature and constantly undergoing metamorphism. Structurally, snow is a granular material characterized by a continuous ice network, formed through cohesion between ice grains, to form

a porous structure. Snow behavior, properties, and processes often fall far outside of those normally encountered in granular materials. Unique properties of snow include its high compressibility.

Once the snow is on the ground, it will settle under its own weight. Recrystallization under stress caused by the weight of the overlying snow becomes predominant, and grains change in size and shape in order to minimize the stress on them with large or favorably oriented grains growing at the expense of others. Increases in density above this initial compression occur primarily due to melting and refreezing, caused by temperatures above freezing or by direct solar radiation. By late spring, snow densities typically reach a value half of water density. This densification of the snow proceeds more slowly after reaching this density and many of the processes become less and less effective.

In many parts of the world, snow is the primary source of water during summer and autumn. Water equivalent is of great interest to water managers wishing to predict spring runoff and the water supply of cities downstream. Sudden melting of snow can cause flooding. Snow is also a source of recreational activity and at the same time turns into a deadly avalanche. Climate is also influenced by snow cover due to its reflection character as compared to other surface materials, and also the absorption of solar radiations.

SNOW BED/SNOW BED VEGETATION

Nadine Konz
Institute of Environmental Geosciences, University of Basel, Basel, Switzerland

Snow beds are defined through the duration of snow cover and snow height leading to an individual geomorphology and a specific microclimatology (Huelber et al., 2006). These conditions lead to an ecological niche for different plants; the snow bed vegetation.

The term snow bed is currently adopted to designate plant communities whose occurrence is determined by the geomorphological situations favoring a long duration of the snow cover (Tomaselli, 1991). One of the most extreme sets of conditions under which plants may grow is those of snow beds. Generally, the snow does not cover the ground to the same depth everywhere: small depressions are filled with snow; ridges are blown free from snow. Places with more snow than a medium depth form the snow beds. Duration of snow cover, character of bedrock, and quantity of available moisture are the three dominating factors that influence the mountain vegetation. The snow cover is generally the one of greatest physiognomic importance (Faegri, 1957). The plant communities of the snow bed belong to the class of *Salicetea herbacea*. These plants are snow covered between seventh and tenth month a year. Snow bed vegetation can be divided into vegetation on siliceous bedrock and limestone. Some examples of snow bed vegetation on siliceous bedrock are *Salicaceae* (e.g., *Salix herbacea*), *Poaceae* (e.g., *Poa alpina*), *Polytrichaceae* (e.g., *Polytrichum sexangulare*), and *Peltigeraceae* (e.g., *Solorina crocea*). Some examples of snow bed vegetation on limestone are *Poaceae* (e.g., *Sesleria albicans*), *Plantaginaceae*, (e.g., *Veronica alpina*), and *Ranunculaceae* (e.g., *Ranunculus alpestris*) (Merz, 2000).

Bibliography

Faegri, K., 1957. Snow-bed vegetation. *Ecology*, **38**, 668–669.
Huelber, K., Gottfried, M., Pauli, H., Reiter, K., Winkler, M., and Grabherr, G., 2006. Phenological responses of snowbed species to snow removal dates in the central alps: implications for climate warming. *Arctic Antarctic and Alpine Research*, **38**, 99–103.
Merz, P., 2000. *Pflanzengesellschaften mitteleuropas und der alpen – erkennen, bestimmen*. Landsberg/Lech: Bewerten.
Tomaselli, M., 1991. The snow-bed vegetation in the Northern Apennines. *Vegetatio*, **94**, 177–189.

SNOW COURSE

A. K. Singh
DIAT (Deemed University), Girinagar, Pune, Maharashtra, India

Snow course consists of a series of manually marked sampling points or locations where depth and snow water equivalent measurements are made by trained observers. It is an established line, usually from several hundred feet to as much as *a mile long*, traversing representative terrain in a mountainous region of appreciable snow accumulation. Snow course length and the frequency of sampling points are defined depending on site specific conditions such as slope, aspect, land cover, and uniformity of snow cover. Snow course data are, however, subject to a systematic bias because the measurements, obtained by inserting a tube through the snowpack to the soil to cut and hold a snow core, tend to underestimate snow water equivalent due to sampling difficulties associated with ground ice and depth hoar. The size of the sampling cutter can also influence accuracy. Besides, other aspects regarding snow course data that must also be taken into account are consistency of equipment, procedures, and measurement locations over time, and the degree to which a real snow cover condition can be represented by a series of point measurements.

Snowmelt is a major source of water supply to areas in temperate zones near mountains that catch and hold winter snow, especially those with a prolonged dry summer. In such places, water equivalent is of great interest to water managers wishing to predict spring runoff and the water supply of cities downstream.

Bibliography

Dressler, K. A., Fassnacht, S. R., and Bales, R. C., 2006. A comparison of snow telemetry and snow course measurements in the Colorado River Basin. *Journal of Hydrometeorology*, **7**(4), 705–712.

SNOW COVER AND SNOWMELT IN FOREST REGIONS

Tobias Jonas[1], Richard Essery[2]
[1]Snow Hydrology Research Group, WSL Institute for Snow and Avalanche Research SLF, Davos, Switzerland
[2]School of GeoSciences, University of Edinburgh, Edinburgh, UK

Definition

Snow cover. Snow that accumulates on the ground due to snow precipitation and snow redistribution processes. Typically used for seasonal snow, excluding firn and ice.
Snowmelt. Snow ablation process and/or meltwater originating from the snow cover.

Introduction

The evolution and ablation of the seasonal snow cover in a forest is very different compared to the snow in open terrain. Snow precipitation is partly intercepted by the canopy, from where the snow may subsequently evaporate directly, melt and drip down, or fall off. The canopy also absorbs shortwave radiation and changes the longwave radiation budget. The presence of trees decelerates wind fields near the snow cover surface and thus constrains the turbulent exchange of heat and moisture. Finally, litter fall from trees (e.g., conifer needles or lichens) can have a significant impact on the snow surface albedo, increasing the absorption of shortwave radiation. Due to these differences, the maximum snow water equivalent and the subsequent amount of melt water can easily differ by some 10% from the respective amounts at neighboring open sites, while melt-out dates may be shifted by several weeks. As boreal and subalpine forests cover large areas of the northern hemisphere land surface, snow-forest processes have an important influence on weather and hydrology, even at hemispheric scales. See also the entry on *Snow and Vegetation Interaction*, which covers related topics from an alternative perspective.

Measuring relevant data

A forest canopy typically features a complex and heterogeneous structure. The canopy density may display spatial variability on different scales, e.g., shortwave radiation and snowfall rates below the canopy can significantly differ on the meter scale. The same applies to the distribution of stems and other parts of the vegetation which emit longwave radiation. Given the spatial complexity of important snow cover energy budget forcing terms, it is not surprising that snow cover thickness inside forests often shows great levels of spatial variation. It is hence difficult to measure "representative" data. In this respect, single point measurements below the canopy are typically useless, and snow depth, snow water equivalent (SWE), or snow accumulation rates are normally measured on transects, grids, snow courses, etc. that represent the area of interest (and the spatial scales to be resolved).

Several setups have been used to measure radiation inside forests. Most commonly, arrays of fix sensors have been used to capture the spatial variability of radiation below the canopy (e.g., Link et al., 2004; Pomeroy et al., 2008). Alternatively, radiation sensors have been moved manually or automatically along ground transects, cables, or rails (Sturm et al., 2005; Stähli et al., 2009). Also, infrared thermography has been used to map the emission of longwave radiation (Pomeroy et al., 2009).

Quantitative measurement of snow interception is challenging. While qualitative interception levels can be gathered from periodic observations (e.g., by webcams), the mass of snow intercepted per unit area is a difficult parameter to obtain. Techniques that have been applied include (a) weighing trees or tree-like structures mounted on or suspended from scales (Hedstrom and Pomeroy, 1998; Storck et al., 2002), (b) optically tracking the vertical position of branches, which bend down under the weight of intercepted snow (Brundl et al., 1999), (c) measuring canopy snow using radar absorption (Gustafsson et al., 2010), or (d) absorbing gamma radiation (Calder, 1990).

As important boundary conditions for snow-forest processes, information about the canopy structure/density is required, usually specified through parameters such as sky-view fraction (SVF; the projected fraction of the sky hemisphere visible from a point below the canopy) and leaf area index (LAI; the total projected leaf area per unit area of ground). Manual or optical methods of measuring canopy parameters (e.g., destructive sampling or hemispherical photography) can be time consuming and subject to large uncertainties (Chen et al., 1997). Airborne laser scanning (LiDAR) offers the possibility of canopy structure mapping at landscape scales (Riaño et al., 2004).

Snow distribution in forests

On the meter scale, forest snow cover is typically heterogeneous. Snow depth patterns often mirror canopy gaps, the distribution of shorter vegetation on the ground and thermal radiation effects in the vicinity of stems. As a useful first-order predictor for such small-scale patterns, the sky-view fraction has been found to correlate well with the maximum SWE below forest canopies of varying density (e.g., Pomeroy et al., 2002; Lundberg et al., 2004; Lopez-Moreno and Latron, 2008). Since denser canopies intercept more snow, locations with higher sky-view fractions generally accumulate more snow on the ground than locations with lower sky-view fractions (within the same stand). Some studies even report forest openings to accumulate more snow than nearby unforested sites (Lopez-Moreno and Latron, 2008).

However, snow distribution patterns within forests are certainly not just driven by interception. In addition to snow accumulation phenomena, spatially variable snow ablation processes also contribute to complex distribution dynamics of snow in forests. Energy budget

considerations are therefore covered in a separate section below in more detail.

Understanding snow distribution dynamics in forests is important, since snow accumulated on the ground directly drives runoff from snowmelt. But also, the fate of snow that is intercepted in the canopy is important to consider for the water balance. A significant part of intercepted snow may be evaporated (e.g., 20–30% in a study by Montesi et al., 2003) and hence does not contribute to runoff. Further information is given in the entry on Interception of Snow.

Energy budget of snow in forests

Insight into the specific and interacting effects of physical forest snow processes can be gained by assessing the energy budget of a forest snow cover (Figure 1).

Terms that counterbalance the rate of change in snowpack heat storage are:

- SWR: Net shortwave radiation
- LWR: Net longwave radiation
- THF: Turbulent heat fluxes (sensible and latent)
- PHF: Heat advected by precipitation
- GHF: Heat exchange with the ground (including advection by meltwater)
- PCH: Energy of snowpack phase changes

At a global scale, forests in regions with seasonal snow have characteristics that are so diverse with respect to canopy structure and ambient conditions that there is no general rule for the relative importance of the terms in the energy balance (but see King et al., 2008). In the following, some of the terms are discussed in more detail.

Shortwave radiation (SWR): Transmission of short wave radiation through a forest canopy is a truly three-dimensional phenomenon. Naturally, canopy structure and density are the main predictors for the transmissivity τ_{SWR}, which is the ratio between the radiation below and above the canopy. The simplest way to describe this relationship adopts Beer's law,

$$\tau_{SWR} = \exp(-\kappa \cdot LAI)$$

where, κ is an empirical extinction parameter related to the orientation and clumping of canopy elements. Such descriptions can be enhanced by additionally accounting, e.g., for (a) solar angle, which affects the path length of direct radiation through the canopy or (b) snow interception, which enhances diffuse radiation below the canopy (Stähli et al., 2009). Moreover, multiple reflection effects can entail increased τ_{SWR} during cloudy weather when diffuse radiation dominates the SWR budget below the canopy; these effects can be accounted for using a two-stream radiative transfer approximation (Niu and Yang, 2004). The net SWR on the other hand is also determined by snow albedo, which is the ratio between reflected and incoming radiation at the snow surface. Albedo generally decreases as a snow surface ages because increasing contaminants in the snow increase absorption of visible radiation and increasing snow grain sizes increase near-infrared absorption. Snow albedos may be lower in forests than in the open due to both decreases in the proportion of visible radiation and increases in litter accumulation under forest canopies (Melloh et al., 2002), although net SWR may still be higher in the open due to the higher incoming shortwave radiation.

Longwave radiation (LWR): A forest snowpack receives longwave radiation from the canopy and from the atmosphere through canopy gaps. Since canopy surface temperatures are often very different from atmospheric temperatures, the sky-view fraction (SVF) is an important parameter for the net LWR budget of the snow cover in semi-closed forests. The simplest way to describe the net LWR is:

$$LWR_{net} = SVF \cdot LWR_{from\ atmosphere} + (1 - SVF) \times LWR_{from\ canopy} - LWR_{from\ snow\ cover}$$

or using the Stefan–Boltzmann law

$$LWR_{net} = SVF \cdot LWR_{from\ atmosphere} + (1 - SVF) \cdot \sigma T_c^4 - \sigma T_s^4$$

where, T_c and T_s denote the temperatures of canopy and snow surface, σ is the Stefan–Boltzmann constant, and the emissivities of canopy and snow surface are approximated to be 1 (both around 0.97). In practice, T_c is often simplified to equal the air temperatures measured below the canopy, while incoming LWR above canopy can be estimated from air temperature, humidity, and cloud cover using bulk formulae (e.g., Flerchinger et al., 2009). These parameterizations have been evaluated against measurements by Essery et al. (2008) and Pomeroy et al. (2009).

Turbulent heat flux (THF): Latent and sensible heat fluxes can constitute important contributions to the energy balance of a forest snow cover (e.g., Li et al., 2008), which

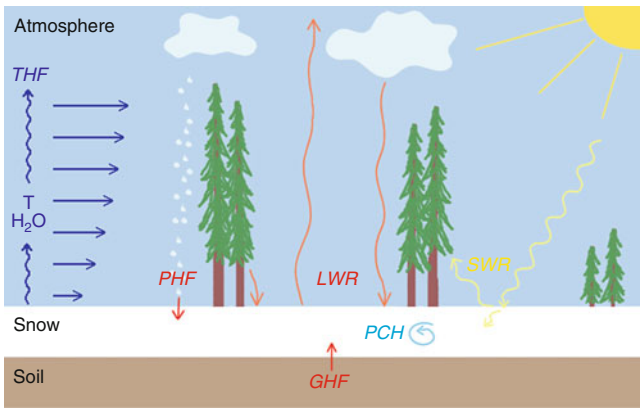

Snow Cover and Snowmelt in Forest Regions, Figure 1 Schematic of the energy budget of snow in forests.

may appear surprising given that wind speeds are typically low inside forests. Estimating turbulent heat fluxes for a forest snow cover is comparatively difficult and imprecise, since it involves a combination of parameterizing wind speeds, temperature, and humidity gradients. However, snow models that incorporate interactions with vegetation/forest do so with differing levels of complexity (Essery et al., 2009). Only a few attempts have been made so far to measure latent and sensible heat fluxes inside forests over snow using eddy covariance (EC) systems (Molotch et al., 2006; Marks et al., 2008), since applying EC systems in such environments is associated with significant uncertainties. More research is certainly needed to improve the understanding and prediction of turbulent heat exchange inside snow-covered forests.

Snowpack modeling for forest regions

Because of the importance of forest snow processes, many snow models have been developed or modified recently to include vegetation canopies. Thirty-three such models, listed by Rutter et al. (2009), participated in the second Snow Model Intercomparison Project (SnowMIP2) by performing simulations driven by meteorological observations for paired open and forested plots at five sites. The models generally perform complete mass and energy balance calculations for forest canopies and snowpacks, but they were primarily evaluated by comparison with measurements of SWE on the ground. Although the evaluation is complicated by uncertainties in meteorological and snowpack observations, the intercomparison revealed a wide range in the ability of models to simulate snow in open and forested situations. On the larger scales used in climate modeling, Roesch (2006) suggested that the models participating in the IPCC Fourth Assessment Report showed difficulties in determining the extent of snow albedo masking by forests.

Summary

Forest snow is subject to very different ambient conditions compared to snow in open terrain. Accumulation patterns are predominantly altered by interception of snow in the canopy, while melting dynamics are driven by complex processes such as the transfer of shortwave and longwave radiation through the canopy and the turbulent transport of heat and water. Today, many snow models try to reproduce interactions between snow and vegetation, emerging from the need to involve forest snow processes in distributed land-surface models.

Bibliography

Brundl, M., Bartelt, P., Schneebeli, M., and Fluhler, H., 1999. Measuring branch defection of spruce branches caused by intercepted snow load. *Hydrological Processes*, **13**, 2357–2369.

Calder, I. R., 1990. *Evaporation in the uplands*. Chichester, UK: Wiley.

Chen, J. M., Rich, P. M., Gower, S. T., Norman, J. M., and Plummer, S., 1997. Leaf area index of boreal forests: theory, techniques, and measurements. *Journal of Geophysical Research-Atmospheres*, **102**, 29429–29443.

Essery, R., Pomeroy, J., Ellis, C., and Link, T., 2008. Modelling longwave radiation to snow beneath forest canopies using hemispherical photography or linear regression. *Hydrological Processes*, **22**, 2788–2800.

Essery, R., Rutter, N., Pomeroy, J., Baxter, R., Stähli, M., Gustafsson, D., Barr, A., Bartlett, P., and Elder, K., 2009. SnowMIP2 – An evaluation of forest snow process simulations. *Bulletin of the American Meteorological Society*, **90**, 1120–1135.

Flerchinger, G. N., Xaio, W., Marks, D., Sauer, T. J., and Yu, Q., 2009. Comparison of algorithms for incoming atmospheric long-wave radiation. *Water Resources Research*, **45**, 13.

Gustafsson, D., Magnusson, J., and Granlund, N., 2010. Impulse radar measurements of snow interception – laboratory tests and field application to a forest stand in northern Sweden. *Cold Regions Science and Technology*, in prep.

Hedstrom, N. R., and Pomeroy, J. W., 1998. Measurements and modelling of snow interception in the boreal forest. *Hydrological Processes*, **12**, 1611–1625.

King, J. C., Pomeroy, J., Gray, D. M., Fierz, C., Föhn, P. M. B., Harding, R. J., Jordan, P., Martin, E., and Plüss, C., 2008. Snow-atmosphere energy and mass balance. In Armstrong, R. A., and Brun, E. (eds.), *Snow and Climate Physical Processes, Surface Energy Exchange and Modeling*. Cambridge: Cambridge University Press, pp. 70–124.

Li, W. P., Luo, Y., Xia, K., and Liu, X., 2008. Simulation of snow processes beneath a boreal Scots pine canopy. *Advances in Atmospheric Sciences*, **25**, 348–360.

Link, T. E., Marks, D., and Hardy, J. P., 2004. A deterministic method to characterize canopy radiative transfer properties. *Hydrological Processes*, **18**, 3583–3594.

Lopez-Moreno, J. I., and Latron, J., 2008. Influence of canopy density on snow distribution in a temperate mountain range. *Hydrological Processes*, **22**, 117–126.

Lundberg, A., Nakai, Y., Thunehed, H., and Halldin, S., 2004. Snow accumulation in forests from ground and remote-sensing data. *Hydrological Processes*, **18**, 1941–1955.

Marks, D., Reba, M., Pomeroy, J., Link, T., Winstral, A., Flerchinger, G., and Elder, K., 2008. Comparing simulated and measured sensible and latent heat fluxes over snow under a pine canopy to improve an energy balance snowmelt model. *Journal of Hydrometeorology*, **9**, 1506–1522.

Melloh, R. A., Hardy, J. P., Bailey, R. N., and Hall, T. J., 2002. An efficient snow albedo model for the open and sub-canopy. *Hydrological Processes*, **16**, 3571–3584.

Molotch, N. P., Blanken, P. D., Williams, M. W., Turnipseed, A. A., Monson, R. K., and Margulis, S. A., 2006. Estimating sublimation of intercepted and sub-canopy snow using eddy covariance systems. *Hydrological Processes*, **21**, 1567–1575.

Montesi, J., Elder, K., Schmidt, R. A., and Davis, R. E., 2003. Sublimation of intercepted snow within a subalpine forest canopy at two elevations. *Journal of Hydrometeorology*, **5**, 763–773.

Niu, G. Y., and Yang, Z. L., 2004. Effects of vegetation canopy processes on snow surface energy and mass balances. *Journal of Geophysical Research-Atmospheres*, **109**, 15.

Pomeroy, J. W., Gray, D. M., Hedstrom, N. R., and Janowicz, J. R., 2002. Prediction of seasonal snow accumulation in cold climate forests. *Hydrological Processes*, **16**, 3543–3558.

Pomeroy, J., Rowlands, A., Hardy, J., Link, T., Marks, D., Essery, R., Sicart, J. E., and Ellis, C., 2008. Spatial variability of shortwave irradiance for snowmelt in forests. *Journal of Hydrometeorology*, **9**, 1482–1490.

Pomeroy, J., Marks, D., Link, T., Ellis, C., Hardy, J., Rowlands, A., and Granger, R., 2009. The impact of coniferous forest

temperature on incoming longwave radiation to melting snow. *Hydrological Processes*, **23**, 2513–2525.
Riaño, D., Valladares, F., Condes, S., and Chuvieco, E., 2004. Estimation of leaf area index and covered ground from airborne laser scanner (Lidar) in two contrasting forests. *Agricultural and Forest Meteorology*, **124**, 269–275.
Roesch, A., 2006. Evaluation of surface albedo and snow cover in AR4 coupled climate models. *Journal of Geophysical Research-Atmospheres*, **111**, 18.
Rutter, N., Essery, R., Pomeroy, J., Altimir, N., Andreadis, K., Baker, I., Barr, A., Bartlett, P., Boone, A., Deng, H. P., Douville, H., Dutra, E., Elder, K., Ellis, C., Feng, X., Gelfan, A., Goodbody, A., Gusev, Y., Gustafsson, D., Hellstrom, R., Hirabayashi, Y., Hirota, T., Jonas, T., Koren, V., Kuragina, A., Lettenmaier, D., Li, W. P., Luce, C., Martin, E., Nasonova, O., Pumpanen, J., Pyles, R. D., Samuelsson, P., Sandells, M., Schadler, G., Shmakin, A., Smirnova, T. G., Stähli, M., Stockli, R., Strasser, U., Su, H., Suzuki, K., Takata, K., Tanaka, K., Thompson, E., Vesala, T., Viterbo, P., Wiltshire, A., Xia, K., Xue, Y. K., and Yamazaki, T., 2009. Evaluation of forest snow processes models (SnowMIP2). *Journal of Geophysical Research-Atmospheres*, **114**, 18.
Stähli, M., Jonas, T., and Gustafsson, D., 2009. The role of snow interception in winter-time radiation processes of a coniferous sub-alpine forest. *Hydrological Processes*, **23**, 2498–2512.
Storck, P., Lettenmaier, D. P., and Bolton, S. M., 2002. Measurement of snow interception and canopy effects on snow accumulation and melt in a mountainous maritime climate, Oregon. *United States. Water Resources Research*, **38**, 16.
Sturm, M., Douglas, T., Racine, C., and Liston, G. E., 2005. Changing snow and shrub conditions affect albedo with global implications. *Journal of Geophysical Research-Biogeosciences*, **110**, 13.

Cross-references

Depletion of Snow Cover
Glacier Mass Balance
Hydrologic Cycle and Snow
Radiative Transfer Modeling
Snow and Vegetation Interaction
Sublimation from Snow and Ice
Surface Energy Balance

SNOW COVER CHANGES IN THE ALPS

Christoph Marty
WSL Institute for Snow and Avalanche Research SLF, Davos, Switzerland

Definition

HS: Snow Depth
RCM: Regional Climate Model
Snow day: A day with a snow depth larger than a given threshold
Winter snow cover duration: Continuous snow depth of at least 1 cm

Introduction

Snow influences life and society in many ways. The amount and duration of snow in the Alps has a high socioeconomic significance in terms of both tourism and hydropower. Many Alpine towns and villages heavily depend on snow, because their economy is dominated up to 90% by winter tourism (Abegg et al., 2007). The vast majority of customers of such ski areas live in the pre-Alpine regions of Switzerland, Austria, Germany, Italy, and France. A longer sequence of almost snowless winters in these heavily populated regions, as was observed between the late 1980s and mid-1990s, caused a discussion about the uniqueness of such a situation and the possible connection to climate change.

Observed changes

The importance of snow for hydrology and tourism in the Alps has led to quite a few studies, which investigated the past variability and trends of the Alpine snow cover. Some of the Alpine countries have a relatively dense network of manual measurement stations available, where daily snow depth and snowfall have been measured with the help of a permanently mounted snow stake, respectively a new snowboard for 50 years or more. This comprehensive dataset and the above-mentioned socioeconomic importance of snow make the Alps a preferred region to investigate changes in snow cover. Remote sensing data of Alpine snow cover have not been used for climatological purposes due to the lack of longer time series and due to the limited data quality, which is caused by the steep topography of the Alps.

In the Swiss Alps, a significant decrease of HS for elevations below 1,300 m asl was observed in the late twentieth century with measurements from more than 100 stations, whereas no significant differences could be detected for high-altitude stations above 2,000 m asl (Scherrer et al., 2004). It was shown that the long-term snow trends in the Swiss Alps are similar for snow depth, the duration of the continuous snow cover and the number of snowfall days (Laternser and Schneebeli, 2003). Earlier investigations concluded that the length of snow season and snow amount have substantially decreased since the mid-1980s, but there have been periods in the records (e.g., 1930s) where snow depth was as low as during the late 1980s (Beniston, 1997). However, a newer study with more data available points out the uniqueness of the series of snow-poor winters over the period of 20 years from 1988 to 2007 (Marty, 2008), in comparison with at least the last 130 years. In particular, it could be shown that the decline is rather caused by an abrupt change than by a continuous decrease. The number of snow days ($HS > 5$ cm) below 800 m asl, for example, dropped by about 50% in the last 20 years compared to the long-term mean before the change.

In the Austrian Alps, an investigation on different snow parameters at 98 long-term stations revealed a more diverse picture (Jurkovic, 2008). The two 20-year periods between 1980 and 2000 and between 1896 and 1916 were compared and tested for changes. Statistical tests detected decreasing trends at the majority of the stations, but

the decline was only significant at the southern Austrian stations. There, a clear decreasing trend was found for the winter snow cover duration and the snow days with HS > 1 cm. A separate analysis of 14 stations with 100 years of data revealed similar results with mostly significantly decreasing snow day trends in southern Austria and no significant trends in the remaining part of the country.

In the Italian Alps, a general decrease in snowfall in the last 20 years of the analyzed time series between 1920 and 2004 could be found using data from 40 stations (Valt et al., 2005).

In the German Alps, a 20–30% reduction of the snow cover duration was found for low-lying areas between 1952 and 1996 (Günther et al., 2006). A smaller reduction was generally observed in higher areas.

In the French Alps, data from only one long-term station at 1,320 m asl was analyzed. There, a clear decreasing trend in the mean snow depth and in the number of days with snow on the ground was detected (Martin and Etchevers, 2005).

Only one study found an increase of snow depth at high altitude based on one station at 2,500 m asl (Beniston et al., 2003), whose data seem to be questionable due to the measurements on a mountain summit and several displacements of the snow stake.

Future changes

Climate models successfully reproduce large-scale parameters such as temperature today. However, investigations on the evolution of the future snowpack under changing climate conditions all battle with the fact that the current climate models have difficulties in representing fine-scaled spatial and temporal variability of snow. Some studies therefore use physical models driven by artificially generated data of future weather to predict the snow depth and duration at local level. Other studies estimate future snow conditions based on a sensitivity analysis of the current variability.

Such a simple approach was chosen by Hantel and Hirtl-Wielke (2007). They assessed the snow-temperature sensitivity in the European Alps based on data of the last 40 years from 268 stations and came to conclusion that the number of snow days (HS > 5 cm) will decrease by 33% per 1°C warming. This corresponds to a reduction of snow cover duration of about 1 month at the height of maximum sensitivity (about 700 m) but falls rapidly above and below that level. The future snow reliability of 666 Alpine ski resorts in six countries was investigated by Abegg et al. (2007). The authors calculated the impact of a 1°C, 2°C, and 4°C temperature increase based on the assumption that the altitudinal limit of natural snow reliability will rise by 150 m per 1°C warming. They concluded that the number of naturally snow-reliable areas would drop by 25% with 1°C, by 40% with 2°C, and by 70% with a 4°C warming.

In the Swiss Alps, the sensitivity of the snow cover to future climate was analyzed for 20 Swiss ski resorts with a more sophisticated approach and came to similar results (Uhlmann et al., 2008). The authors used the HIRHAM RCM model results of the IPCC A2 scenario and an energy balance model to compute future snow reliability. They pointed out that snow will become scarce on the lower ski runs in all resorts and that days with more than the critical 30 cm snow depth will drastically decrease at more than half of the stations. Future changes in two alpine river basins (above 800 m asl) in the Swiss Alps have been investigated with the help of the distributed catchment model WaSiM-ETH (Jasper et al., 2004). A 2.5°C warming and small changes in precipitation were elaborated from 23 regional climate models calculated for the end of the twenty-first century. The authors found a decrease of 70% in the annual mean snow-water equivalent. The duration of continuous snow cover was shortened by about 2 months, while the snow line was raised by about 450 m. A similar study assessed two other alpine river basins (above 1,600 m asl) in the Swiss Alps using the model system Alpine3D and the IPCC A2 and B2 scenarios from 12 RCMs (Bavay et al., 2009). According to these results, the snow volume and the maximum snow-water equivalent at the end of the twenty-first century will be reduced by about 40%. The complete melt of the snow cover will occur about 40 days earlier and the snow line will be shifted by about 900 m, which would be the end of most of the glaciers in these basins.

The future Austrian snow conditions have been analyzed using a simple temperature- and precipitation-dependent snow model by Breiling and Charamza (1999). An assumed 2°C warming and no change in precipitation showed a 50% reduction of snow cover at the mean altitude of residential population in the 85 Austrian districts. The authors also mention that the 2,000 m mark does not seem to be problematic concerning the amount of snow.

For the French Alps, a similar study was undertaken assuming a temperature increase of 1.8°C (Martin and Etchevers, 2005). They used the more elaborated model chain Safran-Crocus, which is usually used for operational avalanche warning and found a 50% reduction of snow depth below 1,500 m asl and 30% snow-covered area in midwinter.

Conclusions

The seasonal snow cover in the Alps is primarily influenced by a high year-to-year variability due to natural large-scale weather patterns. Despite this fact, a general decrease of the snow depth and snow cover duration could be detected since the end of the 1980s for low-lying stations throughout the European Alps. The decline could be linked to anomalous warm winter temperatures in the last 20 years (Scherrer et al., 2004; Marty, 2008), which seem to be unique for at least the last 500 years (Luterbacher et al., 2007).

Regarding future snow cover the two different approaches, the one based on physical models and the other on the current snow-temperature sensitivity, both came to similar results, which, for a 2°C warming, point to a drastic decrease of snow depth and snow-water equivalent of about 40–60% below 1,800 m, a reduction of the snow cover duration of 4–6 weeks and a rise of the snow line by about 300–500 m. According to the RCM projections, the warming in the Alps will be accompanied by a small increase in winter precipitation. Some authors therefore concluded that higher altitudes, where the temperatures are still cold enough for snowfall might experience an increase in snow depth with climate warming. However, the outcomes of two newer studies revealed that the projected increase in winter precipitation over the Alps will not even in the higher resorts compensate for the projected increase in temperature (Uhlmann et al., 2008; Bavay et al., 2009).

Because of the sensitivity of the Alpine snow cover to temperature, the depth, length, and duration of the snow cover is highly influenced by climate change. As warming progresses in future, regions where snowfall is the current norm will increasingly experience rain and the snow on the ground will melt faster. These perspectives leave no doubt that the projected changes will have a large impact on the economic, social, hydrological, and biological systems in the Alpine region.

Bibliography

Abegg, B., Agrawala, S., Crick, F., and de Montfalcon, A., 2007. *Climate change impacts and adaptation in winter tourism. Climate Change in the European Alps*. Paris:OECD: S. Agrawala, pp. 25–60.

Bavay, M., Lehning, M., Jonas, T., and Löwe, H., 2009. Simulations of future snow cover and discharge in Alpine headwater catchments. *Hydrological Processes*, **23**(1), 95–108, doi:10.1002/hyp. 7195.

Beniston, M., 1997. Variatons of snow depth and duration in the Swiss Alps over the last 50 years: Links to changes in large-scale climatic forcings. *Climatic Change*, **36**, 281–300.

Beniston, M., Keller, F., Koffi, B., and Goyette, S., 2003. Estimates of snow accumulation and volume in the Swiss Alps under changing climatic conditions. *Theoretical and Applied Climatology*, **76**(3), 125–140, doi:10.1007/s00704–003–0016–5.

Breiling, M., and Charamza, P., 1999. The impact of global warming on winter tourism and skiing: a regionalised model for Austrian snow conditions. *Regional Environmental Change*, **1**(1), 4–14, doi:10.1007/s101130050003.

Günther, T., Rachner, M., and Matthäus, H., 2006. Langzeitverhalten der Schneedecke in Baden-Württemberg und Bayern. KLIWA-Projekt A 1.1.4: "Flächendeckende Analyse des Langzeitverhaltens verschiedener Schneedeckenparameter in Baden-Württemberg und Bayern. *KLIWA Berichte*. A. KLIWA: 76.

Hantel, M., and Hirtl-Wielke, L.-M., 2007. Sensitivity of Alpine snow cover to European temperature. *International Journal of Climatology*, **27**(10), 1265–1275, doi:10.1002/joc.1472.

Jasper, K., Calanca, D., Gyalistras, D., and Fuhrer, J., 2004. Differential impacts of climate change on the hydrology of two alpine river basins. *Climate Research*, **26**(2), 113–129, doi:10.3354/cr026113.

Jurkovic, A., 2008. Gesamtschneehöhe – Vergleichende Zeitreihenanalyse. *Meteorology*. Vienna: University of Vienna. Magistra der Naturwissenschaften (Mag.rer.nat.).

Laternser, M., and Schneebeli, M., 2003. Long-term snow climate trends of the Swiss Alps (1931–99). *International Journal of Climatology*, **23**(7), 733–750, doi:10.1002/joc.912.

Luterbacher, J. r., Liniger, M. A., Menzel, A., Estrella, N., Della-Marta, P. M., Pfister, C., Rutishauser, T., and Xoplaki, E., 2007. Exceptional European warmth of autumn 2006 and winter 2007: Historical context, the underlying dynamics, and its phenological impacts. *Geophysical Research Letters*, **34**, 10.1029/2007GL029951.

Martin, E., and Etchevers, P., 2005. Impact of climatic changes on snow cover and snow hydrology in the French Alps. In Huber, U. M., Bugmann, H. K. M., and Reasoner, M. A. (eds.), *Global Change and Mountain Regions: An Overview of Current Knowledge*. New York: Springer, pp. 235–242.

Marty, C., 2008. Regime shift of snow days in Switzerland. *Geophys. Res. Lett.* 35. 10.1029/2008GL033998.

Scherrer, S. C., Appenzeller, C., and Laternser, M., 2004. Trends in Swiss Alpine snow days: the role of local- and large-scale climate variability. *Geophysical Research Letters*, **31**, 10.1029/2004GL020255.

Uhlmann, B., Goyette, S., and Beniston, M., 2008. Sensitivity analysis of snow patterns in Swiss ski resorts to shifts in temperature, precipitation and humidity under conditions of climate change. *International Journal of Climatology*, doi:10.1002/joc.1786.

Valt, M., Cagnati, A., Crepaz, A., and Marigo, G., 2005. *Snow precipitation in the last years on Italian Alps*. Zadar, Croatia: International Conference on Alpine Meteorology ICAM.

Cross-references

Alps
Depletion of Snow Cover
Global Outlook of Snowcover, Sea Ice, and Glaciers
Global Warming and its Effect on Snow/Ice/Glaciers

SNOW CRYSTAL STRUCTURE

Kenneth G. Libbrecht
Department of Physics, Caltech, Pasadena, CA, USA

Synonyms

Ice crystal structure; Snow crystal morphology

Definition

Snow Crystal Structure refers to the various morphologies of snow crystals that form from condensing water vapor in the atmosphere.

Introduction

Snow crystals, also called snowflakes, are single crystals of ice that grow from water vapor. They form in copious numbers in the atmosphere and are well known for their elaborate, symmetrical patterns. Figure 1 shows several examples of natural snow crystals.

The origin of the varied structures of snow crystals has been the source of considerable curiosity and scientific study for centuries (for a detailed historical account,

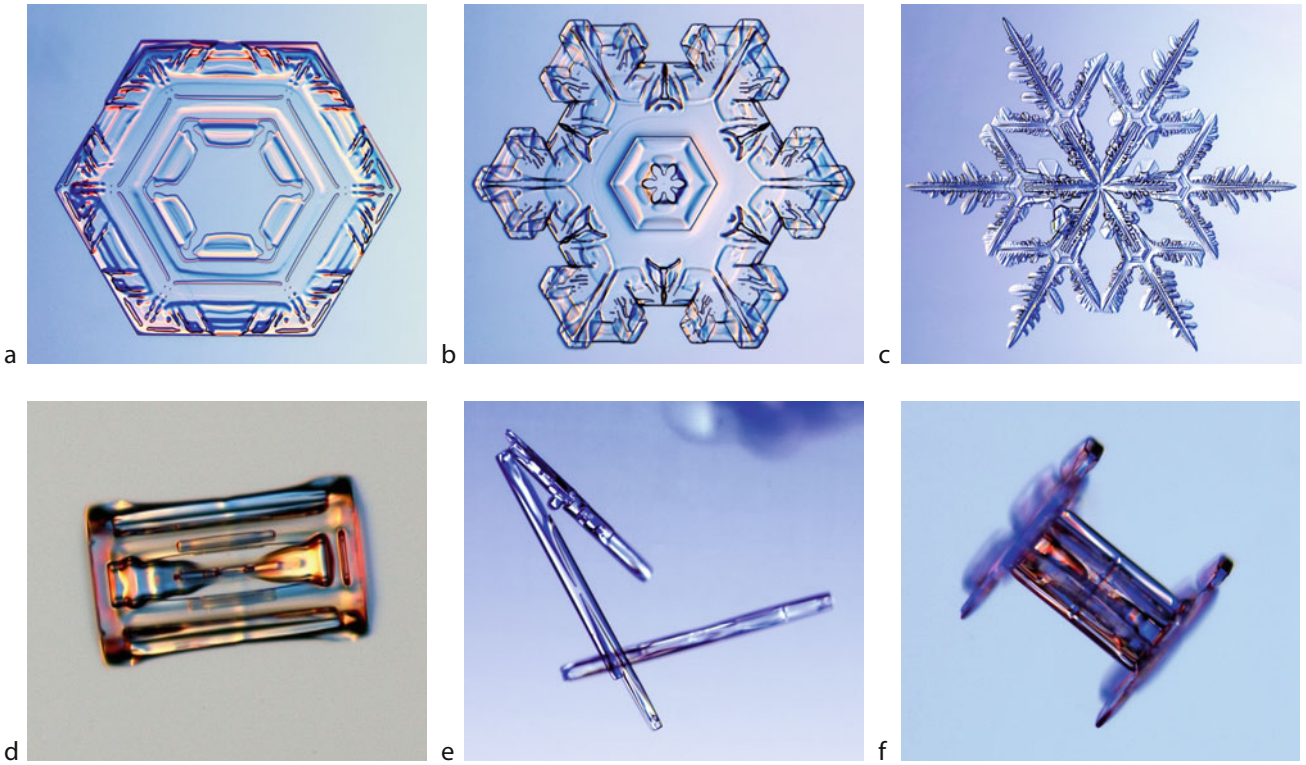

Snow Crystal Structure, Figure 1 Examples of several different morphological types of snow crystals found in natural snowfalls in temperate climates. (**a**) A relatively simple platelike crystal, 1.4 mm from tip to tip, with surface markings. Plates with smooth, featureless facets are less common in nature, except at low temperatures ($T < -20°C$) and low humidities. (**b**) A more elaborate platelike crystal, 2.1 mm from tip to tip, with an unusually high degree of complex symmetry. (**c**) A multibranched stellar dendrite crystal, 3.0 mm from tip to tip. These typically form at higher humidities when the temperature is near $T = -15°C$. (**d**) A simple hexagonal columnar crystal, 0.45 mm in length. Some internal hollowing resulted when the initially hollow ends of the column grew over. (**e**) Needlelike crystals, the largest being 1.1 mm in length. Note one needle grew as a slender hollow column before the ends branched. These crystals only grow near $T = -5°C$. (**f**) A capped column crystal, 0.6 mm in length. This crystal began growing as a stout hollow column, and then platelike stellar crystals grew on the two ends of the column. Photos by the author (Libbrecht, 2003).

see Kobayashi and Kuroda (1987) and Nakaya (1954)). With the development of photography in the late nineteenth century, Wilson Bentley (1931) catalogued several thousand snow crystal images in 1931 that he had acquired over many decades. Bentley's images popularized the snow crystal as a winter icon and were largely responsible for the widespread notion that no two snowflakes are alike.

Faceting

When water molecules condense from the vapor phase onto a growing ice surface, the rate of incorporation into the solid lattice is governed by complex molecular dynamics known as *attachment kinetics* (Libbrecht, 2005). Molecules attach especially slowly to molecularly flat surfaces, which have fewer dangling molecular bonds. As a crystal grows, the faster-growing surfaces fill in more readily, so with time one is left with only the slower growing surfaces, which become the crystal facets.

Faceting is the dominant mechanism determining snow crystal structure when the growth is slow or the crystals are small. The resulting structure is that of a hexagonal prism, with two *basal surfaces* and six *prism surfaces*. The process of faceting is how the geometry of the ice crystal lattice is transferred to the structure of a macroscopic snow crystal.

Branching

Snow crystal growth behavior is typically dominated by attachment kinetics in combination with effects of water molecule diffusion through the air. If we begin with a platelike hexagonal prism crystal, then particle diffusion will bring molecules to the six tips of the hexagon at a slightly faster rate than to the neighboring flat surfaces. With a greater supply of material, the tips grow out, which increases the water supply even more. This positive feedback effect is called the *Mullins–Sekerka instability* (see Saito, 1996; Langer, 1980), and it is a ubiquitous feature of diffusion-limited growth. Much of the complex structure seen in snow crystals ultimately derives from this instability.

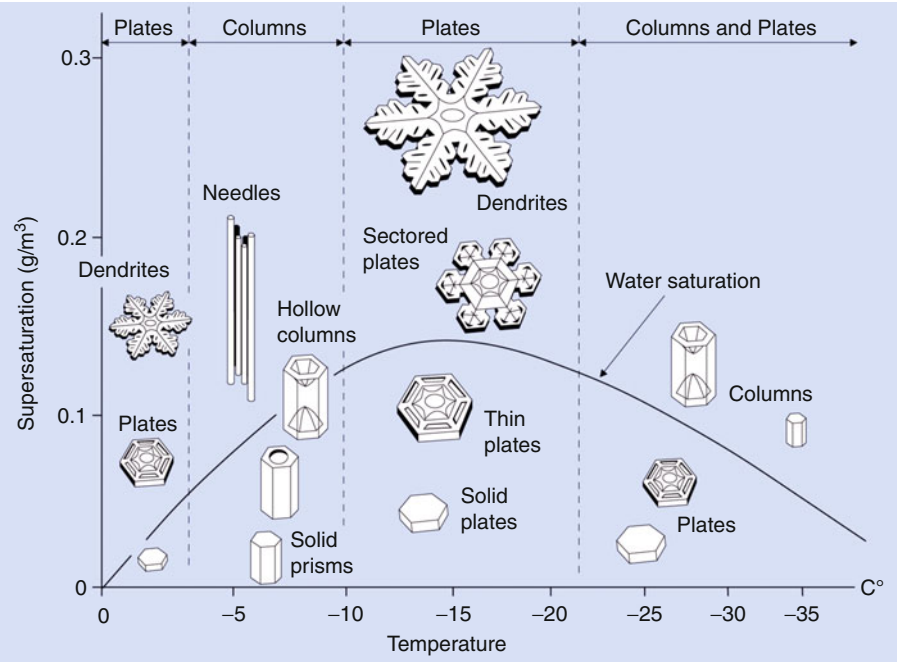

Snow Crystal Structure, Figure 2 The snow crystal morphology diagram, showing different types of snow crystals that grow in air at atmospheric pressure, as a function of temperature and water vapor supersaturation relative to ice. The water saturation line gives the supersaturation of supercooled water, as might be found within a dense cloud. The morphology switches between platelike and columnar forms as a function of temperature, while higher supersaturations produce more complex structures.

Snow crystal morphology diagram

The observed variety of snow crystal forms prompted the first laboratory investigations of snow crystal growth in 1930s. Nakaya (1954) observed the different growth morphologies as a function of ambient temperature and water vapor supersaturation, and he combined these observations into what is now called a *snow crystal morphology diagram*, shown in Figure 2. This diagram refers to snow crystals growing in air at a pressure near 1 bar, so applies to natural snow crystals.

The increase in structural complexity with increasing supersaturation is explained by the mechanics of diffusion-limited growth and the branching instability, but the changing morphology with temperature remains something of a scientific mystery.

Complexity and symmetry

The sensitivity of snow crystal growth to temperature and supersaturation allows a straightforward explanation for the combination of complexity and symmetry seen in many specimens like those shown in Figure 1. When a snow crystal is first nucleated inside a cloud, faceting dictates that the growth initially takes the form of a simple hexagonal prism. Diffusion limits the growth as the crystal becomes larger, and eventually this causes branches to form. Because ice growth is so sensitive to the local environment, it frequently happens that an abrupt change of some kind will cause all six corners of a simple platelike crystal to sprout arms at the same time.

As the growing crystal travels through the cloud, it experiences different temperatures and humidities along the way, and thus the growth behavior changes as a function of time. All six arms, however, experience the same changing conditions as they grow. The result is a rather complex growth pattern for each arm of the crystal, with all six arms developing roughly the same pattern. Under ideal conditions – for which the growth must be unperturbed by collisions with other ice or water particles – a snow crystal can grow into an elaborate, sixfold symmetrical shape, like those shown in Figure 1. Turbulent motions in the atmosphere cause each crystal path to be different, so each grows into a slightly different complex structure.

There are a number of naming conventions for snow crystals as they are falling (e.g., Kobayashi and Kuroda, 1987) and after metamorphosis of the crystals has taken place on the ground (IACS, 2009).

Bibliography

Bentley, W. A., and Humphreys, W. J., 1931. *Snow Crystals*. New York: McGraw-Hill.

IACS Working Group, 2009. International classification for seasonal snow on the ground, IHP-VII technical documents in hydrology N° 83.

Kobayashi, T., and Kuroda, T., 1987. Snow crystals. In Sunagawa, I. (ed.), *Morphology of Crystals–Part B*. Tokyo: Terra Scientific, pp. 645–743.

Langer, J. S., 1980. Instabilities and pattern formation in crystal growth. *Reviews of Modern Physics*, **52**, 1–28.
Libbrecht, K. G., 2003. *The Snowflake: Winter's Secret Beauty*. Stillwater: Voyageur.
Libbrecht, K. G., 2005. The physic of snow crystals. *Reports on Progress in Physics*, **68**, 855–895.
Nakaya, U., 1954. *Snow Crystals: Natural and Artificial*. Cambridge: Harvard University Press.
Saito, Y., 1996. *Statistical Physics of Crystal Growth*. Singapore: World Scientific.

SNOW DEFORMATION

Jerome B. Johnson
Institute of Northern Engineering, University of Alaska Fairbanks, Fairbanks, AK, USA

Synonyms

Snow creep; Snow strain

Definition

Snow deformation. A change in the shape and/or size of snow due to an applied stress.

Introduction

Snow deformation complexity arises because it is composed of ice that exists on the ground near its melting temperature as an intricate three-dimensional porous material formed from new and sintered snow grains that metamorphose over relatively short timescales (Flin et al., 2004; Schneebeli and Sokratov, 2004). Ice exhibits elastic, viscous, viscoelastic, viscoplastic, and brittle deformation that is a function of temperature and loading/deformation rates, and can lead to cohesive failure (Petrenko and Whitworth, 1999). Metamorphism changes the microstructure of snow through the sublimation and diffusion of water molecules from high surface energy surfaces to surfaces with less surface energy or through melting/freezing processes (Bartelt and Buser, 2004; Fierz et al., 2009). Sintering is the process of forming bonds between snow grains by "freezing" the disordered layers on snow grain surfaces that come into contact, or diffusing water molecules to points of contact between snow grains. The size of bonds increase through molecular diffusion of water at rates that increase dramatically as the snow temperature approaches the melting temperature of ice (Blackford, 2007) and with increasing pressure in the bond (Szabo and Schneebeli, 2007). Changes in snow microstructure, and the size of bonds between snow grains, change the mechanical properties of snow that control the deformation response of snow to stress.

Snow microstructure

The microstructure of deposited snow is highly variable because snowflakes take many different forms (Nakaya, 1954). New snow is highly porous with fragile and intricate structures similar to foam materials. Snow self-weight densification and metamorphosis can produce microstructures that consist of random variations of grain and bond sizes or stiff, brittle, vertically oriented large grains connected by small bonds (Figure 1) (Armstrong, 1980; Trabant and Benson, 1972). Melting and refreezing of snow produces clusters of extremely large grains, polycrystals, and bonds (Fierz et al., 2009). As the density of snow increases, its microstructure becomes more uniform with decreasing porosity and heterogeneity.

Continuum-scale uniaxial compression, uniaxial tension, and shear

At the continuum scale, snow subjected to stress or deformation in compression, tension, or shear has fundamentally different deformation paths. Under the influence of uniaxial compressive stresses or deformations, low-density snow ($<$300–400 kg/m^3) will initially deform with little resistance (stress or load). The resistance to deformation increases gradually with density until about 450 kg/m^3 whereupon a dramatic increase in resistance occurs with density. The specific path of deformation and overall resistance to compression depends on snow initial density and microstructure, temperature, and the rate of loading/deformation. At relatively high initial densities, greater than about 500 kg/m^3, resistance to compression is a strong function of density and deformation paths coalesce (Figure 2).

Uniaxial tension at constant temperature causes snow to elongate with increasing resistance to deformation that eventually ends in failure. The form of deformation is a strong function of deformation rate. At high rates of deformation ($>10^{-4}$/s), the resistance to deformation increases rapidly until the snow undergoes a brittle failure (Figure 3a). As the rate of deformation decreases (10^{-5}/s), the resistance to deformation initially increases with strain to a relatively constant value and then decreases with strain as microcracks form. Eventually, microcracks will coalesce to form larger cracks that may gradually expand with deformation or cause the snow to rupture (Figure 3b and c). Higher density snow resists deformation more than lower density snow and will deform to a greater extent than low-density snow. At low deformation rates ($<10^{-6}$/s), the resistance to deformation gradually increases with strain (Figure 3d), eventually forming slow opening cracks (Narita, 1980).

Shear deformation occurs when a plane within snow displaces relative to adjacent parallel planes under the influence of shear stresses or displacements. For low-density snow at low loading/deformation rates, resistance to shear increases with shear displacement, often with an associated decrease in snow volume. The magnitude of resistance to shear, at a given shear displacement increases as stresses acting perpendicular to shear planes increase. As the loading/deformation rate increases, for constant temperature, resistance to shear will increase to a maximum, and then decrease to relatively constant values,

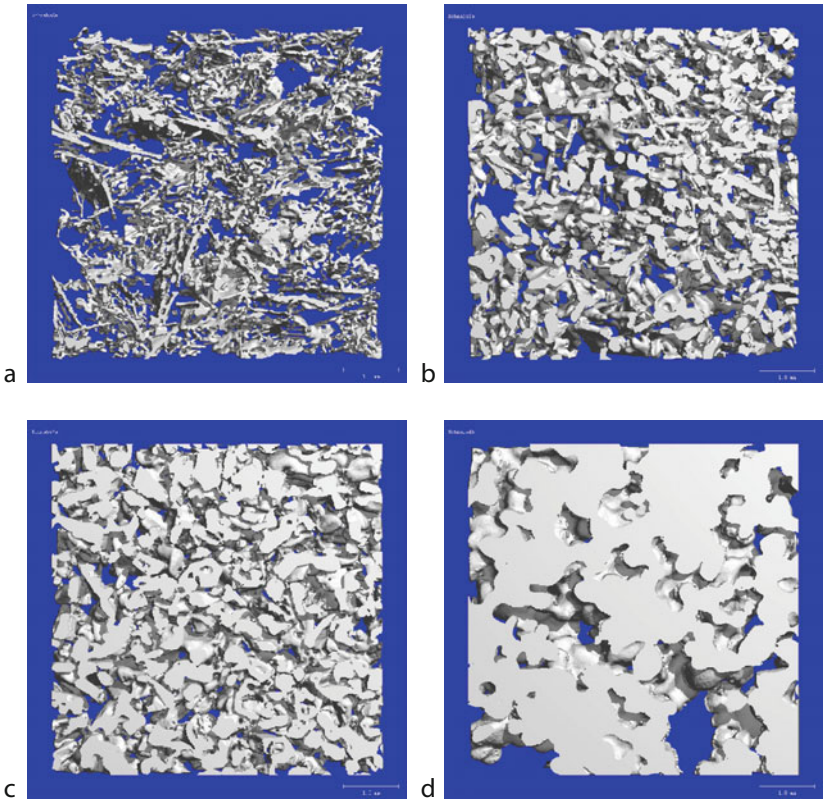

Snow Deformation, Figure 1 Snow microstructure at different stages of metamorphism and sintering. New snow with density $\rho = 110$ kg/m^3 (**a**), equilibrium temperature metamorphosed snow, $\rho = 240$ kg/m^3 (**b**), depth hoar, $\rho = 380$ kg/m^3 (**c**), and high-density snow, $\rho = 610$ kg/m^3 (**d**) (Images: M. Schneebeli, WSL Institute for Snow and Avalanche Research SLF).

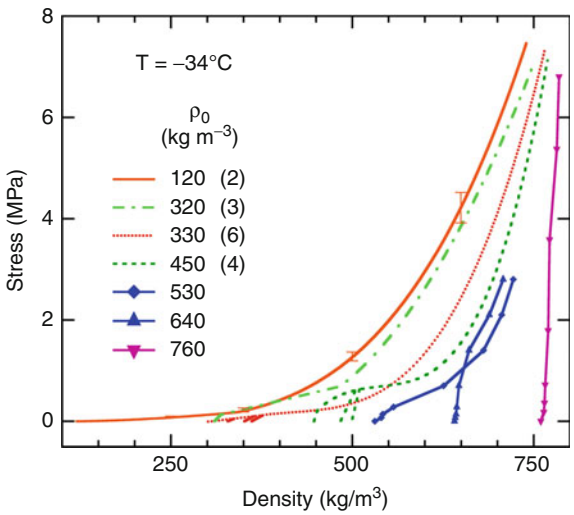

Snow Deformation, Figure 2 Uniaxial compression deformation of snow (Data from Abele and Gow, 1975, 1976). Numbers in parentheses indicate the number of tests.

as shear layers within the snow fail. As temperature increases, resistance to shear decreases. The magnitude of peak shear stresses at failure are functions of the magnitude of the stress perpendicular to the shear planes, temperature, rate of loading/deformation, and density (Figure 4) (McClung, 1977; Montmollin, 1982).

Microstructural and grain-scale processes that control snow deformation

Snow microstructure varies significantly over the range of possible densities from new snow to ice. New snow has no, or very small, bonds connecting grains together (Figure 1a). Metamorphosed snow grains are larger than in new snow (Figure 1b and c). Well-metamorphosed, high-density snow exhibits little microstructural variety, and differences between bond and grain sizes are relatively small (Figure 1d).

The intricate microstructure and small size of bonds compared to grain sizes in low-density snow influences deformation in two important ways. First, loads that cause deformation are not uniformly supported by the microstructural geometry and some geometric pathways support more load than others (Kry, 1975). This means that deformation occurs more rapidly in some parts of the bulk of

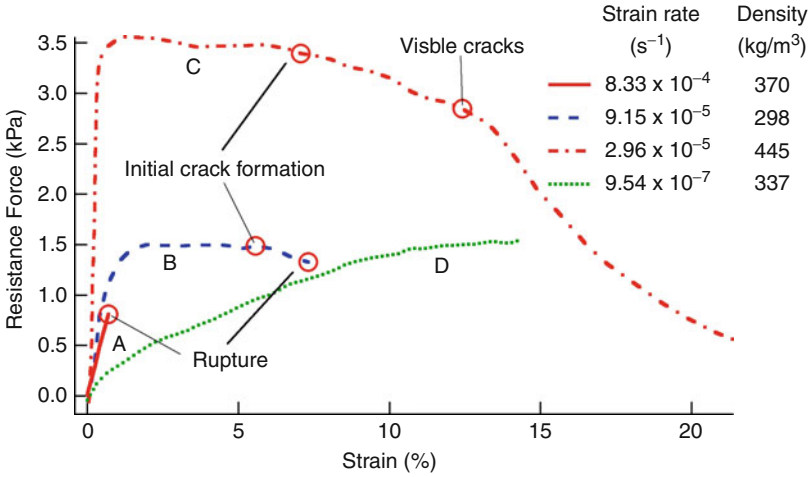

Snow Deformation, Figure 3 Resisting force as a function of uniaxial tension strain (Data from Narita, 1980).

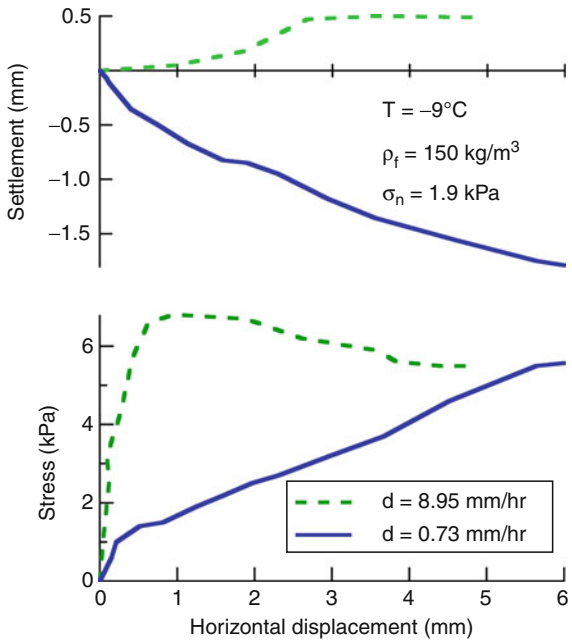

Snow Deformation, Figure 4 Shear stress as a function of horizontal (shear) displacement. Negative settlement indicates densification and positive settlement indicates dilation (Data from McClung, 1977).

snow than in others and that as deformation proceeds more of the microstructure geometry may become involved. Alternatively, as some parts of the microstructure fail, other parts of the microstructure will experience increased loading and deformation. Snow microstructure is more uniform in high-density snow so that stress and deformation will also be more uniform. Secondly, stresses applied to bulk snow concentrate at the bonds with the result that most of the deformation occurs in the bonds, not the grains. As bond sizes approach the size of grains, the distinction between grains and bonds disappears and snow deforms as porous ice.

Grain-scale deformation processes act similarly for deformation in compression, tension, and shear. Differences in the expression of the grain-scale processes at continuum scales are due to the differences in the way the loads are applied. At the grain scale, bonds can be subjected to tension, compression, linear or torsional (twisting) shear, bending, or a combination of those (Johnson and Hopkins, 2005). Tension causes bonds to elongate and thin, and eventually to rupture, while compression causes bonds to thicken. Shear allows grains to move past each other, or rotate in place, via creep deformation while remaining bonded, or sliding if the bond ruptures. Bending is a response to combined tension and compression loads that can eventually lead to rupture. Combined conditions of loading or deformation, such as shear and compression, can cause grains to rotate (Faraday, 1859). Sintering affects grain-scale deformation by changing bond thickness and snow microstructure, especially near the melting temperature where sintering rates are high.

Uniaxial compression

During uniaxial compression, assuming that the rate of loading/deformation and temperature are held constant, the bonds between snow grains can thicken or thin, depending on their orientation to stress. At densities below about 300–400 kg/m^3, grains rearrange through viscous creep in the bonds or fracture of the bonds that permit grains to be displaced with respect to each other. This is a shear deformation process at the grain scale even though the continuum-scale deformation is compression (Shapiro et al., 1997). The process of grain rearrangement is generally accommodated within the pore space of the snow such that confinement of the snow has little effect on deformation (Scapozza and Bartelt, 2003). Sintering continues to operate during deformation, producing changes in the

bonds that can be more important in controlling deformation magnitude and rate than the applied stress, at low loading rates or at high temperatures. As grains rearrange, the microstructure tightens and the density of the snow increases resulting in more grain contacts and new sintered bonds that can produce a wide range of values in the mechanical properties of snow. Often, an *apparent* relationship between density and deformation can be established because both the deformation response of snow to stress and the density depend on the snow microstructure and the form of the bonding/grain contacts. Thus, it is the microstructure and bonding, and not the density, which are important for determining snow deformation response to applied stresses.

At initial densities of between 500 and 700 kg/m^3, snow microstructure makes a transition from complex forms to a form that resembles distributed interconnected pores in an ice matrix. The resistance to uniaxial compression of snow increases significantly as the pore space is no longer able to accommodate snow grain rearrangement. The size of bonds between grains grow to become a significant percentage of the grain size causing stress concentrations to decrease to negligible levels that are related to the ratio of the pore space to the overall volume of ice. At these higher densities, deformation becomes a strong function of density.

Uniaxial tension

Uniaxial tension deformation in relatively low-density snow occurs as viscous creep in bonds, or elastic deformation and rupture of bonds, to allow grains to rearrange in an alignment parallel to the axis of tension. Grains that are initially randomly distributed will undergo shear within their bonds and grain rearrangement to achieve alignment with the tensile stress field. As grains become aligned with the tension axis, bonds will elongate and thin. Bonds will begin to rupture in tension producing progressive failure of the snow at low rates of loading or catastrophic failure of the snow at high loading rates (Narita, 1980). As bonds rupture, stress is transferred to the remaining bonds. As snow density increases, the influence of microstructure decreases, and deformation becomes more ice-like.

Shear

During shear, grains attempt to move past each other along shear planes and may be able to do so without change in volume when grains do not interfere with each other and there are no loads perpendicular to the planes of shearing. When loads act perpendicular to planes of shear, grains will move past each other and fill available pore space, reducing snow volume. If grains interfere with each other during deformation, the grains must fail or the snow volume increase (dilate) to allow grains to rearrange into an easy glide configuration. Increasing the perpendicular loading on a shear plane makes it more difficult for interfering grains to move around each other, thus requiring larger shear stresses to dilate the snow or cause grain failure. For higher-density snow, or at higher loading/deformation rates, interference of grains with each other will cause the deformation resistance to increase to a maximum. At this point, deformation resistance decreases to a relatively constant value determined by the sliding resistance between grains and/or the rates of bond or grain rupture, sintering, and re-sintering (Figure 4).

Conclusions

Snow deformation at the continuum scale is complex because of the cumulative influences of snow microstructures that change under the influence of sintering and multiple grain-scale deformation processes. Sintering and grain-scale deformation are both temperature and loading/deformation rate dependent. Continuum-scale reflections of grain-scale mechanisms in uniaxial compression include decreasing volume with an associated increasing deformation resistance. Uniaxial tension produces an initial increase in deformation resistance as grains align themselves with the axis of tension. Once grains are aligned, bonds will fail as deformation continues, causing the resistance to deformation to decrease and cracks to form in the snow. Resistance to shear deformation increases until grains fail or rearrange themselves to move past neighboring grains. If grains can move into available pore space without interfering with each other, then snow density will increase along with resistance to shear. If grain movement is restricted then resistance will increase to a maximum followed by a decline to a relatively constant value as grains fail or arrange themselves in an easy glide orientation. The importance of microstructure and grain-scale processes decreases with increasing snow density such that, at densities greater than about 500 kg/m^3, deformation mechanisms transition to those associated with porous ice.

Bibliography

Abele, G., and Gow, A., 1975. *Compressibility characteristics of undisturbed snow.* Research Report, USA Cold Regions Research and Engineering Laboratory.

Abele, G., and Gow, A. J., 1976. *Compressibility characteristics of compacted snow.* CRREL Report, USA Cold Regions Research and Engineering Laboratory.

Armstrong, R. L., 1980. An analysis of compressive strain in adjacent temperature-gradient and equi-temperature layers in a natural snow cover. *Journal of Glaciology*, **26**(94), 283–289.

Bartelt, P., and Buser, O., 2004. The principle of minimum entropy production and snow structure. *Journal of Glaciology*, **50**(170), 342–352.

Blackford, J. R., 2007. Sintering and microstructrure of ice: a review. *Journal of Physics. D. Applied Physics*, **40**, R355–R385.

Faraday, M., 1859. On regelation, and on the conservation of force. *Philosophical Magazine*, **17**, 162–169.

Fierz, C. et al., 2009. *The International Classification for Seasonal Snow on the Ground.* IHP-VII Technical documents in hydrology N°83, IACS contribution N°1, UNESCO-IHP, Paris, 80 pp. http://unesdoc.unesco.org/images/0018/001864/186462e.pdf

Flin, F., et al., 2004. Three-dimensional gemoetric measurements of snow microstructural evolution under isothermal conditions. *Annals of Glaciology*, **38**, 39–44.
Johnson, J. B., and Hopkins, M. A., 2005. Identifying microstructural deformation mechanisms in snow using discrete element modeling. *Journal of Glaciology*, **51**, 432–442.
Kry, P. R., 1975. The relationship between the visco-elastic and structural properties of fine-grained snow. *Journal of Glaciology*, **14**(72), 479–500.
McClung, D. M., 1977. Direct simple shear stress tests on snow and their relation to slab avalanche formation. *Journal of Glaciology*, **19**(81), 101–109.
Montmollin, V. d, 1982. Shear tests on snow explained by fast metamorphism. *Journal of Glaciology*, **28**(98), 187–198.
Nakaya, U., 1954. *Snow crystals: natural and artificial*. Cambridge: Harvard University Press.
Narita, H., 1980. Mechanical behavior and structure of snow under uniaxial tensile stress. *Journal of Glaciology*, **26**(94), 275–282.
Petrenko, V. F., and Whitworth, R. W., 1999. *Physics of ice*. New York: Oxford University Press, p. 373.
Scapozza, C., and Bartelt, P., 2003. Triaxial tests on snow at low strain-rate. Part II. Constitutive behavior. *Journal of Glaciology*, **49**(164), 91–101.
Schneebeli, M., and Sokratov, S. A., 2004. Tomography of temperature gradient metamorphism of snow and associated changes in heat condutivity. *Hydrological Processes*, **18**, 3655–3665.
Shapiro, L. H., et al., 1997. *Snow mechanics: review of the state of knowledge and applications.* CRREL Report, Research and Engineering Laboratory, US Army Cold Regions, 35 pp.
Szabo, D., and Schneebeli, M., 2007. Subsecond sintering of ice. *Applied Physics Letters*, **90**, 3.
Trabant, D., and Benson, C., 1972. Field experiments on the development of depth hoar. *Geological Society of America Memoirs*, **135**, 309–322.

Cross-references

Creep
Firn
Seasonal Snow Cover
Snow Density
Snow Grains

SNOW DENSITY

Steven Fassnacht
Snow Hydrology, Watershed Science Program,
Colorado State University, Fort Collins, CO, USA

Definition

Snow density is the ratio of snow water equivalent (SWE) to snow depth. When SWE is given in mm of water and snow depth in m, the units of density are kg m^{-3}.

The density of snow can vary by more than an order of magnitude. The density of freshly fallen snow has been observed to range from 20 kg m^{-3} to 250 kg m^{-3} (e.g., Reek et al., 1992; Fassnacht and Soulis, 2002) and is a function of formation conditions in the clouds and the atmospheric conditions through which the snow crystals fall. Upon reaching the ground, snow crystals begin to metamorphose. Prior to melt, the snow can attain a density of 300 kg m^{-3} (e.g., Fassnacht and Soulis, 2002) to 500 kg m^{-3}, depending on the length of time on the ground, meteorological conditions, and the depth of overlying snow.

Bibliography

Fassnacht, S. R., and Soulis, E. D., 2002. Implications during transitional periods of improvements to the snow processes in the Land Surface Scheme – Hydrological Model WATCLASS. *Atmosphere-Ocean*, **40**(4), 389–403.
Reek, T., Doty, S. R., and Owen, T. W., 1992. A deterministic approach to the validation of historical daily temperature and precipitation data from the cooperative network. *Bulletin of the American Meteorological Society*, **73**, 753–762.

SNOW DEPTH

Gavin Gong
Department of Earth and Environmental Engineering,
Henry Krumb School of Mines, Columbia University,
New York, NY, USA

Definition

The amount of snow on the Earth's surface at a specific point in space and time, measured as the actual vertical distance from the ground surface to the snowpack surface.

Introduction

Snow depth is arguably the most basic and fundamental descriptive feature of snow that resides on the Earth's surface. It is an intuitive measure of the magnitude of a solid precipitation event, for example, "last night's storm dumped 10 in. of snow on the ground". However the familiarity of snow depth belies its spatiotemporal variability, its physiological importance to the cryosphere, hydrosphere, lithosphere, and atmosphere, and also its societal importance as a water resource, especially in a changing climate (Doesken and Judson, 1997).

Snow depth refers to the actual thickness of a snowpack that overlays the surface, and has some important distinctions from other common snow cover descriptors. The binary presence/absence or the spatial extent of snow cover is the most extensively documented feature since it is the easiest to observe. Although snow extent and snow depth are inherently related, their fluctuations do not necessarily coincide in magnitude, timing, or even phase. This distinction is innate at local scales, where snow depth can vary between two different locations within a snow-covered domain, and can vary at a given location throughout the course of its snow season. At broader regional or continental scales, this distinction is often overlooked; for example, a year with a more extensive October snow cover over North America may be incorrectly assumed to have an anomalously deep snowpack throughout the snow-covered region.

Snow water equivalent refers to the depth of water that would result from a melted snowpack. Although this parameter also represents the amount of snow on the ground, it is not interchangeable with snow depth. The difference lies in the highly variable density of snow (typically 50–400 kg m^{-3}) in contrast to the relatively fixed density of liquid water (~1,000 kg m^{-3}). The density of freshly fallen snow depends on the meteorological conditions producing the snowfall event, and the density of a snowpack varies with depth and from seasonal down to hourly timescales even in the absence of melting. Thus, especially during the winter season, snow depth can vary considerably relative to snow water equivalent.

Observed spatial and temporal patterns of variability

Snow depth is represented as a continuous, nonnegative variable defined over an *x, y, t* coordinate system, where *x* and *y* define a location on the land surface (including glaciers and sea ice), and *t* is an instantaneous point in time. Local spatial variability can arise from factors such as heterogeneous precipitation rates, hillslope orientation, vegetation interception, and wind interaction with surface features. On regional scales (e.g., a watershed), the local variations are often averaged out to consider a homogenous snow depth for hydrologic and water resource applications. An important regional phenomenon is lake-effect snow, where atmospheric warming over lakes induces lifting, condensation, and snowfall over downstream land areas, resulting in regions with high snow depth. At the mesoscale, snow depth generally increases with latitude, but orography and proximity to oceans are key geographic determinants. Snow depths tend to be greater over mountain ranges where consistently lower temperatures facilitate solid precipitation and sustain surface snowpacks. The high heat capacity of water has a warming effect on coastal regions, so that Northern Hemisphere snow depth actually decreases with latitude near the Arctic coasts due to reduced snowfall. Hence, maximum snow depths tend to occur in the high-elevation interior of the North American and Eurasian continents (Foster and Davy, 1988).

Temporal variability can occur over multiple timescales. Snow depth can decrease on hourly-daily timescales via ablation processes such as melting, sublimation, and metamorphic transition from crystalline to granular structure which increases snowpack density. Ablation also occurs on weekly-monthly timescales, but is less apparent since periodic snowfall events increase snow depths. The interaction of snowfall and ablation generally lead to a broad delineation of the snow season, into an accumulation period with increasing snow depth, followed by a melt period with decreasing snow depths. On interannual to decadal timescales, snow depth exhibits structured periodicities as well as unstructured random variability, especially at large spatial scales. For example, twentieth century snow depth measurements gridded over North America indicate a decreasing trend from about 1970 to 2000, especially in late winter and early spring, preceded by an increasing trend from about 1900 to 1970 (Ge and Gong, 2008; Dyer and Mote, 2006). Early twenty-first century records do not clearly continue the late twentieth century decreasing trend; hence, the existence of any long-term anthropogenic trend in the snow depth record is ambiguous.

Measurement methods

Snow depth can be easily measured with a ruled stick or snow board inserted through the snowpack, typically to 1 in. or 1 cm precision. The drawbacks of this method are the limitation to point measurements, and the manual effort required and associated inconsistencies (Doesken and Judson, 1997). Nevertheless, it is commonly used for a wide range of scientific and nonscientific activities due to its simplicity and low cost. Snow depth station measurement networks exist throughout North America and Eurasia, and some stations have records dating back for over a century. Recent efforts have been made to interpolate the station measurements into gridded snow depth time series, particularly over North America (Brown, 2000; Dyer and Mote, 2006), which offer a new opportunity to fully characterize the large-scale spatiotemporal variability of snow depth. However, the gridded values can be constrained by irregular station distribution, which can lead to local biases, relatively coarse gridcell resolution that can dampen the true spatial variability, and insufficient accounting of elevation differences. Therefore, individual gridcell values far removed from station observations should be used with caution.

An alternative method for measuring snow depth utilizes remote sensing of electromagnetic waves. At local scales, an ultrasonic sensor is typically mounted on a permanent stand, and measures the time required for an ultrasonic (~50 kHz) pulse to travel through the air down to and back up from the surface. A shorter travel time is indicative of a shorter travel distance due to deeper snow. A temperature probe is also required since the speed of sound is sensitive to air temperature. At the mesoscale, passive microwave sensors mounted onto orbiting satellites are used to measure the degree of scattering caused by snow grains, which can be related to snow depth or snow water equivalent over broad regions (Cavalieri et al., 2004). The principal advantage of satellite remote sensing over station measurements is consistent spatial coverage, but the precision of satellite-based snow depth estimates is still evolving.

Data assimilation has also been used to infer snow depth values at locations far removed from station measurements. Deterministic snowpack models are used to simulate gridcell snow depth based on more readily available meteorological inputs, and model outputs are constrained to match station measurements where

available. Assimilation techniques for snow depth are still developing, but one available product provides daily snow depth for 1 km gridcells over the continental United States dating back to 2003 (NOHRSC, 2004).

Physical processes and modeling

The physical processes that govern snow depth are driven by energy fluxes as well as moisture fluxes (Dingman, 2002). Snow depth, of course, increases directly in response to snowfall events, but this increase can be short-lived if temperatures do not consistently remain below ~0°C. If the snowpack experiences a sustained net energy loss, snowpack temperatures will decrease, ablation will be minimal, and successive snowfall events will accumulate leading to sustained snow depth increases. If the snowpack experiences a net energy gain, snowpack temperatures will increase toward a maximum of ~0°C. During this warming phase, snow depth changes in the absence of snowfall events are minimal since ablation results from sublimation but not evaporation or melting. Even upon reaching ~0°C, snow depth changes are modest at first since initial melting is retained by surface retention onto snow particles within the snowpack; during this ripening period, ablation results from sublimation and evaporation. Only after surface retention has reached capacity does a melt period commence, in which melted snow infiltrates into the underlying soil, and snow depth decreases conspicuously.

Although the energy fluxes are the primary drivers of snow depth, other physical processes can also have an important influence. Wind-driven transport (i.e., blowing snow) during and between snowfall events can spatially redistribute snow depths, affecting sublimation rates and increasing avalanche risks due to locally high accumulations (Pomeroy et al., 2008). Dust deposition onto a snowpack affects snow depths by decreasing the albedo and hence increasing snowmelt rates at the snow surface. Metamorphic processes within a snowpack, such as gravitational settling, refreezing of snowmelt and water vapor transport, result in the densification of a snowpack over time, which can decrease snow depths even in the absence of snowmelt losses.

Mathematical models have been developed to simulate the evolution of a snowpack and its associated physical processes, by solving the governing equations of mass and energy balance for a one-dimensional system comprised of multiple snow and underlying soil layers. Radiative, turbulent, and diffusive energy exchanges are computed between each layer, from specified optical and thermal properties for snow and the underlying soil, and meteorological inputs at the snow–air interface. These fluxes determine the temperature and density of each layer, which in turn control the snowpack accumulation and ablation processes, and the resulting snowpack depth. Examples of such models include SNTHERM, CROCUS, and SNOWPACK, and they are used for a variety of applications from water supply planning to avalanche warning (Rasmus et al., 2007).

Snow depth is also a prominent land surface feature simulated in large-scale climate models, as part of a land surface parameterization scheme. Because of the gridcell structure of most climate models that is very coarse relative to the physical snow accumulation and ablation processes, these snow parameterizations are necessarily simplified. Typically, only a single snow layer is modeled, primary processes such as albedo are computed simply from vegetation type, snow depth, and snow temperature, and other important metamorphic processes such as refreezing are ignored. Recent improvements have increased vertical resolution, improved vertical physics, and incorporated sub-grid-scale heterogeneity to represent snow depth variability within a gridcell. Overall, climate models capture the broad features of the observed land surface snow regime, although ablation processes at low snow depths are a significant source of both scatter between individual models and overall modeling weakness (Slater et al., 2001).

Socioeconomic importance

Land surface snow depth is of tremendous social and economic importance, affecting many sectors such as water supply, agriculture, fishery, forestry, manufacturing, and tourism (Doesken and Judson, 1997; Frederick and Gleick, 1999). The potential influence of insufficient winter snowpack on water supply and drought risk during the subsequent spring and summer seasons is a major concern in the densely populated mid-latitude regions of the world. The lack of water stored in the form of snow also limits agricultural irrigation, creates shortages of water for industrial users, and damages wildlife habitats. Less snow accumulation in winter or early snow melt in spring are also a major reason for more frequent and prolonged forest fires that put ecosystems and humans in peril. Another impact of snow depth is its influence on the tourism sector, in particular skiing and other winter activities that serve as a major contributor to regional economies in many places around the world. Snow depth variations even on a weekly basis can have a direct financial impact on the local ski and snow sports industry and related businesses, while seasonal to interannual variations can affect employment patterns and construction decisions.

Conversely, excessive snow depths can jeopardize livelihoods and disrupt local economies. The consequences of severe snow storms are usually devastating, resulting in power outages, agricultural damage, and property loss (Doesken and Judson, 1997). Deep snowpacks pose an obvious avalanche risk in mountainous areas, and can also be a primary reason for floods when combined with excessive rainfall during the snow melting season, which may require massive evacuations and damage buildings, bridges, dams, and other infrastructure. Rapid melt of deep snowpacks can also trigger landslides and debris flows which could impair downstream water quality, cause

serious soil erosion, and limit agricultural productivity (Frederick and Gleick, 1999).

The SNOTEL system operated by the United States Natural Resources Conservation Service (http://www.wcc.nrcs.usda.gov/snow/about.html) illustrates the socio-economic value of snow depth. This service regularly collects, transmits, and processes snowpack and related climatic data at roughly 2,000 manual and/or automated sites in the western United States and Alaska, as well as streamflow forecasts for about 740 locations. This information is critical to regional water managers and decision makers in these regions, where, winter snowpack represent the largest component of water storage (Mote et al., 2005). It is used to inform crop optimization plans for irrigation-dependent agricultural land, drought management plans for water supply reservoirs, and flood diversion plans for municipalities. It is also used by local businesses to inform staffing, equipment, and other operational decisions.

Climatic relationships

Land surface snow depth is being increasingly recognized for exhibiting physically based relationships with the overlying climate system, distinct from the more widely studied snow extent relationships (Ge et al., 2009). Although the presence of a snow cover is known to suppress local air temperature, deeper snow has been shown to enhance the temperature suppression. Climate modeling studies suggest that snow depth may have a greater impact on the Indian monsoon than snow extent, via alterations to the hydrological cycle and surface energy budget. Extending to larger scales, snow depth anomalies over Siberia have also been found to influence the dominant mode of extratropical North Hemisphere climate variability.

Conversely, large-scale climate teleconnection patterns have been shown to influence snow depth, particularly over North America. Many of these studies are motivated largely by socioeconomic issues such as water supply in the western United States, and therefore use snow water equivalent rather than snow depth as the snow cover metric. These studies have identified various regional-scale statistical relationships with a disparate set of climatic drivers, for example, the Pacific–North American Pattern (PNA), El-Nino Southern Oscillation (ENSO), Pacific Decadal Oscillation (PDO), and the North Atlantic Oscillation (NAO). More recently, a gridded snow depth dataset covering all of North America has been used to identify more coherent continental-scale relationships with climate phenomena that originate in the extratropical North Pacific. Overall, snow depth is emerging from the shadow of the more readily measured snow extent as having meaningful climatic causes and consequences.

Bibliography

Brown, R. D., 2000. Northern hemisphere snow cover variability and change, 1915–1997. *Journal of Climate*, **13**, 2339–2355.

Cavalieri, D., Markus, T., and Comiso, J., 2004. *AMSR-E/Aqua Daily L3 12.5 km Brightness Temperature, Sea Ice Conentration, and Snow Depth Polar Grids V002*. Boulder, CO: National Snow and Ice Data Center. Digital media.

Dingman, S. L., 2002. *Physical Hydrology*. Upper Saddle River, NJ: Prentice-Hall.

Doesken, N. J., and Judson, A., 1997. *The Snow Booklet – A Guide to the Science, Climatology, and Measurement of Snow in the United States*. Fort Collins, CO: Colorado State University.

Dyer, L. J., and Mote, T. L., 2006. Spatial variability and trends in snow depth over North America. *Geophysical Research Letters*, **33**, L16503, doi:10.1029/2006GL027258.

Foster, D. J., and Davy, R. D., 1988. *Global Snow Depth Climatology, USAFETAC/TN-88/006*. Illinois: USAF Environmental Technical Applications Center, Scott Air Force Base.

Frederick, K. D., and Gleick, P. H., 1999. *Water and Global Climate Change: Potential Impacts on U.S. Water Resources*. Washington, DC: Pew Center on Global Climate Change.

Ge, Y., and Gong, G., 2008. Observed Inconsistencies Between Snow Extent and Snow Depth Variability at Regional/Continental Scales. *Journal of Climate*, **21**, 1066–1082.

Ge, Y., Gong, G., and Frei, A., 2009. Physical Mechanisms Linking the Winter Pacific – North American Teleconnection Pattern to Spring North American Snow Depth. *Journal of Climate,* in press.

Mote, P. W., Hamlet, A. F., Clark, M. P., and Lettenmaier, D. P., 2005. Declining Mountain Snowpack in Western North America. *Bulletin of the American Meteorological Society*, **86**, 39–49.

National Operational Hydrologic Remote Sensing Center (NOHRSC), 2004. *Snow Data Assimilation System (SNODAS) Data Products at NSIDC*. Boulder, CO: National Snow and Ice Data Center. Digital Media.

Pomeroy, J. W., Gray, D. M. and Marsh, P., 2008. Studies on Snow Redistribution by Wind and Forest, Snow-Covered Area Depletion, and Frozen Soil Infiltration in Northern and Western Canada. *Cold Region Atmospheric and Hydrologic Studies. The Mackenzie GEWEX Experience. Volume 2: Hydrologic Processes*. doi:10.1007/978-3-540-75136-6_5. 81–96.

Rasmus, S., Gronholm, T., Lehning, M., Rasmus, K., and Kulmala, M., 2007. Validation of the SNOWPACK model in five different snow zones in Finland. *Boreal Environment Research*, **12**, 467–488.

Slater, A. G., et al., 2001. The representation of snow in land surface schemes: results from PILPS 2(d). *Journal of Hydrometeorology*, **2**, 7–25.

Cross-references

Frequency Analysis of Snow Storms
Global Outlook of Snowcover, Sea Ice, and Glaciers
Snow Density
Snow Water Equivalent
Surface Energy Balance

SNOW DRIFT

Richard Bintanja
Royal Netherlands Meteorological Institute (KNMI),
De Bilt, The Netherlands

The process of transporting snow particles due to strong winds is called snowdrift.

In regions with permanent snow cover such as Antarctica, and in regions with seasonal snow cover, blizzards, snowstorms, and snowdrift are common phenomena. Loose surface snow particles are usually present whenever temperatures are below 0°C. When surface winds exceed about 7 m s^{-1}, these particles are picked up by the wind and become airborne. At moderate winds, individual snow particles bounce along the surface – a process called saltation – thereby ejecting more particles at each bounce. This is also referred to as drifting snow, and takes place in the lowest 0.1 m or so of the atmosphere. When wind speeds increase further, the particles become fully detached from the surface. This state of snowdrift is usually referred to as suspension, or blowing snow, and can reach heights of tens to even hundreds of meters. During snowdrifting conditions, individual particles collide, break, and generally become more round while airborne. Starting as snowflakes, they quickly turn into much smaller, rounded particles, which can be more densely stacked when they are deposited again. This process is usually referred to as wind packing.

Persisting winds may transport snow particles tens to hundreds of kilometers before settling down again. The erosion, horizontal transport, and subsequent deposition of snow lead to a significant redistribution of the surface snow, often resulting in surface features like snow dunes. Over the vaste flat snowplains of Antarctica, snow dunes thus formed can reach heights of about 1 m. However, when orography or buildings induce irregular wind patterns, snowdrift can potentially lead to accumulation of tens of meters of snow. Another adverse and potential dangerous effect of snowdrift is the reduced visibility caused by the airborne snow particles; during strong blizzards, the visibility may be reduced to almost zero.

Snowdrift not only involves the transport of snow from one location to the other, it also causes the snowdrifting particles to sublime. Traveling downwind, turbulent updrafts within the snowstorm will keep the particles afloat. Hence, the airborne particles are continuously ventilated, inducing a turbulent moisture flux, or sublimation, which steadily eats away mass from the particle. Snowdrift sublimation is a fairly efficient process, since the airborne particles are ventilated on all sides (in contrast to particles at the surface). This constitutes a two-step mechanism by which the snow surface loses mass: first snow particles are being swept up by the winds, after which they are slowly sublimated away while traveling downstream. Calculations have shown that snowdrift sublimation is generally a significant term in removing mass from the snow surface; averaged over Antarctica, about 15% of all precipitated snow is thus sublimed to water vapor again.

Bibliography

Bintanja, R., 1998. The contribution of snowdrift sublimation to the surface mass balance of Antarctica. *Annals of Glaciology*, **27**, 251–259.

Bintanja, R., 2001. Modification of the wind speed profile caused by snowdrift: results from observations. *Quart J R Meteorol Soc*, **127**, 2417–2434.

SNOW GAUGE

A. K. Singh
DIAT (Deemed University), Girinagar, Pune, Maharashtra, India

A snow gauge is an instrument used by meteorologists and hydrologists to measure the amount of snow precipitation over a set period of time. Snow stakes and simple rulers can be used to determine the depth of the snowpack, though they will not evaluate either its density or liquid equivalent. Snow gauges measure snowfall water equivalent directly. The snow gauge consists of two parts, a copper catchment container and a funnel-shaped gauge. The snow collection container is generally shielded to reduce wind turbulence around the orifice, as shown in Figure 1, and is mounted on a pipe outdoors and is approximately 1.5 m high, far enough above the snow surface to minimize the accumulation of blowing snow in the gauge, while the container is 51.5 cm in length. When snow has fallen the container is removed and replaced with a spare.

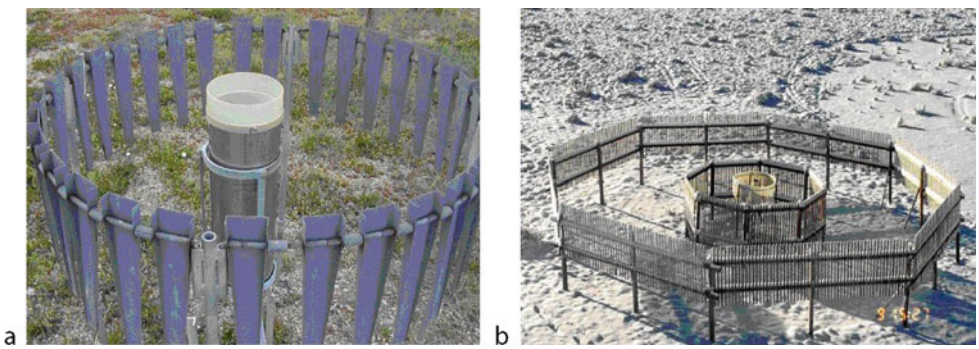

Snow Gauge, Figure 1 Snow gauge. Single alter shield (**a**); double fenced intercomparison reference shield (**b**). (Taken from ams.confex.com/ams/pdfpapers/119076.pdf.)

Snow Gauge, Figure 2 Tipping bucket rain gauges, that is, electric rain/snow gauges (www.omega.com).

The snow is then melted and poured into a measuring glass. While the depth of snow is normally measured in centimeters, the measurement of melted snow (water equivalent) is in millimeters. An estimate of the snow depth can be made by multiplying the water equivalent by ten.

The snow gauge suffers from the problem as that of the rain gauge when conditions are windy as the amount of snow may be under or over reported. Another problem may occur when there is both snowfall and rainfall leading to inaccurate measurement. In all of these cases the observer judgment is of critical importance to ascertain the accuracy of measurement.

Remote reading gauges used by weather stations that work similar to rain gauges have a large catch area that collects a critical weight of snow after which it tips and empties the snow catch. This activates a switch and sends a signal (Figure 2). If the catch container has a heater in it the snow weight is measured accurately. There is a possibility to tip the switch based on volume instead of weight leading to appropriate fill sensing.

Bibliography

Landolt, S. D., and Rasmussen, R. M., National Center for Atmospheric Research, Boulder, CO (taken from ams.confex.com/ams/pdfpapers/119076.pdf).

SNOW GRAINS

Thomas H. Painter
Jet Propulsion Laboratory/Caltech, Pasadena, CA, USA

Definition and introduction

Changes in snow grains and their bonds contribute to changes in snow's albedo, microwave scattering, thermal conductivity, mechanical properties, and gas adsorption. The concept of the snow grain would seem to be easily defined and yet the complexity of the snow matrix and forms resulting from initial conditions and metamorphism renders an exact definition impossible (Mätzler, 1997). This lack of a simple definition results largely because the degree of sintering between the (always) monocrystalline particles varies enormously and concave or highly asymmetric forms are not uncommon. The concept of the snow grain to a remote sensor is substantially different from that to an avalanche forecaster, and their respective defined sizes for the same snow can vary by two orders of magnitude. Here, the concept of snow grains is described through the characterization of shape and size. (Note: sintering is described in the entry on snow bonding.)

We tend to conceptualize snow as a collection of grains because snow precipitates discretely to the Earth's surface and scrapes discretely from a snow pit face (Figure 1). However, the concept of the snow grain is most sound when the degree of metamorphism is modest, and the principal axes of the crystals are similar. The advent of micro-tomography has shown that snow has a much more complex structure than previously thought, and traditional grain-bond models are of little scientific use. Still, grain size and shape is the only possible morphometric measure that can be observed in the field.

Grain shape

In the new International Classification for Seasonal Snow on the Ground (Fierz et al., 2009), the snow grain is defined by its shape and its size. The shape is based mainly on morphological criteria, but also to some degree by its assumed state of metamorphism as described below. This definition relies methodologically on the traditional way of estimating grain size by scraping snow particles from the wall of a snow profile and studying these particles on a gridded black board using a magnifying hand lens or loupe.

The ICSSG (International Classification of Seasonal Snow on the Ground) suggests classification of snow grains according to the following classes: precipitation particles, machine-made snow, decomposing and fragmented precipitation particles, rounded grains, faceted grains, depth hoar, surface hoar, melt forms, and ice formations. As such, the first seven classes are specific to dry snow whereas the last two are specific to a period of

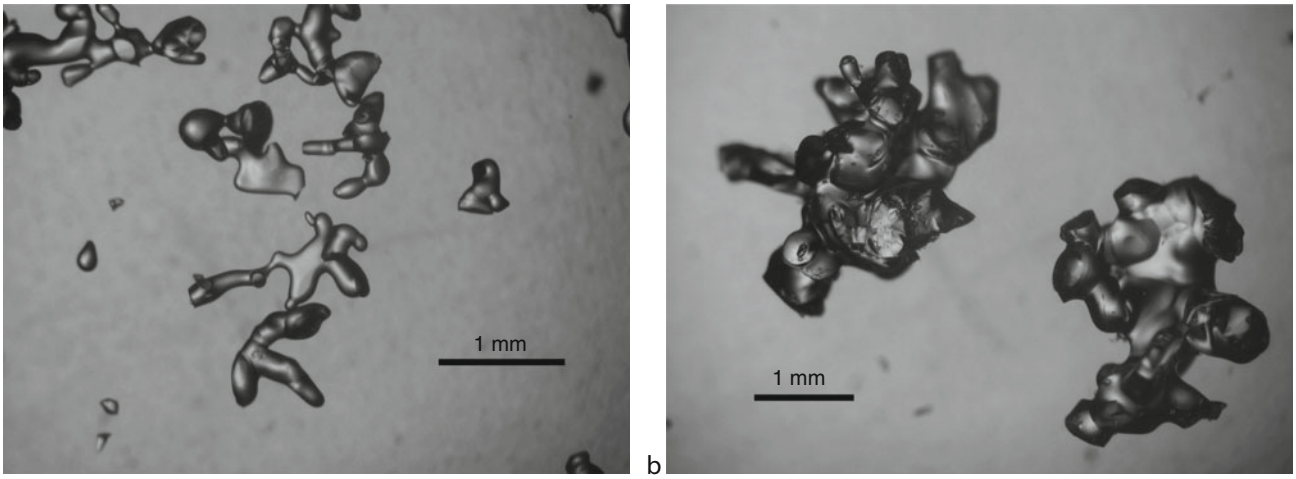

Snow Grains, Figure 1 (**a**) Decomposing precipitation particles from near-surface layer, Mammoth Lakes, California, February, 2001 (Photo: T. H. Painter, from Painter and Dozier (2004), Figure 6). (**b**) Rounded polycrystals from near-surface layer, Mammoth Lakes, California, March, 2001 (Photo: T. H. Painter, from Painter and Dozier (2004), Figure 6).

wet snow. The classes are further divided into subclasses for which the description of the physical process is relied upon to assist in assignment of subclass. These classes and subclasses are used in most applications with little confusion but it is understood that the observations involve human interpretation and as such are inexact.

When modeling radiative transfer and thermal conductivity, these classes are often approximated with analytical forms that resemble atmospheric forms (Macke and Mishchenko, 1996; Mishchenko et al., 1999; Painter and Dozier, 2004) but more detailed treatments are emerging (Kokhanovsky and Zege, 2004). Techniques for automatically retrieving grain shape from X-ray microtomography and digital imagery with the metrics of dendricity (to distinguish "new" from "old" snow) and sphericity (to distinguish faceted from rounded grains) have been demonstrated with modest success (Flin et al., 2005; Bartlett et al., 2008).

Grain size

The complexity of grain shapes and bonds in snow renders the description of grain size difficult. In the ICSSG, the size is defined by the range of the longest extent of a collection of grains. The maximum dimension of a fresh stellar snowflake can be as large as 10 mm whereas the minimum dimension can be as small as 0.05 mm, having an aspect ratio of 200. By contrast, a rounded polycrystal particle that has experienced persistent melt-freeze cycles can be quasi-spherical with a radius of 1 mm (Figure 1b). Without quantitative description of the grain shapes, comparison of single grain sizes for these two particles would be meaningless for any application.

Grain size therefore is often described as the equivalent grain size within the context of application or process. For example, grain size with respect to visible and near-infrared radiative transfer (reflectance, transmission) is described by an optically equivalent grain size, given by the radius of the ice sphere that can represent the optical properties of the observed nonspherical snow. Likewise, equivalent grain size is described for microwave radiative transfer and current efforts are investigating how these equivalent grain sizes are related across the electromagnetic spectrum.

While the concept of "equivalent grain size" is useful from a practical, computational standpoint, a more physically explicit and comparable description of snow grain "size" comes from the specific surface area (SSA). SSA is defined as surface area per unit ice volume ($mm^2/mm^3 = mm^{-1}$) or surface area per unit mass (m^2/kg). The SSA is an essential microstructural parameter for the characterization of sintered materials such as snow, determining radiative properties, adsorption and release of trace gases, and permeability. The radius of the equivalent sphere for a specific surface area is 3/SSA (units of m).

The most fundamental modern method to measure snow SSA is through the determination of adsorption isotherm of gases such as nitrogen or methane (Adamson and Dormant, 1966; Legagneux et al., 2002; Kerbrat et al., 2008). Micro-X-ray tomography and stereology of vertical sections are equally precise (Kerbrat et al., 2008), and have the advantage that they can resolve spatial heterogeneities and very thin layers. Near-infrared photography (Matzl and Schneebeli, 2006) and contact spectroscopy (Painter et al., 2007) likewise give precise results but for the entire snow column at vertical resolutions of <1 mm to ~ 2 cm and far more rapidly than possible with the previous techniques (Figure 2). By resolving heterogeneities and thin layers with these

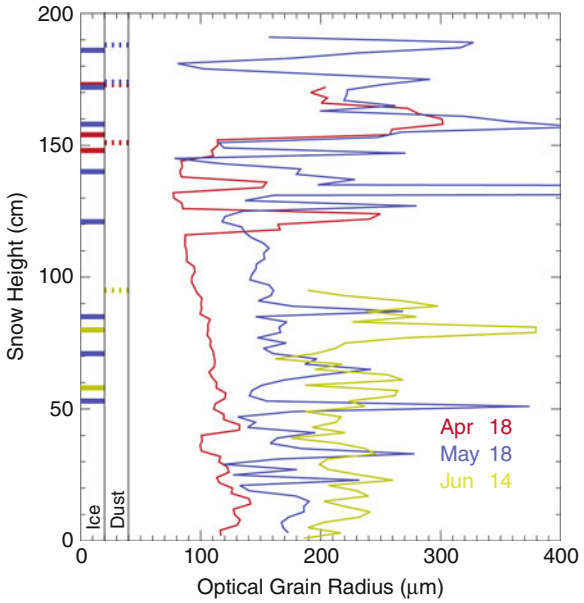

Snow Grains, Figure 2 Optical equivalent grain radius from contact spectroscopy in the San Juan Mountains, Colorado (From Painter et al. (2007), Figure 4).

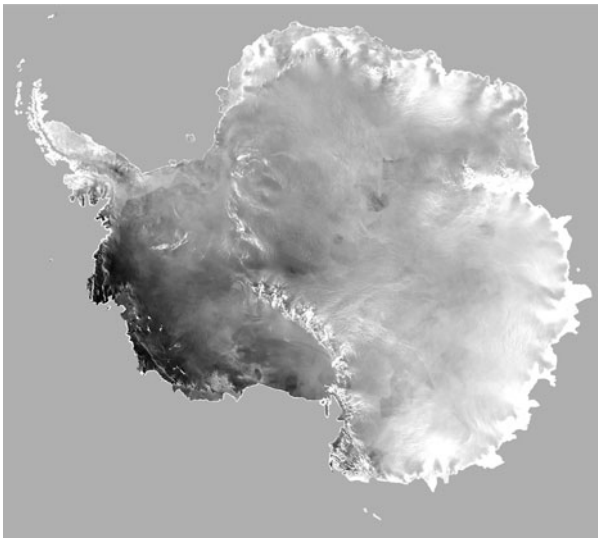

Snow Grains, Figure 3 Optical grain size map of Antarctica from the Mosaic of Antarctica from the NASA Moderate Resolution Imaging Spectroradiometer (MODIS) (Haran et al., 2005; Scambos et al., 2007). The OGS range was 40 μm (*dark*) to 1,100 μm (*light*) in radius (Image courtesy of the National Snow and Ice Data Center [NSIDC]).

techniques, we can better understand the influence on optical and microwave radiative transfer and mechanical properties of the snow column (Painter et al., 2007). These techniques do not presently treat grain shapes but in the future, directional retrievals will facilitate simultaneous retrievals of metrics of grain shape and grain size (Painter et al., 2003).

Remote sensing of snow grains

The spectral reflectance of snow is sensitive to changes in the optical grain size and grain shapes. Because of this sensitivity, multispectral and hyperspectral optical remote sensing from airborne and spaceborne platforms has the capacity to invert the measured reflectance for near-surface, optical grain size (Figure 3). The spatial distribution of optical grain size (which can be inverted for SSA) can be mapped using absolute reflectance at discrete bands in the near infrared (Fily et al., 1997), the integral of ice absorption features from imaging spectrometer data (Nolin and Dozier, 2000), and the general shape of the reflectance spectrum (Scambos et al., 2007; Painter et al., 2009).

Summary

Our understanding of the snow grain has come to more quantitative terms since the seventeenth-century observations by Descartes, Grew, Hooke, and Kepler. Even since the previous International Snow Classification of Seasonal Snow on the Ground in 1990, technological and modeling advances have contributed the X-ray tomograph, portable optical spectroscopy, and performance computing. These most recent technologies have allowed us to explore the three-dimensional structure of snow, specific surface area, and the influences of changes in the concepts of grains on energy and mass transfer. At the time of writing, laboratory, field, and remote sensing experiments are exploring the consistency between wavelength specific equivalent grain sizes and our ability to accurately infer SSA, new reflectance technologies, and relationship between passive and active microwave retrievals of snow water equivalent and our best understanding of the grain.

Bibliography

Adamson, A. W., and Dormant, L. M., 1966. Adsorption of nitrogen on ice at 78 Degrees K. *Journal of the American Chemical Society*, **88**, 2055–2057.

Bartlett, S. J., Rüedi, J.-D., Craig, A., and Fierz, C., 2008. Assessment of techniques for analyzing snow crystals in two dimensions. *Annals of Glaciology*, **48**, 103–112.

Fierz, C., Armstrong, R. L., Durand, Y., Etchevers, P., Greene, E., McClung, D. M., Mishimura, K., Satyawali, P. K., and Sodratov, S. A., 2009. *The International Classification for Seasonal Snow on the Ground*. Paris: UNESCO-IHP.

Fily, M., Bourdelles, B., Dedieu, J. P., and Sergent, C., 1997. Comparison of in situ and Landsat Thematic Mapper derived snow grain characteristics in the Alps. *Remote Sensing of Environment*, **59**(3), 452–460.

Flin, F., Brzoska, J. B., Coeurjolly, D., Pieritz, R. A., Lesaffre, B., Coleou, C., Lamboley, P., Teytaud, O., Vignoles, G. L., and Delesse, J. F., 2005. Adaptive estimation of normals and surface area for discrete 3-D objects: Application to snow binary data from X-ray tomography. *IEEE Transactions on Image Processing*, **14**(5), 585–596.

Haran, T., Bohlander, J., Scambos, T., Painter, T. H., and Fahnestock, M., 2005. *MODIS Mosaic of Antarctica (MOA) Image Map*. Boulder, CO: National Snow and Ice Data Center.
Kerbrat, M., Pinzer, B., Huthwelker, T., Gaggeler, H. W., Ammann, M., and Schneebeli, M., 2008. Measuring the specific surface area of snow with X-ray tomography and gas adsorption: comparison and implications for surface smoothness. *Atmospheric Chemistry and Physics*, **8**(5), 1261–1275.
Kokhanovsky, A. A., and Zege, E. P., 2004. Scattering optics of snow. *Applied Optics*, **43**(7), 1589–1602, doi:10.1364/AO.43.001589.
Legagneux, L., Cabanes, A., and Dominé, F., 2002. Measurement of the specific surface area of 176 snow samples using methane adsorption at 77 K. *Journal of Geophysical Research*, **107**, 4335–4349.
Macke, A., and Mishchenko, M., 1996. Applicability of regular particle shapes in light scattering calculations for atmospheric ice particles. *Applied Optics*, **35**(21), 4291–4296.
Matzl, M., and Schneebeli, M., 2006. Measuring specific surface area of snow by near infrared photography. *Journal of Glaciology*, **52**(179), 558–564.
Mätzler, C., 1997. Autocorrelation functions of granular media with free arrangement of spheres, spherical shells or ellipsoids. *Journal of Applied Physics*, **81**(3), 1509–1517.
Mishchenko, M., Dlugach, J. M., Yanovitskij, E. G., and Zakharova, N. T., 1999. Bidirectional reflectance of flat, optically thick particulate layers: an efficient radiative transfer solution and applications to snow and soil surfaces. *Journal of Quantitative Spectroscopy and Radiative Transfer*, **63**, 409–432.
Nolin, A. W., and Dozier, J., 2000. A hyperspectral method for remotely sensing the grain size of snow. *Remote Sensing of Environment*, **74**(2), 207–216.
Painter, T. H., Paden, B., and Dozier, J., 2003. Automated spectro-goniometer: a spherical-robot for the measurement of the directional reflectance of snow. *Reviews of Scientific Instruments*, **74**(12), 5179–5188.
Painter, T. H., and Dozier, J., 2004, Measurements of the hemispherical-directional reflectance of snow at fine spectral and angular resolution, *Journal of Geophysical Research-Atmospheres*, 109(D18): D1811510.1029/2003JD004458.
Painter, T. H., Molotch, N. P., Cassidy, M. P., Flanner, M. G., and Steffen, K., 2007. Contact spectroscopy for the determination of stratigraphy of snow grain size. *Journal of Glaciology*, **53**(180), 121–127.
Painter, T. H., Rittger, K., McKenzie, C., Slaughter, P., Davis, R. E., and Dozier, J., 2009. Retrieval of subpixel snow covered area, grain size, and albedo from MODIS. *Remote Sensing of Environment*, **113**, 868–879, doi:10.1016/j.rse.2009.01.001.
Scambos, T., Haran, T., Fahnestock, M., Painter, T. H., and Bohlander, J., 2007. MODIS-based Mosaic of Antarctica (MOA) data sets: Continent-wide surface morphology and snow grain size. *Remote Sensing of Environment*, **111**(2–3), 242–257, doi:10.1016/j.rse.2006.12.020.

Cross-references

Albedo
Atmosphere-Snow/Ice Interactions
Dry Snow
Firn
Layering of Snow
Melting Processes
Radiative Transfer Modeling
Snow Crystal Structure
Snow Hydrology
Stratigraphy of Snowpacks

SNOW HYDROLOGY

Sarah Boon, Katie Burles
Department of Geography, University of Lethbridge, Lethbridge, AB, Canada

Definition

Snow hydrology is the study of snow contributions to the hydrologic cycle, particularly snowmelt, meltwater movement within the snowpack, and meltwater contributions to surface runoff.

Snow hydrology processes

The snow accumulation period is characterized by accumulating snow water equivalent (SWE), as observed in many parts of the northern hemisphere and high-elevation locations in the southern hemisphere. During the accumulation period, net energy inputs to the snowpack are negligible: average air temperatures decrease while SWE increases.

The snowmelt period is initiated when air temperatures begin to rise, net energy becomes positive, and SWE begins to decrease. The melt period can be separated into three phases:

1. *Warming*: snowpack temperature increases until the snowpack is isothermal at 0°C.
2. *Ripening*: melt occurs but meltwater remains within the snowpack. At the end of this phase, the snowpack is "ripe": all available pore spaces are saturated with meltwater, and no additional water can be stored (see *Snow Ripening*).
3. *Output*: continuing energy inputs create additional melt. Since the snowpack is saturated, additional melt leaves the pack and contributes to surface hydrology (soil moisture, surface runoff).

The average snowpack may not necessarily follow this exact sequence; in many cases, meltwater is produced at the snow surface prior to the pack becoming isothermal. This meltwater then percolates down through the pack and freezes, releasing latent heat which can act to warm the pack. Alternatively, the snow surface may become isothermal then refreeze until air temperatures increase and melting continues. Snowmelt can be empirically assessed using remote sensing approaches that quantify the areal extent of snowpack and the phase of melt (warming, ripening, output); however, it is difficult to quantify the volume and timing of snowmelt using these approaches (Rango, 1980; Déry et al., 2005; Derksen and MacKay, 2006; Wolken et al., 2009).

Factors influencing snowmelt

The rate and timing of snowmelt is determined mainly by the amount of available energy (Pomeroy and Goodison, 1997), which varies with topography (elevation, aspect), climate and meteorological conditions (maritime,

continental; rain-on-snow events, chinooks), and vegetation cover (open, sub-canopy, shrub, glacier surface). South-facing slopes have higher melt rates than north-facing slopes given increased radiation inputs, while lower elevations melt earlier than high elevations due to higher air temperatures. In maritime climates, rain-on-snow events enhance snowmelt, while in continental climates with frequent föhn (chinook) events, winter melt can occur. Vegetation cover plays a significant role in altering the energy reaching the snow surface, thus melt processes are often divided into open versus forested environments. In open environments (prairie, clear-cut, glacier surface), melt is driven by a combination of both radiative and turbulent fluxes. In forested environments, however, turbulent fluxes are significantly reduced, and radiative fluxes are much more complex. Shrub environments, however, lie between open and forested environments, with reduced longwave radiation inputs relative to a forest, but only slightly reduced turbulent fluxes, and very similar shortwave radiation inputs to open environments.

Snowmelt production: temperature index methods

Snowmelt has historically been calculated using temperature index (degree-day) approaches, which approximate snowmelt as a function of average air temperature (Anderson, 1973):

$$\text{SWE} = M(T_a - T_m) \text{ when } T_a \geq T_m \quad (1)$$

$$\text{SWE} = 0 \text{ when } T_a < T_m \quad (2)$$

where SWE is the snow water equivalent; M is the melt coefficient (also termed melt factor or degree-day factor); and T_a and T_m are the temperature of the atmosphere and snowpack, respectively. This approach assumes that, during melt, $T_m \approx 0°C$, that energy inputs to the pack from longwave and turbulent sources are linear functions of air temperature, and that solar radiation is well correlated with air temperature (Braithwaite, 1984). The melt coefficient can be difficult to determine and is dependent on latitude, elevation, aspect, forest cover, and day of year, all of which must be empirically measured or assumed for various watersheds (Gray and Prowse, 1993). The strength of these models lies in their minimal input data requirements, as air temperature is the most readily available meteorological variable, and their minimal computational requirements. However, these models are highly calibrated (Walter et al., 2005) and are limited to larger spatial scales and longer time periods (i.e., exceeding hourly and daily intervals) (Gray and Prowse, 1993). They are most commonly applied in large-scale watershed models with limited input data; for example, the HBV (Bergström, 1995), SRM (Martinec and Rango, 1986), UBC (Quick and Pipes, 1977), and SWAT (Fontaine et al., 2002) models. Despite their simplistic representation of the snowmelt process, temperature index–based model outputs have been validated in many environments (Beven, 2001).

To improve the physical basis of degree-day models, researchers have defined modified degree-day methods that incorporate additional variables such as snow surface albedo (e.g., Hock, 1999; Pellicciotti et al., 2008). While these models require additional input data and are more computationally intensive than the standard temperature index method, they remain more accessible than energy balance approaches, which can require significant amounts of data and data processing time.

Snowmelt production: energy balance methods

Energy balance models are more complex than temperature index approaches, as they are based on the fundamental physical principles of conservation of energy and mass. Designed for short-term forecasts (e.g., hourly and daily intervals) and highly data intensive (Gray and Prowse, 1993), energy balance models are the most thorough and accurate methods for calculating snowmelt. Figure 1 shows a basic schematic of the vertical energy fluxes during snowmelt in a forested environment. Here we describe the snow surface energy balance in a forested environment, as it is most complex given the ability of the forest canopy (e.g., density, height to live crown, crown depth and diameter, tree condition) to absorb and reflect incoming shortwave radiation, emit longwave radiation, and alter snow surface albedo (Link and Marks, 1999). Forest canopy also increases surface roughness, thereby decreasing wind speeds (Gray and Prowse, 1993).

The energy balance during snowmelt is calculated as:

$$Q_m = Q^* + Q_h + Q_e + Q_g + Q_r - Q_\Theta \quad (3)$$

where: Q_m = energy available for melt; Q^* = net radiation Q_h = convective transport of sensible heat between the air and snowpack; Q_e = latent heat released through condensation of water vapor onto the snowpack or lost through evaporation; Q_g = conduction of heat to the snowpack from the ground; Q_r = advection of heat to the snowpack through rain; Q_θ = rate of change of internal energy per unit surface area per unit time (all in MJ m^{-2} day^{-1}).

Net radiation (Q^*) is the sum of net shortwave (K^*) and net longwave (L^*) radiation fluxes and is the dominant energy flux contributing to snowmelt in forested environments (Link and Marks, 1999; Woo and Giesbrecht, 2000; Koivusalo and Kokkonen, 2002; Spittlehouse and Winkler, 2002). K^* is the total amount of incoming shortwave radiation (K↓) minus outgoing shortwave radiation (K↑). K↓ is representative of the total amount of solar radiation that has reached the ground or snow surface. This includes the portion that is not reflected by clouds or absorbed and scattered by the atmosphere (direct beam [S]), and the portion that is scattered by the atmosphere or above-surface objects such as trees (diffuse solar radiation [D]). K↑ is a function of the surface albedo (α), or reflectivity, which is calculated as the ratio of incoming solar radiation reflected by a surface to the total amount incident on that surface. Albedo declines as snow ages and melts (Table 1), and is also affected by organic debris

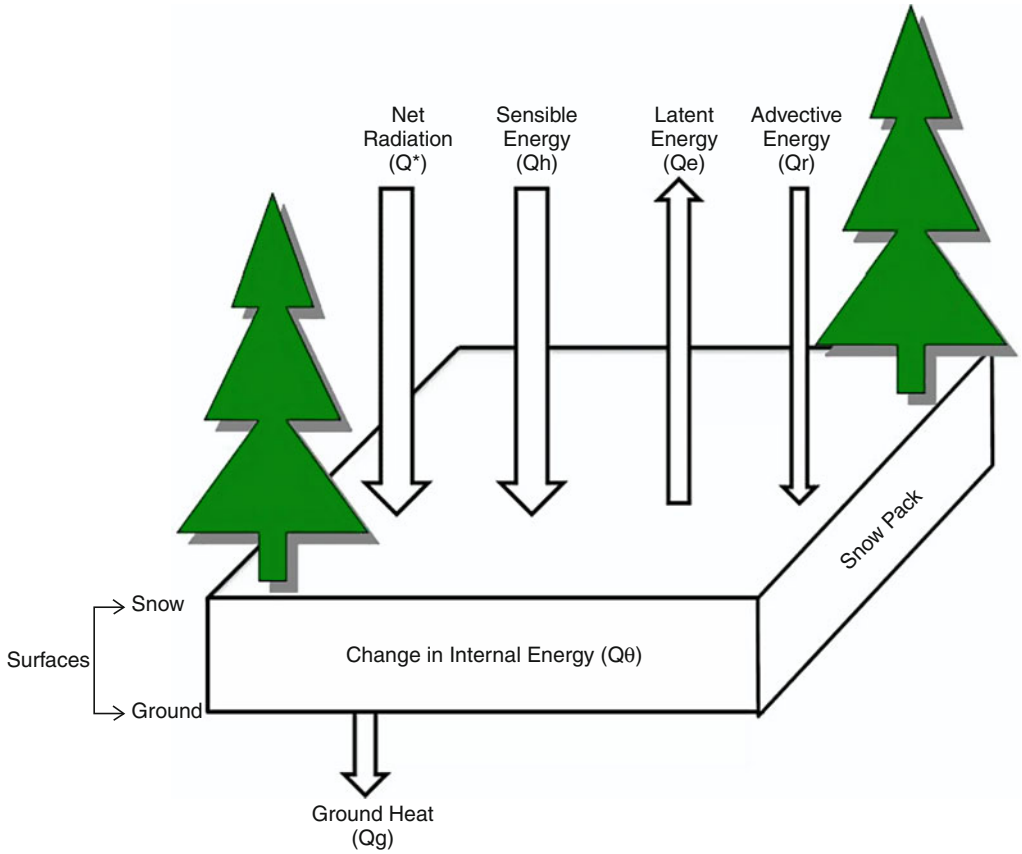

Snow Hydrology, Figure 1 Schematic of vertical energy fluxes in a forested environment (Modified from Gray and Prowse, 1993).

Snow Hydrology, Table 1 Albedo of various surfaces (From Gray and Prowse, 1993)

Surface	Typical range in albedo
New snow	0.80–0.90
Old snow	0.60–0.80
Melting snow-porous-fine grained	0.40–0.60
Forests-conifers, snow	0.25–0.35
Forests-green	0.10–0.20
Water	0.05–0.15
Snow ice	0.30–0.55
Black ice: intact → candled → granulated	0.10→0.40→0.55

accumulating on the snow surface (Link and Marks, 1999; Melloh et al., 2001; Winkler et al., 2010). Albedo can also be significantly affected later in the melt season, when the snowpack becomes patchy and the underlying ground surface is exposed (Liston, 1995). K↓ is not limited to the snow surface, but can penetrate up to 10 cm into the snowpack (Brock et al., 2000) , and reach the ground surface in shallow packs (DeWalle and Rango, 2008) with subsequent implications for the energy balance.

K^* in forested stands can be calculated as:

$$K^* = K \downarrow \tau_c(1 - \alpha) \quad (4)$$

where canopy transmissivity (τ_c) is the amount of K↓ transmitted through the forest canopy (Boon, 2009) and is largely dependent on tree type, stand characteristics, stand age, and stand productivity (Geiger et al., 2003). In coniferous forests, up to 90% of incident shortwave radiation may be absorbed by the canopy (Gray and Prowse, 1993).

L^* is the sum of all longwave radiation emitted by the atmosphere (L↓) minus the amount emitted by the Earth's surface (L↑). In the absence of clouds, L↓ is a function of atmospheric temperature and emissivity (ε), the latter of which is dependent on the vertical distribution of atmospheric temperature, water vapor, and carbon dioxide (Oke, 1988). Periods of low cloud cover increase L↓ from the atmosphere (Gray and Prowse, 1993). L↓ is important for snowmelt in dense forests, where a significant proportion of incident shortwave radiation is absorbed by the canopy and reemitted to the snow surface. As snow can more effectively absorb longwave versus shortwave radiation, this causes higher snowmelt rates near tree trunks (Reifsnyder and Lull, 1965) and results in high

spatial variability in melt rates (Bohren and Thorud, 1973). As with L↓, L↑ is dependent on the temperature and ε of the ground surface (Table 2). In forested environments, L^* at the snow surface is the sum of L↓ from the atmosphere, canopy, and tree stems; and L↑ from the snow surface:

$$L^* = \tau_L L\downarrow + (1-\tau_L)\varepsilon_c \sigma {T_c}^4 + (H_t/H)\varepsilon_t \sigma {T_t}^4 - \varepsilon_{ss}\sigma {T_{ss}}^4 \quad (5)$$

L↓ from the atmosphere and canopy is dependent on the sky view factor (τ_L) which is the proportion of hemisphere visible beneath the forest canopy. L↓ from the canopy is a function of the Stefan–Boltzmann law ($\varepsilon\sigma T^4$); where σ is the Stefan-Boltzmann constant = 5.67×10^{-8} W m^{-2} K^{-4} and the fraction of the hemisphere covered by canopy. L↓ from the tree stems is a function of the ratio of the hypothetical hemisphere surface area affected by longwave radiation from the tree trunk (H_t) and the hypothetical hemispherical area emitting longwave radiation to a point on the snow surface located at a distance from the tree trunk (H), multiplied by the energy emitted by the tree stems (Woo and Giesbrecht, 2000). Finally, L↑ from the snow surface is determined by the temperature and emissivity of the snow surface (Table 2).

The turbulent heat fluxes – sensible (Q_h) and latent (Q_e) heat – represent the exchange of energy between the snow surface and overlying air due to temperature and vapor pressure gradients, respectively (Andreas, 2002). These transfers occur not only at the snow surface, but also within the top few centimeters of the snowpack as wind is "pumped" into the pore spaces of the pack itself (Colbeck, 1997). Under dense forest canopies, where wind speeds are generally low, turbulent heat transfers are small (Woo and Giesbrecht, 2000). However, Q_h and Q_e can dominate the snowpack energy balance under strong warm winds, resulting in high short-term melt rates (Moore, 1983; Hayashi et al., 2005).

These fluxes are calculated as:

$$Q_h = \rho C_a D_k (T_a - T_s s) \quad (6)$$

$$Q_e = \rho \lambda_v D_e \left(\frac{0.622}{P}\right)(e_a - e_{ss}) \quad (7)$$

Snow Hydrology, Table 2 Emissivity of various surfaces (From Oke, 1988)

Surface	Typical emissivity range
Snow old → fresh	0.82–0.99
Forests deciduous bare → leaved	0.97–0.98
Forest coniferous	0.97–0.99
Water	0.92–0.97
Ice	0.92–0.97

where: ρ = density of air (kg m^{-3}); C_a = heat capacity of air (J kg^{-1} K^{-1}); D_h = bulk transfer coefficient for sensible heat (m s^{-1}); T_a, T_{ss} = temperature of the atmosphere and snow surface (°C), respectively; P = atmospheric pressure (kPa); λ_v = latent heat of vaporization (2.48×10^6 J kg^{-1}); D_e = bulk transfer coefficient for latent heat (m s^{-1}); and e_a, e_{ss} = atmospheric and snow surface vapor pressure (kPa), respectively.

The bulk transfer coefficients for latent and sensible heat vary with atmospheric condition. Under neutral atmospheric conditions, $D_h = D_e$ (Price, 1977):

$$D_h = D_e = \frac{k^2 u_a}{\left[\ln\left(\frac{z_a}{z_o}\right)\right]^2} \quad (8)$$

where k is Von Karman's constant (0.40), u_a is the wind speed (m s^{-1}), z_a is the height of the wind measurement (m), and z_o is the roughness length of the snow surface (m). Values of z_o range from 0.0002 to 0.02 m, with the greatest roughness lengths over older snow (Moore, 1983). When atmospheric conditions become highly stratified, the bulk aerodynamic method (Richardson number) is used:

$$R_i = \frac{g(T_a - T_{ss})z_a}{{u_a}^2 T_k} \quad (9)$$

where g is the gravitational acceleration (m s^{-2}) and T_k is the mean temperature of the air layer. Conditions are stable when $R_i > 0$, and unstable when $R_i < 0$. Air temperatures during snowmelt are usually >0°C, resulting in log-linear profiles for wind, temperature, and vapor pressure above the snow surface and stable atmospheric conditions, with $D_m = D_h = D_e$ (Price, 1977; Moore, 1983), calculated as:

$$D_m = D_m/(1 + 10R_i) \quad (10)$$

where D_m is the bulk exchange coefficient for momentum.

Ground heat (Q_g) flux occurs at the base of the snowpack and is estimated using soil temperature and moisture data (Gray and Prowse, 1993). Soil temperature generally increases with depth as a result of energy stored during the summer months and geothermal heat, thus establishing a temperature gradient that results in heat conduction upward to the ground surface and the base of the snowpack:

$$Q_g = k_G\left(\frac{T}{z}\right) \quad (11)$$

where k_G is the thermal conductivity of the soil, which varies spatiotemporally as a function of soil texture, soil density, and moisture content (Oke, 1988); T is the soil temperature (°C); and z is the depth of measurement below the ground surface (m). In comparison with Q^*, Q_h and Q_e, Q_g is relatively small on a daily time step (0–6 W m^{-2}); thus it is either assumed to be negligible, or to be a constant value in the energy balance equation

(USACE, 1956; Melloh, 1999). While the effects of Q_g on snowmelt can be ignored over short time periods (Gray and Prowse, 1993), the cumulative ground heat flux should be considered over entire winter seasons (Pomeroy and Goodison, 1997).

Advective energy (Q_r) is supplied to the snowpack by rainfall during the snowmelt period; the magnitude of the energy contribution depends on the regional climate and the frequency and magnitude of rain-on-snow events (e.g., Storck et al., 2002). Q_r is measured as the ratio between rainfall energy content while airborne (prior to contact with the snow surface) and energy content on reaching thermal equilibrium within the pack (Gray and Prowse, 1993). Two main scenarios are considered: (1) rainfall on an isothermal pack where the rain does not freeze; or (2) rainfall on a frozen pack (<0°C) at which point the rainfall freezes, releasing the heat of fusion (Male and Gray, 1981). These processes are calculated as:

$$Q_r = \rho_w C_w P(T_r - T_{ss}) \tag{12}$$

$$Q_r = \rho_w C_w P(T_r - T_{ss}) + \rho_w \lambda_F P \tag{13}$$

where ρ_w = density of liquid water (~1,000 kg m^{-3}); C_w = specific heat of liquid water (~0.0042 MJ kg^{-1}°C^{-1}); P = rainfall rate (L s^{-1}); T_r = temperature of rain (°C); T_{ss} = temperature of the volume of snow (°C); and λ_F = latent heat of fusion (~0.334 MJ kg^{-1}).

Finally, Q_θ is the rate of change of internal energy in the snowpack (Gray and Prowse, 1993). Within deep snowpacks, Q_θ can be relatively small in comparison to other energy fluxes, and is often considered negligible as snowpack temperature during ablation is ~0°C. However, midday snowmelt followed by overnight freezing can result in large changes in internal energy in both shallow snowpacks and the upper layers of deep packs. Q_θ is calculated as:

$$Q_\theta = (\rho_i C_i + \rho_w C_w + \rho_v C_v)\Delta T_i Z_i \tag{14}$$

where: ρ_i = density of snow and ice (~922 kg m^{-3}); C_i = specific heat of snow and ice (~0.0021 MJ kg^{-1}°C^{-1}); ρ_v = density of water vapor (kg m^{-3}); C_v = specific heat of water vapor (MJ kg^{-1}°C^{-1}); ΔT_i = the change in snow temperature (°C); and Z_i = snow depth (m).

Internal changes in snowpack temperature can also be measured using thermistor strings, or modelled using one-dimensional snow temperature and energy balance models such as SNTHERM (Jordan, 1991; Melloh, 1999).

Once the total energy available for melt (Q_m) is calculated, the total amount of meltwater or snow water equivalent (SWE) (in m) can be calculated as (Pomeroy and Goodison, 1997):

$$\mathrm{SWE} = Q_m/(\rho_w \lambda_F B_i) \tag{15}$$

where the thermal quality of snow (B_i) is the fraction of ice in a unit mass of snow (approximately 0.95–0.97) (Male and Gray, 1981).

Water movement through the snowpack

Once melt is initiated, meltwater can flow through the snowpack as both Darcian flow through an unsaturated porous medium (Colbeck, 1976) and as flow "fingers" that concentrate in particular regions of the pack (Colbeck, 1979; Albert et al., 1999). Water movement is a function of the temperature, structure, and water content of the snowpack (USACE, 1956; Waldner et al., 2004); for example, the presence of ice lenses or weaker snowpack layers can cause preferential flow paths within the pack. Observed time lags between melt onset and runoff production are a function of cold content, the liquid-water-holding capacity of the pack, and meltwater transmission through the snowpack as a function of permeability and gravity (Fountain, 1996; DeWalle and Rango, 2008) (see Cross-references).

Runoff generation from the snowpack

Meltwater outflow is generated from the snowpack once it can no longer hold meltwater within its internal pore spaces. This meltwater is then routed to surface runoff via overland flow, subsurface stormflow, and groundwater flow, the timing of which is critical for basin-scale runoff. Thus, snow hydrology is strongly linked with soil moisture and runoff generation, groundwater recharge, spring freshet, and climate change (see Cross-references).

New directions in snow hydrology

Current snow hydrology research is examining key topics around the relative importance of topography and vegetation cover in driving the snowmelt energy balance. Research suggests that south-facing slopes are more sensitive to changes in forest canopy cover than north-facing slopes, given the role of the canopy in attenuating incoming shortwave radiation and driving fluxes of incident radiation at the snow surface. Research is also detailing the role of forest litter and atmospheric dust on snow surface albedo, the snowmelt energy balance, and subsequent melt and runoff. Shifting weather patterns have increased long-range dust transport from arid/semi-arid regions to mountain snowpacks (Painter et al., 2007), while increasing rates of forest disturbance have enhanced forest litter production and incorporation into the snowpack (Winkler et al., 2010). While both dust and forest litter have significant impacts on snow surface albedo, they behave differently in terms of their effect on spectral albedo – thus new research is examining the spectral reflectance properties of both contaminant types in an effort to quantify their impact on snowmelt and runoff. Additional research is examining the relationship between snow hydrology and soil moisture (Seyfried et al., 2009; Williams et al., 2009), which is critical for determining patterns of runoff generation at the watershed scale (James and Roulet, 2009). Finally, research continues to assess the effects of shifts in air temperature and precipitation amount and type

as a result of climate change, and associated forest cover change, on snow hydrology (Bales et al., 2006; Lundquist et al., 2008; Jost et al., 2009). See Cross-references.

Bibliography

Albert, M., Koh, G., and Perron, F., 1999. Radar investigations of melt pathways in a natural snowpack. *Hydrological Processes*, **13**(18), 2991–3000.

Anderson, E. A., 1973. *National Weather Service River Forecast System – Snow Accumulation and Ablation Model*. NWS Hydro-17. Silver Spring: US Dept. Commerce, NOAA, National Weather Service.

Andreas, E. L., 2002. Parameterizing scalar transfer over snow and ice: A review. *Journal of Hydrometeorology*, **3**(4), 417–432.

Bales, R. C., Molotch, N. P., Painter, T. H., Dettinger, M. D., Rice, R., and Dozier, J., 2006. Mountain hydrology of the western United States. *Water Resources Research*, **42**(8), 13. W08432.

Bergström, S., 1995. The HBV model. In Singh, V. P. (ed.), *Computer Models of Watershed Hydrology*. Colorado: Water Resources Publications, pp. 443–476.

Beven, K. J., 2001. *Rainfall-Runoff Modelling – The Primer*. London: Wiley.

Bohren, C. F., and Thorud, D. B., 1973. Two theoretical models of radiation heat transfer between forest trees and snowpacks. *Agricultural Meteorology*, **11**, 3–16.

Boon, S., 2009. Snow ablation energy balance in a dead forest stand. *Hydrological Processes*, **23**(18), 2600–2610.

Braithwaite, R. J., 1984. Calculation of degree-days for glacier-climate research. *Zeitschrift für Gletscherkunde und Glazialgeologie*, **20**, 1–8.

Brock, B. W., Willis, I. C., and Sharp, M. J., 2000. Measurement and parameterization of albedo variations at Haut glacier d'Arolla, Switzerland. *Journal of Glaciology*, **46**(155), 675–688.

Colbeck, C., 1976. Analysis of water flow in dry snow. *Water Resources Research*, **12**(3), 523–527.

Colbeck, C., 1979. Water flow through heterogeneous snow. *Cold Regions Science and Technology*, **1**(1), 37–45.

Colbeck, C., 1997. Model of wind pumping for layered snow. *Journal of Glaciology*, **43**(143), 60–65.

De Walle, D. R., and Rango, A., 2008. *Principles of Snow Hydrology*. New York: Cambridge University Press, p. 410.

Derksen, C., and MacKay, M., 2006. The Canadian northern boreal snow water equivalent band. *Atmosphere-Ocean*, **44**(3), 305–320.

Déry, S. J., Salomonson, V. V., Stieglitz, M., Hall, D. K., and Appel, I., 2005. An approach to using snow areal depletion curves inferred from MODIS and its application to land surface modelling in Alaska. *Hydrological Processes*, **19**, 2755–2774.

Fontaine, T. A., Cruickshank, T. S., Arnold, J. G., and Hotchkiss, R. H., 2002. Development of a snowfall-snowmelt routine for mountainous terrain for the soil water assessment tool (SWAT). *Journal of Hydrology*, **262**, 209–223.

Fountain, A. G., 1996. The effect of snow and firn hydrology on the physical and chemical characteristics of glacial runoff. *Hydrological Processes*, **10**, 509–521.

Geiger, R., Aron, R. H., and Todhunter, P., 2003. *The climate near the Ground*. Langham: Rowman & Littlefield, p. 584.

Gray, D. M., and Prowse, T. D., 1993. Snow and floating ice. In Maidment, D. (ed.), *Handbook of Hydrology*. New York: McGraw-Hill, pp. 7.1–7.58.

Hayashi, M., Hirota, T., Iwata, Y., and Takayabu, I., 2005. Snowmelt energy balance and its relation to foehn events in Tokachi, Japan. *Journal of the Meteorological Society of Japan*, **93**, 783–798.

Hock, R., 1999. A distributed temperature-index ice- and snowmelt model including potential direct solar radiation. *Journal of Glaciology*, **45**(149), 101–111.

James, A. L., and Roulet, N. T., 2009. Antecedent moisture conditions and catchment morphology as controls on spatial patterns of runoff generation in small forest catchments. *Journal of Hydrology*, **377**, 351–366.

Jordan, R., 1991. A one-dimensional temperature model for a snow cover: technical documentation for SNTHERM89. Hanover, NH: US Army Corps of Engineers, Cold Regions Research and Engineering Lab, Special Report 91-16.

Jost, G., Moore, R. D., Weiler, M., Gluns, D. R., and Alila, Y., 2009. Use of distributed snow measurements to test and improve a snowmelt model for predicting the effect of forest clearcutting. *Journal of Hydrology*, **376**(1–2), 94–106.

Koivusalo, H., and Kokkonen, T., 2002. Snow processes in a forest clearing and in a coniferous forest. *Journal of Hydrology*, **262**, 145–164.

Link, T. E., and Marks, D., 1999. Point simulation of seasonal snowcover dynamics beneath boreal forest canopies. *Journal of Geophysical Research*, **104**(D22), 27841–27857.

Liston, G. E., 1995. Local advection of momentum, heat and moisture during the melt of patchy snow covers. *Journal of Applied Meteorology*, **34**, 1705–1715.

Lundquist, J. D., Neiman, P. J., Martner, B., White, A. B., Gottas, D. J., and Ralph, F. M., 2008. Rain versus snow in the Sierra Nevada, California: Comparing radar and surface observations of melting level. *Journal of Hydrometeorology*, **9**, 194–211.

Male, D. H., and Gray, D. M., 1981. Snowcover ablation and runoff. In Gray, D. M. (ed.), *Handbook of Snow*. New Jersey: The Blackburn Press, pp. 360–430.

Martinec, J., and Rango, A., 1986. Parameter values for snowmelt runoff modeling. *Journal of Hydrology*, **84**, 197–219.

Melloh, R. A., 1999. A synopsis and comparison of selected snowmelt algorithms. Cold Regions Research and Engineering Lab Report 99-8.

Melloh, R. A., Hardy, J. P., Davis, R. E., and Robinson, P. B., 2001. Spectral albedo/reflectance of littered forest snow during the melt season. *Hydrological Processes*, **15**(18), 3409–3422.

Moore, R. D., 1983. A comparison of the snowmelt energy budget in two alpine basins. *Archives of Meteorology, Geophysics and Bioclimatology Series A*, **33**, 1–10.

Oke, T., 1988. *Boundary Layer Climates*. New York: Routledge, p. 464.

Painter, T. H., Barrett, A. P., Landry, C. C., Neff, J. C., Cassidy, M. P., Lawrence, C. R., McBride, K. E., and Farmer, G. L., 2007. Impact of disturbed desert soils on duration of mountain snow cover. *Geophysical Research Letters*, **34**(12), 6. L12502.

Pellicciotti, F., Helbing, J., Rivera, A., Favier, V., Corripio, J., Araos, J., Sicart, J. E., and Carenzo, M., 2008. A study of the energy balance and melt regime on Juncal Norte glacier, semi-arid Andes of central Chile, using melt models of different complexity. *Hydrological Processes*, **22**(19), 3980–3997.

Pomeroy, J. W., and Goodison, B. E., 1997. Winter and Snow. In Bailey, W. G., Oke, T. R., and Rouse, W. R. (eds.), *The Surface Climates of Canada*. Montreal: McGill-Queen's University Press, pp. 68–100.

Price, A. G., 1977. *Snowmelt runoff processes in a subarctic area*. Climatology Research Series No. 10. Montreal: McGill University.

Quick, M. C., and Pipes, A., 1977. UBC watershed model. *Hydrological Sciences Bulletin*, **22**(1), 153–161.

Rango, A., 1980. Remote sensing of snow covered area for runoff modelling. *International Association of Hydrological Sciences*, **129**, 291–297.
Reifsnyder, W. E., and Lull, H. W., 1965. *Radiant energy in relation to the forest*. USDA Agricultural Technical Bulletin No. 1344, 111 pp. (Reprinted by AMS Press, 1979).
Seyfried, M. S., Grant, L. E., Marks, D., Winstral, A., and McNamara, J., 2009. Simulated soil water storage effects on streamflow generation in a mountainous snowmelt environment, Idaho, USA. *Hydrological Processes*, **23**, 858–873.
Spittlehouse, D. L., and Winkler, R. D., 2002. Modelling snowmelt in a forest and clearcut. In *Proceedings 25th Conference on Agricultural and Forest Meteorology*, 20–24 May 2002, Norfolk Virginia. American Meteorological Society, Boston, MA, pp. 121–122.
Storck, P., Lettenmaier, D. P., and Bolton, S., 2002. Measurement of snow interception and canopy effects on snow accumulation and melt in mountainous maritime climate, Oregon, USA. *Water Resources Research*, **38**(11), 1223–1238.
United States Army Corps of Engineers, 1956. *Snow hydrology: summary report of the snow investigations*. US Army Corps of Engineers, North Pacific Division, Portland, OR.
Waldner, P. A., Schneebeli, M., Schultze-Zimmerman, U., and Fluhler, H., 2004. Effect of snow structure on water flow and solute transport. *Hydrological Processes*, **18**(7), 1271–1290.
Walter, M. T., Brooks, E. S., McCool, D. K., King, L. G., Molnau, M., and Boll, J., 2005. Process-based snowmelt modeling: does it require more input data than temperature-index modeling? *Journal of Hydrology*, **300**(1–4), 65–75.
Williams, C. J., McNamara, J. P., and Chandler, D. G., 2009. Controls on the temporal and spatial variability of soil moisture in a mountainous landscape: the signature of snow and complex terrain. *Hydrology and Earth System Sciences*, **13**, 1325–1336.
Winkler, R., Boon, S., Zimonick, B., and Baleshta, K., 2010. Assessing the effects of post pine beetle forest litter on snow albedo. *Hydrological Processes*, **24**, 803–812.
Wolken, G., Sharp, M., and Wang, L., 2009. Snow and ice facies variability and ice layer formation on Canadian Arctic ice caps, 1999–2005. *Journal of Geophysical Research, Earth Surface*, **114**, 14, doi:10.1029/2008JF001173. F03011.
Woo, M., and Giesbrecht, M. A., 2000. Simulation of snowmelt in a subarctic spruce woodland: 1. Tree model. *Water Resources Research*, **36**, 2275–2285.

Cross-references

Albedo
Atmosphere–Snow/Ice Interactions
Degree-Days
Depletion of Snow Cover
Global Warming and its Effect on Snow/Ice/Glaciers
Hydrologic Cycle and Snow
Impacts of Snow and Glaciers on Runoff
Latent Heat of Condensation
Latent Heat of Fusion/Freezing
Latent Heat of Sublimation
Latent Heat of Vaporization/Condensation
Melt Runoff Modeling
Melting Processes
Rain-Induced Snowmelt
Runoff Generation
Snow and Vegetation Interaction
Snow Cover and Snowmelt in Forest Regions
Snow Metamorphism
Snow Ripening
Snow Water Equivalent
Specific Melt Rate

SNOW LAYER

A. K. Singh
DIAT (Deemed University), Girinagar, Pune, Maharashtra, India

Snow cover forms layer by layer (Figure 1), from one storm to another through interaction with atmosphere along with densification, accumulating in high-altitude geographic regions. In order to follow the evolution of a given snow layer, it is necessary to construct a time profile, based on a series of pits excavated through the snow cover at periodic intervals where density, crystal size and type, temperature, and other properties of the individual layers can be analyzed.

Assessing the formation and stability of snow layer is important in the study and prediction of avalanches. Many of the mechanical and thermal properties of snow that are significant to avalanche formation are related to a large extent on snow density. Temperature, crystal type, superimposed load, and temperature gradient all play a role in determining snow density. There is a strength variation in the snowpack due to its multilayered character. The mechanical properties of snow layers determine if it is stable enough to prevent an avalanche. Such stability information requires analysis of snow on avalanche slopes on a regular basis. The snow layers in which depth hoar formation (TG metamorphism) takes place show a distinctly different densification pattern. The density increases very slowly (reflecting the common observation that depth hoar layers undergo little settlement), and

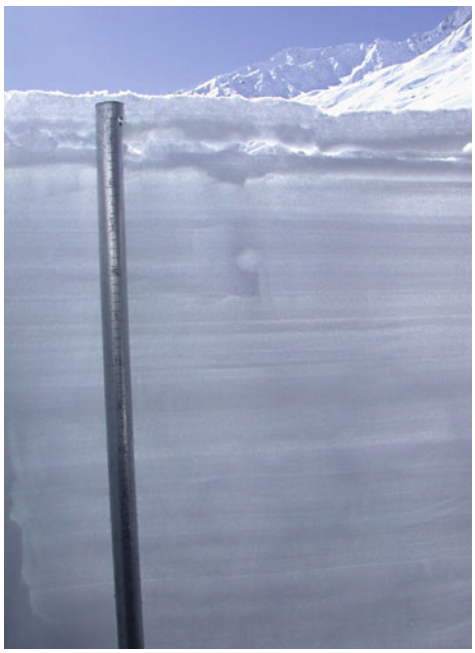

Snow Layer, Figure 1 Snow layers in snow cover.

requires over 100 days to reach a value of 300 kg/m^3. The density values are also of importance in evaluation of forecasting snowmelt runoff as snow covers are important water resources that feed streams and rivers. Snowpacks are also studied in relation to climatic change and global warming.

SNOW LOAD

A. K. Singh
DIAT (Deemed University), Girinagar, Pune, Maharashtra, India

Snow load is the force acting on a structure. Load causes stress, deformation, and displacement in structures. Assessment of its effects is carried out by the methods of structural analysis. Excess load or overloading may cause structural failure. In addition to the load magnitude, its frequency of occurrence, distribution, and nature (static or dynamic) are important factors in design.

The load resulting from the accumulation of snow on a roof in a severe winter must be taken into account in designing buildings in snow-bound hilly regions. The unit weight factor is used in the design of a flat or pitched roof for the probable amount of snow lying upon it. Roof failures in snow-bound regions are often associated with early spring rains, and, therefore, it is advisable to add to the snow load, the load of rainwater also, that might be retained in the snow.

SNOW METAMORPHISM

A. K. Singh
DIAT (Deemed University), Girinagar, Pune, Maharashtra, India

Since snow, in nature, exists close to its melting point, it transforms with time depending on the physical parameters of the snow environment. This process is called metamorphism. Under metamorphism we study change in crystal structure with change in temperature and pressure conditions. Fresh snow crystal is a branched structure (Figure 1a and b), which immediately after touching the ground starts decaying (Figure 1c and d). Researchers have described three types of thermal metamorphism, namely, Equi-temperature (ET) or equilibrium forms,

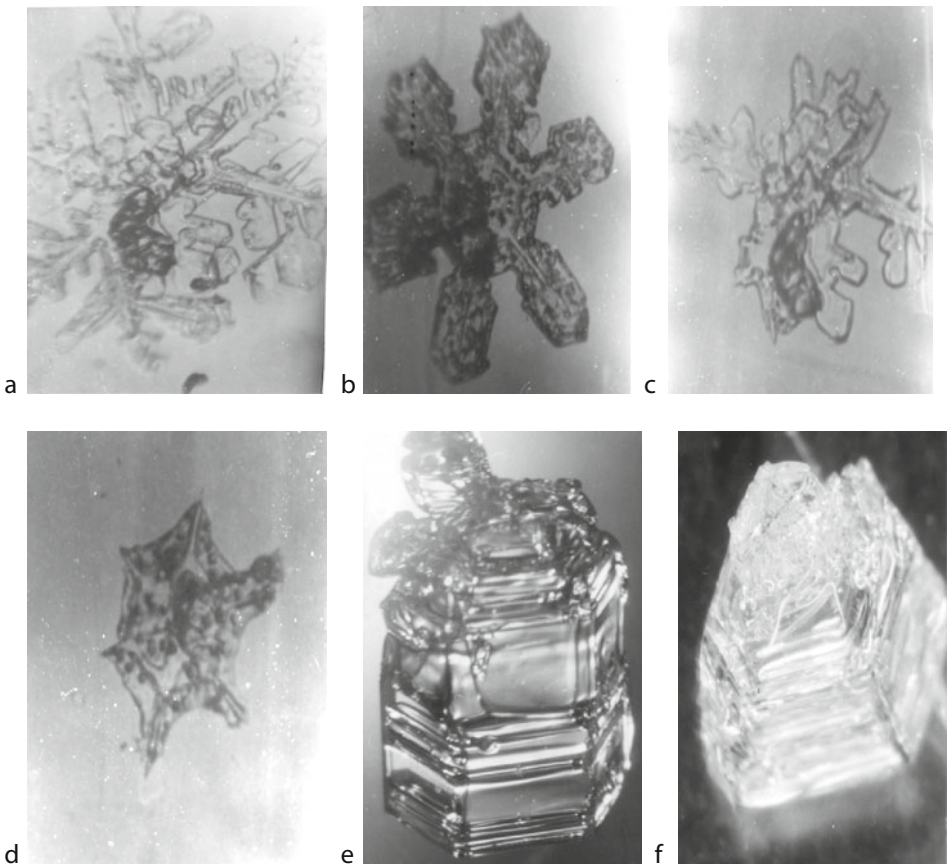

Snow Metamorphism, Figure 1 Snow grains, (**a, b**) new snow (**c, d**) rounding of snow (**e, f**) depth hoar (TG) snow.

Temperature-gradient (TG) metamorphism or kinetic growth forms (Figure 1e and f), and Melt-freeze (MF) metamorphism. Depending upon the temperature and temperature gradient inside snow cover, felt-like crystal may either convert to round or ET or TG grains. In almost all the situations there is fast destruction of branches of fresh snow crystal to felt-like structure. TG metamorphism is the source of weak layer formation in the snow cover and is of importance in avalanche studies and is an active research field in snow and ice community. Metamorphic modification of structure, texture, and density of snow is accompanied by changes in the mechanical properties of snow.

For ET growth, curvature effects are dominant in changing the crystal morphology, and vapor pressure over convex region is higher than that over concave region. Due to this, vapor transfer takes place from convex to concave surface thereby rounding off fresh snow crystal or felt-like crystal. During ET metamorphism the density changes from approximately 80 to 250 kg m^{-3}. Equilibrium form dominates snow pack at low temperature gradients and temperatures above −6°C.The process of equilibrium form goes through various stages, that is, rounding, growth of neck or bond, and further rounding and becoming almost equi-dimensional. This process has great significance in avalanche formation. The rounding of the snow grains and the neck formation tend to increase snow strength in tension, compression, as well as in shear.

For TG growth, if air temperature is very low or snow pack is very shallow, there exists a strong temperature gradient. Vapor migrates from higher temperature to lower temperature regions upwardly. On countering an obstruction or grain the vapor is directly deposited over the grain surface, thereby forming faceted or inverted cup-like crystal structures (Figure 1e and f) that are instrumental to avalanche formation. These depth hoar grains, being angular in character, generally do not bond well and exhibit extremely poor strength in shear. The depth hoar layers have high compressive viscosity and therefore snow density remains constant during formation.

The melt-freeze (MF) process occurs due to cyclic variation in snow surface temperature, resulting in formation of large poly-granular grains after repeated cycles of melting and refreezing and is known as MF metamorphism. In spring, the entire snowpack becomes isothermal near 0°C, however, the temperature varies considerably between day and night, resulting in melting and refreezing.

SNOW MICROSTRUCTURE

Christine Pielmeier
WSL Institute for Snow and Avalanche Research SLF, Warning and Prevention, Davos Dorf, Switzerland

Synonyms

Snow texture

Definition

The most recent definition of snow microstructure is given in the International Classification of Seasonal Snow on the Ground (Fierz et al., 2009, p. 3): "Snow on the ground is a highly porous, sintered material made up of a continuous ice structure and a continuously connected pore space, forming together the snow microstructure." Hence, snow microstructure is the size, shape, and number of structural elements and their arrangement in a sample of snow. A previous definition by Arons and Colbeck (1995) distinguished between snow microstructure and snow texture. They defined snow texture in terms of microstructure and mesostructure. Snow texture combines on the microscale the size and shape of individual ice particles with the three-dimensional arrangement and interconnectedness of the grains and pore spaces in a mesoscale specimen of snow.

Genesis

The microstructure of snow in the atmosphere (new snow) is initially determined by the meteorological (crystal type, snow fall intensity, temperature, wind, radiation) disposition during the snow fall period. After the snow reaches the ground it forms the snowpack. Properties of the ground or of the existing snowpack influence the deposition process. Postdepository metamorphism as well as mechanical and meteorological impacts produce large and persistent changes in the snow microstructure as long as the snowpack exists on the ground. Snow microstructure disappears either by melting of the snowpack or by the transformation of firn to glacial ice.

Relevance of snow microstructure

The snow microstructure is complex, since size, shape, and number of structural elements and their arrangement vary widely spatially and also temporarily in natural snowpacks. Thermodynamic, electromagnetic, and mechanical processes in snow depend highly on the microstructure of snow. Hence, the current state of the snow microstructure itself has a feedback effect on all processes within the snowpack and consequently on the future microstructure.

Measurement and simulation

Traditionally, snow microstructure is approximated by measuring the properties of isolated grains, knowing that it is an incomplete model of the three-dimensional ice-air-matrix (Fierz et al., 2009). Porous materials such as snow can be described by their porosity, specific surface area, and curvature. Recent progress has been made to simulate the thermal, mechanical, and electromagnetic properties of snow (Schneebeli, 2004; Flin and Brzoska, 2008; Kaempfer and Plapp, 2009; Satyawali et al., 2009), and to correlate to specific surface area and porosity (Johnson and Schneebeli, 1999; Matzl and Schneebeli, 2006; Dadic et al., 2008; Toure et al., 2008).

Conclusion

Recent studies show the importance of considering the snow microstructure in order to explain the snow

properties correctly. To improve our knowledge of thermodynamic, electromagnetic, and mechanical processes in snow, the snow microstructure has to be quantified and considered in the analysis and in simulations.

Bibliography

Arons, E. M., and Colbeck, S. C., 1995. Geometry of heat and mass transfer in dry snow: a review of theory and experiment. *Reviews of Geophysics*, **33**(4), 463–493.

Dadic, R., Schneebeli, M., Lehning, M., Hutterli, M. A., and Ohmura, A., 2008. Impact of microstructure of snow on its temperature: a model validation with measurements from summit, Greenland. *Journal of Geophysical Research*, **113**, 11, doi:10.1029/2007JD0009562. D14303.

Fierz, C., Armstrong, R. L., Durand, Y., Etchevers, P., Greene, E., McClung, D. M., Nishimura, K., Satyawali, P. K., and Sokratov, S. A., 2009. *The International Classification for Seasonal Snow on the Ground*. IHP-VII Technical Documents in Hydrology N°83, IACS Contribution N°1, UNESCO-IHP, Paris.

Flin, F., and Brzoska, J.-B., 2008. The temperature-gradient metamorphism of snow: vapour diffusion model and application to tomographic images. *Annals of Glaciology*, **49**, 17–21.

Johnson, J. B., and Schneebeli, M., 1999. Characterizing the micro structural and micro mechanical properties of snow. *Cold Regions Science and Technology*, **30**, 91–100.

Kaempfer, T. U., and Plapp, M., 2009. Phase-field modeling of dry snow metamorphism. *Physical Review E*, **79**(3), 17. 031502.

Matzl, M., and Schneebeli, M., 2006. Measuring specific surface area of snow by near-infrared photography. *Journal of Glaciology*, **52**(179), 558–564.

Satyawali, P. K., Schneebeli, M., Pielmeier, C., Stucki, T., and Singh, A. K., 2009. Preliminary characterization of alpine snow using SnowMicroPen. *Cold Regions Science and Technology*, **55**, 311–320.

Schneebeli, M., 2004. Numerical simulation of elastic stress in the microstructure of snow. *Annals of Glaciology*, **38**, 339–342.

Toure, A. M., Goïta, K., Royer, A., Mätzler, C., and Schneebeli, M., 2008. Near-infrared digital photography to estimate snow correlation length for microwave emission modeling. *Applied Optics*, **47**(36), 6723–6733.

Cross-references

Seasonal Snow Cover
Snow
Snow Crystal Structure
Snow Deformation
Snow Density
Snow Grains
Snow Layer
Snow Metamorphism
Stratigraphy of Snowpacks

SNOW PELLET

A. K. Singh
DIAT (Deemed University), Girinagar, Pune, Maharashtra, India

Snow pellets are symbolized by white ice particles that fall as precipitation, grow by supercooled water, and break apart easily when landing on surface. Falling snow may partially melt and refreeze into a rain drop before it reaches the ground, as shown in Figure 1. These snow pellets are also referred to as sleet. Snow pellets can also occur when snowflakes melt about half way then refreeze as they fall. Soft hail also grows in a way similar to the growth of snow pellets. Snow pellets have whiter appearance than sleet. Snow pellets are typically a few to several millimeters in size and have small air pockets embedded within their structure and have visual remnants of ice crystals unlike sleet.

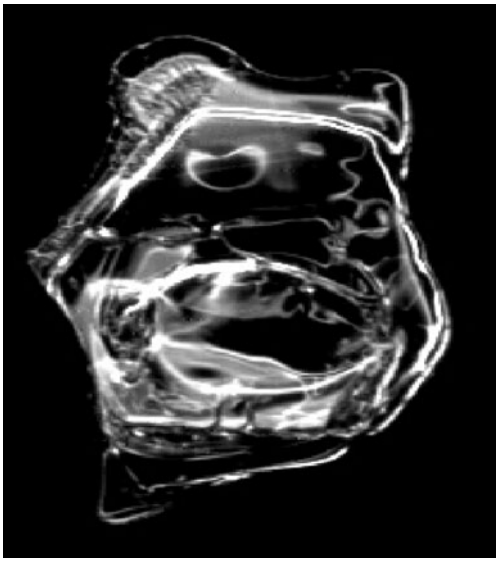

Snow Pellet, Figure 1 An image of partially broken and melt/refreeze snow grain.

SNOW PILLOW

A. K. Singh
DIAT (Deemed University), Girinagar, Pune, Maharashtra, India

The snow pillow provides a point value of the average water equivalent of snow which has accumulated on it. It is based on the detection of the hydrostatic pressure caused by snow. It is a large air mattress filled with an antifreeze fluid (mixture of methyl alcohol and water or a methanol–glycol–water solution, in the ratio of 1:1, having a specific gravity of 1). The fluid pressure responds to changes in the weight of snow on it, and is measured with a manometer or pressure transducer or load cell, as shown in Figure 1. Telemetry data acquisition systems (DAS) can be installed to provide continuous

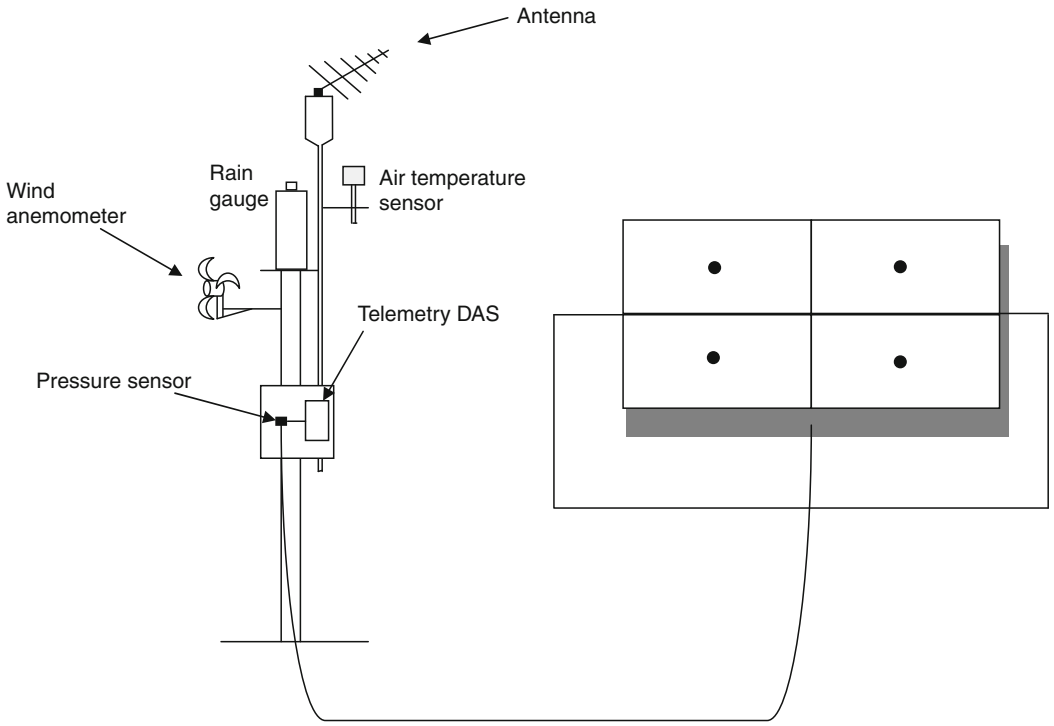

Snow Pillow, Figure 1 Schematic of snow pillow with telemetry data acquisition system.

measurements of water equivalent. Complete system consists of a DAS, a shaft encoder that tracks the movement of the float in the standpipe from the pillow, 12-volt battery for powering and mounted solar panel for recharging the batteries. A float connected to a shaft encoder records the distance the antifreeze is pushed up the standpipe. The DAS contains a transmitter to send the recorded data to the central station. Snow pillows are made up of different materials and come in various shapes and sizes. The stainless steel snow pillows have the problem of repair.

A small pillow used in a deep snow gives a pressure reading indicating a higher snow water equivalent than the actual. As the response of smaller pillows to the added weight of a heavy snowfall on a deep pack is longer than the larger pillows, it can produce an erroneous depth-time distribution for a storm. Intermittent freeze-thaw periods or rain on snow events may lead to the formation of ice layers within the pack, causing bridging, leading to lower values of the recorded water equivalent. In shallow snowpack the diurnal temperature changes may give spurious indications of snowfall or snowmelt due to expansion or contraction of the fluid in the pillow. Pillow sites should be near existing meteorological stations, or snow pillow should be equipped with certain meteorological instruments like precipitation gauge, thermograph, and anemometer.

Snow pillows are powerful tools for the study of precipitation measurements, particularly in mountain areas. It has been reported that pillows provide rough estimates of daily snowmelt losses from the snowpack. Pillow records can also be used to study meltwater formation as a function of climatic parameters. For the purpose of flood forecasting or inflow to reservoirs, it is of utmost importance to choose representative sites after surveying. Combined with measurements of snowmelt runoff, pillow records may also be useful for evaporation from snow cover.

SNOW PIT

A. K. Singh
DIAT (Deemed University), Girinagar, Pune, Maharashtra, India

The snow pit provides information about the stability of snow. It is a trench exposing a flat, vertical snow face from the snow surface to the ground, usually referred to as snow stratigraphy, as shown in Figure 1. Digging a snow pit reveals more about the snowpack structure than is visible from the surface and requires a little more practice and experience. Smoothen the uphill wall until it is vertical

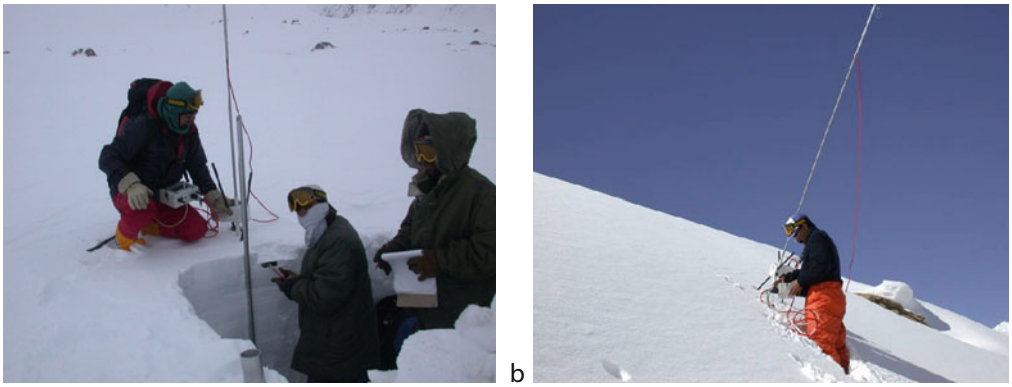

Snow Pit, Figure 1 Image (**a**) snow pit observation in progress, image (**b**) usage of Snow Micro Pen (SMP).

and the different layers of snow can be seen by pressing the snow layer so weak layers can be identified. After preparing the snow pit, temperatures on the data sheet are recorded and markings of each snow layer are done. For each layer, record the crystal size and type, hardness and density. Typical stratigraphy results are shown in Figure 2. The detection of snow layers and their mechanical behavior is most important in the assessment of snow pack stability. It allows study of the characteristics of the different layers of the snowpack that have developed as the snow has changed due to compaction and weather changes. Snow pits are used in mountainous areas to determine if one layer might slip on another causing an avalanche. The most effective snow pits should be dug near potential avalanche starting zones. As snow accumulates and changes over time, it develops layers marked by physical differences that are used to determine the history of the snowpack and are broadly classified as new snow, firn, or depth hoar. The new snow layer consists of new sharp crystals lying loosely on the top of the snow bank that are slowly being compacted by additional falling snow. The firn layer lies just below the new snow layer and consists of crystals that have lost their sharp edges due to evaporation, freezing, and compaction. They are rounded into more sphere-like shapes, during the process of becoming particles of ice. This snow is dense and the grains are more closely bonded together, which increases the mechanical strength of the firn layer. At the bottom of the snowpack lies the depth hoar layer consisting of snow crystals that have transformed (metamorphosed) into lumps of ice through evaporation, condensation, and compaction. This layer is weakly bonded than the firn or new snow layers. The depth hoar layer is loose and grainy and it is often nicknamed as sugar snow.

Many snow pits are not possible over a day by classical methods due to their time-consuming procedure. Recently an automated method has been developed, called SnowMicroPen (SMP) to identify the snow layers and their strength over a large area in a short interval of time. SMP motor and sensor is shown in Figure 3.

Bibliography

http://www.nasa.gov/pdf/186123main_SnowPitProcedures.pdf.

Satyawali, P. K., Pielmeier, C., Stucki, T., and Singh, A. K., 2009. Preliminary characterization of Alpine snow using SnowMicroPen. *Cold Regions Science and Technology*, **55**(3), 311–320.

SNOW RIPENING

A. K. Singh
DIAT (Deemed University), Girinagar, Pune, Maharashtra, India

Snow repining is the transition from a dry, subfreezing snow cover to isothermal snow, which can freely conduct water, that is, snow coming to full development, becoming mature for melt. It is a process during which the snow pack attains a state where it yields meltwater, including warming of the snowpack to 0°C. If the snow is ripe and air temperature is above freezing point, snowmelt occurs, otherwise positive energy first brings down snow to 0°C, that is, satisfying cold content of a few centimeters of top snow.

SNOW SKATING

Ashok Kumar Verma
Department of Geography and Environmental Studies, Cold Regions Research Center, Wilfrid Laurier University, Waterloo, ON, Canada

Synonyms

Ice skating; Roller skating; Skating; Snow boarding

Definition

Skating is defined as the sport where a person glides on the surface of ice or any other surface using the suitable

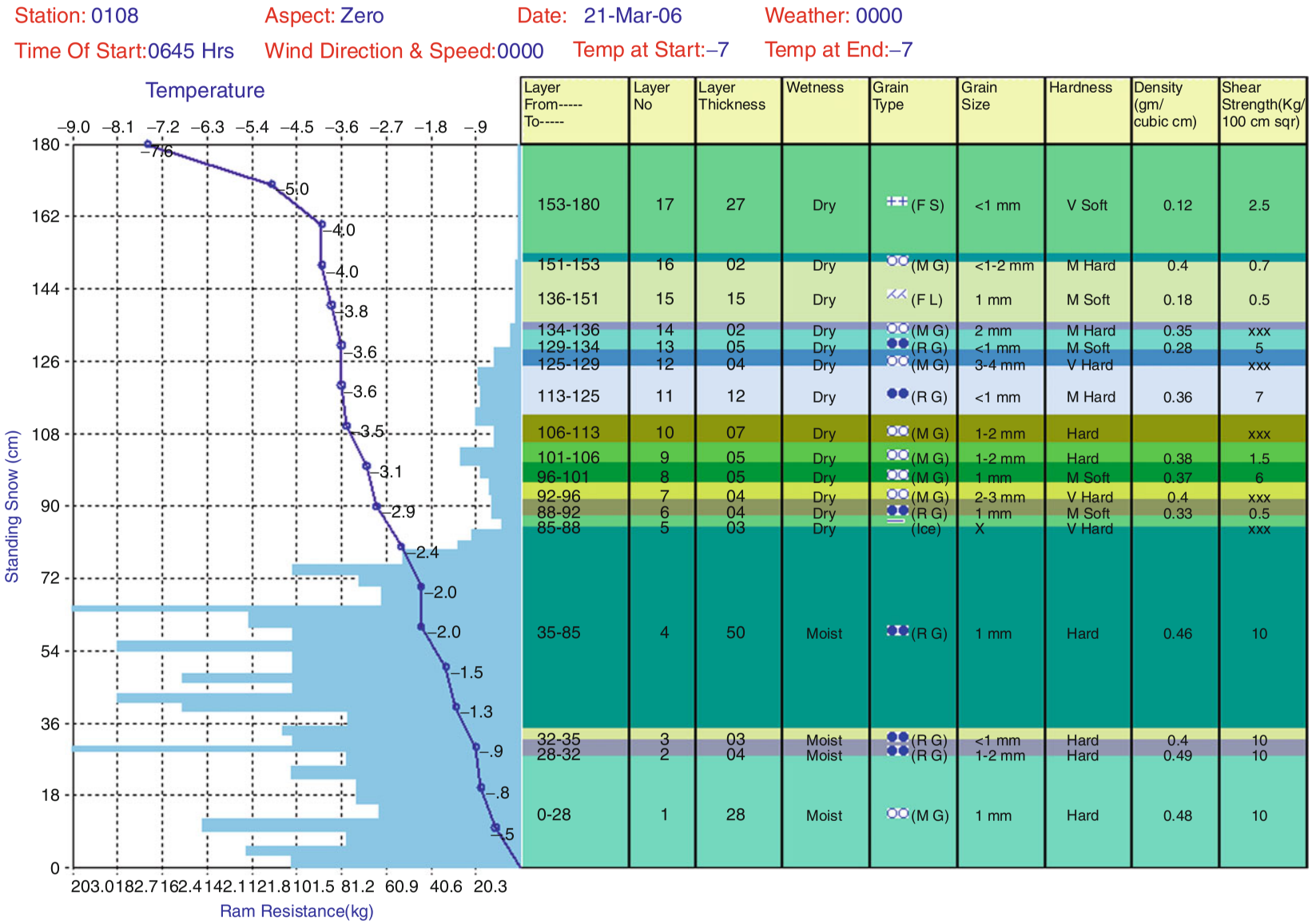

Layer From----- To-----	Layer No	Layer Thickness	Wetness	Grain Type	Grain Size	Hardness	Density (gm/ cubic cm)	Shear Strength(Kg/ 100 cm sqr)
153-180	17	27	Dry	(F S)	<1 mm	V Soft	0.12	2.5
151-153	16	02	Dry	(M G)	<1-2 mm	M Hard	0.4	0.7
136-151	15	15	Dry	(F L)	1 mm	M Soft	0.18	0.5
134-136	14	02	Dry	(M G)	2 mm	M Hard	0.35	xxx
129-134	13	05	Dry	(R G)	<1 mm	M Soft	0.28	5
125-129	12	04	Dry	(M G)	3-4 mm	V Hard		xxx
113-125	11	12	Dry	(R G)	<1 mm	M Hard	0.36	7
106-113	10	07	Dry	(M G)	1-2 mm	Hard		xxx
101-106	9	05	Dry	(M G)	1-2 mm	Hard	0.38	1.5
96-101	8	05	Dry	(M G)	1 mm	M Soft	0.37	6
92-96	7	04	Dry	(M G)	2-3 mm	V Hard	0.4	xxx
88-92	6	04	Dry	(R G)	1 mm	M Soft	0.33	0.5
85-88	5	03	Dry	(Ice)	X	V Hard		xxx
35-85	4	50	Moist	(R G)	1 mm	Hard	0.46	10
32-35	3	03	Moist	(R G)	<1 mm	Hard	0.4	10
28-32	2	04	Moist	(R G)	1-2 mm	Hard	0.49	10
0-28	1	28	Moist	(M G)	1 mm	Hard	0.48	10

Snow Pit, Figure 2 Record of stratigraphy profile with temperature profile, RAM profile, standing snow, temperature, snow type, grain type, etc. (Courtesy snow and Avalanche Study Establishment, SASE.)

Snow Pit, Figure 3 SnowMicroPen (SMP) motor, sensor assembly. (Courtesy Schneebeli, M, SLF, Davos, Switzerland.)

equipment such as bladelike runner or set of wheels attached to the shoe. Skating can be used for leisure activity, traveling, and in different forms of the sports activity as mentioned above in synonyms.

Origin: skating is regarded as the oldest winter sports back in times as long as 4,000 years in southern Finland as studied by Formenti and Minetti (2008). Skating as winter sports was quite famous in the Netherlands and other European countries in present. It is believed that skating in North America is brought by the British personnel during the eighteenth century (Flower, 1976). Earlier, the skates were made up of sharpened, flattened bone strapped to the bottom of the foot. With the advancement of the technology, the skates took form of steel blades, which invented by the Dutch in thirteenth century (Ice skating, 2009). The working principal of ice using skates is quite interesting. The metal blade at the bottom of the skates can glide with little friction over the surface of the ice. But variable leaning and digging of one of its edges into the ice will give skater a better ability to increase the friction and control of the movement.

The present-day skating had taken many forms such as roller skating, skateboard skating, and street skating. These forms use the wheels (often known as "spins") with skateboard instead the typical metal blade shoe. These forms of skating enhanced the outdoor sports activities, which were limited to the presence of snow and ice. Although, skating is a famous sport (winter or street), some hazard associated with this should be avoided as they may lead to serious injuries to head and legs. The practice and training of skate should be performed under suitable guidance and professional supervision.

Bibliography

Flower, R., 1976. *The history of skiing and other winter sports*. Toronto: Methuen.

Formenti, F., and Minetti, L. E., 2008. The first humans travelling on ice: an energy-saving strategy? *Biological Journal of the Linnean Society*, **93**(1), 1–7.

Ice skating, 2009. In *Wikipedia, The Free Encyclopedia*. http://en.wikipedia.org/w/index.php?title = Ice_skating&oldid = 283327568

SNOW SKIING

Ashok Kumar Verma
Department of Geography and Environmental Studies, Cold Regions Research Center, Wilfrid Laurier University, Waterloo, ON, Canada

The word Ski is derived from the Old Norse word "skio," which means split piece of wood or flat log (Flower and Killy, 1977; The History of Skiing, 2009; Skiing and Creation of Norwegian Identity, 1996).

The historical evidence of the ski is found in the Norway and Scandinavian literature that describe the ancient use of skiing for the livelihood (hunting), for military purpose, and as an efficient means of transportation. The oldest and accurate evidence documented in the region of Sweden and Norway dated back to 2,500–4,500 BC by archaeologists. The earliest reference of the skiing as winter sports is found in Procopius (560–559 AD), which mentions the race of Skridfinner – sliding finnes (Flower and Killy, 1977).

Present-day skiing is famous winter sports in all the cold climate countries such as North America, Europe, and some Asian countries and, recognized by the international Olympic organization and International Ski Federation. The worldwide popularity of ski as winter sports can be explained by the fact that the establishment of winter Olympic games for such sports. Over the time, skiing has evolved and divided into several categories and taken different forms of winter sports with respect to location and need namely, Alpine skiing, Backcountry skiing, Randonnee and Telemark skiing. In spite of its popularity as winter sports, the learning of ski by amateurs should be performed under proper guidance and supervision (Skiing, 2009). The ignorance of suitable learning environment and personnel can lead to fatal accidents causing major injuries and in some cases could even lead to death.

Bibliography

Flower, R., and Killy, J. C., 1977. *The History of Skiing and Other Winter Sports*. Toronto: Methuen.

Skiing, 2009. In *Wikipedia*, http://en.wikipedia.org/w/index.php?title=Skiing&oldid=283367370

Skiing, and Creation of Norwegian Identity, 1996. http://www.norway.org/News/archive/1996/199601skiing1.htm

The History of Skiing, 2009. The International Ski History Organisation (ISHA Resources). http://skiinghistory.org/

SNOW STORM

A. K. Singh
DIAT (Deemed University), Girinagar, Pune, Maharashtra, India

Steady snows of significant intensity accompanied by a certain amount of wind are often referred to as snowstorms. A massive snowstorm with strong winds (about 35 mph or more) is known as a blizzard. Snowstorms are usually considered to be less dangerous than ice storms. Mountain snowstorms can produce cornices and avalanches. Standing dead trees can be brought down by the weight of the snow, especially if it is wet or very dense. Even a few inches of dry snow can form drifts, many feet high under windy conditions. An additional danger, following a snowy winter, is spring flooding if the snow melts suddenly due to a dramatic rise in air temperature. Deaths can occur from hypothermia, infections brought on by frostbite, car accidents due to slippery roads, fires or carbon monoxide poisoning due to alternative heating methods after a storm causes a power outage, or heart attacks caused by overexertion while shovelling heavy wet snow.

SNOW AND VEGETATION INTERACTION

Christopher A. Hiemstra[1], Glen E. Liston[2]
[1]Cold Regions Research and Engineering Laboratory (CRREL), U.S. Army Corps of Engineers, ERDC, Fort Wainwright, AK, USA
[2]Cooperative Institute for Research in the Atmosphere, Colorado State University, Fort Collins, CO, USA

Definition

Snow and vegetation interaction describes how the assemblage of plants in an area influences snow accumulation and ablation and the subsequent effects of the snow on plants.

Introduction

Snow and vegetation interact in two principal ways. First, snow accumulation and ablation processes and patterns are influenced by vegetation's physical structure and spatial arrangement. Second, snow deposition and melt patterns affect vegetation's distribution and growth. These interactions take place at fine scales (1 mm to 100 m) and are common to all environments where snow and vegetation coexist. The most striking examples of snow and vegetation interaction are found where high winds, abundant snow, and isolated groups of trees interplay to create snow distributions that vary from 0.5 m to 5 m deep within horizontal distances of 100 m or less.

Vegetation effects on snow

Vegetation influences snow accumulation through canopy interception and by altering wind patterns within and around vegetation. All plants intercept snow to varying degrees as long as leaves, branches, or stems are exposed and there is a surface upon which snow can be deposited (see *Interception of Snow*). The exposed canopy's structure is important in determining the amount of interception and retention that occurs. For example, evergreen trees and shrubs retain leaves in winter; these leaves are densely arranged on their stems and provide abundant horizontal surface area. As a result, these leaves and branches are efficient at intercepting and retaining snow, even in windy locations. In contrast, deciduous trees and shrubs with vertically oriented stems present little surface area for snow interception. Moreover, that branch's surface can be smooth (e.g., aspen and birch) and light winds easily scour snow from the branches.

The rigidity of the plant also plays a role in interception. Branches with a snow burden may droop and jettison snow, or the stems may drop to the snow surface and become buried in the snowpack. Further, a plant's ability to intercept snow may change over time. In grasslands, leaves that were upright and readily intercepted snow in the fall become prostrate by mid-winter due to leaf and stem comminution through high winds, decomposition, and previous snow accumulation.

In areas where snow transport by wind is common, vegetation plays crucial roles in snow transport and resultant snow accumulation patterns. In windy environments, vegetation has a "snow holding depth," defined to be the maximum snow depth captured within and to the lee of the vegetation structure that is not available for wind redistribution (Liston and Elder, 2006). This depth varies as a function of vegetation height, canopy structure, and the spatial arrangement of individual plants. As one would expect, taller vegetation has a higher snow holding depth; in similar conditions, forested areas can retain more snow compared with grassland or alpine and arctic tundra. Structurally, plants with a dense canopy possess a larger snow holding depth compared with spreading plants of identical height. Areas dominated by many plants hold more snow than sparsely vegetated areas. As a general rule, vegetation can capture snow depths within ~60–90% of the plant's height, but this can vary substantially depending on vegetation height, structure, and spatial arrangement. If snow is shallower than the

vegetation's snow holding depth, the snow is generally not available for wind transport and snow redistribution in the environment will be limited. If snow depth exceeds this height and wind is sufficient, snow above the holding depth is available for transport and snow erosion will occur. In the case of taller forests, snow holding depth is almost always higher than actual snow depth.

In snowy and windy landscapes, snow depths frequently vary with dominant vegetation types as snow holding depths change through space. Agricultural areas in winter often feature recently tilled soils holding little-to-no snow while adjacent fields containing stubble from the previous growing season have a snowpack approximating the stubble height. Likewise, natural systems have varying snow holding depths corresponding with shifting vegetation types that exacerbate and emphasize snow–vegetation interactions. Vegetation's ability to produce deep snows is especially evident in upper treeline areas. On Libby Flats at 3,200 m elevation in the North American Rocky Mountains of southeast Wyoming, abundant winter snow precipitation (~71 cm SWE) and high winds (mean = 10 m/s) transport snow to the lee sides of tree patches and lines of trees (ribbon forests; Billings, 1969) that are 4–12 m tall and are maintained by snow deposition patterns (see below). At the end of each winter, 2–7 m of snow accumulate on the lee side of tree islands and ribbon forests and these drifts last well into summer (Figure 1). Trees are embedded in a matrix of subalpine meadow that has a smaller holding depth and acts as a source area for the lee sides of trees (Hiemstra et al., 2006). Drifts produced on the lee of trees in this area have a large effect on vegetation patterns, ecosystem processes, and growing season length (see below).

Vegetation can be used for snow management. On the high plains (shortgrass steppe with <20 cm holding depth) of North America, living snow fences consisting of several rows of trees and shrubs are planted upwind of roads susceptible to drifting snow. These windbreaks can be effective as long as the transplanted trees and shrubs remain vigorous. Additionally, crop stubble will often be left standing in the fields to retain winter snows needed to recharge soil moisture for the next crop.

While vegetation shapes snow accumulation patterns and overall distribution, it also affects snowpack metamorphism and ablation. A canopy influences soil temperatures before the snow arrives and alters subsequent thermal fluxes at the snow-soil interface and snowpack temperature gradients between the soil and upper snow surface. This gradient influences snow metamorphism occurring within the snowpack throughout the winter. Plant leaves, stems, and boles embedded in the snow conduct energy away from or into the snowpack depending on existing temperature gradients between the atmosphere and the ground. In environments where vegetation protrudes above the snowpack, shortwave radiation warms the exposed vegetation and longwave radiation emitted from the vegetation melts snow surrounding the vegetation (see *Snow Cover and Snowmelt in Forest Regions*). Snowpack properties and melting rates change with distance from exposed vegetation as heat islands associated with the vegetation are advected downwind over the remaining snow cover (Liston, 1995). In the Arctic, the snow-free season has arrived 1–9 days decade^{-1} earlier than in the recent past (Chapin et al., 2005) and increased shrub dominance (Sturm et al., 2005) will lengthen the snow-free season and alter energy budgets. In simulations

Snow and Vegetation Interaction, Figure 1 Large snowdrifts formed on the lee side of tree islands remain well into summer on Libby Flats (photo taken July 3, 1998). The prevailing winter wind direction is from left to right. Vegetation not covered by snow is growing, while vegetation covered by the snow awaits its growing season.

of a vegetation shift from shorter arctic tundra to taller arctic shrubland, snow melts 11 days earlier due to enhanced shrub cover and corresponding changes in the surface energy budget (Strack et al., 2007).

Vegetation is not always associated with accelerated snowmelt. A thicker canopy, such as that associated with forested environments, intercepts shortwave radiation above the snowpack and delays snowmelt. Vegetation can enhance the amount of snow in an area by capturing blowing snow and reducing sublimation.

Inasmuch as vegetation affects soil temperatures, snow accumulation patterns, ablation, and sublimation, vegetation can play an important role in resource management and water yield. Since vegetation plays such key roles in governing snow processes and distributions, it is critical to design observations and water resource forecast schemes around predominant vegetation types within watersheds. Further, vegetation can change slowly through succession or land cover change that gradually alters snow–vegetation interactions. Vegetation can also be disturbed (e.g., fire and widespread beetle outbreaks), consequently altering the snow cycle and energy and water budgets.

Snow effects on vegetation

Snow distribution has important implications for vegetation. Prevailing wind direction, snowfall, and resultant snow distribution patterns are often similar year after year (Walker et al., 2001), so that relatively steady-state environmental conditions are produced. These repeating conditions create characteristic spatial variation in ecosystem properties such as growing season length, soil and permafrost temperatures (Zhang, 2005), decomposition (Gilmanov et al., 2004), susceptibility to fungal predation (Cunningham et al., 2006), species composition (Billings, 2000), and primary production (Bowman and Fisk, 2001). Observations show strong correlations among snow season length and timing, temperatures, and vegetation growth (Jonas et al., 2008). Experiments with winter snow-free periods (Bokhorst et al., 2008) and earlier snowmelt dates (Wipf et al., 2009) show the importance of snow in terms of timing and insulation for vegetation. Vegetation exposed to harsh winter temperatures due to mid-winter snowmelt is susceptible to damage, and with advanced snow-free dates and accelerated growth, some plants may be damaged by extreme early-season temperatures before they are hardy.

Alpine vegetation distributions are often depicted in terms of a mesotopographic gradient (Johnson and Billings, 1962), where interplay among snow cover, wind exposure, and topographic position explain vegetation distribution patterns. For example, fellfields dominated by cushion plants are located on windy, snow-free ridge tops, while snowbed vegetation is predominant under long-lived lee-side snowbanks where growing season length is brief. Forest patterns, such as ribbon forests (Billings, 1969), have been explained by an abundance of leeward snow limiting tree survival to create alternating lines of forests and open glades. In areas where snow distributions repeat year after year, those patterns can be mirrored by vegetation distribution patterns and inferences can be made about snow depths based on existing vegetation and ecosystem patterns, and vice versa.

Snow can also physically affect trees by scouring and avalanches. While many plants are buried and protected by snow, taller shrubs and trees protrude above the snowpack and are exposed to saltating and suspended snow moving at and above the snow surface. Blowing snow crystals are abrasive and can damage leaf cuticles. This damage eventually leads to water loss and desiccation that kills plant leaves and meristems (Hadley and Smith, 1986). It is blowing snow that causes winter mortality of tree leaves and creates flagged trees commonly observed at treeline, where the only live branches above the snowpack are on the lee side of the tree's stem. Heavy snowfall events and avalanches can damage branches, produce scars, and uproot trees and the damage can be examined to study avalanche frequencies and distributions.

Summary

Vegetation plays a large role in snow distribution patterns; it interacts with snow through interception, by retaining blowing snow, and by reducing sublimation losses due to blowing snow. Vegetation can accelerate or delay snowmelt depending on canopy characteristics and the amount of incoming energy. In turn, snow affects ecosystem structure and function, including the distribution of vegetation in landscapes. The effect of snow on ecosystems is especially important in areas where most precipitation arrives as snow and growing seasons are relatively short.

Bibliography

Billings, W. D., 1969. Vegetational pattern near alpine timberline as affected by fire-snowdrift interactions. *Vegetatio*, **19**, 192–207.

Billings, W. D., 2000. Alpine vegetation. In Barbour, M. G., and Billings, W. D. (eds.), *North American Terrestrial Vegetation*. Cambridge: Cambridge University Press, pp. 537–572.

Bokhorst, S., Bjerke, J. W., Bowles, F. W., Melillo, J., Callaghan, T. V., and Phoenix, G. K., 2008. Impacts of extreme winter warming in the sub-Arctic: growing season responses of dwarf shrub heathland. *Global Change Biology*, **14**, 2603–2612.

Bowman, W. D., and Fisk, M. C., 2001. Primary production. In Bowman, W. D., and Seastedt, T. R. (eds.), *Structure and Function of An Alpine Ecosystem: Niwot Ridge, Colorado*. Oxford: Oxford University Press, pp. 177–197.

Chapin, F. S., Sturm, M., Serreze, M. C., McFadden, J. P., Key, J. R., Lloyd, A. H., McGuire, A. D., Rupp, T. S., Lynch, A. H., Schimel, J. P., Beringer, J., Chapman, W. L., Epstein, H. E., Euskirchen, E. S., Hinzman, L. D., Jia, G., Ping, C. L., Tape, K. D., Thompson, C. D. C., Walker, D. A., and Welker, J. M., 2005. Role of land-surface changes in Arctic summer warming. *Science*, **310**, 657–660.

Cunningham, C., Zimmermann, N. E., Stoeckli, V., and Bugmann, H., 2006. Growth response of Norway spruce saplings in two forest gaps in the Swiss Alps to artificial browsing, infection with black snow mold, and competition by ground vegetation. *Canadian Journal of Forest Research*, **36**, 2782–2793.

Gilmanov, T. G., Johnson, D. A., Saliendra, N. Z., Svejcar, T. J., Angell, R. F., and Clawson, K. L., 2004. Winter CO_2 fluxes

above sagebrush-steppe ecosystems in Idaho and Oregon. *Agricultural and Forest Meteorology*, **126**, 73–88.
Hadley, J. L., and Smith, W. K., 1986. Wind effects on needles of timberline conifers: seasonal influence on mortality. *Ecology*, **67**, 12–19.
Hiemstra, C. A., Liston, G. E., and Reiners, W. A., 2006. Observing, modelling, and validating snow redistribution by wind in a Wyoming upper treeline landscape. *Ecological Modelling*, **197**, 35–51.
Johnson, P. L., and Billings, W. D., 1962. The alpine vegetation of the Beartooth Plateau in relation to cryopedogenic processes and patterns. *Ecological Monographs*, **32**, 105–133.
Jonas, T., Rixen, C., Sturm, M., Stoeckli, V., 2008. How alpine plant growth is linked to snow cover and climate variability. *Journal of Geophysical Research-Biogeosciences*, **113**, G03013, doi:10.1029/2007JG000680.
Liston, G. E., 1995. Local advection of momentum, heat, and moisture during the melt of patchy snow covers. *Journal of Applied Meteorology*, **34**, 1705–1715.
Liston, G. E., and Elder, K., 2006. A distributed snow-evolution modeling system (SnowModel). *Journal of Hydrometeorology*, **7**, 1259–1276.
Strack, J. E., Pielke Sr., R. A., Liston, G. E., 2007. Arctic tundra shrub invasion and soot deposition: consequences for spring snowmelt and near-surface air temperatures. *Journal of Geophysical Research*, **112**, G04S44, doi:10.1029/2006JG000297.
Sturm, M., Schimel, J., Michaelson, G., Welker, J. M., Oberbauer, S. F., Liston, G. E., Fahnestock, J., and Romanovsky, V. E., 2005. Winter biological processes could help convert arctic tundra to shrubland. *Bioscience*, **55**, 17–26.
Walker, D. A., Billings, W. D., and de Molenaar, J. G., 2001. Snow-vegetation interactions in tundra environments. In Jones, H. G., Pomeroy, J. W., Walker, D. A., and Hoham, R. W. (eds.), *Snow Ecology: An Interdisciplinary Examination of Snow-Covered Ecosystems*. Cambridge: Cambridge University Press, pp. 266–324.
Wipf, S., Stoeckli, V., and Bebi, P., 2009. Winter climate change in alpine tundra: plant responses to changes in snow depth and snowmelt timing. *Climatic Change*, **94**, 105–121.
Zhang, T. J., 2005. Influence of the seasonal snow cover on the ground thermal regime: an overview. *Reviews of Geophysics*, **43**, RG4002, doi:10.1029/2004RG000157.

Cross-references

Global Outlook of Snowcover, Sea Ice, and Glaciers
Hydrologic Cycle and Snow
Melting Processes
Snow Cover and Snowmelt in Forest Regions
Snow Drift

SNOW WATER EQUIVALENT

Michael Durand
Byrd Polar Research Center, Ohio State University, Columbus, OH, USA

Definition

Snow water equivalent (SWE) is the equivalent depth of liquid water that would result from complete melting of a snowpack.

Introduction

In many parts of the world, snowmelt runoff is a critical water resource. It has been estimated that one-sixth of the global population lives in areas where streamflow is dominated by snowmelt runoff (Barrett et al., 2005). For water resource studies, and for applications such as long-term water supply forecasting, the liquid water equivalent stored in a snowpack is the most important quantity of interest, since SWE represents the amount of water that will be available during spring melt.

Snowpack accumulation on land results from atmospheric precipitation as snow. Snowpack is generally composed of air and frozen snow grains, as well as liquid water. At a point in space, snow density varies vertically with depth; the bulk density of the snowpack is defined such that the product of the snow depth and bulk density is equal to the SWE. Due to the presence of air within the matrix of snow grains, bulk density is generally less than that of pure ice, which is 917 kg m^{-3}; thus, SWE is generally less than the snow depth.

Measuring SWE

Manual in situ methods of measuring SWE are of two general types, both of which rely upon measurements of the snow mass, which can be converted to SWE. The first in situ type of SWE measurement is obtained by inserting a hollow pole vertically through the snowpack and into the underlying soil. The mass of the pole and the snow are then measured; as the mass of the pole is known, SWE can then be determined (Dingman, 2002). This method is generally practiced as part of a snow survey. The second type of in situ SWE measurement consists of vertical measurements of snow density at predefined intervals (e.g., 10 cm) through the snowpack. In order to obtain these measurements, a snow pit must be excavated. A snow pit also offers the opportunity to measure snowpack stratigraphy and the snowpack temperature profile in addition to the SWE; excavating a snow pit is generally far more labor intensive than snow surveys.

In contrast to the manual methods of measuring SWE, snow pillows are installed at a remote location, and consist of a pressure sensor that measures the mass of a snowpack that accumulates in a given location. Snow pillows can be configured to transmit snow mass observations to a central location where they can be archived. This approach allows for measurement of SWE in near-real time while obviating the need for potentially dangerous navigation of often complex terrain (e.g., in mountainous areas) by snow surveyors. As an example, the SNOw TELemetry (SNOTEL) network of snow pillows in the Western United States records SWE in several hundred locations (Serreze et al., 1999); data are made publicly available via World Wide Web archival and distribution.

Methods to measure SWE from airborne and spaceborne platforms have been developed over recent decades. For example, terrestrial radiation emitted at microwave frequencies is routinely measured from space by such

platforms as the Advanced Microwave Scanning Radiometer – EOS (AMSR-E) aboard the Terra and Aqua platforms. By observing the attenuation of the radiometric brightness at different microwave frequencies, global estimates of SWE can be inferred, albeit at coarse spatial scales (e.g., Chang et al., 1987). From airborne platforms, measurements of gamma radiation emitted by the earth surface can be used to infer SWE. The SWE retrieval exploits the fact that gamma radiation responds to isotopes in the upper 20 cm of soil; when the soil is covered by snow, the gamma emissions are modulated (Liston et al., 2008). For instance, the National Operational Hydrologic Remote Sensing Center (NOHRSC) in the USA performs regular airborne surveys using gamma radiation measurements (Fritzsche, 1982). Remote sensing of SWE is thus a field that is becoming more mature. Building on this remote sensing heritage, radar measurements at microwave frequencies can be used to infer SWE; the European Space Agency is currently planning the CoreH2O satellite mission to make high spatial resolution global measurements of SWE via microwave radar remote sensing (Rott et al., 2008).

Summary

SWE is an integrated measure of the potential water resources stored in a snowpack. For purposes of water resources planning, it is typically characterized by in situ measurements of snow mass; large-scale estimates are achieved by in situ measurement networks. Remote sensing estimates of SWE are becoming more mature. The upcoming CoreH2O mission has the goal of making high-resolution global measurements of SWE, enabling a significant advance in global cryospheric characterization.

Bibliography

Barrett, T. P., Adam, J. C., and Lettenmaier, D. P., 2005. Potential impacts of a warming climate on water availability in snow-dominated regions. *Nature*, **438**, 303.

Chang, A. T. C., Foster, J., and Hall, D., 1987. Nimbus-7 SMMR derived global snow cover parameters. *Annals of Glaciology*, **9**, 39.

Dingman, S. L., 2002. *Physical Hydrology*. New Jersey: Prentice Hall.

Fritzsche, A. E., 1982. The National Weather Service gamma snow system physics and calibration. Publication No. NWS-8201, EG&G, Inc., Las Vegas, NV, 37 pp.

Liston, G. E., Hiemstra, C. A., Elder, K., and Cline, D. W., 2008. Mesocell study area snow distributions for the Cold Land Processes Experiment (CLPX). *Journal of Hydrometeorology*, **9**, 957.

Rott, H., Cline, D., Duguay, C., Essery, R., Haas, C., Macelloni, G., Malnes, E., Pulliainen, J., Rebhan, H., and Yueh, S., 2008. CoReH2O – A Ku- and X-Band SAR Mission for Snow and Ice Monitoring, Alfred Wegener Institute for Polar and Marine Research: ePIC repository, Germany, 4 pp.

Serreze, M. C., Clark, M. P., Armstrong, R. L., McGinnis, D. A., and Pulwarty, R. S., 1999. Characteristics of the western United States snowpack from snowpack telemetry (SNOTEL) data. *Water Resources Research*, **35**, 2145.

Cross-references

Precipitation
Snow Density
Snow Depth
Snow Grains
Snow Pit
Stratigraphy of Snowpacks
Temperature Profile of Snowpack

SNOWBOARD

Amit Kumar
Department of Geology, Centre of Advanced Study in Geology, Punjab University, Chandigarh, India

The measurement of snow depth is made on the snowboard whose surface is kept free of snow before the snowfall. The snowboard is at least a 40 cm × 40 cm piece of plywood or lightweight metal and is placed on the surface of snow. The board is painted white or covered with while flannel, which provides a reference level for measurements.

Snowboard is also termed as a single thin, constructed with a laminated wood core with a steel edge, attached to the feet to ridden in snowboarding to descend a snow-covered slope area, and used to glide on snow. Snowboards generally have a length between 140 cm and 165 cm and a width between 24 cm and 27 cm. A different variety of snowboards exists according to riding preferences. Throughout the world, skiing sports develop great business in winter season. At high altitude areas, it offers exciting opportunities to develop snowboarding in mountain ranges. To enjoy snowboarding, which is the best sport that has gained immense popularity all over the world, the snowboard has been used worldwide.

SOLIFLUCTION

Stephen J. Walsh, Daniel J. Weiss
Department of Geography, University of North Carolina, Chapel Hill, NC, USA

Definition

Solifluction, the "slow gravitational downslope movement of water saturated, seasonally thawed materials" (Thomas and Goudie, 2000), is most commonly associated with alpine and/or arctic environments where seasonal and diurnal freeze-thaw cycles are prominent drivers of geomorphic activity (French, 1996). It is often coincident with cryoturbation (e.g., frost heaving and needle ice activity), the processes by which surficial materials, including soils and their residual parent materials, are mechanically mixed, moved, and sorted by repeated freezing and thawing. In contrast, solifluction and cryoturbation produce distinct features

including hummocks, stripes, sheets, lobes, and terraces (Matsuoka, 2001). Typically, these features are linear or quasi-linear, may be regularly spaced, and tend to occur parallel to the slope contour. Kessler and Werner (2003) identify the underlying mechanisms responsible for producing striped periglacial patterned ground on hillslopes, as feedback processes related to ice lens and stone transport within freezing soils.

Features and processes

Among identified solifluction features, lobes and terraces are most commonly observed and are frequently associated with alpine periglacial environments (French, 1996). Solifluction lobes and terraces are reported in areas including the Colorado Front Range, USA (Benedict, 1970), New Zealand (Billings and Mark, 1961), the Yukon Territory, Canada (Hugenholtz and Lewkowicz, 2002), Iceland (Douglas and Harrison 1996), the Olympic Mountains of Washington, USA (Hansen-Bristow and Price, 1985), Norway (Matthews et al., 1998), and the Northern Rocky Mountains of Montana, USA (Butler and Malanson, 1989). Solifluction terraces typically consist of flat areas (i.e., treads) covered by coarse materials that are adjacent to sloped areas (i.e., risers) covered by fine materials (Washburn, 1980). In contrast, solifluction lobes have a characteristic curved, lobate form (Benedict, 1970). Both lobes and terraces occur parallel to slope contours and often cover entire hillslopes. When occurring in areas covered by tundra, the alternating areas of surficial materials may produce turf-banked terraces and/or turf-banked lobes as vegetation establishes on the exposed fine materials. Vegetation does not, however, typically establish on the stone-covered treads, probably in response to mechanical disturbance from needle ice activity and frost heaving (Butler et al., 2004; Douglas and Harrison, 1996). Turf-banked terraces and lobes may also form in areas of relic solifluction features that are no longer experiencing downslope movement.

A key factor distinguishing solifluction from other processes influencing the production of periglacial patterned ground is slope angle, as solifluction requires slopes sufficiently gradual to retain water and yet sufficiently steep to allow downslope gravitational movement of materials. Further contributing to this process is permafrost that limits infiltration of water, thereby facilitating saturated conditions. The relationship between slope angle and patterned ground is explored, for example, by Butler and Malanson (1989), who categorize pattern ground types in alpine areas of Glacier National Park, Montana, USA as polygons, turf-banked terraces, and larger terraces dominated by frost shattering. Of these types, solifluction is considered most important for turf-banked terraces that are observed in areas with slope angles ranging from 5 to 22 degrees. This finding concurs with observations from Iceland by Douglas and Harrison (1996), who identify solifluction as the source of downslope movement for turf-banked terraces found on slopes ranging from approximately 5–19°. Likewise, Hansen-Bristow and Price (1985) report on turf-banked terraces in Olympic National Park, Washington, USA, that are coincident with slopes ranging from 5° to 20°. Several other environmental factors are proposed as contributing to the maintenance and formation of solifluction forms. These include a continental climate regime (Hansen-Bristow and Price, 1985), a threshold depth of snow (Hugenholtz and Lewkowicz, 2002), terrace and lobe orientation in relation to prevailing wind and the spatially variable pattern of snow scouring and drifting (Billings and Mark, 1961; Selkirk, 1998; Hugenholtz and Lewkowicz, 2002), mean annual air temperature depth of ice lens formation, slope inclination (Matsuoka, 2001), and presence of permafrost (Butler and Malanson, 1989).

Examples from Glacier National Park, Montana, USA

Solifluction features are often found in association with vegetated surfaces, and these surfaces may play a role in the formation of soliflucted landforms. Vegetation has been found to increase the soil moisture content, prevent rapid downslope movement, insulate the ground surface against extreme temperature, thereby depressing the freezing point of the soil, retarding surface runoff (Hansen-Bristow and Price, 1985), and altering the effective soil depth and stoniness of the soil (Malanson et al., 2002). The relationship between solifluction features and vegetation is not unidirectional, as these features may produce advantageous conditions for distinct vegetation types. For example, Butler et al. (2004) describe exfoliation of turf-banked terrace risers as a source of micro alluvial fans, occurring on stone-covered treads, that serve as seedling establishment sites above the existing alpine treeline. Solifluction features may also encourage tree line advance by providing topographic shelter for seedling establishment (Resler et al., 2005).

Turf-banked terraces found in Glacier National Park, Montana, USA are well described in the literature and provide an illustrative example of solifluction feature characteristics. Figure 1 shows a broad area of solifluction treads and risers on Lee Ridge, Glacier National Park, Montana, USA; Figure 2 is a more localized view of the tread/riser complex in the same geographic area. Turf-banked terraces found in the Park have treads and risers that typically range from less than 1 m to several meters in width. These sites are usually found on slight elevation gradients, with the individual stripes oriented parallel to the contours of the slope. Rock treads are covered with a thin veneer of coarse clasts (i.e., pebbles and cobbles), ranging from 3 to 8 cm in depth, that are typically coated with small populations of lichens, indicating a relict condition (Butler and Malanson, 1989). In contrast, vegetated risers are dominated by sand, silt, and clay (Butler and Malanson, 1989), and are populated by a dense ground cover of alpine tundra flora that is principally comprised of *Dryas octopetala* in association with *Salix reticulata, Carex ruspetris, Korbresia myosuroides, Oxytropis sericea,* and

Solifluction, Figure 1 A regional view of solifluction steps and risers on Lee Ridge, Glacier National Park, Montana, USA.

Solifluction, Figure 2 A local view of solifluction steps and risers on Lee Ridge, Glacier National Park, Montana, USA.

Selaginella densa (Bamberg and Major, 1968). Bamberg and Major (1968) use a soil movement plot to conclude that *Dryas* terraces are stable even though some amount of movement is recorded. This finding is confirmed by Butler and Malanson (1989), who hypothesize that no movement has taken place in the turf-banked terraces since the harsher climate of the neoglacial period. More recently, spatial patterns of turf-banked terraces, and their association with terrain settings, are explored using spatial digital technologies and geostatistical analysis (Walsh et al., 2003a, b).

Summary

Solifluction is a common feature of alpine environments throughout the world. Characterized by turf-banked, terraces and lobes, freeze-thaw conditions, in concert with moderate slope angles, can produce broad landscapes of patterned ground composed of alternating sequences of steps and risers. Vegetation, soil moisture, soil stoniness and depth, cryoturbation, terrain configuration, and climate conditions are among the factors that contribute to the formation of solifluction and dictate its geographic distribution.

Bibliography

Bamberg, S. A., and Major, J., 1968. Ecology of the vegetation and soils associated with calcareous parent materials in three alpine regions of Montana. *Ecological Monographs*, **38**, 127–167.

Benedict, J. B., 1970. Downslope soil movement in a colorado alpine region: rates, processes, and climatic significance. *Arctic and Alpine Research*, **2**, 165–226.

Billings, W. D., and Mark, A. F., 1961. Interactions between alpine tundra vegetation and patterned ground in the mountains of southern New Zealand. *Ecology*, **42**, 18–31.

Butler, D. R., and Malanson, G. P., 1989. Periglagial patterned ground, Waterton-glacier international peace park. *Canada and U.S.A. Zeitschrift fur Geomorphologie*, **33**, 43–57.

Butler, D. R., Malanson, G. P., and Resler, L. M., 2004. Turf-banked terrace tread and risers, turf exfoliation, and possible relationships with advancing treeline. *Catena*, **58**, 259–274.

Douglas, T. D., and Harrison, S., 1996. Turf-banked terraces in öraefi, southeast iceland: morphometry, rates of movement, and environmental controls. *Arctic and Alpine Research*, **28**, 228–236.

French, H. M., 1996. *The Periglacial Environment*. Essex: Longman.

Hansen-Bristow, K. J., and Price, L. W., 1985. Turf-banked terraces in the olympic mountains, Washington, USA. *Arctic and Alpine Research*, **17**, 261–270.

Hugenholtz, C. H., and Lewkowicz, A. G., 2002. Morphometry and Environmental Characteristics of Turf-Banked Solifluction Lobes, Kluane Range, Yukon Territory, Canada. *Permaforst and Periglacial Processes*, **13**, 301–313.

Kessler, M. A., and Werner, B. T., 2003. Self-organization of sorted patterned ground. *Science*, **299**, 380–383.

Malanson, G. P., Butler, D. R., Cairns, D. M., Welsh, T. E., and Resler, L. M., 2002. Variability in an edaphic indicator in alpine tundra. *Catena*, **49**(3), 203–215.

Matsuoka, N., 2001. Solifluction rates, processes and landforms: a global review. *Earth Science Reviews*, **55**, 366–374.

Matthews, J. A., Shakesby, R. A., Berrisford, M. S., and McEwen, L. J., 1998. Periglacial patterned ground on the styggedalsbreen glacier foreland, Jotunheimen, Southern Norway: micro-topographic, paraglacial and geoecological controls. *Permafrost and Periglacial Processes*, **9**, 147–166.

Resler, L. M., Butler, D. R., and Malanson, G. P., 2005. Topographic shelter and conifer establishment and mortality in an alpine environment, Glacier National Park, Montana. *Physical Geography*, **26**, 112–125.

Selkirk, J. M., 1998. Active vegetation-banked terraces on Macquarie Island. *Zeitschrift für Geomorphologie*, **42**, 483–496.

Thomas, D. S. G., and Goudie, A., 2000. *The Dictionary of Physical Geography.* Oxford: Blackwell.

Walsh, S. J., Bian, L., McKnight, S. A., Brown, D. G., and Hammer, E. S., 2003a. Solifluction steps and risers, lee ridge, Glacier National Park, Montana, USA: a scale and pattern analysis. *Geomorphology*, **55**(5 and 6), 381–398.

Walsh, S. J., Butler, D. R., Malanson, G. P., Crews-Meyer, K. A., Messina, J. P., and Xiao, N., 2003b. Mapping, modeling, and visualization of the influences of geomorphic processes on the alpine treeline ecotone, Glacier National Park, Montana, USA. *Geomorphology*, **53**(1–2), 129–145.

Washburn, A. L., 1980. *Geocryology: a survey of periglacial processes environments*. New York: Wiley.

Cross-references

Cryoturbation
Freezing and Thawing Index
Mountain Geomorphology
Periglacial
Permafrost

SOLUTE IN GLACIAL MELTWATERS

Martyn Tranter
Bristol Glaciology Centre, School of Geographical Sciences, University of Bristol, Bristol, UK

Introduction

Solutes in glacial meltwaters are generated by reactions that are comparable with other temperate and tropical latitudes, yet the factors controlling the production of solute are different. Factors controlling chemical weathering in other environments, such as the continual presence of water, soil, and vegetation (Drever, 2003), are not applicable to glacial environments, which are largely frozen for significant periods each year. The residence times of liquid water in glaciated catchments are often low (Knight, 1999), there are thin, skeletal soils at best, and vegetation is either absent or limited (French, 1996). However, glaciated catchments usually have high specific runoff, there are high concentrations of freshly comminuted rock flour, and adsorbed organic matter or surface precipitates that may hinder water-rock interactions are largely absent (Tranter, 2003). In short, the rapid flow of water over fine-grained, recently crushed, reactive mineral surfaces maximizes both the potential rates of chemical weathering and chemical erosion.

Composition of solutes

The chemical composition of glacial runoff from ice sheets, ice caps, and glaciers around the world is shown in Table 1 (after Brown, 2002; Tranter, 2003), which also includes the composition of global mean river water for comparative purposes. Sea salt, largely derived from marine aerosol, is a variable component of glacial runoff, and the dominant non-sea salt ions are Ca^{2+}–HCO_3^-–SO_4^{2-} – Mg^{2+}. The concentration of glacial runoff is usually inverse to discharge – hence low discharge waters are concentrated, whereas high discharge waters are dilute. The concentration of low discharge waters approaches ~1 meq/l (of positive charge) from smaller temperate, lower latitude glaciers, and ~3 meq/l for larger glaciers at higher latitudes. Glacial runoff is usually more dilute than global mean river water, and usually contains more K^+ and less Si for a given specific runoff (Anderson et al., 1997). The Ca^{2+}:Si and HCO_3^-:SO_4^{2-} ratio of glacial meltwaters are high and low, respectively, when compared with the principal world river waters, making glacial runoff an end member of global riverine water (Tranter, 2003). This is because glaciers preferentially weather carbonates and sulfides from the bedrock.

Glacial chemical weathering

The principal reactions that comminuted bedrock undergoes in glaciated terrain are summarized below, assuming that the bedrock is primarily composed of silicates and aluminosilicates.

Solute in Glacial Meltwaters, Table 1 The concentration of major ions in glacial runoff from different regions of the world (after Brown, 2002). Concentrations are reported in μeq/l

Region	Σ^+	Ca^{2+}	Mg^{2+}	Na^+	K^+	HCO_3^-	SO_4^{2-}	Cl^-	Source
Canadian High Arctic	280–3,500	260–2,600	21–640	1–190	0.1–39	210–690	59–3,900	–	1
Antarctica	550–3,100	72–1,300	120–336	360–1,400	0.8–110	91–1,600	34–1,200	0.6–1,000	2
Svalbard	330–1,900	120–1,000	99–540	110–270	5.1–41	110–940	96–760	5–310	3–5
Canadian Rockies	1,300–1,500	960–1,100	290–310	3.7–36	5.8–9.2	890–920	380–520	1.7–25	6
Iceland	170–960	110–350	30–120	30–480	2.8–12	190–570	26–130	30–87	7,8
Himalayas	130–940	75–590	6.6–230	25–65	22–51	200–730	160–410	1–22	9
Norway	20–930	8.8–623	1.6–66	8.3–210	1.0–29	1.4–680	7–140	0.9–190	10
European Alps	37–910	20–640	6–140	4.9–92	5.9–33	11–400	10–240	0.9–92	10, 11, 12
Alaska	670	550	36	25	61	430	260	2	13
Greenland	280–387	130–170	68–98	78–110	5–9	220–340	90–200	16–30	14
Cascades	56–150	35–80	8.3–20	2.5–17	9.7–37	83–100	7.9–29	–	15
Global mean runoff	1,200	670	280	220	33	850	170	160	16

Data sources. 1: Skidmore and Sharp (1999); 2: De Mora et al. (1994); 3: Hodgkins et al. (1997); 4: Hodson et al. (2000); 5: Wadham et al. (1997); 6: Sharp et al. (2002); 7: Raiswell and Thomas (1984); 8: Steinporsson and Oskarsson (1983); 9: Hasnain et al. (1989); 10: Brown (2002); 11: Collins (1979); 12: Thomas and Raiswell (1984); 13: Anderson et al. (2000); 14: Rasch et al., 2000; 15: Axtmann and Stallard, 1995; 16: Livingstone (1963)

Glacial comminution crushes bedrock and exposes the trace reactive components within crystalline aggregates more rapidly than would be the case in temperate and tropical soils, where new minerals are ultimately accessed via solubilization of the crystalline silicate lattices. Hence, glaciers are effective at solubilization of trace reactive components in the bedrock, which include carbonates, sulfides, and fluid inclusions. Laboratory experiments and direct sampling of waters from the glacier bed (Tranter et al., 1997, 2002) show that the initial reactions to occur when dilute snow and ice melt first access glacial flour are carbonate and silicate hydrolysis (Equations 1 and 2). These reactions raise the pH to high values (>9), lower the PCO_2 (to $\sim 10^{-6}$ atms), and maximize the water's potential to adsorb CO_2. Carbonate hydrolysis produces a solution with a Ca^{2+} concentration of ~200 μeq/l, with HCO_3^- the dominant anion.

$$\underset{\text{calcite}}{Ca_{1-x}(Mg_x)CO_3(s)} + H_2O(l) \leftrightarrow (1-x)Ca^{2+}(aq) + x\ Mg^{2+}(aq) + HCO_3^-(aq) + OH^-(aq) \quad (1)$$

$$\underset{\text{K-feldspar}}{KAlSi_3O_8(s)} + H_2O(l) \leftrightarrow \underset{\text{weathered feldspar surface}}{HAlSi_3O_8} + K^+(aq) + OH^-(aq) \quad (2)$$

The relatively dilute meltwater in contact with fine-grained glacial flour promotes the exchange of divalent ions from solution for monovalent ions on surface exchange sites. Hence, some of the Ca^{2+} and Mg^{2+} released from carbonate and silicate hydrolysis is exchanged for Na^+ and K^+.

$$\text{glacial flour} - Na_{(2-z)}, K_z(s) + (1-x)Ca^{2+}(aq) + x\ Mg^{2+}(aq) \leftrightarrow \text{glacial flour} - Ca_{(1-x)}, Mg_x(s) + (2-z)Na^+(aq) + zK^+(aq) \quad (3)$$

The high pH derived from hydrolysis enhances the dissolution of aluminosilicate lattices, since Al and Si become more soluble at pH > 9. Hydrolysis of carbonates results in a solution that is near saturation with calcite and aragonite. It is only in these types of waters that aluminosilicate dissolution is greater than carbonate dissolution. The influx of gases (including CO_2 and O_2), either from the atmosphere or from basal ice, and CO_2 produced by microbial respiration (see below) both lower the pH and the saturation with respect to carbonates. In addition, sulfide oxidation produces acidity (see below). Hence, almost all subglacial meltwaters are undersaturated with respect to calcium carbonate. The rapid dissolution kinetics of carbonates with respect to silicates means that carbonate dissolution continues to have a large impact on meltwater chemistry, despite carbonates being present often in only trace concentrations in the bedrock. For example, Haut Glacier d'Arolla has a bedrock, which is composed of metamorphic silicate rocks. Carbonates and sulfides are present in trace quantities in bedrock samples (0.00–0.58% and <0.005–0.71%, respectively). There are also occasional carbonate veins present in the schistose granite. Despite the bedrock being dominated by silicates, sulfide oxidation in subglacial environments dissolves carbonate to silicate in a ratio of ~5:1 (Tranter et al., 2002), compared to the global average of ~1.3:1 (Holland, 1978).

The acid hydrolysis of silicates and carbonates (Equations 4 and 5) that arises from the dissociation of CO_2 in solution is known as carbonation. Carbonation occurs in a restricted number of subglacial environments because ingress of atmospheric gases to these water-filled environments is restricted. It largely occurs in the major arterial channels at low flow, particularly near the terminus, and at the bottom of crevasses and moulins that reach the bed. Fine-grained sediment is flushed rapidly from these environments, and there is little time for the formation of secondary weathering products, such as clays, to form.

Hence, silicates dissolve incongruently, as crudely represented by Equation 4.

$$\underset{\text{anorthite}}{CaAl_2Si_2O_8(s)} + 2CO_2(aq) + 2H_2O(l) \leftrightarrow Ca^{2+}(aq) + 2HCO_3^-(aq) + \underset{\text{weathered feldspar surfaces}}{H_2Al_2Si_2O_8(s)} \quad (4)$$

$$\underset{\text{calcite}}{Ca_{1-x}(Mg_x)CO_3(s)} + CO_2(aq) + H_2O(l) \leftrightarrow (1-x)Ca^{2+}(aq) + xMg^{2+}(aq) + 2HCO_3(aq) \quad (5)$$

There is a limited body of evidence, which suggests that microbial oxidation of bedrock kerogen occurs (Wadham et al., 2004), and if this is the case, carbonation as a consequence of microbial respiration may occur in debris-rich environments, such as in the distributed drainage system and the channel marginal zone.

$$C_{org}(s) + O_2(aq) + H_2O(l) || CO_2(aq) + H_2O(l) \leftrightarrow H^+(aq) + HCO_3^-(aq) \quad (6)$$

The dominant reaction in subglacial environments is sulfide oxidation, since, following hydrolysis, this is the major reaction that provides protons to solution, so lowering the pH, decreasing the saturation index of carbonates, so allowing more carbonate dissolution (Equation 7). Sulfide oxidation occurs predominantly in debris-rich environments where comminuted bedrock is first in contact with water. It is microbially mediated, occurring several orders of magnitude faster than in sterile systems (Sharp et al., 1999). It consumes oxygen, driving down the pO_2 of the water.

$$\underset{\text{pyrite}}{4FeS_2(s)} + 16Ca_{1-x}(Mg_x)CO_3(s) + 15O_2(aq) + 14H_2O(l) \leftrightarrow 16(1-x)Ca^{2+}(aq) + 16xMg^{2+}(aq) + 16HCO_3^-(aq) + 8SO_4^{2-}(aq) + \underset{\text{ferric oxyhydroxides}}{4Fe(OH)_3(s)} \quad (7)$$

Earlier studies suggested that the limit on sulfide oxidation was the oxygen content of supraglacial melt, since subglacial supplies of oxygen are limited to that released from bubbles in the ice during regelation, the process of basal ice melting and refreezing as it flows around bedrock obstacles. However, studies of water samples from boreholes drilled to the glacier bed show that the SO_4^{2-} concentrations may be two or three times that allowed by the oxygen content of supraglacial meltwaters (Tranter et al., 2002). This suggests that oxidizing agents other than oxygen are present at the glacier bed. It seems very likely that microbially mediated sulfide oxidation drives certain sectors of the bed towards anoxia, and that in these anoxic conditions, Fe(III), rather than O_2, is used as an oxidizing agent (Equation 8). Sources of Fe(III) include the products of the oxidation of pyrite and other Fe(II) silicates in a previous oxic environment, as well as that found in magnetite and hematite.

$$FeS_2(s) + 14Fe^{3+}(aq) + 8H_2O(l) \leftrightarrow 15Fe^{2+}(aq) + 2SO_4^{2-}(aq) + 16H^+(aq) \quad (8)$$

Support for anoxia within subglacial environments comes from the $\delta^{18}O$–SO_4, which is enriched in ^{16}O when sulfide is oxidized in the absence of oxygen (Bottrell and Tranter, 2002).

The realization that there is microbial mediation of certain chemical weathering reactions in subglacial environments (Sharp et al., 1999; Skidmore et al., 2000; Bottrell and Tranter, 2002) has resulted in a paradigm shift, since the types of reactions that may occur in anoxic sectors of the bed include the common redox reactions that occur, for instance, in lake or marine sediments (Drever, 1988). A key difference in glacial systems is that the supply of new or recent organic matter is limited to that inwashed from the glacier surface, such as algae, insects and animal faces, or overridden soils during glacier advance. By contrast, the supply of old organic matter from comminuted rocks is plentiful. Given the thermodynamic instability of organic matter in the presence of O_2 or SO_4^{2-}, it seems likely that microbes will have evolved to colonize subglacial environments and utilize kerogen as an energy source. The first data to support this assertion is stable isotope analysis from Finsterwalderbreen, a small polythermal-based glacier on Svalbard, which has shale as a significant component of its bedrock (Wadham et al., 2004). The $\delta^{18}O$–SO_4 of waters upwelling from subglacial sediments are very enriched in $\delta^{18}O$, and the $\delta^{34}S$ is enriched in ^{34}S, which suggests that cyclical sulfate reduction and oxidation has been occurring. The $\delta^{13}C$ of DIC (dissolved inorganic carbon) is negative, consistent with the assertion that organic matter has been oxidized. Mass balance calculations suggest that a possible source of organic matter is kerogen, but the necromass of dead bacteria cannot be discounted. Whatever is the source of organic matter, sectors of the bed at Finsterwalderbreen are so anoxic that sulfate reduction is occurring (Equation 9).

$$\underset{\text{organic carbon}}{2CH_2O(s)} + SO_4^{2-}(aq) \leftrightarrow 2HCO_3^-(aq) + H_2S(aq) \quad (9)$$

It is possible that methanogenesis occurs under certain ice masses, since methanogens have been isolated from subglacial debris (Skidmore et al., 2000). The low $\delta^{13}C$–CH_4 and high concentration of methane found in gas bubbles within the basal ice of the Greenland Ice Sheet are consistent with there being methanogenesis within the basal organic-rich paleosols.

To date, there are few studies of glacial chemical weathering on bedrock with a significant evaporitic content. Work at John Evans Glacier in the Canadian High Arctic has shown that gypsum is dissolved in some areas of the bed, and that mixing of relatively concentrated Ca^{2+}–SO_4^{2-} waters with more dilute Ca^{2+}–HCO_3^-–SO_4^{2-} waters results in $CaCO_3$ precipitation due to the common ion effect (Skidmore (U. Montana) personal communication, 2010).

A key feature of the above chemical weathering scenarios is that relatively little atmospheric or biogenic CO_2 is involved. Hence, whereas ~23% and ~77% of solutes, excluding recycled sea salt, found in global mean river water is derived from the atmosphere and rock, respectively (Holland, 1978), atmospheric sources account for a maximum of 3–11% of solute in glacial runoff (after Hodson et al., 2000).

Bibliography

Anderson, S. P., Drever, J. I., and Humphrey, N. F., 1997. Chemical weathering in glacial environments. *Geology*, **25**, 399–402.

Anderson, S. P., Drever, J. I., Frost, C. D., and Holden, P., 2000. Chemical weathering in the foreland of a retreating glacier. *Geochimica et Cosmochimica Acta*, **64**, 1173–1189.

Axtmann, E. V., and Stallard, R. F., 1995. Chemical weathering in the South Cascade Glacier Basin, comparison of subglacial and extra-glacial weathering. *IAHS*, **228**, 431–439.

Bottrell, S. H., and Tranter, M., 2002. Sulphide oxidation under partially anoxic conditions at the bed of Haut Glacier d'Arolla, Switzerland. *Hydrological Processes*, **16**, 2363–2368.

Brown, G. H., 2002. Glacier meltwater hydrochemistry. *Applied Geochemistry*, **17**, 855–883.

Collins, D. N., 1979. Hydrochemistry of meltwaters draining from an alpine glacier. *Arctic and Alpine Research*, **11**, 307–324.

De Mora, S. J., Whitehead, R. F., and Gregory, M., 1994. The chemical composition of glacial melt water ponds and streams on the McMurdo Ice Shelf, Antarctica. *Antarctic Science*, **6**, 17–27.

Dokken, T. E., and Jansen, E., 1999. Rapid changes in the mechanism of ocean convection during the last glacial period. *Nature*, **401**, 458–461.

Drever, J. I., 1988. *The Geochemistry of Natural Waters*, 2nd edn. Englewood Cliffs, NJ: Prentice-Hall, 437 pp.

Drever, J. I., 2003. Surface and Ground Water, Weathering, Erosion and Soils. In Holland, H. D., and Turekian, K. K. (eds.), *Treatise on Geochemistry*, Vol. 5, Oxford and San Diego: Elsevier Pergamon.

French, H. M., 1996. *The Periglacial Environment*. 2nd edn. Reading, MA: Addison Wesley Longman, 341 pp.

Hasnain, S. I., Subramanian, V., and Dhanpal, K., 1989. Chemical characteristics and suspended sediment load of meltwaters from a Himalayan glacier in India. *Journal of Hydrology*, **106**, 99–108.

Hodgkins, R., Tranter, M., and Dowdeswell, J. A., 1997. Solute provenance, transport and denudation in a high Arctic glacierised catchment. *Hydrological Processes*, **11**, 1813–1832.

Hodson, A. J., Tranter, M., and Vatne, G., 2000. Contemporary rates of chemical weathering and atmospheric CO_2 sequestration in glaciated catchments: an Arctic perspective. *Earth Surface Processes and Landforms*, **25**, 1447–1471.

Holland, H. D., 1978. *The Chemistry of the Atmosphere and Oceans*. New York: Wiley. 351 pp.

Knight, P. G., 1999. *Glaciers*. Stanley Thornes: Cheltenham, 261 pp.

Livingstone, D. A., 1963. Chemical compositions of rivers and lakes, *U.S. Geological Survey Professional Paper 440-G*, 64 pp.

Raiswell, R., and Thomas, A. G., 1984. Solute acquisition in glacial meltwaters I. Fjällsjökull (south-east Iceland): bulk meltwaters with closed system characteristics. *Journal of Glaciology*, **30**, 35–43.

Rasch, M., Elbering, B., Jakobsen, B. H., and Hasholt, B., 2000. High-resolution measurements of water discharge, sediment, and solute transport in the River Zackenbergelven, Northeast Greenland. *Arctic, Antarctic and Alpine Research*, **32**, 336–345.

Sharp, M., Parkes, J., Cragg, B., Fairchild, I. J., Lamb, H., and Tranter, M., 1999. Bacterial populations at glacier beds and their relationship to rock weathering and carbon cycling. *Geology*, **27**, 107–110.

Sharp, M., Creaser, R. A., and Skidmore, M., 2002. Strontium isotope composition of runoff from a glaciated carbonate terrain. *Geochimica et Cosmochimica Acta*, **66**, 595–614.

Skidmore, M. L., and Sharp, M. J., 1999. Drainage system behaviour of a High-Arctic polythermal glacier. *Annals of Glaciology*, **28**, 209–215.

Skidmore, M. L., Foght, J. M., and Sharp, M. J., 2000. Microbial life beneath a High Arctic Glacier. *Applied Environmental Microbiology*, **66**, 3214–3220.

Steinporsson, S., and Oskarsson, N., 1983. Chemical monitoring of Jokulhaup water in Skeidara and the geothermal system in Grimsvotn, Iceland. *Jökull*, **33**, 73–86.

Thomas, A. G., and Raiswell, R., 1984. Solute acquisition in glacial meltwaters II. Argentiere (French Alps): bulk meltwaters with open system characteristics. *Journal of Glaciology*, **30**, 44–48.

Tranter, M., 2003. Chemical weathering in glacial and proglacial environments. In Holland, H. D., and Turekian, K. K. (eds.), *Treatise on Geochemistry*, Vol. 5, Surface and Ground Water, Weathering, Erosion and Soils (ed. J.I. Drever), pp. 189–205.

Tranter, M., Sharp, M. J., Brown, G. H., Willis, I. C., Hubbard, B. P., Nielsen, M. K., Smart, C. C., Gordon, S., Tulley, M., and Lamb, H. R., 1997. Variability in the chemical composition of in situ subglacial meltwaters. *Hydrological Processes*, **11**, 59–77.

Tranter, M., Sharp, M. J., Lamb, H. R., Brown, G. H., Hubbard, B. P., and Willis, I. C., 2002. Geochemical weathering at the bed of Haut Glacier d'Arolla, Switzerland – a new model. *Hydrological Processes*, **16**, 959–993.

Wadham, J. L., Hodson, A. J., Tranter, M., and Dowdeswell, J. A., 1997. The rate of chemical weathering beneath a quiescent, surge-type, polythermal based glacier, southern Spitsbergen. *Annals of Glaciology*, **24**, 27–31.

Wadham, J. L., Bottrell, S., Tranter, M., and Raiswell, R., 2004. Stable isotope evidence for microbial sulphate reduction at the bed of a polythermal high Arctic glacier. *Earth and Planetary Science Letters*, **219**, 341–355.

SOLUTES IN GLACIER ICE

Renoj Thayyen
Western Himalayan Regional Centre, National Institute of Hydrology, Jammu (J&K), India

Source

Dissolved ions (solute) in the glacier ice are mainly derived from the atmosphere by means of deposition of atmospheric particles on the glacier through precipitation. The deposition of atmospheric particle on the glacier is roughly proportional to their concentration in the atmosphere. Direct deposition of dust particles on the glacier, especially in the accumulation zone is also a major source

of solute in the glacier. At the subglacial zone of the glacier, solute entrainment happens in association with the relegation processes.

Processes

After the deposition in the accumulation zone of the glacier chemical constituents in the snowpack undergo various changes during the freeze thaw cycles. Preferential releases of ionic species from the snowpack occur during the densification processes. Impurities reach the ice grain boundary during recrystallization and reject most of the impurities to meltwater and the new ice formed will be purer. Solute concentration and its characteristics in the glacier ice with respect to the original solute characteristics of the snowpack are determined by the densification environment of the glacier. Glacier ice formation in subzero temperature ensures preservation of snowpack chemical characteristics to a great extent whereas in warmer climate, solute concentration in glacier ice undergoes major changes due to preferential elution processes.

Use

Atmospheric particle or aerosols originate from a variety of natural and manmade sources and chemical compositions of ice core provide good information on atmospheric particulate loading at the time of deposition and act as a good source of information for climate change studies. Radioactive isotopes derived from nuclear or volcanic activity is a very good time marker in the glacier ice.

Bibliography

Souchez, R. A., and Lemmens, M. M., 1987. Solutes. In Gurnell, A. M., and Clark, M. J. (eds.), *Glacio-fluvial Sediment Transfer: An Alpine Perspective*. Wiley: New York, pp. 285–303.

SPECIFIC MELT RATE

Pratap Singh
Tahal Consulting Engineers Ltd, New Delhi, India

The specific melt rate represents the melt rate over unit area and is represented in the unit of mm/day. Prevailing weather condition in a particular area has a control on the specific melt rate. Specific melt rate of snow/ice can be determined by allowing a small block of snow/ice to melt under natural weather conditions and observing the melt runoff and weather condition. Specific melt rate can be computed using energy balance approach or using temperature index approach. In general, empirical relationships are established between specific melt rate and mean daily temperature. The specific melt rate of glaciers ice is higher than that of snow due to lower albedo of ice. While computing the runoff from a snowfed or glacier fed basin, first specific melt rate is estimated and then runoff is derived by multiplying it with the representative area.

STABLE ISOTOPES

Bhishm Kumar
Hydrological Investigation Division, National Institute of Hydrology, Roorkee, Uttarakhand, India

The atoms of an element that do not decay with time or take infinite time to decay are called stable isotopes of that element (See *Oxygen Isotopes* and *Hydrogen Isotopes*).

Stable Isotopes, Table 1 Stable isotopes with their isotope ratio, abundance and commonly measured phases

Isotope	Ratio	% Natural Abundance	Reference (abundance ratio)	Commonly measured phases
^{2}H	$^{2}H/^{1}H$	0.015	VSMOW (1.5575×10^{-4})	H_2O, CH_2O, CH_4, H_2, OH^- minerals
^{3}He	$^{3}He/^{4}He$	0.000138	Atmospheric He (1.3×10^{-6})	He in water or gas, crustal fluids, basalt
^{6}Li	$^{6}Li/^{7}Li$	7.5	L-SVEC (8.32×10^{-2})	Saline waters, rocks
^{11}B	$^{11}B/^{10}B$	80.1	NBS 951 (4.04362)	Saline waters, clays, borate, rocks
^{13}C	$^{13}C/^{12}C$	1.11	VPDB (1.1237×10^{-2})	CO_2, carbonate, DIC, CH_4, organics
^{15}N	$^{15}N/^{14}N$	0.366	AIR N_2 (3.677×10^{-3})	N^2, NH_4^+, NO_3^-, N-organics
^{18}O	$^{18}O/^{16}O$	0.204	VSMOW (2.0052×10^{-3}) VPDB (2.0672×10^{-3})	H_2O,CH_2O,CO_2, sulfates NO_3^-, carbonates, silicates OH^- minerals
^{34}S	$^{34}S/^{32}S$	4.21	CDT (4.5005×10^{-3})	Sulfates, sulfides, H_2S, S-organics
^{37}Cl	$^{37}Cl/^{35}Cl$	24.23	SMOC (0.324)	Saline waters, rocks, evaporates, solvents
^{81}Br	$^{81}Br/^{79}Br$	49.31	SMOB	Developmental for saline waters
^{87}Sr	$^{87}Sr/^{86}Sr$	$^{87}Sr = 7.0$ $^{86}Sr = 9.86$	Absolute ratio measured	Water, carbonates, sulfates, feldspar

Over 2000 isotopes of 92 naturally occurring elements have been identified out of which several hundred are stable isotopes. But for hydrological investigations, we talk much about hydrogen and oxygen stable isotopes. As we know water molecule is made up of two hydrogen atoms and one oxygen atom therefore, many combinations (18) are possible out of which $^{1}H^{1}H^{16}O$, $^{1}HD^{16}O$, $HD^{18}O$, $^{1}H^{1}H^{17}O$, and $^{1}HD^{17}O$ are important. The stable isotopes with their isotope ratio, abundance, and commonly measured phases are listed in Table 1 (Clark and Fritz, 1997).

Bibliography

Clark, I., and Fritz, P., 1997. *Environmental Isotopes in Hydrogeology.* Boca Raton/New York: Lewis.

STAGE-DISCHARGE RELATIONSHIP

Amit Kumar
Centre of Advanced Study in Geology, Department of Geology, Punjab University, Chandigarh, India

Synonyms

Rating curve

Definition

The relationship between the amount of water flowing in a river or stream and stage at any particular point is usually known as stage–discharge relationship. Stage–discharge relationships for flow in rivers and channels are established by concurrent measurements of stage (y) and discharge (Q) (through velocity measurements, dilution methods, or other techniques) and the results are fitted graphically or statistically to yield the development of rating curves. The dynamic relationship between stage and discharge, which is unique to a particular selected station along the river, can be determined via mathematical relationships.

Introduction

Hydrologists, watershed managers are often interested in estimating stream discharge. Discharge is the flow rate of water passing a point on a stream at an instant in time; therefore, continuous flow measurement of river discharge is a hard and expensive task in hydrology. To overcome this problem, the stage reading at hydrometric gauges are permanently taken and the discharge of any time at which the actual discharge is unavailable will be estimated through a developed relationship between discharge and stage. To study the stage–discharge relation and the capability of long-term data in establishing a permanent stage–discharge relationship, and also to determine the best time to measure the discharge of rivers. More accurate values for discharge can be obtained when a permanent gauging station has been established on a stretch of a river where there is a stable relationship between stage and discharge, and this has been measured and recorded. Once this relationship is established, readings need only be taken of stage, because the discharge may then be read from a stage–discharge curve.

Stage–discharge relationship

Hydrological studies relied on stage–discharge relationships to monitor discharge in shallow streams of all depths. Hydrologists would typically get on a time-intensive program to rate a stream using a current meter to measure instantaneous discharge against several different stage events and a rating curve was developed. The stage–discharge relationship is based upon the relationship between stream water depth (stage) and discharge at a cross section. The relationship will be different for every cross section, and will change at a cross section as the cross section changes through time (aggrades or degrades).

The first step is to identify a permanent cross section. The cross section should be in a stable portion of the stream where the intensity of erosion and deposition is less. The second step is to install a stage staff or depth meter in the channel/well at the cross section. The stage staff must be fixed and permanent. Its stability and the cross section are crucial for developing a meaningful stage–discharge relationship. In the next step, the area of cross section of the river at a gauging site and the velocity of flow through the cross-sectional area are to be measured. The applied method at the cross section to estimate discharge over a wide range of value of discharge (low flow to peak flow) is known as area–velocity method. After enough observations, a stage–discharge relationship (equation) can be developed to correlate stage and discharge. Once the stage–discharge relationship is developed, discharge can be computed directly by only monitoring of the water level at the cross section over time. The extrapolation of computed values must be under the range of discharge used to develop such relationships.

If such relationship for a gauging station is and does not change with time constant, the control is said to be permanent. If it changes with time, it is called shifting control.

When measured value of stage and discharge are plotted on arithmetic paper, the result is an approximate parabolic curve, as shown in Figure 1. The curve can be expressed as

$$Q = a(h - h_0)^b \tag{1}$$

In which h_0 is a constant, representing the gauge reading for zero discharge, and a and b are rating curve constant. This relationship can also be expressed graphically by plotting the observed stage against corresponding discharge values in logarithmic paper, the plot is straight line, as shown in Figure 2. The equation becomes

$$\log Q = \log a + b \log(h - h_0) \tag{2}$$

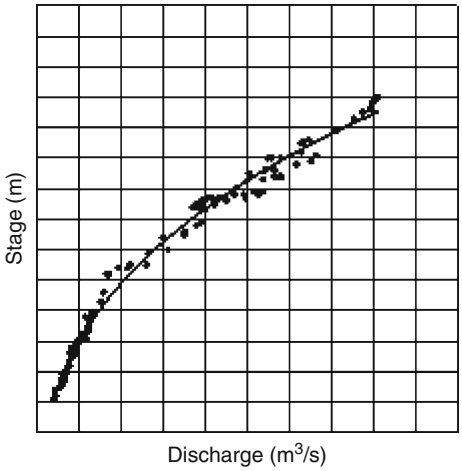

Stage-Discharge Relationship, Figure 1 Stage–discharge relationship curve (*arithmetic plot*).

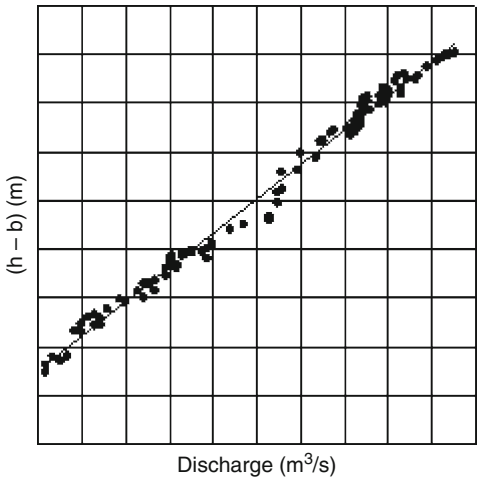

Stage-Discharge Relationship, Figure 2 Stage–discharge relationship curves (*logarithmic plot*).

The best value of constants a and b can be obtained using the least square method; however, constant h_0 must be found beforehand, and this can be estimated in several ways. A trial-and -error method can be used to yield h_0, which then gives the best-fit curve. Another way is to extrapolate the rating curve corresponding to $Q = 0$ and then plot log Q versus log $(h–h_0)$. If the plot is the straight line, then the value of h_0 obtained by extrapolation is acceptable. Otherwise, another value in the neighborhood of the previous value of h_0 is selected and the procedure is repeated.

A graphical method to determine h_0 has been reported by running (Wisler and Brater, 1959). According to this method, Q and h are plotted on arithmetic scale and a

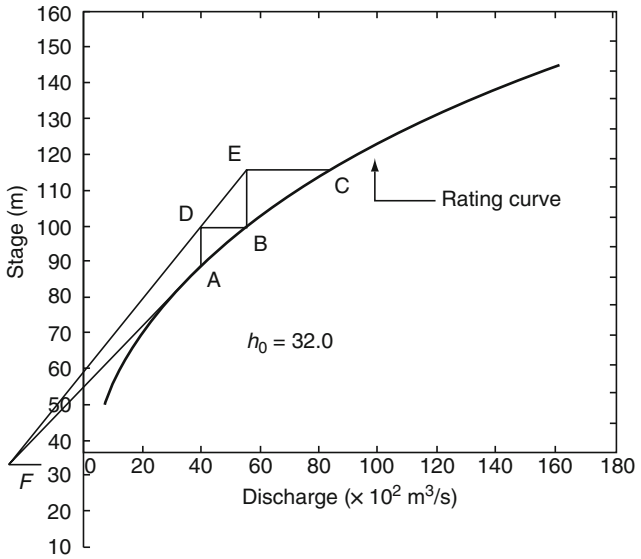

Stage-Discharge Relationship, Figure 3 Running's method for estimation of constant h_0.

smooth curve is drawn through plotted points. In Figure 3, three points, A, B, and C, are selected in such a way that their geometric progression is as follows.

$$\frac{Q_A}{Q} = \frac{Q_B}{Q} \tag{3}$$

The vertical lines are drawn at A and B, and horizontal lines drawn at B and C. Thus, D and E are obtained as intersection points with verticals. Two straight lines are drawn through E and D, and stage–discharge curve is assumed to be a parabola in this method.

Another method of computing h_0 is analytical. From a smooth curve of Q versus h, three values of discharge, Q_1, Q_2, and Q_3, are selected such that $Q_1/Q_2 = Q_2/Q_1$. The corresponding values of stage are h_1, h_2, and h_3. Then, using equation

$$\frac{(h_1 - h_0)^b}{(h_2 - h_0)^b} = \frac{(h_2 - h_0)^b}{(h_3 - h_0)^b} \tag{4}$$

$$\frac{(h_1 - h_0)}{(h_2 - h_0)} = \frac{(h_2 - h_0)}{(h_3 - h_0)} \tag{5}$$

$$h_0 = \frac{h_1 h_3 - {h_2}^2}{h_1 + h_3 - 2h_2} \tag{6}$$

Alternatively, all three parameters, a, b, and h_0, can be obtained by optimization.

The simple rating curve is generally satisfactory for a majority of streams where rapid fluctuation of stage is not experienced at gauging section. The adequacy of the curve is measured by the scatter of data around fitted

curve. When there is a permanent control, the rating curve is essentially permanent. If the rating curve is made using a range of stages from low to high, it can be used to interpolate the discharge for any stage of flow between the measured stages without measuring that flow. It is important to check the stability of the curve by parabolic discharge measurement, and to extend it with each new observed high stage. Changes in channel shape, due to scouring or sedimentation, can change the effect of control and thereby change the rating curve.

For some gauging stations, there may be two or more control each for a particular range of stage. The rating curve for such a station is discontinuous; the point of discontinuity corresponds to the stage reflecting the change in control. An example is the start of submergence of a weir control when the tail water level below the control rises above the lowest point of the control. Even under such conditions, the simple rating curve may be satisfactory if the control is permanent, free of backwater, and the stream slope is steep.

Summary

There have been a number of developments in recent years that have resulted in new and better estimation of stage and discharge relationships. Many types of equipments for both instantaneous measurements of flow and full-time monitoring of ungauged river were to be used for discharge measurements. Discharge is important for the hydrologic studies, considerable efforts to be made to collect this data as WMO recommended norms, by developing number of hygrometry stations in various geographical locations.

Bibliography

Herschy, R. W., 1978. *Hydrometry Principles and Practices*. Chichester, West Sussex: Wiley.

Herschy, R. W., 1985. *Streamflow Measurements*. Lonon and New York: Elsevier Applied Science.

Singh, P., and Singh, V. P., 2001. *Snow and Glacier Hydrology*. Dordrecht: Kluwer Academic.

Wisler, C. O., and Brater, E. F., 1959. *Hydrology*. New York: Wiley.

STATIONARY GLACIER

Renoj Thayyen
Western Himalayan Regional Centre, National Institute of Hydrology, Jammu (J&K), India

Synonyms

Standstill glacier

When horizontal velocity component of a glacier equals the horizontal component of ablation, glacier terminus remains stationery (Boulton, 1986). Glacier margins advance, retreat, or remain stationery in response to the variations in glacier mass balance. Frontal margins of the glacier will remain at same position when $U_{hx} = a_b/\tan \alpha$, where U_{hx} is the horizontal velocity component, a_b is the ablation rate, and α is the glacier surface slope. ($a_b/\tan \alpha$) constitute the horizontal component of ablation. While the position of the glacier termini is stationery, glacier ice itself is in motion but removed from the terminus region at a rate equal to the velocity.

Bibliography

Boulton, G. S., 1986. Push moraines and glacier contact fans in marine and terrestrial environments. *Sedimentology*, **33**, 677–698.

STRATIGRAPHY OF SNOWPACKS

Peter W. Nienow[1], Fay Campbell[2]
[1]School of Geosciences, University of Edinburgh, Edinburgh, UK
[2]Department of Geographical and Earth Sciences, University of Glasgow, Glasgow, UK

Definition

Snowpack stratigraphy. Snowpacks are often characterized by a number of distinctive "stratigraphic" layers in which the properties of the snow vary vertically in terms of density, crystal shape, grain size, and hardness. These individual layers when combined make up the stratigraphy of a snowpack.

Introduction

Any snowpack, whether of a seasonal or multi-year duration, will develop a layered structure (Figure 1) during its formation which will evolve through time. Each layer is formed by the deposition of falling snow, the redistribution of windblown snow, or a combination of these two processes. The initial snowpack is subsequently modified by compaction and thermal metamorphic processes resulting in the gradual densification of the snowpack. Surface melting, percolation, and under certain conditions, refreezing of meltwaters further modifies the snowpack and enhances the rate of densification. Snowpacks are typically heterogeneous with each layer varying in terms of density, crystal shape and grain size with subsequent implications for both porosity and permeability. An understanding of snowpack stratigraphy is important because the complex structure of an individual snowpack affects: (1) its stability, and therefore propensity to fail catastrophically in an avalanche; and (2) the snowpack hydrology (qv *Temperature Profile of Snowpack*) and therefore the rate at which meltwater is released from a given snowpack with implications for the runoff characteristics from snow-covered catchments. Snowpack

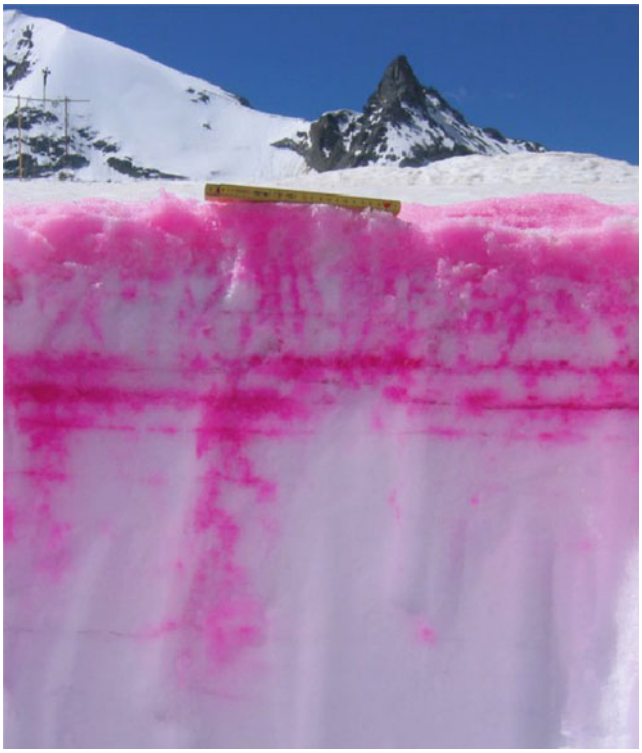

Stratigraphy of Snowpacks, Figure 1 Layered snowpack stratigraphy as revealed in a snow-pit, excavated 1½ h after a dye injection on the snowpack surface at Haut Glacier d'Arolla, Switzerland on 27 June 2004. The ruler at the surface is 20 cm long. (Photo: F. Campbell).

stratigraphy has traditionally been investigated in situ through the excavation of snow-pits and detailed vertical sampling of the snow characteristics of the walls therein (Fierz et al., 2009). More recently, numerical models have been developed to simulate the evolution of snowpack stratigraphy and stability (e.g., Brun et al., 1992; Jordan, 1991; Lehning et al., 2002).

Physical properties of the snowpack

The physical properties of the seasonal snowpack are controlled by processes operating on the snow during its formation in the atmosphere, deposition on the ground, and time on the ground. A thorough understanding of the processes of snowcover formation is therefore critical for understanding how the stratigraphy of a snowpack develops and evolves through time. More comprehensive discussions of snowpack development, characteristics, and processes from deposition to melt are provided by Male (1980), Marsh (2005), Lehning et al. (2002) and Pielmeier and Schneebeli (2003); a summary of those aspects most relevant to snowpack stratigraphy is given here.

Snowpack formation and evolution: dry snow processes

Snow Crystals (qv) forming in the atmosphere take on a range of sizes and a diverse variety of forms depending on the temperature and humidity of the atmosphere at the time of their formation and as they fall to the ground (Male, 1980). Crystal size and shape may be altered by wind action both as snowflakes fall to the ground and once deposited, with *Grains* (qv) broken and abraded into more equidimensional particles (Male, 1980).

As the seasonal snowpack is typically deposited by a series of winter storms, a characteristic layered (qv *Snow Layer*) structure develops, with varying layer properties depending initially on the conditions under which the snow was deposited. Between storms, the snowpack surface may be modified by freezing rain, packing by wind action, or surface melting and refreezing, resulting in the formation of thin, high-density layers which subsequently separate snow strata (Male, 1980). These "ice" layers, though rarely of solid ice, are relatively impermeable compared to the lower density and more permeable snow strata, and play an important role in controlling the physical properties of the snowpack, especially with respect to *Snow Hydrology* (qv) (Colbeck, 1975a; Campbell et al., 2006; Figure 1).

Once on the ground, snowflakes undergo a rapid *Snow Metamorphism* (qv) driven by water vapor gradients between convex and concave surfaces, allowing the snowpack to assume a lower energy state by reducing its total surface area relative to mass. In this process, known as equilibrium growth or equi-temperature metamorphism due to the small temperature gradients under which it takes place (Sommerfeld and LaChappelle, 1970), snowflakes and broken particles can be reduced to more spherical snow grains in a matter of days, and smaller grains melt and disappear as larger grains grow. In this way, grains may attain a diameter of up to 1 mm even while still below 0°C, and the rounding of grains can allow an increase in *Snow Density* (qv) to between 580 and 600 kg m^{-3} (Sommerfeld and LaChappelle, 1970), compared to only 50–70 kg m^{-3} for new snow deposited under calm conditions (Paterson, 1994).

If the snowpack is subject to a temperature gradient, the resulting movement of water vapor between grains that are at different temperatures drives kinetic growth metamorphism, producing characteristic faceted grains known as surface and depth hoar. More detailed information about the processes of equilibrium growth and kinetic growth metamorphism can be found in Sommerfeld and LaChappelle (1970) and Male (1980).

As metamorphism proceeds, the breaking up and rounding of dendritic particles is accompanied by the formation of bonds at points of contact between grains. This process, known as sintering, leads to an increase in snow density and strength. The snowpack, previously a matrix of single crystal or polycrystalline ice grains, becomes a complex three-dimensional network of connected particles (Male, 1980).

Snowpack formation and evolution: the metamorphism of wet snow

When liquid water is first introduced into the snowpack, it initiates a rapid metamorphism, whereby small ice grains are eliminated while larger grains grow rapidly until they reach diameters of 1–2 mm, with important implications for subsequent snowpack strength and hydrology (qv *Snow Hydrology*; *Stratigraphy of Snowpacks*). A thermodynamic analysis of the relationship between grain size and phase equilibrium temperature (Colbeck, 1975b) shows that this process can be understood as the result of differences in the melting temperature of small and large grains caused by the difference in their radii of curvature. Due to their smaller radius of curvature, melting temperature is higher for large grains than for small, and larger grains therefore exist at a higher temperature than smaller grains. This temperature difference drives heat flow by conduction toward the smaller grains. As a result, smaller grains decrease in size and eventually disappear, while larger grains increase in size, conserving the total mass.

The diverse grain forms found in both dry and wet snow at various stages of development are brought together by Fierz et al. (2009) in the International Classification for Seasonal Snow on the Ground. While primarily based on grain morphology, the scheme includes valuable information about the physical processes that lead to different grain types.

Snowpack structure

Metamorphism (qv *Snow Metamorphism*) of the snowpack through both dry and wet processes alters the initial snowpack stratigraphy and ensures that snowpack structure is continuously evolving following the initial deposition of falling or redistributed windblown snow. Investigations of snowpack stratigraphy, through snowpit studies (Fierz et al., 2009), typically reveal a horizontally layered structure in which crystal size, shape, and density vary with depth. These horizontal layers affect the permeability of the snowpack with implications for the transfer of surface meltwaters or liquid precipitation down through the snowpack (Figures 1 and 2). Where percolating meltwaters refreeze at depth, ice layers and ice lenses form. These layers may be spatially extensive where the boundary between two different stratigraphic units within the snowpack is consistent over long horizontal length scales (Pfeffer and Humphrey, 1998). If however the snowpack is characterized by a complex stratigraphy and snowpack permeability with numerous undulating stratigraphic boundaries, often due to the presence of sastrugi and windcrusts, the ice layers will rarely be spatially continuous even at short length scales of <1 m (Parry et al., 2007). The horizontal nature of the snowpack stratigraphy is disrupted by the downward percolation of water, which has been observed to percolate through both arctic and temperate snowpacks, via preferential flow-fingers or pipes (Figure 2) which occupy only a fraction of total snowpack volume but transmit a large proportion of flow (Marsh and Woo, 1984).

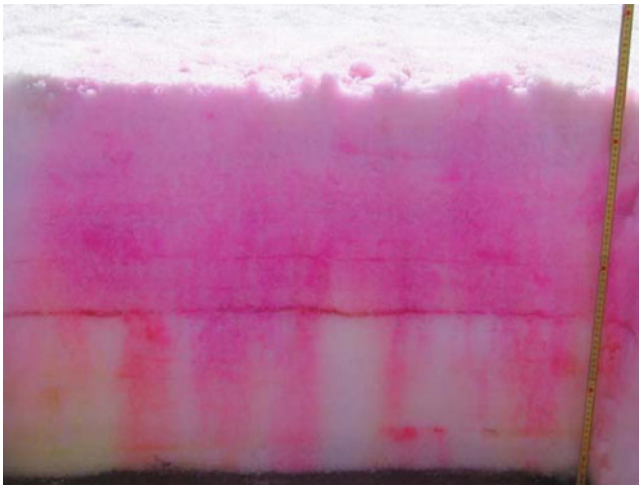

Stratigraphy of Snowpacks, Figure 2 The pattern of percolation as revealed by dye-stained surface meltwater in an excavated snow-pit 2½ h after a dye injection on the snowpack surface at Haut Glacier d'Arolla, Switzerland on 25 July 2004. An ice layer, 30 cm above the glacier surface, retains dye above it allowing continued downward flow through preferential flow-fingers. (Photo: F. Campbell).

The characteristic horizontal layering within a snowpack will affect the strength of the snowpack with implications for snowpack failure and avalanches. For example, the presence of a weakly bonded hoar layer within the snowpack provides a potential failure plane that will shear easily thus promoting the likelihood of an avalanche. As a result, avalanche forecasting is highly dependent on knowledge both of the in situ snowpack stratigraphy and our ability to predict, using models, how snowpack structure (and thus strength) will change through time (Lehning et al., 2002).

Modeling snowpack structure

The physical processes governing snow temperature evolution, grain metamorphism, densification, surface melt, and water transport have been brought together to produce comprehensive snow process models to simulate the energy and mass evolution of a snowpack through time given surface meteorological conditions. Well-established models include CROCUS, developed by the French national meteorological service (Brun et al., 1992), SNTHERM, from the US Army Corps of Engineers Cold Regions Research and Engineering Laboratory (CRREL) (Jordan, 1991), and the Swiss Federal Institute for Snow and Avalanche Research's SNOWPACK (Lehning et al., 2002). In the case of both CROCUS and SNOWPACK, the need for accurate snow stability information for avalanche warning purposes provided the impetus for detailed snowpack modeling, with SNOWPACK in particular including detailed information about snow microstructure

and resulting mechanical stability (Lehning et al., 2002). Advances in numerical modeling and the importance of effective prediction of snowpack stability ensure that investigations of snowpack stratigraphy will continue to be a well-researched area of snow science.

Summary

The processes that are responsible for the development of a snowpack ensure that it is characterized by internal "stratigraphic" layers in which the physical properties such as grain size, crystal type, density, and moisture content vary. Following the initiation of a snowpack as a result of snowfall or redistributed windblown snow, the stratigraphy of the snowpack continuously evolves due to physical compaction and the processes of both dry and wet-snow metamorphism. A detailed physical understanding of the processes that control snowpack stratigraphy is important because its complex structure affects: (1) the stability of the snowpack and its likelihood to fail as an avalanche; and (2) the permeability of the snowpack and the rate at which meltwaters are released from a given snowcover. There are numerous ways to characterize and investigate snowpacks as described in a detailed historical review on "Developments in the Stratigraphy of Snow" by Pielmeier and Schneebeli (2003). In recent decades, developments in both computational power and of the detailed understanding of snowpack processes has resulted in advances, through numerical modeling, in the simulation of the evolution of snowpack stratigraphy and stability (e.g., Brun et al., 1992; Jordan, 1991; Lehning et al., 2002).

Bibliography

Brun, E., David, P., Sudul, M., and Brunot, G., 1992. A numerical model to simulate snowcover stratigraphy for operational avalanche forecasting. *Journal of Glaciology*, **38**, 13–22.

Campbell, F., Nienow, P., and Purves, R., 2006. Role of the supraglacial snowpack in mediating meltwater delivery to the glacier system as inferred from dye tracer investigations. *Hydrological Processes*, **20**, 969–985.

Colbeck, S. C., 1975a. A theory for water flow through a layered snowpack. *Water Resources Research*, **11**(2), 261–266.

Colbeck, S. C., 1975b. Grain and bond growth in wet snow. In *Snow Mechanics: Proceedings of a symposium* held at Grindelwald, April 1974. IAHS Publication. Vol. 114, pp. 51–61.

Fierz, C., Armstrong, R. L., Durand, Y., Etchevers, P., Greene, E., McClung, D. M., Nishimura, K., Satyawali, P. K., and Sokratov, S. A. 2009. The international classification for seasonal snow on the ground. IHP-VII Technical Documents in Hydrology N°83, IACS Contribution N°1, UNESCO-IHP, Paris.

Jordan, R., 1991. A one-dimensional temperature model for a snow cover (91-16). US Army Corps of Engineers Cold Regions Research and Engineering Laboratory, Hanover, New Hampshire

Lehning, M., Bartelt, P., Brown, B., Fierz, C., and Satyawali, P., 2002. A physical SNOWPACK model for the Swiss avalanche warning. Part II: snow microstructure. *Cold Regions Science and Technology*, **35**, 147–167.

Male, D. H., 1980. The seasonal snowcover. In Colbeck, S. C. (ed.), *Dynamics of Snow and Ice Masses*. New York: Academic, pp. 305–395.

Marsh, P., 2005. HSA167 – water flow through snow and firn. In Anderson, M. (ed.), *The Encyclopedia of Hydrological Sciences*. London: Wiley.

Marsh, P., and Woo, M.-K., 1984. Wetting front advance and freezing of meltwater within a snow cover 1. Observations in the Canadian Arctic. *Water Resources Research*, **20**(12), 1853–1864.

Parry, V., Nienow, P., Mair, D., Scott, J., Hubbard, B., Steffen, K., and Wingham, D., 2007. Investigations of meltwater refreezing and density variations in the snowpack and firn within the percolation zone of the Greenland ice sheet. *Annals of Glaciology*, **46**, 61–68.

Paterson, W. S. B., 1994. *The Physics of Glaciers*, 3rd edn. Oxford: Butterworth Heinemann.

Pfeffer, W. T., and Humphrey, N. F., 1998. Formation of ice layers by infiltration and refreezing of meltwater. *Annals of Glaciology*, **26**, 83–91.

Pielmeier, C., and Schneebeli, M., 2003. Developments in the stratigraphy of snow. *Surveys in Geophysics*, **24**, 389–416.

Sommerfeld, R. A., and LaChappelle, E., 1970. The classification of snow metamorphism. *Journal of Glaciology*, **9**(55), 3–17.

Cross-references

Atmosphere-Snow/Ice Interactions
Layering of Snow
Snow Crystal Structure
Snow Density
Snow Grains
Snow Hydrology
Snow Metamorphism
Snow Pit

STREAMFLOW TRENDS IN MOUNTAINOUS REGIONS

Peter Molnar, Paolo Burlando, Francesca Pellicciotti
Institute of Environmental Engineering, ETH Zurich, Zurich, Switzerland

Definition

Streamflow is a hydrological variable measured at a defined river cross-section; it spatially integrates the runoff generating processes in the contributing watershed, including precipitation and air temperature. *Trends in streamflow* are progressive changes in the time series of streamflow that can be detected with *statistical methods* and their statistical significance can be assessed. Mountainous regions are particularly vulnerable to streamflow change because of their high specific runoff and the sensitivity to the distribution of precipitation and air temperature, and the processes of snow accumulation and melt.

Introduction

In the context of *climate change*, precipitation and temperature changes potentially have severe impacts on runoff in mountainous regions where the snowpack, glaciers, and small ice caps play a crucial role in runoff formation.

IPCC (2007) projects that widespread mass losses from glaciers and reductions in snow cover over recent decades will accelerate into the twenty-first century, reducing water availability, hydropower potential, and changing seasonality of flows in regions supplied by meltwater from major mountain ranges. It is therefore important to use statistical methods to detect gradual changes (trends) in streamflow from instrumental records and to attribute these changes to their possible causes.

In most cases, the *attribution* of discovered trends in streamflow to their causes is difficult. Because streamflow measurements integrate the runoff generating processes in the upstream watershed, they reflect not only the seasonal variability in precipitation and temperature, but also the variability in land surface properties (vegetation, soil, topographic characteristics such as slope and aspect, rock cover, glaciers, etc.). The existence of statistically significant trends in streamflow together with other hydroclimatic variables like precipitation and air temperature are an indication but not proof of causality. Only detailed knowledge about the physical processes of runoff formation in the tested basin can provide conclusive evidence.

In mountainous regions, there are additional issues related to *snow and ice*. Precipitation in winter builds the snowpack and contributes to streamflow in the following spring and summer seasons during snowmelt. The effect of temperature changes on the snowpack is therefore crucial for understanding streamflow trends (e.g., Stewart, 2009). Glacier change itself may result in both increasing or decreasing trends in streamflow during a warming trend, depending on the glacier mass balance (e.g., Huss et al., 2008). In the short-term, warming can lead to increased glacier runoff (e.g., Pellicciotti et al., 2010), while in the long-term, glacier recession can decrease the glacier mass to the point where a reduction in glacier runoff can result (e.g., Stahl and Moore, 2006).

An important element in any hydroclimatic trend detection is the choice of the *time period* over which data are tested. Hydroclimatic data generally exhibit variabilities at both short and long timescales. The time period is related to the purpose of the testing and should be chosen carefully so that discovered trends are not attributed erroneously to external factors when in fact they could be part of the natural long-term periodicity (e.g., Cohn and Lins, 2005; Laternser and Schneebeli, 2003). Furthermore, if trends in several variables are to be compared, it is fundamental that the time period is the same for all tested variables.

Methods

Several statistical tests for detecting changes in statistical properties of time series exist. Here, we focus only on the most common ones used in studies of gradual change (i.e., trends not jumps) in hydroclimatic data from the recent literature, with a special focus on streamflow. The details of the tests can be found in any statistical textbook, Helsel and Hirsch (1992) is recommended. Streamflow trend testing consists of four basic steps (Table 1).

Exploratory data analysis

In data preparation, attention should be paid to the type and resolution of data used. It is important to test streamflow for trends at several temporal resolutions. Daily data can indicate shifts in the distribution of streamflow, for example, the frequency of low and high flows (e.g., Birsan et al., 2005), while monthly and seasonal data can indicate the presence of seasonal shifts in the runoff regime, for example, the timing of spring snowmelt (e.g., Zhang et al., 2001). If daily data are available, it is advisable to study trends in quantiles Q_p, that is, daily flows exceeded with a frequency 1-p, for a range of p including minima and maxima on a seasonal basis. This gives an indication of shifts in the distributions of streamflow. Several time periods T should be tested, analyses could also be conducted on moving windows to identify more precisely in time when maximum change occurs (see Pellicciotti et al., 2010, for an effect of different time windows on trend detection). It is important to choose basins that are undisturbed, so that anthropogenic effects such as flow regulation, which are common in some mountain basins used for hydropower production, are ruled out.

Trend computation methods

The objective of testing is to compute a test statistic that quantifies the trend present in the data. In streamflow trend testing, there is a preference for nonparametric methods because the underlying distributions of the data are not known and are often non-normal. The four most common tests are listed in Table 1. Linear regression (LR) and Sen's robust slope estimator (SEN) estimate the magnitude of the trend slope b, which is useful when the magnitude of change itself is of importance. LR should be used only if the trend is linear. The Mann-Kendall (MK) test computes the test static Z and the Spearman rank correlation (RC) the test statistic t. These two tests have similar power and both are nonparametric methods not sensitive to outliers. The MK test is the most widely used test in the literature and is recommended for hydroclimatic data. It is distribution-free and captures linear and nonlinear monotonic trends. However, it is advisable to use more than one test in any trend detection study.

Testing statistical significance

At each site, the computed test statistic (b, Z, t) needs to be tested for its significance. The null hypothesis H_0 of no trend ($b = 0$, $Z = 0$, $t = 0$) is rejected at a chosen significance level α based on the computed test statistic and its distribution. For LR and SEN, the t-ratio is computed and tested with the Student's t distribution, for MK the test statistic Z is tested with the standard normal distribution, for RC the Student's t distribution may be used. In general if the test statistic, e.g., $|Z| > Z_{crit}(1 - \alpha/2)$ for a two-tailed

Streamflow Trends in Mountainous Regions, Table 1 Summary of the streamflow trend detection procedure

Steps and methods	Data/results	Selected references
1. Exploratory data analysis		
• Verifying data quality, aggregating data at different resolutions, computing daily quantiles, visual inspection of time series plots	Q (daily, monthly seasonal, annual) Daily quantiles Q_p	Kundzewicz and Robson (2004) Birsan et al. (2005) Lins and Slack (1999)
• Choice of trend testing time period/s T	Constant T Moving window T	
2. Trend computation methods		
• Trend slope – least squares linear regression, parametric method (LR)	Slope b, st.err. of b	Helsel and Hirsch (1992) Khaliq et al. (2009)
• Trend slope – Sen, nonparametric method (SEN)	Slope b, st.err. of b	
• Mann-Kendall test, nonparametric method (MK)	Test statistic Z	
• Spearman rank correlation test, nonparametric method (RC)	Test statistic t	
3. Testing statistical significance		
• Site significance: testing H_0 for b, Z, t	reject H_0 if $\|Z\| > Z_{crit}\ (1 - \alpha/2)$ $\|t\| > t_{crit}\ (1 - \alpha/2, DF)$	Khaliq et al. (2009) Kundzewicz and Robson (2004) Yue et al. (2002)
• Effect of serial correlation, methods – prewhitening, trend-free prewhitening, variance correction, resampling: permutation, bootstrap	Accounting for ρ	Burn and Elnur (2002) Livezey and Chen (1983) Zhang et al. (2001)
• Field significance: testing for the spatial congruence of site-significant trends in space (block bootstrap, Monte Carlo)	α_f -field significance level	
4. Assessing causality		
• Trend testing of other hydroclimatic data, for the same T (precipitation, temperature, snow, etc.) and examination of relations between variables and test statistics	Multivariate regression	Birsan et al. (2005) Kundzewicz and Robson (2004) Dery and Wood (2005) Lettenmaier et al. (1994)
• Examining dependence on long-term climate (climatic teleconnections)	ENSO, NAO, PDO indexes, etc.	Stahl and Moore (2006) Scherrer and Appenzeller (2004)
• Examining dependence on static basin properties	Assess vulnerability	Laternser and Schneebeli (2003)

test, then H_0 is rejected and it is concluded that the detected trend is statistically significant, that is, it is not likely to be due to random fluctuations, with the probability α of being wrong (Type I error). Sometimes a p-value is reported, that is, the probability that the computed test statistic would occur provided H_0 is true, values of $p < \alpha$ are statistically significant. Commonly used significance levels are $\alpha = 0.05, 0.1$. The power of a test is the test's ability to detect a trend when it really exists. The power is high when the detection error (Type II error) is low. The critical significance levels of the test statistics are affected by serial (auto) correlation in the data. Several methods have been developed to account for this (Table 1), details can be found in the review by Khaliq et al. (2009). The most commonly used method is the Trend-free prewhitening approach (Yue et al., 2002). Serial correlation is not likely to be high in inter-annual hydrological data, however it is advisable to compute the serial correlation coefficient for raw and detrended data to check if it is significantly $\rho > 0$. If serial correlation is an issue, variance correction and resampling methods have been found to perform well. In spatial studies, the field (spatial) significance of trends is tested by resampling (bootstrap) methods in order to identify if the spatial coherence of site-significant trends is nonrandom. For example, this could be the case for streamflow changes driven by large-scale regional climate shifts, the presence of glaciers, etc.

Assessing causality

The attribution of discovered trends in streamflow to their causes may be data-driven (indirect), for example, multivariate regression between streamflow and other hydroclimatic variables, or model-driven (direct), for example, by physically based rainfall-runoff modeling. The most common explanatory variables are precipitation (wet day frequency and intensity) and air temperature (minimum, maximum, mean), but if available, other variables like evaporation, snow cover duration and depth, glacier mass and length, etc. may be used. Long-term climate teleconnections may be examined by correlations with climate indexes such as ENSO, PDO, NAO, etc., which capture large-scale climate variability. Basin vulnerability to streamflow trends may also be examined by multivariate regression of trend statistics with static basin properties, such as basin area, average slope, soil type, rock and glacier coverage, vegetation cover, etc. (e.g., Birsan et al., 2005).

Example

An example of a streamflow trend testing procedure following the steps above is presented for the mountainous Oberried Basin, Simme River, central Switzerland. A 30-year record of daily streamflow (1971–2000) is studied for this 35.7 km^2 basin, which is 34.6% glaciated (Plaine Morte glacier) and has an average altitude of 2,370 m. Daily precipitation data are from the station Boltigen lower in the valley and daily minimum and maximum temperatures are measured at Adelboden in the neighboring valley for the same period.

In step (1) data were quality checked and aggregated to seasonal and annual totals, and seasonal quantiles Q_{min}, $Q_{0.1}$, ..., $Q_{0.9}$, Q_{max} were computed. Mean streamflow appears to be consistently increasing over the study period, especially in the summer (Figure 1a). There is pronounced seasonality typical of glacio-nival regimes, with highest flows in the snow and ice melt period in May-June-July. In step (2) the whole 30-year period was used for trend testing. The LR and MK trend tests were applied to the data and the trend slopes b and test statistic Z were computed. In step (3) statistically significant trends (α = 0.05) were found in Q in all seasons by both LR and MK tests. Quantile analyses showed that summer and spring increases were strongest for low and moderate flows (Figure 1b). But changes were statistically significant in most quantiles. Serial correlation was not present in the detrended data so prewhitening was not conducted. Field significance cannot be tested with one station. Assessing causality in step (4) focused on minimum temperatures T_{min} and precipitation P. Precipitation frequency and mean intensity did not show any meaningful trends in the study period, except for a small increasing trend in winter intensity. Statistically significant trends were however found for minimum temperature increases in spring and summer (Figure 1c). Spring in particular is a sensitive season because minimum temperatures fluctuate around 0°C, so even small increases may increase the likelihood of liquid precipitation and snowmelt. We also focused closer on the 10-year period 1984–1994 (Figure 1) where consistent increases in summer T_{min} were observed jointly with increases in runoff and glacier retreat and no major changes in P. The glacier retreated by almost 400 m between 1971 and 2000.

In summary, the seasonal MK Z for mean P, T_{min}, and Q in Figure 2a shows that temperature increases are likely the dominant reason for increases in streamflow, especially in the spring and summer months when they are

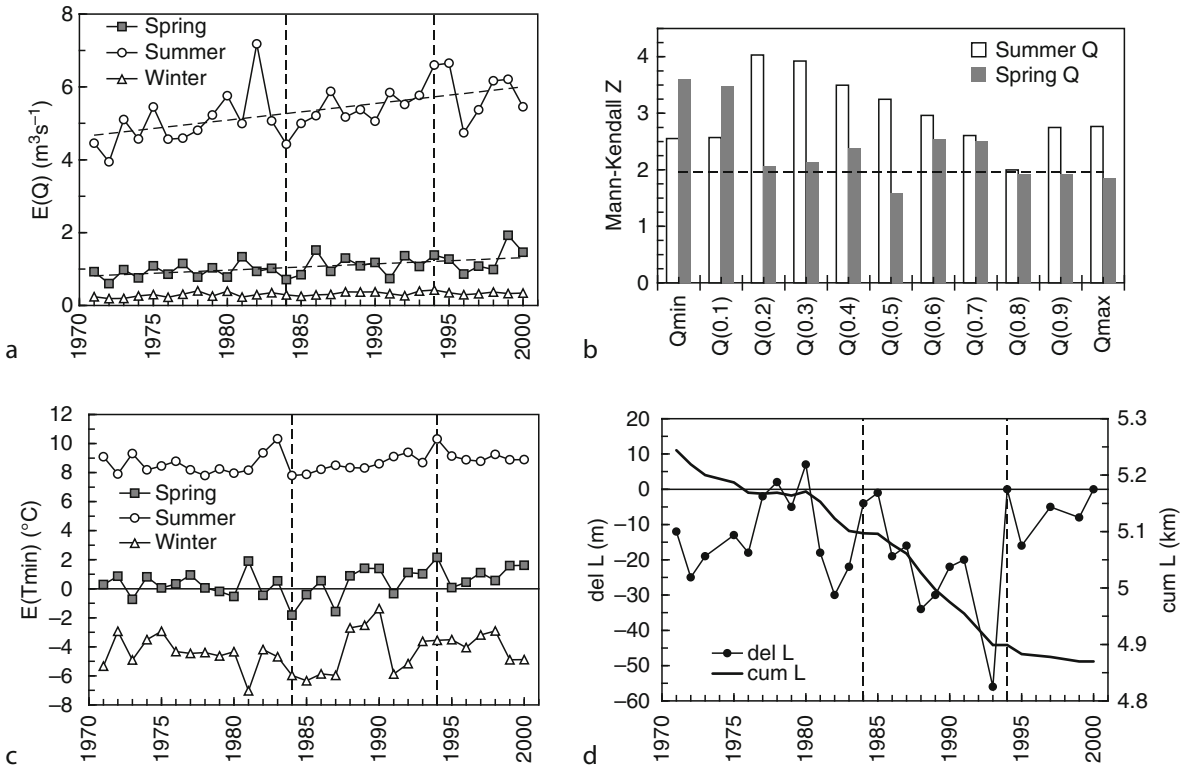

Streamflow Trends in Mountainous Regions, Figure 1 (**a**) Mean daily streamflow for the spring, summer, and winter seasons in Oberried (1971–2000) with linear trend line shown. (**b**) Mann-Kendall test statistics Z for quantiles Q_p of daily flows for the summer and spring seasons (Z_{crit} at α = 0.05 is shown with dashed line). (**c**) Mean minimum daily temperature for the spring, summer, and winter seasons. (**d**) Plaine Morte annual glacier retreat (ΔL) and total glacier length (ΣL) for the studied period (data from Glaciological reports, 1881–2008). Vertical lines show the rapid glacier mass loss period 1984–1994.

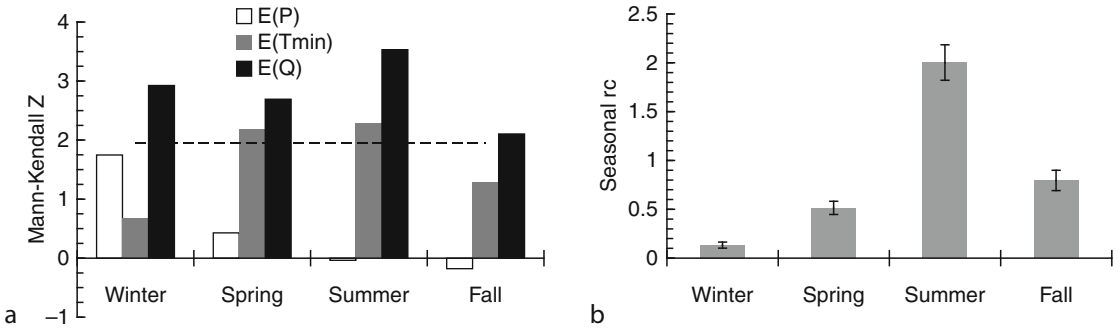

Streamflow Trends in Mountainous Regions, Figure 2 (**a**) Seasonal Mann-Kendall *Z* for mean precipitation, minimum temperature, and streamflow (Z_{crit} at $\alpha = 0.05$ is shown with dashed line). (**b**) Seasonal runoff coefficient (*rc*) computed as the ratio *rc* = E(*Q*)/E(*P*) with error bands due to altitude and wind corrections to convert point gauge precipitation to basin-wide estimates.

statistically significant ($\alpha = 0.05$). Small increases in winter precipitation may also contribute to the snowpack in winter and subsequent snowmelt. In Oberried, like in most mountain basins, the runoff coefficient *rc* (ratio between streamflow and precipitation) is strongly seasonal (Figure 2b). In fact in winter there is very little runoff $rc \approx 0$, while in summer $rc \approx 2$, which means that roughly half of the runoff volume comes from snow accumulated in the previous winter and from glacier melt.

Selected streamflow trend studies

Regional effects

There are large regional differences in streamflow trends in mountainous and/or cold environments, which are confounded by the fact that studies use different time periods. Main commonalities are that streamflow trends are often correlated with large-scale climate patterns (indexes such as NAO, PDO, etc.), with general warming, and less clearly with precipitation changes. For example, increasing trends in *Q* have been observed in the Eurasian Arctic rivers (1936–1999) (Peterson et al., 2002). In Canada, decreases in annual *Q* have been observed in the Pacific Climatic region (1960–1997) (Burn and Elnur, 2002) and in northern Canada (1964–2003) (Dery and Wood, 2005), as well as southern Canada (1967–1996) (Zhang et al., 2001). Predominantly increasing trends in *Q* were found in the continental USA (1944–1993) in particular for moderate and low quantiles, but there was regional variability (Lins and Slack, 1999) and often trends in streamflow were not entirely consistent with changes in precipitation and temperature (1948–1988) (Lettenmaier et al., 1994). Therefore, single site studies of streamflow trends should be examined in their regional context before any extrapolation of the results is made.

Glaciers and snow

In glacierized basins, summer streamflow has been found to increase due to glacier melt (e.g., Birsan et al., 2005; Pellicciotti et al., 2010) but also to decrease in areas where the glacier mass is past the critical point (e.g., Stahl and Moore, 2006). A review of other observations of glacier runoff changes can be found in Casassa et al. (2009). Single site case studies, like our Oberried example above or the study of Ye et al. (2005) of a glacier in Tianshan, show that summer runoff increases are primarily correlated with summer temperature rises and secondarily with precipitation increases. Pellicciotti et al. (2010) demonstrated that spring and summer streamflow increased for selected glacierised basins in the Swiss Alps, in relation to an increase in temperature and decrease in the seasonal snowpack. They also showed a shift in the timing of runoff due to earlier melt onset. However, they found that the magnitude and sign of trends vary with different time periods, in particular for those periods that include phases of positive glacier mass balance. Birsan et al. (2005) found a strong relation between upward streamflow trends and glacier coverage especially for summer moderate and low flow quantiles, which represent the snow and ice-melt contribution to flow. Similarly, Hodgkins (2009) found that higher summer flows were present in glaciated basins compared to non-glaciated ones during a shift from a cold to a warm phase of the PDO. In terms of melt, warming may also result in a shift in the seasonality and timing of flow (Pellicciotti et al., 2010). In several Canadian rivers, ice conditions have been found to begin and end earlier in more recent years (Zhang et al., 2001; Burn and Elnur, 2002). These observations suggest that temperature effects on streamflow trends should be a focus point of any trend detection study in mountainous regions, especially those with glaciers.

Summary

Streamflow trend detection is presented in four steps: (1) exploratory data analysis, (2) trend test methods and statistics, (3) testing for statistical significance, and (4) assessing the causality of streamflow trends. Trend detection is always connected with the choice of a time period, which should reflect the purpose of the analysis and be mindful of long-term climate oscillations that could be present. Streamflow trend attribution in mountainous regions to its causes is nontrivial, because it is difficult to separate the combination of precipitation and

temperature effects on runoff generation in high altitude catchments, the seasonal processes of snow accumulation and delayed snow melt, and the effect of the retreat and thinning of glaciers. A survey of studies highlights that streamflow trends are regionally dependent and should be investigated on a seasonal basis together with changes in precipitation and air temperature in order to capture the essence of streamflow change and its possible causes, in particular in glacierized basins.

Bibliography

Birsan, M. V., Molnar, P., Burlando, P., and Pfaundler, M., 2005. Streamflow trends in Switzerland. *Journal of Hydrology*, **314**, 312–329.

Burn, D. H., and Elnur, M. A. H., 2002. Detection of hydrologic trends and variability. *Journal of Hydrology*, **255**, 107–122.

Casassa, G., Lopez, P., Pouyaud, B., and Escobar, F., 2009. Detection of changes in glacial runoff in alpine basins: examples from North America, the Alps, central Asia and the Andes. *Hydrological Processes*, **23**, 31–41.

Cohn, T. A., and Lins, H. F., 2005. Nature's style: naturally trendy. *Geophysical Research Letters*, **32**, L23402, doi:10.1029/2005GL024476.

Dery, S. J., and Wood, E. F., 2005. Decreasing river discharge in northern Canada. *Geophysical Research Letters*, **32**, L10401, doi:10.1029/2005GL022845.

Glaciological reports (1881–2008). The Swiss Glaciers: Yearbooks of the Cryospheric Commission of the Swiss Academy of Sciences (SCNAT) published since 1964 by VAW, ETH Zurich, No. 1–124, (http://glaciology.ethz.ch/swiss-glaciers/).

Helsel, D. R., and Hirsch, R. M., 1992. Statistical methods in water resources. Studies in Environmental Science 49, Elsevier, Amsterdam, the Netherlands.

Hodgkins, G. A., 2009. Streamflow changes in Alaska between the cool phase (1947–1976) and the warm phase (1977–2006) of the Pacific Decadal Oscillation: the influence of glaciers. *Water Resources Research*, **45**, W06502, doi:10.1029/2008WR007575.

Huss, M., Farinotti, D., Bauder, A., and Funk, M., 2008. Modelling runoff from highly glacierized alpine drainage basins in a changing climate. *Hydrological Processes*, doi:10.1002/hyp.7055.

IPCC, 2007. Climate Change 2007. Fourth Assessment report of the Intergovernmental Panel on Climate Change, Synthesis Report, Geneva, Switzerland, 104 p.

Khaliq, M. N., Ouarda, T. B. M. J., Gachon, P., Sushama, L., and St-Hilaire, A., 2009. Identification of hydrological trends in the presence of serial and cross correlations: A review of selected methods and their application to annual flow regimes of Canadian rivers. *Journal of Hydrology*, **368**, 117–130.

Kundzewicz, Z. W., and Robson, A. J., 2004. Change detection in hydrological records – a review of the methodology. *Hydrological Sciences Journal*, **49**(1), 7–19.

Laternser, M., and Schneebeli, M., 2003. Long-term snow climate trends of the Swiss Alps (1931–99). *International Journal of Climatology*, **23**, 733–750.

Lettenmaier, D. P., Wood, E. F., and Wallis, J. R., 1994. Hydro-climatological trends in the continental US, 1948.88. *Journal of Climate*, **7**(4), 586–607.

Lins, H. F., and Slack, J. R., 1999. Streamflow trends in the United States. *Geophysical Research Letters*, **26**(2), 227–230.

Livezey, R. E., and Chen, W. Y., 1983. Statistical field significance and its determination by Monte Carlo techniques. *Monthly Weather Review*, **111**, 46–59.

Pellicciotti, F., Bauder, A., and Parola, M., 2010. Effect of glaciers on streamflow trends in the Swiss Alps. *Water Resources Research*, doi:10.1029/2009WR009039, in print.

Peterson, B. J., Holmes, R. M., McClelland, J. W., Vörösmarty, C. J., Lammers, R. B., Shiklomanov, A. I., Shiklomanov, I. A., and Rahmstorf, S., 2002. Increasing discharge to the Arctic Ocean. *Science*, **298**, 2171–2173.

Scherrer, S. C., and Appenzeller, C., 2004. Trends in Swiss Alpine snow days: The role of local- and large-scale climate variability. *Geophysical Research Letters*, **31**, L13215, doi:10.1029/2004GL020255.

Stahl, K., and Moore, R. D., 2006. Influence of watershed glacier coverage on summer streamflow in British Columbia. *Canada. Water Resource Research*, **42**, W06201, doi:10.1029/2006WR005022.

Stewart, I. T., 2009. Changes in snowpack and snowmelt runoff for key mountain regions. *Hydrological Processes*, **23**, 78–94.

Ye, B., Yang, D., Jiao, K., Han, T., Jin, Z., Yang, H., and Li, Z., 2005. The Urumqi river source Glacier No. 1, Tiashan, China: changes over the past 45 years. *Geophysical Research Letters*, **32**, L21504, doi:10.1029/2005GL024178.

Yue, S., Pilon, P., Phinney, B., and Cavadias, G., 2002. The influence of autocorrelation on the ability to detect trend in hydrological series. *Hydrological Processes*, **16**, 1807–1829.

Zhang, X., Harvey, K. D., Hogg, W. D., and Yuzyk, T. R., 2001. Trends in Canadian streamflow. *Water Resources Research*, **37**(4), 987–998.

Cross-references

Characteristics of Snow and Glacier Fed Rivers in Mountainous Regions with Special Reference to Himalayan Basins
Climate Change and Glaciers
Glacier Hydrology
Deglaciation
Hydrologic Cycle and Snow
Hydrological Response in Glacierized Basins
Runoff Generation
Runoff Observations
Snow Hydrology
Water Balance in the Glacierized Region

STRUCTURAL GLACIOLOGY

Michael J. Hambrey
Centre for Glaciology, Institute of Geography & Earth Sciences, Aberystwyth University, Aberystwyth, Ceredigion, UK

Synonyms

Glacier structure

Definition

Structural glaciology is the study of depositional and deformational structures in glaciers on all scales.

Structural glaciology

Glaciers demonstrate a wide range of structures that reflect their dynamic behavior. Such structures resemble those in rocks found in mountain belts, and as such, glaciers can serve as large-scale models of rock deformation

(Hambrey and Lawson, 2000). Interest in structural glaciology dates back to the early days of glaciology as a science, when pioneers such as James Forbes and John Tyndall investigated glaciers in the European Alps. However, it took the leap in understanding of the mechanics of glacier flow, triggered by Glen and Nye in the 1950s, and the subsequent introduction of structural geological principles to provide the basis for modern understanding of structures in glaciers.

Today, our knowledge of the structures of valley glaciers is well-founded, but up-scaling these ideas to ice sheets is still in its infancy. Structural glaciology is important not only for understanding glacier dynamics, but also in explaining water-routing through glaciers and glacial depositional landforms.

Glacier structures reflect both ductile and brittle deformation, and sometimes a combination of the two. Interpretation of structures requires consideration of two main concepts. Just as in rocks, ice is subject to multiple phases of deformation, referred to as "polyphase deformation." The early structures form in the upper reaches of the glacier, with later structures forming below and commonly overprinting pre-existing structures, resulting in complex associations of intersecting features. The second concept is that of cumulative (or finite) strain, since structures, once formed, continue to evolve under changing stress regimes. Adding increments of strain gives the cumulative strain, and may reflect both simple shear and pure shear. Such strains are expressed graphically as strain ellipses. They may be determined from direct measurements of velocity or by means of numerical modeling, supported by detailed 3-D mapping in the field (Hambrey and Lawson, 2000).

Before being subject to deformation, glacier ice is generally stratified from the progressive accumulation of snow and its conversion to *firn*. Internal deformation of ice under the action of gravity modifies and overprints this "primary structure." The most important ductile structures are:

- *Foliation*, which is a discontinuously layered structure originating from the simple shear and pure shear of pre-existing inhomogeneities, including stratification (Figure 1).
- *Folds*, which occur on scales from centimeters to kilometers, and reflect progressive compression or shear.
- *Boudinage*, a structure difficult to spot, but having the appearance of a string of sausages (from the French "boudin"); it results from ductility contrasts between different types of ice.
- *Ogives*, which are light and dark bands of clean and dirty ice respectively that commonly form below icefalls.

Brittle structures are dominated by *crevasses* – open V-shaped fractures in the ice, formed where ice is under tensile stress. They can be several tens of meters deep and several meters wide and are the main hazard to travel over glaciers, especially when snow-covered. Related to crevasses are *crevasse traces* which are closed water- or snow-filled crevasses, or tensional veins where the bounding ice walls have not physically separated. In addition, there are a variety of faults illustrating visible displacements, with thrust-faults being of particular importance through their role in recycling debris from the bed. A well illustrated account of glacier structures may be found in Hambrey and Alean (2004) and in their website, www.swisseduc.ch/glaciers/earth_icy_planet/glaciers05-en.html.

Structural Glaciology, Figure 1 Foliation in Gornergletscher, Switzerland, looking down-glacier toward the Matterhorn.

With different parts of a glacier developing their own distinctive suites of structures, depending on whether they are subject to shear, compression, or extension, the resulting structural assemblages may be of considerable complexity. Extensional flow regimes are dominated by crevasses and crevasse traces, the latter especially providing an historical record of dynamic regimes that may no longer exist. Compressive flow regimes, particularly at the base of an icefall typically show longitudinal foliation at the margins and arcuate foliation (derived from crevasse traces) across the middle. Within these structures folds on various scales can be identified. Icefalls may severely modify or even obliterate earlier structures. In the compressive zone near the snout foliation may be folded, whilst low-angle thrusts may develop, all superimposed on the aforementioned assemblages. Surge-type glaciers are a special case, and although they demonstrate all of the above attributes, they are further characterized by looped moraines and pervasive thrusting.

Understanding structures on glaciers aids interpretation of depositional landforms, including moraines dominated by folding and thrusting of ice and sediment, and of longitudinal ridges related to foliation, or transverse ridges related to crevassing. Thus, glacial geomorphological mapping needs to embrace knowledge of structural processes in the glaciers themselves.

Summary

Structural glaciology involves the investigation through mapping and 3-D analysis of the structures observed within glaciers. Analysis follows a structural geological approach on the grounds that glacier ice deforms in a manner resembling processes occurring in metamorphic rocks close to the melting temperature. The original primary structure comprises stratification of snow, firn, and ice in the accumulation area. Secondary structures include both brittle and ductile forms. Of these, brittle structures include crevasses, crevasse traces, faults, and thrusts; whereas ductile structures include foliation, folding, and boudinage. Structural glaciology is of fundamental importance in evaluating debris entrainment and transfer, and the subsequent deposition of sediment as landforms.

Bibliography

For a comprehensive review of structural glaciology

Hambrey, M. J., and Lawson, W., 2000. Structural styles and deformation fields in glaciers: a review. In Maltman, A. J., Hubbard, B., and Hambrey, M. J. (eds.), *Deformation of Glacial Materials*. London: Geological Society Special Publication 176, pp. 59–83.

For a layperson's account of glacier structures

Hambrey, M. J., and Alean, J., 2004. *Glaciers*. Cambridge: Cambridge Univ. Press. Chapter 5.
Illustrating a wide range of glacier structures. Available from World Wide Web: http://www.swisseduc.ch/glaciers/earth_icy_planet/glaciers05-en.html.

Cross-references

Crevasses
Englacial Processes
Forbes Band
Formation and Deformation of Basal Ice
Ogives
Sediment Entrainment, Transport, and Deposition

SUBGLACIAL BOREHOLE INSTRUMENTATION

Philip R. Porter
Division of Geography and Environmental Sciences, School of Life Sciences, University of Hertfordshire, Hatfield, Hertfordshire, UK

Definition

Subglacial borehole instrumentation: Instruments inserted via boreholes into the glacier substrate, usually used to measure basal motion and physical and hydraulic properties of basal sediments.

Introduction

Where glaciers overlie a sedimentary substrate, both sliding (Glacier Sliding) and deformation of subglacial sediments may contribute to total forward motion (Dynamics of Glaciers and Glacier Motion/Ice Velocity), yet the processes that control the partitioning of basal motion between sliding and deformation are not fully understood. This problem has arisen partially due to a lack of in situ monitoring of mechanical and hydrological conditions (Glacier Hydrology) at the ice-bed interface. However, hot-water drilling allows direct access to the ice-bed interface and direct monitoring of the processes of glacier basal motion (Subglacial Processes) is then made possible via the use of instrumented boreholes.

Much of the pioneering work to develop subglacial borehole instrumentation was carried out at Trapridge Glacier, Yukon Territory, Canada. Instruments are installed into the glacier substrate using a borehole percussion hammer, the operation of which is described in detail by Blake et al. (1992). Briefly, this comprises a 2 m long tubular structure around which is mounted a striker or "hammer" that can be repeatedly raised and dropped onto an anvil at the base of the hammer by an operator at the glacier surface. Subglacial instruments are housed within a "sheath" or attached to a "finger" at the base of the hammer below the anvil and the resultant percussive force drives the subglacial instrument progressively deeper into the substrate (see Blake et al., 1992).

This technique has been successfully used to install instruments into the substrate of Trapridge Glacier (e.g., Blake et al., 1992; Blake et al., 1994; Fischer and Clarke, 1997a; Fischer and Clarke, 1997b; Fischer et al., 1999; Kavanaugh and Clarke, 2001), Storglaciaren, Sweden (e.g., Iverson et al., 1994; Hooke et al., 1997; Fischer et al., 1998), Unteraargletscher, Switzerland (Fischer et al., 2001), and Bakaninbreen, Svalbard (e.g., Porter et al., 1997; Porter and Murray, 2001; Murray and Porter, 2001). Inevitably however, there are limitations associated with installing instruments in situ remotely from the surface beneath thick ice, aside from the obvious logistical demands. Firstly, the hot-water drilling process itself is likely to evacuate sediment from the base of the borehole to a depth of several decimeters (Blake et al., 1992) and it will inevitably take some time for sediment to intrude into the resultant void and for hydraulic and sedimentary equilibrium conditions to be reestablished. Secondly, although insertion depth can be monitored at the surface with an estimated accuracy of 0.01 m, exact placement of the sensor with respect to the ice-bed interface will always be unknown and careful interpretation of results is therefore required. Notwithstanding these issues, subglacial borehole instruments have the capacity to yield much useful information concerning basal motion and the factors that control it.

Measuring sliding

In order to effectively assess the relative contributions to glacier motion of sliding and sediment deformation, some independent measure of both these components of flow is required. Drag-spools are simple devices that give a continuous, quantitative measure of basal sliding. These instruments were first deployed beneath Trapridge Glacier (Blake et al., 1994). The drag-spool consists of a miniature multi-turn potentiometer attached to a spool, around which is wound several meters of thin string. This string passes out through a sealed plastic housing and is attached to a brass insertion tip. This tip is anchored in the subglacial sediment using the percussion hammer, while the drag-spool itself remains frozen and fixed into the borehole. As the glacier moves over its bed, the anchor remains fixed within the sediment and string is paid out from the spool. As displacement between drag-spool and anchor increases, progressive rotation of the spool and potentiometer causes a resistance change within the device (Figure 1). This resistance change is logged at the glacier surface and is converted to a glacier sliding rate using calibration data gained prior to installation.

Initial results from Trapridge Glacier indicated that basal sliding accounted for 50–70% of total glacier flow with measured basal sliding rates ranging from 40 to 80 mm d^{-1} and that peak sliding rates corresponded with rises in basal water pressure (as opposed to peak water pressure, Subglacial Drainage System) as recorded by pressure transducers suspended in boreholes (Blake et al., 1994). This latter finding conflicts with observations made elsewhere that peak glacier velocity and peak basal water pressure (Meltwater Pressure) generally coincide (e.g., Iken and Bindschadler, 1986; Kamb et al., 1985; Kamb and Engelhardt, 1987; Hooke et al., 1989). Fischer and Clarke (1997a) suggested that the relationship between sliding rate and rising basal water pressure observed beneath Trapridge Glacier could be explained in terms of "stick-slip" sliding processes operating at the ice-bed interface. As basal water pressure begins to rise, local strain buildup in the ice is released as basal ice decouples from the bed and the resultant increase in basal sliding is registered by drag-spools. However, once this strain is released, further increases in basal water pressure do not result in subsequent increases in the rate of basal sliding.

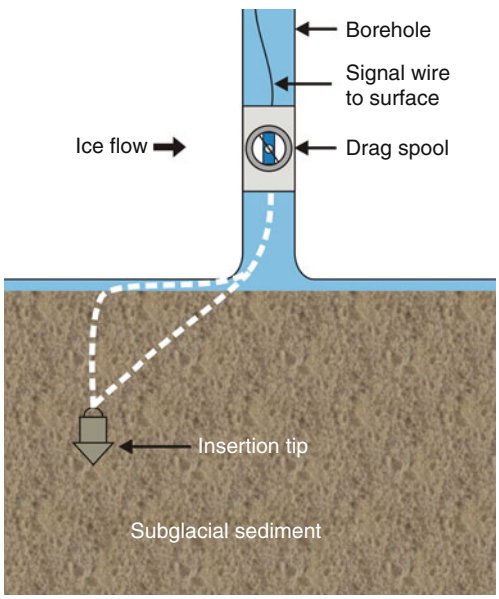

Subglacial Borehole Instrumentation, Figure 1 Conceptual diagram of a drag-spool installed within a borehole. Note the two possible locations for the drag-spool string (dashed white line) that will be dictated by sediment stiffness. Adapted from Blake et al. (1994) and Murray (1998).

Measuring deformation

Measuring the deformation rate of basal sediments is important both in order to assess the contribution of basal sediment deformation to flow and to obtain baseline stress and strain data to enhance understanding of the rheological properties of basal sediments. Qualitative measurements of total strain have been obtained from Trapridge Glacier using a resin filled tube (a "bed cast") inserted into basal sediments. A heating wire catalyzes the resin after several days of monitoring and the resultant deformation of the now-rigid tube once removed from basal sediments provides an indication of the extent of basal sediment deformation (Blake et al., 1992). A development of the bed cast is a rubber rod to which strain gauges are bonded (Blake et al., 1992). The advantage of the rubber rod over the bed cast technique is that a continuous, qualitative measure of strain rate can be obtained.

Quantitative assessment of the deformation rate of basal sediments can be made using strings of tilt cells inserted into basal sediments. A basic assumption is that, once installed, the tilt cell behaves as a clast within the basal sediment, becoming realigned as the sediment deforms. Thus, as the sediment deforms, the cell is tilted (Figure 2). Tilt cells are installed as "strings" of two or three cells allowing assessment of the vertical deformation profile and differentiation of the tilt data time series allows computation of instantaneous strain rates (Blake et al., 1992).

Tilt cells comprise two main designs. Firstly, leaf spring tilt cells comprise two pendulum weights attached to leaf springs orientated perpendicular to one another to which strain gauges are bonded. As the cell is tilted, the pendulum weights flex the leaf springs causing the resistance of the strain gauges to change. This resistance change can be related to angle of tilt once the cell has been calibrated. The operation and calibration of leaf spring tilt cells are described in detail by Blake et al. (1992).

Secondly, electrolytic tilt cells consist of a series of metal electrodes housed in a chamber containing a suitable electrolytic fluid that contacts the electrodes. Electrodes are arranged around a central common

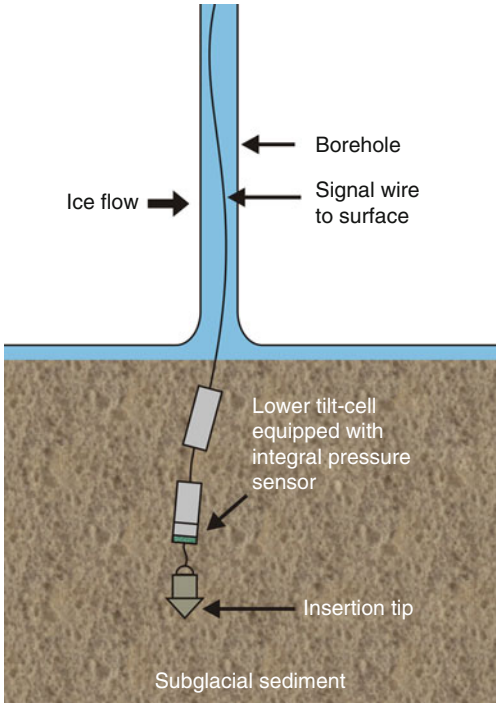

Subglacial Borehole Instrumentation, Figure 2 Conceptual diagram of a string of tilt cells installed within deforming subglacial sediments. Adapted from Murray (1998).

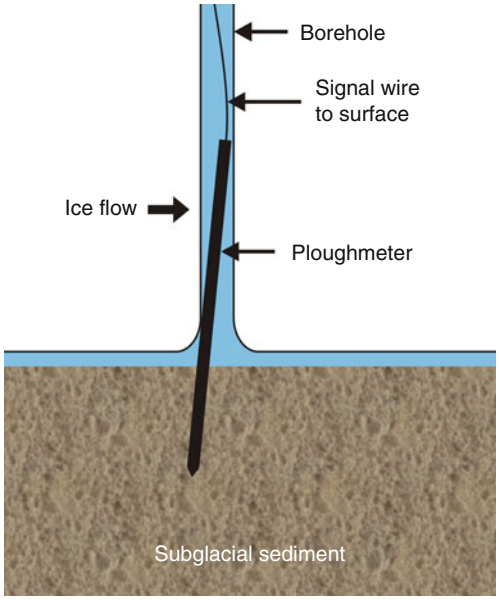

Subglacial Borehole Instrumentation, Figure 3 Conceptual diagram of a ploughmeter installed within a borehole. As the glacier flows over the sedimentary substrate, the ploughmeter is dragged through subglacial sediments. Adapted from Fischer and Clarke (1994) and Murray (1998).

electrode. In a dual-axis cell, four electrodes are mounted around the central electrode at 90° intervals in a "cross" configuration. As the cell is tilted, the outer electrodes either become immersed in, or emerge from the electrolyte depending on their position with respect to the central electrode, while the level of electrolyte in contact with the central electrode remains constant at all times. This has the effect of changing the impedance between electrodes that can be measured as a voltage change and related to angle and direction of tilt once the cell has been calibrated. Full details of the operation and calibration of electrolytic tilt cells are described by Blake et al. (1992) and Porter and Murray (2001). Strings of tilt cells are inserted vertically into basal sediments using a percussion hammer.

Data obtained from tilt cells installed beneath Trapridge Glacier show that subglacial strain rates vary in amplitude and polarity over short timescales. Observed negative strain rates may be a function of extrusion flow (Blake et al., 1992). A development of the basic electrolytic tilt cell was deployed at Bakaninbreen, Svalbard by Porter and Murray (2001). Here, the lowermost cell in each string was equipped with a pore-pressure transducer to allow relationships between sediment strain rates and water pressure fluctuations within deforming sediments to be assessed. At the time of installation, Bakaninbreen was in the late-active phase of a prolonged surge (Glacier Surging). Tilt cells were installed up- and down-glacier of a surge front. In common with observations at Trapridge Glacier, strain rates at Bakaninbreen fluctuated over short timescales, with periods of both positive and negative strain evident in the time series. Strain rates up-glacier of the surge front were an order of magnitude higher than those measured down-glacier of the surge front. Interpretation of tilt cell records indicated that deformation of basal sediments comprised the dominant mode of basal motion. However, in contrast to observations made elsewhere (e.g., Boulton and Hindmarsh, 1987), no consistent relationship between water pressure within basal sediments and strain rate was observed.

Assessing sediment properties

The ploughmeter is a device that enables assessment of properties of subglacial sediments such as viscosity and yield strength, and may also be used to infer sediment texture and assess glacier sliding rates (Fischer and Clarke, 1994; Fischer and Clarke, 1997b). The device consists of a steel rod onto which strain gauges are bonded near one end. It is hammered into the bed, such that all strain gauges are fully immersed into the subglacial sediment. The upper section of the device then becomes trapped in the ice, while the lower portion is dragged through the underlying sediment, effectively acting as an ice-entrained clast (Figure 3). This "plowing" action sets up stresses within the ploughmeter that cause changes in the resistance of the strain gauges that are monitored at the glacier surface and translated into an applied force by application of

calibration data. A full description of the device and its calibration is provided by Fischer and Clarke (1994).

Ploughmeter data makes it possible to obtain estimates of the rheological properties of basal sediments. If sediment is assumed to behave as a Newtonian viscous fluid, then an estimate of viscosity can be obtained. If sediment is assumed to behave as an ideal plastic solid (Plastic Flow and Plastic Deformation), then an estimate of yield strength (Bed Strength) can be obtained. Viscosity estimates gained from Trapridge Glacier range from 3.0×10^{-9} to 3.1×10^{10} Pa s (Fischer and Clarke, 1994), while estimates from ploughmeters installed beneath Bakaninbreen range from 1.1×10^{10} to $4.3\ 10^{10}$ Pa s (Porter, 1997). Applying an idea plastic solid model, yield strength estimates at Trapridge Glacier range from 48 to 57 kPa (Blake et al., 1992) and at Bakaninbreen they range from 6.6 to 411.6 kPa with high recorded values thought to be caused by ploughmeters moving into areas of frozen bed and by implication, areas of high-yield strength sediment (Murray and Porter, 2001). Comparison of calculated basal shear stress and yield strength data gained from ploughmeters at Bakaninbreen, allowed areas where stress exceeds yield strength to be identified (Porter et al., 1997). By implication, these areas are likely to be experiencing basal sediment deformation, an assertion that is supported by subsequent studies (Porter and Murray, 2001). Ploughmeter data has also been used to estimate glacier sliding rate based on clast collision frequency and associated force variations recorded by the device (Fischer and Clarke, 1997b).

The rheological properties of basal sediments have also been measured using a subglacial borehole instrument that has some conceptual similarities with the ploughmeter, dubbed a "dragometer" (Iverson et al., 1994). The device comprises a conical "fish" attached to a wire that runs up to a load cell installed in a metal tube that is trapped in the base of a borehole. The signal recorded by the load cell varies according to the forces applied to the "fish" which in turn relate to the residual strength of the subglacial sediments through which the "fish" is being dragged. A full description of the dragometer is provided by Iverson et al. (1994).

Data obtained from a dragometer installed in the bed of Storglaciären indicate an average residual strength for subglacial sediments of ~55 kPa (Iverson et al., 1994).

Hydraulic properties

Where ploughmeter data is collected alongside basal water pressure data from borehole pressure transducers, conclusions can be drawn regarding both the functioning of the basal hydrological system (e.g., Fischer et al., 1999; Kavanaugh and Clarke, 2001) and the hydraulic properties of basal sediments (e.g., Fischer et al., 1998; Fischer et al., 2001). Ploughmeter records and associated borehole water pressure records from Trapridge Glacier show good correspondence, with diurnal force fluctuations correlating well with large and rapid fluctuations in basal water pressure (Fischer et al., 1999). However, this correlation was observed to be in phase with one ploughmeter and out of phase with another in an adjacent borehole and was thought to arise from the existence of time-varying "sticky spots" beneath the glacier, whereby one ploughmeter is moving through an area where ice-bed coupling is enhanced (a "sticky spot") in response to a reduction of basal water pressure (Fischer et al., 1999).

Subsequent observations at Trapridge Glacier demonstrated that a series of "spring events" resulted in the failure of borehole pressure transducers and yielded significant force responses on ploughmeters, interpreted to result from strong basal motion associated with the establishment of a connected drainage system (Subglacial Drainage System) beneath the glacier (Kavanaugh and Clarke, 2001).

Ploughmeters installed beneath Unteraargletscher, Switzerland also displayed an inverse correlation with basal water pressure recorded by borehole pressure transducers and a significant time lag between the two signals (Fischer et al., 2001). This lag was thought to reflect the time taken for a pressure pulse in the subglacial drainage system to propagate through basal sediments to the insertion depth of the ploughmeter, thereby reducing sediment strength and associated force exerted on the ploughmeter. Assuming this assertion is correct, the hydraulic diffusivity of basal sediments can be estimated and values from Unteraargletscher range from 1.3×10^{-6} to 2.3×10^{-6} $m^2\ s^{-1}$. A similar ploughmeter force–water pressure relationship was measured at Storglaciären (Fischer et al., 1998) and again, using the propagation velocity of water pressure waves through basal sediments, calculated hydraulic diffusivity was found to range from 1.9×10^{-6} to 3.6×10^{-6} $m^2\ s^{-1}$.

Data concerning the hydraulic properties of basal sediments have also been obtained from pressure transducers installed within tilt cells inserted into basal sediments at Bakaninbreen (Porter and Murray, 2001). Here it was found that pore-water pressure fluctuations, as recorded by pore-pressure sensors installed within tilt cells, lagged borehole water pressure fluctuations by 37–49 h. Because the depth of insertion of tilt cells and integral pore-pressure sensor can be measured during installation, it is again possible to estimate hydraulic diffusivity using the propagation velocity of water pressure waves. Diffusivity values at Bakaninbreen range between 1.2×10^{-6} and 5.0×10^{-6} $m^2\ s^{-1}$ and if a value for specific storage of till is assumed then hydraulic conductivity of basal sediments can also be estimated. At Bakaninbreen, diffusivity ranges from 3.2×10^{-7} to 7.7×10^{-8} m s^{-1} which is in good agreement with values derived elsewhere (e.g., Boulton and Dent, 1974; Fountain, 1994; Iverson et al., 1994; Hubbard et al., 1995; Murray and Clarke, 1995). It is interesting to note, however, that at Bakaninbreen there is no clear relationship between basal water pressure fluctuations and strain rate as measured by tilt sensors (Porter and Murray, 2001). Furthermore, ploughmeters also showed only occasional strong relationships with basal water pressure and in contrast to observations made

elsewhere these correlations were mostly positive (Murray and Porter, 2001). At Bakaninbreen, it appears that there is weak coupling between sediment strength and water pressure fluctuations and that force fluctuations recorded by ploughmeters may arise from variations in granulometry (Granulometry) or ice-bed coupling (Murray and Porter, 2001).

Summary

The installation of subglacial borehole instruments has the capacity to yield much useful information concerning basal motion and the properties of basal sediments. Installation of borehole instrumentation is, however, logistically demanding and given inevitable uncertainties over instrument placement with respect to the ice-bed interface when installing remotely beneath thick ice, careful interpretation of results is required.

Bibliography

Blake, E. W., Clarke, G. K. C., and Gérin, M. C., 1992. Tools for examining subglacial bed deformation. *Journal of Glaciology*, **38**(130), 388–396.

Blake, E. W., Fischer, U. H., and Clarke, G. K. C., 1994. Direct measurement of sliding at the glacier bed. *Journal of Glaciology*, **40**(136), 595–599.

Boulton, G. S., and Dent, D. L., 1974. The nature and rates of post-depositional changes in recently deposited till from south-east Iceland. *Geografiska Annaler*, **56A**(3–4), 121–134.

Boulton, G. S., and Hindmarsh, R. C. A., 1987. Sediment deformation beneath glaciers: rheology and geological consequences. *Journal of Geophysical Research*, **92**(B9), 9059–9082.

Fischer, U. H., and Clarke, G. K. C., 1994. Ploughing of subglacial sediment. *Journal of Glaciology*, **40**(134), 97–106.

Fischer, U. H., and Clarke, G. K. C., 1997a. Stick-slip sliding behaviour at the base of a glacier. *Annals of Glaciology*, **24**, 390–396.

Fischer, U. H., and Clarke, G. K. C., 1997b. Clast collision frequency as an indicator of glacier sliding rate. *Journal of Glaciology*, **43**(145), 460–466.

Fischer, U. H., Iverson, N. R., Hanson, B., Hooke, R. Le B, and Jansson, P., 1998. Estimation of hydraulic properties of subglacial till from ploughmeter measurements. *Journal of Glaciology*, **44**(148), 517–522.

Fischer, U. H., Clarke, G. K. C., and Blatter, H., 1999. Evidence for temporally varying 'sticky spots' at the base of Trapridge Glacier, Yukon Territory, Canada. *Journal of Glaciology*, **45**(150), 352–360.

Fischer, U. H., Porter, P. R., Schuler, T., Evans, A. J., and Gudmundsson, G. H., 2001. Hydraulic and mechanical properties of glacial sediments beneath Unteraargletscher, Switzerland: Implications for glacier basal motion. *Hydrological Processes*, **15**(18), 3525–3540.

Fountain, A. G., 1994. Borehole water-level variations and implications for the subglacial hydraulics of South Cascade Glacier, Washington State, USA. *Journal of Glaciology*, **40**(135), 293–304.

Hooke, R. L., Calla, P., Holmlund, P., Nilsson, M., and Stroeven, A., 1989. A 3 year record of seasonal variations in surface velocity, Storglaciaren, Sweden. *Journal of Glaciology*, **35**(120), 235–247.

Hooke, R. Le B, Hanson, B., Iverson, N. R., Jansson, P., and Fischer, U. H., 1997. Rheology of till beneath Storglaciären, Sweden. *Journal of Glaciology*, **43**(143), 172–179.

Hubbard, B. P., Sharp, M. J., Willis, I. C., Nielsen, M. K., and Smart, C. C., 1995. Borehole water-level variation and the structure of the subglacial hydrological system of Haut Glacier d'Arolla, Valais, Switzerland. *Journal of Glaciology*, **41**(139), 572–583.

Iken, A., and Bindschadler, R. A., 1986. Combined measurements of sunglacial water pressure and surface velocity of Findelengletscher, Switzerland: conclusions about drainage system and sliding mechanism. *Journal of Glaciology*, **32**(110), 101–119.

Iverson, N. R., Jansson, P., and Hooke, R. Le B, 1994. In-situ measurement of the strength of deforming subglacial till. *Journal of Glaciology*, **40**(136), 497–503.

Kamb, B., and Engelhardt, H., 1987. Waves of accelerated motion in a glacier approaching surge: the minisurges of Variegated Glacier, Alaska, USA. *Journal of Glaciology*, **33**(113), 27–46.

Kamb, B., Raymond, C. F., Harrison, W. D., Engelhardt, H., Echelmeyer, K. A., Humphrey, N., Brugman, M. M., and Pfeffer, T., 1985. Glacier surge mechanism: 1982–1983 surge of variegated glacier, Alaska. *Science*, **227**(4686), 469–479.

Kavanaugh, J. L., and Clarke, G. K. C., 2001. Abrupt glacier motion and reorganization of basal shear stress following the establishment of a connected drainage system. *Journal of Glaciology*, **47**(158), 472–480.

Murray, T., 1998. Assessing the paradigm shift: deformable glacier beds. *Quaternary Science Reviews*, **16**, 995–1016.

Murray, T., and Clarke, G. K. C., 1995. Black-box modelling of the subglacial water system. *Journal of Glaciology, Journal of Geophysical Research*, **100**(B6), 10,231–10,245.

Murray, T., and Porter, P. R., 2001. Basal conditions beneath a soft-bedded polythermal surge-type glacier: Bakaninbreen, Svalbard. *Quaternary International*, **86**(1), 103–116.

Porter, P. R., 1997. Glacier surging: subglacial sediment deformation and ice-bed coupling. *Unpublished PhD thesis*, University of Leeds.

Porter, P. R., and Murray, T., 2001. Hydrological and mechanical properties of till beneath Bakaninbreen, Svalbard. *Journal of Glaciology*, **47**(157), 167–175.

Porter, P. R., Murray, T., and Dowdeswell, J. A., 1997. Sediment deformation and basal dynamics beneath a glacier surge front: Bakaninbreen, Svalbard. *Annals of Glaciology*, **24**, 21–26.

Cross-references

Bed Strength
Dynamics of Glaciers
Glacier Hydrology
Glacier Motion/Ice Velocity
Glacier Sliding
Glacier Surging
Plastic Flow
Subglacial Drainage System
Subglacial Processes

SUBGLACIAL DRAINAGE SYSTEM

Bryn Hubbard
Centre for Glaciology, Institute of Geography and Earth Sciences, Aberystwyth University, Aberystwyth, Ceredigion, Wales, UK

Synonyms

Basal drainage system; Subglacial hydrological system; Subglacial hydrology

Definition

Subglacial drainage systems are formed from the hydraulic pathways that contain and transfer water located close to the contact between an ice mass and its substrate. These pathways are commonly considered to be spatially discrete, e.g., flowing through dendritic networks of channels, or spatially dispersed, e.g., flowing through diffuse films. The subglacial drainage system can exchange water with the overlying englacial drainage system and the underlying groundwater drainage system. Extensive reviews of subglacial drainage have been provided by, among others, Flowers (2008), Hooke (1989), Hodgkins (1997) and Hubbard and Nienow (1997).

Introduction and significance

The investigation of subglacial hydrology forms an important branch of glaciology. However, it is important to note that well-developed subglacial drainage systems only exist at the bases of those temperate or polythermal ice masses that are at least partly warm based (i.e., are characterized by a basal interface that is melting).

Reconstructing the nature of, and changes in, subglacial drainage is important for several reasons. First, water located at the basal interface of any ice mass exerts a strong control over the way in which that ice mass moves. In general, the presence of subglacial water acts as a lubricating layer, speeding basal motion up by partially decoupling the ice mass from its (otherwise harder and/or rougher) substrate (e.g., Iken and Bindschadler, 1986). It is not only the presence of water that is important here but probably also the quantity of water stored at the glacier bed and its pressure (e.g., Bartholomaus et al., 2008), both of which change at a variety of timescales both across a single ice mass and between different ice masses. Recent so-called dynamic thinning, caused by a postulated increase in the delivery of surface-derived meltwater to the base of Greenland outlet glaciers (Zwally et al., 2002), is considered to be responsible for their speed up and retreat. Similarly, increases in lubricating basal meltwater may be responsible for at least facilitating, if not triggering, rapid speedups during the surge phase of *surge-type* glaciers (e.g., Kamb et al., 1985). Systematic representations of the links between subglacial drainage and ice mass motion are also important to computer modelers to allow them to improve the realism of their models of ice mass response to climate change.

Second, most of the water delivered from ice masses exits via the subglacial drainage system. In different settings and at different times, this water can represent a resource or a hazard. In terms of resource, subglacial water may be tapped directly from the glacier bed or shortly after it leaves the glacier for hydroelectric power generation and/or potable uses. Downstream extraction for domestic use and agricultural irrigation represents crucial supply issues in many populous but otherwise arid areas of the world. Understanding controls over changes in water delivery from glaciers at a variety of timescales is important for scientists to predict future supplies and to inform planners and policymakers. For example, ~2 billion people are dependent on water supplied by rivers that are fed by Himalayan glaciers – many of which are currently receding and are anticipated to continue to do so over the next several decades to centuries. Subglacial drainage can also be more immediately hazardous. *Jökulhlaups*, for example, probably represent the most visible hazard associated with subglacial water delivery. Taking the name from type events in Iceland, jökulhlaups (literally "glacier leaps") are large floods associated with the catastrophic release of water from subglacial lakes located in areas of high geothermal heating (e.g., Bjornsson, 2002). For example, the Grimsvötn jökulhlaup of 1996 discharged ~3 km^3 of meltwater in just over 2 days across its *sandur* (at a peak discharge of ~45,000 $m^3 s^{-1}$), causing an estimated ~US$15 million of infrastructural damage. Understanding the relationships between subglacial drainage and water delivery is therefore important to modelers, engineers, planners, and policymakers.

Third, water may be stored for long periods in isolated subglacial lakes, allowing distinctive microbiological forms to evolve. There are currently believed to be approaching 300 such lakes beneath the Antarctic Ice Sheet alone (Siegert et al., 2005; Smith et al., 2009), the largest known of which is Lake Vostok with surface dimensions of ~200 km and ~50 km, and an approximate volume of 5,400 km^3. In addition to the biological interest provided by these water bodies, research updates revealing ever-larger numbers of such lakes (e.g., Popov and Masolov, 2007) and the existence of hydraulic linkages between them (Fricker et al., 2007; Wingham et al., 2006) will probably transform our understanding of ice sheet drainage and motion over the next few decades.

Methods of empirical investigation

Revealing the dynamic nature of subglacial drainage represents a fundamental challenge for glaciologists. However, gaining direct access to undisturbed meltwater drainage pathways is at best challenging and at worst impossible. Consequently, researchers of subglacial drainage are continually developing and applying new methods and techniques (summarized in Hubbard and Glasser, 2005). Approaches to studying subglacial drainage fall into five broad categories.

1. *Investigations of the quantity and character of meltwater discharged from ice masses*. Analysis of the meltwater flowing from ice masses can provide important information about the subglacial flow pathways that it has followed beneath that ice mass. Simple discharge records, for example, when compared with the timing of water input to the ice mass, can inform on water transit times and water storage within the englacial and subglacial systems. Similarly, analysis of variations in

the fine sediment particles suspended in the water and of the chemical (ionic) composition of the water itself can also provide information relating to how long that water has spent at the glacier bed and under what broad conditions. For example, water that is routed efficiently through large subglacial channels will have little time to interact with reactive subglacial sediments and will be characterized by a rapid and peaked hydrograph. It will also be solute-poor relative to subglacial water that has been routed via diffuse flow pathways. Changes in the ratio of suspended sediment concentration to discharge of subglacially routed waters can be related to changes in subglacial sediment supply, with increases for example indicating the headward growth of channels or the tapping of new areas of the glacier bed (Fenn et al., 1985).

2. *Tracer investigations*. Tracers such as salt or, more commonly fluorescent dye (which can be detected at far lower concentrations and therefore requires lower dosages), can be added to the glacier drainage system at known locations and recorded as it exits the ice mass. The resulting breakthrough curve of dye concentration plotted against time can provide valuable information relating to the flow pathways followed by the water between the input location and the measuring station. For example, a rapidly-reached, narrow and flashy breakthrough curve will represent flow through a hydraulically more efficient, probably channelized, drainage system than a strongly attenuated breakthrough curve. In addition to such qualitative judgments, breakthrough curve analysis can yield quantitative data such as minimum flow speeds (given by dividing the straight-line distance between the input location and the measuring station by the time separating the tracer injection from the measurement) and dispersion (given by an analysis of the spread of the breakthrough curve relative to its velocity) (e.g., Burkimsher, 1983; Nienow et al., 1998).
3. *Proglacial bedrock investigations.* The methods outlined above provide useful information relating to real-time subglacial hydrological processes, but they are spatially integrated over large, and possibly unknown, flow lengths. In contrast, investigations of drainage-related geomorphic features etched into glaciated surfaces provide excellent spatial discrimination but poor temporal discrimination. Such studies can yield important information relating, in particular, to the structure and morphometry of the former subglacial drainage system and its individual flow pathways (e.g., Walder and Hallet, 1979). This information can be used to approximate former subglacial water discharges and pressures, and this information can in turn be used to inform reconstructions of former ice mass movement (e.g., Sharp et al., 1989).
4. *Borehole-based investigations*. Borehole-based investigations of subglacial drainage systems suffer from neither excessive spatial integration nor excessive temporal integration. However, the approach is logistically demanding, typically requiring multiple boreholes to be drilled to the bed of the ice mass concerned and then instrumented. Such boreholes can be created mechanically, which has the advantage of providing ice cores as well as access to the base of the ice mass (but which is logistically demanding and slow, typically yielding meters to tens of meters of borehole length per day), or thermally by pressurized hot water, which provides no ice core but which typically yields hundreds of meters of borehole length per day. Each such borehole provides direct access to a specific location on the ice mass bed, which can be investigated via several techniques. For example, our understanding of the relationship between subglacial drainage and ice mass motion has been revolutionized by synchronous borehole-based measurements of subglacial water pressure and surface measurements of ice velocity (Bartholomaus et al., 2008; Iken and Bindschadler, 1986). Where arrays of such boreholes can be drilled, spatial variability in multiple hydrological properties can be measured at high temporal resolution, providing the most detailed records available to date relating to subglacial drainage (e.g., Hubbard et al., 1995).
5. *Remotely sensed (geophysical and satellite-based) investigations.* The most widespread spatial coverage of information relating to subglacial drainage is supplied by remotely sensed data. However, while this information does provide good spatial coverage, it commonly yields first-order data that need to be interpreted in terms of specific subglacial properties. Such interpretations are rarely unequivocal, although inversion techniques can be used to infer hydrologically modulated variations in basal motion from satellite-based interferometric synthetic aperture radar (InSAR) (e.g., Magnusson et al., 2007). Ice surface radar also has the capacity to identify the presence of water at the ice-bed contact, and repeated radar measurements at a given site have the capacity to reveal changes in the nature of the interface and the distribution of that water (e.g., Smith et al., 2007). Recently, for example, repeat satellite-derived altimetry has revealed spatial variations in the surface elevation of ice masses pointing to coordinated, episodic water transfer between sub-ice lakes (e.g., Carter et al., 2009).

Configuration and change

Subglacial drainage networks are generally considered to fall into one of two broad categories. *Discrete* drainage systems are formed from a network of channels that may be cut upward into the overlying ice (named Röthlisberger channels or R-channels) (Röthlisberger, 1972) or cut downward into the underlying bedrock (named Nye channels or N-channels) (Nye, 1973). These networks are of broadly dendritic form, composed of small feeder streams

linking to create branch streams that in turn join to create a small number of trunk channels, each progressively flowing at low pressure and therefore drawing water from their smaller feeders. In contrast, *distributed* drainage systems form diffuse or anastomosing networks that do not evolve into progressively larger, lower-pressure channels. Such distributed systems can be formed of films, linked cavities, permeating flow through sub-ice sediments, or so-called canals, cut both upward into ice and downward into underlying sediments. These systems generally transfer water more slowly and at higher pressure for a given discharge than do discrete networks. Switching between the two can therefore raise or lower the pressure of subglacial meltwater, and correspondingly, ice motion (e.g., Fowler, 1987).

Controls over the structure of subglacial drainage systems, and of the individual flow pathways that comprise them, can change at a variety of timescales. Many subglacial drainage systems are correspondingly subject to spatial and temporal changes. For example, a change in the configuration of subglacial drainage pathways – from discrete (operating at relatively low pressure) to distributed (operating at relatively high pressure) – has been closely associated with the initiation of glacier surges (e.g., Fowler, 1987; Kamb et al., 1985 above). However, the most commonly recognized changes in subglacial drainage result from meteorological seasonality. Accordingly, the subglacial drainage system beneath mid-latitude valley glaciers can change from a diffuse network through the winter, when minimal and spatially diffuse water inputs derive from basal melting alone, to the summer, when large fluxes of surface meltwater are delivered to the glacier bed via point sources such as crevasses and moulins. However, this drainage system replacement is not instantaneous but time transgressive, with repeated dye tracer studies revealing that the distributed system is gradually replaced in an upglacier direction (dictated by the retreat of the surface snow line) by the channelized system (Nienow et al., 1998). While such wholesale seasonal changes are improbable at larger ice masses, subglacial drainage change is likely where summer surface melting occurs near the margins of large ice sheets, and over decades to centuries at larger ice masses that are subject to changing climatic conditions.

Conclusions

Subglacial drainage systems are important, diverse, and subject to change at various temporal and spatial scales. They are important because they (a) exert a strong influence on the basal motion of ice masses, (b) represent potential hazards and resource, and (c) can form large subglacial lakes. Subglacial drainage systems are diverse because they are composed of flow pathways that can have different specific configurations, which can in turn exist adjacent to each other and change over time. However, investigating the structure and dynamics of subglacial drainage systems is difficult, requiring major logistical effort and continual development of new methods and technologies. Despite these developments, the most pressing challenges that face researchers in the future are similar to those that have confronted researchers in the past. The most fundamental of these is probably still to obtain high (spatial- and temporal-) resolution records of changes in subglacial drainage systems at the ice mass scale, and to determine the physical controls responsible for those changes. This information would then be applied in a structured manner to allow future drainage system changes and meltwater discharges to be predicted. Additionally, perhaps the most interesting developments in the field of our exploration of subglacial drainage systems will come from obtaining the first direct access to major subglacial lakes, as well as their continued geophysical investigation.

Bibliography

Bartholomaus, T. C., et al., 2008. Response of glacier basal motion to transient water storage. *Nature Geoscience*, **1**, 33–37.

Bjornsson, H., 2002. Subglacial lakes and jokulhlaups in Iceland. *Global and Planetary Change*, **35**, 255–271.

Burkimsher, M., 1983. Investigations of glacier hydrological systems using dye tracer techniques: observations at Pasterzengletscher, Austria. *Journal of Glaciology*, **29**, 403–416.

Carter, S. P., et al., 2009. Dynamic distributed drainage implied by the flow evolution of the 1996–1998 Adventure Trench subglacial lake discharge. *Earth and Planetary Science Letters*, **283**, 24–37.

Fenn, C. R., et al., 1985. An evaluation of the use of suspended sediment rating curves for the prediction of suspended sediment concentration in a proglacial stream. *Geografiska Annaler: Series A, Physical Geography*, **67**, 71–82.

Flowers, G. E., 2008. Subglacial modulation of the hydrograph from glacierized basins. *Hydrological Processes*, **22**, 3903–3918.

Fowler, A. C., 1987. A theory of glacier surges. *Journal of Geophysical Research – Solid Earth and Planets*, **92**, 9111–9120.

Fricker, H. A., et al., 2007. An active subglacial water system in West Antarctica mapped from space. *Science*, **315**, 1544–1548.

Hodgkins, R., 1997. Glacier hydrology in Svalbard, Norwegian High Arctic. *Quaternary Science Reviews*, **16**, 957–973.

Hooke, R. L., 1989. Englacial and subglacial hydrology: a qualitative review. *Arctic and Alpine Research*, **21**, 221–233.

Hubbard, B., Glasser, N. F., 2005. *Field Techniques in Glaciology and Glacial Geomorphology*. West Sussex, England: Wiley.

Hubbard, B., and Nienow, P., 1997. Alpine subglacial hydrology. *Quaternary Science Reviews*, **16**, 939–955.

Hubbard, B. P., et al., 1995. Borehole water-level variations and the structure of the subglacial hydrological system of Haut Glacier d'Arolla, Valais, Switzerland. *Journal of Glaciology*, **41**, 572–583.

Iken, A., and Bindschadler, R. A., 1986. Combined measurements of subglacial water pressure and surface velocity of Findelengletscher, Switzerland: conclusions about drainage system and sliding mechanism. *Journal of Glaciology*, **32**, 101–119.

Kamb, B., et al., 1985. Glacier surge mechanism – 1982–1983 surge of variegated glacier, Alaska. *Science*, **227**, 469–479.

Magnusson, E., et al., 2007. The impact of jokulhlaups on basal sliding observed by SAR interferometry on Vatnajokull, Iceland. *Journal of Glaciology*, **53**, 232–240.

Nienow, P., et al., 1998. Seasonal changes in the morphology of the subglacial drainage system, Haut Glacier d'Arolla, Switzerland. *Earth Surface Processes and Landforms*, **23**, 825–843.
Nye, J., 1973. Water at the bed of the glacier. *International Association of Hydrological Sciences Publication*, **95**, 189–194.
Popov, S. V., and Masolov, V. N., 2007. Forty-seven new subglacial lakes in the 0–110 degrees E sector of East Antarctica. *Journal of Glaciology*, **53**, 289–297.
Röthlisberger, H., 1972. Water pressure in intra- and subglacial channels. *Journal of Glaciology*, **11**, 177–204.
Sharp, M., et al., 1989. Structure and Stability of the Former Subglacial Drainage System of the Glacier De Tsanfleuron, Switzerland. *Earth Surface Processes and Landforms*, **14**, 119–134.
Siegert, M. J., et al., 2005. A revised inventory of Antarctic subglacial lakes. *Antarctic Science*, **17**, 453–460.
Smith, A. M., et al., 2007. Rapid erosion, drumlin formation, and changing hydrology beneath an Antarctic ice stream. *Geology*, **35**, 127–130.
Smith, B. E., et al., 2009. An inventory of active subglacial lakes in Antarctica detected by ICESat (2003–2008). *Journal of Glaciology*, **55**, 573–595.
Walder, J. S., and Hallet, B., 1979. Geometry of former subglacial water channels and cavities. *Journal of Glaciology*, **23**, 335–346.
Wingham, D. J., et al., 2006. Rapid discharge connects Antarctic subglacial lakes. *Nature*, **440**, 1033–1036.
Zwally, H. J., et al., 2002. Surface melt-induced acceleration of Greenland ice-sheet flow. *Science*, **297**, 218–222.

Cross-references

Glacier Surging
Subglacial Lakes, Antarctic

SUBGLACIAL LAKES, ANTARCTIC

John C. Priscu
Department of Land Resources and Environmental Sciences, Montana State University, Bozeman, MT, USA

Definition

Subglacial lakes: Water-filled cavities located beneath glaciers and ice sheets

Introduction

Visual observations of what appeared to be floating ice by the crews of Russian aircraft flying missions over the Antarctic continent provide the earliest evidence of subglacial lakes. These observations were later verified by airborne radio-echo sounding, seismic data, and satellite imagery. We now know that more than 150 lakes exist beneath the Antarctic continent, and are connected by networks of subglacial streams and rivers, which may initiate and maintain rapid ice flow and should be considered in ice-sheet mass balance assessments (Siegert, 2000; Siegert et al., 2005). Morphometric data indicate that the volume of Antarctic subglacial lakes alone exceeds 10,000 km^3, with Lake Vostok (~5,400 km^3) and Lake 90° E (1,800 km^3) being the largest (Studinger et al., 2003, 2004). Antarctica lakes may hold over 8% of all lacustrine freshwater on Earth, enough to cover the whole continent with a uniform water layer ~1 m thick. Simple balance calculations reveal that the average water residence time in the subglacial zone of Antarctica is equal to ~1,000 years, which is likely a reflection of low liquid water generation rates coupled with slow rates of drainage of liquid water through subglacial environments (Priscu et al., 2008).

Over 60% of the lakes lie within 50 km of a local ice divide and 88% lie within 100 km of a local divide (Priscu et al., 2008) (Figure 1). The association of subglacial lakes with local ice divides and regions of high hydraulic fluid potential leads to a fundamental question concerning the evolution of subglacial lake environments: Does the evolving ice sheet control the location of subglacial lakes or does the fixed lithospheric character necessary for lake formation (e.g., basal morphology, geothermal flux, or the nature of sub-ice aquifers) constrain the evolution of ice sheet catchments? With the exception of central West Antarctica (where lakes are few), we know little about either the lithospheric character along these catchment boundaries or the history of their migration as discerned from layering within the ice sheet.

Origins of subglacial lakes

Deep subglacial lakes have probably been stable through many glacial cycles and may have developed novel ecosystems, in contrast to the shallower lakes (Dowdeswell and Siegert, 1999, 2002). Although arguments have been made for the tectonic origins of deep subglacial lakes, there continues to be debate about whether subglacial lakes in Antarctica reside in active tectonic basins or along old inactive zones of structural weakness that once provided guidance for subglacial erosion (Bell et al., 2006). Much of East Antarctica, where the majority of subglacial lakes have been found so far, is thought to have assembled 500–800 million years ago. However, our knowledge of the interior of the continent, the distribution of major tectonic boundaries, and old zones of structural weakness is limited due to a paucity of data.

The biology of subglacial systems

Much attention is currently focused on the exciting possibility that the subglacial environments of Antarctica may harbor microbial ecosystems under thousands of meters of ice, which have been isolated from the atmosphere for as long as the continent has been glaciated (20–25 million years). Profiles of prokaryotic cell abundance through the entire Vostok core reveal a two to sevenfold higher cell density in accretion ice than the overlying glacial ice, implying that Lake Vostok is a source of bacterial carbon beneath the ice sheet (Priscu et al., 1999; Christner et al., 2006). Data from the overlying accretion ice have been used to show that bacterial densities within Lake Vostok surface waters should be between 150 and 460 cells mL^{-1}.

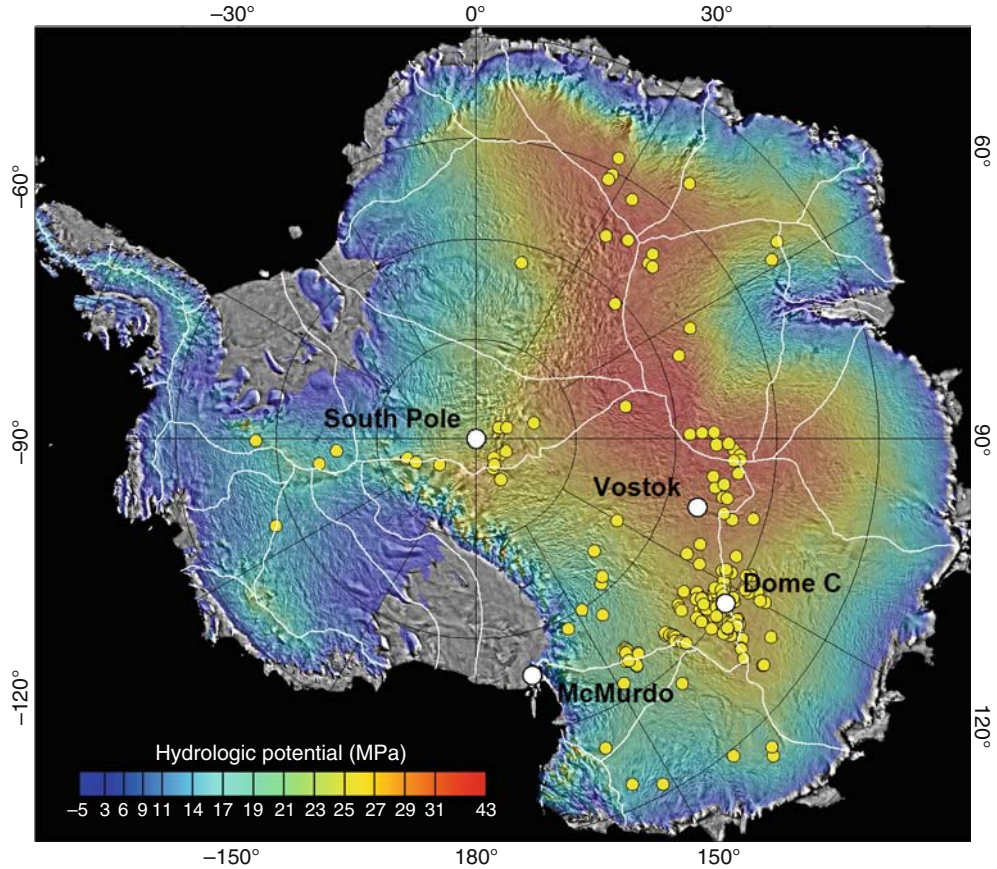

Subglacial Lakes, Antarctic, Figure 1 Map of Antarctica showing location of known subglacial lakes (*yellow circles*) in relation to ice divides (*white lines*) and hydrologic potential (*colored contours*). Modified from Priscu et al., 2008).

These values indicate that Lake Vostok is a highly oligotrophic system supporting relatively low levels of biomass. Sequence data obtained from DNA encoding for small subunit ribosomal RNA revealed that the microorganisms within Lake Vostok do not represent an evolutionarily distinct subglacial biota (Priscu and Christner, 2004). The time scale of isolation within Lake Vostok (>15 $\times 10^6$ year) is not long in terms of bacterial evolution compared to their 3.7 $\times$ 10^9 year history on Earth, and studies of species divergence of other bacteria have shown that species level divergence may take ~100 million years. Evidence for the presence of hydrothermal input is supported by the recent interpretation of He^3:He^4 data from accretion ice, which implies that there may be extensive faulting beneath Lake Vostok, which could introduce geochemical energy sources to the southern part of the lake (Petit et al., 2005). If this emerging picture is correct, Lake Vostok could harbor a unique assemblage of organisms fueled by chemical energy. While it seems inevitable that viable microorganisms from the overlying glacial ice, and in sediment scoured from bedrock adjacent to the lake, are regularly seeded into the lake, the question remains whether these or preexisting microorganisms have established an ecosystem in Lake Vostok. If a microbial ecosystem were found to exist within the water or sediment of these subsurface environments, they would represent one of the most extreme and unusual ecosystems on Earth.

Summary

The past 10 years have seen the study of subglacial lakes go from a curiosity to a focus of scientific research. We now know that more than 150 lakes exist beneath the Antarctic ice sheets, some of which rival the largest surface lakes on our planet in terms of size. These lakes appear to play a role in ice sheet dynamics (Llubes et al., 2006; Bell et al., 2007) and may harbor novel microorganisms, the mediate important microbial transformations. Several national programs plan to penetrate the subglacial environment over the next 5 years (Priscu et al., 2005). Data from these expeditions will yield the first samples from these environments and will change our view of polar regions.

Bibliography

Bell, R. E., Studinger, M., Fahnestock, M. A., and Shuman, A., 2006. Tectonically controlled subglacial lakes on the flanks of the Gamburtsev Subglacial Mountains. *East Antarctica Geophysical Research Letters*, **33**, L02504, doi:10.1029/2005GL025207.

Bell, R. E., Studinger, M., Shuman, A., Fahnestock, M. A., and Joughin, I., 2007. Large subglacial lakes in East Antarctica at the onset of fast-flowing ice streams. *Nature*, **445**, 904–907.

Christner, B. C., Royston-Bishop, G., Foreman, C. M., Arnold, B. R., Tranter, M., Welch, K. A., Lyons, W. B., Tsapin, A. I., Studinger, M., and Priscu, J. C., 2006. Limnological conditions in subglacial Lake Vostok, Antarctica. *Limnology and Oceanography*, **51**, 2485–2501.

Dowdeswell, J. A., and Siegert, M. J., 2002. The physiography of modern Antarctic subglacial lakes. *Global and Planetary Change*, **35**, 221–236.

Dowdeswell, J. A., and Siegert, M. J., 1999. The dimensions and topographic setting of Antarctic subglacial lakes and implications for large-scale water storage beneath continental ice sheets. *Geological Society of America Bulletin*, **111**, 254–263.

Llubes, M., Lanseau, C., and Rémy, F., 2006. Relations between basal condition, subglacial hydrological networks and geothermal flux in Antarctica. *Earth and Planetary Science Letters*, **241**, 655–662.

Petit, J. R., Alekhina, I., and Bulat, S., 2005. Lake Vostok, Antarctica: Exploring a Subglacial Lake and Searching for Life in an Extreme Environment. In Gargaud, M., Barbier, B., Martin, H., and Reisse, J. (eds.), *Lectures in Astrobiology, Vol. I, Series: Advances in Astrobiology and Biogeophysics*. Berlin: Springer, pp. 227–288.

Priscu, J. C., and Christner, B. C., 2004. Earth's icy biosphere. In Bull, A. T. (ed.), *Microbial Biodiversity and Bioprospecting*. Washington, DC: American Society for Microbiology Press, pp. 130–145.

Priscu, J. C., Adams, E. E., Lyons, W. B., Voytek, M. A., Mogk, D. W., Brown, R. L., McKay, C. P., Takacs, C. D., Welch, K. A., Wolf, C. F., Kirstein, J. D., and Avci, R., 1999. Geomicrobiology of subglacial ice above Lake Vostok, Antarctica. *Science*, **286**, 2141–2144.

Priscu, J. C., Kennicutt, M. C., III, Bell, R. E., Bulat, S. A., Ellis-Evans, J. C., Lukin, V. V., Petit, J.-R., Powell, R. D., Siegert, M. J., and Tabacco, I., 2005. Exploring subglacial antarctic lake environments. *EOS, Transactions of the American Geophysical Union*, **86**, 193–197.

Priscu, J. C., Christner, B. C., Foreman, C. M., and Royston-Bishop, G., 2006. Biological Material in Ice Cores. In Elias, S. A. (ed.), *Encyclopedia of Quaternary Sciences, Vol. 2*. UK: Elsevier, pp. 1156–1166.

Priscu, J. C., Tulaczyk, S., Studinger, M., Kennicutt, M. C., II, Christner, B. C., and Foreman, C. M., 2008. Antarctic subglacial water: origin, evolution and ecology. In Vincent, W., and Laybourn-Parry, J. (eds.), *Polar Lakes and Rivers*. UK: Oxford University Press, pp. 119–135.

Siegert, M. J., Carter, S., Tabacco, I., Popov, S., and Blankenship, D. D., 2005. A revised inventory of Antarctic subglacial lakes. *Antarctic Science*, **17**, 453–460.

Siegert, M. J., 2000. Antarctic subglacial lakes. *Earth Science Reviews*, **50**, 29–50.

Studinger, M., Karner, G. D., Bell, R. E., Levin, V., Raymond, C. A., and Tikku, A. A., 2003. Geophysical models for the tectonic framework of the Lake Vostok region, East Antarctica. *Earth and Planetary Science Letters*, **216**, 663–677.

Studinger, M., Bell, R. E., and Tikku, A. A., 2004. Estimating the depth and shape of subglacial Lake Vostok's water cavity from aerogravity data. *Geophysical Research Letters*, **31**, L12401, doi:10.1029/2004GL019801.

SUBGLACIAL PROCESSES

Sean Fitzsimons[1], Reginald Lorrain[2]
[1]Department of Geography, University of Otago, Dunedin, New Zealand
[2]Département des sciences de la Terre et de l'Environnement, Université Libre de Bruxelles, Bruxelles, Belgium

Synonyms

Basal processes; Subglacial sediment deformation

Definition

Subglacial processes are the thermal and mechanical processes immediately above and below the boundary between the ice and glacier bed that control glacier motion and processes of erosion, transportation, and deposition.

Introduction

In glaciology the term subglacial processes encompasses the thermal, mechanical, hydrological, and chemical processes that occur a few meters beneath and above the contact between a glacier and its substrate. These processes are of considerable importance because they determine the behavior of glaciers and ice sheets and are responsible for a range of phenomena that are expressed as spatial and temporal variations in the dynamic behavior of glaciers over a range of scales. Consideration of subglacial processes generally excludes processes that occur beneath floating ice masses. A recent, thorough review of subglacial processes was published by Clarke (2005).

Glacier beds

The nature and complexity of subglacial processes are controlled by the thermal conditions at the bed and by the material properties of the bed. The key thermal boundary condition at a glacier bed is the pressure melting point, which is the melting point of ice adjusted for pressure exerted by the weight of overlying ice. If the temperature is below the pressure melting point the ice is classified as cold-based and there is no bulk meltwater at the bed. In contrast, if the basal temperature is at the pressure melting point the glacier is classified warm-based and meltwater is freely available. Bed materials range from hard beds, which are characterized by lithified materials, to unconsolidated sediments such as till, sands, and gravels (soft beds). An additional complexity is that particles eroded from the bed can become entrained within the base of glaciers to form basal ice, which has mechanical properties that are quite distinct from ice of a meteoric origin (Fitzsimons, 2006). The combination of thermal and mechanical conditions, which can be simplified to three schematic velocity structures, are summarized by Figure 1.

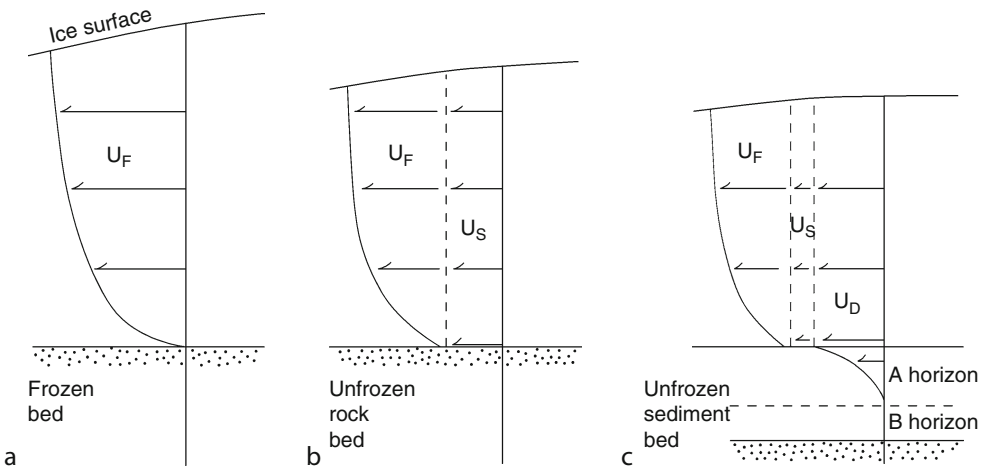

Subglacial Processes, Figure 1 Vertical velocity distributions associated with different thermal and mechanical conditions at glacier beds: (**a**) Shows the velocity distribution associated creep of ice above a frozen bed composed of rock or sediment. (**b**) Shows the velocity profile associated with creep and sliding above a warm rigid bed. (**c**) Shows the velocity profile associated with creep, sliding, and subglacial sediment deformation above a warm deformable bed. From Boulton (1996). Reprinted from the *Journal of Glaciology* with permission of the International Glaciological Society.

Thermal and mechanical processes

Most of our knowledge of subglacial processes comes from warm-based glaciers that have hard or soft beds. Warm, hard-bed glaciers are characterized by well-developed subglacial drainage systems, movement by basal sliding, and relatively high rates of erosion by processes of abrasion and plucking. Warm-based glaciers with soft beds are characterized by either rapid sliding that is facilitated by high subglacial water pressures that can uncouple the glacier from its bed, and/or result in deformation of subglacial sediment due to a decrease in shear strength of unconsolidated sediment caused by high pore water pressure.

An experiment conducted by Boulton (1979) beneath an Icelandic outlet glacier concluded that approximately 90% of glacier motion could be attributed to deformation of the uppermost 0.5 m of saturated till that formed the glacier bed. In such a situation, the "effective bed" of a glacier, that is, the surface below which there is no movement, is below the interface between the ice and the sediment. In the 1980s, seismic studies of active ice streams in Antarctica identified the presence of a layer of porous, saturated material beneath the ice, which was likely to be too weak to rigidly support the weight of the overlying ice, and therefore was probably undergoing deformation (Blankenship et al., 1986; Alley et al., 1986). The possibility that ice streams move principally by deformation of subglacial sediment forced a major rethinking of different chapters of glaciology and glacial geology that has been described as a paradigm shift (Boulton, 1986; Murray, 1997). This major shift in thinking has led to a large volume of published research on the nature of subglacial processes associated with warm-based glaciers underlain by soft beds.

A major focus of research into subglacial sediment deformation has involved investigations into processes beneath fast-flowing ice streams that drain the West Antarctic Ice Sheet. Although the ice streams only account for about 10% of the volume of the ice sheet they make up for up to 90% of the ice discharged to the ocean because they reach speeds of over 1,000 m/year, and are up to 60 km wide and 2,000 m thick. Despite numerous investigations into the basal processes associated with the fast flow of Antarctic ice streams it remains unclear whether the high velocities are sustained by subglacial sediment deformation, by fast sliding of ice over the substratum, or by a combination of both. In addition, studies of formerly glaciated landscapes show that ice streams also form on hard beds (Stokes and Clark, 2003), which suggests that the development of fast ice flow cannot be solely attributed to the presence of warm-based ice and a soft bed. A further complexity in our understanding of ice streams is that velocity can vary considerably over a range of timescales. For example, variations in the surface velocity of Whillans Ice Stream have been attributed to a single tidal cycle that is propagated through an ice shelf (Bindschadler et al., 2003), whereas the Kamb Ice Stream appears to have ceased flowing rapidly about 150 years ago. These studies, together with more recent research on the relationship between surface melting and acceleration of glacier flow (Zwally et al., 2002; Rignot and Kanagaratnam, 2006), demonstrate that the temporal variability of ice stream behavior forms an important component of understanding of the response of glaciers to climate change. The increase in velocity has been attributed to an increase in surface meltwater that rapidly migrates to the bed causing an increase in water pressure, which reduces effective normal stress causing accelerated sliding and/or subglacial sediment deformation.

Studying subglacial processes

Despite the difficulties of gaining direct access to glacier beds numerous successful field experiments have been conducted in such environments. The development of rapid hot-water drilling has facilitated the observation of subglacial conditions using cameras. Hot-water drilling has also enabled the deployment of a range of instruments designed to measure subglacial sediment deformation, sliding, bed strength, basal water pressures, and to sample subglacial sediment. Borehole-based instrumentation for observing and measuring subglacial processes has been reviewed by Fischer and Hubbard (2006).

Experiments have been conducted at Svartisen Subglacial Laboratory beneath Engabreen in Norway where Cohen et al. (2000) installed a concrete obstacle to measure bed shear stress. A later study in the laboratory was conducted by Iverson et al. (2003) who blasted a cavity in the bed and filled with it sediment to simulate subglacial till. After the ice closed over the cavity, the effective normal stress was experimentally controlled by changing the pore water pressure. The results showed that the sediment underwent shear at intermediate pore water pressures and that at higher pressures the ice moved over the till by plowing without deforming the sediment.

Uncertainties and questions raised by field experiments have stimulated laboratory experiments on the behavior of subglacial materials. This work has included direct shear tests on sediment collected from the bed of Antarctic ice streams (Kamb, 1991) and the construction of a ring shear device that permitted study of the mechanical behavior of materials under conditions of high shear strains (Iverson et al., 1997). These experiments concluded that the properties of deforming till exhibit the behavior of Coulomb (frictional) plastic material and that resistance to shear varies linearly with effective normal stress. The spatial and temporal variability of such processes has been highlighted by modeling studies, which suggested that local weakening of subglacial sediment could occur due to high pore water pressures in front of objects being dragged through a bed (Iverson, 1999). Similar measurements have been made with a "ploughmeter" to measure force and subglacial water pressure (Fischer et al., 2001). These data suggest that rapidly sliding glaciers might move by plowing through unconsolidated subglacial sediment rather than by penetrative deformation. Although the full complexity of the behavior of warm-based, soft-bed glaciers has yet to be fully understood, there is a clear consensus that the basal hydrological system controls the transient behavior of coupling between the glacier and its bed and whether movement is achieved by sliding or subglacial sediment deformation.

Our understanding of subglacial processes beneath cold-based glaciers with soft beds has also been advanced recently through a combination of field experiments conducted in tunnels excavated in glaciers, laboratory experiments, and modeling (Echelmeyer and Wang, 1987; Cuffey et al., 2000a, b; Fitzsimons et al., 1999, 2000). These studies have shown that cold-based glaciers can slide and ice-rich subglacial permafrost can be deformed and eroded (Figure 2).

Subglacial Processes, Figure 2 A 4.5 m thick excavation in deforming subglacial permafrost beneath Wright Lower Glacier in the McMurdo Dry Valleys, Antarctica. Measurements over 3 years demonstrate that deformation extends more than 3.5 m beneath the ice-permafrost boundary and that most deformation is accommodated by ice-rich layers between frozen sediment layers. The bolts and stakes have been used to measure strain and velocity over a period of 4 years.

Erosion, transportation, and deposition

In addition to acting as an important control of glacier dynamics, subglacial processes are also responsible for the processes of erosion, transportation and deposition that occur at the beds of glaciers. Exchanges of material between the bed and the glacier have two principal outcomes: the formation of a distinctive type of ice at the base of a glacier (basal ice) and the formation of distinctive erosional and depositional landforms. Basal ice is characterized by a relatively high debris content which frequently results in a stratified or banded appearance, high solute concentrations, and distinctive gas and isotopic composition, all of which distinguish the ice from overlying ice that has a meteoric origin. Studies of the chemistry of ice from the beds of glaciers have yielded new insights into the basal boundary conditions when the basal ice formed (Souchez et al., 1993; Souchez and Lorrain, 1991; Sleewaegen et al., 2003). For example, study of the stable isotope characteristics of basal ice exposed at the edge of the Greenland ice sheet suggested that there is considerable spatial variability in ice sheet erosion processes (Sugden et al., 1987). The presence of solid and dissolved contaminants together with associated changes in crystal structure and size result in markedly different mechanical behavior of basal ice from overlying meteoric ice. As a result, the lower few meters of glaciers are characterized by very high strain rates concentrated within the debris-bearing ice. For example, "amber ice" that occurs at the base of glaciers in the McMurdo dry valleys has been recognized as being soft compared to overlying white ice (Holdsworth and Bull, 1970). Later research on amber ice demonstrated that the small crystal size (<1 mm) is directly related to high strain rates (Cuffey et al., 2000b; Samyn et al., 2005).

The landforms left behind by formerly more extensive glaciers during the Pleistocene are testament to the processes that operate beneath glaciers. A wide variety of landforms have been used in a variety of ways to reconstruct the dimensions, behavior, and impact of glaciers on landscapes. However, there remains considerable uncertainty as to the origin of many distinctive landforms such as drumlins. Theories concerning their origin range from subglacial floods to instabilities in deforming beds to episodic erosion and depositional events. The most recent developments in understanding subglacial landforms have been driven by the acquisition of high definition remotely sensed imagery, both terrestrial and marine, that have permitted detailed mapping of glacial landforms such as lineations and moraines associated with ice streams (O'Cofaigh et al., 2002; Stokes and Clark, 2003).

Summary

The last few decades have seen enormous advances in understanding how glaciers interact with the substrates over which they flow. The central issue in our recently acquired understanding is the role of subglacial water as a means of uncoupling glaciers from their beds whether this is accomplished by rapid sliding, or subglacial sediment deformation. However, we have yet to develop an understanding of how spatial and temporal variability in subglacial processes is translated into the behavior of large glacial systems. Such an understanding is a prerequisite for the development of ice sheet models that parameterize subglacial processes.

Bibliography

Alley, R. B., Blankenship, D. D., Bentley, C. R., and Rooney, S. T., 1986. Deformation of till beneath ice stream B, West Antarctica. *Nature*, **322**, 57–59.

Bindschadler, R. A., King, M. A., Alley, R. B., Anandakrishnam, S., and Padman, L., 2003. Tidally controlled stick-slip discharge of a West Antarctic Ice Stream. *Science*, **301**, 1087–1091.

Blankenship, D. D., Bentley, C. R., Rooney, S. T., and Alley, R. B., 1986. Seismic measurements reveal a saturated porous layer beneath an active Antarctic ice stream. *Nature*, **322**, 54–57.

Boulton, G. S., 1979. Processes of glacier erosion on different substrata. *Journal of Glaciology*, **23**, 15–38.

Boulton, G. S., 1986. A paradigm shift in glaciology? *Nature*, **322**, 18.

Boulton, G. S., 1996. Theory of glacial erosion, transportation and deposition as a consequence of sediment deformation. *Journal of Glaciology*, **42**, 43–62.

Clarke, G. K. C., 2005. Subglacial Processes. *Annual Review of Earth and Planetary Sciences*, **33**, 247–276.

Cohen, D., Hooke, R., Le, B., Iverson, N. R., and Kohler, J., 2000. Sliding of ice past an obstacle at Engabreen, Norway. *Journal of Glaciology*, **46**, 599–610.

Cuffey, K. M., Conway, H., Gades, A., Hallet, B., Lorrain, R., Severinghaus, J. P., Steig, E. J., Vaughn, B., and White, J. W. C., 2000a. Entrainment at cold gacier beds. *Geology*, **28**, 351–354.

Cuffey, K. M., Conway, H., Gades, A., Hallet, B., Raymond, C. F., and Whitlow, S., 2000b. Deformation properties of subfreezing glacier ice: role of crystal size, chemical impurities, and rock particles inferred from in situ measurements. *Journal of Geophysical Research*, **105**(B12), 27,895–27,915.

Echelmeyer, K., and Wang, Z., 1987. Direct observations of basal sliding and deformation of glacial drift at subfreezing temperatures. *Journal of Glaciology*, **33**, 83–98.

Fischer, U. H., and Hubbard, B. P., 2006. Borehole-based subglacial instrumentation. In Knight, P. G. (ed.), *Glacier Science and Environmental Change*. Oxford: Blackwell, pp. 387–394.

Fischer, U. H., Porter, P. R., Schuler, T., Evans, A. J., and Gudmundsson, G. H., 2001. Hydraulic and mechanical properties of glacial sediments beneath Unteraargletscher, Switzerland: implications for glacier motion. *Hydrological Processes*, **15**, 3525–3540.

Fitzsimons, S. J., 2006. Mechanical behaviour and structure of the debris-rich basal ice layer. In Knight, P. G. (ed.), *Glacier Science and Environmental Change*. Oxford: Blackwell, pp. 329–335.

Fitzsimons, S. J., McManus, K. J., and Lorrain, R., 1999. Structure and strength of basal ice and substrate of a dry-based glacier: evidence for substrate deformation at sub-freezing temperatures. *Annals of Glaciology*, **28**, 236–240.

Fitzsimons, S. J., Lorrain, R., and Vandergoes, M., 2000. Behaviour of subglacial sediment and basal ice in a cold-based glacier. In Maltman, A. J., Hambrey, M. J., and Hubbard, B. (eds.), *Deformation of Glacial Materials*. Special Publication 176, Geological Society Publishing House, Bath, pp.181–190.

Holdsworth, G., and Bull, C., 1970. The flow law of cold ice; investigations on Meserve Glacier, Antarctica. *International Association of Hydrological Sciences Publication*, **86**, 204–216.

Iverson, N. R., 1999. Coupling between an glacier and a soft bed: II. Model results. *Journal of Glaciology*, **45**, 41–53.
Iverson, N. R., Baker, R. W., and Hooyer, T. S., 1997. A ring shear device for the study of till deformation: tests on a clayrich and a clay-poor till. *Quaternary Science Reviews*, **16**, 1057–1066.
Iverson, N. R., Cohen, C., and Hooyer, T. S., 2003. Effects of basal debris on glacier flow. *Science*, **301**, 81–84.
Kamb, B., 1991. Rheological nonlinearity and flow instability in the deforming bed mechanism of ice stream motion. *Journal of Geophysical Research*, **96**, 16585–16595.
Murray, T., 1997. Assessing the paradigm shift: deformable beds. *Quaternary Science Reviews*, **16**, 995–1016.
O'Cofaigh, C., Pudsey, C. J., Dowdeswell, J. A., and Morris, P., 2002. Evolution of subglacial bedforms along a paleo-ice stream, Antarctic Peninsula continental shelf. *Geophysical Research Letters*, **29**, 1199, doi:10.1029/2001GL01448.
Rignot, E., and Kanagaratnam, P., 2006. Changes in the velocity structure of the Greenland Ice Sheet. *Science*, **311**, 986–990.
Samyn, D., Svensson, A., Fitzsimons, S., and Lorrain, R., 2005. Ice crystal properties of amber ice and strain enhancement at the base of cold Antarctic glaciers. *Annals of Glaciology*, **40**, 185–190.
Sleewaegen, S., Samyn, D., Fitzsimons, S., and Lorrain, R., 2003. Equifinality of basal ice facies from an Antarctic cold-based glacier. *Annals of Glaciology*, **37**, 257–262.
Souchez, R., and Lorrain, R., 1991. *Ice Composition and Glacier Dynamics*. Berlin: Springer.
Souchez, R., Lemmens, M., Tison, J.-L., Lorrain, R., and Janssens, L., 1993. Reconstruction of basal boundary conditions at the Greenland Ice Sheet margin from gas composition in the ice. *Earth and Planetary Science Letters*, **118**(327–3), 33.
Stokes, C. R., and Clark, C. D., 2003. Laurentide ice streaming on the Canadian Shield: A conflict with the soft-bedded ice stream paradigm. *Geology*, **31**, 347–350.
Sugden, D. E., Knight, P. G., Livesey, N., Lorrain, R. D., Souchez, R. A., Tison, J.-L., and Jouzel, J., 1987. Evidence of two zones of debris entrainment beneath the Greenland ice sheet. *Nature*, **328**, 238–241.
Zwally, H. J., Adalati, W., Herring, T., Larson, K., Saba, J., and Steffen, K., 2002. Surface melt-induced acceleration of Greenland Ice-Sheet flow. *Science*, **297**, 218–222.

Cross-references

Bed Strength
Cold-Based Glaciers
Formation and Deformation of Basal Ice
Glacial Striations
Glacier Motion/Ice Velocity
Landforms of Glacial Erosion
Subglacial Drainage System

SUBGLACIAL VOLCANISM

Hugh Tuffen
Lancaster Environment Centre, Lancaster University, Lancaster, UK

Synonyms

Glaciovolcanism; Ice–volcano interaction

Definition

Strictly, volcanic activity beneath ice sheets or glaciers, but used generally to refer to volcanic eruptions where magma interacts with ice in any form, both on Earth and other planetary bodies (Glaciovolcanism). Subglacial volcanism may occur wherever volcanic vents are covered with bodies of ice, which may include small glaciers on the flanks of stratovolcanoes, substantial regional ice sheets, and even the Martian cryosphere (Smellie, 2000; Ice–Volcano Interactions).

Key localities of subglacial volcanism

Beneath past and present ice sheets: Iceland, Western Antarctic Ice Sheet, Antarctic Peninsula Ice Sheet, British Columbia.

At ice-covered stratovolcanoes: Andes, Cascades, Alaska, Aleutian Islands, Kamchatka

On other planets: Mars

Principal styles of subglacial volcanism

Tuya-building eruptions: Sustained, large-volume eruptions that melt through to the surface of ice sheets, forming distinctive "table mountains." Tuyas commonly consist of pillow lavas overlain by fragmental glassy volcanic deposits (hyaloclastites) that were emplaced within englacial lakes, and capped by subaerial lava flows formed when the ice surface was pierced (Smellie, 2000).

Tindar ridge-forming eruptions: eruptions from volcanic fissures beneath ice sheets that generate elongate ridges of pillow lavas and hyaloclastites. Example: Kalfstindar, Iceland (Smellie, 2000).

Magma–ice interaction at stratovolcanoes: interaction between lava or pyroclastic deposits and ice either on the flanks, or in the summit crater of a stratovolcano (Lescinsky and Fink, 2000).

The composition of magma erupted subglacially ranges from basalt to rhyolite (Smellie, 2000; McGarvie, 2009).

Hazards from subglacial volcanism

Melting of ice and snow can generate devastating meltwater floods (Guðmundsson et al., 1997; Glacier Lake Outburst Floods) and lahars (Major and Newhall, 1989). Explosive magma–meltwater interactions can lead to widespread ash fall.

Interesting features of subglacial volcanism

- The products of past subglacial eruptions can be used to reconstruct paleo-ice thicknesses in Iceland, Antarctica, and elsewhere (Smellie 2008; Ice–Volcano Interactions).
- Deglaciation is known to accelerate rates of volcanism in Iceland and other regions (Sigvaldason et al., 1992).
- Subglacial volcanoes may be an important environment for microbial life on Earth and even on Mars.

Bibliography

Guðmundsson, M. T., Sigmundsson, F., and Björnsson, H., 1997. Ice–volcano interaction of the 1996 Gjálp subglacial eruption, Vatnajökull, Iceland. *Nature*, **389**, 954–957.
Lescinsky, D. T., and Fink, J. H., 2000. Lava and ice interaction at stratovolcanoes: use of characteristic features to determine past glacial events and future volcanic hazards. *Journal of Geophysical Research*, **105**, 23711–23726.
Major, J. J., and Newhall, C. G., 1989. Snow and ice perturbation during historical volcanic eruptions and the formation of lahars and floods. *Bulletin of Volcanology*, **52**, 1–27.
McGarvie, D. W., 2009. Rhyolitic volcano–ice interactions in Iceland. *Journal of Volcanology and Geothermal Research*, **185**, 367–389.
Sigvaldason, G. E., Annertz, K., and Nilsson, M., 1992. Effect of glacier loading/deloading on volcanism: postglacial volcanic production rate of the Dyngjufjöll area, central Iceland. *Bulletin of Volcanology*, **54**, 385–392.
Smellie, J. L., 2000. Subglacial eruptions. In Sigurðsson, H., Houghton, B. F., McNutt, S. R., Rymer, H., and Stix, J. (eds.), *Encyclopaedia of Volcanoes*. London: Academic, pp. 403–418.
Smellie, J. L., 2008. Basaltic subglacial sheet-like sequences: Evidence for two types with different implications for the inferred thickness of associated ice. *Earth Science Reviews*, **88**, 60–88.

Cross-references

Andean Glaciers
Antarctica
Bottom Melting or Undermelt (Ice Shelf)
Glacier Lake Outburst Floods
Iceland Glaciers
Natural Hazards Associated with Glaciers and Permafrost
Subglacial Drainage System

SUBGLACIAL WEATHERING

Markus Konz
Institute of Environmental Engineering, Hydrology and Water Resources Management ETH Zürich, Zurich, Switzerland

Subglacial weathering is the study of mechanical and chemical changes in soil and rocks due to physical (e.g., grinding) and chemical (e.g., dissolution) processes in glacial environments. The subglacial hydrochemistry governs the rates of biogeochemical denudation and carbon cycling. These processes can have a significant impact on global biogeochemical cycles (Jones et al., 2002). Effluent glacier water transports dissolved and suspended matters that have been mobilized due to subglacial weathering and which can be used to determine nutrient and metal export and cycling (Mitchell et al., 2001, 2006; Mitchell and Brown, 2007).

Hydrologists use chemical analysis of glacier water to infer hydrological flow-paths in glacial drainage systems (Brown et al., 1996; Mitchell et al., 2006). The chemical signature of water samples can indicate the configuration and evolution of subglacial drainage systems.

Subglacial environments feature tough conditions for life due to a combination of low temperatures and lack of energy sources. However, recent investigations indicate an important abundance of bacterial populations in this habitat (see Hodson et al., 2008 for a review). The presence of bacteria is important for subglacial weathering reactions and these in turn supply energy to maintain bacterial populations.

Bibliography

Brown, G. H., Sharp, M., and Tranter, M., 1996. Experimental investigations of the weathering of suspended sediment by alpine glacial meltwater. *Hydrological Processes*, **10**, 579–597.
Hodson, A., Anesio, A. M., Tranter, M., Fountain, A., Osborn, M., Priscu, J., Laybourn-Parry, J., and Sattler, B., 2008. Glacial ecosystems. *Ecological Monographs*, **78**(1), 41–67.
Jones, I. W., Munhoven, G., Tranter, M., Huybrects, P., and Sharp, M., 2002. Modelled glacial and non-glacial HCO3 2, Si and Ge fluxes since the LGM: little potential for impact on atmospheric CO2 concentrations and marine Ge:Si ratio. *Global and Planetary Change*, **33**, 139–153.
Mitchell, A. C., and Brown, G. H., 2007. Diurnal hydrologicalphysicochemical controls and sampling methods for minor and trace elements in an alpine glacial hydrological system. *Journal of Hydrology*, **332**, 123–143.
Mitchell, A., Brown, G. H., and Fuge, R., 2001. Minor and trace element export from a glacierised Alpine headwater catchment (Haut Glacier d'Arolla, Switzerland). *Hydrological Processes*, **15**, 3499–3524.
Mitchell, A. C., Brown, G. H., and Fuge, R., 2006. Minor and trace elements as indicators of solute provenance and flow routing in a subglacial hydrological system. *Hydrological Processes*, **20**, 877–897.

SUBLIMATION FROM SNOW AND ICE

A. K. Singh
DIAT (Deemed University), Girinagar, Pune, Maharashtra, India

The process of ice changing directly into vapor without any intermediate liquid stage is often described by sublimation. The opposite of sublimation is "deposition," where water vapor changes directly into ice. The sublimation of ice or snow is driven by an imbalance between the saturation vapor pressure (or vapor density) at a given temperature, and the vapor pressure in the immediate vicinity of an ice surface. Sublimation process in snow controls the grain shape and size. Snow sublimation rate can be defined as the amount of mass lost per unit time and depends on particle surface area to mass ratio, vapor pressure gradients, and rate of air exchange around the snow crystal surface. Typically, these rates are higher when large vapor pressure gradients exist and rapid air exchange occurs.

It is not easy to actually see sublimation occurring, especially for ice. Sublimation occurs more readily when certain weather conditions are present, that is, on a dry and windy day with low relative humidity. Sublimation also occurs more at higher altitudes, where the air pressure is less than at lower altitudes. Sublimation is fairly slow since it takes quite a bit of energy for an ice molecule to escape the solid rigid structure to a gas. Sublimation will be enhanced under direct sunlight since photons of solar energy will add the energy necessary for solid ice molecules to escape. Sublimation will occur even at low sun angles but the amount of sublimation will be very weak. Since sun angle is a minimum at the start of winter and much higher in late winter, the sublimation power of the sun on surface snow will be much higher in late winter as compared to early winter on sunny days.

The sublimation rate of ice or snow has important implications on surface energy balance calculations, mass balance calculations, and studies of snow metamorphism.

Bibliography

Montesi, J., Elder, K., Schmidt, R. A., and Davis, R. E., 2004. Sublimation of Intercepted Snow within a Subalpine Forest Canopy at Two Elevations. *Journal of Hydrometeorology*, **5**(5), 763–773.

Neumann, T. A., Albert, M. R., Engel, C., Courville, Z., and Perron, F., 2009. Sublimation rate and the mass-transfer coefficient for snow sublimation. *International Journal of Heat and Mass Transfer*, **52**, 309–315.

SUMMER ACCUMULATION TYPE GLACIERS

Nozomu Naito
Department of Global Environment Studies, Hiroshima Institute of Technology, Hiroshima, Japan

Synonyms

Summer-accumulation type glacier

Definition

Accumulation. The process of adding of snow or ice to a glacier or its amount. Snowfall is generally the most popular process. In addition, frost, avalanche, refreezing of melt water, and catchment of blowing snow are other possible processes.

Ablation. The process of losing of glacier ice or snow or its amount. Melting is generally the most popular process. Then, evaporation, removal of snow by wind, and calving of icebergs are also possible.

Mass balance. The net mass change of glacier; accumulation subtracting ablation.

Introduction

Classical glaciology was initiated and has been developed through studies on glaciers in Europe and North America, where the main accumulation to the glaciers is snowfall in winter, and the main glacier ablation occurs in summer. The *Mass balance* of the glaciers is usually positive in winter, negative in summer, and then the annual *mass balance* is determined by the deduction of these two seasonal components. On the other hand, glaciers in Asia have been observed to have different characteristics since the 1970s (e.g., Ageta et al., 1980; Xie, 1980). These glaciers receive more accumulation in summer than in winter, and such glaciers have been called as *summer accumulation type glaciers* (Ageta, 1983; Ageta and Higuchi, 1984). In this definition, the periods of summer and winter are not explicitly defined, but they are generally regarded as warm and cold half years, respectively. Because climate in most parts of Asia is influenced by summer monsoon, most of the annual precipitation is concentrated in summer, while winter is cold but is a relatively dry season. Successive studies carried out on glaciers around the Himalayas and Tibetan Plateau have clarified that the *summer accumulation type glaciers* are very sensitive to changes in air temperature, as explained in what follows. Thus, *summer accumulation type glaciers* are considered to be much vulnerable to global warming.

Distribution

Summer accumulation type glaciers are extensively distributed in Asian highland regions influenced by Asian summer monsoon, i.e., the Himalayas, Tibetan Plateau, Qilian Mountains, Kunlun Mountains, Tien Shan, Pamir and so on. The Karakoram, however, is rather influenced by the westerlies, and receives much winter accumulation. In addition to the Asian glaciers, a part of the Andean glaciers are also revealed to be *summer accumulation type*, from an objectively analyzed meteorological datasets (Fujita, 2008).

Characteristics of mass balance

As most of the annual accumulation and ablation occur simultaneously in the same season on *summer accumulation type glaciers*, a change in climatic conditions in summer can induce a more drastic change in the glacier *mass balance* than that in winter. For example, an increase in summer air temperature will usually increase melting of glaciers. On the other hand, it will also decrease the snow fraction in precipitation, thereby decreasing accumulation. Moreover, it will lower the surface *albedo* of glaciers, thereby increasing absorption of solar radiation and melting. Thus, warming in summer has three negative effects on the *mass balance* of *summer accumulation type glaciers* (Ageta, 1983). In usual cases, warming in winter does not have such severe effects on the *mass balance* as warming in summer, because winter temperature is low enough below the melting point of ice.

As follows, the *albedo* effect on *mass balance* is probably the most important feature for *summer accumulation type glaciers*. Snowfall in summer keeps high *albedo* on the glacier surface and depresses melting. Due to this effect, the *equilibrium line altitude*, where the annual *mass*

balance is zero, is quite lowered, compared with a contrasting *winter accumulation type glacier*, which is assumed to have the same climate conditions except for only the seasonality of precipitation (Fujita and Ageta, 2000). In other words, *summer accumulation type glaciers* can exist as they are, owing to summer *accumulation*. In the case of winter accumulation, they should be smaller at higher altitudes or could not exist at all.

Sensitivity to climate changes

The above-mentioned significant characteristics in the *mass balance* of *summer accumulation type glaciers* deduce their high sensitivity to global warming, which have been investigated through numerical experiments. Not only *mass balance* but also dynamical response of *summer accumulation type glaciers* is more sensitive to temperature changes than that of *winter accumulation type glaciers* (Fujita and Ageta, 2000; Naito et al., 2001). On the other hand, the dynamical response to precipitation changes is more sensitive in the *winter accumulation type glaciers* (Naito et al., 2001). Moreover, precipitation seasonality and its concentration have a larger effect on the *mass balance* sensitivity to warming than latitude and the annual amount of precipitation (Fujita, 2008). These results indicate that forecasting the shrinkage of *summer accumulation type glaciers* to global warming requires an adequate consideration of their unique characteristics beyond simply applying any empirical relationship obtained for *winter accumulation type glaciers*.

Summary

Summer accumulation type glaciers receive more snowfall in summer than in winter. They are extensively distributed in Asian highland regions under summer monsoon climate, and parts of Andes. This type of glaciers are likely quite vulnerable to global warming, as decreasing summer snowfall reduces the surface *albedo*, and accelerates melting. In order to evaluate future shrinkages of this type of glaciers, the specific characteristics in their *mass balance* should be taken into account.

Bibliography

Ageta, Y., 1983. Characteristics of mass balance of the summer-accumulation type glacier in the Nepal Himalaya. *Seppyo*, **45**, 81–105 [in Japanese with an English abstract.].

Ageta, Y., and Higuchi, K., 1984. Estimation of mass balance components of a summer-accumulation type glacier in the Nepal Himalaya. *Geografiska Annaler*, **66 A**, 249–255.

Ageta, Y., Ohata, T., Tanaka, Y., Ikegami, K., and Higuchi, K., 1980. Mass balance of Glacier AX010 in Shrong Himal, east Nepal during the summer monsoon season. *Seppyo*, **41**(Special Issue), 34–41.

Fujita, K., 2008. Effect of precipitation seasonality on climatic sensitivity of glacier mass balance. *Earth and Planetary Science Letters*, **276**, 14–19.

Fujita, K., and Ageta, Y., 2000. Effect of summer accumulation on glacier mass balance on Tibetan Plateau revealed by mass-balance model. *Journal of Glaciology*, **46**, 244–252.

Naito, N., Ageta, Y., Nakawo, M., Waddington, E. D., Raymond, C. F., and Conway, H., 2001. Response sensitivity of a summer-accumulation type glacier to climate changes indicated with a glacier fluctuation model. *Bulletin of Glaciological Research*, **18**, 1–8.

Xie, Z., 1980. Mass balance of glaciers and its relationship with characteristics of glaciers. *Journal of Glaciology and Cryopedology*, **2**, 1–10 [in Chinese with an English abstract.].

Cross-references

Albedo
Andean Glaciers
Climate Change and Glaciers
Equilibrium-Line Altitude (ELA)
Glacier Mass Balance
Glaciers of the Karakoram Himalaya
Himalaya
Tibetan Plateau
Winter Accumulation Glacier

SUPER COOLING CLOUDS

P. Pradeep Kumar
Department of Atmospheric and Space Sciences, Pune University, Pune, India

As cloud forms and ascends it may be cooled to temperatures below 0°C. The water drops are expected to freeze, but in natural clouds this may not happen. Whether the water drops will freeze or not depends on the number of ice nuclei present in the cloud. Such drops are called as supercooled drops. For pure water droplets, the homogeneous freezing does not occur till −40°C. Supercooling of clouds till −15°C are not uncommon.

Bibliography

Rogers, R. R., 1979. *A Short Course on Cloud Physics*. New York: Pergamon, p. 234.

SUPERCOOLED WATER

Simon Cook
Centre for Glaciology, Institute of Geography & Earth Sciences, Aberystwyth University, Ceredigion, Wales, UK

Synonyms

Undercooling

Definition

Supercooled water. Water that remains in a liquid state when cooled below its melting (freezing) point.

Introduction

The freezing point of water (or the melting temperature of ice) varies depending upon the ambient pressure, the solute content of the water, whether the water is kept turbulent, and, where water and ice exist in soils or sediments, the interfacial forces between liquid water and ice. Typically, we think of water as a substance whose phase changes from liquid to solid as we cool it to 0°C, but there are several situations within cryospheric environments where water may exist in a liquid state at a temperature below the ambient freezing point. In this situation the water is referred to as being supercooled.

The transition of water to ice

As Block (2003) describes, the transition of water to ice via crystallization involves three stages: (1) supercooling, (2) formation of an ice nucleus, and (3) freezing to produce an ice crystal and growth of an ice front. Solutions supercool to varying degrees before spontaneously freezing. For example, perfectly pure and still water can remain liquid when cooled to approximately −40°C (Davis, 2001). In this supercooled state, liquid water is thermodynamically less stable than ice but it will remain in the liquid phase unless perturbed beyond a certain threshold. Such perturbations to the system could include further cooling, agitation of the water, or introduction of a freezing nucleus such as a sediment grain (seeding).

Pressure

The pressure dependence of the temperature at which ice melts and water freezes is of fundamental consequence to many aspects of cryospheric science. At atmospheric pressure, water will freeze at a temperature of 0°C, but with an increase in ambient pressure, the freezing point is depressed at a rate of 0.072°C per MPa (1 Pa = 1 N per square meter). So, for example, beneath glaciers and ice sheets, the freezing point of water is depressed by the pressure exerted by the ice thickness. The pressure beneath 2,000 m of ice is ∼17.6 MPa giving a melting point of −1.27°C (Benn and Evans, 1998). This pressure-determined melting/freezing temperature is referred to as the pressure melting point. Water at −1.27°C beneath 2,000 m of ice is not considered supercooled because its temperature is in equilibrium with the ambient pressure, but if that water were to flow from this area of high pressure to an area of lower pressure without freezing then it would be supercooled (e.g., Röthlisberger, 1968, 1972; Röthlisberger and Lang, 1987).

Glaciohydraulic Supercooling (qv) is a process that allows subglacial water to exist in a liquid state beneath ice masses in response to such pressure changes, and subsequently for this supercooled water to freeze to the glacier base to produce *basal ice* (qv *Formation and Deformation of Basal Ice*) and clog subglacial watercourses (e.g., Alley et al., 1998; Lawson et al., 1998; Cook et al., 2006). This mechanism of supercooling is implicitly associated with the flow of subglacial water through topographic basins or "overdeepenings." At the base of the overdeepening, the melting temperature is depressed beneath thick ice. As water is forced along a pressure gradient to ascend the reverse slope out of the overdeepening, the pressure melting temperature gradually rises toward 0°C as the overburden pressure decreases beneath thinner ice at the margin. For the water to remain in thermal equilibrium with the overlying temperate ice, the water must also warm as it moves along the gradient of decreasing pressure. Heat can be provided by a variety of potential sources, including: (a) viscous dissipation associated with water flow, (b) geothermal heat flux, (c) basal sliding, and (d) latent heat release if part of the water freezes. However, thermodynamic calculations suggest that if the adverse bed slope is sufficiently steep (more than 1.2–1.7 times the gradient of the ice-surface slope) then the heat generated and the rate of increase in water temperature will be insufficient to match the changing pressure melting point and it will become supercooled (Röthlisberger, 1972; Hooke, 1991; Alley et al., 1998). The minimum gradient of the adverse slope to allow supercooling varies dependent upon the air saturation state of the water. For the water to remain in thermal equilibrium with the overlying temperate ice, some of it must freeze to release latent heat, resulting in the production of *Frazil ice* (qv) (porous aggregates of lozenge-shaped crystals) and *Anchor Ice* (qv) (ice platelets anchored to the glacier or substrate). Sediment-laden water percolates through anchor and frazil ice until pore spaces freeze shut, and subsequent debris – ice segregation produces debris-laden basal ice (Alley et al., 1998; Lawson et al., 1998). The melting of this basal ice is suggested to have important implications for glacial geomorphology and landscape development (e.g., Larson et al., 2006), although there is still much uncertainty about the controls on the temporal and spatial pervasiveness of the process (e.g., Tweed et al., 2005; Cook et al., 2007).

Solutes

The presence of solutes within water may also depress its freezing point. In glaciers, the presence of solutes has an important impact on ice flow. The influence of solutes on the strain rate of glacier ice is variable as different solutes can either harden, soften, or have no effect on the ice (Nakamura and Jones, 1973). However, in situations where high solute concentrations act to depress the freezing point of water between ice crystals, the *Creep* (qv) of glacier ice may be enhanced (e.g., Wolff et al., 1988). Shreve (1984) demonstrated that glacier sliding could also be enhanced by elevated levels of solutes, in this case by sodium chloride (salt).

The depression of the freezing point by salt is of particular significance to sea ice scientists where supercooling and frazil ice formation occur as a result of differences in the salinities of waters. Martin (1981) explains that water becomes supercooled and produces frazil ice in Arctic river mouths or beneath pack ice where a layer of fresh meltwater at its freezing point (0°C) overlies a layer of

seawater at its freezing point (−1.6°C). Between 0.2 to 0.3 m of fresh water ice can grow beneath melting pack ice during the polar summer. Tsang and Hanley (1985) conducted experiments on ice formation for different supercoolings and initial salinities. Their results showed that the rate of frazil ice production was faster in fresh water than in saline water demonstrating that rates of sea ice formation depend to some extent on local salinity levels.

Block (2003) explains how, for terrestrial invertebrates which live in cold environments, solutes are important in maintaining body fluids in a liquid state. These "freeze avoiding" species may possess thermal hysteresis proteins (THPs) which depress the freezing point relative to the melting point of the body fluids, and which may be present together with compatible solutes that act as antifreezes (e.g., polyhydric alcohols and sugars).

Turbulence

The freezing point of water may be depressed by turbulence. This effect can pose a significant problem in rivers where frazil ice growth from turbulent supercooled water interrupts the operation of hydroelectric power stations (Martin, 1981). At low turbulence, frazil ice will float to the surface where it forms a pan, whereas when turbulence is high, frazil ice can be entrained into the flow and be carried to the bottom where it may attach to the channel bed and form anchor ice (Doering et al., 2001). Anchor ice can therefore alter the hydraulic characteristics of the flow. For example, the upper Niagara River experiences flow reductions of 20–30% as a result of anchor ice growth (Arden and Wigle, 1972).

Martin (1981) described how supercooling and frazil ice formation occur at the ocean surface due to the effect of turbulence. For leads (open water less than 100 m wide) and polynyas (width scale larger than 100 m) frazil ice will form where cold winds blow across regions of open water that is at the freezing point, agitating the water. In leads, frazil ice crystals form throughout the open water and are piled up to depths of 0.1–0.3 m at the edge of the lead due to wind and wave action. In polynyas, frazil ice tends to pile up in streaks aligned with wind direction to depths of around 1 m.

Interfacial effects

Soils and sediments encountered within cryospheric environments (i.e., permafrost and subglacial tills) can comprise a mixture of solid particles, air, ice, and liquid water. Supercooled water may exist in such situations as a consequence of solute content but of additional importance is the effect of premelting which itself can result from three related effects:

1. Ice–water interfacial tension – Interfacial tension results at an ice–water interface because of strong intermolecular forces between liquid water molecules at the interface. Hence a thin layer (on the order of nanometres) of supercooled liquid water will separate an ice lens growing in permafrost from a sediment particle (Rempel et al., 2004). Where the ice surface itself is curved, this will tend to promote the supercooling of pore-water that exists between sediment grains close to the ice front (Rempel et al., 2004).
2. Interfacial curvature – Higher interfacial tension is also promoted by enhanced curvature of sediment grains such that the finer grained a sediment is, the higher the curvature of the interface and the greater the depression of the freezing point (Christoffersen and Tulaczyk, 2003a; French, 2007).
3. Adsorption of liquid water onto a solid particle – The mineral properties of the soil particle also affect the thickness of the water layer that may be adsorbed to it (French, 2007). Adsorption refers to the forces that emanate from the particle surface which reduce the free energy of the water film.

Some important consequences of these effects include ice frost heaving in permafrost environments, and glacier motion. The deformation of the ground level in permafrost environments during winter cannot be fully explained by the volumetric expansion of water on freezing. Instead, it is due to the migration of premelted ice within the permafrost to a freezing front to produce segregation ice. The basic forcing mechanism is the repulsion between soil and water particles across the premelted water film which gives rise to low pressure within the water film (Rempel et al., 2004). Thus water in the surroundings is drawn toward the low pressure ice–water freezing interface where it may be frozen to produce segregation ice. Continued growth of the ice lens in this manner causes the ground to rupture – a process typically referred to as frost heaving (Dash et al., 1995).

Christoffersen and Tulaczyk (2003a, b) described a process of basal freeze-on beneath ice streams analogous to the process of frost heave in permafrost environments. In fine-grained subglacial till, water is unable to freeze due to interfacial effects and insufficient space for crystal growth. In polar ice streams, basal temperatures may be reduced by ice thinning, or by fast downward advection of cold surface ice. Reduced basal temperatures are accompanied by a decrease in water pressure at the ice–water interface producing a hydraulic gradient that drives the supercooled pore-water to the freezing front where it freezes to produce basal ice. Dewatering of the till in this manner causes it to consolidate and hence ice stream motion, which had once been accommodated by deformation of the saturated till layer, slows to the point of stagnation.

The existence of liquid water within glacier ice and subfreezing subglacial sediments is of fundamental importance for glacier motion of *Cold-Based Glaciers* (qv) and their geomorphic potential (Waller, 2001). Andersland and Alnouri (1970) demonstrated that at −12°C, frozen sand is much more resistant to loading than frozen clay because liquid water exists between clay particles due to interfacial effects, whereas water is completely frozen in

the sand sample. Echelmeyer and Zhongxiang (1987) suggested similarly that the existence of liquid water within subglacial sediments beneath Urumqi No. 1 Glacier reduced its creep strength by over 100 times relative to ice at a similar stress and temperature, enabling it to deform. This is contrary to previously held assumptions that cold-based glaciers were effectively frozen to their beds and were hence incapable of performing geomorphic work (e.g., Boulton, 1972).

Droplet size

When water is dispersed as tiny droplets in clouds, it can remain in a supercooled state in supercooled clouds. Clouds consist of water droplets at temperatures down to −12°C. *Rime Ice* (qv) may form from such masses of supercooled vapor or from water vapor carried by wind. On glaciers, rime ice development is most rapid in cool, humid conditions on surfaces that are exposed to wind (Benn and Evans, 1998). Rime ice formation can have a major impact on power supplies and telecommunication towers where it grows around cables and structures until they collapse under the additional weight (Makkonen, 2000). Rime ice accretion is also a major consideration in aeronautical engineering because aircraft must be resistant to rime ice formation since they routinely fly through supercooled vapor (Gent et al., 2000).

Summary

Whilst the transition from liquid water to ice is typically considered to occur at 0°C, there are a number of reasons why water can exist in a supercooled liquid state below this freezing point. Furthermore, the existence of supercooled water in the cryosphere has fundamental implications for important phenomena including frost heave of permafrost, glacier motion and dynamics, sea ice formation, the clogging of rivers and hydroelectric power inlets with frazil ice, and the design of power and telecommunications infrastructure and aircraft.

Bibliography

Alley, R. B., Lawson, D. E., Evenson, E. B., Strasser, J. C., and Larson, G. J., 1998. Glaciohydraulic supercooling: a freeze-on mechanism to create stratified, debris-rich basal ice: II theory. *Journal of Glaciology*, **44**, 563–569.

Andersland, O. B., and Alnouri, A., 1970. Time-dependent strength behaviour of frozen soils. *Journal of the Soil Mechanics and Foundations Division*, **SM4**, 1249–1265.

Arden, R. S., and Wigle, T. E., 1972. *Dynamics of Ice Formation in the Upper Niagara River. Proc.: The Role of Snow and Ice in Hydrology*. Banff: IAHS-UNESCO-WHO, pp. 1296–1313.

Benn, D. I., and Evans, D. J. A., 1998. *Glaciers and Glaciation*. London: Arnold.

Block, W., 2003. Water or ice? – the challenge for invertebrate cold survival. *Science Progress*, **86**, 77–101.

Boulton, G. S., 1972. The role of thermal regime in glacial sedimentation. In Price, R. J., and Sugden, D. E. (eds.), *Polar Geomorphology – Institute of British Geographers Special Publication Four*. Oxford: Alden, pp. 1–19.

Christoffersen, P., and Tulaczyk, S., 2003a. Response of subglacial sediments to basal freeze-on: I. Theory and comparison to observations from beneath the West Antarctic ice sheet. *Journal of Geophysical Research*, **108**(B4), 2222.

Christoffersen, P., and Tulaczyk, S., 2003b. Thermodynamics of basal freeze-on: predicting basal and subglacial signatures of stopped ice streams and interstream ridges. *Annals of Glaciology*, **36**, 233–243.

Cook, S. J., Waller, R. I., and Knight, P. G., 2006. Glaciohydraulic supercooling: the process and its significance. *Progress in Physical Geography*, **30**, 577–588.

Cook, S. J., Knight, P. G., Waller, R. I., Robinson, Z. P., and Adam, W. G., 2007. The geography of basal ice and its relationship to glaciohydraulic supercooling: Svínafellsjökull, southeast Iceland. *Quaternary Science Reviews*, **26**, 2309–2315.

Dash, J. G., Fu, H., and Wettlaufer, J. S., 1995. The premelting of ice and its environmental consequences. *Reports on Progress in Physics*, **58**, 115–167.

Davis, N., 2001. *Permafrost: A Guide to Frozen Ground in Transition*. Fairbanks: University of Alaska Press.

Doering, J. C., Bekeris, L. E., Morris, M. P., Dow, K. E., and Girling, W. C., 2001. Laboratory study of anchor ice growth. *Journal of Cold Regions Engineering*, **15**, 60–66.

Echelmeyer, K., and Zhongxiang, W., 1987. Direct observation of basal sliding and deformation of basal drift at sub-freezing temperatures. *Journal of Glaciology*, **33**, 83–98.

French, H. M., 2007. *The Periglacial Environment*. Chichester: Wiley.

Gent, R. W., Dart, N. P., and Cansdale, J. T., 2000. Aircraft icing. *Philosophical Transactions: Mathematical, Physical and Engineering Sciences*, **358**, 2873–2911.

Hooke, R. LeB., 1991. Positive feedbacks associated with erosion of glacial cirques and overdeepenings. *Geological Society of America Bulletin*, **103**, 1104–1108.

Larson, G. J., Lawson, D. E., Evenson, E. B., Alley, R. B., Knudsen, O., Lachniet, M. S., and Goetz, S. L., 2006. Glaciohydraulic supercooling in former ice sheets? *Geomorphology*, **75**, 20–32.

Lawson, D. E., Strasser, J. C., Evenson, E. B., Alley, R. B., Larson, G. J., and Arcone, S. A., 1998. Glaciohydraulic supercooling: a freeze-on mechanism to create stratified, debris-rich basal ice: I field evidence. *Journal of Glaciology*, **44**, 547–562.

Makkonen, L., 2000. Models for the growth of rime, glaze, icicles and wet snow on structures. *Philosophical Transactions: Mathematical, Physical and Engineering Sciences*, **358**, 2913–2939.

Martin, S., 1981. Frazil ice in rivers and oceans. *Annual Review of Fluid Mechanics*, **13**, 379–397.

Nakamura, T., and Jones, S. J., 1973. Mechanical properties of impure ice crystals. In Whalley, W. B., Jones, S. J., and Gold, L. W. (eds.), *Physics and Chemistry of Ice*. Ottawa: Royal Society of Canada, pp. 365–369.

Rempel, A. W., Wettlaufer, J. S., and Worster, M. G., 2004. Premelting dynamics in a continuum model of frost heave. *Journal of Fluid Mechanics*, **498**, 227–244.

Röthlisberger, H., 1968. Erosive processes which are likely to accentuate or reduce the bottom relief of valley glaciers. *International Association of Hydrological Sciences Publication*, **79**, 87–97.

Röthlisberger, H., 1972. Water pressure in intra- and subglacial channels. *Journal of Glaciology*, **11**, 177–202.

Röthlisberger, H., and Lang, H., 1987. Glacial hydrology. In Gurnell, A. M., and Clark, M. J. (eds.), *Glacio-Fluvial Sediment Transfer: An Alpine Perspective*. Chichester: Wiley.

Shreve, R. L., 1984. Glacier sliding at sub-freezing temperatures. *Journal of Glaciology*, **30**, 341–347.

Tsang, G., and Hanley, T. O'. D., 1985. Frazil formation in water of different salinities and supercoolings. *Journal of Glaciology*, **31**, 74–85.

Tweed, F. S., Roberts, M. J., and Russell, A. J., 2005. Hydrologic monitoring of supercooled discharge from Icelandic glaciers. *Quaternary Science Reviews*, **24**, 2308–2318.
Waller, R. I., 2001. The influence of basal processes on the dynamic behaviour of cold-based glaciers. *Quaternary International*, **86**, 117–128.
Wolff, E. W., Mulvaney, R., and Oates, K., 1988. The location of impurities in Antarctic ice. *Annals of Glaciology*, **11**, 194–197.

Cross-references

Anchor Ice
Cold-Based Glaciers
Creep
Formation and Deformation of Basal Ice
Frazil
Glaciohydraulic Supercooling
Rime Ice

SUPRA-GLACIAL DEBRIS ENTRAINMENTS

D. P. Dobhal
Wadia Institute of Himalayan Geology, Dehradun, India

Supra-glacial debris entrainments is defined as an unsorted and unstratified accumulation of sediments carried by the glacier along the bed and valley sides and deposited directly on glacier surface. They may occur by regelation or by the ice simply picking up the debris.

SURFACE ENERGY BALANCE

Michiel Van den Broeke[1], Xavier Fettweis[1,2], Thomas Mölg[3]
[1]Institute for Marine and Atmospheric Research, Utrecht University, Utrecht, Netherlands
[2]Department of Geography, University of Liège, Liège, Belgium
[3]Center for Climate & Cryosphere, University of Innsbruck, Innsbruck, Austria

Definition

The surface energy balance (SEB) describes the partitioning of energy fluxes toward and away from the surface. The local SEB determines the surface temperature of the Earth (T_s) and the associated exchange of energy between the surface and the atmosphere on one hand, and between the surface and the subsurface layers (whether it be soil, rock, water, snow, or ice, see Figure 1) on the other. When the surface consists of snow or ice, the SEB also determines the amount of energy that is available for sublimation and melting/freezing. These processes directly couple the SEB to the *surface mass balance* (SMB). In this entry, we describe the components of the SEB, and give six examples of the annual SEB cycle, all with a permanently snow-/ice-covered surface, but in widely varying geographical settings.

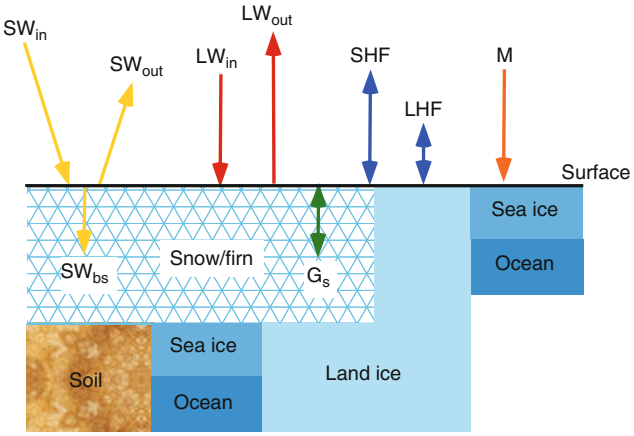

Surface Energy Balance, Figure 1 Components of the surface energy balance of snow, sea ice, and land ice. Length of arrows is only indicative.

Components of the surface energy balance

The SEB is defined as the sum of all fluxes of energy passing each second through a horizontal surface of unit area (Figure 1), with units J s^{-1} m^{-2} or W m^{-2}. *We define fluxes as positive when they are directed toward the surface,* i.e., *when they represent an energy gain for the surface.* For an infinitesimally thin surface layer without heat capacity (sometimes called a *skin layer*), these fluxes *balance,* i.e., their sum equals zero. If we neglect the heat added to the surface by falling snow, rain, or fog droplets, the SEB over a snow/ice surface can be written as:

$$M = SW_{in} + SW_{out} + SW_{bs} + LW_{in} + LW_{out} + SHF + LHF + G_s \left[Wm^{-2}\right] \quad (1)$$

In Equation 1, M is the melting flux when T_s equals 273.15 K, otherwise M = 0. Note that the melting temperature for sea ice surfaces can be lower than 273.15 K because the ice is saline in most cases. If $T_s < 273.15$ K and if there is liquid water available at the surface, M represents the freezing flux.

The abbreviations SW_{in} and SW_{out} represent the incoming and outgoing fluxes of shortwave (solar) radiation, SW_{bs} is the amount of shortwave radiation that is absorbed below the surface. LW_{in} and LW_{out} are the incoming and outgoing fluxes of longwave (terrestrial) radiation. Shortwave and longwave radiation are distinguished on the basis of their wavelength domain, determined from Planck's law by the temperature of the body that emits the radiation. If radiation originates from the surface of the Sun ($T_s \approx 5{,}800$ K), either directly or scattered in the Earth's atmosphere, nearly all energy is confined to wavelengths below 3 μm, hence the name *shortwave radiation*. If the radiation originates from the Earth-atmosphere system ($T_s \approx 200$–300 K), nearly all energy derives from wavelengths greater than 3 μm, hence the name *longwave*

radiation. SW and LW radiation fluxes are measured directly with broadband radiation sensors using selective filters.

At a sufficiently small distance above the surface, in the order of one to several mm, sensible heat exchange (SHF) and latent heat exchange (LHF) between the surface and air occurs predominantly by molecular conduction. Higher in the atmosphere, turbulence occurs as eddies (whirls) that vertically mix momentum, heat, and moisture. Turbulence is more effective in transporting scalars than molecular diffusion (Stull, 1988), and SHF and LHF are dominated by turbulent exchange. That is why they are usually referred to as *turbulent fluxes.*

Finally, G_s is the vertical heat flux below the surface, an expression of the molecular conduction of heat along temperature gradients in the snow/ice. The energy coming from the interior of the Earth, the geothermal heat flux, usually does not exceed 0.1 W m^{-2}, and is incorporated in G_s. The major components of the SEB are discussed separately below.

Shortwave radiation fluxes

When solar radiation impinges on the snow/ice surface, a part is absorbed at the surface, another part is reflected back to the atmosphere, and a third part penetrates to deeper layers and is absorbed below the surface. The net shortwave radiation flux (SW_{net}) is the total amount of shortwave radiation that is absorbed at or below the snow/ice surface. SW_{net} therefore equals the sum of downward (SW_{in}) and upward shortwave radiation (SW_{out}), and drives the daily and annual cycle in most SEB components.

SW_{in} is determined by (a) the amount of solar radiation impinging on the top of the atmosphere, (b) the amount of shortwave radiation that is scattered or absorbed in the atmosphere (depending notably on the cloudiness), and (c) the slope magnitude and orientation of the snow/ice surface. The instantaneous amount of solar radiation impinging on the top of the atmosphere (SW_{TOA}) depends on the solar constant, latitude, time of year, and time of day. Averaged over the year, the geographic poles receive about 40% of the insolation at the equator. But the temporal distribution of this energy is very different for different latitudes. As a rule of thumb, high-latitude (polar) regions experience a small daily cycle and a large annual cycle in SW_{TOA}, while tropical regions experience a large daily cycle and a small annual cycle in SW_{TOA} (Figure 2).

The amount of shortwave radiation that is scattered or absorbed in the atmosphere depends on the optical thickness of the atmosphere, which is mainly a function of vertically integrated water vapor mass and liquid water mass (clouds). The vertically integrated aerosol content also is important for shortwave radiation scattering. In the Polar Regions and for highly elevated tropical glaciers, the water vapor and aerosol content of the atmosphere is relatively low, so that the optical thickness is relatively small and the shortwave radiation intensity at the surface high. Explosive volcanic eruptions reduce the amount of solar energy reaching the surface; the El Chichón and Mount Pinatubo eruptions in 1983 and 1991 significantly impacted the SEB of Greenland (Fettweis, 2007). Glaciers or ice caps that are situated in temperate climates usually experience more cloudy conditions, limiting the amount of shortwave radiation that reaches the surface.

The orientation of glaciers with respect to the sun influences the amount of shortwave radiation impinging on the surface. If a glacier surface is steeply sloping and directed toward the sun, this can greatly enhance the amount of

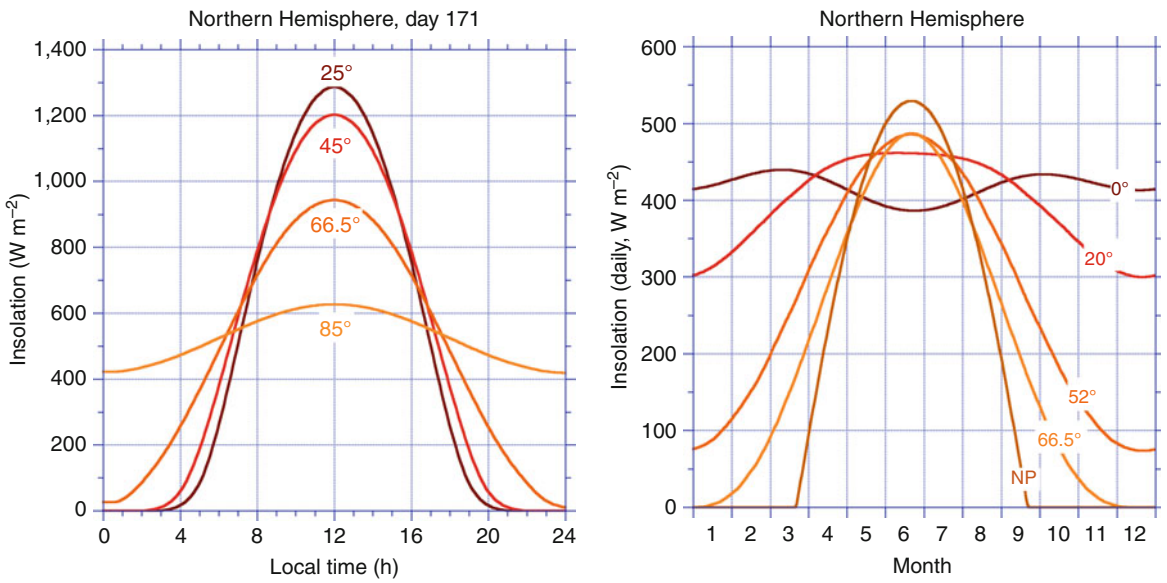

Surface Energy Balance, Figure 2 SW_{in} at the top of the atmosphere. Daily cycle in the northern hemisphere for June 20th (*left*) and annual cycle for the northern hemisphere based on daily means (*right*) of SW_{TOA} for various latitudes.

absorbed solar radiation and hence melting. On the other hand, if the sloping glacier is directed away from the sun, the solar rays hit the surface at an oblique angle, thereby decreasing the amount of shortwave radiation reaching the surface. Moreover, the surface can be shaded for parts of the day, eliminating the direct component of SW_{in}. For glacier melt modeling, the orientation of the glacier surface and the surrounding topography, therefore, needs to be explicitly taken into account (Klok and Oerlemans, 2002).

Part of the absorption (SW_{bs}) takes place below the surface (Grenfell and Maykut, 1977). Typical penetration depths are several cm in fine, dry-grained snow to several decimeters in ice (Brandt and Warren, 1993). This results in heating of the subsurface snow and ice layers (Kuipers Munneke and others, 2009) and may lead to subsurface melting (Van den Broeke and others, 2008b). When calculating the penetration of shortwave radiation in ice/snow, it is essential that the wavelength dependence of shortwave radiation absorption is taken into account, instead of using a bulk-extinction coefficient.

The fraction of shortwave radiation that is absorbed at or below the surface, is determined by the broadband surface albedo α, defined as:

$$\alpha = |SW_{out}|/SW_{in} \quad (2)$$

Snow albedo depends on the thickness, aerial coverage, and physical characteristics of the snow (grainsize, wetness, temperature), the thickness of the snow layer over dark soil and the spectrum and direction of the impinging solar radiation (wavelength distribution, solar zenith angle, ratio of diffuse to direct radiation, see Wiscombe and Warren, 1980, and entry on snow albedo). Clean, dry ice has an albedo of approximately 0.55, while clean, fresh snow has an albedo ~0.85. The albedo of water (<0.1) is much lower than that of snow and ice, and meltwater that accumulates at the snow/ice surface can therefore have a significant impact on its albedo (Greuell, 2000).

Melting leads to rapid growth of snow grains and can lower the snow albedo to values near 0.75, i.e., increasing the amount of absorbed shortwave radiation by ~70% compared to fresh snow. This represents the all-important albedo-melt feedback: melting lowers the albedo, which further enhances melt, etc. Typical low-ranging values of albedo (0.15–0.4) are found over ice and snow with a large dust load. The dust could have been melted out from the ice or blown onto it from the ice-free surroundings (Oerlemans and others, 2009). When seasonal snow or sea ice is replaced by the darker soil or sea surface, the amount of absorbed solar radiation may increase severalfold.

Figure 3 shows the global distribution of annual mean surface albedo, as derived from satellite measurements and radiative transfer modeling. The impact of snow and ice at high latitudes is clearly visible. The highest values (>0.8) are found over the interior dry snow zones of Greenland and Antarctica. The Arctic sea ice cover has a lower albedo, because it is melting for part of the year. The gradual transition toward lower values at mid-latitudes takes place over areas that are covered by seasonal snow or sea ice for part of the year. In the entry on snow albedo, the annual cycle of the albedo of Arctic sea ice is presented.

Longwave radiation fluxes

The net longwave radiation flux (LW_{net}) is the sum of incoming (LW_{in}) and outgoing (LW_{out}) longwave radiation fluxes. Over Greenland, LW_{in} appears the most sensitive SEB component for increased atmospheric concentrations of Greenhouse gases (Fettweis, 2007). Apart from exceptional cases, LW_{net} represents an energy loss for the surface, as the surface is generally warmer and has higher emissivity than the overlying atmosphere.

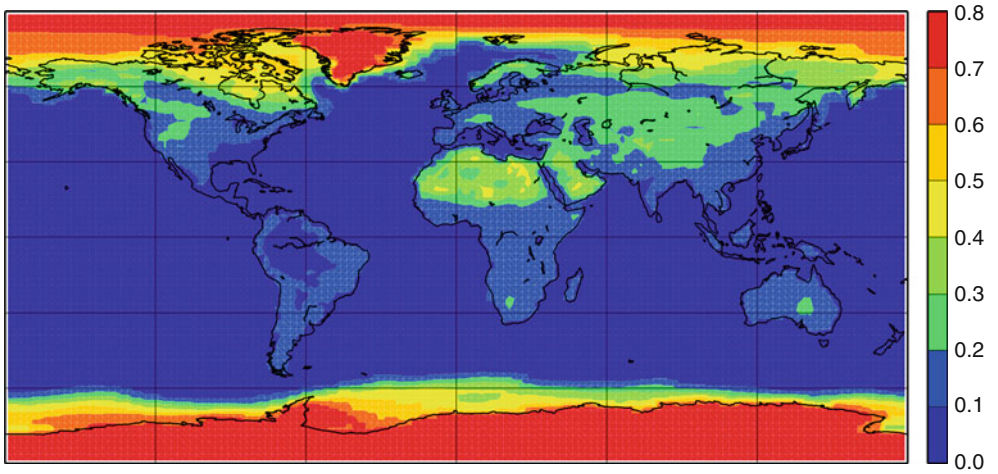

Surface Energy Balance, Figure 3 Satellite-derived surface broadband albedo, annual mean (based on data of Hatzianastassiou and others, 2004).

LW_{in} is determined by the effective emissivity (ε_{eff}) and effective radiation temperature (T_{eff}) of the atmosphere, while LW_{out} is determined by the emissivity (ε_s) and temperature (T_s) of the snow/ice surface. Using the Stephan–Boltzmann law, LW_{net} can be approximated by:

$$LW_{net} = \varepsilon_s \varepsilon_{eff} \sigma T_{eff}^4 - \varepsilon_s \sigma T_s^4 \quad (3)$$

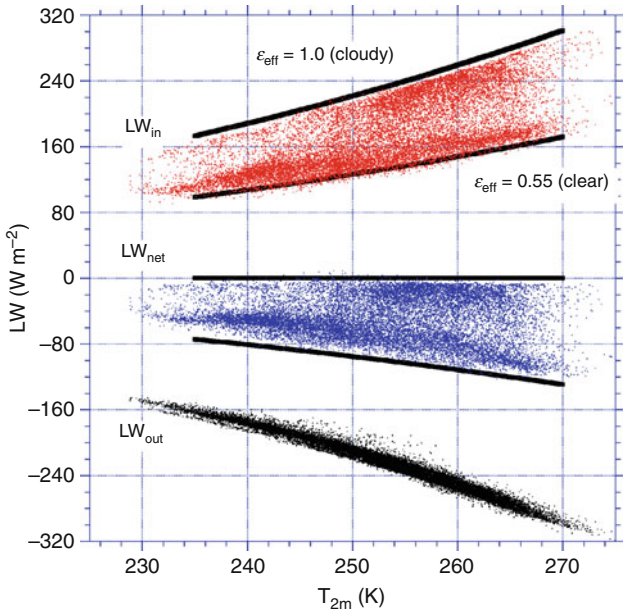

Surface Energy Balance, Figure 4 Observed hourly mean values of LW_{in} (*red dots*), LW_{out} (*black dots*), and LW_{net} (*blue dots*) as well as calculated from empirical formula (black lines, Equation 3) as a function of 2 m temperature for a non-melting location in Antarctica, at 1,100 m a.s.l. The upper and lower bounds of all three cases are for cloudy and clear sky conditions, respectively.

where the Stefan–Boltzmann constant $\sigma = 5.67 \times 10^{-8}$ W m^{-2} K^{-4}.

The surface emissivity of a dry snow surface is close to unity ($\varepsilon_s \approx 0.98$, Wiscombe and Warren, 1980) while the effective emissivity and radiation temperature of the atmosphere are complex functions of the vertical distribution of temperature, moisture, and other atmospheric compounds. In spite of this complexity, some general statements can be made. Under cloudy conditions, $\varepsilon_{eff} \approx 1$, and T_{eff} represents the cloud base temperature. When the cloud base is situated at low elevation, T_{eff} will not deviate much from T_s, so that LW_{net} will be zero or weakly negative. Under clear sky conditions, if 2 m air temperature is used as a measure for effective atmospheric radiative temperature, it is found that ε_{eff} can be approximated by a constant, to be determined empirically. Figure 4 shows an example for a location in Antarctica, where $\varepsilon_{eff} \approx 0.55$ (thick black lines in Figure 4). The resulting expression can be used to estimate LW_{in} and, if T_s is known (or assumed approximately equal to T_{2m}), to estimate LW_{out} and hence LW_{net}. The challenge lies in estimating LW_{in} for partly cloudy conditions, i.e., to interpolate between these two extremes (Kuipers Munneke and others, 2010).

Net radiation flux

Averaged over the year, $R_{net} = SW_{net} + LW_{net}$ is negative over much of the Polar Regions and in some highly elevated plateaus away from the Poles (e.g., the Tibetan Plateau, Figure 5). At these locations, cooling by LW_{net} exceeds warming by SW_{net}. This is remarkable, given that the Sun provides radiative energy for half of the time. The radiation deficit in the Polar Regions can be explained by factors that limit SW_{net}, such as the low Sun angle and the high albedo of the surface that usually consists of snow, glaciers, and sea ice. On the other hand, the snow effectively emits longwave radiation ($\varepsilon_s \approx 1$) while the polar

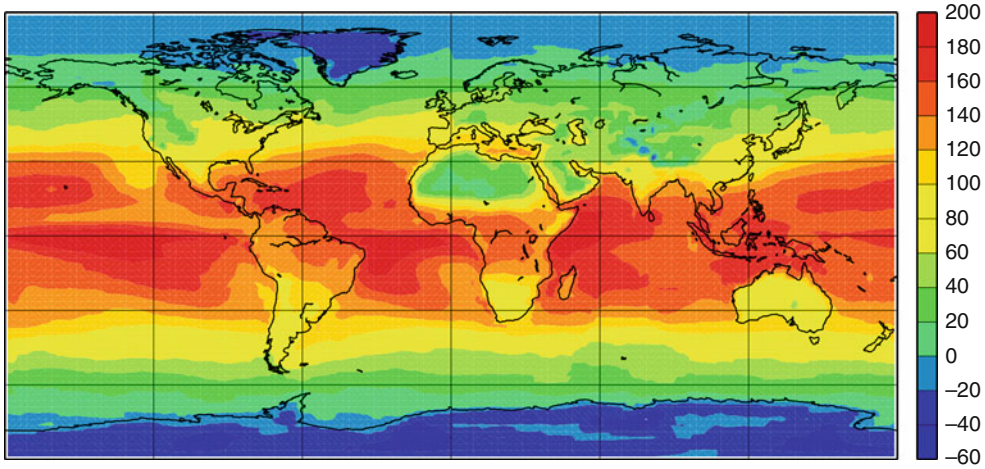

Surface Energy Balance, Figure 5 Annual average surface net radiation in W m^{-2} (*based on data of* Hatzianastassiou and others, 2004).

atmosphere is cold and dry, resulting in small ε_{eff}. This results in relatively strongly negative values of LW_{net}. Even at these sites, R_{net} will become positive around noon during sunny summer days, but when averaged over the year, the radiation balance is negative. Over a semi-infinite snow pack, this radiation deficit must be compensated by the sensible heat flux from the atmosphere, as the heat flux from the snowpack equals approximately zero when averaged over the year (see Section Subsurface heat flux). The latent heat flux is also likely to be small at polar sites (see Section latent heat flux), so that the most likely candidate is a flux of sensible heat from the atmosphere to the surface (next Section "Sensible heat flux"). Over sea ice, heat provided by the ocean through the subsurface heat flux compensates an important part of the radiative heat loss. Over open water in winter, much of the radiative heat loss is invested in cooling the upper ocean layers, resulting in the formation of sea ice.

Sensible heat flux

The turbulent flux of sensible heat, SHF (often referred to as the sensible heat flux), describes heat exchange between the surface and the air above it. In the surface layer, SHF can be directly measured using sonic anemometers that measure rapid (turbulent) fluctuations in temperature and vertical velocity. But these instruments are relatively vulnerable and expensive, which is why the sensible heat flux is often calculated, based on measured profiles of wind and temperature, in combination with surface-layer similarity theory (Stull, 1988). These calculations usually give satisfactory results over melting and non-melting snow and ice surfaces.

The sensible heat flux is directed away from the surface (negative) when the surface is warmer than the air, i.e., under statically unstable conditions in the atmospheric surface layer (SL). This upward heat transport is often referred to as convection. In the Polar Regions, convection is rare, and occurs, for instance, when cold polar air flows over open water, forming characteristic convective cloud straits. Weak convection also occurs during summer at highly elevated sites on the Polar Ice sheets, where temperatures are too low for sublimation to be significant (King and others, 2006).

In general, however, the negative net radiation cools the surface, which then becomes colder than the air above. Therefore, over snow and ice, SHF is commonly positive, i.e., directed toward the surface. The associated cooling of the atmospheric boundary layer often results in a surface-based temperature inversion, in which the temperature increases with height. In regions where the radiative heat loss is quasi-permanent during the Polar Night, i.e., the elevated interior plateaus of the Greenland and Antarctic ice sheets, the surface temperature inversion can become several tens of degrees (e.g., Vostok station in Figure 6). In the coastal areas and in the Arctic (Overland and others, 2000), the radiative cooling is weaker because of the more frequent occurrence of clouds, enhancing incoming longwave radiation, resulting in a weaker surface temperature inversion (e.g., Mawson and Neumayer in Figure 6).

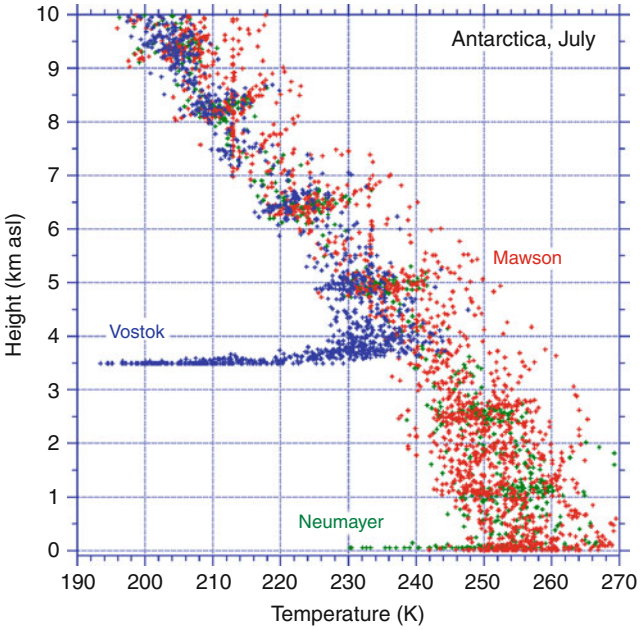

Surface Energy Balance, Figure 6 Wintertime (July) vertical temperature profiles from radiosondes measurements at three Antarctic stations. Atmospheric temperature profiles at South Pole are similar to Vostok.

Under these statically stable conditions, wind shear is a prerequisite for the generation of turbulent heat exchange. Wind shear is enhanced over rough surfaces, such as hummocky sea ice (Andreas and Claffey, 1995); over snow and ice surfaces that are relatively smooth, it requires relatively large wind speeds for the wind shear to become sufficiently large. Over ice sheets and glaciers, which have a sloping surface, this wind shear is often provided by *katabatic* forcing. The cold near-surface air is denser than the air in the free atmosphere at the same elevation, which sets up a horizontal pressure gradient over a sloping surface, forcing *katabatic* or downslope winds. Over the large ice sheets, katabatic winds can be very persistent. Because the katabatic forcing acts along the local slope, katabatic winds have a high *directional constancy.* Because of their direct coupling to the radiative cooling of the surface, katabatic winds efficiently generate the turbulence necessary to keep the sensible heat transport going in the stably stratified atmospheric surface layer.

Latent heat flux

Over a snow/ice surface at freezing temperatures, the latent heat flux (LHF) equals the amount of heat extracted from or added to the surface as a result of sublimation (the phase change from solid to water vapor) or deposition (phase transition from vapor to solid, i.e., rime formation). When the surface is melting and liquid water is available, LHF equals the amount of heat extracted from or added to

the surface as a result of evaporation (the phase change from liquid to gas) or condensation (phase transition from gas to liquid, i.e., dew formation). In mountainous areas and over sea ice, frost formation (from liquid to solid) may also be an important process. All these processes exchange not only heat but also mass with the surface, which couples the surface energy balance to the surface mass balance (the sum of all mass fluxes toward and away from the surface).

The LHF can be directly measured using instruments that measure the absorption of light by water vapor at a specific wavelength. Alternatively, LHF can be calculated using simultaneously measured vertical profiles of wind speed and specific humidity. The latter is often determined from relative humidity measurements, which are difficult to perform over snow and ice (Anderson, 1994).

Temperature plays a pivotal role in the magnitude of LHF through its influence on the moisture content of the air. The maximum moisture content of the air, and therewith its vertical gradients, is tightly coupled to temperature through the Clausius Clapeyron equation. Figure 7 (left) shows specific humidity as a function of 2 m temperature for a non-melting location in East Antarctica. Neglecting the temperature difference between the surface and 2 m for the moment and using the fact that the snow/ice surface is always saturated (i.e., the surface-specific humidity is represented by the upper boundary of the point cloud), the distance of individual points to the upper boundary represents the vertical moisture gradient, and therewith the sublimation potential. The undersaturation and therewith the vertical humidity gradient become small at low temperatures, resulting in low LHF values (Figure 7, right).

In summer, when the surface absorbs solar radiation and heats up, significant sublimation does occur at this site (significantly negative LHF). But even under very favorable conditions, the magnitude of LHF usually does not exceed several tens of W m^{-2}, which are small values compared to the mid-latitudes and tropics, where LHF can attain values of several hundreds of W m^{-2}. But this does not mean that LHF is unimportant for the hydrological cycle at high latitudes. An average LHF of only -1 W m^{-2} still represents a surface mass loss of 11 kg m^{-2}. For areas where snowfall and melt are small, such as the interior of the Greenland and Antarctic ice sheets, this potentially represents a considerable fraction of the annual snowfall.

When snowdrift takes place, sublimation from the surface ceases while the sublimation of drifting snow particles takes over. For snowdrift sublimation, which is thought to be an important term in the mass balance of the Greenland and Antarctic ice sheets and the seasonal snowpack at high northern latitudes (Box and others, 2006; Déry and Yau, 2001), no robust measurement techniques are yet available.

Subsurface heat flux

The subsurface heat flux (G) represents the conduction of heat into the subsurface strata; this flux is mainly driven by molecular conduction and therefore occurs along vertical temperature gradients in the snow/ice, following $G(z) = k\, dT(z)/dz$. The heat conductivity (k) of snow is mainly a function of snow density and grain structure, connecting the low heat conductivity of air ("zero" density snow) to that of ice (red curve in Figure 8). Since snow is

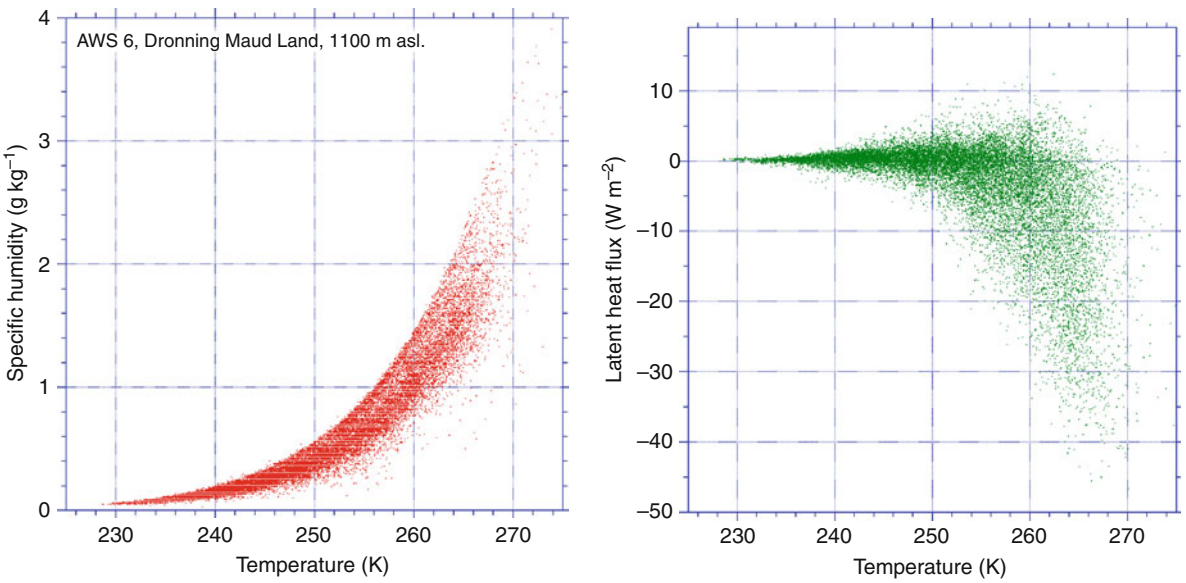

Surface Energy Balance, Figure 7 Observations of hourly 2 m specific humidity (*left*) and calculated latent heat flux LHF (*right*) as a function of 2 m temperature at an automatic weather station in East Antarctica.

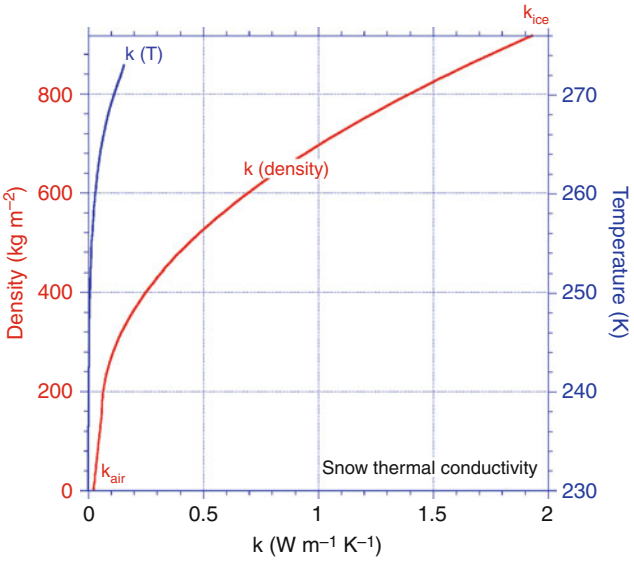

Surface Energy Balance, Figure 8 Value of heat conductivity k in snow is mainly a function of snow density and grain structure (*red curve*). A small part of the heat transport results from internal convection and from sublimation and subsequent deposition elsewhere in the snowpack, mainly a function of temperature (*blue curve*).

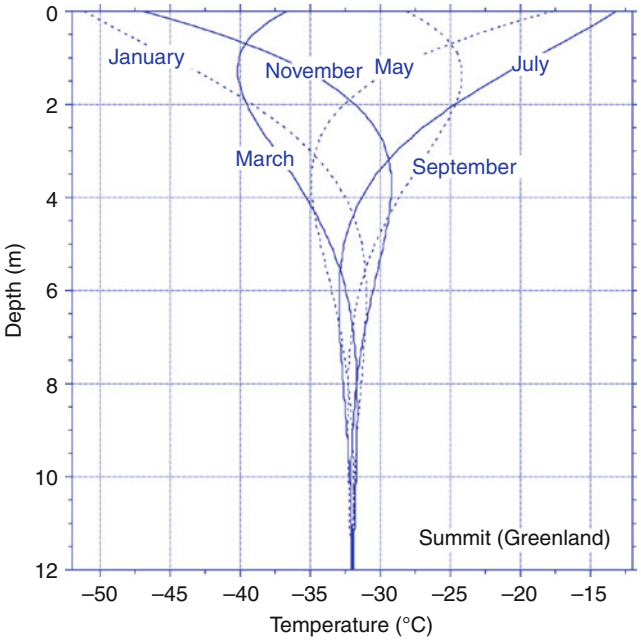

Surface Energy Balance, Figure 9 Theoretical temperature distribution in the snow at Summit, Greenland, forced by a sinusoidal temperature variation at the surface, and assuming a homogeneous snowpack with k = 0.5 W K^{-1} m^{-1}.

a porous medium, a small part of the heat transport results from internal convection and from sublimation and subsequent deposition elsewhere in the snowpack, both processes being a function of temperature (blue curve in Figure 8). This results in an effective heat conductivity that is the sum of conduction and internal convection/deposition.

In the surface energy balance, the surface value of G, G_s, is relevant. Over sea ice, G_s is an important SEB component (see further in this entry). Over a semi-infinite snowpack, G_s will be close to zero when averaged over the year; otherwise the snow layers below the surface would continuously cool or heat up. In the monthly average, G_s will be negative in summer, when the surface is warmer than the subsurface snow layers and heat is transported into the snowpack, and positive in winter, when the temperature gradient is reversed and heat is extracted from the deeper snow layers. But also monthly average values are usually small, typically several W m^{-2}. The real importance of G_s is in the daily cycle of the SEB. At times when turbulence is small, for instance under weak wind conditions, G_s is the only term that can compensate the radiative heat gains/losses; the chain of events is as follows: when the radiation balance becomes strongly positive/negative, and turbulence is weak, the surface temperature will quickly rise/fall. In response, the vertical temperature gradients between the subsurface and the surface will quickly grow, triggering a strongly negative/positive value of G_s, which compensates for the radiative heat exchange.

Because it transports heat, G(z) determines the ice/snow temperature distribution. Figure 9 shows the (theoretical) subsurface temperature distribution at Summit Station at the top of the Greenland ice sheet, as forced by a sinusoidal annual cycle in surface temperature, assuming a homogenous snowpack with constant density. In the absence of melting, the annual temperature variation vanishes below approximately 10 m depth. This means that at those depths, the temperature approximates the annual mean surface temperature. This technique is often used to estimate the annual mean surface temperature in the interior of the large ice sheets, where few observations are available. When melt occurs, the refreezing of the percolating meltwater releases heat into the snowpack and the underlying ice. Under these conditions, the technique of determining annual mean T_s is no longer applicable.

Melting and refreezing

If absorption of solar radiation has heated the snow/ice layers to the melting point, the excess energy produces melting ($M > 0$). The meltwater formed at the surface either runs off (when the surface is impermeable, i.e., ice), or penetrates the snowpack. Sea ice is an intermediate case where the water partly pools at the surface and partly percolates through or flows off the ice into the ocean. In the case of a snow pack, the meltwater may refreeze at some depth where the temperature is still below freezing. This refreezing of meltwater may constitute an important process for the mass balance of glaciers and sea ice

because the ice involved must be melted more than once before it is removed from the glacier. Moreover, upon refreezing, latent heat is released within the snowpack, which alters the subsurface temperature distribution. However, because the heat is released below the surface, as is the case with penetration of shortwave radiation, this heat source is not part of the surface energy balance. It merely influences the SEB through altering the subsurface heat flux by changing the subsurface temperature gradient. Gallée and Duynkerke (1997), for instance, showed that the daily cycle of surface melting and refreezing below the surface significantly impacts the SEB in Greenland. If it is not taken into account, the surface and subsurface temperatures are significantly underestimated.

Annual cycle of SEB over various permanent snow- and ice-covered surfaces

In this section, we discuss the idealized annual cycle, based on monthly means, of the SEB over various permanently snow- and ice-covered surfaces. The coordinates, elevation, surface type and basic climate conditions of these locations during different seasons are summarized in Table 1. For clarity, the annual cycles presented in the following figures have been smoothed using 3-month running means. For details of calculation and variability beyond the mean annual cycle, we refer to the original references.

North pole, arctic basin

While some SEB estimates are available from Russian drifting station and from various US drift stations such as SHEBA (Surface Heat Budget of the Arctic Ocean, Utta and others, 2002; Persson and others, 2002), here we present, for illustrative purposes, the idealized annual cycle of the SEB at the North Pole (90° North, NP), based on model/weather observations combined with an SEB model, assuming 2 m thick sea ice. The NP is situated over a frozen ocean surface that consists of snow-covered sea ice in winter and melting snow/ice in summer (Table 1). The wintertime SEB (Figure 10) is a first-order balance between (longwave) radiative cooling and heating by SHF and G_s. Especially G_s is significant; 30 W m^{-2} is the approximate amount of heat that flows from the warm ocean (−1.8°C) to the sea ice surface (−30°C), when the ice is 2 m thick. Because of the radiative cooling, the sea ice surface is colder than the overlying air, which, in combination with the moderate winds, generates a flux of sensible heat toward the surface. At the sea ice–ocean boundary, a semi-unlimited heat source is available from the deeper ocean. As a result, annual average G_s is significantly positive, driving freezing at the ice/ocean interface.

At these low temperatures, wintertime LHF is negligible. In spring, shortwave radiative heating increases surface temperature and specific humidity, resulting in weak sublimation. At sea level, the summer climate is relatively mild, even this far north, and frequent melting occurs. When melting starts in earnest in summer, the moisture and temperature gradients between the sea ice surface and the overlying air diminish, reducing the magnitude of the turbulent fluxes. Because the temperature gradient between ice surface and ice base also disappears, G_s goes to zero. All the absorbed shortwave radiation is invested in melting. The integrated amount of melt energy represents the removal of approximately 1.5 m of ice, less than the total ice thickness. In spite of bottom melting also taking place, sea ice at the North Pole usually survives the summer melt period, to form multiyear sea ice in the subsequent years.

Ablation zone of the west-greenland ice sheet

The Greenland ice sheet is the second largest ice mass in the world, and its southernmost part is situated in a subarctic climate. A site was selected in the lower ablation zone of the southwestern ice sheet (Table 1) for which reliable, multiyear meteorological observations are available (Van den Broeke et al., 2008a, b). In winter, surface radiative cooling is compensated in first order by SHF, with small contributions from LHF and G_s (Figure 11).

Surface Energy Balance, Table 1 Surface and climate characteristics of some SEB locations

Location name	Coordinates Elevation (m asl)	Surface type		Temperature (°C)		Wind speed (m s^{-1})	
		Summer	*Winter*	*Summer*	*Winter*	*Summer*	*Winter*
North Pole (Sea Ice)	90° N ~0 m	Melting snow/ice	Snow	−2	−30	6	5
West Greenland ablation zone	67° 06′N, 50° 07′ W 500 m	Melting ice	Snow	+3	−20	5	5
Morteratsch glacier	46° 24′ N, 9° 56′ E 2100 m	Melting ice	Snow	+9	−7	6	6
Neumayer (Antarctica)	70° 39′ S, 8° 15′ W 40 m	(Melting) snow	Snow	−5	−25	7	10
South Pole (Antarctica)	90° S 2830 m	Snow	Snow	−30	−60	5	7
		Dry season	*Wet season*	*Dry season*	*Wet season*	*Dry season*	*Wet season*
Kersten glacier (Kilimanjaro)	3° 05′ S, 37° 21′ E 5873 m	Ice	(Melting) snow	−7	−6	4	5

The subsurface heat flux G_s is heating the surface during winter, when the surface temperature is lower than the deeper snowpack temperature (Figure 9). In summer, the surface at this site is continuously at the melting point while the temperature deeper in the snowpack is several degrees lower than the melting point inducing a negative G_s.

Because in summer the air is usually warmer than 0°C, both SHF and LHF are directed toward the melting ice surface, contributing significantly to melt. Because of the sunny climate and relatively high temperatures in this part of Greenland, the total amount of summer ice melt at this site exceeds 4 m, among the largest values found in Greenland. Both SHF and LHF show a double maximum, one in winter and one in summer, which is caused by the double maximum in wind speed. In both seasons, atmospheric cooling through SHF maintains the katabatic winds. In winter, surface radiative cooling maintains the surface temperature deficit, while in summer the melting surface is responsible for a temperature deficit. Over melting ice surfaces, katabatic winds are sometimes called *glacier winds*.

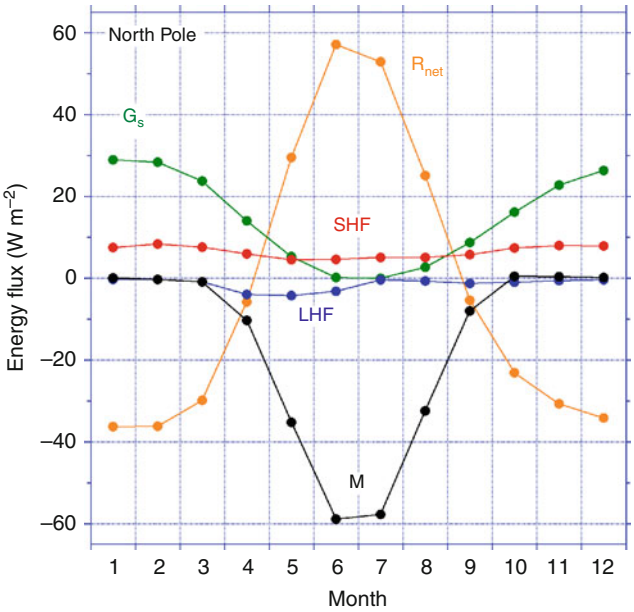

Surface Energy Balance, Figure 10 Annual cycle of SEB components at North Pole in the Arctic basin. Idealized results from model data and observations, assuming 2 m thick sea ice (see text).

Ablation zone of morteratsch glacier, swiss alps

Vadret da Morteratsch is a mid-latitude glacier in Switzerland (Table 1) and has one of the longest uninterrupted SEB records from the surface of a valley glacier (15 years, Oerlemans and others, 2009). The automatic weather station that produced the results shown in Figure 12 is situated in the ablation zone at the tongue of the glacier at 2,100 m asl. The winter SEB (Figure 12) is comparable to the Greenland ablation zone, with radiative heat losses being compensated mainly by SHF. In summer, the glacier tongue is surrounded by ice-free terrain, resulting in high summer air temperatures over the melting ice surface

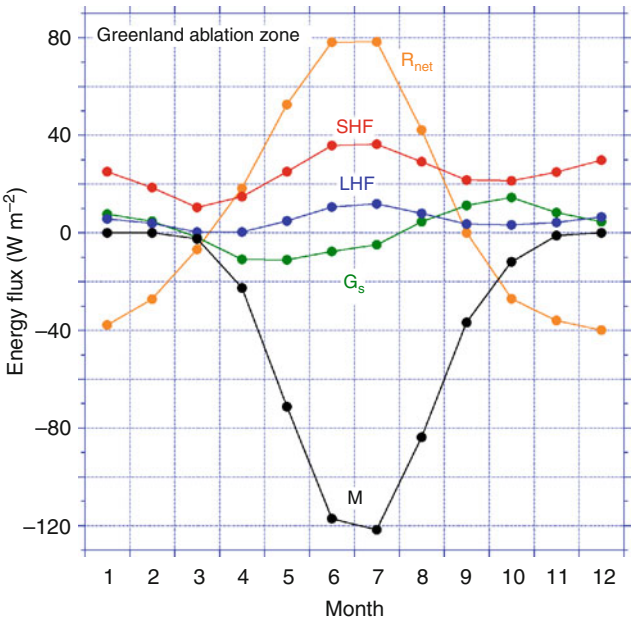

Surface Energy Balance, Figure 11 Annual cycle of SEB components in the lower ablation zone of the ice sheet in southwest Greenland. SEB calculated from 4 years of automatic weather station observations (see text).

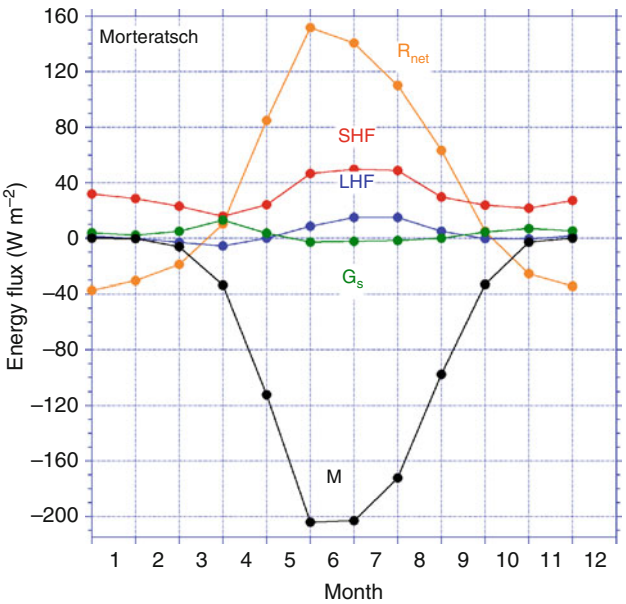

Surface Energy Balance, Figure 12 Annual cycle of SEB components in the ablation zone of the Morteratsch glacier, Switzerland. SEB calculated from 15 years of automatic weather station observations (see text).

(Table 1). This also results in dust accumulation, so that the surface albedo of the ice attains very low values (~0.15). This strongly enhances the absorption of shortwave radiation and therewith surface melting. As a result, R_{net} attains much higher values than in Greenland, while SHF and LHF are comparable, including the double annual maxima. The total melt for this location exceeds 7 m of ice, which has forced a strong retreat of the glacier in recent decades.

Kersten glacier, Kilimanjaro

This tropical glacier is situated between 5,100 and 5,900 m on the southern flank of Kilimanjaro, close to the equator (Table 1). Based on several years of AWS data and distributed energy balance modeling, the SEB, averaged over the entire glacier surface, could be determined (Mölg and others, 2009). The annual cycle (Figure 13) deviates strongly from other locations. As a result of its location close to the equator, the annual cycles in SW_{in} and ambient temperature are small, and thus there is no climatological summer or winter at this site; the seasonal variations are mostly forced by the wet and dry seasons. At these high elevations, the air contains little moisture and sublimation produces an important heat and mass loss year round. In the main wet season (April/May), sublimation strongly decreases. Net radiation is small, because SW_{net} is at a minimum, mainly due to high albedo. At the same time, as the air is moist and cloudy, cooling by LW_{net} is also small, resulting in small net radiation. In the core dry season (June–August) there is hardly any melt and ablation is controlled by sublimation. In these months, cooling by sublimation significantly exceeds warming by R_{net}, so that the surface remains significantly colder than the overlying air and SHF peaks. The most variable part of the year is the wet season around November/December. This season can start in October and last into January/February, but sometimes is totally absent. The occurrence of sublimation and the associated surface cooling is vital for limiting the melt amount throughout the year. Note that, even in the presence of moderate refreezing, melt (575 kg m^{-2} $year^{-1}$) still removes more mass than sublimation (450 kg m^{-2} $year^{-1}$) glacier-wide, because of the much smaller latent heat of fusion compared to evaporation/sublimation. However, at the glacier summit, sublimation dominates and accounts for 75% of the total annual mass loss.

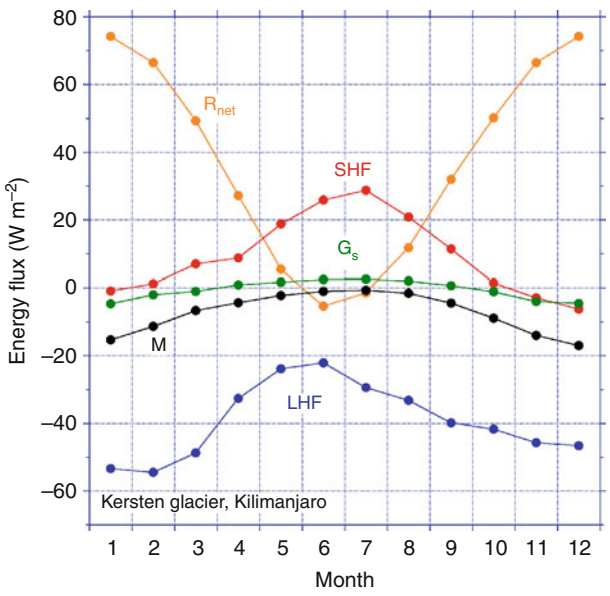

Surface Energy Balance, Figure 13 Annual cycle of SEB components on Kersten glacier, Kilimanjaro, Tanzania. SEB calculated from three years of automatic weather station observations in combination with a distributed energy balance model (see text).

Neumayer, antarctica

Neumayer station (Germany) is situated on Ekstrøm ice shelf in coastal East Antarctica, at approximately 70°S (Table 1). The station is situated relatively far to the north, at low elevation (40 m asl) and close to the Southern Ocean. The nearby ocean is ice-covered in winter, but ice free in summer. Being situated close to the circumpolar pressure trough, Neumayer experiences strong easterly winds year round with frequent occurrence of snowdrift (~40% of the time). The wind maximum in winter is caused by enhanced depression activity, not by katabatic forcing, because Neumayer is situated on a flat ice shelf, which does not allow for significant katabatic forcing. In spite of the proximity of the ocean, Neumayer has a cold climate with only occasional melting around noon during sunny summer days. The SEB (Figure 14) was calculated using 13 years of high-quality meteorological observations (König Langlo and Loose, 2007; Van den Broeke and others, 2009). In the absence of continuous melting, with slow snow metamorphosis, the surface albedo is high year round. Only after prolonged dry periods with daytime melt in summer does the albedo of the snow surface fall below 0.8; as a result, R_{net} is small and the radiation balance only becomes positive in summer. In combination with mild summer temperatures, this allows for significant sublimation (Figure 14). In winter, longwave radiative cooling dominates and is compensated by SHF and in second order by LHF and G_s.

South pole, east antarctica

The geographic South Pole is situated in the vast interior of the East Antarctic ice sheet at an altitude in excess of 2,800 m (Table 1). The South Pole experiences a wintertime surface inversion similar to Vostok Station in Figure 6. Because it is not situated on a dome, the wind climate shows an appreciable wintertime (katabatic) maximum which, because the surface slope is small, is much weaker than those measured over the steeper parts of the ice sheet closer to the coast. Snow metamorphism is slow at these low temperatures, resulting in a year-round high surface albedo. As a result, summertime net radiation is

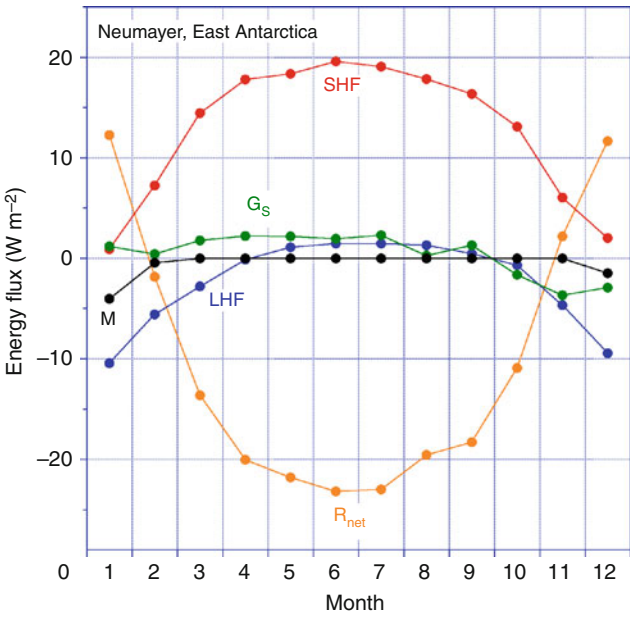

Surface Energy Balance, Figure 14 Annual cycle of SEB components at Neumayer, East Antarctica. SEB calculated based on 13 years of surface observations (see text).

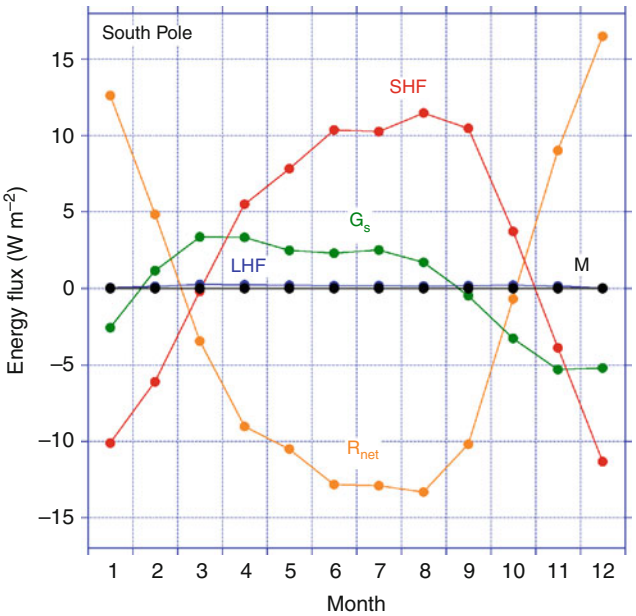

Surface Energy Balance, Figure 15 Annual cycle of SEB components at South Pole, East Antarctica. SEB calculated based on 3 years of surface observations (see text).

small, <15 W m^{-2}, and all fluxes are smaller in magnitude than at Neumayer (Figure 15). Summer temperatures are also too low to allow for significant sublimation to occur. In the absence of this heat sink, surface temperature can rise quickly above the air temperature during sunny summer days, allowing weak convection (negative SHF) and a shallow (~100 m) mixed boundary layer to develop (King and others, 2006; Van As and others, 2006). Because all other fluxes are small, monthly mean G_s becomes a significant component of the SEB at the South Pole, in spite of its small magnitude. The wintertime SEB is comparable to Neumayer, i.e., a first-order balance between radiative cooling and heating by SHF.

Summary

This entry describes the components of the surface energy balance (SEB) over snow and ice: shortwave and longwave radiation, the turbulent fluxes of sensible and latent heat, and the subsurface (conductive) heat flux. If the surface is melting, the sum of these fluxes determines the melt rate. We explicitly describe the idealized mean annual cycle of the surface energy balance components at six locations with permanently ice- or snow-covered surfaces, but with widely varying melt characteristics: sea ice at the North Pole, the ablation zone of the Greenland ice sheet, the ablation zone of the Morteratsch glacier in Switzerland, Kersten Glacier on the Kilimanjaro in Tanzania, Neumayer station in coastal East Antarctica, and South Pole station in interior East Antarctica.

Acknowledgments

We thank Gert König Langlo, Rianne Giesen, and Hans Oerlemans for providing data. Thomas Grenfell and an anonymous reviewer are thanked for improving the original manuscript.

Bibliography

Anderson, P. S., 1994. A method for rescaling humidity sensors at temperatures well below freezing. *Journal of Atmospheric and Oceanic Technology*, **11**, 1388–1391.

Andreas, E. L., and Claffey, K. J., 1995. Air-ice drag coefficients in the western Weddell Sea: 1. Values deduced from profile measurements. *Journal of Geophysical Research*, **100**, 4821–4831.

Box, J., Bromwich, D., Veenhuis, B., Bai, L.-S., Stroeve, J., Rogers, J., Steffen, K., Haran, T., and Wang, S.-H., 2006. Greenland ice sheet surface mass balance variability (1988–2004) from calibrated polar MM5 output. *Journal of Climate*, **19**, 2783–2800.

Brandt, R. E., and Warren, S. G., 1993. Solar heating rates and temperature profiles in Antarctic snow and ice. *Journal of Glaciology*, **39**, 99–110.

Déry, S. J., and Yau, M. K., 2001. Simulation of blowing snow in the Canadian Arctic using a double-moment model. *Boundary-Layer Meteorology*, **99**, 297–316.

Fettweis, X., 2007. Reconstruction of the 1979–2006 Greenland ice sheet surface mass balance using the regional climate model MAR. *The Cryosphere*, **1**, 21–40.

Gallée, H., and Duynkerke, P., 1997. Air-snow interactions and the surface energy and mass balance over the melting zone of west Greenland during GIMEX. *Journal of Geophysical Research*, **102**, 13813–13824.

Grenfell, T. C., and Maykut, G. A., 1977. The optical properties of ice and snow in the Arctic basin. *Journal of Glaciology*, **18**, 445–463.

Greuell, W., 2000. Melt-water accumulation on the surface of the Greenland ice sheet: effect on albedo and mass balance. *Geografiska Annaler*, **82A**, 489–498.
Hatzianastassiou, N., Matsoukas, C., Hatzidimitriou, D., Pavlakis, C., Drakakis, M., and Vardavas, I., 2004. Ten year radiation budget of the Earth: 1984–93. *International Journal of Climatology*, **24**, 1785–1802.
King, J. C., and Connolley, W. M., 1997. Validation of the surface energy balance over the Antarctic ice sheets in the UK meteorological office unified climate model. *J Climate*, **10**, 1273–1287.
King, J. C., Argentini, S. A., and Anderson, P. S., 2006. Contrasts between the summertime surface energy balance and boundary layer structure at Dome C and Halley stations, Antarctica. *Journal of Geophysical Research*, **111**, D02105, doi:10.1029/2005JD006130.
Klok, E. J., and Oerlemans, J., 2002. Model study of the spatial distribution of the energy and mass balance of Morteratschgletscher, Switzerland. *Journal of Glaciology*, **48**, 505–518.
König-Langlo, G. C., and Loose, B., 2007. The meteorological observatory at Neumayer stations (GvN and NM-II). *Antarctica, Polarforschung*, **76**, 25–38.
Kuipers Munneke, P., van den Broeke, M. R., Reijmer, C. H., Helsen, M. M., Boot, W., Schneebeli, M., and Steffen, K., 2009. The role of radiation penetration in the energy budget of the snowpack at Summit, Greenland. *The Cryosphere*, **3**, 155–165.
Kuipers Munneke, P., Reijmer, C. H., and van den Broeke, M. R., 2010. Assessing the retrieval of cloud properties from radiation measurements over snow and ice. *International Journal Climatology*, doi:10.1002/joc.2114.
Mölg, T., Cullen, N. J., Hardy, D. R., Winkler, M., and Kaser, G., 2009. Quantifying climate change in the tropical mid troposphere over East Africa from glacier shrinkage on Kilimanjaro. *Journal of Climate*, **22**, 4162–4181.
Oerlemans, J., Giessen, R. H., and van den Broeke, M. R., 2009. Retreating alpine glaciers: increased melt rates due to accumulation of dust (Vadret da Morteratsch, Switzerland). *Journal of Glaciology*, **55**, 729–736.
Overland, J. E., McNutt, S. L., Groves, J., Salo, S., Andreas, E. L., and Persson, P. O. G., 2000. Regional sensible and radiative heat flux estimates for the winter Arctic during the Surface Heat Budget of the Arctic ocean (SHEBA) experiment. *Journal of Geophysical Research*, **105**, 14093–14102.
Persson, P. O. G., Fairall, C. W., Andreas, E. L., Guest, P. S., and Perovich, D. K., 2002. Measurements near the atmospheric surface flux group tower at SHEBA: near-surface conditions and surface energy budget. *Journal of Geophysical Research*, **107** (C10), 8045, doi:10.1029/2000JC000705.
Stull, R. B., 1988. *An introduction to boundary layer meteorology*. Dordrecht/Boston/London: Kluwer Academic Publishers, p. 666.
Uttal, T., Curry, J. A., McPhee, M. G., Perovich, D. K., Moritz, R. E., Maslanik, J. A., Guest, P. S., Stern, H. L., Moore, J. A., Turenne, R., Heiberg, A., Serreze, M. C., Wylie, D. P., Persson, O. G., Paulson, C. A., Halle, C., Morison, J. H., Wheeler, P. A., Makshtas, A., Welch, H., Shupe, M. D., Intrieri, J. M., Stamnes, K., Lindsey, R. W., Pinkel, R., Pegau, W. S., Stanton, T. P., and Grenfell, T. C., 2002. The surface heat budget of the Arctic. *Bulletin of the American Meteorological Society*, **83**, 255–275.
Van As, D., van den Broeke, M. R., and Helsen, M. M., 2006. Structure and dynamics of the summertime atmospheric boundary layer over the Antarctic plateau, I: measurements and model validation. *Journal of Geophysical Research*, **111**, D007102, doi:10.1029/2005JD005948.
Van den Broeke, M. R., Smeets, C. J. P. P., Ettema, J., van der Veen, C., van de Wal, R. S. W., and Oerlemans, J., 2008a. Partitioning of melt energy and meltwater fluxes in the ablation zone of the west Greenland ice sheet. *The Cryosphere*, **2**, 179–189.
Van den Broeke, M., Smeets, P., Ettema, J., and Munneke, P. K., 2008b. Surface radiation balance in the ablation zone of the west Greenland ice sheet. *Journal of Geophysical Research*, **113**, D13105, doi:10.1029/2007JD009283.
Van den Broeke, M. R., König-Langlo, G., Picard, G., Kuipers Munneke, P., and Lenaerts, J., 2009. Surface energy balance, melt and sublimation at Neumayer station, East Antarctica. *Antarctic Science*, doi:10.1017/S0954102009990538.
Wiscombe, W., and Warren, S., 1980. A model for the spectral albedo of snow I. Pure snow. *Journal of Atmospheric Sciences*, **37**, 2712–2733.

Cross-references

Albedo
Arctic Hydroclimatology
Atmosphere-Snow/Ice Interactions
Climate Change and Glaciers
Degree-Days
Dry Snow
Firn
Glacier Mass Balance
Heat and Mass Transfer in Sea Ice
Ice Sheet
Ice Shelf
Katabatic Wind: In Relation with Snow and Glaciers
Kilimanjaro
Latent Heat of Condensation
Latent Heat of Fusion/Freezing
Latent Heat of Sublimation
Melting Processes
Physical Properties of Snow
Sea Ice
Snow
Snow Density
Snow Drift
Surface Temperature of Snow and Ice
Temperature Profile of Snowpack

SURFACE TEMPERATURE OF SNOW AND ICE

Dorothy K. Hall
Crysopheric Sciences Branch, Greenbelt, MD, USA

Definition

Land-Surface Temperature (LST) – surface temperature measurement from space over land areas, including land ice and snow.

Introduction and background

Thermal infrared (TIR) sensors facilitate surface temperature and melt-condition monitoring over extensive areas of snow and ice (Key and Haefliger, 1992; Stroeve and Steffen, 1998; Comiso, 2006; Hall et al., 2006, 2008a, b), especially when used with complementary satellite-derived passive- and active-microwave data.

The surface temperature (T) is not an intrinsic property of the surface; it varies with external factors such as meteorological conditions. Emissivity *is* an intrinsic property

of the surface and is independent of the temperature (Hook et al., 2007). Emissivity of snow and ice features is far less variable than the range encountered in a wide variety of land surfaces, leading to greater potential accuracies in retrieved land-surface temperature (LST) over snow and ice even when the emissivity is not known precisely. To obtain snow-surface temperatures to an accuracy of 0.01 K, the emissivity must be known to within 0.1% (Stroeve et al., 1996).

Analysis of the Advanced Very High Resolution Radiometer (AVHRR)-derived surface temperature of the Antarctic and Greenland ice sheets, ice caps, and smaller glaciers, available from the early 1980s, provides a method to evaluate melt and general climate trends as a surrogate for, and in addition to, air-temperature records that are obtained from relatively few and scattered in-situ observations (Stroeve and Steffen, 1998; Wang and Key, 2003, 2005a, b; Comiso, 2006). Satellite-derived "clear-sky" surface-temperature data are also useful for the validation of climate models and as input to data-assimilation models. However, AVHRR data, though highly valuable, have been acquired from a variety of instruments over a period >20 years, leading to satellite intercalibration issues. Newer data from the Earth Observation System (EOS) offer promise for validating the overlapping AVHRR record and extending the surface-temperature record over ice-covered areas into the future at a higher spatial resolution with improved instrument calibration.

One way to assess the accuracy of remotely sensed LSTs is to compare the values with in-situ surface temperatures under clear-sky conditions (Hall et al., 2008b). Various factors make that problematic, including the fact that the in-situ observations are point measurements while the satellite-derived observations represent LSTs from a much larger area. Also, in-situ observations from weather stations, and in particular the Greenland Climate Net-work (GC-Net) automatic weather station (AWSs) (Box, 2002) which are generally acquired at some height above the surface so that the measured air temperature must be extrapolated to calculate a surface temperature. That calculation is also affected by meteorological factors such as wind speed, but for higher wind-speed conditions, when the near-surface air is well mixed, near-surface air temperature is very close to the surface temperature. Also the AWS instruments record in-situ data at a "point" while the satellite instruments record data over an area varying in size from: 57 × 57 m Enhanced Thematic Mapper Plus (ETM+), 90 × 90 m Advanced Spaceborne Thermal Emission and Reflection Radiometer (ASTER), or to 1 × 1 km Earth Observing System Moderate Resolution Imaging Spectroradiometer (MODIS). Surface topography and other factors contribute to variability of surface temperature within a pixel, thus the AWS measurements may not be representative of the LST of the pixel as a whole. Without more information on the local spatial patterns, the AWS LST cannot be considered valid ground truth for the satellite measurements, with RMS uncertainty ~2°C or greater (Hall et al., 2008b; Koenig and Hall, in press).

Satellite-derived "clear-sky" LST products were studied from EOS instruments including the MODIS (Wan et al., 2002), the ASTER (Gillespie et al., 1998), and the ETM+ (Barsi et al., 2005) over snow and ice on Greenland. Satellite-derived LSTs were compared with in-situ air-temperature observations from the GC-Net. Results showed that MODIS, ASTER, and ETM+ provide reliable and consistent LSTs under clear-sky conditions and relatively flat terrain over snow and ice targets over a range of temperatures from −40°C to 0°C. The satellite-derived LSTs agree within a relative RMS uncertainty of ~0.5°C. The good agreement among the LSTs derived from the various satellite instruments is especially notable since different spectral channels and different retrieval algorithms are used to calculate LST from the raw satellite data. However accuracies are lower when LSTs are compared with AWS measurements.

Summary

The accuracy of measuring the surface temperature of snow and ice has been assessed. Difficulties are encountered when attempting to validate satellite data covering a large area (e.g., 1 × 1 km) with a point measurement (e.g., using air temperature data from meteorological stations or AWS), but relative validation between EOS IR sensors has provided accuracies of LST measurements over snow and ice of <1°C. To develop a long-term record of "clear-sky" surface temperature, satellite intercalibration remains an issue.

Bibliography

Barsi, J. A., Shott, J. R., Palluconi, F. D., and Hook, S. J., 2005. Validation of a Web-based atmospheric correction tool for single thermal band instruments. In *Proceedings of SPIE*, 5822, SPIE, Bellingham, doi:10.1117/12.619990.

Box, J. E., 2002. Survey of Greenland instrumental temperature records: 1873–2001. *International Journal of Climatology*, **22**, 1829–1847.

Comiso, J. C., 2006. Arctic warming signals from satellite observations. *Weather*, **61**(3), 70–76.

Gillespie, A. R., Rokugawa, S., Matsunaga, T., Cothern, J. S., Hook, S., and Kahle, A. B., 1998. A temperature and emissivity separation algorithm for Advanced Spaceborne Thermal Emission and Reflection Radiometer (ASTER) images. *IEEE Transactions on Geoscience and Remote Sensing*, **36**, 1113–1126.

Gillespie, A., Rokugawa, S., Hook, S. J., Matsunaga, T., and Kahle, A. B., 1999. *The ASTER temperature/emissivity separation algorithm theoretical basis document* (ATBD-AST-03) Version 2.4.

Hall, D. K., Williams, R. S., Jr., Casey, K. A., DiGirolamo, N. E., and Wan, Z., 2006. Satellite-derived, melt-season surface temperature of the Greenland ice sheet (2000–2005) and its relationship to mass balance. *Geophysical Research Letters*, **33**, L11501, doi:10.1029/2006GL026444.

Hall, D. K., Williams, R. S., Jr., Luthcke, S. B., and DiGirolamo, N. E., 2008a. Greenland ice sheet surface temperature, melt and mass loss: 2000–2006. *Journal of Glaciology*, **54**(184), 81–93.

Hall, D. K., Box, J. E., Casey, K. A., Hook, S. J., Shuman, C. A., and Steffen, K., 2008b. Comparison of satellite-derived ice and snow surface temperatures over Greenland from MODIS, ASTER,

ETM+ and in-situ observations. *Remote Sensing of Environment*, **112**(10), 3739–3749, doi:10.1016/j.rse.2008.05.007.
Hook, S. J., Vaughan, R. G., Tonooka, H., and Schladow, S. G., 2007. Absolute radiometric in-flight validation of mid infrared and thermal infrared data from ASTER and MODIS on the Terra spacecraft using the Lake Tahoe, CA/NV, USA, Automated Validation Site. *IEEE Transactions Geoscience and Remote Sensing*, **45**, 1798–1807.
Key, J., and Haefliger, M., 1992. Arctic ice surface temperature retrieval from AVHRR thermal channels. *Journal of Geophysical Research*, **97**(D5), 5885–5893.
Koenig, L. S., and Hall, D. K., in press. Comparison of satellite, thermochron and air temperatures at Summit, Greenland, 1 during the winter of 2008-09. *Journal of Glaciology*.
Stroeve, J., and Steffen, K., 1998. Variability of AVHRR-derived clear-sky surface temperature over the Greenland ice sheet. *Journal of Applied Meteorology*, **37**, 23–31.
Stroeve, J., Haefliger, M., and Steffen, K., 1996. Surface temperature from ERS-1 ATSR infrared thermal satellite data in polar regions. *Journal of Applied Meteorology*, **35**(8), 1231–1239.
Wan, Z., Zhang, Y., Zhang, Q., and Li, Z.-L., 2002. Validation of the land-surface temperature products retrieved from Terra Moderate Resolution Imaging Spectroradiometer data. *Remote Sensing of Environment*, **83**, 163–180.
Wang, X., and Key, J., 2003. Recent trends in Arctic surface, cloud, and radiation properties from space. *Science*, **299**(5613), 1725–1728.
Wang, X., and Key, J., 2005a. Arctic surface, cloud, and radiation properties based on the AVHRR Polar Pathfinder dataset, Part I: Spatial and temporal characteristics. *Journal of Climate*, **18**(14), 2558–2574.
Wang, X., and Key, J., 2005b. Arctic surface, cloud, and radiation properties based on the AVHRR Polar Pathfinder data set, Part II: Recent trends. *Journal of Climate*, **18**(14), 2575–2593.

Cross-references

Albedo
Arctic Hydroclimatology
Temperature Profile of Snowpack

SUSPENDED SEDIMENT CONCENTRATION

Veerle Vanacker
TECLIM, Earth and Life Institute, University of Louvain, Louvain-la-Neuve, BW, Belgium

Definition

Suspended sediment is generally transported within and at the same velocity as the surrounding fluid (water or wind). The stronger the flow and/or the finer the sediment, the greater the amount of sediment that can be suspended by turbulence.

Only the finer fraction (usually silt and clay fraction) of the suspended sediment can be continuously maintained in suspension by the flow turbulence. This fraction is often referred to as "wash load," and is typically not found in significant quantities at the bed surface. Its concentration is usually related to the sediment supply and is difficult to determine theoretically.

Most sediment particles are not continuously suspended, but are continuously settling through the surrounding fluid and may eventually return to the bed. This part of the total suspended sediment is referred to as "bed-material load," and its concentration can be estimated from the hydraulic parameters of the fluid and the composition of the bed material.

History and current techniques

The first measurements of suspended sediment go back at least to the samplings of the Rhone River (France) in the early 1800s (Garcia, 2008). The earliest suspended sediment samples were collected using instantaneous samplers. Later, more sophisticated samplers were developed that could be filled at a selected depth below the water surface.

The first sediment sampling and analytical methods used to differ strongly between the various monitoring programs (Glysson and Gray, 1997). The creation of the Federal Interagency Sedimentation Project (FISP) was important to standardize sediment samplers, sampling, and analytical techniques around the world. At present, a large number of both manually operated samplers and automatic samplers exist. Information on the use and calibration of these samplers can be obtained from the Federal Interagency Sedimentation Project (FISP, 2009).

In addition to these suspended sediment samplers, rapid progress is being made in developing new techniques for measuring the concentration of suspended sediment in fluids. These new methods are commonly based on optical backscatter, optical transmission, focused beam reflectance, laser diffraction, acoustic, nuclear, spectral reflectance, digital optical, and differential pressure principles to capture specific characteristics of the sediment–fluid mixture (Wren et al., 2000). At the moment, several of these advanced techniques still suffer from technical limitations that render their operation difficult in some environments. Continued technological improvements will undoubtedly lead to improved methods to collect data on suspended sediment concentration in the future.

Factors controlling variations in suspended sediment concentration

There is now a wealth of information from case studies worldwide that exemplify the large temporal and spatial variation that exists in suspended sediment concentration. It is becoming increasingly clear that variations in suspended sediment concentrations cannot be explained by natural biophysical factors only such as climate, geology, or topography.

Various studies have clearly shown that sediment fluxes from anthropogenically altered catchments are significant (Walling, 2006). Research at different spatial scales has indicated that humans have accelerated sediment production by agricultural activities, road construction, and intense logging, but have reduced the global sediment delivery to the oceans because of sediment retention in

reservoirs (Hooke, 2000; Syvitski et al., 2005; Vanacker et al., 2007).

In addition to global-scale analyses, simultaneous research on small catchments may contribute to yield complementary information on suspended sediment dynamics that would be difficult to obtain exclusively through large catchment studies.

Conclusions

In recent years, new techniques have been developed that will provide us a wealth of data on suspended sediment concentrations at spatial and temporal resolutions much higher than previously possible. In the future, this information will undoubtedly contribute to better understand the role of anthropogenic disturbances and climate change on terrestrial sediment fluxes.

Bibliography

Federal Interagency Sedimentation Project (FISP), 2009. Federal Interagency Sedimentation Project Home Page. (http://fisp.wes.army.mil, April 2009).

Garcia, M. H., 2008. *Sedimentation engineering: processes, management, modeling and practice.* ASCE Manual and Reports on Engineering Practice No. 110, American Society of Civil Engineers (ASCE).

Glysson, G. D., and Gray, J. R., 1997. Coordination and standardization of federal sedimentation activities. In *Proceedings of the U.S. Geological Survey Sediment Workshop*, Expanding sediment research capabilities in Today's USGS, Reston, Virginia, and Harpers Ferry, West Virginia, February 4–7, 1997. (http://water.usgs.giv/osw/techniques/workshop/glysson.html)

Hooke, R. Le. B., 2000. On the history of humans as geomorphic agents. *Geology*, **28**, 843–846.

Syvitski, J. P. M., Vorosmarty, C. J., Kettner, A. J., and Green, P., 2005. Impacts of humans on the flux of terrestrial sediment to the global coastal ocean. *Science*, **308**, 376–380.

Vanacker, V., Molina, A., Govers, G., Poesen, J., and Deckers, J., 2007. Spatial variation of suspended sediment concentrations in a tropical Andean river system: The Paute river, southern Ecuador. *Geomorphology*, **87**, 53–67.

Walling, D. E., 2006. Human impact on land-ocean sediment transfer by the world's rivers. *Geomorphology*, **79**, 192–216.

Wren, D. G., Barkdoll, B. D., Kuhnle, R. A., and Derrow, R. W., 2000. Field techniques for suspended-sediment measurement. *J Hydraul Eng*, **126**, 97–104.

Cross-references

Sediment Yield
Suspended Sediment Dynamics

SUSPENDED SEDIMENT DYNAMICS

Tim Stott
Physical Geography and Outdoor Education, Liverpool John Moores University, Liverpool, UK

Definition

Suspended sediment. The fine portion of a river or stream's sediment load which is normally carried in suspension. Suspended sediment is usually finer than 2 mm, although this boundary can vary significantly according to the stream's power and turbulence.

Dynamics. The branch of mechanics that deals with the motion and equilibrium of systems under the action of forces, usually from outside the system.

Introduction

Glaciers alternate between phases of accumulation and ablation. It is during ablation phases that most meltwater is discharged from glaciers. Even at low discharges, the meltwater is usually capable of entraining and transporting fine sediment in suspension. The dominant trend over the past few decades is that most glaciers worldwide are out of equilibrium with the current climate and they are slowly adjusting to seasonal changes in precipitation and higher temperatures by showing negative mass balance, significant volume loss, and retreat in most areas. In terms of landscape dynamics, this widespread and rapid retreat of mountain glaciers is revealing new expanses of fresh glacial debris, the stability, dynamics, and potential fluvial transport of which is beginning to gain the attention of research scientists. Meltwater streams and rivers draining glaciers and flowing across the fore field are called pro-glacial streams. Due to the large supply of sediment deposited beneath and in front of glaciers, pro-glacial streams can have high suspended sediment concentrations (SSC) during the peak (summer) melt season and during rainstorms. They are capable of transporting high suspended sediment loads.

Measurement methods

The most common approach to measuring suspended sediment dynamics in pro-glacial streams relies on retrieving discrete water samples at-a-point over time. This can be achieved by lowering a wide-mouthed bottle (usually 1 L capacity) into the flow and retrieving it when full. The highly turbulent nature of the flow usually means that suspended sediment is extremely well mixed and that values sampled at the stream margin will be representative of the whole cross section (see Gurnell et al., 1992). Water samples are then passed through pre-weighed filters (these are normally glass fiber such as Whatman GF/D 8 μm filters) on which the suspended sediment in the water sample is retained. Filters are then oven dried, and the filter plus dry sediment are weighed. The difference in the pre- and post-weight of the filter is due to the suspended sediment in the water sample. The weight of sediment divided by the volume of the water sample gives the SSC which is reported in mg/L. This method is known as the gravimetric method. However, in order to gain any meaningful understanding of suspended sediment dynamics, samples taken at a minimum of 3-hourly intervals are necessary, and most researchers reduce this time to 1 h or less if possible, which can be very labor intensive. Therefore, automatic pumping samplers (Figure 1) are used to


a


b

Suspended Sediment Dynamics, Figure 1 (**a**) Suspended sediment and discharge gauging site with stage board and ISCO automatic water sampler used to retrieve samples from Castle Creek draining the Roberts glacier, Cariboo Mountains, British Columbia with Roberts glacier in background (photo: Tim Stott). (**b**) Researchers filtering water samples retrieved by an ISCO automatic water sampler at Castle Creek which drains the Roberts glacier in background, Cariboo Mountains, British Columbia in summer 2008 (photo: Tim Stott).

Suspended Sediment Dynamics, Figure 2 Glass fiber 7 cm diameter filters which have been used to remove suspended sediment from a sequence on 1-hourly water samples collected in the Torrent du Glacier Noir, Ecrins National Park in SE France during July 2003. NB. The first sample (*top left*) was taken at 14:00 on day 1 and the last (*bottom right*) at 13:00 on day 2. The *top* row (14:00–17:00 on afternoon of day 1) and *bottom* rows (10:00–13:00 on day 2) show much higher SSCs as these will have coincided with times of highest discharge.

automatically pump water samples from the river via a 5–6 m tube (Figure 1a) into a series of 24 bottles (Figure 1b). The sampler is battery powered and the time interval at which samples are pumped can be determined by the operator. Figure 2 shows 24 filters which were collected from an Alpine pro-glacial torrent.

Since stream discharge has been shown to exert an important control over suspended sediment dynamics, this is normally measured at the same time that water samples are retrieved, or maybe even at greater frequency by means of electronic water level sensors such as a pressure transducer. The relationship between SSC and discharge (Q) shown in Figure 3 is known at a rating curve where $SSC = aQ^b$, where a and b are constants representing the intercept and slope of the rating plot, respectively.

Turbidity has successfully been used as a surrogate for SSC in pro-glacial streams (Clifford et al., 1995; Hodgkins, 1999; Irvine-Fynn et al., 2005; Stott and Mount, 2007a, b; Stott et al., 2008). Partech infrared (IR15C) 0–10,000 mg/L range turbidity sensors are a popular choice (Figure 4).

Turbidity sensors, such as the one shown in Figure 4, work by emitting a beam of light which is detected by a photoelectric cell on the opposite side of a gap. The instrument produces a voltage output which is proportional to the amount of light received by the light sensor. When the instrument is deployed in a stream, the proportion of the emitted light which is received by the light sensor is deemed to be proportional to the color or SSC of the stream water. The voltage output is logged by a data logger at any predetermined time interval (e.g., 10 s to 10 min) giving a far greater insight into the dynamics of the suspended sediment. However, in order to make useful meaning of the turbidity voltage data, gravimetrically determined samples are needed in order to calibrate the voltage output of the turbidity sensor (Figure 5).

The turbidity reading is sensitive to the particle size of the suspended sediment passing through the sensor gap which can scatter the light in different ways, hence the less-than-perfect relationship on Figure 4. So, the use of turbidity in pro-glacial streams can be a useful application to gain a more detailed picture of the suspended sediment

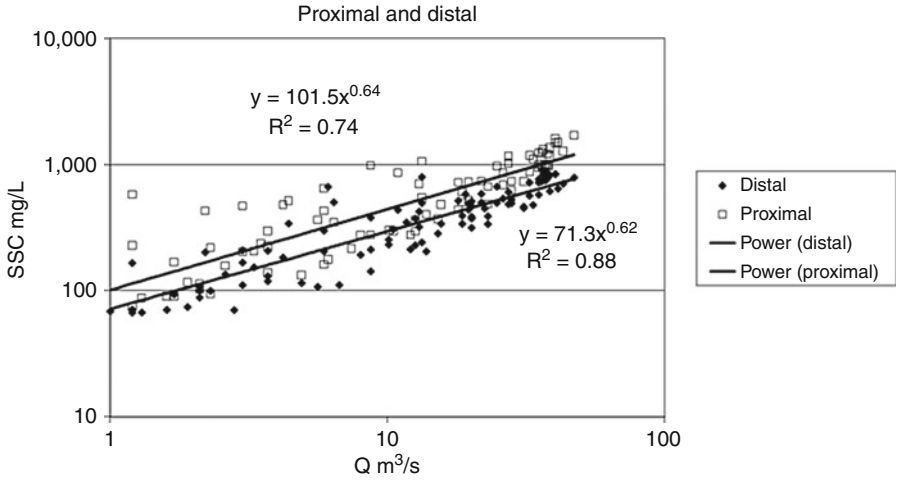

Suspended Sediment Dynamics, Figure 3 Suspended sediment concentration vs discharge rating relationship for proximal (50 m from glacier snout) and distal (600 m from glacier snout) sampling stations in the Ova da Morteratsch, Switzerland (From Stott et al., 2008).

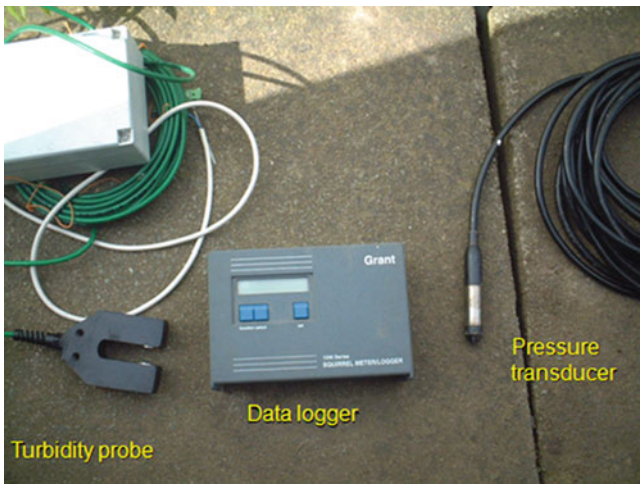

Suspended Sediment Dynamics, Figure 4 Partech turbidity sensor, data logger, and pressure transducer (photo: T. Stott).

dynamics, but it has limitations due to the difficulties of obtaining strong-enough calibration relationships.

Time series investigations

Figure 6 shows a typical time series plot for discharge and SSC predicted from turbidity sensors at two pro-glacial monitoring stations.

The predicted SSC record (Figure 6), while broadly responding to discharge fluctuations, shows SSC to be erratic, particularly at the proximal station. Some of the SSC peaks coincide with discharge peaks but others do not, suggesting that factors other than discharge are controlling SSC variations. One clear diurnal pattern is that discharge minimum consistently occurs at 09:10 each morning, after which it rises rapidly until it peaks sometime between 13:50 (e.g., 8 July) and 18:40 (e.g., 7 July), which seems to depend on the weather conditions (in particular air temperature). The SSC records behave differently, with proximal SSC behaving much more erratically, with greater variation, than the smoother less variable distal SSC. Nevertheless, diurnal variations are clear at both locations. Prior to 12 July, SSC at both stations rises and falls in response to discharge, until a cold weather spell on the night of 9–10 July occurred, when air temperature dropped to almost 0°C followed by cool days on 10 and 11 July causing discharge and SSC to fall. Some rain also fell on 9 and 10 July when daily totals of 24.8 and 1.8 mm were recorded. Warmer temperatures returned on 12 July after which peak discharge climbed steadily each day and a clear SSC exhaustion effect begins to appear. This can be seen clearly in Figure 5 where, following the minimum discharge at 09:10 in the morning, proximal SSC would fall and remain low for up to 6 h, not regaining its 09:10 am level until mid-afternoon, while distal SSC would start and continue to rise from 09:10 am with discharge. This suggests that the suspended sediment source during the morning and early afternoon was the pro-glacial area itself, whereas by mid-afternoon the proximal SSC would overtake the distal SSC suggesting that the suspended sediment source had now switched to the subglacial meltwater once the glacier had started to melt and the supra-, en-, and subglacial conduits had begun to flow. However, despite increasing air temperatures in the latter part of the record (13–19 July), SSC peaks in both proximal and distal records became progressively lower suggesting that the available sediment supply, apparent in the early part of the record, had become exhausted.

Figure 7 shows three examples of hydrographs and sedigraphs (generated using 5-min turbidity data) plotted using data gathered by Stott and Grove (2001) in the

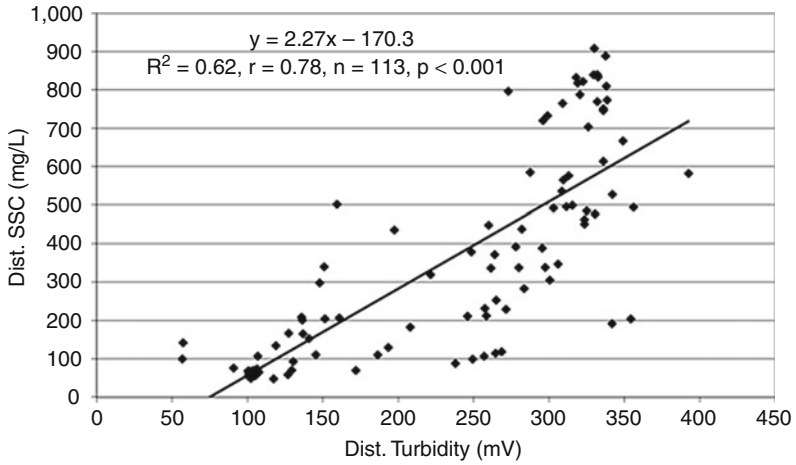

Suspended Sediment Dynamics, Figure 5 Suspended sediment concentration vs turbidity voltage calibration curve for Ova da Morteratsch, Bernina Alps, Switzerland after Stott et al. (2008). Note the large degree of scatter in the relationship.

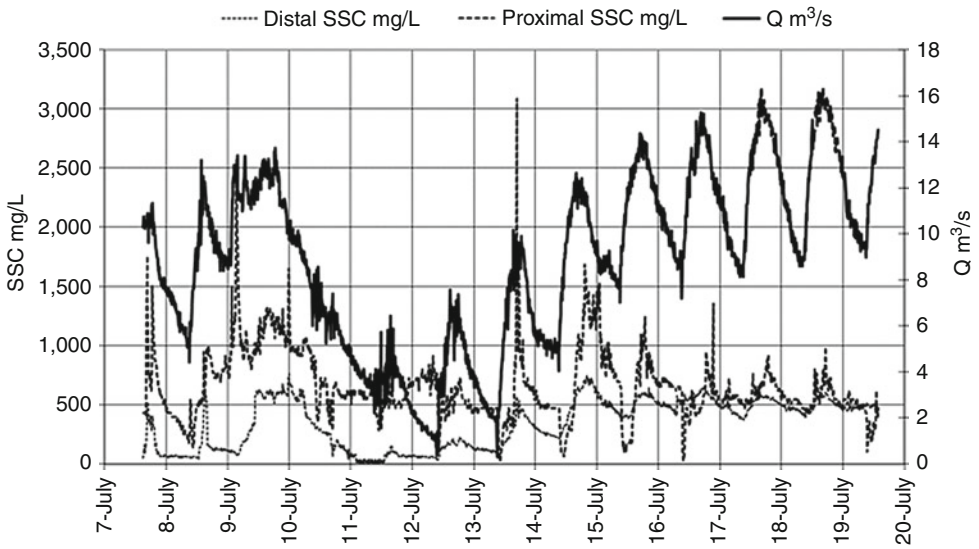

Suspended Sediment Dynamics, Figure 6 Time series plot for discharge and suspended sediment concentration predicted from turbidity sensors at two monitoring stations in the pro-glacial zone of the Morteratsch glacier, Switzerland in July 2007. The proximal station is 50 m from glacier snout, and the distal station is 600 m from the glacier snout (From Stott et al., 2008).

Skeldal River, NE Greenland in the 1998 melt season. At the same monitoring station during the study in August, SSC peaks before (Figure 7a), at the same time as (Figure 7b), and after the main hydrograph peak (Figure 7c).

This means that SSC can have very different values depending on which part of the hydrograph is being examined. For example, in Figure 7a, at a stage of 35 cm on the rising limb of the hydrograph SSC is 750 mg/L whereas when stage is 35 cm on the falling limb, around 10 h later, SSC is 550 mg/L. Where SSC can have different values at the same stage or discharge is known as the hysteresis effect.

Hysteresis

Figure 8 shows two examples of hysteresis loops in the SSC vs Q relationship in the Torrent du Glacier Noir, SE France (data from Stott and Mount, 2007a). Clearly, there is a large amount of scatter in the SSC vs Q relationship during both hydrographs.

However, when the sampling sequence is identified by numbers and the points are traced sequentially by arrows,

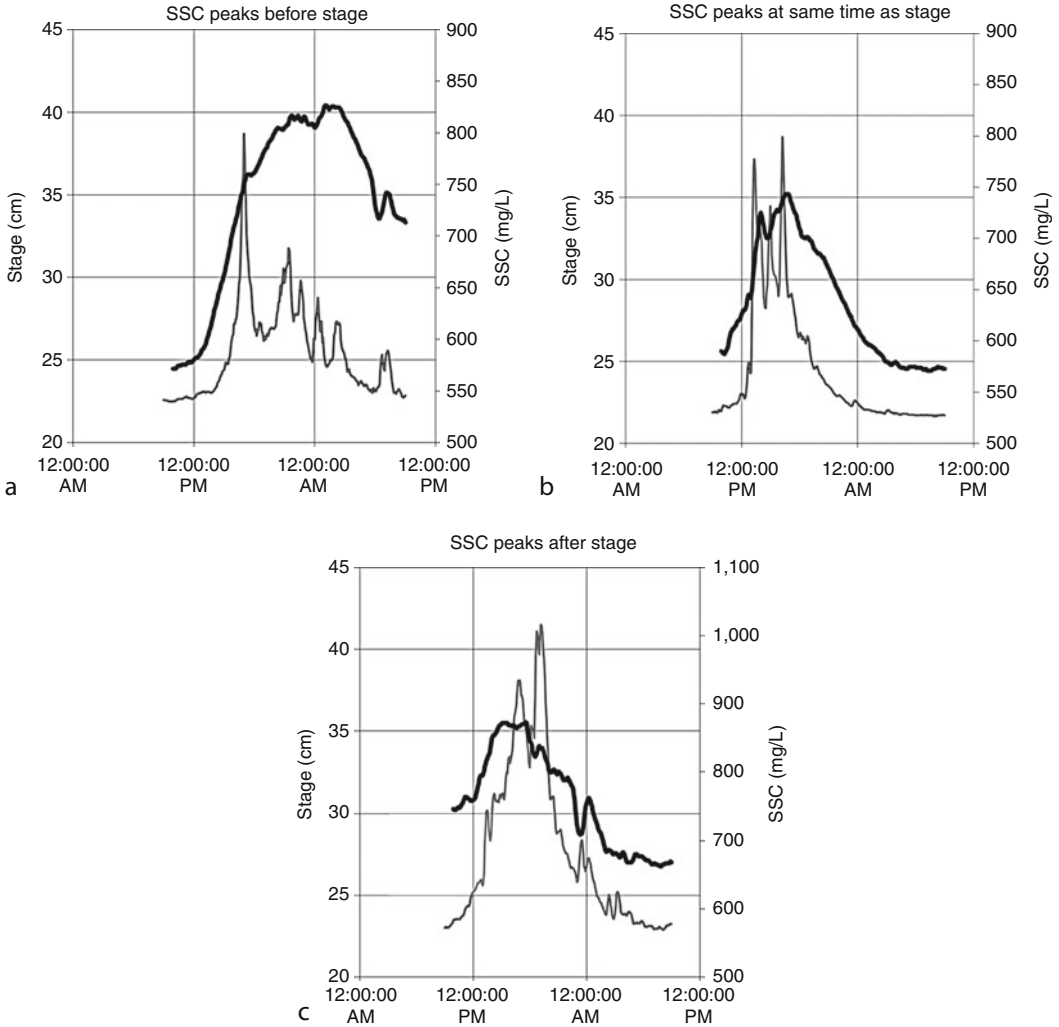

Suspended Sediment Dynamics, Figure 7 River stage (black line) and suspended sediment concentration (gray line) time series plots for the Skeldal River, NE Greenland (5-min data from a study by Stott and Grove, 2001), August 1998.

the loop nature of the hysteresis effect is visible in each of the flood events on 11 and 12 July 2003. While the loops are not perfect (they cross-over), the generally clockwise loop on 11 July (Figure 8a) suggests that SSC peaked before Q, whereas the anticlockwise loop in 12 July (Figure 8b) suggests that SSC peaked after Q.

Current investigations, controversies, and gaps in current knowledge

Future changes in pro-glacial suspended sediment dynamics are likely given the generally agreed forecasts for global warming this century (IPCC, 2007) and the likely continued retreat of glaciers. The consequences are likely to have greatest impact in the less economically developed parts of the world like the Himalaya (Singh et al., 2004) where changes in inputs of sediments to glacier-fed rivers have important implications for water abstraction and drinking water supply. Hydropower (HEP), large and small, is one of the most important of the renewables for electrical power production worldwide, providing 19% of the world's electricity (Paish, 2002) and set to increase. Small-scale hydro which draws water directly from streams and rivers with no dam or water storage, is one of the most cost-effective and environmentally benign energy technologies to be considered for rural electrification in less developed countries. Paish (2002) reports that the European Commission has a target to increase small hydro capacity by 4500 MW (50%) by the year 2010, and notes that turbines need to be protected from all the debris commonly found in rivers. Sediment entering intake pipes can be highly abrasive to turbines resulting in high maintenance and/or repair costs. A better understanding of sediment dynamics, and the likely future, will be important to HEP operators as it will allow planning of sediment flushing events and water intake at times when suspended sediment loads are likely to have least impact.

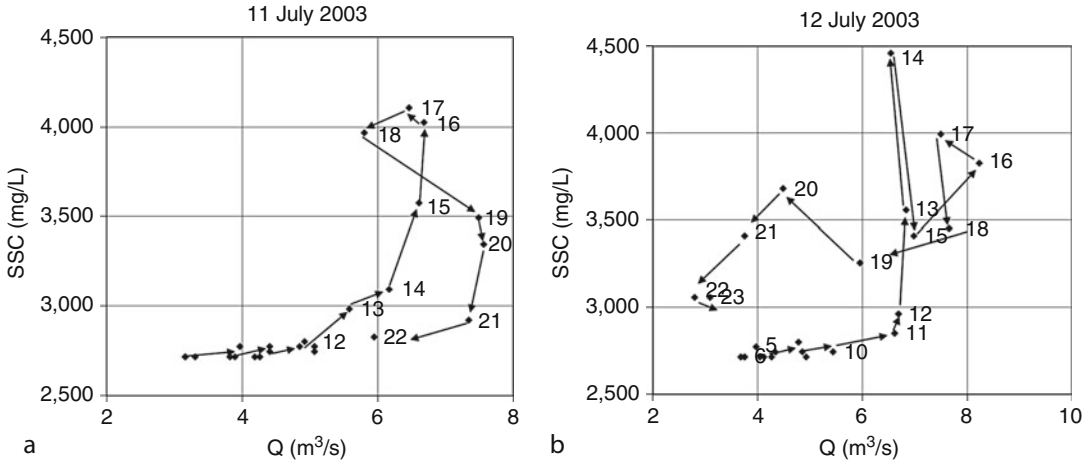

Suspended Sediment Dynamics, Figure 8 Examples of hysteresis loops in the SSC vs Q relationship for 1-hourly samples in the Torrent du Glacier Noir, SE France (data from Stott and Mount, 2007a), (**a**) clockwise on 11 July 2003, (**b**) anticlockwise on 12 July 2003.

High suspended sediment loads from mountain regions can result in sedimentation in lowland rivers which may affect stream ecology. Silt can clog river-bed gravels (Petticrew and Biickert, 1998), which in certain reaches contain salmon spawn so depriving the eggs of vital oxygen, thus jeopardizing successful salmon reproduction. River sedimentation can also impact channel dynamics in lowland river systems by causing decreases in channel capacity which can increase flood potential and lateral erosion, and may require expensive river dredging programs to avert such problems (Owens et al., 2005).

Summary

Suspended sediment dynamics is concerned with the motion and equilibrium of the fine portion of a river or stream's sediment load which is normally carried in suspension. Most meltwater is discharged from glaciers during ablation phases, and even at low discharges the meltwater is usually capable of entraining and transporting fine sediment in suspension, and at peak discharges pro-glacial streams are capable of transporting extremely high suspended sediment loads.

Changes in SSC are measured by collecting water samples in sequence at-a-point over time, then filtering the water through special glass fiber filters and measuring the weight change, known as the gravimetric method. Samples can be retrieved manually by dipping an empty bottle into the flow, or automatically using pumping samplers. Scatter plots of SSC vs Q are known as rating relationships. Turbidity can be used as a surrogate for SSC and has the advantage of being able to automatically scan at high frequency and log voltages to a data logger. However, SSC vs turbidity calibration relationships in pro-glacial streams, like SSC vs Q, tend to be less than perfect. Nevertheless, they can reveal patterns which might otherwise be missed by water sampling programs, and thereby aide interpretation of suspended sediment dynamics in pro-glacial streams. Examination of time series datasets from NE Greenland for SSC and Q show asynchronous SSC and Q patterns, with SSC peaking before, at the same time, and after the hydrograph peak in different flood events. A hysteresis effect in the SSC vs Q rating relationship is demonstrated for the Torrent du Glacier Noir in SE France.

Future changes in pro-glacial suspended sediment dynamics are likely given the generally agreed forecasts for global warming this century. The consequences are likely to be greatest in the less economically developed parts of the world like the Himalaya where glacier-fed rivers supply a high proportion of drinking water. Elsewhere, hydroelectricity generation often relies on abstracting water from glacier-fed rivers and changes in suspended sediment dynamics will have important implications for the timing and amount of abstraction since sediment-laden water causes problems concerned with increased abrasion and scour of pipes and turbines. Silt from pro-glacial zones can clog river-bed gravels downstream where certain reaches contain salmon spawn so depriving the eggs of vital oxygen, thus jeopardizing successful salmon reproduction. River sedimentation can also impact channel dynamics in lowland river systems by causing decreases in channel capacity which can increase flood potential and lateral erosion, and may require expensive river dredging programs to avert such problems.

Bibliography

Clifford, N. J., Richards, K. S., Brown, R. A., and Lane, S. N., 1995. Scales of variation of suspended sediment concentration and turbidity in a glacial meltwater stream. *Geografiska Annaler*, **77A**(1–2), 45–65.

Gurnell, A. M., Clark, M. J., Hill, C. T., and Greenhalgh, J., 1992. Reliability and representativeness of a suspended sediment concentration monitoring programme for a remote alpine proglacial river. In Bogen, J., Walling, D. E., and Day, T. (eds.), Erosion and Sediment Transport Monitoring in River Basins. *Proceedings of the Oslo Symposium* 24–28 August

1992, International Association of Hydrological Sciences Publication, 210, 191–200.
Hodgkins, R., 1999. Controls on suspended sediment transfer at a High-Arctic glacier determined from statistical modelling. *Earth Surface Processes and Landforms*, **24**(1), 1–21.
Hodgkins, R., Cooper, R., Wadham, J., and Tranter, M., 2003. Suspended sediment fluxes in a high-Arctic glacierised catchment: implications for fluvial sediment storage. *Sedimentary Geology*, **162**, 105–117.
IPCC. 2007. *Climate Change 2007: The Physical Science Basis, Contribution of Working Group I to the Fourth Assessment Report of the Intergovernmental Panel on Climate Change*. Fourth Assessment Report of the Intergovernmental Panel on Climate Change, Cambridge University Press. Available at http://www.ipcc.ch/ [accessed 21-10-07].
Irvine-Fynn, T. D. L., Moorman, B. J., Willis, I. C., Sjogren, D. B., Hodson, A. J., Mumford, P. N., Walter, F. S. A., and Williams, J. L. M., 2005. Geocryological processes linked to high Arctic proglacial stream suspended sediment dynamics: examples from Bylot Island, Nunavut, and Spitsbergen, Svalbard. *Hydrological Processes*, **19**(1), 115–135.
Owens, P. N., Batalla, R., Collins, A. J., Gomez, B., Hicks, D. M., Horowitz, A. J., Kondolf, G. M., Marden, M., Page, M. J., Peacock, D. H., Petticrew, E. L., Salomons, W., and Trustrum, N. A., 2005. Fine-grained sediment in river systems: environmental significance and management issues. *River Research and Applications*, **21**, 693–717.
Paish, O., 2002. Small hydro power: technology and current status. *Renewable & Sustainable Energy Reviews*, **6**(6), 537–556.
Petticrew, E. L., and Biickert, S. L. 1998. Characterization of sediment transport and storage in the upstream portion of the Fraser River (British Columbia, Canada). In Modeling Soil Erosion, Sediment Transport and Closely Related Hydrological Processes (*Proceedings of a Symposium held al Vienna*, July 1998). International Association of Hydrological Sciences Publication, **249**, 383–391.
Singh, P., Haritashya, U. K., Ramasastri, K. S., and Kumar, N., 2004. Diurnal variations in discharge and suspended sediment concentration, including runoff-delaying characteristics, of the Gangotri glacier in the Garhwal Himalayas. *Hydrological Processes*, **19**(7), 1445–1457.
Stott, T. A., and Grove, J. R., 2001. Short-term discharge and suspended sediment fluctuations in the proglacial Skeldal River, N. E. Greenland. *Hydrological Processes*, **15**, 407–423.
Stott, T. A., and Mount, N. J., 2007a. Alpine proglacial suspended sediment dynamics in warm and cool ablation seasons: implications for global warming? *Journal of Hydrology*, **332**(3–4), 259–270.
Stott T. A., and Mount, N. J., 2007b. The Impact of Rainstorms on Short-Term Spatial and Temporal Patterns of Suspended Sediment Transfer over A Proglacial Zone, Ecrins National Park, France, in Effects of River Sediments and Channel Processes on Social, Economic and Environmental Safety. In *Proceedings of the Tenth International Symposium on River Sedimentation*, Vol. V, River Sediment in the Environment: 259–266. Moscow. 1–4, August 2007.
Stott, T. A., Nuttall, A., Eden, N., Smith, K., and Maxwell, D., 2008. Suspended sediment dynamics in the Morteratsch proglacial zone, Bernina Alps, Switzerland. *Geografiska Annaler Series A Physical Geography*, **90**(4), 299–313.

Cross-references

Glacier Hydrology
Suspended Sediment Concentration
Suspended Sediment Load

SUSPENDED SEDIMENT LOAD

Amit Kumar
Department of Geology, Centre of Advanced Study in Geology, Punjab University, Chandigarh, India

Synonyms

Wash load

Definition

Almost all the world's streams carry sediment that originates from erosion processes in the basin that feed the streams. Sediment carried in a stream is classified as either suspended load or bed load. The suspended load is the fine-grained (clay and silt) sediment that remains in water during transportation. The bed load consists of the coarser fractions of the sediment (sands and gravels), moves by rolling, sliding, or saltation actions. Coarser sediments will be deposited first and suspended sediment load moves at approximately with the same velocity of the flowing water. From the general point of view, river is a main component of global water cycle and it plays an important role to transport sediment and other matter into the ocean (Garrels et al., 1975; Martin and Meybeck, 1979). In Himalayas, three major river systems: the Ganga, the Brahamputra, and Indus delivered a combined suspended sediment load of the order of 1.8×10^9 ton/year (Meybeck, 1976), which is about 9% of the total annual load carried from the continent to the oceans worldwide. Suspended sediment load can be satisfactory assessed directly from discharge and sediment concentration. Suspended sediment records are also used to estimating erosion rates in mountainous region, where the eroded material is transported as a sediment load.

Bibliography

Benn, D. I., and Evans, D. J. A., 1998. *Glaciers and Glaciation*. London: Arnold.
Garrels, R. M., Mackenzie, F. T., and Hunt, 1975. *Chemical Cycle and the Global Environment*. New York: William Kaufman. 260 pp.
Hambrey, M., and Alean, J., 2004. *Glaciers*, 2nd edn. New York: Cambridge University Press.
Lenzi, M. A., D' Agostino, V., and Billi, P., 1999. Bed-load transport in the instrumented catchment of the Rio Cordon: Part1. Analysis of bed-load records, condition and threshold of bad-load entrainment. *Catena*, **36**, 171–190.
Martin, J. M., and Meybeck, M., 1979. Elemental mass-balance of material carried by major world rivers. *Marine Chemistry*, **7**, 173–206.
Meybeck, M., 1976. Total mineral dissolved transport by world major rivers. *Hydrological Science Bulletin*, **21**, 265–284.
Milliman, J. D., and Meade, R. H., 1983. World-wide delivery of river sediment to the oceans. *Journal of Geology*, **91**, 1–21.

Cross-references

Sediment Entrainment, Transport, and Deposition
Suspended Sediment Load

SYNTHETIC APERTURE RADAR (SAR) INTERFEROMETRY FOR GLACIER MOVEMENT STUDIES

Y. S. Rao
Centre of Studies in Resources Engineering, Indian Institute of Technology, Powai, Mumbai, India

Synonyms

Mapping glacier movement

Definition

Glaciers move due to their own weight and the influence of gravity. Information about the movement of the glacier is very important for understanding the climate change, mass balance, and glacier dynamics. The movement can be measured using surveying techniques (stakes and theodolite), laser ranging, and global positioning systems. All these techniques are confined to a point measurement and consumes time and expensive to measure over large inaccessible and inhospitable areas. Remote sensing techniques are very useful and cost effective to map those areas for glacier movement. Synthetic Aperture Radar Interferometry (InSAR) is a powerful technique for measuring the glacier velocity and strain rate (velocity gradient) with centimeter accuracy. In this technique, the phase difference of two or more SAR images acquired from slightly different orbit positions or view angles and at different times is exploited to obtain topography and surface change due to earthquake, volcano, land subsidence, and glacier velocity mapping.

Introduction

InSAR is widely used to map the velocity of glaciers in Antarctica (Goldstein et al., 1993; Frolich and Doake, 1998) and Greenland (Joughin et al., 1995, 1996; Kwok and Fannestock, 1996; Rignot et al., 1995). However, its applicability to map the velocity of temperate glaciers is challenging due to steep topography, melting of snow, and atmospheric changes between two SAR acquisitions. In spite of these difficulties, InSAR was successfully applied to map the velocity of the temperate and alpine glaciers using ERS-1 and 2 SAR tandem data. The advantage with tandem data is that ERS-1 and 2 satellites with similar SAR system acquired data with a 1-day interval between August 1995 and June 1996. Within a 1-day interval, glacier velocity in many parts of the glacier except at terminus is less than the prescribed limit. The upper limit on differential displacement occurs when the phase change is equal to phase sampling rate in range (Vachon et al., 1996). It means that the change in displacement between adjacent resolution cells must be less than $\lambda/2$. This condition sets the upper limit for the detectable velocity gradient. For example, when ice blocks move more than $\lambda/2$ from one resolution cell to the next, phase cycles are no longer detectable on interferogram and phase unwrapping is impossible. However, if the scene coherence is retained, there is no upper limit on absolute displacement measurement. In order to retain the scene coherence, the upper limit on displacement would be roughly half the resolution cell. For ERS system, the value is 4.8 m/day as the slant range resolution is 9.6 m.

Repeat pass InSAR

Glacier velocity can be mapped using 2-pass and 3-pass differential SAR interferometric (DInSAR) techniques. In 2-pass technique, one image is acquired before an event (earthquake, volcano eruption, land subsidence, landslides, glacier movement, etc.) and another one after an event. A typical SAR interferometer is an extension of famous two slit Young's experiment and is shown in Figure 1a. The phase difference between the two images (i.e., interferogram phase) containing both topography and displacement phase can be written as (Rosen et al., 2000, Massonnet and Feigl, 1998; Madsen and Zebker, 1998)

$$\Delta\phi = -\frac{4\pi}{\lambda}\frac{B_n \delta h}{r \sin\theta} + \frac{4\pi}{\lambda}\delta r \tag{1}$$

where $\Delta\phi$ is the interferogram phase after correcting for flat earth surface phase, B_n is perpendicular baseline, δh is altitude difference between two point targets, λ is the wavelength of the SAR system used, θ is the SAR signal incidence angle, r is slant range distance, and δr is the displacement between the two scene acquisitions.

In order to obtain the displacement due to glacier motion, the first term in Equation 1 representing topography phase is to be removed. For this, one has to obtain the accurate topography information. In February 2000, shuttle radar topography mission (SRTM) flew around the globe for around 11 days and collected digital elevation models (DEMs) of the earth surface except the area around north and south poles. The DEMs derived from the SRTM data are freely available to the public. Using orbital parameters of the two SAR scenes and SRTM digital elevation models, synthetic phase corresponding topography can be obtained. The synthetic phase is subtracted from interferogram to get the differential interferogram, representing only phase due to displacement map. After removing the phase due to topography, the Equation 1 becomes

$$\Delta\phi_{\text{defo}} = \frac{4\pi}{\lambda}\delta r \tag{2}$$

From this equation, displacement corresponding to one phase cycle ($\Delta\phi_{\text{defo}} = 2\pi$, i.e., one fringe in differential interferogram) yields $\lambda/2$. This value for ERS-1&2 is 2.8 cm, SIR-C L-band is 12 cm, and TerraSAR-X is 1.5 cm. The entire procedure for obtaining displacement is shown in Figure 1b.

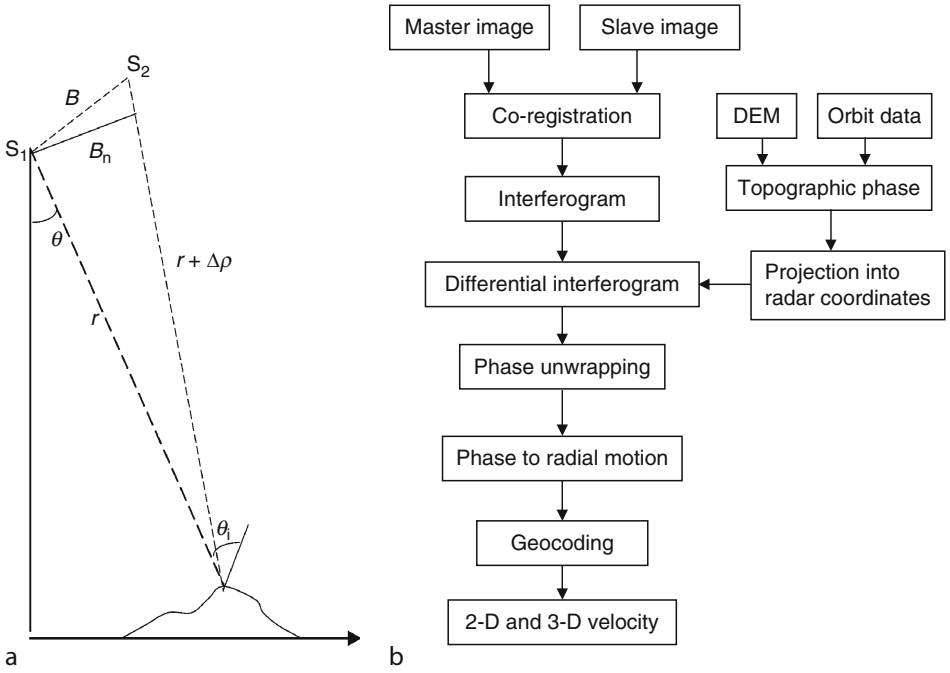

Synthetic Aperture Radar (SAR) Interferometry for Glacier Movement Studies, Figure 1 (**a**) Geometric configuration for InSAR and (**b**) flow diagram for 2-pass differential InSAR for glacier movement.

For typical ERS-1&2 SAR parameters λ = 5.6 cm, r = 850 km, θ = 23° baseline B_n=100 m, the first term (topographic) in Equation 1 becomes

$$\Delta\phi_{\text{topo}} = -0.06756\,\delta h \tag{3}$$

From this equation, the topographic height δh per one phase cycle ($\Delta\phi_{\text{topo}} = 2\pi$) becomes $\delta h = 93$ m. By comparing differential and topographic values, we can say that differential interferometry is 3,321 times greater sensitivity than topography. However, this sensitivity depends on the baseline value and decreases with increasing baseline. That is why DInSAR is better for lower baseline values. If DEM has some error of 30 m, then the error in displacement is about 1 cm (30 m/3,321 ≈ 1 cm).

Error in the baseline also creates an error in differential phase (Vachon et al., 1996). For ERS-1&2 tandem data, the error is about 0.4 cm/day. In addition to these topography and baseline-related errors, atmospheric changes will also affect the accuracy of displacement map (Zebker et al., 1997).

3-pass DInSAR is not useful for mapping the displacement map of temperate glaciers due to large interval (35 days) between two passes and melting of snow. However, this technique was applied by Kwok and Fannestock (1996) and Joughin et al. (1995) with several ERS SAR datasets over Greenland acquired with a 3-day interval to remove motion effects and obtain the topography. In this method, minimum three SAR images are required to form two interferograms. It is important to note that motion should be uniform throughout the acquisition period. By taking the difference of the two interferograms, motion is canceled and the resultant differential phase represents the topography. With this topography information, glacier motion can be obtained after removing the topography-related phase from the interferogram.

Phase coherence

For the analysis of glacier movement using InSAR, information about phase coherence is very important. In the interferometry processing, coherence is one of the products of InSAR technique. Interferometric complex correlation can be written as (Rosen et al., 2000)

$$\gamma = \frac{\langle g_1 g_2^* \rangle}{\sqrt{\langle |g_1|^2 \rangle \langle |g_2|^2 \rangle}}$$

where g_1 and g_2 represent the first and second SAR images, respectively, and angular brackets denote averaging over the ensemble of speckle realizations. The magnitude of the correlation $|\gamma|$ is usually known as coherence and varies from 0 to 1. The causes for the decorrelation between two images are due to temporal, spatial, and thermal noise. The total coherence of the image can be written as (Zebker and Villasenor, 1992)

$$\gamma_{\text{total}} = \gamma_{\text{temporal}}\gamma_{\text{spatial}}\gamma_{\text{thermal}}$$

The spatial decorrelation ($\gamma_{spatial}$) depends on sensor geometry and baseline separation between two acquisitions. The temporal decorrelation ($\gamma_{temporal}$) is due to changes in vegetation growth, snowdrift, snowmelt, glacier motion, permafrost freezing and thawing, soil moisture changes, agricultural practices, etc. that occur during repeat pass acquisition. The decorrelation due to thermal noise is related to signal to noise ratio of the sensor system.

Rignot et al. (1996) observed the coherence over San Rafael glacier, Chile using SIR-C L- and C-band and found that the coherence at L-band is better than C-band with a 1-day interval between two scenes as shown in Figure 2. Coherence is low ($\gamma < 0.4$) on the glacier at C-band, but higher on the plains surrounding Laguna San Rafael. Mountain peaks without vegetation also shows high coherence (γ = 0.7–0.8). The forest area shows low coherence (γ = 0.4–0.6) due to movement of leaves and volume scattering. At L-band, the coherence is high ($\gamma < 0.95$) at low elevations over the forest and also at slow moving part of the ice fields ($\gamma < 0.75$), intermediate over fast moving part of the glacier ($\gamma = 0.5$), moderate ($\gamma = 0.35$) in areas of high shear strain and low ($\gamma < 0.2$) over the open water and shadows. Snowmelting areas also show low coherence.

Using many ERS-1 and 2 tandem datasets, Vachon et al. (1996) and Mattar et al. (1998) observed change in coherence on different dates over Saskatchewan and Athabasca glaciers. It was found that on some dates, coherence is very low even for the tandem data and not useful for InSAR studies. They estimated the coherence using an averaging window size of 50 (azimuth) × 10 (range) samples.

Rao et al. (2008a) observed coherence change over three major Indian Himalayan glaciers, namely, Siachen, Gangotri, and Bara Shigri using ERS-1 and 2 tandem data and ENVISAT ASAR 35-day interval data. Among all these, Siachen glacier showed the highest coherence with ERS-1/2 tandem data acquired in descending pass as shown in Figure 3a. Low coherence was observed over Gangotri and Bara Shigri glaciers using the tandem data and shown in Figure 3b and c. ENVISAT ASAR 35-day interval data also gave good coherence outside glacier area. In glacier area, the coherence is completely lost due to large movement of the glacier within a 35-day interval and also changes in the debris on the glacier due to melting and precipitation. High-resolution TerraSAR-X images over Gangotri glacier with a 11-day interval also give poor coherence for the glacier part due to lower wavelength and fast movement of the glacier. However, good coherence and fringes are observed in the adjacent glacier area.

ALOS PALSAR L-band images over Qinghai-Tebetan plateau with interval 45–90 days also show low coherence over glacier area (Li et al., 2008). But the coherence obtained with a 45-day interval data as shown in Figure 4 is better than that obtained with a 90-day interval data. Due to longer wavelength of PALSAR and winter season, coherence was preserved between images acquired with a 45-day interval.

Intensity, coherence, and speckle-tracking methods

When the loss of coherence is high between interferometric SAR images, differential InSAR cannot be applied. An alternative to DInSAR for the estimation of glacier motion is offset tracking (Strozzi et al., 2002; Pattyn and Derauw, 2002). In the intensity tracking, image offsets in the slant range and azimuth directions are calculated using SAR intensity images, whereas in coherence-tracking method single look complex SAR images are used to calculate coherence and maximized the value by shifting the offset. This is done over entire image by tracking small patches of size 8 × 8 pixels which correspond to 160 m in the ground range and 30 in the azimuth direction for ERS SAR system. The offsets obtained through this procedure are due to orbit configurations and glacier movement. The offsets related to orbital geometry are estimated using precision orbit and ground control points and the offsets related to glacier displacement is separated. The accuracy of the offset-tracking methods is two times less than that we get using DInSAR studies (Strozzi et al., 2002). Advantage of offset-tracking method is that we get two-dimensional velocities in azimuth and range direction, whereas the DInSAR gives only in radar look direction (one direction). Rignot et al. (1996) also used intensity-tracking technique for the estimation of movement in crevasse areas.

Speckle tracking is similar to intensity and coherence tracking. Instead of correlating intensity or coherence between two images, it correlates speckle between two images for observing shifts between two images. The condition for this technique is that coherence between two images is necessary (Gray et al., 2001; Joughin, 2002; Short and Gray, 2004).

Three-dimensional flow estimation

Radar measures the displacement in the line of sight (LOS) direction. One single interferogram gives only one component of velocity. However, the true displacement may lie in any direction. Without additional information, it is not possible to separate horizontal and vertical displacement. Joughin et al. (1998), Mattar et al. (1998), Mohr et al. (1998), and Magnússon et al. (2007) combined the displacements obtained with ascending and descending pass data and surface slope to estimate three-dimensional ice velocity vector. They assumed that glacier flow is parallel to the topographic surface and also ice flows at a steady rate during acquisition of the ascending and descending passes. These assumptions may fail in some cases. The surface-parallel flow assumption fails in the regions of accumulation and ablation areas with bumpy terrain where vertical component motion is large and leads to errors. However, the horizontal component of motion is relatively unaffected by deviations in surface-parallel flow. The required inputs for the calculation of three component velocity vector are surface slope, angular separation of ascending and descending tracks α, and incidence angle (θ_i) which

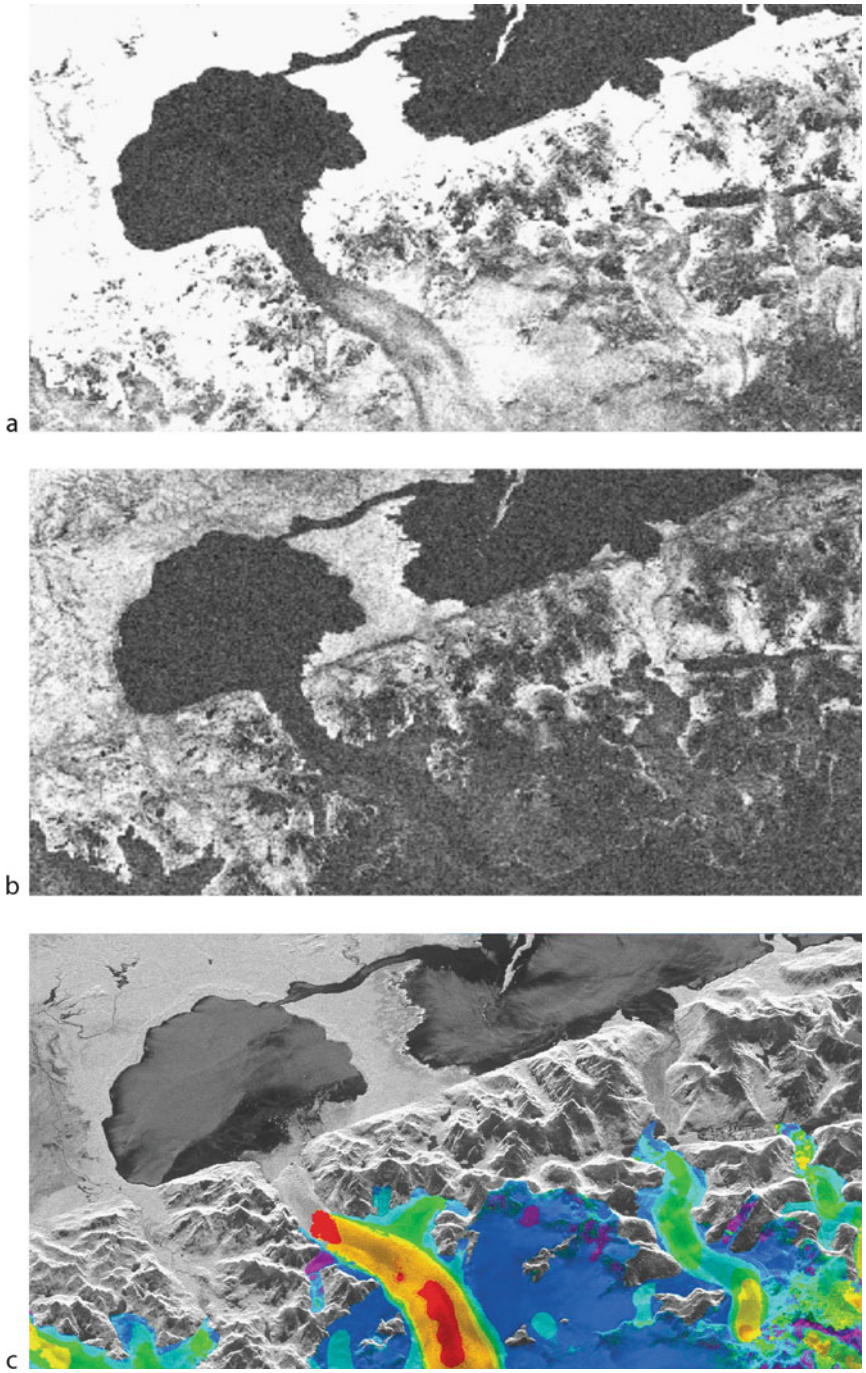

Synthetic Aperture Radar (SAR) Interferometry for Glacier Movement Studies, Figure 2 (**a**) Phase coherence between October 9 and 10, 1994 SIR-C L-band image pair, San Rafael Glacier, Chile. (**b**) phase coherence at C-band, and (**c**) ice motion derived using L-band data in the direction of radar illumination (Rignot et al., 1996). *Light purple* (<–3 cm/day), *purple* (–3 to –0.5 cm/day), *gray* (–0.5 to +0.5 cm/day), *blue* (0.5–3 cm/day), *light blue* (3–20 cm/day), *green* (20–45 cm/day), *yellow* (45–85 cm/day), *orange* (85–180 cm/day), and *red* (>180 cm/day). Negative sign is movement away from the radar and positive sign is movement toward the radar.

is defined with respect to local normal to the ellipsoid as shown in Figure 1, angle between ascending pass direction and reference x-axis and unwrapped phase corresponding to motion (Joughin et al., 1998).

Using single interferogram also, surface displacement can be estimated using range displacement (Vachon et al., 1996). For certain critical angles of surface slope and the direction of slope, the LOS displacement is

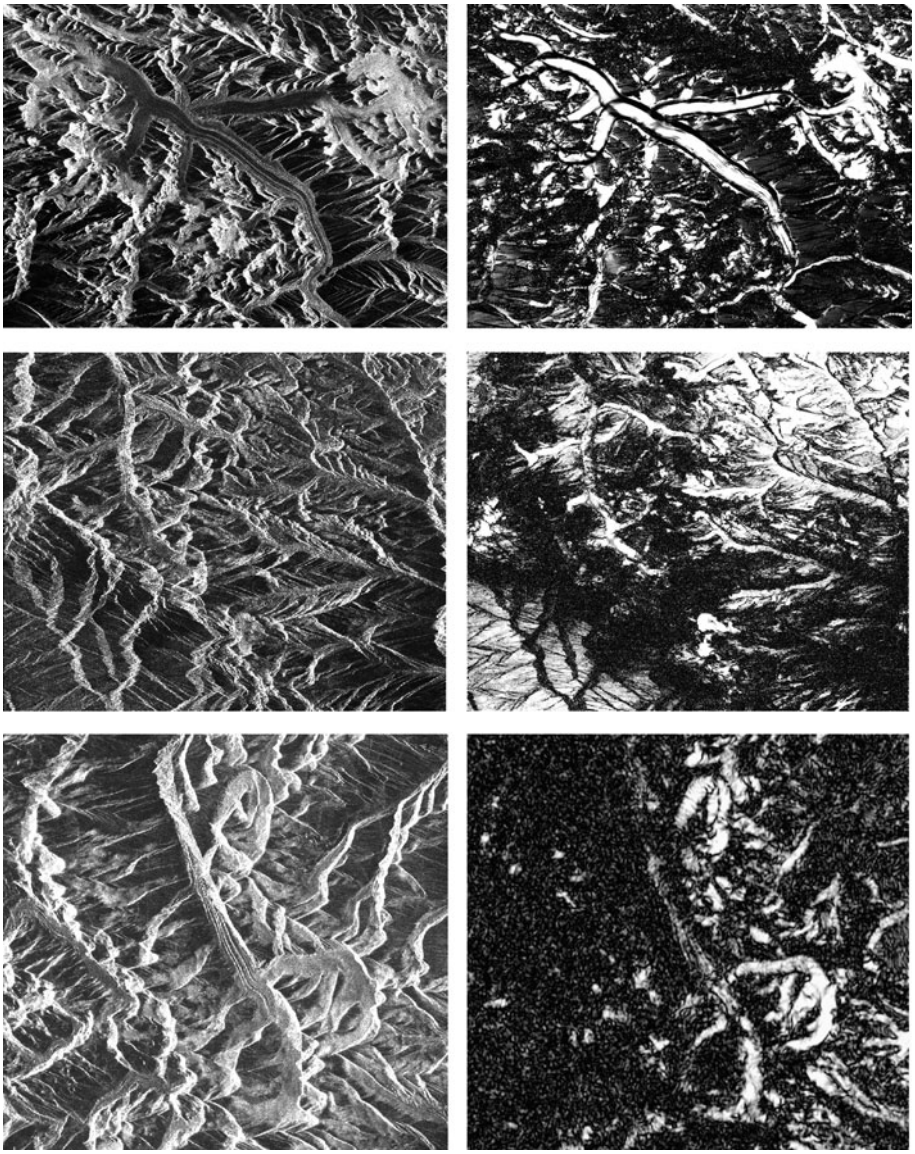

Synthetic Aperture Radar (SAR) Interferometry for Glacier Movement Studies, Figure 3 Interferometric coherence along with SAR intensity images are shown for Siachen (*top*), Gangotri (*middle*), and Bara Shigri (*bottom*) glaciers in Himalaya using ERS-1/2 tandem data.

perpendicular to the glacier displacement and surface displacement tends to infinity. To estimate the displacement from single LOS measurement, the LOS direction relative to displacement is outside the critical range.

Studies on land glaciers

InSAR studies on midlatitude alpine glaciers are very few. Vachon et al. (1996) studied surface displacement of Athabasca and Saskatchewan glaciers using several ERS-1/2 tandem pairs acquired with a 24 h interval. Topography information in the interferogram was removed using the DEM derived using airborne SAR data. The RMS error in their DEM is about 5 m that cause an error of 0.4 cm/day in displacement map at the baseline of 300 m. They also mentioned that the error in the baseline also causes 0.4 cm/day error in displacement map. Mattar et al. (1998) extended the same work and estimated three-dimensional surface flow field using surface-parallel flow assumption by combining ascending and descending passes. The LOS displacement of maximum 18 cm/day was observed for Saskatchewan glacier with ascending pass data, whereas 10 cm/day with descending pass data. The corresponding surface displacement along the center line of the Saskachewan glacier is 35 cm/day.

Rignot et al. (1996) studied San Rafael, Chile glacier using SIR-C L- and C-band October 1994 interferometric

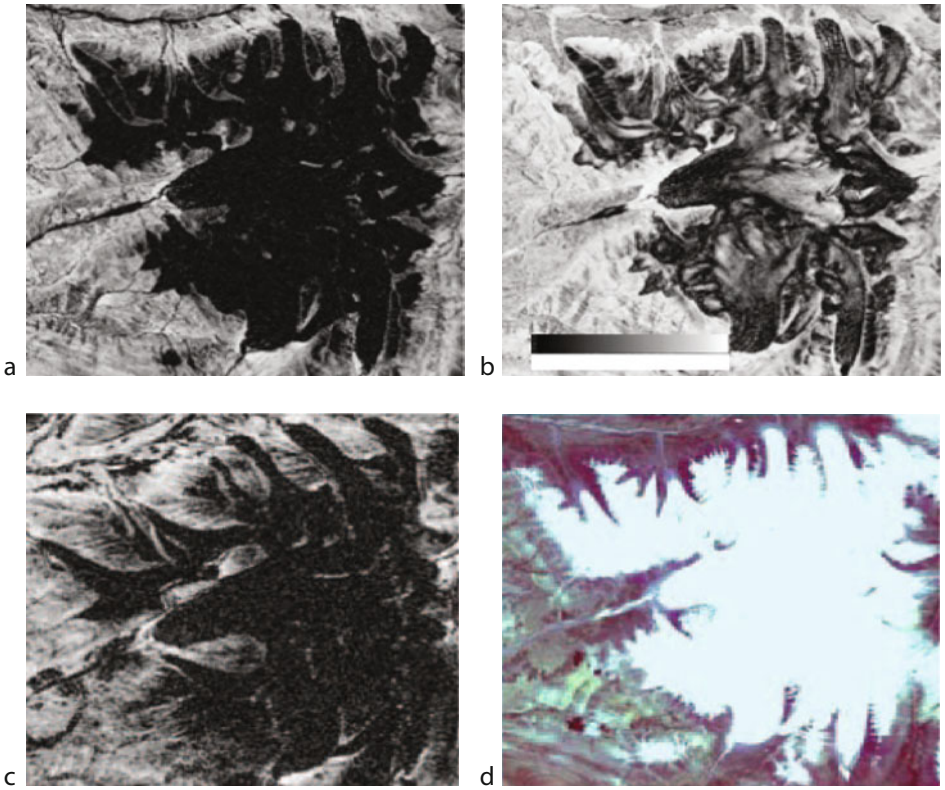

Synthetic Aperture Radar (SAR) Interferometry for Glacier Movement Studies, Figure 4 Phase coherence images over the glacier Dongkemadi in Qinghai-Tibetan plateau. (**a**) ALOS PALSAR pair June 11, 2006 and September 11, 2006 (**b**) ALOS PALSAR pair December 10, 2007 and January 25, 2008, (**c**) ENVISAT ASAR pair July 10, 2007 and August 14, 2007, and (**d**) TM image for the same area (Li et al., 2008).

data acquired with interval of 24 h. Due to shorter wavelength, C-band data did not give good coherence image for this area. However, L-band data preserved the coherence in many parts of the glacier and were used to map the surface topography over the glacier with accuracy of 10 m and measured the ice velocity with a precision of 4 mm/day. The LOS interferometric velocities were converted to surface displacement by assuming a flow direction and complemented by feature-tracking result near the calving front. Ice velocity map in radar LOS direction is shown in Figure 2c. InSAR observed ice velocity at the equilibrium line (1,200 m altitude) is 2.6 m/day (0.85 km/year) and increases rapidly before the glacier enters the narrower terminal valley. Just before 100 m from the calving front, ice velocity reaches 17.5 m/day (6.4 km/year). InSAR could estimate velocities upto 9 m/day. Feature-tracking method was used near the crevasse areas to estimate velocity upto 17.5 m/day. Effective starin-rate map was also generated using velocity map. Forster et al. (1999) studied Europa and Penguin glaciers in Chile using SIR-C L-band data and estimated ice velocity with a precision of 2 cm/day.

Michel and Rignot (1999) used SIR-C L-band October 1994 data to map Moreno glacier in Argentina. Both interferometry and feature tracking based on coherence have been used to map the glacier velocity and found that InSAR can measure ice velocity with a precision of 1.8 cm/day, while feature-tracking method can estimate with an accuracy of 14 cm/day.

Swiss Alpine glacier movement was studied by Strozzi et al. (2003). The glaciers covered in their study were the largest glacier Groβer Aletschgletscher and other glaciers Unteraargletscher, Fieschergletscher, and Grüebu Gletscher. As the ground truth data over Unteraargletscher glacier are available through various methods, interferometric derived LOS displacement map was obtained using ERS-1/2 tandem data for this glacier. The maximum velocity observed at the upper part of the glacier at steeper slopes is 4 cm/day and decreases gradually along the glacier. It was observed that radar is not sensitive to displacement measurement if the glacier flow is perpendicular to the radar look direction. It was suggested that the LOS surface displacement map of the glacier is useful to estimate mass balance distribution using the kinematic boundary condition without the use of ground measurements.

Himalayan glaciers movement

Rao et al. (2004, 2008a, b) mapped the movement of the major Himalayan glaciers, namely, Siachen, Gangotri, and Bara Shigri using ERS-1/2 tandem data. Siachen

glacier is the largest glacier located at higher elevation. It has a length of about 72 km and with varying width. It is the second largest glacier in the world outside the polar region. It feeds the Nubra river (also known as Shaksgam river) that flows parallel to the Karakoram range before entering into Tibet. The trunk glacier and its tributaries are in the form of a vast ice field. Continuous snowfall can be seen during winter periods. The average winter snowfall is about 10.5 m. The temperature varies from −10°C and −50°C. The elevation varies from the snout (3,620 m) to source of the glacier (i.e., Indira col) (5,753 m).

Gangotri glacier is a major source of water for many states of the North India. It is about 25 km long with varying width of 2.5–0.5 km and having many tributary glaciers. Some of these tributary glaciers are in turn having their own tributaries. The elevation over the main glacier varies from terminus (4,000 m) to the source of the glacier (6,000 m). The temperature at the glacier (terminus) varies from 10°C to –20°C. According to many reports, the glacier is retreating at alarming rates (20 m/year).

Bara Shigri glacier lies (N32°10'33", E77°40′09″) on Chandra-Bhaga river basin (Pir Panjal range) in Lahaul-Spiti district of Himachal Pradesh. The glacier is the largest in Himachal Pradesh with a length of 28 km (131 km^2) with elevation changing from terminus (4,000 m) to the source of the glacier (5,500 m). There are several glaciers around this glacier (Chhota Shigri, Hamta, etc.). All these glaciers are covered in one scene of the ERS-1/2 SAR data.

ERS-1/2 tandem data acquired on April 1 and 2, 1996 in descending pass with perpendicular baseline of 110 m and May 2 and 3, 1996 in ascending pass with baseline of 114 m were used to map the surface displacement of Siachen glacier. ERS-1/2 tandem pair acquired on March 25 and 26, 1996 in ascending pass with baseline of 75 m was used for Gangotri glacier studies. ERS-1/2 tandem pair acquired on May 2 and 3, 1996 in ascending pass with perpendicular baseline of 110 m was used to study the Bara Shigri glacier.

To get differential interferometric fringes, one has to follow several the steps given in Figure 1. Topography information from the interferogram was removed using SRTM 3 arc second DEM. Figure 5 shows ERS-1 SAR intensity, interferoram, differential interferogram and ice velocity in the LOS direction for Siachen glacier. Figure 5d shows velocity of the glacier in color. Negative (−) velocities represent movement away from the radar direction and positive (+) represents movement toward the radar direction.

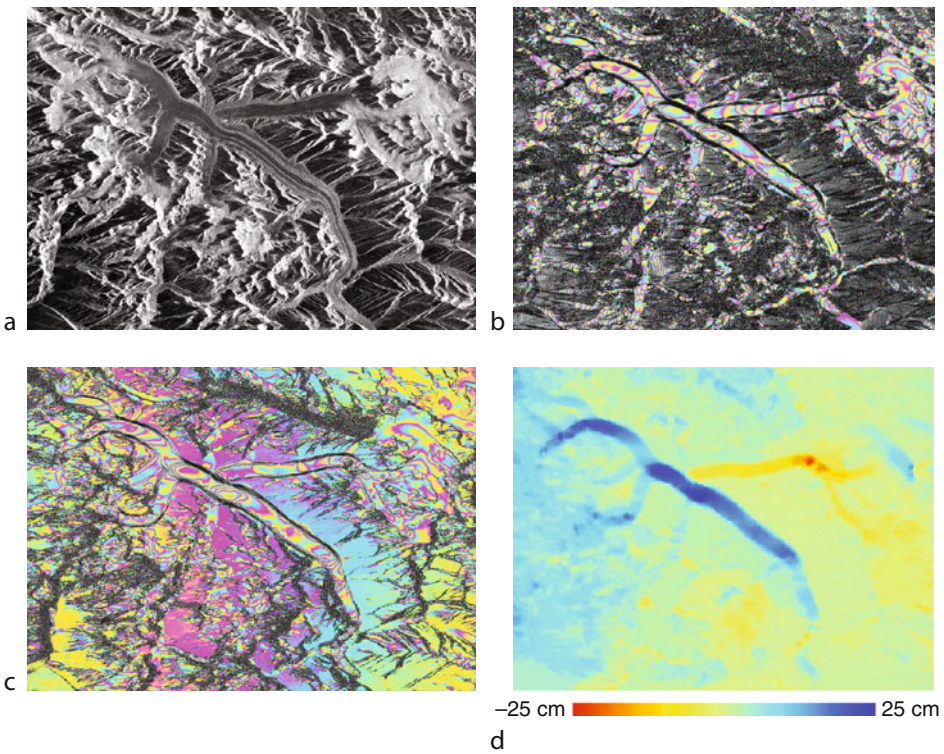

Synthetic Aperture Radar (SAR) Interferometry for Glacier Movement Studies, Figure 5 Synthetic Aperture Radar (SAR) images of April 1 and 2, 1996 acquired by ERS-1 and 2 satellites were processed using interferometric technique for estimating Siachen glacier movement. (**a**) SAR intensity image, (**b**) Interferogram with each fringe representing topographic height of 85 m, (**c**) Differential interferogram with each fringe representing 2.8 cm motion toward the radar direction, and (**d**) Surface displacement map in cm (*dark blue* represents (25 cm/day) movement toward the radar and red represents (–25 cm) away from the radar).

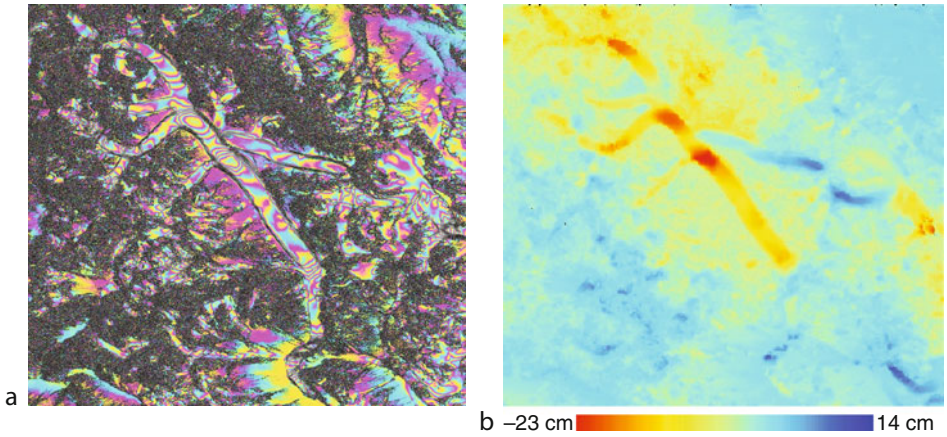

Synthetic Aperture Radar (SAR) Interferometry for Glacier Movement Studies, Figure 6 (**a**) Differential interferogram and (**b**) ice velocity in the radar direction for Siachen glacier obtained using ascending pass of ERS-1/2 SAR tandem data.

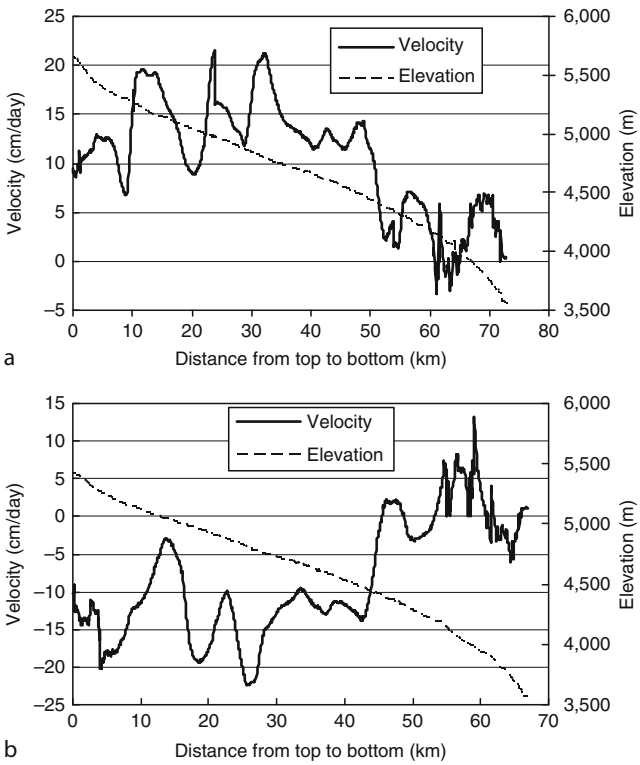

Synthetic Aperture Radar (SAR) Interferometry for Glacier Movement Studies, Figure 7 Ice velocity in the radar direction and surface elevation of Siachen glacier versus the distance from the top to terminus: (**a**) ascending and (**b**) descending pass.

Differential fringes over Siachen are more, particularly at higher elevation and also lower part of the glacier, that is, ablation area. Fringes are not seen at the middle part of the glacier. Above the Siachen glacier, there are small glaciers where fringes are observed. Fringes are also seen at some places where there are no glaciers. It may be due to differences between SRTM DEM and actual elevation present at the ground. At the joining place of tributaries with trunk of the glacier, round-shaped fringes (often called bull eye shape) are observed. It is due to the movement of ice over elevation and through a bump. Maximum number of fringes at the location is about 8 which is equal to 22.4 cm displacement toward the radar direction.

Similarly, differential fringes for ascending pass over Siachen are produced and shown in Figure 6. More differential fringes are seen for this pass particularly at the ablation area indicating that the glacier is moving faster in May than in April. We have also used ENVISAT ASAR datasets with interval of 35 days to 1 year for DInSAR studies. For the 35-day data, complete loss of coherence was observed on the glacier area. To estimate motion using the large interval data, intensity-tracking method can only be used.

Along the middle of the glacier, we took the velocity profile from highest elevation to lowest and shown in Figure 7 for both descending and ascending passes respectively. The X-axis is the distance in pixels down the glacier. Each pixel is about 20 m. In case of Gangotri, we observed positive velocity that indicates the movement of glacier away from the radar direction. For Siachen glacier, the trend of movement along the glacier varies depending on the descending and ascending passes. At the bump of the glacier (525 and 1,000 pixel number), there was steep change in displacement at the glacier. At the bottom of the glacier also, there is variation in the movement. The variation is highest at the ablation zone.

About two to three differential fringes (8.4 cm) were observed for Gangotri area particularly in higher elevation of the glacier. There was also displacement at some other areas due to DEM and baseline errors. Considering the

error in SRTM DEM which is about 30 m, the error in displacement map for Gangotri is less than 1 cm. Although we observed differential fringes for Bara Shigri glacier, we could not obtain displacement map due to phase unwrapping problems. We observed heavy coherence loss at this area. The differential fringes show that the maximum glacier movement is 5 cm/day.

Alaska surge glaciers

Bering glacier is the largest glacier in North American continent with 190 km length. Fatland and Lingle (1998, 2002) analyzed the glacier surge 1993–1995 using intereometric SAR data. Rabus and Fatland (2000) analyzed Black Rapids glacier in Alaska using ERS-1 SAR 3-day interval data. There is not much literature on catastrophic glacier using InSAR.

Summary

InSAR is a power tool for mapping glacier movement with centimeter accuracy at high spatial resolution. All satellite datasets may not be useful for InSAR applications due to large glacier movement, melting of snow, baseline requirements, and atmospheric changes. ERS-1/2 tandem data acquired with a 1-day interval was the best suitable data for mapping glacier movement. Limited data acquired by SIR-C were also used for glacier velocity mapping. For removing the topographic effects in the interferograms, SRTM digital elevation models have been used. Glacier velocity map generated with SAR data is in the line of radar direction. To obtain the three-dimensional velocity map, ascending and descending pass data are combined with an assumption that glacier movement is parallel to topographic surface. As most of the operating satellites give the data at the interval of 11–45 days, applications of InSAR for glacier movement is not feasible. To overcome the difficulty, intensity-, coherence-, and speckle-tracking methods have been used. As the resolution of the present satellites is better than the older satellites, glacier movement of even smaller glaciers can be mapped with greater accuracy.

Bibliography

Fatland, D. R., and Lingle, C. S., 2002. In SAR observations of the 1993–1995 Bering Glacier (Alaska, USA) surge and a surge hypothesis. *Journal of Glaciology*, **48**, 439–451.

Fatland, D. R., and Lingle, C. S., 1998. Analysis of the 1993–1995 Bering glacier (Alaska) surge using differential SAR interferometry. *Journal of Glaciology*, **44**(148), 532–546.

Forster, R. R., Rignot, E., Isacks, B. L., and Jezker, K. C., 1999. Interferometric radar observations of Glaciares Europa and Penguin, Hielo Patagonico Sur, Chile. *Journal of Glaciology*, **45**, 325–337.

Frolich, R. M., and Doake, G. S. M., 1998. Synthetic Aperture radar interferometry over Rutford ice stream and Carlsm inlet, Antarctica. *Journal of Glaciology*, **44**, 77–92.

Goldstein, R. M., Engelhardi, H., Kamb, B., and Frolich, R. M., 1993. Satellite radar interferometry for monitoring ice sheet motion: application to an Antarctic ice stream. *Science*, **262**, 525–1530.

Gray, A. L., Short, N., Mattar, K. E., and Jezek, K. C., 2001. Velocities and flux of the Filchner Ice Shelf and its tributaries determined from speckle tracking interferometry. *Canadian Journal of Remote Sensing*, **27**, 193–206.

Joughin, I., 2002. Ice-sheet velocity mapping: a combined interferometric and speckle tracking approach. *Annals of Glaciology*, **34**, 195–201.

Joughin, I. R., Winebrenner, D. P., and Fahnestock, M. A., 1995. Observations of ice-sheet motion in Greenland using satellite radar interferometry. *Geophysical Research Letters*, **22**, 571–574.

Joughin, I., Kwok, R., and Fahnestock, M., 1996. Estimation of ice sheet motion using satellite radar interferometry: Method and error analysis with application to the Humboldt Glacier, Greenland. *Journal of Glaciology*, **42**, 564–575.

Joughin, I. R., Kwok, R., and Fahnestock, M. A., 1998. Interferometric estimation of three-dimensional ice-flow using ascending and descending passes. *IEEE Transaction on Geosciences and Remote Sensing*, **36**, 25–37.

Kwok, R., and Fannestock, M. S., 1996. Ice sheet motion and topography from radar Interferometry. *IEEE Transaction on Geosciences and Remote Sensing*, **34**, 189–200.

Li, Z., Zhou, J., Tian, B., and Xie, Z., 2008. *The glacier identification using SAR interfermetric and polarimetric information in Qinghai-Tibetan plateau*. IV: Proceedings of IGARSS, pp. 1054–1056.

Madsen, S. N., and Zebker, H., 1998. Imaging radar interferometry. In Hdenderson, F. M., and Lewis, A. J. (eds.), *Principles and Applications of Imaging Radar, Manual of Remote Sensing.* Chapter 6, 3rd edn., Vol. 2, pp. 359–380.

Magnússon, E., Rott, H., Björnsson, H., and Pálsson, F., 2007. The Impact of jökulhlaups on basal sliding observed by SAR interferometry on Vatnajökul, Iceland. *Journal of Glaciology*, **53**, 232–240.

Massonnet, D., and Feigl, K. L., 1998. Radar interferometry and its application to changes in the earth's surface. *Reviews of Geophysics*, **36**, 441–500.

Mattar, E. K., Vachon, P. W., Geudtner, D., and Gray, A. L., 1998. Validation of Alpine glacier velocity measurements using ERS tandem-mission SAR data. *IEEE Transaction on Geosciences and Remote Sensing*, **36**, 974–984.

Michel, R., and Rignot, E., 1999. Flow of Glaciar Moreno, Argentina, from repeat pass shuttle imaging radar images: comparison of the phase correlation method with radar interferometry. *Journal of Glaciology*, **45**, 93–100.

Mohr, J. J., Reeh, N., and Madsen, S. N., 1998. Three-dimensional glacial flow and surface elevation measured with radar interferometry. *Nature*, **391**, 273–276.

Pattyn, F., and Derauw, D., 2002. DInSAR and coherence tracking applied to glaciology: the example of Shirase Glacier. *Journal of Glaciology*, **48**, 559–565.

Rabus, B. T., and Fatland, D. R., 2000. Comparison of SAR-interferometric and surveyed velocities on a mountain glacier: black rapids glacier, Alaska, U.S.A. *Journal of Glaciology*, **46**(152), 119–128.

Rao, Y. S., Venkataraman, G., Rao, K. S., and Snehmani, A., 2004. SAR interferometry for DEM generation and movement studies over Indian Glaciers. *Proceedings of IGARSS*, **2**, 1128–1131.

Rao, Y. S., Singh, G., Venkataraman, G., and Snehmani, A., 2008b. Application of SAR interferometry for DEM generation and movement studies over Himalayna glaciers. In *Proceedings of Natioanl Snow Science Workshop 2008 (NSSW-08)*, held during 11–12 January 2008, pp. 210–217.

Rao, Y. S., Kumar, V., Singh, G., Venkataraman, G., and Snehmani, A., 2008a. The loss of coherence in the InSAR images of Himalayan Glaciers. In *Proceedings of International Workshop on Snow, Ice, Glacier and Avalanches*, held at IIT Bombay during January 7–9, 2008, pp. 232–239.

Rignot, E., Jezek, K. C., and Sohn, H. G., 1995. Ice flow dynamics of the Greenland ice sheet from SAR interferometry. *Geophysical Research Letters*, **22**, 575–578.

Rignot, E., Forster, R., and Isacks, B., 1996. Interferometric observations of Glacier San Rafael. Chile. *Journal of Glaciology*, **42**, 279–291.

Rosen, A. P., Hensley, S., Joughin, I. R., Li, F. K., Madsen, S. N., Rodriguez, E., and Goldstein, R. M., 2000. Synthetic aperture radar interferometry. *Proceeding of IEEE*, **88**, 333–382.

Short, N. H., and Gray, A. L., 2004. Potential for RADARSAT-2 interferometry: glacier monitoring using speckle tracking. *Canadian Journal of Remote Sensing*, **30**, 504–509.

Strozzi, T. A., Luckman, T. M., Wegmüller, U., and Werner, C. L., 2002. Glacier motion estimation using SAR offset-tracking Procedures. *IEEE Transaction on Geosciences and Remote Sensing*, **40**, 2384–2391.

Strozzi, T., Gudmundsson, G. H., and Wegmuller, U., 2003. Estimation of the surface displacement of Swiss Alpine Glaciers using satellite radar interferometry, ERSeL eProceedings 2 1/2003 Observing our Cryosphere from Space: Techniques and Methods for Monitoring Snow and Ice with Regard to Climate Change, CD-ROM, 2003.

Vachon, P. W., Geudtner, D., Mattar, K., Gray, A. L., Brugman, M., and Cumming, I., 1996. Differential SAR interferometry measurements of Athabasca and Saskatchewan glacier flow rate. *Canadian Journal of Remote Sensing*, **22**, 287–296.

Zebker, H. A., and Villasenor, J., 1992. Decorrelation of interferometric radar echoes. *IEEE Transaction on Geosciences and Remote Sensing*, **30**, 950–959.

Zebker, H. A., Rosen, P. A., and Hensley, S., 1997. Atmospheric effects in interferometric synthetic aperture radar surface deformation and topographic maps. *Journal of Geophysical Research*, **102**(B4), 7547–7563.

Cross-references

Glacier Motion/Ice Velocity
Glacier Surging
Optical Remote Sensing of Alpine Glaciers

T

TALIK

Tingjun Zhang
National Snow and Ice Data Center, Cooperative Institute for Research in Environmental Sciences, University of Colorado at Boulder, Boulder, CO, USA

Definition

Talik refers to a layer or body of unfrozen ground occurring in permafrost regions due to a local anomaly in thermal, hydrological, hydrogeological, or hydrochemical conditions (van Everdingen, 1998/2005). This definition has no time restraint; any layer or body of unfrozen ground for a certain period of time in permafrost regions can be classified as a talik, such as an active layer over permafrost, which is unfrozen ground in summer; however, such a layer is not a talik. With some modification, talik is defined as a layer or body of unfrozen ground existing continuously for more than a year in permafrost region. In Russian and Chinese literature, talik mainly refers to unfrozen ground for more than a year in continuous permafrost regions. When the area of unfrozen ground appears to be comparable with or larger than the area of frozen ground, the unfrozen ground is termed as a talik zone.

Talik types

According to its temperature, taliks can be classified into two major types:

1. Noncryotic talik with its temperatures above 0°C
2. Cryotic talik with its temperature below 0°C and forming part of the permafrost

According to its physical position in response to permafrost, taliks can be classified into five major types:

1. Closed talik: a noncryotic talik located below the seasonally frozen layer and above the permafrost table. Closed taliks usually occur underneath a lake, also called "lake talik," or underneath a river called "river talik." Its temperature remains above 0°C because of the heat storage effect of the surface water. Its thickness varies from less than a meter to tens of meters, depending on the age of lakes or river channels.
2. Open talik: a talik that penetrates the permafrost completely, connecting suprapermafrost and subpermafrost water, usually below large rivers or lakes. An unfrozen ground in discontinuous permafrost regions belongs to an open talik type. It may be noncryotic or cryotic.
3. Lateral talik: a talik overlain or underlain by perennially frozen ground; can be noncryotic or cryotic.
4. Isolated talik: a talik entirely surrounded by perennially frozen ground; usually cryotic but may be noncryotic.
5. Transient talik: a talik that is gradually being eliminated by freezing, e.g., the initially noncryotic closed talik below a small lake which, upon draining of the lake, is turned into a transient isolated talik by permafrost aggradation.

According to the physical mechanism responsible for their unfrozen condition, taliks can be classified into five major types:

1. Thermal talik: a noncryotic talik formed under the effect of local surface energy balance. Thermal taliks mainly occur in discontinuous permafrost regions, especially in the southern limits of permafrost regions. In these regions, ground surface receives much higher solar radiation with higher air and ground surface temperatures, resulting in widespread talik formation and distribution. The insulating effect of seasonal snow cover can cause the mean annual ground surface temperature several degrees higher, if there is a thin or no snow cover, resulting in the northward movement of permafrost boundaries and the talik zone.

Vijay P. Singh, Pratap Singh & Umesh K. Haritashya (eds.), *Encyclopedia of Snow, Ice and Glaciers*, DOI 10.1007/978-90-481-2642-2,

2. Hydrothermal talik: a noncryotic talik formed under the warming effect of surface water bodies. Hydrothermal taliks include taliks above subsea permafrost due to the warming effect of seawater, under an estuary due to the heating effect of river and seawater, and under a lake or river. Taliks may be formed under a flood plain due to the effect of irregular but frequent floodwaters. Taliks may also be formed under cold mountain glaciers due to glacier meltwater.
3. Hydrochemical talik: a cryotic talik in which freezing is prevented by mineralized groundwater flowing through the talik.
4. Geothermal talik: a noncryotic talik formed due to thermal anomalies resulting from processes in the earth's interior. The origin of these geothermal anomalies is associated with connective heat transfer by subpermafrost waters under pressure and conductive heat transfer through geothermal heat flux from the earth's interior along active faults and volcanoes.
5. Artificial talik: a noncryotic or cryotic talik formed in the course of human activities in permafrost regions. These taliks are formed under artificial water reservoirs, spoil heaps, and fills of coal- and sulfide-containing rocks, areas with artificial vegetation removal, and infrastructures such as buildings and roads. Artificial taliks can be easily formed in a discontinuous permafrost zone because a small, often rather short-term, change in hear exchange condition on the ground surface is sufficient for taliks to be formed.

Based on the definition of talik given above, any layer or body of unfrozen ground in permafrost regions is talik. According to the International Permafrost Association (IPA) Circum-Arctic Map of Permafrost and Ground-Ice Conditions (Brown et al., 1997), permafrost regions occupy approximately 22.79 million km^2 or 23.9% of the exposed land area of the Northern Hemisphere (Zhang et al., 1999). The actual area underlain by permafrost ranges from 12.21 to 16.98 million km^2 or 12.8–17.8% of the exposed land area in the Northern Hemisphere (Zhang et al., 2000). In this case, the distribution of taliks ranges from 5.81 to 10.58 million km^2 or 6.1–11.1% of the permafrost regions in the Northern Hemisphere. In reality, the talik distribution is much greater than these values since taliks under water (under lakes, rivers, and seawater) and glaciers are not included in these statistics. Taliks above the permafrost table, especially in discontinuous permafrost zones, are also excluded in these estimates. At present, there is no data or information available about the extent of taliks under water and above the permafrost table.

Under global warming scenarios, permafrost boundaries will move northward, resulting in substantial increase in the areal extent of unfrozen ground or taliks in permafrost regions. Taliks under seawater will also expand due to the sea level rise and rapid arctic coastal erosion. Expansion of thaw lake surface area in continuous permafrost zones will result in more talik development. At the same time, widespread taliks may develop over land due to the thickening of the active layer in summer and less soil freezing in winter because of stronger snow insulation effect and high winter air temperatures.

Development of taliks strongly depends on surface and ground water and on the type of water exchange. It is the water that can be considered as an accumulator and carrier of heat and has most effect on ground temperatures and thus the talik formation in permafrost regions. The nature of groundwater movement and the rate of water exchange directly influence the processes of talik formation. In turn, taliks provide channels for groundwater movement and exchange between super-, intra-, and sub-permafrost waters. Taliks and groundwater are strongly coupled in permafrost regions.

Summary

Taliks provide an excellent environment for soil microbial activities that can produce methane from organic materials, such as dead plants and animals trapped in permafrost. It has been reported that methane released from thaw lakes in permafrost regions is a significant source of atmospheric methane (Walter et al., 2007). Development of taliks also has a dramatic impact on vegetative growth, landscape, surface and groundwater hydrology, and human infrastructure.

Bibliography

Brown, J., Ferrians, O. J. Jr., Heginbottom, J. A., and Melnikov, E. S., 1997, *Circum-Arctic Map of Permafrost and Ground-Ice Conditions*. Washington, DC: U.S. Geological Survey. Circum-Pacific Map Series no. CP–45.

van Everdingen, R. (ed.), 1998 revised May 2005. *Multi-Language Glossary Of Permafrost and Related Ground-Ice Terms*. Boulder: National Snow and Ice Data Center/World Data Center for Glaciology.

Walter, K. M., Edwards, M. E., Grosse, G., Zimov, S. A., and Chapin, F. S., III, 2007. Thermokarst lakes as a source of atmospheric CH_4 during the last glaciation. *Science*, **318**, 633–636.

Zhang, T., Barry, R. G., Knowles, K., Heginbottom, J. A., and Brown, J., 1999. Statistics and characteristics of permafrost and ground ice distribution in the Northern Hemisphere. *Polar Geography*, **23**(2), 147–169.

Zhang, T., Heginbottom, J. A., Barry, R. G., and Brown, J., 2000. Further statistics on the distribution of permafrost and ground-ice in the Northern Hemipshere. *Polar Geography*, **24**(2), 126–131.

Cross-references

Permafrost
Permafrost and Climate Interactions

TARN

Himali Panthri
Department of Geology, D.B.S (P.G) College, Dehradun, Uttarakhand, India

Synonyms

Cirque lake

Definition

A tarn is a lake formed within a cirque due to excavation by glacier. Greater thickness and enormous pressure of ice mass at the floor of cirque basin are the causes of formation of tarn. A tarn is generally circular, small, and deep with no major inlet. Usually it is fed by the runoff from the slopes surrounding it. Its boundary is often marked by small moraines.

Bibliography

Fairbridge, R. W. (ed.), 1968. *The Encyclopedia of Geomorphology.* New York: Reinhold Book.

TEMPERATE GLACIERS

Andrew Fountain
Department of Geology, Portland State University, Portland, OR, USA

The term "temperate glacier" originally derives from the geographic classification of glaciers along with tropical, polar, maritime, and so on. While that definition has some currency at the time of this writing, a more nuanced and commonly used definition is that of a glacier that is a "warm glacier" – a glacier that is at its melting temperature throughout except for a seasonal skin effect. This thermal definition of "temperate" is much more descriptive of the glacier than one that defines its geographic zone.

The thermal definition of "temperate glacier" implies the presence of water. If the glacier is at its melting temperature throughout the ice mass then much of its mass loss is through melting. Furthermore, the melt water can be routed through the "warm" body of the glacier, via crevasses and moulins, with minimal freezing, to reach the glacier bed where it is in contact with the substrate of bedrock or sediment. The presence of water at the bed can reach large pressures, often a significant fraction of the weight of the ice, such that it facilitates glacier sliding. A temperate glacier flows by sliding and internal ice deformation at speeds roughly double that of a "cold" glacier that is frozen to the bed and flows by deformation of ice alone.

To accommodate the flux of surface meltwater the glacier evolves a system of passageways through the body of the glacier (englacial) and may be composed of naturally formed conduits and cracks, much like that found in cave systems of karst topography. At the bottom of the glacier, passageways may include conduits and cavities, separations between the ice and bedrock, as well as water flow through sediments.

One can see why the thermal definition of "temperate glacier" has been largely adopted because it explains much more about the glacier and what one might expect, compared to the traditional geographic definition. Temperate glaciers are found from the tropics to the subpolar regions, depending on the elevation of the glacier.

TEMPERATURE LAPSE RATES IN GLACIERIZED BASINS

Shawn J. Marshall, Mira Losic
Department of Geography, University of Calgary, Calgary, AB, Canada

Synonyms

Near-surface lapse rates; Slope lapse rates; Vertical temperature gradients

Definition

Lapse rate. Vertical gradient of an atmospheric variable. Unless specified otherwise, this refers to the rate of change of temperature with altitude, $\partial T/\partial z$.
Free-air lapse rate. Rate of change of atmospheric temperature with height above the ground.
Near-surface temperature. Air temperature measured near the Earth surface, typically at a height of 2 m, using sensors sheltered in a radiation shield. Also known as *screen temperature*.
Near-surface (slope) lapse rate. Rate of change of near-surface temperatures with elevation.

Introduction

Air temperatures at Earth's surface govern many aspects of natural and societal systems. The importance of air temperature in hydrology and glaciology is particularly direct. Snow and ice melt occur when air temperatures rise above 0°C, warm air contributes directly to available melt energy, and the transition from rainfall to snowfall occurs at a temperature close to the freezing point. The spatial and temporal patterns of temperature on the landscape are therefore central to snow hydrology and glacier mass balance.

Despite this importance, there are few long-term measurements of near-surface air temperature in most of the world's mountain regions. It is therefore a challenge to model snow and ice melt in glacierized catchments. Most modelling studies estimate meteorological conditions at the glacier surface based on an extrapolation of station observations from low-elevation (e.g., valley bottom) sites or an interpolation of modelled or reanalyzed climatology (i.e., from regional climate or general circulation models). Because temperature is believed to be more easily extrapolated than other meteorological fields, such as wind and humidity, most large-scale glaciological models are based on temperature index methods such as positive-degree-day (*PDD*) scheme (e.g., Braithwaite, 1995; Jóhannesson et al., 1995). Hock (1999) introduces a combined *PDD*-potential radiation melt model that has come to be broadly applied, while other studies, with a more limited geographic extent, make use of distributed models of the full energy balance (e.g., Arnold et al., 1996).

These models all rely heavily on accurate knowledge of near-surface air temperatures, for both the identification of

the 0°C isotherm (the threshold for melt) and the calculation of melt energy, through cumulative *PDD* or through estimation of sensible and longwave heat fluxes to the glacier surface. There are numerous atmospheric and terrain controls on surface (hence, near-surface) temperatures, such as slope, aspect, and surface type (Carrega, 1995), but elevation is the first-order control. The most common approach in glacier mass balance modelling is therefore based on a constant "lapse rate" correction to linearly extrapolate or interpolate near-surface air temperatures from station data or modelled fields to the site-specific elevations of the glacier surface (e.g., Huybrechts et al., 1991; Jóhannesson et al., 1995; Marshall and Clarke, 1999; Klok and Oerlemans, 2002; Hock, 2003). Calculations of snow and ice melt are extremely sensitive to the choice of lapse rate, and there is frequent confusion between free-air and near-surface temperature gradients with elevation. The next section addresses this, followed by a discussion of some unique properties of the glacier boundary layer. The final section summarizes observations of near-surface temperature lapse rates in glacier environments.

Surface temperature versus free-air lapse rates

There are several mechanisms of heat transfer in the atmosphere and at the surface-atmosphere interface. Absorption of solar radiation drives warming of Earth's surface, giving an average pattern of maximum temperatures at the surface and cooling with height above the ground. Turbulent mixing and convective adjustment processes redistribute this heat through the troposphere. Air mass advection (winds), latent heat exchange (evaporation and condensation of water vapor), and diabatic heating and cooling processes, such as longwave radiation exchange, further distribute this heat energy.

The result of these heat transfer mechanisms is a variable and dynamic temperature structure in the troposphere. Some temporally averaged generalizations are possible, however. Of particular interest here is the vertical temperature gradient in the lower troposphere, classically known as the free-air lapse rate. At the idealized level of an isolated air parcel, the lapse rate is precisely defined by atmospheric thermodynamics. For an unsaturated air parcel that is lifted under free or forced convection, adiabatic expansion gives a rate of cooling of −9.8°C/km. If the air is saturated, cooling induces condensation and latent energy release, which reduces this rate of cooling. The resultant lapse rates vary but are closer to −5°C/km. The amount of warming from latent heat release depends on the extent of condensation, so is greater at high temperatures (e.g., in the tropics or at low altitudes). On average, observed lapse rates in the lower troposphere are −6°C/km to −7°C/km.

These classical values refer to average global conditions. Values deviate from this in specific environments or as a function of the time of day or year. In particular, longwave radiative cooling creates cold surface temperatures overnight and at high latitudes in the winter, setting up near-surface temperature inversions: warming with height above the surface. Horizontal air mass advection and vertical subsidence also affect vertical temperature gradients, introducing a synoptic meteorological influence. The classical values for free-air lapse rates are reasonably representative of free-air conditions for the mean state of the atmosphere. However, the distinction between free-air and surface temperature lapse rates is not always clear in climatological applications (McCutchan, 1983). The change in temperature with elevation is critical in ecological, hydrological, or glaciological studies in mountain regions, but it is the surface or near-surface temperature that is of interest in these applications. The controls of surface temperature are different from those in the free air, however, so it is not clear that the classical free-air lapse rate of −6°C/km to −7°C/km is appropriate.

Surface temperatures are governed by the surface energy balance, with warming or cooling driven by the net radiation balance, sensible and latent heat exchange with the atmosphere, and heat conduction and storage in the subsurface. The terms in the surface energy balance are still sensitive to elevation. For example, incoming longwave radiation and sensible heat generally decrease with altitude, while incoming solar radiation can be higher as a result of less atmospheric absorption. However, the overall surface energy balance does not change with altitude according to, e.g., adiabatic processes in the free atmosphere, so surface temperature lapse rates (also known as "slope" lapse rates) differ. Near-surface or "screen temperature" lapse rates – those that would be measured at, e.g., 2-m height above the ground – closely follow surface temperatures and therefore feel the combined influence of both the surface energy balance and regional free-air conditions. An EOF analysis by Lundquist and Cayan (2007) implicitly isolates these effects in a 2-year study of daily temperatures in the Yosemite Network, an array of stations spanning elevations of ca. 1,200–3,000 m in the US Sierra Nevada.

As observed by Lundquist and Cayan (2007) and many other studies, near-surface temperature lapse rates in mountain environments are highly variable, both temporally and spatially. Based on long-term climatological data (average monthly temperatures) at 589 stations in the Austrian and Italian Alps, Rolland (2003) reports mean annual near-surface temperature lapse rates of −5.4°C/km to −5.8°C/km, with a clear seasonal cycle. Summer values are closer to typical free-air rates, −6.3°C/km to −6.6°C/km. Shea et al. (2004) find similar results in the Canadian Rockies, with a mean annual value of −5.2°C/km, weaker lapse rates in the winter months (−4.6°C/km), and the steepest lapse rates in the spring (−6.0°C/km). In a catchment-scale study in southern Idaho, U.S. Rockies, Blandford et al. (2008)

measure even weaker lapse rates: −2.8°C/km in the winter months, with the strongest monthly lapse rate found in April, −4.9°C/km.

These results imply that, on average, the free atmosphere cools off with altitude more quickly than the surface in mountain environments. There are regional exceptions. For instance, Lundquist and Cayan (2007) report an average annual near-surface lapse rate of −6.8°C/km for stations in the Sierra Nevada, consistent with average free-air lapse rates. Numerous other studies, often based on a small number of stations (e.g., two) or on short-term (e.g., summer) measurements, give widely variable estimates of near-surface lapse rates in mountain regions, with recommended literature values that range from −3°C/km to −10°C/km (de Scally, 1997; Rolland, 2003). de Scally (1997) recommends a summer lapse rate of −7.8°C/km for the Punjab region of Pakistan, steeper than typical free-air values.

Regionally specific values likely need to be measured and applied for most ecological, hydrological, or glaciological applications, but a few generalizations are possible from studies to date. Part of the discrepancy in reported near-surface temperature gradients can be understood as an expected result of the surface environments in question. Where surface environments are similar (e.g., the sites of long-term WMO-standard meteorological stations) and multiyear observations are available, average monthly values of −4°C/km to −6°C/km and the consistent seasonal cycle (weaker winter lapse rates and steeper spring and summer values) appear to be robust results. Winter lapse rates are significantly weaker due to the frequency of low-level temperature inversions, cold air drainage and pooling in valley bottoms, and the weaker influence of solar radiation. Where local lapse rates deviate substantially from these typical rates, this can often be understood in terms of the local surface energy balance. For instance, de Scally (1997) interprets the steep summer lapse rates in the Punjab Himalaya as a result of surface warming on vegetated, snow-free surfaces at the lowest elevations, vs. cold, snow-covered (i.e., high-albedo) environments at the highest elevations. The relatively strong spring lapse rates reported in the North American Rockies (Shea et al., 2004; Blandford et al., 2008) may result from the same effect.

In addition to seasonal cycles, there is substantial diurnal and synoptic variability in near-surface lapse rates (Pepin and Losleben, 2002; Pepin et al., 2005; Marshall et al., 2007; Lundquist and Cayan, 2007; Gardner et al., 2009). Weaker lapse rates are more frequent overnight, again due to the occurrence of cold air drainage and the change in the dominant terms in the surface energy balance, from incoming shortwave radiation during the day to outgoing longwave radiation at night. Consistent altitudinal gradients in the net radiation budget drive greater daytime warming at low elevations, particularly where snow and ice are present at high elevations. The next two sections examine these relevant energy balance processes and their implications for near-surface lapse rates on glaciers.

The glacier boundary layer

For much of the year (and year-round at the world's highest elevations and latitudes), glacier surfaces are snow covered and a glacier's surface environment is generally undifferentiated from that of the surrounding area. The surface energy balance and the atmospheric boundary layer behave similarly to non-glacierized snow-covered regions, although the specific topographic setting of valley glaciers often gives rise to strong, channelized winds in the near-surface boundary layer. This is particularly true for glaciers that drain icefields or ice sheets, as the high-elevation plateaus in such settings are conducive to the formation of cold air masses. Gravitational drainage of this cold air produces downslope, katabatic winds year-round in many glacial settings. This cold-air advection can produce anomalously cool temperatures at low elevations on a glacier, weakening the near-surface lapse rates. Warming from adiabatic compression of the descending air counteracts this effect but does not usually offset it.

In the summer season, glacier surfaces become more interesting and distinct from the surrounding environment. van den Broeke (1997) discusses the meteorology of the "glacier boundary layer" – the near-surface atmospheric conditions on a glacier. Greuell and Bohm (1998) examine temperature variability in this boundary layer on a mid-latitude valley glacier, while Steffen and Box (2001) discuss near-surface meteorological conditions on the Greenland Ice Sheet. On an intermediate scale, Marshall et al. (2007) consider mesoscale patterns of temperature variability on a polar ice field in Arctic Canada.

Several general properties of the glacier boundary layer emerge from these studies. Katabatic winds and the relatively smooth surface of glaciers give the frequent occurrence of a low-level wind speed maximum, within a few meters of the glacier surface, which affects the turbulent heat fluxes and generally cools the lower altitudes of a glacier and weakens near-surface lapse rates, as discussed above. Beyond this influence, near-surface temperatures are primarily governed by the radiation balance and synoptic weather systems. On most ice bodies, spring and summer warming leads to rapid "ripening" of the snowpack to the melting point (0°C), after which point the glacier surface can no longer warm. Overnight refreezing is common on glaciers, with temperatures dipping slightly below 0°C on many nights and for short periods of the summer when cold weather systems pass through, but surface temperatures remain close to 0°C throughout the summer melt season. This acts to limit the atmospheric warming over glaciers, such that they are usually colder than the surrounding environment (e.g., adjacent moraines or rock ridges) during the summer.

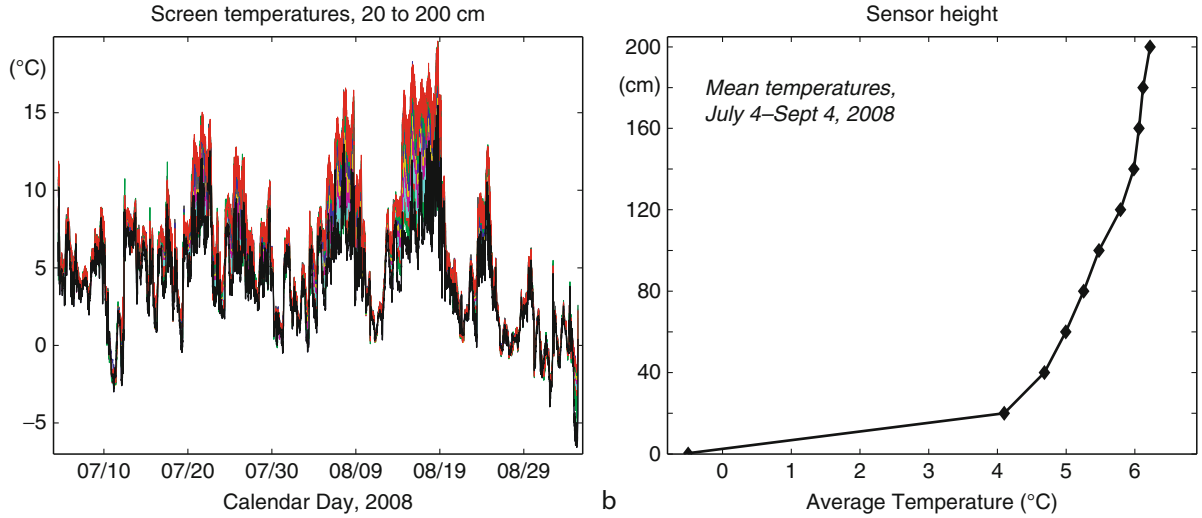

Temperature Lapse Rates in Glacierized Basins, Figure 1 Screen temperatures in the glacier boundary layer, Opabin Glacier, Canadian Rockies. (**a**) Ten-minute temperature data at ten vertical levels (20–200 cm), July 4–Sept 4, 2008. The heavy black line (bottom trace) is at the 20-cm level and, in general, temperatures increase with height. (**b**) Profile of average temperatures at each level for the 62-day period.

In spite of this thermal buffering effect, 2-m temperatures on mid-latitude valley glaciers can warm to temperatures as high as 20°C during the day. Figure 1a illustrates this for a 2-month time series of temperature measurements in the ablation area of the Opabin Glacier in the Canadian Rockies (51.3°N, 116.3°W). This figure plots 10-min data from a set of 10 temperature sensors deployed at heights of 20–200 cm (with 20-cm spacing) in the glacier boundary layer (Losic, 2009). Temperatures increase with height above the surface, as seen in the average temperature profile for the 2-month period (Figure 1b). The sharp, buoyantly stable temperature gradient is typical of the glacier boundary layer during the daytime. This gradient weakens and can reverse overnight.

Near-surface temperature lapse rates in glacier environments

Temperature gradients in the glacier boundary layer have been the subject of several studies, as the near-surface lapse rate is a critical parameter in glacier mass balance models. Braun and Hock (2004) examine this on King George Island, Antarctica and report the frequent occurrence of shallow and inverse (positive) lapse rates, giving average near-surface lapse rates that are well below average free-air values. Jóhannesson et al. (1995) adopt a value of −5.3°C/km for mass balance modelling in Iceland. Steffen and Box (2001) measure −4.0°C/km for the ablation area of Greenland in the month of June, while Box and Rinke (2003) give an updated June–July estimate of −5.0°C/km. Marshall et al. (2007) report on 2 years of data from a network of 25 temperature sensors on the Prince of Wales Icefield, Ellesmere Island, Arctic Canada. The mean annual lapse rate in this study was −3.7°C/km, with a summer value of −4.3°C/km. Similar to non-glacial settings, there is a large degree of synoptic and seasonal variability in daily lapse rates, with a seasonal cycle that reflects that of Rolland (2003).

Gardner et al. (2009) extend this work through an analysis of regional near-surface temperature lapse rates over several icefields in the Canadian high Arctic for the period 1988–2007. They report a mean ablation season (JJA) value of −4.9°C km^{-1} at all sites, along with substantial regional correlation in daily lapse rates. Winter season lapse rates and their regional correlation are weaker. Gardner et al. (2009) also report a correlation between weaker lapse rates and anomalously warm atmospheric conditions, generally associated with southerly air masses and anti-cyclonic flow (ridging over the Canadian Arctic). The seasonal and synoptic variability in near-surface lapse rates may be sufficiently systematic to incorporate in regional-scale snow and ice melt models, although the patterns of variability are certain to be specific to the meteorological and energy balance regime of a particular region.

A multiyear study of near-surface lapse rates in the glacier boundary layer at a mid-latitude valley glacier, the Haig Glacier in the Canadian Rockies (50.7°N, 115.3°W), also reveals average near-surface lapse rates that are weaker than free-air values, but with the opposite seasonal cycle and extreme summer lapse-rate weakening. Figure 2a illustrates this, based on regressions of daily mean temperature vs. elevation from six temperature sensors along the centerline of the Haig Glacier for the period 2001–2009. Shea et al. (2005) and Sinclair and Marshall (2009) describe the field site and instrumentation in detail.

The buffering effect described above – limited heating in the glacier boundary layer due to the maximum surface

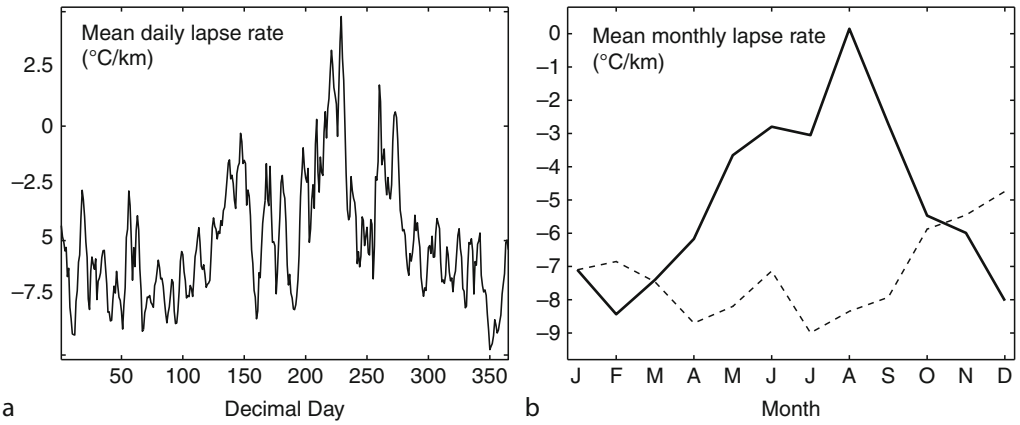

Temperature Lapse Rates in Glacierized Basins, Figure 2 (**a**) Daily average near-surface temperature lapse rates (2001–2009), Haig Glacier, Canadian Rockies (five-point moving average). Values are based on regressions of daily average temperature from a transect of six temperature sensors along the glacier centerline (elevations of 2,530–2,760 m). (**b**) Mean monthly near-surface temperature lapse rates for this period. *Solid line*: the glacier boundary-layer lapse rate, based on the centerline transect. *Dashed line*: calculated from automatic weather stations on the glacier (2,670 m) and in the glacier forefield (2,360 m).

Temperature Lapse Rates in Glacierized Basins, Table 1 Mean seasonal and annual near-surface temperature lapse rates measured on the Haig Glacier, Canadian Rockies, August 2001 to May 2009, °C km^{-1}

	DJF	MAM	JJA	SON	Annual
AWS data	−6.2	−8.1	−8.2	−6.4	−7.2
Glacier transect	−7.9	−5.7	−1.9	−4.7	−5.1

temperature of 0°C – tends to create a more homogeneous boundary layer, weakening summer lapse rates. Downslope winds reinforce this tendency. Mean monthly lapse rates are plotted in Figure 2b (solid line), while seasonal values are given in Table 1: −5.1°C/km annually, weakening to −1.9°C/km in the summer (JJA). The entire glacier surface is at the melting point through this period, and the lapse rates are weakest, with frequent inversions, late in the summer (August) when most snow has melted off the glacier, exposing bare glacier ice. Over the period of record, 2001–2009, the upper accumulation area has been snow-free in August in 5 of 9 years.

Also plotted in Figure 2b are the near-surface lapse rates as determined by the "classical" method of differencing temperatures from two automatic weather stations (AWS sites), one on the upper glacier and one in the glacier forefield. Average daily average temperature gradients through this method are much steeper: −7.2°C/km annually and −8.2°C/km in the summer (Table 1). This is a fundamentally different measure from the lapse rates in the glacier boundary layer; the glacier AWS is on the snow/ice surface, while the forefield AWS is on glacier moraine and is subject to intense summer radiative warming. As discussed by de Scally (1997) for the Punjab Himalaya, this comparison of temperatures on rock vs. a snow/ice surface produces a systematically steep gradient in the summer season.

Caution is needed when interpreting reported lapse rates in glacierized catchments, to ensure that meteorological station environments are comparable. In addition to the different albedo and thermal properties of rock and ice in the example above (i.e., rock can warm above 0°C), stations can be affected by cold air drainage or other microclimatic effects, creating an unrepresentative lapse rates. Regression-based analyses from multiple sites are recommended to minimize this problem. If one is extrapolating temperatures from an off-glacier site, the latter (AWS-derived) lapse rates are probably more appropriate than those measured in the glacier boundary layer. In this case, one needs to differentiate between near-surface lapse rates measured in the valley, forefield, and glacier environments.

Summary

Mean near-surface temperature lapse rates in mountain regions and in the glacier boundary layer are weaker than typical free-air lapse rates. Mean annual values of −4°C/km to −5°C/km are typical of mountain regions and also appear to be representative of summer lapse rates in polar regions. These rates can be much weaker on a melting glacier (bare-ice) surface, as occurs on mid-latitude glaciers in the summer months, as the glacier surface is held at a temperature close to 0°C and relatively homogeneous conditions prevail in the glacier boundary layer. Summer values of ca. −2°C/km are measured on the Haig Glacier and have also been reported on the John Evans Glacier, Ellesmere Island, in the melt season (Gardner et al., 2009).

There is substantial seasonal and synoptic variability in near-surface lapse rates, governed by the surface energy balance, evolution of the surface environment

(e.g., albedo) through the melt season, and the seasonal and synoptic variability of atmospheric conditions. Although the controls and patterns of lapse-rate variability are regionally specific, it is likely that much of the seasonal and synoptic variability in near-surface lapse rates is deterministic and may be possible to include in hydrological and glaciological modelling. Tests of the sensitivity of mass balance models to the choice of lapse rate indicate that this is a first-order control on modelled snow and ice melt, and that application of a fixed, free-air lapse rate can lead to large underestimation of summer melt (Gardner et al., 2009; Marshall and Sharp, 2009).

Bibliography

Arnold, N. S., Willis, I. C., Sharp, M. J., Richards, K. S., and Lawson, M. J., 1996. A distributed surface energy-balance model for a small valley glacier. I. Development and testing for Haut Glacier d'Arolla, Valais, Switzerland. *Journal of Glaciology*, **42**(140), 77–89.

Blandford, T. R., Humes, K. S., Harshburger, B. J., Moore, B. C., Walden, V. P., and Ye, H., 2008. Seasonal and synoptic variations in near-surface air temperature lapse rates in a mountainous basin. *Journal of Applied Meteorology and Climatology*, **47**, 249–261.

Box, J. E., and Rinke, A., 2003. Evaluation of Greenland Ice Sheet surface climate in the HIRHAM regional climate model using automatic weather station data. *Journal of Climate*, **16**, 1302–1319.

Braithwaite, R. J., 1995. Positive degree-day factors for ablation on the Greenland ice sheet studied by energy-balance modelling. *Journal of Glaciology*, **137**(41), 153–160.

Braun, M., and Hock, R., 2004. Spatially distributed surface energy balance and ablation modelling on the ice cap of King George Island (Antarctica). *Global and Planetary Change*, **42**, 45–58.

Carrega, P., 1995. A method for the reconstruction of mountain air temperatures with automatic cartographic applications. *Theoretical and Applied Climatology*, **52**, 69–84.

de Scally, F. A., 1997. Deriving lapse rates of slope air temperature for meltwater runoff modeling in subtropical mountains: an example from the Punjab Himalya, Pakistan. *Mountain Research and Development*, **17**(4), 353–362.

Gardner, A. S., Sharp, M. J., Koerner, R. M., Labine, C., Boon, S., Marshall, S. J., Burgess, D. O., and Lewis, D., 2009. Near-surface temperature lapse rates over Arctic glaciers and their implications for temperature downscaling. *Journal of Climate*, **22**, 4281–4298.

Greuell, W., and Böhm, R., 1998. 2-m temperatures along melting mid-latitude glaciers, and implications for the sensitivity of the mass balance to variations in temperature. *Journal of Glaciology*, **44**(146), 9–20.

Hock, R., 1999. A distributed temperature-index ice- and snowmelt model including potential direct solar radiation. *Journal of Glaciology*, **45**(149), 101–111.

Hock, R., 2003. Temperature index melt modelling in mountain areas. *Journal of Hydrology*, **282**, 104–115.

Huybrechts, P., Letréguilly, A., and Reeh, N., 1991. The Greenland ice sheet and greenhouse warming. *Palaeogeography, Palaeoclimatology, Palaeoecology*, **89**(4), 399–412.

Jóhannesson, T., Sigurdsson, O., Laumann, T., and Kennett, M., 1995. Degree-day glacier mass-balance modelling with application to glaciers in Iceland, Norway, and Greenland. *Journal of Glaciology*, **41**, 345–358.

Klok, E. J., and Oerlemans, J., 2002. Model study of the spatial distribution of the energy and mass balance of Morteratschgletscher, Switzerland. *Journal of Glaciology*, **48**(163), 505–518.

Losic, M., 2009. *On the Turbulent Heat Flux Contributions to Energy Balance at Opabin Glacier*. Yoho National Park, Canada. Unpublished M.Sc. thesis, University of Calgary, 152 pp.

Lundquist, J. D., and Cayan, D. R., 2007. Surface temperature patterns in complex terrain: daily variations and longterm change in the central Sierra Nevada, California. *Journal of Geophysical Research*, **112**, 15, doi:10.1029/2006JD007561 (D11124).

Marshall, S. J., and Clarke, G. K. C., 1999. Ice sheet inception: subgrid hypsometric parameterization of mass balance in an ice sheet model. *Climate Dynamics*, **15**, 533–550.

Marshall, S. J., and Sharp, M. J., 2009. Temperature and melt modelling on the Prince of Wales icefield, Canadian high Arctic. *Journal of Climate*, **22**(6), 1454–1468.

Marshall, S. J., Sharp, M. J., Burgess, D. O., and Anslow, F. S., 2007. Near-surface temperature lapse rate variability on the Prince of Wales icefield, Ellesmere Island, Nunavut: implications for regional-scale temperature downscaling. *International Journal of Climatology*, **27**(3), 385–398.

McCutchan, M. H., 1983. Comparing temperature and humidity on a mountain slope and in the free air nearby. *Monthly Weather Review*, **111**, 836–845.

Pepin, N., and Losleben, M., 2002. Climate change in the Colorado rocky mountains: free air versus surface temperature trends. *International Journal of Climatology*, **22**, 311–329.

Pepin, N., Losleben, M., Hartman, M., and Chowanski, K., 2005. A comparison of SNOTEL and GHCN/CRU surface temperatures with free-air temperatures at high elevations in the western United States: data compatibility and trends. *Journal of Climate*, **18**, 1967–1985.

Rolland, C., 2003. Spatial and seasonal variations of air temperature lapse rates in alpine regions. *Journal of Climate*, **16**, 1032–1046.

Shea, J. M., Marshall, S. J., and Livingston, J. L., 2004. Climate controls on glacier distribution in the Canadian Rockies. *Arctic, Antarctic and Alpine Research*, **36**(2), 272–280.

Shea, J. M., Anslow, F. S., and Marshall, S. J., 2005. Hydrometeorological relationships on the Haig Glacier, Alberta, Canada. *Annals of Glaciology*, **40**, 52–60.

Sinclair, K. E., and Marshall, S. J., 2009. The impact of vapour trajectory on the isotope signal of Canadian rocky mountain snowpacks. *Journal of Glaciology*, **55**(191), 485–498.

Steffen, K., and Box, J., 2001. Surface climatology of the Greenland ice sheet: Greenland climate network 1995–1999. *Journal of Geophysical Research*, **106**, 33951–33964.

van den Broeke, M. R., 1997. Structure and diurnal, variation of the atmospheric boundary layer over a mid-latitude glacier in summer. *Boundary-Layer Meteorology*, **83**, 183–205.

Cross-references

Albedo
Canadian Rockies and Coast Mountains of Canada
Climate Change and Glaciers
Degree-Days
Glacier
Glacier Mass Balance
Greenland Ice Sheet
Himalaya
Katabatic Wind: In Relation With Snow and Glaciers
Melt Runoff Modeling
Moraine
Surface Energy Balance

TEMPERATURE PROFILE OF SNOWPACK

Charles Fierz
WSL Institute for Snow and Avalanche Research SLF, Davos Dorf, Switzerland

Synonyms

Snow temperature distribution

Definition

Snow temperature profiles are records of snow temperatures, T_s, taken within the snowpack along a line vertical or perpendicular to the base, including both snow surface and base temperature, T_{ss} and T_g, respectively (Fierz et al., 2009). Measurement spacing is independent of layer boundaries, usually denser near the surface. Ground surface is in general taken as the base, but on firn fields and glaciers, base refers to the level of either the firn surface or glacier ice. Ground surface temperature, T_g, corresponds to Bottom Temperature of Snow BTS in the field of permafrost.

Significance

A snow temperature profile reflects the temperature distribution within the snowpack at one point in both space and time. Temperature distribution is a consequence of (1) the *snow–atmosphere interactions* at the surface and (2) of ground heat fluxes at the lower boundary (or base) of the snowpack. In addition, energy sinks (melting) and sources (freezing, shortwave radiation) effect temperature distribution and hence the internal energy of the snowpack. In absence of melt-freeze processes, temperature distribution is a signature of the cold content of the snowpack and snow surface temperature reflects the energy balance of the dry snow surface.

Within the snowpack, thermal properties of snow govern the shape and time evolution of the temperature profile. As heat transfer in snow is complex, an "effective" thermal conductivity is usually used to embrace all processes involved. Thermal diffusivity then controls the speed and attenuation of heat waves initiated at or near the surface and propagating through the snowpack. These and other thermal properties of snow are well described in literature (see, e.g., Gray and Male, 1981; Jones et al., 2001; Kaempfer et al., 2005; Armstrong and Brun, 2008). As a result of layering and densification within the snowpack, nonuniform temperature gradients are established that induce water vapor gradients, which in turn drive *snow metamorphism*. Indeed, dry seasonal snowpacks are hardly ever found to be isothermal. Percolating water, however, either from rain or melt at the surface, very efficiently warms up subfreezing snow as it releases latent heat during refreezing. In the end, percolating water leads to an isothermal snowpack at the melting point, that is, the snow temperature reaches 0°C throughout the snowpack. Note that percolating water is seldom an important energy input after this state has been reached.

Finally, spatial variability of the snow cover, e.g., variations in snow depth, strongly influences temperature distribution. This variability mostly results from the interaction of external causes like precipitation and redistribution of snow by wind with topography and vegetation (Schweizer et al., 2008). For example, snowpacks under trees may be shallower than in clearings due to snow interception. Such variations induce lateral heat fluxes within the snowpack, but these are rarely considered in general.

Description of snow temperature profiles

The snow temperature profiles in Figure 1 nicely show the influence of *snow–atmosphere interactions* on the top 50 cm of the snowpack. Starting 18:15 on 23 February 2000, the measurements were done with a specially designed vertical probe pushed downward from the snow surface. IR-thermometers recorded snow surface temperature. The sky was clear up to late in the morning the next day. Under such conditions, one would expect the topmost snow to cool during the night due to long-wave radiation loss. Accordingly, the temperature profile then becomes convex and temperatures near and at the surface are the lowest just before sunrise. In our case, however, the profile recorded around midnight reflected warming of the surface snow. This was due to wind along with raising air temperatures, that is, increasing turbulent heat fluxes, particularly sensible heat. This heat then diffused into the snowpack from the surface. At the surface, however, long-wave radiation losses counterbalanced warming, resulting in a typical Z-shaped profile with a temperature extreme located right below the surface. At 06:05, the heat wave penetrated deeper in the snowpack. In addition, ventilation may also have played a role in this unexpected warming up of the topmost snow made up of decomposing and fragmented precipitation particles.

After sunrise, short wave radiation penetrated the snowpack until about 11:00. The net flux entering the snowpack depends on snow *albedo* that is determined by the properties of the top centimeters of the snowpack. The net shortwave energy then diffused through the snow from the depth at which it was absorbed. The sky being still clear, a Z-shaped or swan-like profile (from French "col de cygne") resulted again. Note, however, that the upper warm extreme of the profile was located somewhat deeper in the snow than the one observed at night. This is a signature of the different energy-delivering mechanisms: heat diffusion in the latter and instantaneous release at depth in the former case.

These temperature profiles also clearly exemplify that heat only slowly penetrates the snow and that heat waves are strongly attenuated with depth. Therefore, below about 30 cm, temperature profiles showed only low-amplitude diurnal cycles that almost disappeared further down. As a consequence, snow is an excellent insulator, a well-known property of this fascinating material.

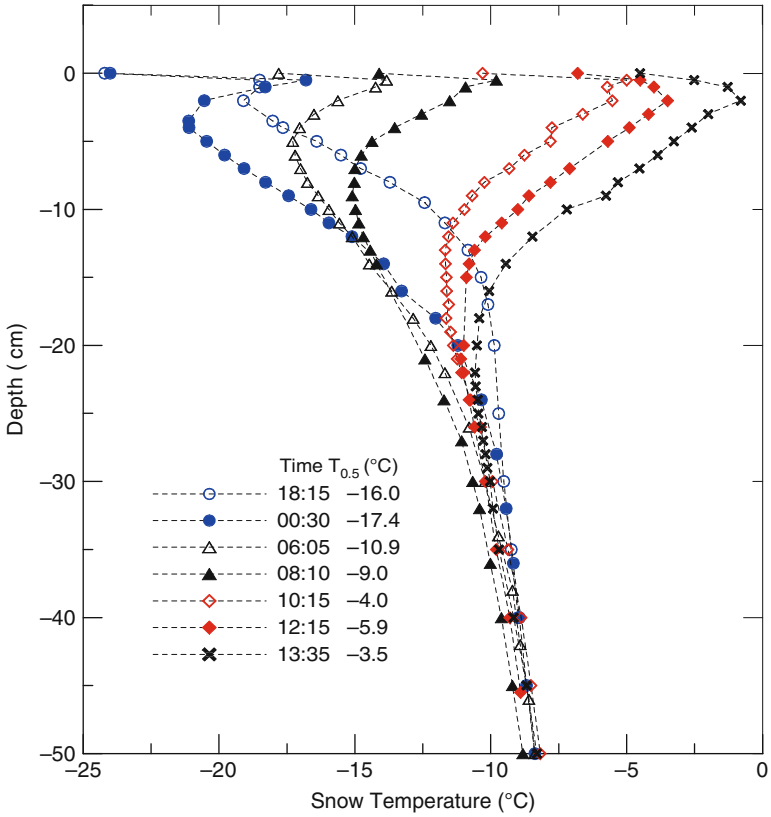

Temperature Profile of Snowpack, Figure 1 Snow temperature profiles measured 23–24 February 2000, on the study plot of the WSL Institute for Snow and Avalanche Research SLF, Weissfluhjoch, 2540 m a.s.l., Davos, Switzerland. The temperature probe was inserted vertically down from the surface.

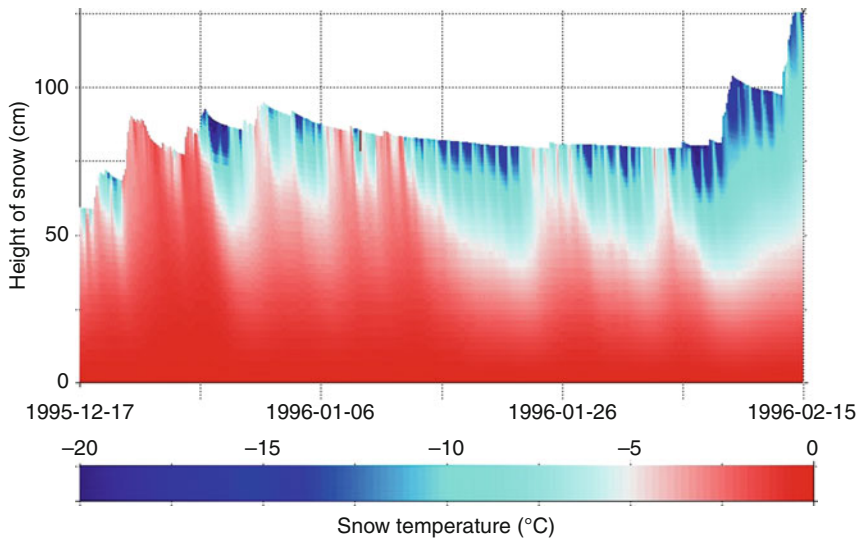

Temperature Profile of Snowpack, Figure 2 Numerical simulation of the temperature distribution within the snowpack. Input data originate from the Weissfluhjoch study plot, 2540 m a.s.l. The model used is SNOWPACK, developed at WSL Institute for Snow and Avalanche Research SLF, Davos, Switzerland.

Modeling the temperature distribution of a snowpack

Snow temperature distribution over time is often simulated with numerical models like SNOWPACK (see, e.g., Lehning and Fierz, 2008). Figure 2 presents one such simulation for part of the winter 1995/96 at Weissfluhjoch, Davos, Switzerland (2540 m a.s.l.). Note that the white "band" in Figure 2 corresponds to about −5°C. The simulation nicely reproduces the characteristic warm and rather slowly varying temperatures near the ground, while close to the surface, the snow experiences the influence of daily changing meteorological conditions. The time delay with depth is also clearly visible as well as the alternation of cold and warm waves travelling through the snowpack.

Measuring snow temperatures

There are various ways to measure temperature profiles in the snowpack. Most of them require first digging a pit and then placing suitable temperature sensors from the side wall (see Figure 3a). If measurements are done manually, the sensor is displaced by the observer and the record represents one point in time. This is the classical way to measure snow temperature profiles. A vertical resolution of a few centimeters can be reached with some uncertainty in the positioning. Furthermore, as seen in Figure 3a, measurements have to be shadowed to avoid the sensor picking up shortwave radiation and reading erroneous temperatures due to self-heating. This problem affects all types of snow temperature measurements down to 20–30 cm, at which depth almost all shortwave radiation will have been absorbed by the snow. Infrared thermography can also be used to take instantaneous shots of temperature profiles. However, the pit wall must be freshly dug out as snow temperature on the pit wall will quickly equilibrate to air temperature prevailing in the pit. Snow surface temperature, however, is best measured with contactless IR-thermometers, avoiding radiation pickup and positioning of sensors at the surface of the snowpack.

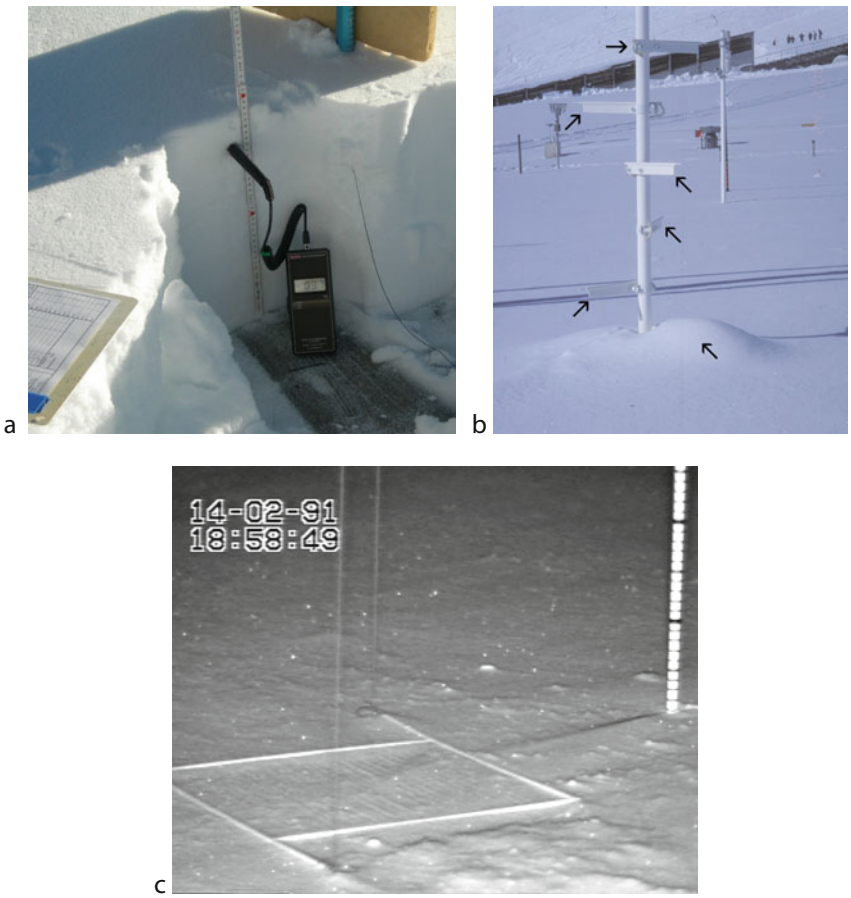

Temperature Profile of Snowpack, Figure 3 Different ways to measure snow temperatures. (**a**) Conventional manual measurement. Note that the surface need to be shaded during measurements performed within the top 10–20 cm of the snowpack. (**b**) Temperature sensors at fixed heights shown by arrows on the pole in the middle of the photo. Note that sensor readings may be effected by the settling snowpack or vice versa. (**c**) Snow harp seen just before being snowed in by the ongoing snowfall. This device records simultaneously height and temperature (Fierz and Lehning, 2001). The fine tungsten wire recording temperature is still visible.

To avoid digging a pit, vertical probes can be used. For example, a specially designed probe was used to measure the profiles shown in Figure 1. In particular, the material supporting the measuring thermocouple has to be chosen such as to avoid heat diffusion from the part of the probe exposed to air and radiation to the probe tip.

If measurements have to be continuous over longer time scales, several sensors can be placed in the pit wall and the pit backfilled. For example, this is often done in polar snowpack studies, for which either several single sensors or strings of either thermistors or thermocouples are used. To measure accurately snow temperatures near the surface, however, careful sensor design is required to reduce both shortwave radiation pickup and differential settling of both snow and sensors (see, e.g., Bakermans and Jamieson, 2006). To know the real position of the sensors during measurements requires back-calculations after removal.

Mounting sensors on fixed structures such as poles avoids the uncertainties in position. However, the supporting structure and the fixed sensors will disturb the free settlement of the snowpack (see Figure 3b) and a perfect contact to the surrounding snow is often questionable. In general, measurements of such sensors not covered by at least 10 cm of snow measured from the undisturbed surface should be discarded. Because of the difficulties involved, few attempts have been made to design sensors capable of recording both their position and the corresponding snow temperature as shown in Figure 3c (Fierz and Lehning, 2001).

Summary

Temperature distribution, more precisely its evolution with time, illustrates what processes are at work within the snowpack. It reflects the current state of the internal energy of the snowpack as a result of energy exchanges at the interfaces with both ground and atmosphere and the interplay with internal heat sinks and sources. Snow temperature profiles are snapshots of snow temperature distribution, both in time and space. Measuring snow temperature profiles over longer period of time requires careful experimental design to be useful for further analysis.

Bibliography

Armstrong, R. L., and Brun, E. (eds.), 2008. *Snow and Climate: Physical Processes, Surface Energy Exchange and Modeling*. Cambridge: Cambridge University Press.

Bakermans, L. A., and Jamieson, B., 2006. Measuring near-surface snow temperature changes over terrain. In *Proceedings ISSW 2006*. International Snow Science Workshop, Telluride, 1–6 October 2006, pp. 377–386.

Fierz, C., and Lehning, M., 2001. Assessment of the microstructure-based snow-cover model SNOWPACK: thermal and mechanical properties. *Cold Regions Science and Technology*, **33**(2–3), 123–131.

Fierz, C., Armstrong, R. L., Durand, Y., Etchevers, P., Greene, E., McClung, D. M., Nishimura, K., Satyawali, P. K., and Sokratov, S. A., 2009. *The International Classification for Seasonal Snow on the Ground*. UNESCO-IHP: Paris. IHP-VII Technical Documents in Hydrology N°83, IACS Contribution N°1, pp. 80.

Gray, D. M., and Male, D. H. (eds.), 1981. *Handbook of Snow*. Toronto: Pergamon Press (reprinted 2004; The Blackburn Press).

Jones, H. G., Pomeroy, J. W., Walker, D. A., and Hoham, R. W. (eds.), 2001. *Snow Ecology: An Interdisciplinary Examination of Snow-Covered Ecosystems*. Cambridge: Cambridge University Press.

Kaempfer, T. U., Schneebeli, M., and Sokratov, S. A., 2005. A microstructural approach to model heat transfer in snow. *Geophysical Research Letters*, **32**(21), L21503, doi:10.1029/2005GL023873.

Lehning, M., and Fierz, C., 2008. Assessment of snow transport in avalanche terrain. *Cold Regions Science and Technology*, **51**, 240–252.

Schweizer, J., Kronholm, K., Jamieson, J. B., and Birkeland, K. W., 2008. Review od spatial variability of snowpack properties and its importance for avalanche formation. *Cold Regions Science and Technology*, **51**, 253–272.

Cross-references

Albedo
Atmosphere–Snow/Ice Interactions
Layering of Snow
Percolation Zone
Snow Metamorphism

TERMINUS

Amit Kumar
Department of Geology, Centre of Advanced Study in Geology, Punjab University, Chandigarh, India

Synonyms

Snout

Definition

Glacier terminus (snout) is the end of a glacier at any given point in time (Figure 1). Although glaciers seem motionless to the observer, in reality they are in very slow motion and the glacier terminus is always either advancing or retreating. The location of the terminus is often directly related to glacier mass balance. The position of a glacier terminus is also affected by localized or regional temperature change over time. Changes in location of a glacier terminus with time are determined by monitoring a glacier's movement. The difference in location of a terminus as measured from its fixed position at different time intervals provides a record of the glacier's movement. Another way of detecting changes in the movement of terminus of glacier is comparing satellite imageries of the glacier's position at different times.

The form of a glacier terminus is determined by many factors. If the glacier is retreating, it is usually gently sloping in form because a melting glacier tends to assume this shape. But there are many conditions that modify this typical shape, including the presence of thermal fields and

Terminus, Figure1 View of Terminus (Gaumukh) of Gangotri glacier in Himalayas.

various stresses that cause cracking and melting response resulting in glacial calving and other diverse forms.

Bibliography

Benn, D. I., and Evans, D. J. A., 1998. *Glaciers and Glaciation*. London: Arnold.
Fairbridge, R. W. (ed.), 1968. *The Encyclopedia of Geomorphology*. New York: Reinhold Book.
Hambrey, M., and Alean, J., 2004. *Glaciers*, 2nd edn. Cambridge: Cambridge University Press.
Thomas, D. S. G., and Goudie, A. (eds.), 2000. *Dictionary of Physical Geography*. Oxford: Blackwell.
Whittow, J. B., 1984. *The Penguin Dictionary of Physical Geography*. London: A. Lane.

Cross-references

Glacier Mass Balance

TERRACES

Amit Kumar
Department of Geology, Centre of Advanced Study in Geology, Chandigarh, Punjab University, India

Synonyms

Kame terrace

Definition

Terrace is generally a series of surfaces in a stream valley, flanking and more or less parallel to the stream flow direction. These surfaces originally formed at or below the level of the stream, and now higher than the present stream. They represent the former valley floors and dissected remnants former flood plain. The melt water from glaciers carries immense amounts of sediment: clay, sand, gravel, and rock fragments. It deposits these sediments, creating a riverbed at the height of the terrace. As the glacier ice recedes, the river transports sediments. The kame terrace is termed as the distinctive landform that is formed when the glacier retreats, the former stream bed is left perched above the deglaciated valley floor.

Bibliography

Fairbridge, R. W. (ed.), 1968. *The Encyclopedia of Geomorphology*. New York: Reinhold Book.
Holmes, A., 1978. *Principles of Physical Geology*. London: English Languages Book Society (ELBS) and Nelson, 730 pp.
Thornbury, W. D., 1961. *Principles of Geomorphology*. New York: Wiley.

Cross-references

Kame and Kettle Topography

THAW WEAKENING

Divya Dudeja
Department of Geology, DBS (P.G.) College, Dehradun, Uttarakhand, India

The ice located in the frozen, frost-susceptible soils of cold regions is subjected to thawing when seasonal or diurnal temperatures rise. Thawing causes saturation of soil by excess water that is restricted from draining due to frozen underlayers. This saturation reduces soil strength due to generation of excess pore pressure and the saturated active

layer becomes substantially weaker and tends to lose bearing capacity. This is called thaw weakening.

Occurrence of thaw weakening depends on frost-susceptible soil, its permeability, poor drainage conditions, and rate of thaw. Knutson (1993) categorized soil in high to low frost-susceptible soils. High frost-susceptible soils are typically coarse silts with less than 40% of particles smaller than 0.002 mm, more than 12% of particles smaller than 0.02 mm, and more than 50% of particles smaller than 0.2 mm.

Depending upon the surface temperature conditions, thawing can proceed downward from the top, or upward from the bottom, or in both directions. During a sudden thaw, melting will proceed almost entirely from the surface downward. This type of thawing leads to extremely poor drainage conditions.

Thaw weakening adversely affect stability of pavements, slopes, and other engineering structures in cold regions. Traffic on thaw-weakened pavements may cause permanent damage onto the surface like rutting, widening of the pavement, cracking, and failure of the pavement.

In order to mitigate the detrimental effects of thaw weakening, the assessment of depth of thawing is a prerequisite that depends in part on the magnitude and duration of the temperature differential below or above freezing at the ground surface. For the depth of thawing, thawing index (TI) is estimated. The air thawing index is the annual summation of the thawing degree-days. A thawing degree-day is defined as the mean daily temperature minus freezing temperature multiplied by 1 day, when the mean daily temperature is above freezing.

$$\mathrm{TI} = \sum (T - T_f) \cdot d$$

where T = mean daily temperature T_f = Thawing temperature (typically 0°C).

The calculated TI can be used to estimate the depth of thawing by modified Berggren formula given as

$$x = 13.15\lambda\left[(k_{avg} n \mathrm{TI})/L\right]^{0.5}$$

Where x = depth of freeze or thaw (m) λ = dimensionless coefficient that takes into consideration the effect of temperature changes in the soil mass k_{avg} = thermal conductivity of soil, average of frozen and unfrozen, W/(m °C) n = surface correction factor for TI, TI = air thawing index or freezing index (°C days), L = Specific volumetric latent heat of fusion (kJ/m^3).

These estimations are helpful in structure designing and mitigating adverse affects of thaw weakening by limiting depth of frost penetration, replacing or modifying frost-susceptible soils, and providing effective drainage.

Bibliography

Knutson, A., 1993. *Frost Action in Soils*. Oslo: Norwegian Road Research Laboratory, p. 40.

Smith, D. W., 1996. *Cold Regions Utilities Monograph.* American Society for Civil Engineering Publications, p.780.

Cross-references

Freezing and Thawing Index
Permafrost

THERMAL INFRARED SENSORS

Anju Chaudhary
Water Resources System Division, National Institute of Hydrology, Roorkee, India

Definition

All matter radiates energy at thermal infrared wavelengths (3–14 μm) during day and night. The infrared radiation region representing the wavelengths from 3–14 μm is called the thermal IR region. Photographic films do not detect thermal IR radiation. Thermal infrared sensors detect and record this thermal radiation as images. Majority of satellites have thermal infrared sensors on board. These sensors operate in the same fashion as visible and near infrared sensors. The signal from thermal IR range of spectrum is significantly weak and presently available sensors are typically less sensitive to it. This leads to sensors with lower resolution and longer dwell time to increase the energy that is integrated. While it is easier to distinguish clouds from the land by visible sensors, more detail inside the clouds is obtained by the infrared sensors. This is useful for studying cloud structure.

Thermal IR images generally record broad spectral bands, typically 8–14 μm for images from aircraft and 10.5–12.5 μm for images from satellites.

Applications

Thermal infrared sensors are used for infrared imaging for both military and civilian purposes. Military applications include target acquisition, surveillance and night vision, homing, and tracking. Nonmilitary uses include thermal efficiency analysis, remote temperature sensing, and weather forecasting. The main advantage of infrared sensors is that it can take images at night, allowing a continuous sequence of weather to be studied.

Thermal infrared sensors are used in the field of climatology. In this field, atmospheric infrared radiation is monitored to detect trends in the energy exchange between the earth and the atmosphere. These trends provide information on long-term changes in the earth's climate. It is one of the primary parameters studied in research into global warming together with solar radiation.

Weather satellites equipped with thermal infrared sensors produce thermal infrared images, which can be used to determine cloud heights and types, to calculate land surface water temperatures, and to locate ocean clouds of gas and dust in our galaxy.

THERMAL REGIME OF ICE-COVERED LAKES

Lars Bengtsson
Department of Water Resources Engineering,
Lund University, Lund, Sweden

Definition

Thermal regime of ice-covered lakes considers the heat fluxes to and from a water body without direct contact with the atmosphere, the temperature distribution over the depth, and how it changes during the ice-covered period.

In the autumn after the surface water is cooled to 4°C and the water has turned over, the warmest water in a lake is that of the highest density. The surface water is colder than the bottom water. If there is a very cold period shortly after turnover, a wind-sheltered lake may freeze-over when the water not far from the surface and downward is still 4°C. In another year, the turnover may be followed by an extended windy period with air temperatures fluctuating around 0°C, resulting in a reduction of the lake water temperature down to considerable depths. The initial temperature profile after freeze-over is quite different for the two situations.

Once a lake has a stable ice cover, the lake water is more or less insulated from the atmosphere. The heat lost to the cold atmosphere is taken from the latent heat released from the ice growth. There is a small sensible heat flux from the water to the underside of the ice. The major heat flux in an ice-covered lake is that from the sediments to the lake water. Heat stored in the sediment from summer to winter is released. The lake water temperature increases in course of the winter (see Figure 1) from Lake Velen in Sweden. Lakes in cold long winter climate tend to be warmer than lakes in milder climate with less stable winters. In the milder climate, the lakes freeze-over later, when they have cooled down throughout the vertical, and also in the milder climate the lake ice may break up several times during winter, allowing wind mixing and heat losses directly to the atmosphere. The bottom temperature is often 4°C already at the time of freeze-up; if not, because of the contribution of heat from the sediments this temperature is approached in the course of the winter. The bottom temperature may even be slightly higher than 4°C, due to diffusion of solutes from muddy sediments.

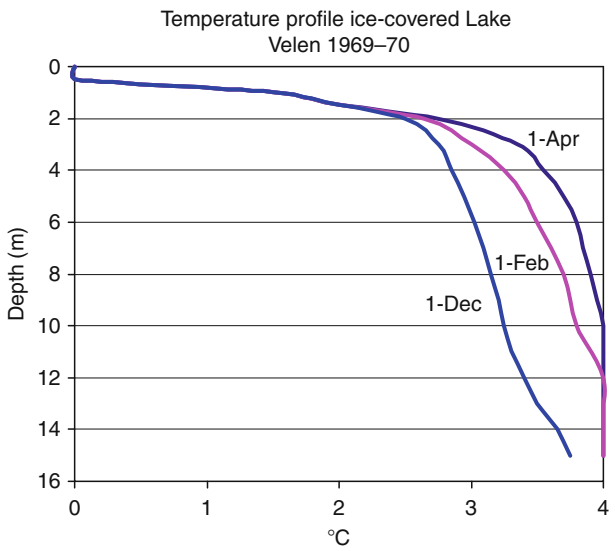

Thermal Regime of Ice-Covered Lakes, Figure 1 Temperature in ice-covered Lake Velen, mean depth 6.5 m, maximum depth 17 m, lake area 2.8 km^2.

The sediments gain heat from the lake water during summer. The sediments are warmer at low water depth than at larger depths, since the surface water is warmer than the bottom water during summer. The heat budget of the sediments in Swedish lakes that develop a thermocline during summer is of the order 10^8 J/m^2 (e.g., corresponding to 2.5°C temperature change in 10 m of water). In the ice-covered period, the surface water is colder than the bottom water. Thus, when heat is released from the sediments to the water during winter, the heat flux is considerably higher in the shallow parts of a lake than at the deeper parts. As heat is released the sediments cool down and the lake water slowly becomes warmer, so the heat flux from the sediments is reduced in course of the winter. The sediment heat flux at shallow water may be in the range 4–10 W/m^2 in early winter and reduce to 1–3 W/m^2 in late winter. At the deep part of a lake it is smaller, 2–3 W/m^2 in early winter, and less than 1 W/m^2 prior to breakup. The warming of the lake water temperature profile over an ice-covered period is shown for Lake Velen in Sweden, Figure 1.

The heat balance of an ice-covered lake is

$$\text{Heat content change} = \text{sediment heat flux} - \text{heat loss to ice} + \text{solar radiation} + \text{heat loss with through} - \text{flow}$$

The heat advection with the through-flow is very small in most lakes, since the river through-flow per unit lake area is small and the temperature of the inflowing river water is very close to 0°C. When the outflow and inflow both are 1 m^3/s in a 5 km^2 large lake, the inflow temperature being 0°C and the outflow temperature 0.5°C, the heat loss is 0.4 W/m^2. In narrow fjord-lakes the flow may be substantial. However, in such lakes a thermocline develops so that the river runs through the lake within a top layer of 0°C temperature.

The sediment heat flux is already mentioned as the most important heat flux. The only heat loss, except the heat loss with outflowing water, is the sensible heat flux from the water to the underside of the ice. A pronounced temperature gradient develops close to the underside of the ice. A viscous sublayer develops. Temperature measurements very close to the ice have shown that the heat flux is 1–2 W/m^2 in most lakes but can be rather much higher

in late spring. Higher midwinter values have been reported from small very shallow lakes.

In spring when the snow on the ice melts, solar radiation can penetrate the ice and heat the water below. The surface water becomes instable. Convection is initiated and a mixed top layer is formed. The temperature gradient next to the ice sharpens and the heat flux to the ice increases. The transmissivity of snow ice is low, but much solar radiation can pass through black ice. Although only a small fraction of the solar radiation reaches the lake water, the flux is higher than the other fluxes in an ice-covered lake. Depending on the ice character and the ice thickness and time of year the solar radiation penetrating the ice is 10–40 W/m^2, partly compensated for by increased heat transfer from the water to the ice.

The knowledge of the thermal conditions in lakes is essential when planning for water intakes, so that desirable water is provided, or planning for discharge of effluents, so that recirculation is avoided. Withdrawal and release of water may affect the thermal conditions. Also regulation of rivers causing winter flows to be higher than the natural ones may influence the temperature in an ice-covered lake; large river flows may result in advective heat losses and cooler lakes.

Bibliography

Ali Maher, O., Uvo, C., and Bengtsson, L., 2005. Comparison between the thermal regime of a shallow ice-covered lake during two extreme NAO winters. *Journal of Hydrometeorology*, **6**(5), 775–783.

Bengtsson, L., and Svensson, T., 1996. Thermal regime of ice covered Swedish lakes. *Nordic Hydrology*, **27**, 39–56.

Bengtsson, L., Malm, J., Tehrzevik, A., Petrov, M., Boyarinov, P., Glinsky, A., and Palshin, N., 1996. Field investigation of winter thermo- and hydrodynamics in a small Karelian lake. *Limnology and Oceanography*, **41**, 1502–1513.

Cross-references

Circulation and Mixing in Ice-Covered Lakes
Ice Covered Lakes

THERMOKARST

Debasmita Misra[1], Ronald P. Daanen[2], Anita M. Thompson[3]
[1]Geological Engineering, College of Engineering and Mines, University of Alaska Fairbanks, Fairbanks, AK, USA
[2]Geophysical Institute, University of Alaska Fairbanks, Fairbanks, AK, USA
[3]Department of Biological Systems Engineering, University of Wisconsin-Madison, Madison, WI, USA

Synonyms

Cave-in lake; Permafrost thaw; Thaw lake

Definition

Karst: The term Karst is usually associated with a characteristic topography formed due to groundwater dissolving sedimentary rocks such as limestone. These characteristics of the topography are usually channels, shafts, caves, tunnels, and sinkholes. The land thus becomes fragile and is susceptible to erosion and pollution.

Thermoerosion: Thermoerosion refers to erosion by water combined with its thermal effect on frozen ground. Small channels can develop into gullies up to several kilometers in length, growing at rates of 10–20 m/year, and in sandy deposits, as fast as 1 m/h. The main climatic factors controlling the intensity of thermoerosion are snow melt regime and summer precipitation. (Source: http://www.cartage.org.lb/en/themes/Sciences/Earthscience/Geology/WaterCycles/Frozenground/Frozenground.htm.)

Thermokarst: Thermokarst refers to a range of characteristic landforms features created in areas of low relief underlain by permafrost with excess ice thaws. These are unevenly distributed and include subsidence of ground with massive ice, water-filled depressions, "drunken" forests, new fens, and other forms of thaw settlement that account for many of the geotechnical and engineering problems encountered in periglacial landscapes. Even where repeated ground freezing takes place, thermokarst features, once formed, are likely to persist. The occurrence of thermokarsts is thus limited to high latitudes or at times in high altitudes of the earth. These features render the land to be susceptible to erosion and degradation. (Source: http://www.cartage.org.lb/en/themes/Sciences/Earthscience/Geology/WaterCycles/Frozenground/Frozenground.htm.)

Introduction

Thermokarst has been described as characteristic landforms that result from thawing of ice-rich permafrost or the melting of massive ice (French, 1976; Washburn, 1980; van Everdingen, 1998). Thermokarst topography forms as ice-rich permafrost thaws, either naturally or anthropogenically, and the ground surface subsides into the resulting voids (Brown and Grave, 1979; Hinzman et al., 1997). The important processes involved in thermokarsting include thawing, ponding, surface and subsurface drainage, surface subsidence, and related erosion. These processes are capable of rapid and extensive modification of the landscape and predicting, preventing, or controlling thermokarst is a major challenge for northern development (Lawson, 1986). The depression formed by thaw settlement is at times occupied by what is termed as a thermokarst lake (also called thaw lake). Typically, such lakes may expand by thermokarst forming processes (Wallace, 1948; Hopkins, 1949; Williams and Smith, 1989; Grosse et al., 2006). Even small disturbances, especially on the surface, that affects the soil thermal regime can initiate thermokarst processes and create related lakes. Many thermokarst ponds and depressions have been

observed across Interior Alaska and Canada in regions of discontinuous permafrost (Jorgenson et al., 2001; Osterkamp et al., 2000; Burn and Smith, 1990).

Permafrost thawing has profound implications for two major reasons. First, large areas of permafrost (about 50% in Alaska) are ice-rich. Permafrost underlies 20–25% of the northern hemisphere land area (Brown et al., 1997). Ice that forms during periods of cold climate frequently constitutes a high proportion (20–30%) of the volume of these frozen soils (Brown et al., 1997). Consequently, melting of permafrost can lead to surface collapse of soils forming thermokarst. When this ice melts, the ground above can subside dramatically. Since these ice deposits are erratically distributed, permafrost thawing can disrupt a level ground surface into a jumble of trenches and pits. Thaw settlement related to permafrost degradation is presently responsible for damage to houses, roads, airports, military installations, pipelines, and other facilities founded on ice-rich permafrost (Osterkamp et al., 1997).

The primary control on local hydrological processes in higher latitudes of the earth is dictated by the presence or absence of permafrost, but it is also influenced by the thickness of the active layer (layer of soil above the permafrost and below the ground surface that freezes and thaws annually) and the total thickness of the underlying permafrost (Hinzman et al., 2001). The permafrost underlying the active layer poses an extremely low permeability barrier and may be compared to poorly drained soils underlain by shale or clay. The inability of soil moisture to infiltrate to deeper underground zones under poorly drained conditions and the previous pore volume expansion due to ice result in super saturated soil moisture regimes in the active layer during the thaw season. Thermokarst can thaw the upper portion of permafrost, the intermediate layer, which is super saturated with ice. The added water and lack of soil structure can lead to highly unstable ground in areas where the super saturated soils could easily detach (active layer detachment slide) and displace the soil from its matrix due to either high hydraulic gradient (or due to high hydrostatic pressure), due to action of gravity on a slope, or a combination of both.

A disturbance to a permafrost environment such as removal of the surface organic layer and installation or removal of a road will modify the surface energy and water balances and change the ground thermal regime often resulting in a deepening of the active layer (Klinger et al., 1983; Waelbroeck, 1993). If during this process ice-rich soils are thawed, catastrophic settling may occur causing formation of a thaw lake or thermokarst (Carter et al., 1987). It has been reported by Greenpeace (http://archive.greenpeace.org/climate/arctic99/reports/perma.html) that thermokarst formations in Alaska have forced the abandonment of a hospital in Kotzebue, are ruining homes and the local schoolhouse in Kipnuk, have required the reconstruction of roads in Fairbanks and airport runways in Deadhorse, and have created large landslides and ground collapse near Tuktoyaktuk and many other places in the Arctic. The second reason for concern is that organic material in thawing permafrost decays rapidly, releasing large quantities of carbon dioxide and methane (Khalil and Pusmussen, 1989; Kvenvolden and Lorenson, 1993; Walter et al., 2006). Moreover, large summer methane releases are closely correlated to warming temperatures.

Hydrology and the related processes of heat and mass transfer are vital linkages between the atmospheric, terrestrial, and aquatic ecosystems. If we do not physically understand this coupling, we will never reach the point where we can understand and predict the impact of disturbance (such as initiation of thermokarsts) or restoration (such as incorporation of the thermal effects of revegetation) (Hinzman et al., 1997). There is a significant lack of understanding of the degree to which the surface energy balance changes in response to disturbance that causes initiation and growth of thermokarsts. Equally important is the impact of alterations in the thermal regime of soils on physical stability and consequently, surficial morphology. This lack of understanding stems from the complex nature of the formation of thermokarsts (Nixon, 1975; Jorgenson et al., 2001).

As a result of the warming of soil temperatures, long-term permafrost degradation has already started at some sites (Federov, 1996; Osterkamp et al., 2000; Jorgenson et al., 2001; Federov and Konstantinov, 2003; Gavriliev and Efremov, 2003) forming thermokarsts in the process. Changes in permafrost regime probably reflect undocumented changes in the thickness or thermal conductance of snow or vegetation, in addition to changes in air temperature (Osterkamp and Romanovsky, 1999). Thermokarst features are developing actively in the zone of discontinuous permafrost (Osterkamp and Romanovsky, 1999), particularly in association with fire and human disturbance, but there are no long-term records from which to detect trends in the regional frequency of thermokarst.

The large observed and predicted future climatic changes will inevitably change the energy and mass fluxes at the land surface and, as a result, the near-surface and subsurface physical conditions in the Arctic and Sub-Arctic. This will trigger changes in ecosystems, hydrology, and infrastructure because the stability of these systems in the north relies on the stability of ice that, so far, holds these systems together. In losing permafrost, we are losing the stability of systems. Thermokarst and related lakes are closely linked to the ground thermal regime and, thus, especially sensitive to changes in boundary conditions. The existence of thermokarst lakes is a clear expression of ground conditions (e.g., thermal regime and ice content). Even small changes in boundary conditions such as climate can be made clearly visible by thermokarst processes. Thermokarst lakes can, therefore, be seen as geo-indicators (Romanovskii et al., 1996).

Phases of a thermokarst

According to Black (1969), "The genesis and evolution of thermokarst depressions and thermokarst lakes remain

some of the least understood cryogenic processes" (Toniolo et al., 2009). The evolution to maturity of a thermokarst has three stages: (1) the origination or initiation, (2) the progression or growth, and (3) the stable formation and expansion of a thaw lake.

Thermokarst initiation

Perhaps the least understood and studied aspect of the thermokarst is its initiation. While it is known that thermokarsts are initiated due to changes in the thermal regime of a permafrost underlain soil due to the thawing of the ice-rich permafrost, these features only occur in certain regimes of the soil and not in all places where thermal imbalance has occurred. This origination or initiation of thermokarst is yet a mystery to scientists and engineers, although such initiation has direct impact on soils, structures, and other engineering aspects of areas underlain by permafrost. Having stated such, it is also difficult to study the initiation of thermokarsts because the process can originate quite suddenly and at times in remote and inaccessible locations. Hence, to our knowledge, there has been no record of the cause of the origination of a thermokarst. Nonlinear processes are similar to the flap of a butterfly, which can cause the formation of a hurricane, and a foot print of a caribou that can cause the formation of a lake. One of the necessary components is ice-rich permafrost close to the surface in the intermediate layer. Further study of these ice-rich layers is necessary to understand catastrophic change in the arctic landscape.

Thermokarsts are crucial to study because they form suddenly and the reason for their initiation is still not well understood. However, some scientists are of the opinion that these thermokarsts could form quickly or may take decades (Hinzman, 2004, Personal Communication). They may respond to disturbance or to a warming climate or some interaction of both. They do have very important implications for engineered structures in higher latitudes, but they are also indicative of a warming climate with broad impacts to huge geographical areas. Whether anthropogenic activities are responsible for such initiation is not well known. With the new highways, bridges and railroads that are being built consistently and the existing structures that influence the permafrost as well as the ground, it is crucial to understand the initiation, progression, and potential impact of the thermokarst.

There are several aspects of the initiation and development of a thermokarst that are not well understood. For example,

- What soil conditions are responsible for initiation of a thermokarst?
- What thermal regime is responsible for such initiation?
- What are the bounding factors that either allow or prohibit progression of a thermokarst?
- What are the factors that contribute to the process and quantity of erosion from a thermokarst?
- What is the quality of the water that emanates from a thermokarst?

It has been hypothesized that the soil gradient (slope) (cf. Strang, 1973), percent of fine materials in soil, the soil bulk density, depth of active layer, and change in thermal regime are variables that affect the initiation of a thermokarst. Additionally, the supersaturation of soil and connectivity to remote groundwater source provides the hydrostatic head and the hydrodynamic force to detach the soil from its matrix and transport it downstream, thus developing the eroded gully.

Although it has not been established, however we hypothesize that the thermokarsts are initiated due to preferential thaw settlement at the top and with a constant source of water at the bottom such as the ones observed in laboratory conditions (Figures 1 and 2). The figures illustrate the time scale thaw settlement in a silty-loam soil with approximately 50% fines. The experimental set up was designed such that we have only top down freezing with a constant source of water from the bottom. Figure 1 shows the completely frozen soil at 9:15 am. Figure 2

Thermokarst, Figure 1 Soil completely frozen at 9:15 am.

Thermokarst, Figure 2 Preferential thaw settlement at room temperature after 5 h of thaw.

shows preferential thaw settlement and channel development at 2:15 pm.

The aspect of underlying permafrost degradation has not been included in the laboratory studies in Figures 1 and 2. However, once the thaw settlement is initiated, the groundwater finds a path to remove the fines from these settled zones to create a gully. This gully is next expanded with more groundwater action and surface abrasion. Sediments removed are transported downstream of the gully thus creating a permanent topographic depression. This aspect or stage of the thermokarst has been studied, although in a very limited context (see Toniolo et al., 2009).

Thermokarst growth

The rapid growth of a thermokarst in Alaska has been studied by Kodial (2005) and Kodial et al. (2005), perhaps for the first time. They speculated that the initiation of the thermokarst was directly related to a major rainfall event with 90 mm of precipitation that occurred over a 2-day period, which triggered the thermal erosion. The thermokarst subsidence occurred when the energy balance at the ground surface was modified, which increased the heat flux to the subsurface layers, thus initiating the thaw of permafrost ice wedges and formation of terrain depression. Toniolo et al. (2009) state, "These depressions may grow due to subsidence over successive summers. When conditions are favorable for water storage, ponding can be significant. The presence of subsurface formations such as pipes and sinkholes may lead to drainage of the stagnant water, depending on the groundwater static level. Gradually shorelines stabilize as the ground subsides. Erosion and sedimentation are final steps in the thermokarst formation process."

The development or growth of a thermokarst is also observed from other physical indicators such as drunken trees, slumping of banks, and submergence of vegetation (Burn, 1992). Dingman (1976) states that rapid and extensive degradation of landforms occur in northern latitudes when significant amount of flowing water comes into contact with ice-rich soil. This subsidence and subsequent increased thermokarst development are amplified by the thermal erosion associated with the flowing water (U.S. Arctic Research Commission Permafrost Task Force, 2003). This process can be best illustrated in Figure 3.

Associated with growth of thermokarst is the yield of higher sediment loads, especially beginning with removal of finer sediments due to melting of ice and the resulting viscous slurry flow out of the soil matrix that would weaken the soil structure followed by abrasion due to ground water or surface water flow through the gully that would remove the coarser particles. Toniolo et al. (2009) report, "The probability that this disturbed terrain will recover to its original stable configuration on the time scale of decades to perhaps centuries is very low, as seen in three intensive study sites located in the National

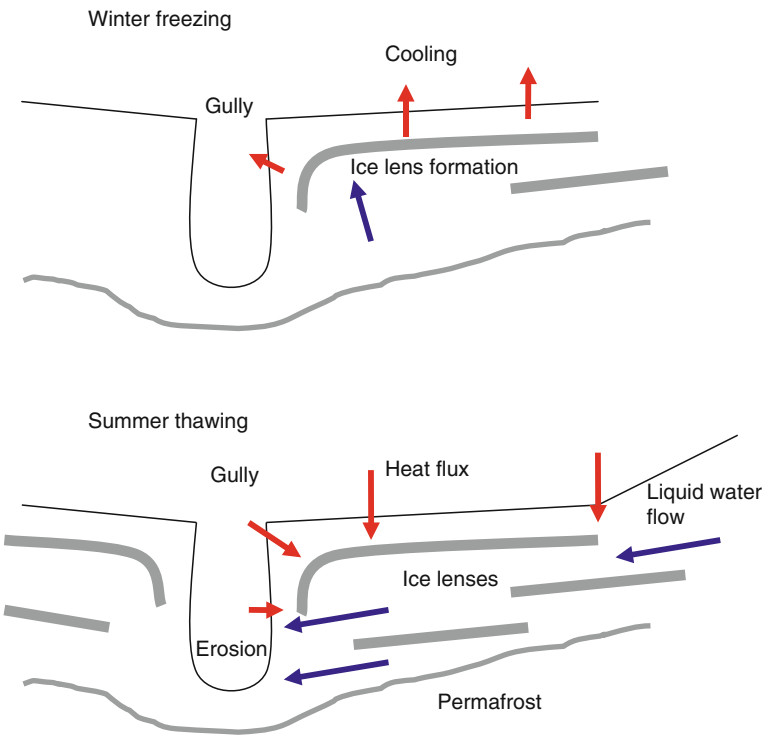

Thermokarst, Figure 3 Schematic representation of Thermokarst growth.

Thermokarst, Figure 4 Photograph of the Caribou-Poker creeks research watershed thermokarst showing profiles from where soil samples were collected and temperature was measured.

Petroleum Reserve-Alaska (Lawson, 1986). Recently, Fortier et al. (2007) observed rapid changes in landscape due to gully evolution in the Bylot Island (Canada). The formation of sinkholes initiated gully evolution in the area. Carey and Woo (2000) described the importance of cryogenic piping in slope runoff. High velocity flows inside the pipes could cause soil destabilization and gully formation."

In order to develop a better understanding of the growth of thermokarst, we collected temperature data and soil samples from the Right and Left Bank profiles of the same thermokarst that was studied by Kodial (2005), Kodial et al. (2005), and Toniolo et al. (2009). A photograph with description of the thermokarst on June 9, 2004 is shown in Figure 4.

At the time (June 9, 2004) the data and samples were obtained, the right bank showed signs of erosion wherein slurries of water rich mud were being pushed out of the bank as shown in Figure 5. As opposed, the left bank at both the locations did not show any sign of erosion due to soil water movement. Rather, the channel carrying the water downstream perhaps had a shearing effect or simply melting of the pore ice at the bottom of the left bank profiles that relieved some of the sediments from the very bottom of the gully. The left bank profiles are shown in Figure 6.

We plotted the temperature (Figure 7) and the percent of fines that passed sieve # 200 (Figure 8) for all three profiles along the depth. While the left bank temperature profiles were all above 32°F, the right bank showed a layer approximately between 5″ and 10″ from the bottom that was above 32°F with the rest being below. The same layer showed a huge decrease in the percent of fine material that has been perhaps removed from the profile due to the flow of water through this zone of the soil. We had observed the slurry in Figure 5 emanating from this layer of the soil. A decrease in the fines from the bottom layer of the left bank near the origin might be due to simple shear action of the stream.

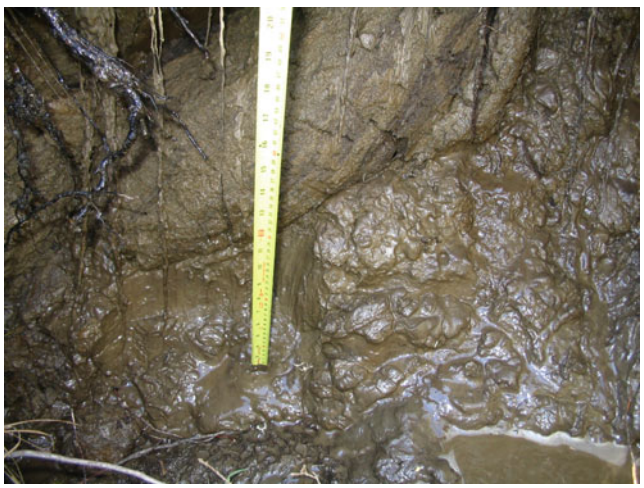

Thermokarst, Figure 5 Soil profile of the right bank eroding face of the gully demonstrating supersaturated soil conditions and slurry detachment from soil matrix under high fluid pressure. (Photograph taken on June 9, 2004 after a few days without any precipitation.)

Our field observations and the results obtained have been extremely helpful in asserting that the process of erosion and sedimentation is driven by the following two factors: (a) the soil gradient and (b) the hydrostatic head in combination with some hydrodynamic force. Degradation of permafrost being a major cause has already been ascertained by many authors as referenced above. The

Thermokarst, Figure 6 Soil profile of the (**a**) Left bank near origin and (**b**) Left bank far from origin. Both the pictures show no supersaturated condition along the profile. Each profile is host to the surface runoff from the gully that out-springs from the vicinity of the Origin and the Right Bank close to the origin. (The photographs were taken on June 9, 2004.)

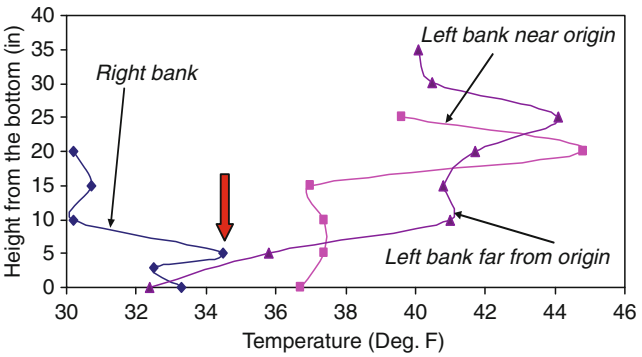

Thermokarst, Figure 7 Temperature of soil layers as sampled on June 9, 2004.

thermal regime undoubtedly plays a major role in the development of the thermokarst. Our field observation of the temperature profile on July 13, 2004 of the right bank of the thermokarst (Figure 9) revealed a completely thawed profile from bottom up. We also did not observe any flow or erosion taking place on that date.

More detailed description of the thermokarst growth and process of sedimentation, fluvio-thermal erosion, interflow, cryogenic piping, and gully development through stabilization is provided in Toniolo et al. (2009). This thermokarst study is to our knowledge the only study that has been done on possible initiation but a detailed growth of an infant thermokarst.

Thaw lake

Thaw lakes or thermokarst lakes are formed once the permafrost underlain soil is completely thawed and the gully is eroded and developed into a permanent lake. This aspect of thermokarst has been quite well studied from an ecological and environmental perspective. Thaw lakes may not develop at all if the topography is not conducive for such development (Kääb and Haeberli, 2001). Thermokarst lakes have been studied for past climate change studies (Bohncke et al., 2008; Walter et al., 2007). The initiation and cause of expansion of thaw lakes were studied extensively by Boiskov (2003). Edwards et al. (2009) studied the impact of thermokarst lakes on carbon and methane cycle in the Arctic. The influence of environment on thermokarst lakes was studied by Kirpotin et al. (2008). There are many more studies on thermokarst lakes in the recent years (e.g., Yoshikawa and Hinzman, 2003).

Summary

Thermokarsts are formed due to degradation of permafrost (increase in active layer thickness) as a result of increase in soil temperature in the Arctic and the sub-Arctic. Soil temperatures are increased due to an increase in air temperature as a result of global warming. However, forest fires and other anthropogenic disturbances may also elevate the soil surface temperature. Thaw settlement related to permafrost degradation is presently responsible for damage to houses, roads, airports, military installations, pipelines, and other facilities founded on ice-rich permafrost.

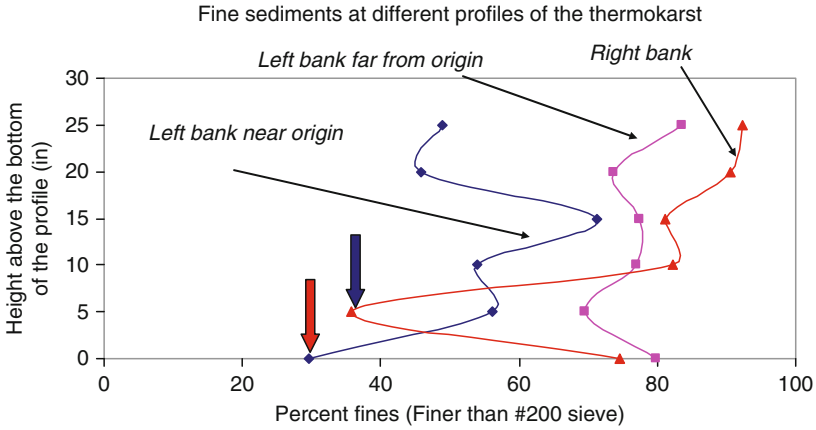

Thermokarst, Figure 8 Percent of fines (finer than #200 sieve) at various depths of the thermokarst as collected on June 9, 2004.

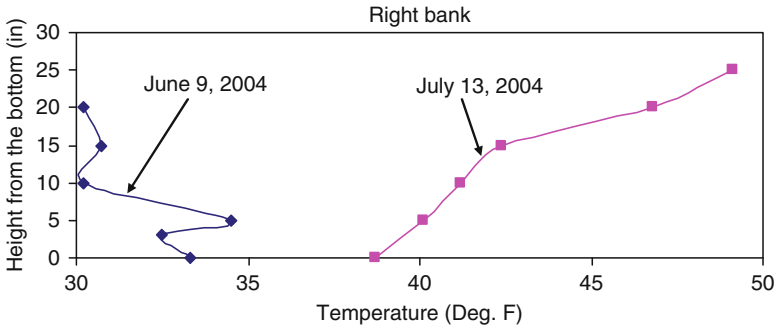

Thermokarst, Figure 9 A comparison of the temperature profiles of the right bank of the thermokarst on two different dates.

There is a significant lack of understanding of the degree to which the surface energy balance changes in response to the disturbance that causes initiation and growth of thermokarsts. Equally important is the impact of alterations in the thermal regime of soils on physical stability and consequently, surficial morphology. This lack of understanding stems from the complex nature of the formation of thermokarsts. There are no long-term records from which to detect trends in the regional frequency of thermokarsts. So far, most thermokarst-related studies have focused mainly on well-developed lakes and related water quality. From the field evidence gathered, we hypothesize that the soil gradient (slope), percent of fine materials in soil, the soil bulk density, depth of active layer, and the change in thermal regime initiates a thermokarst. Additionally, the supersaturation of soil provides the hydrostatic head along with the soil moisture movement providing the hydrodynamic force to detach the soil from its matrix and transport it downstream, thus developing the eroded gully. The thermokarst formation and the sediment moved due to the process cause water quality (both sediment and dissolved organic carbon), hydrologic, and ecological disparity issues. Understanding the physical processes in development and formation of thermokarsts in a climate changing environment and/or in areas of increased anthropogenic disturbance and forest fires is crucial because the understanding developed and the parameters measured could help reduce potential impact on engineered structures or the ecosystem in northern areas.

Bibliography

U.S. Arctic Research Commission Permafrost Task Force, 2003. Climate change, permafrost, and impacts on civil infrastructure. Arlington, VA: U.S. Arctic Research Commission, Special Report 01-03, 62 pp.

Black, R. F., 1969. Thaw depressions and thaw lakes: a review. *Biuletyn Peryglacjalny*, **19**, 131–150.

Bohncke, S. J. P., Bos, J. A. A., Engels, S., Heiri, O., and Kasse, C., 2008. Rapid climatic events as recorded in Middle Weichselian thermokarst lake sediments. *Quaternary Science Reviews*, **27**, 162–174.

Boiskov, N., 2003. Climate and cryogenic processes along linear structures. In Phillips, M., Springman, S. M., and Arenson, L. U. (eds.), *Permafrost: Proceedings of the Eighth International Conference on Permafrost.* Swets and Zeitlinger, Lisse, ISBN 90 5809 582 7.

Brown, J., and Grave, N. A., 1979. Physical and thermal disturbance and protection of permafrost. U.S. Army CRREL, Special Report 79-5. 42pp.

Brown, J., Ferrians, O. J. J., Heginbottom, J. A., and Melnikov, E. S., 1997. International permafrost association circum arctic map of permafrost and ground ice conditions. Washington, DC: U.S. Geological Survey, Circum Pacific Map Series, Map CP 45, Scale 1:10,000,000.

Burn, C. R., 1992. Canadian landform examples – 24: thermokarst lakes. *Canadian Geographer*, **36**(1), 81–85.

Burn, C. R., and Smith, M. W., 1990. Development of thermokarst lakes during the Holocene at sites near Mayo, Yukon Territory. *Permafrost and Periglacial Processes*, **1**(2), 161–176.

Carey, S. K., and Woo, M. K., 2000. The role of soil pipes as a slope runoff mechanism, subarctic Yukon, Canada. *Journal of Hydrology*, **233**(1–4), 206–222.

Carter, L. D., Heginbottom, J. A., and Woo, M. K., 1987. Arctic lowlands. In Graf, W. L. (ed.), *Geomorphic systems of North America*. Boulder, CO: Geological Society of America, Centennial Special Volume 2, pp. 583–628.

Dingman, S. L., 1976. Hydrologic effects of frozen ground: literature review and synthesis. U.S. Army CRREL Special Report, Vol. 218, 55 pp.

Edwards, M., Walter, K., Grosse, G., Plug, L., Slater, L., and Valdes, P., 2009. Arctic thermokarst lakes and the carbon cycle. *Science Highlights PAGES News: Change at the Poles*, **17**(1), 16–18.

Federov, A. N., 1996. Effects of recent climate change on permafrost landscapes in central Sakha. *Polar Geography*, **20**, 99–108.

Federov, A., and Konstantinov, P., 2003. Observations of surface dynamics with thermokarst initiation, Yukechi site, Central Yakutia. In *Proceedings of the VII International Permafrost Conference*, July 21–25, Switzerland, pp. 239–243.

Fortier, D., Allard, M., and Shur, Y., 2007. Observations on rapid drainage system development by thermal erosion of ice wedges on Bylot Island, Canadian Arctic Archipelago. *Permafrost and Periglacial Processes*, **18**, 229–243.

French, H. M., 1976. *The Periglacial Environment*. London and New York: Longman Group Limited, p. 309.

Gavriliev, P. P., and Efremov, P. V., 2003. Effects of cryogenic processes on Yakutian landscapes under climate warming. In *Proceedings of the VII International Permafrost Conference*, July 21–25, Switzerland, pp. 277–282.

Grosse, G., Schirrmeister, L., and Malthus, T. J., 2006. Application of Landsat-7 satellite data and a DEM for the quantification of thermokarst-affected terrain types in the periglacial Lena-Anabar coastal lowland. *Polar Research*, **25**, 51–67.

Hinzman, L. D., Goering, D. J., Li, S., Kinney, T. C., 1997. Numeric simulation of thermokarst formation during disturbance. In Crawford, R. M. M. (ed.), *Disturbance and recovery in Arctic lands: an ecological perspective*. Dordrecht: Kluwer Academic, pp. 621. ISBN: 0-7923-4418-9 NATO Advanced Science Institutes Series: (NATO ASI) Partnership Sub-Series: 2 Environment Volume No. 25.

Hinzman, L. D., Yoshikawa, K., and Kane, D. L., 2001. Hydrologic response and feedbacks to a warmer climate in arctic region. In *Second Wadati Conference on Global Change and Polar Climate*. 7–9 March, Tsukuba, Japan.

Hopkins, D. M., 1949. Thaw lakes and thaw sinks in the Imuruk Lake area, Seward Peninsula, Alaska. *Journal of Geology*, **57**, 119–131.

Jorgenson, M. T., Racine, C. H., Walters, J. C., and Osterkamp, T. E., 2001. Permafrost degradation and ecological changes associated with a warming climate in central Alaska. *Climate Change*, **48**, 551–579.

Kääb, A., and Haeberli, W., 2001. Evolution of a high-mountain thermokarst lake in the Swiss Alps. *Arctic, Antarctic and Alpine Research*, **33**(4), 385–390.

Khalil, M. A. K., and Pusmussen, R. A., 1989. Climate-induced feedbacks for the global cycles of methane and nitrous oxide. *Tellus B*, **41B**(5), 554–559.

Kirpotin, S., Polishchuk, Yu, Zakharova, E., Shirokova, L., Pokrovsky, O., Kolmakova, M., and Dupre, B., 2008. One of the possible mechanisms of thermokarst lakes drainage in West-Siberian North. *International Journal of Environmental Studies*, **65**(5), 631–635.

Klinger, L. F., Walker, D. A., and Webber, P. J., 1983. The effect of gravel roads on Alaskan Arctic Coastal Plain tundra. In *Proceedings of Fourth International Permafrost Conference*, 18–22 July, Fairbanks, AK: University of Alaska and National Academy of Sciences, pp. 628–633.

Kodial, P., 2005. Thermokarst evolution and sediment transport study in the Caribou-Poker creeks research watershed, Alaska, MS Thesis, Fairbanks, AK: University of Alaska Fairbanks, 86 pp.

Kodial, P., Toniolo, H., Hinzman, L., and Yoshikawa, K., 2005. Thermokarst evolution in subarctic Alaska: a study case. In *World Water Resources Conference Proceedings*. ASCE, pp. 173–182.

Kvenvolden, K. A., and Lorenson, T. D., 1993. Methane in permafrost – Preliminary results from coring at Fairbanks, Alaska. *Chemosphere*, **26**(1–4), 609–616.

Lawson, D. E., 1986. Response of permafrost terrain to disturbance: a synthesis of observations from northern Alaska. *Arctic and Alpine Research*, **18**(1), 1–17.

Nixon, J. F., 1975. The role of convective heat transport in the thawing of frozen soils. *Canadian Geotechnical Journal*, **12**, 425–429.

Osterkamp, T. E., and Romanovsky, V. E., 1999. Evidence for warming and thawing of discontinuous permafrost in Alaska. *Permafrost and Periglacial Processes*, **10**, 17–37.

Osterkamp, T. E., Esch, D. C., and Romanovsky, V. E., 1997. Infrastructure: effects of climatic warming on planning, construction and maintenance. In *Proceedings of the BESIS Workshop*. Fairbanks, AK: University of Alaska, pp. 115–127.

Osterkamp, T. E., Viereck, L. A., Shur, Y., Jorgenson, M. T., Racine, C., Doyle, A., and Boone, R. D., 2000. Observations of thermokarst and its impact on boreal forests in Alaska, USA. *Arctic, Antarctic, and Alpine Research*, **32**(3), 303–315.

Romanovskii, N. N., Gravis, G. F., Leibman, M. O., and Melnikov, E., 1996. Periglacial processes as geoindicators in the cryolithozone. In Berger, A. R., and Iams, W. J. (eds.), *Geoindicators: assessing rapid environmental changes in earth systems*. Rotterdam: Balkema, pp. 33–54.

Strang, R. M., 1973. *Studies of vegetation, landform and permafrost in the Mackenzie Valley: some case histories of disturbance*. Information Canada: Ottawa. 49 pp.

Toniolo, H., Kodial, P., Hinzman, L. D., and Yoshikawa, K., 2009. Spatio-temporal evolution of a thermokarst in Interior Alaska. *Cold Regions Science and Technology*, **56**, 39–49.

Van Everdingen, R. O., 1998. *Multi-language glossary of permafrost and related ground-ice terms*. Calgary: International Permafrost Association, University of Calgary.

Waelbroeck, C., 1993. Climate-soil processes in the presence of permafrost: a systems modeling approach. *Ecological Modeling*, **69**, 185–225.

Wallace, R. F., 1948. Cave-in lakes in the Nabesna, Chisana and Tanana River valleys, eastern Alaska. *Journal of Geology*, **56**, 171–181.

Walter, K. M., Zimov, S. A., Chanton, J. P., Verbyla, D., and Chapin, F. S., 2006. Methane bubbling from Siberian thaw lakes as a positive feedback to climate warming. *Nature*, **443**, 71–75.

Walter, K. M., Edwards, M., Grosse, G., Zimov, S. A., and Stuart Chapin III, F., 2007. Thermokarst lakes as a source of atmospheric CH4 during the last deglaciation. *Science*, **318**, 633–636.
Washburn, A. L., 1980. Geocryology. New York: Wiley, Halstead. 406 pp.
Williams, P. J., and Smith, M. W., 1989. *The frozen earth: fundamentals of geocryology.* Cambridge: Cambridge University Press. 306 pp.
Yoshikawa, K., and Hinzman, L. D., 2003. Shrinking thermokarst ponds and groundwater dynamics in discontinuous permafrost near Council, Alaska. *Permafrost and Periglacial Processes*, **14**, 151–160.

Cross-references

Ice Covered Lakes
Permafrost

THINNING OF ARCTIC SEA ICE

Ron Lindsay
Polar Science Center, Applied Physics Laboratory, University of Washington, Seattle, WA, USA

Definition

Sea ice is frozen ocean water that floats on the surface of the sea.

Introduction

In the northern winter, sea ice is found over the entire Arctic Ocean and the peripheral seas such as Hudson Bay, Davis Strait, Barents Sea, and the Bering Sea. More southerly seas also have some ice in the winter such as the Sea of Okhosk or the Gulf of Bothnia. In the summer, ice is found just in the Arctic Ocean and the seas within it, such as the Beaufort, the Chukchi, the East Siberian, the Laptev, and, to a lesser extent, the Kara and Barents seas. It is also found in the passages of the Canadian Archipelago, and along the east coast of Greenland. The typical extent of all winter sea ice in the northern hemisphere is 15.6×10^6 km^2 and in the summer it is 6.7×10^6 km^2 (1979–2008, NSIDC Sea Ice Index, Fetterer et al., 2002). Major changes have been observed recently in the age, thickness, extent, and circulation of Arctic sea ice.

Typical age and thickness

Sea ice ranges in thickness from a few centimeters in newly frozen regions to 30 m or more in pressure ridges, where the ice has been compressed and broken by the force of the winds and currents. The mean thickness in the Arctic Ocean in the winter is 3–4 m and in the summer it is 2–3 m. The ice often fractures to form linear features called *leads* of open water in which thin ice soon forms. The much thicker ice of the *pressure ridges* are formed from the rubble of broken ice floes. The age of ice in the Arctic Ocean ranges from *first-year ice*, less than 1 year old, to ice more than 10 years old, *multiyear ice.* First-year ice is commonly less than 2 m thick except where it has ridged, while multiyear ice is typically 4 or 5 m thick, again except where it has ridged. Ice age is a good proxy for ice thickness for ice less than 4 or 5 years old (Maslanik et al., 2007). Changes in the ice age distribution in the Arctic is a major contributor to the observed thinning trend.

Movement

Sea ice is highly mobile, pushed by the winds, currents, and the *Corriolis force* (from the earth's rotation). In the Arctic Ocean there is a clockwise rotation of the ice in the Pacific sector, called the *Beaufort Gyre* that changes in size and strength from year to year. The *Transpolar Drift Stream* takes ice across the *North Pole* and through *Fram Strait* between Greenland and Svalbard. This is the major point of export of ice from the Arctic Ocean. The ice that moves south along the coast melts before reaching the southern tip of Greenland. Changes in the circulation of the ice have major impacts on the mean ice thickness. In the late 1980s and early 1990s, the wind circulation patterns shifted dramatically as represented by the *Arctic Oscillation* (AO) index. The AO is a hemispheric pattern of variability of the atmospheric sea level pressure that is characterized by relatively low surface pressures in the North Pole region when the AO index is high (Thompson and Wallace, 1998). The AO index shifted to a highly positive mode for several years starting about 1989 and continuing to 1995. This change in the wind circulation patterns caused a large amount of the old thick ice that is normally found north of the Canadian Archipelago and north of Greenland to be flushed out of the Arctic Ocean and south along the east coast of Greenland (Rigor et al., 2002). This change in the circulation was the beginning of an extended period of change for Arctic sea ice in which the ice has grown thinner and the summer extent has been reduced (Lindsay and Zhang, 2005; Lindsay et al., 2009), a change that has continued to the present day.

Recent trends in extent

We have good records of the sea ice extent since the era of passive microwave measurements from satellites began in 1979. The sea ice concentration is measured from thermal emissions from the surface in the microwave region of the spectrum with a spatial resolution of about 25 km for the older instruments. For the first two decades after the beginning of the satellite record, the decline in the late summer ice extent was about –6.9%/decade (in September, the month with the minimum extent, 1979–2000). But in recent years, the decline has accelerated. For the period 1979–2008, the rate is –11.1%/decade (based on data from NSIDC Sea Ice Index, Fetterer et al., 2002). The rate of decline in the winter is less, –2.8%/decade in March from 1979 to 2008 (NSIDC Sea Ice Index, Fetterer et al., 2002) because of the geographical constraints on ocean areas in the Arctic. In 2007, the September mean ice extent fell to 4.3×10^6 km^2, far below the trend line.

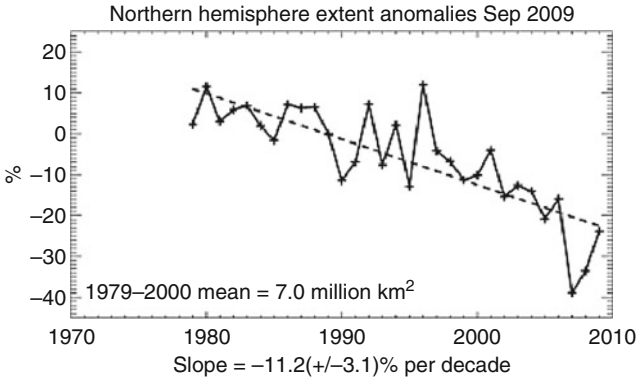

Thinning of Arctic Sea Ice, Figure 1 Northern hemisphere sea ice extent for September (National Snow and Ice Data Center, Sea Ice Index, http://nsidc.org/data/seaice_index).

The large decline in 2007 was due both to the very thin nature of the ice pack after years of thinning and to unusual winds that blew the remaining ice to one side of the Arctic Ocean (Lindsay et al., 2009). The last 2 years have seen a partial recovery with the September 2009 ice extent very near the trend line, but there is large year-to-year variability in the total ice extent (Figure 1).

Recent trends in thickness

Ice thickness in the Arctic can be measured by several different methods. Moored *upward looking sonars* (ULS) measure the ice draft (depth of the bottom of the ice) as the ice passes by above, while submarines use a ULS instrument to measure the draft as it conducts a transect under the ice. The thickness of the ice can also be measured from a satellite using either a laser or radar altimeter. Airborne electromagnetic instruments are also used to measure the ice thickness. The methods used and time periods and areas sampled by the various instruments are quite different.

Ice draft data from U.S. submarines dating back to 1958 have been declassified for a Data Release Area (DRA, see Figure 1) that includes most of the central Arctic Ocean outside of the exclusive economic zones of foreign countries. It covers about 38% of the Arctic Ocean. Within this DRA, Rothrock et al. (1999) found that sea-ice draft data acquired on cruises between 1993 and 1997 was 1.3 m thinner at the end of the melt season than similar data acquired between 1958 and 1976, a decrease of 40% from greater than 3 m to less than 2 m over a roughly 28 year period. Rothrock et al. (2008) analyze a more extensive submarine record for the DRA from 1975 to 2000 (34 cruises). Multiple regressions are used to separate the interannual change, the annual cycle, and the spatial field. The annual mean ice draft declined from a peak of 3.42 m in 1980 to a minimum of 2.29 m in 2000, a decrease of 1.13 m (1.25 m in ice thickness).

Sea ice freeboard (distance of the top snow or ice surface above the surface of the water) and, hence, thickness is measured from space by a laser altimeter on ICESat (Ice, Cloud, and land Elevation Satellite). Kwok et al. (2009) use ICESat-based ice freeboard measurements in the Arctic Ocean to produce basin-scale ice thickness estimates from 1-month-long fall and spring ICESat campaigns from a period of 5 years (2003–2008). They report a basin-wide decline of –0.17 m/year over this period. The ICESat data (for the DRA only) shows that the ice continues to thin at an accelerated rate when compared to the submarine data of Rothrock et al. (2008). Figure 2, from Kwok and Rothrock (2009), shows the winter and summer mean ice thickness for the submarine period (1975–2000) and for the ICESat period (2003–2008) for the DRA.

Recent radar altimeter records from the Envisat satellite for the regions south of 81.5° N show no evidence of short-term preconditioning through ice thinning between 2002 and 2007 but show that, after the record minimum ice extent in 2007, the average ice thickness was reduced, particularly in the Western Arctic (Giles et al., 2008).

Sea ice and global warming

The decline of the ice in the Arctic is likely directly linked to global warming caused by anthropogenic greenhouse gases. As in most of climate science, proof in the mathematical sense is not possible, but virtually all models of the global climate show a drastic reduction in late summer sea ice extent with increasing greenhouse gasses. Some important feedbacks to consider in understanding the reduction in Arctic sea ice include the ice-albedo feedback wherein reduced ice extent exposes more dark ocean waters (compared to the bright ice surface) to sunlight and the increased absorption of solar energy leads to increased ice melt, a positive feedback. A strong negative feedback is the greatly increased rate of ice growth in the winter for thin ice compared to thick ice. Another interesting positive feedback is seen in the average speed of the ice movement. As the ice thins, it becomes weaker and more mobile, deforming more rapidly. Then more ice is readily exported through Fram Strait, further reducing the volume of ice in the Arctic Ocean (Rampal et al., 2009). A negative feedback related to the deformation is found in the increased areas of open water caused by the increased deformation, areas that are then the locations of accelerated ice production.

Antarctica

Sea ice in the southern hemisphere differs from that in the north in several respects. It forms around the periphery of the Antarctic continent at latitudes much farther from the pole. Most of the ice forms and melts each year. Only the ice in the more southerly Weddell Sea and the Ross Sea survives the summer. It also is often covered with so much snow that the weight pushes the top surface of the ice below the water level and the top floods. During the winter, much of the ice is therefore growing on the top

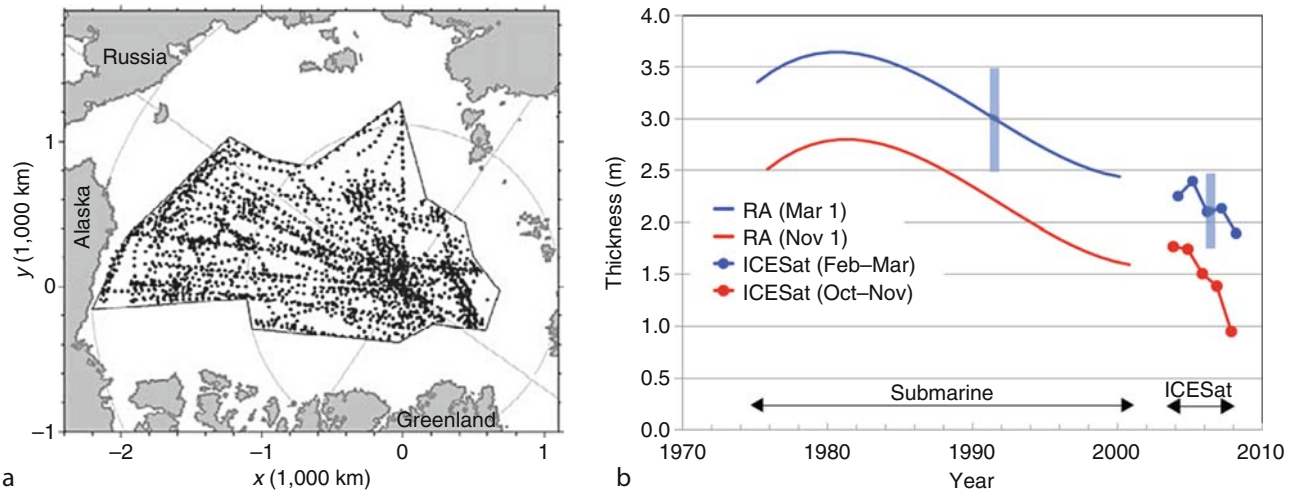

Thinning of Arctic Sea Ice, Figure 2 (**a**) Data points from U.S. Navy cruises used by Rothrock et al. (2008) and the data release area (irregular polygon). (**b**) Interannual changes in winter (*blue*) and summer (*red*) mean ice thickness based on submarine data from the regression equation of Rothrock et al. (2008) and from ICESat laser altimeter data centered on the ICESat campaigns (Kwok et al., 2009). *Blue error bars* show residuals in the regression and quality of ICESat data. Figure from Kwok and Rothrock (2009).

while melting on the bottom, and in the summer most of the melt is from the bottom.

The winter ice extent in Antarctica is slowly increasing in spite of global warming at an annual mean rate of 0.97%/decade (Turner et al., 2009). This increase is linked to changes in the surface wind speeds in specific sectors of the Antarctic coastal regions, changes caused by the springtime loss of ozone in the stratosphere, the so-called ozone hole (Turner et al., 2009). Some areas, such as the Amundsen-Bellinghausen Sea are losing significant amounts of ice while others, such as the Ross Sea, are gaining ice. As the ozone hole dissipates in decades to come, the global warming impact on the Antarctic will likely be seen in a reduction of the sea ice extent.

Summary

The sharp decline in the Arctic mean ice thickness began about 1990, when there was a very significant shift in the wind patterns over the Arctic Ocean for several years linked to changes in the Arctic Oscillation. The wind patterns are no longer so unusual but the ice decline continues due to global warming and feedback mechanisms. The changes in the ice age are clearly observed in satellite measurements that distinguish multiyear ice from first-year ice (Maslanik et al., 2007), while the changes in the thickness are seen in new laser and radar satellite measurements of the ice thickness. Because the sea ice is floating in the ocean, melting of sea ice has negligible impact on sea level, as opposed to land-based ice sheets and glaciers that add mass to the ocean when they melt.

The ice responds strongly to the regional air temperatures and a runaway positive feedback (a tipping point) is not likely. The summer ice extent is likely to continue to decline in the next few decades and to be highly variable from year to year, while winter ice is likely to be extensive for many decades to come because of the thin-ice-rapid-growth feedback and the very large loss of thermal energy from the surface when there is no sunlight in the Arctic.

Bibliography

Fetterer, F., Knowles, K., Meier, W., and Savoie, M., 2002. Updated 2009. *Sea Ice Index*, 1979–2008. Boulder, Colorado, USA: National Snow and Ice Data Center. Digital Media.

Giles, K. A., Laxon, S. W., and Ridout, A. L., 2008. Circumpolar thinning of Arctic sea ice following the 2007 record ice extent minimum. *Geophysical Research Letters*, **35**, L22502, doi:10.1029/2008GL035710.

Kwok, R., and Rothrock, D. A., 2009. Decline in Arctic sea ice thickness from submarine and ICESat records: 1958–2008. *Geophysical Research Letters*, **36**, L15501, doi:10.1029/2009GL039035.

Kwok, R., Cunningham, G. F., Wensnahan, M., Rigor, I., Zwally, H. J., and Yi, D., 2009. Thinning and volume loss of the Arctic Ocean sea ice cover: 2003–2008. *Journal of Geophysical Research*, **114**, C07005, doi:10.1029/2009JC005312.

Lindsay, R. W., and Zhang, J., 2005. The dramatic thinning of arctic sea ice, 1988-2003: have we passed a tipping point? *Journal of Climate*, **18**, 4879–4894.

Lindsay, R. W., Zhang, J., Schweiger, A. J., Steele, M. A., and Stern, H., 2009. Arctic sea ice retreat in 2007 follows thinning trend. *Journal of Climate*, **22**, 165–176, doi:10.1175/2008JCLI2521.

Maslanik, J. A., Fowler, C., Stroeve, J., Drobot, S., Zwally, J., Yi, D., and Emery, W., 2007. A younger, thinner Arctic ice cover: Increased potential for rapid, extensive sea-ice loss. *Geophysical Research Letters*, **34**, L24501, doi:10.1029/2007GL032043.

Rampal, P., Weiss, J., and Marsan, D., 2009. Positive trend in the mean speed and deformation rate of Arctic sea ice, 1979–2007. *Journal of Geophysical Research*, **114**, C05013, doi:10.1029/2008JC005066.

Rigor, I. G., Wallace, J. M., and Colony, R. L., 2002. Response of Sea Ice to the Arctic Oscillation. *Journal of Climate*, **15**(18), 2648–2668.
Rothrock, D. A., Yu, Y., and Maykut, G. A., 1999. Thinning of the Arctic sea-ice cover. *Geophysical Research Letters*, **26**(23), 3469–3472, doi:10.1029/1999GL010863. C05003, doi:10.1029/2007JC004252.
Rothrock, D. A., Percival, D. B., and Wensnahan, M., 2008. The decline in arctic sea-ice thickness: Separating the spatial, annual, and interannual variability in a quarter century of submarine data. *Journal of Geophysical Research*, **113**, C05003, doi:10.1029/2007JC004252.
Thompson, D. W. J., and Wallace, J. M., 1998. The Arctic oscillation signature in the wintertime geopotential height and temperature fields. *Geophysical Research Letters*, **25**, 1297–1300.
Turner, J., Comiso, J. C., Marshall, G. J., Lachlan-Cope, T. A., Bracegirdle, T., Maksym, T., Meredith, M. P., Wang, Z., and Orr, A., 2009. Non-annular atmospheric circulation change induced by stratospheric ozone depletion and its role in the recent increase of Antarctic sea ice extent. *Geophysical Research Letters*, **36**, L08502, doi:10.1029/2009GL037524.

Cross-references

Sea Ice

THINNING OF GLACIERS

Etienne Berthier
LEGOS/CNRS/UPS, Toulouse, France

Definition

Reduction of the glacier thickness

Introduction

A glacier in equilibrium with the climate is characterized by a given geometry. This geometry results from a balance between snow accumulation, ablation (mainly by melting), and the flow that redistributes the mass accumulated at high elevations toward the lower parts of the glacier. If external forcings (climate) or internal forcings (ice flow) change, the geometry of the ice body also evolves. Nowadays, most glaciers around the globe are responding to climate change by a reduction of their thickness. This *thinning* is the topic of the present article. We will describe how the thinning can be measured, what can cause a glacier to thin, and briefly review the thinning of glacierized areas around the globe.

How to measure the thinning of a glacier?

Ice elevation changes can be determined by comparing sequential measurements of the altitude of the glacier surface collected during field, air-borne, and space-borne surveys.

Field surveys provide very accurate elevation change measurements but they generally only cover a limited portion of a glacier. In the French Alps, for example, 4–5 transverse profiles are surveyed yearly on a few selected benchmark glaciers using differential GPS (Vincent et al., 2009). The high accuracy of these field surveys (typical $\pm$ 20–30 cm) allows studying the year-to-year fluctuations in ice thickness. They also provide a precious ground truth reference in order to validate/calibrate air- and space-borne surveys.

Differential digital elevation models (DEMs) derived from *aerial photographs* are considered the most reliable measurement of ice elevation changes over one or several decades (Thibert et al., 2008). This approach is limited by the relatively small coverage of the photographs (30–40 km^2) and is generally restricted to glaciers already monitored in the field. Airborne laser altimetry is also an efficient tool to estimate the volume change of glaciers (Echelmeyer et al., 1996). Its high accuracy in the accumulation area and the possibility to extract thickness changes along longitudinal profiles of large glaciers (Arendt et al., 2002) are the main advantages of this method.

Eventually, ice thinning can also be observed from satellite data by comparing sequential digital elevation models (Berthier et al., 2004), repeat laser profiling (Sauber et al., 2005), or using a combination of both techniques (Kääb, 2008). The challenge consists in measuring a small signal (generally a few meters of elevation changes) from a sensor located a few hundred kilometers above the Earth surface. This challenge is addressed either by having very precise individual elevation measurements (e.g., ICESat laser profiles) or by adjusting some less accurate DEMs on the stable ice-free regions surrounding the ice bodies and then averaging over a large number of pixels (Berthier et al., 2004).

What causes the changes in glacier elevation?

The primary cause of thickness changes are the fluctuations of the glacier surface mass balances. The topic of surface *mass balance* (the difference between accumulation and ablation) is discussed in a different section of this encyclopedia and, thus, is not examined in detail here. The current thinning of most glacier tongues is partly the glacier response to increase in surface ablation (itself a response to rising air temperature). However, other factors than surface mass balances also contribute to glacier thickness changes.

Ice flow variations can also lead to ice elevation changes. A clear illustration is given by the changes experienced by glaciers of the Antarctic Peninsula that drained into the former Larsen B ice shelf which disintegrated in March 2002. The loss of resistive stress due to shelf removal led to a strong acceleration of those glaciers and a rapid lowering (10s m/yr) of their surface (Scambos et al., 2004). The lowering was so fast that stranded ice remained on their margins (Figure 1).

The surge phenomenon illustrates how elevation changes can occur without some changes in the total glacier volume. The life cycle of a surging glacier is characterized by a quiescent phase when ice flow rates are small and mass is accumulated in the reservoir area

Thinning of Glaciers, Figure 1 Stranded ice on the margins of Crane glacier (Antarctic Peninsula). Crane glacier thinned so rapidly after the collapse of the Larsen B ice shelf that ice remained on its flanks. Stranded ice underlies the level of the glacier surface before thinning (© T. Scambos, February 11, 2006).

(Clarke, 1987). During the active phase, ice velocities increase by a factor of 10–100 (or more) leading to a rapid transfer of mass from the upper "reservoir" area to the lower "receiving" area. This active phase results in thinning of the reservoir area and thickening of the receiving area. Many glaciers in Svalbard, Iceland, and Southeast Alaska are surge-type so that, over a short time scale (years to decades), their elevation changes are not directly linked to climate fluctuations.

If part of the glacier is floating on the sea or on a lake, thinning can occur at its base through basal melting. Basal melting rates as high as 40 m/year have been reported for outlet glaciers of the Antarctic and Greenland ice sheets and are an important component of their mass balance (Rignot and Jacobs, 2002). For a grounded glacier, basal melting due to geothermal heat fluxes is generally small, in the order of a few mm/yr. These rates can be much larger if the glacier is located above a volcano. For example, volcanic eruptions and continuous geothermal activity at the bed of the Vatnajökull ice cap (Iceland) accounted for >5% of its overall melting during the late 1990s and early 2000s (Björnsson and Pálsson, 2008).

An elevation change is not necessarily associated with a change in mass or flow of the glacier. It can also be due to a change in the rate at which the snow falling on the surface is metamorphosed into firn (first) and then into ice. For example, if accumulation is maintained at the same level but the atmosphere above the glacier surface gets warmer, the snow metamorphism will be faster and a lowering of the glacier surface will occur. Such mechanisms are difficult to measure and model although they are crucial for a realistic assessment of the mass balance of the polar ice sheets (Helsen et al., 2008).

Recent thinning of glaciers

Most glaciers around the globe are now thinning at a rapid rate (Cogley, 2009) and, between 2003 and 2008, mountain glaciers and ice sheets were the main contributors (85%) to a sea-level rise of 2.5 mm/year (Cazenave et al., 2009). The rare regions where glaciers were in equilibrium or thickening in the 1990s (West of Norway, Iceland, and New Zealand) are now also thinning (on average) and losing mass (Björnsson and Pálsson, 2008; Chinn et al., 2005; Nesje et al., 2008). There is a striking similarity between the patterns of thinning in different regions. As observed in Alaska (Arendt et al., 2002), in Patagonia (Rignot et al., 2003), in the Alps (Berthier et al., 2006; Paul and Haeberli, 2008), and in many other mountain ranges, the thinning of glaciers is maximum at low elevation and limited in their accumulation areas (Figure 2). This is an expected thinning pattern during the retreat phase of mountain glaciers (Schwitter and Raymond, 1993).

Summary or conclusions

Together with their retreat, thinning of glaciers is their most striking response to global warming and explains why they are generally regarded as a symbol of the ongoing global warming. Yet, the number of glaciers whose elevation changes have been actually observed is still too limited. The number is currently growing thanks to some recent advances in our capabilities to measure glacier

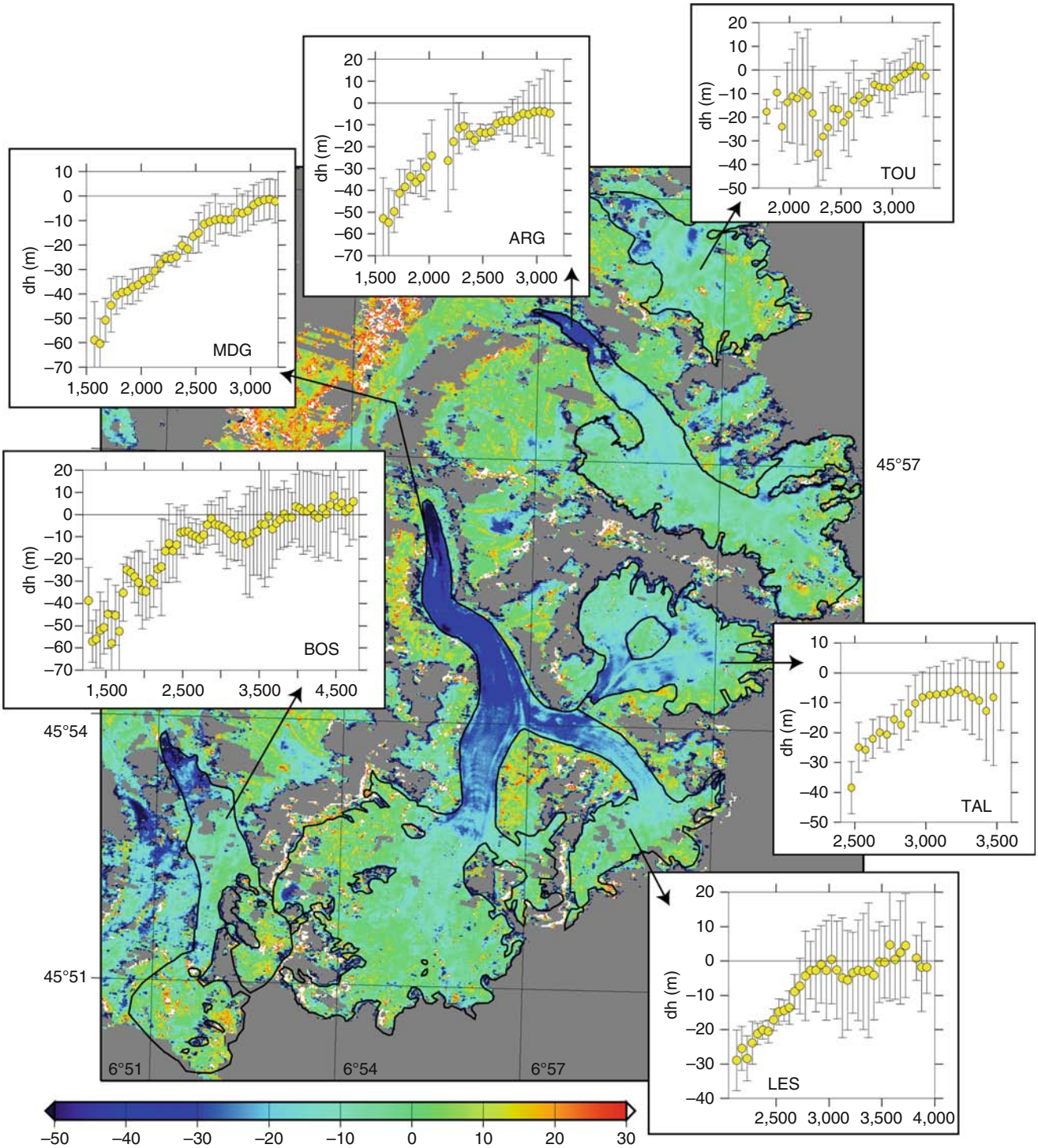

Thinning of Glaciers, Figure 2 Elevation changes in the Mont-Blanc area (French Alps) between 1979 and 2003. Plots of elevation changes as a function of altitudes are given for, from North to South, *TOU* Tour glacier, *ARG* Argentière glacier, *TAL* Talèfre glacier, *MDG* Mer de Glace, *LES* Leschaux glaciers, *BOS* Bossons glacier.

elevation changes, in particular from satellite data (ASTER and SPOT stereo-images, ICESat laser profiles). This capability will even increase in the near future thanks to new satellite missions to be launched in 2010 (and beyond) such as CryoSat-2 (European Space Agency) and Tandem-X (DLR, German Aerospace Center).

Bibliography

Arendt, A. A., Echelmeyer, K. A., Harrison, W. D., Lingle, C. S., and Valentine, V. B., 2002. Rapid wastage of Alaska glaciers and their contribution to rising sea level. *Science*, **297**, 382–386.

Berthier, E., Arnaud, Y., Baratoux, D., Vincent, C., and Remy, F., 2004. Recent rapid thinning of the "Mer de Glace" glacier derived from satellite optical images. *Geophysical Research Letters*, **31**, L17401.

Berthier, E., Arnaud, Y., Vincent, C., and Remy, F., 2006. Biases of SRTM in high-mountain areas: Implications for the monitoring of glacier volume changes. *Geophysical Research Letters*, **33**, L08502.

Björnsson, H., and Pálsson, F., 2008. Icelandic glaciers. *Jökull*, **58**, 365–386.

Cazenave, A., Dominh, K., Guinehut, S., Berthier, E., Llovel, W., Ramillien, G., Ablain, M., and Larnicol, G., 2009. Sea level budget over 2003-2008: A reevaluation from GRACE space gravimetry, satellite altimetry and Argo. *Global and Planetary Change*, **65**, 83–88.

Chinn, T., Winkler, S., Salinger, M. J., and Haakensen, N., 2005. Recent glacier advances in Norway and New Zealand: a comparison of their glaciological and meteorological causes. *Geografiska Annaler*, **87A**, 141–157.

Clarke, G. K. C., 1987. Fast glacier flow: ice streams, surging and tidewater glaciers. *Journal of Geophysical Research*, **92**, 8835–8841.

Cogley, J. G., 2009. Geodetic and direct mass-balance measurements: comparison and joint analysis. *Annals of Glaciology*, **50**, 96–100.

Echelmeyer, K. A., Harrison, W. D., Larsen, C. F., Sapiano, J., Mitchell, J. E., DeMallie, J., Rabus, B., Adalgeirsdottir, G., and Sombardier, L., 1996. Airborne surface profiling of glaciers: A case-study in Alaska. *Journal of Glaciology*, **42**, 538–547.

Helsen, M. M., van den Broeke, M. R., van de Wal, R. S. W., van de Berg, W. J., van Meijgaard, E., Davis, C. H., Li, Y. H., and Goodwin, I., 2008. Elevation changes in Antarctica mainly determined by accumulation variability. *Science*, **320**, 1626–1629.

Kääb, A., 2008. Glacier volume changes using ASTER satellite stereo and ICESat GLAS laser altimetry, A test study on Edgeøya, Eastern Svalbard. *IEEE Transactions on Geoscience and Remote Sensing*, **46**, 2823–2830.

Nesje, A., Bakke, J., Dahl, S. O., Lie, O., and Matthews, J. A., 2008. Norwegian mountain glaciers in the past, present and future. *Global and Planetary Change*, **60**, 10–27.

Paul, F., and Haeberli, W., 2008. Spatial variability of glacier elevation changes in the Swiss Alps obtained from two digital elevation models. *Geophysical Research Letters*, **35**, L21502.

Rignot, E., and Jacobs, S. S., 2002. Rapid bottom melting widespread near Antarctic ice sheet grounding lines. *Science*, **296**, 2020–2023.

Rignot, E., Rivera, A., and Casassa, G., 2003. Contribution of the Patagonia Icefields of South America to sea level rise. *Science*, **302**, 434–437.

Sauber, J., Molnia, B., Carabajal, C., Luthcke, S., and Muskett, R., 2005. Ice elevations and surface change on the Malaspina Glacier, Alaska. *Geophysical Research Letters*, **32**, L23S01.

Scambos, T. A., Bohlander, J. A., Shuman, C. A., and Skvarca, P., 2004. Glacier acceleration and thinning after ice shelf collapse in the Larsen B embayment, Antarctica. *Geophysical Research Letters*, **31**, L18402.

Schwitter, M. P., and Raymond, C. F., 1993. Changes in the longitudinal profiles of glaciers during advance and retreat. *Journal of Glaciology*, **39**, 582–590.

Thibert, E., Blanc, R., Vincent, C., and Eckert, N., 2008. Glaciological and volumetric mass-balance measurements: error analysis over 51 years for Glacier de Sarennes, French Alps. *Journal of Glaciology*, **54**, 522–532.

Vincent, C., Soruco, A., Six, D., and Le Meur, E., 2009. Glacier thickening and decay analysis from 50 years of glaciological observations performed on Glacier d'Argentière, Mont Blanc area, France. *Annals of Glaciology*, **50**, 73–79.

Cross-references

Aerial Photogrammetry for Glacial Monitoring
Climate Change and Glaciers
Digital Elevation Model Generation Over Glacierized Region
Dynamics of Glaciers
Glacier Mass Balance
Sea-Level

TIBETAN PLATEAU

Tandong Yao, Yongqin Liu, Huabiao Zhao, Wusheng Yu
Laboratory of Tibetan Environment Changes and Land Surface Processes (TEL), Institute of Tibetan Plateau Research, Chinese Academy of Sciences, Beijing, China

Definition

The Tibetan Plateau lies between 25°N and 40°N, 74°E and 104°E. It constitutes the world's largest Plateau, covering an area of 2.5 million km^2 that extends from the Pamir Plateau in the west to the Hengduan Mountains in the east; and from the Kunlun Mountains and Qilian Mountains in the north to the Himalaya Mountains in the south. The Tibetan Plateau also includes the highest land mass, with an average elevation of over 4,500 m sometimes called "the roof of the world." It forms one of the major drivers of global climate, referred as the Earth's "third pole." It includes the headwater areas for a series of major Asian rivers, called the "water tower" of east-south Asia. It embraces a unique natural lab for the study of global climatic change and geodynamics, drawing the attention of increasingly more international researchers.

Mountains on the Tibetan plateau

The mountain systems of the Tibetan Plateau have been uplifting rapidly since the late Tertiary and now form the world's highest and largest high mountain region. Towering mountains cover the Tibetan Plateau. Most of the mountains exceed 5,500 m; over 100 mountains rise above 7,000 m. All of the world's 14 mountains higher than 8,000 m rise from the Tibetan Plateau, ten of them in the Himalayan Mountains, the other four in the Karakorum Mountains.

Eight mountain ranges strike east–west across the Plateau, from north to the south, the Aerhchin, Qilian, Eight mountain ranges strike east–west across the Plateau, from north to the south, the Aerhchin, Qilian, Kunlun, Karakorum, Tanggula, Gangdisi, Nyainqentanglha, and Himalayan Mountains. The Himalayan Mountains, meaning "abode of snow," include the planet's highest mountains. The Himalayas run east to west, from Mt. Namcha Barwa (7,756 m) to Nanga Parbat (8,126 m), continuing for about 2,500 km. The average altitude of the Himalayan Mountains exceeds 6,000 m and they include Mount Qomolangma (8,844 m), the world's highest peak. The Karakorum Mountains make up one of the greatest ranges of the world, including K2 (8,611 m), the second highest peak on earth. The Kunlun Mountains runs eastward from the Pamir Plateau, extending more than 2,500 km. The main ridge of the range varies between 6,000 and 6,500 m, including its highest mountain, Mt. Kunlun Goddess (7,167 m). The Tangula Mountains span about 700 km with their main ridge averaging more than 5,000 m, with (6621 m) its tallest peak. The Nyainqentanglha Mountains run 740 km across Tibet, from the Nimu County in the west to Ranwu County in the east. The range's highest peak, Mt. Nyainqentanglha, reaches 7,162 m. The Gangdisi Mountains parallel the Himalayas, extending about 1,100 km. The main peak, Mt. Kailas (6,638 m) owes its sacredness to Tibetan Buddhism and Hinduism. With its unique geographical location and graceful landscape, Kailas is considered the most holy of all mountains. Buddhist pilgrims believe that Mt. Kailas holds the sacred abode of the deity Chakrasamvara and his consort Dorje Phamo. Hindu pilgrims regard it as the throne of the great God Shiva. The 800 km long Qilian Mountains consist of a series of alternating northwest-trending ridges and valleys. Tuanjie Peak (5,808 m) is the highest peak of the range. The Aerhchin Mountains run roughly 1,000 km, forming the boundary of the Tarim Basin the Qaidam Basin. The highest peak, Shulamutage Peak, reaches 6,295 m. The north–south striking Hengduan Mountains lie on the southeastern Plateau and consist of a series of high parallel ranges and deep canyons oriented north to south.

Glaciers on the Tibetan plateau

The Tibetan Plateau encompasses the largest mid-low latitude part of the world currently covered by glaciers. Shi's (2005) Chinese glacier inventory has counted all the glaciers on the Tibetan Plateau. The inventory show that 36,102 existing glaciers on the Plateau, with a total area of 49,688 km^2 and a cumulative ice volume of 4,972 km^3, or a total water equivalent ice volume of 5.04×10^{12} m^3. This immense fresh water reservoir on the Tibetan Plateau could provide 6.16×10^{10} m^3 of water to river runoff (Yang, 1991).

The Kunlun, Nyainqentanglha, Himalayan, and Karakorum Mountains account for over half of the total number of glaciers and ice volume on the Tibetan Plateau (Shi, 2005, 2008). Most of glaciers in the Kunlun Mountains concentrate in the western section. The West Kunlun Mountains (75° 10′–80° 40′ E) contain 6,580 glaciers, with a total area of 10,844 km^2 and a volume of 1,175 km^3, accounting for 85%, 88%, and 92%, respectively, of these numbers for the entire Kunlun Mountains. More than 50% of the glacier covered area of the West Kunlun Mountains contains various valley glaciers. These include the Duofeng Glacier, the largest dendritic valley glacier, with a length of 31 km and an area of over 250 km^2. Many complex valley glaciers and dendritic valley glaciers exist on the northern slopes of the West Kunlun Mountains. However, the southern slopes accommodate numerous flat-topped and outlet glaciers with piedmont lobes. As the glaciers on the northern and southern slopes may originate on the same peak, a glacier composite may form an ice cap, e.g., the Guliya Ice Cap. The maximum length of the Guliya Ice Cap reaches 30.9 km from north to south, and includes a total area of 212 km^2. The average depth of the ice cap has been estimated at over 200 m, with the maximum in excess of 350 m, making it the highest, largest, and coldest ice cap in the mid-low latitudes. A 308.7 m deep ice core has been recovered from the ice cap.

The Nyainqentanglha Mountains contain 7,080 glaciers, with a total area of 10,700 km^2, with two-thirds of the galcier and five-sixths the area lying in the eastern section. The eastern section faces the approaching moist southwest monsoons, which enter the Plateau at the Grand Bend of the Yarlung Zangbo River. The terrain forces the air flow to rise, providing the region with the maximum precipitation and highest moisture on the Plateau, enhancing glacier development. Thirty-two glaciers exceed 10 km in length, with the Kyagqen Glacier largest, at 35.3 km in length and 207 km^2 in area.

Of the Mt. Qomolangma, glaciers cover 1,600 km^2. This zone contains 15 glaciers larger than 20 km^2, and 18 other glaciers larger than 10 km^2. The largest glacier on Qomolangma's northern slope is the Rongbuk Glacier, a dendritic valley glacier consisting of the Middle and West Rongbuk Glaciers, 22.4 km long and covering 85.4 km^2. The largest glacier on the southern slopes is the Ngozumpa Glacier, 23 km in length and 80.8 km^2 in area. A series of seracs lie between 5,300–5,700 m on the Rongbuk Glacier, within a horizontal distance of 6 km. These include embryonic, connected, and isolated seracs, ranging in height from a few meters to 50 m, forming a forest of neve penitentes, under conditions of strong solar radiation, a high angle of incidence, and a dry climate.

Mt. Xixiabangma forms another glaciation center in the Himalayan Mountains. The peaks and sides of the main ridges contain 438 glaciers, with a total glacier area of 1,173 km^2 and an ice volume of 122 km^3. The 20.2 km long Langtang Glacier (covering 58.57 km^2) forms the largest complex valley glacier on Xixiabangma's southern slope. The 14.3 km Daqu Glacier (covering 44 km^2 and holding 8.3 km^3 of ice), is the largest complex valley glacier on the northern slope. Another large valley glacier,

the Dasuopu Glacier (11.0 km long, covering 26.2 km^2, and containing 3.4 km^3 of ice) also sits on the northern slope.

Glaciers in the Karakorum Mountains cover 17,835 km^2, accounting for about 37% of the total mountain area. They cover mainly the western and southwestern portions of the mountains. The Karakorum Mountains within China contain five dendritic glaciers with an area greater than 100 km^2, namely, the Yengisogat, Yulin, Teram Kangri, Gasherbrum, and Kyagar Glaciers. Of these, the Yengisogat Glacier (42.0 km long, covering 380 km^2, and with an ice volume of 116 km^3) ranks as both the longest glacier in China and the one covering the largest area.

The glaciers on the Tibetan Plateau have been retreating continuously under the impact of climatic warming for several recent years. The decrease in glacial volume in the High Asian China falls between 587 km^3 during the past 40 years (Yao et al., 2004).

Lakes on the Tibetan plateau

The Tibetan Plateau includes a fairly high density of lakes, 1,091 of which exceed 1.0 km^2. Lakes cover a total area of more than 400,000 km^2 (Wang and Dou, 1998). Tectonics has controlled the placement of most of the large lakes on the Plateau, while numerous small lakes result from glacial processes. Depending on their sources, these lakes may also be categorized as glacier-fed or non-glacier-fed.

Remote sensing data from the Landsat TM show that 11 lakes on the Plateau exceed 13,300 km^2 (Lu, 2006). The big lakes on the Plateau include: (1) Qinghai Lake, the largest salt lake in China, with a surface elevation of 3,196 m, 67 km wide and 109 km long, covering 4,344 km^2 in 2001, and a maximum depth of 27 m as measured in 1981; (2) Nam Co, the largest holy lake in Tibet, with a surface elevation of 4,718 m, 50 km wide and 78.6 km long, and covering 1962 km^2; (3) Serling Co, a mysterious lake at 4,350 m, with a maximum width of 45.5 km and maximum length of 77.7 km, and a total area of 1,628 km^2; (4) Zhari Namco, a lake with rich fishing resources, at 4,613 m, 26.2 km wide and having a total area of 997 km^2; and (5) Tangra Yumco at 4,528 m, with a width of 19.4 km, length of 71.7 km, and 836 km^2 of total area.

Rivers on the Tibetan plateau

The Tibetan Plateau gives birth to many of the great rivers in Asia, i.e., the Yellow, Yangtze, Mekong, Salween, Ganges, Indus, and Brahmaputra rivers.

The 5,464 km long Yellow River originates in the southwest of the Yoigilangleb Basin on the northern slope of Mount Bayan Har. Water flows down from the Maqu Quguori Divide through Gyaring Lake and Ngoring Lake, before discharging finally into the Maqu and forming the Yellow River.

The Yangtze River ranks as the longest river in China. It has three recognized sources. Its main source, the Tuotuo River, lies in the glacial region of Mt. Geladandong in the Tanggula Mountains, serves as its southern source and the Qumar River as its northern source. These three sources merge into the Tongtian River and form the Jinsha Jiang, which winds over 6,300 km before eventually flowing into the East China Sea in the Pacific Ocean.

The Mekong River (4,500 km in total length) originates on the northern slope of the Tanggula Mountains. It flows down to the Zachu River, joins the Lancang River and merges into Burma to form the Mekong River. The river finally discharges into the South China Sea after passing Laos, Thailand, Cambodia, and Vietnam.

The Salween River (2,690 km long) originates near Dengka Peak to the east of Tanggula Pass. Afterward, it merges into the Nujiang River and becomes the well-known Salween River once it enters Burma, and finally discharges into the Indian Ocean.

Four international rivers originate from Mt. Kailas in the Gangdisi Mountains, named, respectively, after four auspicious animals: the horse, the peacock, the lion, and the elephant. The Maquan River (meaning "Horse Fountain") runs on its eastern side, traveling through the Yarlung Zangbo, the Brahmaputra, and the Ganges rivers before discharging into the Bay of Bengal. On the south, the Kongque River (meaning "Peacock Fountain") flows to the west, running through the Indus River Plain before discharging into the Arabian Sea. The Shiquan River (meaning "Lion Fountain") lies on the north, and joins other rivers to also join the surging Indus River and travels through the Indus River Plain to pour into the Arabian Sea (Xu, 1992).

Ice cores from the Tibetan plateau

Ice core studies have contributed considerably to global change research. These studies have provided not only the information about the past temperature changes, but also about the past precipitation, greenhouse gas concentrations, volcanic activity, desert development, atmospheric circulation intensity, solar activity, biogeochemical cycles, and other worldwide events. Ice core studies on the Tibetan Plateau have made substantial progress over the past 2 decades and have attracted much attention from international geoscientists. Many shallow and deep ice cores have been extracted from the Qilian Mountains, West Kunlun Mountains, Tanggula Range, the Himalayas, and other regions.

The drilling of ice cores on the Tibetan Plateau began on the Dunde Ice Cap in the Qilian Mountains. In 1984, the Byrd Polar Research Center and the Lanzhou Institute of Glaciology and Geocryology (Chinese Academy of Sciences), conducted a cooperative glaciological research program to retrieve and study the Dunde ice cores. Four shallow cores (10.2, 16, 32, and 34.5 m long) and three ice cores to bedrock (139.8, 136.6, and 138.4 m long) were recovered from 1984 to 1987 (Yao and Xie, 1991). Analyses of these ice cores provided a detailed record of climatic and environmental changes in the region since the late Pleistocene (Thompson et al., 1989).

The Guliya ice core was then drilled and yielded the longest record from the middle and low latitudes. The 308.6 m long core was recovered from Guliya Ice Cap in the West Kunlun Mountains in 1991. The ice at the bottom of the core dates from about 760 ka BP. Climatic and environmental changes on several different time scales since the Last Interglacial Stage have been reconstructed from the Guliya ice core (Thompson et al., 1997; Yao et al., 1997, 2001).

The Dasuopu ice core comes from the highest elevation (7,100 m) and was drilled in the Dasuopu Glacier on Mt. Xixabangma, in the middle of the Himalayas. In 1997, three deep ice cores were recovered, with lengths of 160, 150, and 164 m. Analyses of these deep ice cores reveal the evolution of the Indian Monsoon (with high resolution and good quality), the history of the impact of human activities on the environment, and the characteristics of climate change in the middle of the Himalayas (Thompson et al., 2000).

Bibliography

Lu, A., 2006. *Modern Relation Study of Glaciers and Lakes on the Qinghai-Tibet*. Thesis for PhD degree in the Cold and Arid Regions Environment and Engineering Research, CAS (in Chinese).

Shi, Y., 2005. *Chinese Glacier Inventory*. Shanghai: Shanghai Popular Science Press.

Shi, Y., 2008. *Glaciers and Related Environment*. Beijing: Science Press.

Thompson, L. G., Mosley-Thompson, E., Davis, M. E., Bolzan, J. F., Dai, J., Yao, T., Gundestrup, N., Wu, X., Klein, L., and Xie, Z., 1989. Holocene late pleistocene climatic ice core records from Qinghai-Tibetan Plateau. *Science*, **246**, 474–477.

Thompson, L. G., Yao, T., Davis, M. E., Henderson, K. A., Mosley-Thompson, E., Lin, P. N., Beer, J., Synal, H. A., ColeDai, J., and Bolzan, J. F., 1997. Tropical climate instability: the last glacial cycle from a Qinghai-Tibetan ice core. *Science*, **276**, 1821–1825.

Thompson, L. G., Yao, T., Mosley-Thompson, E., Davis, M. E., Henderson, K. A., and Lin, P. N., 2000. A high-resolution millennial record of the South Asian Monsoon from Himalayan ice cores. *Science*, **289**, 1916–1919.

Wang, S., and Dou, H., 1998. *Memoirs of China's Lakes*. Beijing: Science Press.

Xu, H., 1992. *Geography of the Tibet Autonomous Region*. Lhasa: Tibet People's Press, pp. 25–169. in Chinese.

Yang, Z., 1991. *China's Glacier and Water Resources*. Lanzhou: Gangsu Science and Technology Press.

Yao, T. D., 1999. Abrupt climatic changes on the Tibetan Plateau during the Last Ice Age – Comparative study of the Guliya ice core with the Greenland GRIP ice core. *Science in China. Series D: Earth Sciences*, **42**, 358–368.

Yao Tandong, and Xie Zichu, 1991. Dunde ice core and its significance. In *Quaternary Climate and Environment in China*. Beijing: Science Press, pp. 24–31. in Chinese.

Yao, T. D., Jiao, K. Q., Tian, L. D., Yang, Z. H., Shi, W. L., and Thompson, L. G., 1996. Climatic variations since the Little Ice Age recorded in the Guliya ice core. *Science in China. Series D: Earth Sciences*, **39**, 587–596.

Yao, T. D., Thompson, L. G., Shi, Y. F., Qin, D. H., Jiao, K. Q., Yang, Z. H., Tian, L. D., and Thompson, E. M., 1997. Climate variation since the last interglaciation recorded in the Guliya ice core. *Science in China. Series D: Earth Sciences*, **40**, 662–668.

Yao, T. D., Xu, B. Q., and Pu, J. C., 2001. Climatic changes on orbital and sub-orbital time scale recorded by the Guliya ice core in Tibetan Plateau. *Science in China. Series D: Earth Sciences*, **44**, 360–368.

Yao, T. D., Wang, Y. Q., Liu, S. Y., Pu, J. C., Shen, Y. P., and Lu, A. X., 2004. Recent glacial retreat in High Asia in China and its impact on water resource in Northwest China. *Science in China. Series D: Earth Sciences*, **47**, 1065–1075.

TIDEWATER GLACIERS

Andreas Vieli
Department of Geography, Durham University, Durham, UK

Definitions

Calving. Refers in context of glaciers to the mechanism of breaking off of ice blocks from a vertical ice cliff.

Calving rate. The rate of ice loss by calving measured in along flow distance per time unit.

Introduction

Tidewater glaciers are glaciers that terminate in the sea and discharge icebergs to the ocean through the mechanism of calving (Calving Glaciers; VanderVeen, 1996, 2002; Benn et al., 2007). This mechanism of ablation is highly efficient and accounts for 70% of the annual mass transfer from the world's glaciers and ice sheets to the ocean. Tidewater glaciers currently only occur in latitudes higher than 45° and can be found in Alaska, the Canadian Arctic, Greenland, Svalbard, Novaya Zemlya, the Antarctic Peninsula, and to a small extent in Patagonia. The vertical ice cliff at the terminus of a tidewater glacier is usually grounded in temperate regions (e.g., Alaska), but in polar regions they are often floating and form small ice shelves that are laterally confined in fjords (Ice Shelf). Tidewater glaciers that discharge ice from ice caps or ice sheets (Ice Sheet) into coastal fjords are referred to as tidewater outlet glaciers (Outlet Glacier).

Tidewater glaciers are different to land-based valley glaciers (Glacier) in many ways. For tidewater glaciers, the dominant mechanism of ablation is through iceberg calving and surface ablation plays only a minor role in the overall mass balance (Glacier Mass Balance). Such glaciers are characterized by fast flow near their terminus of up to a few kilometers per year and the flow is dominated by basal motion rather than internal ice deformation (Glacier Motion/Ice Velocity and Glacier Sliding). This increased flow toward the glacier terminus causes strong along-flow extension and explains the observed intense crevassing of the glacier surface toward the terminus (Crevasses). Further, along-flow acceleration is caused by enhanced basal motion due to reduced resistance from the glacier bed as the surface approaches the level of flotation toward the terminus (Benn et al., 2007).

In contrast to land-based glaciers or ice sheet margins, fluctuations in terminal positions of tidewater glaciers are not necessarily directly related to changes in climate (Climate Change and Glaciers and Dynamics of Glaciers). For example, the terminus position of Columbia Glacier in Alaska (Figure 1; Alaskan Glaciers) was stable until 1980 located at a shallow morainal bank but then a rapid unstable retreat into deeper water set in, with average retreat rates of almost 2 km/year (VanderVeen, 1996). Over the last two centuries, many other tidewater glaciers in Alaska seem to have gone through such phases of rapid retreat through fjord overdeepenings and restabilization in more shallow water upstream.

Tidewater glacier cycle

This highly nonlinear behavior was first explained by the empirical observation that calving rates are roughly linearly proportional to water depth at the terminus (VanderVeen, 2002; Meier and Post, 1987). Typically, tidewater glaciers terminate at a shallow morainal bank or bedrock sill within the fjord. When the terminus starts to retreat, the water depth increases due to the reverse bed slope and further enhances calving and thereby accelerates the retreat until the fjord gets shallower again. This retreat seems irreversible in that it would require an unrealistic high shift to a more positive surface mass balance for the terminus to readvance over the fjord overdeepening. Many such glaciers erode and deliver a large amount of basal sediment at the terminus. Consequently, they can build up and plow a shallow morainal bank in front of them. This reduces water depth at the terminus and thereby calving rates and eases readvance (Nick et al., 2007), but requires high sedimentation rates and time, typically several decades or centuries. Hubbard and Taku Glacier in Alaska are examples of such an advance mechanism; the latter built up a terminal moraine that almost completely protected the terminus from the marine water and allowed it to readvance 7 km through a 100-m deep fjord over the last 120 years (Motyka and Beget, 1996).

This cyclic behavior of rapid retreat through overdeepenings in a fjord and slow readvance through the build up of a morainal bank is referred to as the "tidewater glacier cycle" (Meier and Post, 1987).

Tidewater glacier dynamics

During the rapid retreat of Columbia Glacier, the flow velocities at the terminus increased almost as much as the calving rates from 2 to 10 km/year. This increase in ice flux leads to a drawdown of the glacier surface. Under the assumption that the ice calves off due to buoyancy forces when the surface approaches the flotation level, this surface lowering leads to a further retreat of the terminus (VanderVeen, 1996, 2002).

Based on this concept a "buoyancy-induced calving model" has been proposed to explain the dynamical behavior of tidewater glaciers (VanderVeen, 1996, 2002).

Tidewater Glaciers, Figure 1 Columbia Glacier in Alaska in 1969 with its stable terminus at a shallow morainal shoal. (Photo: Unknown, 1969.)

The rates of retreat and calving are then a direct result of the flow dynamics and controlled by the rate of thinning of the surface at the terminus. This concept has been successfully tested using a numerical model (Vieli et al., 2001). Results from such a modeling experiment are shown in Figure 2 and illustrate how tidewater glaciers dynamically behave. Initially, the terminus is stable at a topographic high. At time zero of the model experiment, the Equilibrium-Line Altitude (ELA) is raised by 50 m. This shift to a more negative surface mass balance causes the glacier to thin and slowly retreat and eventually, it retreats over the basal high into slightly deeper water. This leads to an increase in flow speed and therefore an increase in ice flux at the terminus that provokes a thinning and further retreat into deeper water and leads to an unstable retreat-thinning feedback. Note the strong increase in flow at the terminus and the resulting peak in calving rates when reaching deeper water (Figure 2a and c). Eventually, the terminus retreats behind the basal low and reaches shallower water that decreases the calving rates, slows down the retreat, decelerates the flow, and stabilizes the terminus again. The main driver of this unstable retreat is a flux instability in the case of a reversed bed slope as similarly proposed on theoretical considerations for explaining the marine ice sheet instability (Schoof, 2007; Marine Ice Sheet).

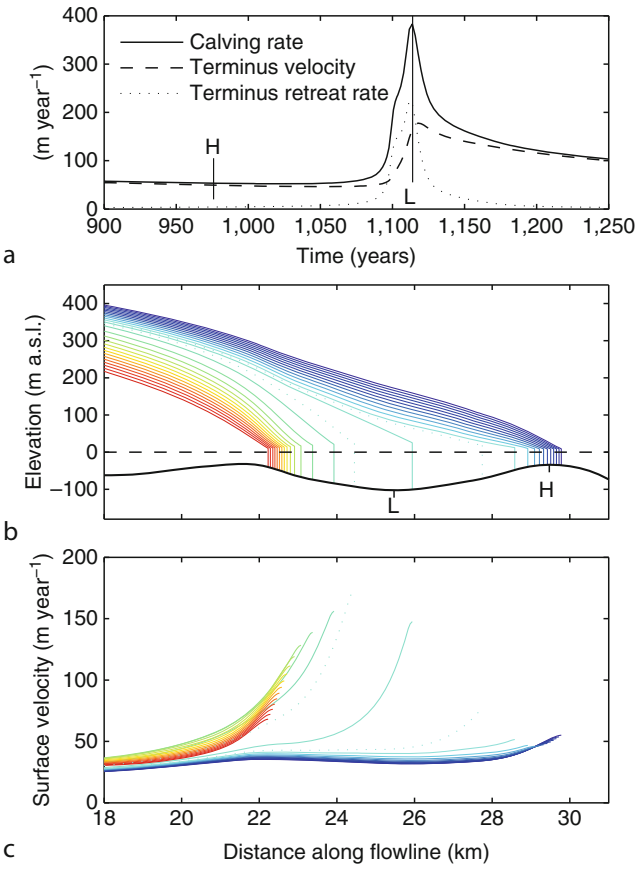

Tidewater Glaciers, Figure 2 Calculated response of a small tidewater glacier to a rise in ELA at time 0. The modeling results are shown from 900 years onward. (**a**) Modeled calving rate (*solid line*), terminus velocity (*dashed line*), and retreat rate (*dotted line*) against model time. Modeled profiles of glacier surface (**b**) and surface velocity (**c**) are shown at 20-year intervals (10 years for *dotted lines*). The lines are color-coded for time and go from dark blue through green and yellow to red. In (**b**), the *solid line* shows bed elevation and the *dashed line* sea level.

This instability can be further enhanced by a positive feedback between subglacial motion and water pressure at the glacier bed. As the surface approaches flotation, the basal water pressure approaches the hydrostatic pressure of the overlying ice and thereby reduces the frictional forces at the glacier bed (Pfeffer, 2007). Variations in glacier width may also affect the stability of a tidewater glacier terminus, with terminus positions being more stable where the glacier channel narrows in the upstream direction.

Glaciers that terminate in freshwater such as a lake behave dynamically very similar to tidewater glaciers, although their calving rates are an order of magnitude lower for the same terminal water depth (Calving Glaciers; Benn et al., 2007).

Tidewater glaciers with a floating tongue

Although the above mechanism has been derived for tidewater glaciers with a grounded terminus, in theory the same dynamical effect occurs for tidewater glaciers with a floating tongue by simply replacing the calving terminus by the grounding line, which defines the point at which the glacier terminus starts to float due to buoyancy forces. This is only true if the floating tongue itself does not provide a significant resistance from lateral friction at the valley walls ("backstress") to the grounded ice upstream. Many outlet glaciers of the Greenland Ice Sheet have floating ice tongues that provide such backstress and act to stabilize the grounding line.

After 3-year phase of strong acceleration, thinning, and retreat related to a basal overdeeping, Helheim Glacier, a major tidewater outlet glacier in East Greenland, started to form a temporary floating ice tongue that slowed the glacier down (Howat et al., 2007) and allowed the terminus to readvance over a basal depression and thereby stabilize its ice tongue. This process reversed the dramatic retreat within a year and on far shorter timescales than considered in the tidewater glacier cycle. A further example illustrating the stabilizing effect of a floating tongue is from Jakobshavn Isbrae, another major tidewater outlet glacier of the Greenland ice sheet. Its recent doubling of flow speed to 13 km/year seems synchronous with the retreat and partial break up of a floating tongue in front of it (Joughin et al., 2004).

Tidewater outlet glaciers

Tidewater outlet glaciers such as Helheim Glacier often terminate in deep ocean fjords and their dynamical behavior appears similar to the rapid and unstable changes of valley tidewater glaciers discussed above (Nick et al., 2009). In Greenland, many such tidewater outlet glaciers are currently undergoing rapid retreat in combination with

a dramatic increase of flow and surface drawdown that both seem to be triggered from the terminus and propagate rapidly inland (Howat et al., 2007; Joughin et al., 2008). These dynamic changes seem to occur synchronously (Rignot and Kanagaratnam, 2006; Howat et al., 2008), suggesting that a common external forcing has acted as a trigger, for example, a regional warming. Indeed, these changes fall into some of the warmest years on record and indications of significantly warmer ocean waters reaching the calving termini have also been found (Holland et al., 2008). Such synchronous behavior and tight link between dynamic changes and climate or ocean are in contrast to the tidewater glacier cycle discussed above.

The recent observations and numerical modeling studies indicate that tidewater outlet glaciers can be extremely sensitive to short-term perturbations at their ocean termini and they react with strong dynamic changes that propagate rapidly inland (Nick et al., 2009). This high dynamic sensitivity and rapid adjustment are a result of the high flow rates and imply that the recently observed dramatic changes in Greenland are likely to reflect short-term fluctuations in climate or ocean conditions and should not necessarily be extrapolated to the future (Howat et al., 2008).

The observed seasonal variations in flow and terminus position of tidewater glaciers, with or without a floating tongue, further support their high sensitivity to short-term changes in climate. The termini of Jakobshavn Isbrae and Columbia Glacier both undergo seasonal cycles of advance and retreat in the order of kilometers per year. Although the short-term variations in tidewater glacier dynamics seem to be related to climate or ocean changes the actual linking mechanisms are not clear but a few potential mechanisms are briefly discussed below.

Triggering mechanisms

Enhanced surface melt in summer may lead to enhanced crevassing through the process of hydrofracturing and thereby weaken the glacier terminus and increase calving (Sohn et al., 1998). Warmer ocean water may increase subaqueous melt at the terminus and provoke more intense calving, or thin the floating tongue and thereby reduce its backstress onto the grounded ice. The onset of acceleration of Jakobshavn Isbrae coincides with the arrival of warmer subsurface ocean water (Holland et al., 2008). For grounded tidewater Glacier LeConte in Alaska, subaqueous melt rates at the calving terminus of 12 m/day have been estimated and demonstrate the potential of ocean melt in influencing calving dynamics (Motyka et al., 2003). Winter Sea Ice that freezes together with icebergs within the fjord ("Sikussak") may provide some backstress onto the calving front and thereby suppress calving. A reduction of winter sea ice duration may therefore increase the annual calving rate (Joughin et al., 2008).

Conclusions

The dynamics of tidewater glaciers is strongly affected by the process of calving and the geometry of the fjord they flow into and is characterized by rapid unstable retreats through basal overdeepenings. Their changes in terminus positions often appear unrelated to changes in climate; however, recent observations indicate that at least on shorter timescales of seasons to a few years tidewater glaciers seem dynamically highly sensitive to fluctuations in climate or ocean conditions. The linking process, however, is still poorly understood and currently subject of intensive research.

Given the high dynamic sensitivity of tidewater glaciers, their potential for rapid changes and their vital role in ice sheet drainage (Ice Sheet Mass Balance), a better understanding of their dynamical behavior, the process of calving and the linking processes to climate are crucial in improving our ability to predict the contribution of glaciers and ice sheets to future sea level (Sea-Level).

Bibliography

Benn, D. I., Warren, C. R., and Mottram, R. H., 2007. Calving processes and the dynamics of calving glaciers. *Earth Science Reviews*, **82**, 143–179.

Holland, D. M., Thomas, R. H., deYoung, B., Ribergaard, M. H., and Lyberth, B., 2008. Acceleration of Jakobshavn Isbræ triggered by warm subsurface ocean waters. *Nature Geoscience*, **1**, 659–664.

Howat, I. M., Joughin, I., and Scambos, T. A., 2007. Rapid changes in ice discharge from Greenland outlet glaciers. *Science*, **315**, 1559–1561.

Howat, I. M., Joughin, I., Fahnestock, M., Smith, B. E., and Scambos, T. A., 2008. Synchronous retreat and acceleration of southeast Greenland outlet glaciers 2000-06: ice dynamics and coupling to climate. *Journal of Glaciology*, **54**, 646–660.

Joughin, I., Abdalati, W., and Fahnestock, M., 2004. Large fluctuations in speed on Greenland's Jakobhavn Isbrae glacier. *Nature*, **432**, 608–610.

Joughin, I., et al., 2008. Seasonal speedup along the Western margin of the Greenland ice sheet. *Science*, **320**, 781–783.

Meier, M. F., and Post, A., 1987. Fast tidewater glaciers. *Journal of Geophysical Research*, **92**(B), 9051–9058.

Motyka, R. J., and Beget, J. E., 1996. aku Glacier, southeast Alaska, U.S.A.: Late Holocene history of a tide-water glacier. *Arctic and Alpine Research*, **28**, 42–51.

Motyka, R. J., Hunter, L., Echelmeyer, K. A., and Connor, C., 2003. Submarine melting at the terminus of a temperate tidewater glacier, LeConte Glacier, Alaska. *Annals of Glaciology*, **36**, 57–65.

Nick, F. M., VanderVeen, C. J., and Oerlemans, J., 2007. Controls on advance of tidewater glaciers: results from numerical modelling applied to Columbia Glacier. *Journal of Geophysical Research*, **112**, F03S24.

Nick, F. M., Vieli, A., Howat, I. M., and Joughin, I., 2009. Large-scale changes in Greenland outlet glacier dynamics triggered at the terminus. *Nature Geoscience*, **2**, 110–114.

Pfeffer, W. T., 2007. A simple mechanism for irreversible tidewater glacier retreat. *Journal of Geophysical Research*, **112**, F03S25.

Rignot, E., and Kanagaratnam, P., 2006. Changes in velocity structure of the Greenland ice sheet. *Science*, **311**, 986–990.

Schoof, C., 2007. Ice sheet grounding line dynamics: steady states, stability, and hysteresis. *Journal of Geophysical Research*, **112**, F03S28.

Sohn, H. G., Jezek, K. C., and Van der Veen, C. J., 1998. Jakobshavn Glacier, West Greenland: 30 years of spaceborne observations. *Geophysical Research Letters*, **25**, 2699–2702.

Unknown, 1969. Columbia Glacier: from the Glacier Photograph collection. Boulder, Colorado USA: National Snow and Ice Data Center/World Data Center for Glaciology. Digital media.

VanderVeen, C. J., 1996. Tidewater calving. *Journal of Glaciology*, **42**, 375–386.
VanderVeen, C. J., 2002. Calving glaciers. *Progress in Physical Geography*, **26**, 96–122.
Vieli, A., Funk, M., and Blatter, H., 2001. Flow dynamics of tidewater glaciers: a numerical modelling approach. *Journal of Glaciology*, **47**, 595–606.

Cross-references

Alaskan Glaciers
Calving Glaciers
Climate Change and Glaciers
Crevasses
Dynamics of Glaciers
Equilibrium-Line Altitude (ELA)
Fjords
Glacier Mass Balance
Glacier Motion/Ice Velocity
Greenland Ice Sheet
Ice Sheet
Ice Sheet Mass Balance
Ice Shelf
Marine Glaciers
Marine Ice Sheet
Outlet Glacier
Patagonia
Sea Ice
Sea-Level

TIEN SHAN GLACIERS

Vladimir Aizen
College of Science, University of Idaho, Moscow, ID, USA

Synonyms

Alpine glaciers; Glaciers of central Asia; Glaciers of Kyrgyzstan, China, Kazakhstan, Uzbekistan; Glaciers of mid-latitudes; Tien Shan Glaciers

Definition

The Alpine glaciers of the mid-latitudes that exist in Tien Shan high mountains in continental climate.

Tien Shan is one of the largest mountain systems in Asia stretching 2,000 km from west to east between 39–46°N and 69–95°E. Glaciers of Tien Shan (Figure 1) spread in altitudinal belt between 2,800 m a.s.l. and 7,400 m a.s.l. and inters one of the major sources of water in central Asia endorheic basins feeding the Aralo-Caspian, Balkhash, Issik Kul, and Tarim hydrographic systems. The glaciers of Tien Shan are supplying water for approximately 50 million populations of Kyrgyzstan, Uzbekistan, Kazakhstan, northern Tajikistan, and Xinjiang supporting the low lands agriculture, urban, and industrial areas. The latest investigations over the whole Tien Shan mountains based on remote sensing data numbers 7,590 glaciers with total area of 13,271.45 and 1,840 km^3 volume of ice (Aizen et al., 2008, 2009). There are different types of glaciers in Tien Shan, from large valley and dendrite glaciers, prevalent in central Tien Shan, to small lobes, niche glaciers in all Tien Shan alpine areas. Large valley glaciers form 82% of the Tien Shan total glacierized area. The South Inylchek (59.5 km long) is the largest Tien Shan glacier located in central Tien Shan, Khan-Tengri glacierized massif that covers 4,320 km^2. The Turkestan type of glaciers nourished by snow avalanches and mass of ice falling from hanging glaciers, are the prevailing glaciers in central Tien Shan, the Khan-Tengri glacierized massif. The mass of the rock falling on the glacier's surface with snow and ice is burying the tongue of the Turkestanian type of glaciers under thick moraine and commonly make glacier ice dead (Kotlyakov, 1984). The flat ice cap glaciers are typical of the Inner Tien Shan high elevated area.

The main factor controlling the glacier regime in Tien Shan is the impact of air temperature that affects the type of precipitation, the duration, and the intensity of snow

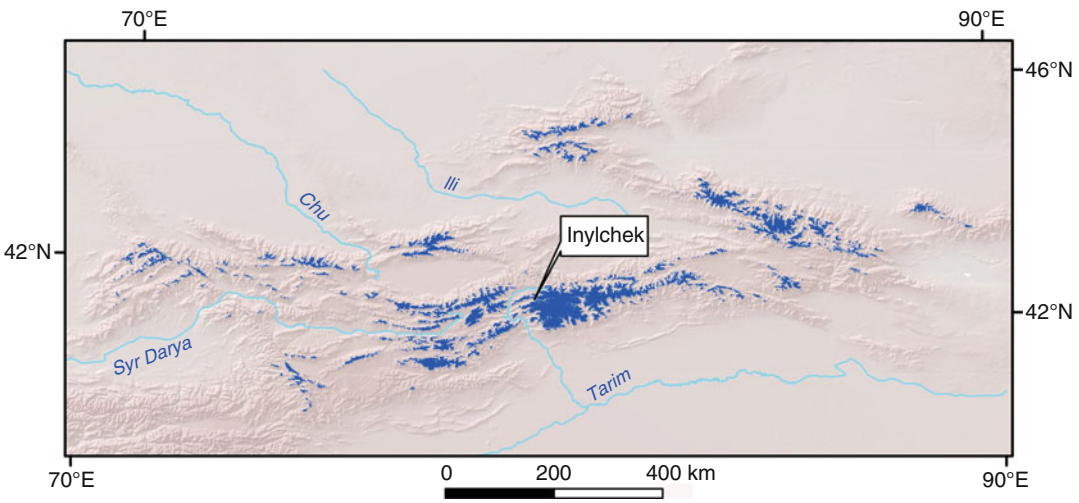

Tien Shan Glaciers, Figure 1 Glaciers of the Tien Shan Mountains.

and ice melt throughout altitudinal belts. The Tien Shan glaciers represent all though glacier ice formation zones, from cold recrystallization at altitudes over 6,000 m to warm infiltration-recrystallization and infiltration-congelation (Aizen et al., 1997). The modern increase of air temperature, which is observed in the Tien Shan's alpine areas, extends the period and intensity of melt not only in the glacier ablation area but also in the upper accumulation areas of the glaciers, which impact on acceleration of glacier recession in Tine Shan particularly from the mid 1970s. The Tien Shan glaciers lost 8.5% of their total area since the 1970s. However, different Tien Shan regions have different rates of glacier recession for the same period. The largest absolute, as well as relative glacier area loss occurred in the northern Tien Shan (−361 km^2, 14.3%), where the annual and seasonal sums of precipitation decreased at elevations above 3,000 m (18.6 mm), and the summer air temperatures increased by 0.44°C. Similar large absolute recession occurred in the inner and central Tien Shan (287 and 244 km^2) (Figure 2) where annual precipitation decreased on −35 mm and summer air temperatures increased on 0.71°C. However, the relative glacier area loss is 10% and 5%, respectively, due to large total glacierized area in inner and central Tien Shan. The least

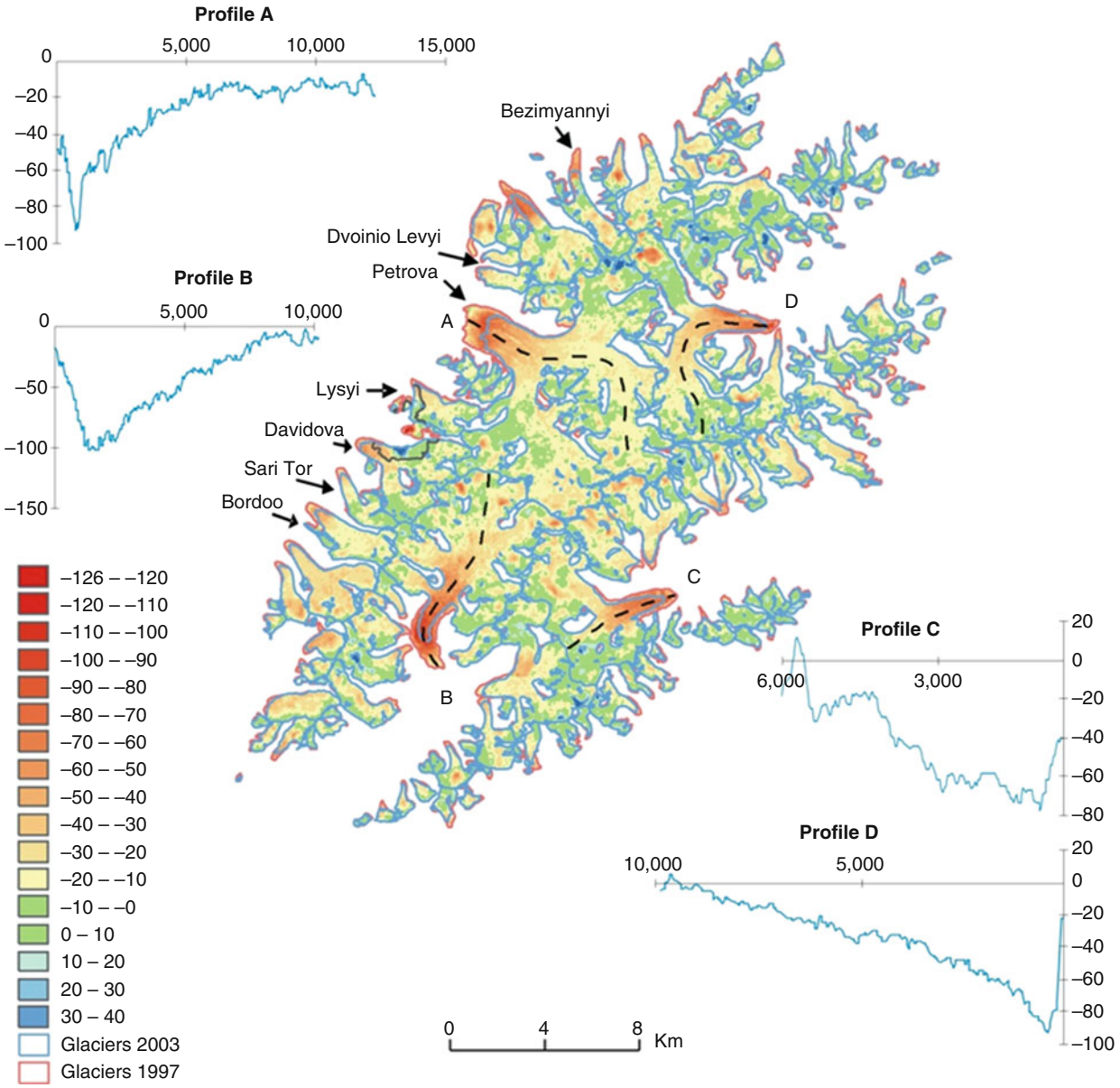

Tien Shan Glaciers, Figure 2 Akshiirak glacierized massif in inner Tien Shan region. Changes in glacier area and surface elevation between 1977 and 2003 (Aizen et al., 2006).

absolute glacier recession occurred in the western Tien Shan (45 km^2), where summer air temperatures increased only by 0.23°C and annual precipitation decreased on 13.4 mm. The eastern Tien Shan lost 196 km^2 of the total glacier area (12%) (Liu et al., 1998; Aizen et al., 2009). The retreat of the Tien Shan glaciers was accompanied by equilibrium line altitude (ELA) with an uplift of 23 m from 4,012 m a.s.l. in 1973 to 4,035 m a.s.l. in 2003. On average, air temperatures in Tien Shan increased on 0.8°C with 7% precipitation decrease at the ELA (Aizen et al., 2008, 2006). Tien Shan glaciers exist in arid continental climate only because of spring-summer or summer maximum precipitation, which increase albedo in periods of glacier melt. Therefore, even a small decrease of precipitation along with increase of air temperature causes acceleration in Tien Shan glacier recession.

Bibliography

Aizen, V. B., Aizen, E. M., Dozier, J., Melack, J., Sexton, D., and Nesterov, V., 1997. Glacial regime of the highest Tien Shan mountains, Pobeda-Khan Tengry massif. *Journal of Glaciology*, **43**(145), 503–512.

Aizen, V. B., Aizen, E. M., Surazakov, A. B., and Kuzmichenok, V. A., 2006. Assessment of glacial area and volume change in Tien Shan (Central Asia) during the last 150 years using Geodetic, Aerial Photo, ASTER and SRTM data. *Annals of Glaciology*, **43**, 202–213.

Aizen, V. B., Aizen, E. M., Surazakov, A. B., and Nikitin, S. A., 2008. Is Central Asia really exsiccated? *Proceedings of AGU Fall Meeting*, San Francisco, GC53C-07.

Aizen, V. B., Aizen, E. M., Surazakov, A. B., and Nikitin, S. A., 2009. Is Central Asia exsiccated? *Journal of Hydrology* (submitted).

Kotlyakov, V. M., 1984. *Glaciologicheskii Slovar' (Glaciological Dictionary)*. Gidrometeoizdat, L., 526p (in Russian).

Liu, S. Y., Ding, Y. J., Wang, N. L., and Xie, Z. C., 1998. Mass Balance Sensitivity to Climate Change of the Glacier No. 1 at the Urumqi River Head, Tien Shan Mts. *Journal of Glaciology and Geocryology*, **20**(1), 9–13.

TILL

Jan A. Piotrowski
Department of Earth and Sciences, University of Aarhus, Aarhus C, Denmark
Department of Geography, University of Sheffield, Sheffield, UK

Synonyms

Boulder clay

Definition

Till. A sediment that has been transported and deposited by or from glacier ice, with little or no sorting by water.
Tillite. A lithified till from a pre-Quaternary glaciation.

Introduction

The term till is older than the glacial theory and has been first used by Scottish country folk to describe coarse, obdurate land, the soil developed on the stony clay that covers much of northern Britain (Flint, 1971). Despite its widespread occurrence in all areas covered by glaciers and ice sheets making it one of the most common sediment in the Northern Hemisphere, its origin and the interpretation of structural and textural characteristics are highly debated. Till is more variable than any other sediment known under a single name (Dreimanis, 1988) and its properties mirror the great complexity of processes involved in erosion, transport, and deposition of geological material by glaciers. For over a century researchers have tried, with variable success, to define diagnostic criteria of different till types and formulate a definition of till that would account for most of its characteristics. One problem is the gap between our understanding of glacial processes based on the study of environments glaciated at present, and the interpretation of the geological product of these processes, that is, a till, formed in the past. This is to a large extent caused by the inaccessibility of glacier beds and, consequently, the perplexing lack of direct observations of till formation. Therefore, reconstructions of till origin often lack reference to modern analogues verified by observation. The till definition given above (after Dreimanis and Lundqvist (1984)) is therefore a broad, descriptive formulation purposely avoiding any specific reference to till properties or the mechanisms of formation.

Till characteristics and classifications

Tills are typically diamicton consisting of a wide range of grain sizes from clay to boulders mixed together in various proportions depending on the rock types overridden by a glacier, transport modes, and the process in which glacial material is released from ice to become sediment. They contain both far-travelled and local components reflecting the flow path of a glacier, and their occurrence unequivocally marks the extent of past glaciers in Earth's history. On a continental scale, tills occur as meter to tens of meters thick sheets often separated by other glacial materials such as clay, silt, sand, and gravel leading to a pronouncedly stratified appearance of glacial sequences consisting of diamictons interbedded with sorted sediments. Besides being essential indicators of past glaciations, tills are important aquitards that influence groundwater flow in the upper lithosphere and they constitute a substrate for diverse engineering activities. The hydrogeological and geotechnical parameters of tills vary according to their lithological composition, texture, structure, and degree of compaction.

Numerous genetic classifications of tills have been proposed, typically based on their environment of formation (subglacial or supraglacial) or the relation to ice movement (formed by active or stagnant ice) (Dreimanis, 1988; Benn and Evans, 1998; Menzies, 2002). As research progresses, the till classification is being simplified merging the various local till types reported in the literature into fewer, more general classes (Evans et al., 2006). It is now

recognized that tills (1) often are hybrids derived from superposition of different processes that operated at a certain place in space during a glaciation (Larsen et al., 2004; Piotrowski et al., 2006), and (2) are typically parts of a glacial continuum characterized by overlapping properties and poorly defined boundaries (Evans, 2007) rendering rigid and complicated classifications unverifiable and unnecessary. The most important glacial processes leading to till formation are lodgement, deformation, melt-out, and flowage.

Lodgement till

This till type is deposited by plastering of glacial debris from the base of a moving glacier onto the substratum by pressure melting and/or other mechanical processes (Dreimanis, 1988). Lodgement occurs at the ice/bed interface (IBI) below active, warm-based glaciers particle by particle or in packages, whenever frictional forces between the debris and the bed overcome adhesion forces keeping the debris in the ice. This does not happen instantaneously and the debris is first dragged along the bed. Boulders dragged over the bedrock generate striations and percussion marks whereas finer-grained material may polish the bedrock. When lodgement occurs on a soft bed, boulders carve characteristic plowing marks in the bed before being liberated from the ice (Clark and Hansel, 1989; Jørgensen and Piotrowski, 2003; Thomason and Iverson, 2008).

Since lodgement tills are deposited from a base of a sliding glacier (or an ice sheet), their various structural elements have consistent orientation caused by the regionally uniform ice movement direction. This refers in particular to the till fabric whereby elongated stones are typically aligned parallel with the ice flow direction, which is the position of least resistance to the flow. Lodgement tills host syndepositional glaciodynamic structures such as slickensides, ribs, wedges (Ehlers and Stephan, 1979), and erosion tails behind boulders (Piotrowski and Kraus, 1997). Frequently, boulders' bottom surfaces bear signature of mechanical attrition imprinted during plowing, and their tops are flattened by abrasion after they have been lodged and the debris-laden ice was moving over them. Striations on the flat upper surfaces of the boulders are oriented parallel to the elongated stones found in the surrounding till matrix. Bullet-shaped boulders occur, with their blunt ends pointing up-glacier (Krüger, 1984). The base of a lodgement till is erosive, reflecting ice movement along the bed before till accretion commenced. Shear planes and subhorizontal fractures (Boulton, 1970; Benn, 1994) may also occur in lodgement tills but they may equally well be found in any other, postdepositionally mobilized tills and therefore their presence cannot be considered diagnostic for any particular process of till formation. Due to abrasion accompanying lodgement, these tills tend to have bimodal grain-size distribution with a distinct peak in the silt fraction caused by grain comminution (Haldorsen, 1981). Unless interrupted by other processes such as basal decoupling and sediment sorting by meltwater, accretion of lodgement tills by gradual release of basal debris together with lateral motion of the ice sole leads to their macroscopically structureless appearance. If porewater drainage from an accreting lodgement till is possible (e.g., through subglacial channels or into a permeable bed below), these tills are overconsolidated by the weight of the overlying ice. However, efficient drainage may be impeded under the ice and the pressurized porewater often prevents consolidation (Piotrowski and Kraus, 1997).

For decades it was assumed that lodgement tills are major components of flat to gently undulating ground moraines covering large areas of previously glaciated continents and are thus the volumetrically most important till type. However, it now appears that the typical volume of material transported englacially may be insufficient for the formation of thick till sequences by pure lodgement alone. Also, clay fraction which sometimes accounts for over 20–30% of these tills is difficult to attribute to lodgement because of the high mobility of this soft, low-strength material. Alternatively, some combination of lodgement and mobilization of the preexisting subglacial material may be considered (see below).

Deformation till and glaciotectonite

Named and described from the geological record by (Elson, 1961), deformation till can be regarded as weak rock or unconsolidated sediment that has been subglacially mobilized from its in situ position, the primary structures deformed or destroyed, and some foreign material admixed (cf. Elson, 1988). This type of till is produced beneath the glacier in the zone called deforming bed, mobile layer, or subglacial traction carpet where soft, dilated sediment, weakened by elevated porewater pressure cannot withstand stresses applied to it by the overriding glacier and starts to deform. Depending on local conditions controlling the sediment strength and ice-bed coupling, the zone of deformation may be in the range of centimeters (Engelhardt and Kamb, 1998) to several meters thick (Boulton, 1996), or it may be absent altogether. Because of the rheologically complex nature of diamictons subjected to stress, there are no universally agreed-upon criteria to distinguish deformation tills that experienced large strain from those that have not (Paterson, 1994). This is particularly true for macroscopically massive tills. The problem of the identification of deformation tills has generated some controversy as to how widespread deforming beds were under past ice sheets (Piotrowski et al., 2001). However, some proxies, as summed up below, help constrain the deformation process and identify its product. It is worth emphasizing that the genesis of deformation tills has consequences reaching far beyond glacial sedimentology alone; it also bears on our understanding of continental-scale debris redistribution by ice sheets and the processes controlling ice sheet stability, movement mechanism, and the

generation of certain landforms such as drumlins and megascale glacial lineations.

It is agreed that progressive deformation leads to sediment mixing and homogenization by mechanically predictable (Weertman, 1968) grain diffusion and advection. Therefore, deformation tills that experienced pervasive strain may be expected to have macroscopically massive appearance while revealing a large spectrum of microstructures when viewed under a microscope (van der Meer, 1993; Menzies, 2000; Hiemstra and Rijsdijk, 2003). If strain was lower, heterogeneities such as pods, lenses and stringers of sorted sediments bounded by smudged contacts with the surrounding till matrix (Hooyer and Iverson, 2000a) may occur. Thin intra-till stringers of sorted sediments produced by tectonism through mobilization and detachment from the bed, partial mixing with till matrix, and finally thinning and attenuation during advection within the deforming bed may be difficult to distinguish from the inclusions of sorted sediments formed by in situ sedimentation in water. Yet, careful examination is highly recommended since the unequivocal identification of tectonic versus sedimentary process may be crucial for the reconstruction of the genesis of the entire sequence of a bedded till. Deformation tills that experienced lower strains will be characterized by well-preserved tectonic layering with flat, overturned folds and rooted structures (Figure 1a). Given the uneven distribution of strain in the vertical profile of a deforming bed with the highest degree of deformation close to the ice sole (Boulton and Hindmarsh, 1987), basal contacts of deformation tills may be expected to be gradational from the undisturbed substratum (Piotrowski et al., 2006). Stress-induced intergranular collisions lead to particle comminution and thus grain-size modification (Boulton et al., 1974), they imprint wear pattern on grain surfaces (Benn, 1994), and generate specific micromorphological features such as in situ crushed quartz grains (Larsen et al., 2006b). Under such conditions, fragile material has low preservation potential and is typically absent in deformation tills, although nearly intact shells have been reported from fine-grained diamictons generated by subglacial deformation (Boulton et al., 1996; Hicock and Dreimanis, 1992).

Fabric signature of deformation tills has been interpreted differently, depending on the rheological model applied to the deformation. Earlier studies suggested that tills behave as viscous materials whereby clasts rotate freely within the matrix (Jeffery-type rotation model) leading to weak fabric strength. Since it was established that tills are more likely to be plastic materials, March-type rotation models have been applied to explain till fabric development (Benn, 1995; Hooyer and Iverson, 2002) whereby elongated particles quickly rotate into a quasi-stable, strain-parallel position and remain there

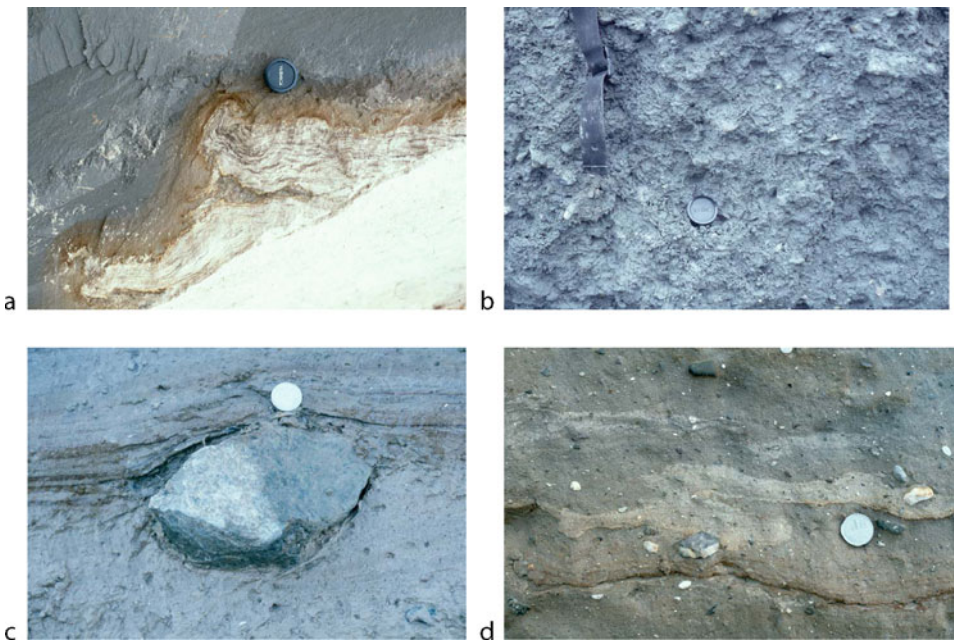

Till, Figure 1 (**a**) Deformation till overlying outwash sand. Note sand mobilization and incipient mixing with till matrix caused by basal shear stress. Stohl cliff, northern Germany. (**b**) Subglacial traction till in a fluted ground moraine recently exposed in front of a retreating glacier. Note the massive appearance of the till. Elisebreen, Spitsbergen. (**c**) Melt-out till. Note the bedded appearance of the till and that the sorted sediment layers are draped over an angular boulder. Dänischer Wohld, northern Germany. (**d**) Flow till. Note the overturned slump-fold (*left* of the coin) and the heterogeneous appearance of the till caused by subaerial washing and flowage. Dänischer Wohld, northern Germany.

irrespective of further advection of till around them. This type of rotation has been confirmed in laboratory experiments (Hooyer and Iverson, 2000b; Hooyer and Iverson, 2002) that demonstrated a rapid evolution of fabrics in a pervasively deforming till, its strong final clustering and up-ice dip of elongated particles (Thomason and Iverson, 2009). These findings, together with strain-rate dependent evolution of microshears (Thomason and Iverson, 2006), can help estimate strain in a till of unknown history (Larsen et al., 2006a) and possibly distinguish it from other till types.

Deformation tills may or may not be overconsolidated. During pervasive deformation, a coarse-grained till is dilated due to grain rotations pulling the sediment skeleton apart whereby pressurized water fills in the enlarged pore spaces and prevents till compaction by the weight of the overlying ice. If porewater drains after the deformation ceases, the till may collapse to a denser state. The thicknesses of deformation tills can be expected to increase toward the ice margin (Evans and Hiemstra, 2005) where the subglacial advection of glacial debris terminates. Deformation tills consist primarily of local material with limited admixture of far-travelled components (Kjær et al., 2003) and occur at the bottom of a till sequence deposited during one glacial cycle.

A rock or sediment that has been deformed by subglacial shearing but retains some of the structural characteristics of the parent material and does not contain any admixture of foreign, ice-transported debris is called glaciotectonite (cf. Benn and Evans, 1998). This term includes comminution till, a dense fine-grained diamict formed by abrasion and crushing of bedrock underneath the ice (Elson, 1988). Ideally, an upward transition from undeformed bed to glaciotectonite and finally deformation till can be expected.

Subglacial traction till

Generated in the same environment (subglacial), under similar conditions (active, warm-based ice), and from similar parent material (any kind of bedrock and sediment overridden by a glacier), deformation and lodgement tills bear numerous common features and often are indistinguishable. Lodgement and deformation frequently coexist. For example, clasts plowing the bed at an early stage of lodgement may deform the bed to a depth of several clast diameters (Tulaczyk, 1999). This can imprint deformation signatures now distributed through the entire till thickness because of the time-transgressive accretion of till accompanied by plowing by clasts progressively emerging from the ice sole. Debris making up the lodgement till should, strictly speaking, remain immobile immediately after it was released from the ice which is difficult to envisage given the very low strength of a fresh till. It is therefore reasonable to consider lodgement and deformation tills as closely related and largely overlapping members of a subglacial continuum, and merge them into one common till type called subglacial traction till (STT) as suggested by Evans et al. (2006) (Figure 1b). The term STT would also include diamicts formed by creep or flowage into cavities on the lee sides of roches moutonnées (lee-side tills of Hillefors (1973)), and sorted sediments locally formed at the IBI due to ice-bed decoupling and washing partly referred to as "subglacial sliding bed deposits" (Evans, 2007).

Processes generating tills under active glaciers and ice sheets depend on the coupling of ice with its bed (e.g., Fischer and Clarke, 2001; Piotrowski et al., 2004), strength of the subglacial sediment, hydrological and thermal conditions and, as such, they vary in time and space which yields a mosaic of features whose interpretation often is contentious. Among several lines of modern research, on-site studies under modern glaciers (e.g., Iverson et al., 1995; Hart et al., 2009) and laboratory experiments (e.g., Iverson et al., 2008) and seem particularly promising in better constraining the origin of active-ice-till properties.

Melt-out till

Melt-out till is an ablation deposit formed by slow, in situ melting of ice. It consists of sediment released by the melting of stagnant or slowly moving debris-rich glacier ice and it is deposited without subsequent transport or deformation (Benn and Evans, 1998). Therefore, melt-out tills are typically formed at a late stage of glaciation when inactive ice melts down and the load it carried is gradually lowered onto the bed. These tills often occur on top of active ice tills and may constitute the bulk of sediment found in ice-disintegration landforms. When ice wastage occurs under cold and dry conditions, sublimation may replace melting and give rise to a specific till type known as sublimation till (Shaw, 1988). Melt-out tills can be generated by ablation at the top or at the bottom of a glacier, but the preservation potential of the latter is higher (Paul and Eyles, 1990). Formation of melt-out tills has been monitored in a modern environment (Lawson, 1981) but the significance of melt-out tills in the sedimentary record of past glaciations is contentious because the volume of englacial debris needed for the production of thick melt-out tills seems larger than it is typically observed in modern ice sheets.

Since the process of passive release of debris from the ice is clearly different from the processes involved in the formation of active-ice till facies, melt-out tills should be comparatively easy to identify. They are characterized by the preservation of original structures inherited from englacial transport, contain clasts of unlithified fragile material and abundant unabraded stones. Melt-out tills have a high proportion of far-travelled material including large, intact rafts of soft bedrock, in some cases transported for hundreds of kilometers. Elongated stones in melt-out tills tend to have high strength of clustering and they are aligned parallel to the ice flow direction as during the preceding englacial transport. The strong fabric can be reduced by stone collisions if ice has high debris

content. Dip angles of elongated stones are smaller than during the englacial transport due to subsequent ice removal causing wholesale volume reduction (Menzies, 2002). Melt-out tills can have undulating bases with little evidence of erosion. Sometimes, melt-out tills are found on top of upward-convex outwash sediments deposited in subglacial cavities that have been subsequently draped by the morainic material released from the ice sole.

Formation of melt-out tills is intimately associated with meltwater, and the diamictic matrix of the till may be occasionally intercalated with layers of sorted sediments such as sand and silt containing subglacial dropstones of various sizes. The contacts between these layers and the till matrix are often gradational which indicates transitions between phases of passive melting of material from the ice base in shallow subglacial cavities under stagnant-water conditions, and episodes of water flow through these cavities leading to lateral transport and sediment sorting. Such shifts in deposition are sometimes recorded as successions of current ripples preserved below the diamictons formed during subsequent melt-out phases (Piotrowski, 1994). An important feature of some melt-out tills are cm-thick, subhorizontal layers of sand that either drape stones in the till matrix (Figure 1c), or are downwarped underneath them. This results from volume reduction during ice melting and can be considered diagnostic for melt-out tills (Shaw, 1979). The drape structures above the stones are symmetrical, that is, lack lateral folding that is characteristic for tills generated by active ice. The layers of sand themselves are formed due to sorting of englacial debris where layers of relatively clean ice melt and release water. Basal decoupling and turbulent flow of meltwater along the IBI may lead to the formation of scour marks underneath boulders embedded in basal ice (Munro-Stasiuk, 2000). Given the ubiquitous presence of water preventing matrix compaction, melt-out tills are unlikely to be overconsolidated.

Despite the well-constrained process of in situ loss of ice from a melting debris-rich glacier, the recognition of past melt-out tills is often controversial with the same properties being attributed either to melting or to deformation (Evans, 2007).

Flow till

For many researchers not a true till but rather an ice-slope colluvium, flow till can be regarded as glacial debris gravitationally redeposited in direct contact with glacier ice (cf. Dreimanis, 1988). Its formation comprises (1) release of morainic material from the ice surface due to melting, (2) gravity-driven flowage along the sloping ice surface, and (3) deposition at the ice margin (Lawson, 1979). The dynamics of the flowage depend primarily on the ice slope angle, water saturation of the material, and the air temperature. Formed during a late stage of ice disintegration, flow tills commonly occur at the top of a till succession generated by a single glaciation and they are found in hummocky ice-disintegration landscapes, kames, and end moraines. They have limited aerial extent and variable thickness.

Flow tills are loosely packed (unless overridden during ice re-advance), coarse-grained diamictons with fine fraction depleted due to meltwater washing on the ice surface. If the washing is intense, flow tills may contain irregular pockets and lenses of sorted sediments, often deformed and partly mixed together with diamictic matrix during the flowage (Figure 1d). Gravitational folds and normal faults triggered by melting of the surrounding ice such as those reported from kames and end moraines are common. Flow tills may have locally strong but regionally inconsistent fabrics with stone orientation governed by the local configuration of the ice slope and the area where the flow stopped.

Conclusions

Considering a small number of features unique to a given till type and the genetic continuity between most types of tills, only a complex study of multiple proxies can help decipher the origin of a certain till. Unfortunately, many of these proxies are open to subjective interpretation by the individual researcher, which leads to disagreement that frequently cannot be resolved using rigorous scientific approach. Recent years have witnessed (1) a rapid development of analytical techniques such as analogue experiments in large ring-shear devices to test the behavior of tills under conditions mimicking those beneath glaciers; (2) advances in studies of till micromorphology to learn more about the small-scale structural diversity of macroscopically massive tills; (3) sophisticated on-site investigations of the ice/bed interface using probes and other devices inserted into the subglacial bed to monitor the behavior of till in its natural environment; and (4) enhanced development of numerical models to simulate till rheology in the context of continental-scale ice sheet dynamics. These fields are also the areas where research will likely be focussed in the near future.

Bibliography

Benn, D. I., 1994. Fluted moraine formation and till genesis below a temperate glacier: Slettmarkbreen, Jotunheimen, Norway. *Sedimentology*, **41**, 279–292.

Benn, D. I., 1995. Fabric signature of till deformation, Breidamerkurjokull, iceland. *Sedimentology*, **42**, 735–747.

Benn, D. I., and Evans, D. J. A., 1998. *Glaciers and Glaciation*. London: Arnold.

Boulton, G. S., 1970. On the deposition of subglacial and melt-out tills at the margins of certain Svalbard glaciers. *Journal of Glaciology*, **9**, 231–245.

Boulton, G. S., 1996. On the origin of till sequences by subglacial sediment deformation beneath mid-latitude ice sheets. *Annals of Glaciology*, **22**, 75–84.

Boulton, G. S., and Hindmarsh, R. C. A., 1987. Sediment deformation beneath glaciers: rheology and geological consequences. *Journal of Geophysical Research*, **92**, 9059–9082.

Boulton, G. S., Dent, D. J., and Morris, E. M., 1974. Subglacial shearing and crushing, and the role of water pressures in tills from south-east iceland. *Geografiska Annaler*, **56A**, 135–145.

Boulton, G. S., Van Der Meer, J. J. M., Hart, J., Beets, D., Ruegg, G. H. J., Van Der Wateren, F. M., and Jarvis, J., 1996. Till and moraine emplacement in a deforming bed surge — an example from a marine environment. *Quaternary Science Reviews*, **15**, 961–987.

Clark, P. U., and Hansel, A. K., 1989. Clast ploughing, lodgement and glacier sliding over a soft glacier bed. *Boreas*, **18**, 201–207.

Dreimanis, A., 1988. Tills, their genetic terminology and classification. In Goldthwait, R. P., and Matsch, C. L. (eds.), *Genetic Classification of Glacigenic Deposits*. Rotterdam: Balkema, pp. 17–84.

Dreimanis, A., and Lundqvist, J., 1984. What should be called till? *Striae*, **20**, 5–10.

Ehlers, J., and Stephan, H. J., 1979. Forms at the base of till strata as indicators of ice movement. *Journal of Glaciology*, **22**, 345–355.

Elson, J., 1961. The geology of tills. In *Proceedings of the 4th Canadian soil mechanics conference*, Commission for Soil and Snow Mechanics, Technical Memoir, Vol. 69, pp. 5–36.

Elson, J., 1988. Comment on glaciotectonite, deformation till and comminution till. In Goldthwait, R. P., and Matsch, C. L. (eds.), *Genetic Classification of Glacigenic Deposits*. Rotterdam: Balkema, pp. 85–88.

Engelhardt, H. F., and Kamb, B., 1998. Sliding velocity of ice stream B. *Journal of Glaciology*, **44**, 223–230.

Evans, D. J. A., 2007. Tills. In Elias, S. A. (ed.), *Encyclopedia of Quaternary Science*. Amsterdam: Balkema, pp. 959–975.

Evans, D. J. A., and Hiemstra, J. F., 2005. Till deposition by glacier submarginal, incremental thickening. *Earth Surface Processes and Landforms*, **30**, 1633–1662.

Evans, D. J. A., Phillips, E. R., Hiemstra, J. F., and Auton, C. A., 2006. Subglacial till: formation, sedimentary characteristics and classification. *Earth Science Reviews*, **78**, 115–176.

Fischer, U., and Clarke, G. K. C., 2001. Review of subglacial hydromechanical coupling: Trapridge glacier, Yukon territory, Canada. *Quaternary International*, **86**, 29–43.

Flint, R. F., 1971. *Glacial and Quaternary Geology*. New York: Wiley.

Haldorsen, S., 1981. Grain-size distribution of subglacial till and its relation to glacial crushing and abrasion. *Boreas*, **10**, 91–105.

Hart, J. K., Rose, J. C., Martinez, K., and Ong, R., 2009. Subglacial clast behaviour and its implication for till fabric development: new results derived from wireless subglacial probe experiments. *Quaternary Science Reviews*, **28**, 597–607.

Hicock, S. R., and Dreimanis, A., 1992. Deformation till in the Great Lakes region: implications for rapid flow along the south-central margin of the Laurentide ice sheet. *Canadian Journal of Earth Sciences*, **29**, 1565–1579.

Hiemstra, J. F., and Rijsdijk, K. F., 2003. Observing artificially induced strain: implications for subglacial deformation. *Journal of Quaternary Science*, **18**, 373–383.

Hillefors, A., 1973. The stratigraphy and genesis of stoss- and lee-side moraines. *Bulletin of the Geological Institute of the University of Uppsala*, **5**, 139–154.

Hooyer, T. S., and Iverson, N. R., 2000a. Diffusive mixing between shearing granular layers: constraints on bed deformation from till contacts. *Journal of Glaciology*, **46**, 641–651.

Hooyer, T. S., and Iverson, N. R., 2000b. Clast-fabric development in a shearing granular material: implications for subglacial till and fault gouge. *Geological Society of America Bulletin*, **112**, 683–692.

Hooyer, T. S., and Iverson, N. R., 2002. Flow mechanism of the Des Moines lobe of the Laurentide ice sheet. *Journal of Glaciology*, **48**, 575–586.

Iverson, N. R., Hanson, B., Hooke, R. L., and Jansson, P., 1995. Flow mechanism of glaciers on soft beds. *Science*, **267**, 80–81.

Iverson, N. R., Hooyer, T. S., Thomason, J. F., Graesch, M., and Shumway, J. R., 2008. The experimental basis for interpreting particle and magnetic fabrics of sheared till. *Earth Surface Processes and Landforms*, **33**, 627–645.

Jørgensen, F., and Piotrowski, J. A., 2003. Signature of the Baltic ice stream on Funen island, Denmark during the Weichselian glaciation. *Boreas*, **32**, 242–255.

Kjær, K. H., Houmark-Nielsen, M., and Richardt, N., 2003. Ice-flow patterns and dispersal of erratics at the southwestern margin of the last Scandinavian ice sheet: signature of palaeo-ice streams. *Boreas*, **32**, 130–148.

Krüger, J., 1984. Clasts with stoss-lee form in lodgement tills: a discussion. *Journal of Glaciology*, **30**, 241–243.

Larsen, N. K., Piotrowski, J. A., and Kronborg, C., 2004. A multiproxy study of a basal till: a time-transgressive accretion and deformation hypothesis. *Journal of Quaternary Science*, **19**, 9–21.

Larsen, N. K., Piotrowski, J. A., and Christiansen, F., 2006a. Microstructures and microshears as proxy for strain in subglacial diamicts: Implications for basal till formation. *Geology*, **34**, 889–892.

Larsen, N. K., Piotrowski, J. A., Christoffersen, P., and Menzies, J., 2006b. Formation and deformation of basal till during a glacier surge; Elisebreen, Svalbard. *Geomorphology*, **81**, 217–234.

Lawson, D. E., 1979. *Sedimentological analysis of the western terminus region of the Matanuska Glacier, Alaska*. CRREL Report 79-9. Hanover, NH.

Lawson, D. E., 1981. Distinguishing characteristics of diamictons at the margin of the Matanuska Glacier, Alaska. *Annals of Glaciology*, **2**, 78–84.

Menzies, J., 2000. Micromorphological analyses of microfabrics and microstructures indicative of deformation processes in glacial sediments. In Maltman, A. J., Hubbard, B., and Hambrey, M. J. (eds.), *Deformation of Glacial Materials*. Geological Society, Special Publication, Vol. 176, pp. 245–257.

Menzies, J., 2002. *Modern and Past Glacial Environments*. Oxford: Butterworth Heinemann.

Munro-Stasiuk, M. J., 2000. Rhythmic till sedimentation: evidence for repeated hydraulic lifting of a stagnant ice mass. *Journal of Sedimentary Research*, **70**, 94–106.

Paterson, W. S. B., 1994. *The Physics of Glaciers*. Oxford: Pergamon.

Paul, M. A., and Eyles, N., 1990. Constraints on the preservation of diamict facies (melt-out tills) at the margins of stagnant glaciers. *Quaternary Science Reviews*, **9**, 51–69.

Piotrowski, J. A., 1994. Waterlain and lodgement till facies of the lower sedimentary complex from the Dänischer-Wohld-Cliff, Schleswig-Holstein, North Germany. In Warren, W. P., and Croot, D. (eds.), *Formation and Deformation of Glacial Deposits*. Rotterdam: Balkema, pp. 3–8.

Piotrowski, J. A., and Kraus, A., 1997. Response of sediment to ice sheet loading in northwestern Germany: effective stresses and glacier bed stability. *Journal of Glaciology*, **43**, 495–502.

Piotrowski, J. A., Mickelson, D. M., Tulaczyk, S., Krzyszkowski, D., and Junge, F., 2001. Were subglacial deforming beds beneath past ice sheets really widespread? *Quaternary International*, **86**, 139–150.

Piotrowski, J. A., Larsen, N. K., and Junge, F. W., 2004. Reflections on soft subglacial beds as a mosaic of deforming and stable spots. *Quaternary Science Reviews*, **23**, 993–1000.

Piotrowski, J. A., Larsen, N. K., Menzies, J., and Wysota, W., 2006. Formation of a subglacial till under transient bed conditions: deposition, deformation, and basal decoupling under a Weichselian ice sheet lobe, central Poland. *Sedimentology*, **53**, 83–106.

Shaw, J., 1979. Genesis of Sveg tills and Rogen moraines of central Sweden: a model of basal melt-out. *Boreas*, **8**, 409–426.

Shaw, J., 1988. Sublimation till. In Goldthwait, R. P., and Matsch, C. L. (eds.), *Genetic Classification of Glacigenic Deposits*. Roterdam: Balkema, pp. 141–142.

Thomason, J. F., and Iverson, N. R., 2006. Microfabric and microshear evolution in deformed till. *Quaternary Science Reviews*, **25**, 1027–1038.
Thomason, J. F., and Iverson, N. R., 2008. A laboratory study of particle ploughing and pore-pressure feedback: a velocity-weakening mechanism for soft glacier beds. *Journal of Glaciology*, **54**, 169–181.
Thomason, J. F., and Iverson, N. R., 2009. Deformation of the Batestown till of the Lake Michigan lobe, Laurentide ice sheet. *Journal of Glaciology*, **55**, 131–146.
Tulaczyk, S., 1999. Ice sliding over weak, fine-grained tills: dependence of ice-till interactions on till granulometry. In Mickelson, D. M., and Attig, J. W. (eds.), *Glacial Processes: Past and Present*. Geological Society of America, Special Paper, Vol. 337, pp. 159–177.
van der Meer, J. J. M., 1993. Microscopic evidence of subglacial deformation. *Quaternary Science Reviews*, **12**, 553–587.
Weertman, J., 1968. Diffusion law for the dispersion of hard particles in an ice matrix that undergoes simple shear deformation. *Journal of Glaciology*, **7**, 161–165.

Cross-references

Glaciogenic Deposits
Moraine
Quaternary Glaciation
Sediment Entrainment, Transport, and Deposition
Subglacial Processes

TOPOGRAPHIC NORMALIZATION OF MULTISPECTRAL SATELLITE IMAGERY

Michael P. Bishop[1], Jeffrey D. Colby[2]
[1]Department of Geography and Geology, University of Nebraska-Omaha, Omaha, NE, USA
[2]Department of Geography and Planning, Appalachian State University, Boone, NC, USA

Synonyms

Anisotropic reflectance correction; Radiometric correction

Definition

Topographic normalization of satellite imagery represents the removal/reduction of multi-scale topographic effects in satellite imagery. Surface spectral reflectance should be representative of land-surface compositional and land-cover structural variations.

Introduction

Earth scientists studying the Earth's cryosphere are increasingly making use of multispectral satellite imagery for assessing land-surface composition and properties, thematic mapping, and change detection (Bishop et al., 2004; Bishop and Shroder, 2004). The availability of new imagery and information extraction technology (i.e., algorithms and pattern recognition approaches), however, does not directly translate into obtaining accurate surface information, as image spectral variability is governed by numerous environmental factors. Consequently, the information content in imagery varies depending upon atmospheric, topographic, surface composition, land-cover structure, and sensor characteristics that collectively determine the nature of the radiation transfer (RT) cascade at any particular location in time. These complexities often dictate the need for image preprocessing and radiometric calibration to convert calibrated digital numbers (DNs) to absolute units of at-sensor spectral radiance, and ultimately to surface spectral reflectance parameters, as many Earth science applications are primarily concerned with surface characterization.

It is widely known that topography plays a significant role in the RT cascade (Holben and Justice, 1981; Bishop and Colby, 2002). Complex topography, which includes extreme relief, steep slopes, and variations in slope azimuth (cardinal direction of slope), directly influence the amount of radiation that reaches the surface (surface irradiance). Altitude variations partially determine the magnitude of atmospheric attenuation. Other multi-scale topographic parameters, in relation to solar geometry, also cause variations in surface irradiance (e.g., shadows). The topography also governs microclimate and surface processes that control surface composition and land-cover structure. Collectively, the topography and surface composition and structure govern surface reflectance, such that the magnitude of surface reflectance varies in all directions (anisotropic reflectance). Surface reflectance is characterized by the bidirectional reflectance distribution function (BRDF). Furthermore, the topography in relation to the sensor's viewing geometry determines the BRDF sampling location, such that the magnitude of reflectance only from this BRDF location will directly propagate into the sensors field-of-view. Atmospheric attenuation and sensor characteristics then determine the magnitude of at-sensor radiance.

Clearly, the RT cascade is inherently complex, and RT interactions between the atmosphere, topography, and the surface must be taken into consideration. The influence of topography on the RT cascade dictates that satellite imagery acquired over complex terrain will exhibit spectral variability that is not representative of surface biophysical conditions. Consequently, satellite imagery frequently exhibits the *topographic effect*, which includes the presence of cast shadows, and spectral variation caused by differential illumination. It is also important to note that the influence of topography on spectral variability is not always visually detectable in imagery, as a particular topographic parameter may have varying degrees of impact on the magnitude of irradiance and reflectance. Therefore, radiometric calibration of satellite imagery requires anisotropic reflectance correction (ARC) to ensure that image reflectance variations are representative of surface-matter composition and structure, rather than indicative of atmospheric, irradiance, and topographic-induced BRDF pattern variations.

Researchers have attempted to remove the topographic effects in satellite imagery using a variety of

methodological approaches. This is generally referred to in the literature as *topographic normalization.* It should be noted, however, that topographic normalization techniques focus on removing/reducing the topographic effect in imagery, although they may not address numerous RT components influenced by topography. Consequently, topographic normalization does not represent comprehensive ARC. To our knowledge, an operational ARC model has yet to be developed to address the inherent complexities of topography and anisotropic reflectance. Therefore, we review the problem of ARC, provide simple guidelines for radiometric calibration, review various topographic normalization approaches, and assess the issues and feasibility of removing topographic effects from satellite multispectral imagery.

Background

Addressing the complex problem of anisotropic reflectance requires an understanding of radiation transfer processes, matter–energy interactions, and RT cascade components. Topography plays a significant role, as it has a multi-scale influence on the RT cascade. Topographic effects, however, have not been accurately characterized or systematically evaluated (Smith et al., 1980; Teillet et al., 1982; Proy et al., 1989; Bishop and Colby, 2002).

Radiation transfer

The passive reflection model of remote sensing is based upon the RT cascade from the Sun to the sensor (Figure 1). Solar irradiance variations occur at several timescales related to solar rotation, magnetic field variations, and sunspot activity. Earth's orbital variations influence the magnitude of irradiance that reaches the top of the Earth's atmosphere (exo-atmospheric irradiance, E^0) at a multitude of temporal scales. The orbital parameters of eccentricity (shape of the elliptical orbit around the Sun), obliquity (tilt of the Earth on its axis), and longitude of perihelion govern solar geometry and the distance between the Earth and the Sun. Consequently, solar and orbital parameters cause variations in the magnitude of E^0 on diurnal, annual, and longer timescales.

The exo-atmospheric irradiance is attenuated by the atmosphere, as numerous processes such as scattering, absorption, and refraction govern the magnitude of attenuation/transmission. This is controlled by atmospheric composition and the temperature/pressure vertical structure. The integrated influence of atmospheric attenuation is related to the optical depth of the atmosphere that is a function of solar geometry and landscape hypsometry (i.e., altitude distribution). Solar geometry, atmospheric, and terrain conditions are coupled to generate other sources of irradiance. Therefore, the topography strongly governs the amount of energy reaching the Earth's surface.

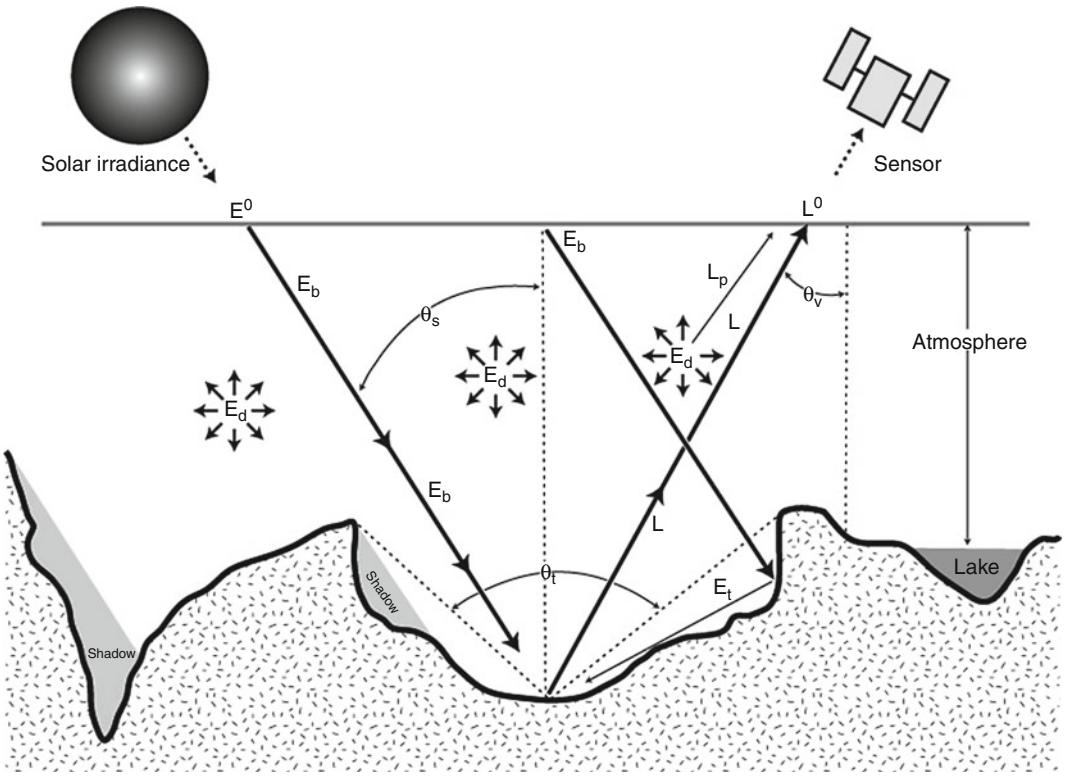

Topographic Normalization of Multispectral Satellite Imagery, Figure 1 Conceptual diagram of the primary radiation transfer components and multi-scale topographic effects.

Surface irradiance

The total spectral irradiance at the Earth's surface (E) is a composite of three irradiance components that are wavelength (λ) dependent such that

$$E(\lambda) = E_b(\lambda) + E_d(\lambda) + E_t(\lambda), \quad (1)$$

where E_b is the direct-beam irradiance component, E_d is the diffuse-skylight irradiance component, and E_t is the adjacent-terrain irradiance component.

The atmosphere attenuates the direct irradiance primarily by gaseous absorption and molecular and aerosol scattering (Chavez, 1996). Therefore, the downward atmospheric transmission ($\tau^{\downarrow}$) is a function of the total optical depth of the atmosphere. In many mountain ranges, extreme relief dictates significant changes in $\tau^{\downarrow}$ over relatively short horizontal distances.

The direct irradiance is also a function of solar and terrain geometry. Local topographic conditions are represented by the incidence angle of illumination (i), such that

$$\begin{aligned}\cos\ i = &\cos\ \theta_s\ \cos(\beta_t) \\ &+ \sin\ \theta_s\ \sin\ \beta_t\ \cos(\phi_t - \phi_s),\end{aligned} \quad (2)$$

where θ_s is the solar zenith angle, ϕ_s is the solar azimuth angle, β_t is the slope angle of the terrain, and ϕ_t is the slope-aspect angle of the terrain.

The value of cos i can be ≤ 0.0, indicating no direct irradiance due to the orientation of the topography. The regional scale topographic relief is not accounted for by Equation 2, and the altitude distribution in the direction of ϕ_s must be considered to determine if a pixel is in shadow (S). Satellite imagery acquired in rugged terrain with relatively high, solar zenith angles and/or steep slopes exhibit cast shadows (Figure 2). The local topography and cast shadows increase the global spectral variance in satellite images, with a decrease in spectral variance associated with shadowed areas. These multi-scale topographic effects are incorporated into E_b as

$$E_b(\lambda) = E^0(\lambda)\tau^{\downarrow}(\lambda)\ \cos\ i\ S. \quad (3)$$

This component can be highly variable over complex mountain terrain.

Atmospheric scattering will produce a hemispherical source of irradiance (E_d, Figure 1). This source is composed of a direct-downward skylight component and a secondary diffuse component caused by multiple interactions between the ground surface and the atmosphere (Iqbal, 1983; Proy et al., 1989). Diffuse-skylight irradiance is influenced by hemispherical shielding of the topography, as a significant part of the hemisphere can be masked by the mesoscale relief. Consequently, only a solid angle of the sky will contribute to E_d, and this angle (θ_t) will change as a function of pixel location and direction. In general, the solid angle will increase with altitude. In mountain environments exhibiting extreme relief and deep valleys, topographic shielding of the solar diffuse irradiance can be significant (Proy et al., 1989). Mesoscale topographic shielding plays less of a role in terrain exhibiting low to moderate relief.

Topographic Normalization of Multispectral Satellite Imagery, Figure 2 ASTER false-color composite (bands 3, 2, 1) depicting the Bualtar Glacier within the Hispar Mustagh region of the Karakoram Himalaya, Pakistan. This subscene exhibits extreme relief and a multitude of surface-cover types. Multi-scale topographic effects include cast shadows, local topographic effects, hemispherical shielding of the topography, and adjacent-terrain influences. Spectral variation caused by the topography is problematic for estimating surface properties and for thematic mapping applications.

The irradiance components E_b and E_d interact with the terrain to generate an adjacent-terrain irradiance component (E_t, Figure 1). This source of irradiance can be highly variable depending upon terrain geometry and surface composition and structure. Furthermore, the hemispherical integration of these factors, dictates the complexity of accounting for this component in mountain environments. Therefore, topographic normalization approaches do not usually account for E_t. Nevertheless, Proy et al. (1989) attempted a first-order approximation to this irradiance component assuming Lambertian reflectance (magnitude of reflectance is equal in all directions).

The contribution of E_t to the total surface irradiance in alpine environments is not accurately known, although it is generally thought to be highly variable, and significant where highly reflective rocks/sediment, vegetation, and ice/snow are prominent.

Surface reflectance

The magnitude of the reflected energy at the surface is determined by the conservation of energy, such that

$$\rho(\lambda) + \alpha(\lambda) + \tau(\lambda) = 1.0, \tag{4}$$

where, ρ, α, and τ represent reflectance, absorption, and transmission, respectively. For opaque objects ($\tau = 0.0$), α is equivalent to the emissivity (ε) of the object, which describes how well the object radiates energy. The reflected surface radiance (L) can be described as

$$L(\lambda) = \rho(\lambda)\left(\frac{\mathrm{E}(\lambda)}{\pi}\right). \tag{5}$$

Equation 5 represents isotropic reflectance (Lambertian). This assumption, however, is not valid in alpine environments due to the topography and biophysical characteristics of alpine landscapes (Smith et al., 1980; Kimes and Kirchner, 1981; Hugli and Frei, 1983; Hall et al., 1988; Dozier, 1989; Aniya et al., 1996; Greuell and de Ruyter de Wildt, 1999).

Given spatiotemporal variations in solar geometry, topography, surface composition, and land-cover structure, surface reflectance in alpine environments is highly anisotropic. It is necessary to characterize the BRDF, which describes the magnitude of reflectance for all combinations of input–output angles. For example, Greuell and de Ruyter de Wildt (1999) measured numerous BRDFs for melting glacier ice in Switzerland. They found that all BRDFs exhibited similar patterns and that the amount of anisotropy increased with an increase in wavelength, with increasing solar zenith angle, and decreasing albedo. Unfortunately, the BRDF is very difficult to accurately measure, especially on inclined surfaces, and more research is required to understand the influences associated with topography, surface-matter mixtures, and land-cover structure. This will require the development and evaluation of RT BRDF models.

The at-sensor radiance (L^0, Figure 1) does not represent the magnitude of L, as it is attenuated by atmospheric effects governed by sensor viewing geometry and topography. Consequently, spectral variations in satellite imagery are differentially influenced by atmospheric effects, topography, and BRDF geometry variations, which are not directly related to surface-matter composition. ARC is required to address these complexities, while topographic normalization usually focuses on reducing multiscale topographic effects related to surface irradiance. The complexity of the problem requires a special emphasis be given to radiometric calibration of satellite data before it can be utilized reliably for environmental information extraction.

The at-sensor radiance values require modification to account for the influence of the atmosphere. Numerous atmospheric-correction models for images have been developed for remote-sensing applications, and they enable the estimation of surface radiance, such that

$$L(\lambda) = \frac{\left(L^0(\lambda) - L_p(\lambda)\right)}{\tau^{\uparrow}(\lambda,\ \theta_v)}, \tag{6}$$

where L_p represents the collective additive path-radiance component caused by the scattering of the direct-beam component into the sensor field-of-view, $\tau^{\uparrow}$ is the beam transmittance of surface reflectance through the atmosphere in the upward direction, and θ_v is the view angle of the sensor. The surface radiance must then be modified to account for topographic effects and BRDF geometry variations.

Topographic normalization

Research into topographic normalization and ARC has been ongoing for 30 years. To date, a comprehensive operational model designed to meet the needs of Earth scientists has yet to emerge. In general, scientists have taken a variety of approaches to reduce spectral variability caused by the topography. The primary approaches include the following.

Spectral feature extraction

Spectral feature extraction methods usually involve linear transformations of the original data to produce *spectral features* that enhance spectral variation related to surface conditions. Techniques such as spectral band ratioing, principal components analysis, and other methods have been shown to reduce the influence of local topographic effects (i.e., cos i and S) in satellite images (Holben and Justice, 1981; Kowalik et al., 1983; Yool et al., 1986; Walsh et al., 1990; Colby, 1991; Conese et al., 1993b; Horsch, 2003). Although such spectral features are relatively easy to generate, research has shown that local topographic effects are still present in the transformed images (Holben and Justice, 1981; Kowalik et al., 1983; Colby, 1991). The limitations of this approach are in the empirical nature of the results, such that they are scene dependent. Furthermore, there are radiometric and technical issues that must be considered.

It is important to account for atmospheric effects such as the additive path-radiance term before ratioing (Kowalik et al., 1983). This dictates that DN values must be converted to radiance and that atmospheric-correction procedures account for optical-depth variations, which are a function of altitude. In addition, information may be lost in areas where cast shadows are present, depending upon solar geometry.

One might also expect that ratioing using visible bands may not be effective due to the influence of the atmosphere. Ekstrand (1996) found this to be the case and indicated that the blue and green spectral bands of Landsat Thematic Mapper Data should not be used in ratios to

remove the topographic effect. Therefore, depending upon topographic conditions and time of image acquisition, spectral feature extraction may or may not be useful for biophysical remote sensing or thematic mapping.

Empirical approaches

Given these difficulties, empirical equations can be used to characterize the relationships between reflectance and topography within a particular scene. Normalizing equations can be generated by sampling cover types and using cos i and regression analysis (Meyer et al., 1983; Civco, 1989; Naugle and Lashlee, 1992; Ekstrand, 1996; Allen, 2000; Riano et al., 2003; Nichol et al., 2006; Wu et al., 2008).

For example, Civco (1989) used a two-stage normalization procedure that included a linear transformation based on an illumination model, and compared samples from northern and southern slopes to known areas of deciduous forest to derive an empirical wavelength-dependent calibration coefficient. In other studies, a statistical-empirical approach reportedly outperformed semi-empirical modeling (Vikhamar et al., 2004; Wu et al., 2008). It has been noted, however, that in steep and highly variable terrain, or when using imagery acquired with high solar zenith angles, empirical corrections may be less reliable (Franklin, 1991), or may not be effective at all wavelengths (Civco, 1989; Naugle and Lashlee, 1992). Empirical functions by their nature are difficult to use, as their complexity must vary to account for variations in topographic conditions (Allen, 2000).

Semi-empirical modeling

The most common approach to topographic normalization is semi-empirical modeling of the influence of topography on spectral response. Although numerous topographic parameters play a role, the parameter, cos i, is considered to be the most significant and proportional to the direct irradiance. It is used in the most common algorithms as described below.

Cosine correction

Topographic effects can be reduced in imagery by accounting for the nature of surface reflectance (Lambertian or non-Lambertian) and the local topographic conditions (Colby, 1991; Ekstrand, 1996; Colby and Keating, 1998). Semi-empirical approaches make use of a digital elevation model (DEM) to account for the local illumination conditions for each pixel, and may assume isotropic upward radiance. Given the Lambertian assumption, the cosine-law correction can be used as follows:

$$L_n(\lambda) = L(\lambda)\left[\frac{\cos\,\theta_s}{\cos\,i}\right], \tag{7}$$

where L_n represents the normalized radiance.

Research indicates that this approach may produce reasonable results for terrain where slope angles and solar zenith angles are relatively low (Smith et al., 1980), although numerous investigators have found that this approach does not work well in more complex topography, as overcorrection occurs (Figure 3), producing an inverse topographic effect (Civco, 1989; Bishop and Colby, 2002). This result can be potentially attributed to not accounting for the diffuse-skylight and adjacent-terrain irradiance components, which can significantly affect E and L (Proy et al., 1989; Trotter, 1998).

C-correction

Teillet et al. (1982) developed a semi-empirical function which is based upon linear regression such that

$$L(\lambda) = \beta \cos i + a, \tag{8}$$

where β is the slope coefficient and a is the Y-intercept of the linear relationship between L and cos i. The correction

Topographic Normalization of Multispectral Satellite Imagery, Figure 3 False-color composite of normalized spectral radiance using the cosine-correction model. The influence of topography has not been removed, and extreme radiance values are generated (overcorrection) because the model does not account for irradiance from the diffuse-skylight and adjacent-terrain irradiance components.

parameter c is used to modify the cosine law as an additive term such that

$$L_n(\lambda) = L(\lambda)\left[\frac{\cos\ \theta_s + c}{\cos\ i + c}\right], \quad (9)$$

where $c = a/\beta$, and is thought to be related to the effects of indirect illumination, presumably from the diffuse-skylight irradiance and the adjacent-terrain irradiance components. It is important to note that c is not a specific physical irradiance component, because the regression analysis may also include spectral variability from atmospheric, land cover, and other multi-scale topographic effects. It does not appear to work very well in complex topography as documented in Figure 4.

Minnaert correction

The Minnaert-correction procedure has been used by a variety of investigators to reduce the topographic effect in imagery (Smith et al., 1980; Justice et al., 1981; Teillet et al., 1982; Colby, 1991; Bishop et al., 1998; Colby and Keating, 1998; Hale and Rock, 2003). The correction procedure makes use of the Minnaert coefficient k, such that

$$L_n(\lambda) = \frac{(L(\lambda)\ \cos\ e)}{(\cos^k\ i \cos^k e)}, \quad (10)$$

where e is the existence angle ($e = \beta_t$ for nadir viewing). As shown here, k represents a globally derived dimensionless coefficient that is wavelength dependent and ranges from 0.0 to 1.0. It is calculated using least-squares regression on the variables x and y, where $x = \log(\cos i \cos e)$ and $y = \log(L \cos e)$. The slope of the regression equation represents k. The correction procedure defaults to the Lambertian assumption when $k = 1.0$.

Although this procedure reduces the topographic effect in imagery (Figure 5), the use of one globally derived k value may not accurately characterize the variability of anisotropic reflectance caused by topography and land cover in complex environments (Bishop and Colby, 2002). Several investigators have found the use of one fixed k value to be inadequate and that a unique k value may be needed for each land-cover class in order to produce statistically significant k values (Estes, 1983; Ekstrand, 1996; Bishop and Colby, 2002).

Topographic Normalization of Multispectral Satellite Imagery, Figure 4 False-color composite of normalized spectral radiance using the C-correction model. This model attempts to account for additional topographic variation globally, and produces better results than with the cosine-correction model. The topographic effects have been reduced, however, local topographic variation is clearly present. This demonstrates that statistical characterization via regression analysis cannot adequately account for topographic effects in complicated terrain. The values of *c* for ASTER VNIR spectral bands are 1.761870, 1.546854, and 1.502178, respectively.

Radiative transfer modeling

Radiation transfer processes can be mathematically characterized to account for photon flux, atmospheric and irradiance components, as well as the BRDF of surface area and volumetric mixtures of surface materials. A number of studies have recognized the importance of accounting for atmosphere-topographic coupling and the diffuse-skylight and adjacent-terrain irradiance components (Dozier, 1980; Kimes and Kirchner, 1981; Proy et al., 1989; Conese et al., 1993a; Duguay, 1993). For such modeling efforts researchers have either developed radiation transfer models (e.g., Dozier, 1980; Proy et al., 1989), or have utilized existing models such as MOTRAN (Berk et al., 1989), 6 S (Vermote et al., 1997) ATCOR (Richter, 1997, 1998), and/or GIS-based solar radiation models (Dubayah and Rich, 1995).

The difficulty in developing and applying a comprehensive physically based RT model for ARC has been noted, as a treatment of all the RT components has not been considered feasible (Hugli and Frei, 1983; Woodham and Gray, 1987; Yang and Vidal, 1990; Duguay and LeDrew, 1992). Therefore, numerous simplifying assumptions are frequently applied, including the small-angle approximation (constant solar geometry), isotropic diffuse-skylight, Lambertian reflectance, and exclusion

Topographic Normalization of Multispectral Satellite Imagery, Figure 5 False-color composite of normalized spectral radiance using the Minnaert-correction model and a global Minnaert coefficient. This model accounts for the exitance angle and anisotropic reflectance. Normalization results appear to be better than the C-correction model in some places, although the C-correction model produces better results in other places. It is clear that the topographic effect has not been effectively removed, as variation in topographic and land-cover conditions cannot be characterized by one Minnaert coefficient, and the topographic effect is evident in the imagery. Explicit modeling of multi-scale topographic effects and radiation transfer modeling are required. The values of *k* for ASTER VNIR spectral band are 0.214693, 0.233699, and 0.241097, respectively.

of E_t. In addition, atmospheric variables are not usually available at the time of image acquisition, and these include temperature, pressure, aerosol, water vapor, ozone, and carbon dioxide vertical profiles. Furthermore, complex surface area and volumetric mixtures of snow, ice, and mineral debris govern the anisotropic nature of the BRDF that governs E_t, and L in the direction of the sensor. Although statistical models of various RT components exist, they do not account for photon fluxes (first principles) given specific atmospheric and surface compositional mixtures.

A physically based operational ARC model requires a BRDF model based upon radiation transport theory. To our knowledge, a fully coupled ARC model that includes atmospheric, topographic, and surface RT BRDF modeling of complex mixtures in alpine environments, has yet to be developed and tested. Additional research is needed in order to better understand the relationship between the surface BRDF and topographic boundary conditions.

Issues and concerns

The complexity of the ARC problem has resulted in the dominance of empirical and semi-empirical approaches to topographic normalization. A multitude of assumptions have been utilized to address many difficult issues related to parameterization schemes and computation (Hugli and Frei, 1983). In general, the issues focus on addressing the anisotropic nature of the RT cascade, and include primary and secondary influences of topography with respect to atmospheric effects, irradiance, and surface reflectance. Furthermore, it is imperative to recognize that the numerous approaches to topographic normalization have not been systematically evaluated in terms of radiometric accuracy.

This raises concerns related to quality of data, standardization of computational methods, and approaches for evaluating normalized imagery.

Data quality

Accurate quantitative characterization of the atmosphere, topography, and surface-cover characteristics are required to determining the utility of a particular topographic normalization technique. For example, accurate geomorphometric parameters (i.e., slope angle and slope-azimuth angle) are required for each pixel, although numerous issues associated with DEM generation need to be taken into consideration. These parameters include DEM resolution, DEM source data, spatial interpolation algorithms, and geomorphometry algorithms (Justice et al., 1981; Teillet et al., 1982; Conese et al., 1993a; Pons and Sole-Sugrafies, 1994; Colby and Keating, 1998; Wu et al., 2008). Similarly, the degree of generalization associated with data collection, as governed by sensor spatial (point-spread function), spectral (spectral-response function), and radiometric characteristics may determine the influence of topography on at-sensor spectral response, and the degree to which a particular technique may reduce topographic effects. Furthermore, geometric preprocessing of satellite imagery may also influence spectral variance.

Standardization

Unfortunately, there are inconsistencies in the computation/estimation of semi-empirical model parameters. For example, a number of techniques have been used to derive the Minnaert coefficient *k*. In addition, different parameterization schemes are utilized. Consequently, investigators must choose from a wide variety of techniques that

have been published, without any assurances as to which approach is best suited for a particular area and topographic complexity.

Given significant variations in landscape complexity, study area characteristics are not systematically reported to enable effective evaluation of methodological approaches. An approach may work in a particular geographic area, but may have little value in another region due to unique terrain and land-cover conditions. Investigators typically assume that their study area represents complex topography, although when compared to a standard, it is clear that there is a wide range of topographic conditions that determine whether an approach will work, as documented by others and our examples of normalized imagery. Consequently, some degree of standardization seems warranted given variations in parameterization schemes and landscape complexity. It is plausible that selected approaches/methods may be appropriate under limited conditions, although this aspect of topographic normalization has not been thoroughly investigated.

Finally, standard diagnostics to determine the ability of a method/approach to actually reduce spectral variability due to multi-scale topographic effects is sorely needed. Current diagnostic methods do not effectively address the spatial variability in spectral reflectance caused by variations in spatial, spectral, and radiometric resolution. Furthermore, data characteristics/quality and landscape complexity determine the degree to which topographic effects will manifest as spectral variation given sensor characteristics.

Image diagnostics

Normalized imagery should exhibit a global reduction in spectral variation caused by multi-scale topographic effects, and local increases in spectral variability within shadowed areas caused by land-cover variation. Unfortunately, the definition of what constitutes acceptable normalization varies by application and/or study area. The most common approach is to examine the visual appearance of imagery to determine if global spectral variation has been reduced. Very few investigators have evaluated local increases in spectral variance. Bishop and Colby (2002) have noted that topographic normalization procedures can alter the spatially dependent variance structure of satellite imagery, such that normalization may result in variance compression (loss of information) that may be visually interpreted as a reduction of topographic effects. It is extremely difficult to objectively assess the scale-dependent spectral variance in imagery via human interpretation. Furthermore, variance compression is the extreme opposite of overcorrection, as discussed in the cosine-correction section.

Another common approach has been to examine the relationship between normalized radiance and cos *i* (Figure 6). This approach enables the identification of statistical trends (linear or nonlinear) that may reveal overcorrection associated with lower cos *i* values. It is assumed that the lack of a statistical trend ($r^2 = 0.0$) is representative of good normalization and removal of topographic effects. This statistical characterization, however, does not necessarily account for topographic variation related to other multi-scale topographic effects that potentially influence atmospheric transmission, cast shadows, hemispherical shielding, and adjacent terrain and viewing geometry, as cos *i* only accounts for local topography. It is plausible that existing topographic effects are masked by compositional and land-cover spectral variation that can vary significantly in mountain environments. To address this would require an examination of spectral variation with altitude and the shielding coefficient, for example, although the nature of the specific relationships might also be masked by surface spectral variability.

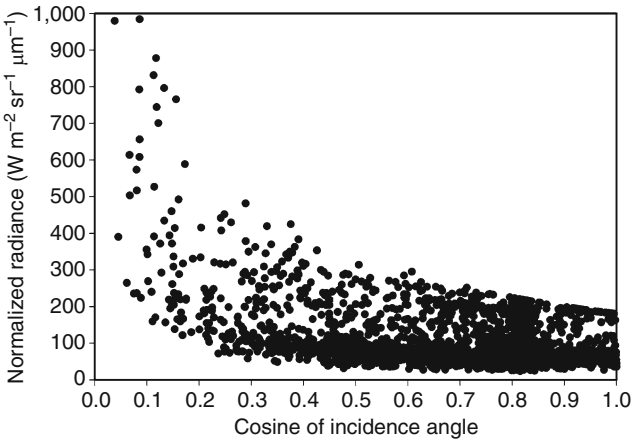

Topographic Normalization of Multispectral Satellite Imagery, Figure 6 Relationship between normalized radiance (cosine correction of ASTER near-infrared band (0.78–0.86 μm) and the cosine of the incidence angle). The cosine-correction procedure generates a nonlinear increase in normalized radiance with decreasing values of cos *i*. This is commonly referred to as overcorrection that is indicative of a topographic bias.

Statistical approaches have also been traditionally used to assess the global reduction in spectral variance. Examples include basic descriptive statistics, analysis of variance, correlation analysis, and more recently, semivariograms. These are used to demonstrate a change in spectral variance, although, with the exception of variogram analysis, these methods do not account for the spatially dependent variance structure. More importantly, however, they do not account for radiometric accuracy.

Finally, many investigators have evaluated topographic normalization techniques based upon the use of pattern recognition and classification accuracies. The assumption is that improved classification accuracies are indicative of effective normalization. This thematic mapping perspective is far removed from the notion of effective normalization of imagery to reduce topographic effects. Fundamentally, the removal of topographic effects represents a radiometric calibration issue, where the focus is

on the magnitude of surface reflectance given the BRDF. Normalization methods alter the magnitude and the spatial variability of spectral reflectance, although it is not known if the magnitude and the spatial variability are consistent with surface-matter property variation.

Thematic mapping using normalized imagery does not adequately address the issue of topographic effects and BRDF variations. Such an approach makes use of spectral variability and statistical separability in *n*-dimensional space, irrespective of changes in surface composition/properties.

Brute-force supervised and unsupervised classification algorithms produce thematic maps, but the classification results are also dependent upon decision rules. Consequently, classification accuracies generated from normalized imagery do not permit direct evaluation of surface reflectance and its spatial variability in terms of radiometric accuracy.

Accuracy assessment

Ultimately, it is important to better understand the anisotropic nature of the surface BRDF in mountain environments. Surface BRDF measurements are required to account for variations related to wavelength, surface composition and structure, solar geometry, and topography. Although difficult to obtain, such measurements need to be compared to radiometrically calibrated imagery (normalized imagery) to ascertain the primary and secondary topographic effects on sensor spectral response. It is also necessary to determine how well various normalization approaches generate radiometrically accurate surface reflectance values.

Without field and scale-dependent assessment of normalized imagery, it is difficult to determine the inherent advantages and disadvantages associated with various methodological approaches. Such field-based and spatial validations have yet to be established. The development and evaluation of RT BRDF models that can address the heterogeneous mixtures of surface materials typically found in mountain environments can greatly assist in better evaluating topographic normalization approaches and the production of validated surface reflectance information products.

Summary and conclusions

Understanding the complex nature of anisotropic reflection and the RT cascade in mountain environments is difficult. Multi-scale topographic effects govern numerous primary and secondary RT components. Consequently, satellite imagery contains scale-dependent spectral variation that is commonly referred to as topographic effects. The removal of spectral variation caused by topography is required to assess surface biophysical conditions and permit accurate thematic mapping. Investigators have utilized a variety of topographic normalization procedures and RT models to accomplish this, with varying degrees of success. To date, an operational model to address the difficulties of ARC has yet to emerge, given the full range of the Earth's topographic complexity.

A simplistic spatial perspective dominates most approaches, with an emphasis on direct irradiance. The nature of the problem dictates the understanding of a multitude of RT parameters in order for operational ARC of satellite imagery to be routinely conducted. This will require an explicit evaluation of time, location, matter–energy interactions, and sensor characteristics. For example, what is the influence of changing orbital parameters on irradiance and solar geometry over specific time periods, and when do these parameters need to be accurately modeled? Given the spatiotemporal variability of solar geometry, when should we not use the small-angle approximation? How does topographic complexity in relation to geographic location influence the utility of topographic normalization methods? What is the error associated with using the Lambertian assumption or statistical models of the BRDF on irradiance and reflection? To what degree does the topography influence the anisotropic nature of the BRDF? Furthermore, to what degree do sensor system characteristics determine the utility of topographic normalization methods? Many of these and other questions have not been definitively answered.

This makes it extremely difficult to determine the implications of using various topographic normalization techniques for a multitude of practical mapping applications in the Earth's cryosphere. The image ratioing method is most frequently used and is very useful for basic glacier ice and snow mapping. Very little research, however, has specifically focused on the many issues that have been previously addressed, in terms of the accuracy and validity of results needed for various alpine research and environmental concerns (e.g., water resources, mountain hazards, climate change). Clearly, more research is warranted.

Bibliography

Allen, T., 2000. Topographic normalization of Landsat Thematic Mapper data in three mountain environments. *GeoCarto International*, **15**(2), 13–19.

Aniya, M., Sato, H., Naruse, R., Skvarca, P., and Casassa, G., 1996. The use of satellite and airborne imagery to inventory outlet glaciers of the southern Patagonia icefield, South America. *Photogrammetric Engineering and Remote Sensing*, **62**(12), 1361–1369.

Berk, A., Bernstein, L. S., and Robertson, D. C., 1989. MOTRAN: a moderate resolution model for LOWTRAN7. Tech. rep., Air Force Geophysical Laboratory, Hanscom AFB.

Bishop, M. P., Barry, R. G., Bush, A. B. G., Copland, L., Dwyer, J. L., Fountain, A. G., Hae-berli, W., Hall, D. K., Kääb, A., Kargel, J. S., Molnia, B. F., Olsenholler, J. A., Paul, F., Raup, B. H., Shroder, J. F., Trabant, D. C., and Wessels, R., 2004. Global land-ice measurements from space (GLIMS): Remote sensing and GIS investigations of the Earth's cryosphere. *Geocarto International*, **19**(2), 57–84.

Bishop, M. P., and Colby, J. D., 2002. Anisotropic reflectance correction of SPOT-3 HRV imagery. *International Journal of Remote Sensing*, **23**(10), 219–222.

Bishop, M. P., and Shroder, J. F., Jr. (eds.), 2004. *Geographic Information Science and Mountain Geomorphology.* Chichester: Springer-Praxis.

Bishop, M. P., Shroder, J. F., Jr., Sloan, V. F., Copland, L., and Colby, J. D., 1998. Remote sensing and GIS technology for

studying lithospheric processes in a mountain environment. *Geocarto International*, **13**(4), 75–87.

Chavez, P. S., Jr., 1996. Image-based atmospheric corrections – revisited and improved. *Photogrammetric Engineering and Remote Sensing*, **62**(9), 1025–1036.

Civco, D. L., 1989. Topographic normalization of landsat thematic mapper digital imagery. *Photogrammetric Engineering and Remote Sensing*, **55**(9), 1303–1309.

Colby, J. D., 1991. Topographic normalization in rugged terrain. *Photogrammetric Engineering and Remote Sensing*, **57**(5), 531–537.

Colby, J. D., and Keating, P. L., 1998. Land cover classification using Landsat TM imagery in the tropical highlands: The influence of anisotropic reflectance. *International Journal of Remote Sensing*, **19**(8), 1459–1500.

Conese, C., Gilabert, M. A., Maselli, F., and Bottai, L., 1993a. Topographic normalization of tm scenes through the use of an atmospheric correction method and digital terrain models. *Photogrammetric Engineering and Remote Sensing*, **59**(12), 1745–1753.

Conese, C., Maracchi, G., and Maselli, F., 1993b. Improvement in maximum likelihood classification performance on highly rugged terrain using principal components analysis. *International Journal of Remote Sensing*, **14**(7), 1371–1382.

Dozier, J., 1980. A clear-sky spectral solar radiation model for snow-covered mountainous terrain. *Water Resources Research*, **16**(4), 709–718.

Dozier, J., 1989. Spectral signature of alpine snow cover from the Landsat Thematic Mapper. *Remote Sensing of Environment*, **28**, 9–22.

Dubayah, R., and Rich, P. M., 1995. Topographic solar radiation models for GIS. *International Journal of Geographical Information Systems*, **9**(4), 405–419.

Duguay, C. R., 1993. Radiation modeling in mountainous terrain: review and status. *Mountain Research and Development*, **13**(4), 339–357.

Duguay, C. R., and LeDrew, E. F., 1992. Estimating surface reflectance and albedo from Landsat-5 Thematic Mapper over rugged terrain. *Photogrammetric Engineering and Remote Sensing*, **58**(5), 551–558.

Ekstrand, S., 1996. Landsat TM-based forest damage assessment: Correction for topographic effects. *Photogrammetric Engineering and Remote Sensing*, **62**(2), 151–161.

Estes, J. E. (ed.), 1983. *Manual of Remote Sensing*, 2nd edn. Falls Church: Sheridan, Vol. 2.

Franklin, S. E., 1991. Image transformations in mountainous terrain and the relationship to surface patterns. *Computers and Geosciences*, **17**(8).

Greuell, W., and de Ruyter de Wildt, M., 1999. Anisotropic reflection by melting glacier ice: measurements and parametrizations in Landsat TM bands 2 and 4. *Remote Sensing of the Environment*, **70**, 265–277.

Hale, S. R., and Rock, B. N., 2003. Impact of topographic normalization on land-cover classification accuracy. *Photogrammetric Engineering and Remote Sensing*, **69**(7), 785–791.

Hall, D. K., Chang, A. T. C., and Siddalingaiah, H., 1988. Reflectances of glaciers as calculated using Landsat-5 Thematic Mapper data. *Remote Sensing of Environment*, **25**, 311–321.

Holben, B. N., and Justice, C. O., 1981. An examination of spectral band ratioing to reduce the topographic effect of remotely sensed data. *International Journal of Remote Sensing*, **2**, 115–123.

Horsch, B., 2003. Modeling the spatial distribution of montane and subalpine forests in the central Alps using digital elevation models. *Ecological Modeling*, **168**(3), 267–282.

Hugli, H., and Frei, W., 1983. Understanding anistropic reflectance in mountainous terrain. *Photogrammetric Engineering and Remote Sensing*, **49**(5), 671–683.

Iqbal, M. (ed.), 1983. *An Introduction to Solar Radiation*. New York: Academic.

Justice, C. O., Wharton, S. W., and Holben, B. N., 1981. Application of digital terrain data to quantify and reduce the topographic effect on Landsat data. *International Journal of Remote Sensing*, **2**(3), 213–230.

Kimes, D. S., and Kirchner, J. A., 1981. Modeling the effects of various radiant transfers in mountainous terrain on sensor response. *IEEE Transactions on Geoscience and Remote Sensing*, **19**(2), 100–108.

Kowalik, W. S., Lyon, R. J. P., and Switzer, P., 1983. The effects of additive radiance terms on ratios of Landsat data. *Photogrammetric Engineering and Remote Sensing*, **49**(5), 659–669.

Meyer, P., Itten, K. I., Kellenberger, T., Sandmeier, S., and Sandmeier, R., 1983. Radiometric corrections of topographically induced effects on Landsat TM data in an alpine environment. *ISPRS Journal of Photogrammetry and Remote Sensing*, **48**(4), 17–28.

Naugle, B. I., and Lashlee, J. D., 1992. Alleviating topographic influences on land-cover classifications for mobility and combat modeling. *Photogrammetric Engineering and Remote Sensing*, **58**(8), 1217–1221.

Nichol, J., Hang, L. K., and Sing, W. M., 2006. Empirical correction of low sun angle images in steeply sloping terrain: a slopematching technique. *International Journal of Remote Sensing*, **27**(3).

Pons, X., and Sole-Sugrafies, L., 1994. A simple radiometric correction model to improve automatic mapping of vegetation from multispectral satellite data. *Remote Sensing of Environment*, **48**(2).

Proy, C., Tanre, D., and Deschamps, P. Y., 1989. Evaluation of topographic effects in remotely sensed data. *Remote Sensing of Environment*, **30**, 21–32.

Riano, D., Chuvieco, E., Salas, J., and Aguado, I., 2003. Assessment of different topographic corrections in Landsat-TM data for mapping vegetation types. *IEEE Transactions on GeoScience and Remote Sensing*, **41**(5).

Richter, R., 1997. Correction of atmosphere and topographic effects for high spatial resolution satellite imagery. *International Journal of Remote Sensing*, **18**(5), 1099–1111.

Richter, R., 1998. Correction of satellite imagery over mountainous terrain. *Applied Optics*, **37**(18), 1099–1111.

Smith, J. A., Lin, T. L., and Ranson, K. J., 1980. The Lambertian assumption and Landsat data. *Photogrammetric Engineering and Remote Sensing*, **46**(9), 1183–1189.

Teillet, P. M., Guindon, B., and Goodenough, D. G., 1982. On the slope-aspect correction of multi-spectral scanner data. *Canadian Journal of Remote Sensing*, **8**(2), 733–741.

Trotter, C. M., 1998. Characterising the topographic effect at red wavelengths using juvenile conifer canopies. *International Journal of Remote Sensing*, **19**(11), 2215–2221.

Vermote, E. F., Tanré, D., Deuzé, J. L., Herman, M., and Morcrette, J., 1997. Second simulation of the satellite signal in the solar spectrum, 6 S: An overview. *IEEE Transactions on Geoscience and Remote Sensing*, **35**(3), 675–686.

Vikhamar, D., Solberg, R., and Seidel, K., 2004. Reflectance modeling of snow-covered forest in hilly terrain. *Photogrammetric Engineering and Remote Sensing*, **70**(9).

Walsh, S. J., Butler, D. R., Brown, D. G., and Bian, L., 1990. Cartographic modeling of snow-avalanche path location within Glacier National Park, Montana. *Photogrammetric Engineering and Remote Sensing*, **56**(5), 615–621.

Woodham, R. J., and Gray, M. H., 1987. An analytic method for radiometric correction of satellite multispectral scanner data. *IEEE Transactions on GeoScience and Remote Sensing*, **25**(3).

Wu, J., Bauer, M. E., Wang, D., and Manson, S. M., 2008. A comparison of illumination geometry-based methods for topographic correction of Quickbird images of an undulant area. *ISPRS Journal of Photogrammetry and Remote Sensing* **63**(2).

Yang, C., and Vidal, A., 1990. Combination of digital elevation models with SPOT-1 HRV multispectral imagery for reflectance factor mapping. *Remote Sensing of Environment*, **32**, 35–45.
Yool, S. R., Star, J. L., Estes, J. E., Botkin, D. B., Eckhardt, D. W., and Davis, F. W., 1986. Performance analysis of image processing algorithms for classification of natural vegetation in the mountains of Southern California. *International Journal of Remote Sensing*, **7**(5).

Cross-references

Digital Image Information Extraction Techniques for Snow Cover Mapping from Remote Sensing Data
Mapping of Internal Glacial Layers
Radiative Transfer Modeling
Topographic Normalization of Multispectral Satellite Imagery

TRANSFORMATIONS OF SNOW AT THE EARTH'S SURFACE AND ITS CLIMATIC AND ENVIRONMENTAL CONSEQUENCES

Florent Domine
Laboratoire de Glaciologie et Géophysique de l'Environnement, CNRS, Saint Martin d'Hères, France

Definition

Snow crystals: Snow crystals are ice crystals formed in the atmosphere by the condensation of water vapor or the freezing of water droplets (i.e., riming).
Snow: Snow can refer either to snow crystals in the atmosphere or to snow on the ground. Here snow means snow on the ground, and the discussion is limited to seasonal snow.
Transformations of snow: Because snow has a high surface-to-volume ratio, it is thermodynamically unstable and undergoes transformations at the Earth's surface. These transformations include densification, sublimation, and changes in physical properties of snow such as specific surface area, albedo and thermal conductivity. Physical changes in snow are regrouped under the term snow metamorphism. Transformations of snow also involve changes in the chemical composition of snow, ice, and glaciers.

Introduction

When the first snow falls on the ground in autumn, it immediately creates an enormous change in the energy balance of the surface: the albedo in the visible spectral range changes from about 0.25 to about 0.95. This produces a forcing at the surface that can exceed 100 W m^{-2}, resulting in a change in the temperature of the air near the surface of several degrees at least. Another effect of this new snow is that it thermally insulates the ground from the cold autumn air, limiting its cooling (Zhang, 2005). If the first snow fall is late in season, the ground will cool more than usual, favoring the preservation of permafrost. These two examples illustrate how snow can affect climate and the environment. Other examples can be found in Armstrong and Brun (2008).

After deposition to the surface, snow undergoes physical changes called metamorphism, which generates numerous types of snow crystals whose classification has been updated by Fierz et al. (2009). In the absence of liquid water, that is, if the snow remains below 0°C, snow metamorphism is caused by the transfer of water vapor between grains (Colbeck, 1982), and results in changes in snow grains sizes, shapes, and bond strength. The physical properties of snow such as albedo and thermal conductivity are affected by metamorphism, and since metamorphism is determined by climatic variables such as temperature, wind speed, and the amount of precipitation, there are some feedback loops between the transformations of snow and climate. This entry examines some of the changes undergone by snow physical properties during metamorphism and discusses a few of the relevant implications for climate and the environment.

Transformations of snow at the Earth's surface

After snow falls on the ground, a temperature gradient ∇T establishes itself between the cold atmosphere (e.g., −10°C) and the ground (e.g., 0°C), producing a gradient in the partial pressure of water vapor, ∇P_{H_2O}. This gradient, in turn, causes water vapor fluxes from the base to the top of the snowpack. At the macroscopic scale, what takes place is the transfer of water vapor from the top of a crystal to the base of the overlying crystal, typically 1 mm further up (Figure 1). If the temperature gradient is greater than 20°C m^{-1}, layers of large hollow depth hoar crystals form, which have very little mechanical strength (Colbeck, 1982). If on the contrary the temperature gradient is less than a few degrees per meter, then water vapor transfer is determined mostly by the Kelvin effect, according to Equation 1

$$P_{H_2O}(r) = P_0 e^{2\gamma V_m / rRT} \quad (1)$$

where $P_{H_2O}(r)$ is the water vapor partial pressure over an ice surface of curvature r, P_0 is the water vapor partial pressure over a flat surface, γ is the ice surface tension (104 mJ m^{-2}), V_m is the molar volume of ice (1.96×10^{-5} m^3 mol^{-1}), R is the gas constant, and T is the temperature in Kelvin. Shapes with a small positive radius of curvature sublimate, and the water vapor produced condenses preferentially in concave spots such as contact points between grains. In this case, cohesive snow layers of small rounded grains form (Colbeck, 1980). These two distinct dry metamorphic regimes have been discussed at length since Sommerfeld and LaChapelle (1970), who called them TG (for temperature gradient) and ET (for equi-temperature) metamorphisms. Water vapor fluxes are much more important under the TG than under the ET regime. For example, if ∇T is such that a change in temperature from −10°C to −15°C over a vertical distance of 25 cm is observed, the resulting water vapor pressure gradient will be ∇P_{H_2O} = 400 Pa m^{-1}. In comparison, under isothermal conditions, ∇P_{H_2O} can be calculated using Equation 1 for the case of a faceted crystal 400 μm in size, and whose edges have

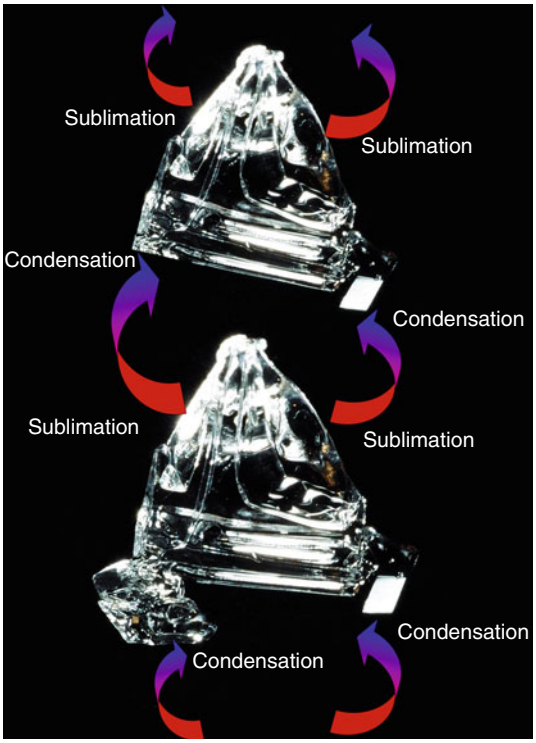

Transformations of Snow at the Earth's Surface and its Climatic and Environmental Consequences, Figure 1 Water vapor transfer between depth hoar crystals during TG metamorphism.

a radius of curvature r = 10 μm. A value ∇P_{H_2O}= 15 Pa m^{-1} is found at −15°C, much lower than under the above TG conditions.

Melting of the snow can also take place. In this case, liquid water accumulates in concaves spots, which increases the mechanical strength of the snow upon refreezing. Grains also grow with each melt-freeze cycle (Colbeck, 1982), so that melt-freeze layers are the hardest layers in a snowpack.

Wind is also involved in metamorphism. Some snow grains become airborne in windy conditions, and they partially sublimate, thus becoming smaller and more rounded. Eventually, grains accumulate in wind-sheltered spots, such as the lee of sastrugi (i.e., snow dunes caused by winds, whose height is often 5–30 cm), and sinter, forming hard layers of small rounded grains called windpacks. The hardness and density of windpacks depend on the speed of the wind event that formed them. Densities of about 500 kg m^{-3} are observed in the Arctic for wind speeds around 30 m s^{-1}.

It has been observed that the growth of depth hoar was considerably hindered in high density snow (Marbouty, 1980). Even though high density depth hoar can form in the Arctic under extreme temperature gradients, such depth hoar has few large grains and many small grains can still be observed. Recent models of snow grain size evolution (Flanner and Zender, 2006) have confirmed that grain growth was slower in high density snow, with the growth rate being close to 0 for a density of 480 kg m^{-3}. It is therefore not sufficient to consider air temperature and ∇T in the snowpack to predict the evolution of snow grain size and morphology. Wind speed, because it largely determines snow density, is also an essential variable.

Climate and changes in snow physical properties

Snow metamorphism is determined by variables such as the temperature of the air, wind speed, and insolation, i.e., climate. Here we review examples of how climatic conditions can affect climate-relevant variables such as specific surface area, albedo, and thermal conductivity. In the following section, we detail examples that integrate some of these physical changes.

Specific surface area and albedo

The specific surface area (SSA) of snow is the surface area per unit mass. It can easily be related to intuitive grain size: if snow grains are assumed to be spheres, then SSA = $6/\rho_{ice}\, d$, where d is the sphere diameter and ρ_{ice} is the density of pure ice (917 kg m^{-3} at 0°C), as detailed in Physical Properties of Snow. Measured values of snow SSA range from 1.9 m^2 kg^{-1} for a melt-freeze crust to 155.8 m^2 kg^{-1} for fresh dendritic snow (Domine et al., 2007a), which translates into d = 3.4 mm and d = 42 μm, respectively.

SSA in part determines snow albedo. In the visible range, albedo is little affected by grain size (see Figure 3 of Physical Properties of Snow), because ice absorbs visible light very weakly, and scattering of light onto the many surfaces provided by the snow crystals will eventually lead to light escaping the snow, with little influence of grain size (see also *Optical Remote Sensing of Alpine Glaciers*). The main variable affecting albedo in the visible is the concentration of light-absorbing impurities such as mineral dust and soot (Warren, 1982). In the near infrared, on the contrary, ice is a moderate to strong absorber of light, so that an infrared photon propagating through solid ice would be absorbed after a few millimeters. In snow, the chance that an infrared photon will be reflected before it is absorbed will be increased by the number of scattering events at the surface of snow crystals, so that snow with smaller grains, that is, with high SSA, will increase the probability that light is reflected before it is absorbed. Snow SSA therefore affects snow albedo in the infrared, while absorbing impurities are responsible for most of the albedo variations in the visible range.

The SSA of fresh snow is often in the range of 50–156 m^2 kg^{-1}. In most cases, the natural evolution of snow is to reduce its surface energy, and SSA therefore almost always decreases with time (Taillandier et al., 2007), even though increases have been observed (Domine et al., 2009). Equations of the form SSA = B − A ln(t + Δt), where t is time and A, B, and Δt are temperature-dependent coefficients, have been proposed by

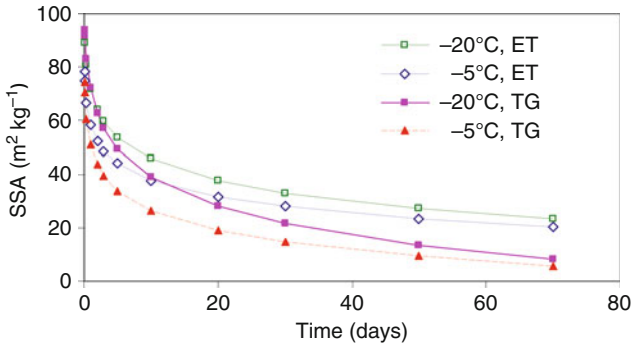

Transformations of Snow at the Earth's Surface and its Climatic and Environmental Consequences, Figure 2 Effect of temperature and of the metamorphic regime on the rate of decrease of snow SSA. Initial SSA values are 100 $m^2\ kg^{-1}$, and the rates of decrease are according to the equations of Taillandier et al. (2007).

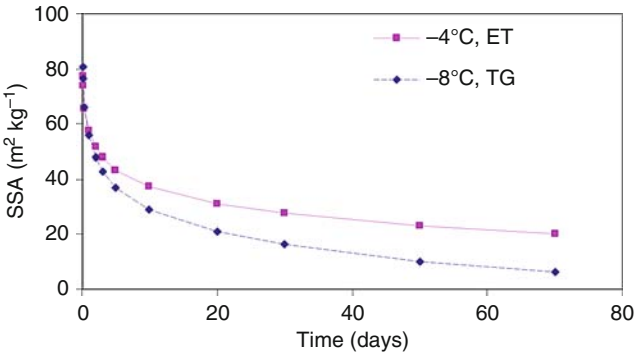

Transformations of Snow at the Earth's Surface and its Climatic and Environmental Consequences, Figure 3 Effect of a simultaneous increase in temperature and total amount of precipitation, producing a change in metamorphic regime from TG to ET, on the rate of decrease of snow SSA. After 10 h time, the SSA of the snow under the warmer conditions is greater than that in colder conditions, indicating a negative climate-snow albedo feedback. Initial SSA values are 100 $m^2\ kg^{-1}$, and the rates of decrease are according to the equations of Taillandier et al. (2007).

Taillandier et al. (2007) to describe the rate of SSA decrease of seasonal snow, as a function of the snow temperature averaged over the time period considered and of the metamorphic regime, TG or ET. Figure 2 shows the decrease of snow SSA according to those equations, for four sets of conditions. As expected, higher temperatures lead to a faster rate of decrease, because P_{H_2O} is greater and therefore metamorphism is faster. The decrease is also faster under TG that under ET conditions, because the greater ∇P_{H_2O} values accelerate metamorphism.

Figure 2 illustrates a positive snow–climate feedback. Warmer temperatures lead to faster snow aging and SSA decrease, that is, a faster albedo decrease and therefore a faster surface warming. The magnitude of this snow aging forcing can be quite large. Radiative transfer calculations using methods detailed in Stamnes et al. (1988) show that decreasing snow SSA from 32.8 to 16.4 $m^2\ kg^{-1}$ would decrease surface reflectance by ~3%, producing a 22 $W\ m^{-2}$ forcing at the tropopause at local noon, 65°N, at the summer solstice. The yearly average forcing under clear sky conditions is about 5 $W\ m^{-2}$, a value comparable to that caused by CO_2 doubling.

Feedbacks between snow SSA and climate can also be negative. A warmer climate will decrease the ∇T in the snowpack and may increase the amount of precipitation, further contributing to a decrease in ∇T. A change in metamorphic regime, from TG to ET, may therefore accompany the temperature increase, and Figure 3 shows that this can lead to a slower rate of decrease in snow SSA. In this case, warming will lead to an albedo increase, and a negative feedback loop then exists. Of course, this is only one aspect of all the processes that can take place, as warming will inevitably be accompanied by a change in the frequency of snowfalls, and therefore in the frequency of presence of fresh snow of high SSA on the surface, of changes in wind storms and wind speeds, etc., so that considerations of temperatures alone do not suffice to quantify snow–climate interactions.

Thermal conductivity

The thermal conductivity of snow k_{snow} relates the heat flux q through the snow to ∇T in the snowpack.

$$q = -k_{snow}\nabla T \tag{2}$$

Heat conduction through ice involves several processes described in Figure 4, including conduction through the snow crystals and through interstitial air. Given that $k_{ice} >> k_{air}$, conduction through the network of interconnected snow grains is often the main heat transfer process in snow (Sturm et al., 1997). Intuitively, one therefore expects the hardest snows to have the greatest thermal conductivity values, even though today no experimental study has related thermal conductivity to mechanical properties, that is, to how snow reacts to an applied force (see *Ram Resistance*). However, Sturm et al. (1997) have shown that there was a strong positive correlation between snow density and thermal conductivity. In seasonal snow, the lowest values are encountered for freshly fallen snow and for depth hoar, with values as low as 0.025 $Wm^{-1}\ K^{-1}$, and the highest values, up to 0.65 $Wm^{-1}\ K^{-1}$, have been measured in windpacks and melt-freeze layers.

Figure 4 illustrates the fact that k_{snow} depends on snow structure. The metamorphic history of the snow, and therefore climate, then determines k_{snow}. Sturm and Johnson (1992) have monitored the evolution of k_{snow} in the taiga snowpack in central Alaska. There, thin snowpacks, cold temperatures, and low wind speeds combine to produce temperature gradients that reach 200 $K\ m^{-1}$ and average about 40 $K\ m^{-1}$. The snowpack therefore transforms almost entirely into depth hoar of low density, typically 200 $kg\ m^{-3}$. Most k_{snow} values that they measured were in the range 0.04–0.09 $W\ m^{-1}\ K^{-1}$, and they observed alternating stages where k_{snow} increased and decreased

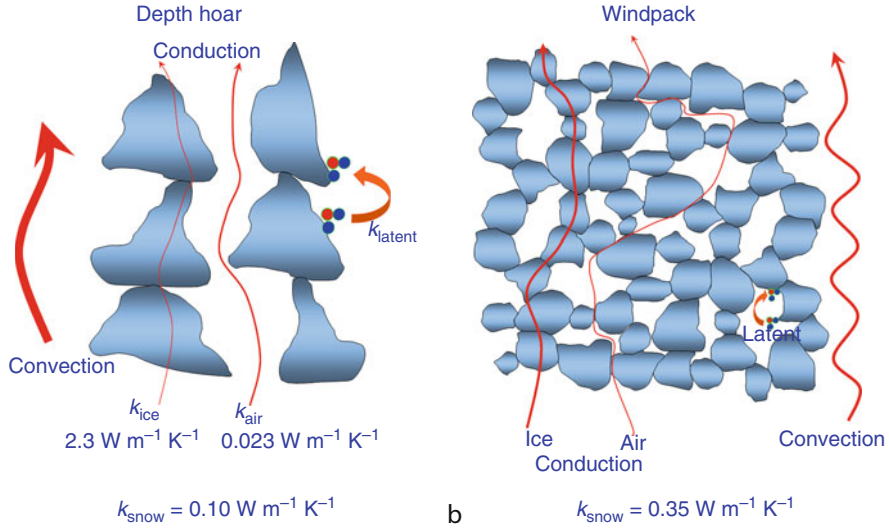

Transformations of Snow at the Earth's Surface and its Climatic and Environmental Consequences, Figure 4 Main processes involved in heat transfer though (**a**) depth hoar and (**b**) windpacked snow. Heat conduction in snow is the result of mainly four processes: (1) heat conduction through the network of interconnected ice crystals; (2) heat conduction through interstitial air; (3) latent heat transfer caused by the sublimation-condensation cycles induced by metamorphism; and (4) air flow through snow, in the form of either convection caused by high temperature gradient in the snow or advection caused by wind blowing over a rough snow surface. Air flow is often not important, latent heat transfer is significant only in depth hoar and the thermal conductivity of ice, k_{ice} = 2.3 W m^{-1} K^{-1} at −10°C is much greater than that of k_{air} = 0.023 W m^{-1} K^{-1} at −10°C. As a result, heat flow in snow mostly results from conduction through the interconnected network of snow crystals, and the thermal conductivity of windpacks is usually much greater than that of depth hoar.

over time. In contrast, Schneebeli and Sokratov (2004) performed experiments where they monitored the evolution of k_{snow} in a small snow chamber for about 10 days. They studied mostly snow samples of moderate to high densities (268–514 kg m^{-3}) that were subjected to ∇T values in the range 25–100 K m^{-1} and observed that k_{snow} increased during metamorphism, because of the growth of intergranular bonds, that facilitated heat conduction.

At present, there is clearly insufficient data to allow a full understanding and prediction of the effect of climatic variables on the value of k_{snow}. However, since depth hoar has the lowest k_{snow} values, while snow formed of small rounded grains and windpacks have moderate to high values, it appears likely that colder temperatures that generate larger temperature gradients will lead to lower k_{snow} values. All other things being equal, warming will then probably lead to increase in k_{snow} values. This will be further enhanced by the more frequent occurrence of melt-freeze layers that have high k_{snow} values.

An obvious consequence is that snow will shield the ground from the effect of cold air less efficiently. Figure 5 illustrates that an increase in temperature of 3°C, if it results in an increase in k_{snow} from 0.07 W m^{-1} K^{-1} (typical of depth hoar) to 0.20 W m^{-1} K^{-1} (typical of small rounded grains), will produce no change in permafrost temperature. As far as ground temperature is concerned, snow in this case therefore produces a negative feedback on warming, that is, the effect of snow is to reduce the effect of warming.

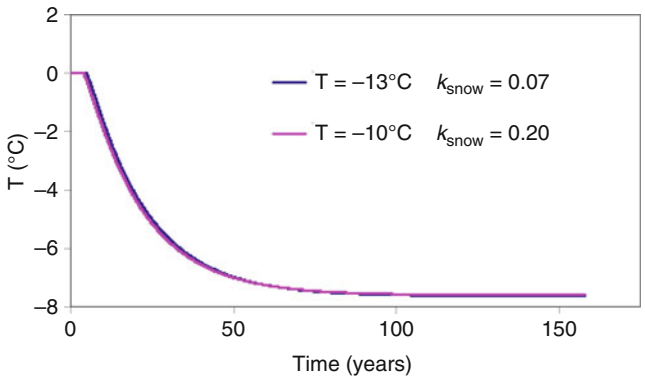

Transformations of Snow at the Earth's Surface and its Climatic and Environmental Consequences, Figure 5 Combined effect of a warming of 3°C and of a change in snow thermal conductivity on permafrost temperature at a depth of 18 m, where seasonal variations are negligible. In the cold scenario, the air temperature shows annual sinusoidal variations of amplitude 40°C with a mean of −13°C. The snowpack lasts from November 1st to June 1st with a maximum height of 60 cm in March, and k_{snow} = 0.07 W m^{-1} K^{-1}. The ground has 25% water content and the mean geothermal flux is 0.06 W m^{-2}. Calculations start in January 2000, with the unfrozen ground at 0°C, and the temperature at 18 m depth takes 80 years to stabilize. The cold scenario has the same characteristics, except that the mean temperature is −10°C and k_{snow} = 0.20 W m^{-1} K^{-1}. The change in k_{snow} therefore compensates a warming of +3°C.

Increases in temperature are however almost always accompanied by other changes, such as changes in wind speed and amount of precipitation, which also cause changes in vegetation. Higher vegetation shelters snow from the effects of wind, hindering the formation of windpacks, which have small grains and a high thermal conductivity, and favoring the formation of depth hoar, which has large grains and a low thermal conductivity, so that warming, when associated with changes in wind speed, can lead to a decrease in k_{snow}. An example of these complex changes is the warming-induced transformation of arctic tundra into boreal forest, also called taiga. This example is detailed in the next section.

Examples of snow–climate interactions

The transformation of tundra to taiga

Warming can facilitate vegetation growth, and the increased presence of shrubs on the Arctic tundra, as well as the transformation of tundra into taiga, have recently been observed (Chapin et al., 2005; Tape et al., 2006). Vegetation in turn shelters snow from wind action, limits its densification, and therefore facilitates depth hoar formation. As a result, the structure of the snowpacks is greatly modified, as shown in a simplified manner in Figure 6. The tundra snowpack is in general comprised of a basal depth hoar layer surmounted by a windpack, as detailed in Physical Properties of Snow. Tundra depth hoar forms from windpacks deposited in autumn that undergo partial sublimation because of the thermal contrast between the warm ground and the rapidly cooling atmosphere. The resulting density decrease allows the growth of depth hoar, but tundra depth hoar often remains fairly hard so that its thermal conductivity is usually moderate, typically k_{snow} = 0.15 W m^{-1} K^{-1}. Subsequent windpacks formed in the winter are much less affected by sublimation because the ground has cooled and the temperature gradient is not sufficient anymore to cause significant sublimation and density decrease. They often do not transform into depth hoar and their thermal conductivity is usually high, typically k_{snow} = 0.40 W m^{-1} K^{-1}. The snowpack thickness is about 40 cm.

In contrast, the taiga snowpack is not subjected to densification by wind. Densification by compaction is in part compensated by vigorous water vapor transfer from the warm base to the colder top of the snowpack (Sturm and Benson, 1997) so that most of the snowpack remains of moderate density, typically 200 kg m^{-3}. Conditions are optimal for the growth of large loosely bonded depth hoar crystals that have a low thermal conductivity, typically k_{snow} = 0.07 W m^{-1} K^{-1}. The changes in snowpack properties can be quantified by calculating the thermal resistance R_T of both snowpacks:

$$R_T = \sum_{i}^{\text{layers}} h_i / k_{\text{snow},i} \tag{3}$$

where h_i is the thickness of layer i. For the tundra, R_T = 1.8 m^2 K W^{-1} while for the taiga, R_T = 7.1 m^2 K W^{-1}, that is, the insulating power of the snowpack is increased almost fourfold. Calculations similar to those shown in Figure 5 show that in that case a warming of 3°C, from a mean temperature of −13°C in the tundra to −10°C in the taiga will eventually result in a permafrost warming of 10°C at a depth of 18 m. It is then clear that in this case, snow will positively feedback on ground temperature.

Other effects will come into play, further strengthening this feedback. Precipitated snow crystals evolve slower on the tundra than on the taiga because of the lower temperature gradient near the surface, so that the SSA of surface snow is about 40 m^2 kg^{-1} on the tundra

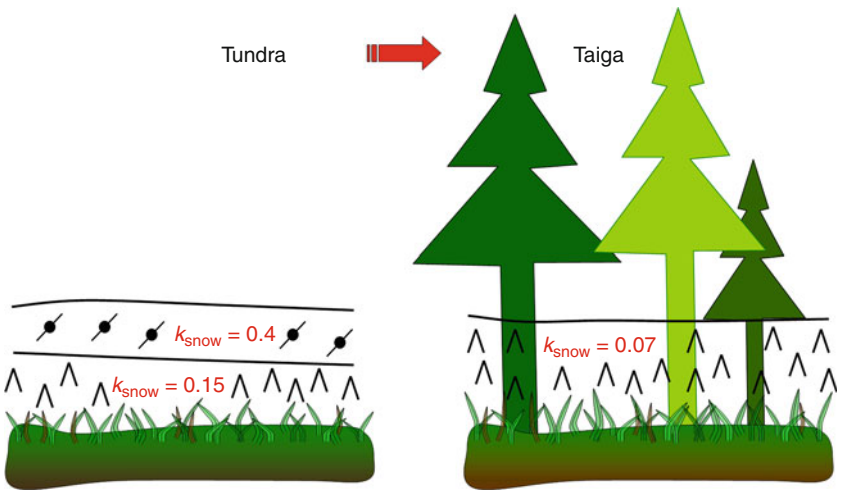

Transformations of Snow at the Earth's Surface and its Climatic and Environmental Consequences, Figure 6 Simplified view of the impact of a vegetation change from tundra to taiga on the snowpack thermal properties. A depth hoar layer of moderate thermal conductivity and a windpack of high thermal conductivity are replaced by a depth hoar layer of low conductivity. The thermal resistance of the snowpack is increased from 1.8 to 7.1 m^2 K W^{-1}.

(Dominé et al., 2002) versus about 30 $m^2\ kg^{-1}$ on the taiga (Taillandier et al., 2006). Taiga snow will therefore often have a lower albedo than tundra snow, enhancing warming. Of course, the presence of vegetation will have an even greater effect on the albedo of the surface, and all these effects will combine and contribute to the observed enhanced warming of boreal regions (Chapin et al., 2005).

Modification of snow on sea ice

The rapid decrease in Arctic sea ice coverage (Comiso and Nishio, 2008) suggests that strong positive feedbacks operate, such as enhanced export of ice through the Fram strait due to easier icepack deformation and migration allowed by a decreased thickness (Rampal et al., 2009). However, other feedbacks involving snow are also likely to take place, as suggested by the observations of Domine et al. (2007b), who studied sea ice thickness and measured snowpack physical properties on the Eastern coast of Spitsbergen for two consecutive years. In 2005, the weather was normal while in 2006, the average winter temperature was almost 6°C warmer. Despite this unusual warmth, sea ice was thicker in 2006, and Figure 7 shows that this was mostly due to the fact that the snow layers had higher k_{snow} values.

The lower R_T value in 2006 (0.7 versus 3.3 $m^2\ K\ W^{-1}$ in 2005) of course led to enhanced ocean cooling, and the thickness of landfast ice (i.e., sea ice that is attached to land and is therefore not drifting) was a bit thicker than in 2005. Domine et al. (2007b) performed simple calculations to explain observations, and these confirmed that changes in snow thermal conductivity could indeed explain thicker ice in 2006. In this case, snow exerted a powerful negative feedback on sea ice growth, as warming alone obviously would lead to the expectation of thinner ice.

Other possible feedbacks

Other physical snow climate feedbacks exist, but have been insufficiently studied or have not received attention. For example, metamorphism affects snow permeability, that is, the ability of snow to allow the flow of air when subjected to a pressure gradient, such as that caused by wind over a rough snow surface. Air flow in the snow transports heat (Albert and Hardy, 1995; Albert and Schultz, 2002). Warmer temperatures, by reducing depth hoar formation and increasing the occurrence of melt-freeze crusts of low permeability, are likely to reduce heat transfer by air flow through snow. Warming-induced changes in snowpack permeability are then expected to reduce ground cooling in the winter and to slow down snowpack melt in the spring.

Chemical processes in snow and Ice can also feedback on climate. For example, vigorous TG metamorphism generate sublimation-condensation cycles that release species dissolved in the ice crystals lattice to the atmosphere. Such species include formaldehyde, HCHO, an oxidant precursor that can enhance aerosol formation. Experiments in Alaska have indeed shown that HCHO concentrations in the natural taiga snowpack decreased as depth hoar formation proceeded, while concentrations were stable when depth hoar formation was suppressed (Domine et al., 2007b). This was achieved by allowing

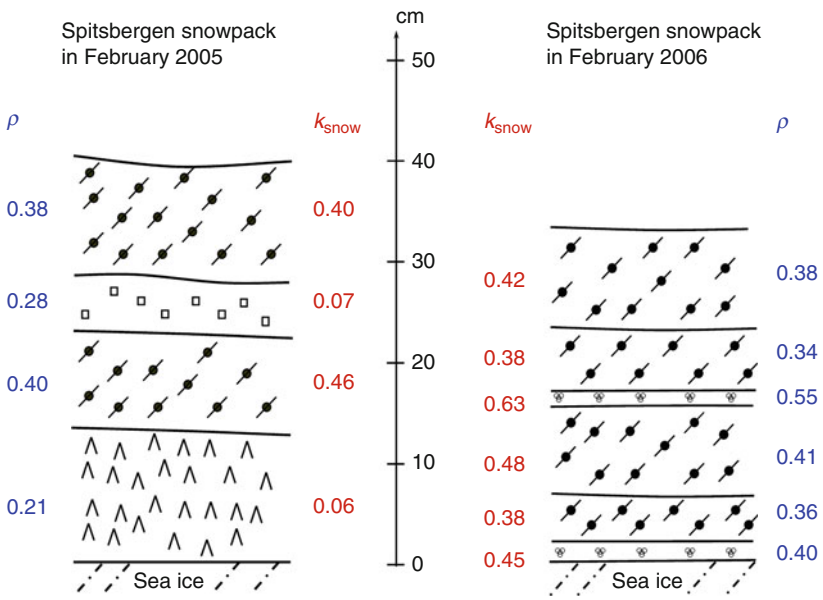

Transformations of Snow at the Earth's Surface and its Climatic and Environmental Consequences, Figure 7 Comparison of the thermal properties and densities of the snowpack on sea ice near Spitsbergen in 2005 (normal winter) and 2006 (warm winter). k_{snow} is the thermal conductivity and ρ is the snow density. In 2005, layers of depth hoar and faceted crystals with moderate k_{snow} values were present, while in 2006, they were absent while melt freeze crusts of high k_{snow} values were present. Windpacks were present during both years. In 2005, $R_T = 3.3\ m^2\ K\ W^{-1}$ while $R_T = 0.7\ m^2\ K\ W^{-1}$ in 2006.

the natural snowpack to form on tables, under which air circulation prevented the establishment of any significant temperature gradient.

Climate-induced changes in snowpack physical properties such as albedo and light penetration (Domine et al., 2008) will also affect the rate of snowpack photochemical reactions (Grannas et al., 2007), therefore modifying the chemical composition of snow, ice, and glaciers, the amount of reactive species released to the atmosphere, the oxidative capacity of the atmosphere and therefore climate through chemistry-climate interactions such as aerosol formation (Ming and Ramaswamy, 2009).

Some snow and vegetation interactions were mentioned earlier. In particular, vegetation impacts snowpack structure by limiting snow blowing and densification. In return, snow and snow–climate interactions impact vegetation by determining the length of the growing season (Jonas et al., 2008) and nutrient cycling such as nitrogen mineralization through influences on soil temperature (Chapin et al., 2005). However, all these complex interactions are only starting to be explored.

Summary

The transformations of seasonal snow at the Earth's surface lead to dramatic changes in snowpack physical properties, including climate-relevant variables such as SSA, albedo, thermal conductivity, and permeability. Physical properties in turn affect chemical processes in the snow, and therefore determine the modification of snow chemical composition. Both snow physical properties and chemical composition impact climate. Examples detailed here illustrate that changes in the thermal conductivity of snow can have locally dramatic effects on ground temperature and sea ice growth. Other studies also show that modulation of surface-atmosphere heat exchanges also affect atmospheric temperature at a global scale (Cook et al., 2008) so that it is becoming clear that snow–climate feedbacks must not be forgotten when attempting to predict future climate change, especially in polar regions. Many of these feedbacks have barely started to be explored, such as those caused by changes in permeability and also feedbacks between snow physics, snow chemistry, and climate. It is anticipated that the near future will lead to a much improved understanding of those fields.

Bibliography

Albert, M. R., and Hardy, J. P., 1995. Ventilation experiments in a dry snow cover. In Tonnessen, K., Williams, M., and Tranter, M. (eds.), *Biogeochemistry of Seasonally Snow-Covered Catchments. Proceedings of a Boulder Symposium, IAHS Publ. N° 228*, pp. 41–49.

Albert, M. R., Grannas, A. M., Bottenheim, J. W., Shepson, P. B., and Perron, F. E., Jr., 2002. Processes and properties of snow–air transfer in the high Arctic with application to interstitial ozone at alert, Canada. *Atmospheric Environment*, **36**, 2779–2787.

Albert, M. R., and Shultz, E. F., 2002. Snow and firn properties and air-snow transport processes at Summit, Greenland. *Atmospheric Environment*, **36**, 2789–2797.

Armstrong, R. L., and Brun, E. (eds.), 2008. *Snow and Climate: Physical Processes, Surface Energy Exchange and Modelling*. Cambridge: Cambridge University Press. 219p.

Chapin, F. S., III, Sturm, M., Serreze, M. C., McFadden, J. P., Key, J. R., Lloyd, A. H., McGuire, A. D., Rupp, T. S., Lynch, A. H., Schimel, J. P., Beringer, J., Chapman, W. L., Epstein, H. E., Euskirchen, E. S., Hinzman, L. D., Jia, G., Ping, C.-L., Tape, K. D., Thompson, C. D. C., Walker, D. A., and Welker, J. M., 2005. Role of land–surface changes in arctic summer warming. *Science*, **310**, 657–660.

Colbeck, S. C., 1980. Thermodynamics of snow metamorphism due to variations in curvature. *Journal of Glaciology*, **26**, 291–301.

Colbeck, S. C., 1982. An overview of seasonal snow metamorphism. *Reviews of Geophysics*, **20**, 45–61.

Comiso, J. C., and Nishio, F., 2008. Trends in the sea ice cover using enhanced and compatible AMSR-E, SSM/I, and SMMR data. *Journal of Geophysical Research-Oceans*, **113**, C02S07.

Cook, B. I., Bonan, G. B., Levis, S., and Epstein, H. E., 2008. The thermoinsulation effect of snow within a climate model. *Climate Dynamics*, **31**, 107–124.

Domine, F., Taillandier, A.-S., and Simpson, W. R., 2007a. A parameterization of the specific surface area of snow in models of snowpack evolution, based on 345 measurements. *Journal of Geophysical Research*, **112**, F02031.

Domine, F., Taillandier, A.-S., Houdier, S., Parrenin, F., Simpson, W. R., and Douglas, T. A., 2007b. Interactions between snow metamorphism and climate: physical and chemical aspects. In Kuhs, W. F. (ed.), *Physics and Chemistry of Ice*. Cambridge, UK: Royal Society of Chemistry, pp. 27–46.

Domine, F., Albert, M., Huthwelker, T., Jacobi, H.-W., Kokhanovsky, A., Lehning, M., Picard, G., and Simpson, W. R., 2008. Snow physics as relevant to snow photochemistry. *Atmospheric Chemistry and Physics*, **8**, 171–208.

Domine, F., Taillandier, A.-S., Cabanes, A., Douglas, T. A., and Sturm, M., 2009. Three examples where the specific surface area of snow increased over time. *The Cryosphere*, **3**, 31–39.

Dominé, F., Cabanes, A., and Legagneux, L., 2002. Structure, microphysics, and surface area of the Arctic snowpack near Alert during ALERT 2000. *Atmospheric Environment*, **36**, 2753–2765.

Fierz, C., Armstrong, R. L., Durand, Y., Etchevers, P., Greene, E., McClung, D. M., Nishimura, K., Satyawali, P. K., and Sokratov, S.A., 2009. The International Classification for Seasonal Snow on the Ground. IHP-VII Technical Documents in Hydrology N°83, UNESCO, Paris, 80p.

Flanner, M. G., and Zender, C. S., 2006. Linking snowpack microphysics and albedo evolution. *Journal of Geophysical Research*, **111**, D12208.

Grannas, A. M., Jones, A. E., Dibb, J., Ammann, M., Anastasio, C., Beine, H. J., Bergin, M., Bottenheim, J., Boxe, C. S., Carver, G., Chen, G., Crawford, J. H., Domine, F., Frey, M. M., Guzmán, M. I., Heard, D. E., Helmig, D., Hoffmann, M. R., Honrath, R. E., Huey, L. G., Hutterli, M., Jacobi, H. W., Klán, P., Lefer, B., McConnell, J., Plane, J., Sander, R., Savarino, J., Shepson, P. B., Simpson, W. R., Sodeau, J. R., von Glasow, R., Weller, R., Wolff, E. W., and Zhu, T., 2007. An overview of snow photochemistry: evidence, mechanisms and impacts. *Atmospheric Chemistry and Physics*, **7**, 4329–4373.

Jonas, T., Rixen, C., Sturm, M., and Stoeckli, V., 2008. How alpine plant growth is linked to snow cover and climate variability. *Journal of Geophysical Research*, **113**, G03013.

Marbouty, D., 1980. An experimental study of temperature gradient metamorphism. *Journal of Glaciology*, **26**, 303–312.

Ming, Y., and Ramaswamy, V., 2009. Nonlinear climate and hydrological responses to aerosol effects. *Journal of Climate*, **22**, 1329–1339.

Rampal, P., Weiss, J., and Marsan, D., 2009. Positive trend in the mean speed and deformation rate of Arctic sea ice, 1979–2007. *Journal of Geophysical Research*, **114**, C05013.
Schneebeli, M., and Sokratov, S. A., 2004. Tomography of temperature gradient metamorphism of snow and associated changes in heat conductivity. *Hydrological Processes*, **18**, 3655–3655.
Sommerfeld, R. A., and LaChapelle, E., 1970. The classification of snow metamorphism. *Journal of Glaciology*, **9**, 3–17.
Stamnes, K., Tsay, S. C., Wiscombe, W., and Jayaweera, K., 1988. Numerically stable algorithm for discrete-ordinate-method radiative transfer in multiple scattering and emitting layered media. *Applied Optics*, **27**, 2502–2509.
Sturm, M., and Benson, C. S., 1997. Vapor transport, grain growth and depth hoar development in the subarctic snow. *Journal of Glaciology*, **43**, 42–59.
Sturm, M., and Johnson, J., 1992. Thermal conductivity measurements of depth hoar. *Journal of Geophysical Research*, **97**, 2129–2139.
Sturm, M., Holmgren, J., König, M., and Morris, K., 1997. The thermal conductivity of snow. *Journal of Glaciology*, **43**, 26–41.
Taillandier, A.-S., Domine, F., Simpson, W. R., Sturm, M., Douglas, T. A., and Severin, K., 2006. Evolution of the Snow Area Index (SAI) of the subarctic snowpack in Central Alaska over a whole season. Consequences for the air to snow transfer of pollutants. *Environmental Science and Technology*, **40**, 7521–7527.
Taillandier, A.-S., Domine, F., Simpson, W. R., Sturm, M., and Douglas, T. A., 2007. The rate of decrease of the specific surface area of dry snow: isothermal versus temperature gradient conditions. *Journal of Geophysical Research*, **112**, F03003.
Tape, K., Sturm, M., and Racine, C., 2006. The evidence for shrub expansion in Northern Alaska and the pan-Arctic. *Global Change Biology*, **12**, 686–702.
Warren, S. G., 1982. Optical properties of snow. *Reviews of Geophysics and Space Physics*, **20**, 67–89.
Zhang, T., 2005. Influence of the seasonal snowcover on the ground thermal regime: an overview. *Reviews of Geophysics*, 43:RG4002.

Cross-references

Albedo
Chemical Composition of Snow, Ice, and Glaciers
Chemical Processes in Snow and Ice
Inverted Cup Depth Hoar Crystals
Optical Remote Sensing of Alpine Glaciers
Permafrost
Physical Properties of Snow
Rime Ice
Seasonal Snow Cover
Snow
Snow and Vegetation Interaction
Snow Crystal Structure
Snow Density
Snow Metamorphism
Snow Storm
Sublimation from Snow and Ice

TRANSIENT SNOWLINE

Markus Konz
ETH Zürich, Institut für Umweltingenieurwissenschaften, Hydrologie und Wasserwirtschaft, Zürich, Switzerland

The term snowline is an umbrella term for different interpretations of the boundary between a snow-covered surface and a snow-free surface with different temporal and spatial focus.

The "transient" snowline determines the boundary at any given time on the ground as well as on the surface of a glacier (Ostrem, 1974). In most regions the transient snowline depicts a seasonal dynamics. It shows a seasonal alternation of altitude with minima at positions near sea level in winter at some locations, and maxima at high altitudes in mountainous environments in summer. The final height of the transient snowline at the end of the melting season is subject to climatic variability and thus varies from year to year.

The snowline can be measured using automatic cameras, aerial photographs, or satellite images, for example, Landsat TM images. Its position is a useful constraint to calibrate hydrological models in alpine environments due to its integral character of precipitation input and melt. In this sense the transient snowline is a highly valuable variable, because it can be determined by remote sensing techniques and does not require ground measurements. This enables assessments of hydrological variables in remote areas.

The average elevation of the transient snowline is called the "climatic" snowline. This parameter is used to classify regions by means of climatic conditions.

Commonly, the boundary between the accumulation zone and the ablation zone on glaciers is expressed by the "annual" snowline (Flint, 1971). It is measured at the end of the melting season. The region below the annual snowline delimits the part of a glacier where melting occurred during the previous season, and it is often referred to as equilibrium line or firn line. Per definition, it is also the line where the glacier mass balance is zero or accumulation is equal to ablation.

The term "orographic" snowline is used for regions outside glaciers where the annual snowline continues on the ground. Both, the annual and the orographic snowlines are controlled by local topography and orientation. A more regional, larger-scale view on the orographic snowline helps to understand the distribution of alpine glaciers. In this context, the term "regional" snowline is used to describe a large area or band varying in width, which represents regional temperature and precipitation conditions (Flint, 1971). It expresses the critical summit elevation, which is necessary for a glacier to arise on a mountain, therefore it is also known as the glaciation level.

Bibliography

Flint, R. F., 1971. *Glacial and Quaternary Geology*. New York: Wiley.
Ostrem, G., 1966. The height of the glaciation limit in southern British Columbia and Alberta. *Geografiska Annaler*, **48A**, 126–138.
Ostrem, G., 1974. Present alpine ice cover. In Ives, J. D., and Barry, R. G. (eds.), *Arctic and Alpine Environments*. London: Menthuen.

TREE-RING INDICATORS OF GLACIER FLUCTUATIONS

Dan J. Smith, Lynn Koehler
Tree-Ring Laboratory, Department of Geography, University of Victoria, Victoria, BC, Canada

Definition

Glacier response to climate change is commonly benchmarked by dating trees overrun and killed during glacial advances (Figures 1 and 2), or by dating trees found growing on moraines formed as glaciers retreat from advanced positions. These traditional dendroglaciologic applications employ dendrochronologic methods to reconstruct past glacier activity. Evolving methodologies, including the construction of proxy glacier mass balance histories from tree rings, are expanding the avenues of glaciological research by using tree-ring indicators to examine the pre-instrumental response of glaciers to changing climates.

Dendroglaciology

Dendroglaciology describes the application of tree-ring dating principles to assign ages to glacial sediments and landforms (Schweingruber, 1988; Luckman, 1998; Smith and Lewis, 2007). Lawrence (1946) pioneered early efforts and numerous researchers subsequently used the total number of annual rings within first-colonizing trees inhabiting deglaciated terrain as a minimum estimate of surface age (McCarthy and Luckman, 1993; Osborn et al., 2007; Koch, 2009). Surveys of the age of the oldest trees colonizing recently deposited moraines provide the chronological control necessary to develop detailed Little Ice Age glacial histories (Heusser, 1956; Smith et al., 1995; Luckman, 2000; Allen and Smith, 2007).

In many settings, retreating glaciers regularly expose the remains of forests buried or killed by past advances (Figures 1 and 2). Dendroglaciology allows for dating the glacier activity recorded by these woody deposits (Luckman, 1993, 1998). This approach to event dating rests foremost on the assumption that trees in the higher latitudes form annual growth rings; and, secondly that the annual tree ring-width vary in response to limiting factors (i.e., temperature and/or precipitation climate) to create distinctive time series (Fritts, 1976).

Tree-ring cross-dates of living and glacially killed trees provide an opportunity to precisely date glacial forefield histories by

- Resolving the year of death of glacially overridden trees by cross-dating, a process that involves comparing ring-width patterns, between living and glacially reworked trees (Osborn et al., 2001; Reyes et al., 2006; Jackson et al., 2008; Barclay et al., 2009a, b).
- Establishing the calendar year of glacial advance into ice-marginal forests, through the selection of trees exhibiting callous tissue, corrasion scars, or reaction wood, which demonstrate abnormal cell development in response to encroaching glacier snouts (Luckman, 1988; Wiles et al., 1996).
- Applying radiometric dating to the perimeter wood of subfossilized samples, when ring-widths fail to cross-date with a master chronology, or when the preservation of wood is poor (Glasser et al., 2002; Wood and Smith, 2004; Allen and Smith, 2007; Barclay et al., 2009a, b).

Tree-Ring Indicators of Glacier Fluctuations, Figure 1 The construction of a Little Ice Age lateral moraine in the British Columbia Coast Mountains killed and buried this 232-year-old subalpine fir tree in 1733 AD.

Tree-Ring Indicators of Glacier Fluctuations, Figure 2 Standing snag located adjacent to the distal slope of Little Ice Age lateral moraine in the British Columbia Coast Mountains. The tree died in 1738 AD, following the deposition of the moraine. Note in the background the growth of subalpine fir trees on the stabilized moraine surface. Counts of the number of annual rings in the oldest cohort of living trees provide a minimum date for surface stabilization following the most recent advance of glacial ice.

Tree-Ring Indicators of Glacier Fluctuations, Figure 3 Excavation of subfossil trees killed and buried in till by an advancing glacier in the British Columbia Coast Mountains. Cross-dates of the annual ring patterns within the trees to a living tree-ring chronology indicate the subfossil boles and branches were entombed in 1815.

- Relating the ring-width patterns of ice marginal trees to glacier-climate fluctuations and moraine building episodes (Bray and Struik, 1963; Matthews, 1977; Pederson et al., 2004; Pelfini et al., 2005; Nesje et al., 2008).

The global recession of glaciers over the last century has led to the exposure of an abundance of cross-datable material (Figure 3). These subfossil remains have successfully been interpreted using dendroglaciology to detail ice front fluctuations (Smith and Desloges, 2000). The annual ring-width patterns of the subfossil wood is measured and compared to the radial growth trends of living tree–ring chronologies (Figure 4). Where the growth trends match over time and cross-date, the perimeter date of the subfossil samples is interpreted to indicate when the glacier was advancing and killing the trees.

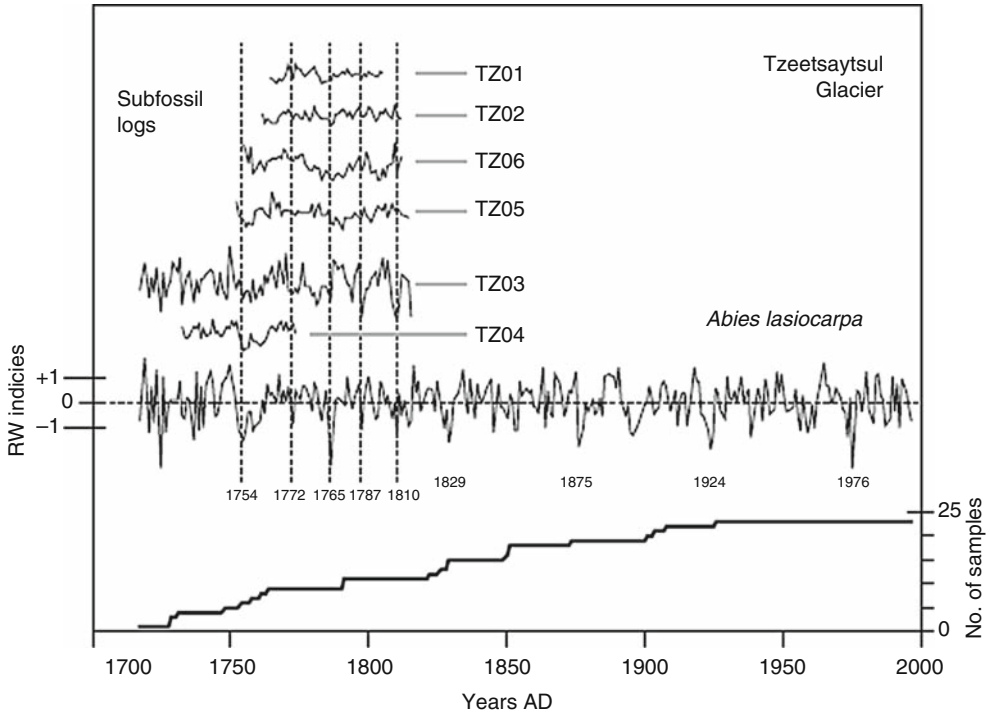

Tree-Ring Indicators of Glacier Fluctuations, Figure 4 Summary of dendroglaciological studies used to date subfossil wood shown in Figure 3. The upper portion of the figure illustrates the duration of cross-dated subfossil samples. While the youngest portion of each record indicates the pith date of the sample, the oldest portion does not necessarily represent the absolute age of the sampled wood due to surface abrasion. The middle portion of the figure illustrates the annual growth trends found in living trees growing in the forest adjacent to the glacier. Dates refer to common pointer years in the chronology and within the subfossil samples. The lower portion of the graph shows the sample depth of the living chronology (from Smith and Desloges, 2000).

Although dendroglaciology benefits from simplicity and low cost, several limitations are worth noting. The success of dendroglaciological research depends upon an abundant supply of wood and subsequent preservation within actively eroding proglacial environments (Allen and Smith, 2007; Koch, 2009). Dendroglaciologic interpretations are also restricted in their temporal range. For example, the success of cross-dating depends upon the longevity of local trees, which often fail to exceed 300–400 years in many subalpine locations (Schweingruber, 1988). Nonetheless, millennial length chronologies are being compiled from subfossil wood that has been preserved in glacial and glaciofluvial sediments that allow for absolute dating of glacier fluctuations over extended time periods (Scuderi, 1987; Barclay et al., 1999, 2009a).

Limitations to dendroglaciological dating arise because: (a) intercepting the pith when coring a tree is rare, especially for large diameter trees (Villalba and Veblen, 1997); (b) extracting cores from the root ball is challenging (McCarthy et al., 1991; Winchester and Harrison, 2000); (c) tree-ring series sometimes contain missing and/or false ring boundaries, resulting in incorrect age determinations; and, most importantly (d) opportunities for determining locally relevant ecesis intervals, the time it takes for seedlings to establish, are often limited by the lack of reliable control surfaces and/or inconsistent colonization rates due to microclimatic effects (Sigafoos and Hendricks, 1969; Villalba et al., 1990; McCarthy and Luckman, 1993; Koch, 2009).

Dendroclimatic mass balance reconstruction

Dendroclimatic investigations focused on climate-sensitive tree species found in glaciated settings offer the opportunity to acquire insights into glacial mass balance changes at decade-to-century timescales. A growing number of studies have demonstrated that a strong relationship exists between the annual ring-width variations of some tree species and glacier ice front fluctuations (Bräuning, 2006; Yang et al., 2008; Borgaonkar et al., 2009). The underlying relationship to climate variability has allowed for the hindcasting of mass balance fluctuations.

Changes in glacier volume reflect the sensitivity of glaciers to changes in climate. Conventional mass balance surveys provide a way to evaluate the long-term impact of climate variability on changes in glacier volume, area, and length (Calmanti et al., 2007). Most mass balance records are sparse and of short duration. Following recognition that the annual radial growth variations of trees are

often significantly correlated to local glacier activity (LaMarche and Fritts, 1971; Yang et al., 2008; Borgaonkar et al., 2009), attention has been directed to developing extended proxy glacier activity records from tree rings.

When examined in detail, mass balance measurements reveal that the winter and summer seasons are marked by peak accumulation and peak ablation phases (Bitz and Battisti, 1999). The same seasonal climates that govern these glaciological relationships influence the growth of tree rings. Climate conditions that promote above-average radial growth (wide rings) are the same conditions that favor glacier ablation (negative mass balance) and retreat (Bray and Struik, 1963; Bräuning, 2006). Conversely, the conditions that result in a shortened growing season and below-average radial growth trees (narrow rings) lead to accumulation, positive mass balance conditions, and glacier advance (Watson and Luckman, 2004; Larocque and Smith, 2005; Calmanti et al., 2007). Recognition of the inverse climatic relationship between tree-ring growth and glacier mass balances indicates it is possible to estimate past mass balance variations from tree-ring data (Leonelli et al., 2008).

A number of different methodological approaches and tree species have been used to explore the potential for reconstructing local and regional mass balance records (Lewis and Smith, 2004; Watson and Luckman, 2004; Larocque and Smith, 2005; Calmanti et al., 2007; Linderholm et al., 2007; Leonelli et al., 2008). Despite their inherent uncertainties, most tree-ring-derived mass balance models appear to provide a good approximation of summer (B_s) and net (B_n) mass balance conditions. Less certain is their ability to fully represent glacier winter balance (B_w) (Linderholm et al., 2007).

As noted by Leonelli et al. (2008), limitations to reconstructing glacier mass balance histories from tree ring chronologies arise because their annual variations are affected by distinct biological and physical processes and because diverse climatic factors may influence them during different periods of the year. It is also likely that the mass balance response of contemporary glaciers to climate is distinct from that of larger Little Ice Age glaciers (i.e., Nesje et al., 2008). If this is the case, mass balance models based upon assumed present-day causal relationships to climate by glaciers and tree growth may bias the reconstructions.

Summary

Dendroglaciological research methodologies provide the evidence necessary to precisely date the glacier activity. Annual ring counts of trees colonizing recently deglaciated terrain provides a spatial record of the glacial retreat patterns, as well as the means to establish chronologies of recent lateral and terminal moraine stabilization.

Dendroglaciologic evidence exposed by retreating glaciers provides an opportunity to develop Holocene glacial records. Since Holocene ice fronts periodically extended below tree line in many regions, advancing and retreating glaciers repeatedly overrode and buried forests beneath till deposits. Cross-dating and radiometric dating of these subfossil deposits provides an opportunity to delineate ice front positions over several millennia.

Tree-growth patterns have been used to reconstruct glacier behavior and mass balance with encouraging results. The extension of current glacier mass balance measurements to several centuries enables a more precise assessment of the impact of past climates on glacial systems.

Bibliography

Allen, S. M., and Smith, D. J., 2007. Late Holocene glacial activity of Bridge Glacier, British Columbia Coast Mountains. *Canadian Journal of Earth Sciences*, **44**, 753–1773.

Barclay, D. J., Wiles, G. C., and Calkin, P. E., 1999. A 1119-yr tree ring-width chronology from Western Prince William Sound, southern Alaska. *Holocene*, **9**, 79–84.

Barclay, D. J., Wiles, G. C., and Calkin, P. E., 2009a. Tree-ring cross-dates for a first millennium AD advance of Tebenkof Glacier, southern Alaska. *Quaternary Research*, **71**, 22–26.

Barclay, D. J., Wiles, G. C., and Calkin, P. E., 2009b. Holocene glacier fluctuations in Alaska. *Quaternary Science Reviews*, **71**, 22–26.

Bitz, C. M., and Battisti, D. S., 1999. Interannual to decadal variability in climate and the glacier mass balance in Washington, Western Canada, and Alaska. *Journal of Climate*, **12**, 3181–3196.

Borgaonkar, H. P., Ram, A., and Sikder, A. B., 2009. Assessment of tree-ring analysis of high-elevation *Cedrus deodara* D. Don from Western Himalaya (India) in relation to climate and glacier fluctuations. *Dendrochronologia*, **27**, 59–69.

Bräuning, A., 2006. Tree-ring evidence of 'Little Ice Age' glacier advances in southern Tibet. *Holocene*, **16**, 369–380.

Bray, J. R., and Struik, G. J., 1963. Forest growth and glacial chronology in eastern British Columbia, and their relation to recent climatic trends. *Canadian Journal of Botany*, **41**, 1245–1271.

Calmanti, S., Motta, L., Turcoc, M., and Provenzaled, A., 2007. Impact of climate variability on Alpine glaciers in northwestern Italy. *International Journal of Climatology*, **27**, 2041–2053.

Fritts, H. C., 1976. *Tree Rings and Climate*. London: Academic, 567pp.

Glasser, N. F., Hambrey, M. J., and Aniya, M., 2002. An advance of Soler Glacier, North Patagonian Icefield, at c. AD 1222–1342. *Holocene*, **12**, 113–120.

Heusser, C. J., 1956. Post-glacial environments in the Canadian Rocky Mountains. *Ecological Monographs*, **26**, 253–302.

Jackson, S. I., Laxton, S. C., and Smith, D. J., 2008. Dendroglaciological evidence for Holocene glacial advances in the Todd Icefield area, northern British Columbia Coast Mountains. *Canadian Journal of Earth Sciences*, **45**, 83–98.

Koch, J., 2009. Improving age estimates for late Holocene glacial landforms using dendrochronology – Some examples from Garibaldi Provincial Park, British Columbia. *Quaternary Geochronology*, **4**, 130–139.

LaMarche, V. C., Jr., and Fritts, H. C., 1971. Tree rings, glacial advance, and climate in the Alps. *Zeitschrift fiir Gletscherkunde und Glazialgeologie*, **7**, 125–131.

Larocque, S. J., and Smith, D. J., 2005. Little Ice Age proxy glacier mass balance records reconstructed from tree rings in the Mt Waddington area, British Columbia Coast Mountains, Canada. *Holocene*, **15**, 748–757.

Lawrence, D. B., 1946. The technique of dating recent prehistoric glacial fluctuations from tree data. *Mazama*, **28**, 57–59.

Leonelli, G., Pelfini, M., and Cherubini, P., 2008. Exploring the potential of tree-ring chronologies from the Trafoi Valley

(Central Italian Alps) to reconstruct glacier mass balance. *Boreas*, **37**, 169–178.
Lewis, D. H., and Smith, D. J., 2004. Dendrochronological mass balance reconstruction, Strathcona Provincial Park, Vancouver Island, British Columbia, Canada. *Arctic, Antarctic, and Alpine Research*, **36**, 598–606.
Linderholm, L. W., Jansson, P., and Chen, D., 2007. A high-resolution reconstruction of Storglaciären mass balance back to 1780/81 using tree-ring data and circulation indices. *Quaternary Research*, **67**, 12–20.
Luckman, B. H., 1988. Dating the moraines and recession of Athabasca and Dome Glaciers, Alberta, Canada. *Arctic and Alpine Research*, **20**, 40–54.
Luckman, B. H., 1993. Glacier fluctuation and tree-ring records for the last millennium in the Canadian Rockies. *Quaternary Science Reviews*, **12**, 441–450.
Luckman, B. H., 1998. Dendroglaciologie dans les Rocheuses du Canada. *Géographie physique et Quaternaire*, **52**, 139–151.
Luckman, B. H., 2000. The Little Ice Age in the Canadian Rockies. *Geomorphology*, **32**, 357–384.
Matthews, J. A., 1977. Glacier and climate fluctuations inferred from tree-growth variations over the last 250 years, central southern Norway. *Boreas*, **6**, 1–24.
McCarthy, D. P., and Luckman, B. H., 1993. Estimating ecesis for tree-ring dating of moraines: a comparative study from the Canadian Cordillera. *Arctic and Alpine Research*, **25**, 61–68.
McCarthy, D. P., Luckman, B. H., and Kelly, P. E., 1991. Sampling-height-age error correction for spruce seedlings in glacial forefields, Canadian Cordillera. *Arctic and Alpine Research*, **23**, 451–455.
Nesje, A., Dahl, S. O., Thun, T., and Nordli, Ø., 2008. The 'Little Ice Age' glacial expansion in western Scandinavia: summer temperature or winter precipitation? *Climate Dynamics*, **30**, 789–801.
Osborn, G. D., Robinson, B. J., and Luckman, B. H., 2001. Holocene and latest Pleistocene fluctuations of Stutfield Glacier. Canadian Rockies, *Canadian Journal of Earth Sciences*, **38**, 1141–1155.
Osborn, G., Menounos, B., Koch, J., Clague, J. J., and Vallis, V., 2007. Multi-proxy record of Holocene glacial history of the Spearhead and Fitzsimmons ranges, southern Coast Mountains, British Columbia. *Quaternary Science Reviews*, **26**, 479–493.
Pederson, G. T., Fagre, D. B., Gray, S. T., and Graumlich, L. J., 2004. Decadal-scale climate drivers for glacial dynamics in Glacier National Park, Montana, USA. *Geophysical Research Letters*, **31**, doi: 10.1029/2004GL019770.
Pelfini, M., Bozzoni, M., and Carton, A., 2005. The contribution of dendroglaciology for the reconstruction of historical fluctuations of Madaccio Glacier (BZ, Italy) and the definition of its scientific attribute and ecological value. *Geophysical Research Abstracts*, **7**, 07462.
Reyes, A. V., Luckman, B. H., Smith, D. J., Clague, J. J., and Van Dorp, R., 2006. Tree-ring dates for the maximum Little Ice Age advance of Kaskawulsh Glacier, St. Elias Mountains, Canada. *Arctic*, **59**, 14–20.
Schweingruber, F. H., 1988. *Tree Rings: Basics and Applications of Dendrochronology.* Dordecht, Holland: Kluwer Academic. 275p.
Scuderi, L. A., 1987. Glacier variations in the Sierra Nevada, California, as related to a 1200-year tree-ring chronology. *Quaternary Research*, **27**, 220–231.
Sigafoos, R. S., and Hendricks, E. L., 1969. The time interval between stabilization of alpine glacial deposits and establishment of tree seedlings. US Geological Survey Professional Paper, **650-B**, B89–B93.
Smith, D. J., and Desloges, J. R., 2000. Little Ice Age history of Tzeetsaytsul Glacier, Tweedsmuir Provincial Park, British Columbia. *Géographie physique et Quaternaire*, **54**, 135–141.
Smith, D. J., and Lewis, D., 2007. Dendroglaciology. In Elias, S. A. (ed.), *Encyclopedia of Quaternary Science*. Amsterdam: Elsevier Scientific, Vol. 2, pp. 986–994.
Smith, D. J., McCarthy, D. P., and Colenutt, M. E., 1995. Little Ice Age glacial activity in Peter Lougheed and Elk Lakes provincial parks, Canadian Rocky Mountains. *Canadian Journal of Earth Sciences*, **32**, 579–589.
Villalba, R., and Veblen, T. T., 1997. Improving estimates of total tree ages based on increment core samples. *Ecoscience*, **4**, 534–542.
Villalba, R., Leiva, J. C., Rubulls, S., Suarez, J., and Lenzano, L., 1990. Climate, tree-ring and glacial fluctuations in the Rio Frias Valle, Rio Negro, Argentina. *Arctic and Alpine Research*, **22**, 215–232.
Watson, W., and Luckman, B. H., 2004. Tree-ring-based mass-balance estimates for the past 300 years at Peyto Glacier, Alberta, Canada. *Quaternary Research*, **62**, 9–18.
Wiles, G. C., Calkin, P. E., and Jacoby, G. C., 1996. Tree-ring analysis and Quaternary geology; principles and recent applications. *Geomorphology*, **16**, 259–272.
Winchester, V., and Harrison, S., 2000. Dendrochronology and lichenometry colonization, growth rates and dating of geomorphological events on the east side of the North Patagonian Icefield, Chile. *Geomorphology*, **34**, 181–194.
Wood, C., and Smith, D. J., 2004. Dendroglaciological evidence for a Neoglacial advance of Saskatchewan Glacier, Banff National Park, Canadian Rocky Mountains. *Tree-Ring Research*, **60**, 59–65.
Yang, B., Bräuning, A., Dong, Z., Zhang, Z., and Keqing, J., 2008. Late Holocene monsoonal temperate glacier fluctuations on the Tibetan Plateau. *Global and Planetary Change*, **60**, 126–140.

Cross-references

Climate Change and Glaciers
Dating Glacial Landforms
Glacier Mass Balance
Holocene Glacier Fluctuations
Little Ice Age

TRIBUTARY GLACIERS

Hester Jiskoot
Department of Geography, University of Lethbridge, Lethbridge, AB, Canada

Synonyms

Confluent glaciers; Merging glaciers; Side glaciers; Tributary ice streams

Definition

A tributary glacier merges into a larger glacier, called trunk glacier, and often contributes mass to this trunk glacier from its separate accumulation basin. When two merging glaciers are of equal size, they are referred to as confluent glaciers rather than tributaries.

In case several tributary glaciers flow into a trunk glacier and some of these tributaries are themselves trunks to higher level tributaries, a glacier system becomes dendritic. At each junction of a tributary and a trunk glacier, the flow regime of one or both glaciers will be affected to some extent by the tributary-trunk interaction. Some of this interaction can have a long-term effect on

ice flow dynamics as well as mass balance, which can be particularly important in ice stream behavior. Where tributary and trunk glaciers join, they are often separated by a medial moraine. This medial moraine debris usually forms a straight line extending toward the trunk glacier terminus, but can also manifest a bulging moraine loop or an elongated teardrop-shaped or sheared-off moraine loop in the case of a glacier surge.

Glacier retreat can cause tributary glaciers to separate from their trunks, resulting in fragmentation of the glacier system into smaller glacier units. This process can lead to the formation of ice-dammed lakes in the gap between the two detached glaciers. If glacier fragmentation occurs where tributary glacier valley floors are at higher elevations than the deeper eroded trunk glacier valleys, hanging valleys will remain.

Bibliography

Gudmundsson, G. H., Iken, A., and Funk, M., 1997. Measurements of ice deformation at the confluence area of Unteraargletscher, Bernese Alps, Switzerland. *Journal of Glaciology*, **43**(145), 548–556.

Hewitt, K., 2007. Tributary glacier surges: an exceptional concentration at Panmah Glacier, Karakoram Himalaya. *Journal of Glaciology*, **53**(181), 181–188.

Joughin, I., Gray, L., Bindschadler, R., Price, S., Morse, D., Hulbe, C., Mattar, K., and Werner, C., 1999. Tributaries of West Antarctic ice streams revealed by Radarsat interferometry. *Science*, **286**, 283–286.

Kargel, J. S., Abrams, M. J., Bishop, M. P., Bush, A., Hamilton, G., Jiskoot, H., Kääb, A., Kieffer, H. H., Lee, E. M., Paul, F., Rau, F., Raup, B., Shroder, J. F., Soltesz, D., Stainforth, D., Stearns, L., and Wessels, R., 2005. Multispectral imaging contributions to Global Land Ice Measurements from Space. *Remote Sensing of Environment*, **99**, 187–219.

U

URBAN SNOW

Lars Bengtsson, Annette Semádeni-Davies
Department of Water Resources Engineering,
Lund University, Lund, Sweden

Definition

Urban snow is simply the snow in urban environments. Snow conditions in settlements and cities are different from those in the country side. Snow is removed by man. Activities within the city influence both the snow characteristics and its distribution, which are usually heterogeneous. The melt occurs at different rates at different places within the city, and at higher rates than in the country side.

Introduction

Settlements may become isolated after extreme snowfalls. River floods caused by melt or by ice jams can inundate towns. Still, it is non-extreme events which usually impact on urban hydrology throughout the winter and into the summer. The presence of snow is inevitable in northern cities. The snow conditions in an urban environment are different from those in the country side. For example, snow falling in the city is often wet, while it is dry in the rural environment. When the snow falls in a built environment, its distribution is influenced by the wind conditions between the buildings. The fallen snow is often removed from many surfaces and piled up at other surfaces or transported out of the city. The snow that remains in the city is affected by how people move over the snow and by dust or other impurities falling onto the snow. The snow is compacted and includes impurities giving it a high density and low albedo. The snow cover is highly heterogeneous.

Melt occurs earlier in the city than outside the city and proceeds at a higher rate than outside the city. It is usually warmer in the city but the enhanced melt is more due to changed radiation conditions. Compacted snow and snow surface with impurities have lower albedo than clean dry fresh snow, and therefore absorbs more solar radiation. Buildings emit longwave radiation. The melt occurs at different rate at different parts of the city depending on exposure to the sun and different snow characteristics. When the snow melts, runoff occurs from surfaces being permeable in summer time. The frozen ground is inundated, preventing water from flowing the shortest possible route to the conduit system, which may lead to flooding. Retention facilities are flooded and may not function as intended when there is a storm. The melt water that infiltrates leaks into the sewage system as the water table rises.

Melt intensities are low (10–20 mm/day) as compared to rain storms (20–40 mm/day for 1 year return period), but the melt continues for several days so the total runoff generated is generally larger. Also the peak flow may be comparable since the contributing area may be larger than for storms when frozen grassed and graveled surfaces contribute to urban runoff, Bengtsson and Westerström (1992). During rain events, when snow is still present in the city, there is runoff from permanently impervious surfaces as well as from snow-covered surfaces on hardly packed frozen ground. Thorolfsson and Brandt (1996) have show an example from Trondheim, Norway, when a rain event with a 15-year return period resulted in a one-in-30-year runoff event.

The water quality of urban snow is poor due to deicing chemicals, regular atmospheric fallout, airborne residue from heating fuels, friction material, oil, exhaust from motor vehicles, animal excrement, and debris from road surfaces and tires. Winter-long accumulation and storage within the snowpack means that melt runoff has a higher pollutant load than rain events. Much of the annual runoff

Vijay P. Singh, Pratap Singh & Umesh K. Haritashya (eds.), *Encyclopedia of Snow, Ice and Glaciers*, DOI 10.1007/978-90-481-2642-2,

load of some pollutants is transported via meltwater (Viklander, 1997). Soluble pollutants are eluted early in the melt period, while particles can be filtered by the soil and remain on the surface after melt or can be mechanically transported by the meltwater runoff. Water quality depends largely on location, population density, and traffic (e.g., Hautala et al., 1985).

The concept of snow water equivalents (SWE) must be used with care for urban environments, since snow in towns is unevenly distributed with varying properties. Snow is almost completely removed from impervious surface to clear roads for traffic, to avoid the buildup of pollutants in the snowpack, and to decrease the risk of spring flooding. Snow accumulates in sheltered areas, whereas the snowpack is thin or nonexistent in exposed areas, especially on south-facing slopes and on roofs. Plowed snow can be stored in close proximity to the area cleared or it can be removed to sites outside the urban area. Private front gardens can have increased snow depths as snow is shoveled from drives and footpaths. Scales in snow hydrology have been discussed by Woo (1998), Blöschl (1999), and Bengtsson and Singh (2000).

Suburban piles of plowed snow tend to be on permeable surfaces such as parks, private gardens, vacant lots, and roadside verges, as shown in Figure 1, whereas they are found on asphalt in the inner city. Snow density and coverage in urban environments are related to land use intensity (e.g., Bengtsson and Westerström, 1992; Buttle and Xu, 1988). Undisturbed snow in Luleå, Sweden, has similar properties to nearby rural snow (density 200–300 kg m^{-3}). Plowed snow in piles and banks has a wide range of density, 250–700 kg m^{-3}, depending on location (Semadeni-Davies 1999).

Urban melt

The energy required for melt is determined from the energy balance for a snowpack:

$$Q_M = Q^* + Q_H + Q_E + Q_P + Q_G - \frac{dE}{dt}$$

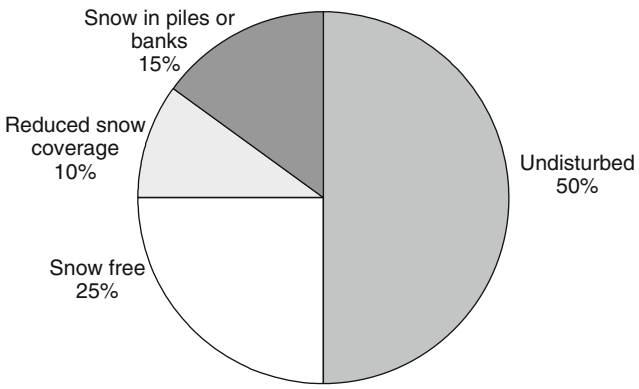

Urban Snow, Figure 1 Areal breakdown of snow cover in a residential suburb, Luleå (1979–1980) (Unpublished from first author).

where Q_M is heat flux density available for melt, Q^* is net radiation flux density, Q_H is turbulent sensible heat flux density, Q_E is turbulent latent heat flux density, Q_P is the advected heat flux from rain, Q_G is the conductive heat flux density to or from the ground, and dE/dt is the change per unit area in the internal energy held in the snow. The heat associated with rain is small as is the heat exchange with the ground. The change of the internal energy can be quite large since it is associated with refreezing of liquid water in the snowpack. The turbulent sensible and latent fluxes (in the order of 10 Wm^{-2}) can be in either direction. The sensible heat flux is related to the wind speed and the temperature difference between the atmosphere and the snow surface. The latent heat flux, sublimation, or condensation depends on the wind speed, the stability of the air, and the vapor pressure difference between the air and the snow surface. The energy balance is dominated by the radiative fluxes. In general, during daytime when melt occurs, sensible heat is an energy gain, while latent heat is an energy loss (Bengtsson, 1980; Male and Granger, 1981). The latent heat of vaporization is 7.5 times greater than the latent heat of fusion, so, even when Q_E is large, the volume of water loss to melt is low. Where there are bare patches or nearby building, which may be heated by the sun, the advection can contribute to increased sensible heat flux (see below).

The snow characteristics and the environment are different in the city than outside the city. Buildings alter the radiation balance. Moisture, aerodynamic, and thermal properties are different. Snow characteristics, distribution, and melt conditions in urban environments are related to land use and snow-handling practices. Snow accumulation and melt conditions form a mosaic over the city. The imperviousness in urban areas is augmented during spring as soils become frozen, saturated, and partly or fully impermeable. The energy balance changes over short distances with snowpack location and land use. Where there is little advection, melt is mostly driven by solar radiation, so the rate of melt depends largely on snow albedo and snow location with respect to the sun. Hence, the energy balance also varies temporally. Like the terrain effects of alpine topography, the surfaces of the "canyon" configuration of buildings interspersed with roads – with its reduced sky view, increased surface area, and multiple reflections – can serve to enhance the energy balance by trapping radiation in some places while others are shaded (Xu and Buttle, 1987; Verseghy and Munro, 1989a, b; Semadeni-Davies and Bengtsson, 1998). The urban surroundings as a whole reflect less shortwave radiation than rural areas partly due to the lower albedo of materials such as wood, brick, and asphalt, and partly due to the building geometry. The melt proceeds at different rate depending much on the degree of urbanization, as is shown with example from Luleå, Sweden, in Figure 2 (Bengtsson and Westerström, 1992).

Urbanization, by altering the land surface, affects radiative, aerodynamic, moisture, and thermal characteristics of the atmosphere. A well-known example is the heat

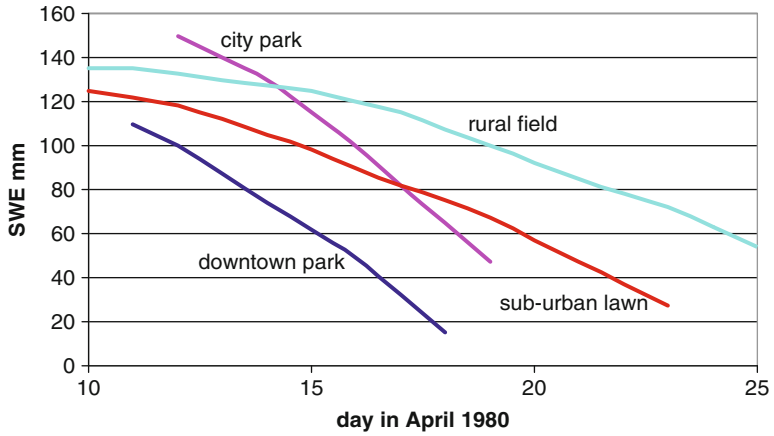

Urban Snow, Figure 2 Reduction of snow water equivalent at four different sites in Luleå, Sweden.

island effect which is related to building materials and artificial heat sources such as fuel combustion. Changes to the radiation balance in urban areas have been addressed by Xu and Buttle (1987), Todhunter et al. (1992), and Semadeni-Davies and Bengtsson (1998) for snowy conditions. They all show that the surfaces of the "canyon" configuration of buildings interspersed with roads can serve to enhance the energy balance by trapping both long- and shortwave radiation, while at the same time reducing shortwave radiation through shading. The maximum effect occurs during sunny days when shortwave radiation is mostly direct beam.

The albedo of urban snow itself is less than rural areas. A reduction from 70% to 40% means that the absorption of solar radiation is doubled. Compaction and the incorporation of gravel, exhaust fumes, debris, litter, and so forth lowers the albedo. In rural areas, albedo ranges from 0.8 for fresh dry snow to 0.6 at the onset of melt and 0.4 for old wet snow (US Army Corps of Engineers, 1956). Undisturbed urban snow has albedo values in this range, but albedo can be as low as 0.1–0.2 near roads (Bengtsson and Westerström, 1992; Semadeni-Davies, 1999).

The atmospheric longwave radiation is higher in a city than in the country side due to increased cloud cover, warmer air temperatures, and aerosols (Rouse et al., 1973). Shortwave radiation is absorbed by buildings and reemitted as longwave radiation. Urban snowpacks receive more longwave radiation than rural snowpacks. Bengtsson and Westerström (1992) measured the average enhancement integrated over 10 m from south-facing buildings to be about 100 W/m^2. In Canada, Xu and Buttle (1987) measured the net radiation in the vicinity of two houses; 8 m away from the buildings the net all-wave radiation could be between 67% and 435% greater than that in open areas. Hence, the location of snow with respect to buildings plays a part in energy availability. Semadeni-Davies et al. (2001) described the radiation balance for Luleå in detail.

Latent and sensible heat fluxes over urban snowpacks are difficult to estimate. Kirnbauer et al. (1994) point out that in complex terrain, notions of stability and roughness length become meaningless so common boundary layer theory cannot be used. Jetting and mixing along city streets (canyons) could cause localized increases in the turbulent fluxes. Advection from warm snow-free surfaces increases energy availability to the snowpack. Research in Arctic tundra with heterogeneous snow coverage showed that advection downwind from snow-free patches can be significant (Liston, 1995; Neumann and Marsh, 1998).

Piles or banks of plowed snow are features of the urban winter landscape located near roads or access ways. The snow is compacted and icy with low albedo. Gravel along with litter, oil, road debris, and exhaust particles is incorporated and airborne pollutants are deposited on the surface. The bulk energy balance of a melting snow pile is discussed and modeled by Sundin et al. (1999). The pile shape greatly influences melt due to high surface exposure per unit area. Gravel particles can cause localized points of melt by absorbing shortwave radiation. While gravel may initially enhance melt, it is possible that as thaw progresses, an insulating crust forms on the snow surface which slows the melt rate. Despite an increase in melt rate, the volume of snow held within piles means that they remain long after other snow is melted.

Snowmelt follows a diurnal pattern relating to energy availability, as seen in Figure 3 from measurements in Luleå by Bengtsson (1983). Since shortwave radiation dominates the energy balance, most melt occurs from shortly after sunrise until sunset with a clear peak at the hours around noon. In a homogeneous snowpack, it takes several hours for the meltwater to move from the surface to the bottom of the pack. However, especially in urban snow preferential flowpaths soon develops, and the required time to move through a ½ m snow cover is not more than an hour or so (Bengtsson, 1982a; Marsh

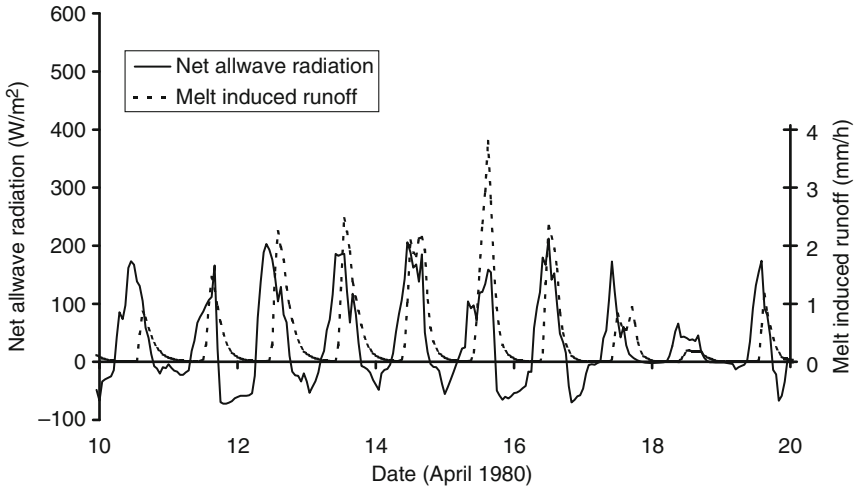

Urban Snow, Figure 3 Runoff measured from an impervious surface showing the diurnal melt phase and how melt runoff lags behind positive net radiation (Luleå, April 1980).

and Woo, 1984). Thus, there is not much delay between surface melt and runoff.

Meltwater reaching permeable surfaces can either infiltrate or flow overland depending on soil structure, moisture, and thermal status. The effective hydraulic permeability in spring is a function of the unfrozen and frozen water content, the fraction being related to the temperature of the soil (Gray and Prowse, 1993). Kane and Stein (1983) pointed out the influence of the moisture content prior to ablation on the storage capacity of the frozen soil and thus on the infiltration capacity and production of overland flow. The role of macro-pore flow is essential. Overland flow of meltwater is rare in forests, where the soil cover is thick and permeable with macro-pores. Espeby (1990) notes the effect of macro-pores on meltwater movement through frozen glacial deposits, stating that infiltration can be rapid. There is a rapid hydraulic coupling of groundwater recharge in upland areas and downhill groundwater discharge and consequent stream response (Thorne et al., 1998).

At the other end of the spectrum, meltwater from snow overlying a compacted urban soil can flow overland (Westerström, 1984; Bengtsson and Westerström, 1992). In comparison to rainfall-induced runoff generation, there is a progressive increase in the area contributing to overland flow during spring. Daytime meltwater infiltration can be followed by cold nights so that the soil infiltration capacity can be lowered by both saturation and freezing. Melt water either freezes in the soil or saturates the soil above an impervious frozen layer. Freezing caused normally permeable gravel and grass surfaces in Luleå to become virtually impervious while infiltration in a nearby forest was relatively unaffected (Engelmark, 1984). Observations from three 200 m^2 snow-covered plots with different surfaces – asphalt, gravel, and grass – showed that at the end of the melt period, overland flow from all three plots was similar. Observations in Norway (Thorolfsson and Brandt, 1996) and Canada (Buttle and Xu, 1988) also show that overland flow is great following melt, despite the fact that asphalted surfaces are snow-free.

Meltwater flows overland via the minor natural drainage system pathways in the city. These are natural irregularities on the ground and often lead onto asphalt surfaces and, in turn, toward inlets into the major drainage conduit system. However, in spring, flow in the storm- and wastewater pipes is often more than can be attributed to overland flow; water also enters indirectly as sewer infiltration (inwards leakage) through pipe cracks and joints. While water reaching pipes directly accounts for quick-flow peaks, sewer infiltration can be equated to the slow or base-flow component of hydrograph. This water may take days or weeks to enter the wastewater system (e.g., Annette Semádeni-Davies, 1998; Hernebring et al., 1997). It influences the water balance of a town for months as shown by Semádeni-Davies and Bengtsson (1999).

Ponds, wetlands, and streams fringed with riparian vegetation offer a natural technique for handling stormwater. However, these systems may function differently during spring than during summer. Marsalek (1991) gives example of detention ponds during thaw. Ponds can remain ice-covered forcing meltwater to flow either over or beneath the ice. In either case, both the storage capacity and ability of suspended solids to settle are lowered.

Snow models

Snowmelt models are used to estimate stormwater runoff. There are three different types of models: temperature index models relating melt solely to air temperature, energy balance models treating the snowpack as a single layer, and energy balance models considering different snow layers and having routines for the water transport through the snowpack. The commonly used temperature index models for rural areas are crude in temporal as

well as spatial resolution. They perform best for large (100 km^2) homogeneous river basins, where time resolution of 1 day or more is sufficient. While energy balance computations at point scale are successful, the transfer of the energy balance models from the point scale to basin scale has not been very successful (Kirnbauer et al., 1994). The simple temperature index method is better able to model average conditions (e.g., Kuchment and Gelfan, 1996). It is, however, not possible to use a temperature index method, also known as degree-day method, to compute melt over short periods, since solar radiation contributes very much to the melting and the solar radiation vary much over the day, as shown in Figure 3.

Temperature indices or the degree-day approach relate melt to the average daily ambient air temperature, simply as $M = C\ (T_a - T_s)$, where the daily melt, M, is in mm day^{-1}, C is the melt-rate factor (mm/°C/day) (degree-day coefficient), T_a is the daily ambient air temperature (°C), and T_s is the threshold melt temperature (°C) most often set to 0°C. The melt-rate factor, C, varies with location and snow characteristics. For open areas it ranges from 2 to 10 mm/°C/day, and for forests it is about 2 mm/°C/day. Routines to simulate retention and refreeze are usually coupled to the method. In the absence of shortwave radiation, the degree-day method is physically sound, Bengtsson (1976), as much of the energy supplied to the snowpack is atmospheric longwave radiation, which is dependent on air temperature as are sensible and latent heat transfers. The method is standard for operational rural models. It is robust and has been applied to a variety of spatial scales and environmental conditions.

It is difficult to relate the degree-day melt-rate factor to different urban locations or time periods, since the factor embodies the total energy availability rather than air temperature. A comparison of melt-rate factors from different environments is given in Table 1. The melt factor can vary over short distances. Increased energy availability results in degree-day melt coefficients that are greater than in rural areas. Westerström (1981) measured two factors in Luleå, corresponding to early (1.7 mm/°C/day) and late thaw (6.5 mm/°C/day). The melt rate generally increases with land use intensity. Bengtsson and Westerström (1992) measured the average melt rate during thaw at two locations within Luleå: undisturbed suburban snow had an average degree-day factor of 6 mm/°C/day, whereas snow in a downtown park had a factor of 8.4 mm/°C/day. Sundin et al. (1999) found that the melt-rate factor of plowed snow piled at snow deposits can be 11 mm/°C/day.

A time step of 1 hour is adequate to estimate stormwater runoff, since melt variations within an hour are small and the runoff is delayed because of the transport through the snowpack. A daily melt routine time step is reasonable when considering infiltration into sewers from soil and groundwater as the lags involved can be in the order of days to weeks (Semadeni-Davies, 1998). In this case, the runoff process does not need to be considered in detail and distribution can be restricted to determining the fractional area of different snow coverage, properties, and exposure.

Urban Snow, Table 1 Degree-day melt-rate factors for different environments (Compiled from Gray and Prowse, 1993; Martinec and Rango, 1986; Bergström, 1995; Kuusisto, 1984; Kuchment and Gelfan, 1996; Bengtsson and Westerström, 1992; and Sundin et al., 1999)

Location	Melt rate, C_m, (mm/°C/day)
Rural (Europe, North America)	
Open fields	2–3.5
Forests	1.5–2.0
Alpine	3.5–6
Prairie	1.5–7
Exposed slopes	5–6
Urban (northern Sweden)	
Suburban	1.5–7
Inner city	1.5–8
Plowed snow in piles	5–11

To be able to compute urban melt at high time resolution without using the full energy balance Sand (1990) tried a modified temperature index model which calculates melt on an hourly basis assuming that melt occurs at positive air temperatures ($T_m = 0$°C). The modified routine was based on Bengtsson's (1984) work and includes a simple term for net shortwave radiation and a fairly advanced refreeze approach (Bengtsson, 1982b):

$$M_h = C_t(T_a) + C_r(1 - \alpha)K \qquad T_a > 0$$

where M_h is the meltwater generated (mm/h), C_t is the temperature melt-rate factor (mm/°C/h), C_r is the radiation melt-rate factor (mm m^2/W/day), α is snow albedo, K is incoming shortwave radiation (W/m^2), and T_a is the air temperature.

$$M_{cc} = R(-T_a t)^{0.5} \qquad T_a \leq 0$$

where M_{cc} is the effective loss of water to melt due to refreeze (mm), that is, the change in internal energy; R is a refreeze coefficient ($mm/°C^{0.5}/h^{0.5}$); and t is the number of hours during which the air temperature is at or below freezing. The amended degree-day method was tested in Trondheim, Norway. Thorolfsson and Sand (1991) found that the routine was able to accurately simulate diurnal changes in meltwater release from. Thorolfsson and Killingtveit (1991) incorporated the melt routine into the HBV model structure (Bergström, 1995). HBV was then applied to several Norwegian urban or partly urbanized catchments. It is, however, not straightforward to find proper values of the factors C_t and C_r, as pointed out by Bengtsson (1984).

When energy balance models are applied, the minimum data requirements for computations are air temperature, incoming shortwave radiation, vapor pressure, and wind speed near the ground (Anderson, 1976; Leavesley, 1989). Even so, many uncertain parameters must be included to compute all fluxes. Energy balance snowmelt

models are largely restricted to research applications. Models of the snowpack energy balance are coupled to simple routines to simulate refreezing within the snowpack. Morris (1983) detailed equations for energy, momentum, and mass flows, which were built into the distributed SHE model. Metamorphosis and water flow were simulated in each layer of the snowpack. It is essential to consider refreezing in all models, also the temperature index approach, since the melt following a cold day or night is much delayed.

Summary

Snow distribution in urban environments is extremely nonuniform. Heterogeneity is mainly artificial due to snow handling, but wind patterns and the variable timing of melt (related to the albedo and solar exposure) also play a role. Within the space of a few meters, there may be snow-free ground, almost untouched snow and banks of plowed snow. Most of the snow falling on permanently impermeable surfaces, such as streets and footpaths, is removed. Activities in the city, in particular traffic, result in fallout of pollutants onto the snow. The atmospheric heat exchange, and therefore the snowmelt rate, is affected by buildings. Large areas of the city are shaded from the sun for at least part of the day. In other areas, the incoming radiation is enhanced by multiple reflections. Snowmelt takes place at different rates and is affected by different elements within an urban area.

Urban meltwater pathways are mostly overland. The infiltration capacity of soils which are permeable in summer can be very much reduced during snowmelt periods. If there is no refreeze, the time for meltwater to flow from the snow surface to the inlets of a conduit is 1 or so hours, refreezing greatly extends this time period. To resolve the melt on hourly basis, some form of energy balance computation is required. If the meltwater input at the bottom of the snowpack is known on an hourly basis, it can be equated to the hourly runoff in the conduit system without any runoff computations. However, the melt rates at different parts of the urban basin must be accounted for by dividing it into elements, each with differing snow and energy characteristics. Thus, snow models must be spatially distributed rather than lumped. Meltwater enters into the urban conduit system either directly from overland flow or indirectly as sewer infiltration. Sewer conduits function as a groundwater drainage system. Recharge-driven sewer infiltration is a slow process. Hence, the contribution of groundwater inflow can be estimated from a degree-day approach or can even be related to the amount of snow available.

Acknowledgments

Much of the text is drawn from two chapters in Urban Drainage in Cold Climates IHP Technical Documents in Hydrology No. 40 Vol. II. UNESCO, Paris (2000). written by the authors.

Bibliography

Anderson, E. A., 1976. *A point energy and mass balance model of snow cover.* NOAA Tech Pep NWS 19, US Dept. Commerce, Washington, DC.

Bengtsson, L., 1976. Snowmelt estimated from energy budget studies. *Nordic Hydrology*, **7**(1), 3–18.

Bengtsson, L., 1980. Evaporation from a snow cover. *Nordic Hydrology*, **11**, 221–234.

Bengtsson, L., 1982a. Percolation of melt water through a snow pack. *Cold Regions Science and Technology*, **6**, 73–81.

Bengtsson, L., 1982b. The importance of refreezing on the diurnal snowmelt cycle with application to a northern Swedish catchment. *Nordic Hydrology*, **13**, 1–12.

Bengtsson, L., 1983. Snowmelt induced urban runoff in northern Sweden. In *Proceedings Stormwater and Water Quality Model Users Group Meeting*. Athens, Georgia, USA, pp. 215–236.

Bengtsson, L., 1984. Modelling snowmelt induced runoff with short time resolution. In *Proceedings of the 3rd International Conference Urban Storm Drainage*, Gothenburg, Sweden. pp. 305–314.

Bengtsson, L., and Westerström, G., 1992. Urban snowmelt and runoff in northern Sweden. *Hydrological Sciences Journal*, **37**, 263–275.

Bengtsson, L., and Singh, V. P., 2000. Model sophistication in relation to scales in snowmelt runoff modeling. *Nordic Hydrology*, **31**, 267–286.

Bergström, S., 1995. The HBV model. In Singh, V. P. (ed.), *Computer Models of Watershed Hydrology.* Highlands Ranch, CO, USA: Water Resources Publications, pp. 443–476.

Blöschl, G., 1999. Scaling issues in snow hydrology. *Hydrological Processes*, **13**(14–15), 2149–2175.

Buttle, J. M., and Xu, F., 1988. Snowmelt runoff in suburban environments. *Nordic Hydrology*, **18**, 19–40.

Buttle, J. M., and Sami, K., 1990. Recharge processes during snowmelt: an isotopic and hydrometric investigation. *Hydrological Processes*, **4**, 343–360.

Engelmark, H., 1984. Infiltration in unsaturated frozen soil. *Nordic Hydrology*, **15**, 243–252.

Espeby, B., 1990. Tracing the origin of natural waters in a glacial till slope during snowmelt. *Journal of Hydrology*, **118**, 107–127.

Gray, D. M., and Prowse, T. D., 1993. Snow and floating ice. In Maidment, D. R. (ed.), *Handbook of Hydrology.* USA: McGraw-Hill.

Hautala, E. L., Rekilä, R., Tarhanen, J., and Ruuskanen, J., 1995. Deposition of motor vehicle emissions and winter maintenance along roadside assessed by snow analysis. *Environmental Pollution*, **87**, 45–49.

Hernebring, C., Marklund, S., and Gustafsson, L.-G., 1997. Modelling of flow components in sewer systems influenced by snowmelt processes using the MouseNAM concept. In *2nd DHI Software User Conference*, Helsingør, Denmark.

Kane, D. L., and Stein, J., 1983. Water movement into seasonally frozen soils. *Water Resources Research*, **19**, 1547–1557.

Kirnbauer, R., Blöschl, G., and Gutknecht, D., 1994. Entering the age of distributed snow models. *Nordic Hydrology*, **25**, 1–24.

Kuchment, L. S., and Gelfan, A. N., 1996. The determination of the snowmelt rate and the melt water outflow from a snow pack for modelling river runoff generation. *Journal of Hydrology*, **179**, 23–36.

Kuusisto, E., 1984. *Snow Accumulation and Snowmelt in Finland.* Publication of the Water Research Institute, National Board of Waters, Finland no. 155.

Leavesley, G. H., 1989. Problems of snowmelt runoff modelling for a variety of physiographic and climatic conditions. *Hydrological Sciences Journal*, **34**(6), 617–634.

Liston, G. E., 1995. Local advection of momentum, heat, and moisture during the melt of patchy snow covers. *Journal of Applied Meteorology*, **17**, 1833–1842.
Male, D. H., and Granger, R. J., 1981. Snow surface energy exchange. *Water Resource Research*, **17**(3), 609–627.
Marsalek, J., 1991. Urban drainage in cold climates: problems, solutions and research needs. In Maksimović, Č. (ed.), *International Conference on Urban Drainage and New Technologies (UDT91),* Dubrovnik, Yugoslavia, Elsevier Applied Science, pp. 299–308.
Marsh, P., and Woo, M.-K., 1984. Wetting front advance and freezing melt water within a snow cover 1. Observations in the Canadian Arctic. *Water Resource Research*, **20**(12), 1853–1864.
Martinec, J., and Rango, A., 1986. Parameter values for snowmelt runoff modelling. *Journal of Hydrology*, **84**, 197–219.
Morris, E. M., 1983. Modelling the flow of mass and energy within a snow pack for hydrological forecasting. *Annals of Glaciology*, **4**, 198–203.
Neumann, N., and Marsh, P., 1998. Local advection of sensible heat in the snowmelt landscape of Arctic tundra. *Hydrological Processes*, **12**, 1547–1560.
Rouse, W. R., Noal, D., and McCutcheon, J., 1973. Radiation, temperature and atmospheric emissivities in a polluted urban atmosphere at Hamilton, Ontario. *Journal of Applied Meteorology*, **12**, 789–807.
Sand, K., 1990. *Modelling Snowmelt Runoff Processes in Temperate and Arctic Environments*. PhD thesis, Trondheim, Division of Hydraulic and Sanitary Engineering, University of Trondheim.
Semádeni-Davies, A. F., 1998. Modelling snowmelt induced waste water inflows. *Nordic Hydrology*, **29**(4/5), 285–302.
Semádeni-Davies, A. F., 1999. Snow-cover heterogeneity in Luleå, Sweden. *Urban Water*, **1**, 39–47.
Semadeni-Davies, A. F., 2000. Representation of snow in urban runoff models. *Journal of Hydrologic Engineering*, **5**(4), 363–370.
Semádeni-Davies, A. F., and Bengtsson, L., 1999. The water balance of a sub-arctic town. *Hydrological Processes*, **13**, 1871–1885.
Semádeni-Davies, A. F., Lundberg, A., and Bengtsson, L., 2001. Radiation balance for snow in the urban environment: a water management perspective. *Cold Regions Science and Technology*, **33**, 59–76.
Semádeni-Davies, A. F., and Bengtsson, L., 1998. Snowmelt sensitivity to radiation in the urban environment. *Hydrological Sciences Journal*, **43**(1), 67–89.
Sundin, E., Andreasson, P., and Viklander, M., 1999. An energy budget approach to urban snow deposit melt. *Nordic Hydrology*, **30**, 39–56.
Thorne, G. A., Laporte, J., and Clerke, D., 1998. The effects of frozen soils on groundwater recharge and discharge in granite rock terrane of the Canadian Shield. *Nordic Hydrology*, **29**, 371–384.
Thorolfsson, S. T., and Killingtveit, Å., 1991. The use of conceptual hydrological models for modelling urban runoff form precipitation and snowmelt. In Maksimović, Č. (ed.), *International Conference on Urban Drainage and New Technologies (UDT91)*, Dubrovnik, Yugoslavia, Elsevier Applied Science, pp. 317–324.
Thorolfsson, S. T., and Brandt, J., 1996. The influence of snowmelt on urban runoff in Norway. In *7th International Conference on Urban Storm Drainage*, Hanover, Germany pp. 133–138.
Thorolfsson, S. T., and Sand, K., 1991. Urban snowmelt research in Norway: measurements and modelling approach. In Maksimović, Č. (ed.), *International Conference on Urban Drainage and New Technologies (UDT91)*, Dubrovnik, Yugoslavia, Elsevier Applied Science, pp. 309–316.
Todhunter, P. E., Xu, F., and Buttle, J. M., 1992. A model of net radiation over suburban snow packs. *Atmospheric Environment*, **26B**(1), 17–27.
U.S. Army Corps of Engineers, 1956. *Snow hydrology. Summary Report of the Snow Investigations.* North Pacific Division, Portland, Oregon, USA.
Verseghy, D. L., and Munro, D. S., 1989b. Sensitivity studies on the calculation of the radiation balance of urban surfaces: I Shortwave radiation. *Boundary-Layer Meteorology*, **46**, 309–331.
Verseghy, D. L., and Munro, D. S., 1989a. Sensitivity studies on the calculation of the radiation balance of urban surfaces: II Longwave radiation. *Boundary-Layer Meteorology*, **48**, 1–18.
Viklander, M., 1997. *Snow Quality in Urban Areas.* Unpublished PhD thesis, LTU-DU 1997:21 SE, Sweden, Luleå University of Technology.
Westerström, G., 1981. Snowmelt runoff from an urban plot. In *Proceedings of the 2nd International Conference on Urban Storm Drainage,* Urbana, Illinois, USA, pp. 452–459.
Westerström, G., 1984. Snowmelt runoff from Porsön residential area. Luleå, Sweden. *3rd International Conference on Urban Storm Drainage*, Gothenburg, Sweden, pp. 315–323.
Woo, M.-K., 1998. Arctic snow cover information for hydrological investigations at various scales. *Nordic Hydrology*, **29**, 245–266.
Xu, F., and Buttle, J. M., 1987. Patterns of net radiation over urban snow packs. In *Proceedings of the Eastern Snow Conference*, Fredericton, Vol. 43, pp. 173–184.

Cross-references

Specific Melt Rate
Physical Properties of Snow
Radiative Transfer Modeling
Snow Grains
Snow Metamorphism
Surface Energy Balance

U-SHAPE VALLEY

Amit Kumar
Department of Geology, Centre of Advanced Study in Geology, Punjab University, Chandigarh, India

Synonyms

Fjord; Glacial trough

Definition

Glacier erosion greatly modifies the shape of that portion of the river valley, which was occupied by glacier commonly known as U-shaped valley. A glacial valley generally differs from a river valley. Glacial valley is deepened and side slopes are steepened so that its cross section is changed from V-shaped to U-shaped. The U-shaped valley is one of the most well-known geomorphologic features of glaciation. (Figure 1 shows a developed U-shaped valley in Himalaya by Gangotri glacier.)

Synonyms: A glacially eroded valley; also called a glacial trough. It may extend to coastal location and in some cases may have been drowned by the post-glaciation rise in sea level; this submerged glaciated valley becomes a fiord.

U-Shape Valley, Figure 1 U-shape glacial valley developed by Gangotri glacier in Himalayas.

Origin: A glacier flows down in a former V-shaped river valley. As the glacier moves, it erodes the side wall and bottom of the valley. The valley becomes U-shaped with steep sides and a flat base.

Bibliography

Benn, D. I., and Evans, D. J. A., 1998. *Glaciers and Glaciation*. London: Arnold.

Bennett, M. R., and Glasser, N. F., 1996. *Glacial Geology: Ice Sheets and Landforms*. Chichester: Wiley.

Hambrey, M., and Alean, J., 2004. *Glaciers*, 2nd edn. Cambridge: Cambridge University Press.

Cross-references

Glacial Erosion

V

VEIN ICE

Chelamallu Hariprasad
Centre for Studies in Resource Engineering, IITB, Mumbai, India

Vein ice is defined as the ice occupying the cracks of soil or rock, below the earth's surface, at which the temperature has been continuously below 0°C for several years at the least. This exists where summer heating fails to reach the base of the layer of frozen ground. Formation of vein ice is the result of thermal contraction cracking.

V-SHAPED VALLEY

Amit Kumar
Department of Geology, Centre of Advanced Study in Geology, Punjab University, Chandigarh, India

Definition

V-shaped valleys are found in the upper part of a river, which is elongate depression of the Earth's surface. Valleys are commonly drained by rivers and slope denudation is typically characterized by the V-shape. Valley evolution is controlled mainly by climate and lithology. The angle of the V-shaped cross section depends on the rate of uplift of rock, the type of rock.

Bibliography

Benn, D. I., and Evans, D. J. A., 1998. *Glaciers and Glaciation*. London: Arnold.

Vijay P. Singh, Pratap Singh & Umesh K. Haritashya (eds.), *Encyclopedia of Snow, Ice and Glaciers*, DOI 10.1007/978-90-481-2642-2,

W

WATER BALANCE IN THE GLACIERIZED REGION

Heidi Escher-Vetter
Commission for Glaciology, Bavarian Academy of Sciences and Humanities, Munich, Germany

Synonyms

Hydrological-balance budget; Hydrological cycle; Water cycle

Definition

Water balance. Relationship between precipitation, evaporation, runoff, and storage for a given catchment.
Glacierized region. Catchment where part of the surface is covered with glaciers.

Introduction

At the Symposium on Glacier Hydrology in Cambridge, 1969, many questions on the topics of water and glaciers were discussed, partly for the first time. Here, Golubev (1973) analyzed the runoff and flow routing for a mountain glacier basin, which was one of the early contributions to this research topic. Some 10 years later, Baumgartner et al. (1983) included the water yield from glaciers in their textbook on the water cycle of the Alps, where they analyzed the reasons and consequences of glacier reduction for the water balance in the climatologic period 1931–1960. Shortly before, Collins (1982) gave an overview of water and mass balance measurements in glacierized drainage basins worldwide for 11 basins with water balance data from 95 glacier regions providing mass balance data.

Determination of water balance

Water balance of glacierized regions differs considerably to that of basins without glaciers. This is due to the fact that glaciers store *solid* and liquid precipitation, as well as meltwater over periods ranging from a few days to centuries and release it during spells of sunny warm weather when no runoff is produced by precipitation. This is the so-called 'compensating effect' of glacial runoff. Chen and Ohmura (1990) have shown that the ratio of summer to annual runoff is smallest and by that the 'compensating effect' largest in basins with 30–50% of ice cover; it increases for higher as well as lower ice cover shares.

In the water balance equation, the glacial influence is accounted for by an additional storage term S, which represents the change of the glacier mass. In a general form, the total balance can be written as

$$P = R + S + E \tag{1}$$

Here, P stands for precipitation, R for runoff, S for the storage term, and E for (net) evaporation. When these quantities are given in mm of water equivalent (mm w.eq.), they represent areal averages for the size of the respective basin. A complete balance is typically obtained for the natural mass balance year, that is, the period between the beginning of October and the end of September of the next calendar year.

There are several possibilities to assess water balance. For one type of investigation, the balance terms are evaluated on the basis of measurements of the individual components. For glaciers with independently determined mass balance data, the storage term S is often the most reliable one, especially when it is based on the direct glaciological method for mass balance determination. The calculation of basin precipitation P typically provides the largest difficulty, in spite of the fact that even in high-mountain regions, there are more precipitation stations than glacier discharge gauges. Discharge records R, on the other hand, succumb to from problems of insufficient calibration or from water losses due to seepage in the ice-free part of the basin. For net evaporation E, there are

Vijay P. Singh, Pratap Singh & Umesh K. Haritashya (eds.), *Encyclopedia of Snow, Ice and Glaciers*, DOI 10.1007/978-90-481-2642-2,

no continuous records available in these remote regions, and numerical values of this typically small quantity are therefore deduced from single experiments. In many studies, E is set constant over the glacier area and longer periods or taken as the residual between precipitation, glacier mass change, and runoff.

Numerous models have been developed to evaluate water balance. Morris (2006) gives a comprehensive overview of the techniques for predicting runoff from glacierized areas. The choice of the appropriate model depends on the available meteorological and geodetic input data and the temporal/spatial scale of the study. Other modeling tools are necessary for headwater sheds with sizes of some 10 km², than for study areas up to 100,000 km². Conceptual models have to be calibrated, whereas physical models are mainly independent from calibration by time series of runoff, for example. Kuhn and Batlogg (1998) use the calibrated OEZ model to determine monthly precipitation sums, based on monthly means of the water balance for 100 m altitudinal steps. A widely used model type is the so-called HBV/ETH runoff model, which is based on daily means of air temperature and daily precipitation sums. It simulates daily discharge and glacier mass balance with a temperature index method, and it is calibrated with measured discharge and glacier mass balance. A detailed description of some model extensions for the special application in glacierized basins is given by Braun et al. (2000). Another concept also uses a temperature index method in a hybrid form including potential solar radiation (Hock, 1999). Verbunt et al. (2003) have taken this approach as a sub-model of WaSiM-ETH to simulate the discharges in three Swiss high alpine basins with different levels of glacierization (Massa, Rhone, and Dischma basins). For these basins, the altitudinal distribution of snowmelt, ice-melt, precipitation, evapotranspiration and total runoff is discussed.

The highest data requirements are posed by gridded energy balance models, which calculate hourly meltwater amounts, and route the runoff through the glacier with a linear reservoir approach. An example for this approach is the so-called PEV model (Escher-Vetter, 2000), developed and applied for Vernagtferner.

Main characteristics of water balance as observed for the Vernagtferner, Oetztal Alps, Austria

In their comprehensive report on glacier storage, Jansson et al. (2003) characterize glaciers with respect to their short-term, intermediate-term, and long-term storage and the respective influence of these processes on glacier hydrology and water balance. The first timescale, that is, hours to days comprises processes like the diurnal runoff cycle. The intermediate-term storage includes seasonal snow cover and firn water storage within periods from months to years and, on the long-term storage scale, changes in glacier volume up to centuries are considered. For the Vernagtferner, the records presented in Figure 1 show the development of the components of water balance for the intermediate to long-term scale.

In Figure 1, annual values of precipitation, runoff, and glacier storage change are presented for the Vernagtferner basin, Central Alps, (2,640–3,630 m a.s.l., 11.44 km²), from 1974/1975 to 2006/2007. Since the 1970s, the glacierized share was reduced from some 81% to 71% in 2008. For this glacier basin, all balance components can be derived from measurements. Hourly values of total basin discharge observations have been available since 1974. Net mass balance has been determined for every year since 1965, and the separation of winter and summer mass balance provides winter precipitation data for the whole period of Vernagtferner (Escher-Vetter et al., 2009). Summer precipitation is recorded with weighing gauges (Escher-Vetter and Siebers, 2007), and E

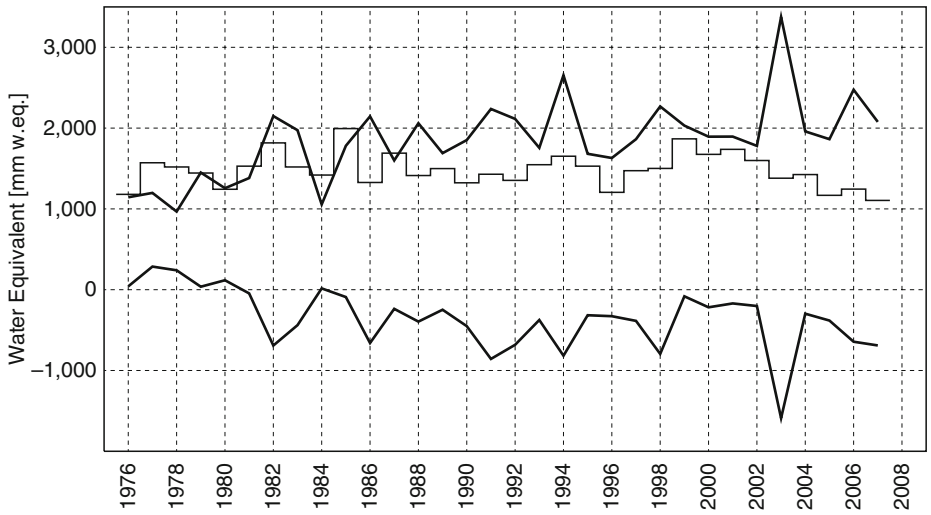

Water Balance in the Glacierized Region, Figure 1 Main components of water balance for the Vernagtferner from 1974/1975 to 2006/2007: basin precipitation (step function), glacier storage change (*lower curve*), and runoff (*upper curve*).

(not included in Figure 1) derived from several experiments on the glacier during the last decades. For the period depicted, runoff amounts have nearly doubled from some 1,000 mm w.eq. up to 2,000 mm w.eq., due to the continuing mass losses, largest in 2003 with 3120 mm w.eq.; basin precipitation, however, does not show any trend. Between June and October 90% of the runoff is recorded (Escher-Vetter and Reinwarth, 1995), and the diurnal variation has increased from 2 to 3 $m^3 s^{-1}$ to more than 10 $m^3 s^{-1}$ over the last 30 years due to the reduction of snow and firn storage capacity.

Water balance studies in different climate regions – Arctic, Central Asia, and South America

The Vernagtferner represents the climate region of the European Alps, where a clear distinction is found between the accumulation period (October to April) and ablation period (May to September). This "Alpine scheme" is also found in Scandinavia, Central Asia, and the Arctic, but not in the Tropics, where accumulation and ablation can occur within the same weather period.

Killingtveit et al. (2003) summarize recent and ongoing water balance studies in Svalbard and comment extensively on the uncertainties of individual terms. For two differently glacierized catchments (Bayelva, 55% of 31 km²/De Geerdalen, 10% of 79 km²), the average water balance terms for the hydrological years 1990/1991 to 2000/2001 amount to P = 624/548 mm w.eq., S = 245/49 mm w.eq., R = −1,050/−539 mm w.eq., and E = −37/−72 mm w.eq. The same quantities for the period 1974/1975 to 2004/2005 for the Vernagtferner are for P = 1,525 mm w.eq., S = 305 mm w.eq., R = −1,790 mm w.eq., E = −120 mm w.eq. (Braun et al., 2007), showing the typically larger quantities in the Central Alps.

For the Indian part of the Satluj basin, Singh and Jain (2002) determined the average contribution of snow and ice melt to runoff from the water balance. For this 22,305 km² Himalayan catchment, the period from 1986 to 1996 was analyzed. The hydrographs at Bakhra Dam show that 83% of the total runoff is recorded between April and September. On an average, 59% of the runoff is contributed by snow and ice melt, emphasizing the importance of glaciers in this large catchment.

For the smaller Beas River basin at the Pandoh Dam (5,278 km², 15% glacierized), Kumar et al. (2007) calculated the water budget for the period 1990–2004. Here, snow- and glacier-melt runoff contributes about 35% of the annual runoff, which reaches its maximum with more than 600 $m^3 s^{-1}$ on average in July and August.

The glacier fed catchments, Yanamarey (1.3 km²) and Uruashraju (3.4 km²) of the Cordillera Blanca, Peru, show the typical features of tropical glacier basins. 35% of the average discharge of the <10% glacierized Querococha basin is provided by glacier melt in February and March (Mark and Seltzer, 2003), and specific discharge for the period 1956–1996 amounts to 870 mm a^{-1}.

For the Zongo Glacier, Peru, Francou et al. (1995) analyzed the monthly components of the water balance with respect to El Niño-Southern Oscillation events from September 1991 to August 1993. For this tropical glacier, the early and late wet season, that is, October–December and March–May, are most important for the annual mass balance in contrast to midlatitude glaciers, where the summer months mainly determine the balance.

Summary and outlook: water balance in glacierized regions under changed climate conditions

Glaciers are important storages of water. They change the water balance of drainage basins considerably, as they shift the precipitation from small-term to long-term periods. In this way, they can become important sources of water for drinking or irrigation purposes, especially in arid regions. The examples from different climate regions (Arctic, Alps, Himalayas, and Andes) show this very clearly. At the present time, these water reservoirs are reduced markedly due to climate change, and complete losses within the next 100 years in some mountainous parts of the world cannot be excluded. This will not only change water balance, but also living conditions for mankind.

Bibliography

Baumgartner, A., Reichel, E., and Weber, G., 1983. *Der Wasserhaushalt der Alpen. Enclosed: Section 5: Influence of glaciers on the water balance of alpine catchments in the period 1931–1960*. Oldenbourg Verlag München Wien, 75–101.

Braun, L. N., Weber, M., and Schulz, M., 2000. Consequences of climate change for runoff from Alpine regions. *Annals of Glaciology*, **31**, 19–25.

Braun, L. N., Escher-Vetter, H., Siebers, M., and Weber, M., 2007. Water balance of the highly glaciated Vernagt basin, Oetztal Alps. In Psenner, R., and Lackner, R. (eds.), *Alpine Space – Man & Environment. Vol. 3: The Water balance of the Alps*. Innsbruck University Press, 33–42.

Chen, J., and Ohmura, A., 1990. On the influence of Alpine glaciers on runoff. In Lang, H., and Musy, A. (eds.), *Hydrology in Mountainous Regions I, Hydrological Measurements, The Water Cycle*. IAHS Publ. No. 193, 117–125.

Collins, D., 1984. Water and mass balance measurements in glacierised drainage basins. *Geografiska Annaler*, **66A**(3), 197–214.

Escher-Vetter, H., 2000. Modelling meltwater production with a distributed energy balance method and runoff using a linear reservoir approach – results from Vernagtferner, Oetztal Alps, for the ablation seasons 1992 to 1995. *Zeitschr. f. Gletscherkd. u. Glazialgeologie*, **36**, 119–150.

Escher-Vetter, H., and Reinwarth, O., 1995. Two decades of runoff measurements (1974 to 1993) at the Pegelstation Vernagtbach/Oetztal Alps. *Zeitschr. f. Gletscherkd. u. Glazialgeologie*, **30**, 53–98.

Escher-Vetter, H., and Siebers, M., 2007. Sensitivity of glacier runoff to summer snowfall events. *Annals of Glaciology*, **46**, 309–315.

Escher-Vetter, H., Kuhn, M., and Weber, M., 2009. Four decades of winter mass balance of Vernagtferner and Hintereisferner, Austria: methodology and results. *Annals of Glaciology*, **50**, 87–95.

Francou, B., Ribstein, P., Saravia, R., and Tiriau, E., 1995. Monthly balance and water discharge of an inter-tropical glacier: Zongo

Glacier, Cordillera Real, Bolivia, 16°S. *Journal of Glaciology*, **41**(137), 61–67.
Golubev, G. N., 1973. Analysis of the run-off and flow routing for a mountain glacier basin. Symposium on Hydrology of Glaciers, Cambridge, 7–13 September 1969, organized by the Glaciological Society. Publication No. 95 de l'association international d'hydrologie Scientifique, 41–50.
Hock, R., 1999. A distributed temperature-index ice- and snowmelt model including potential direct solar radiation. *Journal of Glaciology*, **45**(149), 101–111.
Jansson, P., Hock, R., and Schneider, Th., 2003. The concept of glacier storage: a review. *Journal of Hydrology*, **282**, 116–129.
Killingtveit, Å., Pettersson, L.-E., and Sand, K., 2003. Water balance investigations in Svalbard. *Polar Research*, **22**(2), 161–174.
Kuhn, M., and Batlogg, N., 1998. Glacier runoff in alpine headwaters in a changing climate. In Kovar, K., Tappeiner, U., Peters, N. E., and Craig, R. G. (eds.), *Hydrology. Water Resources and Ecology in Headwaters*, IAHS Publ. No. 248, 79–88.
Kumar, V., Singh, P., and Sing, V., 2007. Snow and glacier melt contribution in the Beas River at Pandoh Dam, Himachal Pradesh. India. *Hydrological Sciences Journal*, **52**(2), 376–388.
Mark, B. G., and Seltzer, G., 2003. Tropical glacier meltwater contribution to stream discharge: a case study in the Cordillera Blanca. Peru. *Journal of Glaciology*, **49**(165), 271–281.
Morris, E., 2006. Techniques for predicting runoff from glacierized areas. In Demuth, M. N., Munro, D. S., and Young, G. J. (eds.), *Peyto Glacier – one century of science.* NHRI Science Report No. 8, ISSN 0843-9052. 203–225.
Singh, P., and Jain, S. K., 2002. Snow and glacier melt in the Satluj River at Bhakra Dam in the western Himalayan region. *Hydrological Sciences Journal*, **47**(1), 93–106.
Verbunt, M., Gurtz, J., Jasper, K., Lang, H., Warmerdam, P., and Zappa, M., 2003. The hydrological role of snow and glaciers in alpine river basins and their distributed modeling. *Journal of Hydrology*, **282**, 36–55.

Cross-references

Discharge/Streamflow
Diurnal Cycle of Runoff
Glacier Hydrology
Glacier Mass Balance
Precipitation

WESTERLIES AND THEIR EFFECTS ON MARITIME ICE CAPS AND GLACIERS

Robert D. McCulloch
School of Biological and Environmental Science, University of Stirling, Stirling, Scotland, UK

Synonyms

Polar convergence zone low pressure storms; Westerly air circulation; Westerly storms

Definition

Westerlies: A meteorological phenomenon where the thermal gradient between the mid-latitudes and the polar regions leads to increased baroclinicity and increased thermal winds in a westerly direction along the polar front in both hemispheres. Warmer mid latitude air mixes with colder polar air at the polar convergence zone leading to the formation of westerly storms, known as the westerlies. The westerlies are further distorted by orography along topographic barriers such as the southern Andes, the Rockies, Norway, and the New Zealand Alps leading to increased precipitation on the western flanks of the mountains and dry conditions on the eastern lee side further characterized by westerly katabatic winds.

Introduction

Air circulating north and south of the subtropical high pressure zones in the northern and southern hemispheres, respectively, generally blows in a westerly direction in both hemispheres, giving rise to the prevailing westerly winds. The temperature gradient between the mid-latitudes and the polar regions leads to the development of the polar front and increases wind speeds and the formation of a jet stream. The ascending air and low pressures at the latitudes of the jet streams are caused by the baroclinic instability of the jet streams, which produce surface convergence and uplift creating low pressure storm cells that may be modified by orography (Barry, 2008). Understanding the behavior of the westerlies and their effect on glaciers is key to understanding the reorganization of hemispheric ocean-atmosphere circulation patterns at the end of the last glaciation because their latitude and strength are influenced by such factors as the strength of the subtropical high pressure and the location of sea ice in the Southern Ocean (Yuan and Martinson, 2000).

During the Northern hemisphere winter (November–January), Arctic sea ice advances and in the Southern Hemisphere the Antarctic sea ice retreats with the rise in the austral summer temperatures. The situation between the poles is reversed during the boreal summer and austral winter (May–July). This seasonal expansion and contraction of sea ice and the strength of the subtropical high lead to latitudinal shifts in the position of the northern and southern polar convergence zone and the polar fronts. The jet streams are dynamically unstable and the position of the polar fronts may also change. This constant shifting northwards or southwards results in different weather patterns. In the northern hemisphere, the polar fronts shift southward to bring winter storms to much of the U.S. In the summer months, the polar front shifts northward and warmer subtropical air circulates farther north.

There is an advantage in exploring the relationship between westerly air circulation and glaciers in southern South America. The mountainous crest of the southern Andes supports ice fields and glaciers that are sensitive to climate and an extensive suite of landforms and sediments are created by processes of glacial erosion and glacial deposition. These provide a record of Quaternary glaciations from which we can infer paleo-climatic change. During the Last Glacial Maximum (LGM), an ice sheet, approximately 1,800 km long, built up along the north–south axis of the Andes (Clapperton, 1993; Figure 1).

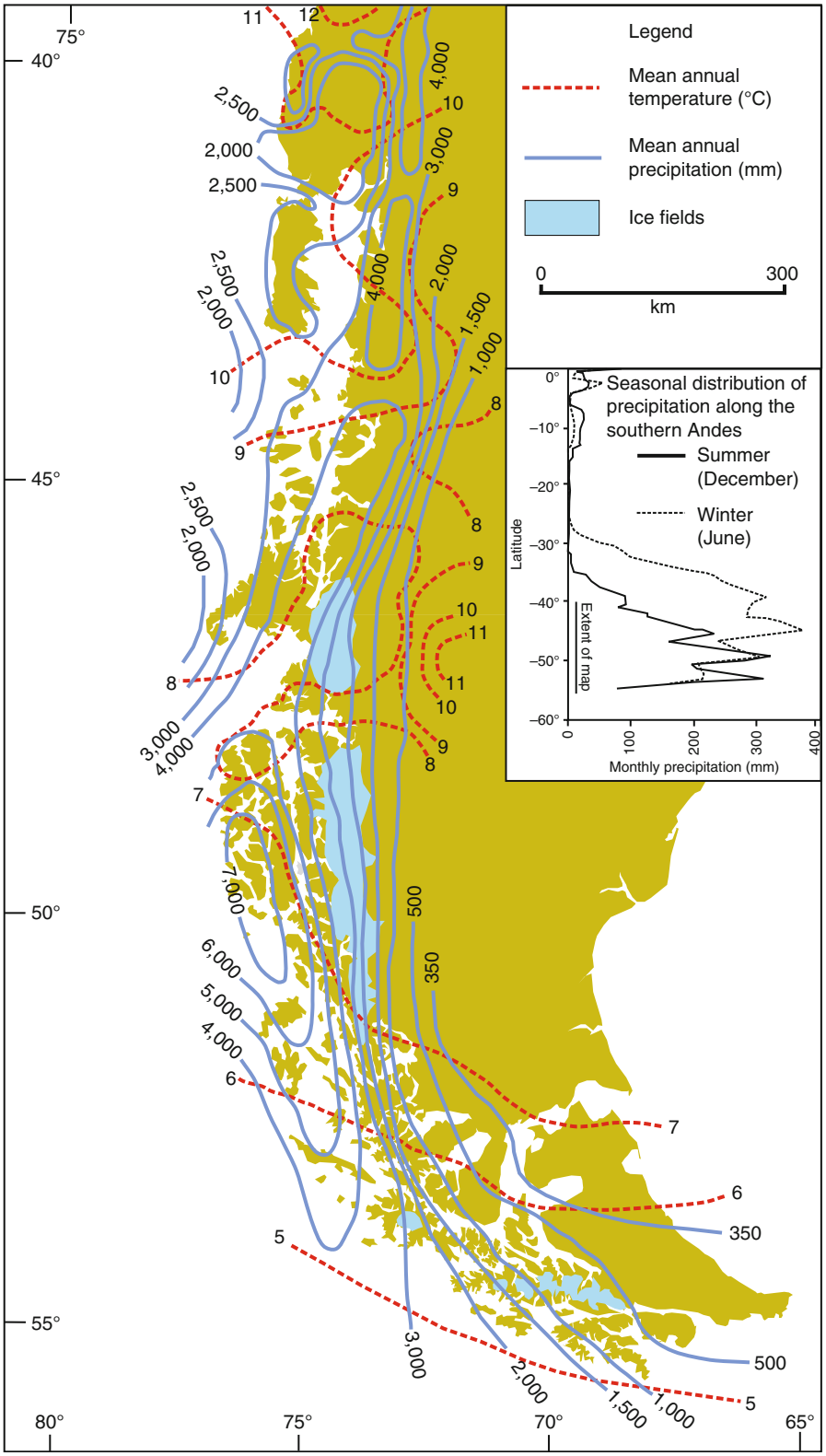

Westerlies and their Effects on Maritime Ice Caps and Glaciers, Figure 1 Climate map of Patagonia indicating the core of the westerly precipitation centered around 50°S. The inset chart indicates the extent of the seasonal latitudinal migration of the westerly precipitation belt (from McCulloch et al., 2000).

In the southern hemisphere, the southern Andes span several climatic zones from subpolar in the south (55°S) to warm temperate in the north (36°S). South of 36°S, the southern Andean mountains lie athwart the southern westerlies and experience precipitation all year from the westerly storms. This zone of westerly storm tracks reaches the southern Chilean coast laden with moisture from the warm Pacific, and the point of maximum precipitation is found at c. 48–50°S (Barry, 2008). Through a combination of frontal and orographic precipitation, the highest rainfall is experienced on the western flanks of the southern Andean Cordillera (Figure 1). This generates a strong lee-effect on the eastern flanks of the Andes seen in the increased dryness of Argentina.

Glacier dynamics are controlled by a complex relationship between elements of the hydrological cycle; temperature, precipitation, cloud cover, wind speed, and humidity (Benn and Evans, 1998). The large amounts of precipitation falling on the high Andean mountains sustains a number of ice fields; the North Patagonian ice field, the larger South Patagonian ice field, and the numerous, though smaller, Cordillera Darwin ice fields. These ice fields are supported by the accumulation of winter precipitation (falling as snow) exceeding the summer ablation, which may affect the entire accumulation area of the ice field. This climatic regime produces temperate maritime ice fields and leads to a rapid turnover of ice through the glacier system. This leads to a greater sensitivity of the ice fields and outlet glaciers to fluctuations in climate and in particular the latitudinal position of the westerly storm tracks (Hulton and Sugden, 1995).

Glaciological modeling experiments and paleoecological evidence suggests that the core of the southern hemisphere westerlies moved north by some 5° latitude during the Last Glacial Maximum (Hulton et al., 2002). Such a migration makes sense in the light of an expansion of sea ice limits during the last glaciation (Lamy et al., 2004) and appears to be necessary to bring the levels of precipitation required to sustain the expanded and continuous Patagonian ice field to the north of the present day North Patagonian ice field. Ice sheet modeling experiments indicate that a reduction in temperature alone is unlikely to have been sufficient to drive glacier advances in the area of the Chilean and Argentine Lake Districts (approximately 42–40°S) (Hulton et al., 2002).

Glaciological modeling also suggests that as the large continuous Patagonian ice sheet formed along the southern Andes, there was a corresponding intensification of the rain shadow to the east of the Andes as the westerly precipitation was forced over a higher and colder topography. Detailed glaciological modeling by Hubbard et al. (2005) has suggested that during the waning stages of the Patagonian ice sheet after c. 14300 ^{14}C years BP, the precipitation from the westerlies was able to drive across or between the reduced and dividing ice fields giving rise to the expansion of smaller mountain glaciers on higher mountain peaks to the east of the main Andean mountain chain.

Following the Last Glacial Maximum (LGM), rapid retreat of the northern extent of the Patagonian ice field and the ensuing spread of humid-temperate vegetation suggests that the westerlies moved south some 1,500–1,800 years after the first step of deglaciation and reached their present latitude (approximately 50°S) by 14300 ^{14}C years BP (McCulloch et al., 2000). It is likely that the westerlies moved south of their present latitude in the early Holocene between 11400 and 9500 ^{14}C years BP, when the Magellan region in the far south of Patagonia, experienced a phase of aridity and increased frequencies in fires (Whitlock et al., 2007). Under such circumstances, the surrounding oceans would have also been warmer and this period coincides with an Antarctic Holocene optimum recognized in the early loss of ice shelves such as that in George VI Sound at the base of the Peninsula (Bentley et al., 2005). A mid-Holocene expansion of humid-temperate vegetation, and glacial landform evidence for Neoglacial glacier advances around the North and South Patagonian ice fields suggest that the core of the westerlies had shifted close to its present day focus at approximately 50°S (McCulloch et al., 2000).

Summary

The distribution of westerly storm tracks in the northern and southern hemisphere is controlled by the intensity of the subtropical high and the extent of polar sea ice. This in turn, when coupled with changes in global temperatures during glacial-interglacial cycles, leads to a greater sensitivity in the behavior of mid to high latitude temperate maritime glaciers due to large fluctuations in precipitation driving changes in the glacier mass balance system.

Bibliography

Barry, R., 2008. *Mountain Weather and Climate*. Cambridge: Cambridge University Press.

Benn, D. I., and Evans, D. J. A., 1998. *Glaciers and Glaciation*. London: Arnold.

Bentley, M. J., Hodgson, D. A., Sugden, D. E., Roberts, S. J., Smith, J. A., Leng, M. J., and Bryant, C., 2005. Early Holocene retreat of George VI ice shelf, Antarctic Peninsula. *Geology*, **33**, 173–176.

Clapperton, C. M., 1993. *Quaternary Geology and Geomorphology of South America*. Amsterdam: Elsevier.

Hubbard, A., Hein, A., Kaplan, M. R., Hulton, N. J., and Glasser, N., 2005. Model reconstruction of Late glacial maximum ice sheet. *Geografiska Annaler*, **87A**(2), 375–391.

Hulton, N. R. J., and Sugden, D. E., 1995. Modeling Mass-balance on Former Maritime Ice Caps – A Patagonian Example. *Annals of Glaciology, Ch. 63*, **21**, 304–310.

Hulton, N. R. J., Purves, R. S., McCulloch, R. D., Sugden, D. E., and Bentley, M. J., 2002. The last glacial maximum and deglaciation of southern South America. *Quaternary Science Reviews*, **21**, 233–241.

Lamy, F., Kaiser, J., Ninnemann, U., Hebbeln, D., Arz, H. W., and Stoner, J., 2004. Antarctic timing of surface water changes off chile and patagonian ice sheet response. *Science*, **304**, 1959–1962.

McCulloch, R. D., Bentley, M. J., Purves, R. S., Hulton, N. R. J., Sugden, D. E., and Clapperton, C. M., 2000. Climatic inferences from glacial and palaeoecological evidence at the last glacial

termination, southern South America. *Journal of Quaternary Science*, **15**, 409–417.
Whitlock, C., Moreno, P. I., and Bartlein, P., 2007. Climatic controls of Holocene fire patterns in southern South America. *Quaternary Research*, **68**, 28–36.
Yuan, X., and Martinson, D. G., 2000. Antarctic sea ice extent variability and its global connectivity. *Journal of Climate*, **13**, 1697–1717.

Cross-references

Climate Change and Glaciers
Glacier
Glacier Mass Balance
Landforms of Glacial Deposition
Landforms of Glacial Erosion
Neoglaciation
Palaeoclimate and Past Glaciations
Patagonia
Quaternary Glaciation
Retreat/Advance of Glaciers
Temperate Glaciers
Winter Accumulation Glacier

WGMS (WORLD GLACIER MONITORING SERVICE)

Wilfried Haeberli
Geography Department, University of Zurich, Zurich, Switzerland

Worldwide collection of information about ongoing glacier changes was initiated in 1894 with the foundation of the International Glacier Commission at the Sixth International Geological Congress in Zurich, Switzerland. In 1986, the World Glacier Monitoring Service (WGMS) started to maintain and continue the collection of information on ongoing glacier changes, when the two former services – PSFG (Permanent Service on Fluctuations of Glaciers) and TTS/WGI (Temporal Technical Secretary/World Glacier Inventory) were combined.

The World Glacier Monitoring Service (WGMS) collects standardized observations on changes in mass, volume, area, and length of glaciers with time (glacier fluctuations), as well as statistical information on the distribution of perennial surface ice in space (glacier inventories). Such glacier fluctuation and inventory data are high priority key variables in climate system monitoring; they form a basis for hydrological modeling with respect to possible effects of atmospheric warming, and provide fundamental information in glaciology, glacial geomorphology, and quaternary geology. The highest information density is found for the Alps and Scandinavia, where long and uninterrupted records are available. Data are published in the biennial Glacier Mass Balance Bulletin and the quinquennial Fluctuations of Glaciers. A recent overview was published by the United Nations Environment Programme (UNEP) and WGMS (Zemp et al., 2008a, b). Together with the GLIMS (Global Land Ice Measurement from Space) initiative and NSIDC (National Snow and Ice Data Center) at Boulder, Colorado, WGMS runs the GTN-G (Global Terrestrial Network for Glaciers) as part of the Global Terrestrial/Climate Observing System (GTOS/GCOS) under the Umbrella of World Meteorological Organization (WMO), Food and Agricultural Organization of the United Nations (FAO), International Council for Science (ICSU), UNEP, and United Nations Educational, Scientific, and Cultural Organization (UNESCO).

Bibliography

Haeberli, W., 2004. Glaciers and ice caps: historical background and strategies of world-wide monitoring. In Bamber, J. L., and Payne, A. J. (eds.), *Mass Balance of the Cryosphere*. Cambridge: Cambridge University Press, pp. 559–578.
Haeberli, W., Hoelzle, M., and Suter, S. (eds.), 1998. Into the second century of worldwide glacier monitoring: prospects and strategies. A contribution to the International Hydrological Programme (IHP) and the Global Environment Monitoring System (GEMS). *UNESCO – Studies and Reports in Hydrology*, 56.
http://nsidc.org/
http://wgms.ch/
http://www.fao.org/gtos/
http://www.glims.org/
Zemp, M., Roer, I., Kääb, A., Hoelzle, M., Paul, F., and Haeberli, W., 2008a. *Global glacier changes: facts and figures*. Nairobi and Zurich: UNEP and WGMS.
Zemp, M., Haeberli, W., Hoelzle, M., and Paul, F., 2008b. Glaciers and ice caps. Terrestrial essential climate variables for climate change assessment, mitigation and adaptation – GTOS Biennial report supplement, FAO, Rome, pp. 22–23.

Cross-references

Climate Change and Glaciers
Glacier
Glacier Mass Balance
Inventory of Glaciers

WINTER ACCUMULATION GLACIER

Amit Kumar
Department of Geology, Centre of Advanced Study in Geology, Punjab University, Chandigarh, India

Winter accumulation glacier

In the high land areas, winter precipitation in the form of snow is the major source to form the glaciers. The glaciers that receive heavy solid precipitation during winter period and also fallen precipitation accumulates over the glacier and adds to its mass, are known as winter accumulation glaciers. In general, majority of glaciers fall under this category. Only a few glaciers have accumulation in summer time. Thus, at the places where accumulation occurs primarily in the winter season and ablation during summer season are commonly known as winter-accumulation type glaciers.

Bibliography

Knight, P. G., 1999. *Glaciers*. Routledge; ISBN: 0-7487-4000-7.

Y

YEAR-ROUND ABLATION PATTERN

Rijan B. Kayastha
Himalayan Cryosphere, Climate and Disaster Research Center (HiCCDRC), Kathmandu University, Dhulikhel, Kavre, Kathmandu, Nepal

Definition

An ablation pattern which shows ablation in a whole year below the equilibrium line is called year-round ablation pattern. Most tropical glaciers show year-round ablation pattern and the seasonality controls accumulation, whereas most Himalayan glaciers in Nepal show summer accumulation as well as ablation type characteristics. Most glaciers in the European Alps are winter accumulation and summer-ablation type glaciers. Year-round ablation pattern occurs only where the seasonal climatic variations is very less, such as on the Puncak Jaya massif in the Indonesian territory of Irian Jaya (4° 05′ S., 137° 11′ E.; 4,884 m).

YOUNGER DRYAS

Sven Lukas
Department of Geography, Queen Mary University of London, London, UK

Synonyms

Deglaciation; Greenland Stadial 1 (GS-1); Lateglacial; Stadial; Termination I

Definition

The Younger Dryas (YD, c. 12.9–11.7 ka) represents the last return to cold, stadial conditions prior to early Holocene warming and is characterized by abrupt climate change. It marks the final phase of Termination I and is also referred to as Greenland Stadial 1 (GS-1).

Introduction

The YD is characterized by abrupt climate change both at its beginning and end (e.g., Alley, 2000; Bakke et al., 2009). This period is the most pronounced of a series of climatic fluctuations following the global last glacial maximum as identified in marine sediment cores (LGM *sensu* Mix et al., 2001). The name YD can be traced back to the occurrence of the plant species *Dryas octopetala* L. (mountain avens) that is particularly abundant in pollen counts obtained from sediment successions deposited after the demise of the last ice sheets in North Western (NW) Europe. Since this plant thrives under arctic and alpine climatic conditions, its prominence in pollen profiles allowed early reconstructions of severe cold conditions in NW Europe as early as the 1930s (Mangerud et al., 1974). The YD forms part of a period referred to as the Lateglacial, which comprises a succession of alternating interstadial (warm) and stadial (cold) phases: the Oldest, Older, and Younger Dryas (stadials) and the Bølling and Allerød (interstadials). Although originally devised in Denmark, the terminology was adopted across NW Europe (cf. Mangerud et al., 1974) and is widely used to this day, albeit with the Bølling and Allerød being referred to as one interstadial complex (cf. Liu et al., 2009). Because this climatostratigraphical terminology is – strictly speaking – only valid for Scandinavia, where it was devised, Lowe et al. (2008) suggest that when making global correlations of climatic events, the YD should be referred to as "Greenland Stadial 1 (GS-1)" to avoid ambiguities regarding synchroneity.

The YD is a key period in the late Quaternary and has been the focus of paleoclimatic research for several decades. This is due to this period (a) having experienced a number of drastic changes that can be observed in

Vijay P. Singh, Pratap Singh & Umesh K. Haritashya (eds.), *Encyclopedia of Snow, Ice and Glaciers*, DOI 10.1007/978-90-481-2642-2,

numerous proxy records, including geomorphological, biological, and chemical changes in terrestrial, ice core, marine, and lacustrine settings and (b) being characterized by very abrupt, or rapid, changes in reconstructed air temperatures. This makes it an ideal role model for rapid climate change that humanity may face (Steffen et al., 2004; Seager and Battisti, 2007).

Characteristics of the Younger Dryas

In order to constrain *rates of change* that may be used as input data for predictive numerical climate models, it is of paramount importance to establish the duration of climatic oscillations using numerical dating methods. Historically, however, the YD has been very difficult to date for two main reasons: Firstly, the period is relatively brief, lasting c.1,200 years, and thus just below the resolution of most dating methods. Secondly, there are a number of problems associated with the most precise dating method in this context, radiocarbon dating; these are the marine reservoir effect and a major radiocarbon plateau, both of which increase the error associated with this method (cf. Walker, 2005) and complicate reliably dating the onset and end of the YD. Because of aforementioned shortcomings, annually resolved records have been extensively studied to fill this gap. Three key records with the required resolution exist, namely ice cores (e.g., Alley, 2000; Rasmussen et al., 2006; Lowe et al., 2008), varved lake sediments (e.g., Brauer et al., 2008) and tree-ring chronologies (e.g., Friedrich et al., 2004).

According to a new chronology that has been constructed by layer counting in the three most highly resolved Greenland ice cores (Rasmussen et al., 2006; Lowe et al., 2008), the YD has been dated to 12,896–11,703 ka GICC05 b2k ("Greenland Ice Core Chronology 2005 before AD2000"). This corresponds well with an age of 11,590 a BP for the end of the YD as identified in the Hohenheim Oak and Pine Chronology from Central Europe (Friedrich et al., 2004).

A number of archives with continuous or near-continuous sedimentation records show similar magnitudes of change both during the beginning and end of the YD; however, temperatures during the first half of the YD, after an initial drop, remained fairly stable (e.g., Brooks and Birks, 2000; Bakke et al., 2009). The second half of the YD saw a much less stable pattern where the temperature regime "flickered" between warmer and colder temperatures before the final transition to the present interglacial (Bakke et al., 2009). Irrespective of the proxies used, the rates of change are of the order of several degrees celsius in a few years to a decade.

Triggers – atmosphere or ocean?

The origin of the YD is still a matter of debate. A widely accepted hypothesis is that its cause lies in a weakening or shutdown of the meridional overturning circulation (MOC) in the North Atlantic (Rahmstorf, 2002; Denton et al., 2005; Tarasov and Peltier, 2005). The original hypothesis holds that large volumes of freshwater, stored in proglacial ice-dammed Lake Agassiz in front of the Laurentide Ice Sheet (Teller et al., 2002), were released suddenly and led to a reduction of the salinity contrasts that drive the MOC (Rahmstorf, 2002). Such sudden inputs of freshwater into the ocean happened periodically during deglaciation, intimately tied to cyclic climatic fluctuations like Heinrich Events (cf. Rahmstorf, 2002), although the exact causal links are still not established.

In recent years, a number of alternatives for the sources and routing of freshwater have been discussed. Tarasov and Peltier (2005), using numerical modeling, strongly suggest that a substantial amount of meltwater and icebergs was most likely discharged into the Arctic Sea. Other potential sources include the release of water from an ice-dammed lake in the hinterland of the Lena and Yana rivers (Spielhagen et al., 2005) or increased meltwater runoff and calving of the Greenland Ice Sheet contributed, perhaps significantly, to YD cooling (Jennings et al., 2006). It is likely that a combination of these sources, perhaps time-transgressively, might be responsible for the episodic input of freshwater into the oceans, leading to the climatic fluctuations observed.

Although the "oceanic trigger hypothesis" remains popular, several problems exist: Firstly, it is disputed whether the MOC is the major conveyor along which heat transport to northerly latitudes, and Europe in particular, occurs (e.g., Seager et al., 2002; Seager and Battisti, 2007). Secondly, the two largest events, labeled meltwater pulse 1a and 1b, occurred several hundreds of years before and after the YD, respectively (Fairbanks, 1989), failing to provide the desired clear link (cf. Wunsch, 2006).

In the light of these discrepancies, changes in atmospheric circulation patterns have been invoked to be a cause, rather than an effect, of rapid climate change and hence of the YD: these changes, possibly initiated by the growth and presence of continental ice sheets during the Quaternary (cf. Wunsch, 2006), together with a dynamical displacement of the sea ice edge (Li et al., 2005; Bakke et al., 2009), could be a key factor in cooling associated with the YD. Air masses moving across the sea ice would have been chilled and deprived of moisture (cf. Brauer et al., 2008), linking well with observations of a windy, cold, and dry YD across Europe and in the Greenland ice cores (cf. Alley, 2000). Although the exact links are at present still only tentative (cf. discussion in Brauer et al., 2008), changes in atmospheric circulation could also explain reconstructed changes in MOC activity since wind shear is known to have an impact on ocean circulation (e.g., Dickson et al., 2000; Seager et al., 2002; Timmermann and Goosse, 2004; Seager and Battisti, 2007). Shifts in seasonality, with stronger cooling during the winter half (cf. Denton et al., 2005; Lie and Paasche, 2006), may be explained through the presence of sea ice as well. In order to solve this debate, more sophisticated climate models and a more systematic use of paleo-wind proxies such as dunes (cf. Kasse, 2002) have been suggested (e.g., Wunsch, 2006).

The most recent hypothesis regarding the triggering mechanism for the YD is the proposal that an extraterrestrial impact (ETI) may have contributed to atmospheric cooling (Firestone et al., 2007).

Global Younger Dryas?

Glacial landforms, most notably ice-marginal moraines, have been extensively used to establish synchronous response to climate change in terrestrial settings. Across Europe, the cooling associated with the YD led to the growth of glaciers in mountain ranges (e.g., Thompson Davis et al., 2009) and a readvance of the Scandinavian ice sheet (e.g., Tschudi et al., 2000).

The existence of the YD cold event in the North Atlantic region is well documented and accepted (cf. Isarin and Renssen, 1999; Seager and Battisti, 2007), apart from a few areas where the evidence remains equivocal, for example, bizarrely, Greenland (cf. Miller, 2008). However, its occurrence and impact has been controversially debated elsewhere on Earth (e.g., Barrows et al., 2008; Lowell and Kelly, 2008; Mahaney et al., 2008). The center of attention in the debate around a global YD event has been whether geomorphological and biological systems responded synchronously to a global trigger or asynchronously to local factors, a question that is highly significant in the context of explaining triggers and forcing of rapid climate change; in particular, it could introduce further uncertainties regarding the prediction of future climate change.

In order to determine whether these events were synchronous or asynchronous, it is necessary to obtain detailed paleoclimatic records from different parts of the world that are independently and securely dated. The key problems in solving this debate are twofold: Firstly, prominent, singular moraine ridges are usually selected for dating, but such landforms are likely to have been subject to postdepositional erosion, therefore not representing the time of glacier retreat but that of landform stabilization (Ice-Cored Moraines). Secondly, glacier response to climate change is in the order of years to decades and depends on a number of local factors (cf. Lukas and Benn, 2006). However, the resolution of cosmogenic surface exposure dating, the method commonly used to date boulders on moraines, is at least one order of magnitude lower than glacier response and also of quite coarse resolution when dating a short period like the YD: within error, ages could place a moraine on the YD-Holocene transition, so that unequivocal dating is not straightforward (cf. Miller, 2008, and references therein). Hence, one could argue that the methodological repertoire is at present insufficient to satisfactorily answer the question of global synchroneity of glacier advances during the YD.

Conclusions

The YD is a central time period characterized by rapid climate change. It is documented in a large number of terrestrial, marine, and lacustrine records.

However, a large number of uncertainties and white spots still exist when compared to more recent periods of glacier advances, for example the "Little Ice Age." This is partly due to the geographical spread of areas investigated (some "type sites" have been covered numerous times, others remain untouched to this day) and partly due to limitations in dating, for example an absence of dateable material, but also problems such as postdepositional erosion that may blur otherwise clearer signals.

Despite having been the focus of much research in the past 30 years, much still remains to be learned – and much exciting research still to be carried out – regarding triggers (atmosphere and/or ocean), extent (amphi-North Atlantic or global), impact on various systems and its power as a tuning-tool for numerical models.

Bibliography

Alley, R. B., 2000. The Younger Dryas cold interval as viewed from central Greenland. *Quaternary Science Reviews*, **19**, 213–226.

Bakke, J., Lie, Ø., Heegaard, E., Dokken, T., Haug, G. H., Birks, H. H., Dulski, P., and Nilsen, T., 2009. Rapid oceanic and atmospheric changes during the Younger Dryas cold period. *Nature Geoscience*, **2**, 202–205.

Barrows, T. T., Lehman, S. J., Fifield, L. K., and De Deckker, P., 2008. Response to Comment on "Absence of cooling in New Zealand and the adjacent ocean during the Younger Dryas Chronozone". *Science*, **320**, 746e.

Brauer, A., Haug, G. H., Dulski, P., Sigman, D. M., and Negendank, J. W. F., 2008. An abrupt wind shift in western Europe at the onset of the Younger Dryas cold period. *Nature Geoscience*, **1**, 520–523.

Brooks, S. J., and Birks, H. J. B., 2000. Chironomid-inferred late-glacial air temperatures at Whitrig Bog, south-east Scotland. *Journal of Quaternary Science*, **15**, 759–764.

Denton, G. H., Alley, R. B., Comer, G. C., and Broecker, W. S., 2005. The role of seasonality in abrupt climate change. *Quaternary Science Reviews*, **24**, 1159–1182.

Dickson, R. R., Osborn, T. J., Hurrell, J. W., Meincke, J., Blindheim, J., Adlandsvik, B., Vinje, T., Alekseev, G., and Maslowski, W., 2000. The Arctic Ocean response to the North Atlantic Oscillation. *Journal of Climate*, **13**, 2671–2696.

Fairbanks, R. G., 1989. A 17,000-year glacio-eustatic sea level record: Influence of glacial melting rates on the Younger Dryas event and deep-ocean circulation. *Nature*, **342**, 637–642.

Firestone, R. B., West, A., Kennett, J. P., Becker, L., Bunch, T. E., Revay, Z. S., Schultz, P. H., Belgya, T., Kennett, D. J., Erlandson, J. M., Dickenson, O. J., Goodyear, A. C., Harris, R. S., Howard, G. A., Kloosterman, J. B., Lechler, P., Mayewski, P. A., Montgomery, J., Poreda, R., Darrah, T., Que Hee, S. S., Smith, A. R., Stich, A., Topping, W., Wittke, J. H., and Wolbach, W. S., 2007. Evidence for an extraterrestrial impact 12, 900 years ago that contributed to the megafaunal extinctions and the Younger Dryas cooling. *Proceedings of the National Academy of Sciences of the United States of America*, **104**, 16016–16021.

Friedrich, M., Remmele, S., Kromer, B., Hofmann, J., Spurk, M., Kaiser, K. F., Orcel, C., and Küppers, M., 2004. The 12, 460-year Hohenheim Oak and Pine tree-ring chronology from Central Europe – a unique annual record for radiocarbon calibration and paleoenvironment reconstructions. *Radiocarbon*, **46**, 1111–1122.

Isarin, R. F. B., and Renssen, H., 1999. Reconstructing and modelling Late Weichselian climates: the Younger Dryas in Europe as a case study. *Earth Science Reviews*, **48**, 1–38.

Jennings, A. E., Hald, M., Smith, M., and Andrews, J. T., 2006. Freshwater forcing from the Greenland Ice Sheet during the Younger Dryas: Evidence from southeastern Greenland shelf cores. *Quaternary Science Reviews*, **25**, 282–298.
Kasse, C., 2002. Sandy aeolian deposits and environments and their relation to climate during the Last Glacial Maximum and Lateglacial in northwest and central Europe. *Progress in Physical Geography*, **26**, 507–532.
Li, C., Battisti, D. S., Schrag, D. P., and Tziperman, E., 2005. Abrupt climate shifts in Greenland due to displacements of the sea ice edge. *Geophysical Research Letters*, **32**, doi: 10.1029/2005gl023492.
Lie, Ø., and Paasche, Ø., 2006. How extreme was northern hemisphere seasonality during the Younger Dryas. *Quaternary Science Reviews*, **25**, 404–407.
Liu, Z., Otto-Bliesner, B. L., He, F., Brady, E. C., Tomas, R., Clark, P. U., Carlson, A. E., Lynch-Stieglitz, J., Curry, W., Brook, E., Erickson, D., Jacob, R., Kutzbach, J., and Cheng, J., 2009. Transient simulation of last deglaciation with a new mechanism for Bølling-Allerød warming. *Science*, **325**, 310–314.
Lowe, J. J., Rasmussen, S. O., Björck, S., Hoek, W. Z., Steffensen, J. P., Walker, M. J. C., and Yu, Z. C., 2008. Synchronisation of palaeoenvironmental events in the North Atlantic region during the Last Termination: a revised protocol recommended by the INTIMATE group. *Quaternary Science Reviews*, **27**, 6–17.
Lowell, T. V., and Kelly, M., 2008. Was the Younger Dryas global? *Science*, **321**, 348–349.
Lukas, S., and Benn, D. I., 2006. Retreat dynamics of Younger Dryas glaciers in the far NW Scottish Highlands reconstructed from moraine sequences. *Scottish Geographical Journal*, **122**, 308–325.
Mahaney, W. C., Milner, M. W., Kalm, V., Dirszowsky, R. W., Hancock, R. G. V., and Beukens, R. P., 2008. Evidence for a Younger Dryas glacial advance in the Andes of northwestern Venezuela. *Geomorphology*, **96**, 199–211.
Mangerud, J., Andersen, S. T., Berglund, B. E., and Donner, J. J., 1974. Quaternary stratigraphy of Norden: a proposal for terminology and classification. *Boreas*, **3**, 109–127.
Miller, G. H., 2008. Greenland's elusive Younger Dryas. *Quaternary Science Reviews*, **27**, 2271–2272.
Mix, A. C., Bard, E., and Schneider, R., 2001. Environmental processes of the ice age: land, oceans, glaciers (EPILOG). *Quaternary Science Reviews*, **20**, 627–657.
Rahmstorf, S., 2002. Ocean circulation and climate during the past 120, 000 years. *Nature*, **419**, 207–214.
Rasmussen, S. O., Andersen, K. K., Svensson, A. M., Steffensen, J. P., Vinther, B. M., Clausen, H. B., Siggaard-Andersen, M.-L., Johnsen, S. J., Larsen, L. B., Dahl-Jensen, D., Bigler, M., Röthlisberger, R., Fischer, H., Goto-Azuma, K., Hansson, M. E., and Ruth, U., 2006. A new Greenland ice core chronology for the last glacial termination. *Geophysical Research Letters*, **111**, doi: 10.1029/2005JD006079
Seager, R., and Battisti, D. S., 2007. Challenges to our understanding of the general circulation: abrupt climate change. In Schneider, T., and Sobel, A. (eds.), *The General Circulation of the Atmosphere*. Princeton: Princeton University Press, pp. 331–371.
Seager, R., Battisti, D. S., Yin, J., Gordon, N., Naik, N. H., Clement, A. C., and Cane, M. A., 2002. Is the Gulf Stream responsible for Europe's mild winters. *Quarterly Journal Royal Meteorological Society*, **128**, 2563–2586.
Spielhagen, R. F., Erlenkeuser, H., and Siegert, C., 2005. History of freshwater runoff across the Laptev Sea (Arctic) during the last deglaciation. *Global and Planetary Change*, **48**, 187–207.
Steffen, W., Sanderson, A., Tyson, P. D., Jäger, J., Matson, P. A., Moore, B., III, Oldfield, F., Richardson, K., Schellnhuber, H. J., Turner, B. L., II, and Wasson, R. J., 2004. *Global Change and the Earth System*. Berlin: Springer.
Tarasov, L., and Peltier, W. R., 2005. Arctic freshwater forcing of the Younger Dryas cold reversal. *Nature*, **435**, 662–665.
Teller, J. T., Leverington, D. W., and Mann, J. D., 2002. Freshwater outbursts to the oceans from glacial Lake Agassiz and their role in climate change during the last deglaciation. *Quaternary Science Reviews*, **21**, 879–887.
Thompson Davis, P., Menounos, B., and Osborn, G., 2009. Holocene and latest Pleistocene alpine glacier fluctuations: A global perspective. *Quaternary Science Reviews* **28**, 2021–2033.
Timmermann, A., and Goosse, H., 2004. Is the wind stress forcing essential for the meridional overturning circulation? *Geophysical Research Letters*, **31**, L04303, doi:10.1029/2003GL018777.
Tschudi, S., Ivy-Ochs, S., Schluchter, C., Kubik, P., and Rainio, H., 2000. Be-10 dating of Younger Dryas Salpausselka I formation in Finland. *Boreas*, **29**, 287–293.
Walker, M. J. C., 2005. *Quaternary Dating Methods*. London: Wiley.
Wunsch, C., 2006. Abrupt climate change: an alternative view. *Quaternary Research*, **65**, 191–203.

Cross-references

Alps
Atmospheric Circulation and Glaciochemical Records
Climate Change and Glaciers
Deglaciation
Glacial/Interglacial Cycles
Holocene Glacier Fluctuations
Ice-Dammed Lakes
Palaeoclimate and Past Glaciations
Pleistocene Epoch
Sea Ice

List of Articles

Table 1 List of category "A" articles

Aerial Photogrammetry for Glacial Monitoring	Hydropower: Hydroelectric Power Generation from Alpine Glacier Melt
Alaskan Glaciers	Ice Age
Albedo	Ice Age Cycles: Data, Models, and Uncertainties
Antarctica	Ice Sheet
Atmosphere-Snow/Ice Interactions	Iceland Glaciers
Automated Glacier Mapping	Impacts of Snow and Glaciers on Runoff
Catastrophic Rock Slope Failures and Mountain Glaciers	Isotope Analysis
Characteristics of Snow and Glacier Fed Rivers in Mountainous Regions with Special Reference to Himalayan Basins	Kilimanjaro
Climate Change and Glaciers	LIDAR in Glaciology
Dating Glacial Landforms	Moraine
Digital Elevation Model Generation over Glacierized Region	Natural Hazards Associated with Glaciers and Permafrost
Digital Image Information Extraction Techniques for Snow Cover Mapping from Remote Sensing Data	Optical Remote Sensing of Alpine Glaciers
Dynamics of Glaciers	Periglacial
Epiglacial Morphology	Permafrost
Equilibrium-Line Altitude (ELA)	Permafrost and Climate Interactions
Estuary Ice Cover	Quaternary Glaciation
Frozen Soil Hydrology	Radar Application in Snow, Ice, and Glaciers
Geochemistry of Snow and Ice	Radiative Transfer Modeling
Glacial Erosion	Reconstruction of the Last Glaciations in the Whole of Asia
Glacial Geomorphology and Landforms Evolution	Retreat/Advance of Glaciers
Glacial/Interglacial Cycles	Rock Glaciers
Glaciation During Times of Enhanced/Reduced Atmospheric Carbon Dioxide	Sediment Entrainment, Transport, and Deposition
Glacier Lake Outburst Floods	SEM Analysis of Glacial Sediments
Glacier Mass Balance	Snow Hydrology
Glacier Motion/Ice Velocity	Surface Energy Balance
Glacier Surging	Suspended Sediment Dynamics
Glaciers of the Karakoram Himalaya	Synthetic Aperture Radar (SAR) Interferometry for Glacier Movement Studies
Glaciotectonic Structures, Landforms, and Processes	Temperature Lapse Rates in Glacierized Basins
Global Outlook of Snowcover, Sea Ice, and Glaciers	Till
Greenland Glaciers Outside the Ice Sheet	Topographic Normalization of Multispectral Satellite Imagery
Ground Penetrating Radar Measurements over Glaciers	Transformations of Snow at the Earth's Surface and its Climatic and Environmental Consequences
Himalaya	Urban Snow

Table 2 List of category "B" articles

Ablation Depression
Alps
Altai-Sayan Glaciers
Andean Glaciers
Anisotropic Ice Flow
Appalachian Glacier Complex in Maritime Canada
Arctic Hydroclimatology
Artificial Production of Snow
Atmospheric Circulation and Glaciochemical Records
Basal Sediment Evacuation by Subglacial Drainage Systems
Base Flow/Groundwater Flow
Benchmark Glacier
Biogeochemistry of Sea Ice
Calving Glaciers
Canadian Rockies and Coast Mountains of Canada
Caucasus Mountains
Chemical Composition of Snow, Ice, and Glaciers
Chemical and Microbe Records in Snow and Ice
Chemical Processes in Snow and Ice
Circulation and Mixing in Ice-Covered Lakes
Cirque Glaciers
Climate Variability and High Altitude Temperature and Precipitation
Cold-Based Glaciers
Creep
Crevasses
Cryoconite
Debris
Debris Thermal Properties and Impact on Ice Ablation
Debris-Covered Glaciers
Deglaciation
Degree-Days
Depletion of Snow Cover
Direct Surface Runoff
Discharge/Streamflow
Diurnal Cycle of Runoff
Dry and Wet Snow Line/Zone
Dye Tracer Investigations of Glacier Hydrology
Englacial Processes
Estimation of Glacier Volume and Volume Change by Scaling Methods
Firn
Fjords
Formation and Deformation of Basal Ice
Frequency Analysis of Snow Storms
Frost
GIS in Glaciology
Glacial Drainage Characteristics
Glacial Ecosystems
Glaciations and Groundwater Flow Systems
Glacier Field Studies: Important Things to Notice
Glacier Hydrology
Glaciohydraulic Supercooling
Glaciology
Global Climate Modeling in Cryospheric Assessment
Global Warming and its Effect on Snow/Ice/Glaciers
GPS in Glaciology, Applications
GRACE in Glaciology
Greenland Ice Sheet
Heat and Mass Transfer in Sea Ice
High Elevation Glacio-Climatology
Himalayan Glaciers in 2010 and 2035
Hindu Kush
Holocene Glacier Fluctuations
Hydrochemical Characteristics of Snow, Ice, and Glaciers
Hydrographs
Hydrologic Cycle and Snow
Hydrological Response in Glacierized Basins
Hydrology of Jökulhlaups
Hypsometry
Ice
Ice Age Development Theory
Ice Caves
Ice Core
Ice Covered Lakes
Ice Dams
Ice Sheet Mass Balance
Ice Shelf
Ice-Cored Moraines
Ice-Dammed Lakes
Ice-Marginal Deposition
Ice-Marginal Processes
Ice-Volcano Interactions
ICESat Data in Glaciological Studies
International Polar Year 2007–2008
Inventory of Glaciers
Inverse Methods in Glaciology
Isotopic Characteristics of Ice, Snow, and Glaciers
Isotopic Fractionation of Freezing Water
Kunlun Mountains
Lake Ellsworth
Lake Vostok
Landforms of Glacial Deposition
Landforms of Glacial Erosion
Landforms of Glacial Transportation
Landscapes of Glacial Erosion
Last Glacial Maximum Glaciation (LGM/LGP) in High Asia (Tibet and Surrounding Mountains)
Lateroglacial Landform Systems
Laurentide Ice Sheet
Mapping of Internal Glacial Layers
Mediterranean Glaciers and Glaciation
Melt Runoff Modeling
Melting Processes
Meltwater Channels
Meltwater Erosion
Meltwater Storage
Microorganisms Associated with Glaciers
Monitoring and Warning Systems
Monsoonal Records Observed from Snow/Ice/Glacier
Mount Everest
Mount Kenya
Mountain Geomorphology
New Zealand Glaciers
Normalized-Difference Snow Index (NDSI)
Orographic Precipitation
Palaeo Glaciofluvial Sediment Systems
Palaeo-Ice Stream
Palaeoclimate and Past Glaciations
Pamirs
Papua
Paraglacial Landscape Transformations
Patagonia
Permafrost on Asteroids
Permafrost Modeling
Physical Properties of Snow
Polythermal Glaciers
Precipitation

Table 2 (Continued)

Proglacial Lakes	Solifluction
Rain-Induced Snowmelt	Solute in Glacial Meltwaters
Rating Curve	Stage-Discharge Relationship
Recession of Discharge	Stratigraphy of Snowpacks
River Ice Hydrology	Streamflow Trends in Mountainous Regions
Rocky Mountains	Structural Glaciology
Runoff Generation	Subglacial Borehole Instrumentation
Runoff Observations	Subglacial Drainage System
Scandinavian Glaciers	Subglacial Lakes, Antarctic
Sea Ice	Subglacial Processes
Sea-Level	Summer Accumulation Type Glaciers
Sediment Budgets	Super Cooling Clouds
Sediment Core and Glacial Environment Reconstruction	Supercooled Water
Sediment Flux Source-To-Sink	Surface Temperature of Snow and Ice
Sediment Gravity Flow	Suspended Sediment Concentration
Sediment Transfer Modeling	Talik
Sediment Yield	Temperature Profile of Snowpack
Siberia	Thermal Regime of Ice-Covered Lakes
Snow Cover and Snowmelt in Forest Regions	Thermokarst
Snow Cover Changes in the Alps	Thinning of Arctic Sea Ice
Snow Crystal Structure	Thinning of Glaciers
Snow Deformation	Tibetan Plateau
Snow Depth	Tidewater Glaciers
Snow Gauge	Tien Shan Glaciers
Snow Grains	Tree-Ring Indicators of Glacier Fluctuations
Snow Microstructure	Water Balance in the Glacierized Region
Snow Pit	Westerlies and their Effects on Maritime Ice Caps and Glaciers
Snow and Vegetation Interaction	Younger Dryas
Snow Water Equivalent	

Table 3 List of category "C" articles

Ablatometer
Acidity of Glacier Ice
Active Ice Wedge
Adfreeze
Anabatic Winds: In Relation with Snow/Glacier Basin
Anchor Ice
Anti-Icing
Anti-Syngenetic Ice Wedge
Artificial Ground Freezing
Bed (Bottom) Topography
Bed Forms (Fluvial)
Bed Roughness
Bed Strength
Blue Ice
Bottom Melting or Undermelt (Ice Shelf)
Brash Ice
Cascade Mountains, USA
Cascade System
Catastrophic Flooding
Catchment Glacier
Cloudburst
Cohesion
Condensation Nuclei
Confluence of Rivers
Congelation Ice
Crack
Critical Temperature
Crush
Crust
Cryodessication
Cryofront
Cryogenesis
Cryogenic Aquiclude
Cryogenic Fabric
Cryolithology
Cryopeg
Cryosol
Cryostatic Pressure
Cryostructure
Cryoturbation
Dead Ice
Deposition from Debris-Rich Ice
Distributary Channels
Diverging Ice Flow
Drift Glacier/Ice/Snow
Dry Snow
Elongation Ratio
Englacial Conduit
Environmental Isotopes
Epigenetic Ice
Erosion of Hard Rock Bed
Erosion Rate
Fast Ice
Finger Rafting
Foliation
Forbes Band
Frazil
Freezing Bottom (Ice Shelf)
Freezing Meltwater
Freezing and Thawing Index
Fresh Water Storage
Frictional Melting
Frozen Toe (Outer Zone of Glacier Snout)
Gelisols
Geocryology
Glacial Erratic
Glacial Grooves
Glacial Overdeepening
Glacial Striations
Glacial Trough
Glacier
Glacier Bird of the Andes
Glacier Cave
Glacier Pothole
Glacier Sliding
Glacier System
Glacier Toe
Glacieret
Glacierization
Glacioeustasy
Glaciofluvial
Glaciogenic Deposits
Glacioisostasy
Glaciolacustrine
Glaciomarine
Glaciostatic Pressure/Stress
Granulometry
Gravel Sheet
Gravitational Mass Movement Deposits
Gravity Flow (Mass Flow)
Gray-White Ice
Ground Ice
Horizontal Component of Ablation
Horizontal Component of Velocity
Hummocks (Peat)
Hydrogen Isotopes
Hysteresis
Ice Apron
Ice Caps
Icefall
Icicle
Icing
Interception of Snow
Interflow
Interstitial Ice
Intrusive Ice
Inversion Layers
Inverted Cup Depth Hoar Crystals
Irreducible Water
Isotopic Signatures
Kame and Kettle Topography
Katabatic Wind: In Relation with Snow and Glaciers
Lake Ice
Laminated Sediments
Latent Heat of Condensation
Latent Heat of Fusion/Freezing
Latent Heat of Sublimation
Latent Heat of Vaporization/Condensation
Lateroglacial
Layering of Snow
Little Ice Age
Lobe
Marginal Channel (Lateral Meltwater Channel)
Marginal Ice Zones
Marine Glaciers
Marine Ice Sheet
Mechanical Weathering
Median Elevation of Glaciers

Table 3 (Continued)

Meltwater Conduit
Meltwater Pressure
Moulins
Negative Temperature Gradient (in Ice)
Neoglaciation
Network of Stakes
Niche Glacier
Novaya Zemlya
Nye (N) Channels
Ogives
Outlet Glacier
Overburden Pressure
Oxygen Isotopes
Palaeo-Channel
Palaeohydrology
Pancake Ice
Paternoster Lakes
Peak Flood Glacier Discharge
Percolation Zone
Perennially Frozen Ground
Permacrete
Permanent/Perpetual Snow Line
Piedmont Glaciers
Pingo
Plastic Deformation
Plastic Flow
Pleistocene Epoch
Plucking
Radioactive Fallout
Radioactive Isotopes
Radioactivity
Ram Resistance
Recession Coefficient
Recrystallization of Ice
Refreezing of Meltwater
Regelation
Remobilization (of Debris)
Resedimentation
Rime Ice
Roche Moutonnees
Röthlisberger (R)-Channels
Runoff Coefficient
Runout Distance
Salinity
Saltation
Seasonal Frost
Seasonal Snow Cover
Sediment Routing
Septa of Englacial Debris
Serac
Slush and Sleet of Snow
Snow
Snow Bed/Snow Bed Vegetation
Snow Course
Snow Density
Snow Drift
Snow Layer
Snow Load
Snow Metamorphism
Snow Pellet
Snow Pillow
Snow Ripening
Snow Skating
Snow Skiing
Snow Storm
Snowboard
Solutes in Glacier Ice
Specific Melt Rate
Stable Isotopes
Stationary Glacier
Subglacial Volcanism
Subglacial Weathering
Sublimation from Snow and Ice
Supra-Glacial Debris Entrainments
Suspended Sediment Load
Tarn
Temperate Glaciers
Terminus
Terraces
Thaw Weakening
Thermal Infrared Sensors
Transient Snowline
Tributary Glaciers
U-Shape Valley
Vein Ice
V-Shaped Valley
WGMS (World Glacier Monitoring Service)
Winter Accumulation Glacier
Year-Round Ablation Pattern

Author Index

Subject Index